PROCEEDINGS

ASNR 2013

NEURORADIOLOGY FOR THE 21ST CENTURY

ASNR 51ST ANNUAL MEETING

SAN DIEGO CONVENTION CENTER | SAN DIEGO, CA | MAY 20 - 23, 2013

ASNR 2013

NEURORADIOLOGY FOR THE 21ST CENTURY

Dear ASNR Members, Visitors, and Neuroscience Colleagues:

It is my pleasure to invite you to the ASNR 51ST Annual Meeting in San Diego, California May 18-23, 2013. President-Elect and Program Committee Chair, Mauricio Castillo, MD, FACR, has planned an exciting symposium and intellectually stimulating Annual Meeting scientific program. The 2013 venue, the San Diego Convention Center is truly remarkable. Located on the San Diego Bay right in the heart of the magnificent downtown San Diego, the Convention Center is only steps away from our headquarters hotel, San Diego Marriott Marquis & Marina.

The Foundation of the ASNR Symposium 2013: New Concepts and Trends in Neuroimaging, will explore new and exciting concepts that include genetics of brain tumors, advances in epilepsy imaging, functional connectivity, neurocognitive disorders in children and adults and financial issues in clinical practice.

The 51ST Annual Meeting will provide informative updates on general neuroradiology and showcase specialty programming from the ASFNR, ASHNR, ASPNR, ASSR, and SNIS. As always, the heart of the meeting will be the invited lectures, original presentations, scientific posters, and educational exhibits.

There will be approximately 34.5 hours of continuing medical education credit available for the ASNR 51ST Annual Meeting (See pages XIV for details). We continue offering Maintenance of Certification (MOC) and Self Assessment Modules (SAM) with interactive audience response technology. We will again feature valuable non-CME "How To Sessions" sponsored by our commercial partners, updating you on the capabilities and use of their hardware and software.

This year, I am also thrilled to introduce a new series of lectures, CSI: San Diego (Computer Sciences and Informatics) formally known as Synaptic Junction Programming.

Among its most valuable functions, the Annual Meeting will be the ideal opportunity to stay connected with friends and colleagues and learn the latest in brain, spine, and head and neck imaging.

I look forward to a great meeting and seeing you in San Diego!

Pamela W Schaefer

Pamela W. Schaefer, MD
ASNR President

Pamela W. Schaefer, MD
ASNR President

GET THE ASNR MOBILE MEETING APP!

Scan to download!

Schedule, Maps, Twitter and more on your mobile device - completely free.

Download **Guidebook** on the Apple App Store or Android Marketplace or visit guidebook.com/getit

Search for the 'ASNR' guide under the Download Guides section of the app.

guidebook

guidebook.com

TABLE OF CONTENTS

I - II ..... 2012 - 2013 ASNR Committees

III ..... AJNR/ASNR Staff

IV ..... General Information

V ..... Important Information for Young Professionals

VI ..... Special Programming

VII - VIII ..... 2013 ASNR Gold Medal Award Recipient

IX ..... 2013 ASNR Honorary Member

IX ..... 2013 J. Arliss Pollock Memorial Lecture

X ..... 2013 ASNR Cornelius G. Dyke Memorial Award Recipient

X ..... 2012-2013 Specialty/Regional Society Awards

XI ..... ASNR 2012 Outstanding Presentation Awards

XII ..... 2013 Women in Neuroradiology Leadership Award

XII ..... 2013 The Foundation of the ASNR Research Scientist Award

XII ..... 2013 The Foundation of the ASNR Comparative Effectiveness Award

XII ..... 2013 The Foundation of the ASNR Scholar Award in Neuroradiology Research

XIII ..... 2013 The Foundation of the ASNR Award for Outstanding Contributions in Research

XIV ..... Continuing Medical Education, Accreditation Statement, Credit Designation Statement and Target Audience

XV ..... ASNR 51ST Annual Meeting Educational Objectives

XVI ..... How-To Sessions

XVII ..... Technical Exhibition Floor Plan

XVIII ..... Technical Exhibition Roster

XIX - XXII ..... Scientific Program Overview

XXIII ..... ASNR Future Annual Meetings

Page 1 - 103 ..... Monday Sessions

Page 104 - 193 ..... Tuesday Sessions

Page 194 - 249 ..... Wednesday Sessions

Page 249 - 335 ..... Thursday Sessions

Page 335 - 395 ..... Electronic Excerptas (EE)

Page 395 - 468 ..... Scientific Posters (P) Printed

Page 468 - 654 ..... Electronic Posters (eP)

Page 654 - 704 ..... Education Exhibits (EdE) Printed

Page 704 - 805 ..... Electronic Education Exhibits (eEdE)

Page 806 - 843 ..... Index of Program Participants

2012-2013 ASNR COMMITTEES

Executive Committee

Pamela W. Schaefer, MD
President

Mauricio Castillo, MD, FACR
President-Elect/Program Chair

Gordon K. Sze, MD
Vice President

Laurie A. Loevner, MD
Treasurer

Jacqueline A. Bello, MD
Secretary & AMA Alternate Delegate, ACR Alternate Representative and ACR Neuro Committee Representative

Pratik Mukherjee, MD, PhD
Research Committee Co-Chair

Pina C. Sanelli, MD, MPH
Research Committee Co-Chair & Evidence Based Medicine Chair

Daniel P. Barboriak, MD
Functional Representative

C. Douglas Phillips, MD, FACR
Head and Neck Representative

Philip M. Meyers, MD
Neurointerventional Surgery Representative

Dennis Shaw, MD
Pediatric Representative

Allan L. Brook, MD
Spine Representative

David B. Hackney, MD, FACR
1st Past President & Parliamentarian

Carolyn Cidis Meltzer, MD, FACR
2nd Past President & ACR Neuro Commission Liaison

John R. Hesselink, MD, FACR
3rd Past President

Robert M. Barr, MD, FACR
Health Policy Chair, Member-At-Large & ACR Representative

Suresh K. Mukherji, MD, FACR
Fellowship Director Chair

Mark E. Mullins, MD, PhD
Education Committee Chair

Adam E. Flanders, MD
Rules Committee Chair

Tina Young Poussaint, MD
Publication Committee Chair

Michele H. Johnson, MD
Membership Committee Chair

Steven Falcone, MD
Delegate to the AMA

James B. Gantenberg, FACHE
ASNR Executive Director/CEO & Commercial Relations Chair

Dikoma C. Shungu, PhD
Research Scientist Chair

Jaime F. Mata, PhD
Research Scientist Representative

Vincent P. Mathews, MD
ABR Trustee (1st)

Robert D. Zimmerman, MD, FACR
ABR Trustee (2nd)

Michael Tyszka, PhD
Physicist Advisor

Nafi Aygun, MD
Physicist Advisor

Vinil N. Shah, MD
Member-In-Training

Howard A. Rowley, MD
Chairman, The Foundation of the ASNR

Pia Maly Sundgren, MD, PhD
International Representative

Program Committee

Mauricio Castillo, MD, FACR
President-Elect/Program Chair

Jacopo Annese, PhD
Robert M. Barr, MD, FACR
Walter S. Bartynski, MD
Norman J. Beauchamp, Jr., MD
Jacqueline A. Bello, MD
Allan L. Brook, MD
Harry J. Cloft, MD, PhD
Colin P. Derdeyn, MD
Girish M. Fatterpekar, MBBS, DNB, MD
Nancy J. Fischbein, MD
John L. Go, MD
P. Ellen Grant, MD
Christopher P. Hess, MD, PhD
Nickoleta L. Hoefling, MD
David F. Kallmes, MD
Lucien M. Levy, MD, PhD
Weili Lin, PhD
Philip M. Meyers, MD
Michelle A. Michel, MD
Suresh K. Mukherji, MD, FACR
Mark E. Mullins, MD, PhD
Thomas P. Naidich, MD
Alexander M. Norbash, MD
A. Orlando Ortiz, MD, MBA, FACR
C. Douglas Phillips, MD, FACR
Whitney B. Pope, MD, PhD
Tina Young Poussaint, MD
Robert M. Quencer, MD
Noriko Salamon, MD
Pina C. Sanelli, MD, MPH
Pamela W. Schaefer, MD
Dennis Shaw, MD
A. Gregory Sorensen, MD
Gordon K. Sze, MD
Chip Truwit, MD
Gregory G. Zaharchuk, MD, PhD

Technical Exhibits Committee

A. Orlando Ortiz, MD, MBA, FACR
Chair

Todd Abruzzo, MD
William G. Bradley, MD, PhD, FACR
Joseph P. Comunale, Jr., MD
Thomas S. Dina, MD
Steven Falcone, MD
John L. Go, MD
Andrei I. Holodny, MD
Timothy J. Kaufmann, MD
Meng Law, MD, MBBS, FRACR
Gregg H. Zoarski, MD

2012-2013 ASNR COMMITTEES

Audio Visual Committee

Edward A. Michals, MD
Chair
Erin Simon Schwartz, MD
Consultant
Andrew G. Bleicher, MD
James Y. Chen, MD
Steven W. Hetts, MD
Jenny K. Hoang, MBBS
Timothy J. Kaufmann, MD
Amy L. Kotsenas, MD
Lucien M. Levy, MD, PhD
Mark E. Mullins, MD, PhD
Hemant A. Parmar, MD
Stuart R. Pomerantz, MD
Frank C. Tong, MD
Achala S. Vagal, MD
Max Wintermark, MD

Education Exhibits Committee

Dheeraj Gandhi, MD
Chair
Stephen Gebarski, MD
Consultant
Ellen G. Hoeffner, MD
Consultant
Ashley H. Aiken, MD
Sameer A. Ansari, MD, PhD
Nafi Aygun, MD
Kathleen A. Barry, MD
Timothy J. Biega, MD
Mary E. Cunnane, MD
Lawrence E. Ginsberg, MD
Ajay Gupta, MD
Benjamin Y. Huang, MD, MPH
Gaurav Jindal, MD
Sangam G. Kanekar, MD, DNB
Rihan Khan, MD
Robert E. Morales, MD
Susan Palasis, MD
Gregory W. Petermann, MD
Jordan M. Prager, MD
Otto Rapalino, MD
Amit M. Saindane, MD
Haris Sair, MD
Gaurang V. Shah, MD
James G. Smirniotopoulos, MD
Maria Vittoria Spampinato, MD
Ashok Srinivasan, MD
Christopher P. Wood, MD
Geoffrey Young, MD

Education Committee

Mark E. Mullins, MD, PhD
Chair
Achala S. Vagal, MD
Vice-Chair
Barton F. Branstetter IV, MD
Consultant
Ashley H. Aiken, MD
Nafi Aygun, MD
Daniel P. Barboriak, MD
Jacqueline A. Bello, MD
Eric C. Bourekas, MD
Jerrold Boxerman, MD
Richard A. Bronen, MD
Dale A. Charletta, MD
Falgun H. Chokshi, MD
Rebecca S. Cornelius, MD
H. Christian Davidson, MD
Richard K. Downs, Sr., MD
Edward J. Escott, MD
Nikdokht Farid, MD
Adam E. Flanders, MD
Melanie B. Fukui, MD
John L. Go, MD
David B. Hackney, MD, FACR
Jenny K. Hoang, MBBS
Chad A. Holder, MD
Steven G. Imbesi, MD
Alisa Kanfi, MD
Andrew Ku, MD
Meng Law, MD, MBBS, FRACR
Laurie A. Loevner, MD
Michael Lubarsky, MD
David S. Martin, MD
Bruce McCandliss, PhD
Gary M. Miller, MD
Gul Moonis, MB, BS
Christopher J. Moran, MD
Toshio Moritani, MD, PhD
Suresh K. Mukherji, MD, FACR
Gerard J. Muro, MD
C. Douglas Phillips, MD, FACR
Edward P. Quigley, III, MD, PhD
Karen L. Salzman, MD
Pina C. Sanelli, MD, MPH
Pamela W. Schaefer, MD
David J. Seidenwurm, MD, FACR
Dennis Shaw, MD
James G. Smirniotopoulos, MD
Jay Starkey, MD
Apostolos John Tsiouris, MD
Achala S. Vagal, MD
Richard H. Wiggins, III, MD, CIIP
Christopher P. Wood, MD
Robert D. Zimmerman, MD, FACR

AJNR STAFF

American Journal of Neuroradiology
Headquarters Office
800 Enterprise Drive, Suite 205
Oak Brook, IL 60523-4216
Telephone: 630-574-1487
Fax: 630-786-6251
Website: http://www.ajnr.org

Karen Halm
Managing Editor
Ext. 238, khalm@asnr.org

Jason Gantenberg
Electronic Publications Manager
Ext. 240, jason@asnr.org

Mary Harder
Editorial Assistant
Ext. 239, mharder@asnr.org

ADDITIONAL EMAIL ADDRESSES

Communications
communications@asnr.org

Economics & Health Policy
healthpolicy@asnr.org

Executive
executive@asnr.org

Finance
finance@asnr.org

Foundation
foundation@asnr.org

Meetings
meetings@asnr.org

Membership
membership@asnr.org

ASNR STAFF

American Society of Neuroradiology
Headquarters Office
800 Enterprise Drive, Suite 205
Oak Brook, IL 60523-4216
Telephone: 630-574-0220
Fax: 630-574-0661
Website: http://www.asnr.org

James B. Gantenberg, FACHE
Executive Director/CEO
Ext. 224, jgantenberg@asnr.org

Arthur An
Educational Technologist
Ext. 241, aan@asnr.org

Angelo Artemakis
Director of Communications and Media Management
Ext. 227, aartemakis@asnr.org

Kenneth Cammarata
Director of Specialty Societies and Member Services
Ext. 226, kcammarata@asnr.org

Tina Cheng, CPA
Director of Finance and Information Systems
Ext. 225, tcheng@asnr.org

Michelle Davies
Meetings & Logistics Assistant
Ext. 232, mdavies@asnr.org

Patricia G. Bingham
Staff Accountant
Ext. 222, pat@asnr.org

Valerie Geisendorfer, CMP
Senior Manager of Scientific Meetings
Ext. 228, vgeisendorfer@asnr.org

Kristine Kulpaka
Membership/Society Coordinator
Ext. 234, kkulpaka@asnr.org

Karen Mansfield
Office Manager/Executive Assistant
Ext. 221, kmansfield@asnr.org

Michael Morrow, MBA
Director of Economics & Health Policy
Ext. 233 , mmorrow@asnr.org

Kelsey Pliner
Meetings Registrar
Ext. 231, kpliner@asnr.org

Lora Di Padova-Tannehill, CMP
Director of Scientific Meetings
Ext. 229, ltannehill@asnr.org

Stephanie Walsh, MBA
Director of Development
Ext. 235, swalsh@asnr.org

GENERAL INFORMATION

Meeting Location

San Diego Convention Center
111 West Harbor Drive
San Diego, CA 92101
619-525-5000

Meeting Registration

Registration is located in the Sails Pavilion of the San Diego Convention Center. The registration desk will be open during the following hours:

Friday, May 17 ..... 5:00 pm - 8:00 pm

Saturday, May 18 through Thursday, May 23 ..... 6:30 am - 6:00 pm

Speaker Ready Room Location & Hours

Room 3 (Upper Level)

Friday, May 17 ..... 5:00 pm - 8:00 pm

Saturday, May 18 through Thursday, May 23 ..... 6:00 am - 6:00 pm

Name Badges

Please wear name badges at all times while you are attending the scientific sessions, social programs, and technical exhibits. Badge colors are identified as follows:

ASNR Members, ASNR Members-In-Training & ASNR Specialty Societies (ASFNR, ASHNR, ASPNR, ASSR & SNIS) ..... Blue
Non-Member ..... Green
Other Professional ..... Yellow
Guest ..... Peach
Exhibitor ..... Gold
Staff ..... Purple

Emergency Service Procedure

STEP 1

SAN DIEGO CONVENTION CENTER

In the event of a medical emergency, please contract Security Control immediately. ASNR attendees may contact Security Control by dialing

- Extension **5911** for life threatening emergency on facility house phones (white in color)
- Extension **5490** for non-life threatening emergency on facility house phones (white in color)
- From a cell phone (or outside the center) dial: **619-525-5911** for life threatening emergency, **619-525-5490** for non-life threatening emergency

*All house phones in San Diego Convention Center are white in color and are located in public corridors and lobbies throughout the center, Security Control will be dispatched directly to your location.

SAN DIEGO MARRIOTT MARQUIS & MARINA HOTEL

In the event of a medical emergency, please contract Security Control immediately. ASNR attendees to contact Security Control by dialing

- Extension **53** for life threatening emergency on facility house phones (beige in color)
- Extension **6100** for non-life threatening emergency on facility house phones (beige in color)
- From a cell phone (or outside the hotel) dial **619-234-1500** and ask for ext **53**

*All house phones in San Diego Marriott Marquis & Marina are beige in color and located throughout all public areas and hallways, Security Control will be dispatched directly to your location.

STEP 2

The caller should provide the following:

1. Determine name of specific meeting room or exhibit hall where the situation has occurred.
2. Identify yourself as an ASNR attendee, reference your exact location, and provide details on the nature of the emergency situation.
3. Provide a brief but concise description of the problem, be prepared to answer any questions that the operator may ask you, and remain on the line.

ASNR Publications Booth: *Lobby 6*

Saturday, May 18 and Sunday, May 19: **7:30 am - 5:00 pm**

Monday, May 20 through Thursday, May 23: **8:30 am - 5:00 pm**

All attendees are invited to stop by the booth any time to tour the AJNR and Neurographics Web sites and AJNR Blog and app.

ASNR Publications

Dr. Mauricio Castillo, *AJNR*'s Editor-in-Chief, will be present at the Journal's booth Monday - Thursday from 11:00 am until noon to answer questions regarding the Journal's online features, listen to suggestions, talk about projects with prospective authors, and advise fellows regarding their future contributions to *AJNR*.

Neurographics

Neurographics is ASNR's quarterly online educational journal, featuring peer-reviewed scientific exhibits and select case reports. *Neurographics* is available free online www.neurographics.org. *Neurographics* Editor Dr. Barton Branstetter IV will be available in the ASNR Publications booth Monday through Wednesday from 11:00 am to noon to answer questions.

EXHIBITS

Scientific Posters, Electronic Posters, Electronic Excerptas, Education Exhibits, and Electronic Education Exhibits

Hall B1 (Ground Level)

Technical Exhibits

Sails Pavilion (Upper Level)

MISCELLANEOUS

How-To Sessions

Ballroom 6AB (Upper Level)

Young Professionals Lounge

Room 16AB (Mezzanine Level)

VIP/The Foundation of the ASNR Donor Lounge

Room 14B (Mezzanine Level)

IMPORTANT INFORMATION FOR YOUNG PROFESSIONALS

(Fellows, Residents, Medical Students and Neuroradiologists in their first three years in practice)

Young Professionals Lounge

Saturday, May 18 - Thursday, May 23, 2013 6:30 am - 6:00 pm

Room 16AB (Mezzanine Level)

Visit the Young Professional Lounge in Room 16AB (Mezzanine Level) open from 6:30 am – 6:00 pm daily from Saturday, May 18 - Thursday, May 23. This will provide a "home base" for Young Professionals to network and share knowledge and experiences throughout the meeting.

Young Professionals Luncheon

Tuesday, May 21 • 12:15 pm - 1:15 pm

Room 16AB (Mezzanine Level)

Join ASNR Leaders for Lunch, at 12:15 pm on Tuesday, May 22, 2013 in Room 16AB (Mezzanine Level).

Young Professionals Sessions

Fellows, Residents, Medical Students and Neuroradiologists in their first three years in practice, the ASNR has designed specific program topics for learning during the ASNR Annual Meeting. You won't want to miss the following session presentations:

Tuesday, May 21

Room 1AB

8:45 am – 10:15 am
Choosing Your Career

Benefits of Academic Medicine
Eric J. Russell, MD, FACR

Benefits of Private Practice
Bidyut K. Pramanik, MD

Negotiating a Position in Academic Medicine: What You Need to Know
Suresh K. Mukherji, MD, FACR

Negotiating a Contract in Private Practice: What You Need to Know
Robert M. Barr, MD, FACR

Why I Did What I Did and Did I Make The Right Decision?
David J. Seidenwurm, MD, FACR

1:15 pm – 2:45 pm
Basics Session: Head and Neck Post-Treatment Imaging

Post Treatment Larynx: The Basics
Suresh K. Mukherji, MD, FACR

Anatomy, Pathology and Post-Treatment Appearance of the Skull Base: The Basics
Stephen E. J. Connor, MB, ChB MRCP, FRCR

Post-Treatment Sinus: The Basics
Varsha M. Joshi, MD

5:00 pm – 6:30 pm
Creating a New Service: How You Can Add Value to Your Practice

MR Spectoscopy
Lara A. Brandao, MD

fMRI
Guarang V. Shah, MD

CT Perfusion
Max Wintermark, MD

MR Perfusion
Michael T. Preece, MD

DTI and Tractography
Neeraj B. Chepuri, MD

SPECIAL PROGRAMMING

2013 Education Exhibits Tour

San Diego Convention Center
Hall B1 (Ground Level)

Monday, May 20 .....12:15 pm – 1:15 pm

Wednesday, May 22 .....12:15 pm – 1:15 pm

You will receive CME credits for participating in the Education Exhibits Tour!

Review Education Exhibits, visual presentation/educational displays designed to further the understanding of Neuroradiology by featuring cutting-edge material or by offering an instructional review of a particular topic. The session will allow for review of visually-oriented educational displays that demonstrate novel and innovative applications for computers in Neuroradiology clinical practice, training and research. Share this educational opportunity with your colleagues and primary Exhibit presenters and exchange in a lively Questions & Answers Session.

Another unique feature not to be missed at the ASNR. See you on the tour!

Case of the Day

San Diego Convention Center
Hall B1 (Ground Level)

Monday, May 20 through Wednesday, May 22

A continuing addition to the ASNR program for the ASNR 51st Annual Meeting is the Case of the Day (COD) program. Led by Drs. Mark Mullins and Achala S. Vagal, COD is scheduled from Monday, May 20 through Wednesday, May 22.

Cases will be presented in Hall B1 at the San Diego Convention Center and will be available in printed poster format as well as on a video loop at a nearby monitor. There will be 6 categories: brain, functional, head & neck, pediatric, spine and vascular/interventional, each with 1 case per day. Answers will be presented on the day following their respective questions.

An online system will be available for submission of preferred diagnoses (links are available through the ASNR Annual Meeting Mobile Application). Be sure to participate in this new interactive programming feature with a limited number of prizes awarded to those participants with highest daily correct responses.

No CME credit is available for this activity.

Annual Meeting Closing Reception

USS Midway Museum in Downtown San Diego

Wednesday, May 22, 2013 ..... 7:00 pm-10:00 pm

Harbored in the serene waters of San Diego Bay is the impressive USS Midway Museum which is the venue for the night's grand event. This is within walking distance from the San Diego Convention Center and the San Diego Marriott Marquis & Marina, the ASNR headquarters hotel.

Largely unaltered from the USS Midway's original operating state, guests can expect a truly genuine experience from the time they enter the ominous hangar bay. Many different exhibits throughout the carrier document her long and proud military service. You will also enjoy everything from docent led mini tours, to flight simulator rides, to a pre-dinner buffet reception on the flight deck. A variety of food and beverage stations will be available to tantalize your taste buds. We look forward to you joining us and experiencing the USS Midway's military tradition while networking and mingling with ASNR meeting attendees and exhibitor representatives throughout the evening's event.

Complimentary round-trip transportation to and from the USS Midway Museum will be provided. Badge required for entry.

CSF Flow Group

San Diego Convention Center
Room 10 (Upper Level)

Thursday, May 23 and Friday, May 24, 2013

The IHIWG (International Hydrocephalus Imaging Working Group) consists of neuroradiologists, neurologists, neurosurgeons, bioengineers, and basic scientists who meet twice a year in conjunction with ASNR and ISHCSF (International Society for Hydrocephalus and CSF Disorders). During our meeting we address all forms of hydrocephalus including DESH (Disproportionately Enlarged Subarachnoid Space Hydrocephalus) with emphasis on imaging NPH. We discuss phase contrast techniques to measure blood and CSF flow out of the brain and to dynamically model it and predict intracranial pressure. We review CSF production and resorption, role of aquaporins, and CSF flow measurements to study Chiari I malformations as well as potential sources of error in our measurements.

We discuss infantile hydrocephalus and benign external hydrocephalus and the role of the latter as a potential cause of NPH later in life. We examine changes in DTI and MR elastography in NPH and discuss related topics such as aqueductal stenosis and pseudotumor cerebri. We debate the value of imaging vs. detailed clinical assessment vs. a high volume tap test vs. saline infusion tests to select NPH patients for shunting.

No CME credit is available for this activity.

AWARDS AND HONORS

ASNR Gold Medal Award

The Gold Medal is intended to foster the highest standards of the American Society of Neuroradiology, recognizing exceptional service and achievement. The Medal is awarded on the basis of both professional and personal excellence, honoring individuals who are superb neuroradiologists, scientists, and/or physicians, and who also are truly outstanding people. Recipients will have consistently extended themselves beyond self-interest to make contributions that have benefited our entire field. The receipts are individuals who are clinicians, researchers, teachers, or neuroradiological statesmen and stateswomen may be considered for the Gold Medal. Candidates are not required to be members of the American Society of Neuroradiology. Nominees should have made extra-ordinary contributions to enhance the development and/or stature of neuroradiology, including service to the Society.

The recipient of the 2013 award is:

Eric J. Russell, MD, FACR

Northwestern University, Chicago, IL

Eric Jay Russell, MD, FSIR, FACR is a Professor of Radiology, Neurosurgery and Otolaryngology at the Feinberg School of Medicine of Northwestern University.

After graduation from Brooklyn College (City University of New York), he attended medical school in Buffalo, where he received the MD degree in 1974 (elected to Alpha Omega Alpha in his junior year). He then returned to New York City and to the Montefiore Hospital and Medical Center and served as an intern in Internal Medicine before completing his residency in Radiology under Harold Jacobson, his role model, Robert D. Zimmerman, who remains a close friend, and Norman Leeds and Thomas Naidich. As a fellow in Neuroradiology at NYU under the direction and guidance of Irvin I. Kricheff, with mentors including Norman Chase, Thomas Bergeron, Richard Pinto and Ajax George, he chose to work closely with Alex Berenstein, who had just arrived at NYU the year before. Interventional Neuroradiology was truly in its infancy in the US, and Alex's commitment and dedication to his patients strongly influenced Dr. Russell to continue this work.

Dr. Russell, as a junior attending in Chicago, benefitted greatly from the mentorship and support of Dr. Michael Huckman, who hired him for his first faculty position, at Rush-Presbyterian-St. Luke's Hospital. With his guidance, Dr. Russell was able to develop an Interventional Neuroradiology service along with his diagnostic responsibilities, as he began his academic career.

Six years later, Dr. Russell was recruited by Lee F. Rogers to become the Director of Neuroradiology at Northwestern across town. For 25 years, Dr. Russell was the director of the Division and also the Neuroradiology fellowship program, helping to recruit and train more than 60 fellows. In the 1990's, Dr. Russell twice served as interim Chair of the Department, before being named the Frederick John Bradd and William Kennedy Professor of Radiology and Chairman of the Department of Radiology at Northwestern University in 2002. During his time as Chair, the department doubled its faculty and its research portfolio. He has advocated for a strong clinical practice in Interventional Radiology, supporting the growth of an internationally recognized IR division and developing an outreach program to provide IR and neurointerventional services at local community hospitals. During a recent medical school leadership transition, he served as Interim President and CEO of the Northwestern Medical Faculty Foundation (NMFF), an academic practice plan with more than 700 full-time physicians, completing this term in 2011 and returning to Chair the Radiology Department a year ago. Dr. Russell has served Neuroradiology at many levels. A long-time board examiner for the ABR, he served on the examiner panel for the first CAQ examination in 1995, and currently serves on the CAQ/MOC examination preparation committee. He served as Scientific Program Chair for Neuroradiology at the annual meeting of the RSNA for several years, and currently serves as the RSNA representative to the Joint Commission Ambulatory Care Committee. He is an ACR fellow, served as editor-in-chief of the Neuroradiology II ACR Syllabus, was a member of the Illinois delegation to the ACR council, and is a long-term member the ACR Standards and Guidelines Committee, serving as lead author for the ACR Guideline for Cervicocerebral Angiography, recently revised.

His service to the ASNR is extensive; serving on numerous committees, and holding several offices including president-elect and program chairman for the 1999 ASNR meeting in San Diego. Importantly, the Ad Hoc Committee for the 1999 Annual Meeting which he chaired, recommended structural changes that were incorporated that year to strengthen the unity of the subspecialty societies by providing for formal input and direction from the sub-specialty societies into the meeting program, a structure that still is in place today.

Dr. Russell was installed as the 37th President of the ASNR on May 25, 1999 at the society's annual meeting in San Diego, and served his term as the 21st century began. Among other accomplishments, he worked with others to establish an ACGME approved neurointerventional training program acceptable to both Radiology and Neurosurgery, and he further supported the efforts of Arliss Pollock, Chair of the ASNR Clinical Practice Committee, to more fully involve the ASNR in socioeconomic activities. Seeing the need for close communication with interventional radiologists, he sat as a member of the SCVIR (now SIR) Executive Council for three years to facilitate communication, guideline development and joint planning. He was elected to fellowship in the SCVIR in 2000. Dr. Russell has served on the editorial boards of Radiology and the AJNR, currently serving a second term on the Radiology board. Dr. Russell also served a three year term as Chairman of the Board on the Neuroradiology Research and Education Foundation (NERF), and helped to shepherd it through the financial crisis of 2008-9. Dr. Russell's fascination with all aspects of the specialty accounts for the breadth of his academic focus, covering the spectrum of our specialty, with more than 140 peer-reviewed publications. Many have an interventional focus (including a highly cited early publication in AJNR on Functional Neuroangiography, stemming from his mentorship by Alex Berenstein and Pierre Lasjaunias while at

AWARDS AND HONORS

ASNR Gold Medal Award (Continued)

NYU). Early work on high resolution CT of the temporal bone, employing one of the first high-resolution CT algorithms (developed by Manlio Abele at NYU), stimulated his interest in Head and Neck Imaging, with subsequent publications that include the first anatomic/pathologic CT imaging study of the lacrimal drainage apparatus. His experience in CT of the head and neck led to his observation that enhancement was common at the margins of cervical disk herniations, improving their conspicuity. His investigations of the anatomical substrates of this enhancement in cadavers led to publications in Radiology, including the first in the US on contrast enhanced CT of the cervical spine in degenerative disease, and subsequently a "state of the art" article in Radiology on Imaging of the Cervical Spine. He was also an early clinical investigator for the pre-approval safety and efficacy trial of the first contrast agent for MR use, gadolinium-DTPA. His success as a local PI led to a first author publication on the Phase II placebo controlled clinical trial of Gd-DTPA (Magnevist), in Radiology. With material collected from the trial, he was one of the first to statistically prove the advantages of contrast-enhanced MRI for detecting cerebral metastases, at a time when many were skeptical that contrast-enhancement was necessary for MRI.

Dr. Russell has been married for more than 30 years to Sandra K. Fernbach, MD, a prominent academic pediatric radiologist who he met during his residency at Montefiore, recently retired. They have two wonderful girls, Gabrielle Robin, an intellectual properties lawyer in NYC and Meredith Jean, a research coordinator in the Department of Pediatrics, Pediatric Oncology practice, at the University of New Mexico Hospitals, married to Andrew Millard, an engineer at Sandia National Laboratory. The Russell's live in the Lincoln Park/Gold Coast area in downtown Chicago.

ASNR 2013

NEURORADIOLOGY FOR THE 21ST CENTURY

AWARDS AND HONORS

ASNR Honorary Member

Dr. Valery N. Kornienko has had a long career as a neuroradiologist in Moscow, Russia. Dr. Kornienko received his internal medicine degree from the Rostov-Don Medical Institute in 1959, and did a postgraduate course in neurosurgery and neuroradiology from 1962-1964. He then spent three years in a Fellowship at Burdenko Neurosurgery Institute, Moscow. Since 1980 he has served as Head of Neuroradiology at Burdenko Neurosurgery Institute, RAMS, Moscow. He has been Professor since 1985.

He has over 500 academic publications and 15 books. His most recent book is a three volume 1288 page textbook titled "Diagnostic Neuroradiology" and was published in 2009 by Springer, in English language. This work was awarded the Burdenko Prize by the Russian Academy of Medical Sciences in 2010. He was also awarded a State Prize for "The development and introduction of the pathogenic methods of diagnosis, prognosis and treatment of traumatic brain injury and its consequences" (1995), and in 2007 the Prize of the Government of the Russian Federation for "Development and implementation of a practice complex reconstructive techniques and minimally invasive neurosurgery in times of peace and military conflict".

This summer the Russian Society of Neuroradiology was founded, and Professor Kornienko was elected the Founding President of the Society.

The recipient of the 2013 award is:

Valery N. Kornienko, MD, PhD

Burdenko Neurosurgery Institute, Moscow, Russia

ASNR J. Arliss Pollock Memorial Lecture

The Pollock Memorial lecture is held in honor of J. Arliss Pollock, MD, a pioneering neuroradiologist who led the ASNR socio-economic and health policy programs for fifteen years. A true visionary, he was one of the first physicians to specialize in neuroradiology in California and the first to introduce cerebral angiography into a community based practice. We are indebted to him for his willingness to carve out a presence for the ASNR in the area of socioeconomics and health policy at a national level. He led the ASNR health policy efforts at the AMA CPT Editorial Panel Advisory Committee and the Relative Value Scale Update Committee (RUC). These highly influential multi-specialty committees create codes for new technologies and procedures and develop values that set the physician reimbursement rates. He served as a liaison to the ACR and AMA and many other societies when consensus was needed. In 2001, he received the ASNR's highest award, the Gold Medal. We dedicate a health policy lecture each year to recognize his exceptional leadership and commitment to neuroradiology.

The presenter of the 2013 lecture is:

Dieter R. Enzmann, MD

David Geffen School of Medicine at UCLA, Los Angeles, CA

"Radiology Value Chain"

Presentation Time: **Tuesday, May 21 - 1:25 pm - 1:50 pm**

Location: **Ballroom 6DE**

AWARDS AND HONORS

ASNR Cornelius G. Dyke Memorial Award

This award was established to honor Cornelius G. Dyke, one of the pioneers in neuroradiology, and is given to a trainee or junior faculty member in neuroradiology for excellence as demonstrated in a paper, which represents original, unpublished research in some aspect of neuroradiology.

The recipient of the 2013 award is:

Presentation Time: **Thursday, May 23 - 10:45am - 10:53am**

Location: **Ballroom 6DE**

Hediyeh Baradaran, MD

Weill Cornell Medical College, New York, New York

"Metabolic Reserve and Stroke Risk in Patients with Carotid Stenosis or Occlusion: A Systematic Review and Meta-Analysis"

Dr. Hediyeh Baradaran is a radiology resident at New York Presbyterian Hospital/Weill Cornell campus. She graduated from Weill Cornell Medical College and completed her internship at the University of Utah Medical Center. Her current research interests include imaging in patients with carotid atherosclerotic disease.

2012-2013 Specialty/Regional Society Awards

The American Society of Neuroradiology is pleased to announce the recipients of the 2012/2013 Special/Regional Society Awards. These individuals were selected by the respective societies as having the best presentation at each society's most recent Annual Meeting.

American Society of Spine Radiology (ASSR) (Mentor Award)

"Diffusion-weighted MRI (DWI) 'claw sign' is Useful in Differentiation of Infectious from Degenerative Modic I Signal Changes of the Spine"

Keyur Patel, MD
The Mount Sinai Medical Center, New York, NY

Eastern Neuroradiological Society (ENRS) (The Norman E. Leeds Award)

"Evaluating CT Perfusion Using Outcome Measures of Delayed Cerebral Ischemia in Aneurysmal Subarachnoid Hemorrhage"

Jana Ivanidze, MD
Weill Cornell Medical College, New York, NY

Southeastern Neuroradiological Society (SENRS)

"Functional Neuroimaging to Characterize the Effect of Chemotherapy on Visual System Development in Children Treated for Retinoblastoma"

Kathleen J. Helton, MD
St. Jude's Children's Research Hospital, Memphis, TN

Western Neuroradiological Society (WNRS) (The Gabriel H. Wilson Award)

"Direct Puncture Treatment of Orbital & Peri-orbital Vascular Malformations"

Gary M. Nesbit, MD
Oregon Health & Science University, Portland, OR

AWARDS AND HONORS

ASNR 2012 Outstanding Presentation Awards

ASNR is pleased to announce the winners of the Outstanding Presentation Awards. The overall quality of the paper and poster presentations at the New York meeting was excellent, and the winners should be commended for their outstanding work. A $1,000 award will be given to the primary author of each winning presentation.

Seven awards were presented in Six categories: in *Adult Brain/General Neuroradiology* (two awards, one awarded by the ASNR, and another awarded by The Foundation of the ASNR), *Functional Neuroradiology, Head and Neck, Interventional* (The Michael Brothers Memorial Award), *Pediatrics* (The Derek Harwood-Nash Award), and *Spine*. Both awards in Adult Brain/General Neuroradiology were selected by a panel of ASNR members under the direction of the Education Committee. The five subspecialty awards were judged by panels selected from each of the specialty societies, including ASFNR, ASHNR, ASPNR, ASSR, and SNIS. We would like to thank all of the judges for their tremendous effort in evaluating the presentations. Congratulations to the winners!

General Neuroradiology

(on behalf of the ASNR)

Paper 37: Cerebrovascular and Functional MR Imaging with the Blood Pool Agent Ferumoxytol: Initial Experience in Normal Subjects

Zaharchuk, G. • Christen, T. • Qiu, D. iNi, W. • Schmiedeskamp, H. • Bammer, R. • Moseley, M.E.

(Stanford University, Stanford, CA)

General Neuroradiology

(on behalf of The Foundation of the ASNR)

Paper 98: Imaging Genomic Mapping in Glioblastoma Multiforme: A Novel Quantitative Merge between Imaging and Genomics. The Creation of a Signature for Tumor Necrosis Using Image Genomic Analysis in 12,764 genes and 555 microRNAs

Colen, R.R.[1] • Mahajan, B.[1] • Bruyere, J.[1] • Jolesz, F.A.[1] • Sathyan, P.[2] • Zinn, P.O.[2]

([1]Brigham and Women's Hospital, Boston, MA,
[2]M.D. Anderson Cancer Center, Houston, TX)

Functional Neuroradiology

Paper 226: Beyond the Tip of the Iceberg: Widespread pH Abnormalities Detected with 31P-MR Spectroscopy in the Normal-Appearing Parenchyma of Patients with Cortical Malformations and Epilepsy

Andrade, C.S.[1] • Otaduy, M.C.G.[1] • Park, E.J.[1] • Valente K.D.R.[1] • Tsunemi, M.H. [2] • Leite, C.C.[1]

([1]Faculdade de Medicina da Universidad de Sao Paulo, Sao Paulo, Brazil,
[2]Universidade Estadual Paulista Julio de Mesquita Filho, Botucatu, Brazil)

Head and Neck Radiology

Paper 327: Repeatability of Pretreatment FDG-PET Compared to Early Treatment-Induced Changes for Head and Neck Cancer

Hoang, J.K. • Peterson, B.L. • Broadwater, G. • Das, S. • Yoo, D. • Brizel, D.D.

(Duke University Medical Center, Durham, NC)

Interventional Neuroradiology

(The Michael Brothers Memorial Award)

Paper 412: Cerecyte Coil Trial: Angiographic and Clinical Outcomes of Endovascular Coiling in Patients with Ruptured and Unruptured Intracranial Aneurysms Treated with Cerecyte Coils Compared with Bare Platinum Coils - Final Results of a Prospective Randomized Trial

Molyneux, A.J.[1] • Fox, A.[2] • Sneade, M. [1] • Clarke, A. [1] • Mehta, Z. [1] • Coley, S.[3]

([1]Oxford University, Oxford, United Kingdim,
[2]Sunybrook Health Sciences, Toronto, ON, Canada,
[3]Royal Hallamshire Hospital, Sheffield, United Kingdom)

Pediatric Neuroradiology

(The Derek Harwood-Nash Award)

Paper 181: Diffusion Tensor Imaging of the Normal Pediatric Spinal Cord Using an Inner-Field-of-View EPI Sequence

Barakat, N.[1] • Mohamed F.[1] • Hunter, L.[2] • Shah, P.[1] • Faro, S.[1] • Samdani, A.[2] • Finsterbusch, J.[3] • Betz, R.[2] • Gaughan, J.[1] • Mulcahey, M.[2]

([1]Temple University, Philadelphia, PA.,
[2]Shriners Hospital for Children, Philadelphia, PA.,
[3]University Medical Center Hamburg-Eppendorf, Hamburg, Germany)

Spine

Paper 523: Vertebral Artery Position in the Setting of Cervical Degenerative Disease: What is a "Safe Position" for Selective Cervical Nerve Root Block?

Fitzgerald, R.T. • Bartynski, W.S.

(University of Pittsburgh, Pittsburgh, PA)

AWARDS AND HONORS

The Foundation of the ASNR Scholar Award in Neuroradiology Research

Since 1995, The Foundation of the ASNR has been in the process of raising funds to support neuroradiology research. This is one of the most important goals of the The Foundation of the ASNR, and of the ASNR as the premier organization for neuroradiology. This award was created for young investigators in the early stages of their careers, to enhance their competency in areas important to the future of neuroradiology, including health services research, physiological imaging and interventional neuroradiology. It also affords the Foundation the opportunity to begin to develop leadership in these areas.

The recipient of the 2013 award is:

Monica Pearl, MD, DABR

Johns Hopkins University School of Medicine, Baltimore, MD

"Highly Selective MRI-Guided Targeting of Intra-arterial Chemotherapeutic Drug Delivery to the Brainstem in a Rabbit Model of Mannitol-Induced Blood Brain Barrier Disruption"

The Foundation of The ASNR Research Scientist Award

The Foundation of the ASNR established the Research Scientist Award to provide research opportunities for PhD investigators to advance the science of neuroradiology. Scientific research is the foundation upon which the clinical practice of neuroradiology is built. Research scientists in partnership with radiologists have traditionally led the development of new imaging technologies and image-guided procedures. The directive of this award is to assist young scientists in their transition to becoming independent investigators in neuroradiology research, as well as to help established investigators initiate new projects with relevance to neuroradiology.

The recipient of the 2013 award is:

Ali Tabesh, PhD

Medical University of South Carolina, Charleston, SC

"Diffusional Kurtosis MRI Evaluation of Medial Temporal Lobe Epilepsy"

The Foundation of the ASNR Comparative Effectiveness Research Award

The Foundation of the ASNR has established the Comparative Effectiveness Research Award to support investigators in the generation and synthesis of evidence that compares the benefits and harms of diagnostic imaging methods or interventions to prevent, diagnose, treat, and monitor a clinical condition or to improve the delivery of care. Comparative effectiveness research (CER) is valuable to clinicians, patients, purchasers, and policy makers in making informed decision that will improve health care at both the individual and population levels. Neuroradiologists have an important role in the development of new imaging technologies and image-guided procedures, as well as in the assessment of these techniques in the clinical care of patients.

No Award in 2013

Women in Neuroradiology Leadership Award

The Foundation of the American Society of Neuroradiology, American College of Radiology, and American Association for Women Radiologists have established an award to provide leadership opportunities for women in neuroradiology. Since neuroradiologists must be leaders in the field and women continue to be underrepresented in neuroradiology, this award is for mid-career women with demonstrated experience and promise for leadership in neuroradiology and/or radiology overall. The objectives are to provide the awardee with additional skills and insights to enhance opportunities for advancement.

The recipient of the 2013 award is:

Pina C. Sanelli, MD, MPH

Weill Cornell Medical College/New York – Presbyterian Hospital, New York, NY

The Foundation of the ASNR Award for Outstanding Contributions in Research

This award, created in 2004 in recognition of Neuroradiologists who have demonstrated consistent excellence and lifelong accomplishment in basic or clinical neuroscience research, particularly funded research from the NIH, NSF, March of Dimes, etc. This award is given to an ASNR senior member over the age of 50 recognized in the neuroradiology field for distinguished long term achievement in basic or clinical research.

The recipient of the 2013 award is:

William P. Dillon, MD

University of California, San Francisco
San Francisco, CA

Dr. William P. Dillon was born and raised in the Bay Area of Northern California. He was the oldest of 4 children, and credits his mother, Mary, for encouraging him to read by taking him to the public library each Saturday and his father, William, for showing him how to throw and catch a baseball. He attended Moreau Catholic High School and graduated from the University of Santa Clara where he studied biology and math. During his undergraduate years he worked at NASA-Ames Research Center in the lab of the late William Mehler, PhD, a master old school neuro-anatomist, who inspired Bill to a life of academia and science. Dr. Dillon graduated from UCLA School of Medicine in Los Angeles, California in 1978. He completed an internship in internal Medicine at Virginia Mason in Seattle, Washington, residency in radiology at the University of Utah (1982) and fellowship in neuroradiology (1983) at UCSF under the direction of Drs. Newton, Norman and Brant-Zawadaski. In 1983, Dr. Dillon joined the faculty of UCSF and advanced through the ranks to Professor of Radiology, Neurology and Neurosurgery. He was appointed neuroradiology section chief in 1992 and in 1997 was named as Vice Chair for Research. In 2004 he was honored with the Elizabeth A. Guillaumin Endowed Professorship of Radiology. In 2007, Dr. Dillon became the Executive Vice-Chair of the Department of Radiology at UCSF.

Dr. Dillon's research interests span several areas in neuroradiology. He began his career at the University of Utah where Dr. Tony Mancuso was an early mentor and inspired Dr. Dillon's work in head and neck radiology. Dr. Dillon's landmark paper on MR of the Nasopharynx was the first to describe the application of MR to head and neck oncology and with colleagues he described the major atrophic patterns on imaging in patients with cranial nerve deficits. Dr. Dillon became interested in MR applications and biomarker development in neurooncology, and helped pioneer the application of MR spectroscopy and perfusion techniques in brain tumor evaluation. Dr. Dillon became interested in the applications of CT and MR perfusion techniques in stroke, and was an early adopter of the stroke protocol that incorporated CTA and CT perfusion for acute stroke detection and management. He led the UCSF core laboratory that helped imbed these techniques in stroke clinical trials. Dr. Dillon turned his interest to spine imaging and therapy in the last decade. His work on the imaging features and treatment of intracranial hypotension brought attention to this disorder to the neuroscience community and with colleagues he described the entity of "pre-syrinx." At UCSF, Dr. Dillon was instrumental in starting the Precision Spine Center at UCSF, where he and colleagues have developed pioneer the use of low dose CT guidance for spine interventions.

Dr. Dillon has authored over 260 manuscripts in peer-reviewed journals, over 30 chapters to medical texts and reviews, and co-edited two Neuroradiology textbooks. For his work, Dr. Dillon has received the Gold Medal Award from the American Society of Head and Neck Radiology (2007), the Francis A. Sooy, M.D. Award for Clinical Excellence from the Department of Otolaryngology (1992), and the 2011 J. Elliott Royer Award for Academic Contributions to Neurology from the San Francisco Neurological Society. He served as Senior Editor of the American Journal of Neuroradiology from 1998-2011, President of the American Society of Head and Neck Radiology in 1993 and President of the ASNR in 2001. He continues to be active in the leadership of both societies, most recently chairing the 2013 strategic plan review for the ASNR.

With his wife, Irene, Dr. Dillon enjoys traveling, hiking, reading, sports and spending time with his three children, Alex, a second year medical student at NYU, Andrea, currently in Chile on a Fulbright fellowship, and Annelise, a sophomore at Stanford University.

CONTINUING MEDICAL EDUCATION (CME)

Take Your Official Continuing Medical Education (CME) Certificate Home With You!

An enhancement of the Continuing Medical Education online evaluation system allows for attendees to print out their official CME certificate for the number of hours claimed during The Foundation of the ASNR Symposium 2013 and ASNR 51ST Annual Meeting and take it with them when they leave. Go to any terminal in the CME Pavilion and follow the simple directions for printing out an official The Foundation of the ASNR Symposium 2013 and ASNR 51ST Annual Meeting CME Certificate.

Following the meeting, the ASNR 2013 CME certificate site will be available online by mid-July for 90 days for attendees to print out their CME certificates.

Please Note: Due to the availability of CME certificates online, certificates will not be mailed to attendees.

Letter of Attendance

If you wish to obtain a Letter of Attendance, please request one at the Registration Desk located in the Sails Pavilion of the San Diego Convention Center.

Continuing this year!

- **Evaluations available online with remote access 24/7 through the meeting**
- **Streamlined format**
- **Open throughout the meeting until Monday, June 10**

CME Pavilion - Room 4AB (Upper Level)

To access the CME evaluation program, scan the barcode on the front of your badge at the reader at one of the terminals and follow the simple directions for selecting and evaluating the sessions you have attended. The CME credit hours awarded to a session will automatically be recorded in your record when the evaluation for a session is completed. Evaluations can be completed at the end of a session, during breaks, at the end of the day or the end of the week, as well as on your personal device. You will be able to view a record of the sessions you have evaluated and the number of CME credit hours earned throughout the program. It will also be possible to print your certificate and transcript to take home with you.

Please Note: To receive CME credit for sessions attended at The Foundation of the ASNR Symposium 2013 and ASNR 51ST Annual Meeting, all evaluations must be entered by Monday, June 10.

Scientific Program and Meeting Evaluation

The 2013 Continuing Medical Education (CME) Pavilion allows online recording of CME credits via the Internet. The improvements have created a faster and more user-friendly system for evaluating sessions and speakers and recording CME hours electronically.

The CME Pavilion is easily accessible in Room 4AB at the San Diego Convention Center. Please complete the evaluations for each session to assist in planning future meetings and to help us maintain accreditation of future programs.

ACCREDITATION STATEMENT

The American Society of Neuroradiology is accredited by the Accreditation Council for Continuing Medical Education (ACCME) to provide continuing medical education for physicians. The American Society of Neuroradiology takes responsibility for the content, quality, and scientific integrity of the CME activity.

CREDIT DESIGNATION STATEMENT

The American Society of Neuroradiology designates this live activity for a maximum of *34.5 AMA PRA Category 1 Credit(s)™*. Physicians should claim only credit commensurate with the extent of their participation in the activity.

TARGET AUDIENCE

The 51ST Annual Meeting is the premier neuroradiology meeting in the world. It is designed for general radiologists who read Neuroradiology studies, dedicated neuroradiologists who strive to better integrate advanced imaging and image-guided diagnostic and therapeutic strategies into daily practice, and scientists who seek better understanding of the current state of these technologies and how they are applied to evaluate the brain, spine, head and neck. All participants will benefit from exchange of ideas with colleagues from around the world. Programming will include invited talks and original presentations of new results in imaging methods and techniques such as MR diffusion, and perfusion-weighted imaging, susceptibility-weighted imaging, magnetic resonance spectroscopy, functional magnetic resonance imaging, MR angiography, CT perfusion, CT angiography, CT interactive construction techniques, dual energy CT, catheter-based angiography and associated therapies, peripheral nerve imaging, image-guided spine interventions, new interventional devices, molecular imaging and positron emission tomography, MR PET, and functional connectivity. Sessions dealing with pediatric neuroradiology, head and neck imaging, diagnostic imaging of the spine and spinal therapeutic interventions, vascular imaging and interventions, functional and molecular imaging, and adult neuroradiology will be offered. There will also be sessions on multiple relevant socioeconomic and practice management issues as well as invited lectures on scientific publishing, best of the Asian-Oceanian Society of Neuroradiology and Head and Neck Radiology, Best of the European Society of Neuroradiology, the Brain Observatory, controversies in Neuroradiology, how the brain thinks, and evidence based imaging in brain trauma among others.

ASNR 51ST OVERALL ANNUAL MEETING EDUCATIONAL OBJECTIVES

OVERALL OBJECTIVES FOR THE 51ST ANNUAL MEETING

After attending the 51ST Annual Meeting, you will be able to:

- Review in MOC and SAM formats current concepts in spine, head and neck, interventional, brain and pediatric neuroimaging.
- Identify current mandates and how future changes in health care policy and socioeconomic factors will affect the practice of neuroradiology both diagnostic and interventional.
- Review new concepts in cerebrovascular disease pertaining to inflammation, vasoconstriction syndrome, dissections, stroke, and aneurysms.
- Describe the imaging findings in diseases and malformations affecting the neck, airway, sinonasal cavities, and base of skull.
- Utilize new Web-based resources, tablets and mobile devices, and computer-assisted diagnosis methods as they relate to neuroradiology.
- List emerging imaging techniques for the vertebral column and spinal cord.
- Discuss newer applications of functional MRI and MR PET.
- Describe the imaging findings in congenital malformations, tumors, and metabolic disorders in children.

Objectives for the Young Professionals Program

- Compare benefits of different types of Neuroradiology practices.
- Explain how to negotiate a contract in different types of neuroradiology practices.
- Review the post treatment changes in all regions of the head and neck.
- Describe how to implement MRS, fMRI, perfusion, and DTI into your practice.

ASNR 2013

NEURORADIOLOGY FOR THE 21ST CENTURY

HOW-TO-SESSIONS - BALLROOM 6AB

In addition to the Technical Exhibition, the leadership of the ASNR is pleased to announce the fifteenth annual slate of instructional How-To forums. These sessions presented in conjunction with major corporate contributors, deal with advances in imaging and procedures as well as principles in Neuroradiology and image information management. How-To Sessions are scheduled throughout the week. The How-To Sessions offer a unique opportunity for Neuroradiologists to discuss technical specialists from the imaging industry. Comments and suggestions from meeting registrants were integrated into this year's format. The sessions vary and include both didactic presentations and demonstrations, all with a strong practical emphasis. A significant portion of each session is devoted to questions and answers.

Monday, May 20 ..... 12:15 pm - 1:15 pm

SIEMENS

Creative Dose Control for Critical Neuro CT - Leveraging New Technology
Lawrence N. Tanenbaum MD, FACR
Mount Sinai Medical Center

Healthcare Today and Tomorrow
David N. Fisher
Siemens Medical Solutions USA, Inc.

Tuesday, May 21 ..... 12:15 pm - 1:15 pm

BRACCO
LIFE FROM INSIDE

Hot Topics in Brain MRI
Standard and Advanced MRI Techniques: Current and Future Applications to Patients with Multiple Sclerosis
Meng Law, MD, MBBS, FRACR
USC Keck School of Medicine and Medical Center

Optimizing Contrast-Enhanced MRI for Tumor Evaluation and Treatment
David S. Enterline, MD
Duke University Medical Center

Wednesday, May 22 ..... 12:15 pm - 1:15 pm

TOSHIBA
Leading Innovation

Advances in High-field Neurological Imaging
Meng Law, MD, MBBS, FRACR
USC Keck School of Medicine and Medical Center

Thursday, May 23 ..... 12:15 pm - 1:15 pm

Olea MEDICAL | Improved diagnosis for life™

Advanced Diffusion & Perfusion MR in Acute Stroke and Stroke-like Syndromes
Juan Pablo Villablanca, MD
David Geffen School of Medicine at UCLA

Advanced Imaging in Neuroradiology: Case Based Review
Lawrence N. Tanenbaum, MD, FACR
Mount Sinai Medical Center

Moderator: Pina C. Sanelli, MD, MPH
Weill Cornell Medical College/New York – Presbyterian Hospital, New York, NY

Please Note: Due to the direct financial support from companies to conduct these sessions, CME credit hours will not be granted for any How-To Sessions

TECHNICAL EXHIBITION HALL

San Diego Convention Center - Sails Pavilion

Exhibit Hours

Monday, May 20 ..... 10:00 am - 4:00 pm
Tuesday, May 21 ..... 10:00 am - 4:00 pm
Wednesday, May 22 ..... 9:00 am - 4:00 pm

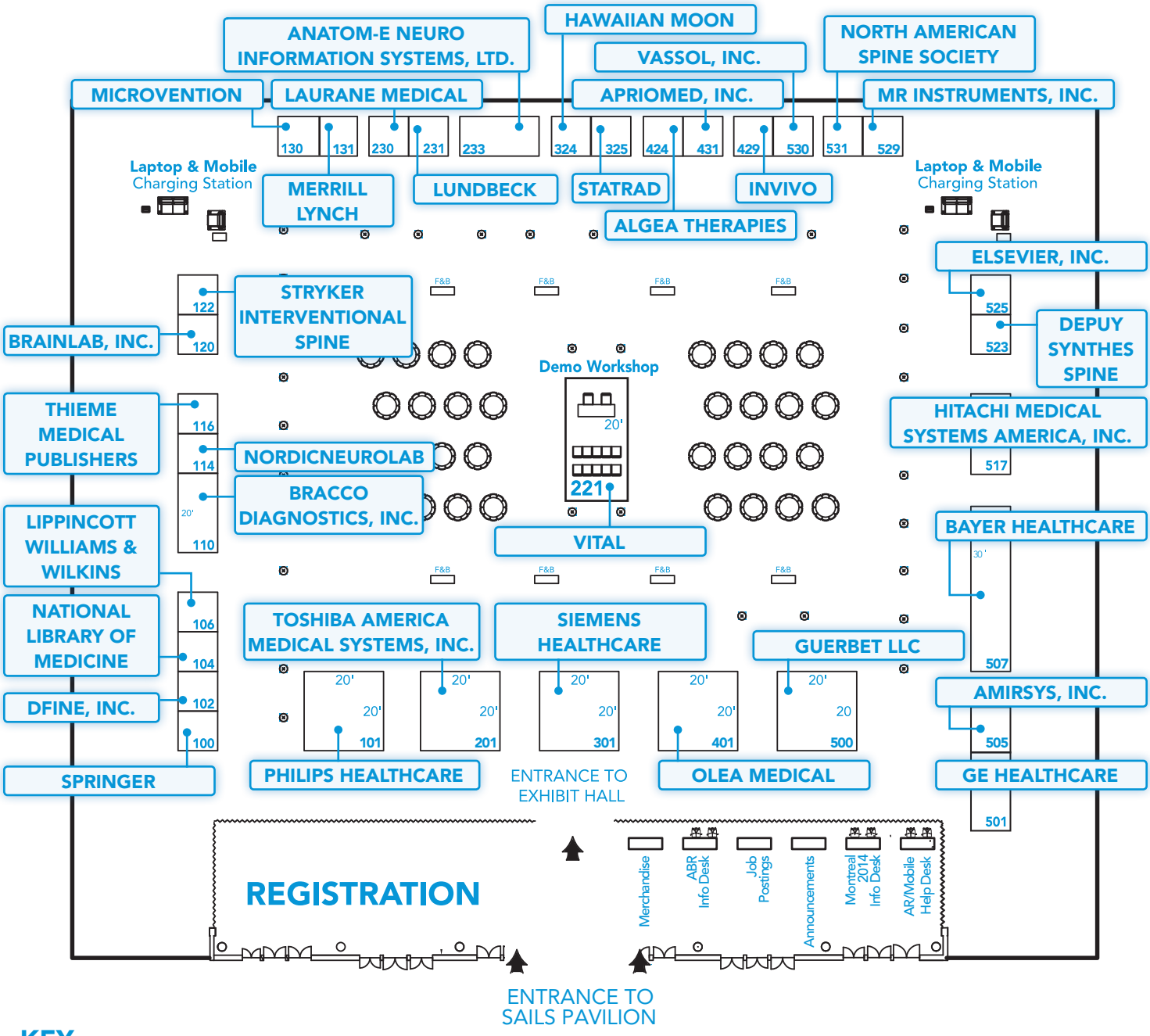

KEY

High Cocktail Tables	Round Tables	Food & Beverage Stations
		F&B

(AS OF 04/19/13)

TECHNICAL EXHIBITS ROSTER

San Diego Convention Center - Sails Pavilion

Monday, May 20 ..... **10:00 am – 4:00 pm**

Tuesday, May 21 ..... **10:00 am – 4:00 pm**

Wednesday, May 22 ..... **9:00 am – 4:00 pm**

ALGEA THERAPIES ..... Booth #424
2560 General Armistead Avenue
Audubon, PA 19403

AMIRSYS, INC ..... Booth #505
2180 South 1300 East, Suite 570
Salt Lake City, UT 84106

ANATOM-E NEURO INFORMATION SYSTEMS, LTD. ..... Booth #233
2047 University Boulevard
Houston, TX 77090

APRIOMED, INC ..... Booth #431
2 Palmer Drive
Londonderry, NH 03053

BAYER HEALTHCARE ..... Booth #507
6 West Belt
Wayne, NJ 07470

BRACCO DIAGNOSTICS INC. ..... Booth #110
259 Prospect Plains Road
Monroe Township, NJ 08831

BRAINLAB ..... Booth #120
3 Westbrook Corporate Center, Suite 400
Westchester, IL 60154

DEPUY SYNTHES SPINE ..... Booth #523
325 Paramount Drive
Raynham, MA 02767

DFINE, INC. ..... Booth #102
3047 Orchard Parkway
San Jose, CA 95134

ELSEVIER INC. ..... Booth #525
1600 JFK Boulevard, Suite 1800
Philadelphia, PA 19103

GE HEALTHCARE ..... Booth #501
PO Box 414
Milwaukee, WI 53201-0414

GUERBET LLC ..... Booth #500
1185 West 2nd Street
Bloomington, IN 47403

HAWAIIAN MOON ..... Booth #324
321 South Missouri Avenue
Clearwater, FL 33756

HITACHI MEDICAL SYSTEMS AMERICA, INC. ..... Booth #517
1959 Summit Commerce Park
Twinsburg, OH 44087

INVIVO ..... Booth #429
N27 W23676 Paul Road
Pewaukee, WI 53072

LAURANE MEDICAL ..... Booth #230
159 Wesley Avenue
Westbrook, CT 06498

LIPPINCOTT WILLIAMS & WILKINS ..... Booth #106

LUNDBECK ..... Booth #231
Ottiliavej 92500 Valby
Denmark

MERRILL LYNCH ..... Booth #131
9560 Wilshire Boulevard, 3rd Floor
Beverly Hills, CA 90212

MICROVENTION ..... Booth #130
1311 Valencia Avenue
Tustin, CA 92780

MR INSTRUMENTS, INC ..... Booth #529
5610 Rowland Road, Suite 145
Minneapolis, MN 55343

NATIONAL LIBRARY OF MEDICINE ..... Booth #104
10833 Le Conte Avenue 12-77CHS Box 951783
Los Angeles, CA 90280

NORDICNEUROLAB ..... Booth #114
234 West Florida Street, Suite 210
Milwaukee, WI 53204

NORTH AMERICAN SPINE SOCIETY ..... Booth #531
7075 Veterans Boulevard
Burr Ridge, IL 60527

OLEA MEDICAL ..... Booth #401
93 Avende Des Sorbiers
La Ciotat, 13600 France

PHILIPS HEALTHCARE ..... Booth #101
22100 Bothell Everett Hwy.
Bothell, WA 98021

SIEMENS HEALTHCARE ..... Booth #301
51 Valley Stream Parkway
Malvern, PA 19355

SPRINGER ..... Booth #100
233 Spring Street
New York, NY 10013

STATRAD ..... Booth #325
13915 Danielson Street, Suite 200
Poway, CA 92064

STRYKER INTERVENTIONAL SPINE ..... Booth #122
4100 East Milham Avenue
Kalamazoo, MI 49001

THIEME MEDICAL PUBLISHERS ..... Booth #116
333 Seventh Avenue
New York, NY 10001

TOSHIBA AMERICA MEDICAL SYSTEMS, INC ..... Booth #201
2441 Michelle Drive
Tustin, CA 92780

VASSOL, INC ..... Booth #530
348 Lathrop Avenue
River Forest, IL 60305-2122

ASNR 51ST ANNUAL MEETING SCIENTIFIC PROGRAM OVERVIEW

Monday through Thursday: ASNR will provide Breakfast, Lunch, and Morning & Afternoon Breaks.
Monday through Wednesday: ASNR will provide Continuous Coffee Service in the Technical Exhibit Hall - Sails Pavilion

Monday May 20, 2013

6:30am - 7:55am	**Continental Breakfast**
7:25am - 7:30am	Opening Remarks
7:30am - 8:30am	(1) Maintenance of Certification Review Session - Spine (AR)
8:45am - 10:15am	(2) SNIS Programming: Acute Ischemic Stroke
8:45am - 10:15am	(3) General Programming: Computation Modeling in Cerebral Aneurysms
8:45am - 10:15am	(4) ASSR Programming: Spinal Cord Syndromes: Clinical Vignettes to Emphasize Anatomic Tracts
8:45am - 10:15am	(5) General Programming: I Don't Want to Read That Study! (SAM)* (AR)
8:45am - 10:15am	(6) General Programming: WFNRS Presents: Highlights of the 24th Annual Meeting of SILAN
10:15am – 10:45am	**Morning Beverage Break**
10:45am - 12:15pm	(7) Parallel Scientific Paper Sessions
	Session 7a Adult Brain: Dementia and Degenerative Disorders I
	Session 7b Functional Imaging I: fMRI and DTI
	Session 7c Adult Brain: Stroke I
	Session 7d Adult Brain: New Techniques and Novel Post Processing I
	Session 7e Spine: New Techniques
12:15pm - 1:15pm	Education Exhibits Tour
12:15pm – 1:15pm	**Lunch Break (Provided)**
12:15pm - 1:15pm	**How-To Session - Siemens**
1:15pm - 2:45pm	(8) General Programming: Reversible Brain Syndromes: PRES, Reversible Cerebral Vasoconstriction Syndrome and Cerebral Venous Thrombosis (SAM)* (AR)
1:15pm - 2:45pm	(9) ASFNR Programming: Advanced Imaging in Neuro-Oncology: Do They Improve Outcome?
1:15pm - 2:45pm	(10) General Programming: Arterial Dissections: Extra- and Intra-Cranial Diagnosis and Treatment (SAM)* (AR)
1:15pm - 2:45pm	(11) General Programming: Scientific Publishing Update
2:45pm – 3:15pm	**Afternoon Beverage Break**
3:15pm - 4:45pm	(13) Parallel Scientific Paper Sessions
	Session 13a Interventional: Aneurysms
	Session 13b Adult Brain: Hemodynamics, Arterial and Venous
	Session 13c Adult Brain: Infectious and Inflammatory Diseases
	Session 13d Spine: Trauma, Other and Spinal Cord
	Session 13e Epilepsy: Adult and Pediatric
5:00pm - 6:30pm	(14) General Programming: Aneurysms: To Leave Alone or Treat
5:00pm - 6:30pm	(15) Advanced Imaging Seminar: MR PET
5:00pm - 6:30pm	(16) SNIS Programming: New Indications. Tumor Treatment
5:00pm - 6:30pm	(17) CSI San Diego: Basics of Tablets
5:00pm - 6:30pm	(18) Parallel Scientific Paper: Excerpta Session: Case Reports and Other Cool Ideas

AR = Audience Response Session

**This module (or activity) meets the ABR's criteria for a self-assessment activity in the ABR Maintenance of Certification program.*

SCIENTIFIC PROGRAM OVERVIEW

Tuesday May 21, 2013

6:30am - 7:55am	**Continental Breakfast**
7:30am - 8:30am	(19) Maintenance of Certification Review Session - Pediatrics (AR)
8:45am - 10:15am	(20) ASFNR/ISMRM Programming: Ultrafast MR Imaging
8:45am - 10:15am	(21) SNIS Programming: New Devices in Interventional Neuroradiology and Their Imaging Appearances
8:45am - 10:15am	(22) ASSR Programming : Next Generation of Imaging the CSF: Myelography, Has the Magic Returned?
8:45am - 10:15am	(23) General Programming: WFNRS Presents the Best of AOSNHNR Peritherapeutic Neuroradiology
8:45am - 10:15am	(24) Young Professionals Programming: Choosing Your Career
10:15am – 10:45am	**Morning Beverage Break**
10:45am - 12:15pm	(25) Parallel Scientific Paper Sessions
	Session 25a Adult Brain: Tumors I: Glioblastoma
	Session 25b Adult Brain: Dementia and Degenerative Disorders II
	Session 25c Adult Brain: Stroke II: Endovascular Recanalization
	Session 25d Functional Imaging II: fMRI and MRS
	Session 25e Socioeconomic: Coding, Quality and Informatics
12:15pm - 1:15pm	**How-To Session - Bracco**
12:15pm - 12:15pm	American Society of Pediatrics Neuroradiology (ASPNR) Annual Business Meeting (members only)
12:15pm – 1:15pm	**Lunch Break (Provided)**
1:15pm - 2:45pm	(26) ASFNR Programming: Memory and the Aging Brain: Imaging Tools Which Will Shape Humanity
1:15pm - 2:45pm	(27) Advanced Imaging Seminar: DWI: Advances in Brain, Spine, and Head and Neck (SAM)* (AR)
1:15pm - 2:45pm	(28) Socioeconomic Programming: Theoretical and Applied Considerations for Radiology in Healthcare Reform
1:15pm - 2:45pm	(29) Special Session: The Brain Observatory
1:15pm - 2:45pm	(30) Young Professionals Programming: Basics Session: Head and Neck Post-Treatment Imaging
2:45pm – 3:15pm	**Afternoon Beverage Break**
3:15pm - 4:45pm	(31) Parallel Scientific Paper Sessions
	Session 31a Intervention: Vascular Malformations: Devices and Treatments
	Session 31b Adult Brain: Tumors II: Gliomas and Imaging Surrogates
	Sessuion 31c Adult Brain: Aneurysms, AVMs and AVFs
	Session 31d Spine: Degenerative, Inflamatory Infectious and Interventions
	Session 31e Pediatrics: Developmental/ Congenital Malformations
5:00pm - 6:30pm	(32) Special Session: Controversies in Neuroradiology
5:00pm - 6:30pm	(33) SNIS Programming: Quality, Workforce and Research
5:00pm - 6:30pm	(34) ASPNR Programming: Metabolic Brain Disorders
5:00pm - 6:30pm	(35) CSI San Diego: Neuroradiology Resources on the Web
5:00pm - 6:30pm	(36) Young Professionals Programming: Creating a New Service: How You Can Add Value to Your Practice

AR = Audience Response Session

**This module (or activity) meets the ABR's criteria for a self-assessment activity in the ABR Maintenance of Certification program.*

SCIENTIFIC PROGRAM OVERVIEW

Wednesday May 22, 2013

6:30am - 7:55am	**Continental Breakfast**
7:30am - 9:00am	(37) General Programming: How Does the Brain Think? From Cytoarchitecture to Neurotransmission and Imaging
9:00am - 9:30am	**Morning Beverage Break**
9:30am - 10:00am	**(38) Keynote Speaker: Imaging as Cash Cow or Cooked Goose? Thriving in a New Era of Neuroradiology** **A. Gregory Sorensen, MD**
10:00am - 10:15am	**(38a) Presidential Address**
10:15am - 10:30am	**(38b) Award Announcements** 2013 Gold Medal Award 2013 Honorary Member Award 2013 The Foundation of the ASNR Outstanding Contribution in Research Award 2013 Women in Neuroradiology Leadership Award 2013 The Foundation of the ASNR Scholar Award in Neuroradiology Research 2013 The Foundation of the ASNR Research Scientist Award 2013 Cornelius G. Dyke Memorial Award 2012 Trainee Award 2012 Outstanding Presentation Awards
10:30am - 11:00am	(38c) ASNR Annual Business Meeting (members only)
11:15am - 12:15pm	(39) Maintenance of Certification Review Session: Brain (AR)
12:15pm - 1:15pm	Education Exhibits Tour
12:15pm - 1:15pm	**How-To Session - Toshiba**
12:15pm – 1:15pm	**Lunch Break (Provided)**
1:15pm - 2:45pm	(40) ASHNR Programming: Evidence-Based Imaging in the Head and Neck
1:15pm - 2:45pm	(41) Special Session: Human Papillomavirus and Head and Neck Cancer
1:15pm - 2:45pm	(42) ASSR/ASFNR Programming: Imaging Tools Which Will Shape Future Spine Imaging
1:15pm - 2:45pm	(43) Socioeconomic Programming
1:15pm - 2:45pm	(44) ASPNR Programming : Pediatric Brain Tumors (SAM)* (AR)
2:45pm - 3:15pm	**Afternoon Beverage Break**
3:15pm - 4:45pm	(45) Parallel Scientific Paper Sessions Session 45a Adult Brain: Stroke III Session 45b Adult Brain: Tumors III: High-Grade Tumors Sessuiom 45c Head and Neck: Orbits, Thyroid and Parathyroid Glands: Evolving Techniques Session 45d Adult Brain: Trauma Session 45e Pediatrics: Perinatal Imaging, Tumors, and Spine
5:00pm - 6:30pm	(46) ASHNR Programming : Contemporary Imaging of the Temporal Bone
5:00pm - 6:30pm	(47) Advanced Imaging Seminar : fMRI: Now and Future
5:00pm - 6:30pm	(48) CSI San Diego: Neuroradiology on the Go: Viewing Studies Outside of Work and Home (Viewers for Phones and Tablets)
5:00pm - 6:30pm	(49) ASPNR Programming : Development and Malformations
5:00pm - 6:30pm	(50) Special Session: WFNRS presents the Best of ESNR

AR = Audience Response Session

**This module (or activity) meets the ABR's criteria for a self-assessment activity in the ABR Maintenance of Certification program.*

SCIENTIFIC PROGRAM OVERVIEW

Thursday April 24, 2013

6:30am - 7:55am	**Continental Breakfast**
7:30am - 8:30am	(51) Maintenance of Certification Review Session - Head and Neck (AR)
8:45am - 10:15am	(52) ASHNR Programming: Everyday Issues in Head and Neck Imaging
8:45am - 10:15am	(53) General Programming: Peripheral Nerve Imaging for the Neuroradiolgist
8:45am - 10:15am	(54) CSI San Diego: Computer-Assisted Diagnosis Review of Available CADs for Radiology
8:45am - 10:15am	(55) General Programming: Cerebrovascular Imaging Update: Foundation of the ASNR Special Session
10:15am – 10:45am	**Morning Beverage Break**
10:45am - 12:15pm	(56) Parallel Scientific Paper Sessions Session 56a Special Session: Regional Societies Award Winners and DTI Session 56b Head and Neck: Cancer and Neoplasm: Advanced Concepts and Techniques Session 56c Adult Brain: Stroke IV: Extracranial Blood Vessels and Infarctions Session 56d Pediatrics: Functional Imaging and New Techniques Session 56e Anatomy and Related Issues
12:15pm - 1:15pm	**How-To Session - Olea Medical**
12:15pm – 1:15pm	**Lunch Break (Provided)**
1:15pm - 2:45pm	(57) Parallel Scientific Paper Sessions Session 57a Head and Neck: Skull Base: Sinonasal, Temporal Bone and Soft Tissue Neck Session 57b Adult Brain: Tumors IV: Glioblastoma Session 57c Pediatrics: Vascular, Congenital Malformations, and Miscellaneous Session 57d Adult Brain: Tumors V: Metastases and Miscellaneous Session 57e Adult Brain: New Techniques and Novel Post Processing II
2:45pm – 3:15pm	**Afternoon Beverage Break**
3:15pm - 4:45pm	(58) ASPNR Programming : Interesting Case Conference (AR)
3:15pm - 4:45pm	(59) ASHNR Programming: Current Concepts and Advances in Head and Neck Cancer Imaging (SAM)* (AR)
3:15pm - 4:45pm	(60) Special Session : Imaging in Mild Traumatic Brain Injury: What is the Evidence?
3:15pm - 4:45pm	(61) General Programming: Neuroimaging: What Is It and How Can it Help Us?
4:45pm - 5:00pm	**(62) Closing Remarks**

AR = Audience Response Session

**This module (or activity) meets the ABR's criteria for a self-assessment activity in the ABR Maintenance of Certification program.*

AMERICAN SOCIETY OF NEURORADIOLOGY
FUTURE ANNUAL MEETINGS

52ND ANNUAL MEETING
May 17 - 22 | Palais des congrés de Montreal

MONTREAL
2014

53RD ANNUAL MEETING
April 25 - 30

Sheraton Chicago Hotel & Towers

CHICAGO
2015

54TH ANNUAL MEETING
May 21 - 26

Washington Marriott Wardman Park

WASHINGTON DC
2016

55TH ANNUAL MEETING
April 22 - 27

Long Beach Convention & Entertainment Center

LONG BEACH
2017

56TH ANNUAL MEETING
May 19 - 24

Vancouver Convention Centre

VANCOUVER
2018

57TH ANNUAL MEETING
May 18 - 23

Hynes Convention Center

BOSTON
2019

Simplify
the MOC Process

Manage
your CME Credits Online

CMEgateway.org

Available to Members of Participating Societies

- American Board of Radiology (ABR)
- American College of Radiology (ACR)
- American Roentgen Ray Society (ARRS)
- American Society of Neuroradiology (ASNR)
- Commnission on Accreditation of Medical Physics Educational Programs, Inc. (CAMPEP)
- Radiological Society of North America (RSNA)
- Society of Interventional Radiology (SIR)
- SNM
- The Society for Pediatric Radiology (SPR)

It's Easy and Free!

Log on to CME Gateway to:

- View or print reports of your CME credits from multiple societies from a single access point.
- Print an aggregated report or certificate from each participating organization.
- Link to SAMs and other tools to help with maintenance of certification.

American Board of Radiology (ABR) participation!

By activating ABR in your organizational profile, your MOC–fulfilling CME and SAM credits can be transferred to your own personalized database on the ABR Web site.

Sign Up Today!

go to CMEgateway.org

PROGRAM CONTRIBUTORS

Platinum Level

Bayer HealthCare

- An educational grant in support of The Foundation of the ASNR Symposium 2013: New Concepts and Trends in Neuroimaging
- Annual educational grant in support of the Self Assessment CME, Maintenance of Certification (MOC) and Self Assessment Modules (SAM)* programming live and as an internet enduring material on the ASNR website
- Performance and Quality Improvement (PQI) Initiative

Gold Level

BRACCO
LIFE FROM INSIDE

SIEMENS

TOSHIBA
Leading Innovation

ViTAL
A Toshiba Medical Systems Group Company

Silver Level

Olea MEDICAL

Improved diagnosis for life™

** This module (or activity) meets the ABR's criteria for a self-assessment activity in the ABR Maintenance of Certification program.*

Note: Scanned images are included in the proceedings. Some submitted images were reduced during editing, thereby decreasing clarity. Also, refer to the Program Planner. Proceedings Content as of 3-29-2013.

Monday Morning

7:25 AM - 7:30 AM
Ballroom 6AB

(0) Opening Remarks

O-1 **7:25 AM - 7:30 AM**

Opening Remarks

Castillo, M.
Univ. Of North Carolina School Of Medicine
Chapel Hill, NC.

Monday Morning

7:30 AM - 8:30 AM
Ballroom 6AB

(1) Maintenance of Certification Review Session - Spine (AR)

O-2 **7:30 AM - 8:00 AM**

Spine - Part I

Ortiz, A.
Winthrop University Hospital
Mineola, NY.

Presentation Summary
This session will cover key topics in diagnostic and interventional Spine radiology using the case method combined with audience participation. Some areas that will be addressed include congenital spine, spine trauma, degenerative spine disease, inflammatory spine disease, spine infection, spine tumors and metabolic spine disease.

O-3 **8:00 AM - 8:30 AM**

Spine - Part II

Riascos, R. F.
University of Texas Medical Branch
Galveston, TX.

Presentation Summary
The MOC of spine will cover six cases that will be discussed with one or two questions per case with companion cases to review the differential diagnosis. The topics covered include trauma, congenital disease, disk pathology, vascular malformations, tumors and neurocutaneous syndromes.

Monday Morning

8:45 AM - 10:15 AM
Ballroom 6AB

(2) SNIS Programming: Acute Ischemic Stroke

O-4 **8:45 AM - 9:15 AM**

IMS-3 Trial Results in Context: Where Do We Go from Here?

Tomsick, T. A.
Univ. Hosp./Univ. Cincinnati College Of Medicine
Cincinnati, OH.

Dr. Tomsick is Professor of Radiology at the University of Cincinnati Medical Center, and was Principal Neurointerventionist for the IMS I, II, and III Trials. He is Past-President of the American Society of Therapeutic and Interventional Neuroradiology (2001-2).

Presentation Summary
The IMS III Trial investigated full-dose IV rtPA versus reduced-dose IV rtPA in treatment of acute ischemic stroke from 2006 to 2012. The trial was halted for futility in April, 2012 after 656 of 900 subjects were enrolled. This presentation will focus on the clinical and revascularization outcomes in the trial, and consider reasons the trial proved futile as designed.

O-5 **9:15 AM - 9:45 AM**

Role of IA Stroke Treatment from the Neuroradiologist's Perspective

Saver, J. L.
David Geffen School of Medicine at UCLA
Los Angeles, CA.

Jeffrey L. Saver, MD is Director of the UCLA Stroke Center and Professor of Neurology at the David Geffen School of Medicine, University of California, Los Angeles. Dr. Saver received his medical degree from Harvard Medical School, and is a graduate of the Harvard-Longwood Neurology Training Program, the University of Iowa Fellowship Program in Behavioral Neurology and Cognitive Neuroscience, and the Brown University Fellowship Program in Vascular Neurology. An author or co-author of over 365 research articles, Dr. Saver's research interests are in acute stroke treatment, stroke prevention, neuroimaging, clinical trial design, and neurocognitive consequences of stroke. Dr. Saver has held numerous leadership positions in international and national stroke studies and organizations. He is the immediate Past Chair of the Stroke Council of the American Heart

Note: Scanned images are included in the proceedings. Some submitted images were reduced during editing, thereby decreasing clarity. Also, refer to the Program Planner. Proceedings Content as of 3-29-2013.

Association/American Stroke Association; Chair of the AHA Stroke Performance Measures Oversight Committee; Co-Chair of the NIH-NINDS Common Data Elements - Stroke Task Force; principal investigator of the NIH-NINDS Field Administration of Stroke Magnesium (FAST-MAG) clinical trial; editorial board member for the journals Stroke, Journal of Stroke and Cerebrovascular Diseases, Journal of Neuroimaging, and Reviews in Neurological Disease; and associate editor of the online textbooks Medlink Neurobase and Emedicine Neurology.

Presentation Summary
Despite the disappointing results of randomized trials of the first generation of endovascular recanalization therapy, noninterventional stroke neurologists recognize the promise and key potential role of catheter-based interventions. Intravenous tissue plasminogen activator is of only modest recanalization efficacy, achieving reperfuson in only 40% of treated patients. As a treatment that can be delivered quickly and that does not potentiate endovascular risk, IV thrombolysis will always play an important role in acute ischemic stroke care. However, it is an intermediate stage therapy, not a final destination. Highly effective second generation endovascular recanalization treatments, such as stent retrievers, are likely to demonstrate benefit in the next wave of randomized trials and become a useful anchor of clinical practice. Intensive efforts to shorten door to puncture and door to clot times are needed for endovascular therapy, following on the models of door to needle time care improvements for stroke and door to balloon time care improvements for acute myocardial ischemia. Once endovascular therapy is definitively shown to be beneficial, regional stroke systems of care will need to evolve to two tier systems, with rational routing of appropriate patients to widely disseminated Primary Stroke Centers and Hub Comprehensive Stroke Centers.

O-6 **9:45 AM - 10:15 AM**

Stroke Imaging: CT, MRI, Perfusion, Where Do We Stand Today?

Gonzalez, R.
Massachusetts General Hospital
Boston, MA.

Presentation Summary
With the development of effective therapies for acute ischemic stroke, a plethora of advanced imaging methods were developed to help triage patients to the most effective therapies. The management of patients with mild symptoms (NIHSS<5, no treatment) and moderate symptoms (NIHSS6-10, IV-tPA if <4.5 hours post ictus, only NCCT imaging essential) are well supported by the evidence. For patients with severe symptoms (NIHSS>10) advanced imaging provides essential information. Evidence-based analyses have shown that NCCT, CTA and DWI are Class I/Level A methods. Perfusion imaging by CT or MRI have been found to be unreliable and are Class IIb. The key parameters for assessing the acute stroke patient in order of importance are: neurologic status, site of occlusion, and size infarct core, which can be determined accurately and reliably with NIHSS, CTA (or MRA) and DWI, respectively. The clinically relevant penumbra in patients with a major anterior circulation occlusion can be deduced by combining the NIHSS score and the DWI lesion volume alone. Theoretical considerations and the inherently poor signal-to-noise ratio make CTP an unreliable, potentially misleading method to substitute for DWI to determine the size of the infarct core, and is unsuitable for patient triage decisions.

Monday Morning

8:45 AM - 10:15 AM
Ballroom 6CF

(3) General Programming: Computation Modeling in Cerebral Aneurysms

O-7 **8:45 AM - 9:15 AM**

Growth and Remodeling in Aneurysms

Robertson, A. M.
University of Pittsburgh
Pittsburgh, PA.

Anne M. Robertson is Associate Professor of Mechanical Engineering and Materials Science and Associate Professor of Bioengineering at the University of Pittsburgh, Pittsburgh, PA. Her research team carries out theoretical, computational and experimental research on cerebral vascular disease and constitutive modeling of soft biological tissues. Her research has been funded by the NIH, NSF, DOE and the Whitaker Foundation. Dr. Robertson has co-authored over 75 publications and is co-author of the book, Hemodynamical Flows: Modeling, Analysis and Simulation, Birkhauswer, 2008. She is a member of the editorial board of the International Journal for Numerical Methods in Biomedical Engineering. Dr. Robertson earned an MS and PhD from the Department of Mechanical Engineering at U.C. Berkeley and was a President's postdoctoral fellow in the Department of Chemical Engineering at U.C. Berkeley. She has held visiting research professorships at the Polictecnico di Milano (Italy), the Instituto Superior Technico in Lisbon (Portugal), the Bernouilli Center at the Swiss Federal Institute of Technology (EPFL, Switzerland), the University of Pisa (Italy) and RWTH University of Aachen (Germany).

Presentation Summary
Intramural cells in the walls of healthy arteries are

Note: Scanned images are included in the proceedings. Some submitted images were reduced during editing, thereby decreasing clarity. Also, refer to the Program Planner. Proceedings Content as of 3-29-2013.

endowed with an ability to maintain the structural integrity of the wall through a continuous process of collagen turnover. Further, these cells have the capacity to remodel the extracellular matrix in response to changes in mechanical and chemical stimuli. The cellular content in the walls of cerebral aneurysms show tremendous heterogeneity across the population and can vary from an endothelialized wall with linearly organized smooth muscle cells (SMCs) to a thin hypocellular wall (e.g., (1; 2)). Diminished cell content and function within the aneurysm wall will hinder, or even prevent, the maintenance and repair of the extracelluar matrix and thereby influence disease progression towards stabilization, growth or rupture (1-3). The nature of the flow dynamics within the aneurysm sac is believed to play a vital role in determining this cell content and therefore, ultimately, the wall strength. In this talk, we will discuss the relationship between cellular content, extracellular matrix and mechanical function in both resected segments of human aneurysm walls as well as the walls of an elastase induced aneurysm model in rabbits (4-6). Consideration also will be given to the vital question of the extent to which the wall structure and content in the elastase induced aneurysms is similar to that of human aneurysms. For this work, collagen and elastin architecture were evaluated using a custom uniaxial loading device, designed to be compatible with a multiphoton microscope (7). Using this device, we were able to simultaneously perform mechanical testing and MPM imaging of the architecture in the aneurysm samples without destructive histological techniques (8). Unruptured human aneurysm domes were assessed at single time points. The growth and remodeling process was evaluated in the elastase-induced aneurysm model by investigating the changing collagen and elastin architecture at four time points.

O-8 **9:15 AM - 9:45 AM**

Computational Fluid Dynamics Pre- and Post-Aneurysm Treatment

Cebral, J. R.
George Mason University
Fairfax, VA.

Juan R. Cebral is a Professor at the Center for Computational Fluid Dynamics, College of Science, George Mason University, in Fairfax, Virginia, USA. He finished his undergraduate studies in Physics at the University of Buenos Aires, Argentina in 1991 and received his PhD in Computational Sciences and Informatics from George Mason University in 1996. He conducts research on image-based computational modeling of cerebral blood flow and aneurysms in close collaboration with clinicians from Inova Fairfax Hospital and other institutions in the USA and around the world. He has co-authored over 60 journal papers, 10 book chapters, and over 150 conference papers. His research has been funded by the National Institutes of Health, the American Heart Association, the Whitaker Foundation as well as industrial partners such as Philips Healthcare and Boston Scientific. He teaches graduate level courses in Fluid Mechanics, High Performance Computing and Foundations of Computational Sciences.

Presentation Summary
This presentation will discuss our investigations of the relationships between hemodynamic conditions created immediately after implantation of flow diverting devices to treat cerebral aneurysms and the long-term outcome of these interventions. These studies are carried out by connecting data from "patient-specific" image-based computational fluid dynamics models and clinical, animal and biological information.

O-9 **9:45 AM - 10:15 AM**

Use of Modeling in the Clinical Setting

Murayama, Y.
Division of Endovascular Neurosurgery, Department of Neurosurgery, Jikei University School of Medicine
Tokyo, JAPAN.

Presentation Summary
Computational fluid dynamics (CFD) has become a prominent subject in the research of cerebral aneurysms. Researchers conduct CFD analysis to understand mechanism of aneurysm rupture or difference between ruptured and unruptured aneurysms. The wall shear stress (WSS), which is the most commonly studied hemodynamic parameter, has been studied intensively. Several new parameters, such as energy loss (EL), oscillatory shear index (OSI), or pressure loss coefficient (PLC) have been introduced. Intensive research using CFD technology has been done; however, no conclusive result has been obtained to anticipate aneurysm rupture. Risk of rupture also is associated with multifactorial factors, such as genetics, or biological factors. Computational fluid dynamics technology also can be used for treatment planning, especially utilization of flow diverters. Furthermore, simulation of such endovascular device development can be performed in the virtual environment. We discuss current status and future of CFD research in the field of interventional neuroradiology.

Note: Scanned images are included in the proceedings. Some submitted images were reduced during editing, thereby decreasing clarity. Also, refer to the Program Planner. Proceedings Content as of 3-29-2013.

Monday Morning

8:45 AM - 10:15 AM
Ballroom 6DE

(4) ASSR Programming: Spinal Cord Syndromes: Clinical Vignettes to Emphasize Anatomic Tracts

O-10 **8:45 AM - 9:15 AM**

Extrinsic Cord Compression. State of the Art Imaging and Classification Schemes

Cianfoni, A.
Neurocenter of Southern Switzerland
Lugano, SWITZERLAND.

Presentation Summary
Spinal cord compression is a pathologic condition, potentially leading to devastating neurologic sequelae, that requires imaging to distinguish among specifically treatable causes. Clinical presentation includes a combination of motor and/or sensory deficit, often pointing to a definable level of involvement, pyramidal syndromes, neuropathic pain, gait disturbance, fever, with variable patterns of progression. There is a wide spectrum of conditions that may compress the spinal cord: degenerative disease, disk herniation and metastatic compression are the most common causes; other conditions include spine trauma, epidural abscess, epidural hematoma and neoplastic conditions other than metastasis. The role of imaging is to establish a radiologic diagnosis, to distinguish intrinsic spinal cord disease from extrinsic compression, to define mechanical spine stability, to evaluate the integrity of neural tissue and to provide further radiologic information if necessary. The spine is a complex anatomical environment, and in the setting of spinal cord compression imaging is required to assess osseous structures and soft tissues, as muscles, disks, ligaments, epidural fat planes, meninges, cerebro-spinal fluid, vessels and spinal cord. The need to image "across anatomical compartments" usually requires more than one imaging technique, with specific technical requirements. Multi-detector CT is progressively replacing plain radiography for the accurate assessment of the osseous spine, and actually is the preferred imaging modality in acute spine trauma. MR imaging is the best imaging modality to assess soft tissues, image the extra-dural, intra-dural and spinal cord compartments. Conventional MR imaging protocols need to be implemented with fat suppression techniques applied to multiplanar T2- and contrast- enhanced T1-weighted sequences. MR imaging helps in predicting neurologic recovery: conventional T1-weighted, T2-weighted and post-contrast images provide macroscopic information including both reversible and irreversible histologic changes. Diffusion tensor imaging (DTI) enables depiction of microstructural changes in the compressed spinal cord, which could further predict tissue viability, potential functional prognosis and patient recovery. The role of CT myelography is reserved to selected cases, when MRI is not feasible or results are unclear but, in the setting of spinal cord compression, intrathecal injection of contrast from below and above the compression level might be necessary to overcome the diagnostic limitations imposed by a myelographic block. Various spinal cord compression conditions will be presented, different in nature, arising from, or involving, different anatomical compartments. Respective best imaging modalities or combinations thereof will be discussed.

O-11 **9:15 AM - 9:45 AM**

Intrinsic Cord Pathology and State of the Art Imaging of Spinal Tracts - I

Van Goethem, J. W.
Antwerp University Hospital
Antwerp (Edegem), BELGIUM.

Presentation Summary
The spinal cord has a complex anatomy with a great concentration of different tracts in a small cross-sectional area. Although intrinsic cord pathology is relatively rare, many different diseases may effect normal spinal cord functioning. Benign intramedullary tumors, mainly astrocytoma and ependymoma, may disrupt normal cord functioning. Also inflammatory and infectious diseases, including multiple sclerosis and different kinds of myelitis will be discussed. A third important group of diseases affecting the spinal cord may provoke extrinsic cord compression or laceration and these can be seen in tumoral pathology, degenerative spinal disease and trauma. In general only magnetic resonance imaging (MRI) allows accurate visualization of intrinsic cord pathology. Previously the focus of imaging was on determining the etiology and the general location of spinal cord lesions. Delineation of gray and white matter is done nowadays in routine imaging. Discriminating the different spinal tracts is still challenging. New techniques, especially diffusion tensor imaging (DTI), however are promising in visualizing individual spinal tracts and, as consequence, lesions to spinal tracts. Techniques to optimize spinal cord DTI will be discussed and this will be illustrated with several examples.

Note: Scanned images are included in the proceedings. Some submitted images were reduced during editing, thereby decreasing clarity. Also, refer to the Program Planner. Proceedings Content as of 3-29-2013.

O-11a **9:15 AM – 9:45 AM**

Intrinsic Cord Pathology and State of the Art Imaging of the Spinal Tracts - II

Van Hecke, W.
icoMetrix
Leuven, BELGIUM.

O-12 **9:45 AM - 10:15 AM**

Vascular Anatomy, Etiologies and Ischemic Syndromes

Patsalides, A.
Weill Cornell Medical College
New York, NY.

Presentation Summary
Arterial anatomy of the spinal cord. Venous anatomy of the spinal cord. Embryology. Anastomosis and clinical implications. Ischemic syndromes.

Monday Morning

8:45 AM - 10:15 AM
Room 5AB

(5) General Programming: I Don't Want to Read That Study! (SAM) (AR)

O-13 **8:45 AM - 9:10 AM**

Tinnitus: Imaging and Clinical Approach to Diagnosis

Phillips, C.
Weill Medical College of Cornell/NY Presbyterian
New York, NY.

Presentation Summary
Tinnitus is an incredibly common condition in the world, and is suffered by countless millions of people in the U.S., some of whom will be referred for imaging evaluation. Tinnitus is the perception of sounds by an individual in the absence of an external sound. It may be a ringing, buzzing, or other monotonous tone. The tone may vary with time, and can be pulse-synchronous, or may be unvarying. Continuous tinnitus is the unvarying form, and pulsatile tinnitus refers to a sound which varies with the cardiac cycle. Tinnitus may be an unremitting problem in patients, and may lead to referral for imaging. In this regard, it is a very problematic item of history for the radiologist, as it is a symptom with an incredibly wide range of potential etiologies. There is little acceptance of a standard imaging algorithm for diagnosing a potential cause of tinnitus. As expected, the pulsatile form may be vascular in nature, and a potential cause may be found more commonly on imaging, but the study to be recommended also is widely debated, without consensus. Continuous tinnitus is a particularly vexing clinical issue. Tinnitus without a radiologic abnormality is likely the most common form of tinnitus, and the radiologist may recommend a perfectly appropriate examination without a discovered diagnosis. Pulsatile tinnitus may be associated with vascular pathology, and with other lesions as well. A reasonable differential diagnosis includes arterial and venous anomalies, vascular neoplasia, and other less common but potentially diagnosable and treatable conditions, such as otospongiosis. Continuous tinnitus can be caused by a very wide range of pathology, including intracranial and IAC neoplasms, TMJ disease, brainstem lesions, intracranial hypotension or hypertension, or simply presbycusis. The diagnostic study ordered may be dependent on clinical factors, such as patient age, onset of symptoms, or potentially causative conditions. CT and MRI may be utilized, and CTA and MRA as well as venous studies may be useful in arriving at a cause. Temporal bone CT studies often are ordered, as are CTA. CT angiography has been proposed as a reasonable “one stop shopping” exam, yielding both vascular information and high quality temporal bone CT studies. However, brainstem, IAC and posterior fossa disease still is best studied with MR with and without contrast.

O-14 **9:10 AM - 9:30 AM**

The Post-Op Temporal Bone

Huang, B. Y.
University of North Carolina
Chapel Hill, NC.

Presentation Summary
In contemporary practice, imaging plays a crucial role in both the pre and postoperative assessment of the diseased ear. In this session, we review the role of imaging following common otologic surgical procedures. The most common procedures of the middle ear and mastoid cavity are performed to address the sequelae of chronic otitis media and Eustachian tube dysfunction or to address stapes fixation in patients with otosclerosis. The term tympanoplasty is used generically to describe surgical procedures within the middle ear performed to eradicate disease and, secondarily, to reconstruct the conductive hearing apparatus. They are performed frequently in conjunction with mastoidectomy and/or ossicular chain reconstruction. The postoperative appearances of temporal bones following tympanoplasty and other middle ear surgeries can vary drastically from case to case depending upon the specific procedures performed; therefore, correlation with the operative note, if available, should be a crucial part of the radiologic assessment. In all cases, the postoperative CT evaluation should include careful assessment of: 1) the status of the ossicular chain and/or reconstruction prostheses; 2) the presence of soft tissue or fluid in the middle ear and mastoid; 3) the

Note: Scanned images are included in the proceedings. Some submitted images were reduced during editing, thereby decreasing clarity. Also, refer to the Program Planner. Proceedings Content as of 3-29-2013.

integrity of the tegmen tympani/mastoideum, lateral semicircular canal, sigmoid plate, and fallopian canal; and 4) the status of the inner ear. In cases in which there is soft tissue in the tympanum or mastoid, MRI can be useful for further tissue characterization. Common surgeries in the inner ear, IAC, and CP angle cistern include cochlear implantation and schwannoma resection. CT and plain radiography are the primary imaging tools used for assessing cochlear implants and adequately demonstrate electrode abnormalities, including electrode misplacement, migration, kinking, and fracture. Schwannomas of the IAC and CP angle typically are approached from one or more of three primary routes: 1) middle cranial fossa; 2) suboccipital; and 3) translabyrinthine. MR imaging is the preferred imaging test to evaluate the totality of tumor resection and to assess for surgical complications, which can include infection, hematoma formation, retraction injury to the temporal lobe or cerebellum, injury to the sigmoid sinus, or injury to the inner ear. Typical imaging features of each of these procedures will be demonstrated, along with examples of common causes of surgical failure or complication.

O-15 **9:30 AM - 9:50 AM**

The Post-Therapy Neck

Curtin, H. D.
Massachusetts Eye & Ear Infirmary
Boston, MA.

Presentation Summary
The post-therapy imaging study of the neck is one of the most avoided examinations in any radiology practice. The anatomy of the neck is normally complex and if distorted by surgery or radiation, the difficulty of image interpretation is magnified significantly. Knowledge of standard surgical resections and reconstruction strategies as well as an understanding of the most common sites of recurrences can help organize the interpretation strategy. Certain changes in the soft tissues are predictable after radiation and should not be confused with recurrence. The pretherapy imaging study and a clear knowledge of the therapeutic history should be considered indispensable resources for the radiologist making the interpretation. Certain surgeries are very standardized. For instance, neck dissections follow predicable patterns. Knowledge of the precise terminology can be confusing. Simply indicating that there has been a neck dissection and noting the structures that have been removed is usually sufficient. The jugular vein and sternocleidomastoid muscle as well as the submandibular gland should be mentioned. In the most limited of dissections only the nodes are removed and the gland, vein and muscle may remain. In this case, the only indicator of the dissection is loss of fat around the vessels. If the accessory nerve (XI) is removed the trapezius and sternocleidomastoid (if remaining) will atrophy. The various flaps used to reconstruction may be swung into place using the original blood supply (pedicled flap) or brought into the surgical site (free flap) from a more distant site and attached to the vessels of the neck. Radiation changes also are predictable with swelling of the aryepiglottic folds and apparent edema in the retropharyngeal space as well as stranding of the fat and linear enhancement of the mucosa. Recurrences are usually in relatively predicable locations along surgical approach path or along the edge of a flap as well as at the primary site. These tend to have more nodular appearance. It is very common that the radiologist must deal with an area of tissue that is indefinite. The radiologist can recommend a short interval follow-up examination or even a biopsy. A PET/CT may be done if the original exam was a CT. Being able to deal with this ambiguity is an important part of the post-therapy imaging of the neck. Not all cases have had surgery or radiation. In some cases, imaging may be performed after chemotherapy to follow the response of a primary tumor or lymph node. A decision must be made regarding continuation of chemotherapy or perhaps whether or not a lymph node dissection is warranted. Such studies usually are done with direct comparison to the recent pretherapy study such as PET/CT performed with very similar techniques and usually are not as difficult to interpret. The choice of examination to follow the patient after therapy is controversial. Many specialized head and neck radiologists rely on contrast-enhanced CT. Others prefer PET/CT as it may increase conspicuity of a recurrence that may not be obvious otherwise. A post-therapy patient with difficulty handling secretions often will have problems with MRI.

Monday Morning

8:45 AM - 10:15 AM
Room 1AB

(6) General Programming: WFNRS Presents: Highlights of the 24th Annual Meeting of SILAN

O-16 **8:45 AM - 8:55 AM**

The Mission, Vision and Trajectory of SILAN

Rojas, R.
Beth Israel Deaconess Medical Center
Brookline, MA.

Presentation Summary
The Mission, Vision, and Trajectory of SILAN. The SILAN Society, whose formal name is "Sociedad Iberolatinoamericana de Neurorradiología Diagnóstica y Terapéutica", is a nonprofit scientific professional organization established in 1988 by the initiative of Dr.

Note: Scanned images are included in the proceedings. Some submitted images were reduced during editing, thereby decreasing clarity. Also, refer to the Program Planner. Proceedings Content as of 3-29-2013.

Juan Taveras and Dr. Fernando Viñuela. The SILAN Society is an inclusive educational society, composed by Spanish and Portuguese-speaking neuroscientists, involved in neuroimaging and neuro-intervention. Its members are neuroradiologists, neurologists, and neurosurgeons from Spain, Portugal, Canada, United States, and all Spanish and Portuguese-speaking countries in America. The goals of the SILAN Society are: • To promote the progress of diagnostic and therapeutic neuroradiology in the member countries. • To develop training programs in neuroradiology, benefiting young talents from the member countries, helping to develop the future generations of neuroimaging and neurointerventional specialists in Latin America, Spain, and Portugal. • To sponsor an annual Scientific Meeting, bringing to a different country each year the latest advances in neuroradiology and neuroscience, through oral communications, scientific exhibits, and educational activities. • To promote the publication of scientific papers in professional journals, emphasizing the participation of young neuroradiologists in training. • To sponsor short-term visiting fellowships and formal training fellowships, in institutions internationally recognized for excellence in the field. Since its establishment, the SILAN Board of Directors had the vision to create various scholarships in diagnostic and interventional neuroradiology. There are currently training scholarships in academic centers in Buenos Aires, Argentina, Barcelona and Zaragoza in Spain, Augusta Georgia, USA, Shreveport Louisiana, USA, and Puerto Rico. The support of our scholarship program has been centered on our recently established SILAN Foundation, created by the initiative of Dr. Alex Berenstein and the SILAN Board of Directors, channeling funds exclusively designated to support and expand our educational mission. The SILAN Society has unfailingly sponsored an annual scientific meeting for the last 25 years, characterized always by high academic standards, acting as the international forum for presenting the latest advances in diagnostic and therapeutic neuroradiology from Europe and Latin America. The SILAN Society is very proud to participate in the 51st Annual Meeting of the American Society of Neuroradiology, presenting some of the highlights of our past conference in Quito, Ecuador in 2012. We want to take this opportunity to invite you to the 25th SILAN Annual Meeting, to be held in Ciudad de Panama on June 17-21, 2013.

O-17 **8:55 AM - 9:15 AM**

Changes that Occur in the Intervertebral Disk in Astronauts Exposed to Zero Gravity

Riascos, R. F.
University of Texas Medical Branch
Galveston, TX.

Presentation Summary
Exposure to microgravity has an effect on the spine of the astronauts, specifically on the intervertebral disks. Astronauts have an increased risk for back pain and intervertebral disk herniation, thought to be a result of the exposure to microgravity. The mechanical forces on the intervertebral disk are different in space, where the lack of cyclic mechanical stressors may reduce the nutrition of the disk, increase its water content and alter the normal configuration of the nucleus pulposus and annulus fibrosus. Disk expansion has been described in astronauts after exposure to prolonged space flight. We will discuss the exercises available to the astronauts in space, and the tests that are performed to detect the cause of these changes in the astronaut population with the terrestrial and in-flight imaging modalities available.

O-18 **9:15 AM - 9:35 AM**

3D STIR and DTI from the Spinal Cord to Peripheral Nerves: Techniques, Tips and Tricks

Vargas, M.
Geneva University Hospital, Neuroradiology
Geneva, SWITZERLAND.

Dr. Vargas was born in Ecuador. She attended secondary school in Ecuador where she graduated summa-cum-laude. She obtained her medical degree in 1994 from the Catholic University of Guayaquil-Ecuador and then worked for one year in the Galapagos-Islands. In 1996 she received a full scholarship from the Swiss government to study radiology at Geneva University. She completed her residency in Radiology in 2001 and achieved radiologist status. She completed a fellowship in neuroradiology at Strasbourg-France in 2002 and returned to Geneva to complete this specialization in 2006. She obtained the title of "Privat Docent" (Assistant Professor) in 2011 and then in 2012 the title of Associated Professor (Charge de Cours) at Geneva University. From 2007 until 2010, she was responsible for the education program in radiology and neuroradiology in the Department of Radiology. She received an award for the management of patients at the MRI unit in 2011. Currently she is Assistant Radiologist, Associated Professor and Head of the MRI section at Geneva University Hospital. Her areas of interest include epilepsy, spinal cord, peripheral nerves, new neuroimaging techniques, PET-MR and management in radiology. She has published more than 70 scientific papers and is also the author of 9 book chapters.

Presentation Summary
The presentation will be divided into two main parts: 3D STIR SPACE and diffusion tensor imaging (DTI). During the presentation the following questions will be answered concerning each technique: What is it? How is it done? What are the limits and clinical indications? Examples of each point mentioned above will be shown at the level of the peripheral nerves and the spinal cord.

Note: Scanned images are included in the proceedings. Some submitted images were reduced during editing, thereby decreasing clarity. Also, refer to the Program Planner. Proceedings Content as of 3-29-2013.

O-19 **9:35 AM - 9:55 AM**

The Good, The Bad and The Ugly of the Flow Diverters for the Treatment of Aneurysms

Diaz, O. M.
The Methodist Hospital
Houston, TX.

Presentation Summary
The Pipeline embolization device (PED) is the only flow diverter FDA-approved on the market today. Flow diverters are tubular stent-like device that are placed within the parent artery crossing the aneurysm neck to divert flow away from the aneurysm to achieve aneurysm occlusion. The advantage of this new modality is seen especially in giant aneurysms, which are very difficult to treat and have a higher incidence of recanalization. As with all stents, dual antiplatelet medication is necessary with its inherent risks that is especially necessary to decrease the incidence of in-stent thrombosis due to the larger lumen of metal. New to this device are delayed aneurysm rupture and intraparenchymal hematoma distal to the aneurysm, which will be discussed.

O-20 **9:55 AM - 10:15 AM**

INR in the Pediatric Population

Berenstein, A.
St. Luke Roosevelt Hospital
New York, NY.

Monday Morning

10:45 AM - 12:15 PM
Ballroom 6AB

(07a) Parallel Scientific Papers: Adult Brain: Dementia and Degenerative Disorders I

O-21 **10:45 AM - 10:53 AM**

Amyloid-β Modulates the Effect of Clusterin on Alzheimer Neurodegeneration

Desikan, R. S.[1]·McEvoy, L.[1]·Thompson, W.[1]·Holland, D.[1]·Brewer, J.[1]·Andreassen, O.[2]·Dale, A.[1]
[1]University of California San Diego, San Diego, CA,
[2]University of Oslo, Oslo, NORWAY.

Purpose
Genome-wide association and biomarker studies indicate that clusterin (CLU) is associated with Alzheimer disease (AD). However, the mechanism by which CLU influences the earliest stages of the Alzheimer disease process is not well understood.

Materials & Methods
We examined 90 cognitively healthy older adults who underwent longitudinal MR imaging and baseline lumbar puncture. Using linear mixed effects models, we evaluated main and interactive effects between CSF CLU and CSF Aβ1-42, and CSF CLU and CSF phospo-tau (p-tau181p) on atrophy rate of the entorhinal cortex. We also examined the relationship between CSF CLU, CSF Aβ1-42, and CSF p-tau181p on atrophy rate of other AD-vulnerable neuroanatomical regions.
Results
We found a significant interaction only between CSF CLU and CSF Aβ1-42 on atrophy rate of the entorhinal cortex and other AD vulnerable regions indicating elevated volume loss in individuals with increased CLU and decreased CSF Aβ1-42. In contrast, we found no interaction between CSF CLU and CSF p-tau181p on brain atrophy.

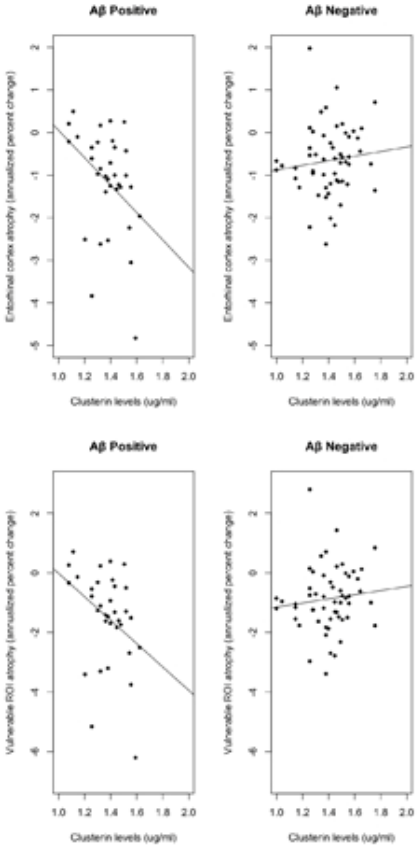

Conclusion
Our findings indicate that in preclinical AD clusterin contributes to AD neurodegeneration predominantly via an Aβ-dependent mechanism.

KEYWORDS: Amyloid, Alzheimer disease, Mild cognitive impairment

Note: Scanned images are included in the proceedings. Some submitted images were reduced during editing, thereby decreasing clarity. Also, refer to the Program Planner. Proceedings Content as of 3-29-2013.

O-22 **10:53 AM - 11:01 AM**

3T MR Spectroscopy Reveals an Imbalance between Excitatory and Inhibitory Neurotransmitters in Amyotrophic Lateral Sclerosis

Foerster, B. R.[1]·Pomper, M. G.[2]·Callaghan, B. C.[1]·Petrou, M.[1]·Edden, R. A. E.[2]·Mohamed, M. A.[2]·Welsh, R. C.[1]·Carlos, R. C.[1]·Barker, P. B.[2]·Feldman, E. L.[1]
[1]University of Michigan, Ann Arbor, MI, [2]Johns Hopkins University, Baltimore, MD.

Purpose
To determine whether there are reductions in γ-aminobutyric acid (GABA) and elevations of glutamate + glutamine (Glx) levels in different brain regions of patients with amyotrophic lateral sclerosis (ALS) using proton magnetic resonance spectroscopy (1H-MRS).
Materials & Methods
Twenty-nine ALS patients and thirty age- and gender-matched healthy controls (HCs) underwent 3T short echo time (TE) and GABA-edited 1H-MRS centered on the left motor cortex (MC) and left subcortical white matter (SWCM). Short TE 1H-MRS also was performed centered on the pons. Data were analyzed using logistic regression, t-tests, and Pearson correlations. Post hoc analyses were performed to investigate differences between riluzole-naïve and riluzole-treated ALS patients.
Results
Amyotrophic lateral sclerosis patients had significantly lower levels of GABA in the MC compared to HCs (P<.01). Amyotrophic lateral sclerosis patients also had significantly lower levels of N-acetylaspartate (NAA) in MC (P<.01), SCWM (P<.05), and pons (P<.01) and higher levels of myo-inositol (mI) in MC (P<.001) and SCWM (P<.01) compared to HCs. Compared to riluzole-treated ALS patients, riluzole-naïve ALS patients had higher levels of Glx in MC (P<.05) and pons (P<.01), higher levels of Cr in MC (P<.001) and SWCM (P=.05), and higher levels of NAA in MC (P<.01).
Conclusion
There are reduced levels of GABA in the motor cortex of ALS patients. There are elevations of Glx in riluzole-naïve ALS patients compared to ALS riluzole-treated patients. These results point to an imbalance between excitatory and inhibitory neurotransmission, contributing to the pathogenesis of ALS.

KEYWORDS: Amyotrophic lateral sclerosis, MR spectrocopy

O-23 **11:01 AM - 11:09 AM**

Sulcal Pattern Analysis Using Earth Mover Distance Differentiates Shunt-Responsive Normal Pressure Hydrocephalus from Alzheimer Disease

Rusinek, H.·Tyagi, V.·Serulle, Y.·Thakur, S.·Nutanson, I.·Gonen, O.·Shepherd, T.·Golomb, J.·George, A.
New York University School of Medicine
New York, NY.

Purpose
In patients with cognitive impairment and dilated ventricles, it can be difficult to differentiate normal pressure hydrocephalus (NPH) from cerebral atrophy associated with Alzheimer disease (AD). Existing radiologic criteria include quantitative volumetry of global gray matter and ventricles, and assessment for hippocampal atrophy. Patterns of sulcal widening also are used to differentiate the two conditions. This study evaluated the quantitative assessment of sulcal size and distribution of sulcal enlargement to distinguish between NPH and AD.
Materials & Methods
Subjects (17 AD, 15 NPH, 11 healthy elderly) received clinical and cognitive evaluation at the NYUMC Aging and Dementia center. High-resolution T1-weighted images (MPRAGE, Siemens 1.5T) from preshunt NPH and AD patients were used. Sulcal masks were obtained by automated segmentation. Masks were partitioned into eight 45^{o} wedges, resulting in a series V(θ), where V is the sulcal CSF volume and θ the polar angle encircling the axial section clockwise (left frontal→left temporal→left parietal→left occipital→right occipital⋯etc). Mean sulcal volume Vavg was computed for each subject and each sector, yielding the relative volume distribution D(θ) = V(θ)/Vavg. Differential earth mover's distance (EMD) measure then was computed for each subject using the NPH group pattern as reference.
Results
Sulcal volume was significantly larger in AD (3.19±0.68, mean±SD) compared to healthy controls (1.79±0.45), p=0.000001, T=6.02. Volume also was increased in NPH (2.87±0.76), p=0.0002, T=4.17 compared to healthy controls, but there was no volume difference between NPH and AD. Sulcal pattern as expressed by EMD, however, differentiated AD (0.482+0.131) from NPH (0.353+0.103), p=0.002, T=3.07 (Figures).

Note: Scanned images are included in the proceedings. Some submitted images were reduced during editing, thereby decreasing clarity. Also, refer to the Program Planner. Proceedings Content as of 3-29-2013.

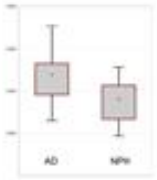

Distribution of sulcal pattern index in AD and NPH groups. Dot = median, box = two middle quartiles, whiskers = minimum and maximum.

Polar plot (in blue) of relative sulcal volume in NPH patients. The green circle indicates homogenous distribution. NPH shows relatively smaller sulci in parietal and temporal lobes, larger sulci in the frontal lobes

Conclusion
Normal pressure hydocephalus is characterized by a predominantly frontal lobe distribution of larger sulci while AD is characterized by a predominately temporal and parietal lobe distribution of large sulci. The observed highly significant pattern difference between NPH and AD patients may help identify candidates for shunt placement.

KEYWORDS: Normal pressure hydrocephalus, Alzheimer disease

O-24 **11:09 AM - 11:17 AM**

Age-Matched Quantitative Atrophy Mapping in a Large Clinical MR Imaging Sample

Wright, B. W.·Anderson, J. S.
University of Utah
Salt Lake City, UT.

Purpose
Although neuroradiologists have long recognized that brains tend to atrophy with age, descriptions of atrophy in radiology reports are seldom more specific than “age-appropriate,” “mild,” “moderate,” or “severe.” Recent work has shown that atrophy in neurodegenerative diseases is not diffuse or random, but rather involves large-scale functional connectivity networks that are correlated with gray matter volume (Seely 2009). Our goals were (1) to identify patterns of atrophy in a large clinical MRI sample and (2) to create age-matched atrophy maps based on these data.
Materials & Methods
Most of the brain MRI exams at our institution currently include an MPRAGE sequence that undergoes brain tissue segmentation using SPM8 software (modulated, normalized). Five hundred (about 40%) of the MRI exams performed during a specified time period met the inclusion criteria of this study: ages 20-80 years, successful segmentation, and no tumor, stroke, or history of intracranial surgery. The tools of source-based morphometry (Xu 2009) were applied to identify independent components with similar covariance across subjects from the segmentation data. A model order of 16 was identified as optimal (Xu 2009) and 10 non-noise components were present by inspection. K-means clustering of voxels in a gray matter restriction mask based on their Z-scores in the independent components produced a 10-cluster parcellation of brain regions showing similar covariance across subjects.
Results
Ten bilaterally symmetric anatomical clusters were identified from the MRI segmentation data, including a frontal cluster, anterior temporal cluster, occipital cluster, and others. Notably, one cluster corresponds anatomically to the posterior nodes of the default mode network, specific brain regions (posterior cingulate/precuneus and bilateral lateral parietal) that demonstrate synchronous activity during rest on fMRI and may be disrupted preferentially in Alzheimer disease. Age-matched atrophy maps based on these 10 clusters appear to be robust to gyral/sulcal variation in individual subjects given the large cluster size.
Conclusion
Based on source-based morphometric analysis of segmented gray matter images from a large clinical MRI sample (n = 500), we have parcellated the brain into 10 clusters that tend to covary similarly across subjects from 20 to 80 years old. Rapidly accessible, evidence-based atrophy maps will enable neuroradiologists to make more specific, clinically relevant observations about quantitative brain atrophy patterns in time consistent with clinical workflow.

KEYWORDS: Brain aging, Brain morphometry, Brain mapping

O-25 **11:17 AM - 11:25 AM**

How Sensitive Are the Proposed Imaging Criteria for the Diagnosis of the Primary Progressive Aphasia?

Sajjadi, S. A.[1]·Sheikh Bahaei, N.[1]·Scoffing, D.[2]·Cross, J.[2]·Gillard, J.[1]·Nestor, P. J.[1]
[1]University of Cambridge, Cambridge, UNITED KINGDOM,
[2]Addenbrooke's Hospital, Cambridge, UNITED KINGDOM.

Purpose
Primary progressive aphasia (PPA) is a major subtype of frontotemporal dementia. It is a clinically and pathologically heterogeneous condition. Nonfluent (nfv), semantic (sv), logopenic (lpv) and mixed PPA are the

Note: Scanned images are included in the proceedings. Some submitted images were reduced during editing, thereby decreasing clarity. Also, refer to the Program Planner. Proceedings Content as of 3-29-2013.

currently recognized variants. To circumvent the uncertainty surrounding the early diagnosis of PPA subtypes on clinical grounds alone, the recent recommendations on classification of PPA have advocated certain patterns of atrophy as supporting features for the diagnosis of PPA variants. Perhaps surprisingly, the recommendations are all based upon group-level statistical comparisons of PPA subjects against control participants. It is, however, unknown whether individual patients present with the prescribed patterns of atrophy. The aim of the present study was to evaluate the utility of the proposed imaging criteria and to assess the neuroradiologists' intra- and inter-rater agreement.
Materials & Methods
The cohort comprised 51 patients with a root diagnosis of PPA and 26 matched control participants. The breakdown of the PPA subjects was 21 svPPA, 14 nfvPPA, 14 mixed PPA, and 2 lvPPA. All study participants were scanned on a Siemens Trio 3T system. T1-weighted anatomical images were acquired using 3D magnetization-prepared, rapid gradient-echo (MPRAGE). Statistical parametric mapping (SPM) implemented in SPM5 was used for group level comparison of patient groups against control participants. Three neuroradiologists - blind to the clinical diagnoses - separately reported all unprocessed T1 sequences. In order to assess intra-observer agreement, 28 scans (N = 7) for each diagnostic group) were duplicated.
Results
There was no statistical difference between the groups for any of the demographic parameters. Assessment of the sensitivity of the proposed imaging markers, based on the lobar distribution of the abnormalities, revealed almost perfect results in the svPPA individuals (Mean: 98%) but low sensitivity in the other PPA variants. Imaging markers were least sensitive for the diagnosis of the nfvPPA participants (Mean: 29%). In terms of the intra-rater agreement values, with the exception of the nfvPPA group the mean kappa values in the other groups were above the widely accepted threshold of 0.6. Pair-wise inter-observer agreement outcome indicated a similar dichotomized pattern of perfect agreement in the svPPA group but only moderate agreement for mixed and nfvPPA.
Conclusion
This study provides the first objective assessment of the utility of the proposed imaging markers in supporting the diagnosis of various PPA variants. While the group level atrophy patterns were in precise agreement with the proposed imaging criteria reliability of the proposed measures at a single-subject level is necessary for determining the diagnostic utility of the proposed criteria.

KEYWORDS: Degenerative, MR imaging brain, Frontotemporal dementia

O-26 **11:25 AM - 11:33 AM**

Objective Criteria Utilizing Unique Midbrain Angle Measurements to Evaluate for Progressive Supranuclear Palsy

Raz, E.[1]·Dietrich, A.[1]·Shields, M.[1]·Pantano, P.[2]·Piattella, C.[2]·Fatterpekar, G.[1]
[1]New York University, New York, NY, [2]Sapienza University, Rome, ITALY.

Purpose
Progressive supranuclear palsy (PSP) is the second most common neurodegenerative cause of parkinsonism (after Parkinson disease). It is characterized by midbrain atrophy, identified qualitatively on imaging as the "hummingbird" sign. However, this appearance is sometimes difficult to assess and also can be seen in patients other than PSP. The purpose of our study was therefore to identify objective measurement criteria to evaluate for midbrain atrophy in routine clinical practice for diagnosing PSP.
Materials & Methods
MR imaging obtained in 15 patients with progressive supranuclear palsy which included a T1-MPRAGE, were identified retrospectively. Thirty healthy age-matched subjects (imaging studies obtained for headache or dizziness with no history of dementia), 15 patients with multiple system atrophy (MSA) and 20 patients with Parkinson disease were used as controls. Two neuroradiologists assessed these studies evaluating three angles: (1) internal ventral cerebral peduncle angle (ivCPA), defined as the angles comprised between the cerebral peduncles, (2) external dorsal cerebral peduncle angle (edCPA), (3) external ventral cerebral peduncle angle (evCPA). The studies were evaluated for any statistically significant difference between the different populations using a t test and an ANOVA. Inter- and intra-observer variability were assessed using a Bland-Altman analysis.
Results
For observer one, the ivCPA, edCPA, and evCPA average measurements were: PSP patients [62º (6.7); 84.6º (13.7); 68.8º (14.6)]; healthy controls [52.2º (9.7); 66.4º (10.8); 81.8º (12.5)]; MSA [55.2º (11.2); 74.2º (14.7); 87.5º (9.4)]; Parkinson disease [54.1º (8.4); 77.3º (9.20); 83º (12.7)]. For observer two, the ivCPA, edCPA, and evCPA average measurements were: PSP patients [75.7º (4.0); 75.7º (4.0); 75.7º (4.0)]; healthy controls [62.2º (7); 59.6º (12.1); 71.5º (13.8)]; MSA [53.4º (7); 75.7º (8.2); 83.4º (4.0)]; Parkinson disease [53.4º (3.0); 73.7º (7.3); 85.7º (9.3)]. A statistically significant difference was noted by both observers in the ivCPA measurements (observer 1: $p<0.001$; observer 2: $p = 0.024$) between PSP and all the other subjects. The other two angles were not significantly difference. The Bland-Altman analysis for inter- and intra-observer variability demonstrated a bias of -6.9º (6.8, -20.4 - 6.7), -25.5º (8.1, -41.8 - -9.2), and -0.6º (11.9, -4.4 - 23.2) for angles ivCPA, edCPA, and evCPA, respectively.
Conclusion
Utilizing unique midbrain angle measurements, especially

Note: Scanned images are included in the proceedings. Some submitted images were reduced during editing, thereby decreasing clarity. Also, refer to the Program Planner. Proceedings Content as of 3-29-2013.

ivCPA measurement, helps to accurately assess for midbrain atrophy in patients with PSP.

KEYWORDS: Parkinson disease, 3D visualization, progressive supranuclear palsy

O-27 **11:33 AM - 11:41 AM**

Brain MR Imaging Findings in Fragile X Premutation Carriers with and without the Fragile X Tremor Ataxia Syndrome

Brunberg, J. A.[1]·Adams, P.[1]·Mu, Y.[2]·Tassone, F.[2]·Seritan, A.[1]·Boyd, A.[1]·Nguyen, D.[2]·Hagerman, P.[2]·Hagerman, R.[1]
[1]University of California Davis, Sacramento, CA, [2]University of California Davis, Davis, CA.

Purpose
FXTAS is diagnosed in aging previously normal relatives of children with mental retardation due to fragile x syndrome, and in elderly patients, having no known family history of childhood cognitive impairment, who present with gait instability, tremor, autonomic instability, neuropathy, and/or cognitive decline. To expand our prior reports of FXTAS-associated MR findings, an independent cohort of control subjects and male fragile-x premutaton carriers, with and without FXTAS, was evaluated.
Materials & Methods
MR imaging was completed in 65 premutation carriers, 52 of whom had FXTAS, and in 37 controls. Clinical neurologic findings sorted the premutation carriers into two groups: those with normal (n = 7) or with only questionable tremor or balance problems (n = 6) who were classified as unaffected, and into those with tremor or balance problems that were mild (n = 13), moderate with occasional falls (n = 19), severe requiring a cane or walker (n = 16), or severe requiring a wheelchair (n = 4), who were classified as having FXTAS. Age, clinical staging, number of CGG repeats in the 5' untranslated X-chromosome region, and psychometric testing were correlated with MR imaging findings. Images were characterized for altered size and T2SI within supratentorial and infratentorial regions of interest. Linear measurements were made of the pons, middle cerebellar peduncles (MCP) and ventricles. Imaging findings in supratentorial and infratentorial ROIs were characterized otherwise as normal or as demonstrating mild, moderate or severe abnormality.
Results
Significant ($p < 0.025$) differences were found between FXTAS and unaffected permutation carriers for the presence of increased T2SI involving MCPs, cerebellar deep WM, pons, subependymal and deep cerebral WM, body and splenium of the corpus callosum, columns of the fornix, and gray and white matter immediately deep to the insular cortex. Significant ($p < 0.025$) volume loss was demonstrated in FXTAS versus unaffected carriers, as enlarged cerebral and cerebellar sulci, as lateral and III ventricular enlargement, as volume loss involving the amygdala and hippocampal gyri, and as diminished dimensions of the pons and MCPs. Mean CGG length was significantly ($p<.0001$) increased in FXTAS (100.3 $\pm$ 18.1) versus asymptomatic carriers (80.8$\pm$ 16.4), and in asymptomatic carriers versus normal controls (28.8 $\pm$ 4.4).
Conclusion
Adult symptomatic fragile-x premutation carriers demonstrate characteristic MRI findings of cerebral, brainstem and cerebellar volume loss, with increased T2SI in MCPs, cerebral and cerebellar WM, in subinsular gray and white matter, and in the body and splenium of the corpus callosum. The presence and severity of imaging findings statistically correlate with clinical staging of tremor and balance dysfunction, with the presence and severity of cognitive and behavioral alterations, and with CGG repeat length in permutation carriers. FXTAS must be included in the differential diagnosis for MR imaging studies obtained on adult subjects presenting with tremor, gait instability and/or cognitive impairment.

KEYWORDS: Degenerative, Encephalopathy

O-28 **11:41 AM - 11:49 AM**

Substantia Nigra in Parkinsonian Disorders: A Multimodal MR Imaging Assessment at 3T

Al-Helli, O.·Massey, L.·De vita, E.·Thornton, J.·Yousry, T.
University College London
London, UNITED KINGDOM.

Purpose
The substantia nigra (SN) is a key nucleus in the pathogenesis, pathology, and treatment of Parkinsonian disorders. It is sometimes difficult to clinically differentiate Parkinson disease (PD) from its mimics - Progressive supranuclear palsy (PSP) and Multi-system atrophy (MSA). We performed a clinico-radiologic, cross-sectional, case-control multimodal MRI study.
Materials & Methods
Fifty-nine subjects were recruited: 20 patients with PD, 20 with PSP and 19 with MSA in addition to 20 age- and gender-matched control subjects were scanned using a multi-sequence MRI protocol that included: multi-echo (3 and 31 echo times) T2 relaxometry, T2* relaxometry and MTR sequences, ROIs were defined on T2-weighted images and transferred to the co-registered T2, T2*, FA and MD maps. SPSS 20.0 for Mac was used for statistical analysis.
Results
There were no between-group differences in age at onset or disease duration. The PSP group had higher clinimetric scores on the Hoehn & Yahr, UPDRS parts II scales. Our T2, T2*, MD and FA values of the STN are comparable to those of previous studies. Values were overlapping between the four subject groups, and did not correlate with age, disease duration or clinimetric scores. T2 obtained using the 31-TE sequence of the posterior part of the SN in the PD patients were significantly lower than in PSP, MSA and

Note: Scanned images are included in the proceedings. Some submitted images were reduced during editing, thereby decreasing clarity. Also, refer to the Program Planner. Proceedings Content as of 3-29-2013.

controls, whereas T2 obtained from 3-TE sequence showed only a trend for lower values. T2* values were lower in the posterior part of the SN in the PD group in comparison to the other groups. However, such difference was not statistically significant. Fractional anisotropy and MD values between disease groups did not show significant differences. Contrary to other studies, we have not found significant correlation between age, duration of disease, clinimetric scales and the measured MRI indices.

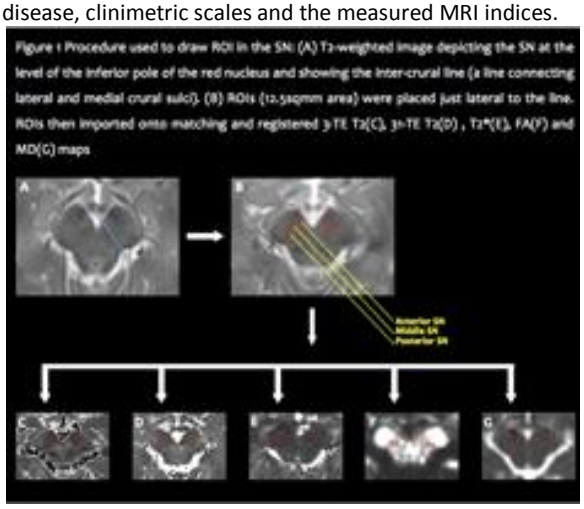

Conclusion

Using 31-TE T2 sequence, there are significant differences in T2 relaxation times in the posterior part of the SN in PD in comparison to control and PSP groups. However, in order to find clinical utility there are several hurdles that need to be overcome including differences in scanning parameters and differences in signal-to-noise ratio between 3T systems at different sites using different systems, and difficulties with reproducing accurate region-of-interest studies between observers particularly in small midbrain structures.

KEYWORDS: 3T, Parkinson disease, Substantia Nigra

O-29 **11:49 AM - 11:57 AM**

Role of Apolipoproteins in Preclinical Alzheimer Disease

Desikan, R. S.[1]·McEvoy, L.[1]·Thompson, W.[1]·Holland, D.[1]·Brewer, J.[1]·Andreassen, O.[2]·Dale, A.[1]
[1]University of California San Diego, San Diego, CA, [2]University of Oslo, Oslo, NORWAY.

Purpose

Epidemiological and genetic studies indicate an association between hypercholesterolemia and Alzheimer disease (AD). Here, we examined the relationship between cerebrospinal fluid (CSF) levels of apolipoproteins (Apo), proteins that bind lipids, and AD-associated neurodegeneration.

Materials & Methods

We examined 90 cognitively healthy older adults who underwent longitudinal MR imaging and baseline lumbar puncture. Using a linear mixed effects model, we evaluated the relationship between CSF levels of Apo A-I, Apo C-III, Apo-D, Apo-E, and Apo-H and entorhinal cortex atrophy rate. We also examined whether an interaction between CSF apolipoprotein levels and CSF $A\beta_{1-42}$, CSF phospo-tau ($p\text{-}tau_{181p}$), and CSF tau effects entorhinal cortex atrophy rate.

Results

We found a significant relationship between CSF Apo C-III and entorhinal cortex atrophy rate. We also found a significant interaction between CSF Apo C-III and CSF $A\beta_{1-42}$ on entorhinal cortex atrophy rate. In the presence of CSF $A\beta_{1-42}$, CSF Apo C-III significantly associated with volume loss of the entorhinal cortex; in the absence of CSF $A\beta_{1-42}$, the relationship between CSF Apo C-III and brain atrophy was not significantly different from zero. We found no interaction between CSF Apo C-III and CSF $p\text{-}tau_{181p}$ or tau on brain atrophy.

Conclusion

Our findings suggest that a synergistic interaction between intracranial lipid biology and amyloid pathology underlies the earliest stages of Alzheimer neurodegeneration. These findings have implications for early AD prevention strategies.

KEYWORDS: Alzheimer disease, Mild cognitive impairment, Inflammation

O-30 **11:57 AM - 12:05 PM**

Application of a Radiologic Severity Score for Brain Amyloid-Related Imaging Abnormality with Edema or Effusion in Phase 3 Clinical Trials of Intravenous Bapineuzumab in Alzheimer Disease

Ketter, N.[1]·Barkhof, F.[2]·Miaux, Y.[3]·Arrighi, H.[1]·Guenzler, V.[1]·Purcell, D.[4]·Gass, A.[5]·Collins, P.[1]·Miloslavsky, M.[1]·McGovern, M.[1]·Morris, K.[1]·Brashear, H.[1]
[1]Janssen Alzheimer Immunotherapy R&D, LLC, South San Francisco, CA, [2]VU University Medical Center, Amsterdam, NETHERLANDS, [3]Synarc, Newark, CA, [4]California Pacific Medical Center, San Francisco, CA, [5]Universitätsklinikum Mannheim, Mannheim, GERMANY.

Purpose

To assess the extent and severity of amyloid-related imaging abnormality with edema (ARIA-E), and other MRI findings in mild to moderate Alzheimer disease patients, in 2 phase 3 placebo-controlled clinical trials of bapineuzumab. Background: ARIA-E is defined by parenchymal or sulcal FLAIR hyperintensity on MRI, consistent with edema or effusion. The relationship of ARIA-E with other MRI findings such as gyral swelling, ARIA-H [(hemosiderin deposition (small HD or microhemorrhages) and Age Related White Matter Changes (ARWMC)] is not well understood.

Materials & Methods

A total of 15,713 MRI scans in 1,331 APOE*E4 noncarriers and 1,121 APOE*E4 carriers were reviewed by five pairs of

Note: Scanned images are included in the proceedings. Some submitted images were reduced during editing, thereby decreasing clarity. Also, refer to the Program Planner. Proceedings Content as of 3-29-2013.

trained neuroradiologists after patients had completed trial participation using a standardized, sequential, locked reading process. Differences in final results within a pair were adjudicated by consensus. The extent and location of sulcal hyperintensity, parenchymal hyperintensity, and gyral swelling were recorded for each brain region in addition to ARIA-H, ARWMC and other findings.
Results
ARIA-E was identified in 243 subjects. The incidence of treatment-emergent ARIA-E was higher in APOE*E4 carriers (active 21.2%; placebo 1.1%) than in noncarriers (active 7.1 %, placebo 0.6%). The mean maximum ARIA-E score was slightly higher in patients treated with the same dose in APOE*E4 noncarriers (14.0) than carriers (12.3); there was a trend towards lower scores when ARIA-E occurred with later infusions in APOE*E4 noncarriers. The overall agreement for the five pairs of neuroradiologists was good for both presence of ARIA-E (kappa 0.73) and ARIA-H (kappa 0.69). For the presence of parenchymal hyperintensity, sulcal hyperintensity and gyral swelling, the kappas were 0.63, 0.72, and 0.70, respectively. Within reader pairs, the intraclass correlation coefficient for severity scores was lowest for gyral swelling, highest for sulcal hyperintensities and intermediate for parenchymal hyperintensities. Gyral swelling was not found in the absence of sulcal/parenchymal hyperintensity. The mean maximum radiologic scores were similar in patients regardless of whether they were dosed through an episode of ARIA-E or not. Patients with pre-existing sHDs at baseline had a higher incidence of ARIA-E. There was a higher incidence of treatment-emergent sHDs in APOE*E4 carriers than noncarriers and a higher incidence with increasing dose in noncarriers. The incidence proportion of ARIA-E was higher in patients with a higher ARWMC score. The presence of radiologic evidence of ARIA-E generally was not associated significant clinical symptoms. Preliminary analyses did not show evidence of ARIA-E-associated decline in cognition or function.
Conclusion
Slightly higher total maximum ARIA-E radiologic scores were noted in APOE*E4 carriers at the equivalent dose; the highest scores were seen with ARIA-E that occurred early in APOE*E4 noncarriers. Bapineuzumab dosing may not need to be withheld in the presence of asymptomatic ARIA-E as continued dosing was not associated with a worse radiologic or clinical outcome. A relationship of the severity of ARIA-E to presence and quantity of amyloid remains to be assessed. The radiologic score of ARIA-E may be a useful parameter when differentiating doses or treatments and the scale provides a reliable quantitative assessment of radiologic severity and location.

KEYWORDS: Alzheimer disease, MR imaging brain, ARIA

O-31 **12:05 PM - 12:13 PM**

Heart Fatty Acid Binding Protein: A Biomarker for Alzheimer Disease

Desikan, R. S.[1]·McEvoy, L.[1]·Thompson, W.[1]·Holland, D.[1]·Brewer, J.[1]·Andreassen, O.[2]·Dale, A.[1]
[1]University of California San Diego, San Diego, CA, [2]University of Oslo, Oslo, NORWAY.

Purpose
Epidemiological and experimental findings suggest a relationship between Alzheimer disease (AD) and dyslipidemia. Here we evaluated the feasibility of using heart fatty acid binding protein (H-FABP), a carrier protein of fatty acids, as a diagnostic and prognostic marker of AD neurodegeneration.
Materials & Methods
We assessed longitudinal structural magnetic resonance imaging and baseline cerebrospinal fluid (CSF) levels of H-FABP, amyloid-β (Aβ1-42), tau and phospho-tau (p-tau181p) in 229 nondemented individuals (90 cognitively normal older adults and 130 memory impaired individuals). For comparison, we also evaluated 69 patients with AD.
Results
Cerebrospinal fluid H-FABP and H-FABP/Aβ levels differentiated patients with AD from cognitively normal older adults. Among individuals with memory impairment, CSF H-FABP/ Aβ1-42 levels significantly predicted time to progress to AD. Among nondemented older individuals, CSF H-FABP levels significantly correlated with CSF levels of Aβ1-42, tau, and p-tau181p and longitudinal atrophy of the entorhinal cortex and other AD-vulnerable brain regions. In a linear mixed effects model, there was a significant interaction between CSF H-FABP and CSF Aβ1-42 on atrophy of the entorhinal cortex and other AD-vulnerable brain regions. In the presence of Aβ1-42, CSF H-FABP was significantly associated with volume loss; in the absence of Aβ1-42, there was no relationship between CSF H-FABP and brain atrophy. There was no interaction between CSF H-FABP and CSF tau or CSF p-tau181p on atrophy of the entorhinal cortex and other AD-vulnerable brain regions.

Note: Scanned images are included in the proceedings. Some submitted images were reduced during editing, thereby decreasing clarity. Also, refer to the Program Planner. Proceedings Content as of 3-29-2013.

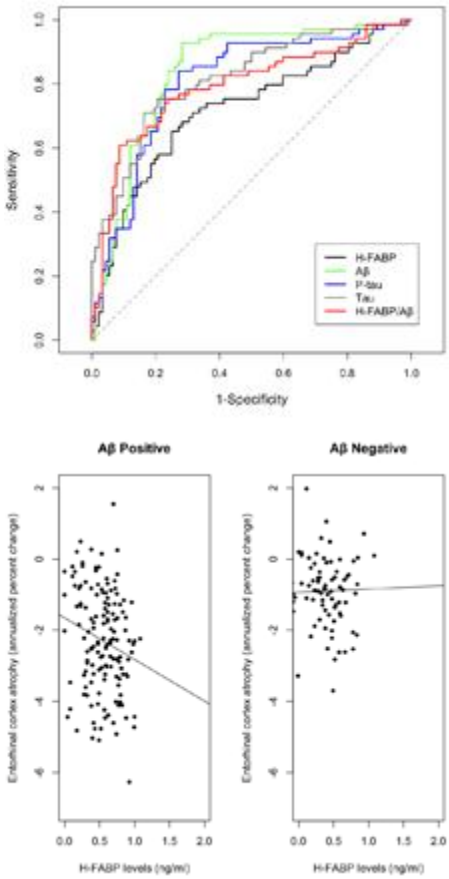

Conclusion
Our findings suggest the diagnostic and prognostic utility of CSF H-FABP and H-FABP/ Aβ1-42 as an AD biomarker. These results also indicate that a synergistic interaction between lipid biology and Aβ pathology underlies Alzheimer neurodegeneration.

KEYWORDS: Alzheimer disease, Mild cognitive impairment, Biomarker

Monday Morning

10:45 AM - 12:15 PM
Ballroom 6CF

(07b) Parallel Scientific Papers: Functional Imaging I: fMRI and DTI

O-32 **10:45 AM - 10:53 AM**

Direct Intracranial Stimulation and Simultaneous Functional MR Imaging Using Implanted Electrodes

Jones, S.·Avitsian, R.·Bhattacharyya, P.·Bulacio, J.·Enatsu, R.·Gonzalez-Martinez, J.·Nair, D.·Najm, I.·Phillips, M.·Zhang, M.
Cleveland Clinic Foundation
Cleveland, OH.

Purpose
Cortico-cortical evoked potentials (CCEPs) use direct intracranial electrical stimulation (DES) and recording to study electrophysiologic connectivity (EC), helping identify the epileptogenic zone (EZ) and networks and guide resective surgery. The fMRI BOLD response also can reveal networks. We present the first investigation of simultaneous BOLD response to DES using stereotactic EEG (SEEG) electrodes. Unlike prior related studies, we compare stimulated EC and BOLD activation throughout the brain, in human subjects and in the context of intractable epilepsy.
Materials & Methods
Epilepsy patients undergoing invasive surgery evaluation were implanted with up to 16 SEEG electrodes. Cortico-cortical evoked potentials were recorded while stimulating the hypothesized EZ and non-EZ control areas (1Hz, 8mA), using the RMS as a measure of EC. During explantation, one electrode remained for stimulation, and fMRI was performed in an intraoperative MRI while under general anesthesia, using a block paradigm for DES. Four acquisitions included 20Hz stimulation of the hypothesized EZ at low (4mA) and high (8 or 15mA) current, with similar control stimulation of distal contacts. Functional MRI analysis used AFNI. Extensive safety testing on phantoms preceded this investigation. Seven patients have been imaged to date.
Results
The figure shows a typical pattern of BOLD activation(threshold $|t| > 3$), with signal changes up to 4%. Stimulated contacts (15mA) were in the medial left orbitofrontal lobe (arrow), deemed in the EZ. There is strong network activation in the limbic system, extending to the hippocampus and lateral orbitofrontal lobe. Also evident is strong negative activation. Cortico-cortical evoked potentials activity at recording contacts showed significant correlation with fMRI *t*-values (r = .45, p = 8.6e-

Note: Scanned images are included in the proceedings. Some submitted images were reduced during editing, thereby decreasing clarity. Also, refer to the Program Planner. Proceedings Content as of 3-29-2013.

6). Other patients also showed activation networks, with varying CCEP-fMRI correlation (*r* between .2 and .6). Activated networks are similar for low and high current stimulation. Two patients showed greater activation when stimulated in the EZ versus non-EZ, while two others showed the opposite pattern. Low frequency stimulation (10Hz and lower) showed no BOLD response.

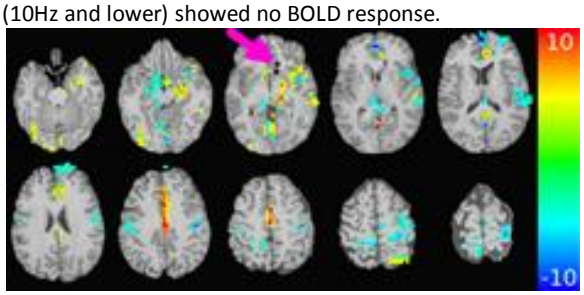

Conclusion
To our knowledge, we present the first simultaneous DES-fMRI experiment in humans with comparison to EC. Further experiments will explore optimal stimulation parameters and effects of the EZ, but early data show stimulated fMRI patterns are consistent with CCEPs. Given the clinical utility of CCEPs and complete spatial coverage afforded by fMRI, this technique has great potential for aiding epilepsy surgery. Studying CCEPs and BOLD in tandem can improve our understanding of both processes, in particular basic mechanisms of BOLD.

KEYWORDS: BOLD fMRI, Intracranial electrodes, Direct Electrical Brain Stimulation

O-33 **10:53 AM - 11:01 AM**

Role of the Secondary Motor and Language Cortices in Postoperative Morbidity and Mortality: A Retrospective Functional MR Imaging Study of Surgical Planning for Patients with Intracranial Tumors

Maksimovic, J. H.·Voss, J.·Meier, T.·Friedel, R.·Prabhakaran, V.
University of Wisconsin
Madison, WI.

Purpose
Functional magnetic resonance imaging (fMRI) commonly is utilized by neurosurgeons to pre-operatively identify brain regions associated with essential behaviors, such as language and motor abilities. This study investigated the relationship between the distance from tumor border area to functional activations in secondary motor and language cortices to patient morbidity and mortality.
Materials & Methods
Subjects were selected from a database of 423 patients who received pre-operative fMRI at the University of Wisconsin Hospital and Clinics between June 1999 and July 2011. Of these, 52 patients had tumors encroaching on the secondary motor area and 72 patients had tumors encroaching on the secondary language area. The lesion-to-activation distance (LAD) was measured in each subject relative to the supplementary motor area for motor tasks and pre-supplementary motor area for language tasks. The LAD were categorized into the following: 1) less than 1 cm, 2) between 1 and 2 cm, and 3) greater than 2 cm. The association between LAD and the incidence of deficits was investigated using Fisher's exact tests of significance. Any record of preoperative or postoperative weakness and/or aphasia was included in the analysis as deficits. Mortality information was collected for all patients using medical records that were cross referenced with multiple sources. The impact of other variables, including age, handedness, gender, and tumor grade also were investigated. In a subset of subjects, logistic regression was performed to identify the likelihood of deficits based on LAD to primary and secondary regions. Finally, Mantel-Cox log-rank tests were performed to determine whether survival time significantly related to LAD to secondary motor and language areas.
Results
A significant association was observed between LAD to the SMA and the incidence of motor deficits, with the percentage of patients with deficits dropping for those in the LAD > 2 cm group. The relationship between LAD to the pSMA and the incidence of language deficits was not significant. Logistic regression demonstrated that the LAD to primary sensorimotor cortex does affect the incidence of motor deficits, but LAD to SMA does not. Finally, we observed no relationship between LAD to secondary regions and patient mortality.
Conclusion
This investigation of the relationship between tumor distance to fMRI responses in secondary language and motor areas shows a significant association with the incidence of language and motor deficits. These results demonstrate that LAD to SMA structures does affect morbidity, although not to the extent of LAD to primary structures. In addition, motor deficits are significantly associated with LAD to secondary structures, but language deficits are not. This should be considered by neurosurgeons for patient consultation and pre-operative planning.

KEYWORDS: fMRI, Neoplasm, Supplemental Motor Area

O-34 **11:01 AM - 11:09 AM**

Changes in Functional MR Imaging Functional Connectivity of Distributed Neural Networks after Selective Thalamic Ablation in Humans

Druzgal, T. J.·Wintermark, M.·Huss, D.·Loomba, J.·Khaled, M.·Frysinger, R.·Monteith, S.·Sperling, S.·Elias, J.
University of Virginia
Charlottesville, VA.

Purpose
Magnetic resonance-guided focused ultrasound (MRgFUS) is an emerging technology for performing targeted

Note: Scanned images are included in the proceedings. Some submitted images were reduced during editing, thereby decreasing clarity. Also, refer to the Program Planner. Proceedings Content as of 3-29-2013.

neurosurgery without skin incisions. In a cohort (n = 15) of patients with essential tremor, we have used MRgFUS to ablate the ventral intermediate nucleus (Vim) of the thalamus corresponding to the dominant hand of each patient. For the majority of our patients, the clinical results of this trial have been striking, immediate, and durable at one-year followup. Compared to the established treatment of deep brain stimulator placement, the MRgFUS technique also provides a unique opportunity to use blood oxygen level dependent (BOLD) functional magnetic resonance imaging (fMRI) to study the effects of focal brain lesions on distributed neural networks.
Materials & Methods
Resting-state BOLD fMRI data and MPRAGE anatomical data were obtained successfully from 14 patients on a Siemens Trio MRI. Data were obtained both before and after unilateral Vim ablation with MRgFUS. The Data Processing Assistant for Resting-State fMRI Advanced Edition (DPARSFA) was used both for data preprocessing and to assess changes in the temporal synchrony of the motor networks as a result of the MRgFUS ablation. DPARSFA preprocessing included steps of: fMRI data realignment, coregistration of anatomical and fMRI data, nuisance covariate regression, and motion scrubbing. After calculation of functional connectivity metrics - such as degree centrality - the output data for each subject was normalized to a standard template brain. If individual voxels within brain regions are characterized as nodes in a larger network, degree centrality of each node can be characterized by the edges connected to each node. The edges in the network are defined by peak cross-correlation of resting state functional MRI time series between individual nodes. The strength of each node is defined as the sum of weights from edges connecting to a node. For an individual voxel, this sort of analysis represents an assay of how closely its activity is tied to activity in the remainder of the brain.
Results
Degree centrality analyses reveal that focal ablation of the Vim nucleus of the thalamus has broad effects in the node strengths throughout the core of the motor network (primary motor cortex, premotor cortex, and cerebellum). In addition, changes in functional connectivity extend to frontal regions not typically described as core motor areas. Several of these frontal regions have been suggested to perform general control and inhibition that modify basic motor phenomena.
Conclusion
These findings begin to suggest mechanisms whereby neurodegeneration of deep gray nuclei (a common theme across several movement disorders) may result in the more subtle cognitive effects associated with conditions such as essential tremor.

KEYWORDS: fMRI, Focused ultrasound, Tremor

O-35 **11:09 AM - 11:17 AM**

Longitudinal Changes in BOLD Functional Connectivity after Mild Traumatic Brain Injury Revealed by Serial Resting-State Functional MR Imaging

Liu, C. J.·Li, Y.·Cooper, S. R.·LaHue, S. C.·Manley, G. T.·Mukherjee, P.
University of California San Francisco
San Francisco, CA.

Purpose
Cognitive impairment following mild traumatic brain injury (mTBI) has been hypothesized to result from disruption of white matter tracts connecting disparate brain regions. We use resting-state functional MRI (fMRI) to investigate longitudinal changes in functional connectivity following mTBI.
Materials & Methods
Twenty-two subjects who have suffered mTBI (Glasgow Coma Scale 13-15 in the Emergency Department), with loss of consciousness less than 30 minutes and post-traumatic amnesia less than 24 hours, underwent resting state fMRI at <2 weeks after the injury and again at six months after the injury. All mTBI patients were imaged on a 3T scanner with a whole-brain 2D multislice single-shot gradient echo blood oxygenation level-dependent (BOLD) sequence (TE 28 ms, TR 2000 ms). Two hundred brain volumes were collected in seven minutes. The data were analyzed after correction for subject motion supplied in the FMRIB Software Library (FSL) toolbox. Fifteen seed regions of interest (ROIs) for computing resting-state networks were chosen from a literature review of BOLD functional connectivity following head trauma. A one-sample randomized test was performed to generate the group level functional connectivity map, with a two-tailed two-sample nonparametric permutation test applied to z-scores on voxels with group significance from the one sample test to examine for statistically significant group differences within subjects between the <2 weeks and six-month time points. The resulting difference maps were thresholded by cluster area size and then corrected for multiple comparisons at a false discovery rate of $p < 0.05$.
Results
Comparisons of the functional connectivity maps of mTBI subjects at <2 weeks versus six months after injury demonstrates decreasing connectivity over time in the right supramarginal gyrus and right precuneus at six months compared to the acute time point. There is increasing connectivity at six months compared to <2 weeks in bilateral orbitofrontal cortex, anterior cingulate gyrus, inferior temporal gyrus, amygdala, caudate, and thalamus.

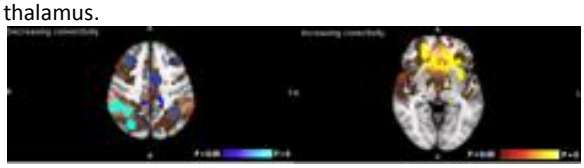

Note: Scanned images are included in the proceedings. Some submitted images were reduced during editing, thereby decreasing clarity. Also, refer to the Program Planner. Proceedings Content as of 3-29-2013.

Conclusion
The serial resting-state fMRI findings demonstrate statistically significant changes in functional connectivity between acute and chronic time points after mTBI. Some regions show decreasing connectivity over time, whereas others show increasing connectivity. These complex patterns may result from both long-term degenerative changes following mTBI as well as compensatory changes such as neuroplasticity.

KEYWORDS: Resting-state fMRI, TBI

O-36 **11:17 AM - 11:25 AM**

Tracking Prediction Error Learning Signals Using Computational Functional MR Imaging in Substance Dependence

Tanabe, J. L.[1]·Reynolds, J.[2]·Krmpotich, T.[1]·Claus, E.[3]·Thompson, L.[1]·Du, Y.[1]·Banich, M.[4]
[1]University of Colorado Denver, Denver, CO, [2]Denver University, Denver, CO, [3]Mind Research Network, Albuquerque, NM, [4]University of Colorado Boulder, Boulder, CO.

Purpose
Substance dependent individuals (SDI) make poor decisions. Goal-directed decision-making depends upon several factors, including how sensitive individuals are to feedback and how well they learn based on such feedback. A physiologic signal known as prediction error (PE) guides decision-making based on feedback, is carried by striatal dopamine, and is hypothesized to be involved in the pathophysiology of drug addiction. *The current study tested the hypothesis that compared to controls, Substance dependent individuals would show altered processing of frontal-striatal PE during goal-directed decision-making.*
Materials & Methods
Thirty-two SDI and 30 controls performed a decision-making task during fMRI scanning. Behavior and fMRI blood-oxygen-level-dependent (BOLD) signal were modeled using a computational model of PE. Tracking of PE was compared across group using a 2-sample t-test. Statistical threshold was set at voxel-level of $p < 0.005$, uncorrected, and $p < 0.01$ whole-brain cluster-corrected, corresponding to an extent threshold of 39 voxels based on 10,000 Monte Carlo simulations.
Results
In controls, trial-to-trial PE tracked most strongly in the striatum and medial OFC consistent with expected loci of prediction error processing and previous model-based fMRI studies (left Figure). Compared to controls, SDI showed weaker tracking of PE in medial OFC (right Figure) and striatum. Substance dependent individuals also showed significantly lower performance on the task.

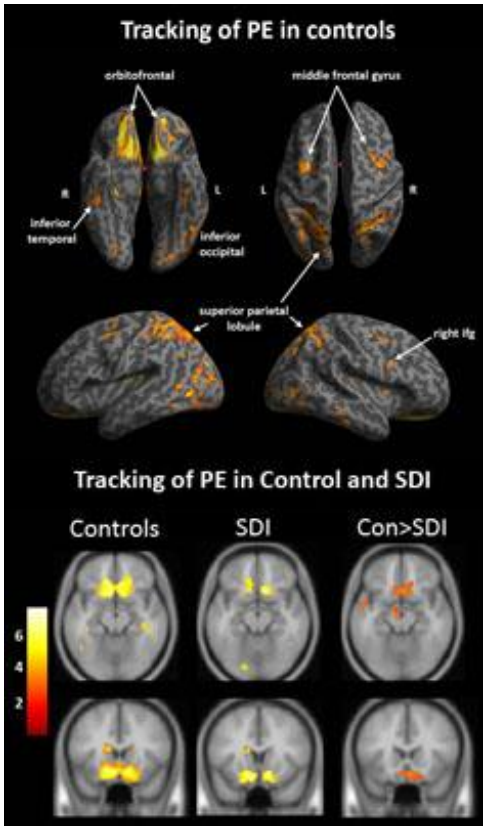

Conclusion
Decreased neural tracking of PE in SDI suggests that learning processes involving frontal-striatal regions may contribute to decision-making deficits in substance dependence. Our findings also suggest that computational model-based fMRI can provide a mechanistic account of learning impairments in clinical populations.

KEYWORDS: Cognition disorders, Psychiatry, computational model

O-37 **11:25 AM - 11:33 AM**

Magnetoencephalography Imaging Reveals Reduced Cortical Activity in Patients with Traumatic Brain Injury During Re-Orienting of Visuospatial Attention

Dale, C. L.·Luks, T. L.·Findlay, A. M.·Tarapore, P. E.·Cooper, S. R.·LaHue, S. C.·Lee, H. A.·Honma, S. M.·Mizuiri, D.·Nagarajan, S. S.·Mukherjee, P.
University of California San Francisco
San Francisco, CA.

Purpose
Traumatic brain injury (TBI) often produces chronic deficits in cognitive function that affect patients' quality of life. To investigate attention-related neural activity differences associated with TBI, we measured whole-head magnetoencephalography (MEG) signals during a cued visuospatial attention task.
Materials & Methods

Note: Scanned images are included in the proceedings. Some submitted images were reduced during editing, thereby decreasing clarity. Also, refer to the Program Planner. Proceedings Content as of 3-29-2013.

Magnetoencephalography data from 19 patients with mild-to-moderate symptomatic TBI and 18 healthy control participants were analyzed using an adaptive spatial filtering technique (NUTMEG, http://bil.ucsf.edu/nutmeg), and coregistered to individual brain anatomy prior to normalizing images for within- and between-group comparisons. We examine high gamma band activity (63-117 Hz) arising from Incongruently- versus Congruently-cued target stimuli.

Results

Using Family-wise Error (FWE) correction for comparisons across voxels, in healthy participants we observe activations in left middle frontal gyrus (LMFG) from 100 to 175 ms, followed by largely concurrent right hemisphere activity from 175 to 300 ms in areas of right inferior parietal sulcus (RIPS), insula, putamen, and superior temporal cortex and, subsequently, at ~325 ms left inferior frontal cortex for a 50 ms period. In these regions, TBI patients exhibited reduced activity relative to healthy participants and, as a group, showed no alternate compensatory pattern of activity that survived the FWE correction threshold. Linear discriminant analyses revealed that activity levels in just two of these five regions, LMFG and RIPS, reliably predicted injury status. Furthermore, activity in LMFG showed negative correlation with both the Head Injury Symptom Checklist for postconcussive syndrome (HISC-PCS) and a measure of cognitive failures.

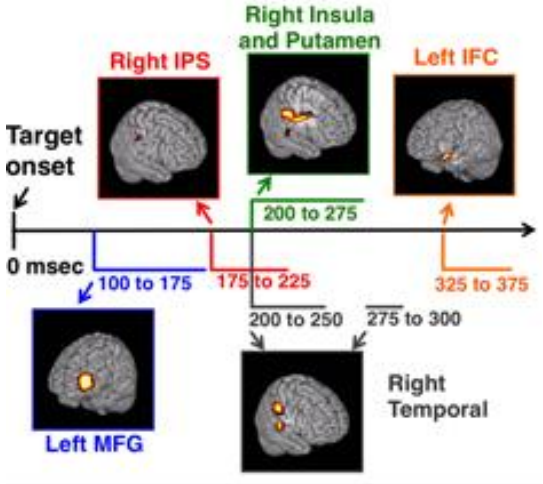

Conclusion

These results suggest reduced activation due to TBI within a frontotemporal high-gamma oscillatory network subserving spatial attention.

KEYWORDS: Traumatic brain injury, MEG, Attention

O-38 **11:33 AM - 11:41 AM**

Regional Abnormally High Aniostropy Predict Better Attention Three Months following Mild Traumatic Brain Injury

Lewkowitz-Shpuntoff, H. M.·Rosenbaum, S.·Kim, N.·Avner, S.·Provataris, J.·Smith, J.·Zimmerman, M.·Lipton, R.·Lipton, M.
Albert Einstein College of Medicine
Bronx, NY.

Purpose

Low fractional aniosotropy (FA) has been widely reported as a manifestation of mild traumatic brain injury (mTBI) pathology. Abnormally high FA also has been reported, but its pathologic and prognostic implications are an area of uncertainty. The purpose of this study was to assess the relationship of abnormally high FA, identified at the time of mTBI, with attention performance three months later.

Materials & Methods

Twenty-four patients meeting diagnostic criteria for mTBI were recruited from a local emergency center, and 40 healthy volunteers were recruited via advertisement. T2-weighted FLAIR and SWI images disclosed no abnormalities. DTI was performed at 3T (32 directions, b = 1000) within two weeks of injury and tests of attention were administered three months post injury using a computer-based battery. Regions of abnormally low FA and abnormally high FA were identified using a voxelwise t-test ($p<0.05$, corrected) comparing the patient and control groups. Additionally, voxelwise Z-score maps were computed for each patient based on the control group, with bootstrap resampling of the variance and thresholding at $p<0.05$, corrected. Predictor variables were the number of voxels of abnormally high or abnormally low FA, both across the entire brain and within regions (frontal, temporal and parietal white matter) expected to be substrates of attention function. Measures derived from occipital white matter and internal capsule served as controls. The association between the number of voxels with abnormally high or low FA and attention was assessed using Spearman's rank correlation analysis.

Results

We detected significant associations between the number of voxels with high FA and better attention performance at three months post injury in the right parietal white matter ($p = .001$, $n = 24$, $R = .647$), the right temporal white matter ($p = .047$, $n = 24$, $R = .408$). No significant association of number of voxels with abnormally high FA and attention was found in the remaining control regions: right internal capsule ($p = .092$, $R = .352$), or the occipital lobes (Right: $p = .773$, $R = .062$ and Left: $p = .775$, $R = .071$) Only one control region, the left internal capsule, showed a significant association with attention ($p = .033$, $n = 24$, $R = .436$).

Conclusion

Higher regional volume of white matter (number of voxels) containing abnormally high FA predicts better attention

Note: Scanned images are included in the proceedings. Some submitted images were reduced during editing, thereby decreasing clarity. Also, refer to the Program Planner. Proceedings Content as of 3-29-2013.

performance three months after mTBI. Supranormal aniosotropy in these regions may indicate a neuroplastic response to the injury rather than injury pathology per se.

KEYWORDS: Mild TBI, Diffusion tensor image, Attention

O-39 **11:41 AM - 11:49 AM**

Relationship between Lesion Distance to Diffusion Tensor Imaging White Matter Tracts and Postoperative Speech Deficits

Holdsworth, R.·Hussain, N.·Greenstein, M.·Huss, D.·Voss, J.·Prabhakaran, V.
University of Wisconsin Hospital
Madison, WI.

Purpose
Prior research, including our own work (Wood et al, 2011), has shown that intracranial mass lesions located within 1-2 cm of an eloquent region of cerebral cortex identified by functional magnetic resonance imaging (fMRI) is associated with increased incidence of postoperative deficits. Our purpose was to see if this relationship also applies to the distance between an intracranial lesion and the specific white matter tracts which connect these functional areas with the hypothesis that lesions less 2 cm from major functional white matter tracts would have an increased incidence of postoperative deficits.
Materials & Methods
In retroprospective fashion, we evaluated 60 patients with an intracranial mass lesion who had both pre-operative DTI mapping and subsequently underwent surgical lesion resection. Distance between the lesion and the superior longitudinal fasciculus, corticospinal tracts, and cingulum were measured using diffuse tensor imaging (DTI) maps overlaid on anatomical MR imaging. Patients with postoperative speech deficits were identified by a systematic review of the electronic medical record.
Results
Of the 60 patients enrolled, 23 patients had postoperative speech deficits, 13 of which were new deficits compared to pre-operative evaluation. Of all patients with postoperative speech deficits, a significantly higher proportion had lesions less than 2 cm from the left superior longitudinal fasciculus ($p = 0.016$). In subgroup analysis of the patients with new postoperative speech deficits, a higher proportion had lesions less than 2 cm from the left superior longitudinal fasciculus which trended towards significance ($p = 0.058$). The odds ratio of having lesions less than 2 cm from the left superior longitudinal fasciculus and all postoperative speech deficits or new postoperative speech deficits were 0.94 ($p<0.001$) and 0.96 ($p = 0.04$), respectively.
Conclusion
Patients with lesions less than 2 cm from the left superior longitudinal fasciculus are more likely to experience postoperative speech deficits. These results are similar to our previous work regarding the distance between an intracranial lesion and a region of eloquent cortex identified by fMRI. Work is ongoing to further evaluate this association and the possible association between lesion distance to other white matter tracts and postoperative deficits; for example, the corticospinal tracts and postoperative motor deficits.

KEYWORDS: Diffusion tensor image, Functional outcome

O-40 **11:49 AM - 11:57 AM**

Changes in Regional White Matter Integrity in the Prefrontal Cortex in Patients with Systemic Lupus Erythematosus

Sundgren, P. C.[1]·Cagnoli, P.[2]·Wang, P.[2]·Schultz, T.[3]·McCune, J.[2]·Schmidt-Wilcke, T.[4]
[1]Lund University, LUND, SWEDEN, [2]University of Michigan, Ann Arbor, MI, [3]Max Planck Institute, Tübingen, GERMANY, [4]Ruhr Universität Bochum, Bochum, GERMANY.

Purpose
Systemic lupus erythematosus (SLE) is an autoimmune connective tissue disease that can affect the central nervous system with neuropsychiatric symptoms variously reported to occur in 25-70% of patients with SLE. Although clinical assessment is the cornerstone of the SLE diagnosis, confirmation of the diagnosis is difficult and presumptive. The purpose was to investigate if regional differences in white matter integrity exist between a) patients with SLE and healthy controls (HCs) and b) between SLE with neuropsychiatric symptoms (NPSLE) and those without neuropsychiatric symptoms (non-NPSLE) patients. The second aim was to test whether it is possible to build a classifier(e.g., a support vector machine) to differentiate between patients with SLE and HCs, respectively between NPSLE and non-NPSLE patients.
Materials & Methods
dMRI images (15 gradient directions at b=800s/mm^2, plus one b=0 image) were obtained, using a 3T MR scanner, of 19 NPSLE patients, 19 SLE and 18 healthy controls HCs. Image preprocessing and statistical analyses were performed using FSL, following the standard TBSS pipeline. A general linear model with threshold-free cluster enhancement was used to assess significant differences between the three groups (HC versus SLE; HC versus NPSLE; non-NPSLE versus NPSLE) while correcting for FWE with permutation testing; age was included as a covariate of no interest. For classification, we used fraction anisotropy (FA) values at all 102,898 skeleton voxels as a feature vector. Fractional anisotropy values in each voxel were weighted by their F score, in order to decrease the weight of voxels less relevant to the classification task. Classification accuracy was estimated by training a linear support vector machine on the resulting vectors in a leave-one-out manner; care was taken to exclude test data from feature weighting via the F score.
Results

Note: Scanned images are included in the proceedings. Some submitted images were reduced during editing, thereby decreasing clarity. Also, refer to the Program Planner. Proceedings Content as of 3-29-2013.

Statistical analyses revealed decreased FA in several regions in the prefrontal white matter both in non-NSLE and NPSLE patients. The regions of significant changes in the NPSLE patients were larger than in the non-NSLE patients. In a post-hoc analysis, those additional areas were found to exhibit an FA decrease also in the non-NPSLE cohort, albeit below the $p<0.05$ significance threshold. Classification analyses revealed a better than chance classification when testing all SLE patients versus HCs (82%), NPSLE patients versus HCs (70%), and non-NPSLE patients versus HC (68%). In all cases, a binomial test rejected the null hypothesis that these results were achieved by chance($p<0.05$). It was not possible to classify non-NPSLE versus NPSLE patients (40% accuracy, not significantly different from chance).
Conclusion
Our data suggest that changes in regional white matter integrity, in terms of a decrease in FA, are present in SLE patients (as compared to HCs) in the prefrontal cortex, especially in NPSLE patients. Fractional anisotropy images in this study were suited to distinguish between SLE patients and HCs, but not between NPSLE and non-NPSLE, which might be indicative of white matter involvement in both types of SLE. Further research is needed to investigate the underlying neurobiology of white matter changes, and to determine whether neurocognitive deficits and fatigue, are related to these changes.

KEYWORDS: Systemic lupus erythematosus, Diffusion tensor image

O-41 **11:57 AM - 12:05 PM**

Evaluation of Functional MR Imaging during Virtual Tennis Playing

Demirci, A.·Demirci, D.·Anik, Y.·Akansel, G.·Kaya, A.
Kocaeli University
Kocaeli, TURKEY.

Purpose
To identify the brain areas activated in viewing and thinking of the response while watching video of tennis play, filmed from the subject's perspective across the opponent, to compare activation areas among tennis players and no players.
Materials & Methods
Via 3T MR scanner, in a block-design, functional MR imaging (fMRI) study, 29 tennis players, 25 sedentary as a control group watched video clips of tennis play. The main stimulus conditions were (1) watch the play and think of what to do subsequently, (2) resting lack of watching. Brain activation regions were delineated and areas under those regions were compared among both groups.
Results
In tennis players activation was seen on optic nerves, optic tractus, lateral geniculate nucleus, occipital cortex, calcarine sulcus, superior temporal gyrus and sulcus, middle temporal gyrus, precuneus, precentral gyrus, midfrontal gyrus, right inferior frontal gyrus, angular gyrus and short gyri of insula. The whole activation areas were significantly greater in tennis players compared with that of the control group ($p = 0.002$). There was a linear moderate significant correlation among activation areas and years of tennis playing ($p = 0.013$, $r = 0.457$).
Conclusion
Perceptual skills improve significantly in tennis players, and this can be shown by fMRI.

KEYWORDS: 3T

O-42 **12:05 PM - 12:13 PM**

Does Gender Affect the Functional MR Activation during Working Memory after mTBI?

Chen, C.·Chen, D.·Liao, Y.·Wang, W.·Ku, J.·Huang, Y.
Taipei Medical University/Shuang Ho Hospital
Taipei, TAIWAN.

Purpose
It is controversial in the literature whether female gender is a protective factor or aggregative factor in mild traumatic brain injury (mTBI). The aim of this study is to evaluate the influence of gender on working memory activation in functional magnetic resonance imaging (fMRI) after mTBI.
Materials & Methods
Research ethics committee approval and patient written informed consent were obtained. Brain activation patterns in response to a working memory task (n-back; 1 and 2-back conditions) were assessed with fMRI on a 3T MR system in 34 mTBI patients (male:female = 1:1) within one month after their injury and in 34 age-matched healthy control subjects (male:female = 1:1). Resting-state fronto-parietal attention network (FPN) also was analyzed by independent component analysis (ICA) method using "Group ICA for fMRI toolbox" (GIFT version 2.0d).
Results
In the male group, the patients had more activation than controls in bi-frontal and bi-parietal regions (in 2b > 1b condition, p-value < 0.001). The male patients had decreased functional connectivity in bilateral FPN than controls. This could be explained by a compensatory working memory activity (i.e., think hard) in male patients due to the disruption of their fronto-parietal connectivity. In the female group, there was no significant signal change between the patients and controls in working memory activation (in 2b > 1b condition, p-value < 0.001).

Note: Scanned images are included in the proceedings. Some submitted images were reduced during editing, thereby decreasing clarity. Also, refer to the Program Planner. Proceedings Content as of 3-29-2013.

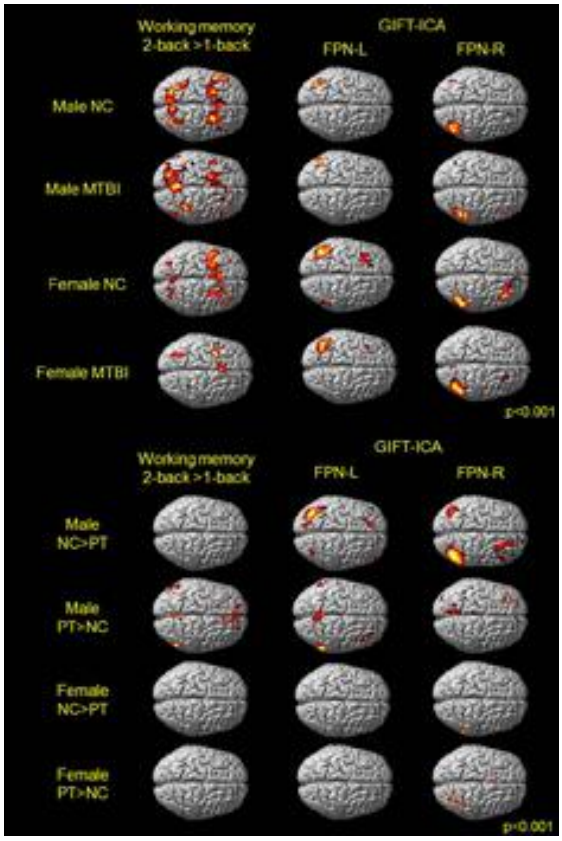

Conclusion

Our result showed that the male patients had increased working memory activation and decreased fronto-parietal connectivity after mTBI. This phenomenon was not observed in the female patients which may suggest female gender to be a protective factor in mTBI.

KEYWORDS: Mild TBI, Sex differences

O-42a **12:13 PM - 12:21 PM**

Diffusion Tensor Imaging in Deep Brain Stimulation Patients at Very Low Radiofrequency Power

Sarkar, S. N.·Papavassiliou, E.·Alterman, R.·Hackney, D. B.·Stormann, J.·Rojas, R.
Beth Israel Deaconess Medical Center, Harvard Medical School
Boston, MA.

Purpose

Due to the unavailability of low RF power (Low-SAR) MRI (0.1 W/kg, FDA approved limit), many patients with implanted deep brain stimulators (DBS) do not benefit from many MR sequences. Sequences including DTI, T2 and fast STIR produce 1-3 W/kg of SAR. The current practice of using atlas-based, indirect targeting of deep brain nuclei is imperfect. Recent reports that claim diffusion tractography improves targeting accuracy, also show significant variation to co-localize the cingulate gyrus targets in depression or thalamic targets for tremor with MR images. Such issues may be resolved if advanced techniques like DTI can be applied routinely at FDA approved low-SAR level for patients with indwelling electrodes. We propose localizing DBS leads by T2 and fast STIR sequences that are more useful for delineating deep nuclear boundaries than conventional MPRAGE followed by superimposing white matter connectivity, all at FDA-approved RF power.

Materials & Methods

Five Parkinson's and two dystonia patients underwent DBS implantation followed by low-SAR MR imaging (≤ 0.1 W/kg, 1.5T) to assess postsurgical accuracy with FSET2 and fastSTIR sequences (resolution 1x1x3mm3, scan time 7 min, 16-24 slices) as well as by 25-direction DTI (resolution 2x2x3mm3, scan time 5 min, 30 slices) in addition to 3D MPRAGE. Three patients also were scanned at high SAR at 3T (pre-DBS surgical planning for implanting 1st DBS). The low-SAR sequences used low refocusing flip angles and stretched RF pulses as proposed in a recent work. Coregistration between diffusion-based fibers and underlying structural T1/T2/fSTIR volumes was done by NordicBrainEX Diffusion/DTI Module *(NordicNeuoLab, Bergen, Norway).* [Figure below, synchronized fibers on T2(left) and on fast STIR(right)].

Results

The signal voids at the metallic leads were 4 mm or three times the lead diameters in 3D T1 MPRAGE and 3 mm or two times the lead diameters in 2D FSE T2 or fastSTIR images. The fractional anisotropies in DTI maps at basal ganglia level were virtually unchanged irrespective of underlying structural image used (MPRAGE or T2 or fast STIR) although the later two delineated deep nuclear boundaries with significantly better G/W contrast. High-SAR (pre-DBS, 3T) and low-SAR (post-DBS, 1.5T) DTI fiber tracts were qualitatively similar with minimal effects from the implanted leads.

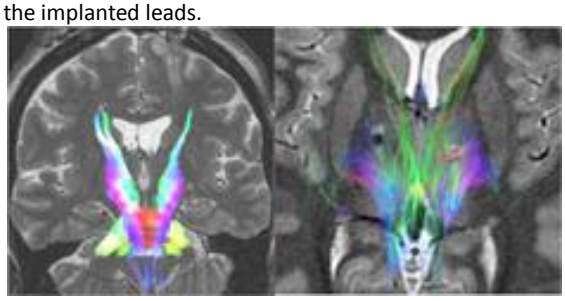

Conclusion

We have demonstrated that it is possible to obtain high resolution, T2 and fast STIR-weighted low-SAR MR images which, combined with tractography, can map changes in brain connectivity in deep gray/white matter areas for patients treated with deep brain stimulation.

KEYWORDS: Parkinson disease, DTI tractography, Deep Brain Stimulation

Note: Scanned images are included in the proceedings. Some submitted images were reduced during editing, thereby decreasing clarity. Also, refer to the Program Planner. Proceedings Content as of 3-29-2013.

O-42b **12:21 PM - 12:29 PM**

MR Imaging Findings in Childhood Posterior Reversible Encephalopathy Syndrome: What is Different Than the Adults?

Donmez, F. Y.·Guleryuz, P.·Agildere, M.
Baskent University
Ankara, TURKEY.

Purpose
Posterior reversible encephalopathy syndrome (PRES) is a clinical scene presenting with convulsion, vision abnormalities, altered mental status and headaches in the presence of an underlying etiology and diagnosis can be made by support of radiologic studies. In this study, we evaluated the MRI findings of PRES in children and compared our findings with that of the known features in adult patients, and find the pathophysiologic reason that may cause the difference.
Materials & Methods
Twenty-nine children (13 male, 16 female, aged 1-17 years, mean age 10 years) diagnosed as PRES clinically and by radiologic workup were reviewed retrospectively. Clinical records were analyzed for the clinical symptoms at the time of MRI study and the underlying etiology. MR images were evaluated for the distribution of the lesions, contrast enhancement, diffusion restriction and any complication such as hemorrhage.
Results
Twenty-four of the patients presented with seizure, five had altered mental status, one patient had vision abnormality and one had ataxia. Underlying etiologies were variable: Chronic renal disease (n:8), leukemia (n:3), lymphoma (n:3), Wilson's disease (n:3), acute hepatitis (n:3), liver transplant recipient (n:3), hemolytic uremic syndrome (n:2), hemophagocytic syndrome (n:2), aplastic anemia (n:1) and metastatic osteosarcoma on chemotherapy regimen (n:1). Mean blood pressure was 130/85. Parietal (90%) and occipital (72%) involvement are the most common findings as expected; however, frontal lobe (66%) edema also is not uncommon, with rates close to occipital involvement. Temporal lobes were only involved if the edema was extensive in all parts of the brain (21%). Isolated temporal lobe involvement in absence of parietooccipital edema was not seen. The most interesting finding was the cerebellar involvement which was present in almost half of the patients (48%) and which was also atypical in adult patients. There were two patients with atypical presentation, with involvement of the thalami and basal ganglia and the brainstem. Contrast enhancement is also another finding which was found more common than the adults (39%). Twenty-six patients had diffusion-weighted imaging, diffusion restriction was seen in four of them (15%) and four patients had hemorrhage (15%); which are almost the same frequencies as in the adults.
Conclusion
The explanation of the posterior involvement related to lack of sympathetic innervation of the arterioles supplied by the vertebrobasilary system also is not entirely correct in children with PRES. However, the increased incidence of cerebellar involvement may show that the posterior circulation in children is more vulnerable than the adults. The contrast enhancement which is seen more common than in the adults may show that the pathophysiology in children may be related to blood-brain barrier breakdown more commonly, which can support the theory of the toxic endothelial injury. Mean blood pressure was not very high in our study group, only some of the children with kidney diseases had hypertension, which also makes it not possible to explained the syndrome solely by hypertensive effects and promote the toxic endothelial injury theory to be more commonly encountered in children with PRES.

KEYWORDS: PRES, Childhood, MR imaging

Monday Morning

10:45 AM - 12:15 PM
Ballroom 6DE

(07c) Parallel Scientific Papers: Adult Brain: Stroke I

O-43 **10:45 AM - 10:53 AM**

CT Angiography in Acute Stroke: A Subgroup Analysis of the Third International Stroke Trial

Mair, G.[1]·Wardlaw, J. M.[2]·Sandercock, P.[2]·Lindley, R.[3]·von Kummer, R.[4]·Farrall, A. J.[2]·IST-3 Collaborative Group
[1]Western General Hospital, Edinburgh, UNITED KINGDOM, [2]University of Edinburgh, Edinburgh, UNITED KINGDOM, [3]University of Sydney, Sydney, AUSTRALIA, [4]Dresden University Stroke Center, Dresden, GERMANY.

Purpose
The Third International Stroke Trial (IST-3) is a multicenter, randomized controlled trial (RCT) testing intravenous thrombolysis (rt-PA 0.9mg/kg) given within six hours of acute ischemic stroke. In addition to prerandomization and follow-up brain imaging performed for all patients, CT angiography was obtained routinely in some centers. We aimed to identify relationships between CT angiography (CTA), early noncontrast CT signs of ischemic stroke, clinical presentation and outcome and whether CTA improved diagnosis or prognosis prediction over noncontrast imaging alone.
Materials & Methods
All IST-3 patients with prerandomization and follow-up noncontrast CT and concurrent CTA were included. A single observer (GM) analyzed the images, blinded to treatment allocation, clinical and follow-up data. On noncontrast CT, we recorded the presence, extent and

Note: Scanned images are included in the proceedings. Some submitted images were reduced during editing, thereby decreasing clarity. Also, refer to the Program Planner. Proceedings Content as of 3-29-2013.

location of ischemia (ASPECT and IST-3 scores) and/or hyperattenuated arteries (HAS). We assessed hemorrhage on follow-up scans. We dichotomized CTA as normal/abnormal. The location/extent of CTA abnormality was graded using validated scales (TICI, TIMI, Clot Burden Score, collateral score). We compared imaging findings with baseline clinical assessments (including National Institutes of Health Stroke Scale - NIHSS, atrial fibrillation - AF) and six-month functional outcome (Oxford Handicap Scale - OHS, death). Significant univariate associations were included in multivariate models.

Results

We included 234 patients (42% male, median age 81 years, IQR 71-86). Follow-up imaging was performed within 48 hours for 92%. Acute ischemia was apparent in 28%, rising to 67% at followup. Hyperattenuated arteries were present in 26%. CT angiogrpahy was abnormal in 40% and was strongly related to HAS ($\chi2 = 80$, $p<0.001$). Acute ischemia was apparent in 47% of those with abnormal CTA, rising to 91% at followup ($\chi2 = 49.0$, $p<0.001$) and compares with rates of 34% and 90% in the presence of HAS. On univariate analysis, those with abnormal CTA were more likely to be older ($p<0.001$), female ($\chi2 = 7.3$, $p = 0.007$) have a shorter time to prerandomization CT ($p = 0.005$), a higher NIHSS ($p<0.001$), be in AF ($\chi2 = 5.2$, $p = 0.023$), have a worse OHS ($p<0.001$), or be dead ($\chi2 = 29$, $p<0.001$) at six months. Similar univariate results were obtained for HAS but relationships were more likely to be statistically significant in the presence of abnormal CTA. A poor collateral supply was associated with lower ASPECT scores ($p = 0.014$) and increased prevalence of acute ischemia on prerandomization scan ($\chi2 = 4.8$, $p=0.028$). Neither CTA findings nor HAS were associated with hemorrhagic transformation post-randomization. Multivariate analysis demonstrated that abnormal CTA (or HAS), increasing age and more severe NIHSS independently predicted both dependency and death at six months. Neither ASPECTS score nor ischemia on noncontrast prerandomization CT were predictive of outcome.

Conclusion

CT angiography may image more completely than noncontrast CT the impact of stroke on the brain by demonstrating low attenuation thrombus and collateralization, thus providing additional prognostic information. Further analyses are now required to determine if this additional information leads to improved outcome after rt-PA, accounting for factors such as delay to treatment, utility and cost of CTA.

KEYWORDS: CTA, Stroke

O-44 **10:53 AM - 11:01 AM**

Utility of CT Perfusion in the Detection of Lacunar Infarction

Das, T.[1,2]·Huynh, T. J.[1]·Eilaghi, A.[1]·Jakubovic, R.[1]·Symons, S. P.[1,2]·Swartz, R.[1]·Aviv, R. I.[1,2]
[1]Sunnybrook Health Sciences Centre, Toronto, ON, CANADA, [2]University of Toronto, Toronto, ON, CANADA.

Purpose

Twenty to 25% of ischemic strokes are lacunar. Lacunar strokes are challenging to detect early and detection remain a limitation of advanced CT stroke protocols including CT perfusion (CTP). There is some evidence of the beneficial role of thrombolysis in lacunar infarction. The purpose of this study is to systematically examine the utility of CT perfusion (CTP) in detecting acute lacunar infarction in the absence of major vessel occlusion.

Materials & Methods

Patients with acute lacunar stroke without vessel occlusion, evaluated with CTP within 4.5 hours of symptom onset, were extracted from a prospective stroke database. Of 450 cases, 170 met the inclusion criteria. CT perfusion was performed on a 64-slice CT scanner (GE Healthcare, Waukesha, WI) with a z-axis spatial coverage of 4 cm. Patients underwent follow-up MRI within 30 days of presentation. Cases in which a diagnosis of infarction was made from follow-up imaging were classified retrospectively as true positive (TP) if detected on the admission CTP or false negative (FN) if not detected on CTP. Ischemia or infarction on CTP was defined as decreased cerebral blood flow and increased mean transit time with or without corresponding decreased cerebral blood volume. Lacunar infarcts were defined as ≤ 15 mm in long axis within the basal ganglia or supratentorial deep white matter. Baseline clinical and radiographic variables including age, gender, NIH Stroke Scale, 3-month modified Rankin score, time to presentation and final infarct size were compared between TPs and FNs.

Results

Thirty-eight percent of all infarcts were classified as lacunar. There were 28% TP and 67% FN cases. The sensitivity of CTP for the detection of lacunar infarcts was 63%. Baseline characteristics between TP and FN lacunar infarcts were compared. True positive cases showed a lower time to presentation compared to FNs (96 ± 29 minutes versus 112 ± 32 minutes $p = 0.04$). There were no significant differences in other measured variables. The added role of CTP over a combination of NCCT and CTA for lacunar infarct detection will be reported.

Conclusion

CT perfusion detects lacunar infarcts with moderate sensitivity but requires the perforator territory to be examined specifically for small CTP defects. However, the lower spatial resolution and inherent noise of CTP remains a challenge. Earlier time to presentation of TP patients may attest to a capsulostriate, rather than a lenticulostriate etiology. In the former, a larger number of

Note: Scanned images are included in the proceedings. Some submitted images were reduced during editing, thereby decreasing clarity. Also, refer to the Program Planner. Proceedings Content as of 3-29-2013.

perforators are affected increasing the size of the CTP defect.

KEYWORDS: Stroke, CT perfusion, Lacunar Infarct

O-45 **11:01 AM - 11:09 AM**

High Frame Rate Dynamic Oxygen Extraction Fraction Changes Using Parameter Assessment by Retrieval from Signal Encoding MR Imaging

Menon, R. G.[1]·Cantrell, C. G.[1]·Walsh, E. G.[2]·Twieg, D. B.[3]·Carroll, T. J.[1]
[1]Northwestern University, Chicago, IL, [2]Brown University, Providence, RI, [3]University of Alabama at Birmingham, Birmingham, AL.

Purpose
Oxygen extraction fraction (OEF) is a crucial perfusion marker and shown to be an independent predictor of stroke. Here we show that we can measure dynamic changes in OEF (OEF reactivity) by inducing mild hypercapnia using a breath-hold experiment. This surrogate measure for cerebrovascular reserve provides complementary information on collateralization, and correlates with favorable outcomes in revascularization therapy.
Materials & Methods
A parameter assessment by retrieval from signal encoding (PARSE)-based MR OEF sequence was implemented on a clinical 3T MR scanner. In a series of five normal volunteers (M/F 3/2, age = 26 ± 10 years) we acquired single slice, 5.0 mm thick, 220 mm x 220 mm FOV, 64 x 64 matrix, resolution = 3 x 3 x 5.0 mm3 2D PARSE images. Volunteers were tested with four conditions: normal breathing, breath-hold at the 1st, 5th and 10th measurement. PARSE acquisitions were taken every three seconds through the breath-hold, for a total of 20 measurements. The frequency change maps were calculated from PARSE reconstructions. Spatial ICA analysis then was performed on these frequency maps to separate out other confounding static effects from the dynamic OEF components.
Results
The change in OEF following a breath-hold experiment is seen in the representative fractional OEF difference maps (Figure 1). The OEF reactivity for different breath-hold conditions is shown in Figure 3. OEF reactivity is seen soon after the breath-hold induced physiologic stress.

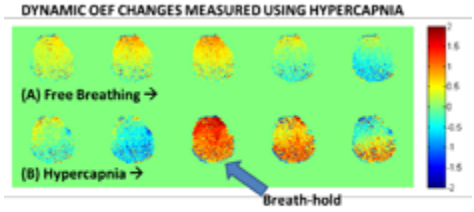

Figure 1: A PARSE acquisition acquired every 3s is used acquire frequency maps that measure dynamic OEF changes that occur during mild hypercapnia. (A) Free Breathing, and (B) Hypercapnia induced by a breath-hold experiment. Shown here are difference maps which have static components removed, to make the dynamic components visible.

Conclusion
While the free-breathing condition ΔOEF does not change measurably, the mild hypercapnic conditions do cause a measurable change in ΔOEF. This technique can provide supplemental information regarding the vascular reserve in patients who typically receive diamox/acetazolamide challenge to determine information on collateralization. The speed of the MR OEF technique allows for multiple measurements in a single breath-hold experiment thus allowing measurement of dynamic OEF changes. Clinical validation of this technique on patients needs to be done to establish the efficacy of this technique.

KEYWORDS: Misery perfusion, Stroke, Oxygen Extraction Fraction

O-46 **11:09 AM - 11:17 AM**

Association between African American Ethnicity, ApoE4 and Lacunar Infarction in the Dallas Heart Study

King, K.[1]·Warren, M.[2]·McColl, R.[1]·Weiner, M.[1]·Peshock, R.[1]
[1]University of Texas Southwestern Medical Center, Dallas, TX, [2]Duke University Medical Center, Durham, NC.

Purpose
African American ethnicity has been associated with a higher prevalence of lacunar infarction, but the etiology for this is unclear. Apolipoprotein E4 (ApoE) may increase stroke risk and in the Dallas Heart Study Brain Aging cohort African Americans have increased ApoE4 allele frequency compared to other ethnicities. We reviewed genetic data and brain MRIs to determine the independent contribution of African American ethnicity and ApoE4 towards odds of lacunar infarction.
Materials & Methods
This IRB-approved HIPAA compliant project examined data from 526 Dallas Heart Study participants 55 or more years of age that underwent genotyping in the first wave of the study in 1999 and brain imaging approximately seven years later. The presence of lacunar infarction was determined from 3T MRI (Achieva; Philips Medical Systems, Best, The Netherlands) of the brain using 3D magnetization prepared rapid acquisition gradient echo, FLAIR and T2. Lacune criteria were size of 3-20 mm, isointense to CSF on T2 and lack of cortical involvement with verification by a neuroradiologist. Logistic regression was performed to evaluate the association between African American ethnicity and presence of lacunar infarction adjusting for age and gender. ApoE4 allele number and African American ethnicity then were examined jointly for their association with lacunar infarction, also adjusting for age and gender.
Results
See table for population characteristics. In a model adjusting for age and gender, African American ethnicity was associated with increased odds of lacunes (OR 2.2, p 0.0375). Number of ApoE4 alleles then was added to the regression model and was significant (OR 2.2, p 0.009)

Note: Scanned images are included in the proceedings. Some submitted images were reduced during editing, thereby decreasing clarity. Also, refer to the Program Planner. Proceedings Content as of 3-29-2013.

while the association with African American ethnicity decreased (OR 1.8, p 0.135).

	African American n = 233	Non African American n = 293 (239 Caucasian, 46 hispanic, 8 other)
Female Gender	142 (60.9%)	174 (59.4%)
Age at MRI	61.2 ± 5.5	61.2 ± 4.6
ApoE4 allele frequency	23.8%	12.0%
Lacunar Infarct Prevalence	20 (8.58%)	12 (4.1%)

Conclusion
African American ethnicity was associated with increased odds of lacunar infarction. When the relative contribution of ApoE4 was evaluated in conjunction with African American ethnicity, it was associated with significant increased odds of lacunar infarction and lessened the association with African American ethnicity. This suggests increased ApoE4 allele frequency may underlie some of the association between African American ethnicity and increased prevalence of lacunar infarction.

KEYWORDS: Genetics, Ethnicity, Lacunar Infarction

O-47 **11:17 AM - 11:25 AM**

Calcified Cerebral Emboli, A "Do Not Miss" Diagnosis: Seventeen Proven Cases and Meta-Analysis of the World Literature

Walker, B. S.·Shah, L. M.·Osborn, A. G.
University of Utah
Salt Lake City, UT.

Purpose
Calcified emboli are a rarely reported but potentially devastating cause of stroke and may be the first manifestation of vascular or cardiac disease. Proper identification can guide treatment towards preventing future embolic events. This study identifies the source, risk factors, and imaging findings of calcified cerebral emboli.
Materials & Methods
A MEDLINE search for calcified AND emboli AND stroke identified 37 cases with imaging findings. Our institutional radiology information system also was searched retrospectively for all noncontrast head CT scans performed between 2001 and 2012 using keywords "calcified" and "emboli." Seventeen cases of calcified cerebral emboli were identified.

Results
A total of 54 cases (61% male and 39% female) were available for analysis. Mean patient age was 64 years. Mean embolus density was 166 HU. Average diameter was 2.5 mm (range 1.0-5.5 mm). Emboli were equally distributed in both hemispheres with 17% bilateral and 35% multiple. Eighty-one percent occurred in the middle cerebral artery distribution. The anterior (9%) and posterior (9%) cerebral arteries were the next most common sites. Presumed embolic sources were aortic stenosis (37%), carotid atherosclerotic plaque (20%), calcific mitral valve (17%), unidentified (9%), and miscellaneous (18%). Repeat imaging demonstrated distal migration of emboli in 11% of cases. Of our 17 cases, 71% were identified correctly as calcified emboli. Twenty-nine percent were misdiagnosed on initial interpretation as hemorrhage or infectious, traumatic, or vascular calcification. Twelve percent were overlooked on preliminary interpretation by the on-call radiology resident.

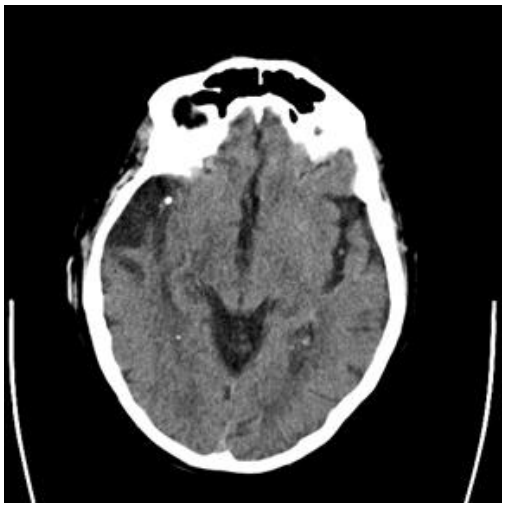

Figure 1. NECT scan in an 81-year-old female shows a calcified embolus in the right MCA with right temporal lobe encephalomalacia from a prior infarct. CT angiography demonstrated a calcific plaque with 70% stenosis of right ICA.
Conclusion
Proper identification of calcified emboli is important for appropriate patient management. Over 60% of calcified cerebral emboli are cardiac in origin. Nearly one quarter of all patients subsequently received aortic valve replacement to prevent further stroke. It is therefore crucial that all patients with calcified cerebral emboli should receive cardiac and extracranial carotid evaluation. Multiple emboli and distal migration suggest that repeat embolization may occur without proper intervention. Of those identified at our institution, nearly one in four initially was overlooked or misdiagnosed. It is imperative that radiologists correctly identify this manifestation of potentially treatable disease.

KEYWORDS: Calcifications, Emboli

Note: Scanned images are included in the proceedings. Some submitted images were reduced during editing, thereby decreasing clarity. Also, refer to the Program Planner. Proceedings Content as of 3-29-2013.

O-48 **11:25 AM - 11:33 AM**

Computed Tomography Perfusion Parameter to Predict Cerebral Hyperperfusion Phenomenon following Carotid Artery Stenting

Takahashi, Y.·Mori, T.·Iwata, T.·Miyazaki, Y.·Nakazaki, M.
Shonan Kamakura General Hospital Stroke Center
Kamakura, JAPAN.

Purpose
Although SPECT is useful for predicting and finding cerebral hyperperfusion phenomenon (CHP) following carotid artery stenting (CAS), there are few institutions that could perform SPECT during peri-CAS period. The purpose of our study is to evaluate whether or not parameters derived from CT perfusion (CTP) used widely can predict CHP.
Materials & Methods
Patients who underwent CTP before elective CAS and SPECT before and immediately after elective CAS in our institution from December 2010 to November 2012. We defined CHP as post-CAS increase of more than 10% of the ratio of cerebral blood flow (CBF) in the territory of the affected middle cerebral artery (MCA) divided by CBF in the ipsilateral cerebellum (MCA/CE ratio) measured by SPECT. We assessed the correlation of pre-CAS CTP's parameters' ratio to MCA/CE ratio change between pre-CAS and post-CAS SPECT. The CTP's parameters' ratio was calculated as (parameters in the affected side divided by in the unaffected side) x 100. CT perfusion parameters we assessed are as follows: time-to-peak (TTP), mean-transit-time (MTT), cerebral blood volume (CBV) and CBF.
Results
Sixty-five patients were analyzed. Pre-CAS TTP ratio ($r = 0.323$, $p = 0.009$) and MTT ratio ($r = 0.317$, $p = 0.010$) showed a significant positive correlation with MCA/CE ratio change. Other parameters (CBV and CBF) had no significant correlation. The cut-off value of pre-CAS TTP and MTT ratio was 1.08 (AUC = 0.81, Sensitivity 85.7%, Specificity 70.0%), 1.05 (AUC = 0.74 Sensitivity 64.3%, Specificity 44.7%) to predict CHP respectively.
Conclusion
Increase of pre-CAS TTP ratio or MTT ratio is probably correlated with CHP following elective CAS.

KEYWORDS: Carotid artery stenting, CT brain perfusion

O-49 **11:33 AM - 11:41 AM**

Improved Agreement of Mismatch Classification in Acute Stroke of Arterial Spin Labeling and Bolus Perfusion-Weighted Imaging at 3T

Zaharchuk, G.·Zun, Z.·Bammer, R.·Moseley, M. E.·Albers, G. W.
Stanford University
Stanford, CA.

Purpose
Arterial spin labeling (ASL) has been proposed as a noncontrast alternative to bolus perfusion-weighted imaging (PWI) for acute stroke patients, enabling perfusion imaging in patients who cannot receive contrast. Studies also suggest that it can assess collateral flow and provide quantitative CBF measurements. However, a prior study at 1.5T showed that ASL overestimates tissue at-risk in patients with mild arterial delays, due to conventional ASL's known sensitivity to slow flow. Signal-to-noise ratio increases and errors due to slow flow decrease at 3T compared to 1.5T. Accordingly, the purpose of this study is to assess the agreement between PWI and ASL for mismatch status at 3T using both pseudocontinuous ASL (pcASL) and a transit-delay insensitive labeling method, velocity-selective ASL (vsASL).
Materials & Methods
This prospective study included all patients scanned at 3T for the evaluation of acute stroke within 48 hours of last seen normal with a positive diffusion-weighted imaging (DWI) lesion. Arterial spin labeling was performed with two separate scans: pseudocontinuous ASL (TR/TE/TL/post-label delay 4400/10/1500/2000 ms) and vsASL (TR/TE/TI 5000/14/1100 ms). Diffusion-weighted imaging and PWI scans were assessed automatically using RAPID software, and patients classified into reperfusion, no mismatch, or mismatch groups based on the DEFUSE-2 criteria. Arterial spin labeling DWI mismatch was assessed by a neuroradiologist blinded to patient history, clinical symptoms, and other imaging. Linear-weighted kappa for agreement between modalities was calculated. After rebinning ASL cases into mismatch versus no mismatch, sensitivity and specificity were determined using PWI as the reference standard.
Results
Thirty-two patients (age: 72 ± 14 years, range 39-105 years, M/F 9/23) were enrolled over a three-month period. Mean DWI and PWI lesion sizes were 11 ± 21 and 17 ± 29 ml, respectively. Twenty-nine and 18 patients received pcASL and vsASL, respectively. Linear-weighted kappa for agreement with PWI-DWI was 0.87 (95% confidence interval: 0.69-1.0) for pcASL and 0.62 (0.24-1) for vsASL. For mismatch versus no mismatch, sensitivity and specificity was 1 (0.46-1) and 0.92 (0.72-0.99) for pcASL; and 0.5 (0.09-1) and 1 (0.73-1) for vsASL. Velocity-selective ASL demonstrated less sensitivity to arterial delay, as predicted theoretically and observed in a prior study in chronic ischemia. Agreement (93% for pcASL and

Note: Scanned images are included in the proceedings. Some submitted images were reduced during editing, thereby decreasing clarity. Also, refer to the Program Planner. Proceedings Content as of 3-29-2013.

89% for vsASL) with PWI was significantly higher than in a prior study performed at 1.5T, presumably due to reduced arrival time effects and higher SNR at 3T.

Agreement of Mismatch Classification by ASL DWI and PWI DWI

	PWI DWI Classification			
pcASL DWI Classification	Reperfusion	No Mismatch	Mismatch	Total
Reperfusion	3	0	0	3
No Mismatch	0	19	0	19
Mismatch	0	2	5	7
Total	3	21	5	29
vsASL DWI Classification	Reperfusion	No Mismatch	Mismatch	Total
Reperfusion	1	1	0	4
No Mismatch	0	12	2	14
Mismatch	0	0	2	2
Total	1	13	4	18

Conclusion

Arterial spin labeling and PWI agree significantly for the determination of mismatch in acute stroke patients at 3T. Velocity-relective ASL is feasible and demonstrates reduced sensitivity to slow flow in ischemic regions compared with pcASL. 3T ASL is a reasonable alternative to PWI as a perfusion modality to determine mismatch status in acute stroke patients.

KEYWORDS: Stroke, Arterial spin labeling

O-50 **11:41 AM - 11:49 AM**

Novel Technique for Oxygen Extraction Fraction Measurement Using PARSE MR Imaging

Menon, R. G.[1]·Walsh, E. G.[2]·Twieg, D. B.[3]·Carroll, T. J.[1]
[1]Northwestern University, Chicago, IL, [2]Brown University, Providence, RI, [3]University of Alabama at Birmingham, Birmingham, AL.

Purpose

Oxygen extraction fraction (OEF) is shown to be an independent predictor of stroke. There is an unmet clinical need for a robust MRI technique to quantify OEF in the brain. A novel, fast, and noninvasive MRI technique to measure OEF is being reported here.

Materials & Methods

We implemented the parameter assessment by retrieval from signal encoding (PARSE) sequence on a clinical 3T MR scanner. Parameter assessment by retrieval from signal encoding uses a more accurate MR signal model and allows the simultaneous estimation of M0, R2* and OEF related frequency changes. We performed sensitivity analysis and numerical simulations and concluded that the technique is sensitive to frequency changes of 4Hz and higher. In a series of five normal volunteers (M/F 3/2, age = 26 ± 10 years) and one arteriovenous malformation (AVM) patient we acquired single slice, 5.0 mm thick, 220 mm x 220 mm FOV, 64 x 64 matrix, resolution = 3 x 3 x 5.0 mm3 2D PARSE data. The frequency change maps calculated from the PARSE reconstruction were processed using ICA analysis to separate static components from the dynamic OEF components.

Results

The mean frequency change for normal subjects was in the range of 15.49 Hz ± 2.77. The mean calculated OEF for the five normal subjects was 36.87 ± 6.60%. The AVM patient exhibited an area of elevated OEF (84.05 ± 4.54%). Figure 1 shows the plot of OEF for normal subjects and the AVM patient, compared to published positron emission tomography (PET) literature.

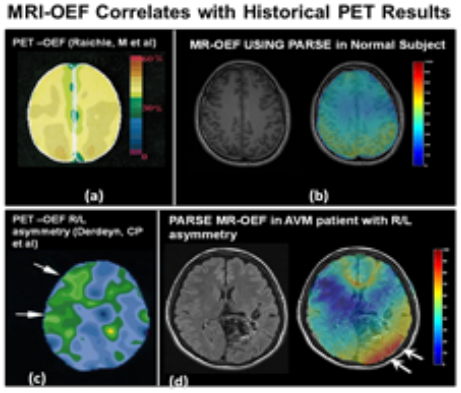

Figure 1: PARSE based MR-OEF images acquired in 5 sec are referenced to anatomic MPRAGE (5:00 min scan) and overlaid (b, d), correlate with expectations based on previously published PET data (a,c)

Conclusion

Note: Scanned images are included in the proceedings. Some submitted images were reduced during editing, thereby decreasing clarity. Also, refer to the Program Planner. Proceedings Content as of 3-29-2013.

The mean OEF for the normal subjects are in close agreement to literature values of PET OEF studies of normative values from Carpenter (35 ± 7%), Yamauchi (42 ± 5%), Diringer (41 ± 6%) and Raichle (40 ± 9%). The AVM patient exhibits elevated OEF proximal to the AVM and "steal" in the distal part of the slice, suggesting that the surrounding tissue may be in distress due to the AVM. The data from PARSE-based studies on our cohort suggest a potential MRI OEF measurement technique. Further patient studies are required to validate the efficacy of this technique as related to assessing the risk in stroke patients.

KEYWORDS: Misery perfusion, Stroke, Oxygen Extraction Fraction

O-51 **11:49 AM - 11:57 AM**

Use of CT- and CBV-ASPECTS in Predicting Clinical Outcomes of Endovascularly Treated Acute Ischemic Strokes

Psychogios, M.·Schramm, P.·Frölich, A. M.·Knauth, M.
University Medicine Goettingen
Goettingen, GERMANY.

Purpose
Patient selection is crucial in the endovascular treatment of acute ischemic stroke patients. Baseline CT images, evaluated with the Alberta Stroke Program Early CT Scale (ASPECTS), are considered significant predictors of outcome. In this study we evaluated CT images and perfusion parameters, analyzed with ASPECTS, as final outcome predictors after endovascular stroke treatment.
Materials & Methods
A previously published cohort of endovascularly treated patients was analyzed. Patients with an occlusion of the M1 segment and multimodal CT imaging were included. CT perfusion data were reconstructed using commercial software. Two experienced neuroradiologists separately reviewed and scored CT and CT perfusion images with the ASPECTS score. Parameters were compared between patients with poor follow-up outcome and with favorable follow-up outcome. Significantly different variables were analyzed further by forward stepwise logistic regression.
Results
Fifty-one patients were included in our study. Baseline characteristics did not differ between patients with favorable and poor outcomes. No significant difference in recanalization status, the various times or CT ASPECTS was demonstrated between the two groups. Significant differences between the two groups were demonstrated for age (P = 0.0049), cerebral blood volume (CBV) ASPECTS (P = 0.0007) and the difference between CBV and cerebral blood flow (CBF) ASPECTS (P = 0.0045). Cerebral blood flow ASPECTS >7 demonstrated the highest sensitivity and specificity for good outcome with 84% and 79%, respectively.
Conclusion
CT perfusion parameters, evaluated with ASPECTS, are significant predictors of outcome and are more sensitive and specific than CT ASPECTS in the prediction of favorable outcome. Use of these parameters in treatment decisions could lead to a reduction of futile recanalizations.

KEYWORDS: Stroke, Cerebral blood volume, ASPECTS

O-52 **11:57 AM - 12:05 PM**

Correlation between Leukoaraiosis Volume and Diabetes

Saba, L.[1]·Raz, E.[2]·Suri, J. S.[3]·Piga, M.[1]
[1]AOU Cagliari, Cagliari, ITALY, [2]University of New York, New York, NY, [3]Biomedical Technologies, Pocatello, ID.

Purpose
The association between diabetes mellitus and leukoaraiosis is uncertain, while the association with hypertension, age and carotid artery stenosis is widely demonstrated. We aim to evaluate the association of white matter hyperintense lesion volume and diabetes in a cohort of patients who underwent an MRI of the brain at our Institution.
Materials & Methods
Fifty-four consecutive patients (mean age 72 ± 9 years, males 42) were recruited prospectively at our Institution before undergoing carotid endarterectomy. The patients were assessed for the presence of vascular risk factors, including diabetes mellitus, hypertension, hyperlipidemia. The patients underwent an admission MRI of the brain which included T2-FLAIR, T2-SE and DWI sequences. FLAIR-leukoaraiosis lesion volume was performed by a neuroradiologist, blinded to the presence of risk factors, using a semi-automated segmentation technique (Jim, Xinapse System, Leicester, UK). Receiver operating characteristic (ROC) analysis was performed to evaluate the AUC of FLAIR-leukoaraiosis lesion volume and number of lesions with respect to the vascular risk factors.
Results
The ROC curve analysis showed an AUC of 0.725 (SE = 0.082 and 95% CI from 0.593 to 0.873) with a statistically significant p value of 0.002 between the presence of diabetes mellitus and the FLAIR-leukoaraiosis lesion volume. In the ROC curve analysis between the presence of diabetes mellitus and number of lesions the AUC was 0.715 (SE = 0.085 and 95% CI from 0.553 to 0.845) with a p value of 0.0119.
Conclusion
Our data demonstrate an association between diabetes mellitus and the volume of the cerebral white matter abnormality.

KEYWORDS: White matter disease

Note: Scanned images are included in the proceedings. Some submitted images were reduced during editing, thereby decreasing clarity. Also, refer to the Program Planner. Proceedings Content as of 3-29-2013.

O-53 **12:05 PM - 12:13 PM**

Low B-Value Diffusion-Weighted Imaging in Cerebral Ischemia: An Initial Experience

Besachio, D. A.·Rassner, U.
University of Utah
Salt Lake City, UT.

Purpose
Diffusion-weighted imaging (DWI) is routine in the evaluation of stroke patients. Signal changes on DWI are caused not only by self-diffusion of water, but also by water movement in vessels. Our purpose is to determine whether low B-value DWI may have some utility in identifying altered perfusion and may allow to identify "tissue-at-risk" in the setting of cerebral ischemia through our understanding of the principle of intra-voxel incoherent motion (IVIM).
Materials & Methods
We retrospectively reviewed six months of inpatient and emergency department brain magnetic resonance images (MRIO where low b-value MRI diffusion sequences (B = 50 s/mm^2) were performed in the setting of stroke evaluation. Low b-value apparent diffusion coefficient (ADC) maps were compared to perfusion imaging when available and with areas of infarct on follow-up imaging.
Results
Our data indicate that low b-value imaging ADC maps are mostly perfusion maps. A larger low b-value ADC abnormality compared to high b-value ADC can indicate tissue at risk beyond classic DWI imaging and correlates with site of infarct on follow-up CT images (Figures 1 and 2). In cases where tissue perfusion is re-established, low b-value ADC map abnormalities normalize. Low b-value images can predict sites at risk of future infarction on follow-up imaging.
Conclusion
Our limited experience with low B-value imaging suggests that decreased ADC values in a low b-value DWI sequence may act as an effective surrogate for cerebral tissue perfusion and can identify tissue at risk as well as normalization of blood flow. Further research with the use of intra-operative MRI during angiography for acute stroke is ongoing.

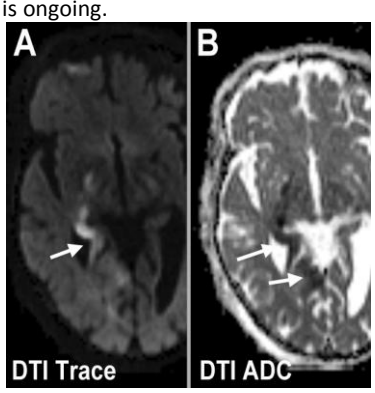

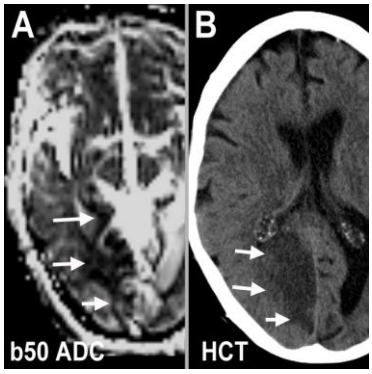

KEYWORDS: Diffusion MR imaging, Stroke

Monday Morning

10:45 AM - 12:15 PM
Room 5AB

(07d) Parallel Scientific Papers: Adult Brain: New Techniques and Novel Post Processing I

O-54 **10:45 AM - 10:53 AM**

Fast 3D Arterial Wall Imaging Using Variable Flip-Angle, Ultralong Echo Train T1 FLAIR

Mazura, J. C.[1]·Fullerton, H. J.[1]·Banerjee, S.[2]·Koon, P. D.[2]·Barkovich, A. J.[1]·Hess, C. P.[1]
[1]University of California San Francisco, San Francisco, CA, [2]GE Global Applied Sciences Laboratory, Menlo Park, CA.

Purpose
Catheter angiography, CTA and MRA permit accurate evaluation of the arterial lumen, but are typically unable to identify abnormalities within the arterial wall. Mural thickening and enhancement on 2D T1 FLAIR arterial wall imaging (AWI) may improve the ability to differentiate among different types of intracranial arteriopathy. However, long scan times and flow artifacts have limited this approach. In this work, we developed a variable flip angle, ultra-long echo train 3D T1 FLAIR FSE pulse sequence for fast, clinically feasible AWI with isotropic 1 mm resolution and applied the technique to patients with various intracranial arterial lesions.
Materials & Methods
A fat-suppressed, pre and postgadolinium 3D T1 CUBE FLAIR imaging protocol was developed and deployed on two 3T GE MR750 scanners for the evaluation of adult and pediatric patients with suspected neurovascular disease. Using parallel acquisition and a variable flip angle schedule optimized for T1 contrast, scan time to achieve 1 mm resolution with whole brain coverage was 4.5 minutes per

Note: Scanned images are included in the proceedings. Some submitted images were reduced during editing, thereby decreasing clarity. Also, refer to the Program Planner. Proceedings Content as of 3-29-2013.

acquisition (TR/TE=600 ms/MIN, ETL=20, ARC acceleration=2, NEX=1). Pre and postgadolinium 2D T1 FLAIR (TR/TE/TI=860/12/2100 ms, ETL=8, ASSET acceleration=2, total scan time = 30 minutes) also was performed in select patients for comparison. Unenhanced images were reviewed for dissection and concentric or eccentric mural thickening and compared to gadolinium-enhanced sequences to detect mural enhancement in five patients with transient childhood arteriopathy (TCA), four with stroke, two with vasculitis, and one with suspected intracranial dissection.

Results

The figure shows one representative positive AWI study, in which mild luminal narrowing on MRA was accompanied by concentric mural enhancement in a 13-year-old with a left lateral lenticulostriate infarct presumed due to TCA. Arterial wall imaging was performed successfully in all patients, and showed unilateral focal arterial enhancement in the supraclinoid ICA and/or MCA in three cases (1 TCA, 1 embolic infarct, and one dissection). Compared to 2-plane 2D T1 FLAIR, the 3D CUBE T1 FLAIR technique reduced imaging time from 30 minutes to under 10 minutes, allowed reformatting in any plane, showed fewer CSF pulsation and vascular pulsatility artifacts, and was less sensitive to cortical venous enhancement.

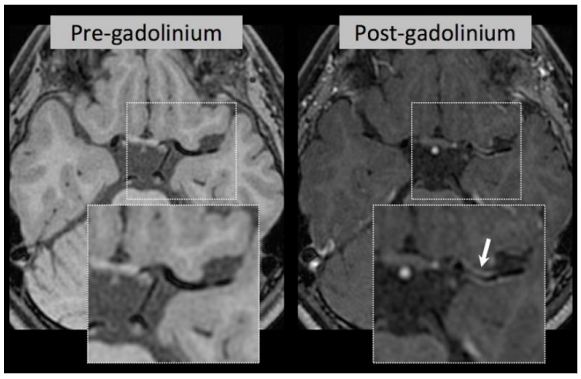

Conclusion

High-quality volumetric AWI can be performed with 1 mm isotropic spatial resolution in under 10 minutes using 3D T1 CUBE FLAIR in order to reveal intracranial arterial wall dissection, thickening and/or enhancement with higher fidelity than 2D T1 FLAIR. This technique shows promise for distinguishing between inflammatory, infectious and other types of intracranial arteriopathy.

KEYWORDS: 3D imaging, Vessel wall

O-55 **10:53 AM - 11:01 AM**

Ultra-High Resolution 0.4 mm Isotropic Structural Imaging of the Human Hippocampus in vivo Utilizing Phase-Cycled bSSFP at 7.0T

Zeineh, M. M.·Parekh, M.·Su, J.·Rutt, B.
Stanford University
Stanford, CA.

Purpose

The hippocampus plays a central role in memory formation and disease entities such as Alzheimer disease and temporal lobe epilepsy. However, it is a complex and intricate structure with many components tightly wrapped and folded, particularly in the anterior hippocampus, or hippocampal head. Hippocampal microstructure is identified best with T2-weighted contrast. However, achieving isotropic high-resolution T2-weighted images is quite difficult, so most hippocampal acquisitions are anisotropic. This complicates segmentation, and has resulted in a myriad of attempts to label the hippocampal head consistently and accurately. This stands in contradistinction to specimen MRI, in which full hippocampal head segmentation is possible at a resolution on the order of 0.2 mm isotropic. Here, we report using balanced steady-state free precession (bSSFP) at 7.0T to achieve 0.4 mm in vivo isotropic resolution with contrast that reveals hippocampal microstructure in clinically achievable scan times.

Materials & Methods

Four subjects provided informed consent in accordance with the IRB for scanning with a GE 7.0T Discovery MR950 scanner using a Nova coil (quadrature transmit, 32-channel receive). After performing high-order B0 shimming to approximately 20 Hz r.m.s. uniformity, we acquired six-eight increments of phase-cycled bSSFP (FIESTA, coronal, BW 62, FOV 17, 420x420, FA 25, TR 8.2 ms, TE 4.1, 0.4 mm slice thickness, 480 slices, 0.5NEX, ARC 1.75x1.75, 5:11 per phase cycle, several seconds of rest between phase cycles). Individual phase cycle images were reconstructed and combined into an initial sum-of-squares (SOS-1). FSL's flirt then was used to coregister each phase cycle to the SOS-1, after which we recombined into a second SOS (SOS-2), and this procedure was repeated once to produce SOS-3. Images were visualized and the hippocampal cell layer stratum radiatum lacunosum moleculare (SRLM) was segmented using itk-SNAP.

Results

The images demonstrated contrast comparable with T2-weighted FSE images with gray-white contrast-enhanced by a significant component of iron contrast. In all subjects, fields CA3 and CA1 of the hippocampal head were readily discernible and separable in coronal section, and the entirety of SRLM could be segmented (Figure 1). Three to four hippocampal digitations were observable in coronal section with fluid in the adjacent hippocampal sulcus. Gray-white contrast in the remainder of the brain was similar to 3D T2 FSE acquisitions.

Note: Scanned images are included in the proceedings. Some submitted images were reduced during editing, thereby decreasing clarity. Also, refer to the Program Planner. Proceedings Content as of 3-29-2013.

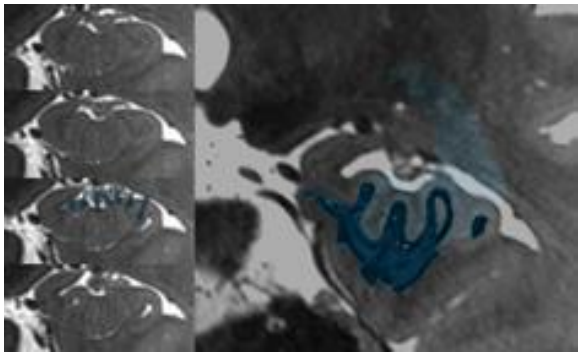

Conclusion
Balanced steady-state free precession provides extremely detailed visualization of hippocampal microstructure only previously possible with ex vivo imaging. This may have applications to and beyond diseases of the medial temporal lobes.

KEYWORDS: 7T, Hippocampus

O-56 **11:01 AM - 11:09 AM**

Silent MR Image Acquisition: Initial Clinical Experience and Assessment of Image Quality

Korosec, F. R.[1]·Rowley, H. A.[1]·Holmes, J. H.[2]·Wang, K.[2]·Thornton, F. J.[1]·Vigen, K. K.[1]·Mckinnon, M. C.[3]·King, K. F.[3]·Akao, J. H.[3]·Wei, S.[3]·Turski, P. A.[1]
[1]University of Wisconsin Madison, Madison, WI, [2]GE Healthcare, Madison, WI, [3]GE Healthcare, Waukesha, WI.

Purpose
Two concerns often expressed by patients undergoing MRI exams are the confined space and the loud noise. The confined space is being addressed by wider bore scanners. Recently, a prototype T1-weighted silent scanning sequence (Silenz, GE Healthcare) has been provided to our institution for internal evaluation in patient volunteers presenting for clinical neurologic MR exams. The goal of this work is to assess the quality and diagnostic capability of images obtained with the T1-weighted Silenz method.
Materials & Methods
Fourteen patients were enrolled in this IRB-approved study. Patients underwent a standard-of-care neurologic MR exam, including a postcontrast, T1-weighted fast gradient-echo scan (BRAVO, GE Healthcare), followed by a T1-weighted Silenz scan. The Silenz scan is a 3D radial acquisition method, in which the gradients are changed minimally during the acquisition in order to minimize the traditional gradient "banging" sounds. Imaging was performed on a 1.5T wide-bore scanner with a 24-channel GEM head-neck coil (Optima MR 450w, GE Healthcare). Imaging parameters for the Silenz scan were: TI=450ms, TE=0.016ms, flip=4°, RBW=±31.3kHz, FOV=256 mm2, matrix=256×256, 1.0 mm isotropic acquisition resolution, and scan time=6:11. Scan times were reduced by using parallel imaging in the conventional acquisition, and moderate radial undersampling in the Silenz acquisition. During the Silenz scan, the sound of the scanner had been measured previously to be slightly (<3dB) above the ambient noise levels in the room.
Results
Example axial images from a patient volunteer with an enhancing meningioma (Figure 1) show similar image quality with both the Silenz acquisition and the conventional method. Quality of the Silenz images was scored by two board-certified neuroradiologists using a scale of 1 to 5 (1=no useful diagnostic information, 2=limited diagnostic value but visible structures, 3=fair/marginal image quality, 4=good image quality but visibly lower SNR or contains artifacts, 5=excellent image quality with minimal if any artifacts). The combined average score from the two radiologists was 3.6. Additionally, the diagnostic capability of the Silenz and conventional fast gradient-echo images was compared (1=conventional more diagnostic, 2=same, 3=Silenz more diagnostic). Both radiologists noted that the images were comparable and this was reflected in their scores (combined average score of 2.0 for the two radiologists). Each acquisition method exhibited unique artifact properties and different signal-to-noise ratios.

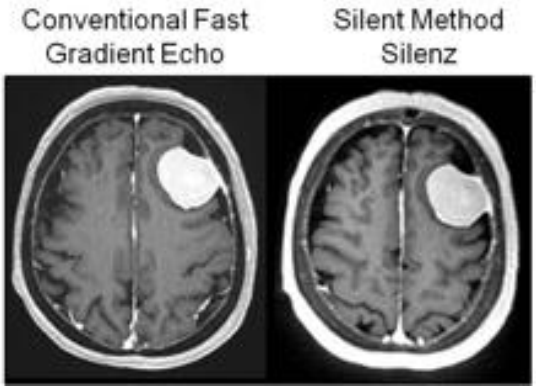

Conclusion
Preliminary results indicate that the T1-weighted Silenz images exhibit good image quality, and diagnostic capabilities similar to those of a conventional T1-weighted fast gradient-echo method, while offering the advantage of silent acquisition.

KEYWORDS: MR imaging, Brain, Silent MR Scanning

O-57 **11:09 AM - 11:17 AM**

Sinogram Affirmed Iterative Reconstruction for Head CT: Effects on Radiation Dose and Image Quality

Rivers-Bowerman, M. D.·Shankar, J.
Dalhousie University
Halifax, NS, CANADA.

Purpose
Iterative reconstruction has been reported to reduce radiation dose in CT, while preserving and even improving

Note: Scanned images are included in the proceedings. Some submitted images were reduced during editing, thereby decreasing clarity. Also, refer to the Program Planner. Proceedings Content as of 3-29-2013.

image quality. The purpose of this study was to evaluate the effects of a commercially available iterative reconstruction algorithm, sinogram affirmed iterative reconstruction (SAFIRE), on radiation dose reduction and quantitative and qualitative measures of image quality for noncontrast head CT.

Materials & Methods

Institutional review board approval was obtained for this retrospective analysis of head CT datasets. For direct comparison of filtered back-projection (FBP) and SAFIRE image reconstruction techniques, fifty consecutive adult patients who underwent noncontrast head CT with SAFIRE were age-matched (± 5 years) with 50 patients who previously underwent noncontrast head CT with FBP. All CT scans were performed on a SOMATOM Definition Flash unit (Siemens Medical Solutions, Germany). Images were reconstructed axially with an H37s medium smooth kernel for FBP and with a J37s medium smooth kernel for SAFIRE. Dose-length products (DLP) were obtained from scanner-generated CT dose reports to estimate patient dose. One reader blinded to reconstruction technique measured gray matter (GM) and white matter (WM) attenuation in each patient with a region-of-interest (ROI) tool. Gray matter-WM signal-to-noise ratios (SNR) and GM-WM contrast-to-noise ratios (CNR) then were calculated from these values. Intra-observer variation was analyzed with a repeatability coefficient. Two readers blinded to reconstruction technique independently evaluated CT datasets for motion, noise, scatter-related artifact, GM-WM differentiation, small structure visibility, and image sharpness with an ordinal scale. Interobserver agreement was evaluated with the kappa statistic. Significance testing of quantitative and qualitative numerical data was performed with the independent samples t-test. Alpha was set at 0.05.

Results

The mean (standard deviation, range) age of the patient population was 57 (20, 21-92) years. With respect to the FBP control group, mean DLP in the SAFIRE test group was significantly reduced from 951 (59, 849-1144) mGy to 803 (77, 654-959) mGy ($P < 0.0001$). The mean ROI area for attenuation measurements was 22.8 (0.8, 18.3-26.3) mm^2 with a repeatability coefficient for ROI attenuation measurements of 1.8 HU. Gray matter SNR significantly increased from 10.0 (1.5, 7.1-15.1) in the FBP group to 15.6 (2.4, 11.1-22.6) in the SAFIRE group ($P < 0.0001$). Similarly, WM SNR increased from 7.3 (1.0, 5.1-9.4) in the FBP group to 10.2 (1.6, 7.4-14.5) in the SAFIRE group ($P < 0.0001$). There was also a significant improvement with SAFIRE for GM-WM CNR which rose from 1.7 (0.3, 0.9-2.5) to 3.1 (0.5, 2.1-4.1) ($P < 0.0001$).

Conclusion

Iterative reconstruction for noncontrast head CT reduces patient radiation dose by 15% for the SAFIRE settings employed at our institution, while significantly reducing image noise and improving contrast resolution.

KEYWORDS: Iterative reconstruction, Radiation dose reduction

O-58 **11:17 AM - 11:25 AM**

Phantom Validation of MR Thermometry Using Proton Resonance Frequency Chemical Shift for Clinical High Field Applications

Dehkharghani, S.[1]·Wei, L.[2]·Pate, K. S.[1]·Magrath, R. P.[3]·Tong, F. C.[1]·Mao, H.[1]·Oshinski, J. N.[1]
[1]Emory University Hospital, Atlanta, GA, [2]Georgia Institute of Technology, Atlanta, GA, [3]Northwestern University, Chicago, IL.

Purpose

Brain temperatures lie at the intersection of complex metabolic and hemodynamic phenomena. The augmentation of ischemic neuronal injury during modest *hyper*thermia, and the well-known neuroprotective effects of *hypo*thermia highlight the importance of brain temperature in CNS disease. Traditional techniques aimed at brain thermometry are restricted by their costly and invasive nature, as well as their highly spatially constrained data collection. Physiologic models of cerebral thermoregulation have thus met with considerable controversy. Noninvasive measures of spatially varying cerebral temperatures represent a crucial step towards the elucidation of cerebral thermoregulation under normal and pathologic conditions, and during thermal therapies. Several nuclear magnetic resonance phenomena show sensitivity to temperature, and have been proposed as means of noninvasive MR thermometry. We report the results of a series of temperature-controlled phantom experiments investigating the sensitivity of single-voxel, point-resolved MR spectroscopy (SVS) as a means of thermometry in a brain cytosol phantom under clinically relevant parameters.

Materials & Methods

An aqueous metabolite solution titrated to physiologic concentrations of neuronal N-acetylaspartate (NAA), lactate (Lac), creatinine (Cre) and choline (Cho) was composed in-house for all phantom studies. The solution was secured within the bore of a 3T Siemens TimTrio whole-body clinical system (Siemens Medical Solutions, Erlangen, Germany); system temperature control and modulation was achieved through a circulating water bath custom designed for the following study, and experimentally validated in an independent series of experiments to ±0.1°C control. ^{1}H-MRS was acquired at static room temperatures (~18.8°C) with partially water-suppressed SVS (Tr=3000ms; Te=30ms; NEX=128; 1.5cc) following manual shimming, with eight repeated measures. Subsequently, in separate experimental sessions, sequential SVS were acquired with similar parameters during modulated temperatures. Spectra were first collected simultaneously during dynamic temperatures between 5-20°C, and in a second experiment between 20-45°C. Metabolite reference

Note: Scanned images are included in the proceedings. Some submitted images were reduced during editing, thereby decreasing clarity. Also, refer to the Program Planner. Proceedings Content as of 3-29-2013.

temperatures from within the solution were collected simultaneously in all experiments at 3-second temporal update from a 4-channel, MR-compatible fiber-optic thermometry system (OpSens OTG-MPK5). Single-voxel spectroscopy thermometry was derived from the known temperature sensitivity of the water-NAA chemical-shift (ΔδH20-NAA), related to the temperature-dependent fluctuation in populations of bound and unbound water species, and approximated at 0.01ppm/°C. Spectra chemical shifts were assigned in java-version magnetic resonance user interface V4.0 (http://www.mrui.uab.es) and LCModel V6.3 (http://s-provencher.com/pages/lcmodel.shtml).

Results

Static MR thermometry sessions acquired by SVS at ambient room temperature (~18.8°C) demonstrated excellent stability and agreement (computed temperature=19.0°C on each of eight repeated measures). Collected spectra were of excellent quality (water line width=8Hz), facilitating frequency assignments and ΔδH20-NAA determination. Single-voxel spectroscopy thermometry acquired across 18 observations during modulated temperatures 20-45°C in two hours demonstrated a linear relationship (R^2=0.95; alpha=0.01±0.0007; RMSE=0.02ppm). Single-voxel spectroscopy thermometry session acquired during temperatures 5-20°C across 19 observations was best approximated by two-parameter model by linear regression (R^2=0.99; alpha=0.01±0.0003; RMSE=0.078ppm).

Conclusion

Noninvasive probes of brain temperature may be of tremendous utility for characterization of cerebral temperatures during ischemia or thermal therapy. Our results validate the accuracy and reproducibility of a simple SVS sequence acquired on a clinical whole body system for accurate, reproducible, and timely brain temperature estimation, and determination of cerebral thermal gradients.

KEYWORDS: Advanced MR imaging, Temperature, spectroscopy

O-59 **11:25 AM - 11:33 AM**

Intra-Arterial Mannitol-Induced Blood-Brain Barrier Disruption in a Rabbit Model: Implications for Chemotherapeutic Drug Delivery in Brainstem Tumors

Pearl, M. S.[1,2]·Janowski, M.[1,3]·Airan, R.[1]·Walczak, P.[1]
[1]The Johns Hopkins University School of Medicine, Baltimore, MD, [2]Children's National Medical Center, Washington, DC, [3]Mossakowski Medical Research Centre, Polish Academy of Sciences, Warsaw 02-106, POLAND.

Purpose

One of the main challenges in brainstem tumor treatment is the poor penetration of chemotherapeutic drugs through an intact blood-brain barrier. This study describes a rabbit model of mannitol-induced blood-brain barrier disruption (BBBD).

Materials & Methods

This protocol was approved by our Institutional Animal Care and Use Committee. Four-French sheaths were placed in the right femoral arteries of 4-kg New Zealand white rabbits. Using a hybrid MRI angiography suite (Miyabi, Siemens), a 4-French catheter was used placed in the left vertebral artery. Through this catheter, a 1.7-French microcatheter was advanced over a 0.014-inch microwire into the left V4 segment or basilar artery under roadmap guidance. All catheters were continuously flushed with heparinized saline. The rabbits were transported to a 3T (Magnetom Trio, Siemens) MRI for dynamic injection and postmannitol administration images of the brain. Coronal T2 (TE/TR = 105/1500), T1 (TE/TR = 9.1/300), and GE-EPI (TE/TR = 30/3000; 60 measurements) images were obtained prior to intra-arterial (IA) mannitol injection. Dynamic EPI images were obtained during IA injection of feraheme (iron oxide nanoparticles, ~20 nm). Intra-arterial mannitol (25%, 0.26 ml/sec for 30 seconds) was delivered in the left V4 segment. After five minutes, gadolinium (Magnevist) was injected intra-arterially (0.5 molar, 0.01ml/sec for 1minute), Evans blue (EB) (2%, 2 ml/kg), known for rapid binding with albumin, was injected intravenously, and coronal T1 postgadolinium images were acquired. The EB staining was evaluated postmortem on brain slices.

Results

Dynamic EPI depicted the perfusion territory following contrast agent injection via the vertebral or basilar artery. Manipulation of the injection rate resulted in differential brain parenchymal coverage. Intra-arterial mannitol produced visible BBBD: diffuse bilateral enhancement of the brainstem, cerebellum and the PCA territory on gadolinium-enhanced T1-weighted images. Necropsy revealed unilateral EB uptake within the brainstem notably smaller than the degree of T1 enhancement.

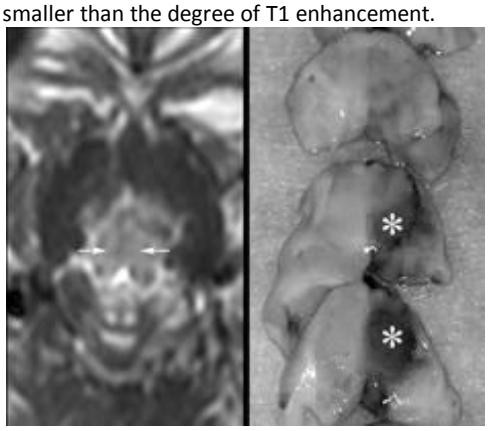

Figure 1. A) Coronal post-gadolinium T1-weighted image demonstrates diffuse bilateral enhancement of the brainstem (arrows). The unenhanced supratentorial brain is seen surrounding the brainstem. B) Selected brain slices show left-sided EB extravasation (asterisks) in the brainstem.

Note: Scanned images are included in the proceedings. Some submitted images were reduced during editing, thereby decreasing clarity. Also, refer to the Program Planner. Proceedings Content as of 3-29-2013.

Conclusion
A transfemoral approach for IA microcatheter delivery of mannitol to the vertebrobasilar system in rabbits is feasible and efficient in producing BBBD. Assessment of BBBD for chemotherapy should consider the size of the therapeutic agent, as differential extravasation across the BBB was seen with gadolinium versus EB.

KEYWORDS: Blood-brain barrier, Vertebral artery

O-60 **11:33 AM - 11:41 AM**

Cone Beam CT Metal Artifact Reduction in the Clinical Evaluation of Stent-Assisted Aneurysm Coiling

Radvany, M. G.[1]·Gundlack, F.[2]·Katz, Z.[1]·Kaminsky, I.[1]·Obrzut, M.[1]·Ehtiati, T.[2]
[1]Johns Hopkins University School of Medicine, Baltimore, MD, [2]Siemens, Princeton, NJ.

Purpose
Cone beam CT (CB CT) imaging is a useful technique for evaluation of intracranial stents. However, after aneurysm coiling there can be a significant amount of metal artifact precluding evaluation of the stent patency as well as residual filling at the base of an aneurysm. This study evaluates a modified reconstruction algorithm to reduce metal artifact and improve stent visualization.
Materials & Methods
We prospectively selected 11 consecutive cases in which patients underwent stent-assisted coiling and CB CT. Using the original data set from the diagnostic angiogram we reconstructed the data using the modified algorithm. The stent/vessel visibility, evidence of artifacts both near and far from the area of interest and overall image quality were evaluated by four interventional neuroradiologists.
Results
In eight of 11 cases there was improved visibility of the parent vessel/stent ($p < 0.01$). In all cases the overall image quality was improved ($p < 0.05$). In all cases there was a reduction in artifact near the area of interest ($p < 0.01$) and in 10 or 11 cases there was decrease in artifact distal from the area of interest ($p<0.05$).

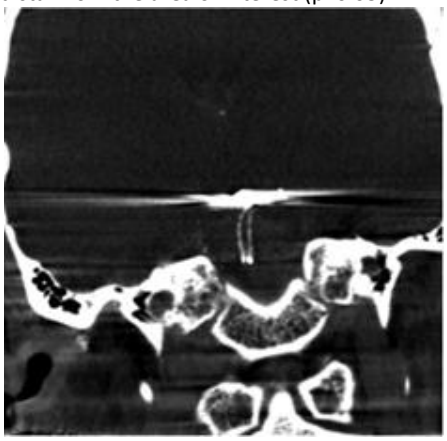

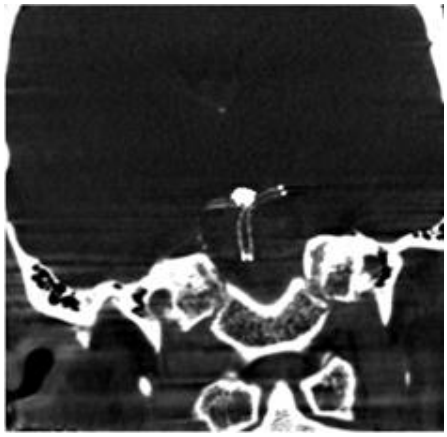

Conclusion
Using a modified reconstruction algorithm to reduce metal artifact can improve image quality and evaluation of stents in stent-assisted coiling of aneurysm.

KEYWORDS: 3-dimensional reconstruction, Artifacts

O-61 **11:41 AM - 11:49 AM**

Evaluation of Cerebral Perfusion Parameters on CT Perfusion Associated with Global Cerebral Edema in Aneurysmal Subarachnoid Hemorrhage

Fodera, V.·Sanelli, P.·Gupta, A.·Baradaran, H.
New York Presbyterian-Weill Cornell
New York, NY.

Purpose
Aneurysmal subarachnoid hemorrhage (SAH) is a devastating disease with severe complications including global cerebral edema (GCE) contributing to functional and cognitive disability. It is well known that GCE occurring during the early stage (day 0-3) independently leads to poor outcomes. However, little is known about mechanisms underlying the development of GCE and its effects on cerebral perfusion. Our aim was to evaluate cerebral perfusion parameters on CTP associated with GCE in aneurysmal SAH.
Materials & Methods
A retrospective study of consecutive SAH patients with CTP performed on admission (day 0-3) admitted from 2008-2010. Presence of GCE was determined on the noncontrast CT (performed concurrently with CTP) by two independent neuroradiologists blinded to all other clinical and imaging data using Claassen's definition: (1) complete or near-complete effacement of the hemispheric sulci and basal cisterns and (2) bilateral disruption of the hemispheric gray-white matter junction at the level of the centrum semiovale. Global cerebral edema was considered present if there was more than 75% sulcal effacement or more than 75% of gray-white matter disruption. CT perfusion was postprocessed into cerebral blood flow (CBF), cerebral blood volume (CBV) and mean transit time (MTT) data using a standardized method.

Note: Scanned images are included in the proceedings. Some submitted images were reduced during editing, thereby decreasing clarity. Also, refer to the Program Planner. Proceedings Content as of 3-29-2013.

Qualitative analysis of CTP maps were performed by two independent blinded neuroradiologists to determine presence of global CTP deficits, defined as diffuse reduction in CBF and/or elevated MTT. Adjudication was performed by a third neuroradiologist. Test characteristics of CTP were calculated and statistical significance was determined by Fisher's exact test.

Results

A total of 45 patients were included in the statistical analysis. There were 42.2% (19/45) patients classified as GCE and 57.8% (26/45) as no GCE. Global perfusion deficits were seen in 52% (10/19) patients with GCE and 7.7% (2/26) without GCE. There is a statistically significant difference in the global perfusion in GCE ($p = 0.0014$) manifesting as diffusely reduced CBF and/or elevated MTT. Figure 1 demonstrates a patient with GCE and global perfusion deficit. Global perfusion deficits had a 53% sensitivity, 92% specificity, 83% positive predictive value and 73% negative predictive value.

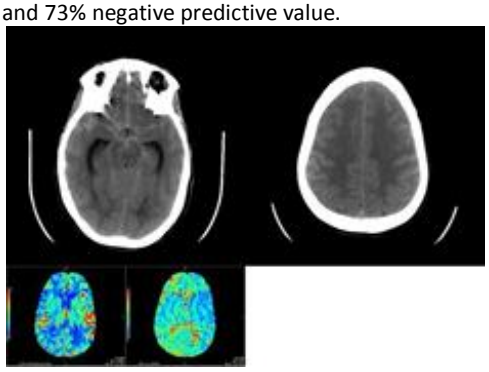

Conclusion

Global perfusion deficits on CTP were statistically increased in GCE patients compared to patients without GCE. CT perfusion has a high specificity and positive predictive value. These initial results support further work in this field to evaluate the effects of GCE on cerebral perfusion and its association with poor outcomes.

KEYWORDS: CT brain perfusion, Aneurysmal subarachnoid hemorrhage

O-62 **11:49 AM - 11:57 AM**

Noninvasive Cerebral MR Thermometry Using Proton Resonance Frequency Chemical Shift in the Nonhuman Primate: Initial Experience and Validation

Dehkharghani, S.[1]·Wei, L.[2]·Oshinski, J. N.[1]·Mao, H.[1]·Magrath, R. P.[3]·Pate, K. S.[1]·Tong, F. C.[1]·Zhang, X.[4]·Howell, L. L.[4]

[1]Emory University Hospital, Atlanta, GA, [2]Emory University, Atlanta, GA, [3]Northwestern University, Evanston, IL, [4]Yerkes National Primate Research Center, Atlanta, GA.

Purpose

Cerebral thermoregulation remains a poorly understood phenomena, due primarily to the costly, invasive, and spatially limited nature of traditional techniques utilizing implanted brain temperature probes. The augmentation of neuronal injury during *hyper*thermia, and the neuroprotective effects of *hypo*thermia highlight the importance of brain temperature in CNS diseases. Among temperature-sensitive NMR phenomena, chemical shift difference between water and the N-acetylaspartate (NAA) methyl resonance ($\Delta\delta_{water\text{-}NAA}$) may be specifically well suited to characterization of cerebral gradients. We report the use of single and multivoxel MR spectroscopy (SVS/MVS) for noninvasive thermometry in the nonhuman primate (NHP) brain under clinically relevant conditions.

Materials & Methods

Imaging was performed on a 3T clinical system (Siemens Tim/Trio). Healthy Rhesus monkeys were obtained from the breeding program of our national primate research center with IAUCAC approval. Rhesus monkeys were selected for their recognition as an excellent surrogate for the modeling of human cerebrovascular diseases. Imaging included SVS collected by point-resolved spectroscopy with partial-water suppression (TR=2500 ms; TE=30 ms; Avg=128). A 10 x10x10 mm^3 voxel was placed juxtacortically near the right operculum, reflecting the anatomical vicinity of ischemic injury imposed by a NHP stroke model under investigation at our institution. Six repeated measurements were acquired successively under identical conditions for determination of $\Delta\delta_{water\text{-}NAA}$. In a separate experimental session, 2D-MVS (TR=2500; TE=84) with 6 repeated measurements was acquired with a 16x16 matrix placed to span the bilateral hemispheres from the sylvian region to the angular gyrus, with outer-volume suppression bands to mitigate lipid contamination. Physiologic monitoring, including rectal thermometry, was maintained on the anesthetized monkey throughout the protocol. Chemical shifts were assigned and analyzed in *j-mrui (http://www.mrui.uab.es)* and LCModel V6.3 *(http://s-provencher.com/pages/lcmodel.shtml)*.

Results

Systemic temperatures were maintained at ~37°C as indicated by rectal thermometry. MR thermometry derived following manual postprocessing of SVS yielded a temperature range 36.7-37.2°C (mean±sd=36.94±0.22). In MVS, separate $\Delta\delta_{water\text{-}NAA}$ values across two adjacent voxels assigned symmetrically in the right/left hemisphere (Figure) were derived from the MVS grid, with systemic temperatures again at ~37.0°C. Adjacent right hemispheric voxels acquired across six observations yielded cerebral temperatures 37.6°C±0.08 and 37.5°C±0.06 and an averaged 37.3°C±0.31 and 38.0°C±0.24 in left hemispheric voxels.

Note: Scanned images are included in the proceedings. Some submitted images were reduced during editing, thereby decreasing clarity. Also, refer to the Program Planner. Proceedings Content as of 3-29-2013.

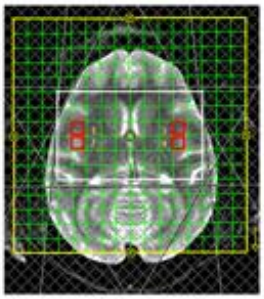

Placement of chemical shift imaging 2D-multi-voxel 16x16 grid for $\Delta\delta_{water\text{-}NAA}$ thermometry. 8 saturation bands placed for suppression of lipid resonance

Temp ($\Delta\delta_{water\text{-}NAA}$) °C

1: 37.5967±0.083	3: 37.2867±0.306
2: 37.5167±0.060	4: 37.9983±0.238

Conclusion
The validation of a noninvasive MR technique for brain temperature monitoring may facilitate the elucidation of complex metabolic and hemodynamic phenomena underlying neuronal injury. Our findings suggest that chemical shift thermometry offers a feasible and reproducible technique of brain thermometry with the potential to probe cerebral thermal gradients noninvasively.

KEYWORDS: Temperature, Animal model, spectroscopy

O-63 **11:57 AM - 12:05 PM**

Evaluation of Normal-Appearing White Matter in Multiple Sclerosis Using Quantitative Susceptibility Mapping

Moriya, J.[1]·Kakeda, S.[1]·Ueda, I.[1]·Watanabe, K.[1]·Murakami, Y.[1]·Ide, S.[1]·Ogasawara, A.[1]·Futatsuya, K.[1]·Sato, T.[1]·Ohnari, N.[1]·Okada, K.[1]·Tsuji, S.[1]·Liu, T.[2]·Wang, Y.[2]·Korogi, Y.[1]
[1]University of Occupational and Environmental Health School of Medicine, Kitakyushu, JAPAN, [2]Weill Cornell Medical College, Ithaca, NY.

Purpose
The recent evidence from histologic studies has shown that the disease processes of multiple sclerosis (MS) involve not only the plaques seen on conventional MR images but also the white matter regions that appear to be normal on such studies. Quantitative susceptibility mapping (QSM) is a novel technique which allows determining the bulk magnetic susceptibility distribution of tissue in vivo from gradient echo magnetic resonance phase images. The purpose of this study was to determine whether the normal-appearing white matter (NAWM) regions surrounding and remote from MS plaques have abnormal magnetic susceptibility value.
Materials & Methods
Conventional MR and QSM imaging examinations were performed in 10 patients with MS and in 10 age-matched control subjects. Quantitative susceptibility mapping was performed for various ranges of echo time by using both the magnitude and phase components in the morphology-enabled dipole inversion method. We evaluated 60 MS plaques larger than 10 mm in diameter in the white matter. Uniform regions of interest (ROI) were placed on the plaques, periplaque white matter (PWM) regions, NAWM regions in the contralateral side of the brain, and WM regions in the control subjects, to obtain QSM values, which were compared across the WM regions (Figure). For ROI placement, PWM was defined as the white matter that was closest to and surrounding the plaque and that did not have abnormal signal intensity on coregistered T2WI and FLAIR images.

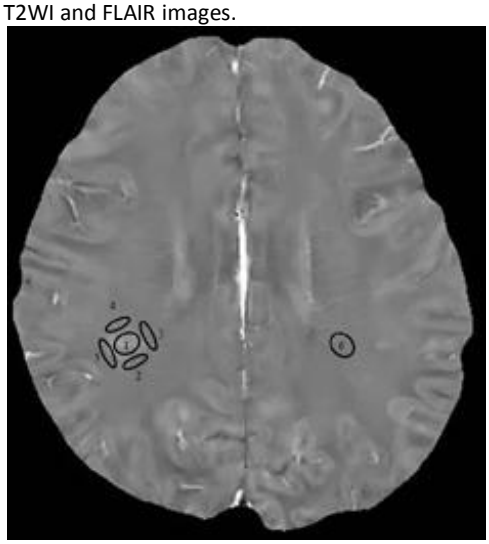

Results
In 50 of 60 plaques, the area of abnormal signal intensity on the QSM images was larger than the size of the corresponding plaque at qualitative visual evaluation of coregistered T2WI and FLAIR images. The mean QSM value was 150.3 ppb for plaques, 132.6 ppb for PWM, 120.3 ppb for NAWM, and 120.3 ppb for WM of control subjects. Significant differences in mean QSM values were observed among all WM regions ($P < .001$ for all comparisons, except QSM value in NAWM versus control subject WM).
Conclusion
The QSM values were abnormal in the periplaque regions in the patients with MS. Quantitative susceptibility mapping may be more accurate than T2WI or FLAIR for assessment of disease burden.

KEYWORDS: Multiple sclerosis plaques, Advanced MR imaging, QSM

Note: Scanned images are included in the proceedings. Some submitted images were reduced during editing, thereby decreasing clarity. Also, refer to the Program Planner. Proceedings Content as of 3-29-2013.

O-64 **12:05 PM - 12:13 PM**

Evaluation of a Bayesian Expert System for Aiding Neuroradiology Diagnoses: A Pilot Study

Tanwar, M.·Herskovits, E. H.·Nasrallah, I. M.·Kundel, H.·Mohan, S.·Li, C.·Lynch, M. C.·Bryan, R.
University of Pennsylvania
Philadelphia, PA.

Purpose
Recently, there has been an explosive growth of digital imaging data, resulting in challenge and opportunity. Contemporary computational techniques can analyze immense amounts of complex data and are being incorporated into decision-support applications. We have developed a prototypical Bayesian expert system that takes input key features (KFs) detected in images and outputs a differential diagnosis (DDx) ranked by posterior probability. We hypothesize that the idealized KFs upon which the model was based and those extracted by radiologists at different levels of training and the DDx lists produced by the model and human readers are similar.
Materials & Methods
Eleven neuroradiological entities (abscess, cerebritis, craniopharyngioma, glioblastoma, hematoma, infarct, metastasis, multiple sclerosis, rhombencephalitis, toxoplasmosis, xanthogranuloma) and normal, were evaluated by a senior neuroradiologist to identify characteristic and idealized imaging KFs and approximate conditional probabilities of these features. These features and probabilities were used to build a Bayesian expert system for differential diagnosis. Two attending neuroradiologists selected a test set of 60 diagnosis-proven MR examinations from our PACS: 5 for each entity. Three diagnosis-blind readers -- attending neuroradiologist, neuroradiology fellow and PGY-3 radiology resident -- reported the KFs and their rank ordered DDx after reviewing each case. We entered each reader's KFs into our model, obtaining a posterior probability ranked DDx list for each case-reader combination. We compared reader's observed KFs to each other and to the ideal disease features, and we compared readers' DDx to those of the model and to each other. We also compared DDx lists to the clinically proven diagnosis. Percentage agreement, kappa statistics, and ROC analysis were used to evaluate human and computer reader performance.
Results
For individual extracted KFs, there was moderate to excellent agreement between the different human readers (57-91%), which was similar to agreement between individual reader KFs and the idealized KFs for the various diseases (42-94%). Inter-reader agreement for each feature was similar to agreement between readers and the model system KFs. The model, using ideal cases (i.e., cases with "classic" features, as determined by a senior neuroradiologist), was in 100% agreement with the known diagnosis. These indicate that the KFs upon which the model system was based are concordant with actual clinical cases. The primary diagnoses of the human readers versus the proven diagnoses showed percent agreement of 77-92% and K = 0.74-0.91. ROC analysis of DDx for human readers (AUC 0.91-0.93) and model output diagnoses based on human extracted KFs (AUC 0.66-0.82) all demonstrated excellent performance.
Conclusion
A prototype neuroradiological decision-support application was developed and evaluated using a small set of clinical neuroradiological MR examinations. Readers selected similar KF values regardless of experience level, probably reflecting our use of readily noticeable findings. There was excellent agreement between each readers' most likely diagnoses and the known diagnosis, with the resident manifesting slightly lower accuracy, probably because our 12 entities are fairly distinct. Further development might render this software suitable for reducing the variability of radiology reports, improving report quality, and increasing the efficiency of practicing radiologists.

KEYWORDS: Computer-aided diagnosis, Informatics, Bayesian network

O-64a **12:13 PM - 12:21 PM**

Time Delayed Contrast-Enhanced MR Imaging Improves Detection of Brain Metastases

Kushnirsky, M.·Katz, J. S.·Knisely, J. P. S.·Schulder, M.·Rosen, L.·Steinklein, J.·Warshall, C.·Nguyen, V.
Hofstra North Shore-LIJ School of Medicine
Manhasset, NY.

Purpose
Contrast-enhanced magnetic resonance imaging (MRI) is the preeminent diagnostic test for brain metastases (BM). Brain metastases detection for stereotactic radiosurgery (SRS) planning may improve with a time delay following administration of a high-relaxivity agent for 1.5T and 3T imaging systems. Metastasis detection with time-delayed MRI was evaluated in this study.
Materials & Methods
Fifty-three volumetric MRI studies from 38 patients undergoing SRS for BM were evaluated. All studies used 0.1 mmol/kg gadobenate dimeglumin (MultiHance®), immediately after injection, followed by two more axial T1 sequences after five minute intervals (final image acquisition commenced 15 minutes after contrast injection). Two studies were motion-limited and excluded. Twu hundred eighty-seven BM were identified. The studies were randomized and examined separately by three radiologists, who were blinded to the temporal sequence. Each recorded the number of BM detected per scan. A Wilcoxon signed-rank test compared BM numbers between scans. One radiologist determined the scan on which BM were defined best.
Results

Note: Scanned images are included in the proceedings. Some submitted images were reduced during editing, thereby decreasing clarity. Also, refer to the Program Planner. Proceedings Content as of 3-29-2013.

The interclass correlations for scans 1, 2, and 3 were 0.7392, 0.7951 and 0.7290, respectively, demonstrating excellent inter-rater reliability. At least one new lesion was detected in the 2nd scan as compared to the 1st in 35.3% of subjects (95% CI: 22.4%-49.9%). The increase in BM numbers between scans 1 and 2 ranged from 1 to 10. At least one new lesion was detected in the 3rd scan as compared to the 2nd in 21.6% of subjects (95% CI: 11.3%-35.3%). The increase in BM numbers between scans 2 and 3 ranged from one to nine. Between scans 1 and 3 additional tumors were seen on 41.2% of scans (increase range 1 to 14). The median increase in tumor number for all comparisons was one. There was a significant increase in number of BM detected from scan 1 to scan 2 ($P < 0.0367$), and from 1 to 3 ($P < 0.0264$). In 34 of the 51 studies (66.7%), the radiologist selected the 3rd scan as providing the clearest tumor definition.

Conclusion

In patients who are being prepared for SRS of brain metastases, delayed MRI after contrast injection revealed an increased number of targets that need treatment. To avoid missing tumors that could be treated at the time of planned SRS, and resultant "treatment failures", we recommend that postcontrast MRI be acquired between 10 and 15 minutes after injection in patients undergoing SRS for treatment of metastatic brain tumors.

KEYWORDS: Contrast enhancement, Metastases, delayed

Monday Morning

10:45 AM - 12:15 PM
Room 1AB

(07e) Parallel Scientific Papers: Spine: New Techniques

O-65 **10:45 AM - 10:53 AM**

Reducing Artifacts in Patients with Implanted Spinal Hardware at 1.5 and 3T Using WARP

Safriel, Y.[1,2]·Dale, B.[3]·Padua, A.[3]
[1]University of South Florida, Belleair Beach, FL, [2]Radiology Associates of Clearwater, Clearwater, FL, [3]Siemens Medical Solutions, Inc., Morrisville, NC.

Purpose

Implanted spinal hardware can create significant artifacts on MRI images due to the change in susceptibility between metal and tissue. This artifact can be particularly severe at 3T as compared with 1.5T. Clinically, the signal loss and distortion may obscure pathology resulting in additional invasive tests. WARP is a work-in-progress designed to reduce these artifacts but has not been evaluated on the spine or at 3T.

Materials & Methods

The study was IRB approved and HIPPA compliant. The WARP sequence is a turbo-spin echo (TSE) sequence that utilizes increased transmit and receive bandwidth and either view angle tilting (VAT) or slice-encoding metal artifact correction (SEMAC) in order to reduce sensitivity to susceptibility variations. All patients with implantable spinal hardware had a routine lumbar MRI and at least one WARP sequence. Routine sequences included a sagittal and axial T2 TSE with restore sequence and T1 TSE sequence.

Results

Twenty-four patients were scanned. The cohort included subjects with lumbar or cervical instrumentation (pedicle screws, disk arthroplasty and plates) scanned on 1.5T or 3T platforms (Siemens, Germany). Hardware composition included stainless steel, titanium, and composites. Sagittal T2 images showed qualitatively greater improvement with the application of metal suppression. Fat-suppressed images showed least improvement. View angle tilting images were superior to SEMAC images. In six patients, the metal suppression improved visualization of pathology. In two patients, metal suppression changed the diagnosis or revealed pathology that was not seen otherwise. In one of those, metal suppression revealed a syrinx that was incompletely seen with the standard sequences. In the other, the metal suppression revealed a small disk fragment and severe central stenosis that previously was obscured.

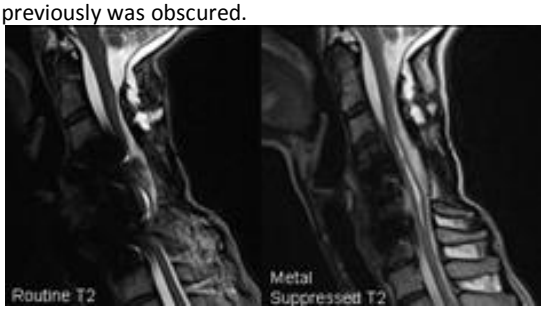

Conclusion

WARP sequences have potential to improve imaging in patients with implanted hardware on both 1.5T and 3T platforms. It also may improve diagnostic confidence possibly reducing the need for invasive procedures such as myelography. Further work is needed to better define the parameters prior to commercial release.

KEYWORDS: Metal artifact, Spinal imaging, 3T

Note: Scanned images are included in the proceedings. Some submitted images were reduced during editing, thereby decreasing clarity. Also, refer to the Program Planner. Proceedings Content as of 3-29-2013.

O-66 **10:53 AM - 11:01 AM**

Single Voxel MR Spectroscopy in Nonherniated Painful, Herniated Painful, and Nonpainful Lumbar Disks

Tanenbaum, L.[1]·Hu, S.[2]·Gornet, M.[3]·Berven, S.[2]·Peacock, J. C.[4]·Lotz, J.[4]·Bradford, D.[4]·Claude, J.[4]·Kane, P.[4]·Schranck, F.[3]·Stewart, D.[5]
[1]Mount Sinai School of Medicine, New York, NY, [2]University of California San Francisco, San Francisco, CA, [3]Orthopedic Center of Saint Louis, Saint Louis, MO, [4]Nocimed, LLC, Redwood City, CA, [5]MRI Partners of Chesterfield, Saint Louis, MO.

Purpose
To evaluate noninvasive in vivo single voxel MR spectroscopy (SVS) via two leading commercial 3T scanners in lumbar disks in diskogenic low back pain (LBP) patients receiving provocative diskography (PD) and asymptomatic volunteers (ASY), and correlate to nonherniated painful (NHP), herniated painful (HP), and nonpainful (NP) disks.
Materials & Methods
Single voxel spectroscopy exams were conducted via CHESS/PRESS SVS pulse sequences on commercial GE Signa and Siemens Verio 3T scanners, each single center, per custom investigational acquisition/postprocessing configurations and protocols developed for each platform. Two hundred twelve of 82 (disks/subjects) acquisitions from both platforms were conducted during the study(79/42 GE; 133/39 Siemens). Developmental technique refinements yielded 167 disk spectra meeting criteria for deterministic diagnostic correlations (74 of 79 disks, GE; 93 of 133 disks Siemens): 14 PD positive(PD+) NHP disks (13 GE; 1 Siemens); 7 PD+ HP disks, including six with significant leg pain(Siemens only); and 146 NP disks(61 GE; 85 Siemens), comprising PD negative (PD-) disks in pain patients and ASY disks. Provocative diskography was performed generally per ISIS guidelines. Proteogylcan(PG), lactic acid (LA), and alanine(AL)-related spectral measures were used for diagnostic algorithm development to correlate to disk types - which was performed independently for disk spectra subgroups acquired via each MR platform, with combined results assessed.
Results
Single voxel spectroscopy-based algorithms using PG and LA measures for both MR platforms resulted in 99.4% overall accuracy in correlating with 159 of the 160 NHP and NP disks, including 13 of 14 NHP disks, and all 146 of the NP disks with no false positives(12/13 NHP and 61/61 NP disks, GE; 1/1 NHP and 85/85 NP disks, Siemens). Of the 93 Siemens-based disk spectra evaluated, SVS signatures for the 7 PD+ HP disks did not differ significantly from the 85 NP disks. However, all 92 Siemens-based HP and NP spectra had a PG/LA ratio > 1, versus a PG/LA ratio < 1 for only the one Siemens-based PD+ NHP disk evaluated. Prior 11T ex vivo analysis of surgically removed disks also demonstrated PG/LA ratios were significantly lower for NHP disks versus NP disks. Nociceptor in-growth into disk nuclei has been observed in NHP disks, but not typically in NP disks - potentially related to inflammation and PG reduction. Increased LA in disks may irritate such intradiskal nociceptors to cause diskogenic LBP. However, annulus fibrosus disruptions of HP disks can irritate external nerves instead, and may allow extradiskal fluid interaction to neutralize intradiskal acidity.
Conclusion
PG and LA-related biomarkers via noninvasive SVS acquisitions in 160 lumbar disks on two commercial 3T scanners differentiated NHP from HP and NP disks with 99.4% accuracy in this study, with 100% positive predictive value and specificity (0 false positives in 146 NP disks), and failing to predict only 1/14 PD+ NHP disk. Quantitative disk SVS may provide a valuable radiology platform for chemical differentiation between these different disk types and pain profiles, and which may help guide clinical management of LBP patients in the future. Further study is warranted to confirm these encouraging findings.

KEYWORDS: MR spectrocopy, Pain, disk degeneration

O-67 **11:01 AM - 11:09 AM**

Comparison of in vivo Quantification of T1ρ in Lumbar Spine Disk Spaces at 3T in Middle-Aged Elite Athletes versus Middle-Aged Sedentary Controls: Initial Findings

Filippi, C. G.[1,2]·Duncan, C. T.[2]·Schlobohm, K.[2]·Gonyea, J. V.[3]·Hipko, S.[3]·Andrews, T.[4]·Watts, R.[3]
[1]Columbia University College of Physicians and Surgeons, New York City, NY, [2]University of Vermont School of Medicine, Burlington, VT, [3]University of Vermont School of Medicine-FAHC, Burlington, VT, [4]Philips Health Care, Cleveland, OH.

Purpose
T1 is an emerging, quantitative MR imaging modality that has been shown to correlate with proteoglycan content. Recent studies at 3T with parallel transmission have shown significant negative correlations of T1 with age at all disk space levels in the lumbar spine in normal controls supporting a potential role for T1 as a biomarker of disk degeneration. Studies have shown higher rates of disk degeneration in elite athletes particularly at L5/S1. The purpose of this study was to compare standard T2-weighted sequences and T1 quantification in middle-aged elite athletes to sedentary age-matched controls to determine if T1 would detect proteoglycan changes between these two groups.
Materials & Methods
Eleven male sedentary subjects (age range 44 to 59 years, mean 49.8 years) and six elite male athletes (age range 48 to 56 years, mean 51.4 years) with no history of chronic back pain or surgery had T1 imaging of the lumbar spine at 3T with parallel transmission. All athletes are marathoners considered elite level by national USA Track and Field parameters for age. For T1, sagittal 3D gradient-echo

Note: Scanned images are included in the proceedings. Some submitted images were reduced during editing, thereby decreasing clarity. Also, refer to the Program Planner. Proceedings Content as of 3-29-2013.

sequence (TR 3.35/TE 1.76) with flip angle 10, matrix 240 mm, 3 mm slice thickness, 18 slices, and five spin lock times of 1/25/50/75/100 msec respectively with a spin lock frequency of 350Hz. Mean T1 values of all lumbar spine disk space levels were quantified. For quantitative analysis, ROIs were placed centrally within the disk space compartments on 100 msec spin lock time sequences. Average and standard deviations of T1 values were calculated using a monoexponential curve fit with baseline correction based on noise values (air). Sagittal T2-weighted images were performed with TR 2800/TE 110 with 240 mm FOV, 3 mm thickness, 18 slices, flip angle 90. From these images, Pfirrmann scores of degenerative grade were determined at all lumbar disk space levels. Student two tail t-test was used to analyze these measures at all disk space levels with significance set to $P < .05$. One neuroradiologist with CAQ and two medical students performed quantification, all blinded. Interobserver and intra-observer variability was determined for T1 with Spearman rank correlation and for Pfirrmann scores with Cohen Kappa statistic.

Results

There were no statistically significant differences in Pfirrmann scores between these groups at any disk space level. Kappa statistic .675 indicated good interrater agreement. Regarding T1, there was a statistically significant lower T1 value in elite athletes at L5-S1 level ($P < .05$). T1 at L5/S1 for elite athletes is 48. 54 +/- 14.74, T1 for sedentary controls was 89.67 +/- 23.42. Spearman correlations for T1 values ranged from .62 to .99.

Conclusion

T1 was significantly lower at L5/S1 in elite athletes, which supports clinical studies, and no significant differences detected on Pfirrmann scores derived from T2-weighted images at this L5-S1 level such that T1 may be a more sensitive biomarker for disk degeneration. Larger studies will be needed to corroborate this preliminary work.

KEYWORDS: Spinal imaging, 3T, T1 Rho

O-68 **11:09 AM - 11:17 AM**

Comparison of Contrast-Enhanced Time-Resolved MR Angiography and Digital Subtraction Angiography for Evaluation of Spinal Vascular Malformations

Boddu, S.·Saindane, A. M.·Dehkharghani, S.·Tong, F.·Dion, J.
Emory University School of Medicine
Atlanta, GA.

Purpose

Spinal vascular malformations (SVMs) can pose a challenge in diagnosis and exact localization. Spinal digital subtraction angiography (DSA) is the gold standard for diagnosis, but can be intensive in time, radiation dose, and contrast dose. Conventional spinal MRI has limited sensitivity for evaluation of SVMs. We hypothesize that multiphasic contrast-enhanced time-resolved MRA (CE-TR-MRA) will have utility for noninvasive diagnosis and pre-angiographic localization of SVMs.

Materials & Methods

Thirty-one consecutive patients who underwent CE-TR-MRA for suspected SVMs presenting over a 24-month period were reviewed. Of these, 17 patients [14 males; median age 65 years (30-80 years)] underwent both CE-TR-MRA and DSA, with DSA performed a median of 11 days (0 - 41 days) after the CE-TR-MRA. Subjects underwent MRA on a 1.5T GE unit using both 3D TOF-MRA and CE-TR-MRA using yime resolved imaging of contrast kinetics (TRICKS) with intravenous administration of a standard dose gadolinium-based contrast agent. Both the CE-TR-MRA and DSA images were evaluated for presence or absence of SVM and location of feeding arterial supply. Contrast-enhanced TR-MRA was evaluated against DSA as the reference standard. Digital subtraction angiography also was evaluated for number of vessels catheterized, contrast volumes, fluoroscopic and procedure time.

Results

Thirteen of 17 CE-TR-MRA studies were of diagnostic quality; four patients had suboptimal MRA from motion artifact. Of the 13 diagnostic studies, six patients were positive for SVM both on CE-TR-MRA and DSA, six patients were negative for SVM on both CE-TR-MRA and DSA and one patient was a false positive on CE-TR-MRA (a nonspecific hypervascular blush from the right L1 level with no shunt pathology on DSA). The sensitivity, specificity, positive and negative predictive values of TR MRA were 100%, 86%, 86% and 100%, respectively. One patient negative on both CE-TR-MRA and DSA had a cavernous malformation on MRI. One patient with an initially negative DSA had a positive CE-TR-MRA for dAVF, confirmed on repeat targeted DSA. The localization of SVM arterial supply on CE-TR-MRA was within one vertebral level on DSA for all patients. Compared to patients with confirmed SVM on CE-TR-MRA, patients with negative and suboptimal CE-TR-MRA had significantly increased number of vessels catheterized (p=0.001) and larger contrast volumes (p=0.0009). No significant difference in fluoroscopic and procedure time were found.

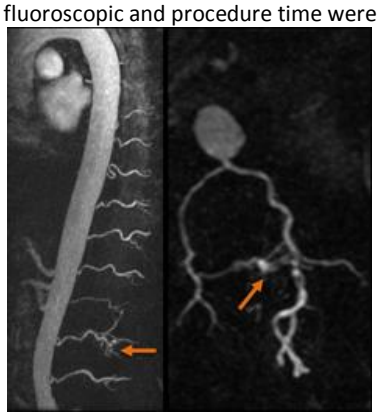

Conclusion

Contrast-enhanced TR-MRA is a reliable noninvasive investigation for the diagnosis and localization of SVMs,

Note: Scanned images are included in the proceedings. Some submitted images were reduced during editing, thereby decreasing clarity. Also, refer to the Program Planner. Proceedings Content as of 3-29-2013.

and is useful prior to DSA to reduce the number of catheterized vessels and contrast volume.

KEYWORDS: 4D MRA, Spinal arteriovenous malformation

O-69 **11:17 AM - 11:25 AM**

Novel Semi-Automatic Algorithm for Spinal Cord Cross-Sectional Area Analysis in Multiple Sclerosis

Bakshi, A. C.·Winston, L.·Saad, Z.·Jacobson, S.·Reich, D. S.·Nair, G.
National Institutes of Health
Bethesda, MD.

Purpose
To quantify spinal cord atrophy in multiple sclerosis (MS) by using a novel semi-automated algorithm that determines cross-sectional area from noninvasive imaging techniques.
Materials & Methods
MR imaging was performed on seven MS patients (two secondary progressive, one primary progressive, three relapsing-remitting, one clinically isolated syndrome, age 43.3 ± 9.2 years, EDSS between 0 and 6.5, five women and two men) and seven healthy controls (44.4 ± 7.5 years, age-matched to MS, five women and two men) on a Siemens 3T Skyra system equipped with a spine array coil. Volumetric images of the cervical and thoracic cord were obtained using a T1-weighted MPRAGE sequence with TR = 3000 ms, TE = 4.5 ms, TI = 750 ms, FA= 8 degrees, and 1 mm isotropic resolution. Cross-sectional area of the cord was calculated by detecting the edge of the spinal cord from slices reformatted perpendicular to the cord at each point between the C1 and C7 vertebral body segments. Total postprocessing time was <5 minutes with minimal user input. Multiple sclerosis patients also underwent disability tests including the Expanded Disability Status Scale (EDSS) and the 9-hole peg test.
Results
The average cross-sectional cervical cord area for MS patients (69.4 ± 12.0 mm2) was significantly lower than that for healthy controls (84.2 ± 10.9 mm2) (t-test, $p < 0.001$). The average cross-sectional area at each point along the cord was also lower for MS patients (Figure). In the MS group, there were negative correlations between the average cross-sectional cervical spinal cord area and the corresponding EDSS score ($r = -0.90$, $p = 0.003$) and 9-hole peg test times ($r = -0.73$, $p = 0.03$), suggesting that cord measures determined through this novel algorithm may be associated with clinical disability.

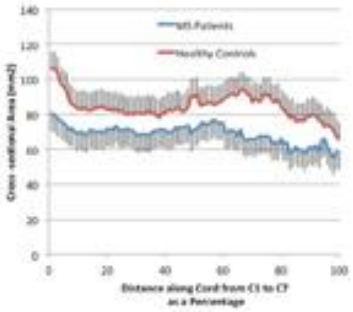

Figure: Cross-sectional cord area for 7 MS patients and 7 healthy controls as a percentage of distance from C1 to C7.

Conclusion
Cross-sectional area measurements acquired through this algorithm correlated inversely with clinical disability scores. These measurements therefore may prove useful as imaging biomarkers of MS progression both in the clinic and in clinical trials. Testing of additional patients as well as expanding these measures to the thoracic spinal cord is underway.

KEYWORDS: Spinal cord, Atrophy

O-70 **11:25 AM - 11:33 AM**

Oxaliplatin-Induced Neuropathy Can Be Demonstrated by Imaging: Molecular Neurography in a Mouse Model

Le Roux, L. G.·Bredow, S.·Schellingerhout, D.
M. D. Anderson Cancer Center
Houston, TX.

Purpose
The purpose of our study was to utilize a new imaging technology, neurography, based on the retrograde transport of a molecular imaging agent, to determine if oxaliplatin neurotoxicity affects retrograde axonal transport.
Materials & Methods
Female adult BALB/c mice (n = 8) were treated with oxaliplatin to a cumulative dose of 30 mg/kg by giving 10 divided intraperitoneal doses using a five days of treatment, five day rest, five day treatment administration paradigm. Animals were imaged at baseline and weekly for 149 days after commencement of therapy. Control animals (n = 8 from 8 to 28 days, n = 4 from 35 to 65 days)) were mock treated with saline and were imaged similarly out to 65 days. All animals received fluorescently labeled TTc-Alexa790 (15 ug in 20 uL) via intramuscular injection into the calf muscles at every imaging session. Fluorescent imaging (Xenogen IVIS 200) was used to image the distribution of TTc over 60 minutes, with ROI measurements taken from the thoracic spine to quantitate fluorescent uptake. Region of interest measurements had background activity subtracted, and were normalized to the signal intensity at time = 0.
Results

Note: Scanned images are included in the proceedings. Some submitted images were reduced during editing, thereby decreasing clarity. Also, refer to the Program Planner. Proceedings Content as of 3-29-2013.

With sham treatment, TTc transport through the sciatic nerve and spinal cord causes the fluorescent signal intensity over the thoracic ROI to gradually increase (Figure, legend indicates number of days after start of study). At 60 minutes the grouped mean normalized fluorescence was 562% (+/-210% SD). With oxaliplatin treatment, transport is abruptly and severely impaired with baseline values of 836%+/-375% falling to 396%+/-140%, 247%+/-63%, 213%+/-58%, 162%+/-46%, 147%+/-63% with each successive week and stabilizing around 175% (+/-45%) for grouped means from 6 weeks out to the end of the study. The difference between normalized fluorescence grouped mean values from 6 weeks after oxaliplatin treatment to the end of study, and control animals is highly statistically significant (T-test $p<0.0001$).
Conclusion
Oxaliplatin causes a rapid and apparently irreversible (to our current followup of 149 days) decrease of retrograde axonal transport in the sciatic nerves and spinal cord, as demonstrated with a neurographic molecular imaging agent.

KEYWORDS: Neurography, Neurotoxicity, Molecular Imaging

O-71 **11:33 AM - 11:41 AM**

Hereditary Transthyretin Familial Amyloid Polyneuropathy: In vivo Detection of Lower Limb Nerve Injury Using High-Resolution MR Neurography

Kollmer, J. C.·Hund, E.·Hornung, B.·Schönland, S.·Hegenbart, U.·Kimmich, C.·Bendszus, M.·Pham, M.
University of Heidelberg
Heidelberg, GERMANY.

Purpose
Transthyretin-familial-amyloid-polyneuropathy (TTR-FAP) is an autosomal-dominant transmitted hereditary disease leading to misfolding and extracellular deposition of the protein transthyretin. It is endemic (e.g., in certain regions of Portugal and Sweden) but very rare in other parts of Europe and the U.S. Clinically, it is a life-threatening multisystemic disorder, presenting mainly with an axonal, distal-symmetric-sensory-motor, small-fiber-polyneuropathy (PNP) in addition to autonomic/cardiac manifestations. Concerning the pathomechanisms of TTR-FAP it is unclear whether the deposited amyloid leads to direct toxic effects or indirect ischemic nerve injury. For the first time, we investigated in vivo amyloid-related nerve-injury by large coverage and high-resolution T2-weighted imaging.
Materials & Methods
We prospectively examined a large sample of 20 patients with genetically confirmed TTR-FAP {13 with manifest PNP [measurements included: complete neurologic examination, scoring for NIS-LL (Neuropathy-Impairment-Score-Lower-Limbs), NDS (Neuropathy-Deficit-Score), NSS (Neuropathy-Symptom-Score), detailed neurographic measurements], and seven neurologic/electrophysiologic asymptomatic-gene-carriers}. These subjects were compared to 60 healthy volunteers, age/gender-matched. Imaging was done on a 3T-MR-scanner (Magnetom/Trio/Siemens) with high-resolution T2-weighted fat-suppressed-sequences separately for each leg and lumbar plexus: 1) axial T2-TSE-fs-sequences from proximal thigh to distal ankle (140 slices/leg; TE/TR 55/5970ms, voxel-size 0.4x0.3x3.5mm); 2) 3D-T2-IR-SPC sequence with axial reformation (50 images) for the lumbar plexus/spinal nerves (TE/TR 202/3000, voxel-size 1.0x1.0x1.0). Manual segmentation of the lumbar plexus/sciatic/tibial/fibular/sural nerve as nerve-tissue-voxels was performed on each axial imaging slice (320/subject). Lesion-voxels then were classified fully automated and operator-independent. Statistical analysis was performed by using nested-two-way-ANOVA and pairwise-contrast-analysis.
Results
Quantitative evaluation of lesion-voxels and pairwise-contrast-analysis showed with strong statistical significance that lesion-voxel-number was markedly higher not only in symptomatic TTR-FAP (28948±5035;$p<0.0001$) but also in asymptomatic gene-carriers (18119±4162;$p=0.02$) compared to healthy controls. Differences in lesion-voxel-number between symptomatic and asymptomatic TTR-FAP also were highly significant ($p<0.0001$). Nested-two-way-ANOVA revealed for lesion-voxel-count a predominant proximal focus (thigh) of nerve lesions (proximal 35290±3275 versus distal 12610±1380;$p<0.0001$).

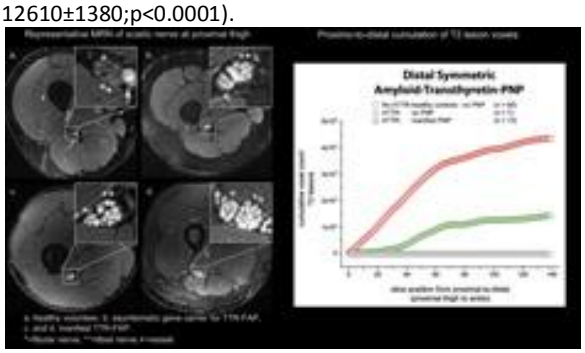

Conclusion
We could show for the first time, that in TTR-FAP, nerve lesions were detectable in vivo by using high-resolution MRN not only in patients with manifest PNP, but also in asymptomatic gene carriers in whom imaging detection precedes clinical/electrophysiologic manifestation. This suggests that MRN can serve as a novel and highly sensitive diagnostic marker even of early asymptomatic stages of TTR-FAP. Furthermore, we found proximal nerve lesions to be more severe than distal lesions in all 20 TTR-FAP subjects. This finding is surprising because symptoms prevail distally (not proximally), pointing towards ischemia rather than metabolic toxicity as major pathomechanism of TTR-induced nerve damage.

Note: Scanned images are included in the proceedings. Some submitted images were reduced during editing, thereby decreasing clarity. Also, refer to the Program Planner. Proceedings Content as of 3-29-2013.

KEYWORDS: MR neurography, Peripheral nerve, Hereditary Amyloidosis

O-72 **11:41 AM - 11:49 AM**

MR Neurography versus Electric Nerve Conduction in Distal Ulnar Nerve Entrapment

Kollmer, J. C.[1]·Dombert, T.[2]·Staub, F.[2]·Bäumer, P.[1]·Bendszus, M.[1]·Pham, M.[1]
[1]University of Heidelberg, Heidelberg, GERMANY, [2]Center for Peripheral Neurosurgery, Dossenheim/Heidelberg, GERMANY.

Purpose
In patients with a suspected peripheral neuropathy it is essential to determine the presence of an underlying nerval lesion, especially if surgical decompression is indicated. The current diagnostic goldstandard are electrophysiologic measurements of nerve function, but even then, the exact localization and detection of nerve entrapment often remains unclear. The clinical relevance and validity of MR neurography (MRN) in determining a neuropathic lesion is still subject of controversial discussions, especially because the underlying histopathologic processes leading to an increased intraneural T2-signal, the major diagnostic sign of MRN, are not completely understood. In this study, we correlated intraneural T2-signal with motor-nerve-conduction, which has never been performed before in any human or experimental study.
Materials & Methods
We prospectively examined 11 patients with confirmed rare ulnar nerve entrapment neuropathy at the wrist and 11 asymptomatic volunteers, matched for age and gender. Imaging was done on a 3T MR-scanner (Magnetom/Verio/Siemens) applying axial T2-weighted fat-suppressed-sequences (TR/TE 3830/60ms, voxel-size 0.2x0.2x2.0mm). Intraneural T2-weighted-signal was evaluated by manually delineating nerve circumference as intraneural region-of-interest (ROI) on each axial imaging slice. To determine contrast-to-noise-ratios (CNR), additional ROIs were placed in the thenar muscles and in the air. Electrophysiologic examinations included distal motor-nerve-conduction of the ulnar nerve measured as distal-motor-latency (dml) to first dorsal-interosseus (IOD I) and abductor digiti minimi muscle.
Results
Electrical-nerve-conduction of the deep motor branch measured as dml to IOD I shows a significant nonlinear correlation with ulnar motor branch T2-signal (mean dml IOD I in patients 5.85 +/-0.66ms (range 3.0-10.3 ms), mean dml IOD I in volunteers 3.28+/-0.10ms (range 2.7-3.8; pathologic if >4.4ms); R^2 = -0.8; p<0.001). T2-weighted-CNR values increase steeply within the range of beginning deceleration of electrical-conduction (up to 5ms) until reaching a plateau within the range of severe conduction slowing (>5ms). Furthermore, ROC-analysis revealed increased nerve T2-signal of the deep motor branch to be a sign of excellent diagnostic performance (area-under-the-curve 0.94; specificity 90%, sensitivity 89.5%).

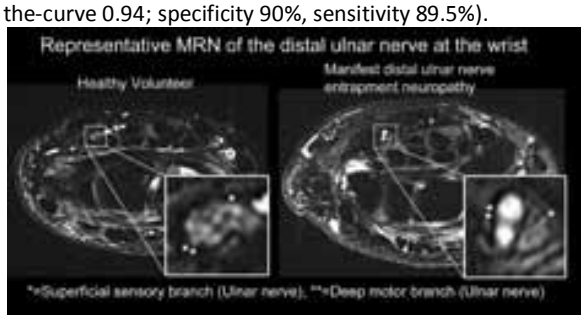

Conclusion
MR neurography serves as an excellent diagnostic test in determining even distal nerve entrapment with involvement of smallest distal nerve branches at the limit of current structural resolution. The strong nonlinear correlation between nerve T2-signal and motor-nerve-conduction with an exponential asymptotic growth underlines that MRN is particularly sensitive for the detection of early stages of focal entrapment neuropathy, whereas nerve conduction during this stage shows only slightly subnormal deceleration. Furthermore, our results support that an increased intraneural T2-signal reflects an underlying clinically relevant pathology.

KEYWORDS: Peripheral nerve, MR neurography, Entrapment Neuropathy

O-73 **11:49 AM - 11:57 AM**

MR Neurography: Anterior Interosseus Nerve Syndrome Is Not a Neuropathy of the Anterior Interosseus Nerve

Pham, M.[1]·Baeumer, P.[1]·Kollmer, J.[1]·Kele, H.[2]·Bendszus, M.[1]
[1]Heidelberg University Hospital, Heidelberg, GERMANY, [2]Center for Peripheral Nerve Disease, Neuer Wall, Hamburg, GERMANY.

Purpose
Anterior-interosseus-nerve-syndrome (AINs) is conceived as entrapment-neuropathy of the anterior-interosseus-nerve trunk (AIN) at mid-forearm level, distal to its exit from median nerve (MN). MR imaging has been used so far to rule out mass lesions compressing AIN and to confirm muscle injury/denervation by increased intramuscular T2-weighted-signal. However, precise determination and localization of the nerve lesion itself by MR-neurography or any other test including electrophysiology has failed so far.
Materials & Methods
In a large prospective cohort of 20 consecutive patients (45.6 ± 10.4 years,15m,5f) the rare AINs was confirmed by standard criteria: acute weakness of terminal thumb and index finger-flexion. All patients and additional 20 healthy controls matched to age/gender underwent extended high-resolution MR-neurography of upper

Note: Scanned images are included in the proceedings. Some submitted images were reduced during editing, thereby decreasing clarity. Also, refer to the Program Planner. Proceedings Content as of 3-29-2013.

arm/elbow/forearm level (15Ch/Transmit-Receive extremity coil, 3x41 slices 2D-T2-TSE, TE/TR 55/5970ms, in-plane resolution/slice thk. 0.3mm/3mm). AIN (forearm) and median nerve (elbow+upper-arm) signal was rated qualitatively as "normal" versus "increased/lesion". Quantitative evaluation was performed after normalization of nerve T2-weighted-signal with respect to adjacent intramuscular T2-weighted-signal (long head/biceps muscle). Three different regions-of-interest were read-out: MN-controls-all-fascicles, MN-patients-lesion-fascicles, MN-patients-normal-fascicles. Predominant lesion focus was determined from maximum intensity of normalized T2-weighted-signal and referenced to humeroradial joint space.

Results

In all AINs patients but none of controls (sensitivity/specificity 100%) proximal lesions of MN-trunk at upper arm (14.4 ± 5.5 cm proximal to humeroradial joint) and not of distal AIN-trunk were found. In all patients proximal lesions involved selectively only certain fascicles at dorsal and ulnar aspect within MN cross-section (Figure). This cross-sectional/fascicular distribution corresponded exactly to the somatotopic organization of the fascicle group destined to become AIN further distally but is not equivalent to AIN itself(Figure). Additionally, multifocality of lesions was observed in the majority of patients. Quantitative evaluation showed that normalized T2-weighted-signal intensity within affected fascicles was increased strongly in all patients (> 1.7 of normalized T2-weighted-signal corresponding to >2SD of controls;p<0.0001) and was normal in other fascicles within MN cross-section not corresponding to AIN fascicle group (p = 0.35).

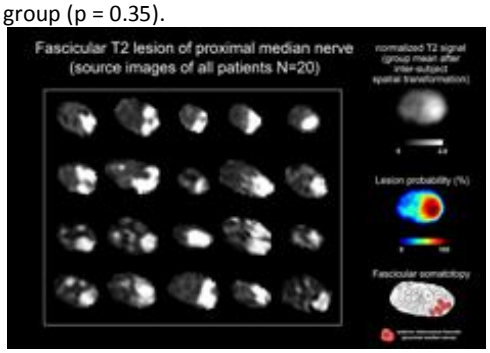

Conclusion

MR neurography could accomplish to determine precise localization of nerve lesions in AINs, which before has not been possible neither by attempts of physical nor electrophysiologic localization. Findings of selective injury to certain but not all fascicles within upper-arm MN trunk and of lesion multifocality rule out entrapment as pathomechanism and saves these patients from inappropriate surgical exploration of AIN. The observation of lesion multifocality in the majority of patients suggests immune-mediated inflammation and not mechanical entrapment as cause.

KEYWORDS: MR neurography, Peripheral nerve, Neuropathy

O-74 **11:57 AM - 12:05 PM**

Early Diabetic Nerve Injury Detected in vivo by Large Coverage Sampling of Nerve T2 Signal

Pham, M.·Hornung, B.·Oikonomou, D.·Weiler, M.·Baeumer, P.·Kollmer, J.·Nawroth, P.·Bendszus, M.
Heidelberg University Hospital
Heidelberg, GERMANY.

Purpose

Distal symmetric diabetic polyneuropathy (DPN) is a very frequent complication of diabetes and the most prevalent neuropathy. DPN causes considerable long-term morbidity. Its pathogenesis remains unclear with two theories competing to explain nerve injury: direct/toxic metabolic injury to distal fibers versus indirect/secondary ischemic injury. To detect in vivo spatial patterns of early DPN would improve differentiation because experimental work indicates that toxic/metabolic effects result in diffuse-distal, whereas ischemia results in proximal injury. Few studies investigated spatial patterns of diabetic nerve injury only analyzing ex vivo samples. We showed previously that severe DPN is detectable in vivo by MR neurography (MRN). Now, with refined image acquisition, data analysis and coil technology, we show the spatial distribution of even early DPN in vivo.

Materials & Methods

Sixty patients confirmed with DPN (59.5±12.2 years. 25f/35m) by physical and electrophysiologic examinations were graded as nonsymptomatic/mild/moderate according to national guidelines. These groups were compared to 60 nondiabetic, age/sex-matched controls. Participants underwent extended MRN acquiring nerve-T2-signal with high spatial resolution and at same time ample anatomical coverage (spinal nerve to ankle,TA 57 min.): 140 axial slices per leg (2D-T2-TSE, TE/TR 55/5970ms, in-plane resolution/slice-thk. 0.3mm/3mm, 15Ch/Tx/Rx Coil), +50 axial slices for spinal nerve and plexus coverage reformatted from 3D-T2-SPC sequence (TE/TR 200/1000). Manual segmentation of nerve tissue voxels (spinal nerves/plexus/sciatic/tibial/fibular/sural) was performed slice-by-slice (320 slices per subject). Lesion voxels were classified in fully automated, operator-independent manner: first, normative distributions of T2-signal was calculated in controls for each slice and nerve. Lesion voxels were identified in patients as statistical outliers at 1.5 of normalized T2-signal which separated best patients from controls.

Results

Nested two-way ANOVA showed strong significance for increasing lesion-voxel count with increasing DPN severity (main effect GROUP:p<0.0001), with proximal (thigh) not distal (ankle) position (main effect POSITION:p<0.0001), and for interaction GROUPxPOSITION (p=0.0003) indicating a proximal-to-distal gradient of injury

Note: Scanned images are included in the proceedings. Some submitted images were reduced during editing, thereby decreasing clarity. Also, refer to the Program Planner. Proceedings Content as of 3-29-2013.

dependent on DPN severity (Figure). Pairwise contrasts for GROUP showed that lesion voxel number in moderate (2527±631,p<0.0001), even in mild (1991±291;p=0.0039) and even in nonsymptomatic DPN (1749±284;p=0.29) were higher than in controls (1518±151,Figure), for POSITION that lesions occurred with predominant proximal not distal focus (proximal:3262±92 vs. distal: 715±34.3;p<0.0001).

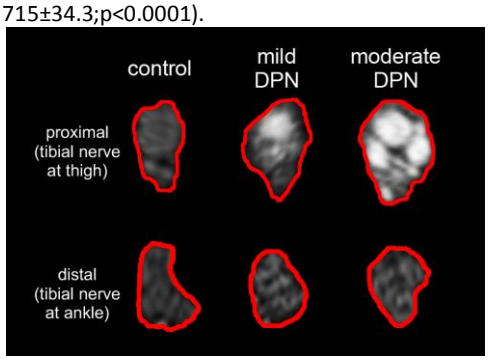

Conclusion

We report for the first time that nerve injury is detectable in vivo by MRN not only in severe but also early/mild DPN; and further, that spatial injury pattern is proximal rather than distal-diffuse suggesting ischemia rather than direct toxicity to nerve as predominant pathomechanism.

KEYWORDS: MR neurography, Diabetes, Neuropathy

O-75 **12:05 PM - 12:13 PM**

DT Imaging Can Detect Even Subclinical Peripheral Nerve Injury

Baumer, P.·Heiland, S.·Weiler, M.·Ruetters, M.·Bartsch, A.·Bendszus, M.·Pham, M.
University of Heidelberg
Heidelberg, GERMANY.

Purpose

Diffusion tensor imaging (DTI) is a promising technique in MR neurography (MRN) for the evaluation of the peripheral nervous system. The main functional parameter obtained by DTI for peripheral nerves is fractional anisotropy (FA). Previous experimental and clinical works have explored the potential of FA as a sensitive parameter for the detection of neuropathy in carpal tunnel syndrome and inflammatory diseases . Fractional anisotropy was shown to correlate with electrophysiologic parameters of distal motor latency and amplitude of action potential in a small number of patients. It is hitherto unclear how sensitive FA is in the detection of neuropathy. We set out to investigate the ability of DTI to detect subclinical nerve injury at the ulnar nerve.

Materials & Methods

MR neurography exams were performed on elbows and wrists (Magnetom Trio, Siemens, 15Ch Tx/Rx Coil) in 30 healthy subjects without a history of peripheral nerve injury. Sequences included a PD/T2-weighted relaxometry (TR 3000ms, TE 13/52ms, slices 18, averages 2, spectral fat-suppression, in-plane-resolution 0.39x0.39x4mm^3, TA 6:23 min) and DTI (TR 3800ms, TE 87ms, b-value 800s/mm^2 encoded in 19 directions, slices 18, averages 2, in-plane-resolution 1.17x1.17x4mm^3, TA 2:43 min). DTI postprocessing was performed on a Siemens Syngo MMWP version VE32B station. Nerves were segmented manually slice-by-slice to obtain nerve T2 and FA values. All subjects also underwent electrodiagnostics including nerve conduction velocities(NCV) for ulnar and median nerves, distal motor latency (dmL), and motor compound action potentials.

Results

Across all subjects, ulnar FA values showed a nadir (minimum 0.46±0.02, mean 0.55±0.02) in the proximal ulnar sulcus where T2 values showed a peak (maximum 197.9±9.4, mean 174.6±7.9)(Figure A). Ten subjects (33%) had decreased NCV across the elbow segment. These exhibited significantly decreased FA values (0.40±0.10, p=0.043) as well as increased T2 values (183.8±60.0, p=0.037) at this position. T2 values did not correlate significantly to NCV. In contrast, both minimum and mean FA values correlated with proximal ulnar NCV (minimum FA r=0.57, p=0.0016, mean FA r=0.41, p=0.031; Figure B). Similar results were obtained for the median nerve in the carpal tunnel with increased T2 signal and decreased FA. Again, T2 values did not correlate with electrophysiologic parameters at the carpal tunnel, but mean FA significantly correlated with dmL (r=-0.41, p=0.029).

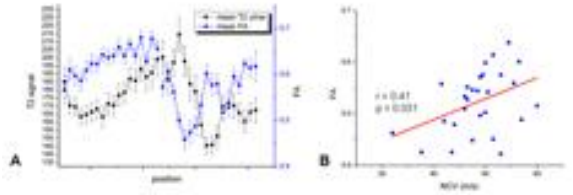

Proximo-distal course of T2 and FA at upper arm and elbow

Correlation between FA vs. NCV at ulnar sulcus

Conclusion

Changes in nerve FA correspond already to subclinical nerve injury. DTI demonstrates stronger correlations to electrodiagnostic parameters and therefore might be even more sensitive than T2-weighted nerve signal in the detection of neuropathy.

KEYWORDS: DTI, Peripheral nerve

Note: Scanned images are included in the proceedings. Some submitted images were reduced during editing, thereby decreasing clarity. Also, refer to the Program Planner. Proceedings Content as of 3-29-2013.

O-76 **12:13 PM - 12:21 PM**

Diffusion Tensor Imaging and Tractography of the Sciatic Nerves in Chronic Inflammatory Demyelinating Polyradiculoneuropathy

Gasparotti, R.·Todeschini, A.·Filosto, M.
University of Brescia Medical School
Brescia, ITALY.

Purpose
Chronic inflammatory demyelinating polyradiculoneuropathy (CIDP) is an acquired peripheral neuropathy of presumed autoimmune etiology. The diagnosis rests upon a combination of clinical, electrodiagnostic and laboratory features. MR imaging showing bilateral hypertrophy of brachial and/or lumbar plexuses may assist the diagnosis. Diffusion tensor imaging (DTI) recently has been proposed as a noninvasive technique to evaluate the peripheral nerve microstructure in vivo. We hypothesized that diffusion tensor tractography (DTT) and measurements of fractional anisotropy (FA) along the sciatic nerves can differentiate patients with CIDP from controls.
Materials & Methods
We performed a 1.5T MRI (Aera, Siemens, Germany) on 10 patients affected by CIDP (mean age 50.2) and 10 age- and sex-matched healthy volunteers (mean age 48.7 years) using the following imaging protocol: a) 3D magnetic resonance neurography (3D MRN) of brachial and lumbosacral plexuses, b) 2D MRN and c) DTI of sciatic nerves at the level of thigh. Diffusion tensor tractography of the sciatic nerves was guided by color-coded FA maps overlaid on high-resolution MRN. The FA values of the tracked segments of the sciatic nerves were compared between the two groups. The sciatic nerve cross-sectional area (CSA) also was measured at the level of mid-thigh on the axial 2D MRN sections. The CSF protein concentration was available for nine patients. T-test and Pearson correlation test were utilized for the statistical analysis. Threshold for significance was defined as $p<0.05$.
Results
In the patient group, plexus hypertrophy and increased signal intensity were detected in 13 out of 20 plexuses (65%) on 3D MRN. Sciatic nerve CSA was increased significantly in CIDP patients (mean 58.50 ± 3.41 mm^2) compared to controls (mean 86.20 ± 22.07) ($p = 0.04$). The sciatic nerve FA values were significantly lower in CIDP patients (mean 0.404, 95% C.I 0.378-0.427) than in healthy volunteers (mean 0.466, 95% C.I. 0.443-0.490) ($p = 0.001$) and inversely correlated with the CSA values ($r = -0.708$, $p = 0.033$). The association between the CSF protein concentration and FA values reached statistical significance ($r = 0.67$, $p = 0.52$).

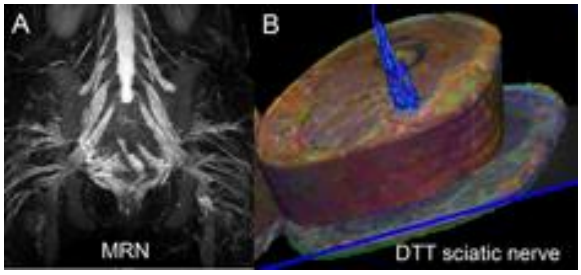

Conclusion
Our preliminary data suggest that a noninvasive DTI assessment of the sciatic nerves may provide clinically useful information in addition to MRN in patients with CIDP. The quantitative assessment of FA can help further characterizing the effects of the disease processes on the structural integrity and directional coherence of the nerve fibers.

KEYWORDS: Peripheral nerve, Diffusion tensor image, MR Neurography

Monday Afternoon

1:15 PM - 2:45 PM
Ballroom 6AB

(8) General Programming: Reversible Brain Syndromes: PRES, Reversible Cerebral Vasoconstriction Syndrome and Cerebral Venous Thrombosis (SAM) (AR)

O-77 **1:15 PM - 1:40 PM**

Posterior Reversible Encephalopathy Syndrome (PRES)

Bartynski, W. S.
Presbyterian University Hospital
Pittsburgh, PA.

Presentation Summary
Posterior reversible encephalopathy syndrome (PRES) is a unique neurotoxic state. Typically the clinical presentation is nonspecific with altered mentation, headache, visual symptoms and seizures most common. The toxicity has been identified most commonly in patients following allogeneic bone marrow or solid organ transplantation, women experiencing preeclampsia or eclampsia, patients with autoimmune conditions such as Lupus, patients with significant infections, sepsis or shock and patients following cancer chemotherapy. The imaging pattern of PRES generally demonstrates vasogenic edema with a

Note: Scanned images are included in the proceedings. Some submitted images were reduced during editing, thereby decreasing clarity. Also, refer to the Program Planner. Proceedings Content as of 3-29-2013.

characteristic distribution in the parietal, occipital and frontal lobes, primarily reflecting the brain watershed areas. The areas of vasogenic edema usually reverse and resolve, hence the concept of "Reversible Encephalopathy". Evidence of vasculopathy can be identified on imaging studies including MRA and catheter angiography and pathophysiology obtained in the acute phase of the process demonstrates evidence of endothelial activation and immune cell trafficking and up-regulation of vascular endothelial growth factor (VEGF) suggesting brain hypoxemia. Clinically, approximately 25-30% of patients have a normal blood pressure at the time of toxicity with mild BP elevation (MAP 105-115 mmHg) seen in approximately 15% and more severe hypertension (MAP>120 mmHg) in approximately 50%. Evidence of systemic inflammatory response syndrome (SIRS) and multi-rgan dysfunction syndrome (MOD) commonly is noted including thrombocytopenia, liver dysfunction, renal dysfunction, pulmonary dysfunction and BP instability (most frequently noted in patients with infection and eclampsia). This talk will review the clinical and imaging features of PRES, focusing on the likely biological factors responsible for the toxicity.These features are important for initial recognition of the toxicity as well as understanding the probable causes of the condition.

O-78 **1:40 PM - 2:00 PM**

Reversible Cerebral Vasoconstriction Syndrome

Gandhi, D.
Johns Hopkins University Hospital
Baltimore, MD.

Presentation Summary
RCVS represents a group of clinical syndromes characterized by severe "thunderclap" headache with or without neurologic deficits and multifocal segmental areas of cerebral arterial narrowing or vasoconstriction that usually resolve within weeks. RCVS is being recognized increasingly as a cause of isolated convexity subarachnoid hemorrhage (cSAH) and must be differentiated from other etiologies of cSAH such as amyloid angiopathy, cortical vein thrombosis and PRES. Several specific clinical, laboratory and neuroimaging findings can assist in differentiating RCVS from SAH-related vasospasm or primary angiitis of CNS (PACNS); diseases with which RCVS often is confused. Acute relapsing thunderclap headaches with or without neurologic deficits, presence of cortical SAH over the convexity, diffuse vasoconstriction involving the distal intracranial vessels (out of proportion to the amount of SAH), near normal CSF analysis and short-term reversibility of vasoconstriction (<3 months) are typical of this entity and help differentiate it from other conditions causing thunderclap headaches. This presentation will summarize the clinical and imaging criteria for the diagnosis of RCVS and review the current literature on this entity.

O-79 **2:00 PM - 2:20 PM**

Cerebral Venous Thrombosis

Spampinato, M.
Medical University of South Carolina
Charleston, SC.

Presentation Summary
Cerebral venous thrombosis is an infrequent but serious disorder accounting for 0.5% of all cerebrovascular accidents. Several predisposing factors have been identified, including congenital and acquired prothrombotic states, while infection remains the most common underlying cause in developing countries. The clinical diagnosis of cerebral venous thrombosis can be difficult because signs and symptoms of this condition are frequently vague and nonspecific, including signs of intracranial hypertension, focal neurologic deficits, seizures, and/or cavernous sinus syndrome. As a result, neuroimaging can be of paramount importance in establishing an early diagnosis of cerebral venous thrombosis, which in turn can significantly decrease the risk of serious complications including stroke or death. Cerebral venous thrombosis should be considered in the differential diagnosis when confronted with unexplained brain edema, especially in young or middle-age patients, in the setting of atypical or unusual headache or stroke-like symptoms, and in the absence of cardiovascular risk factors. The diagnosis of cerebral venous thrombosis usually is established with the use of contrast-enhanced brain MRI and MR venogram, although unenhanced brain CT can sometimes demonstrate findings concerning venous thrombosis. CT venogram also is used increasingly in the emergency setting because it can be performed quickly and offers improved visualization of small venous structures when compared with MR venography. Parenchymal abnormalities seen in cerebral venous thrombosis can include parenchymal swelling, vasogenic and cytotoxic edema, hemorrhage, or gyral enhancement. Even large areas of nonhemorrhagic brain signal abnormality can resolve completely. The radiologist may play an important role in the diagnosis of cerebral venous thrombosis and in monitoring treatment response. Understanding the pathophysiology and imaging characteristics of reversible and nonreversible MR imaging abnormalities can improve patient management and prognosis prediction.

Note: Scanned images are included in the proceedings. Some submitted images were reduced during editing, thereby decreasing clarity. Also, refer to the Program Planner. Proceedings Content as of 3-29-2013.

Monday Afternoon

1:15 PM - 2:45 PM
Ballroom 6CF

(9) ASFNR Programming: Advanced Imaging in Neuro-Oncology: Do They Improve Outcome?

O-80 **1:15 PM - 1:35 PM**

fMRI and DTI

Young, R. J.
Memorial Sloan-Kettering Cancer Center
New York, NY.

Learning Objectives
Upon completion of this presentation, participants will be able to:
1) Review the roles of BOLD fMRI and DTI in the treatment of patients with brain tumors.
2) Present representative motor and language cases where fMRI and DTI impact preoperative planning.
3) Discuss the limitations of fMRI and DTI.
4) Discuss the advantages and disadvantages of tractography.
Presentation Summary
Surgery is an effective treatment for many brain tumor patients with improvements possible in both the length and the quality of patient survival. Blood oxygen level dependent (BOLD) functional MRI (fMRI) and diffusion tensor imaging (DTI) allow the in vivo noninvasive evaluation and mapping of eloquent brain areas. These may provide useful information to facilitate patient counseling, and assist preoperative planning to maximize tumor resection and minimize potential neurologic complications. This lecture will describe the complementary roles of fMRI and DTI and present illustrative motor and language cases. The practical limitations of both techniques also will be discussed, including the unique advantages and disadvantages manifested by tractography

O-81 **1:35 PM - 2:00 PM**

Genomics and Genetics in Gliomas

Colen, R. R.
M.D. Anderson Cancer Center
Houston, TX.

Learning Objectives
Upon completion of this presentation, participants will be able to:
1) understand the field of imaging genomics.
2) understand the application of imaging genomics in brain tumors.
3) understand the use of MRI as a biomarker for underlying genomic composition.
4) understand the role of MRI in personalized medicine for target discovery of therapeutic targets.
5) understand the use of MRI in drug development.
6) understand the research available in imaging genomics.
Presentation Summary
The objective of this course is to introduce the recently emerged field of imaging genomics (radiogenomics) in brain tumors, specifically glioblastoma (GBM). Emphasis will be on the use of imaging in relation to underlying tumor genomics, how to use MRI as a biomarker, surrogate and correlate of tumor genomics as well as the use of MRI as a genomic target discovery tool and its application in therapeutic discovery and drug development.

O-82 **2:00 PM - 2:20 PM**

Nanotechnology

Provenzale, J. M.
Duke Medical Center
Durham, NC.

Presentation Summary
The intent of this presentation is to inform the audience of recent advances of nanotechnology to the central nervous system (CNS). Nanotechnology provides important and interesting new methods to diagnose CNS disease, determine disease extent, deliver therapy, monitor therapeutic response and re-engineer tissue. *Diagnosis.* A number of investigators have used nanoparticles as contrast agents for more sensitive diagnosis of CNS diseases. As an example, presently this author and collaborators at Emory University are studying the use of magnetic iron oxide nanoparticle clusters to identify medulloblastoma cells in the cerebrospinal fluid (CSF) of medulloblastoma patients. The nanoparticles used in this study are coated with a ligand that binds to epidermal growth factor receptor (EGFR), which is highly expressed by medulloblastoma cells. After lumbar puncture to obtain CSF, the nanoparticles are immersed in small quantities of CSF. After the magnetic nanoparticles bind to cells, the nanoparticles can be isolated by application of a magnetic field, thereby allowing identification of tumor cells. *Determination of Disease Extent during Surgery.* One of the major applications of nanotechnology is intra-operative determination of tumor extent, in an attempt to improve surgical margins after tumor removal. Paramagmetic iron-oxide nanoparticles have been used for approximately a decade for intra-operative imaging. These nanoparticles appear to accumulate in intratumoral macrophages and reactive astrocytes; they can be detected on MR imaging for a period of days after intravenous infusion. Using intra-operative MR imaging, the neurosurgeon can assess adequacy of brain tumor resection in real-time. Working with collaborators at

Note: Scanned images are included in the proceedings. Some submitted images were reduced during editing, thereby decreasing clarity. Also, refer to the Program Planner. Proceedings Content as of 3-29-2013.

Emory University and Georgia Institute of Technology, this author has examined the use of a handheld imaging device for detection of fluorescent dyes within tumors. This technique at once offers an alternative to the use of large, stationary imaging devices in the operating room and an alternative to the use of nanoparticles. The process involves the intravenous infusion of the fluorescent marker indocyanine green (ICG) a few hours prior to surgery. Indocyanine green is approved by the FDA for retinal angiography. Workers in our laboratory have found that ICG passively leaks into tumors but not into normal tissue. By using ICG in an off-label manner to assess tumor margins, we have successfully used a handheld laser that emits near-infrared light to identify tumor margins in approximately 12 types of non-CNS tumors during surgery on naturally occurring tumors in canine patients at the University of Georgia, College of Veterinary Medicine. Other types of fluorescent dyes are being explored for use in brain tumors. *Nanoparticles for Drug Delivery.* Another highly promising application of nanoparticles for treating brain tumors is delivery of chemotherapy. Advantages of nanoparticles in this setting include the potential for highly localized deposition of chemotherapy within the tumor as opposed to systemic delivery using standard chemotherapy formulations. For instance, even intravenous administration of nanoparticles could provide a means of specific delivery of the agent by allowing nanoparticles to be preferentially deposited within tumor. A major impediment has been development of nanoparticles that will readily cross the blood-brain barrier, which has been addressed successfully by a number of investigators. The major advantages include the potential for incorporating relatively large amounts of chemotherapy into nanoparticles as well as for delivery of hydrophobic substances that normally might have very limited access to brain tumors because of the blood-brain barrier. By avoiding delivery of chemotherapy to nontarget organs outside the CNS, toxic effects might be minimized and lower doses might be possible. As an example, intravenous use of the chemotherapeutic agent camptothecin has been limited by high rates of systemic toxicity. However, intravenous infusion of camptothecin within polymeric micelles (one form of nanoparticle) allowed the drug to be delivered in amounts sufficient to decrease tumor volumes without development of toxicity. *Tissue Engineering.* Nanoparticles offer the prospect of restructuring the CNS microenvironment and, in some cases, repair damage caused by CNS tissues. For instance, one form of nanoparticle termed a carbon nanotube has been shown to be capable of improving responsiveness of neurons. Nanotubes placed within cultured neuronal networks can affect the collective electrical properties of such networks by promoting electrical “shortcuts” between the proximal and distal components of neurons. Carbon nanotubes also have been shown to be capable of serving as a scaffold for neuronal cell adhesion and growth. Functionalized nanotubes can modulate neuronal growth in a graded manner; positively charged nanoparticles have been shown to promote neurite outgrowth of hippocampal neurons in culture. Finally, nanofiber scaffolds have been developed which can self-assemble within the CNS to promote growth of neuritis. These devices promote formation of a gel-like material which encapsulates neural progenitor cells and promotes differentiation of these cells into mature neuronal cells. Such mechanisms may eventually allow regeneration of CNS tissue in such diseases as multiple sclerosis and neurodegenerative diseases. In summary, a wide range of potential applications of nanotechnology for assessment and therapy of CNS diseases are available. The exact forms in which these possibilities will come to fruition in humans are undetermined at present. However, it appears highly likely that at least some of the initiatives outlined here will play a role in human CNS diseases in one form or another.

O-83 **2:20 PM - 2:45 PM**

Neuro-Oncology Trials

Barboriak, D. P.
Duke University Medical Center
Durham, NC.

Presentation Summary
Clinical trials have a key role in the process of translating advances in imaging into clinical practice. There is increasing demand for "strong evidence" in order to incorporate advanced imaging techniques into clinical practice guidelines and to justify reimbursement from payers. Depending on the maturity of the imaging technology, a variety of trial designs can be justified in order to advance an imaging application toward clinical acceptance. Ultimately, however, a multicenter trial frequently is necessary to provide the strength of evidence needed to change clinical practice. In this talk, possible pathways to translation of imaging technology to clinical practice through a series of trials will be discussed, with a focus on the types of data generated in single center trials that are most helpful in justifying validation in a multicenter trial. Because of the high costs of these trials, there is increasing interest in imaging techniques with proven utility for guiding therapeutic decision-making that leads to improvements in patient outcomes such as quality of life and survival. Not surprisingly, diagnostics (although not necessarily imaging) and treatments have become much more closely linked, and there is increasing emphasis on performance of practice-altering trials that validate the diagnostics and treatment in tandem. This talk also will review the role of imaging for brain tumor evaluation in the current clinical trials environment. The importance of specifying use cases for imaging such as differentiation of pseudoprogression from true progression, differentiation of pseudoresponse from true response, better prediction of patient response to specific treatments, and early identification of treatment success or failure will be discussed. The evolution of imaging assessment from Macdonald criteria to the RANO criteria,

Note: Scanned images are included in the proceedings. Some submitted images were reduced during editing, thereby decreasing clarity. Also, refer to the Program Planner. Proceedings Content as of 3-29-2013.

and future directions for these assessments will be examined. Because of the centrality of treatment as providing the context of advanced imaging assessments, the talk will review current thinking for possible treatment modalities and associated trials, including the use of treatment de-escalation strategies, anti-angiogenic therapies, immunotherapies, and tumor vaccines, among others. In addition, imaging has a central role in target localization for anatomically guided therapies, and current ideas for the use of imaging to delineate tumor volumes for surgical planning and for radiation therapy will be reviewed.

Monday Afternoon

1:15 PM - 2:45 PM
Ballroom 6DE

(10) General Programming: Arterial Dissections: Extra- and Intra-Cranial Diagnosis and Treatment (SAM) (AR)

O-84 **1:15 PM - 1:40 PM**

Diagnosis: MR verses CTA?

Zaharchuk, G. G.
Lucille Packard Children's Hospital at Stanford
Stanford, CA.

Presentation Summary

Cervical arterial dissection is the most common cause of ischemic stroke in the young (patients under 45 years of age). Despite this, it often is not initially suspected due to the sometimes subtle presenting signs, overall infrequent occurrence of stroke in this age group, and the lack of routine neck imaging as part of the stroke workup. However, given the delayed and sometimes devastating presentation of large vessel embolic stroke in these patients, establishing the diagnosis early can have a big impact. Digital subtraction angiography (DSA) traditionally has been the reference standard for diagnosis of cervical artery dissection. However, because of its risk and expense, it has been largely supplanted by noninvasive modalities, including ultrasound, CT/CT angiography, and MRI/MR angiography. Each of these tests has its strengths and limitations. Ultrasound is contrast- and radiation-free, but results are sensitive to technologist skill and there is poor conspicuity of the vertebral arteries. CT/CTA can be acquired rapidly and has high spatial resolution, but involves both radiation and contrast; radiation in particular is a limitation in the widespread use of this technique, as many patients are young. MRI/MRA can document both small amounts of acute ischemia and the pathognomonic "methemoglobin" crescent sign, but suffers from motion-sensitivity and poor accuracy in the vertebral arteries. This talk will review the relative advantages and disadvantages of each of these modalities.

O-85 **1:40 PM - 2:00 PM**

Extracranial Vascular Dissections: Endovascular Treatment

Pride, G.
University of Texas Southwestern Medical Center
Dallas, TX.

Presentation Summary

As a common cause of stroke in young and middle aged individuals[1], Extracranial neurovascular dissection presents an important opportunity for diagnostic and interventional neuroradiologists to positively impact patient care. Timely diagnosis and precise imaging evaluation allows the institution of appropriate therapy that may substantially decrease stroke risk and maximize patient outcomes. Awareness of the etiology, pathophysiology, clinical presentation, imaging findings, prognostic features and multiple treatment options is thus extremely important. Treatment paradigms for Extracranial neurovascular dissections generally lack guidance from large clinical trial data. First line therapy is most commonly medical with interventional or surgical approaches being reserved to select cases. Multidisciplinary approaches often offer the best promise for optimal outcomes. This talk will review treatment paradigms for Extracranial vascular dissections, focusing on endovascular treatment options.

Extracranial cervical dissections may account for 5-22% of ischemic strokes in the young, representing a significant health problem[2]. Most have a high chance for complete healing and are as thus often best managed medically with antithrombotic therapy to prevent thromboembolism. Both antiplatelet and anticoagulant therapies prevent stroke during the healing process[2,3]. Non-randomized studies fail to show superiority of one approach over the other[3]. Randomized comparison trials are currently underway. Imaging and clinical follow-up is critical to document healing. Endovascular treatment for Extracranial dissection may be done as part of acute stroke therapy for tandem lesions or acute occlusion when appropriate[4,5]. More frequently, it is reserved for ongoing neurological ischemic symptoms despite medical therapy, either due to hemodynamic insufficiency or resistant thromboembolism[5]. Other potential indications are persistent significant stenoses on follow-up with limited collateral opportunity or enlarging/ruptured pseudoaneurysms[2]. Treatment strategies include stenting with or without angioplasty, coil embolization, covered stent placement, vascular sacrifice and flow diversion. We will conclude with a discussion of future directions in the endovascular treatment of Extracranial neurovascular dissections and dissecting aneurysms.

Note: Scanned images are included in the proceedings. Some submitted images were reduced during editing, thereby decreasing clarity. Also, refer to the Program Planner. Proceedings Content as of 3-29-2013.

O-86 **2:00 PM - 2:20 PM**

Same Disease, Different Pathology: The Special Case of Intracranial Disssecting Aneurysms - Diagnosis and Treatment

Derdeyn, C. P.
Mallinckrodt Institute
St. Louis, MO.

Presentation Summary
Acute intracranial arterial dissections, particularly distal vertebral or basilar dissections, often present with ischemic symptoms related to thrombo-emboli in the distal circulation or local branch vessel occlusion. In a subset of these patients, the entire wall may be damaged by the dissection and hemorrhage into the subarachnoid space ensues. Dissecting aneurysms are an uncommon but extremely important cause of subarachnoid hemorrhage (SAH): they may be difficult to diagnose, difficult to treat, and carry a very high risk for recurrent hemorrhage. It is important to consider dissecting aneurysms as a cause for SAH if no saccular aneurysm is identified. Dissecting aneurysms often appear as an irregular, nonsaccular aneurysmal enlargement of an intracranial artery. In some cases this is accompanied by focal narrowing. The most common location is the distal vertebral artery at the origin of the posterior inferior cerebellar artery. The supraclinoid carotid or basilar arteries are less commonly affected. Imaging findings may be very subtle, with only minimal irregularity of the arterial contour. This is particularly true of internal carotid “blister” aneurysms. Close angiographic follow up of indeterminant cases is imperative, as these lesions may grow quickly prior to rerupture. The imaging diagnosis requires high-resolution angiographic imaging. Catheter angiography, particularly with 3 dimensional reconstruction, is important if the diagnosis cannot be made with noninvasive imaging. Treatment can be challenging. The most definitive treatment is sacrifice, open surgical or endovascular, of the diseased vessel segment. This is not feasible in some locations without complex bypass procedures. More recently, stents and flow diverters have been used in selected cases with some success. The need for aggressive anti-platelet medications in this setting remains an issue, however.

Monday Afternoon

1:15 PM - 2:45 PM
Room 5AB

(11) General Session: Scientific Publishing Update

O-87 **1:15 PM - 1:45 PM**

Peer Review Systems

Castillo, M.
University Of North Carolina School Of Medicine
Chapel Hill, NC.

Presentation Summary
Journal scientific peer review (PR) as we know it started in the mid 1950s with the invention of the photocopier. Peer review can be un-blinded or blinded and in AJNR we use the double-blinded method. However, this method has been significantly criticized, especially by editors themselves. With the advent of Web 2.0 the possibility of open PR arose and by adding this step one may increase or decrease time to publication. Postpublication open PR does not affect publication schedules and keeps articles fresh by self-renewal due to revisions. Unfortunately, journals have experienced mixed results with these new methods. Parallel to the journal’s efforts, many third party postpublication PR websites have appeared and these commercial for profit sites take advantage of recycling already published material for their own purposes. This lecture reviews these aspects and proposes solutions to the most pressing issues of PR. The lecture will be divided into three parts: historical aspects of PR, open PR, and postpublication PR including blogs and Facebook.

O-88 **1:45 PM - 2:15 PM**

Is What’s Published False?

Kressel, H. Y.
Harvard Medical School
Boston, MA.

Herbert Y. Kressel, M.D., Beth Israel Deaconess Medical Center, Miriam H. Stoneman Professor of Radiology, Harvard Medical School, Editor, Radiology.
Dr. Kressel graduated from the University of Southern California School of Medicine, 1972. He completed internship at the University of Washington Hospitals in Seattle and served as a resident and fellow in diagnostic radiology at the University of California, San Francisco. He joined the section of gastrointestinal radiology at the Hospital of the University of Pennsylvania in 1977, was later appointed Director of MRI and Professor of Radiology. He has served as past president of the Society of Magnetic

Note: Scanned images are included in the proceedings. Some submitted images were reduced during editing, thereby decreasing clarity. Also, refer to the Program Planner. Proceedings Content as of 3-29-2013.

Resonance in Medicine, and on the Editorial Board of many professional journals. Dr. Kressel's major interests are magnetic resonance imaging of the abdomen and pelvis with particular interests in prostate, liver and pancreas. In 1993 Dr. Kressel was appointed Radiologist-In-Chief of the Department of Radiology at the Beth Israel Hospital in Boston, and Miriam H. Stoneman Professor of Radiology at the Harvard Medical School. In February 1998 Dr. Kressel was appointed Chief Medical Officer at Beth Israel Deaconess Medical Center, and continued to serve as Radiologist-in-Chief. In August 1998 Dr. Kressel was appointed President and CEO of Beth Israel Deaconess Medical Center. In January 2000, Dr. Kressel returned to the Radiology Department at Beth Israel Deaconess Medical Center and resumed his role as Radiologist-in-Chief. In 2007, Dr. Kressel was appointed Editor Designate for Radiology, and assumed the role of Editor in January 2008. In 2011 he was awarded the RSNA's Gold Medal.

Presentation Summary
Over the past several decades, concerns have been raised increasingly as to the validity and ability to generalize from published scientific articles. The causes of this problem appears to be multifactorial but include ethical issues, including conflict of interest and redundant publication, and issues relating to the quality of the science and the tendency to over-interpret or "spin" the findings that are being reported. The rate of retraction of scientific manuscripts has grown ten-fold in the past decade. Nearly half of the retractions, unfortunately, are due to some form of misconduct, including plagiarism, redundant publication, and data falsification. There is ample evidence that conflict of interest particularly as it relates to industry sponsored research also contributes to the problem. Despite recent efforts in mandating trial registration before the study begins, and in making the primary data available for review, these commercially driven problems appear to persist. Scientifically, the validity of a result is largely dependent on the statistical power of the study, and the many sources of bias, including publication bias, the apparent desire of journals to publish positive results. Smaller studies, testing multiple variables, and within study flexibility as to designs, outcomes and analyses are all sources of potential problems. Recently a number of investigators have begun to look at "spin" in scientific publications. In a study reviewing over 126 articles on diagnostic performance, a variety of journals with impact factors of 4.0 or greater, 31% had some form of over-interpretation and a much larger number, perhaps as high as 89%, had some evidence of potential over-interpretation including lack of a sample size calculation, lack of a clear test hypothesis, and failure to report confidence intervals in accuracy measurements. To deal with these issues we will need a multifaceted approach including restructuring the incentives in science, encouraging the publication of high quality studies with negative results, promoting Meta-analysis and creating a culture of ethical scientific research throughout the research community.

O-89 **2:15 PM - 2:45 PM**

Metrics: Now and Future

Wilms, G. E.
UZ-Gasthuisberg
Leuven, B-3000, BELGIUM.

Presentation Summary
Publication metrics such as the impact factor (IF) are used to evaluate and rank journals. They are obtained from dividing citations received in one year by the number of papers published in the two previous years. Some influencing of the IF by the editor is possible by encouraging self-citation, choice of article types, open access and publication of themed issues but these are considered as caretaking for the journal rather than manipulation. Disadvantage of the IF as a measure of a journal importance are, besides discipline and language dependence, that the IF is based on high citations of a minority of articles and the absence of evaluation of the real impact on medical practice. Major criticism concerns the use of the IF in the decision of appointment, promotion, tenure and awarding of research grants to individual researchers, since the IF does not apply to a single article nor one author. The h-index, based on the set of the scientist's most cited papers and the number of citations of other publications, seems a more appropriate way of evaluating a scientist or a scientist group. The index is used widely with possible local modifications. Newer indices seem mandatory taking into account the influence of online citation counting such as Google Scholars or CrossRef, online first publications, open access journals and frequency of downloads.

Monday Afternoon

3:15 PM - 4:45 PM
Ballroom 6AB

(13a) Parallel Scientific Papers: Interventional: Aneurysms

O-93 **3:15 PM - 3:23 PM**

Neuropsychologic Deficits and Structural Brain Damage after Aneurysm Treatment in Patients with Good Clinical Outcome

Friedrich, B.·Wostrack, M.·Hammer, K.·Harmening, K.·Meyer, B.·Ryang, Y.·Förschler, A.
Klinikum Rechts der Isar, Technische Universität München
Muenchen, GERMANY.

Note: Scanned images are included in the proceedings. Some submitted images were reduced during editing, thereby decreasing clarity. Also, refer to the Program Planner. Proceedings Content as of 3-29-2013.

Purpose
Despite good neurologic outcome after treatment of cerebral aneurysm with or without preceding subarachnoid hemorrhage (SAH) many patients are complaining about mood disorders and chronic headaches. We aimed to investigate whether the history of SAH or treatment modality are crucial for neuropsychologic deficits and if any specific brain changes are associated with these disorders.
Materials & Methods
Fifty case-matched pairs of patients with or without previous SAH treated by surgical clipping or endovascular coiling are intended to be assessed prospectively by a test battery including Hospital Anxiety and Depression Scale (HADS), Beck depression inventory (BDI) and Headache Impact Test (HIT-6). Additionally, brain MRI including H1-MR spectroscopy and volumetry of the hippocampus as well as DTI measurement are performed. So far, 37 consecutive patients were enrolled: n = 17 with preceding SAH, n =10 incidental, n = 23 with first treatment by clipping, n = 14 first treatment by coiling; MRI was performed in 29 cases.
Results
No substantial differences were found between patients with and without previous SAH in respect of depression, anxiety and headaches. However, we observed significantly higher mean scores in all tests in patients treated surgically versus patients treated by coiling: HADS 13.9 versus 9.7; BDI 13.57 versus 11.26; HIT-6 52.57 versus 48.26, respectively. HADS score significantly increased in patients with multiple aneurysms resulting in multiple treatments: 13.18 versus 9.7 in those with single treatment. Spectroscopy revealed slight reduction of hippocampal Glx in patients with previous SAH: 0.013 versus 0.0109 in non-SAH subjects. All surgically treated patients showed lower mean concentrations of hippocampal NAA (0.00479 versus 0.00946), Glu (0.0065 versus 0.00835) and Glx (0.011 versus 0.013) compared to those treated by coiling. Hippocampal atrophy could be detected in both patients who suffered SAH or were surgically treated, but surgical treatment resulted in a significantly aggravated atrophy. In the DTI measurement the FA values in the hippocampal area were reduced significantly in patients treated by surgical approach compared to endovascular coiling.
Conclusion
Aneurysm surgery seems to be associated with higher morbidity in respect of mood disorders and headaches compared to endovascular treatment independently of preceding SAH. Additionally surgical aneurysm clipping seems to induce a much severe structural damage to the depression-associated hippocampal area than endovascular coiling.

KEYWORDS: Aneurysm treatment, MR imaging

O-94 **3:23 PM - 3:31 PM**

Long-Term Risks of Re-Bleeding and Death after Coiling and Clipping of Ruptured Aneurysms: Results of Followup 10 to 18 Years after Subarachnoid Hemorrhage of Patients Enrolled in the International Subarachnoid Aneurysm Trial

Molyneux, A. J.·Sneade, M.·Birks, J.·Yarnold, J.·Clarke, A.·Kerr, R.
Oxford University
Oxford, UNITED KINGDOM.

Purpose
To report the long-term risk of recurrent subarachnoid hemorrhage and the causes of death in patients enrolled in the International Subarachnoid Aneurysm Trial (ISAT), after coiling or clipping of a ruptured cerebral aneurysm.
Materials & Methods
Two thousand one hundred forty-three patients enrolled in ISAT were followed as a whole cohort for five years. The UK cohort of 1644 patients has been followed up since enroment for between 10 and 18 years based on annual patient questionnaires. All UK patients were flagged with the Office for National Statistics (ONS) and all UK deaths were notified direct to the Trial office together with cause of death. Recurrent SAH was notified by patient questionnaire, direct from the hospital concerned or via ONS cause of death notification.
Results
UK patients alive at one year have been followed for a minimum of 10 years and for a maximum of 18 years after enrollment, with a mean of 14 years. A total of 37 recurrent subarachnoid hemorrhages have occurred between one year and the date of final followup. The total number of follow-up years is now in excess of 20,000 person years. Twenty-one recurrent SAHs have occurred from the original treated target aneurysm, 16 in the patients allocated coiling and five in the patients allocated clipping. Sixteen were from another aneurysm, of these six were from pre-existing aneurysms, one of which had been clipped previously and five that had not been treated. Nine were from new aneurysms and in one patient the source of hemorrhage was unknown. Of the 37 patients with recurrent SAH 16 died within 30 days as a result of the re-bleed. All the causes of death after one year were categorized and the most common causes of delayed mortality were due to cancer and cardiovascular disease unrelated to SAH or its treatment.
Conclusion
The risk of delayed recurrent subarachnoid hemorrhage from the ruptured aneurysm in patients treated by coiling and clipping between 1994 and 2002 is very low. Re-bleeding is more common after coiling than clipping but this risk is of the order of between one and two per thousand per year. The significant initial clinical benefit observed after coiling will never be lost at this rate of aneurysm re-bleeding at any age of presentation.

Note: Scanned images are included in the proceedings. Some submitted images were reduced during editing, thereby decreasing clarity. Also, refer to the Program Planner. Proceedings Content as of 3-29-2013.

KEYWORDS: Aneursym, Long-term followup, subarachnoid hemorrhage

O-95 **3:31 PM - 3:39 PM**

Molecular and Cellular Mechanisms of Aneurysm Occlusion following Flow Diverter Treatment

Kadirvel, R.·Ding, Y.·Dai, D.·Rezek, I.·Lewis, D.·Kallmes, D.
Mayo Clinic College of Medicine
Rochester, MN.

Purpose
Uncertainty regarding the relative importance of flow disruption, thrombus formation in the dome, and endothelialization across the neck impedes our ability to design improved flow diversion devices. The objective of this study was to characterize the progression of healing across aneurysm necks following flow diverter treatment.
Materials & Methods
Rabbit saccular aneurysms were treated with flow diverters. On days one, three, and seven (n=3 at each time point), and at eight weeks (n=9) after implantation, angiography was performed and the aneurysm along with the device-implanted vessel was harvested. Gross examination and histology were performed. *En face* staining was performed for CD-31 (endothelial cells), CD-34 (endothelial progenitor cells), SMA (smooth muscle cells) and inflammatory cells.
Results
Aneurysms remained patent in all subjects at days one and three and remained incompletely occluded at seven days. At eight weeks, complete, near-complete, and incomplete occlusion was noted in four, two, and three aneurysms, respectively. The parent artery segments covered by the flow diverters were completely devoid of endothelial cells at one and three days, but had re-endothelialized by seven days. The struts along the aneurysm necks at one, three, and seven days harbored scattered tissue islands comprised exclusively of inflammatory cells; similar findings were present in the patent areas of the incompletely occluded eight-week samples. Translucent tissue was present along the occluded segments of the aneurysm necks at eight weeks (Figure A). Most of the scattered tissue islands at all-time points consisted of inflammatory cells. However, some tissue islands in the periphery were made up of endothelial cells, which were in continuity with endothelial cells along the parent artery wall (Figures B&C). Histological analysis showed the incompletely occluded aneurysm domes harbored primarily unorganized thrombus. The necks of the completely occluded aneurysms were covered with a thin layer of endothelial cells (Figures D&E). A few, localized, nonendothelialized areas covered with smooth muscle cells were noted (Figure F). The domes were filled with organized thrombus. We did not observe any CD-34$^+$ cells in any aneurysm to suggest that circulating-progenitor cells were the cell of origin in and around the aneurysm neck.

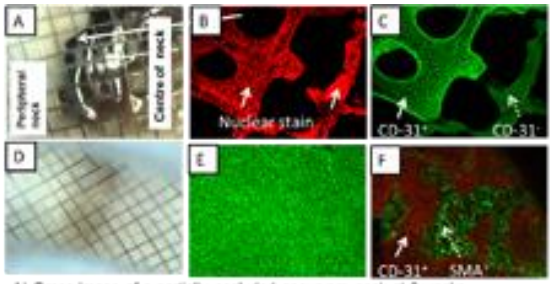

A) Gross image of a partially occluded aneurysm neck at 8 weeks demonstrating scattered tissue islands in the center of the neck. B) Nuclear staining of Figure A confirms the presence of nucleated cells covering the device struts that are in close proximity to the vessel wall. C) Peripheral cells stained CD-31+ (solid arrow) and CD-31- in the neck center (dotted arrow), indicating that endothelial cells are growing from parent vessel out over the aneurysm neck. D) Gross image a completely occluded aneurysm at 8 weeks showing the thick, translucent membrane covering the aneurysm orifice. E) The neck area is mostly endothelialized with CD-31+ cells. F) Smooth muscle cells (SMA+, dotted arrow) reside under both the endothelialized (solid arrow) and non-endothelialized areas.

Conclusion
The initial event following flow diversion treatment is adherence of clusters of inflammatory cells across the aneurysm neck. Endothelialization is relatively delayed and is derived exclusively from cells in the adjacent parent artery. Concurrent with centripetal endothelialization, thrombus formation in the dome and gradually extends down toward the aneurysm neck.

KEYWORDS: Aneursym, Flow diverter

O-96 **3:39 PM - 3:47 PM**

Cerebral Aneurysm Treatment Is Beginning to Shift to Low Volume Centers

Brinjikji, W.·Lanzino, G.·Kallmes, D. F.·Cloft, H. J.
Mayo Clinic
Rochester, MN.

Purpose
A recent expansion of the neurointerventional workforce in the United States could lead to a trend toward cerebral aneurysms being treated increasingly at low volume centers. Such a trend could have a negative impact on patient care because higher volume centers are known to have better outcomes than low volume centers.
Materials & Methods
Using the Nationwide Inpatient Sample, we evaluated trends in aneurysm treatment in the United States from 2001 to 2010. We assessed the following outcomes: 1) number of subarachnoid hemorrhage (SAH) and unruptured aneurysm (UA) patients treated annually by treatment modality from 2001-2010, 2) trends in the proportion of SAH and UA patients treated at high volume centers (≥50 cerebral aneurysms treated per year) from 2001-2010, and 3) the percentage of aneurysm treatment centers treating <50 cerebral aneurysms per year from 2001-2010. Chi-squared testing was used to compare categorical variables.
Results

Note: Scanned images are included in the proceedings. Some submitted images were reduced during editing, thereby decreasing clarity. Also, refer to the Program Planner. Proceedings Content as of 3-29-2013.

The number of SAH patients treated per year increased from 7680 in 2001 to 10970 in 2003. From 2003 to 2010 the number of ruptured aneurysms treated per year has fluctuated between 9291 and 12237. The number of UA patients treated per year increased steadily from 4474 in 2001 to 10720 in 2006, but then has fluctuated between 8304 and 11897 cases from 2006 to 2010. The percentage of SAH patients treated at high volume centers rose from 22% in 2001-2002 to 68% in 2007-2008 and then dropped to 58% in 2009-2010 (P<.0001). The percentage of UA patients treated at high volume centers rose from 38 percent in 2001-2002 to 73% in 2005-2006 and then dropped to 65% in 2009-2010 (P<.0001). The percentage of aneurysm treatment centers with <50 cases/year steadily declined from 99% in 2001 to 85% in 2008 (P<.0001). Since 2008, there has been an increase in the percentage of low volume treatment centers to 91% (P<.0001).

Conclusion

A trend toward fewer cerebral aneurysms being treated in high volume centers in 2009 and 2010 is worrisome, as high volume centers are known to tend to have better outcomes than low volume centers. This trend is likely due to recent expansion of the neurointerventional workforce.

KEYWORDS: Endovascular coiling, Aneursym, Trends

O-97 **3:47 PM - 3:55 PM**

Timing and Nature of Immediate Postoperative Events following Elective Endovascular Aneurysm Treatment: Is Routine Intensive Care Unit Observation Necessary?

Patel, B.·Arias, E. J.·Cross, D. T.·Moran, C. J.·Derdeyn, C. P.
Washington University in St. Louis School of Medicine
St. Louis, MO.

Purpose

Patients with asymptomatic intracranial aneurysms treated with endovascular methods are observed in the postprocedure period for complications, including ischemic and hemorrhagic stroke, cardiac dysfunction and groin access complications. The purpose of this study was to analyze the timing, nature and rate of postoperative events in patients in whom the procedure was completed without apparent intraprocedural complications, and determine whether routine postprocedure monitoring in an intensive care setting is necessary for these patients.

Materials & Methods

Patients who underwent endovascular treatment of unruptured cerebral aneurysms from March 2002 to June 2012 were identified from a prospective case log. Hospital records were reviewed. Admissions for treatment of recurrent aneurysm were included. Postprocedure monitoring for all patients was in a neurologic intensive care unit or 24-hour postanesthesia care unit for a minimum of 24 hours. The presentation, patient characteristics, aneurysm size and location, and form of treatment of each cerebral aneurysm were analyzed. Endovascular procedures included coiling alone, stent-assisted coiling, balloon-assisted coiling, Onyx HD 500 occlusion, and pipeline embolization device with or without coiling. Patients with adverse intraprocedural events including perforation and embolic events were excluded from this analysis. Postprocedural events occurring during hospitalization included intracerebral hemorrhage, stroke, groin hematoma (if resulting in additional treatment or prolonged hospital stay), retroperitoneal hematoma, and cardiac events. The time from the completion of the procedure to event discovery was recorded.

Results

A total of 681 endovascular treatments of unruptured cerebral aneurysms were performed. Nine treatments were excluded from our analysis due to intraprocedural events. Twenty-seven treatments (4.0%) resulted in postprocedure complications: three hemorrhages (one intraventricular hemorrhage, one subarachnoid hemorrhage with intraventricular hemorrhage, and one intraparenchymal hemorrhage), six ischemic strokes, four cardiac events, five retroperitoneal hematomas and nine groin hematomas. The majority (20/27 or 74.0%) of these complications were detected within four hours from the procedure. These included one hemorrhage, four ischemic strokes, four cardiac events, two retroperitoneal hematomas, and nine groin hematomas. All cardiac events and groin hematomas were detected within four hours. In contrast, 14.8% (4/27) of the complications were detected between four to 12 hours, 3.7% (1/27) between 12 and 24 hours, and 7.4% (2/27) more than 24 hours after the procedure. Further analysis of the complications detected greater than four hours from the conclusion of the procedure revealed two minor hemorrhages detected on head CT due to headaches resulting in no permanent deficits, two ischemic strokes with minor deficits requiring inpatient rehab after discharge, and three asymptomatic retroperitoneal hematomas found due to falling hematocrit levels that required no further intervention or treatment.

Conclusion

Patients with uncomplicated endovascular aneurysm intervention require close monitoring for at least four hours. The nature and frequency of complications between four and 24 hours suggests continued in-patient monitoring is useful, but could be performed in a less resource-intensive environment.

KEYWORDS: Aneurysm treatment, Complications

Note: Scanned images are included in the proceedings. Some submitted images were reduced during editing, thereby decreasing clarity. Also, refer to the Program Planner. Proceedings Content as of 3-29-2013.

O-98 **3:55 PM - 4:03 PM**

Safety and Efficacy of a New Device for the Treatment of Wide Neck Bifurcation Aneurysms (pCONus): Preliminary Experience in Eighteen Patients

Aguilar-Pérez, M.[1]·Kurre, W.[1]·Felber, S.[2]·Donauer, E.[3]·Hopf, N.[1]·Bäzner, H.[1]·Henkes, H.[1]
[1]Klinikum Stuttgart, Stuttgart, GERMANY,
[2]Stiftungsklinikum Mittelrhein, Koblenz, GERMANY,
[3]MediClin Krankenhaus Plau am See, Plau am See, GERMANY.

Purpose
Wide neck intracranial bifurcation aneurysms are considered to belong to the subgroup of aneurysms with increased treatment difficulty and risks. The simultaneous use of two or more microcatheters and the use of one or two compliant balloons for temporary sealing of the aneurysm neck while introducing coils are known techniques for the endovascular treatment of these aneurysms. Also the use of intracranial self-expanding stents to create an artificial border between a vessel bifurcation and an aneurysm has shown during the last decade to be a safe and efficacious option. pCONus is a self-expanding, completely retrievable, electrolytically detachable device with a proximal shaft (similar to stents) and four distal petals and with a nylon cross in the distal end of the shaft (Figure 1). The device is made to bridge the orifice of wide neck bifurcation aneurysms in order to allow better control of the coil occlusion. It combines functional elements of “waffle cone” stent deployment and the no longer available TriSpan Neck Bridging Device. The purpose of this study was to evaluate the safety and efficacy of this new device for the treatment of intracranial wide neck bifurcation aneurysms.
Materials & Methods
Eighteen consecutive patients, deemed unsuitable for or refusing microsurgery, underwent an endovascular treatment of intracranial wide neck bifurcation aneurysms using the pCONus device between April 2011 and November 2012. pCONus was used by prescription in highly selected patients. Target vessels included the anterior circulation in 13 (72.3%) and the posterior circulation in five (27.7%). Six patients were treated in the setting of acute subarachnoid hemorrhage (33.3%) and five of the aneurysms showed reperfusion after previous coil occlusion (27.7%).
Results
No technical failure or major complication was encountered. Rupture did not occur during any of the procedures. No premedication was used in the patients with subarachnoid hemorrhage and no thromboembolic complications were observed. After the initial embolization procedure, a 90 to 100% occlusion rate was achieved in all cases but a neck remnant was evident in four patients. Initial follow-up angiography was available in 10 of 18 (55.5%) patients and demonstrated a 90 to 100% occlusion rate in eight (80%). Evident coil compaction was observed in one patient, who underwent a second treatment two months after the first therapeutic session.

Conclusion
The pCONus device allows a controlled coil occlusion of wide neck bifurcation aneurysms, both ruptured and unruptured. Major complications are rare.

KEYWORDS: Aneurysm treatment, Aneurysmal subarachnoid hemorrhage, Bifurcation aneurysms

O-99 **4:03 PM - 4:11 PM**

Stent-Assisted Coiling versus Coiling Alone in Unruptured Intracranial Aneurysms in the MAPS Trial: Safety, Efficacy, and Mid-Term Outcomes

Hetts, S. W.[1]·Turk, A.[2]·English, J.[1]·Prestigiacomo, C.[3]·Nesbit, G.[4]·Mocco, J.[5]·Barnwell, S.[4]·Gobin, Y. P.[6]·Lopes, D.[7]·Ge, G.[8]·Jin, J.[8]·Carroll, K.[8]·Murayama, Y.[9]·Gholkar, A.[1]·Johnston, S. C.[1]·McDougall, C.[10]
[1]University of California San Francisco, San Francisco, CA,
[2]Medical University of South Carolina, Charleston, SC,
[3]University of Medicine & Dentistry of New Jersey, Newark, NJ, [4]Oregon Health and Science University, Portland, OR, [5]Vanderbilt, Nashville, TN, [6]Weill Cornell Medical School, New York, NY, [7]Rush University Medical Center, Chicago, IL, [8]Stryker Neurovascular, Fremont, CA,
[9]Jikei University School of Medicine, Tokyo, JAPAN,
[10]Barrow Neurological Institute, Phoenix, AZ.

Purpose
Stent-assisted coiling (SAC) may result in less aneurysm recanalization but more complications than coiling alone (CA). We evaluated outcomes of SAC in the prospective, multicenter MAPS Trial.
Materials & Methods
Three hundred sixty-one MAPS patients with unruptured intracranial aneurysms (UIAs) were treated per protocol by SAC or CA. Baseline patient and aneurysm characteristics, procedural details, neurologic outcomes, and safety data were analyzed post hoc. An independent core laboratory evaluated angiographic outcomes.
Results
One hundred thirty-seven of 361 patients received a Neuroform stent. Aneurysms treated with SAC had wider necks (62% of SAC versus 33% of CA with necks >4mm, P<0.0001) and lower dome-to-neck ratios (1.5 versus 2.1, p = 0.0001) necks, however. Although complete angiographic obliteration for SAC was similar to CA at 1 year (51.8% versus 44.4%, p = 0.22), angiographic

Note: Scanned images are included in the proceedings. Some submitted images were reduced during editing, thereby decreasing clarity. Also, refer to the Program Planner. Proceedings Content as of 3-29-2013.

worsening was lower for SAC than CA (16.7% versus 33.3%, p = 0.002). The primary endpoint for the MAPS Trial was defined as target aneurysm recurrence (TAR), a composite clinical endpoint consisting of target aneurysm retreatment, delayed intracranial hemorrhage, or death from an unknown cause. At one year of followup, the TAR rate among all UIA was 12/137 (8.8%) for SAC and 19/227 (8.5%) for CA (p = 0.93). Among WNA at one year, the TAR rates were 12/85 (14.1%) and 10/73 (13.7%), respectively (p = 0.94). By two years of followup, 13/137 (9.5%) of SAC and 22/224 (9.8%) of CA patients had had a TAR event (p = 0.92) in the UIA cohort. Similarly, TAR event rates did not differ in the WNA groups at two years, with 13/85 (15.3%) of SAC and 11/73 (15.1%) of CA experiencing a TAR event (p = 0.97).
Conclusion
Stent-assisted coiling was effective in treating UIAs. Stent-assisted coiling correlated with better angiographic outcomes at one year without significantly higher rates of SAEs, death, or disability despite the stented aneurysms having more difficult morphology than coiled aneurysms. Increased ischemic events in SAC as compared to CA warrant attention as the trial continues. Primary clinical outcomes did not differ between the SAC and CA groups either among all UIAs or among WNAs at both one and two years.

KEYWORDS: Aneurysm treatment, Intracranial stenting

O-100 **4:11 PM - 4:19 PM**

Middle Cerebral Artery Aneurysms - Feasibility, Clinical and Anatomical Results of the Endovascular Treatment by WEB Flow Disruption: Preliminary Evaluation in a Multicenter Study

Pierot, L.[1]·Klisch, J.[2]·Cognard, C.[3]·Szikora, I.[4]·Mine, B.[5]·Kadziolka, K.[1]·Sychra, V.[2]·Gbucz, I.[4]·Januel, A.[3]·Lubicz, B.[5]
[1]Hopital Maison-Blanche, Reims, FRANCE, [2]Helios General Hospital, Erfurt, GERMANY, [3]Purpan Hospital, Toulouse, FRANCE, [4]National Institute of Neurosurgery, Budapest, HUNGARY, [5]Erasme University Hospital, Brussels, BELGIUM.

Purpose
The endovascular treatment of middle cerebral artery (MCA) aneurysms with unfavorable anatomy (wide neck, unfavorable morphology) frequently is challenging. Flow disruption using the WEB® is potentially an interesting endovascular treatment for this type of aneurysm. In this multicenter study we report our preliminary experience with this device.
Materials & Methods
Thirty-three patients with 34 MCA aneurysms were treated using the WEB in five European centers. The ability to successfully deploy the WEB, procedural and device related adverse events, morbidity and mortality of the treatment, and short-term angiographic follow-up results were analyzed.
Results
Most treated aneurysms (85.3%) were unruptured, had a size between 5 and 10 mm (85.3%), and a neck size greater or equal to 4 mm (88.2%). The treatment failed in 1/34 aneurysms (2.9%) due to the lack of appropriate size of the device. Treatment was performed exclusively with the WEB in 29/33 (87.9%). Additional treatment (coiling and/or stenting) was used in 4/33 (12.1%). Mortality of the treatment was 0.0% and morbidity 3.1% (intraoperative rupture with mRS 3 at one-month followup). In short-term followup (2 to 12 months), adequate occlusion (total occlusion or neck remnant) was observed in 83.3% of aneurysms.
Conclusion
Flow disruption seems to be a promising technique for the treatment of complex MCA aneurysms, singularly those with a wide neck or unfavorable dome-to-neck ratio. However the analysis of mid- and long-term anatomical results is still needed to confirm the value of this technique.

KEYWORDS: Aneurysm treatment, Endovascular embolization

O-101 **4:19 PM - 4:27 PM**

Safety and Long-Term Efficacy of Flow Diversion versus Standard Coiling in the Treatment of Unruptured Carotido-Ophthalmic Aneurysms: A Preliminary Analysis

Di Maria, F. I.[1]·Clarençon, F.[1]·Sourour, N. A.[1]·Bernat, A.[1]·Biondi, A.[2]·Jean, B.[3]·Chiras, J.[1]
[1]Pitié Salpêtrière Hospital, Paris, FRANCE, [2]CHU Besançon, Besançon, FRANCE, [3]CHU Clermont Ferrand, Clermont Ferrand, FRANCE.

Purpose
Carotido-ophthalmic aneurysms (COA) are challenging lesions often prone to recanalization after endovascular treatment. Flow diversion (FD) is emerging as a new endovascular strategy for the treatment of these aneurysms, its goal being virtually to achieve a stable aneurysm occlusion on a long-term basis. We sought to compare angiographic outcome and complication rates in two groups of patients treated by standard coiling (SC) or FD at our institution over six years.
Materials & Methods
From February 2006 to December 2011, 40 unruptured COAs were treated endovascularly in 38 patients, nine of which were symtomatic. Twenty-six COAs were treated by SC. Balloon-assisted technique was employed in eight cases, stent-assistance in five cases. Flow diverters were deployed in the 14 aneurysms starting June 2009. Additional coiling was performed in four cases. One treated aneurysm was a recurrence after previous standard coiling. Imaging followup was carried out by 3D TOF MRA and DSA at six months and at 12 months respectively, then 3D TOF MRA on a yearly basis.

Note: Scanned images are included in the proceedings. Some submitted images were reduced during editing, thereby decreasing clarity. Also, refer to the Program Planner. Proceedings Content as of 3-29-2013.

Results
Mean followup was 59.2 +/- 35.6 months. No death or permanent morbidity was observed. One thromboembolic event (3.8%) causing transient neurologic motor deficit occurred in the SC group within six hours after the procedure. One homolateral intraparenchimal hemorrhage (7.1%) was observed 10 days after procedure in the FD group, causing transient aphasia and contralateral monoplegia. Clinical outcome was good in all patients. No statistical significance was found in terms of difference in complication rates (p = 0.08). No cases of rebleeding were observed during followup. Partial recanalization was observed during followup (mean 65.3 +/- 27.1 months) in 12 (46.3%) COAs treated by SC (six neck remnants and six residual sacs), leading to retreatment in five (19.2%). Of the five aneurysms coiled by stent-assisted technique, two recanalized at one year. One incompletely treated aneurysm didn't show any increase in the size of the circulating portion over 38 months. On the other hand, in the FD group (mean follow-up time 37.2 +/- 25.4), eight COAs showed complete thrombosis within six months, 13 within 12 months. No recanalization was observed after thrombosis had occurred. One small (5 mm) wide-necked aneurysm remained patent at 24 months and required retreatment by a second flow diverter. The difference in recanalization rate between the two groups in terms of recanalization at followup was statistically significant (p = 0.0004) even when considering only sac remnants and not neck remnants in the SC group (p = 0.002).
Conclusion
Though conducted on a small sample and in a particular subset of aneurysms, this retrospective analysis shows better stability of aneurysmal thrombosis after use of FD compared to SC. The introduction of flow diverters may probably increase the rate of long-lasting complete angiographic occlusion in COAs. However, larger samples and long term followup for FD are needed to better assess complication rates and stability of treatment results.

KEYWORDS: Aneurysm treatment, Flow diverter, carotido-ophthalmic

O-102 **4:27 PM - 4:35 PM**

Luminal Expansion and Narrowing in the Progression of Intracranial Aneurysms

Saloner, D.[1]·Rayz, V.[1]·Lee, W. A.[1]·Faraji, F.[1]·Martin, A.[1]·Young, W. L.[2]·Ko, N.[2]·Lawton, M. T.[2]
[1]VA/University of California San Francisco, San Francisco, CA, [2]University of California San Francisco, San Francisco, CA.

Purpose
This study was designed to investigate changes in lumenal morphology in patients with untreated aneurysms who were imaged serially over time. The aim was to determine individuals who demonstrated outward remodeling of their aneurysms and those where the lumenal geometry narrowed, and to relate those changes to prevalent hemodynamics on patient-specific basis.
Materials & Methods
Eighty-three patients were recruited where a clinical decision was made not to attempt any interventional repair of their aneurysms. These subjects underwent serial MR imaging at intervals of six months on a 1.5T scanner. 3D contrast-enhanced MR angiography was performed to determine the lumenal geometry with 30 second acquisition and with a voxel size of 0.5 mm^3 . In addition, 3D balanced steady state imaging was performed on the identical volume with identical spatial resolution. In selected subjects, 4D MR velocimetry was acquired with 1 mm^3 spatial resolution. Serial studies were co-registered in a three-dimensional space and changes of the lumen were measured on the CE MRA studies, and changes in the outer wall were determined from the balanced steady state images. Numerical computational fluid dynamic simulations were performed to determine the time-varying velocity fields in the aneurysms using patient-specific geometries as determined by CE MRA and inlet flow velocities from the MR velocimetry.
Results
A total of 337 interval studies were performed over the 83 subjects, with each subject having received at least two studies and some as many as nine studies. The error of reproducibility averaged over all subjects was found to be 4.9%. In all subjects, the outer wall of the aneurysm either remained unchanged or demonstrated outward remodeling over time. Twelve percent of the aneurysms showed significant layering of intralumenal thrombus. Of the aneurysms that remained thrombus-free, 15% demonstrated lumenal growth(Figure: ACoA aneurysm). Computational fluid dynamics calculations indicated that locations of growth correlated with areas of the aneurysm that were subjected to low wall shear stress. Regions of thrombus layering were found to correlate with locations where there was low blood shear stress and long residence times adjacent to the aneurysmal wall.

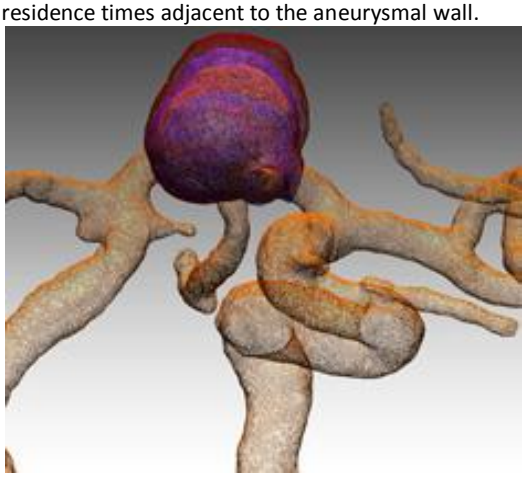

Conclusion
MR imaging is an effective modality for monitoring the

Note: Scanned images are included in the proceedings. Some submitted images were reduced during editing, thereby decreasing clarity. Also, refer to the Program Planner. Proceedings Content as of 3-29-2013.

temporal evolution of aneurysm morphology. These studies indicate that hemodynamics can play an important role in the rate of outward remodeling of the aneurysms and in the likelihood that regions of the anuerysm might layer clot. These studies could potentially lead to improved methods for stratifying patient treatment.

KEYWORDS: 3D imaging, 4D Flow MR

O-103 **4:35 PM - 4:43 PM**

Effects of Circle of Willis Anatomical Variations on Angiographic and Clinical Outcomes of Coiled Anterior Communicating Aneurysms

Tarulli, E.[1]·Sneade, M.[2]·Clarke, A.[2]·Molyneux, A. J.[2]·Fox, A. J.[1]
[1]Sunnybrook Health Sciences Centre, Toronto, ON, CANADA, [2]Oxford Neurovascular and Neuroradiology Research Unit, Oxford, UNITED KINGDOM.

Purpose
To evaluate the effects of circle of Willis anatomical variations on angiographic and clinical outcomes of anterior communicating aneurysm coiling treatment.
Materials & Methods
Anatomical variations and contrast filling of anterior cerebral artery trunks (A1), pericallosal (A2), and anterior communicating (A-com) arteries showed a high rate of aneurysm occurrence for unilateral A1 dominance cases (AJNR 2010;31:186-191). The randomized Cerecyte Coiling Trial (CCT) provides a sub-group of 98 cases with A-com aneurysms compared with 335 cases with other aneurysm locations for analysis of clinical outcome and the stability of aneurysm packing (platinum coil or Cerecyte coil) from follow-up angiography for angiographic outcome (Stroke 2012; 43:2544-2550). Clinical outcomes were assessed categorically by the Modified Rankin Score (mRS) at six months. A-com aneurysm cases are analyzed to relate A1 vessel dominance for treatment results, seeking differences in coil packing stability between cases with balanced A1 pattern and for aneurysms in other locations. Post-coiling angiographic outcomes were categorized immediately after coiling and at delayed followup (five-seven months) determining treatment success as defined in the published CCT results.
Results
A1 dominance was seen in 70% (n = 72) of A-com aneurysms and 30% (n = 31) A1 co-dominant. Treatment success in the A1 dominant group was 56% (n = 39 of 69) compared with 55% (n = 16 of 29) for treatment success for A-com aneurysms with other configurations at five-seven months (five cases lost to followup). These results compare to 57% (n = 190/335) treatment success for other aneurysms in other locations. Using p = 0.05 as a cutoff for the one-sided Fisher exact test there was no statistically significant difference in immediate treatment success rate between any A-com aneurysm configurations versus aneurysms elsewhere (p>0.5). Yet Pearson Chi-square tests comparing the angiographic appearance at baseline and five-seven months followup for the A1-dominant, A-com group showed statistical significance (p = 0.048) with fewer neck remnants (comparing 53% with 38%, n = 38 to n = 26) and more incompletely treated aneurysms with sac filling (comparing 8% with 22%, n = 6 to n = 15) while the completely treated proportion was unchanged (40%, n = 28). There was no statistically significant difference in clinical outcomes between these groups at the five-seven month followup (p = 0.57). No difference was seen for the randomized platinum and Cerecyte coil groups.
Conclusion
A-com aneurysms with A1 dominant circle of Willis configurations with incomplete occlusion at baseline may be less stable at followup than other aneurysms and those with A1 co-dominance despite no difference in clinical outcome at this time point. This supports the hypothesis that the A1 dominant flow into termination aneurysms of the A-com artery contributes to aneurysm formation, growth, and instability of treatment with coil packing.

KEYWORDS: Aneurysm treatment, Anterior communicating aneurysm, Anatomy

Monday Afternoon

3:15 PM - 4:45 PM
Ballroom 6CF

(13b) Parallel Scientific Papers: Adult Brain: Hemodynamics, Arterial and Venous

O-104 **3:15 PM - 3:23 PM**

Hyperperfusion in Carotid Stenting Patients

Aralasmak, A.·Atay, M.·Toprak, H.·Ozdemir, T.·Asıl, T.·Goktekin, O.·Alkan, A.
Bezmialem Vakif University
Fatih/Istanbul, TURKEY.

Purpose
To define hyperperfusion by evaluating pre and poststent CT perfusion studies of carotid stenting patients.
Materials & Methods
Total 29 patients, referred for carotid artery stenting, were enrolled. Sixty-four-channel CT (Toshiba, Aquilion) was used. Prestent CT perfusion studies were performed within one week before stenting. Poststent studies were performed three days after stenting. For CT perfusion, 45 ml contrast agent was administrated after five sn of data acquisition. The injection was performed by automatic injector in the right arm at a rate of 5 ml/s. Following computation of CBV, CBF, MTT and TTP maps, measurements were performed from areas of perfusion

Note: Scanned images are included in the proceedings. Some submitted images were reduced during editing, thereby decreasing clarity. Also, refer to the Program Planner. Proceedings Content as of 3-29-2013.

deficits and corresponding contralateral normal sides. Measurement from watershed regions and putamen were obtained irrespective of perfusion deficit. At least four areas were measured. For CBV, relative CBV (rCBV) were calculated by dividing ipsilateral (stent side) CBV to the contralateral CBV values. Pre and poststent rCBV were calculated separately. Similar calculations were performed for pre and poststent relative CBF (rCBF) and relative MTT (rMTT) values. Additionally for MTT, the different present MTT (dMTTpre) value was calculated by subtracting contralateral MTT from ipsilateral MTT values. Similar calculations were performed by using poststent values for poststent difference MTT (dMTTpost). Finally, average values of measurements were taken into consideration for comparison. Patients with clinical showing of one of the hyperperfusion syndromes except mild headache were accepted as a patient with hyperperfusion syndrome.

Results

Two of 29 (6%) showed clinical hyperperfusion of focal neurologic deficit and seizure after stenting. Their average values and comparing with average values of patients with no clinical hyperperfusion syndrome were given in the table. Only appreciable difference was noted in pre and poststent dMTT values. Six of 29 showed poststent radiologic hyperperfusion noted with increased CBF, increased or spared CBV and shortened MTT values. However, only one of them was symptomatic showing clinical hyperperfusion syndrome.

Hyperperfusion	rCBV pre	rCBF pre	rMTT pre	rCBV post	rCBF post	rMTT post	dMTT pre	dMTT post
-	1.00	1.13	1.28	1.09	1.10	1.16	**0.71**	**0.27**
+	1.09	1.30	1.28	1.00	1.41	1.11	**-0.08**	**-0.49**

Conclusion

After carotid stenting, revascularization of previously hypoperfused areas can cause symptoms such as ipsilateral headache, hypertension, seizure, focal neurologic deficit, brain edema, intracerebral or subarachnoid bleeding and death. Hyperperfusion mostly occurs within three-five days of revascularization. Due to dreadful consequences of hyperperfusion, to anticipate the possibility of hyperperfusion before stenting is critical. In our study, among the perfusion parameters, we found only appreciable difference between the patients with and without clinical hyperperfusion is MTT. Radiologic hyperperfusion does not match the clinical hyperperfusion.

KEYWORDS: Carotid artery stenting, CT perfusion, Hyperperfusion

O-105 **3:23 PM - 3:31 PM**

Comparison of Vasoconstrictive and Vasodilatory Reserve in Patients with Stenosis of Brain-Supplying Arteries

Mandell, D. M.[1]·Poublanc, J.[1]·Pucci, O.[1]·Wong, T.[1]·Sam, K.[1]·Han, J.[1]·Crawley, A.[1]·Duffin, J.[2]·Fisher, J.[1]·Mikulis, D.[1]
[1]University Health Network, Toronto, ON, CANADA, [2]University of Toronto, Toronto, ON, CANADA.

Purpose

In patients with stenosis of brain-supplying arteries and reduced cerebral perfusion pressure, there is reduced capacity for vasodilator-induced augmentation of cerebral blood, that is, reduced cerebrovascular reactivity. Measurement of cerebrovascular reactivity can be useful for risk stratification. While the cerebral vasodilatory response is relatively well known in patient populations, the response of the cerebral vasculature to vasoconstrictive stimuli is less well known. The aim of this study was to compare the magnitude of vasoconstrictive and vasodilatory reactivity in patients with stenosis of brain-supplying arteries.

Materials & Methods

We measured vasoconstrictive and vasodilatory reactivity in 12 patients with arterial steno-occlusive disease using both hypocapnic (vasoconstrictive) and hypercapnic (vasodilatory) stimuli, and blood oxygen level-dependent (BOLD) MR to measure changes in cerebral blood flow. MR imaging was performed on a 3.0 T whole body scanner. Following a T1-weighted three-dimensional sequence for anatomical co-registration, CVR data was acquired with a T2*-weighted single-shot gradient-echo echo-planar sequence during a precisely controlled ramp waveform of end-tidal partial pressure of carbon dioxide (PETCO2) from 30 mm Hg to 50 mm Hg. CVR was calculated as percent change in BOLD MR signal intensity per mm Hg change in PETCO2 on a voxel-wise basis. We segmented the middle cerebral artery territory cortex using an automated algorithm, and calculated mean CVR for the combined MCA segments for each patient. We performed a paired t-test to determine whether there was a difference in magnitude of reactivity for hypocapnic (30 - 40 mm Hg) versus hypercapnic (40 - 50 mm Hg) stimuli. We also analyzed whether baseline (resting) PETCO2 was correlated with the difference between hypocapnic and hypercapnic reactivity.

Results

There was a (nearly significant) trend toward higher vasoconstrictive cerebrovascular reactivity than vasodilatory reactivity (0.17 versus 0.13; two-sided P = 0.052). There was no significant correlation between resting PETCO2 and the difference between hypocapnic and hypercapnic reactivity.

Conclusion

CO2 BOLD MR demonstrates greater vasoconstrictive than vasodilatory reactivity in patients with stenosis of brain-supplying arteries. Further investigation is required to determine whether this difference is due to a normal

Note: Scanned images are included in the proceedings. Some submitted images were reduced during editing, thereby decreasing clarity. Also, refer to the Program Planner. Proceedings Content as of 3-29-2013.

physiologic difference in magnitude of vasoconstrictive and vasodilatory response, or due to the underlying steno-occlusive disease.

KEYWORDS: Hemodynamics

O-106 **3:31 PM - 3:39 PM**

Comparison of Common Carotid, Internal Carotid and Vertebral Arterial Compliance in Young Healthy Controls and Elderly Subjects Directly Measured with 3D Time-of-Flight MR Angiography

Bert, R. J.[1]·Mihlon, F.[2]·Hildreth, K.[1]·Moreau, K.[1]·Schwartz, R.[1]
[1]Univerisity of Colorado Denver, Aurora, CO, [2]Duke University, Durham, NC.

Purpose
Common carotid artery (CCA) compliance decreases with aging and may affect CNS perfusion dynamics. Less is known about internal carotid artery (ICA) and vertebral artery (VA) compliance, as they are difficult to directly measure with ultrasound. We have used cardiac-gated 3D time-of-flight (CG 3D ToF) MRA to directly measure CCA, ICA and VA compliance changes in small cohorts of young and older males and compared these changes to vascular flow waveforms obtained with quantitative phase contrast MRA in the same vessels.
Materials & Methods
We measured CCA, ICA and VA compliance with CG 3D ToF MRA in 10 healthy young men and 10 older men (seven with mild cognitive impairment and three without) as previously described, with a 1.5T system. Comparison ultrasound compliance measurements of the CCA provided controls (3). Quantitative phase-contrast MRA, normal to the vessels, was used to obtain velocity and flow curves. Peak systolic velocity and peak blood flow curves were used to set gates for compliance measurements.
Results
Common carotid artery vascular distension from MRI and ultrasound were reasonably correlated (MRI 0.158 ± 0.049, US 0.125 ± 0.034); R2 = 0.41. There were pronounced compliance differences between CCA (0.171 ± 0.04) and ICA (0.029 ± 0.011) ≈ VA (0.031 ± 0.01) in young healthy controls. The pattern was the same but differences smaller in the 10 older subjects: CCA (0.104 ± 0.04), ICA (0.037 ± 0.026), VA (0.039 ± 0.02). Common carotid artery was reduced in older compared to younger subjects (p<.002) However, there were no differences in ICA (P = 0.71) and VCA (p = 0.17) between older and young adults. However, surprisingly, ICA compliance differences did reach significance between MCI and normal older subjects (p = 0.049), despite the low power. Common carotid artery flow curves broadened and peak flows decreased with age, as compliance decreased.

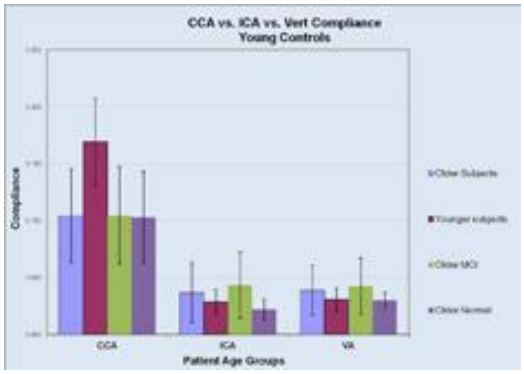

Conclusion
Internal carotid artery and VA are less compliant than CCA in both young healthy controls and older adults. Common carotid artery versus ICA-VA compliance differences narrowed significantly with aging and resulted from decreased CCA compliance alone. In our small sample, MCI and non MCI older subjects demonstrated significant differences in ICA, but not CCA or VA compliance. These results warrant further study to obtain greater statistical power for validation. Current findings suggest that CCA contractility decreases with age, broadening flow curves and decreasing peak flows.

KEYWORDS: Carotid angiography, Compliance, Mild Cognitive Impairment

O-107 **3:39 PM - 3:47 PM**

Hemodynamic Alterations in Cerebral Blood Vessels after Carotid Artery Revascularization: Quantitative Analysis by Using 2-Dimensional Phase-Contrast MR Imaging

Youn, S.[1]·Kim, H.[1]·Lee, J.[2]·Lee, H.[2]
[1]Daegu Catholic University Medical Center, Daegu, KOREA, REPUBLIC OF, [2]Kyungpook National University Hospital, Daegu, KOREA, REPUBLIC OF.

Purpose
While the clinical benefits from carotid artery revascularization (CAR) gained consensus, the understanding of hemodynamic alterations in cerebral blood vessels are still limited. It is unclear whether and how collateral flow and total cerebral blood flow volume ($_{FV}$TCBF) would change after CAR. It also is unknown that the increased intracranial pressure (ICP) and/or cerebral hyperperfusion syndrome may be suggested by flow changes in cerebral veins and cerebrospinal fluid (CSF) in the ischemic brain with significant carotid artery stenosis. The purpose of this study was to evaluate comprehensively the effect of CAR on cerebral arterial and venous flow volume (FV) with 2-dimensional phase-contrast magnetic resonance imaging (2D PC MRI).
Materials & Methods
The 39 carotid artery stenoses in 37 patients (28 men; 70.00 ± 8.58 years old), who were treated by CAR including 32 stentings and seven endarterectomies, were included in this prospective study. From the 2D PC MRI acquired

Note: Scanned images are included in the proceedings. Some submitted images were reduced during editing, thereby decreasing clarity. Also, refer to the Program Planner. Proceedings Content as of 3-29-2013.

before and after the revascularization, time-FV curves were generated with software (Reportcard, GE Healthcare, Milwaukee, WI). The FVs of the arteries, veins and CSF ($_{FV}$CSF) for before and after revascularization were compared with paired T-test. The relationships between the parameters of different locations were correlated with the Pearson correlation.

Results

After revascularization, the mean FV in the treated internal carotid artery ($_{FV}$TxICA; proportion of treated ICA among total FV) increased from 162.06 mL/min (25.80%) to 267.71 mL/min (37.21%; *P*<.001). The mean total FV of patients before revascularization was 638.66 mL/min. CAR increased the $_{FV}$TCBF of patients to 716.72 mL/min (*P*<.001). However, no significant changes were seen in the FV of the contralateral ICA and basilar artery after CAR. The FV of the internal jugular veins, superior sagittal and straight sinuses ($_{FV}$SS+SSS), and transverse sinuses increased after CAR (*P*<.05). Positive relationships were shown between the $_{FV}$TCBF and the $_{FV}$SS+SSS before and after revascularization (*r* = 0.584-0.741, *P*<.001). However, no significant changes were seen in the $_{FV}$CSF after CAR, and there was no patient with suspicion of hyperperfusion syndrome.

Conclusion

Carotid artery revascularization improves effectively the $_{FV}$TCBF by increasing the $_{FV}$TxICA without disturbing the collateral flows. The venous drainages are increased and closely linked to the increased $_{FV}$TCBF. The closed linkage of artery and vein, and interval constant $_{FV}$CSF may suggest our patients' condition with stable ICP. Based on these results, 2D PC MRI is recommended to evaluate the outcomes of CAR quantitatively.

KEYWORDS: Cerebral hemodynamics, Blood flow, carotid artery stenosis

O-108 **3:47 PM - 3:55 PM**

Value of Noncontrast Time-Resolved MR Angiography Using Arterial Spin Labeling in the Diagnosis of Occlusive Disease of the Major Intracranial Arteries

Tsuchiya, K.·Gomyo, M.·Ohara, A.·Shimatani, N.·Nitatori, T.
Kyorin University
Tokyo, JAPAN.

Purpose

Our purpose was to assess the value of noncontrast time-resolved MR angiography developed based on the arterial spin labeling technique in the evaluation of the hemodynamic status of occlusive disease of the major intracranial arteries.

Materials & Methods

The study group comprised a total of 24 patients (16 men and eight women; age range, 15-76 years; mean age, 59 years). Their disease included stenosis or occlusion of the internal carotid artery (five patients), middle cerebral artery (five patients), anterior cerebral artery (one patient), and moyamoya disease (13 patients). Among them, 10 patients were in the status of postbypass surgery. Noncontrast time-resolved MR angiography was performed on a 3T system using a 3D fast field-echo sequence with parameters as follows: TR/TE/FA, 4.5 ms/2.1 ms/15 deg; FOV, 230 × 256 mm; imaging matrix, 256 × 256; slab thickness, 96 mm; and section thickness, 3 mm. As to magnetically label the blood as a tracer, we placed a tag pulse band of 200 mm thickness inferior to the scan slab placing an interval of 17 mm. No cardiac or peripheral pulse gating was used. Changing a labeling delay time by 300-500 ms, we performed three-six scans in the axial plane. Visual assessment regarding the visualization of the stenoocclusive lesion and collateral vessels was performed comparing with 3D time-of-flight (TOF) MR angiograms in all patients using a four-point grading system. Comparison also was done with digital subtraction angiography in 15 patients and brain perfusion single photon emission tomography (SPECT) in 18 patients.

Results

Noncontrast time-resolved MR angiography better depicted the stenoocclusive lesion and collateral vessels than 3D TOF MR angiography in 21 patients (84%) achieving a better result in the assessment by scoring (Wilcoxon rank-sum test, P<0.01). Its findings were comparable with digital subtraction angiography in 14 of the 15 patients and with SPECT in 16 of the 19 patients.

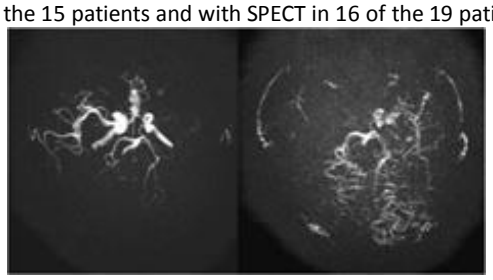

Conclusion

In assessing the hemodynamic status of occlusive diseases of the major intracranial arteries, noncontrast time-resolved MR angiography is superior to 3D TOF MR angiography, while it is equivalent to conventional digital subtraction angiography and SPECT.

KEYWORDS: MR angiography

O-109 **3:55 PM - 4:03 PM**

Validation of Dynamic CT Perfusion Summary Maps in Suspected Hyperacute Middle Cerebral Artery Stroke Patients: Comparison to Early Diffusion-Weighted Images

McKinney, A. M.·Palmer, C.·Jaghadeesan, B.·Truwit, C.
University of Minnesota & Hennepin County Medical Centers
Minneapolis, MN.

Purpose

Accurate CT perfusion (CTP) maps of penumbra and infarct core have been elusive, and are quite variable between postprocessing vendors. Meanwhile, the relatively simple,

Note: Scanned images are included in the proceedings. Some submitted images were reduced during editing, thereby decreasing clarity. Also, refer to the Program Planner. Proceedings Content as of 3-29-2013.

reproducible measurement of infarct volume on DWI MRI has been proposed as a means to select patients for thrombolytic therapy. Our goal was to evaluate the performance of one vendor's dynamic CTP "summary" (penumbra) maps in hyperacute MCA infarcts, as compared to DWI, and to compare the volume of infarct "core" between methods.

Materials & Methods

We identified 1087 64-slice emergent adult CTP examinations performed for stroke over 5.5 years, 244 of which were positive on DWI (DWI+), and 249 negative (DWI-). Forty-three of 244 DWI+ patients were performed <12 hours post-ictus/onset (>1.5 cm size), who were compared to 43/249 DWI patients, also <12 hours onset. Three reviewers separately evaluated both coregistered DWI and CTP "summary" (penumbra) maps, tabulating ASPECTS scores, and being blinded to other CTP parameters and noncontrast CT. The summary maps were generated automatically by a delay-corrected singular value decomposition ("SVD+") method, which automates comparison to contralateral and surrounding cerebrum via thresholds (CBV -40%, TTP>7.0sec., etc.); suspected infarct was colored red, ischemic penumbra yellow, and "normal" cerebrum green. Infarct volumes from the DWI and the CTP summary maps then were measured and correlated.

Results

The maximum diameter of MCA infarcts in the 43 DWI+ patients ranged from 16-142 mm (mean 46.2 mm). Regarding the three reviewers' ASPECTS scores, "interobserver" kappa for infarct "core" ranged from 0.930-0.969 ($p<0.0001$) on DWI, and from 0.943-0.963 ($p<0.0001$) on CTP summary maps; "intraobserver" kappa (comparing DWI to CTP scores) ranged from 0.645-0.737 ($p<0.0001$). The infarct "core" volume on DWI ranged from 1.5-215.6 cc (mean 34.5 cc), and on CTP summary maps was 0-184.5 cc (mean 28.7 cc). The volume of infarct "core" on CTP summary maps correlated excellently with DWI volume (Spearman's $r = 0.928$, $p<0.0001$), while the red+yellow "core+penumbra" region had less correlation($r = 0.766$, $p<0.0001$). Overall, the sensitivity, specificity, and accuracy of the summary maps ranged from 72.1-83.3%, 86.0-95.3%, and 79.1-88.4%, with a PPV of 83.8-94.3%.

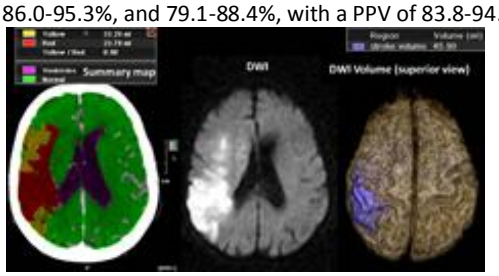

Conclusion

The automated display and volume measurement of infarct "core" on "summary" (penumbra) maps were quite representative of the infarct volume on DWI, with reproducible ASPECT scoring between observers. However, automated penumbra visualization needs prospective validation, and future studies could validate whether infarct "core" volumes on such maps correlate with outcome, in order to augment patient selection for therapy.

KEYWORDS: CT perfusion, Penumbra, Stroke

O-110 **4:03 PM - 4:11 PM**

Delayed MD CT Angiography Significantly Improves Detection of the Spot Sign and Increases Sensitivity for Prediction of In-Hospital Mortality following Intracerebral Hemorrhage

Ciura, V. A.[1]·Ortiz Lievano, J. C.[1]·Brouwers, H. B.[2,3,4]·Rosand, J.[2,3,5]·Goldstein, J. N.[2]·Pomerantz, S. R.[1]·Gonzalez, R. G.[1]·Romero, J. M.[1]
[1]Massachusetts General Hospital, Boston, MA, [2]Massachusetts General Hospital, Harvard Medical School, Boston, MA, [3]Center for Human Genetic Research, Massachusetts General Hospital, Harvard Medical School, Boston, MA, [4]J. Philip Kistler Stroke Research Center, Massachusetts General Hospital, Harvard Medical School, Boston, MA, [5]Hemorrhagic Stroke Research Group, Massachusetts General Hospital, Harvard Medical School, Boston, MA.

Purpose

To determine whether addition of 90 second delayed multidetector computed tomography angiography (MD CTA), in addition to routine first-pass MD CTA in patients with spontaneous intracerebral hemorrhage (ICH) improves detection of the spot sign and increases sensitivity for predicting in-hospital mortality. Previous trials have demonstrated that the spot sign is an independent predictor of hematoma expansion and death. Delayed imaging may capture additional patients at risk of death.

Materials & Methods

We performed a prospective study of consecutive patients enrolled over nine months at a single academic center. Patients were separated into two groups - those with a spot sign and those without. Spot sign positive cases were further subdivided into groups depending on the presence of the spot sign on first pass, delayed, or both CTA acquisitions. Uni- and multivariate logistic regression was performed to assess clinical and neuroimaging covariates (including the spot sign) for relationship with in-hospital mortality. Accuracy measures were calculated to compare first pass and delayed CTA performance.

Results

Of 55 consecutive patients, 16 patients (29%) had a positive spot sign; eight of 16 with spot sign on first pass and delayed CTA, and eight of 16 with spot sign on delayed CTA only. Median baseline hematoma volume for all patients was 43 mL (interquartile range 9 - 79 mL). Twenty-four of 55 (44%) patients died in hospital. Of the patients with a positive spot sign, 13/16 (81%) died in hospital. The odds ratio (OR) of in-hospital mortality if a spot sign was present on first pass CTA was 12.4 (95%

Note: Scanned images are included in the proceedings. Some submitted images were reduced during editing, thereby decreasing clarity. Also, refer to the Program Planner. Proceedings Content as of 3-29-2013.

confidence interval (95% CI) 1.40 - 109.07, p = 0.02), whereas OR of in-hospital mortality if a spot sign was present on delayed CTA was 11.0 (95% CI 2.62 - 46.37, p = 0.0007). The sensitivity for predicting mortality increased from 0.29 to 0.52 with the addition of delayed CTA, while specificity marginally decreased from 0.97 to 0.90. The area under the curve (C-statistic) for the spot sign on first-pass CTA was 0.63 in predicting in-hospital mortality, improved to 0.72 with the addition of delayed CTA. In multivariate analysis, baseline ICH volume and the spot sign were predictive of in-hospital mortality; however, the effect of the spot sign was only significant if present on first pass CTA.

Conclusion

Addition of 90 second delayed CTA to the imaging workup of patients with spontaneous ICH captures additional patients with the spot sign and nearly doubles the sensitivity for predicting in-hospital mortality. This improved sensitivity makes the spot sign a more attractive selection tool for targeting patients that may benefit from early surgical or medical intervention. The spot sign is a dynamic entity that appears to change with time, thus supporting the theory that it represents active ongoing hemorrhage.

KEYWORDS: Intracerebral hemorrhage, Spot sign, Delayed CTA

O-111 **4:11 PM - 4:19 PM**

Presence of CT Angiography Spot Sign Depends on Scan Timing of CT Angiography

Tsukabe, A.･Watanabe, Y.･Tanaka, H.･Nishizawa, M.･Kunitomi, Y.･Yoshiya, K.･Tomiyama, N.
Osaka University Graduate School of Medicine
Suita City, Osaka Prefecture, JAPAN.

Purpose

Morbidity and mortality in spontaneous intracerebral hematoma (ICH) are correlated with hematoma expansion. Recently computed tomography angiography (CTA) spot sign has been reported to be correlated with hematoma expansion and patients' outcome. However, previous studies showed various predictive values, especially in sensitivity for hematoma expansion. One of the reasons for this discrepancy might be the difference of scan timing of CTA. So the purpose of this study is to assess the impact of scan timing on predictive value for hematoma expansion of CTA spot sign from two different arterial phases.

Materials & Methods

Fifty-one consecutive patients with primary ICH who underwent dual-arterial phase CTA within six hours symptom onset, as well as follow-up noncontrast CT (NCCT) before discharge or death between January 2009 and October 2012 were recruited. All CT examinations were performed with 64-detector CT scanner. CT angiography studies were obtained using automatic triggering technique at the level of hyoid with 100 cc contrast media (300 mgI/ml), injection rate of 4 cc/sec and two sequential arterial phases were obtained. Two neuroradiolists reviewed two arterial phases of CTA for spot sign independently. One neuoradiologist reviewed admission and follow-up NCCT for measuring hematoma volume using ABC/2 method in another session. Hematoma expansion was defined as volume increase of hematoma size >20% or >6 ml. Predictive values of CTA spot signs in each phase for hematoma expansion were statistically analyzed respectively.

Results

The number of patients whose hematoma expanded was 15 out of 51 patients. Time difference between two phases of CTA was 11.6 second on average. CT angiography spot sign was depicted in 11/51 patients (21.5%) in early arterial phase, and in 26/51 patients (51.0%) in late arterial phase. Table shows sensitivity, specificity, positive predictive value (PPV), negative predictive value (NPV) and accuracy for hematoma expansion of CTA spot sign in two different arterial phases. Sensitivity and NPV were much better and specificity was worse in late arterial phase than in early arterial phase. Positive predictive value and accuracy were almost not different. In both phases, CTA spot sign was associated with hematoma expansion (in early arterial phase: p = 0.039, in late arterial phase: p < 0.001, Pearson's chi-square test).

	sensitivity	specificity	PPV	NPV	accuracy
early arterial phase	40.0%	86.1%	54.5%	77.5%	72.5%
late arterial phase	93.3%	66.7%	53.8%	96.0%	74.5%

Conclusion

The sensitivity and specificity of CTA spot sign for hematoma expansion showed big difference between two sequential arterial phases. To evaluate the CTA spot sign properly, we must pay more attention to scan timing and scan timing should be coordinated especially when planning the multicenter studies.

KEYWORDS: Intracerebral hemorrhage, CTA, CTA spot sign

Note: Scanned images are included in the proceedings. Some submitted images were reduced during editing, thereby decreasing clarity. Also, refer to the Program Planner. Proceedings Content as of 3-29-2013.

O-112 **4:19 PM - 4:27 PM**

Association of Developmental Venous Anomalies with Perfusion Abnormalities on Arterial Spin Labeling and Bolus Perfusion-Weighted Imaging

Iv, M.·Fischbein, N. J.·Zaharchuk, G.
Stanford University Medical Center
Stanford, CA.

Purpose
While developmental venous anomalies (DVAs) are the most common CNS vascular malformation, how they arise and their relationship to other shunting lesions such as arteriovenous malformations is incompletely understood. Some DVAs are associated with abnormal perfusion parameters on arterial spin label (ASL) and bolus perfusion-weighted imaging (PWI). We investigated the frequency and characteristics of DVA-associated perfusion abnormalities and discuss their potential causes.
Materials & Methods
We reviewed official brain MRI reports to identify all cases of DVAs on studies performed between March 2009 and August 2012 at a single hospital. Developmental venous anomalies' location (infratentorial, supratentorial, deep gray) and perfusion abnormalities on PWI and/or ASL imaging were assessed. 3D FSE pseudocontinous ASL was performed (TR/TE/label time/post-label delay: 4400/10/1500/2000 ms). Perfusion-weighted imaging was acquired with gradient-echo EPI (TR/TE: 1800/40 ms) and 0.1 mmol gadolinium contrast with post-processing using RAPID software. For PWI, conspicuity on separate hemodynamic maps (CBV, CBF, MTT, Tmax) was evaluated. For ASL, abnormality in the DVA itself, adjacent parenchyma, or associated draining vein was recorded.
Results
Six hundred thirty-two cases of DVA were identified. Of these, 121 had both perfusion modalities,15 had PWI alone, and 127 had ASL alone. Most DVAs were located in the supratentorial brain (77%). For cases with ASL imaging, 21/248 (8%) showed abnormalities: abnormal venous signal within a draining vein adjacent to the DVA (2/21, 10%), high signal within the DVA itself (10/21, 47%), and abnormal signal within the parenchyma surrounding the DVA (9/21, 43%) (Figure 1). For PWI, 106/136 (78%) demonstrated abnormalities, typically elevated CBF and CBV and mildly delayed MTT and Tmax that was largely confined to the DVAs themselves

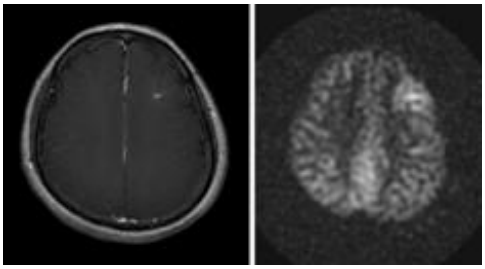

.
Conclusion
This study establishes an estimate of the incidence of perfusion abnormalities associated with DVAs. Perfusion abnormalities in DVAs were common on PWI but uncommon on ASL. Perfusion-weighted imaging findings of mild delay and high CBV are expected; they appear more prominent than the DVA itself likely due to the blooming effects of deoxyhemoglobin with gradient echo EPI acquisition. Developmental venous anomalies with intrinsic ASL signal or signal in draining veins ("venous ASL signal") may represent transitional lesions or small arteriovenous shunts and, as such, may warrant further evaluation with angiography and/or follow-up imaging. A prospective study would be needed to understand more fully the clinical significance of these findings.

KEYWORDS: Developmental venous anomalies, Arterial spin labeling, Perfusion

O-113 **4:27 PM - 4:35 PM**

Volume versus Hounsfield Unit of Thrombus: Which One Determines Hyperattenuated Artery Sign on 5 mm CT?

Kim, E. Y.[1]·Ahn, S. S.[2]·Shin, N. Y.[2]·Carneiro, F.[1]
[1]The University Hospital, Cincinnati, OH, [2]Severance Hospital, Seoul, KOREA, REPUBLIC OF.

Purpose
A recent study claimed that the hyperattenuated artery sign (HAS) on 5 mm nonenhanced CT reflects RBC content of thrombus. It also has been suggested that thrombi with lower HU on 2.5 mm nonenhanced CT are more resistant to pharmacologic lysis. The outcomes also may be affected by the thrombus volume, which is larger in patients with HAS than in those without. Therefore, determination of both the volume and HU of thrombus is important before thrombolytic treatment. As nonenhanced CT images are still reconstructed with 5 mm thickness for evaluation of acute stroke in many hospitals, it may be advantageous to predict both the HU and volume of thrombus on 5 mm nonenhanced CT. The purpose of this study was to assess the difference of HU and volume between thrombi with HAS and without on 5 mm nonenhanced CT using 1.25 mm helical nonenhanced CT.
Materials & Methods
We enrolled 85 patients who underwent both 5 mm sequential and 1.25 mm helical nonenhanced CT, demonstrating anterior circulation artery occlusion on CTA, within six hours of symptom onset. Hyperattenuated artery sign was determined on 5 mm nonenhanced CT. The patients were classified into ICA (ICA terminus/ICA and others), M1, and M2-only occlusion groups. HUs and volumes of thrombi were measured on 1.25 mm nonenhanced CT and were compared between patients with and without HAS identified on 5 mm nonenhanced CT.
Results
Mean thrombus HUs were not significantly different between 53 (62.4%) patients with and 32 (37.6%) without HAS, stratified by occlusion location [ICA group (n = 25):

Note: Scanned images are included in the proceedings. Some submitted images were reduced during editing, thereby decreasing clarity. Also, refer to the Program Planner. Proceedings Content as of 3-29-2013.

53.76±2.74 versus 52.54±3.11 (*P*>0.05); M1 group (n = 40): 51.86± .49 versus 50.56±2.11 (*P*>0.05); M2 group (n = 20): 49.52±2.78 versus 50.39±3.15 (*P*>0.05)]. Mean thrombus volume was significantly larger in patients with HAS compared to those without, except for the M2 group [ICA group: 218.40±151.58 mm^3 versus 71.49±47.41 mm^3 (*P* = 0.007); M1 group: 101.28±88.90 versus 61.90± 32.03 (*P* = 0.036); M2 group: 25.73±23.96 versus 25.21±25.84 (*P*>0.05)]. When further analyzed on 1.25 mm nonenhanced CT, no significant difference of thrombus HU between the patients with and without HAS on 5 mm nonenhanced CT was measured. However, in ICA and M1 occlusions, mean thrombus volume was significantly larger in patients with HAS than in those without.

	HAS-ICA (n = 25)			HAS-M1 (n = 40)			HAS-M2 (n = 20)		
	Present (SD)	Absent (SD)	*P*	Present (SD)	Absent (SD)	*P*	Present (SD)	Absent (SD)	*P*
	N = 20	N = 5		N = 23	N = 17		N = 10	N = 10	
HU	53.76 (2.74)	52.54 (3.11)	>0.05	51.86 (2.49)	50.56 (2.11)	>0.05	49.52 (2.78)	50.39 (3.15)	>0.05
Volume	218.40 (151.58)	71.49 (47.41)	0.007	101.28 (88.90)	61.90 (32.03)	0.036	25.73 (23.96)	25.21 (25.84)	>0.05

Conclusion
Therefore, HAS on 5 mm nonenhanced CT is dependent on thrombus volume, and thin-slice CT images are essential to determine thrombus HU.

KEYWORDS: Acute ischemic stroke, Thrombus imaging

O-114 **4:35 PM - 4:43 PM**

Venous Attenuation CT Sign of Idiopathic Intracranial Hypertension

Ibrahim, Y.[1]·Mironov, O.[2]·Deif, A.[2]·Mangla, R.[2]
[1]Ain Shams University, Cairo, EGYPT, [2]University of Rochester, Rochester, NY.

Purpose
Idiopathic intracranial hypertension (IIH) is a clinical disorder of unknown etiology manifesting with increased intracranial pressure in the absence identifiable cause. Idiopathic intracranial hypertension may exhibit several nonspecific imaging findings including: an empty sella, posterior globe flattening, tortuosity of the optic nerve, and optic nerve sheath distention. Patients with intracranial hypertension (IH) demonstrate intracranial venous sinus attenuation with a characteristic change in contour and caliber of the distal transverse sinus seen on routine noncontrast sagittal reformatted CT images of the brain. We have termed this the venous attenuation sign (VAS). Our purpose is to introduce the venous attenuation sign as a new imaging marker for IIH.
Materials & Methods
The transverse sinuses on sagittal reformatted noncontrast CT 25 patients with IIH and 24 control patients were assessed independently in a blinded fashion by three readers for the presence of a VAS. A present or absent VAS was determined for each patient by each reader, and a consensus result for each patient was determined by unanimity or majority rule. Correlation of the VAS with CT or MR venographic studies was assessed. The presence of traditional cross-sectional findings in patients with IIH also was evaluated.
Results
Using the VAS, the readers correctly identified 96% (24 of 25) of the IIH patients and 83.3% (20 of 24) of the control patients. There was a high rate of agreement among the readers for the interpretation of the VAS. The overall sensitivity of the VAS for the diagnosis of intracranial hypotension was 96%. Specificity also was 83.3%.

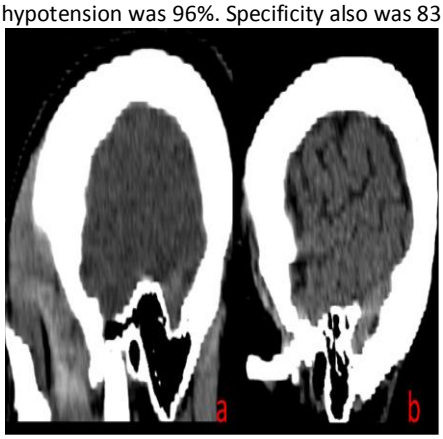

Figure: Noncontrast CT scan sagittal reformatted images at the level of distal transverse sinus. A positive VAS is demonstrated in A in a patient known to have IIH proved by lumbar puncture. Note the sinus is thin. B: shows normal sinus appearance in a control patient with normal CSF pressure on lumbar puncture.
Conclusion
Our study demonstrates the association of several classic imaging findings with IIH and supports the venous attenuation sign as an additional imaging marker which may be incorporated into the evaluation of patients suspected to have this condition.

KEYWORDS: Intracranial hypertension, CT, : Idiopathic intracranial hypertension, empty sell

Note: Scanned images are included in the proceedings. Some submitted images were reduced during editing, thereby decreasing clarity. Also, refer to the Program Planner. Proceedings Content as of 3-29-2013.

Monday Afternoon

3:15 PM - 4:45 PM
Ballroom 6DE

(13c) Parallel Scientific Papers: Adult Brain: Infectious and Inflammatory Diseases

O-115 **3:15 PM - 3:23 PM**

MR Imaging Findings in Fungal Meningitis: A Comparative Categorization of 31 Cases

Joseph, O.[1]·Aulakh, M.[1]·Keyes, D.[2]·Sherry, R.[2]·Karolyi, D. R.[2]
[1]Virginia Tech Carilion School of Medicine, Roanoke, VA, [2]Carilion Clinic, Roanoke, VA.

Purpose

There is a current multistate outbreak of fungal meningitis related to contaminated preservative-free methylprednisolone acetate steroid injections into the spinal area. The purpose of this study was to (1) categorize the magnetic resonance imaging (MRI) findings related to these infections and (2) determine how many of these patients have positive imaging findings based on the subset of patients that are/were being treated at our institution.

Materials & Methods

This study was approved by the Virginia Tech Carilion institutional review board. Patients with fungal meningitis related to contaminated injections were identified by retrospective search of the electronic medical record through consultation with physicians in the infectious disease department. The PACS was searched for MRI examinations of these patients obtained after their contaminated steroid injections. These examinations were reviewed by two experienced board-certified neuroradiologists. The results were categorized based on anatomical site of imaging and findings.

Results

Thirty-three patients were identified with fungal meningitis, of which 31 received MRI exams. The average age of the patients was 61 years with 15 male and 18 female patients. A total of 125 MRI examinations were reviewed. At presentation, 16 patients received spinal MRI exams, 13 of which had positive findings. The three most common spinal MRI findings at presentation were leptomeningeal enhancement (4 focal/nodular, 6 diffuse), clumped nerve rootlets (5), and thecal sac debris (4). During followup, 23 additional spinal MRI exams were performed, 20 of which had positive findings. The three most common findings were leptomeningeal enhancement (8 focal/nodular, 6 diffuse), clumped nerve rootlets (9), and thecal sac debris (7). At presentation, 21 patients received brain MRI exams, nine of which had positive findings. The three most common findings were focal leptomeningeal enhancement (7), foci of restricted diffusion in the occipital horns of the lateral ventricles (6), and posterior circulation infarcts (4). During followup, 18 patients received brain MRI exams, 14 with positive findings. The three most common findings were focal leptomeningeal enhancement (9), posterior circulation infarcts (6), and foci of restricted diffusion in the occipital horns of the lateral ventricles (5). To date, four patients have had negative brain MRI, while three have had negative spinal MRI.

Summary of MRI Findings

SPINE		
		Number of patients
Leptomeningeal enhancement		15
	Diffuse	8
	Focal/nodular	7
Clumped nerve rootlets		10
Thecal sac debris		9
Loculated collection/Abscess		7
Paraspinal muscle enhancement		5
Foci of restricted diffusion in spine		5
Interspinous enhancement		3
Transverse myelitis		1
BRAIN		
Leptomeningeal enhancement		
		11
	Diffuse	0
Foci of restricted diffusion in ventricles	Focal/nodular	11
Posterior circulation infarcts		7
Hydrocephalus		5
		2

Conclusion

Of the 31 patients reviewed, 28 showed positive MR findings. The most common findings on spine MRI were focal and diffuse leptomeningeal enhancement, clumped nerve rootlets, and thecal sac debris. The most common brain MRI findings were focal leptomeningeal enhancement, foci of restricted diffusion in the occipital horns of the lateral ventricles, and posterior circulation infarcts. The categorization of the 31 patients studied resulted in a reproducible spectrum of MRI findings in the brain and spine that would be amenable to interval follow-up MR imaging to evaluate for progression or regression of disease.

KEYWORDS: Meningitis, MR imaging, Fungal

Note: Scanned images are included in the proceedings. Some submitted images were reduced during editing, thereby decreasing clarity. Also, refer to the Program Planner. Proceedings Content as of 3-29-2013.

O-116 **3:23 PM - 3:31 PM**

Differentiation of Pyogenic and Fungal Brain Abscesses with Susceptibility-Weighted Imaging

Antulov, R.[1]·Dolić, K.[2]·Fruehwald-Pallamar, J.[3]·Miletić, D.[1]·Thurnher, M. M.[3]
[1]University Hospital Rijeka, Rijeka, CROATIA, [2]University Hospital Split, Split, CROATIA, [3]Medical University of Vienna, Vienna, AUSTRIA.

Purpose
Conventional magnetic resonance imaging (MRI) techniques are insufficient to determine the causative agent of brain abscesses. Recent studies have shown the value of susceptibility-weighted imaging (SWI) in providing additional information in the assessment of pyogenic abscesses. The goals of this study were: (1) to investigate the value of SWI in the differentiation of fungal and pyogenic brain abscesses; and (2) to analyze the effect of field strength (1.5T versus 3T) on SWI in detecting the specific imaging characteristics of brain abscesses.
Materials & Methods
We retrospectively reviewed the MR studies of 10 patients with pyogenic and five patients with fungal brain abscesses. Conventional MR sequences, DWI, and SWI were performed in all patients. Nine patients underwent MRI examinations on a 3T MR scanner, and six patients on a 1.5T MR scanner. We analyzed the size, number, and location of all abscesses. On T2-weighted images (WI), lesions were assessed for the presence of a hypointense rim. The enhancement on postcontrast T1-weighted imaging was defined as ring-like, nodular or absent. On diffusion-weighted imaging (DWI) lesions were categorized as homogeneously hyperintense or heterogeneous. Lesions on SWI images were described as having central low signal intensity or a low signal intensity rim. Lesions with a low signal intensity rim were characterized as: complete or incomplete; and smooth or irregular. On SWI, all lesions were assessed for the presence of a "dual rim sign".
Results
In 10 patients with pyogenic abscesses, 32 lesions were found, whereas in five patients with fungal abscesses, 28 lesions were detected. The mean size of pyogenic abscesses was 22.45 ± 1.87 mm and 12.61 ± 10.35 mm in fungal abscesses. Patients with pyogenic abscesses had a mean of 3.2 lesions per patient, while the group with fungal abscesses had a mean of 5.6 lesions per patient. On T2-weighted imaging, all pyogenic abscesses and 22/28 fungal abscesses showed a hypointense rim surrounding a central hyperintensity. Complete ring-enhancing lesions were present in all pyogenic abscesses and in 6/28 fungal abscesses, 1/28 fungal abscesses showed an incomplete enhancing rim, 2/28 nodular enhancement and 19/28 no enhancement. A homogeneously hyperintensity on DWI was present in 28/32 pyogenic abscesses, but only in 2/28 fungal abscesses. On SWI, 30/32 pyogenic abscesses had a complete low signal intensity rim. Five fungal abscesses showed a complete low signal rim on SWI. A "dual rim sign" was apparent in all pyogenic abscess scanned on a 3T scanner (6/6). Of the lesions scanned on a 1.5T scanner, none of the pyogenic abscesses (0/26) nor any of the fungal abscesses were positive for a "dual rim sign".
Conclusion
Pyogenic brain abscesses show T2-weighted imaging hyperintense center surrounded by hypointense rim along with the "dual rim sign" on SWI. The "dual rim sign" is a specific feature of pyogenic brain abscesses on a 3T scanner. In fungal abscesses "dual rim sign" will not be present; on SWI a prominent peripheral rim or marked central susceptibility effects will be seen.

KEYWORDS: Brain abscess, Susceptibility-weighted imaging, Dual rim sign

O-117 **3:31 PM - 3:39 PM**

Septic Thrombosis of Cavernous Sinus

Alazzaz, A. A. A.·Alsaadi, A.·Alattas, F.·Malhotra, R. M.·Hassan, A.
King Fahad Hospital
Madinah Monawara, SAUDI ARABIA.

Purpose
Septic cavernous sinus thrombosis is a rare disease and it was considered a fatal condition before the era of antibiotics with a mortality rate reaching 100%. With the use of antibiotics, the mortality rate was decreased dramatically down to 20-30%. The most important predisposing factors for acute septic cavernous sinus thrombosis are facial infections and complicated tooth extraction that are spreading by means of venous extension to the cavernous sinus along the normal drainage system. Our study reviewed four different patients of different ages (ranging from eight months to 64 years) who have been diagnosed having septic cavernous sinus thrombosis on the bases of clinical presentation, laboratory results and radiologic findings.
Materials & Methods
Imaging modalities are playing an important role in the early detection of cavernous sinus thrombosis. CT venogram is the modality of choice for the assessment of CVST especially with the use of the multiplanar reconstruction images.
Results
The most important findings are the visualization of the cavernous sinus filing defect associated with lateral wall expansion on the coronal images.
Conclusion
MR imaging is very useful in the detection and evaluation of septic cavernous sinus thrombosis and associated complications. MR imaging also is as an alternative choice for CT venogram in patients with renal impairment.

KEYWORDS: 1.5T, 1.5T

Note: Scanned images are included in the proceedings. Some submitted images were reduced during editing, thereby decreasing clarity. Also, refer to the Program Planner. Proceedings Content as of 3-29-2013.

O-118 **3:39 PM - 3:47 PM**

Whole Brain In Vivo Quantification of T1ρ of White Matter and Gray Matter in Multiple Sclerosis Patients Compared to Controls: Feasibility Study

Filippi, C. G.[1,2]·Gonyea, J. V.[3]·Hipko, S.[3]·Applebee, A.[3]·Karr, L.[2]·Andrews, T.[4]·Watts, R.[3]
[1]Columbia University, New York, NY, [2]University of Vermont School of Medicine, Burlington, VT, [3]University of Vermont School of Medicine-FAHC, Burlington, VT, [4]Philips Health Care, Cleveland, OH.

Purpose
T1 is an emerging MR imaging modality that is sensitive to anionic exchanges of large bulky molecules (i.e., proteins) determined by the use of spin lock sequence. In demyelinating disease leakage of proteins occurs and has been detected in the brains of MS patients. The purpose of this study is to compare quantitative in vivo measurements of white matter and gray matter at 3T in MS patients compared to age-matched control and to determine if there are any differences in white matter and gray matter and to correlate with disability scores.
Materials & Methods
This is an IRB-approved cross-sectional study of 17 age-matched controls (11 male, 6 female, age 44.5 +/- 10.3) to 14 MS patients (10 female, 4 male, age 44.5 +/- 11.1). Whole-brain T1-weighted images obtained with fluid-attenuated variable flip angle 3D turbo spin-echo technique (spatial resolution 1.8 x 1.8 x 1.8 mm^3). Images acquired with a spin lock frequency of 500HZ and spin lock durations of 0, 20, 40, 60, 80, and 100 ms. Each T1 map was calculated on a single exponential fit to the coregistered T1-weighted images. The T1 map was itself co-registered to T1-weighted 3D TFE anatomical scan. Using unified segmentation (SPM8) of the T1-weighted image, the T1 maps were segmented into white matter (WM) and gray matter (GM) and normalized to MNI space. Major white matter tracts were defined using the JHU atlas while cortical gray matter and juxtacortical white matter were defined by an intersection of the Harvard-Oxford cortical atlas with the subject-specific GM and WM masks respectively. 3D FLAIR (1.2 x 1.2 x 1.2 mm^3) and 3D DIR (1.2 x 1.2 x 1.3 mm^3) were obtained for lesion identification.
Results
T1 values of all the white matter fiber tracts sampled in this cross-section of MS patients as a group (superior and inferior longitudinal fasciculi, inferior frontal occipital fasiculi, anterior thalamic tracts bilaterally, superior longitudinal fasiculi, and forceps minor) were significantly elevated ($P < .002$), particularly the forceps minor and the inferior frontal fasiculus bilaterally. However there was little correlation with EDSS ($r < .042$). In cortical gray matter, group differences between MS patients and controls did not reach statistical significance, but individual areas including insula, paracingulate gyrus, occipital cortex, and Heschl's gyrus showed significantly different T1 values in MS patients ($p < .01$). However, many regions show significant negative correlations with disability scores ($r < -0.6$ to -0.7) in superior, middle, and inferior frontal gyri and precentral and postcentral gyri.
Conclusion
Whole brain quantification of T1 is a feasible, emerging MR modality that detects significant changes in white matter and cortical gyri of MS patients compared to age-matched controls in this initial cross-sectional study.

KEYWORDS: Multiple sclerosis, 3T, T1 Rho

O-119 **3:47 PM - 3:55 PM**

Decreased Frontal Lobe Gray Matter Perfusion in Cognitively Impaired Secondary Progressive Multiple Sclerosis Patients Detected by the Bookend Technique

Aviv, R.[1]·Francis, P.[1]·Tenenbein, R.[1]·O'Connor, P.[2]·Liying, Z.[1]·Eilaghi, A.[1]·Lee, L.[1]·Carroll, T.[3]·Mouannes-Srour, J.[3]·Feinstein, A.[1]
[1]Sunnybrook Health Sciences Centre, Toronto, ON, CANADA, [2]St. Michael's Hospital, Toronto, ON, CANADA, [3]Northwestern University, Chicago, IL.

Purpose
To quantify differences in MRI-based Bookend-derived cerebral perfusion between cognitively impaired and nonimpaired secondary progressive multiple sclerosis (SPMS) patients.
Materials & Methods
Patients were recruited prospectively and assessed using MRI and a standard cognitive battery, the Minimal Assessment of Cognitive Function In Multiple Sclerosis. Patients exhibiting impairment on ≥2 individual tests were classified as cognitively impaired. Healthy controls were recruited prospectively and assessed using MRI to validate Bookend assumptions. Structural and perfusion scans were coregistered and partitioned into anatomical brain regions and tissue compartments. Clinical and radiologic characteristics were compared between patients with and without impairment to identify potential confounders. A Bonferroni adjusted p-value threshold ($p<0.005$) was used for lobar and sublobar level analyses to correct for multiple comparisons.
Results
Thirty-seven SPMS patients (age: 56 ± 9 years, F/M: 23/14) and 10 age- and gender-matched healthy controls were recruited. Bookend assumptions were found to be valid in MS. Gray matter (GM) and white matter quantitative cerebral blood flow and volume (qCBV) all were reduced globally in impaired patients. After adjusting for potential confounders while examining sublobar level perfusion, only GM qCBV was significantly different between cognitive groups, and this hypoperfusion localized to the bilateral medial superior frontal regions and left inferior, middle, and superior frontal regions ($p<0.005$) of impaired patients compared to nonimpaired patients. GM qCBV accounted for 22.5% of the model variance compared to a

Note: Scanned images are included in the proceedings. Some submitted images were reduced during editing, thereby decreasing clarity. Also, refer to the Program Planner. Proceedings Content as of 3-29-2013.

model including only confounders (p = 0.0007).

Table 5: Relationship between cognitive impairment and sublobar GM qCBV

Lobe and Parameter	Estimate	SE	χ^2	*P* Value
Frontal, left (goodness of fit: deviance, *df* = 1.11; Pearson χ^2, *df* = 0.95)				
Intercept	18.7597	4.0521	21.43	<.0001
qCBV				
IF	−0.5396	0.1886	8.19	0.0042[b]
MidF	−0.4740	0.1664	8.11	0.0044[b]
MIF	−0.5185	0.1917	7.32	0.0068
MMidF	−0.4598	0.1668	7.60	0.0058
MSF	−0.4872	0.1708	8.13	0.0043[b]
SF	−0.5387	0.1902	8.02	0.0046[b]
BPF	−17.5403	5.2881	11.00	0.0009[b]
WML volume[a]	0.6301	0.1833	11.82	0.0006[b]
Frontal, right (goodness of fit: deviance, *df* = 1.11; Pearson χ^2, *df* = 0.95)				
Intercept	18.1061	3.9819	20.68	<.0001
qCBV				
IF	−0.5166	0.1986	6.77	0.0093
MidF	−0.4685	0.1719	7.43	0.0064
MIF	−0.5398	0.2100	6.61	0.0101
MMidF	−0.4317	0.1594	7.34	0.0068
MSF	−0.4906	0.1741	7.94	0.0048[b]
SF	−0.5638	0.2039	7.65	0.0057
BPF	−16.5799	5.2116	10.12	0.0015[b]
WML volume[a]	0.6532	0.1843	12.56	0.0004[b]

Note:—IF indicates inferior frontal; MidF, middle frontal; MIF, medial inferior frontal; MmidF, medial middle frontal; MSF, medial superior frontal; SF, superior frontal; WML, white matter lesion.
[a] Natural logarithmic transformation was applied.
[b] Significant result ($P < .005$, Bonferroni adjusted).

Conclusion
Bookend-derived GM qCBV was significantly reduced in cognitively impaired SPMS patients in functionally relevant brain regions.

KEYWORDS: Multiple sclerosis, Cognitive deficit, MRI PWI

O-120 **3:55 PM - 4:03 PM**

Robust Perfusion Deficits in Cognitively Impaired Secondary Progressive Multiple Sclerosis Patients

Francis, P.[1]·Jakubovic, R.[1]·O'Connor, P.[2]·Zhang, L.[1]·Eilaghi, A.[1]·Lee, L.[1]·Carroll, T.[3]·Mouannes-Srour, J.[3]·Feinstein, A.[1]·Aviv, R.[1]
[1]Sunnybrook Health Sciences Centre, Toronto, ON, CANADA, [2]St. Michael's Hospital, Toronto, ON, CANADA, [3]Northwestern University, Chicago, IL.

Purpose
We investigated the impact of cerebral perfusion and brain and lesion volumetry on cognitive performance in 45 secondary progressive multiple sclerosis (SPMS) patients using magnetic resonance imaging.
Materials & Methods
Cognition was assessed using a standard battery, the Minimal Assessment of Cognitive Function In Multiple Sclerosis. Focal (i.e., voxel-wise) analyses of gray matter (GM), white matter (WM), and WM lesion (WML) volume revealed no significant differences between patients with and without cognitive impairment, although global GM volume was significantly decreased and global WML volume was significantly increased in impaired patients. Cerebral perfusion was analyzed using Statistical Parametric Mapping (SPM) and Partial Least Squares (PLS).
Results
Both SPM and PLS demonstrated significantly reduced quantitative cerebral blood volume (qCBV) in the superior medial frontal cortex of impaired patients. Partial least squares also revealed significantly lower qCBV in the bilateral thalami and caudate nuclei of impaired patients and identified a pattern of significantly attenuated quantitative cerebral blood flow similar to that of qCBV. Performance on the Symbol Digit Modalities Test, which assesses information processing speed, correlated most strongly overall with cerebral perfusion.

Table 5: Correlations between predictive variables and brain scores based on either qCBF or qCBV (PLS Analysis)

Predictive Variable	Correlation Coefficient (qCBF)	Correlation Coefficient (qCBV)
Normalized WML volume	−0.71[a]	−0.72[a]
SDMT	−0.56[a]	−0.52[a]
COWAT	−0.54[a]	−0.53[a]
Overall patient impairment	−0.53[a]	−0.53[a]
BVMT-R Delayed Recall	−0.51[a]	−0.51[a]
BVMT-R Total Learning	−0.49[a]	−0.46[a]
JLO	−0.45[a]	−0.43[a]
Normalized GM volume	0.44[a]	0.39[a]
PASAT	−0.41[a]	−0.38[a]
D-KEFS	−0.42[a]	−0.35[a]
CVLT-II Total Learning	−0.34[a]	−0.28[a]
CVLT-II Delayed Recall	−0.28[a]	−0.28

Note:—BVMT-R indicates Brief Visuospatial Memory Test-Revised; COWAT, Controlled Word Association Test; CVLT, California Verbal Learning Test; D-KEFS, Delis-Kaplan Executive Function System; JLO, judgment of line orientation; PASAT, Paced Auditory Serial Addition Test; SDMT, Symbol Digit Modalities Test.
[a] 95% confidence interval does not overlap zero.

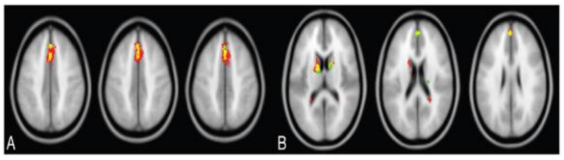

Fig 1. *A*, Decreased qCBV detected by SPM and PLS. Inferior-to-superior arrangement of axial sections with 3 different color overlays. The red overlay represents significantly reduced qCBV in cognitively impaired patients with SPMS identified by SPM alone. The green overlay represents significantly reduced qCBV in the same patients identified by PLS alone. The yellow overlay represents the overlap of the SPM and PLS results and thus significantly reduced qCBV found by both analytic techniques. *B*, Decreased qCBV and qCBF detected by PLS. Inferior-to-superior arrangement of axial sections with 3 different color overlays. The red overlay represents significantly reduced qCBV in cognitively impaired patients with SPMS identified by PLS. The green overlay represents significantly reduced qCBF in the same patients identified by PLS. The yellow overlay represents the overlap of the qCBV and qCBF hypoperfusion.

Conclusion
These results suggest that cognitively impaired SPMS patients exhibit robust perfusion deficits in cortical and subcortical GM and impaired processing speed.

KEYWORDS: Multiple sclerosis, Cognition disorders, MRI PWI

O-121 **4:03 PM - 4:11 PM**

Leptomeningeal Contrast Enhancement in Multiple Sclerosis

Rao, A. T.[1]·Butman, J. A.[2]·Cortese, I. C. M.[2]·Reich, D. S.[2]
[1]George Washington University, Washington, DC, [2]National Institutes of Health, Bethesda, MD.

Purpose
To determine the incidence and characteristics of leptomeningeal inflammation in multiple sclerosis (MS)

Note: Scanned images are included in the proceedings. Some submitted images were reduced during editing, thereby decreasing clarity. Also, refer to the Program Planner. Proceedings Content as of 3-29-2013.

using postcontrast T2-FLAIR imaging.
Materials & Methods
MR imaging scans from natural history protocols in the National Institute of Neurological Disorders and Stroke, obtained between November 2010 and December 2012, were reviewed retrospectively. 3D T2-weighted FLAIR scans were obtained on 3T systems, using phased-array head coils, 5-20 m following intravenous injection of single-dose gadolinium DTPA or gadobutrol. Noncontrast T2-FLAIR scans were available in a subset of patients. Two neuroradiologists (a fellow and an attending with eight years of experience in MS imaging), masked to the clinical diagnosis and findings, evaluated the T2-FLAIR data for presence of leptomeningeal enhancement. If present, enhancement was characterized by location, size, focal versus multifocal versus diffuse, and stability (if multiple datasets were available).
Results
The figure shows a typical example of focal leptomeningeal enhancement in primary progressive MS. Of the 271 participants, 231 (85%) had analyzable postcontrast 3D T2-FLAIR data and adequate clinical characterization. Assigned diagnoses and incidence of leptomeningeal enhancement were: MS (n = 27/167; 16%); other inflammatory neurologic disease (e.g., HTLV-associated myelopathy) (1/20; 4%); noninflammatory neurologic disease (1/26; 5%); no neurologic disease (n = 1/18; 6%). Leptomeningeal enhancement was more common in MS cases compared to all non-MS cases (p = 0.027, Fisher's exact test) and to cases of other neurologic diseases (p = 0.05). No difference was noted between relapsing (12/87; 14%) and progressive (13/75; 17%) forms of MS (p = 0.66). In virtually all cases, enhancement was focal or multifocal rather than diffuse. It was typically found adjacent to <5 cortical gyri and was not associated with nearby subcortical or juxtacortical white matter lesions. In 59% (12/29) of cases with repeated scans over the two-year period, the enhancement pattern was stable over time, whereas in the other 41% (11/57), the pattern fluctuated.

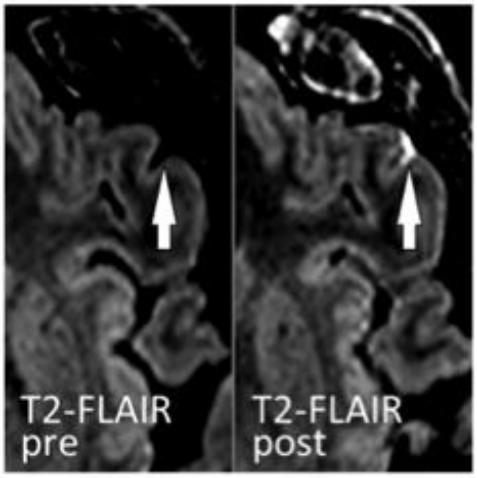

Conclusion
Although relatively infrequent, leptomeningeal enhancement, which may signify the presence of leptomeningeal inflammation, is a robust finding in MS. Leptomeningeal inflammation, which is sometimes organized into lymphoid follicle-like structures, is a pathologically described finding in all stages of MS that appears to be important for the development of cortical, especially subpial, demyelinating lesions. Further characterization of this imaging finding, with respect to clinical disability and other disease characteristics, will shed light on its significance for assessment of disease.

KEYWORDS: Multiple sclerosis, Meningeal, FLAIR

O-122 **4:11 PM - 4:19 PM**

Detection of the Multiple Sclerosis Lesions with Quantitative Susceptibility Mapping: Preliminary Results

Kakeda, S.[1]·Ueda, I.[1]·Watanabe, K.[1]·Moriya, J.[1]·Murakami, Y.[1]·Ide, S.[1]·Ogasawara, A.[1]·Sato, T.[1]·Okada, K.[1]·Tsuji, S.[1]·Liu, T.[2]·Wang, Y.[2]·Korogi, Y.[1]
[1]University of Occupational and Environmental Health School of Medicine, Kitakyushu-shi, JAPAN, [2]Weill Cornell Medical College, Ithaca, NY.

Purpose
Quantitative susceptibility mapping (QSM) is a novel technique which allows determining the bulk magnetic susceptibility distribution of tissue in vivo from gradient-echo magnetic resonance phase images. Our purpose is to compare the detection of multiple sclerosis (MS) lesions with QSM, T2WI, and 2D FLAIR in patients with MS.
Materials & Methods
Conventional MR and QSM imaging examinations were performed in 18 patients (four male, 14 female) with MS. Quantitative susceptibility mapping was performed for various ranges of echo time by using both the magnitude and phase components in the morphology-enabled dipole inversion method. The MS lesions were categorized into five anatomical regions: intracortical, mixed white matter-gray matter, juxtacortical, periventricular white matter, and deep white matter. The numbers of lesions per category were compared between QSM images and conventional MRI (T2WI and FLAIR images).
Results
In 110 (75%) of 146 MS lesions, the area of abnormal signal intensity detected with QSM images was larger than the size of the corresponding lesion at qualitative visual evaluation on coregistered T2WI and FLAIR images. The total number of the detected lesions was 146 for QSM, 182 for T2WI and 178 for FLAIR. The mean numbers of the lesions per category is shown in the table. Quantitative susceptibility mapping was more sensitive than T2WI and FLAIR in detecting the cortical lesions (mean numbers of lesions per patients: 0.28 versus 0.06 and 0.00 for the intracortical lesion, and 0.61 versus 0.11 and 0.06 for the mixed white matter-gray matter lesion, respectively). However, QSM was less sensitive than T2WI and FLAIR

images for the detection of the white matter lesions.

Table Mean Numbers of Lesions per Patients with QSM, T2WI, and FLAIR

	QSM	T2WI	FLAIR
Intracortical	0.28	0.06	0
Mixed WM-GM	0.61	0.11	0.06
Juxtacortical	0.83	1.39	1.33
Periventricular WM	2.44	2.83	2.83
Deep WM	3.94	5.72	5.67
Total	8.1	10.11	9.89

Conclusion
Our preliminary results suggest that MR imaging with QSM may increase the sensitivity in cortical lesion detection, although its sensitivity to white matter lesion detection may be limited.

KEYWORDS: 3T, Multiple sclerosis plaques, QSM

O-123 **4:19 PM - 4:27 PM**

Diffusional Kurtosis Imaging of Normal-Appearing White Matter in Multiple Sclerosis

Spampinato, M.·Pravata, E.·Hatch, N.·Jensen, J.·Helpern, J.·Tabesh, A.
Medical University of South Carolina
Charleston, SC.

Purpose
Our aim was to assess the correlation between measures of brain tissue microstructure in the normal-appearing white matter (NAWM) derived from diffusional kurtosis imaging (DKI) and neurologic disability in multiple sclerosis (MS).
Materials & Methods
Eighteen patients with MS (16 relapsing remitting, two secondary progressive MS, median age + / - SD = 39 years + / - 12 years) underwent brain MRI on a 1.5T scanner. Approval for this retrospective study was obtained from the Institutional Review Board. The MRI protocol included axial FLAIR, 3D T1 MPRAGE, and diffusion-weighted imaging using a twice-refocused echo-planar sequence with three diffusion weightings (b = 0, 1000 and 2000 s/mm2) along 30 diffusion encoding directions (TR = 5500 ms, TE = 100 ms, FOV = 222 ×222 mm2, matrix size = 74 × 74, parallel imaging factor of 2, slice thickness = 3 mm, and 40 axial slices). Diffusional kurtosis imaging allows for estimation of the conventional DTI parametric maps of mean diffusivity (MD), axial diffusivity, radial diffusivity, and fractional anisotropy (FA), as well as the additional diffusional kurtosis metrics of mean kurtosis (MK), axial kurtosis, and radial kurtosis. These maps were obtained using in-house software. Fractional anistotropy (FA) maps were spatially normalized to the standard MNI space using the FMRIB Software Library (FSL) and the resulting transformation was applied to normalize the other maps. The white matter skeleton for each map then was obtained using FSL's Tract-Based Spatial Statistics. Finally, we obtained average values for all diffusion metrics in several regions of the skeleton. The regions consisted of the entire white matter skeleton, corpus callosum (genu, body, and splenium), bilateral corticospinal tracts (CST), and bilateral posterior thalamic radiations (including optic radiations). The white matter regions of interest were obtained from the Johns Hopkins University atlas after masking out T2 hyperintense areas for individual patients. Spearman's rank correlation coefficient was used for assessing the association between the diffusion metrics and expanded disability status scale (EDSS). Results were considered significant when $p < 0.05$.
Results
The median EDSS was 3.25 (range = 1 - 9). Statistically significant correlations were found between the EDSS and CST MD ($r = 0.535$, $p = 0.02$), FA ($r = - 0.488$, $p = 0.04$), radial diffusivity ($r = 0.519$, $p = 0.03$), MK ($r = - 0.555$, $p = 0.02$), and radial kurtosis ($r = - 0.577$, $p = 0.01$). The correlations between EDSS and diffusion metrics in the NAWM skeleton, corpus callosum, and posterior thalamic radiations were not statistically significant.
Conclusion
Diffusional kurtosis imaging can provide information about brain tissue microstructure complementary to that of DTI. Quantitative diffusion metrics are correlated with neurologic disability in MS and can be helpful in the assessment of disease severity, with the potential of guiding patient management.

KEYWORDS: Multiple sclerosis, Diffusional kurtosis imaging

O-124 **4:27 PM - 4:35 PM**

Accumulation of Iron in Multiple Sclerosis in Normal-Appearing Brain Tissue and Lesions

Raz, E.[1]·Branson, B.[1]·Jensen, J.[2]·Fleyscher, L.[3]·Herbert, J.[1]·Grossman, R. I.[1]·Inglese, M.[3]
[1]New York University, New York, NY, [2]Medical University of South Carolina, Charleston, SC, [3]Mount Sinai Hospital, New York, NY.

Purpose
Accumulation of iron can lead to oxidative damage in the brain secondary to the formation of oxygen free radicals and its mesuration may provide insight into progression and severity of multiple sclerosis (MS). Significant differences in iron content between patients and controls using magnetic field correlation (MFC), were found. It has been posited that a portion of the signal may in fact originate from macroscopic interfaces in tissue density. The purpose of the present study is to remove such macroscopic irregularities, and draw a connection between the iron content of lesions and normal-appearing white matter.
Materials & Methods
Twenty-three patients (mean age = 39 years, range 21-61

Note: Scanned images are included in the proceedings. Some submitted images were reduced during editing, thereby decreasing clarity. Also, refer to the Program Planner. Proceedings Content as of 3-29-2013.

years, M=7, F=16, mean disease duration = three years, range 0-13 years) with definite, clinically diagnosed relapsing and remitting MS, and 14 matched controls (mean age = 36 years, range 19-60 years, M/F=5/9), consented to inclusion in our study. Mean EDSS was 1.7 (range 0-4.5). The MFC and Micro estimation have been described previously. An echo-planar spin-echo imaging sequence was used to procure images which contained 48 axial, 1.7 mm thick contiguous sections. The parameters were: bandwidth = 1345 Hz, TR = 3420 ms, TE = 40 ms, matrix = 128*128, FOV = 220*220 mm2, voxel size = 1.719*1.719 mm2. The images were postprocessed for movement correction using Statistical Parametric Mapping (SPM), and macro and micro MFC maps were generated. Multiple ROI were analyzed in both the white and grqy matter including the centrum semiovale, splenium of the corpus callosum, thalamus, putamen, caudate, globus pallidus, red nucleus and hippocampus in all subjects. White matter ROIs were drawn in normal-appearing WM on T2. All white matter lesions greater than 6 mm were identified in the patients and corresponding MFC values were assessed.

Results

When patients to controls were compared in terms of macro MFC, correcting for age and gender, the centrum semiovale [122.89 (29.03) in controls; 141.8 (36.75) in patients; p = 0.05], globus pallidus [835.17 (167.31) in controls; 1009.38 (249.82)in patients; p = 0.006], putamen [338.42 (92.98) in controls 402.42 (102.86) in patients; p = 0.02] were significantly different. When patients to controls were compared in terms of micro MFC, correcting for age and gender, the centrum semiovale [111.66 (29.93) in controls; 130.92 (36.4) in patients; p = 0.05], globus pallidus [762.27 (167.21) in controls; 925.35 (230.23) in patients; p = 0.008] were significantly different. In patients the macro and micro MFC of lesions [respectively 121.44 (67.18) and 105.97 (65.65)] was significant lower than the values for GM.

Conclusion

Quantitative measurement of the macro and micro MFC, hence removing sources of macroscopic irregularities of the field, demonstrates increased MFC values in the white and gray matter in patients with MS, suggesting accumulation of iron.

KEYWORDS: Multiple sclerosis, Iron deposition

O-125 **4:35 PM - 4:43 PM**

Normal-Appearing White Matter Permeability Distinguishes Poor Cognitive Performance in Processing Speed and Working Memory

Eilaghi, A.[1]·Kassner, A.[2]·Sitartchouk, I.[2]·Francis, P. L.[1]·Jakubovic, R.[1]·Feinstein, A.[1]·O'Connor, P. W.[3]·Carroll, T. J.[4]·Mouannes-Srour, J.[4]·Aviv, R. I.[1]

[1]Sunnybrook Health Sciences Centre, Toronto, ON, CANADA, [2]University of Toronto, Toronto, ON, CANADA, [3]St. Michael's Hospital, Toronto, ON, CANADA, [4]Northwestern University, Evanston, IL.

Purpose

Localized blood-brain barrier (BBB) break-down in multiple sclerosis can be quantified using relative recirculation (rR). We hypothesize that severity of BBB breakdown in normal appearing white matter (NAWM) differs between cognitive impaired and unimpaired secondary progressive multiple sclerosis (SPMS) patients particularly in the functional areas of attention and processing speed.

Materials & Methods

The study was research ethics board approved. Cognitive performance was classified as impaired or unimpaired based on the Minimal Assessment of Cognitive Function In MS (MACFIMS) test components. Demographic data, brain parenchymal and white matter lesion fractions, WML and NAWM regions of interest (ROIs) and weighted mean NAWM rR ROIs were compared in cognitively dichotomized groups. Univariate comparison and multivariate logistic regression were used to investigate the association between cognitive test results and NAWM rR ROIs.

Results

The mean (SD) age of 36 SPMS patients studied was 55.9 ± 9.3 years; 13/36 (36%) patients were male. A highly significant difference between NAWM rR and WML rR was present for all patients ($p < 0.001$). Normal appearing white matter rR in impaired patients was significantly lower than unimpaired subjects for SDMT ($p = 0.007$), COWAT ($p = 0.008$), or PASAT ($p = 0.024$) shown in Table 1. EDSS score demonstrated an inverse correlation with NAWM rR (correlation coefficient = -0.319, $p = 0.075$). After adjusting for confounders, significant NAWM rR reduction persisted in impaired patients for SDMT ($p = 0.023$) and PASAT ($p = 0.047$) but not COWAT ($p=0.13$) as presented in Table 2.

Table 1: Univariate comparison of the nonimpaired (NI) and impaired (I) groups. Parameters showing $p<0.3$ in the univariate analysis were included in the multivariate logistic model.

Note: Scanned images are included in the proceedings. Some submitted images were reduced during editing, thereby decreasing clarity. Also, refer to the Program Planner. Proceedings Content as of 3-29-2013.

	SDMT			COWAT			PASAT		
Parameter	NI	I	p value	NI	I	p value	NI	I	P value
NAWM rR	0.066 ±0.011	0.055 ±0.009	**0.007**	0.062 ±0.009	0.051 ±0.007	**0.008**	0.063 ±0.011	0.054 ±0.007	**0.024**
Age (years)	56.6 ±6.2	58.3 ±12.1	0.687	57.7 ±10.5	53.5 ±10.0	0.391	54.5 ±5.7	56.8 ±8.9	0.421
Gender (Male%, Male/Total)	36 (5/14)	36 (8/22)	0.983	41 (11/27)	33 (3/9)	0.334	35 (7/20)	33 (5/15)	0.983
Education (years)	16.2 ±2.3	15.3 ±2.6	0.367	15.7 ±2.8	14.8 ±1.5	0.379	16.1 ±2.5	15.3 ±2.2	0.434
Duration (years)	16.5 ±6.1	21.1 ±13.1	0.55	18.9 ±8.8	19.3 ±11.4	0.922	17.4 ±6.4	20.6 ±10.3	0.34
BDI Median(1^{st}-3^{rd} QR)	6(5-13)	10(7-13)	0.38	8(5-10)	9(2-13)	0.624	7(5-11)	9(6-11)	0.554
EDSS Median(1^{st}-3^{rd} QR)	6 (5.5-6.5)	6.5 (6..0-6.5)	0.32	6.5 (6.0-7.0)	6.5 (6.0-7.5)	0.395	6 (5.6-6.5)	6.5 (6.0-7.0)	0.496
Brain Parenchymal Fraction	81.9 ±3.9	80.1 ±4.3	0.28	80.4 ±4.3	79.9 ±4.7	0.802	81.9 ±4.5	80 ±4.2	0.267
White Matter Fraction	38 ±3.3	36.6 ±2.9	0.27	37.1 ±2.6	35 ±3.0	0.108	37.7 ±3.2	36.5 ±3.1	0.297
White Matter Lesion Fraction	0.6 ±0.7	1.5 ±1.0	**0.02**	1.1 ±1.0	2.6 ±1.6	**0.014**	0.9 ±1.0	1.8 ±1.0	**0.033**
Grey Matter Fraction	41.4 ±1.5	41 ±2.9	0.71	40.8 ±2.6	42.5 ±2.2	0.169	41.8 ±2.2	41 ±3.0	0.971

Table 2: Outcomes of multivariate logistic regression analyses for NAWM rR after controlling for potential confounders. NAWM rR continues to be significantly lower in the impaired group for both SDMT and PASAT tests.

Cognitive Test	Odds Ratio	p value
SDMT	0.177 (5-95%CI; 0.040-0.785)	**0.023**
COWAT	0.662 (5-95%CI;0.002-2.226)	0.130
PASAT1.6	0.053 (5-95%CI; 0.003- 0.961)	**0.047**

Conclusion

Significant NAWM rR reduction exists in cognitively impaired SPMS patients localizing to the domains of processing speed and working memory. Further validation and longitudinal studies are required to study the association between rR, cognition, disease progression and treatment response; however rR could be a useful surrogate for future pharmacologic and rehabilitative strategies targeting cognition.

KEYWORDS: Multiple sclerosis, White matter disease, permeability

Monday Afternoon

3:15 PM - 4:45 PM
Room 5AB

(13d) Parallel Scientific Papers: Spine: Trauma, Other and Spinal Cord

O-127 **3:15 PM - 3:23 PM**

Diffusion Tensor Imaging Tractography for Peripheral Nerve Lesions: Feasibility and Clinical Utility

Narvid, J.·Kliot, M.·Chin, C.
University of California San Francisco
San Francisco, CA.

Purpose

Imaging methods that can visualize nerve fascicles in peripheral nerves are needed. Such techniques would be extremely useful in helping to distinguish axonontmetic nerve injuries which can recover through axonal regeneration from neurotmetic injuries which cannot either due to physical discontinuity in the nerve or intraneural fibrosis which impedes nerve fibers from regenerating. It would also be useful to visualize the spatial relationship of nerve fibers vis-a-vis tumors arising from nerves (nerve sheath tumors) to help determine the surgical resectablility of such masses when clinically appropriate. Due to the geometric distortion that arises from the low phase-encoding bandwidth in single-shot echo-planar imaging (ssEPI), local susceptibility gradients due to tissue interfaces often degrades image quality. In particular, achieving good image quality and spatial resolution with ssEPI diffusion in the spine always has been technically challenging since with conventional 1D slice selective excitation, a large field-of-view (~32-36 cm) has to be prescribed to avoid aliasing artifacts. Encoding such a large FOV with high resolution requires a very long echo-train length, which exacerbates off-resonance artifacts. 2D partially selective RF can be used to limit FOV in the phase-encoding direction and avoid aliasing. We applied rFOV DTI to visualize nerve fibers in the clinical setting of traumatic nerve injuries and peripheral nerve tumors and correlated pre-operative findings with intra-operative electrophysiology.

Materials & Methods

Diffusion tensor imaging datasets were acquired on a 3T whole body MR750 scanner (GE Healthcare, Waukesha) utilizing the reduced field of view (rFOV) diffusion method which employs a 2D spatially selective RF excitation pulse in the ssEPI sequence with 10 direction-encoded images that uses a 2D echo-planar RF pulse to excite and read out a rectangular-shaped field of view. Fourteen patients were evaluated due to either traumatic nerve injury or suspected peripheral nerve sheath tumor. Slices were prescribed sagittally to cover the brachial-plexus. Imaging parameters common to all patients were: TR=3600 ms, TE=52 ms, acquisition matrix=128x64, FOV=24x12 cm, slice thickness=3 mm, 16 slices, b=500 s/mm2, 10 diffusion encoding directions, 10 averages, scan time=nine minutes 30 seconds. Tractography analysis was performed on the DTI images using Brainwave software.

Results

Reduced field of view DTI was used successfully to visualize the displacement and distortion of fascicles

Note: Scanned images are included in the proceedings. Some submitted images were reduced during editing, thereby decreasing clarity. Also, refer to the Program Planner. Proceedings Content as of 3-29-2013.

adjacent to nerve sheath tumors. In four cases, these findings were correlated with intraoperative visual inspection and electrophysiologic testing. All such cases confirmed the location and relation of nerve fibers to tumor, confirming the utility of this technique in pre-operative planning. In eight cases, findings of fascicular discontinuity (the presence and absence of nerve fibers in damaged peripheral nerve) were correlated with EMG findings of nerve injury. All such confirmed the location of injury.
Conclusion
Peripheral nerve tractography using MR DTI can be used to visualize the relationship of nerve fascicles to masses such as nerve sheath tumors which can be helpful in the planning of surgical resection. It also provides useful information following traumatic nerve injuries to help determine the extent of axonal disruption.

KEYWORDS: MR neurography, Diffusion tensor image

O-128 **3:23 PM - 3:31 PM**

Application of 3T Diffusion Tensor Imaging in Sciatic Neuropathy: Comparison to Normative Values

Thawait, G. K.[1]·Farahani, S. J.[1]·Andreisek, G.[2]·Thawait, S. K.[1]·Belzberg, A. J.[1]·Chhabra, A.[1]
[1]Johns Hopkins University School of Medicine, Baltimore, MD, [2]University of Zurich, Zurich, SWITZERLAND.

Purpose
To determine normative diffusion values of the sciatic nerve and compare these values with those in patients with sciatic neuropathy.
Materials & Methods
In this IRB approved study, 37 healthy volunteers with no sciatic neuropathy (19 men and 18 women) and 11 patients with EMG/surgery-proven unilateral sciatic neuropathy (five men and six women) were evaluated. In all the subjects, DTI was performed by utilizing 3T MR and single-shot echo-planar imaging sequence (TR/TE, 11300/ 77ms, b-values-0, 800 and 1000s/mm2; 12 encoding directions). Two readers independently determined fractional anisotropy (FA) and apparent diffusion coefficient (ADC) values of each patient's sciatic nerve with regions of interest (at least 3 mm^2 area) at two locations: at the level of greater sciatic notch, anterior to the piriformis muscle (point A); and outside the pelvis at the level of the ischial spine, behind posterior column of the acetabulum (point B). Paired and unpaired t-test was performed to determine any significant difference in FA and ADC between different sides and locations in the controls and also between the cases and controls. The level of agreement between the readers was determined utilizing inter-class correlation coefficient.
Results
There was 89% and 84% agreement for FA and ADC between two readers. The mean FA and ADC values at point A and point B for right sciatic nerve were, 0.46±0.11 and 1111.973 x $10^{-3}s/mm^2$, and 0.44±0.08 and 1172.17±207.9 x $10^{-3}s/mm^2$ for controls. While the mean FA and ADC for left sciatic nerve in the healthy volunteer were 0.43 ± 0.086 and 1147.33 ± 201.86 x $10^{-3}s/mm^2$ at point A and 0.43 ± 0.082 and 1202.41 ± 247.2 x $10^{-3}s/mm^2$ at point B. These values were 0.37 and 4763.763 x $10^{-3}s/mm^2$ for FA and ADC of the involved side of the cases and 0.31 and 1335.143 x $10^{-3}s/mm^2$ for noninvolved side, respectively. There was a significant difference between controls and patients with sciatic neuropathy (P <0 .005 for both FA and ADC for all observations). Fractional anisotropy and ADC values did not differ between men and women or between points A and B in the healthy group. According to the receiver operating characteristic (ROC) curve, the optimal cutoff value of mean FA value for predicting sciatic neuropathy was 0.34, with sensitivity and specificity of 100% and 69.3% (area under the ROC curve, 0.877; 95% CI, 0.728-1.000). The cutoff point for mean ADC value was 1254.675 x $10^{-3}s/mm^2$, with sensitivity of 91% and specificity of 88% (area under ROC curve, 0.9239; 95% CI, 0.85-0.99).
Conclusion
Decreased FA and increased ADC values have been reported to be important parameters for the diagnosis of carpal tunnel syndrome and cervical radiculopathy in previous studies. Similar trends in these quantitative parameters were observed in this study. Diffusion tensor imaging could be used in the diagnosis of sciatic neuropathies. Alterations in mean FA and ADC values can be used to identify cases with sciatic neuropathy and thus, DTI provides a good noninvasive diagnostic tool in sciatica.

KEYWORDS: 3T, Diffusion tensor image, Magnetic resonance neurography

O-129 **3:31 PM - 3:39 PM**

Idiopathic Spinal Cord Herniation: An Imaging Diagnosis but with a Significant Delay

Carter, B.·Jain, R.·Griffith, B.·Newman, D.·Abdulhak, M.
Henry Ford Health System
Detroit, MI.

Purpose
Idiopathic spinal cord herniation (ISCH) is an under-recognized entity that often is missed on imaging studies and/or ignored by treating physicians leading to a delay in diagnosis. This leads to unnecessary imaging studies, nonimaging diagnostic studies such as EMGs, unnecessary surgeries, and continual office visits. The purpose of this study was to assess the length of delayed diagnosis of ISCH from a patient's original presentation and the associated costs of this entity going unrecognized.
Materials & Methods
A retrospective search was performed using Illuminate software from 6/20/2005 to 12/3/2012 yielding 37 patients that fit the clinical and imaging criteria typically seen in ISCH. Data including patient's age, sex, presenting

Note: Scanned images are included in the proceedings. Some submitted images were reduced during editing, thereby decreasing clarity. Also, refer to the Program Planner. Proceedings Content as of 3-29-2013.

clinical symptoms, number and type of imaging studies performed as part of the workup, EMGs, pain procedures, surgeries, and most importantly, the period of time between the patient's original presentation and receiving the diagnosis of ISCH on imaging were collected.
Results
The most frequent complaints were neck/upper back pain in 70% (26/37), upper/lower extremity numbness/paresthesias/weakness in 49% (18/37), hyperreflexia in 22% (8/37), and burning chest pain in 22% (8/37). The average delay in diagnosis from presentation to imaging was 33 months (0-196 months). Three of these patients underwent dural repair which resulted in improvement of symptoms in each case. There was no change in symptoms in 73% (27/37), worsening of symptoms in 14% (5/37), and improvement in 14% (5/37) when comparing the patient's original presentation and most current office note. There were seven spine surgeries other than dural repair performed in six patients. The only patient to show improvement with surgery other than dural repair received a syrinx decompression and posterior thoracic laminectomy. There was an average of 14 outpatient office visits (1-67) and 1.5 (0-13) inpatient days per patient in which the chief complaint or admission was related to ISCH symptoms. There was also an average of 3.5 MRs (0-23), 1 (0-7) CT/CT myelography, and 1 EMG (0-7) per patient presenting with ISCH.
Conclusion
The symptoms of neck/upper back pain and numbness/paresthesias/pain in the extremities were the most common presentations seen with ISCH and MR was the most common imaging method by which it is diagnosed. There was still a delay of 33 months until this diagnosis was made, leading to repeat office visits and unnecessary surgeries. There was no change or worsening of symptoms in 86% of the patients, some of which had spine surgeries other than dural repair which did not improve the patient's condition. All of the patients that did have repair of the dural rent had improvement in their symptoms. An increase in awareness of ISCH on imaging and as a treatable disease with real symptoms would decrease both the delay in diagnosis/treatment and associated costs. Not only would this lead to improvement in patient care, but reduce national health care expenditures which have skyrocketed in the past decade.

KEYWORDS: Spinal cord, Spinal imaging, Idiopathic spinal cord herniation

O-130 **3:39 PM - 3:47 PM**

Effect of Oscillatory Cerebospinal Fluid Flow on Fluid Movement in the Spinal Cord

Støverud, K. H.[1]·Langtangen, H.[1]·Haughton, V.[2]·Mardal, K.[1]
[1]Simula Research Laboratory, Lysaker, NORWAY,
[2]University of Wisconsin, Madison, WI.

Purpose
Cyclic CSF flow is driven by oscillations in the fluid pressure. The intracranial pressure is closely related to the cardiac cycle and generates pressure waves that travel through the spinal canal. The aim of this study was to investigate whether these pressure waves generate flow in open segments of the central canal assuming a poro-elastic spinal cord.
Materials & Methods
High-resolution diffusion tensor images (DTI) from a sheep cadaveric spinal cord were segmented to create a geometric model. In the segmentation procedure we distinguished between gray and white matter and the central canal. The geometric model was converted into a tetrahedral computational mesh consisting of interconnected nodes. We used continuous pressure measurements from the cranial and lumbal region in a Chiari patient to calculate the wave velocity of the CSF pressure wave. The pressure measurements at the two locations were sampled simultaneously at 200 Hz as described by P. K. Eide. Along the walls of the model we applied a prescribed normal stress and pore pressure calculated from the pressure measurements and representing one cardiac cycle. An open segment of the central canal was modeled by assigning a higher permeability to the central canal than to the surrounding tissue. With the FEniCS toolkit we calculated pressure, displacement and interstitial fluid velocity, assuming the spinal cord to behave as a linear poro-elastic medium.
Results
The antero-posterior and transverse diameter of the model was 0.9 cm and 1.3 cm respectively and the model was 1.7 cm in length. On its surface the central medial fissure was evident. The central canal was between 0.2 and 0.3 mm in diameter. The pressure wave applied along the walls had a velocity of 2 m/s and amplitude of 6 mmHg. Pressure gradients occurred since the pressure wave arrived at different times along the geometric model. In the first part of the cardiac cycle, the pressure increased in the rostral end of the model then caudally. In the second part, the pressure decreased in the rostral end and then caudally. The pressure wave spread inwards from the subarachnoid space towards the central canal. The elastic properties of the spinal cord caused displacements up to 70 µm. In regions of high pressure the tissue is compressed and in region of low pressure the tissue is expanded. Interstitial fluid moved in the direction of lower pressure with velocities ranging from 0.1 to 0.5 µm/s. In the central canal the fluid velocities were several orders of magnitude higher reaching 100 to 200 µm/s.

Note: Scanned images are included in the proceedings. Some submitted images were reduced during editing, thereby decreasing clarity. Also, refer to the Program Planner. Proceedings Content as of 3-29-2013.

Conclusion
Pressure waves in the spinal subarachnoid space generate fluid flow in open segments of the central canal. The possible role of this fluid movement in the genesis of syrinx requires more study.

KEYWORDS: CSF flow, Syringohydromyelia, Poro-elasticity

O-131 **3:47 PM - 3:55 PM**

MR Myelography for Identification of Spinal Cerebrospinal Fluid Leak in Spontaneous Intracranial Hypotension

Chazen, J.·Dillon, W. P.
University of California San Francisco
San Francisco, CA.

Purpose
Spontaneous intracranial hypotension (SIH) is a debilitating disease characterized by low CSF pressure and symptoms of orthostatic headaches. Characteristic imaging findings have been described including diffuse pachymeningeal enhancement and sagging of the brainstem and cerebellar tonsils. Treatment requires precise localization of the site of CSF leak, commonly performed using CT, MR, or nuclear medicine myelography. This study aims to evaluate the benefits of MR myelography using intrathecal gadolinium in the localization of CSF leak.
Materials & Methods
A retrospective review of MR myelogram studies performed over the past five years at our institution. All patients had characteristic clinical and imaging findings for SIH including postural headaches and diffuse pachymeningeal enhancement. MR myelography was performed immediately following CT myelography in all patients using a mixture of 10 mL Omnipaque (iohexol 240 mg/mL) and 0.5 mL Magnevist (gadopentetate dimeglumine 469 mg/mL), instilled intrathecally by lumbar puncture. MR imaging was performed using axial, sagittal, and coronal T1-weighted sequences with fat saturation. Concurrent CT myelography also was performed.
Results
A total of 15 patients were identified from 2007-2012 that met inclusion criteria. All patients had SIH by clinical and imaging criteria and CT myelography performed with subsequent MR myelography. In nine of 15 patients (60%), no CSF leak was found on either CT or MR myelogram. In two of 15 patients (13%), a CSF leak was demonstrated on both CT and MR myelogram and in six of 15 patients (40%) a CSF leak was seen on MR myelogram.

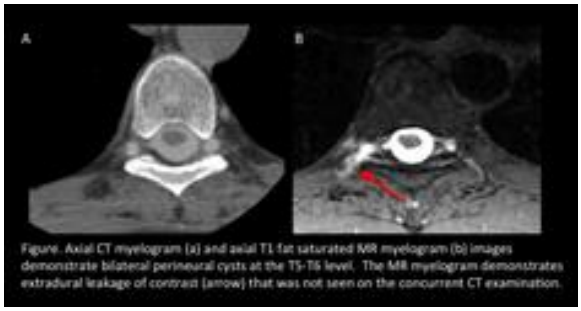

Figure. Axial CT myelogram (a) and axial T1 fat saturated MR myelogram (b) images demonstrate bilateral perineural cysts at the T5-T6 level. The MR myelogram demonstrates extradural leakage of contrast (arrow) that was not seen on the concurrent CT examination.

Conclusion
Our data suggests a significant benefit of MR myelography when investigating CSF leaks with four of 15 patients (27%) showing evidence of CSF leak only on the MR myelogram portion of the examination. These leaks often were subtle and benefitted from the high conspicuity and soft tissue contrast of fat-saturated T1 imaging. Though intrathecal administration remains an FDA off-label use of gadolinium, all patients in this cohort tolerated the medication well without complication. A possible confounding factor is the delayed nature of MR myelography in this cohort, which was performed following the CT portion of the examination, allowing additional time for contrast to diffuse into small leaks. Additionally, MR myelography is most useful in patients without obvious high flow leaks which may be better evaluated by dynamic CT or fluoroscopic myelography. Our data suggest MR myelography with intrathecal gadolinium is a well tolerated examination with significant benefit in the diagnosis of CSF leak.

KEYWORDS: Intracranial hypotension, MR imaging spine, MR myelography

O-132 **3:55 PM - 4:03 PM**

MR Imaging Identification of Anatomical Landmarks to Determine the Correct Thoracic Vertebral Level

Connor, S.·Lung, P.
Kings College Hospital
London, UNITED KINGDOM.

Purpose
Accurate definition of the correct thoracic vertebral level is important for diagnosis and subsequent therapeutic management. MR imaging studies of the thoracic spine occasionally are presented without a cervicothoracic vertebral level "counting scan" in which case localization of vertebral segments may be problematic. This scenario is particularly frequent in the setting of low field or open MRI scanners. Our aim was to describe the anatomical locations of identifiable adjacent bony and soft tissue structures on focused sagittal thoracic spine sequences, and assess their accuracy in estimating the correct thoracic vertebral level.
Materials & Methods
One hundred focused thoracic sagittal T1-weighted and

Note: Scanned images are included in the proceedings. Some submitted images were reduced during editing, thereby decreasing clarity. Also, refer to the Program Planner. Proceedings Content as of 3-29-2013.

T2-weighted MRI studies were analyzed retrospectively by two experienced radiologists. The bone and soft tissue landmarks (including the superior most rib, the aortic arch, the pulmonary trunk, the carina, the sternal notch and the morphology of the superior thoracic vertebrae and spinous processes) were extrapolated to the adjacent vertebral subsegment. The true thoracic vertebral level subsequently was determined and recorded by correlating with a sagittal cervicothoracic "counting scan". Interobserver reproducibility and accuracy of each anatomical landmark in determining a particular thoracic vertebral level was analyzed.

Results

The first rib was identified correctly as articulating with the T1 vertebral body in 98% and 97% of cases. The first long spinous process was identified as C7 in 62% and 80% of studies. The remaining anatomical landmarks produced results where the range was greater than four vertebral levels, localizing to a specific thoracic segment in only 26-71% of cases.

Conclusion

The superior most rib articulated with the T1 vertebral body and can be used as a reliable landmark on focused thoracic spine sagittal sequences for accurately localizing the thoracic vertebral levels in patients without a cervicothoracic "counting scan". Other anatomical landmarks produced inconsistent results and should not be used to define thoracic vertebral levels.

KEYWORDS: Anatomical variation, Spinal imaging

O-133 **4:03 PM - 4:11 PM**

Longitudinally Extensive Spinal Cord Lesions in African American Patients with Neuromyelitis Optica and Neuromyelitis Optica Spectrum Disorder

Mitchell, C. H.·Levy, M.·Pekcevik, Y.·Izbudak, I.
Johns Hopkins Hospital
Baltimore, MD.

Purpose

Neuromyelitis Optica (NMO) is a neuroinflammatory disease causing optic neuritis and transverse myelitis. The autoantibody to aquaporin-4 (NMO-IgG) is 91% specific and 73% sensitive for NMO. Previous examinations on Caucasian and Asian populations found distinctive longitudinally extensive spinal cord lesions (LESCL) in NMO patients by MRI. In Asian populations, there was an association between NMO-IgG positivity and LESCL. In the African American population, this relationship has not been established. The aim of this study is to describe the relationship of NMO-IgG serostatus with LESCL in African Americans.

Materials & Methods

Clinical data and MRIs of 73 consecutive patients with NMO or NMO spectrum disorder diagnosis were reviewed retrospectively with our institutional review boards approval. Longitudinally extensive spinal cord lesions were defined according to the criteria of Misu to involve three or more vertebral body segments on sagittal images with T2 hyperintensity, involvement of the central gray matter on axial images, T1 iso to hypointensity, and lack of contrast enhancement. Lack of contrast enhancement and T1 hypointensity were used to include NMO cases both in the acute and chronic phase.

Results

Of the 73 patients, 81% (59/73) were NMO-IgG positive, 86% (63/73) were female, and 60% (44/73) African American. Of the African American patients, 89% (39/44) had positive NMO-IgG, and 80% (20/25) of NMO-IgG positive African American patients had LESCL. Extension inferiorly from the medulla was seen in 20% (5/25) of the antibody positive African American LESCL patients.

Conclusion

Our study showed an association of LESCL with NMO-IgG positivity as in previous investigations. In the African American population, 80% of antibody positive patients had LESCL. Although we have a selection bias due to our center's patient demographics, our investigation is the first to document a possible susceptibility of the African American population to LESCL in NMO.

KEYWORDS: Neuromyelitis optica, Spinal cord, African American

Note: Scanned images are included in the proceedings. Some submitted images were reduced during editing, thereby decreasing clarity. Also, refer to the Program Planner. Proceedings Content as of 3-29-2013.

O-134 **4:11 PM - 4:19 PM**

Diagnosis of Spinal Drop Metastases on Initial Presentation of Pediatric Brain Tumor Patients Using 3D Volumetric Postcontrast Axial Imaging

Kralik, S. F.[1]·Kamer, A. P.[1]·O'Neill, D. P.[1]·Rodriguez, E.[2]·Ho, C. Y.[1]
[1]Indiana University, Indianapolis, IN, [2]Indiana University School of Medicine, Indianapolis, IN.

Purpose
The purpose of this research was to evaluate MRI with 3D volumetric axial postcontrast imaging in pediatric patients for initial presentation diagnosis of drop metastases from brain tumors. We assessed the effect of replacing standard axial postcontrast T1-weighted spin-echo (SE) with postcontrast axial 3D volumetric T1-weighted sequence with regard to radiologist agreement for presence of drop metastases, image quality, and number of lesions detected.
Materials & Methods
From 1/18/2010 to 1/24/2012, a total of 35 consecutive pediatric patients with a new diagnosis of a brain tumor underwent total spine imaging at 1.5T for evaluation for the presence or absence of drop metastases in the spine prior to therapy. A total of 15 patients were labeled as group 1 whose imaging included postcontrast sagittal and axial T1-weighted SE imaging of the total spine. A total of 20 patients were labeled as group 2 whose imaging included postcontrast sagittal T1-weighted SE imaging and axial 3D T1-weighted postcontrast VIBE (volumetric interpolated breath-hold) sequence replacing postcontrast axial SE. A retrospective independent blinded review of the total spine imaging in groups 1 and 2 was performed by two fellowship trained neuroradiologists (AK, DO). Kappa (K) values were calculated to determine statistical concordance of the diagnosis of drop metastases. Independent reviewer diagnosis was compared to final diagnosis from a dedicated pediatric neuroradiologist, CSF cytology if present, and follow-up imaging.
Results
No false negative MRI was seen in either group. After reviewing the axial postcontrast images for group 1, K-value increased to 0.55 (SD 0.21), which was a statistically significant increase (Student *t*-test p value = 0.01). After reviewing the axial postcontrast images for group 2, K-value increased to 0.70 (SD 0.19), which was a statistically significant increase (Student *t*-test p value = 0.0001). The best possible K-values for group 1 versus group 2 also was statistically significantly different (Student *t*-test p value = 0.03) indicating improved concordance from the use of axial 3D VIBE compared to SE. Image quality (scale 0-5, 5 = best) of the sagittal images for group 1 versus group 2 was not significantly different for the reviewers (*t*-test p value = 0.77). However, image quality of the axial images was significantly better for group 2 versus group 1 (*t*-test p value = 0.002). The number of cases in which the axial images increased the number of lesions detected was two of 15 (13%) cases for group 1 compared to eight of 20 (40%) cases for group 2.
Conclusion
Axial 3D volumetric T1-weighted VIBE postcontrast imaging can be used for a diagnosis of drop metastases on initial presentation of pediatric patients with brain tumors. Compared to routine postcontrast SE axial images, axial 3D T1-weighted postcontrast VIBE further improves concordance between radiologist for diagnosis of drop metastases, consistently demonstrates improved image quality, and increases number of lesions detected. These characteristics are considered an advantage of 3D volumetric imaging compared to routine spin-echo imaging for the diagnosis of drop metastases.

KEYWORDS: Leptomeningeal disease, Pediatric spine

O-135 **4:19 PM - 4:27 PM**

Screening and Detection of Blunt Vertebral Artery Injury in C1/C2 Fractures: Role of Cervical CT/CT Angiography

Payabvash, S.·McKinney, A. M.·Palmer, C.·Truwit, C. T.
University of Minnesota
Minneapolis, MN.

Purpose
Upper cervical spine fractures are associated with increased risk of blunt vertebral artery injury (BVAI), particularly in those with transverse foramen (TF) fracture or subluxations. The purpose of our study was to evaluate the clinical utility of nonenhanced CT (NE CT) and CTA in screening and detection of BVAI in patients with C1 and/or C2 fractures.
Materials & Methods
The imaging and clinical records of all blunt trauma patients who underwent cervical spine NE CT, over a five-year period (8/2006-9/2011) were reviewed retrospectively. All patients with C1 and/or C2 fractures were included in our study. Nonenhanced CT and CTA studies were performed with the 64-multislice Brilliance CT scanner (Philips Medical Systems, Best, Netherlands). Cervical CTA was prompted by cervical fractures involving/adjacent to TF, or with significant subluxation. All CTA studies were reviewed and the BVAI was graded by two neuroradiologists, independently. We determined the inter-rater agreement and independent predictor(s) of BVAI among different patterns of cervical fracture (i.e., concomitant C3-C7 fracture, transverse foraminal fracture, subluxation, condylar fracture, vertebral artery hypoplasia, and comminuted fracture).
Results
There were 210 patients with upper cervical fractures (125 involving C2, 48 involving C1, and 37 involving both C1 and C2). In interpretation of CTAs, there was very good interobserver agreement in detection (kappa=0.93 , $p<0.001$), and grading the BVAI (kappa 0.90 ± 0.05, $p<0001$). From our cohort, 22 patients underwent both CTA and digital subtraction angiography, which showed

Note: Scanned images are included in the proceedings. Some submitted images were reduced during editing, thereby decreasing clarity. Also, refer to the Program Planner. Proceedings Content as of 3-29-2013.

two false-positives for BVAI (one each of grade 1 and grade 2), and one false negative (grade 1). The presence of comminuted cervical fracture was the only independent predictor of BVAI (odds ratio = 3.0 (1.2 - 7.8), (p = 0.026). A clinical follow up of >seven days was available in 191/210 of all patients, and 114/124 who underwent CTA. Only three of 210 patients suffered a posterior circulation stroke. No patients suffered a symptomatic stroke who were negative for BVAI on CTA, or who were not evaluated for BVAI based on our radiologic screening criteria.

Conclusion
Multislice CTA reliably detects symptomatic BVAI in patients with upper cervical fractures or subluxations, although may occasionally miss low-grade, asymptomatic BVAI. Utilization of NE CT criteria (TF involvement or subluxation) may be adequate in deciding whether to perform CTA, as none of our patients who did not undergo CTA suffered a clinically symptomatic stroke.

KEYWORDS: Spinal trauma, CT angiogram, Posterior circulation stroke

O-136 **4:27 PM - 4:35 PM**

Marrow STIR Signal Underestimates Odontoid Fracture Acuity in Older Patients

Lensing, F. D.·Shah, L.·Wiggins, R.
University of Utah Health Sciences Center
Salt Lake City, UT.

Purpose
STIR hyperintensity is used routinely to assess for marrow edema to indicate an acute fracture. However, STIR may not accurately depict the acuity of a C2 fracture in older osteoporotic subjects. This may be explained by the intrinsic structural heterogeneity of the dens with reduced trabecular bone volume and decreased cortical thickness as well as histologic changes that occur with osteoporosis. The overall decreased bone mass reduction of the dens in osteoporotic patients with residual fat in the intertrabecular space may display diminished or absent edema on STIR images with acute injury. This is clinically relevant as there is high fracture nonunion, especially in older osteoporotic patients, when treated with external immobilization if there is delayed treatment. Furthermore, several series favor surgical fixation of C2 fractures in older patients, reporting better results when performed in the acute stage (< six months).
Materials & Methods
The RIS was queried for “C2 fracture,” “dens fracture” and “odontoid fracture” from 2007 to 2012. Those cases with both CT and MRI were included. Patient demographics were recorded. The odontoid fractures were categorized into the three types as initially described by Anderson and D’Alonzo. The images were evaluated for the presence of STIR hyperintensity in the bone marrow and fracture cleft. The angulation of the fracture fragments also was evaluated.
Results
In the study population meeting inclusion criteria, there were 24 females and 22 males with an average age 62.5 years. The odontoid fracture type distribution was 33 Type 2, 12 Type 3 and one Type 1. Though 50% of patients < 60 years old, demonstrated STIR hyperintense marrow signal, only 38% of patients < 60 years old had similar findings (Figure). A trend towards a negative correlation between age and STIR was seen in our group of patients. The average age of patients with a paucity of STIR signal (68.7 years +/- SD 21.6) was greater than that with STIR abnormality (54.4 years +/- 26.1). This age difference was found to be statistically significant (p<0.5).

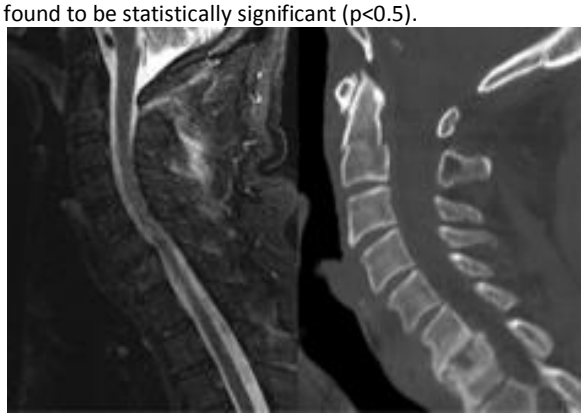

Conclusion
It is critical to be aware of this STIR MR pitfall when assessing the acuity of dens fractures. Patients older than 60 years, particularly with osteoporosis, can have acute odontoid injuries WITHOUT correlative hyperintensity on STIR imaging. Further weight should be placed on multidetector CT findings and clinical history in this setting.

KEYWORDS: Odontoid, MR imaging spine

Note: Scanned images are included in the proceedings. Some submitted images were reduced during editing, thereby decreasing clarity. Also, refer to the Program Planner. Proceedings Content as of 3-29-2013.

O-137 **4:35 PM - 4:43 PM**

Reliability of Diffusion Tensor Imaging Values in Spinal Cord Injury: Analytical Variations and Effects from Injury Severity

Zoltani, Z.[1]·Kamali, A.[2]·Zohrabian, V.[1]·Dresner, M. A.[3]·Gorniak, R. J. T.[1]·Flanders, A. E.[1]
[1]Thomas Jefferson University Hospital, Philadelphia, PA, [2]Cooper Medical Center, Camden, NJ, [3]Philips Medical Systems, Philadelphia, PA.

Purpose
Diffusion tensor imaging (DTI) has potential to improve clinical accuracy in assessing initial neurologic deficit and forecast potential for recovery after spinal cord injury (SCI). Uniformity in the analysis of quantitative DTI data presents a unique challenge in that absolute values of DTI metrics vary considerably in the literature. This calls into question the reliability and reproducibility of spinal cord DTI metrics between studies. Prior studies often incorporate a single measure of DTI values. There are multiple methodologies for analyzing DTI datasets, some of which utilize proprietary algorithms. The purpose of this study was to assess reproducibility of quantitative DTI results when identical datasets are analyzed by two different DTI postprocessing methods and to assess whether the DTI values are potentially less reliable in areas of injury.
Materials & Methods
Twenty-three cervical SCI patients were evaluated on a 1.5T MR (Philips Achieva) within 24 hours of injury. Standard anatomical axial/sagittal SE T1, T2 and GE imaging was performed. Diffusion tensor imaging of the entire cervical spinal cord was performed using 4 mm axial single-shot SE EPI technique (TR/TE: 2500/75 msec; 6 directions; B-value: 800; FOV 20 cm; 8 NEX; scan time: 3:40). Two observers independently traced whole cord regions of interest (ROIs) around a total of 614 discrete axial DTI spinal cord images for each patient using a commercial analytical package (FiberTrak - Philips Medical) and a popular open source toolkit (DTI Studio - Johns Hopkins University). Fractional anisotropy (FA) and apparent diffusion coefficient (ADC) were recorded. Interobserver agreement between ADC and FA values for the two observers was calculated by using Pearson and intraclass correlation coefficients (ICC) while controlling for the patient's American Spinal Injury Association (ASIA) grade and presence/absence of anatomical injury on T2-weighted images.
Results
Distribution of injuries for the 23 patients included ASIA, A (9), B (4), C (4), D (2), unknown (2). Range in FA and ADC values reported were 0.3-0.91 and 0.05-2.2. Overall observer agreement for FA measures was low (0.35, <0.001) but substantially better for ADC measures (0.68, p<0.001). Agreement for values obtained within or outside region of visible injury was similar for FA at 0.34 (p<0.001) whereas agreement for ADC was better in normal-appearing spinal cord (0.77, p<0.001) compared to injured spinal cord (0.63, p<0.001). Agreement for FA measures stratified by ASIA grades were: A:(0.246), B:(0.203), C:(0.23), D:(0.49) and for ADC they were: A:(0.51), B:(0.74), C:(0.76), D:(0.54).
Conclusion
Defining absolute thresholds for DTI parameters in characterizing spinal cord injury may prove difficult because of inherent variations in acquisition, analytical methods and interobserver factors. Relative values may prove more effective to correct for some of these variations. In this regard, minimizing variability introduced through analysis is likely best achieved by central review using a single algorithm.

KEYWORDS: DTI, Cervical spinal cord

Monday Afternoon

3:15 PM - 4:45 PM
Room 1AB

(13e) Parallel Scientific Papers: Epilepsy: Adult and Pediatric

O-139 **3:15 PM - 3:23 PM**

Altered Structural Connectivity in Mesial Temporal Lobe Epilepsy

DeSalvo, M.·Douw, L.·Tanaka, N.·Reinsberger, C.·Stufflebeam, S.
Athinoula A. Martinos Center for Biomedical Imaging Charlestown, MA.

Purpose
Although mesial temporal lobe epilepsy (mTLE) has been theorized to relate to isolated injury of mesiotemporal structures, recent studies have revealed widespread cortical atrophy involving both temporal and extratemporal areas, leading to the concept of mTLE as a "network disease". The default mode network (DMN) consistently has been found to be affected by mTLE in studies of structural and functional connectivity. To our knowledge, this study is the first to use graph theory to compare whole-brain structural connectivity between patients with mTLE and healthy controls using diffusion tensor imaging (DTI) without selecting a priori seed regions or inspecting the results of independent component analysis (ICA).
Materials & Methods
Data were analyzed from 23 patients with left mTLE and 23 healthy controls. MR imaging volumes were segmented into 1000 regions of interest (ROIs) spanning the entire cortex. Whole-brain white matter tractography was performed after voxel-wise tensor calculation. Structural

Note: Scanned images are included in the proceedings. Some submitted images were reduced during editing, thereby decreasing clarity. Also, refer to the Program Planner. Proceedings Content as of 3-29-2013.

connectivity matrices were generated using the pairwise density of connecting fibers between ROIs. Graph theoretical measures were calculated from these matrices and compared using two-sample t-tests.

Results

In patients with mTLE, increased connectivity was observed involving ipsilateral temporal and bilateral precuneus and posterior cingulate cortices, while decreased connectivity was observed among ipsilateral frontal areas (Figure 1). Although network modularity was not significantly different between groups, global efficiency was increased in the setting of mTLE ($p<0.001$). Local clustering and efficiency also were increased in ipsilateral temporoparietal and cingulate cortices($p<0.05$). Modularity analysis showed that the precuneus had a lower within-module z-score of degree ($p<0.05$) but higher participation coefficient ($p<0.05$) in the setting of mTLE.

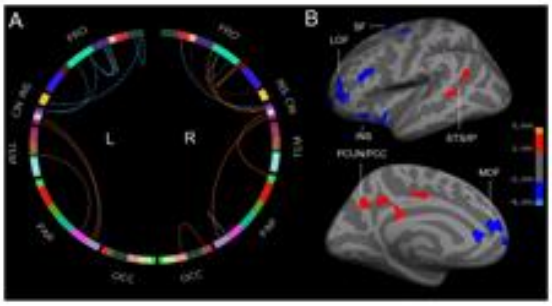

Conclusion

We observed global and local alterations in structural networks of mTLE patients. Increased clustering and efficiency within the ipsilateral temporal lobe suggests increased interconnectedness likely related to aberrant self-reinforcing connectivity due to epileptic activity. In contrast to prior studies, our analysis showed increased structural connectivity between bilateral precuneus and posterior cingulate cortices, which are hub areas within the DMN. Our modularity analysis suggests that posterior DMN areas are connected less densely within the DMN while simultaneously more connected to other modules in mTLE. Similar to prior studies, we found decreased structural connectivity in ipsilateral frontal areas, which may relate to disrupted connectivity in posterior DMN areas. This altered pattern of long-range connectivity may underlie propagation of epileptiform activity that may reinforce an altered mTLE network. This also may lead to distant effects such as cortical thinning in the DMN.

KEYWORDS: DTI tractography, Default mode network, Temporal Lobe Epilepsy

O-140 **3:23 PM - 3:31 PM**

7T MR Imaging of Nonlesional Mesial Temporal Lobe Epilepsy: Comparison to Volumetric Analysis and Clinical MR Imaging

Lin, D.·Trinh, H.·Ratnanather, T.·Bergey, G.·Barker, P.
Johns Hopkins University
Baltimore, MD.

Purpose

MR imaging at 7T offers higher spatial resolution and therefore more detailed depiction of the hippocampus compared to lower field strengths. The purposes of this study were (a) to prospectively evaluate the utility of 7T MRI in patients with mesial temporal lobe epilepsy (mTLE) compared to conventional, lower field MRI, and (b) to compare the results of visual interpretation with quantitative hippocampal volumetrics.

Materials & Methods

Ten surgical candidates with clinically diagnosed mTLE were scanned at 7T (Philips, Best, the Netherlands) using a 32-channel head coil, including high-resolution isotropic 3D MPRAGE whole-brain coverage obtained at 0.6 mm, and coronal T2-weighted images of the temporal lobes. On each scan the mesial temporal structures were evaluated specifically by an attending neuroradiologist for side of abnormality (classified as neither, left, right, or both), and the results were compared with semi-automated analysis of hippocampal volume, as well as findings from routine clinical MRI (1.5T or 3T) and the final clinical diagnosis (a combination of video EEG, intracranial EEG, clinical MRI, PET and histopathology). Kappa (κ) statistics were used to assess concordance between tests.

Results

7T offers superb high-resolution images of the hippocampi, with clear delineation of the CA fields particularly on the T2-weighted images (Figure). There is, however, limited evaluation of the anterior and lateral cortical regions of the temporal lobe related to image blurring and susceptibility artifacts. Neuroradiologic evaluation of combined T1 and T2 7T images showed a good concordance with T1 alone ($\kappa = 0.783$), volumetrics ($\kappa = 0.783$), clinical MRI ($\kappa = 0.600$) and clinical diagnosis ($\kappa = 0.677$). There was a very good concordance between volumetric data and T1 alone at 7T (8 of 10 cases; $\kappa = 0.8$), with hippocampal volume difference ranging from 1.3% to 53.5%. 7T MRI correctly lateralized 7 out of 10 cases based on T1 images, and 8 out of 10 when information from T2 was added; one of the 2 misdiagnosed cases had bilateral involvement based on clinical data. In contrast, clinical MRI had a lower accuracy rate in 6 of 10 cases. A very good concordance was also found between 7T volumetric results and lower field clinical MRI ($\kappa = 0.8$).

Conclusion

Temporal lobe imaging at 7T offers improved spatial resolution and anatomical delineation of hippocampal structures, potentially aiding the presurgical lateralization of epileptic focus with greater accuracy compared to

Note: Scanned images are included in the proceedings. Some submitted images were reduced during editing, thereby decreasing clarity. Also, refer to the Program Planner. Proceedings Content as of 3-29-2013.

clinical MRI performed at 1.5T or 3T. Further study with a larger patient cohort is warranted.

KEYWORDS: 7T, Epilepsy

O-141 **3:31 PM - 3:39 PM**

High-Resolution 7T MR Imaging in the Evaluation of Patients with Intractable Epilepsy

Barker, P. B.·Trinh, H.·Zhu, H.·Ratnanather, T.·Lin, D.·Bergey, G.
Johns Hopkins University
Baltimore, MD.

Purpose
To investigate the use of high-resolution 7T volumetric MRI for identifying lateralized hippocampal abnormalities in patients with drug-resistant partial seizures originating from mesial temporal structures.
Materials & Methods
Seventeen patients with medically intractable epilepsy (10 M, 32 ± 12 years) and nine normal control subjects (6 M, 36 ± 10 years) were recruited. All subjects underwent a 7T MR exam using a 32-channel head coil (Philips, Best, The Netherlands). The protocol included T1-weighted 3D MP-RAGE (0.6 mm isotropic resolution, 300 slices, TI 446 ms, SENSE factor 4) and a coronal multi-slice reduced flip angle FSE T2-weighted sequence (0.5 mm in-plane, 1 mm slice thickness, 40 slices, TR/TE 5000/56 ms, SENSE factor 2). Volumetric images were resliced in orthogonal views and hippocampal volumes determined by manual segmentation. Final diagnosis was based on surface and invasive EEG, clinical evaluation and (when available) pathology.
Results
Of the 17 patients, 11 had clinically defined mesial temporal lobe epilepsy (mTLE), while six had either neocortical or extratemporal epilepsy. Of the patients with mTLE, eight had abnormalities that could be detected in conventional 3T MRI scans. An example of a 7T coronal T2-weighted image in a control subject is shown in Figure 1. In the control group, mean hippocampal volume was 3.52 +/- 0.15 mL, and asymmetry ranged from +5.2% to -7.8%. Patient asymmetries ranged from +42.5% to -53.5%. 7T volumetric measurements correctly lateralized eight of 11 mTLE cases, including two cases with normal 3T MRI scans. Mean hippocampal volumes were significantly smaller than controls in the 3T abnormal MTLE patients (2.54 ± 0.78 ml, P<0.01, ANOVA/Dunnett multiple comparison correction), and showed a trend for reductions in the neocortical/extra-temporal cases (3.08 ± 0.24 ml, P>0.05).

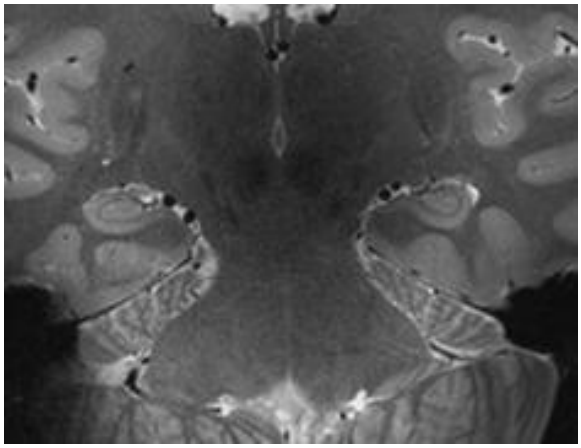

Conclusion
Quantitative, high-resolution, volumetric 7T MRI shows promise in the presurgical evaluation of patients with intractable epilepsy, and may provide lateralizing information in some cases with normal clinical 3T MRI.

KEYWORDS: 7T, Epilepsy

O-142 **3:39 PM - 3:47 PM**

Dark Side of Seizures: Radiologic Clinical Correlation of Negative T2 Shine-Through in Seizure

Chu, E.·Hasso, A.·Handwerker, J.
University of California, Irvine Medical Center
Orange, CA.

Purpose
The magnetic resonance imaging (MRI) phenomenon of “negative T2 shine-through” or "T2 dark-through” refers to lesions that are hypointense on T2-weighted sequences and apparent diffusion coefficient (ADC) maps. It is a rare and often overlooked finding that has been described infrequently in cases of ischemia, hematoma, meningoencephalitis, malignancy, Sturge-Weber, and seizures. The goal of this study is to investigate the significance of this finding in the setting of seizure.
Materials & Methods
We retrospectively reviewed 11 patients whose MRI scans demonstrated “T2 dark-through” that was associated with seizure. Correlation was made with advanced MRI sequences including susceptibility-weighted imaging (SWI), arterial spin labeling (ASL), and perfusion imaging. Correlation was made with their clinical course, laboratory testing, and when available, ancillary testing such as positron emission tomography (PET) and electroencephalography (EEG).
Results
Eleven patients between the ages of three months and 82 years exhibited negative T2 shine-through in the setting of seizure. Three patients were significantly hyperglycemic at the time of their seizures with blood glucose levels ranging from 414 to 505 mg/dL. Three patients had an intracranial

Note: Scanned images are included in the proceedings. Some submitted images were reduced during editing, thereby decreasing clarity. Also, refer to the Program Planner. Proceedings Content as of 3-29-2013.

infectious/inflammatory process. Two patients had an underlying congenital disorder, including Sturge-Weber. Two patients seized in the setting of subdural hematomas. The regions of negative T2 shine-through correlated to hypointensity on SWI, hyperperfusion on ASL imaging, hypermetabolic activity on PET scan, and epileptic activity on EEG. Follow-up imaging showed resolution of the negative T2 shine-through.

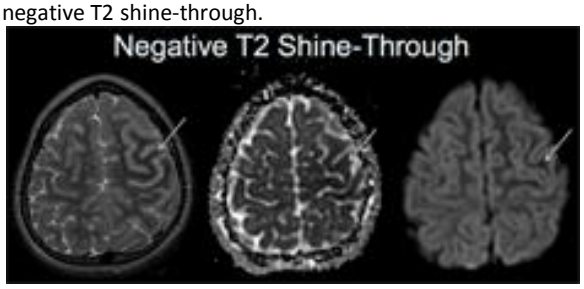

Conclusion
Negative T2 shine-through is a rare transient MRI finding in the setting of seizure that correlates to regions of hyperperfusion, hypermetabolic activity, and epileptic activity in the brain. It was observed in patients with superimposed intracranial processes, such as metabolic disturbances, meningoencephalitis, congenital disorders, and hematomas. This finding may relate to transient ischemia and increased oxygen consumption, especially as it was observed in areas of the brain that may be more metabolically active. Overall, negative T2 shine-through is an under-recognized yet promising finding with associated clinical correlations in the setting of seizure. Continued investigation and followup of this finding could help facilitate diagnosis and management of these patients.

KEYWORDS: Seizure, Restricted diffusion, Negative T2 shine-through, T2 dark-through

O-143 **3:47 PM - 3:55 PM**

Relationship of Brain MR Imaging Findings with Postsurgical Epilepsy Outcome in Children with Malformations of Cortical Development

Kadom, N.·Bansal, S.·Jubouri, S.·Prola Netto, J.·Tryggestad-Codispoti, K.·Gaillard, W. D.
Children's National Medical Center
Washington, DC.

Purpose
To determine if brain MRI variables predict epilepsy outcome after surgical removal of pediatric malformations of cortical development (MCD).
Materials & Methods
Retrospective study, IRB approved. Patients identified from internal epilepsy database. Inclusion criteria: pre-operative brain MRI, availability of surgical pathology. Observers: Five observers: A = pediatric neuroradiologist, B = neuroradiologist, C = radiologist, D = pediatric neurologist, E = neuropathologist. Image analysis performed on GE workstation, Functool. Regions of interest were placed manually by two observers independently. For quantitative analysis (FA, ADC) two ROI locations were placed per patient, one in the normal-appearing white matter closest to the MCD and one in symmetrical position in the contralateral hemisphere. For tractography two ROI locations were placed per patient, one directly over the MCD and one in symmetrical position in the contralateral hemisphere. Statistical analysis with Stata v12.1: Outcome variable was postsurgical state of epilepsy (based on Engel classification): Engel 1) seizure free, Engel 2) rare seizures, Engel 3) worthwhile improvement, and Engel 4) no worthwhile improvement. Predictor variables: quantitative DTI analysis (FA, ADC), conventional MRI signs (bright signal on T2/FLAIR/T1 magnetization transfer, cortical blurring, cortical thickening, radial line), MRI signal patterns (signal variable concatenations), qualitative analysis of fiber tracts (symmetry, color hues), clinical data, pathology data.
Results
We analyzed 29 patients, 16 boys and 13 girls. Mean age at onset of epilepsy, 2.5 years; mean age at surgery, 7.7 years. Postsurgically 12 patients were Engel 1; seven Engel 2; six Engel 3; four Engel 4. All Engel 4 patients had lesions in the left hemisphere, (temporal and extratemporal). All patients had architectural distortion: 17 patients had isolated architectural distortion; there were added dysmorphic cells in two; added dysmorphic cells and balloon cells in five, and added microgyria in five. There was better outcome for patients with T2 bright lesions (χ^2, $p = 0.05$). There was higher FA on the abnormal brain side when compared to the normal side (Wilcoxon signed-rank test, $p = 0.03$), especially in the subgroup with seizure free postsurgical outcome (Wilcoxon signed-rank test, $p = 0.002$). Apparent diffusion coefficient was statistically significantly lower on the abnormal side in the seizure free patient subgroup (Wilcoxon signed-rank test, $p = 0.03$).
Conclusion
Lesions with bright signal on T2 are associated with better postsurgical outcome. Left hemispheric lesions are associated with unfavorable postsurgical outcome, maybe due to less aggressive surgical approach to preserve eloquent cortex. Fractional anisotropy and ADC values from normal-appearing white matter in patients who are seizure-free after surgery showed significant differences between the abnormal and normal side of the brain. We did not find a relationship between MRI signal and pathology findings. MR imaging patterns were not related to postsurgical epilepsy outcomes (Engel). Combination of multiple MRI signal features into patterns did not improve statistical relationships compared to using only bright signal on T2 imaging.

KEYWORDS: Epilepsy, DTI, MR imaging

Note: Scanned images are included in the proceedings. Some submitted images were reduced during editing, thereby decreasing clarity. Also, refer to the Program Planner. Proceedings Content as of 3-29-2013.

O-144 **3:55 PM - 4:03 PM**

MR Imaging Abnormalities in the Resection Region Correlate with Histopathologic Grade, Gliosis Extent, and Postoperative Outcome in Pediatric Cortical Dysplasia

Henkel, D.·Leach, J. L.·Miles, L.·Greiner, H.·Komlos-Kukreja, M.·Holland-Bouley, K.·Zhang, B.·Mangano, F.
Cincinnati Children's Hospital Medical Center
Cincinnati, OH.

Purpose
Cortical dysplasia (CD) is the most common pathology in children with intractable epilepsy. Recent classification schemes have demonstrated differences in clinical behavior, imaging, and outcomes amongst subtypes, mostly in adults. The pathologic basis for imaging findings and how imaging correlates with outcome has been evaluated incompletely in children.
Materials & Methods
Forty-three children with intractable neocortical epilepsy, high quality MR imaging, and CD formed the study cohort. Exclusions included: prior surgery, CD and destructive lesions/tumors, type IIIA CD (HS and adjacent CD), < 6m FU, or age >21 years. Dedicated seizure protocol MRI (3T-37, 1.5T-6) was performed. Image review was blinded to pathology but with knowledge of resection location determined by simultaneously reviewing: postoperative imaging, images of the operative field, grid locations, and operative notes. Each region was evaluated for: abnormal gyral pattern, WM signal, GM signal, cortical thickening, blurred cortical junction, "transmantle" signal, and volume loss. A "MRI score" was calculated for each region (0-7). The resection region was classified as “lesional” (a localized surgical target) or “nonlesional” based upon all imaging features. Neuropathology was reviewed according to 2011 ILAE classification. Cortical gliosis was classified as superficial (sG),or diffuse (dG, involving all layers). Outcome was based on the ILAE scale with 1-3 considered good outcome.
Results
There were 23 males, mean age: 10.2 years (6 months-19 years) and 89 resection regions. There were 50 type I CD, 29 type IIA CD, and 10 type IIB CD. Eleven of 43 (25.6%) had $\geq$2 types of CD. Eighty-four percent (32/38) type II CD versus 18% (8/44) with type I CD, exhibited dG ($p<0.0001$). Lesional findings were significantly more prevalent with type II (51%) versus type I (12%) CD. MR score $\geq$3 was significantly more prevalent in type II versus type I; types IIB versus type I, and type IIB versus type IIA CD. All MR features except localized volume loss, were more common in type II versus type I CD. Only GM signal was more common in type IIB (70%) versus type IIA (17.2%) CD ($p=0.004$). dG was more common in regions that were lesional, MR score $\geq$3, and with all MR features except volume loss. WM signal was most significantly associated with dG. Outcome correlated with CD subtype with 39% of type I CD and 72% of type II CD (100% IIB, 61% IIA), exhibiting good outcome ($p=0.03$). The presence of a lesional MRI abnormality or MR score >3 correlated with good outcome in 78% and 90% of patients respectively ($p<0.03$).
Conclusion
This study provides a detailed correlation between MRI, neuropathology, and outcomes in children with intractable epilepsy using a novel resection site specific evaluation in a large surgical group. Twenty-five percent of our patients had different CD types in different regions mandating a regional analysis approach for imaging pathology correlation in these patients. MR imaging abnormalities and Type II pathology correlated with better outcomes. Type II CD is more detectable by MR and is associated with dG. Improved imaging techniques for detecting CD in children are needed.

KEYWORDS: Cortical dysplasia, MR imaging

O-145 **4:03 PM - 4:11 PM**

Abnormal White Matter Tracts Are Anatomically Related to Reduced Cortical Thickness in Children with Frontal Lobe Epilepsy

Widjaja, E.·Kis, A.·Go, C.·Snead, O.·Smith, M.
Hospital for Sick Children
Toronto, ON, CANADA.

Purpose
Previous research has demonstrated widespread reduction in cortical thickness in children with frontal lobe epilepsy (FLE), which may be related to spread of seizures through the white matter (WM) tracts. The aim of the current study was to assess WM integrity in children with FLE and to evaluate the relation between abnormal WM tracts and cortical thickness.
Materials & Methods
Forty-three children with FLE and normal MRI, and 44 healthy controls were recruited. Twenty-eight patients had left FLE and 15 had right FLE. High-resolution volumetric T1-weighted imaging and diffusion tensor imaging (DTI) were performed in all patients and controls. Whole brain DTI analysis was compared between right and left FLE with controls. Regions of abnormal fractional anisotropy (FA) were used as starting seed for probabilistic tractography. Whole brain cortical thickness was compared between FLE groups and controls. Fractional anisotropy of abnormal tracts was correlated with regions of cortical thickness.
Results
Patients with left FLE had significant FA reductions in left and right superior longitudinal fasciculi (SLF), genu/body and splenium of corpus callosum compared to controls. Patients with right FLE had significant FA reductions in left and right SLF, genu and body of corpus callosum compared to controls. In left FLE, tractography of left SLF overlapped with left precentral, insula, superior temporal, bank of superior temporal sulcus and postcentral reduced cortical thickness; tractography of right SLF overlapped with right supramarginal, superior temporal, middle frontal and

Note: Scanned images are included in the proceedings. Some submitted images were reduced during editing, thereby decreasing clarity. Also, refer to the Program Planner. Proceedings Content as of 3-29-2013.

insula reduced cortical thickness; tractography of genu/body of corpus callosum overlapped with left and right superior frontal and right frontal pole reduced cortical thickness, and splenium of corpus callosum overlapped with left pericalcarine and right precuneus reduced cortical thickness. There was a trend for positive correlation between FA of right SLF with right supramarginal (r= 0.453, p = 0.015) and right insula (r = 0.416, p = 0.028) cortical thickness in left FLE patients. In right FLE, tractography of right SLF overlapped with right insula, postcentral, parstriangularis and superior parietal reduced cortical thickness; tractography of left SLF overlapped with left superior frontal, parsopercularis, superior parietal, precentral, postcentral, supramarginal, superior temporal and insula reduced cortical thickness; tractography of genu of corpus callosum overlapped with left superior frontal and left medial orbitofrontal reduced cortical thickness, and body of corpus callosum overlapped with left superior frontal and left paracentral reduced cortical thickness. There was no significant correlation between FA of WM tracts and regions of reduced cortical thickness in right FLE patients.
Conclusion
We have found abnormal WM both ipsilateral and contralateral to seizure focus in children with FLE. Tractography of abnormal WM demonstrated an anatomical connectivity with regions of reduced cortical thickness, suggesting that spread of seizures through the association tracts beyond the frontal lobes and via the corpus callosum to the contralateral hemisphere may have contributed to widespread reduced cortical thickness.

KEYWORDS: Epilepsy, Diffusion tensor image

O-146 **4:11 PM - 4:19 PM**

Features of Focal Cortical Dysplasias on 7T MR Imaging

Mehan, W. A.·Stemmer-Rachamimov, A.·Ratai, E.·Stufflebeam, S. M.·Caruso, P. A.
The Massachusetts General Hospital
Boston, MA.

Purpose
Malformations of cortical development (MCDs) including focal cortical dysplasias (FCDs) are estimated to cause 40% of cases of medically refractory epilepsy (Guerrini et al., Epileptic Disord 2003); however, MRI at 1.5 and 3T are only 76% sensitive and 53% specific for the characterization of the irritative zone in focal epilepsy (Brodbeck V. Brain 2011) and thus attention has turned to higher field MRI techniques to increase the diagnostic yield of the imaging evaluation. Our goal was to review our experience with pathology proven FCDs imaged preoperatively at 7T in order to determine if there are imaging features specific to 7T imaging that correlate with histopathologic findings.
Materials & Methods
A retrospective review was performed on a series of four patients with medically refractory epilepsy who underwent pre-operative 7T MR imaging between August 2008 to November 2010. Each of the four patients subsequently had surgical resection demonstrating pathology proven FCDs. The MR imaging was performed on a Seimens 7T research magnet; spoiled gradient recalled echo (SPGR), axial and coronal T2, and SWI sequences were performed in each case. Two board certified neuroradiologists and two board certified neuropathologists correlated the 7T MR images of the FCDs with the histopathologic findings together.
Results
The four patients included in the review had a mean age of 23.5 years (range 17 to 38 years). Each patient underwent epilepsy surgery demonstrating pathology-proven focal cortical dysplasia (FCD). Unique 7T imaging features of FCDs included: -linear signal isointense to gray matter that appeared to be arrayed from the cortex toward the subcortical white matter and that corresponded to lines of heterotopic neurons defined histopathologically, -a low signal arcade identified in normal cortex that appeared to be disrupted in dysplastic cortex and that correlated best with the cortical capillary network, and -prominent vessels seen best on SWI, oriented perpendicular to the dysplastic cortex.
Features of FCDs described at 1.5 and 3T such as abnormally thick cortex and blurring of the gray-white matter junction were redemonstrated.
Conclusion
We correlated the 7T MR imaging features of FCDs with histopathology in a series of four patients who underwent surgical resection of pathology proven FCDs, and demonstrated several imaging features of FCDs that we believe to be unique to 7T imaging.

KEYWORDS: 7T, Malformation of cortical

O-147 **4:19 PM - 4:27 PM**

Diffusion Tensor Imaging to Confirm Commissural Disconnection after Corpus Callosotomy

Choudhri, A. F.[1,2]·Whitehead, M. T.[1,2]·McGreggor, A.[1,2]·Einhaus, S.[1,2]·Boop, F. A.[1,2]·Wheless, J. W.[1,2]
[1]University of Tennessee Health Science Center, Memphis, TN, [2]Le Bonheur Children's Hospital, Memphis, TN.

Purpose
Corpus callosum transection can prevent propagation of epileptic discharges; however the procedure can be difficult to perform due to adjacent vasculature and the deep location of the corpus. If seizures persist after surgery, assessment of the efficacy of the transection requires knowledge that the commissural fibers have been disrupted. We evaluated whether diffusion tensor imaging (DTI) and diffusion tensor fiber tracking (DT FT) can assess the degree of callosal transection and determine which white matter pathways remain intact.
Materials & Methods

Note: Scanned images are included in the proceedings. Some submitted images were reduced during editing, thereby decreasing clarity. Also, refer to the Program Planner. Proceedings Content as of 3-29-2013.

Twenty-five patients (15 M, 10 F; age 12.3 ± 7.1 years, range 0.24 to 32.8 years) who underwent prior corpus callosotomy were evaluated with DT FT performed using deterministic and probabilistic techniques. Diffusion tensor imaging was obtained in the axial plane using 15 directions of encoding (n = 18) and 25 directions of encoding (n = 7), with additional coronal plane 25 direction DTI performed in 12 patients. Twelve patients had undergone complete callosal transection, nine patients had partial callosal transection with preservation of the splenium (n = 2) and the splenium and isthmus (n = 5), and four patients had functional hemispherectomies including complete callosal transection. DTI, DT FT, and conventional structural MR imaging were reviewed by two neuroradiologists.

Results

Of patients undergoing complete callosal transection, 17 patients had structural and DT FT evidence of complete transection, and one patient had a small quantity of intact forceps minor fibers within the rostrum on DT FT with transection of the remainder of the corpus callosum. In patients undergoing partial transection, the forceps major was intact in all patients. At least some perirolandic commissural fibers were intact in six of six partial transections where there was sparing of the callosal isthmus.

Conclusion

Diffusion tensor imaging and DT FT aid in the postoperative characterization in patients with callosal transection for seizure control. This can confirm whether the intended fibers have been disconnected, helping planning for possible further surgical intervention versus additional medical therapy.

KEYWORDS: Corpus callosum, DTI tractography, Epilepsy

O-148 **4:27 PM - 4:35 PM**

Minimally Invasive MR Imaging-Guided Stereotactic Laser Thermal Ablation Technique in Neurosurgical Cases; Our Initial Experience

Medina, L.·Chamiraju, P.·Bhatia, S.·Ragheb, J.·Altman, N.·Miller, I.·Pacheco, E.
Miami Children's Hospital
Miami, FL.

Purpose

We present our preliminary experience on nine patients with brain lesions treated with stereotactic placement of laser probe and thermal ablation under MRI guidance.

Materials & Methods

Patient with focal brain lesion on MRI measuring less than 10 centimeters in long axis were selected for the study. Method is FDA approved. Stereotatic placement of the laser probe was done using 3D image guidance. Laser thermal coagulation was performed under continuous MRI guidance. Real time MR thermal images allowed live evaluation of target temperature (50-90^{o}C) and protect surrounding tissues (under 40^{o}C).

Results

Nine patients were enrolled with an age range of 4-20 years. Six patients had cortical dysplasia, one ganglioglioma, one tuberous sclerosis and one recurrent ependymoma. Mean followup was 8.3 months (range 2-16 months).The lesion after ablation showed low T2-weighted signal consistent with protein denaturalization from thermal ablation and halo of surrounding restricted diffusion due to ischemia/infarction. All patients developed perilesional edema after ablation which subsided over few weeks with steroids. Immediate postprocedure headache was seen in nine patients although less than expected in craniotomy patients. Expected unavoidable neurologic deficit was seen in one patient. No other neurologic deficits were seen. In short-term followup, six patients had an improvement in the clinical findings, one required a second ablation for residual lesion with subsequent improvement, two had stable seizures and one had worsening seizures even after ablation.

Conclusion

Minimally invasive laser thermal ablation under MRI guidance can be safely used in a specific group of lesional neurosurgical patients and may be an adequate alternative to open resection. A larger number of patients will need to be studied and long-term followup required before we gauge the adequacy of using laser thermal ablation.

KEYWORDS: Neoplasm

O-149 **4:35 PM - 4:43 PM**

Comparison of an Accelerated 3D Spiral Chemical Shifting Imaging and Single Voxel Spectroscopy at 3T in the Pediatric Age Group

Yazbek, S.·Prabhu, S. P.·Connaughton, P.·Grant, P. E.·Gagoski, B.
Boston Children's Hospital, Harvard Medical School
Boston, MA.

Purpose

With ~20 minutes acquisition times for 3D phase-encoded (PE) chemical shift imaging (CSI) clinically impractical, single voxel spectroscopy (SVS) remains the clinical “workhorse”. However, with no standardized single voxel location to enable comparison to normal data and with lack of spatial coverage limiting ability to assess for regional changes, the tremendous clinical potential of spectroscopy remains unrealized. To overcome lack of efficiency of 3D PE CSI and lack of spatial coverage of SVS, efficient encoding schemes using spiral k-space trajectories have been deployed successfully, enabling acquisition of volumetric CSI in < five minutes. Our aim is to assess feasibility of using 3D spiral CSI routinely in pediatric clinical settings by comparing its reconstructed spectra against SVS spectra.

Materials & Methods

Note: Scanned images are included in the proceedings. Some submitted images were reduced during editing, thereby decreasing clarity. Also, refer to the Program Planner. Proceedings Content as of 3-29-2013.

All experiments were performed on 3T Siemens scanners, using a 32-channel coil. Volumetric spiral CSI obtained spectra from 2cc isotropic voxels. LASER-box excitation was placed entirely within the brain to avoid lipid contamination from the skull. No outer volume suppression bands were used. Acquisition covered bilateral basal ganglia and parieto-occipital white matter. Chemical shift selected pulses were used for water suppression. Acquisition time was *3 minutes* (TR=1.8s, TE=30ms, 3 averages). Single voxel spectroscopy acquisition encoded a 3.4cc (1.5mm isotropic) voxel using conventional PRESS-box excitation, with voxel placement in the left basal ganglia. Acquisition time was *3 minutes* (TR=1.8s, TE=3 ms, averages=100). Higher order shimming was done automatically for all acquisitions. Data was gathered prospectively from 10 random patients presenting for brain MRI. Spectra from left basal ganglia obtained using both techniques were processed with Siemens postprocessing software. Following metabolite ratios were calculated: NAA/Cr, Cho/Cr, Lac/Cr.

Results

The study included seven boys and three girls aged between four days and 10 years. In 9/10 cases, spectral quality of both methods was acceptable. In one case, the SVS spectrum had artifacts due to suboptimal shimming. Considering nine of 10 cases, the *mean ± standard deviation* of the normalized metabolite ratio differences were: NAA/Cr-13.1%±10%, Cho/Cr-17.5%±3.2% and NAA/Cho-17.3%±9.4%. In one subject where lactate peak was detected, Lac/Cr ratios were identical.

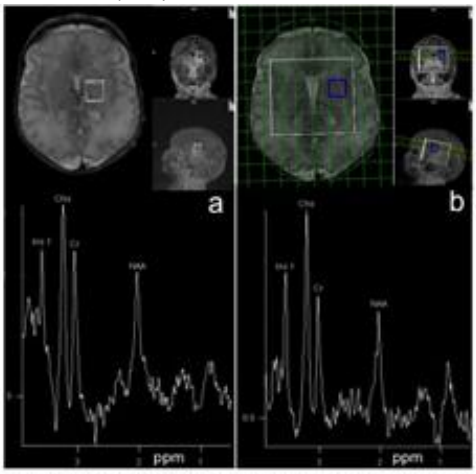

Figure 1. (a) SVS in the left basal ganglia; (b) Spiral CSI spectrum in the left basal ganglia; Also seen is the 3D coverage of spiral CSI

Conclusion

Accelerated 3D CSI is feasible in pediatric patients and can potentially substitute for SVS. 3D CSI can be registered to volumetric acquisitions and offers potential to gather regional and normative group data for reference. Observed differences may be driven primarily by differences in voxel location and size. Future studies will match voxel size and include a larger patient population.

KEYWORDS: 1H MRS, Pediatric brain, 3D spiral CSI

Monday Afternoon

5:00 PM - 6:30 PM
Ballroom 6AB

(14) General Programming: Aneurysms: To Leave Alone or Treat

O-150 **5:00 PM - 5:30 PM**

Deciding Which Unruptured Aneurysm Should Be Treated or Not Treated

Murayama, Y.
Division of Endovascular Neurosurgery, Department of Neurosurgery, Jikei University School of Medicine
Tokyo, JAPAN.

Presentation Summary

Whether or not to treat unruptured intracranial aneurysms (UIAs) depends on various factors, including the risks associated with the natural history of UIAs and those associated with preventive treatment. To date, there are no data from prospective, randomized trials comparing conservative management of UIAs with preventive treatment. The ISUIA and UCAS Japan found a low overall rupture rate and appreciable treatment risks, which could be interpreted to mean that preventive treatment is rarely justified. Larger UIAs, associated with a higher risk of rupture, usually benefit from preventive treatment. However, it is unclear above which aneurysm size there is therapeutic benefit over natural history. Furthermore risk of aneurysmal growth and rupture also is unclear. In this lecture, we discuss the clinical outcome of patients with UIAs that were either managed conservatively or treated preventively.

O-151 **5:30 PM - 6:00 PM**

Which Aneurysms to Treat with Flow Diversion?

Fiorella, D. J.
Stonybrook University Medical Center
Stonybrook, NY.

Presentation Summary

The presentation will review techniques, treatment strategies, results and complications associated with the application of flow diversion to treat brain aneurysms. Case experience will be reviewed with an emphasis upon patient selection.

Note: Scanned images are included in the proceedings. Some submitted images were reduced during editing, thereby decreasing clarity. Also, refer to the Program Planner. Proceedings Content as of 3-29-2013.

O-152 **6:00 PM - 6:30 PM**

Which Recurrent Aneurysms to Treat?

Moran, C. J.
Washington University School Of Medicine
St. Louis, MO.

Presentation Summary
The decision to retreat an aneurysm that has been either surgically clipped or treated endovascularly is strongly dependent upon the reason for the initial treatment. The patient whose aneurysm has previously ruptured will most likely require treatment until the offending aneurysm is obliterated. While there are circumstances that would change this approach, many of these same circumstances apply to the patient with a nonruptured aneurysm being evaluated for recurrence and possible retreatment. There are multiple factors that must be considered in these retreatment decisions. Most are related to the patient and their specific circumstances. Age and life expectancy, vibrancy, and the medical condition of the patient are foremost in these decisions. The location of the aneurysm, the size of the recurrence, and its configuration are significant in the reasoning behind these decisions. The psychosocial aspects of the incompletely treated aneurysm should be remembered as the patient is informed of the results of the recent imaging and subsequent treatment plans. In the follow-up evaluation of patients treated for intracranial aneurysms, the type of evaluation that the patient receives is also important. Magnetic resonance angiography (MRA) with contrast material may provide evidence of flow within treated large aneurysms that may not be detected by CTA or even angiography. The operator must be familiar with the limitations of the imaging modality as well its accuracy. After evaluating the patient who has been found to have a residual or recurrent aneurysm, there are numerous important questions about the aneurysm and the patient that should be answered. Has the aneurysm grown? Over what time period? Is the recurrence due to coil compaction? What is the access? Are adjuncts such as balloons, stents, liquid agents, or flow diversion necessary? If retreatment is undertaken, will the administration of antiplatelet agents be necessary? If so, for how long? Are these agents prudent in this particular patient? Finally the results of the operator with endovascular techniques, particularly with the use of adjunctive devices, must be known so that the complication rate with the proposed retreatment can be compared to the natural history of the aneurysm. In summary, multiple factors must be considered when retreatment of an intracranial aneurysm is being considered. The patient and their particular circumstances, the aneurysm and its particular circumstances, and finally the operator's experiences all combined to make the best decision for the patient. **QUESTIONS:** 1. The most important factor in deciding to retreat an aneurysm is: a. The initial reason for retreatment, b. The age of the patient, c. The configuration of the aneurysm, d. Operator experience. ANSWER: A. 2. Factors important in consideration of retreatment of the recurrent aneurysm include: a. Aneurysm size, b. Aneurysm growth, c. Aneurysm access, d. Operator experience, e. All of the above. ANSWER: E.

Monday Afternoon

5:00 PM - 6:30 PM
Ballroom 6CF

(15) Advanced Imaging Seminar: MR PET

O-153 **5:00 PM - 5:30 PM**

Aspects of PET/MRI Instrumentation

Judenhofer, M. S.
University of California Davis
Davis, CA.

Presentation Summary
In the field of molecular imaging, positron emission tomography (PET) has had great success as a functional imaging modality in major fields like cardiology, oncology and neurology, both in the clinical and the research domain. However, spatial localization of very specifically targeting tracers can be challenging due to the lack of morphologic clues. As a result, PET was combined with x-ray computed tomography (CT) which alleviated the problem of accurate spatial mapping of tracer accumulations. The success of PET/CT has shown that the combination of functional and morphologic information can be superior in difficult or ambiguous situations. A caveat of CT is its limited soft tissue contrast and the significant radiation dose from the x-rays. This is in sharp contrast to magnetic resonance imaging (MRI) where a great variety of tissue contrasts can be obtained and no ionizing radiation is involved. While early attempts to combine PET and MRI were pursued as early as the 1990s, considerable advances in the realm of combined PET/MRI devices have been made possible with the advent of silicon-based and MR compatible light detectors. Even though these light detectors do not always yield the same performance as a PMT and require very sensitive readout electronics, their very compact size allows for directly coupling to scintillators to build PET inserts and facilitates larger axial fields of views which were always hindered by the bulk of optical fibers used in early systems. The good quantification of PET data relies in part on the use of attenuation correction which compensates for the effect of signal underestimation due to absorbed gamma photons in the object being measured. Since this effect is more dominant for larger sized objects, the availability of

Note: Scanned images are included in the proceedings. Some submitted images were reduced during editing, thereby decreasing clarity. Also, refer to the Program Planner. Proceedings Content as of 3-29-2013.

clinical PET/MRI systems calls for methods to obtain this information. Current methods seek to harness the MRI data to derive attenuation correction factors. Since the MR data provide mainly information about 1H-proton distribution which is not directly correlated with tissue density this proves to be a nontrivial task. Current approaches therefore often are based on segmentation and pattern recognition to provide the necessary information. This presentation will provide an overview of past and current developments and challenges of combined PET/MRI systems in both the clinical and preclinical areas with a focus on instrumentation and discussion of methods used for MRI-based PET attenuation correction.

O-154 **5:30 PM - 6:00 PM**

Clinical and Research Applications of PET MR in Brain Imaging

Benzinger, T. L. S.
Mallinckrodt Institute of Radiology
St. Louis, MO.

Presentation Summary
Dual PET MR scanners are now available for human clinical use and offer potential breakthroughs for neurologic imaging. In this presentation, current and future clinical and research applications of PET MR for brain and head and neck imaging will be discussed. PET MR offers several potential advantages over PET CT, including reduced radiation dose, particularly in pediatric patients or patients with an anticipation of multiple PET exams over a lifetime, such as for patients with lymphoma. It combines the physiologic sensitivity of PET tracers, such as FDG, with the resolution and contrast of MR, which may be particularly helpful in cases with small lesions anatomically, such as perineural spread of head and neck tumors. Or, in the case of treated gliomas, the possibility of simultaneous metabolic imaging with FDG combined with dynamic contrast enhancement (DCE) or dynamic susceptibility contrast (DSC) MRI. Although image fusion software for combining separately acquired PET and MRI is available for brain imaging, it is limited in the setting of head and neck cancers, where it is difficult to achieve identical positioning on separate exams. Two commercial designs are now available - one which allows simultaneous and one which provides for sequential PET MR acquisition. Major advantages of simultaneous acquisition are shorter exam times and better coregistration, resulting in less patient burden, particularly in the setting of dementia and advanced oncologic patients, better patient throughput, and potentially offering improved radiosurgical planning. Advantages of the sequential design include fewer artifacts related to the two technologies which might arise from performing PET in an MR environment and vice versa. Issues of attenuation correction, required for quantitative longitudinal studies, are challenging for both designs. PET CT has revolutionized the field of oncologic imaging, particularly for whole body exams. Challenges of PET MR for clinical workflows include development of MR protocols to fit within the PET timing (four-six minutes per station), interpretation of large complex datasets, including data transfers, PACS integration, and specialty readouts, and billing and compensation. Despite these challenges, the potential benefit for clinical patients and research participants are tremendous and are likely to permanently alter the future of neuroradiology.

O-155 **6:00 PM - 6:30 PM**

Hybrid PET/MR Imaging in Neuropsychiatry and Neurooncology

Förster, S.
Technical University Munich
Munich, GERMANY.

Dr. Stefan Forster currently works as an Associate Professor and Head of Neuroimaging at the Department of Nuclear Medicine, Technical University (TU) Munich and is additionally affiliated (PI) to the TUM Neuroimaging Center (TUM-NIC; http://www.tumnic.mri.tum.de/tumnic). He received clinical training in Nuclear Medicine, Radiology and Neuroradiology in two of the most honorable institutions in Germany (LMU and TU Munich). Up to now he has published more than 40 peer-reviewed original articles and more than 40 abstracts. In his recent scientific projects, which were well recognized by the international neuroimaging community ("Young Investigator Award" from SNM Brain Imaging Council 2011 as well as "Georg-von-Hevesy-Preis" from the German Society of Nuclear Medicine 2012), Dr. Forster applied longitudinal FDG- and Amyloid (PiB)-PET as well as MRI in patients with early Alzheimer Disease (AD) and investigated the spread of AD neuropathology in vivo. Currently he receive neurooncologic funding for "Characterization of hypoxic brain tumor regions in high-grade glioma using simultaneous PET/MRI".

Presentation Summary
The research focus is multimodal imaging of the brain using PET and MRI, applying these technologies to neurodegenerative diseases and neurooncology, currently using the worlds first integrated whole-body PET/MRI system.

Note: Scanned images are included in the proceedings. Some submitted images were reduced during editing, thereby decreasing clarity. Also, refer to the Program Planner. Proceedings Content as of 3-29-2013.

Monday Afternoon

5:00 PM - 6:30 PM
Ballroom 6DE

(16) SNIS Programming: New Indications. Tumor Treatment

O-156 **5:00 PM - 5:30 PM**

MRI and US Guided HIFU

Wintermark, M.
University of Virginia
Charlottesville, VA.

Presentation Summary
The concept of high-intensity focused ultrasound will be presented, including its potential brain applications, challenges and limitations.

O-157 **5:30 PM - 6:00 PM**

Intra-Arterial Chemotherapy

Horton, J. A.
Our Lady of Lourdes Hospital
Lafayette, LA.

Presentation Summary
Intra-arterial cis-platinum infusion for treating squamous cell carcinoma (SCC) has been used for some years, but never reached general acceptance. We will be presenting an overview of the technique, its rationale, and a few exemplary cases of this treatment for SCC, inter alia.

O-158 **6:00 PM - 6:30 PM**

Retinoblastoma Therapy

Abruzzo, T.
University of Cincinnati, Neuroscience Institute & Mayfield Clinic
Cincinnati, OH.

Presentation Summary
Selective ophthalmic artery infusion chemotherapy has emerged as an important treatment option for children with retinoblastoma. Interventional neuroradiologists have assumed a primary role in contemporary patient evaluation and management. The clinical features, biology, epidemiology, neuroradiology and oncologic classification of retinoblastoma will be reviewed. Current treatment options will be discussed, emphasizing indications, remission rates, complications, advantages and disadvantages. The evolution of interventional approaches to the management of retinoblastoma will be presented. Variations in technique and adjunctive treatments will be highlighted. The fundamentals of ocular vascular anatomy, which form the guiding principles of selective ophthalmic artery infusion chemotherapy will be illustrated. Technical challenges encountered by neurointerventionalists during selective ophthalmic artery infusion chemotherapy, and related practical solutions will be reviewed. Various strategies for the management of retrograde ophthalmic artery flow will be discussed. Technical advances, which have improved the safety and efficacy of the SOAIC procedure, particularly in patients with challenging anatomy and hemodynamics, will be underscored.

Monday Afternoon

5:00 PM - 6:30 PM
Room 5AB

(17) CSI San Diego: Basics of Tablets

O-159 **5:00 PM - 6:30 PM**

Basics of Tablets

Shah, G. V.
Univ. Michigan Health System
Ann Arbor, MI.

Presentation Summary
The "new online" (Web 2.0) world is here and is expanding rapidly. The digital information, educational resources, communication tools, and networking resources helpful to radiologists have exploded over the past two decades. The rapid adoption rate and integration of mobile technology, especially tablet computing devices by physicians is reshaping the current clinical and radiologic landscape. These devices have sparked a revolution in a variety of arenas, including educational media dissemination, remote patient data access and point of care learning applications and clinical tools. This course gives an overview of tablet computing and communication devices and informs of different platform, products, their capability and suitability to the needs of radiology resident, educator and clinician.

Note: Scanned images are included in the proceedings. Some submitted images were reduced during editing, thereby decreasing clarity. Also, refer to the Program Planner. Proceedings Content as of 3-29-2013.

Monday Afternoon

5:00 PM - 6:30 PM
Room 1AB

(18) Parallel Scientific Papers: Excerpta Session: Case Reports and Other Cool Ideas

O-160 **5:00 PM - 5:05 PM**

Long-Term MR Imaging Signal Change in the Spinal Trigeminal Nucleus and Tract after Ramsay Hunt Syndrome and Trigeminal Herpes Zoster

Clerk-Lamalice, O.·Savage, J.·Fisch, C.
University of Sherbrooke
Sherbrooke, QC, CANADA.

Purpose
Ramsay Hunt syndrome (RHS), an illness caused by varicella zoster virus, refers to the association of a unilateral facial nerve palsy with herpes zoster oticus. Cranial nerve(CN) VIII often is involved and rarely CN V, VI, IX, X, XI and XII. Only four other cases of both RHS and trigeminal herpes zoster have been reported in the literature. We present a case of RHS, multiple CN palsies and trigeminal herpes zoster that developed postherpetic neuralgia(PHN). Longitudinal MRI-signal-intensity abnormalities were followed in the spinal trigeminal nucleus and tract(STNT).
Case Report
A 69-year-old man, on immunosuppressants for a heart transplant, slowly developed dysphagia, sore throat and right otalgia two weeks after a right hemicolectomy. Over the next few days he developed severe right tooth, pinna, and hemifacial pain as well as a lower motor neurone facial paralysis, House-Brackman grade 5/6. Plasma immunosuppressant levels were abnormally high. The patient was treated for RHS with Prednisone and Acyclovir. Vesicular skin lesions appeared gradually over the following days on the right tympanic membrane, and external auditory canal with right audition decrease and vertigo. Nasolaryngoscopy confirmed presence of vesicles on the right hemipharynx, indicating CN IX involvement. The patient also developed vesicular skin lesions and allodynia in the right trigeminal nerve territory. At six months, he had PHN and persistent multiple cranial deficits.
Imaging Findings
MR imaging was performed six weeks and six months after the beginning of symptoms. The initial MRI demonstrated enhancement of the right intratemporal portion of CN VII and swelling of the cisternal portion of CN VII and CN VIII. Right STNT showed initial diffusion restriction and corresponding increase in T2-weighted signal intensity persisting six months after the beginning of symptoms.

Summary
We present a patient with RHS and trigeminal herpes zoster. Transaxonal spread of VZV in the brainstem, between the facial nerve nucleus and STNT, has been hypothesized to explain the rare incidence of both pathologies. This case is interesting because of long-term T2-hyperintensity in the brainstem and the development of PHN. In a study of patients with trigeminal herpes zoster, brainstem signal abnormalities were associated more frequently with PHN. In our case, we believe that the initial severity and intensity of STNT diffusion restriction and T2-weighted hyperintensity relates to the deleterious outcome. Future MR prospective studies should investigate the prognostic value of initial diffusion and T2-weighted signal intensity abnormalities of STNT in patients with RHS and/or trigeminal herpes zoster.

KEYWORDS: Brainstem, Infections, Ramsay Hunt syndrome

O-161 **5:05 PM - 5:10 PM**

West Nile Virus Meningoencephalitis Initially Presenting as Intraparenchymal Hemorrhage in a Hypertensive Patient

Endale, B.·Morales, R.·Steven, A.
University of Maryland Medical Center
Baltimore, MD.

Purpose
To report a case of West Nile virus (WNV) meningoencephalitis initially presenting as intraparenchymal hemorrhage.
Case Report
A 79-year-old male with a past medical history of hypertension and vascular dementia presented with several days of high fevers to 103, shaking chills, and rigidity. Initial examination demonstrated paratonia, meningeal signs including neck stiffness, and a GCS of 11. Blood pressure early in the patient's hospital course was noted to be as high as 170/80 mmHg. Cerebrospinal fluid analysis revealed elevated WBC (265 per mm^3) and protein (134 mg/dL). CT scan revealed a large left temporal lobe intraparenchymal hematoma. MR imaging revealed several predominantly cortical foci of diffusion signal in the right cerebral hemisphere and FLAIR sulcal hyperintensity bilaterally. CT angiography and catheter

Note: Scanned images are included in the proceedings. Some submitted images were reduced during editing, thereby decreasing clarity. Also, refer to the Program Planner. Proceedings Content as of 3-29-2013.

angiogram were negative for underlying vascular anomaly or vasculitis. Cerebrospinal fluid analysis by PCR later revealed WNV infection, and the diagnosis of WNV meningoencephalitis was made. The patient showed improvement in alertness and mental status following treatment with a five-day course of IVIG and blood pressure control.

Imaging Findings

Axial FLAIR MRI reveals a 4.9 x 4.1 cm parenchymal hemorrhage centered in the left temporal lobe. In addition there is extensive sulcal hyperintensity throughout both cerebral hemispheres (Figure 1). Diffusion-weighted images demonstrate multifocal areas of restricted diffusion involving the right insular cortex and medial right occipital lobe (Figure 2). No abnormal parenchymal or leptomeningeal enhancement was shown on postcontrast sequences (not shown).

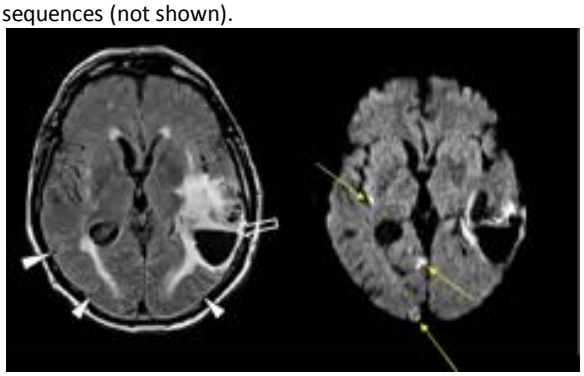

Summary

West Nile virus is a widespread mosquito-borne infectious agent with cases of meningoencephalitis reported throughout the United States. Roughly 1/150 of infected patients will develop CNS syndromes of meningitis, encephalitis, and acute flaccid paralysis/poliomyelitis. Imaging findings are typically absent; however, T2/FLAIR abnormalities in the deep gray matter and brain stem as well as diffusion abnormalities in the white matter including the corona radiata and internal capsule have been described. This patient had several atypical features including predominantly cortical diffusion restriction and leptomeningeal FLAIR signal in addition to intraparenchymal hemorrhage. Our patient also had a history of hypertension which may have made him more prone to develop intraparenchymal hemorrhage. It is still unclear whether the patient suffered from an unusual sudden onset of WNV meningoencephalitis manifested as multifocal infarction/hemorrhage or whether those same areas made the patient more susceptible to developing WNV meningoencephalitis.

KEYWORDS: Meningoencephalitis, Hemorrhage, West Nile virus

O-162 **5:10 PM - 5:15 PM**

Teratoma-Associated Anti-NMDA Receptor Encephalitis

Hong, Y.·Opatowsky, M. J.·O'Connor, J. C.·Layton, K. F.
Baylor University Medical Center
Dallas, TX.

Purpose

To present the clinical course and MRI findings associated with a case of anti-NMDA (N-methyl-D-aspartate) receptor encephalitis.

Case Report

A 20-year-old woman presented with status epilepticus and subsequently was found to have serum anti-NMDA receptor antibodies associated with a pathology-proven benign cystic teratoma of the ovary. Initial MRI findings in this clinical setting were compatible with paraneoplastic limbic encephalitis. Surgical resection of the ovarian teratoma, plasmapheresis, and adjuvant chemotherapy were performed with near complete resolution of MRI findings although status epilepticus persisted and continued clinical decline resulted in eventual withdrawal of advanced supportive care.

Imaging Findings

Initial MRI demonstrated extensive FLAIR signal elevation in the bilateral deep gray nuclei and mesial temporal lobes including the hippocampi, compatible with paraneoplastic limbic encephalitis in the setting of a benign cystic teratoma of the ovary and serum anti-NMDA receptor antibodies. Two weeks after surgical resection of the ovarian teratoma, a repeat MRI demonstrated near complete interval resolution of the initial imaging abnormalities.

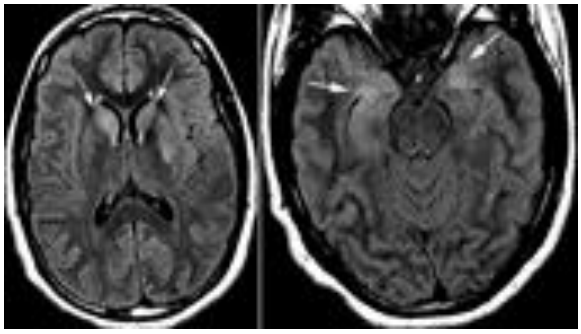

Summary

Although paraneoplastic limbic encephalitis is a well-known entity, the association with anti-NMDA receptor antibodies has been described only recently and appears to be primarily associated with teratomas. The best treatment at this time is thought to be surgical resection of the teratoma with supportive care.

KEYWORDS: Paraneoplastic, Limbic encephalitis, NMDA

Note: Scanned images are included in the proceedings. Some submitted images were reduced during editing, thereby decreasing clarity. Also, refer to the Program Planner. Proceedings Content as of 3-29-2013.

O-163 **5:15 PM - 5:20 PM**

Thirty-Five-Day Old with an Expanding Bruise on the Infants Back

Trinh, V.·Ngo, M.
Kaiser Permanente Los Angeles Medical Center
Los Angeles, CA.

Purpose
To present a case of paraspinal Kaposiform hemangioendothelioma and illustrate the association of this lesion with Kasabach-Merritt phenomenon.
Case Report
A 35-day-old infant without history of trauma found to have an expanding bruise on the back and associated marked thrombocytopenia.
Imaging Findings
X-ray of the spine demonstrates loss of visualization of the right T11/T12 pedicles suggesting erosion. Follow-up postcontrast fat suppressed MRI demonstrates a heterogeneously enhancing right paraspinal mass that has eroded the adjacent pedicle with evidence of retroperitoneal and epidural extension into the spinal canal.

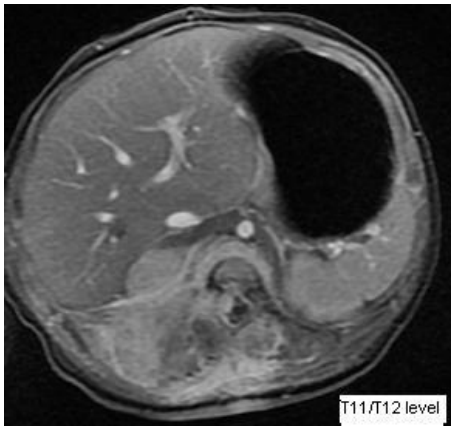

Summary
There is a wide spectrum of pediatric soft-tissue tumors ranging from benign to malignant and/or vascular and nonvascular lesions. The majority of pedatric soft-tissue lesions will be vascular or lymphatic in origin. Kaposiform hemangioendothelioma is a vascular lesion that can be differentiated from a common hemangioma of infancy due to its aggressive nature on imaging and also its association with Kasabach-Meritt pheonomenon (>50% of cases), a profound thrombocytopenia thought related to platelet trapping as the lesion grows in size.

KEYWORDS: Pedicle, Pediatric spine, soft tissue

O-164 **5:20 PM - 5:25 PM**

Imaging Manifestations of Pseudomonas Aeruginosa Chondritis of the Thyroid Cartilage

Howard, E. A.·Gomez, C.·Weprin, L. S.·Opatowski, M. J.
Baylor University Medical Center
Dallas, TX.

Purpose
To describe imaging findings of purulent chondritis of the thyroid cartilage secondary to pseudomonas aeruginosa.
Case Report
A 52-year-old male with end-stage liver disease developed increasing hoarseness over one month. Initial CT of the neck demonstrated mild laryngeal edema. Laryngoscopy showed edematous vocal cords. One month after the first CT, the patient developed acute respiratory distress and CT of the neck showed interval destruction of the thyroid cartilage and replacement by low density collections. Differential considerations included granulomatous, infectious and less likely neoplastic processes. Laryngoscopy and tracheotomy were emergently performed. Biopsies revealed purulent chondritis of the thyroid cartilage, with cultures positive for pseudomonas aeruginosa. Imaging after tracheotomy and intravenous antibiotics showed resolution of abscesses centered at the site of the thyroid cartilage and dissipation of laryngeal edema.
Imaging Findings
CT of the neck performed one month prior to admission

Note: Scanned images are included in the proceedings. Some submitted images were reduced during editing, thereby decreasing clarity. Also, refer to the Program Planner. Proceedings Content as of 3-29-2013.

showed laryngeal edema without cartilaginous destruction. CT of the neck with contrast at the time of admission (Image 1) shows interval worsening of edema of the false cords, aryepiglottic folds and epiglottis. The ventral cords and glottis also demonstrate edema and an ill-defined enhancing 1 cm soft tissue mass at the anterior midline of the glottis. The thyroid cartilage demonstrates interval subtotal replacement by low-density fluid collections with faint rim enhancement. No surrounding inflammatory change or enlarged cervical lymph nodes are seen. Intraoperative images provide correlation for CT findings. Two follow-up CTs of the neck reveal postoperative changes of laryngotomy with evacuation of fluid collections centered at the area of the thyroid cartilage. The enhancing soft tissue component at the glottis had largely resolved.

Summary

Purulent chondritis of the laryngeal cartilages is a rare entity that has been described in case reports as having a subacute clinical course. Etiologies include history of relapsing polychondritis or previous prolonged intubation. Infectious agents previously reported include staphylococcus aureus, aspergillus fumigatus, and a single case report of pseudomonas aeruginosa. Imaging findings in this case are most notable for destruction of the majority of the thyroid cartilage and replacement by low-density collections with mild peripheral enhancement and little surrounding inflammatory change. Due to the subactue time course of PCLC, differential considerations including neoplastic and granulomatous lesions should be considered. This case emphasizes that infectious processes may occur in the laryngeal cartilages, and must be kept in mind and considered a viable differential diagnosis when such imaging findings are encountered.

KEYWORDS: Abscessthyroid cartilage

O-165 **5:25 PM - 5:30 PM**

Eagle Has Landed: Internal Carotid Pseudoaneurysm and Subsequent Stent Erosion Secondary to an Elongated Styloid Process

Burns, P. A.[1]·Almekhlafi, M. A.[1,2]·Yavin, D.[1]·Morrish, W.[1]·Eesa, M.[1]·Goyal, M.[1]·Mitha, A. P.[1]
[1]University of Calgary, Calgary, AB, CANADA, [2]King Abdulaziz University, Jeddah, SAUDI ARABIA.

Purpose

To report an unusual case of post-traumatic internal carotid pseudoaneurysm secondary to Eagle syndrome and subsequent stent erosion by the offending elongated styloid process.

Case Report

A 45-year-old man presented with a two-week history of left-sided neck pain and voice hoarseness after he fell while snowboarding. Examination showed partial left ptosis, tongue deviation to the left and weak left palate elevation. CT angiogram demonstrated a left internal carotid pseudoaneurysm arising from the lateral wall adjacent to the tip of an elongated styloid process(Figure 1). This measured approximately 18 x 15 mm (transverse x craniocaudal) with a 2 mm neck. These findings also were confirmed with catheter angiography. Double antiplatelet therapy was commenced and two days later the pseudoaneurysm was treated using a 7 x 30 mm carotid WALLSTENT (Boston Scientific Corp., Natick, Massachusetts) deployed over the aneurysm neck. An ultrasound performed 24 hours poststenting showed that the majority of the aneurysm was thrombosed, with only a small amount of residual flow. The patient re-presented two weeks later following an episode of transient global amnesia. CT angiography confirmed stent patency; however a focal defect in the stent wall approximate to the styloid process was identified (Figure 2). The pseudoaneurysm was completely thrombosed. A stent fragment embolus was noted within the left parietal lobe, although no focal infarct was seen. This was confirmed with MRI performed on the same day. The styloid process was ultimately resected six weeks later.

Imaging Findings

Note: Scanned images are included in the proceedings. Some submitted images were reduced during editing, thereby decreasing clarity. Also, refer to the Program Planner. Proceedings Content as of 3-29-2013.

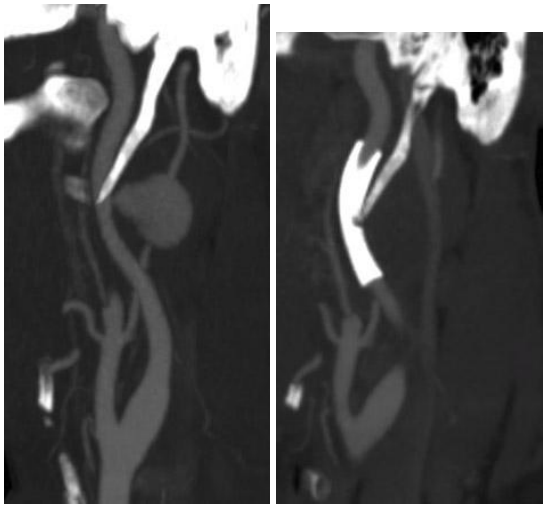

Summary
Vascular complications secondary to Eagle syndrome are unusual and typically involve carotid dissection. Transient ischemic attacks also can occur secondary to stylo-carotid compression. This case illustrates not only the potential for traumatic pseudoaneurysm, but also demonstrates the traumatic effect the elongated styloid process can have on an endovascular stent within a relatively short time frame.

KEYWORDS: Aneurysm formation, Aneurysm treatment, Eagle syndrome

O-166 **5:30 PM - 5:35 PM**

Acute Pyrimethamine Toxicity: MR Imaging Findings

Trunet, S.[1]·Galanaud, D.[1]·Gerber, S.[1]·Jarquin, S.[1]·Henry, C.[2]·Dormont, D.[1]·Leclercq, D.[1]
[1]Hôpital de la Pitié Salpétrière, Paris, FRANCE, [2]Hôpital de Saint Denis, Saint Denis, FRANCE.

Purpose
To present the first reported case of pyrimethamine neurotoxicity. Pyrimethamine commonly is used in the treatment of toxoplasma gondii infections in immunocompromised patients, such as HIV-positive individual. Pyrimethamine is an antifolate drug, like methotrexate. Both molecules interfere with tetrahydrofolic acid synthesis from folic acid by inhibiting the dihydrofolate reductase. Methotrexate can induce acute white matter neurotoxicity with a typical imaging pattern. The pathophysiology of this neurotoxicity is poorly understood, but folate implication is suspected. The purpose of this presentation is: 1. to present the clinical and MRI aspects of pyrimethamine toxicity. 2. Discuss the physiopathology of pyrimethamine and methotrexate toxicity.
Case Report
A 20-year-old immunocompetent woman was addressed to our institution with sudden right hemiparesis associated with confusion and mutism.
Image Findings
An MRI performed the same day showed symmetrical areas of restriction diffusion with discrete high-signal T2 intensity in the centrum semiovale as is commonly observed in acute methotrexate-related leukoencephalopathy: Anamnesis revealed that the patient had been taking pyrimethamine without supplementary folinic acid for the past threee weeks to treat a suspicion of toxoplasmic retinitis. Symptoms resolved completely after folinic acid administration.

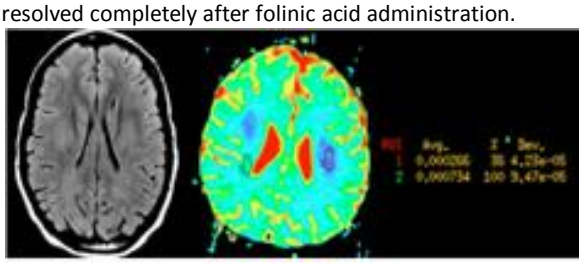

Summary
We present the first reported case of pyrimethamine toxicity in a young adult treated for toxoplasmic retinitis. Clinical presentation and MRI findings were similar to acute methotrexate toxicity: stroke-like episode and symmetrical centrum semiovale restricted diffusion areas. Since both pyrimethamine and methotrexate are antifolate drug, this case report suggests that acute methotrexate neurotoxicity is indeed folate-related.

KEYWORDS: pyrimethamine, intoxication, folinic acid

O-167 **5:35 PM - 5:40 PM**

Chronic Lymphocytic Inflammation with Pontine Perivascular Enhancement Responsive to Steroids

Wang, B.·Fuller, G.·Ketonen, L.
M. D. Anderson Cancer Center
Houston, TX.

Purpose
To illustrate the imaging findings of CLIPPERS, which to our knowledge has not been reported in radiology literature. Our purpose is to raise awareness of the neuroradiology community concerning this unique recently described disease.
Case Report
A 35-year-old right-handed woman with a one-year history of fatigue, generalized aches and low-grade fever was found to have Hodgkin lymphoma. She underwent spine and brain MRI which showed diffuse nodular enhancement. CSF cytology was obtained twice with no evidence of malignancy. The patient underwent biopsy of the meninges and brain parenchyma, which showed reactive perivascular lymphocytic infiltrates consisting primarily of CD3-positive T cells. There was no morphologic or immunophenotypic evidence of Hodgkin lymphoma or of Hodgkin-associated giant cell arteritis.
Imaging Findings

Note: Scanned images are included in the proceedings. Some submitted images were reduced during editing, thereby decreasing clarity. Also, refer to the Program Planner. Proceedings Content as of 3-29-2013.

On the brain MRI, diffuse nodular enhancement is seen extending along the perivascular spaces throughout the brain including along the pituitary stalk. Extensive parenchymal enhancement also is seen throughout brain stem, all compatible with advanced perivascular disease with parenchymal involvement. The CSF spaces on the T2 FLAIR images are well defined, contrary to expected findings in LMD. On the spine MRI, there is diffuse nodular enhancement along the entire spine along with foci of abnormal signal throughout the spinal cord.

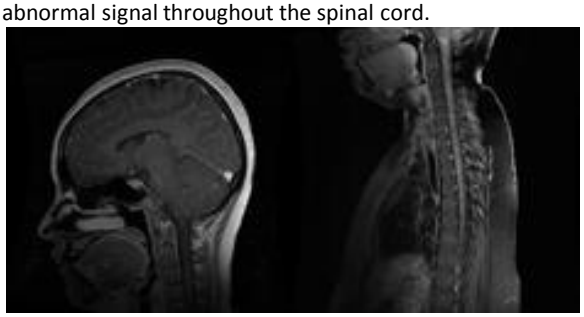

Summary
Chronic lymphocytic inflammation with pontine perivascular enhancement responsive to steroids (CLIPPERS) is a central nervous system (CNS) inflammatory disease that was defined initially in 2010 in a case series of eight patients with common clinical, radiologic, and pathologic features of brainstem involvement that was responsive to and dependent on corticosteroid therapy. The diagnostic criteria for CLIPPERS include the following: (1) episodic brainstem symptoms, (2) characteristic punctuate and curvilinear gadolinium-enhancing lesions peppering the brainstem, especially in the pons, and (3) T-lymphocytic infiltrate with perivascular predominance in brain biopsy specimens. CLIPPERS is a treatable relapsing-remitting disorder without progressive forms. It has been suggested that a diagnosis of CLIPPERS can be made without brain biopsy if the characteristic clinical and MR imaging features are present and if alternative diagnoses are excluded. This particular case has extensive perivascular enhancement involving bilateral cerebral hemispheres and the entire spinal cord, in addition to the characteristic pattern of punctate and curvilinear enhancement peppering the pons. To our knowledge, this recently recognized disease has yet to receive attention in the neuroradiology literature. Although relatively rare, neuroradiologists should be aware of this entity and consider it in the differential diagnosis when the characteristic features are encountered.

KEYWORDS: Brain disease, Spinal cord, CLIPPERS

O-168 **5:40 PM - 5:45 PM**

Inflammatory Progressive Multifocal Leukoencephalopathy following Natalizumab Withdrawal

Hanley-Knutson, K.·Kinder, K.
Santa Barbara Cottage Hospital
Santa Barbara, CA.

Purpose
Natalizumab (Tysabri) is an immunosuppressive drug indicated for treatment of multiple sclerosis and Crohn's disease that has been linked to a number of cases of progressive multifocal leukoencephalopathy (PML). In rare instances, this can progress to inflammatory progressive multifocal leukoencephalopathy (iPML) following discontinuation of the medication.
Case Report
A 38-year-old woman with refractory multiple sclerosis on natalizumab presented to the emergency room with worsening neurologic symptoms. She had an MRI of her brain that was compatible with PML and, as a result, was taken off of natalizumab. She continued to have worsening neurologic symptoms and a follow-up MRI of her brain was concerning for iPML.
Imaging Findings
In addition to baseline MS findings, the initial MRI in the ER revealed new confluent areas of T2/FLAIR hyperintensity in the subcortical white matter in the high right frontal lobe that were volume neutral and did not enhance with contrast. On the MRI performed after stopping natalizumab, the same region of T2/FLAIR hyperintensity had enlarged, demonstrated mass effect on surrounding cortex, and was associated with avid peripheral enhancement.

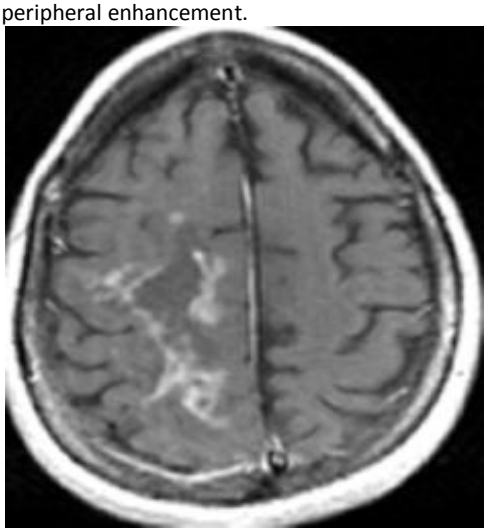

Summary
Progressive multifocal leukoencephalopathy is a demylinating process that results from activation of the JC virus in immunocompromised patients and has been linked to the use of natalizumab and similar immunologic agents. Cessation of immunosuppressive therapy is indicated in the setting of PML, but can result in immune

Note: Scanned images are included in the proceedings. Some submitted images were reduced during editing, thereby decreasing clarity. Also, refer to the Program Planner. Proceedings Content as of 3-29-2013.

reconstitution inflammatory syndrome (IRIS), the CNS manifestation of which is iPML. Progressive multifocal leukoencephalopathy and iPML both preferentially involve the subcortical U-fibers, but can be differentiated on MRI. Specifically, iPML, unlike PML, typically is associated with mass effect and peripheral enhancement, as was seen in this case.

KEYWORDS: Leukoencephalopathy, Multiple sclerosis

O-171 **5:55 PM - 6:00 PM**

Stereotactic Radiosurgery-Induced Cavernoma in Adults: A Rare but Important Entity

Thurlow, P. C.·Goldberg, M. F.
West Penn Allegheny Health System
Pittsburgh, PA.

Purpose
Cavernomas, or cavernous hemangiomas, are CNS vascular lesions comprised of thin-walled, dilated venous channels without intervening brain tissue. A growing and well established literature supports the correlation between childhood radiation to the brain and cavernomas. However, cavernoma formation in adults that have received radiation to the brain is a very rare entity and can represent a diagnostic dilemma. We report a unique and rare case of stereotactic radiosurgery (SRS)-induced cavernoma in an adult. The purpose of this report is to increase the awareness of SRS-induced cavernomas in adults and highlight an unusual presentation of this rare entity.
Case Report
A 77-year-old woman presented 62 months following SRS for a tentorial Borden type-1 dural arteriovenous fistula (AVF) with progressive ataxia and short-term memory loss. MR imaging revealed a left cerebellar mass that was felt to be radiation necrosis with a hemorrhagic component rather than a neoplasm. The patient subsequently underwent third ventriculostomy with symptomatic improvement. Follow-up MRI performed two months later revealed a heterogeneously enhancing mass in the left cerebellum with a large amount of surrounding edema; mass effect resulted in effacement of the fourth ventricle with associated obstructive hydrocephalus. Over the course of the next six months, the mass demonstrated progressively increasing size and mass effect. Owing to the increasing size of the lesion and mass effect with hydrocephalus and cerebellar tonsillar herniation, the decision was made to proceed to primary resection of the mass via suboccipital craniotomy. Surgical pathology of the vascular mass confirmed a diagnosis of cavernous hemangioma.
Imaging Findings
The patient's initial post-radiation MRI demonstrated no abnormality at the site of SRS. Sixty-two months later, when the patient presented with ataxia, there was a 4 x 2 cm heterogeneous enhancing hemorrhagic mass with a large amount of associated edema. Over the next six months, there was progression in size and mass effect, ultimately measuring 6 x 4 cm. The mass demonstrated a heterogeneous "popcorn" appearance with a hypointense rim on T2-weighted images and susceptibility artifact on gradient-echo images. However, given the highly aggressive behavior of this mass, as well as age of the patient at the time of SRS, cavernoma was considered unlikely.

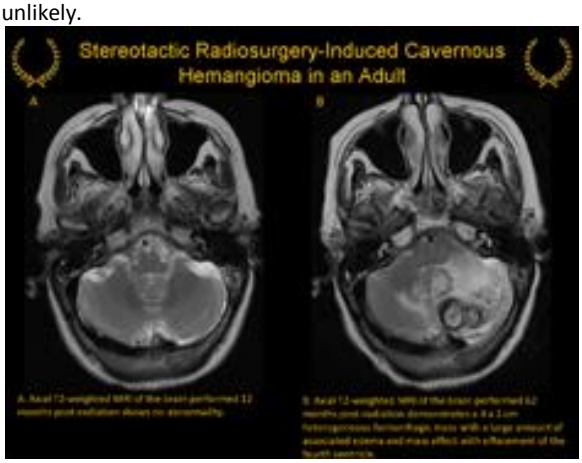

Summary
We present an atypical, highly-aggressive SRS-induced cavernoma. Given increasing role of SRS in clinical practice, the radiologist should be aware of the association between cavernous malformation and radiation therapy when encountering an atypical intracranial mass.

KEYWORDS: Cavernoma, Radiation

O-172 **6:00 PM - 6:05 PM**

Atypical Growth of Persistent Restricted-Diffusion Associated with Atypical Necrosis in Bevacizumab and Radiotherapy-Treated Anaplastic Oligodendroglioma

Chen, J. Y.[1,2]·Lee, R.[1,2]
[1]University of California San Diego Health System, La Jolla, CA, [2]San Diego Veterans Administration Medical Center, La Jolla, CA.

Purpose
Atypical or gelatinous necrosis, manifested by marked restricted diffusion and stippled peripheral enhancement mimicking cellular tumor progression, has been described in high-grade primary neoplasms after treatment with radiation and bevacizumab. A previous case series demonstrated that this atypical necrosis remains stable in volume over a six-month follow-up period, but may increase in volume a median of 23%. The purpose of this submission is to describe a case of atypical growth of atypical necrosis, which increased in volume by approximately 225% during a seven-month follow-up period.
Case Report

Note: Scanned images are included in the proceedings. Some submitted images were reduced during editing, thereby decreasing clarity. Also, refer to the Program Planner. Proceedings Content as of 3-29-2013.

A 43-year-old right-handed male with a right frontal anaplastic oligodendroglioma with a 1p/19q deletion underwent a gross-total surgical resection and was treated with radiotherapy and chemotherapy using temozolomide and subsequently bevacizumab. After 15 months, the patient developed a rim of presumed atypical necrosis around the resection cavity, which subsequently increased in volume over seven and a half months to approximately 225% times the initial volume without developing new clinical symptoms.

Imaging Findings

Fifteen months after beginning therapy, a rim of marked restricted-diffusion with stippled peripheral enhancement developed around the periphery of the resection cavity. The area had low relative blood volume on susceptibility-weighted perfusion and photopenia on FDG-PET, and was thought to represent atypical necrosis. The area of restricted-diffusion and enhancement continued to enlarge on subsequent follow-up MRIs and by 22 1/2 months after beginning therapy, had increased in volume by approximately 225%. There was no significant change in ADC values and perfusion-weighted images again demonstrated low relative blood volume. Subsequent FDG-PET again demonstrated photopenia in the corresponding area.

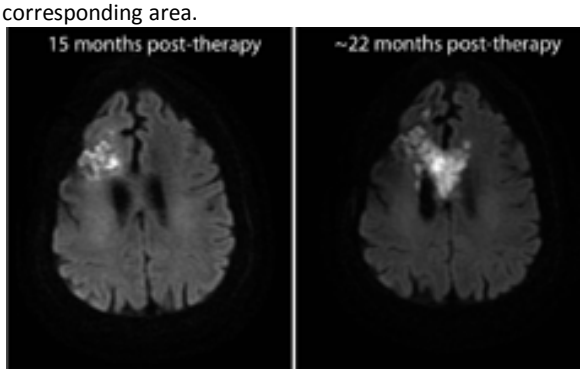

Summary

Atypical necrosis associated with primary neoplasms treated with radiotherapy and bevacizumab may mimic progressive cellular neoplasm due to its marked restricted diffusion. Reports have described stability or mild median enlargement of the necrotic area, this case demonstrates more than doubling of lesion size which did not result in new symptoms or a change in therapy.

KEYWORDS: Necrosis, Tumor-like conditions, bevacizumab

O-173 **6:05 PM - 6:10 PM**

Supplemental Motor Area Syndrome after Colloid Cyst Resection

Hernandez, R. J.·Minja, F. J.
Yale University
New Haven, CT.

Purpose

Revisit the clinical features and radiographic findings of the supplemental motor area (SMA) syndrome. Highlight the anatomical location of the SMA with fMRI correlates and stress the importance of the knowledge of functional anatomy in diagnostic imaging.

Case Report

A 31-year-old gentleman presented to the emergency department with altered awareness. Initial CT demonstrated a hyperdense mass in the third ventricle with obstructive hydrocephalus. MR imaging revealed a corresponding T1 hyperintense cystic mass, with hydrocephalus, and transependymal cerebral spinal fluid flow. A presumptive diagnosis was made of a colloid cyst. The patient underwent shunting and transcallosal resection of the cyst. Postoperatively the patient had a significant left-sided motor deficit. Repeat MRI showed expected postoperative changes and a small area of restricted diffusion in the right paracentral lobule corresponding to the SMA. The restricted diffusion was thought to represent cytotoxic edema secondary to operative retraction. In light of the clinical findings, SMA syndrome was suggested as a diagnosis. By postoperative day four, the patient had improved strength and one month later had completely recovered.

Image Findings

Initial CT without contrast demonstrated a 1.1 cm hyperdense mass in the third ventricle with obstructive hydrocephalus. MR imaging with contrast revealed a corresponding T1 hyperintense cystic mass with hydrocephalus and transependymal cerebral spinal fluid flow. Postoperative MRI with contrast showed a left frontal ventricular shunt catheter, postoperative changes related to transcallosal resection of the cyst, improved hydrocephalus, moderate hemorrhage in the lateral ventricles, and a small area of restricted diffusion in the right medial aspect of the superior frontal gyrus (paracentral lobule) which corresponds to the SMA.

Summary

The SMA syndrome refers to pathology of the SMA producing a contralateral motor deficit which can mimic a pyramidal or motor cortex injury. The syndrome presents with difficulty in initiating movement or apraxia and is most commonly described postoperatively in resected tumors of the SMA. However, in contrast with pyramidal damage most patients have significant recovery with minimal residual deficit. The importance of the SMA is sometimes forgotten and its anatomical location is sometimes misplaced. However, as fMRI becomes more pervasive, the SMA has become increasingly visible as it is

Note: Scanned images are included in the proceedings. Some submitted images were reduced during editing, thereby decreasing clarity. Also, refer to the Program Planner. Proceedings Content as of 3-29-2013.

ubiquitously activated when localizing the motor cortex. It is located in the paracentral lobule or medial aspect of the superior frontal gyrus in what corresponds to the medial aspect of Brodmann area 6. It is thought to have a somatotopic organization and is responsible for the coordination of movement. This case reinforces the benefits of accurate functional anatomical knowledge. When pathology is localized to the SMA, one should report this fact, suggest the potential clinical presentation, and even propose a positive prognosis.

KEYWORDS: fMRI, Adult brain, anatomy

O-174 **6:10 PM - 6:15 PM**

Carotidynia: A Trauma, Infectious or Fluoxetine-Induced Inflammatory Process on Imaging

Feltus, W. Y.[1,2]·Rojas, R.[1,3]·Moonis, G.[1,3]
[1]Beth Israel Deaconess, Boston, MA, [2]Wake Forest School of Medicine, Winston Salem, NC, [3]Harvard Medical School, Boston, MA.

Purpose
Carotidynia is a transient inflammatory condition characterized by unilateral neck pain and enhancing soft tissue thickening surrounding the carotid artery. The cause of the condition remains unknown. Prior to its removal from the classification system of headaches, few reports were published about the radiographic characteristics of carotidynia, which have since provided enough evidence to classify it as a separate and distinct entity.
Case Report
A 21-year-old male presented to the emergency department with sharp pain at the angle of his left jaw which began three weeks prior to being struck in the temple by an elbow. His medical history was significant for use of Symbyax which was discontinued around the time of his presentation. The patient's exam and laboratory workup was also unremarkable except for pain with palpation of the neck on the left. He was discharged three days later with near resolution of his symptoms on oral antibiotics.
Imaging Findings
A CTA of the head and neck was obtained and showed a soft tissue infiltration around the left common and internal carotid artery extending into the parapharyngeal region, compression of the left internal jugular vein with impaired venous drainage, and a small effusion in the retropharyngeal space. An MRI of the head and neck also revealed mild enhancing T2 signaling of the soft tissue density surrounding the left carotid artery, and small reactive cervical lymph nodes with no evidence of an abscess.

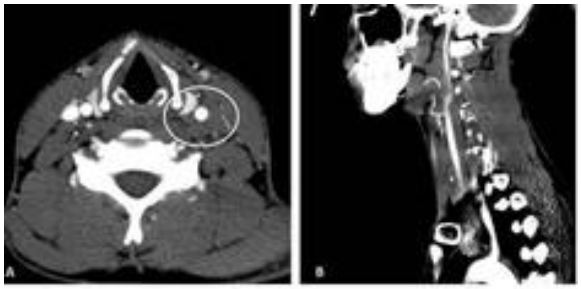

Figure 1. Circumferential soft tissue thickening along the length of the cervical portion of the left carotid artery on contrasted axial (A) and sagittal (B) CTA of the head and neck.

Summary
One case reported fluoxetine-induced carotidynia that resolved with discontinuation of the drug. The exact mechanism is unknown but there have been reports of fluoxetine-induced serum sickness and other hypersensitivity reactions to the medication. Our patient was afebrile with a normal CBC throughout his hospital course. Whether this case is a postinfectious or post-traumatic reaction is unknown. No particular bacteria or pathogen has been isolated in carotidynia, and laboratory values that would indicate an infection are typically normal. The imaging characteristics found in carotidynia separate it from other pathologies of the carotid artery including atherosclerosis, dissections, aneurysms and vasculitis. It is critical to recognize these conditions early on, further warranting a separation of carotidynia from the class of potentially fatal conditions. Although many causes have been linked to the carotidynia, the distinction between this inflammatory condition and other causes of pain in the neck has been provided by its imaging characteristics.

KEYWORDS: Carotid artery, Inflammatory

O-175 **6:15 PM - 6:20 PM**

What Is That Fat Doing in the Thyroid?: Case Discussion and Brief Review of Fat-Containing Lesions of the Thyroid

Fredriksen, J. R.·Morris, J. M.
Mayo Clinic
Rochester, MN.

Purpose
To describe the imaging characteristics of an amyloid goiter and review the rare fat-containing lesions in the thyroid.
Case Report
A 58-year-old male with a past medical history of a renal transplant secondary to chronic glomerulosclerosis and amyloid deposition presented to our institution with an enlarging neck mass in the region of the thyroid. On physical exam he had firm diffuse enlargement of the thyroid gland without nodularity. Clinically and by laboratory testing he was euthyroid. A CT scan was obtained demonstrating diffuse fatty infiltration of an

Note: Scanned images are included in the proceedings. Some submitted images were reduced during editing, thereby decreasing clarity. Also, refer to the Program Planner. Proceedings Content as of 3-29-2013.

enlarged thyroid (see imaging findings). Ultrasound-guided fine needle aspiration yielded amyloid deposits staining with Congo red. Liquid chromatography and mass spectroscopy then was performed on peptides extracted from the tissue staining with Congo red detecting a peptide profile consistent with serum amyloid A type amyloid. The patient was treated conservatively as he was euthyroid at the time.

Imaging Findings

Axial noncontrast CT of the neck with coronal reformats demonstrates diffuse fatty infiltration of a markedly enlarged thyroid. Internal soft tissue nodules and soft tissue stranding was seen within the gland. The lesion extended superiorly bilaterally wrapping posteriorly around the thyroid cartilage into the retropharyngeal space with mass effect on the hypopharynx.

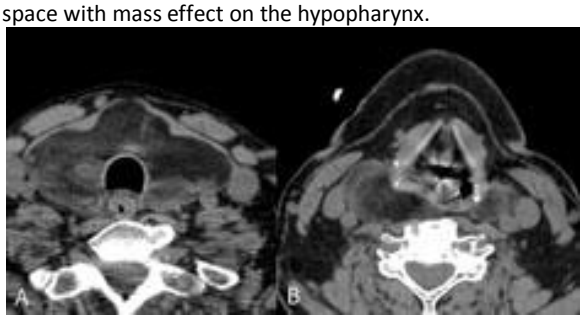

Figure 1.

Summary

Thyroid lesions containing macroscopic fat either radiographically or histopathologically are extremely rare and include amyloid goiter, thryrolipomatosis, liposarcoma, lymphocytic thyroiditis, thyrolipoma/adenolipoma of the thyroid, hamartomatous adiposity of the thyroid, and papillary carcinoma with macroscopic fat. Similarly diffuse enlargement of the thyroid by amyloid infiltration is a rare complication of systemic amyloid and in a minority of these patients can be the presenting sign of systemic disease. These rare lesions have been addressed from a histopathologic standpoint in the medical literature mainly in the form of case reports or small case series. However, little has been written regarding the radiographic evaluation of fat-containing lesions of the thyroid. We present this case to review the findings of amyloid goiter as well as the findings in other fat-containing lesions of the thyroid. Neuroradiologists should be aware that in a patient with known systemic amyloidosis who is euthyroid and has an enlarging thyroid gland that amyloid goiter is high on the differential diagnosis and can present with macroscopic fatty infiltration. FNA may be needed to make the diagnosis and surgery may be necessary due to compressive symptoms.

KEYWORDS: Thyroid, Fat, Amyloid Goiter

O-176 **6:20 PM - 6:25 PM**

Reversible Diffusion Restriction of the Middle Cerebellar Peduncles and Dentate Nucleus in Acute Respiratory Syncytial Virus Cerebellitis

Tang, Y.[1]·Suddarth, B.[1]·Du, X.[2]·Matsumoto, J. A.[3]
[1]Virginia Commonwealth University, Richmond, VA, [2]Hunter Homles Mcguire VA Medical Center, Richmond, VA, [3]University of Virginia, Charlottesville, VA.

Purpose

To report a rare case of acute RSV cerebellitis.

Case Report

A previously healthy three-year-old girl presented with altered mental status and fever after one week of cough and congestion. Nonenhanced head CT was negative except for bilateral mastoid effusions. The lumbar puncture revealed mild CSF pleocytosis, normal protein, glucose, lactate and negative cultures. The nasal aspirate tested positive for RSV. Two days after admission, the patient developed progressive hypotonia and cerebellar mutism. A contrast-enhanced head MRI was suggestive of acute cerebellitis. The patient significantly improved after a five-day course of intravenous methylprednisolone. At the six-month follow-up, she had returned to her baseline.

Imaging Findings

Initial head MRI demonstrated symmetric restricted diffusion of both middle cerebellar peduncles and the right dentate nucleus (Figure). There was corresponding mild FLAIR hyperintensity and no abnormal contrast enhancement. There were no other lesions. Repeat head MRI five days after the initiation of steroid treatment showed resolution of the diffusion and FLAIR abnormalities.

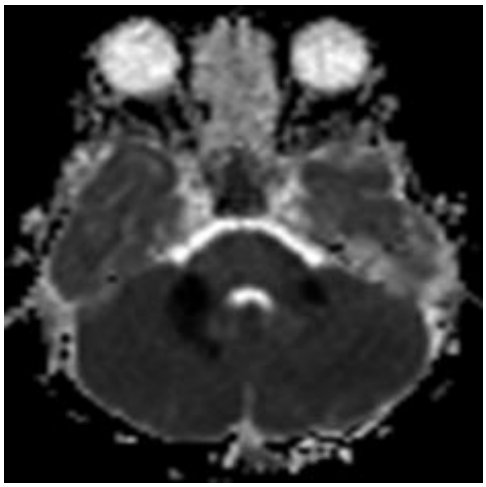

Note: Scanned images are included in the proceedings. Some submitted images were reduced during editing, thereby decreasing clarity. Also, refer to the Program Planner. Proceedings Content as of 3-29-2013.

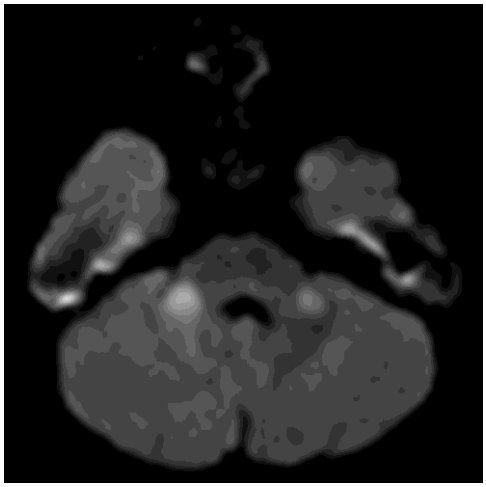

Summary
Acute cerebellitis is a rare postinfectious or postvaccinal inflammatory disorder that can present with fever, headache, altered mental status and cerebellar symptoms. The classic imaging appearance is transient edema involving the gray and white matter of the cerebellar hemispheres. The involvement of dentate nuclei is associated with cerebellar mutism. It is important to recognize that diffusion restriction of the middle cerebellar peduncles or dentate nucleus can be an imaging manifestation of acute cerebellitis, as has been reported previously in cases of rotavirus gastroenteritis. Our case expands these DWI abnormalities to include RSV as an associated pathogen. The transiently reduced diffusion may be due to intramyelinic edema, interstitial edema in tightly packed fibers, or a transient inflammatory infiltrate. Differential diagnoses include acute demyelinating encephalomyelitis (ADEM), infarction of the anterior inferior cerebellar artery (AICA) territories and toxic/metabolic encephalopathies.

KEYWORDS: Cerebellum, Inflammatory, cerebellitis

O-177 **6:25 PM - 6:30 PM**

Utility of Susceptibility-Weighted and Constructive Interference in Steady-State Sequences in the Evaluation of Hydrocephalus in the Newborn

Williams, S. C.·Saigal, G.
University of Miami
Miami, FL.

Purpose
Susceptibility-weighted imaging (SWI) is a magnetic resonance imaging (MRI) technique that is highly sensitive for blood, iron, and calcium deposition in the brain. In certain neonatal neurologic disorders such as traumatic brain injury, coagulation disorders, vascular malformations, cerebral infarction, neoplasms, and neurodegenerative disorders, Susceptibility-weighted imaging has an established role. In the evaluation of hydrocephalus in the newborn, SWI traditionally is not performed. However, in unexplained neonatal hydrocephalus, SWI can play an important role by demonstrating blood products in the ventricles and subarachnoid spaces. Constructive interference in steady state (CISS) is a gradient-echo MRI sequence with increased sensitivity for differentiating cerebrospinal fluid (CSF) intensity from pathologic structures. Constructive interference in steady state provides superior topographic information that helps to delineate the exact location of various cranial pathologies, and is useful in evaluating aqueductal stenosis. The purpose of this exhibit is to demonstrate the utility of SWI and CISS sequences in the evaluation of hydrocephalus in newborns by helping to differentiate congenital aqueductal stenosis from acquired aqueductal stenosis.
Case Report
Five patients underwent conventional MR imaging which demonstrated enlargement of the lateral and third ventricles without enlargement of the fourth ventricle, indicating obstructive hydrocephalus.
Imaging Findings
Etiology of the obstructive hydrocephalus was not determined on standard imaging. Addition of SWI and CISS sequences helped to differentiate acquired aqueductal stenosis from congenital aqueductal stenosis. In three cases, SWI demonstrated hemorrhage along the ventricles and cerebral aqueduct suggesting an acquired cause for the obstructive hydrocephalus. In the remaining two cases, CISS sequence demonstrated a clear narrowing of the cerebral aqueduct to indicate congenital aqueductal stenosis.
Summary
Susceptibility-weighted imaging and CISS are useful sequences in the evaluation of neonatal hydrocephalus at the level of the cerebral aqueduct. Susceptibility-weighted imaging increased the diagnostic sensitivity and specificity of MRI for evaluation of hemorrhage that was not evident on standard sequences. Constructive interference in steady state imaging increased the diagnostic sensitivity for determining congenital aqueductal stenosis in cases where SWI was negative. Therefore, inclusion of SWI and CISS sequences in the standard neonatal brain MRI protocol when evaluating for hydrocephalus should be considered.

KEYWORDS: Hydrocephalus, Aqueductal stenosis, SWI and CISS

Note: Scanned images are included in the proceedings. Some submitted images were reduced during editing, thereby decreasing clarity. Also, refer to the Program Planner. Proceedings Content as of 3-29-2013.

Tuesday Morning

7:30 AM - 8:30 AM
Ballroom 6AB

(19) Maintenance of Certification Review Session – Pediatrics (AR)

O-178 **7:30 AM - 8:00 AM**

Pediatric Brain

Moore, K. R.
Primary Children's Medical Center
Salt Lake City, UT.

Presentation Summary
A series of pediatric brain imaging cases will be presented with correlative differential diagnosis and comprehensive discussion. The cases will be selected to be reasonably representative of patients who may be encountered routinely in a pediatric neuroradiology practice as well as periodically in an adult-oriented neuroradiology practice where pediatric patients are imaged as well. The goal of the presentation is to review common and uncommon presentations of important pediatric neurologic disorders, with differential diagnosis discussion, in order to prepare practicing neuroradiologists for the ABR Neuroradiology recertification exam.

O-179 **8:00 AM - 8:30 AM**

Pediatric Head and Neck

Koch, B. L.
Cincinnati Children's Hospital
Cincinnati, OH.

Presentation Summary
This presentation will focus on the differential diagnosis of neck masses in the pediatric population. A variety of congenital and acquired masses will be reviewed, with emphasis on the variable imaging characteristics and location of lesions, to enable the attendee to more appropriately narrow the differential diagnosis when faced with a neck mass in a child. Congenital lesions such as vascular malformations and branchial apparatus cysts will be reviewed. The International Society for the Study of Vascular Anomalies (ISSVA) classification of vascular lesions will be discussed. In addition, the presentation will review a variety of the more common, and a few uncommon, acquired neck masses that occur in children, such as infantile hemangioma, fibromatosis colli, rhabdomyosarcoma, neuroblastoma and neurofibromas. Finally, the various head and neck manifestations of Neurofibromatosis type 1 will be presented.

Tuesday Morning

8:45 AM - 10:15 AM
Ballroom 6AB

(20) ASFNR/ISMRM Programming: Ultrafast MR Imaging

O-180 **8:45 AM - 9:15 AM**

Current Tools and Concepts for Accelerating Imaging: Parallel Imaging, CS

Roberts, T. P. L.
Children's Hospital of Philadelphia
Philadelphia, PA.

Presentation Summary
This presentation will review the conceptual approaches to faster MRI. As such it will cover the concept of “filling k-space faster”, through shortening TR (transitioning from spin-echo to gradient recalled echo), acquiring multiple lines (FSE/TSE) to single shot approaches (EPI). Approaches capitalizing on certain symmetries of k-space (partial Fourier) will be discussed as well as hybrid approaches (GRASE, HASTE). All sequence approaches will be unified in this theoretical framework. Just when it seems the limits of fast acquisitions have been reached (and only marginal “engineering” improvements are possible), the concept of parallel imaging with multiple receive coils will be introduced (SENSE, GRAPPA), again in the framework of “filling k-space faster”. Finally, a brief introduction to compressed sensing will be presented, again in the unified framework.

O-181 **9:15 AM - 9:45 AM**

What is Compressed Sensing and How Can We Use It?

Nayak, K. S.
University of Southern California
Los Angeles, CA.

Krishna Nayak is an Associate Professor of Electrical Engineering at the University of Southern California (USC), with joint appointments in Biomedical Engineering, Medicine, and Radiology, and is Director of the Magnetic Resonance Engineering Laboratory (http://mrel.usc.edu/). Dr. Nayak received his PhD in Electrical Engineering from Stanford University in 2001, his MS in Electrical Engineering from Stanford in 1996, and BS degrees in Electrical Engineering, Computer Science, and Applied Mathematics from Florida State University in 1995. Dr. Nayak has published 80+ journal papers, 200+ conference papers, and 10+ US patents.

Note: Scanned images are included in the proceedings. Some submitted images were reduced during editing, thereby decreasing clarity. Also, refer to the Program Planner. Proceedings Content as of 3-29-2013.

Presentation Summary
Compressed Sensing is a new method for accelerating the acquisition of medical images that is based on compressibility of resulting images. This talk will review the basic principles of CS (how it works, when it works, what happens when it fails), and will explain in detail several emerging applications in Neuro MRI.

O-182 **9:45 AM - 10:15 AM**

Applications of Compressed Sensing and Dynamic Imaging

Law, M.
Keck Medical Center of the University of Southern California
Los Angeles, CA.

Presentation Summary
The objectives for this lecture are to review some of the applications of compressed sensing (CS) in neuroradiology and dynamic imaging. Below are some techniques which can be utilized for accelerating MRI. Compressed sensing is a method of constrained reconstruction to compress imaging data so that faster imaging times can be obtained. This can be applied to conventional neuroimaging and advanced imaging techniques below. Furthermore, imaging which inherently has spatial and temporal sparsity are ideally suited for CS. These include time-resolved 4D MRA, dynamic contrast-enhanced MRI (DCE MRI) and dynamic susceptibility contrast MRI (DSC MRI). Finally multicontrast and synthetic imaging will be reviewed which is another means of reducing the neuroimaging protocol. **• Fast and Ultrafast MRI Techniques. • Parallel Imaging, View Sharing, Compressed Sensing. • Dynamic Imaging, Airway and Speech Imaging. • Advanced Imaging: Perfusion, DWI, DTI, MR Spectroscopy. • DCE MRI, DSC MRI, Time Resolved MRA. • Multicontrast Imaging, Synthetic Imaging.**

Tuesday Morning

8:45 AM - 10:15 AM
Ballroom 6CF

(21) SNIS Programming: New Devices in Interventional Neuroradiology and Their Imaging Appearances

O-183 **8:45 AM - 9:15 AM**

Flow Diverters: Physiological Purposes in Theory and Practice

Fiorella, D. J.
Stonybrook University Medical Center
Stonybrook, NY.

Presentation Summary
The presentation will discuss preclinical and clinical data which provide insight into the mechanism of action of flow diverters to treat brain aneurysms.

O-184 **9:15 AM - 9:45 AM**

Flow Diverters: Application and Issues

Moran, C. J.
Washington University School Of Medicine
St. Louis, MO.

Presentation Summary
Imaging of the patient treated with flow diversion devices [Pipeline embolization device (PED), eV3 Neurovascular/Covidien, Inc., Minneapolis, MN] has three phases. Preprocedural, intraprocedural, and postprocedure. Each of the imaging modalities [computerized tomography (CT), magnetic resonance imaging (MR), digital subtraction angiography (DSA)] have strengths and weaknesses in evaluating the candidate for flow diversion, undergoing flow diversion, or being followed to determine the adequacy of treatment. In the preprocedure evaluation, CT, CTA, MR, and MRA identify many of the aneurysms suitable for flow diversion. In addition, they depict the relationships of parent arteries to the treatment aneurysm as well as characterizing the lumen and wall. They do not seem to be completely accurate in generating measurements for device sizing. They are very useful in characterizing the brain and other intracranial contents. 2. Most important to intraprocedural imaging is the quality of the digital subtraction image and its accuracy with calibration. Fluoroscopy must be of high quality so that the device can be positioned correctly and deployed. Most equipment has a lower radiation exposure for the fluoroscopic mode and has an available radiographic exposure - which increases the visibility of the device during its deployment. Standard biplane angiographic exposures with a calibration device in place (usually a guiding catheter) allow accurate calibration for device sizing. Rotational angiography (3D) depicts the relationship of the aneurysm, its neck and the parent artery. DynaCT provides the exact relationship of the deployed device to the parent vessel wall. 3. In the postprocedural period, CT is very useful in evaluating the possibility of intracranial hemorrhage without significant artifacts from the deployed PED. Widely windowed CTA can evaluate the patency of the device as well as other vessels. MR is extremely useful to evaluate the brain parenchyma looking for ischemic or thromboembolic

Note: Scanned images are included in the proceedings. Some submitted images were reduced during editing, thereby decreasing clarity. Also, refer to the Program Planner. Proceedings Content as of 3-29-2013.

injuries. MRA is only useful for evaluating flow signal in vessels distant from the PED due to the artifact arising from the PED. In the later postprocedural period, operators have utilized angiography to evaluate the patency of the device, flow into the aneurysm either through the device or with endoleaks, and finally the degree of occlusion of the aneurysm. These evaluations are performed at intervals ranging from 3-6 months and up to a complete aneurysm occlusion. In summary, the imaging modality chosen is based on the phase of the treatment sequence.

O-185 **9:45 AM - 10:15 AM**

Imaging Techniques to Optimize Visualization: What INR Is Looking For

Nesbit, G. M.
Oregon Health & Science University
Portland, OR.

Presentation Summary
The introduction of flow diversion for the treatment of intracranial aneurysms over the past five years has changed the approach to large and wide-necked aneurysms. Flow diversion disrupts intra-aneurysmal flow and encourages aneurysmal thrombosis and progressive angiographic obliteration. Imaging of these devices is designed to determine aneuyrsmal obliteration and evaluation of potential complications. The currently available devices are cobalt chromium and platinum and are conditionally MRI compatible at 1.5 and 3T. Thromboembolic complications and occlusion of perforator vessels are always of concern with endovascular implants, but appear to be very rare, as patients are on dual antiplatelet medication for a variable period and anticoagulation during the procedure. The ideal dosage and duration of antiplatelet therapy in patients undergoing flow diversion and the need for routine antiplatelet sensitivity testing remains controversial. An uncommon but most-feared complication of this technology is delayed aneurysm rupture which usually occurs in the first few weeks, but can be delayed for months. The exact incidence of this is unknown, very low, unpredicatable, but usually confined to very large and giant symptomatic aneurysms. Contrast enhancement within the lumen (indicating lack of complete thrombosis) or of the wall (indicating an inflammatory component) may be of benefit, but needs further study to determine its predictive value. Another complication is distal intraparenchymal hemorrhages. These seem to occur within the first few days after treatment. The etiology of distal intraparenchymal hemorrhage is poorly understood but in part may be due to distal guidewire manipulation in the sometimes difficult delivery of these systems. Imaging followup in patients treated with flow diversion is extremely important is assessing efficacy and risk. Further study of imaging's role in the prediction of potential complications such as delayed rupture and intraparenchymal hemorrhage is recommended.

Tuesday Morning

8:45 AM - 10:15 AM
Ballroom 6DE

(22) ASSR Programming: Next Generation of Imaging the CSF: Myelography, Has the Magic Returned?

O-186 **8:45 AM - 9:15 AM**

Evolution of the Myelograms

Nguyen, D. T. D.
Penn State Hershey University Medical Center
Hershey, PA.

Presentation Summary
The Myelogram study was developed to critique positional status of the thecal sac, spinal cord, and spinal nerve roots decades ago. Its technique has gone through several enhancements through the years, ranging from contrast agents to postprocedure imaging techniques. The study is a minimally invasive procedure that has some limitations and intrinsic risks. Knowledge and recognition of some of these can assist neuroradiologists in minimizing such shortcomings. With such, development of alternate methods to visualize the spinal sac and its contents were developed. Despite the use of these techniques to replace or augment some of its capabilities, the myelogram study still remains a robust study in modern day neuroradiology practice. In this presentation, we will visit: • Myelogram history and techniques. • Myelogram pitfalls. • Advance technique applications.

O-187 **9:15 AM - 9:45 AM**

State of the Art Imaging CT Myelography - Best Indications and MRI Greatest Benefits

Miller, T. S.
Albert Einstein College of Medicine Montefiore
Bronx, NY.

Presentation Summary
Attendees will gain a thorough understanding of myelography. A review the history of myelography will be shared. Indications, contraindications and best practices will be discussed. The current state of the art CT myelography will be presented. Finally, future trends in MRI myelography will be introduced, and MRI will be compared to CT. Myelography originally grew out of

Note: Scanned images are included in the proceedings. Some submitted images were reduced during editing, thereby decreasing clarity. Also, refer to the Program Planner. Proceedings Content as of 3-29-2013.

pneumoencephalography in 1919 when Dandy realized that spinal cord imaging would eventually be accomplished with similar techniques used to image the brain. In 1921 Jacobeus reported successful cord tumor localization, and Dandy reported his experience in 1925. Sicard and Forestier introduced epidurography in 1926 as an x-ray diagnostic method using Lipiodol. Dandy published a series on gas myelography in 1922. Several authors published series on canal access methods. There were issues with gas, and then removal of Lipidol. Both lumbar and cervical access were introduced. Myelography is used to visualize the outline of the spinal cord and subdural space. Multiple agents including gas, lipid soluble: Lipidol, Thorotrast, Pantopaque, and water soluble: Abrodil, Conray, Omnipaque have been used. While originally developed during the pre-MRI plain x-ray era, myelography continues to be used as a problem-solving tool utilizing postinjection CT. Narrowing of the canal and nerve root exit zones is clearly demonstrated on postinjection imaging. Myelography has been shown as superior to MRI in detection of cervical nerve root avulsions. Dynamic or delayed imaging can be used to evaluate cysts in the canal or within the cord. Patients with low-pressure headache syndromes also may be imaged in a delayed or dynamic fashion to delineate CSF leaks. It is in this often young patient group where, due to radiation concerns, off-label use of gadolinium-based agents has gained popularity in MRI myelography.

O-188 **9:45 AM - 10:15 AM**

Gadolinium: A Special Preview of the 21st Century

Tali, E.
Gazi University School of Medicine
Besevler, Ankara, TURKEY.

Presentation Summary
Animal and human studies showed that the intrathecal administration of Gd in the low dose range is a relatively safe procedure without significant side effects at diagnostic dosages. Intrathecally administered GD in animal studies showed no significant change in any of the physiologic or histological parameters examined. A mixture of 0.5 cc (500 mmol/L) Gd and 5 cc of the patient's CSF generally was administrated intrathecally for MR cisternography/myelography (MRCM). No serious side effects or complications were observed related to this technique. Mild transient headache may be the only symptom observed in the first 24 hours following the procedure. This side effect was assumed to be caused by the lumbar puncture instead of intrathecally administered Gd and responds well to oral analgesics. CT cisternography and radioisotope cisternography have been used in the past to evaluate different subarachnoid space pathologies. Conventional myelography is an out-of-date method due to the lack of cross-sectional features and being invasive. Radionuclide cisternography is obsolescent because of its limitation in localization of leak and its difficulties in application. High-resolution CT combined with contrast injection also has been used in detecting different CSF pathologies and especially CSF leakage but turned out to be inadequate in showing the leaks in cases with multiple defects or fractures of the skull base. The most important difficulty that must be overcome in CT cisternography is the restricted distribution of iodinated contrast media in the CSF, the artifacts of the surrounding bones and increasing radiation doses with repeat scans. As MRI provides multiplanar imaging, high contrast-to-noise ratio, thin-section image acquisition, with no bony artifacts and risk of ionizing radiation, it is used more frequently in the setting of CSF leakage. The main advantage of MRI contrast medium compared to CT contrast agents, is their free distribution in the subarachnoid space. These features enable MRCM to readily depict faint or slow flowing CSF fistula, compared to CT cisternography. Meanwhile, MRCM also can be used in any pathology regarding the CSF space such as loculations, adhesions, etc. Although management of arachnoid cysts is still controversial, the detection and characterization of CSF pathway communication or noncommunication with arachnoid cysts by means of MRCM can be useful for surgical planning in symptomatic patients.

Tuesday Morning

8:45 AM - 10:15 AM
Room 5AB

(23) General Programming: WFNRS Presents the Best of AOSNHNR Peritherapeutic Neuroradiology

O-189 **8:45 AM - 9:05 AM**

Physiologic MRI: Surrogate Marker for Lesion Characterization

Toh, C.
Chang Gung Memorial Hospital Chang Gung University
Linkou, TAIWAN.

Dr. Cheng Hong Toh received his education as follows: Radiology Residency and Neuroradiology Fellowship, Department of Medico/Imaging and Intervention, Chang Gung Memorial Hospital, Linkou, Taipei, Taiwan. He is currently Assistant Professor of Radiology, Chang Gung University of Medicine, Department of Medica/Imaging and Intervention, Chang Gung Memorial Hospital, Linou, Taipei, Taiwan. Dr. Toh's academic activities are: Editorial position, 1; Reviewer responsibilities, 2; Book chapter, 1; Articles in peer review journals, 30,· Invited lectures and presentations, 23; scientific exhibits, posters and

Note: Scanned images are included in the proceedings. Some submitted images were reduced during editing, thereby decreasing clarity. Also, refer to the Program Planner. Proceedings Content as of 3-29-2013.

proceedings, 19; Honors, awards and special recognitions, 9; and funded studies, 8. Dr. Toh's research interests ore: Physiologic-based MR techniques (e.g., DTI, SWf and PWI}, CNS tumor imaging, CNS infections, White matter disease and imaging-pathologic correlations. His Website is: https:/ /sites. google. com/site/chtohvc/.

Presentation Summary
Conventional MRI remains the primary imaging modality for noninvasive evaluation of brain lesions. One major limitation of conventional MRI, however, is that it cannot provide physiologic and metabolic information of the lesions. More advanced MR imaging techniques such as diffusion tensor imaging (DTI), dynamic susceptibility contrast-enhanced perfusion-weighted imaging (DSC PWI) and susceptibility-weighted imaging (SWI), hold much promise to fill that role by potentially providing novel physiology-based information. Diffusion tensor imaging provides information on histologic architecture such as cellularity and cellular organization by measuring the directional variation of water diffusivity. Dynamic susceptibility contrast-enhanced PWI assesses the degree of angiogenesis and has been shown to correlate with microvascular proliferation. Susceptibility-weighted imaging is a high-resolution 3D gradient-echo sequence that combines phase and magnitude information to detect magnetic susceptibility differences between adjacent tissues. Its high sensitivity in the detection of paramagnetic and diamagnetic substances such as iron deposits, blood degradation products, and calcifications provides clinically useful information in the evaluation of various disorders. The true strength of physiologic MRI is the ability to provide quantitative surrogate MR markers and depict changes in the internal architecture in the setting of no overall change in the conventional MRI. In this talk, the physics of these physiologic MR techniques will be discussed briefly. The roles of physiologic MRI, particularly in the presurgical workup of common intracranial mass lesions such as gliomas, abscesses, lymphomas, etc. will be presented. The correlations between physiologic MR imaging findings and histopathology will be demonstrated. Finally, the limitations of these MR techniques also will be addressed.

O-190 **9:05 AM - 9:23 AM**

Peritherapeutic Neuroimaging on Brain Tumors

Hirai, T.
Graduate School of Medical Sciences
Kumamoto University
Kumamoto, JAPAN.

Presentation Summary
Peritherapeutic neuroimaging in patients with gliomas has an important role to evaluate structural, hemodynamic, metabolic, cellular, and cytoarchitectural alterations. Although histopathologic assessment remains the reference standard for determining the glioma grade, sampling error, large range of WHO classification and grading systems, inter and intrapathologist variability, and difference in biology within WHO grades of gliomas may result in inadequate evaluation of the entire tumor. Thus, for a final brain tumor diagnosis, neuroimaging studies may provide information in addition to the pathologic assessment. Advanced MR techniques such as diffusion-weighted and perfusion imaging are useful to diagnose and grade gliomas and to assess treatment response and patient prognosis. For diffusion-weighted imaging, it has been suggested that the regions with minimum apparent diffusion coefficients reflect the sites of highest cellularity within heterogeneous tumors, and, therefore, these sites may be of diagnostic value in identifying high-grade tumor components. Perfusion imaging provides information about tumor angiogenesis and is performed with dynamic contrast-enhanced methods or arterial spin labeling techniques. We present and discuss peritherapeutic applications of these neuroimaging techniques especially for tumor grading and prognostic value in patients with gliomas.

O-191 **9:23 AM - 9:41 AM**

Advanced MR Imaging in the Post Therapy Brain Tumor Microenvironment

Kim, H. S.
Asan Medical Center
Seoul, KOREA, REPUBLIC OF.

Dr. Ho Sung Kim (MD, PhD} is assistant professor, Department of Radiology, Division of Neuroradiology, As an Medical Center, Seoul, Korea. Dr. Kim's education is as follows: Han yang University School of Medicine {1993.3 - 1996.2) and Postgraduate: University of Ulsan College of Medicine {2004.3-2006.2). His research interests include advanced CT and MR technologies and imaging processing, especially perfusion MR imaging in brain tumor. Dr. Kim's publication list contains about 40 SCL Papers some of which appeared in Radiology and AJNR.

Presentation Summary
Brain tumor microenvironment has been investigated by a desire to understand, and mitigate, the hypoxic fraction of tumors that are resistant to radiation therapy. The microenvironment within brain tumors is significantly different from that in normal tissues. A major difference is tumor vasculature which results in unbalanced blood supply and significant perfusion heterogeneities, causing tumor hypoxia. It is commonly believed that the hypoxic tumor microenvironment is usually associated with poor perfusion and elevated metabolic rates, respectively. The tumor hypoxia also have important consequences for antitumor therapy and can contribute to the progression of tumors by induction of upregulation of tumor vascularity. Tumor hypoxia can lead to a more aggressive phenotype of tumor cells, with a number of altered behaviors, such as increased metastasis. Hence, tumor

Note: Scanned images are included in the proceedings. Some submitted images were reduced during editing, thereby decreasing clarity. Also, refer to the Program Planner. Proceedings Content as of 3-29-2013.

hypoxia may be essential intermediates in the malignant transformation of low-grade tumor. The most well studied effects of the tumor microenvironment are the inhibition of chemo and radiotherapies. Such physiologic resistance can be caused by direct action of pH and O2 on the therapy or more generally by poor perfusion, which limits the delivery of drugs to the target cells. Resistance to radiotherapy at low pO2 is a direct consequence of the ability of oxygen to propagate radical damage to macromolecules and membranes through the generation of reactive oxygen species. Consequently, hypoxic tumor cells are three to five times more resistant to ionizing radiation compared to well oxygenated cells. Although the mechanisms are unknown, tumor hypoxia incontrovertibly stimulates metastatic behavior by a direct mechanism. This phenomenon is related to expression of vascular endothelial growth factor (VEGF). Many MR imaging techniques including diffusion, perfusion, susceptibility, and BOLD have emerged and allow the interrogation of the brain tumor microenvironment. Studies employing these physiologic imaging methods have provided new insights into the causes and consequences of the hostile tumor microenvironment. Elucidation of pathologic background and imaging correlation will yield further insights into the tumor microenvironment. In this presentation, we attempt to identify various MR imaging techniques, postprocessing and their application to post-treatment brain tumor microenvironment.

O-192 **9:41 AM - 9:59 AM**

Peritherapeutic Functional MR Imaging of Normal Pressure Hydrocephalus: Moving from Research to Clinical Practice

Chen, S.
Tri-Service General Hospital
Taipei, TAIWAN.

Dr. Cheng-Yu Chen was born in 1960. He received his medical degree in the School of Medicine, National Defense Medical Center, Taipei, Taiwan in 1985. Dr. Chen's Professional appointments are: the Executive Dean, National Defense Center, Professor, School of Medicine, National Defense Medical Cent4er, Taipei, 2000. He has served as an editorial board member of the American Journal of Neurology {AJNR) from 2001-2011. He was appointed the section editor, Classic Image, special consultant, AJNR in 2011. Dr. Chen was a member of the scientific program committee, RSNA from 2007-2012 and Editor-in-chief of the Journal of Radiological Science since 2011. He has published several articles in Radiology.

Presentation Summary
Idiopathic normal pressure hydrocephalus (iNPH) has long been recognized as a treatable disease by early shunting with clinically notable improvements, most often on the gait disturbance, followed by the incontinence, and less noticeably the demented symptoms. In the past, efforts have been made on the prediction of shunt responsiveness in iNPH patients, for example, CSF tapping, which, though still being the current standard, is considered invasive. Early studies using noninvasive methods on this regard include MRI measurements of CSF stroke volume by hand drawing regions of interest within the small aqueduct of Sylvius. However, the cut-off value set for the prediction of responsiveness (greater than 42 microL) by Bradley, et al. has not gained wide consensus, partly because the differences in the measurement techniques, imaging parameters, and even the scanners used. More recently, new MR technologies have added to the research realm for iNPH, those including perfusion imaging, diffusion tensor imaging and MR spectroscopy, in addition to the improved phase contrast techniques and objective ROI methods. Independent imaging predictors, such as cerebral blood flow (CBF), loss of vasomotor response in the periventricular WM, mean CSF stroke volume, and distension of the corpus callosum can be measured quantitatively using cutting-edge technology. In this lecture, a short review of the possible etiologic factors for iNPH and the perspectives of using advanced MR imaging to establish the independent predictors potentially useful for clinical applications will be addressed. 1. Noninvasive imaging biomarkers that could be used to differentiate lumbar-drain responded iNPH patients from those unresponded. 2. Early gait disturbance in iNPH, mechanism approach. 3. Incontinence in iNPH as a result of hydrocephalus or ischemia, imaging approach.

O-193 **9:59 AM - 10:07 AM**

MR Voxel-Based Histogram Analysis of Atherosclerotic Basilar Artery in Patients with Isolated Pontine Infarct

Lee, H.
Kyungpook National University Hospital
Daegu, KOREA, REPUBLIC OF.

Dr. Lee was born July 13, 1971. He received his education at Kyungpook National University, School of Medicine from 1992-1997 and at Kyungpook National University, Graduate School from 1998-1999. He received his Doctor of Medicine degree from Kyungpook National University in 2004. Dr. Lee is Associate Professor Deportment of Radiology at Kyungpook National University Hospital (KNUH}, Daegu, South Korea. He is also the Instructor-Assistant Professor (Radiology) at KNUH from 2006.5 to the present. Dr. Lee's interests are Clinical Neuroradiology, Manganese-enhanced MRI (experimental), Thyroid USG. He has published more than 56 articles and has received multiple honors.

Presentation Summary
Each voxel magnetic resonance imaging (MRI) of atherosclerotic vessels represents various tissue components of atherosclerotic plaque according to the physical property of the corresponding tissue. We hypothesized the pattern of voxel-based magnetic

Note: Scanned images are included in the proceedings. Some submitted images were reduced during editing, thereby decreasing clarity. Also, refer to the Program Planner. Proceedings Content as of 3-29-2013.

resonance histogram (MRH) represent the status of atherosclerotic status quantitatively. The aim of this study is to evaluate the usefulness of MRH for atherosclerotic basilar artery in patients with isolated pontine infarction. A total of 42 patients diagnosed with acute isolated pontine infarction (PI) were included and 10 normal healthy volunteers were included as normal controls. Using home-made program (CI image, version 1.0), we analyzed voxel data and calculated the numbers of voxels according to signal intensities from the T1- and T2-weighted MRI of basilar arterial wall. From the histogram, the number of pixels from wall, lumen CSF and brain were defined as Σwall, Σlumen, ΣCSF, and Σbrain. We compared the patterns of histogram between groups of PI with plaque and without plaque. The spectra from the normal healthy control group showed two phasic peaks on spectrum T1-weighted images and multiphasic peaks from T2-weighted images. The spectra from PI with plaque group showed decreased height of the peak from area of the lumen and increased peak from the atherosclerotic plaques. The ratio of area under curve of Σwall/Σlumen were higher in PI with plaque group than PI without plaque on spectrum form T1WI (2.47 versus 1.06, p<0.001) and T2WI (1.22 versus 0.71, p<0.001). We observed a significant difference among the patient with or without pontine infarction and normal control group comparing each histogram. From the MRH of control group, we could get the histograms of wall and lumen and we found that they had their own peak and range in histogram. On base of this histogram, we could compare the histogram of the control group and that of basilar artery with pontine infarction. Also there was no difference in the wall component between patients with plaque and without plaque, whereas the luminal component is much more and has a prominent peak in patients without plaque. Peak in lumen component was not evident in control group and patients with plaque.Therefore, we can identify the wall thickening by atherosclerotic plaques before their impact on the luminogram or even in HRMRI. These findings also suggest that there is ongoing adaptation mechanism of atherosclerotic change, namely “positive remodeling”. Therefore, MRH has several advantages for the evaluation of atherosclerotic plaque. First, it can measure atherosclerotic itself, which makes it possible to evaluate degree of atherosclerotic plaque as well as degree of stenosis. Second, this method is quantitative analysis, which could be useful in follow-up study. Third, it could be a promising method for analysis of the histology of atherosclerotic plaque. Because, the signal intensities of MR depend on the chemical property of voxel, proper acquisition for atherosclerotic plaque could predict vulnerable plaque. In conclusion, this study demonstrated that histogram of basilar arteries in patients with isolated pontine infarction. We thought this method could give the quantitative information for vascular status in atherosclerotic disease.

O-194 **10:07 AM - 10:15 AM**

Utility of Skewness and Kurtosis Derived from MR Perfusion Histogram to Predict Pseudoprogression in Patients with Glioblastoma

Baek, H.
Inje University College of Medicine, Haeundae Paik Hospital
Busan, KOREA, REPUBLIC OF.

Dr. Hye lin Baek received his education at Inje University College of Medicine (2000.3-2006.2) and his Postgraduate from Inje University College of Medicine (2010.3-2012.2). He interned at Busan Paik Hospital (2006.3 -2007.2). He was a resident, Department of Radiology, Busan Paik Hospital {2007.3-2011.2). Dr. Lee then became a Clinical instructor (Fellow): Department of Radiology at Asan Medical Center (2001.3-2012). Currently he is Assistant Professor, Division of Neuroradiology, Department of Radiology, Inje University College of Medicine, Haeundae Paik Hospital. Dr. Baek has published many papers in the Journal of the Korean Society of Radiology, RadioGraphies, Neurointervention, and Radiology.

Presentation Summary
The purpose of this presentation is to test the predictive value of skewness and kurtosis changes of normalized cerebral blood volume (nCBV) during early treatment period for differentiating early tumor progression from pseudoprogression in patients with newly diagnosed glioblastomas. The institutional review board approved this retrospective study. We assessed 135 patients with newly diagnosed glioblastomas who underwent concurrent chemoradiotherapy (CCRT) after surgical resection. Patients who developed new or enlarged contrast-enhancing lesions after CCRT were assessed by conventional and perfusion MR imaging. The percent change of skewness and kurtosis of nCBV histogram between the first and second post-CCRT followup were classified into four categories. Independent predictors of early tumor progression were determined by logistic regression analysis. Of 135 patients, 79 patients had new or enlarged contrast-enhancing lesions after CCRT, and subsequently classified as early tumor progression (n =42, 53.2%) and pseudoprogression (n = 37, 46.8%). Pseudoprogression was observed in 23 of 24 (95.8%) patients in category 1, 10 of 15 (66.7%) in category 2, four of 20 (20.0%) in category 3, and 0 of 20 (0%) in category 4 (Chi-square test, P < 0.0001). The histographic pattern of nCBV was the best independent predictor (odds ratio, 3.51; P = 0.0032) for early tumor progression, representing the largest area under the receiver operating characteristic curve (A_z) (A_z = 0.934; 95% CI: 0.855, 0.977), with a sensitivity of 85.7% and a specificity of 89.2% rather than each percent change of skweness or kurtosis. The change of skewness and kurtosis of nCBV may be a potential imaging biomarker for early treatment response in patients with newly diagnosed glioblastomas.

Note: Scanned images are included in the proceedings. Some submitted images were reduced during editing, thereby decreasing clarity. Also, refer to the Program Planner. Proceedings Content as of 3-29-2013.

Tuesday Morning

8:45 AM - 10:15 AM
Room 1AB

(24) Young Professionals Programming: Choosing Your Career

O-195 **8:45 AM - 9:00 AM**

Benefits of Academic Medicine

Russell, E. J.
Northwestern University
Chicago, IL.

Presentation Summary

Concerning economics, the inducements for residents to opt for private practice include excellent compensation and time off. While academic radiology departments cannot compete directly, since a percentage of earned income must be reinvested in support for research and teaching time, competitive compensation is more prevalent now in academic departments. Furthermore, the involvement of academic radiologists in management roles within the institutions/hospitals/medical schools in which they practice, and connections that develop with other departments through joint educational, research and clinical activities, can provide a more secure practice environment, in this era of "commoditization". Having said that, it is important that the true advantages of an academic career are fully considered when making a career choice. It affords one the opportunity to develop a career where the joys of developing new knowledge through research is supplemented by the time off the clinical schedule given to travel and present your work at national and international meetings, and develop connections with other academic radiologists that can last a lifetime. Furthermore, academic radiologists can focus on a single area of practice. While some may enjoy a more general practice required more often in private groups, market forces and teleradiology companies willing to deliver subspecialty interpretations at all hours are making it less desirable for new radiologists to be a "Jack of all trades but a master of none". Apart from these considerations, there are key factors influencing those who choose an academic career as summarized by Gunderman: 1. *Patient care*: An academic environment best supports state-of-the-art clinical practice, often based on industrial collaborations and translational research. The availability of cutting edge techniques allow faculty to develop the deepest level of expertise. 2. *Intellectual stimulation*: As eloquently stated by Gunderman, "the inquisitive attitude that characterizes good academic radiologists leads them to attend professional meetings, to get involved in organized radiology, and to read research journals regularly, and these are precisely the venues in which new ideas are disseminated." An academic center also facilitates interaction with academicians in other fields and departments, and provides teaching opportunities that further stimulate the teacher ("those who teach a subject understand it better than those who do not"). 3. *Service opportunities*: Academic radiologists, particularly those with an interest in management, can have a significant impact on the future role of radiology in health care delivery and patient care, never more important than it is today to secure the specialty. 4. *The joy of teaching*: Those who have spent time in an academic setting generally say that the most enjoyable and rewarding aspect of their careers is teaching. There is an opportunity to disseminate your knowledge and help patients indirectly by permanently imprinting your "scientific children" with your perspectives and knowledge, a lasting legacy indeed. 5. *Research:* Physicians working in academic centers enjoy a special opportunity to engage in in-depth study of things that puzzle them, and it is deeply satisfying to see the practice of radiology change because your research leads to new information. A career in academic radiology makes the most sense for those who are curious and take pleasure in pursuing knowledge, who enjoy teaching and think they might be good at it, who feel at home in an academic environment where people tend to think critically and creatively about what they do, and who wish to make distinctive leadership contributions in their field.

O-196 **9:00 AM - 9:15 AM**

Benefits of Private Practice

Pramanik, B. K.
Medical Center Radiology Group
Orlando, FL.

Presentation Summary

Private practice radiology offers a number of considerable advantages over academic radiology. One key advantage is personal freedom. There is much more autonomy to make decisions as there is less bureaucracy. The workload is predominantly clinical and there is no research or very little teaching responsibilities. Private practice enables radiologists to capitalize on a broader range of their training. Most private practice radiologists practice general radiology and see a broad range of patients encompassing every radiologic subspecialty and modality. By seeing a breadth of cases, there is more flexibility to adapt. Finally, the major advantage is compensation. Private practice salaries are higher than academic radiology. Moreover, the benefits packages including vacation are frequently more generous.

Note: Scanned images are included in the proceedings. Some submitted images were reduced during editing, thereby decreasing clarity. Also, refer to the Program Planner. Proceedings Content as of 3-29-2013.

O-197 **9:15 AM - 9:30 AM**

Negotiating a Position in Academic Medicine: What You Need to Know

Mukherji, S. K.
University of Michigan Health System
Ann Arbor, MI.

Presentation Summary
The intent of this presentation will be to review important aspects about negotiating an academic radiology position. The attendees will be familiar with important information that will permit them to properly assess different academic opportunities.

O-198 **9:30 AM - 9:45 AM**

Negotiating a Contract in Private Practice: What You Need to Know

Barr, R. M.
Mecklenburg Radiology Associates, P.A.
Charlotte, NC.

Presentation Summary
This will be a practical, "how to" session for attendees preparing to enter the private practice radiology workforce. The basics of the employment contract will be discussed from the perspective of the group practice. The speaker hopes to make up for a lack of legal expertise with a plethora of common-sense advice. The typical steps from recruitment to contracting will be reviewed. The talk will highlight the most important elements of the contract, including the elements that tend to raise the most questions, such as noncompete clauses and tail coverage responsibility. We'll discuss what's typically missing from the contract, and the most common mistakes job seekers make when contracting.

O-199 **9:45 AM - 10:00 AM**

Why I Did What I Did and Did I Make the Right Decision

Seidenwurm, D. J.
Radiological Associates
Sacramento, CA.

Presentation Summary
Choose a career that reflects a realistic assessment of your interests and capabilities, and one that will make you happy based on your priorities in life.

Tuesday Morning

10:45 AM - 12:15 PM
Ballroom 6AB

(25a) Parallel Scientific Papers: Adult Brain: Tumors I: Glioblastoma

O-201 **10:45 AM - 10:53 AM**

Glioblastoma Multiforme: Peritumoral Apparent Diffusion Coefficient Analysis in Prediction of Tumor Volume Recurrence

Chow, D. S.·Lignelli, A.·Qi, J.·Guo, X.·Miloushev, V.·Pisapia, D.·Yun, J.·Canoll, P.·Lassman, A.·Zhao, B.·Filippi, C.
Columbia University
New York, NY.

Purpose
Glioblastoma multiforme (GBM) is an invasive and aggressive tumor. While therapy typically includes maximal surgical resection followed by radiation therapy (XRT) with adjuvant temozolomide (TMZ), rates of recurrence are highly variable. Apparent diffusion coefficient (ADC) maps represent an imaging tool that may be related to prognosis in GBM patients. Low ADC values demonstrate restricted water movement which is suggestive of increased cellular density. Thus, decreased ADC values may correlate to tumor infiltration. We hypothesize that GBM patients with decreased ADC in the peritumoral edema will exhibit a higher amount of tumor regrowth following resection.
Materials & Methods
This retrospective study included patients with native glioblastomas with pre-operative, 24-48 hour postoperative, and 2-3 month follow-up MRIs. All patients received XRT with concurrent TMZ following maximal resection. Two consecutive regions of interests were drawn on pre-operative ADC maps in the (1) immediately adjacent and (2) distant peritumoral FLAIR abnormality. The adjacent ADC value was subtracted from distant ADC value to obtain a subtracted ADC (sADC) value. Therefore, when the immediate peritumoral ADC value was lower than the distant peritumoral ADC values, higher sADC values were obtained. Postoperative tumor volumes were assessed using postcontrast T1-weighted images at 24-48 hours and at 2-3 month followup. Volumes were obtained using a semi-automated algorithm that combines region-based active contours and level set approach. Student's *t*-test was used to compare sADC values between patients with a recurrent tumor volume growth of less than 50% and greater than or equal to 50%. Linear regression analysis also was performed to assess the relationship between peritumoral sADC values and tumor growth by volume. A p-value of < 0.05 was considered statistically

Note: Scanned images are included in the proceedings. Some submitted images were reduced during editing, thereby decreasing clarity. Also, refer to the Program Planner. Proceedings Content as of 3-29-2013.

significant.
Results
A total of 14 patients met inclusion criteria, of which 10 displayed greater than 50% growth on 2-3 month follow-up MRI. The mean sADC in individuals with recurrent tumor volume growth less than 50% and greater than or equal to 50% was -19.8% and 208.3% respectively ($p < 0.01$). Linear regression analyses revealed a significant correlation between sADC values and tumor growth ($p < 0.01$).

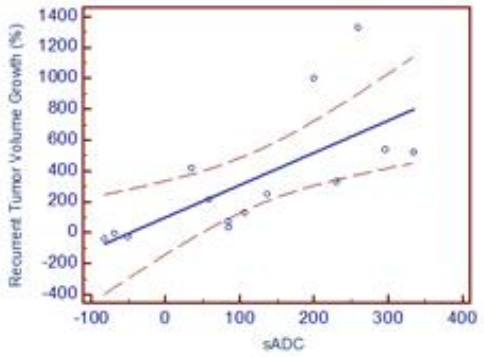

Conclusion
Evaluation of the pre-operative peritumoral ADC potentially can predict the volume of postoperative recurrence within the first 2-3 months of treatment. Additionally, these measurements may represent a potential biomarker for tumor infiltration in the immediate nonenhancing peritumoral region.

KEYWORDS: Glioblastoma, Apparent diffusion coefficient

O-202 **10:53 AM - 11:01 AM**

May the Diffusion Tensor Imaging Metrics Be Used to Predict Survival in Patients with Newly Diagnosed Glioblastoma?: A Preliminary Diffusion Tensor Imaging Histogram Analysis in Glioblastoma

Tian, W.·Liu, X.·Zhong, J.·Ekholm, S.
University of Rochester Medical Center
Rochester, NY.

Purpose
Glioblastoma is the most common malignant primary brain tumor in adults, with median survival of approximately 12-15 months after initial diagnosis. However, occasional long-term survivors have been reported and a subset of patients may show a significant response to therapy. Diffusion tensor imaging (DTI) is a novel noninvasive advanced imaging technique to provide multiple quantitative metrics revealing molecular motion and microstructure information. Although DTI has been shown to be helpful in pre-operative grading of gliomas, its value for predicting survival is still unknown. The purpose of this study is to evaluate the value of DTI derived parameters, and histogram analysis in predicting the survival time in patients with glioblastoma.

Materials & Methods
The study included pre-operative DTI examinations in 34 patients with histologically confirmed glioblastoma (WHO grade IV). Diffusion tensor imaging data were coregistrated to postcontrast T1WI using nordicICE. Region-of-interest (ROIs) was manually delineated to include enhancing tumors. Histogram analysis of FA and MD, age, sex, and Karnofsky performance scale (KPS) were evaluated in overall survival (OS) analysis by the Kaplan-Meier method and Cox proportional hazards regression model. Receiver operating characteristics (ROC) curve analysis was performed for mean FA, maximal FA mean MD and minimal MD in predicting OS of 12 months.
Results
The median survival time in this group is 9.26 ± 1.5 months. Univariate analysis with the Cox proportional hazards model show age, KPS, mean FA, mean MD and minimal MD were associate with survival hazard, the multivariate analysis demonstrated that mean FA and minimal MD were the best predictors after adjusting for age and KPS. Receiver operating characteristics curve analysis showed that mean FA and minimal MD have better area under the curve (0.687 and 0.722 respectively). Discussion: Our preliminary result showed that mean FA, maximal FA mean MD and minimal MD of enhancing glioblastoma could correlate with OS. The mean FA > 0.145 and minimal MD > 0.485 may indicate poorer prognosis.
Conclusion
Our results show mean FA and minimal MD were the best predictors for survival after adjusting for age and KPS. Our study suggested that quantitative histogram analysis of DTI-derived metrics may have potential early predictive value for overall survival (OS) in patients with glioblastomas, warrants further investigation in a large multicenter prospective study.

KEYWORDS: Diffusion tensor image, GBM, survival analysis

O-204 **11:09 AM - 11:17 AM**

Dynamic Contrast-Enhanced Perfusion Imaging for Biopsy-Targeting in Patients with Newly Diagnosed Glioblastoma

Radbruch, A.[1,2]·Decker, C.[1]·Abello, M.[1]·Lutz, K.[1]·Wiestler, B.[1]·Wick, W.[1]·Bendszus, M.[1]·Heiland, S.[1]
[1]University of Heidelberg, Heidelberg, GERMANY, [2]German Cancer Research Center (DKFZ), Heidelberg, GERMANY.

Purpose
Contrast-enhancing areas on T1-weighted images are at present the preferred target for glioma biopsy or resection as they are thought to express the most anaplastic tumor portions. However, the information of this enhancement is limited as it only reflects contrast agent uptake at a single point of time and does not represent kinetic parameters. In brain tumor imaging T1-weighted dynamic contrast-enhanced (DCE) imaging is used mainly to describe the

Note: Scanned images are included in the proceedings. Some submitted images were reduced during editing, thereby decreasing clarity. Also, refer to the Program Planner. Proceedings Content as of 3-29-2013.

status of the blood-brain barrier. We used the pharmacokinetic model introduced by Tofts et al to calculate the transfer constant K^{trans} that is equal to the blood plasma flow per unit volume of tissue. We hypothesized that this approach can separate different tumor compartments even though these compartments may present with comparable signal enhancement on T1-weighted images and thus provide additional information for possible biopsy targets.

Materials & Methods

Images were acquired in the clinical routine workup from 20 patients with newly diagnosed and histologically proven glioblastoma before surgery using a 3T MR system (Magnetom Tim Trio, Siemens Healthcare, Erlangen, Germany). DCE MRI was performed using the following parameters: TR/TE, 5.44/2.47 milliseconds; 40 slices, slice thickness, 3 mm; time resolution, 17.5 seconds; matrix, 256 x 256; FOV, 23 cm x 18 cm,18 measurements, contrast media (0.1 mmol/kg body weight of DOTAREM) infusion rate 3.5 ml/s, starting with the second measurement. We calculated K^{trans} Maps and Maximum Enhancement Maps with in-house developed software. Two experienced neuroradiologists independently evaluated areas presenting either high or low K^{trans} values that presented comparable values on the Maximum Enhancement Map within the enhancing lesion. Two ROIs of the same size were placed in each area and the corresponding values of K^{trans} and the Maximum Enhancement Map were calculated for each voxel within the ROI.

Results

In 17 of 20 patients areas of high and low K^{trans} values that presented comparable enhancement and thus comparable values on the Maximum Enhancement Map could be detected visually. Analysis of these regions revealed significantly different ($p<0.001$) K^{trans} values [(43.25 +/- 25.13 (low K^{trans}) versus 201 +/-67.45 (high K^{trans})] while the corresponding ROIs on the Maximum Enhancement Map did not show any difference [306.6 +/- 110.61 (corresponding ROI for low K^{trans}) versus 315.63 +/- 121.43 (corresponding ROI for high K^{trans})].

Conclusion

K^{trans} Map provides additional information regarding the state of the blood-brain barrier that cannot be visualized on static T1-weighted images. As there is a theoretical basis for a relationship between endothelian permeability and malignancy, it could be beneficial to target voxels that show either only elevated K^{trans} or both - intense enhancement and elevated K^{trans} values. Further studies, especially correlations with biopsies are needed to determine the exact correlation between K^{trans} and malignancy.

KEYWORDS: Glioblastoma, Dynamic contrast-enhanced MR

O-205 **11:17 AM - 11:25 AM**

Cerebral Blood Flow Changes in Glioblastoma Multiforme Patients Undergoing Bevacizumab Treatment Are Seen in Both Tumor and Normal Brain

Andre, J. B.[1]·Nagpal, S.[2]·Hippe, D. S.[1]·Schmiedeskamp, H.[2]·Bammer, R.[2]·Thomas, R.[2]·Straka, M.[2]·Recht, L.[2]·Zaharchuk, G.[2]

[1]University of Washington School of Medicine, Seattle, WA, [2]Stanford University School of Medicine, Stanford, CA.

Purpose

Bevacizumab (Bev), a vascular endothelial growth factor receptor-A antagonist, has been used increasingly for the treatment of recurrent glioblastoma multiforme (GBM). We examine the effects that Bev administration exerts on cerebral blood flow (CBF) contralateral to the tumor in patients with recurrent GBM.

Materials & Methods

Eighteen post-chemoradiation patients with histologically confirmed GBM were treated with Bev and underwent routine tumor imaging at 1.5T and 3T, following informed consent. Pseudocontinuous arterial spin labeling (pCASL) imaging without vessel suppression was serially performed using a 3D background-suppressed fast-spin-echo stack-of-spirals readout module with eight in-plane spiral interleaves. Cerebral blood flow quantification (in mL/100g/min) was performed as described previously using an automated script1. Regions of interest were drawn on pCASL images over tumor regions, symmetrically in the contralateral normal-appearing white matter/tissue, and the contralateral middle cerebral artery (MCA) territory gray matter on an imaging slice 40 mm below the vertex. Changes in CBF from each side within the period before and after Bev administration, and differences between sides for these periods, were evaluated using paired t-tests in eight patients who underwent pCASL imaging during both periods. A linear-mixed model statistical approach with CBF (GBM or contralateral MCA) as the dependent variable and an indicator for Bev treatment period as the independent variable, also was employed in order to utilize all patients, including those with pCASL imaging performed in only one period. To account for any correlation between repeated CBF measurements on the same patient, a random intercept was included and the residual covariance was modeled as a first-order moving average process. The nonparametric bootstrap was applied to assess the difference in change in CBF between the GBM and contralateral sides.

Results

Sixty-three pCASL studies were serially acquired. Pseudocontinuous arterial spin labeling was performed only before and during Bev treatment in eight patients, only during Bev treatment in six patients, only during and after Bev treatment in three patients, and only before Bev treatment in one patient. Initial chemoradiation was performed in all patients, and most patients underwent chemotherapy(most frequently TMZ and/or CCNU, but

Note: Scanned images are included in the proceedings. Some submitted images were reduced during editing, thereby decreasing clarity. Also, refer to the Program Planner. Proceedings Content as of 3-29-2013.

also including others) prior to, or concurrent with Bev treatment. In some, radiation therapy was performed in conjunction with TMZ. Using paired t-tests in eight patients only, significantly lower mean CBF was identified in GBM tumor regions during, compared with before, Bev treatment(p=0.04), while there was a nonsignificant tendency for CBF to be lower in the contralateral MCA territory during the same period (p=0.23). Using a linear mixed model incorporating all patient data to achieve higher statistical power, the trend for lower CBF in the contralateral MCA territory further approached statistical significance (p=0.14) (Figure 1), while the drop in average CBF was found to be significantly greater in GBM compared with contralateral MCA regions(p<0.05).
Conclusion
Bevacizumab appears to preferentially and directly target the tumor vasculature thereby decreasing tumor perfusion, although some mild decrease in global CBF also may occur. A small sample size, prior and concurrent chemo- and radiotherapies, and non-Bev CBF modifiers (such as caffeine) may confound the results.

KEYWORDS: Treatment assessment, Arterial spin labeling, GBM

O-206 **11:25 AM - 11:33 AM**

Differentiation between Gliomas and Brain Metastases Using MR Imaging, Resonance Spectroscopy, Perfusion and Diffusion-Weighted Imaging

Guzmán-De-Villoria, J. A.[1]·Mateos-Pérez, J. M.[1]·Fernández-García, P.[1]·Borrego-Ruiz, P.[1]·Desco, M.[2]
[1]Hospital General Universitario Gregorio Marañón, Madrid, SPAIN, [2]Universidad Carlos III. Instituto de Investigación Sanitaria Gregorio Marañón, Madrid, SPAIN.

Purpose
High-grade gliomas and metastases sometimes appear similar on MR imaging (MRI) but require different treatment strategy. Few attempts have been made to combine different MRI techniques to differentiate between these types of tumors. Our aim was to evaluate the role of MRI, perfusion-weighted imaging (PWI), diffusion-weighted imaging (DWI) and proton spectroscopy (1H-MRS) in the differentiation of brain metastases and gliomas.
Materials & Methods
One hundred ninety-one consecutive patients with an untreated intraaxial brain tumor underwent prospectively conventional MRI, T2*-weighted PWI, DWI (*b* = 2500 s/mm^2) and single voxel 1H-MRS at short (23 ms) and long (144 ms) TE with 1.5 T MR equipment. The gliomas (2 low grade astrocytoma; 7 anaplastic astrocytomas and 72 glioblastomas) and metastases (n = 46) which showed necrosis and enhancement were included in the analysis. The presence of edema, neoformative vessels (neovascularization), and hemorrhage were evaluated with conventional MRI. The relative cerebral blood volume (rCBV) and relative apparent diffusion coefficient (rADC) were calculated by using different regions-of-interest within the enhancing tumoral part and immediate zone of the edema normalized by the contralateral normal-appearing area. Metabolite ratios Cho/Cr; NAA/Cr; Cho/H_2O and NAA/H_2O and the presence of lipids or lactate within the tumor area also were determined. Univariate and multivariate logistic regression analyses were employed to determine the best model for classification.
Results
Significant differences were obtained for the presence of neovascularization (p<0,001), hemorrhage (p = 0.004), lipids (p = 0.046), lactate (p = 0.021) and lower values of NAA/Cr (p<0.04) at long TE in gliomas. The best results were obtained combining the presence of neovascularization, lactate and lipids and low values of NAA/Cr at long TE with an accuracy of 79.3%.
Conclusion
The assessment of some MRI features (neovascularization and hemorrhage) and spectroscopic variables (values of NAA/Cr at long TE, presence of lipids and lactate) could differentiate between gliomas and metastases with similar MRI appearance. However, a conventional analysis of PWI and DWI data do not differentiate between both histologic types due to the overlapping values. This result could explain the controversial published results and may justify the use of high-field MR equipment (≥ 3T) or more sophisticated postprocessing methods.

KEYWORDS: Glioma, Metastases

O-207 **11:33 AM - 11:41 AM**

MR Imaging of Progressive or Recurrent Glioblastoma Multiforme Treated with Laser-Induced Thermal Therapy

Derkatch, S.[1]·McClarty, B.[1]·Tyc, R.[2]·Barnett, G. H.[3]·Sloan, A. E.[4]
[1]University of Manitoba, Winnipeg, MB, CANADA, [2]Monteris Medical Inc., Winnipeg, MB, CANADA, [3]Cleveland Clinic, Cleveland, OH, [4]Case Western Reserve University School of Medicine, Cleveland, OH.

Purpose
Thermal therapy is a cytoreductive modality that can be employed in the treatment of both primary and metastatic intracranial malignancies. The present effort was undertaken with the goal of characterizing immediate and long-term changes to the MRI appearances of glioblastoma multiforme lesions following treatment with MRI-guided, focused laser-induced thermal therapy.
Materials & Methods
A retrospective review was performed of MRI data from 10 patients with progressive or recurrent glioblastoma multiforme enrolled in the phase I trial of an MRI-guided, gas cooled, focused laser interstitial thermal therapy device. Pre and postintervention multisequence MRI images were obtained and analyzed at defined intervals.

Note: Scanned images are included in the proceedings. Some submitted images were reduced during editing, thereby decreasing clarity. Also, refer to the Program Planner. Proceedings Content as of 3-29-2013.

Imaging followup ranged from one to six months.
Results
Distinctive patterns of signal change and evolution were noted on all sequences. A consistent zonal architecture was observed on T1- and T2-weighted images within the confines of the treatment area and this diminished in a generally predictable manner. The margins of the target area were demarcated by a thin rim of enhancement that was evident from the first postoperative days. Many patients ultimately experienced tumor progression related to additional untreated malignant foci but, in all cases, at least a portion of this enhancing rim demonstrated comparative stability. In other patients, this margin persisted to the latest follow-up examination. A transient increase in the volume of the surrounding region of T2 hyperintensity frequently was observed but this rapidly returned to the pretreatment baseline and, in several cases, further improvement was evident. A rim of T1 hyperintensity invariably developed at the periphery of the treated lesion in a delayed fashion and this frequently resolved over a period of two-three months when followup was of suitable duration. Roughly coinciding with the presence of this finding, a thin margin of low signal on gradient-recalled echo images was transiently apparent. Signal abnormalities correlating with restriction of diffusion developed immediately and persisted for one to three months or the most recent examination date.
Conclusion
Progressive or recurrent glioblastoma multiforme lesions treated with focused, laser-induced thermal therapy have characteristic MRI appearances that differ significantly from those of conventional treatment modalities. The variable cooccurrence of complications such as tumor progression and hemorrhage into the necrotic defect provided informative comparisons that may aid in the development of hypotheses regarding the underlying histopathology of laser-induced coagulative necrosis in normal brain parenchyma and tumor. In particular, it is possible that the immediate development and frequent long-term persistence of peripheral enhancement in treated lesions often does not represent residual tumor but rather breakdown of the blood-brain barrier at an immunologically active transition zone between viable and nonviable tissues. These observations are presented with the aim of familiarizing radiologists with expected MRI findings in the ongoing intracranial application of thermal tissue ablation as well as with a view to further research regarding the observed radiopathologic phenomena.

KEYWORDS: Glioblastoma, Laser, MR Imaging

O-208 **11:41 AM - 11:49 AM**

Glioblastoma: Characterization of the Nonenhancing Peritumoral Region Using Resting-State BOLD Functional Connectivity Maps

Chow, D. S.·Filippi, C.·Horenstein, C.·Grinband, J.
Columbia University
New York, NY.

Purpose
Glioblastoma multiforme (GBM) is an invasive and highly aggressive tumor. Though outcomes are highly variable and difficult to predict, there is some consensus that resection provides symptomatic relief and cytotoxic reduction to augment adjuvant therapy. A major limitation for the treatment of GBM has been the ability to differentiate the tumor from surrounding healthy tissue. One means of quantifying the integrity of neural tissue is by assessing the effectiveness of communication between brain regions. Reductions in BOLD functional connectivity have been demonstrated in a wide range of neurologic conditions. In this study, we aim to objectively measure the BOLD functional connectivity, which may represent a potential biomarker for tumor-induced impairment of neural tissue.
Materials & Methods
This was a retrospective review of 13 patients with pathology proven glioblastomas who had resting state BOLD fMRI at 3T prior to tumor resection. Motion correction and slice timing correction was performed on the raw datasets. Functional connectivity (FC) maps were generated. Each voxel time series was correlated to every other voxel in the brain to derive a measure of global functional connectivity. Connectivity maps were coregistered to structural images using FSL. Patterns of functional connectivity within the tumor and peritumoral edema (defined by the peritumoral FLAIR abnormality) were characterized qualitatively and quantitatively.
Results
Peritumoral edema in high-grade gliomas had lower connectivity measures compared to the contralateral normal white matter. The contrast-enhancing tumor region did not show any differences in connectivity when compared to the contralateral normal white matter.

Note: Scanned images are included in the proceedings. Some submitted images were reduced during editing, thereby decreasing clarity. Also, refer to the Program Planner. Proceedings Content as of 3-29-2013.

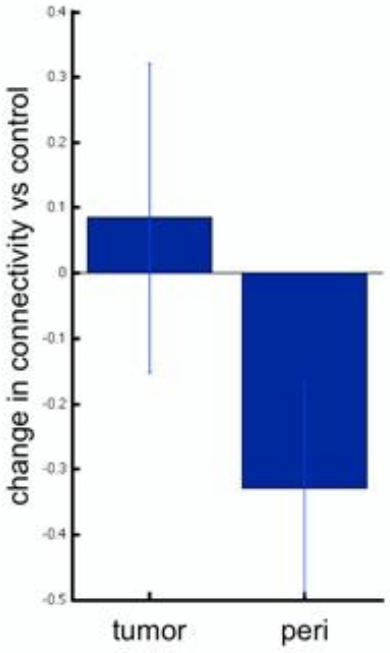

Conclusion
These findings suggest that BOLD functional connectivity maps may provide a potential biomarker for tumor invasion in the nonenhancing peritumoral edema. While the contrast-enhancing tumor region failed to show any differences, this is not unexpected because of loss of vascular regulation in the tumor region. Further study is required to determine whether different classes of tumors are associated with different signatures on these BOLD connectivity maps.

KEYWORDS: Glioblastoma, Functional connectivity MR

O-210 **11:57 AM - 12:05 PM**

Increased Radiosensitivity of IDH1 Mutant Glioblastomas as Demonstrated by Serial Quantitative MR Volumetry

Tran, A. N.[1,2]·Lai, A.[2]·Pope, W. B.[2]·Nghiemphu, P. L.[2]·Cloughesy, T. F.[2]·Ellingson, B. M.[2]
[1]Duke-National University of Singapore, Singapore, SINGAPORE, [2]David Geffen School of Medicine at University of California Los Angeles, Los Angeles, CA.

Purpose
Isocitrate dehydrogenase 1 (IDH1) mutations have been linked to favorable outcomes in patients with glioblastoma multiforme (GBM). A recent study has demonstrated increased radiosensitivity in GBM cell lines that overexpress IDH1 mutant proteins. Therefore, we hypothesized the rate of change in tumor size as measured using serial quantitative MR volumetry would be significantly different between IDH1 mutant (MUT) versus wild-type (WT) GBMs after radiation therapy (RT).

Materials & Methods
All patients in this study signed institutional review board-approved informed consent to have their information in our neuro-oncology database. A total of n = 39 patients were included in this retrospective study with the following criteria: 1) were de novo GBM, 2) had surgery followed by RT and temozolomide only, 3) had IDH1 mutation status sequenced from frozen section samples, 4) had regular postcontrast T1-weighted images (T1+C) and FLAIR or T2-weighted images within six months after starting RT (censored at recurrence). A higher proportion of MUT patients (n = 10) were selected to increase the statistical power. For each serial scan, the regions of contrast enhancement on T1+C and hyperintensity on FLAIR images were manually contoured and the corresponding volumes (VT1+C and VFLAIR) were calculated. Images acquired prior to the start of RT were omitted due to postsurgical edema and swelling. The volumes measured from the scans immediately after RT were used as baseline for normalization. Linear regression models were used to estimate the rate of change in VT1+C and VFLAIR after RT. Kaplan-Meier survival analysis was performed for progression-free survival (PFS).
Results
IDH1 MUT GBMs demonstrated a favorable response to RT as illustrated by 10/10 mutants having a decrease in contrast-enhanced tumor compared to 13/29 wild-types (binomial test p = 0.0003). In the study period, VT1+C and VFLAIR of the IDH1 MUT group changed at -4.8%/week and 0.6%/week respectively, as compared to 4.7%/week and 9.1%/week of the IDH1 WT group (p = 0.0152 for both). Survival analysis showed IDH1 MUT had a significantly longer PFS compared to IDH1 WT GBMs (median PFS of 72.1 months versus eight months, respectively, p = 0.0004).

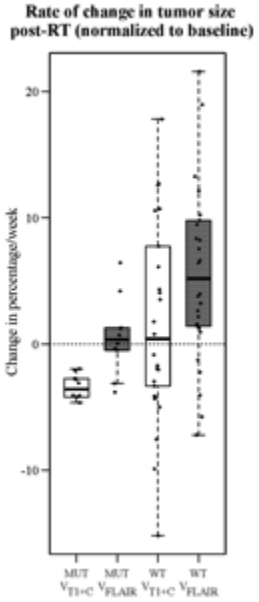

Conclusion
This study supports the hypothesis that IDH1 MUT GBMs

Note: Scanned images are included in the proceedings. Some submitted images were reduced during editing, thereby decreasing clarity. Also, refer to the Program Planner. Proceedings Content as of 3-29-2013.

have increased radiosensitivity compared to WT GBMs as evidenced by the decrease in contrast-enhanced volume (VT1+C) and the stable edema volume (VFLAIR).

KEYWORDS: Glioblastoma, Imaging biomarker, IDH1

O-211 **12:05 PM - 12:13 PM**

Association between Volumetric Imaging Features, Genomic Profile, and Patient Outcome in Glioblastoma: A TCGA Glioma Phenotype Research Group Project

Gutman, D. A.[1]·Holder, C.[1]·Cooper, L.[1]·Dunn, W.[1]·Mikkelsen, T.[2]·Jain, R.[2]·Colen, R.[3]·Jaffe, C.[4]·Saltz, J. H.[1]·Flanders, A.[5]·Brat, D. J.[1]·TCGA Glioma Phenotype Research Group
[1]Emory University, Atlanta, GA, [2]Henry Ford, Detroit, MI, [3]M. D. Anderson Cancer Center, Houston, TX, [4]Boston University, Boston, MA, [5]Thomas Jefferson University, Philadelphia, PA.

Purpose
There is growing interest on the integration of gene expression profiles from tumor biopsies to further classify tumors, although gene expression is influenced not only by the underlying molecular abnormalities driving oncogenesis but also micro- and macro-scale properties. For glioblastoma in particular, neuroimaging provides a unique opportunity to characterize macroscale properties which can affect patient survival as well as genomics. We have previously utilized 2-D semiquantitative imaging features extracted from GBM images to explore these associations. We are now integrating 3D volumetric assessments which we hypothesize will provide a more sensitive measure to evaluate radiogenomic-phenotypic associations.
Materials & Methods
Eighty-nine pre-operative MRI image series were obtained from the Cancer Imaging Archive (TCIA). The postgadolinium T1 image and T2 Flair image were annotated using Velocity AI, a radiotherapy treatment planning system. A contrast-enhancing region (any embedded necrosis) was annotated on the T1 series, and a flair "envelope" consisting of adjacent abnormal signal on the T2 flair were marked up. Annotations subsequently were exported and analyzed using a workflow system developed using niPype to perform volume registration, as well as to calculate the volume of necrosis, contrast enhancement, and edema from the image stack. This framework supports extraction of additional 2D and 3D parameters from the imaging volumes. Genetics data was obtained from the MSKCC cBioPortal, and additional clinical data was obtained from the TCGA archives. Correlations were computed using SAM for genetic correlations, or SPSS. Pathway analysis was performed using Ingenuity Pathway Analysis.
Results
We have previously shown high concordance between measurements obtained via velocity (n = 79, p<0.0001) with independent measures using 3D Slicer in a sample of this data set. A number of volumetric features including overall percentage of necrosis (p<0.001), % of edema (p<0.001) as well as the ratio of contrast enhancement to edema (p<0.003) were associated with poor overall survival. Initial genomics analysis indicated a strong gene set enrichment in the hypoxia-inducible factor signaling (HIF, p<0.0001) and anti-apoptosis pathway (p<0.0159) as a function of the percentage of overall necrosis.
Conclusion
This work further establishes a strong association between macroscopic imaging properties and gene expression. Furthermore, the python-based framework supports the integration of additional imaging features for association studies greatly facilitating our radiogenomic work. We currently are exploring gene signatures associated with both contrast enhancement and edema volumes, as well as characterizing whether relative or absolute measures of imaging properties provide greater sensitivity in the identification of gene/imaging features.

KEYWORDS: Glioblastoma, Gene expression, radiogenomics

Tuesday Morning

10:45 AM - 12:15 PM
Ballroom 6CF

(25b) Parallel Scientific Papers: Adult Brain: Dementia and Degenerative Disorders II

O-212 **10:45 AM - 10:53 AM**

Quantitative Susceptibility Mapping of the Motor Cortex in Upper Motor Neuron Disease

Schweitzer, A. D.[1]·Liu, T.[1]·Zheng, K.[1]·Seedial, S.[1]·Shtilbans, A.[2]·Greene, J.[2]·Shahbazi, M.[2]·Lange, D.[2]·Wang, Y.[1]·Tsiouris, A.[1]
[1]Weill Cornell Medical Center, NewYork Presbyterian Hospital, New York, NY, [2]Hospital for Special Surgery, New York, NY.

Purpose
Specific diagnosis of motor neuron diseases often is difficult due to lack of disease biomarkers. For amyotrophic lateral sclerosis (ALS), there currently exists no quantitative laboratory, imaging, or electrophysiologic test that confirms disease presence or correlates with disease severity. Patients with ALS have been shown to have T2 hypointensity in the motor cortex, possibly due to the T2* effect of deposition of paramagnetic species such as iron. Quantitative susceptibility mapping (QSM) is a novel MRI technique whose pixel intensity directly reflects

Note: Scanned images are included in the proceedings. Some submitted images were reduced during editing, thereby decreasing clarity. Also, refer to the Program Planner. Proceedings Content as of 3-29-2013.

tissue susceptibility. We sought to determine whether patients with motor neuron disease demonstrate increased tissue susceptibility in the motor cortex when compared to a control group.

Materials & Methods

Utilizing a 3.0T MRI system, morphology enabled dipole inversion was used to generate QSM images for seven patients with upper motor neuron disease and 23 control patients. Motor cortices were drawn on axial images in a standardized fashion under the guidance of an experienced neuroradiologist. A semi-automatic program was used to refine the segmentation between motor cortices and adjacent white matter/CSF by applying a threshold. Mean motor cortex susceptibility was calculated, and the Wilcoxon rank sum test was used to evaluate for statistical differences between the groups.

Results

Three patients had clinically confirmed ALS, one had confirmed primary lateral sclerosis (PLS), and three had unspecified upper motor neuron disease (possible ALS). In disease and control groups, mean ages were 58.3 and 56.6 years and percent male were 71% and 57%, respectively. Mean motor cortex susceptibility was found to be significantly higher in patients with motor neuron disease than in control patients (41.6 and 28.5, respectively; p = 0.002). Confirmed cases of ALS had the highest susceptibility and the control group had the lowest susceptibility (Table).

Tissue susceptibility in motor cortex by diagnosis	
Confirmed ALS (n=3)	46.2
Motor neuron disease, possible ALS (n=3)	40.7
Confirmed PLS (n=1)	30.3
Control (n=23)	28.5

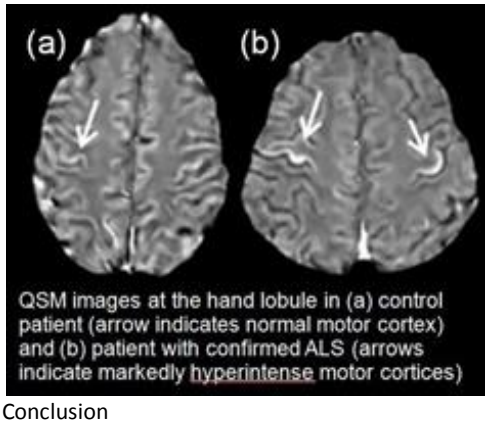

QSM images at the hand lobule in (a) control patient (arrow indicates normal motor cortex) and (b) patient with confirmed ALS (arrows indicate markedly hyperintense motor cortices)

Conclusion

Quantitative susceptibility mapping has the potential to be a quantitative imaging biomarker for patients diagnosed with motor neuron disease. Further study is necessary to determine whether QSM signal in the motor cortex correlates with disease severity in ALS and other motor neuron diseases.

KEYWORDS: Amyotrophic lateral sclerosis, Susceptibility-weighted imaging, Quantitative susceptibility mapping

O-213 **10:53 AM - 11:01 AM**

Cerebral Microbleeds Are Associated with Lower Levels of Cerebrospinal Fluid Beta-Amyloid in Nondemented Elderly Individuals

Chiang, G. C.[1]·Schuff, N.[2]·Weiner, M.[2]
[1]Weill Cornell Medical College-New York Presbyterian Hospital, New York, NY, [2]Veteran Affairs Medical Center, San Francisco, CA.

Purpose

Cerebral microbleeds are four times more likely to be seen in hypertensives than the general population and are associated with white matter hyperintensities on MRI and lacunar infarcts. However, their role in relation to Alzheimer disease (AD) is less clear. A pooled analysis reported that microbleeds are seen in approximately 23% of patients with AD. Pathologically, microbleeds in hypertensives correspond to hemosiderin leakage from abnormal small blood vessels. Conversely, microbleeds in Alzheimer brains are associated with beta-amyloid deposition in vessel walls, or amyloid angiopathy. Furthermore, one study reported that having many microbleeds, greater than seven in this study, correlates with lower beta-amyloid in the cerebrospinal fluid (CSF) and increased brain amyloid deposition, as well as lower scores on the Mini-Mental State Exam (MMSE). The purpose of our analysis was to evaluate the significance of microbleeds in a nondemented cohort without significant vascular comorbidities, for which the Modified Hachinski score was used for screening. Using data from the multicenter Alzheimer's Disease Neuroimaging Initiative (ADNI), we first evaluated whether microbleeds are associated with a hypertensive history, measured blood pressure, age, and APOE4 status. We then evaluated whether microbleeds are associated with CSF biomarkers of Alzheimer disease, namely, beta-amyloid, total tau, and phosphorylated tau. Finally, we evaluated whether microbleeds are associated with memory and overall cognition.

Materials & Methods

Two hundred eighty-six nondemented individuals (90 cognitively normal, 143 with subjective memory complaints, and 53 with mild cognitive impairment) recruited through ADNI underwent a standardized 3T MRI protocol that included 3D MPRAGE and T2* GRE sequences. The number of cerebral microbleeds was visually assessed by a neuroradiologist. All subjects underwent lumbar puncture to determine levels of CSF beta-amyloid, total tau, and phosphorylated tau. Memory

Note: Scanned images are included in the proceedings. Some submitted images were reduced during editing, thereby decreasing clarity. Also, refer to the Program Planner. Proceedings Content as of 3-29-2013.

was assessed using the delayed recall subscores of the Rey Auditory Verbal Learning Test and Logical Memory II subscale. Overall cognition was determined using the MMSE and Alzheimer's Disease Assessment Scale (ADAS). Hippocampal volumes were calculated using Freesurfer segmentation (version 5.1). Multivariate regression was used to test our three aims, using age, gender, education, hypertensive history, measured blood pressure, APOE4 status, and hippocampal volumes as covariates.
Results
Seventy-five of the 286 (26%) of the cohort had at least one cerebral microbleed. The number of microbleeds was associated with age ($p = 0.004$), but not diagnosis group, gender, education, APOE4 status, hypertensive history, or blood pressure. Adjusting for covariates, including hippocampal volumes, the number of microbleeds was negatively associated with CSF beta-amyloid ($p = 0.04$), but not CSF total tau ($p = 0.58$) or CSF phosphorylated tau ($p = 0.8$). The number of microbleeds was not associated with memory or overall cognition.
Conclusion
Microbleeds were not correlated with hypertension in our cohort. Rather, they increased with age and served as independent predictors of CSF beta-amyloid levels, after accounting for APOE4 status and hippocampal volumes. Further research will determine to what degree these microbleeds, suggestive of underlying amyloid angiopathy, adds to the prediction of future development of Alzheimer disease.

KEYWORDS: Cerebral microhemorrhages, Amyloid

O-214 **11:01 AM - 11:09 AM**

Brain T2-Weighted Lesions in Aging: MR Imaging Overestimates Demyelination in Periventricular and Perivascular Areas

Haller, S.·Kovari, E.·Herrmann, F.·Cuvinciuc, V.·Tomm, A.·Zulian, G.·Lovblad, K.·Giannakopoulos, P.·Bouras, C.
University Hospital Geneva
Geneva, SWITZERLAND.

Purpose
Hyperintense T2-weighted brain MRI lesions frequently are seen in healthy elderly people. Whether or not these radiologic lesions correspond to irreversible histologic changes is still a matter of debate. We report the radiopathologic concordance between T2-weighted lesions and neuropathologically confirmed demyelination in the periventricular, perivascular and deep white matter areas.
Materials & Methods
Fifty-nine very old individuals (mean age 80.5 years ± 9.5 years, 54.2% females) with preserved cognitive abilities and normal pre-mortem brain MRI were evaluated independently by three radiologists (T2-weighted lesions) and two neuropathologists (degree of demyelination). Analyses included inter-rater comparisons both within and between neuropathologists and radiologists, multiple regression models controlling for age and MRI autopsy delay and sensitivity/specificity analyses.
Results
Inter-rater reliability was substantial, almost perfect between neuropathologists (kappa 0.66 - 0.88) and slight-moderate between radiologists (kappa 0.18 - 0.46). Discriminating low versus high lesion scores, sensitivity and specificity values were 0.83 and 0.47 for periventricular, but 0.44 and 0.88 for deep white matter lesions. MR imaging overestimates lesion load in the perivascular and periventricular ($p < 0.001$) areas but underestimates it in the deep white matter ($0 < 0.05$).
Conclusion
These observations indicate that MRI assessment of T2-weighted lesions in periventricular/perivascular areas often lead to false positive cases whereas MRI scans positive for T2-weighted lesions in deep white matter correspond to demyelination. This discrepancy might be related to the relatively high water content in the periventricular and perivascular areas and increasing plasma leakage in the elderly favoring increased T2-weighted signal without necessarily neuropathologically confirmed demyelination.

KEYWORDS: Aging, White matter disease

O-215 **11:09 AM - 11:17 AM**

Susceptibility-Weighted MR Imaging in Extrapyramidal Brain Structures Helps Differentiate Different Types of Gait Disorders

Ng, K.[1]·Schneider, E.[1]·Yeoh, C.[1]·Rumpel, H.[1]·Tan, E.[2]·Chan, L.[1]
[1]Singapore General Hospital, Singapore, SINGAPORE,
[2]National Neuroscience Institute, Singapore, SINGAPORE.

Purpose
Poor gait balance is a frequent clinical diagnostic challenge. Most of these patients have gait disorder parkinsonism (PIGD), although the pathophysiologic differences between idiopathic Parkinson disease (PD) and PIGD remains unclear. Various neurodegenerative disorders associated with parkinsonian syndromes have been found to have increased iron content in the basal ganglia. Susceptibility-weighted MRI (SWI) is sensitive to T2* effects and mineralization. In this study, we evaluated for differences in the extrapyramidal brain structures on SWI between PD and PIGD patients and correlated the SWI values with the degree of gait dysfunction.
Materials & Methods
Patients diagnosed with PD and PIGD were recruited from Movements Disorders Clinics by neurologists. After informed consent, the participating subjects were assessed with the Tinetti score (a validated scale for postural instability), and an MRI brain study at 3T. In addition to conventional MR sequences, an SWI sequence (TE/TR/FA 20/33/15) was included. The MR images were read by a neuroradiologist. Ten ROIs were placed in the

Note: Scanned images are included in the proceedings. Some submitted images were reduced during editing, thereby decreasing clarity. Also, refer to the Program Planner. Proceedings Content as of 3-29-2013.

midbrain and basal ganglia by two independent raters blinded to subject data and quantitatively evaluated. A multivariate logistical regression analysis was performed with the SWI values as the dependent variable, and age, gender and vascular risk factors as independent variables. P-values of < 0.05 were considered statistically significant. Clinical correlation of the SWI values with the Tinetti score was done using Pearson's correlation.
Results
Forty patients (21 PD, 19 PIGD) were recruited for the study. The mean age of the PD and PIGD patients was 72 years and 74 years, respectively. The inter-rater reliability between the raters was good (ICC >0.8). The SWI intensity values in all regions were on average lower in PIGD than in PD patients, with the lowest results found in globus pallidum. Multivariate analysis showed statistically significant differences for the putamen between PD and PIGD patients ($p < 0.05$), with a similar trend for the other basal ganglia nuclei. Pearson's correlation analysis showed a statistically significant positive correlation between putaminal hypointensity and the Tinetti total score ($r = 0.389$, $p = 0.05$).
Conclusion
We demonstrated that SWI values in PIGD patients were lower compared to PD, providing new clues to the pathophysiologic differences of these conditions. We also showed that there was a positive correlation between the SWI putaminal hypointensity and the Tinetti score, suggesting that this imaging marker may be useful in prospective evaluation for clinical progression.

KEYWORDS: Gait, Susceptibility-weighted imaging

O-216 **11:17 AM - 11:25 AM**

Caffeine Enhances Task-Related and Functional Connectivity Working Memory Brain Activation in the Elderly

Haller, S.·Rodriguez, C.·Toma, S.·Hofmeister, J.·Sinanaj, I.·Giannakopoulos, P.·Lovblad, K.
University Hospital Geneva
Geneva, SWITZERLAND.

Purpose
Recent evidence indicates that caffeine might be a cognitive normalizer in mild cognitive impairment (MCI) and Alzheimer dementia (AD). Previous studies in young healthy volunteers assessed the complex interaction of caffeine and the BOLD response in fMRI, including cognitive and direct vascular effects. The current investigation in cognitively normal elderly participants complements these previous investigations testing whether caffeine enhances working memory-related brain activation.
Materials & Methods
In a placebo-controlled crossover design, 24 old individuals (mean age 68.8 ± 4.0 years, 17 females) performed a 2-back task. Analyses included task-related general linear model (GLM) and tensorial independent component (TICA) functional connectivity and baseline arterial spin labeling (ASL) perfusion.
Results
There was no significant behavioral difference between caffeine and placebo. Despite a reduction in global perfusion (22.7%, $p<0.001$), caffeine enhanced task-related GLM activation in a distributed network most pronounced in bilateral striatum consistent with the local expression of adenosine receptors. Tensorial independent component functional connectivity was significantly ($p<0.05$) enhanced (Smode + 8.2%) in caffeine versus placebo in a distributed and task-relevant network including working memory and visual areas. The inverse comparison as well as other task irrelevant functional connectivity networks or local perfusion showed no significant change.
Conclusion
Caffeine induced a specific and task-relevant enhancement in both task-related and functional connectivity brain activation. The absence of alterations of task-unrelated functional connectivity networks or local baseline perfusion indicates a specific cognitive effect of caffeine. These results are the basis for further projects in MCI and AD.

KEYWORDS: Aging, caffeine

O-217 **11:25 AM - 11:33 AM**

Comparison between Parkinson Disease with Dementia and Dementia with Lewy Bodies: Evaluation of White Matter Abnormality with Diffusion Tensor Imaging and Tract-Based Spatial Statistics Study

Kim, D.[1]·Kim, S.[1]·Kim, H.[2]·Choi, C.[1]·Kim, H.[1]·Lee, C.[1]
[1]Asan Medical Center, Seoul, KOREA, REPUBLIC OF, [2]Korea Basic Science Institute, Cheongwon, KOREA, REPUBLIC OF.

Purpose
Cognitive impairment and dementia occur commonly in patients with Parkinson disease (PD). Dementia with Lewy bodies (DLB) and PD with dementia (PDD) are two main categories of dementia associated with PD. Although DLB and PDD have different temporal sequence of symptoms and clinical features, pathologic difference is not well understood and there are no known neuroimaging features to differentiate between the two groups. Our purpose is to compare white matter abnormalities in DLB and PDD using diffusion tensor MR imaging and tract-based spatial statistics (TBSS).
Materials & Methods
Diffusion tensor imaging (DTI) was obtained with a 3.0T MR system in age-matched groups of 53 patients with PD, 27 patients with PDD, and 16 patients with DLB. Patients were selected from our Parkinson disease database on the basis of clinical criteria and consensus guidelines. Patients with history of chronic hypertension, diabetes, stroke or head injury, or prominent high signal in the white matter

Note: Scanned images are included in the proceedings. Some submitted images were reduced during editing, thereby decreasing clarity. Also, refer to the Program Planner. Proceedings Content as of 3-29-2013.

on T2-weighted images were excluded from the study. Fractional anisotropy (FA) and mean diffusivity (MD) maps were generated using FDT in the FMRIB's Software Library (FSL) package and processed to perform tract-based comparisons of FA and MD among the three groups using TBSS in FSL. To address multiple comparison issue, this result is corrected for family-wise error using threshold-free cluster enhancement (TFCE) method across the white matter skeleton.

Results

Between PDD and PD groups, both FA and MD maps showed difference in both cingulum, frontal and parietal corona radiata, superior longitudinal fasciculus, corpus callosum, and posterior thalamic radiation. In contrast, between DLB and PD groups, both FA and MD maps showed differences only in the right cerebral peduncle and the right internal capsule. Fractional anisotropy was decreased in the corpus callosum, both side anterior, superior, and posterior corona radiate and both tapetums in PDD group compared to DLB group: in contrast, MD map did not showed significant difference between PDD and DLB groups.

Conclusion

Diffusion tensor imaging with TBSS revealed different extent of white matter abnormality between DLB and PDD groups. Parkinson disease with dementia group showed more wide area of white matter abnormality compared to DLB group.

KEYWORDS: Parkinson disease, Diffusion tensor image, Tract-based spatial statistics

O-218 **11:33 AM - 11:41 AM**

Combined Positron Emission Tomography-MR Imaging for the Evaluation of Suspected Dementia: Initial Experiences and Comparison to Positron Emission Tomography-CT

Shepherd, T. M.·Zhou, Y.·Ding, Y. S.·George, A. E.·Glielmi, C.·Faul, D.·Shulman, M. B.·Boada, F. E.·Friedman, K. P.
New York University Langone Medical Center
New York, NY.

Purpose

MR imaging of patients with cognitive impairment suspected to have neurodegenerative disease can exclude treatable causes such as hemorrhage, tumor or hydrocephalus. Regional hypometabolism on FDG-PET and group-wise differences observed using advanced MRI techniques appear more specific for neurodegenerative diseases. Simultaneous PET and MRI for cognitively-impaired patients may facilitate shortened examination times, PET coregistration to high-resolution anatomical data, temporally-synchronized data collection and increased diagnostic accuracy. We describe initial experiences evaluating patients with suspected dementia using an FDA-approved 3T mMR combined PET/MRI scanner (Siemens Healthcare, Erlangen, Germany) and compare these results to conventional PET-CT to help validate its routine clinical use.

Materials & Methods

Patients with suspected dementia undergoing clinical ^{18}FDG PET-CT were recruited to undergo PET-MRI at a nearby facility. PET-CT utilized a 15-minute PET acquisition on a Siemens mCT with iterative reconstruction, 512x512 matrix, 1.5-mm slice interval and low-dose CT for attenuation correction. PET-MRI were acquired in list-mode for 60 minutes and reconstructed with OSEM, 512x512 matrix, 1.5-mm slice interval and Dixon MR-based attenuation correction. Diagnostic MRI sequences were obtained simultaneously. PET-CT and PET-MRI were interpreted visually and then reinterpreted using MIM-neuro quantitative analysis (Cleveland, OH).

Results

Sequential brain PET-CT and PET-MRI were obtained from six patients with suspected dementia (71.5±10.6 years, 4 males) after a single IV dose of 9.4±0.5 mCi mCi FDG. Mean uptake time for PET-CT and PET-MRI were 66.3±14.2 min and 180.2±23.8 min respectively. PET-CT visual interpretation and scoring of ^{18}FDG uptake indicated two normal studies, one with moderate and three with severe changes associated with Alzheimer disease (hypometabolism in the precuneus, posterior cingulate & medial temporal lobes). Similar patterns of regional ^{18}FDG accumulation were observed in PET-MRI for all six patients without scoring discrepancies compared to PET-CT, although there was apparent decreased cerebellar ^{18}FDG in four of the six patients (Figure). Quantitative analysis of ^{18}FDG uptake relative to normative data demonstrated no other focal regional differences between PET-CT and PET-MRI although this comparison may be limited by the protracted uptake times for PET-MRI data.

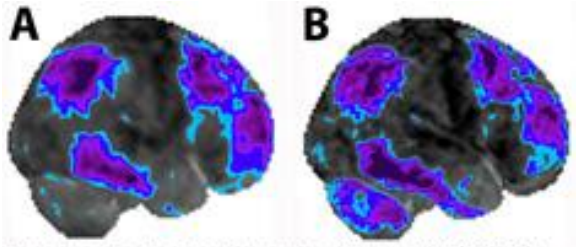

Lateral projection shaded-surface display of PET-CT (A) and PET-MRI (B) data from the same patient with hypo-metabolism relative to normative data in the parietal, temporal and frontal regions. Cerebellar hypometabolism observed in the PET-MRI data (4 of 6 patients) may be from different regional washout kinetics after significantly longer uptake times.

Conclusion

Combined PET-MRI appears feasible and valid for routine clinical evaluation of patients suspected of dementia. Dixon MR-based attenuation correction appears to offer similar quantitative ^{18}FDG uptake results without obvious region-specific limitations. Future work will investigate real-time MRI-based motion correction and further

Note: Scanned images are included in the proceedings. Some submitted images were reduced during editing, thereby decreasing clarity. Also, refer to the Program Planner. Proceedings Content as of 3-29-2013.

refinement of MR-based attenuation correction. It is hoped combined PET-MRI may increase diagnostic accuracy for neurodegenerative diseases in individual patients.

KEYWORDS: Alzheimer disease, PET, PET-MRI

O-219 **11:41 AM - 11:49 AM**

Internal Structures of Globus Pallidus in Patients with Parkinson Disease: Evaluation with Quantitative Susceptibility Mapping

Ide, S.[1]·Kakeda, S.[1]·Ueda, I.[1]·Watanabe, K.[1]·Murakami, Y.[1]·Moriya, J.[1]·Ogasawara, A.[1]·Futatsuya, K.[1]·Sato, T.[1]·Ohnari, N.[1]·Okada, K.[1]·Tsuji, S.[1]·Liu, T.[2]·Wang, Y.[2]·Korogi, Y.[1]
[1]University of Occupational and Environmental Health, Kitakyushu, JAPAN, [2]Cornell University, Ithaca, NY.

Purpose
The globus pallidus (GP) is subdivided into the medial (GPm) and lateral (GPl) segments, and a thin layer in GP, medial medullary lamina (MML), separates the GPm from the GPl. Deep-brain stimulation has shown therapeutic benefits for several neurodegenerative disorders including Parkinson disease (PD); the GPm is one of the targets. Quantitative susceptibility mapping (QSM) is a novel technique which allows determining the bulk magnetic susceptibility distribution of tissue in vivo from gradient echo magnetic resonance phase images. Our objective is to clarify if the QSM can reveal the GPm in PD patients.
Materials & Methods
The conventional MRI as well as QSM and T2*mapping were performed in 19 patients with PD patients and in 15 age-matched normal control (NC) subjects. For the QSM and T2*mapping, the coronal images were acquired covering the entire basal ganglia. The QSM was performed for various ranges of echo time by using both the magnitude and phase components in the morphology-enabled dipole inversion method. Two neuroradiologists evaluated the GP on QSM imaging, T2*mapping and conventional MRI (T2WI and FLAIR), and classified the delineation of the GP into following four grades; Grade 1= GP is not delineated, Grade 2= GP is delineated, but the differentiation of GPm from GPl is poor, Grade 3= Differentiation of GPm from GPl is good, but delineation of MML is unclear, Grade 4= Delineation of MML is clear.
Results
Regarding the visualization of the GP, the image quality with QSM was scored to be Grade 4 in 15 (79%) of 19 PD patients and in seven (47%) of 15 NC subjects, and Grade 3 in 4 (21%) of 19 PD and in eight (53%) of 15 NC (Figure). All study subjects were scored as grade 1 or 2 on conventional MR images. For the mean qualitative image score, QSM were significantly superior to T2*mapping images in both groups (3.80 versus 2.27 in PD patients, $P < 0.05$; 3.40 versus. 2.27 in NC subjects, $P < 0.05$, respectively).

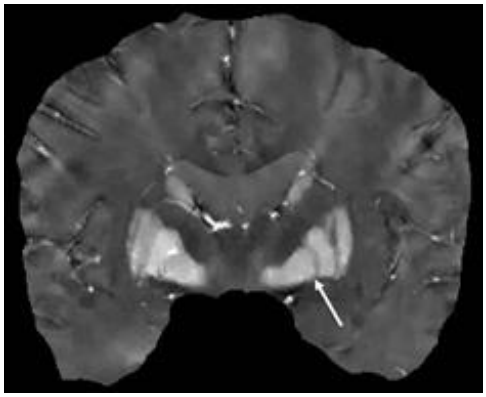

Figure: The QSM image of a parkinson disease patient. On coronal QSM image, the MML separating the GPm from the GPl is clearly seen as a thin low signal intensity layer within the GP (Grade 4).

Conclusion
Quantitative susceptibility mapping technique is able to depict the internal structures of the GP that has been difficult to appreciate on conventional MR imaging; in addition, the QSM showed superior image quality to T2*mapping.

KEYWORDS: Anatomy, Parkinson disease, QSM

O-220 **11:49 AM - 11:57 AM**

Gait Response to Spinal Tap in Normal Pressure Hydrocephalus Is Independent of Cerebrospinal Fluid Volume Removed

Thakur, S.·Serulle, Y.·Rusinek, H.·Nutanson, I.·Tyagi, V.·Tolete, P.·Golomb, J.·Shepherd, T.·George, A.
New York University School of Medicine
New York, NY.

Purpose
Normal pressure hydrocephalus (NPH) is a debilitating disorder characterized by gait instability, cognitive impairment and urinary incontinence. Positive response to cerebrospinal fluid (CSF) removal by spinal tap in NPH patients is an accepted diagnostic marker that predicts positive response to ventricular shunting. To our knowledge, it is unknown whether the amount of CSF removed during the procedure affects gait response. We used longitudinal gait measures to analyze volume of CSF removed as a predictor of gait improvement for a cohort of patients with clinical and imaging findings of NPH.
Materials & Methods
We retrospectively analyzed 72 patients with clinically diagnosed idiopathic NPH who received gait evaluation before and after CSF removal. Patients undergoing spinal tap were placed in prone or prone oblique position. All taps were performed at L2/3 or L1/2 with fluoroscopic assistance using an 18-gauge needle. Evaluation consisted of mean time to walk a fixed distance (WT) and a functional ambulation profile (FAP) score. Evaluation occurred before, immediately after, and 24 hours after CSF

Note: Scanned images are included in the proceedings. Some submitted images were reduced during editing, thereby decreasing clarity. Also, refer to the Program Planner. Proceedings Content as of 3-29-2013.

removal. IBM SPSS 19.0 statistical software (paired t-tests, repeated measures, ANOVA, and regression analyses) was used to examine the relationship between volume of CSF removed and longitudinal changes in WT and FAP. WT and FAP were analyzed as recorded and after logarithmic normalization.

Results

The amount of CSF removed ranged from 15-50 mL. Forty-four out of 72 patients (61%) showed improvement following the spinal tap. There was no relationship [N = 72, R2 = 0.004, p = 0.6, regression slope = 0.0009, 95% confidence interval (-0.0024 - 0.0042)] between the volume of CSF removed and either WT or FAP at either time point (Figure). Analysis limited to responsive patients also showed no correlation between volume and gait response.

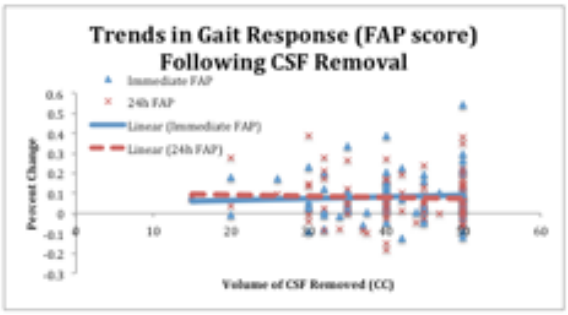

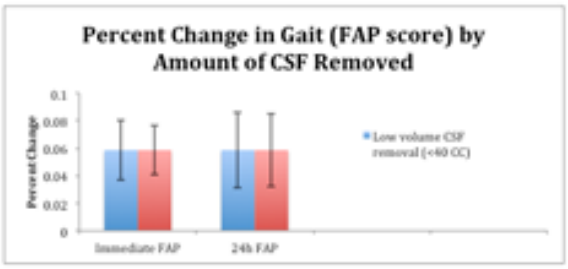

Conclusion

No relationship was demonstrated between the volume of CSF removed and gait improvement following spinal tap.

KEYWORDS: Normal pressure hydrocephalus, Lumbar puncture

O-221 **11:57 AM - 12:05 PM**

Combined Gray Matter Voxel-Based-Morphometry and White Matter Tract-Based Spatial Statistics Analysis in Young First Episode Psychosis Patients with and without Cannabis Consumption

Haller, S.·Curtis, L.·Badan, M.·Bessero, S.·Albom, M.·Chantraine, F.·Alimenti, A.·Lovblad, K.·Giannakopoulos, P.·Merlo, M.
University Hospital Geneva
Geneva, SWITZERLAND.

Purpose

Cannabis consumption is temporally associated with the development of first episode psychosis (FEP). Whether or not the chronic use of this substance induces structural brain changes that may be responsible for the cognitive and psychologic disturbances in this disorder is still a matter of debate. To address this issue, we compared the MRI-assessed gray (GM) and white (WM) changes in young patients with FEP users and nonusers of cannabis.

Materials & Methods

This prospective study included 50 consecutive FEP subjects: 33 users (22.7 ± 4.1 years, four women) and 17 nonusers (23.9 ± 4.2 years, 10 women). Users were further divided into 15 heavy (23.3 ± 4.5 years, two women) and 18 light users (22.2 ± 3.8 years, two women) according to their lifetime cannabis use. Voxel-based morphometry (VBM) analysis of GM and tract-based spatial statistics (TBSS) analysis of WM were performed. Age and gender were used as nonexplanatory coregressors.

Results

There were no suprathreshold differences between user and nonuser groups for both GM and WM parameters. This was also the case when heavy users were considered alone. Multivariate models controlling for age and gender confirmed these findings.

Conclusion

We found no evidence for cannabis consumption-related alterations in GM or WM in FEP subjects. Due to the strict correction for multiple comparisons and sample size, we cannot formally exclude subtle morphometric changes associated with cannabis consumption. However, even if present, such potential alterations would be of low magnitude.

KEYWORDS: Psychiatrycannabis

O-222 **12:05 PM - 12:13 PM**

Corpus Callosum on Diffusion Tensor Imaging in Gait Disorders

Ng, K.[1]·Chan, L.[1]·Rumpel, H.[1]·Tan, E.[2]
[1]Singapore General Hospital, Singapore, SINGAPORE,
[2]National Neuroscience Institute, Singapore, SINGAPORE.

Purpose

Poor gait balance is a frequent clinical diagnostic

Note: Scanned images are included in the proceedings. Some submitted images were reduced during editing, thereby decreasing clarity. Also, refer to the Program Planner. Proceedings Content as of 3-29-2013.

challenge. Most of these patients have gait disorder parkinsonism (PIGD), although the pathophysiologic differences between idiopathic Parkinson disease (PD) and PIGD remains unclear. The integrity of the corpus callosum has been implicated in gait disorders. Diffusion tensor MRI (DTI) is sensitive to microstructural integrity of brain white matter. In this study, we evaluated the integrity of the corpus callosum on DTI between PD and PIGD patients and correlated the DTI values with the degree of gait dysfunction.
Materials & Methods
Patients diagnosed with PD and PIGD were recruited from Movements Disorders Clinics by neurologists. After informed consent, the participating subjects were assessed with the Tinetti score (a validated scale for postural instability), and an MRI brain study at 3T. In addition to conventional MR sequences, a DTI sequence (TR/TE 8200/86, two b values 0 and 800 s/mm2 in 30 noncollinear directions, 128 x 128 matrix, FOV 240 mm) was included. The MR images were read by a neuroradiologist. Regions of interest (ROI) were placed in the genu and splenium of the corpus callosum. In addition, the transcallosal motor tract within the corpus callosum was depicted using the commercially available tractography software based on a deterministic streamline (FACT) approach, connecting two seed regions, one in each right and left motor strip. An ROI also was dropped in the callosal body containing the transcallosal motor tract. The quantitative DTI indices of apparent diffusion coefficient (ADC) and fractional anisotropy (FA) from these ROIs were evaluated and compared between PD and PIGD. Multivariate analysis and clinical correlation of the DTI metrics with the Tinetti score were performed.
Results
Forty patients (21 PD, 19 PIGD) were recruited for the study. The mean age of the PD and PIGD patients was 72 years and 74 years, respectively. The FA values were significantly lower and/or ADC values significantly higher in the callosal body (FA 0.80 versus 0.88, ADC 0.86 versus 0.72 x10-3 mm2/s) and splenium of the corpus callosum (ADC 0.75 versus 0.67 x10-3 mm2/s) in PIGD than in PD patients ($p < 0.05$). Multivariate analysis showed that the FA ($p < 0.05$) and ADC ($p < 0.005$) values in the corpus callosum body differentiated PIGD from PD patients. The callosal body FA values was significantly lower and ADC values significantly higher in PIGD patients with lower Tinetti scores, than those with high scores ($p < 0.05$).
Conclusion
We demonstrated that FA and ADC abnormalities in the callosal body containing the transcallosal motor tract were significantly different between PIGD and PD patients and correlated with the severity of postural instability. This additional differential indicator of gait disability in subjects with parkinsonism may be helpful differentiating PD from those with predominant gait problems.

KEYWORDS: Corpus callosum, Gait, DTI

Tuesday Morning

10:45 AM - 12:15 PM
Ballroom 6DE

(25c) Parallel Scientific Papers: Adult Brain: Stroke II: Endovascular Recanalization

O-223 **10:45 AM - 10:53 AM**

Angioplasty and Stenting of Symptomatic Severe Stenosis of Vertebral and Subclavian Artery: Quantitative Evaluation of Clinical and Hemodynamic Outcome

Chang, F.·Luo, C.·Lirng, J.·Lin, C.·Wu, H.·Hung, S.·Guo, W.·Teng, M.
Taipei Veterans General Hospital/National Yang Ming University, School of Medicine
Taipei, TAIWAN.

Purpose
Angioplasty and stenting (AS) of the severe stenosis of the subclavian and vertebral arteries was reported to be effective in preventing ischemic stroke and improving symptoms of vertebrobasilar insufficiency (VBI). However, the impact of the AS on the hemodynamic of the territory of vertebrobasilar system and improvement of the components of clinical symptoms was not described. This study was designed to evaluate the influence of AS on: 1) hemodynamic change in the territory of vertebrobasilar system by segmented MR perfusion study; 2) clinical change of life quality by DHI (Dizziness Handicap Inventory) and SF-36 (36-Item Short-Form Health Survey) questionnaire.
Materials & Methods
During the past three years, we performed AS in 25 patients of severe stenosis (60-95%, 76.4 ± 10.6%) of vertebral and/or subclavian arteries associated with VBI. All patients finished a 3-time MR perfusion study and life quality questionnaire, including before the AS, and within one month and about six months after the AS. The quantitative MR perfusion study includes the expectation-maximization (EM) algorithm for brain MR segmentations and multi-tissue hemodynamics. We evaluate the rCBV, rCBF & MTT of the midbrain. The contralateral basal ganglion was taken for comparison. The DHI and SF-36 questionnaire are used to evaluate dizziness and health-related quality of life. All data were collected for statistical analysis.
Results
Angioplasty and stenting was successfully done in all of the 25 patients without complications. They included six females and 19 males with average age of 71.9 ± 10.4 (55-85 years old). All patients showed variable degree of

Note: Scanned images are included in the proceedings. Some submitted images were reduced during editing, thereby decreasing clarity. Also, refer to the Program Planner. Proceedings Content as of 3-29-2013.

clinical improvement of the symptoms of vertebrobasilar insufficiency after the management. No restenosis was noted in the followup. Complete 3-time MR perfusion studies were done in 22 patients. Complete 3-time life quality questionnaires (SF-36 and DHI) were done in all 25 patients. On MR perfusion study, the average ratio of MTT, rCBF and rCBV of midbrain to contralateral basal ganglion before AS/ within one month/six months after AS were 1.53 ± 0.44/1.26 ± 0.27/1.36 ± 0.36 (MTT), 0.93 ± 0.22/1.13 ± 0.21/1.03 ± 0.21 (rCBF), 1.33 ± 0.40/1.36 ± 0.24/1.27 ± 0.24 (rCBV). For the SF-36 questionnaire, the results within one month after AS showed no significant difference compared with the preprocedural results. Significant clinical improvement was noted in the six month follow-up of bodily pain (P = 0.019). General health perceptions (P = 0.0153), Vitality (P = 0.0462), Social functioning (P = 0.0149), role problem due to emotional problem (P = 0.0186), mental health (P = 0.0213). The DHI questionnaire showed significant improvement of physical function after treatment within one month (P = 0.0068) and about six months (P = 0.008).
Conclusion
Angioplasty and stenting of the symptomatic stenosis of subclavian/vertebral arteries had improved hemodynamic change of the brainstem with more in MTT and rCBF than in rCBV. The clinical improvement was significant in the delayed function of SF-36 (six months) and recent and delayed physical function in DHI (<one month and six months).

KEYWORDS: Stents, Outcome, MR perfusion

O-224 **10:53 AM - 11:01 AM**

Fate of the Penumbra after Endovascular Mechanical Recanalization

Friedrich, B.·Kertels, O.·Prothmann, S.·Wunderlich, S.·Zimmer, C.·Förschler, A.
Klinikum Rechts der Isar, Technische Universität München Muenchen, GERMANY.

Purpose
In the last years endovascular mechanical recanalization (EMR) has developed to a safe and often used method in the treatment of acute ischemic stroke. In the diagnostic phase perfusion CT often is brought up to visualize the so-called ischemic core - which is reckoned as unrescuable - and the penumbra as rescuable tissue-at-risk. The goal of the present study was to assess the evolution of the infarct compared to the performed perfusion CT and to analyze the clinical and interventional factors determining the fate of the penumbra.
Materials & Methods
All patients receiving EMR in the anterior circulation and receiving a perfusion CT beforehand were identified. Perfusion CTs were fused with postinterventional CCTs and the infarct volume was specified. The clinical parameters, short-time outcome and the interventional result were analyzed and correlated to the infarct size and the results of the perfusion CT.
Results
Sixty patients (32 female) were included in the present study. The mean age was 67 +/- 17 years with a NIHSS of 13.4 +/- 5.9. After EMR 76.7% reached a TICI score of 2b or 3. The final infarct volume was significantly smaller in patients with a TICI score of 2b/3 compared to patients with a less sufficient recanalization (17.9 +/- 3.2 cm3 versus 33.1 +/- 6.3 cm3; p<0.05). Also the final TICI score determined significantly the volume of penumbra rescued. Whereafter TICI 2b/3 recanalization 90.4 +/- 6.4% of the potential infarct size (as calculated by the summation of infarct core and penumbra) could be rescued, in patients with TICI score 2a or less only 70.9 +/- 32.3 of the potential infarct was salvaged (p<0.05). Also the volume of salvaged penumbra determined the short-time outcome expressed by the change in NIHSS. Thirty-one patients improved >4 NIHSS points with 72.1 +/- 9.2 cm3 rescued penumbra, in contrast to four patients where only 18.8 +/- 41.9 cm3 could be rescued and subsequently resulting in their death (p = 0.09).
Conclusion
Endovascular mechanical recanalization is a feasible tool to rescue endangered tissue at risk. Additionally infarct volume is a valuable tool in predicting the short- to mid-term outcome.

KEYWORDS: CT perfusion, Stroke

O-225 **11:01 AM - 11:09 AM**

Does Transfer Status Affect Outcomes in Acute Ischemic Stroke Patients Treated Endovascularly?

Soltanolkotabi, M.[1]·Honarmand, A. R.[1]·Bergman, D.[1]·Shaibani, A.[1]·Hurley, M. C.[1]·Conners, J. J.[2]·Lee, V.[2]·Bernstein, R. A.[1]·Prabhakaran, S. K.[1]·Ansari, S. A.[1]
[1]Northwestern University Feinberg School of Medicine, Chicago, IL, [2]Rush University Medical Center, Chicago, IL.

Purpose
Access to intra-arterial therapy (IAT) for acute ischemic stroke (AIS) is limited to comprehensive stroke centers (CSCs) with timely access deemed critical for success. Inter-hospital transfers represent a growing subset of patients in which outcomes have not been well studied.
Materials & Methods
We retrospectively analyzed consecutive anterior circulation AIS patients that underwent IAT at four institutions from 2006-2011. We excluded patients selected using perfusion imaging. Patient demographics, medical risk factors, presentations, technical, and clinical (NIHSS and mRS scores) outcomes, complications, and mortality were studied. Symptom-onset, groin puncture, and end-of-procedure times were recorded. THRIVE scores were calculated. Successful recanalization was defined as TICI ≥2b. Good functional outcome was defined as mRS 0-2 at 90 days. Patients were categorized into those who were

Note: Scanned images are included in the proceedings. Some submitted images were reduced during editing, thereby decreasing clarity. Also, refer to the Program Planner. Proceedings Content as of 3-29-2013.

transferred from outside institutions and those who presented directly to the CSCs.
Results
Of 116 patients studied, 68 (58.6%) were transferred from outside institutions. Transfers and nontransfers were similar in THRIVE scores (p = 0.300), median symptom-onset to groin puncture times (306 versus 315 minutes; p = 0.572), successful recanalization (p = 0.574), and symptomatic ICH (13.2 versus 10.4, p = 0.776), but differed by age (59 versus 69 years; p = 0.002), prior stroke (3% versus 22%, p = 0.002), cardiac history (17.9 versus 36.6%, p = 0.040), baseline NIHSS (20 versus 17, p = 0.005), and location of occlusion (45.6% versus 22.9% ICA, p = 0.012). Transfer patients had significantly worse outcomes at 90 days (mRS 0-2: 16.2% versus 60.4%, p<0.001). In multivariate analysis, transfer status was an independent predictor of poor functional outcome (adj. OR 0.05, 0.011-0.222), adjusting for relevant covariates.
Conclusion
Transferred AIS patients have worse functional outcomes at 90 days than nontransfers, independent of baseline risk factors, stroke severity, time to IAT, and procedural success/complications. Further investigation should focus on residual factors that may contribute to our findings such as baseline/final infarct volumes, premorbid functional status, and poststroke care including rehabilitation.

KEYWORDS: Acute ischemic stroke, Clinical outcome, Transfer status

O-226 **11:09 AM - 11:17 AM**

Outcome after Mechanical Thrombectomy by Stent Retriever under Conscious Sedation: Comparison between Tandem and Single Occlusion of the Anterior Circulation

Pierot, L.·Soize, S.·Kadziolka, K.·Estrade, L.·Barbe, C.·Serre, I.
Hopital Maison-Blanche
Reims, FRANCE.

Purpose
In acute ischemic stroke patients, tandem ICA/MCA (internal carotid artery/middle cerebral artery) occlusion predicts poor outcome after systemic thrombolysis. We aimed to compare patient's outcome after mechanical thrombectomy of tandem and single anterior circulation occlusion.
Materials & Methods
Consecutive patients with acute ischemic stroke of the anterior circulation who underwent mechanical thrombectomy performed with a stent retriever under conscious sedation in six hours from the symptoms onset were included in a prospective study. Data were collected on clinical, imaging and endovascular findings. Tandem and single occlusions were compared with functional outcome and mortality at three months for primary outcome.
Results
From May 2010 to January 2012, 42 patients with an acute ischemic stroke attributable to MCA and/or ICA occlusion were treated. Eleven patients (26.2%) presented a tandem occlusion and 31 patients (73.8%) a single anterior circulation occlusion. Baseline characteristics were similar between the two groups. Recanalization status did not differ significantly (p = 0.76) but patients with tandem occlusion had a worse functional outcome (p = 0.01), a higher mortality rate at three months (p = 0.03) and higher symptomatic intracranial hemorrhages at 24 hours (p = 0.01).
Conclusion
Tandem lesions predicts poor outcome after mechanical thrombectomy by stent retriever under conscious sedation.

KEYWORDS: Acute ischemic stroke, Mechanical thrombectomy

O-227 **11:17 AM - 11:25 AM**

Acute Stroke Patients Treated with Stent Retrievers in Carotid "T" Occlusions Have Improved Recanalization and Outcome

Lum, C.·Orton, T.·Alhazzaa, M.·Iancu, D.·Lesiuk, H.·Santos, M.·Sharma, M.·Ottawa Stroke Research Group
University of Ottawa
Ottawa, ON, CANADA.

Purpose
Higher recanalization rates have been found with stent-retriever use in acute large vessel stroke compared to prior techniques. We sought to evaluate the efficacy and outcomes in acute stroke patients treated with stent retrievers compared to a previous cohort of patients treated with multiple other recanalization strategies.
Materials & Methods
A retrospective chart review was performed in 60 consecutive patients who underwent intra-arterial therapy for acute stroke at an academic stroke referral center between Jan. 2010-Nov. 2012. The cohort prior to this interval was previously analyzed. We divided this cohort into two groups based on treatment with a stent retriever as first-line strategy (group 1) compared to a nonstent retriever multimodality cohort (group 2). Patient baseline demographic information, recanalization rates, recanalization times and post-treatment morbidity and mortality data were compared between the two groups. A good outcome was defined as a 30-day modified Rankin score $\leq$ 2 or 10-point decrease in NIHSS.
Results
There was no significant difference between the two groups in patient age, gender, intravenous tissue plasminogen activator use or stroke risk factors (diabetes, hypertension, dyslipidemia, smoking, peripheral vascular disease, coronary artery disease, prior stroke or transient

Note: Scanned images are included in the proceedings. Some submitted images were reduced during editing, thereby decreasing clarity. Also, refer to the Program Planner. Proceedings Content as of 3-29-2013.

ischemic attack, severe internal carotid stenosis or atrial fibrillation). Intravenous tPA was administered in 65% and 68%. In group 2, 27% had only ia-tPA, 49% were primarily treated with Penumbra, 16% angioplasty, 3% stent only (ICA dissection) and 5% had failed target lesion access. There was a higher baseline median NIHSS score in the stent-retriever group (18 versus 16, p = 0.034). Twenty-three patients treated primarily with stent retrievers were compared to 37 with a multimodality approach. Overall, there were higher recanalization rates in the stent-retriever group (87% versus 51% group 2, p = 0.005). Good outcomes at 30 days were higher in the stent-retriever group (78% versus 43% group 2, p = 0.008). There was lower mortality in patients treated with stent-retrievers (4% versus 32% in group 2, p = 0.011). There was no significant difference in median time to recanalization (68 versus 79 mins). There was lower mortality (4% versus 32%, p = 0.011) and fewer symptomatic hemorrhages (none versus 11%, p = 0.036) in the stent-retriever group. Terminal carotid "T" occlusions comprised 52% of the stent-retriever cases versus 30% in the group 2 cohort. The proportion of "T" lesions was higher than other reported studies (16%-32%). Recanalization rates were higher in the stent-retriever group (83% versus 38%, p = 0.0123). There were more good outcomes in the stent-retriever group (67% versus 22%, p = 0.036). Mean recanalization times were shorter in patients treated with stent retrievers (69 versus 191 mins, p = 0.0023).

Conclusion

An endovascular strategy employing stent retrievers as the first line revascularization technique improves recanalization rates and good outcomes with reduced morbidity and mortality. In a series with a substantial proportion of carotid "T" occlusions, stent retrievers had higher rates of recanalization, shorter recanalization times and better good outcomes compared to a previous multiple modality approach.

KEYWORDS: Stroke, Endovascular mechanical recanalization

O-228 **11:25 AM - 11:33 AM**

Characteristics and Outcomes of Acute Ischemic Stroke Patients Not Selected for Intra-Arterial Intervention by Perfusion Imaging

Soltanolkotabi, M.·Honarmand, A. R.·Prabhakaran, S. K.·Hurley, M. C.·Shaibani, A.·Ansari, S. A.
Northwestern University Feinberg School of Medicine Chicago, IL.

Purpose

Perfusion imaging has been proposed as an effective modality in selecting acute ischemic stroke (AIS) patients who may benefit from intra-arterial (IA) intervention. We investigated the characteristics and outcomes of patients that were deemed ineligible for IA intervention based on perfusion imaging as compared to those who underwent intervention at our institution.

Materials & Methods

A multicenter retrospective review of all AIS patients who underwent perfusion imaging from February 2010 to August 2012 was conducted. Inclusion criteria were the following: symptom-onset to presentation ≤ eight hours, anterior circulation large vessel occlusion as determined by CT/MR angiography (MCA/ICA occlusions), baseline National Institute of Health Stroke Scale (NIHSS) score ≥ 8. Patients selected or excluded for IA intervention based on CT/MR perfusion imaging profiles (CBV/DWI infarct core < 1/3 MCA territory and mismatch of ischemic penumbra > 20% infarct core) were separated into subgroups for analysis. Patient demographics, cardiac and stroke risk factors, intravenous (iv) tPA utilization, location of occlusion, time from symptom-onset to perfusion imaging, NIHSS and modified Rankin Scores (mRS) scores (baseline, discharge, and 90 days), discharge disposition (home, rehabilitation/nursing home, hospice), and mortality rates were recorded. Good functional outcome was defined as mRS 0-2 at 90 days. Statistical analyses were performed with SPSS 20.0.

Results

One hundred ten eligible AIS patients underwent perfusion imaging of which 62 were excluded from IA intervention (56.4%) based on CT/MR perfusion imaging profiles. Table 1 details patient characteristics and outcomes in the intervention versus nonintervention subgroups.

Note: Scanned images are included in the proceedings. Some submitted images were reduced during editing, thereby decreasing clarity. Also, refer to the Program Planner. Proceedings Content as of 3-29-2013.

	Non-mismatch n=62	Mismatch n= 48	*p Value*
Mean age (yrs)	80.87	74.19	0.04*
Female (%)	40 (64.5%)	(60.4%)	0.89
vessel occlusion	9 (14.5%)	6 (12.5%)	
ICA (%)	53 (85.5%)	(87.5%)	0.91
MCA (%)			
symptom onset	208.13	291.42	0.03*
outside	0	(20.1%)	0.03*
NIHSS	19.35	18.67	0.74
discharge	13.43	9.8	0.02*
IV tPA (%)	40 (64.5%)	(41.7%)	0.04*
hospital stay (d)	5.39	8.44	0.16
Risk factors	33 (53.2%)	(29.2%)	0.04*
Atrial fibrillation	14 (22.6%)	(35.4%)	0.21
DM	28 (45.2%)	(37.5%)	0.23
Hyperlipidemia	52 (83.9%)	(25.0%)	0.03*
HTN	2 (3.2%)	7 (14.6%)	0.05
Smoking			
disposition	2 (3.2%)	9 (18.8%)	0.001*
Home (%)	26 (54.8%)	(41.6%)	0.85
rsing home (%)	34 (42.0%)	(39.6%)	0.87
(%)			
outcome at 90-	20 (35.7%)	(66.7%)	0.001*

Conclusion

Among a large cohort eligible for intervention, mismatch was present in younger patients and fewer vascular risk factors. These data suggest that advanced age and atherosclerotic risk factors may influence rate of progression from ischemia to infarction through decreased cerebrovascular reserve and collateral flow in response to arterial occlusion. Despite earlier time to presentation (imaging) and greater receipt of iv tPA, those without mismatch were six-fold less likely to be discharged to home and half as likely to have independent functional outcomes. However, nearly one third of nonintervention patients achieved functional independence at three months suggesting the need to refine patient selection strategies for IA intervention.

KEYWORDS: Acute ischemic stroke, Outcomes, Perfusion selection

O-229 **11:33 AM - 11:41 AM**

Perfusion-Based Selection Leads to Improved Outcomes Compared with Time-Based Selection for Endovascular Reperfusion Therapy in Acute Ischemic Stroke

Soltanolkotabi, M.[1]·Prabhakaran, S. K.[1]·Honarmand, A. R.[1]·Shaibani, A.[1]·Hurley, M. C.[1]·Curran, Y.[1]·Bernstein, R. A.[1]·Alberts, M. J.[1]·Lee, V. H.[2]·Conners, J. J.[2]·Ansari, S. A.[1]
[1]Northwestern University Feinberg School of Medicine, Chicago, IL, [2]Rush University Medical Center, Chicago, IL.

Purpose

Controversy exists on the role of perfusion imaging-based selection of patients with acute ischemic stroke (AIS) for endovascular reperfusion therapy (ERT). Our hypothesis was that perfusion imaging-based selection would improve functional outcomes at three months compared to time-based selection alone.

Materials & Methods

We reviewed data from consecutive AIS patients treated with ERT at four centers between 2006 and 2011. We excluded patients with initial NIHSS score < 8 and those with posterior circulation occlusions. We collected data on demographics, initial NIHSS score, intravenous tissue plasminogen activator (iv tPA), use of perfusion imaging (CT or MRI), time from onset to groin puncture, initial and final reperfusion grade using the modified TICI scale, procedural complications using ECASS criteria, and functional outcome defined as modified Rankin Scale (mRS) 0-2 at three months. Using univariable statistics and multivariable logistic regression, we assessed whether patients who underwent perfusion imaging had better outcomes than those selected based on time alone. We estimated odds ratios (OR) and 95% confidence intervals (CI) in the final model.

Results

One hundred eighty-five patients (mean age 66.7 years; median NIHSS score 19; MCA occlusion 73% and ICA occlusion 27%) were included. TICI 2b or 3 reperfusion grade was achieved in 49.7% while symptomatic hemorrhage (PH1, PH2, or perforation) occurred in 10.8%. Good outcome at three months was seen in 41.7%. Perfusion imaging was used in 69 (37.3%) patients (45 CT and 24 MRI) and was associated with increased onset-to-groin puncture time (359 versus 298 minutes, P = 0.019). Patients who underwent perfusion imaging also were older (73 versus 63 years, P<0.001). Those who underwent perfusion imaging were more likely to have good outcome (53.6 versus 34.5%, P = 0.011). In multivariable analysis, perfusion imaging remained a predictor of good outcome (adj. OR 2.35, 95% CI 1.17-4.72), independent of initial NIHSS score (adj. OR 0.91, 95% CI 0.86-0.97), TICI 2b or 3 reperfusion (adj. OR 4.94, 95 CI 2.50-9.76), and iv tPA use (adj. OR 2.50, 95% CI 1.26-4.94).

Conclusion

In this multicenter study, AIS patients who underwent perfusion imaging were over two-fold more likely to have good outcome following ERT despite a delay in time to

Note: Scanned images are included in the proceedings. Some submitted images were reduced during editing, thereby decreasing clarity. Also, refer to the Program Planner. Proceedings Content as of 3-29-2013.

treatment and age imbalance between groups. Further studies should continue to address the optimal perfusion imaging thresholds for patient selection for ERT.

KEYWORDS: Actue strokePerfusion selection

O-230 **11:41 AM - 11:49 AM**

Metabolic Syndrome and Outcomes in Patients with Acute Ischemic Stroke Undergoing Endovascular Treatment

Gleason, A. K.[1]·Nahabet, E.[1]·Devulapalli, K.[2]·Hsu, D.[3]
[1]Case Western Reserve University School of Medicine, Cleveland, OH, [2]University Hospitals Case Medical Center, Cleveland, OH, [3]Goodman Campbell Brain and Spine Indiana University, Indianapolis, IN.

Purpose
Previous studies have investigated metabolic associations with regards to stroke presentation and stroke outcomes in patients undergoing stroke treatment with intravenous tissue plasminogen activator (tPA); however, associations between metabolic risk factors and outcomes for patients with acute ischemic stroke treated endovascularly are unknown. The purpose of this study is to identify if metabolic syndrome or its components are predictive of stroke severity and outcomes in patients who underwent endovascular treatment for acute ischemic stroke.
Materials & Methods
A retrospective analysis of a single institution's stroke database collected between January 2008 and March 2011 was conducted. Inclusion criteria included patients undergoing endovascular treatment of acute ischemic stroke through mechanical thrombectomy (MT) and/or intra-arterial tPA (IA-tPA). Metabolic syndrome and its components, as defined by the International Diabetes Federation (IDF) was recorded. Severe stroke was defined as severe if National Institute of Health stroke scale (NIHSS) > 15. Outcome measures included successful vessel recanalization defined by TIMI scores ≥ 2, favorable neurologic outcome (FNO) defined by immediate postprocedural change in NIHSS ≥ 8, and mortality. Outcomes were compared between groups using Chi-Square contingency table analysis. Binary logistic regression models were created to assess predictors of outcome with independent variables chosen if Chi-Square analysis yielded P<0.100.
Results
One hundred fifty-one patients presenting with acute ischemic stroke treated endovascularly. Of these, 32 (21.2%) patients had metabolic syndrome and 91 (60.3%) patients presented with severe stroke. No statistically significant associations were found between incidence of severe stroke and metabolic syndrome or its components. Successful recanalization was achieved in 117 (77.5%) patients. Factors associated with successful recanalization included absence of CHF (OR 0.326, 95% CI: 0.126-0.847), HDL less than 40 (OR 3.32, 95% CI: 1.26-8.75), and combination IA-tPA and mechanical thrombectomy (OR 4.56. 95% CI: 1.36-15.3). Thirty-five (23.2%) patients were found to have an improvement of NIHSS ≥ 8 after treatment. Factors associated with improvement of NIHSS included no prior history of diabetes mellitus (DM) (OR 0.238, 95% CI: 0.060-0.954) and high-density lipoprotein (HDL) less than 40 (OR 3.152: 1.18-8.43). Mortality in this study was 50 (33.1%), with history of DM being predictive of mortality (OR 3.35, 95% CI: 1.28-8.76).
Conclusion
No significant associations between metabolic syndrome and initial stroke severity, recanalization, FNO or mortality were observed. Statistical associations regarding components of metabolic syndrome including HDL and DM were observed in that HDL<40 and no prior history of DM was associated with both successful recanalization and FNO. Only DM was predictive of mortality. To our knowledge, this is the first study to investigate associations between metabolic risk factors and immediate stroke outcomes in patients undergoing endovascular treatment.

KEYWORDS: Stroke, Endovascular therapy

O-231 **11:49 AM - 11:57 AM**

Relationship between Diffusion-Weighted Imaging-ASPECTS before Endovascular Reperfusion Therapy and 90-Day Clinical Outcome in Acute Ischemic Stroke Patients

Nakazaki, M.·Mori, T.·Iwata, T.·Iwata, Y.·Takahashi, Y.
Shonan Kamakura
Kamakura, JAPAN.

Purpose
The purpose of our study was to investigate the relationship between Alberta Stroke Programme Early Computed Tomography Score of MRI/diffusion-weighted imaging (DWI-ASPECTS) before endovascular reperfusion therapy and favorable clinical outcome at 90 days in acute stroke patients.
Materials & Methods
Included in our retrospective analysis were consecutive acute ischemic stroke patients: 1) who admitted one single hospital from January 2004 to March 2012 inclusive with severe neurologic deficit, 2) who underwent emergency MRI screening including DWI, and MRA, which suggested acute internal carotid artery (ICA) or middle cerebral artery (MCA) occlusion, and 3) who underwent emergency endovascular reperfusion therapy from three to eight hours from onset. We evaluated the relationship between DWI-ASPECTS before treatment and favorable clinical outcome defined with a modified Ranking Scale (mRS) of 0 to 2 at 90 days.
Results
Fifty-two patients were included, median age was 80 years old, 24 patients were female, and median NIHSS score was 17. Median DWI-ASPECTS before reperfusion therapy was

Note: Scanned images are included in the proceedings. Some submitted images were reduced during editing, thereby decreasing clarity. Also, refer to the Program Planner. Proceedings Content as of 3-29-2013.

seven (interquartile rage = 5.25-9). Successful recanalization, defined as Thrombolysis in Cerebral Infarction grade 2B or more, was 53%. Diffusion-weighted imaging-ASPECTS before reperfusion therapy was correlated with mRS at 90 days (P<0.001), the higher DWI-ASPECTS was, the better score of mRS at 90 days was. Logistic regression analysis identified DWI-ASPECTS (OR= 1.96, 95% CI=1.08 to 4.45, P= 0.024) as an independent significant predictor of favorable clinical outcome.
Conclusion
Higher DWI-ASPECTS before endovascular reperfusion therapy was an independent determinant for favorable clinical outcome at 90 days in acute ischemic patients with occlusion of the ICA or MCA.

KEYWORDS: Endovascular recanalization therapies, MR imaging/diffusion

O-232 **11:57 AM - 12:05 PM**

T2*-Weighted MR Imaging Reveals Hyperacute Lesional Dynamics after Temporal Occlusion and Reperfusion in a Murine Model

Gersing, A. S.[1]·Eisenbeis, A.[2]·Leypoldt, F.[2]·Siemonsen, S.[2]·Magnus, T.[2]·Zimmer, C.[1]·Fiehler, J.[2]
[1]Klinikum Rechts Der Isar, Technical University Munich, Munich, GERMANY, [2]Universitätsklinikum Hamburg-Eppendorf, Hamburg, GERMANY.

Purpose
We aimed to analyze the growth dynamic of T2*-WI signal intensities under experimental conditions. Onion skin-like lesion expansion was hypothesized, the lesion center exhibiting greatest T2*signal decreases.
Materials & Methods
Thirty mice were i.p. anesthetized and temporal occlusion of middle cerebral artery (MCAO) was induced with occlusion time varying between 40 and 60 minutes. Subsequently, early dynamic T2*-signal changes were examined chronologically utilizing a 3T vertical magnet with a scan every two minutes until 60 minutes after recanalization. Baseline imaging of T2*, qT2 and DWI was acquired. Recanalization was conducted by retracting the occluding filament. Infarct volume were evaluated histopathologically with triphenyltetrazolium chloride (TTC) staining.
Results
Continuous volume growth of the outer layer has been observed during MCAO, while the center layer volume was constant within four or 60 minutes after ischemia (Figure a.). Reperfusion lead to further gradual signal increase with initial signal abnormality in the affected hemisphere compared to the vital hemisphere by 8.8%. Degree of signal increase was associated with occlusion time. Continuous reduction of outer layer volume was found after reperfusion by 8.6% after 60 Minutes (Figure b.). Triphenyltetrazolium chloride staining of final penumbra location correlated with T2*-signal loss. Histologically, the total T2*-lesion was larger than infarct core in 16/18 mice (46.9%).

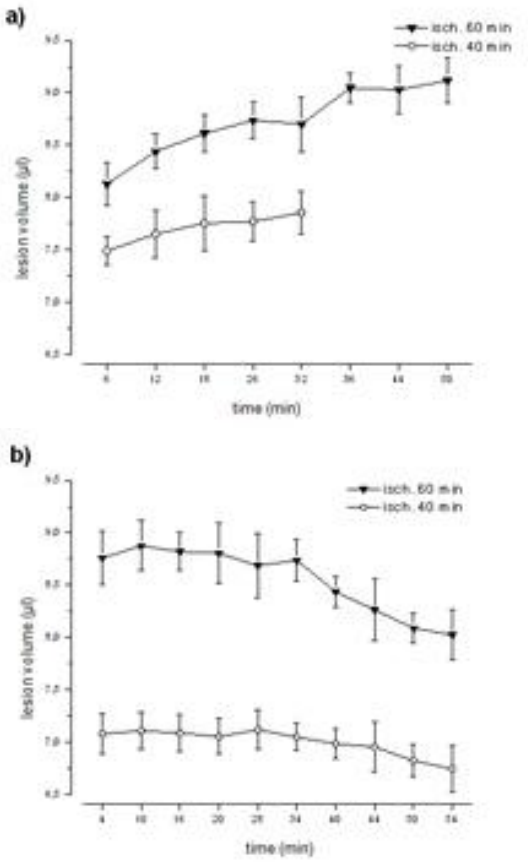

Conclusion
As acute decrease in T2*-signal is attributed to increased local deoxyhemoglobin concentration and is hypothesized to reflect the penumbra on a metabolic level. In the original penumbra concept, the penumbra shrinks from the center by infarct growth while its outer extent is constant. Instead, we observed an increase of the T2*-lesion volume after MCAO and a decrease after reperfusion. The T2*-lesion was larger than the infarct core. It is likely that T2*-WI reflects differences in pathophysiologic states of tissue during ischemia.

KEYWORDS: Acute ischemic stroke, Animal model, T2*-weighted MR imaging

Note: Scanned images are included in the proceedings. Some submitted images were reduced during editing, thereby decreasing clarity. Also, refer to the Program Planner. Proceedings Content as of 3-29-2013.

O-233 **12:05 PM - 12:13 PM**

Achieving Better and Faster Recanalization in Patients with Acute Ischemic Stroke with Dedicated Intra-Aterial Stroke Tool

Shankar, J. J. S.·Conrod, J.
QE II Hospital
Halifax, NS, CANADA.

Purpose
Outcome of patients with acute ischemic stroke (AIS) with proximal occlusion is poor with intravenous thrombolytic therapy. These patients have better outcome with intra-arterial mechanical thrombolysis. The proper tool for mechanical thrombolysis has been debated as more labor-intensive, complicated and much more costly. Despite all the literature available in favor of mechanical thrombolysis, the cost incurred is a big factor in acquisition of these mechanical tools in many institution including ours. This delayed the acquisition of this tool called stent retriever. We assessed the recanalization rate, cost incurred and the outcome of the patients with AIS in our institution in the last two years.
Materials & Methods
From July 2010 to July 2012, we treated 11 patients with acute ischemic stroke with intra-arterial treatment. We procured the stent retriever in November 2011. We treated six patients before November 2011 and six patients after that. Before November 2011 the intra-arterial thrombolysis was done using tPA, microcatheter, microguidewire, intracranial stents and balloons. After November 2011, the intra-arterial thrombolysis was performed using only the stent retriever. We analyzed the recananalization rate, procedure time and equipment cost in all these patients.
Results
The mean procedure time after stent retriever was shorter compared to before stent retriever but it failed to reach significance ($p = 0.076$). The equipment cost before and after stent retriever was not significantly different ($p = 0.69$). The rate of recanalization of the occluded artery after stent retriever was significantly higher ($p = 0.036$).
Conclusion
Adding a dedicated intra-arterial stroke tool improved the outcome of the patients with shorter recanalization time, procedure time, shorter hospital stay, better clinical outcome and with no significant increase in the cost. This suggests that a dedicated mechanical tool for recanalization in selected patients result in better patient outcome without adding any significant cost.

KEYWORDS: Actue stroke, Mechanical thrombectomy

Tuesday Morning

10:45 AM - 12:15 PM
Room 5AB

(25d) Parallel Scientific Papers: Functional Imaging II: fMRI and MRS

O-234 **10:45 AM - 10:53 AM**

More Direct Method for Functional MR Imaging

Tailor, D. R.
University of Pittsburgh
Pittsburgh, PA.

Purpose
Functional MR imaging (fMRI) of the brain has traditionally consisted of T_2^*-weighted imaging which relies on the susceptibility effect of deoxyhemoglobin (the BOLD effect). Since the BOLD signal is several biochemical steps removed from actual metabolism, its use for studying brain function relies on statistical mapping of the imaging data by correlation with the functional stimulation paradigm to indirectly infer neuronal activation. A more direct and perhaps more reliable approach would involve high spatiotemporal resolution brain mapping of oxidative metabolism in response to stimulation. However, there are no techniques presently available that can accomplish this goal. The purpose of this study is to introduce a novel MR approach for high spatiotemporal imaging of relative cerebral metabolic rate of oxygen ($CMRO_2$) and to apply for direct visualization of brain activation without reliance on statistical inference relative to the activation paradigm.
Materials & Methods
Based on our model, the subtraction of high-frequency spin-locked ("high B_1") and low-frequency spin-locked ("low B_1") $T_{1\rho}$-weighted images of the brain directly yields relative $CMRO_2$ on a pixel-by-pixel basis. In accordance with an IRB-approved protocol, three human subjects (two males and one female, ages 23 to 35 years) were visually stimulated using LED goggles flashing at 10Hz for 5s. Both the high and low B_1 images were obtained (TR = 1s, TE = 14 ms, 0.2 x 0.2 x 0.5 mm pixels, NEX =1, ETL = 45, high B_1 frequency = 500 Hz, low B_1 frequency = 250 Hz) within the final 3.2 sec of our five sec visual stimulus, immediately following a control study without stimulation, with an imaging temporal resolution of 3.2s.
Results
Representative data are provided in the graphic file, which consists of a figure demonstrating the control (top left) and experimental (bottom left) $T_{1\rho}$-weighted images of a subject with the color-rendered subtraction of the high and low B_1 images, which is equivalent to the relative

Note: Scanned images are included in the proceedings. Some submitted images were reduced during editing, thereby decreasing clarity. Also, refer to the Program Planner. Proceedings Content as of 3-29-2013.

$CMRO_2$ value in each respective pixel (right column). As expected, the bilateral medial occipital regions consisting of the visual cortex demonstrate elevated relative $CMRO_2$ values in response to visual stimulation. In this particular subject, there appears to be right-side dominance (left side of image) of the visual function.

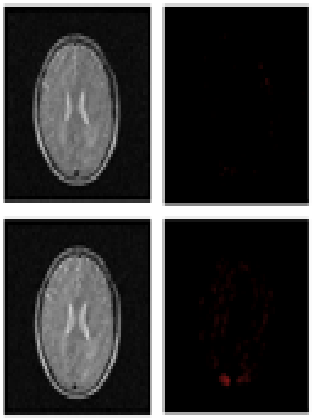

Conclusion

In conclusion, our novel fMRI technique based on $T_{1\rho}$-weighted imaging is capable of high-resolution mapping of brain activation in humans without reliance on statistical inference. This method may provide a more robust alternative to conventional fMRI.

KEYWORDS: 1.5T, Brain mapping, fMRI

O-235 **10:53 AM - 11:01 AM**

Reproducibility of Cerebral Blood Flow Values from Arterial Spin Labeling in Patients with Cognitive Impairment

Karmonik, C.·Pascual, B.·Dulay, M. F.·Spann, B. M.·Grossman, R. G.·Roman, G. C.·Fung, S. H.
The Methodist Hospital Neurological Institute
Houston, TX.

Purpose

To establish confidence limits for longitudinal arterial spin labeling (ASL) perfusion studies in elderly patients evaluated for cognitive impairment by means of test-retest reliability analysis.

Materials & Methods

In a prospective study, two sets of pseudo-continuous ASL (pCASL, post-labeling image delay 2.5 sec to account for possibly increased arterial transit times, GE MR750 3T) image sets were acquired from 30 subjects (patient repositioned during examination, age-range: 62-84 years). Cerebral blood flow (CBF) maps were registered to gray matter (GM, segmented with FSL) maps from 3D anatomical scans and transformed into Talairach space (AFNI) enabling qualitative voxel-based comparisons (entire GM and selected regions from MNI structural atlas) using scatter-plots, quantile-quantile (QQ) plots and box-percentile (BP) plots. Test-retest reliability was quantified with intraclass correlation coefficient (ICC) and standard deviation (SD). Statistical significance of CBF distribution differences were assessed with the Student *t*-test (for mean) and Kolmogorov Smirnov (KS) tests (R statistical language).

Results

Scatter and QQ plots showed good qualitative agreement between both measurements. Box-percentile plots revealed differences in CBF distribution shapes for investigated brain regions (Figure 1). Average ICC values were consistent between entire GM [average: 0.77 (range: 0.9 - 0.5)] and assessed regions (frontal lobe: 0.78 (0.92 - 0.51), parietal: 0.78 (0.91 - 0.40), occipital: 0.74 (0.90 - 0.45), temporal: 0.69 (0.93 - 0.30) and cerebellum: 0.72 (0.91 - 0.41). Average SD was lowest for occipital lobe (7.0 ± 1.7 ml/min/100g) and highest for cerebellum (8.7 ± 2.5 ml/min/100g). Average SD for entire GM was 8.1 ± 2.0 ml/min/100g). P-values for KS tests did not exceed 0.0033 with two exceptions (0.0014 for cerebellum in subject #13 and 0.007, frontal, #15). P-values for Student *t*-test exceeded 0.05 for frontal and parietal lobe each in one subject, for temporal lobe in two subjects and for cerebellum in three subjects.

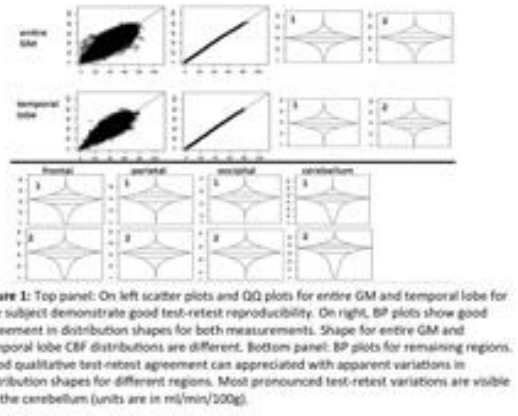

Figure 1: Top panel: On left scatter plots and QQ plots for entire GM and temporal lobe for one subject demonstrate good test-retest reproducibility. On right, BP plots show good agreement in distribution shapes for both measurements. Shape for entire GM and temporal lobe CBF distributions are different. Bottom panel: BP plots for remaining regions. Good qualitative test-retest agreement can appreciated with apparent variations in distribution shapes for different regions. Most pronounced test-retest variations are visible for the cerebellum (units are in ml/min/100g).

Conclusion

Good test-rest reproducibility was found in the investigated patient population. Our results suggest that for statistical significance in longitudinal perfusion studies, observed differences have to exceed 8 ml/min/100g (one standard deviation).

KEYWORDS: Arterial spin labeling, Cognitive deficit

Note: Scanned images are included in the proceedings. Some submitted images were reduced during editing, thereby decreasing clarity. Also, refer to the Program Planner. Proceedings Content as of 3-29-2013.

O-236 **11:01 AM - 11:09 AM**

Quantitative Perfusion Changes in Functional Arterial Spin Labeling MR Imaging during Language and Motor Tasks

Ross, A. B.·Watts, R.·Nickerson, J. P.
University of Vermont/Fletcher Allen Health Care
Burlington, VT.

Purpose
Although arterial spin labeling (ASL) is a well established technique for perfusion brain imaging, it has not yet been used widely for functional imaging paradigms despite certain advantages over traditional BOLD MRI. Specifically, ASL provides quantitative information regarding changes in cerebral blood flow (CBF), is relatively insensitive to signal drift, and may provide more statistical power for certain functional imaging experimental designs. This study compares ASL to the standard of BOLD in classic language and motor tasks and provides normative data regarding quantitative CBF changes within the relevant regions of interest.
Materials & Methods
Seventeen healthy adult volunteers have been recruited to date with the functional tasks consisting of word generation and finger tapping. A simple two-condition block design was used for each sequence. For each functional task, traditional BOLD images were acquired followed by a pseudo-continuous arterial spin labeling acquisition (pCASL) using a protocol similar to Aslan et al. Arterial blood in a slab 20 mm inferior to the imaging volume is magnetically labeled with a labeling duration of 1650 ms and post-labeling delay of 1525 ms. Axial slices are acquired using a 2D echo-planar readout acquisition matrix of 80x80x10 and a resolution of 3x3x5mm3 using a SENSE factor of 2.5. Background suppression and vascular crushers are used to minimize sensitivity to subject motion and intravascular blood. 90 pairs of control and tag images are acquired with a TR of 4s (acquisition time 12 minutes) and TE of 20ms. Data were analyzed using FSL FEAT with full perfusion signal modeling. The BOLD activation maps were used as a guide for generating masks over the hand motor cortex and Broca's area for the finger tapping and word generation tasks, respectively. The masks then were registered into the ASL scan using the SPM suite of tools for Matlab and the quantitative change within the ROI calculated in FSL.
Results
Subject recruitment and data analysis are ongoing with results to date showing that cerebral blood flow increased by 42.83% +/- 15.66 (Mean, Std. Dev.) in the right motor strip and by 44.57% +/- 17.56 in the left motor strip. Broca's area demonstrated a 23.05% +/- 6.13 increase in cerebral blood flow.
Conclusion
Perfusion-based functional imaging using pCASL provides robust and consistent quantitative perfusion information when used for functional activation mapping in motor and language paradigms when compared to BOLD MRI. Normative data for quantitative CBF changes in Broca's area and the motor strip are presented for healthy adult volunteers during word generation and finger tapping tasks respectively. A technique for directly comparing BOLD and ASL scanning paradigms is described in detail. Validation of this quantitative technique may allow for the application of functional MRI in the research setting across differing populations to a greater degree than has been previously achievable with BOLD imaging.

KEYWORDS: Arterial spin labeling, Functional brain mapping

O-237 **11:09 AM - 11:17 AM**

Age Influence in Functional MR Activation during Working Memory after Mild Traumatic Brain Injury

Chen, D.·Wang, W.·Liao, Y.·Hsu, H.·Tseng, Y.·Chen, C.
Taipei Medical University/Shuang Ho Hospital
Taipei, TAIWAN.

Purpose
Mild traumatic brain injury (mTBI)-induced differences in working memory functional activity is observed in several studies. This study aims to evaluate the influence of age on working memory activation in functional MRI after mTBI.
Materials & Methods
Research ethics committee approval and patient written informed consent were obtained. We collected two groups of mTBI patients (age > 50 years and age < 30 years). The older group contains 13 patients (51~68 years; average 57.7 years) and the younger group contains 13 patients (21~29 years; average 24.7 years). Nine normal controls (NC) for the older group (51~68 years; average 60.1 years) and 13 normal controls for the younger group (21~29 years; average 26.1 years) were recruited. Brain activation patterns in response to a working memory task (n-back; 1 and 2-back conditions) were assessed with functional MRI on a 3.0T MR system. Each mTBI subject underwent the first scan within one month after injury. The second scan was repeated at six weeks after the first scan.
Results
In the younger group, the patients had more activations than the controls (2-back>1-back, p-value < 0.01) in the first scan. In the second scan, the working memory activation of the patients returned to be similar with the controls. In the older group, the patients had less activations than the controls (2-back>1-back, p-value < 0.01) in the first scan. In the second scan, however, the working memory activation of the patients further decreased from the first scan.

Note: Scanned images are included in the proceedings. Some submitted images were reduced during editing, thereby decreasing clarity. Also, refer to the Program Planner. Proceedings Content as of 3-29-2013.

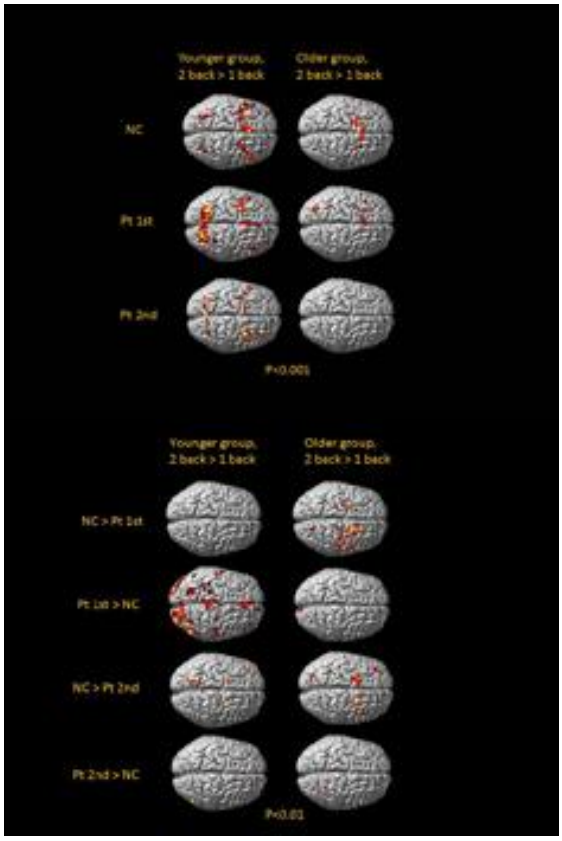

Conclusion

After mTBI, working memory activation of the younger patients increased in the first scan and returned to the baseline after six weeks. The older patients had decreased working memory activation than the controls and did not recover. The result may suggest that younger group has more potential to recover after mTBI while the older group did not.

KEYWORDS: Mild TBI, Aging, Working memory

O-238 **11:17 AM - 11:25 AM**

Default Mode Network Assessment in Patients with Neuromyelitis Optica: A Resting-State Functional MR Imaging Study

Rueda-Lopes, F. C.[1,2]·Miraldi, F.[1]·Domingues, R.[2]·Alves-Leon, S.[1]·Gasparetto, E. L.[1,2]
[1]UFRJ, Rio de Janeiro, BRAZIL, [2]DASA, Rio de Janeiro, BRAZIL.

Purpose

Neuromyelitis optica (NMO) spectrum is an autoimune demyelinating disease usually related to optical neuritis and extensive myelitis. Diffuse white matter damage has been shown, but the cortex was poorly studied in such disease. Our objective was to investigate NMO patients using the resting-state functional magnetic resonance imaging (RS fMRI) compared to the controls, regarding the default-mode network in order to evaluate the cortical adaptations in NMO.

Materials & Methods

We studied 28 NMO spectrum patients (including myelitis, neuritis optica and/or both) mean age 38 years (SD +/- 3,2, 18 female), and also 19 sex- and age-matched controls. All participants signed informed consent. MR imaging was performed in a 1.5T scanner, including 3D T1-weighted images (postprocessed by SIENAX to obtain gray matter (GM), white matter (WM) and total brain volume (BV) and RS fMRI was performed during rest. Functional MRI data were postprocessed using MELODIC, part of FMRIB's Software Library. The fMRI data set was decomposed using independent component analysis (ICA) to identify large-scale patterns of functional connectivity. After that, a "dual-regression" approach was carried out allowing voxel-wise comparisons of resting functional connectivity between both groups. Threshold-free cluster enhancement (TFCE) and p-corrected maps of comparison between both groups were analyzed. Also, the extracted synchronization values of the default-mode network (DMN) of patients and controls were compared and their correlaction with GM volume, WM volume and BV was assessed using Pearson technique. A p-value of 0.05 was considered statistically significant.

Results

Fourteen components were computed in the entire subject group by ICA. Default-mode network was detected clearly among the subjects and was compared between both groups. The evaluation of TFCE maps showed areas of significantly higher synchronization in NMO patients compared to healthy controls in the parietal lobes, precuneus region and also in the right hippocampus ($p<0.01$), which remained after p-correction. Also, controls had areas of higher synchronization in the frontal areas compared to patients in the TFCE maps, which were markedly reduced but still detected after p-correction. The synchronization average value for DMN in patients was 1.373588 (2.429656 SD) and for controls 2.483234 (2.258987 SD) with a p-value of 0.12. These synchronization values had a negative weak correlation with GM volume (-0.03) and a positive correlation with WM volume (0.13) and BV (0.03).

Conclusion

Neuromyelitis optica patients have an increased synchronization during rest in the parietal and precuneus areas of DMN as a form of compensation for the decreased synchronization in the frontal area. The weak correlation of the synchronization values with GM volume is probably due to the maintenance of the cortical and subcortical areas in such disease. The main damage is probably located in the WM tracts, as shown by TBSS and volume studies, corroborating for the correlation between DMN values and WM volume.

KEYWORDS: MR imaging brain, Neuromyelitis optica

Note: Scanned images are included in the proceedings. Some submitted images were reduced during editing, thereby decreasing clarity. Also, refer to the Program Planner. Proceedings Content as of 3-29-2013.

O-239 **11:25 AM - 11:33 AM**

Motor Tongue Representation at the Base of a Novel Sagittal Landmark in the Precentral Gyrus: Introducing the "K"

Tyndall, A. J.[1]·Hartwigsen, G.[2]·Karwacki, G.[1]·Stenzel, F.[1]·Ahlhelm, F.[1]·Stippich, C.[1]
[1]University Hospital Basel, Basel, SWITZERLAND, [2]Language and Aphasia Laboratory, Leipzig, GERMANY.

Purpose
Knowledge of topographical brain anatomy is mandatory in clinical routine and research interpretation, thus identification of characteristic landmarks is fundamental. Landmarks have been described in the axial and sagittal planes, however, the latter is less commonly used in functional studies. The inferior frontal gyrus has a typical M-shape easily identified on sagittal MR images. Adjacent to the pars opercularis, the base of the sensorimotor area abuts this configuration, which typically forms a "K" consisting of the anterior subcentral and inferior precentral sulci, the precentral gyrus, posterior subcentral sulcus, postcentral gyrus and postcentral sulcus that abuts the angular gyrus. Based on the concept of the homunculus, the motor tongue area is located inferior to the motor hand area on the precentral gyrus. As of now, no typical landmark for this area has been described. We aimed to: a) localize the motor tongue area using fMRI and b) describe its anatomical configuration to reliably enable clinicians to identify the base of the precentral gyrus in the sagittal plane based on the resultant anatomical description only.
Materials & Methods
Ten healthy subjects underwent fMRI examination with a tongue motor paradigm using a block design. The M1activation was defined using Spm5. From a cohort of patients of a dementia study (n=33), MPRage datasets were used for morphologic depiction of the "K" performed by two neuroradiologists in consensus. A screenshot with its best depiction was acquired in both hemispheres, which then were presented to three physicians (neurosurgeon, neuroradiology resident and consultant cardiothoracic radiologist), who were requested to locate the precentral gyrus, without further assistance. After this read-out they were informed about the fMRI results of healthy controls and the anatomical formation of the base of the lower convexity ("K"). This read-out then was repeated four weeks later.
Results
In the 10 healthy volunteers, group analysis showed BOLD activation at the base of precentral gyrus in the upper right "arm" of the "K" for the motor tongue paradigm (x=45, y=-7, z=25, MNI space). For the dementia study cohort (n=33), the mean sagittal degree (first lateral slice depicting the cortical surface = 0%; mid-sagittal plane of the brain = 100%) of the chosen sagittal slices best depicting the K-formation was 31.5% (±4.2SD) and 30.4% (±3.8SD) for the right and left hemisphere, respectively. Before anatomical instruction of the "K" formation, the neurosurgeon, neuroradiologist and cardiothoracic radiologist located the precentral gyrus with 91%, 85% and 69% accuracy, respectively. After anatomical instruction, this increased to 100%, 100% and 98%, implying a statistically significant improvement of 10% (p=0.013), 18% (p=0.001) and 44% (p<0.001), respectively.
Conclusion
The motor tongue representation (M1) is found at the base of the lower convexity in the precentral gyrus in the upper arm of a "K" formation. The precentral gyrus can be identified in the sagittal plane via the K-shaped gyral formation with a high accuracy. We consider this a valuable diagnostic asset, especially if other established landmarks are insufficiently identifiable, such as in anatomical deformation due to underlying pathologies.

KEYWORDS: Anatomy, fMRI, Tongue

O-240 **11:33 AM - 11:41 AM**

Altered Resting-State Network Connectivity as a Potential MR Biomarker in Spinocerebellar Ataxia Type 6

Pereira, L. P.·Airan, R.·Sair, H.·Ying, S.
Johns Hopkins Hospital
Baltimore, MD.

Purpose
The cerebellum is known to demonstrate functional co-activation not only with cortical motor areas but also with cognitive networks. In order to test this relationship, we evaluated brain resting state network connectivity in a relatively "pure" cerebellar model of degeneration, spinocerebellar ataxia type 6 (SCA6). Spinocerebellar ataxia type 6 is characterized by both progressive motor impairment and mild cognitive impairment. Patients are expected to demonstrate altered efficiency of internetwork connections between functional modules, in correlation to disease severity.
Materials & Methods
Sixteen patients (age 45 to 70 years) with SCA6 underwent 3T MRI including T1 MPRAGE and seven min BOLD fMRI (TR = 2.5 sec) sequences. Data were preprocessed using FSL (FMRIB, Oxford, UK), SPM8 (Wellcome Trust, UK) and custom MATLAB (Mathworks, MA) scripts to complete slice-timing correction, rigid-body motion correction, segmentation and normalization to a standard template (MNI, 2mm), COMPCOR nuisance regression, bandpass temporal filtering (0.01-1Hz), and spatial smoothing (6 mm Gaussian kernel). Whole-brain gray matter was automatically parcellated into 875 regions of interest (ROIs). For each ROI, the first eigenvariate of voxel timecourses was extracted. Pearson correlation coefficients between each pair of ROI timecourses were calculated across the 875 ROIs. The set of average control correlation coefficients were fed as an undirected weighted adjacency matrix (thresholded at r2 = 0.08) into the infomap modularity algorithm. For each network, the

Note: Scanned images are included in the proceedings. Some submitted images were reduced during editing, thereby decreasing clarity. Also, refer to the Program Planner. Proceedings Content as of 3-29-2013.

intra-network efficiency of the thresholded adjacency sub-matrix was calculated, with a similar measuring applied to the inter-network efficiency. Efficiency was correlated with functional staging for ataxia (FSFA) score, a scale from 0 to 6 that emphasizes mobility.

Results

Functional staging for ataxia is correlated with altered efficiency of internetwork connections within the following functional modules: attention, both inferior and superior cerebellar and pons, limbic, right frontoparietal, ventromedial temporal and inferior temporal gyrus and pons, and medial prefrontal cortex. Of note, the motor network is not involved.

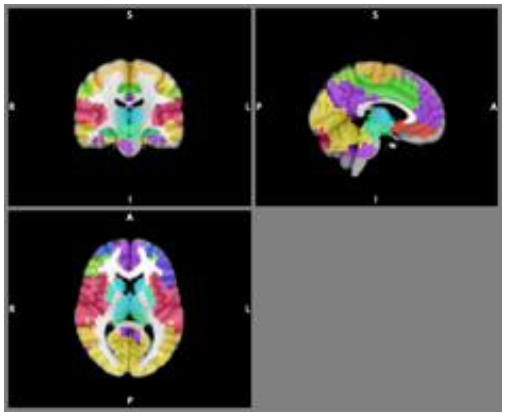

Conclusion

In SCA6, there is altered efficiency of internetwork connections in the cerebellum, brainstem, and frontal and temporal lobes that is consistent with the clinical presentation and is correlated with disease severity. With further validation, resting state network connectivity could have promise as an MR biomarker for functional staging in this genetic model of cerebellar ataxia.

KEYWORDS: Resting-state fMRI, Cerebellum, degeneration

O-241 **11:41 AM - 11:49 AM**

Resting-State Activity in the Left Executive Control Network Is Associated with Behavioral Approach and Is Increased in Substance Dependence

Tanabe, J. L.[1]·Krmpotich, T. D.[1]·Thompson, L. L.[1]·Banich, M. T.[2]·Klenk, A. M.[1]·Tregellas, J. R.[1]

[1]University of Colorado Denver, Aurora, CO, [2]University of Colorado Boulder, Boulder, CO.

Purpose

Individuals with drug addictions report increased willingness to approach rewards. Approach behaviors are thought to involve executive control processes and are more strongly represented in the left compared to right prefrontal cortex. A link between approach behavior and left prefrontal activity has not been shown in the resting brain. We hypothesized that compared to controls, substance-dependent individuals (SDI) would have greater left prefrontal activity in a left executive control network (ECN) at rest.

Materials & Methods

Twenty-five SDI and 25 controls completed a Behavioral Inhibition System/Behavioral Activation System (BIS/BAS) questionnaire and underwent a resting fMRI scan. Group independent component analysis was performed. We used template matching to identify a left ECN component and right ECN component, respectively. Corresponding components were compared across groups using a 2-sample t-test. Maps were set at a threshold of $p<0.005$, uncorrected, with an extent threshold of 35 voxels, corresponding to a whole-brain cluster-corrected level of $p<0.01$. Next, BAS scores were correlated with the magnitude of signal fluctuations in the left ECN and BIS scores with right ECN.

Results

Substance-dependent individuals showed significantly greater activity than controls in the left prefrontal cortex of the left ECN. In contrast, SDI showed less activity than controls in the right prefrontal cortex of the right ECN (top Figure). Behavioral Activation System scores correlated with signal fluctuation in the left ECN (bottom Figure).

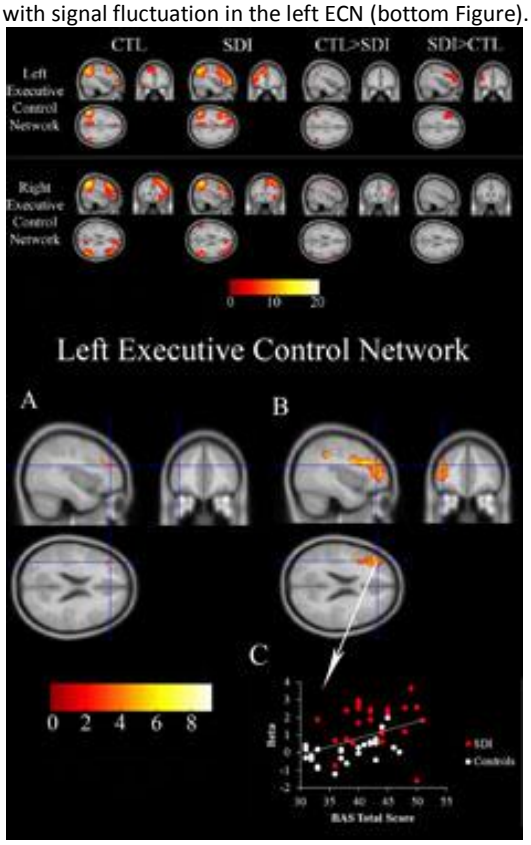

Conclusion

Results from this study suggest that approach tendencies may be related to a left hemispheric ECN at rest. Higher resting-state signal in the left ECN may play a role in heightened approach tendencies that contribute to drug-seeking behavior.

KEYWORDS: Resting-state fMRI

Note: Scanned images are included in the proceedings. Some submitted images were reduced during editing, thereby decreasing clarity. Also, refer to the Program Planner. Proceedings Content as of 3-29-2013.

O-242 **11:49 AM - 11:57 AM**

Is the Normal-Appearing Cerebellum Really Normal?: A H-MR Spectroscopy Study at 3T

Azagra, A.[1]·Beltran-marin, M.[1]·Sadeghi, N.[1]·Manto, M.[1]·Jissendi-Tchofo, P.[2]
[1]Hopital Erasme, Bruxelles, BELGIUM, [2]C.H.U. Lille, Lille, FRANCE.

Purpose
In patients suspected of having a brain lesion on the basis of the neurologic examination, the brain MRI might appear normal, or disclose supratentorial abnormalities whereas the cerebellum is described as normal. Going beyond the morphologic appearance, spectroscopy is the only technique that allows detecting tissular biochemical anomalies, which precede morphologic changes. We aimed at describing metabolic alterations found in the normal-appearing cerebellum of patients with altered neurologic functions, and suggest metabolic ratios thresholds to be used when reading spectra in clinical practice.
Materials & Methods
The study included 32 patients (18F/14M, aged 10-78 years old, mean 37,12) who underwent a brain assessment at 3T. All showed normal-appearing cerebellum on MRI using predefined criteria of reading (two readers). Spectroscopy was performed in all patients and included a single voxel PRESS sequence at short echo time (TE 30-36 msec) within the cerebellum (encompassing the dentate nucleus). The metabolites ratios (Naa/Cr, Cho/Cr, mI/Cr, GlxT/Cr) were calculated and compared with the values obtained in 14 aged-matched controls (group 1), by means of t- and Z score tests. Presence or absence of lactate also was recorded.
Results
The indications for MRI/MRS assessment were: metabolic disease (n = 15; 14 mitochondriopathy, 1 PKU), neurodegenerative processes (n = 5; two Parkinson disease, three cerebellar ataxia), epilepsy (three), cognitive disturbances (two) (1 MCI, one developmental delay), vascular encephalopathy (n = 2), one supratentorial tumor, and three nonspecific neurologic impairment. Eighteen patients showed a totally normal brain (group 2) while 14 patients had supratentorial involvement (group 3). We found significant differences between group 1 and groups 2 and 3 for all the ratios ($p<0.05$). In comparison with the controls, group 2 showed unexpected higher levels of Naa/Cr and mI/Cr ratios ($p<0.01$), with corresponding z scores means at 0.22 and 0.35, while group 3 showed lower Cho/Cr and mI/Cr ($p<0.01$), and strikingly increased GlxT/Cr ($p<0.01$) with z scores means at 0.24, 0.46, and 0.59 respectively.
Conclusion
These findings suggest a probable hyperactivation of the cerebellum in neurologic disturbances with no signal abnormality in the brain, as revealed by an increase of all the metabolites ratios (group 2). In the presence of supratentorial lesions, there is likely an imbalance of the neurotransmitters in the cerebellum as revealed by the striking increase of GlxT/Cr levels. The z scores means may be used as threshold values to interpret the metabolites ratios as abnormal in comparison with a control group.

KEYWORDS: MR spectrocopy, Cerebellum

O-243 **11:57 AM - 12:05 PM**

Comparison of Single Voxel MR Spectroscopy at 3T and 7T

Barker, P. B.[1]·Wijtenburg, S. A.[2]·Gillen, J.[1]·Bonekamp, S.[1]·Rowland, L. M.[2]·Edden, R. A. E.[1]
[1]Johns Hopkins University, Baltimore, MD, [2]University of Maryland, Baltimore, MD.

Purpose
MR spectroscopy (MRS) is believed to benefit from the use of high magnetic field strengths such as 7T; however, to our knowledge, there have been no direct comparisons of 7T MRS to the current clinical standard of 3T. The purpose of this study was to compare 7T to 3T MRS in the same subjects using near identical methodology.
Materials & Methods
Four healthy normal volunteers (2M, 35 ± 7 years) were scanned at both 3T and 7T within a seven-day time period. Spectra were recorded from the anterior cingulate cortex (ACC) and dorsolateral prefrontal cortex (DLPFC) using Philips 3T and 7T scanners running the same operating system, and both equipped with 32-channel head coils. Spectra were recorded with the semi-LASER (sLASER) pulse sequence with the following parameters (3x3x3 cm, TR/TE 3000/32 ms, VAPOR water suppression, 3 kHz adiabatic refocusing pulses, 32 averages). Spectra were analyzed at both field strengths using LCModel software.
Results
Figure 1 shows representative ACC spectra from one subject at both 3T and 7T. Average ACC and DLPFC signal-to-noise ratios (SNR) were 50.1 and 54.8 at 7T, and 33.8 and 35.5 at 3T, respectively. Average line widths were 0.030 ppm (8.9 Hz) and 0.035 ppm (4.5 Hz) at 7T and 3T, respectively. For the major resonances in the spectrum (tCho, tCr, tNAA, mI), average Cramer-Rao lower bounds (CRLB, a measure of the uncertainty of the estimated metabolite concentration) at 7T were between 71-98% of the 3T values, consistent with the improved SNR and resolution at 7T. Some (but not all) other compounds also were more reliably determined at 7T, including glutamate, NAAG, taurine and glutathione.

Note: Scanned images are included in the proceedings. Some submitted images were reduced during editing, thereby decreasing clarity. Also, refer to the Program Planner. Proceedings Content as of 3-29-2013.

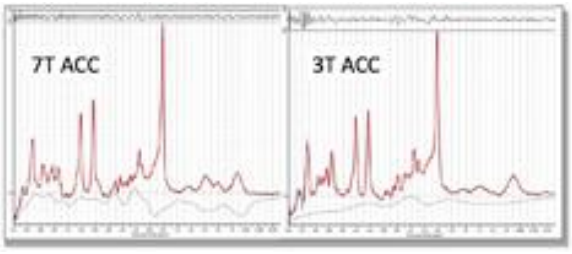

Conclusion
Spectra acquired from cortical gray matter regions show the expected benefit in SNR and reduced uncertainty (CRLBs) at 7T compared to 3T, as well as the ability to accurately detect more compounds at 7T compared to 3T.

KEYWORDS: 7T, MR spectrocopy

O-244 **12:05 PM - 12:13 PM**

MR Proton Spectroscopy of the Brain: Metabolic Imaging Findings in the 1.3 ppm Region Utilizing Ultrashort TE

Boyko, O. B.·Shiroishi, M.·Kim, P. E.·Rajamohan, A.·Rajamohan, A.·Go, J. L.·Lerner, A.·Law, M.
University of Southern California
Los Angeles, CA.

Purpose
To compare the clinical findings in the 1.3 ppm region of ultra-short TE single voxel proton MR spectroscopy (MRS) with standard short TE single voxel proton MRS using either STEAM or PRESS in imaging diseases of the brain.
Materials & Methods
Twenty patients underwent single voxel MR spectroscopy at 1.5T using either STEAM or PRESS for water and fat suppression. MR spectroscopy was acquired with ultrashort STEAM (12-15 msec) and ultrashort PRESS (20, 25 msec) with standard short TE STEAM (20 msec) or standard short TE PRESS (30, 35 msec). The shortest default TR allowed by the scanner was utilized in most cases . The peak heights and/or area under the heights of metabolites identified in the 1.3 ppm region were compared with each TE. TE 144 msec was utilized to identify J-coupling features of metabolites which would indicated lactate.
Results
Ultrashort TE proton MRS was acquired successfully in all patients including the supratentorium and posterior fossa. Outer saturation bands prior to shimming could only be prescribed for ultrashort TE PRESS acquisitions and not STEAM acquisitons. Peak height variability was noted in the 1.3 ppm between the ultrashort STEAM and PRESS compared to standard TE STEAM and PRESS acquisition. Short T1 metabolite such as lipid demonstrated the highest peak height on the ultrashort TE acquisitions both STEAM and PRESS, slightly more apparent with STEAM. Lactate doublet was resolved more readily on standard TE PRESS acquisition.
Conclusion
Brain lesion metabolite such as lipid having a short T1 appears to have the highest peak height with ultra short TE acquisitions. Lactate doublet peak was identified on both ultra short and standard TE MRS. In disease processes of the brain where MRS, delineates a lipid peak at 1.3 ppm, utilization of short TE MRS acquisition may detect the highest peak height.

KEYWORDS: MR spectrocopy, Brain abnormalities

O-244a **12:13 PM - 12:21 PM**

Diagnosis and Surgical Treatment of the Brain Tumors

Murodova, D.·Ahmediev, M. M.
Republican Scientific Center of Neurosurgery
Tashkent, UZBEKISTAN.

Purpose
One of the main trends of modern neurosurgery, is to minimize surgical trauma and improve the quality of life of patients after surgery. The aim of the study. Comparative evaluation of the results of surgical treatment of brain tumors of supratentorial localization method using DT-MRI tractography.
Materials & Methods
We analyzed the results of treatment of 90 patients who were operated under identical conditions. Age of patients was 5-62 years. Surgery was performed under the control of intraoperative monitoring. For noninvasive and more complete removal of the tumor with maximum preservation of pathways using data mechanogram, which allows the surgeon to more accurately determine the amount of tumor resection.This technique made it possible to identify possible ways to access and surgical planning of tumor resection.
Results
These DT-MRI tractography, found that nearly half (56.5%) of primary surgery ended with subtotal removal of the tumor, total tumor removal was possible in 34.8% of cases, the biopsy in 8.7% of cases. Border security resection of the tumor tissue adjacent to the pathways should be at a distance of 5-10 mm from them. However, when the data mechanogram intraoperative monitoring, tracking boundaries resection should be considered intraoperatively shift occurs in the brain. Due to a "shift of the brain" dislocation pathways occurs mainly due to resection and tissue edema, and changes in intracranial pressure. Thus, during the operation the displacement of the center of the white substance formed resection cavity, and the distance from the area of operations to the point of passing the white matter pathways is reduced. Information about the localization pathways and conducted intraoperative monitoring, help plan and implement a more precise surgery, avoiding destruction deployed, as well as swollen and infiltrated tumor tract, increases confidence when working in areas, where the white matter bundles.

Note: Scanned images are included in the proceedings. Some submitted images were reduced during editing, thereby decreasing clarity. Also, refer to the Program Planner. Proceedings Content as of 3-29-2013.

Conclusion
Thus, removal of intracranial tumors under the control of intraoperative monitoring using data from MR tractography, the conditions of intraoperative accuracy and safety of surgery to minimize surgical trauma, helps reduce the risk of neurologic deficit, which determines the efficiency of the operation and the quality of life of patients.

Tuesday Morning

10:45 AM - 12:15 PM
Room 1AB

(25e) Parallel Scientific Papers: Socioeconomic: Coding, Quality and Informatics

O-245 **10:45 AM - 10:53 AM**

Health Policy and Imaging Reimbursement Cuts: How Will You Be Affected and What's Coming Next?

Rehani, B.[1]·Rosman, D.[1]·Romero, J.[1]·Schaefer, P.[1]·Gonzalez, R.[1]·Hirsch, J.[1]·Sherin, C.[2]·Cooper, J.[2]
[1]Massachusetts General Hospital, Boston, MA, [2]American College of Radiology, Washington, DC.

Purpose
Radiology has been affected by decreases in reimbursement for advanced imaging that has been enacted through both federal legislation and regulations. Our aim was to review the decreases that have most affected radiology since 2006 with a specific focus on the current regulations and ongoing health reform.
Materials & Methods
A detailed analysis of the timeline of federal imaging policy starting from the Deficit Reduction Act in 2006 was performed. The existing data and literature concerning the legislation affecting radiology were surveyed. The cumulative impact of decreases in reimbursement was summarized and outlined.
Results
There have been several legislative and regulatory actions since 2006, which have led to decreased reimbursements. These include Multiple Procedure Payment Reduction (MPPR), Medicare Improvements for Patients and Providers Act (MIPPA) and PPACA (Patient Protection and Affordable Act). These legislative and regulatory actions affect reimbursement both directly and indirectly through changes to the Utilization Rate, and the technical and professional components of the Medicare Physician Fee Schedule (MPFS). In addition, the Centers for Medicare and Medicaid Services has mandated code bundling. The cumulative impact of these is significant and is well demonstrated in the attached table (Courtesy: ACR and the Access to Medical Imaging Coalition). For example, the approximate reimbursement for MRI Brain in 2006 was $1118 and is predicted to be $439 dollars in 2013. In neuroimaging, the impact of MPPR may be high due to contiguous organ imaging (e.g., head and neck) as well as imaging of stroke and trauma patients (who are relatively sick and usually undergo multiple exams in a day). On the near horizon are potentially severe cuts to Medicare reimbursement of approximately 30% due to implementation of the Sustainable Growth Rate. On the somewhat more distant horizon are further bundling cuts as CMS turns its screen from codes used together 90% of the time to those used together 75% of the time. Much less predictable are the consequences of at-risk contracts such as Accountable Care Organizations.

Conclusion
Multiple legislative measures in the federal imaging policy have led to a cumulative impact in decreased reimbursements. It is important for neuroradiologists to understand legislation that impacts radiology so that they can appropriately manage their practices and advocate for radiology.
Acknowledgment: Courtesy: Christopher Sherin and Ted Burns, ACR Government Relations Dept., ACR and the Access to Medical Imaging Coalition.

KEYWORDS: EconomicsReimbursements

O-246 **10:53 AM - 11:01 AM**

Transitioning from a Denial to Nondenial Approach to Radiology Benefit Management: Impact on the Utilization of Neuroimaging

Hiatt, M. D.[1]·Johnstad, T. R.[1]·Boyko, O. B.[2]
[1]HealthHelp, Houston, TX, [2]University of Southern California, Los Angeles, CA.

Purpose
In managing the utilization of neuroimaging, traditional pre-authorization, as administered by radiology benefit managers (RBMs), has incorporated payment denial for lack of medical necessity. A new approach in which no denials are issued offers the advantages of diminished

Note: Scanned images are included in the proceedings. Some submitted images were reduced during editing, thereby decreasing clarity. Also, refer to the Program Planner. Proceedings Content as of 3-29-2013.

acrimony between provider and payer and reduced costs and delays related to an appeals process that is no longer needed. Reluctance to adopt a nondenial approach centers on the assumption that the threat of denial is necessary to compel physicians to comply. The aim of this study is to quantify the impact on neuroimaging utilization of replacing a denial approach with a nondenial one.
Materials & Methods
A major health insurance company transitioned from one RBM embracing denials to another eschewing them for its ~80,000 beneficiaries (half of whom were Commercial subscribers and the other half Medicare) in one state in the southwestern U.S. on 1/1/2011. When a procedure request diverged from RBM guidelines, it was denied under the old schema, but approved under the new paradigm. This study focused on CT and MRI of the brain, defined by CPT codes 70450, 70460, 70470, 70551, 70552, and 70553. Utilization, derived from claims data and expressed as units per 1,000 members (UPK), was calculated in the year before (2010) and the year after (2011) implementing the nondenial approach. This same analysis was performed for a contiguous state that employed a nondenial approach in both years.
Results
For the total population, 2,991 neuroimaging procedures were performed in 2010 and 2,861 in 2011, yielding UPKs of 4.63 in 2010 and 4.23 in 2011 for CT and 10.36 in 2010 and 10.13 in 2011 for MRI in the Commercial population, representing decreases of 9 and 2%, respectively, and 26.88 in 2010 and 22.84 in 2011 for CT and 34.36 in 2010 and 32.65 in 2011 for MRI in the Medicare population, representing decreases of 15 and 5%, respectively. Utilization did not similarly decrease in the comparison state.
Conclusion
Transitioning to a nondenial approach yielded no increase in utilization. Providers working in a collaborative environment in which the result of disagreement is to defer to the treating clinician did not cause greater utilization than when they worked in an environment in which the payer retained the "final say". A collaborative approach to utilization management can still "bend the cost curve" without the confrontational atmosphere traditionally associated with such efforts.

KEYWORDS: Utilization management, Utilization rates, Radiology benefit management

O-247 **11:01 AM - 11:09 AM**

Effect of Direct Neuroradiologist Participation in Physician Marketing on Imaging Volumes in Outpatient Radiology

Grignon, L.[1]·Vavricek, J.[1]·Horsley, W.[2]·Murphy, R.[2]·Keiper, M.[1,2]
[1]University of Nebraska Medical Center, Omaha, NE,
[2]Scottsdale Medical Imaging, Scottsdale, AZ.

Purpose
Referring clinicians are the key referral source of imaging studies to an outpatient radiology center. Marketing to referring physicians may have a profound impact on referral patterns, whether marketing is performed by a radiologist or a radiology sales representative. The purpose of this study is to determine the relative impact of direct neuroradiologist participation in marketing on imaging study volumes in outpatient radiology.
Materials & Methods
Baseline monthly physician referral data of CT and MR scans of 19 referring clinicians (neurologists, neurosurgeons and anesthesiologists) to an outpatient radiology group were collected over a six-month period from January to June of 2009. During that time, a nonphysician radiology sales representative made personal visits to the referring physicians' offices every two weeks providing support, substantive education material and personal encounters with clinicians to maximize radiology referrals. From January to June 2010, the same radiology sales representative visited the same referring clinician offices every two weeks but accompanied by a neuroradiologist once a month. The neuroradiologist provided educational lectures, imaging examples, advice and additional substantive personal interaction with referring clinicians during the visits. Monthly CT and MRI referral volumes were collected during this time period as well. The time periods were separated by a year to control for typical seasonal variations of referral patterns. No significant changes or improvements in the radiology group's service parameters such as telecommunications equipment, scheduling or authorization personnel, or quantity of scanners or imaging centers available for scheduling. In addition, no change in the individual referring clinicians' practices occurred between the time periods. The monthly referral volumes of CT and MRI examinations collected for both time periods were compared with the identical month of the corresponding time period for statistical analysis to control for additional potential monthly variations.
Results
The generalized estimating equation (GEE) negative binomial regression with log link was used to fit the scan data to adjust for correlation among the repeated interventions on a single referring clinician. The Tukey post-hoc method was used for pairwise comparisons of results between months in the different time periods. The results demonstrate the relatively dramatic effect of the

Note: Scanned images are included in the proceedings. Some submitted images were reduced during editing, thereby decreasing clarity. Also, refer to the Program Planner. Proceedings Content as of 3-29-2013.

use of a neuroradiologist in garnering increases in imaging referral volumes. Cross-sectional imaging referral volumes were approximately 2.5 times greater during the six-month period utilizing the neuroradiologist for direct physician to physician marketing when compared with the volumes achieved with the sales representative alone. Moreover, this difference was statistically significant for all six months evaluated (p<0.0001).

	Mean scan volume **Year 2009**	Mean scan volume **Year 2010**	
	Sales Representative	Sales Representative + Neuroradiologist	P-value
January	8.47	19.53	<0.0001
February	8.29	20.35	<0.0001
March	8.35	21.00	<0.0001
April	7.65	20.12	<0.0001
May	7.59	18.71	<0.0001
June	5.65	16.12	<0.0001

Conclusion
Direct radiologist participation in physician marketing is an essential tool in creating and maintaining imaging volumes in outpatient radiology.

KEYWORDS: Economics, Marketing

O-248 **11:09 AM - 11:17 AM**

Trends in Advanced Spinal Imaging in the Medicare Population from 2000-2010: Slowing Down the Runaway Train

Zoltani, Z. A.·Zohrabian, V. M.·Parker, L.·Friedman, D. P.
Thomas Jefferson University Hospital
Philadelphia, PA.

Purpose
To examine trends in utilization of spine CT and MR in the Nationwide Medicare population from 2000-2010.
Materials & Methods
The Nationwide Medicare Part B databases for 2000-2010 were queried. Current Procedural Terminology (CPT)® codes were obtained for CT and MR imaging of the cervical, thoracic, and lumbar spines without, with, and with and without contrast. All nine CT CPT codes were combined and all six MRI CPT codes were combined, and analyzed separately. Fee-for-service beneficiary denominators were calculated from the Medicare Advantage market penetration files. Study volume for fee-for-service beneficiaries, utilization rates per 1,000 beneficiaries, and growth rates were calculated. The 2000-2010, pre-Deficit Reduction Act (2000-2005), and DRA/post-DRA (2006-2010) time periods were examined.
Results
The overall volume of spine CT increased by 235% from 2000-2010. There was positive year-to-year growth in overall volume of spine CT throughout the study period, and the rate of growth peaked in 2005 (16.6%), at which point the rate of increase slowed. However, from 2005-2010, the total volume of CT still nearly doubled (655,408 to 1,172,959). The total utilization rate of CT was 11 per 1,000 beneficiaries in 2000 and 33 per 1,000 beneficiaries in 2010 (+212%). The compounded annual growth rate (CAGR) in the pre-DRA and DRA/post-DRA period was nearly uniform, and the CAGR from 2000-2010 was 12.1%. From 2000 to 2010, the overall volume of spine MR increased by 103%, and although positive growth was seen each year from 2000-2009, a drop in total volume was observed in 2009-2010. Nearly all the increase in MR volume was seen from 2000-2005 (1,096,809 to 2,154,589), with flattening of the volume increase from 2006-2010. The total utilization rate of MR was 33 per 1,000 beneficiaries in 2000 and 63 per 1,000 beneficiaries in 2010 (+89%). The CAGR in the pre-DRA period was 10.2% and in the DRA/post-DRA period was 0.3%. The CAGR from 2000-2010 was 6.7%.

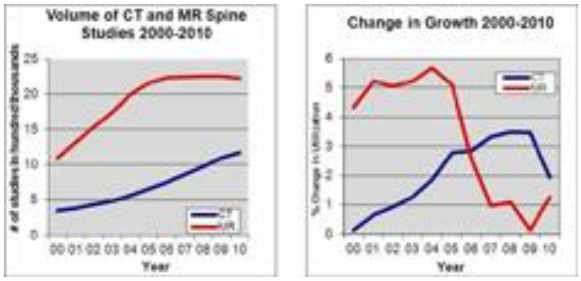

Conclusion
The rate of growth of CT spine in the Medicare population began to slow in 2005, although volume continued to substantially increase. While the rate of growth of spine MR in the Medicare population also grew from 2000-2005, the number of studies performed after 2005 largely reached a plateau. It is speculated that the impending passage of the DRA in early 2006, in combination with increased awareness of the risks of radiation exposure and cost consciousness on the part of patients and physicians, contributed to these trends.

KEYWORDS: Utilization rates

Note: Scanned images are included in the proceedings. Some submitted images were reduced during editing, thereby decreasing clarity. Also, refer to the Program Planner. Proceedings Content as of 3-29-2013.

O-249 **11:17 AM - 11:25 AM**

Pilots to Publications: An Analysis of Preliminary Research Follow-Up in the American Journal of Neuroradiology

Chin, M. S.·Castillo, M.
University of North Carolina
Chapel Hill, NC.

Purpose
There are perceptions, possibly anecdotal, that "pilot" studies lack follow-up to address initial articles' limitations or reinforce its findings. Our purpose was to assess the rate of relevant follow-up publications, whose initial pilot studies were published in the American Journal of Neuroradiology (AJNR).
Materials & Methods
Over a 12-year period (2001 - present), a list of publications from the AJNR electronic archives was obtained with one or more of the following "keywords" in their titles: pilot, initial, preliminary, experimental, and/or exploratory. Using this list, MEDLINE and EMBASE were searched for relevant preceding or subsequent publications, written by one or more of the original authors. Any relevant follow-up papers written by different authors yet based on the original authors' pilot research, were excluded from consideration.
Results
Of 194 pilot articles, 64 (33%) follow-up publications addressed a limitation or expanded upon the preliminary paper. Two or more relevant follow-up publications were seen in 26 (13%) of pilot studies. An additional 29 (15%) follow-up papers applied the pilot research in a different disease and/or clinical setting. Of the 70 translational (animal/in vivo/cadaver) pilot papers, 39% (n = 27) resulted in a follow-up publication, with 10% (n = 7) having two or more follow-up publications. Comparing translational and non-translational research, no statistical significance was seen in percentage of follow-up publications (single follow-up paper, p = 0.27; multiple follow-up papers, p = 0.24). Twenty-five percent (n = 48) of pilot papers were preceded by smaller, yet relevant "pre-pilot" papers by one or more of the same authors, yet lacked one of the "keywords" in their titles. The majority (95%) of pilot papers reflected "positive" results in their findings. The average time to follow-up publication was 19.5 months (SD: 16.2), with an average of 17.7 months (SD: 14.1) for translational research papers. A weakness of this study is the exclusion of potential pilot papers that did not include one of the specified keywords in its title. This paper also does not assess the number of relevant subsequent papers by different authors (based on these authors' pilot papers) or examine the reasons for the lack of follow-up publications in the remaining "pilot" studies (despite reported positive results in the pilot papers).
Conclusion
One third of published AJNR papers with certain "pilot" keywords in their title resulted in follow-up publications and 13% resulted in two or more subsequent papers. No statistical significance was seen between rate of follow-up publications between translational and non-translational research articles.

KEYWORDS: AJNR, Long-term followup, Pilot

O-250 **11:25 AM - 11:33 AM**

Bringing the Reading Room to the People: Evaluation and Efficacy of Relocating the Head & Neck Radiologists Directly into the ENT Clinic

Peterson, R. B.·Corey, A.·Aiken, A.·Baugnon, K. L.·Mattox, D. E.·Hudgins, P. A.
Emory University
Atlanta, GA.

Purpose
At our academic institution, the Head & Neck (HN) radiology reading room recently was integrated into the newly renovated Otolaryngology Outpatient Clinic in an attempt to improve multidisciplinary interaction, customer service, patient treatment planning and appropriateness of radiology examination ordering. The goal of this investigation was to evaluate the referring clinician's perceptions after this change. Additionally, radiology residents, fellows and faculty were surveyed to evaluate the educational benefits and/or deficits to the change.
Materials & Methods
A 10-question survey was designed for health care practitioners, including physicians (MD), nurse practitioners (NP), and physician assistants (PA) involved in our institutional HN Tumor Board (ENT, Hematology/Oncology, Radiation/Oncology, Pathology, Oral Maxillofacial Surgery) as well as other support staff (Nursing, Audiology, Speech Pathology, Social Work, Research, Scheduling, etc). The survey identified the individuals by their specialty, role and whether they were directly affiliated with our institution or an outside referring clinician. Both qualitative and quantitative benchmarks were included to evaluate the daily interaction with radiology before and after the move, the effects of the change on multidisciplinary tumor board/treatment planning and overall practice workflow (exam appropriateness and report turnaround time). Additionally, radiology residents, neuroradiology fellows and HN radiology faculty completed a separate survey to evaluate the educational value of the integration.
Results
Thirty-five responses were returned via an electronic survey from the clinical services. Approximately 58% were from the Department of Otolaryngology at our institution. Ninety-four percent responded that the move was extremely beneficial to their practice. The greatest improvements were in the availability of the HN radiologist for prompt consultation and interpretation of outside images. ENT clinicians reported an increased interaction with the radiologists from 6% to 31%, in the

Note: Scanned images are included in the proceedings. Some submitted images were reduced during editing, thereby decreasing clarity. Also, refer to the Program Planner. Proceedings Content as of 3-29-2013.

"frequently" (defined as multiple times per day) and "regularly" (defined as at least once a day) categories. The most commonly reported interaction with a radiologist was multiple times per week. Respondents also reported a 37.5% improvement in the tumor board productivity after the move into the clinic. More importantly, even though the move was most favorable to the department of Otolaryngology, the other specialties indicated no significant hindrance to their interaction with radiology. Sixteen radiologists responded to our survey with 100% indicating an increase in daily interaction with clinicians (from once per day on average to multiple times a day) compared to other diagnostic subspecialties. The results also indicate an increase in direct patient interaction compared to other nonprocedurally based subspecialties.
Conclusion
Preliminary results demonstrate a significant improvement in the interaction between HN radiologists and referring clinicians without deterring the interaction with other subspecialties. Radiology trainees and faculty report an increased improvement in clinical correlation and educational value of the rotation. Overall, the move has been beneficial for both radiologist and clinician.

KEYWORDS: Clinical applications

O-251 **11:33 AM - 11:41 AM**

Effects of Installing an MR Scanner in the Emergency Department on the Emergency Department Length of Stay for Patients Admitted with Symptoms of Stroke

Babiarz, L. S.·Zan, E.·Urrutia, V.·Hill, P.·Leigh, R.·Lewin, J. S.·Yousem, D. M.
Johns Hopkins Hospital
Baltimore, MD.

Purpose
Patients presenting with stroke-like symptoms (SLS) often undergo MRI. We assessed the effects of installing an MR scanner in the ED on the emergency department length of stay (EDLOS) of patients admitted through the ED with SLS. We hypothesized that MRI availability in the ED increases EDLOS for patients with SLS because of the additional time for the completion o f MR studies prior to admission.
Materials & Methods
Our study was HIPAA compliant and approved by the IRB. We compared patients with SLS seen in the ED and admitted between July 1st and August 15th 2011 and 2012, before (2011) and after (2012) ED MR scanner installation. The overall EDLOS for patients who did and who did not have MRI in the ED was determined. Time intervals between ED registration and MR exam order and completion of MR exam were measured. Comparative statistics and t-tests were computed.
Results
Sixty-seven patients (mean age = 57.8 years, range = 21-87 years; male = 33) with SLS in July/August 2011 and 48 patients (mean age = 59 years, range = 24-87 years; male = 22) in 2012 were seen in the ED. Twenty-one MRs were performed for 10 patients in the ED (14.9%) in 2011 and 28 MRs for 14 patients (29.2%) in 2012. Mean overall EDLOS was 5.17 hours in 2011 and 5.94 hours in 2012 (p-value=0.33, NS). Mean EDLOS for patients who did and did not have an MR in the ED were 6.44 and 4.95 hours (p-value=0.12, NS) in 2011 and 5.90 and 5.91 hours in 2012 (p-value= NS), respectively. The 2012 patients who had MRI in the ED had shorter EDLOS (p-value=0.0006). ED registration to MR exam order time was 138.8 in 2011 and 144.3 minutes in 2012 (p-value=NS). MR exam order to MR exam completion time was 124.2 in 2011 and 97.3 minutes in 2012 (p-value=NS). Patients with SLS seen in the ED in 2011 were diagnosed with: 26 ischemic strokes, 22 TIAs, five hemorrhagic strokes, five migraines, three vertigo, one acute pressure palsy, one retinal artery occlusion, one complex partial seizure, one cranial nerve palsy, one migraine versus TIA, one optic neuritis, one postconcussive syndrome. In 2012, ED patients with SLS were diagnosed with: 21 ischemic strokes, 18 TIAs, three retinal artery occlusions, one hemorrhagic stroke, one conversion disorder, one new intracranial mass, one migraine, one migraine veersus TIA, one venous infarct/sinus thrombosis, one vertigo versus Meniere's disease.
Conclusion
Although not statistically significant, there was an overall trend for patients who presented with SLS in 2012 to have longer EDLOS than those who presented in 2011, before installation of the MR scanner. However this difference was not attributable to performing MR exams in the ED setting as those who had an MR were scanned more quickly and had a shorter LOS in 2012 than in 2011. Further analysis of larger patient samples is needed for confirmation of the benefits of prompt and accurate diagnosing of patients with SLS in the ED with MRI.

KEYWORDS: Actue stroke, Utilization management

O-252 **11:41 AM - 11:49 AM**

Emerging Trends in Critical and Semi-Urgent Notification of Radiologic Findings

Aamodt, D.·Hunt, C. H.·Knudsen, J. M.·Schwartz, K. M.·Diehn, F. E.·Eckel, L. J.·Wood, C. P.
Mayo Clinic
Rochester, MN.

Purpose
To describe trends in communication of critical and semi-urgent findings in a neuroradiology practice using both the telephone and an automated semi-urgent report system.
Materials & Methods
A retrospective review was made of all neuroradiology reports by modality from 1/2005 to 12/2011. Telephone communication of critical findings always has been documented directly within the radiology report at our institution. From 4/2007, an automated process was put in place where a report with a semi-urgent finding could be

Note: Scanned images are included in the proceedings. Some submitted images were reduced during editing, thereby decreasing clarity. Also, refer to the Program Planner. Proceedings Content as of 3-29-2013.

flagged and the clinician notified electronically with verification of receipt. For this study, the number of reports each month in which direct telephone communication was documented and the number of reports that were flagged with the semi-urgent notification system was recorded.
Results
A total of 391895 neuroradiology reports were reviewed from 2005 through 2011 (CT: 1865+/-134; MR: 2800+/-348 per month). Telephone communications for all findings increased from 3.4%+/-0.47 of reports per month in 2005 (CT: 6.3%+/-1.0; MR: 1.8%+/-0.3) to 4.3%+/-0.50 of reports per month in 2011 (CT: 7.1%+/-1.0; MR: 2.1%+/-0.4) ($p<0.0002$). Since successful implementation in 2007, the semi-urgent automated notification system has been used fairly consistently on 1.4%+/-0.3 of reports per month (CT: 0.7%+/-0.3; MR: 1.9%+/-0.5). Interestingly, a telephone call was made to the ordering clinician in 14.2%+/-5.5 of neuroradiology reports per month, in which the automated notification system also was utilized (CT: 21.2%+/-13.2; MR: 12.9%+/-7.3).
Conclusion
There is an increasing trend of telephone communication with clinicians to convey important radiologic findings. A semi-urgent notification system has demonstrated significant sustained use in our busy clinical practice. In a small percentage of reports, both the semi-urgent notification system and direct telephone communication are utilized, potentially leading to inefficiency in the radiologist's and clinician's practice.

KEYWORDS: Quality improvement, Report style, Semi-urgent notification

O-253 **11:49 AM - 11:57 AM**

Effects of Installing an MR Scanner in the Emergency Department on the Hospital Length of Stay for Patients Admitted with Symptoms of Stroke

Babiarz, L. S.·Zan, E.·Urrutia, V.·Hill, P.·Leigh, R.·Lewin, J. S.·Yousem, D. M.
Johns Hopkins Hospital
Baltimore, MD.

Purpose
Patients presenting with stroke-like symptoms (SLS) often undergo MRI evaluation which may be performed in the emergency department (ED) or inpatient setting. We assessed the effects of installing an MR scanner in the ED on the hospital length of stay (HLOS) of patients admitted with SLS through the emergency department. We hypothesized that MRI availability in the ED expedites patient evaluation resulting in shorter HLOS.
Materials & Methods
Our study was HIPAA compliant and approved by the IRB. We compared patients admitted through the ED with SLS between July 1st and August 15th 2011 and 2012, before (2011) and after (2012) ED MR scanner installation. The overall HLOS and HLOS for SLS patients who did and did not undergo MRI evaluation in the ED was determined. Comparative statistics and t-tests were computed.
Results
Sixty-seven patients (mean age = 57.8 years, range = 21-87 years; male = 33) with SLS in July/August 2011 and 48 patients (mean age = 59 years, range = 24-87 years; male = 22) in 2012 were admitted through the ED. Twenty-one MRs were performed for 10 patients (14.9%) in the ED in 2011 and 28 MRs for 14 patients (29.2%) in 2012. Mean overall HLOS was 3.52 days in 2011 and 2.63 days in 2012. Mean HLOS for patients who did and who did not have an MR in the ED was 3.01 and 3.61 days in 2011 and 2.43 and 2.71 days in 2012. For patients seen in 2011, the final diagnoses were: 26 ischemic strokes, 22 TIAs, five hemorrhagic strokes, five migraines, three vertigo, one acute pressure palsy, one retinal artery occlusion, one complex partial seizure, one cranial nerve palsy, one migraine versus TIA, one optic neuritis, one postconcussive syndrome. For 2012 patients, the final diagnoses were: 21 ischemic strokes, 18 TIAs, three retinal artery occlusions, one hemorrhagic stroke, one conversion disorder, one new intracranial mass, one migraine, one migraine versus TIA, one venous infarct/sinus thrombosis, one vertigo versus Meniere's disease.
Conclusion
There was nearly a full day reduction in HLOS for patients admitted through the ED with SLS before (3.52 days) and after (2.63 days) installation of an MRI scanner in the ED with the greatest benefit occurring in those patients in 2012 who had an MR in the ED (HLOS 2.43 days). Further analysis of larger patient samples is needed to confirm the benefits of prompt and accurate diagnosing of patients with SLS in the ED with MRI.

KEYWORDS: Actue stroke, Utilization management

O-254 **11:57 AM - 12:05 PM**

Demographics of Providers Who Order Neuroimaging Procedures for Medicaid Patients

Boyko, O. B.[1]·Hiatt, M. D.[2]·Malkan, P. R.[2]
[1]University of Southern California, Los Angeles, CA,
[2]HealthHelp, Houston, TX.

Purpose
To characterize the types of providers who order neuroimaging for Medicaid patients.
Materials & Methods
Requests for pre-authorization of neuroimaging under the utilization management of a radiology benefit manager since the inception of such management in the state of New York for its approximately 875,000 Medicaid beneficiaries were reviewed retrospectively to ascertain the proportion of requests initiated by (a) physician assistants (PAs) and nurse practitioners (NPs), (b) family and general practitioners (FPs and GPs, respectively), and (c) neurologists, neurosurgeons, and psychiatrists to

Note: Scanned images are included in the proceedings. Some submitted images were reduced during editing, thereby decreasing clarity. Also, refer to the Program Planner. Proceedings Content as of 3-29-2013.

understand how Medicaid patients are being served. The time period spanned from April 2011 to October 2012. The neuroimaging procedures of interest were comprised of CT and MRI of the brain, defined by CPT codes 70450, 70460, and 70470 for CT and 70551, 70552, and 70553 for MRI.
Results
During the 1.5 years of review, 17,691 requests for neuroimaging, comprised of 4,593 CTs and 13,098 MRIs, were initiated for 14,876 unique patients. Considering those requests submitted by providers pertaining to just the three categories of interest, 7% were from PAs and NPs, 30% from FPs and GPs, and 63% from neurologists, neurosurgeons, and psychiatrists.
Conclusion
The recent preponderance of PA, NP, FP, and GP involvement in ordering neuroimaging for Medicaid patients may be a harbinger of the nature of care to come under the Affordable Care Act, which may largely rely on Medicaid to provide health insurance coverage to over 30 million more Americans. This initial analysis also may serve as a baseline against which to compare presumed even greater reliance on PAs and NPs in the future.

KEYWORDS: Utilization management, Utilization rates, Radiology benefit management

O-255 **12:05 PM - 12:13 PM**

Patient Protection and Affordable Care Act: What You Need to Know as a Radiologist?

Rehani, B.·Rosman, D.·Romero, J.·Schaefer, P.·Gonzalez, R.·Hirsch, J.
Massachusetts General Hospital
Boston, MA.

Purpose
To understand the basics of health care reform, mechanisms by which PPACA expands health care coverage and how PPACA pays for its coverage. To outline in comprehensible terms PPACA's effect on consumers, on neuroradiologists specifically and radiology at large.
Materials & Methods
The PPACA legislation was studied extensively and key elements of health reform are summarized. The pertinent legislation that has a potential to directly impact radiologists was studied.
Results
PPACA expands coverage to nearly all U.S. citizens and legal residents through two principle mechanisms: a mandate to require most U.S. citizens and legal residents to purchase health insurance; and an expansion of Medicaid. Each of these mechanisms achieves approximately half of the 30+MM people who will be newly insured due to the Act. The insurance products are made available on a state by state basis through insurance exchanges and the mandate is enforced through the tax code. Individuals who do not meet the expanded criteria for Medicaid and who meet other income eligibility criteria (from 133%-400% of federal poverty level) will be given subsidies for purchase of insurance on the exchange. Other important components of PPACA include cost controls, incentives to form Accountable Care Organizations and health plan regulation. Specific to radiology is legislation that includes utilization rate, self-referral, appropriateness criteria and a 2.3% excise tax on medical devices.
Conclusion
There are many unanswered questions regarding the implementation of PPACA and a general lack of awareness about how health reform will impact radiology. After detailed study of the legislation, there are specific key points which can help simplify the understanding of PPACA for neuroradiologists both in academic and private practice settings.

KEYWORDS: Economics, Utilization rates, PPACA

Tuesday Afternoon

12:15 PM – 1:15 PM
Room 1AB

Business Meeting

American Society of Pediatric Neuroradiology (ASPNR) Annual Business Meeting (members only)

Tuesday Afternoon

1:15 PM - 2:45 PM
Ballroom 6AB

(26) ASFNR Programming: Memory and The Aging Brain: Imaging Tools Which Will Shape Humanity

O-256 **1:15 PM - 1:45 PM**

Alzheimer: Clues, Causation and Clues

Small, S.
Columbia University
New York, NY.

After graduating from NYU with a BA in experimental psychology, Dr. Small began the MD/PhD program at Columbia University in Eric Kandel's laboratory. Discovering that he enjoyed patient care more than he

Note: Scanned images are included in the proceedings. Some submitted images were reduced during editing, thereby decreasing clarity. Also, refer to the Program Planner. Proceedings Content as of 3-29-2013.

anticipated, he decided to focus exclusively on his medical training. After completing a medical internship at UCLA, a neurology residency and chief residency at Columbia, and a fellowship with Richard Mayeux, Dr. Small "returned" to research. Informed by his prior experience studying neuronal physiology and pathophysiology he began a research program at Columbia dedicated to investigating intractable disorders of the brain. Taking a decidedly top-down approach, he optimized brain imaging tools designed to pinpoint brain dysfunction in human patients and mouse models of disease. More recently, Dr. Small has combined brain imaging with gene-expression technologies to uncover novel molecular defects underlying Alzheimer disease and aging. Dr. Small is the recipient of numerous awards, including the Beeson Scholar Award in Aging Research from the American Federation on Aging, the McKnight Neuroscience of Brain Disorders Award, the Derek Denny-Brown Young Neurological Scholar Award from the American Neurological Association, and the Lamport Award for Excellence in Clinical Science Research from Columbia University.

Presentation Summary
Alzheimer disease, like all diseases of the brain, manifests with regional vulnerability. Pinpointing brain regions vulnerable and resistant to a disease is important for understanding underlying mechanisms. In this presentation I will begin by briefly reviewing a variant of fMRI that uses "cerebral blood volume" to map brain metabolism, and which has features well suited for identifying anatomical patterns of hippocampal vulnerability in patients and animal model. Then, I will discuss how this fMRI variant has been applied to patients, nonhuman primates, and mouse models to identify a pattern of hippocampal vulnerability that distinguishes Alzheimer disease from aging. Next, I will review recent imaging studies in humans and mice, which suggests how the disease spreads over time. Finally, I will show how the pattern of vulnerability has been used to uncover a pathogenic molecular pathway that has opened up a novel avenue of drug discovery.

O-257 **1:45 PM - 2:15 PM**

Translational Imaging Strategies for Therapy in AD

Petrella, J. R.
Duke University Medical Center
Durham, NC.

Presentation Summary
As neuroradiologists, our role in the workup of the dementia patient has been limited. This is primarily driven by the lack of effective treatment options and limitations of our imaging tools. Over the past 100 years, we have made tremendous strides in our understanding of the genetic, molecular, cellular basis of AD. We now know that the pathology underlying AD is present years, if not decades, prior to development of symptoms. Unfortunately, current therapies are symptomatic only, directed at slowing progression of cognitive decline for a limited time. The search for a true disease-modifying therapy continues and many clinical trials are underway. Current outcome measures are based on cognitive tests which are relatively insensitive to disease progression, requiring long trials with large numbers of participants. Biomarkers, including neuroimaging, have great potential to increase the power of clinical trials through greater effect sizes. This approach is based on matching the imaging methodology with therapeutic mechanism. The multicenter ADNI trial aims at identification and characterization of such biomarkers for clinical trials. Perhaps one of the most important advances over the past decade has been the development of in vivo imaging probes targeted to amyloid beta protein. One such agent has been approved by the FDA and other similar agents are in late stage clinical trials. These agents show great potential for enriching samples in clinical trials of anti-amyloid agents. Volumetric imaging measures to quantitate cerebral volume loss in a variety of critical brain structures correlate well with cognitive decline as well as with tau pathology, suggesting that they might serve as accurate surrogate markers of neurodegeneration. Recent development of automated, highly reproducible volumetric methods has increased the availability and practicality of these tools. Use of such techniques in early phase clinical trials is expected to significantly decrease the duration and number of subjects in such trials and greatly increase the rate at which candidate drugs can be brought to testing in larger phase III trials.Though recent failures of several phase III trials employing anti-amyloid therapies in patients with AD has thrown the amyloid hypothesis in question, this approach may still be effective earlier in the disease, before significant neurodegeneration has taken place. The National Institute on Aging is currently funding three national trials of anti-amyloid therapies in asymptomatic, at-risk subjects, in which neuroimaging biomarkers will be used for sample enrichment and outcome measures.

O-258 **2:15 PM - 2:45 PM**

Neurodegenerative Disorders and Resting fMRI

Sunaert, S.
University of Leuven
Leuven, BELGIUM.

Stefan Sunaert is a senior clinical investigator of the Research Foundation - Flanders. He is Professor of Radiology at University of Leuven/BE and attending physician in Neuroradiology. He heads a research group that investigates the functional and structural organization of the normal and pathological human brain by the combination of functional MRI and diffusion tensor imaging. He has published over 100 peer-reviewed international papers. He was section editor 'Functional and molecular imaging' of the journal Neuroradiology, course

Note: Scanned images are included in the proceedings. Some submitted images were reduced during editing, thereby decreasing clarity. Also, refer to the Program Planner. Proceedings Content as of 3-29-2013.

director of the ESMRMB - School of MRI on clinical fMRI, past member of the Postgraduate Educational Program (PEP) of the European Congress of Radiology 2010 (European Society for Radiology), past member of the Annual Meeting Program Committee (AMPC) of the international society of magnetic resonance imaging in medicine (ISMRM), and member of the organizing faculty of the ECNR and Erasmus Courses. Finally, he was the winner of the Horlait-Dapsens Medical Scholarship 2001, the Nomination of Excellence for the Sixth Lucien Appel Prize for Neuroradiology 2002, winner of the ECR 2004 Research & Education Fund, and winner of the Outstanding Teaching Award of the ISMRM in 2008 and 2011.

Presentation Summary
Resting state functional MRI allows to study brain functional connectivity. The study of altered connectivity in neurodegenerative disease will be discussed.

Tuesday Afternoon

1:15 PM - 2:45 PM
Ballroom 6CF

(27) Advanced Imaging Seminar: DWI: Advances in Brain, Spine, and Head and Neck (SAM) (AR)

O-259 **1:15 PM - 1:40 PM**

Diffusion Imaging of the Brain: My BFF Sequence

Filippi, C. G.
Columbia University Medical College of Physicians and Surgeons
New York, NY.

Learning Objectives
Upon completion of this presentation, participants will be able to:
1) Describe diffusion-weighted imaging (DWI) techniques and define the quantitative parameters derived from these sequences including age-related and normative, regional-related values.
2) Demonstrate key diagnostic applications of DWI beyond stroke imaging, specifically intracranial infections, neoplasm, and demyelinating diseases.
3) Explore the emerging use of DWI in novel applications such as the analysis of brain tumor histopathologic grade and assessment of treatment response.
Presentation Summary
Diffusion-weighted imaging has become an important part of routine brain magnetic resonance (MR) imaging. The molecular motion of protons within brain tissue is impeded or influenced by interactions with cell membranes as well as intracellular and extracellular structures. Within any given voxel, average diffusion can be quantified by apparent diffusion coefficient, the volume-averaged rate of propagation of water molecules as they interact with cellular structures within that voxel. In ordered anatomical structures like axons and white matter fiber tracts, diffusion is highly oriented, or anisotropic, and can be exploited for diffusion tensor imaging (DTI). By acquiring diffusion-sensitized images along multiple noncollinear directions, at least six and typically up to 32, one can determine the fractional anisotropy of white matter as well as its major and minor eigenvalues (or equivalently, axial and radial diffusivity). Together these parameters can be used to make inferences about the integrity of white matter microstructure. Quantitative DTI is an intense focus of ongoing neuroimaging research because more accurate quantitative in vivo neuroimaging biomarkers are necessary for prognostication and as outcome measures for treatment management and efficacy in a number of neurologic disorders. The high sensitivity and specificity of diffusion imaging for the detection of acute infarction has fundamentally altered neuroimaging practice. Diffusion-weighted imaging is not simply a stroke-related sequence, however, as DWI and DTI are helpful in the diagnosis of many other neurologic diseases. Diffusion-weighted imaging is particularly useful in the diagnosis of intracranial infections like pyogenic abscess, septic embolism, herpes encephalitis, and prion disease. The role of DWI in the evaluation of brain tumors also is evolving rapidly. Not only can DWI readily distinguish epidermoid from arachnoid cysts, but the technique also is being increasingly used to aid in the histologic grading of pediatric and adult tumors. There is heightened interest in the use of DWI and DTI as a way to monitor therapeutic response to treatment, assess recurrence of brain neoplasms, and better predict the long-term course of disease. Diffusion-weighted imaging also plays an important role in the evaluation of inflammatory, dysmyelinating, and demyelinating diseases. This presentation will briefly define DWI and DTI and the quantitative metrics derived from these sequences, and discuss age-related and regional variations in mean diffusivity and fractional anisotropy. Characteristic examples of DWI in intracranial infections, brain tumors, and demyelinating diseases will be presented along with novel uses and applications of DWI in these and other neurologic disorders, which will highlight emerging advances in this technique.

Note: Scanned images are included in the proceedings. Some submitted images were reduced during editing, thereby decreasing clarity. Also, refer to the Program Planner. Proceedings Content as of 3-29-2013.

O-260 **1:40 PM - 2:00 PM**

What Does Diffusion Mircroscopy Tell Us About Diffusion In Vivo?

Shepherd, T. M.
New York University Medical Center
New York, NY.

Presentation Summary

Diffusion microscopy of ex vivo nervous tissue enjoys several important experimental advantages that have proven useful to investigate the biophysical basis for water diffusion observed during clinical diffusion MRI. Unlike MRI in clinical practice, isolated tissue samples without motion are well suited to time-intensive, complex acquisitions using high-field narrow-bore research magnets, gradients and optimized coil designs without tissue heating limitations. Quantitative 3D data obtained from diffusion microscopy are less time- and labor-intensive to obtain than histology, and more amenable to modeling of nervous tissue properties and connectivity in normal and diseased states. This presentation will summarize the key underlying biophysical determinants of diffusion and discuss how these features should color the interpretation of clinical MR diffusion imaging studies. Landmark MR microscopy studies in specimens demonstrate that water diffusion in nervous tissue is affected by a number of biophysical properties of tissue, including the distribution of water within the intra and extracellular compartments (and their respective T2 values), extracellular tortuosity, restriction or hindrance from semi-permeable membranes and the rate of water exchange across the cell membrane. While it is not entirely incorrect to ascribe diffusion changes observed during ischemia, to simple cell swelling, for example, it should be recognized that this simple process alone most likely affects all these properties simultaneously. Determining the precise contributions from each of these factors to the diffusion signal during ischemic stroke is difficult and potentially intractable given the dynamic changes that occur in real time. The contribution from different factors also varies significantly across disease states. Importantly, diffusion microscopy also has proven that the coherent ordering of intact axonal membranes, not myelin, is the dominant contribution to diffusion anisotropy observed with clinical diffusion MRI in large bundles of white matter. It follows that observed microstructural coherences, such as from the ordered orientations of large pyramidal neurons and their dendritic arborization, also result in significant diffusion anisotropy. Thus, diffusion microscopy may be able to investigate the functional organization of clinically important structures, such as the cortex or hippocampus, and thereby provide a standard by which to better interpret normal and abnormal organization of these structures in the individual patient. This exciting development has the potential to enable diffusion MRI detection of early changes in connectivity related to neurologic disease.

O-261 **2:00 PM - 2:20 PM**

Diffusion Imaging Outside the Brain: Challenges and Applications

Hess, C. P.
University of California, San Francisco
Mill Valley, CA.

Presentation Summary

The past two decades have seen MR diffusion imaging transform from laboratory curio to standard of practice for a number of routine indications for clinical brain imaging. However, the application of this technique outside of the brain has yet to gain widespread acceptance.
Although there exist many scenarios for which diffusion imaging is helpful or even necessary to establish a diagnosis in the spinal cord, peripheral nervous system, soft tissues, or osseous structures, diffusion-weighted imaging (DWI) and diffusion tensor imaging (DTI) are more technically challenging to acquire and frequently difficult to interpret in these areas of the body. Similar to its use in the brain, diffusion imaging in other body regions can be integrated with other conventional MR contrast mechanisms to enhance tissue contrast and/or by itself to provide a quantitative probe of tissue microstructure. The most widely used quantitative diffusion parameter, apparent diffusion coefficient, represents an important adjunct for distinguishing between benign and aggressive soft tissue masses, permits accurate identification of recurrent cholesteatoma in the postoperative temporal bone, and serves as a valuable benchmark for assessing treatment response in head and neck oncologic imaging. Beyond these applications, DWI and DTI are also useful for improving visualization and characterization of nerve and spinal cord lesions, and for enhancing sensitivity to osseous and soft tissue metastatic disease. This presentation will focus on current and emerging extracranial applications of diffusion imaging in neuroradiology, using case studies to illustrate how the technique can be effectively implemented in the clinical setting and used for head and neck, spine, and nerve imaging. In this context, the relative strengths and limitations of different presently available approaches for DWI and DTI, including single-shot and multi-shot, PROPELLER, reduced field-of-view, and other volume suppressed echo-planar pulse sequences will be presented.

Note: Scanned images are included in the proceedings. Some submitted images were reduced during editing, thereby decreasing clarity. Also, refer to the Program Planner. Proceedings Content as of 3-29-2013.

Tuesday Afternoon

1:15 PM - 2:45 PM
Ballroom 6DE

(28) Socioeconomic Programming: Theoretical and Applied Considerations for Radiology in Healthcare Reform

O-262a **1:15 PM – 1:25 PM**

2013 J. Arliss Pollock Memorial Lecture Introduction and Presentation

Turski, Patrick A.

O-262 **1:25 PM - 1:50 PM**

Radiology Value Chain - 2013 J. Arliss Pollock, MD Memorial Lecture Award Recipient

Enzmann, D. R.
David Geffen School Of Medicine at UCLA
Los Angeles, CA.

Presentation Summary
A simplified view of the diagnostic radiology value chain defines components vulnerable to significant change. Some of these changes are disruptive and some are opportunities to improve productivity, to add value, or to mitigate the risk of commoditization. The radiology business model must define new ways to add value either by increasing productivity or by creating new services. This may initiate an evolution of diagnostic radiology from a professional service into an information business. These two models differ fundamentally. Areas of symbiosis between diagnostic and interventional radiology are proffered as a potential for expanding radiology's value proposition by reframing image-guided therapy into image information-guided interventions (iiGI). Overall the value chain in radiology's business model is evolving from a technical orientation to an image-based, personalized precision diagnostic and therapeutic patient care orientation.

O-263 **1:50 PM - 2:15 PM**

Cost Centers and Service Lines

Rasmussen, P. A.
Cleveland Clinic Foundation
Cleveland, OH.

Dr. Rasmussen is director of the Cerebrovascular Center, Cleveland Clinic. He received his education, Medical Degree, Neurosurgical Training at the University of Wisconsin. Dr. Rasmussen is Fellowship-trained in cerebrovascular microsurgery and endovascular neurosurgery. His current interests include systems development for comprehensive stroke care.

Presentation Summary
Cerebrovascular disease and stroke care demands a multidisciplinary approach to deliver high-quality and cost-effective care. One model of such health are delivery, a disease-based center concept, sharing a unified service line reporting model will be discussed. As a real life example, our experience at the Cleveland Clinic will be presented.

O-264 **2:15 PM 240 PM**

Stent and Thrombolysis Code Bundling

Barr, J. D.
La Jolla Radiology
San Diego, CA.

Tuesday Afternoon

1:15 PM - 2:45 PM
Room 5AB

(29) General Programming: Special Session: The Brain Observatory

O-265 **1:15 PM - 1:45 PM**

Patient H.M. and the UCSD Digital Brain Library

Annese, J.
The Brain Observatory
San Diego; Department of Radiology University of California San Diego
San Diego, CA.

Presentation Summary
The Digital Brain Library project is an effort to catalog the morphologic variability of human brains in relation to cognition and behavior and understand how aging and disease affect the dynamics of structure-function relationships. Subjects that are recruited in the local community undergo annual neuroimaging sessions and neuropsychologic assessments. Intelligence and personality tests also are administered in the context of the longitudinal evaluation. The impact of the study is maximized by the consent of research participants to donate their brains for follow-up postmortem examination. These cases provide the extraordinary opportunity to combine noninvasive neuroimaging (conducted in vivo) with postmortem neuropathologic analyses; and consequently afford the direct correlation of neuroimaging and behavioral markers and cellular-level

Note: Scanned images are included in the proceedings. Some submitted images were reduced during editing, thereby decreasing clarity. Also, refer to the Program Planner. Proceedings Content as of 3-29-2013.

structural information. This success is in part due to the fact that research subjects also are given the choice to participate in a personal autobiographical interview that covers major elements of the patients life experience. The distinguishing feature of the "Digital Brain Library" is the fact that it collects 2-dimensional (2D) and 3-dimensional (3D) data from multiple neuroimaging modalities and spanning a very wide range of file sizes and levels of resolution. Given the sheer size of the image collection relative to each individual brain, it is obvious that the resource cannot be utilized efficiently by any single researcher or clinician; instead, it is essential to create the infrastructure for a larger collaborative environment. We present new strategies in data sharing and data visualization that are poised to maximize the use and scientific impact of a novel multimodal neuroimaging archive. One of the Digital Brain Library's most notable archived cases is that of the amnesic patient H.M. who underwent a medio-temporal lobotomy in 1953 to alleviate his severe epileptic seizures; unexpectedly, the operation created a profound state of anterograde amnesia while all other cognitive functions were preserved. His case became a landmark in the behavioral sciences, because for the first time it was clear that the hippocampus and medial temporal lobe structures were essential to store and retrieve memories. A complete histological atlas of the brain of patient H.M. was created representing a centralized archive of information that would be available to researchers worldwide. The goal of the digital collection is to provide a commensurate scope of neuroanatomical data relative for corroborating an unprecedented amount of neurobehavioral investigations that spanned over 50 years.

O-266 **1:45 PM - 2:15 PM**

Computational and Visualization Strategies Involved in the Correlation of Multimodal Neuroimaging at Multiple Levels of Resolution

Bartsch, H.
University of California San Diego
San Diego, CA.

Hauke Bartsch studied computer science in Germany and got his PhD in 2003 with work on computations of lateral connection in primary visual cortex. He has since worked in the medical industry on 3D image processing and PACS/HIS/RIS systems. Since 2011 he shares his passion for advanced image analysis between The Brain Observatory and the Multi-modal Imaging Laboratories at the University of California San Diego, Department of Radiology. In his spare time he enjoys reading and building robots with his two kids.

Presentation Summary
The correlation between different neuroimaging modalities that entail qualitatively different image data and at different scales of resolution presents serious computational challenges. Nevertheless, the correct integration of information obtained from non invasive clinical MRI and histological features underlying MRI signal is crucial for the interpretation of clinical radiologic scans and proper diagnosis and treatment (Annese, 2012). We have developed a computational workflow that operates in 2D and 3D for the processing, analysis, and visualization of neuroimaging data. The workflow is intended to organize cellular-level parameters contained histological images based on the original geometry of the brain. In practice, each individual patient who participates in The Digital Brain Library undergoes regular MRI scans (longitudinal imaging) and behavioral testing. When the patient dies, the brain undergoes a series of postmortem scans (in situ and ex-situ) before it is processed, in one piece, histologically (Bartsch et al., 2012). The process generates a series of stacked anatomical images (blockface imaging) and corresponding tissue slices. The latter are stained to reveal neuropathologic features and digitized at approximately 0.4 µm/pixel. Therefore the image size to contend with varies from matrices of 256x256 pixels (clinical MRI; < 100 MB on disk) to over 400,000x400,000 pixels (50GB on disk). In addition, the bit depth and information contained in the image vary considerably (gray scale radiologic images versus 16 bit color anatomical and histological images). The pipeline developed at The Brain Observatory includes processing steps that convert 2D blockface and histological images into 3D volume data sets. These are registered to the original MRI via nonlinear registration techniques, so that quantitative analyses conducted at the microscopic level can be "projected" onto the clinical images. For example, we quantify age- and disease-related changes in microscopic fiber architecture underlying regions of white matter hyper-intensities localized by MRI and DTI. Finally, the inspection of radiologic scans, anatomical structures, and large-scale histological montages is achieved by 2D and 3D visualization strategies that feed into a web-based resource accessible to other investigators. The portal also contains cognitive and behavioral measures together with a large number of imaging-related parameters (neuroimaging markers) derived by atlas-based image processing tools like FSL and FreeSurfer. The portal was designed to evaluate correlations between the diverse imaging data and scores obtained with previous neuropsychologic testing.

O-267 **2:15 PM - 2:45 PM**

Exploring Correlations between Neuroimaging Markers and Complex Traits in Essential Tremor

Klaming, R.
University of California San Diego
San Diego, CA.

Ruth Klaming graduated cum laude with a Master of Science in Neuropsychology from Maastricht University in the Netherlands. She currently works as a research

Note: Scanned images are included in the proceedings. Some submitted images were reduced during editing, thereby decreasing clarity. Also, refer to the Program Planner. Proceedings Content as of 3-29-2013.

associate at The Brain Observatory, University of California San Diego where she is responsible for neuropsychologic assessments and neuroimaging for the Digital Brain Library project. Mrs. Klaming is a PhD candidate at the Vrije University of Amsterdam working on a collaborative longitudinal study on healthy aging conducted by The Brain Observatory and the Vrije University of Amsterdam.

Presentation Summary
Essential tremor (ET) is one of the most common movement disorders yet its underlying pathophysiology is still unclear making a correct diagnosis and effective treatment extremely difficult (Louis, 2005). In addition to motor symptoms, mild cognitive deficits are common in ET patients. Although ET can occur at any age, it is more prevalent amongst elderly; hence, dissociating age-related brain atrophy and cognitive decline from changes that are specific to ET is challenging. The cerebellum is implicated in motor and higher cognitive functions, supported by its extensive connections with several brain regions, including the prefrontal cortex. This makes the cerebellum a likely area affected by ET. However, the precise nature of cerebellar involvement in the pathophysiology of ET and the possibility that imaging the cerebellum might provide specific noninvasive biomarkers of the disease remains to be established. We have explored a novel MRI parameter in a cohort of well characterized ET patients who are enrolled in the Digital Brain Library project. The gyrification Index (GI) is defined as the ratio between the cortex that lies on the surface and that which is buried in the depth of the sulci. The GI is therefore an index of gray matter loss, separate from overall changes in volume (which could be due to gray and/or white matter atrophy). The comparison of the GI of the cerebral cortex with that of the cerebellum could reveal abnormal rates of atrophy distinct from age-related cerebral structural changes. The analysis of specific neuroimaging markers like the GI is associated with the results of neuropsychologic assessments and individual measures of tremor symptomatology. Complex behavioral scores are combined with neuroimaging data in the framework provided by the Digital Brain Library, making it possible to explore the relationship between behavioral and structural changes specific to ET.

Tuesday Afternoon

1:15 PM - 2:45 PM
Room 1AB

(30) Young Professionals Programming: Basics Session: Head and Neck Post-Treatment Imaging

O-268 **1:15 PM - 1:45 PM**

Post-Treatment Larynx: The Basics

Mukherji, S. K.
University of Michigan Health System
Ann Arbor, MI.

Presentation Summary
The presentation will review the post-treatment imaging changes following surgical and nonsurgical organ preservation therapy. This presentation will review the surgical procedures and the expected surgical changes. It also will review the expected changes following radiation therapy.

O-269 **1:45 PM - 2:15 PM**

Anatomy, Pathology and Post-Treatment Appearance of the Skull Base: The Basics

Connor, S. E. J.
King's College Hospital
London, UNITED KINGDOM.

Dr. Steve Connor is a consultant neuroradiologist and head and neck radiologist at King's College Hospital and Guy's and St Thomas' Hospital, London, UK. He underwent a neuroradiology fellowship at King's College Hospital and gained head and neck radiology subspecialty training at the Royal National Nose, Throat and Ear Hospital. He has a busy head and neck radiology practice with a particular interest in otology, skull base and maxillofacial imaging. He is deputy editor for three journals and has written three book chapters. He has written over 20 original papers as first author, and has published over 90 peer-reviewed articles. He is vice-chairman of the British Society of Head and Neck Imaging. He has given numerous invited lectures at ENT and radiology meetings, and he reviews the national ENT imaging guidelines and training curriculum.

Presentation Summary
CT and MRI are the principle imaging modalities used to evaluate the skull base, and they are complementary in the diagnosis and staging of skull base lesions. A detailed understanding of the skull base anatomy helps the radiologist predict the likely origin of pathologic tissue, anticipate patterns of disease spread and identify critical

Note: Scanned images are included in the proceedings. Some submitted images were reduced during editing, thereby decreasing clarity. Also, refer to the Program Planner. Proceedings Content as of 3-29-2013.

anatomical structures at risk. The skull base is traditionally divided into anterior, central and posterior parts and there are numerous associated important neurovascular structures. The radiologic differential diagnosis can be formulated by identifying the specific location of the lesion within the skull base, and then can be refined by recognizing typical imaging appearances. Some examples at specific sites will be used for illustration. There are some lesions which have specific or highly suggestive imaging findings which will obviate biopsy whilst there are some entities which should be identified as “don’t touch” lesions, either because they are normal variants/pseudolesions or because biopsy will be perilous. Even if the imaging findings are nonspecific, there are important generic aspects, such as cystic/solid or benign/aggressive imaging features which are likely to influence treatment planning. The radiologist should identify the anatomical structures adjacent to the lesion, and in particular those which offer potential pathways for spread or which may be endangered by the disease or its treatment. There are some useful imaging criteria which may be used to assess the involvement of such structures (e.g., vascular⋯). The extent of pathologic tissue is critical for staging and planning of appropriate therapies, and an awareness of the potential patterns of spread and the differing appearances of invaded tissues (e.g., bone marrow, dura, perineural) will help the radiologist define the extent of pathology. Pretreatment imaging helps define tumor volumes for radiotherapy planning and guides the appropriate surgical approach (e.g., external versus endoscopic resection . Post-treatment imaging of the skull base is used for the detection of residual or progressive disease or to demonstrate complications of treatment. It is particularly challenging to evaluate since reconstructions and foreign substances, together with the distorted and altered post-treatment tissue (e.g., secondary to scarring, denervation or irradiation) may mimic disease. Normal post-treatment imaging appearances will be presented, together with imaging features of treatment complications (e.g., ??? radionecrosis,cephalocele) and some imaging features which may be helpful in more difficult cases.

O-270 **2:15 PM - 2:45 PM**

Post-Treatment Sinus: The Basics

Joshi, V. M.
Apollo Hospital
Hyderabad, INDIA.

Presentation Summary
Interpretation of CT and MRI scans showing post-treatment changes in the paranasal sinuses often is a diagnostic challenge. Knowledge of the basic disease process, the type of treatment or surgery performed on the patient, and the anticipated imaging appearances of the sinuses after the therapy allow accurate assessment and may prevent misinterpretation of post-treatment changes as recurrent disease. In this talk, we will review the various treatment options for sino-nasal diseases, the choice of imaging modalities to assess the post-treatment sinus, the CT and MRI acquisition protocols and the optimal time interval after the therapy to perform the imaging study. We will discuss the spectrum of expected surgical changes found on postoperative imaging of paranasal sinuses after various functional endoscopic procedures and their common surgical complications. The talk also will focus on the anticipated imaging appearances after surgery and irradiation for sinonasal tumors and the postoperative imaging evaluation of myocutaneous flaps used for reconstructive surgery. The sole intent of the discussion will be to familiarize ourselves with the basic expected imaging changes in the paranasal sinuses following therapy to enable optimal interpretation and differentiate post-treatment changes from recurrent disease.

Tuesday Afternoon

3:15 PM - 4:45 PM
Ballroom 6AB

(31a) Parallel Scientific Papers: Interventional: Vascular Malformations: Devices and Treatments

O-271 **3:15 PM - 3:23 PM**

Flow Diverter Stents in Bifurcation Aneurysms: Is It Safe?

Saleme, S.·Ayoub, D.·Ponomarjova, S.·Mounayer, C.
University Hospital of Limoges
Limoges, FRANCE.

Purpose
We report our experience with flow diverters (FD) in the treatment of aneurysms in artery bifurcations beyond the level of the circle of Willis.
Materials & Methods
A total of 21 bifurcation aneurysms were treated with FD, 42.8% (9/21) at the middle cerebral artery bifurcation, 28.6% (6/21) at the anterior communicating complex, 14.3% (3/21) at the pericallosal artery, and 14.3% (3/21) at the internal carotid bifurcation. Twenty-eight flow diverter stents were deployed (1.3 FD/aneurysm). Aneurysm sizes varied from 1 mm to 20 mm (6 mm average). Nine out of 21 aneurysms (42.8%) have been treated previously by coiling or stent+coiling. All patients but four (17/21, 81.0%) had MRI 24-48 hours after the procedure. MR imaging at six months was performed in 8/21 (38%) patients. Control angiography at six months was obtained in 13/21 (62.0%).
Results

Note: Scanned images are included in the proceedings. Some submitted images were reduced during editing, thereby decreasing clarity. Also, refer to the Program Planner. Proceedings Content as of 3-29-2013.

Twenty-one aneurysms were treated flow diverters in artery bifurcations (19/21, 90.5% saccular; 2/21, 9.5% blister-like). There were no failures of stent deployment but in one case (4.8%) balloon angioplasty was necessary for the perfect opening of the stent. Reversible neurologic complications were noted in 9.5% (2/21), and permanent neurologic complications in 4.8% (1/21, mRS of 2). There was no mortality. MR imaging at 24-48 hours showed micro embolic spots at diffusion in 35.3% (6/17), all asymptomatic, and ischemic lesions in the territory of the shunted branch in 17.6% (3/17), two of which had reversible symptoms. MR imaging at six months showed no new ischemic lesion in 87.5% (7/8) and a junctional infarct (12.5%, 1/8) responsible for a transient facial paralysis due to occlusion of the MCA frontal branch covered by a FD , probably in relation to flow competition. Control angiography at six months showed complete occlusion of the aneurysm in 92.3%(12/13) and residual sac in 7.7%(1/13).
Conclusion
Aneurysms in artery bifurcations beyond the level of the circle of Willis are amenable to treatment by flow diverters in selective cases.

KEYWORDS: Flow diverter, Aneurysm treatment, Bifurcation

O-272 **3:23 PM - 3:31 PM**

MR Imaging Findings of Intracranial Dural Arteriovenous Fistula with Venous Hypertension

Ting, W.[1]·Tsai, F.[2,3]·Guo, W.[1]·Pan, H.[1]·Shiau, C.[1]
[1]Taipei Veterans General Hospital, Taipei, TAIWAN, [2]Taipei Medical University, Taipei, TAIWAN, [3]University California at Irvine, Irvine, CA.

Purpose
The study was aimed to correlate the digital subtraction angiography (DSA) and magnetic resonance imaging (MRI) findings of intracranial dural arteriovenous fistula (ICDAVF) focusing on their relation to intracranial venous hypertension and to find out the feasibility of using the imaging findings as a predictor of therapeutic effects.
Materials & Methods
From 2003 to 2010, totally 91 cases of intracranial dural arteriovenous fistula treated by Gamma Knife radiosurgery were included, (Cognard classification: 24 type I, 24 IIA, 15 IIB, 9 III, 19 IV). Integrated stereotactic MRI and DSA were used for radiosurgical targeting. Follow-up MRI at a six-month interval was undertaken after radiosurgery. Once the ICDAVF became regressed on MRI, DSA was performed to verify the therapeutic result. The patients were followed up 122 (6-122) months. Two neuroradiologists reviewed all DSA and MRI, retrospectively, and recorded the imaging findings on consensus.
Results
Three abnormal MRI findings were observed: Prominent Peri-Optic Nerve Subarachnoid Space (PONS) in 75% (68/91), mesial temporal lobe swelling (MTS) in 19% (17/91), and venous hypertension-related subcortical white matter changes (SWM) in 32% (31/91) of the cases. Stratified by the Cognard classification, type IIB ICDAVF had the highest incidence of PONS (13/15, 87%) and MTS (6/15, 40%). Type III had the highest incidence of SWM (9/9, 100%). But there was no significant difference in incidence of the imaging findings among the types and locations of ICDAVF. Three abnormal DSA findings were observed, namely, internal jugular vein hypoplasia (IJVH), sinus thrombosis (ST), and anterior drainage (AD). Cases with all three abnormal findings showed higher incidence of PONS (81.1% versus 70.4%; 77.2% versus 70.6%; 92.9% versus 45.7%) and MTS (32.4% versus 9.3%; 26.3% versus 5.9%; 19.6% versus 17.1%). Subcortical white matter changes occurred more in cases with IJVH (54.1% versus 16.7%) and AD (35.7% versus 25.7%) but less in cases with ST (29.8% versus 35.3%). In the 68 cases presented PONS, three cases lost followup, among the rest, 54 cases showed regression of ICDAVF by TOF MRA or DSA and 52 of them showed regression of PONS (Figure). The other 11 cases showed, yet, no improvement of ICDAVF in the follow-up periods and persistent PONS.

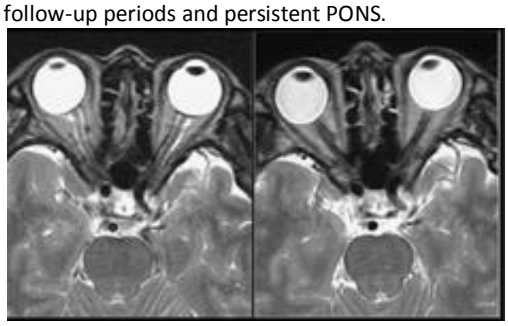

Conclusion
Peri-optic nerve swelling (PONS) depicted by MRI was a highly specific finding of ICDAVF. It was most likely related to the venous hypertension that stemmed from the associated IVJH, ST or AD. PONS is also a good predictor of radiosurgical effects in ICDAVF.

KEYWORDS: dAVF, Gamma knife, Venous hypertension

O-273 **3:31 PM - 3:39 PM**

Brain Arteriovenous Malformation Treatment by Venous Approach

Saleme, S.·Ponomarjova, S.·Ayoub, D.·Mounayer, C.
University Hospital of Limoges
Limoges, FRANCE.

Purpose
We report our experience in the treatment of brain AVMs by Onyx using the venous approach.
Materials & Methods
From February 2008 to December 2012 a total of eight brain AVMs (BAVM) were treated by Onyx via the venous approach. This technique was chosen when there was no other therapeutic solution for hemorrhagic BAVMs with

small nidus and, for almost all cases (7/8, 87.5%) with deep venous drainage. There were four men and four women with a mean age of 39.5 years (range, 12-57 years). In 50.0% (4/8) of cases the BAVM was treated by venous approach alone and in 50.0% (4/8) by both venous and arterial approach.
Results
The complete obliteration of the nidus was achieved in 75% (6/8). We deplored one (1/8, 12.5%) procedure-related complication by venous perforation during microcatheterism that was immediately controlled by Onyx injection, resulting in intraventricular hemorrhage with no clinical consequence. All patients remained clinically stable with unchanged modified Rankin Scale.
Conclusion
The transvenous approach using Onyx for the management of BAVMs is shown to be an efficient and safe alternative treatment in cases with no other conventional therapeutic choice and when some anatomical considerations are respected.

KEYWORDS: Arteriovenous malformation, Treatment assessment, Onyx

O-274 **3:39 PM - 3:47 PM**

Pretreatment Predicting Factors of Symptomatic Adverse Effects with Linear Accelerator or Gamma Knife Treatment of Arteriovenous Malformations

Machnowska, M. H.·Taeshineetanakul, P.·Geibprasert, S.·Menezes, R.·Agid, R.·Schwartz, M.·Krings, T.·Terbrugge, K.
University of Toronto
Toronto, ON, CANADA.

Purpose
To identify the angioarchitectural, dosimetric and vascular predictors of symptomatic post-radiation T2 signal change in patients with arteriovenous malformations treated with radiosurgery.
Materials & Methods
The charts of 211 consecutive patients with arteriovenous malformations treated with either gamma knife radiosurgery or linear accelerator radiosurgery between 2000-2009 were reviewed retrospectively. One hundered sixty-eight patients had a minimum of 12 months of clinical and radiologic followup following the procedure and complete dosage data. A symptomatic adverse effect was considered as new or worsening focal or global neurologic deficits including worsening of headaches, visual symptoms, increased seizure frequency, worsening of seizure activity, or motor and sensory symptoms. Pretreatment characteristics and dosimetric variables were analyzed to identify predictors of adverse radiation effects.
Results
One hundred forty-one patients had no clinical symptomatic complications. Twenty patients had global or focal neurologic deficits attributed to symptomatic edema; four patients had a hemorrhagic complication; two patients had arterial ischemia, one in the region of the AVM and the other remote from the AVM; one patient was diagnosed with radiation necrosis. We found that the variables associated with development of symptomatic edema included an asymptomatic or nonhemorrhagic symptomatic presentation compared to presentation with hemorrhage, $p = 0.001$, the presence of venous rerouting compared to the lack of venous rerouting, $p = 0.031$; OR (95% CI) = 3.25 (1.20, 8.80); radiosurgery with GKS compared to radiosurgery with LINAC $p = 0.012$; OR (95% CI) = 4.58 (1.28, 16.32); and the presence of more than one draining vein compared to a single draining vein $p = 0.032$; OR (95% CI) = 2.82 (1.06, 7.50). Sex, AVM size, flow rate through the AVM, the number of dominant feeders, perinidal angiogenesis, nidus type, drainage pattern, focal venous pouches, and eloquence did not correspond statistically to the presence of symptoms.
Conclusion
We postulated that the greater number of isocenters used with gamma knife radiosurgery may be responsible for the greater number of adverse radiation effects with this modality compared to linear accelerator radiosurgery. We found that AVMs with greater venous complexity and therefore instability resulted in more adverse treatment outcomes, suggesting that AVM angioarchitecture should be considered when making treatment decisions.

KEYWORDS: Arteriovenous malformation

O-275 **3:47 PM - 3:55 PM**

Posterior Fossa Arteriovenous Malformations More Frequently Present with Prenidal Aneurysm Rupture

Kouznetsov, E.·Raymond, J.·Weill, A.·Ghostine, J.·Roy, D.
l'Hôpital Notre-Dame du CHUM
Montréal, QC, CANADA.

Purpose
A controversy exists regarding natural history and treatment of AVM-related prenidal aneurysms. We conducted a retrospective review of 233 consecutive AVM cases in order to examine whether or not we could corroborate previously reported findings, suggesting that posterior fossa AVMs more frequently presented with a prenidal aneurysm rupture.
Materials & Methods
Medical records of all patients with cerebral AVMs seen at Notre Dame Hospital (Montreal, QC, Canada) between April 2001 and August 2012 were reviewed. All fossa and only two of those had a nonhemorrhagic presentation. Twelve out of 22 hemorrhagic posterior fossa AVMs (55%) had a prenidal aneurysm-related hemorrhage, whereas only five out of 135 (3.7%) hemorrhagic supratentorial AVMs presented with a prenidal aneurysm hemorrhage ($Z = 7$; $p < 0.001$).
Results

Note: Scanned images are included in the proceedings. Some submitted images were reduced during editing, thereby decreasing clarity. Also, refer to the Program Planner. Proceedings Content as of 3-29-2013.

Out of 233 AVMs, 24 (10%) were in the posterior cases with a prenidal aneurysm as the main hemorrhagic source were identified. We compared prenidal aneurysm-related rupture rates between supra and infratentorial AVMs.
Conclusion
Posterior fossa AVMs present much more frequently with a prenidal aneurysm rupture than supratentorial AVMs. Our data support more aggressive management of these aneurysms, especially when complete AVM excision is not possible.

KEYWORDS: Aneurysm rupture, AVM, prenidal aneurysms

O-276 **3:55 PM - 4:03 PM**

Endovascular Treatment of Hypoglossal-Clival Dural Arteriovenous Fistula

Liu, H.[1]·Hsu, Y.[2]·Lee, C.[1]·Wang, Y.[1]
[1]National Taiwan University Hospital, Taipei, TAIWAN, [2]Cheng-Hsin Hospital, Taipei, TAIWAN.

Purpose
To report our experience about the treatment of hypoglossal-clival DAVF.
Materials & Methods
From the databank of our institute, we found a total of 17 patients suffered from hypoglossal-clival dural arteriovenous fistula (AVF). They were eight males and nine females and their ages ranged from 43 to 77 years old (mean = 56 years old). Two of them associated with transverse sinus dural AVF. Sixteen patients had pulsating tinnitus and one mainly presented with dementia which may be caused by her transverse sinus DAVF. Three of them associated with eye congestion symptoms due to drainage to the cavernous sinuses.
Results
Of the 17 patients, seven were treated with transvenous approach alone, three with transarterial approach alone (one with onyx and one with coiling), and five with transvenous approach with adjuvant transarterial approach with NBCA or particles. Two patients received no treatment but the lesion had obliterated spontaneously on the follow-up images. The immediate post-treatment was excellent. No evidence of clinical or imaging residual/recurrence in 16 patients, while one treated with onyx had minimal residual without subjective symptom.
Conclusion
Endovascular treatment provides is safe, feasible, and excellent treatment for hypoglossal-clival AVF. Transvascular coiling is a better approach in long-term aspect.

KEYWORDS: Dural arteriovenous fistula, Endovascular management

O-277 **4:03 PM - 4:11 PM**

Comparative Efficacy of Intra-Arterial Cone-Beam CT Angiography Relative to Biplane Digital Subtraction Angiography in the Evaluation of Intracranial and Spinal Arteriovenous Fistulas

Honarmand, A. R.[1]·Gemmete, J. J.[2]·Soltanolkoltabi, M.[1]·Hurley, M. C.[1]·Chaudhary, N.[2]·Pandey, A. S.[2]·Shaibani, A.[1]·Ansari, S. A.[1]
[1]Northwestern University Feinberg School of Medicine, Chicago, IL, [2]University of Michigan Health System, Ann Arbor, MI.

Purpose
Digital subtraction angiography (DSA) is considered the standard for characterization of intracranial/spinal arteriovenous fistulas (AVFs). Although DSA offers superior spatial and temporal resolution, it is limited by 2D planar imaging. Prior reports described the value of intra-arterial cone-beam CT angiography (IACBCTA) in the anatomical localization of intracranial/spinal dural AVFs, but a comparative analysis is lacking. We directly paralleled these modalities to assess the relative IACBCTA efficacy in the anatomical identification/localization of AVFs and utility for surgical/endovascular treatment planning.
Materials & Methods
Patients with intracranial/spinal AVFs underwent biplane DSA and IACBCTA procedures (AXIOM-Artis FlatDetector Biplane-Angiosuite, Siemens) at two institutions with identical contrast injection, radiation exposure, and postprocessing techniques. Images were reviewed retrospectively and independently by two neurointerventionalists on a de-identified PACS workstation. Observers were blinded to clinical information and reviewed both DSA and IACBCTA images in tandem, obtained from the same IA injection. Qualitative image analysis was performed based on the level of delineation on a scale of 1-3 (3: Excellent/Good with minimal attenuation; 2: Moderate, relevant visibility with restrictions; 1: Poor, nondiagnostic). The following parameters were scored: a) Arterial feeders, b) Venous drainers and course, c) Fistula site, d) Adjacent anatomical landmarks for cross-sectional localization, and e) Overall diagnostic value for interpretation. Differences between the scores were defined as the IACBCTA efficacy value. For evaluation of IACBTA treatment planning efficacy, observers described the treatment strategy at the end of DSA and IACBCTA grading respectively and scored its adjunctive value: altered or more confident treatment plan versus no value. Wilcoxon signed rank and Mann-Whitney U tests compared scores of image quality parameters. Interobserver agreement was assessed using Spearman correlation coefficient. P value <0.05 was considered statistically significant.
Results
Thirty-two consecutive patients [22M/10F, mean age 60.9±12.4 years (29-83 years)] were studied. Intracranial AVFs were classified as Cognard type I (n=3), type II (n=11),

Note: Scanned images are included in the proceedings. Some submitted images were reduced during editing, thereby decreasing clarity. Also, refer to the Program Planner. Proceedings Content as of 3-29-2013.

type III (n=3), type IV(n=1) and metameric dural/pial (n=5). Spinal AVFs were limited to Anson-Spetzler type I (n=9). Despite moderate interobserver agreement for IACBCTA overall efficacy value (rho=0.4, P=0.02), no significant difference was observed between efficacy values (P = 0.6). Both observers assigned significantly higher scores to IACBCTA for overall diagnostic value (both observers: P<0.001). No significant differences were observed between DSA and IACBCTA scores while evaluating arterial feeders (observer 1: P=0.3, observer 2: P=0.6) or venous drainers (observer 1: P=0.08, observer 2: P=0.15). Both readers assigned higher scores to IACBCTA when evaluating the fistula site (observer 1: P <0.0001, observer 2: P=0.0003) and adjacent anatomical landmarks/cross-sectional localization(both observers: P<0.0001). In 30/32 cases, both observers noted that IACBCTA did not alter the treatment plan; but provided a more confident endovascular or surgical treatment approach. Both observers altered their treatment plan from an endovascular approach to microsurgery in one case based on IACBCTA.

Conclusion

IACBCTA adjunctively improves the anatomical delineation of AVFs, particularly in terms of fistula site and localization; biplane DSA may be equally sensitive for arterial feeder and venous drainer identification. IACBCTA confers a more confident endovascular or surgical treatment approach when performed in conjunction with DSA.

KEYWORDS: Flat-detector cone-beam CT, DSA, Arteriovenous fistula

O-278 **4:11 PM - 4:19 PM**

Ophthalmic Artery Patency and Clinical Followup after Placement of Pipeline Embolization Device

Raz, E.·Tanweer, O.·Becske, T.·Shapiro, M.·Zumofen, D.·Riina, H.·Nelson, P. K.
New York University
New York, NY.

Purpose

Flow diversion of aneurysms with the pipeline embolization device (PED) has been shown to be an effective treatment option for intracranial aneurysms. Concerns for patency of branch arteries that are covered by a PED have been raised. We aim to examine the patency of the ophthalmic artery and clinical sequelae of occlusion in treatment of intracranial aneurysms with PEDs.

Materials & Methods

A prospective study was performed for all patients undergoing treatment of an internal carotid artery aneurysm where a PED was used and covered the neck of the ophthalmic artery and followup was available. Age, gender, type of aneurysm, number of PEDs used, ophthalmic artery flow on follow-up angiograms, P2Y12 platelet function test results and ophthalmologic exam data were collected. At the followup, the time interval from the procedure, the complete or partial aneurysm occlusion, P2Y12 and ophthalmologic exam were recorded.

Results

The study included 58 patients (M/F ratio = 6/52; mean age 60.2 ± 11.9 years) who had at least one PED placed covering the ostium of the ophthalmic artery. A total of 127 PED were implanted successfully in the 58 patients covering the ophthalmic artery (median 2; range 1-4). The last followup available was performed at 14.5 (11.5) months on average (range 1.9-59.6 months). At followup, 47 out of 58 (81.0%) aneurysms were occluded. Functional impairment of the ophthalmic artery was noted in 12 cases (20.7%): in seven cases the flow within the ophthalmic artery was noted to be slow, in four cases the ophthalmic artery was closed and in one case, proximal stenosis was noted. In all cases of occlusion, reconstitution of the ophthalmic artery was noted via external carotid supply and in one case from the meningohypophyseal trunk. No new visual deficits or complaints were noted in patients with occlusions. No significant difference on the number of PED covering the neck of the ophthalmic artery was present between the two patient groups(p=0.354). No correlation was found between monitoring platelet functionality and ophthalmic artery patency (p=0.782).

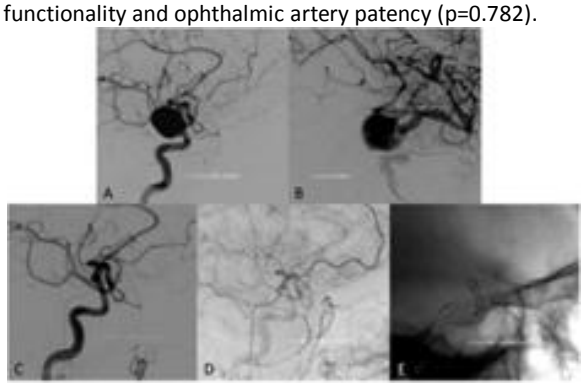

Figure: Baseline images (A-B) demonstrating a paraophthalmic aneurysm with preserved ophthalmic artery flow. One year followup after PED (C-D-E): complete occlusion of the aneurysm; ophthalmic artery origin occluded; reconstitution of flow via the left middle meningeal artery.

Conclusion

In our case series, 20.7% of the ophthalmic arteries were found to be occluded or exhibiting diminished flow on follow-up angiography. None of these changes were found to have clinical sequelae.

KEYWORDS: Aneurysm treatment, Aneurysm embolization

Note: Scanned images are included in the proceedings. Some submitted images were reduced during editing, thereby decreasing clarity. Also, refer to the Program Planner. Proceedings Content as of 3-29-2013.

O-279 **4:19 PM - 4:27 PM**

Bigger Is Not Always Better: Unexpectedly High Radiation Doses Using Flat Panel Detectors with Increasing Magnification

Lin, S. J.[1]·Badve, C.[2]·Vidal, L. L. M.[2]·Jordan, D. W.[2]·Blackham, K. A.[2]
[1]Case Western Reserve University School of Medicine, Cleveland, OH, [2]University Hospitals, Case Western Reserve University, Cleveland, OH.

Purpose
Flat panel detector units (FPDs) are a new alternative to image intensifiers (II) and ostensibly have a number of advantages; however, the design and operation of the technology is not commonly understood. The large field of view of the detector may result in excessive magnification to visualize small structures. This study evaluates the dose performance of an FPD at various magnification levels which also are known as fields of view (FOV) to quantify dose changes. A small field of view indicates a higher magnification.
Materials & Methods
Measurements were performed on a biplane Philips Allura Xper FD 20/20 (flat detector) system in the AP plane only at different FOV: 42 cm, 22 cm and 15 cm, utilizing clinically typical modes: fluoroscopy (15 frames/second) and digital subtraction angiography modes of 3, 4, and 6 frames/second. Skin-entrance dosimetry was performed with an Unfors Xi R/F detector placed under a CTDI head phantom. Secondly, simulated dosimetry at various locations on the head was measured using thermoluminescent dosimetry (TLD) chips placed on a RANDO head phantom. A fluoroscopic system resolution test tool was used to visually evaluate image resolution at the three levels of magnification.
Results
For FPD fluoroscopy, skin dose rates increased by factors greater than the predicted scaling of 1/FOV with increasing magnification. For acquisition modes, the skin dose effect of magnification paralleled the predicted values of $1/FOV^2$ that is typical for image intensifiers. This resulted in skin dose rates much higher than the predicted scaling of 1/FOV typically associated with FPD-based equipment. Measurements at multiple locations on a head phantom indicated that for fluoroscopy at magnification factors of 1.0-1.9, the increase in radiation output is partially offset by the irradiation of less tissue (i.e., smaller FOV), including minimizing irradiation of the eyes and areas potentially overlapped by the lateral plane. At magnification factors of 2.0 and higher, however, the summed dose from the measurement locations still increases dramatically despite the smaller region of irradiation. The fluoroscopic image spatial resolution check demonstrated expected results for magnification modes that do and do not used pixel binning. As to how this relates to a particular clinical use: an acquisition run performed at six frames/sec with a 15 cm FOV (i.e., for evaluation of arteriovenous fistula) results in a skin dose 16.8 times larger than a run at three frames/sec with a 42 cm FOV (i.e., routine diagnostic run). Not including the effect of the increased frame rate, this is three times the dose increase that commonly would be predicted for an FPD at this magnification using 1/FOV scaling.
Conclusion
Radiation dose rates increase much more than predicted when using FPD at high magnification. Optimal use of this equipment requires operator awareness of the dose-magnification relationship for a given FPD technology. As with any system, the performance and dose delivery should not be assumed optimal by solely relying on factory settings; imaging preferences at the operator level may need to be revised.

KEYWORDS: Flat panel detector, Dosimetry, Image intensifiers

O-280 **4:27 PM - 4:35 PM**

Long-Term Followup in a Consecutive Series of Patients with Intracranial Aneurysms Treated by Flow Diverter Stents

Biondi, A.·Pomero, E.·Macovei, I.·Jirari, M.·Cattin, F.
Besancon University Hospital
Besancon, FRANCE.

Purpose
To evaluate long-term follow-up clinical and angiographic results in a consecutive series of patients with intracranial aneurysms treated using a flow diverter stent.
Materials & Methods
Sixty-three patients (ranging in age from 16 to 79 years, mean age 52 years) with 76 unruptured or recanalized intracranial aneurysms treated by a flow diverter stent were included in the study. Thirty-four out of 63 patients were symptomatic. Seventy-seven percent of lesions were large or giant. At total, 78 stents were deployed (from 1 to 3 per patient). Six patients with adjacent aneurysms (from 1 to 4) were treated by only one stent. Flow diverter stents were Silk Stent (Balt company) in 10 aneurysms, Pipeline Stent (ev3 company) in 50 and Surpass stent in 16. In four cases, coils also were positioned within the aneurysm sac immediately before the deployment of the stent. After the procedure and at one-year followup, angiographic results were evaluated using the Kamran score (Grade 0 - no change in endosaccular flow; Grade 1 - residual contrast filling, greater than 50%; Grade 2 - residual sac filling, less than 50% of pretreatment aneurysm volume; Grade 3 - residual filling confined to the neck region, and not extending beyond the width of neck; Grade 4 - no residual filling (i.e., complete obliteration of the aneurysm). Technical and clinical complications were recorded systematically. All patients underwent long-term MR follow-up studies.
Results
At 1-3-year followup, improvement or cure of the

Note: Scanned images are included in the proceedings. Some submitted images were reduced during editing, thereby decreasing clarity. Also, refer to the Program Planner. Proceedings Content as of 3-29-2013.

compressive syndrome was observed in 80% of patients. Complete occlusion was observed in 92 % of patients. At three month followup, asymptomatic parent artery stenosis (>50%) was observed in three patients. Occlusion of small aneurysms seems to need more time in relation to large/giants lesions. Immediate complications included one regressive hemiparesis in a patient with a severe groin hematoma. Transient worsening of mass effect syndrome in eight patients with one case of persistent ophthalmoparesis. At one month, one patient died because of cataclysmic hemorrhage during surgical treatment of a tumor. Due to worsened clinical conditions, the patient underwent surgery only 10 days after the discontinuation of the antiplatelet treatment. One patient had a regressive hemiparesis and speech disturbances at one year after stopping aspirin. Five days after the intervention, one patient bled and died. Correlations with long-term follow-up MR studies are under analysis.
Conclusion
Our results confirm that the use of flow diverter stents is a very promising technique in some configurations of intracranial aneurysms, especially in large or giant lesions. However, more experience and long-term followup is needed in order to define the indications of these new stents.

KEYWORDS: Aneursym, Interventional, Stenting

O-281 **4:35 PM - 4:43 PM**

Association of Intralesional and Juxtapositioned Developmental Venous Anomalies in Patients with Capillary Telangiectasia: Observations from a Large, Single Center Series

Trimble, C. R.·Gandhi, D.
University of Maryland School of Medicine
Baltimore, MD.

Purpose
Capillary telangiectasias are “angiographically occult” vascular lesions and often identified incidentally as small areas of blush-like enhancement primarily within the pons on postcontrast brain MR imaging. Though generally considered benign entities, there is controversy regarding their etiology and clinical significance. In our experience, we have noted that many of the capillary telangiectasias may harbor an intralesional developmental venous anomaly (DVA). We hypothesize that there is a significant and perhaps causal association between DVA and capillary telangiectasia.
Materials & Methods
Forty-four patients (16 male and 28 female) with capillary telangiectasia were identified from a phrase search of a diagnostic MRI database during a 24-month period. Following retrospective image analysis, 20 patients were excluded due to lack of identification of the capillary telangiectasia, presence of co-existent demyelinating disease, or intracranial malignancy. The 24 remaining patients had lesions that had imaging appearance consistent with capillary telangiectasias. A detailed review of imaging studies was performed by two radiologists with specific attention to the presence of DVA within or adjacent to the capillary telangiectasia.
Results
Capillary telangiectasias were seen primarily in the pons (15/24 cases), but also in the basal ganglia (2/24), thalamus (1/24), subcortical white matter (3/24), tectum (1/24), and superior cervical spinal cord (1/24). Developmental venous anomalies were visualized within the capillary telangiectasia in 13/24 cases and juxtaposed to the capillary telangiectasia in 2/24 patients. Capillary telangiectasias with high diagnostic confidence of associated DVA demonstrated larger cross-sectional areas (average 54.4 mm2) compared with capillary telangiectasias without associated DVAs (average 12.2 mm2) ($p = .03$ paired T test).

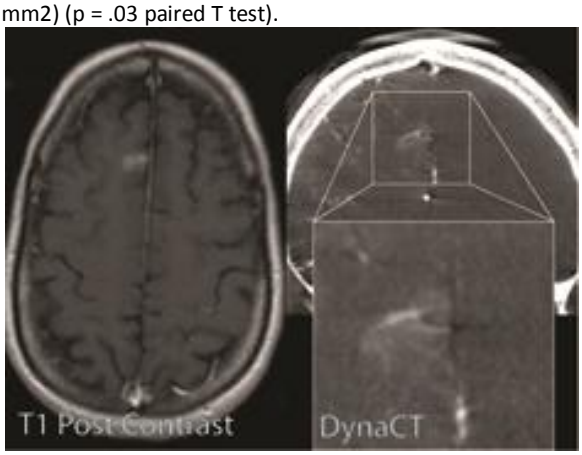

Conclusion
This retrospective case analysis demonstrates that association between DVAs and capillary telangiectasias may be stronger than previously reported. Our data also lend support to the possibility that capillary telangiectasias may represent a manifestation of local venous hypertension from DVAs.

KEYWORDS: Developmental venous anomaliesCapillary telangiectasia

Note: Scanned images are included in the proceedings. Some submitted images were reduced during editing, thereby decreasing clarity. Also, refer to the Program Planner. Proceedings Content as of 3-29-2013.

Tuesday Afternoon

3:15 PM - 4:45 PM
Ballroom 6CF

(31b) Parallel Scientific Papers: Adult Brain: Tumors II: Gliomas and Imaging Surrogates

O-282 **3:15 PM - 3:23 PM**

Predicting Recurrent Glioma versus Treatment-Related Necrosis Using Multiparameter Advanced MR Imaging: Accurate and Cost-Effective Clinical Decision-Making

Hamilton, J. D.·Jackson, E. F.·Leeds, N. E.·Ketonen, L.·Schellingerhout, D.·Jones, J.·Tatum, L. S.·Hou, P.·Evans, D. T.·Underwood, M. L.·Jones, J. R.·Reed, B. J.·Hash, S.·Steele, J.·Albright, H. W.·Kumar, A. J.
The University of Texas M. D. Anderson Cancer Center
Houston, TX.

Purpose
To reduce the amount of unnecessary brain surgeries or biopsies of patients with treatment-related brain necrosis and no residual viable high-grade glial tumor by utilizing physiologic MRI sequences, and doing so in an efficient and cost-effective manner.
Materials & Methods
As part of an on-going clinical protocol, patients 1) with history of histologically proven glioma brain tumor, 2) treated with radiation therapy >six months prior and often surgery/chemotherapy, 3) who developed a new enhancing lesion within the radiation field, were prospectively imaged to determine recurrent glioma versus treatment-related brain necrosis. For this study, we concentrated on the patients with 4) biopsy or resection within 60 days of imaging. The protocol, which began in 2009, includes dynamic contrast-enhanced (DCE) and dynamic susceptibility contrast (DSC) perfusion, diffusion tensor and multivoxel spectroscopy in addition to conventional imaging (scan time <75 minutes, postprocessing ~30 minutes). At the beginning of 2011, multiple changes to the protocol occurred based on review of earlier results, this included changes to our techniques (e.g., DSC perfusion), data processing (e.g., for DCE perfusion), and novel cut-off values. We also learned which values were important in which situations (e.g., Avastin makes DCE values less reliable). To evaluate the refinements of the prospectively prescribed imaging protocol, data from January 2009 -September 2010 were gathered for the baseline and compared to June 2011-June 2012 after the refinements. Pathology and radiology reports were graded on a five-point scale from pure tumor (1) to mixture to pure treatment effects (5). Radiologist reports were considered accurate if within a point of pathology. The cost of all care (surgery, chemotherapy, hospitalization, etc.) for patients beginning from the date of MRI scan through 90 days follow-up was tabulated. Inflation estimates derived from U.S. Department of Labor Statistics adjusted the line item costs. Fisher exact test compared group differences by pathology.
Results
In the baseline group, 110 patients were imaged, 33 fulfilled the inclusion criteria including biopsy/surgery within 60 days of imaging and 11 of those were found to have no residual brain tumor with only treatment effects. After the protocol was refined, 103 patients were imaged, 29 had biopsy/surgery and 1 of those were found to have no residual brain tumor but only treatment changes (p = 0.003 between baseline and after refinements). Similarly, the accuracy of radiology reports increased from 72% (24/33 cases accurate) to 97% (28/29). After costs were adjusted for inflation and outliers were censored, the average total cost for the 110 baseline patients imaged was $28,447 and $24,507 for the 103 patients imaged after the refinements, a cost savings of about $3,900 per patient.
Conclusion
Refining a physiologic MRI protocol improved the accuracy of imaging diagnosis to >95% making surgical intervention for treatment effect unnecessary and reducing the overall patient care costs. This required an experienced team (MR technologists, physicists and neuroradiologists) with a small additional scanning and postprocessing time (<1 hour more than conventional imaging). This data provide justification for a prospective multicenter clinical trial.

KEYWORDS: Glioma recurrence, Necrosis, Cost-effective

O-283 **3:23 PM - 3:31 PM**

Evaluation of T2* Dynamic Susceptibiliy-Based Contrast-Enhanced and T1 Dynamic Contrast-Enhanced Perfusion and Permeability Imaging in Glioma Grading

Santarosa, C.·Castellano, A.·Politi, L. S.·Terreni, M. R.·Leoncini, G.·Falini, A.·Anzalone, N.
Ospedale San Raffaele
Milano, ITALY.

Purpose
T2*-weighted dynamic susceptibility-based contrast-enhanced (DSC) MR perfusion technique offer an estimate of relative cerebral blood volume (rCBV), established to predict glioma grading. Nevertheless limitations of DSC technique due to high sensitivity to susceptibility effects are well known. Our purpose was to evaluate, in comparison with DSC, a more recent T1-based perfusion technique, dynamic contrast-enhanced (DCE). Two parameters are derivable from DCE: fractional plasma volume (fVp) and volume transfer coefficient (Ktrans), respectively, an estimate of vessel compartment volume and an estimate of vessel permeability. Dynamic

Note: Scanned images are included in the proceedings. Some submitted images were reduced during editing, thereby decreasing clarity. Also, refer to the Program Planner. Proceedings Content as of 3-29-2013.

susceptibility-based contrast-enhanced and DCE-derived parameters were correlated with WHO histologic grading.
Materials & Methods
Ten patients affected by glioma (including both astrocytic and olidendroglial histotypes) underwent DSC and DCE perfusion MR imaging with a 3.0T scanner (Achieva, Philips). NordicIce software was used for postprocessing. Parameters were measured through hotspot-based method, from region of interest (ROI) of the maximal abnormality within the lesion, and through histogram-based method, from ROI including the whole lesion volume. Mean-Median-Standard deviation-Skewness-Kurtosis were considered as distribution frequency descriptive indices. Spearman rank correlations evaluated associations beetween rCBV-fVp-Ktrans parameters and histologic WHO grade.
Results
Through "hotspots-based" method, correlation WHO grade-fVp ($p = 0.001$) and WHO grade-Ktrans ($p = 0.001$) from DCE was more significant than correlation WHO grade-rCBV from DSC ($p = 0.067$). Through "histogram-based" method, for each parameter all the frequency distribution descriptive indices resulted to be almost equally correlated with WHO grading.
Conclusion
Our preliminary results seem to indicate that: 1. Vp parameter is more related than rCBV to WHO grading, with both measurement method; 2. Ktrans parameter correlates with WHO grading too. If confirmed by a larger sample, these results could lead to consider DCE preferable to DSC in noninvasive grading of gliomas.

KEYWORDS: Glioma, Brain perfusion

O-284 **3:31 PM - 3:39 PM**

Spatial Variation of Apparent Diffusion Coefficient and Fractional Anisotropy within Nonenhancing Components of Glioblastomas as a Function of Distance from Enhancing Tumor: Predicting Clinical Outcome - A TCGA Glioma Phenotype Research Project

Hwang, S. N.[1]·Holder, C. A.[2]·Gutman, D.[2]·Jain, R.[3]·Wintermark, M.[4]·Colen, R. R.[5]·Saltz, J.[2]·Brat, D. J.[2]·Jaffe, C.[6]·Flanders, A. E.[7]·The TCGA Glioma Phenotype Research Group
[1]St Jude Children's Research Hospital, Memphis, TN, [2]Emory University, Atlanta, GA, [3]Henry Ford Hospital, Detroit, MI, [4]University of Virginia, Charlottesville, VA, [5]M. D. Anderson Cancer Center, Houston, TX, [6]Boston University, Boston, MA, [7]Thomas Jefferson University, Philadelphia, PA.

Purpose
Explore the variation of apparent diffusion coefficient (ADC) and fractional anisotropy (FA) within the nonenhancing component of glioblastomas as a function of distance from enhancing tumor. MR diffusion parameters of glioblastomas have been described previously in the literature; however, the goal of the current work is to more completely characterize the spatial variation of these parameters to improve the classification of glioblastomas and to predict clinical outcome.
Materials & Methods
As part of The Cancer Genome Atlas (TCGA) MRI characterization project of the National Cancer Institute, the multi-institutional TCGA Glioma Phenotype Research Group has been investigating MRI, including diffusion and diffusion tensor imaging, as a means of predicting clinical outcomes for glioblastoma patients. For the current work, a previously described interactive machine learning method for segmenting MRI of glioblastomas into various components, including nonenhancing and enhancing tumor, was applied. A Euclidian distance transform was performed to compute the distance from enhancing tumor. Volumes of interest (VOIs) containing nonenhancing tumor were generated at increasing distances from enhancing tumor: 0 to 2 mm, 2 to 4 mm, 4 to 6 mm, and 6 to 8 mm from enhancing tumor. Fractional anisotropy and ADC were computed for the VOIs. Thirty-five of the tumors have been processed thus far. Clinical outcomes including days of survival were obtained from the publicly available TCGA data. Analysis of variance and Kaplan-Meier survival analysis were performed. For initial analysis, tumors were divided into two groups based on the medians of the parameters (e.g., high ADC versus low ADC).
Results
A suggestion of a minimal increase in ADC was noted with greater distance from enhancing tumor, but was only statistically significant ($p<0.05$) between the volumes of tumor 0 to 2 mm compared to 4 to 6 mm and between 2 to 4 mm compared to 4 to 6 mm. In the subset of tumors currently evaluated, no significant difference in survival was identified between tumors with high FA versus low FA. However, tumors with high ADC in enhancing tumor demonstrated significantly longer survival ($p = 0.004$, 543 days versus 187 days). High ADC in nonenhancing tumor adjacent to enhancing tumor (within 0 to 2 mm) also was associated with longer survival ($p = 0.03$, 654 versus 357 days). In the next layer of nonenhancing tumor (2 to 4 mm from enhancing tumor), there was only a suggestion of improved survival with higher ADC ($p = 0.052$).
Conclusion
Low ADC within enhancing tumor and the immediately adjacent nonenhancing tumor may help predict survival in patients with glioblastoma. The threshold value preliminarily identified is approximately 1.2×10^{-3} mm^2 s^{-1}. These findings suggest a more sophisticated method of characterizing the spatial variations of MR diffusion parameters may be helpful in predicting clinical outcomes.

KEYWORDS: Glioblastoma, Brain neoplasms, Diffusion

Note: Scanned images are included in the proceedings. Some submitted images were reduced during editing, thereby decreasing clarity. Also, refer to the Program Planner. Proceedings Content as of 3-29-2013.

O-285 **3:39 PM - 3:47 PM**

Perfusion Imaging Genomic Mapping Uncovers Potential Genomic Targets Involved in Angiogenesis and Invasion

Colen, R. R.·Abrol, T.·Zinn, P. O.
M. D. Anderson Cancer Center
Houston, TX.

Purpose
To create an imaging genomic map, linking MR imaging traits with gene- and miRNA expression profiles, in patients with GBM to determine genomic correlates of a MR perfusion radiophenotype to possibly find new genomic targets for GBM treatment. Increases in angiogenesis demonstrate increases on MRI perfusion relative cerebral blood volume (rCBV) maps. Increases in angiogenesis are seen in patients with highly aggressive and hypervascular tumors. Here, we present the first study examining in a quantitative way perfusion imaging genomics in GBM to determine novel and targetable angiogenic biomarkers in GBM.
Materials & Methods
We identified 30 GBM patients from The Cancer Genome Atlas (TCGA) who had both genetic- expression profiles and neuroimaging. All morphologic image analyses were done using slicer 3.6 (slicer.org) and functional analysis using NordicIce, and reviewed in consensus by two neuroradiologists. Quantitative perfusion parameters where obtain using the region of interest (ROI) method. Regions of interest were placed in the previously segmented regions of contrast enhancement, necrosis, and nonenhancing perilesional FLAIR hyperintensity - the latter reflecting a mixture of edema/tumor infiltration. Biostatistics analysis was performed for gene and miRNA sets whereas the median CBV values of each of the segmented regions were taken as the cutoff to define high and low groups. These groups then were analyzed by Comparative Marker Selection (Broad Inst.). Among the whole gene set the most upregulated mRNAs/miRNAs, were analyzed with ingenuity pathway analysis (IPA).
Results
Ingenuity pathway analysis identified molecular networks, as well as canonical and functional pathways highly associated with cancer, angiogenesis, and invasion in those patients with high tumor rCBV.
Conclusion
The perfusion radiophenotype identified genes and miRNAs and corresponding molecular networks that were highly associated with angiogenesis and invasion. By these means we were able to identify possible key genes and miRNAs involved in the latter regulation. The uncovered genes and miRNAs represent new insight into tumors with high perfusion seen on MRI and the underlying molecular mechanisms in GBM for growth and treatment response.

KEYWORDS: Imaging genomics, Gene expression, perfusion

O-286 **3:47 PM - 3:55 PM**

Small- and High-Molecular-Weight Contrast Agents for MR Perfusion Imaging in Cerebral Neoplasms

Varallyay, C. G.[1]·Nesbit, E.[1]·Fu, R.[1]·Gahramanov, S.[1]·Muldoon, L. L.[1]·Li, X.[1]·Rooney, W.[1]·Neuwelt, E. A.[1,2]
[1]Oregon Health Sciences University, Portland, OR,
[2]Department of Veterans Affairs Medical Center, Portland, OR.

Purpose
Using ferumoxytol, a high-molecular-weight iron oxide contrast agent for perfusion MR imaging of brain neoplasms has potential benefits. Being a blood pool agent, theoretically no leakage correction is needed for relative cerebral blood volume (rCBV) calculation. Also, its high transverse relaxivity helps avoiding pronounced T1 effects on the dynamic susceptibility contrast (DSC) imaging. The purpose of this study was to compare rCBV values obtained using gadoteridol versus ferumoxytol in patients with cerebral neoplasms. Relative CBV was calculated in normal-appearing brain areas and in malignant tumors.
Materials & Methods
We analyzed 96 human brain MRI studies acquired in three similar research protocols between 2008 and 2011. Each of them included DSC perfusion measurements on two consecutive days; first with gadoteridol (0,1 mmol/l), and a day later with ferumoxytol (1 or 2 mg/kg). Dynamic susceptibility contrast scans used gradient-echo echo-planar acquisition with a short echo time (20 ms) to reduce susceptibility artifacts and image distortions. Cerebral blood volume maps were calculated in three different ways for each contrast agent; without leakage correction, with mathematical correction for T1 effects only or for combined T1 and T2 effects. Relative CBV values in the normal-appearing thalamus and putamen, as well as in enhancing tumor and tumor hotspots were obtained and compared between contrast agents and leakage correction methods using linear mixed effects model. Results are presented as mean (standard deviation).
Results
Leakage correction for T1 effects substantially increased the mean rCBV values obtained with gadoteridol in enhancing tumors from 1.36 (1.39) to 2.46 (1.41), and in tumor hot spots from 1.99 (1.33) to 3.41 (1.46), $P<0.0001$, but resulted in minimal change in values obtained with ferumoxytol [2.11 (1.22) to 2.18 (1.23) and 3.4 (1.29) to 3.47 (1.29) respectively]. Furthermore, normal-appearing brain assessed with gadoteridol also was affected by leakage correction for T1 effects, most prominently in the putamen, where rCBV increased from 1.28 (0.26) to 1.53 (0.28), $P<0.0001$. Additional correction for T2 effects resulted in a less prominent decrease of T1 corrected rCBV in the tumor and the thalamus, similarly for either contrast agent.

Note: Scanned images are included in the proceedings. Some submitted images were reduced during editing, thereby decreasing clarity. Also, refer to the Program Planner. Proceedings Content as of 3-29-2013.

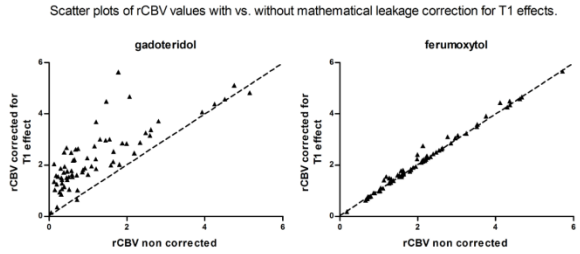

Conclusion
While leakage correction for T1 effects is necessary when assessing rCBV of tumors using gadoteridol, no T1 correction is necessary for ferumoxytol. Correcting for T2 effects is less important in acquisitions with shorter echo times. Mathematical leakage correction can alter rCBV measurement in the normal brain regions and tumors, which is not necessarily attributed to contrast agent leakage.

KEYWORDS: Brain neoplasms, Contrast agents, Ferumoxytol

O-287 **3:55 PM - 4:03 PM**

Deformation Field Morphometry as a Surrogate Imaging Biomarker for Tumor Growth and Infiltration Rate Quantification in Diffuse Gliomas

Ellingson, B. M.·Cloughesy, T. F.·Lai, A.·Nghiemphu, P. L.·Pope, W. B.
David Geffen School of Medicine at University of California Los Angeles
Los Angeles, CA.

Purpose
Brain tumor growth characteristics are estimated traditionally by volumetry; however, a new technique was developed recently for examining subtle changes in the structure of the brain over time in patients with neurodegenerative diseases called “deformation field morphometry” (DFM). Deformation field morphometry mapping involves quantification of the nonlinear (elastic) deformation fields resulting from serial image registration. In the current study we explored DFM mapping as a method for quantifying “tissue expansion velocity” and “volume growth rate” in patients with low grade diffuse gliomas (LGGs) and recurrent glioblastoma (GBM).
Materials & Methods
Deformation field morphometry maps were constructed for both tissue expansion velocity (v) and volume growth rate (ρ) using the deformation field information extracted from nonlinear (elastic) registration of serial 3D MR images (pre or postcontrast T1-weighted or T2-weighted) in the same patient over time. The FMRIB nonlinear registration tool (FNIRT) was used for nonlinear registration. The deformation warp field vector $U(t) = Ux + Uy + Uz$ for each voxel denotes the local displacement direction and magnitude of the tissue at time t during a patient’s clinical course, taken with respect to another scan date (usually the most recent). The “tissue expansion velocity”, v, was calculated as: $v = ||U(t)||/dt \cong ||U(t)||/\Delta t$, where Δt is the time between scans and $||U(t)||$ is the deformation warp field vector magnitude for each image voxel. The “volume growth rate”, ρ, was estimated from the rate of change in the Jacobian determinant, or $\rho = [\det(J(t))-1]/dt \cong [\det(J(t)-1]/\Delta t$, where again Δt is the time between sequential scans.
Results
In patients with suspected tumor progression (GBM) or malignant transformation (LGGs, Figure 1), DFM maps of expansion velocity and growth rate were able to isolate and quantify loci of proliferative tumor. Positron emission tomography scans confirmed spatial specificity in many cases. Regions of elevated expansion velocity appeared slightly outside of FLAIR abnormal regions, suggesting these maps may be useful for localizing infiltrating tumor. Vector fields from DFM data appeared to define the directionality of tumor spread across the brain. Subtle mass effect from slow growing tumor was easily quantified using expansion velocity and growth rate estimates. Changes in tissue expansion velocity and volume growth rates also can be used to quantify localized response to various therapies.

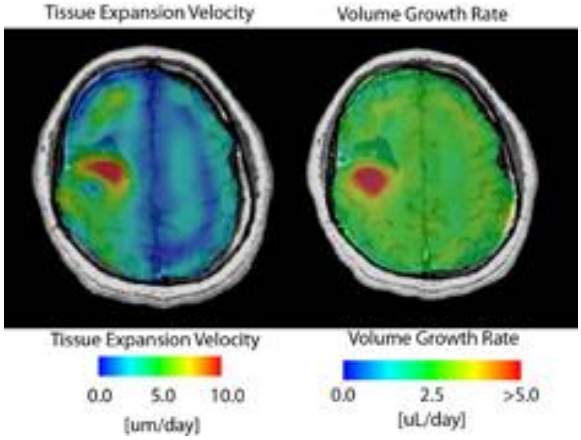

Conclusion
Deformation field morphometry-derived estimates of tumor expansion velocity and volume growth rate are a novel clinical tool for noninvasive quantification of tumor growth dynamics.

KEYWORDS: Glioma, Imaging biomarker, Deformation Field Morphometry

Note: Scanned images are included in the proceedings. Some submitted images were reduced during editing, thereby decreasing clarity. Also, refer to the Program Planner. Proceedings Content as of 3-29-2013.

O-288 **4:03 PM - 4:11 PM**

Identifying the Mesenchymal Molecular Subtype of Glioblastoma Using Quantitative Volumetric Analysis of Anatomical MR Images

Naeini, K. M.[1]·Pope, W. B.[1]·Cloughesy, T. F.[1]·Harris, R. J.[1,1]·Lai, A.[1]·Eskin, A.[1]·Chowdhury, R.[1]·Phillips, H. S.[2]·Behbahanian, Y.[1]·Nghiemphu, P. L.[1]·Ellingson, B. M.[1]
[1]David Geffen School of Medicine at University of California Los Angeles, Los Angeles, CA, [2]Genentech, Inc., San Francisco, CA.

Purpose
To explore the relationship between radiographic imaging features and glioblastoma (GBM) molecular subtypes, specifically identifying radiologic biomarkers for identifying the mesenchymal (MES) phenotype from non-MES GBMs.
Materials & Methods
A total of 47 patients with histologically confirmed de novo GBM, molecular data, and presurgical, postcontrast T1-weighted and T2-weighted/T2-weighted FLAIR images available were enrolled in this study. The volume of contrast enhancement, central necrosis, and T2 hyperintensity were measured. The ratio of [FLAIR/(enhancement+necrosis)] was calculated. Gene expression subclassification was performed according to standard protocols and subtypes. Subtype names were chosen based on the expression of signature genes: proneural (PN), proliferative (PROLIF) and MES.
Results
A statistically significant difference was observed between the different GBM subtypes when examining the combined volume of contrast enhancement and central necrosis. Specifically, the MES phenotypes, having a median volume of 47cc, had a significantly higher volume of contrast enhancement and necrosis compared with the PN and PROLIF subtypes, which each had a median volume around 2.7cc. The volume ratio of T2/FLAIR hyperintensity to the combined volume of contrast enhancement and central necrosis was statistically different between the different GBM phenotypes. Specifically, the MES phenotype had a statistically lower ratio than both the PN and PROLIF phenotypes. This difference also was confirmed when the PN and PROLIF phenotypes were pooled into a single non-MES group. This ratio was a very strong predictor of the MES phenotype, showing a sensitivity of 83% and a specificity of 87% using a cutoff of 2.3.

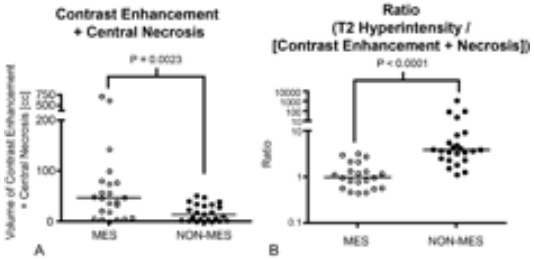

Conclusion
The ratio of T2/FLAIR volume to contrast-enhancing and necrotic volume is more effective than any of the other factors in stratifying between MES and non-MES subtypes. This study suggests that the volume ratio can be used as a biomarker for GBM subtype, and by extension, survival.

KEYWORDS: Imaging genomics, Glioblastoma

O-289 **4:11 PM - 4:19 PM**

Multiparametric Imaging Model to Accurately Predict Extent of Invasion of High-Grade Gliomas

Durst, C.·Raghavan, P.·Tustison, N.·Patrie, J.·Cupino, A.·Xin, W.·Wintermark, M.
University of Virginia
Charlottesville, VA.

Purpose
Despite advances in the surgical and oncologic approach to high-grade gliomas, the prognosis remains poor. Some hypothesize that a more complete initial surgical resection might improve outcome. The exact extent of high-grade gliomas is difficult to define on MRI. Postcontrast T1-weighted images underestimate and T2-weighted images overestimate the true tumor extent. Prior studies have evaluated the role of diffusion-weighted imaging (DWI), diffusion tensor imaging (DTI), magnetic resonance spectroscopy (MRS) and perfusion-weighted imaging (PWI), in the prediction of extent of local invasion. Although these studies have shown improved accuracy compared to conventional MRI, each has its limitations. This study combines the advantages from multiple conventional and advanced imaging techniques in an effort to provide the neurosurgeon and neuro-oncologist with a multiparametric imaging model that can reliably differentiate tumor margins from surrounding edema.
Materials & Methods
Ten patients with preliminary imaging findings suggestive of a high-grade glioma were enrolled in a prospective study. Each patient underwent a MRI using precontrast T1, T2, FLAIR, gradient echo, DWI, DTI, arterial spin labeling (ASL), and postcontrast T1 and PWI. Each patient then underwent stereotactic biopsies at prespecified points along the biopsy tract. The biopsy sites were coregistered to the imaging sequences so that imaging values could be ascribed to each biopsy site. The imaging values were analyzed against the measured cell density of each biopsy sample as the gold standard. From these data, a statistical multiparametric predictive model was developed using principle component analysis to predict the cell density associated with an infiltrative tumor.
Results
The major components of the model included the mean diffusivity, fractional anisotropy numerator and denominator, contrast transfer coefficient (Ktrans), mean transfer time, and time to peak. A multivariate generalized estimating equation analysis demonstrates an intercept near 0, a slope of approximately 45 degrees, and a

Note: Scanned images are included in the proceedings. Some submitted images were reduced during editing, thereby decreasing clarity. Also, refer to the Program Planner. Proceedings Content as of 3-29-2013.

coefficient of determination of 0.56. A subject specific model of goodness of fit shows that most patients' data are distributed along the curve. A probability plot of the residuals versus the expected order statistics yields a Filliben correlation of 0.976.

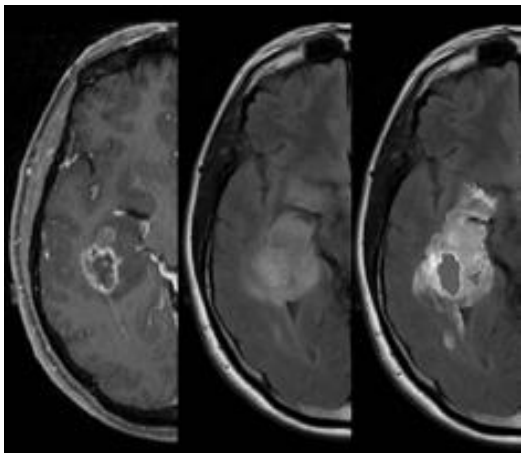

Conclusion

Our proposed multivariate imaging model can predict cell density of the tumor and surrounding tissue, providing the neuroradiologist, neurosurgeon, and neuro-oncologist with valuable information regarding the extent of infiltrative high-grade gliomas. Further validation studies are required to assess whether this would facilitate surgical and radiation planning, improving patients' outcome.

KEYWORDS: Glioma, Advanced MR imaging, Model

O-290 **4:19 PM - 4:27 PM**

Neurosurgical Resection of Malignant Gliomas Guided by 5-Aminolevulinic Acid Reduces Post-Op Residual Tumor Volume

Holder, C. A.[1]·Hadjipanayis, C. G.[1]·Cordova, J. S.[1]·Hwang, S. N.[2]·Gutman, D. A.[1]·Schreibmann, E.[1]·Danish, H.[1]·Shu, H. G.[1]·Olson, J. J.[1]·Shim, H.[1]
[1]Emory University School of Medicine, Atlanta, GA, [2]St. Jude Children's Research Hospital, Memphis, TN.

Purpose

Malignant gliomas (WHO grade III and IV) are infiltrative primary brain neoplasms with high morbidity and mortality. Surgery remains first line therapy. Completeness of resection and minimization of tumor burden is recognized as a prognostic factor in survival. A significant survival advantage has been seen with as little as 78% resection, and stepwise improvement in survival was evident; however, defining the margins of malignant gliomas at surgery is very difficult due to their infiltrative nature. The purpose of this study was to evaluate the utility of 5-aminolevulinic acid (5-ALA) as an intra-operative fluorescent detection agent by quantitative volumetric measurement of enhancing tumors before and after surgery, in order to determine whether the use of 5-ALA during surgical resection reduces postoperative residual enhancing tumor volume.

Materials & Methods

Malignant glioma cells express biosynthetic pathways that produce protoporphorin IX (PpIX) from 5-ALA. Oral administration of 5-ALA (20 mg/kg) leads to selective accumulation of PpIX in tumor cells. Following excitation with blue light (λ = 400 nm) emitted from a special filter attachment on the operative microscope, the PpIX, which has accumulated selectively in malignant cells, emits a red-violet light of 635 nm. The neurosurgeon then is able to resect the red-violet tumor tissue. Patients with suspected malignant gliomas were enrolled into this IRB-approved study and administered 5-ALA orally four hours prior to surgery. At the time of this abstract, tumor resection has been performed in 18 patients administered 5-ALA or placebo, followed by high-resolution postoperative MRI at 48 hours (including T1-weighted images pre and postgadolinium). Eighteen control patients with matching tumor location and size also were selected. To assess quantitatively the 5-ALA-guided surgery, an FDA 510k-approved software package (Velocity AI) which allows the display, annotation, volume-rendering, registration, and fusion of multimodality medical images was used. The software allows the coregistration of multimodality image datasets; placement of regions-of-interest (ROIs); and calculation, display, and report of relative differences in voxel intensities, radiation dose distributions, or other values within those regions. To estimate the tumor volume before surgery, coarse ROIs were drawn around the tumor and the software was used to semi-automatically segment volumes of hyperintensity (enhancing tumor), as well as hypointensity within the rim of hyperintensity (central necrosis). To estimate the residual tumor postsurgery, subtracted images were produced by subtracting coregistered, postresection, pre and postgadolinium T1-weighted images, correcting for postoperative blood accumulation.

Results

The average tumor resection without 5-ALA-guidance was 81.1%, leaving 18.9% residual tumor (standard error = 4.4). That of 5-ALA-guidance was 91.4%, leaving 8.6% residual tumor (standard error = 1.5). Two-tailed, two sample T-test $p = 0.03269$.

Conclusion

Use of oral 5-ALA for guidance of surgical resection of malignant gliomas reduces the postoperative residual enhancing tumor volume, as determined by semi-automated 3D tumor volume measurements. This improvement is important, since it is believed to be necessary to resect greater than 90% of a malignant glioma in order to make a meaningful difference in patient survival. Thus, the use of 5-ALA for surgical guidance may significantly improve patient outcomes.

KEYWORDS: Glioblastoma, Surgery

Note: Scanned images are included in the proceedings. Some submitted images were reduced during editing, thereby decreasing clarity. Also, refer to the Program Planner. Proceedings Content as of 3-29-2013.

O-292 **4:35 PM - 4:43 PM**

Correlation of Morphologic and Physiologic Phenotype of the Nonenhancing Component of Glioblastoma with Patient Survival and Genomic Expression: A TCGA Glioma Phenotype Research Group Project

Jain, R.[1]·Poisson, L.[1]·Khalil, K.[1]·Scarpace, L.[1]·Hwang, S. N.[2]·Gutman, D.[2]·Wintermark, M.[3]·Colen, R. R.[4]·Kirby, J.[5]·Freymann, J.[5]·Rubin, D.[6]·Jaffe, C.[7]·Mikkelsen, T.[1]·Flanders, A.[8]
[1]Henry Ford Health System, Detroit, MI, [2]Emory University, Atlanta, GA, [3]University of Virginia, Charlottesville, VA, [4]Brigham & Womens Hospital, Boston, MA, [5]TCIA/TCGA, St. Louis, MO, [6]Stanford University, Stanford, CA, [7]Boston University, Boston, MA, [8]Thomas Jefferson University Hospital, Philadelphia, PA.

Purpose
Traditionally the focus of treatment planning, response assessment and patient prognosis has been based on evaluation of contrast-enhancing component (contrast-enhancing lesion, CEL) in GBMs. However, non-enhancing component (Non-enhancing lesion, NEL) of GBM also contains important information about tumor and its surrounding environment which is indicative of tumor invasiveness and aggressiveness. The purpose of this study was to correlate morphologic (MRI features) and physiologic phenotype (rCBV) of the NEL in patients with GBM, as well as key genomic markers with patient survival.
Materials & Methods
Forty-five patients had DSC T2* MR perfusion data, and a detailed assessment of the various morphologic features of NEL (percentage NEL, proportion of edema, definition of margins of NEL, T1/FLAIR ratio, deep white matter involvement, NEL crossing the midline) available from The Cancer Imaging Archive (TCIA). Relative cerebral blood volume (rCBVNEL), a physiologic measure of the NEL also was measured. Mutation and copy number variation in the key oncogneic genes EGFR, PDGFRA, PTEN and TP53 were used to stratify patient groups. Correlation of the phenotypic and the genotypic expression of GBM with overall and progression-free survival were done.
Results
We observed that worsening overall survival (log-rank p=0.0145) and progression-free survival (log-rank p=0.0223) are each associated with increasing rCBVNEL. Also associated with increased risk of death or progression in our study were the following morphologic features: Minimal (<5%) edema (OS p=0.0424; PF, p=0.0296) and NEL crossing the midline (OS, p=0.012; PF, p=0.055). The level of rCBVNEL was increased on average in tumors with poorly defined NEL margins compared to those with well defined margins (two-sample t-test p=0.0317). Using a survival regression tree that allowed selection of predictors from the dichotomized rCBVNEL measure and various morphologic features listed in the methods above we found that the overall survival can be well described using the rCBVNEL measure with the high group further divided by the T1/FLAIR ratio (log-rank p=0.0228) with mixed and infiltrative descriptions having worse survival. Interestingly, the T1/FLAIR ratio is not significantly predictive of overall survival when used alone (p=0.288). Remarkably, this split shows a difference in median survival of over one year between the lowest (median 0.50 years, 95%CI: 0.37 - inf) and highest (median: 1.62 years, 95% CI: 1.14 - 2.27) groups. We also noticed that rCBVNEL remains a prognostic indicator within various patient groups which were stratified based on genomic expression, especially within the wild-type EGFR group (log-rank p=0.0085) compared to the altered group (log-rank p=0.6400).
Conclusion
Morphologic features of NEL and genomic alterations of the tumor provide important prognostic information, yet the additional information gained from the hemodynamic parameter of NEL (rCBVNEL) seems to make it a very important prognostic biomarker in patients with GBM. This analysis also raises the question if surgical resection for GBMs should extend beyond the CEL margins for better patient prognosis and also to have a better understanding of tumor biology, which in future may guide therapy decisions based on combined results of morphologic and physiologic phenotypic expression of the tumor as well as tumor genomics.

KEYWORDS: Glioblastoma, Diffusion MR imaging, blood volume

Tuesday Afternoon

3:15 PM - 4:45 PM
Ballroom 6DE

(31c) Parallel Scientific Papers: Adult Brain: Aneurysms, AVMs and AVFs

O-293 **3:15 PM - 3:23 PM**

Simulation of Hemodynamic Parameters in Cerebral Aneurysms and on Virtual Flow Diverter Devices Using a Dedicated Computational Fluid Dynamics Prototype System: First Experiences

Karmonik, C.[1]·Chintalapani, G.[2]·Rangel-Castilla, L.[1]·Redel, T.[2]·Diaz, O.[1]·Klucznik, R.[1]·Zhang, Y. J.[1]·Grossman, R. G.[1]
[1]The Methodist Hospital Neurological Institute, Houston, TX, [2]Siemens AX, Forchheim, GERMANY.

Purpose
To demonstrate the enhanced value in using a dedicated computational fluid dynamics (CFD) prototype system for assessing flow, wall shear stress and pressures in cerebral

Note: Scanned images are included in the proceedings. Some submitted images were reduced during editing, thereby decreasing clarity. Also, refer to the Program Planner. Proceedings Content as of 3-29-2013.

aneurysms and on virtual flow diverter devices with comparison to phase contrast magnetic resonance imaging (pcMRI).

Materials & Methods

Hemodynamic parameters including streamlines, velocities and wall shear stress were calculated in 18 cerebral aneurysms with a dedicated CFD prototype system (Siemens AX) using 3D digital subtraction angiographic (DSA) data. Simulation results were compared to CFD results obtained with a commercial solver (Fluent, Ansys, Inc) and with phase contrast magnetic resonance (pcMRI) measurements in a subset of six aneurysms. In a subset of nine aneurysms, virtual flow diverters were placed into the calculated velocity field and pressures on these devices were determined. In one case, post-treatment MRI measurements and fluoroscopic images were available for direct comparison to pressures onto the flow diverter/wall calculated with CFD.

Results

The user-optimized interface for preprocessing the 3D DSA allows the creation of computational meshes on average in less than 15 minutes. Simulation time for two cardiac cycles was in the order of several hours, steady state simulation needed less than 30 minutes. Results from the CFD prototype compared favorably with results from the commercial solver and with the pcMRI measurements (Figure 1). Calculation of forces on the virtual flow diverter revealed focal maxima of pressures. Comparison with post-treatment treatment images in one case showed correlation of focal pressure zone with remnant inflow jet into the aneurysm.

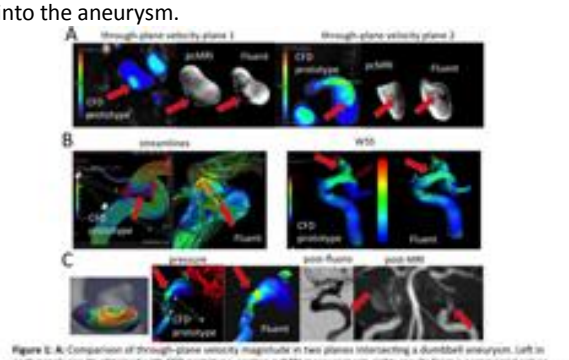

Figure 1: A: Comparison of through-plane velocity magnitude in two planes intersecting a dumbbell aneurysm. Left in each panel: results obtained with CFD prototype, center: pcMRI measurement, right: results from a commercial solver. Common features are marked by red arrows. B: Streamlines and wall shear stress (WSS). Left in each panel: results from CFD prototype, right: results from a commercial solver. C: On left, calculated forces on virtual flow diverter placed into a cerebral aneurysm (red: focal region of high pressure) are illustrated. Center: Pressure on aneurysm wall (coinciding with location of flow diverter). Red arrows indicate focal region of high pressure. Right: Post-treatment fluoroscopic image and post-MRI. Arrows indicate remnant inflow jet into aneurysm originating at approximately same position as location of focal pressure region visualized with CFD.

Conclusion

The use of a dedicated system facilitates CFD simulations and analysis of results. Enhanced value is demonstrated for the evaluation of pressures on virtual flow diverters.

KEYWORDS: Aneursym, 3D visualization

O-294 **3:23 PM - 3:31 PM**

Predicting Outcomes Based on Imaging in Aneurysmal Subarachnoid Hemorrhage

Robinson, C. L.·Hurtado Rua, S.·Gupta, A.·Sanelli, P. C.
Weill Cornell Medical College
New York, NY.

Purpose

Delayed cerebral ischemia (DCI) is a serious complication of aneurysmal subarachnoid hemorrhage (SAH) leading to disability and death. Currently, several imaging modalities are used in clinical practice to detect DCI. At times, there is not good agreement amongst imaging exams for determining DCI, leading to variability in diagnosis and management decisions. Our aim was to evaluate the predictive abilities for clinical outcomes using CT perfusion (CTP) and transcranial doppler sonography (TCD) in symptomatic and asymptomatic patients.

Materials & Methods

A retrospective study of consecutive SAH patients enrolled in an IRB-approved clinical trial was performed. Inclusion criteria were patients with SAH who had CTP and TCD performed. Symptomatic patients were determined by clinical assessment for focal neurologic deficits (such as aphasia, hemiparesis, hemiplegia, etc). The CTP studies were evaluated by two neuroradiologists blinded to all other data to determine perfusion deficits, defined as focal areas of reduced cerebral blood flow and/or elevated mean transit time. Transcranial doppler sonography findings supporting vasospasm were determined by the clinical reports. Clinical outcomes were obtained from medical record review for patients who recovered without neurologic deficits (mRs = 0-2), disability (mRs = 3-5) and death (mRs = 6). A multinomial logistic regression model was developed and fitted to determine the prediction probabilities with 95% confidence intervals (CI) for each outcome based on the imaging findings for both symptomatic and asymptomatic patients.

Results

A total of 97 patients were included in the statistical analysis; 73% (71/97) were female and 27% (26/97) were male. The mean age is 50.5 years (range 28-80 years). The predictive probabilities (95% CI) of the CTP and TCD data in symptomatic and asymptomatic patients are displayed in Table 1. Symptomatic patients with CTP deficits demonstrate statistically significant lower recovery and higher disability and death compared to patients without CTP deficits. Additionally, asymptomatic patients with CTP deficits also demonstrate statistically significant lower recovery and higher disability and death compared to patients without CTP deficits. However, symptomatic patients with TCD deficits do not have significantly different outcomes compared to patients without TCD deficits. Similar findings also are seen in asymptomatic patients.

Table 1: Prediction probabilities and 95% CI

Note: Scanned images are included in the proceedings. Some submitted images were reduced during editing, thereby decreasing clarity. Also, refer to the Program Planner. Proceedings Content as of 3-29-2013.

	CTP		TCD	
	Deficit	NO deficit	Deficit	NO deficit
Symptomatic:				
Recovery	51% (47-55%)	79% (75-82%)	59% (55-63%)	53% (49-57%)
Disability	39% (35-43%)	16% (14-19%)	32% (28-35%)	38% (34-42%)
Death	10% (8-13%)	5% (3-7%)	9% (7-11%)	9% (7-11%)
Asymptomatic:				
Recovery	77% (74-81%)	92% (90-94%)	90% (88-93%)	87% (85-90%)
Disability	19% (16-22%)	6% (4-8%)	8% (6-10%)	11% (8-13%)
Death	4% (2-5%)	1% (0.5-2%)	2% (1-3%)	2% (1-3%)

Conclusion

CT perfusion provides predictive information for outcomes in both symptomatic and asymptomatic patients. However, TCD as a predictor for clinical outcomes of recovery, disability, and death does not offer much information in symptomatic or asymptomatic patients. Thus, CTP may be helpful for guiding patient management and treatment decisions in the clinical setting.

KEYWORDS: CT brain perfusion, Aneurysmal subarachnoid hemorrhage

O-295 **3:31 PM - 3:39 PM**

Cerebral Aneurysm Wall Permeability: A New Marker for Detecting Rupture Risk

Vakil, P.[1]·Ansari, S. A.[1]·Schnell, S.[1]·Wasliewski, M.[1]·Batjer, H.[2]·Bendok, B. R.[1]·Eddleman, C. S.[3]·Markl, M.[1]·Carroll, T. J.[1]
[1]Northwestern University, Chicago, IL, [2]Northwestern University, Dallas, TX, [3]University of Texas Southwestern, Dallas, TX.

Purpose

Cerebral aneurysms pose a significant risk to the public with incidence estimates of up to 6%. Aneurysms larger than 10 mm generally are considered dangerous; however, many aneurysms smaller than 10 mm are known to rupture, highlighting the need for more quantifiable, and noninvasive metrics that may distinguish progressing aneurysms from stable ones. We studied aneurysm wall permeability to intravascular contrast agent using dynamic contrast-enhanced (DCE) MRI as a new metric for assessing rupture risk.

Materials & Methods

With IRB approval, we used a standard DCE MRI protocol to measure contrast agent leakage through the aneurysm wall in 12 patients with angiographically confirmed saccular cerebral aneurysms . Using Tofts's contrast leakage model we quantified the contrast agent leakage rate (k_{trans}) and the leakage space volume (v_l), and compared these parameters against aneurysm size and aspect ratio, well established morphologic markers of rupture risk. We incorporated a vascular term given by the arterial input function (AIF) into Toft's model such that $C(t) = vAIF(t) + (1-v)c_{Tofts}(t)$ where v is the proportion of voxel volume containing vascular signal ($v \leq 1$) and c_{Tofts} is Tofts's classic model given by $C_{Tofts}(t) = Dk_{trans}*sum\{a_i[exp(-m_3t)-exp(-m_it)]/[m_i-m_3],i=1,2\}$ with dose D, $m_3= k_{trans}/v_l$, $m_1= 0.144\ min^{-1}$ and $m_2= 0.0111\ min^{-1}$. Regions of interest were drawn in the CSF adjacent to the aneurysm wall to calculate mean k_{trans} and v_l for each patient. Aneurysm morphology was assessed using CT angiography.

Results

Twelve patients (8W,4M; mean age = 67.5 years ± 10.2; range, 56-76 years) were recruited. The mean contrast leakage rate, k_{trans}, through the aneurysm wall was significantly larger compared to healthy parent vessels ($0.20 \pm 0.17\ min^{-1}$ vs $0.04 \pm 0.03\ min^{1}$, p = 0.0030 student *t*-test). Similarly the leakage volume, v_l, adjacent to the aneurysm was significantly larger compared to the healthy parent (46 ± 28% vs. 12 ± 11%, p<0.001). Figure 1 shows k_{trans} parametric map superimposed on the same slice of a T1-weighted contrast-enhanced anatomical image of a 56-year-old woman with a 1.4 cm aneurysm on the left internal carotid artery. Furthermore, we found that both k_{trans} (R = 0.597,p = 0.040) and v_l (R = 0.712,p = 0.0093) correlated strongly with aneurysm size, indicating that wall permeability modeling may be a useful metric for clinicians in assessing aneurysm rupture risk.

Conclusion

Our preliminary studies in patients with unruptured cerebral aneurysms indicate that DCE MRI kinetic modeling of aneurysm leakage provides quantitative metrics which correlate with classical rupture risk criteria.

KEYWORDS: Aneurysm rupture, Aneurysmal subarachnoid hemorrhage, Aneurysm Risk Stratification

Note: Scanned images are included in the proceedings. Some submitted images were reduced during editing, thereby decreasing clarity. Also, refer to the Program Planner. Proceedings Content as of 3-29-2013.

O-296 **3:39 PM - 3:47 PM**

Comparison of Two Patient Groups from the Same Geographic Population: Incidental Brain Aneurysms and Patients with Subarachnoid Hemorrhage. What Annual Rate of Hemorrhage Does the Population Prevalence and Observed Number of Ruptures Support?

Miller, T. S.
Montefiore Medical Center
Bronx, NY.

Purpose
To compare the incidence and size of ruptured and incidental unruptured aneurysms in a single urban population at a single center. Some unruptured cerebral aneurysms are more likely to rupture than others and should be treated when discovered. Appropriate management of patients with small (< 1 cm) unruptured cerebral aneurysms is debatable. Prospective studies indicate a rupture rate near zero for a given small aneurysm, while retrospective series demonstrate that most observed ruptured aneurysms are small. Does the population prevalence of small aneurysms support the expected rupture rate of <1% per year?
Materials & Methods
Charts, reports from CT scans, MRI/MRA exams, and angiograms for patients with both a diagnosis of subarachnoid hemorrhage and incidentally detected cerebral aneurysms at a single center between January 2006 and December 2011 were reviewed. Demographics, aneurysm size and location were recorded.
Results
For subarachnoid hemorrhage 370 consecutive patients were included. For incidental aneurysms 20,000 reports were reviewed. Sixty-four percent were female, mean combined age was 51 years (Range 10-91, SD 14). The ruptured cohort included 279 patients with (75%) ruptured cerebral aneurysms. The unruptured cohort included 13,000 unique patients with 800 aneurysms. The mean age of patients with aneurysms was 52 (SD 14.5, Range 17-91). The average size of the aneurysms was 6.08 mm (SD 3.2), 92% were < 10 mm.

270 Ruptured Aneurysms patients w/ Bronx Zip: **92%<10mm**

Average Size	5.68 mm
Median	5.78 mm

Location	Number	Size mm	%
Acomm	77	5.34	29%
Pcomm	56	6.22	21%
ICA	45	7.37	17%
MCA	45	6.38	17%
ACA	5	5	2%
Ant Choridal	12	5.08	4%
Basilar	10	7.33	4%
PICA	10	4.75	4%
Pericalossal	9	6.33	3%
PCA	1	3	0.4%
Total	270		

Results: 800 Aneurysms

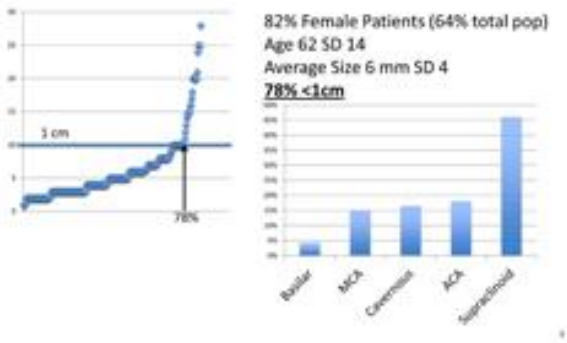

Conclusion
In a single population, 85% of incidental aneurysms were < 8 mm in size. Seventy-eight percent of aneurysmal SAH were due to aneurysms <=7 mm, and 90% < 10 mm. The population consists of 1 million adults. A prevalence rate of 6% (double expected) was identified. The population prevalence supports the observed rate of subarachnoid hemorrhage in the same population.

KEYWORDS: Aneurysm sizes, Prevalence

O-297 **3:47 PM - 3:55 PM**

Comparison of the Evaluation of Cerebral Aneurysm of High-Resolution Time-of-Flight MR Angiography at 3.0T and Conventional MR Angiography. Correlation with Standard Digital Subtraction Angiography: A Study of 50 Aneurysms

Lee, A.·Sohn, C.·Yoon, T.·Han, M.·Jung, S.·Yoo, I.·Kim, S.
Seoul National University Hospital
Seoul, KOREA, REPUBLIC OF.

Purpose
1. To evaluate accuracy of 3T HR MRA in detecting aneurysm compared with conventional MRA (C MRA) 2. To prove potential diagnostic advantage of HR MRA using correlation with DSA.
Materials & Methods
Thirty-seven patients with 50 possible aneurysms on C MRA were underwent 3T HR MRA and DSA. The protocols of HR MRA were following: TR 29.0, TE 4.6, matrix 512x512, FOV 20cm, and thickness 0.5mm with 8-channel head coil. Two blinded neuroradiologists reviewed C MRA and HR MRA in the detection of aneurysms, independently. For each possible aneurysm, readers recorded the location and their level of confidence with a 5 point scale [pseudolesion (A), definite infundibulum (B), suspicious infundibulum (C), suspicious aneurysm (D), and definite aneurysm (E)]. VR DSA were obtained and used as the standard of reference. The accuracy was calculated in addition to the sensitivity and specificity of HR MRA compared to C MRA. In particular, cases with advantage of

Note: Scanned images are included in the proceedings. Some submitted images were reduced during editing, thereby decreasing clarity. Also, refer to the Program Planner. Proceedings Content as of 3-29-2013.

detection on HR MRA were evaluated in detail.
Results
Among 50 possible aneurysms in 37 patients on C MRA, DSA revealed 38 aneurysms in 26 patients and no aneurysm or ID in 12 cases in 11 patients. Multiple aneurysms were 24 cases in 11 patients. On HR MRA, two reviewers exactly detected each 42, 40 cases, superior to C MRA (39, 38 cases). On the lesion-based evaluation, accuracy, sensitivity, and specificity of were 90.5%, 92.5, and 85.3% on HR MRA and 72.1%, 85.5%, and 50.3% on C MRA, respectively. Each three and five suspicious aneurysm on C MRA were recategorized as definite aneurysm on HR MRA. Each eight and 10 suspicious aneurysmal lesion on C MRA, revealed as infundibular dilatation on HR MRA, correlated with DSA.

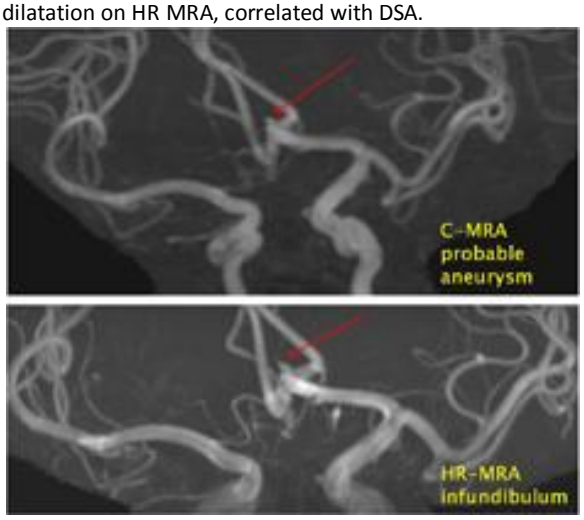

Conclusion
High-resolution MRA had a high accuracy, sensitivity and specificity for the detection of intracranial aneurysms, comparing C MRA. In equivocal aneurysm on C MRA, HR MRA can be a useful tool and replace DSA.

KEYWORDS: MR angiography, Aneursym, Infundibulum

O-298 **3:55 PM - 4:03 PM**

Evaluation and Optimization of Cerebral CT Angiography Using Model-Based Iterative Reconstruction for Evaluation of Treated Aneurysms: A Phantom Study

Perez, F. A.·Ramos, M.·McCallum, S.·Mengesha, B.·Mossa-Basha, M.·Fink, K. R.·Anzai, Y.·Andre, J.
University of Washington
Seattle, WA.

Purpose
Radiation dose is of particular concern in patients where frequent surveillance CT examinations are performed, including those with treated cerebral aneurysms who undergo routine follow-up CT angiograms. Advancements in CT technology, such as new reconstruction algorithms, are designed to reduce radiation dose while maintaining diagnostic accuracy. Moreover, innovative CT reconstruction algorithms may be helpful to reduce artifacts such as metal from aneurysm clips and coils thereby improving diagnostic accuracy while potentially reducing radiation dose. A phantom CTA study was performed to evaluate the performance of and optimize scanning parameters for a new clinically available model-based iterative reconstruction algorithm, Veo (trademarked; GE Healthcare, Milwaukee, WI), using simulated aneurysms treated with medical grade metallic coils or clips.
Materials & Methods
An in-house phantom was constructed consisting of a human cadaver skull containing agar and catheter tubing filled with 3.5 mg iodine/ml Omni350 contrast and arranged in a configuration to simulate aneurysms treated with coils or clips. Multiple CT scans of the phantom were acquired on a GE Discovery CT750HD scanner with varying mA, kV, pitch, and rotation speed. Each scan subsequently was reconstructed using both traditional filtered back projection and model-based iterative reconstruction (Veo). Three board-certified, fellowship-trained, neuroradiology faculty scored image quality, blinded to CTA technique, using Likert-type items based on coil/clip artifact, aneurysm visualization, confidence in measuring residual aneurysm, quality of artery lumen visualization, and overall diagnostic quality. Differences were evaluated with multifactorial ANOVA using R Statistical Programming Language.
Results
Model-based iterative reconstruction was associated with increased aneurysm clip/coil artifact, decreased confidence in measuring residual aneurysm, and decreased visualization of the artery lumen compared to filtered back projection reconstruction ($p < 0.05$) of CTA data acquired at the same radiation doses.
Conclusion
Reducing radiation exposure in patients undergoing repeat head CTA for routine surveillance of treated aneurysms is an important goal. The use of model-based iterative reconstruction algorithms for the evaluation of treated aneurysms requires additional optimization to achieve diagnostic quality similar to standard filtered back projection reconstruction at a fixed radiation dose.

KEYWORDS: Aneursym, CTA

O-299 **4:03 PM - 4:11 PM**

Reangiography after Perimesencephalic Subarachnoid Hemorrhage

Ringelstein, A.·Mueller, O.·Moenninghoff, C.·Timchenko, O.·Sure, U.·Forsting, M.·Schlamann, M.
University Hospital Essen
Essen, GERMANY.

Purpose
This study aimed to determine the yield of DSA for the

Note: Scanned images are included in the proceedings. Some submitted images were reduced during editing, thereby decreasing clarity. Also, refer to the Program Planner. Proceedings Content as of 3-29-2013.

detection of causative vascular lesions in patients with perimesencephalic SAH and negative initial noninvasive and invasive neurovascular examinations (CTA, DSA and MRA).
Materials & Methods
We examined the yield of repetitive DSA for the detection of causative vascular lesions in 750 patients presenting to our institution with SAH and 30 of them with a perimesencephalic pattern of the subarachnoidal blood and negative initial noninvasive and invasive neurovascular examinations during a 10-year period.
Results
Repetitive DSA demonstrated a causative vascular lesion in one patient (3.3 %). In all other patients no causative vascular lesion was found.
Conclusion
Repetitive DSA shows a bleeding source after initially negative imaging diagnostics in some rare cases. Such finding has a therapeutic and prognostic impact. Usually, aneurysms in the posterior circulation are diagnosed and bear a higher rebleeding risk. Therefore, we believe that a repetitive DSA should be recommended in patients with perimesencephalic SAH, even under consideration of the risk of a second invasive diagnostic angiography itself.

KEYWORDS: Aneursym, Catheter angiography

O-300 **4:11 PM - 4:19 PM**

Prediction of Outcome of Brain Arteriovenous Malformations following Stereotactic Radiosurgery Based on the Angiographic Characteristics at Presentation

Tang, Y.·Fleetwood, I.·Shankar, J.
QEII Health Science Centre
Halifax, NS, CANADA.

Purpose
Stereotactic radiosurgery is the mainstay of treatment for brain arteriovenous malformations (BAVMs). Still, the outcome of radiosurgery is not consistent and some BAVMs do not respond. The purpose of our study was to determine if we can predict the outcome of stereotactic radiosurgery in BAVMs based on their angiographic characteristics at presentation.
Materials & Methods
A retrospective review of all patients who underwent stereotactic radiosurgery for BAVMs at our institution between 1999 and 2009 was carried out. Patients with catheter angiograms prior to radiosurgery and at least three years following radiosurgery were included. Various angiographic characteristics of the BAVMs were studied. Patients' outcomes were classified as achieving complete obliteration, incomplete response, or no change of their BAVMs on the 3-year follow-up angiogram. The association between the angiographic characteristics of the BAVMs at presentation and their outcome following radiosurgery was analyzed using binomial logistic regression.
Results
A total of 75 BAVMs were treated with radiosurgery during this time period. Only 46 of these fulfilled our inclusion criteria. These BAVMs were followed for a median of 38 months (mean 49 months). Twenty-eight (61%) of the BAVMs that were analyzed achieved complete angiographic obliteration at three years following radiosurgery, 16 (35%) had partial response, and two (4%) were unchanged. The location of the BAVM ($p = 0.006$), size of the feeding artery ($p = 0.047$), presence of a deep draining vein ($p = 0.029$), and pseudophlebitic pattern ($p = 0.019$) showed significant correlation with incomplete response. Pial vein less than 3 cm ($p = 0.059$) and venous ectasia ($p = 0.082$) showed a trend towards correlation with incomplete response, but failed to reach statistical significance.
Conclusion
The initial angiographic characteristics of BAVMs may predict the outcome following stereotactic radiotherapy. Deeper draining vein, certain locations, and venous congestion may predict incomplete response to radiotherapy.

KEYWORDS: Arteriovenous malformation, Angiogram

O-301 **4:19 PM - 4:27 PM**

Absolute Hemodynamic Quantification in Cerebral Arteriovenous Malformations Using 4D Flow MR Imaging: A Preliminary Study

Honarmand, A. R.[1]·Wu, C.[2]·Entezari, P.[1]·Vakil, P.[2]·Patel, B.[1]·Bendok, B.[1]·Batjer, H.[3]·Carroll, T.[2]·Markl, M.[2]·Ansari, S. A.[1]
[1]Northwestern University Feinberg School of Medicine, Chicago, IL, [2]Northwestern University, Chicago, IL, [3]University of Texas Southwestern, Dallas, TX.

Purpose
Hemodynamic characterization of arteriovenous malformations (AVMs) may have implications for risk stratification. Gross visualization and quantification of intracranial AVM flow dynamics have been investigated using various methods including computational flow dynamics and 4D flow MRI. In this study, we aimed to selectively quantify arterial feeder hemodynamics in a cohort of cerebral AVMs of different Spetzler-Martin grades (SMG) using 4D flow MRI.
Materials & Methods
Following IRB approval, eight patients with documented intracranial AVMs were selected for baseline 4D flow MRI at 1.5T or 3T MR systems (Siemens, Germany) for a prospective study. Flow quantification was performed using ECG gated three-directional velocity encoding with full 3D coverage of the AVM nidus, feeding and draining vessels, and contralateral equivalent normal arteries. 4D flow MRI was acquired in an axial oblique 3D volume using flip angle of 15°, VENC: 100 cm/s, spatial resolution = $(1.2\text{-}1.6)^3 mm^3$, and temporal resolution: 44 ms. Data analysis

Note: Scanned images are included in the proceedings. Some submitted images were reduced during editing, thereby decreasing clarity. Also, refer to the Program Planner. Proceedings Content as of 3-29-2013.

included 3D visualization of the velocity data and flow quantification using time integrated 3D pathlines positioned orthogonal to the vessel by a commercially available software (Ensight, CEI, Inc. Apex, NC). Peak velocity (m/s), net flow (ml/cycle), forward flow (ml/cycle), retrograde flow (ml/cycle), and regurgitation (%) were quantified retrospectively and compared at two levels: arterial AVM feeders and normal contralateral equivalent arteries.

Results

Eight patients (5M/3F with mean age 23.9 ± 18) with AVMs ranging from SMG 1 (1 patient), SMG 2 (5 patients), SMG 3 (1 patient), SMG 4 (1 patient) were selected for analysis. Peak velocity and net flow of AVM arterial feeders were quantified as the following: 0.35 m/s, 0.7 ml/cycle; 0.62 ± 0.16 m/s, 3.9 ± 2.4 ml/cycle (mean ± SD); 1.25 m/s, 4.05 ml/cycle; 1.84 m/s, 6.11 ml/cycle; in AVM SMGs 1, 2, 3, and 4 respectively. Normal contralateral equivalent artery peak velocity and net flow were measured as the following: 0.23 m/s, 0.31 ml/cycle; 0.52 ± 0.26 m/s, 3.54 ± 2.48 ml/cycle (mean ± SD); 0.57 m/s, 3.22 ml/cycle; 0.72 m/s, 4.42 ml/cycle in AVM SMGs 1, 2, 3, and 4 respectively. No retrograde flow or regurgitation was noted in either arterial feeders or normal contralateral equivalent arteries.

Conclusion

Quantified hemodynamic parameters of peak velocity and net flow were higher in all AVM feeders compared with normal contralateral equivalent controls. Additionally, increasing peak velocity and net flow correlated with higher SMG grading that may be secondary to larger and high flow lesions. Our preliminary results demonstrate the feasibility and sensitivity of 4D flow MRI in quantitative monitoring of hemodynamic parameters of cerebral AVMs. These findings may have implications in novel characterization schemes for risk stratification based on quantitative flow analysis.

KEYWORDS: 4D Flow MR, Arteriovenous malformation

O-302 **4:27 PM - 4:35 PM**

Diagnosis and Followup of Intracranial Dural Arteriovenous Fistulae Using Contrast-Enhanced Time-Resolved MR Angiography

Boddu, S.·Saindane, A. M.·Dehkharghani, S.·Tong, F.·Dion, J.
Emory University School of Medicine
Atlanta, GA.

Purpose

Digital subtraction angiography (DSA) remains the gold standard for diagnosis and followup of intracranial dural arteriovenous fistulae(dAVF). Recent improvements in MRA have shown utility for evaluation of intracranial dAVF. We hypothesize that multiphasic contrast-enhanced time-resolved MRA (CE-TR-MRA) with high spatial and temporal resolution will provide a reliable and effective noninvasive method for diagnosis and followup of dAVF.

Materials & Methods

Twenty-five consecutive patients [18 male, median age 64 years (38-84 years)]with known or suspected intracranial dAVFs over a 24-month period were reviewed. Each patient underwent both MRA and DSA with a median lag of 0 days(0-144 days). MR angiography was performed on a 1.5T GE unit using both 3D-TOF-MRA and CE-TR-MRA using time-resolved imaging of contrast kinetics(TRICKS) with intravenous administration of a standard dose gadolinium-based contrast agent. Ten dynamic phases with submillimeter in-plane resolution and four-second temporal resolution were obtained. MR angiography and DSA studies were reviewed for presence or absence of dAVF, laterality, site, arterial feeders, venous drainage, and venous sinus occlusion. Confidence in the MRA findings also was evaluated. Concordance between the techniques evaluated with DSA as the reference standard.

Results

The 25 patients harbored 29 dAVFs(one patient had three fistulae and two patients had two fistulae each). Sixteen of 25 patients were for initial diagnosis or followup of untreated dAVFs. On both CE-TR-MRA and DSA: 2/16 had no dAVF, 1/16 had spontaneous closure of a previously known Borden type 1 dAVF, 12/16 had Borden Type 1 dAVF and 1/16 with Borden type 3. All patients with untreated dAVF had conclusive reports on CE-TR-MRA except 1/16 with artifact from prior craniotomy, where DSA was recommended to confirm absence of dAVF. Nine of 25 patients had followup after treatment(Borden type 1 (n=2), Borden type 2 (n=4) and Borden type 3(n=3). Eight of 10 dAVFs remained occluded and one had recurrence of treated Borden type 3 fistula demonstrated on both CE-TR-MRA and DSA. Contrast-enhanced TR-MRA for all post-treatment follow-up patients was deemed conclusive. Contrast-enhanced TR-MRA was concordant with DSA for Borden type in the evaluation of both untreated dAVF and followup of treated dAVF in all cases. Both 3D-TOF-MRA and CE-TR-MRA were limited in detection of smaller arterial feeders, specifically of ICA(e.g., meningohypophyseal trunk).

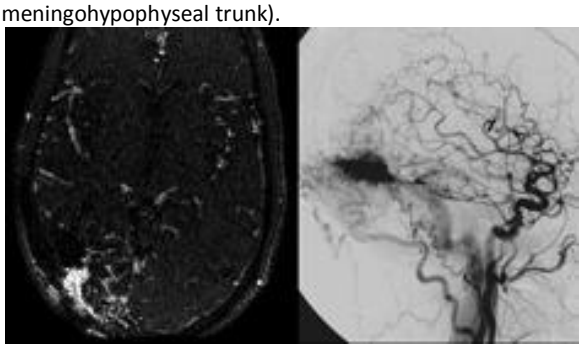

Conclusion

Contrast-enhanced TR-MRA is a reliable noninvasive technique for the diagnosis and followup of intracranial dAVF with excellent correlation with DSA. We recommend

Note: Scanned images are included in the proceedings. Some submitted images were reduced during editing, thereby decreasing clarity. Also, refer to the Program Planner. Proceedings Content as of 3-29-2013.

CE-TR-MRA as a first line investigation for diagnosis and to guide followup.

KEYWORDS: 4D MRA, Arteriovenous fistulas

O-303 **4:35 PM - 4:43 PM**

Longitudinally-Followed, Unruptured Aneurysms Exhibit Morphologic and Hemodynamic Changes in Progression towards Rupture

Chien, A.·Vinuela, F.
David Geffen School of Medicine at the University of California Los Angeles
Los Angeles, CA.

Purpose
Due to limited information about aneurysm natural history and the mechanisms underlying aneurysm rupture, choosing the appropriate management strategy for an unruptured aneurysm is challenging. Research based on aneurysm morphology and hemodynamics has found that certain aneurysm shapes and flow properties may relate to aneurysm rupture. With this study, we address whether morphology and blood flow change as an aneurysm progresses towards rupture. Hypothesis: The morphologic and hemodynamic properties of an unruptured aneurysm change in the progression towards rupture.
Materials & Methods
We conducted a retrospective study using unruptured aneurysms diagnosed in our center but not treated. Aneurysms with 3D images recorded at least one year prior to rupture and at the date of rupture were selected. Three aneurysms with initial size 11.6, 7.7, and 6.7 mm located at the posterior communicating arteries were analyzed. For each aneurysm, patient-specific hemodynamic analysis was performed to simulate the flow pattern, and 3D morphologic analysis was used to examine evidence of geometrical changes between unruptured and ruptured states.
Results
All of the aneurysms increased in size (averaging 1.9 mm) and surface area (averaging 32.6%). The figure shows a representative result of a 6.7 mm aneurysm in the unruptured state (left) and rupture two years later at 11 mm (right). Distinct changes in curvature (top), wall shear stress (middle) and flow pattern (bottom) were observed. The center bottom figure presents the original flow superimposed on the ruptured aneurysm shape, showing a prominent change in morphology at the impingement area.

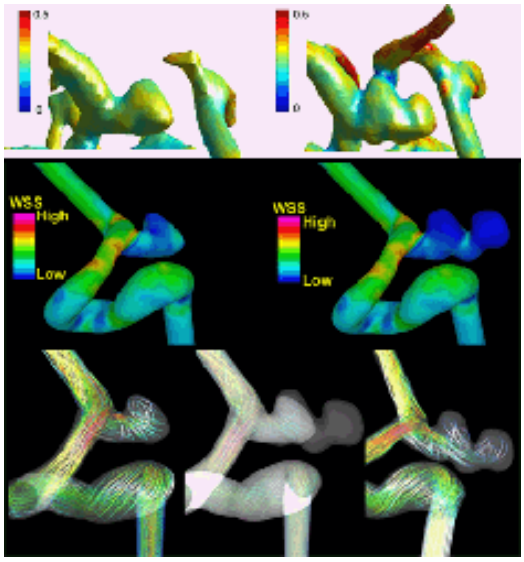

Conclusion
Changes in shape and flow properties were found between unruptured and ruptured states. Through morphologic analysis, we found such changes were not limited to blebs and included the aneurysm body, suggesting certain changes in shape and flow might progressively increase aneurysms rupture risk.

KEYWORDS: Morphology, Hemodynamics, aneurysm rupture

Tuesday Afternoon

3:15 PM - 4:45 PM
Room 5AB

(31d) Parallel Scientific Papers: Spine: Degenerative, Inflammatory Infectious and Interventions

O-304 **3:15 PM - 3:23 PM**

Diffusion Tensor Imaging Predicts Functional Impairment in Mild to Moderate Cervical Spondylotic Myelopathy

Ellingson, B. M.[1]·Holly, L. T.[1]·Grinstead, J.[2]·Salamon, N.[1]
[1]David Geffen School of Medicine at the University of California Los Angeles, Los Angeles, CA, [2]Siemens Healthcare, Portland, OR.

Purpose
The purpose of the current study was to implement DTI as a biomarker for microstructural integrity and functional impairment in patients with cervical spondylosis with or without myelopathy.
Materials & Methods
All patients in this study signed institutional review board-

Note: Scanned images are included in the proceedings. Some submitted images were reduced during editing, thereby decreasing clarity. Also, refer to the Program Planner. Proceedings Content as of 3-29-2013.

approved informed consent. Forty-eight patients with cervical spondylosis with or without myelomalacia underwent 3T MRI of the cervical spinal cord. A zoomed-EPI technique and custom 2D spatially selective RF excitation pulse were used for DTI measurements of the spinal cord. Fractional anisotropy (FA), mean diffusivity (MD), transverse and longitudinal apparent diffusion coefficient (tADC and lADC), measured longitudinal anisotropy (MA1 = lADC-MD), and the standard deviation of primary eigenvector orientation were evaluated at the site of compression.

Results

Average FA, tADC, MA1, and the standard deviation of primary eigenvector orientation at the spinal level of highest compression were correlated linearly with modified Japanese Orthopedic Association (mJOA) score ($P<0.01$). A combined index consisting of anterior-posterior spinal cord diameter, FA, tADC, MA1, standard deviation of primary eigenvector orientation, and the presence of T2 hyperintensity within the spinal cord accurately predicted functional impairment in mild-to-moderate CSM ($R2=0.6843$, $P<0.0001$). Receiver-operator characteristic (ROC) analysis suggested FA, MA1, and the composite index could identify stenosis patients with mild to moderate symptoms with a relatively high sensitivity and specificity.

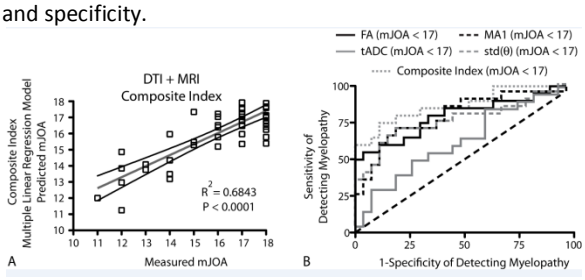

Conclusion

Results support the use of DTI as an imaging biomarker for predicting functional impairment in patients with cervical spondylosis. Additionally, a composite index consisting of standard MRI features combined with DTI anisotropy, diffusivity, and directional information can be used to more accurately predict neurologic impairment in patients with mild to moderate CSM and may potentially provide a means for selection of favorable surgical candidates.

KEYWORDS: Cervical myelopathy, Diffusion tensor image

O-305 **3:23 PM - 3:31 PM**

Optimized T1-MPRAGE Sequence for Better Visualization of Spinal Cord Multiple Sclerosis Lesions at 3T

Nair, G.[1]·Absinta, M.[1,2]·Reich, D. S.[1,3]
[1]National Institutes of Health, Bethesda, MD, [2]San Raffaele Scientific Institute, Vita-Salute San Raffaele University, Milan, ITALY, [3]Johns Hopkins University, Baltimore, MD.

Purpose

Cord lesions are highly prevalent in multiple sclerosis (MS), and their visualization can help both in diagnosis and patient followup. However, the sensitivity of MRI to spinal cord lesions remains poor, primarily due to suboptimal contrast between lesions and normal-appearing cord. Here, we propose an optimized 3D magnetization prepared rapid gradient-echo (MPRAGE) sequence for improved detection of MS lesions in the cord at 3T.

Materials & Methods

Images were acquired using fast spin echo (T2 FSE), short-tau inversion recovery (STIR), T1-GRE (for T1 mapping), and MPRAGE (T1-MPRAGE) in the sagittal plane, and T2*-weighted scans in the axial plane, on 39 MS patients (Age: 50 ± 12 years; disease duration 14 ± 11 years, EDSS range 1-7) and seven healthy volunteers (Age: 44 ± 7 yeara). Two observers qualitatively evaluated the images for lesion conspicuity. Lesions seen between the C1 and C4 segments in 10 randomly selected MS patients were further evaluated quantitatively for contrast-to-noise ratio between lesion and normal--appearing cord, and for lesion burden.

Results

Spinal cord lesions were more conspicuous on the optimized T1-MPRAGE sequence than any other sequence tested (Figures). In a more detailed analysis of 10 cases, the lesions were almost three times more conspicuous ($p<<0.001$), and the total lesion volume was two times greater ($p<0.05$, $n=10$), in the T1-MPRAGE sequence compared to the standard STIR sequence. Correlation of clinical disability (EDSS) with lesion load from each sequence also demonstrated the importance of the improved lesion conspicuity with T1-MPRAGE.

Note: Scanned images are included in the proceedings. Some submitted images were reduced during editing, thereby decreasing clarity. Also, refer to the Program Planner. Proceedings Content as of 3-29-2013.

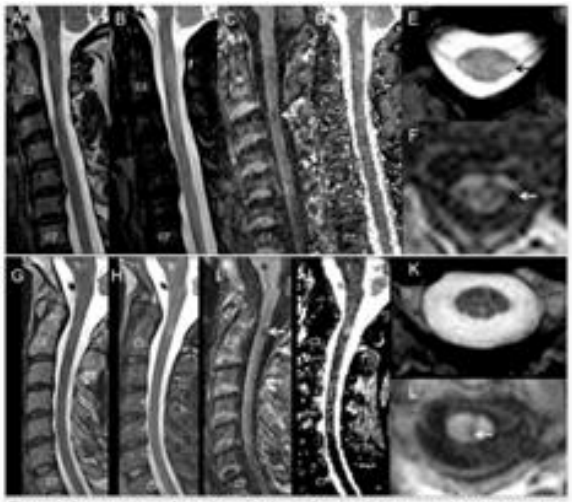

Figure 1: A comparison of imaging techniques for visualizing cervical cord lesions in a 45 y.o. woman (A through F) and a 43 y.o. man (G – L), both with relapsing-remitting MS. T1-weighted MPRAGE (C and I) performed better than routine clinical T2-weighted fast spin echo (A and G), short-TI inversion recovery (STIR, B and H), and multi-echo recombined gradient echo (MERGE, E and K) for visualizing lesions. Quantitative T1-maps of the cervical cord (D and J), generated using a multiple flip angle gradient echo sequence, showed the lesions as hyperintense. The lesions were also visible on axially reformatted T1-MPRAGE images (F and L).

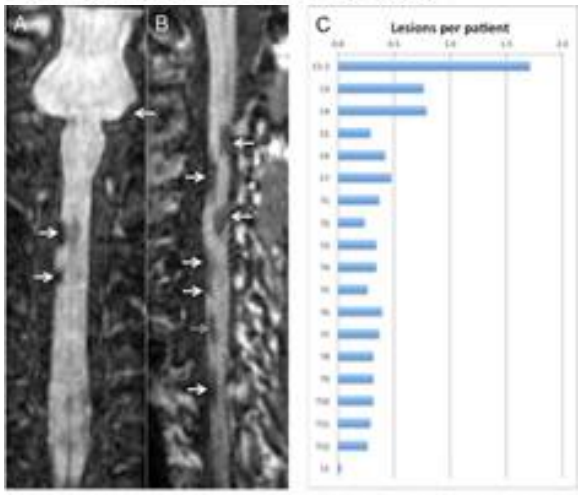

Figure 2: Coronal (A) and curved-reformatted (B) images from the T1-weighted MPRAGE sequence in the cervical cord of two patients, showing lesions mainly on the surface of the cord (white arrows) and a lesion that appears to be completely within the cord (grey arrow). (C) Rate of occurrence of lesions per spinal cord segment as read by the raters using all scans acquired in the MS population studied herein (39 MS patients, Age: 50 ± 12 y; disease duration 14 ± 11 y, EDSS range 1-7).

Conclusion

The optimized T1-MPRAGE sequence described here improves the reliability of lesion visualization and estimation of lesion burden, especially when used in conjunction with other well established clinical sequences.

KEYWORDS: Multiple sclerosis plaques, MRI spine, Visualizing spinal cord lesions

O-306 **3:31 PM - 3:39 PM**

Predictive Value of Nerve Root Sleeve Diverticula and Cerebrospinal Fluid Leak on Postmyelographic CT for the Development of Postmyelographic Headache

Alhilali, L. M.·Thomas, A.·Piper, S.·Fakhran, S.
University of Pittsburgh Medical Center
Pittsburgh, PA.

Purpose

To determine if evidence of nerve root sleeve diverticula or CSF leakage on postmyelogram CT is useful in predicting subsequent headache in patients undergoing myelography.

Materials & Methods

Three hundred fifty-eight lumbar and 195 cervical myelograms were performed consecutively by one operator (SP), via a lumbar approach, with a 22-gauge spinal needle and identical postmyelography care (three hours of bed rest with head of bed less than 30 degrees, encouragement of oral intake of fluids). Postmyelogram CT studies were reviewed retrospectively at each disk level bilaterally for evidence of either nerve root sleeve diverticula or CSF leak using the following scoring system: (1) nerve root sleeve diverticulum not extending beyond the lateral vertebral body margin, (2) nerve root sleeve diverticulum extending beyond the lateral vertebral body margin, (3) leak of contrast into the periradicular soft tissues, (4) epidural collection of contrast material. Two scores were obtained for each level (left and right) and the total score of either the lumbar or cervical spine was calculated for each patient. Patients were excluded who had evidence during the procedure of epidural or mixed injection of contrast. Results on CT myelogram were correlated with findings on telephone followup performed for postmyelogram symptoms two days after the procedure as well as any subsequent clinical followup.

Results

Inter-rater reliability for scoring nerve root sleeve diverticula and CSF leaks was substantial (Fleiss Kappa = 0.85, 95% confidence interval 0.74-0.96). Headaches were reported by 15 (4.2%) and 10 (5.1%) patients who underwent lumbar and cervical myelograms, respectively. No significant difference was found in the concentration of intrathecal contrast material used between patients with and without headaches who had undergone either lumbar ($p = 0.14$) or cervical ($p = 0.91$) myelography. Total scores were significantly higher for patients with headaches who had undergone lumbar ($p<0.0001$) and cervical ($p<0.0001$) myelography compared to patients without headaches that had undergone the same procedure. Patients with headaches were significantly younger than those without headaches ($p = 0.003$ and $p = 0.0002$ for lumbar and cervical myelography patients, respectively) and the group of patients with headaches had a significantly greater proportion of females ($p = 0.03$ and $p = 0.02$ for lumbar and cervical myelography patients, respectively). Furthermore, using multiple regression analysis, an

Note: Scanned images are included in the proceedings. Some submitted images were reduced during editing, thereby decreasing clarity. Also, refer to the Program Planner. Proceedings Content as of 3-29-2013.

epidural collection of contrast material was found to be independently correlated with postmyelography headache (p =0.03) in the lumbar spine.
Conclusion
In patients undergoing myelography, a lumbar epidural collection of contrast is associated with postmyelographic headache. Furthermore, patients with postmyelographic headaches are more likely to have nerve root sleeve diverticula and extrathecal contrast extravasation than patients without headache.

KEYWORDS: Myelography, CSF leak

O-307 **3:39 PM - 3:47 PM**

Fluoroscopic-Guided Lumbar Puncture: Fluoro Time and Implications of Body-Mass Index: A Baseline Study

Boddu, S. R.·Fountain, A. J.·Saindane, A. M.·Applegate, K.·Corey, A. S.
Emory University Hospital
Atlanta, GA.

Purpose
Fluoroscopic-guided lumbar puncture is an alternative to the bedside lumbar puncture in challenging patients. This is a less traumatic procedure, which decreases the false positive results, thus preventing the unnecessary subsequent investigations. There are no published guidelines for the acceptable range of fluoroscopic time for lumbar puncture. The study is aimed to obtain baseline fluoroscopic time ranges for lumbar puncture and their variability based on body-mass index (BMI). We also tested the hypothesis that fluoroscopic time of lumbar puncture increase with increasing BMI.
Materials & Methods
Retrospective review of all patients who underwent fluoroscopic-guided lumbar puncture at four hospitals over a one-year period (July 2011 - June 2012) was performed. Procedure logbooks and electronic medical records were accessed for variables such as patient demographics, clinical indication, BMI, and fluoroscopic time. Based on the federal obesity guidelines issued by National Heart Lung and Blood Institute patients were categorized as normal (18.5 - 24.9), over weight (25 - 29.9) , obese (30 - 39.9) or as extremely obese (≥ 40). Subgroups based on the clinical indication included: infection, inflammation, neoplasm, cognitive decline, hemorrhage, idiopathic intracranial hypertension (IIH) and miscellaneous. Logarithmic conversion of fluoroscopic times was performed to render normal distribution to the data. Fluoroscopic times were calculated for each subgroup and chi-square analysis was performed.
Results
Three hundred fifteen (mean age 47.6 years, range18-92, 35% male) fluoroscopic-guided lumbar procedures were performed. Twenty-two patients were excluded due to insufficient data. The mean BMI was higher in female patients (33.8 kg/ m; range: 21.6 - 69.4) than males (30.2 kg/m2; range: 19 - 51.8). Fourteen neuroradiologists and 25 residents/fellows participated. Mean fluoroscopic time for lumbar puncture in our study population was 1.18 minutes (standard deviation: 0.94). The details of each subgroup fluoroscopic times were summarized in Table 1. When the patient population was categorized by clinical indication for the study, we found that the IIH subgroup had the maximum mean BMI of 40.2; (range: 24-55.8) and corresponding maximum mean fluoroscopic time of 1.34 minutes (range: 0.2 - 6.2). The fluoroscopic times are significantly higher among the obese (P = 0.002) and extremely obese (P = 0.0001) in comparison to patients with normal BMI.

Table:1

S.No	BMI	Mean	Median	Standard Error of Mean	95% CI
1	18.5 - 24.9	1.012	0.7	0.14	±0.260.75 - 1.27
2	25 - 29.9	1.075	0.7	0.10	±0.210.87 - 1.28
3	30 - 39.9	1.195	0.7	0.10	±0.21.0 - 1.39
4	≥ 40	1.374	1.1	0.11	±0.221.16 - 1.59

Conclusion
In our study population, the fluoroscopic time for lumbar puncture increases with the increase in patient body-mass index (BMI). Idiopathic intracranial hypertension (IIH) is the single clinical indication with highest fluoroscopic procedure time, presumably related to the maximum mean BMI of this subgroup. This study contributes to literature by providing the baseline fluoroscopic times for lumbar puncture based on body-mass index (BMI) and clinical indication. We suggest use of this data as an initial benchmark in the evaluation of individual and department performance as monitored at our institution.

KEYWORDS: Fluoroscopic-guided lumbar punctureBody-Mass index

Note: Scanned images are included in the proceedings. Some submitted images were reduced during editing, thereby decreasing clarity. Also, refer to the Program Planner. Proceedings Content as of 3-29-2013.

O-308 **3:47 PM - 3:55 PM**

Determination of Optimal Contrast Concentration for CT-Guided Spine Procedures

Abbott, M. F.·Abbott, D.·Hoang, J. K.·Kranz, P. G.
Duke University
Durham, NC.

Purpose
Contrast frequently is used in CT-guided procedures to ensure proper needle placement. Once injected, however, undiluted contrast often obscures the needle tip, making subsequent needle repositioning more difficult. As a result, several authors have advocated the use of dilute contrast during various CT-guided procedures, including spine interventional procedures. To our knowledge, the optimal contrast dilution has not been established. The purpose of this investigation is to establish the optimal contrast dilution for CT-guided spine procedures.
Materials & Methods
We assessed optimal contrast concentration using both in vitro and in vivo methods, based on various dilutions of commercially available contrast containing 200 mg/mL iodine (Isovue-M 200) with preservative-free sterile saline. First, a phantom containing a 22-gauge needle surrounded by various contrast dilutions from 33 to 200 mg/mL iodine was imaged, and images were scored for needle visibility. Based on these results, a prospective study was performed in which patients presenting for CT-guided interlaminar or transforaminal epidural steroid injections were randomized to one of four contrast concentrations: 66, 100, 133, or 150 mg/mL iodine. Images from the procedure were scored for needle visibility and tissue contrast using a 5-point scale by a blinded neuroradiologist. Generalized estimating equations were utilized to assess the effect of contrast concentration on visibility.
Results
In the phantom study, contrast concentrations of 150 mg/mL or higher unacceptably obscured the needle. In the in vivo study, 42 patients who received a total of 60 injections were enrolled. There was a strong association between contrast concentration and needle visibility ($p = 0.0002$). Of the four concentrations, 100 mg/mL was optimal for allowing needle visualization and providing sufficient tissue contrast, with no instances of unacceptably dilute or concentrated contrast. A concentration of 66 mg/mL resulted in 3/17 cases of insufficient tissue contrast, while 133 and 150 mg/mL resulted in 11/13 and 7/14 cases respectively where the needle was unacceptably obscured by contrast. There was a statistically significant improvement in needle visibility at 100 mg/mL compared with 133 mg/mL ($p = 0.0012$).

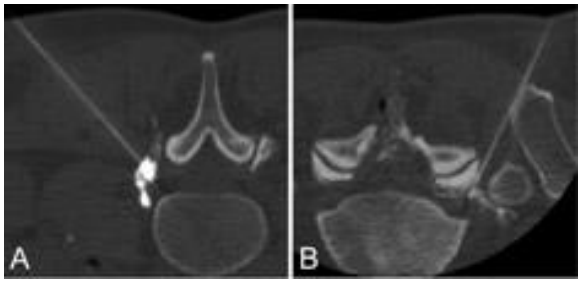

Figure. Effect of contrast concentration on needle visibility. A, Undiluted contrast (200 mg/mL iodine) obscures the needle tip, hindering repositioning. B, Dilute contrast (100 mg/mL iodine) allows visualization of the needle tip while providing acceptable tissue contrast.
Conclusion
For CT-guided spine procedures requiring contrast, the optimal contrast concentration is 100 mg/mL iodine. Use of dilute contrast in such procedures improves needle visibility.

KEYWORDS: Spine interventions, Contrast agents

O-309 **3:55 PM - 4:03 PM**

Incorporating Spinal Pain Management Procedures into Neuroradiology Fellowship

Delfyett, W. T.[1]·Wo, S.[2]·Agarwal, V.[1]
[1]University of Pittsburgh Medical College/Presbyterian-Shadyside, Pittsburgh, PA, [2]University of Pittsburgh School of Medicine, Pittsburgh, PA.

Purpose
The performance of spinal pain management procedures (SPMPs) crosses several specialties. Local referral patterns and competition may all contribute to the spinal pain management patient volumes that neuroradiologists may encounter. Data suggests increasing utilization of multiple modalities the treatment of back pain. At our institution a dedicated neuroradiology spinal pain management service has experienced increases in annual patient encounters of 12-23% annually over the past three years, an increase in volume which parallels volume increases previously reported. The purpose of this study is to assess the methods by which neuroradiology fellowship training programs provide the ACGME required instruction in the performance of spinal pain management procedures in light of increasing patient volumes and competition from other specialties.
Materials & Methods
An IRB approved survey using Survey Monkey was distributed twice to all physicians designated as neuroradiology fellowship directors by the ASNR approximately eight weeks apart. The types of spinal pain management procedures performed as part of neuroradiology fellowship as well as volumes of these procedures were queried along with the manner in which these procedures are incorporated into fellowship

Note: Scanned images are included in the proceedings. Some submitted images were reduced during editing, thereby decreasing clarity. Also, refer to the Program Planner. Proceedings Content as of 3-29-2013.

training. Information regarding which other specialties perform these SPMPs also was requested.
Results
Of 100 surveys 44% response rate was achieved. Among responders; 49% incorporate SPMPs as part of an interventional rotation, 33% incorporate SPMPs as part of a diagnostic rotation, 18% have dedicated spinal intervention services/fellow rotations, 21% have fellows rotate on other services within or external to radiology, 9% provide experience in an elective manner and 9% report no incorporation into fellowship. The volumes of these procedures which the fellows perform was reported between 0-10 cases; for cervical epidural injections 90%, cervical nerve root blocks 84%, lumbar epidural injections 50%, lumbar nerve root blocks 47%, and disk aspirations/intradiscal procedures 67%. Competing services were reported to be; Anesthesia/Pain medicine 90%, Physical Medicine and Rehabilitation medicine 37%, Orthopedics 12%, Neurosurgery 5%, and Neurology 3%. As part of postgraduate surveys, performance of individual spinal pain management procedures were reported as practice needs by 15-35% of graduates according to fellowship directors with the highest reported need for lumbar epidural steroid injections, 35%.
Conclusion
Among responding fellowship directors, the manner in which SPMPs are incorporated into fellowship was found to be heterogeneous, likely related to center specific considerations. Up to 9% report no incorporation of SPMIs into fellowship training despite ACGME requirement. Considering increasing patient volumes and increasing interest in conservative therapies for back pain, neuroradiology fellowship training experience in SPMP remains important to clinical practice as was found on postgraduate surveys. Neuroradiology fellowship program requirements do not specify numerical minima for SPMPs, but the numbers of cases reported are in range of the ACGME specified procedural minima defined for fellowship programs in pain medicine, a source of primary competition. Although center specific considerations often dictate how these procedures are incorporated into fellowship training, a variety of methods may be used, and potential target procedural minima likely can be achieved in the vast majority of neuroradiology fellowship training experiences.

KEYWORDS: Spine injections, Educational, Fellowship Training

O-310 **4:03 PM - 4:11 PM**

Spinal Cord Stimulators in Outpatient Interventional Neuroradiology Practice

Georgy, M.[1]·Padwal, J.[2]·Georgy, B.[3]
[1]Canyon Crest Academy, San Diego, CA, [2]University of California San Diego, San Diego, CA, [3]San Diego Imaging, University of California San Diego, San Diego, CA.

Purpose
Spinal cord stimulation is a known modality for treatment of chronic back and neck pain. Traditionally, spine surgeons and pain physicians perform those procedures. We are reporting our experience in performing neuromodulation procedures in an out-patient interventional radiology practice.
Materials & Methods
Retrospective analysis of medical records of all trial and permanent implantation patients over a period of four years was performed after obtaining IRB approval. Forty-five patients (32 males and 13 females with median age of 47 years) were included in the study. Primary diagnoses were: 23 cases of failed back or neck surgery syndrome, 12 cases with spinal stenosis, four cases of axial pain, three cases with reflux sympathetic dystrophy, one case of peripheral vascular disease, one case of phantom limb and one case of postconcussion syndrome.
Results
Thirty-four trials were performed in outpatient clinic while 11 trials were performed in hospital outpatient's settings. Trial periods were 3-7 days. Twenty-seven patients (60%) who reported 50% or more pain relief underwent a permanent implantation. An interventional neuroradiologist performed 17 implantations, while spine surgeons performed 10 implantations. Twenty-three implants were epidural (19 lumbar and 4 cervical) while four cases were subcutaneous. During follow-up period, three patients had infections (13%) and required removal of the device and two cases (8%) reported lead migration.
Conclusion
Neuromodulation procedures can be performed safely in an outpatient interventional radiology setting. Complication rates and trial to implant ratio are similar to published data.

KEYWORDS: Vertebral augmentation, Vertebral compression fractures, cement

Note: Scanned images are included in the proceedings. Some submitted images were reduced during editing, thereby decreasing clarity. Also, refer to the Program Planner. Proceedings Content as of 3-29-2013.

O-311 **4:11 PM - 4:19 PM**

Targeted Radiofrequency Ablation of Malignant Spine Lesions before Cement Augmentation Using Novel Bipolar Navigational Device

Georgy, B.
San Diego Imaging, University of California San Diego
San Diego, CA.

Purpose
Report early clinical experience of targeted radiofrequency ablation (t-RFA) followed by cement augmentation in malignant lesions of the spine using a novel bipolar RF ablation system, purpose built for minimally invasive procedures in the axial skeleton.
Materials & Methods
Twenty-five spinal lesions in 15 patients with different malignant etiologies were included after IRB approval. The STAR Tumor Ablation System includes a robust, articulating, navigational osteotome, containing an extensible electrode. The device is bipolar and contains two thermocouples (TC) positioned at 10 and 20 mm from center of the ablation zone to permit real-time monitoring of the ablation zone. Radiofrequency-warmed cement augmentation via the same guiding cannula was performed after lesion ablation.
Results
All procedures were performed safely with no complications or thermal injury. Ablation time ranged from 1.5-6 minutes. Maximum recorded temperature was 65°C at the distal TC and 50°C at the proximal TC (10 and 20 mm from the center of the ablation zone, respectively). Thermocouples on the electrode were used to confirm re-establishment of core temperature prior to cement augmentation. Postprocedure CT showed no significant cement leakage. Average VAS scores dropped from seven preprocedure to 4.7 postprocedure. Average ODQ scores improved from 25.8 to 18 postprocedure. Decreased tumor volume and decreased metabolic activity was confirmed by MRI and PET scan, respectively.
Conclusion
Targeted RF ablation followed by RF-warmed high viscosity cement augmentation was performed successfully in this series of malignant spinal lesions. Improvement in pain and functional status was noted in all patients. The STAR Tumor Ablation System permitted minimally invasive access to all lesions, regardless of location. Proximal and distal TCs allowed accurate monitoring of the temperature inside the vertebral body to avoid complications of nearby vital structures. Targeted delivery of high viscosity cement following ablation via the same guiding cannula provided vertebral stability.

KEYWORDS: Vertebral augmentation, Vertebral compression fractures, radiofrequency ablation and spine tumors

O-312 **4:19 PM - 4:27 PM**

Balloon Kyphoplasty and Radiofrequency Kyphoplasty in Treatment of Patients with Osteoporotic Compression Fractures

Bornemann, R.·Jansen, T. R.·Otten, L. A.·Kabir, K.·Wirtz, D. C.·Pflugmacher, R.
Universitätsklinikum Bonn
Bonn, GERMANY.

Purpose
Since the 1990s, balloon kyphoplasty has been proven as an effective method of treating patients with painful vertebral compression fractures (VCF). However, due to the low viscosity of the PMMA cement uncontrollable cement leakage with corresponding risks often is the focus of discussions on this procedure. The radiofrequency kyphoplasty (RFK) is an innovative procedure available since 2009, for which an ultrahigh viscosity cement is used. It also offers the advantage of over 30 minutes' constant processing time. For the statistical comparison of the two methods clinical and radiologic data of two larger patient groups were evaluated.
Materials & Methods
As part of the surgical treatment of patients with conservative therapy-resistant osteoporotic vertebral fractures a prospective study of RFK was performed between 2009 and September 2010. From the clinical aspect, measurement parameters for efficacy and safety were the course of pain intensity using the VAS (0 to 100 mm) and the ODI (0-100%). For the radiologic outcome the increase in the middle and anterior parts of the treated vertebra and also the reduction of kyphosis after surgery and after 6, 12 and 24 months were evaluated. Furthermore, the extent of cement extrusion and the duration of operation time were compared. There were two groups of patients chosen with the same indication, and with the same average VAS prior to treatment. For the BKP the Kyphon ® technology was used. For the BKP group the same parameters like in the first group were evaluated (matched pairs). To compare the data statistically parametric and nonparametric tests were applied.
Results
For the radiofrequency kyphoplasty group (RFK) 101 patients were recruited, and for the balloon kyphoplasty group (BKP) 101 appropriate patients were selected. In 47% of the RFK patients and in 45% of the BKP patients more than one vertebral body were treated (thoracic or lumbar).Prior to treatment 85 mm on the VAS were calculated in both groups. The decrease in VAS values was (RFK versus BKP) immediately after surgery, 56 mm versus 55 mm ($p = 0.02$), and after 6, 12 and 24 months ($p<0.001$). In both groups improvements in the Oswestry scores were registered after 6, 12 and 24 months without a statistically significant difference. In both groups, the middle part of the vertebral bodies was increased by an average of 3 mm. Radiofrequency yielded a decrease in the average kyphosis angle of 4.6, the BKP resulted in

about 3.9 degrees. Concerning cement leakage a key difference in favor of the radiofrequency kyphoplasty was detected (5.9% versus 26.7%; p <0.0001). For RFK a significant shorter duration of operation time was calculated (28 versus 49 min; p<0.001).
Conclusion
The RFK has proven to be a clinically very effective procedure that does somewhat better than BKP in long-lasting pain relief. No differences could be detected regarding improvement of functioning and the mean restoration of mid- and anterior-vertebral height. As the safety aspect is concerned the RFK offers the advantage of a statistically significant lower proportion of cement extrusion.

KEYWORDS: Osteoporosis, Kyphoplasty, Vertebral compression fracture

O-313 **4:27 PM - 4:35 PM**

Multiple Myeloma: Radiofrequency Kyphoplasty versus Conservative Care in the Treatment of Osteolytic Vertebral Fractures

Bornemann, R.·Jansen, T. R.·Kabir, K.·Wirtz, D. C.·Pflugmacher, R.
Universitätsklinikum Bonn
Bonn, GERMANY.

Purpose
Radiofrequency kyphoplasty (RFK) provides a minimally invasive procedure to treat vertebral compression fractures (VCF) due to osteoporosis, trauma or tumor. Painful osteolytic vertebral fractures due to multiple myeloma often are treated conservatively. Patients suffer from pain and immobilization. There is still a controversial discussion how to treat osteolytic vertebral fractures. Conservative care is the default approach, despite lack of evidence. Radiofrequency kyphoplasty uses ultrahigh viscosity cement to stabilize the fracture. The aims of this study were to compare RFK to conservative care and to evaluate two patient groups which were treated with RFK or conservatively. The control group of conservative care results by patients who denied a surgical intervention. All patients were followed for six months. All patients were seen every six weeks.
Materials & Methods
Patients with painful osteolytic vertebral compression fractures due to multiple myeloma were offered surgical treatment by RFK. Patients which agreed were treated within three days, patients who denied were treated conservatively (analgesics, bracing and physiotherapy). They then wereoffered the choice of continuing conservative care or crossing over to radiofrequency kyphoplasty, after six and 12 weeks. All patients, in the RFK or conservative care group, were treated by the oncologist and received chemotherapy when necessary. Clinical success was defined as: 1) VAS pain improvement ≥ 2.0) final VAS pain ≤ 5.0) no functional worsening on ODI. Ninety patients (51 females and 39 males) with 162 osteolytic vertebral fractures were treated with RFK using the StabiliT Vertebral Augmentation System (Dfine Inc, San Jose, CA). Seventy-eight patients could be followed up to six months. Forty-eight patients (29 females and 19 males) with 92 vertebrae initially were treated conservatively. After six weeks 22 out of 48 patients and after 12 weeks 12 out of 48 patients decided to cross over to RFK. Thirty-four out of 48 patients made a crossover to RFK. Forty-four patients could be followed up to six months.
Results
In the RFK group the median pain scores (VAS) (p<0.001) and the ODI (p<0.001) improved significantly from pre- to post-treatment and maintained at three and six months followup. Postoperative, three and six months follow-up RFK stabilized the vertebral height and avoided further kyphotic deformity. After six months 76 out of 78 patients met the criteria for clinical success. In the conservative group only one out of 48 patients after the initial six weeks of conservative care met the criteria for clinical success and median VAS improvement was two. After 12 weeks of conservative care, only three patients met the criteria for clinical success, and median VAS improvement was two. Further the radiologic data showed a significant height loss and increase in kyphotic deformity in comparison to RFK.
Conclusion
For the vast majority of patients, conservative care did not provide meaningful clinical improvement. Nearly all patients who underwent RFK had rapid substantial improvement. Surgery was clearly much more effective than conservative care and should be offered to patients sooner. Further RFK did not interrupt or delay chemotherapy or radiation therapy!

KEYWORDS: Multiple myeloma, Kyphoplasty, conservative care

O-314 **4:35 PM - 4:43 PM**

Sacral Radiofrequency Neurolysis for the Management of Sacroiliac Joint-Related Pain: A Comparison of Three Techniques

Ortiz, A.[1]·Golovac, S.[2]
[1]Winthrop University Hospital, Mineola, NY, [2]Space Coast Pain Institute, Merritt Island, FL.

Purpose
To compare the utility, efficacy and safety of three different sacral denervation techniques in the management of sacroiliac joint (SIJ) pain that is refractory to conservative medical management.
Materials & Methods
Forty-seven patients who met eligibility criteria including at least 7/10 sacroiliac joint-related pain, on either over the counter or prescribed analgesic therapy, and with a favorable, but temporary response to image-guided percutaneous sacroiliac joint anesthetic/steroid injections underwent a total of 50 fluoroscopy-guided sacral RF

Note: Scanned images are included in the proceedings. Some submitted images were reduced during editing, thereby decreasing clarity. Also, refer to the Program Planner. Proceedings Content as of 3-29-2013.

procedures over a 2½-year period. The three types of radiofrequency procedures were cooled RF, bipolar RF and multilesion RF. Patient followup was conducted at three week, three month and one year intervals. The following parameters were recorded: clinical presentation, procedure time, fluoroscopy time, type of anesthesia, complications and pre and postnumeric pain scores and analgesic requirements. The latter was categorized as 0: no analgesics, 1: over the counter analgesics or 2: prescribed analgesics. IRB approval was obtained for this project.

Results

Eight patients, four male and four female, with an average age of 76.5 years underwent cooled RF (average procedure time 2.5 hours and average fluoroscopy time 10 minutes). All patients in this group were followed to one year and experienced complete relief of their SIJ pain. Twenty patients, 15 female and five male, and an average age of 74 years had 28 bipolar RF procedures (five patients had bilateral procedures; average procedure time 1.5 hours and average fluoroscopy time six minutes). All but two experienced significant pain relief by one-year followup. Nineteen patients, 13 female and six male, with an average age of 68.5 years underwent multilesion RF (average procedure time 30 minutes and average fluoroscopy time 1.5 minutes). All patients in this group have been followed to at least three weeks, and are pain free. No major complications were encountered in any patient group; one patient in the multilesion RF group experienced transient neuritis at the treatment site, which responded to conservative management. Thirty-one patients had either prior spine surgical interventions and/or hip replacement surgery.

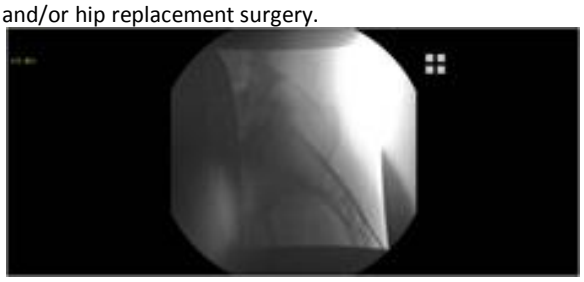

Conclusion

All sacral RF procedures were effective in providing pain relief with a reasonable safety profile in properly selected patients. The sacral multi-RF procedure, however, was more efficient. Long-term results with the latter technology are still pending.

KEYWORDS: Sacroiliac, Pain

Tuesday Afternoon

3:15 PM - 4:45 PM
Room 1AB

(31e) Parallel Scientific Papers: Pediatrics: Developmental/ Congenital Malformations

O-315 **3:15 PM - 3:23 PM**

Gene-Brain-Behavior Relationships in Tuberous Sclerosis Complex: Focus on Radial Migration Lines

van Eeghen, A. M.·Ortiz Teran, L.·Johnson, J.·Pulsifer, M. B.·Thiele, E. A.·Caruso, P.
Massachusetts General Hospital
Boston, MA.

Purpose

The search for neuroradiologic biomarkers in TSC has resulted in varying findings on tubers and white matter (WM) microstructure. Although radial migration lines (RMLs) are the main radiologic WM feature in TSC and are associated with DTI abnormalities, their contribution to the neuroanatomical and neurocognitive phenotype has been understudied. Our aims were to include radial migration lines (RMLs) and normal-appearing WM (NAWM) features in a comprehensive evaluation of the neuroradiologic endophenotype, and to compare macrostructural and microstructural characteristics with genotype and neurodevelopmental outcomes.

Materials & Methods

MR images of 30 patients with TSC, including volumetric thin-section FLAIR imaging and DTI, were evaluated for frequencies of tubers, RMLs, subependymal nodules (SENs), and sub-ependymal giant cell tumors (SGCTs) per hemispheric lobe. Cerebellar lesions were counted. Fractional anisotropy(FA) and apparent diffusion coefficients(ADCs) were measured of the largest tuber, largest RML, and in the NAWM of each hemispheric lobe. Whole brain NAWM DTI indices were compared with 16 control patients. Relationships between neuroanatomical features were explored, and compared with genotype, epilepsy variables, intellectual/developmental quotients, and prospectively collected data on autistic features and global psychologic functioning. Linear regression analysis was performed to identify a predictive neuroanatomical biomarker for intelligence.

Results

A mean of 47 RMLs (range 4-86), 27 tubers (range 1-76) and 10 (range 0-22) SENs were found per patient. Radial migration lines greatly outnumbered tubers, and tubers generally were connected to an RML. Cerebellar lesions were associated with occurrence of SGCTs, and with more

Note: Scanned images are included in the proceedings. Some submitted images were reduced during editing, thereby decreasing clarity. Also, refer to the Program Planner. Proceedings Content as of 3-29-2013.

severe macrostructural and microstructural features. Lesion frequencies covaried with DTI indices of the largest tuber and RML, but not with NAWM FA or ADC. Normal-appearing WM FA and ADC values of TSC patients were similar to control patients (p=0.26). However, mean FA values of NAWM were significantly associated with the ADC of the largest tuber(p=0.01) and showed a trend towards association with the ADC of the largest RML(p=0.09). All lesion frequencies were significantly associated with level of autistic features, intelligence and age of seizure onset (p<0.05 for all), but NAWM FA and ADC values were not. Of all lesion types, RML frequency showed the strongest associations with intelligence quotients and autistic features (p<0.01). Of the microstructural lesion indices, only RML ADC was significantly associated with intelligence. Linear regression analysis did not yield a unique neuroanatomical biomarker. Distinct genotype-neuroradiologic phenotype associations were observed, with significantly more lesions with more disturbed DTI indices associated with truncating TSC2 mutations compared with patients with TSC1 or TSC2 missense mutations.

Conclusion

Radial migration lines represent the major WM abnormality in TSC and were unvariably, in great frequency, and diffusely present. Normal-appearing WM showed normal DTI outcomes; the association between NAWM FA and lesion ADCs may reflect disrupted axon packing interfering with normal axon guidance mechanisms. Tubers, SENs, RMLs and lesion FA/ADC values covaried strongly together, with genotype and with neurobehavioral outcomes, providing a robust neuroradiologic endophenotype. Until more sophisticated biomarkers such as whole brain DTI are established, SENs may provide a crude but practical biomarker to stratify patients for early intervention or SGCT monitoring.

KEYWORDS: Tuberous sclerosis, Neuropsychiatry, Anatomy

O-316 **3:23 PM - 3:31 PM**

Normal Developmental Myelination Pattern of Callosal Splenium Commissural Fibers on MR Imaging in Children Three to Six Months of Age

Whitehead, M. T.·Raju, A.·Choudhri, A. F.
University of Tennessee Health Sciences Center/LeBonheur Children's Hospital
Memphis, TN.

Purpose

The purpose of this study is to depict the specific developmental callosal splenium MR myelination pattern and distinguish the normal transient mid splenium hypointensity from pathologic splenium lesions.

Materials & Methods

We reviewed 131 consecutive brain MRIs of patients between the ages of three-six months who presented to a single academic children's hospital over a one-year period. Examinations without diffusion tensor images, preterm patients (<38 weeks gestation), patients with severe hydrocephalus, and patients with substantial volume loss were excluded. A total of 50 patients' (ages 3-6 months) MRIs that included sagittal 3D T1-weighted (T1WI) FSPGR (Fast spoiled gradient echo), axial T1 FLAIR, axial T2-weighted (T2WI) fast spin echo, axial T2/FLAIR, and axial diffusion tensor images with 15 encoding directions were reviewed. Regions and degree of callosal splenium, isthmus, and posterior body myelination manifested by T1 and T2 shortening were evaluated. The maximum area of specific regions of T1 prolongation in the developing splenium were measured in the sagittal plane. Tractography was performed with seeds placed over the posterior, mid, and anterior splenium to define the primary origin, destination, and course of traversing commisural fibers.

Results

The splenium signal intensity was significantly different in patients ages three-six months with distinct age-related trends. On T1WI, diffuse hypointense signal was present in nearly all (9/10) three-month-old patients, mixed signal with geographic hypointensity in the mid splenium was present in nearly all (15/16) four-month-old patients, and a mixed mildly heterogenous signal was seen in nearly all six-month-old patients (9/10). Signal intensity was more variable in the five-month-old patients. Tractography revealed three distinct white matter tract populations located in the posterior, mid, and anterior splenium, respectively: medial occipital fibers, medial temporal fibers, and high parietal fibers.

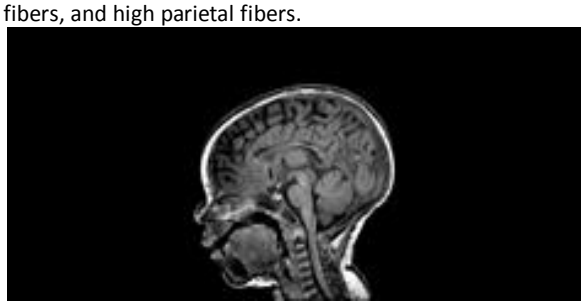

Conclusion

Specific commissural fiber components of the callosal splenium myelinate at different time periods. The transient developmental mid splenium hypointensity on T1WI corresponds to small fiber tracts from associative cortex, principally originating and terminating from the medial temporal lobes. Heterogenous splenium signal alteration in patients ages three-six months is a normal developmental phenomenon that should not be confused with pathologic lesions.

KEYWORDS: Myelination, Corpus callosum

Note: Scanned images are included in the proceedings. Some submitted images were reduced during editing, thereby decreasing clarity. Also, refer to the Program Planner. Proceedings Content as of 3-29-2013.

O-317 **3:31 PM - 3:39 PM**

Hipoccampal Malformations in Copy Number Gains of 15q11-q13

Boronat, S.·Thibert, R.·Mehan, W.·Caruso, P.
Massachusetts General Hospital
Boston, MA.

Purpose
Gain of gene dosage of 15q11-q13, either as an interstitial duplication or triplication of the maternal allele or as an isodicentric marker chromosome [idic (15)] has been associated with global developmental delay, autistic spectrum disorder, psychiatric disease, and epilepsy. MR images in these patients have been reported as normal or having nonspecific findings such as a thin corpus callosum. The purpose of this study is to characterize the neuroimaging features of eight patients with this genotype.
Materials & Methods
A retrospective review was performed of the charts of 37 patients affected by isodicentric (15) or interstitial duplication of 15q11-q13. 8 MR inages were available for review: seven patients had an isodicentric (15) and one had an interstitial duplication. The pertinent literature was reviewed.
Results
Seven patients had hippocampal malformations and one patient had mesiotemporal sclerosis. One patient had hypoplasia of the posterior corpus callosum and one had an abnormally thin corpus callosum. One had dilatation of the central ependymal canal from C5 through T1. In the MRI literature, the most frequently reported finding in copy number gain of 15q11-q13 is hypoplasia of the corpus callosum. Although hippocampal malformation has been reported in the neuropathologic literature in copy number gain of 15q11-q13, our study represents the largest series of patients with MRI findings yet to be reported.
Conclusion
Hippocampal malformation is the most frequent finding in neurodevelopmental disorders due to copy number gain at 15q11-q13. This feature may be related to some of the clinical features presented by these patients such as the high incidence of epilepsy and sudden unexpected death.

KEYWORDS: Hippocampus

O-318 **3:39 PM - 3:47 PM**

Prenatal Pattern Analysis and 3D Modeling in Callosal Agenesis

Kasprian, G. J.·Langs, G.·Dittrich, E.·Brugger, P. C.·Prayer, D.
Medical University of Vienna
Vienna, AUSTRIA.

Purpose
To detect and describe abnormalities and differences in cortical folding patterns of fetuses with callosal agenesis (CCA).
Materials & Methods
Three orthogonal T2-weighted sequences (1.5T, slice thickness 4.4 mm, FOV 230 mm, TE = 140 ms) of 21 fetuses with isolated, partial and associated forms of CCA were analyzed retrospectively. 2D pattern analysis consisted of cortical contour delineation (coronal plane) and 2D shape modeling using a multivariate Gaussian model. For 3D modeling, the axial, coronal and sagittal sequences of each subject were reconstructed into an isotropic high-resolution volume. Afterwards, a semi-supervised image processing algorithm is applied to retrieve segmentations of the cortical surfaces for all cases. Based on these segmentations, the symmetry of the 3D shapes was evaluated in terms of shape variation on left and right hemispheres, respectively. Results were compared to 21 age-matched fetuses with normal cerebral development.
Results
Hemispheric asymmetry patterns are less pronounced in the acallosal group of fetuses as demonstrated by 2D pattern analysis. Hemispheric asymmetries were less pronounced in the perisylvian brain regions in CCA cases. 3D modeling readily could visualize the dynamic cortical folding patterns in CCA fetuses and could detect subtle differences in comparison to normal controls.
Conclusion
2D and 3D modeling and pattern analysis are computerized, quantitative methods to detect even subtle differences of atypical cortical folding patterns in fetuses with CCA. In future these tools may be further suitable to differentiate cases of isolated CCA with adverse neurodevelopmental outcome from those with close to normal development.

KEYWORDS: Fetal brain development, Fetal MR imaging, Callosal Agenesis

Note: Scanned images are included in the proceedings. Some submitted images were reduced during editing, thereby decreasing clarity. Also, refer to the Program Planner. Proceedings Content as of 3-29-2013.

O-319 **3:47 PM - 3:55 PM**

Monitoring Craniocervical Junction Abnormalities in Osteogenesis Imperfecta Using Plain Radiography and MR Imaging Techniques

Williams, F.·Connolly, D. J. A.
Royal Hallamshire Hospital Sheffield
Sheffield, UNITED KINGDOM.

Purpose
Osteogenesis imperfecta (OI) is an inherited disorder of collagen metabolism with a prevalence of 1 in 10 000-20 000 worldwide. The genetic defect leads to defective bone mineralization and hence weakened and fragile bones unable to withstand normal biomechanical forces. This is of significance at the base of skull and cranio-cervical junction where the weight of the developing brain leads to platybasia-a flattening of the skull base and basilar impression where there is protrusion of the uppermost vertebral structures into the cranium and invagination in which there is lowering of the cranial base. These can lead to serious morbidity and mortality. We aim to study a group of children with OI in order to provide radiologic markers of increasing severity in an effort to predict when intervention is necessary by use of both radiography and MRI which is especially relevant as the children age.
Materials & Methods
Children with OI who were referred to Department of Paediatric Metabolic Bone Disease, Sheffield Children's NHS Foundation Trust and Academic Unit of Child Health, University of Sheffield, United Kingdom were identified by retrospective review of the database. Their demographic and clinical data were collated. All patients underwent genetic testing, serial plain radiography and MR imaging of the skull base and cranio-cervical junction as both initial diagnostic studies and subsequent followup. The MR imaging was reviewed and 2D flow analysis of CSF mechanics at the craniocervical junction was performed in the Academic Department of Radiology, Sheffield.
Results
Thirty-eight patients were identified presenting over a four-year period from 2008-2012. The age range was two years to 23 years. Radiographic analysis was performed on the presentation and follow-up series with respect to the basal angle and the presence or absence of basilar invagination. The majority of patients (34/38) had radiographic evidence of platybasia at diagnosis. In the remaining four cases this subsequently developed on follow-up imaging. Correlation with MRI was made using a modified basal angle measuring technique and evidence was seen of this in 37 patients. Subsequent followup showed progression to varying degrees of invagination in 30 patients. In addition 2D flow analysis of CSF mechanics at the craniocervical junction was obtained in each patient. This demonstrated evidence of significant alteration in CSF flow in 15/38 patients who were patients with the most significant radiologic progression, five of whom had demonstrated evidence of syrinx formation.
Conclusion
Craniocervical abnormalities can be confidently diagnosed on both plain radiography and magnetic resonance imaging and can be used as a guide for future followup of such patients. In addition, the use of CSF flow analysis techniques can be used to monitor and predict eventual brainstem compressive complications and thus be used as a guide for surgical intervention.

KEYWORDS: Cranio-cervical junction, Basilar invagination

O-320 **3:55 PM - 4:03 PM**

Unique Brain MR Imaging Findings in Two Siblings with Prosaposin Deficiency

Stence, N. V.[1]·Fenton, L. Z.[1]·Lindsay, A.[2]·Lovell, M.[1]·Manchester, D.[1]
[1]Children's Hospital Colorado, Aurora, CO, [2]University of Colorado Denver, Aurora, CO.

Purpose
Prosaposin deficiency (pSap-d) is a rare, neonatal neurovisceral lipid storage disorder described in few case reports. A single report has described brain MRI findings. The prosaposin protein (PSAP) is a product of *PSAP*, a >39 kb gene located on chromosome 10. Prosaposin protein is a lysosomal precursor protein for four sphingolipid activator proteins, the sapopsins, which are indispensible for normal lysosomal catabolism. Prior case reports of pSap-d have described a syndrome of rapid neurologic deterioration and death in the neonatal period. We describe the history and imaging of two siblings with nearly identical unique brain MRI findings who declined precipitously after birth and died in the neonatal period. One was diagnosed with pSap-d at autopsy with genetic testing.
Materials & Methods
A chart review and review of MRI brain imaging findings was conducted in two siblings diagnosed with pSap-d.
Results
Clinical Histories: The first infant was born at 38 weeks gestation and was noted to be hypotonic, jittery, and a poor feeder immediately after birth. A brain MRI was obtained at DOL 9 for onset of seizures. His course deteriorated precipitously and he died at day of life (DOL) 20. His sibling was born at 37 weeks of gestation, and was transferred to the NICU on DOL 2 for poor feeding. Brain MRI was obtained at DOL 3, showing findings similar to her brother. She deteriorated rapidly and died at DOL 53.
Imaging: Brain MRI findings are similar in both siblings. Gray matter intensity nodules were distributed diffusely throughout the periventricular white matter, focally concentrated adjacent to the lateral ventricle atria. Multiple gyri were abnormally enlarged and few in number, with an appearance suggestive of pachygyria. However, the cortex was abnormally thin, and the white matter was diffusely T2 hyperintense (Figure 1). Post mortem: Autopsy was performed in the second infant.

Note: Scanned images are included in the proceedings. Some submitted images were reduced during editing, thereby decreasing clarity. Also, refer to the Program Planner. Proceedings Content as of 3-29-2013.

Brain examination revealed heterotopic neurons in the molecular layer of cortex and white matter, simplification of gyral pattern, microcephaly, islands of engorged histiocytes and near complete loss of white matter in the cerebrum. Genetic testing confirmed a compound heterozygous mutation in *PSAP*.

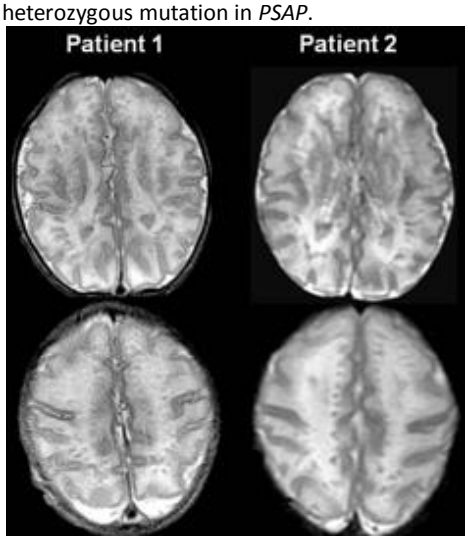

Conclusion

Siblings with pSap-d demonstrated identical unique brain MRI findings of gray matter intensity heterotopic nodules, abnormally enlarged and sparse gyri, cortical thinning, and abnormal white matter hyperintensity. This unique combination of findings could suggest the diagnosis of this rare disorder in the appropriate clinical setting.

KEYWORDS: Pediatric brain, Congenital brain malformations, Storage Disorders

O-321 **4:03 PM - 4:11 PM**

Neuroimaging Findings in Twenty-Five Children with Isolated and Associated Hemimegalencephaly

Bosemani, T.[1]·Boltshauser, E.[2]·Staudt, M.[3]·Flores-Sarnat, L.[4]·Buerki, S.[5]·Pieper, T.[3]·Sarnat, H. B.[4]·Wei, X.[4]·Hartman, A. L.[1]·Huisman, T. A. G. M.[1]·Poretti, A.[1]
[1]The Johns Hopkins University School of Medicine, Baltimore, MD, [2]University Children's Hospital, Zurich, SWITZERLAND, [3]Epilepsy Center for Children and Adolescents, Schön Klinik, Vogtareuth, GERMANY, [4]University of Calgary and Alberta Children's Hospital, Calgary, AB, CANADA, [5]University Children's Hospital, Berne, SWITZERLAND.

Purpose

Hemimegalencephaly (HME) is a rare congenital hamartomatous malformation characterized by excessive growth limited to one cerebral hemisphere. Hemimegalencephaly may occur in isolation or be associated with neurocutaneous syndromes. Typical neuroimaging findings in HME include enlargement of the affected cerebral hemisphere with a dysplastic and thickened cortex, abnormal signal intensity and increased volume of the ipsilateral white matter, and enlargement of the lateral ventricle. We aim to evaluate the differences between isolated and associated HME with respect to neuroimaging findings including degree of severity of HME and involvement of cranial nerves and intracranial vessels.

Materials & Methods

MR images of 25 children (13 males and 12 females) with HME were included in this study. At the time of MRI, the median patient age was 0.8 years (range one day to 9.8 years). MR imaging findings were reviewed retrospectively. We used the anatomical grading of severity reported by Flores-Sarnat. Additionally, all MR images were evaluated qualitatively for asymmetry in size of cranial nerves, intracranial vessels, and posterior fossa structures.

Results

Hemimegalencephaly was isolated in 17 children. In eight patients, HME was associated with neurocutaneous syndromes including epidermal nevus syndrome (n = 4), megalencephaly-capillary malformation (n = 2), Klippel-Trenaunay syndrome (n = 1), and hemicorporal hypertorphy (n = 1). The severity of HME was classified as Grade 1 (mild) in 7/25 (28%, four associated), Grade 2 (moderate) in 11/25 (44%, two associated) and Grade 3 (severe) in 7/25 (28%, two associated). We were not able to identify and evaluate all studied structures in each patient. This is reflected in the denominator of the following ratios. The ipsilateral olfactory bulb, trigeminal and optic nerves were enlarged in 4/19 (21%, one associated), 1/18 (6%, one), and 1/25 children (4%, one), respectively. Asymmetric dilatation was observed in the ipsilateral meningeal vessels in 14/25 patients (56%, seven), ipsilateral anterior and middle cerebral arteries in 8/25 (32%, two), ipsilateral internal cerebral vein in 5/24 (21%, two), and ipsilateral posterior cerebral artery in 5/25 (20%, two). Ipsilateral enlargement of the cerebellum and middle cerebellar peduncles was present in 4/25 patients (16%, four and three, respectively). Reduction in size of the ipsilateral cerebral peduncle was found in 6/25 (24%, one).

Conclusion

In children with HME, ipsilateral enlargement of structures other than the involved cerebral parenchyma is present, particularly the olfactory bulb, meningeal vessels, cerebral vessels, hemicerebellum and middle cerebellar peduncles. Ipsilateral enlargement of the trigeminal and optic nerves, meningeal vessels, hemicerebellum and middle cerebellar peduncles were more frequent in children with associated HME compared to the isolated group. However, the associated group tended to be milder in terms of anatomical degree of severity. Reduction in size of the ipsilateral cerebral peduncle was present only in children with Grade 2 or 3 HME and mostly associated with involvement of the temporo-parietal lobe. Reduction in size of the ipsilateral cerebral peduncles seems to be a secondary finding, most likely due to Wallerian degeneration.

Note: Scanned images are included in the proceedings. Some submitted images were reduced during editing, thereby decreasing clarity. Also, refer to the Program Planner. Proceedings Content as of 3-29-2013.

KEYWORDS: Hemimegalencephaly, MR imaging brain, Children

O-322 **4:11 PM - 4:19 PM**

Ataxia, Cognitive Impairment, and Ocular Motor Apraxia with Cerebellar Cysts and Dysplasia: A New Form of Dystroglycanopathy?

Poretti, A.[1]·Huisman, T. A. G. M.[1]·Bertini, E.[2]·Boltshauser, E.[3]
[1]The Johns Hopkins Medical School, Baltimore, MD,
[2]Ospedale Pediatrico Bambino Gesù, Rome, ITALY,
[3]University Children's Hospital, Zurich, SWITZERLAND.

Purpose
Cerebellar cysts are a rare finding in pediatric neuroimaging and are rather characteristic for congenital muscular dystrophies (CMD) due to impaired glycosylation of alpha dystroglycan. We aim to evaluate the MRI spectrum, characterize neurologic/ophthalmologic features and cognitive outcome and report genetic analysis in seven children (including three siblings) with an apparently new syndrome characterized by cerebellar cysts.
Materials & Methods
All images were qualitatively evaluated for infra and supratentorial abnormalities. Data about neurologic and ophthalmologic features and outcome were collected from clinical history and follow-up examination. *POMT1*, *POMT2*, *POMGnT1*, *FKRP*, *FKTN*, *LARGE*, and *GPR56* genes were screened in all patients. In three children a SNP 6.0-Array also was performed.
Results
The seven patients included four males and three females. At a mean age of 7.2 years (range 3.5 to 13.5 years), cognitive impairment and ataxia were found in all patients, ocular motor apraxia in six, and severe myopia in three. Qualitative MR evaluation showed cerebellar cysts in the cerebellar hemispheres and vermis in all patients. Additional MR findings included cerebellar dysplasia and an enlarged fourth ventricle in all children, vermian hypoplasia and brain stem morphologic abnormalities in six, and an elongated and squared shape of the fourth ventricle in five. In all patients, no mutations were found in the *POMT1*, *POMT2*, *POMGnT1*, *FKRP*, *FKTN*, *LARGE*, and *GPR56* genes. The SNP array showed no pathogenetic imbalances in all children evaluated.
Conclusion
The seven children share the same clinical and neuroimaging phenotype including cognitive impairment, ataxia, ocular motor apraxia, cerebellar cysts, and cerebellar dysplasia. These are features of dystroglycanopathies. However, weakness, a key feature of CMD, was not a finding. Additionally, no mutations were found within the known dystroglycanopathy genes. Therefore, we suggest that the reported clinical and neuroimaging phenotype may represent a new syndrome related to the dystroglycanopathy spectrum.

KEYWORDS: Cerebellum, MR imaging brain, Cerebellar cysts

O-323 **4:19 PM - 4:27 PM**

Midbrain-Hindbrain Involvement in Septo-Optic Dysplasia

Severino, M.·Allegri, A.·Roviglione, B.·Pistorio, A.·Maghnie, M.·Rossi, A.
Gaslini Children's Hospital
Genova, ITALY.

Purpose
The diagnosis of septo-optic dysplasia (SOD) requires at least two features of the classical triad: (i) optic nerve hypoplasia, (ii) pituitary hormone abnormalities, and (iii) midline brain defects. Midbrain-hindbrain involvement has not been described well, despite mutations of genes (i.e., OTX2 and FGF8) regulating brainstem anteroposterior (AP) patterning in SOD patients. We aimed to describe midbrain-hindbrain involvement in SOD and to identify possible clinical-neuroimaging correlations.
Materials & Methods
We studied 38 SOD patients with MRI (mean age 61 months, 21 males). Patients were categorized subjectively based on the presence (group A, 21 patients) or absence (group B, 17 patients) of visible brainstem anomalies. We then measured height and AP diameter of midbrain, pons, and medulla, AP midbrain/pons diameter (M/P ratio), vermian height, and tegmento-vermian angle, and compared the results with a database of 114 normal age- and gender-matched controls. Differences between groups were evaluated with nonparametric ANOVA test (Kruskal-Wallis) and the results were corrected a-posteriori according to Bonferroni (p_B). Furthermore, patients were subdivided based on the presence of midline anomalies in three subtypes: group I (septal agenesis, 23 patients), group II (abnormal corpus callosum, seven patients), and group III (no midline brain defects, eight patients), and the association between brainstem and midline abnormalities was investigated (Fischer exact test). Finally, we studied the association between brainstem involvement and clinical features (Chi-square and Fisher exact tests).
Results
Septo-optic dysplasia patients with brainstem abnormalities (group A) presented reduced AP pons diameter compared to controls (p_B<0.0001) and to group B (p_B=0.012), and higher M/P ratio compared to controls (p_B<0.0001) and to group B (p_B<0.0001); their AP medulla oblongata diameter (p_B=0.001), height of the pons (p_B=0.00072) and of the vermis (p_B=0.0009) were shorter than controls. Six out of 21 patients with brainstem abnormalities (group A) presented thickening of the quadrigeminal plate with aqueductal stenosis and triventricular hydrocephalus (surgically treated in all patients), and three of them also had agenesis of the epithalamus (i.e., pineal gland, habenular trigone and posterior commissure). There was a statistically significant

Note: Scanned images are included in the proceedings. Some submitted images were reduced during editing, thereby decreasing clarity. Also, refer to the Program Planner. Proceedings Content as of 3-29-2013.

association between brainstem abnormalities and corpus callosum dysgenesis (p = 0.011) and developmental delay (p = 0.035), respectively.
Conclusion
Midbrain-hindbrain abnormalities are a significant, albeit under-recognized, component of the SOD spectrum. Patients with these abnormalities are more likely to present with developmental delay.

KEYWORDS: Septo-Optic dysplasia, Brainstem, MR imaging

O-324 **4:27 PM - 4:35 PM**

Pituitary Hypoplasia with Absence of Internal Carotid Artery: Report of Two Cases

Nath, J.·Bawa, P.·Neimark, M.
SUNY Health Science Center at Brooklyn
Brooklyn, NY.

Purpose
We report two cases of a rare association of congenital pituitary hypoplasia with absence of left internal carotid artery.
Materials & Methods
A four-year-old Indian American girl with short stature, hypothyroidism and neurodevelopmental delay was evaluated for pituitary hypoplasia. MR imaging of brain and sella revealed absence of anterior pituitary gland with absence of normal flow-void of left internal carotid artery (LICA). MR angiography demonstrated absence of LICA in carotid canal with an anomalous intracavernous communication from right ICA supplying distal cavernous and supraclinoid LICA. A two-year-old boy with multiple congenital anomalies including VSD and single incisor underwent MR imaging of brain and sella. MR imaging demonstrated a small anterior pituitary gland suggestive of pituitary hypoplasia. Normal flow void of LICA was not seen. A prominent flow void was seen arising from cavernous right ICA and continuing as distal LICA supplying left anterior circulation.
Results
Association of congenital pituitary hypoplasia with ICA agenesis and trans-sellar anastomosis, an extremely uncommon anomaly.
Conclusion
The internal carotid artery develops in the 4^{th} embryonic week while the pituitary primordial develops in 3^{rd} to 4^{th} week. Rare association of absence of one internal carotid artery and pituitary hypoplasia suggests a possible relationship of these two anomaly. Only a few case reports of this entity are reported in literature. Absence of internal carotid artery with pituitary hypoplasia may describe a new disease entity.

KEYWORDS: Pituitary gland, Carotid artery, Pituitary hypoplasia

O-325 **4:35 PM - 4:43 PM**

MR Imaging of the Fetal Brain Using a Rapid 3D Steady-State Sequence

Williams, F.[1]·Griffiths, P. D.[1]·Jarvis, D.[2]·McQuillan, H.[2]·Paley, M.[2]·Armitage, P.[2]
[1]Royal Hallamshire Hospital Sheffield, Sheffield, UNITED KINGDOM, [2]University of Sheffield, Sheffield, UNITED KINGDOM.

Purpose
To evaluate the capacity of a rapid T2-weighted 3D sequence to diagnose fetal brain abnormalities by comparing the results with current 2D methods. We also have made assessments of the estimates of energy deposition using those methods.
Materials & Methods
Fifty pregnant women were included in this study under the guidance of the institutional review board. All of their fetuses had suspected brain abnormalities on ante-natal ultrasonography or were at increased risk of a brain malformation based on the results of an earlier pregnancy. All of the fetuses had a routine MR protocol that includes three orthogonal plane single-shot fast spin-echo and 2D steady-state sequences. In addition, a 3D rapid steady-state sequence of the fetal brain was performed (acquisition time approximately 40s) and the standard and 3D sequences were reported independently and the results compared. The SAR predicted by the scanner was recorded in 12 cases in order to estimate the energy deposited by the three sequences.
Results
The 3D rapid steady-state sequences produced diagnostic quality images in 41/50 (82%) of cases. All of the failures were in second trimester fetuses (9/26 - 35% failure rate). There was a discrepancy between the standard report and findings using the 3D sequence in 2/41 of the fetuses with good quality 3D imaging. The predicted SAR deposition of the 3D steady-state sequences was comparable to the single-shot fast spin-echo sequence.
Conclusion
Our initial assessments of a 3D rapid steady-state sequence to image the fetus are encouraging in terms of diagnostic information and acceptable energy deposition values. The high failure rate in second trimester fetuses probably relates to greater mobility of the smaller fetuses and improvements in the 3D sequence are required in terms of reduced acquisition time and higher resolution.

KEYWORDS: In utero MR, Fetal MR imaging

Note: Scanned images are included in the proceedings. Some submitted images were reduced during editing, thereby decreasing clarity. Also, refer to the Program Planner. Proceedings Content as of 3-29-2013.

Tuesday Afternoon

5:00 PM - 6:30 PM
Ballroom 6AB

(32) Special Session: Controversies in Neuroradiology

O-326 **5:00 PM - 5:30 PM**

Brain Imaging Controversies: DTI in the Clinic: To Be or Not To Be

O-327

Pro

Roberts, T. P. L.
Children's Hospital of Philadelphia
Philadelphia, PA.

Presentation Summary
Diffusion imaging with MRI (including DTI, HARDI ...) provides at least two valuable technological advances: 1. fiber tracking of white matter pathways and structural connectivity, 2. microstructural characterization of regional white matter. Although, in many cases, "ground truth" interpretation is currently lacking, utility in characterizing pathology is clearly evident and can in many settings be of value in diagnosis, prognosis and treatment planning as well as in the study of processes of development and degeneration, once again placing the radiologist in a critical role at the interface of basic and clinical science, at the junction of technology and medicine.

O-328

Con

Mukherjee, P.
University of California San Francisco
San Francisco, CA.

O-329

Brain Imaging Controversies: CCSVI: Is There Venous Insufficiency in MS or Not?

O-330

Pro

Zaharchuk, G. G.
Lucille Packard Children's Hospital at Stanford
Stanford, CA.

O-331

Con

Field, A. S.
University of Wisconsin
Madison, WI.

Presentation Summary
Chronic cerebrospinal venous insufficiency (CCSVI) is a controversial, hypothetical condition recently proposed (Zamboni, et al.) to be an etiological factor in the pathogenesis of multiple sclerosis (MS); specifically, it has been suggested that the neuroimmunologic cascade of events that produces the focal plaques and diffuse neurodegeneration characteristic of MS is somehow triggered or promoted by chronically insufficient venous drainage from the brain and spinal cord. This idea is now the subject of intensive study and debate, not only with respect to its scientific merits but also regarding the ethical questions surrounding unproven therapies for incurable diseases (such as the “Liberation Procedure” for MS) and the roles of government, media, and public discourse in setting priorities for medical research. Chronic cerebrospinal venous insufficiency, dubbed “The Big Idea” by Dr. Zamboni, set off a social-media-fueled firestorm when it was first proposed in 2009 but the notion that MS has a vascular etiology dates back many decades. It has fallen out of favor for many valid reasons, not the least of which is the overwhelming and ever-growing mountain of evidence over the past few decades that MS is primarily an auto-immune disease. The CCSVI hypothesis thus resurrected an old debate between the vascular and immune theorists. The initial studies supporting the CCSVI hypothesis were lacking in proper blinding and control procedures, and yielded what seemed like impossibly perfect results, heightening levels of skepticism and making the debate especially contentious. Since then, other research groups have weighed in with several additional studies, some well blinded and controlled, some not. A recent meta-analysis found even the better studies to be highly inconsistent, yet still concluded that a link between venous abnormalities and MS may indeed exist. In the meantime, even in the absence of definitive proof that CCSVI not only exists as a genuine clinical entity but is causative rather than an epiphenomenon, clinical trials are ongoing to study the safety and effectiveness of venous angioplasty for MS. Most concerning is the fact that many patients are being treated outside of any clinical trial, with a few procedures leading to disastrous complications. The CCSVI debate is highly relevant to neuroradiologists as the diagnosis is based on imaging of the venous system, whether by ultrasound, computed tomography, magnetic resonance, or catheter angiography. Much of the discussion now surrounds not only the entity of CCSVI itself but the relative merits and drawbacks of the various imaging modalities in making this controversial diagnosis. The remarkably wide range of normal variation in venous anatomy and physiology also is central to the debate. This

Note: Scanned images are included in the proceedings. Some submitted images were reduced during editing, thereby decreasing clarity. Also, refer to the Program Planner. Proceedings Content as of 3-29-2013.

presentation will put the "con" into the CCSVI controversy; the studies to date will be summarized and the presenter will show, by a preponderance of the evidence (as the lawyers like to say), that CCSVI is a proverbial blind alley in the search for an MS cure. Disclaimer: Please note that the presenter was assigned to the "con" side of this debate by the session organizers. He is currently the PI on a carefully blinded CCSVI study funded by the National Multiple Sclerosis Society, which he is conducting with no preconceived expectations; he will let the data speak for themselves when they become available.

O-332 **5:30 PM - 6:00 PM**

Spine Imaging Controversies: Is There Value in Vertebroplasty?

O-333

Pro

Bartynski, W. S.
Presbyterian University Hospital
Pittsburgh, PA.

O-334

Con

Ortiz, A.
Winthrop University Hospital
Mineola, NY.

O-335

Spine Imaging Controversies: Disk Nomenclature - Does It Matter?

O-336

Pro

Williams, A. L.
Medical College of Wisconsin
Milwaukee, WI.

O-337

Con

Falcone, S.
University of Miami
Miami, FL.

O-338 **6:00 PM - 6:30 PM**

Head and Neck Controversies: To Fat-Sat or Not to Fat-Sat: Post Contrast Perineural Tumor

O-339

Pro

Shatzkes, D. R.
Lenox Hill Hospital
New York, NY.

Presentation Summary
The search for perineural tumor spread (PNTS) is one of the most challenging undertakings of the head and neck radiologist. It requires detailed knowledge of anatomy and tumor behavior, and intense scrutiny of imaging studies. Optimizing technique is critical. While all agree that contrast-enhanced MRI is the modality of choice for detecting PNTS, there is some disagreement with regard to the optimal sequences utilized. The controversy revolves around the skull base, and the fact that this area, which includes the foramina that transmit the cranial nerves between the extracranial and intracranial compartments, is composed of bone and air-containing structures, both of which can incite susceptibility artifact. These artifacts may be exaggerated when fat-suppression techniques are applied. On the flip side, high signal fat within skull base marrow, the neural foramina, and in the soft tissues below the skull base may serve to diminish conspicuity of pathologic contrast enhancement within cranial nerves, one of the imaging hallmarks of PNTS. It is my opinion, and one I believe is shared by the majority of my colleagues, that the benefits of fat-suppression, with indisputable advantage along the extracranial course of the cranial nerves, outweigh its costs. This differential has increased since my highly esteemed colleague Dr. Curtin wrote his editorial on the topic in 2004. Though the use of 3T scanners has increased in the interim, improvements in fat-suppression techniques have reduced the prevalence and severity of degradation by susceptibility artifact. Additionally, most protocols utilized in H&N tumor mapping and the search for PNTS include a contrast-enhanced whole brain sequence which provides an opportunity to assess skull base foramina and associated intracranial structures like the cavernous sinuses and Meckel cave in the absence of fat suppression. In summary, the increased conspicuity of the enhancing cranial nerve against suppressed fat of the skull base marrow and adjacent fatty soft tissues is worth the cost of the negligible increase in susceptibility artifact due to fat suppression. Let's see what Dr. Curtin has to say. It's always worth hearing.

Note: Scanned images are included in the proceedings. Some submitted images were reduced during editing, thereby decreasing clarity. Also, refer to the Program Planner. Proceedings Content as of 3-29-2013.

O-340

Con

Curtin, H. D.
Massachusetts Eye & Ear Infirmary
Boston, MA.

O-341

Head and Neck Controversies: To Gad or Not to Gad: IAC Imaging

O-342

Pro

Dillon, W. P.
University of California
San Francisco Med Center
San Francisco, CA.

O-343

Con

Harnsberger, H.
University of Utah
Salt Lake City, UT.

Tuesday Afternoon

5:00 PM - 6:30 PM
Ballroom 6CF

(33) SNIS Programming: Quality, Workforce and Research

O-344 **5:00 PM - 5:25 PM**

Quality in Radiology

Blackmore, C.
Virginia Mason Medical Center
Seattle, WA.

Presentation Summary
Higher quality in radiology is an opportunity to improve care and lower costs. In this presentation, I will discuss the multiple aspects of quality in radiology, both technical and professional, including how quality can be measured at the individual and institutional levels. I also will relate radiology quality to national trends and initiatives, contrasting a quality driven health care market from one driven solely by cost. Finally, I will highlight opportunities for quality improvement projects, and how radiologists can both be involved with and benefit from quality initiatives.

O-345 **5:25 PM - 5:50 PM**

Work Force Analysis for INR

Cloft, H. J.
Mayo Clinic
Rochester, MN.

Presentation Summary
Estimates of neurointerventional workforce supply and demand will be discussed.

O-346 **5:50 PM - 6:15 PM**

Clinical Trials in INR

Derdeyn, C. P.
Mallinckrodt Institute
St. Louis, MO.

Presentation Summary
The clear challenge facing medicine in general is proving the value of what we do: for us in neuroradiology that means the value of imaging and image-guided intervention in improving patient outcomes. In the past, we have been focused on innovation and bringing new imaging techniques and interventional devices to the clinical arena. This is important and this activity was rewarded under the fee for service model. Accountable care organizations, presently being piloted, will reward the system for the outcome of individual patients. These systems will make decisions regarding individual patient care based on what has been proven to improve outcome. This may be algorithm-based. We know that what we do has enormous impact on patient care and patient outcomes. For much of what we do, however, we lack high-level evidence that this is the case. Clinical trials, and in particular randomized clinical trials, are the coin of the realm for proving efficacy. In this talk, I will focus on why randomized trials are so important, using recent examples of studies in our domain with profound impact. Nonrandomized trials and registries may identify subgroups with better outcomes, but this does not necessarily reflect a benefit from a procedure. The recent endovascular stroke trials are a case in point. There is great interest in comparative effectiveness research as well. How these types of studies might work in the cerebrovascular is not clear, but are important to consider. Finally, we will review areas for future research in stroke and cerebrovascular disease relevant to our field.

Note: Scanned images are included in the proceedings. Some submitted images were reduced during editing, thereby decreasing clarity. Also, refer to the Program Planner. Proceedings Content as of 3-29-2013.

Tuesday Afternoon

5:00 PM - 6:30 PM
Ballroom 6DE

(34) ASPNR Programming: Metabolic Brain Disorders

O-347 **5:00 PM - 5:30 PM**

Lysosomal/Peroxisomal Disorders

Pruthi, S.
Monroe Carell Jr. Children's Hospital
Nashville, TN.

Learning Objectives
Upon completion of this presentation, participants will be able to:
1) Know the classification of various lysosomal and peroxisomal disorders.
2) Understand key clinical presenting features and possible treatment options available for some of the common diseases in each group.
3) Review critical neuroimaging features of the common diseases in each group, and the role of advanced neuroimaging techniques in the assessment of these entities.

O-348 **5:30 PM - 6:00 PM**

Disorders of Amino and Organic Acid Metabolism

Parmar, H. A.
University of Michigan
Ann Arbor, MI.

Learning Objectives
Upon completion of this presentation, participants will be able to:
1) Know spectrum of diseases presenting as either amino acidurias or organic acidurias.
2) Understand basic metabolic reason for some of the common diseases in each group and understand their clinical presentations.
3) Review critical neuroimaging features of the common diseases in each section.
Presentation Summary
The common diseases (but not limited) to be discussed will include: propionic and methylmalonic acidemia, glutaric aciduria type I, L-2 hydroxyglutaric aciduria, maple syrup urine disease (MSUD), phenylketonuria (PKU) and different forms of urea cycle disorders.

O-349 **6:00 PM - 6:30 PM**

MR Patterns and Translational Research in Two New Entities of Mitochondrial Encephalomyelopathy

Valk, J.
Free University Hospital
Amsterdam, NETHERLANDS.

Jaap Valk, MD, PhD received his education from the State University, Leiden and Stichting Klinisch Hoger Onderwijs Rotterdam. Dr. Valk is curently a neuroradiologist at MRI Centrum, Amsterdam, Rotterdam. He is credited with more than 15 books on neuroradiological, psychiatrical and radiological subjects and has published more than 200 scientific articles in leading journals. Dr. Valk has had postgraduate courses and given invited lectures at many conferences. He is a member of 15 (Dutch, European, American and other International) Scientific Organizations. Dr. Valk was Knighted by the Queen of the Netherlands, June 2006: Knight in the order of the Dutch Lion (Ridder in de Orde van de Nederlandsew Leeuw).

Presentation Summary
Systematic and computer-assisted MRI Pattern Recognition helped us to detect a number of so far unclassified white matter disorders (Marjo van der Knaap, Jaap Valk: Myelination and Myelin disorders, 3d edition, Springer Verlag, Berlin). This was followed by research into genetics and analysis of disease mechanisms. In this presentation we will focus on two newly described mitochondrial disorders with autosomal recessive inheritance, LBSL (leukoencephalopathy with brain stem and spinal involvement and elevated lactate) and LTBL (leukoencephalopathy with thalamic and brain stem involvement and elevated lactate), of which the mutated genes were identified. Long-term followup showed unexpected phenotypic variation.

Tuesday Afternoon

5:00 PM - 6:30 PM
Room 5AB

(35) CSI San Diego: Neuroradiology Resources on the Web

O-350 **5:00 PM - 5:45 PM**

Neuroradiologists Resources on the Web

Wiggins, R. H.
University of Utah Health Sciences Center
Salt Lake City, UT.

Presentation Summary
Neuroradiologists Resources on the Web. This review will

Note: Scanned images are included in the proceedings. Some submitted images were reduced during editing, thereby decreasing clarity. Also, refer to the Program Planner. Proceedings Content as of 3-29-2013.

discuss and review Internet resources that may be helpful for the neuroradiologist, and mobile applications and hardware that may be helpful for the neuoradiologist.

O-351 **5:45 PM - 6:30 PM**

RSNA MIRC Teaching Files on Tablets

Flanders, A. E.
Thomas Jefferson University Hospital
Philadelphia, PA.

Presentation Summary
This presentation will provide an overview of the traditional radiology teaching file and the transition to web-based solutions in the now filmless radiology department. The presentation will feature the RSNAs MIRC Teaching File System software which is freely available and provides a feature-rich turnkey solution to anonymize images and author teaching file cases. It uses a patient-centric workflow that automatically organizes cases with multiple exams into a coherent chronological timeline. The software features an easy-to-use basic and advanced authoring template system and an automatic anonymizer for DICOM data as well as burned-in pixel data. It has a powerful data engine which can search for combinations of metadata in large collections and display the most relevant cases in seconds. There are modules for creation of self-study quizzes and a feature for creating conferences through a "shopping-cart" model. Moreover, the software has functionality to share cases locally or to your myRSNA account. Cases can be exported individually to the user desktop as individual images or as a Powerpoint file which can be used directly. The participant will have the opportunity to "kick-the-tires" of the RSNAs public MIRC Teaching File portal which catalogs cases from a number of public libraries worldwide. The participant also will learn about the online MIRC resources which provide easy-to-follow instructions for obtaining and installing the software, setup and configuration as well as authoring and searching. Participants should bring their favorite wireless device to the session (preferably a laptop or a slate) to maximize the experience.

Tuesday Afternoon

5:00 PM - 6:30 PM
Room 1AB

(36) Young Professionals Programming: Creating a New Service: How You Can Add Value to Your Practice

O-352 **5:00 PM - 5:15 PM**

MR Spectroscopy

Brandao, L. A.
Clinica Radiologica Luis Felippe Mattoso
Rio De Janeiro, BRAZIL.

Presentation Summary
The first thing we will discuss in this presentation is what we need to start the service. The answer for that question is motivation! We want to do it. And the reason for that is because we know magnetic resonance spectroscopy (MRS) really makes a difference in many clinical situations! Magnetic resonance spectroscopy (MRS) is a useful technique to further access various intracranial diseases, particularly to specifically determine which major category of disease is manifest by the observed lesion (neoplastic, inflammatory, ischemic⋯). A few disease processes such as Canavan's disease and nonketotic hyperglycemia have distinct MRS profiles that may allow the precise diagnosis. In the case of rim-enhancing lesions, the spectral pattern permits differentiation of pyogenic abscess from tumors by demonstrating the presence of amino acid peak (0.9 ppm) in abscesses. MR spectroscopy not only helps to distinguish infective from noninfective lesions but also may give information on the type of infective agent, which may guide the clinician to initiate appropriate antibiotic therapy, while the pus culture results are awaited. So, when appropriately incorporating MRS into the neuroradiologic evaluation, this technique will produce relevant information to radiologists and clinicians for their understanding of adult and pediatric neurologically based disease processes. Now that we have demonstrated MRS is a powerful technique that can improve our diagnostic capability, in order to implement MRS in our practice, we need be familiar with some technical issues, such as: 1-Magnetic field strengths - since the main objective of proton MRS is to detect weak signals from metabolites, a minimum of 1.5T is advised; 2-Protons (^{1}H) are the most used nuclei for clinical applications of MRS in the human brain; 3-Single voxel and multivoxel MRS- what should be my choice? 4-PRESS x STEAM- which one is better? 5-What is necessary to obtain a diagnostic quality spectra? All of the previously mentioned issues will be addressed. Finally,

Note: Scanned images are included in the proceedings. Some submitted images were reduced during editing, thereby decreasing clarity. Also, refer to the Program Planner. Proceedings Content as of 3-29-2013.

to implement MRS in our service we also need to be familiar with the main metabolites and their meaning. We need to know spectra is age specific, parameter specific and region specific, which means the metabolites observed in the spectra are related to patient's age, the technique employed in terms of TE and TR and the region where the voxel was placed. Finally, we need to know that some differences will be observed in the spectra obtained in a 1.5T x 3T. Now, we can get started!

O-353 **5:15 PM - 5:30 PM**

fMRI

Shah, G. V.
University of Michigan
Ann Arbor, MI.

Presentation Summary
Mapping of various brain functions before surgery was mainly by structural MRI and surface anatomy. Physiologic tests like WADA could determine laterality of brain for language function, but was deemed invasive, expensive and elaborate. Intraoperative electrocorticography and direct cortical electrical stimulation (DCES) are very precise tests, but utilize much precious OR time, require a large team and can be challenging, especially for language function. Advent of fMRI has allowed detailed mapping of various brain functions and fusing them with structural images result in precise localization. This is an attractive alternative to more invasive and elaborate older tests for brain mapping. Having a clinical fMRI service can add a great value to a clinical radiology service; it can enhance its utility and engender greater confidence in radiologists' ability to help a neurosurgeon. However, the changeover poses challenges for both the radiologist and the neurosurgeon. The challenges include logistical challenges, scheduling challenges and personnel challenges. Technical issues related to conducting the test, postprocessing the test and delivering the test to neurosurgical navigation program should be resolved beforehand. There is a diverse vendor pool for different moving parts and components of the operation, which should be integrated well. Matters related to operational efficiency, physician communication and education also should be resolved in an efficient manner. Addressing and overcoming these challenges while starting a new fMRI service, while imparting excellent fMRI maps can win the trust and confidence of referring physicians and translate in increased efficiency and enhanced work flow.

O-354 **5:30 PM - 5:45 PM**

CT Perfusion

Wintermark, M.
University of Virginia
Charlottesville, VA.

Presentation Summary
I will present a practical approach to implement a new imaging service at an institution, taking perfusion CT as an example.

O-355 **5:45 PM - 6:00 PM**

MR Perfusion

Preece, M. T.
Radiology Imaging Associates
Denver, CO.

Presentation Summary
MR perfusion imaging can be a simple and valuable adjunct in tumor analysis. A pragmatic approach to the interpretation of MR perfusion imaging as it relates to tumor will be presented, particularly geared toward the private practice radiologist. Discussion will include basic perfusion principles as well as several examples from clinical practice.

O-356 **6:00 PM - 6:15 PM**

DTI and Tractography

Chepuri, N. B.
Abbott-Northwestern Hospital
Minneapolis, MN.

Presentation Summary
I will discuss the methods that can be used to successfully implement an advanced MRI algorithm such as DTI into a private radiology practice.

Note: Scanned images are included in the proceedings. Some submitted images were reduced during editing, thereby decreasing clarity. Also, refer to the Program Planner. Proceedings Content as of 3-29-2013.

Wednesday Morning

7:30 AM - 9:00 AM
Ballroom 6AB

(37) General Programming: How Does the Brain Think? From Cytoarchitecture to Neurotransmission and Imaging

O-357 **7:30 AM - 8:00 AM**

Cortical Chemoarchitecture

Zilles, K.
Institute of Neuroscience and Medicine
Jülich, GERMANY.

Presentation Summary

Transmitter receptors are key molecules of neurotransmission and connectivity. Their *regionally specific distribution patterns* differ between sensory, motor and multimodal association areas as well as between various areas within each of these major functional groups. The receptor-based regional segregation of the cerebral cortex is further differentiated by the *layer specific distribution patterns* of receptor densities. Thus, mapping of transmitter receptor distributions provides data for understanding the molecular basis of cortical organization and connectivity. Borders of cortical areas and layers can be precisely defined by localized changes of the density of single or multiple receptor types calculated in single cortical layers or averaged over all layers. In most cases, receptorarchitectonic borders are found at precisely the same positions, where borders are also detectable in cytoarchitectonic, axonal tracing or functional neuroimaging studies as well as analysis of fibrearchitecture. This finding underlines the representation of connectional aspects by receptor distribution patterns. Receptorarchitectonics can also reveal hitherto unknown cortical areas (e.g., in the Broca region). Furthermore, distribution patterns of multiple receptors in each single area show a specific balance between the various receptors, i.e. the "receptor fingerprint". The cluster analysis of fingerprints of cortical areas reveals segregated systems belonging to different functional modalities and embedded in a hierarchical organization.

The thalamic input to the primary sensory cortical areas terminates in layer IV and supragranular layers. We hypothesized, that this connectional aspect of is reflected by laminar distribution of receptors in all primary sensory areas. Very high densities of $GABA_A$, muscarinic M2 and α_2 receptors are found in the supragranular layers and particularly layer IV of the primary visual, auditory and somatosensory cortex. The cholinergic nicotinic receptor is nearly exclusively expressed in layer IV of the primary visual, auditory, and somatosensory areas. In sharp contrast to these primary sensory areas, adjoining secondary sensory areas display significantly lower densities of $GABA_A$, muscarinic M2 and α_2 receptors, but markedly higher densities of other receptors. Motor and multimodal cortices have a completely different, but regionally typical laminar distribution pattern.

In conclusion, regional and laminar multiple receptor distribution patterns provide a comprehensive overview of known and novel organizational principles of cortical connectivity.

O-358 **8:00 AM - 8:30 AM**

Specific Brain Circuits, Default Networks and Task Networks

Schmahmann, J. D.
Massachusetts General Hospital and Harvard Medical School
Boston, MA.

Dr. Jeremy D. Schmahmann is Professor of Neurology at Harvard Medical School and Neurologist at the Massachusetts General Hospital where he is Director of the Ataxia Unit, a member of the Cognitive Behavioral Neurology Unit, and Director of the Laboratory for Neuroanatomy and Cerebellar Neurobiology. He received his medical degree with distinction at the University of Cape Town, completed residency in the Neurological Unit of Boston City Hospital, and postdoctoral fellowship in the Department of Anatomy and Neurobiology at Boston University. Dr. Schmahmann's research focuses on anatomical substrates of cognition. He pioneered the role of the cerebellum in intellect and emotion, and received the Norman Geschwind Prize in 2000 from the American Academy of Neurology and the Behavioral Neurology Society, and the American Neurological Association's Distinguished Neurology Teacher Award in 2008. He is a Fellow of the American Academy of Neurology, and the American Neuropsychiatric Association. He has been cited in The Best Doctors in America since 1996. His >175 publications include The Cerebellum and Cognition (Academic Press), MRI Atlas of the Human Cerebellum (Academic Press), Fiber Pathways of the Brain (Oxford University Press), Cerebellar Disorders in Children (Mac Keith Press), and Handbook of the Cerebellum and Cerebellar Disorders (Springer).

Presentation Summary

It is premature to believe that we know precisely how or why humans are endowed with the inner workings of the mind. There is sufficient anatomical, imaging, and clinical evidence available however, to allow for a consideration of the neural basis of the mental operations essential for thought. The constituent elements of the neural basis of

Note: Scanned images are included in the proceedings. Some submitted images were reduced during editing, thereby decreasing clarity. Also, refer to the Program Planner. Proceedings Content as of 3-29-2013.

thought are the 20 billion neurons of the cerebral cortex arranged in multiple distinct areas and characterized extensively with respect to their morphologic and cellular specialization, the remaining 80 billion or so neurons of the subcortical nuclei and cerebellum, and the white matter paths that link these geographically distant areas into distributed neural circuits. The evidence from anatomical investigations in nonhuman primates of the existence and functional properties of these circuits receives support from functional MRI studies in humans showing activations in interconnected brain areas by task-specific conditions, and from resting-state functional connectivity MRI studies that reveal networks of brain areas active during the apparent brain-idling state and during directed cognitive processes. These functional studies are supported by the identification using diffusion tensor MRI in humans of white matter tracts that link cortical and subcortical areas, producing results in agreement also with analyses of these pathways in nonhuman primates. The question of how the vast, complex, and intricate neural architecture of the brain subserves as elusive a concept as thought is both intriguing and vexing. This lecture will attempt to address this question by considering first what we mean by thought, drawing on the insights of educators and philosophers. Next we will review the general and specific principles of brain organization (Schmahmann and Pandya 2006, 2008) and the nature of cortico-cortical and selected subcortical connections. We will draw on the principles of anatomical organization of the brain to provide an approach to understanding how the nervous system functions to support emotion, as well as trivial, contemplative and reflective thought, and deductive reasoning. Finally, we will discuss selected clinical scenarios that provide empirical evidence in support of these notions.

O-359 **8:30 AM - 9:00 AM**

Different Types of Neurotransmission

Naidich, T. P.
Mount Sinai Medical Center
New York, NY.

Presentation Summary
Thought is the net result of the underlying architecture of the brain cortex (cytoarchitecture) and white matter (myeloarchitecture), the distribution of neurotransmitter receptors within the brain (chemoarchitecture), and the pattern of interconnecting regions that make up the multiple circuits and hubs of the brain (connectivity). This session explores the regional specializations of gray and white matter that are the anatomical underpinnings of thought, extends these to the synaptic, bulk transmission and electrical synchronizations by which regions communicate, and presents our current theories as to how these interact to achieve the task-directed activity, emotional feelings and cognitive accomplishments that are the human mind.

Wednesday Morning

9:30 AM - 10:00 AM
Ballroom 6AB

(38) Keynote Speaker

O-360 **9:30 AM - 9:50 AM**

Imaging as Cash Cow or Cooked Goose? Thriving in a New Era of Neuroradiology

Sorensen, A.
Siemens Healthcare
Malvern, PA.

Imaging has had a very strong track record of innovation but also is perceived as being an expensive and often overused family of technologies. What does the future hold for imaging? How will evolving reimbursement models impact the demand for what neuroradiologists do? What are the key steps we as a specialty need to take in order to remain relevant in the years ahead? This presentation will discuss potential answers to these questions based on the evolving framework of medical care in the United States.

Wednesday Morning

10:00 AM - 10:15 AM
Ballroom 6AB

(38a) ASNR Presidential Address – Pamela W. Schaefer, MD

O-361 **10:00 AM - 10:15 AM**

Presidental Address

Wednesday Morning

10:15 AM - 10:30 AM
Ballroom 6AB

(38b) Award Announcements

O-362

Gold Medal Award

Note: Scanned images are included in the proceedings. Some submitted images were reduced during editing, thereby decreasing clarity. Also, refer to the Program Planner. Proceedings Content as of 3-29-2013.

O-363

Honorary Member Award

Wednesday Morning

10:30 AM - 11:00 AM
Ballroom 6AB

(38c) ASNR Annual Business Meeting (members only)

O-367 **10:30 AM - 11:00 AM**

ASNR Annual Business Meeting (members only)

Wednesday Morning

11:15 AM - 12:15 PM
Ballroom 6AB

(39) Maintenance of Certification Review Session: Brain (AR)

O-368 **11:15 AM - 11:45 AM**

Brain - Part I: Brain Tumor: Imaging Pearls

Fatterpekar, G. M.
New York University School of Medicine
New York, NY.

Learning Objectives
Upon completion of this presentation, participants will be able to:
1) Highlight distinguishing features of vasogenic and cytotoxic edema.
2) Discuss important tumor mimics including subacute infarction, vasculitis, inflammatory and demyelinating conditions. Provide the attendee with certain key distinguishing features to help differentiate tumor mimics from tumor.
3) Discuss imaging features to distinguish primary neuroglial neoplasms from metastasis.
4) Discuss imaging features to distinguish low-grade from high-grade neoplasms.
5) Discuss key imaging features that can help the neuroradiologist suggest the pathology of the underlying neoplasm.
6) Discuss tumor recurrence from treatment-induced changes including pseudoprogression and pseudoresponse.

O-369 **11:45 AM - 12:15 PM**

Brain - Part II

Filippi, C. G.
Columbia University College of Physicians and Surgeons
New York City, NY.

Learning Objectives
Upon competion of this presentation, participants will be able to:
1) Describe classic imaging findings and clinical presentations of both common and uncommon demyelinating diseases of the brain.
2) Explore the role of MR imaging in disease management in demyelinating disease and the utility of advanced neuroimaging techniques in framing differential diagnoses.
Presentation Summary
This session will present cases of demyelinating disease of the central nervous system beginning with a classic case of multiple sclerosis (MS) in which discussion will focus on reviewing the most recent revised McDonald Criteria in 2010 as well as considering newer MR techniques to address cortical lesion detection. Current issues in therapy and the use of MR in patient management are going to be highlighted. Additionally, more challenging cases of multiple sclerosis will be shown including tumefactive MS lesions and Marburg variant or malignant multiple sclerosis. In these cases, there will be emphasis on the use or potential shortcomings of advanced imaging techniques that may help in shaping the differential diagnosis. Complications of new therapies for MS including progressive multifocal leukoencephalopathy (PML) and immune reconstitution inflammatory syndrome (IRIS) associated with cessation of therapy following PML development will be featured. In the classic differential of multiple sclerosis, there are other considerations. Additional cases that are grouped in MS traditionally include Lyme and acute disseminated encephalomyelitis (ADEM), and there will be a discussion on current thinking in ADEM. Neuromyelitis optica (NMO), long considered a variant of MS, will be featured as a case because NMO is being recast currently as a distinct entity with its own unique diagnostic criteria. Lastly, a final case of Susac syndrome will be shown as it is commonly misdiagnosed as MS or ADEM, and its classic clinical features and imaging findings will be demonstrated.

Note: Scanned images are included in the proceedings. Some submitted images were reduced during editing, thereby decreasing clarity. Also, refer to the Program Planner. Proceedings Content as of 3-29-2013.

Wednesday Afternoon

1:15 PM - 2:45 PM
Ballroom 6AB

(40) ASHNR Programming: Evidence-Based Imaging in the Head and Neck

O-370 **1:15 PM - 1:45 PM**

Evaluation of the Patient with a Thyroid Mass: Best Practices

Aiken, A. H.
Emory University Hospital
Atlanta, GA.

Presentation Summary
The evaluation of thyroid nodules and masses is a broad, complex and controversial topic. This presentation aims to look at the current evidence for three of the most common clinical scenarios: 1. Incidental thyroid nodule on CT or MRI: When to recommend ultrasound or biopsy? 2. Palpable thyroid mass: What is the best test? 3. Preoperative evaluation of a thyroid mass with cancer diagnosis: What is the best test? Thyroid nodules are extremely common, with approximately 50% at autopsy. Most of these nodules are less than a centimeter. Thyroid cancer also is common, but not nearly as common as thyroid nodules, with approximately 2-5% at autopsy. Thyroid cancer incidence is on the rise without a significant change in mortality rate. There is some evidence that a rising incidence of subcentimeter papillary thyroid cancer results from increased detection on CT. There are no current guidelines for the management of these extremely common incidental thyroid nodules. This presentation will review the current literature and suggest some practical guidelines to help radiologists decide how to report these nodules. The combination of size criteria and clinical risk factors such as age is the best approach to date. The common practice of using a 10 mm size threshold alone to recommend ultrasound (US) is arbitrary and results in excessive work-up of these incidental nodules, cost and patient anxiety. Current evidence suggests that a stratification approach, incorporating aggressive imaging findings, age younger than 35-40 years, and a15 mm cutoff for triaging work-up, may reduce this excess work-up of benign ITNs while capturing the same proportion of thyroid malignancies. Ultrasound is the study of choice for the evaluation of an intrathyroidal mass or nodule. CT has no signs that help to differentiate malignant from benign thyroid nodules and is therefore not the study of choice. The Society of Radiologists in Ultrasound (SRU) has developed ultrasound criteria to determine high- risk nodules and prompt fine needle aspiration (FNA) for diagnosis. The SRU recommends FNA for the following US characteristics: 1. >1 cm & microcalcification. 2. > 1.5 cm solid or coarse calcifications. 3. > 2 cm mixed solid & cystic components. 4. Nodule w/ substantial growth. 5. Nodule w/ abnormal cervical lymph nodes. The American Thyroid association (ATA) guidelines also currently recommend ultrasound as the preoperative study of choice for evaluation of uncomplicated thyroid cancer. However, cross-sectional imaging should be recommended for cases with: 1. Aggressive pathology. 2. Clinical signs of extra-thyroidal extension: vocal cord palsy, fixed mass, dysphagia, respiratory symptoms, etc. 3. Lateral compartment lymphadenopathy by palpation or ultrasound. Many thyroid cancer experts also would consider cross-sectional imaging for ultrasound or palpable central compartment lymphadenopathy.

O-371 **1:45 PM - 2:15 PM**

Imaging Evaluation of CSF Leak: What Study to Order

Hudgins, P. A.
Emory University School of Medicine
Atlanta, GA.

Presentation Summary
Evidence-Based Practice: integration of individual clinical expertise, patient values, and the best research evidence into the decision-making process for patient care. For diagnosis of CSF leak EB research is lacking for virtually every modality we currently use! Therefore, discussion of imaging modalities that follows is based on individual clinical experience/expertise. Our approach was developed by consensus between ENT and Neurological Surgical Departments and Head and Neck Radiology Section. **Cerebrospinal fluid (CSF) leak** is defined as extradural CSF extending through a dural and arachnoid defect, into the paranasal sinus cavities, nasopharynx, mastoid air cells or middle ear cavity. Intraspinal CSF leak can occur either through a tear in a nerve root sleeve or directly through meninges, and clinical presentation is usually a low pressure headache syndrome . Only CSF leaks above the foramen magnum will be discussed. **Rhinorrhea:** CSF leak into the nasal cavity or paranasal sinuses. **Otorrhea:** CSF leak into mastoids or middle ear cavity. **Clinical presentation** is variable, but common symptoms are oto or rhinorrhea and patient often complains of a salty taste or nasal drip that does not respond to nasal vasoconstrictors. Chronic mastoid or middle ear opacification unresponsive to tympanostomy tubes, is presenting complaint when the leak is in the tegmen tympani or mastoideum. If the leak is high volume, daily low pressure headaches may occur, worse at the end of the day. Prior to modern imaging techniques and improved recognition of the syndrome, meningitis was common, but current rates are probably lower than 10%. However, meningitis is a dreaded complication with dramatic neurologic sequelae. **Etiology for CSF leak** is

Note: Scanned images are included in the proceedings. Some submitted images were reduced during editing, thereby decreasing clarity. Also, refer to the Program Planner. Proceedings Content as of 3-29-2013.

either congenital or acquired. **Congenital leaks** usually are due to a meningocele or meningoencephalocele and generally manifest early in life. Inner ear anomalies may be associated with peri or endolymph leaking into the middle ear, often mixed with CSF. **Acquired leaks** are much more common. Postoperative and post-traumatic leaks account for > 60% of all leaks. Spontaneous leaks are increasing in frequency, especially in the United States where average BMI is rising. **Diagnosis** can be straightforward, or difficult and complicated. It is critical that the presence of a leak be proven prior to imaging, and the first step should be to collect 1-2 ccs to check for ***B_2*-transferrin or Beta-trace protein, specific to CSF,** for immunoelectrophoresis protein assay. **Imaging should not be used to diagnose a CSF leak, but to find the source of the leak. PICO: Problem/Intervention/Comparison/Outcome PICO:** Known CSF leak/Diagnostic test/ 1) nuclear medicine cisternogram vs 2) high-resolution CT versus 3) CT-cisternogram versus 4) MRI brain versus 5) MR-cisternogram versus 6) intrathecal gadolinium cisternogram. **Nuclear medicine - cisternogram.** Rarely necessary, only in questionable cases. Limitations: patient must be actively leaking, lacks anatomical detail. **High-resolution computed tomographic (CT) scan of skull base**, including cribriform plate, ethmoid sinus roof, all walls of sphenoid sinus, mastoid complex, region of geniculate ganglion and middle ear complexes. Include tympanic cavity even if rhinorrhea and not otorrhea is described. Technique is critical, must be thin-section, no patient motion, bone algorithm. Reformations in all planes, even oblique, to assess for skull base bony defect. Careful review on work-station, as skull base defect may be small. Standard sagittal and coronal reformations may not be best plane to display defect. **Imaging findings:** Bone defect, fluid in dependent portion of sinus, or mucosal thickening at level of defect from CSF beneath intact mucoperiosteum. Bi-dimensional measurement of defect, precise description of location help plan repair. Active leak at time of study NOT required. **CT-cisternogram.** Only required if > 1 bone defect present on noncontrast CT, or if confirmation is requested by surgeon. Pt must be actively leaking or leak can be exacerbated by Trendelenburg position or other maneuver on day of study. Start with non-contrast high-resolution CT. LP - 5-7 ccs intrathecal contrast, placement confirmed at fluoroscopy. Perform provocative maneuvers to see leak. Repeat CT, prone coronal, within one hour of LP, so contrast will pool in dependent portion of sinus, mastoid or middle ear, or nasal cavity. Prone position may exacerbate leak by increasing intracranial pressure. For difficult or small leaks, repeat high-resolution CT, supine, after prone study so that reformations can be performed. Review soft tissue algorithm to assess for meningocele. **MRI brain and cisternogram.** Should not be primary diagnostic modality. Always obtain MR to see if soft tissue in sinus is from intra-cranial compartment, ie, meningocele, or meningoencephalocele. Encephalocele or meningocele usually associated with encephalomalacia at site. Dural enhancement with contrast MR is not uncommon and does not always mean meningitis is present. **Intrathecal gadolinium.** Promising early results with this technique suggest high sensitivity for detecting skull base and spinal leaks. Pre-LP do T1 and T2 imaging through skull base in three planes. 0.5 ml intrathecal gadolinium. Repeat scans with T1 fat saturation techniques after LP. Scans can be obtained up to 24 hours after LP to enable detecting low volume leaks.

O-372 **2:15 PM - 2:45 PM**

Imaging of Hyperparathyroidism: An Era of Modalities and Multiple Phases

Hoang, J. K.
Duke University Medical Center
Durham, NC.

Presentation Summary
1. The role of parathyroid imaging is to accurately localize the parathyroid adenoma in eutopic and ectopic locations, and to detect multiglandular disease. The traditional modalities for parathyroid imaging are cervical ultrasound and nuclear scintigraphy. 4D CT has advantages common to both ultrasound and scintigraphy and is useful as a second-line investigation. 2. The 4D CT protocol is comprised of multiple phases (typically two to four phases) and reformatted images in three planes. 3. Characteristic enhancement pattern for a parathyroid adenoma on 4D CT is peak enhancement on an arterial phase, washout of contrast from the arterial to delayed phase and low attenuation on the noncontrast images. The morphologic imaging findings are central low attenuation change, lobulated margins, and a feeding artery or enlarged draining vein. 4. Interpretation of parathyroid imaging is challenging because of ectopic lesions, multiglandular disease, and lesion mimics such as thyroid nodules and lymph nodes. The radiologist's ability to detect a parathyroid lesion on 4D-CT and differentiate it from mimics can be increased with appreciation of the typical enhancement characteristics and morphologic features.

Note: Scanned images are included in the proceedings. Some submitted images were reduced during editing, thereby decreasing clarity. Also, refer to the Program Planner. Proceedings Content as of 3-29-2013.

Wednesday Afternoon

1:15 PM - 2:45 PM
Ballroom 6CF

(41) Special Session: Human Papillomavirus and Head and Neck Cancer

O-373 **1:15 PM - 1:35 PM**

The Epidemic of HPV-Associated Oropharyngeal Cancer

Sturgis, E. M.
The University of Texas M.D. Anderson Cancer Center
Houston, TX.

Dr. Sturgis joined the faculty of the Department of Head & Neck Surgery as assistant professor with a joint appointment in Epidemiology at The University of Texas M.D. Anderson Cancer Center in 2000. He completed a Master of Public Health in 2004 and was promoted to associate professor with tenure in 2005 and full professor with tenure in 2010. His principal research interests are human papillomavirus and molecular epidemiology of carcinomas of the head and neck region. His work has generated numerous interviews with the lay press, including mention in U.S.News and World Report, the New York Times, and the Wall Street Journal. Additionally, he has explored these trends and potential genetic risk factors for HPV-associated cancers in additional publications. His principal clinical interests are sarcomas of the head and neck region and differentiated thyroid cancer. He has over 190 peer-reviewed publications and over 40 invited reviews/book chapters. He has been/is principal investigator on a NIH R03, an American Thyroid Association grant, a Fanconi Anemia Research Fund grant and project leader on a NIH U01 grant, as well as co-investigator on 3 NIH R01 and 2 NIH SPORE grants, co-mentor on a NIH K07 and recipient of three career development awards.

Presentation Summary
This presentation will review the epidemiology of the epidemic of human papillomavirus (HPV)-associated oropharyngeal cancer. This discussion will cover the basics of HPV oncogenesis as well as the behaviors associated with this disease. The typical clinical presentation of HPV-associated oropharyngeal cancer will be reviewed. Much of this presentation will cover the dramatic demographic shifts and public health impact of the rising incidence in oropharyngeal cancer in the U.S.

O-374 **1:35 PM - 1:55 PM**

Imaging of HPV-Related Oropharyngeal Cancer

Ginsberg, L. E.
M.D. Anderson Cancer Center
Houston, TX.

Presentation Summary
HPV-associated oropharyngeal squamous cell carcinoma is an increasingly recognized and distinct clinic-pathologic entity. This presentation will review the MD Anderson experience of imaging findings associated with this malignancy, to include characteristics that may distinguish the HPV +ive vs. HPV –ive primary malignancy, the issue of cystic nodal metastases typical of this diagnosis and the associated problem of misdiagnosis, and finally, the imaging spectrum of atypical nodal patterns and distant metastatic sites that are increasingly being observed with HPV-associated oropharyngeal cancer.

O-375 **1:55 PM - 2:15 PM**

Treatment Implications of HPV-Associated Oropharyngeal Malignancy

Rosenthal, D. I.
The University of Texas M.D. Anderson
Houston, TX.

Presentation Summary
There is an epidemic of oropharynx cancer and a shift in demographics from tobacco-related to HPV-related.
The standard AJCC staging system based on TNM categories is no longer predictive of prognosis in the HPV era.
I will discuss treatment selection including RT, chemotherapy, and surgery. New techniques including endoscopic surgery and proton therapy will be discussed.
Since patients with HPV+ oropharynx cancers have a better prognosis than tobacco-related cancers, current clinical trials focusing on treatment de-intensification to reduce toxicities and promote better functionality will be discussed.

Note: Scanned images are included in the proceedings. Some submitted images were reduced during editing, thereby decreasing clarity. Also, refer to the Program Planner. Proceedings Content as of 3-29-2013.

Wednesday Afternoon

1:15 PM - 2:45 PM
Ballroom 6DE

(42) ASSR/ASFNR Programming: Imaging Tools Which Will Shape Future Spine Imaging

O-376 **1:15 PM - 1:40 PM**

The Future of Spinal Imaging: Is There Still Room for Plain Films?

Van Goethem, J. W.
Antwerp University Hospital
Antwerp (Edegem), BELGIUM.

Presentation Summary

A plethora of imaging techniques is available to visualize the spine. The most recent techniques, especially magnetic resonance imaging (MRI), allow in detail visualization of spinal structures and have been able to depict spinal pathology in detail and accurately. Awareness of the possible harmful effects of ionizing radiation used in diagnostic spinal imaging have further weakened the position of plain film spinal imaging as an imaging modality. One might wonder if there is still room for plain film spinal imaging in 2013. In this presentation I will emphasize situations where plain films still have a key role in spinal imaging. Using new technical developments radiation levels can be kept to a minimum. Careful use of plain films for well defined indications is still very valuable in the diagnostic work up of several disease entities. Moreover, plain films are still the only imaging method, besides niche techniques, allowing to image the patient standing with optional flexion/extension films. I will show imaging algorithms that will allow radiologists to determine exactly for what indications plain film spine imaging should be used today.

O-377 **1:40 PM - 2:00 PM**

Advanced Imaging: The Next 50 Years

Thurnher, M. M.
Medical University Vienna
Vienna, AUSTRIA.

Presentation Summary

Findings on conventional MRI in spinal cord diseases are not specific to the severity of cord damage and are unable to discriminate potentially reversible edema and/or ischemia from irreversible changes. Despite significant expansion of imaging capabilities, the spinal cord has continued to pose great challenges. The introduction of high-field MRI has substantially altered spinal cord imaging. *DTI metrics* and *fiber tracking (FT)* allow more accurate characterization of intrinsic integrity of tissues including cellular density and architecture. After initial technical problems, good solutions that have overcome some of the initial challenges have helped to incorporate DWI and DTI into everyday clinical MR routine. *Perfusion MR imaging (PWI)* may provide a significant advantage in the diagnosis of neoplastic or infectious processes in the spine. *Ultrafast MRI* has been shown to drastically decrease scan time. Today, we're just at the beginning of "Sci-Fi spinal imaging". It is more than a prophecy that the next generation imaging techniques will provide an excellent set of biomarkers for understanding diseases of the spinal cord.

O-378 **2:00 PM - 2:20 PM**

Novel Imaging of Disks

Hackney, D. B.
Beth Israel Deaconess Medical Center
Boston, MA.

David Hackney is Chief of Neuroradiology at Beth Israel Deaconess Medical Center and Professor of Radiology and Assistant Dean for Faculty Development at Harvard Medical School. He has served HMS in numerous capacities including co-chairing the Faculty Development Working Group for the Medical Education Reform process, and chairing the Faculty Diversity Committee. Dr. Hackney has published over 170 original manuscripts, as well as editorials, reviews and chapters, and hundreds of abstracts. His academic work has focused on spine and spinal cord imaging, with particular interest in MR imaging of spinal cord injury. ***He has served on numerous NIH federal advisory boards including the Trauma Task Force, the Medical Imaging Study Section (MEDI-regular member) for the Center for Scientific Review, the Training Grant and Career Development Committee (NST-regular member) for NINDS, and special emphasis panels for the NCI. He also has served as a member of the federal Food and Drug Administration, Radiological Devices Panel, Medical Devices Advisory Committee, for which he is now a Consultant. He was also a member of Veteran's Administration State of the Art Conference on Traumatic Brain injury.*** *He is a Past President of the American Society of Neuroradiology, and a fellow of the American College of Radiology and the International Society of Magnetic Resonance in Medicine. He consistently appears on lay "Best Doctors" lists. Dr. Hackney's primary research interest concerns MR imaging of spinal cord injury.*

Presentation Summary

Many years of study of the intervertebral disk, and advances in MR imaging in the last few decades, have shed considerable light on the complex degenerative process. It is clear that the changes in the composition of the disk are closely related to the stresses to which it is subjected and its nutrition. The disk loses its constituent

Note: Scanned images are included in the proceedings. Some submitted images were reduced during editing, thereby decreasing clarity. Also, refer to the Program Planner. Proceedings Content as of 3-29-2013.

glyclosaminoglycans (GAG), loses water, and collagen and macromolecular degradation products accumulate in this nearly avascular tissue. All of the above alter the MR characteristics of the disk in reproducible ways. This means that we now have the ability to predict the macromolecular composition of the disk by employing a combination of MR methods. Even more exciting, there has been substantial progress in understanding the mechanical function of the disk, how it is changed by degeneration, and how degeneration progresses. With the ability to interrogate not only composition, but also structure, we can begin to predict degradation of disk function with MR. This opens the possibility of individualized treatment, better prediction of disease progression in the absence of treatment, and the response to therapy. Among the methods we will consider are approaches to estimating the content of water and GAG, integrity of the annulus fibrosus, mechanical stiffness and damping coefficient of the disk, and responses to loading. We will discuss T2, T1 and proton density maps, along with sodium imaging, magnetization transfer, chemical exchange saturation transfer (CEST), and diffusion methods.

O-379 **2:20 PM - 2:45 PM**

Ultra High Field and Novel MR Imaging in the Human CNS

Atkinson, I. C.
University of Illinois at Chicago
Chicago, IL.

Presentation Summary
The major challenge of healthcare today is the containment of costs without compromise of quality of care and hopefully with improved patient outcome. Imaging has been blamed as one of the cost drivers. This economic perspective requiring “more for less” may appear at odds with the introduction of new MR technologies, such as ultra-high field 7.0 and 9.4T MR scanners, hyperpolarization and quantitative metabolic MR imaging. However, this is only if these new technologies address the same clinical questions. A less pessimistic strategy is to address more pertinent clinical questions beyond those available from proton MR imaging. Metabolic MR imaging based on 23-sodium, 17-oxygen, 13-carbon, 31-phosphorus and 39-potassium have been demonstrated in the human and clinical applications are being evaluated. Quantification of signals into bioscales rather than image contrast allows numerical modeling that can provide valuable insight into disease processes not possible with anatomical imaging. Quantitative sodium imaging that provides direct measurement of tissue viability and cell density at clinically useful spatial resolution in less than 10 minutes will be demonstrated as a prototypical bioscale in the clinical setting of brain tumor management. But how will cost be managed? Technologies that can assess treatment responses in near real-time (i.e., during treatment) address the question of whether the therapy is appropriate. Patients who do not respond can be triaged into more effective therapies. Costs of ineffective and often expensive treatments thereby can be avoided early and the patient does not suffer untoward consequences of inappropriate therapy needlessly. Decisions as to treatment protocols no longer have to be based on population studies where survival is the clinical outcome measure but rather true personalized medical care can be delivered. Costs of such new technology are covered by the redistribution of costs from ineffective treatments and improved patient outcome. These new quantitative metabolic MR imaging methodologies will be described in relation to clinically relevant diseases of the central nervous system where better information can facilitate more effective medical management. Replacement of existing less effective procedures may be expected to make these new technologies cost neutral.

O-379a **2:45 PM - 2:53 PM**

Diffusion-Weighted MRI “Claw Sign” in Differentiation of Infectious from Degenerative Disease – ASSR Mentor Award Winner

Patel, K.·Poplawski, M.·Pawha, P.·Naidich, T.·Tanenbaum, L. N.
The Mount Sinai Medical Center
New York, NY.

Purpose
Modic signal changes, a common observation in MR imaging, are signal intensity findings in vertebral body marrow adjacent to the endplates of degenerative disks. Type II and III patterns are easy to recognize and indicative of chronic degenerative disease. Type I Modic change is more likely to be clinically symptomatic and characterized by decreased signal on T1WI and increased signal on T2WI that can be difficult to differentiate from and often suggestive of vertebral osteomyelitis and diskitis (1). Of late, diffusion-weighted MR imaging (DWI) has been shown to be a useful tool in imaging of osseous and epidural spinal lesions, including spinal infection (2). In this retrospective observational study of patients who were referred for spinal MRI, we characterize and correlate the MRI appearance of spinal levels in patients with Modic I signal changes, and in patients with confirmed spinal infection, with particular attention to the presence or absence of the DWI “claw sign”.
Materials & Methods
Seventy-four patients with Modic I type endplate abnormalities were selected and classified into three groups: clinically confirmed diskitis/osteomyelitis (n=21), degenerative Modic I change (n=33), and suggestive of infection but clinically disproved (n=20). Each abnormal spinal level was evaluated in terms of MR endplate and disc signal changes, enhancement, and appearance on DWI (b value of 500s/mm2). The presence of diffusion “claw sign” was scored on a scale of 1=definite,

Note: Scanned images are included in the proceedings. Some submitted images were reduced during editing, thereby decreasing clarity. Also, refer to the Program Planner. Proceedings Content as of 3-29-2013.

2=probable, 3=questionable, 4=absent (diffuse DWI signal).
Results
Type I changes in the absence of infection invariably correlated with a characteristic DWI "claw sign" of high diffusion signal at the boundary of the proliferative marrow process and the normal marrow, while patients with type I Modic signal and confirmed spondylodiskitis exhibited significant absence of the "claw sign" on DWI (average "claw" score of 1.21±0.07 vs. 3.67±0.17, p<0.01). Similarly, the group in which infection was initially suggested, but subsequently discounted, had an average score of 1.45±0.13. Suggestion of infection seemed to be related to the presence of high T2 signal in the disk space, which in this study had a high sensitivity, but low specificity for infection. On the other hand, absence of the "claw sign" (combined score 3 and 4) had a high sensitivity (90%), specificity (98%) and predictive values for infection.
Conclusion
DWI offers powerful characterization information in patients with Type I Modic MR signal changes and assists in the differentiation of degenerative disease from spondylodiskitis of the spine.

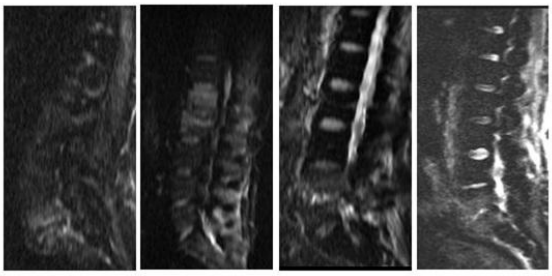

Wednesday Afternoon

1:15 PM - 2:45 PM
Room 5AB

(43) Socioeconomic Programming

O-380 **1:15 PM - 1:40 PM**

Performance Measures and PQI

Seidenwurm, D. J.
Radiological Associates
Sacramento, CA.

Presentation Summary
Performance measures are employed to improve patient care, especially in areas where gaps in care are documented in the literature. Performance measures in neuroradiology attempt to specify quality care in a manner that is reproducible among various practice sites, actionable by the measured physician, and, most importantly, relevant to the practice of neuroradiology and not excessively burdensome to report. Performance measures are based on high quality evidence as distilled in multispecialty guidelines, and tested in clinical settings prior to introduction. Performance measures are retired when all sites achieve a high level of performance, a uniform threshold is reached and remains stable, or if new evidence or clinical priorities change the ratio of benefit to cost in quality improvement.

O-381 **1:40 PM - 2:05 PM**

Accountable Care Organizations

Beauchamp, N. J.
University of Washington
Seattle, WA.

Norman J. Beauchamp Jr, MD, MHS, is Professor and Chairman of the Department of Radiology at the University of Washington. He holds degrees from Michigan State University (BS in Biology, MD) and The Johns Hopkins School of Public Health (MHS). He is also a Professor of Neurological Surgery and Industrial Engineering at the University of Washington. Dr. Beauchamp completed his radiology residency, neuroradiology fellowship and neurointerventional training at The Johns Hopkins Medical Institution. He joined the faculty at Johns Hopkins in 1996. While at Johns Hopkins, he served as Vice Chairman for Clinical Operations and Interim Chairman. In 2002, he assumed the role of Chairman of the Department of Radiology at the University of Washington. During his tenure, he also has served as President of the UW Physician Practice. Dr. Beauchamp's area of research emphasis has been in developing and applying MRI-based

Note: Scanned images are included in the proceedings. Some submitted images were reduced during editing, thereby decreasing clarity. Also, refer to the Program Planner. Proceedings Content as of 3-29-2013.

advanced imaging techniques to extend the treatment window in acute stroke as well as using imaging to identify risk predictors of stroke and dementia. He was the recipient of the American Society of Neuroradiology Basic Science Fellowship Award and the American Roentgen Ray Society Scholarship. He is the Director of the Epidemiologic Studies Image Analysis Center in the Department of Radiology at the UW. The center has been primarily funded by the NIH National Heart, Lung and Brain Institute and at present is involved in the analysis of three multicenter cohort studies enrolling over 6000 individuals. He has served as a grant reviewer for the NIH, the RSNA R and E Foundation, and currently is on the grant selection Committee for the Walter H. Coulter Foundation Translational Research Partnership Awards in Bioengineering at the University of Washington. He has served as the Chair of the Radiology Research Alliance and as Chair of the Coalition for Bioimaging Research. His efforts as an educator have been lecturing in his area of research focus, participating in Radiology Society educational efforts, and in developing future leaders in Radiology. Pursuant to this, he recently co-edited the book, Radiology Business Practice, How to Succeed. He served on the Editorial Board for the journal Radiology. He has served as Chair of the American Roentgen Ray Society Education/CME Committee. Dr. Beauchamp is currently serving on the Board of Directors of the Society of Chairs of Academic Radiology Departments, The Executive Council of the American Roentgen Ray Society and previously was on the Board of the Association of University Radiologists. He is the incoming President of the American Roentgen Ray Society and President-elect of the Society of Chairs of Academic Radiology Departments.

Presentation Summary
The role of the neuroradiologist in an accountable care organization requires a greater focus on partnership, leadership and integration of care. In this presentation, we will emphasize essential tactics to ensure success in our new health care environment.

O-382 **2:05 PM - 2:30 PM**

RUC and CPT

Donovan, W. D.
William W. Backus Hospital
Norwich, CT.

Presentation Summary
Review and discuss radiology reimbursement issues, with emphasis on Medicare policy changes, RUC activity, and sequestration issues (if necessary).

Wednesday Afternoon

1:15 PM - 2:45 PM
Room 1AB

(44) ASPNR Programming: Pediatric Brain Tumors (SAM) (AR)

O-384 **1:15 PM - 1:40 PM**

Infratentorial Tumors

Poussaint, T.
Boston Children's Hospital
Boston, MA.

Presentation Summary
Brain tumors are the most common solid pediatric tumors and are the leading cause of death in children from solid tumors. The estimated incidence of all childhood primary brain and central nervous system (CNS) tumors is 5.1 cases per 100,000 person-years. Approximately 4,300 new cases of childhood primary nonmalignant and malignant brain and central nervous system tumors will be diagnosed in the United States in 2013.(CBTRUS). Supratentorial tumors are most common in the first 2-3 years of life and infratentorial tumors are most common from age 4-10 years. In children older than 10 years, supratentorial and infratentorial are of equal frequency. When infratentorial tumors involve the posterior fossa they may present with the clinical symptoms of ataxia, dysmetria, headache, nausea, vomiting, neck pain or extraocular muscle impairment. If the tumor involves the brainstem, children may present with extraocular muscle impairment, facial paresis, swallowing problems, hemiparesis, quadriparesis, ataxia or dysmetria. The common posterior fossa tumors of childhood include medulloblastoma, cerebellar astrocytoma, brainstem glioma, and ependymoma. Less frequently diagnosed posterior fossa tumors in children are atypical teratoid/rhabdoid (ATRT) tumors, hemangioblastoma, dermoid-epidermoid tumors, acoustic schwannomas, meningioma, enteric cysts, teratoma and skull base tumors. Improvements in imaging, especially MR, has resulted in improved detection and treatment planning. The understanding of the known molecular genetics, histopathologic and imaging features of some of these tumors, including medulloblastoma, will be reviewed.

Note: Scanned images are included in the proceedings. Some submitted images were reduced during editing, thereby decreasing clarity. Also, refer to the Program Planner. Proceedings Content as of 3-29-2013.

O-385 **1:40 PM - 2:00 PM**

Supratentorial Tumors

Koral, K.
University of Texas Southwestern Medical Center at Dallas
Dallas, TX.

Presentation Summary
Approximately one-half of the pediatric brain tumors are supratentorial. The histopathology of pediatric supratentorial tumors are more varied compared to the cerebellar and brainstem tumors. In addition to the density/signal characteristics of the tumor, the age of the patient and location of the tumor are equally important parameters in forming a relatively short differential diagnosis. It is helpful to categorize the supratentorial tumors into i) Cerebral hemispheric tumors, ii) Sellar/ Suprasellar tumors, iii) Pineal region tumors while generating a differential diagnosis. Astrocytomas are the most common tumors of the supratentorial compartment, pilocytic astrocytomas (WHO grade 1) comprising the majority of them. The supratentorial pilocytic astrocytomas tend to be in the optic-hypothalamic region and are associated with neurofibromatosis type I. Intense enhancement of the solid component and cyst formation are features observed in more than one-half of the pilocytic astrocytomas. Facilitated diffusion is encountered almost universally in pilocytic astrocytomas and may be a valuable adjunct in diagnosis. Other less common astrocytomas include WHO grade 2 tumors such as pleomorphic xanthoastrocytoma and pilomyxoid astroctyoma. Anaplastic astrocytoma (WHO grade 3) is seen uncommonly in children. Gangiogliomas (usually WHO grade 1) is a peripheral tumor of the supratentorial compartment, such as desmoplastic infantile gangliogliomas (DIG) and dysembroplastic neuroepithelial tumors (DNET). Embryonal tumors (e.g., primitive neuroectodermal tumor, atypical teratoid/ rhabdoid tumor) generally show restricted diffusion. Craniopharyngioma is typically associated with cysts and calcifications of the sellar and suprasellar region in children. Germinoma and Langerhans cell histiocytosis of the suprasellar region generally present with diabetes insipidus and nonvisualization of T1 shortening of neurohypophysis. Pineal region tumors include germ cell tumors (e.g., germinoma) and pineal parenchymal tumors (e.g., pineoblastoma).

O-386 **2:00 PM - 2:20 PM**

Effects of Treatment

Rollins, N. K.
Childrens Medical Center
Dallas, TX.

Presentation Summary
In comparison to adults, pediatric brain tumors are rare. However, nearly 20% of pediatric solid tumors arise in the brain. Pediatric brain tumors differ from those seen in adults with respect to location and histologic type. Intracranial metastases from extracranial malignancies and CNS lymphoma are rare in children while the high-grade glial tumors of the cerebral hemisphere seen in adults are uncommon in children in whom infratentorial tumors of embryonal (e.g., PNET, medulloblastoma, etc.) and neuroepithelial tumors predominate. Neurotoxicity associated with pediatric brain tumors may result from the neurosurgical intervention, hydrocephalus, chemotherapy, and/or radiotherapy as many pediatric CNS tumors require radiation therapy for control. Conformational radiation therapy limits exposure of normal regional brain while maintaining or improving local tumor and potentially limiting the toxic effects of radiation on normal brain. As in adults, high-dose conformational radiation therapy may be associated with frank radiation-necrosis that simulates recurrent tumor, although radiation necrosis in uncommon in children. Medulloblastoma/PNET and atypical rhabdoid tumors (ATRT) are associated with occult leptomeningeal disease and tumor recurrence after chemotherapy. Whole brain irradiation with a boost to the tumor bed is needed either once the patient has reached three years of age or earlier if tumor progresses during chemotherapy. Radiation necrosis is a focal process within the tumor bed while radiation neurotoxicity is a global process. Radiation necrosis may present with seizures, altered mental status, neurologic dysfunction similar to that at initial presentation with the tumor, and signs of increased ICP. Diffuse radiation neurotoxicity may be acute, early delayed, or late onset and delayed. Acute neurotoxicity occurs one-six weeks after irradiation and presents with an acute encephalopathy. Early delayed changes occur one-four months after radiotherapy. Affected patients may be sleepy, encephalopathic, and show signs of increased ICP. Acute and early delayed complications are steroid responsive. Late delayed neurotoxicity occurs months to years after treatment and is associated with cognitive decline, personality changes, and gait disturbances and does not improve with steroid therapy. Radiotherapy is particularly deleterious to infants and children under three years of age. Younger age at time of treatment, larger port size, higher dose, and larger number of treatments contribute to the well known cognitive, endocrine and neurologic sequel; the most devastating long-term deficits are neurocognitive. Acute neurotoxicity and significant late treatment effects in long-term survivors of pediatric brain tumors are a substantial burden for patients, their families, and society and a major goal of pediatric cancer therapy is to maintain or improve cure rates while decreasing neurotoxicity. Discussion of neurotoxicity resulting from treatment of childhood cancer is incomplete without considering childhood acute lymphoblastic leukemia (ALL), one of the most common malignancies of childhood and more common than brain tumors. ALL is treated with methotrexate (MTX); a cell cycle-specific agent that inhibits the enzyme dihydrofolate reductase, preventing the conversion of folic acid to

Note: Scanned images are included in the proceedings. Some submitted images were reduced during editing, thereby decreasing clarity. Also, refer to the Program Planner. Proceedings Content as of 3-29-2013.

tetrahydrofolic acid and inhibiting cell replication. Both high-dose intravenous MTX and intrathecal MTX are associated with demyelination, white matter necrosis, loss of oligodendroglia, axonal swelling, microcystic encephalomalacia, and atrophy relatively selective for the deep cerebral white matter. MTX also causes a relative excess of homocysteine, a byproduct of the folate deficiency, which may be responsible for small vessel vasculopathy. L-asparaginase is thought to deprive leukemic cells of the essential amino acid L-asparagine thereby disrupting cell replication. Additional neurotoxic effects of L-asparaginase result from chemotherapy-induced transient protein S deficiency and coagulopathy, leading to intracranial venous and/or arterial thrombosis and hemorrhage; usually intraparenchymal. Potential host factors responsible for heightened sensitivity to MTX and L-asparaginase toxicity include age, sex, race, associated syndromic condition, and pharmacogenetics. Primary chromosomal abnormalities of leukemic cells are known to be associated with different prognoses and genetic polymorphisms encoding for drug-metabolizing enzymes, transporters, and receptors may account for variable sensitivity to toxic side effects. Multi-agent chemotherapy in combination with 1800-2400 Gy cranial irradiation prevents overt CNS relapse at the price of significant neurotoxicity. Cranial irradiation has been replaced with intensive intrathecal and systemic chemotherapy, with low CNS relapse rates. Indications for CNS radiation include CNS disease at presentation, CNS relapse, and unacceptable MTX neurotoxicity.

Wednesday Afternoon

3:15 PM - 4:45 PM
Ballroom 6AB

(45a) Parallel Scientific Papers: Adult Brain: Stroke III

O-387 **3:15 PM - 3:23 PM**

Gaussian Filter versus Downsizing with Antialiasing: Which One is Better to Improve Contrast-to-Noise Ratio of Early Ischemic Change on Noncontrast CT?

Kim, E. Y.[1]·Ahn, S. S.[2]·Shin, N. Y.[2]·Carneiro, F.[1]
[1]The University Hospital, Cincinnati, OH, [2]Severance Hospital, Seoul, KOREA, REPUBLIC OF.

Purpose
It has been documented that early ischemic changes on admission noncontrast CT (NCCT) quantified using ASPECTS to predict outcomes after intra-arterial therapy. However, it has been reported that interobserver reliability of ASPECTS is limited. The low-contrast resolution of NCCT is inherently lower than MRI due to its higher noise. Gaussian filter or downsizing with antialiasing can reduce noise, resulting in improvement of contrast-to-noise ratio (CNR), which may ultimately improve interobserver reliability. However, there has been no comparison study between the two methods. The purpose of this study was to compare the CNRs of normal-appearing gray matter (cortex/basal ganglia; NAGM), normal-appearing white matter (NAWM), and early ischemic change in the cortex and/or basal ganglia among the original images, Gaussian-filtered images, and 128×128-downsized images.
Materials & Methods
We enrolled 30 patients who underwent 5 mm sequential NCCT of the head, demonstrating occlusion in the ICA, M1, and/or M2 on CTA, within six hours of symptom onset. The original 512×512 matrix NCCT DICOM images were processed with Gaussian filter of sigma 2.0 (G2) and 2.5 (G2.5) and downsized with antialiasing to 128×128 matrix images. Regions of interest were drawn in the NAGM, NAWM, and the cortex/basal ganglia showing early ischemic changes in all image sets. The CNR was calculated using the standard deviation of the normal-appearing gray/white matter. Repeated measures ANOVA were conducted for statistical analysis.
Results
The mean CNR between the NAGM and NAWM was 2.12 ± 0.46 in original images, 6.38 ± 1.44 in G2 images, 7.66 ± 2.41 in G2.5 images, and 4.12 ± 0.94 in downsized images (P<0.0001). There were significant differences among the four image sets in post hoc analysis (P<0.0001). The mean CNR between the NAGM and contralateral cortex/basal ganglia showing early ischemic changes was 0.73 ± 0.41 in original images, 1.81 ± 0.95 in G2 images, 2.05 ± 1.09 in G2.5 images, and 0.98 ± 0.59 in downsized images (P<0.0001). There were significant differences among the four image sets in post hoc analysis except for between G2 and G2.5 images.

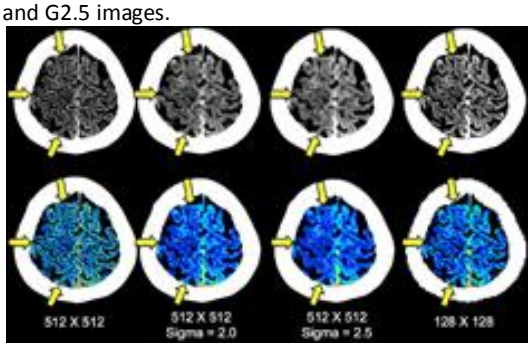

Conclusion
The Gaussian-filtered or downsized NCTT images demonstrate significantly improved CNRs between the NAGM and NAWM, and NAGM and contralateral cortex/basal ganglia with early ischemic changes, which may help improve interobserver reliability of ASPECTS. Gaussian filter is better than downsizing with antialiasing in terms of improvement of CNR.

KEYWORDS: Acute stroke, Postprocessing

Note: Scanned images are included in the proceedings. Some submitted images were reduced during editing, thereby decreasing clarity. Also, refer to the Program Planner. Proceedings Content as of 3-29-2013.

O-388 **3:23 PM - 3:31 PM**

Effect of CT Perfusion Deconvolution Algorithms on Estimation of Penumbra and Ischemic Core in Middle Cerebral Artery Stroke

Nicholson, A.·Hwang, S.·Dehkharghani, S.
Emory Healthcare
Atlanta, GA.

Purpose
Qualitative cerebral blood flow (CBF) maps and quantitative relative cerebral blood flow (rCBV) measurements are used to predict final infarct volume in acute stroke patients. Phantom and clinical studies have shown significant differences in perfusion metrics such as rCBF, when computed with different deconvolution algorithms. In particular, singular value decomposition methods of deconvolution (often used in clinical perfusion analysis software) are known to have varying sensitivities to benign arrival-time delay, which can result in the overestimation of hypoperfused tissue. Our aim is to determine if a correlation exists between CBV abnormality and final infarct core on follow-up MRI and to investigate the degree to which this correlation is affected by the use of different deconvolution algorithms.
Materials & Methods
After institutional review board approval, a consecutive series of acute stroke patients with middle cerebral artery occlusion (MCAO) were characterized retrospectively. Patients were selected who received CTA and CTP of the head in the setting of their acute presentation, per our standard clinical protocol. From these patients we selected those who had a follow-up brain MRI within 28 days of presentation. Seventeen patients met these criteria (mean age 63.5 years, 40% male, mean NIHSS 17.7). Subjects were characterized by the duration of stroke-like symptoms, lateralization of clinical findings, and NIH stroke scale. CT perfusion data were analyzed with freely available independent software (Perfusion Mismatch Analyzer: http://asist.umin.jp/index-e.htm). Three separate perfusion datasets were obtained for each patient: using standard (sSVD), delay-insensitive block-circulant SVD (bSVD), and delay-corrected (dSVD) deconvolution algorithms. User-generated ROIs were placed on the CBF maps generated by each of these techniques. Lesion volumes as well as mean Tmax values (by bSVD technique) were computed for each ROI. Manual ROIs also were placed on the MRI images (DWI for MRIs obtained 0-7 days after presentation and FLAIR for MRIs obtained 7-28 days after presentation). Repeated measure analysis of variance was performed to identify significant differences among the different methods of perfusion computation.
Results
Correlation (R2) values between the volume of CBV abnormality and that of the DWI abnormality were 0.7243 for sSVD, 0.7605 for dSVD, and 0.8948 for bSVD. Average rTmax values in the region of CBF abnormality were 272.7% for sSVD, 163.6% for dSVD, and 351.3% for bSVD.
Conclusion
Correlation between volume of CBV abnormality and final infarct volume was highest with bSVD and lowest with sSVD. This is supportive of the concept that delay-sensitive sSVD will overestimate hypoperfusion secondary to benign arrival-time delay, whereas delay-insensitive bSVD values are more reflective of true tissue perfusion. Relative values of Tmax were higher in bSVD than in the other deconvolution algorithms as a result of the inclusion of less benign oligemia in lesion selections. For future studies we plan to coregister the MR images with the perfusion maps to directly measure perfusion parameters in the area of infarct core, as well as incorporate threshold-generated ROIs in the measurement of abnormal rCBF volumes.

KEYWORDS: Brain perfusion, Deconvolution

O-389 **3:31 PM - 3:39 PM**

Degree of Anterior Insula Infarction at Admission Is the Strongest Predictor of Infarct Growth in Endovascular-Treated Stroke Patients without Recanalization

Morais, L. M. T.·Kamalian, S.·Borgie, R. C.·Payabvash, S.·Franceschi, A. M.·Schaefer, P. W.·Yoo, A. J.·Lev, M. H.
Massachusetts General Hospital
Boston, MA.

Purpose
Admission core infarct volumes greater than 70 ml on diffusion-weighted-imaging (DWI) are an established marker for poor stroke outcome. Previous pilot studies also have suggested a strong correlation between stroke severity and degree of insula infarction. We hypothesized that percent insula infarction is associated more strongly with poor tissue outcome in proximal occlusive-stroke patients treated with intra-arterial therapy (IAT) than is admission DWI lesion volume.
Materials & Methods
We identified 74 consecutive IAT patients who presented with acute middle cerebral artery (MCA) occlusion. Two experienced neuroradiologists rated the admission DWI scans according to percent anterior and posterior insula infarction using a 4-point scale (normal, <50%, >50%, 100%). Admission DWI and follow-up MRI core infarct volumes were segmented independently, and infarct growth determined. Following IAT, patients were stratified into good (TICI 2/3) versus poor (TICI 0/1) recanalization groups. Univariate (spearman rank correlation) and multivariate regression analyses were performed to determine the relationship between admission imaging and clinical variables, and final infarct volume/growth in each of the revascularization groups.
Results
There were 23/74 (31%) patients with no/poor revascularization (TICI 0/1) and 51/74 (69%) with good/excellent revascularization (TICI 2/3). For the poor recanalization group, percent anterior insula infarct was

Note: Scanned images are included in the proceedings. Some submitted images were reduced during editing, thereby decreasing clarity. Also, refer to the Program Planner. Proceedings Content as of 3-29-2013.

the *only* predictor of infarct growth for both the uni- and multivariate analyses (spearman rho = 0.43, p = 0.04). Predictors of final infarct volume in this group included age, anterior/posterior/total insula percent infarct, and admission DWI lesion volume (all p<0.05). For the good recanalization group, admission NIHSS score was the *only* predictor of infarct growth for both the uni- and multivariate analyses (spearman rho = 0.34, p = 0.02). Predictors of final infarct volume in this group included anterior/posterior/total insula percent infarct, and admission DWI lesion volume (all p<0.05). Overall, there were 26/74 (35%) with anterior insula infarct >50% and 48/74 (65%) without. These dichotomized anterior insular infarct groups were matched for mean admission NIHSS score and time-to-imaging (p = 0.3 and 0.4, respectively), however mean final infarct volume and infarct growth were lower in the <50% anterior insula infarct group (78+/-55 ml versus 166+/-104 ml, p<0.0001 for volume, and 66+/-81 ml versus 114+/-95 ml, p<0.03 for growth).

Conclusion

In this highly selected endovascular-treated cohort, percent anterior insula infarction at admission was the *only* independent predictor of infarct growth in patients without significant revascularization. We speculate that anterior insula infarction may be a stronger surrogate for overall stroke severity than is DWI lesion volume, because the unique vascular supply of this location reflects the combined effects of not only the degree of superior division MCA occlusion, but also of the quality of collateral flow from both the anterior and inferior MCA divisions (as well as that of other pial collateral sources). Future studies with CT or MR perfusion imaging will determine if radiographic penumbral flow markers (not available for our current study) more strongly correlate with infarct growth than does the “clinical penumbra” (i.e., NIHSS score) in IAT patients *with* significant recanalization.

KEYWORDS: Stroke, Insula, DWI

O-390 **3:39 PM - 3:47 PM**

Pseudo-Continuous Arterial Spin Labeling Perfusion in Acute Ischemic Syndrome: A Feasibility Study

Nael, K.[1]·Meshksar, A.[1]·Khan, R.[1]·Carmody, R.[1]·Salamon, N.[2]
[1]University of Arizona Medical Center, Tucson, AZ,
[2]University of California Los Angeles, Los Angeles, CA.

Purpose

To evaluate the feasibility of a modified arterial spin-labeled (ASL) perfusion in patients with acute ischemic syndrome (AIS) and to compare the results with dynamic susceptibility contrast (DSC) perfusion.

Materials & Methods

Forty-five patients (28M, age: 38-90 years old) with AIS who underwent both ASL and DSC perfusion imaging were evaluated retrospectively. For ASL we used a pseudo-continuous (PCASL) pulse sequence with optimized image readout using a 3D GRASE (gradient and spin echo) and background suppression. A total of 30 pairs of tag and control images was obtained in four minutes using a two-second post-labeling delay and a labeling pulse duration of 1.5 seconds. Arterial spin-labeled cerebral blood flow (CBF) and DSC time-to-peak (TTP) and CBF maps were evaluated for image quality, presence and type of perfusion abnormality. In addition diffusion-perfusion mismatch was evaluated on each modality and patients were categorized into two categories of perfusion-diffusion mismatch using a modified version of Diffusion and Perfusion Imaging Evaluation for Understanding Stroke Evolution (DEFUSE) criteria: 1) Mismatch: perfusion abnormality volume > 1.5 (150%) of DWI lesion volume; 2) Matched: perfusion abnormality volume < 1.5 (150%) of DWI lesion volume. Wilcoxon test was used to evaluate the differences in image quality scores and Kappa test for interobserver and intermodality agreement.

Results

Dynamic susceptibility contrast and ASL studies were rated of diagnostic image quality in 96% and 94% of patients respectively with interobserver agreement of k = 0.81 for DSC and 0.72 for ASL. The image quality of ASL, although diagnostic, was rated significantly lower than for DSC (p = 0.005). There was no significant difference between the image quality of studies acquired at 3T versus 1.5T for DSC (p = 0.3) or ASL (p = 0.1). In all (30/45) patients who had DWI positive lesion, both DSC and ASL showed a type of perfusion abnormality without disagreement. Among 15 patients without DWI lesion, three patients had regional perfusion deficit on both DSC and ASL indicative of true nature of ischemia. The ASL-DWI mismatch classification agreed with TTP-DWI in 27 of 30 cases with $\kappa = 0.71$, 95% CI, 0.52-0.87. The agreement between the ASL-DWI and CBF-DWI was lower with agreement in 23 of 30 cases yielding a $\kappa = 0.46$, 95% CI, 0.23-0.76). In all discrepant cases, the disagreement was due to overestimation of hypoperfused lesion on ASL than on corresponding DSC maps.

Conclusion

The described ASL protocol is feasible in the assessment of perfusion deficit in patients with AIS and can provide an alternative method in evaluation of patients who cannot receive gadolinium. However the ASL technique as currently used still underperforms DSC method with lower image quality and only moderate agreement for mismatch classification mainly due to overestimation of hypoperfusion. Further improvement in ASL methodology such as faster sequence design and arterial transit delay insensitive techniques such as velocity selective ASL is needed before ASL can be incorporated as a major perfusion modality in large clinical scale.

KEYWORDS: Acute ischemic stroke, ASL, DSC, MR Perfusion

Note: Scanned images are included in the proceedings. Some submitted images were reduced during editing, thereby decreasing clarity. Also, refer to the Program Planner. Proceedings Content as of 3-29-2013.

O-391 **3:47 PM - 3:55 PM**

Susceptibility-Weighted Imaging at 3T Is Superior to Time-of-Flight Angiography for the Detection of Peripheral Thrombi in Patients with Acute Stroke

Radbruch, A.[1,2]·Mucke, J.[1]·Schlemmer, H.[2]·Heiland, S.[1]·Bendszus, M.[1]·Rohde, S.[1]
[1]University of Heidelberg, Heidelberg, GERMANY, [2]German Cancer Research Center (DKFZ), Heidelberg, GERMANY.

Purpose
Time-of-flight (TOF) angiography detects occlusion or stenosis of arteries in patients with acute ischemic stroke due to the absence of blood flow in the occluded vessel, depicted as loss of signal. In contrast susceptibility-weighted imaging (SWI) enables intravascular clot imaging in terms of the susceptibility vessel sign (SVS). Susceptibility vessel sign is defined as a hypointensity within the occluded vessel with a greater diameter than the one of the contralateral vessel, which occurs due to the high sensitivity of SWI sequences for blood products. The aim of this study was to compare the diagnostic accuracy of both methods regarding the determination of vessel occlusion in patients with acute stroke.
Materials & Methods
Ninety-four patients who presented clinical symptoms for acute stroke (NIHSS>2) and displayed a region of impaired perfusion on the time to peak perfusion map determined by dynamic susceptibility contrast perfusion images (TE 35, TR 1920, FoV 240, slice thickness 5 mm, 75 dynamic scans, injection of 0.1 mmol/kg DOTAREM with bolus technique after the third frame followed by 20ml of NaCl solution) in the area of the anterior(ACA), middle (M1, M1/M2, M2/M3) or posterior (PCA) cerebral artery were included prior to thrombolytic therapy. For all patients TOF angiography and SWI at 3T were assessed with respect to delineation of SVS on SWI and vessel occlusion or stenosis on TOF angiography.
Results
Eighty-seven of 94 patients displayed a clearly definable SVS on SWI within the affected artery. In 72 patients the SVS could be correlated with occlusion or stenosis observed on the TOF angiography (1 ACA, 36 M1, 13 M1/M2, 12 M2/M3, 10 PCA). No patient displayed occlusion or stenosis on TOF angiography without a correlate on SWI. Fifteen patients displayed SVS on SWI (14 M2, 1 M1) without any sign for occlusion on the TOF angiography(Figure 1). Sensitivity for detection of embolic occlusion within major vessel segments(e.g., M1, ACA and PCA) was 97% for SWI and 96% for TOF angiography. In contrast sensitivity for detection of embolic occlusion within M2/M3 was 84% for SWI and 39% for TOF angiography.

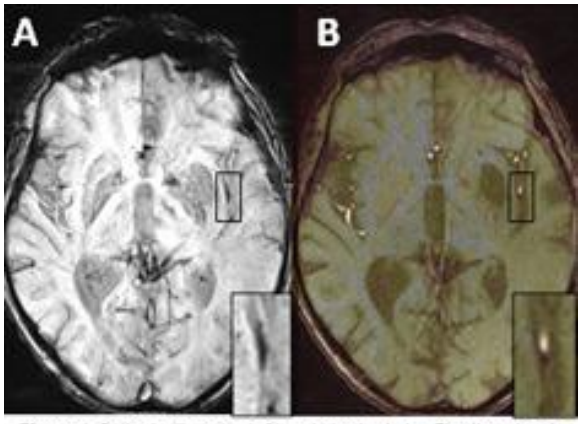

Figure 1. Patient with acute left-hemispheric-stroke. The thrombus in the peripheral segment of the MCA can be visualized clearly on SWI (A). Coregistration of SWI and TOF-angiography (B) highlights the TOF-angiography signal within the SVS.

Conclusion
Susceptibility-weighted imaging and TOF angiography provide equal results for the detection of proximal thrombemboli while SWI is superior for the detection of peripheral clots. Since TOF angiography can provide additional information for stroke identification and classification due to peripheral vessel rarefaction we suggest a combined analysis of TOF angiography and SWI for vascular assessment of ischemic stroke.

KEYWORDS: Thrombus imaging, Susceptibility-weighted imaging

O-392 **3:55 PM - 4:03 PM**

Blood Flow "Oversupply" following EC-IC By-Pass?

Mikulis, D. J.[1]·Al Harbi, M.[1]·Mandell, D. M.[1]·Poublanc, J.[1]·Wong, T.[1]·Crawley, A. P.[1]·Fisher, J. A.[2]
[1]Toronto Western Hospital, Toronto, ON, CANADA, [2]Toronto General Hospital, Toronto, ON, CANADA.

Purpose
The EC-IC by-pass procedure can significantly improve blood flow in the MCA territory secondary to proximal large vessel steno-occlusive disease. In spite of this, no advantage over medical management for treatment of steno-occlusive disease has been observed. EC-IC by-pass however remains a treatment option for medical failures. Flow dynamics before and after EC-IC by-pass has been studied, but, to our knowledge, there are no reports that describe persistent steal physiology despite restoration in blood flow.
Materials & Methods
Ten patients with moyamoya disease who had cerebrovascular reserve (CVR) studies before and after EC-IC by-pass surgery were identified retrospectively in a database of over 600 CVR studies. 3T TOF MRA, phase-contrast by-pass flow assessment (NOVA), and whole brain blood flow mapping using ASL (GE Healthcare, Milwaukee) were performed in 12 by-passed hemispheres.

Note: Scanned images are included in the proceedings. Some submitted images were reduced during editing, thereby decreasing clarity. Also, refer to the Program Planner. Proceedings Content as of 3-29-2013.

Cerebrovascular reserve was obtained using a BOLD MRI EPI sequence during precision control of arterial CO2 to achieve two brief CO2 elevations of 10 mmHg above resting levels. Whole brain CVR maps were generated following linear regression of end-tidal CO2 waveforms with CVR = % BOLD signal/mmHg CO2.

Results

All patients had evidence of steal physiology in the by-pass territory prior to surgery. All by-passes were patent post surgery. Seven by-passes with by-pass flow in the range of 30-90 ml/min showed conversion of steal physiology to positive vascular reactivity. Of the five patients without CVR improvement, two showed by-pass flow of 30 ml/min or less, but two unexpectedly showed the highest by-pass flow in the group (> 90 ml/min - Figure 1). One patient in this latter subgroup showed resting blood flow on ASL that was two std devs. above normal (age-matched).

Figure 1

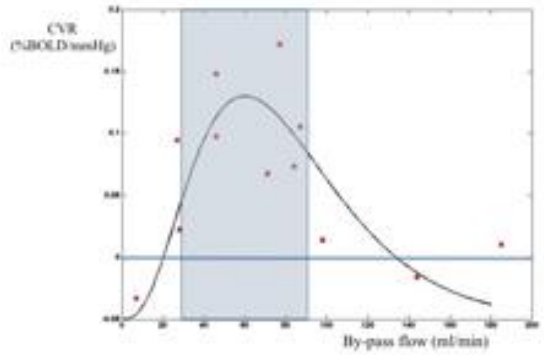

Conclusion

The data suggest that high by-pass flows may overwhelm the MCA territory such that recovery of vascular reserve fails to occur. This can be associated with elevated resting blood flow reflecting the failure of the reserve mechanism to re-establish blood flow control. The significance of this physiology is uncertain as there have not been adverse events reported in these patients at this time.

KEYWORDS: EC-IC bypass, Blood flow, Cerebrovascular reserve

O-393 **4:03 PM - 4:11 PM**

High-Resolution MR Imaging in Large Vessel Occlusions

Hui, F. K.[1]·Jones, S. S.[1]·Obusez, E. C.[1]·Zhu, X.[2]·Uchino, K.[1]·Hussain, S.[1]·Lou, X.[3]·Jiang, W.[4]
[1]Cleveland Clinic Foundation, Cleveland, OH, [2]China-Japan Friendship Hospital, Beijing, CHINA, [3]Chinese People's Liberation Army General Hospital, Beijing, CHINA, [4]The Second Artillery General Hospital, Beijing, CHINA.

Purpose

Large vessel occlusions are an important cause of ischemic stroke. Imaging goals center on identifying the site of occlusion, the size of ischemic core and the size of ischemic penumbra. The etiology of the occlusion typically is inferred by history and demographics, or subacutely during investigation for shunt, hypercoagulable state or other causes. Current generation vascular imaging is based primarily on lumenography. Contours of the vessel lumen on lumenography may suggest the presence of atherosclerosis, dissection or thrombus. High-resolution MRI (HRMR) techniques can characterize wall morphology in the presence of an occlusion, which may impact clinical care by better definition of intra-occlusion wall characteristics as well as downstream vasculature normally confounded by the lack of antegrade flow.

Materials & Methods

The High Resolution MRI database of Cleveland Clinic and Beijing Tiantan Hospital were reviewed to identify patients with large vessel occlusions on lumenography, performed with diagnostic quality high-resolution MRI imaging. Clinical data were reviewed for each patient, and images analyzed by experienced neuroradiologists at both institutions. Where possible, conventional angiography/lumenography was reviewed for comparison.

Results

Nine patients with large vessel cerebral artery occlusions were identified in whom high-resolution MRI characteristics were reviewed and categorized. Images were correlated with demographics, risk factors, and the working diagnosis of each case.

Table : Vessel Wall Imaging

Patient	Lumenography	HRMR Findings	Presumed Diagnosis	Excluded
1	Right MCA occlusion	The occlusion site showed thickening wall with enhancement.	Atherosclerosis	Clot, vasculitis, dissection
2	Right MCA occlusion	The occlusion showed the enhanced eccentric plaque without lumen. The proximal or distal sites showed thickening wall and circle enhancement.	Atherosclerosis	Clot, vasculitis, dissection
3	Right MCA occlusion	plaque without lumen. The proximal or distal sites showed eccentric thickening wall.	Atherosclerosis	Clot, vasculitis, dissection
4	Right MCA occlusion	The occlusion showed the enhanced eccentric plaque without lumen. The proximal or distal sites showed thickening wall and circle enhancement.	Atherosclerosis	
5	Occlusion Basilar, no flow in post PICA V4. Flow down Basilar from PCOMs	Focal, irregular enhancement of proximal basilar artery with intermediate signal material without outer vessel narrowing. Shows slow flow (White Snake) in the bilateral post PICA V4, implying patency of the distal vertebral artery.	Atherosclerosisvs focal dissection.	Pure Clot/Vasculitis
6	L M1 occlusion with leptomeningeal collaterals	L M1 narrowing/occlusion with circumferential enhancement	Atherosclerosis/Inflammation	Clot/Dissection
7	R Vertoccluded past C4 with trickle flow from L V4 to narrow Basilar artery	R V4 Filling defect (clot) from C2 horizontal segment to Basilar. Concomitant mid basilar narrowing of both inner and outer diameter with enhancement.	Thrombus filling R V4 segment and proximal basilar artery, with coincident basilar artery atherosclerosis.	
8	L P1 occlusion, L V4 irregular narrowing	L V4 flap, narrowing, enhancement with P1 filling defect in a low flow enhanced area.	Dissection plus clot	Pure Clot /Vasculitis/Atherosclerosis
9	R ICA occlusion with cessation of flow at the cavernous segment	Dissection and subintimal blood is seen at the supraclinoid ICA with wall enhancement of the adjacent ICA proximally and distally. The ICA lumen was smaller than expected.	Dissection	Pure Embolic Event, Atherstenosis

Note: Scanned images are included in the proceedings. Some submitted images were reduced during editing, thereby decreasing clarity. Also, refer to the Program Planner. Proceedings Content as of 3-29-2013.

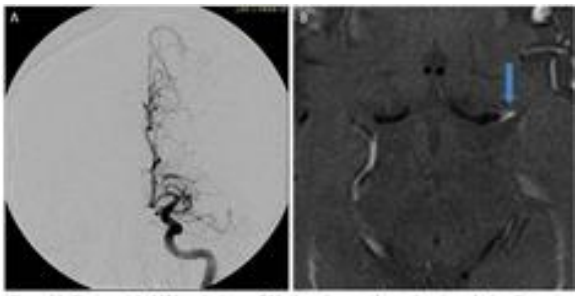

Figure 1A: Shows a right MCA occlusion on DSA, thrombus vs atherosclerotic occlusion. Figure 1B Shows that it is not a thrombus . Concentric wall enhancement and thickening , however, uncertain if atherosclerotic or vasculopathic.

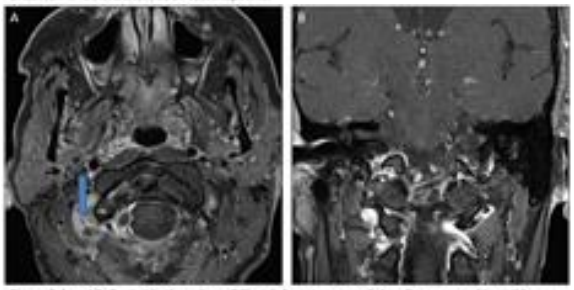

Figure 2 A and B: Probable thrombus : Filling defects in areas of slow flow are starkly visible. Limited experience with these findings makes differential characteristics in post contrast imaging uncertain.

Conclusion
High-resolution MR of vascular occlusions can identify wall characteristics as well as characterize the course and caliber of the vasculature distal to the occluded segment. This information may be useful in determining preferred approaches for endovascular revascularization.

KEYWORDS: 3T, Arterial occlusion, High Resolution Magnetic Resonance Imaging

O-394 **4:11 PM - 4:19 PM**

Echo-Planar Fluid Attenuated Inversion Recovery in Patients with Acute Stroke: A Comparative Analysis with Fluid Attenuated Inversion Recovery

Meshksar, A.·Khan, R.·Carmody, R.·Erly, W.·Kubal, W.·Nael, K.
University of Arizona Medical Center
Tucson, AZ.

Purpose
To prospectively evaluate the diagnostic performance of an EPI-FLAIR sequence in evaluation of acute stroke with potential reduction in scan time and compare the result with conventional FLAIR images.
Materials & Methods
Thirty-four consecutive patients (18 F, 16 M, age range: 32-96 years old) with clinical suspicion of acute stroke were evaluated prospectively with an acute stroke protocol which encompassed both conventional FLAIR (subsequently referred to as FLAIR) and EPI-FLAIR imaging. Using an EPI sequence with integration of parallel acquisition (GRAPPA x 2), EPI-FLAIR images were acquired in 50 seconds compared to three minute acquisition time for FLAIR imaging. Image quality was evaluated by two neuroradiologists independently and in different sessions using a 1-4 grading scale. In addition the images were assessed to determine the presence of hyperintensity on FLAIR and EPI-FLAIR images and compared to the DWI abnormality and rated as concordant or discordant. The DWI images were coregistered with FLAIR and EPI-FLAIR images and the signal intensity ratio (SIR) of the lesion to contralateral normal white matter were calculated for both FLAIR and EPI-FLAIR. Interobserver and intermodality agreement and correlation were tested with Kappa and Spearman Rank correlation respectively. The quantitative analysis was performed utilizing a t test.
Results
Except for two studies that were deemed nondiagnostic (one due to motion artifact and the other due to susceptibility artifact related to dental braces), all studies were rated as being of diagnostic quality by both observers and without significant difference in image quality scores ($p = 0.4$). The interobserver agreement for image quality scores was excellent for both FLAIR ($k = 0.85$) and EPI-FLAIR ($k = 0.80$). Twelve patients did not have infarction (DWI lesion). In 22 patients with acute infarction (+DWI lesion), FLAIR and EPI-FLAIR agreed in 19 (86%) with good correlation ($r = 0.94$, 95% confidence interval: 0.89-0.97). In only three patients (14%) EPI-FLAIR was discordant with FLAIR and unable to show hyperintensity detected on both FLAIR and DWI. The mean ± SD of the SIR values on EPI-FLAIR and FLAIR for DWI positive lesions were 1.20 ± 0.1 and 1.27 ± 0.16 respectively ($p = 0.1$) and concordant with a recently published clinical trial. In three discordant cases, despite subjective discrepancy, there was no statistically significant difference between mean SIR values of FLAIR (1.22) and EPI-FLAIR (1.13) ($P = 0.10$).
Conclusion
The described EPI-FLAIR sequence is feasible with acceptable qualitative and quantitative results in comparison to routine FLAIR images for evaluation of patients with acute stroke. EPI-FLAIR can be implemented in acute stroke MR protocol resulting in much needed reduction in scan time for these patients.

KEYWORDS: Stroke, Echo planar imaging, EPI-FLAIR

O-395 **4:19 PM - 4:27 PM**

CT Perfusion in the Halifax Acute Stroke Imaging Study

Shankar, J. J. S.·Langlands, G.·Phillips, S.
QE II Hospital
Halifax, NS, CANADA.

Purpose
The thrombolytic time window for treatment of acute ischemic stroke (AIS) is based on time and not on the tissue involved. Different time window for different patients have been suggested based on different clinical scenario. So to make a proper judgement regarding

Note: Scanned images are included in the proceedings. Some submitted images were reduced during editing, thereby decreasing clarity. Also, refer to the Program Planner. Proceedings Content as of 3-29-2013.

thrombolysis in acute stroke we need to evaluate the tissue window. CT perfusion has been a valuable and widely available tool for the assessment of tissue at risk in cases or AIS. But due to limited experience in many centers including ours, we decided to first evaluate the parameters of CT perfusion in relation to follow-up imaging. Our hypothesis was that the final volume of infarcted brain on follow-up imaging will not be smaller than that predicted by the cerebral blood volume (CBV) parameter on CTP imaging performed at the time of AIS.
Materials & Methods
We retrospectively analyzed our prospectively kept acute stroke database. The study was approved by the institutional ethics committee. We analyzed patients admitted to our hospital between April 1st and August 31st, 2012 with symptoms of AIS and had CTP done at their hospital arrival. We calculated the ASPECT score on plain head CT at baseline, lesion on cerebral blood flow, volume, time to peak maps and CT angiogram source images (SI) and volume of final infarct size on follow-up CT or diffusion imaging, whichever was available. The volume was calculated manually on the PACS work station. The lesion volume on different CTP parameters and SI data then were correlated with the final infarct volume. This analysis was done by three observers - a fellowship trained neuroradiologist, a stroke neurologist with more than 20 years experience in the field and a medical student with two weeks training in the analysis of acute stroke imaging including CTP. Paired t test, regression analysis and correlation analysis were done. A p value of <0.05 was considered significant. The interobserver variability also was analyzed.
Results
We had a total of 84 patients with AIS and CTP at admission in this time period. Out of these only 38 patients met all the criteria for final analysis. There was no significant difference between CTP CBV or SI and follow-up MRI/CT lesion volume (P>0.05). Lesion volumes were greater on time to peak (TTP) and cerebral blood flow (CBF) CTP images compared to follow-up MRI/CT (P<0.05). The correlation coefficient (r) between lesion volume on TTP, CBF, CBV or SI to follow-up lesion volume on MRI/CT was 0.41, 0.78, 0.81 and 0.70 respectively (correct to two significant figures). Regression analysis between each imaging parameter's ischemic volume at admission and final infarct volume found that the CBV correlated best with the final infarct volume (R2 = 0.6591).
Conclusion
Results from the Halifax Acute Stroke Imaging Study (HASIS) confirms our hypothesis that admission CTP and SI in suspected AIS patients can predict final infarct volume, where final volume of infarcted brain will not be smaller than that predicted by CTP CBV.

KEYWORDS: Actue stroke, CT perfusion

O-396 **4:27 PM - 4:35 PM**

Acute Cerebral Infarction Is Strongly Associated with Increased Prominence of Ipsilateral Deep Medullary Veins on Susceptibility-Weighted Imaging

Salehi, B.·Jacobson, J.·Oyoyo, U.·Kido, D.
Loma Linda University Medical Center
Loma Linda, CA.

Purpose
During ischemia, oxygen dissociates from iron atoms in hemoglobin, forming deoxyhemoglobin, a paramagnetic molecule that acts as a negative contrast agent on susceptibility-weighted imaging (SWI). Accordingly, dramatic changes in oxygen saturation of venous vascularity are reflected on SWI by the blood oxygen level dependent (BOLD) effect. Our purpose is to determine the association between prominence of cerebral deep medullary veins (DMV) in SWI and the presence of recent cerebral infarct.
Materials & Methods
Under an IRB waiver, a cohort of 22 consecutive cases of acute stroke with SWI with brain imaging obtained in the first week after initial symptoms. Controls were 27 normal volunteers with brain MRI using the same 1.5T scanner. Two neuroradiologists reviewed SWI of the all cases and controls; DMV prominence was determined for each cerebral hemisphere using a 7-point ordinal visual scale. Demographic information as well as the length of hospital stays, as an index for clinical outcome, were collected from the medical record. Differences in DMV prominence per hemisphere between stroke patients and controls were assessed using Chi Square and Mann-Whitney tests.
Results
Stroke cases were 21.7 times more likely than normal controls to present with deep medullary vein asymmetry (OR, 95% CI: 2.48, 189.1). Deep medullary veins of the partially infarcted hemisphere were more prominent compared to normal hemisphere, resulting in the asymmetric appearance (Figure). Among the cases, those presenting with asymmetric DMVs were older compared to stroke cases without (median, 62 years versus 56 years); however, this was not statistically significant (Median test, p = 0.67). Male stroke patients were 5.6 times more likely than female stroke patients to present with asymmetric medullary veins (OR, 95% CI: 0.814, 38.5). No correlation between prominence of the deep medullary veins and length of hospital stay was observed.

Note: Scanned images are included in the proceedings. Some submitted images were reduced during editing, thereby decreasing clarity. Also, refer to the Program Planner. Proceedings Content as of 3-29-2013.

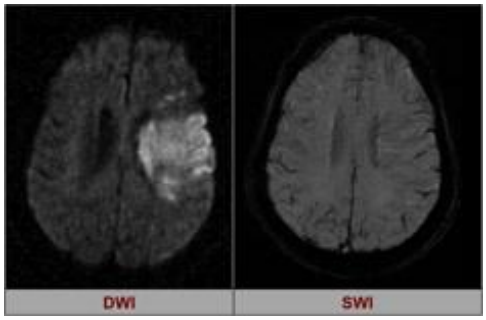

Conclusion
In the setting of acute cerebral infarct, ispilateral deep medullary veins (DMVs) appear larger and darker on susceptibility-weighted imaging resulting in asymmetric appearance compared to the normal hemisphere. This asymmetric prominence of DMVs likely is mediated by elevated deoxyhemoglobin on the infarcted region.

KEYWORDS: Actue stroke, Susceptibility-weighted imaging, Deep Medullary Veins

O-397 **4:35 PM - 4:43 PM**

CT Permeability in Prediction of Hemorrhagic Transformation following Acute Ischemic Stroke

Shankar, J. J. S.·Cobb, A.
QE II Hospital
Halifax, NS, CANADA.

Purpose
The thrombolytic therapy is the mainstay of treatment of acute ischemic stroke (AIS). The hemorrhagic complication is one of the most important complications following treatment of AIS. It will be useful to have a tool which can predict the hemorrhagic complication in these patients at presentation. CT perfusion (CTP) has been a valuable and widely available tool for the assessment of tissue at risk in cases or AIS. The data of CTP can be used to extract information of CT permeability, which has been described by some studies to be useful in predicting the hemorrhagic transformation. Our hypothesis was that the permeability surface area product will be able to predict the hemorrhagic transformation on follow-up scan in patients with AIS.
Materials & Methods
We retrospectively analyzed our prospectively kept acute stroke database. The study was approved by the institutional ethics committee. We analyzed patients admitted to our hospital between April 1st and August 31st, 2012 with symptoms of AIS and had CTP done at their hospital arrival. We calculated the permeability surface area product in addition to the other routine CTP parameters. Paired t test was done to compare the permeability ratio between patients with and without hemorrhagic transformation. A p value of <0.05 was considered significant. Sensitivity, specificity, positive and negative predictive values also were calculated for a certain cut off value.
Results
We had total of 84 patients with AIS and CTP at admission in this time period. Out of these only 38 patients had a follow-up imaging done in our institution. Out of these permeability could be calculated for 14 patients. The relative permeability was calculated as a ratio of permeability on the side of AIS versus that on the contralateral side at the same level. Patients with hemorrhagic transformation on follow-up scan had significantly higher (p = 0.001) relative permeability compared to patients with no hemorrhagic transformation on followup. For a relative permeability cut off of 1.5, the sensitivity, specificity, positive and negative predictive values were 85.7%.
Conclusion
Our study confirms our hypothesis that the permeability surface area product can predict the hemorrhagic transformation on follow=up scans in patients with AIS. This showed high sensitivity, specificity, positive and negative predictive values at relative permeability cut off of 1.5.

KEYWORDS: Actue stroke, CT perfusion, CT Permeability

Wednesday Afternoon

3:15 PM - 4:45 PM
Ballroom 6CF

(45b) Parallel Scientific Papers: Adult Brain: Tumors III: High-Grade Tumors

O-398 **3:15 PM - 3:23 PM**

Histogram Analysis of Dynamic Susceptibility Contrast Perfusion MR Images in Oligodendroglial Tumors: Correlation between Cerebral Blood Volume, Grade and Angiogenic Subtypes According to 1p19q Status

Kim, B.·Kim, S.·Jung, H.·Kim, H.·Cha, J.·Kim, K.·Jeon, P.·Kim, H.·Byun, H.
Samsung Medical Center
Seoul, KOREA, REPUBLIC OF.

Purpose
Grading of oligodendroglial tumors using MR images have low predictive accuracy given that low-grade tumors exhibit heterogeneous patterns of blood flow in different patients. And degree of oligodendroglial vascularity is associated with loss of heterozygosity (LOH) on 1p/19q. The aim of this study was, first, to analyze histogram of MR perfusion images of oligodendroglial tumors in grading histopathologic subtype and, second, to assess the difference of distribution of relative cerebral blood volume

Note: Scanned images are included in the proceedings. Some submitted images were reduced during editing, thereby decreasing clarity. Also, refer to the Program Planner. Proceedings Content as of 3-29-2013.

(rCBV) values in subtype of oligodendroglial tumors according to 1p/19q status.
Materials & Methods
Thirty-three patients (20 women, 13 men; mean age, 47.4 years; range, 23 - 75 years) with histologically confirmed oligodendroglial tumors underwent preoperative dynamic susceptibility contrast MR imaging at 3.0T and were analyzed retrospectively. Patients were classified by histopathologic grade (high- and low-grade) and stratified into two cytogenetic groups: 1p or 1p and 19q LOH (Group 1), and 19q LOH only on intact alleles (Group 2). Routine rCBV measurements were obtained from ROIs of the whole tumors. Mann-Whitney tests compared the utility of histogram parameters of rCBV values for histoapathologic grading and identification of cytogenetic subtypes.
Results
Of the 33 patients, 22 was classified to Group 1 (9 low-grade, 13 high-grade) and 11 was identified to Group 2 (five low-grade, six high-grade). High-grade tumors were showing relatively low kurtosis and skewness of rCBV values than low-grade ones, signifying that high-grade ones have a tendency of heterogeneous and predominant distribution of high rCBV values on its rCBV histogram (P = .038 and P = .035, respectively). In each Group 1 and 2, high-grade subtypes also showed relatively low kurtosis and skewness of rCBV values than low-grade subtypes, implying the similar tendency of high rCBV values distribution. In addition, Group 1 showed relatively low kurtosis and skewness of rCBV values than those of Group 2. Mean, mode and maximum value of rCBV, however, showed statistically insignificant difference (P > .05).
Conclusion
The rCBV histogram analysis showed somewhat different distribution of rCBV values between low- and high-grade oligodendroglial tumors despite most overlapping histogram parameter. And our results showed that role of 1p/19q LOH in angiogenesis of tumor vascularity, which have an effect on the difference of rCBV value distribution.

KEYWORDS: Oligodendroglioma, MR perfusion-weighted imaging, Histogram

O-399 **3:23 PM - 3:31 PM**

MR Susceptibility-Weighted Contrast-Enhanced Perfusion Imaging and Diffusion Tensor Imaging Patterns in Patients with Progressive/Recurrent Glioblastomas after Bevacizumab Treatment

Liu, X.[1]·Tian, W.[2]·Hussain, A.[2]·Ekholm, S.[1]
[1]University of Rochester School of Medicine & Dentistry, Rochester, NY, [2]University of Rochester Medical Center, Rochester, NY.

Purpose
Bevacizumab is the humanized monoclonal antibody that blocks vascular endothelial growth factor (VEGF) and inhibits angiogenesis, and has been used widely in patients with glioblastomas. However, Bevacizumab-induced MRI changes are still full of conflicting controversies, including advanced imaging techniques of MR dynamic susceptibility-weighted contrast-enhanced MR perfusion imaging (DSC PWI) and diffusion imaging. For example, new restricted diffusion followed by Bevacizumab treatment is thought be a good response in some studies, but other studies thought this was indication of tumor progression. Some studies found that decreased cerebral blood volume (rCBV) is a good therapeutic response after Bevacizumab treatment, in contrast, some researcher thought that elevated blood perfusion responded to antiangiogenic therapy, and subsequently increase survival in such patients. Therefore, the purpose of this study was to evaluate patterns of DSC PWI and diffusion tensor imaging (DTI) in patients with progressive/recurrent glioblastomas after Bevacizumab treatment.
Materials & Methods
Fifty-two cases with pathology or radiologic confirmed progressive/recurrent glioblastomas after Bevacizumab treatment were reviewed. Serial DSC PWI and DTI examinations were performed after Bevacizumab treatment. The maximal rCBV ratios and minimal apparent diffusion coefficient (ADC) value in the examinations when the glioblastomas presenting minimal enhancement after Bevacizumab treatment and recurrence/progression were evaluated.
Results
The mean maximal rCBV ratio of reference in glioblastomas after Bevacizumab treatment was 1.65 ± 0.52; there were 41 patients with the mean maximal rCBV ratio of recurrent/progressive glioblastomas significantly higher, 6.11 ± 4.58, *p* value of paired t test was 0.013. There were 11 patients whose maximal rCBV ratio at recurrence/progression was relatively lower, 1.26 ± 0.29, without significant difference compared to reference, *p* = 0.71. All patients showed new restricted diffusion after Bevacizumab treatment. The mean minimal ADC value of reference was 0.49 ± 0.17, the mean minimal ADC value of 41 and 11 patients at recurrence/progression were 0.63 ± 0.19 and 0.71 ± 0.57 respectively, and there was no significant difference compared to reference, *p* value of 0.22 and 0.09 respectively. Discussion: The recurrent/progressive glioblastomas after Bevacizumab could present two types of perfusion changes, re-increased high rCBV and unchanged low rCBV. In contrast, the minimal ADC alone may have limited value in detecting recurrence/progression after Bevacizumab treatment.
Conclusion
Our preliminary result shows that there were different patterns of MR PWI/DTI changes in recurrent/progressive glioblastomas after Bevacizumab treatment. Combing multiple imaging biomarkers is necessary for imaging interpretation.

KEYWORDS: Glioblastoma, Pseudoresponse, Bevacizumab

Note: Scanned images are included in the proceedings. Some submitted images were reduced during editing, thereby decreasing clarity. Also, refer to the Program Planner. Proceedings Content as of 3-29-2013.

O-400 **3:31 PM - 3:39 PM**

Diffusional Kurtosis MR Imaging in the Evaluation of Gliomas

Spampinato, M.·Manzoor, M.·Rumboldt, Z.·Kereshi, B.·Jensen, J.·Helpern, J.·Tabesh, A.
Medical University of South Carolina
Charleston, SC.

Purpose
Our aim was to assess microstructural differences between glioblastoma multiforme (GBM) and non-GBM gliomas, with the hypothesis that diffusional kurtosis metrics will differ between GBM and other gliomas.
Materials & Methods
Eleven treatment-naïve adult subjects with pathology proven gliomas, six GBM (WHO grade IV) and five non-GBM (1 WHO grade I; 1 grade II; 3 grade III), were identified retrospectively. All subjects had undergone a preoperative MRI including a twice-refocused spin-echo echo-planar imaging diffusion sequence (b values = 0, 1000, 2000 s/mm^2 with 30 noncollinear gradient directions for each nonzero b value). A tumor volume-of-interest (VOI) including the entire solid portion of the mass was manually outlined on FLAIR images. A VOI was drawn within the contralateral normal-appearing white matter (NAWM). Average mean kurtosis (MK) and mean diffusivity (MD) values within the tumor were obtained using in-house software and normalized to the contralateral NAWM values. Mann-Whitney test and receiver operating characteristic (ROC) curves were used for statistical analyses.
Results
Mean unnormalized MK was significantly different (p = 0.045) between GBM (mean +/-SD = 0.73 +/- 0.08) and non-GBM (0.60+/-0.10) neoplasms. Mean normalized MK, as well as unnormalized and normalized MD were not statistically significantly different between groups. The area under the ROC curve for MK was 0.75 (95% confidence interval = 0.456-1). A threshold MK value of 0.62 provided a sensitivity of 83.3% and specificity of 67% in the identification of GBM. A threshold MK value of 0.72 had a sensitivity of 50% and a specificity of 83.3% in the identification of GBM.
Conclusion
Greater microstructural complexity of GBM can be detected using diffusion imaging. Diffusional kurtosis imaging has potential applications in the noninvasive assessment of tumor grade.

KEYWORDS: Glioma, Diffusion kurtosis imaging

O-401 **3:39 PM - 3:47 PM**

Apparent Diffusion Coefficient Histogram Analysis Is a Predictive, Not Prognostic, Imaging Biomarker for Recurrent Glioblastoma Treated with Bevacizumab

Ellingson, B. M.[1]·Shebjam, S.[2]·Kim, H. J.[1]·Harris, R. J.[1]·Woodworth, D. C.[1]·Pope, W. B.[1]·Lai, A.[1]·Nghiemphu, P. L.[1]·Mason, W. P.[2]·Cloughesy, T. F.[1]
[1]David Geffen School of Medicine at the University of California Los Angeles, Los Angeles, CA, [2]University of Toronto, Toronto, ON, CANADA.

Purpose
Bevacizumab is now the standard of care for treatment of recurrent glioblastoma in the United States. Apparent diffusion coefficient (ADC) histogram analysis has been shown to be a valuable imaging biomarker for predicting the response of recurrent glioblastoma to bevacizumab; however, no studies have compared pretreatment ADC histogram analysis between bevacizumab and a matched cohort of patients that were never exposed to bevacizumab during their treatment history. The purpose of the current study was to determine whether ADC histogram analysis performed prior to treatment in recurrent glioblastoma is a predictive (bevacizumab-specific) or prognostic (treatment independent) biomarker of response to bevacizumab.
Materials & Methods
All patients in this study signed institutional review board-approved informed consent. A total of n = 89 recurrent glioblastoma patients from UCLA treated with bevacizumab and n = 43 recurrent glioblastoma patients from the University of Toronto that were treated with a variety of chemotherapies and never exposed to bevacizumab were included in this retrospective study. In all patients, ADC values within pretreatment contrast-enhancing ROIs were extracted and the resulting histogram was fitted to a mixed model with a double Gaussian distribution. The mean value of ADC in the lower Gaussian curve (ADCL) was used as the primary biomarker of interest. Cox proportional hazards model and Log-rank tests were used for survival analysis.
Results
Cox multivariate regression analysis accounting for the interaction between bevacizumab- and nonbevacizumab-treated patients suggested the ability for ADCL to predict PFS and OS is dependent on treatment (P = 0.045 and P = 0.003, respectively). Cox regression suggested bevacizumab-treated recurrent glioblastoma with pretreatment ADCL>1.2um2/ms had a significantly longer overall survival (OS) compared with bevacizumab-treated patients with ADCL1.2um2/ms (P<0.025). Univariate analysis suggested an ADCL value of 1.2um2/ms stratified short and long-term progression-free (PFS) and OS in bevacizumab-treated patients (Log-rank, P = 0.009 and P = 0.0103, respectively); however, no differences in PFS or OS were observed in the nonbevacizumab-treated cohort (Log-rank, P = 0.0562 and 0.3737, respectively).

Note: Scanned images are included in the proceedings. Some submitted images were reduced during editing, thereby decreasing clarity. Also, refer to the Program Planner. Proceedings Content as of 3-29-2013.

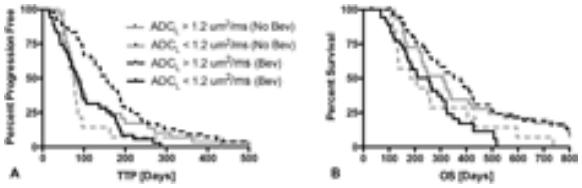

Conclusion
Together, results suggest ADCL extracted from ADC histogram analysis is a predictive, not prognostic, imaging biomarker for stratifying PFS and OS in bevacizumab-treated recurrent glioblastoma.

KEYWORDS: Glioblastoma, Imaging biomarker

O-402 **3:47 PM - 3:55 PM**

Elemental Brain Volumes Derived from Cytoarchitectonics and Crossing White Matter Tracts Are an Independent Predictor of Mortality for Glioma with Improved Understanding of Infiltration

Hamilton, J. D.[1]·Kumar, V. A.[1]·Schellingerhout, D.[1]·Shah, K.[1]·Chi, L.[1]·Hunter, J.[2]·Naidich, T. P.[3]·Chavalli, L.[1]·Leeds, N. E.[1]·Prabhu, S.[1]·Kumar, A. J.[1]·Hayman, L. A.[4]
[1]M. D. Anderson Cancer Center, Houston, TX, [2]Texas Children's Hospital, Houston, TX, [3]The Mount Sinai Hospital, New York, NY, [4]Anatom-e Information Systems, Houston, TX.

Purpose
Previous reports have hinted that there are elemental brain volumes (EBV) that guide glioma spread, beyond gyral and sulcal anatomy. We investigate how this can be used to define if the tumor is growing or spreading, and confirm these observations with survival data.
Materials & Methods
Seventy-four patients with diffuse gliomas (Grade II-IV) with pre and postoperative MR imaging and at least two years of followup were reviewed retrospectively from the year 2005. Tumors were determined to be "growth pattern" if they were confined to the archicortex or neocortex and if neocortical were located in a single EBV, defined by architectonics and white matter branching. Extension beyond these regions through the crossing, deep white matter fibers of the corona radiata and sagittal striatum was considered "spread pattern" by a consensus of three-nine neuroradiologists, blinded to survival data. This determination was compared to other previous reported single and multiparameter survival criteria (e.g., age, Karnofsky performance, size, extent of resection, enhancement, tumor grade, etc.) to determine its utility and independence from other criteria. (Please note that the construction of this atlas and its use for specific brain locations are submitted to this meeting as a separate communication).
Results
Determining if a glioma is growth versus spread pattern was an independent predictor of mortality (p = 0.007), regardless of tumor grade or size. Although spread pattern was more likely to be multifocal (p = 0.004), it was a better predictor of mortality than multifocality. As a single criterion these patterns had similar performance to a previously verified multiparameter criteria (VAK criteria) and its addition improved all post-hoc multiparameter modeling.

Coronal and sagittal T1 post-contrast images of a 45 year African American female with a multifocal glioblastoma confined to EBV associated with Brodmann area 6, who survived 24 months after diagnosis (Initial KPS 90).

Conclusion
The survival data provide evidence that this parcellation strategy to define glioma growth patterns is useful. This strategy worked particularly well for common glioma locations such as near the central sulcus and sylvian fissures but may need refinements in less common locations, such as the occipital lobe. Crossing deep white matter tract creating a net-like barrier to spread may explain these observation but other hypothesis such as the localized genomic signature and stem cell migration patterns have yet to be tested.

KEYWORDS: Glioma, Shape analysis, Survival

O-403 **3:55 PM - 4:03 PM**

Longitudinal MR Spectroscopic Imaging in a Cohort of Newly Diagnosed Glioblastoma Patients Receiving Adjuvant Antiangiogenic Therapy

Andronesi, O.[1,2]·Borra, R.[1,2]·Gerstner, E.[1,2]·Marjanska, M.[3]·Batchelor, T.[1,2]·Rosen, B.[1,2]
[1]Massachusetts General Hospital, Boston, MA, [2]Harvard Medical School, Boston, MA, [3]University of Minnesota, Minneapolis, MN.

Purpose
The aims of this longitudinal imaging study were to establish: a) if a vascular normalization "window" occurs in newly diagnosed glioblastoma patients treated with a combination of antiangiogenic and standard chemoradiation therapy, b) the metabolic consequences of such normalization, c) the mechanisms of tumor response and relapse.
Materials & Methods
Multimodal MR imaging at 3T has been performed with structural, perfusion, diffusion and spectroscopic imaging. A group of 40 glioblastoma patients treated with cediranib

Note: Scanned images are included in the proceedings. Some submitted images were reduced during editing, thereby decreasing clarity. Also, refer to the Program Planner. Proceedings Content as of 3-29-2013.

(oral pan-VEGF receptor tyrosine kinase inhibitor) and standard chemoradiation were scanned serially: two baselines (days -5 and -1), weekly during six weeks of chemoradiation, and then monthly until disease progression or patient went off study. MR spectroscopic imaging (MRSI) was acquired with an optimized low power adiabatic sequence using LASER (Localization by Adiabatic SElective Refocusing). Acquisition parameters were repetition time (TR) of 1.5 s, echo time (TE) of 45 ms, single slice, matrix size 16x20, 10 mm in plane resolution, 15 mm slice thickness. Spectral data were interpolated to a matrix of 32x32 and subsequently fitted by LCModel software. Mean concentrations of six metabolites (N-acetyl-aspartate (NAA), total choline (tCho), creatine (Cre), myo-inositol (mIns), lactate (Lac) and lipids (Lip)) were calculated within tumor regions of interest (ROI) and in normally appearing white matter.

Results

Here we include preliminary results on 11 patients. We observed differences in metabolic time courses in tumors measured by MRSI as compared to changes in tumor contrast-enhanced T1-weighted (ce-T1w) images. In some patients with reduction of tumor ce-T1w the levels of tCho increased throughout the course of the treatment. The ratio of mean tumor Cho to mean Cre in the normal-appearing white matter ($tCho_{tumor}$ / $Cre_{healthy}$) seems to identify two subgroups of patients, one group showing 75% increase, while second group a 25% reduction of this ratio. The ratio of mean tumor Lac to mean healthy Cre (Lac_{tumor} / $Cre_{healthy}$) appears to increase towards the end of chemoradiation.

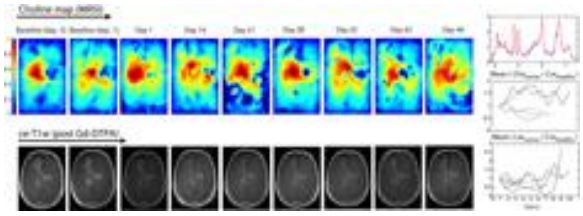

Conclusion

Choline and lactate are metabolic biomarkers that have been associated with tumor proliferation and hypoxia, respectively. Our data suggest that metabolic MRSI provides complementary information to functional and structural MRI that could help in better understanding and predicting response to combined antiangiogenic and chemoradiation therapy in newly diagnosed glioblastoma patients. Further statistical analysis of all patients aiming to correlate metabolic, permeability, perfusion, diffusion and clinical endpoints is undergoing.

KEYWORDS: Glioblastoma, MR spectrocopy, Antiangiogenic therapy

O-404 **4:03 PM - 4:11 PM**

Repeatability of MR-Based Vessel Caliber Estimates in Brain Tumor Imaging

Polaskova, P.[1,2]·Emblem, K. E.[3]·Jafari-Khouzani, K.[1,2]·Kalpathy-Cramer, J.[1,2]·Batchelor, T. T.[4]·Gerstner, E. R.[4]·Rosen, B. R.[1,2]·Stufflebeam, S. M.[1,2]
[1]Massachusetts General Hospital, Charlestown, MA, [2]A.A. Martinos Center for Biomedical Imaging, Charlestown, MA, [3]Oslo University Hospital/Rikshospitalet, Oslo, NORWAY, [4]Massachusetts General Hospital, Boston, MA.

Purpose

Vessel caliber estimation by dynamic susceptibility contrast (DSC) MRI is an emerging technique for assessment of tumor vasculature and knowledge of the repeatability of the technique is critical for monitoring of therapy effectiveness. Using double baseline scans acquired as part of a clinical study in newly diagnosed glioblastoma (nGBMs) patients, we compared the repeatability of two methods for estimation of vessel caliber. Method A uses the ratio of cerebral blood volume (CBV) from contrast-enhanced gradient-echo (R_2*) and spin-echo (R_2) DSC images. Method B provides a semiquantitative vessel caliber index (VCI), correcting for regional diffusion coefficients and blood flow.

Materials & Methods

Thirty-three patients with nGBMs were included in this IRB-approved study after signing informed consent. Two baseline scans were acquired before treatment onset, two-four days apart. In addition to conventional MRI (pre/postcontrast T_1-weighted, FLAIR), DSC MRI was acquired as follows: 100 volumes combined gradient-echo (GE) and spin-echo (SE) EPI sequence; TE 31 ms and 94 ms, TR 1.48s, 0.1 mmol/kg of Gd-DTPA was injected at 5 cc/s after ~81s of imaging and predose of Gd-DTPA (0.1 mmol/kg) was used to minimize T_1 effects from contrast agent extravasation. Apparent diffusion coefficient (ADC) maps were obtained from diffusion-weighted MRI with 42 directions, b = 0/700 mm^2/s. Tumor ROIs were drawn by a neuroradiologist, outlining contrast-enhancing tumor on T1-weighted postcontrast images, and coregistered to DSC images using rigid coregistration. After correction for contrast agent leakage, vessel caliber maps were estimated as follows: Method A: $\Delta R_2^*/\Delta R_2$ ratio maps obtained from GE and SE CBV maps. Method B: First, a voxel-by-voxel 'Q' value was obtained by fitting the linear dependence of $\Delta R_2^*/\Delta R_2^{3/2}$ during the bolus passage. Second, VCI was estimated by the equation: $VCI = 0.867*(ADC*CBV)^{1/2}*Q$. For measures of repeatability we used intraclass correlation coefficient (ICC) and Spearman's rank correlation coefficient.

Results

The ICC for Method A was 0.5189 and for Method B 0.8993. The Spearman's rank correlation coefficient was 0.7214 ($p<.001$) for Method A and 0.865 ($p<.001$) for Method B. Figure 1 shows the scatter plots for the two methods as well as corresponding example vessel caliber

Note: Scanned images are included in the proceedings. Some submitted images were reduced during editing, thereby decreasing clarity. Also, refer to the Program Planner. Proceedings Content as of 3-29-2013.

image.

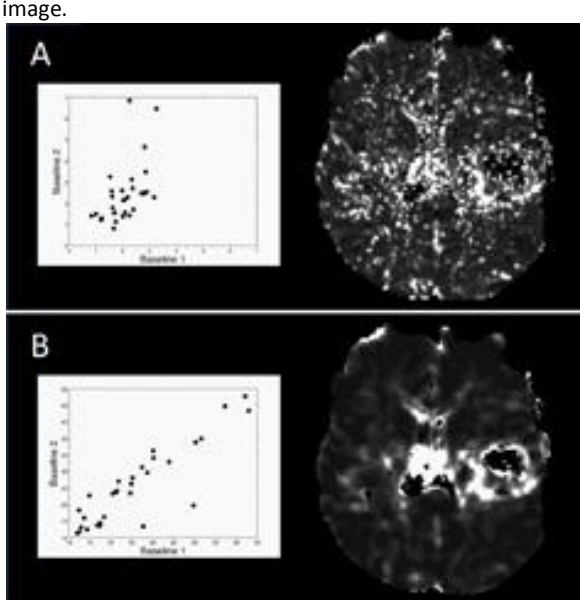

Conclusion

Although the ΔR2*/ΔR2 ratio (Method A) is simple and easily implemented, Method B provides semiquantitative estimate of the vessel caliber with higher repeatability. This makes Method B a good candidate for use as a tumor imaging biomarker, especially in monitoring the vascular response of brain tumors to antiangiogenic therapeutic agents.

KEYWORDS: Dynamic susceptibility contrast-enhanced, Glioblastoma, Vessel size

O-405 **4:11 PM - 4:19 PM**

Early Changes in Relative Cerebral Blood Volume Obtained Using Ferumoxytol-Based Dynamic Susceptibility Contrast MR Perfusion in High-Grade Glial Neoplasms Treated with Bevacizumab

Prola Netto, J.[1]·Varallyay, C. G.[1]·Hamilton, B. E.[1]·Gahramanov, S.[1]·Fu, R.[1]·Nasseri, M.[1]·Neuwelt, E. A.[1,2]
[1]Oregon Health & Science University, Portland, OR, [2]Department of Veterans Affairs Medical Center, Portland, OR.

Purpose

Tumor neovascularization, as an important characteristic of high-grade gliomas, has become a target for anti-angiogenic treatment with bevacizumab. Dynamic susceptibility contrast (DSC)-based perfusion MRI using gadolinium-based contrast agents (GBCA) frequently is used on surveillance imaging to help evaluate active disease. Ferumoxytol, a high molecular weight iron oxide nanoparticle can be used to perform DSC-perfusion MRI, and minimizes errors caused by contrast leak, providing a more reliable measure of relative cerebral blood volume (rCBV) without the need for correction algorithm or preloading dose as is necessary with GBCA-based DSC-perfusion. The aim of this study is to determine early changes in rCBV obtained by using ferumoxytol-based DSC MR perfusion in high-grade glioma patients treated with bevacizumab.

Materials & Methods

Patients were enrolled from a prospective imaging study with brain tumors approved by the institutional review board. Informed written consent was obtained from all patients. Inclusion criteria for our study were patients with histologically proven high-grade glioma which received bevacizumab therapy after standard chemoradiation and underwent ferumoxytol MR perfusion before and after bevacizumab. Bevacizumab was given for clinical and/or radiographic progression in all patients. Anatomical axial T1 spin echo-weighted scans pre and postgadoteridol were acquired. Dynamic susceptibility contrast MR perfusion was performed in a 3T scanner using a 1mg/kg ferumoxytol bolus administered intravenously. Gadolinium-based contrast agents-enhanced axial T1 spin echo and DSC perfusion scans were coregistered before and after bevacizumab in each patient. Regions of interests (ROIs) were drawn manually to include the entire initially enhancing tumor on a representative axial slice. Mean and standard deviation of rCBV values were obtained, and histogram analysis performed. Histograms consisted of 20 bins of rCBV value sizes of 0.5 ranging from 0 to 9.5. Hypo-perfused subvolumes were defined as those areas with rCBV ≤ 0.75 and hyper-perfused as those with rCBV ≥ 1.75.

Results

A total of 27 enhancing masses in 23 patients were analyzed. The mean time of the first scan before bevacizumab was 15 days (range 1-70) and the first post-treatment scan was 27 days after bevacizumab (range 12-50). Mean rCBV in the enhancing area pre-bevacizumab was 1.29, significantly decreasing to 0.91 and 0.93 after bevacizumab administration when the ROI was drawn in the enhancing area pre- and post-bevacizumab ($p = 0.02$ and $p = 0.03$ respectively). Histogram analysis demonstrated a significant increase in the proportion of hypo-perfused voxels from 43% pre-bevacizumab to 56% post-bevacizumab ($p = 0.002$). There was a decrease in the proportion of hyper-perfused voxels from 27% pre-bevacizumab to 19% post-bevacizumab that was not statistically significant($p = 0.08$).

Conclusion

Changes in ferumoxytol-based DSC perfusion can be seen early after bevacizumab administration, with overall decrease in the mean rCBV in the enhancing area. This difference is due mainly to an increased proportion of hypo-perfused voxels rather than a decrease in the hyper-perfused voxels. These preliminary findings may indicate that bevacizumab does not mask the presence of areas of high rCBV and its administration should not be delayed in patients undergoing MR perfusion for evaluation of new or increasing areas of enhancement.

Note: Scanned images are included in the proceedings. Some submitted images were reduced during editing, thereby decreasing clarity. Also, refer to the Program Planner. Proceedings Content as of 3-29-2013.

KEYWORDS: Brain neoplasms, MR imaging perfusion, Ferumoxytol

O-406 **4:19 PM - 4:27 PM**

Spatial Correlation between Apparent Diffusion Coefficient and [18F]-FDOPA Positron Emission Tomography Uptake in Diffuse Gliomas

Leu, K.·Cloughesy, T. F.·Lai, A.·Nghiemphu, P. L.·Chen, W.·Czernin, J.·Pope, W. B.·Ellingson, B. M.
David Geffen School of Medicine at the University of California Los Angeles
Los Angeles, CA.

Purpose
To investigate the relationship apparent diffusion coefficients (ADC) and positron emission tomography (PET) L-3,4-Dihydroxy-6-18F-fluoro-phenyl-alanine (18F-FDOPA) uptake in gliomas.
Materials & Methods
A total of n = 28 patients with histologically confirmed gliomas [World Health Organization (WHO) grades II-IV] who had a T2-weighted/fluid-attenuated inversion recovery (FLAIR) and a diffusion-weighted magnetic resonance image (MRI) scan within three months of the 18F-FDOPA scan were enrolled in this study. Tumor regions were identified via hyperintensities on the T2/FLAIR scans. 18F-FDOPA and ADC maps for each patient were registered to a baseline T2/FLAIR volumetric image using an affine transformation. 18F-FDOPA uptake "hotpots" were defined as areas with uptake greater than the basal ganglia. Apparent diffusion coefficients values were captured within areas of T2/FLAIR lesions that overlapped with the PET "hotspots", called FLAIR(+), and those that did not, FLAIR(-). All statistical tests performed were two-tailed, paired t-tests.
Results
Median ADC was not found to be significantly different between 18F-FDOPA hot or cold spots within FLAIR ROIs [1.28um2/ms in FLAIR(+) versus 1.30um2/ms in FLAIR(-)]. In fact, only 13/28 patients had a lower median ADC in the FLAIR(+) regions. Overall, minimum ADC was significantly higher in the FLAIR(+) regions ($p<0.0001$). A similar trend was found among those with positive tumor recurrence at the time of MR and PET scanning, with only around half of patients illustrating a lower median ADC in FLAIR(+) regions. Interestingly, 10/12 patients who had scans while in the midst of their treatment regimens had a higher median ADC in the FLAIR(+) regions. In a few cases, 18F-FDOPA PET hotspots also were found outside of the T2/FLAIR lesions (Figure 1).

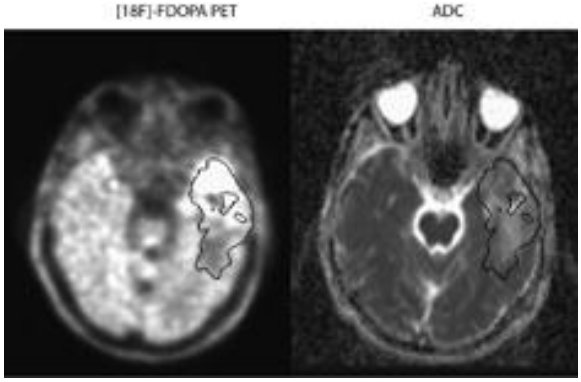

Conclusion
In general, regions with low ADC and elevated 18F-FDOPA PET appear to be spatially independent, suggesting ADC and 18F-FDOPA PET may provide complimentary information about tumor cellularity and metabolism, respectively. Minimum ADC was higher in FLAIR(+) compared with FLAIR(-) regions, suggesting the most metabolically active portions of the tumor may correspond to less dense, but more mobile tumor cells.

KEYWORDS: Glioma, PET, Diffusion

O-407 **4:27 PM - 4:35 PM**

Postoperative Perfusion-Weighted MR Imaging and Tumor Progression/Recurrence in High-Grade Gliomas

Adapa, P.·White, M. L.·Zhang, Y.·Aizenberg, M. R.·Shonka, N.·Kazmi, S. A. J.·Yu, F.
University of Nebraska Medical Center
Omaha, NE.

Purpose
Utilizing the immediate postoperative perfusion-weighted imaging (PWI) MR exams for the prediction of tumor progression and recurrence of primary brain tumors is a novel concept. The current standard of postoperative MRI enhancement for analyzing residual tumor is known to be limited secondary to enhancement from postsurgical changes. This effect can be ameliorated but not completely eliminated with early scanning. Also, enhancement of a tumor does not evaluate angiogenesis. There can be areas of increased tumor angiogenesis that do not have blood-brain barrier breakdown and enhancement. Postoperative perfusion analysis of brain tumor patients allows for an evaluation of the remaining abnormal tumor angiogenesis which likely indicates areas of higher grade tumor. This study evaluates the immediate postoperative PWI for predicting tumor progression and recurrence in subjects with intracranial high-grade gliomas (HGG). The hypothesis is that HGG subjects with elevated PWI postsurgery will have earlier tumor progression/recurrence.
Materials & Methods
This is a single institution retrospective study investigating

Note: Scanned images are included in the proceedings. Some submitted images were reduced during editing, thereby decreasing clarity. Also, refer to the Program Planner. Proceedings Content as of 3-29-2013.

the clinical utility of PWI analyzing when tumor progression/recurrence in HGG will occur. Thirty subjects, 15 males and 15 females, age range from 29-82 years (mean = 55 years) and with pathology proven Grade III and IV gliomas were analyzed. Six subjects were excluded from the final analysis due to the presence of motion artifacts or early loss to followup. The immediate postoperative MRI examinations included T1W pre and postcontrast, T2* PWI at 1.5T or 3.0T. Cerebral blood volume (CBV) maps of the T2* PWI were analyzed for areas of high perfusion. Maximum areas of CBV were measured and a ratio was calculated for this value (rCBV) versus a similar location in the opposite hemisphere. If no areas of elevated perfusion were noted then a maximum rCBV value of one was used indicating perfusion was the same as normal brain. Each of the subjects underwent postoperative chemotherapy and/or radiation therapy per standard of care. Time to recurrence was recorded as the date on which an MRI examination first demonstrated changes that were determined to be recurrence. Subjects' follow-up imaging, pathologic records and clinical records were evaluated to confirm progression/recurrence of HGG. A nonparametric Wilcoxon rank sum test was used for comparing the median values of maximum rCBV in subjects with progression/recurrence before 200 days or after 200 days.
Results
The maximum rCBV (median = 3.8) for subjects that had progression/recurrence of HGG in <200 days was significantly higher than the rCBV (median = 1) in subjects with recurrence/progression in >200 days ($p = 0.0018$). There were six cases that had not recurred with follow-up times of 213-433 days. These were placed in the > 200 day group for analysis.
Conclusion
Greater residual maximum rCBV postoperatively was associated with shorter time to progression and recurrence of HGG. This suggests that areas of residual elevated rCBV after surgery might need to be considered for more aggressive therapy. Protocol for treatment of postoperative residual high rCBV tissue remains to be determined and will be the subject of future studies.

KEYWORDS: Glioma recurrence, MR perfusion-weighted imaging

O-408 **4:35 PM - 4:43 PM**

Early Postoperative Diffusion-Weighted Imaging and Perfusion-Weighted Imaging Are Adjuvant Imaging Tools in Differentiating between Pseudo-Progression and Progression in Patients with Glioblastoma Treated with Temozolomide and Radiotherapy

Liu, X.[1]·Tian, W.[2]·Wang, H.[1]·Ekholm, S.[1]
[1]University of Rochester School of Medicine & Dentistry, Rochester, NY, [2]University of Rochester Medical Center, Rochester, NY.

Purpose
Radiotherapy and concurrent/adjuvant temozolomide treatment is gold standard regimen for patients with newly diagnosed glioblastomas. However, this treatment protocol may induce up to 20-50% patients presenting pseudoprogression within six months after radiation/temozolomide treatment, which is difficult to be distinguished from true tumor progression on conventional MRI. Previous literatures reported that the restricted diffusion in the early postoperative MRI (<72 hours after operation) of such glioblastoma patients indicates the postoperative injuries, which subsequently transfer into pseudoprogression. Therefore, the purpose of this study is to differentiate between the pseudo-progression and true tumor progression based on early postoperative diffusion-weighted imaging and perfusion-weighted imaging.
Materials & Methods
A total of 41 cases of glioblastomas with dynamic susceptibility contrast perfusion-weighted imaging and diffusion-weighted imaging acquired within postoperative 72 hours after resection were included in this study. Nine of the cases had to be excluded due to unacceptable imaging artifacts. Areas with visually detected low apparent diffusion coefficient (ADC) and increased relative cerebral blood volume (rCBV) in the peri-resection cavity regions were detected. Sequential MRI examinations at one month and six months after radiation/temozolomide treatment were performed to determine if these areas of enhancement represented pseudoprogression or true progression by means of the McDonald criteria. The difference of initial ADC and rCBV values in these pseudoprogression and tumor progression was evaluated with the Mann-Whitney U test.
Results
There were 48 postoperative peri-resection cavity regions with reduced ADC value, 33 among of them (68.8 %, mean ADC value 0.656 ± 0.324; rCBV value 0.597 ± 0.312), showed pseudoprogression on follow-up contrast enhancement T1WI, 15 areas (31.2%, mean ADC value 0.597 ± 0.268, p value = 0.33; rCBV value 1.83 ± 0.46, $p<0.001$) showed tumor progression. In addition, there were 12 true tumor progression regions with increased early postoperative rCBV value (1.61 ± 0.27), but without reduced ADC value (1.13 ± 0.35). Discussion: Our preliminary results showed that early postoperative

Note: Scanned images are included in the proceedings. Some submitted images were reduced during editing, thereby decreasing clarity. Also, refer to the Program Planner. Proceedings Content as of 3-29-2013.

restricted diffusion alone has limited value in differentiating between the pseudo-progression and true tumor progression. However, the areas with early postoperative high rCBV are prone to progress as true tumor progression.
Conclusion
Our findings suggest that early postoperative increased rCBV value may be a useful novel imaging biomarker in differentiating between the pseudo-progression and true tumor progression in patients with glioblastomas treated with radiation and temozolomide.

KEYWORDS: Glioblastoma, Pseudoprogression, progression

Wednesday Afternoon

3:15 PM - 4:45 PM
Ballroom 6DE

(45c) Parallel Scientific Papers: Head and Neck: Orbits, Thyroid and Parathyroid Glands: Evolving Techniques

O-409 **3:15 PM - 3:23 PM**

Imaging Findings in Children Referred for Horner's Syndrome

Kadom, N.·Jubouri, S.
Children's National Medical Center
Washington, DC.

Purpose
To determine the spectrum of pathology found in children referred for imaging workup of Horner's syndrome.
Materials & Methods
Retrospective study, IRB approved. There was a single observer (radiology resident) who identified patients using a word search software tool (Montage) for radiology reports from 1991-2012. Search criteria were reports with a positive history of Horner's and an imaging study that was either a computed tomography (CT) or magnetic resonance imaging (MRI). Medical records search for clinical and ophthalmology data also was performed. The following variables were recorded: type of imaging study (CT versus MR, complete exam covering levels of first-third order lesions versus only partial anatomical coverage), age at time of imaging, age at time of Horner's onset, side of Horner's, ophthalmology findings (cocaine test, miosis, ptosis, anhydrosis, other), level of pathology based on final diagnosis (1st , 2nd and 3rd order), final diagnosis. Descriptive statistics with Stata v12.1.
Results
There were 69 patients, 31 boys and 38 girls. Mean age at the time of onset of Horner's syndrome was 3.7 years, mean age at time of imaging was 4.1 years. Side of Horner's was right in 31, left in 24, bilateral in one and unknown in 13. The majority of patients had documented miosis (n = 45), followed by ptosis (n = 43). Cocaine test was positive in seven, anhydrosis was not present in two patients and in all others not documented as positive. The most commonly performed imaging study was a complete MRI (n = 49), followed by partial MRI (n = 10), partial CT (n = 6) and complete CT (n = 4). There were 14 different diagnoses in 27 patients with a documented diagnosis of Horner's: congenital (n = 4), physiologic (n = 4), postinflammatory (n = 4), Chiari (n = 2), CN III palsy (n = 2), brain insult (n = 2), resolved (n = 2), vascular (n = 1), neuroblastoma (n = 1), brain tumor (n = 1), fetal injury (n = 1), autism (n = 1). Of note, 10 patients had ectopic cervical thymus but there was not enough documentation to see if this was clinically considered to be the cause of Horner's syndrome.
Conclusion
Rarely children presenting with Horner's syndrome may have malignant disease, such as neuroblastoma or brain tumor. Pathology accounting for Horner's syndrome in children can be found at any anatomical level corresponding to 1st, 2nd and 3rd order neurons. Therefore, every child with unexplained Horner's syndrome should undergo an imaging study that covers all anatomical levels. Vascular malformations causing Horner's can occur in children and therefore vascular imaging (CT angiogram, MR arteriogram) should be included in the imaging protocol. Due to radiation exposure concerns in children and better ability of MRI to detect subtle anomalies of the cavernous sinus, spinal cord and brain parenchyma, MRI should be the preferred imaging modality.

KEYWORDS: CT, MR imaging, Horner's syndrome

O-410 **3:23 PM - 3:31 PM**

Visual Pathway Damage in Leber's Hereditary Optic Neuropathy: A Quantitative 3T MR Imaging Analysis

Politi, L. S.[1]·Montechiari, M.[1]·Ciasca, P.[2]·Iadanza, A.[1]·Bianchi Marzoli, S.[2]·Falini, A.[1]
[1]San Raffaele Scientific Institute, Milan, ITALY, [2]Auxologico Scientific Institute, Milan, ITALY.

Purpose
Leber's Hereditary Optic Neuropathy (LHON) is a rare genetic disease associated with mutations of mitocondrial DNA. MR imaging (MRI) findings in LHON are reported anecdotally, with contradictory results. The goals of this study were: i) to analyze the MRI findings in brain of LHON patients; ii) quantify size and T2 signal intensity changes along the anterior visual pathway (AVP); iii) correlate size and signal changes to genotype and to clinical and instrumental neuro-ophthalmologic parameters.

Note: Scanned images are included in the proceedings. Some submitted images were reduced during editing, thereby decreasing clarity. Also, refer to the Program Planner. Proceedings Content as of 3-29-2013.

Materials & Methods
Nineteen [16 late-chronic (LC), 3 early-chronic (EC)] genetically confirmed LHON patients and 12 age- and sex-matched healthy controls (HC) underwent a complete neuro-ophthalmologic evaluation with visual acuity, visual field and peripapillary retinal nerve fiber layer (PRNFL) measurements and, on the same day, a 3T MRI examination. FSE T2, FLAIR, T2 SPIR and 3D-FFE T1 sequences were acquired. For each participant, brain lesion load was measured. Optic chiasm (OC) area and T2 signal were quantified on T2 coronal slices; intracranial optic nerves (ON) and optic tracts (OT) were similarly measured 6 mm ventrally and dorsally to the optic chiasm. For each subject the T2 signal intensities of the AVP were normalized to the genu of the corpus callosum and signal intensity ratios (SIRs) were obtained. The intraorbital ON and nerve sheath diameters were measured 9 mm dorsal to posterior pole of ocular globe. Mann-Whitney and Kruskal-Wallis tests were employed for statistical analyses; correlations between MRI results and neuro-ophthalmologic features were performed with Spearman's correlation and nonlinear regression analysis.
Results
White matter (WM) lesions were detected in 8/16 LC and 1/3 EC patients, without significant correlation among lesion load and visual impairment severity or PRNFL thickness. One LC patient presented selective T2 alterations of both Meyer's loops. T2 SIRs of intracranial ON, OC and OT were higher ($p \leq .001$) in patients compared to HC, but were not significantly different between LC and EC. Optic nerve, OC and OT were significantly smaller ($p \leq .001$) in LC compared to HC. A larger ($p = .009$) OC was found in EC than in HC. Average PRNFL of LHON correlated ($p \leq .001$) with size measurements of omolateral intracranial ON ($\rho = .771$), OC ($\rho = .833$) and controlateral OT ($\rho = .722$). A negative nonlinear correlation ($p \leq .001$) was found between AVP size measurements and disease duration [intraorbital ON ($\rho = -.861$), intracranial ON ($\rho = -.549$), OC ($\rho = -.908$) and OT ($\rho = -.640$)]. No correlation was observed between MRI parameters and genotype.
Conclusion
White matter lesion load did not correlate to the degree of visual impairment. In both LC and EC patients, significant SIRs increase was present along the AVP, probably due to edema and/or Wallerian degeneration. Anterior visual pathway size was decreased significantly in LC; conversely, the OC was swollen in EC. These findings may suggest a time-dependent evolution (edema followed by degeneration?) and may explain the contradictory results reported in literature, probably related to different phases of the disease. Anterior visual pathway size significantly correlated to average PRNFL measurement and inversely correlated to disease duration. Thus MRI can be useful in monitoring disease course and quantifying AVP changes in future clinical trials.

KEYWORDS: Optic nerve, Optic chiasm, LHON

O-411 **3:31 PM - 3:39 PM**

Morning Glory Disk Anomaly: Characteristic Orbital Findings at MR Imaging

Ellika, S. K.·Robson, C. D.·Heidary, G.·Paldino, M. J.
Childrens Hospital Boston
Boston, MA.

Purpose
The morning glory disk anomaly (MGDA) is a congenital optic nerve abnormality characterized by a funnel-shaped excavation of the posterior globe that incorporates the optic disk. Establishing the diagnosis of MGDA is crucial to guide appropriate ophthalmic management and to prompt a search for associated intracranial abnormalities. Although findings in MGDA at cross-sectional imaging have been reported in several case studies, reports of at most two patients do not allow an understanding of the consistency with which individual findings occur in this clinical setting. Furthermore, in our experience, the orbital findings of MGDA at high quality imaging are not only highly characteristic for this entity but are also of greater breadth than what has been reported previously. The goal of this study, therefore, is to characterize the spectrum and frequency of orbital findings in a series of patients with MGDA using MRI.
Materials & Methods
Pediatric patients with a diagnosis of MGDA confirmed at ophthalmologic exam were identified retrospectively. Imaging was reviewed by two pediatric neuroradiologists for: 1. Funnel-shaped morphology of the optic disk; 2. Elevation of the adjacent retinal surface; 3. Abnormal tissue associated with the distal intraorbital segment of the optic nerve (ipsilateral to the MGDA); 4. Effacement of the subarachnoid spaces of the distal optic nerve sheath resulting from this abnormal tissue; 5. Fat within the distal optic nerve sheath; 6. Enhancement within the distal optic nerve; 7. Discontinuity of the posterior uveoscleral coat at the optic nerve insertion.
Results
Six patients (age range: 8 months to 2 years) comprised the study group. MR imaging demonstrated three findings in all patients: 1. funnel-shaped morphology of the posterior optic disk (arrow, Figure1) with elevation of the adjacent disk margins in all patients; 2. abnormal tissue associated with the distal intraorbital segment of the ipsilateral optic nerve(arrowhead, Figure 1); this tissue was associated with effacement of the subarachnoid spaces; 3. discontinuity of the posterior uveoscleral coat. These findings were not observed in any of the unaffected globes of the study patients. Less consistent orbital findings included: 1. Fatty infiltration of the distal optic nerve sheath(n=3). 2. Enhancement within the distal optic nerve (n=2). 3. Small size of the globe containing the MGDA (n=2).

Note: Scanned images are included in the proceedings. Some submitted images were reduced during editing, thereby decreasing clarity. Also, refer to the Program Planner. Proceedings Content as of 3-29-2013.

Conclusion
Here we demonstrate several consistent orbital features of MGDA at MRI. These findings may allow for accurate differentiation from other ocular anomalies and have the potential to guide appropriate management of this patient population.

KEYWORDS: Optic nervemorning glory syndrome; morning glory disc anomaly

O-412 **3:39 PM - 3:47 PM**

Normal MR Imaging Appearance of the LR-SR Band in One Hundred Consecutive Patients

Patel, S. H.[1,2]·Juliano, A.[1]·Moonis, G.[1]·Kazlas, M.[1]·Cunnane, M.[1]
[1]Massachusetts Eye and Ear Infirmary, Boston, MA, [2]Massachusetts General Hospital, Boston, MA.

Purpose
Orbital connective tissues are being recognized increasingly for their functional role in eye motility. Such structures include rectus muscle pulleys, which surround and inflect extraocular muscle paths, as well as the connective tissue bands which couple the pulley's actions to one another. One connective tissue band which recently has been investigated is the lateral rectus-superior rectus band (LR-SR Band). In myopic strabismus fixus or "heavy eye syndrome," it is hypothesized that degeneration of the LR-SR band allows inferior slippage of the lateral rectus muscle, producing characteristic esotropia and hypotropia. However, at present the evidence is preliminary, and no radiologic study has defined the normal MRI appearance of the LR-SR band. The purpose of this study is to characterize the normal 3T MRI appearance of the LR-SR band in patients without myopic strabismus fixus.
Materials & Methods
One hundred consecutive patients who underwent orbital MRI examinations at our institution from June 2012 - October 2012 were chosen. Exclusion criteria included: clinical diagnosis of myopic strabismus fixus; pathology affecting location of the LR-SR band; high axial myopia; staphyloma; strabismus unexplained by another cause. Characterization of the LR-SR band was performed on coronal non-fat suppressed T1-weighted images and coronal short tau inversion recovery (STIR) sequences.
Results
Of the selected 100 patients, 61 were female and 39 male, with average age of 49.6 ± 16.4 years. The LR-SR band was identified as an arc-like hypointense structure extending from the superior margin of the lateral rectus muscle to the lateral aspect of the superior rectus/levator palpebrae complex in 198 out of 200 imaged orbits (99%) on the coronal T1-weighted sequences, and 156 out of the 200 imaged orbits (78%) on the coronal STIR sequences. One hundred ninety-four of the 198 visible LR-SR bands (98%) appeared as a continuous, uninterrupted structure, and four out of the 198 visible LR-SR bands (2%) appeared as a discontinuous structure. The appearance of the band was identical on T1-weighted sequences without or with intravenous contrast. In 36 out of the 198 visible bands (18.2%), the posterior aspect of the band demonstrated superolateral bowing. In 155 out of the 200 orbits (77.5%), a distinct levator palpebrae superioris aponeurosis was visible that was clearly separable from the LR-SR band.
Conclusion
The LR-SR band is a readily identifiable structure on 3T MRI imaging of the orbit, most reproducibly seen on nonfat suppressed coronal T1-weighted imaging as a continuous, arc-like, hypointense structure extending from the superior margin of the lateral rectus to the lateral margin of the superior rectus/levator palpebrae muscle complex. The band usually is distinguishable from the levator palpebrae superioris aponeurosis, and occasionally demonstrates superolateral bowing of its posterior segment.

KEYWORDS: OrbitsLR-SR Band

O-413 **3:47 PM - 3:55 PM**

Contrast-Enhanced Radial 3D Fat-Suppressed T1-Weighted Gradient Echo (Radial-VIBE) Sequence: A Viable and Potentially Superior Alternative to Conventional T1-MPRAGE with Water Excitation and Fat-Suppressed Contrast-Enhanced T1-Weighted Sequence for Evaluation of the Orbit

Bangiyev, L.[1]·Raz, E.[1]·Block, T.[1]·Hagiwara, M.[1]·Yu, E.[2]·Fatterpekar, G. M.[1]
[1]New York University Langone Medical Center, New York, NY, [2]University of Toronto, Toronto, ON, CANADA.

Purpose
Contrast-enhanced fat-suppressed T1-weighted (T1W-FS) sequence and T1-MPRAGE with water excitation (WE) are routinely obtained to evaluate orbit pathology. However, this sequence can be marred by multiple artifacts. The purpose of our study was to evaluate the role of contrast-enhanced Radial-VIBE sequence when evaluating orbital studies and compare with routinely acquired sequences.
Materials & Methods
A retrospective study was performed in 46 patients (age 1-

Note: Scanned images are included in the proceedings. Some submitted images were reduced during editing, thereby decreasing clarity. Also, refer to the Program Planner. Proceedings Content as of 3-29-2013.

81 years) who underwent contrast-enhanced MRI orbital studies on a 1.5T system. Each of these patients were evaluated with the Radial-VIBE, T1 MPRAGE-WE and contrast-enhanced T1W-FS studies. The free-breathing Radial-VIBE sequence was acquired with the following: slice thickness=0.8 mm; flip angle=12°; TR=4.57 ms; TE=2.06 ms; Matrix=256x256; Field of view=250x250 cm2. Two radiologists blinded to acquisition scheme evaluated multiple parameters of image quality including motion artifact, fat-suppression, clarity of scleral enhancement, clarity of vessels, clarity of muscles, clarity of optic nerve, clarity of brain parenchyma, and conspicuity of pathology. Each of these parameters was assessed on a 5-point scale with a higher score indicating more optimal exam. Mix-model analysis of variance was performed to compare the results. An interobserver variability assessment was performed using a Cohen K.

Results

Using a Kruskal Wallis test, we compared the results of axial Radial-VIBE, axial T1-MPRAGE and axial T1W-FS and we found significant higher values for all the parameters for the axial VIBE ($p<0.0001$). We compared the reconstructed Radial-VIBE and the coronal and T1W-FS using a Mann-Whitney U test and we found a significant difference with significant higher values for all the parameters for the coronal reconstructed Radial-VIBE ($p<0.0001$). Interobserver agreement in the qualitative evaluation using a Cohen's kappa analysis demonstrated average fair to good agreement for the following variables: motion artifacts=0.745, fat-suppression=0.678, clarity of scleral enhancement=0.688, clarity of vessels=0.655, clarity of muscles=0.675, clarity of nerves=0.518, clarity of brain parenchyma=0.710, pathology conspicuity=0.590. In addition, the obtained Radial-VIBE images can be reconstructed in multiple planes and can be evaluated for dynamic temporal assessment which is another significant advantage of this technique.

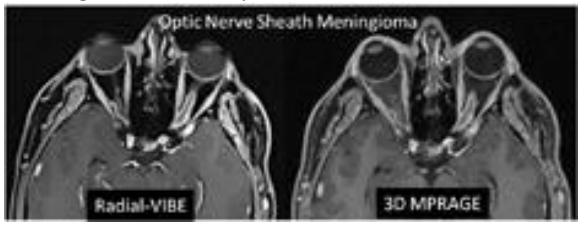

Image Quality Parameter Scores for Each Reader and Sequence (Mean +/- SD)

	Reader 1 Ax VIBE	Reader 1 Ax MPRAGE	Reader 1 Ax FS T1W	Reader 1 Cor FS T1W	Reader 1 Cor VIBE	Reader 2 Ax VIBE	Reader 2 Ax MPRAGE	Reader 2 Ax FS T1W	Reader 2 Cor FS T1W	Reader 2 Cor VIBE
Motion artifact	5±0	3.98±0.649	4.07±0.73	4.59±0.56	5.0±0	4.91±0.285	3.72±0.72	3.93±0.616	4.31±0.535	4.97±0.177
Fat-suppression	4.65±0.795	3.8±1.003	3.29±0.914	3.81±0.644	4.78±0.42	4.63±0.711	3.59±0.777	3.5±1.019	3.81±0.592	4.78±0.491
Scleral enhancement	5±0	4.76±0.431	4.14±0.864	3.72±0.523	5.0±0	4.96±0.206	4.3±0.695	4.0±0.784	3.94±0.759	4.97±0.177
Clarity of vessels	4.89±0.315	3.52±0.658	2.79±0.426	3.0±0.359	4.84±0.369	4.93±0.25	3.83±0.608	3.14±0.663	3.41±0.712	4.97±0.177
Clarity of muscles	4.98±0.147	4.22±0.786	4.57±0.514	4.44±0.669	5.0±0	4.89±0.315	4.13±0.778	4.07±0.73	4.22±0.491	4.94±0.246
Clarity of optic nerve	5±0	3.76±0.899	2.64±0.633	3.38±0.707	5.0±0	4.85±0.363	3.7±0.84	3.36±0.745	3.53±0.671	4.91±0.298
Clarity of brain parenchyma	4.67±0.474	4.87±0.341	2.21±0.579	2.16±0.369	4.72±0.457	4.33±0.519	4.35±0.604	2.29±0.469	2.38±0.492	4.5±0.568
conspicuity of pathology	4.71±0.854	3.96±1.071	3.6±1.075	3.22±1.166	4.67±0.97	4.74±0.526	3.86±0.891	3.4±0.699	3.67±0.767	4.61±0.979

Conclusion

Radial-VIBE sequence is a viable and potentially superior alternative to conventional T1-MPRAGE and T1W-FS sequence.

KEYWORDS: Orbits, 3D imaging, Radial VIBE

O-414 **3:55 PM - 4:03 PM**

4D CT: How Many Phases Do We Need?

Mahajan, A.·Kadivar, K.·Gafton, A. R.·Sze, G.
Yale School of Medicine
New Haven, CT.

Purpose

4D CT recently has been purported as the imaging modality of choice for localization of parathyroid adenomas. This has been a recently described technique, where multiphase CT acquisitions are obtained after contrast administration, through the neck and upper chest. With increased number of scans through the upper neck and chest, there is increased radiation exposure to the thyroid gland. To avoid this, it would be ideal to curtail the study to the minimum number of phases required to obtain the desired information and avoid unnecessary radiation.

Materials & Methods

This is a retrospective evaluation of patients with primary hyperparathyroidism due to parathyroid adenoma. All patients underwent surgery and had clinical cure after surgery. Fifty-six patients with parathyroid adenomas were included in the study. The patients were scanned from the angle of the mandible to the tracheal carina. The scans were evaluated by two board-certified radiologists and each phase was scored according to the quality of information provided (0 - No Valuable information, 1 - Helpful information was obtained to assist in diagnosis and 2 - Diagnostic information). The scan protocols included a 5-phase, 4-phase and a 3-phase protocol. The 5-phase protocol included an initial noncontrast and 4 subsequent phases (30, 90, 150 and 420 secs after contrast administration) while the 4-phase protocol had an initial noncontrast and 3 postcontrast phases - 30, 90, 150 secs). Some patients also had a 3-phase study (1 Noncontrast and 2 postcontrast phases - 30 and 90 secs after contrast administration). Coronal and sagittal reformats were obtained after 1.25 mm reconstructions.

Results

Fifty-six patients with solitary or multiple adenomas were included in the study - 14 patients underwent the 5-phase protocol, 40 patients had 4-phase study and two patients had a 3-phase study. Noncontrast scan was found useful in 18 patients (32%), the arterial phase was helpful in 43 (77%) of patients, the 90 sec scan was helpful in 10 cases (18%), the 150 sec scan was helpful in one patients while the 420 sec scan did not add any additional information in the patient. Coronal reformats were helpful in 20% of patients to identify inferior parathyroid and ectopic mediastinal adenomas, which were hard to identify on the axial scans.

Note: Scanned images are included in the proceedings. Some submitted images were reduced during editing, thereby decreasing clarity. Also, refer to the Program Planner. Proceedings Content as of 3-29-2013.

Conclusion
4D CT is a helpful study in diagnosing parathyroid pathology. Noncontrast and the early arterial phase were the most useful in making the diagnosis. The 90 sec phase helped in identifying lesions missed on the arterial phase; however, the 150 and 240 sec phases were not helpful in providing any incremental value in diagnosis. The coronal reformats also were helpful in identifying inferior and ectopic mediastinal parathyroid adenomas.

KEYWORDS: 4D CT, Parathyroid

O-415 **4:03 PM - 4:11 PM**

Polar Vessel: A Sign of Parathyroid Lesions on 4D CT

Bahl, M.[1]·Muzaffar, M.[2]·Vij, G.[1]·Scheri, R. P.[1]·Hoang, J. K.[1]
[1]Duke University Hospital, Durham, NC, [2]Carle Clinic, Urbana, IL.

Purpose
The characteristic sign of a parathyroid adenoma on multiphase parathyroid CT (4D CT) is enhancement on the arterial phase and washout on the venous phase. A second sign, the "polar vessel" sign, has been reported on ultrasound but is underappreciated on 4D CT. The purpose of this study is to determine the prevalence of the polar vessel sign on 4D CT and to determine features of parathyroid lesions that are associated with this sign.
Materials & Methods
We performed a retrospective review of consecutive patients with pathologically proven parathyroid lesions who had 4D CT between 2008 and 2012 at two institutions. Thirty-one patients (25 females, mean age 58 years, range 15-83 years) were identified for review after excluding six studies with poor image quality and/or lesions too small to be seen. 4D CT images were reviewed for the presence of the polar vessel sign (enlarged feeding artery or draining vein) and a second vascular finding of an enlarged ipsilateral inferior thyroidal artery. The parathyroid lesions also were characterized by location, CT dimensions, gross pathology weight, and arterial phase imaging attenuation (HU). The presence of the polar vessel sign on 4D CT was correlated with these characteristics.
Results
Four of 31 (13%) patients had multiglandular disease and five of 31 (16%) had lesions in ectopic locations. There were a total of 35 parathyroid lesions with a mean lesion weight of 0.66 g (SD 0.65 g), mean maximal CT diameter of 11.4 mm (SD 4.9 mm), and mean arterial attenuation of 156 HU (SD 55 HU). The polar vessel sign was seen in 26/35 (74%) of lesions. Compared to lesions without an associated polar vessel, lesions with a polar vessel had statistically significant higher mean maximum diameters (13.0 and 6.7 mm, $p < 0.01$) and higher arterial phase attenuation (172 HU and 109 HU, $p < 0.01$). There were no differences in location or gross pathology weight of lesions with or without the polar vessel. An enlarged inferior thyroidal artery was seen in only 3/28 (11%) patients with unilateral disease.

Conclusion
The polar vessel sign is present in three-quarters of parathyroid lesions on 4D CT and is more common in larger lesions and lesions with greater arterial phase enhancement. Radiologists can use the polar vessel sign on 4D CT to increase diagnostic confidence for candidate parathyroid lesions.

KEYWORDS: Parathyroid, 4D CT

O-416 **4:11 PM - 4:19 PM**

Dynamic CT for Parathyroid Disease: How Many Phases Do We Really Need?

Raghavan, P.·Durst, C.·Ornan, D.·Muherjee, S.·Patrie, J.·Xi, W.·Wintermark, M.·Shada, A.·Hanks, J. B.·Smith, P. W.
University of Virginia
Charlottesville, VA.

Purpose
Dynamic 4D CT has emerged as a reliable tool in the detection of parathyroid adenomas. A standard 4D protocol involves obtaining unenhanced (U), arterial (A), early (EV) and delayed venous (DV) phase images of the neck. Recent papers have attempted to eliminate one or more phases in order to decrease radiation dose. Our study aims to determine the ideal combination of phases that would minimize radiation dose without sacrificing diagnostic accuracy.
Materials & Methods
The records of 29 patients with primary hyperparathyroidism were reviewed. All patients had undergone preoperative 4D CT followed by surgical exploration. Four neuroradiologists blinded to the surgical outcome reviewed the imaging studies in five combinations (1- unenhanced and arterial phase; 2- unenhanced, arterial and early venous; 3- all four phases; 4- arterial alone: 5- arterial and early venous phases) with an interval of at least seven days between each review. The accuracy of interpretation in lateralizing an

Note: Scanned images are included in the proceedings. Some submitted images were reduced during editing, thereby decreasing clarity. Also, refer to the Program Planner. Proceedings Content as of 3-29-2013.

abnormality to the side of the neck (Right, Left, Ectopic) and to a quadrant in the neck (Right and Left upper, Right and Left lower) was evaluated via binomial generalized estimating equation models.

Results

There was no statistically significant difference between the different combinations of phases in their ability to lateralize adenomas or to localize them to a quadrant (p = 0.930 and 0.969, respectively). The accuracy of each combination is summarized in the tables below.

TABLE 1. Estimated reader vs surgeon diagnostic agreement in lateralization of adenomas(%)

COMBINATION	ESTIMATED DIAGNOSTIC AGREEMENT	LOWER 95% CONFIDENCE LIMIT	UPPER 95%CONFIDENCE LIMIT
U,A	89.9	84.6	93.6
U,A,EV	87.9	83	91.6
U,A,EV,DV	89.9	84.8	93.5
A	89.7	84.4	93.3
A,EV	90.5	85.3	94.0

TABLE 2 Estimated reader vs surgeon diagnostic agreement in localization of adenomas to a quadrant (

COMBINATION	ESTIMATED DIAGNOSTIC AGREEMENT	LOWER 95% CONFIDENCE INTERVAL	UPPER 95%CONFIDENCE INTERVAL
U,A	87.2	83.2	90.4
U,A,EV	86.0	82.0	89.3
U,A,EV,DV	87.9	83.8	91.1
A	87.1	82.7	90.5
A,EV	87.2	82.9	90.6

Conclusion

Our findings indicate that four-phase acquisition is unnecessary and adequate diagnostic accuracy may be achievable by obtaining arterial phase images alone, with the advantage of a 75% reduction in radiation dose.

KEYWORDS: 4D CT, Parathyroid

O-417 **4:19 PM - 4:27 PM**

What to Do with the Incidental Thyroid Nodule on CT and MR Imaging?: A Survey of Radiologists' Reporting Practices

Riofrio, A. D.·Bashir, M.·Hoang, J. K.
Duke University Medical Center
Durham, NC.

Purpose

Incidental thyroid nodules (ITN) commonly are seen on imaging. There currently are no widely accepted guidelines for reporting ITN seen on CT and MRI. The aim of this study is to determine current reporting practices for radiologists from different subspecialties and practice types.

Materials & Methods

A survey was designed to query radiologists about their reporting practices for 14 scenarios of ITN differing in nodule size (8, 10, and 15 mm), multiplicity of nodules, age and gender of the patient, and presence of nonmetastatic lung cancer. The five possible choices for each scenario were A) do not report, B) leave in body of report, C) report in impression without recommendation, D) recommend ultrasound +/- biopsy, and E) no consistent practice. The survey was sent electronically to three groups: Group A - radiologists in all subspecialties at an academic institution, Group B - radiologists attending the ACR Head & Neck radiology course (predominantly private practice radiologists), and Group C - ASNR member radiologists (predominantly neuroradiologists). Responses were evaluated for the most commonly selected decision for each scenario and the proportion of radiologists choosing that decision. If the three groups chose the same decision for a given scenario, it indicated high agreement *between* the groups. Agreement *within* the same group was measured by the proportion of responses that selected the decision(High ≥75%, Moderate 50-74%, Low 25-49%, and Poor <25%). Demographic inquiries included years in practice, subspecialty training, and current practice type.

Results

One hundred fifty-three radiologists participated in the survey, including 41 in Group A, 28 in Group B, and 84 in Group C. Table 1 shows the responses for Groups A-C and agreement within each group. Management of 15 mm nodules was most uniform between the groups with all choosing "recommend ultrasound." There was also at least moderate agreement for this response within each group. The scenarios with least agreement between the groups

Note: Scanned images are included in the proceedings. Some submitted images were reduced during editing, thereby decreasing clarity. Also, refer to the Program Planner. Proceedings Content as of 3-29-2013.

and lowest concordance within groups were 8 mm nodules in adults, 10 mm nodule in 60-year-old females, multiple nodules, and a nodule with lung cancer history.

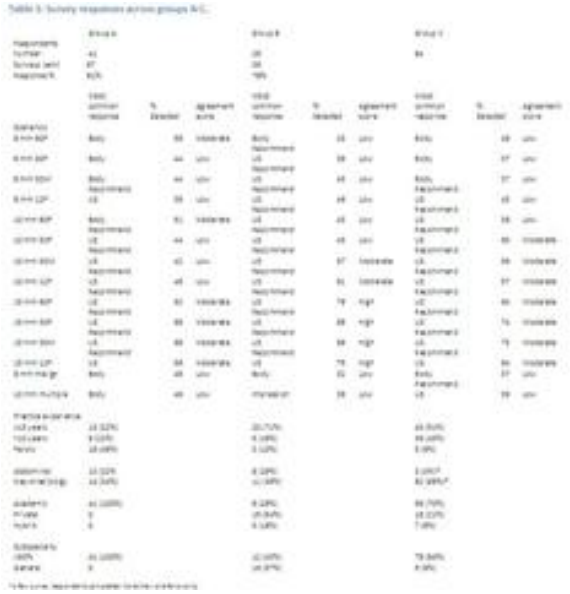

Conclusion

Radiologist practices in reporting ITN on CT and MRI in adults vary widely, especially for nodules less than 15 mm, patients with multiple nodules, and nodules in oncology patients. Guidelines for the standardization of reporting practices may help alleviate radiologist uncertainty and provide consistency for referring clinicians. This survey may serve as one step towards the creation of such guidelines.

KEYWORDS: Incidental findings, Thyroid

O-418 **4:27 PM - 4:35 PM**

Incidental Thyroid Nodules Detected on Imaging: Can Workup Be Reduced by Using the Society of Radiologists in Ultrasound Guidelines and the 3-Tier System?

Hobbs, H. A.·Bahl, M.·Nelson, R. C.·Kranz, P. G.·Esclamado, R. M.·Hoang, J. K.
Duke University
Durham, NC.

Purpose

Incidental thyroid nodules (ITN) on imaging can be a challenging problem for radiologists and clinicians. However, guidelines can help to direct ITN workup. The Society of Radiologists in Ultrasound (SRU) published sonographic recommendations to direct FNA, and recently a 3-tiered system was proposed for workup of thyroid nodules seen on CT, PET and MRI. The intentions of both guidelines are, not to diagnose all cancers, but to diagnose "*clinically significant"* cancers, while avoiding unnecessary tests and surgery in patients with benign nodules. The aim of this study was to determine the number of nodule workups that could be reduced and the malignancies that would be missed if the SRU recommendations and 3-tier system were applied to imaging-detected ITN.

Materials & Methods

This is a retrospective study of 390 consecutive patients who underwent ultrasound-guided thyroid FNA from July 2010 to June 2011. Medical records were reviewed for patients with ITN first detected on imaging studies and their subsequent pathology results. The imaging studies that lead to the detection of the ITNs were reviewed by two radiologists. Readers recorded characteristics of the ITN and whether nodules met criteria per guidelines. Incidental thyroid nodules seen on ultrasound were categorized by SRU recommendations which includes solid nodules ≥15 mm, or nodules with microcalcifications ≥10 mm, coarse calcifications ≥15 mm, and solid-cystic component ≥20 mm. The 3-tiered system was applied to ITN seen on CT, MR and PET/CT. It recommends sonographic workup of nodules with high risk imaging features(suspicious lymph nodes, local invasion, PET focal metabolic activity), high risk history(age <35 years, active metastatic disease), or solid nodules ≥15 mm.

Results

There were 114/390(29%) patients(78 female, 36 male, mean age 60 years, range 14-91) documented as having nodules first detected incidentally by imaging studies. The prevalence of malignancy in nodules based on cytopathology and confirmed at surgery was 8/114(7%). Imaging studies were available for review on 108/114 patients. Of 108 patients, 47 were incidentally detected on ultrasound and the other 61 were seen on CT(37), MRI(11), and PET/CT(13). The SRU recommendations were applied to 47 patients with ITN detected by ultrasound (thyroid, parathyroid, and carotid ultrasound). This group had four malignancies. Fourteen patients did not meet SRU recommendations for workup and would not have undergone FNA. In these 14 patients, SRU recommendations missed one cancer which was a localized papillary thyroid carcinoma. The 3-tier system was used to categorize 61 patients with ITN on CT, MRI and PET/CT. This group also had four malignancies. Twenty-one patients did not meet criteria for the 3-tier system and would not have proceeded with sonographic workup if the system had been applied. There were no missed malignancies in the 21 patients.

Conclusion

Imaging is a common source for ITN, but the prevalence of malignancy in nodules receiving biopsy is low. The 3-tiered system and SRU recommendations can be used as guidelines for managing ITN and can reduce 31% of nodule workups. The SRU recommendations only missed one malignancy which was not aggressive by histological type, size and stage.

KEYWORDS: Thyroid, Incidental findings

Note: Scanned images are included in the proceedings. Some submitted images were reduced during editing, thereby decreasing clarity. Also, refer to the Program Planner. Proceedings Content as of 3-29-2013.

O-419 **4:35 PM - 4:43 PM**

Endovascular Treatment of Head & Neck Arteriovenous Malformations

Dmytriw, A. A.·terBrugge, K. G.·Agid, R.
Toronto Western Hospital
Toronto, ON, CANADA.

Presentation Summary
Purpose: Head & Neck arteriovenous malformations (H&N AVM) are associated with considerable clinical and psychosocial burden and present a significant treatment challenge. We evaluated the presentation, response to treatment and outcome of patients with H&N AVM treated by endovascular means at our institution.
Materials and Methods: Patients with H&N AVM treated by endovascular means in our institution over a 19-year period (from 1993 to 2012) were evaluated retrospectively. These included AVMs involved the scalp, orbit, maxillofacial, and upper neck localizations. Patient's clinical files, radiological images, catheter angiograms and surgical reports were reviewed.
Results: 48 patients with H&N AVM (29 females, 19 males, 23 small, 25 large) were treated with endovascular therapy. Females were more likely to have large AVMs (1.5:1) and were twice more likely to present with hemorrhage. The goals of treatment were defined as curative (n=14), palliative (n=20) or pre-surgical (n=14). The total number of endovascular treatment sessions was 134 (average of 2.8 sessions per patient). Various approaches and embolization materials were used. The goal of treatment was met in 81.25% (39/48) of cases with cure in 25% (12/48). 16.7% (8/48) of patients were cured by embolization alone, 8.3% (4/48) cured by planned post embolization surgical excision. All cured lesions were small. (7/48) patients suffered transient, and 6% (3/48) suffered permanent treatment complications.
Conclusion: Endovascular treatment is effective for H&N AVMs and relatively safe. It is particularly effective for symptom palliation and as pre-surgical aid prior to surgery of large lesions. Embolization is curative in small lesions. In patients with large non-curable H&N AVMs endovascular therapy is often the only option.

KEYWORDS: Arteriovenous

Wednesday Afternoon

3:15 PM - 4:45 PM
Room 5AB

(45d) Parallel Scientific Papers: Adult Brain: Trauma

O-419 **3:15 PM - 3:23 PM**

Resting-State Networks in Traumatic Brain Injury

Lin, L. Y.·Mac Donald, C. L.·Lee, M. H.·Snyder, A. Z.·Brody, D. L.·Shimony, J. S.
Washington University School of Medicine
St. Louis, MO.

Purpose
Survivors of traumatic brain injury (TBI) suffer cognitive dysfunction especially in tasks that depend on memory and control of attention. It is thought that the axonal injury and consequent disruption of functional networks contributes to the cognitive dysfunction. Resting-state fMRI (rsfMRI) is well established as a modality for evaluating the integrity of functional neural networks. Previous studies have shown reduced functional connectivity within the default mode network (DMN) associated with impaired attention in patients with TBI. The goal of this study was to investigate changes in several resting state networks in five severe and 11 moderate chronic TBI patients using a fuzzy-c-means clustering algorithm.
Materials & Methods
Sixteen patients with clinically diagnosed chronic TBI (ages 18-50) and 16 controls matched for age and handedness were scanned in a 3T Allegra MRI scanner (Siemens, Erlangen, Germany). Following previously described protocols, we acquired rsfMRI (4 cubic mm voxels, 438 frames), high-resolution MPRAGE and T2-weighted fast spin-echo scans. Postprocessing included compensation for asynchronous slice timing, retrospective correction for head motion and atlas transformation. A voxel-by-voxel correlation matrix was analyzed for each patient and averaged across the three groups (control, moderate, and severe). The fuzzy-c-means clustering algorithm was used to classify each group's averaged correlation matrix into seven resting state networks. The resulting connectivity maps were compared across groups.
Results
Differences were noted in several networks. The default mode network (Figure 1A: control; 1B: moderate TBI; 1C:severe TBI) showed decreased weight in the medial pre-frontal cortex and increased weight in lateral parietal and occipital cortices, and these changes varied with severity of injury. The dorsal and ventral attention networks showed loss in symmetry, most notably in the severe TBI patients. The language network showed decreased cortical weights with preservation of weights in deep nuclear structures. The fronto-parietal control network showed losses in deep nuclear and occipital cortex, and preservation in pre-frontal cortex.

Note: Scanned images are included in the proceedings. Some submitted images were reduced during editing, thereby decreasing clarity. Also, refer to the Program Planner. Proceedings Content as of 3-29-2013.

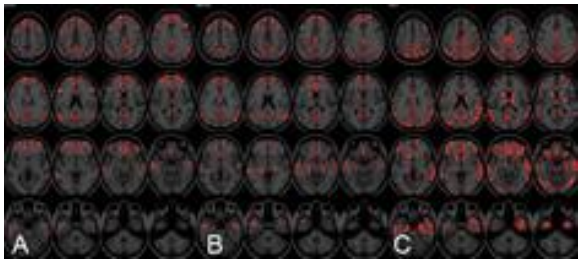

Conclusion
These findings provide preliminary information regarding changes in resting state networks in patients with moderate and severe TBI. The changes in the default mode network and the attention networks may help us understand the cognitive dysfunction in patients with severe TBI. Loss of symmetry in the attention networks suggests corpus callosal disruption interfering with interhemispheric communication. Further investigation is needed to quantify the extent of changes and to correlate these with changes with formal cognitive measures and with clinical outcomes.

KEYWORDS: Brain trauma, fMRI

O-420 **3:23 PM - 3:31 PM**

Assessment of Severe Traumatic Brain Injury with Quantitative Diffusion Tensor Imaging: A Five-Year Prospective Cohort

Khalilzadeh, O.[1]·Dinkel, J.[1]·Perlbarg, V.[2]·Gupta, R.[1]·Puybasset, L.[3]·Galanaud, D.[3]
[1]Massachusetts General Hospital, Boston, MA, [2]Université Pierre et Marie Curie-Paris, Paris, FRANCE, [3]Pitié Salpêtrière Hospital, Paris, FRANCE.

Purpose
Prediction of outcome in survivors of severe traumatic brain injury (TBI) is a major clinical challenge. There is not sufficient evidence on the long-term white matter brain changes in patients who survive after severe TBI. In this study, we used quantitative diffusion tensor imaging (DTI) to evaluate brain changes in 20 different white matter tracts over a span of five years after the injury. We assessed the prognostic value of DTI in prediction of long-term neurologic outcome in severe TBI patients.
Materials & Methods
This study was approved by the institutional review board of our hospital. Sixteen long-term survivors of severe TBI underwent brain MRI at three time-points: within the first six weeks after the injury, year two and year five post-TBI. Eight controls also were scanned at baseline and at two-year interval. The local diffusion parameters, namely, fractional anisotropy (FA), axial diffusivity and radial diffusivity (Lt), were calculated in each patient and control. The DTI parameters were calculated in 20 different brain regions, and were normalized using a set of controls. The changes in DTI values were compared between the three time-points. The association of DTI changes with patients' clinical outcome was also assessed.
Results
The baseline FA (or Lt) values were significantly lower (or higher) at genu/body of corpus callosum and right/left corona radiata in the patients as compared to the controls. In these regions, FA (or Lt) values were significantly lower (or higher) at the year two scan in comparison with the baseline values in TBI patients. After the year two time point, there was stabilization and no significant difference was observed between year two and year five. The normalized baseline FA cut-point of 0.87 at genu of corpus callosum was 80% sensitive and 70% specific in prediction of neurologic sequelae (such as amnesia, aphasia and motor dysfunction).
Conclusion
Fractional anisotropy and Lt changes in genu/body of corpus callosum and corona radiata have prognostic value in prediction of long-term neurologic sequelae in patients with severe TBI. These changes remain stable after two years from the injury, which points to little long-term postinjury repair and plasticity.

KEYWORDS: Traumatic brain injury, Diffusion tensor image, Quantitative MR imaging

O-421 **3:31 PM - 3:39 PM**

Individualized Analysis is a Better Predictor of Persistent Postconcussive Symptoms than Group Analysis: Potential Importance of Individual Variation

Rosenbaum, S. B.·Kim, N.·Smith, J.·Lewkowitz-Shpuntoff, H.·Provataris, J.·Zimmerman, M. E.·Lipton, R. B.·Branch, C. A.·Lipton, M.
Albert Einstein College of Medicine
Bronx, NY.

Purpose
At one-year post-mild traumatic brain injury (mTBI), as many as 80% of patients experience at least one persistent postconcussive symptom, and 30% meet criteria for a postconcussion syndrome diagnosis. Biomarkers that forecast long-term outcome at the time of injury do not exist. Low fractional anisotropy (FA) corresponds to traumatic axonal injury and is associated with worse outcomes. Previously, we have shown that there are associations between early DTI measures and persistent postconcussive symptoms, but it is not clear that these techniques can accurately discriminate between those with good versus poor outcomes. The purpose of this study was to compare a voxelwise, single-subject analysis of FA to a standard voxelwise group comparison (t-test),for their effectiveness in classifying patients as postconcussion syndrome positive [PCS (+)] versus postconcussion syndrome negative [PCS(-)], at one year post-injury.
Materials & Methods
This study was conducted with IRB approval and written,

Note: Scanned images are included in the proceedings. Some submitted images were reduced during editing, thereby decreasing clarity. Also, refer to the Program Planner. Proceedings Content as of 3-29-2013.

informed consent, and complied with HIPAA. We enrolled 25 mTBI patients from a local emergency center and 40 healthy controls. 3T DTI (b=1000, 32 directions) was performed within two weeks of injury, and symptoms were assessed at one year post-injury, using the Rivermead Post-Concussion Symptom Questionnaire. Subjects who met ICD-10 diagnostic criteria for PCS were classified as PCS (+) and those who did not as PCS (-). Fractional anisotropy maps were regression-adjusted for age, gender and years education. Regions of abnormally low FA were identified using a voxelwise t-test ($p<0.05$ corrected) comparing the patient and control groups. Additionally, voxelwise Z-score maps were computed for each patient based on the control group, with bootstrap resampling of the variance and thresholding at $p<0.05$. Mean FA, RD, MD and AD across all voxels of abnormally low FA was calculated for each patient, for each method. Stepwise discriminant function analysis was used to determine which imaging predictors correctly classified subjects as PCS(+) versus PCS(-) at one year post-mTBI.
Results
Ten patients (40%) were classified as PCS (+). Mean FA across all voxels with abnormally low FA identified by the voxelwise t-test analysis discriminated between PCS(+) and PCS(-) (Wilks' lambda=0.822,p=0.035), correctly classifying 64.0% of cases (sensitivity=60.0%, specificity=66.7%). Mean FA and mean RD across all voxels of abnormally low FA identified for each patient by the voxelwise Z-score analysis significantly discriminated between PCS(+) and PCS(-) (Wilks' lambda=0.403, p<.000), correctly classifying 90.9% of cases, (sensitivity=78.8%, specificity=100%).
Conclusion
Abnormally low FA within two weeks of injury, identified using an individualized single-subject Z-score method, more accurately classified subjects as PCS(+) versus PCS(-) than a voxelwise group comparison. Because the individualized analysis is sensitive to intersubject spatial heterogeneity of abnormalities, it may better capture the full extent of mTBI pathology in each individual patient, and therefore predicts outcome (PCS) with a higher degree of accuracy. Moreover, the discriminant function more accurately classified subjects according to PCS diagnosis when using both RD and FA as predictors. This suggests that RD, which may indicate more severe TAI pathology, is an important element for prognostic models in mTBI. Larger-scale studies are necessary to confirm and generalize these findings.

KEYWORDS: Mild TBI, DTI, postconcussive Symptoms

O-422 **3:39 PM - 3:47 PM**

Sex Differences in White Matter Abnormalities after Mild Traumatic Brain Injury on Diffusion Tensor Imaging: Localization and Correlation with Outcome

Alhilali, L. M.·Yaeger, K.·Fakhran, S.
University of Pittsburgh
Pittsburgh, PA.

Purpose
Many factors have been associated with clinical outcome after mild traumatic brain injury (mTBI); among the most controversial is gender. A possible neuroprotective effect of progesterone has been offered for anecdotal evidence of better outcomes in females. The purpose of this study was to evaluate sex differences in diffusion tensor (DTI) white matter abnormalities after mTBI using tract-based spatial statistics (TBSS) and compare associated clinical outcomes.
Materials & Methods
Diffusion tensor imaging was performed in 64 mTBI patients (42 males, 22 females) and 21 controls (10 males, 11 females) with normal conventional MRI. Neuropsychologic evaluation of mTBI patients was performed with the Immediate Post-Concussion Assessment and Cognitive Testing (ImPACT test). Fractional anisotropy (FA) maps for controls and mTBI patients were each aligned to a template with nonlinear alignment and projected onto two separate representative white matter skeletons, derived from each group's aligned images using Functional MRI (fMRI) of the Brain (FMRIB) Software Library package. Voxel-wise comparisons of FA between males and females were performed for controls and mTBI patients, using nonparametric randomized permutation tests with general linear model and multiple comparison correction. Clinical outcomes were assessed with serial neuropsychologic evaluation with the ImPACT test.
Results
Male and female groups were not significantly different in age in either the control ($p = 0.30$) or mTBI ($p = 0.34$) groups. Male and female mTBI patients did not have significantly different initial ImPACT symptom scores ($p = 0.33$). Males in the mTBI group had significantly decreased FA values in the uncinate fasciculi bilaterally compared to females ($p<0.05$), a tract connecting the frontal and temporal regions, two regions which demonstrate the highest concentration of extra-hypothalamic progesterone receptors. This difference was not seen in the control group. Male mTBI patients had a significantly longer time to symptom resolution ($p = 0.04$) compared to females. Time to symptom resolution strongly correlated with sex ($p = 0.004$), but did not correlate with initial symptom severity in either males ($p = 0.73$) or females ($p = 0.99$).
Conclusion
Relative sparing of the uncinate fasciculus is seen in females compared to males after mTBI, with gender being

Note: Scanned images are included in the proceedings. Some submitted images were reduced during editing, thereby decreasing clarity. Also, refer to the Program Planner. Proceedings Content as of 3-29-2013.

a stronger predictor of time to clinical recovery than initial symptom severity.

KEYWORDS: Mild TBI, Diffusion tensor image

O-423 **3:47 PM - 3:55 PM**

Microbleeding and Cerebral Volume Reduction in Diffuse Axonal Injury Patients between One and Twelve Months of Trauma

Feltrin, F. S.[1]·Leite, C. C.[1]·Zaninotto, A. L. C.[2]·Guirado, V. M. P.[2]·Andrade, A. F.[2]·Teixeira, M. J.[2]·Cerri, G. G.[1]·Nascimento, S.[1]
[1]INRAD - HCFMUSP, São Paulo, BRAZIL, [2]HCFMUSP, São Paulo, BRAZIL.

Purpose
Evaluate the white matter atrophy and correlate it to the number of lesions acording to the microbleed anatomical and rating scale (MARS).
Materials & Methods
Approval for this study was obtained from the Institutional Research Ethics Committee and written informed consent was obtained from all subjects. Eleven subjects (5 male; age, 22.1 ± 2.0 years; range, 19 - 32 years) with a history of moderate or severe traumatic brain injury (TBI) were evaluated after 2, 6 and 12 months from the traumatic event by using MR imaging. Images were acquired at a 3.0T MR imaging scanner (Phillips Achieva, Best, The Netherlands). Patients were assessed by T2* and T1 3DFSPGR sequences. Automatic assessment of brain volumes were performed with FreeSurfer (http://surfer.nmr.mgh.harvard.edu/fswiki). The T2* images were evaluated by two radiologists and stratified according to the MARS scale. To assess correlations between the MARS scale, neuropsychologic data and volumetry, we used the Pearson correlation rank.
Results
The average white matter volume reduction was 5.20% (+/-1.4) in 12 months. The lesion number according to the MARS scale was 69 (+/- 65) microbleeds. The inverse order digit span was 3.8 (+/- 1.87). We found a significant correlation between the MARS scale and the volume loss in the first year.
Conclusion
The diffuse axonal injury first grading scale is the Adams and Genarelli scale, which divides the patients into three groups. However, there are big differences in the number of lesions inside each group. The MAARS scale is a new way to rate those patients according to the number of lesions, and here we show that this scale shows strong correlations with the volume loss of white matter in the first year.

KEYWORDS: 3T, TBI, Volumetry

O-424 **3:55 PM - 4:03 PM**

Microhemorrhage Detection in Traumatic Brain Injury Using Ultrafast Segmented Echo-Planar High-Resolution Susceptibility-Weighted Imaging Using Susceptibility-Weighted Imaging

Butman, J. A.[1]·Wang, W.[2]·Li, N.[2]·Pham, D. L.[2]
[1]The Clinical Center of the NIH, Bethesda, MD, [2]Center for Neuroscience and Regenerative Medicine, Bethesda, MD.

Purpose
Dramatic acceleration of GRE can be performed with segmented EPI (segEPI). Therefore, we sought to determine whether accelerated high resolution (0.5×0.5×2) SWI using 3D segEPI GRE covering the whole head (72 slices) can substitute for traditionally implemented 3D GRE SWI for the detection of traumatic intracranial microhemorrhages in routine clinical use.
Materials & Methods
3D GRE and 3D segEPI SWI were performed in 46 consecutive patients enrolled in a natural history study of traumatic brain injury on a 3T system. Scan times were 9m47s for the 3D GRE and 1m30s for the 3D segEPI SWI. Contrast and acceleration parameters for the GRE were TR=64/TE=25/FA=20°/GRAPPA=2 and for the segEPI were TR=40/TE=25/FA=15°/ETL=15. Geometric parameters were matrix 448×343, resolution 0.5×0.5×2 mm and (72 slices). Phase emphasis was applied by (i) global phase unwrapping procedure (ii) followed by high pass filtering (iii) multiplication of the magnitude and filtered phase. Microbleeds were counted in two separate sessions separated by over two weeks. The order of presentation of GRE and segEPI between the two sessions and the case order were randomized. Magnitude, filtered phase, phase emphasized SWI and minimum intensity projections were available.
Results
Microbleed counts with the two methods were correlated (slope=0.84, r2=0.96). Using the 3D GRE, the number of microbleeds was slightly higher 13.7± range=0-179 than for 3D segEP1, 10.7± range 0-171 p=0.014. Patients were classified as TBI+ or TBI- based on the presence or absence of microbleeds. Half (23) of the 46 TBI patients were positive by both methods, and 16/46 were negative. Discordance was present in seven, five positive on 3D GRE only and two positive on segEPI only. Diagnostic classification agreement between the two tests was good (kappa = 0.69).

Note: Scanned images are included in the proceedings. Some submitted images were reduced during editing, thereby decreasing clarity. Also, refer to the Program Planner. Proceedings Content as of 3-29-2013.

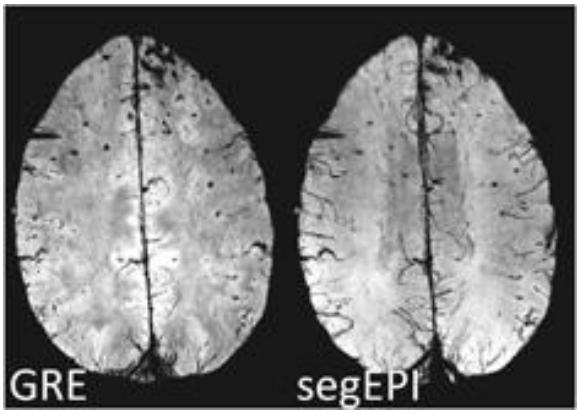

Conclusion
Dramatic acceleration of SWI imaging can be obtained by incorporating segmented EPI into the traditional 3D GRE sequence. For the particular parameters chosen in this study, an over 6-fold acceleration was achieved allowing high resolution 0.5×0.5×2 mm voxels covering the whole brain (72 slices) in 1½ minutes. Here we show that both methods perform comparably in the detection of microbleeds. In classifying patients with TBI based on detection of microbleeds, both methods show good agreement. Because there is no gold standard, it is not clear whether the high degree of image quality and the high level of concordance between the two methods indicate that segEPI can replace GRE for detection of microhemorrhage when time constraints are critical.

KEYWORDS: 3T, Microbleeds

O-425 **4:03 PM - 4:11 PM**

White Matter Microstructural Injury in Mild Traumatic Brain Injury: Findings Relative to Timing of Injury

Agarwal, V.[1]·Wo, S.[2]·Henry, L.[1]·Kontos, A. P.[1]·Collins, M. W.[1]·Delfyett, W. T.[1]
[1]University of Pittsburgh Medical Center, Pittsburgh, PA, [2]University of Pittsburgh School of Medicine, Pittsburgh, PA.

Purpose
Mild traumatic brain injuries (mTBI), or concussions, remain a challenging and controversial neurologic injury. Conventional magnetic resonance imaging (MRI) of mTBI often is normal and there is currently no reliable biomarker. Diffusion tensor imaging (DTI) has been suggested as a potential imaging biomarker of mTBI. Previous DTI studies in mTBI have shown varying results; some studies demonstrate decreases in fractional anisotropy (FA) following mTBI while others demonstrate no change or even an increase in FA. This variability may be multifactorial and in part may be related to timing of imaging relative to injury. The purpose of this study is to document the presence of microstructural white matter damage in patients with mTBI with reference to the timing of imaging relative to injury.
Materials & Methods
An IRB approved, HIPAA compliant retrospective analysis of DTI data (1.5T; 25 directions; b=1000) was performed on 248 patients who underwent MR imaging as part of evaluation for concussion over the past five years at our institution. Demographic, clinical data including date of injury and neurocognitive test results (ImPACT) were recorded. Timing of injury relative to scanning was defined as acute (within three days), subacute (three-21 days) and chronic (greater than 21 days). Comparison was made to healthy control DTI data (N=38) obtained from the International Consortium for Brain Mapping (ICBM) online database. After initial postprocessing including eddy current correction, FA images derived from DTI were compared using whole brain histogram analysis and voxelwise analysis using Tract-Based Spatial Statistics (TBSS). Fractional anisotropy data were projected onto a white matter skeleton and between-group statistical analysis performed. Voxel clusters of significant between-group differences were overlaid onto the mean FA map with threshold set for corrected p-value of 0.01.
Results
Of the 248 patients, clinical data were available on 149 patients (36% female; age range 10-63 years with average age 24.1 years). There were two patients scanned in the acute phase, 40 in the subacute phase and 110 in the chronic phase. Histograms of white matter FA show an overall shift towards lower FA in concussed patients compared with controls for all three groups. There was a slightly greater shift in the histogram curve of FA in the acute phase compared with the subacute and chronic phases. Tract-Based Spatial Statistics analysis showed areas of significantly decreased FA ($p < 0.01$) in the corpus callosum and deep frontal white matter for acute, subacute and chronic cases.
Conclusion
We present the largest known overall series of mTBI patients evaluated with DTI to date. Regardless of the timing of injury relative to scanning, microstructural white matter injury in patients with mTBI is evidenced by an overall shift to decreased white matter FA in concussed patients compared with controls. While certain specific anatomical areas (corpus callosum and deep frontal white matter) demonstrate significant decreases in FA, our data suggest that in the setting of mTBI, global decreases in white matter FA accompany these more focally affected areas.

KEYWORDS: Mild TBI, Diffusion tensor image, Concussion

Note: Scanned images are included in the proceedings. Some submitted images were reduced during editing, thereby decreasing clarity. Also, refer to the Program Planner. Proceedings Content as of 3-29-2013.

O-426 **4:11 PM - 4:19 PM**

Diffusion Tensor and Susceptibility-Weighted Imaging Assessment of National Football League Players

Niogi, S. N.[1]·Luther, N.[1]·Kutner, K.[1]·Christos, P. J.[1]·Shetty, T.[2]·Barnes, R.[3]·Weiss, L.[3]·Warren, R. F.[2]·Rodeo, S. A.[2]·Zimmerman, R. D.[1]·Tsiouris, A. J.[1]·Härtl, R.[1]
[1]Weill Cornell Medical College, New York, NY, [2]Hospital for Special Surgery, New York, NY, [3]New York Giants Professional Football Organization, New York, NY.

Purpose
Given the heightened awareness and concern of the potential somewhat intuitive risks associated with sports-related concussion, there is a justifiable need to better understand the anatomical and functional changes that may occur. Unlike other cases of isolated concussion such as motor vehicle accidents, athletic competition has the added risk factor of repetitive head injuries over the lifetime of a career. Elucidating the extent of traumatic brain injury (TBI) at the professional level, with the longest exposure and presumably greatest cumulative risk of TBI, may help define post-traumatic anatomical changes at the most extreme levels of play. The purpose of this study was to identify whether anatomical changes occurred in National Football League (NFL) players measurable by magnetic resonance diffusion-tensor imaging (DTI) and susceptibility-weighted imaging (SWI).
Materials & Methods
New York Giants Professional football players with and without a history of concussion and normal controls underwent conventional clinical magnetic resonance imaging (MRI) in addition to DTI and SWI. In a prospective fashion, players with concussion during gameplay were assessed by a study neurologist, underwent ImPACT neurocognitive testing, and MRI including DTI and SWI within one week of injury. Diffusion tensor imaging analysis was performed by both region-of-interest (ROI) and voxel-based methodologies. For ROI analysis, comparison of Z-score distributions of player fractional anisotropy (FA) values to normals was performed in 11 high-risk tracts based on prior studies. Voxel-based analysis was performed to compare players to controls, players with concussion history to players without concussion history, and players with greater than four years of professional experience to those less.
Results
Thirty-one players were enrolled. Twenty-one had positive concussion history, including 12 players who suffered an acute concussion. Mean playing experience was 3.1 years. When FA was compared in players to 22 controls, no significant decrease in Z-score distributions was found. No difference was seen in either ROI or voxel-based analysis when subgroups of players with acute concussion history and players with ≥4 years of professional football experience were compared to normals. No player had an FA value >2.5 standard deviations below the normals' means. Susceptibility-weighted imaging revealed chronic microhemorrhage in one player.
Conclusion
Difffusion tensor imaging and SWI revealed no significant evidence of white matter injury or acute microhemorrhage in professional football players with acute concussion or chronic concussion history. Additionally, no differences in white matter integrity were seen in players based on years of experience. Diffusion tensor imaging, while promising, remains under development and continues to be an investigational technique in the assessment of TBI. Clinical decision-making should not be based on this modality at present. Susceptibility-weighted imaging continues to be a critical tool for clinical assessment to detect diffuse axonal injury-related microhemorrhage and other abnormalities, but is likely insensitive to possible subtle changes seen with mild football-related concussion.

KEYWORDS: Traumatic brain injury, Diffusion tensor image

O-427 **4:19 PM - 4:27 PM**

National Football League Hard Knocks: Fractured Inter-Network Connectivity in Subjects with Remote Repetitive Mild Traumatic Brain Injury

Airan, R. D.·Coughlin, J. M.·Sair, H. I.·Pomper, M. G.
Johns Hopkins Medical Institutions
Baltimore, MD.

Purpose
High profile cases of former National Football League (NFL) players demonstrating behavioral dysfunction decades after play have generated interest in understanding the late sequelae of chronic traumatic encephalopathy (CTE). Pathologic and structural brain abnormalities have been described in those known to have suffered repeated concussions. However, brain functional sequelae have been less clearly delineated. Here, we analyze resting-state functional connectivity in former NFL athletes to determine potential functional endophenotypes of CTE.
Materials & Methods
NFL players (n=14; ages 52-74) and age/sex-matched controls (n=4) underwent 3T MRI including T1 MPRAGE and seven minute eyes closed, resting awake BOLD fMRI (TR=2sec) sequences. Data were preprocessed using FSL (FMRIB, Oxford, UK), SPM8 (Wellcome Trust, UK) and custom MATLAB (Mathworks, MA) scripts to complete slice-timing correction, rigid-body motion correction, segmentation and normalization to the MNI 2mm template, COMPCOR nuisance regression, bandpass temporal filtering (0.01-1Hz), and spatial smoothing (6mm Gaussian kernel). Whole brain gray matter was parcellated automatically into 875 regions of interest (ROIs). For each ROI, the first eigenvariate of voxel timecourses was extracted. Pearson correlation coefficients between each pair of the 875 ROI timecourses were calculated. The set of average control correlation coefficients were fed as an undirected weighted adjacency matrix (thresholded at r^2=0.08) into the infomap modularity algorithm. For each

Note: Scanned images are included in the proceedings. Some submitted images were reduced during editing, thereby decreasing clarity. Also, refer to the Program Planner. Proceedings Content as of 3-29-2013.

network, the intranetwork efficiency of the thresholded adjacency submatrix was calculated, with a similar measure applied to the internetwork efficiency.

Results

As shown in the figure, 19 networks spanning all of brain gray matter were found that are consistent with those demonstrated in the literature, without using any a priori information of expected network structure. (Figure, *top*: representative midsagittal slice of network modules overlayed onto a standard template). The differences in network efficiency between NFL players and controls for each pair of networks (Figure, *bottom*: red indicates decreased internetwork efficiency in NFL players) show that this population of NFL players has trend-wise reduced overall internetwork efficiency, with significantly ($p<0.05$) increased efficiency between the temporal default mode and limbic networks, and between parahippocampal and ventral sensorimotor networks. Intranetwork efficiency is relatively preserved.

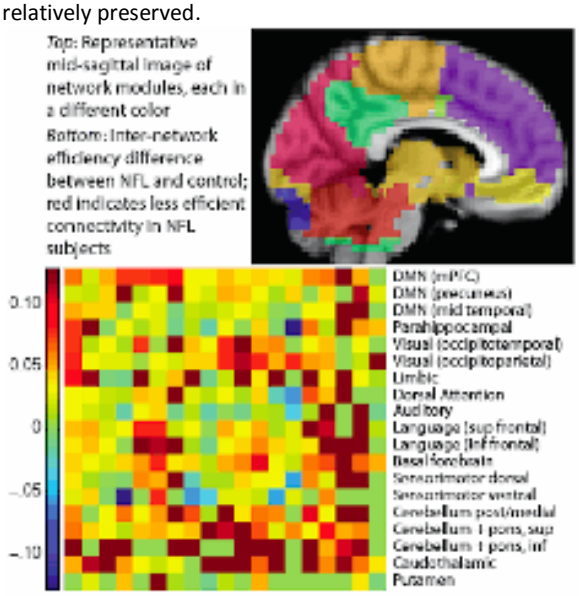

Conclusion

NFL players show reduced overall internetwork efficiency with focally significant increases in limbic-temporal and parahippocampal-ventral sensorimotor connectivity. This fracturing of normal connectivity patterns into temporoparietal subnetworks may provide a functional substrate of CTE. Further studies will assess the potential diagnostic performance of fractured internetwork efficiency for predicting neurocognitive and affective dysfunction in patients at risk for CTE.

KEYWORDS: Brain trauma, Connectivity, Chronic Traumatic Encephalomalacia

O-428 **4:27 PM - 4:35 PM**

Brain Iron Estimation Using Magnetic Field Correlation and Relaxation Rate in Mild Traumatic Brain Injury

Savino, M. R.·Zhou, Y.·Novikov, D. S.·Lui, Y. W.
New York University Langone Medical Center
New York, NY.

Purpose

Magnetic field correlation (MFC) is a novel MR imaging technique that quantifies magnetic field inhomogeneities (MFI) at the mesoscopic scale, commensurate with cell dimensions (~1-10 µm). In brain, the MFIs are caused, among other factors, by iron. We recently showed increased thalamic MFC in patients with mild traumatic brain injury (MTBI), believed to reflect neuropathologic iron. In this study, we aim to show correlation between MFC and tissue relaxation R2* and R2 rates in these patients, to further validate MFC as a reliable MFI metric.

Materials & Methods

Recruited were eight patients with clinically defined MTBI 1 year postinjury and six age-matched, healthy controls. A Siemens 3T MR scanner was used with an asymmetric spin echo (ASE) pulse sequence (TR/TE=3420/40ms; time shifts t_s=0, -4ms, and -16ms; isotropic resolution=1.72mm; 48 axial slices, four averages) for MFC estimation. For R2 estimation, zero shift images with TE=34 ms also were obtained. A 3D gradient echo (GRE) obtained with multi-echo (ME) acquisition and first-order 3D flow-compensated was acquired with eight TEs ranging from 6.12 to 41.82 ms and echo spacing of 5.1 ms (TR=60 ms, flip angle=20°, voxel size=0.5×0.5×1.0 mm^3). Bilateral thalami were outlined manually on three continuous slices as regions of interest (ROI) for each subject. Magnetic field correlation was calculated with inhouse software and initial R2* was estimated by monoexponential fitting. The signal time curve then was visually inspected to assess for constancy of R2*.

Results

MFC_{total}=MFC_{meso}+MFC_{macro} contains the contributions from mesoscopic MFIs and macroscopic B_0 inhomogeneities. Both the MFC_{total} ($P<0.05$) and MFC_{meso} ($P<0.01$) were increased significantly in the thalami of MTBI patients compared to controls. Moreover, there was significant correlation between the MFC_{meso} and R2* values ($r=0.76$, $P=0.03$), and a trend between MFC_{total} and R2* ($r=0.65$, $P=0.08$), in MTBI patients. The time dependence of the R2* relaxation is fairly monoexponential for controls, yet strongly non-monoexponential through at least TE=50 ms in MTBI patients (Figure 1). No significant correlations existed in the control group or between the molecular relaxation rate R2 and MFC.

Note: Scanned images are included in the proceedings. Some submitted images were reduced during editing, thereby decreasing clarity. Also, refer to the Program Planner. Proceedings Content as of 3-29-2013.

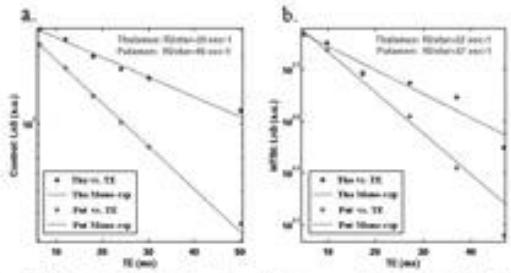

Figure 1. Multi-echo R2* relaxation. Examples from control subject (a) and MTBI patient (b). In the control, R2* signal decay is practically monoexponential, whereas in the MTBI patient, R2* signal is non-monoexponential in both deep gray matter structures. The rate R2*, estimated as the slope of the signal decay as a function of (TE), does not appear to be constant in the MTBI group through TE=50 ms, indicating that there are magnetic field inhomogeneities on the mesoscopic level of at least the size of ~10 μm, presumed to be caused by the presence of abnormal iron clustering at a cellular level.

Conclusion

This study shows an association between the mesoscopic contribution to MFC and R2* in patients one year after MTBI, supporting the utility of MFC in brain imaging. Microscopic (molecular) and macroscopic MFIs are essentially uniform within a single voxel, therefore the non-monoexponential R2* signal decay seen in MTBI subjects further validates the presence of iron-induced MFI on a cellular level, revealed by MFC_{meso}.

KEYWORDS: Mild TBI, Iron, Transverse relaxation

O-429 **4:35 PM - 4:43 PM**

Role of Low-Dose Nonenhanced Brain CT in the Neurosurgical and Neurologic Intensive Care Unit

Hoch, M.[1]·Sethi, V.[2]·Shah, P.[1]·O'Connor, E.[1]·Hershey, B.[1]·Ali, S.[1]·Dass, C.[1]
[1]Temple University Hospital, Philadelphia, PA, [2]Temple University Medical School, Philadelphia, PA.

Purpose

To identify a patient population subject to serial short-term follow-up CT evaluation that may benefit from low dose CT examination. Most neurosurgical/neurologic intensive care unit (NICU) patients undergo multiple serial CT scans during a single hospitalization. After the initial routine scan, we explored if low dose follow-up scans could effectively evaluate NICU patients without sacrificing diagnostic accuracy.

Materials & Methods

Following IRB approval, a retrospective chart review was performed identifying 19 NICU patients (ages 18-73 years, mean 49 years) who had three axial nonenhanced brain CT examinations within a span of 72 hours in the following sequence: initial routine dose, followed by low dose, and finally routine dose. Included studies showed a persistent finding on the initial and final scans. From these routine and low dose scans, 59 unique pairs of comparative individual slices were selected (Figure 1). Two board-certified neuroradiologists, each blinded to the scan parameters and patient information evaluated the selected slices. The readers were asked if each image was diagnostically acceptable for interpretation and to note the presence or absence of the following findings: infarction, hemorrhage, herniation, and catheter location. All CT scans were performed on Siemens Sensation 16- or 64-slice machines. Routine scans were acquired with mAs ≥ 310 and collimation of 1.2 - 1.5 mm, while low-dose scans had mAs ≤ 280 and collimation of 5 mm. All other imaging parameters including 120 kVp were kept constant. Regions of interest placed over gray and white matter were obtained from each slice to calculate contrast-to-noise ratios (CNR).

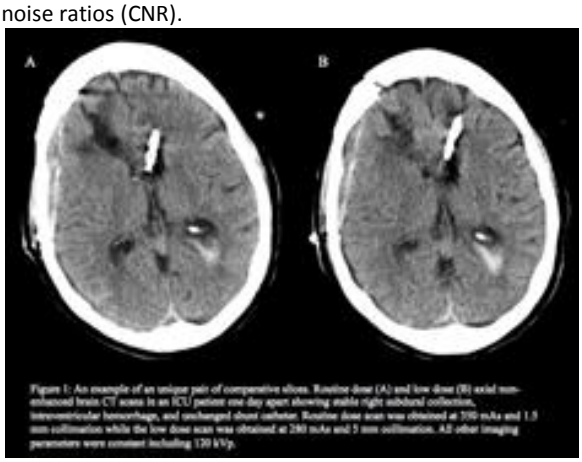

Results

There was very high (95.3%) interobserver agreement in identifying pertinent findings on routine and low dose brain CT examinations among the sampled NICU patients (Table 1). Compared to routine dose, low dose CT imaging delivered a 26.07% reduction in average CTDIvol. Despite an average CNR reduction of 29.23%, low-dose imaging provided equal if not better diagnostic accuracy.

Table 1: Findings Made on Routine vs Low Dose CT

	Routine Dose			Low Dose		
	Reader 1	Reader 2	Concordance	Reader 1	Reader 2	Concordance
Venticular Catheter/ICP Monitor Location	10	10	100%	10	10	100%
Midline Herniation	17	20	85%	19	19	100%
Extracranial Herniation	4	4	100%	4	3	75%
Infarction	15	16	94%	17	17	100%
Intra-axial Hemorrhage	30	31	97%	31	30	97%
Extra-axial Hemorrhage	32	32	100%	38	37	97%

Conclusion

Low-dose brain CT is diagnostically acceptable when applied to the adult NICU population, emphasizing the concept of ALARA (As Low As Reasonably Achievable).

Note: Scanned images are included in the proceedings. Some submitted images were reduced during editing, thereby decreasing clarity. Also, refer to the Program Planner. Proceedings Content as of 3-29-2013.

Further collaboration with referring clinicians may allow development of additional dose reduction protocols.

KEYWORDS: Radiation dose reduction, Protocols, ALARA

Wednesday Afternoon

3:15 PM - 4:45 PM
Room 1AB

(45e) Parallel Scientific Papers: Pediatrics: Perinatal Imaging, Tumors, and Spine

O-430 **3:15 PM - 3:23 PM**

MR Imaging Findings of Preterm Infants with Surgical versus Medical Necrotizing Enterocolitis

Ramos, Y. M.·Kline-Fath, B.·Merhar, S.
Cincinnati Children's Hospital
Cincinnati, OH.

Purpose
To evaluate the degree of brain injury on MRI in infants with medically managed necrotizing enterocolitis (NEC) versus those with spontaneous intestinal perforation/surgically managed NEC. Since patients with surgically managed NEC have worse neurodevelopmental outcomes than those with medically managed NEC (Hintz et al 2005), and poor neurodevelopmental outcomes have been associated strongly with abnormal MRI findings (Miller 2005, Woodward 2006), we hypothesize that the surgical group will demonstrate more severe injury on MRI.
Materials & Methods
Term equivalent brain MRI was performed on all surviving preterm infants with NEC at our institution during the period of July 2011 to October 2012. The studies were reviewed by two pediatric neuroradiologists blinded to all clinical information except postconceptual age at the time of scan. A brain injury scale modified from Miller et al (2005) was utilized to grade intracranial injury. MR imaging findings evaluated included white matter injury, ventriculomegaly, intraventricular hemorrhage, cerebellar hemorrhage and size of extra-axial spaces. Multiple linear regressions were performed in SAS comparing clinical variables with brain injury score as the continuous outcome.
Results
A total of 20 infants were evaluated (11 in the medical group and nine in the surgical group). Birth weight ($p = 0.06$) and gestational age (GA) ($p = 0.046$) were correlated with total brain injury score. On multiple linear regression analysis, after controlling for GA, the brain injury scores were significantly higher in the surgical group versus the medical group ($p = 0.01$). When the sites of injury were compared directly, it was noted that infants in the surgical group statistically had more white matter injury ($p = 0.01$) and greater ventriculomegaly ($p = 0.04$) than those in the medical group.
Conclusion
Infants with surgical NEC have more severe brain injury on MRI at term equivalent age than infants with medical NEC, which likely explains the poorer neurodevelopmental outcomes in the surgical group. In addition, infants with NEC requiring surgery have increased white matter injury and ventriculomegaly. The higher white matter injury may support microglia activation from more severe infection/inflammation resulting in injury to oligodendryocyte progenitors.

KEYWORDS: Neonatal MR imaging, Prematurity, White matter injury

O-431 **3:23 PM - 3:31 PM**

Predictive Value of NICHD Neonatal MR Imaging Scoring Criteria for Neurodevelopmental Outcome at Twenty-Four Months after Therapeutic Hypothermia

Rollins, N. K.[1]·Morriss, M. C.[1]·Sanchez, P.[1]·Heyne, R.[1]·Chalak, L.[2]
[1]Childrens Medical Center, Dallas, TX, [2]University Texas Southwestern Medical Center, Dallas, TX.

Purpose
MR imaging is an imaging surrogate for neurodevelopmental problems in survivors of perinatal hypoxic-ischemic injury (HIE). The NICHD Neonatal Research Network (NRN) recently has revised the MRI criteria for assessing brain injury after HIE treated with whole-body cooling; criteria to be used in subsequent randomized controlled trials of deeper longer cooling. We evaluated the predictive value of the NICHD NRN scoring criteria.
Materials & Methods
Prospective cohort of inborn infants (≥36 weeks' gestation) with perinatal academia s/p cooling for moderate/severe HIE at a single institution from 10/2005-10/2010. Perinatal MRI (T1 SE or FLAIR, T2 FSE, and DWI b = 1000) were scored by two pediatric neuroradiologists blinded to outcome using NICHD-NRN MRI scores (Shankaran, 2012): 0 = negative, 1a = "minimal cerebral lesions only with no basal ganglia/thalami (BGT) or watershed (WS) lesions"; 1b = "more extensive cerebral lesions without BGT or WS lesions"; MRI scores 2a = "any BGT or WS lesions without additional cerebral lesions"; score 2b = "any BGT or WS lesions with additional cerebral lesions" and score 3 = "hemispheric devastation". Primary outcome measure was BSID-III scores in cognitive, language and motor domains at 18-24 months: < 70 = severe and 70-85 = moderate disability respectively; >85 = normal. Sensitivity, specificity, and positive and negative predictive values were calculated.

Note: Scanned images are included in the proceedings. Some submitted images were reduced during editing, thereby decreasing clarity. Also, refer to the Program Planner. Proceedings Content as of 3-29-2013.

Results

There were 90 newborns; 10 (11%) died and 68/80 (85%) underwent MRI at eight (median) days of age followed by BSID-III at 18-24 months of age. MR imaging was 0 in 36 (53%) patients; five (14%) had BSID scores <85 in cognitive or language but not motor domains. Eighteen (26%) had MRI scores 1a-b; eight had BSID scores <85 in cognitive or language domains. Fourteen (20%) had MRI scores 2a, b, or 3; BSID scores were <85 in all and <70 in 10 (93%) which consistently affected motor domains. Table 1 indicates predictive values; MRI scores of 2 a&b and 3 were 100% predictive of any abnormal outcome while lesser degrees of brain injury has lower specificity and positive predictive value. However, a normal MRI was not consistently associated with a normal outcome.

Table 1.

Predictive Value of NRN MRI scoring system

	Sensitivity	Specificity	PPV	NPV
MRI score >0	81%	62%	40%	92%
MRI score 2a or >	62%	92%	71%	89%

Conclusion

In this clinical setting, seemingly minor degrees of WMI may be associated with significant problems in cognition and language but not motor domains in early childhood. Higher MRI scores are highly predictive of abnormal outcome with cognitive and motor deficits in early childhood.

KEYWORDS: Hypothermia, Hypoxia

O-432 **3:31 PM - 3:39 PM**

Tract-Based Mean Apparent Diffusion Coefficient in Hypoxic-Ischemic Encephalopathy as a Predictor of Outcome at Thirty-Two Months

de Macedo Rodrigues, K.[1]·Jacob, F.[1]·Fons Estupina, M.[1]·McLean, A.[2]·Paldino, M.[1]·Khwaja, O.[1]·Soul, J.[1]·Stamoulis, C.[1]·Grant, P.[1]
[1]Boston Children's Hospital, Boston, MA, [2]Brigham and Women's Hospital, Boston, MA.

Purpose

Perinatal hypoxic-ischemic encephalopathy (HIE) remains a major cause of disability in the U.S. and worldwide. Many studies have tried to identify imaging-based biomarkers, particularly from diffusion-weighted images, which may be predictive of clinical outcome in patients with HIE. We previously have investigated mean apparent diffusion coefficient (ADC)and fractional anisotropy (FA) of the corticospinal tract (CST), inferior fronto-occipital fasciculum (IFOF), corpus callosum (CC) and its subdivisions (genu: GCC, splenium: SCC) derived from tractography as a predictor of gross motor outcome at 14 months of age. In this study, we investigated these parameters as potential predictor of combined motor and cognitive outcomes.

Materials & Methods

We retrospectively evaluated 21 term neonates with a clinical diagnosis of HIE and that had undergone MRI within the four days of life, including diffusion tensor imaging with 30 noncollinear directions suitable for tractography reconstruction. Six neonates with similar imaging data collected within the first five days of life, and no diagnosis of HIE were included as normative controls. Tractography was reconstructed using Diffusion Toolkit.Tracts were manually dissected on TrackVis. Clinical data were gathered by means of chart review. Presence of seizures was noted, and clinical outcome was classified as good/bad based on the NICHD hypothermia trial classification. No disability or mild disability was considered as good outcome whereas moderate or severe disability or death, considered as bad outcome. Logistic regression models were developed to assess the correlation between clinical outcomes and imaging parameters. Statistical analysis was performed in Matlab.The study was approved by the Committee on Clinical Investigation at Boston Children's Hospital.

Results

Mean age at scan was 2.3 days for the HIE group and 4.7 days for the control group. Seven neonates in the HIE group had bad outcomes and 14 had good outcomes. Median age at last clinical evaluation was 32.5 months (range 7-48 months). Sixteen infants with HIE had abnormal MRIs and five had normal MRIs. Eight neonates had seizures. Mean ADC of right and left CST and left IFOF were found to be statistically significant predictors of clinical outcome. Similarly, mean ADC of the same tracts also were statistically significant predictors of seizures, which suggests that the presence of seizures may potentiate ADC decreases. Finally, mean ADC of GCC, left CST and right CST were statistically distinct in HIE patients with normal MRI, HIE patients with abnormal MRI, and controls. This suggests that dispite the appearance of a normal ADC map, for at least some tracts, HIE patients have statistically distinct ADC from controls.

Conclusion

Our findings suggest that mean ADC of left CST, right CST and LIFOF may be predictors of outcome at 32.5 month of age after perinatal HIE. Since it represents the entire white matter tract, tractography reconstruction is potentially more robust than the highly subjective two-dimensional ROI placement on ADC maps. Finally, our results suggest that clinical read can potentially miss areas of significantly decreased ADC and a more quantitative evaluation is desired.

KEYWORDS: Neonatal MR imaging, DTI tractography, Hypoxic-ischemic encephalopathy

Note: Scanned images are included in the proceedings. Some submitted images were reduced during editing, thereby decreasing clarity. Also, refer to the Program Planner. Proceedings Content as of 3-29-2013.

O-433 **3:39 PM - 3:47 PM**

Role of Cranial Ultrasound in Predicting Cerebrovascular Complications in Pediatric Patients Treated with Extracorporeal Membrane Oxygenation

Alqahtani, E.·Zamora, C.·Bembea, M.·Berkowitz, I.·Carson, K. A.·Huisman, T. A. G. M.·Tekes, A.
The Johns Hopkins University
Baltimore, MD.

Purpose

Extracorporeal membrane oxygenation (ECMO) is used in the treatment of cardiopulmonary failure in children who fail to respond to maximal medical treatment. Patients on ECMO are at high risk of cerebrovascular complications (CVC) due to systemic heparinization, sepsis, acidosis, young age and carotid artery cannulation. We aim to evaluate the value of resistive index (RI) measurements in the anterior cerebral artery to predict CVC such as intracranial hemorrhage (ICH) and ischemic events in children with ECMO.

Materials & Methods

The institutional review board approved this study. Data were collected retrospectively from 2008 to 2012. A retrospective chart review of patients ≤ 3 months old who received ECMO and head ultrasound (US) with baseline and compression RI measurements between 2008 and 2012 was conducted. RI measurements were acquired utilizing curved and linear array transducers in the sagittal plane through the anterior fontanelle. Two RI measurements were obtained; gentle transducer pressure on the anterior fontanelle was applied for 3-5 seconds during the second measurement. Gender, gestational age, method of delivery, age at cannulation, type of ECMO, duration and indication for ECMO were obtained from patients' records. Association between different outcome, clinical variables and RI measurements were assessed using Kruskal-Wallis, Cochran-Armitage, and Fisher's exact tests.

Results

Thirty-six patients were included in the study (Table 1). Twenty-seven patients had no complications. Nine patients developed CVC (ICH n=6, and ischemia n=3). All US findings were confirmed by a CT or MRI. Only the age at initiation of ECMO had statistically significant correlation with increased risk of CVC (P<0.05). The incidence of CVC was 38% (exact 95%CI=19-59%) for ECMO at age 0-2 days, and 0% (exact 95% CI=0-26%) for ECMO at age > 2 days - Fisher's exact p=0.02. The difference between the baseline and compression RI values and the percent change on the first day of ECMO were statistically significant between CVC and no complications groups (p=0.03 and p=0.02 respectively) (Table 2), with an odd ratio of 13.35 and 95% confidence interval of 2.28-infinity. In pairwise comparisons, the significant difference was between the ICH group and the other two groups.

Table 1: Clinical characteristics of patients treated with ECMO

		No CVC n= 27	ICH n=6	Ischemia n=3	P value
Gender	Male	13 (48%)	5 (83%)	1 (33%)	
	Female	14 (52%)	1 (17%)	2 (67%)	0.32
Gestational age, weeks	Median	39.1	38.9	37.4	
	Range	(36.7-41.6)	(38.0-39.9)	(34.4-39.3)	0.25
Method of delivery	Vaginal	15 (56%)	3 (50%)	3 (100%)	
	Cesarean section	12 (44%)	3 (50%)	0 (0%)	0.39
Age at ECMO intiation, days	Median	2	1	2	
	Range	(1-60)	(0-2)	(0-2)	0.04
Type of ECMO	Venoaterial	22 (81%)	6 (100%)	3 (100%)	
	Venovenous	5 (19%)	0 (0%)	0 (0%)	0.72
Duration of ECMO, days	Median	6	9	8	
	Range	(1-38)	(3-24)	(7-11)	0.65
Indication for ECMO	Congenital diaphragmatic hernia	7 (26%)	2 (33%)	1 (33%)	0.86
	Congenital heart disease	6 (22%)	0 (0%)	1 (33%)	
	Meconium aspiration	5 (5%)	2 (33%)	0 (0%)	
	Pulmonary hypertension	4 (4%)	1 (17%)	0 (0%)	
	Other	5 (26%)	1 (17%)	1 (33%)	
CVC: Cerebrovascular complications					
ICH: Intracranial hemorrhage					

Table 2: Day 1 RI measurements in children treated with ECMO

		No CVC n= 27	ICH n=6	Ischemia n=3	P value
Baseline RI	Median	0.54	0.63	0.45	
	Range	(0.28-0.86)	(0.46-0.84)	(0.34-0.68)	0.23
Compression RI	Median	0.55	0.5	0.45	
	Range	(0.27-0.85)	(0.33-0.58)	(0.43-0.63)	0.61
Difference in RI (Baseline RI - compression RI)	Median	0.01	0.06	0	
	Range	(-0.13-0.24)	(0.03-0.11)	(-0.05-0.09)	0.03
Percent change ((Baseline RI - compression RI)/Baseline RI)	Median	1.64	14.40%	0.00%	
	Range	(-25.00-50.00)	(5.77-26.83%)	(-7.35-26.47%)	0.02
RI: Resistive index					
CVC: Cerebrovascular complications					
ICH: Intracranial hemorrhage					

Conclusion

Initiation of ECMO in the first two days of life sets a higher risk for possible CVC. Differences between baseline RI and compression RI as well as their percent change on the first day of ECMO can be predictive of ICH. These results should be validated in future with larger prospective studies.

KEYWORDS: Hemorrhage, Ultrasonography, ECMO, resistive index

Note: Scanned images are included in the proceedings. Some submitted images were reduced during editing, thereby decreasing clarity. Also, refer to the Program Planner. Proceedings Content as of 3-29-2013.

O-434 **3:47 PM - 3:55 PM**

Reproducibility, Reliability, and Utility of ABC/2 in Calculating Infarct Volumes in the Perinatal Arterial Ischemic Stroke Population

Mirsky, D. M.[1]·Stence, N. V.[1]·Bernard, T. J.[1]·Armstrong-Wells, J.[2]
[1]Children's Hospital Colorado, Aurora, CO, [2]University of Colorado Denver, Aurora, CO.

Purpose
Perinatal arterial ischemic stroke (PAS) is a leading cause of lasting disability. Similar to adult stroke, counseling and prognostic decisions are based off of initial infarct volume on neuroimaging. These decisions may be time-dependent, necessitating a quick, accurate estimation of true infarct volume. ABC/2 method is a fast and reproducible way to calculate infarct volume in adult and childhood acute hemorrhagic stroke. It has been shown, however, to overestimate true infarct volume in the adult arterial ischemic stroke population. Therefore, we sought to determine the accuracy and reproducibility of ABC/2 in assessing acute infarct volume with diffusion-weighted imaging in PAS. Our ultimate goal is to use these data as a platform for further studies looking into the true clinical utility of ABC/2 volumes in our unique population.
Materials & Methods
We reviewed all PAS cases in our prospective cohort study from 08/01/2000 - 1/01/2012. We studied 25 consecutive patients with acute ischemic stroke. The criteria for acute symptomatic PAS included: 1) documented clinical presentation consistent with PAS such as seizure or encephalopathy; 2) MRI showing infarction in an arterial distribution with an acuity consistent with the neurologic signs and symptoms; and 3) greater than 28 weeks gestational age and less than 28 days of life. Two blinded pediatric neuroradiologists (DMM & NVS) determined volumes with the ABC/2 method, and the results were compared with those of the gold standard (manual planimetric method). Given the homogeneity of head circumferences in our study population, we did not adjust for total brain volumes (ABC/XYZ). Data were log transformed to approximate normal distribution in our samples. Student's *t*-test and Mann-Whitney U were used when appropriate, while linear regression was utilized to assess correlation between methods. A p-value of < 0.05 was considered significant.
Results
There were no differences in mean values between ABC/2 and planimetric volume calculations (mean 46 cm^3 versus 32 cm^3, respectively, $p = 0.01$), with good correlation ($R2 = 0.84$). However, the ABC/2 technique overestimated infarct volume by a median false increase (variable ABC/2 volume minus planimetric volume) of 8 cm^3 representing a 61% increase over the value of the gold standard (variable ABC/2 volume over planimetric volume).
Conclusion
Similar to other stroke populations, in the perinatal arterial ischemic stroke population, ABC/2 is a quick and reproducible way for clinicians to calculate stroke volume in the emergent setting. However, given that it consistently overestimates the true infarct volume compared to the gold standard planimetric volume method, caution should be used when relying solely on ABC/2 for prognostic counseling. Therefore, further studies are warranted to validate the true implications of ABC/2 calculation, risk assessment, and outcomes after PAS.

KEYWORDS: Infarct, Neonatal

O-435 **3:55 PM - 4:03 PM**

Diffusion Tensor Imaging of Pediatric Intramedullary Spinal Cord Neoplasms Characterizes Tumor Margins and Predicts Resectability but not Histology

Choudhri, A. F.[1,2]·Whitehead, M. T.[1,2]·Montgomery, B. K.[3]·Boop, F. A.[1,2]
[1]University of Tennessee Health Science Center, Memphis, TN, [2]Le Bonheur Children's Hospital, Memphis, TN, [3]University of Missouri-Kansas City, Kansas City, MO.

Purpose
Diffusion tensor imaging (DTI) and diffusion tensor fiber tracking (DT FT) are valuable tools for mapping white matter pathways in the brain, which more recently have been applied to the spinal cord. Previous work has suggested that DT FT on intramedullary spinal cord neoplasms (ICN) in adults can differentiate astrocytomas from ependymomas as astrocytomas due to infiltration of fibers by astrocytomas and splaying by ependymomas. We sought to determine whether DT FT can aid in characterizing the margins and predicting the histology of pediatric ICN.
Materials & Methods
Six children (5M/1F, age 4-18 years) with ICN were evaluated with preoperative DTI and DT FT. Diffusion tensor imaging was performed using axial and sagittal acquisition with 20 ($n = 3$) and 25 ($n = 3$) noncollinear directions of encoding with 2 mm slice intervals and a 128 x 128 matrix. Concomitant conventional MR imaging without and with gadolinium administration was performed. All DT FT was processed prospectively by a neuroradiologist and reviewed with the neurosurgeon prior to surgical resection.
Results
Diffusion tensor fiber tracking showed splaying of cord fibers in six of six pediatric ICN, without evidence of infiltration. Histology was pilocytic astrocytoma in five patients and ependymoma in one. Postoperative MRI revealed gross-total resection in six of six patients. All patients had improved postoperative neurologic symptoms, without new neurologic deficit.
Conclusion
Diffusion tensor fiber tracking can aid in preoperative planning of ICN by confirming a discrete margin of a lesion.

Note: Scanned images are included in the proceedings. Some submitted images were reduced during editing, thereby decreasing clarity. Also, refer to the Program Planner. Proceedings Content as of 3-29-2013.

Diffusion tensor fiber tracking cannot predict tumor histology in a pediatric population. Prior adult studies which suggest DT FT can predict histology likely were related to the infiltrative nature of adult cord astrocytomas rather than a true histologic distinction. Splaying of fibers without infiltration on DT FT suggests discrete margins which may allow attempt at gross-total resection.

KEYWORDS: Spinal neoplasm, Diffusion tensor image, pediatric

O-436 **4:03 PM - 4:11 PM**

Functional Diffusion Mapping of the Heterogeneous Response to Immunotherapy in Pediatric Brainstem Gliomas: Initial Experience

Furtado, A. D.[1]·Ceschin, R.[1]·Young Poussaint, T.[2]·Ellingson, B. M.[3]·Okada, H.[1]·Jakacki, R.[1]·Pollack, I. F.[1]·Panigrahy, A.[1]
[1]Children's Hospital of Pittsburgh of the University of Pittsburgh Medical Center, Pittsburgh, PA, [2]Boston Children's Hospital, Pittsburgh, PA, [3]University of California Los Angeles, Los Angeles, CA.

Purpose
Little is known about imaging patterns of treatment response in immunotherapy of pediatric brain tumors. Diffusion MRI measures water mobility at the microstructural level within tissue, and has been shown to be a sensitive and earlier indicator of response to therapy. Functional diffusion mapping (FDM) is a novel method for quantifying heterogeneous tumor response by calculating voxel-wise changes in ADC; however, FDM techniques have never been applied to pediatric brain tumors nor have they been applied to examine immunotherapy response. The purpose of this study was to: (1) describe the incidence of tumor necrosis in immunotherapy of pediatric brainstem gliomas and (2) apply FDM techniques to examine serial ADC changes in the prenecrotic regions.
Materials & Methods
Newly diagnosed HLA (human leukocyte antigen) A2-positive brainstem gliomas were treated prospectively with immunotherapy after radiotherapy. Cystic necrosis was defined by focal T2 signal hyperintensity similar in signal intensity to CSF. Functional diffusion maps were created by coregistering ADC maps on post-treatment time points to a baseline pretreatment ADC map, then performing voxel-wise subtraction. Voxels were labeled red, blue, or green based on whether ADC increased, decreased, or did not change beyond a preset threshold (Figure 1 - bottom row).
Results
A total of 16 patients with newly diagnosed brainstem gliomas were included in this study (eight boys, eight girls, mean age = eight years). Approximately 37% of patients demonstrated necrosis at baseline, 75% of patients developed new areas of necrosis during immunotherapy, and 56% of the developing new necrotic areas were characterized as large uni-focal lesions (Figure 1 - top row - square). In a subset of patients, FDMs demonstrated elevated ADC values in the prenecrotic regions that eventually developed cystic necrosis (Figure 1 - bottom row).

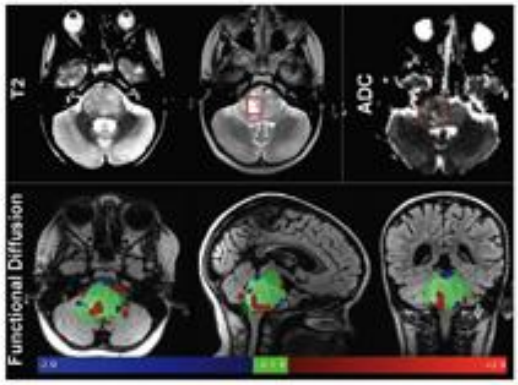

Conclusion
Immunotherapy of pediatric brainstem gliomas is associated with a heterogeneous tumor response characterized by a high incidence of subsequent cystic/necrotic lesions. Functional diffusion mapping techniques may aid in the microstructural characterization of the evolution of prenecrotic regions which can improve our knowledge of response metrics using this novel therapy.

KEYWORDS: Pediatric brain tumors, Diffusion MR imaging

O-437 **4:11 PM - 4:19 PM**

3T Intra-Operative MR Imaging Results in Improved Gross-Total-Resection Rates in the Management of Pediatric Central Nervous System Neoplasms

Choudhri, A. F.[1,2]·Auschwitz, T.[1]·Whitehead, M. T.[1,2]·Klimo, P.[1,2]·Boop, F. A.[1,2]
[1]University of Tennessee Health Science Center, Memphis, TN, [2]Le Bonheur Children's Hospital, Memphis, TN.

Purpose
High field strength intra-operative magnetic resonance imaging (iMRI) has emerged as a powerful adjunct for resection of brain tumors. However, its exact role has not yet been firmly established. We analyzed a prospective database after installation of a 3T iMRI at a tertiary care children's hospital to determine the impact this technology had on the surgical management of a variety of tumors in children.
Materials & Methods
We evaluated 18 consecutive months of patients undergoing brain tumor resection after installation of a 3T iMRI (IMRIS, Winnipeg, Canada) in a children's hospital. Tumor location, histology, surgical approach, OR time, presence and volume of residual tumor, need for tumor

Note: Scanned images are included in the proceedings. Some submitted images were reduced during editing, thereby decreasing clarity. Also, refer to the Program Planner. Proceedings Content as of 3-29-2013.

and nontumor-related reoperation, and anesthesia and MRI-related complications were evaluated.
Results
One hundred thirty-five patients (52 females) underwent iMRI-guided surgery. Of these, 115 were 18 years or younger (mean 8.6 ± 4.7 years). There were 60 posterior fossa tumors. The most common tumors were pilocytic astrocytoma (28%) and medulloblastoma (20%). An average of 1.2 scans were performed per patient (maximum four intraoperative scans). There were no MRI-related safety issues. Additional tumor was resected after scanning in 24% of patients. Ninety-five percent of patients with a preoperative goal of gross-total resection achieved this goal. The 30-day reoperation rate was 0% and no patient required another postoperative MRI scan during the same hospital stay. Challenges included interpreting linear enhancement along the resection cavity, interpreting images after multiple boluses of contrast and image-distortion due to patient positioning.
Conclusion
Intra-operative MRI is safe and reduces the need for early reoperation or repeat sedation for postoperative scans in children with brain tumors. There is a learning curve with this technology that applies to all members of the OR team. By allowing a reduced postoperative disease burden, this hopefully will improve the efficacy of adjunct chemotherapy and radiation and translate into improved long-term patient survival.

KEYWORDS: Pediatric neoplasms, 3T, intraoperative MR imaging

O-438 **4:19 PM - 4:27 PM**

Diagnostic Accuracy of Diffusion Tensor Imaging for Pediatric Cervical Spinal Cord Injury

Barakat, N.[1]·Mulcahey, M.[2]·Gaughan, J.[1]·Shah, P.[1]·Faro, S.[1]·Samdani, A.[2]·Mohamed, F.[1]
[1]Temple University, Philadelphia, PA, [2]Shriners Hospitals for Children, Philadelphia, PA.

Purpose
Spinal cord DTI data can be obtained reliably in healthy children and children with spinal cord injuries (SCI) using inner field-of-view imaging, and shows moderate to good validity against MRI and International Standards for Neurological Classification of SCI(ISNCSCI). Sacral sparing endpoint is important in determining conversion from complete to incomplete injury but is difficult to evaluate in children. The purpose of this study was to evaluate the predictive validity of DTI by examining its diagnostic accuracy for pediatric SCI.
Materials & Methods
Thirty-five subjects were scanned using a 3T scanner: 25 controls(age 13.4±3.9 years) and 10 patients(age=13.5±4.6 years) with cervical SCI. Subjects/parents provided written informed assent and consent. Diffusion tensor imaging was performed using an inner field-of-view pulse sequence. Diffusion tensor imaging indices(FA,AD,RD) were extracted from regions of interest drawn at axial slices along the cervical spinal cord. MR imaging findings were classified “normal” or “abnormal” if increased intramedullary signal on T2-weighted images were seen with or without cord atrophy. Patients were evaluated using ISNCSCI and underwent examination of muscle strength, sensation and sacral sparing. Mean values were compared by group (controls, SCI with intact clinical endpoint, SCI with absent clinical endpoint) and by cord region (motor level, MRI level and regions above/below motor and MRI level of injury). The clinical endpoints used to group subjects with SCI were anal contraction(AC), deep anal pressure(DAP) and S4-5 sensation. Single and multiple variable logistic regressions were used to analyze DTI parameters as predictors of DAP,AC,S4-5 sensation, motor level and MRI level of injury. Specificity, sensitivity, receiver operating characteristics area under the curve(ROC AUC) and corresponding 95% confidence intervals (CI) were calculated(Table). Resampling methods were used to validate estimates from the final models.
Results
There were significant differences in FA between controls, SCI group with intact sacral sparing and SCI group with absent sacral sparing ($p<0.003$). AD values were significantly different among controls, SCI group with AC and SCI group without AC ($p<0.003$). However, for the remaining comparisons of both AD and RD, differences were significant only between controls and SCI group with absent DAP and S4-5 sensation($p<0.003$). There was strong association between FA,AD,RD,AC,DAP,S4-5 sensation, MRI findings and severity of injury. Univariate analysis indicated FA to be the strongest predictor of each clinical endpoint. However, DTI values in combination showed strongest diagnostic accuracy for predicting the presence of AC (AD,RD), DAP(FA), S4-5 sensation (FA,RD), motor level (FA,AD,RD) and MRI level (FA,AD,RD). Bootstrap and Jackknife median values indicated consistency of the parameter estimates.

Multivariate Analysis showing specificity, sensitivity, ROC AUC and 95% CI

	Predictor	Specificity (95% CI)	Sensitivity (95% CI)	ROC AUC (95% CI)
Anal Contraction (AC)	AD,RD	0.74 (0.71,0.77)	0.80 (0.75,0.84)	0.93 (0.91,0.94)
Deep Anal Pressure (DAP)	FA	0.53 (0.50,0.56)	0.70 (0.60,0.79)	0.88 (0.85,0.90)
S4-5	FA,RD	0.81 (0.78,0.83)	0.80 (0.75,0.85)	0.93 (0.92,0.95)
Motor Level	FA,AD,RD	0.67 (0.65,0.70)	0.85 (0.78,0.90)	0.92 (0.91,0.94)
MRI Level	FA,AD,RD	0.83 (0.80,0.85)	0.89 (0,84, 0.93)	0.92 (0.90,0.94)

Note: Scanned images are included in the proceedings. Some submitted images were reduced during editing, thereby decreasing clarity. Also, refer to the Program Planner. Proceedings Content as of 3-29-2013.

Conclusion
Our observation that FA values differ between subjects with SCI who have sacral sparing and those who do not have sacral sparing is novel and has important clinical relevance as this endpoint has low validity and reliability in children.

KEYWORDS: Diffusion tensor image, Pediatric spine, Clinical correlation/ASIA

O-439 **4:27 PM - 4:35 PM**

Correlation of Pediatric Spinal Cord Atrophy Measures with Diffusion Tensor Imaging Metrics

Barakat, N.[1]·Covington, A.[1]·Shah, P.[1]·Faro, S.[1]·Mulcahey, M.[2]·Mohamed, F.[1]
[1]Temple University, Philadelphia, PA, [2]Shriners Hospitals for Children, Philadelphia, PA.

Purpose
Spinal cord injuries (SCI) can cause anterograde retrograde spinal cord degeneration, gliosis and disruption of spinal cord tracts, which can ultimately result in spinal cord atrophy. Diffusion tensor imaging (DTI) parameters can be used to evaluate the microstructure of the spinal cord and yield additional quantitative information characterizing the degree of injury. The aim of this study was to evaluate the correlation between DTI parameters and tissue volume in children with and without SCI.
Materials & Methods
Twenty age-matched subjects (mean age=12.9 years); 10 controls and 10 with SCI were recruited. Subjects/parents provided written informed assent and consent. Diffusion tensor imaging data were acquired on a 3.0T MR scanner using inner field-of-Imaging to cover the cervical spinal cord (C1-T1). Diffusion tensor imaging parameters included: 20 directions, b=1000s/mm^2, voxel size=1.2x1.2x3mm^3, axial slices=35-45, TR=6100-8000ms, TE=115 ms, averages=3 and TA=7 min. T1- and T2-weighted scans also were performed. Anesthesia, cardiac and/or respiratory gating were not used. Motion correction of the DTI images was performed. Tensor estimation was done using MedINRIA. Regions of interest (ROIs) were drawn at axial slice location. Fractional anisotropy (FA), axial diffusivity (AD) and radial diffusivity (RD) were extracted. Spinal cord volume (mm^3) was measured on axial FSE T2-weighted images using Analyze software. Intramedullary lesions were included and extramedullary lesions were excluded. Regions of interest were drawn so that there was a consistent sparing of the outer margin of the spinal cord that represented approximately one voxel width to minimize volume averaging with the CSF. Regions of interest were reviewed and edited by a board-certified neuroradiologist. Correlations between FA, AD, RD and volume were established using Pearson's correlation in JMP SAS.
Results
In patients FA values showed a strong positive correlation with atrophy measures (r=+0.6, p<0.001). A strong negative correlation was seen between RD values and cord volume (r = -0.4, p<0.001) (Figure). Axial diffusivity values had moderate negative relationship with atrophy (r=-0.3, p<0.001). No correlations were observed in the controls group (r<0.01, p<0.6) for all DTI metrics.

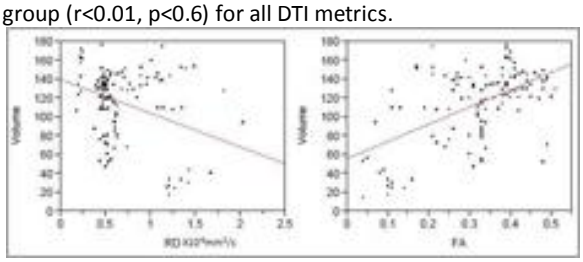

Figure. Pearson's correlation between DTI metrics (FA, RD) and atrophy volume measures.
Conclusion
Our findings showed moderate to strong correlation between DTI metrics and spinal cord volume in children with SCI. Fractional anisotropy showed positive correlation with atrophy measures, in contradistinction to RD and AD which showed negative correlations. These preliminary results are very promising and warrant further analysis with various clinical endpoints.

KEYWORDS: Atrophy, Diffusion tensor image, SCI

O-440 **4:35 PM - 4:43 PM**

Wallerian Degeneration in Pediatric Spinal Cord Injury Using Diffusion Tensor Imaging

Barakat, N.[1]·Faro, S.[1]·Shah, P.[1]·Gaughan, J.[1]·Mulcahey, M.[2]·Mohamed, F.[1]
[1]Temple University, Philadelphia, PA, [2]Shriners Hospitals for Children, Philadelphia, PA.

Purpose
Previous studies have shown that diffusion tensor imaging (DTI) data of the cervical spinal cord can be obtained reliably in typically developing children and children with spinal cord injuries (SCI) using inner field-of-view imaging, and that DTI indices showed moderate to good validity against MRI at injury level. However, in addition to damage at the lesion site, the spinal cord undergoes degeneration above (retrograde) and/or below (antegrade) the point of injury. The purpose of this study was to evaluate the sensitivity of DTI in assessing the extent of Wallerian degeneration in pediatric spinal cord injury.
Materials & Methods
Ten patients with SCI (mean age = 13.5 ± 4.6 years, time since injury = 7.09 ± 3.95) were scanned using a 3T scanner. Mode of injury level = C4. Subjects and parents provided written informed assent and consent. Diffusion tensor imaging, T1- and T2-weighted scans were obtained. Imaging parameters included: 20 diffusion directions, b = 1000s/mm2, voxel size = 1.2x1.2x3mm3, axial slices = 35-

Note: Scanned images are included in the proceedings. Some submitted images were reduced during editing, thereby decreasing clarity. Also, refer to the Program Planner. Proceedings Content as of 3-29-2013.

45 (depending on the subject's height), TR = 6100-8000 ms, TE = 115 ms, number of averages = 3 and acquisition time = 6-7 min. Motion correction was performed using Automatic Image Registration. Tensor estimation was done using MedINRIA. Fractional anisotropy, AD and RD values were extracted from regions of interest drawn at axial slice locations (disk levels and middle portions of cervical vertebral body). The highest spinal cord level of abnormality defined by MRI was assigned 0 and levels above were +1, +2, +3, etc., levels below were assigned -1, -2, -3⋯ etc. The approximate distance between level 0 and ±1 was 9 mm. Differences in mean DTI parameters were compared between cervical levels above and below the level of injury using ANOVA for repeated measures. Non-normally distributed data were transformed to ranks.
Results
There were no statistically significant differences in FA and RD mean values between injury site (level 0) and spinal cord levels above and below injury ($p>0.05$). There were no significant differences in AD values at and below injury site ($p>0.05$). However, significant differences were observed in AD values between injury site and levels above injury level ($p<0.05$).
Conclusion
In summary, FA and RD were sensitive in detecting diffusion abnormalities distant to the site of injury, suggesting retrograde and antegrade Wallerian degeneration, even at levels with normal MRI findings.

KEYWORDS: Pediatric spine, Diffusion tensor image, Wallerian degeneration

Wednesday Afternoon

5:00 PM - 6:30 PM
Ballroom 6AB

(46) ASHNR Programming: Contemporary Imaging of the Temporal Bone

O-441 **5:00 PM - 5:30 PM**

Clinically Based Anatomy of the Temporal Bone

Chapman, P. R.
University of Alabama Birmingham
Birmingham, AL.

Presentation Summary
Presentation will review the practical anatomy of the temporal bone as it pertains to routine CT and MRI imaging of the temporal bone. The presentation will address the fundamental techniques required for CT and MRI imaging, discuss the limits of each modality, and focus on the detailed radiologic anatomy the internal auditory canal, the inner ear, and middle ear. Emphasis will be placed on distinguishing normal appearance and normal variations from subtle or early pathologic processes.

O-442 **5:30 PM - 6:00 PM**

A Geographic Approach to Infectious and Inflammatory Disease of the Temporal Bone

Shatzkes, D. R.
Lenox Hill Hospital
New York, NY.

Presentation Summary
Though the presentation will generally follow the advertised geographic approach, there are several truisms that are worth remembering with regard to temporal bone inflammation: •The middle ear and mastoid cavities can be considered an extension of the upper respiratory tract, connected via the Eustachian tube and lined by similar mucosa. These cavities, in turn, connect to air cells elsewhere in the temporal bone, most notably at the petrous apex. Hence, a similar pattern of inflammatory disease will affect air cells at all of these sites. •The external ear and auditory canal are covered by skin rather than mucosa. Thus, inflammatory (and neoplastic) processes at these sites are more aligned with disease affecting the skin elsewhere in the body. •While inflammatory disease of the temporal bone can be classified broadly into acute and chronic processes, it is important to remember that these generally DO NOT represent a continuum. **Acute otomastoiditis (AOM)** is caused by a bacterial infection of the middle ear. Children are predisposed because of the orientation and length of their Eustachian tubes, and the presence of adenoids. Uncomplicated AOM is rarely imaged. **Chronic otomastoiditis (COM)** is virtually synonymous with chronic Eustachian tube obstruction or dysfunction; infection is rarely present. Chronic otomastoiditis can be further broadly classified as cholesteatomatous or noncholesteatomatous COM. Some of the site-specific entities that will be discussed are: 1. External Ear: - Acute: acute otitis externa, necrotizing otitis externa; - Chronic: Cholesteatoma, keratosis obturans, exostoses. 2. Tympanomastoid Cavity: - Acute: AOM complications including coalescent mastoiditis, sigmoid sinus thrombosis, intracerebral abscess; - Chronic: o Cholesteatoma: Pars flaccida, pars tensa, o Noncholesteatomatous COM: granulation tissue, cholesterol granuloma, ossicular fixation/erosion. 3. Inner Ear: - Acute: Labyrinthitis (viral, bacterial, luetic, mycotic); - Chronic: Labyrinthitis ossificans. 4. Petrous Apex: - Acute: Petrous apicitis; - Chronic: Cholesterol granuloma, cholesteatoma, mucocele.

Note: Scanned images are included in the proceedings. Some submitted images were reduced during editing, thereby decreasing clarity. Also, refer to the Program Planner. Proceedings Content as of 3-29-2013.

O-443 **6:00 PM - 6:30 PM**

Tumors of the Temporal Bone: From EAC to IAC

Harnsberger, H.
University Of Utah
Salt Lake City, UT.

Presentation Summary
In this presentation an anatomy-based differential diagnosis list of tumors for the external auditory canal (EAC), middle ear, inner ear, and facial nerve will be reviewed. In each location the clinical presentation, specific imaging findings of each tumor and differential diagnosis features will be presented. Where possible, characteristic imaging findings unique to a specific tumor will be highlighted. By area benign and malignant tumors reviewed include: 1. External auditory canal, Benign: Exostoses, osteoma. Malignant: EAC squamous cell carcinoma. 2. Middle ear, Benign: Glomus tympanicum and jugulare paraganglioma, facial nerve schwannoma, adenoma and meningioma, Langerhans cell histiocytosis. Malignant: Rhabdomyosarcoma. 3. Inner ear, Benign: Intralabyrinthine schwannoma, endolymphatic sac tumor, meningioma. 4. Facial nerve, Benign: Facial nerve schwannoma, facial nerve hemangioma (venous malformation). Malignant: Perineural parotid malignancy.

Wednesday Afternoon

5:00 PM - 6:30 PM
Ballroom 6CF

(47) Advanced Imaging Seminar: fMRI: Now and Future

O-444 **5:00 PM - 5:30 PM**

Segregation and Wiring of the Brain

Wedeen, V.
Massachusetts General Hospital
Charlestown, MA.

O-445 **5:30 PM - 6:00 PM**

Default Networks and Related Imaging

Rosen, B. R.
Massachusetts General Hospital
Charlestown, MA.

Bruce R. Rosen, MD, PhD is Professor of Radiology, Harvard Medical School and Director, Athinoula A. Martinos Biomedical Imaging Center, Massachusetts General Hospital. Dr. Rosen received his AB (Astronomy) degree from Harvard University, Cambridge, MAin 1977; his MS (Physics) degree from Massachusetts Institute of Technology, Cambridge, MA in 1980; his MD degree from Hahne mann Medical College & Hospital, Philadelphia, PA in 1982 and his PhD from Harvard/MIT Division of Health Sciences in 1984. Dr. Rosen's research focuses on the development and application of physiological and functional NMR techniques to address basic biological and clinical questions. He has held many positions on various Boards in the medical community and received more than six Honors from various organizations. Dr. Rosen has had articles published in at least 15 peer-reviewed publications.

O-446 **6:00 PM - 6:30 PM**

Future of fMRI: From Animals to Humans

Polimeni, J. R.
Massachusetts General Hospital
Charlestown, MA.

Jonathan R. Polimeni, Ph.D., is an Instructor in Radiology at Harvard Medical School and an Assistant in Biomedical Engineering in the Department of Radiology of the Massachusetts General Hospital. Dr. Polimeni received his B.S. in Electrical and Computer Engineering from the Johns Hopkins University. He received his Ph.D. in Electrical and Computer Engineering from Boston University where he worked in the Computational Neuroscience and Computer Vision Laboratory under Professor Eric Schwartz. His Ph.D. work was in the measurement and modeling of visuotopic maps in macaque and human visual cortex. His postdoctoral work was at the Athinoula A. Martinos Center for Biomedical Imaging at the Massachusetts General Hospital within the Imaging Physics group under Prof. Lawrence Wald. He joined the faculty of the Martinos Center in 2010. In 2011 he was awarded an NIH Career Development Award (K01) from the National Institute of Biomedical Imaging and Bioengineering. His research focuses on the development and application of high-resolution 7T fMRI, the characterization of the spatial specificity of the fMRI signals, and on the study of the functional architecture of the human visual cortex. He is currently working on testing whether the hemodynamic response is regulated finely enough to support cortical layer-specific fMRI.

Presentation Summary
What are the spatial resolution and temporal resolution of fMRI achievable today, and what are the resolution limits? This presentation will provide an overview of new technologic advances in fMRI acquisition techniques together with recent discoveries into the physiologic mechanisms of blood flow regulation in the cerebral cortex. The goals of the presentation will be to examine how tightly coupled the hemodynamic response may be to neural activity at fine scales and how to leverage knowledge of cerebral vascular anatomy and physiology to obtain accurate measurements of brain activity with fMRI. Cutting-edge optical imaging techniques used in animal models have provided valuable new insights into cerebral

Note: Scanned images are included in the proceedings. Some submitted images were reduced during editing, thereby decreasing clarity. Also, refer to the Program Planner. Proceedings Content as of 3-29-2013.

hemodynamics, and the data suggest that the blood flow response to neural activity may be much more finely controlled than previously believed. As technologies such as ultrahigh-field MRI and massively parallel receive coil arrays become more common, this tight coupling between neural activity and blood flow can be exploited to provide more faithful representations of neuronal population responses with fMRI. During this presentation, we will review some recent studies that have achieved high spatial and temporal accuracy with fMRI. As an example we will consider a new line of inquiry into the possibility of a cortical layer-specific fMRI response. Throughout, we will point out the current limitations of fMRI and discuss how emerging technology can help to further increase the accuracy into the future.

Wednesday Afternoon

5:00 PM - 6:30 PM
Ballroom 6DE

(48) CSI San Diego: Neuroradiology on the Go: Viewing Studies Outside of Work and Home (Viewers for Phones and Tablets)

O-447 **5:00 PM - 5:45 PM**

Neuroradiologists on the Go

Phillips, C.
Weill Medical College of Cornell/New York Presbyterian
New York, NY.

Presentation Summary
Tinnitus is an incredibly common condition in the world, and is suffered by countless millions of people in the U.S., some of whom will be referred for imaging evaluation. Tinnitus is the perception of sounds by an individual in the absence of an external sound. It may be a ringing, buzzing, or other monotonous tone. The tone may vary with time, and can be pulse-synchronous, or may be unvarying. Continuous tinnitus is the unvarying form, and pulsatile tinnitus refers to a sound which varies with the cardiac cycle. Tinnitus may be an unremitting problem in patients, and may lead to referral for imaging. In this regard, it is a very problematic item of history for the radiologist, as it is a symptom with an incredibly wide range of potential etiologies. There is little acceptance of a standard imaging algorithm for diagnosing a potential cause of tinnitus. As expected, the pulsatile form may be vascular in nature, and a potential cause may be found more commonly on imaging, but the study to be recommended also is widely debated, without consensus. Continuous tinnitus is a particularly vexing clinical issue. Tinnitus without a radiologic abnormality is likely the most common form of tinnitus, and the radiologist may recommend a perfectly appropriate examination without a discovered diagnosis. Pulsatile tinnitus may be associated with vascular pathology, and with other lesions as well. A reasonable differential diagnosis includes arterial and venous anomalies, vascular neoplasia, and other less common but potentially diagnosable and treatable conditions, such as otospongiosis. Continuous tinnitus can be caused by a very wide range of pathology, including intracranial and IAC neoplasms, TMJ disease, brainstem lesions, intracranial hypotension or hypertension, or simply presbycusis. The diagnostic study ordered may be dependent on clinical factors, such as patient age, onset of symptoms, or potentially causative conditions. CT and MRI may be utilized, and CTA and MRA as well as venous studies may be useful in arriving at a cause. Temporal bone CT studies often are ordered, as are CTA. CT angiography has been proposed as a reasonable “one stop shopping” exam, yielding both vascular information and high quality temporal bone CT studies. However, brainstem, IAC and posterior fossa disease still is best studied with MR with and without contrast.

O-448 **5:45 PM - 6:30 PM**

Postprocessing on the Go

Quigley, E. P.
University of Utah Medical Center
Salt Lake City, UT.

Presentation Summary
Target Audience: Radiologists, Fellows, Residents, and Medical Students. Objectives: Presentation will review the currently available imaging tools for remote basic and advanced visualization of imaging studies. Different hardware platforms ranging from laptops, tablets, minitablets, and smart phone and commercially available and open source software packages will be discussed in a vendor neutral environment. Topics will include utilization of remote access, desktop emulators, and thick and thin client options. Advanced visualization capabilities such as 3D, volume and surface rendering capabilities will be reviewed. Medicolegal and information security implications will be introduced. Take your practice on the go!

Note: Scanned images are included in the proceedings. Some submitted images were reduced during editing, thereby decreasing clarity. Also, refer to the Program Planner. Proceedings Content as of 3-29-2013.

Wednesday Afternoon

5:00 PM - 6:30 PM
Room 5AB

(49) ASPNR Programming: Development and Malformations

O-449 **5:00 PM - 5:30 PM**

Hindbrain and Midbrain Development

Barkovich, A.
University of California San Francisco Medical Center
San Francisco, CA.

Presentation Summary

Although the brain stem and cerebellum often are not scrutinized as carefully as the cerebrum, malformations of these structures are not uncommon. An understanding of these structures is best achieved by a general understanding of the anatomy of the structures of the brain stem and cerebellum, the steps involved in their formation and the most important genes involved in these steps. This presentation will give a brief overview of development and anatomy, followed by a classification of malformations that is based upon disturbances in normal development. I. Malformations secondary to early anteroposterior and dorsoventral patterning defects, or to misspecification of mid-hindbrain germinal zones. A. Anteroposterior patterning defects: 1. Gain, loss or transformation of the diencephalon and midbrain. 2. Gain, loss or transformation of the midbrain and rhombomere 1. 3. Gain, loss or transformation of lower hindbrain structures. B. Dorsoventral patterning defects: 1. Defects of alar and basal ventricular zones. 2. Defects of alar ventricular zones only. 3. Defects of basal ventricular zones only. II. Malformations associated with later generalized developmental disorders that significantly affect the brainstem and cerebellum (and have pathogenesis at least partly understood). A. Developmental encephalopathies associated with mid-hindbrain malformations. B. Mesenchymal-neurepithelial signalling defects associated with mid-hindbrain malformations (includes Dandy-Walker malformations). C. Malformations of neuronal and glial proliferation that prominently affect the brainstem and cerebellum. D. Malformation of neuronal migration that prominently affect the brainstem and cerebellum: 1. Lissencephaly with cerebellar hypoplasia. 2. Neuronal heterotopia with prominent brainstem and cerebellar hypoplasia. 3. Polymicrogyria with cerebellar hypoplasia. 4. Malformations with basement membrane and neuronal migration deficits. E. Diffuse molar tooth type dysplasias associated with defects in ciliary proteins (Joubert and related syndromes): 1. Syndromes affecting the brain with low frequency involvement of the retina and kidney. 2. Syndromes affecting the brain, eyes, kidneys, liver and variable other systems. III. Localized brain malformations that significantly affect the brainstem and cerebellum (pathogenesis partly or largely understood, includes local proliferation, cell specification, migration and axonal guidance). A. Multiple levels of mid-hindbrain. B. Midbrain malformations. C. Malformations of rhombomere 1 including cerebellar malformations. D. Pons malformations. E. Medulla malformations. IV. Combined hypoplasia and atrophy in putative prenatal onset degenerative disorders. A. Pontocerebellar hypoplasia. B. Mid-hindbrain malformations with congenital disorders of glycosylation. C. Other metabolic disorders with cerebellar or brainstem hypoplasia or disruption. D. Cerebellar hemisphere hypoplasia (rare, more commonly acquired than genetic, often associated with clefts or cortical malformation).

O-450 **5:30 PM - 6:00 PM**

Genetic-Phenotype Correlations in Hindbrain/Midbrain Malformations - Part I

Ishak, G. E.
Seattle Children's Hospital
Seattle, WA.

Presentation Summary

Malformations of the midbrain and hindbrain (MBHB) are relatively under appreciated due to historical difficulties with imaging and pathologic evaluation. Recent improvements in neuroimaging, neuropathology and neurogenetics have made it possible to distinguish many developmental disorders of the MBHB, revealing their substantial contribution to neurodevelopmental dysfunction. We will present a case-based overview of common MBHB malformations including clinical presentation, imaging features, diagnostic work up and genetic causes of some malformations. Disorders will include pontocerebellar hypoplasias, dystroglycanopathies, tubulinopathies, rhombencephalosynapsis, Joubert syndrome, and other disorders that are relatively common or have added to the understanding of human brain development. Identifying specific disorders has important implications for additional diagnostic work up, prognosis, recurrence risk and medical monitoring for complications. We also will highlight recent advances in imaging and genetics applied to MBHB malformations. The information provided will increase recognition of specific imaging features of MBHB malformations, as well as promote a broader understanding of the clinical implications of these diagnoses.

Note: Scanned images are included in the proceedings. Some submitted images were reduced during editing, thereby decreasing clarity. Also, refer to the Program Planner. Proceedings Content as of 3-29-2013.

O-451 **6:00 PM - 6:30 PM**

Genetic-Phenotype Correlations in Hindbrain/Midbrain Malformations - Part II

Doherty, D.
University of Washington
Seattle, WA.

Presentation Summary
Malformations of the midbrain and hindbrain (MBHB) are relatively under appreciated due to historical difficulties with imaging and pathologic evaluation. Recent improvements in neuroimaging, neuropathology and neurogenetics have made it possible to distinguish many developmental disorders of the MBHB, revealing their substantial contribution to neurodevelopmental dysfunction. We will present a case-based overview of common MBHB malformations including clinical presentation, imaging features, diagnostic work up and genetic causes of some malformations. Disorders will include the pontocerebellar hypoplasias, dystroglycanopathies, tubulinopathies, rhombencephalosynapsis, Joubert syndrome, and other disorders that are relatively common or have added to the understanding of human brain development. Identifying specific disorders has important implications for additional diagnostic work up, prognosis, recurrence risk and medical monitoring for complications. We also will highlight recent advances in imaging and genetics applied to MBHB malformations. The information provided will increase the recognition specific imaging features of MBHB malformations, as well as promote a broader understanding of the clinical implications of these diagnoses.

Wednesday Afternoon

5:00 PM - 6:30 PM
Room 1AB

(50) General Session: Special Session: WFNRS presents the Best of ESNR

O-452 **5:00 PM - 5:08 PM**

Susceptibility-Weighted MR Imaging in Multiple Sclerosis

Auger, C.
Hospital Vall D'Hebron
Barcelona, SPAIN.

Dr. Cristina Auger was born in Barcelona in 1968. She is a full-time neuroradiologist, who gained her MD in 1992 at the University of Barcelona. After formal training in Radiology, she became staff pediatric neuroradiologist at the Department of Radiology at Vall d'Hebron Hospital (Barcelona, Spain). In 2005, she became staff neuroradiologist at the Department of Radiology at University Hospital Vall d'Hebron, and since 2010 Head of Neuroradiology at the MR unit in the same institution. She is author or co-author of 10 original papers published in peer-reviewed journals. Her main interests are multiple sclerosis and neurooncology.

Presentation Summary
Histological stains have shown that various neurologic and psychiatric disorders, including Alzheimer disease, Huntington disease, and Parkinson disease may be associated with elevated focal accumulations of iron. Abnormal iron accumulation also has been detected pathologically in reactive microglia, ameboid microglia, and macrophages in the brain of multiple sclerosis (MS), although it is not yet clear if this accumulation is implicated in MS pathology or merely reflects an epiphenomenon. Several MR techniques have been proposed for in vivo assessment of iron content in central nervous system tissues. The basic principle behind all these techniques is the interaction between high-molecular-weight iron complexes such as ferritin or hemosiderin and water molecules, which leads to decreased T2 and T2* relaxation times in iron-laden tissues. Susceptibility-weighted imaging (SWI), is one of these techniques, which compared to others has the advantage of easily being implemented in clinical practice. Susceptibility-weighted imaging combines magnitude and phase images to enhance contrast, and has shown high sensitivity in demonstrating iron in the form of hemosiderin or ferritin within brain tissue. Recent experience with the implementation of SWI at 3.0T in the routine diagnostic workup of MS has shown that most focal chronic, and acute, demyelinating lesions can be depicted as areas of low signal intensity likely representing iron deposition. In future studies, quantitative MRI analyses of brain iron in a clinical follow-up setting might help to elucidate the implication of iron accumulation in MS. Susceptibility-weighted imaging also takes advantage of the magnetic susceptibility effects from paramagnetic deoxygenated hemoglobin. Using deoxyhemoglobin as an intrinsic contrast agent, SWI affords to acquire images that can be used to visualize venous structures. The quantitative measures of the number of detected venous structures on SWI have show a significant reduction of periventricular white matter venous vasculature visibility in MS patients as compared to healthy control subjects, likely indicating reduced metabolism or morphologic changes of venous vasculature. This observation supports the hypothesis that vascular abnormalities play a role in the pathogenesis of MS. Nevertheless, additional studies are required before SWI can be considered a biomarker in MS. These additional studies should demonstrate their reproducibility, sensitivity to disease evolution and treatment changes, and their value in reflecting and predicting the accumulation of irreversible disability. All

Note: Scanned images are included in the proceedings. Some submitted images were reduced during editing, thereby decreasing clarity. Also, refer to the Program Planner. Proceedings Content as of 3-29-2013.

these necessary efforts are especially important nowadays, when there is a growing interest in developing neuroprotective or regenerative agents in MS, which consequently demands new imaging strategies for achieving and monitoring the neurodegenerative component of MS.

O-453 **5:08 PM - 5:23 PM**

MRI in New Multiple Sclerosis Lesions

Rovira, A.
Hospital Vall d'Hebron
Barcelona, SPAIN.

Presentation Summary

Disease activity in multiple sclerosis (MS) is strongly linked to the formation of new lesions, which comprises a complex sequence of inflammatory, degenerative and reparative processes. However there is dissociation between disease activity (clinical or radiologic) and progression, a phenomenon that can be explained by a process of exhaustion of both structural and functional redundancies (as demonstrated with functional MRI) that increasingly prevents repair and recovery. Conventional magnetic resonance (MR) imaging techniques, such as T2-weighted and gadolinium-enhanced T1-weighted sequences, which are highly sensitive in demonstrating the spatial and temporal dissemination of demyelinating plaques in the brain and spinal cord in MS, can provide a quantitative assessment of inflammatory activity and lesion load in patients suffering from this disease, and are being used increasingly in monitoring disease activity and progression not only in clinical trials but also in individual patients. Serial analysis of new lesion formation by means of MR imaging provides relevant data related to both inflammatory activity and repair mechanisms, which should be considered for assessing specific therapeutic effects of new treatments (anti-inflammatory, neuroprotective, regenerative). Longitudinal and cross-sectional MR studies have shown that contrast enhancement occurs in almost all new MS plaques in patients with relapsing-remitting MS or secondary progressive MS and can sometimes be detected even before the onset of clinical symptoms. New contrast-enhancing lesions are nearly always associated with a hyperintense lesion in the same location on T2-weighted images. The extent of these new T2 lesions usually contract over time (3-5 months) and their intensity is reduced as edema resolves and some tissue repair occurs, leaving a much smaller T2 permanent “footprint” of the prior inflammatory event. Serial changes in lesion intensity and size on contrast-enhanced T1-weighted, and on unenhanced T1- and T2-weighted sequences are two related but temporally disjoined processes, as after cessation of gadolinium uptake transient significant T1/T2 changes T2 exists over a 3-6 months period. According to these changes MS lesion formation and activity can be divided into two phases: an acute phase characterized by contrast uptake reflecting blood-brain barrier disruption, and a subacute phase characterized by changes in lesion signal intensity and size on unenhanced T1- and T2-weighted images. Characteristics of the subacute phase of lesion formation reflect the balance between injury and repair capacity, and changes in this behavior may represent a shift from inflammatory toward degenerative disease activity and greater proximity to a progressive stage of the disease.

O-454 **5:23 PM - 5:53 PM**

Individual Level Classification Analyses of Brain MRI in Neurodegenerative Diseases

Haller, S.
University Hospital Geneva
Geneva, SWITZERLAND.

Dr. Haller received his MD from medical school at the University of Tübingen, Germany. He completed the MS at the Max Planck Research School of Neural and Behavioral Tübingen, Germany. He specialized in Radiology and diagnostic Neuroradiology at the University Hospital of Basel, Switzerland. Thereafter, he completed his Privatdozent (venia docendi, senior lecturer) in Neuroradiology at the University Hospital Geneva, Switzerland. Currently, he is senior staff Neuroradiologist at the University Hospital Geneva, Switzerland, with a special interest in advanced neuroimaging techniques in particular in the domains of neurodegenerative and neurovascular diseases. Dr. Haller has received several awards from the European Society of Neuroradiology (ESNR) and at least five awards from the Swiss Society of Radiology (SSR).

Presentation Summary

Overview - This presentation will discuss recent advances in early and individual detection of neurodegenerative diseases, in particular Alzheimer dementia (AD) based on support vector machine (SVM) pattern recognition analyses. Background - The incidence of AD is increasing. Standard MR imaging is performed routinely in the work up of dementias notably to exclude other diseases such as normal pressure hydrocephalus or meningioma, which are present in approximately 1% of cases. The typical atrophy of the hippocampus and bi-parietal cortex is only a late sign, hence visual inspection of standard MRI is cases noncontributive in most cases in the early phase of neurodegeneration. Challenge - Mild cognitive impairment (MCI) is a state of impaired cognition, which does not yet fulfill the criteria for dementia. Mild cognitive impairment is a very heterogeneous group, and only about 50% of MCI cases will progress to develop dementia. This means that in a classic therapeutic trial, 50% of MCI cases will remain stable even without treatment. The challenge is to identify those MCI cases who will progress later on at an individual basis with respect to both individual patient care and potential treatment trials. Group level versus individual

Note: Scanned images are included in the proceedings. Some submitted images were reduced during editing, thereby decreasing clarity. Also, refer to the Program Planner. Proceedings Content as of 3-29-2013.

level analyses - Typical advanced image analysis techniques of gray matter (e.g., voxel-based morphometry, VBM) or white matter (e.g., tract-based spatial statistics, TBSS) are group level comparisons. While such analyses are fascinating from a research perspective identifying disease-related changes in brain morphometry, these results cannot be applied to clinical practice for the identification of individual patients. Individual level classification analyses such as support vector machines (SVM) are fundamentally different approaches aiming to identify individual cases. The basic principle of such pattern recognition analyses can be illustrated in the example of face recognition. A single feature, for example the nose, is generally not sufficient to detect an individual subject - even though the nose might show group differences. In contrast, individual faces can be identified by the combination of multiple features such as nose, ear, chin, eyebrow, etc. even though each feature per se is not necessarily significantly different between groups. Conclusion - The current presentation will discuss principles of individual level classification analyses and results to identify progressive versus stable MCI based on diffusion tensor imaging (DTI) white matter (accuracy up to 95%) and susceptibility-weighted imaging (SWI) iron deposition (accuracy up to 85%). Finally, future perspectives for multimodal individual level classification analyses will be discussed.

O-455 **5:53 PM - 6:00 PM**

Focal Hypoperfusion in Early Dementia as Assessed with Arterial Spin Labeling MRI

Steketee, R.
University Medical Center Rotterdam
Rotterdam, NETHERLANDS.

Rebecca Steketee has a master's degree in neuropsychology and cognitive neuroscience and is currently a PhD student at the department of Radiology at Erasmus MC - University Medical Center, Rotterdam, the Netherlands. She investigates the use of advanced MR neuroimaging techniques in the diagnosis of early dementia, with a particular interest in arterial spin labeling (ASL) MRI.

Presentation Summary
Early diagnosis of dementia is challenging as brain atrophy may not yet be apparent. Changes in cerebral blood flow (CBF) preceding atrophy may be detected with arterial spin labeling (ASL). This study aims to assess ASL for diagnosing early dementia. Fifteen patients with suspected diagnosis of dementia (mean age 63 years, seven male, mean Mini Mental State Examination 26) and 15 controls (mean age 59 years, eight male) underwent 3D PCASL and T1-weighted MR scanning at 3T (GE Healthcare, U.S.). Data were coregistered and normalized using SPM8 (London, UK). Region of interest (ROI) analysis of the CBF maps, masked for gray matter only, was performed with MarsBaR (Marseilles, FR), in regions involved in dementia and regions initially spared. Mean CBF values were compared between groups using 2-sample t-tests. Age and gender were not different between groups ($p>0.05$). Mean CBF values in dementia-related brain regions were significantly lower in patients than controls ($p<0.05$, right/left medial temporal lobe: 30/30 versus 37/38; right/left precuneus: 29/29 versus 43/42; right/left posterior cingulum: 35/34 versus 56/58 ml/100cc GM/min). No difference was found in regions not implicated in dementia (right/left precentral gyrus: 29/30 versus 35/36; right/left occipital gyri: 24/25 versus 31/29 ml/100cc GM/min for patients and controls respectively). Patterns of hypoperfusion assessed with ASL in early dementia are concordant with those in established dementia and those assessed with positron emission tomography, indicating the contribution of ASL in the early diagnosis of dementia. Future aims are to assess ASL for early differentiation between types of dementia.

O-456 **6:00 PM - 6:15 PM**

Arterial Spin Labeling MRI in Clinical Practice: Current and Future Applications

Smits, M.
Erasmus Medical Center - University Medical Centre Rotterdam
Rotterdam, NETHERLANDS.

Marion Smits is Associate Professor of Neuroradiology and combines her clinical work as a neuroradiologist with scientific research into advanced MR neuroimaging, such as functional MRI, diffusion tensor imaging (DTI) and perfusion imaging. She uses these techniques to visualize the brain's function and microstructure, and to study pathophysiological and regenerative processes in a variety of neurological diseases, such as stroke, dementia and brain tumors. Marion combines her clinical expertise with scientific research and active participation in key European organisations, including the European Society of Radiology (ESR), the European Society for Magnetic Resonance in Medicine and Biology (ESMRMB), European Organisation for Research and Treatment of Cancer (EORTC) and the European Institute for Biomedical Imaging Research (EIBIR). On a national level she is core member of the Young Health Council of the Netherlands, an advisory organ to the Dutch Ministry of Health. As permanent faculty member of several European and national course organisations she lectures frequently on advanced MR neuroimaging. She is Course Director of the European School of MRI fMRI&DTI course, and has been elected Scientific Programme Committee chair of the ESMRMB scientific annual meeting 2015 in Edinburgh (UK). Full list of publications: www.marionsmits.net/publications LinkedIn: nl.linkedin.com/in/marionsmits

Presentation Summary
Arterial spin labeling (ASL) is a noninvasive MRI technique

Note: Scanned images are included in the proceedings. Some submitted images were reduced during editing, thereby decreasing clarity. Also, refer to the Program Planner. Proceedings Content as of 3-29-2013.

with which cerebral blood flow (CBF) can be measured quantitatively. It uses inversion or saturation pulses to label arterial blood. Two images of the brain are acquired: one without and one with labeling of arterial blood. By subtracting the two images, all static signal is cancelled out, resulting in an image of labeled spins only. Although the first publications of ASL MRI date over 10 years back, it is only now that ASL is commercially available on MRI systems from all major vendors and is making its way into clinical practice. The main areas of interest for current and future clinical application of ASL MRI of the brain are dementia, cerebrovascular disease and neuro-oncology. Arterial spin labeling is proposed as a diagnostic alternative to fluorodeoxy-D-glucose (FDG) PET in the workup of dementia patients. Arterial spin labeling has several advantages over FDG PET. Crucially, it can be added easily to the routinely performed structural MRI examination. Feasibility studies show that ASL provides reliable CBF maps in dementia. In patients with established Alzheimer disease and frontotemporal dementia, hypoperfusion patterns are seen that are similar to hypometabolism patterns seen with FDG PET. Current and future studies in this field will need to demonstrate the validity of ASL in the diagnostic workgup of the individual patient, early in the disease process. In cerebrovascular disease, ASL is of particular interest owing to its quantitative nature as well as its capability to determine cerebral arterial territories using vessel-selective techniques. In acute stroke, the source of the collateral blood supply in the penumbra may be visualized, which then can be targeted selectively with thrombolytic and neuroprotective agents. In chronic cerebrovascular disease, the extent and severity of compromised cerebral perfusion can be visualized, which may be used to guide therapeutic or preventative intervention. Arterial spin labeling has further clinical potential for the detection and follow up of arteriovenous malformations, depicting increased venous flow due to arteriovenous shunting. Studies on ASL in brain tumor imaging indicate a high correlation between areas of increased CBF as measured with ASL, and increased cerebral blood volume as measured with dynamic susceptibility contrast-enhanced perfusion imaging. Major advantages of ASL for brain tumor imaging are the fact that CBF measurements are not influenced by breakdown of the blood-brain barrier, as well as its quantitative nature, facilitating multicenter and longitudinal studies.

O-457 **6:15 PM - 6:30 PM**

Neuroradiology in Translational Medicine

Politi, L. S.
San Raffaele Scientific Institute
Milano, ITALY.

Dr. L. S. Politi received his degree in medicine and surgery at the University of Catania in 1988. He performed his residency at the Radiology Department of the Faculty of Medicine, University of Florence from November 1198-November 2002. He was a Clinical Assistant, followed by a Senior Clinical Assistant, Neuroradiology Department, San Raffaele Hospital and Scientific Institute, Milan, Italy. Dr. Politi currently is Head of Clinical Unit, Neuroradiology Department, San Raffaele Hospital and Scientific Institute, Milan, Italy. He is also Group Leader of the Neuroradiology Department and Coordinator of Neuroimaging Research at the Preclinical MRI facility, Imaging Core. He is currently Assistant Professor, Vita-Salute at San Raffaele. Dr. Politi received the Lucien Appel Prize of the European Society of Neuroradiology in 2006.

Presentation Summary
We will present MR-based cellular and molecular imaging techniques for monitoring stem cell transplantation in neurologic diseases. We will discuss optimal conditions for dynamic MR visualization of murine and human neural and hematopoietic stem cell homing to disease sites in the brain and other target organs of several mouse models of human disease, and how these preclinical results can be exploited to monitor the first patients enrolled in stem cell-transplantation trials. Further, we will underline how the results obtained in preclinical neuroimaging experiments can give a precious contribution in the design of new clinical trials, in terms of definition of cell doses, route of administration, therapeutic window and mechanisms of action.

Thursday Morning

7:30 AM - 8:30 AM
Ballroom 6AB

(51) Maintenance of Certification Review Session - Head and Neck (AR)

O-458 **7:30 AM - 8:00 AM**

Head and Neck - Part I

Komakula, S. T.
Stanford University
Stanford, CA.

Presentation Summary
I will be showing interesting cases of the head and neck with a focus on differential diagnoses and key imaging characteristics of regional pathology.

Note: Scanned images are included in the proceedings. Some submitted images were reduced during editing, thereby decreasing clarity. Also, refer to the Program Planner. Proceedings Content as of 3-29-2013.

O-459 **8:00 AM - 8:30 AM**

Head and Neck - Part II

Fischbein, N. J.
Stanford University
Stanford, CA.

Presentation Summary
In this presentation we will review a selection of difficult head and neck cases, along with companion case examples, to reinforce knowledge of head and neck anatomy and imaging pathology.

Thursday Morning

8:45 AM - 10:15 AM
Ballroom 6AB

(52) ASHNR Programming: Everyday Issues in Head and Neck Imaging

O-460 **8:45 AM - 9:15 AM**

Diagnoses Not to Miss in the Head and Neck

Michel, M. A.
Medical College of Wisconsin/Froedtert Hospital
Milwaukee, WI.

Presentation Summary
Although it is important to recognize and correctly diagnose all pathology within the head and neck, there are several diagnoses that are particularly important NOT to miss. In the time allotted for this talk, not all of the important conditions can be discuss, so I have selected a few based upon my opinion and the collective opinions of my head and neck colleagues. The conditions were not selected based upon how commonly they occur, but because they are frequently missed or misinterpreted, because early recognition may prevent morbidity and mortality to the patient, or because making the correct diagnosis on imaging can significantly alter the way the patient is managed. Diagnoses given honorable mention, but not discussed in detail include: 1) Calcific prevertebral tendonitis; 2) Bisphosphonate-related osteonecrosis of the jaws; 3) Enlarged vestibular aqueduct syndrome; 4) Complications of otomastoiditis; 5) Otosclerosis; 6) Isolated sphenoid sinus disease; and 7) Mylohyoid muscle defect containing salivary tissue. **Fibro-osseous Lesions on MRI.** The term "fibro-osseous" (FO) generally refers to a class of benign bony abnormalities and they are common in the craniofacial skeleton. The histologies most often included in this group include osteomas, ossifying fibromas, and fibrous dysplasia. They can have very similar appearances on imaging and on pathology, particularly when they have a mix of both fibrous and osseous components. The MR imaging appearance of FO lesions can be confusing. Depending upon the amount of fibrous tissue present, they can appear quite heterogeneous and variably enhance. When there are large ossified portions, these areas can be very hypointense and mimic air signal. Many of the FO lesions do not require treatment and making the diagnosis correctly with imaging may spare the patient any unnecessary procedure. **Invasive Fungal Sinusitis.** Invasive fungal sinusitis (IFS) is important to diagnosis early and it may progress rapidly and has a high mortality rate. Invasive fungal sinusitis occurs in immunocompromised patients or in patients with other predisposing conditions. Although bone erosion may be present, one of the main pathways of spread beyond the sinonasal cavities is via the blood vessels (angioinvasive). Because of this, complications of vascular narrowing, dissection, and vessel occlusion, in addition to soft tissue destruction, are not uncommon. Fungal processes may demonstrate foci of hypointense long-TR signal on MRI due to the presence of fungal hyphae and metal chelates. Fungal disease also can appear mass-like and may be confused for neoplasm. Therefore, it is important to include IFS in the differential diagnosis of a sinonasal mass lesion if the patient is immunocompromised. **Non-Hodgkin Lymphoma in the H&N.** There are multiple forms of Non-Hodgkin lymphoma in the head and neck. Lymphoma may involve the cervical nodes, the non-nodal lymphatic tissues of Waldeyer ring, or extralymphatic tissues. The most common type seen in the U.S. is the B-cell type. It is an important diagnosis because the imaging features can be suggestive of the diagnosis and it is treated nonsurgically, therefore imaging can guide management. Lymphomas are pliable soft tissue masses and tend to mold themselves around normal structures. Lymphoma can have variable effects on adjacent bone, causing either benign-appearing remodeling or more aggressive, malignant-appearing destruction. Because they are highly cellular tumors with increased nuclear to cytoplasmic ratios, lymphomas may be somewhat hyperdense to other soft tissues on CT, show hypointense signal on long-TR MR sequences, and enhance homogeneously after contrast administration. **Perineural Tumor Spread.** Identifying perineural tumor spread (PNTS) in patients with head and neck malignancy is the job of the head and neck imager. Not only does the presence of PNTS change the patient's prognosis and alter the therapy they may receive, the presence of PNTS may be suggestive of the histology of the tumor. The 5^{th} and 7^{th} cranial nerves are involved most frequently and the most common primary neoplasms include squamous cell carcinoma, adenoid cystic carcinoma, melanoma, and lymphoma. Perineural tumor spread is associated with an increased incidence of local tumor recurrence, development of metastatic disease, and decreased five-year survival. The trigeminal nerve is involved most often by cancers of the facial skin, oral cavity, and nasopharynx. Facial nerve involvement is seen with parotid malignancies and cancers involving the external auditory canal and skin

Note: Scanned images are included in the proceedings. Some submitted images were reduced during editing, thereby decreasing clarity. Also, refer to the Program Planner. Proceedings Content as of 3-29-2013.

around the auricle. Signs of PNTS on imaging include thickening and increased enhancement of the nerve, foraminal enlargement, and denervation changes in the musculature supplied by the nerve. **Cystic Adenopathy versus 2nd Branchial Cleft Cyst.** One of the most common presentations of HPV positive oropharyngeal (OP) carcinoma is the development of a new node in an adult patient. The vast majority of patients with stage III or IV HPV+ OP cancers have adenopathy at presentation and these tumors have a tendency to produce necrotic/cystic nodes and the primary tumor may be very small. These nodes can occur in a location similar to a 2nd branchial cleft cyst and can be mistaken for a congenital cyst. Although the two can have a very similar imaging appearance, one should make the diagnosis of a branchial cleft cyst in an adult patient with a new neck mass with caution and consider and OP malignancies regardless of whether or not there is a smoking history. **Odontogenic Sinusitis.** An odontogenic source of sinusitis should be suspected if predominantly or exclusively unilateral maxillary sinus disease is present on imaging. The inflammation results from odontogenic disease in the alveolar ridge, usually from the molar teeth. Typically periapical lucency is noted around the root of the tooth that is the source of the inflammation and a fistula from the periapical lucency to the alveolar recess of the maxillary sinus may be seen. It is important for the radiologist to identify the odontogenic source of the sinus disease as treatment must address the diseased tooth. Treatment of the sinus alone may be a cause of surgical failure and recurrent disease.
Retropharyngeal Adenopathy. The presence of retropharyngeal adenopathy may upstage a patient in the setting of neoplastic disease and may put a patient at risk for the development of a retropharyngeal abscess in the setting of infection. It is the job of the radiologist to identify pathologic retropharyngeal space (RPS) nodes as they cannot be seen or palpated clinically. Squamous cell carcinoma is the most common primary histology to involve the RPS lymph nodes and the nasopharynx is the most common primary site of neoplasia to involve these nodes. The RPS nodes are a primary drainage pathway for the sinonasal (SN) cavities, so scrutiny of the RPS is necessary in patients with SN cancers.

O-461 **9:15 AM - 9:45 AM**

Mimics and Misses in the Head and Neck

Ginsberg, L. E.
M.D. Anderson Cancer Center
Houston, TX.

Presentation Summary
Mimics and Misses are inherent to the practice of head and neck radiology. Though categorizing and reviewing misses of mine and others will not prevent all future misses, nevertheless such a review is instructional (and entertaining). This presentation, emphasizing head and neck cancer, will seek to list common mistakes, calling attention to underlying root causes, and offering strategies that may help to avoid them. In addition to missing lesions, subject material will include mimics of pathology and misinterpretations.

O-462 **9:45 AM - 10:15 AM**

Findings in the Chest on Neck CT: What to Do!

Elicker, B. M.
UCSF Medical Center
San Francisco, CA.

Dr. Elicker completed medical school at New York Medical College and a residency in diagnostic radiology at Yale/New Haven hospital. After completing a fellowship in thoracic imaging at the University of California, San Francisco he joined the faculty. He is currently the chief of Cardiac and Pulmonary imaging at UCSF and is very active in lung cancer imaging. He is a two time recipient of the UCSF Hideyo Minagi outstanding teaching award.

Presentation Summary
Introduction - Neck CTs often include significant portions of the upper lungs. Neuroradiologists should have an understanding of common findings in the lungs and their significance, including the need for additional testing. This lecture will focus and two categories of findings: incidental lung nodules and inflammatory diseases that may be seen in the upper lobes. *Nodules* - Lung nodules are a common incidental finding that may be seen in up to 50% of patients. Greater than 95% of nodules are benign, even in patients with a cigarette smoking history, however malignancy is always a consideration. Several imaging features are diagnostic of benignity and do not require any additional evaluation or follow-up imaging. These include benign patterns of calcification (diffuse, central, ring-like or popcorn), the presence of fat and greater than two years of stability. When these features are absent, the role of CT is to determine the likelihood of malignancy. In general nodules that are likely malignant undergo immediate workup (biopsy, bronchoscopy, surgery, etc.) and nodules that are likely benign get followed with CT. Features suggestive of malignancy include large size (average diameter >1.5 cm), spiculated border and growth. Ground glass attenuation nodules have a much higher risk of malignancy compared to solid nodules, however these malignancies tend to be more indolent and are often followed with CT. If a nodule is seen in the lung apices on a neck CT, it is reasonable to recommend an immediate dedicated chest CT as a baseline. There are two exceptions to this rule in which case follow up is not necessary: 1. Solid nodule ≤4 mm in patients at low risk for malignancy (nonsmoker, no history of malignancy). 2. Ground glass nodules ≤5 mm (regardless of whether they are a smoker or nonsmoker). *Inflammatory diseases* - Active inflammatory or infiltrative processes may be diffuse or may preferentially involve the upper lungs. Diffuse processes include infection (usually viral or PCP),

Note: Scanned images are included in the proceedings. Some submitted images were reduced during editing, thereby decreasing clarity. Also, refer to the Program Planner. Proceedings Content as of 3-29-2013.

pulmonary edema, acute respiratory distress syndrome (i.e., ARDS) and hemorrhage. On CT these are usually indistinguishable from one another and typical findings include symmetric bilateral ground glass opacity and consolidation. Processes that may predominant in the upper lungs include bacterial pneumonia, granulomatous infections (tuberculosis, histoplasmosis and coccidioidomycosis) and sarcoidosis. The neuroradiologist should be able to distinguish active inflammation in the upper lungs from scarring due to old/inactive disease. Scarring presents as linear or band-like opacities that extend to the pleura. Distortion of the normal lung architecture and traction bronchiectasis often are associated. Consolidation and/or multiple small nodules are the most common findings seen in inflammatory processes that predominate in the upper lobes. Cavitation within areas of consolidation often is seen with granulomatous infections. The nodules of infection usually involve the airways. A centrilobular distribution is typical of endobronchial spread of infection. Centrilobular nodules involve the central portion of the lung and are located at least 5-10 mm from the pleura. Sarcoidosis, in contrast, shows a lymphatic distribution of small nodules. Nodules are clustered in the subpleural lung, and around the central airways and arteries.

Thursday Morning

8:45 AM - 10:15 AM
Ballroom 6CF

(53) General Programming: Peripheral Nerve Imaging for the Neuroradiologist

O-463 **8:45 AM - 9:15 AM**

MR Neurography Techniques

Chhabra, A.
Johns Hopkins University Hospital
Baltimore, MD.

Avneesh Chhabra is a clinical scientist and is Assistant Professor Radiology & Orthopedic Surgery at the MSK section, Diagnostic Division of Russell H. Morgan Department of Radiology & Radiological Sciences, Johns Hopkins University, Baltimore, MD. He is double boarded in Radiology from Delhi University, India and Drexel University, Philadelphia, PA. Dr. Chhabra received his MSK Radiology fellowship from Temple University, Philadelphia, PA. Dr. Chhabra is multi-specialty trained with expertise in MSK, Body and Neuro imaging. During his tenure at Johns Hopkins, he has cultivated high-resolution MR Neurography. He has received several research grants, including the prestigious GERRAF fellowship to study the clinical impact of these techniques. He has received multiple travel grants and awards at national and international conferences, including the young investigator award at the Society of Skeletal Radiology meeting in 2011. Dr. Chhabra has published more than 70 peer-reviewed articles, has given more than 100 presentations, written multiple book chapters, and the 1st book on MR Neurography.

O-464 **9:15 AM - 9:45 AM**

Lumbosacral Plexus and Pelvis

Carrino, J. A.
Johns Hopkins University School of Medicine
Baltimore, MD.

Presentation Summary
To present the 3T MR characteristics of the lumbosacral plexus and several clinically relevant pelvic branch nerves, including normal anatomy, clinical syndromes, and a range of nerve pathologies.

O-465 **9:45 AM - 10:15 AM**

Extremity Nerve Imaging

Amrami, K. K.
Mayo Clinic Radiology
Rochester, MN.

Dr. Kimberly A. Amrami is currently Professor of Radiology, College of Medicine, Mayo Clinic. Dr. Amrami's education is as follows: She received a BA degree from the University of Minnesota in Hebrew Language and Literature; a BS degree from the University of Minnesota in Secondary Education with an Elementary endorsement; an MD degree from the University of Minnesota. Also at the University of Minnesota she performed a Residency in Diagnostic Radiology and at Mayo Clinic in Rochester a Fellowship in Musculoskeletal Radiology. Dr. Amrami has board certifications as follows: American Board of Radiology (Diagnostic Radiology); National Board of Medical Examiners (Diplomate). Certifications from Mayo Clinic include: Quality Academy (Mayo Clinic Quality Fellow: Bronze Level Certification and Silver Level Certification). Dr. Amrami has received more than 15 Honors and Awards, received at least 9 professional positions and major appointments. She has held and continues to hold many professional and community memberships, as well as societies and services. Her Journal responsibilities have included such titles as Associate Editor, Contributing Editor, Editorial Board Member, and peer reviewer. At Mayo Clinic, Dr. Amrami holds various administrative responsibilities and committee memberships along with various other activities.

Presentation Summary
Imaging of peripheral nerves has been revolutionized by

Note: Scanned images are included in the proceedings. Some submitted images were reduced during editing, thereby decreasing clarity. Also, refer to the Program Planner. Proceedings Content as of 3-29-2013.

the advent of MR neurography. This technique emphasizes imaging the nerve itself rather than inferring nerve involvement based on changes in muscles in a given nerve territory. MR neurography requires strict attention to technique and the use of the best available tools. The core imaging principles include high-resolution imaging at full or high field strength, use of the best available receiver coils and high-resolution T1- and T2-weighted imaging with robust fat suppression for fluid sensitive sequence. More recent advances include the use of diffusion-weighted imaging and tractography as well as novel pulse sequences which selectively suppress background signal, including vascular signal. Nerve imaging in the extremities can be complicated by challenges in locating pathology based on clinical exam or EMG, both of which are operator dependent. An EMG indicating radial nerve pathology may not include precise localization so that imaging may involve looking at multiple segments (i.e., arm, elbow or forearm). In the lower extremities, for example, a clinical foot drop could be caused by an abnormality in the lumbosacral plexus, the peroneal division of the sciatic nerve - or anywhere along the common or deep peroneal nerve. The use of all available information is imperative and knowledge of the nerve anatomy of the extremities is critical. When the lesion is located characterization should include high-resolution T1- and T2-weighted image with robust fat suppression for the T2-weighted sequences. Multiple planes may be needed to fully characterize a lesion and the judicious use of contrast often is helpful in distinguishing inflammatory lesions such as CIDP from tumors or perineurioma. Lesions should be characterized as single or multiple and the distribution notes. The effect of primary nerve pathology on downstream musculature also is an important clue as to what exactly is causing the problem. Common primary lesions include benign neurogenic tumors. Malignant tumors, either primary or metastatic, do occur although with less frequency. Another common problem in extremity nerve imaging is nerve entrapment with or without the development of a traumatic neuroma or neuroma in continuity. Trauma of all kinds can affect peripheral nerves from mechanical irritation due to healing fractures to actual nerve transections. Access to the complete medical record can help narrow the differential. Imaging peripheral nerves in the extremities can be a complex and sometimes frustrating process but successful imaging can add significantly to patient care - especially when localization and characterization of a lesion is sought prior to targeted biopsy. High-resolution MRI also often can characterize benign neurogenic lesions with a degree of confidence that often obviates the need for biopsy. When close attention is paid to technique and when the exam is tailored to the need of the individual patient and clinical problem MRI can add tremendous value for patient care.

Thursday Morning

8:45 AM - 10:15 AM
Ballroom 6DE

(54) CSI San Diego: Computer-Assisted Diagnosis Review of Available CADs for Radiology

O-466 **8:45 AM - 9:30 AM**

Point Counterpoint Discussion - Part I

Bryan, R.
University of Pennsylvania Health System
Philadelphia, PA.

Presentation Summary
Please see abstract submitted by Dr. Michel Bilello that covers our joint session.

O-467 **9:30 AM - 10:15 AM**

Point Counterpoint Discussion - Part II

Bilello, M.
University of Pennsylvania
Philadelphia, PA.

Presentation Summary
The basic process of medical image analysis, whether by radiologist or computer, consists of the extraction of key features (KFs) from the image, and the subsequent development of a differential diagnosis (DDx). The KFs derive from signal, spatial or temporal domains of image data, and usually represent the critical abnormal visual "Findings" of the study. The DDx is simply the list of diseases most compatible with the KFs of the image. Human KF extraction is based on pattern recognition, which depends on deconstruction and parallel processing of image data in multiple pathways of the human visual system. Human DDx development typically depends on the heuristic inference of disease likelihood, given image KFs. While probably not obligatory, computer KF extraction and DDx development can be, and often is, implemented in a remarkably comparable fashion to human image analysis processes. The computer is programmed to deconstruct image data into separate domains that are processed in a parallel fashion in order to extract the same KFs that a human observer might report. Then, through a separate inference engine such as a Bayesian network, neural network or rule-based algorithm, the computer can generate a DDx similar to that of a radiologist. This and the following presentation will elaborate on the principles of image analysis and illustrate the similarity of human and computational image analysis processes. A critical aspect of medical image analysis relates to temporal changes,

Note: Scanned images are included in the proceedings. Some submitted images were reduced during editing, thereby decreasing clarity. Also, refer to the Program Planner. Proceedings Content as of 3-29-2013.

such as the growth or regression of lesions such as MS or tumor over time. This is a task particularly well suited to computer analysis whereby the computer program is not necessarily required to make a diagnosis, but rather tracks changes over time of a known disease entity. We will review how temporal changes are detected by computer, including the need to perform registration (i.e., bring image information from one time point to another). We will present a practical example of such a system, a locally developed program for the detection of change in lesion load in multiple sclerosis. Finally, after reviewing the general properties of radiology CAD systems, we will show examples of current computer image analysis software applied to neuroradiology, found in the scientific literature or available from commercial vendors.

Thursday Morning

8:45 AM - 10:15 AM
Room 5AB

(55) General Programming: Cerebrovascular Imaging Update: Foundation of the ASNR Special Session

O-486 **8:45 AM - 9:00 AM**

Introduction and Overview

Rowley, H. A.
University of Wisconsin
Madison, WI.

O-496 **9:00 AM - 9:25 AM**

Advances in Arterial Spin Labeling - Recipient of the Scholar Award 2009-2010

Zaharchuk, G.
Stanford University
Stanford, CA.

Presentation Summary
In this presentation, I will discuss the rapidly growing field of noncontrast arterial spin labeling (ASL) for use in brain imaging applications. This will include a discussion of "second generation" ASL, performed with pseudocontinuous labeling, 3D readout, and background suppression. When these things are brought together, the result is higher SNR whole brain perfusion imaging with minimal susceptibility artifacts and fast imaging times, making it an easy and useful sequence to apply in clinical patients. I will emphasize the flexibility of the ASL method, which has the potential to measure not just brain perfusion, but also to identify collaterals, to map vascular perfusion territories, and to identify small arteriovenous malformations (AVMs). I will present examples of how ASL can be used clinically in a diverse group of clinical conditions, including stroke, seizure, AVM, dural AVF, and brain tumors. Finally, I will address differences between vendor implementations and review the consensus statement on the recommended parameters for clinical ASL based on the recent ISMRM Perfusion Workshop.

O-470 **9:25 AM - 9:50 AM**

Diffusion and Perfusion Imaging: What Should We Be Doing and Why?

Lev, M. H.
Massachusetts General Hospital
Boston, MA.

Presentation Summary
The role and evidence for advanced CT and MR imaging in the diagnosis, therapeutic triage, management, and prognosis of acute ischemic stroke patients will be reviewed. Reference: Lev MH. Perfusion imaging of acute stroke: its role in current and future clinical practice.

O-471 **9:50 AM - 10:15 AM**

Assessing Cerebrovascular Reserve Capacity in Carotid Steno-Occlusive Disease

Derdeyn, C. P.
Mallinckrodt Institute
St. Louis, MO.

Presentation Summary
Patients with atherosclerotic occlusive disease may have reduced flow to the distal territory, owing to poor sources of collateral flow. Conversely, many patients with occlusive disease, even complete occlusion, have normal flow owing to good collateral sources. When perfusion pressure - the difference between mean arterial pressure and the venous backpressure - falls in any arterial territory, the brain and brain vasculature may compensate through two mechanisms. The first is arterial dilation and the second is an increase in the amount of oxygen removed from the blood. Autoregulatory vasodilation is a response by penetrating capacitance arterioles to either reductions in arterial pressure or reduced arterial oxygen content. Neuronal, muscular, and physiologic factors are involved in this complex reflex. Arterial resistance is reduced, allowing flow to continue at near normal rates over a wide range of pressures. At some threshold point, however, further reductions in pressure exceed the ability of vasodilation to compensate and flow will fall passively as a function of pressure. This situation is known as autoregulatory failure. The primary compensatory reflex to reduced blood flow is an increase in tissue oxygen extraction. For a given tissue metabolic rate for oxygen consumption, a reduction in the delivery of oxygen (cerebral blood flow, CBF) will require an increase in the

Note: Scanned images are included in the proceedings. Some submitted images were reduced during editing, thereby decreasing clarity. Also, refer to the Program Planner. Proceedings Content as of 3-29-2013.

amount of oxygen extracted by the blood (oxygen extraction fraction, OEF). Normal OEF is 30 to 40% and this can increase instantaneously to up to 80%. The precise mechanism by which this occurs is not clear. Oxygen is not transported and reaches the brain tissue by passive diffusion. Tissue oxygen tensions are not reduced when flow falls. It is likely that OEF increases owing to a constant flux of oxygen between the tissue and the blood. When flow falls, there is a relative increase in the amount of oxygen that is used by the brain. In humans, these compensatory mechanisms are identified by several different physiologic imaging methods. Paired flow tests assess the ability of the cerebrovasculature to increase blood flow or blood velocity to a vasodilatory stimulus. If flow fails to increase, pre-existing autoregulatory vasodilation is inferred. Static measurements of cerebral blood flow, blood volume, and mean transit time are another method for identifying the presence of autoregulatory vasodilation. Finally, OEF may be measured directly. It is critical to note that these methods are not interchangeable - different physiologic mechanisms are being assessed. Several of these techniques have been tested as predictors of future stroke risk. The data linking hemodynamic impairment and the risk for future stroke will be reviewed.

Thursday Morning

10:45 AM - 12:15 PM
Ballroom 6AB

(56a) Parallel Scientific Papers: Special Session: Regional Societies Award Winners and DTI

O-472 **10:45 AM - 10:53 AM**

Evaluating CT Perfusion Using Outcome Measures of Delayed Cerebral Ischemia in Aneurysmal Subarachnoid Hemorrhage: ENRS Award Winner

Ivanidze, J.·Anumula, N.·Johnson, C. E.·Comunale, J. P.·Tsiouris, A. J.·Riina, H. A.·Segal, A. Z.·Stieg, P. E.·Zimmerman, R. D.·Mushlin, A. I.·Sanelli, P. C.
New York Presbyterian Hospital
New York, NY.

Purpose
Delayed cerebral ischemia (DCI) is a serious complication following aneurysmal SAH and remains a leading cause of morbidity and mortality. Our aim was to evaluate CTP in aneurysmal SAH by using outcome measures of DCI.
Materials & Methods
This was a retrospective study of consecutive patients with SAH enrolled in a prospective institutional review board-approved clinical accuracy trial. Qualitative CTP deficits were determined by twi neuroradiologists blinded to clinical and imaging data. Quantitative CTP was performed by using a standardized protocol with region-of-interest placement sampling of the cortex. Primary outcome measures were permanent neurologic deficits and infarction. The secondary outcome measure was DCI, defined as clinical deterioration. CT perfusion test characteristics (95% CI) were determined for each outcome measure. Statistical significance was calculated by using the Fisher exact and Student *t* tests. Receiver operating characteristics curves were generated to determine accuracy and threshold analysis.
Results
Ninety-six patients were included. Permanent neurologic deficits developed in 33% (32/96). CT perfusion deficits were seen in 78% (25/32) of those who developed permanent neurologic deficits and 34% (22/64) of those without (P < .0001). CT perfusion deficits had 78% (61%-89%) sensitivity, 66% (53%-76%) specificity, and 53% (39%-67%) positive and 86% (73%-93%) negative predictive values. Infarction occurred in 18% (17/96). CT perfusion deficits were seen in 88% (15/17) of those who developed infarction (Figure 1) and 41% (32/79) of those without (P = .0004). CT perfusion deficits had an 88% (66%-97%) sensitivity, 59% (48%-70%) specificity, and 32% (20%-46%) positive and 96% (86%-99%) negative predictive values. Table 1 demonstrates the quantitative CBF, CBV and MTT values for the primary outcome measures of permanent neurologic deficits and infarction. DCI was diagnosed in 50% (48/96). CT perfusion deficits were seen in 81% (39/48) of patients with DCI and in 17% (8/48) of those without (P < .0001). CT perfusion deficits had 81% (68%-90%) sensitivity, 83% (70%-91%) specificity, and 83% (70%-91%) positive and 82% (69%-90%) negative predictive values. Quantitative CTP revealed significantly reduced CBF and prolonged MTT for DCI, permanent neurologic deficits, and infarction. Receiver operating characteristics analysis showed that CBF and MTT had the highest accuracy. Table 2 demonstrates the quantitative CBF, CBV and MTT values for the secondary outcome measure of DCI.
Conclusion
CT perfusion may add prognostic information regarding DCI and poor outcomes in aneurysmal SAH.
Acknowledgment: This research was made possible by Grant Number 5K23NS058387-04 from the National Institute of Neurological Disorders and Stroke (NINDS), a component of the National Institutes of Health (NIH). Its contents are solely the responsibility of the authors and do not necessarily represent the official view of NINDS or NIH.

KEYWORDS: CT perfusion

Note: Scanned images are included in the proceedings. Some submitted images were reduced during editing, thereby decreasing clarity. Also, refer to the Program Planner. Proceedings Content as of 3-29-2013.

O-473 **10:53 AM - 11:01 AM**

Functional Neuroimaging to Characterize the Effect of Chemotherapy on Visual System Development in Children Treated for Retinoblastoma: SENRS Award Winner

Helton, K. J.·Demtchouk, V.·Parra, C. A.·Scoggins, M.·Zou, P.·Lin, Y.·Qaddoumi, I.·Wilson, M.·Ogg, R.
St. Jude Children's Research Hospital
Memphis, TN.

Purpose
Retinoblastoma (RB) is the most common intraocular tumor in childhood, and fatal when untreated. Treatment coincides temporally with the rapid development of the eyes and central nervous system. Little is known about the influence of chemotherapy (CX) on visual development; we hypothesized that the functional MRI (fMRI) can characterize the effects of CX on vision.
Materials & Methods
After IRB approval, fMRI was used to longitudinally investigate primary visual cortex (V1) response to photic stimulation in 60 children being treated for RB [41 unilateral (UL), 19 bilateral (BL), median age at diagnosis 13.3 months], for a total of 225 exams. After baseline fMRI, enucleation was performed on patients with advanced UL or BL disease and patients were staged. Stratum A was early stage UL or BL, and received low dose CX. Stratum B was advanced stage BL and received aggressive CX. Stratum C was advance stage UL, with low risk receiving no CX(C-), and intermediate and high risk receiving aggressive CX(C+).
Results
As reported previously (Barb, et al., IOVS 2011), fMRI response in V1 was predominantly negative in the anterior region of V1 (blue overlay in figure, typical patient), with more variable positive in posterior region of V1 (red overlay in figure). Mean values of activation parameters are summarized in the figure. Mixed-effect modeling showed a significant effect of CX on both the peak fMRI response ($p < .001$) and the volume of cortex activated ($p = 0.002$), but only the activated volume was significantly affected by stratum ($p = .03$).
Conclusion
Primary visual cortex fMRI response was decreased after exposure to chemotherapy in children treated for RB. Functional neuroimaging will be useful to evaluate the impact of disease and treatment on visual system development in children with RB. Additional research is needed to clarify the effects of CX on cortical activation and the neural-hemodynamic coupling that mediates fMRI signals.Clinical relevance/application: The clinical decision to enucleate for RB disease control versus preserve the eye for vision is difficult. Functional MRI can clarify visual function; understanding CX effects on vision is critical.

KEYWORDS: Chemotherapy

O-474 **11:01 AM - 11:09 AM**

Direct Puncture Treatment of Orbital and Peri-Orbital Vascular Malformations: WNRS Award Winner

Nesbit, G. M.·Priest, R.·Ng, J. D.·Hamilton, B. H.
Oregon Health and Science University
Portland, OR.

Purpose
Vascular malformations of the orbit are difficult to treat due to the complex anatomy and the tendency of these low-flow lesions to decompress at surgery. Direct puncture and treatment may provide alternatives in the management of these lesions.
Materials & Methods
Retrospective review of the INR database revealed 17 orbital or periorbital vascular malformations treated with direct puncture and instillation of a therapeutic agent from 2003 - 2012. Specific diagnosis was based on clinical, pathologic, and therapeutic response features. A chart review of these patients and their specific followup was undertaken. Complete response was defined as complete removal of the malformation and/or eradication of any symptoms present to treatment. A partial response was defined as improved but continuing symptoms or problems arising from the lesion. No response was defined as no improvement in symptoms and need for ongoing or further intervention. Complications of the treatment were defined as a worse symptoms at 30 days and classified as temporary or permanent.
Results
The lesions consisted of two lymphatic and 15 venous malformations. The intra-orbital needle placement was performed with ultrasound guidance in two and Xper-CT guidance in nine patients, and, in the periorbital lesions involving the eyelids or sclera, ultrasound on manual palpation was used. The sclerosant used was doxycycline in the lymphatic malformations, and either alcohol, sotradecol, in one case with coils and thrombin, or bleomycin. Overall, 15 of 17 had a complete or parital response with two having no response. Postoperative orbital swelling was seen in the majority of patients, which resolved within 4-10 days, with mild diplopia note due to mass effect. No visual loss or ophthalmoplegia was seen and no complications noted.
Conclusion
Direct puncture and injection of a sclerosant appears to be a viable alternative to surgical resection in symptomatic lymphatic and venous malformations of the orbit and periorbita, and has become the first-line of treatment at our institution.

KEYWORDS: Orbits

Note: Scanned images are included in the proceedings. Some submitted images were reduced during editing, thereby decreasing clarity. Also, refer to the Program Planner. Proceedings Content as of 3-29-2013.

O-475 **11:09 AM - 11:17 AM**

Comparative Analysis between the Cross Sign versus Apparent Diffusion Coefficient and Fractional Anisotropy Measurements for the Detection and Monitoring of Multiple System Atrophy

Park, J.·Guzman, R.·Sayre, J.·Perlman, S.·Ellingson, B.·Fogel, B.·Salamon, N.
University of California Los Angeles
Los Angeles, CA.

Purpose
To determine retrospectively if quantitative diffusion tensor imaging (DTI) metrics of white matter integrity are superior to conventional magnetic resonance imaging (MRI) findings for detecting abnormalities in patients with multiple system atrophy (MSA). We also sought to determine if there was a temporal relationship between time elapsed from disease onset and the presence of a cross sign.
Materials & Methods
Conventional MRI images from 31 patients (with a total of 50 studies) with clinical diagnoses of MSA-P and MSA-C were interpreted by a neuroradiologist for the presence or absence of the cross sign. An expert neurologist determined the clinical diagnosis, as well as ataxia severity and asymmetry for each patient. For quantitative analysis, we compared apparent diffusion coefficient (ADC) and fractional anisotropy (FA) values in the pons, and middle cerebellar peduncles of 19 patients who also had concurrent DTI examinations (four patients had repeat studies, resulting in 23 studies total). Apparent diffusion coefficient and FA values were compared to normal controls. Analysis was conducted using a region of interest method. A statistical comparison of the cross sign and DTI values was performed using a McNemar's Chi-square test. Furthermore, for the four patients who had repeat DTI examinations (mean two years after first study), a paired samples T-test was performed to determine if there were significant changes in FA and ADC. Correlation of imaging findings with clinical ataxia scores was performed.
Results
Average patient age at time of first imaging study was 59.7 years (range 47-75 years). For all 50 traditional MRI examinations (performed mean 4.2 years from symptom onset), the cross sign was present in 80% of patients (found to be more reliable after two years from initial symptom onset (Table). Apparent diffusion coefficient and FA values in the pons and middle cerebellar peduncles were significantly higher in MSA patients than in controls. In patients with both quantitative ADC/FA analysis and traditional MRI studies (n=19), changes in ADC and FA were significantly more sensitive than the presence of the cross sign (p=.025). In addition, in the four patients with serial DTI studies, significant decreases in FA values were noted in the pons (p=.046) and the middle cerebellar peduncles (p=0.18).

Relationship between time elapsed from symptom onset with presence of the cross sign

Number of years elapsed from diagnosis	0-2	3-5	6+
Positive cross sign/total studies performed(% positive)	9/14 (64%)	21/24 (87%)	10/12 (83%)

Conclusion
While the cross sign is classically associated with MSA, it has limited sensitivity, particularly in the first two years from symptom onset. Apparent diffusion coefficient and FA values in the pons and middle cerebellar peduncles detected early pathologic involvement prior to the development of the cross sign. Furthermore in a small sample size, significant decreases in FA were seen over time. Quantitative DTI in conjunction with traditional MRI offers a valuable tool to improve the detection of MSA, as well as to potentially monitor disease progression.

KEYWORDS: Diffusion tensor image, Neurodegenerative

O-476 **11:17 AM - 11:25 AM**

Use of Tractography in Normal Pressure Hydrocephalus

Solomon, D. L.[1]·Mian, A. Z.[1]·Killiany, R. J.[1]·Solomon, M. A.[2]·Koo, B. B.[1]
[1]Boston University School of Medicine, Boston, MA, [2]Los Gatos MRI, Los Gatos, CA.

Purpose
Normal pressure hydrocephalus (NPH) is a clinical diagnosis with no formal definition. Normal pressure hydrocephalus classically is described as a clinical triad of gait abnormality, dementia, and urinary incontinence. Few patients present with all three symptoms, leaving clinicians to rely on a “preponderance of evidence” approach, involving weighing triad symptoms with radiologic findings, CSF opening pressure, and response to Tap Test, external lumbar CSF drainage, lumbar infusion test, and finally shunting. Apart from searching for enlarged ventricles out of proportion to sulcal atrophy, Evan's ratios greater than 0.3, and callosal angles greater than 40 degrees, radiologists are primarily engaged in a process of exclusion for NPH cases. This study proposes tractography as a tool for radiologists to consider when evaluating suspected NPH patients.
Materials & Methods
A retrospective study of 17 patients over age 55, nine classified as “definite” or “probable NPH” by referring physicians and eight normal controls, who underwent brain MRI imaging in a 3T magnet. Diffusion tensor imaging and tractography data were acquired using Philips Fibertrak software, postprocessing was done using FMRIB

Note: Scanned images are included in the proceedings. Some submitted images were reduced during editing, thereby decreasing clarity. Also, refer to the Program Planner. Proceedings Content as of 3-29-2013.

Software Library (FSL), and fractional anisotropy (FA) comparisons were performed using tract-based spatial statisics (TBSS).

Results

Normal pressure hydrocephalus patients were found to have higher FA values than normal controls in the upper corticospinal tract and lower FA values in the corpus callosum, to $p \leq 0.05$ levels, consistent with previous reports. Normal versus NPH FA values in the corpus callosum are 0.72 and 0.60, respectively, while normal versus NPH values in the upper corticospinal tract are 0.45 and 0.63, respectively. Normal pressure hydrocephalus tractography images were characterized with a distinct "heart-shaped" artifactual sign.

NPH Normal

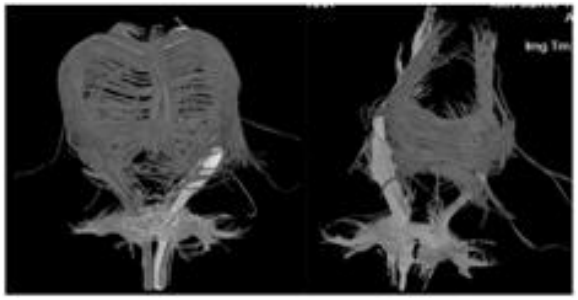

Conclusion

We believe, using probabilistic tractography techniques, there is artifactual connection between the callosal radiation fiber analogs and the fiber analogs of the corticospinal tract when the pressure effects of NPH cause a decrease in FA values of the callosal radiations and an increase in the FA values the corticospinal tract. Since the "heart-shaped" tractography pattern does not appear in Alzheimer disease, which also demonsrates ventricular enlargement, tractography may provide radiologists a new clinical tool for evaluation of patients under suspicion of NPH.

KEYWORDS: Normal pressure hydrocephalus, Fiber tracking, Diffusion Tensor Imaging

O-477 **11:25 AM - 11:33 AM**

Neuritis Optica Evaluation: A Functional and Structural MR Imaging Study

Rueda-Lopes, F. C.[1,2]·Miraldi, F.[1,2]·Bahia, P.[2]·Domingues, R.[1]·Alves-Leon, S.[2]·Gasparetto, E. L.[1,2]
[1]DASA, Rio de Janeiro, BRAZIL, [2]UFRJ, Rio de Janeiro, BRAZIL.

Purpose

Severe neuritis optica (NO) is a hallmark of neuromyelitis optica (NMO). Multiple bilateral attacks or a single one may lead to blindness. Still, the majority of patients partially recover somehow after attacks, probably due to the degree of the visual tract impairment. Our objective was to investigate NMO patients using the resting-state functional magnetic resonance imaging (RS fMRI) and structural analysis compared to the controls, regarding the visual network, in order to evaluate the cortical adaptations in NMO and also its structural damage.

Materials & Methods

We studied 28 NMO spectrum patients [myelitis (6), NO (22)] [mean age 38 years (SD +/- 3,2, 18 female)], and also 19 sex- and age-matched controls. All participants signed informed consent. MR imaging was performed in a 1.5T scanner, including diffusion tensor imaging (DTI) in 30 directions and RS fMRI was performed during rest. Diffusion tensor imaging data were postprocessed using tract-based spatial statistics (TBSS) to aligned all patients and obtain fractional anisotropy (FA) values from the visual pathway. Functional MRI data were postprocessed using MELODIC, part of FSL4.1. The fMRI data set was decomposed using independent component analysis (ICA) to identify large-scale patterns of functional connectivity. After that, a "dual-regression" approach was carried out allowing voxel-wise comparisons of resting functional connectivity between groups, generating threshold-free cluster enhancement (tfce) and p-corrected maps of comparison. Synchronization values of the visual network of patients and controls were compared and their correlation with FA from the visual pathway was assessed, using Pearson. A p-value of 0.05 was considered statistically significant.

Results

Fourteen components were computed in the entire subject group by ICA. Visual network was clearly detected among the subjects and was compared between both groups. There were increased synchronization values in the whole occipital cortex in NMO patients compared to controls ($p<0.01$) in both maps. The average synchronization value in patients was 3.484238 (2.700344 SD) compared to controls,119129 (1.411825 SD), with a p-value of 0.05. The DTI data were obtained from 23 patients, including patients without clinical NO. A total of 15 events of NO on each side (30 in total) were evaluated. The average FA value in the right visual pathway was 0.60 (0.03 SD) and in the left side 0.59(0.03 SD), p-value of 0.56. A weak negative correlation was obtained between synchronization visual network value and right FA (-0.013) and it was positive in the left side (0.075). A positive correlation was obtained between right ON and right FA(0.17) and negative with left ON and left FA (-0.05).

Conclusion

Neuromyelitis optica patients have higher synchronization values found in the occipital cortex in patients compared to controls, as a form of compensation for the NO. Although the correlations between clinical symptoms, structural damage and functional compensation obtained were weak, they all point toward a more subtle structural damage on the right side (as the correlation between NO and FA is higher) and thus a more difficult functional compensation (as the correlation between fMRI and FA is

Note: Scanned images are included in the proceedings. Some submitted images were reduced during editing, thereby decreasing clarity. Also, refer to the Program Planner. Proceedings Content as of 3-29-2013.

negative - more structural damage, less fMRI compensation).

KEYWORDS: MR imaging brain, Neuromyelitis optica

O-478 11:33 AM - 11:41 AM

Effect of Extrinsic Variables on Diffusion Tensor Parameters in White Matter

Khalilzadeh, O.[1]·Dinkel, J.[1]·Perlbarg, V.[2]·Galanaud, D.[3]·Puybasset, L.[3]·Gupta, R.[1]
[1]Massachusetts General Hospital, Boston, MA, [2]Université Pierre et Marie Curie-Paris, Paris, FRANCE, [3]Pitié Salpêtrière Hospital, Paris, FRANCE.

Purpose
Quantitative diffusion tensor imaging (DTI) of brain is becoming increasingly popular in neuroradiology practice. Several factors including patients' demographics, scanner type, and imaging protocol can significantly alter DTI measurements, making them incomparable. Even for a single scanner, the echo time (TE) affects DTI measures. To make quantitative DTI clinically useful as a measure of disease, methods to normalize diffusion parameters are essential. This study evaluates the affect of extrinsic parameters such as TE, age, head positioning, and motion on the measured diffusion parameters in a well balanced clinical setting, using data of a single scanner.
Materials & Methods
This study was approved by the institutional review board (IRB#: 2012P002245) of Massachusetts General Hospital. Diffusion tensor imaging data of 204 consecutive subjects, who were scanned over a period of three months using a single MR scanner (GE Medical Systems, Milwaukee, WI) in the emergency department, were analyzed. Repetition time (TR), field strength, type of head coil, slice thickness, number of diffusion directions, and b values were similar for all scans; different scans ranged in the TE from 85 ms to 102 ms. Only subjects with normal MRI finding were included in this study, and patients with DTI artifacts were excluded. Using a custom-designed automated software package, DTI parameters, namely, fractional anisotropy (FA), axial diffusivity (L1) and radial diffusivity (Lt), were calculated in 20 different white matter brain regions. The dependence of these parameters on TE, age, head rotation angle, and head motions was analyzed.
Results
There was a significant ($p<0.01$) positive association between TE and FA in different white matter regions including left ($r = 0.466$) and right ($r = 0.470$) corona radiata, left ($r = 0.369$) and right ($r = 0.428$) external capsule, left ($r = 0.469$) and right ($r = 0.499$) cerebral peduncle, internal capsule and body of corpus callosum ($r = 0.350$). Radial diffusivity was inversely associated ($p<0.01$) with TE in these regions. There was a significant ($p<0.05$) negative association between mean head motions (or age) and FA. A prediction model based on TE, age, head angle rotation and head motion could account for up to 65% of variance in FA measurements of different white matter regions. In subjects with low head motions (less than median), age<50, and less than 10 degrees head rotation this model could predict up to 74% of variance in FA measurements.
Conclusion
In clinical practice, DTI parameters of the white matter are dependent on several factors such as TE, age, head rotation angle, and head motion, which contribute to measurement variability. A model to normalize DTI measures can curtail this variability by as much as 74%.

KEYWORDS: Diffusion tensor image, MR imaging, Echo Time

O-479 11:41 AM - 11:49 AM

Diffusion Tensor Imaging Detects Microstructural Reorganization in the Brain Associated with Chronic Irritable Bowel Syndrome

Ellingson, B. M.·Mayer, E.·Harris, R. J.·Ashe-McNally, C.·Naliboff, B.·Labus, J. S.·Tillisch, K.
David Geffen School of Medicine at the University of California Los Angeles
Los Angeles, CA.

Purpose
Irritable bowel syndrome (IBS) is a common gastrointestinal disorder characterized by recurring abdominal pain associated with alterations in bowel habits. The purpose of the current study was to determine whether patients with chronic visceral pain associated with IBS have microstructural differences in the brain, as measured using diffusion tensor imaging (DTI), compared with healthy control subjects (HCs), indicative of long-term neural reorganization of chronic pain pathways and regions associated with sensory integration.
Materials & Methods
All patients in this study signed institutional review board-approved informed consent. Diffusion tensor imaging was performed in a large sample of phenotyped IBS ($n = 33$) and HCs ($n = 93$) in using a 64 direction acquisition protocol with $b = 1000s/mm2$. Irritable bowel syndrome patients were phenotyped by gender, symptom severity, and symptom duration. Voxel-wise DTI comparisons including symptom and gender covariates were performed in areas of white matter and central gray matter regions. Probabilistic tractography was performed between relevant structures associated with chronic pain pathways and the number of fiber tracts were compared between IBS and HCs.
Results
Patients had lower FA in thalamic regions, in the basal ganglia (globus pallidus, putamen) and in sensory/motor association/integration regions (suggestive of reduced directional coherence) as well as higher FA in frontal lobe regions and the corpus callosum (suggestive of increased directional coherence). Irritable bowel syndrome patients

Note: Scanned images are included in the proceedings. Some submitted images were reduced during editing, thereby decreasing clarity. Also, refer to the Program Planner. Proceedings Content as of 3-29-2013.

also had reduced ADC within the globus pallidus and higher ADC in the thalamus, internal capsule, and coronal radiata projecting to the sensory/motor regions. Sex differences in FA and MD also were observed in IBS patients, but not HCs. Probabilistic tractography confirmed a higher degree of connectivity in pathways between the thalamus and prefrontal cortex passing through the anterior cinculate cortex (ACC), as well as the connectivity between the medial dorsal thalamic nuclei and ACC. Symptom severity was found to be negatively correlated with FA in the globus pallidus (P = 0.0397), number of fiber tracts found connecting the thalamus and primary sensory cortex (P = 0.0209), and the log transformed number of fibers connecting the thalamus and insula (P = 0.0466), and positively correlated with ADC in the white matter regions adjacent to the primary sensory cortex (P = 0.0190).
Conclusion
Together, these results support the hypothesis that patients with chronically recurring visceral pain from IBS have long-term microstructural changes within the brain, particular in regions associated with integration of sensory information and corticothalamic modulation.

KEYWORDS: Diffusion tensor image, Chronic pain, Irritable Bowel Syndrome

O-480 **11:49 AM - 11:57 AM**

Transcranial Magnetic Stimulation and Magnetic Resonance with Diffusion Tensor Imaging in Amyotrophic Lateral Sclerosis Patients: Combination and Correlations of their Measurements

Stecco, A.·Nasuelli, N.·Mazzini, L.·Cantello, R.·Perchinunno, M.·Carriero, A.
ASU Maggiore della Carità
Novara, ITALY.

Purpose
To determine the diagnostic accuracy of MRI with DTI and TMS with MEPs in UMN assessment in ALS patients; secondary goal to assess if there is a correlations between DTI metric and MEPs.
Materials & Methods
Seventeen patients (10 males and seven females; age range 25-74 years, mean 47) affected by ALS, underwent a TMS and MRI DTI evaluation within 30 days, during their follow-up evaluation. Nine of them had a clinical presentation at upper limbs, five at lower limbs, four as a bulbar type. Twelve were classified (El Escorial) as definite ALS, three probable ALS and two possible, with a ALS-FRS range of 17-40, mean of 33. By TMS, cortical motor threshold (MT) at rest, central motor conduction time (CMCT), cortical MEPs and spinal MEPs have been recorded. MR imaging DTI acquisitions have been performed with a 64 directions oriented tensor, on a 1.5T magnet, without ECG/PPU trigger. The DTI has been acquired on the brain with a 8-channels Head Sense Coil. Diffusion tensor imaging postprocessing has been conducted on a dedicate workstation loaded with proprietary DTI and FiberTracking software, and a two-observer (in consensus), voxel-by-voxel single-point ROI-based analysis on the following several anatomical levels: semioval centers (SC), internal capsule - posterior limb (IC), cerebral pedicle (PED), pons (PON). The color-coded FA map and a 3DT1-weighted axial image served as reference for ROI positioning assistance. Fractional anisotropy and ADC values have been recorded and compared to an institutional healthy volunteers database already existing. Statistical analysis has been carried out by mean of Wilcoxon-Mann-Whitney test and Cochrane Q test, together with sensitivity assessment. SAS v.8.2 and Excel 2007 have been adopted.
Results
Only the internal capsule level FA measurements (mean FA = 0.64) differed statistically from the mean and range (0.74; 0.67-0.81) of values from the control data. Sensitivity assessment of MEPs (with or without a clinical sign) and DTI, showed a slight superiority of DTI if compared to MEPs alone, but when MEPs are combined with the clinical sign show a better sensitivity. The same behavior and results showed for TCMC.

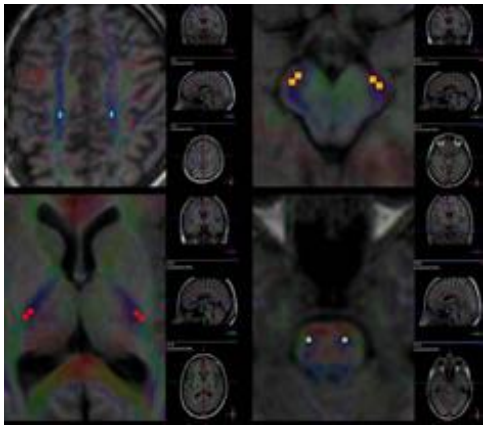

Conclusion
MEPs TCMC and DTI with FA measurement at the internal capsule level, appear to study with the same sensitivity the quality of cortico-spinal tract in ALS patients in evaluating UMN. The clinical signs, if present, add sensitivity to TMS evaluation.

KEYWORDS: DTI, ALS, TMS

Note: Scanned images are included in the proceedings. Some submitted images were reduced during editing, thereby decreasing clarity. Also, refer to the Program Planner. Proceedings Content as of 3-29-2013.

O-481 **11:57 AM - 12:05 PM**

Cerebral Hyperintense White Matter Lesions: Does Increasing Lesion Volume Correlate with Decreased White Matter Fractional Anisotropy?

Cecava, N.[1]·Sherman, P.[1]·Kochunov, P.[2]·McGuire, S.[1]
[1]San Antonio Military Health System, San Antonio, TX, [2]University of Texas Health Science Center at San Antonio, San Antonio, TX.

Purpose
Disease-related and idiopathic, age-related hyperintense white matter (HWM) lesions commonly are encountered on brain magnetic resonance imaging, but their clinical significance often is difficult to discern. Fractional anisotropy (FA) obtained with diffusion tensor imaging (DTI) is a marker for white matter neural tract integrity. This study aims to evaluate the relationship between HWM lesion volume and location-matched FA in a normative population and a population of high altitude U2 pilots following repeated hypobaric exposure with clinical and imaging evidence of neurologic insult.
Materials & Methods
MR FLAIR HWM lesion volume in the frontal lobes and FA in corona radiata were compared in subjects in two separate cohorts: (1) 101 U-2 pilots with history of repeated hypobaric exposure and (2) 89 normative subjects matched for age and education to the pilot cohort. Sixty-six of 101 U-2 pilots had HWM lesions and 52 of 89 normative subjects had HWM lesions. Previous data analysis established a statistically significant elevation in total HWM lesion volume within the pilot cohort as compared to the normative cohort. The imaging data were collected using a 3T MRI scanner and high-resolution (1mm isotropic) 3D FLAIR and DTI sequences. Data analysis included a Spearman's rank-order correlation and statistical significance evaluation.
Results
Increasing frontal HWM lesion volume did not correspond with a statistically significant decrease in corona radiata FA in either cohort. The Spearman's correlation suggested a random relationship of HWM lesion volume and FA (U2 pilot cohort: ρ (99) = -0.028, P =0.781) (Normative cohort: ρ (87) = -0.182, P = 0.088).
Conclusion
Hyperintense whit matter lesions long have been considered to be markers of white matter injury, whether from a known insult or aging. Some authors have postulated that decreased FA may be an early marker in progressive white matter tract damage, with HWM being a latter marker in the injury spectrum. However, this study suggests FA and HWM lesions may not have a strict inverse relationship in either a normative population or a population with pathologically increased HWM lesions such as the studied U-2 pilot population. Further studies will be necessary to evaluate the dynamics of FA in normal aging and in the acute and chronic phases following neurologic injury.

KEYWORDS: Fractional anisotropy, White matter disease

O-482 **12:05 PM - 12:13 PM**

Diffusion Tensor Imaging and Multiple Sclerosis: Patterns of Diffusion Abnormality

Suri, A. K.[1,2]·Fleysher, R.[1]·Wagshul, M. E.[1]·Lipton, M. L.[1,3]
[1]Albert Einstein College of Medicine, Bronx, NY, [2]Bronx Psychiatric Center, Bronx, NY, [3]Montefiore Medical Center, Bronx, NY.

Purpose
Access the concordance of signal abnormalities observed on T2W FLAIR images with the distribution of abnormal fractional anisotropy (FA) individual multiple sclerosis (MS) patients.
Materials & Methods
Imaging of five MS patients was performed at 3T, including T2-weighted FLAIR (TR/TI/TE; 11000, 2800, 125 ms) and diffusion tensor imaging (DTI) (2mm isotropic resolution, 32 directions, b=1000). Fractional anisotropy and T2W-FLAIR images were coregistered to the MNI atlas using a nonlinear procedure. A voxelwise one versus many t-Test ($p<0.01$; 100 voxel cluster size) was performed in each MS patient with comparison of FA and MD images to a group of 40 normal individuals. Lesion location was assessed by two CAQ certified neuroradiologists to determine the degree of concordance between abnormalities shown by T2W FLAIR, FA and MD.
Results
Hyperintensities were detected on T2W FLAIR images in callososeptal and periventricular regions and the brainstem, as expected in MS. Areas of both abnormally low and abnormally high FA were detected in all patients in these areas and in the corticospinal tracts (posterior limb of the internal capsule, corona radiata), corpus callosum and cerebellum. Many of the hyperintensities were concordant with areas of abnormal FA. However, overlap was generally only partial, with areas of abnormal FA generally exceeding the size of colocated hyperintensities. Additional areas of abnormal FA were detected in regions that appeared normal on T2W FLAIR images. Some areas of hyperintensity were present in the absence of colocated diffusion abnormalities. Abnormally high MD was detected in the posterior limb of the internal capsule, brainstem, cerebellum, fornices and the peripheral cerebral white matter.

Note: Scanned images are included in the proceedings. Some submitted images were reduced during editing, thereby decreasing clarity. Also, refer to the Program Planner. Proceedings Content as of 3-29-2013.

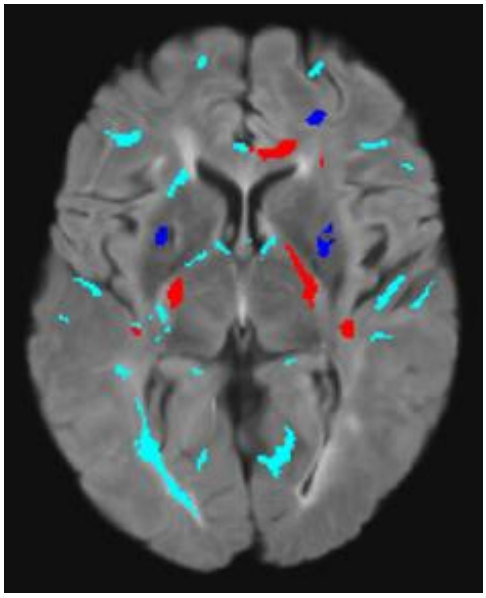

Figure 1. T2W FLAIR image of an MS patient showing hyperintensities in the periventricular white matter and multiple areas of abnormally low FA (red), high FA (blue) and high MD (aqua).

Conclusion

Abnormal white matter anisotropy is detectable in individual MS patients and provides both complementary information colocated with typical hyperintensities as well as abnormalities in normal-appearing white matter.

KEYWORDS: DTI, Multiple sclerosis

Thursday Morning

10:45 AM - 12:15 PM
Ballroom 6CF

(56b) Parallel Scientific Papers: Head and Neck: Cancer and Neoplasm: Advanced Concepts and Techniques

O-483 **10:45 AM - 10:53 AM**

Head and Neck Paragangliomas in the Setting of SDHx Germline Mutations: A Distinct Radiologic and Clinical Entity

Cloran, F. J.·Fishbein, L.·Nathanson, K.·Seol, J.·Pryma, D.·Loevner, L.
University of Pennsylvania
Philadelphia, PA.

Purpose

A subset of head and neck paragangliomas (HNPGLs) harbor a germline mutation in one of the *Succinate Dehydrogenase* (*SDH*) subunit genes. While the imaging characteristics of sporadic head and neck paragangliomas (HNPGLs) have been well described, their behavior in the setting of *SDHx* germline mutations is not well understood and may be associated with different imaging characteristics. The aim of this study is to assess the imaging manifestations of HNPGLs in patients with germline mutations in an *SDHx* gene.

Materials & Methods

Medical records of 140 patients were reviewed who had paragangliomas (PGLs) and underwent genetic testing at our institution from January 2004 through December 2012. Thirty-eight of the 140 patients (27%) had HNPGLs. Pathologic confirmation of HNPGLs was available in 31 of these patients; the remaining 7 patients had either characteristic imaging findings for PGL and/or had tissue sampling from other sites consistent with synchronous or metastatic disease. CT and MR data as well as molecular imaging (In-111 Octreoscan, I-123 MIBG and PET-CT) data were reviewed in this cohort.

Results

SDHx germline mutations were found in 24 of 38 (63%) patients with HNPGLs (*SDHD* n=15; *SDHB* n=8; *SDHC* n=1). Of the 24 patients with *SDHx* mutations, there were a total of 38 HNPGLs. Eleven patients (46%) with *SDHx* mutations had multiple HNPGLs, while patients without a mutation did not have multiple HNPGLs. Of the 24 patients with HNPGLs and *SDHx* mutations, five (21%) had metastatic disease (nodal n=2, distant n=3), which was similar to the presence of metastatic disease in patients without a mutation (3/14 patients, 21%). Of patients with mutations and head and neck tumors, nine (38%) had thoracic and/or abdominal paragangliomas, compared to only one patient without a mutation. Morphologically, the CT and MR appearance of individual HNPGLs in patients with *SDHx* mutations was similar to sporadic HNPGLs without a mutation. Of 18 patients in our cohort who underwent molecular imaging, 8/18 HNPGLs (44%) showed uptake on I-123 MIBG imaging, and 7/9 HNPGLs (77%) showed uptake on In-111 Octreoscan. Two patients had both In-111 Octreoscan and I-123 MIBG imaging which showed their HNPGLs were avid on In-111 but not on I-123 imaging.

Conclusion

Our results suggest that *SDHx* mutations may be present in greater than 60% of patients with HNPGLs. The presence of multiple HNPGLs is indicative of an *SDHx* mutation. Over one-third of patients with HNPGL and a *SDHx* mutation harbor a synchronous thoracic or abdominal tumor, while this appears rare in patients without a mutation. Our data on patients with HNPGLs suggest that the incidence of metastatic disease related to their HNPGL is not clearly different from their sporadic (non-*SDHx* mutation) counterparts. Given the prevalence of *SDHx* mutations with HNPGLs, genetic counseling may be indicated in patients and their first degree relatives when a mutation exists. Furthermore, our results suggest that patients with

Note: Scanned images are included in the proceedings. Some submitted images were reduced during editing, thereby decreasing clarity. Also, refer to the Program Planner. Proceedings Content as of 3-29-2013.

the mutation and HNPGLs have a greater than 33% chance of thoracic and abdominal PGL and should have dedicated imaging of these regions.

KEYWORDS: Paraganglioma, Genetics, SDH

O-484 **10:53 AM - 11:01 AM**

Exponential Growth in Thyroid Cancer: Trends in Incidence and Association with CT Imaging

Hoang, J. K.[1]·Roy Choudhury, K.[1]·Lyman, G.[1]·Eastwood, J.[1]·Wnuk, N.[1]·Esclamado, R.[1]·Nguyen, X.[2]
[1]Duke University Medical Center, Durham, NC, [2]The Ohio State University Medical Center, Columbus, OH.

Purpose
The incidence of thyroid cancer has increased in the United States since the 1980s. The trend is due to an "*apparent*" increase in incidence from increased diagnostic scrutiny, resulting in increased diagnosis of small clinically insignificant cancers. The aim of this study is to determine the recent trends in incidence of thyroid cancer, and to evaluate the relationship between CT scans volume and thyroid cancer incidence.
Materials & Methods
This retrospective cohort study utilized national databases for thyroid cancer and CT imaging volume. Thyroid cancer data for 1983 to 2009 were obtained from the National Cancer Institute's Surveillance, Epidemiology, and End Results (SEER) database. Data on inpatient and outpatient CT imaging volume for 1993 to 2006 in the United States were obtained from the National Council of Radiation Protection and Measurements Report No. 16. Trends in thyroid cancer incidence were modeled for overall incidence and mortality and as a function of patient age and gender as well as tumor histology, size and stage. Simple regression analysis was performed to evaluate the relative impact of annual CT scans on thyroid cancer incidence.
Results
In 2009 the incidence of thyroid cancer was 14 per 100,000, and was almost double the incidence in 2000. The growth in incidence is exponential without significant change in mortality from thyroid cancer(Figure). The subgroup with the highest growth in incidence was subcentimeter papillary carcinoma with 11.8% growth per year resulting in doubling in incidence every 6.2 years. There was a very strong linear relationship between annual CT scan volume and incidence of subcentimeter papillary carcinoma ($r = 0.987$, $p<0.0001$). This is particularly significant given that growth in incidence of subcentimeter papillary carcinoma is not linear, but is exponential. We evaluated other tumor sizes and histologies for their relationship with annual CT volume and found high correlation coefficients, but the slopes of the regression line were smaller compared to subcentimeter papillary carcinoma.

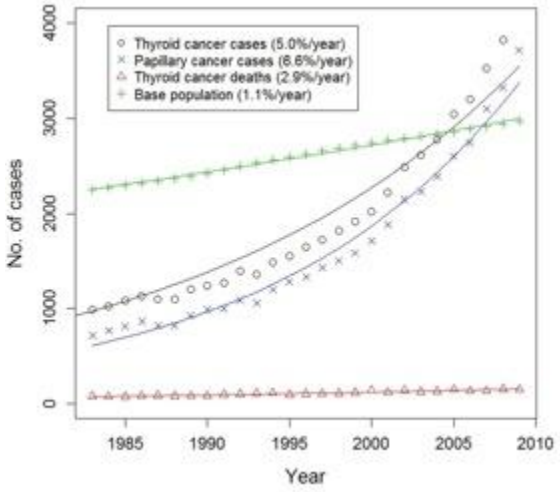

Conclusion
The incidence of small nonpalpable thyroid cancer is growing at an exponential rate without a significant change in mortality rate. This supports the theory of apparent increase in incidence due to increased diagnostic scrutiny. There is a strong relationship between the incidence of subcentimeter papillary carcinomas and CT imaging volume over time. Since CT imaging may be a major source for detection of incidental thyroid cancers, future work should focus on establishing evidence-based and cost-effective guidelines for workup of thyroid nodules seen on CT.

KEYWORDS: Thyroid, CT, malignancy

O-485 **11:01 AM - 11:09 AM**

Estimates of Clinical Cost Savings for New, Better Performing Criteria for Diagnosis of Persistent Nodal Metastases after Treatment for Oropharyngeal Carcinoma

Ahmed, S.·Jones, J.·Steele, J.·Sandulache, V. C.·Ow, T. J.·Skinner, H. D.·Rao, A.·Ginsberg, L. E.·Kumar, A. J.·Myers, J. N.·Hamilton, J. D.
M. D. Anderson Cancer Center
Houston, TX.

Purpose
A recent publication (Hamilton, et al.) demonstrated how new CT diagnostic criteria ("NECk REaD") improved the accuracy of best radiologic practice for diagnosing persistent nodal metastases after definitive treatment for oropharyngeal carcinoma. The economic ramifications of reducing the number of nodal dissections in this previously studied patient group are assessed.
Materials & Methods
One hundred thirty-eight patients who had 1) a diagnosis of oropharyngeal carcinoma between 2002 and 2008, 2) who received definitive radiation therapy +/- chemotherapy, and 3) had pre- and post-therapy CT

Note: Scanned images are included in the proceedings. Some submitted images were reduced during editing, thereby decreasing clarity. Also, refer to the Program Planner. Proceedings Content as of 3-29-2013.

imaging were assessed retrospectively. The cost of all care (surgery, radiation therapy, chemotherapy, hospitalization, etc.) was gathered from a database for patients beginning from the start of radiation therapy through 90 days after nodal dissection. Inflation estimates derived from U.S. Department of Labor statistics adjusted the line item costs to the current standards. The cost of nodal dissection was estimated as all the costs associated with the day of surgery +/- one day. The thirty patients placed at lowest risk (score of 0 or 1; all found to be pathologically negative) by the "NECk REaD" criteria (1 point for necrosis, new calcification, ring enhancement, extranodal disease on pre-therapy CT, and diameter decrease of <50%, with two additional points for new necrosis) had the nodal dissection cost subtracted from the total as an estimate of the economic impact of improved diagnostic accuracy. Records were assessed to see if the new criteria changed the imaging diagnosis compared to the radiologist report.
Results
The average patient cost was ~$64,000. The average cost of the nodal dissection for the 30 patients with the lowest scores was ~$12,000. Of the 30 patients with the lowest scores, 21 had radiology reports that were positive or equivocal for persistent nodal metastases contrary to the NECk REaD Criteria, while nine had negative reports and received planned neck dissections. If the 21 patients' neck dissection costs are subtracted there is an average clinical cost savings of $1,836 per patient and if all 30 patients are used, the savings is $2,622. Interestingly, the five patients with the highest NECk REaD Criteria scores (score >5), all of whom had positive lymph nodes by pathology, had higher average costs (~$106,000) mainly due to three patients with additional chemotherapy or complications with care.
Conclusion
This study shows the economic savings resulting from incremental improvements in diagnostic accuracy. A minimal investment of radiologist time can have substantial impact on the cost of clinical care. Although the CT criteria improves the triaging of these patients with high-risk going straight to nodal dissection and low-risk to observation, there remains a large "intermediate-risk" group (105/137) where additional testing is warranted. The complimentary role of tests such as PET CT and image-guided needle biopsy in this "intermediate" group needs to be explored. Applying new CT diagnostic criteria to evaluate for persistent nodal metastases following definitive radiation +/- chemotherapy results in average clinical cost savings of up to $2600 per patient.

KEYWORDS: Oropharynx, Lymph node metastasis, Cost-effective

O-486 **11:09 AM - 11:17 AM**

Comparison of PET/CECT with CECT or PET/CT Alone for Detection of Recurrent Laryngeal Cancer after Radiation Treatment

Lloyd Baugnon, K.·Chokshi, F. H.·Karagulle Kendi, A. T.·Viamonte, C. A.·Harrison, C. E.·Hudgins, P. A.
Emory University School of Medicine
Atlanta, GA.

Purpose
Positron emission tomography (PET) with computed tomography (PET/CT) has shown promise detecting recurrent laryngeal carcinoma, with improved sensitivity over contrast-enhanced CT (CECT) alone. Our hypothesis is that PET/CECT improves the diagnosis of recurrent or persistent laryngeal cancer, and reader confidence, particularly for less experienced readers.
Materials & Methods
Data warehouse query for patients undergoing PET/CECT for laryngeal cancer was performed with IRB approval. Inclusion criteria included: 1. PET/CT with CECT at our tertiary care facility. 2. History of laryngeal or hypopharyngeal malignancy, treated with radiation therapy, with or without chemotherapy. 3. Either > 6 months of clinical/imaging followup, or pathologic diagnosis to confirm positive or negative imaging study. Each combined PET/CECT yielded three separate studies: Contrast-enhanced CT of the neck, PET/CT, and PET/CECT. For each, the primary site and nodal disease were assessed on a 1-4 scale (1 = no disease, 4 = definite recurrent/residual tumor). The CECT was interpreted independently, blinded to PET results, by two neuroradiologists (NR), at different stages of training. The PET/CT was interpreted independently by two nuclear medicine (NM) physicians, blinded initially to CECT result, also at different levels of training. A final interpretation using both studies was made to determine if the impression was altered or reader confidence was improved. Score of 1 or 2 was considered a negative test, and 3 or 4 was considered a positive test. Sensitivity, specificity, PPV, NPV, and accuracy of each imaging modality, each reader, and the percent of cases with altered interpretations per reader were calculated.
Results
Twenty-five patients were included, ranging from T1 to T4b laryngeal or hypopharyngeal tumors. Imaging was performed at two to 240 months (median of 7 months) after completion of radiation therapy. Fifteen of 25 cases were positive for recurrence at the primary site, proven by biopsy in 13/15. Four of 25 patients had recurrent lymphadenopathy. When PET/CT was combined with CECT, the diagnostic accuracy for recurrent disease improved from 60% to 76% for NR reader 1 (with less experience), and from 76% to 84% for NR reader 2 (the more experienced reader). Staging for primary site and/or nodal disease on CECT changed 56% and 48% of the time with the PET information. When adding CECT information

Note: Scanned images are included in the proceedings. Some submitted images were reduced during editing, thereby decreasing clarity. Also, refer to the Program Planner. Proceedings Content as of 3-29-2013.

to the PET/CT, the accuracy improved from 80 to 84% and 84 to 88% for the two NM readers. There was only one case when CECT prompted the NM physician to completely change the interpretation. Overall, combined CECT and PET/CT interpretation improved confidence in 82% of the cases in the NR group and in 70% of the cases in the NM group. False negative and false positive interpretations on the combined PET/CT interpretations were uncommon and were more common in the inexperienced readers.
Conclusion
Combined PET/CECT is the most accurate imaging modality to assess for recurrence of laryngeal or hypopharyngeal cancer in the post-treatment setting, particularly when compared to CECT alone in the hands of a less experienced radiologist.

KEYWORDS: PET/CT, Cancer, Laryngeal

O-487 **11:17 AM - 11:25 AM**

Extra-Capsular Spread: Accuracy of Preoperative CT and MR Imaging Prediction of Extra-Capsular Spread in Oral Cavity Squamous Cell Carcinoma Lymph Node Metastases

Poliashenko, S. M.·Aiken, A.·Chen, A.·Baugnon, K.·Corey, A.·Hudgins, P.
Emory University School of Medicine
Atlanta, GA.

Purpose
Extra-capsular spread (ECS) is a poor prognostic indicator for patients with head and neck squamous cell carcinoma (SCC). The accepted gold standard for confirmation of ECS is pathology. However, the imaging diagnosis alone may be used to determine treatment in oropharyngeal SCC (OPSCC), as presence of pathologic ECS is an indication for postoperative chemoradiation rather than radiation alone. In addition, the imaging diagnosis of ECS is important in the consideration of primary surgical management for T1 or T2 OPSCC. Radiologic evidence of ECS may sway the decision from primary surgical therapy to primary concurrent chemoradiation. The impact of pretreatment ECS radiologic findings highlights the need to re-evaluate the accuracy of the imaging diagnosis of ECS as previous reports range from 62.5% - 80.9% sensitivity and 60% - 72.7% specificity. Imaging features such as nodal necrosis and large lymph node size have been reported to increase in chance of ECS. Nodal dissection is considered standard treatment for patients with oral cavity SCC, and therefore pathologic confirmation of ECS is available. This study aims to (1) evaluate the accuracy of computed tomographic (CT) and magnetic resonance (MR) imaging to diagnose ECS in oral cavity SCC as a proxy for OPSCC, and (2) to assess the correlation of radiographic lymph node necrosis and size with histopathologic ECS.
Materials & Methods
Our retrospective project had IRB approval. Inclusion criteria were: 1. CT or MR imaging at our tertiary referral Cancer Institute or adequate available outside imaging. 2. Neck dissection with pathology comment on ECS. 3. Re-review for ECS by 2 CAQ neuroradiologists if not documented in report. 4. Radiographic N0-N3 staged necks. An electronic search of the imaging data warehouse for ICD-9 codes for oral cavity cancer between 2007-2012, yielded 137 patients who met these inclusion criteria. Radiology reports were used to document lymph node size and necrosis. Two experienced head and neck radiologists blindly reviewed the cases for evidence of ECS based upon irregular borders, adjacent fat stranding and invasion of adjacent structures. The histopathology reports were reviewed as the gold standard for ECS.
Results
Radiographic evaluation of these 137 patients identified 18/137 thought to be positive for ECS. Pathologic analysis of the 137 patients showed 27 (19.7%) were positive for ECS and 110/137 (80.3%) were negative for ECS. The sensitivity and specificity of CT and MR imaging for ECS was 51.9% and 96.4% respectively. Radiologic nodal necrosis was present in 64% of cases with histopathologic positive ECS, and in only 7% of ECS negative cases with a strong association between the two(P=<.001). There was no significant association between lymph node size and ECS (P = .20).
Conclusion
Although CT and MR imaging specificity for predicting ECS is high, the sensitivity is low. If radiographic ECS is present, there is a high likelihood that ECS will be confirmed histopathologically. Lymph node necrosis is a predictive indicator of histopathologic ECS. CT and MR imaging for the determination of ECS preoperatively may lack the sensitivity for use in determining nonsurgical management decisions in OPSCC.

KEYWORDS: Lymph node metastasisaccuracy

O-488 **11:25 AM - 11:33 AM**

Volume CT Perfusion in Squamous Cell Carcinoma of the Head and Neck: Does Added Locoregional Lymph Node Perfusion Information Aid in Predicting Therapy Response?

Amrhein, T. J.[1]·Massari, F.[1]·Kolić, K.[2]·Canstein, C.[1]·Rumboldt, Z.[1]
[1]Medical University of South Carolina, Charleston, SC, [2]KBC Split, Split, CROATIA.

Purpose
To investigate the utility of volume CT perfusion (VCTP) in predicting the response of squamous cell carcinoma (SCC) of the head and neck to chemoradiation therapy.
Materials & Methods
CT perfusion (CTP) in SCC of the head and neck has been shown to have predictive value for response to chemoradiation therapy. However, traditional CTP methods have been limited in their craniocaudal coverage precluding evaluation of both the primary neoplasm and

Note: Scanned images are included in the proceedings. Some submitted images were reduced during editing, thereby decreasing clarity. Also, refer to the Program Planner. Proceedings Content as of 3-29-2013.

nodal disease during the same acquisition. Volume CT perfusion provides a much larger area of perfusion coverage in the z-axis, which allows for assessment of both the primary lesion as well as locoregional nodal disease. In this prospective single institution study, 23 treatment-naïve patients with pathology proven SCC underwent VCTP of the neck on a 128-slice MDCT scanner using a continuous periodic table motion technique that provided 14 cm of craniocaudal coverage. Single separate regions of interest (ROI) were placed on the primary neoplasm as well as on areas of prominent locoregional nodal disease. Regions of interest were placed in areas of clear enhancement that were associated with solid tissue and did not contain a major vessel. The following perfusion parameters were calculated using a deconvolution algorithm: blood volume (BV), blood flow (BF), mean transit time (MTT), and capillary permeability (CP).
Results
Two patients had SCC of unknown primary precluding comparison between the primary lesion and nodal perfusion values. The remaining 21 patients had nine oral cavity, six oropharyngeal and three laryngeal cancers, with four primary lesions in other locations. The mean values for BF, BV, and CP were on average lower in lymph nodes than in primary lesions (73 versus 102.4, 10.9 versus 15, 29.6 versus 30.3, respectively). Blood flow, BV, and CP were highest in oral cavity cancers, both for the primary site and lymph nodes. Nine scans demonstrated perfusion values within locoregional lymph nodes that were similar to those found within the primary malignancy. The remaining 12 scans demonstrated lymph node perfusion values different from those of the primary neoplasm: nodal BF was more than 50% higher in four cases, while it was over 50% lower in eight patients, all of which had oropharyngeal or oral cavity neoplasms.
Conclusion
There are prominent differences in metastatic nodal CT perfusion values compared to the primary tumor in some patients. Continued patient followup over the duration of the study with attention to relationships between perfusion values and treatment responses will help to elucidate the potential prognostic role of VPCT in SCC of the head and neck. Concomitant nodal perfusion information may provide further insight into subtypes of disease and aid in future patient management and therapeutic decision making.

KEYWORDS: CT perfusion, Squamous cell carcinoma, Neck Neoplasm

O-489 **11:33 AM - 11:41 AM**

Pretreatment Perfusion-Weighted MR Imaging and Diffusion-Weighted MR Imaging in Local Failure Prediction in Oropharyngeal or Hypopharyngeal Squamous Cell Carcinoma Treated with Chemoradiotherapy

Ng, S. H.·Toh, C. H.·Wong, H. F.
Chang Gung Memorial Hospital
Taiwan, TAIWAN.

Purpose
To determine the utility of dynamic contrast-enhanced perfusion-weighted MRI (DCE PWI) and diffusion-weighted MRI (DWI) in predicting local failure of oropharyngeal or hypopharyngeal squamous cell carcinoma (OHSCC) treated with chemoradiotherapy.
Materials & Methods
Between July 2008 and December 2010, patients with newly diagnosed OHSCC scheduled for chemoradiotherapy with curative intent were eligible in this prospective study. Dynamic contrast-enhanced PWI was acquired using a 3D spoiled gradient-echo sequence while DWI was acquired using a modified Stejskal-Tanner diffusion gradient pulsing scheme. Regions of interest were drawn on the primary tumor by the experienced head and neck radiologist with the aid of the T2-weighted and T1-weighted postcontrast MR images. The visible necrosis regions were excluded for the evaluation. The relationship of local failure with clinical and imaging data, including age, hemoglobin level, T-stage, N-stage as well as tumor location, gross tumor volume (GTV), transfer constant (Ktrans), volume of blood plasma (Vp) and volume of extracellular extravascular space (Ve) of PWI, and apparent diffusion coefficient (ADC) of DWI of the primary tumor was analyzed using logistic regression analyses. The patients also were categorized into two groups: local control and local failure. Age, Ktrans, Ve, Vp, ADC, and GTV were compared between local control and local failure using the t-test. The T stage, N stage, and tumor location were analyzed for association with local failure using Fisher's exact test. Receiver operating characteristic (ROC) curve analysis was performed to determine the value that best predicted local failure.
Results
Seventy-eight OHSCC patients were enrolled, in whom 20 were excluded for the analysis because of small or unevaluable lesion, artifact on DWI/PWI images, or death before the definite diagnosis of treatment failure could be determined. Therefore, there were 58 patients (29 oropharynx, 29 hypopharynx; 4 women and 54 men, 48.5 ± 9.7 years of age) with successful pretreatment PWI and DWI available for analysis. With the median follow-up time of 18.2 months, 17 of the 58 patients had local failure while the other 41 patients achieved local control. In the univariate analysis, only pretreatment tumor Ktrans were significantly associated with local failure ($p = 0.03$). Similarly, only the pretreatment tumor Ktrans value of the local control group (0.68 minutes-1) was significantly

Note: Scanned images are included in the proceedings. Some submitted images were reduced during editing, thereby decreasing clarity. Also, refer to the Program Planner. Proceedings Content as of 3-29-2013.

higher (P = .01) than that of the local failure group (0.45 minutes-1). The ROC analysis resulted in a threshold Ktrans value of 0.46 minutes-1 that attained 70.6% sensitivity and 82.9% specificity for the prediction of local failure.
Conclusion
Our results suggest that pretreatment tumor Ktrans of PWI could be a potential noninvasive indicator of local failure in OHSCC treated with chemoradiotherapy. Pretreatment Ve, Vp, ADC, and GTV measurements did not predict treatment response.

KEYWORDS: MR perfusion-weighted imaging, Head and neck, pharyngeal neoplasms

O-490 **11:41 AM - 11:49 AM**

Feasibility of Volume CT Perfusion in Squamous Cell Carcinoma of the Head and Neck

Massari, F.[1]·Amrhein, T. J.[1]·Canstein, C.[1]·Vavro, H.[2]·Rumboldt, Z.[1]
[1]Medical University of South Carolina, Charleston, SC, [2]KB Dubrava, Zagreb, CROATIA.

Purpose
To investigate the feasibility of volume perfusion CT (VP CT) in the assessment of both primary and locoregional nodal disease in squamous cell carcinoma (SCC) of the head and neck.
Materials & Methods
Twenty-three treatment-naïve patients with proven SCC underwent VP CT. Images were acquired on a 128-slice multidetector CT with the following parameters: 80 kVp, 150 mAs, 54 seconds, scan delay of six seconds following intravenous administration of 40 mL of iohexol (350 mgI/mL) at 4mL/sec followed by a saline chaser of 50 mL at 4 mL/sec. A total of 35 scans were acquired per patient using a continuous periodic table motion technique providing z-axis coverage of 14 cm. Completed scans were reviewed for the inclusion of the primary lesion and locoregional nodal disease, and for the presence of artifacts. Perfusion maps were created using a deconvolution algorithm with placement of regions of interest (ROI) over the primary neoplasm as well as lymph nodes concerning for metastatic involvement. Region of interest placement was chosen in areas devoid of imaging findings of necrosis or blood vessels. Capillary permeability (CP), blood volume (BV), blood flow (BF), and mean transit time (MTT) perfusion parameters were recorded.
Results
All patients successfully completed the exam, without adverse events or substantial patient discomfort. Fourteen scans demonstrated streak artifact from dental amalgam. This was significant in one case precluding perfusion assessment of a known oral cavity primary lesion. Only one scan demonstrated considerable motion artifact despite automatic motion correction during postprocessing. Sixteen out of 22 scans had z-axis coverage extending from the paranasal sinuses to below the laryngeal cartilage. Of the six scans remaining scans, five terminated at the mid-aspect of the arytenoid cartilage and one at the level of the hyoid. Perfusion data from additional locoregional nodal disease was acquired in 22 of 22 scans. Mean values (±SD) obtained for the primary lesions were as follows: CP 30.0(±23.3), BV 14.9(±7.4), BF 102.4(±48.6), and MTT 10.4(±6.2). Mean values obtained for lymph nodes: CP 28.1(±11.6), BV 11.7(±4.3), BF 70.6(±36.3), and MTT 13.0(±7.8).

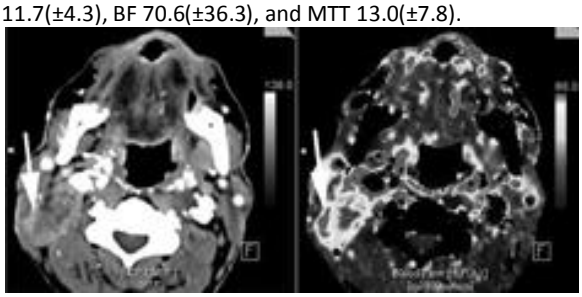

Conclusion
Volume perfusion CT in the head and neck is feasible and, due to the large volume of coverage, it is capable of providing perfusion information for both the primary lesion and locoregional nodal disease during a single acquisition.

KEYWORDS: CT perfusion, Squamous cell carcinoma, Neck Neoplasm

O-491 **11:49 AM - 11:57 AM**

Does Extrinsic Tongue Muscle Involvement Carry a Higher Risk of Local Failure Regardless of Size?: A Preliminary Report

Poliashenko, S.·Aiken, A.·Chen, A.·Baugnon, K.·Corey, A.·Hudgins, P.
Emory University School of Medicine
Atlanta, GA.

Purpose
The American Joint Committee on Cancer (AJCC) staging system for oral cavity (OC) squamous cell carcinoma (SCC) upstages a tumor, regardless of size, to T4a if there is cortical bone invasion or extrinsic tongue muscles (ETM). Extrinsic tongue muscle invasion was added to stage T4 classification of OC tumors in 1988, and is now included in T4a stage in the current 7th edition. Little has been published on the association of ETM invasion with surgical outcomes and prognosis. Our aim was to evaluate the significance of T4a stage due to either cortical bone or ETM invasion, and ETM invasion alone as factors on prognosis.
Materials & Methods
Our project had Institutional Review Board approval. Inclusion criteria for this project were: 1. T4a OC SCC. 2. Computed tomographic (CT) or magnetic resonance (MR) imaging interpretation at our tertiary referral Cancer Institute or available outside imaging. 3. Surgical resection

Note: Scanned images are included in the proceedings. Some submitted images were reduced during editing, thereby decreasing clarity. Also, refer to the Program Planner. Proceedings Content as of 3-29-2013.

at our institution. 4. Minimum of six months of clinical or radiographic followup (for recurrence analysis). An electronic search of our imaging data warehouse for ICD-9 codes for OC SCC between 2007 and 2012 yielded 59 T4a patients who met the above inclusion criteria. Fifty T1-T3 tumors from the same database were used as size-matched controls. Two CAQ neuroradiologists blindly reviewed the images for T stage, presence of ETM and cortical bone invasion. Status of surgical margins and local recurrences were noted from radiology, clinical, and pathology reports for the duration of the patients' followup.

Results

Eighty-eight percent (52/59) T4a patients versus 92% (46/50) T1-T3 control patients had negative surgical margins. Thirty-nine of 52 T4a patients and 34/46 controls had six months or greater follow-up time**.** Sixteen of 39 T4a patients were positive for ETM invasion alone, Nineteen of 39 were positive for cortical bone invasion alone and 4/37 were positive for both. Fifty-three percent of T1-3 and 82% of T4a patients were treated with adjuvant radiation therapy. Overall, 11/39 (28.2%) of T4a patients versus 5/34 (14.7%) of T1-3 patients had local recurrence (P =.164). T4a patients did not have a significantly different local recurrence rate as compared to size-matched controls at 0-2 cm (2/6 versus 0/7), 2-4 cm (6/21 versus 5/19), and 4 cm or greater (3/12 versus 0/8), (P=.192)(P=.873)(P=.242). Overall, 5/16 (31.3%) of T4a patients with ETM invasion alone versus 5/34 (14.7%) of T1-3 controls had local recurrence (P=.256). Extrinsic tongue muscle invasion alone did not have a significantly different local recurrence rate as compared to size-matched controls at 0-2 cm (0/2 versus 0/7), 2-4 cm (4/8 versus 5/19), and 4 cm or greater (1/6 versus 0/8), (P=.99)(P=.375)(P=.429).

Conclusion

This preliminary study suggests that T4a cases have similar successful resection rates with negative margins compared to control T1-3 patients. Overall, patients staged with T4a based on the presence of ETM involvement alone had a higher rate of local recurrence than controls; however this difference was not statistically significant. Further investigation with a larger sample size would be needed to confirm this trend.

KEYWORDS: Oral cavity, Prognosis

O-492 **11:57 AM - 12:05 PM**

Apparent Diffusion Coefficient Histogram Analysis of Salivary Gland Tumors

Saito, N.[1]·Nakahira, M.[1]·Obara, M.[2]·Chang, Y.[3]·Uchino, A.[1]·Kimura, F.[1]·Sakai, O.[3]

[1]Saitama International Medical Center, Saitama, JAPAN, [2]Philips Electronics Japan, Tokyo, JAPAN, [3]Boston Medical Center, Boston University School of Medicine, Boston, MA.

Purpose

Histogram parameters such as skewness and kurtosis represent nongausian measures of differences in tissue heterogeneity. In evaluating pathologic types of salivary gland tumors, mean apparent diffusion coefficient (ADC) value has been used most commonly. However ADC histogram analysis could provide a better assessment of tumors by quantifying tissue heterogeneity characteristics caused by cyst, hemorrhage, and necrosis. The purpose of this study is to assess whether ADC histogram analysis can help identify pathologic types and differentiate between benign and malignant tumors in salivary gland.

Materials & Methods

Clinical history and imaging data of 27 patients with 28 salivary gland tumors (15 females, 12 males: 11 pleomorphic adenomas, 11 Warthin's tumors, 6 primary malignant salivary gland tumors) who underwent MR imaging prior to biopsy or surgical resection between April 2011 and November 2012 were evaluated retrospectively. MR imaging including diffusion-weighted imaging performed using a 3T MR scanner. The regions of interest were drawn manually along the entire tumor on each slice to generate ADC histogram. Peak ADC value, skewness, and kurtosis were extracted from the histograms. The differences in the parameters among tumor types were evaluated by Kruskal-Wallis test.

Results

Apparent diffusion coefficient histograms of the representative cases are demonstrated in the Figure. Significant differences were noted among three lesion types (pleomorphic adenoma, Warthin's tumor, and malignancy) in terms of skewness (p = 0.02) and peak ADC value (p = 0.01). There were no significant differences among the lesion types in kurtosis; however they tended to be higher in Warthin's tumor and pleomorphic adenoma than in malignant tumor.

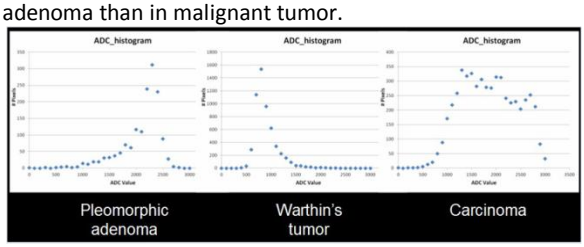

Conclusion

Pleomorphic adenoma, Warthin's tumor, and primary malignant salivary gland neoplasms could be differentiated

Note: Scanned images are included in the proceedings. Some submitted images were reduced during editing, thereby decreasing clarity. Also, refer to the Program Planner. Proceedings Content as of 3-29-2013.

based on skewness and peak ADC values. Apparent diffusion coefficient histogram analysis may be useful in determining lesion pathologic types in patients with salivary gland tumors.

KEYWORDS: Salivary gland, ADC, Histogram

O-493 **12:05 PM - 12:13 PM**

Palliative Cryoablation of Metastatic Tumors Involving the Face

Morris, J. M.·Callstrom, M. R.
Mayo Clinic
Rochester, MN.

Purpose
To demonstrate the feasibility and technique of treating metastatic lesions to the face with percutaneous CT-guided cryoablation. Additionally to share techniques we have learned in avoiding critical structures such as nerves, uninvolved mucosa, and skin.
Materials & Methods
Palliative CT-guided cryoablation of metastatic lesions involving the face were reviewed retrospectively. The lesions were treated with 2-5 Endocare cryoprobes using a standard freeze, passive thaw, and freeze cycle. Patients then were evaluated for palliative relief of symptoms. Specifically we reviewed clinical outcomes, equipment used, techniques to avoid critical structures, and hospital stay length.
Results
Two patients underwent cryoablation of the face both for local control of tumor burden and palliative relief of symptoms. Patient one is a 77-year-old female with metastatic lung adenocarcinoma with direct extension into the liver and a lesion in the left buccal space refractive to radiation and chemotherapy. She developed sever pain and trismus and could not open her mouth to eat. Cryoablation of the lesion was performed under general anesthesia and CT guidance using 2 perc 15 Endocare cryoprobes. A small catheter was placed beneath the dermis and warm saline instilled to displace the overlying skin preventing frostbite injury. Patient had no complications, near immediate improvement in her pain and trismus and was discharged home on postprocedure day three. She was able to continue oral intake while undergoing the remaining chemotherapy treatments. Patient two is a 42-year-old female diagnosed with metastatic clear cell renal cell cancer. While undergoing radiation treatment to the brain, hip, and shoulder she developed a rapidly enlarging lesion involving the right mandible growing into the oral cavity with perineural tumor spread along the inferior alveolar nerve. Patient wished to undergo treatment but was not a surgical candidate. Cryoablation of the lesion was performed under general anesthesia and CT guidance using 5 perc 24 Endocare cryoprobes. A bite block and gauze were used to displace the uninvolved maxilla and spare all gingival surfaces not involved. Postprocedurally patient had complete paresthesia in the distribution of the inferior alveolar nerve but was able to open her mouth with decreased pain and decreased trismus allowing oral nutrition. She was discharged from the hospital on postprocedure day.
Conclusion
Cryoablation is used at our institution as part of a multidisciplinary approach in patients with metastatic and primary cancer in various organ systems for both local control and palliative treatment. We present two patients treated by our service to demonstrate the feasibility and techniques used in percutaneous CT-guided cryoablation of the jaw and of the masticator/buccal space. These cases demonstrate the ability of cryoablation to palliatively treat metastatic facial lesions safely. In both cases oral nutritional requirements while on chemotherapy were of concern and surgical options were not feasible. The primary goal was local tumor control but secondary goals of reducing trismus, reducing pain, and increasing ability to eat were of vital importance in these patients. Future studies will be required to determine the potential of cryoablation in the head and neck.

KEYWORDS: Face, Metastases, Cryoablation

Thursday Morning

10:45 AM - 12:15 PM
Ballroom 6DE

(56c) Parallel Scientific Papers: Adult Brain: Stroke IV: Extracranial Blood Vessels and Infarctions

O-494 **10:45 AM - 10:53 AM**

Metabolic Reserve and Stroke Risk in Patients with Carotid Stenosis or Occlusion: A Systematic Review and Meta-Analysis of the Predictive Role of Increased Brain Oxygen Extraction Fraction – Dyke Award Winner

Baradaran, H.·Gupta, A.·Schweitzer, A. D.·Hurtado Rua, S. M.·Delgado, D.·Wright, D.·Sanelli, P. C.
Weill Cornell Medical College
New York, NY.

Purpose
Impaired metabolic reserve defined by increased oxygen extraction fraction (OEF) on positron emission tomography (PET) is considered a risk factor for stroke in patients with internal carotid artery (ICA) steno-occlusive disease. However, the predictive ability of OEF has been questioned since the early termination of the Carotid

Note: Scanned images are included in the proceedings. Some submitted images were reduced during editing, thereby decreasing clarity. Also, refer to the Program Planner. Proceedings Content as of 3-29-2013.

Occlusion Surgery Study (COSS) which used abnormal OEF hemispheric ratios as a key inclusion criterion. We need to re-evaluate OEF's association with stroke outcomes and solidify our understanding of PET-based OEF testing as a possible metric by which newer MRI measures of oxygen metabolism may be compared. To accomplish this, we performed a systematic review and meta-analysis to summarize the association between increased OEF and stroke risk in patients with ICA steno-occlusive disease.

Materials & Methods

We performed a comprehensive literature search evaluating the association of increased OEF to future stroke in patients with high-grade ICA stenosis or occlusion. We included studies with baseline PET-based OEF testing measures and at least one-year followup with ipsilateral stroke as the primary outcome. We performed subset analyses based on OEF testing method (absolute versus hemispheric ratio), disease site (ICA versus ICA plus middle cerebral artery), and presence of symptoms (all symptomatic versus all asymptomatic). A meta-analysis with assessment of study heterogeneity and publication bias was performed. Results were presented in a forest plot and summarized using a random-effects model.

Results

Seven studies with 430 patients met the inclusion criteria for systematic review after screening 2,158 studies. Six of seven studies with a total of 331 unique patients with mean followup of 31.1 months were amenable to meta-analysis. We found a significant positive relationship between abnormal OEF and future ipsilateral stroke with a pooled random effects odds ratio (OR) of 6.04 (95% CI, 2.58-14.12) (Figure, OR on logarithmic scale). There was no statistically significant difference in the OR in the subset analyses divided by testing method, disease site, and presence of symptoms. Measures of heterogeneity showed mild heterogeneity between studies (I-squared statistic=0, 95% CI, 0 to 38.34) and no statistically significant publication bias (Begg-Mazumdar, p-value=1.00).

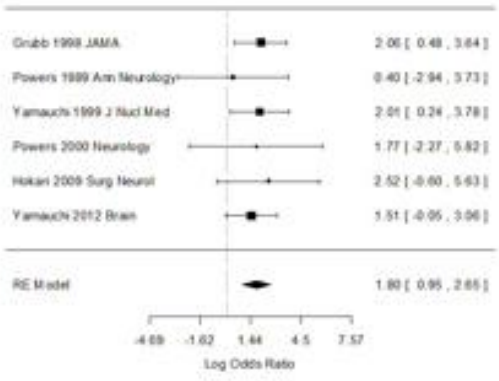

Conclusion

Abnormal OEF remains a powerful predictor of stroke in carotid stenosis or occlusion. These results indicate there is insufficient evidence that the failure of the COSS trial is due to a failure of OEF methodology. Furthermore, our results suggest that PET-based OEF testing is a valuable gold standard by which studies of MRI surrogates of oxygen metabolism can be compared.

KEYWORDS: Meta analysis, Misery perfusion

O-495 **10:53 AM - 11:01 AM**

Carotid Intraplaque Hemorrhage: Increased Stroke Risk in Stenotic and Ulcerated Plaque

McNally, J. S.·Kim, S.·Roberts, J.·Parker, D.·Treiman, G. S.
University of Utah
Salt Lake City, UT.

Purpose

Carotid atherosclerosis accounts for 20-30% of the >690,000 strokes occurring annually in the United States, according to the American Heart Association 2012 update. Stroke risk stratification based primarily on carotid stenosis and plaque morphology results in many unnecessary surgeries on asymptomatic patients each year. Lumen evaluation does not detect unstable plaque components such as carotid intraplaque hemorrhage (IPH), which may account for the disconnect between carotid stroke risk estimates and treatment recommendations. The purpose of this study was to determine if carotid IPH modifies stroke risk with traditional markers of plaque vulnerability.

Materials & Methods

Over two years, 159 patients with suspected acute stroke were imaged with MR brain and MRA neck. Carotid MRA was used to measure traditional markers of vulnerable plaque including stenosis, ulceration and intraluminal thrombus. As shown in the figure, IPH was detected with the magnetization prepared rapid acquisition gradient-recalled echo (MPRAGE) sequence. Nonlacunar ipsilateral ischemic strokes were detected with brain diffusion tensor imaging (DTI). This provided 318 carotid artery and ipsilateral brain images for analysis. Forty-eight arteries were excluded due to extracarotid sources of brain ischemia and four were excluded due to carotid occlusion. Two hundred sixty-six arteries were eligible for data analysis.

Results

Carotid IPH was associated with acute territorial ischemic events [relative risk(RR)=6.4*, 95% confidence interval (CI)=4.3-8.7]. This was similar to the risk associated with >70% stenosis (RR=4.4*, CI=2.8-5.9), ulceration (RR=3.8*, CI=2.4-5.6), and intraluminal thrombus (RR=5.7*, CI=3.6-5.7). Carotid IPH was associated with ulceration (RR=7.2*, 4.5-13.8) and >70% stenosis (6.0*, CI=2.6-13.8). There was a trend toward association with intraluminal thrombus, but this did not reach significance (RR=2.7, CI=0.9-5.6, p=0.056). In addition, the presence of IPH further modified the risk of stroke in >70% stenosis (RR=2.2$^{\#}$, CI=1.1-2.2) and ulceration (RR=2.3$^{\#}$, CI=1.1-6.1). Interestingly, IPH did not modify the stroke risk in the setting of intraluminal

Note: Scanned images are included in the proceedings. Some submitted images were reduced during editing, thereby decreasing clarity. Also, refer to the Program Planner. Proceedings Content as of 3-29-2013.

thrombus (RR=1.0), since all patients with intraluminal thrombus had acute ischemic events (PPV=100%). (*p<0.001, $^{\#}$p<0.05).

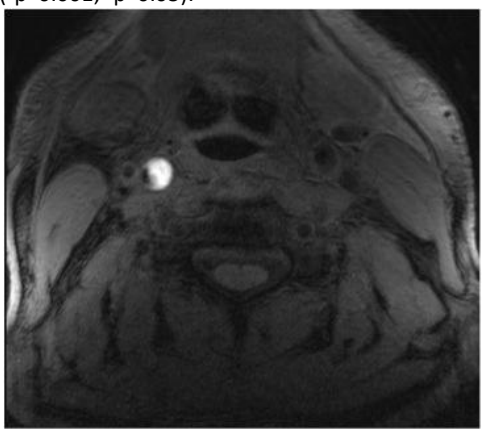

Conclusion

In this retrospective study, carotid IPH was found to be an independent risk factor for ischemic stroke. This risk was on par with historic markers of plaque vulnerability including high-grade stenosis, ulceration, and intraluminal thrombus. Importantly, IPH modified stroke risk in the presence of >70% stenosis and ulceration. These results strongly argue against using plaque stenosis and morphology as sole determinates of stroke risk. By detecting IPH and refining stroke risk, carotid MRI will play an important role optimizing treatment and eliminating unneeded operations.

KEYWORDS: Intraplaque hemorrhage, Acute ischemic stroke

O-496 **11:01 AM - 11:09 AM**

Can CT Angiography Plaque Segmentation Predict *Recurrent* Events in Patients Presenting Initially with Stroke and TIA?: Evaluation in Moderate 50-70% Stenosis

Lum, C.·Perry, J.·Duan, S.·Sharma, M.·Ottawa Hospital Research Institute
University of Ottawa
Ottawa, ON, CANADA.

Purpose

CT angiography plaque segmentation techniques now are readily available via thin-client software and recently have been used to categorize carotid plaque volumetrically into lipid, fibrous and calcific components. Lipid-rich plaques are considered more vulnerable than calcified plaques and may be a target for revascularization techniques. In our centre, CTA is the preferred vascular imaging technique in acute stroke or TIA. Plaque component analysis has not been performed in patients presenting initially with TIA or stroke and moderate 50-70% stenosis. Plaque volume has been suggested to be a better predictor than stenosis measurements. Our objective was to determine if individual plaque components or plaque volumes in symptomatic patients with moderate stenosis can predict future recurrent ischemic events.

Materials & Methods

Between Nov 2006-Aug 2011, 2612 consecutive patients with TIA or minor stroke assessed in the emergency department at two large tertiary care hospitals were evaluated in a specialized stroke clinic. These patients were enrolled prospectively and assessed for subsequent TIA or stroke at 90 days by a blinded adjudication committee. All patients received a screening Doppler and a CTA was performed on those with stenosis. Patients with moderate stenosis on CTA were included in the current analysis. We segmented the carotid plaque in a semi-automated fashion (Terarecon) by a radiologist blinded to clinical outcome. The volume and percentage composition of plaques were calculated using the following HU thresholds: lipid<60, fibrous≤130, calcium>130.

Results

There were 102 patients with moderate stenosis: 28 patients had recurrent TIA/stroke versus 74 without. Mean plaque volume was greater in patients with recurrent stroke versus those without (1.66 versus 1.03 cm^3; p = 0.0007). Recurrent strokes had larger plaque volumes than recurrent TIAs (1.66 versus 1.06 cm^3; p = 0.0055). Receiver operating charcteristic analysis using an optimal threshold plaque volume of 1.1 cm^3 had a sensitivity = 87.5%, specificity = 66.3%, AUC = 0.78(p = 0.0004) for distinguishing recurrent strokes at followup from asymptomatics. There was no significant difference in proportion of lipid, fibrous and calcium in patients with versus those without recurrent symptoms (0.28 versus 0.26; 0.33 versus 0.31; 0.40 versus 0.42).

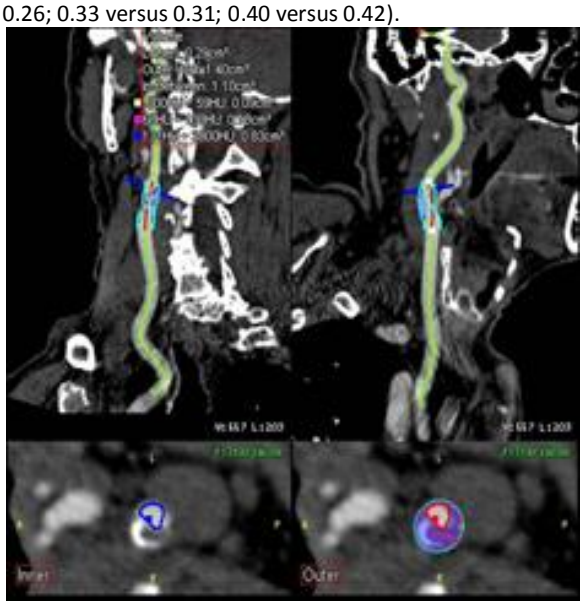

Conclusion

Patients presenting with TIA/stroke and moderate stenosis do not have a CTA plaque composition signature that predicts risk of future events. However, plaque volume is larger in patients who develop recurrent stroke. A

Note: Scanned images are included in the proceedings. Some submitted images were reduced during editing, thereby decreasing clarity. Also, refer to the Program Planner. Proceedings Content as of 3-29-2013.

threshold of > 1.1 cm^3 may be helpful for predicting recurrent stroke in a prospective study.

KEYWORDS: CT angiogram, Plaque imaging, recurrent stroke or TIA

O-497 **11:09 AM - 11:17 AM**

How to Manage Proximal Internal Carotid Artery Thrombus Identified on CT Angiography and MR Angiography in the Workup of Acute Stroke or Transient Ischemic Attack

Lum, C.·Jaberi, A.·Thornhill, R.·Stefanski, P.·Petrcich, W.·Momoli, F.·Iancu, D.·Dowlatshahi, D.·Ottawa Stroke Research Group
University of Ottawa/Ottawa Hospital Research Institute
Ottawa, ON, CANADA.

Purpose
Luminal filling defects at the ICA origin imaged in the workup of stroke/TIA may be due to an ulcerated plaque or rarely, free-floating thrombus (FFT). Accurate identification of FFT is critical because of the potential for distal embolization. There is a paucity of CTA/MRA imaging literature on FFT and its evolution, mostly described in single case reports. Controversy exists regarding its acute management: urgent endarterectomy versus medication. At our institution, we treat suspected FFT with antiplatelets or anticoagulation and perform imaging to evaluate its evolution. We have collected a large series of patients with suspected FFT. The purpose of our study was to describe the imaging appearance at presentation, evolution with therapy, clinical variables and mimics of FFT.
Materials & Methods
Twenty-five consecutive patients with suspected FFT, defined as proximal ICA filling defects in the axial plane surrounded by contrast, were identified at the ICA origin on CTA and MRA. Cases were collected prospectively between Feb 2008-May 2012 at an academic stroke center. Patient demographics, imaging features and clinical data were analyzed using univariate statistics. Free-floating thrombus was measured in the cranial-caudal dimension(finger length) by a vascular neuroradiologist blinded to clinical outcome. Filling defects resolving on follow-up imaging were defined as true+ FFT. Recursive partitioning analysis was performed to identify potential predictors for FFT. ROC analysis was performed to determine a threshold measurement for FFT.
Results
There were 24 cases imaged with CTA, one with MRA. Median follow-up CTA was at five days. Patients were managed medically with antiplatelets(28%), full anticoagulation(48%) or both(24%). In 20 patients(80%), the suspected FFT resolved or significantly improved; in five(20%) there was no change. There was no clinical deterioration on medical therapy. True+ FFT filling defects extended more cranially than false+ cases[7.25 mm(4.47-17.00 IQR) versus 4.30 mm(2.10-4.42 IQR), p=0.023]. Ipsilateral underlying stenosis was seen in 60%, the majority(83%) of stenoses measuring <50%. Using recursive partitioning, we found the presence of filling defects had a sensitivity of 85%, but low specificity=24%. ROC analysis using a threshold of 4.8 mm(finger length) improved performance with a sensitivity of 65%, specificity of 100% and AUC of 0.84(p<0.0001) for distinguishing FFT+ from FFT-(underlying plaque) cases.

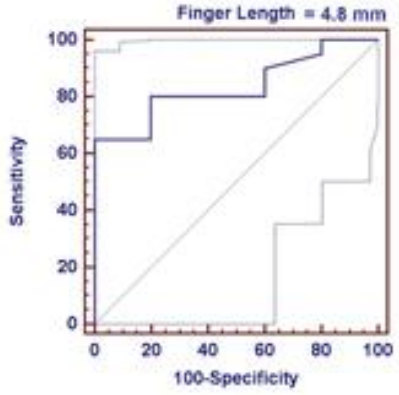

Conclusion
Suspected FFT on CTA resolves with antiplatelet and/or anticoagulant therapy without associated morbidity. A filling defect in the proximal ICA that extends cranially for >4.8mm is more likely to be FFT rather than ulcerated plaque. A prospective trial evaluating this threshold is warranted.

KEYWORDS: CTA, Thrombus imaging

O-498 **11:17 AM - 11:25 AM**

Association between Cervical Spine or Skull Base Fracture and Blunt Cerebrovascular Injury

Buch, K.·Nguyen, T.·Mahoney, E.·Libby, B.·Calner, P.·Burke, P.·Mian, A.
Boston Medical Center
Boston, MA.

Purpose
Blunt cerebrovascular injuries (BCVI) are associated with high morbidity and mortality and can lead to neurologic deficits. Prompt diagnosis and treatment of BCVI can limit the associated morbidity and mortality. While digital subtraction angiography has been the gold standard for diagnosing these injuries, computed tomographic angiography (CTA) is employed increasingly for evaluation in blunt trauma patients. The established criteria for recommending patients receiving CTA for evaluation of possible injury are broad, potentially exposing patients to unneeded radiation. The goal of this study was to examine the prevalence of vascular injury in patients with blunt trauma on CTA examination and to determine which

Note: Scanned images are included in the proceedings. Some submitted images were reduced during editing, thereby decreasing clarity. Also, refer to the Program Planner. Proceedings Content as of 3-29-2013.

presentations have the highest rates of vascular injury.
Materials & Methods
From 2007-2010, we instituted prospectively a protocol to screen trauma patients for blunt cerebrovascular injury following a predefined set of criteria at a Level I Trauma University Hospital. CT angiography studies were helically acquired at 1.25 mm slice thickness on 64 detector row CT scanners. The corresponding electronic medical records were reviewed on all subjects, including the initial patient presentation and hospital course. Statistical analysis of imaging and clinical data were performed using a Fisher test. The study was approved by the IRB.
Results
Four hundred thirty-nine patients were reviewed retrospectively for the presence of vascular injury. A positive CTA was defined as presence of vasospasm (n = 10) and dissection (n = 38) and found in 48/439 (10.9%) patients. Cervical spine or skull base fractures were present in 40/48 (83.3%) positive CTAs compared to 267/391 (68.2%) negative CTAs (p = 0.02). Three patients had a dissection in more than one artery. Thirty-eight of 48 patients (79.2%) had a diagnosis of dissection and 10/48 patients (20.8%) had a diagnosis of vasospasm. Thirty-two of 38 (84.2%) patients had both dissection and fractures compared to 6/38 patients (15.8%) with dissection without fracture. There was a significant correlation between dissection and fracture (p = 0.0016). Twenty-two of 439 patients (5%) presented with neurologic deficits attributed to cerebral contusion (10 patients), cerebral injury (six patients), cervical spine hematomas (two patients), and cervical spine cord injury (one patient). In three patients there was no obvious cerebrospinal injury to account for neurologic deficit. Thirteen of 22 patients (59%) with neurologic deficits had fractures. All 13 of these patients with neurologic deficits and fractures had positive CTAs. There was a significant correlation between neurologic deficits and positive CTA (p = 0.0001). No statistically significant correlation between neurologic deficits and underlying fractures (p = 0.66).
Conclusion
The presence of a blunt cerebrovascular injury is correlated with the presence of a cervical and/or skullbase fracture. There is also a correlation between blunt trauma with neurologic deficits and underlying vascular injuries with or without fractures. Patients with blunt trauma presenting with cervical spine and skull base fractures or focal neurologic deficits should have rapid CTA evaluation for suspected underlying vascular injury.

KEYWORDS: CTA, Balloon angioplasty, cerebrovascular injury

O-499 **11:25 AM - 11:33 AM**

CT Angiography for Screening of Complicated Atherosclerotic Carotid Plaque: American Heart Association Type VI Lesions as Defined by MR Imaging

Trelles, M.[1]·Buchholz, M.[2]·Schindler, A.[2]·Bayer-Karpinska, A.[2]·Dichgans, M.[2]·Reiser, M. F.[2]·Nikolaou, K.[2]·Saam, T.[2]
[1]University of Texas Medical Branch at Galveston, Galveston, TX, [2]Ludwig-Maximilians-University Hospital, Munich, GERMANY.

Purpose
High-resolution carotid MRI can accurately identify complicated American Heart Association lesion type VI (AHA-LT6) plaques, which are characterized by thrombus, hemorrhage or a ruptured fibrous cap. The purpose of this study is to evaluate whether CTA can be used as screening tool to predict the presence or absence of AHA-LT6 as defined by high-resolution MRI.
Materials & Methods
Fifty-one patients with suspected ischemic stroke or TIA with carotid CTA and high-resolution carotid MRI performed within 14 days of the event or admission from April 2008 to December 2010 were reviewed. Vessels with stents or occlusion were excluded (n=2). Each carotid artery was classified according to the MRI-based AHA lesion type classification. The maximum wall thickness, maximum soft plaque component thickness, maximum calcified component thickness and plaque density (if thickness of the soft plaque component >2 mm) was obtained from the CTA.
Results
Twenty-three out of 100 vessels had a complicated AHA-LT6 plaque by MRI representing presence of intraplaque hemorrhage, thrombus and/or a ruptured fibrous cap. The average maximum wall thickness and the maximum thickness of the soft plaque component of complicated plaques was significantly higher compared to noncomplicated plaques (5.3±0.4 versus 3.9±0.3 mm; P<0.001 and 4.7±0.5 versus 2.2±0.3 mm, P<0.001, respectively). The mean soft plaque component density did not differ significantly between complicated and noncomplicated plaques (60±12 HU versus 72±12 HU; P=0.12). The maximum soft plaque component thickness proved the best discriminating factor to predict a complicated plaque by MRI with a relative operating characteristics area under the curve (ROC-AUC) of 0.897 ± 0.063. Maximum wall thickness performed less adequately with ROC-AUC of 0.81 ± 0.084. Hard plaque component thickness and HU measurements did not prove to be of diagnostic help. Utilization of maximum, minimum and average HU value made no difference in the discriminatory power. The optimal sensitivity and specificity for detection of complicated plaque by MRI was achieved with a soft plaque component thickness threshold of 4.4mm (sensitivity:0.65, specificity:0.94, PPV:0.75 and NPP:0.9). No complicated plaque had a soft tissue plaque thickness lower than 2.2 mm (NPV:1) and no simple

Note: Scanned images are included in the proceedings. Some submitted images were reduced during editing, thereby decreasing clarity. Also, refer to the Program Planner. Proceedings Content as of 3-29-2013.

(noncomplicated) plaque had a thickness greater than 5.6 mm (PPV:1).

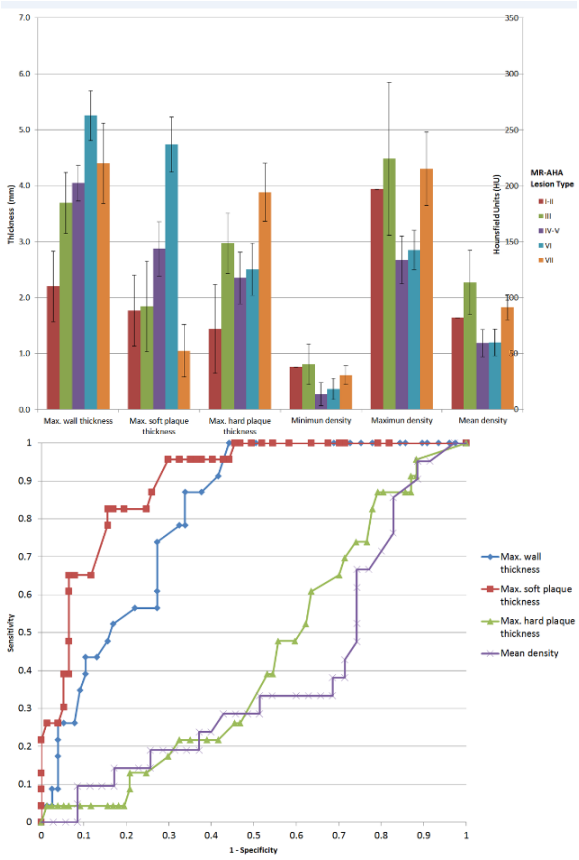

Conclusion

This study demonstrates that CTA can be used as a screening tool to predict the presence/absence of complicated AHA-LT6. Maximum soft plaque component thickness has the best discriminatory power with a threshold of 2.2 mm representing little to no probability of a complicated AHA-LT6 plaque.

KEYWORDS: Carotid plaque, Atherosclerosis

O-500 **11:33 AM - 11:41 AM**

Stenosis Asymmetry Index between Symptomatic and Asymptomatic Patients in the Analysis of Carotid Arteries with Severe Stenosis

Saba, L.[1]·Montisci, R.[1]·Raz, E.[2]·Porcu, M.[1]·Fatterpekar, G.[2]·Piga, M.[1]
[1]AOU Cagliari, Cagliari, ITALY, [2]University of New York, New York, NY.

Purpose

Extracranial carotid artery stenosis is accepted as a significant risk factor for cerebrovascular events. The purpose of this work was to compare the stenosis asymmetry index (SAI) in symptomatic and asymptomatic patients with a severe stenosis of carotid arteries.

Materials & Methods

Eighty-five consecutive symptomatic patients (males 52; median age 67 years) and 85 consecutive nonsymptomatic patients matched for gender and age, were analyzed by using a 40 detector-row CT angiography. Stenosis degree of 340 carotids was calculated according to NASCET method. Only patients with at least one carotid stenosis > 70% NASCET were included. For each patient, the ratio between the most severe stenosis and the contralateral was calculated to obtain the SAI. Wilcoxon test was applied to evaluate difference between asymmetry index in symptomatic and asymptomatic group. Receiver operating characteristic (ROC) curve also was calculated.

Results

Fourteen patients were excluded because of a stenosis < 70% NASCET. Results of our study indicate a mean SAI of 1.44 (95% CI 1.34 -1.53) in asymptomatic group and a mean SAI of 1.88 (95% CI 1.72 - 1.92) in the symptomatic group with a statistically significant difference (p value = 0.0018). The ROC curve analysis indicated that an SAI value of 1.8 has a specificity of 87% for the presence of cerebral symptoms whereas to have a sensitivity of 90% we should use a 1.5 SAI.

Conclusion

Our results indicate that the SAI can be used as further parameter to stratify the stroke risk related to carotid artery in those patients with a NASCET stenosis > 70%.

KEYWORDS: Carotid, CTA

O-501 **11:41 AM - 11:49 AM**

Is There an Association between Carotid Artery Dissection and Vessel Tortuosity?

Saba, L.[1]·Raz, E.[2]·Argiolas, G. M.[3]·Fatterpekar, G.[2]·Suri, J. S.[4]·Siotto, P.[3]·Piga, M.[1]
[1]AOU Cagliari, Cagliari, ITALY, [2]University of New York, New York, NY, [3]Ospdale Brotzu, Cagliari, ITALY, [4]Biomedical Technologies, Pocatello, ID.

Purpose

Carotid artery dissection is an important cause of ischemic stroke in all age groups, in particular young subjects. The purpose of this work was to assess whether there is an association between the presence of carotid artery dissection (CAD) and vessel tortuosity.

Materials & Methods

In this multicentric analysis, one hundred three patients (males 62; median age 58 years) with CT/MR diagnosis of CAD of internal carotid artery were analyzed retrospectively. The vessel tortuosity was evaluated and when present was categorized as tortuous, kinking, coiling. For each patient both right and left side were considered for a total number of 206 in order to have a similar number of case control. Fisher's exact test was applied to test the association between tortuosity, kinking, coiling, dissection and the side affected by CAD.

Results

Note: Scanned images are included in the proceedings. Some submitted images were reduced during editing, thereby decreasing clarity. Also, refer to the Program Planner. Proceedings Content as of 3-29-2013.

No patients were excluded and Fisher's test showed that there was a statistically significant association between the CAD and kinking (p = 0.009) and coiling (p = 0.046) whereas no statistically significant difference was found with the vessel tortuosity (p = 0.304). We found that the side (left or right) plays a statistically significant role in the risk of CAD (p = 0.0001).
Conclusion
The presence of kinking and coiling are statistically significantly associated with an increased risk to CAD. The underlying causes that determine the increased risk of CAD may therefore be genetic predisposition or geometrical ones. The CADs show a statistically significant association with the left side.

KEYWORDS: Carotid artery, CTA

O-502 **11:49 AM - 11:57 AM**

Localized Gray Matter Changes in Acute Stroke

Gupta, J.·Young, B.·La, C.·Reiter, P.·Jensen, M.·Chacon, M.·Sattin, J.·Nair, V. A.·Prabhakaran, V.
University of Wisconsin
Madison, WI.

Purpose
Global gray matter volume decreases linearly with age.There is evidence that changes in subcortical gray matter volume is associated with cognitive impairment after ischemic stroke (3-6 months). We investigated 1) gray matter differences between acute noncortical stroke patients, patients with risk factors for stroke, and healthy controls and 2) gray matter changes associated with behavioral performance after a stroke.
Materials & Methods
Patients with acute stroke (N = 11, noncortical ischemic stroke within seven days of stroke onset, mean age 58 years, six M), patients with risk factors for stroke (N = 5, mean age 69 years, three M) and age-matched healthy controls (N = 17, mean age = 56 years, 10 M) were scanned on a GE 3T MRI scanner. High-resolution 3D T1-weighted whole brain BRAVO FSPGR images were collected with: repetition time TR = 8.13 ms, echo time TE = 3.18 ms, flip angle = 12,156 slices, voxel resolution 1 mm isotropic. The subjects also performed a letter fluency task (word generation-FAS task) which was collected outside the scanner and corrected for age and education. Gray matter changes were assessed using VBM8 toolbox and SPM8 in Matlab. Further groupwise gray matter volume changes and cortical thickness in areas of interest also were analyzed using Freesurfer in a subset of five noncortical stroke (average age 56 years, three M) and 13 healthy controls (average age 56 years, seven M).
Results
There was a significant group difference between acute noncortical stroke patients and healthy controls on the verbal task (p<.05) with patients scoring less (mean score = 35) than healthy controls (mean score = 49). Two sample t tests indicated significant group differences between strokes and controls in gray matter volume in regions of bilateral inferior temporal, bilateral middle temporal, right post central, and right lingual gyrus (p<.001 (uncorrected), extent threshold 20 voxels). Analysis with verbal fluency score as covariate identified differences in the left inferior temporal and left middle temporal regions (p<.001 (unc), extent threshold 20 voxels).There were no significant differences between healthy controls and patients with risk factors for stroke. In a subset of patients, Freesurfer analysis of cortical thickness and volume showed a significant difference in left inferior temporal cortical thickness at p<.007 (unc) and Lt transverse temporal volume at p<.02 (unc).
Conclusion
There are localized cortical gray matter changes notably in the temporal lobe in acute periods of noncortical stroke patients showing significant association with verbal fluency deficits in these patients. This suggests that acute noncortical stroke may induce cortical regional changes in gray matter volume. This could be attributed to remote effects of stroke as well as chronic changes due to risk factors for stroke. Further studies will test this and compare stroke patients with patients with risk factors for stroke.

KEYWORDS: Stroke, MR imaging brain

O-503 **11:57 AM - 12:05 PM**

Penumbra Imaging in Patients with Acute Stroke Using Susceptibility-Weighted MR Imaging

Radbruch, A.[1]·Mucke, J.[1]·Graf, M.[2]·Floca, R.[2]·Schlemmer, H.[2]·Heiland, S.[1]·Bendszus, M.[1]·Rohde, S.[1]
[1]University of Heidelberg, Heidelberg, GERMANY, [2]German Cancer Research Center (DKFZ), Heidelberg, GERMANY.

Purpose
Although increasingly used for the clinical management of patients with acute ischemic stroke the mismatch concept, based on MR perfusion and diffusion imaging, has come under debate, since it is reported that time to peak (TTP) maps, generated from PWI, tend to overestimate the tissue at risk. Susceptibility-weighted imaging (SWI) has been reported to enable the identification of the tissue at risk in patients with acute ischemic stroke due to the visualization of hypointense vessels within the hypoxic area. The aim of this study was to assess size of the penumbra determined by either SWI or TTP perfusion maps and calculate their intersection.
Materials & Methods
Seventy patients with ischemic infarction proved by clinical symptoms (NIHSS>2) and a reduced perfusion on the TTP perfusion map determined by dynamic susceptibility contrast perfusion images (TE 35, TR 1920, FoV 240, 75 dynamic scans, injection of 0.1 mmol/kg DOTAREM with bolus technique after the third frame followed by 20 ml of NaCl solution) were included. Alterations of SWI were

Note: Scanned images are included in the proceedings. Some submitted images were reduced during editing, thereby decreasing clarity. Also, refer to the Program Planner. Proceedings Content as of 3-29-2013.

defined as a conglomeration of vessels presenting a higher diameter than vessels on the contralateral, nonischemic hemisphere (Figure). Regions of altered SWI, restricted diffusion on diffusion-weighted images (DWI) and reduced perfusion on PWI were delineated manually on SWI, apparent diffusion coefficient (ADC) DWI and TTP maps. Subsequently, the maps were coregistered automatically and intersections of the determined regions were calculated and visualized using in-house developed software.

Results

In all patients the area of SWI alterations could be delineated. Mean size of the delineated SWI region (2994.8 mm^2±1097.3) was significantly smaller than size of the delineated TTP maps (3626.6 mm^2±1315.5) ($p>0.0001$) but significantly larger than areas on ADC diffusion maps (1396.6 mm^2±1102.0) ($p>0.0001$). Median intersection of TTP and SWI was 73.6%±28.6% of the delineated TTP area, SWI and ADC intersected on 34.0%±32.1% of the size of SWI area.

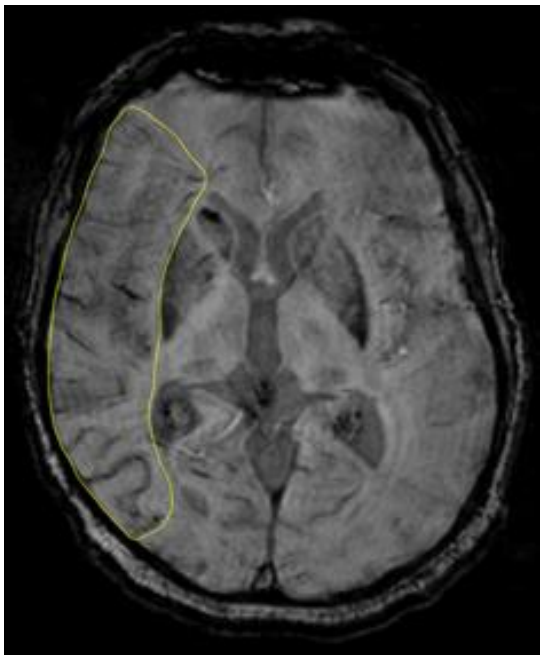

Conclusion

Since the identified region on SWI was significantly smaller than on the TTP map, that supposedly overestimates the tissue at risk, SWI may determine the size of the penumbra more accurately. Further studies are required to clarify the pathomechanism of SWI alterations and verify our findings considering follow-up images and patient outcome. Until then SWI provides a valuable tool in addition to PWI for penumbra estimation and treatment decision. Since SWI does not require contrast agent injection, it can be used in patients with contraindications to contrast agents.

KEYWORDS: Penumbra, Susceptibility-weighted imaging

O-504 **12:05 PM - 12:13 PM**

High Baseline CT ASPECTS Correlates with Perfusion-Based Patient Selection, but May Be Poor Discriminator of Functional Outcomes

Honarmand, A. R.·Soltanolkotabi, M.·Prabhakaran, S.·Hurley, M. C.·Shaibani, A.·Rahman, O.·Ansari, S. A.
Northwestern University Feinberg School of Medicine
Chicago, IL.

Purpose

Appropriate patient selection in acute ischemic stroke (AIS) is central for improving patient outcomes following intra-arterial (IA) reperfusion therapy (thrombolysis/mechanical thrombectomy). Perfusion imaging with CTP/MR DWI-PWI has been utilized increasingly to identify subpopulations with acceptable risk-benefit profiles for reperfusion, avoiding futile or harmful recanalization. Earlier studies reported to have prognostic value of baseline Alberta Stroke Program Early CT Score (ASPECTS) of >7 in determining good functional outcomes following IA reperfusion. We investigated baseline CT ASPECTS in AIS patients selected for IA reperfusion therapy based on perfusion mismatch profiles. Furthermore, we studied the predictive value of CT ASPECTS for clinical outcomes following recanalization.

Materials & Methods

In a multicenter review, all AIS patients that underwent IA thrombolysis/thrombectomy between January 2010 and September 2012 were studied retrospectively for the following inclusion criteria: baseline NIHSS >8, presentation <8 hours from symptom onset, CTA/MRA verified M1-M2 MCA occlusion, and favorable perfusion (CTP/MR DWI-PWI) mismatch profile. Patient demographics, medical comorbidities, time from symptom onset to recanalization, final recanalization (TICI scale), and clinical outcomes (90 day modified Rankin Scale) were obtained. One neuroradiologist conducted blinded scoring of ASPECTS for all baseline noncontrast CT scans. For evaluation of inter-rater reliability, scores by another neuroradiologist were used and analyzed using Intraclass Correlation Coefficient (ICC) and Bland and Altman method. ASPECTS scores were dichotomized into >7 and ≤7 for primary analysis. Chi-square, Mann-Whitney U and student *t* tests were used for univariate analyses as appropriate. To obtain the optimal cut-off ASPECTS for discriminating patients with favorable outcomes, receiver operating characteristic (ROC) curve analysis was performed.

Results

Fifty-six consecutive patients (29 male/27 female patients with mean age of 71±16 years) met inclusion criteria for analysis. Successful recanalization (TICI > 2b/3) was achieved in 34 patients (60.7%), highly correlating with good functional outcomes (mRS 0-2) in 36 patients (64.3%) ($P < 0.005$). No significant difference was observed between ASPECTS reading ($P=0.6$) with good inter-rater reliability (ICC=0.80, 95% confidence interval: 0.63 to

Note: Scanned images are included in the proceedings. Some submitted images were reduced during editing, thereby decreasing clarity. Also, refer to the Program Planner. Proceedings Content as of 3-29-2013.

0.87). No significant differences were observed in baseline characteristics between groups with ASPECTS >7 (37 patients) and ≤7 (19 patients) (age, P=0.9; sex, P=0.9; baseline NIHSS score, P=0.3; diabetes, P=1.0; atrial fibrillation, P=0.5; hyperlipidemia, P=1.0; hypertension, P=0.5; time from symptom onset to recanalization, P=0.1). Relatively high ASPECTS correlated with perfusion-based patient selection with mean and median baseline ASPECTS of eight. However, no significant correlation was observed between baseline ASPECTS and final clinical outcomes (P=0.6). Additionally, baseline ASPECTS score >7 did not correlate with final outcome in patients with successful recanalization (P=0.4). The ROC curve analysis demonstrated a cut-off point of eight for discrimination of final outcome, but with poor predictive value (sensitivity=47.1%; specificity=68.7%; P=0.7, AUC=0.52).
Conclusion
Our results indicate favorable baseline CT ASPECTS correlate with favorable perfusion mismatch profiles and may represent an equivalent surrogate for primary patient selection in IA reperfusion therapy. However, CT ASPECTS did not clearly predict good functional outcomes independent of recanalization, suggesting other confounding variables such as core infarct volume versus eloquence may impact clinical outcomes and have to be elucidated.

KEYWORDS: ASPECTS, Stroke, Functional outcome

Thursday Morning

10:45 AM - 12:15 PM
Room 5AB

(56d) Parallel Scientific Papers: Pediatrics: Functional Imaging and New Techniques

O-505 **10:45 AM - 10:53 AM**

Structural Connectivity Alterations in Brain Networks in Pediatric Hydrocephalus: A Pilot Study

Jones, B. V.[1]·Shimony, J. S.[2]·McKinstry, R. C.[2]·Mangano, F. T.[1]·Limbrisk, D. D.[2]·Nash, T.[1]·Simpson, S.[1]·Rajagopal, A.[1]·Holland, S. K.[1]·Phillips, J. M.[1]·Powell, S. K.[2]·Mercer, D.[2]·Altaye, M.[1]·Yuan, W.[1]
[1]Cincinnati Children's Hospital, Cincinnati, OH,
[2]Washington University School of Medicine, St. Louis, MO.

Purpose
This study seeks to investigate the impact of brain injury as reflected in the topological features of brain networks in children with hydrocephalus (HCP). Increased intracranial pressure and ventriculomegaly in HCP can lead to white matter structural displacement and distortion. Resulting damage has been found in multiple areas in the brain, especially in major white matter tracts that connect and transfer information among functional brain regions. The goal of this study was to investigate structural network connectivity in children with HCP using graph theoretical analysis. It was hypothesized that both global and regional topological connectivity features of brain networks in children with HCP are abnormal compared to controls.
Materials & Methods
Three groups of children were included in the study. (Group 1: controls, n = 10, age 1.1-6 years; Group 2: HCP patients before CSF diversion surgery, n = 4, age 2.1-16.2 years; Group 3: HCP patients 3-12 months after CSF diversion surgery, n = 5, age = 1.6-16.3 years). Informed consents or assent were obtained during the enrollment. Diffusion tensor imaging (DTI) data were acquired on 1.5T scanners using a single-shot EPI sequence (TR/TE = 9400/93.2 msec; resolution = 2.5 mm iso, 15 directions, b = 1000). The structural connectivity data processing and analysis pipeline followed the methodology described by Ferreira et al. Five global connectivity measures (global coefficient, characteristic path length, clustering coefficient, small-worldness, modularity) and four regional connectivity measures (degree, betweeness centrality, nodal clustering coefficient, regional coefficient) were calculated. Group comparisons were made between Group 1 with Groups 2 and 3 separately, using Mann-Whitney U-test at significance level of $p<0.05$.
Results
Global network measures - Compared to the controls, no significant change was found for the Group 2 in any of the global network measures. There was statistically significant decrease in the normalized clustering coefficient ($p = 0.02$), modularity ($p = 0.007$), and a trend of decrease in the small-worldness ($p = 0.07$) in Group 3. Regional network Measures - Extensive brain network regions were found to have significant changes in the regional network measures. In both Group 2 and Group 3, cingulate gyrus and the middle occipital lobe gyrus were found to have significant changes (or at least at trend level) in all the four regional network measures examined. Initial results also showed that the change in the measure of nodal degree was region specific: the cingulate gyrus in both patient groups had a significantly higher nodal degree than the controls, while the mid-occipital lobe gyrus in both patient groups had significantly lower nodal degree than the controls.
Conclusion
Our data showed that graph theoretical analysis using DTI data is sensitive in the detection of abnormalities of brain network connectivity at both global and regional levels, providing a new avenue in quantifying brain damage in children with hydrocephalus.

KEYWORDS: Hydrocephalus, DTI, Connectivity, Graph Theory

Note: Scanned images are included in the proceedings. Some submitted images were reduced during editing, thereby decreasing clarity. Also, refer to the Program Planner. Proceedings Content as of 3-29-2013.

O-506 **10:53 AM - 11:01 AM**

Reorganization of the Remaining Brain after Hemispherectomy: A Diffusion Tensor Imaging Study

Meoded, A.·Faria, A. V.·Bastian, A. J.·Jallo, G.·Hartman, A. L.·Mori, S.·Huisman, T. A. G. M.·Poretti, A.
Johns Hopkins Hospital
Baltimore, MD.

Purpose
Hemispherectomy should reduce the burden of seizures and the general dysfunction in children with severe or progressive unilateral cortical epilepsy. Etiologies of intractable seizures requiring hemispherectomy include congenital (e.g., hemimegalencephaly) and postnatally acquired (e.g., Rasmussen encephalitis) causes. In a large cohort of patients after hemispherectomy, we aimed to evaluate the architecture of 1) projection (e.g., corona radiate), association [e.g., cingulum, supero-fronto-occipital fasciculus (SFO)], and commissural (e.g., corpus callosum) white matter fibers and 2) cortical and deep gray matter structures of the remaining, nonaffected cerebral hemisphere.
Materials & Methods
The inclusion criteria were: 1) Status posthemispherectomy and 2) availability of postsurgical DTI data. Diffusion tensor imaging data were acquired using 1.5/3T MR scanner. Age- and gender-matched controls were selected from our pediatric DTI database. Diffusion tensor imaging postprocessing including atlas (ABA)- and voxel (VBA)-based analysis was performed using MRI Studio software. With ABA we measured fractional anisotropy (FA), mean (MD), axial (AD), and radial (RD) diffusivity of the projection, association and commissural white matter fibers and FA of the cortical and deep gray matter of the remaining hemisphere. One-way ANOVA and Tukey's significant difference test were used to access differences between patients and controls. With VBA we assessed DTI metrics' differences between patients and healthy controls using a two-sample *t*-test.
Results
Nineteen patients (mean age 13.3 years) and 21 age- and gender-matched healthy controls (mean age 12.5 years) were included in the study. Mean age at surgery and time since surgery were 4.15 and 7.12 years, respectively. Eleven patients had a congenital, eight patients a postnatally acquired pathology requiring hemispherectomy. Compared to controls, in patients the ABA revealed 1) lower FA values in the anterior (ACR) and posterior corona radiata (congenital), cingulum (congenital<acquired), and callosal genu, body and splenium (congenital), 2) higher MD values in the cingulum and callosal genu and splenium (congenital and acquired), SFO, congenital) and callosal corpus (acquired), 3) lower AD values in the callosal genu and splenium (congenital) and cingulum (acquired), and 4) higher RD values in the callosal genu, corpus, and splenium (congenital and acquired), SFO and ACR (congenital), and cingulum (acquired). ABA of the gray matter structures showed reduced FA values in the superior frontal, temporal, parietal, occipital, pre and postcentral, and cingulate gyri in patients compared to controls. Compared to ABA, VBA showed similar FA and more pronounced MD and RD changes for the studied structures.
Conclusion
Using DTI, we were able to quantifiy brain reorganization within the remaining cerebral hemisphere after hemispherectomy. A decrease in FA and AD and increase in RD and MD of the white matter fibers reflects secondary Wallerian degeneration. Wallerian degeneration appears to be more severe in commissural and association, than projection fibers. A decrease in FA values in gray matter structures most likely is explained by increased unoccupied interecellular space. This might be due to a change in neuronal cell density and/or be the result of reduced cortical neuropil.

KEYWORDS: Cerebral cortex, Hemimegalencephaly, Rasmussen syndrome

O-507 **11:01 AM - 11:09 AM**

Reorganization of the Infratentorial White Matter Tracts after Hemispherectomy: A Diffusion Tensor Imaging Study

Meoded, A.[1]·Faria, A. V.[1]·Bastian, A. J.[2]·Jallo, G.[1]·Hartman, A. L.[1]·Mori, S.[1]·Huisman, T. A. G. M.[1]·Poretti, A.[1]
[1]Johns Hopkins Hospital, Baltimore, MD, [2]The Kennedy Krieger Institute, Baltimore, MD.

Purpose
Hemispherectomy aims to reduce the burden of seizures and the general dysfunction in children with severe or progressive unilateral cortical epilepsy. Etiologies of intractable seizures requiring hemispherectomy include congenital (e.g., hemimegalencephaly) and postnatally acquired (e.g., Rasmussen encephalitis) causes. Little is known about the reorganization of the infratentorial white matter tracts after hemispherectomy. In a large cohort of patients after hemispherectomy, we aimed 1) To evaluate differences in DTI metrics and volume between the ipsi-/contra-lesional corticospinal tract (CST), medial lemniscus (ML), middle cerebellar peduncle (MCP), and cerebellar hemisphere and 2) To correlate the values of the studied parameters with the age at and time since surgery.
Materials & Methods
The inclusion criteria were: 1) Status posthemispherectomy and 2) availability of postsurgical diffusion tensor imaging (DTI) data. DTI data were acquired using 1.5/3T MR scanner. Different acquisition protocols were used. DTI postprocessing included atlas (ABA)- and voxel (VBA)-based analysis and was performed using MRI Studio software. With ABA we measured the volume, fractional anisotropy (FA), mean (MD), axial (AD), and radial (RD) of the bilateral CST, ML, and MCP and the size of the cerebellar hemispheres. Symmetry between

Note: Scanned images are included in the proceedings. Some submitted images were reduced during editing, thereby decreasing clarity. Also, refer to the Program Planner. Proceedings Content as of 3-29-2013.

ipsi-/contra-lesional structures was determined with the laterality index, LI = (ipsi-contra)/(ipsi+contra). One-way ANOVA and Tukey's significant difference test were used to analyze data obtained from ABA. Spearman's rank correlation test was used to correlate age at/time since surgery with DTI metrics/volume of the studied structures. With VBA we assessed DTI metrics' differences between patients and healthy controls using a two-sample *t*-test.
Results
Nineteen patients (mean age 13.3 years) and 21 age- and gender-matched healthy controls (mean age 12.5 years) were included in the study. Mean age at surgery and time since surgery were 4.15 and 7.12 years, respectively. Eleven patients had a congenital, eight patients a postnatally acquired etiology for hemispherectomy. For the CST, ABA showed a significantly negative LI for volume, FA, and AD (=smaller volume and lower values ipsi-lesionally) and positive LI for MD and RD (=higher values ipsi-lesionally) for patients (acquired>congenital) compared to controls. A significantly positive LI of the cerebellar volume (=smaller size contra-lesionally) and negative LI for MD and RD (=higher values contra-lesionally) of the MCP was found for patients (congenital) compared to controls. An older age at surgery correlated significantly with a smaller volume and positive LI for MD and RD values of the contra-lesional cerebellar hemisphere and MCP, respectively. VBA confirmed the results of atlas-based analysis.
Conclusion
Our findings demonstrate the ability of DTI to quantify brain reorganization after hemispherectomy. A decrease in volume, FA, and AD and increase in RD of the ipsi-lesional CST reflects secondary Wallerian degeneration. Wallerian degeneration seems to be more severe in acquired than congenital etiologies for hemispherectomy. A smaller volume of the contra-lesional cerebellar hemisphere represents crossed cerebro-cerebellar diaschisis (CCCD). CCCD is secondary to Wallerian degeneration involving the main contra-lesional afferent cerebellar pathway (MCP) and is shown by increased MD and RD values. CCCD seems to be more severe in older patients at surgery reflecting higher reorganization in younger patients.

KEYWORDS: MR imaging brain, Brainstem, hemispherectomy

O-508 **11:09 AM - 11:17 AM**

7T MR Spectroscopy in Healthy Children: Relationship between Neuropsychologic Performance, N-Acetylaspartate and Glutamate Concentrations

Horska, A.[1]·Wang, X.[1]·Ryan, M.[2]·Denckla, M.[2]·Barker, P.[1]·Mahone, E. M.[2]
[1]Johns Hopkins University, Baltimore, MD, [2]Kennedy Krieger Institute, Baltimore, MD.

Purpose
Maturation of the prefrontal and frontal-striatal systems in children is paralleled by development of higher-order cognitive functions. As disruption of neural circuits involving the frontal cortex and its striatal-thalamic-cerebellar connections may contribute to development of neuropsychiatric disorders, studies in healthy children may help to interpret findings in patients. The goal of this ^{1}H MRS study was to evaluate the relationship between frontal, premotor, and striatal concentrations of the neuronal marker N-acetylaspartate (NAA) and the neurotransmitter glutamate (Glu) and neurobehavioral assessment in healthy children.
Materials & Methods
A group of 20 healthy children 5-10 years old (mean age 7.3 ± 1.6 years, eight boys) participated in this IRB-approved study. The neuropsychologic evaluation included tests of IQ, language, reading, neuromotor function, attention, working memory (verbal, spatial), and visual perception. MR imaging (3D-MPRAGE) and single voxel ^{1}H MRS (STEAM, TR/TE/TM = 3000/14/26 ms, SW = 3000 Hz, 2048 data points, NS = 96 and NS = 4 for water-unsuppressed spectra, voxel volume = 5-9 ml) were performed at 7T using a 32-channel volume head coil. Spectra were acquired in the left hemisphere in the anterior cingulate (ACC), dorsolateral prefrontal cortex (DLPFC), premotor cortex (PMC), and the striatum (STR). Metabolite concentrations were evaluated using the LCModel and were corrected for CSF. General linear model ANOVA was applied to examine the relationship between neuropsychologic performance and concentrations of NAA and Glu and the concentration ratios Glu/creatine (Cr) and NAA/Cr, controlling for age.
Results
On the test of auditory working memory, the performance improved with increasing NAA in the DLPFC and STR (both $p<0.05$), but was not associated with Glu concentration, Glu/Cr and NAA/Cr ratios. There was a significant correlation between motor performance (PANESS) and Glu, such that children with poorer performance on the measures of motor speed and response inhibition had higher Glu and NAA concentrations in the PMC and in the striatum, respectively (all $p<0.05$). No significant associations between motor performance and Glu/Cr or NAA/Cr ratios were detected. We also tested for a correlation between NAA and Glu concentrations; in all regions, a strong positive correlation was found (all $p<0.0001$).
Conclusion
In typically developing children, the hypothesized relationship between NAA concentration and cognitive performance followed the anticipated direction on the test of auditory working memory but not on the test of motor performance. In studies including adult patients, higher Glu levels were reported with better cognitive performance, while lower Glu concentration with improving performance was detected in our study. More data thus are needed to explain this apparent discrepancy, which may be due in part to examination of only healthy children in our study, although the positive correlation

Note: Scanned images are included in the proceedings. Some submitted images were reduced during editing, thereby decreasing clarity. Also, refer to the Program Planner. Proceedings Content as of 3-29-2013.

between gray matter Glu and NAA concentrations is in agreement with results in healthy adults (hippocampal region). Future plans include comparisons between healthy children and patients with neuropsychologic disorders (e.g., ADHD).

KEYWORDS: 1H MRS, 7T

O-509 **11:17 AM - 11:25 AM**

Development of Structural Brain Networks and Network-Driven Cortical Modules

Tymofiyeva, O.·Hess, C. P.·Ziv, E.·Lee, P. N.·Glass, H. C.·Ferriero, D. M.·Barkovich, A. J.·Xu, D.
University of California San Francisco
San Francisco, CA.

Purpose
Perinatal disease and premature birth affect more than one in 10 of all babies born around the world and put infants at risk of adverse neurodevelopmental outcome. Application of effective therapies in a timely and targeted manner depends on our ability to detect and monitor individual deviations from anticipated normal developmental trajectories. MR imaging connectomics enables noninvasive mapping of brain networks. However, mapping the developing newborn brain networks poses challenges, since atlases commonly used for brain parcellation might not match with function and anatomy during early brain development. The purpose of this study was to examine the maturational changes of the cortical connectome using a template-free network-driven analysis of white matter connectivity.
Materials & Methods
Diffusion MRI was performed in eight prematurely born neonates (gestational age at birth 27-30 weeks, at scan 31-40 weeks), eight term-born neonates, and 10 six-month-old infants; the two latter groups had transient encephalopathy at birth but no clinical or imaging evidence of brain injury. Seven healthy adults (age 24-31 years) were included to represent the mature brain. The subjects were scanned on a 3T MR scanner using SE EPI with a FOV=24-25.6cm, 128×128, slice thickness 1.8-2mm, 30 directions, b=600s/mm2 for preterm babies, b=700s/mm2 for term and six-month-olds, and b=1000s/mm2 for adults. To assess structural networks, the “baby connectome” framework was employed, which included data quality assurance, deterministic whole-brain fiber tractography (Figure A), and template-free parcellation of the brain surface into 100 nodes based on equal area sphere partitioning. The resulting networks (Figure B) were assessed using the Brain Connectivity Toolbox. To identify modules, the spectral community detection algorithm was applied.
Results
The optimal number of modules was relatively consistent in all groups: 5-6 modules in the preterm group, 5-7 modules in the term-born neonates, 5-8 modules in the six-month-old infants, and 5-7 modules in the adults. In Figure C, we selectively show the obtained network-driven segmentation of the cortex into five modules for subjects from all age groups that showed a similar pattern. We also observed increasing brain network integration and decreasing segregation with age in term-born subjects, consistent with previous findings in the late developing human brain.

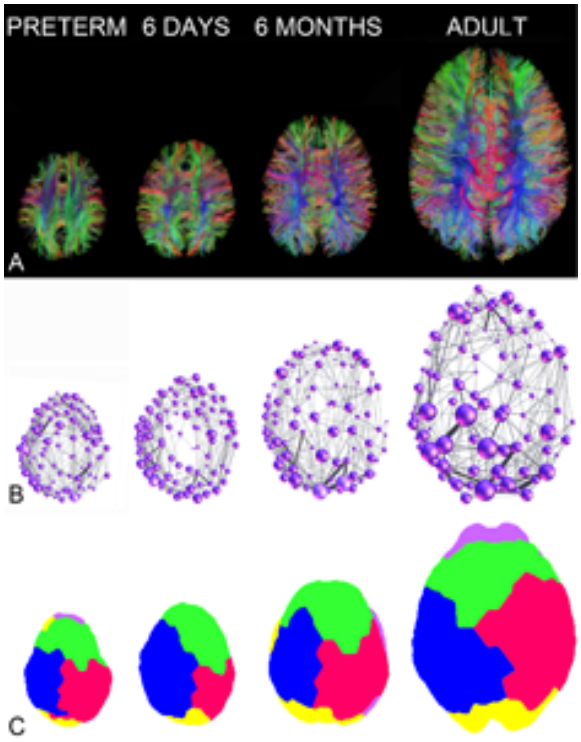

Conclusion
In this study, we explored how the structural brain network nodes can be grouped into modules without any prior anatomical information and observed a basic modular network topology that is present in the brain from the first days of life.

KEYWORDS: Connectivity, Diffusion MR imaging, Connectome

O-510 **11:25 AM - 11:33 AM**

Myelination Age: Establishing Normal Ranges for Myelination Status during Development Using a Histogram-Based Fractional Anisotropy Metric

Chin, E. M.[1]·Choudhri, A. F.[1,2]
[1]University of Tennessee Health Science Center, Memphis, TN, [2]Le Bonheur Children's Hospital, Memphis, TN.

Purpose
Conventional MR imaging typically shows near complete myelin maturation by approximately three years of age; however, it is known that myelin maturation progresses into adolescence. Research studies have shown changes in

Note: Scanned images are included in the proceedings. Some submitted images were reduced during editing, thereby decreasing clarity. Also, refer to the Program Planner. Proceedings Content as of 3-29-2013.

myelination, as determined by diffusion tensor imaging (DTI); however, measures such as mean fractional anisotropy (FA) have shown high variance making quantitative determination of age-appropriateness of myelination status difficult. We have applied a newly developed algorithm to measure fractional myelination (FM), a scanner-independent reproducible measure resistant to partial volume effects to a population of children with normal MRI scans to establish normal ranges throughout development.

Materials & Methods

This HIPAA compliant retrospective study was performed after IRB approval. Five hundred consecutive MRI scans on children under 18 years of age were evaluated. Studies were excluded if there was any definable structural abnormality as determined by neuroradiologist review. All studies has a volumetric T1-weighted sequence, as well as DTI with 15 noncollinear directions of encoding, a b-value of 1000 msec and a single b-0 acquisition. Registration and segmentation were performed within SPM. Fractional anisotropy was analyzed for intracranial white matter as a whole. Fractional myelination with optimized parameters then was calculated based on the FA histograms of each patient. A nomogram of FM over age then was calculated based on an exponential model FM(FA,t)=FM_max - A*exp(-t/tau) with 5th and 95th percentile bounds based on a Student's t-distribution.

Results

Two hundred seventy-five datasets met inclusion criteria and were able to be analyzed successfully. Fractional anisotropy shows exponential convergence to adult values with age, in agreement with previous studies. Similarly, fractional myelination, or the ratio of maturely myelinated white matter as a percentage of total white matter volume also increases throughout childhood before asymptotically approaching adult values. Using FM, we have created a nomogram for assessment of myelination status.

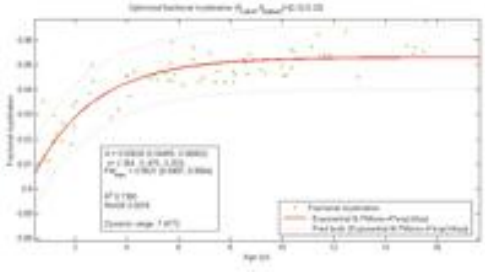

Conclusion

Statistical analysis of DTI metrics confirms the ability to follow myelin maturation from birth through adolescence. Reference values based on statistical analysis of DTI metrics may allow identification of myelination anomalies in a clinical setting. Difffusion tensor imaigng appears to be a more sensitive and reproducible method of assessing myelination than conventional T1- and T2-weighted sequences, and this may serve as the foundation for automated myelination age determination.

KEYWORDS: Myelination, Diffusion tensor image, normal development

O-511 **11:33 AM - 11:41 AM**

Brain Diffusion Tensor Imaging and Volumetric Analysis in Young Children with Autism Spectrum Disorder

Pichiecchio, A.[1]·Carigi, T.[1,2]·Bergsland, N.[1,2]·Palesi, F.[2]·Di Perri, C.[1]·Lucignani, G.[3]·Rossi, G.[1]·Balottin, U.[1,2]·Bastianello, S.[1,2]

[1]Neurological National Institute I.R.C.C.S., Pavia, ITALY, [2]University of Pavia, Pavia, ITALY, [3]University La Sapienza, Rome, ITALY.

Purpose

Since the hypothesis of autism as a disconnection syndrome has been proposed, advanced MRI techniques have taken a great part in its research. Nevertheless, although autism is considered a very early onset disorder, few diffusion tensor imaging (DTI) and volumetric studies focused on the first years of life. We aimed to investigate whether DTI metrics and volumetric analysis could detect regional abnormalities in young autism spectrum disorder (ASD) children.

Materials & Methods

A sample of 22 pre-school ASD children (mean age 44.45 months ± 10.6) and 10 age-matched controls were selected and underwent a conventional and advanced MRI protocol (1.5T), including DTI with 15 directions and 3D T1-weighted imaging. The Diffusion Trackvis Toolkit was used to compute fractional anisotropy (FA) and mean diffusivity (MD) from DTI images, for each voxel in the brain. A region-specific DTI analysis also was performed in the following brain regions: both frontal, parietal, temporal and occipital lobes, cerebellum, amygdale, hippocampi and corpus callosum. Whole brain tissue (BT), white matter (WM) and gray matter (GM) FA and MD histograms also were extracted. Cortical reconstruction and volumetric segmentation was performed with the FreeSurfer image analysis suite. Considering the small sample size, we considered more appropriate to perform a group comparison with the nonparametric Mann-Whitney test. Due to the exploratory nature of the study, a nominal p value of less than 0.05 was considered significant.

Results

No significant differences between ASD and controls were found neither in mean BT, WM and GM volumes nor in the region-specific volumetric analysis. Group comparison of FA and MD mean values and other histogram metrics for both WM and GM only showed significant differences in GM FA (FA mean: p = 0.026; peak height: p = 0.020; skewness: p = 0.041; kurtosis: p = 0.029). Diffusion tensor imaging region-specific group comparison showed significant reduced values in the following regions in ASD children with respect to controls: GM FA in all supratentorial regions analyzed, namely left and right frontal lobe (p = 0.006 and 0.001), left and right parietal lobe (p = 0.010 and 0.003), left and right temporal lobe (p

Note: Scanned images are included in the proceedings. Some submitted images were reduced during editing, thereby decreasing clarity. Also, refer to the Program Planner. Proceedings Content as of 3-29-2013.

= 0.008 and 0.009), left and right occipital lobe (p = 0.001), left and right hippocampi (p = 0.033 and p = 0.016), right amygdale (p = 0.037) and cerebellar hemispheres (p = 0.004); WM FA in the occipital lobes (p = 0.029 and 0.041) and cerebellum (p = 0.001 and 0.003); MD only in the right cerebellum, both for WM (p = 0.016) and GM (p = 0.041).
Conclusion
Volumetric analysis revealed no significant differences between ASD children and controls, while our DTI results suggest an early involvement of both cerebellum and supratentorial GM in young ASD children, with FA being the most sensitive parameter. Further investigation on a larger sample is warranted in order to confirm a potential primary role of GM changes to white matter ones in the complex etiopathogenesis of ASD and to correlate radiologic data to clinical findings.

KEYWORDS: Diffusion tensor image, Autism spectrum disorder, Volumetric analysis

O-512 **11:41 AM - 11:49 AM**

Investigation of Pediatric Magnetoencephalographic Networks Using Meta-Independent Component Analysis

Davenport, E. M.[1]·Whitlow, C. T.[1]·Powers, A.[1]·Thompson, M. M.[2]·Rawley, J.[2]·McGowin, I.[2]·Alberto, G.[2]·Bungo, T.[2]·Godwin, D.[2]·Urban, J. E.[2]·Stitzel, J.[2]·Maldjian, J. A.[1]
[1]Wake Forest University School of Medicine, Winston-Salem, NC, [2]Wake Forest University, Winston-Salem, NC.

Purpose
Magnetoencephalography (MEG) is a noninvasive form of functional brain imaging that can be used to further understand brain function. Independent component analysis (ICA) can be used to decompose the mixture of signals from recorded MEG data into multiple independent components representing networks. Meta-ICA is a newly described method to extract networks common across all spectral bands. The purpose of this study is to use Meta-ICA to identify common MEG networks across spectral bands in a group of pediatric subjects.
Materials & Methods
An institutional ethics committee approved this study. Eighteen normal male subjects aged 16-18 years were scanned using a 3T Siemens Skyra scanner using a 32 channel head coil for collection of structural anatomical MRI data. Eight minutes of, eyes open, resting-state MEG data were acquired for each subject using a 275 channel CTF whole-head system. Using an in-house automated pipeline, all data were baseline corrected, filtered for 60Hz line noise, down-sampled to 100Hz, and band-pass filtered into five frequency bands (δ: 0-4Hz, θ: 4-8Hz, α: 8-13hz, β: 13-30Hz, γ: 30-50Hz). Artifacts from head motion, and muscles also were removed. Magnetoencephalography data then were projected into source space at 5 mm resolution using a scalar beamformer with leadfield correction for noise normalization. The Hilbert envelope was computed, and data were down-sampled to 1Hz. These data then were used as the input for Meta-ICA. For each frequency band, the data from each subject was concatenated into a matrix, X, where each row represented a timecourse for a single voxel across all subjects. Twenty-five independent components, S, for each frequency range were estimated from this matrix using FastICA. The 25 estimated components for each frequency range then were concatenated into a matrix where each column represented a single timepoint across all bands and components. Finally, 10 independent components, G, were estimated from this matrix using FastICA.
Results
Figure 1 demonstrates the spatial representation of three of these 10 components, which are representative of all subjects across all bands and time. The components appear to represent portions of the visual, auditory, and default mode networks, in addition to other regions common across spectral bands.

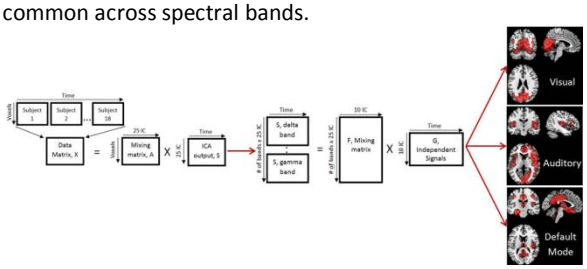

Conclusion
The application of Meta-ICA analysis to MEG data from pediatric subjects revealed specific networks bearing similarity with those found in other studies of network connectivity. The data demonstrates the utility of Meta-ICA when analyzing MEG data to compare networks in pediatric subjects across spectral bands.

KEYWORDS: MEG, Pediatric brain

O-513 **11:49 AM - 11:57 AM**

Retrospective Study of the Impact of a Perception-Based Anisotropic Diffusion Filter on Image Quality in Low-Dose Pediatric Head CT

Tang, E. R.·Li, B.·Sakai, O.·Barest, G.·Setty, B.·Mian, A.
Boston University/Medical Center
Boston, MA.

Purpose
To retrospectively study the impact of a unique perception-based anisotropic diffusion filter (pADF), which uses a structural similarity measure based on visual components (luminance, contrast, structure), on noise and reader-assessed image quality in low-dose pediatric head CT.
Materials & Methods
Ten pediatric patients (ages: 1 to14 years), who underwent brain CT and MRI within one month, were selected after IRB approval. Brain CT images were

Note: Scanned images are included in the proceedings. Some submitted images were reduced during editing, thereby decreasing clarity. Also, refer to the Program Planner. Proceedings Content as of 3-29-2013.

obtained with axial 5mm (brain kernel) and 1.25mm (bone kernel) sections using a 64-multidetector CT. CT dose index, dose-length product, and major CT brain findings (confirmed when possible by MRI) were recorded for each patient. pADF processing (Imsonic Corp.) was applied to images for each patient. The nonprocessed paired brain/bone series and the pADF-processed series were anonymized and randomized. Three neuroradiologists graded the each series on a 5-point scale for noise, contrast, resolution, and overall image quality (1=nondiagnostic to 5=exceptional). Standard deviations (SDs) for noise also were recorded (based on Hounsfield units) in 6x6mm regions of interest at the lenticular nucleus and periventricular white matter.

Results

Quantitative noise SDs of the pADF-processed images for the brain and bone kernel reconstructions were significantly lower than in the nonprocessed images, measured at the lenticular nucleus (brain: 2.44 versus 3.94, p<0.01; bone: 28.42 versus 38.55, p<0.01) and at the periventricular white matter (brain: 2.14 versus 3.65, p<0.01; bone: 25.73 versus 36.26, p<0.01). For bone reconstructions, the pADF-processed series resulted in a slight but statistically significant improvement in reader-assessed scores for resolution (4.52±0.59 versus 4.17±0.75, p=0.02), particularly for low-dose CT (score improvement by average of 0.28 when compared to standard-dose CT, p=0.03). There also were slightly improved scores in contrast (4.39±0.58 versus 4.20±0.71, p=0.58) and overall image quality (4.26±0.62 versus 4.00±0.64, p=0.07) for pADF-processed bone images, though not statistically significant (p>0.05). For brain reconstructions, the pADF-processed series resulted in a slight but statistically significant decrease in reader-assessed scores for overall image quality (3.22±0.74 versus 3.73±0.66, p=0.08). Slightly decreased scores for contrast (3.39±0.84 versus 3.73±0.78, p=0.09) and resolution (3.57±0.59 versus 3.80±0.66, p=0.08) for pADF-processed brain images were not statistically significant (p>0.05). Aside from the bone resolution scores, the other qualitative reader-assessed changes were less pronounced at low-dose CT than standard-dose CT, though differences were not statistically significant (see table below).

Reader-assessed image score changes for pADF- versus nonprocessed CT, in standard- versus low-dose CT.

Reader-assessed image factor (kernel)	Standard-dose CT score change (pADF-processed - nonprocessed)	Low-dose CT score change (pADF-processed - nonprocessed)	Difference in score change by dose (Standard-dose CT - low-dose CT)
Resolution (bone)	0.143 (p=0.409)	0.286 (p=0.032)	-0.143 (p=0.498)
Contrast (bone)	0.143 (p=0.456)	0.143 (p=0.297)	0 (p=1)
Overall image quality (bone)	0.429 (p=0.095)	0.143 (p=0.409)	0.286 (p=0.343)
Resolution (brain)	-0.431 (p=0.156)	-0.287 (p=0.179)	-0.144 (p=0.687)
Contrast (brain)	-0.445 (p=0.236)	-0.297 (p=0.262)	-0.148 (p=0.740)
Overall image quality (brain)	-0.877 (p=0.058)	-0.364 (p=0.242)	-0.513 (p=0.337)

Conclusion

pADF-processing shows statistically significant quantitative reduction in CT noise for both brain and bone reconstructions. pADF-processing demonstrates particular promise for bone-kernel CT images, resulting in a statistically significant improvement in reader-assessed resolution, especially in the low-dose CT group. There is, however, a slight decrease in reader-assessed overall image quality for the pADF processed brain kernel CT imaging. Ongoing studies are underway to confirm these findings, as well as the impact of pADF-processing on CT imaging of other structures.

KEYWORDS: CT, Radiation dose reduction

O-514 **11:57 AM - 12:05 PM**

Adaptive Statistical Iterative Reconstruction: Reducing Dose while Preserving Image Quality in the Pediatric Head CT Examination

McKnight, C. D.·Ibrahim, M.·Watcharotone, K.·Baer, A.·Wright, R.·Parmar, H.
University of Michigan
Ann Arbor, MI.

Purpose

Over the last decade there has been escalating concern regarding the increasing radiation exposure stemming from computed tomography, particularly in children. Adaptive statistical iterative reconstruction (ASIR) is a relatively newer and promising tool to reduce radiation dose while preserving image quality. While encouraging results have been found in adult head and chest and body imaging, validation of this technique in pediatric population is limited due to very small sample size in the previous study. The purpose of our study was to retrospectively compare the image quality and radiation dose of pediatric head CT examinations obtained with ASIR compared to pediatric head CT examinations without ASIR in a large patient population.

Materials & Methods

Retrospective analysis was performed on 82 pediatric head CT examinations. This group included 33 pediatric

head CT examinations obtained with ASIR and 49 pediatric head CT examinations without ASIR. Qualitative analysis consisted of independent assessment by two radiologists in a blinded manner of gray-white differentiation, sharpness and overall diagnostic quality. Quantitative analysis consisted of standardized measurement of attenuation and the standard deviation at the bilateral centrum semiovale and cerebellar white matter. Dose length product (DLP) was recorded on all examinations.
Results
The average DLP value of the ASIR group was 352.0 mGy-cm while the average DLP for the non-ASIR group was 545.5 mGy-cm, representing a statistically significant 35% reduction in DLP in the ASIR group ($p < 0.01$). Radiologist assessment of gray-white differentiation, sharpness and overall diagnostic quality in ASIR examinations was not significantly different compared to non-ASIR examinations. Quantitative analysis revealed a slightly increased average attenuation in the bilateral cerebellar white matter on ASIR examinations (Right 28.1 HU, Left 27.7 HU) as compared to non-ASIR examinations (Right 26.1 HU, Left 25.7 HU) ($p < 0.01$), though no corresponding significant difference was seen in the centrum semiovale.
Conclusion
The use of ASIR in pediatric head CT examinations allows for a 35% reduction in radiation dose without significantly affecting image quality.

KEYWORDS: Dose reduction

O-515 **12:05 PM - 12:13 PM**

Value of Transcranial-Enhanced Ultrasound in Newborns: Initial Experience

Kastler, A.[1,2]·Manzoni, P.[3]·Chapuy, S.[3]·Cattin, F.[3]·Biondi, A.[3]·Kastler, B.[3,2]
[1]University Hospital, Clermont ferrand, FRANCE, [2]I4S Laboratory EA 4268, Franche Comte University, FRANCE, [3]University Hospital, Besançon, FRANCE.

Purpose
To assess the feasibility and value of transcranial-enhanced ultrasound (TCEUS) in various neurologic conditions in newborns.
Materials & Methods
Local Institutional Review Board approval was obtained and written informed consent was waived. Sixteen newborns who underwent a total of 20 TCEUS were included in this retrospective study from June 2009 to February 2012. All TCEUS were performed by one trained operator on an Acuson Sequoia ® U.S. ™ system. Second generation contrast material (SonoVue, Bracco ®) was used. Transcranial-enhanced ultrasound imaging findings were compared with those of conventional transcranial ultrasound and CT/MRI findings when available.
Results
Mean gestational age was 32.6 weeks (range 25 to 41 weeks). Ten out of the 16 included new borns (66%) were premature. Eleven of 18 ETFC were performed within 10 days of life. In 18 out the 20 performed examinations, TCEUS showed brain perfusion abnormalities which were not depicted on nonenhanced TCUS (ischemic: nine cases, hypoperfusion: eight cases, CDR: one case). Two newborns had negative TCEUS findings. MR imaging or CT scans were available for comparison in 12 of 16 patients. A good correlation between TCEUS and either MRI or CT findings was found in 10 out of 12 initial TCEUS (correlation with MRI: three cases, CT: one case, CT and MRI: six cases).
Conclusion
Transcranial-enhanced ultrasound appears as a potential bedside accessible nonionizing alternative imaging modality in the assessment of emergency neonatal brain injury. It provides additional information compared to nonenhanced TCUS, especially in the field of brain perfusion assessment.

KEYWORDS: Ultrasonography, Neonatal, Contrast Agents

Thursday Morning

10:45 AM - 12:15 PM
Room 1AB

(56e) Parallel Scientific Papers: Anatomy and Related Issues

O-516 **10:45 AM - 10:53 AM**

Visualization of the Medial and Lateral Geniculate Nucleus with Phase Difference Enhanced Imaging

Kitajima, M.·Hirai, T.·Shigematsu, Y.·Yoneda, T.·Komi, M.·Azuma, M.·Iryou, Y.·Nishimura, S.·Yamashita, Y.
Kumamoto University
Kumamoto, JAPAN.

Purpose
The medial geniculate nucleus (MGN) and lateral geniculate nucleus (LGN) are the specific nuclei that relay hearing and vision, respectively. Although there is increasing interest in the morphometry of the MGN and LGN, imaging methods for precisely identifying the two nuclei have not been sufficiently developed. The purpose of this study was to compare the delineation of the MGN and LGN among phase difference enhanced (PADRE) imaging on which the phase difference between the target and surrounding tissue was selected in order to enhance the contrast of the target tissue, 2D T2-weighted image (T2WI), short TI inversion recovery (STIR), proton density-weighted image (PD) and diffusion tensor imaging (DTI).
Materials & Methods
We recruited 10 healthy volunteers (six men, four women; ages, 28 - 47 years, mean, 36.8 ± 6.7 years) for this study. Phase difference enhanced images created from 3D high-

Note: Scanned images are included in the proceedings. Some submitted images were reduced during editing, thereby decreasing clarity. Also, refer to the Program Planner. Proceedings Content as of 3-29-2013.

resolution T1 FFE images, 2D T2WI, STIR, PD and DTI were obtained. To elucidate the visibility of the boundary of MGN and LGN, two neuroradiologists consensually assessed PADRE, 2D T2WI, STIR, PD and DTI by referring to Schltenbrand-Wahren atlas. They used a 4-point scale as follows: grade 0, no visible boundary of MGN and LGN; grade 1, vaguely visible boundary; grade 2, mostly obvious boundary; and grade 3, obvious boundary with clear delineation of MGN and LGN. We compared the visibility of MGN and LGN among five sequences statistically.

Results

The visibility of MGN and LGN was grade 3 in all volunteers on PADRE. There were statistically significant differences for visibility of the MGN and LGN between PADRE and the other four sequences ($p<0.01$). Boundary structures of the MGN and LGN consisted of low intensity white matter tracts including the zona lateralis, cerebral peduncle, lateral lemniscus and brachium colliculi superioris. The MGN was found dorsal to the lateral lemniscus, while the LGN existed medial to the zona lateralis and dorsal to the cerebral peduncle. The brachium colliculi superioris was found between the MGN and LGN. The MGN and LGN were identified in 30% and 60% for STIR, and 25% and 55% on PD, respectively. They were not identified on T2WI and DTI in all volunteers.

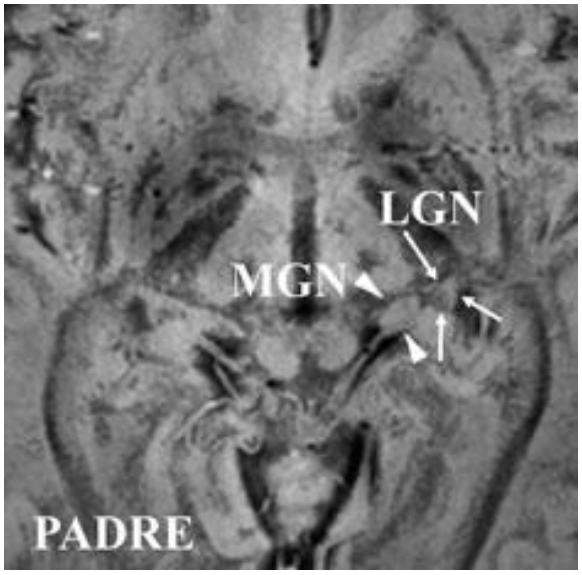

Conclusion

The delineation of MGN and LGN on PADRE was superior to that on STIR, PD, DTI or T2WI.

KEYWORDS: Anatomy, 3 T, thalamus

O-517 **10:53 AM - 11:01 AM**

Observing the Cerebral Autoregulation of Cerebral Blood Flow in Simulated Normotensive Hypovolemia Using Incremental Increases of Lower Body Negative Pressure and Phase-Contrast MR Imaging

Cain, J. R.·Brodie, S.·Sinha, R.·Stivaros, S.·Jackson, A.
University of Manchester
Manchester, UNITED KINGDOM.

Purpose

Classical cerebrovascular autoregulation maintains cerebral blood flow (CBF) during fluctuations in cerebral perfusion pressure. Stimuli which cause a decrease in blood volume while blood pressure is maintained are normotensive hypovolemic challenges. An equivalent stimulus to a tilt-table test can be reproduced by lower body negative pressure (LBNP) of -20mmHg, applying an external vacuum to the lower limbs and torso. Higher levels of negative pressure hypovolemic states also can be simulated eventually resulting in syncope. Understanding the relationship between cardiac output and CBF in normotensive hypovolemic patients has implications for the management of trauma patients.

Materials & Methods

Eleven healthy male volunteers (21-24 years) underwent imaging with a 3T MR scanner with their legs and lower torso within the Manchester MRI compatible LBNP chamber. Quantitative phase-contrast angiography (PCA) acquisitions were used to measuring total blood inflow from internal carotid and basilar arteries middle cerebral arteries(MCA) and flow in both the ascending and descending aorta. Data were acquired at 10mmHg increments from baseline to -50 mmHg. Heart rate (continuous) and blood pressure(intermittent) was measured during the experiment.

Results

Increases in heart rate were seen from -20mmHg LBNP, mean arterial pressure did not decrease until -50mmHg, two of the 11 subjects had pre-syncope episodes at -50 mmHg. A 65.5% decrease ($P<0.01$) in CBF and a 63.6% ($P<0.01$) decrease in cardiac output were observed at -50mmHg LBNP. The decrease in CBF was proportional to the cardiac output up to LBNP of -20mmHg. At pressures between -20mmHg and -40mmHg there was a relative preservation of CBF in relation to cardiac output. MCA flow was maintained until -50mmHg LBNP.

Note: Scanned images are included in the proceedings. Some submitted images were reduced during editing, thereby decreasing clarity. Also, refer to the Program Planner. Proceedings Content as of 3-29-2013.

All values are mean ±S.E.M *P<0.05, ** P<0.01

LBNP level (mmHg)	0 (Control)	-10	-20	-30	-40	-50
Heart rate (bpm)	56±3	57±4	60±4**	62±4**	69±5**	80±5**
Systolic BP (mm Hg)	115±2	114+2	112±2	110±2**	110±2**	110±3**
Diastolic BP (mm Hg)	63±3	63±2	63±2	63±2	63±3	64±3
Ascending aorta flow (l/min)	6.87±.70	6.53±0.69	5.43±0.62*	4.22±0.66*	3.52±0.50*	2.50±0.35*
Descending aorta flow (l/min)	4.51±0.61	4.19±0.71	3.56±0.63*	2.63±0.52*	2.10±0.39*	1.43±0.25*
MCA flow (l/min)	0.15±0.03	0.15±0.02	0.15±0.02	0.13±0.02	0.13±0.03	0.07±0.01*
CBF (l/min)	0.87±0.09	0.83±0.10	0.72±0.08*	0.67±0.10*	0.61±0.10*	0.30±0.06*

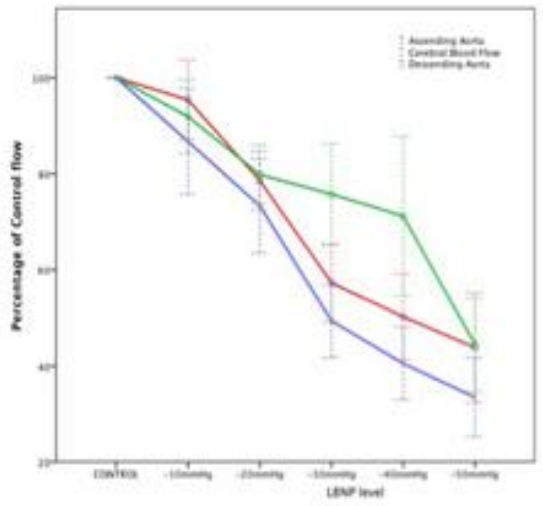

Conclusion

These results add to the classic autoregulation model by describing normotensive autoregulation. They suggest an increase in cerebral vascular resistance comparable to the resistance increase seen peripherally up to -20mmHg. At higher levels of LBNP (-20mmHg to -40mmHg) relative sparing of the cerebral circulation is noted in association with early small changes in systolic blood pressure suggesting that “classic” pressure-based autoregulatory mechanisms are active. While mean arterial pressure remain constant, decompensation seen at -50mmHg LBNP suggests failure of pressure-based autoregulation at this level of hypovolemia.

KEYWORDS: Cerebral blood flow, Autoregulation

O-518 **11:01 AM - 11:09 AM**

Enhanced Detection of Cerebral Venous Anatomy with Susceptibility-Weighted Imaging at 7T

Ge, Y.[1]·Zaman, O.[2]·Lu, H.[3]·Haacke, E.[2]·Grossman, R. I.[1]
[1]New York University Langone Medical Center, New York City, NY, [2]Wayne State University School of Medicine, Detroit, MI, [3]University of Texas Southwestern Medical Center, Dallas, TX.

Purpose

The cerebral venous system consists of superficial and deep venous systems which drain blood following oxygenation of tissues into internal jugular veins. Compared to the well studied cerebral arterial system on MR angiography, the complex venous system is still largely under-investigated with in vivo imaging. This study was to describe the cerebral venous anatomy using susceptibility-weighted imaging (SWI) at 7T MR with enhanced visualization of small venules and their draining courses on SWI venography.

Materials & Methods

Five healthy volunteers (age: 22~40 years old) underwent 7T MR imaging with the use of a 24-element head coil array. High-resolution SWI (a 3D gradient-echo imaging with all-direction flow compensation) MR venography with in-plane resolution of 0.21mm was performed. The slice thickness is 2mm. Susceptibility-weighted imaging minimal intensity projection (mIP) images over variable slice numbers (8~32) were created with phase multiplication algorithm to enhance venous structure contrast. The images were acquired in both transverse and sagittal planes. Using a schematic diagram as a template, we systematically reviewed the resulting venograms in each plane for detection of cerebral veins from both superficial and deep systems.

Results

In addition to the major dural venous sinuses (i.e., superior/inferior sagittal sinuses, straight sinus, occipital sinus and transverse sinuses), the optimized 7T SWI (TR/TE/FA = 40ms/16ms/25°) venography also distinguished nicely the superficial and deep systems with enhanced detection of small branches of veins and their draining courses. Figure 1 showed deep (A) and superficial (B) venous systems. The deep system (A) contains three major veins - great vein of Galen (1), internal cerebral vein (2), and basal veins (3); and the basal vein is formed with small veins (not marked) collecting deep cerebral regions. The internal cerebral vein is formed from the merger of the atrial veins (4), choroid (5), thalamostriate veins (6-9) and septal veins (10). The superficial system (B) contains superior sagittal sinus (1) that drains blood of cerebral hemisphere and is formed by parietal (2,3,7), frontal (4,5), and occipital veins (8) as well as the vein of trolard, vein of Labbe, and pre/post central and central veins (shown on separate saggital views).

Note: Scanned images are included in the proceedings. Some submitted images were reduced during editing, thereby decreasing clarity. Also, refer to the Program Planner. Proceedings Content as of 3-29-2013.

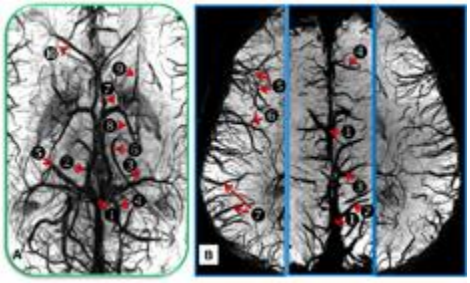

Conclusion
7T SWI venography has great potential to produce a superior venous anatomy (i.e., from venous to collecting veins to sinuses) images to systematically study cerebral venous vasculature in vivo. This may aid in improved detection, visualization, and localization of brain diseases of venous malformations, venous thrombosis, and/or abnormalities.

KEYWORDS: 7T, Venous anatomy, susceptibility-weighted imaging

O-519 **11:09 AM - 11:17 AM**

Correlation of Arcuate Fasciculus Dominance with Hand Dominance: Does Right-Handed Group Have Left Arcuate Fasciculus Dominance?

Chung, G.·Kwak, H.·Hwang, S.
Chonbuk National University
Jeonju, KOREA, REPUBLIC OF.

Purpose
Arcuate fasciculus (AF) is a direct white matter connection that runs medially between Braca's and Wernicke's area. For more than a century, neurologists have hypothesized that the AF carries signals that are essential for language function; however, the exact function and anatomical pathway is highly controversial. It is known in right-handed patient group, almost 99% of them have left hemispheric dominance, but in contrast, the left-handed patient group has only 50-60% of right hemispheric dominance. We hypothesized there will be a relationship between AF and hemispheric dominance, and in this study, we want to evaluate it by using diffusion tensor imaging (DTI).
Materials & Methods
Twenty-two healthy volunteers (11 right-handed, 11 left-handed, mean ages were 28.3 and 24.6 years, respectively, 12 women, 10 men) were studied with conventional MR imaging and DTI. Dominant hand was confirmed by Edinburgh handedness inventory. Using 3T MRI and DTIStudio program, AF fiber tracking was performed in ExploreDTI (A. Leemans, Antwerp, Belgium), using a deterministic streamline method. Fractional anisotropy (FA) and fiber number (FN) of both (right and left) AF fibers of each group were measured by DTIstudio program and then after, we measured LI [lateralization index = (left-right)/(left+right)] to compare right and left AF fiber.
Results
1. Right-handed group: Ten of 11 of right-handed group has positive LI, that means 91% of right-handed group has left dominant AF. Only one has negative LI. So the average of LI was 0.47 and 0.016 in fiber's number and fiber's FA respectively. We compared the number of both fibers and it was significantly left side dominant (p =0.039), but FA of both fibers was insignificantly different (p = 0.0537). 2. Left-handed group: Four of 11 of left-handed group has negative LI, that means only 36% of left-handed group has right dominant AF. Other 64% of left-handed group has positive LI, left dominant AF. So the average of LI was 0.12 and 0.006 in fiber's number and fiber's FA respectively. We compared number of both AF and it was not significantly dominant in any side (p = 0.453), but FA of both fibers was insignificantly different (p = 0.2696).
Conclusion
We demonstrated right-handed group significantly has left dominant AF, in number. But FA was not significant, and this means the number of fibers express well about dominance. Also left-handed group has no dominant AF, and it was well correlated with Edinburgh test.

KEYWORDS: Arcuate fasciculus, DTI tractography

O-520 **11:17 AM - 11:25 AM**

Lesion Mimic: Dilated Anterior Temporal Lobe Virchow Robin Spaces on 3T MR Imaging

Weisman, N. J.·Thakur, M.·Bronen, R.
Yale New Haven Hospital
New Haven, CT.

Purpose
As imaging of seizure patient has evolved with the introduction of 3T MRI, high-resolution coronal imaging sometimes reveals prominent subcortical T2-weighted hyperintensities in the anterior temporal lobes, particularly in young children. While most of these findings are suspected to be secondary to perivascular (Virchow-Robin) spaces, this study sought to determine the significance and frequency of these findings.
Materials & Methods
Coronal T2-weighted and FLAIR images performed on 3.0T scanners were reviewed retrospectively to determine the frequency and distribution of anterior temporal lobe subcortical hyperintensities. High-resolution thin section MR images from 60 seizure patients (mean age = 10.5 years, range 2 -29 years) were compared to 20 control subjects imaged for pituitary conditions (mean age = 20.4 years, range 9-35 years) by three CAQ certified/eligible neuroradiologists using a consensus interpretation method. For each subject, coronal images of each temporal lobe from the anterior pole to the uncal recess were divided into four quadrants. The number of positive quadrant slices then was tallied to determine the prominence and extent of these findings; these were assessed using Student's *t*-test and Pearson correlation statistics.

Note: Scanned images are included in the proceedings. Some submitted images were reduced during editing, thereby decreasing clarity. Also, refer to the Program Planner. Proceedings Content as of 3-29-2013.

Results

T2 hyperintensities at the gray-white matter junction were common in both seizure and control groups, with a prevalence of 99% (79/80 patients) and 95% (19/20 controls). There was no significant difference in the number of positive quadrant slices between seizure patients and controls (29.6 versus 28.6, p = 0.84). A moderately strong inverse relationship between the number of positive quadrant slices and age was found, with Pearson correlation of -0.54 for seizure patients and -0.71 for controls (Graph). There was also a significant difference in prominence of hyperintensities when separated into groups above and below 16 years of age, with an increased number of positive quadrant slices noted in the younger age group ($p<0.01$ for patients and $p<0.0001$ for controls). Confluent T2 hyperintensities, mimicking a pathologic lesion, were encountered in 8.3% (5/60) of seizure patients and 5% (1/20) of control subjects.

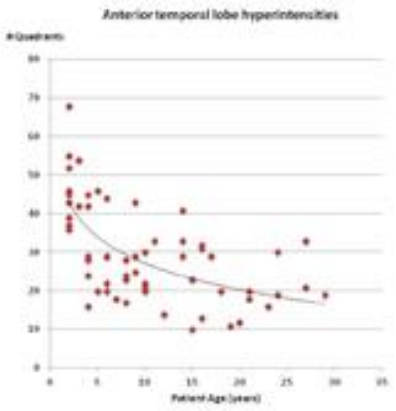

Conclusion

Anterior temporal lobe subcortical hyperintensities are almost universally present on high-resolution 3T coronal imaging in both seizure and control subjects, particularly in younger children. These findings likely represent dilated perivascular spaces. One should be aware that prominent hyperintensities may occur in young children and should not be confused with a pathologic abnormality. Location, signal intensity and adjacent findings should help distinguish confluent perivascular spaces from true abnormalities.

KEYWORDS: 3T, Seizure, Virchow Robin Spaces Anterior Temporal Lobes

O-521 **11:25 AM - 11:33 AM**

Shrinkage of the Petrous Carotid Canal following Application of Selverstone Clamps

Bag, A. K.·Chapman, P.·Cure, J.·Fisher, W.·Zaza, A.
University of Alabama at Birmingham
Birmingham, AL.

Purpose

Narrowing of the petrous carotid canal is believed to be of developmental origin due to a congenitally small internal carotid artery. We have observed gradual narrowing of the ipsilateral carotid canal after Selverstone clamping of the common carotid artery to treat giant cavernous carotid aneurysms. The purpose of this study was to confirm the hypothesis that the carotid canal shrinks compared to the control side in response to iatrogenic narrowing of the common carotid artery with Selverstone clamps. We also hypothesized that iatrogenic narrowing of the carotid would be accompanied by compensatory enlargement of the contralateral ICA.

Materials & Methods

We retrospectively reviewed imaging studies from 21 patients who had clamping of the common carotid artery to treat giant cavernous aneurysm. We measured the pre- and post-therapy (2-6 years after the initial scan) petrous carotid canal diameter as well as anterior-posterior (AP) and transverse diameter of the opening of the entrance of the carotid canal in 21 patients with Selverstone clamping. We also measured (using the same technique) petrous carotid canal diameter as well as anterior-posterior and transverse diameter of the opening of the entrance of the carotid canal at the time of diagnosis and at the latest followup (2-6 years after the first scan) in another 21 patients who were followed up for untreated small MCA bifurcation aneurysm. The diameter of the contralateral cervical ICA was measured just proximal to its entry into the carotid canal.

Results

There was no statistically significant difference between the pre- and post-treatment carotid canal diameters in the control group. However, the pre- and post-treatment measurements were significantly different in the Selverstone group. The rate of change of diameters also was significantly different between the cases and control. There was no statistically significant change in the diameter of the contralateral ICA after Selverstone clamp application.

Conclusion

Narrowing of the carotid canal can be acquired. Canal diameter shrinks over time in response to iatrogenic narrowing/occlusion of ipsilateral common carotid artery. This suggests that a small carotid canal diameter may not in isolation reliably distinguish a congenitally hypoplastic carotid from acquired carotid stenosis.

KEYWORDS: CT angiogram, Carotid artery, Carotid canal

Note: Scanned images are included in the proceedings. Some submitted images were reduced during editing, thereby decreasing clarity. Also, refer to the Program Planner. Proceedings Content as of 3-29-2013.

O-522 **11:33 AM - 11:41 AM**

Automated Quantitation of Globe Flattening by MR Imaging in Idiopathic Intracranial Hypertension

Alperin, N.·Bagci, A.·Lam, B. B.·Sklar, E.
University of Miami
Miami, FL.

Purpose
To develop a fully automated method for assessing globe flattening and nerve protrusion by MRI, and to determine association with papilledema grade and intraocular pressure in patients with idiopathic intracranial hypertension (IIH).
Materials & Methods
Seven women with newly diagnosed untreated IIH and six healthy women of similar age, and BMI were studied by MRI. The diagnosis of IIH was made using the modified Dandy criteria. The mean and SD of papilledema grade (using the Frisen scale) in the seven IIH patients were 2.0 ± 0.96 with a range of 1-4. The MR images were acquired with 1.5 and 3T scanners (Symphony and Trio; Siemens, Erlangen, Germany). MRIs were performed before the diagnostic spinal tap and at one week after the spinal tap. All of the patients were treated with acetazolamide after the spinal tap. The MRI exam included heavily T2-weighted 3D volumetric MRI scan covering both eye globes with 0.6 mm isotropic resolution. The automated quantitative 3D method provides two objective measures: 1) "globe flatness measure (GFM)" depicting overall flatness of the posterior wall of the eye, and 2) "nerve protrusion measure (NPM)"- depicting degree of optic nerve protrusion. Globe flatness measure value of one represents a perfectly spherical posterior globe wall and a lower number represents a higher degree of globe flattening.
Results
Mean and SD values of the GFMs and NPMs in the healthy controls were 0.947 ± 0.015, and 0.986 ± 0.009, respectively. These measures in IIH patients were significantly lower 0.897 ± 0.028 and 0.961 ± 0.017, (p = 0.0001 and 0.00012), respectively. Nerve protrusion measure but not GFM correlated significantly with the degree of papilledema (contingency coefficient of 0.757, p = 0.0033). On the other hand, intraocular pressure was more strongly associated with GFM. Following treatment with acetazolamide, significant improvement was found in the GFM (0.900 ± 0.031 versus 0.930 ± 0.020, p = 0.04). The improvement in NPM did not reach statistical significance (0.961 ± 0.020 versus 0.976 ± 0.002, p = 0.09).

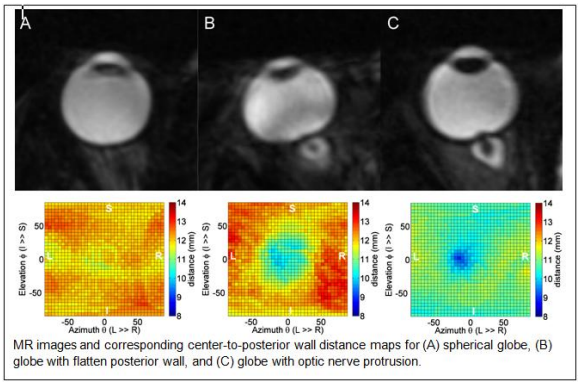

MR images and corresponding center-to-posterior wall distance maps for (A) spherical globe, (B) globe with flatten posterior wall, and (C) globe with optic nerve protrusion.

Conclusion
Automated MRI-derived globe flattening and optic nerve protrusion measures provide reliable and objective quantitative measures of anatomical changes associated with papilledema and increased intracranial pressure. Globe flatness measure and NPM provide complementing information related to the influence of elevated ICP on visual alterations.

KEYWORDS: Eye, Pseudotumor cerebrii, papilledema

O-523 **11:41 AM - 11:49 AM**

Persistent Trigeminal Artery: Modern Characterization Using High-Resolution MR Imaging, MR Angiography and CT Angiography

Lensing, F. D.·Fourgas, E.·McNally, S.·Schabel, A.·Shah, L.·Wiggins, R.·Quiqley, E.
University of Utah Health Sciences Center
Salt Lake City, UT.

Purpose
The persistent trigeminal artery (PTA) is the most common carotid-basilar anastamosis. Persistent trigeminal artery usually is discovered incidentally on MRI and CT angiography (CTA) studies. Persistent trigeminal artery, however, becomes critically relevant in neurovascular intervention. We will review the imaging anatomy of the PTA and demonstrate the value of high-resolution MRA and CTA in characterizing this anomalous vessel.
Materials & Methods
We performed a search of the Radiology Information System (RIS) for the term "trigeminal artery" over a 10-year period (2002-2012). We retrospectively reviewed the imaging studies in 12 patients with incidental persistent trigeminal artery at our institution over the past 10 years. These imaging studies included MRI, MRA, CTA and cerebral angiograms. Special attention was directed to defining the relationship of the PTA and the posterior communicating artery to determine the Saltzman type.
Results
All cases of persistent trigeminal artery were associated with hypoplastic intracranial vertebral arteries and basilar artery proximal to the anastamosis. Of the 12 patients,

Note: Scanned images are included in the proceedings. Some submitted images were reduced during editing, thereby decreasing clarity. Also, refer to the Program Planner. Proceedings Content as of 3-29-2013.

seven were female and five were male. The age range was 39-77 years and the mean age was 60 years. Persistent trigeminal arteries were distributed evenly between left and right. Seven of the cases had Saltzman type I, and five of the cases had Saltzman type II PTAs. Eleven of 12 patients had lateral PTAs and one of 12 had a medial PTA. One of the patients had a dural arteriovenous fistula on the contralateral side and one of the patients had a left posterior communicating aneurysm on the ipsilateral side. Two of 12 of the patients presented with vertiginous or stroke-like symptoms. Thin section CTA was performed in 6/12 (Figure). High-resolution MR imaging [defined as three-dimensional T1 or T2 (Figure) weighted imaging, time of flight magnetic resonance angiography or thin section T2-weighted imaging] was obtained in 8/12. The PTA was adequately characterized in 12/12 cases. The determination of Saltzman type was possible in 100%.

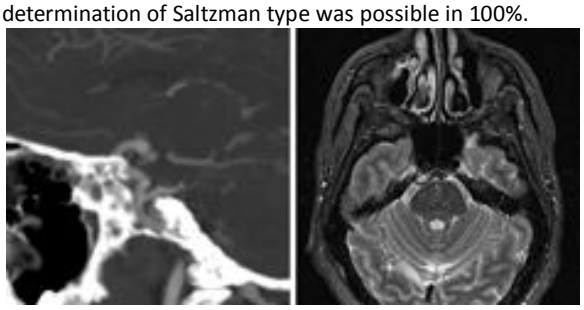

Conclusion

When a hypoplastic posterior circulation is encountered, a persistent carotid-basilar anastamosis should be suspected. The most common persistent carotid-basilar anastamosis is the PTA. High-resolution CT angiography and MRI/MRA provide useful adjuncts in characterizing the relationship of the PTA to the PCA and determining the Saltzman type. If small vertebral and proximal basilar arteries are detected on routine imaging, an abnormal vessel at the level of the persistent trigeminal artery should prompt a high resolution CT or MR evaluation to better characterize this anomalous vessel.

KEYWORDS: Anatomical variation, High-resolution imaging

O-524 **11:49 AM - 11:57 AM**

MR-Based Measurement of Spinal Cord Motion during Flexion of the Spine: Implications for Intradural Spinal Cord Stimulator Systems

Smittkamp, C. A.[1]·Viljoen, S.[1]·Dalm, B. D.[1]·Wilson, S.[1]·Reddy, C. G.[1]·Gillies, G. T.[2]·Howard, M. A.[1]
[1]University of Iowa, Iowa City, IA, [2]University of Virginia, Charlottesville, VA.

Purpose

We are developing the Human Spinal Cord Modulation System (HSCMS) as a new means of delivering electrical stimuli directly to the pial surface of the spinal cord for treatment of intractable pain via neuromodulation of targeted dorsal column pathways. To optimize device performance and avoid risk of injury to the spinal cord, the HSCMS implant must remain in gentle yet direct contact with the spinal cord even as it moves within the spinal canal. Functional anatomical knowledge of the spinal cord movement within the spinal canal therefore is needed to inform design requirements for the HSCMS. We have conducted an experiment to assess this movement at the anticipated lower thoracic location of the HSCMS.

Materials & Methods

The lower thoracic cord in healthy volunteers was imaged in both supine neutral and supine maximal spinal flexion positions. A bariatric MR was utilized as its larger bore size could accommodate volunteers while in the flexed position. CISS pulse sequences were selected for their high spatial frequency, allowing for the most accurate measurements. The distance between the T10 dorsal nerve root entry zone (DREZ) and T11 DREZ on the cord surface was measured in flexed and neutral positions and used as an assessment of spinal cord compression/expansion along the cranial-caudal axis. Next, the distance from the T10 DREZ to the inferior aspect of the T10 pedicle was measured. The difference in this measurement between flexed and neutral position is a measurement of cranial-caudal movement of the cord within the canal. Finally, a similar measurement was made on the conus tip to assess cranial-caudal movement at the distal-most cord.

Results

The inter-DREZ distance across all patients between the neutral and flexion positions ranged from -2.0 mm to +6.7 mm, with a mean and standard deviation of 3.5 ± 2.6 mm. The measured change in the pedicle-to-DREZ distance across all patients between the neutral and flexion positions ranged from 1.9 mm to 18.0 mm, with a mean and standard deviation of 8.5 ± 6.0 mm. The mean and standard deviation for the rostral-caudal conus movement was found to be 6.4 ± 4.1 mm within an overall range of 1.1 to 11.4 mm.

Conclusion

Although mean values for cranial-caudal movement and compression/expansion are calculated and reported as intended, much more interesting results are seen when evaluating the ranges of measurements obtained. An unexpected result was immense intersubject variability in how the spinal cord accommodates maximal flexion. Some subjects have nearly two centimeters of cranial cord movement with very little stretching while others have almost no cord movement while stretching over 25% along the measured segment. Because the spinal cord's structure and anchoring elements vary somewhat over its length, some difference in degree of motion and stretch is expected. Our measurement data further suggests that the intersubject variance in these quantities can be quite large even over a localized segment of the cord. Our findings thus highlight the need for the HSCMS design to accommodate large patient-to-patient variations in spinal cord dynamic movement properties.

Note: Scanned images are included in the proceedings. Some submitted images were reduced during editing, thereby decreasing clarity. Also, refer to the Program Planner. Proceedings Content as of 3-29-2013.

KEYWORDS: Spinal imaging, Spinal cord, movement

O-525 **11:57 AM - 12:05 PM**

Postmortem Radiology-Pathology Correlation of Recurrent Tumor after Bevacizumab Treatment and Apparent Diffusion Coefficient

Weinstein, G.·Wu, J.·Mignano, J.·Linendoll, N.·Do-Dai, D.·Madan, N.
Tufts Medical Center
Boston, MA.

Purpose
After the introduction of bevacizumab (BV) in the treatment of glioblastome multiforme (GBM), it has become increasingly difficult to separate post-treatment changes from recurrent tumor. This is because BV, an anti-angiogenesis agent, often results in recurrent tumor which doesn't enhance on Gadolinium -enhanced MRI. This study sought to determine if apparent diffusion coefficient (ADC) correlated with residual tumor when compared to histologic evaluation in patients with GBM treated with bevacizumab.
Materials & Methods
Eleven patients with GBM treated with bevacizumab consented to postmortem autopsy and inclusion in the current study. The last in vivo MRI was co-registered with a postmortem MRI, and multiple histologic samples were selected based on the presence of FLAIR signal abnormality on the in vivo MRI. Regions of interest (ROI) correlating with the areas of histologic sampling were made on the ADC maps. Histologic analysis was made by a neuropathologist, who graded the amount of tumor present in the region of interest as either absent, low, medium or high-grade (utilizing similar criteria as used to distinguish Grade 2 through 4 astrocytomas). The association between tumor grade and ADC then was evaluated using a mixed linear model with a fixed tumor grade effect and a random subject effect to account for the correlated nature of the data (R software).
Results
An overall trend was identified such that ROIs in regions without tumor had the lowest ADC values (mean 945 x 10-6 mm2/s) compared to those with low (mean 984 x 10-6 mm2/s), medium (mean 1034 x 10-6 mm2/s) or high-grade (mean 1057 x 10-6 mm2/s). A significant association was found between tumor grade and ADC, with a statistically significant difference between regions where no tumor was observed and regions where high-grade tumor was observed ($p = 0.016$). Sensitivity to outliers analysis was performed leading to the same conclusions.
Conclusion
In the setting of GBM treated with BV, higher ADC values are more predictive of tumor recurrence. However, given the high degree of variability, while this is true on a statistical basis, great care must be taken in interpreting ADC images in an individual patient. While in and of itself, ADC is not able to predict tumor recurrence, it may prove to be a useful biomarker when combined with other laboratory, immunohistochemical, clinical and/or MRI data.

KEYWORDS: Glioblastoma, ADC, bevacizumab

O-526 **12:05 PM - 12:13 PM**

Novel Finding of Optic Nerve Central T2 Hypointensity Utilizing 3T MR Imaging

Heymann, J. C.·Hakimelahi, R.·Uribe Acosta, T. E.·Cotes, C. C.·Riascos, R.
University of Texas Medical Branch
Galveston, TX.

Purpose
The improved signal-to-noise ratio of 3T MRI creates opportunities to visualize detailed anatomical features within the optic nerve. We unexpectedly observed a central T2 hypointensity within the optic nerve on MR studies obtained as a part of the NASA Flight Medicine Visual Impairment/Intracranial Pressure Protocol, which had not been described previously.
Materials & Methods
Twenty-one astronauts (two females) who had undergone MRI of the orbits with direct coronal T2 sequences between 2010 and 2012 were included retrospectively. In total, 42 eyes were evaluated. Two astronauts were in training without previous missions to the International Space Station (ISS) and exposure to microgravity. Assessments were done on direct coronal T2 fat-saturated fast-spin-echo pulse sequences obtained by a 3T MR scanner.
Results
A central T2 hypointensity was observed in 100% of both right and left eyes. It was completely visualized throughout the nerve course in 15 right eyes (71.4%) and in 19 left eyes (90.5%). The two astronauts not yet exposed to microgravity also show the central T2 hypointensity throughout bilateral optic nerves. A cylindrical T2 hyperintensity also was present in bilateral eyes in all astronauts.
Conclusion
Previous literature describes a central T2 hyperintensity at the center of the optic nerve when imaged with 1.5T MRI. In our study, we describe a new finding seen in all study participants: a central T2 hypointensity in the epicenter of the previously described hyperintensity with the increased resolution made possible by 3T imaging. We speculate that this T2 hypointensity may represent flow voids caused by the central retinal vessels. Further research is necessary to determine if changes regarding this anatomical finding could potentially predict or be seen in certain disease states affecting the central nervous system. Although this finding was seen in the two astronauts not yet exposed to microgravity, further evaluation of a normal population is needed.

Note: Scanned images are included in the proceedings. Some submitted images were reduced during editing, thereby decreasing clarity. Also, refer to the Program Planner. Proceedings Content as of 3-29-2013.

KEYWORDS: Optic nerve, 3T, Hypointensity

O-527 **12:13 PM - 12:21 PM**

Human Embryonic Serial Anatomy: Bulbar and Pontine Venous System in Relation with the Lower Cranial Nerves

Tonnelet, R.[1]·Lhuaire, M.[2]·Labrousse, M.[2]·Braun, M.[1]
[1]Université de Lorraine, Nancy, FRANCE, [2]Université de Champagne, Reims, FRANCE.

Purpose
Since the mid 1950s, very little work has been done to contribute to a better understanding of venous vasculature development during embryogenesis. We present a new analysis method with multiplanar reformation process based on microscopic sections. This presentation focuses on the brain stem arachnoido-pial venous anastomoses evolutive morphology.
Materials & Methods
High resolution numerized microscopic continuous sections (10 to 20 µ) from Carnegie stage XIX to XXIII human embryo were used. Specific image treatment was the following : binarization- thresholding-labellization, rigid shifting, median filtration (cubic matrix) (resolution 10 µm/pixel) ; DICOM format images (1000 to 4000) are exported for post-treatment process depending on the embryonic stage and size. Angiographic rendering was obtained thanks to the eosine/hematoxylin red cell fixation within the vessels.
Results
At first step, we confirmed the embryonic status relatively to the Carnegie classification in assessing the cochlear canal orientation. The evolutive morphology of the brain stem primitive venous network is presented; at stage XIX, the initial longitudinal veins are separated from the caudal plexus. During the next stages, we demonstrate how they connected to transverse pial anastomoses. The next period (i.e., the early and late postembryonic period) show these intrinsic pial veins lying between the arteries and the brain surface leading to a progressive simplication pattern. During the stages XX to XXIII, we present the changing morphology of the trijeminal ganglion venous plexus and the relationships with CN XII, XI and X. The venous and arterial patterns are presented thanks to the possibilities of the computer program. These organizations are compared to the Padget and Streeter works.

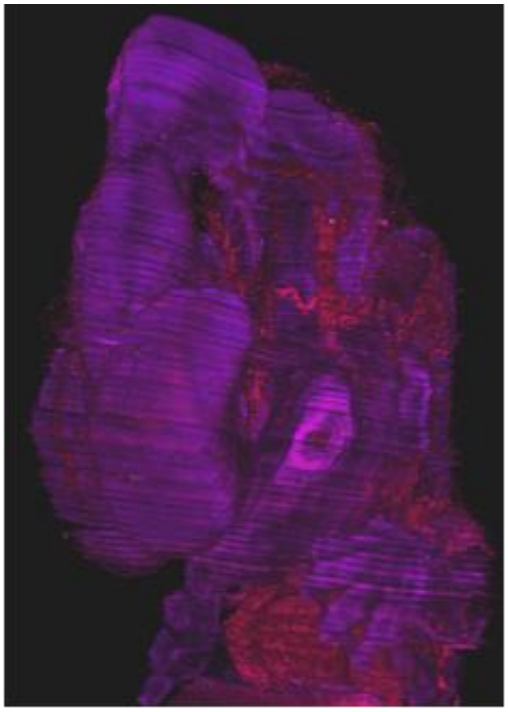

Conclusion
We present the preliminary work of the bulbar and pontine venous embryogenesis using 3D and angiographic rendering at the early postembryonic stages and their relationships with the lower cranial nerves and ganglionic plexux and the vertebral arteries and collaterals.

KEYWORDS: Embryology, Cranial nerves, veins

Thursday Afternoon

1:15 PM - 2:45 PM
Ballroom 6AB

(57a) Parallel Scientific Papers: Head and Neck: Skull Base: Sinonasal, Temporal Bone and Soft Tissue Neck

O-528 **1:15 PM - 1:23 PM**

Distinguishing Laryngeal Tuberculosis from Cancer by CT: A Practical Approach

Fourgas, E.[1]·Eid, M.[2]·Harnsberger, R.[1]·Wiggins, R.[1]
[1]University of Utah, Salt Lake City, UT, [2]Alexandria University, Alexandria, EGYPT.

Purpose
Tuberculosis (TB) of the larynx is a rare form of extra-pulmonary tuberculosis which can mimic laryngeal

Note: Scanned images are included in the proceedings. Some submitted images were reduced during editing, thereby decreasing clarity. Also, refer to the Program Planner. Proceedings Content as of 3-29-2013.

carcinoma. Because of the high infectivity of laryngeal TB, early diagnosis will alert the examining physician to the possibility of this entity, outline the extent of the disease and avoid unnecessary biopsies. The purpose of this presentation is to demonstrate the CT features of laryngeal tuberculosis and identify characteristics that help differentiate it from laryngeal carcinoma.

Materials & Methods

We retrospectively reviewed CT studies in 12 patients with laryngeal tuberculosis over a three-year period. Biopsy was performed on three patients on initial endoscopic examination. The diagnosis was established by sputum culture and complete resolution on imaging and endoscopic followup in the properly treated patients.

Results

The most common CT findings were diffuse edema and thickening of the aryepiglottic folds, vocal cords, paralaryngeal spaces and epiglottis without a focal mass (Figure). Destruction or sclerosis of the laryngeal cartilage was not present. Seven patients had associated lymphadenopathy in the mediastinum and neck including the deep cervical chain and retropharynx. In six of these patients the lymph nodes were necrotic. Three of the patients had asymmetric enhancement of the nasopharynx and one patient had abnormal enhancement and thickening of the soft palate. One patient had an associated cold abscess in the right palatine tonsil. Vocal cord mobility was not impaired in the properly treated cases. One key finding in all cases was the detection of classical CT features of active pulmonary tuberculosis.

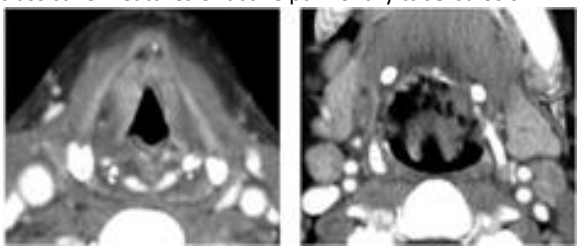

Conclusion

The most important imaging features that aid in differentiating laryngeal tuberculosis from carcinoma are the bilateral and diffuse involvement of the anterior larynx without destruction of the laryngeal architecture and without a focal mass in the setting of pulmonary TB. The presence of associated necrotic lymph nodes, often at sites different from the expected lymphatic drainage of the larynx, also can differentiate it from laryngeal carcinoma. Additional involvement of the soft palate, nasopharyngeal mucosa and palatine tonsils provides other clues in supporting the diagnosis of tuberculosis and these structures should be evaluated carefully. Vocal cord mobility is spared in the properly treated cases of laryngeal TB whereas it often is compromised in laryngeal carcinoma.

KEYWORDS: Tuberculosis, Larynx

O-529 **1:23 PM - 1:31 PM**

Yield of CT Examinations of the Neck in Patients with Globus Sensation

Alhilali, L. M.·Seo, S.·Branstetter, B.·Fakhran, S.
University of Pittsburgh
Pittsburgh, PA.

Purpose

To determine diagnostic and therapeutic efficacy of CT examinations of the neck in patients with isolated globus sensation.

Materials & Methods

We retrospectively identified patients presenting with globus sensation from January 2005 to December 2012 who underwent a CT examination of the neck. We excluded patients with a history of head and neck cancer or other known primary malignancy. We calculated the proportion of patients with abnormal findings on CT, tabulated the nature of the abnormality, and reviewed the medical records to determine whether imaging changed management.

Results

Seventy-five patients undergoing CT examinations of the neck were included (38 females, 37 males; mean age 53.3 years, range 12-91 years). Two patients demonstrated significant imaging findings that related to the history of globus sensation (2.7% diagnostic efficacy, 95% confidence interval 0.5-10.2%). One patient had prominent anterior cervical osteophytes and the second demonstrated an infected thyroglossal duct cyst. Of these, only the study with the infected thyroglossal duct cyst resulted in a change in clinical management (1.3% therapeutic efficacy, 95% confidence interval 0.1-8.2%). Incidental CT findings felt unrelated to globus sensation were six thyroid nodules, three thyroid goiters and a periapical dental abscess. On subsequent clinical followup 20 patients (26.7%) were found to have gastroesophageal reflux disease and three were found to have infectious pharyngitis (4.0%). The majority of the studies were ordered by otolaryngologists (36.0%) or primary care physicians (30.7%). Although emergency physicians only ordered 13 studies (17.3%), both of the studies with significant findings related to globus sensation were emergency department patients.

Conclusion

CT examinations of the neck in patients with isolated globus sensation are unlikely to identify clinically significant imaging findings and are very unlikely to result in a change in clinical management, with an overall therapeutic efficacy of 1.3%. Thus, the routine use of CT examinations of the neck in the evaluation of the patient with isolated globus sensation cannot be recommended.

KEYWORDS: CT, Head and neck

Note: Scanned images are included in the proceedings. Some submitted images were reduced during editing, thereby decreasing clarity. Also, refer to the Program Planner. Proceedings Content as of 3-29-2013.

O-530 **1:31 PM - 1:39 PM**

Imaging Manifestations of Nasopharyngeal Carcinoma Subdivided by Histologic Subtype and Epstein Barr Virus Serology

Russell, D. P.·Baugnon, K. L.·Aiken, A. H.·Hudgins, P.·Muller, S.·Corey, A.
Emory University
Atlanta, GA.

Purpose
Nasopharyngeal carcinoma (NPC) has a distinct behavior compared to other head and neck cancers, particularly in regard to pathogenesis, risk factors, and treatment. Nonkeratinizing NPC has a known association with Epstein Barr virus (EBV) and often a better prognosis, while the keratinizing form, although a separate entity, is more akin to squamous cell carcinoma, with an association with alcohol and tobacco use. The purpose of this study is to review our experience with NPC, and assess for imaging trends based upon the histologic subtype and EBV serology.
Materials & Methods
Twenty-eight cases of biopsy-proven nasopharyngeal carcinoma (NPC) from 2002 through 2012 were reviewed retrospectively by two CAQ neuroradiologists. Inclusion criteria included: 1) Pathologic diagnosis of nasopharyngeal carcinoma, 2) Pretreatment CT and/or MR imaging available for review, 3) EBV serology results for cases of nonkeratinizing carcinoma. The patients were organized into three groups: keratinizing, Epstein Barr positive nonkeratinizing, and EBV negative nonkeratinizing. The pretreatment images were reviewed with regard to primary tumor volume, T stage, N status, lymph node size and number, and degree of intracranial extent. The size of the largest lymph node and number of nodes (0-3, or >3 = extensive) was recorded. Intracranial extent was further subdivided into perineural spread and frank involvement of the sella or prepontine cistern.
Results
Twenty-eight cases of NPC were subdivided into six cases of keratinizing subtype, and 22 nonkeratinizing, most of which (15) were EBV positive. The majority of cases were T4 (15/28, 53%), and N2 at diagnosis (17/28, 60%), and most (64%) had the number of lymph nodes classified as "extensive"; this was greatest in the keratinizing subtype (5/6, 83%). There was no statistically significant difference in the mean diameter of the largest lymph node amongst subtypes. The mean tumor volume was greatest in the keratinizing group, with a mean volume 36.3 cc, compared to EBV positive nonkeratinizing (29.2 cc) and EBV negative nonkeratinizing (16.4 cc). The degree of sphenoid sinus and nasal cavity involvement was greatest in the EBV positive nonkeratinizing subtype, at 50 and 53% respectively compared to EBV negative nonkeratinizing (14 and 0%) and keratinizing (20 and 0%). Similarly, while not statistically significant, there were greater numbers of cases of intracranial extension (including perineural spread and prepontine cistern/sellar extension) in the EBV positive nonkeratinizing subtype (60% and 27%), compared to EBV negative nonkeratinizing (43% and 14%) and keratinizing subtype (50% and 0%).
Conclusion
There were no statistically significant differences between the imaging appearances of the different histologic subtypes of NPC, possibly related to the power of the study, although trends were observed. The keratinizing subtype was more likely to have extensive lymphadenopathy. However, the degree of intracranial extent and local invasion (including sphenoid sinus and/or nasal cavity involvement) was greatest in the EBV positive nonkeratinizing subtype. No significant difference between the groups could be identified with regard to T stage, N status, or largest pathologic lymph node mean diameter.

KEYWORDS: Nasopharyngeal carcinoma (NPC)

O-531 **1:39 PM - 1:47 PM**

Imaging Surrogates of Increased Intracranial Pressure Are Associated with Spontaneous Cerebrospinal Fluid Leaks

Espinoza, F. V.·Madan, G.·Cohn, E.·Zanation, A.·Senior, B.·Ebert, C.·Castillo, M.·Huang, B.
University of North Carolina
Chapel Hill, NC.

Purpose
The etiology of spontaneous cerebrospinal fluid (CSF) leak is poorly understood, but evidence suggests that intracranial hypertension (IH) plays a causative role. The purpose of this study was to determine whether imaging surrogates of IH are seen more commonly with spontaneous than nonspontaneous CSF leaks both overall and at specific leak sites.
Materials & Methods
A retrospective chart and imaging review of adult patients presenting to our institution with new CSF leaks between 2001 and 2012 was performed. Inclusion criteria included a previously untreated CSF leak or encephalocele confirmed either surgically or with a positive beta-2 transferrin assay and a dedicated maxillofacial CT performed at time of diagnosis. Ninety-eight patients meeting these criteria were identified, and were classified as having spontaneous (SL) or nonspontaneous leaks (NSL, postsurgical or postraumatic). The site of leak (sphenoid, cribriform/ethmoid, frontal), determined intraoperatively, also was recorded. CT images were reviewed by a single blinded neuroradiologist who estimated the midsagittal sellar area and the number (0, 1-5, 6-10, >10) and maximal size of arachnoid pits in the greater sphenoid wing and temporal bone. Seventy-five patients also underwent brain MRI which was evaluated for the presence of an empty or partially empty sella. Group comparisons were made using Student *t*-tests for continuous variables and 2-tailed Fisher exact tests for categorical variables, with $p<0.05$ indicating a statistically significant result.

Note: Scanned images are included in the proceedings. Some submitted images were reduced during editing, thereby decreasing clarity. Also, refer to the Program Planner. Proceedings Content as of 3-29-2013.

Results
There were 62 SL and 36 NSL patients. Among SL patients, 41.9% of leaks were sphenoid, 51.6% cribriform/ethmoid, and 6.5% frontal. In the NSL group, 19.4% of leaks were sphenoid, 52.8% cribriform/ethmoid, and 16.7% frontal, while in four patients (11.1%) the site of leak was not identified surgically. Mean midsagittal sellar area was significantly higher overall in the SL group (131.7 mm^3 versus 95.8 mm^3, $p<0.001$). When the site of the leak was taken into account, the mean sellar area was higher in all locations in the SL group, but only significantly so in those with cribriform/ethmoid leaks (130.6 mm^3 versus 91.5 mm^3, $p=0.001$). Among those undergoing MRI, 60.8% of SL patients compared to only 33.3% of NSL patients were deemed to have an empty or partially empty sella ($p=0.046$), but significant differences were not seen at individual leak sites. Arachnoid pits were significantly more likely to be identified in SL patients than in NSL patients (72.6% versus 38.9%, $p=0.001$), and SL patients also tended to show more arachnoid pits. Arachnoid pits were more common among SL patients for all CSF leak sites, but significantly so only for those with sphenoid leaks (84.6% versus 28.6%, $p=0.009$). Among SL patients, arachnoid pits were significantly more common with sphenoid leaks than with cribriform/ethmoid leaks (84.6% versus 59.4%, $p=0.046$).
Conclusion
Three imaging parameters are more likely to be associated with SL than NSL. These include the appearance of an empty sella on MRI, the presence and number of arachnoid pits, and a larger sellar area. Interestingly, increased sella size is associated with leaks in the cribriform/ethmoid area, and the presence of arachnoid pits is associated with sphenoid leaks.

KEYWORDS: Cerebrospinal fluid, Leak, arachnoid granulations

O-532 **1:47 PM - 1:55 PM**

Temporal MR Imaging Evaluation of Endoscopic Multilayer Cranial Defect Reconstruction Utilizing Pedicled Nasoseptal Flap

Learned, K. O.·Adappa, N. D.·Lee, L. Y. K.·Palmer, J. N.·Newman, J. G.·Loevner, L. A.
University of Pennsylvania
Philadelphia, PA.

Purpose
Endoscopic endonasal approach (EEA) is evolving as the surgical approach of choice for resection of a spectrum of skull base pathology beyond sellar lesions. Successful endoscopic closure of the surgically created cranial defect routinely necessitates multilayer reconstruction utilizing inlay free grafts (fat packing, collagen matrix dural graft, and/or fascia lata) and mucosal onlay pedicled nasoseptal flap (NSF) based on the sphenopalatine artery. Kang et al described the characteristic enhancing C-shaped configuration of NSFs in the sphenoidectomy bed on immediate postoperative imaging following trans-sphenoidal hypophysectomy. However, the MR imaging features of the cranial defect reconstructions remain poorly understood and recognized, and frequently mistaken for neoplasm. This study aims to evaluate the normal imaging evolution of skull base reconstruction utilizing NSFs.
Materials & Methods
We retrospectively reviewed unenhanced and enhanced brain MRIs of patients following EEAs and multilayer skull base reconstructions utilizing NSFs. Nasoseptal flaps and free grafts were evaluated for temporal changes in signal intensity, enhancement, thickness, and configuration. Imaging findings were correlated with clinical followup.
Results
Eighteen patients with reconstructions utilizing 22 onlay NSFs with a combination of inlay free grafts had follow-up MRIs (2-41 months). All 18 reconstructions retracted into the skull base defects. All nine intracranial fat grafts showed progressive resorption with 50% reduction in the fat by six months and near complete resorption by 14 months. All six collagen matrix dural inlays remained $\leq$ 2 mm in size, similar to immediate postoperative exams. By 3-6 months, all six inlay fascia lata and 22 onlay NSFs demonstrated mature imaging features with little or no further change on subsequent imaging. The initial variable T2 signal and nonenhancing fascia lata became T2 hypointense, solidly enhanced and decreased in thickness by 50% (range 2-6 mm, mean 5 mm). The initial enhancement of viable NSFs persisted but the flap thickness decreased by 20-30% (range 2-7 mm, mean 5 mm). The distinct C-shaped arc and vascular pedicle leading toward the sphenopalatine foramen seen on immediate postoperative imaging were not defined as clearly due to incorporation of the flap into the denuded skull base, as well as evolving changes in signal characteristics in the sinus contents. The flap location remained unchanged. All four nonviable NSFs showed no enhancement and 1-5 mm enhancing granulation and mucosalization occurred by 2-3 months. In 25% of patients, the NSFs were misinterpreted for neoplasm.
Conclusion
Maturation and stability of multilayer endoscopic skull base reconstruction utilizing NSF appears to occur on MR imaging within 3-6 months after surgery. Identification and an understanding of the normal evolution and appearance of NSF reconstructions are essential for accurate image interpretation and to avoid its misinterpretation for neoplasm.

KEYWORDS: Skull base neoplasm, Postoperative findings, Endoscopic

Note: Scanned images are included in the proceedings. Some submitted images were reduced during editing, thereby decreasing clarity. Also, refer to the Program Planner. Proceedings Content as of 3-29-2013.

O-533 **1:55 PM - 2:03 PM**

Prognostic Imaging Factor in Acute Invasive Fungal Infection of the Sinonasal Cavity: MR Sign of Transosseous Nonenhancing Defect

Kim, J.[1]·Choi, Y.[1]·Park, S.[2]·Yun, T.[1]·Choi, S.[1]·Sohn, C.[1]·Ryoo, I.[1]·Kim, S.[2]
[1]Seoul National University Hospital, Seoul, KOREA, REPUBLIC OF, [2]Seoul National University Boramae Hospital, Seoul, KOREA, REPUBLIC OF.

Purpose
Acute invasive fungal infection of the sinonasal cavity is a fatal disease that necessitates early diagnosis and treatment. However, its imaging characteristics have not been demonstrated clearly. The purpose of our study was to describe its imaging characteristics and to determine the prognostic imaging factors along with pathologic correlation.
Materials & Methods
CT and MR images of 22 consecutive patients (12 men and 10 women; age range, 2-75 years, mean age, 53 years) with acute invasive fungal infection of the sinonasal cavity were evaluated retrospectively, with particular attention to the location, bone destruction, periantral soft tissue infiltration, signal intensity and enhancement pattern on MR, with a review of the clinical records and pathologic slides. The patient age, underlying disease, immune status, performance of surgical debridement, fungus isolated, and imaging features were assessed to identify factors affecting survival by using Kaplan-Meier survival curves, the log-rank test, and the multivariate Cox proportional hazards model.
Results
Seventeen patients were immunocompromised and five patients were immunocompetent. All of them showed extrasinonasal involvement as follows; orbit (n = 10), cavernous sinus (n = 7), brain parenchyma (n = 7), masticator space (n = 3), and oral cavity (n = 1). There were bony destruction on CT in 12 (55%) patients and periantral soft tissue infiltration on CT or MR in all patients. MR showed homogeneous enhancement with low signal intensity on T2-weighted image in seven (32%) patients and transosseous nonenhancing defect in nine (41%) patients. MR sign of transosseous nonenhancing defect has not been reported and was characterized by nonenhancing round or ovoid lesion involving bony structure and periosseous soft tissue as well as primarily infected sinonasal cavity with preservation of bone integrity on CT and MR. It was correlated pathologically with coagulative necrosis by fungal angioinvasion. The MR sign was found to be an independent prognostic factor for mortality in patient with acute invasive fungal infection (hazard ratio = 4.481; 95% confidence interval (CI), 1.140-17.619). In addition, the group with the MR sign showed significantly lower survival rate than the group without the MR sign (P = 0.011).

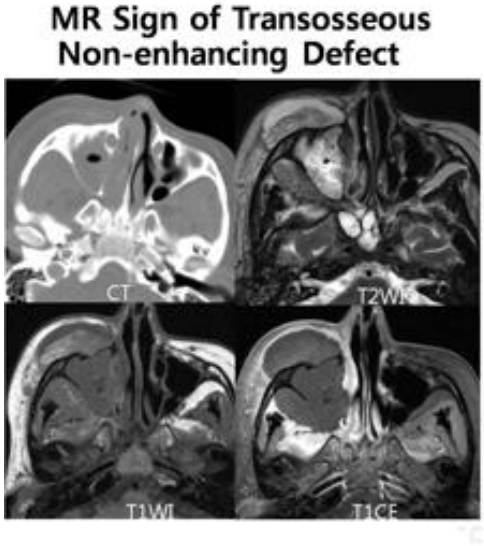

Conclusion
Periantral soft tissue infiltration is a common imaging finding of the acute invasive fungal infection. MR sign of transosseous nonenhancing defect frequently is found and a unique prognostic imaging factor.

KEYWORDS: Fungal disease, MR imaging

O-534 **2:03 PM - 2:11 PM**

Trends and Safety of Endovascular Treatment of Epistaxis: A Study of the Nationwide Inpatient Sample 2003-2010

Brinjikji, W.·Kallmes, D. F.·Cloft, H. J.
Mayo Clinic
Rochester, MN.

Purpose
Patients presenting with epistaxis that is refractory to anterior and posterior packing of the nasal cavity often require more invasive measures to control their bleeding. Surgical ligation of culprit vessels has historically been the primary treatment modality in these cases; however, endovascular embolization has emerged as a viable alternative and adjunct. Using a large administrative database, we sought to determine trends in the surgical and endovascular management of epistaxis and to determine outcomes and complications associated with endovascular treatment of epistaxis.
Materials & Methods
Using the Nationwide Inpatient Sample from 2003-2010, patients with a primary diagnosis of epistaxis were selected using the *International Classification of Diseases 9th Revision* (ICD-9) diagnostic code 7847. Patients undergoing surgical ligation were identified using ICD-9 procedure codes 210.3-210.7 and patients undergoing endovascular embolization were identified using ICD-9 procedure codes 397.2 and 397.9. Trends in utilization of these procedures from 2003-2010 were examined.

Note: Scanned images are included in the proceedings. Some submitted images were reduced during editing, thereby decreasing clarity. Also, refer to the Program Planner. Proceedings Content as of 3-29-2013.

Patients were stratified into three groups: 1) patients undergoing surgical ligation, 2) patients undergoing endovascular embolization and 3) patients undergoing both surgical ligation and endovascular embolization. Demographic variables and comorbidities were compared across groups. The following outcomes were assessed: in-hospital mortality, postoperative stroke, transient ischemic attack, hematoma and length of stay.
Results
A total of 69410 patients underwent surgical and/or endovascular treatment for epistaxis between 2003 and 2010. 64289 (92.6%) patients underwent surgical ligation alone for epistaxis during this time period compared to 4440 (6.4%) undergoing endovascular embolization alone and 681 (1.0%) undergoing both endovascular embolization and surgical ligation. Utilization of endovascular embolization for epistaxis increased from 2.8% of cases in 2003 to 10.7% of cases in 2010 (P<.0001). Patients undergoing endovascular embolization were significantly younger than those undergoing surgical ligation (59.1 ± 41.5 compared to 65.6 ± 42.9, P<.0001). Patients undergoing endovascular embolization were significantly more likely to have head and neck cancers (3.7%, 162/4440 compared to 0.8%, 498/64289, P<.0001) and hereditary hemorrhagic telangiectasia (2.2%, 96/4440 compared to 0.8%, 513/64289, P<.0001). Mortality rates between the two groups were similar (2.1%, 93/4440 compared to 2.1%, 1328/64289, P = 0.89). Patients undergoing endovascular embolization had significantly higher rates of stroke (0.9%, 41/4440 compared to 0.1%, 34/64289, P<.0001) and hematoma (1.9%, 83/4440 compared to 0.4%, 239/64289, P<.0001). Length of stay was similar between the two groups (5.5 ± 18.6 days compared to 5.4 ± 15.5 days, P = 0.68).
Conclusion
Utilization of endovascular embolization for treatment of epistaxis increased significantly between 2003 and 2010. Perioperative mortality rates and length of stay of endovascular embolization and surgical ligation patients are similar. However, stroke rates for patients treated with endovascular embolization are higher than those of patients with surgical ligation. More research is needed to determine which patients would benefit most from endovascular embolization compared to surgical ligation.

KEYWORDS: Endovascular therapy, ENT, Epistaxis

O-535 **2:11 PM - 2:19 PM**

"Boomerang" Malleus-Incus Complex in Congenital Aural Atresia

Mukherjee, S.·Raghavan, P.·Kesser, B.
University of Virginia Health System
Charlottesville, VA.

Purpose
Patients with congenital aural atresia (CAA) have numerous associated external and middle ear abnormalities, many of which have critical implications for atresia repair and reconstructive surgery. The purpose of this study is to describe a specific fusion deformity of the malleus and incus, appearing as a “boomerang” on axial computed tomography (CT) scans, and to discuss the clinical and surgical relevance of this anomaly.
Materials & Methods
We retrospectively reviewed the charts of 18 CAA patients with the boomerang malleus-incus complex to characterize the radiographic features, to report the associated surgical findings, and to analyze postoperative hearing gains. The following imaging features were reviewed: presence of the malleus-incus fusion, the characteristic shape, attachment to stapes superstructure, and attachment to the tympanic fallopian canal.
Results
The "Boomerang” deformity always was associated with attachment of the dysplastic incus to the tympanic fallopian canal rather than to the stapes superstructure; the stapes capitulum was absent in all cases. These findings were confirmed at surgery. The ossicular deformity required removal of the boomerang malleus-incus complex with partial ossicular replacement prosthesis (PORP) reconstruction in all cases. Hearing improved significantly after surgery.

Axial (A and B) and coronal (C) CT images show the characteristic malleus incus “boomerang” fusion abnormality (A), the attachment of the incus to the fallopian canal (B) and the absent incudostapedial joint and stapes capitulum (C) at the oval window.
Conclusion
The “boomerang” malleus-incus deformity is an easily identifiable, important preoperative finding on CT imaging in patients with Congenital Aural Atresia and is associated consistently with absence of the stapes capitulum and attachment of the incus to the fallopian canal. The "boomerang" deformity requires a challenging reconstruction, one that invariably requires an ossicular prosthesis (PORP) given the lack of an incudostapedial joint. Previous work has shown that use of an ossicular prosthesis yields inferior hearing results when compared to using the patient's intact ossicular chain. Recognition of this entity preoperatively enables the surgeon to prepare for the PORP procedure.This important finding must be communicated to the referring surgeon for optimal clinical decision making, surgical planning, and patient counseling.

KEYWORDS: Atresia, Temporal bone, CT

Note: Scanned images are included in the proceedings. Some submitted images were reduced during editing, thereby decreasing clarity. Also, refer to the Program Planner. Proceedings Content as of 3-29-2013.

O-536 **2:19 PM - 2:27 PM**

Identification of Endolymphatic Hydrops in Meniere's Disease Utilizing Delayed Postcontrast 3D FLAIR and Fused 3D FLAIR and CISS Color Maps

Hagiwara, M.[1]·McGorty, K.[2]·Wu, X.[1]·Nusbaum, A. O.[1]·Reaume, J.[1]·Roland, J. T.[1]·Schmit-Hoffman, J.[1]·Babb, J. S.[1]·Roehm, P. C.[1]·Fatterpekar, G. M.[1]
[1]New York University School of Medicine, New York, NY, [2]Columbia-Presbyterian Medical Center, New York, NY.

Purpose
Gadolinium contrast material has been shown to accumulate in the perilymphatic space four hours after intravenous administration. The preferential enhancement of the perilymphatic space allows for detection of the nonenhancing endolymphatic hydrops present in patients with Meniere's disease. The aim of this study was to evaluate the diagnostic utility of delayed postcontrast high-resolution FLAIR images as well as a color map of fused postcontrast FLAIR and CISS images in the identification of endolymphatic hydrops in patients with Meniere's disease.
Materials & Methods
Four hours after the intravenous administration of contrast, 3D FLAIR and CISS sequences of the inner ears were obtained on a 3T magnet in eight patients with Meniere's disease and five volunteer controls. Patients were asked to fill out a questionnaire regarding the side of involvement, symptomatology, date of initial presentation, and date of most recent episode. Color maps were generated upon fused 3D FLAIR and CISS images. Two neuroradiologists blinded to the clinical history independently reviewed the images of both inner ears (right and left) for test and control subjects; both the standard gray-scale FLAIR images and the fused color map images were reviewed independently. Agreement between readers was assessed using a kappa coefficient. Ordinal logistic regression statistical analysis was performed.
Results
Interevaluator reliability was excellent for the two independent and blinded radiologists who evaluated the scans (kappa = 0.69 for gray scale images, kappa = 0.796 for fused color map). There was no significant difference between the unaffected ears of patients with Meniere's disease and the inner ears of controls, and therefore, the two groups were combined into one unaffected ear category. According to ordinal logistic regression for correlated data, there was significant correlation between the gray scale images and color map images with the categorization of involvement ($p = 0.002$). The gray scale 3D FLAIR images demonstrated 60% sensitivity and 96.9% specificity, and the fused color map images demonstrated 78.6% sensitivity and 93.3% specificity. All patients with false negative results on the gray scale and/or color map images reported time of initial presentation to be within the past two years, whereas all of the true positive results were in patients with reported initial presentation of greater than three years prior (range 3-28 years).
Conclusion
3D FLAIR images of the inner ears obtained four hours after the administration of intravenous contrast is potentially a useful diagnostic tool in the evaluation of patients with Meniere's disease. The technique demonstrated good interobserver agreement, and the fused 3D FLAIR-CISS color map images increased diagnostic accuracy. The diagnostic accuracy proved greatest in patients with a longer history of symptomatology of greater than three years.

KEYWORDS: Meniere, FLAIR, color map

O-537 **2:27 PM - 2:35 PM**

CT Findings for Diagnosis and Complications of Temporal Bone Osteoradionecrosis

Ahmed, S.[1]·Gupta, N.[2]·Hamilton, J.[1]·Garden, A.[1]·Gidley, P.[1]·Ginsberg, L.[1]
[1]University of Texas M. D. Anderson Cancer Center, Houston, TX, [2]University of Texas Houston Medical School, Houston, TX.

Purpose
The temporal bone (TB) is included in the radiation field when treating tumors of the nasopharynx, retromolar trigone, external ear, and parotid glands. Osteoradionecrosis (ORN) of the TB is a delayed, but serious complication that may arise in a small number of patients. Patients present with hearing loss, otalgia, otorrhea, and even gross tissue extrusion. Despite an incidence of 2-12% with irradiated parotid tumors, no large series of cases describing CT findings in patients with TB ORN exists in the radiology literature. The goal of this study is to describe CT findings in patients with clinical osteoradionecrosis.
Materials & Methods
Twenty patients with (1) radiation field that included the TB, (2) no evidence of tumor recurrence, and with (3) clinical diagnosis of TB ORN made between 9/10/2002 and 2/20/12 were included for review. High-resolution CT scans were evaluated by a neuroradiologist for bony, soft tissue, and intracranial abnormalities. Retrospective chart review of therapy administered was used to assign a clinical grade of mild (observation), moderate (antibiotics/hyperbaric oxygen), or severe (surgery). P values were calculated using Fisher's exact test (two-tailed).
Results
Radiation therapy had been administered for two SCCa of the skin, five primary parotid malignancies , four metastatic SCCa to the parotid, four nasopharyngeal carcinoma, two melanoma, one basal cell carcinoma, and two SCCa of the retromolar trigone. Radiation dose to the primary tumor ranged from 30 to 75.6 Gy. Time to onset of ORN from completion of RT was two years to 22 years

Note: Scanned images are included in the proceedings. Some submitted images were reduced during editing, thereby decreasing clarity. Also, refer to the Program Planner. Proceedings Content as of 3-29-2013.

(median = 7 years). Clinical grade: mild = 7/20 patients, moderate = 8/20, and severe = 5/20. Please refer to Table 1 for description of CT findings. Of the 20 patients evaluated, 19 demonstrated exposed bone on clinical exam, 17 had otorrhea, 11 had hearing loss, and 10 complained of otalgia. Of the seven patients with clinically mild ORN, none demonstrated enhancing soft tissue or air within deep spaces, while each of these findings was present in six of 13 patients with a clinical grade of moderate or severe ORN. Three patients developed an abscess; one infratemporal fossa abscess, one Bezold's abscess, and one intracranial (temporal lobe) abscess.

Table 1. CT Findings

Clinical grade	External auditory canal erosion	Mastoid effusion	Mastoid bony Coalescence	Enhancing soft-tissue	Air within deep spaces	TMJ-condylar erosion
Mild (7)	6	6	1	0	0	0
Moderate (8)	6	7	1	3	3	2
Severe (5)	5	5	3	3	3	1
TOTAL (20)	17	18	5	6	6	3

Conclusion

Mastoid effusion and EAC erosions commonly are seen with TB ORN. Enhancing soft tissue (p = 0.05) and air within deep spaces (p = 0.05) are more likely to be seen with clinically moderate or severe TB ORN. TMJ-condylar erosion and mastoid bony coalescence also can be seen with TB ORN. Intracranial and soft tissue abscesses are serious complications that can arise. Knowledge of the CT findings and potential complications associated with temporal bone osteoradionecrosis is important for the neuroradiologist who must differentiate from tumor recurrence, with which ORN may be confused.

KEYWORDS: Radiation toxicity, Temporal bone

O-538 **2:35 PM - 2:43 PM**

Persistent Craniopharyngeal Canal and Its Spectrum of Pathology

Abele, T. A.[1]·Salzman, K. L.[1]·Harnsberger, H. R.[1]·Glastonbury, C. M.[2]
[1]University of Utah, Salt Lake City, UT, [2]University of California San Francisco, San Francisco, CA.

Purpose

The craniopharyngeal canal is an embryonic remnant extending from the sella turcica floor to the anterosuperior roof of the nasopharynx. While formation of the canal is disputed, evidence supports its origin from incomplete closure of Rathke's pouch, the precursor of the anterior pituitary gland. Lesions related to the persistent craniopharyngeal canal are varied, ranging from small incidental canals to ectopic tumors of the adenohypophysis and associated embryonic tissues. We reviewed a series of persistent craniopharyngeal canals in an effort to improve diagnosis of this embryonic remnant and highlight the range of associated pathologic lesions. In addition, we examine the embryology and relevant literature of the craniopharyngeal canal to refine understanding of this rare entity.

Materials & Methods

Two neuroradiologists reviewed available clinical and imaging data of a series of persistent craniopharyngeal canals from multiple institutions. All cases had cross-sectional imaging studies, either CT, MRI, or both. The length and diameter at the midpoint of the canal were recorded when available. Imaging evaluation also was directed to position and morphology of the pituitary gland and associated cephalocele or neoplasm. Clinical data including presenting symptom and presence of pituitary dysfunction or other congenital malformations were reviewed.

Results

Twenty-nine patients aged 1 day - 66 years were included. Small (AP diameter range: 0.7-1.0 mm) incidental canals were observed in 31% (9/29) of patients. Medium (3.5-4.4 mm) sized canals with inferiorly displaced pituitary tissue (Figure 1) were seen in 24% (7/29) of patients. Seventeen percent (5/29) of patients had large (7.7-13.5 mm) canals associated with cephaloceles (Figure 2) while 28% (8/29) had associated tumors, including pituitary adenoma, craniopharyngioma, dermoid, teratoma, and glioma. The medium sized canals and large canals with cephaloceles all contained identifiable anterior pituitary tissue. Persistent craniopharyngeal canals are associated with pituitary dysfunction (6/29) and other congenital malformations (7/29).

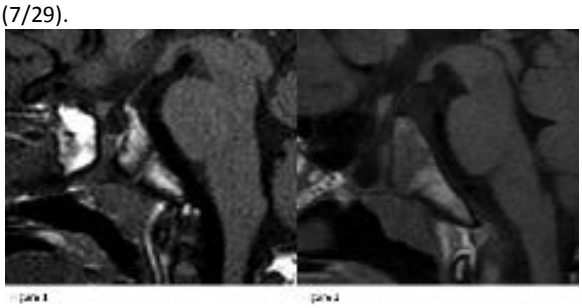

Conclusion

Persistent craniopharyngeal canal is an important entity to consider in the differential diagnosis of nasopharyngeal or midline skull base lesions. Persistent craniopharyngeal canals can be divided into four types: (1) small incidental canals (2) medium sized canals with displaced or ectopic pituitary tissue, (3) large canals with associated cephaloceles, and (4) canals containing epithelial tumors of the adenohypophysis and associated embryonic tissues. Accurate diagnosis can distinguish lesions requiring surgery from those that do not. In our series the medium and large craniopharyngeal canals invariably contained pituitary tissue, which is important in surgical management of these lesions to avoid iatrogenic hypopituitarism.

Note: Scanned images are included in the proceedings. Some submitted images were reduced during editing, thereby decreasing clarity. Also, refer to the Program Planner. Proceedings Content as of 3-29-2013.

KEYWORDS: Midline developmental anomalies, Embryology, Craniopharyngeal canal

Thursday Afternoon

1:15 PM - 2:45 PM
Ballroom 6CF

(57b) Parallel Scientific Papers: Adult Brain: Tumors IV: Glioblastoma

O-539 **1:15 PM - 1:23 PM**

Imaging Genomics: Correlation of Invasive Genomic Composition and Patient Survival Using Qualitative and Quantitative MR Imaging Parameters: A TCGA Glioma Phenotype Research Group Project

Colen, R. R.[1]·Abrol, T.[1]·Gutman, D. A.[2]·Hwang, S. N.[2]·Wintermark, M.[3]·Jain, R.[4]·Jilwan-Nicolas, M.[3]·Chen, J. Y.[5,6]·Raghavan, P.[3]·Holder, C. A.[2]·Rubin, D.[7]·Huang, E.[8]·Kirby, J.[8]·Freymann, J.[8]·Jaffe, C. C.[9]·Flanders, A.[10]·TCGA Glioma Phenotype Research Group·Zinn, P. O.[1]
[1]M. D. Anderson Cancer Center, Houston, TX, [2]Emory University, Atlanta, GA, [3]University of Virginia, Charlottesville, VA, [4]Henry Ford, Detroit, MI, [5]University of California San Diego Health System, San Diego, CA, [6]San Diego Medical Center, San Diego, CA, [7]Stanford University, Stanford, CA, [8]NCI/NIH, Bethesda, MD, [9]NCI/NIH, Rockville, MD, [10]Thomas Jefferson University Hospital, Philadelphia, PA.

Purpose
To identify the invasive MRI characteristics in GBM and the implicated genes and microRNAs associated with these invasive features. Preoperative qualitative imaging data reflective of invasive tumor grown patterns have been documented. These include the presence of either T1 contrast enhancement or increase T2/FLAIR hyperintensity involving the basal ganglia, corpus callosum (unilateral, bilateral, or contralateral,) or brainstem; the presence of subependymal enhancement; the presence of pial enhancement; and a peritumoral nonenhancing FLAIR hyperintensity. Tumor volumetry of the nonenhancing FLAIR hyperintensity also has been validated to reflect increase tumor invasion.
Materials & Methods
A total of 78 treatment-naïve GBM patients whom had both gene- and microRNA expression profiles and pretreatment MR neuroimaging were analyzed. Each image (T1 axial image both before and after gadolinium contrast administration, and axial T2/FLAIR image) was qualitatively assessed by at least three independent neuroradiologists. The standardized VASARI feature set criteria was used for qualitatively visual assessment of key features of invasion (presence of either T1 contrast enhancement of increase T2/FLAIR hyperintensity involving the basal ganglia, corpus callosum (unilateral, bilateral, or contralateral) or brainstem; the presence of subependymal enhancement; and the presence of pial enhancement; and a peritumoral nonenhancing FLAIR hyperintensity). For quantitative assessment, we performed volumetric analysis using the 3D Slicer platform to quantitatively measure actual volumes of each individual region. The flair-volume, contrast-enhancing region, and necrotic core were segmented independently and verified by a trained neuroradiologist experienced in tumor volumetry.
Results
Quantitative tumor volumetry was the strongest predictor of tumor invasive genomic targets such as POSTN ($p<.001$), a known invasive gene implicated in GBM. Qualitative features did not demonstrate similar correlations. Both qualitative and quantitative invasive signatures were predictive of patient survival. This was strongest using the qualitative parameter of involvement of the corpus callosum.
Conclusion
Invasive features of MRI as determined by both qualitative and quantitative assessment reflect tumor compositions which have genes involved in invasion. However, quantitative tumor volumetry of nonenhancing FLAIR hyperintensity continues to be the strongest predictor of highly invasive tumors and genes involved in invasion.

KEYWORDS: Imaging genomics, Genomic mapping, glioblastoma

O-540 **1:23 PM - 1:31 PM**

Evaluation of T2* Dynamic Susceptibility-Based Contrast-Enhanced and T1 Dynamic Contrast-Enhanced Perfusion Imaging in Glioma Grading: Comparison between Two Estimates of Vessel Compartment Volume, T2* DSC-rCBV and T1 DCE-fVp

Santarosa, C.·Castellano, A.·Politi, L. S.·Terreni, M. R.·Leoncini, G.·Falini, A.·Anzalone, N.
Ospedale San Raffaele
Milano, ITALY.

Purpose
The role of relative cerebral blood volume (rCBV) from T2*-weighted dynamic susceptibility-based contrast-enhanced (DSC) MR perfusion imaging in glioma grading is established. Nevertheless limitations of DSC technique due to high sensitivity to susceptibility effects are well known. Our aim was to evaluate an alternative parameter, named fractional plasma volume (fVp), derived from a T1-weighted perfusion technique, dynamic contrast-enhanced (DCE) MR perfusion imaging. We compared estimations of vessel compartment volume given by rCBV and fVp and determined their correlation with histologic

Note: Scanned images are included in the proceedings. Some submitted images were reduced during editing, thereby decreasing clarity. Also, refer to the Program Planner. Proceedings Content as of 3-29-2013.

WHO grade.
Materials & Methods
Thirteen patients with untreated brain gliomas (including both astrocytic and oligodendroglial histotypes) underwent DSC and DCE perfusion MR imaging with a 3.0T MRI scanner (Achieva, Philips). NordicIce software (NordicImagingLab) was used for postprocessing. Measurements of both parameters were obtained, through hotspot method, from ROI of the maximal abnormality within the lesion. Estimations of rCBVmax and fVpmax were reciprocally compared after normalization for their respective highest value in our sample. Spearman rank correlation measured associations between both parameters and histologic WHO grade.
Results
Mean values of both parameters were significantly different between low-grade gliomas (LGG) and high-grade gliomas (HGG) (LGG rCBVmax mean: 1.45; HGG rCBVmax mean: 4.44) (LGG fVpmax mean: 1.3; HGG fVpmax mean: 8.6). Normalized rCBVmax and Vpmax values were very close to each other in all cases, except for a low-grade fronto-mesial oligoastrocytoma (normalized-rCBVmax: 0.9, rCBVmax: 5; normalized-Vpmax: 0.23, Vpmax: 2.8). Correlation beetween Vpmax and WHO grade was more significant (p: 0.000) than that between rCBVmax and WHO grade (p:0.011).

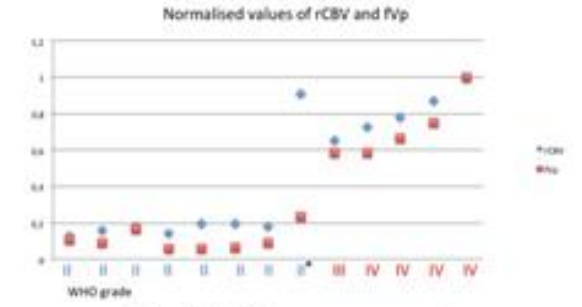

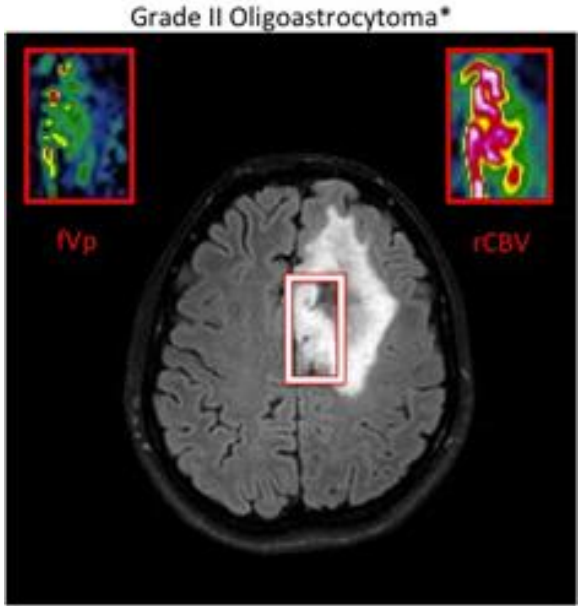

Conclusion
Our preliminary results suggest that fVp is as reliable as rCBV in glioma noninvasive grading. Benefit of fVp seems to emerge when superficial brain lesions, affected by macrovessels-associated susceptibility effects, are evaluated.

KEYWORDS: Glioma, Brain perfusion

O-541 **1:31 PM - 1:39 PM**

Intensity-Normalized T1 Subtraction Maps Improve Quantification of Contrast-Enhancing Tumor Burden and Predict Survival in Recurrent Glioblastoma Treated with Bevacizumab: Evaluation in a Single Institution and a Multicenter Clinical Trial

Woodworth, D. C.·Cloughesy, T. F.·Kim, H. J.·Cloughesy, J. N.·Harris, R. J.·Lai, A.·Nghiemphu, P. L.·Pope, W. B.·Ellingson, B. M.
David Geffen School of Medicine at University of California Los Angeles
Los Angeles, CA.

Purpose
In anti-angiogenic therapy for glioblastoma multiforme (GBM) patients, decreased vascular permeability and the resultant decrease in contrast enhancement in T1-weighted postcontrast MRI scans complicate treatment response assessment. The purpose of this study was to determine whether ΔT1 maps (intensity-normalized precontrast T1-weighted images subtracted from T1 postcontrast-weighted images) improve the ability to quantify contrast enhancing tumor burden and predict response in glioblastoma patients treated with bevacizumab as evaluated in both a single institution and a multicenter clinical trial.
Materials & Methods
A total of 100 patients from UCLA and 165 patients from a multicenter clinical trial (BRAIN trial) with recurrent GBM undergoing treatment with bevacizumab (Avastin; Genetech) were enrolled in this study. Pre (T1) and postcontrast T1-weighted images (T1+C) were intensity-normalized, then T1 precontrast images were subtracted from respective T1 postcontrast images, resulting in ΔT1 maps highlighting regions of subtly enhancing tumor. Tumor volumes were calculated based on regions of ΔT1 hyperintensity. Additionally, tumor volumes on standard postcontrast images were contoured for comparison.
Results
After treatment with bevacizumab, T1+C scans exhibited almost complete reduction of enhancement in more than 80% of patients; however, ΔT1 maps clearly demarcated regions of residual contrast enhancement. A pretreatment ΔT1 map-defined volume of contrast-enhancing tumor >15cc was used to identify short-term progression-free (PFS; UCLA, Log-rank, P = 0.0302; BRAIN trial, Log-rank, P = 0.0005, Cox, P = 0.001) and overall survivors (OS; UCLA,

Note: Scanned images are included in the proceedings. Some submitted images were reduced during editing, thereby decreasing clarity. Also, refer to the Program Planner. Proceedings Content as of 3-29-2013.

Log-rank, P = 0.0184; BRAIN, Log-rank, P = 0.0001, Cox, P7.5cc was used to identify short-term PFS (UCLA, Log-rank, P = 0.0089; BRAIN, Log-rank, P<0.0001, Cox, P<0.001) and OS (UCLA, Log-rank, P = 0.0204; BRAIN, Log-rank, P<0.0001, Cox, P<0.001). Additionally, a >25% decrease in enhancing volume identified long-term PFS (UCLA, Log-rank, P = 0.0041; BRAIN, Log-rank, P = 0.0030); however, this change could only stratify OS in the single institution data (UCLA, Log-rank, P = 0.0110) but not in the clinical trial data (BRAIN, Log-rank, P = 0.0509). Cox regression including interaction tests suggests a significant predictive advantage of ΔT1 maps compared with standard T1+C-defined volumes for both PFS and OS.

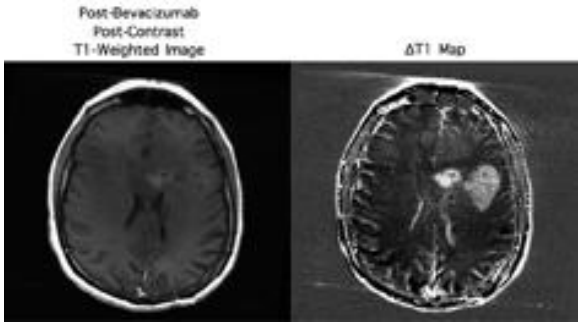

Conclusion
The ΔT1 mapping technique improves visualization and quantification of tumor burden in evaluation of response to anti-angiogenic therapy. Initial, residual, and the change in ΔT1 map-defined contrast enhancement before and after bevacizumab are all predictors of response and survival in recurrent GBM.

KEYWORDS: Glioblastoma, Imaging biomarker

O-542 **1:39 PM - 1:47 PM**

Tumor Boundary Mapping: A Novel Technique for Assessing Tumor Heterogeneity and Deriving a Predictive Biomarker of Outcomes in Glioblastoma Multiforme

Thompson, G.[1]·Mills, S. J.[2]·Jackson, A.[1]
[1]University of Manchester, Manchester, UNITED KINGDOM, [2]Salford Royal NHS Foundation Trust, Salford, UNITED KINGDOM.

Purpose
Glioblastoma multiform (GBM) is the most aggressive primary brain tumor, with dismal clinical outcomes despite advances in chemoradiotherapy. Failure is most commonly adjacent to the original tumor site, occurring within the radiotherapy planning field in the majority of cases. This has been attributed to the presence of microinvasive infiltrating disease - undetectable by standard clinical MR sequences - emanating from the visible, solid tumor edge. These cells exhibit a migratory rather than mitotic phenotype, and are more radioresistant. We previously have presented a modified imaging biomarker of the tumor edge which was based on the boundary change in apparent diffusion coefficient (ADC) between solid enhancing tumor and surrounding parenchyma. This ADC transition coefficient (ATC) was hypothesized to represent tumor invasiveness, and was found to be predictive of overall survival in a retrospective cohort of 22 GBM. An updated technique in which the tumor surface was mapped in three dimensions (ATC-3D) rather than in select axial points in 2D was developed and tested in a prospective validation cohort.
Materials & Methods
Twenty-four patients with subsequently histologically-proven GBM were imaged at 3T prior to surgery. The tumor surface was manually delineated in 3D on a 1mm isotropic postcontrast image. This was coregistered to a 2mm isotropic ADC map from 15-direction DTI. Tumor surface normal vectors were calculated for each surface voxel (Figure), and the ATC was derived. A summary mean ATC was taken as the ATC-3D. This produced both a summary tumor value for comparison with time to progression (TTP) using Cox regression analysis, and a map denoting tumor surface heterogeneity as a function of local ATC. Permeability and quantitative magnetization transfer imaging also were acquired, and spatial correlations were investigated between the local ATC-3D and a variety of vascular and structural imaging parameters.
Results
ATC-3D was predictive of TTP in the prospective cohort (HR=0.986;p=0.028). Spatial correlations also were described between ATC-3D and boundary K^{trans} and v_e from DCE-MRI, and RM_0^A from qMT (p<0.0005).

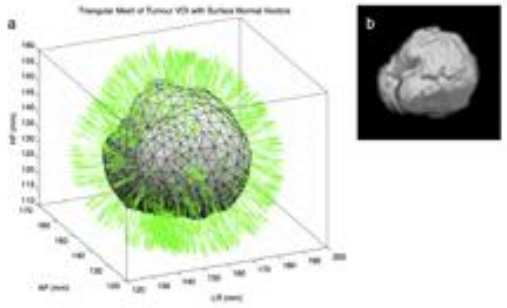

Conclusion
Presented here is a prospective validation study of a novel imaging biomarker which predicts clinical outcomes in GBM based on the tumor surface diffusion characteristics. This tumor boundary mapping has implications for treatment decisions and may be useful for stratifying patients at presentation. Furthermore, there is added value for identifying areas of differential tumor invasiveness and vascularity, particularly in combination with other advanced imaging parameters, which may help guide surgery and radiotherapy to improve outcomes.

KEYWORDS: Glioblastoma, Biomarkers

Note: Scanned images are included in the proceedings. Some submitted images were reduced during editing, thereby decreasing clarity. Also, refer to the Program Planner. Proceedings Content as of 3-29-2013.

O-543 **1:47 PM - 1:55 PM**

Perfusion MR Imaging Outperforms Diffusion MR Imaging in Differentiating Radiation Injury from Recurrent Tumor in Treated High-Grade Gliomas

Prager, A. J.·Martinez, N.·Zhang, Z.·Beal, K.·Young, R.
Memorial Sloan Kettering Cancer Center
New York, NY.

Purpose
The objective was to assess the utility of diffusion-weighted imaging (DWI) and dynamic susceptibility contrast (DSC) perfusion imaging in differentiating between post-treatment change and recurrent tumor in patients with high-grade gliomas (HGGs).
Materials & Methods
We retrospectively examined 68 consecutive patients with HGGs (primary glioblastoma and anaplastic astrocytoma) who received standard treatment consisting of surgical resection followed by radiation therapy with temozolomide, and then developed increasing enhancing mass lesions indeterminate for radiation injury or recurrent tumor. All patients underwent surgical resection of their indeterminate lesions with diagnosis assigned by pathology results as: radiation injury (no tumor cells) or recurrent tumor (any amount of tumor cells). MR imaging before repeat surgery included contrast T1-weighted imaging, DWI with ADC maps and DSC perfusion imaging. Region-of-interest (ROI) analysis was performed by manually drawing an ROI around the entire contrast-enhancing lesion while excluding areas of necrosis and hemorrhage, then applied to the ADC and DSC maps to calculate ADC_{mean} and $rCBV_{lesion}$ values. In addition, up to four small ROIs (approximately 50mm^2) were placed within the contrast-enhancing lesion to calculate ADC_{ROI}, $rCBV_{ROI,}$ percentage signal recovery (PSR_{ROI}), and relative PH (rPH). Statistical analysis was performed with Wilcoxon rank sum tests with false discovery rate corrected p values for multiple comparisons (ADC p = .05/3 = .0167 and rCBV p = .05/4 = 0.0125). Receiver operating characteristics (ROC) curves also were calculated.
Results
Eleven of the 68 patients (16%) had radiation injury, while 57 patients (84%) had recurrent tumor only (n = 18) or recurrent tumor mixed with treatment effects (n = 36). ADC_{mean} was significantly lower for recurrent tumor group (median = 0.00138 mm^2/s) than for radiation injury (median = 0.00157 mm^2/s) with p = 0.005. $rCBV_{lesion}$ was significantly higher for recurrent tumor (median = 1.81) than for radiation injury (median = 1.02) with p = 0.003. $rCBV_{roi}$ also was significantly different between recurrent tumor (median = 2.98) and radiation injury (median = 1.7) with p = 0.011. The area under the ROC curve (AUC) for distinguishing between radiation injury and recurrent tumor was 0.75 for ADC_{mean} and 0.86 for $rCBV_{roi}$. An ADC_{mean} threshold of 0.0014 had a sensitivity of 53.6 and specificity of 90.9, while an $rCBV_{lesion}$ threshold of 1.27 had the best sensitivity (86.8) and specificity (83.8) overall.
Conclusion
Higher perfusion and lower diffusion were seen in recurrent tumor compared to radiation injury groups. Perfusion showed the best sensitivity and specificity, and $rCBV_{lesion}$ outperformed ADC_{mean} in differentiating radiation injury from recurrent tumor in patients with HGGs. Measuring the entire lesion on a single slice performed better than small fixed ROIs.

KEYWORDS: Adult gliomas

O-544 **1:55 PM - 2:03 PM**

Alterations in Functional Connectivity of the Default Mode Network in Malignant Glioma Patients as Measured by Pseudo Resting-State Functional MR Imaging

Harris, R. J.·Bookheimer, S.·Cloughesy, T. F.·Pope, W. B.·Ellingson, B. M.
David Geffen School of Medicine at University of California Los Angeles
Los Angeles, CA.

Purpose
Recent fMRI experiments have shown that correlated fluctuations of the BOLD signal within specific brain regions occur in the absence of stimuli, a phenomenon known as “resting-state networks”. The most prevalent of these is the default mode network (DMN), with nodes appearing in the anterior cingulate cortex (ACC), posterior cingulate cortex (PCC), left lateral parietal cortex (LLPC), and right lateral parietal cortex (RLPC). We hypothesize that malignant gliomas infiltrating anatomical regions adjacent to a node of the DMN will cause decreased functional connectivity between DMN nodes across the entire network, including distal nodes not anatomically affected by bulk tumor.
Materials & Methods
Twenty-four malignant glioma patients with presurgical task-activation fMRI data and data from nine healthy control subjects (Group 1) were included in this study. Ten patients had tumor in the left hemisphere outside DMN nodes (Group 2) and 13 had tumors in the LLPC node (Group 3). Functional tasks were regressed out of the block paradigm, leaving the “pseudo”-resting state fMRI signal. Four ROIs corresponding to the primary notes of the DMN were placed using a standard DMN template. Quantification of “functional connectivity” between nodes was determined using a Pearson’s correlation coefficient, R, between the averaged DMN ICA time series data for each pairs of nodes. This correlation coefficient then was compared across groups and nodes.
Results
In general, functional connectivity as measured using the correlation coefficient was suppressed in tumor patients (Groups 2 and 3) when compared with controls (Group 1). Specifically, functional connectivity (R-value) was significantly different across groups (2-way ANOVA,

Note: Scanned images are included in the proceedings. Some submitted images were reduced during editing, thereby decreasing clarity. Also, refer to the Program Planner. Proceedings Content as of 3-29-2013.

P<0.0001), but not across nodes (P = 0.503). Bonferroni-corrected post-tests showed no difference in connectivity between groups for any of the individual nodes. A one-way ANOVA and Tukey's multiple comparisons test confirmed a significant difference between the connectivity of normal controls (Group 1) versus tumor patients (Groups 2 and 3; P<0.05). No significant difference in functional connectivity was observed between patients that had tumors in or outside the LLPC node (P>0.05); however, patients with tumors inside the LLPC node tended to have a lower connectivity compared to patients with tumors outside this node.

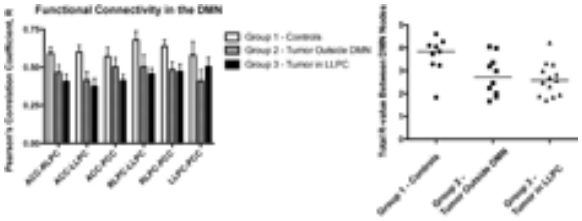

Conclusion
This study supports the hypothesis that diffusely infiltrating malignant gliomas globally impair functional connectivity within the DMN. Additionally, tumors localized to a node within the DMN tended to decrease connectivity to a larger extent than tumors outside these regions.

KEYWORDS: Brain neoplasms, Resting-state fMRI

O-545 **2:03 PM - 2:11 PM**

Results of the First Study Validating MR Imaging as a Screening Tool for Genomic Target Discovery for Therapeutic Drug Development

Colen, R. R.[1]·Zinn, P. O.[1,2]
[1]M. D. Anderson Cancer Center, Houston, TX, [2]Baylor College of Medicine, Houston, TX.

Purpose
The search for an effective therapy of glioblastoma multiforme (GBM) continues. Imaging genomics, a newly emerged field, links gene expression profiles with MRI phenotypes (Zinn et al, 2011). MRI-FLAIR was found to correlate with cellular invasion in GBM; thus, whole genome quantitative imaging analysis can reveal functional microRNA-gene regulatory networks as novel targets for cellular invasion in GBM.
Materials & Methods
We performed radiogenomic mapping of MRI and corresponding genomic data in 78 TCGA patients. The top microRNA-gene regulatory network was validated biologically by luciferase reporter assays, gain and loss of function using tet-inducible lentiviral microRNA expression systems, as well as si/shRNA, small molecule inhibitor/recombindant protein in vitro experiments and in vivo orthotopic xenograft models. Small animal 7T MRI-T2/FLAIR was used for imaging-genomic validations.
Results
The top up-regulated gene in high invasion MRI phenotypes was PERIOSTIN (POSTN). The top down-regulated microRNA (miR-219) was validated to bind to POSTN. Glioblastoma-derived stem cells (GSCs) from high FLAIR GBM patients correlated with levels of POSTN and increased invasion in vitro and in orthotopic xenograft tumor models on histological sections and MRI. Functionally, miR-219 overexpression reduced POSTN protein levels, while recombinant POSTN, neutralizing antibody, and shRNA experiments significantly altered cellular invasion in vitro and in vivo. MRI-T2/FLAIR signal highly correlated with POSTN levels and the degree of cellular invasion in orthotopic xenograft models. Furthermore, high POSTN and a high POSTN/miR-219 signature resulted in decreased survival and shorter time to progression (P<0.0001) in 511 GBM patients.

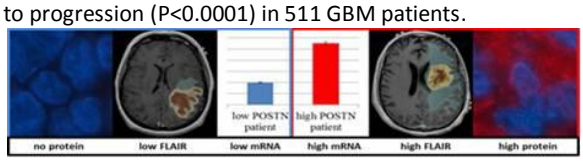

Conclusion
In this study, we validated a novel noninvasive diagnostic method to screen for functional networks of cellular invasion. POSTN inhibition can be a novel therapeutic approach to target invasion in GBM. Furthermore, targeted individualized molecular therapies can be based on diagnostic imaging-genomics and can be monitored throughout the treatment period.

KEYWORDS: Glioblastoma, Genomic mapping, imaging genomics

O-546 **2:11 PM - 2:19 PM**

Combining Diffusion and Perfusion to Differentiate Tumor from Bevacizumab-Related Restricted Diffusion

Farid, N.[1]·Almeida-Freitas, D.[1,2]·White, N. S.[1]·McDonald, C. R.[1]·Muller, K. A.[1]·VandenBerg, S. R.[1]·Dale, A. M.[1]
[1]University of California San Diego, San Diego, CA, [2]University of Sao Paulo, Sao Paulo, BRAZIL.

Purpose
With the increasing use of antiangiogenic agents in the treatment of high-grade gliomas and to a lesser extent in the treatment of brain metastases, we are becoming increasingly aware of distinctive imaging findings seen in a subset of patients treated with these agents. Of particular interest is the development of regions of marked and persistent restricted diffusion which have been shown previously to correlate with improved outcomes. Histopathologic data from these regions reveal areas of atypical gelatinous necrosis rather than viable tumor. Our goal was to quantify the degree of restricted diffusion and the cerebral blood volume (CBV) within these "pseudostroke" lesions (i.e., regions of marked persistent restricted diffusion) in order to develop an algorithm by

Note: Scanned images are included in the proceedings. Some submitted images were reduced during editing, thereby decreasing clarity. Also, refer to the Program Planner. Proceedings Content as of 3-29-2013.

which to differentiate these lesions from viable tumor.
Materials & Methods
Five patients with high-grade glioma and one patient with brain metastasis from NSCLC who developed pseudostroke lesions after the initiation of bevacizumab were included in this study. Five presurgical, treatment-naïve controls with high-grade glioma also were included. Restriction-spectrum imaging (RSI), an advanced DWI technique, was used to create RSI-cellularity maps (RSI-CM) and these were coregistered with CBV maps. Within the pseudostroke lesions, mean RSI-CM intensity values and mean CBV values were calculated and compared to that of the presurgical high-grade gliomas as well as to that of the contralateral NAWM.
Results
Mean RSI-CM intensity values were significantly higher in patients with pseudostroke lesions compared to the treatment-naïve high-grade glioma controls ($p < .05$). Furthermore, mean CBV values were significantly lower in patients with pseudostroke lesions compared to the contralateral NAWM ($p < .01$). Of note, in one patient with a presumed nodule of viable tumor within a large pseudostroke lesion, there was focal increased CBV within this nodule. Histopathologic evaluation of one of the pseudostroke lesions demonstrated necrotic tissue as well as scattered inactive tumor cells.

Fig 1: 45 year old female with GBM who developed a "pseudostroke" lesion which persisted for 11 months after initiation of bevacizumab. Presumed nodule of viable tumor in the right frontal lobe within the pseudostroke lesion which demonstrates elevated CBV and FDG avidity.

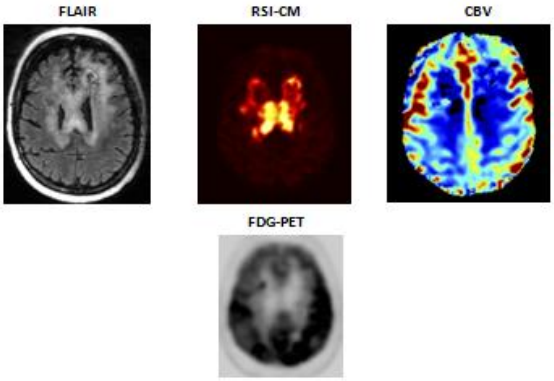

Conclusion
When evaluating areas of restricted diffusion in patients with high-grade glioma or brain metastases treated with bevacizumab, one can utilize the RSI-CM intensity values and the CBV values in order to determine whether these areas represent predominantly necrotic tissue related to bevacizumab treatment or viable tumor. Bevacizumab-related restricted diffusion demonstrates RSI-CM intensity values greater than tumor and CBV values lower than the contralateral NAWM.

KEYWORDS: Neoplasm, Diffusion-weighted imaging, MR Perfusion

O-547 **2:19 PM - 2:27 PM**

High-Grade Gliomas and Solitary Metastases: Differentiation by Using Peritumoral Perfusion and Proton Spectroscopic MR Imaging

Sparacia, G.[1]·Sparacia, B.[1]·Robusto, V.[2]·Gadde, J.[3]·Iaia, A.[3]
[1]University of Palermo, Palermo, ITALY, [2]University of Messina, Palermo, ITALY, [3]Christiana Care Health System, Newark, DE.

Purpose
To evaluate whether peritumoral perfusion-weighted and proton spectroscopic MR imaging can be used in preoperative grading and differentiation of primary gliomas and solitary metastases.
Materials & Methods
Ten low-grade gliomas, eight high-grade gliomas, and five metastases were prospectively evaluated by MR imaging, dynamic susceptibility contrast-enhanced perfusion imaging and single-voxel proton MR spectroscopy before surgical resection or stereotactic biopsy. Normalized rCBV values from peritumoral areas were calculated by using regions of interest (ROIs) of 2cm2 drawn around the nonenhancing peritumoral T2 lesion and the contrast-enhancing lesion. Metabolite ratios were measured from peritumoral areas. Tumor grade determined with normalized rCBV values and MR spectroscopy from peritumoral areas was compared with that from histopathologic grading. A ROC analysis was performed to determine which parameters best increased diagnostic accuracy in grading and differentiation of primary gliomas and solitary metastases.
Results
The mean differences of rCBV values between low-grade gliomas and high-grade gliomas ($P < .001$); high-grade gliomas and metastases ($P < .001$); and low-grade gliomas and metastases ($P < .001$) were significant. A clear rCBV cutoff value of 2.6 was detected for differentiation of low-grade gliomas (1.6) versus high-grade gliomas (3.4). Cutoff rCBV values of 1.1 and 1.98 were quite effective in differentiation of metastases from low-grade gliomas and high-grade gliomas, respectively. The overall efficacy of rCBV was higher in grading than in differentiation. Choline to creatine ratio in the peritumoral regions of high-grade gliomas were significantly higher than they were in the metastases. NAA/Cr tumor ratio of <0.44 has the higher probability for a neoplasm to be a high-grade glioma.
Conclusion
Although conventional MR imaging characteristics of solitary metastases and primary gliomas may sometimes be similar, the peritumoral perfusion-weighted and spectroscopic MR imaging enable distinction between the two. Moreover perfusion-weighted imaging technique is complementary technique for glioma grading.

KEYWORDS: Glioma, Metastases, Perfusion MR Imaging, MR Spectroscopy

Note: Scanned images are included in the proceedings. Some submitted images were reduced during editing, thereby decreasing clarity. Also, refer to the Program Planner. Proceedings Content as of 3-29-2013.

O-548 **2:27 PM - 2:35 PM**

Semi-Automated Measurement of Recurrent and Residual Disease in Glioblastoma Multiforme: A Potential New Objective Metric

Chow, D.·Qi, J.·Guo, X.·Mathew, N.·Miloushev, V.·Filippi, C.·Zhao, B.·Lignelli, A.
Columbia University
New York, NY.

Purpose
Glioblastoma multiforme (GBM) is an invasive and highly aggressive tumor. Though outcomes are highly variable and difficult to predict, there is some consensus that resection provides symptomatic relief and cytotoxic reduction to augment adjuvant therapy. A limitation in postoperative monitoring has been the lack of objective measures to quantify residual and recurrent disease. Automated computer-assisted analysis of contrast-enhancing tissue represents a potential tool to aid the radiologist in following these patients. In this study, we aim to describe our initial results when comparing automated measures to neuroradiologists' reports.
Materials & Methods
This retrospective study included patients with native glioblastomas with postoperative MR imaging in the immediate 24-48 hour and two-three month follow-up period. All patients received XRT with concurrent TMZ following maximal resection. Tumor contours were delineated on immediate and two-month postsurgery contrast-enhanced T1-weighted images using a semi-automated algorithm that combines the region-based active contours and level set approach. Discrepancies between neuroradiologists' reports and automated detection measurements were assessed. Radiologist reports were divided into decrease enhancement, no significant change, or increase/new enhancement.
Results
A total of 21 patients were included in the study. Decreased enhancement, no significant change, and increased/new enhancement was seen in 14.3% (3/21), 19.0% (4/21), and 66.7% (14/21) of patients respectively. Within these categories, automated detection showed discrepancy in 0% (0/3) of patients with decreased enhancement, 100% (4/4) of patients with no significant change, and 14.3% (2/14) of patients with increased/new enhancement.
Conclusion
Our initial results reveal high concordance between the radiologist report and automated techniques in patients with decreasing enhancement and increasing/new enhancement. The discrepancy seen in patients with no significant change likely stems from the fact that small changes often are attributed to difference in technique. This highlights that automated and objective measures may be important for following patients after glioblastomas resection to potentially monitor and direct patient-specific management.

KEYWORDS: Glioblastoma, Computer-aided diagnosis

O-549 **2:35 PM - 2:43 PM**

Bevacizumab: Radiation Combination Produces Restricted Diffusion on MR Imaging

Hesselink, J. R.·Barkovich, M.·Farid, N.·Kesari, S.
University of California San Diego Medical Center
San Diego, CA.

Purpose
To evaluate the effect of bevacizumab on the diffusion properties of irradiated brain gliomas.
Materials & Methods
Imaging studies and medical records of 39 patients undergoing treatment for brain tumors were reviewed to determine the cause of diffusion restriction on post-treatment MRI.
Results
Diffusion restriction on MRI was found in eight patients with cerebral gliomas. All patients received radiation followed by bevacizumab therapy. The diffusion restriction appeared three-four weeks after starting the bevacizumab therapy and persisted up to 18 months. The areas of restricted diffusion showed low T1 and mildly increased T2 signal intensity, no contrast enhancement, and low cerebral blood volume on perfusion MRI. Restricted diffusion typically was observed in areas of the tumor that received relatively high doses of radiation. Areas of restricted diffusion were not metabolically active on MR spectroscopy or PET. One brain biopsy and another autopsy revealed radiation necrosis.
Conclusion
Bevacizumab treatment in combination with radiation therapy of cerebral gliomas is associated with restricted diffusion on MRI.

KEYWORDS: Adult gliomas, DWI

Note: Scanned images are included in the proceedings. Some submitted images were reduced during editing, thereby decreasing clarity. Also, refer to the Program Planner. Proceedings Content as of 3-29-2013.

Thursday Afternoon

1:15 PM - 2:45 PM
Ballroom 6DE

(57c) Parallel Scientific Papers: Pediatrics: Vascular, Congenital Malformations, and Miscellaneous

O-550 **1:15 PM - 1:23 PM**

Thrombosis of Dural Venous Sinuses in Fetuses: Imaging Manifestations and Clinical Outcome

Shifrin, A.[1]·Feygin, T.[2]·Licht, D. J.[2]·Bilaniuk, L. T.[2]·Vossough, A.[2]·Pollock, A. N.[2]·Zimmerman, R. A.[2]
[1]Mount Auburn Hospital, Cambridge, MA, [2]The Children's Hospital of Philadelphia, Philadelphia, PA.

Purpose
To describe imaging findings in a series of cases of fetal dural venous sinus thrombosis on fetal US and MR, and to evaluate the clinical outcomes of these patients on short- and long-term postnatal followup.
Materials & Methods
The cases for this study were selected retrospectively from fetal MR imaging performed at the Children's Hospital of Philadelphia between 2002 and 2012 on a 1.5T scanner for suspected fetal anomalies on obstetric ultrasound. All selected cases demonstrated an abnormal fetal MR appearance of the dural venous sinuses.
Results
A total of 12 cases of suspected fetal dural venous sinus thrombosis was identified on MR. Gestational age at the time of diagnosis varied from 19 to 34 weeks. The indications for fetal MR were varied, including one case of cleft lip and palate, one case of cervical lymphangioma, two cases of arachnoid cyst, three cases of vermian hypoplasia, and five cases of suspected intracranial hemorrhage and possible thrombosis. In seven cases, dural venous sinus thrombosis was an unexpected imaging finding. There was variable extent of thrombosis among these 12 cases, from isolated thrombus in the torcula to massive thrombus of the sagittal, transverse, and straight sinuses as well as the internal cerebral veins. Five cases were further complicated by the presence of mild hydrocephalus. None of the cases revealed any parenchymal changes. Of these 12 cases, nine had postnatal follow-up imaging at our institution. The duration of follow-up imaging varied from three months to five years. All nine of these patients did not show any developmental or neurologic deficit. Postnatal imaging demonstrated spontaneous resolution of dural venous thrombus in three patients, with small residual thrombus apparent in one patient, which did not result in any clinical complication. Two patients were found to have associated venous malformations: one fetal MR showed presence of additional extra-axial venous anomalies which persisted on postnatal follow-up imaging, while another case demonstrated extensive developmental venous anomalies in the posterior fossa, likely a compensatory mechanism for in utero venous obstruction. Workup of coagulopathy in all of the mothers and children was negative.
Conclusion
It is important to recognize the imaging manifestations of this unusual pattern of fetal dural venous sinus thrombosis. Fetal MR provides accurate information about thrombus extension and possible complications, such as mild hydrocephalus, and presence of additional venous anomalies. In our case series, fetal dural venous sinus thrombosis has an apparent favorable long-term clinical outcome.

KEYWORDS: Fetal intracerebral hemorrhage, Dural sinus thrombosis, Fetal MR

O-551 **1:23 PM - 1:31 PM**

Screening CT Angiography for Pediatric Blunt Cerebrovascular Injury, with Emphasis on the Cervical "Seatbelt Sign"

Desai, N. K.·Chokshi, F. H.·Kang, J.
Emory University
Atlanta, GA.

Purpose
Despite its low incidence (0.03%-0.09%), blunt cerebrovascular injury (BCVI) has potentially catastrophic neurologic outcomes. There are currently, however, no standard screening guidelines to evaluate BCVI in children, especially those with a cervical "seatbelt sign"; this is a physical sign that often prompts clinicians to pursue CT angiography (CTA) of the neck. The purpose of this retrospective study is to further understand the risk factors associated with BCVI by examining various clinical and radiologic findings on CTA of the neck and adjunct imaging studies.
Materials & Methods
IRB approval was obtained. From a secure database of trauma patients at a level 1 pediatric trauma center, radiology reports between 2002 and 2012 were queried for the keywords "CTA Neck." The electronic medical record (EMR) was reviewed for pertinent clinical history, including mechanism of injury, Glasgow Coma Scale (GCS), and physical exam findings. Reports from adjunct radiographic, CT, and MR imaging studies performed during the initial trauma encounter were reviewed for internal carotid (ICA), common carotid (CCA), and vertebral artery (VA) injury, intracranial hemorrhage (ICH), and fractures of the cervical spine, skull base, maxillofacial region, ribs, and clavicle. Patients with penetrating injury or without history of trauma were excluded. Findings were recorded by two neuroradiologists. Data were analyzed for

Note: Scanned images are included in the proceedings. Some submitted images were reduced during editing, thereby decreasing clarity. Also, refer to the Program Planner. Proceedings Content as of 3-29-2013.

both descriptive and inference-based statistics.
Results
Over the ten-year period, 463 patients underwent CTA of the neck for various indications, of which 136 had blunt neck trauma. Eighty-six were involved in motor vehicle collisions (MVC). Nine vessels (n = 4 VA, n = 4 ICA, n = 1 CCA) in eight total patients ultimately were diagnosed with various grades (I-IV) of BCVI representing 5.8% of the screened population. Two patients with vertebral artery (VA) injury had no cervical spine fractures, whereas both c-spine fractures and VA injury were found in two additional patients. Although not statistically significant, patients with BCVI had a higher tendency to have additional traumatic injuries, primarily basilar skull fractures (p-value 0.22) and ICH (p-value 0.27). All patients with BCVI had at least one injury. One patient developed infarction in this series; another had nonlocalizing neurologic complaints. Of 42 patients having documented cervical “seatbelt sign” from MVC, none had BCVI.
Conclusion
Blunt cerebrovascular injury is a very uncommon occurrence in the pediatric trauma population. Although no single risk factor was statistically significant in predicting vascular injury in this series, there was a tendency for those with vascular injury to have multiple risk factors, especially basilar skull fractures and ICH. One of the most common indications for neck CTA, the cervical “seatbelt sign”, was not associated with BCVI. These findings suggest that the cervical “seatbelt sign” in children may not be an appropriate reason to perform neck CTA, especially if it is found in isolation. In the current climate of radiation awareness and ALARA (As Low As Reasonably Achievable), cessation of screening CTA of the neck for BCVI may help us “image gently.” Larger, multicenter trials of BCVI should be undertaken before continuing this screening practice.

KEYWORDS: CT angiogram, Pediatric cerebrovascular disease

O-552 **1:31 PM - 1:39 PM**

Brain Parenchymal Signal Abnormalities Associated with Developmental Venous Anomalies in Children and Adolescents

Linscott, L.·Jones, B.·Leach, J. L.
Cincinnati Children's Hospital Medical Center
Cincinnati, OH.

Purpose
Developmental venous anomalies (DVAs) frequently are identified on MR imaging of the brain and typically are considered normal anatomical variants. Developmental venous anomalies can be associated with cavernous malformations (CMs), venous infarction, and signal abnormalities. Associated signal abnormalities have been evaluated in adults but not in children. This study was performed to evaluate the prevalence of brain parenchymal abnormalities subjacent to DVAs in children and adolescents, correlating with DVA morphology and location. This complements previous studies in adults and contributes to our understanding of the natural history of DVAs.
Materials & Methods
Two hundred eighty-five patients with developmental venous anomalies identified on contrast-enhanced brain MRI from 11/2008 - 11/2012 were identified using a radiology database search engine. The examinations were reviewed by a neuroradiologist and pediatric radiology fellow and data were collected regarding the following: location, depth, direction of draining vein, associated cavernous malformations, and associated increased signal intensity on FLAIR and T2-weighted images.
Developmental venous anomalies morphology was described using a previously published system. Exclusions included: subjects with diseases causing multifocal parenchymal signal abnormalities (e.g., TS and NF type 1), surgery or tumor in the DVA drainage territory, Sturge-Weber syndrome, or dural AV fistulas.
Results
Of the 285 subjects identified, 172 met inclusion criteria. Mean age was 11.5 years (+/- 6.3 years) with 91 males and 81 females. In these 172 subjects, 193 DVAs were identified. Of these 193 DVAs, 11 (5.7%) had associated cavernous malformations. Twenty-eight (14.5%) of the 193 DVAs had associated signal-intensity abnormalities in their drainage territory. Six of the 28 DVAs with signal-intensity abnormalities were associated with cavernous malformations. After excluding the DVAs with associated CMs, an adjusted prevalence of 22/182 (12.1%) for associated signal-intensity abnormalities was obtained. Twenty-one of 148 (14.2%) of lobar DVAs had associated signal versus 1/38 (2.6%) of nonlobar DVAs (p = 0.05). Seven of 26 (27%) periventricular DVAs had associated signal abnormalities versus 7/94 (7.4%) juxtacortical or subcortical DVAs (p = 0.02). Fifteen of 69 (21.7%) deep or bidirectional draining DVAs had associated signal abnormalities versus 7/118 (6%) superficial draining DVAs (p = 0.002). The mean age of subjects with DVAs associated with signal abnormalities was 8.3 years versus 11.5 years in subjects without associated signal abnormalities (p = 0.045). There was a trend toward more males with signal abnormalities than females, but this was not statistically significant (p = 0.34).
Conclusion
Signal abnormalities detectable by standard clinical MR images were identified in 12.1% of consecutively identified DVAs. This is similar to the prevalence identified in prior investigations of adult patients, suggesting the underlying pathology of these signal abnormalities arises early in human development. Etiology of these signal intensity abnormalities remains unclear, but may be related to early vascular insult leading to formation of the DVA or secondary to altered vessel hemodynamics in the DVA drainage territory. Signal intensity abnormalities are

Note: Scanned images are included in the proceedings. Some submitted images were reduced during editing, thereby decreasing clarity. Also, refer to the Program Planner. Proceedings Content as of 3-29-2013.

associated more commonly with younger age, lobar location, periventricular depth, and deep venous drainage.

KEYWORDS: Developmental venous anomalies, Venous drainage

O-553 **1:39 PM - 1:47 PM**

Loss of Gray-White Matter Differentiation of the Temporal Pole in Children with Temporal Lobe Epilepsy: A Neuroradiologic Blind Spot

Desai, N. K.·Olson, L.·Saindane, A. M.
Emory University
Atlanta, GA.

Purpose
Temporal lobe epilepsy (TLE) in children may be secondary to a variety of neoplastic and non-neoplastic causes. An especially subtle finding in some patients with TLE is blurring of the gray-white junction (GWJ) at the temporal pole, with or without mesial temporal sclerosis (MTS), suggesting regional gliosis and/or dysplasia. The purpose of this study was to evaluate the salient MRI and PET findings of this often overlooked entity.
Materials & Methods
Retrospective query of radiology reports was performed using the keyword “anterior temporal” and “temporal pole” for studies between 2008-2012 at a tertiary pediatric referral center after IRB approval. MR imaging and PET examinations were reviewed in a blinded fashion by a pediatric neuroradiologist. After review, patients with all pathologies not resulting in primary blurring of the GWJ at the temporal pole, such as discrete mass lesions, were excluded. Any lesion extending beyond the temporal lobe also was excluded. Each imaging report also was reviewed at a separate session. The electronic medical charts of those patients with blurred gray-white matter at the temporal pole were reviewed for pertinent seizure history.
Results
Five hundred seventy-eight patient reports over a five-year period were retrieved. Five hundred twelve patients were excluded before image review as the temporal pole was being referred to in an insignificant manner. Sixty additional patients were excluded secondary to discrete well defined pathology suggestive of neoplasm, well defined cortical dysplasia and vascular malformations. After exclusion criteria, six total patients remained, all of whom had subtle blurring of the GWJ at the temporal pole. One patient had bilateral findings. This finding was identified prospectively on the initial MRI examination in only one patient (16.7%). Two patients also had coexisting MTS. In two patients, the blurred GWJ could not be identified even in retrospect, one presumably because of immature myelination. In the other patient, even at 3.83 years of age the finding was not present but became apparent at 6.42 years of age. Four patients underwent PET, all of which demonstrated asymmetric, ipsilateral temporal pole hypometabolism. One patient had no medical records at our institution. Average age of seizure onset in five of the remaining patients was 2.03 years. All five patients were diagnosed with complex partial seizures with EEG confirming temporal lobe origin. Three are currently well controlled with antiepileptic drugs, whereas two eventually underwent hippocampectomy with anterior temporal lobectomy. Both of the latter patients are now seizure-free. In one patient, histopathology revealed normal brain parenchyma, a not uncommon scenario per recent literature. In the second patient, a diagnosis of focal cortical dysplasia type IA was made.
Conclusion
Children with TLE may present with a variety of temporal lobe pathologies. An uncommon entity that may occur with or without MTS, is that of subtle gray-white matter blurring at the temporal pole, a finding that may go unrecognized. Recognition of this entity, representative of a primary cortical dysplasia and/or reactive gliosis, is crucial to the eventual care of pediatric patients with refractory TLE that may undergo resection.

KEYWORDS: Pediatric epilepsy, Epilepsy

O-554 **1:47 PM - 1:55 PM**

Comparison of Fetal Central Nervous System Biometric Values in the Second and Third Trimester in Four Fetal Groups: Normal, Ventriculomegaly, Open Spinal Dysraphism and Agenesis of the Corpus Callosum

Fanou, E. M.[1]·Batty, R.[2]·Griffiths, P.[2]
[1]University Hospital of North Staffordshire, Stoke-on-Trent, UNITED KINGDOM, [2]University of Sheffield, Sheffield, UNITED KINGDOM.

Purpose
To compare the biometric values of the fetal head on in utero MR (iuMR) at two time points in four fetal groups: normal (N), ventriculomegaly (VM), open spinal dysraphism (OSD) and agenesis of the corpus callosum (ACC).
Materials & Methods
Blinded retrospective measurements of the trigones of the lateral ventricles, bony posterior fossa surface area and cerebellar vermis (in the midsagittal plane), maximum transcerebellar diameter and skull circumference were undertaken in gestationally age-matched fetuses in the second and third trimester.
Results
On-going study. Thirty-six fetuses have been included at present (n = eight agenesis of the corpus callosum, n = 12 open spinal dysraphism, n = seven ventriculomegaly, n = nine normal). We aim to correlate the head biometrics with the gestational age and also correlate range of values between the normal and abnormal groups. Preliminary results from the second trimester are presented in Table 1 and from the third trimester in Table 2 with the mean values and standard deviation (SD).

Note: Scanned images are included in the proceedings. Some submitted images were reduced during editing, thereby decreasing clarity. Also, refer to the Program Planner. Proceedings Content as of 3-29-2013.

Table 1

Parameter Fetal Anomaly	Skull circumference (cm)	Trigone diameter (mm)	Superior-inferior vermis (cm)	Surface area of bony posterior fossa (mm²)	Transcerebellar Diameter (cm)
VM	20.7	11.6	1.09	391	2.07
(SD)	-1.43	-1.6	-0.09	-68	-0.16
ACC	20.8	10.5	1.11	379	2.14
(SD)	-1.37	-3.2	-0.14	-55	-0.14
N	21.52	6.7	1.18	376	2.34
(SD)	-1.14	-1.8	-0.08	-21	-0.21
OSD	19.26	11.8	1.11	219	1.86
(SD)	-1.8	-3.7	-0.16	-38	-0.24

Table 2

Parameter Fetal Anomaly	Skull circumference (cm)	Trigone diameter (mm)	Superior-inferior vermis (cm)	Surface area of bony posterior fossa (mm²)	Transcere bellar Diameter (cm)
VM	31.01	10.9	1.92	813	3.67
(SD)	-1.29	-3	-0.2	-122	-0.3
ACC	31.6	15.6	2.02	797	3.68
(SD)	-2.71	-4.7	-0.16	-201	-0.36
N	29.81	6.1	1.86	773	3.72
(SD)	-1.15	-2.3	-0.23	-55	-0.3
OSD	29	16	2.33	506	3.11
(SD)	-1.83	-6.7	-0.28	-77	-0.37

Conclusion

In progress. Th*e preliminary results show altered bony surface area of the posterior fossa in the OSD fetuses in both trimesters. Regarding the trigones of the lateral ventricles, in the second trimester on average there is ventriculomegaly in the VM, ACC and OSD groups, with the largest ventricles seen on average in the latter group. In the third trimester there is significant increase in the size of the ventricles in the OSD and ACC groups. In the VM group however, on average the trigones can return to the upper limit of normal or borderline ventriculomegaly. The superior inferior dimension of the vermis is increased slightly in the OSD group in the third trimester and when compared to the other groups likely due to elongation of the vermis due to anterior posterior compression.

KEYWORDS: Fetal MR imaging

O-555 **1:55 PM - 2:03 PM**

De Novo, Progressive, Multiple, and Recurrent Intracranial Dural Arteriovenous Fistulas: Characteristics and Outcomes

Tsai, T.·Cooke, D. L.·Amans, M. R.·Kim, W. T.·Stout, C.·McSwain, H.·Dowd, C. F.·Higashida, R. T.·Halbach, V. V.·Hetts, S. W.
University of California San Francisco
San Francisco, CA.

Purpose

Although many intracranial dural arteriovenous fistulas (DAVFs) are straightforward to treat, de novo and rapidly progressive ("runaway" or "malignant") DAVFs are more complex, often requiring multiple treatment sessions with suboptimal results. As these are rare entities, we sought to review our experience in the treatment of de novo and progressive DAVFs in order to better understand predictors of disease progression.

Materials & Methods

Under an IRB-approved protocol, 29 patients with multiple, recurrent, de novo, or progressive DAVFs were identified from our quaternary referral hospital's neurointerventional radiology database of 578 patients treated for intracranial DAVFs between 1986 and 2012. One patient with acute traumatic carotid cavernous fistulas was excluded. Patient demographics, clinical presentation, lesion angioarchitecture, treatment approaches, and clinical outcomes were categorized and assessed. Categorical variables were analyzed with odds ratios and 2-sided Fisher's exact tests.

Results

We compared 28 patients with multiple, recurrent, de novo, or progressive DAVFs to 550 DAVF patients without such features. Whereas 18/28 (64%) of patients with multiple, recurrent, de novo, or progressive DAVFs were female, 283/550 (51%) without such features were female (OR 1.7, 95% CI 0.73-4.2, p=0.24). Mean age at presentation in the multiple, recurrent, de novo, or progressive DAVF group was 42±23 years (range 2 months to 77 years) compared to 52±20 years (range 1 day to 87 years) for the entire DAVF cohort. The most common presenting signs and symptoms of the 28 patients treated for multiple, recurrent, de novo, or progressive DAVFs were headache (50%), cranial neuropathy (46%), tinnitus (36%), visual changes (32%), and intracranial hemorrhage (29%). Fifty-nine DAVFs were identified in these 28 patients. Location of fistulas included transverse/sigmoid sinus in 18 (64%), superior sagittal sinus in eight (29%), torcula in six (21%), cavernous sinus in five (18%), marginal sinus in five (18%), and petrosal sinus in two patients (7%). Eight patients had DAVFs in other intracranial locations. Number of interventions per patient ranged from 2 to 19 (mean 5.5, median 4.5). All 28 patients were treated endovascularly; 15 (54%) also were treated with surgery. Embolic agents included coils in 25 patients (89%), ethanol in 23 (82%), polyvinyl alcohol in 21 (75%), N-butyl cyanoacrylate in 10 (36%), and Onyx in five (18%). One hundred fifty-three transarterial, transvenous, and surgical interventions were performed. The time between diagnosis of DAVF and last imaging ranged from 10 days to 21 years. At last followup, 10 patients (36%) had no symptoms or residual DAVFs, 15 patients (54%) had neurologic symptoms and/or residual DAVFs, and three patients(11%) had died due to intracranial hemorrhage or refractory elevations in intracranial pressure related to intracranial venous hypertension. A total of 19/28 patients had de novo or rapidly progressive DAVFs (68%) with all three deaths occurring in that group. No deaths were recorded in the other nine patients with only recurrent or

Note: Scanned images are included in the proceedings. Some submitted images were reduced during editing, thereby decreasing clarity. Also, refer to the Program Planner. Proceedings Content as of 3-29-2013.

multiple DAVFs.
Conclusion
De novo or rapidly progressive DAVFs constituted 3% of all intracranial DAVF cases treated at our institution. Among these patients, despite aggressive endovascular and surgical care, a minority followed a malignant clinical course.

KEYWORDS: Dural arteriovenous fistula, Pediatric cerebrovascular disease

O-556 **2:03 PM - 2:11 PM**

Brainstem Infarcts in Children

Rollins, N. K.[1]·Plumb, P.[1]·Pride, L.[2]·Dowling, M.[2]
[1]Childrens Medical Center, Dallas, TX, [2]University of Texas Southwestern Medical Center, Dallas, TX.

Purpose
Brainstem infarcts in children differ clinically from those in adults and are sufficiently uncommon that the diagnosis may be delayed. We report a single institution series over 10 years.
Materials & Methods
An IRB-approved query of our institution database yielded 13 patients with brainstem infarcts from 2001-2012. Medical records were reviewed for presenting symptoms; quantitative measure of stroke severity using the Pediatric NIH Stroke Scale (PedNIHSS); findings by MRI/A and catheter angiography; etiology, and outcome using the Pediatric Stroke Outcome Measures (PSOM).
Results
There were 9M/4F; nine months -17 years. Seven patients presented with involuntary rhythmic movements, four with hemiparesis, and three with altered mental status. Time to diagnosis ranged from 12 hours to five days; three patients had orthodontia resulting in suboptimal DWI and MRA. MR imaging showed isolated pontine infarcts in four; and midbrain, pontomesencephalic, or ponto-medullary in one each. Five had pontine infarcts with other posterior circulation infarcts; two had infarcts of different ages. MR angiography showed basilar artery (BA) occlusion in six of nine patients without a vertebral artery (VA) dissection in three; one of five had bilateral distal VA occlusion. Three patients had a VA dissection without BA thrombosis while MRA was normal in two. Catheter angiography showed VA dissection in four of nine; and hypoplasia of VA ipsilateral to the medullary infarct, and multiple peripheral posterior circulation emboli of unclear etiology in one patient each. Onset of symptoms was related temporally to sports in seven; most often football; six had no clear etiology. Management included initial heparinization unless contraindicated, with conversion to long-term anticoagulation or antiplatelet therapy based on results of vascular imaging, echocardiography, and coagulation profile; cardiac ECHO was normal in all patients. Maximum PedNIHSS ranged from 1-34 and was < 10 in seven patients; three in one, 10-20 in two, and > 20 in four. NIHSS with BA occlusion ranged from 5-34. Four patients progressed to locked-in state of which one died after withdrawal of support, one required gastrostomy and tracheotomy, one underwent successful clot extraction; and one survived. Of the 12 survivors, nine have been followed for > six months; PSOM ranges from 0- 4.5. In eight, PSOM is <2.5 and six are <1.0.
Conclusion
Prompt diagnosis of pediatric brainstem infarcts may be delayed by misleading symptoms and absence of risk factors while orthodontia may limit MR diagnosis. Even with BA occlusion and high initial severity, outcome tends to be good if systemic anticoagulation is started promptly.

KEYWORDS: Acute stroke, Brainstem

O-557 **2:11 PM - 2:19 PM**

Diagnosis of Hemimegaencephaly Using in utero MR Imaging

Williams, F.[1]·Griffiths, P. D.[2]
[1]Royal Hallamshire Hospital, Sheffield, Sheffield, UNITED KINGDOM, [2]University of Sheffield, Sheffield, UNITED KINGDOM.

Purpose
Hemimegalencephaly (HME) is a rare disorder characterized by abnormal overgrowth of one cerebral hemisphere. The purpose of this paper is to review our experience of diagnosing HME using in utero magnetic resonance imaging (MRI).
Materials & Methods
The MR imaging database in the Academic Unit of Radiology, University of Sheffield was searched using "Hemimegalencephaly" and "in utero MR" as search terms. The ante-natal histories and reports of ultrasound imaging were reviewed as well as the in utero magnetic resonance images.
Results
Nine cases of fetal hemimegaencephaly were located. One case was referred from ultrasound with the diagnosis of hemimegaencephaly, one as a "complex brain malformation" and one as "mass lesion". The other six were referred as "unilateral ventriculomegaly". A common finding in fetuses imaged in the second trimester was disruption of the normal "transient structures" found in the developing cerebral hemispheres.
Conclusion
Hemimegaencephaly is a difficult diagnosis to make on antenatal ultrasound and in utero magnetic resonance imaging should be considered in cases of unilateral ventriculomegaly diagnosed on ultrasound. Disruption of the transient structures of the cerebral hemispheres is a common finding on in utero magnetic resonance imaging and can sometimes produce mass-like appearances in the region of the germinal matrix/ganglionic eminence.

KEYWORDS: Fetal, Fetal MR imaging

Note: Scanned images are included in the proceedings. Some submitted images were reduced during editing, thereby decreasing clarity. Also, refer to the Program Planner. Proceedings Content as of 3-29-2013.

O-558 **2:19 PM - 2:27 PM**

Transverse Sinus Stenosis in Patients with Chiari I Malformation

Saindane, A. M.·Bruce, B. B.·Desai, N. K.·Newman, N. J.·Biousse, V.
Emory University School of Medicine
Atlanta, GA.

Purpose
The Chiari I malformation (CM) frequently presents with headaches which may or may not be related to elevated intracranial pressure (ICP). Transverse sinus stenosis (TSS) nearly always is present in patients with idiopathic intracranial hypertension (IIH), presumably reflecting elevated ICP. The purpose of this study was to determine whether patients with the CM have a higher frequency of TSS than controls.
Materials & Methods
Twenty-two cases of CM and 76 age- and gender-matched controls without presenting symptoms of headache or visual disturbance were identified. All patients underwent standardized contrast-enhanced MRI including a postcontrast 3D T1-weighted dataset from which maximum intensity projections and curved reformats of the transverse sinuses were generated. Two readers blinded to the patient's diagnosis evaluated MRIs for presence or absence of TSS, and for orbital and skull base findings traditionally described in association with IIH. Cerebellar tonsillar position and morphology was noted. MRI findings were compared between the two groups.
Results
Median cerebellar tonsillar position was 12 mm below the foramen magnum in the CM group (17/22 peg-like in morphology), and 2 mm above the foramen magnum in controls (0/76 peg-like in morphology). While only 1/76 controls had TSS, 9/22 patients with CM had TSS. The odds of a CM patient having TSS was 25 times that of controls ($p<0.001$), and of having increased optic nerve (ON) sheath CSF was 6.8 ($p = 0.002$). Scleral flattening and skull base cephaloceles were present significantly more frequently among patients with CM than controls ($p<0.03$). No differences in frequency of ON head protrusion, ON head enhancement, vertical tortuosity of the ON, or pituitary flattening/sellar expansion were noted between the two groups. The figure depicts: A. 34-year-old female with Chiari I malformation with bilateral TSS, and B. 39-year-old male control with normal tonsillar position and normal appearance of transverse sinuses.

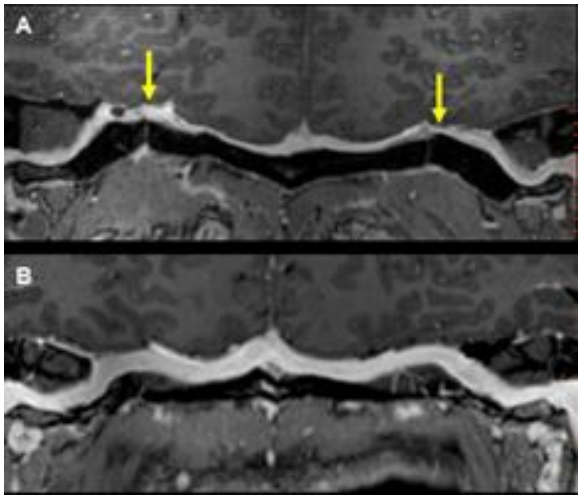

Conclusion
Patients with CM have significantly higher likelihood of TSS and some orbital findings traditionally associated with IIH, suggesting that at least a subset of CM patients have elevated ICP.

KEYWORDS: Chiari malformation type 1, Venous stenosis

O-559 **2:27 PM - 2:35 PM**

Diffusion Tensor Imaging in Chiari Type I Malformation

Eshetu, T.·Meoded, A.·Jallo, G. I.·Carson, B. S.·Huisman, T. A. G. M.·Poretti, A.
The Johns Hopkins University School of Medicine
Baltimore, MD.

Purpose
The Chiari I malformation (CI) is defined by at least 5 mm of herniation of the cerebellar tonsils below the foramen magnum. Children with CI may present with different neurologic symptoms including headaches, neck pain and vertigo, or may be asymptomatic. On conventional MRI, differentiation between symptomatic and asymptomatic forms of CI is limited. We used diffusion tensor imaging (DTI) to study the integrity of the brainstem and cerebellar white matter tracts in children with CI.
Materials & Methods
The inclusion criteria were 1) isolated CI and 2) availability of high-quality presurgical DTI data. DTI data were acquired on a 1.5T MR scanner. Balanced pairs of diffusion gradients were applied along 20 orthogonal directions with a b value of 0/800s/mm2; TR/TE=8500/86ms, slice thickness=2.0mm, FOV=240×240mm; matrix=192×192. DTI postprocessing was performed off-line using MRI-Studio software. FA, color-coded maps, eigenvectors and eigenvalues were calculated after rigid transformation for adjustment of the position and rotation of images. Mean (MD), axial (AD) and radial (RD) diffusivity maps were generated. The quantitative analysis of FA, MD, AD and RD was performed. Regions of interest (ROI) were positioned

Note: Scanned images are included in the proceedings. Some submitted images were reduced during editing, thereby decreasing clarity. Also, refer to the Program Planner. Proceedings Content as of 3-29-2013.

manually on the pontine corticospinal tracts (CST), medial lemnisci (ML), and middle cerebellar peduncles (MCP). An additional cross-sectional ROI was drawn at the level of the lower brainstem. For each anatomical structure, three ROIs were drawn on different MR slices and the median value was calculated. The same postprocessing was performed twice by the first and once by the second author. Generalized linear mixed effects models were used to evaluate the differences between asymptomatic and symptomatic children for each region and DTI scalar. These models were performed from the inter-rater and intra-rater perspectives and intraclass correlation coefficients were calculated to assess these effects.
Results
Between September 2010 and April 2012, MR images were acquired in 197 children with CI in our tertiary pediatric hospital. The majority of the patients were excluded because of 1) absence of DTI data, 2) severe artifacts, and 3) incorrect DTI acquisition parameters. Fifteen patients met the inclusion criteria (10 males, 5 females). Nine children were asymptomatic, six symptomatic. Median age of the patients was 6.43 years (mean age 7.18 years, range 2.87 to 15.34 years). Interclass correlation showed an interclass correlation coefficient > 0.8 for the majority of the DTI scalars. In the left MCPs, FA values were significantly higher (P=0.02), while MD (P=0.02) and RD (P=0.02) values were significantly lower for symptomatic versus asymptomatic patients. In the right MCPs, RD values were significantly lower in symptomatic versus asymptomatic patients (P=0.03), while a marginally significant difference was found for MD values (lower in symptomatic than asymptomatic patients, P=0.05).
Conclusion
This study suggests that MCPs may play a role in CI. Involvement of MCP in CI was shown previously in a study comparing pre and postsurgical FA and MD values. Higher FA values and lower MD and RD values in symptomatic versus asymptomatic patients are unexpected. Further studies of larger cohorts of CI patients are needed to elucidate the significance of these results.

KEYWORDS: Chiari malformation type 1, Diffusion tensor image

O-560 **2:35 PM - 2:43 PM**

Prenatal Diagnosis of Lissencephaly Using in utero MR Imaging

Williams, F.·Griffiths, P. D.
Royal Hallamshire Hospital Sheffield
Sheffield, UNITED KINGDOM.

Purpose
Lissencephaly is a rare disorder of cortical developmental with a prevalence of one in 100,000 live births per annum. Clear genetic links have been established and the risk is increased if a previous pregnancy was affected. Lissencephaly is a challenging prenatal diagnosis to make. Our purpose was to add to the experience of in utero magnetic resonance imaging in the diagnosis of prenatal lissencephaly and to establish whether in utero magnetic resonance imaging can provide a confident diagnosis of fetal lissencephaly during the second trimester of pregnancy especially in at-risk pregnancies where a previous diagnosis was made.
Materials & Methods
Twenty pregnant women who previously had carried a child with proven lissencephaly were recruited. Magnetic resonance (MR) imaging was performed three times during the pregnancy, at around 20 weeks, 25 weeks and 30 weeks gestation. In utero magnetic resonance imaging was carried out in the Academic Unit of Radiology at the Royal Hallamshire Hospital, Sheffield. Additionally, the cases were followed up with clinical data obtained on those that progressed to term and were delivered and postmortem data obtained on those that did not. The information then was used to corroborate the in utero magnetic resonance imaging findings.
Results
Eighteen cases progressed to term, one underwent termination of the pregnancy and one miscarried during the process. Six cases were identified as having in utero magnetic resonance imaging features suggestive of lissencephaly including the two cases which did not progress to term. Of the two cases that did not proceed to term lissencephaly was confirmed on postmortem diagnosis confirming the initial radiologic diagnosis. The remaining cases had lissencephalic features confirmed on postnatal imaging and were moderately to severely mentally disabled.
Conclusion
Lissencephaly is a rare diagnosis and poses diagnostic difficulties. In utero magnetic resonance imaging provides an excellent diagnostic tool for the assessment of the fetal brain and can be used with a degree of confidence in the prenatal diagnosis of lissencephaly.

KEYWORDS: In utero MR, Fetal MR imaging, Fetal brain development

Note: Scanned images are included in the proceedings. Some submitted images were reduced during editing, thereby decreasing clarity. Also, refer to the Program Planner. Proceedings Content as of 3-29-2013.

Thursday Afternoon

1:15 PM - 2:45 PM
Room 5AB

(57d) Parallel Scientific Papers: Adult Brain: Tumors V: Metastases and Miscellaneous

O-561 **1:15 PM - 1:23 PM**

Intra-Arterial MR Perfusion Analysis of Meningiomas: Comparison to Intravenous MR Perfusion and Digital Subtraction Angiography

Lum, M. A.·Martin, A. J.·Saloner, D.·Hetts, S. W.
University of California San Francisco
San Francisco, CA.

Purpose
Pre-operative embolization can prevent excessive blood loss during intracranial meningioma resection. The degree of embolization safely achievable is determined largely by tumor blood supply, with branches of the internal carotid artery (ICA) less amenable to embolization than those of the external carotid artery (ECA). Tumor supply from pial arteries is not safe for embolization. We sought to determine if intra-arterial (IA) and intravenous (IV) perfusion MRI could characterize meningioma blood supply as sensitively as digital subtraction angiography (DSA).
Materials & Methods
Studies were performed in a combined XMR suite comprised of an x-ray angiography unit and 1.5T MR scanner, permitting intraprocedural patient movement between the two imaging modalities. Patients underwent meningioma embolization, evaluated with IV and IA T2* dynamic susceptibility contrast perfusion MR pre-embolization. Intra-arterial perfusion was performed by injecting dilute contrast (5mM Magnevist) into the ECA and common carotid artery (CCA). Twelve patients with IA CCA and ECA data were selected for detailed region-of-interest (ROI) analysis. Based on DSA, 18 ROIs were uniformly drawn on pre-operative CCA images representing ECA dural (n=11), ICA dural (n=4), and pial (n=3) supplies. From these ROIs, perfusion curves were generated with the following parameters extracted: peak-height, full-width at half-maximum (FWHM), and time to percent signal recovery for 50%-60% (TSR50-60%). One-sided t-tests were used to analyze ROI data.
Results
No differences in peak-height (p=0.66), FWHM (p=0.78), TSR50% (p=0.41), and TSR60% (p=0.55) were found between ECA and ICA dural ROIs. On that basis, ICA and ECA dural ROIs were combined and compared to pial ROIs. Pial ROIs demonstrated shorter FWHM (t=7.9s versus t=16.9s, p=0.025), shorter TSR50% (t=5.2s versus 12.6s, p=0.043), and shorter TSR60% (t=6.5s versus t=16.4s, p=0.046). No difference in peak-height was found. A selected patient whose meningioma supply was characterized on DSA as mixed dural-pial demonstrated decreasing FWHM and TSR50-60% as ROIs moved from dural to pial on CCA and ECA runs with the opposite trend observed on IV perfusion (see Figure).

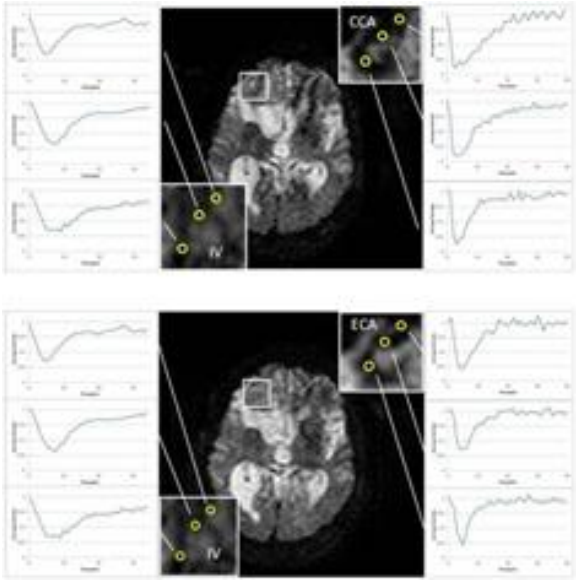

Conclusion
No difference in MR perfusion measures of ICA and ECA dural supplies was found. However, perfusion curve analysis confirms greater "leakiness" among dural supplies when compared to pial supplies as quantified by differences in FWHM, TSR50%, and TSR60%. These IA MR perfusion measures can identify ICA pial supply not amenable to embolization. Intravenous perfusion imaging in the selected patients did not capture the difference between dural and pial supply, thus limiting its ability to triage patients to pre-operative embolization.

KEYWORDS: Meningioma, Interventional MR imaging, Intra-arterial perfusion imaging

O-562 **1:23 PM - 1:31 PM**

Treatment Response in Metastatic Brain Tumor following Gamma-Knife Radiosurgery: Utility of Initial and Final Area under the Curve Ratio of Dynamic Contrast-Enhanced T1-Weighted Perfusion MR Imaging

Suh, C.·Kim, D.·Kim, H.·Kim, S.·Kang, S.·Choi, C.
Asan Medical Center
Seoul, KOREA, REPUBLIC OF.

Purpose
To determine the utility of initial and final area under the curves ratio (AUCR) derived from dynamic contrast-

Note: Scanned images are included in the proceedings. Some submitted images were reduced during editing, thereby decreasing clarity. Also, refer to the Program Planner. Proceedings Content as of 3-29-2013.

enhanced (DCE) perfusion MR imaging for the prediction of treatment response in metastatic brain tumor following gamma-knife radiosurgery (GKRS).

Materials & Methods

Our institutional review board approved this retrospective study. Sixty-two consecutive patients with metastatic brain tumor, who showed enlarged, contrast-enhancing lesions within the radiation field following GKRS, were assessed using conventional and DCE perfusion MR imaging. Histogram parameters of AUCR, including mean AUCR at higher curve ($mAUCR_H$) and 50^{th}($AUCR_{50}$), 75^{th} ($AUCR_{75}$) and 90^{th} ($AUCR_{90}$) percentiles of cumulative AUCR histograms, were correlated with the final clinicoradiologic diagnosis and were compared with normalized cerebral blood volume (nCBV) derived from dynamic susceptibility contrast (DSC) perfusion MR imaging with respect to correlation coefficient and diagnostic accuracy. The best predictor for differentiating tumor progression (TP) from radiation necrosis (RN) was determined by receiver operating characteristic (ROC) curve analyses.

Results

Study patients were stratified into TP (*n* = 25, 40.3%) and RN (*n* = 37, 59.7%) groups. There were statistically significant differences of $mAUCR_H$, $AUCR_{50}$, $AUCR_{75}$, and $AUCR_{90}$ between the two groups ($P < .001$, each). Receiver operating characteristic curve analyses showed the $mAUCR_H$ to be the best single predictor of TP, with a sensitivity of 92.3% and a specificity of 86.1%. $AUCR_{50}$ was found to be the most specific predictor of TP, with a sensitivity of 85.6% and a specificity of 87.5%. A significant positive correlation was found for AUCR with nCBV among all study patients ($r = 0.76$, $P < .001$).

Conclusion

A bimodal histogram analysis of AUCR derived from DCE perfusion MR imaging can be a potential, noninvasive imaging biomarker for monitoring treatment response in patients with metastatic tumors after GKRS.

KEYWORDS: Dynamic contrast enhancement, Metastases, radiation necrosis

O-563 **1:31 PM - 1:39 PM**

Lymphomatosis Cerebri: Multimodal MR Imaging Findings

Trunet, S.·Leclercq, D.·Galanaud, D.·Hoang, K.·Mokhtari, K.·Gerber, S.·Martin-Duverneuil, N.
Hôpital de la Pitié Salpétrière
Paris, FRANCE.

Purpose

Lymphomatosis cerebri (LC) is a rare subtype of cerebral non-Hodgkin lymphoma which is assumed to be caused by widespread infiltration of the white matter by lymphoma cells. The most common symptoms at onset are personality changes, cognitive deficit, and gait ataxia, mimicking dementia. On MRI, the observed extensive white matter changes can be mistaken for subcortical ischemic vascular dementia, infectious leukoencephalitis, or gliomatosis cerebri. The features of lymphomatosis cerebri on multimodal imaging including perfusion and spectroscopy have not be reported. The purpose of this presentation is: 1. to present the MRI aspects of pathologically confirmed LC with conventional MRI, spectroscopy and perfusion. 2. Determine whether conventional imaging, perfusion and spectroscopy can help distinguish LC from other leukoencephalopathy.

Materials & Methods

We retrospectively reviewed the MRI findings, clinical information and pathology reports of four patients presenting with LC between 2006 and 2012 treated in our institution. All patients underwent a multimodal MRI protocol including at least T2-weighted images, FLAIR images, T1-weighted images with and without gadolinium injection, diffusion-weighted images, MR perfusion and spectroscopy (TE: 35ms, 144ms). Maximal rCBV (relative cerebral blood volume), and rCBF were obtained using the software provided by the manufacturer (Functool, General Electric, Milwaukee, WI).

Results

Patients were two male and two female. Average age at diagnosis was 65 years. Extensive diffuse leukoencephalopathy in both hemispheres was present, with no or minimal mass effect in four patients. White matter changes extended in the subcortical and deep white matter in four patients, the splenium of the corpus callosum in three patients, the middle cerebellar peduncle in three patients and along the corticospinal track in two patients. Lenticular nuclei were involved in two patients. The cortex was spared. Lesions were in high T2 signal, low T1 signal and high diffusion signal without restriction of the ADC. Spectroscopy sequences showed a mild choline peak, decreased NAA and the presence of lactates. No lipids were measured. In perfusion sequences, rCBV values were normal and there was no blood-brain barrier disruption. One patient presented small foci of enhancement without perfusion anomalies.

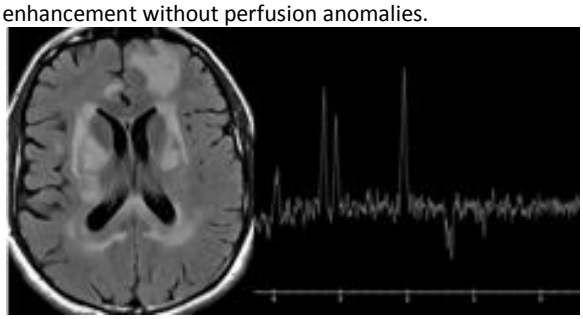

Conclusion

We present the first reported results of multimodal MRI in primary lymphomatosis cerebri in four patients. We confirm a MR pattern markedly different from what is observed in more conventional brain lymphoma, with extensive and diffuse leukoencephalopathy without evidence of blood-brain barrier disruption, no or minimal

Note: Scanned images are included in the proceedings. Some submitted images were reduced during editing, thereby decreasing clarity. Also, refer to the Program Planner. Proceedings Content as of 3-29-2013.

contrast enhancement, no restriction of ADC and no increased free lipids on MR spectroscopy.

KEYWORDS: Lymphoma, Leukoencephalopathy, MR imaging perfusion, MR spectroscopy

O-564 **1:39 PM - 1:47 PM**

Correlation between MR Imaging Findings and Visual Field Exam in Optic Chiasm Compression

Tavares, F. C.·Zan, E.·Boland, M.·Ying, H.·Yousem, D. M.
Johns Hopkins Institution
Baltimore, MD.

Purpose
To our knowledge there is no MR imaging-based literature demonstrating the relation between extrinsic optic chiasm compression and the manifold visual field defects experienced by the patients. Classically, bitemporal hemianopia (BTH) has been described in pituitary macroadenomas with clinical manifestation of partial blindness where the outer half of right and left visual fields is missing. We sought to determine the incidence of visual field deficits in patients with pituitary macroadenomas and to assess which imaging findings best predicted visual field deficits in this patient population.
Materials & Methods
This study was HIPAA compliant and approved by the institutional IRB. We retrospectively evaluated 50 patients with pathology proven macroadenoma and optic chiasm displacement recorded on MRI. In these patients we reviewed the the visual field exam (VFE) charts, MRI reports and electronic medical record notes. The MRI studies were re-evaluated by two neuroradiologists for imaging findings in a blinded fashion, as the reviewers were unaware of the visual deficits at the time of image review.
Results
In 36/50 (70%) patients, MRI showed optic chiasm compression by the macroadenoma with clinical correlation of BTH. MR imaging was able to lateralize the compression to being greater on the left or the right in 11/35 (31%) patients which corresponded to the patients' reported symptoms of visual loss and to VFE lateralization of BTH. In 14/50 (30%) there was elevation of the optic chiasm by the mass. Nine of 14 (64%) had normal VFE whereas 5/14 (36%) had either left- or right-sided temporal or nasal hemianopia. In 3/5 cases we were able to demonstrate the CSF cleft between the pituitary mass and either left or right side of the optic chiasm which corresponded to unilateral temporal hemianopia on VFE (Figure 1). Twenty-four of 50 (48%) patients had initial symptoms related to vision and, of those, 20/24 (83%) complained of various degrees of BTH. Four patients had complaints of visual deficits but on testing had normal VFE. However, of 26 patients whose initial symptoms were other than visual problems, BTH was evident in 16/26 (65%) by ophthalmologic examination.

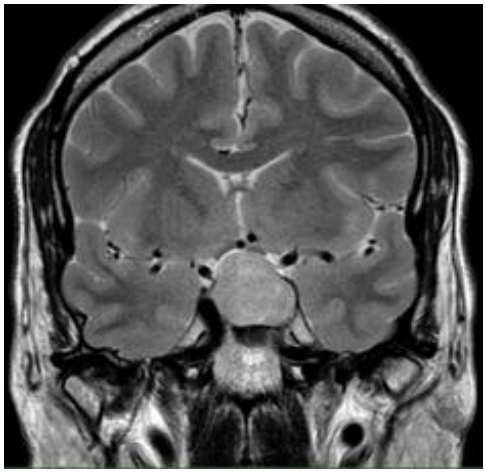

Conclusion
Most patients with pituitary adenomas and optic chiasm displacement have BTH on VFE (36/50=72%). MR imaging sometimes shows optic chiasm elevation but the patient does not have BTH; in fact nine of 50 such patients have normal visual fields. Lateralization on MRI corresponds well to vision deficits on the side of the optic chiasm compressed.

KEYWORDS: Pituitary adenoma, MR imaging, Bitemporal hemianopia, Visual Field Exam

O-565 **1:47 PM - 1:55 PM**

Imaging Profile of Dysembryoplastic Neuroepithelial Tumors

Mironov, A.·Ayeni, S.·Brumback, R.
Creighton University Medical Center
Omaha, NE.

Purpose
Dysembryoplastic neuroepithelial tumors (DNETs) represent developmental glio-neuronal tumors most common inflected by intractable epilepsy. The glial lineages are composed by astrocytic and oligodendroglial phenotypes; the neuronal component is composed of both more mature, ganglionic cells and more immature population of cells with a neurocytic appearance. The study includes 13 cases treated by surgical and conservative approaches. The purpose is to assemble the radiologic features with relation to morphology in unique classification according to the literature and own experience.
Materials & Methods
Clinical, imaging and pathologic features of 13 patients with complex partial seizure disorders featuring DNET (aged 12-45 years) were reviewed. They underwent CT, MR and angiographic studies. In eight cases histological studies were obtained. All patients were followed up to 10 years.
Results
The imaging exhibits a versatile morphologic spectrum and

Note: Scanned images are included in the proceedings. Some submitted images were reduced during editing, thereby decreasing clarity. Also, refer to the Program Planner. Proceedings Content as of 3-29-2013.

could be divided into four groups: 1) Well-circumscribed inhomogeneous temporo-occipital located hypointense of T1 and hyperintense on T2 lesions. The central part was multinodular with multicystic appearance and calcifications. They showed intensive nodular patchy contrast enhancement (two cases). 2) Multicystic cortical lesions restricted in mesial regions limited to one lobe with associated cortical dysgenesis. They showed uniform appearance with small multiple cystic areas hypointense on T1 and FLAIR and hyperintense on T2 without contrast enhancement (seven cases). 3) Diffuse multicystic and nodular not circumscribed lesions with variable cortical and subcortical extension and preferred mesial orientation; they were not demarcated and did not show contrast enhancement, harboring the same signal behavior as Group 2 lesions; they had diffuse appearance and involved more than one lobe with frequent cortical dysgenesis (three cases). 4) Mixed DNET and ganglioglioma with extended ossifications. The MR imaging discovered a complex brain malformation in left parietal-occipital area with cortical dysgenesis. A poorly circumscribed mass with mild inhomogeneous contrast enhancement inside of the massive ossification was identified as DNET and another smaller well circumscribed cortical mass with strong homogeneous enhancement represented a ganglioglioma (one case).

Conclusion

Three pathologic features characterize DNETs: glioneuronal element, nodular component and associated cortical dysplasia. The occurrence in young but matured brain implies the persistence of certain types of neural progenitor cells, which usually are expected in the subventricular zone, the hippocampal dentate fascia, and the cortical subpial layer. The glioneuronal fraction contains neuronal and glial cells with different mucoid substance accumulation. This implies the multicystic appearance with cortical/subcortical and mesial location for the majority of lesions. The second and the third group are composed dominantly of glioneuronal component and emphasize unique imaging findings without contrast enhancement. The nodular component is variable and may contain neurons, astrocytes, and oligodendrocytes associated with cortical dysplasia, which implies the inhomogeneous solid appearance in first and forth groups. The mixed appearance of DNET and ganglioglioma is due to the common embryogenesis from subpial granular layer.

KEYWORDS: Dysembryoplastic neuroepithelial tumor, Brain development

O-566 **1:55 PM - 2:03 PM**

Use of MR Imaging in Predicting Surgical Resectability of Pituitary Adenomas with Parasellar Involvement

Connor, S.[1]·Hogarth, K.[2]·Wilson, F.[3]
[1]Kings College Hospital, London, UNITED KINGDOM, [2]John Radcliffe Hospital, Oxford, UNITED KINGDOM, [3]Starship Hospital, Auckland, NEW ZEALAND.

Purpose

To evaluate preoperative magnetic resonance (MR) imaging in its ability to predict complete removal of parasellar pituitary adenoma (PA) on postoperative MRI. Criteria for the radiologic assessment of parasellar involvement of pituitary adenomas have been defined previously (Cottier et al, 2000 and Vieira et al 2006) but no previous study has evaluated these imaging criteria for their value in predicting the likelihood of achieving a complete surgical resection as assessed by postoperative imaging.

Materials & Methods

Three hundred fifty-four patients with a histological diagnosis of pituitary macroadenoma were operated on at King's College Hospital between December 2004 and January 2010. Both pre and postoperative imaging was available for 49 patients with clear unilateral parasellar involvement (28 male, 21 female; mean age = 53 years, range 23-85, SD = 15 years) remained in the study. Pre and postoperative MR images were reviewed retrospectively by two neuroradiologists and a consensus was obtained. All of the images of pituitary tumors with parasellar involvement were evaluated according to criteria previously described by Cottier et al 2000 and Vieira et al 2006. The postoperative images then were evaluated for residual tumor as defined by signal abnormality in the same location as, or continuous with, the tumor shown on the preoperative images and with the same signal characteristics as the tumor tissue. Preoperative and postoperative MR findings were compared using the Fisher's exact test. *P* values of less than 0.05 were considered to indicate statistical significance. The odds ratio for incomplete resection/indeterminate outcome for each significant criterion was obtained by logistic regression.

Results

Only two MRI criteria reached statistical significance (Table 1). These were the nondepiction of the inferolateral and lateral compartments of the cavernous sinus. The results for the percentage of the intracavernous carotid surrounded by tumor were evaluated with a rank sum test, which also reached significance. The odds ratios indicate that nondepiction of the lateral venous compartment means that a partial/indeterminate outcome is six times more likely and that for every quarter increase of encasement of the intracavernous carotid, the likelihood of a partial/indeterminate outcome is increased 3.4 times. A 50% encasement of the intracavernous carotid by tumor would make a partial/indeterminate result 6.8 times more

Note: Scanned images are included in the proceedings. Some submitted images were reduced during editing, thereby decreasing clarity. Also, refer to the Program Planner. Proceedings Content as of 3-29-2013.

likely.
Table 1

MR imaging criterion	Fisher's exact score
Total encasement of cavernous carotid	0.056
Displacement of cavernous ICA	0.361
Asymmetry of the right/left CS compartments	0.51
Non-depiction of the superior compartment of the CS	0.117
Non-depiction of the carotid sulcus compartment of the CS	0.182
Non-depiction of the inferolateral compartment of the CS	0.001
Non-depiction of the lateral compartment of the CS	0.001
Lateral bulging of the lateral dural venous wall	0.228
Crossing the intercarotid lines	0.188

Conclusion
Three MR imaging features are useful in predicting the complete removal of the parasellar component of a pituitary adenoma as assessed by pos-operative MRI: (1) involvement of the lateral compartment of the cavernous sinus (2) involvement of the inferolateral compartment of the cavernous sinus and (3) tumor surrounding the intracavernous carotid by 50%.

KEYWORDS: Pituitary adenoma, Parasellar, magnetic resonance imaging

O-567 **2:03 PM - 2:11 PM**

Neuroepithelial Tumors of the Temporal Lobe: Relevance of Limbic Involvement to Histopathology and Tumor Biology

Capizzano, A. A.·Chaudhry, U.·Moritani, T.·Kirby, P.
University of Iowa Hospitals & Clinics
Iowa City, IA.

Purpose
To evaluate distinctive pathologic and clinical features of limbic versus nonlimbic neuroepithelial tumors of the temporal lobe.
Materials & Methods
IRB approved retrospective study between 2005 and July 2012. A search of pathologic reports of primary temporal lobe tumors excluding glioblastoma was performed. Cases with preoperative MRI were included. Based upon tumor extension on preoperative MRI, cases were divided into limbic and nonlimbic tumors after the limbic lobe definition of Heimer and van Hoesen. Limbic tumors were further categorized according to groups proposed byYasargil into: 1. mediobasal temporal (MBT), 2. insular-temporo-opercular (I-TO) and 3. frontoorbital-insular-temporopolar (FO-I-TP). MR imaging protocols included axial T1- and T2-weighted, FLAIR, GRE and DWI sequences and axial, coronal and sagittal postcontrast T1-weighted images acquired in 1.5 and 3T clinical scanners.
Results
Fifty cases were included with mean age at diagnosis 38 ± 19.9 years with 14 women and 36 men. Pathologic diagnoses were: 20 anaplastic astrocytomas, 11 gangliogliomas, eight astrocytomas WHO grade II, three pilocytic astrocytomas, two dysembryoplastic neuroepithelial tumors, two oligodendrogliomas grade II, two anaplastic oligodendrogliomas, one low-grade glioneuronal tumor and one atypical extraventricular neurocytoma. Thirty-six tumors were limbic centered (16 MBT, 11 I-TO, 8 FO-I-TP, 1 pantemporal) and 14 involved nonlimbic regions. There were no differences between limbic and nonlimbic tumors in age, sex, pathologic diagnosis and presentation with seizures. When considering three subtypes of temporal lobe limbic tumors, there was a significant difference in glial versus neuronal differentiation (Chi-Square = 7.8, df 2, p = 0.02) with MBT tumors having more frequent neuronal differentiation (50%) compared to I-TO (0%) and FO-I-TP (25%). Furthermore, taking only the eight tumors confined to the hippocampal-amygdala allocortex, seven (87%) had neuronal differentiation versus 36% in 14 nonlimbic tumors ($p<0.05$). When comparing low-grade (WHO I and II) versus high-grade (WHO III) tumors, there were significant differences for age and neuronal versus glial differentiation ($p<0.01$) but not for limbic location or subtype. Neuronal differentiation correlated with lower grade (0.49, $p<0.01$) and younger age (0.52, $p<0.01$). Limbic tumors had less gadolinium enhancement compared to extralimbic tumors including all diagnoses ($p<0.01$) and when comparing only anaplastic astrocytomas ($p<0.05$).
Conclusion
Limbic involvement of neuroepithelial tumors was proven relevant by Yasargil from a neurosurgical perspective regarding routes for tumor spread and surgical approach. Mediobasal temporal limbic tumors had more frequent neuronal differentiation than other limbic or extralimbic temporal lobe tumors. This may result from lesion proximity to the neurogenic subgranular zone of the hippocampus. Neuronal differentiation was maximal in

Note: Scanned images are included in the proceedings. Some submitted images were reduced during editing, thereby decreasing clarity. Also, refer to the Program Planner. Proceedings Content as of 3-29-2013.

hippocampal-amygdala and lowest in insular-temporal tumors. Neuronal differentiation correlated with lower tumor grade and younger age at diagnosis. Furthermore, limbic tumors displayed less gadolinium enhancement on MRI compared to extralimbic tumors. Therefore, consideration of tumor anatomy in relationship to the limbic lobe boundaries is important for the neuroradiologist considering differential diagnoses. In conclusion, although neglected in modern literature, the category of limbic tumors has distinct biologic features which may prove relevant for diagnosis and management.

KEYWORDS: Primary CNS neoplasms, Limbic system

O-568 **2:11 PM - 2:19 PM**

Utility of SPGR versus Fast-SPGR Imaging in the Detection of Brain Metastasis for Pre-Gamma-Knife Planning

Lee, J. H.·Keller, I. A.·Basak, S.·Hargreaves, E. L.·Danish, S. F.
University of Medicine and Dentistry of New Jersey
New Brunswick, NJ.

Purpose
Prior to performing gamma-knife surgery, a gadolinium-enhanced spoiled gradient (SPGR) recall MRI of the brain is performed for localization of intracranial metastasis (IM). SPGR performed on the day of surgery has been shown to detect additional IM that are not seen initially on a conventional outpatient postcontrast axial T1WI (T1+c) and can be considered the gold standard for detecting metastatic lesions. Detection of additional lesions on the day of the procedure potentially renders a patient ineligible for a radiosurgical option. While an SPGR sequence improves surgical planning, its long total scan time makes it impractical to use in all patients with suspected IM for screening purposes. To address this issue, a faster SPGR sequence (f-SPGR), with decreased spatial resolution, was developed to compete with SPGR. This study aims to investigate if f-SPGR can provide adequate resolution for lesion detection without overburdening the outpatient throughput.
Materials & Methods
A retrospective chart review was performed with a subject pool chosen from within the gamma-knife treatment population who underwent the SPGR (28 minutes), f-SPGR (8 minutes), and T1+c (5 minutes) sequences prior to gamma- knife treatment. Four independent observers (two neuroradiologists, one neurosurgeon, and one radiology resident) reviewed SPGR, f-SPGR, and T1+c images for detection of IM. Diagnosis was obtained from independent review by the four observers with SPGR being the gold standard. The f-SPGR sequence was compared against the SPGR and T1+c sequences in its ability to detect IM.
Results
Twenty-five total patients (eight men; 17 women; mean age 57 years) with 27 total scans were evaluated. An average of 181.0 lesions was identified per observer on the SPGR sequences. The overall detection rate was not statistically different for the SPGR versus the f-SPGR sequences (182.7 lesions; 100.0% of SPGR; $p = 0.096$). However, there was a statistically significant increase in the overall detection rate for both the f-SPGR and SPGR versus the T1+c sequences (166.0 lesions; 90.9% of f-SPGR, $p = 0.001$; 91.7% of SPGR; $p = 0.002$). There was no increase in the number of extra lesions detected in f-SPGR versus SPGR. But, there was an observed increase in the number of extra lesions detected in f-SPGR versus T1+c (extra lesions detected in 14 studies; 51.9% increase).
Conclusion
Misclassification of patients with brain metastasis remains a significant outpatient challenge. Fast-SPGR is a statistically comparable alternative to SPGR in its ability to detect IM, but has the added advantage of having an overall scan time savings of 20 minutes. Fast-SPGR provides a statistical advantage over T1+c in IM detection with only an added cost of three extra minutes of scan time. Therefore, f-SPGR provides a viable solution to the "lesions that we can't see" concept without significantly affecting outpatient throughput.

KEYWORDS: Gamma knife, Brain metastases, SPGR

O-569 **2:19 PM - 2:27 PM**

Assessment of Irradiated Brain Metastases by Dynamic Contrast-Enhanced MR Imaging

Almeida-Freitas, D. B.[1]·Pinho, M. C.[2]·Leite, C. C.[1]
[1]Universidade de São Paulo, São Paulo, BRAZIL, [2]University of Texas Southwestern Medical Center, Dallas, TX.

Purpose
Radiological criteria to evaluate the response of brain metastases to stereotactic radiosurgery (SRS) on the early post-treatment period have not been well established. The most used approach for this purpose is tumor size, which may increase as a result of both early radiation-related changes and tumor progression. The rule of dynamic contrast-enhanced (DCE) MRI, a technique that provides additional information about blood-brain barrier integrity, has not been characterized for assessment of irradiated brain metastases. The objectives of this study are to evaluate the effect of SRS on the transfer coefficient (Ktrans) of cerebral metastasis using DCE MRI and to correlate early Ktrans measurements with long-term treatment outcomes.
Materials & Methods
Twenty-six adult patients with a total of 34 cerebral metastases underwent T1-weighted DCE MRI in a 1.5T magnet prior to SRS and four to eight weeks post-treatment. Parametric maps were generated and Ktrans measurements were determined with a region-of-interest analysis. Mean Ktrans prior and after SRS were compared using generalized estimation equation to take into account the correlation between the different metastasis within

the same individual. Early Ktrans changes were correlated with tumor volume changes at long-term MRI followup (> 20 weeks).
Results
The mean (SD) Ktrans value was 0.13 (0.01) at the baseline and 0.08 (0.01) after treatment ($p < 0.001$). The reduction of Ktrans values was correlated with tumor volume reduction at long-term MRI followup ($r = 0.46$; $p = 0.04$). Local control was observed in 73% of the brain metastases, and a decrease in Ktrans was four times more frequent in these cases compared to the progression group ($p = 0.04$).
Conclusion
Stereotactic radiosurgery was associated with a reduction of Ktrans values of the cerebral metastases in the early post-treatment period. Ktrans changes were correlated with tumor volume at long-term MRI followup. These results suggest that Ktrans evaluation with DCE MRI may be a valuable biomarker in the early post-treatment period to predict long-term tumor volumes. Precocious assessment of treatment response is clinically desirable to select unresponsive patients for alternative therapies.

KEYWORDS: Permeability MR imaging, Metastases, Radiosurgery

O-570 **2:27 PM - 2:35 PM**

Neuroimaging Features of Leptomeningeal Carcinomatosis

Raz, E.[1]·Knopp, E.[1]·Wu, S.[1]·Zagzag, D.[1]·Saba, L.[2]·Hygino da Cruz, L.[3]·Fatterpekar, G.[1]
[1]New York University, New York, NY, [2]Cagliari University, Cagliari, ITALY, [3]Federal University of Rio de Janeiro, Rio de Janeiro, BRAZIL.

Purpose
Leptomeningeal carcinomatosis (LC) is a rare presentation of solid tumors, occurring in up to 5% of all patients with cancer. Prognostic factors for LC are cerebrospinal fluid (CSF) proteins, the Karnofsky performance status scale and the time from diagnosis of primary tumor. However, there is only sparse radio-pathologic correlation of LC. The purpose of our study was to correlate the incidence of LC with the primary tumor organ, the incidence of presence of associated intraparenchymal metastasis and determine if the extent of LC influenced the prognosis.
Materials & Methods
We retrospectively evaluated MRI positive studies of 131 pathology proven cases of LC in patients with a known primary tumor (excluding primary tumors of the brain and spinal cord). Gender, age, primary tumor, location of the leptomeningeal disease, presence of parenchymal metastases, CSF findings, categorization of the different histotypes, underlying molecular signature, and the overall survival of these patients.
Results
We evaluated 131 patients (M:F = 58:73) with MRI evidence of LC. Mean age was 55.8 (+/- 15.2) years. The most common types of tumor were breast (n = 47; 35.8%), lung (n = 35; 26.7%), melanoma (n = 18; 13.7%), hematologic malignancies including lymphoma and leukemia (n = 12; 9.1%) and others including thyroid, GI tract (n = 19; 14.5). LC was noted to be positive in 29 cases (22.1%) in the spinal canal, in 39 cases in the supratentorial compartment (29.7%), in 16 cases in the infratentorial (12.2%), and in 47 both compartments were involved (35.8%). The incidence of infratentorial location was more common among patients with breast cancer compared to the other primary tumors (chi square test $p<0.0001$). Forty-nine patients (37.4%) had parenchymal CNS metastases. There was no an association between the presence of intraparenchymal CNS metastases and leptomeningeal disease. There was no statistically significant difference between the extent of LC and the overall prognosis. Data will be presented regarding the CSF findings, categorization of the different histotypes and different molecular signatures.
Conclusion
We establish the radiopathologic correlation of LC in a large retrospective cohort of patients. Specifically, the most common type of tumor with imaging evidence of LC is breast, and simultaneous involvement of supra and infratentorial compartment is most common. There is no association between the presence of intraparenchymal CNS metastasis and LC. There was no statistically significant difference between the extent of LC and the overall prognosis.

KEYWORDS: Leptomeningeal disease, Brain neoplasms

O-571 **2:35 PM - 2:43 PM**

Intracranial Post-Transplant Lymphoproliferative Disorder: Review of Imaging Findings with Clinical and Pathologic Correlation

Waters, J.·Parmar, H. A.·Ibrahim, M.·McKeever, P.·Junck, L.
University of Michigan
Ann Arbor, MI.

Purpose
Post-transplant lymphoproliferative disorder (PTLD) is a well recognized complication of organ transplantation. Epstein-Barr virus (EBV) has a causative role, with more than 90% of tumors associated with EBV. The actual incidence of PTLD is variable, based on recipient's age, type of organ transplanted and the duration and extent of immunosuppression. Predominant or isolated involvement of central nervous system (CNS) with PTLD is considered very rare. Since the first description in 1970, only about 45 cases or so are reported in literature, most of which are in the clinical journals with little if any emphasis on the imaging features. The aim of this study is to identify all cases of CNS PTLD at a single institution and review their MRI findings with clinical and pathologic correlation.
Materials & Methods

Note: Scanned images are included in the proceedings. Some submitted images were reduced during editing, thereby decreasing clarity. Also, refer to the Program Planner. Proceedings Content as of 3-29-2013.

A total of seven patients with intracranial PTLD diagnosed at the University of Michigan from 2004 through 2012 were reviewed retrospectively. Lesions were diagnosed by brain biopsy (four patients), at autopsy (one patient), and by biopsy of extracranial PTLD (two patients). Clinical characteristics recorded include type of transplantation, time since transplant at presentation, presence of extracranial PTLD, and follow-up details. MR imaging characteristics investigated included number of lesions, lesion location (supratentorial or infratentorial), T1 and T2 signal characteristics, enhancement pattern on postcontrast T1-weighted images, and pattern of diffusion restriction (if any).

Results

Transplant	Time since transplant at diagnosis (months)	Solitary or multiple lesions	Lesion location	T1 (with respect to gray matter)	T2 (with respect to gray matter)	Enhancement	Diffusion restriction	Extracranial PTLD documented	Follow-up
Renal	64	Solitary	Infratentorial	Hypointense	Slightly hyperintense	Rim with internal enhancing nodule	Peripheral	No	Expired 5 months after diagnosis
Renal	81	Multiple	Supratentorial	Hypointense	Slightly hyperintense	Rim	None	No	Alive at 52 months with no evidence of disease
Renal	12–106 (patient with two transplants 94 months apart)	Solitary	Supratentorial	Internally hypointense with rim of hyperintensity	Internally hyperintense with rim of hypointensity	Rim	Internal and peripheral	No	Alive at 28 months
Cardiac	4 months	Multiple	Supratentorial and Infratentorial	Hypointense	Hyperintense	Solid enhancing and nonenhancing	Internal and peripheral in enhancing lesions	Right supraclavicular lymph node	Expired 14 months after diagnosis
Cardiac	8 months	Multiple	Supratentorial and infratentorial	Hypointense	Hypointense	Rim enhancement and nonenhancing	Internal and peripheral	Stomach, Cecum and transverse colon, right lower pulmonary lobe	Expired 5 months after diagnosis
Cardiac	42 months	Multiple	Supratentorial	Hypointense and isointense	Hyperintense	Solid nodular	Throughout	No	Alive 47 months after diagnosis
Bone marrow	4 months	Multiple	Supratentorial and Infratentorial	Hypointense	Hyperintense	Rim and patchy internal	Internal and peripheral in different lesions	Left cervical lymph node and stomach	Expired 9 months after diagnosis

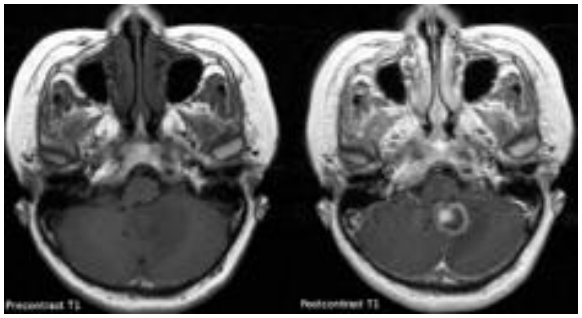

Conclusion

Lesions proven to be CNS PTLD on tissue sampling occurred as both single and multiple lesions in both the supratentorial and infratentorial compartments. The predominant imaging pattern is represented by a T1 hypointense, T2 hyperintense, peripherally enhancing lesion with restricted diffusion corresponding to the areas of enhancement. These imaging features differ from those typically associated with intracranial lymphoma, which usually demonstrate a homogeneous pattern of contrast enhancement and diffusion restriction. In patients with a history of transplantation, lesions with these imaging characteristics should be considered highly-suspicious for PTLD, irrespective of diagnosed PTLD diagnosed elsewhere.

KEYWORDS: Posttransplant lymphoproliferative disorder, Epstein Barr virus

Thursday Afternoon

1:15 PM - 2:45 PM
Room 1AB

(57e) Parallel Scientific Papers: Adult Brain; New Techniques and Novel Post Processing II

O-572 **1:15 PM - 1:23 PM**

Locally Linear Embedding: Applications in Neuroimaging

Starkey, J.·Liu, X.·Schuff, N.
University of California San Francisco
San Francisco, CA.

Purpose

Locally linear embedding (LLE) is a statistical method that allows for simplification of complex datasets from multiple dimensions to fewer dimensions. It was introduced in 2000 and has been employed in applications such as facial recognition. Recently, its utility in medicine has been recognized. Although modern machine learning algorithms are being used increasingly in neuroradiology, such as the prediction of Alzheimer disease (AD) from structural MRI, finding a good representation for multivariate brain MRI features in which their essential structure is revealed and easily extractable has been difficult. Because LLE is an unsupervised algorithm, no assumptions need to be made regarding the model of potentially complex relationships of sampled data. We aimed to apply LLE to Alzheimer disease and Parkinson disease classification and introduce this method to members of the ASNR.

Materials & Methods

Using LLE, we transformed regional brain volume and cortical thickness calculated by Free Surfer to a locally linear space with fewer dimensions, while also utilizing the global nonlinear data structure. The embedded brain features then were used to train a classifier for predicting future conversion to AD based on a baseline MRI. We tested the approach on 413 individuals from the Alzheimer's Disease Neuroimaging Initiative (ADNI) who had baseline MRI scans and complete clinical followups over three years with the following diagnoses: Cognitively normal (CN; n = 137), stable mild cognitive impairment (s-MCI; n = 93), MCI converters to AD (c-MCI, n = 97), and AD (n = 86). We also tested the approach on 100 individuals from the Parkinson's Progression Markers Initiative (PPMI) who had baseline MRI scans with the following diagnoses: Health control (HC; n = 40) and Parkinson disease (PD; n = 60).

Note: Scanned images are included in the proceedings. Some submitted images were reduced during editing, thereby decreasing clarity. Also, refer to the Program Planner. Proceedings Content as of 3-29-2013.

Results

In AD, we found classifications using embedded MRI features generally outperformed ($p < 0.05$) classifications using the original features directly. Moreover, the improvement from LLE was not limited to a particular classifier but worked equally well for regularized logistic regressions, support vector machines, and linear discriminant analysis. Most strikingly, using LLE significantly improved ($p = 0.003$) predictions of MCI subjects who converted to AD within three years and those who remained stable (accuracy/sensitivity/specificity: = 0.69/0.58/0.82), whereas predictions using the original features performed no better than chance (accuracy/sensitivity/specificity: = 0.51/0.57/0.45). Preliminary results suggest that original MRI features are unhelpful in PD and regularized logistic regressions also perform no better than chance. The LLE analysis is pending but will be completed in the next month, well in advance of the May meeting.

Conclusion

Locally linear embedding is an effective tool for classification studies of AD using multivariate MRI data. The improvement in predicting conversion to AD in MCI could have important implications for health management and for powering therapeutic trials by targeting nondemented subjects who will later convert to AD. Additionally, LLE is a promising method of classification in other neurologic diseases.

KEYWORDS: Alzheimer disease, Parkinson disease, Mild Cognitive Impairement, Prediction

O-573 **1:23 PM - 1:31 PM**

Phantom Study on Radiation Effective Doses of Cerebral Blood Volume Measurement Using Flat-Detector Digital Subtraction Angiography

Guo, W.[1,2]·Lin, C.[1,2]·Chen, W.[2]·Hung, S.[1,2]·Chu, W.[1]·Chiu, C.[1]·Wu, T.[2]
[1]Taipei Veterans General Hospital, Taipei, TAIWAN, [2]National Yang-Ming University, Taipei, TAIWAN.

Purpose

Quantitative x-ray digital subtraction angiography (DSA) and cerebral blood volume measurement using flat-detector (FD) DSA is feasible, currently. However, the effective radiation dose remains one of the major concerns. We aimed to estimate effective dose that involved in cerebral blood volume measurement using FD DSA.

Materials & Methods

A radiation experiment using an anthropomorphic phantom (Rando Alderson phantom; Radiology Support Devices, Long Beach, CA) on a biplane FD DSA suite (AXIOM-Artis®, Siemens Healthcare, Erlangen, Germany) was conducted. A clinical DSA imaging protocol (one 8-second rotational mask run with 60 frames/second followed by another 8-second rotational contrast medium filled run with same frame rate) for cerebral parenchyma blood volume measurement (syngo DynaPBV® Neuro, Siemens Healthcare, Erlangen, Germany) was used. The scanning parameters were: 73 kV, 483-555 mA, 4.0-4.1 ms, 48 cm field-of-view (FOV). Two PBV scan ranges, 8-cm slab (slab-PBV, from sella turcica to convexity) and whole brain PBV, were undertaken. 80 lithium fluoride thermo-luminescent dosimeters (TLDs) (TLD-100H, Bicron-Harshaw, Solon, OH) divided into 22 organ sites were embedded in the phantom. We followed the guidelines of International Commission on Radiation Protection Number 103 (ICRP-103) to measure the effective dose. For comparison, repeated two CT scans on the same phantom and TLDs distribution were performed on a 256 slice multidetector CT, (MDCT, Brilliance *i*CT®, Phillips Healthcare, Best, Netherland). A clinical CT perfusion (CTP) scanning protocol was used. The parameters were: 8 cm scan coverage identical to slab-PBV, 5 mm slice thickness, 64x1.25 mm collimation, 20x20 cm FOV, 80 kVp, 250 mA, 100 mAs, 0.4 second tube rotation time, scan interval of 1.5 seconds and lasted for one minute.

Results

The dose area product/entrance skin dose was 2631.6 μGym^2/228 mGy and 6884.4 μGym^2/240 mGy for slab-PBV and whole brain PBV, respectively. The effective dose was 0.84±0.56 and 4.18±0.90 mSv (ICRP-103), respectively for slab-PBV and whole brain PBV. As a comparison, the dose length product of MDCT CTP was 1177.3-1232.9 mGy*cm, equivalent to the effective dose of 2.46-2.58 mSv. The effective dose of MDCT CTP measured by TLDs was 2.55±1.60 to 2.84±1.54 mSv (ICRP-103).

Slab-PBV Scanning Results

Organ Sites	TLD Absorbed Dose (mGy)	
	Mean	Std.
Brain	49.70406	34.55499
Salivary gland	2.47033	0.11095
Thyroid	1.01696	0.34852
Esophagus	0.55624	0.08993
Lung	0.32083	0.03462
Breast	0.00000	0.00000
Liver	0.04034	0.01180
Stomach	0.04375	0.02060
Colon	0.00315	0.00445
Bladder	0.02758	0.02118
Gonad	0.03285	0.01976
Rib	0.49922	0.04345
T-spine	0.56879	0.26982
L-spine	0.02085	0.02368
Pelvis	0.02019	0.02856
Bone surface	0.27726	0.11926
Skin (eye)	48.53140	51.66365
Skin (thorax)	0.19365	0.02834
Skin (abdomen)	0.03365	0.01844
Heart	0.11176	0.04788
Kidney	0.07258	0.00786
Small intestine	0.04844	0.08489
TLD Effective Dose (mSv)	**0.84**	**0.56**

Conclusion

The effective dose measurement presented in the study is reliable and reproducible. Cerebral PBV® measurement

Note: Scanned images are included in the proceedings. Some submitted images were reduced during editing, thereby decreasing clarity. Also, refer to the Program Planner. Proceedings Content as of 3-29-2013.

using FD DSA is a dose-saving imaging protocol. The effective radiation dose of slab-PBV is about one-third of MDCT CTP. Taking the advantages of on-site and immediate morphologic imaging availability, saving of procedural time and patient transportation, FD-DSA slab-PBV is recommended.

KEYWORDS: Cerebral blood volume, DSA, Dyna CT

O-574 **1:31 PM - 1:39 PM**

Modeling the Pattern of Contrast Extravasation in Acute Intracerebral Hemorrhage Using Dynamic Contrast-Enhanced MR Imaging

Liu, R. T.[1,2]·Huynh, T. J.[1,2]·Huang, Y.[1]·Rideout-Gros, S.[1]·Van Slyke, P.[1]·Dumont, D.[1]·Hynynen, K.[1]·Aviv, R. I.[1]
[1]Sunnybrook Health Sciences Centre, Toronto, ON, CANADA, [2]University of Toronto, Toronto, ON, CANADA.

Purpose
Intrahematoma contrast extravasation in spontaneous intracerebral hemorrhage (ICH), coined the spot sign, has been shown to predict subsequent hematoma expansion and poor clinical outcomes. The dynamic relationship of the site of active contrast extravasation and the influence on the pattern of ICH formation are poorly understood. We used an animal model of acute ICH with contrast extravasation to characterize the dynamic pattern and rate of contrast extravasation.
Materials & Methods
Intracerebral hemorrhage was created within the basal ganglia in five yorkshire pigs utilizing a novel ICH animal model permitting real-time observation of contrast extravasation with dynamic contrast-enhanced (DCE) MRI (3T Signa MR750; GE Healthcare). Dynamic contrast-enhanced MRI was performed after intravenous bolus injection of Gadobutrol (Bayer Healthcare) utilizing a 3D T1-weighted spoiled gradient-recalled echo sequence with total acquisition time of 12 minutes. A 10-second temporal resolution was employed allowing dynamic visualization of hematoma growth. Contrast extravasation volume was measured using computerized planimetry (MIPAV, version 5.3; National Institutes of Health) at each time point. Spatial vector analysis was used to characterize asymmetric extravasation and hematoma growth. Vectors at each time point determined the rate of expansion along three-dimensional axes. Temporal phases of growth and stability were defined by maximizing the coefficient of determination for period of growth while minimizing the gradient for periods of stability. Rate of contrast extravasation was calculated using in-house software using a Patlak model (IDL, version 6.1; RSI, Boulder, Colorado).
Results
The ICH animal model exhibited asymmetric growth and variable rates of expansion. Initial rate of contrast extravasation was 8.9±3.4 ml/100g/min. A triphasic pattern of ICH growth was seen (Figure 1) with rapid initial average diameter expansion (156±17%) in the primary phase, followed by relative stability in the secondary phase. The tertiary phase was associated with further overall expansion (30±12%). In the primary phase, expansion in the superior-inferior (SI) plane outpaced the growth in the anterior-posterior (AP) plane (4.0±1.2 mm/min versus 1.2±0.3 mm/min; t-test p=0.003). In the tertiary phase, diameter expansion was greatest in the AP plane and was similar to the AP growth demonstrated in the primary phase (t-test p=0.126).

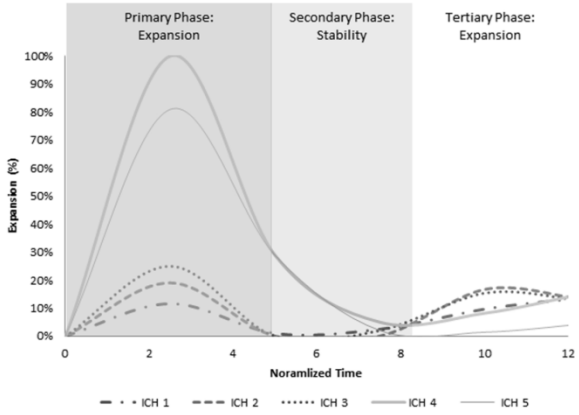

Figure 1. Percentage of contrast extravasation volume in the medial-lateral axes versus normalized time
Conclusion
A novel model of ICH formation demonstrating contrast extravasation is feasible and provides real-time study of the dynamics and rate of contrast extravasation. These data facilitate the understanding of rate and pattern of ICH formation.

KEYWORDS: Intracerebral hemorrhage, Contrast extravasation

O-575 **1:39 PM - 1:47 PM**

Time of Arrival Parametric Maps and Sliding Window Virtual Bolus Images Derived from High-Resolution Whole Brain Contrast-Enhanced 4D MR Angiography Improve the Display of Arteriovenous Malformation Vascular Anatomy and Flow Characteristics

Maksimovic, J.·Wu, Y.·Johnson, K.·Loecher, M.·Mistretta, C.·Turski, P. A.
University of Wisconsin
Madison, WI.

Purpose
Time-of-arrival (TOA) maps can be derived from high-resolution 4D MRA datasets to provide a qualitative description of contrast material arrival time in each voxel. The purpose of this project is to determine whether TOA-enhanced 4D MRA and/or virtual bolus imaging improve the characterization of brain AMVs.
Materials & Methods
High-resolution whole brain contrast-enhanced 4D MRA

Note: Scanned images are included in the proceedings. Some submitted images were reduced during editing, thereby decreasing clarity. Also, refer to the Program Planner. Proceedings Content as of 3-29-2013.

exams with subsecond temporal resolution were acquired by using radial acquisition and highly constrained projection reconstruction (4D CE HYPR MRA) in seven AVM patients. The TOA maps are based on signal intensity changes over time for each voxel. The TOA for each voxel was defined as the time point when the signal intensity reached 20% of its maximum. The TOA maps were generated, color encoded and then multiplied with the time-resolved contrast-enhanced MRA images at each time frame to form new 4D MRA images (TOA-enhanced 4D MRA) which not only represent the contrast enhancement of vessels at different time frames, but also contain the contrast arrival times with defined color encoding. In addition, each time frame also can be weighted by a Gaussian distribution in the time domain to form a virtual 4D bolus map. This 4D bolus map was then color coded and multiplied with the 4D MRA images to form a DSA-like virtual bolus, where at each time frame, only vessels with certain TOA values within the defined bolus length appear.

Results

4D MRA, TOA maps and virtual bolus images from seven AVM patients were scored by two observers for diagnostic confidence (0-100%) for detecting AVM arterial feeders, nidus and draining veins using DSA as the reference standard. For both observers, six of seven of the TOA maps improved identification of the arterial feeders and made evaluation of the nidus and venous drainage easier in all seven cases. The virtual bolus images improved the delineation of the venous drainage in five of seven patients. Figure 1 demonstrates axial projection 4D MRA (top row), TOA-enhanced 4D MRA (second row) and virtual bolus (bottom row).

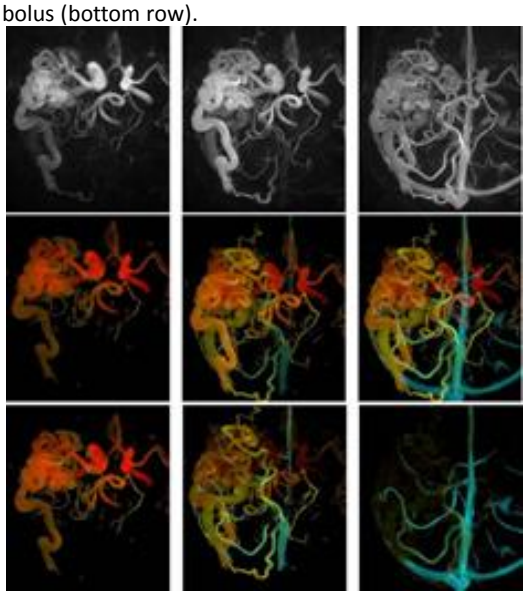

Conclusion

TOA-enhanced 4D MRA provide serial images and time of arrival maps in one simple display. Our preliminary results suggest that TOA mapping improved delineation of the arterial supply, nidus and venous drainage in AVM patients. Virtual bolus images isolate the venous structures by providing better arterial/venous separation.

KEYWORDS: 4D MRA, AVM, Time of Arrival Parametric Maps

O-576 **1:47 PM - 1:55 PM**

Quiet PROPELLER MR Techniques Provide Equivalent Quality for Routine Brain MR Imaging

Corcuera Solano, I.[1]·Gui, D.[2]·Gaddipati, A.[2]·Tanenbaum, L.[1]
[1]Mount Sinai School of Medicine, New York, NY, [2]GE Healthcare, Waukesha, WI.

Purpose

Switching of magnetic field gradients is the primary source of acoustic noise in MRI. Sound pressure levels (SPL) can run as high as 100-120 dB, potentially producing physical discomfort and at least temporary hearing loss, mandating hearing protection. To date two methods have been used to reduce noise - dampen/isolate the gradient coil from the patient bore, or reduce switching rate. Both methods have drawbacks, the first resulting in reduction of bore space and the second reducing performance. New technology has made quieter techniques feasible which range from as low as 80 dB (1/10000 as loud) to nearly silent. The purpose of this study is to evaluate the quality of “Quiet” MR FSE acquisitions in comparison to techniques in current day to day practice in imaging of the brain.

Materials & Methods

This novel ”Quiet” method reduces acoustic noise levels approximately 30 dB for T2 and T2 FLAIR PROPELLER employing an acoustic noise model to optimize gradient waveforms while minimizing the impact on scan time. An additional 180 degree preparation is used to minimize the effect on image quality. Fifty patients were scanned with preclinical “Quiet” techniques in addition to routine T2 and T2 FLAIR PROPELLER imaging sequences on a clinical 1.5T MR scanner. Conventional and “Quiet” PROPELLER FSE images were reviewed retrospectively by two experienced neuroradiologists who qualitatively assessed image quality for contrast resolution, artifact and, when appropriate, lesion conspicuity.

Results

“Quiet” PROPELLER T2 and T2 FLAIR were comparable in quality to conventional PROPELLER acquisitions with no significant tradeoffs aside from longer scan times.

Note: Scanned images are included in the proceedings. Some submitted images were reduced during editing, thereby decreasing clarity. Also, refer to the Program Planner. Proceedings Content as of 3-29-2013.

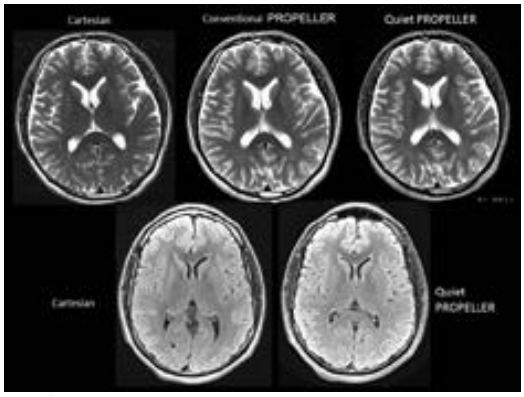

Conclusion
"Quiet" PROPELLER T2 and T2 FLAIR provide equivalent quality at comfortable sound pressure levels and can replace conventional sequences for routine evaluations of the brain.

KEYWORDS: Brain, MR imaging safety, Quiet

O-577 **1:55 PM - 2:03 PM**

Surface-Based Analyses of Brain Cortical Features in Patients with Periventricular Nodular Heterotopia

Beltran-marin, M.[1]·Azagra, A.[1]·Sadeghi, N.[1]·Jissendi-Tchofo, P.[2]
[1]Erasme Hospital, Brussels, BELGIUM, [2]Lille University Hospital, Lille, FRANCE.

Purpose
First, to analyze brain cortical features, including thickness (CT), complexity in terms of gyration and sulcation (CC) and intracortical intensity gradient (CG) in patients with periventricular nodular heterotopia (PNH) and, secondly, to correlate the volume and topography of the heterotopic gray matter with the white matter volume (WMV) and cortical gray matter volume (GMV) of the affected hemisphere.
Materials & Methods
The brain cortex of 14 patients (six M/eight F, mean age 33 years) with PNH and 28 healthy controls (16 M/12 F, mean 25.5 years) were analyzed after an automatic segmentation processed by FreeSurfer, using a 3D T1 sequence. Surface features such as CT, CC and CG were extracted. The heterotopic gray matter was segmented manually in every patient side by side and corresponding volumes were calculated. The surface features variations were assessed using z scores, intraindividually and as compared with the control group. The correlations between the volume and topography (0 = absent, 1 = anterior, 2 = osterior, 3 = diffuse from anterior to posterior) of the heterotopic gray matter with the white matter (WMV) and cortical gray matter volume (GMV) of the affected hemisphere were obtained using the Pearson's test.
Results
Seven patients had bilateral PNH, three on in the right hemisphere (rh) and four on the left (lh). PNH were located anteriorly (four), posteriorly (five) and diffusely (four). Auto z scores did not show significant variations of cortical features intraindividually (z>2, z<-2). The comparisons with the control group showed various pattern of differences. Areas of increased and decreased (z>3, z<-3) CT were found in the affected hemispheres involving prefrontal, central, parietal and temporal cortices. The CC was increased more often in various areas including, the prefrontal, orbitofrontal, anterior cingulated and temporal lateral cortices (z>3, z<-3). We found only subtle and seldom differences in the CG in temporal and prefrontal cortices (z>3, z<-3). The volume of PNH was correlated inversely with the GMV of the affected hemisphere (r= -0,26 -lh; r= -0,41 -rh). Eventually, the WMV likely was more reduced in anterior PNH while the GMV was more reduced in diffuse PNH.

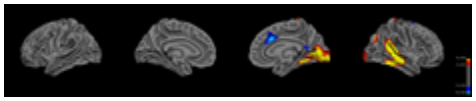

Conclusion
Periventricular nodular heterotopia causes alterations of brain cortical features in individuals, which likely are related to the impaired cortical development. Thickness, complexity and gradient of the cortices are altered at different degrees and areas. The PNH volume likely is more associated with diminished gray matter than reduced white matter.

KEYWORDS: 3D imaging, Brain development, Periventricular Nodular Heterotopia

O-578 **2:03 PM - 2:11 PM**

Dynamic Contrast-Enhanced MR Imaging: Measuring Permeability on MR Imaging as a Novel Biomarker of Human Cerebral Cavernous Malformations

Shah, A.·Mikati, A.·Li, L.·Shenkar, R.·Zhao, L.·Guo, X.·Gao, J.·Shi, C.·Dey, M.·Awad, I.·Christoforidis, G.
University of Chicago
Chicago, IL.

Purpose
Patients with familial cerebral cavernous malformations (CCM) have one of three gene mutations and display multiple cavernomas whereas patients with sporadic CCM typically harbor one lesion. Data from murine haploinsufficient models suggest that these gene mutations play a role in dysfunction of the interendothelial cell junction proteins, demonstrate increased vascular permeability on Evans blue dye studies and that restoration of normal permeability by Rho kinase inhibition is associated with decreased lesion burden. Thus a marker for permeability could serve as a target for treatment. This study sought to replicate findings in heterozygous mice by determining if permeability within cavernomas and permeability within unaffected brain differed between patients with familial and sporadic CCM

Note: Scanned images are included in the proceedings. Some submitted images were reduced during editing, thereby decreasing clarity. Also, refer to the Program Planner. Proceedings Content as of 3-29-2013.

using dynamic contrast-enhanced (DCE) magnetic resonance imaging (MRI).

Materials & Methods

Thirteen patients with either sporadic (five patients) or familial (eight patients) cavernomas were imaged using 3.0T Philips Achieva MRI (Philips Medical Systems) and an eight-element phased array receiver head coil. A saturation recovery gradient recalled sequence was used both for an initial T1 measurement and for the subsequent dynamic imaging. Each slice was acquired after application of a nonselective saturation prepulse with a saturation time delay (TD). T1 measurements were derived from 10 TD values varying from 120 ms to 10 seconds. Gadodiamide (0.05mmol/kg) was injected at 4mL/sec followed by 20mL saline. Arterial input function was obtained using a slice specifically acquired perpendicular to a major arterial vessel (carotid or basilar) identified on MR angiography. Permeability maps were derived using a one compartment Patlak model on Matlab. Mean measurements by two independent observers were obtained by drawing regions-of-interest within cavernomas as well as gray and white matter near and distant (>2cm) from the cavernoma.

Results

Permeability measures are summarized in Figure 1. For each category, mean permeability was significantly higher in the familial versus sporadic cases ($P < 0.05$, Student *t*-test). Significant, interobserver difference was only present when measuring gray matter far from the lesion ($p<0.001$).

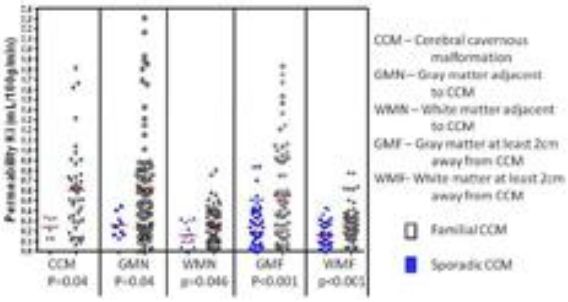

Figure 1: Comparison of permeability in patients with familial and sporadic CCM

Conclusion

Pilot data presented here suggest that patients with familial CCM compared to patients with sporadic CCM have increased permeability on DCE MRI both within the CCM and nonaffected brain. Further studies will be needed to determine if permeability on DCE MRI predicts bleeding risk and if treatments which reduce permeability affect the natural course of CCM formation and hemorrhage.

KEYWORDS: Permeability MR imaging, Cavernous malformation

O-579 **2:11 PM - 2:19 PM**

T1-Weighted 3D Fast Spin-Echo: CUBE MR Outperforms 2D Imaging of the Pituitary and Parasellar Region

Lien, R. J.[1]·Black, A.[2]·Pawha, P. S.[1]·Naidich, T. P.[1]·Tanenbaum, L. N.[1]

[1]Mount Sinai Hospital, New York, NY, [2]Bard College at Simon's Rock, Great Barrington, MA.

Purpose

The relatively thick slices provided by conventional 2D MR techniques are limited by volume averaging, which may obscure small pituitary lesions and suboptimally delineate parasellar structures. Gap-free, thin-slice 3D acquisitions reduce volume averaging, but typically employ GRE techniques that suffer from susceptibility artifacts at the bone-air-soft tissue interfaces of the skull base. The purpose of this study was to show how a novel T1-weighted 3D FSE sequence (CUBE) might outperform conventional 2D FSE techniques for contrast-enhanced imaging of the pituitary and parasellar region.

Materials & Methods

Ninety-one patients were scanned with CUBE (50% overlapped 1 mm slices) and conventional 2D FSE (2.5 mm thickness with a 0.8 mm gap) on a clinical 3.0T MR scanner. Images were reviewed retrospectively by two experienced neuroradiologists, who graded the degree of delineation of the infundibulum, optic apparatus and medial wall of the cavernous sinus, as well as the degree of artifact at the sellar floor from one (poorest) to five (best). The degree of lesion conspicuity or confidence in lesion exclusion was graded on a similar scale.

Results

CUBE demonstrated improved image quality compared to the conventional 2D sequence, and was better or equal to the 2D in 84% and 86% of the cases for readers A and B. Both readers graded the degree of artifact at the sellar floor as less problematic on 3D (mean score of 3.2/3.2 on 2D and 4.3/3.9 on 3D for readers A and B). The readers graded the infundibulum as being better visualized on 3D (mean of 3.0/2.7 on 2D and 4.1/3.6 on 3D for readers A and B). The optic apparatus was graded as being slightly better visualized on 3D (mean of 3.2/2.9 on 2D and 3.7/3.0 for readers A and B). The medial wall of the cavernous sinus was graded as better visualized on 3D (mean of 2.5/3.0 on 2D and 3.6/3.6 on 3D for readers A and B). The degree of conspicuity of a lesion and confidence in excluding a lesion was also greater on 3D (mean of 3.6/2.9 on 2D and 4.3/3.4 for readers A and B).

Note: Scanned images are included in the proceedings. Some submitted images were reduced during editing, thereby decreasing clarity. Also, refer to the Program Planner. Proceedings Content as of 3-29-2013.

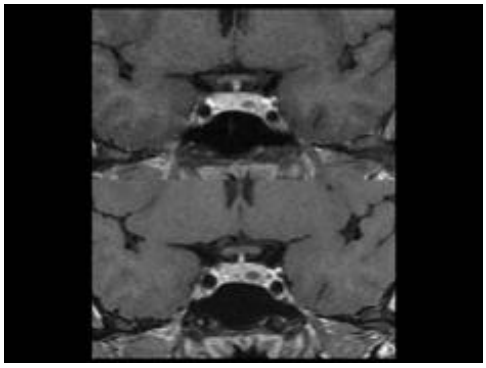

Conclusion
CUBE provides superior quality with thinner slices and diminished artifact, and can replace conventional 2D FSE sequences for routine evaluations of the pituitary and parasellar region.

KEYWORDS: Pituitary gland, 3D imaging

O-580 **2:19 PM - 2:27 PM**

"Silent-Zero TE" MR Techniques Provide Equivalent Quality for Routine T1-Weighted MR Imaging of the Brain

Corcuera Solano, I.[1]·McKinnon, G.[2]·Sun, W.[2]·Akao, J.[2]·King, K.[2]·Tanenbaum, L.[1]
[1]Mount Sinai School of Medicine, New York, NY, [2]GE Healthcare, Waukesha, WI.

Purpose
Switching of magnetic field gradients is the primary source of acoustic noise in MRI. Sound pressure levels (SPL) can run as high as 100-120 dB, potentially producing physical discomfort and at least temporary hearing loss, and mandating hearing protection. To date two methods have been used to reduce noise - dampen/isolate the gradient coil from the patient bore, or reduce switching rate. Both methods have drawbacks, the first resulting in reduction of bore space and the second reducing performance. New technology has made quieter techniques feasible which range from as low as 80 dB (1/10000 as loud) to nearly silent. The purpose of this study is to evaluate the quality of nearly silent MR T1-weighted (T1W) GRE acquisitions in comparison to techniques in current day to day practice in imaging of the brain.
Materials & Methods
This novel technique is an essentially silent 3D isotropic gradient echo acquisition with a nearly zero TE and low flip angles. It uses a 3D spiral radial sampling scheme with no in-plane phase and frequency direction, as well as no slice selection phase. Due to the K-Space trajectory and data sampling scheme, the gradient steps are relatively small, accounting for the extremely quiet behavior. An inversion Prep pulse is used to generate T1-weighted contrast similar to BRAVO IR-FSPGR. In addition because of the non-Cartesian nature of the acquisition fat suppression is needed to reduce the effects from chemical shift. Fifty patients were scanned with this pre-clinical "Silent" T1 technique in addition to routine T1-weighted imaging approaches on a clinical 1.5T MR scanner. Conventional and "Quiet" images were reviewed retrospectively by two experienced neuroradiologists who qualitatively assessed image quality for contrast resolution, artifact and, when appropriate, lesion conspicuity.
Results
"Silent" T1-weighted scans were comparable in quality to conventional T1-weighted acquisitions.

Conclusion
"Silent" T1-weighted scans provide equivalent quality at nearly zero sound pressure levels and can replace conventional sequences for routine T1-weighted evaluations of the brain.

KEYWORDS: Brain, 3D imaging, Silent

O-581 **2:27 PM - 2:35 PM**

Development of an Automated Quantitation Method for Cerebrospinal Fluid Dynamics in the Cerebral Ventricles and the Spinal Subarachnoid Space Using MR Imaging Spin Labeling Technique

Shiodera, T.[1]·Nitta, S.[1]·Takeguchi, T.[1]·Yui, M.[2]·Yamashita, Y.[2]·Yamamoto, T.[2]·Yamada, S.[3]
[1]Toshiba Corporation, Kawasaki, JAPAN, [2]Toshiba Medical Systems Corporation, Tochigi, JAPAN, [3]Tokai University Oiso Hospital, Kanagawa, JAPAN.

Purpose
Using the time-spatial labeling inversion pulse (Time-SLIP) technique, a regional cerebrospinal fluid (CSF) dynamics can be traced without using contrast medium. Previous studies have evaluated visual assessments of CSF dynamics using the Time-SLIP technique. The objective of this study is automated quantitation of CSF dynamics in the cerebral ventricles and the spinal subarachnoid space using the Time-SLIP technique.
Materials & Methods
A series of 2D images with incremental inversion recovery times was obtained using 1.5T MRI scanner with Time-SLIP sequence. Observation regions were the foramen Monro,

Note: Scanned images are included in the proceedings. Some submitted images were reduced during editing, thereby decreasing clarity. Also, refer to the Program Planner. Proceedings Content as of 3-29-2013.

the prepontine cisterns, the aqueduct of Sylvius and the spinal subarachnoid space. These regions of interest were automatically outlined based on signal intensity analysis and shape of region. Subsequently, labeled CSF regions were further detected using the image binarization method. Average speed of the labeled CSF region was calculated using a regression line fitting. To evaluate the proposed method, experiments comparing the average speed and visual assessment by three neurosurgeons were conducted. Correlations between the proposed method and manual annotations of the average speed were evaluated in the spinal subarachnoid space.

Results

Seventy-nine datasets including 76 patients with various diseases (idiopathic normal pressure hydrocephalus, secondary normal pressure hydrocephalus, cerebral infarction, etc.) and three healthy volunteers for intracranial CSF dynamics, and 19 datasets from three healthy volunteers for the spinal subarachnoid CSF dynamics were studied. The proposed method detected the labeled CSF dynamics as shown in Figure 1. For cerebral ventricles, Table 2 shows correlation of the average speed between visual assessment and the automated quantitation method in these regions. Concordance ratios were 87 to 91%. For the spinal subarachnoid space, the correlation factor between the proposed method and manual annotations was R2 = 0.83 ($p < 0.001$). The processing time was less than three seconds.

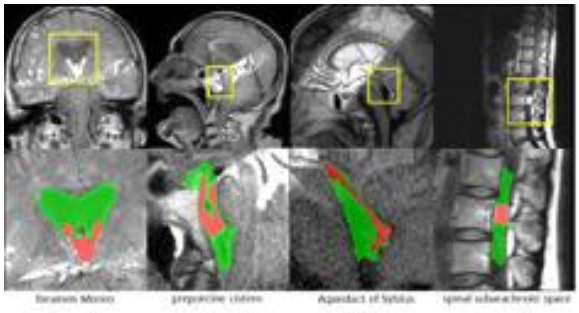

comparison results between average speed and visual assessment

observation region	visual assessment results by neurosurgeons / average speed by the proposed method [mm/sec.]		
foremen Monro	no reflux	slow reflux	normal reflux
	0.40 ± 0.30	1.20 ± 0.62	3.06 ± 0.45
prepontine cisterns	no movement	normal movement	-
	0.55 ± 0.25	1.23 ± 0.49	-
aqueduct of Sylvius	slow movement	normal movement	fast movement
	0.22 ± 0.26	1.09 ± 0.54	3.68 ± 1.66

Conclusion

This paper presented a new automated quantitative method of CSF dynamics using the Time-SLIP technique.

KEYWORDS: Cerebrospinal fluid, MR imaging, image post-processing technique

O-582 **2:35 PM - 2:43 PM**

Correction of Cerebral Blood Volume Perfusion Maps from T1 Leakage Effect Allows a Better Correlation of Perfusion Dynamic Susceptibility Contrast MR Imaging with Histopathologic Glioma Grading and an Estimation of Vascular Permeability

Viry, F.[1]·Galanaud, D.[1]·Mitulescu, A.[2]·Chaibi, Y.[2]·Reina, V.[1]·Leclercq, D.[1]·Dormont, D.[1]
[1]Pitié-Salpêtrière Hospital, Paris, FRANCE, [2]Olea Medical, La Ciotat, FRANCE.

Purpose

Capillary proliferation is a major histopathologic criterion in glioma grade determination, known to correlate with CBV. However, in case of blood-brain barrier (BBB) disruption, contrast agent extravascular leakage increases the signal in voxels inducing underestimation of CBV. Sophisticated mathematical models taking into account BBB disruption and arterial input function (AIF) can be used to correct this misestimation and enable permeability constant K2 calculation. We hypothesized that CBV corrected from vascular leakage can better differentiate glioma grade than uncorrected CBV and that K2 increases with glioma grade.

Materials & Methods

Fifty-four patients with steretotaxic biopsy-confirmed gliomas (20 WHO grade II, 13 grade III and 21 grade IV) explored by multimodal MR imaging including dynamic susceptibility contrast (DSC) gradient-echo perfusion MR (1.5T-3T) were included retrospectively. Preprocessing included motion correction, automatic AIF determination and leakage correction (Perfscape/Neuroscape-Olea Medical). Perfusion maps including relative CBV (corrected/uncorrected), relative CBF and K2 were calculated. Regions-of-interest were delineated within the tumor (biopsy site), and in the symetrical contralateral normal-appearing region.

Results

Differences in corrected rCBV were stastistically significant ($p<0.05$) between grade II-IV, III-IV, II-III (nonparametric Steel-Dwass test). Uncorrected rCBV does not statistically differentiate grades II-III. K2 could only differentiate grade II-IV. Corrected rCBV had a stronger correlation to glioma grade than uncorrected rCBV (Spearman $r = 0.73$ and $r = 0.66$ respectively, $p<0.01$). K2 was correlated weakly to glioma grade ($r = 0.34$, $p<0.01$).

Conclusion

Taking into account BBB disruption in DSC perfusion imaging improves glioma grades differentiation with rCBV. K2 has a weak correlation with glioma grade, which could

Note: Scanned images are included in the proceedings. Some submitted images were reduced during editing, thereby decreasing clarity. Also, refer to the Program Planner. Proceedings Content as of 3-29-2013.

be explained partly by the heterogenous parameters of DSC sequences in this study.

KEYWORDS: Permeability MR imaging, Glioma, CBV coreaction, Perfusion

O-582 **2:35 PM - 2:43 PM**

Correction of Cerebral Blood Volume Perfusion Maps from T1 Leakage Effect Allows a Better Correlation of Perfusion Dynamic Susceptibility Contrast MR Imaging with Histopathologic Glioma Grading and an Estimation of Vascular Permeability

Viry, F.[1]·Galanaud, D.[1]·Mitulescu, A.[2]·Chaibi, Y.[2]·Reina, V.[1]·Leclercq, D.[1]·Dormont, D.[1]
[1]Pitié-Salpêtrière Hospital, Paris, FRANCE, [2]Olea Medical, La Ciotat, FRANCE.

Purpose
Capillary proliferation is a major histopathologic criterion in glioma grade determination, known to correlate with CBV. However, in case of blood-brain barrier (BBB) disruption, contrast agent extravascular leakage increases the signal in voxels inducing underestimation of CBV. Sophisticated mathematical models taking into account BBB disruption and arterial input function (AIF) can be used to correct this misestimation and enable permeability constant K2 calculation. We hypothesized that CBV corrected from vascular leakage can better differentiate glioma grade than uncorrected CBV and that K2 increases with glioma grade.
Materials & Methods
Fifty-four patients with steretotaxic biopsy-confirmed gliomas (20 WHO grade II, 13 grade III and 21 grade IV) explored by multimodal MR imaging including dynamic susceptibility contrast (DSC) gradient-echo perfusion MR (1.5T-3T) were included retrospectively. Preprocessing included motion correction, automatic AIF determination and leakage correction (Perfscape/Neuroscape-Olea Medical). Perfusion maps including relative CBV (corrected/uncorrected), relative CBF and K2 were calculated. Regions-of-interest were delineated within the tumor (biopsy site), and in the symetrical contralateral normal-appearing region.
Results
Differences in corrected rCBV were stastistically significant ($p<0.05$) between grade II-IV, III-IV, II-III (nonparametric Steel-Dwass test). Uncorrected rCBV does not statistically differentiate grades II-III. K2 could only differentiate grade II-IV. Corrected rCBV had a stronger correlation to glioma grade than uncorrected rCBV (Spearman $r = 0.73$ and $r = 0.66$ respectively, $p<0.01$). K2 was correlated weakly to glioma grade ($r = 0.34$, $p<0.01$).
Conclusion
Taking into account BBB disruption in DSC perfusion imaging improves glioma grades differentiation with rCBV. K2 has a weak correlation with glioma grade, which could

be explained partly by the heterogenous parameters of DSC sequences in this study.

KEYWORDS: Permeability MR imaging, Glioma, CBV coreaction, Perfusion

Thursday Afternoon

3:15 PM - 4:45 PM
Ballroom 6AB

(58) ASPNR Programming: Interesting Case Conference (AR)

O-583 **3:15 PM - 4:45 PM**

Interesting Cases

Thursday Afternoon

3:15 PM - 4:45 PM
Ballroom 6CF

(59) ASHNR Programming: Current Concepts and Advances in Head and Neck Cancer Imaging (SAM) (AR)

O-585 **3:15 PM - 3:50 PM**

Applications for PET Imaging: Current Applications and Best Practices

Loevner, L. A.
University of Pennsylvania Medical Center
Philadelphia, PA.

Presentation Summary
The strengths and potential pitfalls of FDG-positron emission tomographic imaging in patients with head and neck cancer, especially those who have undergone surgery and/or chemotherapy and irradiation will be reviewed. Positron emission tomography (PET) currently is performed using the radiopharmaceutical ^{18}F-FDG, a D-glucose analog. The increased vascularity of tumors and glucose metabolism by malignant cells result in preferential uptake of FDG by tumor cells. The inability to process the metabolites of the modified glucose molecule causes intracellular accumulation of F^{18} containing radioisotopes. This metabolism has been invaluable in the evaluation of many cancer patients, and PET plays a pivotal role in the diagnosis, staging, and restaging of head and neck oncology patients. The ability to assess the functional status of tissue with FDG-PET has been remarkable, and addresses this well known limitation of

Note: Scanned images are included in the proceedings. Some submitted images were reduced during editing, thereby decreasing clarity. Also, refer to the Program Planner. Proceedings Content as of 3-29-2013.

conventional cross-sectional CT and MR imaging. Conversely, the excellent spacial resolution and the ability to analyze the relationship of neoplasms relative to critical adjacent structures on CT and MR imaging is a very important adjuvant to, and limitation of PET. This presentation will emphasize physiologic variations seen in PET imaging with particular attention to those seen in the treated neck, and will illustrate the complimentary roles that PET and cross-sectional imaging play in assessing patients with newly diagnosed and treated head and neck cancer. **Evaluating Head and Neck Cancer.** Direct visualization combined with endoscopy is very sensitive in evaluating the mucosa of the aerodigestive tract. However, submucosal infiltration of the deep spaces of the head and neck is difficult to detect on physical and endoscopic examination unless there are symptoms to suggest that such spread is present. As a result, patients often are clinically understaged. CT and MR play a critical role in delineating the extent of deep tumor spread. The need for and type of surgery and the use of chemotherapy and irradiation are guided by the site of origin of the primary tumor and staging at the time of clinical presentation. One of the major limitations of cross-sectional CT and MR imaging is that they are morphologic studies that look at the structure of organs; however, often do not identify regions of biologically active tumor in areas that are morphologically relatively normal in appearance. Surgery, irradiation, and increasingly adjuvant chemotherapy are the arsenal for treating head and neck cancer and result in altered anatomy related to surgical absence of tissue, anatomical distortions, as well as inflammatory changes both in the site of the primary tumor as well as in the lateral neck treated for regional nodal metastases. It can be difficult even for an experienced radiologist to reliably distinguish post-treatment changes and its complications from tumor due to the overlapping densities and intensities of muscle, tumor, edema, and inflammation on CT and MR imaging, respectively. FDG-PET plays a critical role in further assessing these patients. In patients with head and neck cancer, an important factor in determining prognosis, treatment, and long-term survival is the identification of regional nodal metastases. Necrosis within cervical lymph nodes usually is indicative of the presence of metastatic disease. At least 10% of cervical lymph nodes harboring cancer are normal by CT and MR imaging criteria (not enlarged and with normal architectural features). FDG-PET frequently detects metabolic activity in cancer-harboring nodes that are normal on conventional imaging. Such identification frequently alters management. For example, detection of contralateral nodal metastases on PET not suspected clinically or on conventional imaging may result in a neck dissection. The inability to consistently identify small osseous and solid organ metastases is another limitation of CT and MR imaging. Detection of distant metastases may determine that a patient is no longer a surgical candidate. **Limitations of FDG-PET in Evaluating Head and Neck Cancer.** While PET has dramatically improved the detection of tumor(s), it is of paramount importance to understand and recognize the limitations of PET which include but are not limited to spatial resolution, anatomical localization, and physiologic variations in FDG distribution and uptake. Other potential issues with PET include reduced or absent uptake in tumors that are largely cystic or necrotic, and very importantly, some neoplasms are of histologic types that frequently do not take up FDG glucose. Imaging with FDG-PET alone has the limitations of reduced spacial resolution and suboptimal anatomical localization. PET may identify a neoplasm at the skull base, but the resolution is such that it cannot illustrate the involvement of prevertebral muscle, the encasement of the carotid artery, or the contiguous intracranial extension. The most significant contribution that CT has added to the combined PET-CT study is the ability to accurately localize regions of FDG uptake. Everything that is “hot” is not always cancer, and this has particular significance in the head and neck. There are a spectrum of physiologic variations in the distribution of FDG radiotracer that may result in regions of normal, avid FDG uptake. These variations in FDG distribution are compounded and even more complex in patients who have been treated for head and neck cancer. The altered anatomy from surgery results in functional and compensatory differences that change the pattern of radioisotope uptake on FDG-PET images. A solid understanding of both the post-treatment anatomy and the biology of head and neck cancer based on its site of origin in the aerodigestive tract, typical patterns of lymph node metastases, as well as post-treatment anatomy and expected variations in radiotracer distribution is essential to provide accurate interpretations of PET scans and avoid interpretive errors. Physiologic variations of FDG uptake and distribution in the treated neck may occur in the lymphoid tissue of Waldeyer’s ring (mistaken for tumors), the salivary glands**,** within brown fat, as well as in muscles (including the true vocal cords, skeletal muscles, and oral cavity tongue). A common pitfall of PET is the misinterpretation of uptake in a submandibular gland for a malignant lymph node when the contralateral gland is surgically absent as part of a neck dissection. The uptake of FDG in brown adipose tissue (fat) may serve as another potential source of false positive FDG-PET interpretations. Brown fat plays an important role in cold-induced and weight-loss induced thermogenesis. It is frequently formed in patients with rapid weight loss, such as patients being treated for cancer, and is more common in the winter. It also is more common in children and in women. The brown color of the fat is likely related to its vascularity and increased mitochondrial density. FDG uptake in metabolic brown adipose tissue is explained by the presence of glucose transporters. Brown fat commonly occurs bilaterally and often symmetrically. It has a propensity to occur in the mediastinum, paravertebral and intercostals regions, the lateral neck, supraclavicular fossa, axilla, and the abdomen**.** Uptake in metabolically active brown fat may be misinterpreted as tumor, especially when

Note: Scanned images are included in the proceedings. Some submitted images were reduced during editing, thereby decreasing clarity. Also, refer to the Program Planner. Proceedings Content as of 3-29-2013.

deposited in an asymmetric pattern. Fused PET-CT images are useful in avoiding this pitfall by precisely localizing the focal FDG uptake to regions of hypoattenuating fat. Some muscles in the neck that may be common have physiologic uptake include the spinal cervicalis and splenius capitus muscles, the prevertebral muscles (longus colli and longus capitus), and the scalene muscles. To minimize skeletal muscle uptake, it is important that the patient be at rest prior to imaging. Muscular uptake may be symmetric or asymmetric, and usually is elongated in appearance on sagittal and coronal reconstructed PET images. In treated necks patients often compensate for surgical absence of muscles, nerve injury, and pain by using different muscle(s). Asymmetric uptake in these compensatory muscles may be misinterpreted as pathologic lymph nodes. Mucositis occurs in patients managed with irradiation and chemotherapy. These patients often have continual tongue motion in order to manage dry mouth and oral secretions frequently resulting in physiologic uptake in the tongue which should not be misinterpreted as neoplasm. Clinical correlation and manual palpation by the clinical subspecialists are necessary. Another common misinterpretation is in the setting of hemi-tongue paralysis and denervation in which the contra-lateral functioning side of the tongue may show physiologic FDG uptake that is misinterpreted as oral cavity tumor. In patients with vocal cord paralysis there often is normal physiologic uptake in the contralateral vocal cord which frequently is misinterpreted as a glottic cancer. Review of cross-sectional imaging frequently shows the secondary findings of vocal cord paralysis including dilatation of the ipsilateral piriform sinus, vallecula and laryngeal ventricle. These findings as well as patient history will assist in avoiding this false positive pitfall. Sequelae of treatment and its complications also may result in false positive interpretations on PET-CT imaging. Specifically, inflammation frequently seen with radiation therapy, early radiation necrosis, and infection-abscess formation may result in FDG uptake that can be mistaken for recurrent or residual neoplasm. Knowledge of the timing of irradiation and type of surgery if performed is critical when assessing the PET images. While PET is very sensitive in this scenario, it is not specific in the early weeks to months immediately following treatment where tumor, treatment sequela and complications of treatment may be FDG avid and may have overlapping appearances on the CT portion of the study. Specificity on PET imaging increases with time, and usually FDG uptake 12 weeks or more out of therapy is worrisome for the presence of neoplasm. The presence of air in the involved soft tissues on the CT scan is an important associated finding and should raise concern for infection or radiation necrosis. Reparative bone formation in patients that have undergone surgical placement of reconstructive grafts, such as positioning of a mandibular implant following a partial mandibulectomy, also can result in physiologic uptake of FDG. Other potential pitfalls of FDG-PET in the treated neck include inability to detect hypermetabolic activity in cancer-harboring nodes. Reduced or absent FDG avidity within nodes harboring cancer may be related to multiple factors including low cellularity, cystic adenopathy, or in lymph nodes that are primarily necrotic. While the majority of malignant neoplasms in the head and neck are squamous cell carcinomas and are FDG avid, there are other neoplasms that do not always show FDG avidity, and one must be aware of these when ordering and interpreting PET-CT studies. Neoplasms that may not always demonstrate FDG avidity include mucinous adenocarcinomas, salivary tumors especially adenoid cystic and mucoepidermoid carcinomas, and thyroid cancers (iodine avid differentiated cancers and some medullary cancers).

O-586 **3:50 PM - 4:25 PM**

Advanced Techniques and Biologic Imaging of Head and Neck Cancer

Srinivasan, A.
University of Michigan Health System
Ann Arbor, MI.

Presentation Summary

Accurate assessment of the neck after surgery or chemoradiation of head and neck malignancies is important. Detection of residual neoplasm and/or early recurrences negatively impact patient outcome. However, conventional imaging in the post-therapy neck presents challenges due to the distortion of anatomical boundaries and the frequent presence of grafts or flaps, which can result in both false positive and false negative interpretations. Biologic imaging, which can be defined as imaging of biologic processes such as perfusion of a tissue or its metabolic status, has the potential to detect malignant disease at a much earlier stage than conventional imaging alone, and therefore is gaining interest in more institutions. Preliminary studies also have suggested that biologic imaging may play a role in prediction of response to therapies, thus allowing individualization of management strategies rather than follow a "one-for-all" approach. The different biologic imaging modalities including CT perfusion, MR perfusion, diffusion-weighted MRI, MR spectroscopy and dual energy CT will be introduced with discussion of the parameters measured on each modality and its specific role in assessment of the pre and post-treatment neck. Diffusion imaging in the head and neck has shown promise in many clinical scenarios that include differentiation of benign and malignant pathologies, identification of metastatic lymph nodes in a patient with known primary neck tumor, differentiation of recurrent malignancy and benign post-therapeutic change, and prediction and monitoring of response to chemoradiation. MR and CT perfusion measure physiologic parameters that can help in prediction and monitoring of response to chemoradiation and stratify patients into complete and poor responders. Prediction of response to chemoradiation during early stages of therapy can be crucial since this would be the

Note: Scanned images are included in the proceedings. Some submitted images were reduced during editing, thereby decreasing clarity. Also, refer to the Program Planner. Proceedings Content as of 3-29-2013.

first step towards developing modified treatment strategies (e.g., escalated radiation doses) in potentially unresponsive patients. The recent introduction of dual energy CT has opened the possibility of better tissue characterization on CT through material density analysis and this may help in differentiation of benign and malignant tissues. The primary challenge that the head and neck radiologist is faced with on a daily basis is identification of residual or recurrent neoplasm within the treated neck. While there are some conventional imaging features such as increase in size, appearance of new enhancement and perineural spread that suggest presence of malignancy, often it is challenging to assess the treated neck. Diffusion-weighted imaging has shown promise in multiple studies with the ADC value in recurrent tumor consistently being lower than in nonmalignant granulation tissue. Adequate and accurate knowledge of the anatomical and functional status of head and neck cancer is essential to understanding the prognosis, making the right treatment options and a more accurate assessment of the post-treatment lesion. However, it should be remembered that the information derived from biologic imaging modalities cannot be interpreted in isolation and the anatomical and functional information need to be synthesized together for a comprehensive assessment of head and neck cancer.

Thursday Afternoon

3:15 PM - 4:45 PM
Ballroom 6DE

(60) Special Session: Imaging in Mild Traumatic Brain Injury: What Is the Evidence?

O-587 **3:15 PM - 3:30 PM**

Clinical Practice Guidelines and Appropriateness Criteria

Sanelli, P. C.
Weill Medical College of Cornell University
New York, NY.

Presentation Summary
A review of the appropriateness criteria for imaging in mild traumatic brain injury will be presented.

O-588 **3:30 PM - 3:50 PM**

Standard Imaging Techniques for Mild Traumatic Brain Injury

Anzai, Y.
University of Washington
Seattle, WA.

Presentation Summary
Traumatic brain injury (TBI) is a highly prevalent and a leading cause of death and disability among young adults. The CDC estimated that there are approximately 1.5 million people suffering from TBI annually and 75% of them sustain mild TBI. The common etiologies of TBI include motor vehicle accident, motorcycle accidents, fall, and assaults. The vast majority of TBI is so-called mild TBI. Although many mTBI have a predictable favorable course requiring few if any special medical attention, some mTBI patients suffer from impaired memory, attention, executive function as well as emotional instability. One of the major challenges related to diagnosis and management of mTBI is lack of clear consensus as to the definition of mTBI. The terms used to describe mTBI are “concussion”, mild TBI, minor TBI, minimal TBI, and grade 1 TBI. Some use mTBI and concussion interchangeably, and others don't. Some include GCS 13 under mild TBI, and others suggest excluding GCS 13 from mild TBI. Some include negative CT as an inclusion criterion for mTBI, thus presence of structural abnormality indicate at least moderate TBI. American Congress of Rehabilitation Medicine (ACRM) defines a diagnosis of mTBI, of which at least one of the followings must be present: 1) Loss of consciousness of less than 30 min and GCS score of 13-15 after the period of loss of consciousness, 2) Loss of memory of the event immediately before or after the accident (event) with posttraumatic amnesia of less than 24 hours, 3) Any alternation in mental state at the time of accident. CDC conceptual definition of mild TBI includes one of the following signs and symptoms: 1) Any period of transient confusion, disorientation, or impaired consciousness, 2) Any period of dysfunction of memory around the time of injury, 3) Observed signs of other neurologic or neuropsychologic dysfunction, 4) Any period of loss of consciousness lasting 30 min or less. The definition includes patients with CT abnormality or focal neurologic symptoms, though they suggest distinguishing such cases with imaging or neurologic abnormality from those without for outcome assessment. VA and DOD definition of mTBI are: a traumatically induced injury and or physiologic disruption of brain function as a result of an external force and include: 1) Loss of consciousness (LOC) less than 30 min, 2) Alternation of mental state less than 24 hours, 3) Post-traumatic amnesia (PTA) up to one day, 4) GCS score 13-15, 5) Normal structural imaging (i.e., Head CT). It is important to notice up to 15% of TBI patients with GCS score of 14 or 15 will have an acute intracranial injury on noncontrast head CT. Advanced imaging studies such as fMRI, DTI, PET, and EEG are not

Note: Scanned images are included in the proceedings. Some submitted images were reduced during editing, thereby decreasing clarity. Also, refer to the Program Planner. Proceedings Content as of 3-29-2013.

considered currently accepted criteria for measuring severity of TBI in the clinical setting. Evidence-based practice guidelines by the ACEP-CDC (American College of Emergency Physician)-(Centers of Disease Control and Prevention) summarize the current evidence for mTBI. Critical analysis of the medical literatures using MEDLINE and the Cochrane Database from January 2000 to 2007 were reviewed, limited to English literatures, human study, and age 16 years or older. We will focus on the following critical questions: 1) Which patients with acute mTBI should have a noncontrast head CT in ED? Patients with LOC or PTA only if one of the following is present: Headache, vomiting, age >60, drug and alcohol intoxication, short-term memory deficit, physical evidence of trauma above clavicle, post-traumatic seizure, GCS less than 15, focal neurologic deficit, or coagulopathy. Both New Orleans Criteria (NOC) and Canadian Head CT Rule (CHTR) have 100% sensitivity in identifying lesions requiring neurosurgical intervention, though specificity was higher in CHT (37%) than NOC (5.6%). Other major prediction rules include NICE (National Institute for Health and Clinical Excellence), and NCRFNS (Neurotraumatology Committee of the World Federation of Neurosurgical Societies. 2) Is there a role of MRI over noncontrast CT in the ED evaluation of a patient with acute mTBI? There is no evidence-based recommendation of the routine use of brain MRI in acute TBI clinical setting, as compared with CT. Several studies compared brain MR with head CT and documented that MR revealed 10-57% more lesions than noncontrast head CT. These findings include small hemorrhagic or nonhemorrhagic contusion, small extra-axial hematoma, and diffuse axonal injury. None of the studies demonstrated clinical relevance of these abnormal MR in the timeframe relevant for the disposition of patients at ED. One of the added complexities is the difference in timing of CT and MR. In addition to the routine brain MR including FLAIR, T2, DWI, and SWI (susceptibility-weighted imaging) or GRE (gradient echo imaging), DTI has been reported to correlate well with severity of postconcussion symptoms. Diffusion tensor imaging is currently largely a research tool and requires further investigation before the implementation of DTI in clinical care for individual patient level. Nevertheless, many mTBI patients remain symptomatic and face difficulty in returning to daily activity or work for weeks or months, despite lack of abnormality in conventional imaging. The damage caused in mTBI and concussion patients are beyond the resolution or sensitivity of current morphologic imaging studies. The pathophysiology of mTBI/Concussion is likely at molecular, cellular and synaptic level. We must investigate advanced imaging techniques that are sensitive and robust enough to detect these axonal and synaptic changes in an individual patient in order to better refine mTBI.

O-589 **3:50 PM - 4:10 PM**

Advanced Imaging Using Diffusion Tensor Imaging

Lipton, M. L.
Albert Einstein College of Medicine
Bronx, NY.

Presentation Summary
Diffusion tensor imaging (DTI) is an area of much interest for the evaluation of traumatic brain injury (TBI) because of its ability to assess axonal microstructure, the brain substrate of traumatic axonal injury (TAI). This presentation will summarize the literature applying DTI to TBI and assess it in light of evidence-based medicine standards, with comparison to the level of evidence supporting other neuroradiologic applications.

O-590 **4:10 PM - 4:25 PM**

Structural and Functional Connectivity in Mild Traumatic Brain Injury (Recipient of the Basic Science Research Award 2001-2002)

Mukherjee, P.
University of California San Francisco
San Francisco, CA.

Presentation Summary
Diffusion tensor imaging (DTI) of traumatic brain injury is not yet ready for prime time in the reading room.

Thursday Afternoon

3:15 PM - 4:45 PM
Room 5AB

(61) General Session: Neuroimaging: What Is It and How Can It Help Us?

O-591 **3:15 PM - 3:45 PM**

Introduction to Neuroimaging

Lake, D.
University of Michigan-Flint
Flint, MI.

Dr. Dan Lake is a Marketing Lecturer at the University of Michigan-Flint's School of Management. Dan has taught marketing, advertising and consumer behavior for eleven years following a decade of professional marketing-related experience at Ford Motor Company, U.S. Steel Corporation and McCann-Erickson Worldwide Advertising. Dan's research interests include celebrity/athlete endorsements and the impact of "committed 'fandom'" on consumers cognitive and affective responses to negative publicity. Dan

Note: Scanned images are included in the proceedings. Some submitted images were reduced during editing, thereby decreasing clarity. Also, refer to the Program Planner. Proceedings Content as of 3-29-2013.

is completing his PhD this year at Michigan State University following studying at Michigan State University, Northwestern University and The University of Chicago.

Presentation Summary
Dr. Lake will be setting the foundation of marketing core topics and current trends in research/practice, including the cognitive consumer decision-making process (consumer behavior). Dr. Lake will discuss how marketing researchers struggle to accurately measure and account for the real reasons behind consumer purchases as most individuals claim not to be formally influenced by advertising and marketing strategies.

O-592 **3:45 PM - 4:15 PM**

The Role of Imaging Techniques (MR, PET, etc.) Used in Neuromarketing

Kilts, C.
University of Arkansas for Medical Sciences
Little Rock, AR.

Dr. Kilts is currently the founding Director of the UAMS Brain Imaging Research Center (BIRC), a human neuroscience and neuroimaging technology application resource in the Psychiatric Research Institute. He has had a long-standing interest in the modes of neural information processing related to human mental health and illness. While at Emory University he created collaborative relationships with faculty in the Goizueta Business School and with a commercial marketing and strategic planning entity that focused on the application of fMRI technology in business problem-solving. These enterprises resulted in published articles in the NY Times, Harvard Business Review, and peer-reviewed publications in scientific journals on the topic of business neuroscience.

Presentation Summary
This presentation will discuss the history of the academic roots of the field of neuromarketing or the application of brain imaging technology to the understanding of consumer choice behavior. This multimodal imaging science has led to both commercial and academic representations of neuromarketing. I will discuss my personal experiences in developing a collaborative enterprise in business neuroscience and neuroimaging, the response of the anti-business "consumer advocates", and our functional magnetic resonance imaging studies of the business neuroscience topics of moral reasoning, cognitive fitness and strategic ability. This discussion will conclude with a critical assessment of the place of neuromarketing research in academic medical center settings, the confining and charged properties of the term, and the scientific and societal value of a going forward research program in business neuroscience.

O-593 **4:15 PM - 4:45 PM**

What is the Role of our Neuroradiology in Neuromarketing?

Holodny, A. I.
Memorial Sloan-Kettering Cancer Center
New York, NY.

Presentation Summary
Functional MRI (fMRI) currently is used clinically for mapping of essential areas of the brain (e.g., language and motor) prior to brain tumor surgery. This use has associated CTP codes, is covered by insurance and is rapidly becoming the standard of care. However, the vast majority of fMRI manuscripts in the scientific literature currently study the neuroanatomical and functional basis of normal brain function (such as linguistics, development, decision-making, ethics and religion) as well as neurologic disorders outside of brain tumors (such as psychiatric disorders, MS or cortical reorganization after neurologic insults). Hence, it is essential for neuroradiologist to understand these new delineations of brain function and incorporate them into routine clinical reports. For example, instead of reporting a "left frontal lobe metastasis", a neuroradiologist should incorporate the clinically relevant functional anatomy into the report, for example, "metastasis in the pars triangularis, in the expected location of Broca's area." Neuromarketing uses fMRI (as well as other technologies) to study the responses of the brain to optimize various marketing strategies. Neuromarketing has been used by many major corporations; however, it does have its detractors. Notwithstanding, it is essential for neuroradiologist to understand how fMRI scans are being used by others outside of their immediate professional community as well as the functional neuroanatomy underlying these principles of neuromarketing.

Note: Scanned images are included in the proceedings. Some submitted images were reduced during editing, thereby decreasing clarity. Also, refer to the Program Planner. Proceedings Content as of 3-29-2013.

Thursday Afternoon

4:45 PM - 5:00 PM
Ballroom 6AB

(62) Closing Remarks –
Mauricio Castillo, MD, FACR,
ASNR 2013 President

O-594 **4:45 PM - 5:00 PM**

Closing Remarks

Monday, May 20 – Wednesday, May 22
6:30 AM – 9:00 PM
Thursday, May 23
6:30 AM – 3:00 PM
Hall B1

Electronic Excerpta (EE) 1 - 35

EE1-Adult Brain

Note: A missing printed number indicates an abstract has been withdrawn.

EE-1

Intraprocedural C-Arm Computed Tomography Perfusion as Assessing Method for Balloon Occlusion Test: A Case Report

Zhang, Y.[1]·Yang, Z.[1]·Huang, Q.[1]·Hong, B.[1]·Liu, J.[1]·Ye, H.[2]
[1]Center of Clinical Neuroscience, Shanghai, CHINA,
[2]Siemens China, Shanghai, CHINA.

Purpose
To treat some complex lesions, such as intracranial huge aneurysm, traumatic fistula or tumor, it may be necessary to block off a vessel. In such situation, balloon occlusion test (BOT) is required before carotid sacrifice. There have been several reports on strokes after carotid ligation in patients who even had been identified with adequate collateral flow by preoperative BOT. A case tolerated BOT test, but with abnormal cerebral blood volume (CBV) maps generated by intraprocedural C-arm computed tomography (CACT) perfusion is reported. The potential value of CACT CBV measurement for BOT is discussed.
Case Report
A 47-year-old female admitted to our institute. A giant intracranial aneurysm located at the ophthalmic segment of the left internal carotid artery (L-ICA) was demonstrated. A treatment of L-ICA occlusion was adopted. Before the procedure, a BOT was performed. During the BOT, no neurologic impairments were found. A CACT perfusion (syngo DynaPBV Neuro, Siemens, Germany) also was performed to check the perfusion status during the BOT. Since the patient can tolerate the BOT, L-ICA occlusion was performed. The patient's postoperative status was almost uneventful, but three days later, she suffered paroxysmal slurred speech. CT perfusion showed abnormal in perfusion. The diffusion-weighted MR demonstrated an acute infarction in left parietal lobe. With intensive medical care, no further neurologic impairments occurred and the patient was discharged a week later.
Imaging Findings
The intraprocedural CACT perfusion showed there was a relative hypopefusion in the hemisphere with balloon occlusion (Figure). The CT perfusion three days postprocedure showed prolonged time-to-peak (TTP) and mean transit time (MTT) in the occlusion side, as well as decreased cerebral blood flow (CBF) and minor increased CBV, which was a typical sign of early phase of ischemia (Figure).

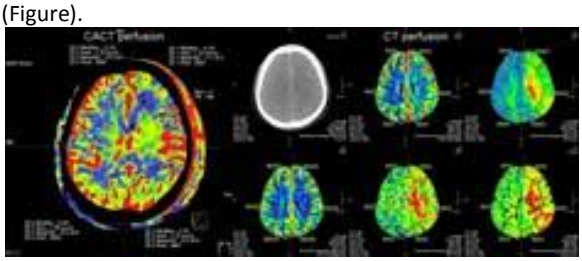

Summary
This case demonstrated that the classic BOT might not be enough to ensure the safety of the carotid sacrifice treatment. The intraprocedural CBV measurements by CACT could detect ischemia during the BOT at an early phase. It may have a good prediction value to detect the patients with high risk of ischemia after carotid occlusion. Large scale clinical trials are needed to evaluate its value.

KEYWORDS: C-arm CT CBV, Balloon test occlusion

EE-2

Rare Case of Amyloidoma in Patient with Plasma Cell Dyscrasia

Javadi, P.·Coffey, M.·Patel, T.·Etesami, M.·Blackham, K.
University Hospital Case Medical Center
Cleveland, OH.

Purpose
Tumefactive amyloid deposition is the rarest form of amyloid deposition disease in the brain. This case highlights and reviews common imaging findings of this disease entity.

Note: Scanned images are included in the proceedings. Some submitted images were reduced during editing, thereby decreasing clarity. Also, refer to the Program Planner. Proceedings Content as of 3-29-2013.

Case Report
A 65-year-old female with three months history of memory loss underwent a CT of the head which revealed a left frontal white matter lesion. This finding was confirmed with MRI and the patient underwent stereotactic-guided brain biopsy for the left frontal lesion. The specimen showed abundance of amyloid deposition which demonstrated positive congo red stain and lambda light chain. The patient was diagnosed with monoclonal gammopathy of unknown significance (MGUS) following bone biopsy. Patient developed an episode of small right-sided frontal intraparenchymal hemorrhage seven months after the initial presentation, from which she subsequently recovered.
Imaging Findings
Initial precontrast CT images of the head revealed diffuse patchy white matter changes which were most pronounced within the left cerebral hemisphere. Focal enhancing white matter lesion was seen in the posterior left frontal lobe on postcontrast CT images. MR imaging confirmed this white matter lesion which was hypointense on T1 and T2 and showed irregular, radiating enhancement extending to the left lateral ventricle.

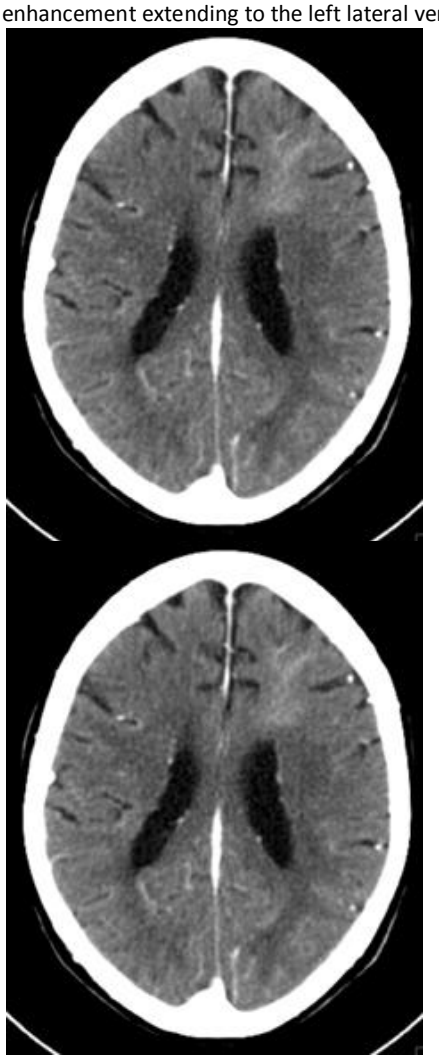

Summary
Amyloidoma should be included in the differential diagnosis of supratentorial white matter lesions without significant mass effect. Imaging findings include irregular, radiating, enhancing margins extending to the lateral ventricles.

KEYWORDS: Amyloid, Brain neoplasms, Amyloidoma

EE-3

Clinical Significance of Mammillary Body Enhancement in Wernicke Encephalopathy: Two Case Reports

Konno, Y.
Yamagata University
Yamagata, JAPAN.

Purpose
To share two cases of acute Wernicke encephalopathy in which the only abnormal finding on MRI was abnormal enhancement of the mammillary bodies.
Case Report
[Case 1] A 75-year-old woman presented at our hospital with bilateral double vision. She had undergone radical pancreaticoduodenectomy for treatment of cholangiocarcinoma. The neurologic examination at the hospital revealed divergence palsy and mild cognitive impairment. The only detectable abnormal finding on MRI with contrast enhancement was diffuse symmetric enhancement of the mammillary bodies (Figure). Acute Wernicke encephalopathy was proposed and a decrease in serum thiamine level was confirmed. With continued thiamine administration, the patient returned to a normal life without any after-effects. [Case 2] A 40-year-old man with high levels of alcohol intake was transported to the emergency room. He had experienced double vision for the preceding month. His consciousness was lucid. A physical examination disclosed extorsion restrictions of both eyeballs, lateral gaze nystagmus, gait ataxia, dysesthesia in bilateral lower limbs, muscle weakness and disappearance of the deep tendon reflex. Acute Wernicke encephalopathy was suspected, and his serum thiamine level was observed to have decreased. MR imaging with contrast enhancement revealed a highly intense gadolinium enhancement only in the mammillary bodies. With continued thiamine administration, he left the hospital without serious after-effects such as memory defects.
Imaging Findings
In two cases of Wernicke encephalopathy, mammillary body enhancement alone was detected on MRI. Considering the high frequency with which mammillary bodies are damaged in Wernicke encephalopathy, abnormal enhancement of this region on MRI will be an important first sign as it becomes more generally known.

Note: Scanned images are included in the proceedings. Some submitted images were reduced during editing, thereby decreasing clarity. Also, refer to the Program Planner. Proceedings Content as of 3-29-2013.

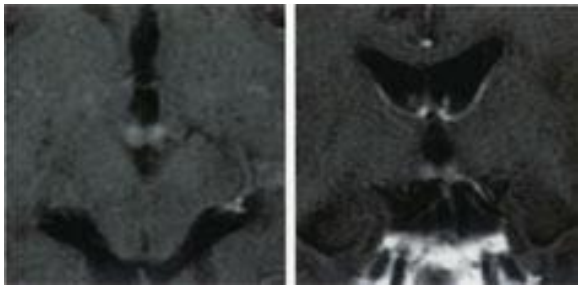

Summary
In two cases of Wernicke encephalopathy in which the initial symptom was double vision, the only abnormal finding on MRI was abnormal enhancement of the mammillary bodies. The mammillary bodies are the region most vulnerable to abnormal enhancement. Because MRI with contrast enhancement can detect such abnormal enhancement at an early stage, it should be performed more often on patients with oculomotor disorder to avoid underdiagnosis of Wernicke encephalopathy.

KEYWORDS: Wernicke encephalopathy, mammillary body

EE-4

Cavernous Sinus Amyloidoma

Patel, S. H.·Barry, K. A.·Patel, S. R.·Wang, A. M.·Al-Hakim, M. M.
William Beaumont Hospital
Royal Oak, MI.

Purpose
To the best of our knowledge, this is the first pathologically proven case of an amyloidoma presenting in this unusual location. We report this rare case of an amyloidoma involving the cavernous sinus and Meckel's cave in a patient who presented with trigeminal neuralgia. Central nervous system amyloidomas are extremely uncommon and usually present as supratentorial masses and cortical senile plaques. This unique case report allows the reader to consider amyloidoma in the broad differential of cavernous sinus masses.
Case Report
A 43-year-old female with no significant past medical history presented with new-onset left facial pain and numbness in the distribution of all three branches of the trigeminal nerve. Further investigation by magnetic resonance imaging (MRI) revealed a homogeneously enhancing mass involving and expanding the left cavernous sinus and Meckel's cave with extension to the left foramen ovale and rotundum. The usual differential diagnosis was offered including trigeminal schwannoma, meningioma, pseudotumor, sarcoidosis, lymphoma, and perineural tumor spread. The patient underwent elective surgery for diagnosis and resection of the mass. A left temporal craniotomy was performed with a left preauricular middle fossa approach, which revealed the lesion involving the left cavernous sinus and Meckel's cave with intradural extension. A gross total resection of the lesion was carried out and the specimens were sent for histopathologic analysis. The specimens showed scattered benign ganglion cells and fragments of nerve embedded in a pink acellular material and special staining with Congo red showed apple green birefringence under polarized light, consistent with amyloidoma. After surgery, the patient had resolution of the preoperative left facial pain. However, left facial numbness persisted, greatest over the V1 and V2 areas and milder over the V3 distribution. Further investigation for systemic amyloidosis or multiple myeloma was negative.
Imaging Findings
MR imaging examination of the internal auditory canals (IACs) demonstrated a homogeneously enhancing T2 hypointense and T1 isointense mass measuring 24 mm x 9 mm in the left cavernous sinus extending to Meckel's cave and the foramen ovale and rotundum.

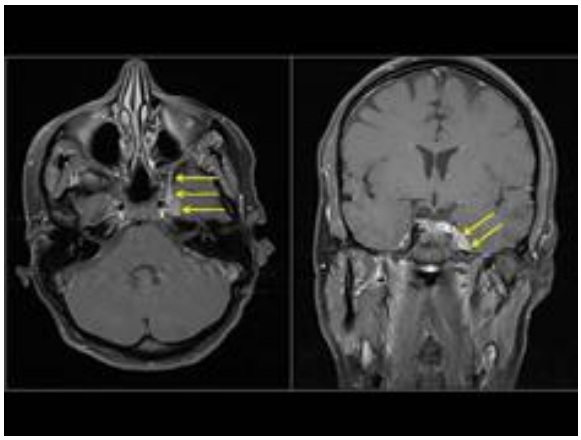

Summary
Although it is extremely unusual, amyloid deposition can involve the cavernous sinus and present as a cause of trigeminal neuralgia. Therefore, amyloidoma should be considered in the broad differential diagnosis of a mass lesion affecting the cavernous sinus.

KEYWORDS: Amyloid, Cavernous sinus

EE-5

Paradoxical Migrating Cyst: An Unusual Presentation of Intraventricular Neurocysticercosis with a Coincidental Pituitary Adenoma

Ghosh, S.·Al-Khalili, R.·Liu, J. K.·Slasky, S. E.
University of Medicine & Dentistry of New Jersey/New Jersey Medical School
Newark, NJ.

Purpose
We present a novel case of intraventricular neurocysticercosis with paradoxical transaqueductal migration of the cyst from the cerebral aqueduct to the

Note: Scanned images are included in the proceedings. Some submitted images were reduced during editing, thereby decreasing clarity. Also, refer to the Program Planner. Proceedings Content as of 3-29-2013.

fourth ventricle shortly after ventricular drain placement for acute hydrocephalus with the presence of a coincidental sellar/suprasellar mass.
Case Report
A 26-year-old previously healthy man who recently immigrated from Ecuador, presented with headache and altered mental status for two days. Over the course of two hours in the emergency department the patient became obtunded having sluggish dilated pupils.
Imaging Findings
CT of the head without contrast showed dilatation of the third and lateral ventricles, consistent with obstructive hydrocephalus at the level of the cerebral aqueduct. A focus of calcification was noted in the cerebral aqueduct. A small cystic lesion within the right parietal lobe also was seen. MR imaging of the brain showed a 6.7 mm ovoid lesion in the aqueduct of Sylvius, demonstrating T1 shortening. A 4 mm ring-enhancing lesion in the right postcentral sulcus and a similar 2 mm lesion in the left frontal lobe were seen. There was also a 2.4 cm mixed solid and cystic sellar and suprasellar lesion, exerting mass-effect on the optic chiasm and optic nerves. An external ventricular drain was placed emergently to relieve the hydrocephalus and resulted in significant improvement in the neurologic exam. A repeat MRI was performed about 48 hours after the initial MRI for operative planning, for resection of the pituitary mass. The MRI demonstrated migration of the aqueductal lesion to the fourth ventricle. Hydrocephalus had improved. The mixed solid and cystic sellar and suprasellar lesion was unchanged in size and configuration. The patient underwent endoscopic endonasal transsphenoidal resection of the pituitary mass and surgical pathology confirmed the diagnosis of a pituitary adenoma.

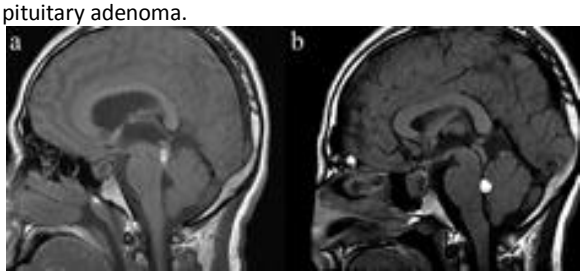

Summary
Our case demonstrates that the intraventricular cysts of neurocysticercosis can migrate in a paradoxical fashion in the setting of cerebrospinal fluid diversion. This resulted in spontaneous relief of obstruction at the cerebral aqueduct, thus restoring normal CSF pathways and precluding the need for permanent CSF shunting. Migrating cysts present a unique challenge to preoperative planning for cyst removal, potentially resulting in surgical exploration of the incorrect ventricular cavity. Additionally, although the presence of a sellar and suprasellar mass in a patient with known neurocysticercosis should raise clinical suspicion for the possibility of sellar neurocysticercosis, pituitary macroadenoma is a more common entity and a more likely etiology for a sellar lesion.

KEYWORDS: Parasite, Pituitary gland

EE-6

MR Imaging Review of West Nile Virus Neuroinvasive Disease

Brace, J. A.·Scott, H. D.·Yetkin, Z. F.·Mendelsohn, D. B.
University of Texas Southwestern Medical Center
Dallas, TX.

Purpose
For 2012, Centers for Disease Control reported a record 5,245 cases of West Nile virus (WNV), including 236 deaths. Of these, 2,663 (51%) were classified as neuroinvasive in the form of meningitis or encephalitis with or without acute flaccid paralysis. A third of cases (1,714) were reported in Texas with 76 related deaths; 35 alone in the Dallas-Fort Worth metropolitan area. On the heels of such an unprecedented epidemic, we provide review (n = 3) of the MR imaging findings of West Nile neuroinvasive disease (WNND) from confirmed 2012 cases at our institution in Dallas, Texas along with a literature review.
Case Report
1: Brain MR in a 43-year-old immunocompromised male showed abnormal FLAIR and T2 signal within the bilateral basal ganglia, thalami, medial temporal lobes, cerebral peduncles and dorsal pons without restricted diffusion. Cerebrospinal fluid (CSF) and serum were positive for West Nile IgM. 2: Brain MR in a 30-year-old female demonstrated scattered foci of nonspecific FLAIR signal within the bilateral cerebral white matter without restricted diffusion. Abnormal FLAIR signal and leptomeningeal enhancement also was seen within the bilateral parietal, occipital, and cerebellar sulci. LP demonstrated mild protein elevation and moderate pleocytosis with lymphocytic predominance. CSF and serum were both positive for West Nile IgM. 3: Lumbar spine MR in a 74-year-old elderly female with left lower extremity weakness revealed smooth enhancement of the cauda equina. Cerebrospinal fluid was positive for West Nile IgG; serum was positive for both West Nile IgG and IgM.
Imaging Findings
Abnormal MR findings in patients with WNND are nonspecific but not uncommon. Studies by Ali and Petropoulou show nearly 70% of patients had abnormal MR findings. Ali defined five MR imaging patterns including: 1) normal; 2) isolated abnormalities of diffusion restriction within white matter; 3) hyperintensity on T2 and FLAIR in the lobar gray and white matter, cerebellum, basal ganglia, thalamus and internal capsule, pons and midbrain; 4) meningeal involvement; and 5) spinal cord and cauda equine/nerve root involvement. Petropoulou noticed that diffusion weighted imaging may be useful in

Note: Scanned images are included in the proceedings. Some submitted images were reduced during editing, thereby decreasing clarity. Also, refer to the Program Planner. Proceedings Content as of 3-29-2013.

the early detection of inflammation when FLAIR abnormalities are absent. CT is normal in most cases of WNV.

Summary

It is important for the radiologist to have an awareness of the MR imaging findings, though nonspecific, in West Nile neuroinvasive disease especially when factors such as season, geographic area, and exposure to mosquitoes are known. Larger retrospective or prospective studies are needed to correlate the above MR findings with clinical presentation, course, and outcome to determine their prognostic importance. The potential role of environmental factors in the 2012 West Nile virus outbreak raises the concern that changes in climate may lead to disease propagation and more serious outbreaks of mosquito-borne diseases.

KEYWORDS: Encephalitis, West Nile virus

EE-7

Progressive Left-Sided Headache: Ophthalmoplegia and Visual Loss Secondary to Left Cavernous and Orbital Aspergillosis

Al-Jaber, A.·Harb, J. G.
Oakland University William Beaumont School of Medicine
Royal Oak, MI.

Purpose

Headache is one of the most frequently encountered health issues causing patients to seek medical attention. Additionally, it is a symptom of a long list of common and uncommon medical conditions. We present an unusual case of left cavernous sinus and orbital aspergillosis causing ophthalmoplegia and necrotizing optic neuritis.

Case Report

The patient's clinical history, physical examination, laboratory results, radiographic and intra-operative findings were reviewed.

Imaging Findings

A 67-year-old Caucasian female presented to her primary care physician with worsening left-sided headache and visual changes for three months. The patient had a past medical history of asthma, chronic renal failure, hypertension, and hyperthyroidism. Full workup including blood and CSF testing, ophthalmic exam, CT and MRI of the brain and orbits were obtained. The MRI showed a large lesion in the left sphenoid wing, extending into the sphenoid sinus as well as along the cavernous sinus and anteriorly into the orbital apex. Subsequently, trans-sphenoidal biopsy of the left cavernous sinus was performed and the pathology specimen showed evidence of chronic inflammatory changes without definite malignancy. Due to the patient's critical symptomatology and the need for a definitive diagnosis, she underwent surgical resection. Portions of the skull base mass involving the anterior and middle cranial fossa as well as the left cavernous sinus and left orbit were resected. Final pathology of the specimen showed evidence of invasive aspergillosis. The patient was started on Amphotericin and Voriconazole. During her hospital stay, she reported improvement of the headache. However, there was no significant change in her left ophthalmoplegia and visual loss.

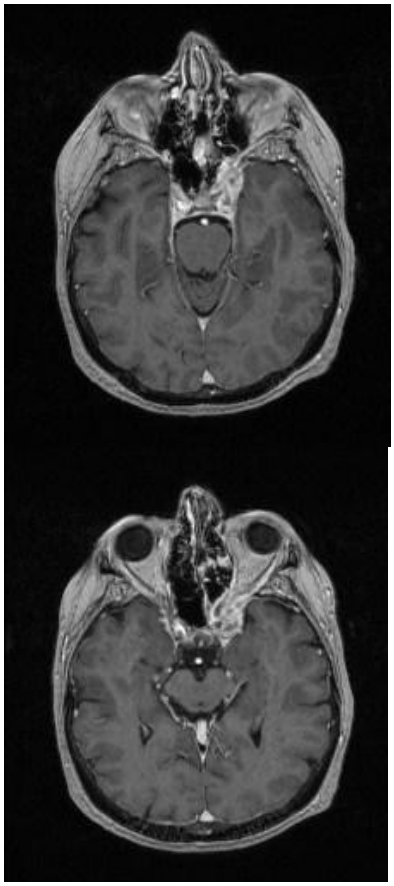

Summary

Cavernous and orbital aspergillosis is a rare cause of headache, ophthalmoplegia, and visual loss. This disease requires a prompt diagnosis as well as adequate management and early intervention in order to avoid serious complications.

KEYWORDS: Fungal disease, Cavernous sinus, Orbital

EE-8

West Nile Virus Encephalitis and Its Mimickers

Bermudez Allende, M. Z.·Hijaz, T.·Futterer, S.·Lester, M.·Oustwani, C.
Northwestern Memorial Medical Center
Chicago, IL.

Purpose

There has been a recent, much publicized increase in the number of reported cases of West Nile virus (WNV) encephalitis in the United States. We review the clinical features and magnetic resonance imaging (MRI) findings in

Note: Scanned images are included in the proceedings. Some submitted images were reduced during editing, thereby decreasing clarity. Also, refer to the Program Planner. Proceedings Content as of 3-29-2013.

three patients at our institution with confirmed WNV infection in order to increase radiologists' awareness of and familiarity with this entity.
Case Report
We describe three patients who initially presented to our institution with fever, diarrhea, mood disturbance, and progressive weakness and were ultimately confirmed to have WNV infection by the presence of cerebrospinal fluid IgM to the virus. All three patients underwent initial computed tomography (CT) and MRI, and we review the imaging findings of WNV encephalitis in each patient. We also discuss the imaging findings of several mimickers, such as thrombosis of the internal cerebral veins and thalamic glioma.
Imaging Findings
West Nile virus is a mosquito-borne flavivirus that can cause meningitis, encephalitis, and myelitis, sometimes leading to significant morbidity and mortality. Many infected individuals are asymptomatic, and those who do present clinically often do so in a nonspecific manner, with flu-like symptoms, headache, malaise, myalgia, and fatigue. Consequently, the diagnosis of WNV encephalitis can be elusive, although the findings on magnetic resonance imaging (MRI) of the brain may increase the likelihood of early, accurate diagnosis. Head CT in all three of our patients was normal. On MRI, all three patients demonstrated enlargement of the thalamus with accompanying hyperintense T2/FLAIR signal, with varying degrees of extension of the signal abnormality into the brainstem and basal ganglia. Two patients demonstrated restricted diffusion, and one had rim enhancement of the thalamic signal abnormality. West Nile virus infection was confirmed in all three patients by cerebrospinal fluid IgM. The Centers for Disease Control (CDC) have reported an increase in U.S. cases of WNV in 2012. In light of this increased incidence and the nonspecific clinical presentation of the disease, it is important that radiologists be familiar with the imaging findings of WNV in order to be able to include it in a useful differential diagnosis.
Summary
The clinical presentation of WNV encephalitis, a serious illness, is usually nonspecific. Particularly given a recent increase in reported cases of this entity in the U.S., radiologists should be aware of its typical imaging findings in order to facilitate its rapid and accurate diagnosis.

KEYWORDS: Encephalitis, Infections, Virus

EE-9

Rare Case of Rosai-Dorfman Disease Presenting as an Isolated Intracranial Mass

Javadi, P.·Coffey, M.·Patel, T.·Etesami, M.·Blackham, K.
University Hospital Case Medical Center
Cleveland, OH.

Purpose
Rosai-Dorfman disease is a rare benign histiocyte proliferative disorder, predominantly involving cervical lymph nodes, but also affecting the skin, upper respiratory tract, and paranasal sinuses. Isolated intracranial involvement without nodal and sinus disease as presented here is extremely uncommon.
Case Report
A 52-year-old female with history of stroke presented with new onset transient left-sided parasthesia and weakness. Head CT revealed an extra-axial mass in the posterior right parietal region with associated irregularity of the skull and soft tissue thickening of the scalp. MR imaging of the brain confirmed a homogeneously enhancing meningeal mass with calvarial and subgaleal extension. The patient underwent a right parieto-occipital craniotomy and mesh repair with resection of the tumor for presumed diagnosis of meningioma. Evaluation of the pathologic specimen revealed histocytes with immunologic staining confirming diagnosis of Rosai-Dorfman disease. Postoperative course was uncomplicated and follow-up imaging to date failed to show any evidence of recurrence.
Imaging Findings
CT of the head revealed a hyperdense extra-axial convex mass in the posterior right parietal region with associated lucency and irregularity of overlying skull and subgaleal extension through the defect in the soft tissue of the scalp. The lesion demonstrated isointense signal on T2WI, low signal on T1WI, and avid enhancement on T1 postcontrast images.

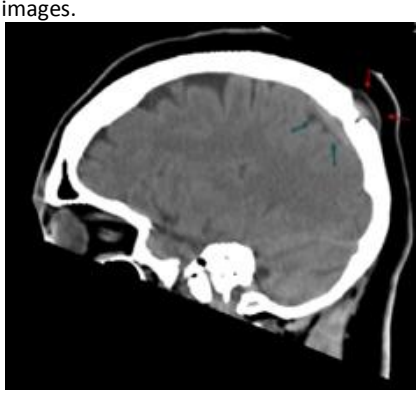

Note: Scanned images are included in the proceedings. Some submitted images were reduced during editing, thereby decreasing clarity. Also, refer to the Program Planner. Proceedings Content as of 3-29-2013.

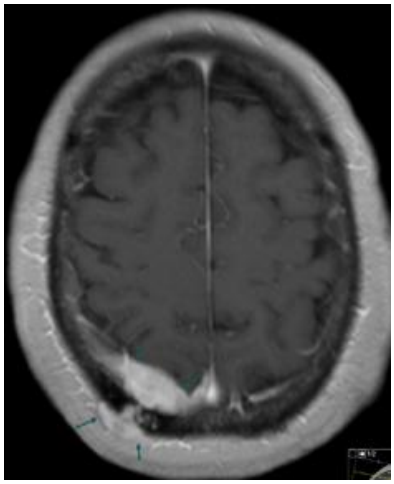

Summary
Rare case of extra-axial mass mimicking meningioma highlights the fact that Rosai-Dorfman disease should be included in the differential consideration when osteolysis and soft tissue extension to the scalp is present.

KEYWORDS: Dural, Meningioma, Rosai-Dorfman

EE-10

MR Imaging Findings in Central Nervous System Hemophagocytic Lymphohistiocytosis

Bezerra, R.·Berkowitz, F.·Toaff, J.·Lee, E.
Georgetown University Hospital
Washington, DC.

Purpose
To describe the imaging findings of three cases of hemophagocytic lymphohistiocytosis (HLH), one of which demonstrates a distinctive triad of imaging findings.
Case Report
We present three patients with bone marrow biopsy proven HLH: Patient 1: 54-year-old gentleman with history of hypertension, diabetes mellitus and chronic alcohol abuse, presented with acute episode of confusion and fever. Lab workup revealed pancytopenia, hyperferritinemia and increased liver functions. Patient 2: 21-year-old female with a past medical history of depression and malaria with several recent admissions due to fevers and chills was admitted with acute kidney failure, pneumonia and respiratory failure and developed seizures and multisystem organ failure. High ferritin and ammonia levels were found. Patient 3: 39-year-old man with a history of ankylosing spondylitis and recently diagnosed systemic lupus erythematosus was admitted due to several weeks of sinusitis, fever, blurred vision and weight loss (9 kg over 3 months). He was found to have sustained endgaze nystagmus bilaterally. Lab workup revealed pancytopenia, hyperferritinemia and increased liver functions.
Imaging Findings
Patient 1: FLAIR hyperintense lesions in the periventricular white matter, most of them along the perivenular spaces, corpus callosum (one lesion with restricted diffusion), internal capsules, middle cerebellar peduncles. In addition, there is an enhancing T2 hyperintense lesion in the left caudate nucleus. Patient 2: FLAIR hyperintense nonrestricting left parietal cortical and subcortical lesion with microhemorrhages, as well as symmetric T2 hyperintense signal in the basal ganglia, insula and cingulate gyrus. Patient 3: Scattered areas of leptomeningeal enhancement, multiple FLAIR hyperintense nonenhancing nonrestricting foci in the deep gray matter bilaterally, some of which are associated with perivascular enhancement.
Summary
Hemophagocytic lymphohistiocytosis is a rare disorder, characterized by proliferation of benign lymphocytes and histiocytes in multiple organs, with CNS involvement in 10-73%. Three progressively severe neuropathologic stages include leptomeningeal infiltration with lymphocytes and macrophages (stage 1), perivascular infiltrates (stage 2) and massive tissue infiltration of lymphocytes and histiocytes and tissue necrosis (stage 3). Reported brain imaging findings include parenchymal atrophy, leptomeningeal and perivascular enhancement, parenchymal T2 hyperintense lesions which may demonstrate nodular or ring enhancement as well as restricted diffusion, parenchymal calcifications and subdural fluid collections. Our first case matches previously described imaging findings, with deep gray matter abnormalities and periventricular white matter lesions along the periventricular spaces, sometimes associated with demyelination. The second patient demonstrates findings suggestive of HLH with a cortical and subcortical lesion. In addition, symmetric deep gray matter T2 hyperintensity is compatible with hyperammonemia. When imaging findings consist of focal parenchymal abnormality accompanied by enhancement along the perivascular spaces, especially with adjacent meningeal enhancement, as demonstrated in our third patient, the differential diagnosis is usually between sarcoidosis and lymphoma. Our third case shows that HLH should be added as a diagnostic consideration. Patients presenting with neurologic symptoms in HLH, may demonstrate expected imaging findings reflecting primary neural HLH infiltration, as well as complications from extensive multiorgan involvement in HLH.

KEYWORDS: MR imaging brain, Hemophagocytic lymphohistiocytosis

Note: Scanned images are included in the proceedings. Some submitted images were reduced during editing, thereby decreasing clarity. Also, refer to the Program Planner. Proceedings Content as of 3-29-2013.

EE-11

Pachymeningitis and Choroid Plexus Granulomas in ANCA-Associated Vasculitis: A Report of Two Cases

McDonnell, O.·Khaleel, Z.
Sir Charles Gairdner Hospital
Perth, AUSTRALIA.

Purpose
ANCA vasculitides are rare and are associated with multiple clinical syndromes. Central nervous systen involvement is rare with incidence reported between 10-40% and has various clinical and imaging manifestations. We present two cases of known ANCA positive vasculitis, one patient with Wegener's granulomatosis and one with microscopic polyangiitis, who presented with new onset neurologic symptoms and the unusual MR imaging findings of pachymeningitis and choroid plexus granulomas.
Case Report
Two patients with known Wegener's granulomatosis and microscopic polyangiitis presented acutely with neurologic symptoms. Case 1, a 71-year-old female was admitted to hospital complaining of increasing nausea, vertigo and ataxia. She had a previous diagnosis of Wegener's granulomatosis confirmed on renal and lung biopsy and was C ANCA positive. At time of admission she was on maintenance treatment with prednisolone and azathioprine. Case 2, a 58-year-old female, had a two-year history of systemic MPO ANCA positive vasculitis microscopic polyangiitis. She was admitted with a 2-week history of mania, pressured speech, grandiose delusions and agitation. She was on maintenance prednisolone 2mg daily at time of admission. Both patients were afrebile and clinical examination was unremarkable. Apart from mildly elevated ESR and CRP all blood and cerebrospinal fluid laboratory investigations were unremarkable.
Imaging Findings
MR imaging in each case demonstrated T2 hypointense dural thickening and enhancement and enhancing choroid plexus lesions presumed to represent granulomas. In case 1 MRI head demonstrated several enhancing T2 hypointense mass lesions in relation to the choroid plexus within the fourth ventricle and foramina of Lushka and temporal horns and bilaterally in the frontal meninges and anterior falx cerebri. In case 2 MRI demonstrated abnormal T2 hypointense dural thickening and enhancement in the anterior cranial fossa bilaterally related to the central falx and an enhancing ovoid T2 hypointense mass within the right foramen of Lushka with secondary brain parenchymal edema.
Summary
Central nervous systen involvement is unusual in ANCA vasculitis and we present two symptomatic cases with combination of dural and choroid plexus involvement demonstrated at MRI which regressed following immunosuppressive therapy. There are few reported cases of these imaging findings. There are only two reported cases of choroid plexus granulomas in Wegener's granulomatosis. Although pachymeningitis has been reported previously in microscopic polyangiitis choroid plexus involvement has not been reported previously in microscopic polyangiitis.

KEYWORDS: Adult brain, Wegener's granulomatosis, Microscopic polyangiitis

EE-12

Diffusion Restriction in Metronidazole Neurotoxicity

Torres, F.·Wang, S.·Lerner, A.·Go, J.·Hoque, K.·Rajamohan, A.
University of Southern California
Los Angeles, CA.

Purpose
We will present a case of metronidazole-induced neurotoxicity demonstrating unusual imaging features that are distributed topographically in the previously described pattern.
Case Report
A 45-year-old Chinese female with a history of gallbladder neuroendocrine cancer presented with fever, abdominal pain and elevated alkaline phosphatase and total bilirubin. The patient then was started on metronidazole for presumed cholangitis after endoscopic evaluation. After receiving a total of two grams of metronidazole a day for a total of 20 days, she was found unresponsive and an MR of her brain was performed.
Imaging Findings
MR imaging demonstrated diffuse increased T2/FLAIR hyperintensity throughout the white matter of the bilateral cerebral hemispheres, splenium of the corpus callosum, posterior limb of internal capsules, dorsomedial thalamic nuclei, midbrain, dorsal pons, vestibular nuclei, facial nuclei, and dorsal medulla. In addition, there is associated symmetric restricted diffusion representing cytotoxic edema within the subcortical and periventricular white matter of the cerebral hemispheres, as well as within the dentate nuclei.

Note: Scanned images are included in the proceedings. Some submitted images were reduced during editing, thereby decreasing clarity. Also, refer to the Program Planner. Proceedings Content as of 3-29-2013.

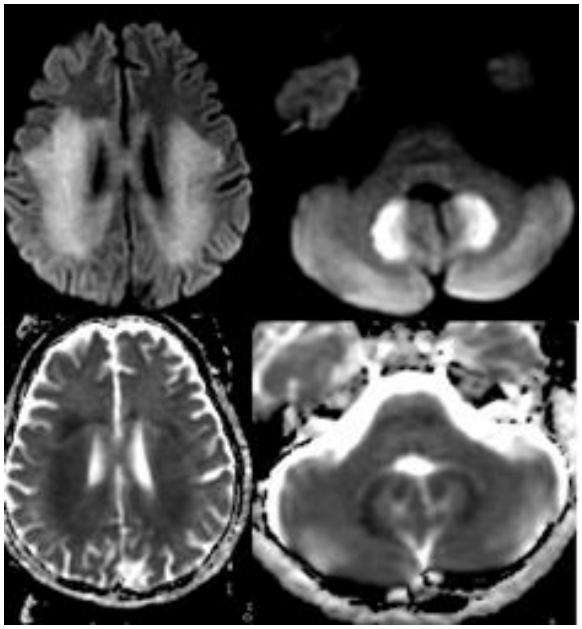

Summary
Metronidazole-induced encephalopathy (MIE) is a rare toxicity that has been described previously as presenting with symmetric areas of vasogenic edema with a topographic distribution involving the dentate nuclei, midbrain, dorsal pons, splenium of the corpus callosum, and dorsal medulla with minimal to no involvement of the cerebral white matter. Our case of metronidazole-induced encephalopathy demonstrates pronounced restricted diffusion within the dentate nuclei, as well as an unusual amount of involvement of the cerebral white matter, which also demonstrated cytotoxic edema. As the exact pathophysiology of MIE is unknown, we hope our case can aid in future studies investigating the exact cause MIE.

KEYWORDS: Diffusion-weighted imaging, Medication, metronidazole-induced encephalopathy

EE-13

Silicon! Could It Be in Our Heads?

Djoukhadar, I. A.[1]·Cosgrive, J.[2]·Jameison, s.[2]·Warren, D. J.[1]
[1]Leeds Radiology Academy, Leeds, UNITED KINGDOM,
[2]Leeds Teaching Hospitals, Leeds, UNITED KINGDOM.

Purpose
To describe the radiologic findings of silicon oil migration into the ventricular system following treatment of retinal detachment.
Case Report
A 74-year-old female presented to the neurology outpatient clinic with six-month history of right-sided headache. She had a history of left phthisis bulbi, which occurred following multiple attempted surgical repairs for retinal detachment 20 years ago. She wore a cosmetic lens over the left eye. Her neurologic examination was unremarkable.
Imaging Findings
Initial unenhanced CT examination demonstrated a high attenuation abnormality in the left orbit replacing the vitreous with posterior extension along the optic nerve and two further foci of high attenuation in the suprasellar region and in the frontal horn of the right lateral ventricle. A subsequent MRI at two weeks interval showed abnormal high T2, intermediate T1 material within the globe and in the left optic nerve. The abnormality had a low T2 signal rim and showed signal suppression on T1 fat saturated imaging. Similar abnormality was seen in the suprasellar region. Interestingly the previously seen lesion in the right frontal horn has migrated posteriorly to lie adjacent to the medial aspect of the right choroid plexus within the right collateral trigone. The signal characteristics demonstrated on both the CT and MRI are consistent with silicone oil migration from the vitreous cavity into the optic nerve and subsequently into the subarachnoid space.

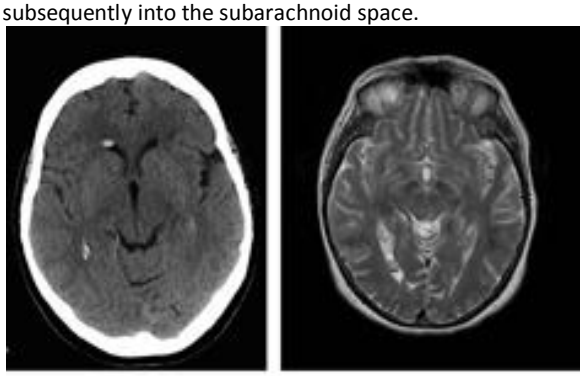

Unenhanced CT and T2 Axial images demonstrating the moving nature of the silicon oil deposit

Summary
This case report highlights an unusual radiologic presentation of silicon oil migration following oil endotamponade for retinal detachment. This is a rare but recognized complication. It is important to be aware that intra-orbital silicon oil can migrate into the ventricular system so that imaging findings in this rare situation can be diagnosed confidently without the need for unnecessary patient distress or invasive investigations.

KEYWORDS: Orbits, Abnormalities, Silicone

EE-14

Chronic Lymphocytic Inflammation with Pontine Perivascular Enhancement Responsive to Steroids

Grigg, A.·Bray, M.·Hart, B.
University of New Mexico
Albuquerque, NM.

Purpose
Only a handful of reports have presented the neuroimaging findings of a recently described disease termed chronic lymphocytic inflammation with pontine

Note: Scanned images are included in the proceedings. Some submitted images were reduced during editing, thereby decreasing clarity. Also, refer to the Program Planner. Proceedings Content as of 3-29-2013.

perivascular enhancement responsive to steroids (CLIPPERS). The purpose of this study is to describe the clinical and neuroimaging findings in a case of CLIPPERS.
Case Report
A 21-year-old male noticed diplopia and general weakness with a subacute onset three weeks prior to admission. Additionally, he developed facial tingling and paraesthesia in his fingertips. His past medical history and family history were unremarkable. Neurologic examination on admission revealed a cerebellar syndrome with minimal gait and stance ataxia, as well as left cranial nerve VI palsy. The remainder of the neurologic examination was normal. Extensive systemic workup included the following: complete blood count; renal and liver function; sedimentation rate; antinuclear antibody; IgG for MS; HIV, viral, fungal and tuberculosis serologies. All tests were all within normal limits or negative. Treatment: After MRI and due to the progressively worsening diplopia, the patient was started on high-dose oral prednisolone. There was a dramatic clinical improvement within one week, followed by improvement on follow-up MR imaging. Discussion: CLIPPERS is a recently described, perhaps underdiagnosed, treatable inflammatory brainstem CNS disease. Exclusion of various inflammatory, infectious and paraneoplastic disorders is necessary before this diagnosis should be considered. The pathogenesis of CLIPPERS is unknown. The clinical response to immunosuppressive therapies suggests an autoimmune or other inflammatory mediated pathogenesis.
Imaging Findings
MR imaging (T2-weighted images) revealed multiple punctate hyperintensities in the pons, medulla, cerebellum and upper cervical spinal cord with corresponding curvilinear enhancement on T1 imaging (Figure1). The largest single lesion measured approximately six mm in greatest dimension, but most lesions measured between one and three mm. The majority of lesions were clustered in and around the pons. Follow-up MRI 10 days later showed marked improvement (Figure 2).
Summary
This excerpta presents the neuroimaging and clinical findings of a recently described disease termed chronic lymphocytic inflammation with pontine perivascular enhancement responsive to steroids (CLIPPERS). The described imaging findings must be correlated with the clinical features along with exclusion of other inflammatory and infectious process to arrive at an accurate diagnosis. Awareness of this entity may help the radiologist differentiate this disease process from other brainstem disorders and possibly save the patient from an unnecessary brain biopsy.

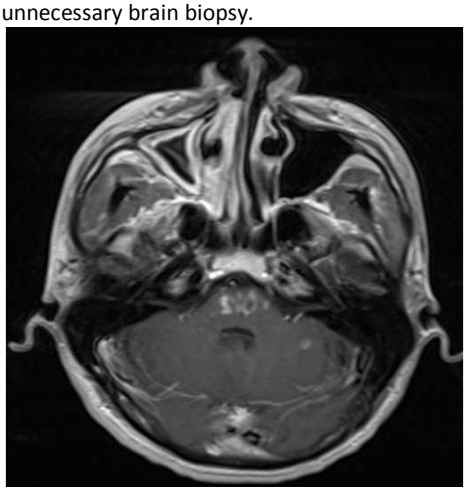

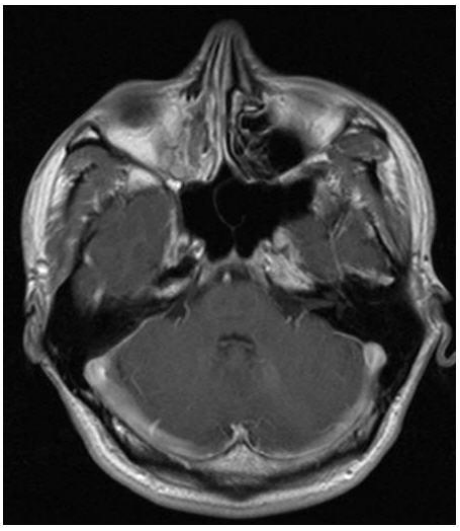

KEYWORDS: Inflammatory, Brainstem, CLIPPERS

EE-15

Inexorably Progressive Balo's Concentric Sclerosis: Sequential MR Imaging of Dramatic Lesion Growth and an Educational Review of Imaging Manifestations

Matys, T.[1]·Wing, L.[1]·Zaccagna, F.[1]·Antoun, N.[1]·Massoud, T. F.[2]
[1]Addenbrooke's Hospital, Cambridge, UNITED KINGDOM,
[2]University of Cambridge, Cambridge, UNITED KINGDOM.

Purpose
Balo's concentric sclerosis (BCS) is a variant of multiple sclerosis. Its pathologic hallmarks are large demyelinated lesions characterized by a peculiar pattern of alternating layers of preserved and destroyed myelin. MR imaging has made diagnosis of BCS rings possible, and early treatment has markedly improved its prognosis. Balo's concentric sclerosis remains a rare disease. Until eight years ago there were only 60 cases reported in the literature. We present a unique case of treatment refractory BCS

Note: Scanned images are included in the proceedings. Some submitted images were reduced during editing, thereby decreasing clarity. Also, refer to the Program Planner. Proceedings Content as of 3-29-2013.

highlighting unusual and rapidly progressive imaging manifestations.

Case Report

A 52-year-old Caucasian male presented with a three-week history of progressive leg weakness. He had no sensory deficit, but had an upper motor neurone weakness affecting his left leg. Outpatient head CT[Imaging 1] followed by MRI [Imaging 2] confirmed the diagnosis of BCS. He was admitted to hospital three weeks later when clinically worse. Brain MRI[Imaging 3] showed slight progression in size of the right cerebral lesion. Soon his lateralizing signs progressed. He was treated with steroids and five days of plasma exchange with stabilization of his weakness. Over the following three months, his clinical condition gradually deteriorated. MR images performed at one, two, and three months[Imaging 4-6] after admission demonstrated further progression. He was treated with six cycles of cyclophosphamide, during which his symptoms continued to progress, including cognitive impairment and no improvement in motor symptoms. Azathioprine was started but subsequently stopped 10 months after initial presentation. MR imaging [Imaging 7] demonstrated significant progression of disease. A five-day course of monoclonal antibody treatment and IV steroids then was attempted, followed by maintenance steroids, but there was no change clinically. He became significantly disabled. There was further MRI[Imaging 8] progression of disease during a period of neurorehabilitation, but he subsequently died 15 months after initial presentation.

Imaging Findings

CT scan [Imaging 1] initially revealed an ill-defined small nonenhancing area of hypodensity in the medial right centrum semiovale, thought to be a likely low-grade tumor. MR imaging followed shortly [Imaging 2], and revealed a classic T2 hyperintense lesion of BCS. Peripheral rings showed enhancement and restricted diffusion. Subsequent follow-up imaging [Imaging 3-8] over the next 14 months revealed dramatic lesion growth and invasion of brain. This involved first the entire white matter of the right cerebral hemisphere with some minor sparing in the occipital lobe, and some T2 hyperintensity also in deep gray nuclei. This was followed by spread through the genu of the corpus callosum and rapid involvement of most white matter of the anterior left frontal lobe prior to patient death. Widespread areas of patchy and linear enhancement and restricted diffusion were still present at the advancing front of the disease.

Summary

We present a rare case of devastatingly progressive BCS refractory to treatment and resulting in patient death within 15 months of presentation. Imaging findings were initially typical, but its inexorable spread through the brain has resulted in dramatic imaging findings that are seldom viewed by neuroradiologists. In this exhibit we also review literature accounts of BCS contrast enhancement, DWI, and MRS.

KEYWORDS: Multiple sclerosis, MR plaque imaging

EE-16

Chronic Lymphocytic Inflammation with Pontine Perivascular Enhancement Responsive to Steroids Syndrome with Infratentorial and Supratentorial Involvement: A Case Report

Yan, Z.·Hoefling, N.·Peyster, R.·Chaudhry, A.
SUNY at Stony Brook
Stony Brook, NY.

Purpose

Previously reported cases of chronic lymphocytic inflammation with pontine perivascular enhancement responsive to steroids (CLIPPERS) syndrome have described only infratentorial involvement. We present a unique case of CLIPPERS syndrome that demonstrates both supratentorial and infratentorial involvement.

Case Report

A 70-year-old female presented with progressive right lower extremity weakness and multiple episodes of falls. Initial MRI showed abnormal contrast enhancement in the supratentorial, pontine and cerebellar white matter. The patient's symptoms markedly improved with five day course of intravenous corticosteroids. Follow-up MRI demonstrated resolution of abnormal enhancement.

Imaging Findings

Ill defined patchy areas of T2 and FLAIR hyperintensities are noted in pons, middle cerebellar peduncles and adjacent cerebellar white matter and also in cerebral white matter bilaterally, left greater than right, without mass effect. On postcontrast images, there is linear and mild nodular enhancement within those T2 and FLAIR hyperintensities along the perivascular spaces.

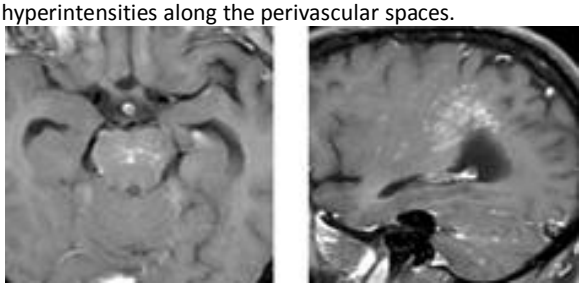

Summary

Chronic lymphocytic inflammation with pontine perivascular enhancement responsive to steroids is a rare and new entity with evolving definition. All reported cases to date have shown exclusive involvement of the posterior fossa. To the best of our knowledge, we present the first case of this syndrome that also demonstrates supratentorial involvement.

KEYWORDS: Brain abnormalities

Note: Scanned images are included in the proceedings. Some submitted images were reduced during editing, thereby decreasing clarity. Also, refer to the Program Planner. Proceedings Content as of 3-29-2013.

EE-17

Hippocampi en Fuego

Romano, J.[1]·Banker, P.[2]
[1]Montefiore Medical Center, Bronx, NY, [2]University of California Los Angeles, Los Angeles, CA.

Purpose
To illustrate a unique imaging finding and a diagnostic problem. We present a case of restricted diffusion in both hippocampi exclusive of other brain regions in a patient with a multifactorial history.
Case Report
A 58-year-old female with prior history of severe depression and multiple suicide attempts was brought to the ED in an unresponsive state. The patient had been taking acetaminophen/oxycodone, and zolpidem, the amounts unknown. The patient's prescription medications included a dopaminergic medication (Carbidopa/Levodopa) for intermittent parkinsonian symptoms of tremor and gait disturbance, selective serotonin reuptake inhibitors (citalopram and sertraline) for depression, and diazepam for anxiety. On exam by EMS, the patient was tachycardic and tachypneic with normal blood pressure. In the ED, she was found to be hypoglycemic, hypoxic, and in hypokalemic lactic acidosis. She was intubated shortly after presentation for respiratory failure. Laboratory evaluation revealed evidence of liver failure with elevated levels of acetaminophen, for which she was treated with N-acetylcysteine. The patient's hospital course was notable for persistent short-term memory loss without focal neurologic deficit. She did not have witnessed seizures or seizure history.
Imaging Findings
The patient presented with symmetric intense restricted diffusion throughout the entire hippocampi bilaterally without involvement of other brain regions.

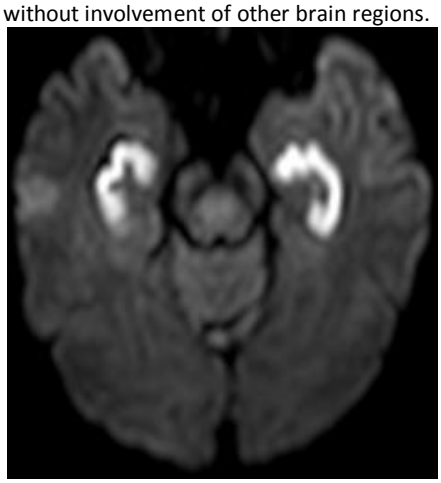

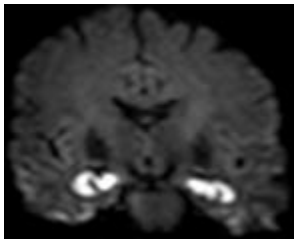

Summary
We illustrate a distinct noteworthy diffusion MRI appearance for which the etiology is not clear. We analyze possible causes for this finding considering diseases that manifest restricted diffusion and occur in the hippocampus (e.g., infarction, hypoxia, peri-ictal signal changes, hypoglycemic encephalopathy and limbic encephalitis). Cases of this kind illustrate a gap in our knowledge between our comprehension of imaging manifestations of disease and what we can see in our practices. As such, this is a fertile opportunity toward improving our understanding.

KEYWORDS: Hippocampus, Diffusion-weighted imaging

EE-18

Basic and Advanced Perfusion-Weighted Imaging, Diffusion Tensor Imaging and Spectroscopic Imaging of a Case of Balò's Concentric Sclerosis: Description of a Case and Literature Review

Stecco, A.·Ripellino, P.·Leone, M.·Cantello, R.·Perchinunno, M.·Carriero, A.
ASU Maggiore della Carità
Novara, ITALY.

Purpose
Balo's concentric sclerosis is a rare variant of multiple sclerosis which can mimic tumor or stroke lesions.
Case Report
We report the case of a 51-year-old woman who was admitted to our department in January 2012 for a slowly increasing right hemiparesis with right brisk deep tendon reflexes. She suffered from Sjogren syndrome and HBV hepatitis (healthy carrier). At patient's admittance the brain MRI showed a concentric ring lesion in the FLAIR sequence and in the T2-weighted image. The lesion was surrounded by a wide vasogenic edema and appeared hypointense in sagittal T1-weighted image, without gadolinium enhancement. We then performed, on a 1.5 T magnet with an 8-channel sense head coil, an advanced MRI study of the lesion which included spectroscopical and perfusional analysis. Single voxel spectroscopy detected a high ratio of Cho/NAA and a double pick of lactate lipids.
Imaging Findings
Perfusion with DSCE technique and calculation of CBV, CBF, MTT maps, showed, after post-processing by arterial input fraction, a central layer (red box) more perfused compared to the surrounding areas, confirming the hypothesis that Balò's lesions usually surround a vessel.

Note: Scanned images are included in the proceedings. Some submitted images were reduced during editing, thereby decreasing clarity. Also, refer to the Program Planner. Proceedings Content as of 3-29-2013.

Cerebrospinal fluid analysis detected oligoclonal bands, without anti-aquaporin-4 antibodies. High-dose iv methylprednisolone was started (1g/day for 10 days) and followed by oral prednisone (1mg/kg/day for two months, then slowly tapered) with concomitant lamivudine as antiviral prophylaxis. The right hemiparesis fully recovered after two weeks and has not relapse after six months, as also documented by follow-up MR scans.

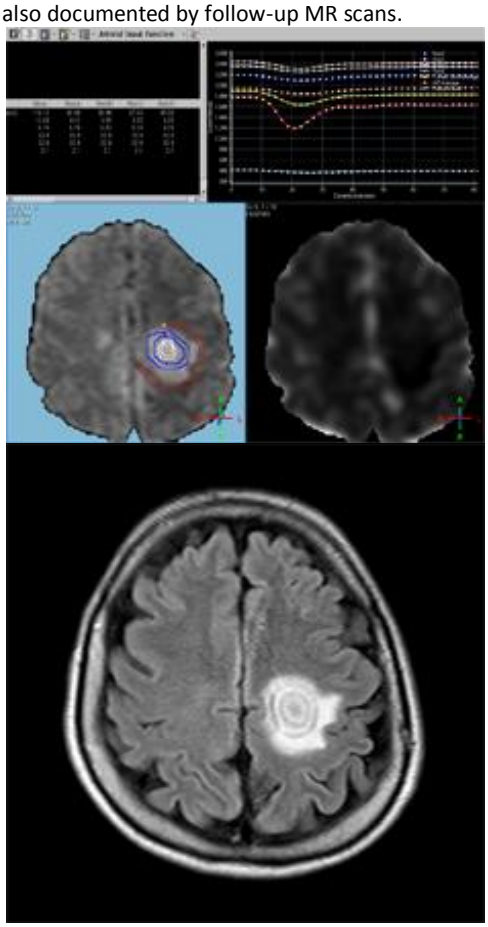

Summary

Balo's concentric sclerosis is a rare variant of multiple sclerosis which can mimic tumor or stroke. It has a well known aspect on MR conventional images, although with advanced techniques is possible to retrieve more structural features.

KEYWORDS: MR spectrocopy, MR perfusion-weighted imaging, multiple sclerosis

EE-19

Amyloid Angitis: Spectrum of Imaging Findings

Kalra, V. B.·Rao, B.·Gibson, J.·Malhotra, A.
Yale University
New Haven, CT.

Purpose

Amyloid angitis is an uncommon entity separate from amyloid angiopathy, and acts as a clinical subset of primary central nervous system vasculitis, responsive to immunosuppression. We present three biopsy-proven cases spanning the spectrum of imaging findings - extensive leukoencephalopathy, focal nonenhancing tumefactive mass lesion, and lobar hemorrhage.

Case Report

Patient #1. A 78-year-old male with one year history of abnormal hand movements, unusual behaviors, and personality changes. MR demonstrated confluent areas of leukoencephalopathy in the right parietal, occipital, and temporal lobes with associated punctate cerebral microhemmorahges. Clinically, there was suspicion for gliomatosis cerebri. MR spectroscopy was not done and there was no immediate response to dexamethasone. Biopsy was performed and showed granulomatous angitis with transmural vasculitis at sites of amyloid deposition - findings consistent with amyloid angitis. Patient #2. A 48-year-old male with new onset generalized seizures. MR demonstrated a right occiptotemporal mass-like lesion. The patient received dexamethasone and phenytoin which decreased the size of the mass. Biopsy showed granulomatous angitis with transmural vasculitis at sites of amyloid deposition - findings consistent with amyloid angitis. Patient #3. A 72-year-old female with history of endometrial carcinoma had two episodes of altered vision two days prior to acute onset left-sided numbness and right-sided headache. The patient underwent CT and MR which demonstrated an isolated posterior right temporal lobar intraparenchymal hemorrhage. CT angiography was normal. Resection was performed secondary to concern for an underlying mass lesion. Pathology showed granulomatous angitis with transmural vasculitis at sites of amyloid deposition - findings consistent with amyloid angitis.

Imaging Findings

Patient #1. MR demonstrates confluent areas of T2/FLAIR hyperintensity in the right parietal, occipital, and temporal lobes with associated regional punctate microhemmorhages and sulcal effacement. These areas had no postcontrast enhancement. MR spectroscopy was not performed and there was no significant change in imaging findings on an MR done four days later while the patient was on dexamethasone. Patient #2. MR demonstrates a right occipitotemporal mass-like area of T2/FLAIR signal abnormality that measured 2.5 x 2.1 cm. There was no postcontrast enhancement or abnormality on spectroscopy. Three months following biopsy, the lesion had markedly decreased in size, measuring 0.8 x 0.8 cm. Patient #3. MR demonstrates an isolated posterior right temporal lobar intraparenchymal hemorrhage. No significant postcontrast enhancement was seen. No punctate areas of microhemmorhage were seen. MR spectroscopy and perfusion showed no abnormalities. No vascular lesions were seen on CT angiography.

Summary

We present three cases reflecting the spectrum of findings seen in amyloid angitis ranging from confluent multilobar

Note: Scanned images are included in the proceedings. Some submitted images were reduced during editing, thereby decreasing clarity. Also, refer to the Program Planner. Proceedings Content as of 3-29-2013.

T2 signal abnormalities resembling gliomatosis cerebri to nonenhancing tumefactive lesions to nonspecific appearing lobar hemorrhages. Lesions resembling gliomatosis cerebri can be distinguished by presence of punctate foci of susceptibility and normal spectroscopy findings and lesions resembling tumefactive lesions can be distinguished from amyloidomas and malignancy by lack of enhancement and normal MR spectroscopy findings. When supportive imaging findings are seen, it is important to suggest the diagnosis as these patients can respond to immunosuppression and biopsy can be avoided.

KEYWORDS: Amyloid, Arteriopathy

EE-20

Confounding Clinical Presentation of Acute Hemorrhagic Leukoencephalitis in Adulthood

Chakraborty, A. K.·Keiper, M. D.·White, M. L.·Helvey, J. T.·Poage, D. P.
University of Nebraska Medical Center
Omaha, NE.

Purpose
Acute hemorrhagic leukoencephalitis (AHL) is a rapidly progressive form of acute disseminating encephalomyelitis (ADEM) generally affecting children and young adults. Acute hemorrhagic leukoencephalitis is relatively rare in middle age and later adulthood and can be a difficult diagnosis based on its protean radiographic findings and radiographic overlap with many more common diseases of adulthood. The neuroradiologist has the unique opportunity to suggest this diagnosis in the appropriate clinical and radiographic setting and provide early potential treatment options for an extremely aggressive and typically fulminant disease process.
Case Report
A 55-year-old gentleman presented to the Emergency Department with rapid onset altered mental status, left-sided weakness and malignant hypertension. MR imaging demonstrated posterior fossa and bihemispheric findings suggestive of somewhat atypical PRES, although additional diagnoses were entertained. Following successful treatment of malignant hypertension, the patient's clinical status did not improve prompting a repeat MR examination demonstrating progressive findings in a radiographic pattern more suggestive of hemorrhagic ADEM (AHL) or other hemorrhagic viral encephalitis. Despite high-dose steroid therapy, the patient deteriorated on hospital day 10 due to progressive development of cerebral swelling and herniation and ultimately expired. An autopsy was performed and confirmed severe cerebral edema, extensive white matter abnormality and scattered petechial hemorrhage most consistent with hemorrhagic leukoencephalitis.
Imaging Findings
Admission brain MRI demonstrated bilateral predominately subcortical hemispheric white matter T2 signal intensity abnormality with additional bilateral signal intensity abnormality and somewhat restricted diffusion in the deep gray nuclei. Additional T2 signal intensity abnormality was noted in the brainstem and cerebellum. Brain MRI on hospital day #5 demonstrated progressive T2 signal abnormality and mass effect in the brain stem, brachium pontis, internal capsules, deep gray nuclei and hemispheric white matter in a pattern suggestive of demyelination. Scattered regions of mildly restricted diffusion and petechial hemorrhage involving the brainstem and internal capsules were noted. Brain MRI hospital day #10 demonstrated marked progression of edema, cerebral swelling, mass effect and herniation. Autopsy demonstrated severe cerebral edema and petechial hemorrhage in the midbrain, pons and medulla.

Summary
Acute hemorrhagic leukoencephalitis is a rare entity particularly in middle aged and elderly adults. Knowledge of the radiographic pattern and presenting findings of AHL allows the neuroradiologist to consider this rare diagnosis over more common diseases of adulthood and potentially provide early therapy for a typically fulminating disease process.

KEYWORDS: Hemorrhage, Leukoencephalopathy

EE-21

Chordoid Glioma Involving Posterior Body of Corpus Callosum

Wang, B.·Ketonen, L.
M. D. Anderson Cancer Center
Houston, TX.

Purpose
To illustrate the imaging findings of a case of chordoid glioma involving the posterior body of corpus callosum, which to our knowledge has not been reported in the literature. Our purpose is to raise awareness of the neuroradiology community concerning this extremely unusual location of a rare tumor that typically occurs in the region of the hypothalamus/anterior third ventricle.
Case Report
A 55-year-old right-handed man developed seizure-like episodes on 2/21/2010 and was evaluated at an outside ER where he underwent a CT followed by an MRI, which revealed an enhancing mass in the posterior corpus callosum. A very limited biopsy was performed, and

Note: Scanned images are included in the proceedings. Some submitted images were reduced during editing, thereby decreasing clarity. Also, refer to the Program Planner. Proceedings Content as of 3-29-2013.

pathology was read as low grade glioma. The physicians at the outside facility felt clinically that the mass was behaving like a high grade glioma, so he was treated with chemoradiation. On followup MRI, there was progressive enhancement around the corpus callosum. Stereotactic biopsy of the lesion was performed at our institution which demonstrated chordoid glioma, perivascular mononuclear infiltrate, and gliosis.

Imaging Findings

On CT, there is low density involving the posterior corpus callosum extending into the bilateral periventricular white matter, suggestive of underlying tumor. On MRI, there is a homogeneously enhancing lesion in the posterior body and splenium of the corpus callosum. Extensive T2 FLAIR hyperintensity involves the posterior corpus callosum and adjacent brain parenchyma around the occipital horns and in the posterior centrum semiovale. Diffusion-weighted imaging demonstrates no restricted diffusion within the tumor.

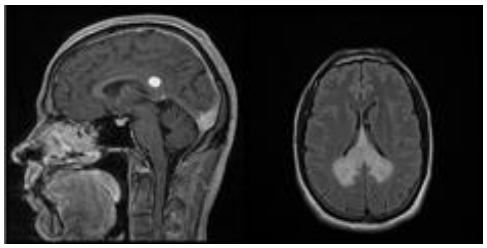

Summary

Chordoid glioma is a rare pathologic entity that has been added to the World Health Organization glioma classification scheme. This neoplasm normally occurs in the region of the hypothalamus/anterior third ventricle. Distinctive imaging characteristics are its consistent location, ovoid shape, hyperdensity on CT scans, and uniform intense contrast enhancement. When present, mass effect causing vasogenic edema tends to be bilaterally symmetrical. We illustrate the imaging findings of a case of chordoid glioma involving posterior body of corpus callosum, which to our knowledge has not been reported in the literature. Despite its rarity, neuroradiologists should be aware of this extremely unusual location of this rare neoplasm and consider it in the differential diagnosis when the characteristic features are encountered.

KEYWORDS: Glioma, Corpus callosum, chordoid

EE-22

Isolated Multi-Intraventricular Rosai-Dorfman Disease

Palacios, W.[1]·Nidecker, A.[2]·Bobinski, M.[2]·Boggan, J.[2]·Shahlaie, K.[2]·Borys, E.[2]
[1]University of California Davis School of Medicine, Sacramento, CA, [2]University of California Davis Medical Center, Sacramento, CA.

Purpose

To report the first case of isolated multi-intraventricular Rosai-Dorfman disease.

Case Report

A 35-year-old woman was evaluated at a different institution in March 2011 for acute onset of persistent, severe headaches. Computed tomography (CT) of the head and subsequent magnetic resonance (MR) imaging of the brain revealed an intraventricular mass, most suspicious for tumor. Two concurrent tissue biopsies were nondiagnostic. She presented at our institution in February 2012 with worsening symptoms. MR imaging of the brain showed interval increase in size of the intraventricular mass. It was centered in the third ventricle extending into the lateral ventricles and was homogenously isointense on T1- and hyperintense on T2-weighted images. Additional lesions were identified in the right temporal horn and left foramen of Luschka. On CT of the brain, the mass was heterogeneous in attenuation with predominantly hyperdense components. A three-section tissue biopsy revealed benign histiocytic infiltrates by positive CD68 and S-100 staining with emperipolesis and a mixture of lymphocytes and plasma cells by positive CD20 and CD3 staining in a fibrotic background, most consistent with Rosai-Dorfman disease.

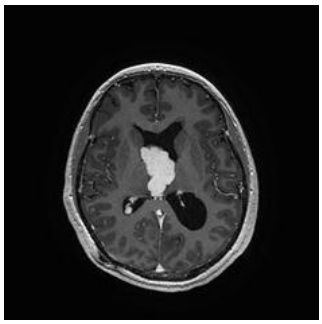

Summary

Rosai-Dorfman disease is also known as sinus histiocytosis with massive lymphadenopathy. It is a rare benign disorder. Isolated extranodal Rosai-Dorfman disease is more rare with isolated intracranial Rosai-Dorfman disease even more so. Only one case has been reported of isolated single intraventricular variant. We report the first case of isolated multi-intraventricular Rosai-Dorfman disease. Management for intracranial disease is low-dose radiotherapy. The disease is most often indistinguishable from a meningioma but has a wide radiographic differential ranging from metastasis to glioma, the management of each just as varied and very much different from treatment for Rosai-Dorfman disease. As such, the recognition and consideration of Rosai-Dorfman disease in all its various forms is essential to avoid improper and unnecessary invasive therapies.

KEYWORDS: Rosai-Dorfman disease, Histiocytosis

Note: Scanned images are included in the proceedings. Some submitted images were reduced during editing, thereby decreasing clarity. Also, refer to the Program Planner. Proceedings Content as of 3-29-2013.

EE-23

MR Imaging Findings in an Extra-Axial Mass Mimicking a Meningioma in an HIV Positive Patient

Lopez, M.·Moonis, G.
Beth Israel Deaconness Medical Center
Boston, MA.

Purpose
Describe the MRI findings in an HIV positive patient with Epstein-Barr virus-related smooth muscle tumor (EBV-SMT) of the CNS which mimicked a meningioma.
Case Report
Our patient was a 50-year-old woman diagnosed with HIV in 10/1991 following a eye examination which revealed CMV retinitis. This patient also had history of a left occipital meningioma, stable for many years and developed rectal and vaginal carcinomas for which she was treated over the preceding years. In 08/2011, in one of her follow-up MRI examinations for her known left occipital meningioma, a new extra-axial mass in the right parietal lobe measuring 9 mm AP x 16 mm TR x 10 mm SI was seen and thought to be an additional meningioma. In the follow-up examination of 08/01/12, the lesion demonstrated rapid growth and measured 15 mm AP x 21 mm TR x 17 mm SI with increased surrounding parenchymal edema (images 1 and 2). Given its rapid growth and associated edema, the lesion was resected. The final pathology report was EBV-associated smooth muscle tumor.
Imaging Findings
This lesion demonstrated signal isointense to gray matter on T2-weighted images, with mild hypointensity on T1-weighted images, and diffuse homogeneous enhancement in the postcontrast images.

Summary
Patients with HIV are known to develop Epstein-Barr virus-related smooth muscle tumor in any organ. However, the most common location is in the CNS. Epstein-Barr virus-related smooth muscle tumor also occurs in immunosuppressed patients (post-transplantation, common variable immunodeficiency syndrome). Pathogenesis appears to be related to infection and transformation of smooth muscle cells by EBV. The mechanism by which EBV enters into the smooth muscle cell is not clear. However, once the tumor is present, they have shown to have different degrees of aggressiveness and thus clinical outcomes, as in some cases these tumors can be fatal. Therefore, when presented with a mass like CNS lesion in a patient with HIV, one must consider EBV-related smooth muscle tumor in the differential.

KEYWORDS: Extra-axial, Masses, meningioma mimicker

EE-24

Giant Intradiploic Epidermoid Cyst of the Parietal Bone

Sundblad, A.·Ralston, M.·Livingston, B.·Florman, J.
Maine Medical Center
Portland, ME.

Purpose
Intracranial epidermoid cysts are rare congenital tumors of ectodermal origin representing 0.2-1.8% of all primary intracranial tumors. They grow slowly as the squamous epithelial lining sheds keratin and cholesterol debris. We report a giant intradiploic epidermoid cyst resulting in profound deformity of the brain without neurologic deficit.
Case Report
A 38-year-old Filipino male presented with intermittent headaches and no focal neurologic symptoms. Noncontrast head CT revealed a large, heterogeneous, extradural right parietal mass measuring 8.5 x 6.1 x 7.4 cm with resultant shift of midline structures by 1.5 cm and uncal herniation. MR imaging demonstrated heterogeneous signal on T1 and T2 with incomplete suppression on FLAIR and marked increased signal on DWI. Postgadolinium and perfusion imaging showed a thin rim of enhancement with absence of internal blood flow. Right parietal craniectomy revealed an extradural mass, soft and mixed in color. Histologically, the mass was lined with squamous epithelium and mostly composed of keratin debris. Areas of ruptured wall were present with foreign body giant cell reaction.
Imaging Findings
On CT, epidermoid cysts typically are well defined hypoattenuating masses that do not enhance. On MR, most epidermoid cysts are isointense or slightly hyperintense to CSF on T1 and T2. Often, they are distinguished from arachnoid cysts by incomplete suppression on FLAIR and high signal intensity on diffusion-weighted images. The characteristic diffusion-weighted appearance is thought to be on the basis of high 2D planar anisotropy, which could be attributed to the well structured orientation of keratin filaments.

Note: Scanned images are included in the proceedings. Some submitted images were reduced during editing, thereby decreasing clarity. Also, refer to the Program Planner. Proceedings Content as of 3-29-2013.

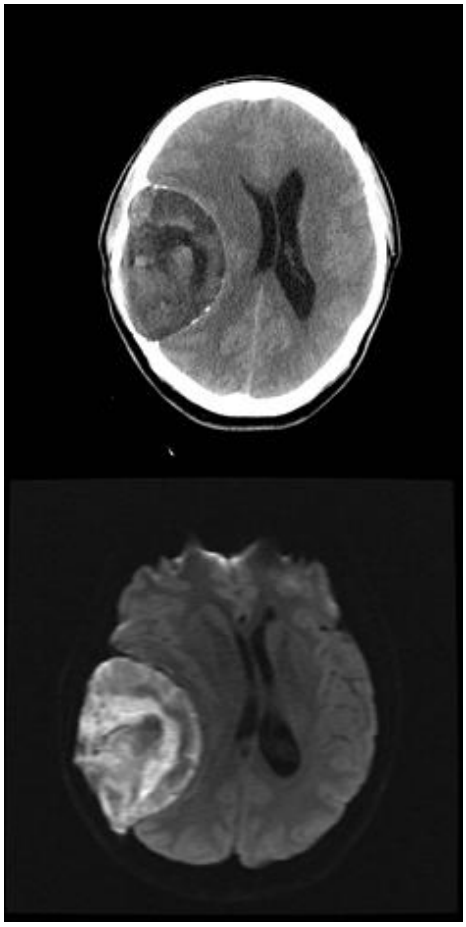

Summary
Extradural epidermoid cysts are slow growing tumors that may cause profound deformity of the brain without significant neurologic impairment. While high signal on DWI and incomplete suppression on FLAIR are the most relevant MR imaging features, absence of blood flow on MR perfusion increases diagnostic confidence.

KEYWORDS: Epidermoid

EE-25

Isolated Cystic Schwannoma of the Hypoglossal Nerve

Marashi, K. B.·Nickell, L. T.·Coimbra, C.·Barnett, D.·Layton, K. F.·Opatowsky, M. J.
Baylor University Medical Center
Dallas, TX.

Purpose
We present an unusual case of a large hypoglossal nerve schwannoma.
Case Report
A 52-year-old man presented with a several month history of intermittent, progressively worsening dizziness and vertigo. He also described new onset headaches, fatigue, difficulty walking down stairs, and difficulty maintaining his lane while driving his car. Physical examination revealed impaired tandem walking. An MRI of the brain demonstrated a large, extra-axial cystic mass centered near the left foramen of Luschka with extension into the ipsilateral hypoglossal canal (Figures 1 and 2). Surgical resection confirmed that the lesion arose from the left hypoglossal nerve at the level of the hypoglossal canal. Pathologic analysis was consistent with a WHO Grade 1 schwannoma.
Imaging Findings

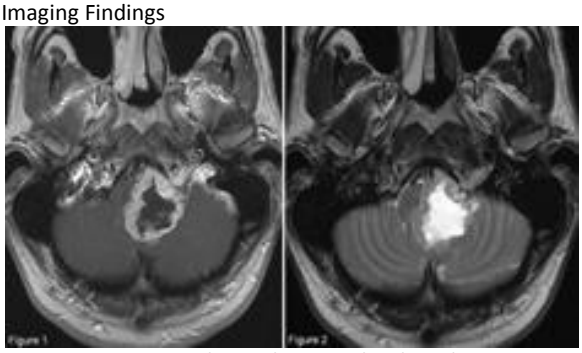

Figure 1: Contrast-enhanced T1-weighted axial MR image of the posterior fossa shows a mass within the left foramen magnum that exhibits thick and irregular enhancement. Figure 2: T2-weighted axial MR image through the same region reveals signal hyperintensity in a more cystic portion of the tumor.

Summary
Schwannomas account for six to eight percent of all intracranial neoplasms. Of these, vestibular schwannomas are the most common, followed by trigeminal and facial schwannomas. Even less frequent are schwannomas arising from the glossopharyngeal, vagus, and spinal accessory nerves. Schwannomas of the oculomotor, trochlear, abducens, and hypoglossal nerves are rare. We present this unusual case of a large, isolated schwannoma of the left hypoglossal nerve.

KEYWORDS: Schwannoma, Hypoglossal nerve

EE-26

MR Imaging of Heavily Calcified Meningioma on 1.5 and 3T: Difference in T1 Signal and Degree of Contrast Enhancement

Wilms, G. E. R.·Demaerel, P.·Sunaert, S.
UZLeuven
Leuven, BELGIUM.

Purpose
To compare the T1-signal and the degree of contrast enhancement of heavily calcified meningioma on 1.5 and 3T magnets.
Case Report
We retrospectively studied the MRI of seven patients with 10 heavily calcified meningiomas in whom T1-weighted images before and after contrast administration were available both on a 1.5 and a 3T magnet.
Imaging Findings

Note: Scanned images are included in the proceedings. Some submitted images were reduced during editing, thereby decreasing clarity. Also, refer to the Program Planner. Proceedings Content as of 3-29-2013.

On the 1.5T studies all calcified meningiomas displayed some degree of T1 hyperintensity. After contrast administration there was intense enhancement that was homogeneous in the majority of patients. On the 3T studies all calcified meningiomas were strongly T1 hypointense. After contrast administration the enhancement was definitely less pronounced. In all but one patient the calcified meningiomas were more strongly hypointense on T2-weighted sequences on the 3T than on the 1.5T study.

Summary

There is a clear difference between the T1-signal and the degree of contrast enhancement of heavily calcified meningioma on 1.5 and 3T magnets, with a more prononunced T1 hypointensity and a lesser degree of contrast enhancement on the 3T studies. We postulate that the T1 hypointensity and the lesser degree of enhancement on 3T are due to a T2 shine through effect. Changes in T1 signal or degree of contrast enhancement in a calcified meningioma between 1.5 and 3T do not reflect pathologicl changes or changes in the vascularity of the lesions, but are due to technical factors.

KEYWORDS: 3 T, Calcifications, meningioma

EE-27

Pituicytoma: Case Report and Literature Review

Liu, H.·Sitton, C. W.·Papasozomenos, S.
University of Texas Health Science Center at Houston
Houston, TX.

Purpose

To present a case of pituicytoma, a rare primary tumor of the neurohypophysis, of which to date only 32 cases have been reported in the literature, along with its imaging features with pathologic correlation.

Case Report

A 44-year-old male with headache, fatigue, vision changes, and decreased libido presented to an endocrinologist where he was found to have bitemporal hemianopsia on exam. Endocrine studies were normal except for a low testosterone level.

Imaging Findings

MR imaging showed a well circumscribed, ovoid, suprasellar mass centered about the pituitary stalk that was slightly hypointense on T1, hyperintense on T2, with peripheral flow voids and marked homogenous enhancement following intravenous administration of Gd-DTPA. The mass displaced the optic chiasm anteriorly and splayed the optic tracts laterally, contacting but not encasing the internal carotid arteries.

Summary

Pituicytoma, although rare, has characteristic MR findings, and inclusion within a preoperative differential diagnosis may help the neurosurgeons manage the highly vascular nature of this tumor with prior embolization.

KEYWORDS: Pituitary gland, Neoplasm, pituicytoma

EE-28

Role of Prone CT in the Diagnosis of Silicone Oil Intraventricular Migration after Intraocular Tamponade: Case Report

Carneiro, F.[1]·Carneiro, F.[2]·Daher Vaz, N.[3]
[1]University of Cincinnati, Cincinnati, OH, [2]Universidade de São Paulo, São Paulo, BRAZIL, [3]Hospital Santa Marcelina - Cidade Tiradentes, São Paulo, BRAZIL.

Purpose

To present the imaging findings of intraventricular silicone oil and emphasize the role of prone imaging as an important diagnostic tool.

Case Report

A 54-year-old man with history of hepatic insufficiency was admitted due to disorientation. A diagnosis of hepatic encephalopathy was suggested, and noncontrast head computed tomography (NCCT) was performed to rule out other causes. A previous history of left eye vitrectomy with silicone oil tamponed to treat retinal detachment was obtained.

Image Findings

Noncontrast head computed tomography demonstrated hyperattenuating material filling the left eye vitreous space, within the optic nerve sheath, and within the frontal horns of the lateral ventricles (Figure A,B). Magnetic resonance imaging (MRI) demonstrated hyperintensity in T1-weighted images (T1WI) and hypointensity in T2-weighted images (T2WI). Both T1WI and T2WI depicted crescent-shaped bands in the silicone oil-aqueous interface representing chemical shift artifact. No diffusion restriction or contrast enhancement was demonstrated. On Prone NCCT, the hyperattenuating material previously located in the frontal horns migrated to the occipital horns (Figure C,D) confirming the low specific gravity of the material in comparison to the cerebrospinal fluid, consistent with silicone fluid.

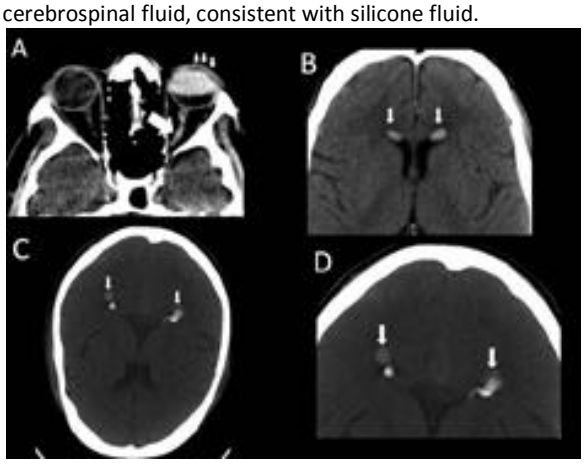

Summary

Silicone oil is a popular agent used to treat retinal

Note: Scanned images are included in the proceedings. Some submitted images were reduced during editing, thereby decreasing clarity. Also, refer to the Program Planner. Proceedings Content as of 3-29-2013.

detachment. Intraventricular migration is rare, but recently has been reported in the medical literature. The mechanism is not totally clear, but some authors have suggested that atrophy of the optic disk associated with elevated intraocular pressure could lead to migration of the silicone oil through the optic nerve sheath that communicates with the subarachnoid space. Silicone oil has been described as hyperattenuating on NCCT with Hounsfield units in the range of blood. Jabbour et al described a case where the NCCT was misdiagnosed as intraventricular hemorrhage. Our MRI findings are in according to the ones described previously. Specific silicone MRI and MR spectroscopy for silicone oil also have been described. Reported MRI and MRS findings likely help assure definitive diagnosis, and might prove highly specific if further investigated. Nondependent, intraventricular CT hyperattenuation likely will not be misdiagnosed as hemorrhagic lesions, particularly if we note the orbital findings and patient history. Prone CT is able to depict the low specific gravity of the oil agent. Due to its low cost and less complexity when compared to MRI and MRS techniques, supine and prone NCCT is the first option in order to confirm the presence of silicone oil in the ventricular system.

KEYWORDS: CT, Ventricles, Silicone-oil

EE-29

Pitfalls in the Diagnosis of Superior Sagittal Sinus Thrombosis: The *Anterior* Delta Sign

Venkatesh, R. M.·Hasso, A. N.·Handwerker, J.
University of California Irvine Medical Center
Orange, CA.

Purpose
Although the "delta" sign is commonly associated with superior sagittal thrombosis, attention often is placed primarily on the posterior superior sagittal sinus on axial CT head images. Anterior "delta" signs are more neglected, particularly near the vertex, and vigilance to this particular area is needed to identify subtle thrombosis. Appropriate imaging protocols are essential for diagnostic accuracy. MR imaging sequences optimally include SWI with phase imaging and GRE sequences as well as thin cut sagittal T1 pre and postcontrast sequences. Computed tomography head optimally should include the vertex as well as additional imaging in the coronal and sagittal planes.
Case Report
This is a 37-year-old right-handed female with no significant past medical history who presents with complaints of worsening headache to an outside hospital. After initial workup with noncontrast CT head, the patient worsened and developed right arm weakness. MR imaging without and with contrast of the brain (axial and sagittal T1 and T2, postcontrast axial T1) consequently was obtained at the outside facility and interpreted as presumed left posterior parietal brain mass. Patient was transferred to our hospital for workup and possible resection of “brain mass”.
Imaging Findings
In retrospect, the initial outside hospital CT (single axial plane, vertex not completely imaged), shows a hyperdense anterior superior sagittal sinus near the vertex and incompletely seen hyperdense vertex cortical veins. Additional small focus of subtle edema is present in the adjacent high right frontal lobe. Subsequently, repeat imaging at our institution (including MRI without and with contrast of the brain and MRV) show anterior superior sagittal sinus thrombosis as well as dilated vertex cortical veins with right supplementary motor area and left posterior parietal lobar hemorrhage, most prominently identified on SWI sequence.

Summary
Although classically superior sagittal sinus thrombosis is associated with the “empty delta sign” on contrast-enhanced CT or contrast-enhanced MR T1WI, radiologists tend to focus primarily on the posterior aspect of the sinus on axial images. Attention should be made to the anterior aspect of the superior sagittal sinus on axial images, especially near the vertex, as potential blind spots in the evaluation for dural sinus thrombosis. Additionally, appropriate imaging protocols are necessary to help confirm the presence of associated venous infarction.

KEYWORDS: Venous sinus thrombosis, Pitfalls, venous infarction

EE-30

Multifocal Intracranial Arterial Stenoses - A Challenging Diagnosis: Case Report and Review of the Literature

McNeill, G. J.·Scott, C. J.·Heran, M. K. S.
Vancouver General Hospital
Vancouver, BC, CANADA.

Purpose
The etiology of multifocal intracranial arterial stenosis is often straightforward based on patient demographics, clinical presentation and typical imaging features. A subset

Note: Scanned images are included in the proceedings. Some submitted images were reduced during editing, thereby decreasing clarity. Also, refer to the Program Planner. Proceedings Content as of 3-29-2013.

of patients exists in whom the etiology of such a finding is not readily apparent. In this scenario, the diagnosis often is difficult. This exhibit will discuss the clinical presentation and imaging findings of the possible etiologies of multifocal intracranial arterial stenosis, using a case discussion as a framework. Entities such as atherosclerosis, reversible cerebral vasoconstriction syndrome, arteritis and vasospasm as well as rare causes will be discussed.
Case Report
A 45-year-old male nonsmoker presented with headache and right hemiplegia. His neurologic symptoms took a fluctuating course with persistent headache but a constellation of different localizing signs. He showed no improvement with anticoagulation or intra-arterial vasodilators but slow improvement following the instigation of immunosuppressive therapy. As a consequence, a diagnosis of central nervous system arteritis was reached.
Imaging Findings
Initial noncontrast CT brain showed no changes of acute ischemia. Computed tomography angiogram performed at presentation showed multifocal large and small vessel stenoses. A severe stenosis of the left M1 segment of his middle cerebral artery was considered responsible for his initial neurologic deficit. These stenoses were confirmed at catheter angiography at which time they proved resistant to intra-arterial vasodilators. Serial imaging demonstrated persistence of intracranial stenoses as well as development of multi-territory infarcts demonstrated at MRI by diffusion-weighted imaging.
Summary
The etiology of multifocal intracranial arterial stenoses can be difficult to ascertain. Using a case presentation as a framework, this exhibit has reviewed the imaging features of both common and rare diagnoses, with emphasis placed on the helpful discriminatory features.

KEYWORDS: Stenosis

EE-31

Isolated Thrombosis of the Deep Medullary Cerebral Veins

San Millan, D.[1]·Bonvin, C.[1]·Gailloud, P.[2]
[1]Hospital of Sion, Sion, SWITZERLAND, [2]The Johns Hopkins Hospital, Baltimore, MD.

Purpose
To report two cases of isolated cerebral deep medullary venous thrombosis.
Case Report
Case 1. A 20 year-old normotensive female with no past medical history presented with an acute episode of left sided hemiparesis and dysarthria in a setting of thunder clap headache. Hemiparesis and dysarthria resolved after 30 minutes. Cardiovascular risk factors included active smoking and oral contraception. The patient was discharged with no persistent neurologic deficit and persistent headache, which resolved over the following weeks. Thrombophilia workup was negative. Noncontrast CT demonstrated linear hyperintensities oriented along the perivascular spaces from the right putamen through the deep white matter to the supero-external angle of the lateral ventricle, suggesting thrombosis of the superior striated veins. Contrast CT did not disclose deep venous system, cortical or dural venous sinus thrombosis. On initial MRI, these linear hyperintensities showed restricted diffusion and susceptibility artifact on SWI. There was locoregional hyperintensity on FLAIR without restricted diffusion consistent with vasogenic edema and several foci of punctate susceptibility artifact consistent with parenchymal hemorrhage in the right putamen and deep white matter. No intraparenchymal or meningeal enhancement was disclosed. Gadolinium-enhanced 3D T1 and phlebography sequences and catheter angiography failed to reveal intracranial thrombosis, particularly of the deep venous system. Follow-up MRI at one and five months demonstrated progressive decrease of the white matter edema with persistence of several foci of FLAIR hyperintensity on the last MRI consistent with gliosis. The linear susceptibility artifacts consistent with superior striated vein thrombosis were found on all follow-up MRIs though restricted diffusion had disappeared. Case 2. A 39-year-old normotensive female with no past medical history presented with severe acute headache, transient dysarthria, lower extremity weakness, left facial paralysis and left upper extremity paresthesia. Cardiovascular risk factors included active smoking, oral contraception and dyslipidemia. The patient was discharged after three days with no persistent neurologic deficit or headache. Aside from a 3 mm putaminal hemorrhage on initial noncontrast CT and MRI, imaging findings were identical to those described in case 1. MR imaging performed three days after the initial imaging workup demonstrated T1-weighted hyperintensity consistent with methemoglobin within the signal changes thought to represent superior striated vein thrombosis.
Imaging Findings
Findings on follow-up MRI performed two years after the initial episode were identical to those in case 1.
Summary
The two cases described above are thought to be consistent with isolated cerebral deep medullary venous thrombosis (superior striated veins) presenting with acute headache (thunderclap headache in case 1) and transient neurologic deficit occurring in two young female smokers under oral contraception. Diagnosis was based on CT and MRI findings consistent with acute clot in the trajectory of the superior striated veins along with locoregional deep white matter edema and punctate hemorrhages, in a setting of predisposing factors for venous thrombosis. Conservative treatment without anticoagulation was opted in both cases. Clinical evolution was favorable with resolution of neurologic symptoms including headache. To the best of our knowledge isolated cerebral deep

Note: Scanned images are included in the proceedings. Some submitted images were reduced during editing, thereby decreasing clarity. Also, refer to the Program Planner. Proceedings Content as of 3-29-2013.

medullary venous thrombosis has not been reported previously in adults.

KEYWORDS: Venous infarction, Cerebral venous thrombosis, deep medullary veins

EE-32

Why Is This Patient Such an Air Head?

Urdaneta-Moncada, A. R.·Helmer, E.·Wong, A.
Kaiser Permanente Los Angeles Medical Center
Los Angeles, CA.

Purpose
To illustrate an unusual case of direct barotrauma to the brain, from inappropriate CPAP use, causing tension hydropneumocephalus.
Case Report
An 88-year-old male with history of obstructive sleep apnea (OSA) presents with worsening headaches and three days of altered mental status. Patient was afebrile and without any focal motor or sensory deficits. Head CT demonstrated extensive pneumocephalus with intraventricular extension and moderate hydrocephalus (Figure 1), initially of unclear cause. Five weeks earlier, the patient had undergone transnasal surgical biopsy of a right sphenoid bone lesion, complicated by CSF leakage that subsequently was repaired (Figure 2). It was later revealed that, after surgery, the patient had used CPAP at home for his OSA against medical advice. It then became clear that the tension hydropneumocephalus seen on our admission reflected direct barotrauma to the brain as a result of positive pressure ventilation into a postsurgical skull base defect which had not yet healed. The dissection of gas through the brain parenchyma into the ventricular system was felt to be due to postsurgical adhesions between the skullbase defect and the overlying brain surface. As the patient was not clinically infected, he was treated conservatively and followed with serial head CTs, which showed marked decrease in pneumocephalus and resolved hydrocephalus by the time of discharge.

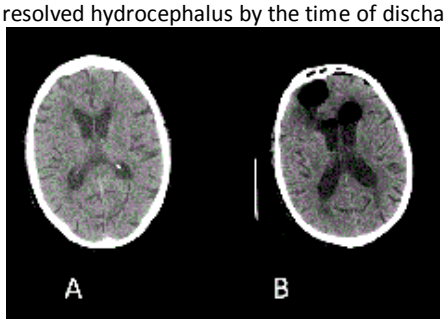

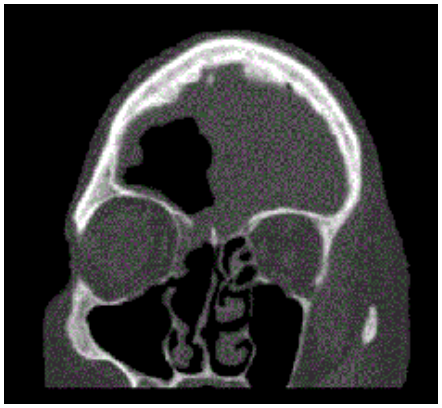

Imaging Findings
1. A: Axial image presurgery, demonstrating normal ventricular size. B: Axial image at admission, demonstrating tension hydropneumocephalus. 2. Coronal reformat, demonstrating surgical defect through the right cribriform plate and pneumocephalus.
Summary
Pneumocephalus is a known consequence of skullbase surgery or trauma. Several cases of positive pressure-induced tension pneumocephalus are reported in the literature. However, to our knowledge, no case of tension pneumocephalus with intraventricular extension and hydrocephalus is documented before. This case illustrates the dangers of using positive pressure ventilation soon after skullbase surgery.

KEYWORDS: Adult brain, Pneumocephalus, Barotrauma

EE-33

Evaluation of Isodense Subdural Hemorrhages

Kohler, N.·Felsberg, G.
Florida Hospital
Orlando, FL.

Purpose
The purpose of this case report is to review the CT and MRI findings in patients with isodense subdural hemorrhages (SDH) on initial CT examination.
Case Report
A 66-year-old male with a past medical history of hypertension, hyperlipidemia and bipolar disorder presented with a history of worsening headaches. On review, the patient denied a history of speech, visual or balance disturbances. He denied vertigo or neurologic deficits. He stated he had a history of fall two weeks previously.
Imaging Findings
The initial scan demonstrates bilateral ill-defined fluid collections which were isodense to cortical gray matter. Follow-up MR imaging demonstrates hypointense subdural fluid collections on T2-weighted imaging.
Summary
Isodense SDH remain a problem for clinicians and

Note: Scanned images are included in the proceedings. Some submitted images were reduced during editing, thereby decreasing clarity. Also, refer to the Program Planner. Proceedings Content as of 3-29-2013.

radiologists in the initial screening evaluation for hemorrhage. Patients with SDH may present initially with a headache and a benign neurologic exam but may quickly deteriorate. Timely diagnosis and treatment is important. In particular, this patient initially underwent a diagnostic MRI and was determined to be neurologically stable. Shortly after he suffered a neurologic decline and underwent emergency decompression. Subdural hemorrhages on CT evaluation have been categorized based on the age of the hematoma, namely, acute (0-7 days), subacute (8-22 days), and chronic (>22 days). A previous study of 429 patients with SDHs found that 98.6% of patients with acute hemorrhages were hyperdense. In patients with subacute hemorrhages, 45.7% were hypodense, 42.9% were isodense and 11.4% were hyperdense. The majority of chronic SDHs were isodense, 73.2% with the remainder hypodense, 21.1%. The large percentage of patients presenting with isodense SDHs remain a diagnostic quandary for radiologists. Diagnosis on plain CT can be difficult due to hemorrhage isodensity to cortex. CT scanning with contrast has been proposed for rapid diagnosis of SDH as subacute or chronic subdural hematomas result in blood-brain barrier breakdown with enhancing margins easily detected. When the diagnosis of SDH is unclear, MRI may be performed in lieu of CT with contrast as was the case for this patient. A retrospective study classified the imaging findings of SDH in 1.5T scanners. Subdural hemorrhages were categorized as acute (one week and two weeks and <one month) and chronic (>one month). Acute SDHs were characterized by hypointensity on long TR/TE images. Early subacute SDHs were noted to have a rim of high signal intensity with a surrounding center of low intensity on long TR/TE images. In late subacute SDHs, there was high signal intensity on all pulse sequences. Chronic SDHs were found to have variable intensity ranging from hypointense to isointense to relative gray matter on short TR/TE imaging.

KEYWORDS: Brain hemorrhage, Subdural hemorrhage, isodense

EE-34

Remote Cerebellar Hemorrhage after Lumbar Drain Placement: Review of a Case

Koohi, Y.·Mukherjee, S.·Matsumoto, J.
University of Virginia Health System
Charlottesville, VA.

Purpose
Intracerebral hemorrhage remote from the site of surgery is an infrequent complication, which has been described after neurosurgical procedures. Remote cerebellar hemorrhage (RCH) has been described following supratentorial and spinal surgery. The most accepted explanation for the occurrence of RCH is the development of cerebrospinal fluid (CSF) hypotension, which in turn leads to sagging of the cerebellum and stretching of the cerebellar veins with subsequent bleeding. Whether stretching leads to occlusion or rupture of bridging cerebellar veins, with resultant hemorrhagic venous infarction or direct hemorrhage remains unclear. Remote cerebellar hemorrhage usually occurs in the superior aspect of the cerebellum following the cerebellar folia in a pattern that has been termed the “zebra sign”. We present a case of RCH in a patient following lumbar drain placement, an uncommon etiology for this rare entity.
Case Report
The patient is a 61-year-old male who was admitted to the hospital for elective open repair of a type III thoracoabdominal aortic aneurysm. The patient underwent intraoperative placement of a lumbar drain. On postoperative day (POD)1, the patient was weaned off sedation and extubated. Upon awakening, the patient was noted to have paraplegia of his lower extremities. The patient was reintubated shortly after extubation due to respiratory distress. MR imaging of the thoracolumbar spine revealed cord infarct extending from T8 to the conus. The patient was started on corticosteroids and lumbar drain remained in place to maintain intracranial pressure (ICP) at 0-5 mm Hg. On POD2, the patient’s lumbar drain was removed without incident. On POD 3, the patient failed to recover his neurologic exam after sedation was weaned. There was concern for an acute intracranial process. Stat head CT revealed hemorrhage in the bilateral cerebellar hemispheres, in a peculiar linear pattern extending across the superior cerebellum and vermis. Blood products appeared to have both an intra- and extra-axial component. This pattern was thought to be most consistent with remote cerebellar hemorrhage following CSF loss related to lumbar drain. Unfortunately, the patient suffered hypoxic ischemic failure and continued to deteriorate neurologically. The patient was extubated and transitioned to comfort care only. He expired on POD 11.
Imaging Findings
Noncontrasted CT of the brain revealed hyperdensity extending in a linear and streaky pattern across the bilateral superior cerebellar hemispheres, compatible with acute hemorrhage. MR imaging, MRA and MRV of the brain was performed shortly after, and ruled out an underlying vascular malformation or dural venous sinus thrombosis as the etiology of the hemorrhage. There was hypointense T2 signal extending across the cerebellar hemispheres with mild adjacent parenchymal edema and mass effect upon the fourth ventricle. There was no hydrocephalus. Several follow-up head CTs did not demonstrate any new hemorrhage.
Summary
Remote cerebellar hemorrhage has been described with supratentorial craniotomy and spinal surgery complicated by dural tear. Intraoperative or postoperative loss of CSF has been proposed as the etiology of this complication. We present a case of RCH following large volume CSF drainage as a result of lumbar drain placement, an unusual etiology of this entity.

Note: Scanned images are included in the proceedings. Some submitted images were reduced during editing, thereby decreasing clarity. Also, refer to the Program Planner. Proceedings Content as of 3-29-2013.

KEYWORDS: Cerebellar, Hemorrhage, Cerebrospinal fluid loss

EE-35

Cerebral Fat Embolism in a Patient with Sickle Cell Anemia/Beta Thalassemia in the Setting of Acute Chest Syndrome and Active Parvovirus B19 Infection

Witkosky, M.·Mossa-Basha, M.
University of Washington
Seattle, WA.

Purpose
We describe the MRI findings in a case of pathology proven cerebral fat embolism in the setting of sickle cell anemia/beta thalassemia and active parvovirus (PV) B19 infection. This is followed by a discussion of relevant pathophysiology.
Case Report
A 27-year-old male patient with sickle cell anemia/beta thalassemia initially presented to the ER with back and chest pain, typical of his prior episodes of acute chest syndrome. Over two days, the patient's consciousness slowly decreased to the point of unresponsiveness. Initial MRI of the brain is described below. The patient's mental status continued to deteriorate, and eight days later repeat MRI brain showed the findings described below. Prognosis was made of a vegetative state and the decision was made to extubate the patient, shortly after which he expired. Post mortem evaluation demonstrated multiple intravascular lesions (consistent with fat) within the brain parenchyma, lungs, and renal glomeruli. Serum PVB19 PCR was positive.
Imaging Findings
Initial MRI brain two days after initial presentation: multiple foci of restricted diffusion involving the striatocapsular region and thalami. Follow-up MRI: diffuse leukoencephalopathy, involving the supratentorial and infratentorial white matter. Susceptibility-weighted imaging shows innumerable foci of susceptibility throughout the white matter, representing tiny hemorrhages. Findings are highly suggestive of cerebral fat embolism syndrome.
Summary
Clinical presentation of cerebral fat embolism is variable including lethargy, delirium, seizures, and coma. In the setting of sickle cell anemia/beta thalassemia, the origin of fat emboli is thought to be the result of vaso-occlusive marrow necrosis, with fat emboli then released into the bloodstream. PVB19 infection can cause an aplastic crisis in patients with chronic hemolytic anemia. This process may be complicated by severe acute lung injury and death in individuals with thalassemia, through the mechanism of fat embolism syndrome associated with bone marrow necrosis. An association of PV B19 infection with marrow necrosis has been recognized, although it is unknown if the virus results in primary marrow necrosis or whether viral injury to the lung results in systemic hypoxemia with resultant increased sickling and subsequent increased marrow necrosis. Petechial hemorrhages throughout the cerebral white matter are the classic histologic lesions suggestive of cerebral fat embolism; however, these are nonspecific and also can be seen in carbon monoxide poisoning, air embolism, and head trauma.The petechial hemorrhages are thought to represent small hemorrhagic embolic infarcts with occlusive fat embolus resulting in vessel wall rupture. Typical MRI findings in cerebral fat embolism include multiple micro-infarcts with punctuate hyperintense foci on T2 and DWI images in the cerebral white matter, basal ganglia, thalami, brainstem, and cerebellum. More confluent hyperinetense T2 and DWI lesions can be seen. Numerous petechial hemorrhages can be seen on heme-sensitive sequences. These microhemorrhages are better depicted on SWI as opposed to GRE images. In conclusion, early diagnosis of hemoglobinopathies and a better understanding of prevention and transmission of PV B19, may result in decreased morbidity and mortality associated with the neurologic sequelae of cerebral fat embolism syndrome.

KEYWORDS: Fat emboli, MR imaging brain, parvovirus B19

Monday, May 20 – Wednesday, May 22
6:30 AM – 9:00 PM
Thursday, May 23
6:30 AM – 3:00 PM
Hall B1

Electronic Excerpta (EE) 36 - 37a

EE2-Anatomy

Note: A missing printed number indicates an abstract has been withdrawn.

EE-36

Angiographic Characterization of a Duplicated Posterior Communicating Artery Variant Associated with a Persistent Primitive Fetal Posterior Cerebral Artery

Honarmand, A. R.·Seth, R.·Hurley, M. C.·Shaibani, A.·Ansari, S. A.
Northwestern University Feinberg School of Medicine
Chicago, IL.

Purpose
Anatomical knowledge is essential for the detection of important neurovascular variants such as duplications, persistent fetal arteries, and fenestrations that may be

Note: Scanned images are included in the proceedings. Some submitted images were reduced during editing, thereby decreasing clarity. Also, refer to the Program Planner. Proceedings Content as of 3-29-2013.

crucial in the pre-operative angiographic evaluation of neurovascular disease. We describe and angiographically elucidate a unique duplication variant of the posterior communicating artery (PcomA) associated with a persistent primitive fetal posterior cerebral artery (PCA) using 3D DSA.

Case Report

A 67-year-old male with a history of fall was diagnosed with prepotine and interpeduncular SAH on CT head study. Digital subtraction angiography (DSA) was performed for further evaluation to exclude underlying neurovascular pathology.

Imaging Findings

Standard AP/lateral and 3D rotational DSA images of the anterior intracranial circulation revealed a duplicated right fetal PCA superior to the right PcomA, providing isolated supply to the posterior temporal branch. The anterior choroidal artery also arose separately from a common origin of the duplicated fetal posterior cerebral artery. Additionally, right vertebral artery DSA images demonstrated minimal opacification of the hypoplastic, but patent right P1 segment contributing to the right PCA distribution in addition to the dominant collateral supply from the right PcomA. However, there was no communication from either the PcomA or P1 segment to the duplicated fetal PCA or its isolated supply to the posterior temporal branch.

Summary

The PcomA, also referred to as “caudal ramus” of the internal carotid artery (ICA), embryogically belongs to the anterior circulation. PcomA variants have been described with several types of anomalies and morphologies including hypoplasia, aplasia/atresia, different lengths and courses, fetal configuration of the PCA branching directly from the ICA, vessels originating from the PcomA (e.g., anterior choroidal artery), fenestration, and partial or complete duplication. A vessel arising independently from ICA distal to the PcomA is termed duplicated PcomAs or duplicated PCAs by different authors. It is exceedingly rare (0.2% at surgical dissection) and has been reported in association with bilateral fetal PCAs and PcomA aneurysm. A few surgical cases of a PcomA duplication variant associated with a persistent primitive PCA have been described, in which one of the arteries arises from the ICA and courses as an isolated temporal artery without joining the PCA. To the best of our knowledge, angiographic characterization of this duplicated PcomA variant (with a persistent primitive PCA) has never been shown. Isolated posterior temporal supply from a persistent primitive PCA versus the native PCA distribution may be an important finding to recognize prior to surgical and endovascular interventions.

KEYWORDS: Anatomical variation, 3D DSA, duplicated posterior communicating artery

EE-37

Fenestration of the Cervical Internal Carotid Artery: Rare Anatomical Variant or Uncommon Presentation of a Common Disorder?

Berberian, G. H.·Federer, G. E.·Burd, D. A.
St. Vincent Hospital
Worcester, MA.

Purpose

We report a case of cervical segment internal carotid artery (ICA) fenestration with contralateral persistent trigeminal artery (PTA) in a 47-year-old female during a workup of transient ischemic attack with ipsilateral weakness and numbness. Fenestration of the cervical ICA is thought to be an extremely rare anatomical variant with only few previously reported cases. Previous authors have even questioned the validity of some true cervical ICA fenestrations, citing a lack of sufficient underlying embryologic explanation. They felt reported angiographic findings instead represented acquired pseudofenetration of dissecting aneurysm, a common cause of stroke in young and middle-aged patients. Our patient presented with symptoms supporting a diagnosis of ICA dissection. Her imaging findings, however, lacked expected supporting pathologic details such as irregular contours, asymmetric limb caliber, intramural hematoma or wall thickening. We describe both the potential congenital and pathologic origins of cervical ICA true and

Note: Scanned images are included in the proceedings. Some submitted images were reduced during editing, thereby decreasing clarity. Also, refer to the Program Planner. Proceedings Content as of 3-29-2013.

pseudofenestrations, present viewpoints both in support of and opposition to true ICA fenestrations with discussion of the expected clinical symptoms and imaging findings, and review the potential imaging pitfalls and mimics of these two discordant diagnoses. Additionally, PTA is an uncommon but well described persistent communication between the carotid artery and vertebrobasilar circulation due to failure of regression of the embryologic trigeminal artery. This is seen in 0.02-0.6% of cerebral angiograms. While PTA is associated with other vascular anomalies such as intracranial aneurysm and vascular malformations, we find no previous report associating it with an ICA fenestration.

Case Report

A 47-year-old female presented with mild occipital headache and left-sided paresthesias of her leg, arm, and face. A left-sided facial droop was reported by the patient's colleagues. She recalled a single episode of lower extremity tingling and weakness with subsequent resolution three years prior. On examination, facial droop had resolved and strength was normal.

Imaging Findings

3D time-of-flight MRA images with maximum intensity projection revealed a 9 mm length fenestration of the left distal cervical ICA with symmetric and smooth 2.5 mm dual channels without wall thickening or intramural hematoma. The bilateral cervical ICAs were dysplastic cephalad to this anomaly. Additionally, an anomalous artery was identified arising from the cavernous C4 segment of the right ICA, extending posteriorly to the basilar artery as a Saltzman type 1 persistent trigeminal artery.

Summary

We report a case of two contralateral anatomical variants. Persistent trigeminal artery is an uncommon but well described finding. Cervical segment ICA true fenestration is, however, quite rare and controversial. The origin of this debate is discussed, both supporting and opposing views are presented, and the potential imaging pitfalls are reviewed.

KEYWORDS: Carotid artery, Fenestration

EE-37a

What Defines Persistent Primitive Ophthalmic Arteries?: A Report of Five Anatomical Variants

Gregg, L.[1]·San Millán, D.[2]·Tamargo, R. J.[1]·Gailloud, P.[1]
[1]Johns Hopkins University School of Medicine, Baltimore, MD, [2]Hospital of Sion, Sion, Valais, Switzerland, SWITZERLAND.

Purpose

Understanding anomalous ophthalmic artery (OA) origins is essential in preventing inadvertent passage of embolic material into important ophthalmic branches during endovascular procedures. We report four observations of OA origin variants and three cases of infraoptic anterior cerebral arteries (ACA). The vessels involved in these variations include the primitive ventral and dorsal OA, the primitive maxillary artery (MA), and the primitive olfactory artery (OlfA). The criteria allowing the identification of these embryonic vessels are discussed.

Case Report

Seven observations of anatomical anomalies derived from variations of four embryonic arteries involved in the formation of the OA are reported.

Imaging Findings

Four types of variants are described: (i) OA from the cavernous segment of the internal carotid artery (ICA) (case 1, primitive MA), (ii) OAs from the distal supraclinoid ICA (cases 2 and 3, primitive ventral or dorsal OA), (iii) OA from the ACA (case 4, primitive OlfA), and (iv) infraoptic ACAs (cases 5 to 7, primitive MA and OlfA).

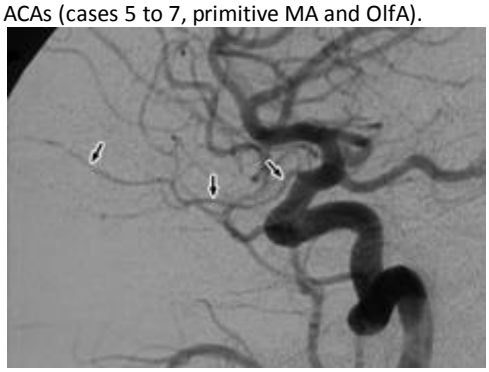

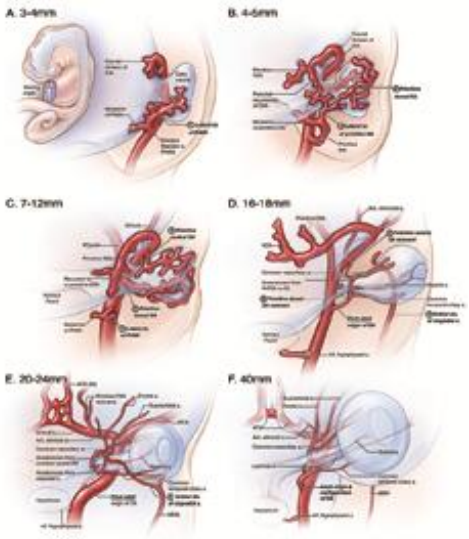

Figures

1. OA (arrows) originating from the distal supraclinoid ICA
2. Development of the OA

Summary

Prior to the formation of the adult OA, the primitive MA, primitive dorsal and ventral OAs, and primitive OlfA contribute to the capillary network surrounding the developing eye. Four types of anomalies derived from these vessels are described. Previously reported OA origin variants and the development of the orbital vasculature are reviewed. Erroneous criteria currently used to identify

Note: Scanned images are included in the proceedings. Some submitted images were reduced during editing, thereby decreasing clarity. Also, refer to the Program Planner. Proceedings Content as of 3-29-2013.

persistent primitive OAs are discussed. An OA arising from the cavernous segment of the ICA likely derives from the primitive MA, while an OA arising from the ACA represents the persistence of a branch of the primitive OlfA. The confusion between these variants and a persistent primitive ventral or dorsal OA appears to result from misinterpretation of the literature concerning the development of the cranial arteries.

KEYWORDS: Ophthalmic artery, Anatomical variation, persistent embryonic vasculature

Monday, May 20 – Wednesday, May 22
6:30 AM – 9:00 PM
Thursday, May 23
6:30 AM – 3:00 PM
Hall B1

Electronic Excerpta (EE) 38 - 54a

EE3-Head and Neck

Note: A missing printed number indicates an abstract has been withdrawn.

EE-38

Venous Invasion of a Salivary Gland Mass as the First Presentation of Metastatic Renal Cell Carcinoma

Maralani, P. J.·Mohan, S.·Loevner, L. A.·Jhala, N. C.
University of Pennsylvania
Philadelphia, PA.

Purpose
We review the imaging findings of a 64-year-old otherwise healthy female who presented with left facial swelling. Imaging findings demonstrated multiple salivary gland masses. The mass in the left parotid gland was associated with venous invasion into the retro-mandibular and facial veins and into the left internal jugular vein (IJV). Based on the venous invasion, the diagnosis of metastatic renal cell carcinoma was suggested on imaging, which subsequently was confirmed on systemic workup and pathology.
Case Report
Our patient is a 64-year-old female with a history of hypertension controlled by thiazide diuretics who presented to an outside physician with swelling in the left side of the face of unknown duration. There was no sign of facial nerve deficit or other significant past medical or surgical history. Outside institution contrast-enhanced neck CT scan demonstrated multiple masses in bilateral parotid glands, left submandibular gland and in the right lobe of the thyroid gland. The patient then was referred to our institution for further management.
Imaging Findings
Contrast-enhanced MRI of the neck demonstrated a 2.8 cm mass involving the superficial and deep lobes of the left parotid gland, a 1.0 cm mass in the right parotid gland, several masses in the left submandibular gland the largest one measuring 2.0 cm and a 3.0 cm mass in the right lobe of the thyroid gland. The masses were slightly hyperintense compared to skeletal muscle on T1- and T2-weighted images with mild restricted diffusion and showed avid postcontrast enhancement. There was no pathologic neck lymphadenopathy. The mass in the left parotid demonstrated invasion and extension to the left retro-mandibular and facial veins extending to the left IJV. Based on this finding and multiplicity of the masses imaging diagnosis of metastatic renal cell carcinoma was proposed. The patient subsequently underwent contrast-enhanced CT of the abdomen and pelvis which demonstrated a 9 x 7 x 6 cm vascular enhancing mass in the right kidney with no extension to the right renal vein. Biopsy of the salivary gland masses and nephrectomy specimen both confirmed clear cell renal cell carcinoma.
Summary
This case signifies two important imaging findings. Firstly, multiplicity of masses should raise suspicion for metastatic disease with the renal cell carcinoma being the most common source for distant metastasis to the thyroid. Secondly, venous invasion of a mass is a known characteristic of the renal cell carcinoma. Although venous invasion can occur in other neoplasms such as hepatocellular carcinoma, renal cell carcinoma is the most common to present in this fashion with remote metastasis.

KEYWORDS: Salivary gland, Thyroid, Renal cell carcinoma

EE-39

Rare Submandibular Bronchopulmonary Foregut Cystic Malformation Mimicking a Lymphatic Malformation

Gross Kelly, T. C.[1,2]·Subramanian, S.[1]·Moe, D.[1,2]·North, P. E.[3,2]·Chun, R. H.[1,2]
[1]Children's Hospital of Wisconsin, Milwaukee, WI, [2]Medical College of Wisconsin, Milwaukee, WI, [3]Wisconsin Children's Hospital, Milwaukee, WI.

Purpose
Bronchopulmonary foregut cystic malformation (BFCM) is an uncommon cause of a cystic neck mass, as they usually are found in chest and abdomen. The imaging features are nonspecific and preoperative diagnosis is usually difficult. We present an unusual case of BPFCM that presented as a multiseptated cystic lesion in the submandibular and sublingual space mimicking a lymphatic malformation.
Case Report
A 31/2-year-old girl presented with recurrent swelling of the left submandibular gland region. When she was one

Note: Scanned images are included in the proceedings. Some submitted images were reduced during editing, thereby decreasing clarity. Also, refer to the Program Planner. Proceedings Content as of 3-29-2013.

year old a lump was noted in the same area, but it spontaneously decompressed. Based upon the current MRI findings, a lymphatic malformation was suspected. A ranula was felt to be less likely as no lesion could be palpated along the floor of the mouth. She underwent three sclerotherapy attempts but the lesion persisted and swelling increased. Therefore, the lesion finally was surgically excised. Surgical pathology results revealed that the lesion was a rare bronchopulmonary foregut cystic malformation (BPFCM).

Imaging Findings

MR imaging examination revealed a septated cystic lesion within the left submandibular space extending into the left sublingual space. The left submandibular gland was displaced laterally. Ultrasound revealed a cystic mass without solid components. Using Picibanil and ultrasound guidance three sclerotherapy attempts were made.

Summary

Given the findings in this case, we suggest that BPFCM should be added to the list of diagnostic possibilities when encountering a mulitseptated cystic lesion in the submandibular space.

KEYWORDS: Masses, Cystic neck mass, submandibular space

EE-40

Hypervascular Mass at the Carotid Bifurcation: Not Always a Carotid Body Tumor

Ibrahim, H.·Sepahdari, A.
University of California Los Angeles
Los Angeles, CA.

Purpose

We present a series of three cases of hypervascular carotid bifurcation-region masses mimicking carotid paraganglioma [i.e., carotid body tumor (CBT)], and a companion case of a true CBT. Relevant anatomy of the carotid space is reviewed, including position of traversing cranial nerves, the sympathetic chain, vessels, and paraganglia. The imaging features of CBT are reviewed, and the phenomena of hypervascular schwannomas and low vagal paragangliomas (i.e., those occurring below the typical location of the inferior nodose ganglion) are discussed.

Case Report

Three adult patients with hypervascular neck masses were referred to our hospital with presumptive diagnoses of CBT. These lesions were surgically proven to be a sympathetic chain schwannoma, vagal schwannoma and vagal paraganglioma. In each case, a careful review of the images was able to suggest sympathetic chain or vagal origin of these lesions.

Imaging Findings

Characteristic imaging features of CBTs are well established on noncontrast and contrast-enhanced MRI, and also on conventional angiography. These include avid contrast enhancement, a “salt-and-pepper” appearance on MRI, and splaying of the internal and external carotid arteries at the carotid bifurcation. Catheter angiography is able to demonstrate a vascular blush, and tumor supply by enlarged branches of the external carotid artery, which are amenable to preoperative embolization. The hypervascular carotid bifurcation region masses in our case series showed the typical signal characteristics described, and also separated the internal and external carotid arteries, but were not centered at the carotid bifurcation. The sympathetic chain lesion displaced both the internal and carotid arteries laterally, while the vagal lesions anteriorly displaced the internal and external carotid arteries while posteriorly displacing the internal jugular vein.

Note: Scanned images are included in the proceedings. Some submitted images were reduced during editing, thereby decreasing clarity. Also, refer to the Program Planner. Proceedings Content as of 3-29-2013.

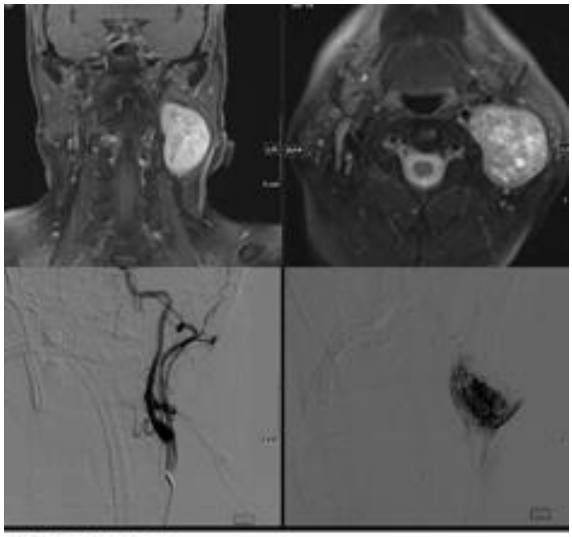

Vagal schwannoma.
Fig 1a. T2-weighted coronal and axial MR images of the neck at the level of the carotid bifurcation demonstrating a heterogenously hyperintense mass.
Fig 1b. Angiography (AP view) of the left CCA and selective ECA branch injection demonstrates a hypervascular mass displacing the ECA medially, but absence of splaying of the ICA/ECA that is seen with carotid body tumors.

Summary
Carotid body tumors classically present as hypervascular masses at the carotid bifurcation. This well known feature may cause a reflexive diagnosis of any hypervascular mass in that region as a CBT. The therapeutic and prognostic implications of an erroneous imaging diagnosis are important. All neuroradiologists should be familiar with detailed anatomy of the carotid space, differential considerations of hypervascular tumors in that region, and how to distinguish them on imaging.

KEYWORDS: Glomus tumors, Neck masses

EE-41

Bilateral Inferior Alveolar Nerve Enlargement

Kumar, S.[1,2]·Ginsberg, L. E.[2]
[1]Baylor College of Medicine, Houston, TX, [2]The University of Texas M. D. Anderson Cancer Center, Houston, TX.

Purpose
We present an unusual case of bilateral inferior alveolar nerve enlargement.
Case Report
A 30-year-old, asymptomatic female presented to the dentist office for routine care. Bilateral enlarged mandibular canal was noticed in her routine panoramic radiograph and the patient was referred for imaging evaluation. There was no sensory neuropathy referable to the mandible, and no prior history of trauma.
Imaging Findings
MR imaging of the face with intravenous contrast was obtained to assess the extent of potential disease and for further characterization. There was bilateral widening of the mandibular canal (L>R) with an "onion- bulb" like configuration, presumably caused by enlarged inferior alveolar nerves. The enlarged nerves were isointense to muscle on T1 and markedly hyperintense on T2 without any enhancement. The mandibular and mental foramen were intact. Panoramic radiograph shows fusiform enlargement of both mandibular canals.

Summary
Bilateral enlargement of intramandibular inferior alveolar nerve without enhancement in an asymptomatic patient was presumed to be hypertrophic neuropathy. Nonenhancement is atypical for peripheral nerve sheath tumor with MR imaging. Hypertrophic neuropathy is a well known condition of the peripheral nerves. They rarely have involved cranial nerves including the trigeminal and vestibulocochlear nerves. There has been only one case of isolated unilateral hypertrophic neuropathy of inferior alveolar nerve reported in the literature. However, our case is unique because of bilateral inferior alveolar nerve enlargement. In localized hypertrophic neuropathy there is slow progressive loss of motor function and sensation in the distribution of a single nerve. Our patient is presently asymptomatic and an asymptomatic variant has not been described in the literature. Because of potential for development of neurologic symptoms in the future, a detailed neurologic workup and close observation are planned.

KEYWORDS: Hypertrophic neuropathy, Inferior alveolar nerve

EE-42

Intraneural Perineurioma of the Trigeminal Nerve Presenting as Recurrent Headache

DeLoia, S. P.·Branstetter, B. F.·Clark, K. H.
University of Pittsburgh Medical Center
Pittsburgh, PA.

Purpose
Perineurioma is a rare neoplasm of the nerve sheath that most commonly is associated with peripheral nerves of the extremities. We present a rare case of the intraneural variant of this lesion arising from the trigeminal nerve.

Note: Scanned images are included in the proceedings. Some submitted images were reduced during editing, thereby decreasing clarity. Also, refer to the Program Planner. Proceedings Content as of 3-29-2013.

Case Report
A 36-year-old Caucasian male with no significant past medical history presented with two years intermittent left-sided headaches. When the headaches progressed in frequency and intensity, the patient underwent unsuccessful medical therapy for presumed migraines, after which MRI of the brain was performed. MR imaging revealed a complex lesion centered in the cisternal segment of the left trigeminal nerve, and a presumptive diagnosis of trigeminal schwannoma was rendered. The patient was referred to neurosurgery for endoscopic transsphenoidal debulking, with final pathology revealing intraneural perineuroma. Incomplete symptomatic relief was reported following surgery. Stereotactic radiosurgery is planned to control residual tumor.
Imaging Findings
Multiple MR examinations reveal a lobular, heterogenous lesion extending from the cisternal segment of the left trigeminal nerve through Meckel's cave and into the left cavernous sinus. There were regions of high T2 signal with minimal enhancement, and other regions with intermediate T2 signal and moderate enhancement. Involvement of the second and third branches of the fifth cranial nerve also was demonstrated, as tumor spread through the foramen ovale and foramen rotundum. A largely cystic component extended into the left pterygopalatine fossa.
Summary
A rare case of intraneural perineurioma of the trigeminal nerve is presented, with symptoms of trigeminal neuralgia correlated to tumor involvement of the second and third branches. The imaging findings and pathologic characteristics are described to illustrate the nature of this unique neoplasm. We also review the pathologic classification of nerve sheath tumors with attention to their different radiologic appearances.

KEYWORDS: Perineural, Trigeminal nerve

EE-43

Review of MR Imaging Features of Herpes Zoster Opthalmicus

Rehmani, R.·Gandhi, S.
North Shore University Medical Center
Manhasset, NY.

Purpose
To illustrate subtle and often overlooked imaging features of herpes zoster opthalmicus on MRI.
Case Report
A 69-year-old female presented with intractable left eye pain and ocular migraines for one week. She went on to develop vesicular rash along the left medial canthus. Clinical diagnosis of herpetic neuralgia was made. Initial orbit and brain MRI were normal. However, she returned two weeks later with worsening left ocular pain with new onset ptosis, opthalmoplegia and photophobia. However, a repeat follow-up brain MRI demonstrated multitude of intracranial and left orbital findings.
Imaging Findings
MR imaging findings showed loss of normal hyperintense T2 CSF signal within the left optic nerve sheath and evidence of retrobulbar perioptic enhancement. Left orbit also demonstrated extraocular myositis, stranding of the retrobulbar fat and proptosis. Postcontrast intracranial transneural enhancement also was noted in the left Meckel's cave and the left proximal trigeminal nerve.

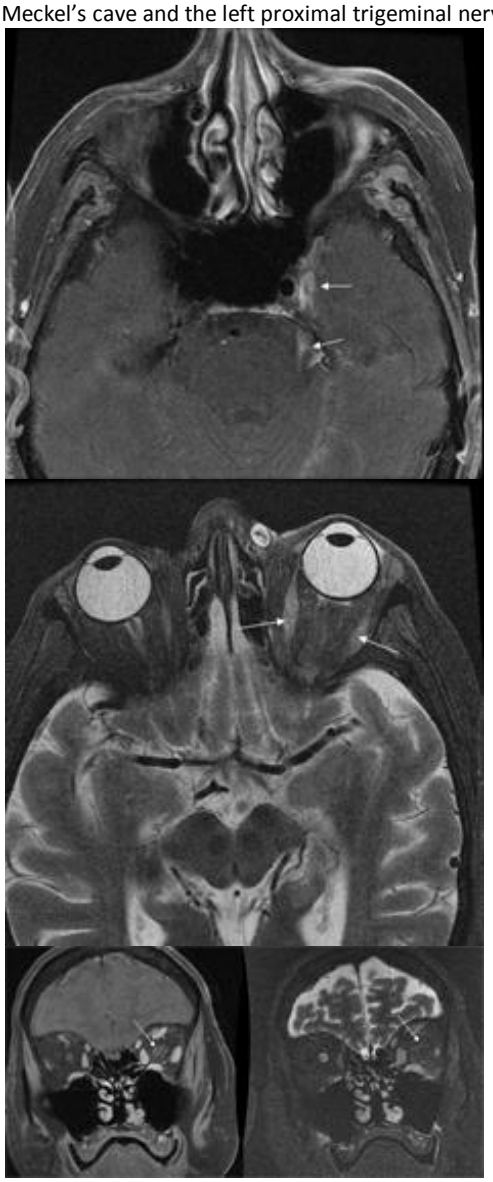

Summary
Herpes zoster opthalmicus is a rare entity and can progress to complications such as acute retinal necrosis which can drastically alter the clinical outcome and patient management. This case outlines the key orbital and intracranial imaging checklist for herpes zoster infection.

KEYWORDS: Orbits, Optic nerve, orbital myositis

Note: Scanned images are included in the proceedings. Some submitted images were reduced during editing, thereby decreasing clarity. Also, refer to the Program Planner. Proceedings Content as of 3-29-2013.

EE-44

Isolated Rheumatoid Arthritis of the Atlanto-Occipital Joint Confused with Migraine

Kozic, D.·Bjelan, M.·Njagulj, V.·Lucic, M.·Koprivsek, K.
University of Novi Sad School of Medicine
Novi Sad, SERBIA.

Purpose
The aim of this report is to demonstrate imaging findings of isolated rheumatoid arthritis (RA) of atlanto-occipital joint that was presented clinically as atypical migraine.
Case Report
Magnetic resonance imaging (MRI) was performed in a 52-year-old woman with a several years long history of the left hemicranial pain, most compatible with migraine. The pain was accompanied with left eye "tunnel vision". The duration of pain was between 48-72 hours, approximately three times per month. No positive response to treatment was evident. The patient also complained of chronic muscle stiffness and tightness in the left suboccipital region. The presence of synovial effusion without erosions of the joint's facets was revealed on MRI most consistent with RA (Figure a,b). No lesions within the brain parenchyma were evident. Laboratory screening was ordered. Rheumatoid factor was significantly positive, >80 IU/ml (normal range 0-20 IU/ml). Clinical examination, performed after MRI study, detected no involvement of other joints.

Summary
Isolated RA of atlanto-occipital or atlantoaxial joints easily could be associated with misdiagnosis and mistreatment. MR imaging became important imaging tool that has had the ability to assess simultaneously all relevant structures in inflammatory joint disease - the synovium, cartilage, bone, ligaments, tendons, tendon sheaths and the presence of synovial fluid.

KEYWORDS: Rheumatoid arthritis, MR imaging

EE-45

Optimized Imaging of Atlantooccipital Synovial Cysts Compressing the Hypoglossal Nerve

Rydberg, C. H.·Lane, J. I.
Mayo Clinic
Rochester, MN.

Purpose
Isolated unilateral hypoglossal nerve palsy is a rare condition. When imaging reveals a cystic mass in the hypoglossal canal, a synovial cyst arising from the atlanto-occipital joint may be misdiagnosed as the more common cystic schwannoma. We offer suggestions for detecting and correctly diagnosing this rare lesion.
Case Report
A 64-year-old man presents with a one-year history of progressive dysarthria, dysphagia, and right tongue hemiatrophy. Electromyography confirmed denervation of the genioglossus muscle.
Imaging Findings
CT and MRI demonstrate expansion of the right hypoglossal canal by a cystic mass with minimial peripheral enhancement suggesting a hypoglossal schwannoma with cystic degeneration. Axial 3D gradient (FIESTA) sequence shows the cystic mass within the hypoglossal canal (Image A) and the continuity of the cyst with the atlanto-occipital joint (Image B). A 3D FSET2 (Cube) sequence parallel to the hypoglossal canal confirms the cyst as arising from the atlanto-occipital joint and extending cephalad to exit through the hypoglossal canal (Image C).

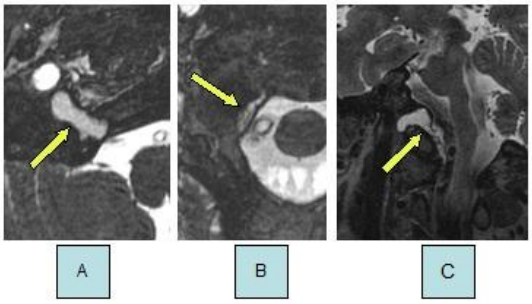

Summary
Isolated unilateral hypoglossal nerve palsy is a rare condition. Differential diagnosis includes hypoglossal schwannoma, meningioma, metastasis, epidermoid, jugulotympanic paraganglioma, dural AVF, solitary fibrous tumor, and synovial cyst arising from either the atlanto-occipital or atlanto-axial joint. If a cystic mass with minimal or no periperal enhancement is discovered, a cystic schwannoma or synovial cyst is the most likely diagnosis. To differentiate, an axial 3D gradient (FIESTA) sequence and 3D FSET2 (Cube) images obtained/reformatted parallel to the hypoglossal canal can demonstrate the origin of the synovial cyst from a joint space. Correct diagnosis allows correct treatment - stabilization, rather than an unnecessary intradural exploratory surgery.

Note: Scanned images are included in the proceedings. Some submitted images were reduced during editing, thereby decreasing clarity. Also, refer to the Program Planner. Proceedings Content as of 3-29-2013.

KEYWORDS: Cyst, Cranio-cervical junction, hypoglossal nerve palsy

EE-46

Tongue Twisted

Darflinger, R. J.·Wong, A.
Kaiser Permanente Los Angeles Medical College
Los Angeles, CA.

Purpose
Illustrate a rarely seen etiology for cranial nerve XII palsy: dissection of the internal carotid artery with pseudoaneurysm formation at the level of the hypoglossal canal.
Case Report
A 61-year-old male with history of hypertension presents with 10 days of left occipital headaches radiating to the neck, and dysphagia, initially treated unsuccessfully for muscle spasm. Subsequent evaluation showed leftward tongue and uvular deviation, and left tongue hemiatrophy with fasciculations.
Imaging Findings
Brain MRI showed asymmetry of the left genioglossus muscle (Figure 1). Laryngoscopy confirmed left tongue atrophy, ipsilateral deviation, and left palate asymmetry; however, no mass was seen. Subsequent CTA demonstrated a left ICA dissection at the craniocervical junction with a 10 mm tortuous dissecting pseudoaneurysm at the level of the hypoglossal canal, effacing the soft tissue planes in the area of the exiting hypoglossal nerve (Figure 1). The aneurysm was confirmed with cerebral angiography (Figure 2) and treated with stent placement. The patient's tongue deviation was resolved at one-month followup.

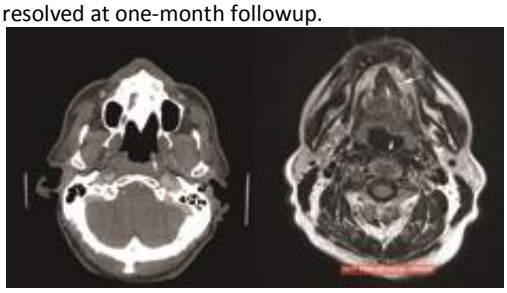

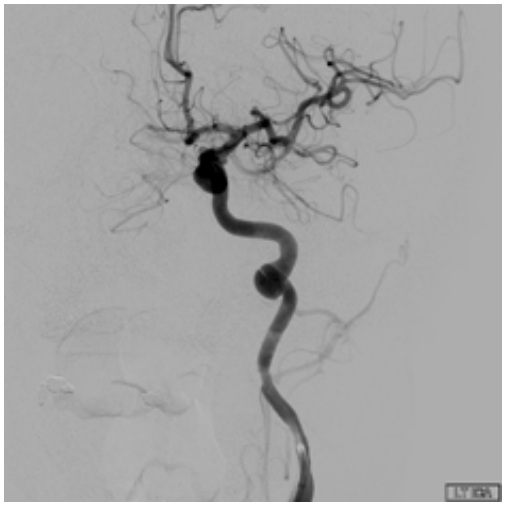

Summary
Hypoglossal (CN XII) palsies can be due to a variety of conditions, with more common etiologies including ischemia, CNS neoplasm, demyelination disease, nasopharyngeal carcinoma, and metastases. Lesions causing this deficit can be located anywhere from the level of the CN XII nucleus at the medullary tectum to the base of the tongue. Dissection and pseudoaneurysm of the ICA is a rarely reported etiology. This case illustrates the importance of considering vascular causes when interpreting imaging studies, including MR imaging, for CN XII palsy.

KEYWORDS: Dissecting aneurysm, Carotid artery, hypoglossal nerve

EE-47

Patient with Incidental Ectopic Retropharyngeal Thyroid Tissue Found to Have Hashimoto's Thyroiditis

Wrubel, G. L.[1]·Juliano, A. F.[2]
[1]Brigham and Women's Hospital, Boston, MA,
[2]Massachusetts Eye and Ear Infirmary, Boston, MA.

Purpose
Ectopic thyroid tissue should be considered in the differential diagnosis of a neck mass which is similar density to thyroid gland on noncontrast CT. This case report highlights that the spectrum of pathology affecting the thyroid gland (e.g., infection, auto-immune disease, neoplasm, etc.) also can affect ectopic thyroid.
Case Report
This 56-year-old male was incidentally found to have a retropharyngeal mass on MRI while being worked up for a musculoskeletal complaint. Initial neck imaging showed a large enhancing right-sided retropharyngeal mass. A fine needle aspiration revealed normal thyroid tissue. The patient returned one month later with odynophagia. Repeat imaging demonstrated an interval increase in size of the retropharyneal mass which exhibited new heterogeneity concerning for infection or less likely

Note: Scanned images are included in the proceedings. Some submitted images were reduced during editing, thereby decreasing clarity. Also, refer to the Program Planner. Proceedings Content as of 3-29-2013.

malignancy. Following empiric antibiotic therapy, the patients symptoms resolved and the mass returned to its baseline appearance on CT. For definitive diagnosis, the patient was taken to the OR for resection. Chronic lymphocytic thyroiditis was diagnosed on pathology.
Imaging Findings
This patients' initial contrast-enhanced neck CT showed a homogeneously enhancing right-sided retropharyngeal mass that minimally extended into the right parapharyngeal space. Normal-appearing thyroid was identified within the infrahyoid visceral space. Repeat imaging when the patient acutely presented with odynophagia showed an interval increase in size of the mass which exhibited new heterogeneous enhancement and resulted in mass effect on the oropharynx. There was adjacent lymphadenopathy and oropharyngeal mucosal thickening and enhancement. Multiple new foci of hypoattenuation throughout the mass and surrounding the mass were suggestive of phlegmon or developing abscess. A follow-up CT after the patients empiric antibiotic course showed the retropharyngeal mass to be similar in appearance to the baseline CT.

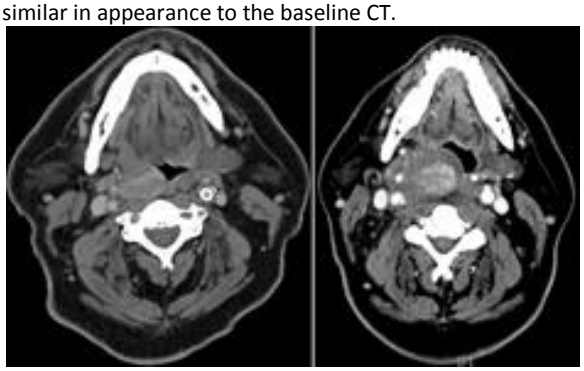

Summary
Ectopic thyroid tissue is reported in seven percent of adults. The majority of ectopic thyroid tissue occurs along the course of the thyroglossal duct or along the 4th brachial pouches. Rarely, ectopic thyroid tissue may occur in unusual locations such as the retropharyngeal space, mediastinum, pericardium, etc. A few case reports of Hashimoto's thyroiditis involving struma ovarii and multinodular goiters extending into the retropharyngeal space have been described in the literature with no previously described case involving incidental ectopic retropharyngeal thyroid tissue. This case report demonstrates that ectopic thyroid tissue should be considered in the differential diagnosis of a neck mass that has thyroid tissue characteristics on CT and that ectopic thyroid tissue can harbor the same pathology affecting normal thyroid gland.

KEYWORDS: Ectopic thyroid, Hashimoto's

EE-48

Youngest Reported Case of Anaplastic Thyroid Cancer

Morozova, L.·Gibson, T.·LaFranchi, S.·Shindo, M.·Sauer, D.·Stork, L.·Pollock, J.
Oregon Health and Science University
Portland, OR.

Purpose
Describe the history, clinical presentation, and imaging findings of the youngest reported female with anaplastic thyroid cancer (ATC).
Case Report
A previously healthy 13-year-old girl was brought to medical attention after discovering a rapidly enlarging right neck mass. The patient reported recent development of "breathy" voice and occasional cough while drinking liquids. There was no hemoptysis, dyspnea, wheezing, or dysphagia. On physical examination, there was a 4 cm minimally mobile hard right neck mass, extending from the right thyroid. The patient also had enlarged right deep cervical lymph nodes and right vocal cord paralysis. FNA of the lesion yielded poorly differentiated carcinoma. The patient underwent CECT scan of the neck and PET scan which demonstrated large right thyroid mass with multiple FDG avid, enlarged, hypodense cervical, mediastinal, and hilar lymph nodes. The patient underwent total thyroidectomy and bilateral modified radical neck dissection. The pathology revealed poorly differentiated thyroid carcinoma with extensive lymphatic and vascular invasion. Metastatic deposits were found in 14/70 regional lymph nodes. The patient proceeded to systemic chemotherapy and subsequently to palliative radiation therapy, but continued to decline. Follow-up imaging demonstrated development of osseous and rapid progression of pulmonary metastasis and hospice referral was made.
Imaging Findings
CECT neck: enlarged and heterogeneous thyroid gland with multiple hypodense and enlarged lymph nodes in the cervical, mediastinal and hilar regions. PET/CT: increased FDG metabolism in both thyroid lobes with extensive metastasis to bilateral cervical, mediastinal, and hylar lymph nodes. Multiple pulmonary nodules were seen on low dose CT scan but only the largest pulmonary nodule in the left lower lobe demonstrates increased metabolic activity.
Summary
Anaplastic thyroid cancer is a very aggressive and deadly cancer that is typically seen in the elderly. This entity should be considered in any patient who presents with a rapidly enlarging neck mass.

KEYWORDS: Thyroid, Neoplasm, anaplastic

Note: Scanned images are included in the proceedings. Some submitted images were reduced during editing, thereby decreasing clarity. Also, refer to the Program Planner. Proceedings Content as of 3-29-2013.

EE-49

Two Cases with Ulcerative Colitis Presenting Acute, Localized Myositis in the Neck

Nakatsuka, T.·KItamura, N.·Inaoka, T.·Terada, H.
Toho University
Sakura, JAPAN.

Purpose
We recently encountered two cases with ulcerative colitis presenting acute, localized myositis in the neck under an immunosuppressive therapy. To our knowledge there is no previous report describing inflammatory bowel disease (IBD)-related myositis in the neck. We report these cases.
Case Report
Cases were a female patient in her 30s with four-year history of ulcerative colitis and a male patient in his 10s with six-month history of ulcerative colitis. Both of them presented with neck pain and fever. CT scan and MRI revealed swelling and T2-prolongation of neck muscles in both cases. Infliximab therapy in the first case and steroid therapy in the second case for ulcerative colitis resolved their neck symptoms.
Summary
From 25 to 40 percent of cases with IBDs, including ulcerative colitis and Crohn's disease, may be associated with extraintestinal manifestations, of which musculoskeletal manifestations are the most common. Arthritis is common in patients with IBDs, but myositis is quite rare.

KEYWORDS: Inflammatory

EE-50

Anaplastic Lymphoma Kinase-Positive Anaplastic Large Cell Lymphoma of the Anterior Skull Base

Jamshidi, P.[1]·Chen, J. Y.[2,3]·Wang, H.[2]·Chen, C. C.[2]
[1]University of California at San Diego, La Jolla, CA,
[2]University of California San Diego Health System, La Jolla, CA, [3]San Diego Veterans Adminstration, La Jolla, CA.

Purpose
To describe an unusual case of an anaplastic lymphoma kinase (ALK)-positive anaplastic large cell lymphoma (ALCL) and highlight its multimodal imaging features and interdisciplinary approach to diagnosis and management. ALK(+) ALCL is a rare peripheral T-cell lymphoma, accounting for approximately 3% of adult nonHodgkin lymphomas (NHL). To the best of our knowledge, this is the first report in which the presentation was an aggressive mass involving upper nasal cavity and anterior skull base.
Case Report
A 28-year-old Asian female presented with a three-month history of nasal congestion culminating in epistaxis. Physical examination was notable for a tissue mass obstructing nasal cavity and the sphenoid sinus. CT and MR imaging revealed a lesion primarily involving the upper nasal cavity extending intracranially through the cribriform plates into the anterior cranial fossa. Preoperative biopsy of the mass proved to be an ALK(+) ALCL based on histological and immunohistochemical profiles, thus obviating need for invasive surgical resection. The tumor mass shrank significantly after two cycles of chemotherapy supplemented with radiation therapy. The patient achieved clinical remission and remained neurologically stable throughout the treatment.
Imaging Findings
MR imaging of the orbital and nasal region demonstrated a homogenous and well-defined mass, with mild homogenous enhancement and mild restricted diffusion, expanding and filling both nasal cavities and extending intracranially through the cribriform plates, with thick dural enhancement, as well as extension through the clivus into the prepontine cistern. The mass encased the right cavernous carotid artery in the cavernous sinus. There was expansile remodeling of the nasal cavity, with lateral deviation of the medial orbital walls with mass effect on the lateral rectus muscles and compression of the orbital apices and intra-orbital optic nerves, likely contributing to the patient's lack of vision in the left eye. Pathologically enlarged right retropharyngeal lymph node with conspicuous left retropharyngeal lymph nodes as well as upper level IB/II lymph nodes, were compatible with either a typical pattern of esthesioneuroblastoma nodal metastases or lymphoma. Maxillofacial CT scan confirmed the MR imaging findings and bony erosion of the anterior clivus, bilateral medial sphenoid bones, and left clinoid process. Although the constellation of tumor location, characteristics of radiologic findings as well as the pattern of bony and regional lymph node involvement is helpful in narrowing down the differential diagnosis to lymphoma or ethesioblastoma, the clinical management of these entities is dramatically different, and biopsy is required for definitive diagnosis to guide management.
Summary
To our best knowledge, this is the first case of an ALK(+) ALCL that presented as an aggressive upper nasal cavity and anterior skull base lesion. This case highlights the importance of multimodality approaches including preoperative imaging and tissue biopsy for definitive diagnosis in order to optimize treatment options and achieve best clinical outcome.

KEYWORDS: Lymphoma, Nasal mass, Mimic

Note: Scanned images are included in the proceedings. Some submitted images were reduced during editing, thereby decreasing clarity. Also, refer to the Program Planner. Proceedings Content as of 3-29-2013.

EE-51

Inflammatory Pseudotumors of the Head and Neck: A Pictorial Review

Koohi, Y.·Raghavan, P.
University of Virginia Health System
Charlottesville, VA.

Purpose
Inflammatory pseudotumor (IPT) is a nonneoplastic process, consisting of inflammatory cells with a variable fibrous response, and can arise in almost any organ, most frequently involving the lungs, abdominal organs and orbits. Inflammatory pseudotumors can mimic a malignant tumor both radiologically and clinically. Inflammatory pseudotumors in the head and neck region most frequently involve the orbit, with sinonasal involvement being relatively rare. The purpose of this exhibit is to present the imaging findings of inflammatory pseudotumors of the head and neck on CT and MRI, utilizing a variety of cases from our institution. Several of the presented cases involve the maxillary sinus, where we have noted distinct bony changes of the maxillary antrum. Pathologic findings in several of these cases demonstrate borderline increased IgG4 positive plasma cells, and these lesions may in fact represent IgG4-related sclerosing lesions.
Case Report
A number of cases will be presented, including a 20-year-old male with left medial orbital mass and left maxillary sinus mass, with biopsy of both lesions revealing fibrosis and chronic inflammation with borderline increased IgG4 positive plasma cells in the orbital lesion. A 45-year-old female presented with a right medial orbital mass and right maxillary sinus mass. Biopsy of the maxillary sinus mass revealed sclerosing inflammatory lesion with question of IgG4-related sclerosing lesion. A 35-year-old female presented with a left maxillary and left buccal space lesion. Biopsy of the maxillary lesion showed tumefactive fibroinflammatory lesion. A 10-year-old female presented with left nasal cavity and left orbital mass. Pathology revealed inflammatory myofibroblastic tumor.
Imaging Findings
The presented cases with maxillary sinus involvement all show distinct bony changes of the maxillary antrum, with thickened, sclerotic bone on CT. MR imaging followup in several patients showed hypointense T2 signal of the soft tissue components, characteristic for fibrous-type tumors. Interestingly, one of the presented patients with maxillary sinus involvement also had unilateral pachymeningeal enhancement, thought to be related to idiopathic hypertrophic pachymeningitis. This entity may in fact represent central nervous system involvement with IgG4-related sclerosing disease.
Summary
Inflammatory pseudotumor is still a poorly understood entity and has many synonyms. Recently it has been proposed that IgG4-related sclerosing lesions may have been described previously as inflammatory pseudotumors. Treatment with corticosteroids represents first line treatment for inflammatory pseudotumors.

KEYWORDS: Inflammatory pseudotumor, Head and neck

EE-52

Is That Just a Nasal Polyp? Or Is That a Meningoencephalocele Extending Through the Frontal Sinus?

Krishnan, A.·Al-Jaber, A.·Zakalik, K.·Rontal, D.
William Beaumont Hospital
Royal Oak, MI.

Purpose
Nasal polyps are common findings both clinically and on imaging. The predominant fluid nature of these lesions can be well seen on both MRI and on CT. Anterior skull-based cephaloceles can rarely present as intranasal masses. It is even rarer to find a meningocele traversing the frontal sinus drainage pathway into the nasal cavity and then proceeding into the nasopharynx, thereby mimicking a frontal sinonasal polyp.
Case Report
A 60-year-old female patient with a prolonged history of nasal stuffiness and sinusitis was scheduled for an endoscopic sinus surgery. Outside sinus CT had demonstrated a long polypoid structure in the nasal cavity extending into the nasopharynx. Fortunately, in the preoperative area, the images were reviewed with radiology and concern was raised for an intracranial abnormality. The surgery was rescheduled. After review of multiple head MRIs, a diagnosis was made and a combined approach by ENT and neurosurgery to extract both the nasal mass and repair the frontal sinus and frontal lobe abnormality was adopted. Intraoperative pictures documenting the surgery also were obtained.
Imaging Findings
Prior head MRI images demonstrated an irregular inferior frontal lobe indenting the frontal sinus through a defect in the posterior wall of the sinus. Subsequent studies revealed gradual increase in the size of the frontal sinus encephalocele that extended further inferiorly in the frontal sinus. At its distal aspect, a fluid-filled structure was seen exiting the sinus into the nasal cavity. The final MRI and CT obtained before surgery demonstrated a long fluid-filled structure in the nasal cavity extending from the frontal sinus into the posterior choana and finally into the nasopharynx. As the encephalocele portion itself was small and restricted to the frontal sinus, it was this meningocele portion that initially had been thought to represent a long sinonasal polyp.
Summary
Herniation of brain, meninges, and CSF via skull base defects can lead to masses that mimic nasal and sinus lesions. Accurate cross-sectional imaging, particularly

Note: Scanned images are included in the proceedings. Some submitted images were reduced during editing, thereby decreasing clarity. Also, refer to the Program Planner. Proceedings Content as of 3-29-2013.

coronal MR images help separate intracranial lesions from primary nasal lesions by assessing for skull base defects. However, this particular case illustrates that the abnormality can occur even via the frontal sinus drainage pathway. In this case, the cephalocele gained access into the frontal sinus through a defect in the posterior wall of the sinus and then utilized the natural frontal sinus drainage pathway to extend into the nasal cavity and progressively grow. The sinusitis that the patient suffered may have been a post-obstructive process to this condition or even unrelated to this condition. In either case, a serious complication may have resulted if the large nasal lesion had not been tied to the frontal lobe abnormality. The value of closely evaluating the adjacent intracranial contents on sinus CT is critical to both the neuroradiologist and to the clinician and is depicted in this case.

KEYWORDS: Meningocele, Nasal mass, frontal sinus

EE-53

Organized Hematoma of the Maxillary Sinus: 2.5-Year Followup

Fujita, A.[1]·Fujii, H.[1]·Sung, E.[2]·Sakai, O.[2]·Sugimoto, H.[1]
[1]Jichi Medical University, School of Medicine, Shimotsuke, JAPAN, [2]Boston University, Boston Medical Center, Boston, MA.

Purpose
Treatment for nasopharyngeal carcinoma.
Case Report
A 72-year-old male presented with nasal obstruction and pharyngeal pain. He was diagnosed with a large nasopharyngeal carcinoma, and initial CT and MR imaging incidentally found a mass-like lesion in the right maxillary. Treatment for nasopharyngeal carcinoma was prioritized and the patient underwent chemoradiation therapy, without intervention to the right maxillary sinus lesion. After completion of the treatment for nasopharyngeal carcinoma, he was imaged by MRI periodically for surveillance. The maxillary sinus lesion showed gradual increase in size, and the patient suffered from epistaxis. He underwent endoscopic sinus surgery 2.5 years after the initial diagnosis of the maxillary sinus lesion, and the histopathologic diagnosis of organized hematoma of the maxillary sinus was obtained.
Imaging Findings
The mass-like lesion of the right maxillary sinus showed heterogeneous signal with peripheral low signal rim on T2-weighted images. Postcontrast T1-weighted images showed multinodular marked enhancement within the lesion corresponding to areas of high signal intensity on T2-weighted images. The surveillance MR studies demonstrated gradual increase in size of the lesion, and CT demonstrated progressive osseous erosion/destruction of the sinus wall, as well as calcifications. Histopathologic specimen confirmed an organized hematoma, and demonstrated vascular rich components which corresponded to areas of high T2 signal and avid enhancement.
Summary
Organized hematoma of the maxillary sinus is a rare benign condition, which is often difficult to differentiate from malignancies. Our case report demonstrates the natural progression of the organized hematoma over the course of 2.5 years, where it was seen to gradually increase in size and result in osseous destruction. Given this progression of disease when left untreated, elective surgery should be considered for definitive management of organized hematoma of the maxillary sinus.

KEYWORDS: CT, MR imaging, organized hematoma

EE-54

Extramedullary Hematopoiesis of the Paranasal Sinuses Associated with Moyamoya Syndrome in Sickle Cell Disease

Ozgür, A.·Kara, E.·Çabuk, G.·Unal, S.·Nass Duce, M.
Mersin University
Mersin, TURKEY.

Purpose
To present magnetic resonance imaging (MRI) and diffusion-weighted imaging (DWI) findings of extramedullary hematopoiesis (EMH) of the paranasal sinuses in a patient with sickle cell disease who has concomitant moyamoya syndrome.
Case Report
A 10-year-old male with known sickle cell disease was evaluated for headache with cerebral MRI and DWI.
Imaging Findings
Cerebral MRI revealed findings consistent with moyamoya such as tapering of both distal internal carotid arteries, collateral vessels within the ambient cisterns and engorged pial vessels causing typical "ivy sign". In addition; homogeneous soft tissue masses filling the entire cavities of both maxillary and sphenoidal sinuses were detected. The masses demonstrated signal intensity similiar to those of red marrow within the craniofacial bony structures on all pulse sequences. Diffusion-weighted imaging showed restricted diffusion within the masses and craniofacial bone marrow with similiar signal intensity and ADC values. Extramedullary hematopoiesis was the final diagnosis on the basis of these imaging findings.

Note: Scanned images are included in the proceedings. Some submitted images were reduced during editing, thereby decreasing clarity. Also, refer to the Program Planner. Proceedings Content as of 3-29-2013.

Summary
Extramedullary hematopoiesis occurs in chronic anemic conditions as a result of increased need for blood production. It commonly is seen in spleen, liver and lymph nodes. Involvement of paranasal sinuses is a rare entity with only a few case reports in the literature. To our knowledge this is the first report of EMH of the paranasal sinuses associated with moyamoya syndrome in sickle cell disease although it seems to be a coincidental finding. Diagnosis of EMH should be considered in the presence of a homogeneous soft tissue mass arising from the paranasal sinus if the mass and the intramedullary red marrow have similiar signal intensity and enhancement pattern.

KEYWORDS: Sinonasal disease, Sickle cell disease, extramedullary hematopoiesis

EE-54a

Pressurized Rapid Sequence Digital Subtraction Sialography for Characterizing Salivary Ductal Injury and Sialocele Formation

Horsburgh, A.[1,2]·Antoun, N.[1]·Massoud, T. F.[1,3]
[1]Addenbrooke's Hospital, Cambridge, UNITED KINGDOM,
[2]Queen's Hospital, Romford, UNITED KINGDOM,
[3]University of Cambridge, Cambridge, UNITED KINGDOM.

Purpose
A sialocele is a subcutaneous cavity with an inflammatory pseudo capsule, containing saliva that accumulates following continuous secretion with no adequate drainage. Sialoceles occur secondary to trauma, infection or as iatrogenic complications in up to 10% of partial superficial parotidectomies. Van Sickles classified ductal injuries into three types: Type A: Intraglandular (proximal to masseter). Type B: Ductal injury (over masseter). Type C: Ductal injury (distal to masseter). Failure to distinguish between these different subtypes of parotid ductal injuries can lead to inappropriate management and increased risk of long-term complications. The imaging of sialoceles and the accurate localization of ductal injuries can be complex, and includes the use of sialography, ultrasonography, CT and MRI. We present a patient who suffered damage to Stenson's duct following a partial parotidectomy. This case is unusual as iatrogenic injuries to Stensen's duct after parotidectomy are much less common than those occurring to intraglandular ducts. We found that by using a modified digital subtraction sialography technique we were able to accurately demonstrate the location of the salivary duct injury.
Case Report
A 26-year-old male underwent an apparently uneventful superficial parotidectomy for a benign myoepithelial adenoma of the left accessory parotid gland. Following surgery he noticed a recurrent postprandial painless and fluctuant swelling at the left angle of mandible region. A sialogram at this time using a pressurized rapid sequence digital subtraction showed significant extravasation of contrast medium due to a lacerated proximal main parotid duct into a large sialocele confirming the presence of an iatrogenic Van Sickles type B injury. This was managed conservatively by regular aspirations and pressure bandages every few days for a month, at the end of which the swelling subsided.
Imaging Findings
An initial attempted parotid sialogram using a standard gentle injection of contrast medium was unhelpful in that there was an arrest of the column of contrast in mid-duct. A slightly more forceful injection revealed a slow extra-luminal trickle of contrast medium in the immediate vicinity of the duct occlusion, which suggested a likely ductal injury, but its relation to the mandibular swelling was still not apparent. A more pressurized injection concurrent with digital subtraction images at 3 frames/second demonstrated a significant extravasation of contrast medium due to a postsurgical lacerated main parotid duct. The contrast medium jetted into a large multiloculated sialocele consisting of two locules, each measuring 6 cm in size, extending laterally into the subcutaneous tissues at the left angle of the mandible.
Summary
Failure to distinguish different subtypes of parotid ductal injuries can lead to suboptimal clinical management. Sialography is best used in cases where the ductal injury may have been overlooked resulting in sialocele formation. Sialographic technique normally requires gentle injection of contrast medium so as not to cause ductal injury or excessive acinarization of the salivary gland. However, this case illustrates the use of pressurized sialography as a useful method for locating and characterizing the site of duct injury, which may not be appreciated easily on conventional sialography or cross-sectional imaging.

KEYWORDS: Parotid gland

Note: Scanned images are included in the proceedings. Some submitted images were reduced during editing, thereby decreasing clarity. Also, refer to the Program Planner. Proceedings Content as of 3-29-2013.

Monday, May 20 – Wednesday, May 22
6:30 AM – 9:00 PM
Thursday, May 23
6:30 AM – 3:00 PM
Hall B1

Electronic Excerpta (EE) 55 - 60

EE4-Interventional

Note: A missing printed number indicates an abstract has been withdrawn.

EE-55

Endovascular Treatment of an Iatrogenic Carotid-Cavernous Fistula with Pseudoaneurysm after Trans-Sphenoidal Pituitary Resection

Murph, D.·Lankford, D.·Chaljub, G.·von Ritschl, R.
University of Texas Medical Branch
Galveston, TX.

Purpose
Endovascular stent-assisted coil embolization utilizing Neuroform stent and Guglielmi detachable coils provided a safe and effective treatment of an iatrogenic carotid-cavernous fistula with pseudoaneurysm after trans-sphenoidal pituitary resection.
Case Report
A 35-year-old female with pituitary macroadenoma presented with excessive bleeding during trans-sphenoidal surgery at the lateral resection margin. Right cavernous internal carotid artery injury was suspected. Subsequent neuroangiography revealed a medial 6 mm pseudoaneurysm and early filling of the superior opthalmic vein suggestive of a carotid-cavernous fistula. A Neuroform stent was placed across the pseudoaneurysm neck with subsequent Guglielmi detachable coil embolization. Follow-up carotid angiography demonstrated successful pseudoaneurysm embolization.
Imaging Findings
Digital subtraction angiography, right ICA (Day 1): A focal irregularity was present at the anterior and medial aspect of the right internal carotid artery at its cavernous portion. This may have represented mild vasospasm or intimal injury at this portion of the artery that lay in close proximity to the surgical area. No active bleeding was seen at this time. Digital subtraction angiography, right ICA (Day 2): The right internal carotid artery was patent with expected branching intracranially. A medial 6 mm pseudoaneurysm had developed since the previous exam. In addition, early filling of the superior opthalmic vein suggested a carotid-cavernous fistula. Neurointervention: A 6 French guiding catheter was placed into the proximal right internal carotid artery. A 4.5 x 20 mm Neuroform stent then was placed across the pseudoaneurysm neck. A microwire was left in place, over which an SL-10 angled microcatheter was advanced into the pseudoaneurysm. Guglielmi detachable coils (1-3 x 6; 1-2 x 3; 2-2 x 1) were placed into the pseudoaneurysm. Subsequent angiographic runs showed minimal residual lumen and significant improvement of the carotid-cavernous fistula with only trace filling. Digital subtraction angiography, Right ICA, follow up: Successful right internal carotid artery pseudoaneurysm embolization without significant residual lumen was noted. The right ICA stent remained patent with minimal narrowing of the lumen. No residual carotid-cavernous fistula was identified.

Summary
Pseudoaneurysm formation in the cavernous portion of the ICA during trans-sphenoidal pituitary resection is a rarely reported complication with significant morbidity and mortality. With stent-assisted coil embolization using Neuroform stent and Guglielmi detachable coils, complete obliteration of an iatrogenic pseudoaneurysm was attained as well as complete resolution of its associated carotid-cavernous fistula.

KEYWORDS: Intracranial stenting, Aneurysm embolization, arteriography

EE-56

Endovascular Treatment of a Symptomatic Dissecting Vertebral Artery Pseudoaneurysm after Chiropractic Manipulation

Murph, D.·Tran, B.·Lankford, D.·Chaljub, G.·von Ritschl, R.
University of Texas Medical Branch
Galveston, TX.

Purpose
Dissecting pseudoaneurysm of the extracranial vertebral

Note: Scanned images are included in the proceedings. Some submitted images were reduced during editing, thereby decreasing clarity. Also, refer to the Program Planner. Proceedings Content as of 3-29-2013.

artery is an injury that can be sustained by trauma to the cervical spine. Endovascular techniques such as stent-assisted coil embolization can be utilized to treat these traumatic injuries in symptomatic patients.
Case Report
History: A 25-year-old female presented after chiropractic manipulation with severe neck pain. She was later found to be aphasic and unable to move extremities. She was admitted to the trauma service and was given methylprednisolone 30mg/kg. Physical exam: Responsive, alert and oriented X3 with GCS of 15, Pupils equal, round, reactive to light, Nystagmus and left lateral gaze, 2/5 strength in BLE, 4/5 strength in BUE, Absent Babinski sign, Sensation was intact throughout, Rectal tone was normal.
Imaging Findings
MR imaging brain with and with contrast: Multiple small lesions were scattered throughout the cerebellum (more prominent on the left), including the cerebellar gray matter, and also are present within the left pons and left medulla. The lesions had increased intensity on T2-weighted and FLAIR, and were hypointense on T1 with no enhancement on the postcontrast images. These lesions were hyperintense on diffusion-weighted imaging and hypointense on the ADC map. Digital subtraction angiography: A dissection involving the distal extracranial segment of the left vertebral artery resulted in severe flow-limiting stenosis of this artery. This extended from C3 to C1 level. A 6 mm pseudoaneurysm was present at C1/C2 level in relation to this dissection.
Neurointervention: GDC embolization of left vertebral artery dissecting pseudoaneurysm: Two 4.5 x 30 mm Neuroform stents were deployed across the neck of the pseudoaneurysm with jailed-microcatheter technique. The aneurysm was subsequently GDC embolized. Follow-up angiography showed good flow and expected intracranial branching of the left vertebral artery. Digital subtraction angiography, 2-year followup: The left vertebral artery demonstrated expected flow intracranially with good filling of the posterior circulation. The pseudoaneurysm at the level of C1/C2 remained coiled and the (2) stents remained patent. A trivial amount of residual was noted in the proximal neck of the pseudoaneurysm; however, this was markedly improved since previous study. There were no major branch vessel occlusion or significant stenosis.

Summary
Dissecting pseudoaneurysm of the extracranial vertebral artery is a well described injury that can be complicated by significant stenosis as well embolic infarcts. We present the case of a symptomatic patient after chiropractic manipulation, complicated by findings of multiple posterior fossa infarcts, that was amenable to endovascular therapy by stent-assisted coiling.

KEYWORDS: 3D angiography, 1.5T, traumatic pseudoaneurysm

EE-57

Staged Endovascular Management of a Complex Intraorbital Arteriovenous Malformation

Metwalli, Z. A.·Yevich, S. M.·Lee, S. R.·Benndorf, G.
Baylor College of Medicine
Houston, TX.

Purpose
Orbital arteriovenous malformations (AVM) are often part of more extensive intracranial or facial vascular malformations. They can cause exophthalmos, conjunctival injection, visual problems, and rarely intraorbital hemorrhage. Management can be challenging and consists of surgical removal, endovascular treatment, or a combination thereof. We report our experience with a patient that presented with a complex intraorbital AVM successfully treated with staged transarterial embolization.
Case Report
A 56-year-old woman with a past medical history of smoking, alcoholic cirrhosis, and thrombocytopenia presented with progressive left exophthalmos and conjunctival injection of several months duration. Imaging revealed a high-flow intraorbital AVM. Over the next year, the patient reported subjective worsening in diplopia, exophthalmos and conjunctival injection. On clinical exam, there was mild proptosis, mild afferent pupillary defect, mild hyperemia, normal vision, and elevated intraocular pressure (25 mmHg). Staged embolization procedures over

Note: Scanned images are included in the proceedings. Some submitted images were reduced during editing, thereby decreasing clarity. Also, refer to the Program Planner. Proceedings Content as of 3-29-2013.

the course of two years were performed and resulted in successful endovascular occlusion of the AVM. Intraocular pressure normalized (14mmHg) and conjunctival injection and exophthalmos improved. Two weeks after initial treatment, the patient developed progressive vision loss due to central retinal vein occlusion. Residual acuity was 20/100 and remained unchanged during post-treatment period.

Imaging Findings

MR imaging and CTA revealed an intraconal orbital vascular mass adjacent to the region of the medial rectus muscle. Digital subtraction angiography revealed a high-flow intraorbital AVM with a nidus supplied by muscular branches of the ophthalmic artery and drained primarily via the superior ophthalmic vein (SOV). Initial intranidal glue (NBCA) injections resulted in 40% occlusion with subsequent progressive occlusion to 80%. Decrease of the arteriovenous shunting lead to unexpected thrombosis of the SOV necessitating heparinization, and shrinkage of two flow-related intraorbital aneurysms. Two additional selective embolization procedures within a 12-month period resulted in complete occlusion of the AVM. An additional small dural AV shunt arising from the proximal ophthalmic artery caused residual venous congestion.

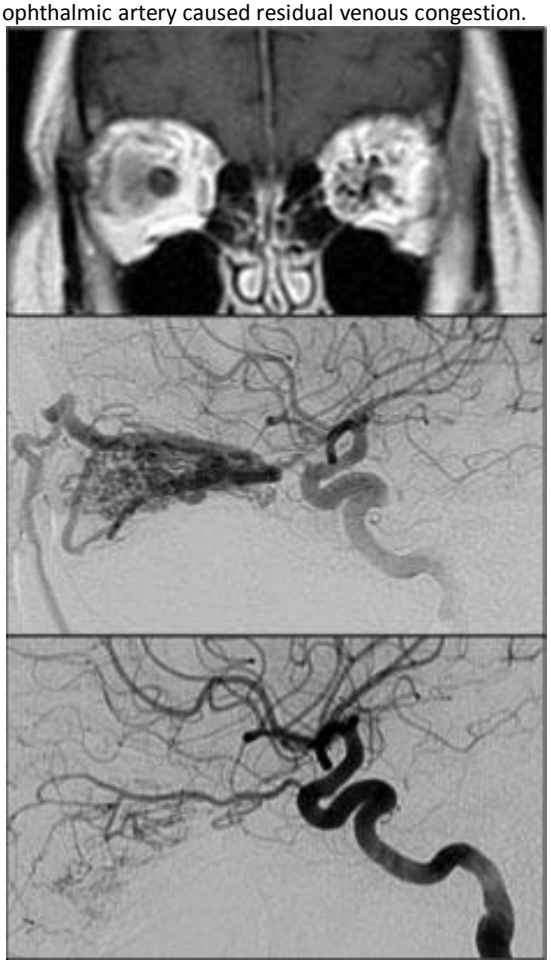

Summary

Orbital AVMs are rare lesions and pose a challenge for treatment. Although surgical resection by fronto-ortibal craniotomy is the conventional treatment, a more comprehensive multidisciplinary approach, which involves ophthalmology, neurosurgery, and neurointerventional radiology allows for optimal management of these complex and rare lesions. Endovascular treatment of intraorbital AVMs can be performed successfully in selected patients either preoperatively or as a primary therapy. We suggest a staged approach to endovascular occlusion of the AVM. However, patients must be counseled regarding the risks of SOV thrombosis worsening of their vision. Concomitant anticoagulation is advised.

KEYWORDS: Arteriovenous malformation, Orbits

EE-58

Glue Embolization of Pelvic Varices in a Patient with Iliac Vein Compression Syndrome Prior to Sacral Chordoma Resection

Scott, C. J.·Heran, M. K. S.·Dea, N.·McNeill, G. J.
Vancouver General Hospital
Vancouver, BC, CANADA.

Purpose

To present a unique case of successful glue embolization of pelvic varices prior to en bloc sacral chordoma resection.

Case Report

A 69-year-old male with sacral chordoma. The patient had a co-existing right common iliac artery aneurysm with compression of the left common iliac vein leading to extensive presacral venous collaterals. These varices significantly increased perioperative bleeding risk and threatened the ability to perform an en bloc resection.

Imaging Findings

Transvenous N-butyl-2-cyanoacrylate (Histocryl) embolization of presacral varices was performed successfully via right common femoral venous approach. Surgical excision subsequently was achieved with minimal intraoperative blood loss and without further complications.

Summary

Preoperative venous embolization is a novel treatment option in patients with presacral varices prior to sacral tumor resection.

KEYWORDS: Chordoma, Venous obstruction, Embolization

Note: Scanned images are included in the proceedings. Some submitted images were reduced during editing, thereby decreasing clarity. Also, refer to the Program Planner. Proceedings Content as of 3-29-2013.

EE-59

Double Embolic Protection during Carotid Artery Stenting with Persistent Hypoglossal Artery

Hou, S.·Silva, C. F.·Kuhn, A. L.·Wakhloo, A. K.
University of Masschusetts Medical Center
Worcester, MA.

Purpose
A persistent hypoglossal artery (PHA) is an extremely rare embryonic carotid-basilar artery anastomosis. Although its presence is usually asymptomatic, it may complicate surgical and interventional procedures used in the treatment of carotid disease. Here we present a highly unique case of carotid artery stenosis with extension into a PHA. Additionally, a novel approach in treating this lesion was employed by stenting and angioplasty while protecting both the anterior and posterior cerebral circulations.
Case Report
A 63-year-old woman presented with a 13-year history of intermittent numbness and weakness involving the left upper extremities and a seven-year history of right-sided pulsatile tinnitus, but her symptoms had increased in frequency prior to her hospitalization. The patient was neurologically intact upon admission. Carotid artery stenting was seen as more technically feasible and safer because it allowed for protection of the anterior and posterior circulations using distal protection devices. The patient tolerated the procedure well, and the hospital course was uneventful. All symptoms of left upper extremity paresthesia and auditory pulsations had resolved completely postprocedure, and the patient was discharged home the next day.
Imaging Findings
Computed tomography angiograms (CTA) of the head and neck and digital subtraction angiography (DSA) (Figure 1A) showed a calcified atherosclerotic plaque involving the proximal right ICA leading to 75% stenosis. The stenosis was just proximal to the origin of the PHA, which arose from the ICA at C2 vertebral body level and continued to the intracranial cavity anterior to the right occipital condyle. The PHA then merged with the left vertebral artery to form the basilar artery, and was the dominant supply to the posterior circulation. At 6-month followup DSA (Figure 1B) the stented vessel segment remained patent without any significant intimal hyperplasia. The patient has been asymptomatic and has not experienced any auditory bruit since the intervention.

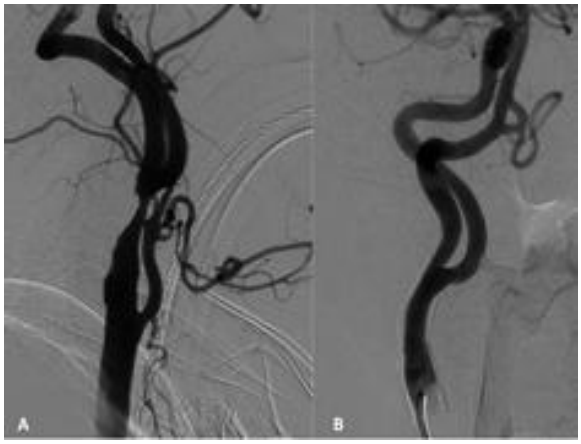

Summary
Carotid artery stenting involving the ICA and origin of the PHA presents a challenge for distal embolic protection (i.e., treatment can be complicated by the necessity to protect both the PHA and the ICA during the intervention). We suggest jailing of one of the protection devices during stent placement enabling simultaneous protection of both the anterior and posterior cerebral circulations.

KEYWORDS: Carotid stenosis, Carotid stent-assisted angioplasty, persistent hypoglossal artery

EE-60

Retrieval of a Fractured Coil Using the Solitaire FR Revascularization Device

Saad, A. F.[1]·Winters, R. R.[2]·Haithcock, J. A.[1]·Layton, K. F.[1]
[1]Baylor University Medical Center, Dallas, TX, [2]Texas Tech University Health Sciences Center, Lubbock, TX.

Purpose
The purpose of this excerpta is to describe the novel use of the Solitaire FR revascularization device (Ev3, Irvine, CA, USA) in the retrieval of a fractured coil.
Case Report
A 52-year-old woman with multiple incidentally discovered cerebral aneurysms was referred for endovascular treatment. During the coiling of a right middle cerebral artery (MCA) bifurcation aneurysm a coil was partially deployed with unsatisfactory placement. During subsequent retraction of the coil for repositioning the coil fractured and was unable to be withdrawn, lodging in the M1 segment of the MCA (Figure 1). Attempts were made to retrieve the coil fragment using a microsnare device without success. A Solitaire FR revascularization device then was deployed in the distal M1 segment with successful engagement of the coil fragment and subsequent successful retrieval. The patient's additional right posterior communicating artery origin aneurysm was coiled successfully, and she awoke without neurologic deficit and was discharged home the next day.
Imaging Findings

Note: Scanned images are included in the proceedings. Some submitted images were reduced during editing, thereby decreasing clarity. Also, refer to the Program Planner. Proceedings Content as of 3-29-2013.

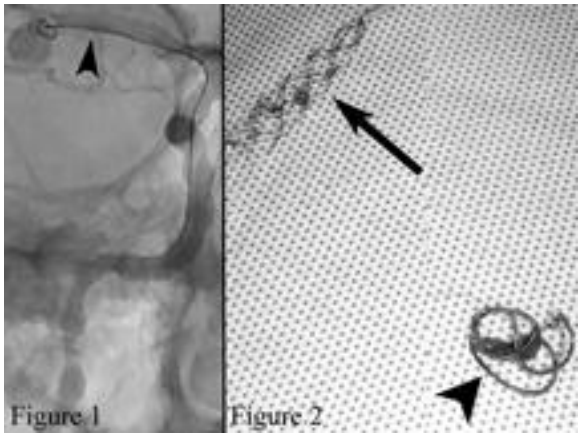

Figure 1: Unsubtracted right internal carotid artery (ICA) injection demonstrates fractured coil (arrowhead) with tip situated within the MCA bifurcation aneurysm in addition to diffuse catheter induced spasm. Figure 2: Coil fragment (arrowhead) is seen following successful retrieval with the Solitaire device (arrow).

Summary

The displacement or less frequent fracture of coils used in the treatment of cerebral aneurysms is an uncommon complication that can have potentially dire results. The use of snare devices has been advocated with favorable results; however in cases of technical failure alternative methods are limited. Reports have shown efficacy of additional devices such as the Alligator retriever (Ev3, Irvine, CA, USA) and MERCI retrieval device (Concentric Medical, Mountain View, CA, USA). We present a case of coil fracture with failure of subsequent microsnare retrieval attempts, followed by successful retrieval using the Solitaire FR revascularization device. The Solitaire stent-retriever, although designed for clot retrieval, may be an additional viable option in the retrieval of fractured or displaced coils. Further experience will be necessary to demonstrate consistent efficacy and safety.

KEYWORDS: Stents, Coils, retrieval

Monday, May 20 – Wednesday, May 22
6:30 AM – 9:00 PM
Thursday, May 23
6:30 AM – 3:00 PM
Hall B1

Electronic Excerpta (EE) 61 - 73

EE5-Pediatrics

Note: A missing printed number indicates an abstract has been withdrawn.

EE-61

Neuroradiologic Findings in a Patient with Wolfram Syndrome: A Case Report

Leake, D. R.
Austin Radiological Association
Austin, TX.

Purpose

Wolfram syndrome is a rare autosomal recessive disorder first described in 1938 by Wolfram and Wagener. The disease consists of diabetes insipidus, diabetes mellitus, optic atrophy, and deafness (acronym DIDMOAD). Wolfram syndrome is caused by WFS1 gene mutation leading to dysfunction of homeostasis of the endoplasmic reticulum. Only a few cases have been described in the radiology literature. Neuroradiologic findings include optic nerve/chiasm atrophy, absent or reduced normal pituitary bright spot on T1, cerebellar and brainstem atrophy, and abnormal T2 hyperintensity in the pons, peritrigonal white matter, and frontal/occipital cortex.

Case Report

The patient is an 18-year-old male diagnosed with optic atrophy and diabetes mellitus at age four. He presented with a large midline pelvic mass. Ultrasound exam demonstrated bladder distension and bilateral hydronephrosis. Subsequently, patient was admitted to the hospital, and workup revealed polyuria/diabetes insipidus in addition to the patient's known diabetes mellitus/optic atrophy. No deafness was noted. Genetic Testing of Wolfram Syndrome 1/Wolframin, WFS1 Sequencing was confirmatory for Wolfram syndrome.

Image Findings

Neuroradiologic findings include bilateral optic nerve and chiasm atrophy, absence of posterior pituitary bright spot on T1, and abnormal T2 hyperintensity of the pons. Septum pellucidum was present.

Note: Scanned images are included in the proceedings. Some submitted images were reduced during editing, thereby decreasing clarity. Also, refer to the Program Planner. Proceedings Content as of 3-29-2013.

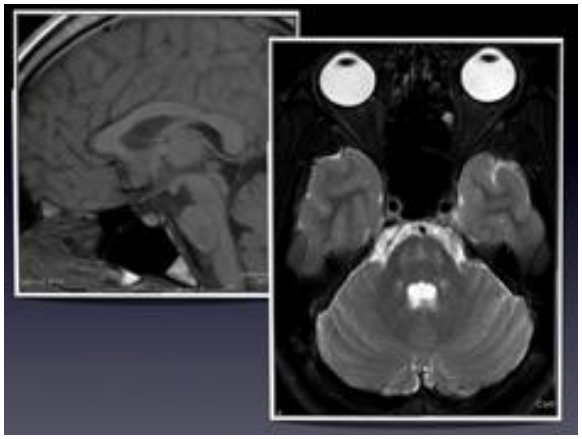

Summary
The purpose of this report was to describe the neuroradiologic findings of a rare case of Wolfram syndrome. Knowledge of the clinical and neuroradiologic findings may lead to earlier diagnosis and treatment of this disease.

KEYWORDS: Metabolic, Optic chiasm, Wolfram Syndrome

EE-62

An Unusual Case of Progressive Multifocal Leukoencephalopathy in a Child with Acute Lymphocytic Leukemia

Mair, Y. H.·Adas, R. A. A.·Almehdar, A. S.
King Abdul-Aziz Medical City
Jeddah, SAUDI ARABIA.

Purpose
To present a case of progressive multifocal leukoencephalopathy (PML) in a child diagnosed with acute lymphocytic leukemia (ALL) five months prior.
Case Report
A three-year-old girl with a known case of ALL presented to the clinic three days after intrathecal injection of methotrexate with right-sided clonic jerks and mouth twitching. A CT scan and an MRI of the brain were performed. The imaging differential diagnosis suggested changes of chemotherapy toxicity versus encephalitis. During her first few days in the hospital, the patient continued to have repeated attacks of seizure with deterioration in the level of consciousness dropping her GCS from 15/15 to 3/15 within a course of three days. She was intubated and shifted to the PICU. During her PICU admission, she developed left-sided seizures and was put on combined antiepileptic medications. She also developed severe hyponatremia which gradually was corrected. Initial CSF analysis was negative and blood and urine cultures were unremarkable. Attempts to treat methotrexate toxicity were ineffective and another MRI was requested. The second MRI showed progression of the lesions with interval development of bilateral abnormalities. The diagnosis of PML was suspected by the neuroradiologist and a CD4 count was requested. A second CSF sample was acquired for JC virus PCR analysis. The CD4 count was < 80 cells/mm3. Although the CSF JC virus PCR was negative, the diagnosis of PML was made. During the following weeks the patient continued to decline demonstrating uncontrollable seizures and enlarging lesions on serial MR studies. She died in the PICU 54 days after admission.
Imaging Findings
The initial CT scan of the brain demonstrated a large left basal ganglia and subinsular hypodensity, with no significant mass effect. The MRI done afterwards showed an ill-defined hyperintense FLAIR change in the left basal ganglia with no diffusion restriction or enhancement. The MRI performed six days later showed marked enlargement of the central gray and white matter lesions without mass effect, enhancement or diffusion restriction. Spectroscopy demonstrated low NAA levels within the lesions compared to unaffected areas. Newer lesions in the brain stem, cerebellum and subcortical white matter were developing over the course of her hospital stay.
Summary
Progressive multifocal leukoencephalopathy is a severe lethal form of demyelinating disease caused by reactivation of the JC virus due to severe immunodeficiency. Very few cases have been reported in children and often were associated with HIV. MR imaging typically shows areas of asymmetric high signal intensity in the periventricular and subcortical white matter. The lack of mass effect, enhancement and diffusion restriction is often a helpful imaging clue. The clinical picture along with the imaging and immunologic findings are often enough to diagnose PML. Knowledge of this entity and its possible occurrence in children is very important since early diagnosis may impact patient survival.

KEYWORDS: Leukemia, PML

EE-63

Concurrent Spontaneous High-Flow Vertebral Arteriovenous Fistula and Reversal of Basilar Artery Flow in a Pediatric Patient: An Extremely Rare Entity

Honarmand, A. R.[1]·Soltanolkoltabi, M.[1]·Ansari, S. A.[1]·Rahman, O.[1]·Schoeneman, S. E.[2]·Hurley, M. C.[1]·Alden, T. D.[2]·Shaibani, A.[1]
[1]Northwestern University Feinberg School of Medicine, Chicago, IL, [2]Ann & Robert H. Lurie Children's Hospital of Chicago, Chicago, IL.

Purpose
High-flow vertebral artery arteriovenous fistula (VAVF) and concurrent steal from intracranial arteries or contralateral vertebral artery is a well known phenomenon; however, to the best of our knowledge, association with basilar artery (BA) steal in the pediatric population has not been reported. Our purpose is to describe a unique

Note: Scanned images are included in the proceedings. Some submitted images were reduced during editing, thereby decreasing clarity. Also, refer to the Program Planner. Proceedings Content as of 3-29-2013.

asymptomatic presentation of a spontaneous high-flow VAVF in a child associated with flow reversal in the BA treated with endovascular coil embolization.

Case Report

An 8-year-old boy presented to the emergency department with fever and lethargy. No relevant clinical signs or symptoms were noted except for a prominent palpable pulse on the right side of the neck. There was no history of trauma to the head and neck or connective tissue disorders.

Imaging Findings

Following primary MR imaging, digital subtraction angiography (DSA) demonstrated a high-flow AVF between the distal portion of the right cervical VA at the level of the proximal transverse foramen of C2, draining into a very large recipient paraspinous venous pouch. Significant enlargement of the right VA was observed at and above the level of the shunt with retrograde supply across the hypertrophied left VA and vertebrobasilar junction into the right VA V4 segment. Selective DSA also demonstrated an enlarged right deep cervical artery supplying the AVF and an enlarged left costocervical trunk augmenting collateral supply to the left VA (Figure A). There was no antegrade visualization of the BA from either the vertebral or costocervical/thyrocervical injections, due to the significant steal towards the AVF. Right internal carotid DSA demonstrated reversal of flow in the BA via a large right posterior communicating artery (Figures B).

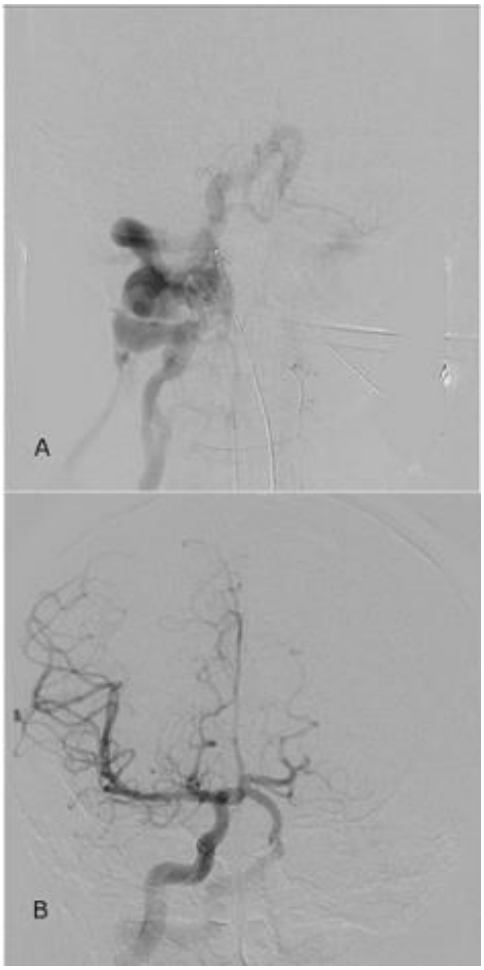

Summary

Reversal of BA flow is an uncommonly described entity and has been described in rare complicated cases of intracranial VA dissections, vertebrobasilar occlusions, giant cell arteritis, and bilateral subclavian steal phenomenon. It indicates both very high-flow arteriovenous shunting and patent posterior communicating arteries to compensate for vertebrobasilar insufficiency. Although reversed basilar flow has been associated with significant neurologic symptoms in patients suffering from subclavian steal phenomenon, it may be asymptomatic as in our case and emphasizes the robust collateral network often present in children. Understanding of complex AVF anatomy, controlled complete obliteration of the VAVF while preserving the parent VA, restoration of antegrade flow in the vertebrobasilar circulation, and strict hemodynamic and blood pressure monitoring are essential in order to obtain technical success and minimize complications.

KEYWORDS: Vertebral artery anomalies, Basilar artery, reversal of flow

Note: Scanned images are included in the proceedings. Some submitted images were reduced during editing, thereby decreasing clarity. Also, refer to the Program Planner. Proceedings Content as of 3-29-2013.

EE-64

Absence of a Cervical Nerve Root Mimicking Erb's Palsy in a Two-Month-Old Girl

Chung, M.[1]·Park, J.[1]·Valencia, H.[2]·Lefton, D.[1]·Grossman, J. A.[2]
[1]St. Luke's Roosevelt Hospital, New York, NY, [2]Miami Children's Hospital, Miami, FL.

Purpose
To report the importance of MRI techniques in the evaluation of an infant with a presumed upper brachial plexus injury that actually demonstrated congenital absence of a ventral cervical nerve root.
Case Report
A 4-month-old girl was seen to evaluate an upper plexus birth palsy. Noncontrast MRI at 10 months was performed and the standard T1- and T2-weighted sequences were obtained in multiple planes. Additionally, thin-section fast imaging employing steady state acquisition (FIESTA) T2-weighted images were acquired. The MRI demonstrated nonvisualization of the left C5 nerve root within the cal sac(Figure 1). There was no evidence of trauma, as evidenced by the absence of a pseudomeningocele, granulation tissue, or reparative neuroma formation. Additionally, there was no evidence of cervical disk herniation, spinal stenosis, or subluxation/dislocation of the humeral heads. Electrodiagnostic studies at 11 months of age failed to demonstrate evidence of a cervical root trauma lesion, but instead revealed lack of both denervation and reinnervation of C5 muscles with a lack of muscle fibers, consistent with the absence of ventral motor neurons. Surgical exploration at 15 months of age demonstrated no evidence of trauma and severe hypoplasia of C5 with minor underdevelopment of C6. Cortical sensory responses were absent with C5 stimulation but present with C6 stimulation. Since the surgery, limited recovery of upper trunk(C5-C6) motor function has occurred.

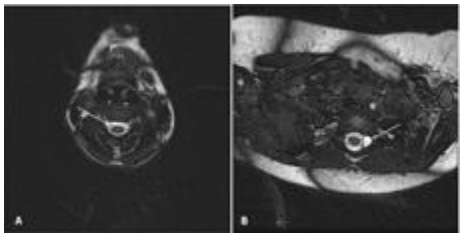

Figure. A. FIESTA sequence demonstrating nonvisualization of the ventral left C5 nerve root; arrow indicates normal ventral right C5 nerve root. B: FIESTA sequence demonstrating pseudomeningocele at the level of brachial plexus injury (arrow).
Imaging Findings
This case demonstrates a rare congenital abnormality that mimicked Erb's palsy clinically. The absence of the left C5 nerve root could be secondary to nerve root avulsion from birth trauma, but there was no associated pseudomeningocele, visible scar tissue, or reparative neuroma formation to corroborate this connection. The root absence was confirmed with electrodiagnostic studies and surgical exploration. Review of the literature shows no recorded cases demonstrating this type of congenital absence.
Summary
The case also demonstrates the importance of MRI in the preoperative workup. The FIESTA sequence is extremely useful in visualizing the individual cervical nerve roots and the pseudomeningocele, which is a key diagnostic feature of brachial plexus injury. The standard T1- and T2-weighted sequences are useful in detecting abnormal periscalene soft tissues on the side of injury. This tissue has been proven to correlate histologically with scar tissue and reparative neuromas.

KEYWORDS: Brachial plexus, Congenital anomalies

EE-65

Diffusion Tensor Tractography for Understanding Complex Brain Fiber Connectivity in Holoprosencephaly: A Unique Case Presentation

Adapa, P.·White, M. L.·Keiper, M. D.·Zhang, Y.
University of Nebraska Medical Center
Omaha, NE.

Purpose
Holoprosencephaly is a disorder of abnormal or noncleavage of the cerebral hemispheres accompanied by midline structural abnormalities. We present a case of severe holoprosencephaly without a dorsal cyst. Diffusion tensor tractography (DTT) was performed and demonstrates marked white matter tract abnormalities in the brainstem, basal ganglia and cerebral hemispheres.
Case Report
A two-day-old full-term female neonate underwent conventional MRI of the brain along with diffusion tensor imaging due to intrauterine diagnosis of Sonic Hedgehog gene mutation, holoprosencephaly and facial anomalies. Family history was also positive for Sonic Hedgehog gene mutation and holoprosencephaly. Multiple intracranial abnormalities were identified on the MRI.
Imaging Findings
There was alobar holoprosencephaly with diffuse lissencephaly, large monoventricle, no dorsal cyst and minimal posterior midline cleavage. Fused midline deep gray nuclei without a third ventricle were seen. Deformed brainstem was present. Cerebellar hemispheres and fourth ventricle were grossly unremarkable. A single optic nerve originating from the brain bifurcated into two globes that were grossly malformed. Diffusion tensor tractography was performed which revealed abnormal anteroposterior hemispheric white matter fibers in anterior cerebral hemisphere with no evidence of crossing fibers (Figure A, green). In the posterior cerebral hemisphere the fibers were oriented more right to left and mostly terminated at the midline with a few posterior crossing fibers (Figure A,

Note: Scanned images are included in the proceedings. Some submitted images were reduced during editing, thereby decreasing clarity. Also, refer to the Program Planner. Proceedings Content as of 3-29-2013.

orange and blue). In the brain stem (Figure B) no fibers extending cranial-caudal were identified. No definite corticospinal tracts were identified. Laterally in the fused brainstem and basal ganglia there were fibers running AP (Figure B, pink and blue) that demonstrated crossing which are of unknown origin but potentially represent corticospinal tracts. There was a midline group of fibers that might be the medial lemnisci running predominantly AP with some crossing identified (Figure B, green). Yellow fibers (Figure B) originated from the mono-optic nerve. Rudimentary middle cerebellar peduncles also were identified by DTT.

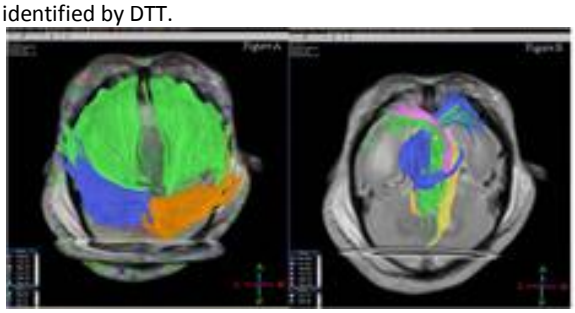

Summary
Diffusion tensor tractography helps in evaluating the complex brain fiber connectivity in subjects with holoprosencephaly. These findings may help with neurodevelopment assessment and prognostication that may otherwise not be available with conventional neuroimaging.

KEYWORDS: Congenital anomalies, Diffusion tensor image, Holoprosencephaly

EE-66

Term Newborn Found to Have Intraventricular Hemorrhage

Trinh, V.·Fong, C. L.
Kaiser Permanente Los Angeles Medical Center
Los Angeles, CA.

Purpose
Discuss the differential diagnosis of brain tumors found in the neonatal period. We present a rare case of neonatal atypical teratoid rhabdoid tumor (ATRT).
Case Report
One-day-old term newborn found to have intraventricular hemorrhage on ultrasound. A CT and MRI were ordered to evaluate for possible arteriovenous malformation.
Imaging Findings
Left thalamic enhancing mass with evidence of intraventricular hemorrhage and hydrocephalus. No calcifications noted on CT.

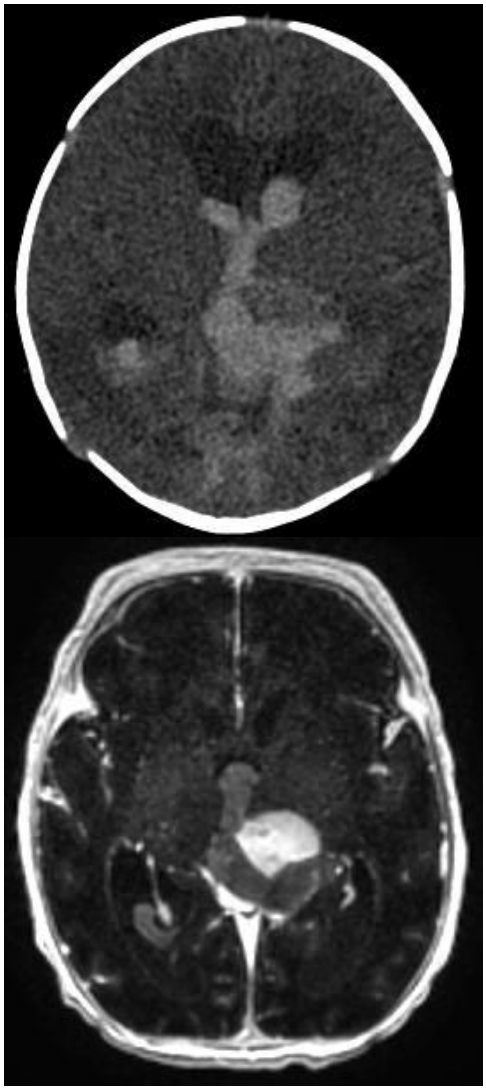

DDx of Neonatal Brain Tumors

Neuroepithelial	PNET and Glial tumors including Astrocytoma, GBM, Choroid plexus papilloma (atrium lateral ventricle), ependymoma
Germ Cell Tumor	Teratoma (coarse calcifications), germinoma
Others (less than 6%)	ATRT, ganglioglioma, medulloepithelioma, angioblastic meningioma

Summary
Neonatal brain tumors are described as tumors found in the first two months of life. The differential diagnosis of neonatal brain tumors primarily includes neuroepithelial

Note: Scanned images are included in the proceedings. Some submitted images were reduced during editing, thereby decreasing clarity. Also, refer to the Program Planner. Proceedings Content as of 3-29-2013.

tumors and germ cell tumors. Atypical teratoid rhabdoid tumors (ATRT) generally have been described in infancy and young children with one case series showing a typical age range from four months to 15 years. We present a neonatal case of ATRT to be included in the differential diagnosis of a neonatal brain tumor. Most neonatal tumors will be difficult to differentiate on imaging alone; however certain tumors such as the potentially resectable choroid plexus papilloma typically seen in the atrium of the lateral ventricle or teratoma with coarse calcifications should be mentioned. Atypical teratoid rhabdoid tumor cannot be differentiated from other locally aggressive lesions such as PNET on imaging and the determination is made by specific immunohistochemical markers and by detection of genetic deletions and/or mutations.

KEYWORDS: Neonatal, ATRT

EE-67

Alveolar Soft Part Sarcoma: Adolescent Presenting with Headache and New Mediastinal Bruit

Schenning, R. C.·Vajtai, P. L.·Troxell, M. L.·Pollock, J. M.·Hopkins, K. L.
Oregon Health and Science University
Portland, OR.

Purpose
Alveolar soft part sarcoma (ASPS) is a rare soft tissue sarcoma occurring primarily in the second and third decades of life. Almost all cases arise in or adjacent to skeletal muscle, most often in the thigh and buttocks, and commonly have symptomatic metastasis in brain, lung, and bone at presentation. The purpose of this abstract is to illustrate the typical intracranial imaging features of ASPS metastases to the brain with a very unusual primary neoplasm arising in the mediastinum.
Case Report
A previously healthy 13-year-old girl presented with five-day history of headache unresponsive to nonsteroidal anti-inflammatory drugs. Physical exam was unremarkable except for a new mediastinal bruit on auscultation. Initial chest radiograph revealed a large left mediastinal mass, which on contrast-enhanced chest CT was seen to be hypervascular with large peripheral vessels and central necrosis. Numerous pulmonary nodules were present, which were pathology-proven metastatic ASPS. Subsequent neuroimaging workup consisted of a contrast-enhanced head CT and brain MRI with DSC perfusion and spectroscopy.
Imaging Findings
Contrast-enhanced head CT revealed a homogeneously enhancing left parietal mass measuring 3.3 cm x 3.0 cm x 3.7 cm, with large feeding arteries from the left middle cerebral artery. Circumferential vasogenic edema and mass effect on the left lateral ventricle were present. On MRI, the well circumscribed left parietal mass was minimally T1 hyperintense, T2 hyperintense, and homogeneously enhancing, with no evidence of necrosis, hemorrhage, or diffusion restriction. Large flow voids were present within the mass and radiating from its lateral margin. The mass demonstrated increased peripheral tumor blood volume and flow on DSC perfusion imaging. Single voxel MR spectroscopy revealed a highly elevated choline-to-creatine ratio, no lactate peak, and an undetectable NAA peak, consistent with a non-neuronal, non-necrotic neoplasm with high cell turnover.
Summary
The imaging appearance of both primary and metastatic ASPS reflects rich vascularity, with large intra and peritumoral vessels being a characteristic feature, regardless of imaging modality or anatomical location. Despite ASPS being rare, the diagnosis should be considered in adolescents and young adults when typical imaging features are present. In this case we present the typical intracranial imaging findings arising from an unreported primary mediastinal origin.

KEYWORDS: MR imaging brain, Brain metastases, Alveolar Soft Part Sarcoma

EE-68

Pilomyxoid Astrocytoma: An Uncommon Tumor in an Atypical Location

Garger, A. V.·Anderson, R. C. E.·Needle, M.·Feldstein, N. A.·Garvin, J.·Filippi, C. G.·Millar, W. S.
Columbia University/New York Presbyterian Medical Center
New York, NY.

Purpose
To demonstrate the unusual MRI features of an exophytic pilomyxoid astrocytoma (PMA) arising from the medulla.
Case Report
A 4-year-old previously healthy girl was brought to a neurologist with a four-week history of increasing right-sided extremity weakness, tongue rolling when speaking, and left eyelid ptosis without headache or visual changes. She had experienced several episodes of emesis three weeks prior, which resolved. An MRI exam demonstrated a heterogeneous, exophytic, partly solid mass with significant cystic components emanating from the medulla. The initial differential based on MRI signal characteristics included pilocytic astrocytoma, ependymoma, hemangioblastoma, medulloblastoma, brainstem glioma or an atypical infection, since she recently had been exposed to a relative with tuberculosis. A PPD was placed, which was subsequently negative. Additional imaging of the spine demonstrated no evidence of metastatic dissemination. Biopsy/partial resection results demonstrated a low-grade glial neoplasm with features consistent with pilomyxoid astrocytoma. Further treatment with multiple cycles of chemotherapy resulted in a progressive decrease in the size of the mass and subjective improvement of right-sided weakness.

Note: Scanned images are included in the proceedings. Some submitted images were reduced during editing, thereby decreasing clarity. Also, refer to the Program Planner. Proceedings Content as of 3-29-2013.

Imaging Findings

A well delineated, exophytic mass with solid and cystic components in the anterior medulla produced circumferential compression of the surrounding parenchyma, partial effacement of the 4th ventricle and posterior displacement of the brainstem and inferior vermis. After administration of gadolinium, the solid component demonstrated heterogeneous enhancement. There was no evidence of satellite or metastatic lesions.

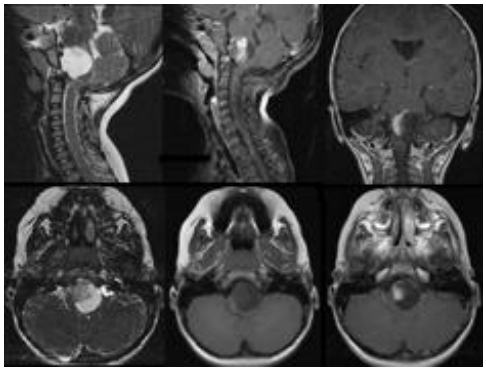

Figure 1: From left upper corner clockwise; sagittal T2; fat-sat sagittal T1C+; coronal T1 C+; axial T1 C+; axial T1 C-; axial T2

Summary

Pilomyxoid astrocytoma (PMA) was described initially as a variant of pilocytic astrocytoma in 1999, and subsequently recognized by the WHO as a distinct grade II tumor in 2007. Most reported cases of PMA are in the hypothalamus/optic chiasm or cerebellum. Less typical locations include the cerebrum , spinal cord and 4th ventricle. This case appears to be the first biopsy-proven primary occurrence of PMA in the medulla. Secondary metastatic involvement of the medulla was reported in only two prior cases. Pilomyxoid astrocytoma should always be considered in the differential diagnosis of posterior fossa masses.

KEYWORDS: Pilocytic astrocytoma, Pediatric brain, Pilomyxoid astrocytoma

EE-70

Uncrossed Sensori-Motor Tracts: Horizontal Gaze Palsy with Progressive Scoliosis with Diffusion Tensor Imaging and Functional MR Imaging Evaluation

Seshadri, R.[1]·PS, B.[2]·Kulkarni, G. B.[2]·Upadhyay, N.[2]
[1]Sri Ramachandra Medical College, Chennai, INDIA,
[2]National Institute of Mental Health and Neurosciences, Bangalore, INDIA.

Purpose

Contralateral control of the body by the cerebral hemispheres forms the basis of neurophysiologic functioning. Here we are presenting two unusual cases of defective neuronal wiring in the brainstem leading to ipsilateral control of the body by the cerebral hemispheres. Horizontal gaze palsy with progressive scoliosis (HGPPS) is a rare autosomal recessive disorder caused by defective ROBO-3 gene, leading to nondecussation of cortico-spinal tracts, posterior column-medial lemniscus tracts, medial longitudinal fasciculus and other commissural fibers in the rhombencephalon, causing congenital absence of conjugate horizontal eye movement and progressive scoliosis developing during childhood. Yet, neurologically, these patients are remarkably intact except for horizontal gaze palsy and progressive scoliosis. This suggests apparently normal sensori-motor integration although on the ipsilateral side of the body.

Case Reports

A 8-year-old boy born of consanguineous-marriage, presented with regression of language milestones following seizures for six months and right torticollis. A 14-year-old girl born of consanguineous marriage presented with delay in motor milestones and progressively increasing scoliosis. Both had horizontal gaze palsy, progressive scoliosis and right facial hemiatrophy. The boy also had torticollis.

Imaging Findings

MR imaging in both patients revealed brainstem hypoplasia, split pons, butterfly medulla, uncrossed sensori-motor axons on DTI (Figure A) and ipsilateral sensori-motor activation on fMRI studies (Figure B). On DTI, abnormalities were seen at the level of pons as well (absence of posterior strip of transverse pontine fibers). Differential diagnoses clinically include Duane syndrome and Mobius syndrome. In Duane's syndrome there will be selective absence of motor neurons in the abducent nuclei. Hence there will be absence of the abducens nerve on MRI (CISS3D). In Mobius syndrome, there will be absence of both the abducent and the facial nuclei. So the patient presents with facial diplegia associated with horizontal gaze palsy. MR imaging will demonstrate brainstem hypoplasia with straightening of the fourth ventricle floor due to absence of the facial colliculi and absence of the abducens nerves.

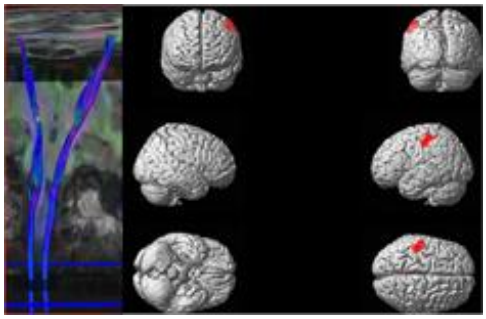

Summary

MR imaging may play a critical role on the precocious diagnosis of HGPPS by showing the maldevelopment of the brain stem, uncrossed sensorimotor tracts (DTI) and ipsilateral activations on fMRI. Early diagnosis of this congenital entity may be important to apply supportive therapies to prevent rapid progression of scoliosis and prevent unnecessary further investigations.

Note: Scanned images are included in the proceedings. Some submitted images were reduced during editing, thereby decreasing clarity. Also, refer to the Program Planner. Proceedings Content as of 3-29-2013.

KEYWORDS: BOLD fMRI, DTI tractography, HGPPS

EE-71

Imaging Evaluation of Meniere's Disease in Children

Vasani, D.·Malhotra, A.
Yale University School of Medicine
New Haven, CT.

Purpose
To identify and assess the reliability of an imaging finding associated with Meniere's disease in pediatric patients.
Case Report
We report a case of a 10-year-old boy with fluctuating hearing loss. Imaging evaluation with CT of temporal bones was performed, as requested by the patient's referring pediatric otolaryngologist.
Imaging Findings
Thin section axial CT imaging of the temporal bones with multiplanar reformatted images in our patient demonstrated nonvisualization of the vestibular aqueduct bilaterally. Previous studies have indicated that vestibular aqueduct size is smaller in patients with Meniere's disease in comparison to control patients and that in approximately 30% of patients with Meniere's disease the vestibular aqueduct is nonvisible. However, to our knowledge, the expected visibility of the vestibular aqueduct in pediatric patients had not been studied. To that end, we reviewed 10 randomly chosen "normal" CT examinations of the temporal bones performed between 2009-2012, of patients between the ages of eight-12 years old. This retrospective review confirmed that the vestibular aqueduct typically is well seen on thin section CT imaging of the temporal bones, even in pediatric patients.
Summary
We demonstrate the expected visibility of the vestibular aqueduct in pediatric patients. Thus, in patient's in whom Meneire's disease is clinically suspected, the absence of visualization of the vestibular aqueducts may reliably be used as supportive evidence towards that diagnosis.

KEYWORDS: Meniere, Temporal bone, vestibular aqueduct

EE-72

Neovascularization and Hemorrhagic Transformation of Cerebellar Tubers in Tuberous Sclerosis Complex

Banker, P.·Rodrigues, D.·Salamon, N.
University of California Los Angeles
Los Angeles, CA.

Purpose
To describe a case of tuberous sclerosis complex (TSC) with cerebellar lesions that experienced changes in signal and morphology over time, including development of neovascularization and hemorrhage, suggesting an alternate pathogenesis of cerebellar tubers that differs from the natural course of cerebral tubers.
Case Report
A 14-year-old boy with history of TSC with right cerebellar tubers that demonstrated changes in size, signal, and content over time with eventual hemorrhagic transformation. He was diagnosed initially at one month of age when noted to have left-sided lip smacking and twitching of the left arm. Bleeding of the cerebellar tuber was discovered when the patient presented with ataxia. MR imaging over an 11-year period from ages two to 13 was reviewed for the patient. A retrospective review of MR imaging from 61 pediatric and young adult patients with TSC found 15 patients with cerebellar lesions (24.6%). The UCLA cohort showed 17 total cerebellar tubers of which six underwent change over time, including our case of hemorrhage. Tuberous sclerosis complex is an inherited systemic disease with prominent CNS, cutaneous, and visceral manifestations. Cerebellar tubers are uncommon, occurring 24-28% of the time in TSC. While Vaughn et al. recently have described cerebellar tubers to evolve with time, the development of adjacent vascularity and propensity for bleeding has never been reported.
Imaging Findings
MR imaging of the brain in our patient at the time of presentation demonstrated at least 25 cerebral tubers, bilateral subependymal nodules, and a right cerebellar tuber. His right cerebellar tuber initially showed T1 hypointensity, T2/FLAIR hyperintensity, enhancement, but no calcification or prominent cortical vessels. Over time, this lesion developed a new cortical vessel, adjacent focal parenchymal atrophy, and calcification. This lesion was found to ultimately hemorrhage about 11 years after its discovery. The hemorrhage bed on follow-up MRI was smaller.

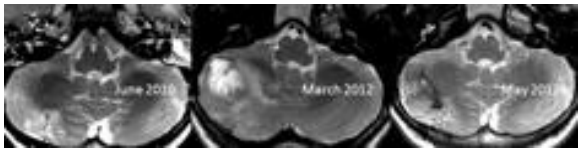

Summary
Tuberous sclerosis complex is a unique neurophakomatosis with diverse manifestations. We describe specific progressive changes in cerebellar tubers in TSC and propose that these changes may have prognostic importance, especially as seen in our case of neovascularization and hemorrhage. Unlike cerebral tubers, which tend to remain stable, the morphologic evolution and vascular development of cerebellar tubers suggests that an alternate pathogenesis may play a role in the progression of these lesions.

KEYWORDS: Tuberous sclerosis, Cerebellar, hemorrhage

Note: Scanned images are included in the proceedings. Some submitted images were reduced during editing, thereby decreasing clarity. Also, refer to the Program Planner. Proceedings Content as of 3-29-2013.

EE-73

Safety and Efficacy of Onyx Embolization for Pediatric Spinal Perimedullary (Type IV) Fistula

Honarmand, A. R.[1]·Soltanolkoltabi, M.[1]·Ansari, S. A.[1]·Schoeneman, S. E.[2]·Patel, B.[1]·Hurley, M. C.[1]·Tadanori Tomita, T.[2]·Shaibani, A.[1]
[1]Northwestern University Feinberg School of Medicine, Chicago, IL, [2]Ann & Robert H. Lurie Children's Hospital of Chicago, Chicago, IL.

Purpose
Several endovascular embolic agents have been utilized for permanent obliteration of perimedullary spinal arteriovenous fistulas (sAVFs) in children; however, endovascular embolization using ethylene vinyl alcohol copolymer (Onyx) has not been widely described in treatment of this type of spinal lesion in the pediatric population. We describe the usefulness of Onyx in endovascular embolization of two pediatric high-flow perimedullary sAVFs.
Case Report
Case 1: During evaluation of a 7-year-old boy presenting with abdominal pain, incidental intraspinal vascular abnormalities were detected on a contrast-enhanced CT abdomen/pelvis study. Subsequent MRI revealed dilated vascular flow voids predominantly along the ventral surface of the spinal cord extending from the lower thoracic level to the cauda equina appearing to be intradural but extramedullary and suggestive of a perimedullary sAVF. The patient had been completely asymptomatic. Physical examination was normal except for an audible bruit in the lower back by auscultation. Case 2: A 17-year-old boy with a history of a cervico-spinal arteriovenous malformation presented with right lower extremity pain and progressive ambulatory disturbance. On physical examination he was noted to have considerable right lower extremity weakness associated with tactile and proprioception deficits [modified Rankin Scale (mRS) score: 4].
Imaging Findings
Case 1: Spinal digital subtraction angiography (DSA) demonstrated a high flow intradural AVF at the L3-4 level with multiple feeders (an extremely hypertrophied anterior spinal artery arising from the left T9 intercostal and two enlarged radiculomedullary arteries arising from each lateral sacral artery respectively), classified as a perimedullary AVF (subtype B). Using detachable platinum coils and Onyx 18, progressive embolization of the fistula was initiated in the efferent recipient vein with embolic reflux proximally across the fistulous site and into the distal afferent components of the three major feeding arteries for obliteration. Postembolization spinal DSA one week later revealed a second separate perimedullary AVF subtype A supplied by the PSA which was resected surgically due to the small caliber of the posterior spinal artery supplying this AVF. Case 2: Spinal DSA demonstrated a high-flow dorsal perimedullary sAVF (subtype C) at C7-T1 level with a large recipient venous varix invaginating into the substance of the cervical cord posteriorly. The lesion was supplied entirely from the PSA and the recipient varix drained superiorly into the dorsal longitudinal spinal veins exiting via the petrosal veins, superior petrosal sinuses, and sigmoid sinuses respectively. Embolization of the AVF was performed utilizing Onyx 34 to occlude the proximal venous efferent, with controlled reflux into the fistulous site and distal afferent of several arterial feeders. The patient achieved significant clinical improvement after one year (mRS score: 2).
Summary
To the best of our knowledge, Onyx has been applied in only one case of a perimedullary sAVF embolization in the pediatric population. Although the safety of Onyx in individuals less than 18 years of age has not yet been well established, we believe Onyx embolization could be performed with high degree of safety and efficacy in treatment of spinal perimedullary AVFs in the pediatric population.

KEYWORDS: Perimedullary fistula, Endovascular embolization, Onyx

Monday, May 20 – Wednesday, May 22
6:30 AM – 9:00 PM
Thursday, May 23
6:30 AM – 3:00 PM
Hall B1

Electronic Excerpta (EE) 74 - 90

EE6-Spine

Note: A missing printed number indicates an abstract has been withdrawn.

EE-74

Nonenhancing Diskitis and Epidural Abscess in an Immunocompromised Patient: A Case Report

Carr, C. M.·Diehn, F. E.·Kaufmann, T. J.
Mayo Clinic
Rochester, MN.

Purpose
To review an atypical, nonenhancing presentation of lumbar diskitis and epidural abscess in an immuncompromised patient.
Case Report

Note: Scanned images are included in the proceedings. Some submitted images were reduced during editing, thereby decreasing clarity. Also, refer to the Program Planner. Proceedings Content as of 3-29-2013.

A 61-year-old male with Wegener's granulomatosis and ankylosing spondylitis, immunosuppressed with high-dose prednisone, rituximab, and plasma exchange, was hospitalized for staphylococcus aureus sepsis from a urinary tract source and worsening back pain. A lumbar spine MRI scan raised concern for diskitis with epidural and paraspinal abscess at the lower two lumbar levels, but there were atypical imaging features. Overnight, the patient developed urinary retention, fecal incontinence, and decreased rectal tone. Repeat lumbar spine MRI showed slight progression of the epidural fluid collection. The patient underwent lumbar decompressive surgery that day, and purulent material which cultured positive for S. aureus was evacuated from the epidural space. A S. aureus-positive psoas abscess also was identified and drained. The patient was ultimately discharged on IV antibiotics.

Imaging Findings

Lumbar spine MRI (Figure 1A: FSE T2-weighted; 1B: post-gadolinium T1-weighted with fat saturation) depicted epidural (arrows) and anterior paraspinal (arrowheads) fluid collections centered around L4-5, and abnormal T2 hyperintensity within the L4-5 and L5-S1 intervertebral disks, compatible with diskitis and abscess formation. There was minimal generalized edema-type signal in the L4 through S1 vertebral body marrow best seen on fat-saturated T2-weighted images (not shown). Sagittal fat-saturated T1-weighted post-gadolinium images (Figure 1B) depicted no significant enhancement around the epidural fluid collection, nor in the vertebral body marrow about the L4-L5 and L5-S1 discs, nor in these disc spaces themselves. Notably, a degenerative vacuum phenomenon was present within these discs on an abdominal CT scan from one month prior, but was no longer present on an abdominal CT scan at admission. Admission abdominal CT also showed a new right psoas abscess adjacent to the L4-L5 level.

Summary

We present a case of nonenhancing lumbar diskitis and epidural and paraspinal abscess. The diagnosis of diskitis and epidural abscess is typically supported by associated enhancement on gadolinium contrast-enhanced MRI but may be absent in patients who are substantially immunocompromised and may not be able to mount the inflammatory response necessary to produce such enhancement. It is important to look for other signs to suggest infection, such as intradiskal hyperintense signal on T2-weighted images, epidural and paraspinal fluid collections, and loss of degenerative disk vacuum phenomenon, so as not to delay the diagnosis.

KEYWORDS: Diskitis, Contrast enhancement

EE-75

Rare Case of IgG4-Related Hypertrophic Pachymeningitis Involving the Spine with Spinal Cord Compression

Patro, S. N.·Torres, C.·Zwicker, J.
The Ottawa Hospital
Ottawa, ON, CANADA.

Purpose

To present the clinical and imaging features of a patient with IgG4-related hypertrophic pachymeningitis in the thoracic spinal cord that led to spinal cord compression. To discuss the rare central nervous system manifestation of IgG4 related disease.

Case Report

A 58-year-old woman presented with pain in the periscapular region followed by numbness in the feet which extended up the torso over several days. An MRI with gadolinium demonstrated circumferential epidural-dural lesion from C7 toT7 causing spinal cord compression. This was felt to represent a dural-based process, probably inflammatory myofibroblastic tumor, lymphoma or metastases. A CT of the chest/abdomen and pelvis demonstrated no neoplasm. At followup two months later, the patient's symptoms persisted. Repeat MRI showed no change. Three months later, the patient reported a two-week history of leg weakness and profound spasticity in the lower extremities. MR imaging with gadolinium demonstrated circumferential thickening of the dura from C7-T7 which was hypointense on T1- and T2-weighted imaging and enhanced homogeneously. A decompressive T2-T4 laminectomy with excision of the hypertrophied dura was performed. On histopathology the epidural/dural tissue was negative for microorganisms, malignancy, and stromal reaction with the smooth muscle actin antibody and was consistent with idiopathic hypertrophic pachymeningitis. Special staining of the tissue with IgG4 showed positive result. She had no clinical or laboratory findings of active connective tissue disorder, except positive rheumatoid factor. Ten months postoperatively, she complained of increasing numbness in the legs. Repeat MRI demonstrated progression of the disease. She was treated with high dose prednisone and methotrexate. Within days her symptoms improved and follow-up MRI demonstrated significantly improved dural thickening.

Imaging Findings

Note: Scanned images are included in the proceedings. Some submitted images were reduced during editing, thereby decreasing clarity. Also, refer to the Program Planner. Proceedings Content as of 3-29-2013.

The initial MRI with gadolinium showed concentric epidural-dural lesion from C7 to T7, causing spinal cord compression. Follow-up MRI at two months interval showed no change. Three months later with worsening of symptoms a repeat MRI showed hypointense circumferential dural thickening on T1- and T2-weighted images with postcontrast enhancement. Ten months following decompressive surgery she again developed increasing leg numbness. Repeat MRI showed progression of dural thickening and compression of spinal cord at T5 level. Following treatment with steroid and methotrexate the symptoms and MRI findings showed significant improvement.

Summary

Prominent dural thickening isolated to the spine may be a manifestation of a systemic infectious/inflammatory or neoplastic process. Rare cases will be diagnosed pathologically as inflammatory pseudotumor, inflammatory myofibroblastic tumor, or idiopathic hypertrophic pachymeningitis. IgG4-related pachymeningitis is a very rare condition with only few case reports in the literature. The pathophysiology and pathogenesis still are not understood completely to date; however the favorable response to steroids suggests a benign and treatable condition. Abundant IgG4 immunostaining of the pathologic tissue and increased serum IgG4 concentration, as in our case helps in clinching the diagnosis of this disease. We strongly suggest that the IgG4-related sclerosing disease should always be considered in the differential diagnosis of patients with pachymeningitis.

KEYWORDS: Pachymeningitis, MR imaging, idiopathic, IgG4

EE-76

MR Imaging of Sporotrichosis Meningitis in a Nonimmunocompromised Adult

Lai, L.·Moritani, T.·Kirby, P.
University of Iowa Hospital and Clinics
Iowa City, IA.

Purpose

To demonstrate MRI findings of an unusual presentation of sporotrichosis as isolated nodular meningitis in a nonimmunocompromised adult.

Case Report

A 22-year-old male construction worker presented with headache, vomiting, and severe lower back pain several months after a motor vehicle accident where he sustained multiple fractures including facial, cervical vertebrae, and ankle fractures. Past medical history included intravenous drug use. Brain and lumbar spine MRI showed meningeal enhancement and enhancing nodules throughout the thoracolumbar spine. Lumbar puncture showed WBC 1980 cells (73% neutrophils, 27% lymphocytes), total protein 720 mg/dl, and glucose <20 mg/dl, negative CSF and AFB stains, and negative bacterial and fungal cultures. Multiple serologic studies for fungal, inflammatory, and viral etiologies were negative. The only positive CSF serologic study was sporothrix with a weakly positive 1:4 antibody titer. Dural biopsy performed at the T11-12 level showed acute and chronic inflammation with necrosis. Gomori Methenamine silver stain showed single septate fungal hypha. Patient initially was treated empirically for tuberculosis but returned one month later with worsening back pain, urinary retention, and lower extremity weakness. Given the positive sporothrix antibody titers, therapy was switched to sporotrichosis treatment with two weeks of amphotericin followed by voriconazole. The patient clinically improved back to baseline. Five months later, lumbar puncture was normal and MRI showed decreased meningeal enhancement.

Imaging Findings

Brain MRI showed meningeal enhancement of the prepontine cistern and right ambient cistern. T2 (Figure, left) and postcontrast (Figure, right) spine MRI showed enhancing intradural, extramedullary nodules with low peripheral T2 signal and central cystic components in the thoracolumbar spine. Differential was fungal or tuberculosis meningitis. Increased T2 cord signal from T8 to the conus was consistent with cord edema.

Summary

Sporotrichosis is a subacute-chronic fungal infection, usually caused by inoculation of soil/moss containing sporothrix schenckii fungi into the skin or subcutaneous lymphatics. Rarely, sporotrichosis can involve the meninges, usually in immunocompromised patients. Obtaining a positive CSF culture of sporothrix is difficult, which can result in delay in treatment. In this case, CSF cultures were negative for sporothrix, but the positive CSF antibody titer, fungal hypha on dural biopsy, and clinical improvement with amphotericin strongly suggested the diagnosis of sporotrichosis. The differential for nodular meningeal enhancement should include fungal meningitis like sporotrichosis. There has been no prior literature on MRI imaging of sporothrix spinal meningitis. We report the MRI features of a rare case of meningeal sporotrichosis in a nonimmunocompromised adult.

Note: Scanned images are included in the proceedings. Some submitted images were reduced during editing, thereby decreasing clarity. Also, refer to the Program Planner. Proceedings Content as of 3-29-2013.

KEYWORDS: Spinal imaging, Meningitis, sporotrichosis

EE-77

Osseous Metastasis of the Spine with Superimposed Osteomyelitis

Gandhe, A. R.·Mohiuddin, J.·Rao, N.·Patel, F.·Flanders, A. E.
Thomas Jefferson University Hospital
Philadelphia, PA.

Purpose
To review the rare occurrence of osteomyelitis and osseous metastasis occurring simultaneously in the spine and to discuss the imaging features. Very few cases of osseous metastasis with coexistent/superimposed infection have been reported in the literature. We report a unique case of osteomyelitis superimposed on vertebral metastasis with associated epidural abscess.
Case Report
A 57-year-old man presented with left-sided headache, neck pain and melanotic stools for three weeks. Imaging demonstrated a destructive enhancing lesion in the occipital bone with epidural extension and edema in the left occipital lobe. On metastatic workup, he was found to have carcinoma of the colon, lymphadenopathy and a lytic lesion in T6 vertebra. Biopsy of the colon demonstrated adenocarcinoma. He underwent resection of the occipital mass which represented metastatic disease. Three weeks later, he presented with abdominal pain. CT demonstrated a lytic lesion with new, innumerable foci of gas throughout T7 vertebral body. Lytic changes and foci of gas also were present in C7 and T5 vertebra and the right fifth rib. There were foci of gas in the epidural space at T6 and in the paraspinal soft tissues. Due to numerous, small foci of intraosseous gas, paraspinal soft tissue gas and gram negative bacteremia, osteomyelitis was considered more likely. Metastatic disease was considered less likely. MR imaging of the spine demonstrated a rim-enhancing epidural collection throughout the thoracic spine, causing mass effect on the spinal cord. Abnormal marrow replacement, enhancement and numerous foci of gas was present in T7 vertebra with a paraspinal soft tissue abscess. There were other scattered marrow replacing lesions in the spine. The patient underwent surgery for evacuation of the epidural abscess, T7 corpectomy and posterior fixation. Histopathology of T7 vertebra demonstrated adenocarcinoma metastasis from the colon with signet ring cells. Culture from T7 vertebra demonstrated Bacteroides fragilis. The patient declined further treatment and was sent to hospice.

Summary
Osseous metastasis with superimposed/coexistent osteomyelitis is extremely uncommon documented in only several published case reports. Both osteomyelitis and metastases show abnormal marrow replacement on MRI and can demonstrate lytic lesions on CT. Isolated foci of gas in primary or secondary bone tumors is extremely unusual. However, the presence of small foci of intraosseous gas strongly suggests osteomyelitis, particularly in the presence of gas in the surrounding soft tissues. In the case of known osseous metastases, the presence of this pattern of intraosseous gas should raise the possibility of coexistent infection.

KEYWORDS: Osteomyelitis, Metastases, abscess

EE-78

CT-Guided Transforaminal Ventral Epidural Blood Patch for the Treatment of Intracranial Hypotension

Park, J.·Yoo, B.·Villablanca, J. P.
University of California Los Angeles
Los Angeles, CA.

Purpose
To illustrate the novel technique of treating a ventral cerebrospinal fluid (CSF) leak utilizing a transforaminal blood patch delivered directly into the ventral epidural CSF collection. To our best knowledge the application of this technique under CT guidance has not been reported previously.
Case Report
A 35-year-old male presented with debilitating headaches secondary to recurrent ventral CSF leak, which did not respond to dorsal blood patch. Prior imaging revealed evidence of intracranial hypotension and a large chronic ventral CSF collection. He underwent an exploratory multilevel laminotomy that was unsuccessful in identifying the precise location of patient's dural tear. The patient underwent an additional CT myelogram, which suggested

Note: Scanned images are included in the proceedings. Some submitted images were reduced during editing, thereby decreasing clarity. Also, refer to the Program Planner. Proceedings Content as of 3-29-2013.

that the site of leakage was approximately at the mid-thoracic level. A decision was made to place a transforaminal epidural blood patch directly into the collection under CT guidance. The technique may be applied as follows: Spinal myelography is performed as usual under fluoroscopic guidance. The patient then is transferred to the CT gantry table and placed prone. Using intermittent low-dose CT guidance, the ventral epidural collection is accessed via transforaminal approach at site of maximal thickness. Following confirmation of needle tip position within the epidural CSF collection, the fluid contents within the fluid collection are aspirated and measured. Incremental, volume-matched, ventral epidural blood patching then is performed under direct intermittent CT visualization using sterile peripheral venous blood until the ventral chamber is completely filled. Twenty-four to 48 hours of supine lumbar drainage postprocedure may be performed. The advantages over fluoroscopically guided techniques include direct visualization of target collection in ventral epidural space, direct visualization of critical neurovascular structures to be avoided(vertebral artery, spinal cord, spinal nerves), and direct visualization of access into, and injection of blood into the ventral epidural collection, maximizing technical success and potential therapeutic benefit.

Imaging Findings

Image A: Intraprocedural prone axial CT images demonstrates spinal needle placed via right transforaminal posterior lateral approach at T6 with needle tip within ventral epidural CSF collection filled with contrast. VES indicates ventral epidural space; VSS, ventral subarachnoid space. Image B: Sagittal postprocedural CT demonstrates ventral epidural space now filled with isodense peripheral venous blood, previously filled with high density contrast. C indicates cord.

Summary

In properly selected patients, CT-guided transforaminal blood patching may serve as a safe and effective alternative to extensive multilevel corpectomy and surgical exploration for the treatment of symptomatic intracranial hypotension caused by ventral epidural CSF leak.

KEYWORDS: Intracranial hypotension, Blood patch

EE-79

Chordoma Mimicking the Imaging Appearance of a Neurofibroma Extending through the Neural Foramen

Mohiuddin, J.·Gandhe, A. R.·Flanders, A. E.
Thomas Jefferson University Hospital
Philadelphia, PA.

Purpose

To review the rare appearance of a chordoma presenting as an extradural mass exiting through an expanded neural foramen and mimicking the appearance of a nerve sheath tumor such as a neurofibroma. CT-guided biopsy confirmed the diagnosis of chordoma with tumor cells having a vacuolated, "physaliphorous" appearance and showed positive immunohistochemical staining. To our knowledge, this is the eleventh reported case of chordoma presenting as a mass expanding the neural foramen. Making the correct diagnosis prior to surgery is important as radical resection of chordoma is required to reduce the risk of local recurrence.

Case Report

A 24-year-old female presented with significant neck pain as well as a history of bilateral hand numbness and tingling and some mild weakness in the bilateral hands. She also complained of difficulty with fine motor activities. She denied any bowel or bladder dysfunction but was noted to be ataxic. The patient had no significant past medical history. No sensory deficit was found on physical examination. No motor deficits were found, apart from 3+ muscle strength involving the triceps, wrist extensors, and finger flexion on the right (compared to 4+ strength on the left). Hand intrinsics were 3+ bilaterally. Given the neck pain and upper extremity weakness, MRI of the cervical spine was performed. This showed a large epidural tumor extending from C3 to C6, exiting through the neural foramina and causing some bony destruction predominantly at C4.

Imaging Findings

The preliminary diagnosis by imaging was made of neurofibroma or lymphoma. In the absence of a history of neurofibromatosis, CT-guided biopsy was arranged. The core biopsy showed cords of cells with eosinophilic cytoplasm situated in a myxoid matrix. Many tumor cells had a vacuolated, "physaliphorous" appearance. Tumor cells showed positive immunohistochemical staining and the diagnosis of chordoma was made. The patient underwent radical resection with cervical decompression, including sacrificing the encased right vertebral artery. She tolerated the procedure well with no complications. To date, the patient has not had evidence of recurrence, although she still complains of pain.

Summary

Morbidity and mortality regarding chordoma usually is related to local recurrence rather than distant metastasis. Therefore, en-bloc resection is necessary to prevent residual tumor or seeding of the surgical tract, and this underscores the importance of a correct preoperative

Note: Scanned images are included in the proceedings. Some submitted images were reduced during editing, thereby decreasing clarity. Also, refer to the Program Planner. Proceedings Content as of 3-29-2013.

diagnosis. Although the MRI findings in our case were felt to be characteristic of a plexiform neurofibroma, the absence of a history of neurofibromatosis and the ability to safely target the large paraspinal component of the mass led to a biopsy that better informed the type of surgical treatment. Thus, we report to our knowledge the eleventh reported case of a chordoma presenting as a mass expanding the neural foramen and mimicking the more characteristic appearance of a nerve sheath tumor.

KEYWORDS: Chordoma, Neurofibromatosis, Mimic

EE-80

Primary Intradural Extramedullary Anaplastic Ependymoma: Report of a Case and Review of the Literature

Koohi, Y.·Durst, C.·Raghavan, P.·Nicolas-Jilwan, M.
University of Virginia
Charlottesville, VA.

Purpose
Primary intradural extramedullary ependymomas are extremely rare and develop from ectopic ependymal cell nests. There are approximately 19 reported cases in the literature, the vast majority of which are low grade with very few reported primarily anaplastic tumors at presentation. Approximately 80% of affected patients are females. To the best of our knowledge, there is to date no reported case of an anaplastic intradural extramedullary ependymoma with diffuse leptomeningeal dissemination at the time of presentation. We present a unique case of a grade III intradural extramedullary ependymoma in a 23-year-old male with extensive leptomeningeal dissemination at the time of diagnosis.
Case Report
The patient is a 23-year-old male who presented with neck pain radiating to the left arm associated with left upper extremity weakness and paresthesias. A cervical spine MRI revealed an intradural extramedullary tumor in the ventral thecal sac at C4 to C7 levels with severe cord compression, mild cord edema, and associated diffuse leptomeningeal nodularity and enhancement. The patient was started on steroids but presented a few weeks later with left foot drop and urinary retention. Imaging of the remainder of the neural axis revealed diffuse leptomeningeal dissemination at the thoracolumbar levels without imaging evidence of intracranial spread. A C4-C7 laminoplasty and tumor debulking were performed. The tumor was very adherent to the nerve roots and resection was subtotal. No cord or dural invasion was present. Postoperatively, the patient's symptoms improved with only mild residual weakness and numbness in the left upper extremity.
Imaging Findings
Cervical spine MRI at presentation shows a mildly heterogeneous avidly enhancing intradural extramedullary tumor in the ventral thecal sac spanning the C4 through C7 levels, eccentrically situated on the left without extradural extension. The tumor had a wide base along the dura. It caused severe cord compression with only mild cord edema. There was diffuse associated leptemeningeal nodularity and enhancement at the cervical, thoracic, and lumbar levels. No intracranial leptomeningeal enhancement was noted. There was no evidence of lymphadenopathy in the included portions of the neck, chest, and abdomen or abnormal bone marrow signal to suggest metastatic disease. While the patient's age would strongly favor metastatic lymphoma, the discrete amount of cord edema, lack of other evidence of metastasis, and the broad dural base and location of the lesion suggested a preliminary diagnosis of an atypical meningioma.
Summary
Intradural extramedullary ependymomas are extremely rare and most commonly low grade (WHO grade II) tumors. They frequently are misdiagnosed as meningiomas on preoperative imaging. Very few cases of primarily anaplastic tumors have been described previously in the literature, the majority of higher grade tumors showing extradural components. Our case illustrates one of these primarily anaplastic tumors with the unique feature of associated leptomeningeal dissemination at the time of presentation and lack of extramedullary extension. Although very rare, anaplastic extramedullary ependymomas should be included in the differential diagnosis of intradural extramedullary tumors with unusual features.

KEYWORDS: Ependymoma, Cervical spine, extramedullary

EE-81

Epidural Chondrosarcoma from the Intervertebral Disk without Osseous Abnormalities

Kalra, V. B.·Gibson, J.·Malhotra, A.
Yale University
New Haven, CT.

Purpose
Chondrosarcoma in the spine is an uncommon entity, and when present, usually demonstrates osseous findings of scalloping, cortical disruption, and periosteal reaction. We present two cases that appear as isolated epidural masses arising from the intervertebral disk level with intact adjacent vertebrae.
Case Reports
Patient #1 - 74-year-old woman with leg weakness and back pain underwent a T11-T12 decompressive laminectomy for a ventral epidural lesion thought to represent a meningioma. MR imaging showed that she had severe spinal canal stenosis from the ventral epidural mass with its epicenter at the T11-T12 disk space. The lesion was mildly hyperintense on T2, hypointense on T1, and had punctate foci of enhancement. A year later, she redeveloped leg weakness, had similar MR findings, and underwent subtotal tumor excision. Pathology showed pleomorphic multinucleate chondrocytes consistent with

Note: Scanned images are included in the proceedings. Some submitted images were reduced during editing, thereby decreasing clarity. Also, refer to the Program Planner. Proceedings Content as of 3-29-2013.

low-grade chondrosarcoma. Two years later, she developed compression fractures with retropulsion and underwent T11 and T12 anterior corpectomy, five CyberKnife treatments, and vertebroplasty of lower thoracic spine with instrumented fusion from T8-L5. T11-T12 diskectomy demonstrated the same pathology - low-grade chondrosarcoma. Patient #2 - 64-year-old man with lower back and leg pain with a L4-L5 posterior decompression for a ventral epidural lesion. MR imaging showed a ventral epidural mass at the L4-L5 disk space level causing severe spinal canal stenosis. The lesion was hyperintense on T2 and hypointense on T1. Pathology showed pleomorphic multinucleate chondrocytes consistent with low-grade chondrosarcoma.The mass grew slowly over six years to extend to the one higher disk space with no significant change in degree of spinal canal stenosis. There was also extension through multiple adjacent neural foramina.

Imaging Findings

Patient #1 - MR imaging demonstrates a 3 cm T2 hyperintense and T1 hypointense lesion in the epidural space with the epicenter at the T11-T12 disk space. The lesion demonstrated multiple punctate foci of enhancement. There were no associated osseous abnormalities. The T11-T12 intervertebral disk was unremarkable. CT demonstrated vague calcifications within the lesion. No significant growth was seen over one year prior to tumor resection and no recurrence was seen as of four years after resection. Patient #2 - MR imaging demonstrates a 4.8 cm x 1.1 cm T2 hyperintense and T1 hypointense lesion in the epidural space with the epicenter at the L4-L5 disk space. There were no associated osseous abnormalities. The L4-L5 intervertebral disk demonstrated degenerative changes similar to those seen at adjacent levels. CT demonstrated vague calcifications within the lesion. Six years later, the lesion grew slightly, 1 cm cranially and through the adjacent neuroforamina.

Summary

We present two cases of previously unreported low-grade chondrosarcomas isolated to the epidural space with their epicenters at intervertebral disks and no osseous involvement. Chondrosarcoma should be included in the differential of epidural lesions even if there is no osseous involvement, especially if CT demonstrates matrix calcifications and the lesion has its epicenter at an intervertebral disk.

KEYWORDS: Spinal neoplasm, Disk

EE-82

Intraosseous Glomus Tumor of the Thoracic Spine

Fong, C. L.·Ngo, M.
Kaiser Permanente Los Angeles
Los Angeles, CA.

Purpose

The purpose of this case report is to demonstrate the findings of an intraosseous spinal glomus tumor.

Case Report

Intraosseous spinal glomus tumors are extremely rare entities. This case is of an 89-year-old male who presented to the ER with worsening gait.

Imaging Findings

CT imaging demonstrates a lytic lesion. MR imaging demonstrates an avidly enhancing markedly T2 hyperintense mass with a salt and pepper appearance due to flow voids. The mass has epidural and paravertebral extension.

Summary

In summary, intraosseous glomus tumors of the spine are extremely rare neoplasms that have a classic MR appearance similar to glomus tumors of the head and neck.

KEYWORDS: Spinal neoplasm, CT, glomus

EE-83

Spinal Epidural Chondrosarcoma from the Intervertebral Disk without Osseous Abnormalities

Kalra, V.·Gibson, J.·Malhotra, A.
Yale University
New Haven, CT.

Purpose

Chondrosarcoma in the spine is an uncommon entity, and when present, usually demonstrates osseous findings of scalloping, cortical disruption, and periosteal reaction. We present two cases that appear as isolated epidural masses

arising from the intervertebral disk level with intact adjacent vertebrae.
Case Report
Patient #1 - 74-year-old woman with leg weakness and back pain underwent a T11-T12 decompressive laminectomy for a ventral epidural lesion thought to represent a meningioma. MR imaging showed that she had severe spinal canal stenosis from the ventral epidural mass with its epicenter at the T11-T12 disk space. The lesion was mildly hyperintense on T2, hypointense on T1, and had punctate foci of enhancement. A year later, she redeveloped leg weakness, had similar MR findings, and underwent subtotal tumor excision. Pathology showed pleomorphic multinucleate chondrocytes consistent with low-grade chondrosarcoma. Two years later, she developed compression fractures with retropulsion and underwent T11 and T12 anterior corpectomy, five CyberKnife treatments, and vertebroplasty of lower thoracic spine with instrumented fusion from T8-L5. T11-T12 diskectomy demonstrated the same pathology - low-grade chondrosarcoma. Patient #2 - 64-year-old man with lower back and leg pain with a L4-L5 posterior decompression for a ventral epidural lesion. MR imaging showed a ventral epidural mass at the L4-L5 disk space level causing severe spinal canal stenosis. The lesion was hyperintense on T2 and hypointense on T1. Pathology showed pleomorphic multinucleate chondrocytes consistent with low-grade chondrosarcoma.The mass grew slowly over six years to extend to the one higher disk space with no significant change in degree of spinal canal stenosis. There was also extension through multiple adjacent neural foramina.
Imaging Findings
Patient #1 - MR demonstrates a 3 cm T2 hyperintense and T1 hypointense lesion in the epidural space with the epicenter at the T11-T12 disk space. The lesion demonstrated multiple punctate foci of enhancement. There were no associated osseous abnormalities. The T11-T12 intervertebral disk was unremarkable. CT demonstrated vague calcifications within the lesion. No significant growth was seen over one year prior to tumor resection and no recurrence was seen as of four years after resection. Patient #2 - MR demonstrates a 4.8 cm x 1.1 cm T2 hyperintense and T1 hypointense lesion in the epidural space with the epicenter at the L4-L5 disk space. There were no associated osseous abnormalities. The L4-L5 intervertebral disk demonstrated degenerative changes similar to those seen at adjacent levels. CT demonstrated vague calcifications within the lesion. Six years later, the lesion grew slightly, 1 cm cranially and through the adjacent neuroforamina.
Summary
We present two cases of previously unreported low-grade chondrosarcomas isolated to the epidural space with their epicenters at intervertebral disks and no osseous involvement. Chondrosarcoma should be included in the differential of epidural lesions even if there is no osseous involvement, especially if CT demonstrates matrix calcifications and the lesion has its epicenter at an intervertebral disk.

KEYWORDS: Chondrosarcoma, epidural

EE-84

Feasibility of Placement of an Anterior Cervical Epidural Blood Patch for Spontaneous Intracranial Hypotension Secondary to a Ventral Dural Tear

Park, J. K.·Yoo, B.·Villablanca, J. P.
University of California Los Angeles
Los Angeles, CA.

Purpose
To illustrate a detailed guide for the novel technique of placing an anterior cervical blood patch for a large cervical ventral cerebrospinal fluid (CSF) leak.
Case Report
A 41-year-old man presented one year after onset of debilitating post-traumatic positional headaches with imaging evidence of intracranial hypotension. Before presentation at our center, he was treated unsuccessfully with multiple lumbar epidural blood patches (EBP) at outside hospitals. CT myelogram demonstrated a large ventral epidural contrast collection secondary to dural tear in the cervical spine. Given the large size of the collection and unknown exact location of dural injury it was thought that exploring the ventral spinal column would require morbid surgery and extensive vertebrectomies, and an anterior EBP approach was performed. Following supine placement on the fluoroscopy table, the C5-C6 disk space was identified and increasing digital pressure was applied in the right anterior neck to displace the carotid sheath laterally, and the esophagus and trachea medially. A spinal needle then was advanced through the target disk under fluoroscopy, with entry just right of midline. After confirmation of needle tip placement in the ventral epidural space with myelographic contrast and gentle CSF aspiration, fresh sterile peripheral blood was slowly injected into the collection without complication. Subsequently 72 hours of lumbar drainage was performed utilizing a lumbar drainage catheter. Our patient experienced marked symptomatic improvement and no complications.
Imaging Findings
Image 1 - Preprocedural sagittal CT myelogram demonstrates a large and continuous ventral epidural contrast collection extending from the C3-C4 through thoracic levels. While the exact site of communication with the ventral subarachnoid space (VSS) could not be identified, both a contrast-attenuation gradient and the largest cross-sectional area of the epidural collection were seen in the lower cervical region, suggesting cervical leakage site. VES indicates ventral epidural space; C, cord.
Image 2 - Lateral fluoroscopic image demonstrating the needle traversing the C5-6 disk space, with tip in the ventral epidural collection/space (VES). D indicates ventral

Note: Scanned images are included in the proceedings. Some submitted images were reduced during editing, thereby decreasing clarity. Also, refer to the Program Planner. Proceedings Content as of 3-29-2013.

dura outlined by myelographic contrast.

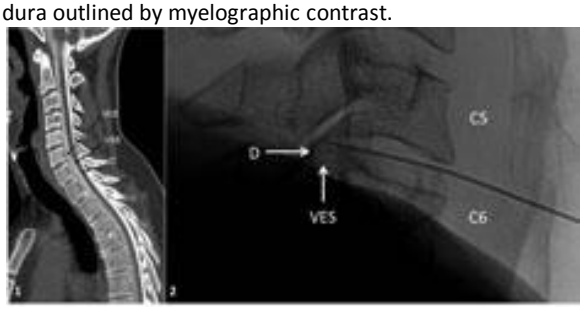

Summary
We present, to our knowledge, the first case of the placement of an anterior EBP for the treatment of SIH from a cervical ventral dural tear. We suggest that in appropriately selected patients with refractory ventral cervical CSF leaks, the anterior technique can be performed safely.

KEYWORDS: Intracranial hypotension, Blood patch

EE-85

Rare Intraperitoneal Cerebrospinal Fluid Leak: A Unique Therapeutic Approach with Sacral Transforaminal Epidural Blood Patch

Fortes, M. C.·Jindal, G.·Miller, T.·Gandhi, D.
University of Maryland
Baltimore, MD.

Purpose
To report a case of severe intracranial hypotension secondary to Tarlov cyst intraperitoneal CSF leak, treated with CT-guided sacral transforaminal blood patch.
Case Report
A 41-years-old healthy male presented to the Emergency Department with a three weeks history of increasing headaches. Patient denied trauma, antiplatelets or anticoagulants. Normal laboratorial workup. Initial imaging evaluation of the head was performed with noncontrast CT and CT angiogram. A cerebral angiogram followed. A CT myelogram and MRI of the spine then were performed. A diagnosis of subdural hematoma secondary to intracranial hypotension was made. A CSF leak adjacent to a Tarlov cyst was identified. To avoid open surgery, a minimally invasive approach was chosen. A CT-guided right S2-3 transforaminal epidural blood patch was performed. After the procedure, patient's symptoms steadily improved and completely resolved in the following week. Follow-up nuclear imaging confirmed complete resolution of the CSF leak.
Imaging Findings
Noncontrast CT of the head demonstrated a subdural hematoma. CT angiogram of the head showed no vascular abnormalities. Cerebral angiography was also negative. MR imaging of the spine showed a 15 mm Tarlov cyst at the S2-3 level. Also seen was free fluid in the peritoneal cavity. CT myelogram demonstrated an area of CSF leakage, adjacent to the Tarlov cyst, at the level of the right S2 nerve root, extending inferiorly beyond the nerve sheath and towards the piriformis muscle and abdominal cavity. CT-guided epidural blood patch with injection of 0.5 ml of Ominipaque 180 contrast confirmed the leakage and again showed contrast along the right S2 nerve and into the right piriformis muscle. Indium-111 radiotracer was injected to the thecal sac 24 hours postepidural blood patch. Planar gamma camera imaging acquisition showed no residual CSF leak.

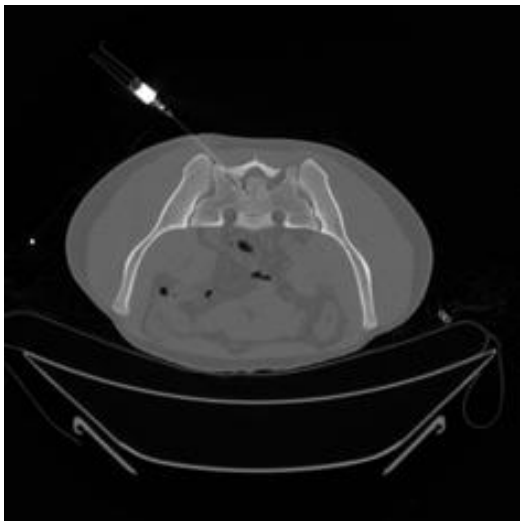

Summary
Cerebrospinal fluid leakage to the peritoneal cavity is a rare finding. Tarlov cyst rupture causing severe intracranial hypotension with subdural hematoma formation is managed more commonly with open surgical repair. We report our experience in a successful attempt of performing a less invasive CT-guided epidural blood patch as an alternative to open surgery.

KEYWORDS: Intracranial hypotension, Subdural hemorrhage, Tarlov cyst

EE-86

Technique for CT Localization of Site of Leakage in Patients with Symptomatic Ventral Cerebrospinal Fluid Leaks

Yoo, B. Y.·Park, J. K.·Bentson, J.·Villablanca, J. P.
Ronald Reagan University of California Los Angeles Medical Center
Los Angeles, CA.

Purpose
To illustrate a novel technique for the detection of the site of leakage of cerebrospinal fluid (CSF) into the ventral epidural space utilizing the "chalice" technique.
Case Report
A 35-year-old male with debilitating headaches and imaging findings of intracranial hypotension secondary to

Note: Scanned images are included in the proceedings. Some submitted images were reduced during editing, thereby decreasing clarity. Also, refer to the Program Planner. Proceedings Content as of 3-29-2013.

recurrent ventral CSF leak. Imaging revealed a large ventral CSF leak from C3 to L1. However, conventional and CT myelography, nuclear cisternography and surgical exploration did not localize the site of leakage. We utilized a novel “chalice” technique to localize the site of CSF leakage, as follows: A lumbar drain is placed into the CSF space using fluoroscopic guidance at the midpoint of the segment of interest. The patient then is placed in the supine position, utilizing the “chalice” technique [i.e., creation of an asymmetric kyphotic deformity at the mid thoracic spine (or appropriate spine segment) by using cervical and lumbar bolsters]. The subarachnoid space then is incrementally filled with small amounts of myelographic dye (Omnipaque-240) via the lumbar drain. Contrast begins to pool progressively in the dependent portion of the subarachnoid space. Intermittent, low dose CT scanning then is used to detect the vertebral level at which contrast opacification of the ventral epidural collection first occurs, as the dye “spills over” from the subarachnoid space into the ventral epidural collection, through the ventral dural defect. Once identified, a targeted surgical repair or blood patch of the dural defect can be performed.

Imaging Findings

Sagittal and axial CT images of the thoracic spine during intermittent injection of contrast through a lumbar drain into the subarachnoid space. Initial injection (B, E) demonstrates a column of dye in the SAS, without contrast filling of the VES. Subsequent injection of dye (C, F) demonstrates cephalad progression of contrast, with filling of the VES first noted when the dye in the SAS reached the T3 level, suggesting T3 as the level of the leak. VES = ventral epidural space; SAS = subarachnoid space; C = spinal cord; LD = lumbar drain.

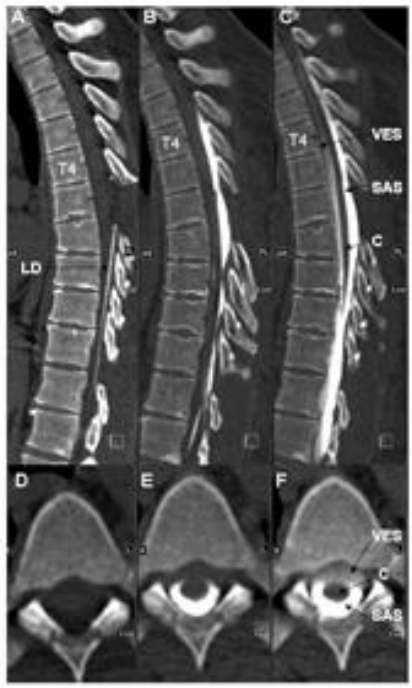

Summary

When traditional methods have failed, the “Chalice" technique may be an effective method to identify the level of a ventral CSF by using low-dose CT monitoring of sequential filling of the subarachnoid space until the “spill-over” location is identified.

KEYWORDS: CSF leak, Myelography, intracranial hypotension

EE-87

Extradural Glioependymal Cyst: A Rare Cause of Spinal Cord Compression

Griffith, B.·Patel, S.·Abdulhak, M.·Gutierrez, J.
Henry Ford Hospital
Detroit, MI.

Purpose

Glioependymal cysts are rare congenital lesions of the central nervous system. While occurring in the spine, the lesions are typically intradural in location. This excerpta describes a rare case of an extradural glioependymal cyst causing compression of the thecal sac and cauda equina.

Case Report

We present a case of a 46-year-old man presenting with one to two-year history of bilateral lower extremity weakness and right foot drop. While the symptom onset was gradual, there had been noticeable worsening over the past year. The patient also complained of numbness, tingling, an a pressure sensation in the lower extremities.

Note: Scanned images are included in the proceedings. Some submitted images were reduced during editing, thereby decreasing clarity. Also, refer to the Program Planner. Proceedings Content as of 3-29-2013.

Electromyography demonstrated bilateral L1-S1 polyradiculopathies, worse on the right. The patient underwent a T11-L2 decompressive laminectomy at which time a thin, semitransparent epidural cyst was removed. Pathology demonstrated a cyst lined by flat cuboidal cells, which were strongly GFAP-positive with focal, intraluminal thick strands forming heaps of GFAP-positive tissue. The cells lining the cavity were EMA and CK negative. These findings are consistent with a glioependymal cyst. Following surgery and rehabilitation, the patient had mild persistent leg weakness.

Imaging Findings

Lumbar spine MR demonstrates a large T2 hyperintense/T1 hypointense extradural cystic lesion (Figure 1) along the posterior spinal canal extending from T12 to L3 with compression of the thecal sac and cauda equina. Bony remodeling and intraforaminal extension with foraminal widening also are present. CT myelogram redemonstrates the large extradural cystic lesion with slow filling of contrast on delayed images indicating communication with the thecal sac (Figure 2).

Summary

Glioependymal cysts are rare, congenital, non-neoplastic lesions of the CNS, lined by a single layer of cuboidal or columnar epithelium. Lesions are thought to be developmental in origin, arising from displaced ependymal cells that become isolated from the neural tube floor plate during embryogenesis. While rare, there are a number of case reports detailing both intra and extramedullary intradural lesions. To the best of our knowledge, this is only the second reported case of an extradural lesion, perhaps secondary to a dural defect permitting its extradural development. In conclusion, glioependymal cysts, while rare, should be considered in the differential diagnosis of extradural cystic spinal lesions.

KEYWORDS: Ependymal cyst, Extradural

EE-88

Spinal Metastasis of Intracranial Primary Malignant Peripheral Nerve Sheath Tumor

Gandhe, A. R.·Mohiuddin, J.·Patel, F.·Talekar, K.·Flanders, A. E.
Thomas Jefferson University Hospital
Philadelphia, PA.

Purpose

To review the drop metastasis from intracranial malignant peripheral nerve sheath tumors (MPNST). Intracranial malignant peripheral nerve sheath tumors are extremely rare; less than 50 cases have been reported in the literature. Drop metastasis from intracranial MPNSTs had been described in only three prior reports. Two patients had a history of cranial radiation in childhood and one had malignant conversion of a vestibular schwannoma. We report the first case of de novo primary intracranial MPNSTs with drop metastasis to spine.

Case Report

A 27-year-old male presented with left facial weakness, hand numbness and severe headache for one week. His past medical history was significant for malignant rhabdomyosarcoma of the left thigh at the age of four, treated with chemotherapy and radiation. Though exact details of prior treatment were not available, there was no history of brain metastasis and radiation. CT scan and MRI of the brain demonstrated a left cerebellopontine angle hemorrhagic, enhancing, extra-axial mass lesion, causing compression on the 4th ventricle and obstructive hydrocephalus. Workup for metastasis was negative. Patient underwent uneventful resection with significant improvement in symptoms. Ventriculoperitoneal shunt also was placed for hydrocephalus. Pathology revealed a sarcoma most compatible with a malignant peripheral nerve sheath tumor. The patient then began a course of radiation therapy. Approximately three months later, he presented with neck and upper back pain with tingling in feet. An MRI of the spine demonstrated an intramedullary hemorrhagic enhancing mass lesion at C2 in the cervical spine and a smaller intramedullary enhancing lesion at T10 in the thoracic spine. The patient underwent immediate resection of the cervical lesion. Histopathology was consistent with MPNST, similar to the intracranial tumor. There was no residual tumor on immediate postoperative MRI. Three weeks later, he returned with a rapid onset of quadriparesis. MR imaging of the cervical spine demonstrated a recurrent hemorrhagic intramedullary mass at C3-C4. He underwent re-resection and was sent to rehabilitation.

Note: Scanned images are included in the proceedings. Some submitted images were reduced during editing, thereby decreasing clarity. Also, refer to the Program Planner. Proceedings Content as of 3-29-2013.

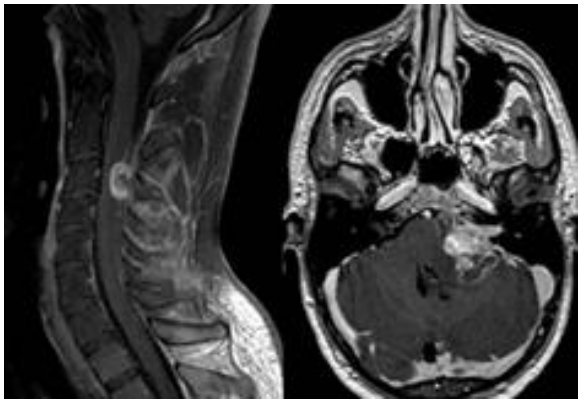

Summary
Intracranial MPNST is a very rare entity with a poor prognosis. It is a very aggressive tumor with a very high recurrence rate even after gross total resection. Only three cases of this kind have been reported previously, probably related to short life span after presentation. This is first case of de novo primary intracranial Malignant peripheral nerve sheath tumors with drop metastasis. Malignant peripheral nerve sheath tumors is a diagnostic consideration in the setting of a rapidly growing hemorrhagic extra-axial mass lesion.

KEYWORDS: Nerve sheath tumor, Metastases

EE-89

Perineural Spread of Malignant Mesothelioma with Spinal Cord Involvement

Newman, S. A.·Mohan, S.·Melhem, E. R.
Hospital of the University of Pennsylvania
Philadelphia, PA.

Purpose
We report a rare presentation of malignant mesothelioma with perineural spread of neoplasm along an intercostal nerve to invade the parenchyma of the spinal cord.
Case Report
Our patient is a 76-year-old man with previously biopsy-proven malignant mesothelioma who was undergoing palliative chemoradiation therapy. He presented with acute onset of urinary retention, bilateral lower extremity weakness and parasthesias with a new thoracic sensory level on neurologic examination. There were no pre-existent focal neurologic deficits. MR imaging scan of the thoracic spine demonstrated a pleural mass invading the left posterior chest wall with perineural spread along the left 6th intercostal nerve to involve the left T6 nerve root and parenchyma of the spinal cord. Based on the history and findings, the imaging diagnosis of malignant mesothelioma with extramedullary and intramedullary spinal cord involvement via perineural spread was proposed. The patient was started on steroids and underwent targeted proton therapy to the thoracic spine followed by fractionated daily radiation therapy, with improvement of bilateral lower extremity strength and sensation. Follow-up MRI performed one month later demonstrated decreased size of the enhancing intramedullary mass with decreased mass effect.
Imaging Findings
Contrast-enhanced MRI of the thoracic spine demonstrated a 5.8 cm pleural mass invading the left posterior chest wall, including the 6th, 7th, and 8th ribs and the left lateral paraspinous soft tissues, extending through the left T6-7 neural foramen contiguously involving the left lateral epidural space/dura mater, in continuity with enhancing intradural, extramedullary mass, with associated thickening and enhancement of the dorsal and ventral nerve roots. There was associated enhancing intramedullary mass in the thoracic cord, measuring 7 mm transverse by 7 mm anteroposterior by 38 mm craniocaudad, spanning the T5 and T6 levels, with extensive cord edema spanning from T4 through T9 (Figure).

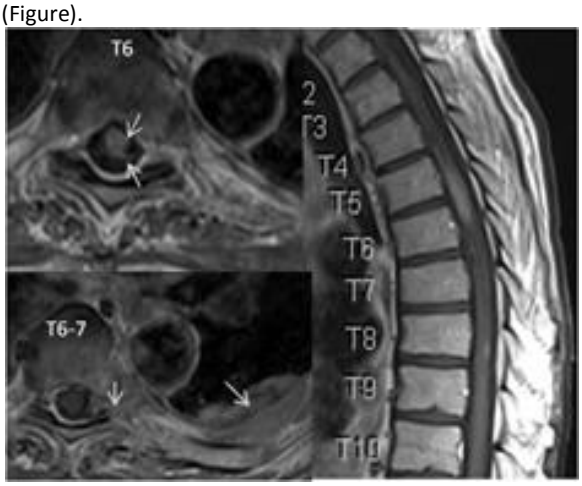

Summary
This case demonstrates the rarely reported finding of intramedullary involvement of the spinal cord via perineural spread by malignant mesothelioma.

KEYWORDS: Perineural, Intradural mass, malignant mesothelioma

EE-90

Synovial Osteochondromatosis of the Craniocervical Junction with Spinal Cord Compression

Garger, A. V.·Zacharia, B. E.·Bruce, J. N.·Ross, R. L.·Lignelli, A. A.
Columbia University New York Presbyterian Medical Center
New York, NY.

Purpose
To report a rare case of synovial osteochondromatosis resulting in cervical spinal cord compression.
Case Report

Note: Scanned images are included in the proceedings. Some submitted images were reduced during editing, thereby decreasing clarity. Also, refer to the Program Planner. Proceedings Content as of 3-29-2013.

An 82-year-old man presented with progressive right upper extremity weakness and diminished dexterity. MR imaging demonstrated a 2.1 x 1.5 cm, well circumscribed, nonenhancing, extramedullary mass at the level of the dens, markedly compressing the spinal cord. Magnetic susceptibility artifacts in the mass were suggestive of calcifications. Image-based differential included calcified meningioma, chordoma, synovial osteochondromatosis, chondrosarcoma, retro-odontoid psudotumor and dural metastasis. A right far lateral exposure was utilized to approach the lesion and grossly the tumor was avascular and soft. Pathology demonstrated dense fibrous and cartilaginous makeup with features consistent with synovial osteochondromatosis. Postoperative MRI demonstrated residual T2 signal abnormality of the spinal cord consistent with edema or myelomalacia. The patient underwent inpatient rehabilitation and has subjective improvement of his right arm deficits at two months followup.

Imaging Findings

A large mass was identified which demonstrated heterogeneous low T1 and T2 signal, as well as mild peripheral enhancement. The mass was severely compressing the spinal cord at the level of the dens (Figure 1: Axial and Sagittal T1 post contrast).

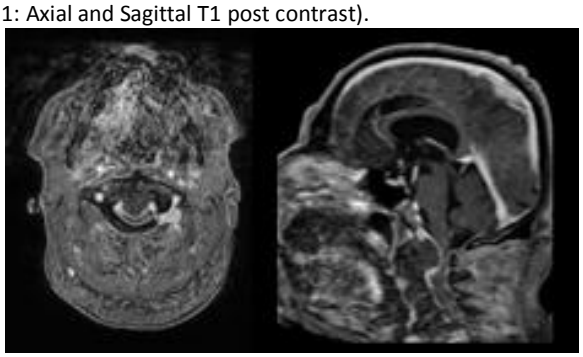

Summary

Synovial osteochondromatosis can occur anywhere synovium is found, yet it is rarely found outside of large joint spaces. Our search of English language literature found only 11 cases of spinal synovial osteochondromatosis. Of these, seven were paravertebral, resulting in nerve root compression and radiculopathy. One lumbar spinal canal mass compressed the cauda equina, and one spinal canal mass at the C1-C2 level was not compressive. Two cases of spinal cord compression by synovial osteochondromatosis have been described in the thoracic spine and cervical spine. Our case is only the second described instance of cervical spinal cord compression from synovial osteochondromatosis.

KEYWORDS: Cervical, Cranio-cervical junction, Osteochondromatosis

Monday, May 20 – Wednesday, May 22
6:30 AM – 9:00 PM
Thursday, May 23
6:30 AM – 3:00 PM
Hall B1

Scientific Posters Printed 1 - 71

P1-Adult Brain

Note: A missing printed number indicates an abstract has been withdrawn.

P-1

Correlation of Vasospasm on CTA and CTP Perfusion Deficits

Vora, A. P.
Weill Cornell
New York, NY.

Purpose

Following aneurysmal subarachnoid hemorrhage (a-SAH), vasospasm and delayed cerebral ischemia (DCI) are major contributors to poor clinical outcomes. Vasospasm, defined as arterial narrowing on angiographic imaging studies, is thought to lead to perfusion deficits in the distal vascular territory. Perfusion deficits on CT perfusion (CTP) have been shown to be related to DCI. It is questioned whether angiographic vasospasm is related directly to perfusion deficits. The purpose of this study was to correlate arterial vasospasm on CT angiography (CTA) and perfusion deficits on CTP.

Materials & Methods

A retrospective study of consecutive a-SAH patients admitted from January 2005 to December 2011 was performed. Inclusion criteria were a-SAH patients who received concurrent CTA and CTP following aneurysm rupture. CT angiographies were reviewed by two independent neuroradiologists, blinded to all clinical and imaging data, to determine the presence or absence of vasospasm and its degree defined as mild (stenosis 75%). For cases of disagreement, a third neuroradiologist reviewed the CTA as a tie-breaker. CT perfusions were reviewed by two independent neuroradiologists, blinded to all clinical and imaging data, to determine the qualitative presence or absence of a perfusion deficit. Perfusion deficits were defined as focal areas of reduced cerebral blood flow and/or elevated mean transit time. Quantitative CTP analysis was performed by region-of-interest (ROI) placement in each vascular territory using a

Note: Scanned images are included in the proceedings. Some submitted images were reduced during editing, thereby decreasing clarity. Also, refer to the Program Planner. Proceedings Content as of 3-29-2013.

standardized method. Statistical analysis included agreement rates measured by Kappa statistic and McNemar chi-square test. The mean CTP values were compared using analysis of variance.
Results
A total of 50 patients with concurrent CTA and CTP were studied with 298 vascular territories examined. The overall agreement rate is considered as none-slight (Kappa = 0.055). Seventy-three percent (218/298) of vascular territories did not demonstrate CTP deficits. Of these territories, 85% (185/218) had none/mild vasospasm and 15% (33/218) had moderate/severe vasospasm on concurrent CTA. Twenty-seven percent (80/298) of territories had CTP deficits, 80% (64/80) had none/mild vasospasm and 20% (16/80) had moderate/severe vasospasm on concurrent CTA. The McNemar chi-square test reveals a statistically significant p-value (0.002319) indicating the disagreement is not spread evenly in these two groups. Table 1 demonstrates the mean quantitative CTP values for patients with none/mild vasospasm compared to moderate/severe vasospasm. There was no statistically significant difference between these CTP parameters.

Mean for the quantitative CTP parameters

CTP parameter	None/Mild vasospasm n=249	Moderate/Severe vasospasm n=49
CBF (mL/100 gm/min)	38.5	39.0
CBV (mL/100 gm)	2.06	2.28
MTT (sec)	5.54	5.61

Conclusion
Our results show no statistically significant correlation between the degree of vasospasm on CTA and qualitative or quantitative CTP deficits in the corresponding vascular territory. Disagreement between the CTA and CTP was more pronounced when a CTP deficit was present indicating that the CTP deficit may be due to causes other than vasospasm on CTA. However, when there was no CTP deficit present, there was improved agreement between CTA and CTP.

KEYWORDS: Aneurysmal subarachnoid hemorrhage, Cerebral angiography

P-2

Cerebral Vascular Lesions: Diagnostic Value of 4D Dynamic Contrast-Enhanced MR Angiography Compared with 3D Time-of-Flight MR Angiography

Cheng, Y.·Chen, H.·Wu, C.·Chen, W.·Chen, C.
Taichung Veterans General Hospital, Taiwan
Taichung, TAIWAN.

Purpose
For early diagnosis and evaluation of cerebral vascular lesions such as arteriovenous malformation (AVM) and arteriovenous fistula (AVF), digital subtraction angiography (DSA) has remained a gold standard diagnostic method. The aim of this study was to analyze the value of different magnetic resonance angiographic images, 4D dynamic contrast-enhanced MRA (D MRA) and time-of-flight magnetic resonance angiography (TOF MRA), to identify their effect on evaluating cerebral vascular lesions.
Materials & Methods
A total of 47 patients with AVM or AVF at their initial evaluation or for followup after treatment were included in this study. Dynamic MRA and TOF examinations were performed simultaneously with conventional angiography as standard references. Two experienced neuroradiologists reviewed the images to compare the diagnosis accuracy, arterial feeder and venous drainage between these two MRA methods. Interobserver and intermodality agreement was assessed by Wilcoxsin Rank sum test.
Results
Almost all vascular lesions (86.7%) were diagnosed correctly using D MRA. However, the MIP TOF MRA only detected 62.2% of the lesions. There is a statistically significant difference regarding the lesion diagnostic accuracy ($p = 0.012$), arterial feeder ($p = 0.01$) and venous drainage identification ($p = 0.000$) between D MRA and TOF MRA. Dynamic MRA is superior to MIP TOF MRA for lesion assessment.
Conclusion
Dynamic MRA proved to be a reliable screening modality and follow-up method for cerebral vascular lesions with higher accuracy and consistency with DSA as compared to TOF MRA.

KEYWORDS: 4D MRA, AVM, TOF MRA

Note: Scanned images are included in the proceedings. Some submitted images were reduced during editing, thereby decreasing clarity. Also, refer to the Program Planner. Proceedings Content as of 3-29-2013.

P-3

Migraine with Visual Aura Due to Occipital Arteriovenous Malformation: Multimodal Imaging Investigation in a Case Series and Review of the Literature

Piccardi, B.[1,2]·La Piana, R.[1]·Klein, D.[1]·Mok, K.[1]·Chen, J.[1]·del Pilar Cortes, M.[1]·Tampieri, D.[1]
[1]Montreal Neurological Institute and Hospital, Montreal, QC, CANADA, [2]University of Florence, Florence, ITALY.

Purpose
Migraine with visual aura (MwVA) is a common presentation for occipital arteriovenous malformation (AVM) with a prevalence ranging between 5% and 28%. This phenomenon seems to be correlated with a state of neuronal hyperexcitability and increases the susceptibility to develop cortical spreading depression, the electrophysiologic correlate of the visual aura. We present a case series of five patients with MwVA attributed to occipital AVM according to the International Classification of Headache Disorders 2nd Edition (ICHD-II). These patients were part of a larger series of 29 cases with AVM referred to our center from 2008 to 2012 for unruptured AVM. Our results emphasize the importance of using a comprehensive protocol that integrates the clinical data with the functional and hemodynamic studies in patients with AVM and MwVA.
Materials & Methods
A comprehensive protocol integrating neurologic examination, ophthalmologic evaluation and neuroimaging was performed. A battery of functional magnetic resonance imaging (fMRI) tasks was administered to all five patients to identify brain regions activated during the performance of visual, motor, sensory and language tasks.
Results
In our series of subjects with AVM, headache was the presenting symptom in 34% (10/29). In this cohort, MwVA always was associated with an occipital localization of the AVM (5/29; 17.2%). In all five patients, the headache was ipsilateral to the lesion while the visual aura was localized in the contralateral visual hemifield. The visual aura was typical in three of them (lasting less than one hour, preceding the headache). In two patients the visual symptoms were often unrelated to headache, triggered by bright light and/or, black and white alternating pattern and lasting more than one hour. In two cases symptoms of visual dysperception other than visual aura were reported. The ophthalmologic examination was normal in all five patients: no evidence of visual field deficit or reduced visual acuity. Of these five patients, only one underwent endovascular treatment. In all patients, the pattern of activation on the fMRI differed from what is observed in healthy controls and showed a more diffuse and complex pattern. In addition, on visual functional imaging tasks, we observed that, despite a normal neurophthalmologic exam, the occipital region affected by the AVM showed a reduction in activation as compared to the unaffected hemisphere. Most interestingly, when stimuli were presented to each visual field, there was an absence of activity in the affected region.
Conclusion
Our study highlights the importance of integrating the clinical information with functional neuroimaging findings in the evaluation of patients with occipital AVM. Although the results are still preliminary, functional imaging data showed unexpected asymmetrical activation in the affected visual cortex despite normal neurophthalmologic exam. These results may be correlated with the important and somewhat unusual visual aura presented by these patients. The combined use of multiple imaging modalities may contribute to a better understanding of this phenomenon and may provide useful information to guide the treatment choice.

KEYWORDS: Arteriovenous malformation, MR imaging brain, migraine with visual aura

P-4

Differentiation between Jugular Venous Reflux and Cavernous Dural Arteriovenous Fistula on Routine Brain MR Imaging and MR Angiography

Lee, D.[1]·Kim, E.[2]
[1]Seoul Medical Center, Seoul, KOREA, REPUBLIC OF, [2]Seoul National University Bundang Hospital, Gyeonggi-do, KOREA, REPUBLIC OF.

Purpose
Both jugular venous reflux (JVR) and DAVF manifest as unusual venous signals in the cavernous sinus and its vicinity on TOF MRA. We investigated brain MR imaging and MRA findings that might distinguish JVR from cavernous DAVF.
Materials & Methods
Forty-one patients with JVR and 26 with cavernous DAVF underwent MR imaging and MRA. We assessed the following findings: sidedness and location of unusual venous signals on intracranial TOF MRA; signal intensity of the proximal jugular vein on T2WI; early opacification of the cavernous sinus in the arterial phase of CE MRA; sidedness of jugular venous drainage in the arteriovenous phase of CE MRA; retrograde jugular venous flow on neck TOF MRA.
Results
Unusual venous signals were seen on the left side in 73% of the JVR and 58% of the DAVF patients; involvement of the cavernous sinus was found in 12% of the JVR and 100% of the DAVF patients. Increased signal intensity in the ipsilateral jugular vein on T2WI was found in 73% of the JVR and 4% of the DAVF patients. Early opacification of the cavernous sinus in the arterial phase of CE MRA, ipsilateral jugular venous drainage in the arteriovenous phase of CE MRA, and ipsilateral retrograde jugular venous flow on neck TOF MRA were found in 0%, 0%, and 63%, respectively, of the JVR patients and in 100%, 100%, and

Note: Scanned images are included in the proceedings. Some submitted images were reduced during editing, thereby decreasing clarity. Also, refer to the Program Planner. Proceedings Content as of 3-29-2013.

0%, respectively, of the cavernous DAVF patients.
Conclusion
Jugular venous reflux and DAVF are associated with different findings from MR imaging and MRA. The CE MRA findings are the most useful for distinguishing between JVR and cavernous DAVF.

KEYWORDS: MR imaging/MR angiography, dAVF, jugular venous reflux

P-5

Diffusion-Weighted Imaging Cortico-Subcortical Spread Reflects Cognitive-Motor Deterioration in Four Creutzfeldt Jakob Disease Cases

Vitali, P.[1]·Caverzasi, E.[2]·Alvisi, E.[1]·Pan, M.[1]·Bini, P.[1]·Costa, A.[1]·Ceroni, M.[1]·Pingue, V.[3]·Geschwind, M.[2]·Bastianello, S.[1]
[1]IRCCS Neurological Institute Mondino, Pavia, ITALY, [2]University of California San Francisco, San Francisco, CA, [3]IRCCS Institute Maugeri, Pavia, ITALY.

Purpose
In Creutzfeldt-Jackob disease (CJD), diffusion-weighted imaging (DWI) MR hyperintensities are highly sensitive and specific to the cortical and subcortical involvement. Because of the rapidly fatal cognitive and motor deterioration, the pattern of DWI hyperintensities spread during the disease progression has been poorly described. In the present study, four patients with rapidly progressive dementia and subsequently path-proven sCJD were longitudinally scanned (at last three times) during the disease course.
Materials & Methods
Four sCJD patients (three females, 71-77 years old) were scanned in three institutions (Mondino, Maugeri, UCSF) by 1.5T MRI scanners, always including DWI (b = 0, 1000) sequences. In all four cases, clinical and MRI criteria at the presentation were suggestive for sCJD, subsequently pathologically proven at autopsy. In all four cases, behavioral and cognitive signs preceded motor signs, with late myoclonus occurrence. Because the gray matter hyperintensities typically are more evident at the DWI than at FLAIR images, only DWI and ADC maps are presented here, to show the cortico-subcortical spreading of abnormalities with diffusion restriction.
Results
In all four CJD cases presented here, longitudinal scans showed spread of DWI hyperintensities in the cortex ("cortical ribboning", typically sparing precentral gyrus) and subsequent subcortical involvement, with typical antero-posterior gradient in the striatum.

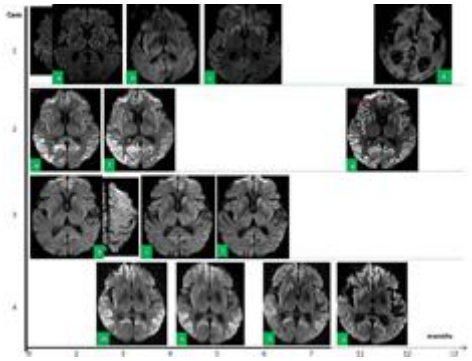

Figure1: Longitudinal DWI. CR = cortical ribboning, SH = striatum hyperintensity. Case 1: (a) right CR; (b) + right SH; (c) bilateral CR/SH; (d) hyperintensities disappearance, Case 2: (e) bilateral CR; (f) + right CR; (g) bilateral CR/SH, Case 3: (h) left CR; (i) + left SH; (l) bilateral CR/SH, and Case 4: (m) bilateral CR (n-o-p) + increasing bilateral SH
Conclusion
Although in cross-sectional studies the pattern of cortico-subcortical involvement varies considerably among different sCJD cases, this longitudinal study shows that the early cortical involvement with subsequent subcortical (striatum) involvement may be the more typical pattern of progression. This is in accordance with the finding that cognitive and behavioral signs typically precede motor signs.

KEYWORDS: Creutzfeldt-Jakob disease, DWI

P-6

Are Initial Brain Abnormalities in Neurologic Form of Wilson's Disease Compatible with Toxic Myelinolysis?

Kozic, D.[1]·Petrović, I.[2]·Kostic, V. S.[2]
[1]University of Novi Sad School of Medicine, Novi Sad, SERBIA, [2]Institute of Neurology, Belgrade, SERBIA.

Purpose
The purpose of the study was to estimate the nature of the brain lesions in Wilson's disease (WD), that usually in radiologic practice are interpreted as gliosis, spongy degeneration and necrosis. We evaluated the resolution of brain lesions in patients with WD during the long-term chelating therapy by magnetic resonance imaging (MRI) and a possible significance of the time latency from the initial symptoms of the disease to the introduction of such therapy.
Materials & Methods
Initial brain MRI was performed in 37 patients with neurologic presentation of WD. Fourteen patients were reexamined with MRI during the followup of 5.7±1.3 years. Pseudoparkinsonian, cerebellar and dystonic symptoms were evident in 45%, 70% and 35% of patients, respectively.
Results
Putamen affected 78% of patients, but in 100% of those with dystonia. Correlation between putaminal affection

Note: Scanned images are included in the proceedings. Some submitted images were reduced during editing, thereby decreasing clarity. Also, refer to the Program Planner. Proceedings Content as of 3-29-2013.

and dystonic presentation was statistically significant (p = 0.035). Complete resolution of putaminal lesions was observed in 60% of patients in whom initiation of decoppering treatment started less than two years after initial symptoms and in none of the patients with late diagnosis and treatment initiation (two to five years after symptoms onset), p = 0.024. There was a significant difference between these two groups regarding complete resolution of brain stem lesions (p = 0.005). Complete resolution of midbrain, pontine base and pontine periaqueductal zone lesions was observed in 66%, 100% and 100% of patients in whom initiation of decoppering treatment started less than two years after initial symptoms and in 20%, 20% and 25% of the patients with late diagnosis and treatment initiation, respectively.
Conclusion
The likelihood of complete resolution of brain stem and putaminal lesions in WD appears to be significantly higher if adequate treatment is initiated earlier in the course of the disease. If the correct diagnosis and adequate treatment have not been established within the period shorter than two years from initial symptoms, permanent clinical impairment associated with irreversible lesions within the brain parenchyma could be expected. Since in 100% of patients initial examination revealed frank symmetry of the lesions and that the majority of them were almost completely reversible if marked latency of adequate treatment had not existed, reversible myelinolysis associated with copper toxicity might have been the initial morphologic process. If untreated on time, consequent transformation into gliosis, necrosis and cystic degeneration seemed to appear.

KEYWORDS: Wilson's disease

P-7

Brain MR Imaging Signature of White and Gray Matter Changes in Hereditary Spastic Paraparesis

Aghakhanyan, G.[1,2]·Vavla, M.[3]·Frijia, F.[2]·Martino, N.[4]·Baratto, A.[4]·De Marchi, D.[2]·De Cori, S.[2]·Lombardo, F.[2]·Paparella, G.[3]·Canapicchi, R.[2]·Martinuzzi, A.[3]·Montanaro, D.[2]
[1]Institute of Life Sciences, Scuola Superiore Sant'Anna, Pisa, ITALY, [2]Fondazione CNR/Regione Toscana G. Monasterio, Pisa, ITALY, [3]Medea Scientific Institute, Conegliano and Bosisio Parini (TV), ITALY, [4]U.O. of Radiology, MRI Unit, O.C.- ULSS7, Conegliano (TV), ITALY.

Purpose
We aimed to investigate voxel-wised changes in gray and white matter microstructures in a group of Hereditary Spastic Paraparesis (HSP) patients (spastic gait locus: SPG4, SPG5, SPG3a, SPG10) and their correlates with clinical scores, disease onset and duration.
Materials & Methods
Diffusion tensor imaging (DTI) and high-resolution T1-weighted structural images were acquired in 14 HSP patients and 14 age-matched controls. Voxel-wise changes in gray matter (GM) volume and topography have been studied by voxel-based morphometry. Two patients were excluded from DTI analysis due to imaging artifacts. Multiple DTI indexes (fractional anisotropy, FA; mean diffusivity, MD; radial and axial diffusivities, RD and AD) were elaborated by tract-based spatial statistic (TBSS), part of FSL 4.1.1v. Data were analyzed accounting age and gender as a nuisance covariates. Family-wise error rate was controlled and significant differences were set up at alpha < 0.05. Correlation analysis were performed between gray/white matter changes and disease onset, disease duration, functional independence measure (FIM) and clinical spastic paraplegia rating scale (SPRS).
Results
We found bilateral GM volumetric reduction restricted in prefrontal cortex (p<0.005, uncorrected). Nevertheless, no cluster was survived after correcting for multiple comparison, probably due to small number of patients. Tract-based spatial statistic analysis revealed widespread alteration of DTI indexes: increase MD (p<0.05, corrected), decrease FA (p<0.01, corrected), and increase RD (p<0.005, corrected). No changes were observed in AD. We identified widespread inverse relationship between FA and SPRS scores (p<0.05, corrected). We did not find any relation between GM reduction and clinical scores, but correlation analysis revealed inverse relationship between reduction of GM volume and disease onset (r = -0.3), but not with disease duration.

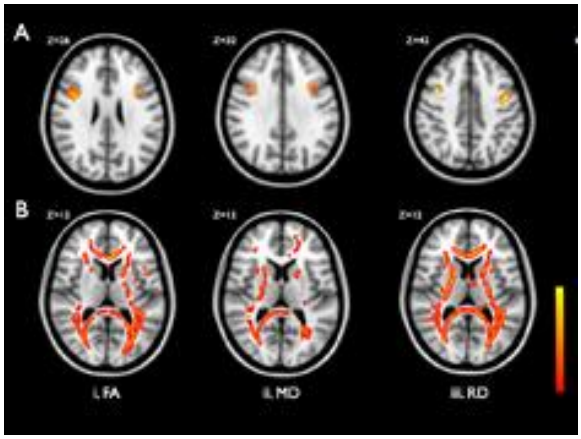

Figure 1: Results of voxelwise analysis showing (A) areas of gray matter volumetric reduction and (B) multiple DTI index maps with decreased FA (i), increased MD (ii) and increased RD (iii) in HSP patients after comparison with age- and sex- matched controls. Results are represented on the MNI152 2mm and 1 mm templates respectively with z axis coordinates (in mm) above each image.
Conclusion
We demonstrated widespread multiple DTI index abnormalities and bilateral clusters of volumetric reduction in prefrontal GM in HSP patients applying quantitative MRI measurements. Fractional anisotropy was voxel-wise correlated with spastic paraplegia rating

Note: Scanned images are included in the proceedings. Some submitted images were reduced during editing, thereby decreasing clarity. Also, refer to the Program Planner. Proceedings Content as of 3-29-2013.

scale (SPRS), indicating that DTI could be a sensitive MRI marker for clinical severity measurement. More research should be performed to reveal the clinical significance of GM abnormalities in HSP patients.

KEYWORDS: Advanced MR imaging, MR imaging brain, Hereditary Spastic Paraplegia; HSP; MND

P-8

Late Life Obesity and Brain Structure in a Community Cohort

Raji, C.[1]·Boyle, C.[2]·Erickson, K. I.[2]·Lopez, O.[3]·Becker, J. T.[3]·Gach, H.[3]·Longstreth, W. T.[4]·Kuller, L. H.[5]·Carmichael, O. T.[6]·Thompson, P. M.[2]
[1]University of California Los Angeles, Los Angeles, CA, [2]University of California Los Angeles Medical Center, Los Angeles, CA, [3]University of Pittsburgh Medical Center, Pittsburgh, PA, [4]University of Washington, Seattle, WA, [5]University of Pittsburgh Graduate School of Public Health, Los Angeles, CA, [6]University of California Davis, Davis, CA.

Purpose
Alzheimer disease affects over 30 million persons worldwide and obesity is an important lifestyle factor that can modify risk. We have shown in a smaller study that increased body mass index is associated with lower brain volume in cognitively normal elderly individuals. Here we assessed how higher body mass index affects brain structure in a much larger cohort of elderly individuals who were cognitively normal or had Alzheimer dementia.
Materials & Methods
We studied 963 subjects - 104 with Alzheimer dementia (AD), 135 with mild cognitive impairment (MCI), and 724 healthy elderly controls with an average age of 78 years and age range 69-95 years. These subjects were drawn from the multi-site Cardiovascular Health Study, a population-based cohort study based in Pittsburgh Pennsylvania, Hagerstown Maryland, Winston-Salem North Carolina, and Sacramento California. We acquired volumetric T1-weighted spoiled gradient-echo MR brain images and performed tensor-based morphometry (TBM) to quantitatively assess regional brain volumes. We then performed a multivariate analysis, regressing body mass index (BMI) on brain structure while accounting for covariates including age, sex, diagnosis of MCI or AD, study site, and physical activity as assessed by the number of city blocks walked per week.
Results
People with higher BMI have a greater burden of gray and white matter atrophy and ventricular dilatation, even after controlling for other factors such as age, sex, diagnosis, and study site. Body mass index-associated volume loss is shown in Figure 1. The top row of images represents p-value maps from our analysis and the bottom row represents beta values from the regression analysis. Increased BMI was associated with atrophy in the frontal lobes including the orbital frontal cortex and the cingulate (shown in color). These results did not vary as a function of co-morbid MCI/AD or physical activity.

Conclusion
This is one of the largest-ever voxel-based studies of a human population. Body mass index was associated with brain atrophy with no detectable dependency on diagnosis, and, in this study, no dependence on self-reported physical activity.

KEYWORDS: Alzheimer disease, Brain aging

P-9

Should We Assess Atrophy of the Mammillothalamic Tracts in Alzheimer Disease? A Preliminary Study of their Conspicuity and Age-Related Morphometry on Axial 3T MR Imaging

Horsburgh, A.[1,2]·Antoun, N.[1]·Massoud, T. F.[1,3]
[1]Addenbrooke's Hospital, Cambridge, UNITED KINGDOM, [2]Queen's Hospital, Romford, UNITED KINGDOM, [3]University of Cambridge, Cambridge, UNITED KINGDOM.

Purpose
Defining age-related structural alterations in normal brain is an important prelude for studies to identify potential imaging biomarkers for the earlier detection of neurodegenerative disorders. Many limbic structures have been demonstrated to atrophy in Alzheimer disease. It is known that transneuronal degeneration occurs more commonly in "closed neuronal systems" such as the circuit of Papez. Despite existing evidence for atrophy of the fornix and mammillary bodies in Alzheimer disease, and these being part of the Papez circuit, the projections from the mammillary bodies to the anterior thalamic nuclei [i.e., the mamillothalamic tracts (MTTs, bundles of Vicq d'Azyr) have not been studied in Alzheimer disease previously]. The MTTs are known to play a part in memory formation and studies of patients with Wernike's encephalopathy have demonstrated impairment in MTT functional connectivity. Prior preliminary functional MTT studies were performed in humans using diffusion tensor tractography, and limited studies of the MTTs have been performed using conventional structural MRI. We preliminarily studied the conspicuity and age-related

Note: Scanned images are included in the proceedings. Some submitted images were reduced during editing, thereby decreasing clarity. Also, refer to the Program Planner. Proceedings Content as of 3-29-2013.

changes in the MTTs on axial 3T brain MRI in healthy subjects prior to future evaluation in patients with Alzheimer disease.
Materials & Methods
We retrospectively analyzed the standardized MRI images of 147 patients. We used magnified T2-weighted axial images for analysis of MTT visualization, and specifically assessed conspicuity, signal intensity, size (using electronic callipers), shape, location, and symmetry of the MTTs. We used a Student's *t*-test for independent samples to statistically compare the MTT size in young and older patient groups, with significance at $p<0.05$. The effect of independent variables (gender and side) also was tested on the dependent variable (MTT size) using regression analysis.
Results
The younger age group (<60 years, mean age 39 years) comprised 62 patients (M:F = 50:50), and the older age group (>60 years, mean age 72 years) were 85 patients (M:F = 30:70). Mean transit times were visualized in 85% in the young, and 72% in the older. Etat criblé precluded detection of the MTTs in several of the over 70s. Right MTTs in the young were a mean 1.09 mm^2, and left MTTs were 1.30 mm^2. Right MTTs in the older were a mean 0.87 mm^2, and left MTTs were 1.08 mm^2. None of the independent variables affected variation in MTT size. There were no statistical differences in the MTT sizes between young and older age groups.
Conclusion
This is the first report of baseline age- and gender-related changes in cross-sectional dimensions of the MTTs, made possible by their greater conspicuity on 3T MRI. Additional studies in Alzheimer disease will determine if MTTs characteristics and morphometrics might be useful biomarkers in assessing disease progression and response to potential disease modifying treatments agents.

KEYWORDS: Alzheimer disease, Neurodegenerative, mammillothalamic tract

P-10

Added Diagnostic Utility of MR Spectroscopy to Diffusion Tensor Imaging in Amyotrophic Lateral Sclerosis

Foerster, B. R.[1]·Carlos, R. C.[1]·Dwamena, B. A.[1]·Petrou, M.[1]·Callaghan, B. C.[1]·Edden, R. A. E.[2]·Mohamed, M. A.[2]·Welsh, R. C.[1]·Barker, P. B.[2]·Feldman, E. L.[1]·Pomper, M. G.[2]
[1]University of Michigan, Ann Arbor, MI, [2]Johns Hopkins University, Baltimore, MD.

Purpose
To explore the added diagnostic utility of magnetic resonance spectroscopy (MRS) including MRS spectral-editing techniques to diffusion tensor imaging (DTI) in the setting of amyotrophic lateral sclerosis (ALS).
Materials & Methods
Twenty-nine ALS patients and thirty age- and gender-matched healthy controls (HCs) underwent 3T DTI as well as short echo time and GABA-edited ^{1}H-MRS centered on the left motor cortex. Subjects also underwent 3T 15 direction diffusion tensor imaging. Tractography of the bilateral corticospinal tracts was performed using ExploreDTI to calculate average fractional anisotropy (FA) values. Data were analyzed using logistic regression, t-tests and receiver operating characteristic curve analyses including leave-one-out cross validation techniques.
Results
Using the DTI FA data (model 1), the area under the curve (AUC) is 0.80. Using DTI, MRS myo-Inositol and MRS GABA data combined (model 2), the AUC is 0.92 and significantly greater than model 1 (P = .03). Model 1 sensitivity, specificity, positive likelihood ratio and negative likelihood ratio values are 0.90, 0.67, 2.72 and 0.15 respectively. Model 2 sensitivity, specificity, positive likelihood ratio and negative likelihood ratio values are 0.83, 0.89, 7.55 and 0.19 respectively.

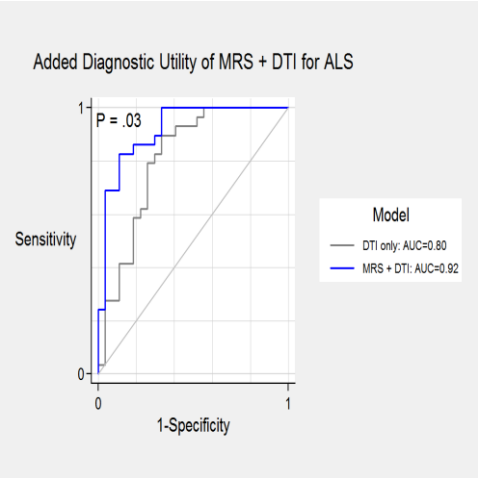

Conclusion
There is a significant increase in the diagnostic accuracy of advanced MRI techniques to diagnose ALS by combining MRS and DTI techniques. These results indicate that a combination of complementary advanced neuroimaging methods offer significant potential as an ALS diagnostic biomarker although additional research efforts are required for optimization and validation.

KEYWORDS: Amyotrophic lateral sclerosis, Diffusion tensor image, magnetic resonance spectroscopy

Note: Scanned images are included in the proceedings. Some submitted images were reduced during editing, thereby decreasing clarity. Also, refer to the Program Planner. Proceedings Content as of 3-29-2013.

P-11

Comparison of the Anatomical Volume and Cortical Thickness Measurements between the Subjects with Mild Leukoaraiosis and Control

Liu, H.[1]·Yang, C.[1]·Lee, C.[1]·Chen, S.[2]·Huang, A.[2]·Liu, M.[2]
[1]National Taiwan University Hospital, Taipei, TAIWAN, [2]Center for Dynamical Biomarkers and Translational Medicine, National Central University, Jhongli, TAIWAN.

Purpose
FreeSurfer is a well known software package to measure cerebral cortical volume and thickness. Leukoaraiosis is the nonspecific changes in the cerebral white matter frequently seen on CT and MRI in aged individuals. Mild leukoaraiosis is a common finding in subjects after mid-age.
Materials & Methods
We compared the results of cerebral cortex and volume in different anatomical locations in 48 subjects with mild leukoaraiosis shown on the FLAIR and T2-weighted images to 67 subjects with normal MR images. They were 75 women (normal = 43, mean age = 54.0 years old, SD = 8.9; leukoaraiosis = 32, mean age = 62.7 years old, SD = 8.9) and 40 men (normal = 24, mean age = 52.0 years old, SD = 8.9; leukoaraiosis = 16, mean age = 61.8 years old, SD = 6.3). The periventricular hyperintensity and deep white matter hyperintensity were graded according to Fazekas et al. The exclusion criteria; evidence of psychiatric illness within the past two years, including substance abuse, a history of recreational drug use in the previous six months, a history of CNS disease or brain injury, any MR imaging abnormality checked by two experienced neuroradiologists. MR scans were acquired with a 1.5T scanner (GE Healthcare, Wisconsin, USA). Coronal T1-weighted images were obtained using an MP-RAGE sequence with TR = 8.9 msec, TE = 2.99 msec, TI = 600 ms and a flip angle of 12. The slice thickness was 0.9 mm with no interslice gap. The image matrix was 256 x 256.
Results
No statistic difference between the two groups in age. On cortical volume measurement in left cerebral hemisphere, the measurement was significantly smaller in leukoaraiosis group in six regions (precuneus, lateral orbital frontal, superior parietal, superior frontal, rostral middle frontal, and pars opercularis), and significantly larger in eight regions (pericalcarine, inferior temporal, pars triangularis, postcentral, isthmus cingulate, superior frontal, insula, and medial orbitofrontal). In the right hemisphere, the measurement was significantly smaller in leukoaraiosis group in six regions (precuneus and isthmus cingulated), and significantly larger in 10 regions (pericalcarine, posterior cingulate, insula, inferior parietal, cuneus, parahippocampal, inferior temporal, inferior parietal, and caudal anterior cingulate). On cortical thickness measurement in left cerebral hemisphere, the measurement was significantly smaller in leukoaraiosis group in four regions (precuneus, superior parietal, superior frontal, and pars opercularis), and significantly larger in nine regions (pars triangularis, isthmus cingulate, inferior temporal, caudal anterior cingulated, insula, precentral, rostral middle frontal, medial orbitofrontal, and pericalcarine). In the right hemisphere, the measurement was significantly smaller in leukoaraiosis group in one region (supramarginal), and significantly larger in five regions (pericalcarine, insula, precuneus, posterior cingulate, and inferior parietal).
Conclusion
Leukoaraiosis has effect on the cortical volume and thickness. The change is variable in different locations.

KEYWORDS: Volumetric measurements, Cortical thickness, leukoaraiosis

P-12

MR Imaging Findings in Anderson-Fabry Disease

Borri, M. L.[1]·Mendes, C. S. C.[2]·Rand, M. H.[2]·Feliciano, P.[2]·Kyosen, S. O.[2]·Wolosker, A. M. B.[1]·Martins, A. M.[3]
[1]UNIFESP - São Luiz - Fleury, São Paulo, BRAZIL, [2]IGEIM, São Paulo, BRAZIL, [3]IGEIM - UNIFESP, São Paulo, BRAZIL.

Purpose
Anderson-Fabry disease (AFD) is an X- linked glycosomal storage disorder caused by deficiency of alpha-galactosidase A. As a consequence, there is accumulation of glycosphingolipids in blood vessels, central and peripheral autonomic nervous system. In the central nervous system, diffuse storage occurs in the cerebral vasculature and neurons. Brain MRI often are abnormal. Neuroradiologic findings include periventricular white matter signal intensity abnormalities, lacunar infarcts, large ischemic cerebral infarctions, and posterior thalamus involvement so-called “pulvinar sign“. The aim of the study was to describe brain MRI findings of 10 patients with AFD, seven male patients and three female patients, ages 12 to 60 years old (median age 34.7 years).
Materials & Methods
The brain MRIs of 10 patients were analyzed retrospectively. Seven patients were under treatment with enzyme replacement therapy (ERT).
Results
Brain MRIs were abnormal in all patients. The most frequent finding was Virchow-Robin spaces enlargement in six patients (4 M/2 F). Mild cortical atrophy was present in five (4 M/1 F), calcification or metallic deposits in deep gray matter (1 M/ 1 F), cerebral atrophy and microangiopathy in two males; hypersignal in FLAIR/T2 in pulvinar in three male patients, white matter lesion in four (2 M/2 F); enlargement of lateral ventricles in three (1 M/2 F); microcalcifications in left thalamus in one female patient, hypersignal in T1 in pulvinar, and hypersignal in T2 in medium cerebral peduncle in one male patient.

Note: Scanned images are included in the proceedings. Some submitted images were reduced during editing, thereby decreasing clarity. Also, refer to the Program Planner. Proceedings Content as of 3-29-2013.

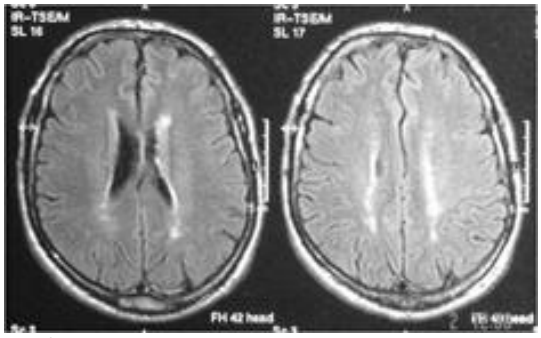

Conclusion
We evaluated 10 patients with AFD to describe neuroradiologic findings. The MR imaging studies described images mainly in small vessel pathology, but no large stroke. All images had alterations, mainly in older patients. The presentation of this disease may be sudden or gradual, and the features permanent or transient, often with exacerbations affecting distant parts of the nervous system, making the diagnosis difficult. MR images are now recognized to be the method of choice and important in monitoring patients with AFD in all ages.

KEYWORDS: Metabolic, Microvascular disease, MRI pulvinar sign

P-13

Stem Cell Effect on Cognitive Status of Patients with Multiple Sclerosis

Sych, N. S.
Cell Therapy Center EmCell
Kiev, UKRAINE.

Purpose
Cognitive impairments in multiple sclerosis (MS) traditionally have received little attention, although they are different and rather frequent (45-70% of cases). Marked intellectual impairment (dementia) occurs at later stages of MS, in 20-30% of cases. Goal: Study effects of fetal stem cells on cognitive impairment in MS patients.
Materials & Methods
The study included 27 MS patients, 12 men and 15 women aged 24 - 59 years (mean age 42, 23 ± 9.04 years), with 6-10 years of disease history: relapsing-remitting - 14, secondary-progressive - 8, progressive remitting - 2, primary progressive - 3. EDSS score varied from 3.5 to 6.5 points. Multiple sclerosis was confirmed in accordance to McDonald's criteria. Mini-Mental State Examination (MMSE) and Isaac's test were used for neuropsychologic examination. All patients underwent transplantation of hematopoietic and nonhematopoietic fetal stem cells (FSC) harvested from germ layers of internal organs of 4-8 weeks old legally aborted fetuses. Neurologic checkup and neuropsychologic assessment were performed before FSC transplantation and three months after the treatment. For ethical reasons, effectiveness of the previous treatment was the major selection criterion as patients were resistant to most conventional MS therapies [MS disease modifying drugs (Copaxone, Avonex, Betaferon), corticosteroids, plasmapheresis]. Statistical processing was performed with Statistika v.6.0.
Results
Fetal stem cell treatment resulted in significant cognitive improvements on MMSE - 26.95 ± 0.30 versus 23.89 ± 0.51 at baseline, $p < 0.05$. The Isaacs Set Test (IST) assessed verbal fluency by measuring the ability to generate lists of words in four semantic categories. In MS patients, the average before the treatment was 31.6 ± 6.0 out of 40 points, and it increased to 35.9 ± 2.5 three months after the treatment, $p < 0.05$.
Conclusion
Fetal stem cell treatment resulted in significant cognitive improvement on MMSE and IST. Our experience showed that FSC therapy is a promising method of treatment for MS patients with cognitive impairment. Cognitive improvement in these patients can be associated with improved cerebral circulation and capillary network development.

KEYWORDS: Acute disseminated encephalomyelitis, Clinical applications, stem cell

P-14

New-Onset Seizures: Appropriate Workup and Example Etiologies

Spirer, D. J.·Gorman, D.·Nemeth, A. J.
Northwestern University
Chicago, IL.

Purpose
This education exhibit will discuss a work-up plan for a patient with a clinical presentation of "new-onset seizures" and numerous pathologies that can result in new-onset seizures.
Materials & Methods
From the available neurology and radiology literature, we collected imaging of numerous etiologies that may result in new-onset seizures. The cases were culled from a combination of patients with a history of new seizure activity encountered during clinical practice, and also utilizing a database search of the electronic medical record for cases illustrative of possible etiologies of new-onset seizures. Additional background information was obtained from the neurology faculty who specialize in epilepsy.
Results
When faced with the clinical information of a patient who presents with new-onset seizures, a first step per the American Academy of Neurology practice guidelines is to obtain an immediate noncontrast CT in the emergency setting (Neurology 2007; 69: 1772-1778). This will guide appropriate acute management, especially if there is an abnormal neurologic examination, predisposing history, or focal seizure onset. Following the acute setting, brain imaging with MR imaging pre and postcontrast with the

Note: Scanned images are included in the proceedings. Some submitted images were reduced during editing, thereby decreasing clarity. Also, refer to the Program Planner. Proceedings Content as of 3-29-2013.

minimum axial T1 pre and postcontrast, T2, FLAIR, and diffusion imaging was found to be helpful. Coronal T1, T2, FLAIR imaging is additionally useful to evaluate for developmental abnormalities, mesial temporal sclerosis, temporal or frontal lobe abnormalities. New-onset seizures can have numerous etiologies. A categorization divides etiologies into primary neurologic disorders and systemic disorders. Primary neurologic disorders include: idiopathic epilepsy, febrile seizures, trauma, stroke, mesial temporal sclerosis, gray matter heterotopia or other developmental abnormalities, vascular malformations, mass lesions, infection including meningitis, encephalitis, or HIV encephalopathy. Systemic etiologies are many and include electrolyte abnormalities, metabolic derangements, organ failure, drug toxicities, global ischemia, hypertensive encephalopathy, eclampsia, hyperthermia, and porphyria.

Conclusion

New-onset seizures are a common reason for neurologic imaging. The radiologist should recommend a CT in the emergency setting and follow-up MR imaging to obtain more details. Etiologies include primary neurologic disorders and systemic disorders. There are numerous potential etiologies for seizure activity that should be considered in the differential diagnosis when evaluating the imaging findings. These etiologies have traditionally been discussed individually, and in this educational exhibit, our approach is to explore what various pathologies a radiologist may expect to find at imaging given the clinical presentation of new-onset seizures.

KEYWORDS: Seizure, Brain abnormalities, new-onset

P-15

Characterization of Focal Cortical Dysplasia Using Diffusion-Weighted Imaging

Steeman, R. R. M.[1]·Besseling, R. M. H.[1]·Damen, M. M. J.[2]·Hoeberigs, M. C.[1]·Jansen, J. F. A.[1]·Backes, W. H.[1]·Hofman, P. A. M.[1,3]
[1]Maastricht University Medical Center, Maastricht, NETHERLANDS, [2]Máxima Medical Center, Veldhoven, NETHERLANDS, [3]Epilepsy Centre Kempenhaeghe, Heeze, NETHERLANDS.

Purpose

Epilepsy is one of the common neurologic syndromes with a lifetime incidence of 2-4%: approximately 50% of these patients suffer from partial seizures. Neuroimaging is used to determine cortical (gray matter) abnormalities related to these seizures. However, in up to 74% of patients with location related (partial) seizures, MRI shows no abnormalities. It is assumed that the majority of these patients have a small focal cortical dysplasia. Detecting these lesions is of clinical importance since in patients with intractable epilepsy, resection may be the only viable therapeutic option, with excellent prognosis for seizure control. The goal of this study is to achieve a more sensitive method for detecting malformations of cortical development by using diffusion-weighted (rather than conventional structural) imaging (DWI) to assess the possible extension of focal cortical dysplasias (FCDs) in the underlying white matter (WM).

Materials & Methods

Sixteen FCD patients underwent MR imaging at 3T including T1 and FLAIR sequences and DWI (128 gradient directions, b=1500s/mm^2) for diffusion tensor imaging (DTI) and tractography. A white matter segmentation mask was employed to confine the region of interest (ROI) to white matter only. Three patients were excluded because the ROI in the dysplasia was outside the WM-mask. A systematic pattern of spherical ROIs was placed in and around the FCD as seen on FLAIR. Contralateral homologues ROIs were defined using landmarks on structural scans and tractograms to bilaterally match the cortical folding as well as the underlying fiber architecture. The extent of FCDs was investigated using concentric expansion of the ROIs. We evaluated fractional anisotropy (FA) and apparent diffusion coefficient (ADC) of the ROIs.

Results

In the center of the FCD, with respect to contralateral normal-appearing white matter, the ADC values were increased in 11/13 patients and the FA values were decreased in 10/13. These effects were significant at the group level (paired t-test, p=0.013 and p=0.047, respectively). In the surrounding tissue, ADC values were increased in 15/57 (26%) of the ROIs ($p<0.05$), and FA was decreased in 10/57 (18%) of ROIs ($p<0.05$). Apparent diffusion coefficient values were decreased in 9/57 (16%) and FA values in 1/57 (2%). There was no significant extent of DWI abnormalities beyond the lesions visible on FLAIR images.

Conclusion

Within FCD, aberrant diffusion properties (increased ADC values and decreased FA values) were measured. No DTI abnormalities were found in surrounding tissue and no significant extent of the lesion on DWI compared to the conventional structural imaging was measured. After optimizing ROI positions using tractography and anatomical landmarks, no interhemispheric differences in FA and ADC were observed outside the FLAIR-derived lesion. This implies the application of simple DTI measures does not increase the sensitivity for the detection of FCDs. Our findings confirm the hypothesis that FCDs are localized lesions, which also is supported by the good seizure outcome after focal resection. This does not fully preclude underlying white matter abnormalities and other, more complex, diffusion properties such as apparent fiber density (AFD) or kurtosis may reveal more subtle white matter abnormalities related to FCD.

KEYWORDS: Focal cortical dysplasia, Diffusion-weighted imaging, epilepsy

Note: Scanned images are included in the proceedings. Some submitted images were reduced during editing, thereby decreasing clarity. Also, refer to the Program Planner. Proceedings Content as of 3-29-2013.

P-16

Functional Integrity Markers in Epilepsy from Functional MR Imaging at Rest

Ascencio, J.[1]·Ochoa, J.[1,2]·Velásquez, J.[3]
[1]Instituto Neurológico de Colombia, Medellin, COLOMBIA,
[2]Universidad de Antioquia, Medellín, COLOMBIA,
[3]Universidad de Antioquia, Medellin, COLOMBIA.

Purpose
To present the findings in a group of patients with epilepsy from functional MRI at rest using two techniques: (i) functional connectivity measured by graph theory and (ii) neuronal activity index from fractional Amplitude of Low-Frequency Fluctuation (ALFF).
Materials & Methods
Using equipment operating at 1.5T and 3T (Siemens, Erlangen) volumetric sequence (MPRAGE TR = 11 ms, TE = 5.2 ms, FA = 15, thickness = 1 mm, matrix = 224 x 256, 176 slices per volume) and T2 EPI sequence sensitive to BOLD effect (TR = 2700 ms, TE = 30 ms, FA = 90, thickness = 3 mm, matrix = 64 x 64, 32 slices per volume covering the entire cerebral cortex) in 20 lesional epilepsy patients divided into two groups: 10 with epilepsy for hippocampal sclerosis and 10 extratemporal epilepsy were performed. Maps of fALFF are calculated from functional imaging, using the tool DPARSFA, and maps of the measure of the degree obtained by graph theory using our own algorithms. The proposed graph has 20092 nodes corresponding to all of the cerebral gray matter from a resolution of 4 mm. For comparison we used masks defined in AAL atlas and compared, for all the patients, the lesional region against his contralateral region.
Results
In all patients the degree value is decreased in the lesional area. The reduction allows significant asymmetry indices between the lesional region and the contralateral region to be obtain. The asymmetry obtained by fALFF is not significant for the subjects studied.
Conclusion
The analysis of the morphology of the BOLD signal in the epileptogenic area, evaluated indirectly in the graphs approach through the correlation of pathologic signal against all the other signals in the cerebral cortex, is a better marker of neuronal dysfunction than the neuronal activity index measured by fALFF.

KEYWORDS: Functional connectivity, Graph theory, epilepsy

P-17

Opposite Effects on White Matter Microstructure of Reciprocal Deletions versus Duplications at the 16p11.2 Chromosomal Locus

Owen, J. P.·Bukshpun, P.·Pojman, N.·Sherr, E.·Mukherjee, P.
University of California San Francisco
San Francisco, CA.

Purpose
The chromosomal region 16p11.2 is strongly linked to autism, schizophrenia and other neurologic disorders caused by deletions or duplications at this locus. There is evidence of “mirroring” in the phenotypes of deletion mutations versus duplication mutations; for instance, individuals with deletions are more likely to have macrocephaly and be overweight, while individuals with duplications tend to have smaller head sizes and be thin. In this study, we use diffusion-tensor imaging (DTI) to investigate abnormal white matter microstructure associated with 16p11.2 duplications and deletions.
Materials & Methods
3T DTI was acquired in 10 subjects with 16p11.2 duplication (mean age 34.5±15.9 years, eight male) and 11 subjects with 16p11.2 deletion (mean age 21.3±14.5, five males). Twenty-one healthy controls matched for age and gender with the probands also were imaged. Diffusion tensor was performed at 2.2mm isotropic voxel resolution with 64 encoding directions at b = 1000 s/mm2. FSL was used to calculate fractional anisotropy (FA), axial diffusivity (AD) and radial diffusivity (RD). Nonparametric permutation testing from tract-based spatial statistics (TBSS) was used to detect significant group differences in the white matter of the whole brain ($p<0.05$), corrected for multiple voxel-wise comparisons with threshold-free cluster enhancement.
Results
We found opposite changes in white matter microstructure of the duplication and deletion cohorts. The duplications have decreased FA compared to matched controls in the body of the corpus callosum and the right forceps major as shown in Figure 1(a). Significantly increased RD also was detected in these regions. Conversely, the deletions have increased FA throughout the supratentorial white matter compared to matched controls, including the corpus callosum, internal capsule, anterior thalamic radiations, and superior longitudinal fasciculus, as shown in Figure 1(b). Axial diffusivity was also significantly increased in the majority of the same voxels.

Note: Scanned images are included in the proceedings. Some submitted images were reduced during editing, thereby decreasing clarity. Also, refer to the Program Planner. Proceedings Content as of 3-29-2013.

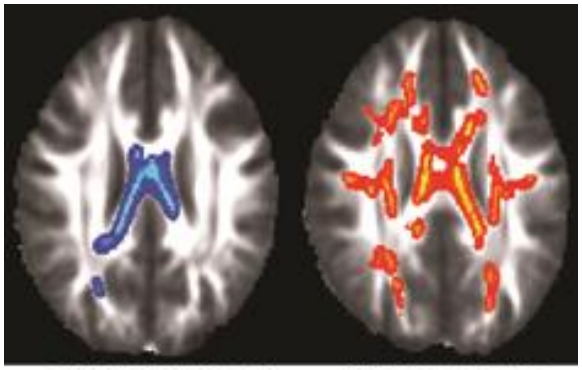

Figure 1: White matter voxels with significantly decreased FA in duplications in blue (a) and significantly increased FA in deletions in red (b).

Conclusion

To our knowledge, this is the first demonstration of mutations at the same genetic locus producing opposite effects on white matter anisotropy. Hence, the "mirror phenotypes" of 16p11.2 deletions versus duplications seem to extend to the microstructure of white matter. Although abnormally reduced FA is found in many disorders, the finding in 16p11.2 deletions of abnormally elevated FA is rare. One such recent example, although with much less spatial extent of increased anisotropy, is Williams syndrome. This work motivates further research into how genes at the 16p11.2 locus govern white matter microstructure and also into how these gene-brain relationships affect behavior and cognitive abilities in subjects with 16p11.2 mutations.

KEYWORDS: Gene deletion, Neurogenetics, 16p11.2

P-18

Evaluation of Hemodynamic Status and Vasodilatory Capacity to Hypercapnia State: Value of Arterial Spin Labeling Perfusion and Susceptibility-Weighted Imaging on 3T

Kishi, T.･Iida, E.･Furukawa, M.･Kato, M.･Matsunaga, N.
Yamaguchi University
Ube, JAPAN.

Purpose

Hypercapnia state is known as a factor that increases the cerebral blood flow (CBF). The purpose of this study is to assess the quantitative analysis using arterial spin labeling (ASL) perfusion and susceptibility-weighted image (SWI) for evaluating hemodynamic status and vasodilatory capacity under hypercapnia and resting state with monitoring end-tidal CO_2($ETCO_2$).

Materials & Methods

Twenty-one healthy volunteers (14 men, 7 women; mean age of 28 years) underwent ASL perfusion and SWI on 3T MRI under two resting states (resting 1 and resting 2) and hypercapnia state. Hypercapnia state was induced by hypoventilation with monitoring $ETCO_2$. On ASL perfusion, CBF values in hypercapnia and resting state were recorded at the level of corona radiata. Then the increase rate of CBF (%ΔCBF) between hypercapnia and resting state was calculated. On SWI, the average signal intensity of the whole brain parenchyma was recorded at the same level for both hypercapnia and resting state. The signal intensity ratio was compared among hypercapnia, resting 1, and resting 2. Using subtraction images, the area of signal increase between hypercapnia state and resting 1 was compared with that between resting 2 and resting 1.

Results

Mean $ETCO_2$ was 35.7 mmHg in resting 1, 36.0 mmHg in resting 2, and 44.3 mmHg in hypercapnia state. Mean $ETCO_2$ in resting 1 and resting 2 was not significantly different (P = 0.25). CBF in hypercapnia state was significantly higher than CBF in resting 1 (27.7 ml/100g/min and 22.5 ml/100g/min , respectively: P<0.001). %ΔCBF between hypercapnia and resting 1 was 24.9 ± 17.7%. On SWI, signal intensity ratio between hypercapnia state and resting 1 was 1.48 ± 1.64%, which was significantly higher than that between resting 2 and resting 1 (-0.37 ± 0.91%: P<0.001). On subtraction images, area of signal increase was 37.9 ± 8.0% between hypercapnia state and resting 1, which was significantly larger than that between resting 2 and resting 1 (18.8% ± 7.3 %: P<0.001).

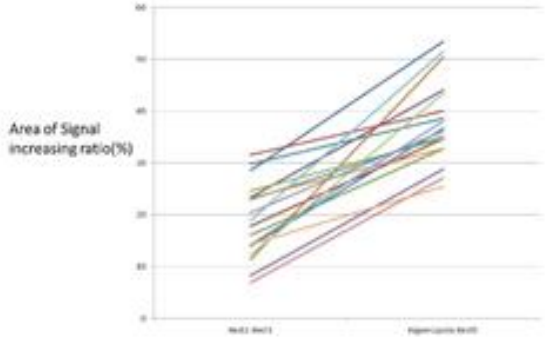

Conclusion

Arterial spin labeling perfusion and SWI combined with hypercapnia state are less invasive valuable tools to assess the hemodynamic status. Subtraction image of SWI sensitively reflects the area of increased CBF and vasodilatory response.

KEYWORDS: Cerebral blood flow, Susceptibility-weighted imaging, MR imaging

Note: Scanned images are included in the proceedings. Some submitted images were reduced during editing, thereby decreasing clarity. Also, refer to the Program Planner. Proceedings Content as of 3-29-2013.

P-19

Structural Connectome of the Human Brain in Agenesis of the Corpus Callosum

Owen, J. P.[1]·Li, Y.[1]·Ziv, E.[1]·Strominger, Z.[1]·Gold, J.[1]·Bukshpun, P.[1]·Wakahiro, M.[1]·Friedman, E.[2]·Sherr, E.[1]·Mukherjee, P.[1]
[1]University of California San Francisco, San Francisco, CA, [2]University of California Berkeley, Berkeley, CA.

Purpose
Adopting a network perspective, the structural connectome reveals the large-scale white matter connectivity of the human brain. Connectomics has great potential for elucidating abnormal connectivity in congenital brain malformations, especially axonal pathfinding disorders. Agenesis of the corpus callosum (AgCC), a prototypical human disorder of axon guidance, is one of the most common brain malformations. In AgCC the fibers that would normally have comprised the corpus callosum instead form Probst bundles, large white matter tracts that course anterior-posterior within each cerebral hemisphere. In this exploratory study, the structural connectome of AgCC is mapped and compared to that of the normal human brain.
Materials & Methods
Seven subjects with AgCC (four male, three female; mean age 24.3 ± 14.2 years) and 11 healthy volunteers (six male, five female; mean age 24.9 ± 9.1 years) were included in this study. Diffusion imaging was performed at 3T with 55 diffusion-encoding directions, at b = 1000 s/mm^2, and 1.8 mm isotropic resolution. FREESURFER was used to segment each subject's T1-weighted MRI; into cortical and subcortical labels. These labels were used as seed regions for probabilistic tractography using FSL's probtrackx2 to create whole brain connectomes. The network measures (degree, betweenness, clustering coefficient, local efficiency, efficiency, cost, and characteristic path length) were computed for the individual networks in each group and statistics were used to assess group differences. We also calculated metrics of consistency for the connection strengths and module assignments. We tested for statistically significant different connection strengths in one module, the “structural core” of the cerebral cortex. A “virtual Probstotomy” was performed on the AgCC subjects to assess the contribution of the Probst bundles to the AgCC connectome.
Results
Our quantitative investigations reveal four major findings. First, global connectivity is abnormally reduced in AgCC, but local connectivity is increased (Table 1). Second, the network topology of AgCC is more variable in both the connection strengths and the module assignments than that of the normal human connectome. Third, modularity analysis reveals that many of the tracts that comprise the structural core of the cerebral cortex have relatively weak connectivity in AgCC, especially the cingulate bundles bilaterally. Finally, virtual lesions of the Probst bundles in the AgCC connectome demonstrate that there is consistency across subjects in many of the connections generated by these ectopic white matter tracts, and that they are a mixture of cortical and subcortical fibers.

Network Metric	Control	AgCC
Mean degree	17.7±2.2	16.7±2.6
Characteristic path length	1.98±0.09	2.21±0.10*
Mean normalized betweenness	0.025±0.002	0.031±0.002*
Global efficiency	0.57±0.03	0.53±0.03*
Mean local efficiency	0.79±0.01	0.83±0.03*
Mean clustering coefficient	0.59±0.02	0.67±0.04*

Table 1: Network metrics applied to individual connectomes,
* denotes statistically different than controls (p<0.05)

Conclusion
Together, these observations demonstrate that structural connectivity in AgCC is much more complex than is currently understood from prior studies using gross anatomical imaging or even diffusion tractography studies of specific fiber pathways. Connectomics has great potential to more comprehensively elucidate the malformed human brain and advance our understanding of normal and abnormal brain development.

KEYWORDS: Malformation of cortical, Autism spectrum disorder, Connectome

P-20

Association between Clinical Measures and Florbetapir F18 PET Amyloid Neuroimaging in Mild and Moderate Alzheimer Dementia

Witte, M. M.[1]·Trzepacz, P.[1,2]·Case, M.[1]·Yu, P.[1]·Hochstetler, H.[1]·Quinlivan, M.[3]·Sundell, K.[4]·Henley, D.[4,2]
[1]Lilly USA, LLC, Indianapolis, IN, [2]Indiana University School of Medicine, Indianapolis, IN, [3]Eli Lilly Australia, West Ryde, AUSTRALIA, [4]Lilly Research Laboratories, Indianapolis, IN.

Purpose
Alzheimer disease (AD) is challenging to diagnose clinically, with the sensitivity of clinical criteria by experts reported to range from 71-87% and specificity from 44.3-70.8%. We compared demographic and neuropsychiatric

Note: Scanned images are included in the proceedings. Some submitted images were reduced during editing, thereby decreasing clarity. Also, refer to the Program Planner. Proceedings Content as of 3-29-2013.

characteristics between those with and without PET evidence of amyloid plaque in clinically-diagnosed AD dementia patients recruited for clinical trials. We sought to identify clinical variables to identify patients at risk of being mistakenly diagnosed with AD.
Materials & Methods
A subset of patients (199/2,648) pooled from two AD anti-amyloid drug trials with identical inclusion criteria participated in an optional amyloid-PET neuroimaging addendum with florbetapir F18 (FBP). The trials enrolled patients ≥55 years of age with clinically-diagnosed mild or moderate AD dementia using NINCDS/ADRDA criteria. Exclusion criteria included stroke, unstable medical illness, substance abuse/dependence, major depression, or vascular dementia. Prior to receiving study drug, patients underwent FBP-PET and were administered the following rating scales: Alzheimer's Disease Assessment Scale-cognitive subscale 14-item version (ADAS-Cog14), Alzheimer's Disease Cooperative Study Activities of Daily Living Inventory (ADCS-ADL), Clinical Dementia Rating (CDR), Mini Mental-State Exam (MMSE), 12-item Neuropsychiatric Inventory (NPI-12), and Geriatric Depression Scale (GDS). Patients with a composite cortical (frontal, temporal, parietal , precuneus, anterior cingulate, and posterior cingulate regions) standardized uptake value ratio (SUVR) <1.1 using whole cerebellum as the reference region were categorized as having a negative scan. Categorical data were compared using Fisher's exact test, means using ANOVA.
Results
In this clinically-diagnosed sample, 35 (18%) patients were FBP-PET negative for amyloid plaque. These patients performed significantly better than FBP-PET positive patients on the ADAS-Cog14 [mean (SD, range): 26.8 (12.4, 8 - 63) vs. 34.1 (10.7, 11-63); p<.001] and the MMSE [mean (SD, range): 24.0 93.21, 15 - 300 vs. 21.0 93.98, 13-300; p<.001] and were significantly more likely to be categorized as having mild dementia (86% vs. 59%, p=.003). FBP-PET negative patients performed statistically worse on the GDS [mean (SD, range): 2.23 (1.70, 0 - 6) vs. 1.51 (1.42, 0 - 7); p=.010], although the scores were well below the cutoff for syndromal depression. No differences were found on the ADCS-ADL, CDR, or NPI-12. Patients in the two groups had similar mean age and years of education, though a greater proportion of FBP-PET negative patients were male (63% vs. 42%; p=.039). A significantly lower proportion of FBP-PET negative patients were carriers for the ApoE4 allele (heterozygous/homozygous: 15%/3% vs. 47%/21%; p<.001). Neither age (r= -0.002; p=.980) nor years of education (r=-0.008; p=.915) were found to correlate significantly with SUVR.
Conclusion
Although diagnosed by expert clinicians, about 18% of patients in this study had FBP-PET results inconsistent with a diagnosis of AD. While these groups were significantly different on some cognitive measures and APOE4 status, there was a large degree of overlap in the results such that no variable could be relied upon by clinicians to distinguish the subgroup of patients who appear to have AD but in fact lack corresponding AD neuropathology. This study highlights the importance of amyloid neuroimaging in the AD diagnostic matrix, even during diagnosis by dementia experts.

KEYWORDS: Alzheimer disease, PET, florbetapir

P-21

Underestimation of Regional Cerebral Blood Flow by Arterial Spin Labeling MR Imaging in Elderly Persons

Wada, A.·Hara, A.·Ohsone, F.·Kitahara, H.·Matsunaga, H.·Yamamoto, K.·Okubo, T.
Teikyo University Chiba Medical Center
Ichihara, JAPAN.

Purpose
In arterial spin labeling (ASL), post labeling delay (PLD) has a major influence to the regional cerebral blood flow (CBF) measurement. In elderly, aging-related change extends the arterial transit time (ATT) and an adaptation of inadequate PLD, which is shorter than ATT, may underestimate the regional CBF. This study aimed to investigate the validity of the conventional PLD setting in healthy elderly and suggest an efficacy of longer PLD adaptation.
Materials & Methods
Quantitative CBF measurement with ASL was performed in 11 healthy elderly (three male, eight female, mean age 65.5 years) with two different PLD (conventional 1525 msec and longer 2525 msec). ASL was performed with pulsed continuous labeling technique by using 3T MR unit. Group analysis with paired t-test was performed about regional CBF value at 18 region of interest set to the standardized three-dimensional CBF data by NEUROSTAT software. P value < 0.05 was defined as a statistically significant difference.
Results
Only conventional PLD revealed a hypo-perfusion at lateral parietal lobe and occipital lobe and significant difference of regional CBF value was recognized associated with PLD difference (p<0.05). Moreover, longer PLD was superior about the homogeneity of perfusion signal.

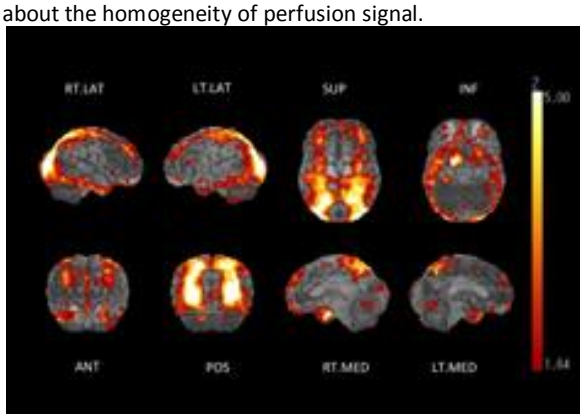

Note: Scanned images are included in the proceedings. Some submitted images were reduced during editing, thereby decreasing clarity. Also, refer to the Program Planner. Proceedings Content as of 3-29-2013.

(Figure) Result of group analysis with paired t-test of regional CBF quantitation. Surface projection of Z-score on standard brain shows the relative hypo-perfusion area in conventional PLD of 1525 msec compared with longer PLD of 2525 msec. Significant relative hypoperfusion is represented at bilateral parietooccipital lobes.

Conclusion

In elderly, ASL with conventional PLD may induce a false hypo-perfusion at rostral region of the brain. This underestimation may impair the ASL diagnosability about cognitive disorders (such as Alzheimer disease, Lewy body disease and Parkinson disease). In elderly, longer PLD is recommended as a default setting of ASL.

KEYWORDS: 3 T, Arterial spin labeling

P-22

Test-Retest Reliability of Computational Network Measures Derived from the Structural Connectome of the Human Brain

Owen, J. P.[1]·Ziv, E.[1]·Bukshpun, P.[1]·Pojman, N.[1]·Wakahiro, M.[1]·Berman, J.[2]·Roberts, T.[2]·Sherr, E.[1]·Mukherjee, P.[1]
[1]University of California San Francisco, San Francisco, CA, [2]Childrens Hospital of Philadelphia, Philadelphia, PA.

Purpose

Structural MR connectomics holds promise for improving diagnosis, outcome prediction and treatment monitoring of many neurodevelopmental, psychiatric and neurodegenerative disorders for which there is currently no clinical utility of MR imaging. Before network metrics computed from a particular processing pipeline can be applied in a clinical setting, the precision and normative intersubject variation must be understood. The reproducibility of commonly used graph theoretic measures is investigated, as applied to the structural connectome of healthy adult volunteers, using standard MRI acquisition parameters and a widely used connectome processing pipeline.

Materials & Methods

Ten healthy control subjects were scanned twice at Site 1 and five healthy controls were scanned once at Site 1 and once at Site 2. MR imaging was performed on a 3T TIM Trio MR scanner(Siemens, Erlangen, Germany) at each site. Whole-brain diffusion imaging was performed with 30 diffusion-encoding directions, at b=1000 s/mm^2, and 2mm isotropic resolution. FSL's probtrack2 was used to perform probabilistic HARDI tractography to create whole-brain connectomes. Global graph metrics: mean degree (K), characteristic path length (L), clustering coefficient (C), mean betweenness (B), global efficiency (E), and mean local efficiency (E_{loc}) are calculated for unweighted and weighted connectomes and at two levels of granularity of the connectome: 82-node parcellation from FreeSurfer and atlas-free parcellation consisting of 1000 cortical nodes. Intraclass correlation coefficient (ICC) and coefficient of variation (CV%) were used as measures of precision and variability. The consistency of the unweighted and weighted edges and the module assignments also are computed for the 82-node connectomes.

Results

In Table 1, we report low CV% and high ICC values for the unweighted network metrics applied to both the 82-node and 1000-nodes connectomes. Only ICC and CV% for C and E calculated for the 82-node connectomes (intrasite) are not significant. The weighted metrics have similar CV% and ICC values, although weighted characteristic path length stands out as a less reproducible metric with a CV% of 34.75 for the 82-node connectome. We also find that the unweighted and weighted edges and module assignments are reproducible intra and intersite.

	82-Node Connectome		1000-Node Connectome	
Intrasite	CV%	ICC	CV%	ICC
K	3.21*	0.89*	2.89*	0.78*
L	1.44*	0.92*	2.96*	0.79*
C	3.40	0.51	1.12*	0.78*
B	2.73*	0.90*	4.89*	0.79*
E	1.18*	0.92*	2.58*	0.78*
E_{loc}	1.79	0.54	0.42*	0.75*
Intersite	CV%	ICC	CV%	ICC
K	6.26*	0.79*	3.81*	0.89*
L	2.26*	0.82*	1.98*	0.94*
C	3.05	0.59*	0.94*	0.88*
B	4.00*	0.82	3.31*	0.94*
E	1.94*	0.84*	1.74*	0.94*
E_{loc}	1.61	0.63*	0.42*	0.87*

CV% and ICC values for unweighted network metrics, * denotes p<0.05.

Conclusion

Note: Scanned images are included in the proceedings. Some submitted images were reduced during editing, thereby decreasing clarity. Also, refer to the Program Planner. Proceedings Content as of 3-29-2013.

Overall, the results demonstrate good to excellent test-retest reliability for the graph analytics in both the intrasite and intersite datasets. The weighted and unweighted global network metrics applied to the 1000-node connectome yield better reproducibility than as applied to the 82-node connectomes. ICC and CV% values indicate, in general, better reproducibility and precision than the findings of other connectome variability papers. This improvement is most likely due to methodologic differences, including tractography algorithm and thresholding. The findings reported here indicate that computational network metrics from this structural connectome pipeline have sufficient precision to be tested as potential biomarkers for diagnosis, prognosis, and monitoring of interventions in neurologic and psychiatric diseases.

KEYWORDS: Connectivity, Diffusion-weighted imaging, Connectome

P-23

Patterns of Diffusivity Changes at the Anterior Cingulum in Patients with Dementia with Lewy Bodies and Alzheimer Disease: Diffusion Tensor Imaging Analysis

Suzuki, M.[1]·Motoi, Y.[1]·Kamagata, K.[1]·Kosuge, M.[1]·Kamiya, K.[1,2]·Sato, K.[1,2]·Shimoji, K.[1]·Hori, M.[1]·Nakanishi, A.[1]·Sasai, K.[1]·Hattori, N.[1]·Aoki, S.[1]
[1]Juntendo University, Bunkyo-ku Tokyo, JAPAN, [2]Tokyo University, Bunkyo-ku Tokyo, JAPAN.

Purpose
To identify the patterns of diffusivity changes at the anterior cingulum in patients with dementia with Lewy bodies (DLB) and Alzheimer disease (AD) and to determine whether diffusion tensor MRI (DTI) is complementary to structural MRI in depicting the tissue abnormalities characteristic of DLB and AD.
Materials & Methods
We studied clinically diagnosed age-, gender-matched subjects with DLB (n = 8), subjects with AD (n = 16) in a case-control study. The brains of all patients were examined with a 3T MR imaging unit and an 8-channel array-receiving head coil for sensitivity encoding parallel imaging. After regular structural images acquisition, diffusion tensor images were obtained. Maps of FA and MD were computed by using dTV II and Volume-One 1.72 (http://www.volume-one.org), developed by Masutani, et al. We performed diffusion tensor tractography of the anterior and posterior cingulate fiber tracts (CFTs) and also the corticospinal tracts as a control procedure. Tract measurements performed by two of the authors, were blinded to the disease status of the subjects. The anterior and posterior CFTs were voxelized, and mean diffusivity (MD), fractional anisotropy (FA), axial diffusivity (AD), radial diffusivity (RD) values in co-registered voxels were calculated. Student's *t*-test was used to compare the averaged values of MD, FA, AD, and RD between DLB patients and AD patients. A Bonferroni correction was applied for the number of comparisons (n = 2: (anterior CFTs, posterior CFTs), setting the level of significance at $P < 0.05/2 = 0.025$).
Results
Fractional anisotropy and RD measured in the anterior CFTs was significantly lower in patients with DLB compared with AD (P = .022, 0.004, respectively). There were no significant diffusion differences in the posterior CFTs, corticospinal tracts between the groups.
Conclusion
Diffusivity measurements were complementary to structural MRI, demonstrating that measures of diffusivity diffusion tensor MRI are valuable tools for characterizing the tissue abnormalities. In a present study, the result demonstrated the feasibility to differentiate DLB and AD by measuring anterior CFTs.

KEYWORDS: Diffusion tensor image, White matter tracts

P-24

Longitudinal Diffusion MR Imaging Evaluation in Rabbit White Matter after Cerebral Hemisphere Radiation Exposure

Shen, C.[1,2]·Li, Z.[2]·Chen, T.[2]·Tyan, Y.[1,1]·Weng, J.[2]
[1]Chung Shan Medical University Hospital, Taichung, TAIWAN, [2]Chung Shan Medical University, Taichung, TAIWAN.

Purpose
We used a linear accelerator as the source of radiation to establish an adult rabbit model for single-dose cerebral hemisphere exposure radiation-induced brain injury, and afterward, longitudinally evaluated the changes in white matter (external capsule) on a 1.5T clinical MR scanner by using T2WI and DTI indices. We hoped that this experimental model can be used to evaluate the neuro-toxic adverse effects of irradiation treatment.
Materials & Methods
Five male New Zealand rabbits of one year of age received irradiation of 30 Gy (collimations = 4 cm x 5 cm) to the right hemi-brain with a single highly collimated 6MV photon beam from a Varian CL21EX linear accelerator (Varian, Palo Alto, CA, USA) under anesthesia. Brain MRI examinations were performed before irradiation and at 1st to 48th week postirradiation (totally 12 time points) on a 1.5T MR scanner (Sonata, Siemens, Erlangen, Germany) with double loop array coils. Whole brain coronal T2WI were obtained using TR/TE = 4330/114 ms, resolution = 0.19 x 0.39 x 1.5 mm3, number of slices = 30. Diffusion tensor imaging data were acquired using a multislice, single-shot spin-echo EPI sequence with TR/TE = 2900/128 ms, resolution = 0.78 x 0.78 x 2 mm3, number of slices = 12 (contiguously from the genu of the corpus callosum to the end of the cerebrum). They were obtained using 12 diffusion-encoding directions with b values changing from 0 to 2,000 s/mm2. In data analysis, FA, MD, AD and RD

Note: Scanned images are included in the proceedings. Some submitted images were reduced during editing, thereby decreasing clarity. Also, refer to the Program Planner. Proceedings Content as of 3-29-2013.

maps were first calculated from DTI data using DSI studio (NTU, Taiwan). Using imageJ (NIH, USA), ROIs were drawn manually on three consecutive slices of the DTI maps and the T2WI. All the results were expressed as mean ± standard error (SE), and the ratios of right (injury)/left (control) were calculated for statistical analysis. Paired t-test was used to detect statistical differences between the pre and the postirradiation time points. A p-value of <0.05 was considered to indicate statistical significance. After 48 week of MRI scans, rabbits were sacrificed for histopathologic evaluation, and stained with H&E and LFB.
Results
Diffusion tensor imaging indices showed a continuing decrease followed by a gradual recovery in the FA R/L ratio during the follow-up time points, and the differences reached statistical significance at the 8th week (p-value = 0.0193) and the 12th week (p-value = 0.0373) postirradiation. The gradual increase was followed by recovery in the RD and the MD R/L ratios and the AD R/L ratio showed a decrease at the 2nd week and the 32nd week postirradiation. On T2WI, there was a continuing, gradual decrease at all the follow-up time points, but the differences did not reach a statistical significance at any of them. One rabbit showed significant radiation-related alterations in irradiated right external capsule with large areas of confluent coagulation necrosis and loss of the myelin sheath in both the H&E and LFB sections.
Conclusion
Our quantitative results suggested the DTI characteristics are more sensitive than T2WI and can reflect pathologic changes in radiation-induced brain white matter injury.

KEYWORDS: Diffusion tensor image, Radiation injury, rabbit model

P-25

Investigation of the Auricular Acupoint-Cortical Associations Using Resting State Connectivity Functional MR Imaging

Bhatnagar, P.·Firbank, M.·Blee, P.·English, P.·Butteriss, D.·Birchall, D.
Royal Victoria Infirmary
Newcastle upon Tyne, UNITED KINGDOM.

Purpose
Mapping of cortical activation during traditional acupuncture has demonstrated specific and reproducible associations. To date, all fMRI studies have related to traditional acupuncture during active stimulation. Auricular acupuncture is a subtype that is widely used within Eastern traditional medicine, but currently there are no systematic studies of the effects of auricular acupuncture on fMRI, particularly relating to resting state connectivity. The aim of this study was to map the effect of a specific auricular acupuncture paradigm using resting state connectivity fMRI.
Materials & Methods
Ten healthy subjects (age range 25-45 years, with equal males and females) underwent a baseline fMRI (3T scanner). Then they had a session of auricular acupuncture by an acupuncturist specializing in auricular techniques. Three acupoints were treated for 30 minutes on the left ear of each subject in turn: Master Cerebral LM7 (anterior ear lobe), Autonomic Point LM1 (anterior helix) and Shen Men LM16 (antihelix body). This was followed immediately with a further second fMRI scan. Functional data were motion corrected, high pass filtered (0.01 Hz) and smoothed with a 5 mm filter. Independent component analysis (ICA) was performed on all rest runs using FSL-MELODIC package. The set of spatial maps from the group-average analysis was used to generate subject-specific versions of the spatial maps and associated timeseries using dual regression (Beckmann09, Filippini09). For each subject, the group-average set of spatial maps was regressed into the subject's 4D space-time dataset. This resulted in a set of subject-specific timeseries, one per group-level spatial map. Next, the timeseries were regressed into the same 4D dataset, resulting in a set of subject-specific spatial maps, one per group-level spatial map. We then tested for differences within the subjects pre vs postacupuncture using FSL's randomized permutation-testing tool. Comparisons were considered significant at p <0.05 corrected for multiple comparisons using the threshold-free cluster enhancement method.
Results
The independent component analysis identified a number of components similar to previously reported resting networks (e. g., Figure 1). Preliminary analysis showed activation within the lateral temporal lobes, hippocampal formation, subfrontal cortex and prerolandic frontal cortex. Further analyses are underway to identify specific subregional activation, and to map differences pre and postauricular acupuncture. These results will be presented in full.

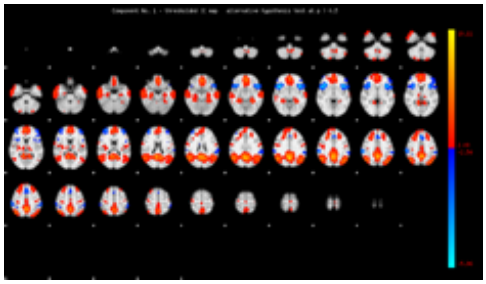

Conclusion
This study represents the first demonstration of the resting state connectivity fMRI findings associated with a specific auricular acupuncture paradigm. This represents the first step in the comprehensive mapping of auricular acupoint-cortical associations.

KEYWORDS: Functional connectivity MR, acupuncture

Note: Scanned images are included in the proceedings. Some submitted images were reduced during editing, thereby decreasing clarity. Also, refer to the Program Planner. Proceedings Content as of 3-29-2013.

P-26

Cognitive Impairment in Patients with Idiopathic Generalized Epilepsy: Functional MR Imaging and Diffusion Tensor Imaging Analysis of 20 Cases

Garcia, L. A. L.·Amaro, E.
Hospital das Clínicas da Faculdade de Medicina de São Paulo
Sao Paulo, BRAZIL.

Purpose
Evaluate cognitive impairment in patients with idiopathic generalized epilepsies (IGE) using functional MRI (fMRI) and diffusion tensor image (DTI), comparing healthy volunteers and IGE patients. Idiopathic generalized epilesies are a group of epileptic syndromes composed by juvenile myoclonic epilepsy, typical absence epilepsy, awakening idiopathic generalized epilepsy and nonspecified IGE. Their clinical presentations are characterized by primarily generalized seizures and specific generalized electroencephalographic patterns. These patients tends to control their seizures and have normal cognitive performance and neuroimaging exams.
Materials & Methods
Patients with IGE (20 right-handed patients, 16 women, age range 16 to 50 years, average age 31 years) were compared to healthy volunteers (24 right-handed patients, 13 women, age range 18 to 63 years, average age 32.5 years). Data were acquired usign a 3T scanner (Philips - The Nederlands), with a gradient BOLD echoplanar volumetric sequence, aligned to the ACPC line, matrix 128 x 128, voxel 3 x 3 x 3 mm, with event-related paradigms designed to investigate memory and language, each lasting about 3.5 minutes, with balanced and radomized stimuli, and echoplanar diffusion tensor images, matrix 128 x 128, voxel 2 x 2 x 2 mm, 32 directions, repeated twice. Data analysis was performed by FSL software, with a nonparametric statistical inference approach and motion correction. Comparison among both groups (patients vs controls) was performed with a significance level of $p<0.05$.
Results
Patients with IGE had a significantly worse BOLD activation, mainly at bilateral parietal and occipital (cuneus and precuneus) lobes in response to paradigms sequence when compared to control group. The white matter malfunction showed by Tract-Based Spatial Statistics (TBSS) of DTI data was almost generalized.
Conclusion
Differences among both groups (patients vs controls) to specific cognitive tasks evaluated by fMRI were observed and suggested a less cognitive performance in IGE patients. The impairment of cerebral white matter could imply disconnections between several areas in brain, as a result of prolonged seizures or as a characteristic of the disease.

KEYWORDS: Epilepsy, fMRI, DTI, memory, language, cognitive, TBSS

P-27

Long-Term Neuropsychologic Sequelae in HIV Seronegative Cryptococcal Meningoencephalitis with and without VP Shunt: A Cine MR Imaging Study

Chen, M.[1]·Lu, C.[1]·Wang, H.[1]·Chen, H.[1]·Tsai, N.[1]·Li, S.[1]·Hsu, N.[2]·Lin, W.[3]·Kung, C.[1]·Lin, W.[1]
[1]Kaohsiung Chang Gung Memorial Hospital, Kaohsiung City, TAIWAN, [2]Yuan's General Hospital, Kaohsiung City, TAIWAN, [3]Chiayi Chang Gung Memorial Hospital, Chiayi County, TAIWAN.

Purpose
Hydrocephalus is common in cryptococcal meningoencephalitis and ventriculo-peritoneal shunt is the management. Cine MRI was applied to evaluate the effect of initial disease severity on long-term CSF flow dynamics and the associated neuropsychologic sequelae in cryptococcal meningoencephalitis patients with and without ventriculo-peritoneal shunt.
Materials & Methods
Eighteen HIV-negative cryptococcal meningoencephalitis patients (10 ventriculo-peritoneal shunt vs. eight without ventriculo-peritoneal shunt) and 32 age- and sex-matched healthy volunteers were included. All subjects underwent complete neurologic examination and neuropsychologic test. Cine MRI was conducted to evaluate CSF flow parameters. Correlations among initial CSF laboratory analysis, imaging findings, present CSF flow parameters, and present neuropsychologic scores were analyzed.
Results
The patients without shunt had higher average flow than controls ($F = 3.516$, $p = 0.038$), suggesting chronic hydrocephalus. The initial higher Evan ratio was associated with higher positive ($r = 0.974$, $p = 0.026$)/negative ($r = 0.983$, $p = 0.017$) peak velocities. Lower CSF glucose level was associated with higher positive ($r = -0.984$, $p = 0.016$)/negative ($r = -0.964$, $p = 0.036$) flow. Worse CSF flow parameters were correlated with poorer performance in attention, picture arrangement, short-term memory, and drawing. The patients with shunt have better results in the block design, orientation, and short-term memory although they had more severe initial presentation.

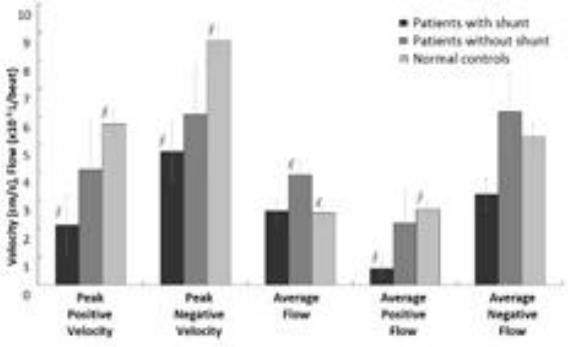

Note: Scanned images are included in the proceedings. Some submitted images were reduced during editing, thereby decreasing clarity. Also, refer to the Program Planner. Proceedings Content as of 3-29-2013.

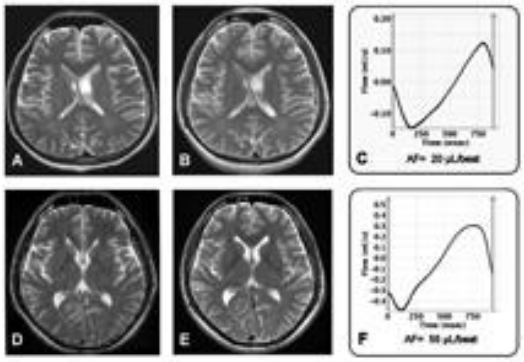

Conclusion
The ventriculo-peritoneal shunts in cryptococcal meningoencephalitis patients do not only save lives but promote long-term cognition function. Cine MRI is useful for unveiling the possibility of chronic hydrocephalus in cryptococcal meningoencephalitis patients that may lead to neuropsychologic deficits.

KEYWORDS: Cerebrospinal fluid, Cryptococcal meningitis, cine MR imaging

P-28

Natalizumab-Associated Progressive Multifocal Leukoencephalopathy during Multiple Sclerosis Treatment and Consecutive Immune Reconstitution Inflammatory Syndrome: Are There Lessons from Continuous Monitoring of Magnetization Transfer?

Krueger, K. W.[1]·Krueger, P.[2]·Hild, M.[1]·Nowak, A.[1]
[1]Neurologische Gemeinschaftspraxis Hennef, Hennef, GERMANY, [2]University of Geneva, Geneva, SWITZERLAND.

Purpose
Progressive multifocal leukoencephalopathy(PML) can occur as a devastating and potentially lethal complication of long-term administration of natalizumab in patients with multiple sclerosis(MS). There is an urgent need for new diagnostic tools to predict the occurrence of PML and its evolution and course in individual patients. As the magnetization transfer ratio(MTR) can be regarded as a marker for myelin integrity we examined whether continuous monitoring of MTR can contribute towards (i) improved risk assessment of patients with MS under long-term natalizumab and (ii) successful management of PML.
Materials & Methods
We present specific imaging data and results of continuous MTR monitoring in a single 44-year-old female with relapsing-remitting MS(RRMS) during the course of natalizumab-associated PML and subsequent immune reconstitution inflammatory syndrome(IRIS), as well as 19, 13 and 7 months prior to the diagnosis. The patient had received natalizumab for 62 months and was clinically inconspicuous at PML diagnosis. We use a PD-weighted SE sequence for longitudinal registration of MTR in our routine MR protocol for all MS patients: TR = 1710 ms, TE = 30 ms, NSA = 1 before and after an off-resonance MT pulse at 1.5T. Using the FDA-approved software package, NordicICE, consecutive MTR histograms of whole brain, normal-appearing white and gray matter as well as FLAIR- and contrast-enhancing lesions are obtained for subsequent statistical analysis.
Results
Using Kolmogorov-Smirnov and Mann-Whitney tests for equality of distributions, we observed a gradual and significant($p<0.0001$) MTR decrease(leftward shift of the MTR histograms) 19, 13 and 7 months before PML diagnosis both in the future PML lesion and in the whole brain. Relying on ANOVA, we confirmed this result by documenting a significant decrease($p<0.0001$) in average MTR over time. During PML-IRIS the MTR histograms of the specific lesion showed a further and significant($p<0.0001$) MTR decrease and exhibited a bimodal shape. A clear trend towards this unfavorable distribution was apparent at diagnosis when neither clinical signs of PML-IRIS nor gadolinium enhancement were visible. At followup the subsequent gadolinium-enhancing areas of the specific lesion seemed to contribute almost exclusively towards the growing second peak with very low MTR values. Concerning anti-inflammatory prednisolone therapy there was a striking difference in outcome between "core" components of the lesion detected incidentally at diagnosis and those detected later during followup. While the first went straight into apoptosis with cortical skeletonization, the areas from later PML spreading at 11-week followup(being treated relatively "timely") soon showed fading enhancement, almost no apoptosis and a significantly($p<0.0001$) better improvement of MTR at 24-week followup.
Conclusion
Patient-specific databases with consecutive MTR data might enable us to improve the risk assessment of natalizumab therapy in RRMS. In natalizumab-associated PML-IRIS, consecutive MTR monitoring seems to anticipate alarming signs of gadolinium enhancement with its poor prognosis early, and is strongly supportive of a timely and prolonged prednisolone use. Our consecutive MTR results further suggest that there is only a small time window for successful anti-inflammatory therapy of natalizumab-associated PML-IRIS with iv and prolonged oral prednisolone concerning an outcome with little apoptosis and favorable MTR values over time.

KEYWORDS: Magnetization transfer imaging, Multiple sclerosis, progressive multifocal leukoencephalopathy

Note: Scanned images are included in the proceedings. Some submitted images were reduced during editing, thereby decreasing clarity. Also, refer to the Program Planner. Proceedings Content as of 3-29-2013.

P-29

Multiplanar Morphometrics of the Optic Chiasm: Feasibility of a Novel MR Imaging Index for Assessing White Matter Atrophy in Multiple Sclerosis

Zaccagna, F.[1]·Matys, T.[1]·Wing, L.[1]·Horsburgh, A.[1]·Antoun, N.[1]·Massoud, T. F.[2]
[1]Addenbrooke's Hospital, Cambridge, UNITED KINGDOM,
[2]University of Cambridge, Cambridge, UNITED KINGDOM.

Purpose
New MRI measurements of brain volume may improve specificity in determining long-term progression of multiple sclerosis (MS). Since sophisticated MRI techniques are laborious, the simple "corpus callosum index" was suggested as a marker for brain atrophy in MS. However, this is limited by inter-subject variations in morphology, including sex differences and handedness. Therefore, in this feasibility study we focused on the optic chiasm (OC). This white matter (WM) structure is related to the optic nerves (ONs), which are known to atrophy in MS, and is readily accessible for measurement on routine brain MRI. We aimed to initially obtain detailed morphometrics in normal and MS patients. We then tested the hypothesis that statistically smaller OCs are present in MS owing to atrophy, aiding in eventual derivation of a simple and potentially clinically useful "optic chiasm index" for evaluation of WM atrophy in MS patients.
Materials & Methods
We retrospectively evaluated standard brain MRIs of 100 patients, 50 with unspecified MS histories, and 50 with normal findings. An observer blinded to clinical data electronically measured eight OC morphometrics on axial T2WIs: its width, A/P diameter, diameters of each ON and optic tract (OT), and angles between individual ONs and OTs. The OC height was measured on midsagittal T1WIs. We also measured the Evans' index to factor for global cerebral atrophy. We expressed continuous values as mean ± SD (min-max; 95% CI). For statistical comparison of clinical characteristics we used an unpaired sample t-test, and for differences in measured parameters between the two cohorts we used the Mann-Whitney test for independent samples (significance set at p-value <0.05).
Results
Three patients were excluded owing to global atrophy. The MS group (M:F=14:34) had a mean age of 36.5 years; the control group (M:F=20:29) had a mean age of 46 years; this age difference was statistically significant. Mean OC width, A/P diameter and height in patients with MS were, respectively, 11.6±0.9 mm (10.3-13.3mm; CI 11.2-12.1), 2.73±0.55mm (2-4mm; CI 2.47-2.98) and 2.18±0.34mm (1.7-3mm; CI 2.03-2.3). In the normal OC group the values were 12.1±1.34mm (10-14.5mm; CI 11.5-12.6), 3.51±0.7mm (2-5mm; CI 3.19-3.83) and 2.3±0.27mm (1.8-3mm; CI 2.2-2.4). There were statistically significant differences between MS and normal patients for A/P diameter (p=0.001) and height (p=0.003), but not for width (p=0.237). As expected, the ONs were significantly smaller in MS (p=0.001), as were the OTs (p=0.004). Consequent to OC atrophy, the angle between each ON was significantly wider (p=0.011) in MS, but not between each OT.
Conclusion
The anterior visual pathway may offer a compelling model for evaluation of demyelinating disease elsewhere in the CNS. The OC is significantly atrophic when examined in a mixed cohort of MS patients. We plan to mathematically derive a clinically useful "optic chiasm index" upon further analysis of stratified and larger MS patient groups. Future studies also will address whether correlation with quantitative MRI of the OC (e.g., using DTI and MTR) can predict future disability in a clinically useful fashion.

KEYWORDS: Multiple sclerosis, Morphometry, optic chiasm

P-30

MR Imaging Evaluation in Patients of Primary Central Nervous System Vasculitis of Indian Origin

Garg, A.·Goyal, V.·Gaikwad, S.·Mishra, N. K.·Bhatia, R.·Shukla, G.·Sharma, M. C.
All India Institute of Medical Sciences
New Delhi, INDIA.

Purpose
To evaluate MR imaging findings in patients of primary central nervous system vasculitis (PCNSV) of Indian origin.
Materials & Methods
Between January 2007 and November 2012, 30 patients (M: F=25:5) suspected of having primary CNS vasculitis based on multiple intracranial hemorrhages and punctate-linear enhancement on MR imaging were included in this study. Patients with secondary vasculitis/reversible vasoconstriction syndrome were excluded from the study.
Results
In 30 patients (male: 25, female: 5) the median age at diagnosis was 28 years (range 15 to 48 years); 47% of patients were in the third decade. Seizure (62%) was most common presenting complaint followed by focal neurologic deficits (50%) and headache (42%). Of 18 biopsies done in 16 patients,10 biopsies were positive (granulomatous vasculitis - eight, lymphocytic vasculitis - two). The rest of the 20 patients were diagnosed as PCNSV based on findings on multiple hemorrhages and enhancement characteristics along with negative vasculitis workup. In brain MRI, most common finding was diffuse discrete to confluent WM lesions in both supra and infratentorial compartments. Lesions in bilateral MCA vascular territorial distribution were seen in 92.4%, while bilateral cerebellar involvement, especially in PICA territory, was seen in 52.8%. In brainstem, pons was most common site for involvement. Hemorrhages, microhemorrhages and/or macrohemorrhages, were seen in all but one patient. Extent and distribution of hemorrhages was better seen on SWI imaging as

Note: Scanned images are included in the proceedings. Some submitted images were reduced during editing, thereby decreasing clarity. Also, refer to the Program Planner. Proceedings Content as of 3-29-2013.

compared to routine gradient imaging sequence (GRE*). Time-of-flight/contrast-enhanced MRA of COW, done in 22 patients, did not show any vascular abnormality. Spinal cord imaging, done in 12 patients (with only spinal symptoms - eight patients, brain symptoms but no spinal symptoms - four patients), showed single/multifocal dorsal cord lesions in 10 patients. Peripheral enhancement was seen in 4/10 spinal cord lesions. All patients with symptoms of spinal cord involvement (eight patients) had multiple asymptomatic brain lesions on imaging. IADSA done in 11 patients was noncontributory except psueoaneurysm in left M2 segment in one case of peripheral SAH and venous phase abnormalities in four patients.

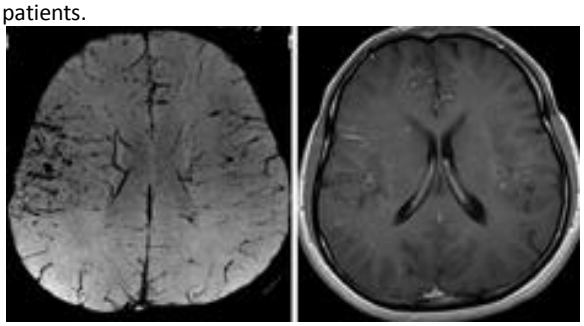

Conclusion

Bilateral supratentorial and infratentorial WM lesions with areas of microhemorrhage and/or macrohemorrhages and punctate and linear enhancements may suggest diagnosis of primary CNS vasculitis after excluding secondary vasculitis/RCVS. Concurrent spinal cord involvement, seen in 33% patients (symptomatic or asymptomatic), is significantly higher compared with existing literature. All symptomatic patients with spinal cord involvement should undergo MRI brain. All suspected PCNSV patients on brain MRI should be screened for spinal cord.

KEYWORDS: Vessel wall, MR imaging brain, vasculitis, primary CNS angitis

P-31

Natalizumab-Associated Progressive Multifocal Leukoencephalopathy during Multiple Sclerosis Treatment: Can Consecutive Monitoring of Magnetization Transfer Improve the Individual Risk Assessment?

Krueger, K. W.[1]·Krueger, P.[2]·Hild, M.[1]·Nowak, A.[1]
[1]Neurologische Gemeinschaftspraxis Hennef, Hennef, GERMANY, [2]University of Geneva, Geneva, SWITZERLAND.

Purpose

Progressive multifocal leukoencephalopathy(PML) can occur as a devastating and potentially lethal complication of long-term administration of natalizumab in patients with multiple sclerosis(MS). There is an urgent need for new diagnostic tools to predict the occurrence of PML and its evolution and course in individual patients. As, within limits, the magnetization transfer ratio(MTR) can be regarded as a marker for myelin integrity, we examined whether continuous monitoring of MTR can contribute towards an improved risk assessment of patients with MS under long-term natalizumab.

Materials & Methods

We present specific results of continuous MTR monitoring in a single 44 year-old female patient with relapsing-remitting MS and natalizumab-associated PML 19, 13 and 6 months prior to and at the incidental diagnosis of PML. The patient had received natalizumab for 62 months and was clinically completely inconspicuous at diagnosis. We used a PD-weighted SE sequence for longitudinal registration of MTR: TR=1710 ms, TE=30 ms, NSA=1 before and after an off-resonance MT pulse at 1.5T. After manual and software-assisted coregistration, consecutive MTR histograms were obtained retrospectively for the specific PML-suspicious lesion as well as for the whole brain using the FDA-approved software package NordicICE.

Results

Using Kolmogorov-Smirnov and Mann-Whitney Tests for equality of distributions, we found a significant and consecutive decrease of the MTR($p<0.0001$) between all examinations in the voxel of the future PML region. Furthermore a less pronounced but significant decrease ($p<0.0001$) of MTR in total brain voxel could be shown when starting from the baseline examination 19 months prior to diagnosis. Relying on ANOVA, we confirmed these results by documenting a significant decrease($p<0.0001$) in average MTR over time.

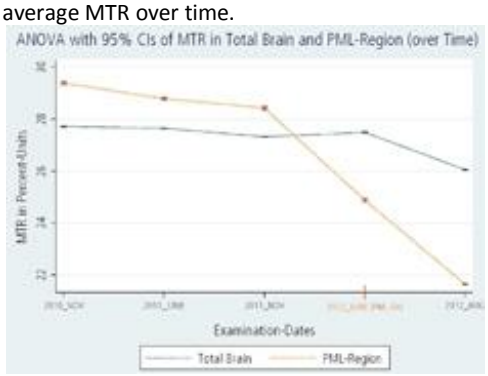

Conclusion

Longitudinal MTR databases can be created for individual patients under identical examination parameters with reasonable effort, and the technique seems suitable for routine MRI scan procedures. In our completely inconspicuous RRMS patient a MTR decrease preceded MRI manifestation, and finally, clinical manifestation of natalizumab-associated PML by several months. Given the known insidious beginnings of PML and our lack of reliable markers for an early diagnosis, we suspect that a continuous and significant decrease of total brain MTR may be an early red flag for upcoming PML. It should prompt cessation of natalizumab therapy and lead to further diagnostic steps to exclude imminent PML. Hence, longitudinal MTR monitoring seems well suited for an improved risk assessment of MS patients under long-term

Note: Scanned images are included in the proceedings. Some submitted images were reduced during editing, thereby decreasing clarity. Also, refer to the Program Planner. Proceedings Content as of 3-29-2013.

natalizumab, but further analysis of larger longitudinal datasets must validate these preliminary results.

KEYWORDS: Magnetization transfer imaging, Multiple sclerosis, Progressive multifocal leukoencephalopathy

P-32

MR Imaging Appearance of Multiple Sclerosis Correlated to CSF, Age, and Clinical Exam Findings

O'Dell, M. C.·Harshman, B.
Florida Hospital
Orlando, FL.

Purpose
Multiple sclerosis(MS) is the most common demyelinating disease and has an extremely variable course, often making early diagnosis difficult. The purpose of this exhibit is to review how MRI appearances correlate to cerebrospinal fluid(CSF) results and physical exam findings in patients with MS among all age groups.
Materials & Methods
We performed a retrospective review of patients who underwent contrast-enhanced MRI of the brain that suggested a demyelinating process or where MS was considered from clinical exam findings. Search included scans from 1.5T and 3T units. Our sample size was 1004 patients, ages 2-92, 754 females, 250 males. The electronic medical record was reviewed for final diagnosis, CSF results (oligoclonal bands, IgG levels), overall MR lesion burden and location (laterality, infra vs. supratentorial, central vs. peripheral), and clinical findings (medical history and neurologic exam).
Results
Pediatric patients diagnosed with MS revealed oligoclonal bands in the CSF with nearly 100% specificity and sensitivity. Almost all presented with leg or facial weakness and a high percentage had both supra and infratentorial involvement. Lesion burden nearly universally increased over time mostly in the supratentorial space. Patients older than 55 years typically had more confluent and extensive supratentorial white matter changes than those with more common degenerative white matter processes such as diabetes or hypertension. Symptoms were more generalized and often overlapped with chronic processes (ischemia, infarcts). The small number of older patients with infratentorial lesions suggests higher morbidity and/or mortality than those with infratentorial involvement.

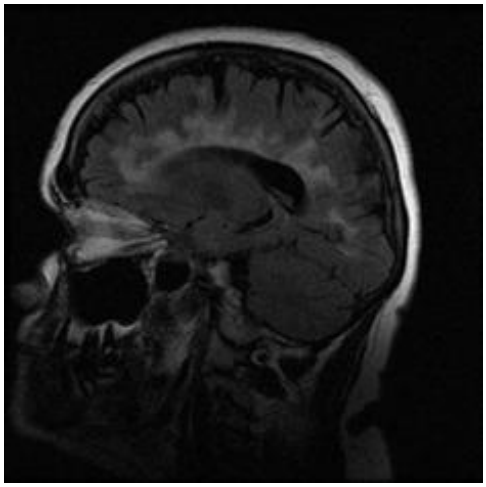

64 yo with advanced plaque burden, no infratentorial involvement

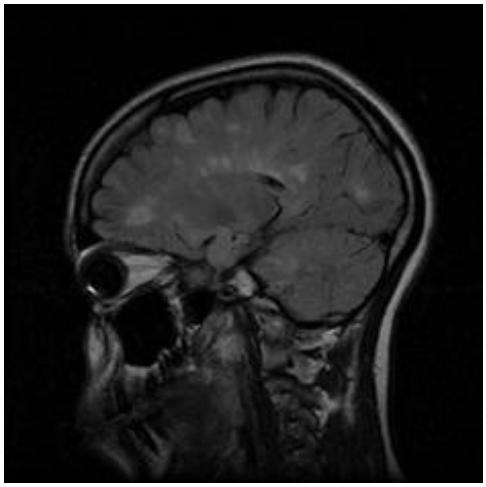

19 yo with advanced plaque burden with both supra- and infratentorial involvement
Conclusion
Multiple sclerosis has a variable course with multiple factors contributing to the typical MR appearance. Our exhibit reviews how the typical MR appearance correlates to CSF results and physical exam findings in patients with MS.

KEYWORDS: Multiple sclerosis, Multiple sclerosis plaques

P-33

Feasibility of T1 Rho Mapping of Intracranial Tumors and Tumor-Related Edema

Villanueva-Meyer, J.[1]·Barajas, R.[1]·Cha, S.[1]·Chen, W.[2]·Shankaranarayanan, A.[2]·Koon, P.[2]
[1]University of California San Francisco, San Francisco, CA,
[2]GE Global Applied Science Lab, Menlo Park, CA.

Purpose
Edema related to intracranial brain tumors is an important cause of morbidity and reflects heterogeneous

Note: Scanned images are included in the proceedings. Some submitted images were reduced during editing, thereby decreasing clarity. Also, refer to the Program Planner. Proceedings Content as of 3-29-2013.

pathophysiology of underlying tumor. More accurate and quantitative assessment of tumor-related edema may allow preoperative diagnosis of histologic subtype of brain tumor and differentiation between vasogenic and infiltrative edema associated with nonglial and glial tumors, respectively. The purpose of this study was to evaluate the use of quantitative T1rho mapping to differentiate different types of tumor related edema.
Materials & Methods
Our study patient group included nine patients with glioma grade I-III, five patients with glioblastoma multiforme (GBM), three patients with metastases, two patients with meningioma, and five normal subjects. All preoperative MRI examinations including 3D T1rho were performed on a 3T scanner. Three-dimensional T1rho imaging parameters were: 0.9 x 0.9 x 1.6 mm resolution, 280 x 196 mm FOV, 120 slices, 0.5 NEX, 2X ARC parallel imaging along phase encoding direction. Six acquisitions were acquired for T1rho quantification. For T1rho, spin-lock frequency was 500Hz, Time of Spin Lock (TSLs) = 2,10, 40, 60, 80, 100 ms and total acquisition time of 3.5 min. T1rho values in regions of contrast enhancement, peritumoral white matter T2 abnormality, and unaffected white matter were obtained. Additionally, T1rho values in different regions of white matter were recorded in healthy volunteers.
Results
T1rho values in vasogenic edema associated with metastasis or meningioma were statistically higher than infiltrative edema related to GBM (199.78 $\pm$ 31.87 versus 133.62 $\pm$ 24.51 with P = 0.01). However, T1rho values amongst grade I-III gliomas, GBM, and metastasis/meningioma were not statistically significant (138.31 $\pm$ 25.0 versus 128.1 $\pm$ 24.47 versus 113.47 $\pm$ 27.94 with P = 0.27).

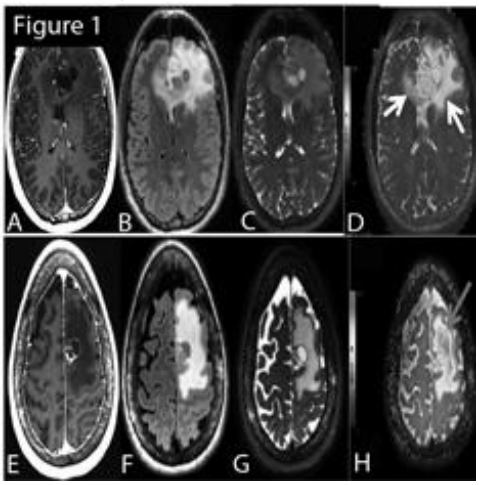

Figure. Diffuse glioma grade III (A-D) and metastatic brain cancer (E-H). (A,E) postcontrast T1-SPGR; (B,F) FLAIR; (C,G) T2-FSE, (D,H) T1rho maps. Vasogenic edema in metastatic cancer shows higher T1rho values in the range of 200-350 msec (gray arrow) than those of invasive edema in diffuse glioma (white arrows).

Conclusion
Our preliminary study demonstrates the feasibility and potential role of 3D T1rho imaging in quantitative assessment of edema related to intracranial tumors. Quantitative T1rho values were significantly different between vasogenic edema and infiltrative edema associated with metastasis and gliomas, respectively. Direct correlation between T1rho values and tissue based on image-guided biopsy is needed for histopathologic validation.

KEYWORDS: Cancer, MR imaging

P-35

Intrinsic Enhancement from the Necrotic Component of Ring-Enhancing Lesions: A Key Imaging Feature to Distinguish Necrotic Tumors from Abscesses

Wilner, A.·Zagzag, D.·Knopp, E.·Narayana, A.·Parker, E.·Golfinos, J.·Fatterpekar, G.
New York University Langone Medical Center
New York, NY.

Purpose
Diffusion-weighted imaging (DWI) is the imaging sequence of choice to differentiate necrotic tumors from abscesses. However, intralesional hemorrhage and diffusion restriction in certain metastatic lesions can limit utility of DWI. The purpose of our study was to evaluate enhancement characteristics from within the necrotic component of these lesions to distinguish tumors from abscesses.
Materials & Methods
A retrospective study evaluating 50 centrally necrotic, peripherally enhancing lesions, including 41 necrotic tumors and nine abscesses was performed. These lesions were evaluated for ADC value and intrinsic enhancement characteristics from the necrotic component of these lesions.
Results
Apparent diffusion coefficient (ADC) from 7/41 necrotic tumors could not be evaluated due to hemorrhage. The remaining 34 tumors demonstrated mean ADC of 2.45 + 0.16 x 10-3mm2s-1. Of these, two patients with metastatic adenocarcinoma demonstrated restricted diffusion with mean ADC 0.94 + 0.16 mm2s-1. Among the abscesses, three of nine patients demonstrated hemorrhage. The remaining six abscesses demonstrated mean ADC of 0.71 + 0.15 x 10-3mm2s-1. Based on the t-test, a statistically significant difference ($p<0.001$) in ADC values could be demonstrated between necrotic tumors and abscesses. However, presence of hemorrhage in seven tumors and three abscesses, and restricted diffusion in two metastases limited the role of ADC evaluation in 12/50 cases. In terms of enhancement characteristics, all tumors demonstrated intrinsic linear-nodular enhancing septations, presumed regressing vessels from central necrotic component. Only one of nine abscesses demonstrated such intrinsic

Note: Scanned images are included in the proceedings. Some submitted images were reduced during editing, thereby decreasing clarity. Also, refer to the Program Planner. Proceedings Content as of 3-29-2013.

enhancing septations. Based on ROC analysis, intrinsic enhancement from the necrotic component of tumor was found to be more sensitive than ADC to distinguish abscesses from necrotic tumors.
Conclusion
Intrinsic linear-nodular enhancement from necrotic component of the tumor is more sensitive than ADC to distinguish abscesses from tumors. According to our literature search, this is the first article which mentions the role of intrinsic enhancement as a key imaging feature to distinguish necrotic tumors from abscesses.

KEYWORDS: Tumor-like conditions, Abscess, necrosis

P-36

Neuroimaging Markers of Treatment-Associated Neurotoxicity in Glioblastoma Patients Undergoing Brain Radiation and Temozolomide Chemotherapy

Prust, M. J.[1]·Kalpathy-Cramer, J.[2]·Poloskova, P.[2]·Jarafi-Khouzani, K.[2]·Gerstner, E. R.[2,3]·Dietrich, J.[3]
[1]Harvard Medical School, Boston, MA, [2]Martinos Center for Biomedical Imaging, Massachusetts General Hospital, Harvard Medical School, Boston, MA, [3]Stephen E. and Catherine Pappas Center for Neuro-Oncology, Massachusetts General Hospital, Boston, MA.

Purpose
Systemic chemotherapy and brain irradiation are associated with neurocognitive impairment in cancer patients during and after treatment. Up to 70% of cancer survivors experience higher-order cognitive deficits and difficulty performing at pretreatment levels in their personal and professional lives. Prior work suggests that injury to neural stem cells (NSC) and progenitor cells in the hippocampal dentate gyrus and the subventricular zone may play a role in the pathogenesis of chronic neurologic deficits in cancer survivors. Investigation into the effects of treatment on healthy brain tissue is needed to identify markers of potential neurotoxicity and guide future efforts at neuroprotection. Here, we used structural MRI to explore patterns of neurotoxic injury in NSC-associated brain regions within a cohort of glioblastoma patients undergoing chemotherapy and radiation.
Materials & Methods
We longitudinally examined volumetric parameters within germinal zones and nontumor regions in 14 GBM patients receiving daily temozolomide (TMZ) chemotherapy and brain irradiation for six weeks, followed by monthly TMZ. In an IRB-approved study, patients underwent weekly MRI during chemoradiation and monthly thereafter up to six months. Using high-resolution MEMPRAGE images, we constructed regions of interest (ROIs) within the lateral ventricles and hippocampus on patients' baseline images and used nonrigid coregistration to map these ROIs onto subsequent images collected across the treatment period. Ventricular volumetric analysis was restricted to the anterior aspects of the lateral ventricles, a region of low tumor burden within our sample to avoid confounding by resolving tumor pressure during treatment. Hippocampal volumetric analysis was conducted within the hemisphere of lowest tumor burden.
Results
Subjects remaining in treatment beyond the six-week chemoradiation period (N=12) showed mean ventricular dilatation of 39.0% (SD: 22.0%; range: 6.8-67.1%) at final study visit (see Figure 1 for sample sizes at each time point). Percent volume change was not associated with tumor volume changes. We found no significant hippocampal volume changes.

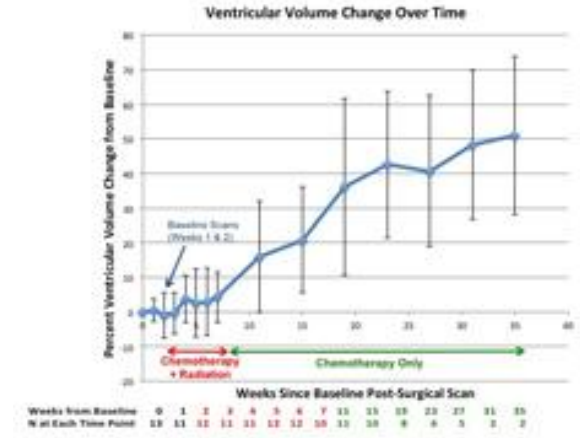

Conclusion
We present evidence of treatment-associated, nontumor anatomical brain changes in patients receiving chemotherapy and irradiation. While preliminary, these data highlight the need for further exploration of treatment-associated brain changes and their underlying pathophysiologic mechanisms. Specifically, patient attrition within our sample and lack of comparison subjects leaves uncertain whether early exposure to chemoradiation initiates an ongoing neurodegenerative process, or whether phenotype severity depends on sustained exposure to chemotherapy over many months. Additionally, future prospective trials employing sensitive neuropsychologic measures are needed to assess the relationship between treatment-associated brain changes and functional neurocognitive sequelae.

KEYWORDS: Neurotoxicity, Chemotherapy

Note: Scanned images are included in the proceedings. Some submitted images were reduced during editing, thereby decreasing clarity. Also, refer to the Program Planner. Proceedings Content as of 3-29-2013.

P-37

Intracranial Tumor Extravascular Extracellular Space: Is There a Correlation between Apparent Diffusion Coefficient and the Extravascular-Extracellular Volume Fraction in Human Meningioma and Cerebral Lymphoma?

Huhdanpaa, H.[1]·Hwang, D. H.[1]·Muradyan, N.[2]·Cen, S.[1]·Torres, F.[1]·Lerner, A.[1]·Commins, D. L.[1]·Rajamohan, A.[1]·Go, J. L.[1]·Law, M.[1]·Shiroishi, M. S.[1]
[1]Keck School of Medicine, University of Southern California, Los Angeles, CA, [2]iCAD, Inc, Nashua, NH.

Purpose
The apparent diffusion coefficient (ADC) determined from diffusion MR imaging can give an impression of the extravascular-extracellular space (EES) and has been shown to be inversely correlated with tumor cell density. The extravascular-extracellular volume fraction (v_e) derived from dynamic contrast-enhanced (DCE) MRI is theorized to provide an estimate of the size of a tumor's EES. Therefore, by logical extension, a positive correlation should be observed between ADC and v_e. The purpose of this study was to determine if there may be a correlation between ADC and v_e as well as with other DCE metrics such as the blood-brain barrier transfer constant (K^{trans}), K_{ep} (K^{trans}/v_e), fractional plasma volume (v_p) and the initial area under the contrast agent concentration-time curve (iAUC) in cerebral lymphomas and meningiomas.
Materials & Methods
Four cerebral lymphomas and five meningiomas were evaluated retrospectively. Diffusion tensor imaging and DCE images were acquired during the same MRI exam. Dynamic contrast-enhanced MR images were postprocessed on an iCAD workstation, a semiautomated image analysis suite. Metrics extracted from DCE MRI were: v_e, v_p, K^{trans}, K_{ep}, and iAUC. Apparent diffusion coefficient maps were extracted automatically from diffusion imaging by the clinical MR scanner software. Dynamic contrast-enhamced and diffusion images were c-registered in SPM to the SPGR using T1 maps and EPI scans. Apparent diffusion doefficient values were interpolated using a concatenated transform into DCE space. Regions of interest were drawn in DCE coordinates on a single slice for the purposes of this study. Voxel-wise correlation pattern between ADC and DCE parameters were examined using scatter plots and tested by random effect model (SAS HPMIXED-High Performance Mixed Model) incorporating both within and between subject variations. Mean and median were extracted for patient level analysis using Spearman correlation.
Results
There was no statistically significant correlation from voxel-wise analysis using random effect modeling. The correlation coefficient between ADC and v_e, K^{trans}, iAUC, K_{ep}, v_e, v_p are -0.01, 0.05, -0.01, 0.05, -0.01, -0.03 respectively. No statistical significance was found in patient level analysis for both mean and median values. The strongest correlation coefficient found was 0.38 between median ADC and median v_e with p=0.32.
Conclusion
Preliminary results showed no correlation between ADC and v_e or any other DCE MRI metrics in meningioma or lymphomas using either mean/median or voxel-by-voxel data. This is in agreement with the only known published study in intracranial tumors by Mills et al. in glioblastomas which also found no correlation between ADC and v_e. This suggests that though ADC and v_e are thought to reflect the size of the EES, our current understanding of these metrics is incomplete. Similarly, no relationship appears to exist between ADC and the other DCE metrics. However, methodologic limitations could be important confounders.

KEYWORDS: Brain neoplasms, Dynamic contrast-enhanced MR, diffusion MR imaging

P-38

Imaging Features of a Gelatin-Thrombin Matrix Hemostatic Agent in the Intracranial Surgical Bed: A Unique Space-Occupying Pseudomass

Hyder, I. Z.·Learned, K. O.·Bagley, L. J.·Dolinskas, C. A.·Han, S. S.·Lee, J. Y.
University of Pennsylvania Health System
Philadelphia, PA.

Purpose
Hemostatic agents are used frequently in neurosurgical procedures due to the particular importance of adequate intracranial hemostasis. Gelatin-thrombin matrix (FloSeal Matrix; Baxter Healthcare Corporation, Fremont, CA, U.S.A.) is an absorbable bovine gelatin-human thrombin composite. Its advantages include fast preparation, easy delivery with syringe applicator to various surgical beds, hydrophilic matrix allowing effective adherence to wet surgical field, and effectiveness in coagulopathic disorders. Even though its intracranial neurosurgical application is well published, its unique postoperative radiographic imaging appearance has been scarcely described and potentially can be mistaken for retained foreign body, abscess and/or neoplasm. The immediate postoperative CT and MR imaging appearance and evolution with time of gelatin-thrombin matrix in the intracranial operative beds are investigated.
Materials & Methods
The postoperative CT and MR imaging studies of four consecutive patients (one man, three women, mean age 54 years) who underwent surgical resection of hemorrhagic brain metastases and were treated intraoperatively with FloSeal for hemostasis were reviewed retrospectively (September 2011- December 2012). The surgical beds were evaluated for size, internal architecture, CT attenuation, MR signal intensity and enhancement during the immediate postoperative period (within 48 hours of surgery) and at subsequent followup (within one week to ten months). Imaging findings were correlated with surgical technique and clinical followup.

Note: Scanned images are included in the proceedings. Some submitted images were reduced during editing, thereby decreasing clarity. Also, refer to the Program Planner. Proceedings Content as of 3-29-2013.

Results

During the immediate postoperative period, FloSeal within all operative beds appeared as space-occupying material with hypoattenuation similar to (or lower than) fat on CT imaging and distinctive T2-hypointense speckles in a background of T2 hyperintensity. Within one week, all operative beds appeared to be filled with fluid density material (on CT), and the T2-hypointense speckles noted on MRI resolved. By 4-6 weeks, the initial T1 hypointensity changed to T1 hyperintensity, and the sizes of the surgical cavities decreased only 20-30% in all cases. Two patients with longer followup demonstrated complete surgical bed collapse by six months. FloSeal within the operative cavities demonstrated T2 and FLAIR hyperintensity, facilitated diffusion and lack of enhancement on all MR imaging studies.

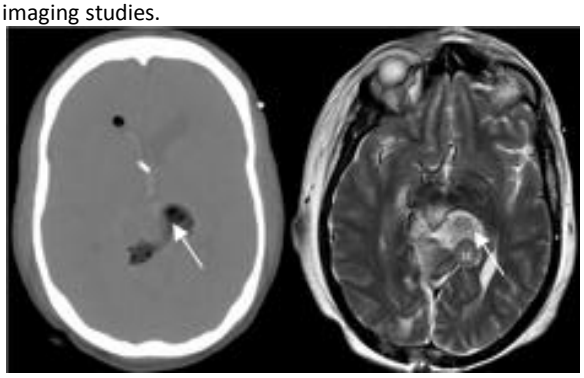

Conclusion

Gelatin-thrombin matrix FloSeal has distinctive fat-like hypoattenuation on CT and T2 hypointense speckles on MR in the intracranial surgical beds during the immediate postoperative period. FloSeal with its unique space-occupying appearance should not be mistaken for retained nonabsorbable surgical material, abscess, hematoma or neoplasm.

KEYWORDS: Postoperative findings, Tumor-like conditions, hemostatic agent

P-39

Apparent Diffusion Coefficient and Fractional Anisotropy Values of the Lateral Ventricles and Corpus Callosum in Patients with Leptomeningeal Metastatic Disease

Liu, H.[1]·Wang, J.[2]·Suki, D.[2]·Guha-Thakurta, N.[2]·Chi, T. L.[2]·Ketonen, L. M.[2]·Mayer, R. R.[3]·Weinberg, J. S.[2]·Debnam, J. M.[2]
[1]University of Texas Health Science Center at Houston, Houston, TX, [2]University of Texas M. D. Anderson Cancer Center, Houston, TX, [3]Baylor College of Medicine, Houston, TX.

Purpose

Leptomeningeal disease (LMD) is the dissemination of cancer cells throughout the subarachnoid space, diagnosed by imaging or cerebrospinal fluid (CSF) analysis. On MRI, the magnitude of fluid diffusion within the voxel is measured by the apparent diffusion coeffecient (ADC). A low ADC value indicates that molecular movement in the sampled tissue is restricted, while a high value for ADC indicates that the tissue has free diffusion. The purpose of this study was to evaluate the ADC values of intraventricular CSF and of the corpus callosum, with the hypothesis being that the ADC values will differ between the patients with LMD and controls.

Materials & Methods

The ADC values were measured in 47 patients with LMD confirmed by cytological evaluation of the cerebrospinal fluid, and for control in 40 patients with a history of cancer, but no clinical or radiologic evidence of LMD. Measurements were taken in the atrium of the lateral ventricles, as well as the genu and splenium of corpus callosum in both groups and compared. The Kruskal-Wallis test was used for the statistical analysis.

Results

The mean ADC value in the right and left lateral ventricle in the patients with LMD were 3.20E-09 and 3.24E-09, respectively, compared to 3.04E-09 and 3.03E-09 in the control group (p= 0.016 and 0.002, respectively). No significant difference in ADC values was noted between LMD and control groups for measurements obtained in the genu and splenium of the corpus callosum.

Conclusion

The ADC values in patients with LMD are significantly different than in the control group without LMD, while ADC values in the corpus callosum are not significantly different. Future applications in patients with LMD may include ADC measurement in the lateral ventricles to assess treatment response.

KEYWORDS: Leptomeningeal disease, Apparent diffusion coefficient, lateral ventricles

P-40

Susceptibility-Weighted Imaging Characteristics of Brain Metastases

Marquez, J. C.[1,2,3]·Medina, F. J.[1,4]·Castillo, M.[1]
[1]University of North Carolina at Chapel Hill, Chapel Hill, NC, [2]Resonancia Magnética del Country, Bogotá, COLOMBIA, [3]Pontificia Universidad Javeriana - Hospital Universitario San Ignacio, Bogotá, COLOMBIA, [4]Fundación Valle de Lili, Cali, COLOMBIA.

Purpose

Hemorrhagic brain metastases are not infrequently encountered using only conventional MRI sequences. We utilized SWI in brain metastases to determine the incidence of hemorrhage in them and the effect of treatment type on presence of blood.

Materials & Methods

We retrospectively reviewed SWI in 635 brain metastases in 81 patients. Four hundred eleven metastases had undergone treatment (radiosurgery, gamma knife,

Note: Scanned images are included in the proceedings. Some submitted images were reduced during editing, thereby decreasing clarity. Also, refer to the Program Planner. Proceedings Content as of 3-29-2013.

radiotherapy, chemotherapy). In order of frequency, primary tumors were nonsmall cell lung cancer (N = 318), breast (N = 95), ovary (N = 50), melanoma (N = 2), sinonasal undifferentiated carcinoma (N = 30), renal cell carcinoma (N = 25), endometrial carcinoma (N = 21), colon cancer (N = 15), small cell carcinoma (N = 13), pancreas (N = 12), pharynx squamous cell carcinoma (N = 8), adrenal cancer (N = 5), thyroid cancer (N = 3), and mixed germ cell testicular tumor (N = 1). The SWI lesions were evaluated by two radiologists and hypointensities representing hemorrhage were recorded as present or absent. Hemorrhage was correlated with presence or not of treatment and its type. Each lesion was measured in two dimensions on the axial plane.

Results

Of the 635 brain lesions evaluated 56.45% showed hemorrhage on SWI. Most of the treated lesions demonstrated blooming, and bigger lesions tend to show more hemorrhage than smaller lesions. Of lesions 10 mm or more in size, 82.3% (163/198) showed hemorrhage and those 15 mm or more in size, 93.9% (77/82) had hemorrhage. In contrast, only 40.6% (101/249) of lesions measuring 5 mm or less showed hemorrhage. Metastases from colon (100%), melanoma (84.4%), and renal cell cancer (92%) showed the higher rates of hemorrhage. Eighty-six percent of metastases treated with radiosurgery alone showed hemorrhage and 82% of those treated with combined radiosurgery and radiotherapy showed hemorrhage. In contrast, 39% of lesions treated with chemotherapy alone showed hemorrhage and 63% and 60% of those treated with radiotherapy alone combined radiation therapy and chemotherapy respectively showed hemorrhage.

Conclusion

Overall more than one-half of brain metastases contained hemorrhage, particularly larger ones. Metastases from melanoma, kidney, and colon were more likely to bleed. The incidence of hemorrhage after treatment ranged from 39-86% being more common in those receiving radiosurgery.

KEYWORDS: Brain metastases, Susceptibility-weighted imaging, hemorrhage

P-41

Role of Dynamic Susceptibility Contrast Perfusion MR Imaging in Selecting Patients with Meningiomas for Preoperative Embolization

Toh, C.·Wei, K.·Peng, Y.·Wong, H.·Ng, S.·Chen, Y.·Wu, Y.
Chang Gung Memorial Hospital
Linkou, TAIWAN.

Purpose

Preoperative embolization is considered a useful adjuvant therapy in meningiomas as it may reduce intraoperative blood loss during subsequent tumor resection. It typically is performed on meningiomas with increased angiographic tumor vascularity and feeders arising from ECA branches. The relationship between relative CBV derived from DSC perfusion and angiographic vascularity on DSA of meningiomas has never been investigated. We aimed to differentiate meningiomas of different angiographic vascularity by using DSC perfusion MRI.

Materials & Methods

Relative CBV were measured in enhancing tumor portions and contralateral NAWM of 32 meningiomas. The CBV ratios were calculated by dividing the tumor values to those obtained from contralateral NAWM. The angiographic vascularity of meningioma was graded as follows: 0 indicated none; 1, minimal; 2, moderate; and 3, exuberant. Embolization would not be necessary for meningiomas with grade 0 or 1 vascularity. Spearman correlations were used to investigate associations between CBV ratios and angiographic vascularity grades. Comparisons of CBV between meningiomas with low (grades 1 and 2) and high (grades 3 and 4) angiographic vascularity were done by using a two-sample t test. The diagnostic performance of DSC perfusion MRI in differentiating meningiomas with low vascularity from those with high vascularity was assessed with ROC curve analysis.

Results

There were no correlations between angiographic vascularity and the size or location of meningiomas. Statistically significant correlations were observed between angiographic vascularity grades and CBV ($r = 0.867$; $P < .001$). The CBV of meningiomas with low vascularity ($5.59 \pm .01$) were significantly ($P < .001$) lower than those of high vascularity (14.97 ± 7.73). In differentiating between meningiomas of low and high vascularity, the diagnostic performance of CBV, in terms of AUC, was 0.927.

Conclusion

Dynamic susceptibility contrast perfusion MRI can differentiate meningiomas of different angiographic vascularity. Dynamic susceptibility contrast perfusion MRI can serve as a noninvasive tool to evaluate the vascularity of meningiomas prior to catheter angiography, and aid in selecting patients for preoperative embolization.

KEYWORDS: Meningioma, MR perfusion-weighted imaging

P-42

Using Image-Based Statistical Probes to Query Imaging Archives

You, K.·Butman, J. A.
The Clinical Center of the National Institutes of Health
Bethesda, MD.

Purpose

Querying image databases for certain image features typically requires that an observer has coded or classified the images in some manner. This is a time-consuming process requiring an expert reader. Therefore, most image

Note: Scanned images are included in the proceedings. Some submitted images were reduced during editing, thereby decreasing clarity. Also, refer to the Program Planner. Proceedings Content as of 3-29-2013.

databases (e.g., those on hospital PACS systems) have not been coded in such a manner. Our goal was to generate a probe capable of identifying studies in a brain tumor image database that contained nonartifactual sites of diffusion restriction, thereby streamlining data collection for future analysis.

Materials & Methods

Isotropic diffusion-weighted image (DWI) datasets (n = 7354) obtained on all brain tumor patients (n = 1074) were automatically transferred to an archive, registered into a patient-specific space and stored in Analyze format. To develop a probe of this dataset, an arbitrary sample of 50 DWI data volumes was selected. Signal intensities were normalized (median) and the volumes were affine registered to a base image using nine degrees of freedom. From this data, the probe generated the voxel-wise mean and z-scores at each voxel (in a manner analogous to fMRI analysis). Next, each individual DWI was tested against the probe, and the number of voxels exceeding various z-score thresholds was recorded. Independently, each dataset was classified as DWI positive or negative by an expert. Receiver-operating characteristic curves were generated by varying the the z-score threshold as well as the number of voxels exceeding the threshold. Based on the results of this analysis, criteria were selected and the database was probed.

Results

The probe performed well when compared to the gold standard, with the area under the ROC curves ranging from 0.80 to 0.87 depending on the standard deviation selected. The probe was most effective when counting voxels with standard deviation 3 (area under ROC curve = 0.87) or 4 (area under ROC curve = 0.86) above the mean. When the t-scores were calculated using a mean and standard deviation from a separate sample of 50 diffusion-weighted images, the probe on the initial 50 diffusion-weighted images was similarly effective. The area under the ROC curves ranged from 0.75 to 0.85. However, the probe was less effective when performed on images in which the signal intensity of the signal abnormality was lower and closer to the surrounding voxels. In a probe on a sample of 50 images with this characteristic, the area under the ROC curves ranged from 0.24 to 0.33.

Conclusion

Diffusion abnormalities are characterized by large signal differences between lesion and normal brain in DWI. Identification of studies in which diffusion abnormalities are present in an image archive is feasible with statistical probes. However, because of susceptibility effects, high signal due to signal pileup is found on nearly every image. In order to identify studies in which diffusion abnormalities are present, we developed a statistically based probe that is relatively insensitive to these false positive results. Such probes are necessary to extract data from massive image archives as it is impractical to use expert observers in this role.

KEYWORDS: Informatics, DWI

P-43

Diffusion Tensor Imaging in Patients with Recurrent Neoplasm versus Treatment Effect

Masch, W. R.[1]·Wang, P.[1]·Chenevert, T. L.[1]·Junck, L. R.[1]·Tsien, C.[1]·Heth, J.[1]·Wang, A.[1]·Sundgren, P. C. M.[2,1]
[1]University of Michigan, Ann Arbor, MI, [2]Lund University, Lund, SWEDEN.

Purpose

The purpose of this study is to retrospectively analyze the diffusion-tensor imaging (DTI) characteristics of new enhancing lesions in patients with brain neoplasms who have undergone radiation therapy and chemotherapy in an attempt to radiologically differentiate recurrent tumor from treatment-related injury.

Materials & Methods

Ten patients with new contrast-enhancing lesions who previously had undergone treatment with surgery, chemotherapy and radiation therapy for a brain neoplasm were examined with diffusion tensor magnetic resonance (MR) imaging. Apparent diffusion coefficients (ADCs), fractional anisotropy (FA) values, and eigenvalues were measured on maps generated from isotropic DW images in the following areas: the enhancing lesion, the perilesional edema, and the contralateral normal-appearing white matter. Magnetic resonance spectroscopy (MRS) data were used in guiding surgical biopsy/resection of the lesions as well as in the placement of the region of interest cursor such that the portion of the enhancing lesion with the most malignant MRS signal was measured. Radiation necrosis versus tumor recurrence was determined by histologic evaluation in nine patients and by clinical course in one patient. Between group differences in ADC, FA, and eigenvalues were compared using a two-sample t-test.

Results

Of the 10 patients enrolled, five had glioblastoma multiforme, four had a glioma, and one had metastatic disease (ages 20-62 years; 1 F/9M). The treatment-related injury group was composed of five patients and the recurrent tumor group was composed of five patients. Apparent diffusion coefficient values in the contrast-enhancing lesions trended higher (P = 0.15) for the recurrence group (mean +/- S.D. = 1.16×10^{-3} +/- 0.24×10^{-3}) in comparison to the treatment-related injury group (mean +/- S.D. = 0.90×10^{-3} +/- 0.27×10^{-3}). The principal eigenvalues ($\lambda\|$) in the contrast-enhancing lesions also trended higher (P = 0.10) for the recurrence group (mean +/- S.D. = 1.42×10^{-3} +/- 0.31×10^{-3}) in comparison to the treatment-related injury group (mean +/ - S.D. = 1.05×10^{-3} +/- 0.31×10^{-3}).

Conclusion

The assessment of DTI characteristics of new contrast-enhancing lesions in patients with previously treated brain neoplasms, particularly evaluation of the ADC and eigenvalues, may be helpful in differentiating recurrent neoplasm from treatment-related injury.

Note: Scanned images are included in the proceedings. Some submitted images were reduced during editing, thereby decreasing clarity. Also, refer to the Program Planner. Proceedings Content as of 3-29-2013.

KEYWORDS: DTI, Neoplasm recurrence, diagnosis

P-44

Renovate Enhancement Developed in Low-Grade Glioma Revealed No Malignant Transformation: Imaging and Pathologic Correlation

Kawamura, Y.·Hadeishi, H.·Narita, M.·Hoshi, K.
Kameda Medical Center
Chiba, JAPAN.

Purpose
Transformation from low-grade “diffuse” astrocytoma to high-grade has been accepted as a natural progression. However, in this study authors observed the renovate enhancement in three patients whose previous MRI had shown a lack of enhancement and following operation revealed no histologic malignancy. The mechanism of the altered enhancement of low-grade astrocytoma was discussed.
Materials & Methods
Three patients (age 17, 22 and 25 yeara, one man and two women) known to have well circumscribed nonenhancing brain tumor had been followed up more than three years on MRI with 1.5T and 3T magnet (Signa, GE, USA). T1-weighted images (SE, TR/TE/NEX: 333-483/14-20/2), T2-weighted images (FSE, TR/TE /NEX: 3200-3500/83-100/2), FLAIR images (FSE, TR/TE/TI /NEX: 10002/125/220/1), and EPI diffusion weighted images (TR/TE /NEX: 5000/101/1, *b* = 1000) were obtained. For contrast-enhanced MRI, 0.1 mmol/kg of gadolinium-DTPA was injected intravenously. Enhanced CT was performed with 64-raw-unit (Aquillion 64, Toshiba, Japan) The patient's age, sex, main symptoms, tumor location and follow-up duration are summarized in Table 1. Histopathologic examination was performed with HE staining and immunohistochemical staining such as GFAP, S-100, occludin (ZYMED; vascular endothelial tight junction marker), CD45R0 (DAKO; T cell marker), CD20cy (DAKO; B cell marker), anti-CD31 (DAKO; microvascular density).
Results
Clearly demarcated ovoid lesions were demonstrated as high intensity on T2-weighted and FLAIR images and as homogeneous low intensity on T1-weighted images in case 1 (Figure 1, left). Diffusion-weighted images did not show high intensity in all cases. Well circumscribed ring enhancement (Figure 1, right; arrow) developed on follow-up MRI taken three years later. Punctate enhancement was revealed within (case 2) and adjoining to nonenhancing portion (case 3). Total surgical removal was performed subsequently according to the renovate contrast enhancement seen on MRI. Microscopic examination did not show significant cellular atipia, mitosis, tumor neovascularity and tumor necrosis. In case 1, the immunohistochimical examination confirmed intact vascular endothelial tight junction in enhancing portion of the tumor with infiltration of B-cell lymphocytes and macrophage. In cases 2 and 3, the vascular endothelial tight junction marker (occludin) was negative in contrast to positive staining of occludin in the nonenhancing portion of the tumor.

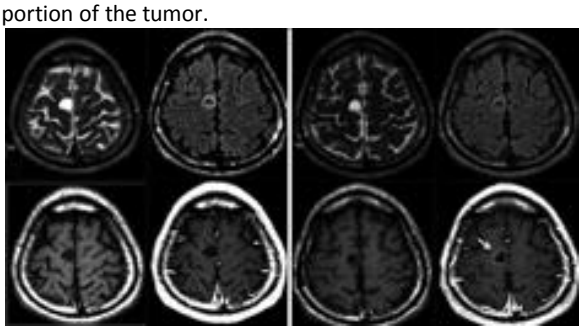

Conclusion
Our result indicates that the new onset of enhancement in previously nonenhancing low-grade astrocytomas do not necessarily imply the histologic deterioration but could be influenced by the change of vascular endothelial tight junction and/or infiltration of inflammatory cells.

KEYWORDS: Brain neoplasms, 3 T

P-45

Usefulness of SPACE T2-Weighted Images in Diagnosing Small Pituitary Adenoma: Comparison with Dynamic-Enhanced T1-Weighted Images

Ahn, K.·Choi, H.·Jung, S.·Kim, B.
College of Medicine, The Catholic University of Korea
Seoul, KOREA, REPUBLIC OF.

Purpose
Although dynamic-enhanced T1-weighted images have been accepted as the best imaging technique to detect pituitary microadenoma, frequently there have been difficulties to make correct diagnosis when the imaging findings were vague due to regional susceptibility or insufficient contrast between the lesion and normal gland. Sampling perfection with application optimized contrasts by using different flip angle evolution (SPACE) T2-weighted images are three-dimensional imaging techniques based on fast spin-echo method, thus very thin slice images with compatible signal to noise ratio are possible with allowable scanning time. The purpose of this study is to know the usefulness of SPACE-T2-weighted images in diagnosing small pituitary adenoma, especially for microadenoma.
Materials & Methods
Total 28 patients with small pituitary adenoma (< 2 cm, including 16 microadenomas) who underwent dynamic-enhanced T1-weighted images and SPACE T2-weighted images together were recruited in our study. As controls, 21 patients without any lesion in pituitary gland were included. Two experienced radiologists reviewed both dynamic-enhanced T1-weighted images and SPACE T2-weighted images independently to detect adenoma in the pituitary gland. To score the lesion conspicuity four point

Note: Scanned images are included in the proceedings. Some submitted images were reduced during editing, thereby decreasing clarity. Also, refer to the Program Planner. Proceedings Content as of 3-29-2013.

scale (0-3) was used and the sensitivity, specificity and diagnostic accuracy of both imaging techniques were evaluated.
Results
No significant difference between average score of dynamic T1-weighted images and SPACE T2-weighted images was noted (1.55 versus 1.43, $p = 0.5$). SPACE T2-weighted images showed similar sensitivity to the dynamic-enhanced T1-weighted images (85.7% 92.9%, respectively) in detecting small pituitary adenoma. The specificity of SPACE T2-weighted images was superior to that of dynamic-enhanced T1-weighted images (100% 95.2%, respectively). On SPACE T2-weighted images the signal intensities of pituitary adenomas were variable (high, low and isointense signal intensities in 14, 11 and 3 cases, respectively).
Conclusion
SPACE T2-weighted images showed similar sensitivity and superior specificity to dynamic-enhanced T1-weighted images in diagnosing small pituitary adenoma. Considering that infusion of MR contrast medium was not used in SPACE T2-weighted images, there are very encouraging results. SPACE T2-weighted images can be used as a very good complementary imaging technique to diagnose small pituitary adenoma in clinically concerned patients.

KEYWORDS: 3D imaging, Pituitary adenoma

P-46

Evaluation of a Bayesian Expert System for Aiding Neuroradiology Diagnoses: A Pilot Study

Tanwar, M.·Herskovits, E. H.·Nasrallah, I. M.·Kundel, H.·Mohan, S.·Li, C.·Lynch, M. C.·Bryan, R.
University of Pennsylvania
Philadelphia, PA.

Purpose
Recently, there has been an explosive growth of digital imaging data, resulting in challenge and opportunity. Contemporary computational techniques can analyze immense amounts of complex data and are being incorporated into decision-support applications. We have developed a prototypical Bayesian expert system that takes input key features (KFs) detected in images and outputs a differential diagnosis (DDx) ranked by posterior probability. We hypothesize that the idealized KFs upon which the model was based and those extracted by radiologists at different levels of training and the DDx lists produced by the model and human readers are similar.
Materials & Methods
Eleven neuroradiological entities (abscess, cerebritis, craniopharyngioma, glioblastoma, hematoma, infarct, metastasis, multiple sclerosis, rhombencephalitis, toxoplasmosis, xanthogranuloma) and normal, were evaluated by a senior neuroradiologist to identify characteristic and idealized imaging KFs and approximate conditional probabilities of these features. These features and probabilities were used to build a Bayesian expert system for differential diagnosis. Two attending neuroradiologists selected a test set of 60 diagnosis-proven MR examinations from our PACS: 5 for each entity. Three diagnosis-blind readers -- attending neuroradiologist, neuroradiology fellow and PGY-3 radiology resident -- reported the KFs and their rank ordered DDx after reviewing each case. We entered each reader's KFs into our model, obtaining a posterior probability ranked DDx list for each case-reader combination. We compared reader's observed KFs to each other and to the ideal disease features, and we compared readers' DDx to those of the model and to each other. We also compared DDx lists to the clinically proven diagnosis. Percentage agreement, kappa statistics, and ROC analysis were used to evaluate human and computer reader performance.
Results
For individual extracted KFs, there was moderate to excellent agreement between the different human readers (57-91%), which was similar to agreement between individual reader KFs and the idealized KFs for the various diseases (42-94%). Inter-reader agreement for each feature was similar to agreement between readers and the model system KFs. The model, using ideal cases (i.e., cases with "classic" features, as determined by a senior neuroradiologist), was in 100% agreement with the known diagnosis. These indicate that the KFs upon which the model system was based are concordant with actual clinical cases. The primary diagnoses of the human readers versus the proven diagnoses showed percent agreement of 77-92% and K = 0.74-0.91. ROC analysis of DDx for human readers (AUC 0.91-0.93) and model output diagnoses based on human extracted KFs (AUC 0.66-0.82) all demonstrated excellent performance.
Conclusion
A prototype neuroradiological decision-support application was developed and evaluated using a small set of clinical neuroradiological MR examinations. Readers selected similar KF values regardless of experience level, probably reflecting our use of readily noticeable findings. There was excellent agreement between each readers' most likely diagnoses and the known diagnosis, with the resident manifesting slightly lower accuracy, probably because our 12 entities are fairly distinct. Further development might render this software suitable for reducing the variability of radiology reports, improving report quality, and increasing the efficiency of practicing radiologists.

KEYWORDS: Computer-aided diagnosis, Informatics, Bayesian network

Note: Scanned images are included in the proceedings. Some submitted images were reduced during editing, thereby decreasing clarity. Also, refer to the Program Planner. Proceedings Content as of 3-29-2013.

P-47

Evaluating Ventriculostomy Catheter Position and Patency Using High-Resolution MR Imaging Techniques

Eckart, D.·Solomon, D.·Moghekar, A.·Rigamonti, D.·Blitz, A.
Johns Hopkins Hospital
Baltimore, MD.

Purpose
We present the result of two years of clinical experience using high-resolution MRI techniques to characterize the position and patency of ventriculostomy tubes during the evaluation of shunted hydrocephalus.
Materials & Methods
Clinical MRI examinations performed at our institution were tailored for evaluation of shunted hydrocephalus, using isotropic high-resolution heavily T2-weighted imaging (CISS) and T1-weighted sequences (VIBE) with and without intravenous gadolinium contrast. After obtaining IRB approval, the MRI examinations of patients with ventriculostomy tubes who had undergone an MRI protocol including high-resolution imaging were reviewed restrospectively by two radiologists. Twenty-one cases met our inclusion criteria. The catheter position and location of the side holes were assessed. The patency of the lumen was evaluated by documenting the presence or absence of internal debris. Additionally, three-dimension reformations were performed to best depict the course and position of the catheter.
Results
Using high-resolution MRI with attention to the ventriculostomy catheter, excellent visualization of side-hole position was observed in 17/21 cases. In seven of 16 cases, debris was visible in the catheter lumen, suggesting obstruction. Three-dimensional MRI reconstructions better depicted the course and position of the ventriculostomy catheters relative to conventional imaging, aiding the neurosurgical service in management of shunted hydrocephalus patients.

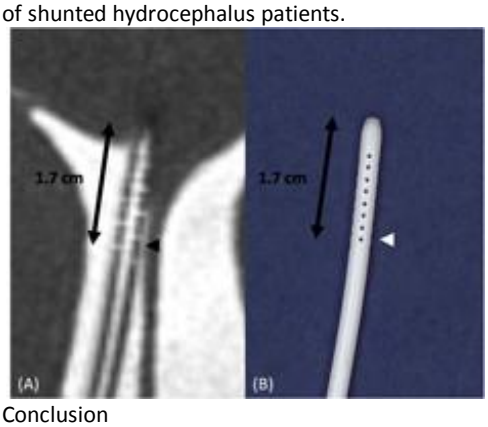

Conclusion
Despite the frequency of shunt malfunction and malpositioning, MRI often is not utilized to its full potential to evaluate the position and patency of the proximal ventriculostomy catheter itself. Using high-resolution techniques and multiplanar reformations, sublties of catheter position, side-hole location, and the presence luminal debris (patency) can be assessed with greater sensitivity.

KEYWORDS: Hydrocephalus, Shunt, ventriculostomy

P-48

Usefulness of RESOLVE Multi-Shot, Diffusion-Weighted Imaging in Clinical Practice

Ahn, K.·Choi, H.·Jung, S.·Kim, B.
College of Medicine, The Catholic University of Korea
Seoul, KOREA, REPUBLIC OF.

Purpose
Although single-shot echo-planar imaging is well established as the method of choice for clinical diffusion-weighted imaging, it is prone to artifacts due to susceptibility changes at tissue interfaces and has a limited spatial resolution. RESOLVE multi-shot, diffusion-weighted imaging is based upon the readout-segmented EPI method, which has been modified to incorporate 2D navigator phase correction and navigator-based reacquisition. It provides a robust correction for motion-induced phase artifact in allowable scan time. The purpose of our study is to evaluate the usefulness of RESOLVE in detecting small acute infarction in routine practice by comparing image quality and detecting rate between RESOLVE and conventional single-shot diffusion imaging.
Materials & Methods
Twenty healthy volunteers and 39 consecutive patients with total 337 infarct lesions were recruited and underwent RESOLVE and single-shot diffusion imaging. In control group, overall image qualities of both techniques were evaluated qualitatively and compared at level of anterior and middle skull base. In 39 patients with infarctions, the number of small acute infarctions less than 1 cm was counted on two sequences for quantitative comparisons.
Results
On overall image quality comparison, RESOLVE showed significant superior quality to single-shot diffusion imaging ($p < 0.01$). On quantitative comparisons in patients with small acute infarctions, total 294 lesions were detected on single-shot diffusion-weighted imaging. However, with RESOLVE technique 43 additional lesions were detected.
Conclusion
RESOLVE multi-shot, diffusion-weighted imaging for acquiring high-resolution diffusion images showed low susceptibility and T*2 blurring and a robust correction for motion-induced artifact. The technique provides significant image quality improvement compared with single-shot diffusion imaging in detecting small size acute infarction in the brain.

KEYWORDS: Diffusion-weighted imaging, Infarct

Note: Scanned images are included in the proceedings. Some submitted images were reduced during editing, thereby decreasing clarity. Also, refer to the Program Planner. Proceedings Content as of 3-29-2013.

P-49

Qualitative Evaluation of Dual-Energy Head CT in Comparison with Conventional Head CT

Hwang, W. D.·Mossa-Basha, M.·Andre, J. B.·Culberton, S.·Ramos, M.·Anzai, Y.
University of Washington
Seattle, WA.

Purpose
1) To determine the optimal monochromatic energy levels for supratentorial brain and posterior fossa, based on blinded-reader analysis. 2) To perform quality analysis of dual-energy CT over conventional polychromatic CT. 3) To quantify the radiation dose of dual-energy CT gemstone spectral imaging (GSI) unenhanced head CT and conventional CT.
Materials & Methods
From July 25 to October 24, 2012, approximately 153 patients were scanned with dual-energy 64-channel MDCT scanner, GE Discovery CT750HD, in GSI mode. Patients with pathology such as MCA territory infarct and posterior fossa tumor were excluded from the study. A total of 20 patients scanned at regular dose GSI and 19 patients scanned at low dose GSI, with recent comparison study (within one year) on the same Discovery scanner in non-GSI mode, were included in the study. Scans were reconstructed at monochromatic viewing levels from 60 to 80 kev, at 2 kev intervals. These along with a recent comparison study (control) were viewed simultaneously for each patient on an independent workstation by a blinded attending neuroradiologist. The reader was asked to grade each energy level and the control study on three parameters, insular cortex differentiation, posterior fossa artifact, and overall study noise, on a scale of 0 to 5, 0 being nondiagnostic, 5 being superior quality.
Results
Overall optimal viewing energy was determined to be 62 kev for regular dose and 72 kev for low dose GSI CT. Posterior fossa image quality was determined to be best at 80 kev at both regular and low dose. No significant reduction in image quality was found with either regular or low dose dual-energy CT over conventional CT. Posterior fossa image quality was found to be superior with both regular and low dose dual-energy CT over conventional CT. Conventional CTs were all scanned at 140 kvp and 330 mA, with a CTDI dose 43.81 +/- 1.61 mGy. Regular dose GSI CTs were scanned at 140 kvp and 630 mA, with a CTDI of 36.74 +/- 1.21 mGy, representing a mean dose reduction of 16% over conventional CT. Low dose GSI CTs were scanned at 140 kvp and 360 mA, with a CTDI of 28.16 +/- 0.88 mGy, representing a mean dose reduction of 36% over conventional CT.
Conclusion
There is a significant dose benefit in performing dual-energy GSI head CT with current reconstruction algorithms at regular or low dose compared with conventional CT. There was no significant degradation in subjective image quality observed in direct comparison of dual-energy with conventional CT. Optimal monochromatic viewing energy was found to be 62 kev for regular dose and 72 kev for low-dose dual-energy CT. There was an improvement in posterior fossa artifact reduction and image quality with GSI. Thus, GSI is a viable alternative to conventional polychromatic unenhanced head CT in the clinical setting.

KEYWORDS: Dual-energy CT, Dual energy spectral, radiation dose

P-50

Assessment of C-Arm Cerebral Blood Volume Maps Obtained through Aortic Arch Injection with 50% and 30% Diluted Contrast Medium

Itokawa, H.·Moriya, M.·Fujimoto, M.·Tomita, Y.·Okamoto, N.·Kikuchi, N.·Shibata, N.·Awane, A.
Kasai Shoikai Hospital
Tokyo, JAPAN.

Purpose
Recent studies have demonstrated the feasibility of C-arm cerebral blood volume (CBV) maps obtained via intravenous contrast injection. For patients undergoing diagnostic angiography or endovascular treatment, intra-arterial injection may provide a viable approach for reducing the amount of contrast medium used during C-arm CBV imaging. The purpose of this study was to assess the feasibility of C-arm CBV maps obtained through aortic arch injection at 50% and 30% diluted contrast medium, and to compare these maps with CT perfusion (CTP) CBV.
Materials & Methods
Twenty-seven patients with normal perfusion on CTP CBV were enrolled in this study. Standard CTP study was performed on a 64-section CT scanner (Aquillion, Toshiba, Japan). For each patient, C-arm CBV images (syngo neuro PBV IR, Siemens AG, Forchheim, Germany) then were acquired via a flat-detector angiographic system (Artis zee BA, Siemens AG, Forchheim, Germany). C-arm CBV requires two rotational acquisitions, the first without contrast injection, and the second with a delay after the start of contrast injection in order to achieve steady state of contrast flow in the brain parenchyma. The delay was timed individually in each patient via a test bolus injection. All studies were performed via aortic arch injection with 4F diagnostic catheter positioned directly above the aortic valve. Depending on the injection delay, 75-100 ml of diluted contrast medium was injected at a rate of 5ml/s. Patients were divided into two groups; Group A (17 patients) for which 50% diluted contrast was used, and Group B (10 patients) for which 30% diluted contrast was used. The acquired data were reconstructed on a separate workstation (syngo XWP VB 15D, Siemens AG, Forchheim, Germany). C-arm CBV and CTP CBV were manually coregistered, and regions of interest (ROIs) subsequently

Note: Scanned images are included in the proceedings. Some submitted images were reduced during editing, thereby decreasing clarity. Also, refer to the Program Planner. Proceedings Content as of 3-29-2013.

were placed in the anterior cerebral artery (ACA), middle cerebral artery (MCA), posterior cerebral artery (PCA) territories and basal ganglia (BG).
Results
C-arm CBV with aortic arch injection was technically successful, without complications, and image quality was adequate for evaluation in all patients. No significant differentiation of image quality was observed between groups A and B. C-arm CBV values for groups A and B were higher than CTP CBV values (p0.05). C-arm CBV right/left ratios in ACA and MCA were slightly higher than those for CTP CBV; however, these differences did not reach statistical significance (0.01<p<0.05). The same tendency was observed in Group A and Group B. A maximum of 30 ml of contrast was used for C-arm CBV imaging in Group B, compared to 60 ml of contrast for intravenous injection C-arm CBV or CTP CBV.
Conclusion
Preliminary results indicate that aortic-arch injection of 30% diluted contrast medium generates C-arm CBV maps that are comparable to those obtained with 50% diluted contrast medium, with the advantage of lower contrast dosage requirement. C-arm CBV with 30% diluted contrast medium may provide clinically useful information for the patient management.

KEYWORDS: C-arm CT CBV

P-51

New Multispectral MR Imaging Technique for White Matter Lesion Detection and Classification

Chen, C. C. C.[1]·Chen, H.[2]·Chai, J.[1]·Lee, S.[1]·Yang, C.[1]·Chang, C.[3]
[1]Taichung Veterans General Hospital, Taichung, TAIWAN, [2]Hungkuang University, Taichung, TAIWAN, [3]University of Maryland, Baltimore County, Baltimore, MD.

Purpose
White matter lesions (WML) commonly are found in elderly subjects and are associated with cognitive decline and dementia. Magnetic resonance imaging (MRI) has become an important imaging modality for understanding and managing several aspects of WML. WML exhibit almost the same hyper-signals in T2-weighted MRI, and hypo-signals in T1-weighted MRI, with respect to normal WM intensities. Many studies measure WML volume using a single MR sequence or combining sequences. Such approaches include probabilistic methods, neural networks, and the expectation-maximization algorithm. These methods demand complex computational efforts to achieve good performance. In this study, we developed a new multispectral approach, called constrained energy minimization (CEM), to overcome these difficulties for a study of WML detection. The CEM has shown great success in hyperspectral target detection and classification. It was designed based on a premise that no background information is required for target detection. The aim of this study is to introduce a new multispectral approach for the validation of WML volumetry.
Materials & Methods
Synthetic data from the BrainWeb database was used to evaluate the accuracy of WMLs volume measurements by using the proposed method to analyze three sets of T1-weighted, T2-weighted and proton density images. The parameter setting includes three noise levels of 0%, 1%, and 3% for brain with lesions. Let **d** be the spectral signature of WML. The goal is to design a finite impulse response (FIR) linear filter specified by an ***L***-dimensional vector $\mathbf{w} = (w_1, w_2, \cdots, w_L)$ that passes the desired signature **d** by constraining its direction while minimizing its output energy that are caused by signal source vectors with directions other than the constrained direction. The value of resulting from CEM method represents the estimated abundance fraction of the object signature **d** contained in the image pixel. As a result, the image generated by the CEM filter is generally gray scale where the gray level value of each image pixel reflects the detected amount of the abundance fraction of the desired object present in the pixel. The object detection then is performed based on the resulting gray scale image and classification is carried out by detecting the desired objects in separate images. In order to conduct a quantitative study and compare with the ground truth, we convert the CEM-generated abundance fractional images to binary images. In this study, the adaptive threshold is used for the cutoff abundance fraction threshold value to convert CEM results to binary images. The Tanimoto index was measured to statistically evaluate the results of the WML volumes with the ground truth data of the synthetic brain images.
Results
The mean TI values of WML in synthetic MR images with noise level 0%, 1%, and 3% were separately 0.88, 0.86, and 0.82. The preliminary results demonstrated the proposed technique would be effective.
Conclusion
Our experimental results revealed significantly high accuracy of the CEM method in classification of synthetic brain WML data. The proposed method could effectively enhance the detection and classification of brain lesions.

KEYWORDS: Computer-aided diagnosis, White matter disease, multispectral MR imaging

P-52

Evaluation of Cerebral Perfusion Parameters on CT Perfusion Associated with Global Cerebral Edema in Aneurysmal Subarachnoid Hemorrhage

Fodera, V.·Sanelli, P.·Gupta, A.·Baradaran, H.
New York Presbyterian-Weill Cornell
Colonia, NJ.

Purpose
Aneurysmal subarachnoid hemorrhage (SAH) is a devastating disease with severe complications including

Note: Scanned images are included in the proceedings. Some submitted images were reduced during editing, thereby decreasing clarity. Also, refer to the Program Planner. Proceedings Content as of 3-29-2013.

global cerebral edema (GCE) contributing to functional and cognitive disability. It is well known that GCE occurring during the early stage (day 0-3) independently leads to poor outcomes. However, little is known about mechanisms underlying the development of GCE and its effects on cerebral perfusion. Our aim was to evaluate cerebral perfusion parameters on CTP associated with GCE in aneurysmal SAH.

Materials & Methods

A retrospective study of consecutive SAH patients with CTP performed on admission (day 0-3) admitted from 2008-2010. Presence of GCE was determined on the noncontrast CT (performed concurrently with CTP) by two independent neuroradiologists blinded to all other clinical and imaging data using Claassen's definition: (1) complete or near-complete effacement of the hemispheric sulci and basal cisterns and (2) bilateral disruption of the hemispheric gray-white matter junction at the level of the centrum semiovale. Global cerebral edema was considered present if there was more than 75% sulcal effacement or more than 75% of gray-white matter disruption. CTP was postprocessed into cerebral blood flow (CBF), cerebral blood volume (CBV) and mean transit time (MTT) data using a standardized method. Qualitative analysis of CTP maps was performed by two independent blinded neuroradiologists to determine presence of global CTP deficits, defined as diffuse reduction in CBF and/or elevated MTT. Adjudication was performed by a third neuroradiologist. Test characteristics of CTP were calculated and statistical significance was determined by Fisher's exact test.

Results

A total of 45 patients were included in the statistical analysis. There were 42.2% (19/45) patients classified as GCE and 57.8% (26/45) as no GCE. Global perfusion deficits were seen in 52% (10/19) patients with GCE and 7.7% (2/26) without GCE. There is a statistically significant difference in the global perfusion in GCE ($p = 0.0014$) manifesting as diffusely reduced CBF and/or elevated MTT. Figure 1 demonstrates a patient with GCE and global perfusion deficit. Global perfusion deficits had a 53% sensitivity, 92% specificity, 83% positive predictive value and 73% negative predictive value.

Conclusion

Global perfusion deficits on CTP were statistically increased in GCE patients compared to patients without GCE. CTP has a high specificity and positive predictive value. These initial results support further work in this field to evaluate the effects of GCE on cerebral perfusion and its association with poor outcomes.

KEYWORDS: Aneurysmal subarachnoid hemorrhage, Cerebral edema, CT perfusion

P-53

Development of an MR Compatible Circulating Water Bath for Phantom Temperature Control: Design, Experimental Validation, and Applications in Neuroimaging Research

Pate, K.·Dehkharghani, S.·Magrath, R.·Wei, L.·Mao, H.·Tong, F.·Oshinski, J.
Emory University
Atlanta, GA.

Purpose

Refined temperature control is of paramount importance when probing phenomena sensitive to dynamic system temperatures, with widespread implications in neuroimaging research. Circulating water baths coupled to temperature control systems are used extensively throughout in vitro and in vivo magnetic resonance (MR) research for regulating temperature; however, commercially available products may be prohibitively costly. We propose that with limited components and experimental modeling, exquisite temperature control with an MR-compatible system can be achieved at nominal costs. Herein we report the design of a highly refined temperature control system constructed for optimization of MR thermometry sequences in a brain cytosol phantom.

Materials & Methods

Basic construction consists of a 48-quart basin, submersible pump, two ball-valves, six-liter plastic bin, and tubing. Temperature was controlled by a proportional-integral-derivative (PID) controller connected to a 1000W heating element within the basin. The circulator was designed to control brain cytosol phantom temperatures during 1H-spectroscopy (MRS) and water phase-contrast (PC) measurements. The submersible pump was placed in the basin, powering the inflow into a bath housing the phantom in the MR scanner. The basin remained outside the scanner room, accessing the bath through a wall port. Water return to the basin was achieved by establishing a siphon, and the outflow rate was controlled by a ball-valve at the terminal end. A steady state waterline was demarcated in the basin, ensuring safe control of the phantom bath level in the scanner. Total system cost was approximately $180.00.

Results

The temperature difference between basin water and phantom was used to determine a relationship that modeled the time-dependant temperature response in the phantom. The model requires an input sequence of temperatures for the water in the basin, as well as initial phantom temperature. System accuracy was tested by a PID input sequence ramping phantom temperatures from 23 - 42°C over two hours. The phantom then was placed in the MRI scanner where actual reference temperatures were recorded via MR-compatible fiber optic probes (OpSens OTG-MPK5) during simultaneous MRS and PC MR thermometry (Figure 1). System testing confirmed stability and control over the range of target temperatures (± 0.1°C

Note: Scanned images are included in the proceedings. Some submitted images were reduced during editing, thereby decreasing clarity. Also, refer to the Program Planner. Proceedings Content as of 3-29-2013.

over 20 minutes).

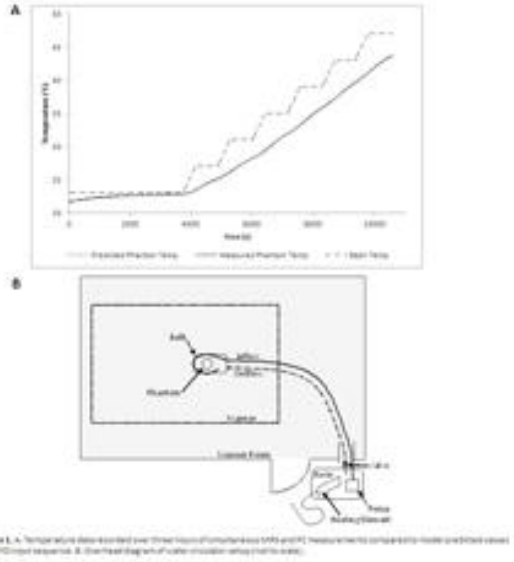

Conclusion

Preliminary testing for MR thermography techniques in the brain requires a refined system for temperature control. We show that construction of an MR-compatible system with predictable control is readily achievable at nominal comparative costs, affording examination of MR protocols for temperature measurement across a broad range of temperatures.

KEYWORDS: Temperature, Semiquantitative, MR thermometry

P-54

Comparison of the Macintosh Operation System and Grid Computing System on Anatomical Volume and Cortical Thickness Measurements

Liu, H.[1]·Chen, S.[1,2]·Yang, C.[1]·Huang, A.[2]·Liu, M.[2]
[1]National Taiwan University Hospital, Taipei, TAIWAN, [2]Center for Dynamical Biomarkers and Translational Medicine, National Central University, Jhongli, TAIWAN.

Purpose

FreeSurfer is a well known software package to measure cerebral cortical volume and thickness. However, it is CPU-intensive (20-30 hours per brain for a full segmentation). Grid computing is a loosely coupled, heterogeneous dispersing computer resources from multiple domains but dedicate to a particular application. Grid computing is faster than a single computer in the factors of the total number of computers in the grid.

Materials & Methods

We compared the results of cerebral cortex and volume in different anatomical locations in 118 subjects obtained from a Macintosh computer and a Grid computing (consisted of 48 personal computers with same configurations). They were 71 women (age mean = 45.9 years old, SD = 16.1) and 47 men (age mean = 42.8 years old, SD = 17.4). The exclusion criteria: evidence of psychiatric illness within the past two years, including substance abuse, a history of recreational drug use in the previous six months, a history of CNS disease or brain injury, any MR imaging abnormalities checked by two experienced neuroradiologists. MR scans were acquired with a 1.5T scanner (GE Healthcare, Wisconsin, USA). Coronal T1-weighted images were obtained using an MP-RAGE sequence with TR = 8.9 msec, TE = 2.99 msec, TI = 600 ms and a flip angle of 12. The slice thickness was 0.9 mm with no interslice gap. The image matrix was 256 x 256. The FreeSurfer comprises two main processing streams, a volume-based stream and a surface-based stream. The volume-based stream is designed to assign a neuroanatomical label to each (sub) cortical voxel, whereas the surface-based stream is developed to derive the white and pial surfaces from which, among others, cortical volumes and cortical thickness (CT) are derived. Both of them used the version 5.1.

Results

No statistic difference found between the two computing methods in all of the 42 subcortical and 68 cortical regions in volume and thickness measurement. The p ranged between 0.772 to 1.

Conclusion

With grid computing, we can obtain the volume and cortical thickness of different cerebral anatomical regions much faster than one computer with comparable results.

KEYWORDS: 1.5T, Anatomical results

P-55

Detection of Pituitary Incidentalomas on High Spatial Resolution 3D MR Imaging: Detection Rate, Size and Distribution

Tavares, F. C.·Zan, E.·Aygum, N.·Blitz, A. M.
Johns Hopkins Hospital
Baltimore, MD.

Purpose

3D high-resolution MRI (HR MRI) may increase sensitivity for small lesions of the skull base. In certain cases the detection of pituitary microadenomas remains challenging, due partly to their small size. We hypothesized that detection of small pituitary incidentalomas, as a proxy for symptomatic microadenomas, would increase using high-resolution images.

Materials & Methods

We retrospectively studied the rate of pituitary incidentalomas in 101 patients who underwent HR MRI. The protocol included isotropic 0.6 mm CISS and 0.8 mm VIBE sequences, which were reviewed for focal signal abnormality within the pituitary gland.

Results

We excluded 41 cases due to known/clinically suspected

Note: Scanned images are included in the proceedings. Some submitted images were reduced during editing, thereby decreasing clarity. Also, refer to the Program Planner. Proceedings Content as of 3-29-2013.

pituitary pathology, prior surgery or pituitary region radiation. The pituitary was normal in 50 subjects, while 10 (20%) demonstrated focal signal abnormalities, with no quadrant predilection. We found five (10%) enhancing (Figure1) pituitary masses (minimum size of 1.9 x 1.4 mm) and five (10%) nonenhancing lesions (Figure 2), the latter classified as pars intermedia cysts (minimum size of 0.9 x 0.7 mm).

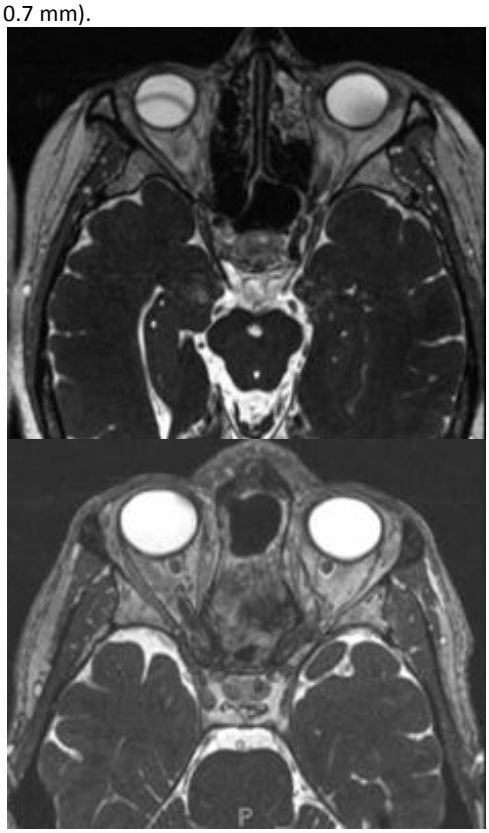

Conclusion
To our knowledge, the minimum size of incidentalomas detected on 3D MRI has not been studied. The reported incidence of pituitary incidentalomas is up to 27% in autopsy cases and 22.5% in diagnostic images. Although our initial cohort did not show a higher incidence, smaller abnormalities were detected than typically are seen on standard imaging.

KEYWORDS: High-resolution imaging, Pituitary gland, Incidentaloma

P-56

Rapid Determination of Perfusion Deficits for Acute Stroke Triage Using CT Perfusion

Chang, J. P.·Parekh, N.·Cantrell, C.·Gallagher, T.·Carroll, T. J.
Northwestern University
Chicago, IL.

Purpose
To develop and validate improved computed tomographic cerebral perfusion (CTP) images. We hypothesize that CTP, which parameterize altered perfusion in a setting of acute ischemic stroke, can be more easily implemented and better quantified using an arterial input function (AIF) independent, first moment of time (FMT) analysis, than more commonly used AIF dependent deconvolution analysis methods, which are subject to well known bolus delay and dispersion effects.
Materials & Methods
Retrospective review of patients (n=50) on PACS who received a CTP over a two-year period (1/2010-9/2012) and selected 10 consecutive patients who also received a follow-up head CT at least 10 days following the stroke. No patients in this study underwent thrombolysis (chemical or mechanical) in the time between CTP and follow-up imaging. Parametric images of relative cerebral blood flow (rCBF), relative cerebral blood volume (CBV), and mean transit time (MTT) color maps were obtained using standard deconvolutional methods with AIFs selected by a trained operator. The images then were reprocessed using a fully automated, nondeconvolutional method and FMT color maps were obtained and compared to the corresponding MTT maps. Differences in lesion conspicuity were quantified between MTT and our proposed approach based on an "asymmetry index" which quantified R/L asymmetry in a less objective manner than visual inspection. Discrepancies between MTT and FMT results were adjudicated through independent, blinded review of the follow-up CT images by two radiologists to determine which method was more predictive of final stroke volume.
Results
Preliminary results demonstrate that qualitatively, FMT has excellent concordance with the AIF dependent MTT. Mean absolute asymmetry scores were 0.104 and 0.185 for FMT and MTT respectively. Student *t*-test was calculated from the mean asymmetry index and demonstrates subtle statistically significant difference between FMT and MTT (p value=0.046). Qualitative evaluation demonstrates that FMT more closely matches the final stroke volume.

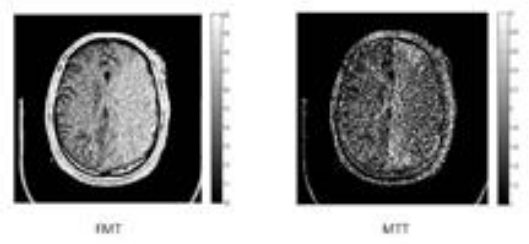

Conclusion
Using a fully automated, AIF independent,

Note: Scanned images are included in the proceedings. Some submitted images were reduced during editing, thereby decreasing clarity. Also, refer to the Program Planner. Proceedings Content as of 3-29-2013.

nondeconvolutional method for identification of perfusion abnormalities is equivalent to standard MTT deconvolutional methods currently available without the inherent limitations of AIFs. Preliminary results also demonstrate that FMT has qualitatively higher specificity than MTT in predicting final stroke volume. Our method, as an adjunct to standard methods, has the potential to save precious time during an acute stroke workup, leading to a higher probability of salvageable brain tissue, and in situations of acute infarct, better predict the final stroke volume, allowing for more specific and personalized after stroke care planning.

KEYWORDS: CT brain perfusion, Postprocessing, first moment of time

P-57

Cerebrovascular Plaques: Association with Cerebral Microbleeds and Cerebrovascular Ischemic Events

Park, D.[1,2]·Lee, Y.[2]·Lee, S.[2]·Park, C.[1,2]
[1]Hanyang University Guri Hospital, Guri-si, KOREA, REPUBLIC OF, [2]College of Medicine, Hanyang University, Seoul, KOREA, REPUBLIC OF.

Purpose
The purpose of this study is to evaluate the correlation of cerebrovascular plaque characters, the presence of cerebral microbleeds (CMBs) and cerebrovascular ischemic (CVI) events.
Materials & Methods
Thirty-five consecutive patients (18 men; 17 women; mean age, 62.1 years) underwent vessel wall MRI studies including high-resolution T1-, T2-, proton density, and contrast-enhanced T1-weighted images and MR angiography for cerebrovascular plaque at 3T. Cerebral microbleeds were studied using T2*-weighted GRE sequences and/or susceptibility-weighted images. Plaques are characterized based on their composition. Intraplaque hemorrhage (IPH) and adventitial enhancement (AE) are categorized by T1 and T2 hyperintensity and contrast enhancement. Patients are classified with recent CVI events. Chi-square and multiple logistic regression analyses, as well as ROCs, are calculated.
Results
Intraplaque hemorrhage and AE are present in 29% and 82% of patients, which are associated with recent CVI events (P value < 0.05). The prevalence of CMBs is 21%, which is significantly higher in the patients with recent CVI events (P value < 0.05). A statistically significant association is observed between the presences of IPH, AE and CMBs (P value < 0.05). Correlation analysis demonstrates an association between the number of CMBs and the recent CVI events (P value < 0.05).
Conclusion
In conclusion, there is an association between the presence of IPH, AE, CMBs and recent CVI events. The presence of CMBs may represent an indicator of cerebrovascular symptom severity.

KEYWORDS: MR plaque imaging, Stroke

P-58

Desmoteplase in Acute Ischemic Stroke: Role of Imaging in the Ongoing DIAS-3 and DIAS-4 Clinical Trials

Albers, G. W.[1]·von Kummer, R.[2]·Truelsen, T.[3]
[1]Stanford University Stroke Center, Palo Alto, CA, [2]Technical University, Dresden, GERMANY, [3]Lundbeck A/S, Valby, DENMARK.

Purpose
Thrombolytic treatment of acute ischemic stroke (AIS) patients should be focused on those who are likely to benefit from thrombolysis and tissue reperfusion and unlikely to be harmed. It is logical that only patients with thrombo-embolic arterial occlusion can benefit who have not yet had major cerebral ischemic injury of the arterial territory affected. In the three completed trials within the Desmoteplase In Acute Ischemic Stroke (DIAS) clinical trial program, MRI and perfusion/diffusion mismatch failed to select patients for thrombolytic treatment. Desmoteplase is a novel, highly fibrin-specific thrombolytic agent. Here we review the results of the completed clinical trials, and provide the rationale for patient selection based on nonenhanced CT and CTA or DWI and MRA in the ongoing trials based on imaging.
Materials & Methods
Publications on completed trials and status update given by the sponsor on ongoing trials.
Results
In the two phase II trials (DIAS, DEDAS), desmoteplase had acceptable safety profiles, and showed superior reperfusion compared to placebo in patients selected by perfusion/diffusion mismatch. While the DIAS-2 phase III trial also supported the safety profile of desmoteplase, it did not replicate the positive efficacy findings. Clinical response was 47% and 36% for 90 and 125 µg/kg desmoteplase, respectively, and 46% for placebo. In DIAS-2, it appeared however, that 70% of the mismatch-selected patients presented with normal flow or low-grade stenosis (TIMI 2-3) at screening. Post-hoc analyses of the completed DIAS, DEDAS and DIAS-2 trials showed that desmoteplase was superior to placebo in patients presenting with TIMI 0-1 (occlusion or high-grade stenosis [OR 4.1 (1.4-12.3)], in contrast to TIMI 2-3 [OR 1.1 (0.5-2.4)]. These findings provided the basis for the design of the ongoing DIAS-3 and DIAS-4 phase III trials (n=880 in total). The objective of both trials is to evaluate the safety and efficacy of a single IV bolus injection of 90 µg/kg desmoteplase given 3-9 hours after onset of AIS. Patients are included with TIMI 0-1 in proximal cerebral arteries as assessed by MR or CT angiography. Signs of extensive early infarction on CT or MRI is an exclusion. Primary efficacy parameter is achieving a modified Rankin Scale score 0-2

Note: Scanned images are included in the proceedings. Some submitted images were reduced during editing, thereby decreasing clarity. Also, refer to the Program Planner. Proceedings Content as of 3-29-2013.

at day 90. Other outcomes include NIHSS score, recanalization in patients with follow-up angiography, and clinical outcome in patients with core lesion <25 mL, or with perfusion/diffusion mismatch. Safety outcomes comprise mortality, symptomatic ICH, symptomatic ischemic edema, and other major hemorrhagic events. Mid-2012, total enrollment in DIAS-3 and DIAS-4 passed 500. DIAS-3 enrolls patients originating from sites in Europe, Asia and Australia; DIAS-4 from Europe, Latin America and North America.
Conclusion
The results of the DIAS clinical trial program will be important for physicians and patients with AIS in need of a safe and effective treatment in a time-window of up to nine hours.

KEYWORDS: Acute ischemic stroke, Thrombolysis, desmoteplase

P-59

Clinical Neuroimaging in the Second Century of Life: Evidence for Altered Susceptibility to Age-Related Processes

O'Dowd, S. M.[1]·Chu, T.[2]·Taylor, T. R.[1]·Dineen, R. A.[2]
[1]Nottingham University Hospitals NHS Trust, Nottingham, UNITED KINGDOM, [2]University of Nottingham, Nottingham, UNITED KINGDOM.

Purpose
The World Health Organization predicts a 1000% increase in centenarian numbers globally by 2050, but neuroimaging changes in extreme old age are not well characterized. Epidemiological research shows that 85% of centenarians have avoided or delayed the onset of major age-related diseases. We model age-related neuroimaging changes [white matter lesions (WML) and cerebral atrophy] in a cohort of 60 to 100+ year-olds to test if these increase linearly or nonlinearly, and test the hypothesis that mean WML and atrophy scores in centenarians will fall below the expected mean based on linear modelling.
Materials & Methods
Retrospective cross-sectional study of clinically acquired cranial CT scans from 40 centenarians (34 female, mean age 101.7 years, range 100.0-110.6), and cohorts aged 60, 70, 80 and 90 years (n = 40 each group) matched for gender and type of presentation. Two neuroradiogists, blinded to all demographics, independently rated the cranial CT scans using validated published scales for global cortical atrophy (GCA; scored 0-3) and WML burden (scored 0-3 for right and left frontal and parietal regions, maximum score of 12). We assessed the possibility of nonlinear association between age-related neuroimaging changes and chronological age in a linear regression model. To test the stated hypothesis, we estimated the deviation of the observed mean WML or GCA score at 100 years from the group mean predicted by the linear models and tested for the significance of their differences.
Results
Each increase of 10 years in age was associated with 0.43 increase in GCA score (95% CI: 0.38-0.48, P<0.01) and 1.92 increase in WML score (95% CI: 1.62-2.23, P<0.01). There was insufficient evidence to support a nonlinear relationship for age-related increases in WML (P = 0.14) or GCA (P = 0.74) scores [Figure: Relationship between WML (left) and GCA (right) scores and age; Circle size proportional to number of patients; Solid line: regression model with age as continuous explanatory variable; Dotted line: regression model with age as categorical variable]. For centenarians, the observed mean total WML score was 1.77 units (95% CI: -3.27 to -0.27, P = 0.02) lower than the predicted mean score but the corresponding difference for mean GCA score was not statistically significant.

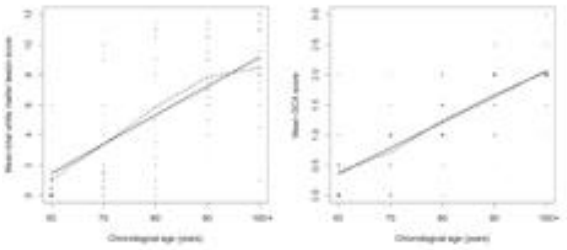

Conclusion
Atrophy and WML burden increase with age linearly. However, centenarian's mean WML scores were lower than expected from a linear trend, partially supporting the proposed hypothesis and the notion that biological aging mechanisms may be inherently different in centenarians.

KEYWORDS: Aging, Atrophy, white matter lesions

P-60

Detection of Crossed Cerebellar Diaschisis in Patients with Acute Cerebral Infarction by CT Perfusion Using 320-Detector Row CT

Kinoshita, T.·Kinoshita, F.·Umetsu, A.
Research Institute of Brain and Blood Vessels-Akita Akita, JAPAN.

Purpose
Crossed cerebellar diaschisis (CCD) is characterized by a reduction in blood flow and oxidative metabolism in the cerebellar hemisphere contralateral to a supratentorial lesion. Crossed cerebellar diaschisis consistently results from circuit inactivation, such as cerebral infarction. Whole brain CT perfusion analysis using 320-detector row CT permits the identification of remote effect perfusion abnormalities. The purpose of this study was to assess the detection of CCD after acute middle cerebral artery (MCA) infarction using 320-detector row CT.
Materials & Methods
Consecutive 24 patients with unilateral MCA infarction in less than six hours from the onset of symptoms were

Note: Scanned images are included in the proceedings. Some submitted images were reduced during editing, thereby decreasing clarity. Also, refer to the Program Planner. Proceedings Content as of 3-29-2013.

included. We excluded patients with abnormalities in the posterior fossa on unenhanced CT. CT perfusion study was performed using a 320-detector row CT. Image acquisition was performed as a dynamic contrast material-enhanced scan covering the entire brain. Perfusion maps were generated using CTP analysis software. CT perfusion color maps including cerebral blood flow (CBF) and cerebral blood volume (CBV) of the whole brain were obtained. The degree of CCD was measured on one axial cut representing the highest cerebellar asymmetry. Asymmetry index (AI) was calculated as a difference in the value between unaffected and affected cerebellar hemisphere divided by the value in the unaffected cerebellar hemisphere. Patients with AI more than 0.1 and those with AI equal to 0.1 or less than 0.1 were classified as CCD-positive and CCD-negative, respectively.

Results

Complete coverage of the posterior fossa was acquired in CT perfusion study in all patients. A total of 17 of 24 patients were identified to demonstrate asymmetrical cerebellar blood flow. In the remaining seven patients, CCD was negative at both CBF and CBV maps. Among the 17 CCD-positive patients at CBF maps, AI was 0.151 ± 0.034. Asymmetrical cerebellar blood volume was demonstrated in 10 patients. Among the 10 CCD-positive patients at CBV maps, AI was 0.154 ± 0.036.

Conclusion

Our results suggest that both CBF and CBV maps can evaluate CCD induced by acute MCA infarction. Cerebral blood flow maps are more sensitive than CBV maps for the detection of CCD. CT perfusion using 320-detector row CT is helpful in identifying CCD.

KEYWORDS: 320 detector row, Crossed cerebellar diaschisis, cerebral infarction

P-61

MR-Based Oxygen Extraction Fraction Using Spatial Independent Component Analysis of Breath-Hold PARSE Acquisitions

Cantrell, C. G.·Menon, R. G.·Vakil, P.·Johnathan, S.·Carroll, T. J.
Northwestern University
Chicago, IL.

Purpose

Cerebral oxygen extraction fraction (OEF) has been shown to be an independent predictor of stroke risk. Increased hemispheric OEF was linked to poor long-term outcomes. We have developed a means of quantifying OEF with MRI using PARSE. Observation of OEF alteration under mild physiologic stress induced by breath-holding reflects cerebrovascular reserve which may provide complimentary information on collateralization, and correlate with favorable outcome to revascularization therapy. We present an analysis of breath-hold MR OEF images using spatial independent component analysis (sICA). Traditionally, ICA analysis is performed in the time domain and component selection is motivated by anatomical landmarking and often manual selection, and the associated biases. We present here a sICA analysis of raw free-induction decay signals, which is completely independent of the normal bias associated with anatomical landmarking.

Materials & Methods

PARSE acquisitions acquired a 2D k-space volume using a well described rosette trajectory in 65 ms. By acquiring 20 PARSE datasets (1/5 seconds) and inducing a short 15 second breathhold we are able to observe frequency shifts (δω) resulting from increased deoxyhemoglobin in the draining veins of the head, similar to BOLD contrast. These 4-10 Hz shifts are denoised using sICA with spatial coordinates defined as the length along the PARSE readout and temporal domain being the 20 time points separated by ΔT=5 s. Spatial ICA uses blind-source separation to extract time courses, which correspond to bulk signal enhancement associated with the breath hold. Only the time courses that showed an enhancement of greater than 20% during breath hold were used to reconstruct the denoised free-induction decay signal; allowing us to create a signal containing only the dynamic components affected by the induced stress.

Results

Figure 1 shows a comparison between 20 consecutive MR OEF images created before and after sICA analysis. Though little can be deduced from the time course created before denoising, the sICA images clearly show a frontal shift in OEF during the period of induced stress followed by a return to the baseline after the stress is removed.

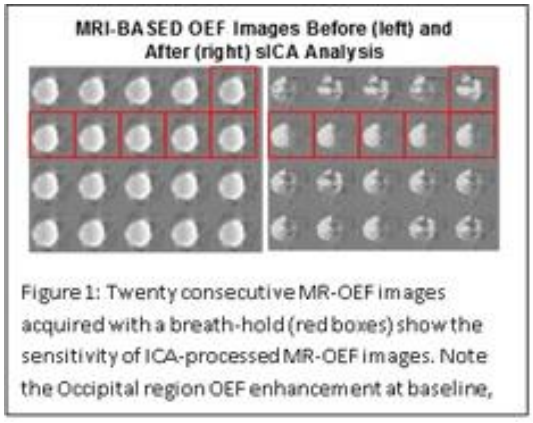

Figure 1: Twenty consecutive MR-OEF images acquired with a breath-hold (red boxes) show the sensitivity of ICA-processed MR-OEF images. Note the Occipital region OEF enhancement at baseline,

Conclusion

We have found that MR PARSE has high sensitivity to frequency shifts induced by transient alterations in deoxyhemoglobin. The use of ICA to extract and quantify cerebrovascular reactivity represents a new simple, noncontrast approach to stratifying patients toward therapies to prevent stroke.

Acknowledgements: NIH/NIBIB T32 EB005170, NIH/NHLBI R01 HL088437.

KEYWORDS: Oxygen, Brain and stroke

Note: Scanned images are included in the proceedings. Some submitted images were reduced during editing, thereby decreasing clarity. Also, refer to the Program Planner. Proceedings Content as of 3-29-2013.

P-62

Comparison of CT and MR Imaging ASPECTS Score in Acute Ischemic Stroke

Nguyen, T.·Culbertson, C. J.·Lau, H.·Masoud, H.·Romero, R. J.·Norbash, A. M.·Mian, A.
Boston Medical Center
Boston, MA.

Purpose
Acute ischemic stroke (AIS) patients with small area of infarction by imaging, but severe clinical deficits are potential candidates for endovascular treatment. However, brain CT may not be as accurate as MRI in determining the area of core infarction. We aimed to compare brain CT and MRI-defined area of core infarct in patients who were candidates for acute stroke intervention, based on calculation of ASPECTS scores.
Materials & Methods
Patients with AIS between August 2007 to July 2012 were reviewed retrospectively. Inclusion criteria were AIS with NIHSS $\geq$ 8 and brain CT/MRI performed within four hours of symptom onset. A neuroradiologist (AM) and vascular neurologist (TN) independently rated 71 CT and MRI ASPECTS scores on two separate occasions. Discrepancy was defined as frequency of mismatch of ASPECTS score dichotomized as <7 versus $\geq$7.
Results
Eight hundred sixty-six AIS patients presented during the study period. Five hundred twenty-one were excluded due to NIHSS <8. Two hundred sixty-seven patients did not have brain imaging within four hours, and seven were excluded due to infarctions in multiple cerebral arterial territories, yielding 71 patients eligible for the study. Of the 71 patients [39 women, mean age (+/- SD) 69 years $\pm$ 4 years] mean NIHSS was 15 $\pm$ 1. A large vessel occlusion (LVO) was present in 52%. Interval between CT and MRI was 90 minutes (n = 25 patients), three hours (n = 61 patients), and four hours (n = 71). Inter-rater observer agreement for ASPECTS score $\geq$ 7 and <7 showed good reliability for CT (k = 0.62) and MRI (k = 0.67). CT MRI discrepancy was associated with presence of LVO ($p<0.003$), but not associated with age, time delay between imaging studies, or time from symptom onset. Among patients with LVO, concordant frequency for good CT and MRI ASPECTS score ($\geq$7) was 56% for the neuroradiologist rater, and 51% for the neurologist rater.
Conclusion
In a subset of patients with acute ischemic stroke, discrepancy between CT and MRI-based ASPECTS score was seen in nearly half of the cases, and more frequent in the presence of large vessel occlusion.

KEYWORDS: ASPECTS, Stroke, comparison

P-63

Pooled Assessment of Computed Tomography Interpretation in the STRokE DOC Telestroke Network: Agreement between Spoke Radiologist, Hub Vascular Neurologist, and Central Read

Spokoyny, I.[1]·Raman, R.[1]·Ernstrom, K.[1]·Demaerschalk, B. M.[2]·Lyden, P. D.[3]·Hemmen, T. M.[1]·Guzik, A. K.[1]·Chen, J. Y.[1,4]·Meyer, B. C.[1]
[1]University of California San Diego, San Diego, CA, [2]Mayo Clinic, Phoenix, AZ, [3]Cedars Sinai Medical Center, Los Angeles, CA, [4]San Diego VA Medical Center, San Diego, CA.

Purpose
The American Stroke Association guidelines emphasize the need for high-quality studies assessing agreement of radiologists and nonradiologists engaged in emergency telestroke decision-making. The objective of this pooled analysis is to determine the level of agreement between central read and each of two groups (spoke hospital radiologists and hub hospital vascular neurologists/tele-strokologists), in interpreting brain CT scans of patients presenting to telestroke hospitals with acute stroke.
Materials & Methods
The Stroke Team Remote Evaluation Using a Digital Observation Camera (STRokE DOC and STRokE DOC-AZ TIME) trials were prospective, randomized, outcome-blinded trials comparing audiovisual telemedicine with teleradiology stroke evaluations to telephone-only consultations. These two trials assessed eligibility for IV rt-PA and correctness of decision-making for two hubs and six spokes. In each trial, the subjects' CT scans were interpreted by the hub tele-strokologist in the telemedicine arm, and by the spoke radiologist in the telephone arm. In this analysis, a central read was performed for each trial by adjudicating committees blinded to treatment arm and outcome. The data were pooled and results reported for the entire population. Baseline characteristics were compared between hub sites. Kappa statistics and exact percent agreement rates were used to assess interobserver agreement for acute-stroke-related radiographic issues such as contraindication to rt-PA, presence of ICH, SAH, SDH, tumor, hyperdense artery, acute stroke and normal scan.
Results
Two hundred sixty-one subjects who underwent assignment to telemedicine or telephone and had CT reads completed were analyzed. The overall agreement for presence of radiologic contraindications to thrombolysis was excellent (95.4%, κ = 0.74, 95%CI 0.59-0.88) and was slightly higher for hub tele-strokologist (96.2%, κ=0.81, 95%CI 0.64-0.97) than for spoke radiologist (94.7%, κ=.64, 95%CI 0.39-0.88) when each was compared to central read. When excluding patients in whom the degree of early ischemic changes was the reason for potential radiographic contraindication to rt-PA, the agreement was even stronger (98.3%), with 100% tele-strokologist agreement with central read. For the rt-PA treated subset

Note: Scanned images are included in the proceedings. Some submitted images were reduced during editing, thereby decreasing clarity. Also, refer to the Program Planner. Proceedings Content as of 3-29-2013.

(N=65), overall agreement was 98.5%, and tele-strokologist agreement with central read again reached 100%. Secondary outcomes included agreement on presence of: normal scan (74.6%, 77.1%), acute stroke (74.6%, 77.9%), intracerebral hemorrhage (99.2%, 98.5%), subarachnoid hemorrhage (98.5%, 96.9%), subdural hematoma (100%, 100%), tumor (100%, 97.7%), and hyperdense artery (93.8%, 88.5%) for hub tele-strokologist and spoke radiologist respectively, versus central read.
Conclusion
In the context of a combined telestroke network designed to assess patients with acute stroke syndromes, this pooled analysis found that both tele-strokologists and spoke radiologists had excellent central agreement in identifying radiologic contraindication to rt-PA treatment. The agreement was slightly higher for tele-strokologists. This effect also was seen in the rt-PA treated subset. When excluding those CT scans with more significant degree of early ischemic changes (where rt-PA treatment is potentially controversial even amongst experts), the agreement between tele-strokologists and central read was perfect. These pooled findings demonstrate, in a larger sample size, that tele-strokologists are effectively able to interpret brain CT scans for the purpose of determining appropriateness of rt-PA administration in the setting of acute stroke.

KEYWORDS: Acute stroke, CT and stroke, telemedicine

P-64

Regionally Specific Cortical Thickness Differences in Acute Stroke

Young, B. M.·Nair, V. A.·La, C.·Gupta, J.·Dabbs, K.·Reiter, P.·Nadkarni, T.·Chacon, M.·Jensen, M. B.·Sattin, J.·Prabhakaran, V.
University of Wisconsin Madison
Madison, WI.

Purpose
Cortical thickness changes after stroke are not well documented with little known about associations between cortical thickness and behavioral performance in the acute stage. Given the relationship between cortical thickness and cognitive performance in healthy aging and disease populations (e.g., multiple sclerosis), we examined if a similar relationship exists in acute stroke.
Materials & Methods
Twenty patients with acute ischemic stroke were scanned within seven days of stroke onset on a General Electric 3T MRI scanner. High-resolution whole brain 3D T1-weighted BRAVO FSPGR 1mm isotropic images were collected and then processed with Freesurfer version 5.1.0. Eleven acute stroke patients' (average age = 63 years, seven M, seven cortical stroke) data were further analyzed after inspection for correct cortical surface reconstruction. Age-matched healthy controls (n = 15, average age = 57 years, six M) were scanned with the same parameters. We looked for differences in the correlation between cortical thickness and letter fluency performance, controlling for age. Letter fluency (word generation) measures were collected outside the scanner and corrected for age and education.
Results
There was a significant difference in the correlation between cortical thickness and age ($p<0.01$, uncorrected), with patients showing more thinning in the rostral middle frontal region. Analyses investigating cortical thickness-verbal fluency correlations identified the left inferior temporal region as correlated with performance with significant differences ($p<.003$, uncorrected) between patients (average thickness = 2.6 mm) and normals (= 2.9 mm). Cortical thinning was associated with poorer performance and also seen in patients in the right insular ($p<.003$, uncorrected) regions.
Conclusion
Cortical thinning changes that have occurred over chronic time periods have been associated with cognitive performance in other disease populations. These results suggest that regional cortical thinning changes can be seen even in the acute time period after a stroke and may be predictors of cognitive performance.

KEYWORDS: Cortical thickness, Acute stroke

P-65

Value of the 3D Arterial Spin Labeling MR Imaging for Evaluating the Cerebral Perfusion in Patients with Cerebrovascular Stenosis: A Comparative Study with 123I-Iodoamphetamine Single Photon Emission CT

Furukawa, M.·Iida, E.·Matsunaga, N.
Yamaguchi University
Ube, JAPAN.

Purpose
Arterial spin labeling (ASL) MR imaging is an emerging technique for noninvasive measurement of cerebral perfusion. 3D-gradient and spin-echo (GRASE) ASL can produce higher signal-to-noise ratio perfusion images with a high spatial resolution compared with 2D-multislice echo-planar imaging. The purpose of this study is to investigate the value of 3D ASL MR imaging for cerebral blood flow (CBF) assessment in patients with cerebrovascular stenosis.
Materials & Methods
Forty-three patients with unilateral or bilateral cerebrovascular stenosis underwent CBF evaluation by 3D ASL and 123I-iodoamphetamine (IMP) SPECT within a mean interval of four days (range: 0-30 days). All patients had no history of vascular surgery such as CEA or CAS, and did not have a major cortical infarction in the internal carotid artery (ICA) territory on conventional MR imaging. 3D-GRASE ASL was performed on a 3T MR unit with following parameters ((FOV 256 mm, matrix 64 x 64, 32 slices, TR/TE/TI 5,000/16/1,800 msec, FA 180 degree). Quantitative CBF and cerebrovascular reserve (CVR)

Note: Scanned images are included in the proceedings. Some submitted images were reduced during editing, thereby decreasing clarity. Also, refer to the Program Planner. Proceedings Content as of 3-29-2013.

measurement by 123I-IMP-SPECT with a dual table autoradiography method was used as a standard reference. Side-by-side difference on 3D ASL MR imaging was evaluated visually by two radiologists, and those were compared with the SPECT findings for the MCA territory.
Results
Among total 43 patients, 26 patients had unilateral ICA or middle cerebral artery (MCA) stenosis, and the remaining 17 patients had bilateral stenosis on MR angiography. On rest SPECT scans, 20 patients showed >10% CBF difference between bilateral MCA territory, and 29 patients showed >5% CBF difference. On 3D ASL, 36 patients showed visual CBF difference between bilateral MCA territory. When a cut-off value of 10% was used on 123I-IMP-SPECT, the sensitivity, specificity, and diagnostic accuracy of 3D ASL were 90%, 21.7%, and 53.5%, respectively. When a cut-off value of 5% was used, the sensitivity, specificity, and diagnostic accuracy of 3D ASL were 86.2%, 21.4%, and 65.1%, respectively. Among 23 patients whose CBF difference was less than 10% on rest 123I-IMP-SPECT, 18 patients showed a side-by-side difference on 3D ASL, and 10 patients in those 18 patients (55.6%) showed >10% CBF difference on acetazolamide challenge 123I-IMP-SPECT.
Conclusion
Although 3D ASL MR imaging showed a low specificity, that might include the potentials for predicting the CVR. Three-dimensional ASL MR imaging is clinically applicable, especially as a noninvasive screening examination.

KEYWORDS: Arterial spin labeling, Cerebrovascular disease, SPECT

P-66

Uniform Extent and Degree of Cerebral Ischemia after Middle Cererbral Artery Occlusion in Rats: Use of Prospective 4.7T Diffusion MR Imaging

Yi, K.[1]·Cha, S.[1]·Lee, S.[1]·Lee, C.[2]·Lee, S.[3]
[1]Chungbuk National University Hospital, Cheongju, KOREA, REPUBLIC OF, [2]Korea Basic Science Institute, Cheonwon, KOREA, REPUBLIC OF, [3]Korea Research Institute of Bioscience and Biotechnology, Cheongwon, KOREA, REPUBLIC OF.

Purpose
For the translational research to evaluate therapeutic potential of any agent, there should be rat models with cerebral ischemia/infarction of very similar characteristics. And yet previous reports revealed middle cerebral artery occlusion (MCAO) models in rats presented very diverse results of cerebral infarction with the use of either sutures or macrospheres. This experimental study was to produce brain infarctions with uniform extent and level of ischemic damage after MCAO in rats.
Materials & Methods
A total of 19 rats were subject to left MCAO using the suture technique. Immediately after occlusion, the animals were transferred into an MRI scanner (4.7T) and diffusion-weighted imaging (DWI) of axial and coronal planes was repeated every 10 minutes to postocclusion 125 minutes (11 times). Every first MR imaging was started 15 minutes after stroke onset. Immediately after each DWI, the apparent diffusion coefficient (ADC) values were determined in the ischemic lesions and compared to the unaffected contralateral hemisphere. Successful MCAO was defined when the whole left MCA territory showed ADC abnormality on the first postocclusion DWI at 15 minutes.
Results
Territorial infarction was induced successfully in nine rats (9/19, 47.4%), and MCAOs in 10 rats were classified as failure. On initial postocclusion MR imaging at 15 minutes, the ADC values of the affected lesions were significantly lower than those of contralateral hemispheres (mean relative ADC value=0.77 ± 0.06), and remained stable in seven rats; however in two rats the ADC values decreased and reached lowest plateau in 45 and 55 minutes, respectively. Thus seven out of 19 MCAO cases had brain infarctions with very similar MR characteristics of lesion extent and temporal evolution of ADC abnormality.

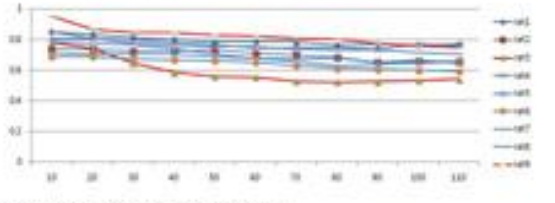

Fig 1. Temporal changes of relative ADC values.
In the ischemic lesions after left MCAO in nine cases, initially defined as successful, relative ADC values of the two showed different pattern of temporal evolution (red line) comparing to the those of the remaining seven (blue line).

Conclusion
Applying prospective diffusion MRI and judging the success of modeling very early on after MCAO, we could exclude any inhomogeneity of brain infarctions and produce uniform extent and level of ischemic damage in rats. This technique would make it possible to obtain homogenous group of murine stroke models for the translational research.

KEYWORDS: Actue stroke, MR imaging/diffusion, rat

P-67

Institution of Dedicated Acute Stroke Protocol Helped in Achieving Target Door-to-CT Time and Thereby Faster Delivery of Thrombolytic Therapy

Strathearn, L.·Simpkin, W.·Phillips, S.·Shankar, J.
QE II Hospital
Halifax, NS, CANADA.

Purpose
Benefit of thrombolytic therapy for acute ischemic stroke is time dependent - earlier the better. Outcome of thrombolytic therapy depends on size of baseline infarct.

Note: Scanned images are included in the proceedings. Some submitted images were reduced during editing, thereby decreasing clarity. Also, refer to the Program Planner. Proceedings Content as of 3-29-2013.

Optimal outcomes can be accomplished by rapid assessment of salvagable brain - penumbra and early treatment. Institution of proper Acute Stroke Protocol (ASP) helps expedite the whole process of imaging and therapy. We designed an Acute Stroke Protocol to facilitate this in eligible patients. The target Door-to-CT time was kept at 25 minutes. We assessed Door-to-CT time in our institution and its effect on patient's management and compared this before and after the institution of the Acute Stroke Protocol.
Materials & Methods
In November 2011, a group of health professionals designed an algorithm to standardize and expedite early imaging and management of patients who access Emergency Health Service for suspected acute ischemic stroke. Imaging paradigm included plain CT head, CT perfusion and CT angiogram of head as opposed to only plain CT head before Acute Stroke Protocol. A series of training lectures were organized for CT technologists and radiology residents on Acute Stroke Protocol imaging protocol. A database was prospectively collected to track outcomes. The Acute Stroke Protocol was launched on April 1, 2012. Door-to-CT and Door-to-Needle time were assessed as parameter for smooth and successful functioning of our Acute Stroke Protocol. Two sample t tests and ANOVA are used to compare these parameters before and after the institution of the Acute Stroke Protocol. p value less than 0.05 was considered significant.
Results
In first quartile of operation, 16 patients received thrombolytic therapy within significantly shorter Door-to-Needle time (p = 0.005; median-75 minutes) after arrival in the Emergency Department. Mean Door-to-CT time (24 minutes) was significantly shorter (p = 0.013) than that in previous nine months before ASP.
Conclusion
In Acute Stroke Protocol, added imaging provided better assessment of penumbra within significantly shorter Door-to-CT time. Proper education and awareness for technologists was critical in exceeding our goal of 25 minutes in the very first quartile. This resulted in better patient care. Regular auditing is important in smooth functioning of Acute Stroke Protocol.

KEYWORDS: Acute ischemic stroke, CT perfusion, acute stroke protocol

P-68

Post-Traumatic Focal Cortical Encephalomalacia Predicted by Focal Cortical Diffusion Abnormalities on Acute MR Imaging

Butman, J. A.[1]·Pham, D. L.[2]·Magrath, E.[2]·Latour, L. L.[3]
[1]The Clinical Center of the NIH, Bethesda, MD, [2]Center for Neuroscience and Regenerative Medicine, Bethesda, MD, [3]National Institute of Neurological Disorders and Stroke, Bethesda, MD.

Purpose
To demonstrate that post-traumatic focal cortical encephalomalacia (FCE) identified on MRI 1-3 m following mild to moderate TBI is preceded by anatomically correlated sites of focal cortical diffusion abnormality (FCDA) on acute MRI obtained within 48 hours of the TBI.
Materials & Methods
Patients (n = 38) with head injury presenting to the Trauma/ED were enrolled in the Center for Neuroscience and Regenerative Medicine Traumatic Head Injury Neurioimaging Classification (THINC) study. MR imaging was obtained within 48 hours of injury and at 1-3 month followup. MR imaging included a 3D T1 IR SPGR (~ 1 mm isotropic), and isotropic trace diffusion-weighted images (isoDWI), computed from 15 direction b=1000 DTI obtained at 3.5 mm slice thickness. First, follow-up 3D T1 images were reviewed to identify focal cortical encephalomalacia (FCE). Next, the acute isoDWI were evaluated for sites of hyperintensity involving the cortical gray matter. Finally, the cases of discordance between the two interpretations were reviewed with all imaging data available to understand the basis for the discordance.
Results
A total of 18 sites of FCE were identified on the follow-up 3D T1 in five patients. Focal cortical encephalomalacia was characterized by complete loss of the ribbon of cortical gray matter such that white matter was “exposed” to CSF at 17/18 sites. One site demonstrated cortical thinning. In the five patients with FCE, the acute MRI demonstrated corresponding sites of FCDA(Figure). In two patients, FCDA was present acutely, but no FCE was identified on the follow-up MRI, even in retrospect. No patients with FCE on the follow-up scan had a normal acute isoDWI. In 24 patients, no FCE or FCDA was identified. Thus, FCE was highly associated with FCDA (P=0.00012, Fisher’s exact test).

Note: Scanned images are included in the proceedings. Some submitted images were reduced during editing, thereby decreasing clarity. Also, refer to the Program Planner. Proceedings Content as of 3-29-2013.

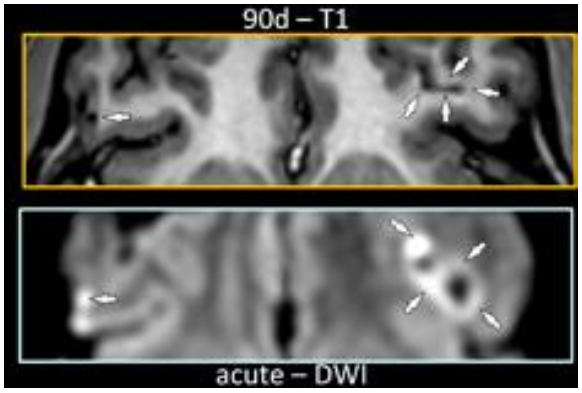

Conclusion
Much attention has been directed towards the white matter injuries that result from TBI as well as to global/quantitative measures of atrophy. Here we identify focal cortical gray matter encephalomalacia as a relatively common consequence of mild to moderate TBI. In most cases, the presence of FCDA developed into sites of FCE, whereas no FCE developed when FCDA was initially absent. In a manner analogous to the evolution of ischemic stroke, FCDA represents cytotoxic edema which can be identified readily by acute diffusion-weighted MRI, and, as in stroke, evolves to encephalomalacia. Thus, FCDA may represent gray matter "at risk" and represent a salvageable target for therapeutic intervention, motivating the use of MRI in the acute TBI setting.

KEYWORDS: Diffusion-weighted imaging, Cortical thickness

P-69

Cervical Arterial Dissection: Presentation, Treatment and Outcome over a 5-Year Period at a Level I Trauma Center

Bagga, S.·Pastel, D. A.
Dartmouth Hitchcock Medical Center
Lebanon, NH, NH.

Purpose
Arterial dissections of the extracranial carotid and vertebral arteries occurs when a small tear forms in the innermost lining of the arterial wall. Blood enters the space between the inner and outer layers of the vessel, causing stenosis, complete occlusion or pseudoaneurym formation. Dissections, which are either traumatic or spontaneous in origin, are recognized as an underdiagnosed but serious cause of morbidity. With the increasing use of noninvasive imaging, including magnetic resonance and computed tomography angiography, the diagnosis of vascular dissection has increased in frequency. The combined incidence of both vertebral artery dissection (VAD) and carotid artery dissection (CAD) is estimated to be 2.6 per 100,000. Among all extracranial cervical artery dissections, CAD is 3-5 times more common than VAD.The incidence of carotid artery dissection as a result of blunt injuries (mainly high-speed motor vehicle accidents) ranges from less than 1% to 3%.The goal of identifying arterial dissections is to prevent cerebral infarctions. Management options include observation, medical therapy and endovascular intervention. Challenges remain, as no clear cut evidence-based guidelines exist about treatment and followup of these patients. The purpose of this retrospective study is to better understand the presentation, treatment and outcome in patients diagnosed with arterial neck dissections at a level I trauma center over a five-year period.
Materials & Methods
The RIS database will searched using keyword "Dissection" on all CTAs and MRAs performed for trauma between January 2006 and January 2011. Followup for all patients will be at least one year. The following data information will be collected through the electronic medical record system: location and severity of dissection (six), clinical or imaging evidence of for acute infarctions, findings on subsequent vascular neck imaging studies, and any medical or invasive treatments received for the vascular injury. The data will be de-identified as it is collected and a unique, encrypted study ID will be assigned to each case. Subgroup analysis of the treated vs. nontreated groups will be performed.
Results
Neuroimaging is helping in early diagnosis and treatment of cervical arterial dissections.
Conclusion
Our study will report the presentation, management, and outcome of patients with cervical arterial dissections and possibly identify features and treatments that predict favorable outcome.

KEYWORDS: Arterial dissection, CT angiogram, CT, MRA CARIT, vertabral artery dissecton

P-70

High-Resolution MR Characteristics of Reversible Cerebral Vasoconstriction Syndrome

Obusez, E. C.·Cerejo, R.·Hajj-ali, R.·Hui, F.·Jones, S.
Cleveland Clinic Foundation
Cleveland, OH.

Purpose
High-resolution 3T MR imaging and MR angiography (HRMR) is an emerging tool for evaluating intracranial arterial disease. Diagnostic imaging considerations for reversible cerebral vasoconstriction syndrome (RCVS) traditionally include imaging of cerebral vessels with catheter angiography, CT or MR angiography, which focus on the arterial lumen. Other work demonstrates the advantage of HRMR in providing additional information about the arterial wall. However, followup of RCVS with HRMR has not been studied. The aim of this study was to determine HRMR vessel wall characteristics of RCVS during followup.

Note: Scanned images are included in the proceedings. Some submitted images were reduced during editing, thereby decreasing clarity. Also, refer to the Program Planner. Proceedings Content as of 3-29-2013.

Materials & Methods

All patients at our institution with a diagnosis of RCVS that underwent HRMR were identified and retrospectively studied. High-resolution vessel wall imaging protocol included black-blood contrast-enhanced T1-weighted sequence with fat suppression and time-of-flight MRA of the circle of Willis. Clinical and demographic data and vessel wall characteristics including enhancement, wall thickening, and lumen narrowing, were collected.

Results

Thirteen patients with a mean age of 44.2 years were diagnosed with RCVS and underwent HRMR. Vessel wall findings during initial imaging included four patients with mild uniform wall thickening and enhancement, six patients with nonenhancing uniform wall thickening, two patients with no abnormality and one patient with only narrowing. All patients had clinical followup. Nine patients had follow-up imaging with median follow-up imaging period of two months of which eight showed improved imaging findings.

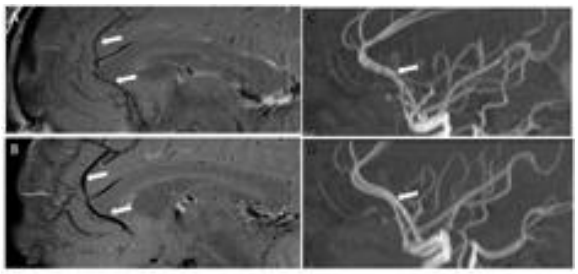

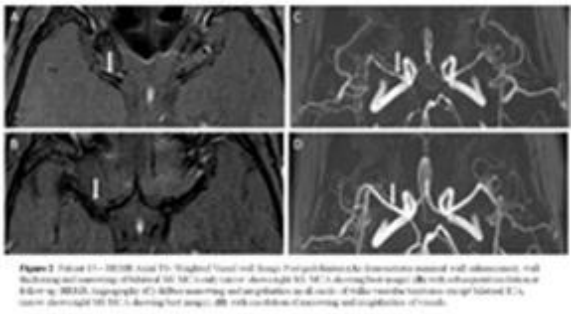

Conclusion

HRMR shows that uniform vessel wall thickening and luminal narrowing without or with mild enhancement are characteristics of RCVS.

Table: Follow-Up HRMR Vessel Wall Imaging Characteristics

		1st HRMR (MRI and MRA)					2nd HRMR (MRI and MRA)			
Follow Up	Vessel	Enhancement	Thickening	Narrowing	MRA	Treatment	Enhancement	Thickening	Narrowing	MRA
2	Bilateral M1	No	Yes	Yes	Normal	Verapamil	No	No	No	Normal
1	Bilateral M1, A2, A3	Minimal	Yes	Yes	Irregularity Bilateral A2, A3	Steroids, Verapamil	No	No	No	Improved Irregularity A2, A3
NA	None	No	No	No	Normal	Verapamil	NA	NA	NA	NA
NA	Bilateral ACA, MCA, PCA	Minimal	Yes	Yes	Irregularity Bilateral MCA, PCA	Steroids, Verapamil	NA	NA	NA	NA
0.5	Bilateral A2, A3, Right P1	No	Yes	Yes	Irregularity Bilateral Clinoid ICA	Verapamil	No	No	No	Normal
4	Bilateral A1, M1, P1	Minimal	Yes	Yes	Irregularity, Narrowing Bilateral A1, M1, P1	Verapamil	Minimal	Yes	No	Subtle Left M1 Narrowing
2	Bilateral A1, A2, Left P1	No	Yes	Yes	Irregularity Bilateral A1, A2, Left P1	Verapamil	No	No	No	Normal
2	Left A1, M3	No	Yes	Yes	Stenosis, Narrowing Left M3	Verapamil	No	Yes	Yes	Normal
7	Bilateral M1, Left A2	No	Yes	Yes	Narrowing Left A2	Steroids	No	No	No	Normal
NA	Right M1	No	No	Yes	Narrowing Right M1	Nimodipine , Verapamil	NA	NA	NA	NA
0	Bilateral M1	No	Yes	Yes	Normal	Nimodipine , Verapamil,	No	No	No	Normal
NA	None	No	No	No	Normal	Verapamil	NA	NA	NA	NA
3	Bilateral ACA, MCA, PCA, ICA Terminus	Minimal	Yes	Yes	Narrowing, Irregularity Bilateral ACA, MCA, PCA, ICA Terminus	Steroids, Verapamil	No	No	No	Normal

KEYWORDS: 3 T, Reversible cerebral vasoconstriction, high-resolution MR imaging

P-71

Evaluation of Gadobenate Dimeglumine for Contrast-Enhanced MR Angiography

Pirovano, G.[1]·Kirchin, M.[2]·Parker, J. R.[1]
[1]Bracco Diagnostics Inc., Monroe, NJ, [2]Bracco Imaging, Milan, ITALY.

Purpose

Gadobenate dimeglumine is a higher relaxivity paramagnetic MR contrast agent currently approved in 48 countries for MRI of the brain and spine at an iv dose of 0.1 mmol/kg bodyweight and in certain countries for liver imaging at a dose of 0.05-0.1 mmol/kg. In the United States, this agent also is approved for magnetic resonance angiography (CE MRA) in adult patients with known or suspected renal or aorto-ilio-femoral occlusive vascular disease at a dose of 0.1 mmol/kg. As part of the registration of this agent with the US FDA, we identified and summarized published clinical studies on the use of this agent for contrast-enhanced magnetic resonance angiography (CE MRA).

Materials & Methods

We performed a Medline search using the terms “Multihance OR gadobenate dimeglumine or BOPTA” AND “magnetic resonance angiography or MRA”. Initially 168 citations were identified. After review to eliminate abstracts, animal studies, reviews, technical reports, and papers without original data, 96 original clinical publications were identified. These 96 papers were tabulated, evaluated and summarized.

Results

Publications reported on dosing of gadobenate dimeglumine, scanning optimization, comparisons with unenhanced MRA or carotid DSA, and comparisons with other gadolinium agents. In addition to the supraaortic arteries, represented by 21 published studies, all other major vascular territories were represented in the literature (peripheral = 22, abdominal = 17, thoracic or pulmonary = 9, whole body MRA = 8, coronary = 7, liver = 4, upper extremities = 4, multiple territories = 4). Most

Note: Scanned images are included in the proceedings. Some submitted images were reduced during editing, thereby decreasing clarity. Also, refer to the Program Planner. Proceedings Content as of 3-29-2013.

neuroradiology studies used a dose of 0.1 mmol/kg bodyweight, although higher doses were sometimes reported in coronary, whole body, or peripheral MRA studies. Twenty-two studies reported comparative data. Most were intra-individual crossover studies in which each patient received gadobenate dimeglumine and another gadolinium agent in two separate exams. The comparators were gadopentetate dimeglumine (nine studies), gadofosveset (four studies), gadobutrol (three studies), gadoterate meglumine (three studies), and gadodiamide (two studies). In one study gadobenate dimeglumine was compared to both gadopentetate dimeglumine and gadobutrol. Typically, comparative studies reported better enhancement with gadobenate dimeglumine versus the comparator agent, despite the fact that in several studies a higher dose of comparator agent was given. No differences in safety were evident in any of the published papers with the other gadolinium agents.
Conclusion
Published clinical studies support the safe and effective use of gadobenate dimeglumine at a dose of 0.1 mmol/kg for CE MRA of supra-aortic vessels as well as a number of "below the heart" applications. Comparative trials suggest gadobenate dimeglumine may be administered at a lower dose that conventional ECF agents for CE MRA as a result of its higher relaxivity.

KEYWORDS: 3D angiography, Arteriography

Monday, May 20 – Wednesday, May 22
6:30 AM – 9:00 PM
Thursday, May 23
6:30 AM – 3:00 PM
Hall B1

Scientific Posters Printed 72 - 77

P2-Anatomy

Note: A missing printed number indicates an abstract has been withdrawn.

P-72

Aqueduct of Sylvius: 3T MR Imaging Morphology and Morphometry with Neuroendoscopic Relevance

Matys, T.[1]·Horsburgh, A.[1]·Kirollos, R. W.[1]·Antoun, N.[1]·Massoud, T. F.[2]
[1]Addenbrooke's Hospital, Cambridge, UNITED KINGDOM, [2]University of Cambridge, Cambridge, UNITED KINGDOM.

Purpose
Neuroendoscopic aqueductoplasty with optional stent placement is a therapeutic consideration for hydrocephalus due to a membranous or short segment stenosis of the aqueduct of Sylvius (AqSylv), as well as for decompression of an isolated fourth ventricle. The procedure can be performed through a transfrontal approach passing through foramen of Monro and the third ventricle, or a suboccipital trans-foramen magnum fourth ventricular approach. The few studies to date investigating the normal dimensions and contour of the AqSylv, which would be highly relevant to the above procedures, have been performed on cadavers or fresh-frozen specimens prone to shrinkage errors and distortion of normal anatomy. The aim of this study was to obtain precise in vivo morphometry of the normal AqSylv using high-resolution 3T MR images.
Materials & Methods
We retrospectively analyzed magnified midsagittal T1-weighted 3T MR images of 100 patients with normal brain imaging findings, aged 13-83 years (45 men and 55 women). We measured widths of the AqSylv pars anterior, ampulla, pars posterior, narrowest point, and its length. We recorded angulation of AqSylv relative to the intercommissural AC-PC line, angulation between the caudad and rostral part of the AqSylv, and its angulation relative to the fourth ventricle. We statistically determined age- and sex-related changes in AqSylv morphometry.
Results
Mean morphometric parameters of the AqSylv were as follows: width of the pars anterior 1.1 mm, ampulla 1.2 mm, pars posterior 1.4 mm, length 14.1 mm, narrowest point 0.9 mm. The entry into the AqSylv from the third ventricle was at a mean 26° angle to the AC-PC line. AqSylv then followed a gentle curve concave ventrally so that its caudad part was at a mean 32° angle to the rostral segment. The caudad segment was at a mean 18° angle to the forth ventricular floor. Diameters of the ampulla and pars posterior were slightly larger in males, but the other measurements were comparable between sexes. The widths generally correlated positively, and length correlated negatively with Evans' index (a surrogate marker for ventricular volume) and age; therefore, with increasing age and enlargement of the ventricular system, the AqSylv widens and shortens. However, AqSylv maintained its angles with age. There was a negative correlation between the AqSylv widths and length (apart from width of pars posterior), so that wider aqueducts also were shorter, and tended to be more curved. There was a

Note: Scanned images are included in the proceedings. Some submitted images were reduced during editing, thereby decreasing clarity. Also, refer to the Program Planner. Proceedings Content as of 3-29-2013.

strong negative correlation between the rostral-caudad angle of AqSylv and angles of entry from the third or fourth ventricle, so that a steeper entry into the AqSylv from either ventricle is associated with less curvature along its course.

Conclusion

We present the first normative MRI dimensions of AqSylv obtained in vivo which, importantly, are at variance with published cadaveric morphometrics. We also present age- and sex-related changes in AqSylv size and curvature, and internal correlations between morphometric size parameters. Reported data are valuable in guiding neuroendoscopic management of hydrocephalus and aqueductal stenosis. Awareness of these normal morphometrics also is highly useful when stent placement is an option during aqueductoplasty.

KEYWORDS: Anatomy, Morphometry, aqueduct, aqueductal stenosis, neuroendoscopy

P-73

Foramina of Monro: A New Look at 3D Spatial Configuration Based on Multiplanar 3T MR Imaging Morphometry Relevant to Neuroendoscopy

Matys, T.[1]·Horsburgh, A.[1]·Kirollos, R. W.[1]·Antoun, N.[1]·Massoud, T. F.[2]
[1]Addenbrooke's Hospital, Cambridge, UNITED KINGDOM, [2]University of Cambridge, Cambridge, UNITED KINGDOM.

Purpose

Connections between lateral and third ventricles have been confusingly characterized as either one or two foramina of Monro (FoM), and described as either Y-shaped, or T-shaped. This inconsistency is perpetuated on routine neuroimaging because standard orthogonal MRI projections do not match true anatomical spatial configurations of FoM, thus depicting them in a foreshortened or distorted manner. Knowledge of the precise 3D configuration of FoM has important implications for neuroendoscopic practice of traversing FoM (e.g., when creating third ventriculostomy). We therefore studied normal 3T MRI morphometry of FoM to establish detailed differences in shape and size on standard orthogonal imaging planes versus more representative features on 3D imaging in their true anatomical spatial orientation.

Materials & Methods

We first retrospectively reviewed standard 2D coronal T1-weighted images in 100 normal patients obtained on 3T MRI, and measured FoM minimal width, angle between the right and left FoM, their separation (fornix width), and length. We established the angle at which coronal images were acquired in relation to the intercommissural (AC-PC) line. We then repeated measurements on retrospective 3D FSPGR datasets from 50 separate patients (see Table). Measurements on these images were performed twice, in the plane replicating the standard coronal 2D plane, and also in the true anatomical plane of FoM obtained by 3D image manipulation of the coronal plane along a transverse line traversing FoM.

Results

Two-dimensional coronal images were acquired at 81±6° relative to AC-PC line; for morphometric data see Table. There was high concordance between 2D and 3D morphometrics in the plane replicating the standard coronal plane (set at 81°). The true anatomical plane of FoM was found at 31°±8° relative to AC-PC line. The minimal width of the FoM (2.4±0.5 mm) in this plane was significantly less than that apparent on standard coronal images (2.9±0.8 mm), and the angle between the two FoMs was larger (74±7° vs. 61±7°) owing to greater curvature of the thalamus forming the postero-infero-lateral wall of FoM. Interestingly, the mean length of FoM in its anatomical plane equaled its mean width (and in 61% of patients was actually larger), suggesting that in many instances the interventricular connections could perhaps be described as short "canals" rather than "foramina".

	2D coronal	3D coronal	3D anatomical
Age (years)	47 ± 16 (13-83)	48 ± 24 (19-82)	48 ± 24 (19-82)
Evans index	0.23 ± 0.04 (0.12-0.29)	0.23 ± 0.03 (0.19-0.29)	0.23 ± 0.03 (0.19-0.29)
Plane angle vs AC-PC (deg)	81 ± 6 (65-100)	81 (set)	31 ± 8 (20-39)
FoM minimal width (mm)	2.9 ± 0.6 (1.3-5.6)	2.9 ± 0.8 (1.6-4.8)	2.4 ± 0.5 * (1.2-4.0)
FoM length (mm)	2.3 ± 0.5 (1.0-3.7)	2.4 ± 0.5 (1.7-3.9)	2.4 ± 0.5 (1.6-4.0)
Fornix width (mm)	3.1 ± 0.7 (1.7-3.6)	2.8 ± 0.6 (1.9-4.2)	3.0 ± 0.9 (1.9-4.3)
FoM angle (deg)	58 ± 8 (36-84)	61 ± 7 (43-71)	74 ± 7 * (60-84)

Table: Patients' characteristics and morphometrics of FoM [mean ± SD (range)]. * p<0.001 vs. 3D coronal.

Conclusion

We provide the first detailed normal MRI morphometrics for FoM and show that: 1) their true size and orientation differ from those perceived on standard coronal images; 2) the right and left FoMs are clearly separate with V-shaped orientation; 3) each FoM is angled about 30°, 60°, and 35° to the axial (AC-PC line), coronal, and sagittal planes respectively; and 4) FoMs often have a 3D spatial configuration resembling short canals. Planning of neuroendoscopic procedures should ideally rely on 3D datasets and not standard 2D images.

KEYWORDS: Anatomy, Morphometry, Monro foramen, neuroendoscopy

Note: Scanned images are included in the proceedings. Some submitted images were reduced during editing, thereby decreasing clarity. Also, refer to the Program Planner. Proceedings Content as of 3-29-2013.

P-74

Engraftment of Human Mesenchymal Stem Cells in a Rat Photothrombotic Cerebral Infarction Model: Comparison of Intra-Arterial and Intravenous Infusion Using MR Imaging and Pathologic Analysis

Byun, J.[1]·Kwak, B.[1]·Kim, J.[1]·Jung, J.[1]·Ha, B.[1]·Park, S.[1]·Shim, J.[1]·Kim, H.[2]
[1]Chung-Ang University Hospital, Seoul, KOREA, REPUBLIC OF, [2]Samsung Medical Center, Seoul, KOREA, REPUBLIC OF.

Purpose
To evaluate that administration routes affect the early stage migration of transplanted human bone marrow-derived mesenchymal stem cells (hBM-MSCs) in acute brain infarction.
Materials & Methods
Male Sprague-Dawley rats (n = 40) were subjected to photothrombotic infarction. Three days after photothrombotic infarction, rats were randomly allocated to one of four experimental groups (IA group: n = 12, IV group: n = 12, superparamagnetic iron oxide (SPIO) group: n = 8, control group: n = 8). All groups were subdivided into 1-, 6-, 24-, and 48-hour groups according to time point of sacrifice. MR images of rat brain were obtained prior to and at 1, 6, 24, and 48 hours postimplantation. After final MRI, rats were sacrificed and grafted cells were analyzed in brain and lung specimen.
Results
Grafted cells appeared as dark signal intensity regions at the infarction. In IA group, dark signals in infarction were more prominent compared with IV group. On Prussian blue staining, IA administration showed substantially increased migration and a large number of transplanted hBMMSCs in the target brain than IV administration.
Conclusion
IA transplantation results in superior delivery and sustained presence of hBM-MSCs in 48-hour group (five days after brain infarction) compared to IV transplantation.

KEYWORDS: Stem cell, Infarct

P-75

Signal Intensity of Normal Facial Nerves on Post-Contrast T1-Weighted Images at 3T: Comparison of 2D and 3D Pulse Sequences

Haneda, J.[1]·Ishikawa, K.[2]·Okamoto, K.[3]·Sato, T.[1]
[1]Nagaoka Chuo General Hospital, Nagaoka, JAPAN, [2]Niigata University, Niigata, JAPAN, [3]Brain Research Institute Niigata University, Niigata, JAPAN.

Purpose
Magnetic resonance imaging (MRI) is an important tool for investigating diseases affecting facial nerves. Recently, 3T MRI has become common in our daily clinical practice and proper sequences must be selected. Gradient echo-based 3D T1WIs commonly are used and have less partial volume effect with thinner slices than 2D T1WI. However, gradient echo-based 3D T1WIs show susceptibility artifacts due to mastoid pneumatization, which may impede visualization of the facial nerves. We visually compared the signal intensity of normal facial nerves on 3D T1WI with that on conventional 2D T1WI.
Materials & Methods
We retrospectively reviewed 124 normal facial nerves of 62 patients, including 32 patients(21 men, 11 women; mean age, 52.72 years) with postcontrast 3D T1WI and 30 patients(12 men, 18 women; mean age, 50.03 years) with postcontrast 2D T1WI obtained at our hospital from 2009 to 2012. Cases with clinical facial palsy, cerebello-pontine angle tumor, and a past history of intracranial surgery or radiation therapy were excluded in this study. MR imaging was performed on a 3T imager(Magnetom Verio, Siemens) with a 32-channel head coil. Spin-echo T1WI(slice thickness, 3mm; slice gap, 0mm) and fast low angle shot(FLASH) (slice thickness, 1mm; slice gap, 0mm) were used for 2D and 3D T1WI, respectively. Two radiologists evaluated the signal intensity of the facial nerves in agreement using a 4-scale visual score as follows: 1, hypointense to temporal gray matter; 2, isointense to temporal gray matter; 3, isointense to temporal white matter; 4, hyperintense to temporal white matter in the same plane. Visual scores were examined by two radiologists in the five facial nerve segments as follows: the intrameatal segment (Im), labyrinthine segment (Lb), geniculate ganglion (GG), horizontal segment (Hz) and vertical segment (Vt). We compared the visual scores in each segment on 3D T1WI with those on 2D T1WI via relative to an identified distribution (RIDIT) analysis.
Results
Visual scales in each segment on 2D T1WI and 3D T1WI are shown in Table 1. The scores in the Im, Lb, and GG on 3D-T1WI were significantly higher than those on 2D T1WI (P<0.01 for each segment), whereas the scores in the Hz on 3D T1WI were significantly lower than those on 2D T1WI (P<0.01). There were no significant differences between the scores in the Vt on 3D T1WI and 2D T1WI. Image quality was adequate for diagnosis.
Table 1. Visual scale results on 2D T1WI and 3D T1WI for each normal facial nerve segment

	Im		Lb		GG		Hz		Vt	
scale	2D	3D	2D	3D	2D	3D	2D	3D	2D	3D
1	0	0	6	1	8	0	5	53	1	0
2	12	0	30	0	0	3	6	9	0	0
3	44	20	23	39	18	7	37	2	2	0
4	4	44	1	24	34	54	12	0	57	64

Conclusion
The signal intensity of the facial nerve was higher on Gd-enhanced 3D T1WI compared to that on Gd-enhanced 2D T1WI in the Im, Lb, and GG segment, but the intensity of

Note: Scanned images are included in the proceedings. Some submitted images were reduced during editing, thereby decreasing clarity. Also, refer to the Program Planner. Proceedings Content as of 3-29-2013.

that in the Hz segment was higher on 2D T1WI than that on 3D T1WI.

KEYWORDS: Facial nerve, 3 T

P-76

Subfrontal Neuroendoscopic Approach to the Anterior Wall of the Third Ventricle: An Applied 3T MR Imaging Morphometric Study

Matys, T.[1]·Horsburgh, A.[1]·Kirollos, R. W.[1]·Antoun, N.[1]·Massoud, T. F.[2]
[1]Addenbrooke's Hospital, Cambridge, UNITED KINGDOM, [2]University of Cambridge, Cambridge, UNITED KINGDOM.

Purpose
Detailed neuroimaging analysis can be critical for accurate characterization of regional anatomy of the anterior third ventricle, an area of substantial neurosurgical importance. The lamina terminalis (LT), the main structure in the anterior third ventricular wall, can provide an access window for removal of intraventricular tumors, and may be fenestrated during treatment of aneurysmal subarachnoid hemorrhage to prevent ensuing hydrocephalus. More recently, neuroendoscopic opening of the LT via the subfrontal supraorbital approach has been suggested as an advantageous alternative to conventional third ventricular floor fenestration in internal shunting of obstructive hydrocephalus. The anatomy of this anterior third ventricle region has been studied previously on cadavers; this however requires organ fixation and is potentially prone to shrinkage errors. In this study we use high-resolution 3T MRI to obtain more accurate in vivo morphometric measurements of the anterior third ventricular structures of relevance to subfrontal neuroendoscopy.
Materials & Methods
We retrospectively analyzed magnified midsagittal T1-weighted 3T MR images of 50 patients (25 men and 25 women) with normal brain imaging findings, with a mean age of 49 years (range 19-82 years). We measured the following: distances from the frontal pole to the recommended site of fenestration of LT in its inferior third (FP-LT) and to the genu of the corpus callosum (FP-CC), length of LT (LLT), width and depth of the optic recess (ORW and ORD), width and height of the anterior commissure (ACW and ACH), distances from the optic chiasm to the anterior commissure (OC-AC), mammillary bodies (OC-MB) and posterior commissure (OC-PC), and distance between the LT and mammillary bodies (LT-MB). We statistically determined potential correlations between morphometric categories, and age- and sex-related changes in these parameters using Pearson's correlation.
Results
Morphometrics for the various distances are shown in the Table. There were no significant age- or sex-related changes in these measurements. Except for the obvious correlation between LLT and OC-AC (r=0.661, p<0.001), there was only a weak positive correlation between LLT and FP-CC (Pearson's r = 0.601, p<0.01), but not with any of the other measured parameters. The flow voids of the anterior cerebral/anterior communicating artery complex were invariably seen adjacent to the optic chiasm and lower third of the LT. However, components of this complex and their spatial relationships were not unraveled with any confidence on these standard midsagittal images alone.

Parameter	Mean ± SD (mm)	Min-Max (mm)
FP-LT	58.4 ± 4.4	49.8-67.7
FP-CC	35.8 ± 4.7	27.1-45.8
LLT	11.1 ± 1.5	7.8-14.1
ORW	2.9 ± 0.7	1.7-4.3
ORD	3.3 ± 0.9	1.4-4.8
ACW	2.7 ± 0.5	1.7-3.9
ACH	2.9 ± 0.6	1.6-4.0
OC-AC	8.9 ± 1.0	6.9-11.4
OC-MB	7.4 ± 1.1	5.4-9.3
OC-PC	27.7 ± 1.7	24.4-31.5
LT-MB	10.7 ± 1.1	8.4-12.8

Conclusion
We provide the first detailed in vivo morphometric analysis of the anterior third ventricular region, including the distance of the LT to the frontal poles. These baseline data are relevant and useful for accurate MRI planning of neuroendoscopic and neurosurgical procedures in this region.

KEYWORDS: Anatomy, Morphometry, neuroendoscopy, lamina terminalis, third ventricle

P-77

Extraoccular Muscle Morphometrics Relative to Anthropometric Features: Evaluation of Potentially Novel MR Imaging Indices for Assessing Graves' Ophthalmopathy

Wing, L.[1]·Matys, T.[1]·Horsburgh, A.[1]·Antoun, N.[1]·Massoud, T. F.[2]
[1]Addenbrooke's Hospital, Cambridge, UNITED KINGDOM, [2]University of Cambridge, Cambridge, UNITED KINGDOM.

Purpose
Thyroid orbitopathy is the most common extathyroidal manifestation of Grave's disease. MRI is useful for studying edematous swelling and fibroblast proliferation within thickened extraoccular muscles (EOMs: IR, MR, SR, LR) that form part of the Graves' ophthalmopathy (GO) spectrum. Amongst several MRI parameters, cross-sectional areas of EOMs, used as valid surrogates for EOM volumes, have been regarded as useful simple variables for diagnosis and monitoring the course of GO treatment. It was shown

Note: Scanned images are included in the proceedings. Some submitted images were reduced during editing, thereby decreasing clarity. Also, refer to the Program Planner. Proceedings Content as of 3-29-2013.

previously that normative morphometrics of the EOMs poorly correlate with age and sex alone, but no prior studies have factored in the potential variation in dimensions of normal and dysythyroid EOMs with patient anthropometric features (AFs). In this feasibility study we initially obtained detailed morphometrics of EOMs in normal and GO patients. We then tested the hypothesis that correlation with several patient AFs would result in more refined imaging indices for GO than possible without factoring in individual patient variations in dimensions of orbits and heads.

Materials & Methods

We retrospectively evaluated 102 standard multiplanar MRI studies of the orbits and brain (i.e., 204 orbits), 52 in patients with GO and 50 with normal findings. An observer blinded to clinical data and using electronic calipers manually traced and measured cross-sectional area at maximum belly thickness for each rectus muscle on coronal T2WIs. We then recorded seven AFs on each study on axial and coronal images: interzygomatic distance, biparietal distance, fronto-occipital distance, orbital width, orbital depth, greatest orbital height, and greatest horizontal ocular diameter, bilaterally when required. We statistically correlated rectus muscle areas and AFs using unpaired t-test and Pearson's correlation coefficient (significance set at p-value <0.05).

Results

The GO group (M:F=13:39) had a mean age 57.8 years; the control group (M:F=22:28) had a mean age 46.6 years. Age and sex did not statistically influence muscle size or AFs. There was no significant difference between AFs of patients in GO and control groups. Mean cross-sectional areas of rectus muscles in the GO group were: IR=55.3mm^2, MR=43.0mm^2, SR=40.2mm^2, and LR=25.9mm^2. Mean cross-sectional areas of rectus muscles in the control group were IR=25.1mm^2, MR=27.0mm^2, SR=22.5mm^2, and LR=17.3mm^2. All rectus muscles were significantly larger in the GO group compared to control group (P<0.0001). There was no significant correlation between each AF and the combined rectus muscle area in either group. Therefore, combined rectus muscle cross-sectional area was 1.79-fold greater in the GO group, and when this was divided by each AF, the ratios similarly ranged from 1.54- to 1.82-fold higher in the GO group compared to the controls.

Conclusion

This is the first study investigating variation in sizes of the EOMs with AFs. In adults, the size of EOMs, whether in normal patients or in those affected by GO, did not statistically correlate with the AFs, as similarly established previously for other independent factors such as age and sex. Potentially new indices derived in this study for characterizing rectus muscle size relative to AFs in patients with GO did not confer any advantage over measuring muscle morphometrics alone.

KEYWORDS: Morphometry, Thyroid-associated orbitopathy

Monday, May 20 – Wednesday, May 22
6:30 AM – 9:00 PM
Thursday, May 23
6:30 AM – 3:00 PM
Hall B1

Scientific Posters Printed 78 - 86

P3-Head and Neck

Note: A missing printed number indicates an abstract has been withdrawn.

P-78

Accuracy of Coronal Contrast-Enhanced Fat-Suppressed FLAIR in Detecting Acute Optic Neuritis and Its Sequela

Iyer, V. R.·McKinney, A. M.·Rykken, J. B.
University of Minnesota
Minneapolis, MN.

Purpose

Optic neuritis (ON), remains a clinical diagnosis, in which brain/orbital MRI is primarily utilized to detect brain lesions or to exclude other orbital pathology. Axial FLAIR images have been found to have higher specificity but lower sensitivity than contrast-enhanced T1-weighted images (T1WI), the current imaging standard, in detecting acute optic neuritis (ON). By using newer FLAIR techniques, detection of acute ON or its sequela, may be improved. The purpose of this study is to determine the accuracy of coronal contrast-enhanced fat-suppressed FLAIR (CE-FS-FLAIR) images in detecting ON.

Materials & Methods

Internal review board approval was obtained. The clinical data and MRI examinations of 44 patients who underwent 1.5T brain MRI to rule out or evaluate demyelinating disease, which included a CE-FS-FLAIR sequence, were reviewed retrospectively. Each patient underwent 3mm coronal CE-FS-FLAIR as part of a new "Multiple Sclerosis brain" protocol at our institution over a two-year period. Two staff neuroradiologists independently evaluated the CE-FS-FLAIR sequence, recording "+", "-", or "+/-" (indeterminate) for abnormality of each of the 44 patients' optic nerve (for a total of 88 nerves); these images were reviewed twice by each reviewer at different sittings. These results were correlated with the clinical history of ON in each optic nerve.

Results

There were 15 controls without demyelinating disease or ON, 26 patients suffering a demyelinating disease (10 of

Note: Scanned images are included in the proceedings. Some submitted images were reduced during editing, thereby decreasing clarity. Also, refer to the Program Planner. Proceedings Content as of 3-29-2013.

whom suffered ON), and three patients with ON but no demyelinating disease. Thus, 31 patients did not have any history of ON, while 13 patients were clinically positive for ON, affecting 19 of the study's 88 optic nerves. Between reviewers, the sensitivity ranged from 74-100%, specificity from 75-93%, and the overall accuracy 80-91%. The PPV was 52.8-73.7%; the NPV was 91.4-100%. The reviewers called "+/-" (indeterminate) in 5-8/88 optic nerves, typically when the fat suppression was compromised near the orbital apex. Interobserver kappa was 0.59 ($p<0.0001$). Intraobserver kappa ranged from 0.54-0.741 ($p<0.0001$).

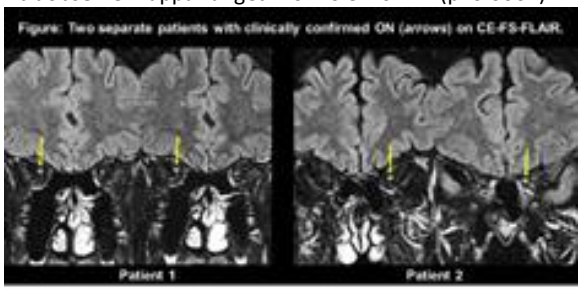

Conclusion
Coronal CE-FS-FLAIR images are relatively accurate in determining ON, with a particularly high NPV. This sequence could be an adjunct to postcontrast, fat-suppressed T1WI in evaluating ON patients with suspected demyelinating disease. However, it would be optimal for future studies to directly compare CE-FS-FLAIR to T1WI, and to compare both sequences to the clinical data, both in patients suffering demyelinating disease as well as in controls.

KEYWORDS: Optic nerve, Multiple sclerosis, contrast-enhanced FLAIR

P-79

MR Imaging of Fasciocutaneous and Myocutaneous Flap Reconstruction following Orbital Exenteration

Sedrak, P.[1]·Lee, P. S.[1]·Guha-Thakurta, N.[2]·Chang, E. I.[2]·Ginsberg, L. E.[2]·Esmaeli, B.[2]·Debnam, J. M.[2]
[1]The University of Texas at Houston, Houston, TX, [2]The University of Texas M. D. Anderson Cancer Center, Houston, TX.

Purpose
Complex free flap reconstruction may be performed following orbital exenteration for the treatment of tumors involving the orbit. The purpose of this study was to review the MR imaging findings of fasciocutaneous and myocutaneous flap reconstructions in this patient population.
Materials & Methods
The patient demographics and MR imaging findings of 28 patients who underwent fasciocutaneous or myocutaneous flap reconstruction following orbital exenteration were reviewed retrospectively. The soft tissue or muscular component of the flaps was assessed for enhancement pattern, T2 signal intensity, and size of the flap on initial postoperative and follow-up imaging.
Results
Twelve fasciocutaneous flaps were placed in 12 patients (6 men and 6 women), age range 5-75 years (median 50 years) and 16 myocutaneous flaps were placed in 16 patients (10 men and 6 women), age range 16-78 years (median 48.5 years). The type of orbital flap reconstruction included anterolateral thigh (ALT) (n = 13), radial forearm (n = 7), rectus abdominis (n = 5), deep inferior epigastric perforator (DIEP) (n = 1), serratus anterior (n = 1), and latissimus dorsi (n = 1). The soft tissue component of the fasciocutaneous flaps enhanced in 11 of the 12 cases and was either homogeneous (n = 5) or patchy (n = 6). The enhancement decreased over time in 5 of 10 flaps on followup. Eleven of 12 fasciocutaneous flaps were T2 hyperintense, and nine of 10 flaps that were assessed on follow-up studies decreased in size over time. The enhancement of the muscular component of the myocutaneous flaps was either homogeneous (n = 5), patchy (n = 5), linear (n = 4), or none (n = 2); this decreased over time in six flaps. On T2, the flaps were hyperintense (n = 15) or isointense (n = 1). Three of the 16 flaps decreased in size over time.
Conclusion
The soft tissue and muscular components of fasciocutaneous and myocutaneous orbital flaps are usually T2 hyperintense and demonstrate at least some degree of enhancement after surgery. This enhancement may persist or decrease over time. The soft tissue associated with fasciocutaneous flaps on initial imaging is likely to retract secondary to resolution of postoperative changes such as edema. Neuroradiologists, surgeons and oncologists involved in the care of patients following orbital exenteration with flap reconstruction should become familiar with the imaging findings of these complex flap reconstructions at baseline and on follow-up evaluations.

KEYWORDS: Orbital tumor, MR imaging

P-80

CT and MR Imaging Patterns of Chordoma and Chondrosarcoma of the Skull Base and Spine before and after Treatment with Proton Beam Radiation

Wycliffe, N. D.·Holness, S.·Suarez, K.·Oyoyo, U.·Loredo, L.·Kido, D.
Loma Linda University Medical Center
Loma Linda, CA.

Purpose
The purpose of this study was to identify CT and MR imaging patterns, frequency of location and the effect of location on the success rate of surgical resection and proton beam radiation treatment for chordoma and chondrosarcoma of the skull base and spine.

Note: Scanned images are included in the proceedings. Some submitted images were reduced during editing, thereby decreasing clarity. Also, refer to the Program Planner. Proceedings Content as of 3-29-2013.

Materials & Methods
This study is IRB and HIPPA compliant. This is a retrospective review of all the available CT and MR imaging of cases of chordoma and chondrosarcoma treated at our Proton Beam Radiation Treatment Facility at Loma Linda University Medical Center from January 1, 1992 to June 30, 2011. CT and MR of 424 cases of chordoma and 190 cases of chondrosarcoma were reviewed by two medical students and one CAQ certified neuroradiologist. Tumor location, preoperative, postoperative and post-treatment size of the tumor, presence of calcification in CT, T2 brightness in MRI and contrast enhancement pattern were recorded. Tumor type, location, initial tumor size, postoperative and post-treatment tumor size were correlated to survival data during the study period.
Results
Patient population included 255 males and 169 females with chordoma (age 2-85 years, mean 48.2 years) and 108 males and 82 females with chondrosarcoma (age 8-83 years, mean 45.5 years). During the study period alive:dead:lost to follow-up numbers for chordoma were 216:173:35 and chondrosarcoma 114:52:24. Chordoma had higher prevalence in skull base (SB) 36.76%, cranio-cervical junction (CCJ) 19.6%, cervical spine (CS)16.18% and sacro-coccygeal spine (SCS)16.67% than thoracic (TS) 3.92% and lumbar spine (LS) 6.86%. Chondrosarcoma had higher prevalence in skull base 65.22% and thoracic spine 21.74% than cranio-cervical junction 3.26%, cervical spine 3.26%, lumbar spine 2.17% and sacro-coccygeal spine 4.35%. Significant imaging features: for chordoma were, midline 67.66%, heterogeneous T2 hyper intensity 69.7%, no clacification70.6%, heterogeneous contrast enhancement 96%, and for chondrosarcoma were, off midline 80.2%, calcification 59.74%, contrast enhancement 98.5% (16.6% homogeneous). Death rates were higher with chordoma compared to chondrosarcoma in SB (31% vs.15.4%), CCJ(16.7% vs.7/7%), CS(31% vs.7.7%) and LS(14.3% vs.0%) and death rate was higher for Chondrosarcoma compared to Chordoma in TS(69.2% vs.7.1%). Positive correlation was seen with higher preoperative, post operative and post treatment tumor volume in both CT and MRI and death during the study period compared to those who were alive. Patients in the alive category showed increased reduction of tumor volume in the postoperative and post-treatment scan compared to those who died, for chordoma in SB, CCJ, and CS and in postoperative scan for chondrosarcoma in SB and TS. For chordoma, mean postoperative tumor resection volumes were higher in SB and CS compared to CCJ. Post-treatment tumor volume was difficult to assess in the spine for metallic hardware related artifacts.
Conclusion
Imaging characteristics overlap between chordoma and chondrosarcoma in the skull base and spine; however location, calcification and enhancement pattern are helpful in differentiating them. Higher reduction of tumor volume in postoperative scans show positive correlation with increased reduction of tumor volume in postproton beam radiation treatment scans and longer survival. Postsurgical tumor volume reduction was proportionately lower in CCJ compared to SB and CS in our study.

KEYWORDS: Chordoma, Chondrosarcoma, proton therapy, skull base, craniocervical, spine

P-81

Head and Neck Imaging of Chronic Recurrent Multifocal Osteomyelitis

Sargar, K.·Kao, S.·Sato, Y.·Ferguson, P.·Singh, A.
University of Iowa Hospitals
Iowa City, IA.

Purpose
1. To demonstrate various imaging features of chronic recurrent multifocal osteomyelitis (CRMO) in head and neck region. 2. To discuss key imaging features to differentiate CRMO from other differential diagnoses such as infection and neoplasms.
Materials & Methods
Chronic recurrent multifocal osteomyelitis is noninfectious osteomyelitis seen in pediatric population. Most common sites of involvement are metaphysis of long bones, clavicle, mandible, vertebrae and pelvis. Typical imaging pattern of involvement in clavicles and mandible is very helpful for the diagnosis of this entity. Though extremity involvement is common in CRMO, involvement of clavicles and mandible is important differentiating point between CRMO and infection. We are demonstrating radiographic, MRI, CT and nuclear scan imaging features of two prototype sites of CRMO (i.e., clavicles and mandibles). There are two phases of CRMO - active and reparative. Imaging appearance can also be helpful to suggest the phase of disease. Lack of abscess, fistula sequestrum and significant soft tissue involvement and aggressive periosteal reaction are key features to differentiate CRMO from infectious osteomyelitis and neoplasms.
Results
Though CRMO is diagnosis of exclusion, radiologists can suggest diagnosis based on imaging appearance. It is necessary to differentiate CRMO from infections and neoplasms as treatment approach and prognosis is entirely different.

Note: Scanned images are included in the proceedings. Some submitted images were reduced during editing, thereby decreasing clarity. Also, refer to the Program Planner. Proceedings Content as of 3-29-2013.

Conclusion
CRMO is noninfectious osteomyelitis in pediatric population with typical involvement of clavicles and mandibles in head and neck region. Various key features on imaging of head and neck region are helpful to differentiate chronic recurrent multifocal osteomyelitis from infection and neoplasms. Differentiation of CRMO from these entities is essential in view of treatment and prognostication.

KEYWORDS: Head and neck, Osteomyelitis, chronic recurrent multifocal osteomyelitis

P-82

Cervical Lymph Node Metastasis from Papillary Thyroid Carcinoma: Spectrum of Ultrasonographic Findings

Kumar, S.[1]·Edeiken-Monroe, B. S.[2]·Debnam, J. M.[2]
[1]Baylor College of Medicine, Houston, TX, [2]The University of Texas M. D. Anderson Cancer Center, Houston, TX.

Purpose
Knowledge of the presence of cervical lymph node metastasis in papillary thyroid carcinoma is imperative for appropriate management. The purpose of this study was to evaluate the ultrasonographic (US) appearance of metastatic cervical adenopathy in the setting of papillary thyroid carcinoma (PTC).
Materials & Methods
The clinical data, imaging studies, and US-guided biopsy results from lymph node metastasis in patients with PTC were reviewed retrospectively. Inclusion criteria included an US of the soft tissues of the neck and accompanying US-guided fine needle aspiration (FNA) biopsy documenting metastatic cervical adenopathy. The indication for US imaging, appearance of the metastatic lymph nodes including degree of vascular flow and the presence calcification, and the treatment were reviewed.
Results
Cervical lymph node metastasis is associated with primary and recurrent PTC. Lymph nodes of concern are detected during clinical examination, US examination for thyroid nodules, and during evaluation of abnormal lymph nodes incidentally detected on alternate imaging modalities and routine surveillance following thyroidectomy. The metastatic lymph nodes are hypoechoic with distortion or absence of the normal central fatty echogenic hilum. Disorganized vascular flow, punctate calcification and a cystic component may be present raising concern for metastasis. Reactive lymph nodes cannot be distinguished from metastatic adenopathy based on US characteristics and thus, US-guided FNA is required for diagnosis. Surgical resection often is performed on documented pathologic lymph nodes in the soft tissues of the neck.
Conclusion
Cervical nodal metastases from PTC should be suspected in the presence of alteration or absence of the central echogenic hilum, distortion of the normal hilar vascularity, calcification and cystic change. An US-guided FNA is necessary to document metastasis and to facilitate presurgical planning.

KEYWORDS: Thyroid, Metastases, ultrasound

P-83

Bump on the Forehead: The Differential Diagnosis of Pott's Puffy Tumor

Espinoza, F. V.·Castillo, M.
University of North Carolina
Chapel Hill, NC.

Purpose
The classic description of Pott's puffy tumor is that of a patient presenting with a bump on the forehead due to chronic osteomyelitis of the frontal bones due to underlying frontal sinus infection. This presentation is not unique to this condition and imaging becomes essential for finding a specific etiology. Illustrative cases are presented to demonstrate the range of conditions that present with forehead bumps. We provide a differential diagnosis, and discuss their complications.
Materials & Methods
Examples of diverse conditions presenting as forehead lumps from our teaching files (2002-2012) using both MRI and CT were chosen. Each entity was reviewed and a differential diagnosis generated. Complications from these entities are addressed.
Results
A review of the case files has shown that many categories

Note: Scanned images are included in the proceedings. Some submitted images were reduced during editing, thereby decreasing clarity. Also, refer to the Program Planner. Proceedings Content as of 3-29-2013.

of disease including infection (tubercular, pyogenic), traumatic, tumor, inflammatory (mucocele, polyposis) and vascular as well as developmental anomalies (encephaloceles, dermoids) can present as a bump on the forehead. Diagnostic imaging provides the necessary information to differentiate among these and triage the patient to the correct treatment. Imaging is also helpful in the evaluation of complications arising from these entities.
Conclusion
Patients presenting with Pott's puffy tumor or a forehead bump should undergo CT and possibly MRI to determine the nature of the lesion and choose the appropriate treatment. Evaluation of the underlying bone and frontal sinus is indispensable as many entities arising in them present with bump on the forehead.

KEYWORDS: Abscess, Masses, Pott's puffy tumor

P-84

Usefulness of High-Resolution Three-Dimensional Diffusion-Weighted Imaging of Middle Ear Cholesteatoma: Compared to Single-Shot Echo-Planar Diffusion-Weighted Imaging

Yamashita, K.[1]·Yoshiura, T.[1]·Hiwatashi, A.[1]·Obara, M.[2]·Togao, O.[1]·Matsumoto, N.[1]·Kikuchi, K.[1]·Honda, H.[1]
[1]Kyushu University, Fukuoka, JAPAN, [2]Philips Electronics Japan, Tokyo, JAPAN.

Purpose
To prospectively evaluate the usefulness of a newly developed high-resolution three-dimensional diffusion-weighted imaging method, turbo field-echo with diffusion-sensitized driven-equilibrium (DSDE TFE) in diagnosing middle-ear cholesteatoma by comparing it to conventional single-shot echo-planar diffusion-weighted imaging (SS EP DWI).
Materials & Methods
Institutional review board approval and informed consent from all participants were obtained. We studied 30 patients with preoperatively suspected acquired cholesteatoma. Each patient underwent an MR examination including both SS EP DWI and DSDE TFE using a 3.0 T MR scanner. Images of the 30 patients (60 temporal bones including 30 with and 30 without cholesteatoma) were reviewed by two independent neuroradiologists. The confidence level for the presence of cholesteatoma was graded on a scale of 0-2 (0 = none, 1 = equivocal, 2 = definite). Interobserver agreement as well as sensitivity, specificity, and accuracy for detection were assessed for the two reviewers.
Results
Excellent interobserver agreement was shown for DSDE TFE ($\kappa = 0.821$) whereas fair agreement was obtained for SS EP DWI ($\kappa = 0.416$). Turbo field-echo with diffusion-sensitized driven-equilibrium was associated with significantly higher sensitivity (83.3 %) and accuracy (90.0 %) compared to SS EP DWI (sensitivity = 35.0 %, accuracy = 66.7 %; $p<0.05$). No significant difference was found in specificity (96.7 % for DSDE TFE, 98.3% for SS EP DWI).
Conclusion
With increased spatial resolution and reduced susceptibility artifacts, DSDE TFE improves the accuracy in diagnosing acquired middle ear cholesteatomas compared to SS EP DWI.

KEYWORDS: Cholesteatoma, Diffusion-weighted imaging, 3D

P-85

Usefulness of Contrast-Enhanced 3D T1 VISTA for Diagnosis of Facial Neuritis: Compared with Contrast-Enhanced T1 Turbo Spin-Echo Imaging

Ryu, C.[1]·Choi, W.[1]·Jahng, G.[2]·Lee, K.[1]
[1]Kyung Hee University Hospital, Seoul, KOREA, REPUBLIC OF, [2]Kyung Hee University Hospital at Gangdong, Seoul, KOREA, REPUBLIC OF.

Purpose
Three-dimensional reformatted images are promising technique. It offers improved anatomical accuracy with minimal flow artifact and thinner sections without gaps between slices when compared with conventional 2D imaging. The purpose of this study was to evaluate the usefulness of the contrast-enhanced 3D T1-weighted VISTA fat-suppression (CE T1 VISTA) sequence when compared to contrast-enhanced T1-weighted turbo spin-echo images (CE T1 TSE) sequence in patients with facial neuritis.
Materials & Methods
The study enrolled 32 consecutive patients (21 females, mean age: 52.4 years ± 13.6, 25 right lesions) who underwent internal auditory canal (IAC) MR imaging for Bell's palsy. Internal auditory canal MR scanning including CE T1 VISTA and CE T1 TSE and was performed in all patients by use of 3T scanner. Scan order of CE T1 VISTA and CE T1 TSE were performed randomly. Contrast-enhanced T1 VISTA was performed with the following parameters: TR, 350 ms; TE, 19.51 ms; matrix, 360 x 299; field of view, 113 x 180; section thickness, 1 mm; total scan time, 3 min 4 sec. Parameters of CE T1 TSE are as follow: TR, 568.82 ms; TE, 11.00 ms; matrix, 256 x 205; field of view, 180 x 200; section thickness, 2 mm; total scan time, 3 min 36 sec. The signal intensity was measured from three segments (canalicular, labyrinthine, and anterior genu) of the facial nerve by drawing ROI along the affected side and normal side in each segment. We compared quantitative lesion-to-normal contrast ratio of two MR sequences with paired t-test.
Results
In all three segments, the lesion-to-normal contrast ratios on CE T1 VISTA (canalicular: 2.22 ; labyrinthine: 2.02 ; anterior genu: 1.99) were greater than those on CE T1 TSE (canalicular: 2.17 ; labyrinthine: 1.72 ; anterior genu: 1.68). Labyrinthine and anterior genu segment were significantly

Note: Scanned images are included in the proceedings. Some submitted images were reduced during editing, thereby decreasing clarity. Also, refer to the Program Planner. Proceedings Content as of 3-29-2013.

higher lesion-to-normal contrast ratios on CE T1 VISTA SPAIR in patients with facial neuritis (labyrinthine: P= 0.030; anterior genu: P = 0.004).
Conclusion
Contrast-enhanced T1 VISTA was significantly superior to CE T1 TSE regarding image contrast between lesion and normal facial nerve. By using CE T1 VISTA image, diagnostic performance of facial neuritis can be improved.

KEYWORDS: Facial nerve, 3 T

P-86

Novel Method of 3D Image Analysis of High-Resolution Cone-Beam CT and Multislice CT for the Detection of Semicircular Canal Dehiscence

Eibenberger, K.[1,2,3]·Carey, J. P.[2]·Ehtiati, T.[4]·Trevino, C.[2,5]·Haslwanter, T.[1]
[1]University of Applied Sciences Upper Austria, Linz, AUSTRIA, [2]Johns Hopkins University School of Medicine, Baltimore, MD, [3]Johannes Kepler University, Linz, AUSTRIA, [4]Siemens Corporation, Baltimore, MD, [5]Escuela de Medicina Ignacio A. Santos, Monterrey, MEXICO.

Purpose
In semicircular canal dehiscence (SCD), multislice CT (MSCT) scans tend to overestimate the size of dehiscence and skew the ascertainment toward dehiscence when thin bone may remain; therefore we present an objective method to detect inhomogenities in temporal bones, based on comparison of radiodensity variance in regions of interest (ROIs).
Materials & Methods
We simulated the problem of detecting a dehiscence in the superior canal (SC) by building a bone cement phantom containing holes(0.4-0.1mm). In addition, a cadaveric head specimen was used to create an anatomical model for a "borderline" SCD: a middle fossa craniotomy was performed and the SC was drilled to the point of translucency. Tomographic scans were acquired on MSCT(Toshiba Aquilion64, step-mode, 0.5mm collimation, 135kVp, 250mA) and cone-beam CT (CBCT) with high-resolution secondary reconstructions (HR CBCT, Siemens Artis zee C-Arm-syngo HR-Dyna CT, 89kVp, 140mA, 20s scan time, 1x1 binning prototype). Variances of radiodensity in bone cement ROI scans containing a hole were compared with variances in regions without holes(Figure A). This technique was applied to detect the artificial dehiscence on the cadaveric head: we collected radiodensities from a row of 30 voxels along a path from the lumen of the SC orthogonally out toward the middle cranial fossa. This linear ROI was compared with a spherical ROI covering only the lumen of the SC(Figure B). Variance of radiodensity in each ROI was compared with the Fligner-Killeen test. Dehiscence(absence of bone) was rejected if the variances were not different (p≥0.05).
Results
Holes in bone cement and intact bone over the SC was detected by comparing the homogeneity of variance. HR CBCT, CBCT and MSCT detected a hole in bone cement<0.1mm (p=0.0001 for 0.1mm, HR CBCT). For thin bone over the cadaveric SC, the method rejected the existence of dehiscence with p=0.6922 with HR CBCT.

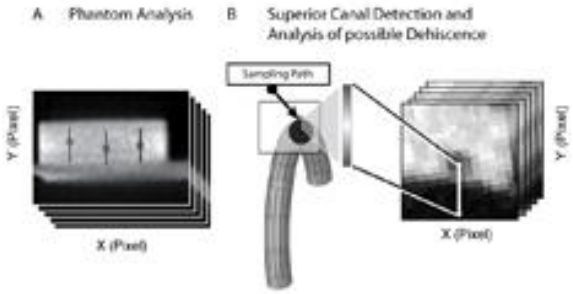

Conclusion
We have shown that with CT an approach comparing radiodensity variance in ROIs is capable of detecting a 0.1mm hole in dense, homogeneous bone. If the variance in radiodensity along a path from the center of the canal to the outside exceeds the variance found inside the lumen, then it is likely that some bone remains over the canal, and dehiscence can be rejected. Moreover, this method can be used to objectively compare the spatial resolution of different CT scanners for the problem of SCD. Further clinical evaluation is required to assess the results of this method for correct diagnosis of SCD.

KEYWORDS: Cone-beam computed tomography, Semicircular canal dehiscence, spatial resolution

Monday, May 20 – Wednesday, May 22
6:30 AM – 9:00 PM
Thursday, May 23
6:30 AM – 3:00 PM
Hall B1

Scientific Posters Printed 87 - 95

P4-Interventional

Note: A missing printed number indicates an abstract has been withdrawn.

Note: Scanned images are included in the proceedings. Some submitted images were reduced during editing, thereby decreasing clarity. Also, refer to the Program Planner. Proceedings Content as of 3-29-2013.

P-87

320-Row Multidetector CT Angiography and Digital Subtraction Angiography in the Evaluation of Cerebral Vasospasm after Subarachnoid Hemorrhage

Hebert, J.·Roncarolo, F.·Tampieri, D.·Cortes, M. D. P.
Montreal Neurological Institute
Montreal, QC, CANADA.

Purpose
To determine if 320-row multidetector CT angiography is a reliable technique to assess cerebral vasospasm following subarachnoid hemorrhage by comparing it with the gold-standard DSA.
Materials & Methods
Diameters of 54 arteries were measured retrospectively on both CTA and DSA in eight patients who were diagnosed with cerebral vasospasm following an aneurysmal subarachnoid hemorrhage. Digital subtraction angiography was performed within 24 hours following CTA. Statistical analysis was performed to determine the correlation between the arterial diameters measured by both techniques.
Results
The quantitative approach used in this study to determine the correlation between 320-row MDCT angiography and DSA showed excellent interobserver reliability. There was however no statistically significant correlations between arterial diameters taken on CTA and DSA. CT angiogrqaphy tended to show smaller arterial diameters in the anterior circulation of the circle of Willis when compared with DSA.
Conclusion
The results of this study suggest that 320-row multidetector CT angiography may overestimate the degree of vasospasm in the anterior circulation. The method used by this study, which is unique in that it adopted a quantitative approach, proved to be reliable as suggested by the good interobserver reliability and should be repeated with a greater sample size.

KEYWORDS: 320 detector row, Cerebral angiography, cerebral vasospasm

P-88

Detection of True Aneurysm Using High-Resolution Time-of-Flight MR Angiography at 3.0T: Correlation with Standard Digital Subtraction Angiography

Lee, A.·Sohn, C.·Han, M.·Yoon, T.·Kang, H.·Jung, S.·Yoo, I.·Kim, S.
Seoul National University Hospital
Seoul, KOREA, REPUBLIC OF.

Purpose
1. To evaluate accuracy of 3T high-resolution MRA in detecting aneurysm compared with conventional MRA. 2. To prove potential diagnostic advantage of high-resolution MRA using correlation with DSA.
Materials & Methods
Thirty-two patients with 43 possible aneurysms on conventional MRA underwent 3T high-resolution MRA and DSA. The protocols of high-resolution MRA were following: TR 29.0, TE 4.6, matrix 512 x 512, FOV 20 cm, and thickness 0.5 mm with 8-channel head coil. Two blinded neuroradiologists reviewed conventional MRA and high-resolution MRA in the detection of aneurysms, independently. For each possible aneurysm, readers recorded the location and their level of confidence with a three point scale (0:no, 1:suspicious, and 2:definite aneurysm). Two dimensional or VR DSA were obtained and used as the standard of reference. The accuracy was calculated in addition to the sensitivity and specificity of high-resolution MRA compared to conventional MRA. In particular, cases with advantage of detection on high-resolution MRA were evaluated in detail.
Results
Digital subtraction angiography revealed 35 aneurysms in 25 patients and no aneurysm or ID in eight cases in seven patients. Multiple aneurysms were 12 cases in eight patients. On high-resolution MRA, reviewers exactly detected 40, 37 cases, superior to conventional MRA (29, 32 cases). On the lesion-based evaluation, accuracy, sensitivity, and specificity of were 89.5%, 91.5, and 81.3% on high-resolution MRA and 72.1%, 81.5%, and 31.3% on conventional MRA, respectively. Each three and five suspicious aneurysm on conventional MRA were recategorized as definite aneurysm.

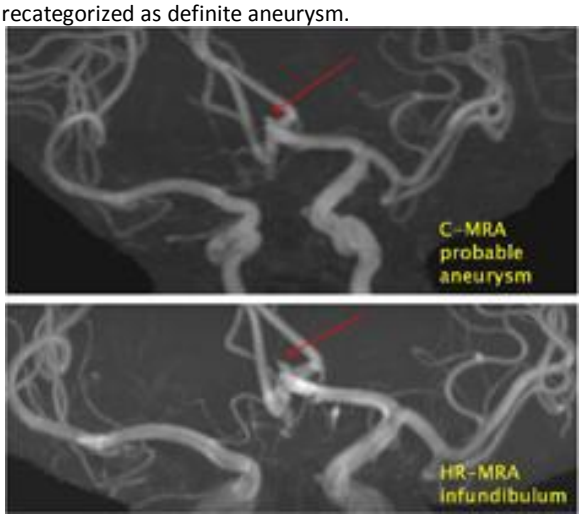

Conclusion
High-resolution MRA had a high accuracy, sensitivity and specificity for the detection of intracranial aneurysms, comparing conventional MRA. In equivocal aneurysm on conventional MRA, high-resolution MRA can be a useful tool and replace DSA.

KEYWORDS: Aneursym, Infundibulum

Note: Scanned images are included in the proceedings. Some submitted images were reduced during editing, thereby decreasing clarity. Also, refer to the Program Planner. Proceedings Content as of 3-29-2013.

P-89

Onyx Embolization of Dural Arteriovenous Fistulas Using a New Dual Arterial Pedicle Catheterization Technique

Miller, T. R.·Gandhi, D.·Jindal, G.
University of Maryland
Baltimore, MD.

Purpose
Embolization of dural arteriovenous fistulas with Onyx (eV3, inc.) has proven to be safe and effective. However, when a microcatheter cannot be navigated distally in the arterial pedicle due to either small vessel size or proximal tortuosity, the standard "plug-and-push" technique of Onyx embolization can be challenging. In these instances, formation of an occlusive plug of Onyx around the microcatheter tip prior to forward flow of the liquid embolic agent is essential to achieving subsequent distal penetration and lesion closure. We present a new technique for forming this crucial plug of Onyx utilizing a second microcatheter navigated alongside the first.
Materials & Methods
A series of cases consisting of four patients with dural arteriovenous fistulas was collected at our institution and one other, all of which had small, and/or, tortuous arterial feeders that prevented distal navigation of the microcatheter to a position close to the fistula. All patients were male, age over 50, who presented over a two-year period. Clinical presentations included pulsatile tinnitus (two) and hemorrhagic stroke (two). All patients had undergone prior fistula treatment using standard Onyx embolization technique, without complete fistula closure. Using the dual arterial pedicle catheterization technique, two microcatheters were navigated into the arterial pedicle of interest. Onyx 34 then was injected via the proximal microcatheter, forming an occlusive plug around the more distal catheter. Fistula embolization then proceeded by injection of Onyx 18 via the distal microcatheter.
Results
Fistula location varied, with one located parasagittally near the vertex, while the remaining lesions were in the posterior fossa. Arterial supply was primarily from external carotid artery branches; two patients also had supply from vertebral artery dural branches. Three fistula had associated cortical venous reflux. In three patients, the dual arterial pedicle catheterization technique resulted in complete obliteration of the fistula. In the fourth patient, the technique resulted in good penetration of the lesion, but there was residual mild arteriovenous shunting from other feeders that has required subsequent treatment.

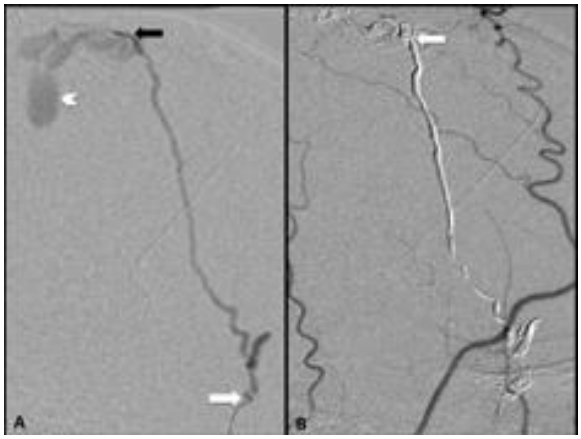

Conclusion
Our experience demonstrates the utility of using a second microcatheter to form an occlusive Onyx plug proximally in an arterial pedicle prior to dural fistula embolization. This technique appears well suited when working in small, and/or tortuous arterial pedicles. This technique also may prove advantageous in embolization of cerebral arteriovenous malformations under similar circumstances. Further experience is necessary to fully assess the technique's potential for enhancing Onyx embolization of vascular malformations.

KEYWORDS: Dural arteriovenous fistula, Embolization, Onyx

P-90

Strategy of Endovasucular Treatment for Dural Arteriovenous Fistulas of Cavernous Sinus Using 320-Row Area-Detector Computed Tomography

Kiura, Y.·Okazaki, T.·Sakamoto, S.·Matsushige, T.·Shinagawa, K.·Ichinose, N.·Kurisu, K.
Hiroshima University
Hiroshima, JAPAN.

Purpose
In transvenous embolization (TVE) for cavernous sinus dural arteriovenous fistula (CSdAVF), the main access route to lesion is the inferior petrosal sinus (IPS). However, the IPS often is occluded. In such cases, it is important to know substitute access routes before treatment. As a new imaging modality, 320-row area detector computed tomography (320ADCT) offers a short scan time and superior spatial resolution compared to conventional CT. The aim of this study is to examine an utility of 320ADCT and treatment strategies on CSdAVF.
Materials & Methods
Since July 2010, 320ADCT was obtained in five patients with CSdAVF treated with endovascular treatment. We performed 320ADCT preoperatively and divided results into arterial phase, late arterial phase and venous phase. We then judged the relationships between draining veins

Note: Scanned images are included in the proceedings. Some submitted images were reduced during editing, thereby decreasing clarity. Also, refer to the Program Planner. Proceedings Content as of 3-29-2013.

and the normal venous system.
Results
Imaging results allowed us to grasp the lengths of the occluded portion of the IPS and the confluence of the IPS and internal jugular vein, helping us to open up the occluded IPS.
Conclusion
Use of 320ADCT angiography helped diagnose CSdAVF and facilitated successful treatment planning.

KEYWORDS: 4D CT angiography, Dural arteriovenous fistula

P-91

Spontaneous Thrombosis without Associated Hemorrhage Revealing a Brain Arteriovenous Malformation: A Rare Presentation

Clarençon, F.[1]·Cao, C.[2]·Sourour, N.[1]·Di Maria, F.[1]·Nouet, A.[1]·Reina, V.[1]·Cornu, P.[1]·Chiras, J.[1]
[1]Pitié-Salpêtrière Hospital, Paris, FRANCE, [2]University Hospital of Dijon, Dijon, FRANCE.

Purpose
To detail a rare presentation of brain arteriovenous malformation (bAVM): the thrombosis of the draining vein without subsequent hemorrhage, and to review the literature on this rare occurrence.
Materials & Methods
Brain arteriovenous malformations are serious vascular malformations that may be responsible for intracranial bleeding. One of the main pathomechanism that can lead to bAVM rupture is thrombosis of the main draining vein. Exceptionally, thrombosis of the venous drainage may occur without subsequent hemorrhage and be revealed by headache or neurologic deficit related to venous congestion. The recognition of such “prerupture” stage is of tremendous importance to plan treatment in emergency. A 31-year-old male was attended in our department for severe headache associated with right hemiparesis and slight aphasia. Brain CT scan and MRI showed abnormal vascular network with a huge cortical venous thrombosis. Perivenous edema also was observed. No intracranial hemorrhage was depicted however. The diagnosis of spontaneous thrombosis of the draining vein in a parietal AVM was considered. The DSA confirmed the diagnosis. Endovascular treatment with NBCA injection allowed for a 2/3 exclusion of the nidus volume.
Results
The patient fully recovered from his neurologic deficits. An additional Gamma-knife radiosurgery is planned.
Conclusion
Spontaneous thrombosis of the draining vein may occur without any hemorrhage and reveal bAVM. Neurosurgeons as well as interventional neuroradiologists should be aware of this rare bAVM presentation in order to treat in emergency the malformation before bleeding.

KEYWORDS: Arteriovenous malformation, Thrombosis

P-92

Endovascular Salvage of Intra-Operative Iatrogenic Complications Involving the Internal Carotid Artery Related to Surgery of the Sellar and Parasellar Regions

Griauzde, J.·Chaudhary, N.·Pandey, A. S.·Sullivan, S. E.·McKean, E. L.·Gemmete, J. J.
University of Michigan Health System
Ann Arbor, MI.

Purpose
To present our experience with acute endovascular management of intra-operative complications involving the internal carotid artery (ICA) related to surgery of the sellar and parasellar regions.
Materials & Methods
We retrospectively reviewed the clinical and operative records, imaging, and postoperative course of patients with intra-operative iatrogenic ICA injury related to surgery involving the sellar and parasellar regions. We subsequently reviewed prior reports of similar complications and their management.
Results
In total, four patient cases with iatrogenic operative injury to the ICA were identified. There were three males and one female. The average age was 52 years. Two patients had a pituitary macroadenoma, one had a complex recurrent planum meningioma, and one had a chondrosarcoma with suprasellar extension. In all four cases the tumor was either compressing or surrounding the affected ICA. Two patients had undergone previous operations and had altered anatomy and extensive calcification. Three of the cases presented with acute obvious carotid bleeding in the surgical field and one presented with loss of pulse of the ICA. Three patients underwent emergent placement of Jostent Graftmaster stents (Abbott Vascular; Santa Clara, CA) for repair of their ICA injury. The first patient required subsequent additional stent placement for improved stent to vessel wall apposition and had residual intermittent unilateral blurred vision. A second patient was at his neurologic baseline at followup. A third patient failed stent placement and required ICA sacrifice because of persistent hemorrhage. This patient passed away six days after the procedure. The final patient experienced an intra-operative ICA stroke. This patient was treated with suction thrombectomy using a Penumbra device (Penumbra Inc; Alameda, CA), intra-arterial tissue plasminogen activator (tPA) and ReoPro (Eli Lilly; Indianapolis, IN) followed by Wingspan stent placement (Stryker Neurovascular; Freemont, CA) for persistent vessel narrowing caused by intraluminal tumor invasion or thrombus. The patient’s course was further complicated by intraprocedural in-stent thrombosis, requiring subsequent balloon angioplasty and additional administrations of tPA and ReoPro. The patient needed subsequent emergent craniotomy for subdural and

Note: Scanned images are included in the proceedings. Some submitted images were reduced during editing, thereby decreasing clarity. Also, refer to the Program Planner. Proceedings Content as of 3-29-2013.

epidural hematomas. At followup, the patient had mild cognitive deficits and difficulty with writing, but was otherwise at his neurologic base line. His craniotomy bone flap has been replaced.

Conclusion

Intra-operative vascular injury involving the ICA from surgery of the sellar and parasellar regions is uncommon, but when it occurs, management must be immediate and definitive to maximize patient survival and minimize morbidity. Endovascular therapies including covered stent placement, suction thrombectomy, and intra-arterial thrombolysis with adjuvant ReoPro have been reported. Our experience supports the viability of these therapies in the acute management of intra-operative ICA injury.

KEYWORDS: Internal carotid artery, Iatrogenic, acute management

P-93

Utility of Temporary Balloon Occlusion Testing in Prediction of Outcomes following Permanent Parent Vessel Sacrifice

Whisenant, J. T.·Derdeyn, C. P.·Cross, D. T.·Moran, C. J.
Mallinckrodt Institute of Radiology
St. Louis, MO.

Purpose

To review the utility of the temporary balloon occlusion (TBO) test as it pertains to prediction of patient outcomes following permanent parent vessel occlusion. Patients often undergo TBO testing as part of the diagnostic workup prior to permanent parent vessel sacrifice. We perform a three-part test that includes intraprocedural neurologic assessment, neuroangiographic evaluation of the adequacy of collateral flow, and 99m-Tc-Bicisate administration during temporary balloon occlusion. Pending the TBO test results, parent vessel occlusion may be performed; and this patient population is at risk for post-parent vessel sacrifice ischemic complications, such as TIA, stroke, and death.

Materials & Methods

Data were reviewed retrospectively from all patients who underwent ICA TBO from March 2002 to December 2011. Patients then were subdivided into those that underwent permanent ICA occlusion and those that did not. Data from those that underwent permanent ICA occlusion were collected over the succeeding six months for the occurrence of three primary outcomes: transient ischemic attack (TIA), ischemic stroke (CVA), and death. In the subgroup of patients with a CVA following the parent vessel occlusion, additional data were collected in the following areas: 1) type of parent vessel sacrifice (open v. endovascular), 2) timing of symptom onset (procedural, early postop, late postop), and 3) type/location of infarct. Based on these factors, a mechanism of the event was postulated (thromboembolic v. hemodynamic).

Results

One hundred fifty ICA TBOs were performed between March 2002 and December 2011. Thirty-six went on to have permanent endovascular or surgical ICA occlusion. In the group that had parent vessel sacrifice, there were the following outcomes: five TIAs (13.9%), six CVAs (16.7%), and three deaths (7.3% - all due to underlying malignancy). Of the nine patients with ischemic complications (i.e., TIA or CVA) after the parent vessel sacrifice, eight had SPECT performed and all eight were normal or had “fixed” defects, seven had angiography performed and six of the seven were interpreted as normal, and all nine had clinical neurologic assessment performed and all nine passed. Of the six patients with CVA, four are postulated to be hemodynamic in etiology, one is postulated to be thromboembolic in etiology, and one is of indeterminate etiology (hemodynamic or thromboembolic).

Timing and Type of Ischemic Stroke Following Parent Vessel Sacrifice

Age	TBO Angio	SPECT	TBO Neuro Exam	Method of Sacrifice	Time Onset of CVA	Mechanism of CVA	Symptoms
78	Not Done	Pass	Pass	Endovascular	early post-op (hours/days)	Hemodynamic/Embolic - single centrum semiovale by CT	Mild RUE weakness
44	Pass	Pass	Pass	Open Surgical	early post-op (hours/days)	Hemodynamic	Mild weakness - complete recovery at later follow up
51	Pass	Not Done	Pass	Endovascular	early post-op (hours/days)	Hemodynamic - Centrum Semiovale	L hemiplegia, R facial droop
64	Fail	Pass	Pass	Open Surgical	early post-op (hours/days)	Hemodynamic - Centrum Semiovale	LUE weakness persistent at f/up 4 months later
86	Pass	Pass	Pass	Endovascular	late post-op (weeks/months)	Thromboembolic - stump	LUE/LLE weakness and L sided neglect
73	Not Done	Pass	Pass	Endovascular	early post-op (hours/days)	Hemodynamic	R hemiplegia, R facial weakness, aphasia

Conclusion

The rate of ischemic stroke following ICA sacrifice in patients who have “passed” TBO testing is higher than expected. The majority of ischemic strokes affected the deep white matter of the centrum semiovale and occurred in the early or late postop period supporting a hemodynamic etiology. The SPECT and angiographic testing appears to be more effective in assessing cortical flow than assessing flow to the deep white matter.

KEYWORDS: Balloon test occlusion, Hemodynamics

P-94

Conscious Sedation versus General Anesthesia: A Comparison of Outcomes for Acute Ischemic Stroke Patients Receiving Endovascular Treatment

Chao, R.·Vachhani, J.·Talkad, A.·Meagher, S.
University of Illinois College of Medicine at Peoria
Peoria, IL.

Purpose

Endovascular treatment of acute ischemic stroke has two options for sedation: general anesthesia (GA) and conscious sedation (CS). General anesthesia immobilizes the patient and allows greater control over the patient’s vitals and pain, while CS is faster and allows neurologic evaluation during the procedure. There are few studies comparing patient outcomes for the use of CS versus GA. The purpose of this study is to compare the clinical outcomes between the two methods of sedation. We

Note: Scanned images are included in the proceedings. Some submitted images were reduced during editing, thereby decreasing clarity. Also, refer to the Program Planner. Proceedings Content as of 3-29-2013.

hypothesize that there will be no difference in patient outcomes between the two groups.
Materials & Methods
Medical records from a cohort of adult patients who have undergone digital subtraction angiogram (DSA) after acute ischemic stroke since 2009 were examined retrospectively for the type of sedation used and clinical outcomes as measured by National Institutes of Health Stroke Scale (NIHSS) score and a modified Rankin Scale Score (mRS). National Institutes of Health Stroke Scale and mRS scores were collected at admission and at 90-day followup. Other data collected include use of intravenous tissue plasminogen activator (tPA), length of hospital stay, and discharge disposition. Types of intervention include the use of intra-arterial tPA, mechanical thrombectomy, angioplasty, and stent placement. Patients below 18 years of age and those with incomplete documentation were excluded from the study.
Results
Between January 2009 and January 2012, 123 patients underwent DSA for ischemic stroke and met inclusion criteria. Of these patients, 56 received GA and 67 received CS. The GA cohort had a mean admit NIHSS score of 17.68 ± 7.11 and admit mRS of 4.34 ± 0.64. At 90-day followup, the NIHSS score was 3.29 ± 3.43 and mRS 1.86 ± 1.12. The CS cohort had mean admit NIHSS score of 15.56 ± 6.91 and mean mRS of 4.18 ± 0.90. At 90-day followup, the NIHSS score was 3.70 ± 4.74 and mean mRS of 1.71 ± 1.48. There was no statistically significant difference between the GA and CS groups at admission or 90 days.
Conclusion
There was no appreciable difference in outcomes in patients who had GA versus CS while undergoing DSA after ischemic stroke as measured by NIHSS scores and mRS.

KEYWORDS: Stroke, Interventional, anesthesia

P-95

Use of Solitaire Retrieval Device in Wake-Up Strokes: Saint Luke's Neuroscience Institute Experience

Akhtar, N.[1]·Holloway, W.[1]·Martin, C.[1]·Rymer, M.[1]·Akhtar, E.[1]·Chakravarthy, V.[2]
[1]Saint Luke's Neuroscience Institute, Kansas City, MO, [2]University of Missouri-Kansas City School of Medicine, Kansas City, MO.

Purpose
Wake-up strokes at Saint Luke's Neuroscience Institute present unique therapeutic challenge and most of them were denied any interventional treatment due to unknown time of onset. We started intervention on wake-up strokes after incorporation of CT perfusion in our stroke treatment algorithm in 2009. The presenting noncontrast CT of the head had to be normal or show changes of ischemia in less than one third of vascular territory. The CT perfusion should be favorable with preserved blood volume and relative preservation of cerebral blood flow. The presenting NIHSS score should be significant as well.
Materials & Methods
Since approval of Solitaire retrieval device by the Federal Drug Administration in the United States we had treated 31 patients since March 2012 with Solitaire device with adjunct intravenous TPA (i/v TPA), intra-arterial TPA (i/a TPA). Out of these 31 patients, nine patients were wake-up strokes involving the anterior circulation. Three patients with wake-up vertebra-basilar strokes were excluded. The average age was 72.6 years (range 39-92 years). There were six males and three females. The average presenting NIHS score was 16.1 (range from 8 to 25). The location of clot was seven in the middle cerebral artery M1/M2, one with T occlusion and one with ICA occlusion. In all cases the Solitaire device was utilized with no i/v or i/a TPA. One patient needed ICA stenting for acute carotid occlusion. Average fluoroscopy time was 21.47 minutes (range 10-47 minutes). Average total procedure time was 73.66 minutes (range 41-180 minutes). Number of passes were nine passes in one patient, four passes in one patient, two passes in one patient and one pass in six patients. The postprocedure TICI score was 2b in one patient and 3 in eight patients. One patient had intracranial hemorrhage (PH2). This patient expired. There was no embolization in uninvolved territories. The average NIHSS score at discharge was 5.44 (range 0-20), excluding two patients who expired. Thirty day Modified Rankin Score (MRS) was two patients expired, five in one patient, and two in three patients, and one in three patients. This shows favorable outcome of Modified Rankin Score of 0-2 in six patients.
Conclusion
In conclusion, wake-up strokes are a challenging group of patients which can be treated if carefully selected. High technical success rate is possible after availability of mechanical retrieval devices like the Solitaire device and adjunct treatment with TPA is not needed in these patients decreasing the risk of complications.

KEYWORDS: Wake-up stroke, Thrombectomy, solitaire

Note: Scanned images are included in the proceedings. Some submitted images were reduced during editing, thereby decreasing clarity. Also, refer to the Program Planner. Proceedings Content as of 3-29-2013.

Monday, May 20 – Wednesday, May 22
6:30 AM – 9:00 PM
Thursday, May 23
6:30 AM – 3:00 PM
Hall B1

Scientific Posters Printed 96 - 105a

P5-Pediatrics

Note: A missing printed number indicates an abstract has been withdrawn.

P-96

Arrested Pneumatization of Sphenoid Sinus in Children

Penta, M.[1]·Koral, K.[1,2]
[1]University of Texas Southwestern Medical Center, Dallas, TX, [2]Children's Medical Center, Dallas, TX.

Purpose
Arrested sphenoid sinus pneumatization is a relatively common benign developmental variant in children that may occasionally be confused with significant skull base pathology when unrecognized. The purpose of this study is to review the imaging findings of arrested pneumatization of the sphenoid sinus as seen on MRI and describe the frequency of arrested sphenoid sinus pneumatization in children.
Materials & Methods
Institutional review board approval was obtained for this retrospective study. Brain MR examinations of 316 consecutive patients performed in 2012 were reviewed. Patients with presumed abnormalities of bone marrow, skull base surgery, and history of chemotherapy or radiation therapy and examinations without a coronal T2-weighted sequence were excluded. There were 101 patients (58 male) included in the study. The mean age was 8.41 years (0.67-17.37). Presence of arrested sphenoid sinus pneumatization, described as a focus of increased signal with hypointense corticated margins on coronal T2-weighted spin-echo images, was recorded by a pediatric neuroradiologist. When present, the greatest orthogonal dimensions of the arrested sphenoid sinus pneumatization were noted.
Results
Arrested sphenoid sinus pneumatization was present in 16 (15.8%) of the patients. When present, the mean area of the arrested sphenoid pneumatization was 132 mm2 (SD = 219, min-max = 6-798).

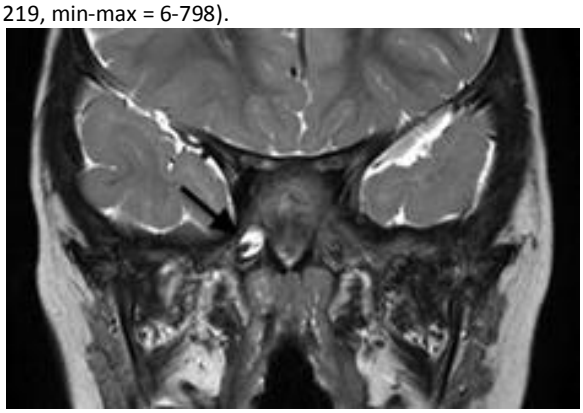

Figure: Coronal T2-weighted image of two-year-old male shows a 8.0 x 4.9 mm delineated T2 hyperintense focus in the right sphenoid body.
Conclusion
Regions of corticated T2 prolongation are seen relatively frequently on normal pediatric brain MR examinations and can be attributed to arrested sphenoid sinus pneumatization. Recognition of this benign developmental variant is important in avoiding unnecessary anxiety, further imaging, and procedures, especially in children with known malignancies.

KEYWORDS: Bone marrow, Pseudomass, skull base

P-97

MR-Guided Laser Ablation of Nonlesional, Nonmesial Temporal Lobe Epileptic Foci in Patients with Medically Refractory Seizures Utilizing Magnetoencephalographic Localization and Surface Electroencephalogram Recording

Ghassemi, A.·Ciricillo, S.·Krishnan, A.·Chez, M.
Sutter Neuroscience Institute
Sacramento, CA.

Purpose
Medically refractory epilepsy affects approximately 300,000 patients in the United States. Early surgery reduces long-term impact and comorbidities, improving quality of life. Fear of an open craniotomy combined with more extratemporal foci in pediatric cases may delay surgical options. Often, as in our series, electroencephalogram (EEG) tracing localization does not correlate with any obvious 3T MRI lesion. We present a less invasive technique, combining EEG, magnetic source imaging (MSI) and functional MR imaging (fMRI) combined with BrainLab localization to enable minimally invasive MRI-guided stereotactic laser ablation (SLA) of epileptogenic foci.
Materials & Methods
Eight medically refractory epilepsy patients (seven to 20 years, median age 12.2 years, Table 1), were evaluated with video EEG, fMRI, MSI and PET and 3T MRI. Six

Note: Scanned images are included in the proceedings. Some submitted images were reduced during editing, thereby decreasing clarity. Also, refer to the Program Planner. Proceedings Content as of 3-29-2013.

patients had cognitive and behavioral issues making craniotomy for intracranial electrode localization difficult. Three had focal interictal dipole localization that were in regions where traditional surgical intervention would have caused potential collateral damage. Focal abnormalities on EEG were correlated with MSI and PET scan data (Table 1). All underwent SLA (Visualase, Inc.) with frameless navigation (BrainLab, Inc). All had intraoperative EEG monitoring via MR compatible plastic electrodes (Ives) placed over cranial surface above ablated region.

Results

The patients showed resolution (n=7) or diminished number (n=1) of pre-ablation spikes on intraprocedure EEG taken immediately postablation. They were all discharged on postsurgery day one (n=6) or 2 (n=2). To date, the three patients with frontal seizures remained seizure free, off medications, and two have a normal EEG. The dominant posterior temporal patient is seizure free, and the two occipital patients with multiple probes had seizure resolution and EEG normalization. No new visual, cognitive, or motor deficits occurred.

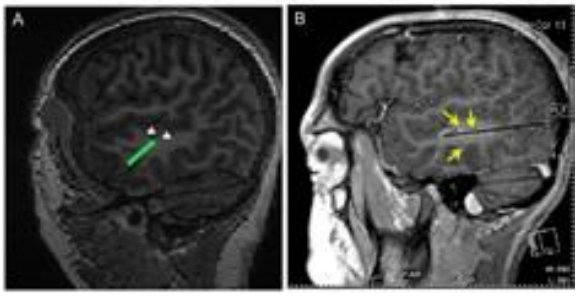

Table 1. Patient Characteristics

Patient #	Age	Sex	MEG Dipole Location	PET Activity	Cognitive Deficit
1	11	M	Left Frontal	N/A	Autism
2	9	M	Right Frontal	N/A	Autism ADHD
3	19	F	Right Middle Temporal Gyrus	N/A	Cognitive Delay Noonan Variant
4	14	F	Right Frontal	N/A	ADHD
5	11	F	Left Inferior Cingulate	Left Inferior Parietal	LD ADHD
6	7	F	N/A	Left Occipital Temporal	Autism Cognitive Delay
7	12	M	Right Occipital Temporal	N/A	Cognitive Delay Autism
8	20	F	Left Superior Temporal	N/A	None

Conclusion

SLA can be an alternative surgical treatment for refractory epilepsy and may allow earlier intervention in temporal or nontemporal cortex foci. Coordinating MSI, fMRI, and surface EEG allows patients to avoid open craniotomy or invasive intracranial EEG electrode placement. Intraoperative laser probe localization via Brainlab guidance permitted accurate ablation of targeted epileptogenic cortex. Surface EEG activity pre- and post-SLA confirmed a decrease in epileptiform discharges.

KEYWORDS: Epilepsy, Laser

P-98

Abnormal White Matter Microstructure of Posterior Cerebral Tracts Correlates with Sensory Dysfunction, Impaired Multisensory Integration and Inattention in Children with Sensory Processing Disorders

Owen, J. P.·Marco, E.·Fourie, E.·Desai, S.·Harris, J.·Hill, S.·Mukherjee, P.
University of California San Francisco
San Francisco, CA.

Purpose

Sensory processing disorders (SPD) affect 5-16% of school-aged children and cause long-term deficits in intellectual and social development. Current theories of SPD implicate primary sensory cortical areas and higher-order multisensory integration (MSI) cortical regions. The role of white matter in SPD has not been investigated previously. We hypothesize that reduced microstructural integrity of white matter fibers in primary sensory tracts and/or in tracts projecting to multimodal association areas may result in impaired sensory processing, MSI, and motor planning and the inability to suppress distracting stimuli.

Materials & Methods

3T DTI was acquired in 16 boys with SPD and 24 age-, gender-, handedness- and IQ-matched typically developing controls (TDC). All subjects were ages 8-11 years with a full-scale IQ > 70. Auditory, tactile, visual, multisensory, and inattention scores for all subjects were collected using the Sensory Profile, a parent questionnaire. DTI was performed at 2.2 mm isotropic voxel resolution with 64 encoding directions at b=2000 s/mm2. FSL was used to calculate fractional anisotropy (FA), mean diffusivity (MD) and radial diffusivity (RD). Nonparametric permutation testing from tract-based spatial statistics(TBSS) was used to detect significant group differences in the white matter of the whole brain and to detect regions where DTI parameters were significantly correlated with behavioral variables ($p<0.05$, corrected for multiple voxel-wise comparisons).

Results

Significant decreases in FA as well as increases in MD and RD were found in areas of cerebral white matter in the SPD cohort relative to TDC, primarily in posterior white matter tracts including the splenium and posterior body of the corpus callosum, the bilateral posterior corona radiata and the bilateral posterior thalamic radiations, including

Note: Scanned images are included in the proceedings. Some submitted images were reduced during editing, thereby decreasing clarity. Also, refer to the Program Planner. Proceedings Content as of 3-29-2013.

the optic radiations. Significant positive correlations were observed between FA of specific frontal and posterior cerebral tracts and the auditory, multisensory, and inattention scores (r=0.51-0.78; p<0.001). (See Figure 1 for a representative example.) Conversely, negative correlations were detected between RD and the multisensory and inattention scores (r=0.61-0.71; p<0.001).

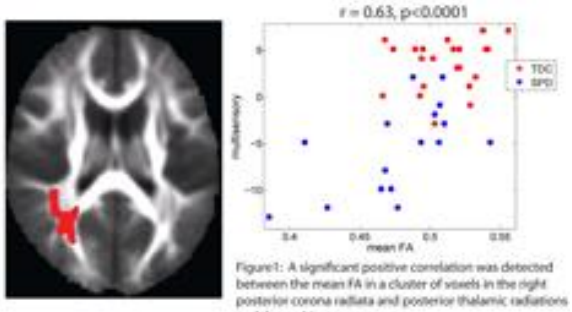

Figure1: A significant positive correlation was detected between the mean FA in a cluster of voxels in the right posterior corona radiata and posterior thalamic radiations and the multisensory score.

Conclusion

We demonstrate reduced white matter microstructural integrity in SPD patients and that DTI microstructural parameters in posterior tracts correlate strongly with sensory dysfunction and abnormal MSI, while left frontal tract integrity correlates specifically with a measure of inattention. These findings suggest abnormal white matter as a biological basis for SPD and help to distinguish SPD from overlapping clinical conditions such as autism and ADHD. Using brain-behavior correlations, we hope to move towards a more individualized understanding and treatment of children with sensory processing differences.

KEYWORDS: Autism spectrum disorder, Pediatric brain, sensory processing disorders

P-99

Maturation of the Brain Stem and Cerebellar White Matter Tracts from the Neonatal Period to Adolescence: A Diffusion Tensor Imaging Study

Poretti, A.·Meoded, A.·Yoshida, S.·Huisman, T. A. G.
The Johns Hopkins Medical School
Baltimore, MD.

Purpose

Diffusion tensor imaging (DTI) allows to study the normal development of white matter tracts. Several studies focused on the supratentorial white matter tracts. Almost no data are available about the temporal changes of DTI scalars for the infratentorial white matter tracts during the progressing myelination. We evaluated the quantitative changes of fractional anisotropy (FA) and mean (MD), axial (AD), and radial (RD) diffusivity within the brain stem and cerebellar white matter tracts from the neonatal period to adolescence.

Materials & Methods

We selected 96 subjects (47 females, 49 males, age three days to 17.9 years) with normal brain anatomy and absence of neurologic disorders. Single-shot spin-echo, echo-planar axial DTI sequences were acquired on a 1.5T MR scanner. Balanced pairs of diffusion gradients were applied along 20 orthogonal directions. Atlas-based analysis with parcellation of the brain in 130 regions was performed using MRI Studio software. The following infratentorial white matter tracts were evaluated: corticospinal tract, medial lemniscus, and superior, middle, and inferior cerebellar peduncles.

Results

For all white matter tracts, an increase of FA and decrease of MD, RD, and less pronounced, AD values were seen over time. For all white matter tracts, changes in DTI parameters were higher for the youngest subjects (younger than 12 months of age). Additionally, changes in DTI parameters, particularly MD, RD and AD, differed depending on the studied white matter tracts and were higher for the corticospinal tracts and middle cerebellar peduncles compared to medial lemnisci and superior and inferior cerebellar peduncles.

Conclusion

The changes in DTI parameters correlate well with the normal myelination and developmental processes. The most pronounced changes were seen in white matter tracts that myelinate later. We report on normative values for pediatric DTI parameters of the infratentorial white matter tracts using atlas-based analysis.

KEYWORDS: Diffusion tensor image, Cerebellum, brain stem; Atla- based analysis; myelination

P-100

Longitudinal Comparison of Diffusion Tensor Imaging Values in Neonates with Hypoxic Ischemic Encephalopathy Undergoing Hypothermia Treatment

Lee, P. N.·Tymofiyeva, O.·Glass, H.·Bonifacio, S.·Ferriero, D.·Barkovich, J.·Xu, D.
University of California San Francisco
San Francisco, CA.

Purpose

Diffusion tensor imaging (DTI) is a valuable tool for studying brain development in infants with hypoxic ischemic encephalopathy (HIE). Low apparent diffusion coefficient (ADC) values due to injury can be detected before abnormalities are seen on conventional anatomical MR imaging, these have prognostic value in neonates with HIE. We studied neonates with HIE by evaluating the DTI values at approximately four days of life and at six months and correlated these to outcome status at six months. A longitudinal comparison then was performed to determine changes over time across outcome groups.

Materials & Methods

Comprehensive MRI exams with DTI were performed at approximately four days and again at six months of life for 36 newborns with HIE who underwent hypothermia

Note: Scanned images are included in the proceedings. Some submitted images were reduced during editing, thereby decreasing clarity. Also, refer to the Program Planner. Proceedings Content as of 3-29-2013.

treatment. All subjects were examined by a pediatric neurologist at six months of age and were neurologically evaluated using a Neuromotor Scoring (NMS) system validated at our institution. Thirty-six percent of the patients had abnormal neurologic outcome with a NMS≥2. A basal ganglia (BG), thalamus (TH), parietal white matter (PWM), cortical spinal tract (CST), and posterior limb of the internal capsule (PLIC) regions of interest (ROI) were drawn bilaterally on the ADC maps. Left and right ROIs were statistically similar and were combined for analysis. The difference between the late and early scans was used for the longitudinal comparison. Linear regression with age correction was performed.

Results

Infants with abnormal outcome had higher ADC values in all regions, with significant differences in the PWM (p=0.03) and CST (p=0.01) regions at the neonatal scan. At six months, significantly higher ADC in the abnormal group was found only in the PLIC (p=0.05). The abnormal cohort showed a significantly steeper change over time in the PWM (p=0.03) and CST (p=0.01) (Chart 1).

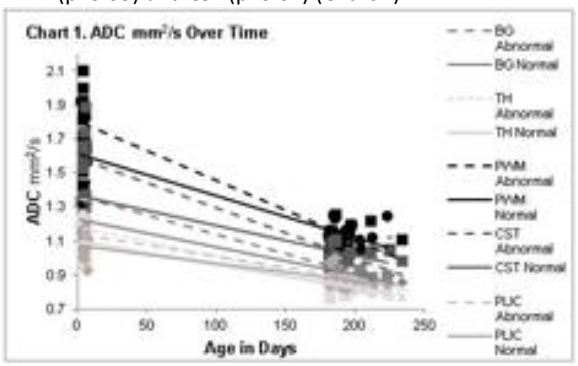

Conclusion

Apparent diffusion coefficient values in subjects with abnormal outcome approached those of subjects with normal outcome by the six month time point, though elevated ADC was still seen in the PLIC on the six month scan. It is interesting to note that prior studies with uncooled neonates showed reduced diffusion in regions of injury, while the current study showed increased diffusion; the reason for the increased diffusivity after cooling is being investigated. Given that hypothermia provides incomplete neuroprotection, this technique may be useful in choosing which subjects will benefit from additional neuroprotective therapies.

KEYWORDS: Hypoxia, Hypothermia

P-101

Diffusion Tensor Imaging in Hypoxic Ischemic Encephalopathy Treated with Therapeutic Hypotheremia

Niogi, S. N.·Rosenbaum, D.·Perlman, J.·Heier, L.·Kovanlikaya, A.
Weill Cornell Medical College
New York, NY.

Purpose

Perinatal hypoxic-ischemic encephalopathy causes significant disability in newborns and accounts for about 25% of children with cerebral palsy. As of yet, there is no reliable biomarker to predict which of these infants will have poor outcome. Diffusion tensor imaging (DTI) is more sensitive to white matter changes than conventional clinical MRI and can possibly detect subtle variations in white matter in these infants which may better assess severity. In the current study, we use DTI to evaluate white matter integrity in a priori selected regions to predict clinical outcome.

Materials & Methods

Subjects included 19 infants that were imaged between six and nine days of age. Subjects underwent therapeutic hypothermia and were examined at 18-24 months to assess clinical outcome. Subjects were divided into good outcome (neurologic normal) or poor outcome (death or motor/cognitive abnormalities). Subjects were scored with the Bayley Scale of Infant Development. Diffusion tensor imaging was performed using a 1.5T MRI GE scanner using a 33 gradient direction sequence. A semi-automated region of interest (ROI) approach, the Reproducible Objective Quantification Scheme (ROQS) was adopted to test 12 specific tracts selected in an a priori fashion based on prior studies. As a post-hoc test, 3D tractograms of these pathways also were created using home-grown software adopting a streamlined technique. Fractional anisotropy (FA) for the ROIs and tractograms of these tracts were correlated with the Bayley score and FA from subjects in good and poor outcome groups was compared using 2-tailed nonparametric statistics.

Results

White matter integrity measured by FA of the anterior limb of the internal capsule (ALIC) bilaterally, the left posterior limb of the internal capsule (PLIC), and forceps major (FM) bilaterally predict clinical outcome from both 2D ROI and tractogram measurements (statistics from 2D ROIs: right ALIC $p = 0.012$, left ALIC $p = 0.014$, left PLIC $p = 0.035$, right FM $p = 0.009$, left FM $p = 0.002$). The FM tract bilaterally also correlated with Bayley Scores of development (right FM $r = 0.62$, $p = 0.016$, left FM $r = 0.70$, $p = 0.009$). Conventional clinical MRI and other clinical measures cannot adequately predict outcome in infants that have suffered hypoxic-ischemic encephalopathy. However, DTI is sensitive to subtle microstructural changes overlooked by conventional imaging. As shown in this study, variations in white matter integrity in specific pathways (the ALIC, PLIC, and FM) can predict clinical

Note: Scanned images are included in the proceedings. Some submitted images were reduced during editing, thereby decreasing clarity. Also, refer to the Program Planner. Proceedings Content as of 3-29-2013.

outcome after treatment with therapeutic hypothermia.
Conclusion
Diffusion tensor imaging detects subtle variations in white matter and can be performed to possibly predict outcome following therapeutic hypothermia in infants suffering from hypoxic-ischemic encephalopathy, one of the predominate causes of cerebral palsy.

KEYWORDS: Pediatric brain, DTI

P-102

MR Imaging and Spectroscopy Findings in Perinatal Hypoxic-Ischemic Injury following Whole Body Cooling

Kitamura, G.·Bartnik-Olson, B. L.·Merritt, T. A.·Peverini, R.·Kido, D.·Wycliffe, N.·Oyoyo, U.
Loma Linda University
Loma Linda, CA.

Purpose
To determine whether neonates with perinatal hypoxic-ischemic injury (HII) who underwent whole body cooling demonstrated fewer imaging abnormalities when compared to noncooled neonates.
Materials & Methods
A retrospective chart review revealed 39 neonates with HII who underwent 72 hours of whole body cooling (HII/HT+) and 20 neonates with HII who did not undergo whole body cooling (HII/HT-). Inclusion and exclusion criteria for whole body cooling were similar to those in the literature. Magnetic resonance spectroscopy (MRS), magnetic resonance imaging (MRI), and susceptibility-weighted imaging (SWI) data were acquired between 0-20 days after birth. In addition, nine healthy neonates imaged within the same time frame were included in the study as a control group. MR spectroscopy values analyzed included N-acetyl aspartate (NAA), creatine (Cr), choline (Cho), myo-inositol (Ins), and lactate (lac) in the mid-occipital gray matter (OGM), basal ganglia (BG) and thalami (TH). MR imaigng findings were assessed using the previously validated Barkovich scores evaluating T1, T2, proton density (PD), and diffusion-weighted imaging (DWI) findings in the basal ganglia (BG), watershed region (W) and combined basal ganglia-watershed region (BGW). Susceptibility-weighted imaging findings were analyzed using a 7-point ordinal scale evaluating the prominence of cerebral deep medullary veins (POV). Neurologic outcome at discharge was evaluated with the previously validated outcome-predicting encephalopathy score. A *p*-value less than 0.05 was considered to be statistically significant.
Results
There was no significant difference in demographic or discharge variables among the control, HII/HT+, and HII/HT- groups, except with the Miller encephalopathy score, which was higher in the HII/HT- group. Compared to the HII/HT- group, fewer neonates in the HII/HT+ group had lactate detected in the OGM and TH. N-acetyl aspartate level in the OGM and NAA/Cho ratio in the TH also were higher in the HII/HT+ group when compared to the HII/HT- group. The HII/HT+ group demonstrated lower MRI Barkovich scores compared to the HII/HT- group. The HII/HT- group demonstrated a higher number of patients with abnormal POV values when compared to the HII/HT+ group.
Conclusion
Neonates with hypoxic-ischemic injury undergoing whole body cooling demonstrated differences in MRI, MRS, and SWI imaging findings when compared to neonates with hypoxic-ischemic injury who did not undergo whole body cooling. These findings may represent the alteration in cerebral metabolism that occurs with whole body cooling, and may be utilized in the workup of neonates with hypoxic-ischemic injury.

KEYWORDS: Hypoxia

P-103

Institutional Choroid Plexus Tumor Apparent Diffusion Coefficient Histogram Analysis and Comparison of Tumor Grade Values

Kamer, A. P.·Cardinal, J.·Ho, C.
Indiana University School of Medicine
Indianapolis, IN.

Purpose
To evaluate the utility of diffusion-weighted imaging (DWI) in discriminating choroid plexus tumor grade using quantitative analysis with whole-tumor ADC histograms.
Materials & Methods
This study was granted exemption status by our Institutional Review Board. MR imaging data were collected retrospectively for choroid plexus tumors at our institution that had a tissue diagnosis and preoperative DWI. Whole-tumor regions of interest were hand drawn on the apparent diffusion coefficient (ADC) maps for each tumor, and the ADC value was automatically extracted for each included voxel using an in-house MATLAB script. Individual whole-tumor ADC and WHO grade group summation ADC histograms were generated. Statistical metrics were calculated for each tumor including average, standard deviation, skew, kurtosis, and several percentiles. The metrics for the two tumor grades were compared with each other using unpaired, two-tailed Student *t*-test to evaluate for statistically significant differences or trends.
Results
Seventeen WHO grade I (mean age, 5.4 years; range, 2 months - 42 years) and three WHO grade III (mean age, 6 months; range, 3 months -1 year) choroid plexus tumors were included. Mean ADC values for WHO III tumors (1.26 x 10-3 mm2/s) tended to be lower than those for WHO I tumors (1.59 x 10-3 mm2/s), but without statistical significance (P = 0.21). Percentile measures and peak location also tended lower in WHO III tumors, but without statistical significance. Skew and kurtosis, measures of asymmetry and peakedness respectively, revealed no clear

Note: Scanned images are included in the proceedings. Some submitted images were reduced during editing, thereby decreasing clarity. Also, refer to the Program Planner. Proceedings Content as of 3-29-2013.

trends (P=0.32 and P=0.57, respectively). Nearly all individual tumor histograms demonstrated a single dominant peak, while the normalized WHO grade group summation histograms demonstrated bimodal distributions. Individual tumors tended to have relatively low variance in ADC values compared to higher variance in ADC values grouped by tumor grade.

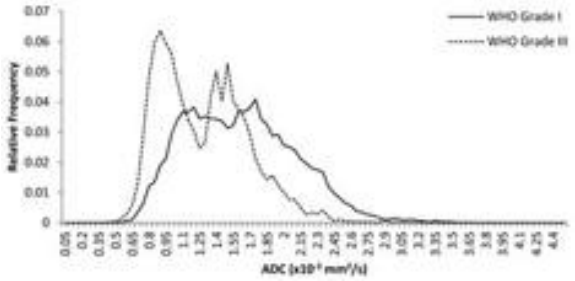

Conclusion
Assessment is limited given only three WHO grade III choroid plexus tumors; however, our results suggest that DWI and quantitative analysis of whole tumor ADC distribution is not clinically useful for discriminating choroid plexus tumor grade. Different ADC peaks for two populations of WHO grade I tumors suggests the presence of two separate subsets of papillomas. Additional research may further clarify these findings.

KEYWORDS: ADC, Choroid plexus, neoplasm

P-104

Primary Brain Tumors in the First Year of Life: What Is Rare and What Is Common?

Decarie, J.·Bernier Turmel, F.
Hopital Ste-Justine
Montreal, QC, CANADA.

Purpose
The purpose of this study is to present a retrospective analysis of primary brain tumor types in children less than one year old treated at a large tertiary care pediatric center. Our goal was to determine the number, the histologic distribution, and the location of primary brain tumors in the first year of life and compare our results with data previously reported.
Materials & Methods
A retrospective study was made of primary brain tumor patients presenting in the first year of life at Saint-Justine Hospital between 2002 and 2012. Nineteen cases were identified through the Pediatric Oncology Service registry. The following data were compiled for each case: Age of patient at time of diagnosis, dimensions of tumor, location and histologic type.
Results
In our study, supratentorial tumors were the most frequent location (74%) and astrocytomas, predominantly benign, represented 52% of all tumors, data in agreement with the literature. Teratoma, suprasellar/thalamic astrocytoma, atypical teratoid rhabdoid tumor, ependymoma, choroid plexus tumor and craniopharyngioma are the most commonly reported types in the literature. However, 42% of our cases are not considered as typical tumor for this age group and 26% of our cases fall in the group of rare tumors. Our series suggests that the spectrum of histologic types is wider than previously reported and that some histologic types considered before as rarities should be included in the differential diagnosis of primary brain tumor for this age group.
Table 1: Histologic types distribution

Histological types	No. of patients (%)
Pilocytic Astrocytoma (WHO grade I)	7 (37)
Pilomyxoid Astrocytoma (WHO grade II)	1 (5)
Anaplastic Astrocytoma (WHO grade III)	2 (11)
Choroid Plexus Papilloma (WHO grade I)	1 (5)
Atypical Choroid Plexus Papilloma (WHO grade II)	1 (5)
Choroid Plexus Carcinoma (WHO grade III)	1 (5)
Medulloblastoma	1 (5)
Pineoblastoma	1 (5)
Pituitary Blastoma	1 (5)
Atypical Teratoid /Rhabdoid Tumor	1 (5)
Desmoplastic Neuroepithelial Tumors	2 (11)

Conclusion
Our study suggests that the spectrum of histologic types of primary brain tumors encountered during the first year of life should be expanded to include types previously reported as rare or very rare as 42% of our cases belonged to that group.

KEYWORDS: Pediatric brain tumors, Epidemiology

Note: Scanned images are included in the proceedings. Some submitted images were reduced during editing, thereby decreasing clarity. Also, refer to the Program Planner. Proceedings Content as of 3-29-2013.

P-105

Radiation Dose Reduction and Protocol Optimization for Pediatric Head CT in Evaluation of Ventricular Size

Gabriel, S.·Eckel, L. J.·Wood, C. P.·Thielen, K. R.·DeLone, D. R.·Krecke, K. N.·Luetmer, P. H.·Bruesewitz, M. R.·McCollough, C. H.·Kofler, J. M.·Yu, L.
Mayo Clinic
Rochester, MN.

Purpose
Radiation dose is an important concern for public health, especially for pediatric patients. In recent times, rapid MR has been promoted as an alternative to CT for evaluation of ventricular size in patients with treated, long-term hydrocephalus. However, MR is not routinely available during off hours or at all institutions. Given this and the sizable number of pediatric patients with treated, long-term hydrocephalus who often need status evaluation of their ventricular size, additional radiation reduction in CT was investigated as a viable imaging alternative. The objective of this work was to determine the minimum radiation dose that still adequately evaluates ventricular size in this pediatric population.
Materials & Methods
Raw data from clinical pediatric head CTs performed on a 128-slice CT scanner (Definition Flash, Siemens Healthcare) was collected and transferred to an external workstation. The exams included five heads on pediatric patients, ranging in age from six months to 14 years. Using a validated noise insertion tool developed at our institute, three different noise levels were inserted into each raw dataset, resulting in unique datasets simulating 50%, 25%, and 10% of the original dose level. Each dataset was reconstructed using both original filtered-back projection (FBP) and sinogram affirmative iterative reconstruction (SAFIRE) methods. For each case, each dose level and reconstruction method, both soft tissue and bone kernel images were produced. Eighty different images were generated (five patients x four dose levels x two reconstruction methods x two kernels) and then independently evaluated by experienced neuroradiologists who were blinded to the dose and reconstruction method. The radiologists indicated which of the 80 images provided acceptable image quality, thereby allowing the lowest acceptable dose to be determined.
Results
Both the soft-tissue and bone reconstruction images reduced to 10% of the original dose were deemed clinically acceptable to the group of neuroradiologists. No perceptible difference between reconstruction methods was detected. Based on the results from reconstruction, the average CTDIvol for patients was reduced by 90% from 26.6 mGy ± 12.1 mGy to approximately 2.7 mGy. Using the conversion factor for a five-year-old patient, the dose was effectively reduced to 0.16 mSv, roughly equivalent to that of a chest radiograph.
Conclusion
A novel noise insertion tool to simulate reduced-dose exams from existing patient exams was validated. Dose reductions of 90% were realized while maintaining acceptable image quality to answer the specific clinical question of ventricular size. At such reduced CT doses, long patient term patient radiation exposure is significantly reduced, workflow efficiency is improved (including avoiding patient transport to a facility with a MRI scanner) and exposures to MRI safety risks reduced utilizing CT as a reasonable alternative to emergent MRI.

KEYWORDS: Radiation dose reduction, Ventricles, pediatric

P-105a

Usefulness of T2 Star/Susceptibility-Weighted Imaging for Detection of Cavernous Angioma after Cranial Irradiation for Treatment of Embryonal Tumors

Yamasaki, F.·Watanabe, Y.·Takayasu, T.·Nosaka, R.·Akiyama, Y.·Saito, T.·Sugiyama, K.·Kurisu, K.
Hiroshima University Hospital
Hiroshima, JAPAN.

Purpose
The incidence of cavernous angiomas after cranial irradiation is unclear as is the role of T2*- or susceptibility-weighted imaging in their diagnosis. We investigated the incidence of cavernous angioma after cranial irradiation using T2*- or susceptibility-weighted imaging.
Materials & Methods
Between 1990 and 2011, 34 patients with embryonal tumors (22 medulloblastomas, six primitive neuroectodermal tumors, six pineoblastomas) were treated at our institution; 31 received cranio-spinal irradiation. All underwent surveillance MRI studies at least once a year. The diagnosis of cavernous angioma was based solely on MRI results. None of the patients underwent surgery for cavernous angioma and none of the lesions were confirmed histologically.
Results
At the time of the last surveillance studied 20 patients were alive and disease-free. Among them, 12 had developed cavernous angiomas after cranial irradiation, in nine patients there were multiple cavernous angiomas. Three patients developed symptomatic lesions (headache/diplopia/abducens palsy); their cavernous angiomas were classified as Zabramski type 3 or 4.

Note: Scanned images are included in the proceedings. Some submitted images were reduced during editing, thereby decreasing clarity. Also, refer to the Program Planner. Proceedings Content as of 3-29-2013.

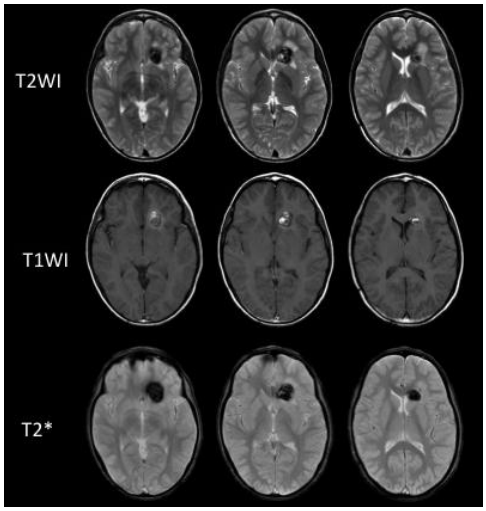

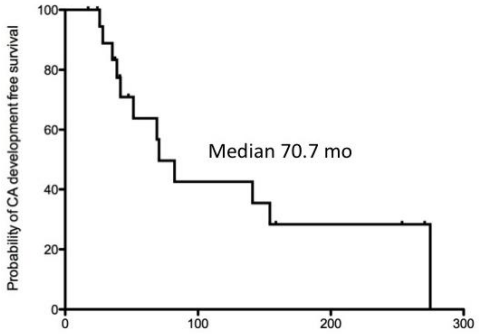

Conclusion
We attribute the higher incidence of cavernous angioma after cranial irradiation in our studies - rather than earlier studies - to our use of T2*- or susceptibility-weighted imaging. Based on our experience we recommend that T2*- or susceptibility-weighted imaging be included in follow-up studies of patients treated by cranial irradiation.

KEYWORDS: Cavernoma, Radiation toxicity, medullobastoma

Monday, May 20 – Wednesday, May 22
6:30 AM – 9:00 PM
Thursday, May 23
6:30 AM – 3:00 PM
Hall B1

Scientific Posters Printed 106 - 108

P6-Socioeconomics

Note: A missing printed number indicates an abstract has been withdrawn.

P-106

Survey into the Prevalence of Radiation-Induced Lens Injury (Cataracts) in Interventional Neuroradiologists

Djoukhadar, I. A.[1]·Jeeva, I.[2]·Chang, B.[2]·Patankar, T.[1]·Goddard, A.[1]
[1]Leeds Radiology Academy, Leeds, UNITED KINGDOM,
[2]Leeds Teaching Hospitals, Leeds, UNITED KINGDOM.

Purpose
Observational study to assess the prevalence of radiation-induced cataract in neurointerventionists.
Materials & Methods
All delegates present at a national neuroradiology conference (Leeds, UK) were invited for a vision check and dilated pupil examination to assess for the presence of cataracts. Examination was performed by a slit lamp and the Lens Opacity Classification System (LOCS-III) was used to assess disease severity. All neurointerventionists with at least two years or a minimum of 50 procedures experience were invited to take part. Exclusion criteria included ocular comorbidities and allergy to Tropicamide or Phenylephrine.
Results
A total of 15 participants took part with age range of 32 - 59 years and male to female ratio of 13:2. Nine doctors were compliant with eye protective goggles. Seven of 15 participants had a cataract that was considered more than the age-matched control. However, only two had visually significant cataracts. This group did not need surgery as vision improved with the use of glasses. The prevalence of cataracts in the goggles-compliant group was three of nine and for the noncompliant group four of six.
Conclusion
This small-scale study shed some light on the prevalence of “radio-cataract” among interventional

Note: Scanned images are included in the proceedings. Some submitted images were reduced during editing, thereby decreasing clarity. Also, refer to the Program Planner. Proceedings Content as of 3-29-2013.

neuroradiologists. Further study with a larger number of participants would be useful in determining the true disease incidence.

KEYWORDS: Radiation injury, cataract

P-107

Lessons Learned from Restructuring MR Imaging Patient Scheduling: A Quality Improvement Project

Ametlli, V.·Wessman, B.·Stickney, K.·Hartzog, J.·Davis, M.·Scarpace, L.·Bower, L.·Faulkner, M.·Remer, S.·Jain, R.
Henry Ford Health System
Detroit, MI.

Purpose
Scheduling a magnetic resonance imaging (MRI) study requires a lot of preparation before an appointment slot can be given to a patient. The one-year transformation from paper to electronic ordering of imaging exams and development of an electronic protocol application at our institution greatly improved processing quality but did not remove barriers to provide patients with same-day MRI appointments. Difficulties in scheduling same-day appointments resulted from varying time for appointments depending on the study and availability of MRI equipment, prior insurance authorization check, proper patient screening and backlog of appointments to schedule. A Lean process improvement team was assembled with the purpose of improving the turnaround time for scheduling an MRI from an average of 4.8 days to same day through process redesign, maximizing resources and elimination of waste. The purpose of this presentation will be to describe this process in detail, discuss the hurdles we faced and our results.
Materials & Methods
A team comprised of key process stakeholders from customer service representatives, technologists, specialty clinic nurses, neuroradiologists, project facilitators, computer analysts and MRI leadership used the PDCA cycle and Lean tools as the foundation to guide the continuous improvement journey. The team mapped current state process and with patient involvement identified opportunities for improvements. Development of key process measures along with baseline data collection guided direction and prioritization of efforts. Five subgroups were formed and met on a weekly basis during the six-month project period to implement action plans. Leveraging home-grown electronic systems assisted in timely data analysis and implementation of electronic changes. On-going communication to team members and staff assisted in ownership and engagement in solving problems.
Results
Through redesigning scheduling process, revision of MRI sequencing protocols, standardizing scheduling blocks, automating exam timing, decreasing radiologist time to protocol order (days to hours), development of service standards and optimization of pre-authorization process, the improvement team was able to streamline steps to schedule the appointment and reduce turnaround time for scheduling from 4.8 days to same day. The improvements benefited patients and especially clinics such as Neurosurgery, who were dependent on the patient completing their study in a timely manner to assist with treatment plan. Process efficiency gains resulted in reducing financial cost by 3 FTEs, a cost saving of $120,000/year.
Conclusion
The commitment from leadership in supporting establishment of a multidisciplinary team combined with using a structured problem-solving methodology allowed the team to produce results that exceeded the area benchmark of 72 hours for an MRI appointment. The combined innovative changes provided financial savings but most importantly the project team spread a culture of problem-solving and improvement in the department. To ensure changes are sustained over time, key process owners are tracking and taking action as needed. The efficiency gains in standardization of exam timings are being spread across the Health System as it prepares to roll-out a new Electronic Medical Record system. Readers will gain an understanding of how to apply Lean methodology to develop a patient-centered scheduling model.

KEYWORDS: Quality assurance, Quality improvement, Lean

P-108

Quality Efforts Centered on Mitigating Clinical Impact of an Unusual MR Imaging Artifact

Watson, R. E.[1]·Welker, K. M.[1]·Wood, C. P.[1]·Miller, G. M.[1]·Prescott, S. L.[1]·Kollasch, P. D.[2]
[1]Mayo Clinic, Rochester, MN, [2]Siemens Healthcare, Malvern, PA.

Purpose
To describe a clinical scenario in which a coordinated effort including neuroradiologists, quality office personnel at the departmental and institutional level, medical physicists, and vendor applications specialists quickly mitigated the potential clinical impact of a previously unrecognized artifact in MRI. These efforts identified that the artifact was produced when a new abdomen-optimized flow compensation technique on T1 3D turbo spin-echo with variable flip angle (T1 SPACE) images was used in the brain. The artifact manifested by subtle pseudoenhancing "lesions" in patients with concomitant T2 signal hyperintensities in the brain. A culture of safety focus facilitated rapid and thorough addressing of the issue.
Materials & Methods
A new flow-compensation method utilized in abdominal imaging to reduce signal from blood flow in the liver on T2 STIR imaging was applied to gadolinium-enhanced T1

Note: Scanned images are included in the proceedings. Some submitted images were reduced during editing, thereby decreasing clarity. Also, refer to the Program Planner. Proceedings Content as of 3-29-2013.

SPACE images of the brain to decrease dural venous sinus pulsation artifact. Preliminary studies in volunteers demonstrated decreased pulsation artifact and no apparent image degradation. This technique then was implemented clinically for contrast-enhanced brain studies. After approximately six weeks of use the possibility of subtle pseudo-enhancement was recognized. This prompted a medical physics, vendor applications specialist, and quality office investigation of the 108 contrast-enhanced clinical brain exams during this period that included the new post-gadolinium T1 SPACE flow compensation technique. 26 neuroradiologists reviewed these cases to assess for potential spurious conclusions that may have been a result of this artifact. When needed, the electronic medical record was reviewed and referring clinicians contacted.

Results

The inclusion of the new flow compensation technique on contrast-enhanced T1 SPACE images produced variable subtle pseudo ring enhancement about the periphery of T2 hyperintense foci. This included around areas of presumed leukoaraiosis, demyelinating plaques and other lesions. In one case, there were ring-enhancing pseudolesions surrounding sites of T2 hyperintensity in both cerebral hemispheres which resulted in a differential diagnosis of parasitic, infectious, embolic, or neoplastic etiologies. This prompted additional clinical investigation and body CT, MR, and US studies, spine MRI, as well as a lumbar puncture. In another case, despite the presence of pseudo enhancement about some lesions, there were other lesions with presumed true enhancement and clinical management was not altered. The first patient described above returned for additional imaging including T1 SPACE sequences performed with and without the new flow compensation, and both before and after intravenous gadolinium contrast administration. This demonstrated that the T1 hyperintensity about T2 hyperintense foci was present and unchanged both before and after IV gadolinium administration, confirming that this was due to artifact. Quality office personnel at both the departmental and institutional level closely monitored the analysis through its completion.

Conclusion

This clinical scenario illustrates the value to patient safety of coordinated collaborative work between radiologists, medical physicists, quality experts, along with vendor support specialists to quickly problem-solve a previously unknown imaging artifact and the extent of its clinical impact.

KEYWORDS: Contrast-enhanced MR imaging, Artifacts

Monday, May 20 – Wednesday, May 22
6:30 AM – 9:00 PM
Thursday, May 23
6:30 AM – 3:00 PM
Hall B1

Scientific Posters Printed 109 - 113

P7-Spine

Note: A missing printed number indicates an abstract has been withdrawn.

P-109

Efficacy of CT-Guided Blood Patch for Treatment for Intracranial Hypotension: Our Experience

Chai, B. B.·Huang, R. Y.
Brigham and Women's Hospital
Boston, MA.

Purpose

Blood patch is the mainstay treatment for spontaneous intracranial hypotension (SIH). Although targeted blood patch has been shown to have greater efficacy compared to blinded blood patch, a significant number of patients presenting with SIH have an unknown leak site despite imaging workup. We retrospectively evaluated 24 patients with SIH in our institution from 2009-2012 who have had a negative total spine CT myelography and evaluated the success rate of symptom improvement and symptom recurrence following lumbar blood patch alone, upper thoracic spine blood patch alone, or successive lumbar blood patch and upper thoracic blood patch.

KEYWORDS: Spinal CSF leak, Blood patch

P-110

Can Radiofrequency Kyphoplasty Improve the Pulmonary Function?

Pflugmacher, R.·Bornemann, R.·Jansen, T. R.·Kabir, K.·Wirtz, D. C.
Universitätsklinikum Bonn
Bonn, GERMANY.

Purpose

Vertebral compression fractures not only reduce the activities of daily living (ADL) because of pain, they also cause respiratory dysfunction. This study investigates the

Note: Scanned images are included in the proceedings. Some submitted images were reduced during editing, thereby decreasing clarity. Also, refer to the Program Planner. Proceedings Content as of 3-29-2013.

impact of radiofrequency kyphoplasty treatment not only on the reduction of back pain and the restoration of vertebral body height, but also on pulmonary function.
Materials & Methods
Twelve patients (six male; mean age 67.6 ± 10.4 years) with vertebral compression fractures at the lumbar spine L1 (n = 7) or L2 (n = 5) were treated by radiofrequency kyphoplasty. The Oswestry Disability Index (ODI) and back pain, assessed by the visual analog scale (VAS; 10 cm), were evaluated by each patient one day before the procedure and 30 days after the procedure. The vertebral body height at anterior, medial and posterior aspect was measured one day before the procedure, one day after the procedure and 30 days after the procedure. For evaluation of pulmonary function a spirometer was used to determine the one-second forced expiratory volume (FEV1) and the peak expiratory flow (PEF), one day before the procedure, one day after the procedure and 30 days after the procedure.
Results
The treatment of vertebral compression fractures via radiofrequency kyphoplasty led to significant reduction of back pain (VAS) 30 days after treatment compared with one day before, 77.6 ± 14,4 (mean ± standard deviation) and 17.2 ± 27,1, respectively. The ODI decreased significantly from 74.7 ± 13.6% one day before the procedure to 21.0 ± 16.2% 30 days after the procedure. There was considerable restoration of vertebral body height one day after the procedure with mean values of 2.8 mm, 3.7 mm and 0.3 mm at the anterior, medial and posterior aspect, respectively. Vertebral body height decreased minimally 30 days after the procedure; however there still was notable restoration in comparison to one day before the procedure by 1.0 mm at the anterior, 1.8 mm at the medial and 0.0 mm at the posterior aspect. There was minimal improvement of pulmonary function as early as one day after the procedure and significant values were obtained 30 days after the procedure ($p<0.01$). The improvement of FEV1 one day after the procedure compared with one day before was 0.1 l/s and 30 days after the procedure compared with one day before 0.4 l/s. The PEF improved one day after the procedure compared with one day before by 50.6 l/min and 30 days after the procedure compared with one day before by 75.2 l/min.
Conclusion
The treatment of vertebral compression fractures at the lumbar spine by radiofrequency kyphoplasty, not only restored the vertebral body height, reduced pain or improved ODI, but also improved pulmonary function significantly.

KEYWORDS: Kyphoplasty, Osteoporosis, lung function

P-111

Is There an Association between Abnormal MR Imaging Signal Intensity of the Nerves around the Elbow Joint and Professional Baseball Pitching?

Thawait, S. K.[1]·Farahani, S. J.[2]·Thawait, G. K.[2]·Demehri, S.[2]·Chhabra, A.[2]
[1]Bridgeport Hospital, Bridgeport, CT, [2]Johns Hopkins Hospital, Baltimore, MD.

Purpose
Repetitive micro-trauma due to frequent throwing results in increased susceptibility to peripheral nerve injury in professional baseball pitchers. The purpose of this study is to evaluate the association between abnormal T2 hyperintensity of the peripheral nerves around the elbow joint and professional baseball pitching.
Materials & Methods
Axial fat-saturated T2W images were reviewed retrospectively for presence of abnormal T2 hyperintensity of the radial, median and ulnar nerve around the elbow joint, which was defined as similar or higher signal intensity than the adjacent vessels. Following the blinded review of MR images, the frequency of abnormal T2 hyperintensity of the nerve was calculated in professional pitchers and nonpitchers. A univariate model was designed to examine the probability of significant difference in these two groups. To adjust for the effect of confounding factors and not normality of data distribution, a multivariate regression model was used.
Results
Out of 96 MRI examinations reviewed, 74 were found to be satisfactory. Thirty-four subjects (11 F, 23 M; age 49±15 years) were nonpitchers, while 40 subjects (1 F, 39 M; age 24±5.8 years) were professional pitchers. Radial nerve hyperintensity was seen in 2/34 (6%) of the nonpitchers and 9/40 (23%) of the pitchers (p value 0.06). Median nerve hyperintensity was seen in 3/34 (8%) of the nonpitchers and 10/40 (25%) of the pitchers (p value 0.05). Ulnar nerve hyperintensity was seen in 13/34 (38%) of the nonpitchers and 19/40 (47.5%) of the pitchers (p value 0.42). T2 hyperintensity of median and radial nerves were close to being significant. After adjusting the model for age and sex as a confounding factor and not normality of median and redial nerve data distribution, no significant difference between the professional pitchers and nonpitchers in terms of frequency of hyper-intensity of the selected nerves was detected.

Note: Scanned images are included in the proceedings. Some submitted images were reduced during editing, thereby decreasing clarity. Also, refer to the Program Planner. Proceedings Content as of 3-29-2013.

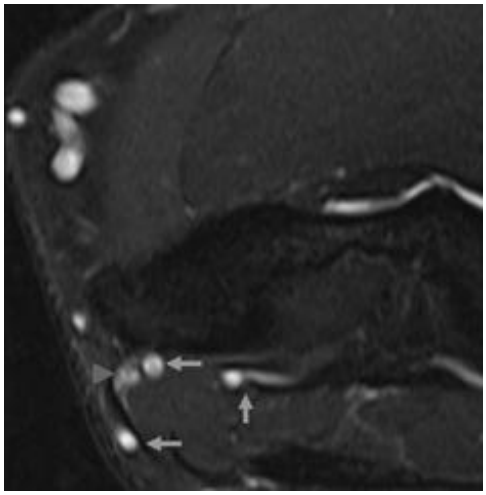

Figure: Axial fat-saturated PD image shows increased signal intensity of ulnar nerve (arrowhead), almost equal to signal intensity of adjacent vessels (arrows) in a professional baseball pitcher.

Conclusion

The results indicate that abnormal T2 hyperintensity of peripheral nerves around the elbow joint is seen commonly in professional pitchers, although the difference was not significant statistically. A larger sample with normal asymptomatic population which will serve as control cases might be helpful in examining the possible association. This finding of hyperintensity of peripheral nerves should be included in the report as early recognition and appropriate therapy may prevent further neurologic damage and permanent irreversible neuropathy.

KEYWORDS: Nerve imaging, Neurography, peripheral nerve MR imaging

P-112

Structure-Function Relationship in Healthy and Myelopathic Spinal Cord: A Combined Diffusion Tensor Imaging and Functional MR Imaging Study

Cui, J.·Li, X.·Luk, D.·Hu, Y.
The University of Hong Kong
Hong Kong, HONG KONG.

Purpose

Currently magnetic resonance imaging (MRI) plays an important role in the diagnosis of cervical spinal cord disorders [e.g., cervical spondylotic myelopathy (CSM)]. The conventional T1- and T2-weighted MRI has provided great benefits in terms of rapid, noninvasive and accurate imaging of cord morphology. However, it is reported that the morphologic and signal change do not necessarily correlate with functional behavior and clinical symptoms. Recently, diffusion tensor imaging (DTI) and blood oxygen level-dependent (BOLD) MR imaging has been developed rapidly to investigate the microstructure and functional behavior of the spinal cord. In this study, we aim to combine the anatomical, functional and diffusion tensor MRI to explore the relationship between function and structure in healthy and myelopathic cervical spinal cord.

Materials & Methods

A total of twenty subjects were recruited with written informed consent, including 14 healthy subjects (age=56±13 years) and six CSM patients (age=67±14 years). Anatomical T2-weighted, diffusion tensor and functional MRI were scanned covering the whole cervical spinal cord from C1 to C7 on a 3T MR system. Cross-sectional area, compression ratio, fractional anisotropy, axial diffusivity, radial diffusivity and BOLD signal change were measured (Figure 1).

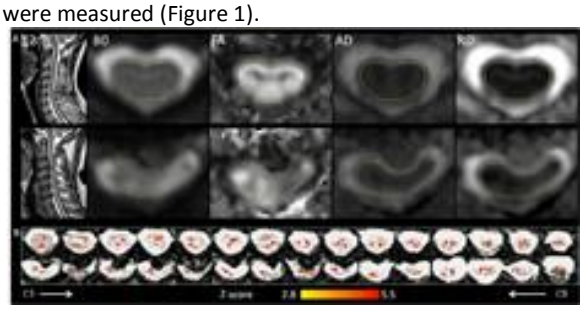

Results

The result showed that BOLD signal change in response to somatosensory stimuli was significantly higher in myelopathic cord (7.86±0.95%) compared to healthy cord (5.52±0.21%) ($p<0.01$). Significant differences were detected between healthy and myelopathic cord for: cross-sectional area (Healthy: 81.78±15.59; CSM: 61.35±14.71, $p<0.05$), compression ratio (Healthy: 58.33±13.03%; CSM: 51.51±10.13%, $p<0.05$), fractional anisotropy (Healthy: 0.65±0.07; CSM: 0.53±0.10, $p<0.01$) and radial anisotropy (Healthy: $0.63\pm0.12\times10^{-3}$ mm^2/s; CSM: $1.05\pm0.47\times10^{-3}$ mm^2/s, $p<0.01$). There was no significant difference of axial diffusivity between healthy subjects and CSM patients (Healthy: $1.71\pm0.14\times10^{-3}$ mm^2/s; CSM: $1.73\pm0.13\times10^{-3}$ mm^2/s) ($p>0.05$). BOLD signal change indicated a much stronger correlation with FA value (Healthy: $r=0.4887$, $p=0.0764$; CSM: $r=-0.8938$, $p=0.0163$) and RD value (Healthy: $r=-0.5348$; $p=0.0488$; CSM: $r=0.8239$; $p=0.0438$) compared to that with compression ratio or cross-sectional area.

Conclusion

Our results indicate that diffusion tensor measurement provides a more accurate estimation of spinal cord functional behavior than morphometry. Moreover, greater microstructural damage was significantly and linearly correlated with enhanced activation in myelopathic cord, which implies the functional reorganization in CSM. This study demonstrates a quantitative relationship between the extent of structural integrity and functional response in healthy and myelopathic cord, which might provide a promising method to gain additional insight into the role of structural damage and functional reorganization in the spinal cord diseases.

Note: Scanned images are included in the proceedings. Some submitted images were reduced during editing, thereby decreasing clarity. Also, refer to the Program Planner. Proceedings Content as of 3-29-2013.

KEYWORDS: Diffusion tensor image, BOLD fMRI

P-113

Retrospective Validation of a Rapid Lumbar Spine MR Protocol for Assessment of Patients with Acute Atraumatic Cord Compression Presenting to the Emergency Room

Boe, D. L.[1]·Farquhar, T.[2]·Greenwood, M.[2]·Herbst, T.[2]·Zimmerman, D.[2]·Bansal, A.[2]
[1]Hartford Hospital, Hartford, CT, [2]Hartford Hospital, Rocky Hill, CT.

Purpose
Nontraumatic acute spinal cord injury (NT/SCI) and cauda equina syndrome are medical emergencies that if not identified and treated early can lead to permanent neurologic deficits. MR imaging is strongly recommended for diagnosis and prognosis of acute spinal cord injury and can be used to direct clinical decision-making; sagittal T2 sequences are of particular diagnostic utility. There are many etiologies of acute NT/SCI, including spinal stenosis, bulky disk herniation, compression from a mass, infection, and vascular compromise. Delay in treatment can result in permanent neurologic deficits. The ideal protocol should be both sufficiently informative, yet not time-consuming to perform or interpret. Utilization of MRI continues to increase, particularly in the ER setting. The purpose of this study is to optimize and retrospectively validate an MRI protocol for acute NT/SCI for the emergency department at Hartford Hospital, a busy tertiary care hospital that triages over 100,000 patients/year in the ED. A rapid protocol could reduce the time to patient treatment, facilitate the clinician's ability to obtain an MRI for more patients in general, as well as for patients who are medically unstable, and decrease overall cost by reducing scan time.
Materials & Methods
Sagittal T1 (noncontrast) and T2 sequences from 30 consecutive MRI examinations of the lumbar spine ordered from the emergency department for NT/SCI were pulled from the Hartford Hospital PACS, without regard to whether the studies initially had been performed with or without contrast. Four radiologists (two experienced neuroradiologists, DLZ and MMG, and two experienced radiologists with subspecialties other than neuroradiology, TF and TH) were blinded to the clinical and demographic information of the subjects as well as the previous interpretation. Their interpretations based on the sagittal T1 and T2 sequences only were compared with the original interpretations (DLB and AB).
Results
The overall accuracy of all readers was extremely high, ranging from 83-90%. There was substantial agreement between readers as well (Cohen's kappa of 0.71 between neuroradiologists and 0.77 between non-neuroradiologists). When noncontrast studies were evaluated separately, performance was significantly better, with accuracy rates ranging from 91-100%. In particular, both neuroradiologists were 100% accurate with all noncontrast exams. Accuracy on studies initially performed with contrast ranged from 74-84%.
Conclusion
A lumbar MRI protocol limited to sagittal T1- and T2-weighted sequences for assessment of acute atraumatic NT/SCI presenting to the ER is a robust technique with high interobserver agreement across radiologists in multiple subspecialties. This protocol can accurately diagnose specific etiologies of acute NT/SCI, especially for exams that are requested without gadolinium contrast. Implementation of this protocol in the ED setting has the potential to reduce the time to treatment for patients, limit patient morbidity and mortality, facilitate a clinician's ability to obtain an MRI for more patients, and decrease overall cost by reducing scan time.

KEYWORDS: Spinal imaging, MR imaging spine

P-114

Utility of CT-Guided Bone Biopsy for Vertebral Osteomyelitis

Bauml, J. A.·Bosman, S. A.·Hansra, N.·Saran, N.
University of Illinois at Chicago Medical Center
Chicago, IL.

Purpose
CT-guided bone biopsy has been advocated as a useful tool to aid in the diagnosis and treatment of suspected vertebral osteomyelitis. No large review study providing convincing evidence supporting this practice is available. This single institution retrospective study is aimed at providing concrete data to help guide the discussion and debate over the usefulness of image-guided bone biopsy for vertebral osteomyelitis.
Materials & Methods
Data pertaining to vertebral body bone biopsies performed from January 2003 to March 2011 at the University of Illinois Hospital Chicago was compiled. Antibiotic regimens/treatment plans (prebiopsy) for the patients undergoing biopsy were recorded. Alterations in treatment plan based on the results of these biopsies were analyzed. The study design was that of a retrospective chart review.
Results
Of the 109 total vertebral body biopsies performed during the study period, 72 were performed for clinically or radiologically suspected cases of vertebral osteomyelitis. Fifty of these patients with clinically diagnosed osteomyelitis had negative culture results. Of the patients with negative culture results, the biopsy changed management in one case, but that change was based on unexpected pathology rather than culture results. In seven patients the biopsies never yielded a diagnostic culture. The total number of positive culture results from these 72 biopsies was 15. Two of those patients were lost to

Note: Scanned images are included in the proceedings. Some submitted images were reduced during editing, thereby decreasing clarity. Also, refer to the Program Planner. Proceedings Content as of 3-29-2013.

followup. Out of the 13 remaining patients, the treatment plan for nine was changed based on the results. Four out of nine were not on prebiopsy antibiotics and were started on tailored therapy. Five out of nine patients' preexisting antibiotic regimens were tailored. Of the 65 specimens that were successfully cultured by microbiology, 15 cultures were positive. This corresponds to a culture positivity rate of 23%. In summary, nine patients who underwent biopsy had their management changed on the basis of the microbiology report. However, the other 57/72 (87.5%) patients who underwent biopsy for culture did not have their treatment changed as a result.

Vertebral biopsies performed by radiology for suspected osteomyelitis 1/2003 to 3/2011

	N	% of total	N Culture result changed treatment	% Treatment changed
Osteo suspected clinically and biopsy ordered	72		9/72	12.5%
Biopsy sample successfully obtained	70	97.2%	9/70	12.9%
Positive Culture	15	23.1%	9/15	60.0%
Negative Culture	50	76.9%	0/50	0.0%
Error in transfer*	4			
Improper preparation**	1			

*Pathology was performed on specimen but the specimen was not received by microbiology
** Specimen sent in formalin and unable to be used for culture

Conclusion
Because (1) image-guided bone biopsies fail to provide an etiologic microorganism in most cases of clinically suspected osteomyelitis-diskitis and (2) in the setting of positive culture results broad-spectrum antibiotics often are continued unchanged, and (3) osteomyelitis is a clinical diagnosis and therefore a negative culture does not allow one to cease antibiotics in suspected cases: bone biopsy may not be a useful tool to guide treatment except in cases in which there is high clinical suspicion of an atypical organism such as tuberculosis.

KEYWORDS: Osteomyelitis, Biopsies, CT-guidance

Monday, May 20 – Wednesday, May 22
6:30 AM – 9:00 PM
Thursday, May 23
6:30 AM – 3:00 PM
Hall B1

Electronic Posters (ePosters)
1 - 101b

ePI-Adult Brain

Note: A missing printed number indicates an abstract has been withdrawn.

eP-1

Clinical Assessment of Improved Motion Sensitized Driven Equilibrium Prepared T1-Weighted Black-Blood Imaging for Intracranial Aneurysms

Maeda, M.[1]·Inoue, K.[1]·Umino, M.[1]·Yamahata, T.[1]·Suwa, A.[2]·Sakuma, H.[1]
[1]Mie University School of Medicine, Tsu, JAPAN, [2]Philips Electronics Japan, Tokyo, JAPAN.

Purpose
Thrombotic aneurysm can cause complicating events at the time of the intravascular or surgical treatment. Therefore, the precise detection of thrombus is of value for treatment strategies. Black-blood imaging (BBI) has been proposed for the assessment of vessel wall abnormalities. However, current BBI techniques provide insufficient images because of flow-related artifacts, particularly in intracranial vessels. This study is intended to evaluate the flow suppression capability of improved motion sensitized driven equilibrium (iMSDE) prepared sequence compared with standard BBI in patients with intracranial aneurysms.
Materials & Methods
Thirty-two patients with intracranial aneurysms were studied using 3T (Achieva; Philips Co.). The aneurysm diameter was 13.2 $\pm$ 7.1 mm. Black-blood imaging techniques included the standard 3D T1-weighted fast SE (VISTA) and the iMSDE-prepared VISTA. Visual assessment for flow suppression was performed using a four-point score. Quantitative assessment was achieved using the contrast ratio between the luminal signal within the aneurysm and adjacent brain parenchyma.
Results
Visual assessment showed that the iMSDE-prepared VISTA

Note: Scanned images are included in the proceedings. Some submitted images were reduced during editing, thereby decreasing clarity. Also, refer to the Program Planner. Proceedings Content as of 3-29-2013.

was significantly higher in scores than the standard VISTA (p<0.01). The signals inside aneurysms, particularly with diameter greater than 9 mm, were suppressed more strongly using iMSDE, indicating that the vessel wall boundary was more clearly visualized and that the thrombus was more definitely depicted if present (Figure). Quantitative assessment revealed that the iMSDE-prepared VISTA provided a significantly better contrast ratio than the standard VISTA did (p<0.01).

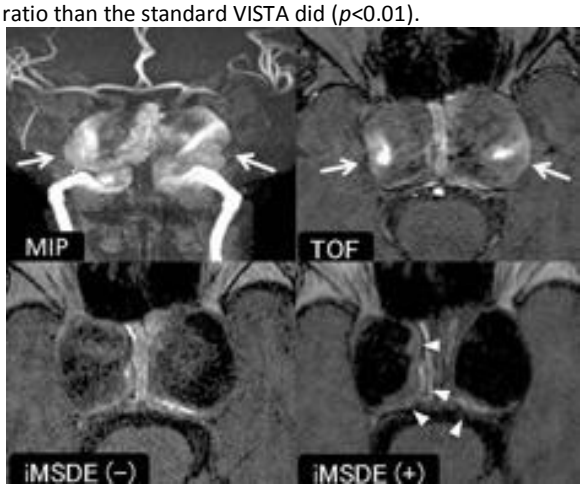

Conclusion

The iMSDE-prepared BBI was able to suppress the signal of intracranial aneurysms more strongly than the standard BBI can. Improved motion sensitized driven equilibrium-prepared BBI appeared to be more suitable for detection of thrombus within intracranial aneurysms.

KEYWORDS: 3 T, Aneursym, black-blood imaging

eP-2

Volume of Interest C-Arm CT Imaging during Endovascular Treatment of Aneurysms: A Comparison of Various Truncation Correction Algorithms

Chintalapani, G.[1]·Chinnadurai, P.[1]·Shaltoni, H.[2]·Morsi, H.[2]·Mawad, M. E.[3]
[1]Siemens Medical Solutions USA Inc., Hoffman Estates, IL, [2]St. Luke's Episcopal Health System, Houston, TX, [3]Baylor College of Medicine, Houston, TX.

Purpose

Volume of interest (VOI) imaging allows additional and repeated C-arm CT acquisitions during the endovascular treatment without significant increase in radiation exposure (70-80% reduction in dose), thus providing real-time 3D information of the device deployment status and vessel wall apposition during the procedure. However, current VOI reconstruction techniques suffer from severe truncation artifacts because of the smaller field of view. Hence, we propose to evaluate three different truncation correction algorithms developed for VOI imaging.

Materials & Methods

Volume of interest images were obtained in 10 patients undergoing endovascular treatment of intracranial aneurysms. 20s-DR DynaCT (Axiom Artis zee, Siemens AG, Forchheim, Germany) images were acquired by iso-centering around the implanted device with the x-ray source collimated on the VOI (approximately 12% size of the full volume). The VOI images were reconstructed using three different offline prototype reconstruction algorithms (Water Cylinder, ATRACT 1D, and ATRACT 2D) that correct for truncation artifacts. The resulting VOI reconstructions were compared to secondary reconstructions from full volume C-arm CT images using image similarity metric, in particular structural similarity index metric (scale of 0-1, with 0 being completely dissimilar images and 1 being exactly similar images).

Results

Qualitative analysis shows that the VOI images are comparable to the secondary reconstructions from a full volume image (Figure 1). Quantitative comparison of image similarity metric between the prototype VOI reconstructions and the ground truth reconstruction (from full head acquisition) show a similarity index of 0.7, 0.72, and 0.74 respectively. Moreover, the similarity metric for high contrast objects such as flow diverters, stents etc. is very close to 1 (Figure 1).

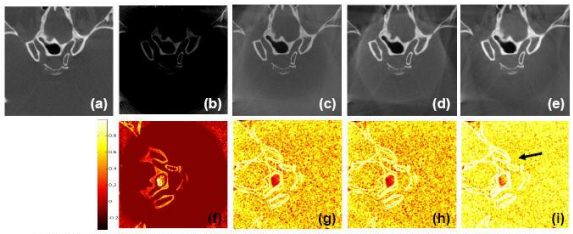

Fig 1. (a) secondary reconstruction from full head scan, (b) standard reconstruction of a VOI acquisition, (c)-(e) prototype reconstructions with truncation correction algorithms for VOI acquisition, (f) structural similarity index between (b) and (a), (g) structural similarity index between (c) and (a), (h) structural similarity index between (d) and (a), and (i) structural similarity index between (e) and (a). Note the high contrast objects such as flow diverter and bones have a similarity index close to 1.

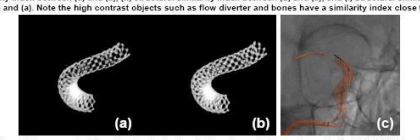

Fig 2. (a) VRT rendering of the segmented flow diverter device from full head acquisition as shown in Fig 1(a), (b) VRT rendering of the segmented flow diverter device from VOI reconstruction with truncation correction as shown in Fig 1(c), (c) An example of segmented flow diverter device overlaid on fluoroscopic images for further image guidance.

Conclusion

All three proposed truncation correction algorithms for VOI imaging perform almost similarly resulting in high quality 3D images of the object of interest (especially high contrast structures like stents, pipeline embolization devices, etc). Volume of interest imaging during endovascular treatment of aneurysms can provide immediate feedback on the device deployment status and the vessel wall apposition. In addition, 3D image of the deployed device can be segmented and overlaid on 2D fluoroscopy for image guidance through the rest of the procedure.

KEYWORDS: Aneurysm treatment, 3D computed tomography, volume of interest imaging

Note: Scanned images are included in the proceedings. Some submitted images were reduced during editing, thereby decreasing clarity. Also, refer to the Program Planner. Proceedings Content as of 3-29-2013.

eP-3

Serial MR Findings of Giant and Large Internal Carotid Aneurysms after Endovascular Parent Artery Occlusion

Morikawa, M.·Enokizono, M.·Koike, H.·Uetani, M.·Hayashi, K.·Horie, N.·Fukuda, S.·Nagata, I.
Nagasaki University
Nagasaki, JAPAN.

Purpose
The aim of this retrospective study was to evaluate the serial MR findings of giant and large internal carotid aneurysms after endovascular parent artery occlusion.
Materials & Methods
Between 2003 and 2011, we treated 12 patients of giant/large internal carotid aneurysm, including 11 unruptured and one ruptured at our institution. Maximum diameter of the aneurysm ranged from 18 to 65 mm (average of 31 mm). Nine of the 12 patients presented with diplopia, one with reduced visual acuity, one with massive nasal bleeding, and remaining one with no symptom. Proximal parent artery occlusion with rough packing of the aneurysm was performed in eight unruptured aneurysms, trapping with rough packing in three unruptured aneurysms and trapping without packing in one ruptured aneurysm. Total 82 MRI/MRA were performed in the follow-up period ranging from14 to 71 months. We evaluated the change of size and signal intensity (SI) of the aneurysms after endovascular treatment.
Results
Reduction of the aneurysm size was observed in 10 of 12 treated aneurysms during follow-up period. The volume of these 10 aneurysms fell to 20-75% of its initial value 8 to 61 months after treatment. In six of the 10 aneurysms, MR was performed within four days after endovascular treatment, and these aneurysms demonstrated high SI on T1-weighted image (T1WI), and low or mixed high/low SI on T2-weighted image (T2WI). As reduction in size of the 10 of 12 aneurysms, high SI areas within the aneurysms on T1WI became iso to low SI, and low or mixed SI on T2WI gave high SI. In remaining two of 12 treated aneurysms, the size of the aneurysms was unchanged or increased up to 15%, and high SI foci on T1WI and low SI foci on T2WI appeared in different region of the aneurysms during follow-up period. Digital subtraction angiography confirmed the recanalization of these two aneurysms.

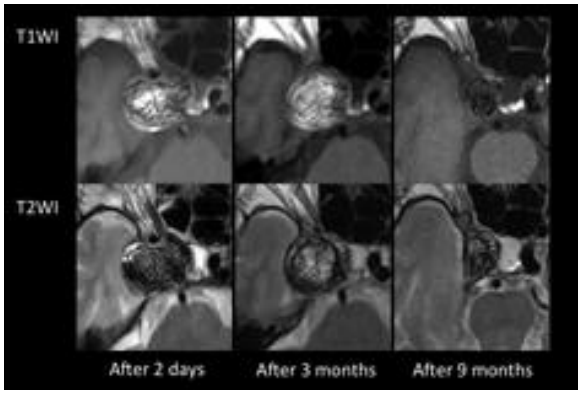

Conclusion
Signal intensity of aneurysms after parent artery occlusion had demonstrated low SI on T1WI and high SI on T2WI with shrinkage of the aneurysms. Appearance of high SI foci on T1WI and low SI foci on T2WI in the aneurysm after treatment indicates recanalization within the aneurysm.

KEYWORDS: 1.5T, 3 T

eP-4

Evaluating Parenchymal Abnormalities Associated with Developmental Venous Anomalies Identified by Susceptibility-Weighted Imaging at 3T

Umino, M.[1]·Maeda, M.[1]·Matsuura, K.[2]·Sakuma, H.[1]
[1]Mie University School of Medicine, Tsu, JAPAN, [2]Suzuka Kaisei Hospital, Suzuka, JAPAN.

Purpose
Since the introduction of susceptibility weighted imaging (SWI), developmental venous anomaly (DVA) has been more incidentally encountered in clinical practice. Susceptibility-weighted imaging enables better visualization of DVAs without requiring any contrast medium. The parenchyma drained by DVA is generally normal, but a few reports have described associated parenchymal abnormalities near DVA, including high signal lesions of the white matter and hemorrhage and/or cavernous hemangioma. More recently, Santucci et al. reported the prevalence of high signal lesions associated with DVAs as 7.8%. However, no report has described the prevalence of brain parenchymal abnormalities associated with DVAs that were identified using SWI. This study is intended to evaluate the prevalence of brain parenchymal abnormalities associated with DVAs identified using SWI at 3T.
Materials & Methods
During January 2008 - November 2012, all brain MR imaging cases studied with SWI at 3T MR machines were reviewed at our hospital and one branch hospital, among which 124 DVAs were identified by SWI. Of those DVAs, 11 DVAs were excluded because abnormal parenchymal findings associated with DVAs could not be determined as a result of underlying white matter changes such as

Note: Scanned images are included in the proceedings. Some submitted images were reduced during editing, thereby decreasing clarity. Also, refer to the Program Planner. Proceedings Content as of 3-29-2013.

ischemic leukoaraiosis. Eventually, 113 DVAs in 112 patients (46 male, 66 female, mean age 55.4 years) were enrolled in this study. We investigated the presence or absence of parenchymal high signal intensities on 2D or 3D FLAIR, as well as hemorrhage and/or cavernous hemangioma on SWI associated with DVAs.

Results

Associated high signal lesions were found in 35 of 113 DVAs (30.9%). A mean maximum diameter of high signal lesions was 12.7 ± 8.1 mm (range 2-33 mm), and high signal lesions typically surrounded DVAs. In four of the 35 DVAs, 3D FLAIR showed a small high signal spot along with DVAs (Figure 1). Concomitant hemorrhage and/or cavernous hemangioma possibly related to DVAs were found in 21 out of 113 DVAs (18.5%). High signal lesions and hemorrhage and/or cavernous hemangioma were found in seven of 113 DVAs (6%).

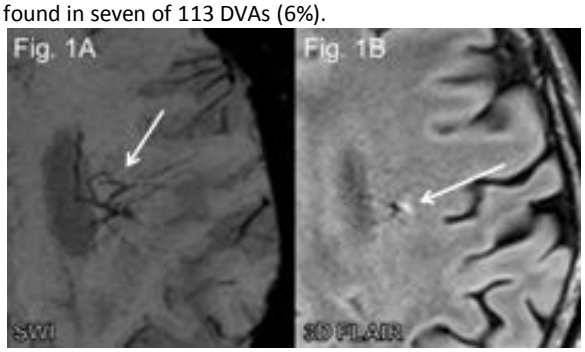

Conclusion

The prevalence of brain parenchymal high signal lesions associated with DVAs might be higher than that reported previously (30.9% vs. 7.8%). Our results suggest that a small high signal spot along with DVAs might be an early finding of associated parenchymal high signal lesions.

KEYWORDS: Developmental venous anomalies, Susceptibility-weighted imaging, associated parenchymal lesions

eP-5

Can 3D Time-of-Flight MR Angiography at 3T Replace Digital Subtraction Angiography in the Characterization of Intracranial Dural Arteriovenous Fistulas?

Hirai, T.·Azuma, M.·Kitajima, M.·Shigematsu, Y.·Kai, Y.·Yamashita, Y.
Kumamoto University
Kumamoto, JAPAN.

Purpose

Since the quality and spatial resolution of images acquired by unenhanced three-dimensional (3D) time-of-flight (TOF) MR angiography (MRA) are improved on 3T MR units, it may replace digital subtraction angiography (DSA) for certain diagnostic purposes in patients with intracranial dural arteriovenous fistulas (DAVF). The purpose of this study was to test the hypothesis that unenhanced 3D TOF MRA at 3T yields the similar characterization of intracranial DAVFs as DSA.

Materials & Methods

Twenty-six consecutive patients with intracranial DAVF (13 women, 13 men; aged 35 - 76 years, mean 60 years) underwent 3D TOF MRA at 3.0T and DSA. The parameters for 3D TOF MRA were TR/TE 20 ms/3.5 ms, flip angle 20°, field of view 20 x 20 cm, matrix 512 x 512, slab 5 chunks, voxel size 0.39 x 0.39 x 1.0 mm (reconstructed voxel size 0.25 x 0.25 x 0.5 mm), parallel imaging factor 2, acquisition time 4 min 48 sec. When a lesion was located at the top of the head, another MRA slab was rostrally added using the same parameters. The main arterial feeders, fistula site, and venous drainage pattern were inspected by two independent observers on 3D TOF MRI and by two other independent readers on DSA. According to the Borden's classification, DAVF drainage was recorded as type 1, drainage directly into the dural venous sinus; type 2, drainage into the dural venous sinus with cortical venous reflux; and type 3, drainage directly into subarachnoid veins. Interobserver and intermodality agreements were assessed by *k* statistics.

Results

At DSA, 13 fistulas were located at the cavernous sinus, six at the transverse sigmoid sinus, two at the hypoglossal canal, two at the superior sagittal sinus, and three at other sites. Interobserver agreement was very good for the main arterial feeders (k = 0.83), excellent for the fistula site (k = 0.94), and very good for the venous drainage pattern (k = 0.88). Intermodality agreement was very good for the main arterial feeders (k = 0.89), the fistula site (k = 0.90), and the venous drainage (k = 0.81).

Conclusion

As unenhanced 3D TOF MRA at 3T is a reliable tool for the evaluation of intracranial DAVF, it may replace DSA to some extent in the characterization of intracranial DAVFs.

KEYWORDS: MR angiography, 3 T, dural AVF

eP-6

Target Delineation for Radiosurgery of a Small Brain Arteriovenous Malformation Using High-Resolution Contrast-Enhanced Cone-Beam CT

van der Bom, I. M. J.·Gounis, M. J.·Ding, L.·Kuhn, A.·Goff, D.·Puri, A. S.·Wakhloo, A. K.
University of Massachusetts
Worcester, MA.

Purpose

Radiosurgery has shown to be a very effective treatment option for brain arteriovenous malformations (bAVMs). Currently, the gold standard technique for diagnostic and follow-up imaging is digital subtraction angiography (DSA). Although this modality provides excellent spatial and temporal resolution, radiosurgery planning using DSA can be tedious as it only provides 2D spatial information. Here we propose the use of high-resolution contrast-enhanced

Note: Scanned images are included in the proceedings. Some submitted images were reduced during editing, thereby decreasing clarity. Also, refer to the Program Planner. Proceedings Content as of 3-29-2013.

cone-beam computed tomography (VasoCT) data, acquired with an angiographic c-arm system, as a 3D planning dataset.

Materials & Methods

Magnetic resonance imaging (MRI), simulation CT, and VasoCT were acquired of a patient with a micro-bAVM of the superior colliculus prior to radiosurgery treatment. Unlike DSA or VasoCT, MRI or CTA did not show the bAVM. VasoCT imaging was performed with a flat-panel, bi-plane c-arm system (Philips Healthcare) using a reduced detector format of 22 × 22 cm^2 in a non-binned mode. During the acquisition, 20% iodinated contrast agent was administered (2 ml/s for a total of 64 ml) into the right vertebral artery using a 5 Fr catheter. Volumetric data were generated (matrix: 512 × 512 × 512; voxel: 0.13 × 0.13 × 0.13 mm^3) using a reconstruction algorithm which allows for visualization of detailed structures at the cost of lower signal-to-noise. All image data were imported into a treatment planning system (Eclipse, Varian Medical Systems) and co-registered. Target delineation was performed on VasoCT slices by an experienced neuroradiologist and dose planning was performed accordingly. The patient received four radiosurgery treatments of 5 Gy on a Trilogy accelerator.

Results

Ten months after final radiosurgery session, the patient underwent a follow-up imaging by catheter angiography showing a complete obliteration of the bAVM and no untoward effects of the radiation treatment. In Figure A the anterior-posterior DSA is given that demonstrates a 3 mm left superior colliculus/pituitary bAVM (asterix). A maximum intensity projection of 5 mm coronal slab of VasoCT data is given in Figure B, in which the bAVM nidus (asterix), the arterial supply through cerebellar arteries and venous drainage trough left superior collicular vein into the vein of Galen are visible.

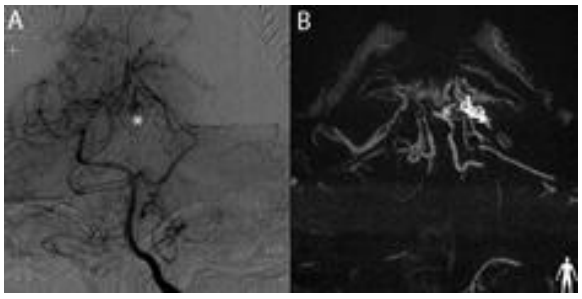

Conclusion

High-resolution contrast-enhanced cone-beam CT has shown to be a feasible method for direct target delineation for radiosurgery in 3D. The nidus of the micro-bAVM was readily visible on VasoCT data and acquisition and including the complementary image data was adopted easily into the standard workflow of radiosurgery.

KEYWORDS: Flat-detector cone-beam CT, Radiation therapy, target delineation

eP-7

Cognitive Impairment in Nondemented ALS and PLS Patients: A Combined Neuropsychologic, DTI and Morphologic Study

Meoded, A.·Kwan, J. Y.·Peters, T. L.·Huey, E. D.·Danielian, L. E.·Morrissette, A.·Wu, T.·Grafman, J.·Floeter, M. K.
National Institute of Neurological Disorders and Stroke, National Institutes of Health
Bethesda, MD.

Purpose

Many patients with amyotrophic lateral sclerosis (ALS) develop impaired executive function, which requires integrity of fronto-temporal networks, and behavioral impairment, suggestive of dysfunction in limbic networks. Primary lateral sclerosis(PLS) is a rare form of motor neuron disorder in which cognitive function has been less well studied than in ALS. The aims of our study were: 1) to explore correlations between DTI metrics of association and commissural tracts and deficits in performance of particular cognitive tests, 2) to explore correlations between gray matter volumetric changes and deficits in performance of cognitive tests, and 3) to compare DTI metrics in patients with and without cognitive and behavioral changes.

Materials & Methods

Seventeen patients who fulfilled Pringle's criteria for PLS, thirteen patients with probable or definite ALS by revised El Escorial criteria, and seventeen age-matched healthy controls participated in the study. In patients, neuropsychologic testing consisted of the Delis-Kaplan Executive Function Scale (D-KEFS) and Mattis Dementia Rating Scale (DRS). On all subjects, structural MRI and DTI was performed. DTI postprocessing included atlas-based analysis (ABA) using MRI Studio software. With this method we measured the fractional anisotropy (FA), mean (MD), axial (AD), and radial (RD) of selected white matter tracts. Voxel-based morphometry was performed using SPM8 in order to assess differences of gray matter volume. Correlations between diffusion properties of selected association and commissural white matter tracts and cognitive performance were analyzed for the patient group as a whole. This model assessed three components derived from the D-KEFS: Fluency, Sorting, and Trails; the DRS total T-score; and DRS memory T-score. In addition, we compared DTI metrics in patients with and without cognitive (ALSci) and behavioral (ALSbi) changes.

Results

Significant associations were found between the total DRS score and FA in the right cingulum and increased RD of the left inferior fronto-occipital-fasciculus. The DRS memory subscore was associated with increased AD of the left and the right IFO and with FA in the right posterior thalamic radiation. Among the executive function tests, the only significant correlation was between verbal fluency and AD of the superior longitudinal fasciculus. Volumetric analysis demonstrated reduced gray matter volume in ALS patients

Note: Scanned images are included in the proceedings. Some submitted images were reduced during editing, thereby decreasing clarity. Also, refer to the Program Planner. Proceedings Content as of 3-29-2013.

in the right pre and postcentral gyrus and in PLS patients in the left supplementary motor area, paracentral lobule, mid cingulum, superior frontal, and precentral gyrus, and in the right pre and postcentral and middle frontal gyrus. However, there was no correlation between volume loss in these areas and neuropsychologic measures. Finally, we found higher FA and lower RD in the right cingulum in patients with ALSci ($p = 0.0106$). In patients with ALSbi, higher FA was seen in the left cingulum ($p = 0.0049$) and lower RD in the right cingulum ($p = 0.0087$).
Conclusion
Changes in diffusion metrics in selected white matter tracts were associated with a decline in global and selected cognitive measures. The involvement of long association fibers together with commissural tracts supports the theory of dysfunction of multiple networks and regions, not only the well-known fronto-temporal but also occipital and parietal areas.

KEYWORDS: Amyotrophic lateral sclerosis, Cognitive deficit, diffusion tensor imaging

eP-8

Susceptibility-Weighted Imaging Phase Values of the Whole Gray and White Matter in Patients with Multiple Sclerosis and Neuromyelitis Optica: A Comparative Study with Controls

Itagiba, V. G. A.[1]·Lopes-Rueda, F. C.[1]·Doring, T.[1]·Domingues, R. C.[1]·Bahia, P. V.[2]·Leon, S. V. A.[2]·Gasparetto, E. L.[1]
[1]DASA- Diagnósticos da América, Rio de Janeiro, BRAZIL, [2]Universidade Federal do Rio de Janeiro, Rio de Janeiro, BRAZIL.

Purpose
To analyze the phase change on susceptibility-weighted imaging (SWI)-filtered phase images in the whole gray and white matter (WM) of multiple sclerosis (MS) and neuromyelitis optica (NMO) patients compared to healthy controls (HC). First, we sought to create a reliable, reproducible and highly automated framework for structure-specific analysis of SWI-filtered phase images. Second we aim to apply this technique to groups of MS and NMO patients and HC in order to analyze the phase change in the whole gray matter (GM) and WM, of these groups.
Materials & Methods
Sixteen relapsing-remitting multiple sclerosis (RRMS) patients, nine NMO patients and 24 HC were imaged on a 1.5T scanner. A postprocessing method was used to create single automated generated masks for the whole GM and WM. Radian values (RV) were determined for the whole GM and WM of MS and NMO patients and HC.
Results
A significant difference ($p = 0.0182$) was detected between the RV of the GM of MS patients and HC. No significant difference was detected when comparing the RV of the WM of MS patients and HC ($p = 0.1416$). There also was no significant difference of the RV of the GM ($p = 0.6966$) and WM ($p = 0.9282$) when comparing NMO patients and HC, neither when comparing NMO and MS patients GM ($p = 0.5352$) and WM ($p = 0.5222$).
Conclusion
We were able to assess the whole GM and WM of MS and NMO patients and we found a significant difference between the RV of the GM in MS patients compared to HC. The possibility of having a single mask including the whole GM and WM would improve the iron overload detection. Future studies should focus on testing this method with a larger cohort, in order to improve the technique and to demonstrate its utility. Clinical relevance statement: This postprocessing method is fast, easy to execute and provides a wider range of information of the whole brain's phase changes what would improve the iron overload detection.

KEYWORDS: Multiple sclerosis, Neuromyelitis optica, gray white matter

eP-9

Cortical Thickness Changes over the Entire Lifespan

Santos, A. C.·Cunha, H. H.·Escorsi-Rosset, S.·Salmon, C. E. G.
University of Sao Paulo
Ribeirao Preto - SP, BRAZIL.

Purpose
After birth a maturation process including myelination and cortical thickness reduction occur at a fast rate, followed by a slow but steady cortical thinning over the entire lifespan. At the end, in the aging brain, a new acceleration occurs in specific regions. While these age-related changes in gray matter volume have been studied extensively, less has been done using newer morphologic indexes, such as cortical thickness and surface area and the studies usually focus on subjects older than 19 years. However, cumulative evidence also indicates that this atrophy is not uniform, and significant heterogeneity of age effects is observed across brain regions. The interpretation of this heterogeneity is complicated by the many variables involved during the entire aging process, mainly the known cellular maturation changes that occur between childhood and adolescence (i.e., myelination, synaptic pruning) which is the cause of most previous research in this area. On the other hand, it is very important to understand how the brain changes as a function of aging. The aim of the present study was to address this problem by testing the consistency of age effects in a unique and general way, from childhood to old age, discussing the interactions between the ages and separating the aging in two moments: maturation and aging itself.
Materials & Methods
Brain imaging data were collected from 143 control subjects (6 - 86 years old); 72 men. All imaging data were

Note: Scanned images are included in the proceedings. Some submitted images were reduced during editing, thereby decreasing clarity. Also, refer to the Program Planner. Proceedings Content as of 3-29-2013.

acquired using a 8-channel head coil on a 3T Philips Achieva X-Series, including a T1-w MPRAGE sequence with whole brain coverage and isotropic voxel of 1 mm^3. All images were processed using FreeSurfer v5.1.0 (http://surfer.nmr.mgh.harvard.edu/) which performs a reconstruction of the cortical surface and uses some automated approaches to parcel and measure thickness, gray matter volume and surface area. The cortical surface was divided into 74 different areas in each hemisphere. Mean thickness then was extracted for each brain region from each individual subject's brain image in its native space. We separated the whole process in two stages: maturation and aging, and computed the best threshold for each region, allowing identifying when those processes begin, their velocities and the relation to aging. Age effects on all data were analyzed using a Java Software constructed specifically to support and optimize the resolution of this study. The software uses the Apache Commons Mathematics Library to handle the regressions and all statistical operations required and MySQL as the main database. Beside age comparison in specific regions, we analyze sex differences in the age effects.
Results
Our data are in according with previous studies pointing to a different rate of growing and decrease of each single brain region.
Conclusion
Because brain regions have different compositions of neurons in the laminar cortex it is possible to think about different neuronal rate of maturation and senescence which might have importance in the understanding of neuronal death in different degenerative diseases.

KEYWORDS: Cortical thickness, Brain development, brain aging

eP-10

Association between Cognitive Decline and Structural Connections in Patients with Mild Cognitive Impairment

Prescott, J. W.·Guidon, A.·Liu, C.·Doraiswamy, P. M.·Petrella, J. R.·The Alzheimer's Disease Neuroimaging Initiative
Duke University Hospital
Durham, NC.

Purpose
The hypothesis of the current study is that the number of structural connections in cortical regions involved in Alzheimer disease (AD) decreases with decreasing cognitive performance, as measured by the mini mental status exam (MMSE) clinical score, in patients with mild cognitive impairment (MCI).
Materials & Methods
1. Subjects included in the analysis were those newly enrolled in the ADNI2 study who were assigned to either the early MCI or late MCI cohorts, and who had baseline DTI scans available. 2. The ADNI2 protocol describes the acquisition protocols in depth. 3. Each subject's baseline SPGR anatomical images were segmented using FreeSurfer "freesurferaparc" parcellation, producing 83 regions of interest. 4. The b0 DTI scans were registered to the anatomical scans using FSL. Fiber tractography then was used to derive structural connectome maps using the Connectome Mapper Toolkit (CMTK). 5. The anatomical parcellation labels then were registered to the connectome map. The strength, or number of structural fibers connected to an anatomical region, and the degree, or number of other cortical regions connected to an anatomical region, then were analyzed in seven anatomical regions, or "nodes", in each brain hemisphere: precuneus, posterior cingulate, parahippocampus, entorhinal, inferior temporal, superior parietal, and superior frontal. These regions were selected because of their known association with AD pathology. A linear regression analysis was performed on the node strength and degree in each anatomical region and MMSE score at baseline.
Results
There were 45 ADNI2 subjects (29 males, 15 females) in the MCI cohorts that had baseline DTI and anatomical SPGR scans available at the time of the analysis. The average age was 71.5 ± 12.3. The average MMSE score was 27.6 ± 1.8. There were significant associations (p less than 0.05) between node strength and MMSE in left posterior cingulate and borderline significant associations (p less than 0.10) in right posterior cingulate, left entorhinal, and left superior parietal regions. There were no significant associations between node degree and MMSE. All regions which demonstrated significant or borderline significant associations had a positive association, such that the node strength decreased as the MMSE score decreased (signifying cognitive decline). In the left and right posterior cingulate regions, patients with high MMSE scores (greater than 28) did have more high strength connectivities (greater than 200) than those with lower MMSE scores (less than 25) - 11:2 in the left and 12:1 in the right. However, the best fit linear regressions did not characterize the data well across the entire MMSE spectrum (R-squared less than 0.10 for all regions).
Conclusion
Although there may be decreases in the structural connections of the posterior cingulate regions that track over the entire range of decreasing cognitive performance in patients with MCI, the largest differences are between patients with high MMSE scores (greater than 28) and those with low MMSE scores (less than 25). This relationship can be analyzed further as more MCI patient data are added to the ADNI2 database, particularly longitudinal scans.

KEYWORDS: Alzheimer disease, Structural network

Note: Scanned images are included in the proceedings. Some submitted images were reduced during editing, thereby decreasing clarity. Also, refer to the Program Planner. Proceedings Content as of 3-29-2013.

eP-11

Multimodal MR Imaging of Single versus Multiple Domain Amnestic Mild Cognitive Impairment

Abdel Razek, A.·Tantawy, A.·Elkhateb, M.·Elsayed, M.
Mansoura University Hospital
Mansoura, EGYPT.

Purpose
To differentiate between single domain and multiple domain subtypes of amnestic mild cognitive impairment (MCI) with MR imaging.
Materials & Methods
Prospective study was conducted upon 50 patients with multiple domain (n = 38) and single domain (n = 12) amnestic MCI (65 ± 5 years, 38 male, 12 female). They underwent T1-weighted 3D magnetization prepared rapid gradient echo (MP-RAGE) sequence, diffusion MR weighted imaging with B value of 0, 500 and 1000 s/mm2 and multivoxel MR spectroscopy of the brain with TE of 270 ms. The apparent diffusion coefficient (ADC) value, the volume and metabolic ratios of different regions of the brain of multiple domain and single domain MCI were calculated. Statistical analysis was done.
Results
There was significant difference in the ADC value of the parietal region (P = 0.01), Ch/Cr ratio of the parietal regions (P = 0.02), and volume of the hippocampus (P = 0.03) and amygdale (P = 0.05) between single domain and multiple domain amnestic. The best combination for differentiation was ADC value and Ch/Cr ratio of parietal region. The cutoff value of ADC, Cr/cr ratio and volume were 0.78, 284, 0.83 with areas under the curve of 0.883, 0.893, and 0.821 respectively.
Conclusion
We concluded that the combination of ADC value and Ch/Cr ratio of the parietal region is a promising noninvasive imaging parameter used for differentiating multiple domains from single domain amnestic MCI.

KEYWORDS: MR imaging/diffusion

eP-12

Decoding the Superior Parietal Lobule Connections of the Superior Longitudinal Fasciculus in the Human Brain: A High-Resolution Diffusion Tensor Tractography Study on 3T

Kamali, A.[1,2]·Flanders, A. E.[3]·Hasan, K.[4]
[1]University of Medicine and Dentistry of New Jersey, Camden, NJ, [2]Cooper University Hospital, Camden, NJ, [3]Thomas Jefferson University Hospital, Philadelphia, PA, [4]University of Texas Medical School Houston, Houston, TX.

Purpose
Inferior parietal lobule connections of the language pathways such as the middle longitudinal fasciculus (MdLF) and temporoparietal connections of the superior longitudinal fasciculus (TP SLF) have been described in the literature. Extensive crossing fibers at the corona radiata at the level of the lateral ventricles as well as lack of adequate imaging sensitivity and spatial resolution, so far, impeded depiction of superior parietal lobule connections of the temporoparietal language pathways in prior diffusion tensor imaging studies. This work aimed to explore the acuity and feasibility of visualization of white matter substructure of the human language pathways connecting the temporal lobe with the superior parietal lobule using a high-resolution diffusion tensor imaging technique and deterministic tractography approach.
Materials & Methods
Subjects**:** Five healthy men (age range 24-37 years) were studied and written informed consent was obtained from all subjects. Conventional and DT-MRI Acquisition: Data were acquired using a Philips 3.0T Intera system using a SENSE receive head coil. Diffusion-weighted image (DWI) data were acquired axially using a single-shot multi-slice 2D spin-echo diffusion with the balanced *Icosa21* tensor encoding scheme. The b-factor = 500 sec mm-2, TR/TE = 14460/60 msec, FOV = 256 mm x 256 mm and slice thickness/gap/#slices = 1 mm/0 mm/120. The EPI phase encoding used a SENSE k-space undersampling factor of two, with an effective k-space matrix of 112 x 112 and an image matrix after zero-filling of 256 x 256.
Results
Numerous anatomical details in the brain white matter connectivity have been undetectable or poorly detectable due to discrepancy of scale between the microstructural anatomy and inadequate image resolution and sensitivity used in diffusion tensor imaging. Using higher resolution combined with higher magnetic field reduced the partial volume effects and incoherency within the voxel. This allowed us to trace the superior parietal lobule connections of the temporoparietal pathways and reveal more anatomical details of the temporoparietal language pathways. In our experience these superior parietal lobule connections of the temporoparietal fibers are not traceable using slice thickness ~ 3 mm. This is attributable to mixing of fibers in different orientations within the voxel leading to lack of adequate anisotropy in larger voxel volume which was solved by using thinner slices and smaller voxel volume.
Conclusion
In this report we demonstrate for the first time the feasibility of in vivo tracing the superior parietal lobule connections of the temporoparietal pathways using high-resolution diffusion tensor tractography.

KEYWORDS: 3 T, Diffusion tensor image, high-resolution, superior longitudinal fasciculus

Note: Scanned images are included in the proceedings. Some submitted images were reduced during editing, thereby decreasing clarity. Also, refer to the Program Planner. Proceedings Content as of 3-29-2013.

eP-13

Functional and Structural Connectivity Helps to Detect and Understand Alzheimer Disease

Santos, A. C.·Rondinoni, C.·Rolo, J.·Escorsi-Rosset, S.·Salmon, C. E. G.
University of Sao Paulo
Ribeirao Preto - SP, BRAZIL.

Purpose
Previous reports show decreased BOLD signal in the anterior and posterior cingulate regions of the DMN in older participants (Broyd et al., 2009). Although these are core areas in the maintenance of brain connectivity, basal areas like the hippocampus and lateral temporal cortex play a role in the default network (Greicius et al., 2004). Here, we sought to identify spatial differences in functional connectivity as seed for effective connectivity calculation. Tractography on AD patients and normal control data sets was used to identify disease-related deviations of brain structural connectivity. Our aim was to verify the relationship between functional/effective and structural variability as disease progresses.
Materials & Methods
A group of 26 elderly were recruited for this study. Mean age for experimental group was 74 years old (s.d. 4.5). Functional data gathered from a control group was used as age-paired controls for comparison of effective connectivity (n = 13, mean age 71, s.d. 7.8). Patients were diagnosed as Alzheimer patients as confirmed by a specialist examination (mean CDR = 1, mean MMSE = 16). The research protocol was approved by the local Ethical Committee and all participants signed an informed consent. Resting state functional images were acquired in an Achieva 3T MRI scanner (Philips, The Netherlands) using a noise-attenuated EPI. Tridimensional T1-weighted images were acquired for functional coregistration. Functional data were submitted to preprocessing and Independent Component Analysis (ICA) in BrainVoyager QX (Brain Innovations, The Netherlands). Procedures for group ICA are described elsewhere (Esposito et al., 2005). Granger causality processing (Roebroek et al., 2005) on volumes-of-interest time courses were accomplished with seeds located in each hippocampus (Talairach coordinates +/- 21, -24,13). Granger causality maps were defined by the probability of GCM values being different from zero inside each group. These maps (p-value < 0.05, clusters > 50 voxels) were taken as an indication of whole-brain differences in effective connectivity for controls and patients.
Results
Group-wise comparison between Default-Mode Network maps showed differences in the right mesial temporal cortex (BA 28, 35,36) and dorsal attentional areas. Granger causality maps showed differences in areas related to attentional processing and auditory stimulus integration. Results point to an association between normal aging and differences in effective connectivity related to AD.
Conclusion
We identified differences between controls and Alzheimer disease patients by analyzing functional data. Data may be useful in giving indications about the progress of the disease, possibly pointing to candidate areas as markers for Alzheimer disease.

KEYWORDS: fMRI, Alzheimer disease, connectivity

eP-14

In Vivo MR Spectroscopy of Bilateral Hippocampi in HIV-Seropositive or Neurosyphilis Patients at 3T

Chiu, P.[1]·Chan, Y.[2]·Chan, Q.[3]·Mak, H.[1]
[1]The University of Hong Kong, Hong Kong, HONG KONG, [2]Social Hygiene Service, Centre for Health Protection, Department of Health, Hong Kong, HONG KONG, [3]Philips Healthcare, Hong Kong, HONG KONG.

Purpose
As a result of changing sexual behaviors which led to the human immunodeficiency virus (HIV) epidemic, neurosyphilis (NS) also has experienced a worldwide resurgence and the infections are often concurrent. Mild cognitive impairment has been observed in early stages of neurosyphilis. In this study, magnetic resonance spectroscopy (MRS) was used to investigate the effect of neurosyphilis on the bilateral hippocampi of HIV-positive patients.
Materials & Methods
Experiments were performed on 12 cognitively normal patients (Mini-mental-state-examination ≥ 28; age: 42 ± 12.66 years) with HIV-seropositive or neurosyphilis positive (status defined by the 2010 Sexually Transmitted Diseases Treatment Guidelines by the Centers for Disease Control and Prevention). Of the 12 patients, six were HIV-seropositive with NS, four were HIV-seropositive without NS and two were HIV-seronegative with NS. Twenty-one healthy age-matched controls also were recruited. A 3.0T MR scanner was used (Achieva, Philips Healthcare) with an 8-channel SENSE head coil. Single-voxel-spectroscopy with short echo-time (TE) 38 ms, repetition time (TR) 2000 ms was employed. Single voxels of size 2.5 cm x 1.5 cm x 1cm were placed in the left and right hippocampi with point-resolved spectroscopy (PRESS) as volume selection method. MR spectroscopy data were analyzed with offline software jMRUI version 4.0 using absolute quantification based on quantum estimation (QUEST). Choline (Cho), creatine (Cre) and N-acetylaspartate (NAA) levels were investigated with internal water as reference. Cerebrospinal fluid normalization was done. Metabolic ratios of the above metabolites also were calculated. SPSS 18.0 was employed for statistical analysis using 2-sample t-test. The level of significance was $p<0.05$.
Results
Table 1. Mean values with standard deviations of metabolites obtained from HIV patients with or without NS, NS patients with or without HIV and their respective

Note: Scanned images are included in the proceedings. Some submitted images were reduced during editing, thereby decreasing clarity. Also, refer to the Program Planner. Proceedings Content as of 3-29-2013.

age-matched controls (NC) for left hippocampus (LH) and right hippocampus (RH).

	HIV with and without NS (NC n = 16, patients n = 10)				NS with and without HIV (NC n = 21, patients n = 8)			
	LH		RH		LH		RH	
	NC	Patient	NC	Patient	NC	Patient	NC	Patient
Cr ($mmol^{1-n_S}$)	3.54±0.39	3.79±0.56	4.97±0.77	3.78±0.64	3.61±0.43	4.10±0.53	4.85±0.68	3.88±0.58
		↑		↓↓		↑		↓↓
Cho ($mmol^{1-n_S}$)	0.62±0.10	0.70±0.06	1.24±0.19	0.72±0.12	0.63±0.10	0.73±0.11	1.23±0.20	0.70±0.09
		-		↓↓		↑		↓↓
NAA ($mmol^{1-n_S}$)	6.84±0.93	6.03±0.55	5.03±0.86	5.13±1.67	6.85±0.90	5.57±1.23	4.99±0.88	5.69±0.45
		↓↓		-		↓↓		↑↑
Cho/Cr	0.18±0.03	0.19±0.03	0.25±0.03	0.19±0.03	0.18±0.03	0.18±0.31	0.25±0.03	0.18±0.03
		-		↓↓		-		↓↓
NAA/Cr	1.96±0.41	1.63±0.31	1.02±0.12	1.38±0.53	1.93±0.39	1.40±0.43	1.03±0.15	1.50±0.29
		↓↓		↑↑		↓		↑↑
Cr/Cho	5.85±1.02	5.49±0.94	4.04±0.48	5.30±1.03	5.83±1.06	5.67±1.00	3.99±0.53	5.62±1.05
		-		↑↑		-		↑↑
NAA/Cho	11.35±2.73	8.72±0.10	4.08±0.53	7.29±2.71	11.09±2.48	7.70±1.99	4.10±0.52	8.23±1.03
		↓↓		↑↑		↓↓		↑↑

Cr: creatine, Cho: choline, NAA: N-acetyl aspartate, $mmol^{1-n_S}$: millimoles per kilogram brain tissue
↑: significant increase compared to control, p<0.05;
↑↑: significant increase compared to control, p<0.01;
↓: significant decrease compared to control, p<0.05;
↓↓: significant decrease compared to control, p<0.01;
-: no significant change compared to control

In LH, there are significant decreases in NAA/Cr and NAA/Cho between both subject groups compared to controls. However, there are significant increases NAA/Cr and NAA/Cho in the RH in both groups compared to controls. Interestingly, distinct asymmetry of metabolic ratios was observed in both LH and RH of the diseased cohorts.

Conclusion

Because of the limited sample size, there is a high degree of overlapping in both subject groups and could surely limit the detection of any differences between the groups. However, both subject groups showed asymmetrical patterns of metabolic ratios in the left and right hippocampi compared to controls. Decrease in NAA/Cr indicates neuronal loss and such targeted cell death in the left hippocampus of both subject groups warrants further investigation in a larger cohort. Although the MMSE scores were normal in the diseased subjects, very early cognitive impairment could not be detected by these psychologic scores but might be reflected by left hippocampal metabolite derangement.

KEYWORDS: Human immunodeficiency virus, 1H MRS, neurosyphilis

eP-15

Glutamate, GABA and NAAG in Medicated Patients with Obsessive-Compulsive Disorder

Mohamed, M. A.·Puts, N.·Brasic, J.·Uy, M.·Intrapiromkul, J.·Nestadt, G.·Edden, R.·Barker, P.
Johns Hopkins University
Baltimore, MD.

Purpose

Cortical excitability reflects a balance between excitation (glutamatergic) and inhibition (GABAergic). The purpose of this study was to use magnetic response spectroscopy (MRS) to determine if the inhibitory GABAergic and the excitatory glutamatergic systems are abnormal in obsessive-compulsive disorder (OCD), and are different in patients who do or do not respond to treatment with selective serotonin reuptake inhibitors (SSRIs).

Materials & Methods

Forty OCD patients (18 females, 22 males, age range 21 to 67 years) and 20 age- and gender-matched controls were included in this study. Nineteen patients were SSRI responders, 17 were SSRI nonresponders, and four were treatment naïve. All patients fulfilled Diagnostic and Statistical Manual of Mental Disorders (DSM-IV) criteria for OCD and Yale-Brown Obsessive Compulsive (YBOCS) score. Responders were defined as patients who had a 35% or greater reduction in their YBOCS score after a 10-week trial of any appropriate SSRI. All studies were performed on a Philips Achieva 3T system using a 32-channel head coil. Subjects underwent single voxel MRS (4.0x3.0x2.5 cm voxel, TR/TE=2000/35 ms) acquired from the anterior cingulate cortex (ACC) and the basal ganglia/thalamus (BG/TH) with and without water suppression. MEGA-PRESS experiments were performed for N- acetyl aspartate (NAA) and NAA-glutamate (NAAG) and γ-amino butyric acid (GABA). Metabolites concentrations were determined using the GANNET program (gabamrs.blogspot.com) for GABA, NAA and NAAG and LCModel for glutamate (Glu), glutamine (Gln), NAA, creatine (Cr), myoinositol (mI), Gln and choline (Cho) [both glycerophosphocholine (GPC) and phosphocholine (PC)] concentrations and ratios. One-way ANOVA and t tests with correction for multiple comparisons were performed between controls, SSRI responders and nonresponders controlling for age and gender.

Results

Anterior cingulate cortex NAA and NAA+NAAG concentrations were higher in younger subjects as compared to older (P<0.006, P<0.003 respectively) with no gender differences. Basal ganglia/thalamus GPC and GPC+PC was higher in males compared to females (P<0.01, P<0.02 respectively) and showed a trend increase in their concentrations in older subjects (P<0.06, P<0.02 respectively). Obsessive-compulsive disorder patients showed lower BG/TH Glu+Gln(Glx)/Cr compared to controls (P<0.03); however, the significance was lost when age and gender were co-varied for. There were no significant differences in Glu, mI, Cho, NAA, NAAG, GABA/Cr between the 3 groups. Discussion: In this study, there were no significant differences between medicated OCD patients and controls; also no differences were found between SSRI responders and nonresponders. This is in contrast to a previous 1.5T MRS study which showed a significant decrease in orbitofrontal white matter Glx and which correlated with OCD symptom severity. Other studies have found higher CSF Glu levels in drug-naïve OCD. Furthermore, a recent 3T MRS study found that unmedicated OCD patients did not have any Glx

Note: Scanned images are included in the proceedings. Some submitted images were reduced during editing, thereby decreasing clarity. Also, refer to the Program Planner. Proceedings Content as of 3-29-2013.

abnormalities in the medial prefrontal cortex; however, they may have decreased GABA levels.
Conclusion
The current study did not find any significant differences in compounds related to the glutamatergic or GABAergic systems (Glu, NAAG, GABA) in the ACC and BG/TH between OCD patients and controls when co-varying for age and gender. The role of MRS in OCD remains to be determined.

KEYWORDS: 1H MRS, Obsessive-compulsive disorder, glutamate GABA NAAG

eP-16

Diffusion Abnormalities in Corpus Callosum of Patients with Refractory Epilepsy Associated with Hippocampal Sclerosis

Lyra, K. P. d.·Chaim, K. T.·Park, E. J.·Rimkus, C. M.·Castro, L. H. M.·Leite, C. C.·Otaduy, M. C. G.
Instituto de Radiologia da Faculdade de Medicina
Sao Paulo, BRAZIL.

Purpose
Corpus callosum (CC) is the most important white matter tract that connects homologous areas of the left and the right cerebral cortex and has been implicated in propagation of epileptic activity. The goal of our study is to detect diffusivity abnormalities in specific areas of the CC in hippocampal sclerosis (HS) patients using diffusion tensor imaging (DTI).
Materials & Methods
Thirty-eight patients with medically refractory epilepsy with HS (16 right- and 22 left-sided) and 24 healthy volunteers were included. MR imaging was acquired with a 3T magnet (Philips® Achieva), including structural conventional imaging and high-resolution (2 mm x 2 mm x 2 mm with 32 gradient directions) DTI. T1-weighted volumetric images were analyzed using a specific algorithm implemented in Freesurfer software, to segment the CC in five subregions named as anterior, midanterior, central, midposterior and posterior. By using Bioimagesuite® and Fsl® softwares, fractional anisotropy (FA) and mean diffusivity (MD) maps were coregistered with segmented T1-images and then diffusion indices were obtained from each CC subregion. We considered a value of p <0,05 statistically significant.
Results
Our study showed that, when compared to controls, the FA was lowest (Figure 1) and MD (mm²/s) higher (Table 1) at posterior, mid-posterior and anterior subregions of the CC.

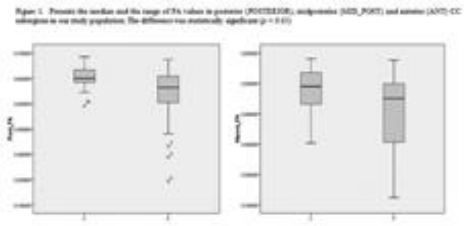

Table 1: Mean diffusivity values in patients and healthy volunteers with p values.

	Posterior	Mid-Post	Central	Mid-Ant	Anterior
Patients	1,11124339	1,17045813	0,98032463	1,05074339	1,01180550
Controls	1,00544904	1,04272488	0,93432958	0,97812492	0,94491379
p value	0,012	0,015	0,126	0,091	0,042

Conclusion
These regional diffusion abnormalities in CC are probably secondary to seizures propagation along specific pathways that are anatomically linked to epileptogenic temporal lobes like dorsal hippocampal commissure, providing pathologic changes and secondary white matter degeneration.

KEYWORDS: Diffusion tensor image, 3 T, hippocampal sclerosis

eP-17

Differentiation of Pyogenic Brain Abscesses from Necrotic Glioblastomas and Cystic Metastatic Brain Tumors: Comparisons of Diagnostic Performance of Dynamic Susceptibility Contrast-Enhanced Perfusion MR Imaging before and after Mathematic Contrast Leakage Correction

Toh, C.·Wei, K.·Chang, C.·Ng, S.·Wong, H.·Chen, Y.·Wu, Y.·Peng, Y.
Chang Gung Memorial Hospital
Linkou, Taipei, TAIWAN.

Purpose
To compare the diagnostic performance of dynamic susceptibility contrast (DSC) perfusion MRI before and after mathematic contrast leakage correction in differentiating pyogenic brain abscesses from glioblastomas and/or metastatic brain tumors.
Materials & Methods
Cerebral blood volume (CBV), leakage-corrected CBV and leakage coefficient K_2 were measured in enhancing rims,

Note: Scanned images are included in the proceedings. Some submitted images were reduced during editing, thereby decreasing clarity. Also, refer to the Program Planner. Proceedings Content as of 3-29-2013.

perifocal edema and contralateral NAWM of 17 abscesses, 19 glioblastomas and 20 metastases, respectively. The CBV and corrected CBV were normalized by dividing the values in the enhancing rims or edema to those of contralateral NAWM. For each study group, a paired t test was used to compare the K_2 of the enhancing rims or edema with those of NAWM, as well as between CBV and corrected CBV of the enhancing rims or edema. Comparisons of CBV, corrected CBV and K_2 among the three groups were done by using ANOVA. The diagnostic performance of CBV and corrected CBV was assessed with ROC curve analysis.
Results
The CBV and corrected CBV in the enhancing rim of abscesses were significantly lower than those of glioblastomas or metastases. In differentiating abscesses from glioblastomas and/or metastases, the AUC values of corrected CBV were higher than those of CBV but their differences were not statistically significant.
Conclusion
Abscesses can be differentiated from glioblastomas and/or metastases with CBV or corrected CBV measured in their enhancing rims. The diagnostic performance of corrected CBV seems to be better than CBV. But, there is no evidence that mathematic contrast leakage correction improves the diagnostic performance of CBV.

KEYWORDS: Abscess, MR imaging perfusion

eP-18

Intracranial Manifestations of *Cryptococcus gattii* Infection

Burke, A. G.[1]·Riccelli, L. P.[1]·Allen, H. N.[2]·Anderson, J. C.[1]
[1]Oregon Health & Science University, Portland, OR,
[2]University of Wisconsin Hospitals and Clinics, Madison, WI.

Purpose
Until 1999, most human *Cryptococcus gattii* (Cg) infections were reported from Australia and other tropical and subtropical regions, including parts of Africa, Asia, the Mediterranean, South America, and southern California. During 1999, Cg began appearing in animals and humans on Vancouver Island and, beginning in 2004, among mainland British Columbia residents who had no exposure to Vancouver Island. The two human infections reported from Oregon in 2004 and 2005 were from Cg. Neither patient had traveled to Vancouver Island or any other known Cg-endemic area. Risk factors for Cg infection in the United States appear to include both immunocompromised and exposure to specific regions of environmental fungal colonization. Cryptococcus gattii infections in Australia have been shown to have higher rates of mass-like lesions than *Cryptococcus neoformans* (Cn), and similar findings have been reported anecdotally in British Columbia and the U.S. Pacific Northwest. These mass-like lesions in immunocompetent patients may be easily confused with intracranial neoplasm, particularly when the clinical index of suspicion for infection is low. This study evaluates the initial intracranial MR imaging findings of Cg infections in order to establish the incidence of Cg cryptococcoma formation and to characterize potential distinguishing characteristics from Cn infection.
Materials & Methods
Imaging studies from 62 patients with Cg infection between November 2004 and February 2012 were obtained from the Oregon Public Health Department, of which 23 patients had MR brain imaging at the time of initial diagnosis. MR brain images were de-identified and three fellowship-trained neuroradiologists independently reviewed the images and cataloged intracranial findings. The study received IRB approval from the Oregon Public Health Department and an IRB waiver from Oregon Health & Science University.
Results
Twenty-two of 23 (96%) of initial MR brain examinations exhibited pathology. Nodules were present in 11 cases (50%), ranging in size from 3 mm to greater than 30 mm in diameter, with eight of these 11 having cyst-like, nodular enlargement of the basal ganglia perivascular spaces. Cyst-like basal ganglia lesions were less likely to enhance than parenchymal nodules. Parenchymal nodules greater than 25 mm diameter occurred in three cases and showed mass-like characteristics with two of these three cases showing heterogeneous enhancement of the lesions. None of the nodules or masses showed diffusion restriction. Leptomeningeal involvement included FLAIR signal abnormality in three cases, nodular enhancement in one case, and smooth enhancement in one case. None of the patients showed hydrocephalus, intraventricular nodules, or pachymeningeal abnormalities.
Conclusion
Intracranial manifestations of Cg infection in this study of patients in Oregon since 2004 range from leptomeningeal enhancement to cystic dilatation of basal ganglia perivascular spaces to large enhancing, solid masses (cryptococcomas). Given the increasing number of Cg infections in the Pacific Northwest and the likelihood of infected both immunocompromised and immunocompetent patients initially presenting with intracranial cryptococcomas that mimic neoplastic processes, Cg infection should be increasingly considered as a differential diagnosis in patients initially thought to have intracranial neoplasm to expedite diagnosis and treatment.

KEYWORDS: Cryptococcoma, MR imaging brain, gattii

Note: Scanned images are included in the proceedings. Some submitted images were reduced during editing, thereby decreasing clarity. Also, refer to the Program Planner. Proceedings Content as of 3-29-2013.

eP-19

Assessment of Deep Gray Matter Volume in Patients with Neuromyelitis Optica

Miraldi, F.·Rueda, F.·Alves-Leon, S. V.·Gasparetto, E. L.
Federal University of Rio de Janeiro
Rio de Janeiro, BRAZIL.

Purpose
Neuromyelitis optica (NMO) is a common demyelinating disease with spinal cord and optic nerve injury. Recently, brain involvement has been described, including typical lesions, normal appearing white matter widespread damage and even some cortical compensations for these structural damage. White matter loss associated with cognitive impairment already has been described, but the deep gray matter (DGM) was poorly studied. Our aim is to evaluate DMG volume in NMO using advanced neuroimaging techniques.
Materials & Methods
The study population included 27 patients with NMO spectrum, including neuritis optica and/or myelitis (18 female, 38 mean age) and 17 controls (13 female, 42 mean age) with no brain lesion on MRI or neurologic disorder. MR imaging of the brain was conducted on a 1.5T scanner using T1WI 3D. Then, FIRST, part of FSL4.1 (FMRIB, Oxford, UK) was applied as a postprocessing software for calculation of volume of the hippocampus, amigdalas, putamen, thalamus and caudate nucleus. Statistical analysis included the Kolmogorov-Smirnov test to evaluate the normal distribution of the values and two-tailed paired Student's *t*-test for the comparison of DGM volumes. A *p*-value equal or less than 0.05 was considered statistically significant.
Results
The comparison between DGM volumes in NMO and controls were respectively: left thalamus (7148 cm^3 vs. 7335 cm^3, p = 0.33), right thalamus (6988 cm^3 vs. 7090 cm^3, p = 0.42), left caudate (3308 cm^3 vs. 3236 cm^3, p = 0.91), right caudate (3219 cm^3 vs. 3308 cm^3, p = 0.50), left putamen (4480 vs. 5048 cm^3, p = 0.07), right putamen (4372 cm^3 vs. 4911 cm^3, p = 0.08), left hippocampus (3526 cm^3 vs. 3755 cm^3, p = 0.20), right hippocampus (3591 cm^3 vs. 3913 cm^3, p = 0.06), left amigdala (1310 cm^3 vs. 1254 cm^3, p = 0.73) and right amigdala (1277 cm^3 vs. 1265 cm^3, p = 0.79).
Conclusion
No significant difference was verified in the comparison between DMG volumes in NMO and controls, which is in agreement with the predominant white matter involvement in NMO as well as the absence of cortical gray matter findings using 7.0 T MRI. The NMO mechanism of pathogenesis might somehow preserve gray matter from damage.

KEYWORDS: Neuromyelitis optica, Basal ganglia

eP-20

IgG4-Related Inflammatory Lymphproliferative Disease Involved Intracranial as well as the Head and Neck: Imaging Findings and Clinical Features

Kawamura, Y.·Nakaji, S.·Kikuchi, Y.·Sezaki, T.
Kameda Medical Center
Chiba, JAPAN.

Purpose
IgG4-related disease has been encountered and diagnosed such as autoimmune pancreatitis (AIP), retroperitoneal fibromatosis (RF), and sclerosing cholangitis that may involve the head, neck, and brain and the radiologic features and clinical characteristics of IgG4-related disease are discussed.
Materials & Methods
Five patients with autoimmune disorders were evaluated for head and neck lesions by MDCT (Toshiba, Aquilion 64) and MRI (SIEMENS, Avanto 1.5T). Patient 1: 61-year-old woman with RF, complained of right orbital discomfort. Patient 2: 67-year-old man with RF and patient 3: 62-year-old woman with AIP revealed bilateral painless salivary glands swelling. Patient 4: 76-year-old man with RF, and suspicious sclerosing cholangitis evaluated for orbital mass. Patient 5: 73-year-old man with RF, complained of chronic headache.
Results
In patient 1, MRI demonstrated homogeneously enhancing soft-tissue mass involving the skull base (Figure 1) along with the second and the third divisions of right trigeminal nerve. In patients 2 and 3, CT and MRI showed symmetric enlargement of salivary glands with homogeneous enhancement. In patient 4, hypointensity lesion in left infraorbital canal on T2-weighted images was seen (Figure 2). In patient 5, MRI demonstrated the dural thickening and enhancement.

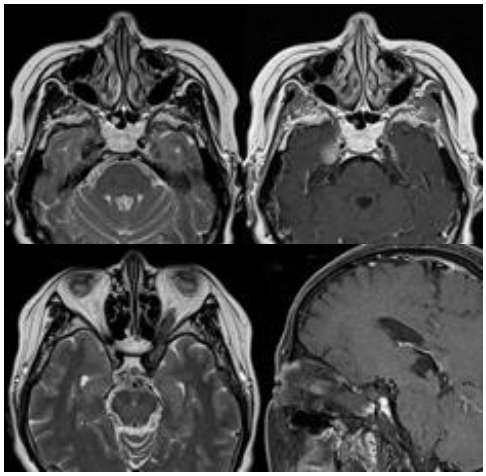

Discussion
Recent study indicated that the autoimmune disorders affecting the lacrimal and salivary glands, Mikulicz disease, was IgG4 involvement in their pathogenesis. Tthe lacrimal and salivary swelling without symptom was seen in

Note: Scanned images are included in the proceedings. Some submitted images were reduced during editing, thereby decreasing clarity. Also, refer to the Program Planner. Proceedings Content as of 3-29-2013.

patients 2, 3 and 4 during the clinical followup for IgG4-related disease. Soft tissue mass extended along meninges and the cranial nerves such as the trigeminal nerve. Symptoms are not severe - even MRI and CT show marked abnormality. In the majority of cases, steroid therapy is effective.

Conclusion

Careful interpretation of MRI is helpful to suspect the uncommon IgG4-related disease and to lead the IgG4 measurement as well as to reduce the risk of the invasive biopsy planning.

KEYWORDS: 1.5T, Autoimmune

eP-21

Chronic Lymphocytic Inflammation with Pontine Perivascular Enhancement Responsive to Steroids: Case Report

Le, N. T.·Buckingham, C. L.
Vanderbilt University Medical Center
Nashville, TN.

Purpose

Chronic lymphocytic inflammation with pontine perivascular enhancement responsive to steroids (CLIPPERS) was first described by Pittock and colleagues in 2010, and a follow-up study on long-term outcome by Taieb and colleagues was published in 2012. CLIPPERS is a distinct steroid-responsive brainstem encephalitis with characteristic MRI findings. It has been proposed that once other diagnoses have been excluded, CLIPPERS can be diagnosed and treated based solely on clinical and radiologic findings without pathologic confirmation. We report three cases to further support that CLIPPERS, though new, is a definable inflammatory CNS disease.

Materials & Methods

We reviewed the medical records and imaging studies of three patients diagnosed with presumed CLIPPERS.

Results

Case 1: A 36-year-old female presented with left-sided weakness, right vision loss, and speech difficulty for six months. Brain MRI showed ill-defined T2-hyperintensity in the middle cerebellar peduncles, pons with small areas of enhancement in the pons. The patient received five days IV methylprednisolone with marginal improvement in the left-sided weakness. Case 2: A 62-year-old male presented with three months of falls and diplopia. Exam revealed lurching gait, hip flexor weakness, dysmetria, and horizontal nystagmus. Brain MRI showed T2-hyperintensity and patchy enhancement in the middle cerebellar peduncles, pons, and the cervicomedullary junction. The patient was treated with five days IV methylprednisolone. He had significant improvement with almost complete resolution of diplopia, nystagmus, dysmetria, ataxia and weakness. Follow-up MRI showed interval improvement. The patient is currently on long-term steroids and Imuran to prevent relapse. Case 3: A 53-year old male presented with numbness in the right face and body, and weakness in the left leg. MR imaging showed small ring-enhancing nodules with surrounding T2-hyperintensity centered in the left middle cerebellar peduncle. He improved after one dose of IV steroid, and was later treated with additional courses of steroid. Due to progression on MRI, biopsy was performed showing perivascular lymphocytes and reactive gliosis.

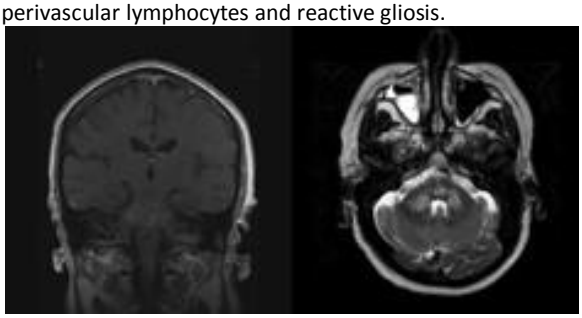

Conclusion

The clinical presentation and MRI findings in these patients with presumed CLIPPERS are similar to those previously described. Most reported cases involve the pons and middle cerebellar peduncles with linear and punctuate enhancement. Many cases have supratentorial involvement or myelitis and some required biopsy to exclude other etiologies. Ideally the diagnosis could be made based on clinical and imaging features. Awareness on the part of radiologists will aid the early diagnosis and treatment of CLIPPERS. More experience will be required to establish diagnostic criteria.

KEYWORDS: Brain abnormalities, Autoimmune, CLIIPPERS

eP-22

Imaging of Meningiomas on 3D FLAIR at 3T MR Imaging

Enokizono, M.[1]·Morikawa, M.[1]·Ideguchi, R.[2]·Uetani, M.[1]·Horie, N.[1]·Matsuo, T.[1]·Nagata, I.[1]·Hayashi, T.[1]·Honda, S.[1]
[1]Nagasaki University Graduate School of Biomedical Sciences, Nagasaki, JAPAN, [2]Nagasaki Municipal Hospital, Nagasaki, JAPAN.

Purpose

FLAIR imaging after contrast medium injection has been shown to be an efficacious method, especially in the delineation of meningeal lesions including meningoencephalitis and leptomeningeal metastases. The purpose of this study is to evaluate the usefulness of noncontrast-enhanced (NE) and contrast-enhanced (CE) 3D FLAIR imaging for meningiomas at 3T MRI.

Materials & Methods

The subjects are 20 patients with intracranial meningioma who underwent tumor excision and histologically confirmed. Two neuroradiologists retrospectively evaluated the preoperative MRI findings including tumor size, the characteristics of tumor-brain interface, the

Note: Scanned images are included in the proceedings. Some submitted images were reduced during editing, thereby decreasing clarity. Also, refer to the Program Planner. Proceedings Content as of 3-29-2013.

degree of peritumoral brain edema, and rim enhancement (RE) compared with CE 3D fast SPGR. The vascular supply also was evaluated from the preoperative digital subtraction angiography (DSA). Neurosurgeon who had performed the surgery evaluated the degree of tumor-brain adhesion during surgery. In addition, we also studied five schwannomas, also common extra-axial tumor, which underwent tumor excision.

Results

Rim enhancement was observed in 18/20 meningiomas (90%) on CE 3D FLAIR, which exhibited a high signal intensity compared to the tumor parenchyma, while in 9/20 meningiomas (45%) on CE 3D fast SPGR. No RE was seen in schwannomas. In meningiomas, no correlation was found between RE and other factors, including the severity of tumor-brain adhesion, histologic grading. However, RE tended to be more highlighted in the group with pial supply on DSA. The cases with severe tumor-brain adhesion demonstrated the lack of a hypointense marginal line at the tumor-brain interface on NE 3D FLAIR.

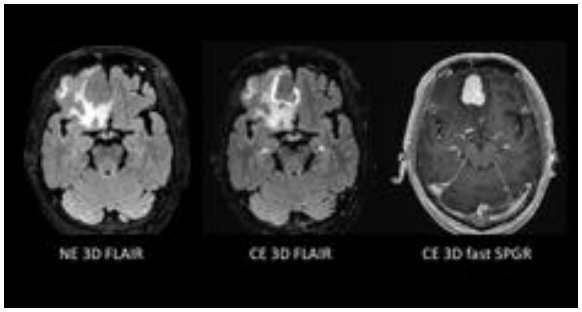

Conclusion

Rim enhancement may represent pial supplies of the tumors and be expected to be helpful to differentiate meningiomas from schwannomas. We also suggest that NE 3D FLAIR is useful MR sequence for predicting adhesion between meningioma and the brain interface.

KEYWORDS: 3 T, 3D imaging, meningioma

eP-23

MR Perfusion in Gliomas Using Arterial Spin Labeling: Comparison with T2* Dynamic Susceptibility Contrast-Enhanced Technique

Cebeci, H.[1]·Buyukkaya, R.[2]·Aydin, O.[1]·Hakyemez, B.[1]
[1]Uludağ University, Bursa, TURKEY, [2]Duzce University, Duzce, TURKEY.

Purpose

Perfusion MRI with the T2* dynamic-susceptibility contrast (DSC) method is used widely to assess the perfusion of gliomas and the degree of tumor angiogenesis. Arterial spin labeling (ASL) is a relatively new, noncontrast perfusion MRI method which uses magnetically labeled arterial blood water protons as an endogenous tracer of flow. The aim of our study was to evaluate efficiency of perfusion in gliomas using ASL and comparison of ASL method with T2* DSC perfusion MRI.

Materials & Methods

Our study included 17 male and 16 female patients who were diagnosed as primer glial tumors between August 2011 and October 2012. Seventeen tumors were glioblastomas, two each were grade 3 oligodendroglioma, one each was grade 3 astrocytoma, four each were grade 2 oligodendroglioma, nine each were grade 2 astrocytoma. All arterial spin labeling and T2* DSC perfusion MR imaging studies were performed on a 3T MR imaging system (Achieva 3.0 Tx; Philips, Best, The Netherlands) by using a 32-channel head coil. Arterial spin labeling technique was performed with pseudocontinuous arterial spin labeling (PCASL). T2* DSC MRI was performed for all tumors by using a first-passage gadopentetate dimeglumine T2*-weighted gradient-echo single-shot echo-planar sequence followed by conventional MRI. Cerebral blood flow (CBF) and cerebral blood volume (CBV) maps were created from PCASL and T2*DSC, respectively. Relative signal intensity (SI) on PCASL images and rCBV value on T2*DSC perfusion maps were measured. The quantitative measures of the lesions were obtained by dividing the values obtained from the normal contralateral hemisphere. One observer placed region of interest (ROI) within solid tumor components where it was thought that high perfusion values would be found; he also placed ROI in the contralateral reference brain on ASL and T2* DSC maps. For statistical analysis Mann-Whitney testing was carried out. A p value of less than 0.05 indicated a statistically significant difference. The correlation between PCASL and T2*DSC and glioma grade was assessed using Pearson correlation analysis.

Results

Thirty-three target lesions (1 lesion per patient) in 33 patients were evaluated. Twenty-two of of lesions were high-grade, 11 each were low-grade lesions according to WHO classification. Signal intensity value on PCASL and rCBV on T2*DSC perfusions were significantly higher for high-grade glial tumors than low-grade tumors ($p<0.001$). There was correlation between signal intensity on PCASL and rCBV on T2*DSC perfusion (Pearson correlation = 0.783, $p < 0.001$).

Conclusion

Arterial spin labeling is a noncontrast perfusion MR imaging method, as an alternative to T2* DSC perfusion. Arterial spin labeling technique is useful in the preoperative assessment of the histopathologic grade of gliomas.

KEYWORDS: Arterial spin labeling, Dynamic susceptibility contrast-enhanced, glioma

Note: Scanned images are included in the proceedings. Some submitted images were reduced during editing, thereby decreasing clarity. Also, refer to the Program Planner. Proceedings Content as of 3-29-2013.

eP-24

Utility of Proton MR Spectroscopy in Differentiating Atypical Primary Central Nervous System Lymphoma from Tumefactive Demyelinating Lesions

Kim, S.[1]·Lu, S.[1,2]·Kim, D.[1]·Kim, H.[1]·Choi, C.[1]·Lim, Y.[1]
[1]Asan Medical Center, Seoul, KOREA, REPUBLIC OF, [2]The First Affiliated Hospital of Nanjing Medical Univerisity, Nanjing, CHINA.

Purpose
Primary central nervous system lymphomas (PCNSLs) usually can be differentiated from tumefactive demyelinating lesions (TDLs) by using conventional MRI, perfusion MRI and proton magnetic resonance spectroscopy (^{1}H-MRS). However, when PCNSLs show atypical MR features, it is often very difficult to differentiate from TDLs and the role ^{1}H-MRS in differentiating between the two conditions is not known well. This study aimed to investigate the usefulness of ^{1}H-MRS in differentiating PCNSLs with atypical MRI features from TDLs.
Materials & Methods
Twenty PCNSLs with atypical MRI features and 21 TDLs were enrolled in this study. Inclusion criteria for atypical MRI features of PCNSLs were necrosis (n = 4), hemorrhage (n = 5), ring enhancement (n = 4), patchy infiltrative enhancement (n = 11), streaky enhancement (n= 3) or absent contrast enhancement (n = 2) with more than one pattern in some cases. Primary central nervous system lymphomas with typical nodular enhancement pattern were excluded. All PCNSLs and six TDLs were histopathologically confirmed while 15 TDLs were clinically diagnosed. In all cases ^{1}H-MRS obtained with single voxel, intermediate TE (144 ms) point-resolved spectroscopy (PRESS) technique were available and retrospectively analyzed. Metabolites assessed were Choline (Cho), Creatine (Cr), N-acetyl-aspartate (NAA), lipid and lactate. Cho/Cr and Cho/NAA ratios were calculated. Lipid and/or lactate peak (lip-lac) was assessed visually and categorized into five grades by comparing the height of the peaks with that of Cr peak. Proton magnetic resonance spectroscopy findings were compared between the atypical PCNSLs and TDLs. Thresholds were selected with receiver operating characteristic (ROC) curves.
Results
Discrepancies between atypical PCNSLs and TDLs were found in Cho/Cr ratio ($P < 0.01$) and Cho/NAA ratio ($P < 0.01$). Lip-lac grade also was higher in atypical PCNSLs than in TDLs, but the difference was not statistically significant ($P = 0.054$). However, high lip-lac grades (> grade 3) were observed mainly in atypical PCNSLs (6/7) and only in one necrotic TDL (1/7). Lymphoma rather than TDL was suggested when Cho/Cr ratio was more than 2.45 (sensitivity 70.0, specificity 71.4), or Cho/NAA ratio was more than 1.75 (sensitivity 90.0, specificity 76.2). In two cases of nonenhancing PCNSLs ^{1}H-MRS revealed spectrums similar to those of TDLs.
Conclusion
Proton magnetic resonance spectroscopy seems to be useful for differentiating PCNSLs with atypical MRI features from TDLs. Cho/NAA and Cho/Cr ratios were significantly higher in PCNSLs than in TDLs and lip-lac grade showed a tendency to be higher in PCNSLs.

KEYWORDS: Lymphoma, 1H MRS

eP-25

Diffuse Gliomas: Does Perfusion and Diffusion MR Imaging Correlate with Overall Survival?

Ramos, A.·Hilario, A.·Perez Nuñez, A.·Salvador, E.·Hernandez Lain, A.·Lagares, A.·Sepulveda, J.
Hospital Universitario 12 de Octubre
Madrid, SPAIN.

Purpose
Diffuse gliomas comprise the second most common primary CNS neoplasms. The prognosis for this heterogeneous group of tumors is determined mainly by histologic grade. The aim of this work is to evaluate the relationship between rCBV and ADC values with overall survival in a group of patients with diffuse gliomas.
Materials & Methods
We conducted a retrospective analysis of 162 histologically confirmed diffuse gliomas. The samples were classified as low-grade and high-grade according to the 2007 WHO Classification of Tumors of the CNS. Dynamic contrast-enhanced T2*-weighted GE EPI were acquired during the first pass of a gadolinium contrast agent. On the color-coded rCBV maps, we selected the maximum rCBV for quantitative analysis. Diffusion-weighted imaging included an axial single-shot SE EPI sequence (b=1000 s/mm^2). Five circular ROIs were placed over the whole tumor to select the region of minimum ADC. The end point of the study was overall survival, which was measured from the date of initial diagnosis to the last follow-up visit or death. To simplify the analysis, rCBV and ADC values were classified as low or high based on a cut-off value obtained from the ROC curves. This cut-off value was ≥1.74 for rCBV and ≤1.185.10^{-3} mm^2/s for ADC. Each of the parameters (histologic grade, rCBV and ADC) was first evaluated univariately by constructing probability curves according to the Kaplan-Meier method and comparing them by the log rank test. The cut-off level chosen for overall survival was their median value. Variables achieving a p value of less than 0.05 in the univariate analysis, together with histologic diagnosis, subsequently were introduced in a multivariate regression analysis (Cox model).
Results
The median survival was 38 months for grade III and 14 months for grade IV gliomas. Analyzing the rCBV values, the median survival was 50 months for low perfusion gliomas and 12 months (9.2-14.81) for high perfusion (rCBV≥1.74) tumors (p=0.001). According to the ADC values, tumors with ADC≤1.185.10^{-3} mm^2/s had a median

Note: Scanned images are included in the proceedings. Some submitted images were reduced during editing, thereby decreasing clarity. Also, refer to the Program Planner. Proceedings Content as of 3-29-2013.

survival time of 12 months (9.22-14.78) ($p<0.001$). When we considered the group of high-grade gliomas, tumors with high perfusion values had a median survival of 11 months, while those gliomas with rCBV<1.74 had a median survival time of 50 months. If we classified tumors on the basis of the cell type, we found that median survival of astrocytomas differs significantly depending on the ADC and rCBV values. In astrocytomas, rCBV≥1.74 and ADC≤1.185.10^{-3} mm^2/s values correlated to a worse prognosis. In oligodendrogliomas, ADC and rCBV values did not have a significant relationship to overall survival. In the multivariate regression analysis we found that rCBV predicts the overall survival of diffuse gliomas regardless of histologic grade.

Conclusion

Although the survival of diffuse gliomas is determined by tumor histology, we have demonstrated that rCBV predicts the overall survival of diffuse gliomas regardless of histologic grade. In our series, perfusion and diffusion MRI correlated to patient overall survival. High-grade gliomas with high perfusion values experienced a worse outcome. The median survival of astrocytomas differed significantly depending on the ADC and rCBV values.

KEYWORDS: Glioma, Diffusion MR imaging, perfusion

eP-26

Differentiating Grade II from Grade III Nonenhancing Astrocytomas and Oligodendrogliomas Using Arterial Spin Labeling Perfusion MR: Comparison of Cerebrovascular Reactivity to Acetazolamide - Initial Experience

Lee, J. S.[1]·Wang, S.[1]·Mohan, S.[1]·Melhem, E. R.[2]
[1]Hospital of the University of Pennsylvania, Philadelphia, PA, [2]University of Maryland Medical Center, Baltimore, MD.

Purpose

While contrast-enhanced MRI is a valuable tool in assessing tumor malignancy, a significant proportion of gliomas do not enhance. Assessment of the histologic grade of nonenhancing gliomas may be aided by evaluation of the cerebrovascular reserve (CVR), a measure of the degree of cerebral perfusion increase in response to a cerebral vasodilator. We hypothesize that higher grade gliomas will have lower CVR compared to lower grade gliomas due to greater metabolic demand. Therefore the reactivity of tumor vessels to vasodilators may provide a noninvasive marker of malignancy grade. Acetazolamide is a carbonic anhydrase inhibitor that acts as a cerebral vasodilator and is known to increase cerebral blood flow (CBF). In this study, we evaluate CBF changes after acetazolamide injection in patients with nonenhancing brain tumors, and determine if there is a correlation between tumor grade and CBF changes.

Materials & Methods

Four patients (ages 31-64 years, 3 males, 1 female) with nonenhancing astrocytomas or oligodendrogliomas were included in this study. A pseudo-continuous ASL sequence was used for the perfusion scan. Interleaved images with and without labeling were acquired using a spin-echo EPI sequence. Using a 3T Siemens TrioTim, the sequence parameters were as follows: TR/TE = 4000/28 ms, FOV = 220 x 220 mm^2, number of sections = 16, slice thickness 5 mm, matrix = 96 x 96, labeling delay = 1200 ms, labeling duration = 1500 ms. Total acquisition time was 5:32 minutes. Arterial spin labeling was acquired before and after injection of 1g of acetazolamide IV. The raw ASL data were realigned, smoothed, and labeled, and control scans were subtracted to obtain CBF data. A 3D mask was drawn over the FLAIR abnormality. Difference of CBF values before and after acetazolamide was injected was computed.

Results

One patient with pathology proven Grade II oligodendroglioma demonstrated modest increase of CBF (2 to 3%) after acetazolamide administration (Figure1). In contrast, the remaining three patients with Grade III astrocytomas all demonstrated no significant difference in CBF.

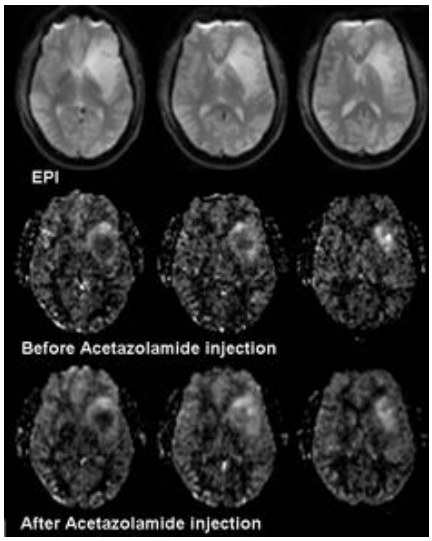

Conclusion

Our preliminary results demonstrate the feasibility of using acetazolamide to evaluate the status of CVR in nonenhancing astrocytomas. Low-grade gliomas tend to have higher cerebrovascular reactivity compared with high-grade gliomas. A larger number of patients will be required to draw definitive conclusions regarding the relationships between tumor grade and vascular reactivity.

KEYWORDS: Astrocytoma, Cerebrovascular reserve, acetazolamide

Note: Scanned images are included in the proceedings. Some submitted images were reduced during editing, thereby decreasing clarity. Also, refer to the Program Planner. Proceedings Content as of 3-29-2013.

eP-27

FDG-PET Imaging for Diagnosis of Pineal Parenchymal Tumors and Germinoma

Kakigi, T.
Kyoto University Graduate School of Medicine
Kyoto, JAPAN.

Purpose
Our aim of this study was to evaluate if it is possible to identify histologic types of pineal parenchymal tumors, which are including pineocytoma, pineal parenchymal tumor with intermediate differentiation (PPTID) and pineoblastoma, and to differentiate pineal parenchymal tumors from germinomas using FDG-PET imaging.
Materials & Methods
We enrolled eight patients who had FDG-PET imaging with histologic verification of pineal parenchymal tumors (five patients) and germinomas (three patients) retrospectively from July 2008 to June 2012. We measured SUVmean and SUVmax of tumors and analyzed them using Mann-Whitney U test.
Results
No significant correlation was found between FDG uptake and tumor grading of pineal parenchymal tumors. However, we found a significant difference between pineal parenchymal tumors and germinomas. SUVmax and SUVmean of germinomas were less than those of pineal parenchymal tumors (p = 0.036 for both).

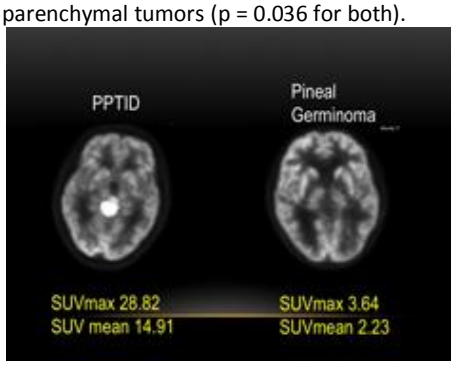

Results of Mann-Whitney test for SUVmean

	PPTmean	Gmean
No.	5	3
Lowest Value	4.73	2.23
Highest Value	14.91	3.36
Median	5.56	2.88

Results of Mann-Whitney test for SUVmax

	PPTmax	Gmax
No.	5	3
Lowest Value	6.51	3.64
Highest Value	28.82	4.09
Median	7.72	3.78

Conclusion
FDG-PET imaging could not differentiate the histology among the pineal parenchymal tumors. However, we proved the diagnostic utility of FDG-PET imaging to differentiate between pineal parenchymal tumors and germinoma.

KEYWORDS: Pineal cell tumor, Germinoma, FDG-PET/CT

eP-28

Precontrast and Postcontrast Susceptibility-Weighted Imaging Grading Performance in Intra-Axial Brain Lesions

Aydin, O.[1]·Buyukkaya, R.[2]·Cebeci, H.[1]·Hakyemez, B.[1]
[1]Uludağ University, Bursa, TURKEY, [2]Düzce University, Duzce, TURKEY.

Purpose
It has been reported that susceptibility-weighted imaging (SWI) may be use for grading brain tumors. The purpose of this study was to compared noncontrast susceptibility-weighted imaging (SWI) and contrast-enhanced SWI in the evaluation of intra-axial tumors.
Materials & Methods
There are different grading methods in the literature. Quantitative analysis was performed by a grading system based on the degree of intratumoral susceptibility signals (ITSS). Fifty-three patients having intra-axial tumors (n = 15 low grade, n = 19 GBM, n = 14 metastases, n = 2 lymphoma and n = 3 abscess) participated in this study. All of the patients underwent both noncontrast SWI and contrast-enhanced SWI at 3T Philips MRI system with 32-channel head coil. Venous BOLD sequence was performed. This sequence is flow-compensated T2 star-weighted 3D gradient-echo sequence. The imaging parameters are as follows: TR/TE, 21/29 ms; flip angle, 10°; FOV, 220 X 220 mm; section thickness, 0.6 mm; ETL, 1 k-space; NEX 2. Susceptibility-weighted imaging tumor grading methods are used - both SWI and contrast-enhanced SWI. The differences between the two groups were analyzed statistically.
Results
Contrast to noise ratio (CNR) of postcontrast SW images

Note: Scanned images are included in the proceedings. Some submitted images were reduced during editing, thereby decreasing clarity. Also, refer to the Program Planner. Proceedings Content as of 3-29-2013.

higer than precontrast SWI and also high-grade tumors showed bright enhancement surrounding the tumor due to breakdown of the blood-brain barrier but there was no statistical difference between precontrast and postcontrast SWI grading (P<0.05).

TABLE 1: For semiquantitative analysis, the degree of ILSS was divided into 4 grades

Grading Method			*Patients number*
Grade 0	No ILSS	SWI	12
		CE-SWI	10
Grade 1	1-5 ILSS	SWI	9
		CE-SWI	8
Grade 2	6-10 ILSS	SWI	11
		CE-SWI	5
Grade 3	>10 ILSS	SWI	26
		CE-SWI	35

ILSS: Intralesional susceptibility signal

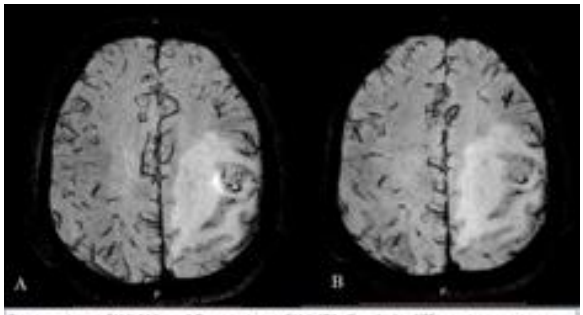

Postcontrast SWI (A) and Precontrast SWI (B). Grade is different same tumor

Conclusion
Susceptibility-weighted imaging at 3T and 32-channel head coil is a useful method to analyze and grade intra-axial lesions. Postcontrast SWI is not superior to precontrast SWI for grading tumors.

KEYWORDS: Susceptibility-weighted imaging, Masses

eP-29

Comparison of the Value of CT Perfusion and MR Perfusion in the Differential Diagnosis of Intra-Axial Brain Tumors

Gomyo, M.[1]·Tsuchiya, K.[1]·Ohara, A.[1]·Tateishi, H.[1]·Koyanagi, M.[2]·Kobayashi, K.[2]·Nitatori, T.[1]
[1]Kyorin University, Mitaka, JAPAN, [2]Kyorin University Hospital, Mitaka, JAPAN.

Purpose
Differential diagnosis of brain tumors before surgery is important for the determination of a way of treatment as well as for the assessment of patient prognosis. Perfusion imaging is a technique that can visualize blood flow in tissue and is reportedly useful for evaluation of tumor characteristics. We comparatively assessed CT perfusion (CTP) and MR perfusion (MRP), which can visualize tumor perfusion quantitatively and semiquantitatively respectively, in the differential diagnosis of intra-axial brain tumors.
Materials & Methods
We performed CTP and MRP in patients with preoperative intra-axial brain tumor that afterwards was histologically diagnosed following resection or biopsy. CT perfusion was performed in 64 patients including high-grade glioma (HGG, n = 32), low-grade glioma (LGG, n = 8), primary central nervous system lymphoma (PCNSL, n = 5), and brain metastasis (n = 19). MR perfusion was performed in 60 patients including HGG (n = 36), LGG (n = 9), PCNSL (n = 5), and brain metastasis (n = 10). Both CTP and MRP were performed in 41 patients that included HGG (n = 23), LGG (n = 5), PCNSL (n = 4), and brain metastasis (n = 9). In CTP, we calculated CBV, CBF and MTT ratios by dividing CBV, CBF and MTT values of the solid component of tumor by that of contra-lateral normal white matter. In MRP, we visually scored CBV, CBF and MTT of the tumor by comparing with the contra-lateral normal white matter. We made comparison of perfusion measurements between CTP and MRP along with comparison among tumor groups.
Results
At both CTP and MRP, HGG and brain metastasis were higher in CBV and CBF than LGG and PCNSL, and brain metastasis was higher in MTT than HGG and LGG. At CTP, PCNSL was higher in CBV and MTT than LGG and higher in MTT than HGG.
Conclusion
Cerebral blood volume and CBF are of value to distinguish between HGG or brain metastasis and LGG or PCNSL, and MTT is useful to distinguish between HGG and brain metastasis at both CTP and MRP. On the other hand, CBV and MTT at CTP can distinguish between PCNSL and LGG.

KEYWORDS: CT perfusion, MR perfusion-weighted imaging, brain tumor

Note: Scanned images are included in the proceedings. Some submitted images were reduced during editing, thereby decreasing clarity. Also, refer to the Program Planner. Proceedings Content as of 3-29-2013.

eP-30

Diffusional Kurtosis Imaging of the Optic Pathways between Multiple Sclerosis and Neuromyelitis Optica

Yoshida, M.[1]·Hori, M.[1]·Yokoyama, K.[1]·Suzuki, M.[1]·Kamagata, K.[1]·Kyogoku, S.[1]·Kamiya, K.[1]·Sato, K.[1]·Aoki, S.[1]·Masutani, Y.[2]
[1]Juntendo University School of Medicine, Tokyo, JAPAN, [2]Graduate School of Medicine, The University of Tokyo, Tokyo, JAPAN.

Purpose
To evaluate differences in diffusional changes of the optic pathways between multiple sclerosis (MS) and neuromyelitis optica (NMO) using a new method, diffusional kurtosis imaging (DKI).
Materials & Methods
Five patients with known MS, five patients with known NMO, and five healthy volunteers participated in this study. Diffusional kurtosis imaging was performed on a 3T MR scanner. Diffusion metric maps were calculated by using the free software dTV II. FZRx (Image Computing and Analysis Laboratory, Department of Radiology, The University of Tokyo). Fractional anisotropy (FA) and apparent diffusion coefficient (ADC) maps of the conventional model and mean kurtosis (MK) maps were computed. The optic tracts (OT) and optic radiations (OR) of patients and controls were analyzed using a tract-specific analysis. The figure shows an example of tractography of the optic pathway.

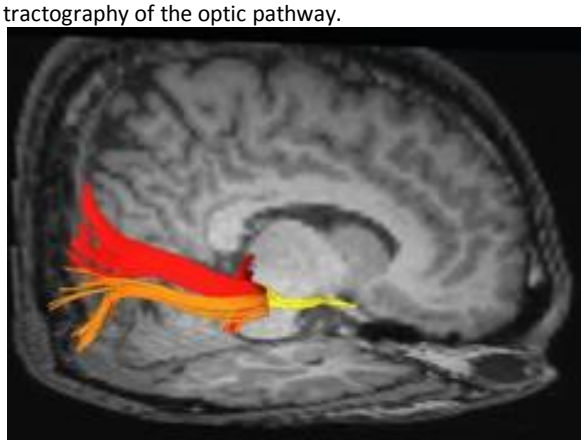

Results
The MK, FA, and ADC of the bilateral OR and OT are shown in the table. The MK in the right and bilateral OT was significantly lower in the NMO group than in the MS group ($P < 0.01$). The MK was significantly lower in the bilateral OR of MS patients than of controls ($P < 0.05$). The MK in the right and bilateral OT was significantly lower in NMO patients than in controls ($P < 0.01$). The mean FA in the right and bilateral OR also was significantly decreased in NMO patients ($P < 0.05$).

The MK, FA, and ADC of the bilateral OR and OT (mean value ± SD)

	MK		FA		ADC(10^{-3} mm^2/s)	
	OR	OT	OR	OT	OR	OT
control	0.862 ± 0.080	0.623 ± 0.042	0.483 ± 0.035	0.313 ± 0.025	0.849 ± 0.127	1.355 ± 0.144
MS	0.742 ± 0.103*	0.610 ± 0.073	0.456 ± 0.022	0.336 ± 0.034	0.913 ± 0.067	1.433 ± 0.363
NMO	0.787 ± 0.077	0.488 ± 0.033**	0.417 ± 0.023*	0.316 ± 0.021	0.876 ± 0.066	1.522 ± 0.305

Conclusion
Diffusional kurtosis imaging may be a more sensitive biomarker to differentiate between MS and NMO than conventional diffusional evaluations, such as diffusion tensor imaging. Each disease produces distinctive diffusional abnormalities of the optic pathways

KEYWORDS: Diffusion kurtosis imaging, Brain white matter

eP-31

Basal Ganglia Calcifications on Quantitative Susceptibility Mapping Images: Paramagnetic Susceptibility Property

Sohn, C.[1]·Kim, J.[1]·Choi, S.[1]·Yun, T.[1]·Han, M.[1]·Wang, Y.[2]
[1]Seoul National University Hospital, Seoul, KOREA, REPUBLIC OF, [2]Cornell University, New York, NY.

Purpose
The majority of intracranial calcifications outside the basal ganglia are diamagnetic. One study reported that almost all calcifications of basal ganglia have paramagnetic susceptibility property in GRE phase image. But, corrected phase images or susceptibility-weighted images cannot clearly differentiate hemorrhage from calcifications that are located in basal ganglia. We demonstrate that quantitative susceptibility mapping (QSM) images can differentiate basal ganglia calcifications that have paramagnetic property from diamagnetic calcifications.
Materials & Methods
Twenty-four patients (women n = 11, mean age = 53 years) were examined with multi-echo T2*-GRE imaging. Imaging was performed at 1.5T (HDXT, GE Healthcare, Milwaukee, WI, USA) with 8-channel head coil. Quantitative susceptibility mapping was reconstructed by using morphology-enabled dipole inversion (MEDI) method.

Note: Scanned images are included in the proceedings. Some submitted images were reduced during editing, thereby decreasing clarity. Also, refer to the Program Planner. Proceedings Content as of 3-29-2013.

Underlying disease processes in these patients included brain tumor (n = 11), cerebral infarction (n = 2), cerebral aneurysm (n = 2), and other (n = 8). Presence or absence of calcification was detected by visually inspecting the CT images. Intracranial calcifications (n = 71) were studied in the 24 patients. Outside basal ganglia calcifications (n = 63) and basal ganglia calcifications (n = 8) were enrolled. Susceptibility property was evaluated by using QSM in all calcific lesions.
Results
All outside basal ganglia calcifications (n = 63) had diamagnetic property (negative susceptibility), but eight basal ganglia calcifications had paramagnetic property (positive susceptibility). Even positive susceptibility signal intensity like calcification was detected at uncalcified basal ganglia (n = 7) that did not have calcific density by CT.
Conclusion
Quantitative susceptibility mapping images clearly visualized basal ganglia calcifications, which was paramagnetic.

KEYWORDS: Calcifications, Susceptibility-weighted imaging, basal ganglia

eP-32

Susceptibility-Weighted Imaging: New MR Sequences in Daily Practice - A Pictorial Essay

Kang, H.
Seoul Veterans Hospital
Seoul, KOREA, REPUBLIC OF.

Purpose
Susceptibility-weighted imaging (SWI) magnetic resonance (MR) sequences are three-dimensional (3D) spoiled gradient-echo sequences that provide a high sensitivity for the detection of blood degradation products, calcifications, and iron deposits. This pictorial review is aimed at illustrating and discussing its main clinical applications.
Materials & Methods
Susceptibility-weighted imaging is based on high-resolution, 3D, fully velocity-compensated gradient-echo sequences using both magnitude and phase images. A phase mask obtained from the MR phase images is multiplied with magnitude images in order to increase the visualization of the smaller veins and other sources of susceptibility effects, which are displayed at best after postprocessing of the 3D dataset with the minimal intensity projection (minIP) algorithm. A total of 82 patients underwent MR examinations that included SWI on a 3.0T MR imager were enrolled. Among the 82 patients, 31 showed developmental venous anomaly, 11 patients showed cavernous malformation, 11 showed calcifications in various pathologic conditions, 10 showed susceptibility vessel sign, eight showed brain tumor, five showed microbleeds, two showed diffuse axonal injury, two showed arteriovenous malformation, one showed moyamoya disease, and one showed Parkinson disease.
Results
Susceptibility-weighted imaging is very useful in developmental venous anomaly and cavernous malformation, in characterizing brain tumors and degenerative diseases of the brain, in detecting cerebral microbleeds and in recognizing calcifications in various pathologic conditions. The phase images are especially useful in differentiating between paramagnetic susceptibility effects of blood and diamagnetic effects of calcium. Susceptibility-weighted imaging also can be used to evaluate changes in iron content in neurodegenerative disorders and to predict stroke evolution.
Conclusion
Susceptibility-weighted imaging is useful in differentiating and characterizing diverse brain disorders.

KEYWORDS: MR imaging brain, Advanced MR imaging, susceptibility-weighted imaging

eP-33

Quantitative Assessment of Susceptibility of the Motor Cortex by Using Quantitative Susceptibility Mapping

Hirai, T.[1]·Azuma, M.[1]·Kitajima, M.[1]·Yamashita, Y.[1]·Liu, T.[2]·Wang, Y.[2]
[1]Kumamoto University, Kumamoto, JAPAN, [2]Weill Cornell Medical College, New York, NY.

Purpose
Quantitative susceptibility mapping (QSM) is a novel postprocessing technique which allows the calculation of the bulk magnetic susceptibility distribution of tissue in vivo from gradient echo MR phase images. It has been proved that paramagnetic iron is the predominant source of susceptibility variations in deep gray matter. The purpose of this study was to determine the course of mean magnetic susceptibility in the motor cortex with age by using QSM.
Materials & Methods
All MR studies were performed with a multiecho gradient-echo sequence at a 3.0T Siemens scanner. The study population consisted of 40 cerebral hemispheres of 20 healthy subjects (10 females, 10 males; 26-72 years; mean age, 43 years). Quantitative susceptibility mapping was performed by using both the magnitude and phase components from all TEs in the morphology-enabled dipole inversion method. The mean of susceptibility over a region containing a hand motor area in the motor cortex was estimated on QSM images as its total susceptibility. It also was performed for the superior frontal cortex (SFC). Measurement differences were assessed by using the Student-*t* test and the *F* test; $P < 0.05$ was considered to indicate a statistically significant difference.
Results
The measured mean susceptibility with QSM was significantly higher for the motor cortex than the SFC ($P <$ 0.01). The mean susceptibility in the motor cortex and SFC

Note: Scanned images are included in the proceedings. Some submitted images were reduced during editing, thereby decreasing clarity. Also, refer to the Program Planner. Proceedings Content as of 3-29-2013.

increased with advancing age; the mean and standard deviation of the mean susceptibility for these structures at the 5th decade was 56 ± 13 ppb and 18 ± 7.6 ppb, respectively. After the age of 50 years, an increase in mean susceptibility was subtle. With respect to latenality in the motor cortex, no differences were found between left and right hemispheres.

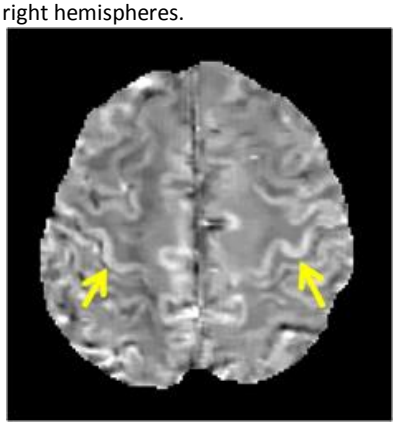

Conclusion

On QSM, the mean susceptibility in the motor cortex increased with advancing age. This probably reflects differences in the concentration of nonheme iron, which is consistent with the putative iron concentrations reported in the hallmark study by Hallgren and Sourander.

KEYWORDS: Aging, 3 T, QSM

eP-34

Advantages and Disadvantages among Noncontrast Time-of -Flight, Contrast-Enhanced Time-of-Flight and Contrast-Enhanced Dynamic Techniques in Cerebral MR Angiography: A Comparison Study

Hsieh, K.[1]·Cheung, W.[1]·Schob, S.[2]
[1]Far Eastern Memorial Hospital, New Taipei City, TAIWAN,
[2]Martin-Luther University, Halle-Wittenberg, GERMANY.

Purpose

Nowadays, magnetic resonance angiography (MRA) is one of the best imaging techniques for detecting intracranial vascular diseases, such as stenosis, aneurysm or other vascular malformations. The current routine MRA protocols include both contrast-enhanced dynamic MRA and noncontrast-enhanced time-of-flight (plain TOF) MRA. However, poor spatial resolution of the contrast-enhanced dynamic MRA is subject to miss small vascular lesions whose sizes are within a few millimeters. Besides, several studies have demonstrated that the administration of contrast agent was beneficial in MRA image for enhancing the diagnosis of intracranial vascular lesions. Because the conventional TOF MRA is not a contrast medium-based protocol, we assessed the hypothesis that contrast-enhanced TOF MRA may do better than the other two conventional MRA protocols. The purpose of this study is to compare the advantages and shortages among plain TOF, contrast-enhanced TOF and contrast-enhanced dynamic MRA and find out the most appropriate technique.

Materials & Methods

Subjects: This prospective, institutional review board-approved study with informed consent assessed MRA imaging of 30 adults with a mean age of 51 years (ranging from 24 to 64 years, 25 men and 5 women). None of them had any known CNS disease. MRI examination and analysis: Three sets of MRA images were collected on a 1.5T MR system, including noncontrast-enhanced TOF MRA, contrast-enhanced TOF MRA and contrast-enhanced dynamic MRA. Arterial image quality (AIQ) scores for 15 different medial to small-sized intracranial arteries were rated by the consensus of two radiologists with a Likart scoring system. The contrast-noise ratio of bilateral middle cerebral arterial trunks (MCAT) also was obtained. Kruskal-Wallis method of ANOVA was used to compare the IQ scores and CNRs at the three types of MRA techniques.

Results

Significantly better visualization ($p<0.001$) of intracranial arteries from the AIQ scores of contrast-enhanced TOF (20.17 ± 3.74) than plain TOF (16.63 ± 3.54) and contrast-enhanced dynamic MRA (13.10 ± 3.20) was found. There also was better MCAT CNR of contrast-enhanced TOF (61.09 ± 10.26) and plain TOF (74.11± 14.04) than contrast-enhanced dynamic MRA (43.29 ± 13.01; $p<0.05$). The CNR of contrast-enhanced TOF is less than that of plain TOF but did not reach statistical significance ($p>0.05$). The visualized intracranial veins on contrast-enhanced TOF MRA do not influence the depictions of the visualized cerebral arteries.

Conclusion

Contrast-enhanced TOF has more potential to depict the smaller intracranial vascular branches and lesions than other MRA techniques. However, the MCAT CNR obtained is comparable in either contrast-enhanced TOF or plain TOF.

KEYWORDS: MRA techniques, 1.5T

eP-35

Susceptibility-Weighted MR Imaging: A Better Technique in the Detection of Capillary Telangiectasia when Compared to T2*-Gradient Echo

De Bruin, D. E.·Chaudhry, U. S.·Policeni, B. A.
University of Iowa Hospitals and Clinics
Iowa City, IA.

Purpose

Enhancing lesions on brain MRI can present a diagnostic quandary as both benign lesions such as capillary telangiectasia (BCT) and pathologic lesions such as demyelination or metastatic disease may appear similar. Stagnation of blood in the low-flow venous channels of BCTs results in susceptibility effect secondary to the increase in local deoxyhemoglobin. Both T2*-gradient echo imaging (GRE) and susceptibility-weighted imaging

Note: Scanned images are included in the proceedings. Some submitted images were reduced during editing, thereby decreasing clarity. Also, refer to the Program Planner. Proceedings Content as of 3-29-2013.

have been demonstrated previously as valuable in the diagnosis of BCT. Because susceptibility-weighted imaging (SWI) is more sensitive to susceptibility changes than GRE, we aim to demonstrate an increased diagnostic value of SWI compared to GRE in making the diagnosis of BCT.
Materials & Methods
We retrospectively reviewed the MR images of 17 patients with a presumed diagnosis of BCT who were examined from June 2010 to September 2012. All patients had undergone MR imaging at 1.5T with T1, T2, FLAIR, GRE, SWI, and gadolinium-enhanced T1 sequences. Lesions were evaluated for the presence or absence of signal abnormality on each particular sequence.
Results
All 17 CBTs demonstrated distinct signal-intensity loss on SWI compared to 7/17 (41%) showing signal-intensity loss on GRE. The increased frequency of detection using SWI versus GRE is statistically significant ($z = 2.85$, $p < 0.01$; $\chi^2 = 8.10$, $p < 0.01$). Six of the lesions showed signal-intensity intensity changes on T1 and/or T2 while the remaining lesions were isointense to normal brain.

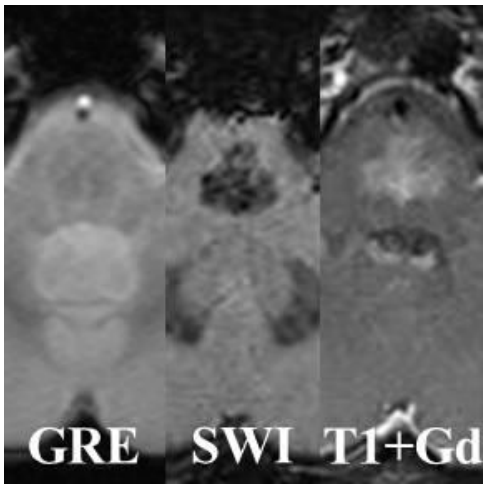

Conclusion
Benign capillary telangiectasias are more conspicuous on SWI than GRE and other precontrast MR imaging. In our review, there were no cases where GRE was positive and SWI was negative. Susceptibility-weighted imaging is a valuable tool in diagnosing these benign lesions which may otherwise be occult on noncontrast MR imaging, and should serve to increase diagnostic confidence.

KEYWORDS: Susceptibility-weighted imaging, Capillary malformation

eP-36

Detection of Quantitative Differences in Cerebral Perfusion Parameters in Symptomatic versus Asymptomatic Intracranial Atherosclerotic Disease Using the Bookend Technique

Korutz, A. W.[1]·Vakil, P.[2]·Hurley, M.[1]·Shaibani, A.[1]·Carroll, T. J.[1,2]·Ansari, S.[1]
[1]Northwestern University, Feinberg School of Medicine, Chicago, IL, [2]Northwestern University, Evanston, IL.

Purpose
Intracranial atherosclerotic disease (ICAD) is associated with significant morbidity. Surgical/endovascular intervention has been relegated to patients that fail optimum medical management, but there is no risk stratification scheme to identify susceptible populations prior to presenting with refractory strokes. We studied differences in quantitative cerebral blood flow (qCBF), cerebral blood volume (qCBV) and mean transit time (qMTT) measurements between vascular territories with and without acute infarcts in patients with advanced ICAD.
Materials & Methods
We retrospectively identified 10 patients (4 male, 6 female; 66 +/- 13 years old) with moderate to severe intracranial stenoses (>50% in the supraclinoid ICA, ACA, MCA or PCA) on MRA, that also underwent a quantitative SCALE DSC-MR PWI scan (Bookend technique) at presentation. Vascular territories were divided into subgroups containing acute infarcts on MR DWI versus those with no infarcts. Exclusion criteria included presumed disease from central emboli, existing encephalomacia > 50% of the volume of the vascular territory, prior angioplasty/stenting or vascular bypass on the affected side. After imaging sequences for each patient were coregistered to a standard 3-D imaging space, vascular territories were automatically segmented using a MATLAB script. In order to assess the hemodynamic parameters of viable brain parenchyma, acute infarcts as well as encephalomalacic regions related to chronic infarcts within each vascular territory were manually excluded by drawing ROIs on B1000 and T2 imaging sequences, respectively. Quantitative cerebral blood flow, qCBV and qMTT values were generated for each vascular distribution from the SCALE PWI scan and combined values were compared using a two-tailed Student's *t*-test.
Results
Ten vascular territories (1 ACA, 6 MCA and 3 PCA) were included in the subgroup with infarcts and 11 vascular territories (5 MCA and 6 PCA) were included in the infarct-free subgroup. The mean qCBF, qCBV and qMTT values for territories containing infarcts were 31.1 +/- 1.6 mL/min/100g, 3.3 +/- 0.3 mL/100g and 6.3 +/- 0.5 sec, respectively. The mean qCBF, qCBV and qMTT values for the territories without infarcts were 37.6 +/- 1.4 mL/min/100g, 4.3 +/- 0.4 mL/100g and 6.8 +/- 0.4 seconds, respectively. Differences between qCBF and qCBV values

Note: Scanned images are included in the proceedings. Some submitted images were reduced during editing, thereby decreasing clarity. Also, refer to the Program Planner. Proceedings Content as of 3-29-2013.

were both statistically significant ($p < 0.01$ and < 0.05, respectively). Differences in mean transit time between the two experimental groups was not significant.
Conclusion
Significant differences in qCBF and qCBV exist between vascular territories with and without acute infarcts in patients with advanced ICAD. Although no significant qMTT differences exist between these two groups, values are elevated when compared to published norms. Our findings suggest that prolongation of time-based metrics alone is not an effective indicator of the risk for infarct progression in patients with advanced ICAD. Quantitative CBF and CBV values utilizing vascular territory analysis may allow the characterization of the stages of hemodynamic failure and hence detection of unstable, refractory intracranial stenoses.

KEYWORDS: MR perfusion-weighted imaging, Stroke

eP-37

Intravenous tPA Alone versus Intravenous tPA Combined with Interventional Treatment in Patients with M3 and M4 Occlusions

Carneiro, F.·Tomsick, T.·Broderick, J.·The IMS Investigators
University of Cincinnati
Cincinnati, OH.

Purpose
M3 and M4 occlusions of the middle cerebral artery (MCA) have demonstrated a better prognosis even without recanalization when compared to proximal occlusions of the more proximal anterior circulation. Moreover these lesions are technically more difficult to treat by interventional means with lower rates of recanalization and probably more prone to complications related to the interventional procedure. The purpose of this study was to preliminarily compare the outcomes of bridging therapy (IV tPA plus interventional intra-arterial treatment) versus IV tPA alone in subjects enrolled in the Interventional Management of Stroke (IMS) I,II studies that presented with M3 and M4 occlusions. Data from IMS III Trial also will be presented.
Materials & Methods
All subjects received 0.6 mg/kg of IV tPA before cerebral DSA. Sixteen subjects demonstrated M3 and M4 occlusions confirmed by subsequent cerebral digital subtraction angiography (DSA). Seven subjects were treated with additional IA therapy via microcatheter, in a nonrandomized fashion according to operator preference.
Results
Sixteen subjects demonstrated M3 or M4 occlusions on postintravenous-rtPA arteriography. Additional IA rtPA treatment via standard microcatheter was performed in seven (43.7%). No additional interventional treatment was performed in nine (56.2%). The modified Rankin Scale (mRS) 0-2 outcomes in the IV/IA or IV-only groups were similar. Recanalization occurred in 42% of IV/IA-treated patients. There was no difference in the mRS 0-2 between subjects that recanalized, and those that did not. There were no symptomatic intraparenchymal hemorrhages. New occlusions in the IA-treated group occurred in one subject. There were no deaths with M3 and M4 occlusions.
Conclusion
Based on recanalization and clinical outcome, IV/IA therapy of M3 and M4 occlusions may offer no clinical benefit when compared to IV tPA itself. Interventional treatment of distal MCA occlusions has the potential to increase adverse events. Data from IMS III Trial also will be presented to support or refute these hypotheses.

KEYWORDS: Interventional, Stroke, M3 and M4 occlusions

eP-38

Predictive Value of Positive Remodeling and Stenosis of Proximal Internal Carotid Artery for Cerebral Ischemic Lesions: Assessment of CT Angiography and Brain MR Imaging

Seo, H.[1]·Kim, J.[2]·Jin, K.[3]·Kim, H.[1]·Chung, S.[1]·Choi, S.[1]
[1]Seoul National University Hospital Healthcare System Gangnam Center, Seoul, KOREA, REPUBLIC OF, [2]Seoul National University Hospital, Seoul, KOREA, REPUBLIC OF, [3]Seoul Metropolitan Government-Seoul National University Boramae Medical Center, Seoul, KOREA, REPUBLIC OF.

Purpose
In coronary artery disease, positive remodeling of arterial wall is a well known factor related to acute coronary syndrome. However, there is lack of study in carotid artery. Therefore, the aim of this study is to assess the predictive value of positive remodeling at proximal interval carotid artery compared to stenosis.
Materials & Methods
We enrolled 2424 patients who had carotid CT angiographies from October 2003 to December 2011. We included patients who had brain MRI after CT angiography. Among these patients, we excluded patients who had neck infection/inflammation, history of head and neck cancer or hematologic malignancy, history of radiation in the neck, trauma in the neck, Takayasu's arteritis, dissection, Ehlers-Danlos syndrome or moyamoya disease. We analyzed CT angiography and brain MRI in the final 316 patients. We assessed the affected side of carotid artery, carotid artery diameter at the narrowest level, the proximal and just distal diameter of stenotic lesion, characteristics of plaque and presence of tandem lesions in the ipsilateral distal artery throughout the intracranial arteries. We also assessed presence and severity of small vessel disease, presence of borderzone infarction, lacunar infarction and large vessel disease. We also searched the reports of perfusion study, if patients had undergone brain SPECT scans or MRI perfusion studies. We assessed the lesions by their side. We defined positive remodeling index as ratio of the largest diameter at the narrowest portion and mean

Note: Scanned images are included in the proceedings. Some submitted images were reduced during editing, thereby decreasing clarity. Also, refer to the Program Planner. Proceedings Content as of 3-29-2013.

diameter (average between proximal and just distal diameters). For grade of stenosis, we used both NASCET and ECST criteria. Chi square test, Student *t*-test and ANOVA test was performed using SPSS program. We analyzed significant factors related to brain lesion using multivariable analysis.
Results
Only 158 patients had proximal internal carotid lesions on CT angiography. There were 98 male and 60 female patients (average age 69.5 years). There were follow-up MRI scans in 98 patients. There were 93 patients with cerebral ischemic lesions, 68 patients with cerebral ischemic lesions except small vessel disease and 24 patients with borderzone infarct. There was no significant correlation between the narrowest diameter or the largest diameter at the narrowest level and mean diameter ($p>.05$). Mean diameter of carotid artery showed significant difference in patients with or without any type of ischemic lesions including small vessel disease ($p = .028$). Severity of stenosis assessed by ECST showed statistical significance in patients with any type of cerebral ischemic lesions ($p = .036$). However, only RI had statistical significance in patients who had cerebral ischemic lesions except small vessel disease ($p = .037$). In the perfusion study, perfusion abnormality was significantly different according to RI and the presence of stenosis was more than 70% in ECST criteria ($p<.042$).
Conclusion
Only RI had statistical significance in patients with cerebral ischemic lesion except small vessel disease. RI and stenosis was related to perfusion abnormality. Positive remodeling of carotid artery could be predictive factor for cerebral ischemic lesion.

KEYWORDS: Carotid plaque, Carotid artery stenosis, cerebral ischemic lesion

eP-39

Comparison of 4D CT Angiography with MR Angiography in Acute Ischemic Stroke Patients with Probable Internal Carotid Artery Occlusion

Miyazaki, Y.･Mori, T.･Iwata, T.･Nakazaki, M.･Takahashi, Y.
Shonan Kamakura General Hospital
Kamakura, Kanagawa, JAPAN.

Purpose
Emergency MR angiography (MRA) can provide useful information to find the internal carotid artery (ICA) occlusion in an acute stroke setting. However, the usefulness of four-dimensional CT angiography (4D CTA) using 320-row area detector CT remains uncertain for emergency diagnosis of cerebral vasculature in acute ischemic stroke. The aim of our retrospective study was to investigate whether or not there were some differences between 4D CTA and MRA findings in acute ischemic stroke patients with probable internal carotid artery occlusion.
Materials & Methods
Included for analysis were acute ischemic stroke patients: 1) who were admitted to our institution within 24 hours of stroke onset from September 2010 to November 2012, 2) who underwent 4D CTA within 24 hours following emergency MRA on admission and 3) in whom the affected ICA absolutely was not visualized in MRA. We compared 4D CTA findings with MRA findings.
Results
During study period, 948 acute stroke patients were admitted within 24 hours of stroke onset and emergency MRA showed no visualization of the affected ICA in 75 of them. Among the 75 patients, 51 patients underwent 4D CTA following MRA. The 4D CTA demonstrated delayed antegrade flow of the affected ICA in 14 patients (27%) and the affected ICA supplied by collateral flow in eight (16%). In the rest (57%, 29/51), 4D CTA could not visualize the affected ICA at all.
Conclusion
In an acute stroke setting, 4D CTA can provide more accurate information of the affected ICA which absolutely is not visualized in MRA.

KEYWORDS: 4D CTA, Acute ischemic stroke, internal carotid artery occlusion

eP-40

Assessment of Crossed-Cerebellar Diaschisis for Internal Carotid Artery Occlusion on Cerebral Perfusion MR Imaging Using Arterial Spin Labeling

Hiratsuka, Y.[1]･Kikuchi, K.[1]･Yokoyama, R.[1]･Mochizuki, T.[1]･Miki, H.[2]
[1]Ehime University, Toon, JAPAN, [2]Ehime Prefectural Central Hospital, Matsuyama, JAPAN.

Purpose
Crossed-cerebellar diaschisis (CCD) is thought to be caused by an interruption of the corticopontocerebellar fibers resulting in the depression of neuronal metabolism and activity displayed as the reduced blood flow in the cerebellar hemisphere contralateral to a supratentorial hypoperfusion. Several studies have reported the incidence of CCD on perfusion MRI using dynamic susceptibility contrast (DSC) technique; however, the reproducibility of CCD was lower than that previously reported in the SPECT or PET studies. Arterial spin labeling (ASL) is an alternative method of perfusion MR imaging for blood flow measurement. This technique is noninvasive and enables us to evaluate the cerebral blood flow without contrast media. Arterial spin labeling is becoming a new clinical neuroimaging tool for evaluating the intracranial blood flow dynamics. There were few reports that described CCD on perfusion MRI using ASL, and the purpose of this study is to evaluate the detectability of crossed-cerebellar diaschisis on perfusion MRI using ASL with making reference to the 123I-IMP SPECT images.
Materials & Methods

Note: Scanned images are included in the proceedings. Some submitted images were reduced during editing, thereby decreasing clarity. Also, refer to the Program Planner. Proceedings Content as of 3-29-2013.

Fifteen patients that had suspected ICA stenosis/occlusion and underwent MR examinations including ASL perfusion imaging were analyzed retrospectively. Arterial spin labeling perfusion images of MRI were acquired with a 1.5T MRI system (GE Healthcare), using a 3D ASL sequence with a pulsed continuous ASL technique and spiral fast spin-echo readout. Imaging parameters for 3D ASL were as follows: FOV: 240 x 240 mm, 128 x 128 matrix, 30 slices with a slice thickness of 4 mm and 4 mm spacing, TR/TE: 5000/10.5 ms, NEX: 3, spiral scan with 8 arms, 1450 ms of labeling time and 2025 ms of postlabeling delay. All of these patients also were scanned by 123I-IMP SPECT and those results were used as the reference. Evaluation of CCD was obtained by two radiologists on display.
Results
In 15 cases with ICA disorder, most cases had shown the decrease of CBF on the ipsilateral side of cerebral hemisphere. Three cases of those also were shown the decrease of contralateral cerebellar hemisphere, and we have estimated the lesion as the expression of CCD. In addition, CCD also was confirmed on 123I-IMP images in all three cases. On the contrary, the cases that CCD could not be detected on SPECT images were not recognized on MR perfusion images, and the results of two examinations were completely corresponding.
Conclusion
In this study, MR perfusion using ASL technique could clearly depict the CCD with high accuracy and the result was compatible with that of SPECT images. MR perfusion with ASL will be a viable alternative to SPECT to study the phenomenon and clinical consequences of supratentorial ischemic change with CCD.

KEYWORDS: ASL, Crossed cerebellar diaschisis, SPECT

eP-41

Eclamptic Encephalopathy and Cerebral Hemorrhage with HELLP Syndrome

Kajlwara, Y.･Seyama, G.･Takechi, A.･Sogabe, T.
Matsuyama Red Cross Hospital
Matsuyama, Ehime, JAPAN.

Purpose
To illustrate a severe eclamptic encephalopathy (posterior reversible encephalopathy) including corpus callosum and cerebral hemorrhage with HELLP syndrome.
Materials & Methods
A 27-year-old primigravida at the 25th week of gestation presented with sudden consciousness disturbance. Her blood pressure was 190/130 mmHg. A plain CT scan of the head showed caudate hemorrhage with severe intraventricular casting and abnormal low density areas in bilateral basal ganglia and right parietal lobe. The blood examination showed HELLP syndrome with hemolytic anemia, elevated liver enzymes, and low platelet count.
Results
We performed emergency ventricular drainage for ventricle hemorrhage and emergency Caesarean delivery for HELLP syndrome. After Caesarean delivery, her blood exam data were improved dramatically. However, consciousness disturbance was persistent. MR imaging revealed multiple hyperintense lesions on T2-weighted and FLAIR images, involving bilateral basal ganglia, the subcortical white matter of the right parietal lobe, and posterior four fifth area of corpus callosum. After three weeks, her consciousness level improved gently. Transient callosal disconnection syndrome caused by corpus callosum lesion occurred during recovery. A follow-up MRI showed almost complete resolution of the abnormal signals with only slight hyperintensities on T2-weighted image in the corpse callosum.
Conclusion
Neuroimaging studies in eclampsia have shown reversible lesions of low density on CT and high-intensity on T2-weighted MRI in the subcortical white matter and basal ganglia. We reported very rare eclamptic encephalopathy case including corpus callosum.

KEYWORDS: Posterior reversible encephalopathy, Acute stroke

eP-42

Nonhuman Primate Model of Transient Focal Stroke with Similar Level of Cerebral Ischemia

Cha, S.[1]･Lee, S.[2]･Lee, H.[3]･Lee, S.[1]･Yi, K.[1]
[1]Chung Buk National University Hospital, Cheongju, KOREA, REPUBLIC OF, [2]National Primate Research Center, Ochang, KOREA, REPUBLIC OF, [3]Chung-Ang University College of Medicine, Seoul, KOREA, REPUBLIC OF.

Purpose
Among the research of nonhuman primates (NHPs), a few models of transient focal cerebral ischemia were documented. There is no NHP model which reproduce infarction lesions of similar characteristics such as location and temporal evolution of ADC abnormality. This is to establish a nonhuman primate (NHP) model of transient focal cerebral ischemia with perfusion-diffusion match using transient endovascular occlusion of middle cerebral artery (MCAO) branch and repeated diffusion MRIs and to observe temporal changes of diffusion abnormality.
Materials & Methods
In each of four rhesus monkeys, proximal M2 branch of right MCA were endovascularly occluded under general anesthesia. Immediately after arterial occlusion, each animal was imaged repeatedly with 3T MRI. When territorial diffusion abnormality did not grow for 30 minutes on consecutive MRIs, occluded artery was recanalized by removing intra-arterial device from the animal which remained in the MR magnet. Patency of the right MCA was confirmed on follow-up MRA. The temporal evolution of lesion volume and apparent diffusion coefficient (ADC) in the ischemic lesions were investigated.
Results

Note: Scanned images are included in the proceedings. Some submitted images were reduced during editing, thereby decreasing clarity. Also, refer to the Program Planner. Proceedings Content as of 3-29-2013.

The duration of arterial occlusion was 50, 80, 100, 120 minutes, respectively. Focal infarction volume was initially at 30 minutes after ischemia, 35.87%, 11.15%, 8.66%, 13.71% of ipsilateral hemisphere (average = 17.35%), peak volume prior to the recanalization was 37.85%, 12.41%, 14.68%, 19.76% (average = 21.18%), respectively. After the reperfusion, in three cases, lesion volume decreased to 13.21%, 3.42%, 2.27% (average = 6.30%) at six hours.

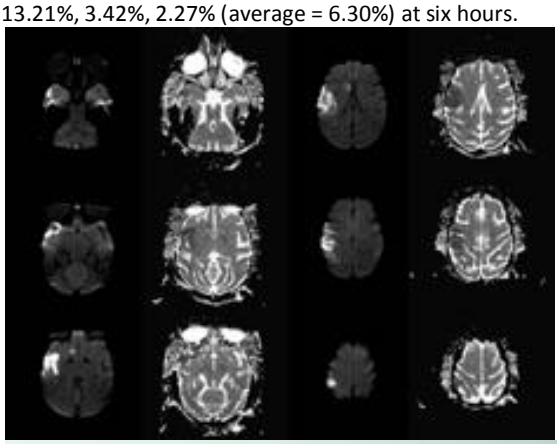

Conclusion

Using temporary endovascular arterial occlusion, serial diffusion MRI and variable duration of transient focal cerebral ischemia, we developed a NHP model of with minimal perfusion-diffusion mismatch. This preliminary experience would lead to establish the NHP stroke model with localized hemispheric infarction of similar damage level.

KEYWORDS: Animal model, Infarct, nonhuman primate

eP-43

Volumetric CT for the Assessment of Moderate and Severe Traumatic Head Injury: Prognostic Value and Reliability Analysis

Ramos, A.·Lagares, A.·Hilario, A.·Salvador, E.·Millan, J. M.·Fernandez Alen, J.·Gomez, P.
Hospital Universitario 12 de Octubre
Madrid, SPAIN.

Purpose

The objectives of this study are to evaluate the feasibility and reliability of volumetric CT for the initial assessment of traumatic brain injury and to determine its prognostic value in relation to other commonly used prognostic factors.

Materials & Methods

A prospective series of 210 patients suffering moderate to severe traumatic brain injury consecutively admitted to Hospital 12 de Octubre between January 2010 to May 2012 were included in the study. Patients were admitted in the ICU and were managed according to standard protocols consistent with international guidelines. All demographic and clinical variables related to prognosis were recorded at admission, as well as the development of raised intracranial pressure and the need for surgical treatment. Outcome was determined six months after injury using the Glasgow Outcome Scale. Initial and control CTs were classified by the TCDB classification and evaluated by the use of Analyze software and the volume of the different hemorrhagic lesions were calculated using region of interest volume (ROI). Also midline shift displacement was assessed, as well as cisternal effacement. The first CT scans were evaluated by two independent observers in order to assess interobserver variability. For appraising the inter-rater reliability of volumetric measurements of the different lesions evaluated as well as the total hemorrhagic volume interclass correlation coefficients (ICC) were used as well as the methodology proposed by Bland and Altman. The relation of individual hemorrhagic lesions and different prognostic factors as well as the total volume of hemorrhagic lesions in the worst CT with outcome was determined by means of Mann-Whitney U tests. Logistic regression analysis was used for predicting outcome using quantitative CT data adjusted by other prognostic factors.

Results

Interobserver reliability was high for the different traumatic hemorrhagic lesions except from traumatic subarachnoid hemorrhage (ICC = 0.6). Subarachnoid hemorrhage, subdural hematoma, intracerebral hematoma and total hemorrhagic volumes were significantly related to a worse prognosis in the univariate analysis. Total hemorrhagic volume had a higher discriminatory capacity then TCDB classification of injury after adjusting for other prognostic factors in the multivariate analysis.

Conclusion

Note: Scanned images are included in the proceedings. Some submitted images were reduced during editing, thereby decreasing clarity. Also, refer to the Program Planner. Proceedings Content as of 3-29-2013.

Quantitative CT is a novel approach for assessing lesional burden in different cerebral pathologies. Its application in head injury patients is feasible, reliable and could improve outcome prediction.

KEYWORDS: Brain trauma, Volumetric analysis

eP-44

Cranio-Cervical Vascular Dissections: A Three-Year Retrospective Analysis of Distribution Patterns and Incidence Using CT Angiography as a Screening Tool at Level I Trauma Center

Chong, J. J. R.·Hanagandi, P. B.·Bessissow, A.·Chankowsky, J.·del Carpio-O'Donovan, R.
McGill University
Montreal, QC, CANADA.

Purpose
To retrospectively analyze the incidence and distribution of vertebral, carotid, extracranial, and intracranial dissections in patients presenting with blunt and penetrating head and neck trauma.
Materials & Methods
Retrospective analysis of 771 patients from January 2009 to December 2011 assessed at a tertiary academic trauma center emergency department was performed. Patients who underwent CT examinations were suspected of cervico-facial, calvarial and skull base fractures and presented with blunt, penetrating, and high velocity injuries. Examinations were evaluated for soft tissue and osseous injuries, as well as intracranial hemorrhage followed by CTA of the head and neck. All examinations were performed with 64 slice MDCT (LightSpeed VCT, General Electric) using standard parameters (120 Kvp, 300 mAs, 0.625 mm slice thickness, 25-35 cm FOV, 0.9 - 1.0 pitch, 60-75 ml nonionic iodinated contrast). Omnipaque 300 was administered intravenously with an automated pressure injector at a flow rate of 4 mL/second and scanned from the arch of aorta to the level of the corona radiata with helical acquisition and bolus tracking technique. Axial, coronal and sagittal images were reformatted at 2.5 mm slice thickness.
Results
A total of 771 patients, 498 male and 273 female, between the ages of 17 to 94 years were evaluated. Twelve definite, and 18 suspected dissections were identified of which 11 were vertebral, five were carotid, and one was intracranial. The overall incidence of vertebral versus carotid dissections was estimated to be 0.8 - 1.4% versus 0.6%. The incidence of extracranial versus intracranial dissections was 1.4 - 2.1% versus 0.1%. Incidental findings were made in an additional 43 cases, predominantly composed of atherosclerotic stenoses and intracranial aneurysms.
Conclusion
Post-traumatic cranio-cervical vascular dissections are a rare but clinically significant entity and CTA as an emergency screening tool significantly influences patient management, risk stratification and the need for any further vascular intervention in patients with post-traumatic cranio-cervical dissection.

KEYWORDS: Carotid dissection, Dissection

eP-45

Imaging of Carotid Artery Plaque Remodelling

Saba, L.[1]·Raz, E.[2]·Suri, J.[3]·Suri, J.[3]·Fatterpekar, G.[2]·Piga, M.[1]
[1]AOU Cagliari, Cagliari, ITALY, [2]University of New York, New York, NY, [3]Biomedical Technologies, Pocatello, ID.

Purpose
The concept of remodelling indicates the morphologic and ultra-structural variation of a plaque in the time. Plaques change and it is possible that some determinants of instability are transitory. In this work our purpose was to understand the physiopathology of plaque remodelling and to review CT, MR and US imaging findings of this phenomenon.
Materials & Methods
Content organization: 1) To review the concept of carotid artery plaque remodelling, 2) The biomechanical effect of plaque eccentricity, 3) MR, CT, and US imaging findings of carotid artery plaque follow up that demonstrate the plaque remodelling, 4) Limits and potentialities and risk of MR, CT and US in the followup of the carotid artery plaque, 5) Presentation of relevant cases.
Results
The unique geometrical configuration and flow properties of the carotid bifurcation contribute to the formation of atherosclerotic plaque that may markedly change over time.
Conclusion
Currently, imaging techniques can identify and characterize the plaque remodelling and in particular the use of MR allows to precisely distinguish plaque components and characteristics and to identify the plaque's changes.

KEYWORDS: Carotid plaque

eP-46

Assessment and Optimization of Dual Energy CT Angiography for Evaluation of Treated Aneurysms: A Phantom Study

Andre, J. B.·Perez, F. A.·Ramos, M.·Fink, K. R.·Mossa-Basha, M.·Mengesha, B.·McCallum, S.·Hippe, D. S.·Anzai, Y.
University of Washington School of Medicine
Seattle, WA.

Purpose
Conventional computed tomography angiography (CTA) is used routinely to evaluate the surgical and endovascular treatment of intracranial aneurysms, yet suffers from

Note: Scanned images are included in the proceedings. Some submitted images were reduced during editing, thereby decreasing clarity. Also, refer to the Program Planner. Proceedings Content as of 3-29-2013.

potentially significant beam-hardening artifact and can compromise identification of residual or recurrent aneurysms. CT advancements, such as dual energy CTA (DE CTA), may help to reduce beam-hardening artifact in patients following aneurysm treatment. Using a phantom model, Gemstone Spectral Imaging (GSI) DE CTA was evaluated and optimized for the imaging of treated intracranial aneurysms.

Materials & Methods

A CTA phantom was constructed utilizing a preserved human cranium. Catheter tubing (Edwards Lifesciences, Irvine, CA) was filled with 3.5 mg iodine/mL iohexol iodinated contrast medium (350 mgI/ml; GE Healthcare Ireland, Cork, Ireland) and configured to form four orthogonal intersections to simulate a vessel and adjacent aneurysm. A medical grade endovascular coil or aneurysm clip then was placed at each of these four simulated aneurysm locations. The calvaria, tubing and coil/clip assemblies then were embedded in agar. CT data were acquired on a Discovery CT750 HD scanner (GE Healthcare, Milwaukee, WI), including baseline data acquired using standard institutional CTA parameters (140 kVp, 330 mA, 0.5:1 pitch, and rotation speed of 0.5 sec; total estimated CTDI was 72.32 mGy) and DE CTA data with parameters matched for radiation dose using fast kV-switching GSI between 40 and 140 keV (140 kVp, 630 mA, 0.5:1 pitch, and rotation speed of 0.5 sec; or 140 kVp, 260 mA, 0.5:1 pitch, and rotation time of 0.8 sec). Sets of images were generated at virtual monochromatic energy levels of 40, 60, 77, and 140 keV and evaluated by three blinded neuroradiologists for assessment of subjective image quality using the following Likert-type items: 1) extent of beam hardening artifact, 2) quality of aneurysm visualization, 3) confidence in aneurysm measurement, 4) quality of artery lumen visualization, and 5) overall diagnostic quality. Differences were evaluated with two-factor ANOVA using R 2.14.1.

Results

Sixty-eight sets of orthogonally reformatted images were evaluated. Compared to conventional CTA, DE CTA was associated with increased artifact, decreased aneurysm visualization, decreased aneurysm measurement confidence, decreased artery lumen visualization, and decreased overall subjective diagnostic quality ($p < 0.05$). Image quality differences were most apparent using a 140 keV monochromatic energy level compared to standard CTA; 40 keV monochromatic images tended to score similar to the conventional CTA, though generally somewhat lower.

Conclusion

When compared with standard CTA parameters, evaluation for residual or recurrent aneurysms with GSI-based DE CTA, using monochromatic energy levels of 40, 60, 77, and 140 keV, is associated with reduced subjective image quality. Additional optimization could be helpful to improve image quality of DE CTA for evaluating treated aneurysms.

KEYWORDS: Aneursym, Dual-energy CT, Gemstone Spectral Imaging

eP-47

MR Imaging and Diffusion Tensor Imaging Markers of Brainstem Sagging in Frontotemporal Brain Sagging Syndrome

Lai, L.·Capizzano, A. A.·Kim, J.·Moritani, T.·Pinzon Jimenez, O.
University of Iowa Hospital and Clinics
Iowa City, IA.

Purpose

Frontotemporal brain sagging syndrome (FBSS) is a recently described, rare presentation of spontaneous intracranial hypotension (SIH) with features of frontotemporal dementia (FTD). The purpose of this study is to determine imaging characteristics that distinguish FBSS from classic SIH, thus shedding light on the pathophysiology of this intriguing condition.

Materials & Methods

Brain MRI and DTI were compared between age- and sex-matched groups of patients with FBSS (n = 3), classic SIH (n = 5), and normal controls (n = 6). Frontotemporal brain sagging syndrome had clinical symptoms of FTD (cognitive decline and affective disorders) combined with brainstem signs and MRI findings of marked brain sagging without frontotemporal atrophy. One patient's neuropathologic exam showed no FTD. Spontaneous intracranial hypotension patients had positional headaches, low opening pressure and brain imaging consistent with SIH, but no FTD-like symptoms. AP midbrain diameter (AP) and pontomammillary distance (PM) were compared (Figure). Exploratory DTI analysis was performed by spatially transforming MRI data into a standard template and analyzed using the tract-based spatial statistics method.

Results

Symptom duration was longer in FBSS (43.7 months) than for SIH (4.2 months) ($p<0.01$). Meningeal enhancement and subdural collections occurred more frequently in SIH than FBSS ($p<0.05$). Increased anterior-posterior (AP) diameter of the midbrain and shortened pontomammillary (PM) distance were significantly different across groups ($p<0.05$) (Figure). The AP/PM ratio ("FBSS index") discriminated between patient groups without overlap. Frontotemporal brain sagging syndrome had higher FA values at the superior cerebellar peduncle and lower FA values in the cerebral peduncle ($p<0.05$) compared to controls.

Note: Scanned images are included in the proceedings. Some submitted images were reduced during editing, thereby decreasing clarity. Also, refer to the Program Planner. Proceedings Content as of 3-29-2013.

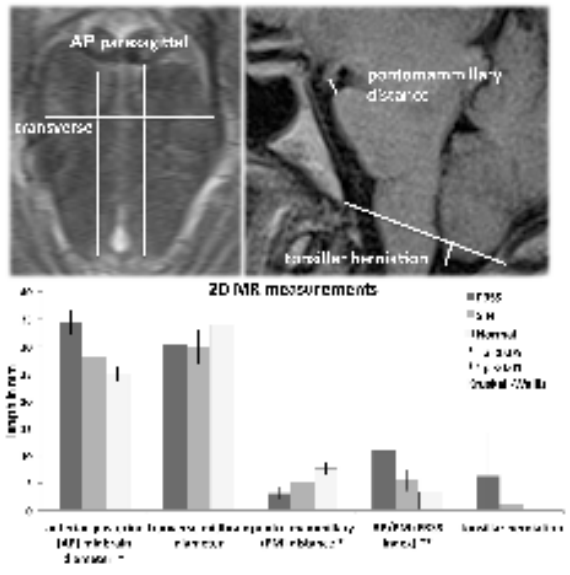

Conclusion

There are significant morphologic and DTI differences between FBSS and SIH or normal controls. The FBSS index can help distinguish SIH alone from FBSS. Frontotemporal brain sagging syndrome also had longer symptom duration and fewer subdural collections and meningeal enhancement compared to SIH group. Diffusion tensor imaging suggests stretching of mesencephalic and upper brainstem neural fibers in FBSS. The Monro-Kellie doctrine explains classic SIH imaging findings of compensatory meningeal enhancement and subdural collections. Frontotemporal brain sagging syndrome is a more chronic and severe brain sagging syndrome where those compensatory mechanisms might be insufficient to prevent neural tissue stretching across the tentorial incissura. Frontotemporal brain sagging syndrome often is confused with FTD although it also includes subcortical symptoms such as hypersomnia, dysphagia and ataxia. Given the potential reversibility of FBSS, distinction from FTD is paramount.

KEYWORDS: Intracranial hypotension, Midbrain, frontotemporal brain sagging syndrome

eP-48

Relationship between MR Imaging Findings and Clinical Diagnosis in Patients with Suspected Normal Pressure Hydrocephalus

Caverzasi, E.·Santos, M.·Sha, S. J.·Geschwind, M. D.·Seider, T.·Miller, B. L.·Henry, R. G.·Hess, C. P.
University of California San Francisco
San Francisco, CA.

Purpose

Normal pressure hydrocephalus (NPH) is a poorly understood and controversial entity for which imaging plays an important role. A number of studies have posited various MRI features as supporting the diagnosis of NPH, but limited work has been done to assess the relationship between imaging findings and clinical diagnosis after evaluation by dementia specialists. In this work, we assessed the prevalence of different clinical and imaging findings in a cohort of patients referred for MRI suspicion of NPH.

Materials & Methods

We retrospectively reviewed records and brain MRI for 80 patients referred to our tertiary behavioral neurology clinic between 2005 and 2012 for suspected NPH based on MRI. Data abstracted included age, gender, presenting symptoms (cognitive deficit, gait apraxia, and/or urinary incontinence) and assigned clinical diagnosis. Patients shunted or who received other prior neurosurgical intervention were excluded, as were patients with evidence of obstructing lesions and/or absent or poor-quality MRI. Blinded to clinical information, radiologists reviewed the brain MRI closest in time to the clinical evaluation (± 6 months) for findings with a reported association with NPH, including Evans index (EI) > 0.3, callosal angle (CA) < 40°, evidence for extra-ventricular CSF obstruction (gaping sulci, narrowed vertex CSF spaces, and/or disproportionately enlarged sylvian fissures), and distended third ventricular contours (abnormal rotation of the third ventricular and chiasmatic lines, mamillopontine or mamillocommissural distance). Periventricular T2 signal also was assessed using the Fazekas scale and dichotomized as either mild (F0 or F1) or significant (F2 or F3). The prevalence of demographic features, clinical findings and imaging signs was assessed for patients diagnosed with possible NPH after clinical evaluation and compared to patients assigned alternative diagnoses.

Results

Forty-four patients were included and divided into groups with or without possible NPH based on clinical impression. All patients with possible NPH were considered for further evaluation (large volume tap, lumbar subarachnoid drain and/or ventriculoperitoneal shunt). Univariable logistic regression showed no difference in demographic variables, clinical presentation or MRI findings between the two groups (Table 1). The diagnosis of NPH was more frequent when cognitive, urinary and gait abnormalities occurred together ($p = 0.5$) or when urinary symptoms occurred alone ($p = 0.05$).

Note: Scanned images are included in the proceedings. Some submitted images were reduced during editing, thereby decreasing clarity. Also, refer to the Program Planner. Proceedings Content as of 3-29-2013.

TABLE. Demographic, Clinical and MRI Findings		Clinical Diagnosis	
		Possible NPH	Other diagnosis
Demographic	Age (years)	76.7(+/-11)	77.8(+/-10)
	Gender (M:F)	14:10	14:06
Clinical	Cognitive deficit	1	0.9
	Urinary incontinence	1	0.6 *
	Gait apraxia	1	1
	Evans index > 0.3	1	1
MRI	Callosal angle < 40°	0.11	0.2
	CSF obstruction	0.44	0.5
	Abnormal third contour	0.4	0.6
	Significant periventricular T2	0.56	0.3
	* statistically significant		

Conclusion

Although MRI is used for the identification and referral of patients with possible NPH, individual imaging findings reported to be associated with the diagnosis may not have a significant relationship to clinical impression by dementia specialists. Further analysis and studies are needed.

KEYWORDS: NPH, MR imaging brain

eP-49

Neuroradiologic Phenotype in Wernicke Encephalopathy Is Age-Related

Zuccoli, G.[1]·Crowley, H.[1]·Gallucci, M.[2]·Nardone, R.[3]·Fitzgerald, R. T.[4]·Tabarki, B.[5]
[1]Children's Hospital of Pittsburgh, Pittsburgh, PA, [2]University of L'Aquila, L'Aquila, ITALY, [3]Franz Tappeiner, Meran, ITALY, [4]University of Arkansas for Medical Sciences, Little Rock, AR, [5]Riyadh Hospital, Riyadh, SAUDI ARABIA.

Purpose

Wernicke encephalopathy (WE) is a rare neurologic disorder resulting from a vitamin B1 deficiency. Early detection and treatment is critical to this disorder because clinical symptoms can be resolved with thiamine supplementation. Brain energy requirements are age-related and thiamine is actively involved in brain energy metabolism. Based on this knowledge, we speculate that areas of high metabolic demand will have a higher rate of involvement in Wernicke encephalopathy in children than adults, therefore the neuroradiologic phenotype of Wernicke encephalopathy may be age-related.

Materials & Methods

A review of the literature was performed on October 14, 2012 using a PubMed/Ovid search of “Wernicke encephalopathy” “Wernicke-Korsakoff,” “Korsakoff Syndrome,” “Wernicke Disease,” “Wernicke-Korsakoff Syndrome,” “Wernicke Syndrome,” and “Thiamine deficiency”. The search included all ages and all studies in which MRI was part of the diagnostic process. Published images were reviewed for selective deep nuclei involvement, a finding first described by the literature in 2001.

Results

A total of 246 cases of WE described by MRI were evaluated. In the adult population, 114/216 (53%) of cases showed periaqueductal gray matter involvement. In 105/216 (49%) the mammillary bodies were involved. In 155/216 (72%) the periventricular region of the third ventricle and thalamus was involved. In 18/216 (8%) the cortex was involved. In 16/216 (7%) the basal ganglia were involved. In 3/216 (1%) the corpus callosum was involved. In 14/216 (6%) the cerebellum was involved. In 93/216 (43%) the brainstem was involved. Of the pediatric population, 15/30 (50%) of the cases showed periaqueductal gray matter involvement. In 15/30 (50%) the mammillary bodies were involved. In 20/30 (67%) the periventricular region of the third ventricle and thalamus was involved. In 7/30 (23%) the cortex was involved. In 13/30 (43%) the basal ganglia were involved. In 7/30 (23%) the brainstem was involved. In 1/30 (3%) the cerebellum was involved. No involvement of the corpus callosum was seen.

Conclusion

Our findings show that the typically affected regions: periaqueductal gray matter, mammillary bodies, and the thalamus do not differ significantly between adults and children. There is, however, a strong prevalence of striatal structure involvement in children, likely reflecting higher thiamine metabolic demands in these anatomical structures correlating with the brain maturation process.

KEYWORDS: Wernicke encephalopathy, MR imaging brain, thiamine deficiency

eP-50

Preliminary Cognitive Functional Imaging Study of Patients with Early Diabetes

Tian, W.[1]·Liu, X.[1]·Xie, J.[2]
[1]University of Rochester Medical Center, Rochester, NY, [2]Peking University Medical Center, 3rd Hospital, Beijing, CHINA.

Purpose

To evaluate cognitive dysfunction in early diabetes

Note: Scanned images are included in the proceedings. Some submitted images were reduced during editing, thereby decreasing clarity. Also, refer to the Program Planner. Proceedings Content as of 3-29-2013.

patients with psychologic tests and fMRI. To analyze MR spectroscopy change in prefrontal cortex (PFC).
Materials & Methods
Twenty patients with early type 2 diabetes mellitus and 15 demographically similar, healthy subjects were enrolled. All subjects with microalbuminuria, hypoglycemia and ketonic acidosis, visible cerebral lesions on MR were ruled out. Wechsler memory scale-revised (WMS-R), trail making test A and the personality and affective states were assessed in both groups. Then nback task fMRI and single-voxel MRS with TE 30 on bilateral PFC were performed. The statistical differences of neuropsychologic tests and MRS result between the two groups were evaluated. The fMRI data were analyzed by SPM2.
Results
(1) Psychologic tests showed that the scores of cognitive tests in diabetes group were significantly lower than those in control group. Diabetic patients were more depressive and anxious than controls. (2) Functional MRI examinations revealed that the activation pattern in diabetes group was similar to the control group, but less activation in frontal, parietal lobe and cerebellar was demonstrated. There was additional activation in right temporal lobe(including inferior temporal gyrus and parahippocampus gyrus) and anterior cingulate cortex in diabetes group. (3) MR spectroscopy data showed that compared with the control group, the value of Glx/(Cho +Cr) was elevated in bilateral PFC, that the value of Cho/Cr were decreased in the right side, and that the value of NAA/Cho, Glx/Cho, Glx/Cr were elevated in the right side. Transit memory was negatively correlated with Glx/Cho (F=-0.546, p value =0.013) and Glx/(Cr+Cho) (F=-0.471, p value = 0.036). The number of errors in trail making test A was positively related to NAA/Cr.

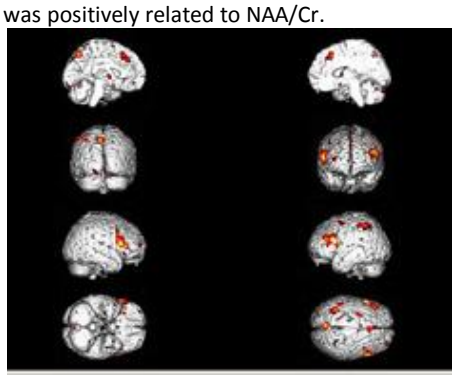

Figure: Localized brain area with decreased activation in patients group.
Conclusion
Early type 2 diabetic patients have cognitive dysfunction, especially decreased memory at verbal working memory. The fMRI using nback test shows the hypofunction in PFC, which plays an important role in cognitive dysfunction and the emotional abnormality in diabetic patients. The value of NAA in PFC is not significantly decreased. However Glx elevation may represent the disregulation of Glx metabolism and/or the neuron apoptosis caused by Glx accumulation. Increase of Glx and the degeneration of choline neuron system, which may be part of the pathophysiologic basis of PFC hypofunction.

KEYWORDS: Cognitive deficit, Diabetes, fMRI and MR spectroscopy

eP-51

Analysis of Association between Cerebral Microbleeds and Volume of White Matter Lesion

Saba, L.[1]·Raz, E.[2]·Suri, J.[3]·Fatterpekar, G.[2]·Piga, M.[1]
[1]AOU Cagliari, Cagliari, ITALY, [2]University of New York, New York, NY, [3]Biomedical Technologies, Pocatello, ID.

Purpose
Cerebral microbleeds (CMB), as visualized on T2*-weighted images, have been detected in patients with ischemic stroke. We hypothesize that CMB are an expression of leukoaraiosis. Our aim is to evaluate the correlation between CMB and a volumetric measure of white matter hyperintensity, as measured with a semiautomatic technique.
Materials & Methods
We prospectively analyzed 54 consecutive patients (mean age 72 ± 9 years, males 42) with carotid artery stenosis recruited at our Institution before undergoing carotid endarterectomy. The patients underwent an admission brain MRI of the brain which included T2-FLAIR, T2-SE, T2*-GE and DWI sequences. A neuroradiologist performed the evaluation of CMB (dicotomic presence/absence and number) as well as FLAIR-leukoaraiosis lesion volume using a semi-automated segmentation technique (Jim, Xinapse System, Leicester, UK). Pearson correlation was conducted to identify correlation between the CMB and the FLAIR-leukoaraiosis lesion volume. Mann-Whitney U was used to test the amount of leukoaraiosis in the subgroups CMB+ and CMB-.
Results
Among the 54 patients, 26% had CMBs. Pearson correlation found a statistically significant association between the volume of leukoaraiosis and the presence of CMB (rho = 0.377, p value 0.0005) and between the number of white matter lesions and leukoaraiosis (rho = 0.295, p value 0.0071). The Mann-Whitney U test confirmed that the amount of leukoaraiosis in the subgroup with CMB was higher compared to the subgroup without CMB (p = 0.0005) as well as the number of lesion (p value = 0.0062).
Conclusion
The presence of CMB is correlated with the volume of white matter hyperintensity, in turn associated with a higher incidence of ischemic stroke.

KEYWORDS: White matter disease, Cerebral microhemorrhages

Note: Scanned images are included in the proceedings. Some submitted images were reduced during editing, thereby decreasing clarity. Also, refer to the Program Planner. Proceedings Content as of 3-29-2013.

eP-52

Glioma Angiogenesis, Angiogenic Switch and Perfusion Imaging: Understanding the Relationship of Tumor Blood Volume and Leakiness with Increasing Tumor Grade

Griffith, B.·Jain, R.·Khalil, K.·Nagpal, P.·Scarpace, L.·Mikkelsen, T.·Bagher-Ebadian, H.·Schultz, L.
Henry Ford Health System
Detroit, MI.

Purpose
The purpose of this study was to provide an imaging correlate to the changes occurring at the microvasculature level during the complex process of angiogenesis in gliomas. This was accomplished through the relationship of in vivo assessment of vascular parameters [i.e., tumor blood volume (cerebral blood volume, CBV) and tumor leakiness (permeability surface area product, PS)].
Materials & Methods
A total of 123 patients with pathologically proven neoplastic (n=106; WHO grade IV=45, grade III=18 and grade II=13, recurrent high-grade gliomas=30) and non-neoplastic (n=17; radiation necrosis, RN=12, tumefactive demyelinating lesions, TDL=5) lesions underwent preoperative perfusion CT (PCT). Regression analyses were done to assess the rate of change between CBV and PS and test whether these rates (or slopes) differed for the distinct lesion groups. In addition for the WHO grades, the ratio of CBV to PS was computed and compared using analysis of variance (ANOVA) methods. All statistical testing was done at the 0.05 level.
Results
The rate of change in CBV with respect to PS was highest for grade II gliomas followed by grade III and then grade IV (1.64 vs 0.91 versus 0.27, respectively) (Figure 1). The difference in rate of change was significant between grade III and IV (p=0.003) and showed a trend for grades II and IV (p=0.098). The difference between grades II and III was not significant (p=0.386). The rate of change for recurrent tumors was even smaller than the WHO grade gliomas (slope=0.14). When assessing the ratio of CBV to PS, the ratios were the highest for grade II and lowest for grade IV (Figure 2). The pairwise difference between all three groups was significant (p < 0.001 for all).

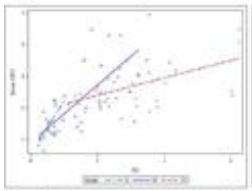

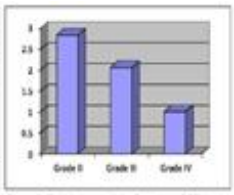

Conclusion
Gliomas have a complex and heterogeneous vasculature, relying on angiogenesis to maintain an adequate blood supply. Developing imaging methods capable of providing insight into this process is critical to better understanding these tumors. It has been shown that CBV and PS correlate with different aspects of vascular histology and hence, may change at different rates as tumors progress to higher grades. This study suggests that CBV and PS can serve as imaging correlates to changes occurring at the microvasculature level, providing an in vivo means of assessing the stepwise progression of angiogenesis. Eventual incorporation of these vascular parameters as potential biomarkers will be important to the development and evaluation of current and new therapies.

KEYWORDS: Glioma, Angiogenesis, perfusion imaging

eP-53

Comparison of Manually Selected Arterial Input Function and Standard Radiologic Arterial Input Function in Dynamic Contrast-Enhanced T1 MR Imaging Estimation of Tumor Kinetics Using Nested Model Selection Approach

Chwang, W. B.·Jain, R.·Nejad-Davarani, S. P.·Vanslooten, A.·Schultz, L.·Arbab, A. S.·Bagher-Ebadian, H.
Henry Ford Health System
Detroit, MI.

Purpose
The purpose of this study is to compare the results of using a standard radiologic arterial input function (SRAIF) versus a manually selected arterial input function (MSAIF) in dynamic contrast-enhanced (DCE) MR image analysis. These two AIFs were used to estimate permeability parameters such as extracellular-extravascular space volume (ve), plasma volume (vp) and forward vascular transfer constant (Ktrans) in rat brain tumors. Two contrast agents (Gd DTPA and Gadofosveset) with different molecular sizes were used.
Materials & Methods
Nine Fisher 344 female rats were inoculated intracerebrally with 9L gliosarcoma cells, and imaging was done using either gadofosveset or gadolinium-diethylenetriaminepentaacetic acid (Gd DTPA), once on the 13th and once on 14th day after inoculation. Animals were scanned on a GE 3T clinical system (Signa Excite, GE health) using a 50 mm (diameter) × 108 mm RF rung length small animal imaging coil (Litzcage small animal imaging system, Doty Scientific Inc.). A set of T1-pre, DCE T1-weighted, and T1 post images were acquired in each experiment. Multiple flip angle (2°, 5°, 10°, 15°, 20° and 25°) fast 3D spoiled gradient-echo (3D SPGRE) images were obtained, for a total scan time of 15 minutes. Gadofosveset was administered at 0.12 ml/kg (0.03 mmol/kg) and Gd DTPA was administered at 0.2 ml/kg (0.1 mmol/kg). A nested model selection (NMS) approach was used to estimate permeability parameters from DCE MR experiments. Resting (precontrast) T1 map was used to calculate the relaxivity change (ΔR1). Toft's extended model and its reduced forms were used to explain the behavior of contrast concentration of each voxel for estimating permeability parameters such as ve, vp, and Ktrans. F-Statistic was used to select the best model for

Note: Scanned images are included in the proceedings. Some submitted images were reduced during editing, thereby decreasing clarity. Also, refer to the Program Planner. Proceedings Content as of 3-29-2013.

each voxel. All analyses were done using SRAIF and MSAIF. The MSAIFs were selected by an expert radiologist, and the SRAIF is the result of a previously reported study. Both AIFs were calibrated to blood relaxivity and normalized to white matter.

Results

There was high correlation between the Ktrans values calculated for each contrast agent, using the two AIF profiles (ICC = 0.95 and 0.94 for Gadofosveset and Gd DTPA respectively); however, the mean Ktrans was considerably different for the contrast agents due to their different molecular size. Even though the mean values of ve and vp using the same AIF are in strong agreement for both contrast agents, these values have a lower correlation between the two AIF profiles (for ve, ICC = 0.39 and 0.42 for Gadofosveset and GD DTPA respectively and for vp, ICC = 0.0077 and 0.56).

Conclusion

In this study, we assessed variations of calculated permeability parameters (ve, vp and Ktrans) when estimated using two different AIF profiles (MSAIF and SRAIF). For each contrast agent, the results show less variation in Ktrans, since it is directly related to the time trace of contrast concentration for both AIFs. However, ve and vp are more susceptible to the AIF profile change. These results show the importance, sensitivity and biasing level of each estimated permeability parameter against different AIF profiles.

KEYWORDS: Arterial input function, MR imaging brain, diffusion contrast enhanced

eP-54

Regional Cerebral Blood Flow in Depression: Arterial Spin Labeling Magnetic Resonance Study

Kaichi, Y.[1]·Higaki, T.[1]·Nakamura, Y.[1]·Honda, Y.[1]·Komoto, D.[1]·Date, S.[1]·Awai, K.[1]·Akiyama, Y.[2]·Okamoto, Y.[1]·Yamawaki, S.[1]
[1]Hiroshima University, Hiroshima, JAPAN, [2]Hiroshima University Hospital, Hiroshima, JAPAN.

Purpose

Findings in the limited number of studies that addressed changes in cerebral blood flow (CBF) in depressed individuals are inconsistent. We investigated changes in CBF using arterial spin labeling (ASL) MR imaging (MRI) in depressed and healthy persons.

Materials & Methods

Our study included 58 participants, 27 were healthy and 21 suffered from depression. They underwent imaging on a 3T MRI system between February and October 2012. Arterial spin labeling and echo-planar images were subtracted and averaged to yield perfusion-weighted images. Region-of-interest (ROI) analysis was applied to the bilateral hippocampi, thalami, caudate nuclei, lentiform nuclei, cortex, and white matter. To reduce potential interindividual variability in CBF we normalized all CBF ROI data by dividing each participant's ROI data by his/her global mean CBF value of the white matter. Group differences in CBF and their associations with clinical features were examined.

Results

Non-normalized CBF in all ROI except the bilateral thalami was significantly lower in depressed than healthy individuals. The bilateral thalamic normalized CBF was significantly higher in depressed than healthy individuals (left: p = 0.005, right: p = 0.008). There was a significant correlation between the bilateral thalamic normalized CBF and the Beck Depression Index scores in depressed patients (left: r = -0.62, right: r = -0.47).

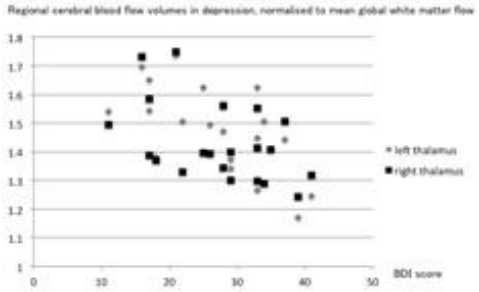

Conclusion

In patients suffering from depression CBF in most parts of the brain was decreased. The effect of depression on the CBF of the bilateral thalami was minimal.

KEYWORDS: Arterial spin labeling, Cerebral blood flow, depression

eP-55

Comparison of Subcortical Volumes in Patients with Ischemic Stroke or Risk Factors for Stroke Using Manual Tracing Versus FreeSurfer Automated Segmentation

Krishnaraj, M.·Gupta, J.·Martens, N.·Kleefisch, C. J.·Nair, V. A.·Zeng, H.·Masodkar, K.·Abellaneda, A.·Jensen, M.·Chacon, M.·Sattin, J.·Prabhakaran, V.
University of Wisconsin
Madison, WI.

Purpose

Subcortical volume comparisons with manual versus automated segmentation methods have not been well studied. The objective of our study was to evaluate any differences between manual and FreeSurfer-automated segmentation for computing volumes of subcortical structures. Further, we compared volumes of subcortical structures between patients with ischemic stroke, patients with risk factors for stroke, and age-matched healthy controls.

Materials & Methods

Forty-one patients were scanned within seven days of onset of ischemic stroke (mean age = 61.1 years), 13 patients with stroke risk factors (mean age = 66.2 years) and 31 healthy controls (mean age = 56.6 years) were scanned on a GE 3T MRI scanner. Whole brain 3D T1-

Note: Scanned images are included in the proceedings. Some submitted images were reduced during editing, thereby decreasing clarity. Also, refer to the Program Planner. Proceedings Content as of 3-29-2013.

weighted BRAVO FSPGR images were collected and volumes (cc) of eight subcortical structures (right and left putamen, caudate, pallidum, and thalamus) were generated with either expert manual tracing via MRIcroN or with FreeSurfer-Linux-centos4-stable-pub-version 5.1.0. A two-sample t-test was used for statistical comparison of computed volumes derived from manual tracing versus automated segmentation. Next, subcortical structure volumes computed by manual tracing between healthy controls, patients with ischemic stroke and patients with risk factors for stroke were analyzed with t-tests and compared. Finally, we utilized Dice's coefficient (DSC) as a statistical means to compare the volumes of overlap between the methods of segmentation. Values for DSC range from zero (indicating no spatial overlap) and one (signifying complete overlap). We utilized a DSC of greater than 0.700 as recommended by Zijdenbos et al (1994) to indicate a good overlap.

Results

There were no statistically significant differences (corrected $p<0.006$) between manual tracings and FreeSurfer for six out of eight subcortical structures in controls, five out of eight structures in patients with stroke risk factors, and four out of eight structures in patients with stroke. When comparing manually traced controls with patients with risk factors for stroke and ischemic stroke, only the right thalamus and right pallidum showed statistically significant differences in their computed volumes (corrected $p<0.006$). Dice's coefficient revealed good overlap in seven out of eight subcortical structures in controls, six out of eight structures in patients with stroke risk factors and only four out of eight structures for patients with stroke (DSC>0.700).

Conclusion

Our results suggest that there are increasing differences in volumes computed by expert manual tracing in comparison to automated FreeSurfer segmentation with increasing levels of vascular disease severity (stroke patients > patients with risk factors for stroke > normals). Overall significant differences were seen in the volumes of subcortical structures when comparing healthy subjects with patients with ischemic stroke or risk factors for stroke.

KEYWORDS: Morphometry, Volumetric analysis, Automated segmentation

eP-56

Intravascular (Blood Pool) Contrast Agent and Dynamic Contrast-Enhanced T1 MR Imaging Using Nested Model Selection: Rat Brain Tumor Kinetics

Chwang, W. B.·Jain, R.·Nejad-Davarani, S.·Iskander, A.·Vanslooten, A.·Schultz, L.·Arbab, A.·Bagher-Ebadian, H.
Henry Ford Health System
Detroit, MI.

Purpose

The purpose of this study was to investigate parameters of vascular physiology -- plasma volume (vp), forward vascular transfer constant (Ktrans), and volume of the extravascular extracellular space (ve) in a rat glioma model using two different contrast agents, an intravascular (blood pool) agent (gadofosveset) and an extravascular agent (gadolinium-diethylenetriaminepentaacetic acid, Gd-DTPA). These parameters were estimated using dynamic contrast-enhanced (DCE) T1 nested model selection (NMS)1.

Materials & Methods

Dynamic contrast-enhanced T1 MRI studies were done in nine Fisher 344 rats inoculated intracerebrally with 9L gliosarcoma cells. Animals were scanned using both gadofosveset and Gd-DTPA, 24 hours apart. For DCE MRI, multi flip angle (2 to 35) fast SPGR 3D images were obtained to create T1 maps. Dynamic T1-weighted images were obtained for 15 minutes using a fixed 30-degree flip angle. vp, Ktrans, and ve were estimated using NMS from the DCE data1, using a standardized arterial input function. Descriptive statistics were computed for the two contrast agents, as well as for the whole lesion and the central core. Nonparametric Wilcoxon signed rank tests were done, and intra-class correlation coefficients (ICC) were computed to assess the agreement or reliability between the two contrast agents.

Results

For the whole lesion, Ktrans measures were significantly lower ($p = 0.0039$) using gadofosveset compared to Gd-DTPA, and there was almost perfect agreement between the two contrast agents. Both ve and vp, measurements were not statistically different, and there was almost perfect agreement for ve and substantial agreement for vp. For the central core, Ktrans was significantly lower ($p = 0.0039$) using gadofosveset compared to Gd-DTPA, with substantial agreement. No difference was observed between the contrast agents for ve and vp. Substantial agreement was observed for vp, but not for ve which showed poor agreement.

Note: Scanned images are included in the proceedings. Some submitted images were reduced during editing, thereby decreasing clarity. Also, refer to the Program Planner. Proceedings Content as of 3-29-2013.

Table 1. Whole lesion analysis in 9 animals scanned with Gadofosveset as well as Gd-DTPA

	Contrast agent	Mean (SD)	p-value	ICC	Agreement
Ktrans (min-1)	Gadofosveset Gd-DTPA	0.025 (0.008)0.046 (0.011)	0.0039	0.848	Almost perfect
ve (%)	Gadofosveset Gd-DTPA	22.7 (4.7)23.6 (5.6)	0.425	0.880	Almost perfect
vp (% or ml/100 g)	Gadofosveset Gd-DTPA	1.5 (0.5)1.6 (0.4)	0.25	0.798	Substantial

Conclusion

Both ve and vp can be measured accurately whether we use an extravascular or intravascular contrast agent in an animal glioma model. Ktrans measurements were significantly lower using a blood pool contrast agent due to the much larger size of the albumin-bound contrast agent, and these were measured with very good accuracy using NMS in DCE MRI. The goal of this research is to demonstrate the stability of NMS in DCE MRI for measurement of these important vascular physiology markers which can provide important information about the tumor microenvironment, and hence, could potentially expand their role into prognostic or predictive imaging biomarkers, an area of very active clinical interest.

KEYWORDS: MR imaging, MR imaging brain, Nested Model Selection

eP-57

"Functional" MR Imaging Protocol for Treatment Decision, Presurgical Planning and Imaging-Guided Surgery of Brain Space-Occupying Lesions

Katsaros, V. K.[1,2]·Papanikolaou, N.[3]·Liouta, E.[2]·Hermoye, L.[4]·Stranjalis, G.[2]

[1]St. Savvas Anti-Cancer Oncology Hospital, Athens, GREECE, [2]University of Athens, School of Medicine, Evangelismos Hospital, Athens, GREECE, [3]STEP-C, Crete, GREECE, [4]Imagilys, Brussels, BELGIUM.

Purpose

To demonstrate our "functional" MRI protocol for treatment decision, presurgical planning, imaging-guided surgery and treatment monitoring of brain tumors and space-occupying lesions.

Materials & Methods

From September 2011 until today, 167 patients (212 examinations) with suspicion of brain tumor were evaluated presurgically, as well as postsurgically (45 patients). Our evaluation protocol included neuropsychologic tests, structural MRI (3D-T1 W, FLAIR, and T2 W), SWI, fMRI, diffusion and perfusion MRI, as well as spectroscopy on a 1.5T magnet before surgery and 3/12 months followup after surgery, radio and/or chemotherapy. The fMRI paradigms were selected according to the neuropsychologic results. The acquired and postprocessed data from structural, functional and DTI tractography sequences were used for differential diagnosis and treatment decision. If surgical approach was chosen (biopsy, ablative or gross total excision) data were transferred to the neuronavigation system and were used for presurgical planning and for "functional" imaging-guided surgery. In all operated cases the pathologic correlation was available.

Results

Thirty-two patients were excluded of the study either because they did not co-operate very well resulting in poor image quality, or because brain tumor was excluded. Our cohort (135 patients) comprised of 21 cases with low-grade gliomas, 44 high-grade gliomas, one DNET, five lymphomas, 31 meningiomas, two cavernomas, one DVM, 27 metastases (5 solitary), two colloid cysts and one postinfectious angiitis. Using a “validated algorithm” for intra-axial brain tumors we were able to establish the correct presurgical diagnosis in 132/135 patients (97.8%). In 77 patients the combination of neuropsychologic and neuroimaging evaluation emerged the need for surgery. The "functional" imaging-guided surgery in most of the tumors allowed gross total excision especially in the groups of low-grade gliomas and meningiomas.

"Validated algorithm" illustrates order of methods used to diagnose and differentiate intraaxial masses. Each method provides an answer to a specific question, which is used as a discriminator to distinguish lesions. 1.1/1000 mm^2 /ADC = $1.1x10^{-3}$ mm^2/sec ADC=apparent diffusion coefficient, CE=contrast material enhanced, Cho=choline, NAA=N-acetylaspartate, rCBV=relative cerebral blood volume, TDL=tumefactive demyelinating lesion.

Radiology 2007; 243:539-550

Conclusion

"Functional" MRI approach in combination with neuropsychologic evaluation is an invaluable tool for differential diagnosis, treatment decision, planning and guiding the surgery, as well as for treatment monitoring, thus providing the best health-care management of patients with brain space-occupying lesions.

KEYWORDS: Brain neoplasms, Functional brain mapping, Image-guided neurosurgery

Note: Scanned images are included in the proceedings. Some submitted images were reduced during editing, thereby decreasing clarity. Also, refer to the Program Planner. Proceedings Content as of 3-29-2013.

eP-58

Transcranial Magnetic Stimulation and Magnetic Resonance with Diffusion Tensor Imaging in Amyotrophic Lateral Sclerosis Patients: Combination and Correlations of their Measurements

Stecco, A.·Nasuelli, N.·Mazzini, L.·Cantello, R.·Perchinunno, M.·Carriero, A.
ASU Maggiore della Carità
Novara, ITALY.

Purpose
To determine the diagnostic accuracy of MRI with DTI and TMS with MEPs in UMN assessment in ALS patients; secondary goal to assess if there is a correlations between DTI metric and MEPs.
Materials & Methods
Seventeen patients (10 males and seven females; age range 25-74 years, mean 47) affected by ALS, underwent a TMS and MRI DTI evaluation within 30 days, during their follow-up evaluation. Nine of them had a clinical presentation at upper limbs, five at lower limbs, four as a bulbar type. Twelve were classified (El Escorial) as definite ALS, three probable ALS and two possible, with a ALS-FRS range of 17-40, mean of 33. By TMS, cortical motor threshold (MT) at rest, central motor conduction time (CMCT), cortical MEPs and spinal MEPs have been recorded. MR imaging DTI acquisitions have been performed with a 64 directions oriented tensor, on a 1.5T magnet, without ECG/PPU trigger. The DTI has been acquired on the brain with a 8-channels Head Sense Coil. Diffusion tensor imaging postprocessing has been conducted on a dedicate workstation loaded with proprietary DTI and FiberTracking software, and a two-observer (in consensus), voxel-by-voxel single-point ROI-based analysis on the following several anatomical levels: semioval centers (SC), internal capsule - posterior limb (IC), cerebral pedicle (PED), pons (PON). The color-coded FA map and a 3DT1-weighted axial image served as reference for ROI positioning assistance. Fractional anisotropy and ADC values have been recorded and compared to an institutional healthy volunteers database already existing. Statistical analysis has been carried out by mean of Wilcoxon-Mann-Whitney test and Cochrane Q test, together with sensitivity assessment. SAS v.8.2 and Excel 2007 have been adopted.
Results
Only the internal capsule level FA measurements (mean FA = 0.64) differed statistically from the mean and range (0.74; 0.67-0.81) of values from the control data. Sensitivity assessment of MEPs (with or without a clinical sign) and DTI, showed a slight superiority of DTI if compared to MEPs alone, but when MEPs are combined with the clinical sign show a better sensitivity. The same behavior and results showed for TCMC.

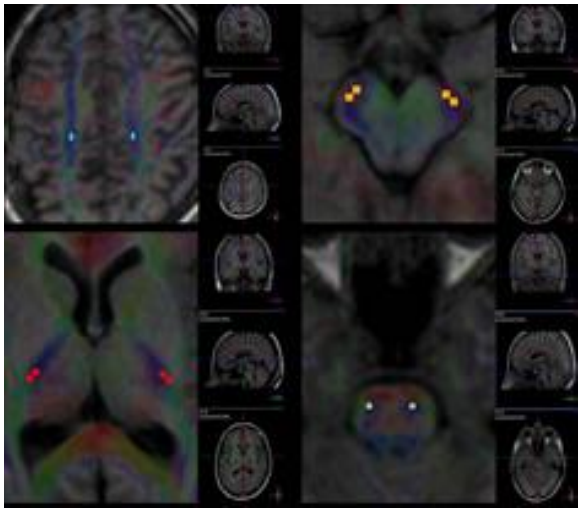

Conclusion
MEPs TCMC and DTI with FA measurement at the internal capsule level, appear to study with the same sensitivity the quality of cortico-spinal tract in ALS patients in evaluating UMN. The clinical signs, if present, add sensitivity to TMS evaluation.

KEYWORDS: DTI, ALS, TMS

eP-59

Visualization of Cerebrospinal Fluid Dynamics in Physiologic and Pathophysiologic Condition Using MR Imaging Arterial Spin Labeling Technique

Yamada, S.[1]·Miyazaki, M.[2]·McComb, G. J.[3]
[1]Tokai University Oiso Hospital, Oiso Naka-gun Kanagawa, JAPAN, [2]Toshiba Medical Research Institute USA, Vernon Hills, IL, [3]Childrens Hospital of Los Angeles, Los Angeles, CA.

Purpose
Cerebrospinal fluid (CSF) flow has been studied using cardiac-gated phase contrast MRI for a decade. This technique, however, allows depiction of "to-and-fro" motion only within one cardiac cycle. We have developed a time spatial labeling inversion pulse (time-SLIP) technique that permits CSF flow observation over a 1-6 sec period. Using this method we have investigated the hydrodynamics of CSF flow in normal volunteers and its alterations in pathophysiologic conditions.
Materials & Methods
The time-SLIP technique was used on healthy volunteers and patients with CSF-related disorders using a 1.5T and 3T MRI scanner. Using a scan time of 3-6 min, time-SLIP was applied to the region of the aqueduct of Sylvius, foramen of Monro and prepontine cisterns.
Results
Active exchange of CSF between the lateral and third ventricles and between the third and fourth ventricles was observed in all normal volunteers. These CSF exchanges

Note: Scanned images are included in the proceedings. Some submitted images were reduced during editing, thereby decreasing clarity. Also, refer to the Program Planner. Proceedings Content as of 3-29-2013.

were absent in the presence of hydrocephalus. Aqueductal CSF flow was nonexistent in the presence of aqueductal occlusion. Exaggerated turbulent CSF flow was observed at the aqueduct with both hydrocephalus except in the presence of aqueductal occlusion. Cerebrospinal fluid flow between the cyst and basal cistern were observed after the surgical internal fenestration for temporal arachnoid cyst. Large pulsatile CSF movement could be observed at the subarachnoid space at the cranio-cervical junction in normal volunteers. In patients with hydorsyringomyelia this pulsatile flow was disturbed.

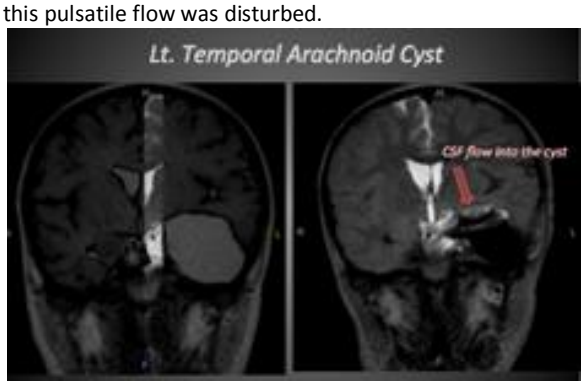

Conclusion
Using a MRI time-SLIP technique, CSF movements in normal and altered conditions are observable and will add to our understanding of normal and pathophysiologic situations.

KEYWORDS: Cerebrospinal fluid, Arachnoid cyst, spin labeling

eP-60

MR Findings in Patients with Nocardia Brain Abscess

Kubal, W. S.·Shastri, R.
University of Arizona
Tucson, AZ.

Purpose
Nocardia brain abscesses are relatively uncommon comprising approximately 2% of all brain abscesses. Retrospective literature review found only 120 cases reported between 1950 and 1993. The more current literature consists of small series and case reports often with few if any descriptions of MR findings. Unfortunately, nocardial infection carries a high mortality rate reaching 34% and is considered the most lethal of all brain abscesses caused by microorganisms. The purpose of this report is to illustrate the MR findings of this uncommon but highly lethal intracranial infection.
Materials & Methods
Retrospective review yielded eight patients with nocardial brain abscess. This study was HIPAA compliant and approved by the local IRB. Each patient had at least one MR obtained on a high field unit. Each patient had histologically proven nocardial infection.
Results
The eight patients ranged in age from 19 to 74 years. Six were male and two were female. Three were transplant patients and two had a pre-existing malignancy. In all patients lesions were either multicentric and/or a conglomerate multilobular mass. All lesions were characterized by peripheral enhancement and surrounding vasogenic edema. Larger lesions showed central nonenhancement, rim that was dark on T2 sequences and central restricted diffusion. One patient demonstrated leptomeningeal enhancement that extended to involve the spinal cord. Gradient-echo imaging was performed as part of each exam; no hemorrhage was seen. Diffusion tensor imaging was performed in one patient and showed infiltration and attenuation of white matter tracts.
Conclusion
Nocardia brain abscesses have imaging findings of a typical pyogenic infection. Given their propensity to occur in immune suppressed patients or in patients with pre-existing malignancy, the restricted diffusion is particularly useful in distinguishing them from intracranial neoplasm. The radiologist should be aware that the lesions often are multicentric and that leptomeningeal spread of disease may occur.

KEYWORDS: Brain abscess, Nocardia

eP-61

Evaluation of Dawson's Fingers in Neuromyelitis Optica Spectrum Disorders and Multiple Sclerosis: A Case-Control Study

Raz, E.[1]·Saba, L.[2]·Kister, I.[1]·Fatterpekar, G.[1]·Herbert, J.[1]·Omari, M.[1]·Lui, Y. W.[1]·Loh, J.[1]
[1]New York University, New York, NY, [2]University of Cagliari, Cagliari, ITALY.

Purpose
There are no studies that examine differences in the periventricular lesional pattern or the frequency of Dawson's fingers in MS and neuromyelitis optica spectrum disorders (NMOsd). To compare the periventricular lesional pattern and the presence of Dawson's fingers in MS and NMOsd.
Materials & Methods
MR imaging of 20 NMO and 40 matched MS patients were evaluated. Two neuroradiologists evaluated the periventricular lesions on FLAIR images (A = no lesions; B = smooth periventricular linear hyperintensity, focal or diffuse; C = discrete periventricular lesions with or without smooth periventricular linear hyperintensity; D = diffuse irregular confluent hyperintensity) and the presence of Dawson's fingers. Group comparisons and inter-reader agreement statistics were performed.
Results
Periventricular patterns: Reader 1, A-B: NMOsd = 17/20; MS = 2/40; C-D: NMOsd = 3/20; MS = 38/40; Reader 2, A-B: NMOsd = 16/20; MS = 2/40; C-D: NMOsd = 4/20; MS =

Note: Scanned images are included in the proceedings. Some submitted images were reduced during editing, thereby decreasing clarity. Also, refer to the Program Planner. Proceedings Content as of 3-29-2013.

38/40. Presence of Dawson's fingers: Reader 1 = 0/20 NMOsd; 37/40 MS. Reader 2 = 1/20 NMOsd; 31/40 MS. A significant difference between the two groups of patients ($p<0.001$) was found. Inter-reader agreement for periventricular pattern description and detection of Dawson's fingers was respectively good (k = 0.604) and very good (k = 0.763).
Conclusion
Certain periventricular lesional patterns are more common in NMO than MS. Dawson's fingers are more common in MS. Evaluation of sagittal FLAIR can help in the differential diagnosis between these two entities.

KEYWORDS: Multiple sclerosis, Neuromyelitis optica

eP-62

Brain Medullary Veins Visibility with Susceptibility-Weighted MR Imaging in Clinically Isolated Syndromes and Relapsing-Remitting Multiple Sclerosis

Rovira, A.·Aymerich, F. X.·Auger, C.·Huerga, E.·Mitjana, R.·Tintore, M.·Alonso, J.·Montalban, X.
Hospital Vall d'Hebron
Barcelona, SPAIN.

Purpose
Susceptibility-weighted imaging (SWI) is a novel MR technique that allows visualizing veins in the brain due to an inverse BOLD effect. Previous studies have described that relapsing-remitting multiple sclerosis (RRMS) patients show in SWI images a significantly reduced visibility of periventricular white matter veins compared to healthy controls (HC), with a negative correlation with T2 lesion load. In this work we propose to extend these studies to patients presenting with clinically isolated syndrome (CIS), who represent the earliest stage of possible multiple sclerosis (MS).
Materials & Methods
One hundred one subjects (17 HC; 48 CIS; 36 RRMS) were examined with 3T MRI (T2 and SWI). Susceptibility-weighted images were acquired using a 3 mm-slice thickness transverse GE sequence (TR/TE = 32 ms/24.6 ms). A home-developed algorithm was used to detect vein pixels in eight rectangular supraventricular white matter ROIs.
Results
Twenty-eight (58%) CIS patients had subclinical brain lesions (pCIS), whereas 20 (42%) had not (nPCIS). There were significant differences in the number of vein pixels among HC, RRMS and CIS groups ($p = 0.047$). Dunnett's test only showed significant difference comparing RRMS versus HC ($p = 0.033$). However, pCIS showed a significant lower number of vein pixels than nPCIS ($p = 0.028$). No significant correlation was observed between T2 lesion load and number of veins pixels.
Conclusion
Clinically isolated syndrome and RRMS patients showed in supraventricular white matter regions a decrease in the number of vein pixels, which is associated with the presence, but not with the volume, of T2 lesions. This finding likely reflects an increase BOLD effect (decrease in deoxihemoglobin) and supports the concept of a widespread hypometabolic process in MS.

KEYWORDS: Multiple sclerosis, Susceptibility-weighted imaging

eP-63

Progressive Multifocal Leukoencephalopathy in HIV and non-HIV Hosts with Prominent Inflammatory Changes

Lin, D.·Zessler, A.
Johns Hopkins University
Baltimore, MD.

Purpose
Progressive multifocal leukoencephalopathy (PML) is a rare and frequently fatal demyelinating disease caused by the JC polyomavirus. It predominantly affects patients in immunosuppressed states, and therefore is associated with a wide range of diseases including HIV, transplant recipients, monoclonal antibody therapy, and diverse rheumatic, oncological, and hematologic diseases. The purpose of this study is to review the MRI findings in patients with PML in a HIV and non-HIV setting, as well as to correlate with clinical course and final diagnosis.
Materials & Methods
Ten patients with acute neurologic symptoms, including four patients with HIV and clinical question of immune reconstitution inflammatory syndrome (IRIS), and six patients without HIV, underwent clinical MRI. Among the six non-HIV patients, two had SLE, two had lymphoma (one cutaneous T-cell and one follicular), one had Wegener's granulomatosis, and one had renal transplant. All patients were confirmed to have PML either by CSF analysis with PCR, or brain biopsy. The imaging findings were re-analyzed retrospectively and compared to the clinical radiology reports and clinical findings.
Results
While most of the cases show mass-like FLAIR hyperintense lesions with little or no mass effect similar to the classic findings of PML, there are features indicating a less typical component of active inflammation or demyelination in this cohort. Fifty percent (two in HIV and three in non-HIV) of the 10 patients showed gadolinium contrast enhancement of the PML lesion, and 50% (three in HIV and two in non-HIV) show restricted diffusion predominantly along the rim of the lesion. At least in two cases mild DWI hyperintensity was evident but accompanied by ADC hyperintensity suggestive of facilitated diffusion. In two cases there were cortical gray matter in addition to white matter involvement, and in three cases the deep gray matter also was involved. Extensive vasogenic edema with moderate mass effect was evident in two patients (one HIV). In one HIV patient with PML-IRIS, 1H-MRS revealed prominently elevated

Note: Scanned images are included in the proceedings. Some submitted images were reduced during editing, thereby decreasing clarity. Also, refer to the Program Planner. Proceedings Content as of 3-29-2013.

Cho/Cr and Cho/NAA ratios with a presence of lactate consistent with inflammation or demyelination. In the same patient brain biopsy was performed, with histopathology revealing more inflammation, lymphoplasmacytic, than in the classic case of PML. Because of the less typical neuroimaging findings, the initial radiology report suggested the diagnosis of subacute infarcts in two of 10 cases, and provided CNS lymphoma as a differential diagnosis in three cases as well as infiltrating astrocytoma or other CNS infection in two cases.
Conclusion
Prominent inflammation occurring in PML, often in the setting of IRIS with HAART therapy in HIV hosts as well as non-HIV patients, can have unusual neuroimaging findings including contrast enhancement, cytotoxic edema, mass effect, and gray matter involvement. It is particularly important to recognize these findings and to suggest the diagnosis given appropriate clinical findings.

KEYWORDS: Leukoencephalopathy, Immune reconstitution inflammatory, PML

eP-64

Neuropsychiatric Systemic Lupus Erythematosus: Prediction of Subsequent Development of Brain Lesions with MR Imaging

Futatsuya, K.[1]·Kakeda, S.[1]·Kaichi, Y.[2]·Moriya, J.[1]·Ohnari, N.[1]·Saito, K.[1]·Tanaka, Y.[1]·Korogi, Y.[1]
[1]University of Occupational and Environmental Health, Yahatanishi-ku, Kitakyushu, JAPAN, [2]Hiroshima University, Hiroshima, JAPAN.

Purpose
Systemic lupus erythematosus (SLE) is an autoimmune disease that is frequently manifested by involvement in the central nervous system, and the antiphospholipid syndrome (APS) may affect the incidence and pathogenesis of cerebrovascular diseases in the SLE patients. Cerebral infarctions, cortical atrophy, and multifocal gray matter and/or white matter lesions frequently are observed at MR imaging in patients with SLE, and the subsequent development of these lesions is seen in some patients. In this study, we assessed whether the clinical or initial MRI findings help predict the subsequent development of the brain lesions in SLE patients.
Materials & Methods
Of the 256 SLE patients that underwent MRI, we identified 91 patients with follow-up MRI. From them, we enrolled 64 patients less than 50 years old to avoid the effect of age-related cerebrovascular diseases. By two radiologists, the initial MRI findings were reviewed and categorized as follows; large territorial infarctions, lacunar infarctions, localized cortical infarctions, watershed infarctions,micro-embolisms, basal ganglia lesions, callosal lesions, white matter hyper intensities, and hemorrhages on T2-weighted and/or FLAIR images. Similarly,we also classified the follow-up MRI findings. Based on the MRI findings, the 64 patients were divided into the following three groups; group A, the patients had no lesion at both initial and follow-up MRI; group B, the patients had the lesions at initial MRI, but no new lesions at follow-up MRI; group C, the patients had the lesions at initial MRI and a new lesion at follow-up MRI.
Results
The numbers of the patients in each group were 18 for groupA, 32 for group B, and 14 for group C. In follow-up MRI, we found the 19 new lesions in group C; large territorial infarction (n = 1), lacunar infarctions (3), localized cortical infarctions (4), watershed infarctions (2), micro-embolism (1), basal ganglia lesions (2), and white matter hyper intensities (6). The prevalence of the patients with APS was more common in the group C (10/14: 71%) than in the group A (3/18: 17%) and group B (7/32:22%). At initial MRI, localized cortical infarction (50% versus 9%, $p < 0.001$) and lacunar infarction (50% versus 0%, $p < 0.05$) were significantly more common in group C than in group B. For the prevalence of the other findings at initial MRI, there were no statistically significant differences between the groups.
Conclusion
In SLE patients, the presence of APS as well as localized cortical infarction and lacunar infarction at the initial MRI may be predictors for the subsequent development of brain lesions.

KEYWORDS: Cerebral infarction, FLAIR, SLE,APS

eP-65

Posterior Reversible Encephalopathy Syndrome and the Brainstem: Features of Infratentorial-Predominant Posterior Reversible Encephalopathy Syndrome

Fitzgerald, R. T.·Samant, R. S.·Burgin, K.·Kumar, M.·Ramakrishnaiah, R. H.·Van Hemert, R.·Angtuaco, E. J.
University of Arkansas for Medical Sciences
Little Rock, AR.

Purpose
Posterior reversible encephalopathy syndrome (PRES) is a clinico-radiologic neurotoxic process that typically occurs in a setting of immune dysregulation accompanied by hypertension. Typical distribution of signal abnormality on MR involves the subcortical white matter of the parieto-occipital and posterior frontal regions. Atypical patterns of PRES involvement, including those involving the infratentorial brain, are well known; however, changes in these regions often are superimposed upon the more typical sites of involvement. We describe six cases that manifested with predominant involvement of the brainstem and cerebellum and lacked the classic pattern of supratentorial involvement, thus potentially obscuring a diagnosis of PRES from the unwary radiologist.
Materials & Methods
An institutional database of PRES patients was created

Note: Scanned images are included in the proceedings. Some submitted images were reduced during editing, thereby decreasing clarity. Also, refer to the Program Planner. Proceedings Content as of 3-29-2013.

through an IRB-approved search of the electronic record from 2007-2012. MR images were reviewed and classified by two neuroradiologists. Clinical data were collected through review of existing electronic medical records.
Results
Six cases among a database of 85 PRES patients treated at our institution between 2007 and 2012 displayed an atypical distribution of FLAIR/T2 signal abnormality predominantly involving the brainstem and/or cerebellum. In these patients, signal abnormalities within the supratentorial brain, when present, showed a predominantly periventricular distribution rather than the classically described and more commonly encountered peripheral, subcortical distribution. In three cases, the pattern of periventricular involvement was reminiscent of a demyelinating process. Four of six patients presented with severe hypertension. Additional predisposing factors included systemic lupus erythematosus (1) and sepsis (2). Presenting symptoms included altered mental status (4), visual disturbance (2), headache (2), and seizure (2). Five of six patients presented with renal dysfunction. One patient died and the remainder showed complete resolution of presenting symptoms at discharge.

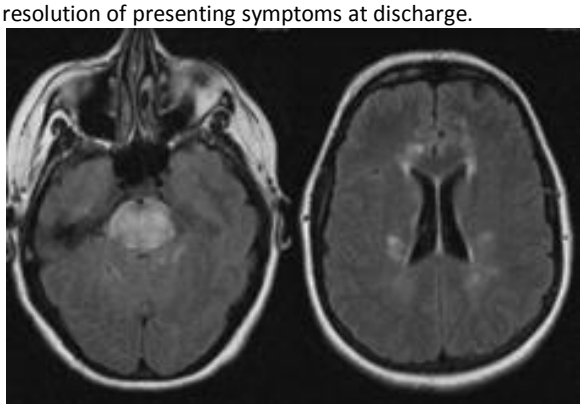

Conclusion
In contrast to the typical pattern of FLAIR signal abnormality in PRES, patients with brainstem/cerebellar-predominant PRES may manifest supratentorial changes in a periventricular distribution that, in some cases, mimics the appearance of a demyelinating process. Predisposing clinical factors in this cohort were similar to those encountered in the PRES population as a whole.

KEYWORDS: Posterior reversible encephalopathy, Encephalopathy, Brainstem

eP-66

Delayed Neuroimaging Findings of Gadolinium Imaging of Brain Disease Using Gadobenate Dimeglumine: A Higher Relaxivity Contrast Agent

Boyko, O. B.·Shiroishi, M.·Lerner, A.·Kim, P. E.·Zee, C.·LAW, M.
University of Southern California
Los Angeles, CA.

Purpose
To demonstrate the clinical imaging findings of delayed T1 and/or FLAIR imaging at 1.5T using a higher relaxivity contrast agent (HRCA) gadolinium contrast agent gadobenate dimeglumine (MultiHance®).
Materials & Methods
Twenty-five patients who had delayed imaging after completion of routine postgadolinium sequences were reviewed. Delayed imaging was do either to repeat T1 and/or FLAIR localized images for MR spectroscopy acquisition or other clinical reasons for the patient to be brought back to the MRI suite. Delayed time ranged from 12 minutes to 26 hours.
Results
As expected 22 cases where imaging was acquired within one hour of contrast administration demonstrated continued enhancement of lesions. Unexpectedly two lesions imaged 12 hours postcontrast administration (abscess and glioma) demonstrated delayed gadolinium enhancement and persisting enhancement.
Conclusion
Higher relaxivity contrast agents are now available for neuroimaging and a possible clinical neuroimaging pitfall of delayed/continued enhancement can occur which is not to be mistaken for blood products and hemorrhage.

KEYWORDS: Contrast enhancement, Contrast, Higher Relaxivity Gadolinium Contrast

eP-67

Peritumoral Edema and Apparent Diffusion Coefficient Characteristics of Angiomatous and Microcystic Meningiomas Are Distinct from Other Low-Grade Meningiomas as well as Atypical and Anaplastic Meningiomas

Azizyan, A.·Eboli, P.·Drazin, D.·Maya, M.·Bannykh, S.
Cedars Sinai Medical Center
Los Angeles, CA.

Purpose
To determine whether meningiomas of angiomatous or microcystic histology have MRI features which are unique from other types of low-grade meningiomas and from meningiomas of high-grade. In particular, we tested whether ADC values can reliably separate biologically aggressive and low-grade meningiomas in the preoperative setting.

Note: Scanned images are included in the proceedings. Some submitted images were reduced during editing, thereby decreasing clarity. Also, refer to the Program Planner. Proceedings Content as of 3-29-2013.

Materials & Methods
Preoperative MRIs of 71 patients with meningiomas were reviewed. Based on histologic characteristics, the tumors were categorized into three groups. Group 1 contained 12 pure microcystic, three pure angiomatoid and seven mixed, angiomatoid and microcystic tumors. Group 2 included WHO grade II and WHO grade III tumors, 28 of which were classified as atypical and nine as anaplastic. Group 3 included WHO grade I meningiomas without angiomatoid or microcystic features. Two reviewers determined maximum tumoral apparent diffusion coefficient (ADC) and cerebral blood volume (CBV) by placing a standardized region of interest within each meningioma. Apparent diffusion coefficient values were normalized to values in the lateral ventricles. Peritumoral edema index was measured as the volume of edema plus tumor divided by tumor volume.

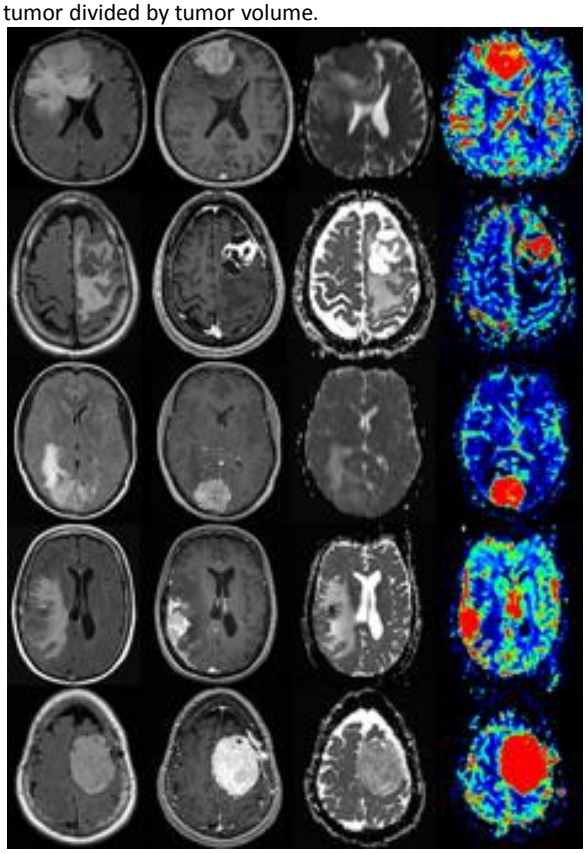

Figure: Group 1 (rows 1 and 2), Group 2 (rows 3 and 4) and Group 3 (row 5).

Results
Group 1 and group 2 meningiomas had significantly higher edema volume indices when compared to the group 3 tumors ($p = 0.003$ between group 1 and 3, $p<0.0001$ between group 2 and 3). There was no significant difference in edema index between group 1 and 2. The ADC values in the biologically aggressive group 2 were significantly higher than either of the two benign groups (1and 3), with p values of 0.0007 and 0.001 respectively. There was no statistically significant difference in the tumoral CBV values between the three groups.

Conclusion
WHO grade I meningiomas of angiomatoid and microcystic histology demonstrate a significantly higher edema index when compared to the rest of the WHO grade I meningiomas studied. Furthermore, the edema index of angiomatoid and microcystic meningiomas fails to distinguish them from the biologically aggressive WHO II and WHO III tumors of group 2. Internal ADC values can reliably distinguish the aggressive group of meningiomas from both groups of low-grade meningiomas.

KEYWORDS: Meningioma, MR imaging

eP-68

MR Imaging Diffusion Characteristics in Glioblastoma with Primitive Neuroectodermal Tumor-Like Components: An Uncommon Tumor Subtype

Ali, S.·Joseph, N. M.·Perry, A.·Cha, S.
University of California San Francisco
San Francisco, CA.

Purpose
Glioblastoma multiforme (GBM) with primitive neuroectodermal tumor (PNET) components is an uncommon variant of GBM with pathology demonstrating sharply demarcated hypercellular nodules with primitive-appearing cells with high nuclear-to-cytoplasmic ratios, markedly hyperchromatic nuclei, and high mitotic rates in a background of infiltrating glial neoplasm. Recent studies describe PNET-like clinical behavior in these patients--with significantly increased propensity for CSF dissemination compared to conventional GBMs and a benefit of "PNET-like" platinum-based chemotherapy upfront or after having failed conventional GBM-type treatment (radiation and temozolomide). Few reports in the literature have described areas of reduced diffusion on MRI of patients with GBM-PNET, and given areas of hypercellularity in the PNET components on pathology, it is not surprising reduced diffusion would be seen on MRI. No study however has quantified the ADC values of these patients and compared them with diffusion characteristics of conventional GBMs. The purpose of this presentation is to quantitatively evaluate the DWI characteristics of GBM with PNET features and compare with published ADC values of conventional GBMs.

Materials & Methods
Eight patients with brain biopsy specimens yielding GBM with PNET features were referred to UCSF Pathology service for consultation. MR images of these patients were reviewed retrospectively. Diffusion-weighted imaging sequences were analyzed with multiple regions of interests placed within nonhemorrhagic areas of the tumor, and ADC values were measured. Results were compared to published data of ADC in pathology-proven conventional GBM cases from our institution.

Results

Note: Scanned images are included in the proceedings. Some submitted images were reduced during editing, thereby decreasing clarity. Also, refer to the Program Planner. Proceedings Content as of 3-29-2013.

Reduced ADC was seen in patients with GBM with PNET components with a mean 691 x 10^-6 mm2/sec (range 345 to 963) compared to previously published means of 1140 and 1610 x 10^-6 mm2/sec in the enhancing and nonenhancing components of conventional GBMs, respectively.

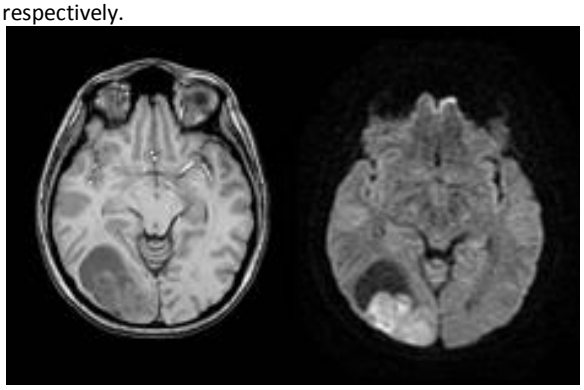

Figure: Axial diffusion-weighted (b1000) and post-gadolinium T1-weighted images demonstrating enhancing right occipital mass with significantly reduced diffusion in the solid component of the tumor. Apparent diffusion coefficient map not shown. Biopsy revealed GBM with PNET components.

Conclusion

We report significantly reduced ADC values in patients with GBM with PNET components compared to conventional GBMs. If demonstrated in a larger sample, when areas of reduced diffusion are seen on MRI in a high-grade glioma, a thorough histologic examination for presence of PNET components can be advocated, as patients with GBM-PNET may have a higher chance of developing CSF dissemination and may benefit for PNET-like chemotherapy.

KEYWORDS: GBM, Diffusion-weighted imaging, PNET

eP-69

MR Spectroscopy Detects Tumor Recurrence in Patients Treated with Bevacizumab

Hesselink, J. R.·Barkovich, M.·Almutairi, A.·Farid, N.·Kesari, S.
University of California San Diego Medial Center
San Diego, CA.

Purpose

To compare MR spectroscopy (MRS) with MR imaging and perfusion for detecting tumor recurrence in patients treated with bevacizumab.

Materials & Methods

Imaging studies and medical records of 39 patients undergoing treatment for brain tumors were reviewed. Seven patients who were being treated with bevacizumab and followed with MR imaging, MRS, and MR perfusion were included in the study. The three MR methods were evaluated independently for evidence of tumor recurrence. Brain tumors included five glioblastomas (GBM), one grade II gemistocytic astrocytoma, and one anaplastic oligodendroglioma on initial biopsy that was upgraded to a GBM after subtotal surgical resection.

Results

Elevated choline was observed in six patients, adjacent to the original tumor site in five and in the opposite hemisphere in one patient. The duration of bevacizumab therapy before MRS ranged from one to 18 months. Tumor recurrence was confirmed by biopsy in two patients, autopsy of one patient, and by clinical disease progression in the other three patients. The cerebral blood volume was minimally increased in only one patient. Increased T2 signal and gadolinium enhancement was noted in three patients, but they had been off bevacizumab for two and three months, respectively. The one patient with no choline elevation was clinically diagnosed with severe radiation necrosis.

Conclusion

In patients treated with bevacizumab, MRS was superior to MR imaging and perfusion for detecting tumor recurrence. Unlike T2 edema, contrast enhancement, and perfusion, the metabolic measures of MRS are not affected by bevacizumab.

KEYWORDS: Neoplasm recurrence, diagnosis, 1H MRS

eP-70

Assessment of Vascular Density in Glial Tumors Using Time-of-Flight MR Angiography at 7T: Initial Experience

Atchie, B.·Pinho, M.·Jiang, F.·Malloy, C.·Maher, E.·King, K.
University of Texas Southwestern Medical Center
Dallas, TX.

Purpose

Tumor vasoproliferation is a central part of tumor grading and with the advent of ultrahigh field strength MRI, novel approaches in the assessment of tumoral vascularity currently are under investigation. It has been shown that vascularity detected by ultrahigh field MRI correlates with post-mortem pathology in glioblastomas, but the prognostic value and potential treatment implications related to vascularity detected by these noninvasive means remains unknown. Because noninvasive monitoring of gliomas is a significant clinical problem, the possibility that vascular characteristics could serve as a biomarker is worth investigation. We aim to add to this body of knowledge by providing our experience with a unique technique in assesing the vascular density in glial tumors at 7T.

Materials & Methods

The study was institutional review board approved and HIPAA compliant. Nineteen subjects with biopsy proven glial neoplasms were evaluated on a 7T Philips Achieva scanner. Four patients were excluded from the sample for confounding factors related to large amounts of hemorrhage or necrosis (three patients) or prior surgery

Note: Scanned images are included in the proceedings. Some submitted images were reduced during editing, thereby decreasing clarity. Also, refer to the Program Planner. Proceedings Content as of 3-29-2013.

(one patient). The remaining 15 subjects were evaluated per the following protocol; 3D TOF MRA and FLAIR sequences were performed on each patient and evaluated by three independent blinded radiologists. If the tumor was felt to demonstrate abnormal tumoral vascularity a 1.0 cm^2 ROI was chosen by the reviewer and placed over what was subjectively felt to represent the most vascular portion of the tumor. The numbers of abnormal vessels then were tallied according to a predetermined criterion and recorded along with the location of the ROI. Calculated vascular density then was correlated to the grade of the tumor.

Results

There was interobserver consistency when it came to determining the most vascular portion of a given tumor, with 18 of 23 ROIs placed within <1 cm of one another. For tumors determined to have definitely abnormal vasculature the mean vessel density was 12.7 vessels/cm^2 for grade IV, 5.6 vessels/cm^2 for grade III, and 4.8 vessels/cm^2 for grade I-II tumors. Although a trend towards greater vascular density was noted for higher grade neoplasms, groupwise correlations did not hold statistical significance due to the fact that half of the grade IV tumors failed to demonstrate any abnormal vascularity at all.

Conclusion

7T MRA depicts finely detailed images of tumor vascularity in primary brain tumors when present. Although high vascular density was a very specific finding for grade IV tumors, our correlations with grade did not reach significance due to a striking dichotomy in the observable vascularity of glioblastomas, with half of these tumors being avascular at MRA. These surprising findings warrant future investigation and may have implications in defining subsets of patients with different tumor genetics, response to therapy, and ultimately survival rates.

KEYWORDS: Glioma, MR angiography, 7 T, MRA techniques

eP-72

Histopathologic Evaluation of High-Grade Brain Tumors Infiltration Using High-Order Diffusion Tensor Imaging

Stefani, T.·Pereira, B.·Coste, A.·Khalil, T.·Chabert, E.·Kemeny, J. L.·Boyer, L.·Jean, B.
University Hospital Clermont-Ferrand
Clermont-Ferrand, FRANCE.

Purpose

Delineation of high-grade brain tumor is critical for treatment planning and prognosis but remains challenging using conventional MRI sequences. The aim of this study was to evaluate the peripheral white matter infiltration of high-grade brain tumors using high-order diffusion tensor imaging.

Materials & Methods

Local IRB approval and informed consent from patients were obtained. Seven patients were prospectively included and underwent 3T clinical MRI scans. MR imaging protocol included T2-WI, FLAIR, T2GRE, 3D gradient-echo sequences before and after contrast media injection and an EPI diffusion tensor sequence with 60 directions of gradient sampling (b = 3000). Patients then underwent surgical stereotactic tumor biopsy targeted with Leksell frame, according to standard procedure. An extra biopsy was performed in normal-appearing white matter adjacent to the tumor along the biopsy pathway. Histopathologic analysis of the biopsy was done using immunologic markers such as MAP2, Ki67 in order to estimate the percentage of tumor infiltration. Analysis of DT MRI datasets was done using in-house software for high order tensor resolution and generalized anisotropy (GA), generalized variance (GV), mean diffusion (MD) estimation at the exact coordinates of the biopsy sites. Finally a statistical analysis (Spearman correlation) was used to correlate GA, GV, MD and the infiltration percentage.

Results

There were significant correlation between the GA ($r = -0.956$ $p<0.05$) and GV ($r = -0.956$ $p<0.05$) values of tumor adjacent normal-appearing white matter and tumor infiltration percentage. Mean diffusion showed no significant correlation ($r = 0.598$ $p>0.1$) with infiltration percentage.

Conclusion

Our results show that GA and GV measurements derived from high-order diffusion tensor estimation are well correlated to tumor infiltration. Therefore the identification of high-grade brain tumor borders may be more accurate using high-order diffusion tensor imaging.

KEYWORDS: DTI, Brain neoplasms, high order; generalized anisotropy

eP-73

Can T1-Weighted Gradient Echo MR Scans Differentiate between Intra and Extracellular Ferumoxytol Enhancement?

Varallyay, C. G.[1]·Muldoon, L. L.[1]·Neuwelt, E. A.[1,2]
[1]Oregon Health & Science University, Portland, OR,
[2]Department of Veterans Affairs Medical Center, Portland, OR.

Purpose

Ferumoxytol, a long circulating iron oxide nanoparticle has been approved by the Food and Drug Administration for iron replacement in patients with kidney failure. Due to its T1 and T2 relaxation time shortening effects it can be used (off label) as an MRI contrast agent. Early after injection it acts as a blood pool agent, and shows peak contrast enhancement 24 hours after administration. Ferumoxytol is eliminated from the plasma through the reticulo-endothelial system, by uptake of mononuclear cells mainly in the liver, spleen and bone marrow. The internalized ferumoxytol particles, clustered in lysosomes, exhibit a

Note: Scanned images are included in the proceedings. Some submitted images were reduced during editing, thereby decreasing clarity. Also, refer to the Program Planner. Proceedings Content as of 3-29-2013.

substantially increased transverse relaxivity causing signal loss in gradient echo T1-weighted images. This differs from the hyperintense enhancement of extracellular particles. The purpose of this study was to analyze the potentials of ferumoxytol in assessing extra and intracellular contrast agent accumulation.
Materials & Methods
T1-weighted sagittal gradient echo brain MRIs were reviewed before and 24 hours after intravenous ferumoxytol injection in 39 patients with brain neoplasms. The administered doses were 2 mg/kg, 4 mg/kg or 510 mg ferumoxytol (13 patients in each dose group). Signal changes were analyzed in regions of interests in the second cervical vertebral body, in enhancing brain lesions and in the pons for reference.
Results
There was a dose-dependent signal decrease in the bone marrow in the spine 24 hours postferumoxytol injection, whereas increased signal was found in the CNS lesions. Figure 1 shows images of a representative case, a patient with glioblastoma. There is an avid signal increase in the region of the tumor 24 hours post-injection, combined with marked signal decrease of the bone marrow in the vertebral bodies of C2 and C3. This signal decrease most likely represents intracellular contrast agent. This patient already had received the same dose of ferumoxytol three months earlier with some residual signal loss in the vertebral bodies seen on the left image (the baseline image from three months before is not shown). The signal decrease in areas of low concentration residual iron oxide in the vertebral bodies suggests that signal changes caused by ferumoxytol (hyper versus hypointense) cannot be explained solely with concentration differences.

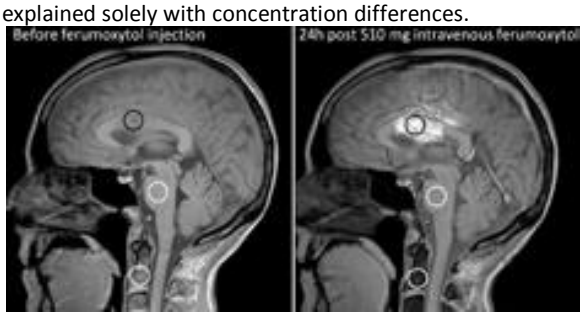

Conclusion
Using the clinically applicable dose up to 510 mg ferumoxytol and T1-weighted gradient echo sequences may help differentiate between mainly intracellular versus mainly interstitial contrast enhancement.

KEYWORDS: Contrast enhancement, Brain neoplasms, Ferumoxytol

eP-74

"Soap Bubble" Pattern Precedes Macrocystic Changes in Acoustic Neuromas within Three Months of Stereotactic Radiosurgery

Delman, B. N.[1]·Carai, A.[1,2]·Germano, I.[1]
[1]Mt. Sinai Medical Center, New York, NY, [2]Presidio Ospedaliero Marino, Caligari, ITALY.

Purpose
To identify the pattern of changes in intralesional enhancement that acoustic neuromas undergo in the months following stereotactic radiosurgery (SRS).
Materials & Methods
We evaluated 24 patients with acoustic neuromas diagnosed by MRI for changes in tumor quality and size following SRS. Standard imaging protocol includes either thin-section or volumetric post-gadolinium images. Measurements of tumor volume were obtained in axial and coronal planes by calculating the sum of cross-sectional area on each image. Enhancement pattern for each tumor at three months was characterized in terms of "soap-bubble" appearance: a) "no bubble", indicating homogeneous enhancement; b) "microbubbles," indicating reduced intensity following contrast without discrete cavities; and c) "large bubbles," reflecting discrete cavities.
Results
The most common pattern was microbubbles, seen in 18/24 (75%) at three months. This was manifest as a nearly ground glass pattern centrally reflecting overall reduction in enhancement in the center of neuromas with sparing at the periphery. Large bubbles were seen in 4/24 (17%), and the no bubble pattern was identified in 2/24 (8%). Regarding volume changes, there was approximately 34% expansion of the tumors on average at three months, reflecting a significant portion of the enlargement that is typically seen in the first six months exams compared with baseline studies.
Conclusion
We believe the "microbubble" pattern reflects early fine cavitary change that is particularly prominent at three months. The imaging appearance is proposed to reflect volume averaging between i) small cavitary areas that do not enhance, and ii) surrounding parenchyma that does enhance. We further propose that the large bubble pattern represents one end of the transformation spectrum, in which microcavities coalesce into larger nonenhancing portions. At the other end of the spectrum are the lesions which lack bubbles, which may be evolving more slowly but which may go on to develop cavitation later.

KEYWORDS: Acoustic schwannoma, Radiation effects

Note: Scanned images are included in the proceedings. Some submitted images were reduced during editing, thereby decreasing clarity. Also, refer to the Program Planner. Proceedings Content as of 3-29-2013.

eP-75

MR Perfusion in Diagnosis of Intraparenchymal Hematoma with Underlying Tumors

Shankar, J. J. S.
QE II Hospital
Halifax, NS, CANADA.

Purpose
The intracranial hematoma could be either idiopathic/primary or secondary to underlying malignant tumors. The imaging appearance gets complicated due to the presence of a large hematoma. The usual sequence of investigation for intraparenchymal hematoma in our institution is plain head CT and MRI with gadolinium to rule out underlying etiology of the tumor. Most of the time the MRI is done in the subacute phase of the hematoma. Due to T1 hyperintensity of the hematoma and patchy enhancement of the hematoma, detection of underlying tumor is extremely difficult. We describe findings of MR perfusion (MRP) done in patients with intraparenchymal hematoma.
Materials & Methods
A retrospective review of MRP in consecutive patients who had MR perfusion done for the investigation of intraparenchymal hematoma in last six months. Routine, postgadolinium images and MR perfusion of these patients were analyzed for possibility of underlying tumor as a possible cause of hematoma. All these patients were followed up on imaging or were operated upon for evacuation of hematoma. Perfusion parameters of cerebral blood volume (CBV) and cerebral blood flow (CBF) and presence and pattern (nodular versus peripheral) of enhancement were recorded for each patient. Sensitivity, specificity, positive and negative predictive values were calculated for each of these parameters to predict the diagnosis of the tumor on followup.
Results
Total of 10 patients (M 7; F 3; Mean age: 61.7 years) with lobar hematoma underwent MRP. The sensitivity, specificity, positive and negative predictive value of both increased CBF and CBV was all 100%. Sensitivity, specificity, positive and negative predictive value for presence of enhancement on postcontrast images were 80, 20, 50, 50%. Sensitivity, specificity, positive and negative predictive value of presence of nodular pattern of enhancement on the postcontrast study were all 60%.
Conclusion
MR perfusion showed very high sensitivity and specificity for diagnosis of underlying tumor as the cause of hematoma. Presence of enhancement also was highly sensitive by had a very low specificity. Since most of these patients undergo MRI brain with gadolinium on a routine basis, the addition of MR perfusion will help in increasing the sensitivity and specificity in the diagnosis of underlying tumor. To our knowledge, we are the first to report the role of MRP in identifying underlying tumor in cases of intraparenchymal hematomas.

KEYWORDS: Brain hemorrhage, Brain neoplasms, MR Perfusion

eP-76

Intravoxel Incoherent Motion MR Imaging for Differentiating Glioblastoma Multiforme from Primary Cerebral Nervous System Lymphoma

Suh, C.·Kim, H.·Lee, S.·Kim, N.·Choi, C.·Kim, S.
Asan Medical Center
Seoul, KOREA, REPUBLIC OF.

Purpose
There has been a resurgent interest in intravoxel incoherent motion (IVIM) MR imaging to obtain perfusion as well as diffusion information on lesions, in which the diffusion was modeled as Gaussian diffusion. We tested the predictive value of the perfusion and diffusion parameters derived from IVIM MR imaging in order to differentiate glioblastoma multiforme (GBM) from primary cerebral nervous system lymphoma (PCNSL). In addition, we aimed to evaluate the relation between IVIM MR imaging parameters and dynamic susceptibility contrast (DSC), dynamic contrast enhanced (DCE) MR perfusion imaging parameters.
Materials & Methods
The institutional review board of our institution approved this study and prior written informed consent for routine brain tumor MR imaging was obtained from all patients. Fifty-nine consecutive patients (33 men, 26 women, mean age 54.5 years) who had pathologically confirmed GBM and PCNSL prior to any treatment, were assessed using IVIM MR imaging. The IVIM method is based on a bi-exponential fit (*) of the relative signal obtained with the Stejskal-Tanner diffusion sequence for multiple b-values, which permits the extraction of the perfusion fraction (*f*) and the diffusion coefficient (D). We acquired 16 different b-values (0, 10, 20, 40, 60, 80, 100, 120, 140, 160, 180, 200, 300, 500, 700, 900 sec/mm2) that are acquired in three orthogonal directions using a 3T MR scanner and a 32-multichannel receiver head coil. Thus, this work is to evaluate the effect of different b-values on IVIM *f* and D for differentiating GBM from PCNSL. The best predictor for differentiating GBM from PCNSL was determined by receiver operating characteristic (ROC) curve analyses. We used maximum normalized cerebral blood volume (nCBVmax) from DSC MR perfusion imaging and maximum initial area under the curve at first 60 sec (IAUC60max) from DCE MR perfusion imaging to evaluate the correlation with IVIM MR perfusion parameters. Pearson's correlation analysis was used to assess the relation between *f*, D, and nCBVmax, IAUC60max.
Results
We enrolled 38 patients (64.4%) with GBM and 21 patients (35.6%) with PCNSL. The *f* was significantly higher in glioblastoma group (mean ± SD; 0.119 ± 0.024) than in PCNSL group (mean ± SD; 0.056 ± 0.013) ($p < 0.001$; 95% confidence interval: 0.0519, 0.0746). The D did not

Note: Scanned images are included in the proceedings. Some submitted images were reduced during editing, thereby decreasing clarity. Also, refer to the Program Planner. Proceedings Content as of 3-29-2013.

significantly differ between two groups (P = 0.144). ROC curve analyses showed *f* to be an excellent predictor of differentiating glioblastoma multiforme from PCNSL (AUC, 0990; 95% confidence interval: 0.973, 1.000; cut-off value, 0.075), with a sensitivity of 97.4% and a specificity of 90.5% and a positive predictive value of 94.9% and a negative predictive value of 95.0%. Excellent correlation between *f* and nCBVmax ($p < 0.001$, r=0.832), good correlation between *f* and IAUC60max ($p < 0.001$, r=0.575) were found for all cases.

Conclusion

The perfusion-fraction (*f*) from IVIM MR imaging can be a potential, noninvasive imaging biomarker for differentiating GBM from PCNSL. Major advantages of IVIM MR imaging are acquisition of perfusion and diffusion imaging simultaneously, independence of intravenous contrast injection, and acquisition of true diffusion imaging separated from the perfusion effects.

KEYWORDS: Glioblastoma, Lymphoma, Intravoxel Incoherent Motion MR Imaging

eP-77

Physiologic MR Imaging for Assessment of Nonenhancing T2 Signal Abnormalities before or after Treatment of Brain Tumors: Myoinositol and Apparent Diffusion Coefficient Values May Be More Helpful than Choline Ratios and Perfusion Imaging

Ison, C.·Kumar, A. J.·Ketonen, L.·Schellingerhout, D.·Jackson, E. F.·Hou, P.·Hamilton, J. D.
M. D. Anderson Cancer Center
Houston, TX.

Purpose

Contrast-enhanced MRI has been a mainstay in the evaluation of intracranial neoplasms, prior to and after management with surgery, radiotherapy and chemotherapy. The pattern and degree of enhancement have been utilized in order to characterize or distinguish malignant neoplasms from low-grade tumors and treatment-related changes. However, since up to a third of malignant intracranial neoplasms do not enhance, and treatment-related changes such as gliosis may not enhance, further diagnostic procedures are needed to better characterize nonenhancing lesions. Therefore, the purpose of the study was to evaluate the utility of various advanced quantitative MR imaging biomarkers in patients with nonenhancing gliomas and treatment-related changes.

Materials & Methods

Twenty-five patients who underwent advanced brain tumor MR imaging for suspected intracranial neoplasm, based on nonenhancing T2 signal abnormalities, were identified retrospectively. Advanced imaging sequences that were acquired included: diffusion tensor imaging, gradient echo dynamic susceptibility contrast (DSC) perfusion imaging, and MR spectroscopy utilizing echo times of 35 and 144 ms. The specific metrics evaluated included DSC negative enhancement integral, DSC relative cerebral blood volume, Cho/Cr ratio, Cho/NAA ratio, myoinositol greater the 75% of the creatine peak height and the apparent diffusion coefficient (ADC) value. The accuracy of the overall protocol in distinguishing between treatment effects, low-grade (I & II) tumor, intermediate-grade (III) tumor, and high-grade (IV) tumor was assessed based on radiologist report, following determination of the actual histologic diagnosis, or if pathology was lacking whether the presumed diagnosis was confirmed based on three-six months of follow-up imaging (e.g., treatment changes resolved). In addition, the individual parameters between these groups were tested with the Fisher's exact test for discrete variables and the unpaired Students *t*-test for continuous variables.

Results

Of the presumed diagnosis, five cases of treatment effects were suspected (two of which were histologically sampled); four cases of high-grade tumor were suspected (two sampled); four cases of intermediate grade tumor were suspected (three sampled); and 12 cases of low-grade tumor were suspected (seven sampled). Overall, the nonenhanced advanced brain tumor imaging protocol had an accuracy of 12/14 (86%) based on the histopathologic diagnosis. The presumed diagnosis accuracy based on follow-up imaging or actual histopathologic diagnosis was 22/25 (88%). All inaccuracies were in the first half of patients imaged. Among the individual imaging parameters, the presence of an elevated myoinositol peak had the greatest degree of accuracy in distinguishing low-grade tumors (92%) from treatment-related effects (0%; $p = 0.0008$) and distinguishing low-grade tumors from high-grade tumors (25%; $p = 0.05$) and there was a trend for distinguishing between low-grade tumors versus combined intermediate and high-grade tumors (50%; $p = 0.06$). Apparent diffusion coefficient values were useful in distinguishing low-grade tumors versus treatment effects (1.5+/-0.5 versus 0.87+/-0.43xe-3 mm^2/s; $p = 0.02$). The other individual advanced brain imaging parameters were not significantly different between groups.

Conclusion

Advanced brain tumor MR imaging for nonenhancing lesions demonstrated a high degree of accuracy in distinguishing between the different tumor grades and treatment effects. Myoinositol and ADC values were the best predictor of histologic diagnosis.

KEYWORDS: Glioma, Radiation injury, Non-enhancing

Note: Scanned images are included in the proceedings. Some submitted images were reduced during editing, thereby decreasing clarity. Also, refer to the Program Planner. Proceedings Content as of 3-29-2013.

eP-78

Development of an Automated Quantitation Method for Cerebrospinal Fluid Dynamics in the Cerebral Ventricles and the Spinal Subarachnoid Space Using MR Imaging Spin Labeling Technique

Shiodera, T.[1]·Nitta, S.[1]·Takeguchi, T.[1]·Yui, M.[2]·Yamashita, Y.[2]·Yamamoto, T.[2]·Yamada, S.[3]
[1]Toshiba Corporation, Kawasaki, JAPAN, [2]Toshiba Medical Systems Corporation, Tochigi, JAPAN, [3]Tokai University Oiso Hospital, Kanagawa, JAPAN.

Purpose
Using the time-spatial labeling inversion pulse (Time-SLIP) technique, a regional cerebrospinal fluid (CSF) dynamics can be traced without using contrast medium. Previous studies have evaluated visual assessments of CSF dynamics using the Time-SLIP technique. The objective of this study is automated quantitation of CSF dynamics in the cerebral ventricles and the spinal subarachnoid space using the Time-SLIP technique.
Materials & Methods
A series of 2D images with incremental inversion recovery times was obtained using 1.5T MRI scanner with Time-SLIP sequence. Observation regions were the foramen Monro, the prepontine cisterns, the aqueduct of Sylvius and the spinal subarachnoid space. These regions of interest were automatically outlined based on signal intensity analysis and shape of region. Subsequently, labeled CSF regions were further detected using the image binarization method. Average speed of the labeled CSF region was calculated using a regression line fitting. To evaluate the proposed method, experiments comparing the average speed and visual assessment by three neurosurgeons were conducted. Correlations between the proposed method and manual annotations of the average speed were evaluated in the spinal subarachnoid space.
Results
Seventy-nine datasets including 76 patients with various diseases (idiopathic normal pressure hydrocephalus, secondary normal pressure hydrocephalus, cerebral infarction, etc.) and three healthy volunteers for intracranial CSF dynamics, and 19 datasets from three healthy volunteers for the spinal subarachnoid CSF dynamics were studied. The proposed method detected the labeled CSF dynamics as shown in Figure 1. For cerebral ventricles, Table 2 shows correlation of the average speed between visual assessment and the automated quantitation method in these regions. Concordance ratios were 87 to 91%. For the spinal subarachnoid space, the correlation factor between the proposed method and manual annotations was $R2 = 0.83$ ($p < 0.001$). The processing time was less than three seconds.

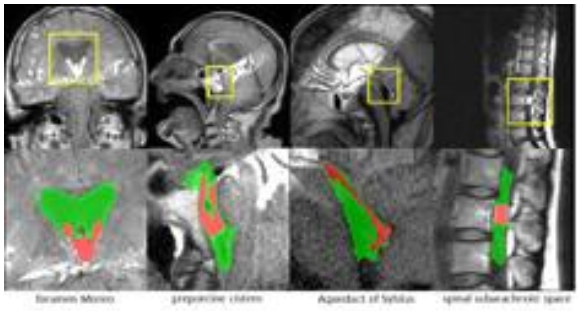

comparison results between average speed and visual assessment

observation region	visual assessment results by neurosurgeons / average speed by the proposed method [mm/sec.]		
foremen Monro	no reflux	slow reflux	normal reflux
	0.40 ± 0.30	1.20 ± 0.62	3.06 ± 0.45
prepontine cisterns	no movement	normal movement	-
	0.55 ± 0.25	1.23 ± 0.49	-
aqueduct of Sylvius	slow movement	normal movement	fast movement
	0.22 ± 0.26	1.09 ± 0.54	3.68 ± 1.66

Conclusion
This paper presented a new automated quantitative method of CSF dynamics using the Time-SLIP technique.

KEYWORDS: Cerebrospinal fluid, MR imaging, image post-processing technique

Note: Scanned images are included in the proceedings. Some submitted images were reduced during editing, thereby decreasing clarity. Also, refer to the Program Planner. Proceedings Content as of 3-29-2013.

eP-79

Feasibility of Creating Intracranial MR Angiography Maximum Intensity Projections Using Automated Processing Tools

Dobre, M. C.[1]·Seeger, C.[2]·Brost, A.[2]·Fischbein, N.[1]·Han, Z.[2]·Maclaren, J.[2]·Vos, S. B.[2]·Hornegger, J.[3]·Bammer, R.[2]
[1]Stanford Hospitals and Clinics, Stanford, CA, [2]Stanford University, Stanford, CA, [3]Friedrich Alexander University Erlangen Nuremberg, Erlangen, GERMANY.

Purpose
The process of manually creating rotational maximum intensity projection (MIP) images of the intracranial vessels is performed by MR technologists at our institution and is laborious, time-consuming and inefficient. It may take as long at 10 minutes to complete these reformats depending on the experience of the technologist and the number of desired projections, and on occasion the technologist may fail to create MIPs when they are distracted by more pressing patient care needs. Software that could automatically generate MIPs from source MRA data would improve MR technologist workflow and efficiency and should produce reliably available images of consistent quality.
Materials & Methods
We implemented a software package (RAPID) which is able to automatically process raw MRA data based on a cutout MIP ROI from an atlas which is registered to an individual patient. We tested this software in the clinical setting on MRA data acquired using standard time-of-flight (TOF) techniques on clinical 1.5T and 3.0T scanners. A board-certified radiologist and a board-certified neuroradiologist jointly reviewed and qualitatively compared 32 MIPs of the COW obtained in both the inpatient and outpatient setting between 10/01/2012 and 10/26/2012.
Results
RAPID generates five different rotational MIPs: entire circulation, anterior circulation, posterior circulation, anterior left Circulation and anterior right circulation of the circle of Willis (COW). Out of 32 MRAs, RAPID created equal or better quality MIPs in all but three instances, two of which were scored as only minor quality flaws. In 11 instances RAPID generated MIPs which offered clearer visualization of the posterior circulation and were less error-prone in patients who had complete vessel occlusion, such as patients with Moyamoya. Figure 1 shows a MIP of the COW created by an MR technologist with an artificial defect in the right PCA (arrow) and the comparison MIP generated by RAPID without this error.

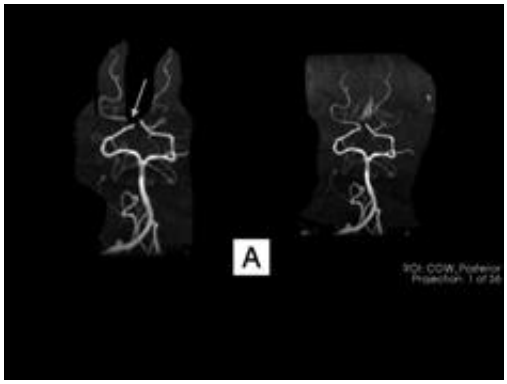

Conclusion
The RAPID software successfully created rotational MIPs of the COW from MRAs obtained using standard TOF techniques on clinical scanners. These MIPs were equivalent in almost all instances to or of better quality than MIPs created by the MR technologist. Introducing fully automated, software generated MIPs into clinical practice is possible and may results in improved technologist workflow and fewer interpretive errors by the radiologist.

KEYWORDS: 3-dimensional reconstruction, Maximum intensity projection, MRA

eP-80

Assessment of Image Quality of Half Dose CT Scans Utilizing SafeCT Processing

Agarwal, V.·Delfyett, W. T.·Hughes, M. A.·Mettenburg, J. M.·Shah, R. R.·Tailor, D. R.·Deible, C. R.
University of Pittsburgh Medical Center
Pittsburgh, PA.

Purpose
There has been exponential growth in the use of CT imaging in the past decade due to technical advances, improved diagnostic accuracy and medico legal pressures. CT is now an indispensable part of diagnostic medicine. Although it has replaced more invasive and expensive tests, the growth in CT use has been accompanied by an unavoidable increase in cumulative radiation exposure. There is a clear need for simple yet effective ways to reduce dose while maintaining diagnostic image quality. The purpose of this study is to evaluate the use of a three-dimensional, nonlinear, postprocessing reconstruction noise reduction algorithm (SafeCT, MedicVision) to determine whether radiation dose can be decreased without compromising diagnostic image quality.
Materials & Methods
Under an IRB-approved protocol, adult patients scheduled for clinically indicated noncontrast CT exams of the head underwent a second, half dose CT scan following the clinical exam. The tube current for the research scan was adjusted to have 50% lower dose than the clinical scan. The low dose data then were reconstructed with a three-

Note: Scanned images are included in the proceedings. Some submitted images were reduced during editing, thereby decreasing clarity. Also, refer to the Program Planner. Proceedings Content as of 3-29-2013.

dimensional, nonlinear, postprocessing reconstruction noise reduction algorithm (SafeCT, MedicVision). Each SafeCT processed exam then was displayed side by side with its full dose counterpart in random left/right order blinded to 5 CAQ neuroradiologist reviewers. For each exam, reviewers rated the images based on five questions about image quality and diagnostic value on a scale of one to five. The results then were unblinded and converted into a five-point scale where scores above three indicated superiority of the SafeCT processed exam and scores below three indicated superiority of the full dose exam.
Results
A total of 33 patients were enrolled and underwent both full dose and half dose noncontrast CT examinations of the head. Median and mean values were computed for each reviewer by each question. A bootstrap method then was used to compute the 95% confidence interval for the mean. In this study, a response value equal to three emphasizes that the two methods are equivalent. In fact based on mean values as well as the median, most raters gave a value of three for each question meaning they consider both methods as being equivalent based on rating questionnaires definition. The 95% confidence interval for the majority of reviewers and questions were narrow suggesting that the variability of ratings was very small. Higher variability was seen for one of the five reviewers for all questions as well as for question number five for all reviewers.
Conclusion
Although there is slight variability amongst the raters, the ratings of the reviewers are close to the value of three as indicated by both the mean and the median suggesting that there is no statistically significant difference between the full dose and half dose scans in terms of image quality and diagnostic acceptability. Therefore, the three-dimensional, nonlinear, postprocessing reconstruction noise reduction algorithm (SafeCT, MedicVision) used in this study can be a simple yet effective strategy to reduce radiation dose while maintaining diagnostic image quality.

KEYWORDS: Radiation dose reduction, CT

eP-81

Silent Ultrashort TE MR Imaging: Initial Experiences with a New Clinical Sequence

DeLano, M. C.[1,2,3]·Sun, W.[4]·Akao, J.[4]·McKinnon, G.[4]·Close, O.[1]·King, K.[4]
[1]Michigan State University, Grand Rapids, MI, [2]Advanced Radiology Services, PC, Grand Rapids, MI, [3]Spectrum Health, Grand Rapids, MI, [4]General Electric Health Care, Waukesha, WI.

Purpose
Acoustic noise of MR imaging has important safety and comfort implications, particularly when imaging at higher field strength. Pioneering work by Bydder et al explored the use of ultrashort TE imaging in multiple body regions. We report the clinical feasibility of brain imaging with silent ultrashort TE 3D T1- and T2-weighted commercial sequences at 3T, and discuss the associated image contrast features and patient acceptance.
Materials & Methods
Seven consecutive patients scheduled for routine pre and postcontrast MR of the brain were recruited for evaluation of these sequences in preparation for FDA 510K submission for use on a commercial 3T MR system (GE Healthcare MR 750W, Waukesha, WI). Multiple weightings were obtained and image quality and contrast features were compared to conventional sequences. Patient tolerance and experience with the silent sequences was assessed subjectively at the end of the scanning session.
Results
Gray-white differentiation, lesion to background contrast, and contrast enhancement features of the silent sequences demonstrated comparable conspicuity to conventional sequences. There was no statistical difference in the volume or intensity of enhancing tissue following intravenous contrast between the Silent T1 and conventional Bravo T1 sequences in those patients with enhancing lesions. Signal to noise was less with the silent sequences. All patients preferred the silent sequences to the conventional sequences.

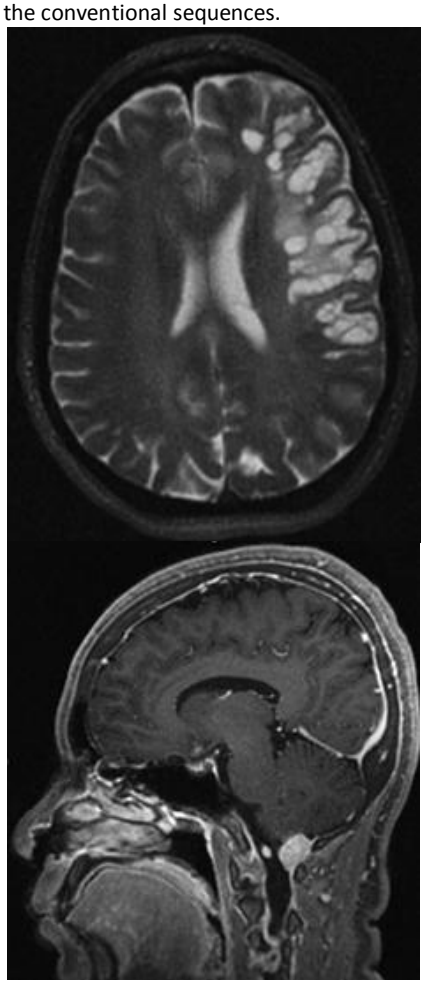

Note: Scanned images are included in the proceedings. Some submitted images were reduced during editing, thereby decreasing clarity. Also, refer to the Program Planner. Proceedings Content as of 3-29-2013.

Figures: Silent T2 with left frontal dilated perivascular spaces and Silent T1 postcontrast with foramen magnum meningioma.

Conclusion

Robust silent imaging can be performed with multiple weightings at 3T with comparable image contrast features to conventional 2D and 3D volumetric sequences. Reduction or elimination of noise improves patient acceptance, facilitates interaction with and monitoring of patients during scanning. These features may be helpful in reducing anxiety and improving acceptance of MR evaluation and warrant further investigation.

KEYWORDS: MR imaging, 3D imaging

eP-82

Feasibility of Utilizing Gadoxetate Disodium (Eovist) as a Cranial Contrast Agent: Preliminary Experience in Renally-Impaired Patients Requiring Brain Imaging

Pezeshk, P.·McKinney, A. M.·Rykken, J.
University of Minnesota
Minneapolis, MN.

Purpose

Nephrogenic systemic fibrosis (NSF) occurs in severely renally-impaired patients receiving intravenous gadolinium-based contrast agents (GBCA), particularly the Group 1 "nonionic linear" agents, but has not been reported in newly approved Group 3 agents, such as gadoxetate disodium (“Eovist”, Bayer Healthcare Pharmaceuticals, Wayne, NJ). Eovist has been claimed to be effective at lower, approved doses of GBCA (0.025 mmol/kg, ¼ of recommended standard dose) per the manufacturer, while other factors could mitigate the development of NSF in at-risk patients receiving Eovist such as: 1) "class" (it is ionic), 2) stability: (it has the highest thermodynamic and conditional stability in an FDA-approved GBCA, although macrocyclic agents have higher “kinetic” stability), and 3) it is the only FDA-approved GBCA with 50-50% renal-biliary/hepatic excretion. As Eovist has traditionally been utilized only for body imaging, our purpose was to evaluate the feasibility of visualizing enhancement of cranial structures utilizing Eovist in patients in whom using GBCA was medically necessary.

Materials & Methods

Over a 2-year period, intravenous Eovist was administered in 11 patients for a 10 cc dose postcontrast MRI (two with normal GFR due to sensitivity to other agents, and nine with renal impairment, performed out of medical necessity), imaged by 1.5T axial and coronal 5 mm-thick postcontrast gradient-echo T1WI (five minute delay). The images were reviewed separately by three staff neuroradiologists, scoring the presence/absence of enhancement of 11 structures [+, -, or +/- (indeterminate)]. Two patients underwent concomitant spine imaging.

Results

The mean patient age was 66.2 years, and the GFR range for the nine patients with renal impairment was 20-43 over the month leading up to the MRI. All three reviewers noted avid, definite enhancement in all 11 patients (100%) within the: cavernous sinuses, transverse sinuses, cavernous sinus, straight sinus, superior sagittal sinus, and nasal/ethmoidal mucosa; the sphenoparietal sinus (82-91%), internal cerebral veins (91-100%), pituitary infundibulum (64-91%), choroid plexi(64-82%), and middle cerebral arteries (65-73%) enhanced with lesser frequencies. Interobserver kappa was excellent, ranging from 0.613-0.732, p<0.0001. Only one of these 11 patients exhibited an enhancing cranial abnormality (meningioma). In two patients also undergoing spine imaging, the abnormalities (meningioma and metastasis) in both were well visualized, and the basivertebral plexi avidly enhanced.

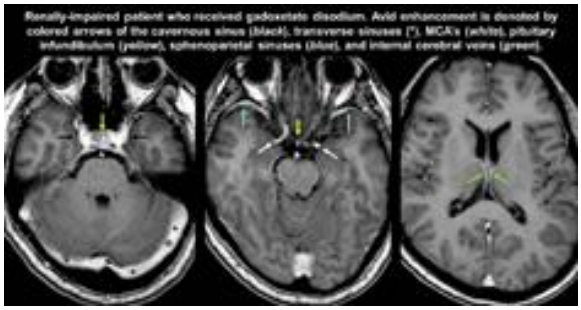

Conclusion

Eovist may be a feasible alternative contrast agent for brain MR imaging. However, future studies should compare to controls, assess efficacy in assessing enhancing cranial lesions, and should prospectively assess the safety of this agent in renally impaired patients.

KEYWORDS: Contrast enhancement, Gadoxetate Disodium

eP-83

Initial and Final Area under the Curves Ratio Derived from Dynamic Contrast-Enhanced T1-Weighted Perfusion MR Imaging in Pathologically Proven Recurrent Glioblastomas

Chung, W.[1]·Kim, H.[1]·Jahng, G.[2]·Kim, N.[1]·Kim, S.[1]·Kim, D.[1]
[1]University of Ulsan College of Medicine, Asan Medical Center, Seoul, KOREA, REPUBLIC OF, [2]Kyunghee University School of Medicine, Seoul, KOREA, REPUBLIC OF.

Purpose

To determine whether an initial and final area under the curves ratio (AUCR) derived from dynamic contrast-enhanced (DCE) perfusion MR imaging can be a imaging biomarker for distinguishing recurrent glioblastoma (RGM) from radiation necrosis (RN) and to compare diagnostic accuracy with commonly used model-free DCE parameters.

Materials & Methods

Note: Scanned images are included in the proceedings. Some submitted images were reduced during editing, thereby decreasing clarity. Also, refer to the Program Planner. Proceedings Content as of 3-29-2013.

Our institutional review board approved this retrospective study. Fifty-seven consecutive patients who had pathologically confirmed RGM or RN were assessed using conventional and DCE MR imaging. Bimodal histogram parameters of initial area under the curve at 30 sec (IAUC30), at 60 sec (IAUC60), and at 120 sec (IAUC120) and AUCR, which included mean value at higher curve ($mIAUC30_H$, $mIAUC60_H$, $mIAUC120_H$, and $mAUCR_H$) and 90th percentile cumulative histogram cutoffs ($_{90th}$IAUC30, $_{90th}$IAUC60, $_{90th}$IAUC120, and $_{90th}$AUCR), were calculated and were correlated with the final pathology. The best predictor for differentiating RGM from RN was determined by receiver operating characteristic (ROC) curve analyses.

Results

Fifty-seven study patients were classified as having either RGM (n = 32, 56.1%) or RN (n = 25, 43.9%). There were not significant differences between the two groups with respect to demographic data. There were statistically significant differences in all of the IAUC and AUCR parameters between the RGM and the RN patient groups ($P < .05$, each). Receiver operating characteristic curve analyses showed the $mAUCR_H$ to be the best single predictor of RGM, with a sensitivity of 95.2% and a specificity of 89.7%.

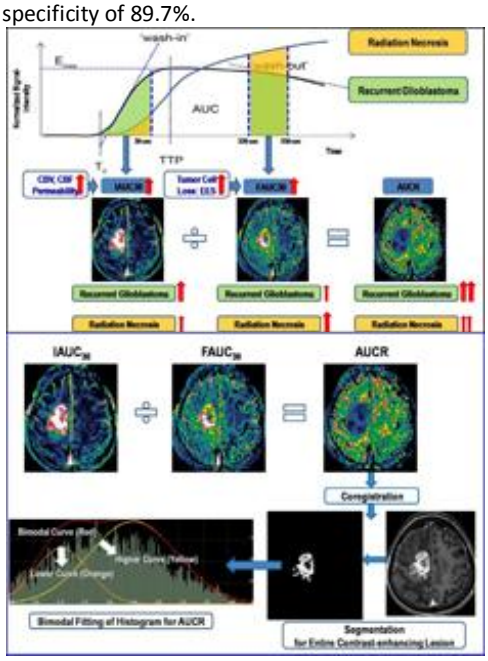

Conclusion

A bimodal histogram analysis of AUCR derived from DCE perfusion MR imaging can be a potential, noninvasive imaging biomarker for differentiating RGM form RN.

KEYWORDS: Dynamic contrast-enhanced MR, Glioblastoma

eP-84

RASER: a pulse sequence for whole-brain bolus tracking at high frame rates

Jonathan, S. V.[1]·Vakil, P.[1]·Jeong, Y. I.[1]·Menon,, R. G.[2]·Ansari, S. A.[1]·Hurley, M. C.[1]·Bendok, B. R.[1]·Carroll, T. J.[1]
[1]Northwestern University, Chicago, IL, [2]Feinberg School of Medicine, Chicago, IL.

Purpose

Current DSC MRI bolus tracking implementations use a temporal resolution of no more than two sec to adequately characterize a contrast agent bolus, with tradeoffs in SNR, spatial resolution, and volume coverage. We introduce 3D RAZIR, a pulse sequence that obtains 76-slice whole-brain perfusion measurements at 1.7 mm^3 isotropic voxel resolution despite using a temporal resolution of 10.3 sec for bolus tracking.

Materials & Methods

Sequence design: 3D RAZIR uses in-plane radial sampling and through-plane 3D GRE EPI Cartesian sampling to produce a cylindrical *k*-space(Figure 1). Consecutive volumes are acquired in 10.3 sec for bolus tracking. Dynamic bolus information is recovered at 160 msec per frame prior to perfusion analysis using sliding window reconstruction. *Subjects*: One patient with angiographically-confirmed Moyamoya disease was recruited with IRB approval. *Image acquisition*: In vivo bolus tracking was performed using 3D RAZIR and a typical 2D GRE EPI pulse sequence(voxel size 1.7 × 1.7 × 5.0 mm^3) as a reference standard with a 3.0 T MR scanner (Tim Trio, Siemens AG, Erlangen, Germany). 3D RAZIR scan parameters: second injection, TE/TR = 36/81 ms, flip angle = 45°, slices = 76, voxel size = 1.7 × 1.7 × 1.7 mm^3, repetitions = 12. Images were acquired with a single-dose injection of 0.1 mmol/kg Gd DTPA at 4 mL/sec. *Data analysis*: Sliding window reconstruction was used to increase the reconstructed frame rate of 3D RAZIR from 10.3 sec to 0.16 sec per measurement using a sliding window factor of 64 before perfusion analysis. Both acquisitions were processed using a stand-alone program in Matlab to produce parametric maps of relative cerebral blood flow(rCBF), relative cerebral blood volume(rCBV), and mean transit time (MTT).

Results

Figure 2 compares coronal, sagittal, and axial perfusion maps in 3D RAZIR(top) and the 2D GRE EPI reference (bottom). Increased coverage in 3D RAZIR allows for fine resolution of the perfusion metrics in the through-plane direction while the reference is blurred. Using an ROI analysis, we obtained gray/white matter CBF ratios of 2.38 in the reference and 2.18 in 3D RAZIR, in close agreement with literature values.

Note: Scanned images are included in the proceedings. Some submitted images were reduced during editing, thereby decreasing clarity. Also, refer to the Program Planner. Proceedings Content as of 3-29-2013.

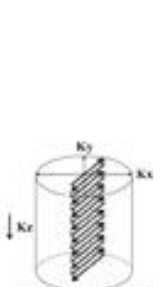

FIGURE 1. In-plane radial and through-plane Cartesian sampling is used to produce a cylindrical 3D *k*-space. Each TR acquires a single radial view in-plane during which all *k*$_z$ partitions are sampled using a 3D GRE-EPI readout.

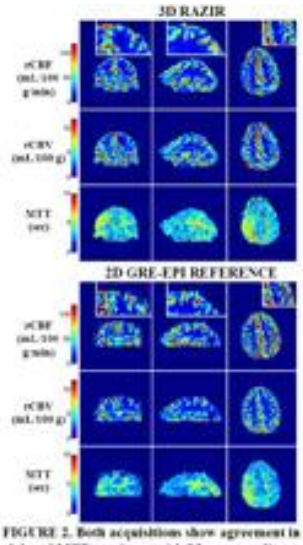

FIGURE 2. Both acquisitions show agreement in contrast and delayed MTT consistent with Moyamoya disease. 3D RAZIR more clearly illustrates the pathology with isotropic voxels.

Conclusion
3D RAZIR is able to obtain whole-brain perfusion measurements with good reference standard agreement. Sliding window reconstruction permits the use of an extended temporal acquisition window without sacrificing SNR for bolus tracking. To our knowledge, no other perfusion technique is able to obtain a spatial resolution higher than our technique without the use of parallel imaging.

KEYWORDS: DSC MR imaging, Brain perfusion

eP-85

Digital Subtraction CT Angiography of the Brain: Evaluation of Postcontrast Venous Phase Mask versus Precontrast Mask

Mends, F.·Davis, A.
New York University-Langone Medical Center
New York, NY.

Purpose
Digital subtraction CT angiography (DS CTA) is improved by using a precontrast low-dose CT mask to subtract bone from the images during postprocessing. Unfortunately, patient movement may occur during the delay between the precontrast mask and the completion of the CTA and can be further exacerbated by the administration of intravenous contrast. A previous study suggested that a postcontrast, venous-phase mask for cervical CTA may be utilized as an alternative, but did not compare directly with standard technique. We evaluated the feasibility of using a postcontrast, venous-phase, low-dose mask for cerebral DS CTA. This simplified technique may reduce patient motion degradation and enhance image quality by improved bone subtraction. This approach has the added advantage of the postcontrast CT mask serving as a diagnostic CT venogram or postcontrast head CT if standard acquisition parameters are used.
Materials & Methods
Fifteen cerebral DS CTA studies performed with a low-dose, postcontrast, venous-phase mask and 15 studies performed with a standard low-dose, precontrast mask were acquired during the study period. Imaging was performed on a 64-slice CT scanner (GE-VCT, Milwaukee WI). Other than mask timing all acquisition parameters were identical. Postprocessing was performed with *syngo* Via NeuroDSA(Siemens Medical Solutions, Erlangen, Germany) utilizing factory default settings. Subtracted volume rendered technique and maximum intensity projection radial rotating images from each group were created with identical postprocessing parameters. The quality of bone subtraction and vessel appearance were graded using predetermined criteria by three independent blinded observers. The arterial and venous opacification (HU) was measured at the most dense supraclinoid ICA and the torcula respectively utilizing the source images for all studies. Radiation dose and mask delay time was determined. These parameters were compared with image quality to determine the optimal time delay for postcontrast mask acquisition.
Results
Analysis of observer data suggests equivalent bone subtraction utilizing either pre or postcontrast mask technique. Vascular image quality particularly for segments adjacent to bone is equivalent. Medium and small vessel detail is preserved. Mean total radiation dose is slightly higher for the venous mask group. Mask delay time ranged from 21-67 seconds, mean 44 seconds. Postcontrast mask inadvertent arterial subtraction occurred in only one case in which the mask was obtained at a 23-second delay and arterial opacification remained dense measuring 299 HU. All other postcontrast mask arterial and venous HU measurements were less than 200 HU at 24-second delay or greater. This is well below the default bone removal threshold of 300 HU.
Conclusion
Simplified postcontrast venous-phase mask for cerebral DS CTA provides bone subtraction and vascular conspicuity equivalent to standard technique using a precontrast mask. The slight difference in radiation dose could introduce bias although the effect is thought to be negligible. Optimal time for the postcontrast mask is highly variable secondary to individual hemodynamic differences. The one inadvertent arterial subtraction artifact observed here supports using an approximate 45-second delay. Use of a low-dose protocol maintains ALARA standards. A postcontrast mask can provide additional information via a diagnostic CT venogram or contrast-enhanced parenchymal study if desired.

KEYWORDS: CTA, Postprocessing, Bone subtraction

Note: Scanned images are included in the proceedings. Some submitted images were reduced during editing, thereby decreasing clarity. Also, refer to the Program Planner. Proceedings Content as of 3-29-2013.

eP-86

Can *Shape Analysis* Differentiate Proximal Internal Carotid Artery *Thrombus* from Atherosclerotic *Plaque* in Patients Evaluated with CT Angiography for Stroke or Transient Ischemic Attack?

Lum, C.·Thornhill, R.·Jaberi, A.·Stefanski, P.·Torres, C.·Petrcich, W.·Momoli, F.·Dowlatshahi, D.·Ottawa Stroke Research Group (OSRG)
University of Ottawa-Ottawa Hospital Research Institute
Ottawa, ON, CANADA.

Purpose
Patients presenting with transient ischemic attack or stroke imaged with CTA rarely demonstrate free-floating intraluminal thrombus (FFT). It is difficult to distinguish FFT from carotid plaque, but the distinction is critical as management differs. Visually, FFT has been described as appearing more elongated as opposed to plaque. However, there are false positives using only qualitative criteria. More advanced imaging analysis techniques such as shape analysis have been used for evaluation of hippocampi but have not been applied to CTA findings. There is sparse ultrasound literature evaluating shape analysis of carotid plaque morphology as an attempt to better stratify patients with stenosis. Ex vivo analysis of endarterecomy specimens has been performed to evaluate simple criteria such as ulcers and smoothness. Shape analysis has not been used to analyze vascular pathology identified on CTA. Thus, our goal was to apply shape analysis techniques to a population with vascular disease identified on CTA. Our study was to determine whether quantitative shape analysis can accurately differentiate FFT from atherosclerotic plaque.
Materials & Methods
Following Institutional Review Board approval, we collected 23 consecutive cases of suspected carotid FFT seen on CTA (13 men, 65 ± 10 years; 10 women, 65.5 ± 8.8 years). True positive FFT cases (FFT+) were defined as filling defects resolving with anticoagulant therapy versus false positives (FFT-), which remained unchanged and were categorized as plaque. "Virtual endarterectomy" was performed independently by two fellowship-trained neuroradiologists. By consensus, the 3D lesion volumes were extracted from CTA source images and shape descriptors were computed. The five most discriminative features were used to construct ROC curves and to generate three machine learning classifiers. Average classification accuracy was determined by cross-validation.
Results
Follow-up imaging confirmed 16 FFT+ and 7 FFT- cases. Five shape descriptors delineated FFT+ from FFT- cases (two for axial, one for coronal and two for sagittal planes). The logistic regression model produced from combining all five shape features demonstrated a sensitivity of 87.5%, specificity of 71.4%, with an AUC = 0.85 ± 0.09. Average accuracy for each classifier ranged from 65.2-76.4%.

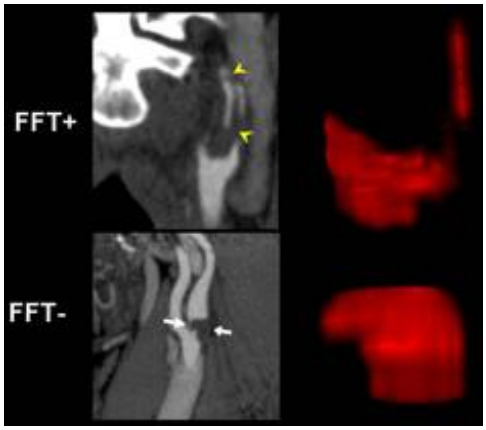

Conclusion
We identified five quantitative shape descriptors of carotid FFT. This 3D shape "signature" shows potential for supplementing conventional lesion characterization in cases of suspected FFT.

KEYWORDS: Carotid artery, Thrombus imaging

eP-87

Susceptibility-Weighted MR Imaging: A Better Technique in the Detection of Capillary Telangiectasia when Compared to T2*-Gradient Echo

De Bruin, D. E.·Chaudhry, U. S.·Policeni, B. A.
University of Iowa Hospitals and Clinics
Iowa City, IA.

Purpose
Enhancing lesions on brain MRI can present a diagnostic quandary as both benign lesions such as capillary telangiectasia (BCT) and pathologic lesions such as demyelination or metastatic disease may appear similar. Stagnation of blood in the low-flow venous channels of BCTs results in susceptibility effect secondary to the increase in local deoxyhemoglobin. Both T2*-gradient-echo imaging (GRE) and susceptibility-weighted imaging previously have been demonstrated as valuable in the diagnosis of BCT. Because susceptibility-weighted imaging (SWI) is more sensitive to susceptibility changes than GRE, we aim to demonstrate an increased diagnostic value of SWI compared to GRE in making the diagnosis of BCT.
Materials & Methods
We retrospectively reviewed the MR images of 17 patients with a presumed diagnosis of BCT who were examined from June 2010 to September 2012. All patients had undergone MR imaging at 1.5T with T1, T2, FLAIR, GRE, SWI, and gadolinium-enhanced T1 sequences. Lesions were evaluated for the presence or absence of signal abnormality on each particular sequence.
Results
All 17 CBTs demonstrated distinct signal-intensity loss on SWI compared to 7/17 (41%) showing signal-intensity loss on GRE. The increased frequency of detection using SWI versus GRE is statistically significant ($z = 2.85$, $p < 0.01$; $\chi^2 =$

Note: Scanned images are included in the proceedings. Some submitted images were reduced during editing, thereby decreasing clarity. Also, refer to the Program Planner. Proceedings Content as of 3-29-2013.

8.10, $p < 0.01$). Six of the lesions showed signal intensity changes on T1 and/or T2 while the remaining lesions were isointense to normal brain.

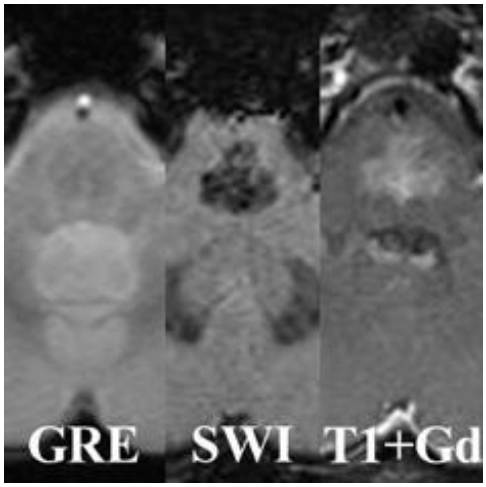

Conclusion

Capillary telangiectasias are more conspicuous on SWI than GRE and other precontrast MR imaging. In our review, there were no cases where GRE was positive and SWI was negative. Susceptibility-weighted imaging is a valuable tool in diagnosing these benign lesions which may otherwise be occult on noncontrast MR imaging, and should serve to increase diagnostic confidence.

KEYWORDS: Susceptibility-weighted imaging, Capillary malformation

eP-88

Evaluation of Enhancing Multiple Sclerosis Brain Lesions with 3D T2 FLAIR and T1 Sequences

Stanton, C. L.[1]·Shapiro, M.[1,2,3]
[1]University of Miami, Miami, FL, [2]University of Central Florida, Orlando, FL, [3]Neuroimaging Winter Park, Winter Park, FL.

Purpose

To compare the relative utility of postcontrast 3D T2 FLAIR with 2D T1 spin echo (SE) or 3D T1 turbo spin echo (TSE) for the evaluation of enhancing lesions in patients with multiple sclerosis (MS).

Materials & Methods

One hundred patients were prospectively recruited based upon sequential presentation to undergo MRI for known or suspected MS at the outpatient imaging center Neuroimaging Winter Park (from December 2011 to December 2012). Scanning was performed on a Siemen's Verio 32-channel 3T machine. All 100 patients underwent standard MS protocol which included administration of intravenous contrast (0.05 mmol/kg gadopentetate dimeglumine) with subsequent acqusition of 3D T2 FLAIR followed by either 2D T1 SE or 3D T1 TSE sequences. Independent readers included an experienced CAQ neuroradiologist and a PGY4 radiology resident. Out of 100, a total of 14 patients (aged 16 to 53 years, one male) demonstrated a combined 34 enhancing lesions deemed to represent active MS plaques. These were categorized with respect to size, location, and relative conspicuity on a previously established four-point scale - with "0" being not visible, "1" being barely visible, "2" being clearly visible and "3" being strikingly visible. Differences in lesion conspicuity were compared using Wilcoxon ranked sum test and interobserver variability was compared using kappa statistics.

Results

p-value testing overall difference between FLAIR and T1 for reader 1: .0953. p-value testing overall difference between FLAIR and T1 for reader 2: .0708. *p-values were computed using a paired Wilcoxon ranked sum test. *Interobserver Variability* - k score for lesion conspicuity was .62 for the T1 sequence (good reproducibility) and .62 (good reproducibility) for the FLAIR sequence.

Lesion Conspicuity	# of Lesions	T1 *Mean Conspicuity (SD)*	3D T2 FLAIR *Mean Conspicuity (SD))*	p-value
Lesion size				
<5mm	26	1.96 (.58)	2.13 (.66)	NS
5-20mm	7	2.36 (.48)	2.56 (.45)	NS
Lesion location				
Cortical/Subcortical	5	2.20 (.57)	2.50 (.45)	NS
Periventricular WM	13	2.08 (.45)	2.30 (.48)	.09
Callosal/Pericallosal	4	1.88 (.63)	1.88 (.63)	NS
Deep WM	6	2.00 (.84)	2.08 (1.11)	NS
Posterior Fossa	5	2.00 (.71)	2.40 (.55)	NS

Conclusion

While comparison of enhancing MS lesions in overall conspicuity as well as in subgroup analysis did not meet statistical significance between the sequences this was likely due to a limited sample size. Despite this, we experienced instances where 3D T2 FLAIR was relatively more sensitive for detection particularly of subtle

Note: Scanned images are included in the proceedings. Some submitted images were reduced during editing, thereby decreasing clarity. Also, refer to the Program Planner. Proceedings Content as of 3-29-2013.

subcortical lesions, a finding which has been suggested previously. As with noncontrast 3D T2 FLAIR, postcontrast 3D T2 FLAIR is certainly valuable for MS lesion localization. While T2 prolongation is the predominant mechanism for T2 FLAIR signal hyperintensity, T1 shortening from gadolinium also contributes. The frequent presence of T2 prolongation in both active and inactive MS lesions emphasizes that pre and postcontrast T1 sequences remain essential for confirming enhancement. As suggested by its utility in assessing other pathologies, we feel that acquisition of a postcontrast T2 FLAIR should be considered as a replacement to precontrast T2 FLAIR in standard MS protocols and our good interobserver reproducibility suggests a useful model to potentially assess this in larger studies.

KEYWORDS: 3 T, Multiple sclerosis plaques

eP-89

Normal Pattern of Intracranial Enhancement on Postcontrast FLAIR MR Imaging

Morales, H.·Radhakrishnan, R.·Vagal, A.·Qi, Z.
University of Cincinnati
Cincinnati, OH.

Purpose
Postcontrast FLAIR (CE FLAIR) has shown to be a valuable imaging modality in the assessment of lepto-meningeal disease. There is also increased interest in its use for acute stroke and tumors. Despite this, there is limited literature evaluating the normal pattern of enhancement on CE FLAIR in the adult brain. Our aim is to describe the normally enhancing structures on CE FLAIR, thus giving a reference point to avoid diagnostic pitfalls.
Materials & Methods
After institutional IRB approval, 44 patients (mean age: 48.3 ± 15 years) who had pre and postcontrast FLAIR images were selected between April and May 2012. All these patients had a normal MRI brain study. Two neuroradiologists and one radiologist-in-training evaluated the structures that showed enhancement on CEFLAIR and contrast T1-WI (CE T1). Areas that showed enhancement on CE FLAIR and no enhancement on CE T1 also were evaluated.
Results
Enhancement in the choroid plexus and the pituitary infundibulum was seen on CE FLAIR in all cases. Enhancement in the cavernous sinus (75%; 33/44) and pineal gland (75%; 33/44) was seen in the majority of cases. The pituitary gland (40.9%; 18/44) and nasal mucosa/turbinates (31.8%; 14/44) showed enhancement in some cases. Rarely, enhancement in the jugular bulbs (9%; 4/44), cortical veins (4.5%; 2/44) and dural sinuses (2.3%; 1/44) also was seen. In some cases, carotid arteries at the skull base (65.9%; 29/44) and the arteries of the circle of Willis (15.9%; 7/44) showed enhancement on CE T1, but none of these regions enhanced on CE FLAIR. Subtle ocular enhancement (choroid) was seen in most cases on CE T1 (79.5%; 35/44), no cases were found on CE FLAIR. Four cases of cystic pineal gland showed enhancement only on CE FLAIR.

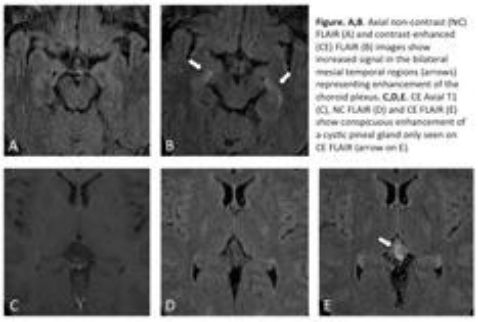

Conclusion
Radiologists should be aware of the normal T1-shortening effect (positive enhancement) of gadolinium on CE FLAIR in the described structures. These findings can be used as a reference to avoid misinterpretations. For instance, increased signal in the mesial temporal region on CE FLAIR should not be confused for abnormal signal as this most likely represents choroid plexus enhancement; on the other hand, enhancement of the cortical veins, dural sinuses or the globes should prompt a search for pathology. Minimal leakage of gadolinium appears responsible for the enhancement only seen on CE FLAIR in some cystic pineal glands.

KEYWORDS: FLAIR, Contrast enhancement

eP-90

Safety and Efficacy of Gadoterate Meglumine in MR Imaging in Adult and Pediatric Patients with Central Nervous System Lesions

Maravilla, K.·SENTIO Investigators Group
University of Washington
Seattle, WA.

Purpose
To demonstrate superiority of gadoterate meglumine-enhanced MRI over unenhanced images for visualization of brain and spinal lesions (including tumor, vascular, inflammatory or infectious diseases) in adults and children.
Materials & Methods
Multicenter, randomized, double-blind, fixed-sequence [unenhanced T1 and T2 MRI followed by either gadoterate meglumine (Dotarem, 0.1 mmol/kg) or gadopentetate dimeglumine (Magnevist, 0.1 mmol/kg) T1-enhanced MRI], active comparator study (SENTIO study). Pediatric patients (aged ≥ two years) were assigned to the gadoterate meglumine group only. MR images of all patients were read by three off-site blinded independent readers. All patients also were evaluated by one on-site radiologist. The primary endpoint was lesion visualization with gadoterate meglumine-enhanced MRI comparing unenhanced images in up to five of the largest lesions

Note: Scanned images are included in the proceedings. Some submitted images were reduced during editing, thereby decreasing clarity. Also, refer to the Program Planner. Proceedings Content as of 3-29-2013.

utilizing three co-primary endpoints: border delineation, internal morphology and degree of contrast enhancement. For each of the three endpoints, a score was computed by summing all lesion scores for a given patient. Each co-primary endpoint then was analyzed using a multiple regression model. Main secondary criteria were evaluated on-site for: lesion visualization, level of diagnostic confidence, image quality, signal intensity, number of lesions, comparison of gadoterate meglumine and gadopentetate dimeglumine for efficacy and clinical safety [including adverse events (AEs), injection site tolerance, changes in vital signs, electrocardiogram recordings and laboratory measures].

Results

A total of 402 patients were evaluable: 364 adults (245 gadoterate meglumine, 119 gadopentetate dimeglumine) and 38 children. The primary endpoint (lesion visualization postgadoterate meglumine enhanced MRI) as well as all three co-primary endpoints were significantly superior ($p<0.001$) for all independent readers when comparing enhanced images to unenhanced images (Table 1). This superiority of gadoterate meglumine enhanced imaging also was confirmed in analyses of all secondary endpoints by on-site evaluators. No statistically significant differences between gadoterate meglumine and gadopentetate dimeglumine were observed for all three co-primary variables for the three independent readers. Analysis of the pediatric group for all three independent readers showed mean scores for each of the three co-primary endpoints were higher for “enhanced” compared to “unenhanced” images. Both contrast agents were well tolerated. Related AEs were reported in 3.8% adult gadoterate meglumine and in 7.7% gadopentetate dimeglumine patients. The most common AEs were injection site pain, headache and nausea. No related serious AEs occurred.

Table 1: Lesion visualization scores with gadoterate meglumine (enhanced vs unenhanced images) in adults

	Gadoterate meglumine					
Readers	**Reader 1**		**Reader 2**		**Reader 3**	
Modality	**Unenhanced**	**Enhanced**	**Unenhanced**	**Enhanced**	**Unenhanced**	**Enhanced**
N (Patients)	**224**	**230**	**224**	**230**	**222**	**235**
Border Delineation Score						
Mean (SD)	1.06 (1.23)	3.30 (2.64)	1.62 (1.43)	4.49 (2.94)	1.43 (1.29)	2.54 (2.30)
Estimate*	1.09	3.35	1.65	4.57	1.43	2.58
Variation Paired-Pre*		2.26		2.92		1.15
Prob>T*	<0.001		<0.001		<0.001	
Internal Morphology Score						
Mean (SD)	0.97 (1.05)	3.70 (2.63)	1.76 (1.24)	4.49 (2.93)	1.45 (1.13)	2.93 (2.30)
Estimate*	0.97	3.72	1.8	4.57	1.42	2.96
Variation Paired-Pre*		2.75		2.77		1.54
Prob>T*	<0.001		<0.001		<0.001	
Contrast Enhancement Score						
Mean (SD)	0.01 (0.20)	3.11 (2.52)	0.01 (0.15)	3.73 (2.67)	0.01 (0.13)	2.95 (2.44)
Estimate*	0.05	3.18	0.05	3.81	0.02	3.01
Variation Paired-Pre*		3.13		3.76		2.99
Prob>T*	<0.001		<0.001		<0.001	

* Regression Model

Conclusion

Gadoterate meglumine significantly improved lesion visualization over unenhanced MRI alone for CNS lesions. A good general safety profile of gadoterate meglumine also was confirmed in adults and in children.

KEYWORDS: Contrast-enhanced MR imaging, MR imaging brain, Gadolinium

eP-91

Quantative Volumetric Followup of Patients with Acoustic Neurinomas

Shreiber, R.·Shreter, R.·Goldsher, D.
Rambam Medical Center
Haifa, ISRAEL.

Purpose

Serial MR studies of patients with acoustic neurinoma (AN) is vital in followup and evaluation of the efficacy of surgical or radiation treatment. The current method to evaluate the tumor size, based on linear measurements - this technique is evaluator-dependent, and requires repeating of the measurements by the same observer for best assessment of tumor progression. To enhance accuracy and objectivity of tumor measurements, we use software-generated volumetric measurements in follow-up studies of patients with AN.

Materials & Methods

All patients that were treated in our hospital for AN and had at least two follow-up MR studies in the last three years were included in the study. Semi-automated registration, segmentation and volumetric measurements at all points in time were performed using a new lesion managment package in the PACS system (Carestream Health, Rochester, NY). Correction of the automatic

Note: Scanned images are included in the proceedings. Some submitted images were reduced during editing, thereby decreasing clarity. Also, refer to the Program Planner. Proceedings Content as of 3-29-2013.

segmentation was done using a live-wire software available on the same package. Each patient was reviewed by two experienced neuroradiologists, who performed postprocessing and lesion measurements. We compared the results obtained from the two independent measurements. Time-for-volume measurements, including refinement of the measurements, were recorded. T1-weighted axial or coronal sequences with gadolinium, were used.

Results

Nineteen patients (11 females and eight males) who were treated and followed up in our hospital were reviewed retrospectively. Age range was 27-76 years (mean = 55.7 years) at the time of the last follow-up study. Two to nine studies per patient (mean 3.9) were examined. The research included a total of 78 studies. The software segmented the lesions successfully in all 78 exams. Average volume of the AN was 2.074 mm^3 (range 0.43 to 19.51 mm^3), average largest linear dimension of the lesions was 24.24 mm (range 10.1 to 40.9). Postprocessing time was completed in less than one minute per lesion including corrections of the automatic segmentation. The difference of the volumetric measurements between the observers in all studies was less than 14% which corresponds to a linear accuracy of 4.4%. As lesions size was larger the difference in size between the observers was smaller.

Conclusion

Volumetric semi-automatic measurements of AC lesions allow accurate assessment for the followup of these patients. The possibility of registration between the exams further improves the confidence of the user in assessing tumor progression. Larger tumors that usually are more difficult for comparisons had better agreement between the observers.

KEYWORDS: Acoustic schwannoma, Postprocessing, Lesions followup

eP-92

Assessment of Iterative Reconstruction Levels on Pathology Detection in Reduced Dose CT Brain

Neelakantan, A.[1]·Iqbal, A.[1]·Aitken, S.[1]·Andrew, R.[2]·Forbes, K. P.[1]

[1]Institute of Neurological Sciences Glasgow, Glasgow, UNITED KINGDOM, [2]Philips Centre, Guildford Business Park Guildford, Surrey, UNITED KINGDOM.

Purpose

Acceptance of the ALARA (As-Low-As-Reasonably-Achievable) principle necessitates that imaging is performed with the lowest possible radiation dose. Recent studies have demonstrated the value of iterative reconstruction (IR) technology in reducing radiation dose in CT of the brain whilst maintaining image quality in normal subjects; however to the best of our knowledge no other studies have examined pathologic areas. We set out to determine the diagnostic impact of varying levels of IR on reduced dose CT brain in subjects with intracranial pathology.

Materials & Methods

Thirty subjects (mean age 59.2 years, SD20.69; 16M; 14F) with intracranial pathology [cerebral infarct: acute (n = 8), chronic (n = 5), intracranial hemorrhage (n = 5), subarachnoid hemorrhage (n = 3), abscess (n = 2), Chiari (n = 1) and tumors (n = 6)] were identified from consecutive patients who had undergone CT brain with reduced dose (Philips, Brilliance 64 scanner, 64 slice, 200 mAs, 120 kVp, 1 mm slice thickness, 25 noncontrast, five contrast examinations). Data were reconstructed using a variety of iDose (Philips) IR and filtered back projection (FBP) blends (iDose 0-5, varying from 100% FBP to 60% IR). Datasets were blinded analyzed qualitatively by two neuroradiologists, who declared their preferred image dataset for pathology detection (Philips Advantage workstation; axial 4 mm slices, window width of 70HU and center of 35 HU). Interobserver variability was measured by using linear-weighted kappa statistic. Quantitative assessment of image noise (SD) and contrast-to-noise ratio (CNR) of pathology to background were measured and correlated to iDose level.

Results

Qualitative assessment yielded a mean preference of iDose level 2.8 +/- 0.85 for pathology detection (iDose 2: 30% IR, 70% FBP; iDose 3: 40% IR, 60% FBP) (observer 1: mean 3.1+/-1.0; observer 2: mean 2.6 +/-1.1; kappa: 0.11). No lesion/diagnosis was missed on any of the reconstructions. Quantitative assessment demonstrated reducing noise ($r2 = 0.98$;$P<0.05$) and increasing CNR of pathology to background, with increasing iDose level ($r2 = 0.97$;$P<0.05$).

Conclusion

Iterative reconstruction is a valuable technique for routine brain CT imaging, allowing detection of pathology at reduced dose. Data confirms reduced noise and improved CNR of pathology with increasing levels of IR blends. However, subjective assessment suggests that this may not be the only important factor in radiologic interpretation, with radiologist preference for moderate levels of IR, although variable between individuals. This may reflect the smoother, more uniform appearances of higher IR levels.

KEYWORDS: Dose reduction

Note: Scanned images are included in the proceedings. Some submitted images were reduced during editing, thereby decreasing clarity. Also, refer to the Program Planner. Proceedings Content as of 3-29-2013.

eP-93

Relationship between Brain-Derived Neurotrophic Factor Gene Polymorphism and Brain Volume in Major Depressive Disorder: Voxel-Based Morphology Analysis of Brain MR Imaging

Ide, S.[1]·Kakeda, S.[1]·Watanabe, K.[1]·Yoshimura, R.[1]·Abe, O.[2]·Nakamura, J.[1]·Korogi, Y.[1]
[1]University of Occupational and Environmental Health, Kitakyushu, JAPAN, [2]Nihon University School of Medicine, Tokyo, JAPAN.

Purpose
A brain-derived neurotrophic factor (BDNF) potentiates release of dopamine, response to emotionally salient environmental stimuli. The polymorphism of the BDNF gene Val66Met confers genetic susceptibility to a range of major depressive disorder (MDD), and has been found to impact brain morphology. The presence of a Met66 substitution leads to decreased secretion of BDNF at the synapse, and it follows that Met66 allele carriers (either Met-carriers) should have smaller brain volumes than Val/Val homozygotes (Val/Val-carriers). To our knowledge, however, no report has demonstrated that there is a significant volumetric difference in the gray matter between the Val/Val-carriers and either Met-carriers in MDD patients. We investigated the relationship between the brain volume and polymorphism of the BDNF gene in MDD using a voxel-based morphometry (VBM) analysis of brain MRI data.
Materials & Methods
Thirty patients with MDD (17 males, 13 females; mean age 44.9 ± 13.0 years; age range 22-67 years) and age- and sex-matched 30 healthy subjects (17 males, 13 females; mean age 43.7 ± 12.6 years; age range 20-65 years) were divided into the following four groups according to the BDNF gene polymorphism; MDD patients with either Met-carriers (n = 25), MDD patients with Val/Val-carriers (n = 5), healthy subjects with either Met-carriers (n = 20), and healthy subjects with Val/Val-carriers (n = 10). The MR imaging data were obtained with all cases using 3D SPGR (a three-dimensional fast spoiled gradient recalled acquisition with steady state) at 3T MRI. Image processing for VBM was conducted using SPM8 (Statistical Parametric Mapping 8). The DARTEL (Diffeomorphic Anatomical Registration Through Exponential Lie Algebra) toolbox was used in a high-dimensional normalization protocol. The VBM was used to analyze the significance for between-group differences of MRI data.
Results
The comparison between MDD patients and healthy subjects demonstrated the significant genotype-diagnosis interaction on GM volume in the left middle frontal gyrus (composition of prefrontal cortex). Furthermore, in MDD patients, the volume of the left middle frontal gyrus also was significantly smaller for the Met-carriers than for the Val/Val-carriers (P<.05) (Figure).

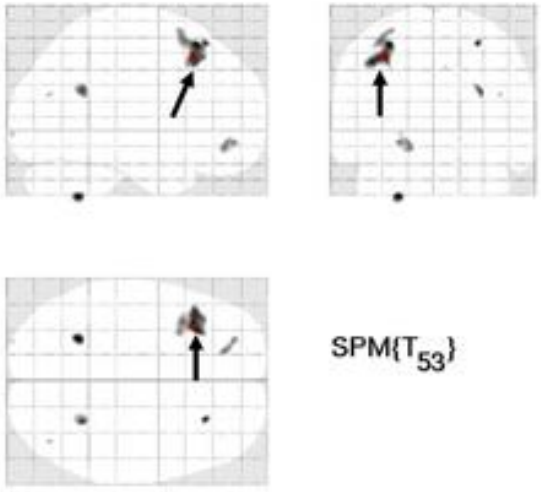

Figure: The region (arrows) shows a significant GM volume decrease in the MDD patients with Met-carriers in comparison to those with Val/Val-carriers (p<0.05).
Conclusion
The polymorphism of BDNF gene was associated with atrophy of the prefrontal cortex in MDD patients, which may relate to manifestation of MDD.

KEYWORDS: Brain volume, Volumetric analysis

eP-94

Comparison of Cerebral Blood Flow on Perfusion MR Imaging by Using Arterial Spin Labeling and Dynamic Susceptibility Contrast in Brain Tumors

Tsuchiya, K.·Ohara, A.·Gomyo, M.·Tateishi, H.·Nitatori, T.
Kyorin University
Tokyo, JAPAN.

Purpose
Arterial spin labeling (ASL) is a technique that can visualize cerebral blood flow (CBF) by electromagnetically labeling arterial flow. To assess the feasibility of ASL perfusion in the diagnosis of brain tumors, we compared CBF by using ASL and that by using dynamic susceptibility contrast (DSC) imaging that has been an established technique.
Materials & Methods
We visually compared perfusion maps by the two methods in 17 cases (seven men and 10 women; age range, 21-76 years; mean, 54.2 years) of preoperative brain tumor. Their lesions included glioblastoma (six cases), metastasis (two cases), meningioma (two cases), primary central nervous system lymphoma (PCNSL, two cases), and others [anaplastic oligoastrocytoma (AOA), two cases; diffuse astrocytoma, oligodendroglioma, and choroid plexus papilloma, one case each]. Perfusion imaging by both ASL and DSC was performed on the same session using a 3T system. Arterial spin labeling was performed using a pulsed ASL sequence with scanning parameters as follows:

Note: Scanned images are included in the proceedings. Some submitted images were reduced during editing, thereby decreasing clarity. Also, refer to the Program Planner. Proceedings Content as of 3-29-2013.

TR/TE/TI (labeling delay time)/FA, 6.0 ms/2.1 ms/220 ms/15 deg; FOV, 256 × 256 mm; imaging matrix, 64 × 64; section thickness, 6 mm; number of sections, 15; NEX, 4; acceleration factor, 2.0; and acquisition time, 3 min 24 sec. Dynamic susceptibility contrast perfusion MR imaging scans were acquired with a single-shot field-echo echo-planar imaging sequence (TR/TE/FA, 2000 ms/25 ms/90 deg; FOV, 240 × 240 mm; matrix, 128 × 96; section thickness, 5 mm; number of sections, 17; number of scans, 30; acquisition time, 1 min) in combination with a bolus injection of Gd-based contrast agent.

Results

In 11 of the 17 cases (average age, 56.9 years), CBF by the two methods were equivalent. In four cases (two cases of metastasis and each one case of glioblastoma and oligodendroglioma; average age, 52.5 years), CBF by ASL was less than that by DSC, while the former apparently was greater in two cases (each one case of PCNSL and AOA; average age, 53 years). No statistical difference in the age was found among the three groups.

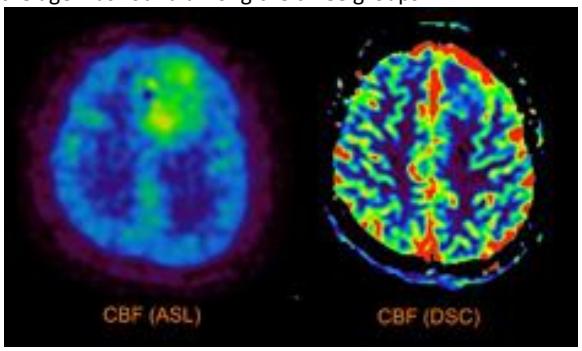

Conclusion

Discrepancy often is found between CBF by ASL and that by DSC. This may be caused by difference in tumor hemodynamic characteristics and also be related to the labeling delay time in ASL.

KEYWORDS: Brain neoplasms, MR perfusion-weighted imaging

eP-95

Comparative Effectiveness of Unruptured Cerebral Aneurysm Therapies: Propensity Score Analysis of Clipping versus Coiling

McDonald, J. S.·McDonald, R. J.·Kallmes, D. F.·Lanzino, G.·Cloft, H. J.
Mayo Clinic
Rochester, MN.

Purpose

Endovascular therapy has increasingly become the most common treatment for unruptured cerebral aneurysms in the United States. We evaluated a national, multi-hospital database to examine recent utilization trends and compare peri-procedural outcomes between clipping and coiling treatments of unruptured aneurysms.

Materials & Methods

The Premier Perspective database was used to identify patients hospitalized between 2006-2011 for unruptured cerebral aneurysm who underwent clipping or coiling therapy. A logistic propensity score was generated for each patient using relevant patient, procedure, and hospital variables, representing the probability of receiving clipping. Covariate balance was assessed using conditional logistic regression. Following propensity score adjustment using 1:1 matching methods, the risk of in-hospital mortality and morbidity was compared between clipping and coiling cohorts.

Results

A total of 4899 unruptured aneurysm patients (1388 clipping, 3551 coiling) treated at 120 hospitals were identified. Following propensity score adjustment, clipping patients had a similar likelihood of in-hospital mortality [OR = 1.43 (95% CI 0.49-4.44), p =.47] but a significantly higher likelihood of unfavorable outcomes including discharge to long-term care [OR = 4.78 (95% CI 3.51-6.58), p<.0001], ischemic complications [OR = 3.42 (95% CI 2.39-4.99), p<.0001], hemorrhagic complications [OR = 2.16 (95% CI 1.33-3.57), p<.0001], postoperative neurologic complications [OR = 3.39 (95% CI 2.25-5.22), p<.0001], and ventriculostomy [OR = 2.10 (95% CI 1.01-4.61), p = .0320] compared to coiling patients.

Conclusion

Among patients treated for unruptured intracranial aneurysms in a large sample of hospitals in the United States, clipping was associated with similar mortality risk but significantly higher peri-procedural morbidity risk compared to coiling.

KEYWORDS: Aneurysm embolization, Aneurysm treatment, Propensity Score Adjustment

eP-96

Comparative Effectiveness of Ruptured Cerebral Aneurysm Therapies: Propensity Score Analysis of Clipping versus Coiling

McDonald, R. J.·McDonald, J. S.·Kallmes, D. F.·Lanzino, G.·Cloft, H. J.
Mayo Clinic
Rochester, MN.

Purpose

The relative merits of treating ruptured aneurysms with clipping versus coiling continue to be a topic of debate. We evaluated a national, multihospital patient database to examine recent trends in ruptured aneurysm therapies and to compare peri-procedural outcomes between clipping and coiling treatments.

Materials & Methods

The Premier Perspective database was used to identify patients hospitalized between 2006 and 2011 for ruptured aneurysm who underwent clipping or coiling therapy. A

Note: Scanned images are included in the proceedings. Some submitted images were reduced during editing, thereby decreasing clarity. Also, refer to the Program Planner. Proceedings Content as of 3-29-2013.

propensity score model, representing the probability of receiving clipping, was generated for each patient using relevant patient and hospital variables. Covariate balance was assessed using conditional logistic regression. Following greedy-type matching of the propensity score, the risk of in-hospital mortality and morbidity was compared between clipping and coiling cohorts.
Results
A total of 5229 ruptured aneurysm patients (1228 clipping, 4001 coiling) treated at 125 hospitals were identified. Clipping therapy frequency decreased from 27% in 2006 to 21% in 2011. Following propensity score adjustment, in-hospital mortality risk was similar between groups [OR = 0.94 (95% CI 0.73-1.21) p = .62]. However, unfavorable outcomes were more common in following clipping compared to coiling, including discharge to long-term care [OR = 1.32 (95% CI 1.12-1.56) p = .0006], ischemic complications [OR = 1.51 (95% CI 1.24-1.83); p = .0009], neurologic complications [OR = 1.64 (95% CI 1.18-2.27); p = .0018], and other surgical complications [OR = 1.55 (95% CI 1.05-2.33); p = .0240].
Conclusion
This study of a database of multiple hospitals in the United States demonstrates that clipping of ruptured cerebral aneurysms resulted in greater adjusted morbidity compared to coiling.

KEYWORDS: Aneurysmal subarachnoid hemorrhage, Aneurysm embolization, Aneurysm clipping

eP-97

An "EKG for the Brain": Electrical Impedance Spectroscopy for Brain Injury

Kamalian, S.·Rosenthal, E. S.·Bonmassar, G.·Borgie, R. C.·Schwamm, L. H.·Lev, M. H.
Massachusetts General Hospital
Boston, MA.

Purpose
Electrical impedance spectroscopy (EIS) is novel, portable, easy-to-implement device that aims to provide rapid, affordable point-of-care detection, assessment, and monitoring of acute brain injury. An adaptation of "passive" electroencephalography (EEG), EIS relies on noninvasive measurement and modeling of the conduction of minute electrical currents applied transcranially across a spectrum of frequencies. Our purpose was to test the feasibility of EIS to distinguish the impedance differences between normal subjects and brain injury attributable to acute/subacute intracranial hemorrhage or subacute ischemic stroke.
Materials & Methods
We performed a prospective, observational, proof-of-principle study of 15 patients admitted to our Neurosciences Intensive Care Unit for ischemic stroke or intracranial hemorrhage compared to four healthy volunteers. Subjects underwent five minutes of EIS recordings. Electrical impedance spectroscopy device delivers small white-noise current through a pair of stimulation electrodes. Voltage is recorded across three bilaterally symmetric pairs according to 10-20 standard EEG system. The transfer function between the white-noise current input and the recorded voltages was estimated for each recording electrode. Log-log plot of the estimated impedance difference of bipolar ipsilateral neighbor electrodes plotted across the 100Hz to100kHz frequency, which is normalized at 100Hz (Figure 1). The impedance variances, among referenced channels, were recorded at 10 and 40 kHz.
Results
Comparing patients with healthy controls (Figure 1): intrasubject variance among all channels (bipolar to ipsilateral neighboring electrodes) for impedance at 10 kHz, were significantly different (p = 0.02) and area under the curve of ROC analysis was 85% with 80% sensitivity, 100% specificity at 10 kHz (p = 0.0002). Intrasubject variance among all channels for impedance at 40 kHz also were significantly different (p = 0.03) and area under the curve was 87% with 80% sensitivity, 100% specificity at 40 kHz (p<0.0001).

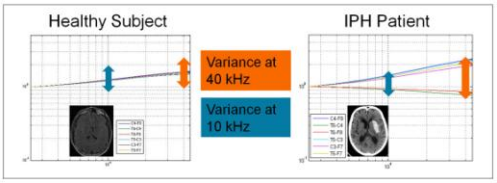

Conclusion
Electrical impedance spectroscopy device is a promising, noninvasive, portable imaging modality that has the potential to be applied in clinical practice to triage patients with acute brain injuries in the battlefield, sportfield and ambulance. Moreover EIS has the potential to be utilized as a brain-monitoring device in Neuro ICU patients to detect new changes in the intracranial pathology.

KEYWORDS: Stroke, Devices

eP-98

Accuracy and Interobserver Reliability of CT Angiography Spot Sign Detection in Acute Intracerebral Hemorrhage by Physician Specialty and Training Level: A Prospective Multicenter Study

Huynh, T. J.[1]·Gladstone, D. J.[1]·Flaherty, M. L.[2]·Broderick, J. P.[2]·Demchuk, A. M.[3]·Dowlatshahi, D.[4]·Meretoja, A.[5]·Davis, S. M.[5]·Mitchell, P.[5]·Tomlinson, G. A.[1]·Chia, T. L.[1]·Symons, S. P.[1]·Aviv, R. I.[1]
[1]University of Toronto, Toronto, ON, CANADA, [2]University of Cincinnati, Cincinnati, OH, [3]University of Calgary, Calgary, AB, CANADA, [4]University of Ottawa, Ottawa, ON, CANADA, [5]Royal Melbourne Hospital, Melbourne, AUSTRALIA.

Purpose
Rapid, accurate, and reliable identification of the CT

Note: Scanned images are included in the proceedings. Some submitted images were reduced during editing, thereby decreasing clarity. Also, refer to the Program Planner. Proceedings Content as of 3-29-2013.

angiography (CTA) spot sign is required to identify patients with intracerebral hemorrhage (ICH) for potential acute hemostatic therapy in clinical trials. We sought to assess the accuracy and interobserver agreement for spot sign identification among neurologists, emergency physicians and neuroradiologists stratified by clinical training level.
Materials & Methods
A total of 120 physicians (48 staff neurologists, 58 neurology fellows; four emergency physicians, three emergency fellows; five staff neuroradiologists, two neuroradiology fellows) underwent web-based CTA spot sign identification training and imaging certification needed to enroll patients in three clinical trials targeting spot-positive ICH patients for hemostatic therapy (STOP-IT, SPOTLIGHT, STOP-AUST). As part of the certification process, 10 ICH cases (five spot-positive, five spot-negative including two spot mimics) were presented to physicians to assess for spot sign presence, spot number, and presence of spot mimic. Representative cases were chosen from our institutional ICH database and true spot-positivity was determined by consensus by three experienced staff neuroradiologists not included in the analysis. Physician accuracy, sensitivity, specificity and time to spot identification were determined. Differences in accuracy, sensitivity, and specificity by clinical specialty and training level were compared with Kruskal-Wallis and Wilcoxon rank sum tests. Interobserver agreement was examined by specialty and training level with the Fleiss multirater kappa statistic.
Results
For spot-positive cases, median (range) spot number, maximum axial spot size, and spot attenuation was one (1-12), four (3.1 - 10.7) mm, and 203 (201 - 496) HU, respectively. Mean (SD) overall accuracy was 87 ± 11% and was similar among neurologists, emergency physicians, and neuroradiologists (87 ± 11%, 87 ± 8%, and 93 ± 8% respectively; p = 0.192). Sensitivity and specificity also was similar among specialties (p = 0.353 and 0.358 respectively). Overall sensitivity for spot detection was reduced compared to specificity (79 ± 19% and 95 ± 11% respectively, p<0.001). Accuracy of staff compared to fellows demonstrated no significant difference (p = 0.125). Overall agreement among staff was substantial (k = 0.63, 95% CI 0.61 - 0.65) and was highest among neuroradiologists (k = 0.79, 95% CI 0.60 - 0.99) compared to neurologists (k = 0.59, 95% CI 0.58 - 0.60) and emergency physicians (k = 0.59, 95% CI 0.46 - 0.73). Median time to spot identification was 2.0 minutes (interquartile range, 1.4 - 3.2 minutes) and was similar among specialties (p = 0.348). True spot signs that were incorrectly classified were most commonly interpreted as spot mimics (p<0.001). When true spots were correctly identified, 80% of responses correctly identified presence of single or multiple spots.
Conclusion
Accuracy for spot identification is high across all specialties with substantial interobserver reliability. High accuracy and agreement is critical for recruitment into ongoing clinical studies.

KEYWORDS: Intracerebral hemorrhage, CTA, Interobserver Agreement, Spot Sign

eP-99

Community Hospital Experience with Utility of CT Angiography in Acute Intraparenchymal Hemorrhage

Metting, S. W.·Alexander, M. D.·Pandit, R. P.·Patel, M. R.
Santa Clara Valley Medical Center
San Jose, CA.

Purpose
Intraparenchymal hemorrhage (IPH) can result from various etiologies, many of which can be diagnosed by noninvasive CT angiography. Given the potentially grave consequences of such hemorrhage, particularly if progression of primary hemorrhage or re-hemorrhage occur, exclusion of underlying pathology is warranted. Although computed tomographic angiography (CTA) is being increasing utilized in the assessment of IPH, often in an emergent setting, the utility, value, and optimal timing of the study remains to be evaluated.
Materials & Methods
A retrospective analysis identified all CTAs performed at a high volume community hospital from January 2001 through November 2012 performed for IPH based on review of the radiology PACS report. These were cross-referenced against unenhanced CTs with demonstrated IPH. Demographic data, presence of trauma, and imaging results were evaluated including presence of hemorrhage and underlying lesions. Analysis of patients with CTA performed for IPH was conducted to investigate differences in rates and types of positive angiographic findings when comparing between certain variables like age, sex, and associated trauma.
Results
One thousand four hundred ninety-one CTAs were performed for 1344 patients during the study period, of which analysis was completed for 549 patients at the time of this submission. Of the analyzed cases, IPH was present in 63 (11.5%) cases. Thirty-seven (58.7%) of these patients were men. Among these patients, trauma had occurred in 26 (41.3%) patients. Mean age was statistically significantly younger among patients with trauma compared to those without (41.5 years versus 53.3 years, respectively, p = 0.017). Abnormality in addition to intracranial hemorrhage was identified in eight (30.8%) patients with trauma and 13 (35.1%) patients without (p = 0.722). Rates of underlying aneurysms in the setting of IPH were higher in the atraumatic cohort compared to patients with trauma (24% versus 3.8%, respectively, p = 0.07). Other pathologic processes identified included arteriovenous malformation, vessel injury with active extravasation, dissection, vasospasm, vessel occlusion, and venous sinus thrombosis. No statistically significant

Note: Scanned images are included in the proceedings. Some submitted images were reduced during editing, thereby decreasing clarity. Also, refer to the Program Planner. Proceedings Content as of 3-29-2013.

differences were identified between groups with relation to these other processes.

Conclusion

Intraparenchymal hemorrhage may result from underlying causative processes that must be identified to properly guide treatment. CT angiographs play a role for detection of such pathology, yet little large-scale evaluation of these techniques has been performed to date. Eleven and one-half percent of CTAs performed in the current series demonstrated IPH, and one in three patients with IPH had identifiable underlying pathology. Multiple types of pathology were identified, with aneurysms being most common. Aneurysms were much more likely to occur in people without concomitant trauma than those with. Patients with IPH who have experienced trauma tend to be younger than those who have not. Further analysis of the utility of CTA in the setting of IPH is warranted, particularly with respect to changes in management and affects on outcomes.

KEYWORDS: Hemorrhage, CT angiogram

eP-100

Role of Low-Dose Nonenhanced Brain CT in the Neurosurgical and Neurologic Intensive Care Unit

Hoch, M.[1]·Sethi, V.[2]·Shah, P.[1]·O'Connor, E.[1]·Hershey, B.[1]·Ali, S.[1]·Dass, C.[1]
[1]Temple University Hospital, Philadelphia, PA, [2]Temple University Medical School, Philadelphia, PA.

Purpose

To identify a patient population subject to serial short-term follow-up CT evaluation that may benefit from low dose CT examination. Most neurosurgical/neurologic intensive care unit (NICU) patients undergo multiple serial CT scans during a single hospitalization. After the initial routine scan, we explored if low dose follow-up scans could effectively evaluate NICU patients without sacrificing diagnostic accuracy.

Materials & Methods

Following IRB approval, a retrospective chart review was performed identifying 19 NICU patients (ages 18-73 years, mean 49 years) who had three axial nonenhanced brain CT examinations within a span of 72 hours in the following sequence: initial routine dose, followed by low dose, and finally routine dose. Included studies showed a persistent finding on the initial and final scans. From these routine and low dose scans, 59 unique pairs of comparative individual slices were selected (Figure 1). Two board-certified neuroradiologists, each blinded to the scan parameters and patient information evaluated the selected slices. The readers were asked if each image was diagnostically acceptable for interpretation and to note the presence or absence of the following findings: infarction, hemorrhage, herniation, and catheter location. All CT scans were performed on Siemens Sensation 16- or 64-slice machines. Routine scans were acquired with mAs ≥ 310 and collimation of 1.2 - 1.5 mm, while low-dose scans had mAs ≤ 280 and collimation of 5 mm. All other imaging parameters including 120 kVp were kept constant. Regions of interest placed over gray and white matter were obtained from each slice to calculate contrast-to-noise ratios (CNR).

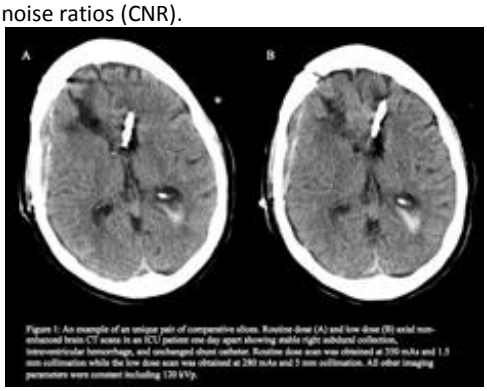

Figure 1: An example of an unique pair of comparative slices. Routine dose (A) and low dose (B) axial non-enhanced brain CT scans in an ICU patient one day apart showing stable right subdural collection, intraventricular hemorrhage, and unchanged ghost catheter. Routine dose scan was obtained at 310 mAs and 1.5 mm collimation while the low dose scan was obtained at 280 mAs and 5 mm collimation. All other imaging parameters were constant including 120 kVp.

Results

There was very high (95.3%) interobserver agreement in identifying pertinent findings on routine and low dose brain CT examinations among the sampled NICU patients (Table 1). Compared to routine dose, low dose CT imaging delivered a 26.07% reduction in average CTDIvol. Despite an average CNR reduction of 29.23%, low-dose imaging provided equal if not better diagnostic accuracy.

Table 1: Findings Made on Routine vs Low Dose CT

	Routine Dose			Low Dose		
	Reader 1	Reader 2	Concordance	Reader 1	Reader 2	Concordance
Venticular Catheter/ICP Monitor Location	10	10	100%	10	10	100%
Midline Herniation	17	20	85%	19	19	100%
Extracranial Herniation	4	4	100%	4	3	75%
Infarction	15	16	94%	17	17	100%
Intra-axial Hemorrhage	30	31	97%	31	30	97%
Extra-axial Hemorrhage	32	32	100%	38	37	97%

Conclusion

Low-dose brain CT is diagnostically acceptable when applied to the adult NICU population, emphasizing the concept of ALARA (As Low As Reasonably Achievable). Further collaboration with referring clinicians may allow development of additional dose reduction protocols.

KEYWORDS: Radiation dose reduction, Protocols, ALARA

eP-101

Improved Quality and Diagnostic Confidence Achieved by Use of Dose-Reduced Gadolinium Blood Pool Agents for Time-Resolved Intracranial MR Angiography

Dehkharghani, S.·Boddu, S. R.·Saindane, A.
Emory University Hospital
Atlanta, GA.

Purpose

Time-resolved MR angiographic (TR MRA) techniques

Note: Scanned images are included in the proceedings. Some submitted images were reduced during editing, thereby decreasing clarity. Also, refer to the Program Planner. Proceedings Content as of 3-29-2013.

using bolus injection of paramagnetic contrast agents to shorten blood T1 have been employed to evaluate the intracranial vasculature. Standard contrast agents have limited blood pool residence times, thus the rationale for the development of highly protein bound blood-pool agents (BPA) with higher T1 relaxivity and longer intravascular residence, theoretically affording improved image quality with smaller administered doses. This study compares the diagnostic quality of the BPA gadofosveset trisodium (Ablavar) to a standard agent gadobenate dimeglumine (Multihance) for intracranial TR MRA.
Materials & Methods
One hundred datasets were acquired in patients with known or suspected cerebrovascular abnormalities on a clinical 1.5T GE system with time resolved imaging of contrast kinetics (TRICKS) using a standardized protocol. Patients were administered recommended, weight-based doses of Multihance at 0.1 mmol/kg or Ablavar at 0.03 mmol/kg. Two neuroradiologists blinded to the administered agent analyzed images in consensus as follows: Peak arterial and venous enhancement were identified from maximum intensity projections, noting the presence or absence of a nonvenous-contaminated arteriographic phase. Axial source data corresponding to peak arterial and venous phases subsequently were reviewed for quality of enhancement, with attention to six vascular segments: 1) cavernous/supraclinoid internal carotid arteries (ICA); 2) middle cerebral artery (MCA) M1 segment; 3) MCA M2 branches; 4) MCA M3 branches; 5) deep cerebral veins; and 6) dural venous sinuses. Images also were evaluated for artifact-related degradation.
Results
Fifty patients were present in both the Ablavar and Multihance groups. All datasets were complete and deemed satisfactory for assessment. No significant differences were found between agents in their generation of uncontaminated arteriograms. Datasets using the BPA Ablavar, at a lower dose of gadolinium, were rated to be of significantly greater diagnostic quality than Multihance across all interrogated arterial segments including: ICA (p=0.019), M1 (p=0.05), M2 (p=0.003), and M3(p<0.01). Datasets using Ablavar were rated as having significantly better enhancement of the deep venous structures (p=0.016), but not for dural venous sinuses. The frequency of artifacts did not differ significantly between agents. The figure demonstrates the improved quality in peak arterial enhancement using Ablavar in a patient scanned on separate occasions with both contrast agents.

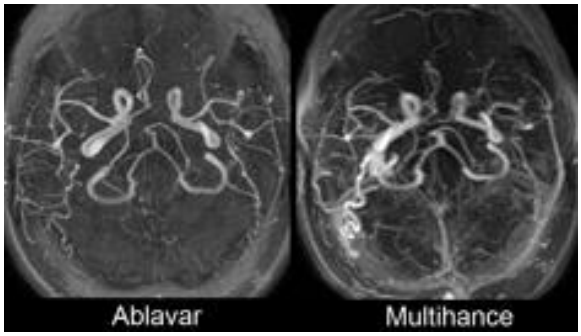

Conclusion
The BPA Ablavar provides superior evaluation of the smaller intracranial arterial and venous structures in TR MRA than Multihance, at a substantially lower dose of gadolinium. This is attributed to the higher relaxivity and pharmacokinetic advantages of BPAs for TR MRA.

KEYWORDS: MR angiography, Blood pool, Time-resolved imaging

eP-101a

Usefulness of Gadolinium-Enhanced Fast Fluid Attenuated Inversion Recovery MR Imaging in Patients with Head Injury

Park, S.[1,2]·Kim, S.[1]
[1]Boramae Medical Center, Seoul, KOREA, REPUBLIC OF, [2]Seoul National University College of Medicine, Seoul, KOREA, REPUBLIC OF.

Purpose
The purpose of this study was to investigate the clinical utility of gadolinium-enhanced fluid attenuated inversion recovery (FLAIR) magnetic resonance (MR) imaging of the brain in patients with head injury.
Materials & Methods
In 70 consecutive patients with head injury referred for gadolinium-enhanced fast fluid attenuated inversion recovery (FLAIR) MR imaging were performed before and after administration of gadopentetate dimeglumine (0.1 mmol per kilogram of body weight). Pre and postcontrast images were evaluated to determine the presence of abnormal contrast enhancement.
Results
Thirty-six of 70 studies showed dural enhancement on post FLAIR images. Diffuse dural enhancement of the whole brain was seen in 10 studies. Seventeen cases demonstrated localized dural enhancement in the location of abnormal localized enhancement of the dura mater correlated with the injured area. In nine studies, falx cerebri only was enhanced. Compared with postcontrast T1-weighted images, postcontrast FLAIR images showed more dural enhancement in 19 patients, an equal number in 10, and fewer lesions in six. Dural enhancement on postcontrast FLAIR images was statistically correlated with the existence of subarachnoid hemorrhage, subdural

Note: Scanned images are included in the proceedings. Some submitted images were reduced during editing, thereby decreasing clarity. Also, refer to the Program Planner. Proceedings Content as of 3-29-2013.

hemorrhage, post-traumatic loss of consciousness and transient amnesia. (p = 0.005, 0.041, 0.000, 0.032)
Conclusion
Postcontrast FLAIR images well presents dural enhancement in patients with head injury. Moreover the presence of abnormal dural enhancement on postcontrast FLAIR images might imply considerable head injury. So, radiologists should pay more attention to detecting traumatic brain lesion such as small amount of subdural hemorrhage or subarachnoid hemorrhage in case abnormal dural enhancement is shown.

KEYWORDS: Neurotrauma, Brain trauma

eP-101b

Outcome Prediction in Patients with Glioblastoma Multiforme Using Clinical Features, MR Imaging, and Genetic Biomarkers

Nicolasjilwan, M.[1]·Ying, H.[2]·Chunhua, Y.[2]·Meerzaman, D.[2]·Raghavan, P.[1]·Gutman, D.[3]·Huang, S.[3]·Holder, C.[3]·Chen, J.[4]·Freymann, J.[5]·Kirby, J.[5]·Jaffe, C.[6]
[1]University of Virginia, Charlottesville, VA, [2]National Cancer Institute, Bethesda, MD, [3]Emory University Hospital, Atlanta, GA, [4]University of California San Diego, San Diego, CA, [5]SAIC-Frederick, Inc., Frederick, MD, [6]Boston University School of Medicine, Boston, MA.

Purpose
Recent advances in glioblastoma treatment have geared current research into identification of different categories of biomarkers that can predict patient outcome, and consequently may impact therapeutic decisions through the selection of more aggressive therapies for the tumors with the worse prognosis. The impact of clinical factors on patient outcome and the correlation between MR imaging features of GBM and survival have been reported previously in the literature. Similarly, the association between genomic biomarkers and patient outcome has received growing attention, in particular with the recent introduction of antiangiogenetic drugs. The purpose of our study was to incorporate clinical factors, imaging biomarkers, and tumor gene expression into a statistical model that would potentially constitute a more robust predictor of patient survival than either individual data.
Materials & Methods
The study was conducted as part of the TCGA effort supported by the National Cancer Institute (http://www.cancergenome.nih.gov/). MRI images of 70 GBM patients were reviewed by six neuroradiologists using the VASARI scoring system. The patients' clinical and genetic data were available through the TCGA website. Patient outcome was measured in terms of survival time. The correlation between different categories of biomarkers and survival was evaluated using Cox regression models.
Results
On multivariate analysis, the only features that correlated significantly to survival were: 1) in terms of clinical factors: chemotherapy; 2) in terms of imaging: proportion of tumor enhancing, and 3) in terms of genetics: expression of the gene HRAS. The incremental addition of these three biomarkers into Cox regression models results in an incremental increase in the prediction strength in terms of survival, with the model including clinical, imaging and genetic variables having the highest predictive accuracy.
Conclusion
A combination of clinical factors, VASARI imaging features, and tumor genes predicts survival of patients with GBM. This information may be valuable, as more treatments become available, in directing a more individually tailored therapeutic approach.

KEYWORDS: Glioblastoma, Gene expression, imaging biomarker

Monday, May 20 – Wednesday, May 22
6:30 AM – 9:00 PM
Thursday, May 23
6:30 AM – 3:00 PM
Hall B1

Electronic Posters (ePosters) 102 – 107

ePosters

Note: A missing printed number indicates an abstract has been withdrawn.

eP-102

Sub-Pial Hemorrhage: Is This an Unusual but Distinct Distribution of Intracranial Hemorrhage?

Matheus, G.·Enterkin, J.·Bartynski, W.
Medical University of South Carolina
Charleston, SC.

Purpose
To demonstrate representative cases of superficial parenchymal hemorrhage with unique imaging features consistent with a sub-pial distribution. Based on these cases we will further discuss the anatomical and physiologic characteristics of the axial and extra-axial spaces with emphasis upon the sub-pial region through both a descriptive and pictorial approach.
Materials & Methods
Five patients were identified with CT and MR imaging demonstrating intracranial hemorrhage with an unusual

Note: Scanned images are included in the proceedings. Some submitted images were reduced during editing, thereby decreasing clarity. Also, refer to the Program Planner. Proceedings Content as of 3-29-2013.

distribution suggestive of a sub-pial location (4 adults and 1 infant). Clinical context included: trauma [three patients; nonenhanced head CT (NEHCT)], postaneurysm rupture (one patient; NEHCT), and one 9-month-old infant with a parietal hemorrhage of unclear etiology (NEHCT and MRI). Review of the current literature regarding imaging findings, epidemiology, potential consequences, and the anatomy of sub-pial hemorrhage also was conducted.
Results
All of the patients demonstrated the unique imaging pattern including: 1) hemorrhage localized along the brain surface, 2) focal and distinct mass effect upon the adjacent cortical gyri and 3) associated focal sulcal expansion. Hemorrhage locations included frontal lobe, temporal lobe and parietal region. Surface hemorrhage was not free and/or mobile in the subarachnoid space. Confusion with subdural hemorrhage was common. In two of the cases the displaced cortex showed focal hypodensity on NEHCT and with MR imaging demonstrating abnormal signal of the displaced cortex on both T1- and T2-weighted images with associated reduced diffusion. Literature review demonstrates a few cases of localized leptomeningeal/superficial parenchymal distribution intracranial hemorrhage, which has been described in both adults and term newborns. Multiple speculative etiologies are proposed without a definitive consensus for the atypical distribution of the hemorrhage. All of the cases described in the literature with longitudinal follow-up imaging resulted in subsequent encephalomalacia. The sub-pial region has been shown anatomically to represent a poorly distensible space that resides between the pia mater and glia limitans on the brain surface. Arteries and veins cross this space which also contains bundles of collagen fibers extending into the trabecula of the subarachnoid space.
Conclusion
The sub-pial space is a distinct space that can be affected by intracranial hemorrhage. Localized hematomas may form in this space with unique imaging features. These hemorrhages may be associated with adjacent brain parenchymal injury - either primary (i.e., from contusion) or secondary (related to decreased distensibility of this space with resultant compression and/or sequela of direct blood product toxicity to the glia limitans and cortex). A more complete understanding of this atypical hemorrhagic pattern may in turn affect the approach to clinical management.

KEYWORDS: Hemorrhage, Brain hemorrhage

eP-103

Incidence of Petrous Apex Cephalocele in Patients with Empty Sella

Jamjoom, D. Z.·Alorainy, I. A.
College of Medicine, King Saud University
Riyadh, SAUDI ARABIA.

Purpose
Petrous apex cephalocele (PAC) is a rare lesion that has been linked to empty sella in several case reports. The primary aim of this study is to document the incidence of PAC in patients with empty sella and examine the correlation between the size of these two lesions, in an attempt to better understand the underlying etiology of PAC. The secondary aim of this study is to document the imaging characteristics of PAC in a large cohort.
Materials & Methods
We found 275 patients with the terms "empty sella" in our radiology report database for the period from January 2005 to December 2011. A total of 214 patients met our inclusion criteria. Retrospective analysis of patients' head CT and/or MRI was performed by two radiologists independently.
Results
Petrous apex cephalocele was found in 33 (15.4%) patients (age range 17 to74 years), and 32 of these were females. Bilateral PAC was more common and seen in 25 patients. There was a statistically significant correlation between the size of empty sella and PAC on the left side. On imaging, all PAC lesions were continuous with the posterolateral aspect of Meckel's cave causing smooth erosion on the anterior part the petrous apex. Lesions followed fluid signal on both CT and MRI.
Conclusion
Petrous apex cephalocele is seen in 15% of patients with empty sella, and in the majority it is bilateral.

KEYWORDS: Petrous apex, Normal variant, meningocele

eP-104

Normal Variability in the Morphology of the Lumbar Disk Annuli and their Adjacent Endplates

Engel, C. W.·Martinez, C. R.·Ford, J. M.·Davy-Jow, S. L.·Decker, S. J.
University of South Florida Morsani College of Medicine
Tampa, FL.

Purpose
Variation in the morphology of the posterior margin of the lumbar annuli has not been thoroughly described. Our aim was to determine the normal shape of the posterior lumbar disk annuli and their adjacent endplates through the CT evaluation of normal lumbar spines in a select population of young adults.
Materials & Methods
Two reviewers retrospectively selected 60 CT scans of the

Note: Scanned images are included in the proceedings. Some submitted images were reduced during editing, thereby decreasing clarity. Also, refer to the Program Planner. Proceedings Content as of 3-29-2013.

abdomen/pelvis (average age = 27.25 years) from a large pool of young adults who presented to an outpatient diagnostic center for evaluation of possible abdominal and/or pelvic pathology. Exclusion criteria included congenital spinal variations/anomalies, scoliosis, prior trauma, degenerative disk or facet disease, disk protrusion, and spondylolisthesis. Three-dimensional models of the lumbar vertebrae and disks were rendered from original raw data, and the curvatures of the posterior margins of the disks and endplates were measured using 3D modeling software.

Results

With positive values reflecting anterior concavity and negative values reflecting posterior convexity, posterior disk curvature was 0.53 ± 0.19 cm^{-1} at L1L2, 0.38 ± 0.16 cm^{-1} at L2L3, 0.30 ± 0.18 cm^{-1} at L3L4, 0.07 ± 0.20 cm^{-1} at L4L5, and -0.20 ± 0.22 cm^{-1} at L5S1 (mean ± 1 SD). The superior endplate curvatures were 0.56 ± 0.14 cm^{-1} at L1L2, 0.42 ± 0.18 cm^{-1} at L2L3, 0.26 ± 0.17 cm^{-1} at L3L4, 0.02 ± 0.17 cm^{-1} at L4L5, and -0.17 ± 0.16 cm^{-1} at L5S1. The inferior endplate curvatures were 0.64 ± 0.18 cm^{-1} at L1L2, 0.50 ± 0.19 cm^{-1} at L2L3, 0.40 ± 0.18 cm^{-1} at L3L4, 0.17 ± 0.20 cm^{-1} at L4L5, and -0.02 ± 0.28 cm^{-1} at L5S1.

Conclusion

There is a normal variation in the shape of the posterior lumbar disk annuli as well as their adjacent endplates. This variation is subtle, with decreasing anterior concavity from L1L2 to L5S1 that usually results in posterior convexity at L5S1 and often at L4L5. The understanding of this normal variation in lumbar disk shape is important in order to avoid a false positive diagnosis of a disk bulge, particularly at L4L5 and L5S1.

KEYWORDS: Lumbar spine, Disk, curvature

eP-105

Acute Cerebral Edema in CT Negative Patients with Traumatic Head Injury

Butman, J. A.[1,2]·Pham, D. L.[2]·Knutson, A.[2]·Latour, L. L.[3]
[1]The Clinical Center of the NIH, Bethesda, MD, [2]Center for Neuroscience and Regenerative Medicine, Bethesda, MD, [3]National Institute of Neurological Disorders and Stroke, Bethesda, MD.

Purpose

To report diffuse acute cerebral edema as a common consequence of traumatic head injury (THI) in patients with negative head CT.

Materials & Methods

Subjects enrolled in the THINC (Traumatic Head Injury Neuroimaging Classification) study were included with i) negative CT on admission, ii) acute MRI 5% was used to classify individuals as “positive” for acute cerebral edema and the association between edema and MR+ was tested using Fisher’s exact test. <0.05 was considered significant.

Results

Seventy-four subjects met criteria. Overall, ventricles increased in size between the two time points (dV = 2.3%, p<0.0001). Subjects found to be MR+ (n = 41) had a larger dV as compared to those were MR- (3.2% vs 1.1%, p = 0.02). There were 12 of 41 (28%) MR+ subjects classified as having acute edema using the 5% threshold in comparison to 3 of 33 (9%) of MR- subjects, p = 0.04.

Conclusion

Diffuse cerebral edema is a known consequence of THI, but is generally not possible to diagnose acutely unless severe. In this study, we identify a relatively rapid and significant decrease in brain volume between MRI scans performed over the first week, in THI patients with a negative CT scan. We propose that this change is due to resolution of the acute edema induced by the THI, and not due to volume loss, as atrophy would not be expected in this time frame. Cerebral edema was more prevalent and of a higher degree in MR+ patients as compared with MR- patients. Furthermore, we found a subgroup of MR- patients with changes in volume strongly suggestive of acute edema, despite otherwise normal imaging. The clinical implications of this finding remain to be elucidated. Methods to detect diffuse edema at a single time need to be developed.

KEYWORDS: Traumatic brain injury, Diffuse axonal injury

eP-106

Diagnostic Yield of Imaging Evaluations for Suspected Horner’s Syndrome

Delfyett, W. T.·Hein, A.·Chang Sen, L.·Rath, T. J.·Yu, J.
University of Pittsburgh Medical Center Presbyterian-Shadyside
Pittsburgh, PA.

Purpose

Horner's syndrome (ptosis, miosis, anhidrosis) results from a lesion involving the well defined oculosympathetic pathway. Suggested imaging work-up algorithms have been reported in the literature for suspected lesions at each level of the oculosympathetic pathway. However, the radiographic evaluation of suspected Horner's syndrome frequently is negative. The purpose of this study is to evaluate the diagnostic yield of the radiographic workup of suspected Horner's syndrome at adult UPMC facilities and to identify clinical characteristics of patients referred for imaging evaluation.

Materials & Methods

An IRB-approved retrospective search of the electronic medical record was performed for all adult UPMC facilities between 01/01/06 and 08/25/11, for keywords; Horner's or oculosympathetic palsy as a provided indication for imaging. The records of the clinical exam which prompted the imaging evaluation were reviewed by an ophthalmology fellow specifically for documented ptosis, miosis, anhidrosis, clinical presentation, and use of eye-drop testing. All radiographic studies were reviewed in a blinded fashion by a CAQ-certified neuroradiologist.

Note: Scanned images are included in the proceedings. Some submitted images were reduced during editing, thereby decreasing clarity. Also, refer to the Program Planner. Proceedings Content as of 3-29-2013.

Studies were categorized as (1) negative, (2) lesion probably related to Horner's syndrome, and (3) lesion definitely causing Horner's syndrome. Categories two and three are considered positive in determining diagnostic yield.
Results
Retrospective medical record search yielded 155 patient evaluations for one or more of the keywords. These constituted 309 exams as determined by CPT codes. Services who provided patient referral were ophthalmology 30%, neurology 24%, internal medicine/primary care 21%, emergency medicine 14%, otolaryngology 2%, surgery 1%, neurosurgery <1%, 7% referring specialty was unclear. In 17 patients (10%) an overlap in symptoms was found and the imaging evaluation was not performed for a clinical Horner's syndrome. Clinical records were unavailable for 60 patients. Upon review of all imaging studies, 21 patient evaluations (14%) were deemed positive. For the subset in which clinical records were available, there were 18 positive cases (19%). Presenting symptoms included ptosis (73%), miosis (71%), and mnhidrosis (6%), ptosis and miosis (52%), and (4%) had ptosis, miosis and anhidrosis. Twenty-five patients (16%) had documented pharmacologic eye-drop testing. Positive radiographic evaluations included; eight carotid dissections, two carotid aneurysms, two lung adenocarcinomas, two midbrain strokes, one lung apex and chest wall invasive aspergillosis, two soft tissue abnormalities of the neck, two skull base lesions and one cervical cord metastasis.
Conclusion
Overall radiographic positive yield in the radiographic evaluation of Horner's syndrome at adult UPMC facilities was 14% for the study period. The ordered imaging workups were found to be heterogeneous across referring specialties. The low number of patients that met all components of Horner's syndrome (4%) suggests that partial Horner's syndromes may be very common or that many patients may be labeled "Horner's" who rather display an overlap in symptoms. There are acute clinical scenarios and known medical conditions which will guide the evaluation of Horner's syndrome aimed at excluding acutely life-threatening conditions such as vascular dissections. However, in an environment of increased utilization review and pre-approval processes, there may be a potential expanded role for relatively inexpensive pharmacologic eye-drop testing in more chronic patients in order to tailor imaging evaluations.

KEYWORDS: Horner's syndrome, CT, MR imaging

eP-107

Neurographic Imaging with a Molecular Probe

Schellingerhout, D.·Bredow, S.·Le Roux, L.
M. D. Anderson Cancer Center
Houston, TX.

Purpose
To develop an agent for imaging retrograde axonal transport in nerve tissues based on the optical labeling of a nontoxic fragment of tetanus toxin.
Materials & Methods
A His-tagged recombinant tetanus toxin fragment C (TTc) was produced in E.coli, purified, and labeled with Alexa fluorophors for optical imaging studies. Gel electrophoresis (SDS-PAGE) and quantitative immunodetection studies were performed. Cell uptake studies were performed to assess in vitro efficacy. Labeled TTc was injected into the calf muscles of C57bl and Balb/C mice, and Wistar rats, and imaging performed with the IVIS 200 (Xenogen). In situ validation was performed with laser scanning confocal microscope FV 1000 (Olympus) utilizing intact glycerol mounted samples, and cryo-sections.
Results
Gel electrophoresis and quantitative immunodetection indicated that the integrity and immune reactivity of the protein was preserved after labeling. Cell uptake assays indicated robust uptake in differentiated PC12 cells. In vivo optical imaging demonstrated the uptake of TTc-Alexa in the sciatic nerve and spinal cord. Progressive uptake and transport of the agent could be seen along the course of the sciatic nerve and spinal cord. Confocal microscopy studies on intact excised nerve segments and cryosections confirmed the compound uptake in nerve fascicles of the sciatic nerve. Axonal nerve uptake and superficial lymphatic uptake were clearly distinguishable, and transport was shown to be nerve-specific. Immunohistochemistry on cord sections demonstrated the presence of the agent in spinal cord neurons.
Conclusion
Fluorescently labeled TTc is taken up into motor nerve endings after intramuscular injection, and is retrogradely transported in nerve axons. This process can be demonstrated with noninvasive in vivo imaging, and allows nerve anatomy and function to be studied.

KEYWORDS: Nerve imaging, Neurography, molecular imaging

Note: Scanned images are included in the proceedings. Some submitted images were reduced during editing, thereby decreasing clarity. Also, refer to the Program Planner. Proceedings Content as of 3-29-2013.

Monday, May 20 – Wednesday, May 22
6:30 AM – 9:00 PM
Thursday, May 23
6:30 AM – 3:00 PM
Hall B1

Electronic Posters (ePosters)
108 - 146

eP3-Head and Neck

Note: A missing printed number indicates an abstract has been withdrawn.

eP-108

IDEAL T2-Weighted Imaging Assessment of Oculomotor Nerve Impairment

Koike, H.[1]·Morikawa, M.[1]·Enokizono, M.[1]·Uetani, M.[1]·Nakashima, H.[1]·Motomura, M.[1]·Ideguchi, R.[2]
[1]Nagasaki University School of Medicine, Nagasaki, JAPAN, [2]Nagasaki Municipal Hospital, Nagasaki, JAPAN.

Purpose
Several studies have reported usefulness of MRI in diagnosis of disease presenting with oculomotor nerve (CN3) palsy. But few studies have documented pathologic characteristics of CN3 on MRI. Iterative decomposition of water and fat with echo asymmetric and least-squares estimation (IDEAL) has been shown to effectively suppress fat, even in the presence of magnetic field inhomogeneity. Therefore, IDEAL sequence is expected to improve visualization of CN3 in cavernous sinus and apex of orbit. Our object is to evaluate the utility of IDEAL T2-weighted image (T2WI) for detection of oculomotor pathology, and for differentiating CN3 disease from other related disease.
Materials & Methods
We retrospectively examined 17 patients presenting with CN3 palsy or similar symptoms (five men, 12 women; age range: 23 - 88 years) between 2010 and 2012 at our hospital. Seven of the 17 patients had inflammatory disease (six oculomotor neuritis, and one radiation injury), six patients had compression of CN3 (three aneurysms, two after transvenous embolization for carotid cavernous sinus fistula, and one meningioma) and four patients had muscular disease (two myasthenia gravis, one Basedow's disease, one idiopathic external ophthalmoplegia). All MR examinations were performed using a 3T MR scanner with an 8-channel head coil. Coronal IDEAL T2WI was performed with the following parameter: TR/TE = 3400-4000/82-88 ms, FOV = 12 × 12 cm, matrix = 320 × 160, thickness = 2.5 mm). Regions of interest (ROI) of CN3, genu of corpus callosum and extraocular muscles were drawn. Signal intensity (SI) in the ROIs was measured and the SI ratio (SIR, SI of oculomotor nerve/SI of genu of corpus callosum) was calculated. Nine of 17 patients underwent contrast-enhanced coronal T1WI with fat suppression (CE-T1WI), and the SI ratios were also calculated.
Results
On IDEAL T2WI, the SIR of the affected and normal side of CN3 was 1.47 vs 0.95 ($p<0.05$) in the inflammatory disease, 1.53 vs 0.88 ($p<0.05$) in the compression disease, and 0.98 vs 0.77 in the muscular disease, respectively. On CE-T1WI, the SIR of the affected side and normal side of CN3 was 1.49 vs 1.02 ($p<0.05$) in the inflammatory disease, and 0.99 vs 1.08 in the compression disease. In five of six patients of oculomotor neuritis, high signal intensity in extraocular muscles due to denervation atrophy was observed.

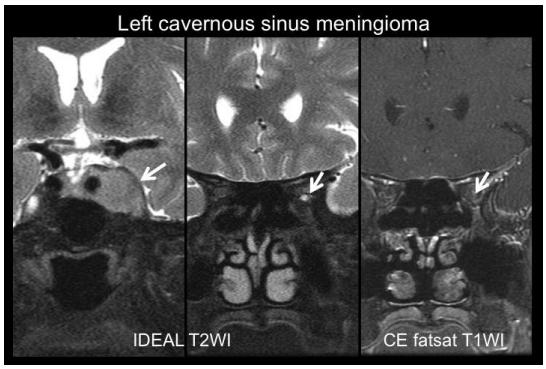

Conclusion
IDEAL T2WI can offer clear images of CN3 abnormalities in disease presenting with CN3 palsy. The use of a contrast agent can distinguish the cause of CN3 palsy.

KEYWORDS: Oculomotor, 3T

eP-109

Can We Halt Vision Loss In Idiopathic Intracranial Hypertension with Venous Stenosis?

Seshadri, R.[1]·HR, A.[2]
[1]Sri Ramachandra Medical College, Chennai, INDIA, [2]National Institute of Mental Health and Neurosciences, Bangalore, INDIA.

Purpose
Idiopathic-intracranial-hypertension (IIH) is a disease entity of exclusion characterized by raised intracranial tension (ICT) with no obvious mass lesion or venous sinus thrombosis. It is characterized with intractable headaches, visual obscurations, papilledema; mainly affects obese women of child-bearing age. Multiple pathophysiologic mechanisms have been proposed to explain the increased intracranial pressure (ICP). In a subset of patients, venous sinus stenosis with a significant pressure gradient has been recognized. Three-dimensional phase contrast MRV,

Note: Scanned images are included in the proceedings. Some submitted images were reduced during editing, thereby decreasing clarity. Also, refer to the Program Planner. Proceedings Content as of 3-29-2013.

contrast-enhanced MRV, cerebral angiography, retrograde venography and manometry help in identification of this subset of patients. The major problem caused by IIH is insidious painless loss of vision which can be halted and reversed to a certain extent, if detected and intervened early. The purpose of this study was to study the effectiveness of venous-sinus stenting in treating IIH due to venous-stenosis.

Materials & Methods

It was a prospective study. Ethical clearance was obtained. Inclusion criteria: Patients diagnosed with IIH, refractory to medical therapy and having venous stenosis with significant pressure-gradient(>/=10 mm of Hg). Exclusion criteria: Patients responding to medical management or venous stenosis with pressure-gradient of less than 10 mm of Hg or venous-sinus thrombosis or intracranial space-occupying lesions. All patients underwent detailed clinical, imaging and ophthalmologic examinations; CSF-analysis, CSF-pressure recording; vasculitic workup. Those fitting the inclusion criteria underwent DSA and manometry. Patients with significant pressure gradient (>/=10 mm of Hg) in venous sinuses were stented with self-expandable stents and pressure difference was recorded poststenting. Postintervention, clinical and ophthalmologic evaluations were performed, and repeat DSA with manometry was performed on followup.

Results

All of the six patients were females (age-range:15- 40 years; weight: 60-88 Kg; BMI: 29-37) (Table 1; Figure 1).

Results of Venous sinus stenting in IIH

case	CSF Pressure	Pre-Stenting visual acuity	Papilledema Right	Papilledema Left	Pre-Stenting Pressure Gradient-mm Hg	Post-Stenting Pressure Gradient-mm Hg	Post-Stenting. Papilledema Right	Post-Stenting Papilledema Left	Post-Stenting visual acuity	Post-Stenting Blurring
1	230	Normal	Present	Present	33	0	Improved	Improved	Normal	Resolved
2	100	Normal	Present	Present	30	4	Improved	Improved	Normal	Resolved
3	200	Normal	Present	Present	30	0	Improved	Improved	Normal	Resolved
4	400	Reduced	Atrophy	Present	32	1	Atrophy	Improved	Improved	Resolved
5	330	Reduced	Atrophy	Atrophy	15	2	Atrophy	Atrophy	Improved	Resolved
6	360	Normal	Present	Present	16	2	Improved	Improved	Normal	Resolved

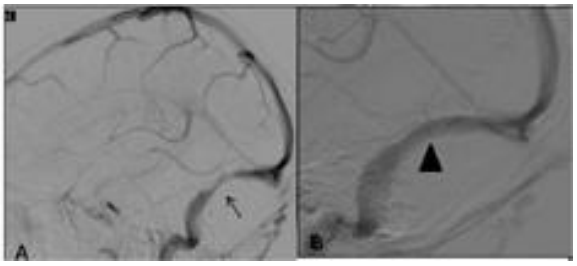

Conclusion

This study clearly shows that whenever the cause of IIH is a stenosed venous sinus with a significant pressure gradient across the stenosis, stenting definitely helps in normalization of ICP with dramatic relief of symptoms. So it should be a primary modality of treatment in cases of significant venous-sinus stenosis refractory to medical management as it helps in halting the progression of visual loss due to raised ICP.

KEYWORDS: Intracranial hypertension, Stents, IIH, Manometry, DSA

eP-110

Update on the Sonographic NASCET Index: A Revised Doppler Parameter for Assessment of Internal Carotid Artery Stenosis

Nayak, N. B.[1]·Abdulla, A.[2]·Huang, J.[3]·Hathout, G.[1,3]
[1]University of California Los Angeles, Los Angeles, CA, [2]2David Geffen School of Medicine at University of California, Los Angeles, CA, [3]Greater Los Angeles-West Los Angeles Veterans Administration Medical Center, Los Angeles, CA.

Purpose

Sonography using either a single peak systolic velocity (PSV) measurement alone or the ICA-CCA velocity ratio does not accurately reflect the North American Symptomatic Carotid Endarterectomy Trial (NASCET)-style methodology for assessing carotid artery stenosis. In a previous paper, a new Doppler parameter, the sonographic NASCET index (SNI), was derived by using the PSV at both the stenotic proximal ICA and distal normal ICA to calculate an ultrasound index directly analogous to NASCET methodology. Correlation between SNI and angiography was found to be greater than that of PSV and angiography, with better accuracy in predicting stenosis of 70% or greater. However, all these parameters use only a single time-point velocity measurement, at the peak of the cardiac cycle, which does not take into account complex changes affecting the Doppler waveform as a whole, such as increased diastolic flow in more narrow occlusions. We have devised an updated SNI, revised to integrate the true volume within the vessel at both the stenotic proximal ICA and distal normal ICA over the entire cardiac cycle, and to calculate a NASCET-style measurement of carotid stenosis.

Materials & Methods

Inclusion criteria were established as: angiographically proven carotid stenoses of 40-95%, measured proximal and distal internal carotid artery Doppler PSV values and correlating Doppler waveform images. Occlusions and near-occlusions were specifically excluded. Doppler and angiographic data meeting the inclusion criteria from 25 carotid bifurcations were identified; actual angiographic stenoses ranged from 40-92%. The integral of the area under the Doppler waveform curves was tabulated at both the proximal and distal internal carotid arteries to calculate the revised SNI for each vessel. Peak systolic velocity, ICA-CCA ratio, and SNI were correlated with angiography by using linear regression analysis. Accuracies of SNI and PSV in predicting stenoses of 70% or greater were compared at two thresholds.

Results

Correlation with angiography was found to be significantly better with SNI than either PSV or the ICA-CCA ratio (r^2 = 0.48 vs.0.22; r^2 = 0.48 vs. 0.16). Peak systolic velocity and SNI values that corresponded to 70% angiographic stenosis

Note: Scanned images are included in the proceedings. Some submitted images were reduced during editing, thereby decreasing clarity. Also, refer to the Program Planner. Proceedings Content as of 3-29-2013.

were 296.5 cm/s and 42.4, respectively. The accuracy of PSV of 296.5 cm/s or greater in predicting stenosis of 70% or greater was 68%, compared with 80% for SNI of 42.4 or greater. The SNI value that corresponded to a PSV threshold of 230 cm/s, the threshold used in our ultrasound laboratory, was 34.4. The accuracy of PSV of 230 cm/s or greater in predicting hemodynamically significant stenosis was 72%, compared with 88% for SNI of 34.4 or greater.
Conclusion
When compared to conventional methodology of inferring the degree of stenosis from elevations of PSV in the stenotic segment without reference to the more normal distal ICA, or using the ICA-CCA ratio (comparing the stenotic segment to the CCA), the revised SNI correlates more closely with angiographic stenosis and is significantly more accurate in predicting stenosis of 70% or greater.

KEYWORDS: Carotid artery stenosis, Ultrasonography

eP-111

Diagnostic Accuracy of 64-Slice Multidetector CT Angiography in the Assessment of in-Stent Restenosis after Vertebral Artery Ostium Stenting

Yoo, W.[1]·Lee, Y.[1]·Kim, K.[2]·Kim, B.[3]
[1]Bucheon St. Mary's Hospital, Bucheon, KOREA, REPUBLIC OF, [2]Incheon St. Mary's Hospital, Incheon, KOREA, REPUBLIC OF, [3]Seoul St. Mary's Hospital, Seoul, KOREA, REPUBLIC OF.

Purpose
The aim of our study was to assess the diagnostic accuracy of 64-slice multidetector computed tomography angiography (CTA) for the detection of in-stent restenosis (ISR) after vertebral artery ostium (VAO) stenting and to compare these with conventional angiography.
Materials & Methods
Sixty-one stents of 54 patients (34 men, 20 women; mean age, 64 years; range, 48-82 years) were evaluated with 64-slice MDCT angiography. Three sets of images were reconstructed with three different convolution kernels. We assessed diagnostic accuracy for ISR (≥50% diameter narrowing) of VAO stents with CTA in comparison with conventional angiography as the reference standard. The mean interval between initial stent implantation and follow-up CTA was 8.2 ± 3.1 months (range, 3.7-20.4 months). The median interval between CTA and conventional angiography was one day (range, 0-24 days). Evaluations were performed by two observers who were blinded to the results of conventional angiography. Sensitivity, specificity, and positive and negative predictive values were calculated.
Results
By CTA, 52 stents (85.2%) were assessable and nine stents (14.8%) were not assessable. For assessable stents, with CTA, six of seven stents with ISR on conventional angiography were diagnosed correctly. The sensitivity, specificity, and positive predictive value, and negative predictive values for all stents were 90.0%, 84.3%, 52.9%, and 97.7%. However, when excluding unassessable stents, values were 85.7%, 95.6%, 75.0%, and 97.7%. There was no significant difference between CTA and conventional angiography for the detection of ISR after VAO stenting (McNemar test, p = 1.00).
Conclusion
Sixty-four-slice MDCT angiography has high diagnostic value for ruling out significant in-stent restenosis after VAO stenting with high negative predictive value.

KEYWORDS: CT angiogram, Stents

eP-112

Monochromatic Imaging with Parametric X-ray: A Basic Study

Sekiya, K.[1]·Kaneda, T.[1]·Suemitsu, M.[1]·Hayakawa, Y.[2]·Sakae, T.[1]
[1]Nihon University School of Dentistry at Matsudo, Chiba, JAPAN, [2]Nihon University, Chiba, JAPAN.

Purpose
Parametric radiation-based x-ray (PXR), one of the pioneering studies using accelerator, is studied and expected for a new x-ray source with unique features different from conventional x-ray. In the Laboratory for Electron Beam Research and Application institute of quantum science (LEBRA), the PXR is generated with relatively a small linear accelerator (125MeV) and silicon crystal. The LEBRA-PXR has several unique characteristics, such as a tuneable wavelength, a nearly perfect mono-chromatid, a nearly perfect parallel beam, and high spatial coherence. All of these features are effective for the x-ray imaging and absorption studies. The purpose of this study was to evaluate the potential of LEBRA-PXR as a new x-ray source modality for imaging diagnosis.
Materials & Methods
The subject was a dog mandibular tissue with melanoma. Simple x-ray images were taken with LEBRA-PXR in several wavelengths (12 keV, 15 keV, 18 keV, 21 keV, 24 keV, 27 keV, 30 keV). An energy-subtracted image was generated with the image with the lowest wavelength PXR and the image with the shortest wavelength PXR. The subject was cut, H&E stained, and viewed with a microscope. As a control, an image was taken with conventional x-ray (42 kV, 125 mA, 40 msec; effective energy 21 keV). X-ray images were compared with the histopathologic images.
Results
Compared to conventional x-ray, LEBRA-PXR images showed contrast related to different wavelengths, reflecting histologic differences between tissues. Energy subtraction imaging with LEBRA-PXR offered more information of the lesion with regard to energy absorption coefficient of the tissues.

Note: Scanned images are included in the proceedings. Some submitted images were reduced during editing, thereby decreasing clarity. Also, refer to the Program Planner. Proceedings Content as of 3-29-2013.

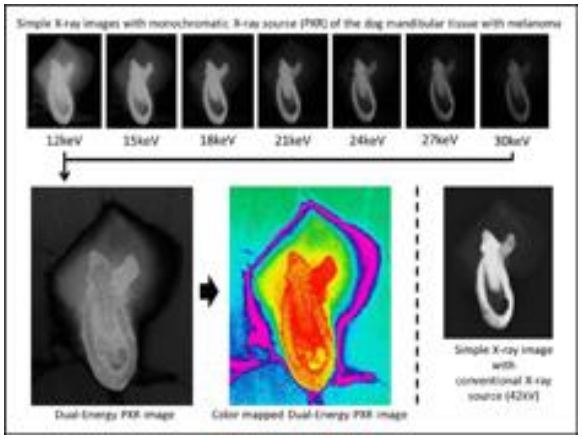

Conclusion
Using LEBRA-PXR, nearly perfect monochromatic x-ray source imaging, the images displayed different contrasts from conventional x-ray. Therefore, LEBRA-PXR may be useful for diagnostic imaging as a new x-ray source.
Acknowledgement: This study was supported by a grant from MEXT (Japan) KAKENHI Grant Number S0801032).

KEYWORDS: Dual energy spectral, Phase contrast imaging, parametric x-ray

eP-113

Vascular Mapping of the External Carotid Artery System: Comparison of the Visibility between CT Angiography with 64-Slice Multidetector CT and 3D Time-of-Flight MR Angiography at 3T

Iida, E.･Furukawa, M.･Kudomi, S.･Kato, M.･Kishi, T.･Matsunaga, N.
Yamaguchi University Graduate School of Medicine Ube, JAPAN.

Purpose
The knowledge of a patient's individual vascular mapping of the external carotid artery (ECA) system would benefit interventional radiologists for treatment planning in the head and neck disorders. The spatial resolution of CT angiography (CTA) has improved, and CTA with volume-rendering (VR) technique allows for assessment of vascular anatomy of the ECA systems. Time-of-flight MR angiography (TOF MRA) is less invasive and might be an alternative option, but saturation effects often lead to signal reduction of the ECA branches and may influence their visibility. The purpose of this study is to compare the visibility of major branches of the ECA between CTA and TOF MRA by using VR images.
Materials & Methods
Ten patients with head and neck tumor underwent both CTA with 64-slice multidetector CT and three-dimensional TOF MRA on 3T before common carotid arteriography and treatment with interventional radiology. Volume-rendering images of CTA and MRA were reconstructed by two independent radiologists. With two-dimensional digital subtraction angiography (DSA) and three-dimensional rotational DSA of common carotid artery as reference standard, the presence and the length from the origin were evaluated for the following 11 ECA branches (superior thyroid artery, lingual artery, facial artery, ascending pharyngeal artery, occipital artery, posterior auricular artery, internal maxillary artery, middle meningeal artery, accessory meningeal artery, superficial temporal artery and transverse facial artery) on VR images of CTA and MRA. The length from the origin of each artery was graded on a five-point scale (0: none, 1: less than 1 cm, 2: less than 2 cm, 3: less than 3 cm, 4: 3 cm or longer). Wilcoxon signed-rank test was used to determine differences between CTA and TOF MRA. A two-sided value of $P<0.05$ was considered significant.
Results
Two hundred eight branches of 19 ECA in 10 patients (total) were evaluated. For the presence of those branches, 152 branches (73.1%) were identified on CTA, while 181 branches (87.0%) were identified on TOF MRA ($P<0.05$). TOF MRA was superior to CTA in two branches (ascending pharyngeal artery and middle meningeal artery), while there was no statistically significant difference between CTA and TOF MRA in the remaining nine branches. For the length from the origin of each branch, mean score of all branches was 2.63 ± 1.77 for CTA and 2.75 ± 1.47 for TOF MRA, and there was no significant difference. CT angiography was superior to TOF MRA in two branches (superior thyroid artery and lingual artery), while TOF MRA was superior to CTA in two branches (ascending pharyngeal artery and middle meningeal artery). There was no significant difference between CTA and TOF MRA in the remaining seven branches.
Conclusion
Three-dimensional TOF MRA with VR is a noninvasive tool that can provide details of ECA branches, and would be an alternative option for treatment planning of interventional radiology in the head and neck disorders.

KEYWORDS: MR angiography, External carotid artery

eP-114

Correlation between Cyst Content CT Value and Microvessel Density in Keratocystic Odontogenic Tumor of the Mandible

Sekiya, K.[1,2]･Suemitsu, M.[1,2]･Kuno, H.[2]･Satake, M.[2]･Kaneda, T.[1]
[1]Nihon University School of Dentistry at Matsudo, Chiba, JAPAN, [2]National Cancer Center Hospital East, Chiba, JAPAN.

Purpose
Keratocystic odontogenic tumor is a locally aggressive developmental cystic neoplasm with a high recurrence rate. Previous studies have indicated that microvessel density is a histopathologic parameter that can be

Note: Scanned images are included in the proceedings. Some submitted images were reduced during editing, thereby decreasing clarity. Also, refer to the Program Planner. Proceedings Content as of 3-29-2013.

indicative of lesion activity. Measurement of the CT value of the cyst content is a simple method for assessing the proportions of the various components. The present study was conducted to investigate the correlation between the CT value and microvessel density in keratocystic odontogenic tumor of the mandible.

Materials & Methods

Nineteen subjects with histopathologically confirmed keratocystic odontogenic tumor who underwent preoperative CT examinations between April 2006 and November 2011 were enrolled in this retrospective study. There were nine males (47%) and 10 females (53%), ranging in age from 11 to 70 years (median, 39 years). The average cyst content CT values for all subjects were measured on axial noncontrast CT images of the lesions. The subjects were divided into two groups according to the presence or absence of high CT value spot. The high CT value spot was defined as higher than 90 HU, by reference to previous studies. Histopathologically, microvessel densities in all subjects were also measured on slides immunohistochemically stained with CD34 antibody (Figure 1). Statistical analysis of the correlation between the cyst content CT value and microvessel density was carried out using Pearman's rank correlation coefficient. The significance of differences in microvessel density between the two groups discriminated according to the highest CT value for the cyst content was tested using the Mann-Whitney U test.

Results

The average cyst content CT value was 31.1 ± 14.3 HU, and five subjects (26%) had the high CT value spot. The average microvessel density was 9.3 ± 3.8 per 40000 μm. Cyst content CT values were correlated with the microvessel density of the lesions (r = .48, P = .036) (Figure 2). Subjects who had high CT values spot showed a significantly higher microvessel density in the lesions (P < .05).

Conclusion

It is suggested that the cyst content CT value is correlated with microvessel density in keratocystic odontogenic tumor of the mandible, and therefore may be applicable as a parameter for prediction of local aggressiveness and potential for recurrence.

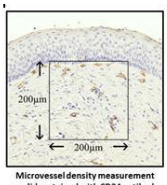

Microvessel density measurement on slides stained with CD34 antibody

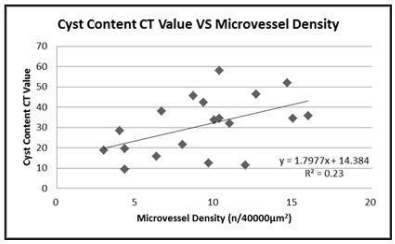

KEYWORDS: CT, Odontogenic, microvessel density

eP-115

Assessment of Follow-Up Ultrasonography and Clinical Improvement among Infants with Congenital Muscular Torticollis

Park, H. J.
Sungkyunkwan University School of Medicine, Kangbuk Samsung Hospital
Seoul, KOREA, REPUBLIC OF.

Purpose

To evaluate whether a new ultrasonographic assessment method that utilizes the muscular thickness ratio of the SCM can help quantify the outcome of rehabilitation therapy for patients with congenital muscular torticollis (CMT).

Materials & Methods

We evaluated 48 patients (M:F = 17:31; mean age, 3.9 months) who were diagnosed with CMT and who underwent initial and follow-up ultrasonography. The ratio of the thickness of the involved SCM to the thickness of the intact SCM ("SCM thickness ratio") was calculated. A scoring system based on the range of motion of the neck was used to assess clinical improvement. The correlations between clinical improvement and the thickness of the involved muscle, the difference in involved muscle thickness, the SCM thickness ratio, and the difference in the SCM thickness ratio were evaluated with Spearman rank correlations.

Results

Follow-up Cheng scores were higher than initial scores, which indicate clinical resolution (followup, 4.90; initial, 3.38). The SCM thickness ratio at followup was lower than at the initial evaluation (followup, 1.29-1.34; initial, 1.65-1.77). Intra and interobserver agreements were excellent. Most variables were moderately correlated with clinical improvement (correlation coefficients: 0.36-0.509). R1 showed the highest correlation with clinical improvement (0.481 and 0.509), followed by the initial maximal thickness of the SCM (0.434 and 0.488). ΔP (P1-P2) and ΔR showed similar correlation coefficients with clinical improvement.

Conclusion

Measurement of the SCM thickness ratio appears to overcome the problem of a false positive diagnosis of clinical aggravation of CMT resulting from physiologic growth. R1 and ΔR are accurate, objective measurements that can be used in the management of CMT.

KEYWORDS: Congenital, Ultrasonography

Note: Scanned images are included in the proceedings. Some submitted images were reduced during editing, thereby decreasing clarity. Also, refer to the Program Planner. Proceedings Content as of 3-29-2013.

eP-116

Ultrasound Predictors of Thyroid Malignancy: Correlating with Ultrasound-Guided Biopsy and Thyroidectomy

Chen, B. T.·Jain, A. B.·Dagis, A.·Vora, L.·Maghami, E.·Salehian, B.
City of Hope Medical Center
Duarte, CA.

Purpose
Thyroid ultrasound has been used extensively for evaluation of thyroid nodules. Well documented ultrasound features associated with thyroid malignancy include micro or macro calcifications, poorly defined margin, hypoechogenicity, taller-than-wide shape and hypervascularity. Ultrasound features of thyroid nodules play important role in clinical management. The purpose of this study is to determine the prevalence of thyroid malignancy, and to evaluate ultrasound predictors of thyroid malignancy. This study compared the ultrasound features with ultrasound-guided biopsy results. It further tested the ultrasound predictors in the subset patients who went on to have thyroidectomy.
Materials & Methods
All consecutive ultrasound-guided thyroid biopsy procedures from 1/2007 to 12/2011 were reviewed retrospectively for ultrasound characteristics and ultrasound-guided biopsy results. Pathology reports from the subset of patients who went on to have hemi/total thyroidectomy also were reviewed. Multivariate logistic regression models were constructed for testing predictors of malignancy. All p values were reported significant at less than 0.05 from either Fisher's exact test or from Wilcoxon test.
Results
A total of 461 thyroid nodules in 350 patients underwent ultrasound-guided thyroid biopsy procedures during the study interval. Of these, 32 (7%) nodules were excluded from the study due to inadequate sampling, leaving 429 nodules available (median age 58 years ranging from 14 to 88, female 80% versus male 20%). Surgical excision with hemi/total thyroidectomy was performed in 105 (24.5%) thyroid nodules. Of the 429 biopsies, 38 (9%) were reported as malignant or suspicious for malignancy. Male patients have significantly higher chance of malignancy found in biopsy compared to females [(19% versus 6%, p = 0.001 in Fisher's exact test), Odds ratio (95% Confidence Interval): 2.74 (1.24, 6.02)]. Ultrasound features that significantly predict malignancy on biopsy included: ultrasound micro calcifications with p <0.001 and Odds ratio (95% confidence interval): 7.16 (2.95, 17.4), Ultrasound coarse or eggshell calcification in thyroid biopsy with p = 0.002 and Odds ratio (95% confidence interval): 4.49 (1.77, 11.4). Thyroid nodule size and other ultrasound features such as hypoechogenicity, increased vascularity, taller-than-wider, and ill-defined margins are weak predictors of thyroid malignancy. In the subset cohort with subsequent hemi/total thyroidectomy (n = 105), ultrasound biopsy results significantly predict malignancy in surgery with p<<0.0001, Odds ratio and confidence interval: 67.3 (18.3, 248). Ultrasound microcalcification predicts malignancy in surgery with p = 0.02, Odds ratio and confidence interval: 3.33 (1.24, 8.93). Ultrasound coarse or eggshell calcification predicts malignancy with p = 0.0006, Odds ratio and confidence interval: 8.48 (2.48, 28.9). Ultrasound hypoechogenicity predicts malignancy in surgery with p = 0.02, Odds ratio and confidence interval: 4.49 (1.23, 16.3). Ultrasound nodule shape predicts malignancy with p = 0.05, Odds ratio and confidence interval: 5.40 (0.99, 29.4).
Conclusion
The prevalence of thyroid malignancy in our cohort is 9% on biopsy. Micro, coarse or eggshell calcifications significantly predict malignancy on biopsy, which is further validated in the subset cohort with subsequent thyroidectomy. Male patients have significantly higher chance of malignancy found in biopsy compared to females. Ultrasound biopsy results significantly predict malignancy in surgery.

KEYWORDS: Thyroid, Ultrasonography, thyroid nodules

eP-117

Effect of Radiotherapy on Dynamic Contrast-Enhanced Perfusion Parameters in the Head and Neck

Ishiyama, M.[1]·Richards, T.[1]·Parvathaneni, U.[1]·Furukawa, M.[2]·Anzai, Y.[1]
[1]University of Washington, Seattle, WA, [2]Yamguchi University, Yamaguchi, JAPAN.

Purpose
Dynamic contrast-enhanced (DCE) MRI allows us to obtain quantitative information of microvascular environment. Dynamic contrast-enhanced MR has the potential to differentiate malignant from benign tumors, post-treatment changes from recurrent tumors, and predict treatment response. Chemoradiotherapy is often the primary treatment for advanced stage head and neck cancer. Radiotherapy (RT) may alter the microvascular profile in tumors and the surrounding normal tissues. To interpret DCE MR changes in posttreatment patients, it is essential to understand the impact of radiation on the perfusion parameters of normal head and neck tissues. The aim of this study was to investigate the effects of radiotherapy on the DCE MRI perfusion parameters of the microvascular environment of the normal tissue among patients with previously treated head and neck cancer.
Materials & Methods
Thirty-three patients (27 men and 10 women, mean age; 55.9 years) who underwent DCE MRI for evaluation of head and neck cancer were enrolled retrospectively in this study. Nine patients were treated previously with RT to the head and neck region. Mean time from completion of the therapy to DCE MRI was 23.9 months. Dynamic contrast-enhanced MRI protocol was based on 3D T1-

Note: Scanned images are included in the proceedings. Some submitted images were reduced during editing, thereby decreasing clarity. Also, refer to the Program Planner. Proceedings Content as of 3-29-2013.

weighted acquisition with time resolution of 2.6 seconds and total acquisition time of 4 minutes 17 seconds (100 dynamic volumes). Quantitative values including permeability surface area (PS) and tumor blood volume (BV) (estimated as area under intensity curve) were obtained from eight locations in the normal tissue. Permeability surface area parameters were obtained using a modified Tofts model. The quantitative values were compared between patient with and without RT, as well as duration after the completion of RT. Wilcoxon signed-rank test was used for analysis.
Results
The number of examined structures depended on the range of scan in each patient because not all of the study covered entire head and neck region. Quantitative values were obtained from the parotid gland (n = 27), submandibular gland (n = 22), tongue (n = 21), floor of mouth (n = 18), medial pterygoid muscle (n = 23), palatine tonsil (n = 25), posterior cervical muscles (n = 31), and cervical spinal cord (n = 33). There were no statistical differences between patients with and without radiotherapy in PS and BV in each location. No statistical difference was observed in PS and BV between patients less than one year from the completion of RT and more than one year from RT.
Conclusion
Radiotherapy has little effect on PS and BV in the normal tissues of the head and neck region. This suggests validity of using ratio between tumor and normal muscles, salivary gland tissues, spinal cords, or palatine tonsil in the head and neck.

KEYWORDS: Dynamic contrast-enhanced MR, Permeability MR imaging

eP-118

Clinical Usefulness of ^{18}F-FDG PET/CT and CT/MR Imaging for Detecting Nodal Metastasis in Patients with Hypopharyngeal Cancer

Kim, J.·Shin, N.·Kim, K.·Lee, J.·Koh, Y.
Yonsei University College of Medicine
Seoul, KOREA, REPUBLIC OF.

Purpose
To assess the clinical usefulness of ^{18}F-FDG PET/CT and CT/MRI for preoperative planning of contralateral neck dissection in patients with hypopharyngeal squamous cell carcinoma (SCC).
Materials & Methods
In total, 35 hypopharyngeal SCC patients who underwent primary site resection with uni or bilateral neck node dissection were evaluated retrospectively. No patient had distant metastasis or history of prior treatment. Every patient underwent PET CT and CT/MRI, and histopathologic analysis was used as the gold standard for assessment of each imaging technique.
Results
Of the 45 patients, 35 (77.8%) had neck node metastasis and 12 (26.7%) had contralateral neck node metastasis. On a level-by-level basis, the accuracy of PET CT for nodal metastases was higher than that of CT/MRI (89.0% vs. 94.0%, p = 0.046). In addition, although three (13.0%) of the 23 patients with palpably negative neck (N0) showed contralateral neck node metastasis, the patients who showed no evidence of ipsilateral nodal metastasis on PET CT and CT/MRI revealed no occult contralateral neck metastasis.
Conclusion
^{18}F-FDG PET/CT has additional values for the preoperative prediction of nodal metastasis in patients with hypopharyngeal cancer. In clinically N0 patients, ^{18}F-FDG PET/CT may prevent them from undergoing unnecessary contralateral neck dissection.

KEYWORDS: Head and neck, PET/CT, lymph node metastasis

eP-119

Clinical Usefulness of ^{18}F-FDG PET/CT for Detecting Nodal Metastasis in Patient with Oropharyngeal Cancer Compared to CT/MR Imaging

Kim, J.·Kim, I.·Choi, Y.·Sohn, B.·Lee, J.·Koh, Y.
Yonsei University College of Medicine
Seoul, KOREA, REPUBLIC OF.

Purpose
To investigate the clinical usefulness of ^{18}F-FDG PET/CT for the preoperative prediction of nodal metastasis in clinically N0 patients with oropharyngeal squamous cell carcinoma (SCC), by comparing with CT and/or MRI.
Materials & Methods
In total, 118 oropharyngeal SCC patients who underwent primary site resection with uni or bilateral neck node dissection were evaluated retrospectively. No patient had distant metastasis or history of prior treatment. Every patient underwent PET CT and CT/MRI, and histopathologic analysis was used as the gold standard for assessment of each imaging technique.
Results
On a patient-by-patient basis, the accuracy of PET CT for nodal metastases was higher than that of CT (77.6% vs. 68.9%, p = 0.015) and MRI (77.6% vs. 66.7%, p = 0.003). Visual correlation of CT/MRI and PET CT yields slightly higher accuracy than CT (73.5% vs. 68.9%, p = 0.020) or MRI alone (73.5% vs. 66.7%, p = 0.028). In addition, 49 (41.5%) of our 118 patients showed clinically negative neck (N0), and the sensitivity for occult neck node metastases in N0 patients was 59.1% in CT, 50.0% in MRI, and 64.0% in PET CT. Ten patients (20.4%) were falsely negative in CT/MRI and nine (18.4%) were falsely negative in PET CT.
Conclusion
Positron emission tomography CT was more accurate than CT/MRI for detecting neck node metastasis of oropharyngeal SCC. In clinically N0 patients, as the

Note: Scanned images are included in the proceedings. Some submitted images were reduced during editing, thereby decreasing clarity. Also, refer to the Program Planner. Proceedings Content as of 3-29-2013.

sensitivity of PET CT as well as CT/MRI was still low, elective neck node dissection should be followed.

KEYWORDS: Oropharynx, PET/CT, lymph node metastasis

eP-120

Native versus Radiation-Induced Soft Tissue Sarcomas of the Head and Neck

Eliahou, R.·Learned, K.·Lustig, R.·Alonso-Basanta, M.·Loevner, L.
Hospital of University of Pennsylvania
Philadelphia, PA.

Purpose
Sarcomas of the head and neck in adults are uncommon accounting for approximately 0.1% of annual malignancies in the U.S. Radiation-induced sarcoma of the head and neck is a rare, late complication of radiation therapy. Native and radiation-induced sarcomas are different clinical entities with different clinical course and management. Radiation-induced sarcomas are treated primarily with surgical excision and have a poor prognosis. The purpose of this study is to evaluate and compare the imaging findings of native versus radiation-induced head and neck sarcomas.
Materials & Methods
We retrospectively reviewed our institution sarcoma database from 2002- 2012 to identify patients with head and neck sarcomas for whom we had CT and/or MR imaging from their initial presentation. Their imaging and medical records including histopathology, clinical course, and radiation dose/protocol for those sarcomas that were radiation-induced were reviewed. The masses were evaluated for anatomical locations, borders, size, and tissue characterization (CT attenuation, T1 and T2 signal intensity, and enhancement).
Results
Eight patients had native head and neck sarcomas (four male, four female, mean age 60 years) and eight patients had radiation-induced sarcomas (four male, four female, mean age 57 years). The radiation-induced sarcoma group received a mean total radiation dose of 68 Gy and had a mean latency period for the development of the sarcoma in the irradiated field of 13 years. The most common primary diagnosis treated with radiation was nasopharyngeal squamous cell carcinoma in three of eight patients. The most common sarcoma histopathology for both groups was soft tissue spindle cell sarcoma (seven of eight in the radiation group, five of eight in the native group). Most sarcomas were high-grade (six of eight in the native group, and eight of eight in the radiation group). The most common anatomical location of adult sarcomas was skull base occurring in six of eight in the radiation group and three of eight for the native group. Enhancing large masses (4.1 cm average size for both groups) was typical. For the native group, six of eight masses were well circumscribed, none necrotic, three of eight involved bone with chronic as well as focal permeative changes. For the radiation group, all sarcomas had poorly defined margins, necrosis was seen in 50%, and six of eight were associated with permeative bone erosion.
Conclusion
Native and postradiation sarcomas of the head are uncommon, and are different clinical entities. Although imaging findings are not pathognomonic and share some similarities, radiation-induced masses have infiltrative margins, necrosis is frequent as is permeative bone destruction, compared to native tumors which are more circumscribed, frequently solid, with less aggressive bone changes. In the radiated group high clinical suspicion for treatment-induced sarcoma in the appropriate setting is important, as these are not uncommonly initially misinterpreted for neoplastic recurrence.

KEYWORDS: Neck masses, Radiation injury, sarcoma

eP-121

Differentiation of Recurrent Tumor from Postradiation Changes on DCE MR Perfusion in the Head and Neck Region

Ishiyama, M.[1]·Parvathaneni, U.[1]·Richards, T.[1]·Furukawa, M.[2]·Anzai, Y.[1]
[1]University of Washington, Seattle, WA, [2]Yamaguchi University, Yamaguchi, JAPAN.

Purpose
Conventional MR or CT imaging has limitations in differentiating post-treatment changes from recurrent tumors following chemoradiotherapy among head and neck (HN) cancer patients. Dynamic contrast-enhanced (DCE) MRI potentially serves as surrogate of microvascular environment, such as leakiness of blood vessels or microvascular density. We hypothesize that DCE parameters such as permeability surface area (PS) and tumor blood volume (BV) (estimated as area under intensity curve) are useful in differentiating a recurrent tumor from post-treatment inflammation or fibrosis. The purpose of this study is to investigate the usefulness of quantitative microvascular parameters in head and neck cancers.
Materials & Methods
This retrospective study included consecutive 29 patients (22 men and seven women, mean age: 56.2 years) who underwent DCE MRI on a 3T scanner. Of 29 patients, 16 patients had newly diagnosed biopsy-proven untreated primary HN cancers, seven patients had biopsy-proven recurrent HN cancers, and six patients had benign post-treatment enhancement confirmed by clinical follow-up examinations. Dynamic contrast-enhanced MRI protocol was based on 3D T1-weighted acquisition with time resolution of 2.6 seconds and total acquisition time of 4 minutes 17 seconds (100 dynamic volumes). An experienced radiologist drew regions of interest to include entire lesion using conventional MR images as anatomical

Note: Scanned images are included in the proceedings. Some submitted images were reduced during editing, thereby decreasing clarity. Also, refer to the Program Planner. Proceedings Content as of 3-29-2013.

reference. Four points in the internal carotid artery were selected and averaged for the arterial input function. Quantitative values including PS and blood volume (BV) were calculated on in-house software (modified Tofts model) and they were compared between the tumor group (primary and recurrent HN cancers) and the nontumor group (benign post-treatment enhancement). Wilcoxon signed-rank test was used for analysis.
Results
Permeability surface areas were 2.4 x 10 -4 +/- 1.6 10 -4 (mean ± SD) in the tumor group (n = 23) and 4.8 x 10 -4 +/- 8.3 10 -4 in the nontumor (post-treatment) group (n = 6). There was a statistically significant difference (p = 0.03) between the two groups (p = 0.03). In contrast, no statistically significant difference was observed in BV between these two groups (p = 0.085).
Conclusion
Post-treatment changes in the head and neck region had markedly high permeability property. There was no significant difference in BV between tumors and post-treatment changes.

KEYWORDS: Dynamic contrast-enhanced MR, Permeability MR imaging

eP-122

Assessment of the Necrosis in the Cervical Lymph Nodes: Diagnostic Value of Contrast-Enhanced Ultrasonography Compared with Enhanced CT and Pathologic Findings

Kato, M.·Iida, E.·Furukawa, M.·Fujita, T.·Tanabe, M.·Oga, A.·Matsunaga, N.
Yamaguchi University
Ube, JAPAN.

Purpose
In the lymph node staging of head and neck squamous cell carcinoma (HNSCC), central necrosis is a characteristic feature suggesting metastatic nodes. Contrast-enhanced ultrasonography (CE US) provides sensitive vascular flow images, and we hypothesized that CE US would improve diagnostic accuracy for the detection of necrotic nodes. The purpose of this study is to assess the value of CE US for identifying the nodal necrosis compared with that of contrast-enhanced CT (CECT), which is widely used for nodal staging.
Materials & Methods
Consecutive 17 patients (age range: 42-91 years; mean age, 66 years) with histologically proven HNSCC were included in this study. Both CE US and CE CT were performed for preoperative nodal staging, and the interval among imaging examinations and operation was within 1 month (mean interval between both examination: 9.4 days, mean interval between first examination and operation: 21.4 days). Two radiologists independently reviewed images regarding the presence of nodal necrosis with a four-point grading scale. Those findings were compared with pathologic findings, which were used as a standard reference, for each individual node. Interobserver and intermodality agreements were calculated. The diagnostic performance of each modality for detecting the necrotic lymph node was analyzed, and compared statistically. ROC analysis also was performed.
Results
Ten of 17 patients had metastatic nodes. Of the total of 53 dissected lymph nodes, 17 nodes were metastatic nodes and 14 of them had necrosis on pathology. The mean short-axis diameter of necrotic nodes was 5.4 mm (range ±3.4 mm). Regarding the evaluation of nodal necrosis, the interobserver agreement was excellent on both modalities (CE US: κ = 0.91, CE CT: κ= 0.94), and the intermodality agreements also were excellent (reviewer 1: κ = 0.90, reviewer 2: κ= 0.92). The sensitivity, specificity, positive predictive value, negative predictive value, and diagnostic accuracy was 93%, 95%, 87%, 97%, 93% on CE US, and 93%, 92%, 81%, 97%, 91% on CE CT, respectively. Between both modalities, there was no significant difference for the diagnostic performance. On ROC analysis, the value of area under the curve was 0.93 on CE US and 0.94 on CE CT, respectively.

A 59 year-old patient with carcinoma of lower gingiva. Low attenuation area is seen in the superior deep cervical lymph node on CECT (A) and corresponds to hypoecholcanea on CEUS (B). A necrotic lymph node metastasis is pathologically confirmed.

Conclusion
Although ultrasonography has some shortcomings such as operator dependency, CE US showed a highly diagnostic performance for identifying necrosis in the metastatic lymph nodes without any radiation exposure. Combined diagnostic criteria with CE US may be a powerful diagnostic tool for lymph node staging in HNSCC.

KEYWORDS: Lymph node metastasis, Ultrasonography

eP-123

Invasive Fungal Sinusitis with Aspergillosis in an Immunocompetent Patient

Iqbal, S.·Joshi, A.·Zuberi, A.·Iqbal, M.
University of Kansas School of Medicine Wichita
Wichita, KS.

Purpose
Invasive fungal sinusitis with Aspergillus rarely has been

Note: Scanned images are included in the proceedings. Some submitted images were reduced during editing, thereby decreasing clarity. Also, refer to the Program Planner. Proceedings Content as of 3-29-2013.

described in an immunocompetent patient.
Materials & Methods
CT imaging details the invasive nature of Aspergillus epidentered in the maxillary sinus and subsequently invading through to the nasal cavity with destruction of nasal trubinates, bony nasal septum, as well as the soft palate. Additionally, a full clinical workup of the patient is presented to explore etiologies and underlying conditions for the patient's presentation. She presents to the ER with "a hole in the roof of my mouth." Detailed history, extensive hematologic workup in order to exclude any immunodeficiency, and biopsy for pathologic diagnosis were reviewed. Follow-up imaging also was obtained at our institution.
Results
CT Imaging of a young healthy female patient demonstrates an invasive, destructive process, epicentered in the maxillary sinuses with destruction of the nasal turbinates, nasal septum, and soft palate. The samples sent to pathology obtained by the otolaryngologist, confirmed the destructive nature of the infection and the smears were positive for a fungal etiology, which grew out Aspergillus. No congenital or acquired immunodeficiencies were found upon extensive hematologic workup.

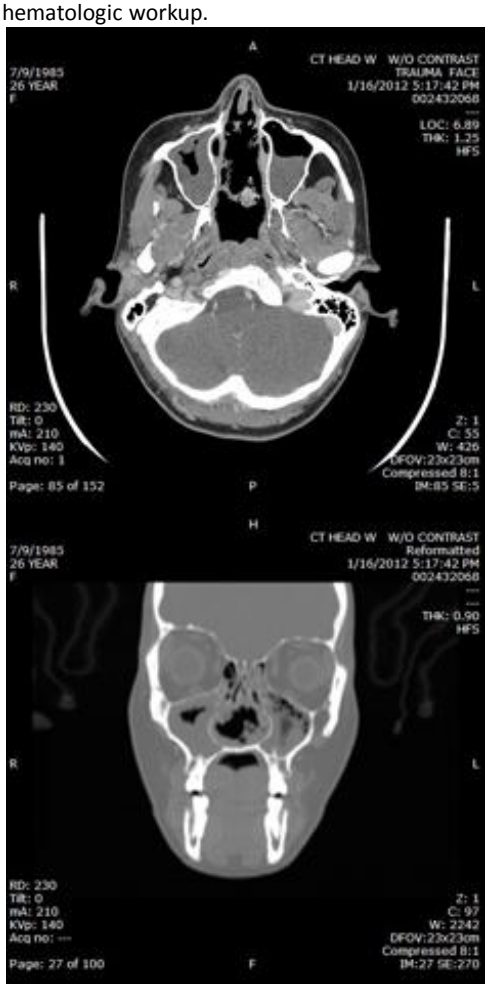

Conclusion
We describe an unusual case of invasive Aspergillus sinusitis in a pregnant patient with otherwise no immunodeficiencies. Our hypothesis is that her chronic use of cephalexin for acne may have altered the sinonasal flora, predisposing her to develop invasive Aspergillus sinusitis.

KEYWORDS: Sinonasal disease, Invasive fungal, immunocompetent

eP-124

Clinical Significance of Incidental Torus Tubarius Calcification

Buch, K.[1]·Nadgir, R.[1]·Ozonoff, A.[2]·Sodagari, F.[1]·Sakai, O.[1]
[1]Boston Medical Center, Boston, MA, [2]Harvard School of Public Health, Boston, MA.

Purpose
Calcification of the torus tubarius rarely has been reported in the literature. Histopathologic studies previously have described cases of Eustachian tube calcification and describe an association with increasing patient age. To our knowledge, a large study examining the prevalence of torus tubarius calcification and potential clinical significance on an unrestricted patient population using thin-section CT has not been reported.
Materials & Methods
Following IRB approval, 1000 patients were included in this study and consecutive noncontrast brain CT scans between January 2011 and February 2011 were reviewed retrospectively for presence of torus tubarius calcifications. Note was made as to whether these calcifications were unilateral versus bilateral. Studies were acquired axially at 1.25 mm slice thickness on 64-detector row CT scanners. Electronic medical records were reviewed on all subjects, and clinical parameters including age, gender, random glucose, hemoglobin A1C, alkaline phosphatase levels, and chronic medical conditions including diagnosis of diabetes, alcoholism, HIV, and renal disease were recorded. Severely motion-limited studies, follow-up examinations if performed, and subjects with limited clinical data were excluded. Statistical analysis of imaging and clinical data was performed using a Fisher test.
Results
Study population consisted of 974 patients with 459 males (mean age, 51 years) and 515 females (mean age, 54 years), ranging in age from 1 month to 100 years. Seven patients out of 974 were found to have torus tubarius calcifications with an overall prevalence of 0.7%. Four out of seven patients had bilateral calcification of the torus tubarius (57.1%) compared to three out of seven patients with unilateral calcification of the torus tubarius (42.9%). There was no statistically significant correlation between diabetes mellitus, HIV or renal disease and prevalence of torus tubarius calcification. There was an increased

Note: Scanned images are included in the proceedings. Some submitted images were reduced during editing, thereby decreasing clarity. Also, refer to the Program Planner. Proceedings Content as of 3-29-2013.

prevalence of elevated alkaline phosphatase in patients with torus tubarius calcification; however, after controlling for age and gender there was no statistically significant correlation. There was no statistically significant correlation between patient age and presence of torus tubarius calcification.
Conclusion
Calcification of the torus tubarius is rare with an overall prevalence of 0.7%, based on the largest series to date on an unrestricted population using thinner section CT imaging. While the clinical significance remains uncertain, there is no statistically significant association between the presence of torus tubarius calcification and common medical conditions or increase in age.

KEYWORDS: Calcifications, Incidental findings, Torus Tubarius

eP-125

CT Findings in Zygomatic Complex Fractures with Trismus

Johnson, J. M.[1]·Morgan, J. N.[2]·Troulis, M.[1]·Rubin, P.[3]·Caruso, P. A.[1]
[1]Massachusetts General Hospital, Boston, MA, [2]Brigham and Women's Hospital, Boston, MA, [3]Boston Eye Physicians and Surgeons, Boston, MA.

Purpose
To review the CT imaging findings in patients with zygomatic complex fractures (ZCF) to determine if certain findings are predictive for the development of trauma-induced trismus.
Materials & Methods
CT images of 30 patients (8 female), age range 14-85 years, with zygomatic complex fractures were reviewed. Patients with mandibular fractures were excluded. The CT imaging for each patient was reviewed and the following elements were recorded: fracture or intactness of the zygoma, the zygomatic sutures, the maxilla, the sphenoid bone and the temporal bone and the relationship of fracture fragments to the mandible and zygomatic arch. Evaluation also was performed on the relationship of the fracture components and regional soft tissues and muscles of mastication.
Results
Sixteen of the 30 patients reported trismus. Two measurements were statistically significant in relationship to the presence of trismus. A measure of retroposition of the zygomatic body between the fractured side and the contralateral normal side revealed a difference of 4.44 mm, (± 3.12) in the trismus group compared to 2.43 mm (± 1.88) in the group without trismus (p = 0.04). The difference of the distance between the coronoid process of the mandible and the zygomaticomaxillary suture between the fractured side and the contralateral normal side was 4.13 mm (± 3.03) in the group with trismus and 2.21 mm (± 1.93) in the group without trismus (p = 0.05).

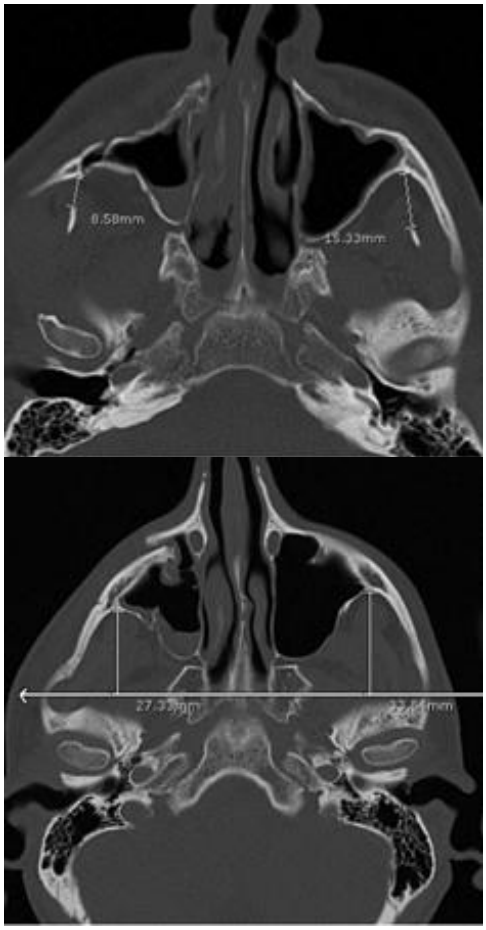

Conclusion
Greater degrees of retroposition of the zygomatic body and narrowing of the space between the zygomaticomaxillary suture and the coronoid process are associated with trismus in the setting of ZCF. These elements should be evaluated routinely in this type of injury.

KEYWORDS: Facial fractures, CT, Trismus

eP-126

Identifying the Malignant Parotid Neoplasm: Evaluation of Imaging Characteristics

Klatt-Cromwell, C. N.·Pina, S.·Chiu, W.·Jewells, V.·Hackman, T. G.
University of North Carolina Chapel Hill
Chapel Hill, NC.

Purpose
Parotid gland masses are comprised of a diverse array of lesions encompassing many benign and malignant entities. While approximately 85% of all tumors are thought to be benign, such as pleomorphic adenomas and Warthin's tumors, the remaining lesions include various malignancies and metastatic disease. With the aggressive behavior of some malignancies, including mucoepidermoid carcinoma

Note: Scanned images are included in the proceedings. Some submitted images were reduced during editing, thereby decreasing clarity. Also, refer to the Program Planner. Proceedings Content as of 3-29-2013.

(ME), acinic cell carcinoma (ACC), adenoid cystic carcinoma (ADC), and carcinoma ex pleomorphic adenoma (CPA), earlier detection is of paramount importance. There is limited discussion in the literature regarding characteristic CT findings for these pathologies and their predictive nature. We hypothesize usage of standardized grading characteristics on imaging may help predict the presence of malignancy pre-operatively. Therefore, the aim of this study was to identify the imaging characteristics of parotid masses that may more accurately diagnose and classify malignant lesions.

Materials & Methods

Retrospective cohort study evaluating patients identified to have parotid masses based on pathology record search over a five-year period. Inclusion criteria were all patients presenting with parotid masses with CT imaging. Lesions of skin origin with parotid infiltration were excluded. Using a blinded approach, patients' pathology reports and imaging were assessed and classified by independent physicians. Three imaging characteristics were used to assess the cohort. Each patients' parotid mass was evaluated for the presence of the following characteristics: lobulated appearance, poorly-defined borders, and infiltration (finger-like projections). Pathology specimens were assessed for final pathologic grading, evidence of infiltration, and margin status. Univariable and multivariable logistic regression models were used to evaluate the association between imaging characteristics and malignancy.

Results

Two hundred eighty-five patients, 129 females and 156 males, ages 7-92 years were identified with parotid masses. Two hundred twenty-nine patients were found to meet all inclusion criteria to undergo analysis. Of these, 80 patients (35%) had malignancies, including 27 (34%) ME, 13 (16%) ACC, 5 (6%) CPA, and 2 (3%) ADC. Results from univariable models demonstrate that infiltration (p<.0001) and margin definition (p=0.01) are significantly associated with malignancy. Those with infiltrative front are 12 times more likely to be associated with malignancy [OR=12 (95% CI: 5.5-26)]. Patients with poorly defined borders are two times more likely to represent malignancy [OR=2 (95% CI: 1.2-3.6)]. Assessing three characteristics together, infiltrative front remains strongly associated with the malignancy (p<.0001).

Table 1: Multivariate Analysis

Model Covariates	Total (N=229)	Malignant (N=80)	Benign (N=149)	Chi-Square	P-Value	Odds Ratio	Lower 95%	Upper 95%
Poorly Defined Margins	94	42	52	2.6159	0.1058	1.79	0.88	3.62
Lobulated Appearance	169	57	112	2.7168	0.0993	0.58	0.31	1.11
Infiltrative Front	47	37	10	36.9214	<0.001	11.86	5.34	26.34

Conclusion

Parotid masses represent a diverse group of lesions with variable imaging characteristics. Our analysis revealed strong correlation between two characteristics (infiltrative front and poor margin definition) and malignancy. We would advocate for these grading characteristics to be used pre-operatively in counseling for potential malignancy. Of note, ACC and CPA showed better margin definition, which we hypothesize may be due to the indolent growth of acinic cell and the benign origin of carcinoma ex pleomorphic adenomas.

KEYWORDS: Parotid gland, CT

eP-127

Zoomed EPI Diffusion Tensor Imaging of the Optic Nerve

Shah, P. N.·Covington, A.·Middleton, D.·Mohamed, F.
Temple University
Philadelphia, PA.

Purpose

The purpose of the study was to (a) image optic nerve (ON) in normal adults using a new zoomed DTI technique and (b) to optimize the DTI imaging parameters and provide a reliable method of DTI ON imaging for clinical use.

Materials & Methods

Twelve subjects (ages 25-50 years) without clinical evidence of ON pathology were recruited on a volunteer basis. All the subjects were instructed to fixate their eyes to a marker inside the 12-channel head coil during DTI scanning. Initially a sagittal scout T1 followed by conventional FSE T2-weighted scans of the orbit were obtained. A zoomed EPI technique DTI sequence was installed and optimized for imaging the optic nerve on a 3.0T Siemens Verio MR scanner. The following scan parameters were used to obtain high-resolution images of the orbits: 6 directions, b=800s/mm^2, voxel size=1.7x1.7x1.5 mm^3, axial slices=10, TR=6100-8000 ms, TE=94 ms, averages=16. This pulse sequence is based on a single shot echo planar (EPI) sequence with spatially selective 2D RF excitations. The data were transferred to an independent workstation for postprocessing. Tensor estimation was performed using MedINRIA software (www-sop.inria.fr/asclepios/software/MedINRIA/). Various DTI indices were calculated for ROIs drawn at every axial slice location along each individual ON: fractional anisotropy (FA), axial diffusivity (AD), radial diffusivity (RD), and mean diffusivity (MD) were measured. Each ON was located on the b0 image and a ROI was manually drawn on the corresponding FA map to include the middle portion of the ON verified by a board certified neuroradiologist.

Results

Imaging with the zoomed DTI sequence resulted in reliable DTI data of the ON (Figure 1). Qualitative examination of the images demonstrated reduced eddy current and motion distortions. A total of 23 ON were included in the data analysis. In one subject the ON on one side demonstrated severe distortion and hence not included in the analysis. Subjects showed mean ± standard deviation: FA=0.43±0.06, AD=1.04±0.22x10^{-3}mm^2/s,

Note: Scanned images are included in the proceedings. Some submitted images were reduced during editing, thereby decreasing clarity. Also, refer to the Program Planner. Proceedings Content as of 3-29-2013.

RD=0.52±0.13x10^{-3} mm^2/s, MD=0.69±0.15x10^{-3} mm^2/s. The total scan time for DT imaging was under 5:30 min.

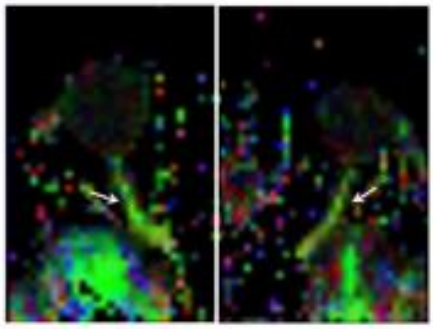

Figure 1: Fractional anisotropic images of the right and left optic nerve (white arrows) in a healthy volunteer using a zoomed DTI technique

Conclusion

This study demonstrates that reliable DT parameters of the optic nerve can be obtained in a reasonable time frame utilizing standard MR imaging equipment. Future studies with clinical pathology of the ON are warranted.

KEYWORDS: Optic nerve, Diffusion tensor image, 3T Zoomed EPI technique

eP-128

3T MR Characterization of the Optic Nerve Sheath in Astronauts

Hakimelahi, R.[1]·Riascos, R.[1]·Hasan, K. M.[2]·Heymann, J. C.[1]·Cotes, C. C.[1]·Sargsyan, A.[3]·Alperin, N.[4]·Kramer, L. A.[2]
[1]University of Texas Medical Branch, Galveston, TX, [2]University of Texas Medical School at Houston, Houston, TX, [3]Wyle, Houston, TX, [4]University of Miami, Miami, FL.

Purpose

Monitoring changes in the optic nerve (OND) and/or optic nerve sheath diameters (ONSD) on MR images has been used to evaluate patients with elevated intracranial pressure (EICP). We sought to compare and evaluate the physical dimensions of the optic nerve and the sheath in astronauts previously exposed to microgravity using 3T MRI with the assumption that exposure to microgravity can increase intracranial pressure due to cephalad fluid shift.

Materials & Methods

Twenty-seven astronauts (three females), with previous missions to the International Space Station (ISS) ranged between 14-382 days and who underwent MRI of the orbits between 2010 and 2012 were identified retrospectively. Fourteen astronauts were scanned before and after their most recent missions. The repeat scans were treated independently because of differences in microgravity exposure. In total, 40 scans (80 eyes) were evaluated. Seventeen astronauts were categorized as short-duration (< 30 days) and 23 as long-duration (≥30 days) based on cumulative microgravity exposure. The measurements were done 3 mm behind the fovea on axial and sagittal isovolumetric T2-3D-TSE sequences.

Results

No statistically significant difference was identified between the short and long mission groups in OND and ONSD of either eye. Both OND and ONSD were significantly longer in vertical directions than in the horizontal directions for both groups. A statistically significant difference between the axial and sagittal diameters also was observed in both eyes in the whole study population (p = 0.000) (Table 1).

Table 1. Comparison of axial and sagittal measurement in OND and ONSD.

	Axial	Sagittal	P Value
All OND Right	0.28 ± 0.01	0.31 ± 0.01	0.000
All ONSD Right	0.67 ± 0.02	0.70 ± 0.02	0.000
All OND Left	0.29 ± 0.01	0.32 ± 0.01	0.000
All ONSD Left	0.65 ± 0.01	0.69 ± 0.01	0.000
Short-Duration Microgravity Exposure OND Right	0.27 ± 0.01	0.30 ± 0.01	0.003
Short-Duration Microgravity Exposure ONSD Right	0.64 ± 0.02	0.67 ± 0.02	0.021
Short-Duration Microgravity Exposure OND Left	0.64 ± 0.02	0.32 ± 0.01	0.000
Short-Duration Microgravity Exposure ONSD Left	0.66 ± 0.02	0.71 ± 0.02	0.000
Long-Duration Microgravity Exposure OND Right	0.29 ± 0.01	0.32 ± 0.02	0.026
Long-Duration Microgravity Exposure ONSD Right	0.69 ± 0.03	0.72 ± 0.03	0.000
Long-Duration Microgravity Exposure OND Left	0.29 ± 0.01	0.31 ± 0.01	0.010
Long-Duration Microgravity Exposure ONSD Left	0.65 ± 0.02	0.67 ± 0.02	0.001

Note: Scanned images are included in the proceedings. Some submitted images were reduced during editing, thereby decreasing clarity. Also, refer to the Program Planner. Proceedings Content as of 3-29-2013.

Conclusion
These findings suggest a slightly elliptically shaped optic nerve/sheath in this population which theoretically could also be seen in other patient populations with different degrees of EICP. If this were found to be correct, it would be advisable to measure the optic nerve/sheath on coronal images. Shape of the nerve can be identified easily on the coronal views and both axial and sagittal diameters can be measured on the same slice to identify the largest diameter. We did not find any significant difference in OND or ONSD between the astronauts with short-duration and long-duration microgravity exposure. This might be due to a small sample size and consequent low statistical power.

KEYWORDS: Optic nerve, 3T, Aerospace medicine

eP-129

Diffusivity of Intraorbital Malignant Lymphoma versus IgG4-Related Disease: 3D Turbo Field Echo with Diffusion-Sensitized Driven Equilibrium Preparation Technique

Hiwatashi, A.[1]·Yoshiura, T.[1]·Togao, O.[1]·Yamashita, K.[1]·Kikuchi, K.[1]·Honda, H.[1]·Obara, M.[2]
[1]Kyushu University, Fukuoka, JAPAN, [2]Philips Electronics Japan, Tokyo, JAPAN.

Purpose
It is difficult to evaluate diffusivity of the intraorbital structures using echo planar (EP) imaging. 3D turbo field echo with diffusion-sensitized driven-equilibrium preparation (DSDE TFE) is a novel non-EP technique for diffusion-weighted imaging (DWI). The purpose of this study was to differentiate intraorbital malignant lymphoma (ML) from IgG4 related disease (IgG4-RD) using the apparent diffusion coefficient (ADC) derived from DSDE TFE.
Materials & Methods
Fifteen patients with ML and eight with IgG4-RDs were imaged with DSDE TFE. Motion probing gradients were conducted at one direction (A-P) with b values of 0 and 500 s/mm^2. The imaging voxel size was 1.5x1.5x1.5 mm^3. Apparent diffusion coefficient was measured in the lesions. Signal intensity compared to normal gray matter on T1-weighted images, fat suppressed T2-weighted images and fat suppressed postcontrast T1-weighted images also was measured. Statistical analyses were performed with Mann-Whitney U test.
Results
Intraorbital lesions were clearly visualized on DSDE TFE without obvious geometrical distortion. Apparent diffusion coefficient of ML (1.24 ± 0.50 x 10^{-3} mm^2/s; mean ± standard deviation) was significantly lower than that of IgG4-RD (1.67 ± 0.84 x 10^{-3} mm^2/s; P < 0.05). Conventional sequences could not separate ML from IgG4-RD (0.92 ± 0.18 versus 0.94 ± 0.21 on T1-weighted images, 0.92 ± 0.17 versus 0.95 ± 0.14 on T2-weighted images, and 2.03 ± 0.35 versus 2.30 ± 0.58 on postcontrast T1-weighted images, for ML and IgG4-RD, respectively; P > 0.05).

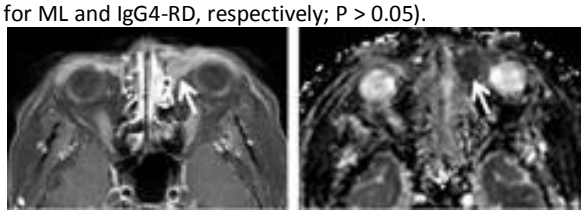

Figure: A 69-year-old male with lymphoma. Postcontrast fat-suppressed T1WI shows enhancing lesion in the left epicanthus (left, arrow). Apparent diffusion coefficient map shows restricted diffusion in the lesion (right, arrow).
Conclusion
Apparent diffusion coefficient derived from DSDE TFE help differentiate ML from IgG4-RD.

KEYWORDS: 3T, ADC

eP-130

A Novel MR Imaging-Based Prognostic Classification Identifies Distinct Molecular Subgroups in Glioblastoma Multiforme

Colen, R. R.[1]·Mahajan, B.[2]·Sathyan, P.[1]·Kumar, A. J.[1]·Majumder, S.[1]·Hegi, M.[3]·Zinn, P. O.[4]
[1]M. D. Anderson Cancer Center, Houston, TX, [2]Brigham and Women's Hospital, Boston, MA, [3]University of Lausanne, Lausanne Switzerland, SWITZERLAND, [4]Baylor College of Medicine, Houston, TX.

Purpose
Several studies have established glioblastoma multiforme (GBM) prognostic and predictive models based on age, Karnofsky Performance Status (KPS), extent of resection, MGMT methylation, CIMP or IDH1 status. However, these parameters either have little connection to the underlying tumor biology and/or can only be determined by invasive measures. Thus, we present a novel clinically relevant imaging-genomic GBM classification based on tumor volume, patient age, and KPS (VAK) that can be determined upon patient admission.
Materials & Methods
We quantitatively analyzed the volumes of 78 GBM patient MRIs present in The Cancer Imaging Archive (TCIA) corresponding to patients in The Cancer Genome Atlas (TCGA) with VAK annotation. The variables then were combined using a simple 3-point scoring system to form the VAK classification. A validation set (N = 64) from both the TCGA and Rembrandt databases was used to confirm the classification.
Results
The image-based VAK-A and VAK-B classes showed significant median survival differences in discovery (P = 0.007) and validation sets (P = 0.008). A molecular gene signature comprised of a total of 25 genes and microRNAs was significantly associated with the classes and predicted survival in an independent validation set (P = 0.001). A

Note: Scanned images are included in the proceedings. Some submitted images were reduced during editing, thereby decreasing clarity. Also, refer to the Program Planner. Proceedings Content as of 3-29-2013.

favorable MGMT promoter methylation status resulted in a 10.5 months additional survival benefit for VAK-A compared to VAK-B patients.

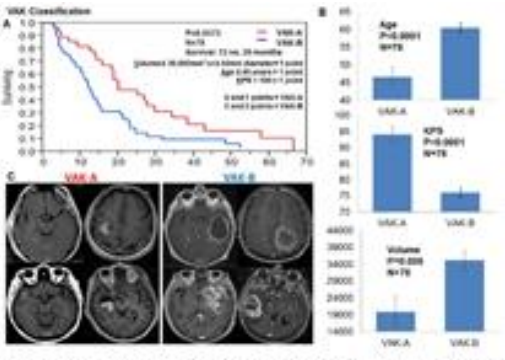

Volume, Age, KPS (VAK)- A and B classes showing **(A)** Kaplan Meier survival plot **(B)** Mean volume, Age, and KPS in VAK-A and VAK-B classes and **(C)** representative MRI images for VAK-A and VAK-B patients.

Conclusion

The noninvasive, image inclusive VAK classification with its implication of VAK-specific molecular regulatory networks, can serve as a very robust initial prognostic tool, clinical trial selection criteria, and important step toward the refinement of personalized therapy for GBM patients. A highly prognostic and predictive imaging genomic GBM classification that implies distinct genomic and possibly targetable molecular pathways can be a major advancement in personalized therapy.

KEYWORDS: GBM, Biomarkers, imaging genomics

eP-131

Accuracy of a Multinomial Logistic Regression Model in Identifying Parathyroid Adenoma on 4D CT

Hito, R.[1]·Kelly, H. R.[1]·Ginat, D. T.[1]·Hamberg, L. M.[2]·Hunter, G. J.[1]

[1]Massachusetts General Hospital, Boston, MA, [2]Brigham and Women's Hospital, Boston, MA.

Purpose

To investigate the accuracy of a 3-covariate multinomial logistic regression model in discriminating between parathyroid adenoma and nonadenomatous tissues as seen on presurgical localization scans using 4-dimensional computed tomography (4D CT).

Materials & Methods

Informed consent was waived by the institutional review body for this chart review study. From January through November 2012 there were 125 patients with biochemically documented hyperparathyroidism who underwent three-phase, contrast-enhanced 4D CT. Thirty-two did not proceed to surgery. Twenty were from outside institutions and follow-up information was not available. In the remaining 73 (13 men, 60 women: mean ages 61 and 61.3 years, respectively) surgical records were reviewed and the site(s) of the removed tissue identified. Using these locations as reference data, regions of interest (ROIs) were placed on these tissues on the 4D CT images. Hounsfield unit (HU) values from the ROIs were entered into an Excel worksheet where the probability that the surgically removed tissue was parathyroid adenoma was calculated using the logistic regression model, previously defined in an independent patient cohort. Probabilities over 50% were taken to mean parathyroid adenoma. The accuracy, sensitivity and positive predictive values of the model for identifying parathyroid adenoma were determined.

Results

There were 83 potentially abnormal surgical samples collected from 73 patients. Pathology identified 77 parathyroid adenomas and six thyroid lesions. The logistic regression model predicted 75 parathyroid adenomas. Seventy-four were correctly classified (true positive) and one was misclassified by the model (false positive). The model classified three true parathyroid adenomas as thyroid (n = 1) or lymph node (n = 2) (false negative). The remaining five lesions were classified correctly by the model as not parathyroid tissue (true negative). The accuracy, sensitivity and positive predictive values for the model were 95.2, 96.1 and 98.7 % respectively. Figure 1 demonstrates the distribution of the data along the model curve.

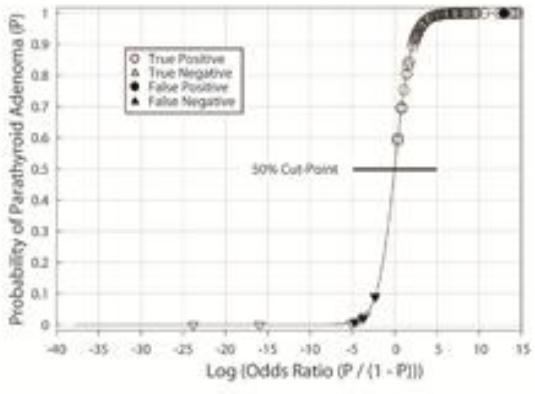

Conclusion

A 3-covariate multinomial logistic regression model using HU values from a three phase 4D CT scan protocol demonstrates that utilization of this model can allow for parathyroid tissue to be reliably discriminated from local mimics with high sensitivity and positive predictive value. Vascular thyroid nodules may behave indistinguishably from parathyroid adenoma and their interpretation remains challenging. Cystic parathyroid lesions and small lesions in regions of the scan that are noisy also may be challenging and application of the model under these circumstances must be performed cautiously.

KEYWORDS: 4D CT, Parathyroid, tissue characterization

Note: Scanned images are included in the proceedings. Some submitted images were reduced during editing, thereby decreasing clarity. Also, refer to the Program Planner. Proceedings Content as of 3-29-2013.

eP-132

Imaging-Genomic Necrosis Mapping Reveals Gender-Specific Survival and Molecular Determinants in Glioblastoma Multiforme

Colen, R. R.[1]·Changlai, T.[1]·Sathyan, P.[1]·Gutman, D.[2]·Zinn, P. O.[3]
[1]M. D. Anderson Cancer Center, Houston, TX, [2]Emory University, Atlanta, GA, [3]Baylor College of Medicine, Houston, TX.

Purpose
Despite recent discoveries of new molecular targets and pathways, the search for an effective therapy for glioblastoma (GBM) continues. A newly emerged field, imaging genomics, links gene expression profiles with MRI phenotypes. Cell death in GBM can either be associated with tumor suppressor or oncogenes, since increased cell death can be caused by an aggressive cellular growth (lack of oxygen/nutrients) or by the presence of tumor suppressor genes inducing apoptosis. Thus, an imaging genomic necrosis screen has the potential to uncover novel molecular determinants of cell death in GBMs. Here, we present the first comprehensive radiogenomic analysis using quantitative necrosis MRI volumetrics and large-scale gene- and microRNA expression profiling in GBM.
Materials & Methods
Based on The Cancer Genome Atlas (TCGA) and The Cancer Imaging Archive (TCIA) gene, microRNA, and quantitative MR imaging data sets were created in 78 patients. Top concordant genes and microRNAs correlated with high necrosis volumes were further analyzed using Ingenuity Pathway Analysis and cognate microRNA-gene networks created.
Results
Female patients demonstrated significantly lower volumes of necrosis than male patients. Thus, a gender specific analysis was chosen and revealed that female patients with high necrosis had a significantly shorter survival compared to both females with lower necrosis or males with high necrosis, while survival in males was similar in patients with high versus low tumor necrosis. The genomic analysis revealed that predominantly oncogenic pathways were associated with necrosis in female patients, while male patients showed a strong association with tumor suppressor pathways, while gender independent necrosis pathways showed equal distribution of both tumor suppressors and oncogenes.
Conclusion
Here, we propose a novel diagnostic method to screen for molecular correlates of necrosis in GBM. Our findings have potential therapeutic significance since the understanding of cell death molecular gene and microRNA signatures can improve therapy and patient survival in GBM.

KEYWORDS: GBM

eP-133

A New Simplified CT-Guided Approach for Greater Occipital Nerve Infiltration in the Management of Arnold's Neuralgia: Preliminary Results in Twenty-One Procedures

Kastler, A.[1,2]·Onana, Y.[3]·Aubry, S.[3,2]·Kastler, B.[3,2]
[1]University Hospital, Clermont Ferrand, FRANCE, [2]I4S Laboratory EA 4268, Franche Comte University, FRANCE, [3]University Hospital, Besançon, FRANCE.

Purpose
To evaluate the efficacy of a new simplified CT-guided approach in the management of greater occipital nerve infiltration.
Materials & Methods
A total of 17 patients (five men, 17 women, with a mean age of 45 years) who underwent 21 procedures were included in this retrospective study between March 2012 and November 2012. All included patients suffered from severe greater occipital nerve neuralgia refractory to conventional specific treatments. Procedures were performed under CT guidance and local anesthesia. Initial nonenhanced planning CT was performed from C0 to C2. Infiltration of greater occipital nerve was performed exclusively at the most superficial site at the first bend of the GON between inferior obliquus capitis and semispinalis capitis muscles facing C1-C2 level, using a 22G needle. A mixture of fast- and slow-acting anesthetic (1.5 mL lidocaine hydrochloride 1% and 3 mL ropivacain hydrochloride 0.25%) then was injected followed by the injection of 1.5 ml of cortivazol at predefined target site. Pain was evaluated on VAS scores immediately before and after procedure and on a monthly basis following procedure. Technical success was defined by the ability to accurately position needle tip at target site. Clinical success was defined by pain relief greater than or equal to 50% lasting for at least one month.
Results
Mean pain prior procedure was 7.65/10. Patients suffered from unilateral pain in 13 of 17 cases (right, n = 7, left, n = 6) and bilateral pain in four cases. Technical success of procedure was 100%. Mean procedure time was 10-15 minutes. Clinical success rate was 86% (18/21 procedures, 2/17 patients). In case of clinical success, mean pain relief duration following procedure was 3.25 months (1-6 months).
Conclusion
This novel simplified CT-guided infiltration approach appears to be effective in the management of refractory Arnold's neuralgia. With this new technique, infiltration of the GON is safer, faster and technically easier compared to other previously described techniques.

KEYWORDS: Infiltration, CT, Headache, Arnold Neuralgia

Note: Scanned images are included in the proceedings. Some submitted images were reduced during editing, thereby decreasing clarity. Also, refer to the Program Planner. Proceedings Content as of 3-29-2013.

eP-134

Reducing Banding Artifact in Balanced Steady-State Free Precession MR Imaging of the Inner Ear Using a Novel Shim Cycling Technique

Abele, T. A.·Kim, S. E.·Roberts, J. A.·Hadley, J. R.·Parker, D. L.·Wiggins, R. H.
University of Utah
Salt Lake City, UT.

Purpose
Balanced steady-state free precession (bSSFP) magnetic resonance (MR) imaging provides high-resolution cisternographic evaluation of the cerebellopontine angle/internal auditory canal (CPA/IAC) and inner ear but is limited by banding artifact associated with variations in the main magnetic field. Inner ear imaging with bSSFP is especially prone to banding artifact given the long TR required for high resolution and magnetic susceptibility related to the surrounding temporal bone. We have developed a novel shim cycling technique that reduces 3D bSSFP banding artifact by combining multiple image volumes acquired with different shim currents to create a uniform composite volume. The purpose of this study is to demonstrate marked reduction in banding artifact using our shim cycling technique in high-resolution 3D bSSFP imaging of the inner ear.
Materials & Methods
MR imaging of the inner ears of a healthy human volunteer was performed on a Siemens 3T TIM Trio using a custom built 4-channel coil (2 channels overlying each external ear). After initial adjustment of the volume shims, transmit voltage, and center frequency, seven 3D bSSFP (TrueFISP) image volumes were acquired. Between each volume acquisition the x-shim was altered, so that successive sets of images had different banding artifact locations. 3D bSSFP parameters were: TE/TR=3.4/6.8 ms, FA=50 degrees, FOV=160 x 160 mm2, matrix = 384 x 384 x 48, total scan time=14 minutes. Acquisition voxel dimension was 0.4 mm isotropic and displayed as 0.2 mm isotropic after zero-filled interpolation. To create the composite volume a median filter was applied along the shim steps with a width equal to the number of shim cycling volumes.
Results
Standard 3D bSSFP images demonstrated banding artifact in the apical turn of the cochlea and anterior wall of the internal auditory canal (arrows, Figure A). Shim cycled 3D bSSFP images (Figure B) at a similar plane showed marked reduction in banding artifact with improved delineation of the osseous architecture of the cochlea, cochlear and vestibular nerves, and anterior inferior cerebellar artery within the CPA/IAC.

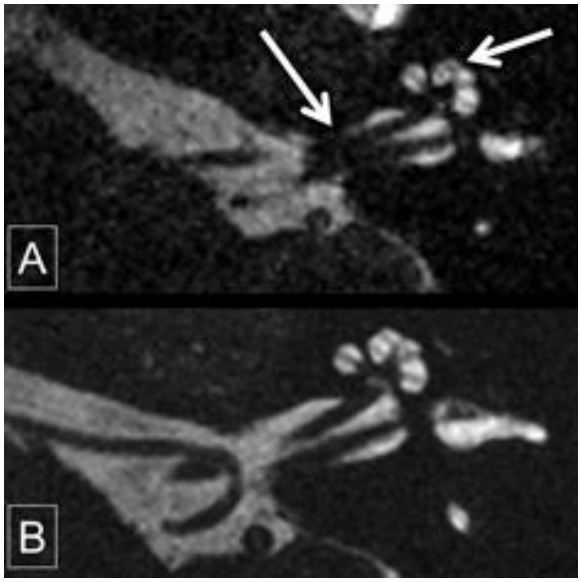

Conclusion
Preliminary results demonstrate that composite shim cycled 3D bSSFP has markedly reduced banding artifact compared to a standard 3D bSSFP sequence. This technique has potential to significantly improve CPA/IAC and inner ear imaging with better detection of vestibular schwannomas and vascular loops, advanced characterization of inner ear microstructure, and reduced pseudolesions related to banding artifact. Future directions include comparison to other artifact reduction techniques and prospective evaluation of inner ear pathology.

KEYWORDS: Inner ear, MR imaging, banding artifact

eP-135

Quantitative Volumetric Analysis of Venous and Lymphatic Malformations of the Head and Neck to Assess Response to Percutaneous Sclerotherapy

Alexander, M. D.[1]·McTaggart, R. A.[2]·Choudhri, O. A.[2]·Wu, A.[3]·Ross, M.[4]·Do, H. M.[2]
[1]Santa Clara Valley Medical Center, San Jose, CA, [2]Stanford University School of Medicine, Stanford, CA, [3]New York University, New York City, NY, [4]George Washington University, Washington, DC.

Purpose
Percutaneous sclerotherapy is used widely to treat venous and lymphatic malformations, but no superior sclerosant has been identified. Studies evaluating efficacy of various sclerosants have relied heavily on qualitative and subjective measures such as cosmetic changes and patient satisfaction. This study describes and evaluates a novel quantitative technique for the evaluation of these lesions that may be employed in future research to define the best treatment agents.

Note: Scanned images are included in the proceedings. Some submitted images were reduced during editing, thereby decreasing clarity. Also, refer to the Program Planner. Proceedings Content as of 3-29-2013.

Materials & Methods
Prospectively maintained procedure records were queried retrospectively to identify all patients with vascular malformations who underwent percutaneous sclerotherapy in the interventional neuroradiology department of a major academic medical center. Lesions were characterized as venous or lymphatic malformations according to the Mulliken and Glowacki classification. Medical records and images were reviewed to record demographic information, clinical and imaging characteristics of the lesions, all treatment sessions and modalities, and clinical response. Initial diagnostic and clinical data were used to classify lesion size by apparent size and degree of visible asymmetry due to the lesion. Size was categorized as not visible, small, medium, or large. Most recent clinical outcome was categorized as excellent, good, fair, or poor in keeping with previously reported classification schemes. Lesion volume was calculated using T2-weighted images for all available studies using Aquarius iNtuition version 4.4.6 (Terarecon, Foster City, CA). Due to a broad spectrum of patient age, volumes were normalized by body mass at time of diagnosis. Additionally, macrocystic and microcystic components of lesions were measured. Pearson coefficients (rho) were calculated to identify correlation between clinical and volumetric measures. Student's *t*-tests were performed to compare dichotomized groups based on lesion characteristics.
Results
Thirty-five patients were identified, undergoing a total of 75 sessions of percutaneous sclerotherapy. At the time of analysis complete records were available for review of 70 such interventions. Analysis of initial volumetric data compared to clinical measures was possible for 30 patients, and this yielded statistically significant correlation (rho = 0.359, p = 0.036). In those patients for whom data were available, an inverse correlation was found between initial lesion volume and qualitative clinical response to treatment (rho = -0.493, p = 0.027).
Conclusion
Previous research into percutaneous sclerotherapy for venous and lymphatic malformations of the head and neck has relied almost exclusively on qualitative clinical measures. The current study demonstrates the feasibility of volumetric analysis of such lesions based on magnetic resonance images. A significant correlation was seen between initial volumetric data and clinical measures of lesion size. The volumetric analysis also demonstrated an inverse correlation between initial lesion volume and clinical response to treatment. As further comparisons of various sclerosants are conducted to determine which agent is most effective, quantitative methods such as those described in this study should be utilized in addition to qualitative clinical results.

KEYWORDS: Venous malformations, Head and neck, percutaneous sclerotherapy

eP-136

Incidental Thyroid Nodules on CT: Evaluation of Risk Categorization Methods for Workup of Nodules

Nguyen, X. V.[1,2]·Roy Choudhury, K.[1]·Eastwood, J. D.[1]·Lyman, G. H.[1]·Esclamado, R. M.[1]·Werner, J. D.[1]·Hoang, J. K.[1]
[1]Duke University Medical Center, Durham, NC, [2]The Ohio State University Wexner Medical Center, Columbus, OH.

Purpose
Thyroid nodules are common incidental findings on CT, but there are no clear guidelines regarding their further diagnostic workup. This study compares the performance of two risk categorization methods of selecting CT-detected incidental thyroid nodules (ITN) for workup.
Materials & Methods
The two categorization methods were Method A, which was based on nodule size ≥10 mm, and Method B, which was a three-tiered system based on aggressive imaging features, age <35 years and size ≥15 mm. In Part 1, the two categorization methods were applied to thyroid cancers in the National Cancer Institute's SEER database to compare the cancer capture rates and survival. In Part 2, 755 CT neck scans at our institution were reviewed retrospectively for the presence of ITNs ≥5 mm, and the same two categorization methods were applied to the CT cases to compare the number of patients that would theoretically meet criteria for workup. Comparisons of proportions of subjects captured under Methods A and B were made using McNemar's test.
Results
For 84,720 subjects in the SEER database, Methods A and B each captured 74% (62,708/84,720 and 62,586/84,720, respectively) of malignancies. SEER subjects that would not have met criteria for further workup by both methods had equally excellent 10-year cause-specific and relative survival of >99%. For Part 2, the prevalence of ITN ≥5 mm at our institution was 133/755 (18%). The number of ITN that would be recommended for workup by Method A was 57/133 (43%) compared to 31/133 (23%) for Method B ($p<0.0005$).
Conclusion
Compared to using a 10-mm size cutoff, the 3-tiered risk stratification method identifies fewer ITN for workup but captures the same proportion of cancers in a national database and shows no difference in missing high-mortality cancers.

KEYWORDS: Thyroid, Epidemiology

Note: Scanned images are included in the proceedings. Some submitted images were reduced during editing, thereby decreasing clarity. Also, refer to the Program Planner. Proceedings Content as of 3-29-2013.

eP-137

Applying the Society of Radiologists in Ultrasound Recommendations for FNA of Thyroid Nodules: Effect on Workup, Malignancy Detection and Costs

Hobbs, H. A.·Bahl, M.·Nelson, R. C.·Eastwood, J. D.·Esclamado, R. M.·Hoang, J. K.
Duke University
Durham, NC.

Purpose
The Society of Radiologists in Ultrasound (SRU) developed sonographic recommendations for thyroid nodules that should undergo FNA. The intention of the guidelines was not to diagnose all cancer, but to diagnose "clinically significant " cancers while avoiding unnecessary tests and surgery in patients with benign nodules. The goal of this study was to determine the tests and surgeries that could be saved and the malignancies that would be missed if thyroid biopsies were performed according to SRU recommendations. A secondary aim was to estimate costs saved if SRU recommendations were utilized.
Materials & Methods
This is a retrospective study of 400 consecutive ultrasound-guided thyroid FNA encounters from July 2010 to June 2011. All nodules receiving biopsy were categorized as SRU positive (SRU+) or negative (SRU-) based on the sonographic findings. The SRU recommendations include solid nodules ≥15 mm, nodules with microcalcifications ≥10 mm, coarse calcifications ≥15 mm, and solid-cystic component ≥20 mm. Medical records were reviewed for pathology and management. Pathology was defined by surgical pathology result if available and FNA cytopathology if the patient did not have surgery. All malignancies were confirmed at surgery and were further followed for stage of disease, treatment response and overall survival. Cost estimates for SRU- patients were based on the reimbursement fee for procedural and pathology CPT codes according to 2012 Medicare Reimbursement Schedule.
Results
Four hundred biopsy encounters were for 390 patients and 560 nodules. Table 1 shows the final pathology results and management for SRU+ and SRU- groups. SRU- group represented 87/400 (21%) biopsy encounters and included five surgical resections for benign disease. Malignancy rate in the SRU+ and SRU- groups was 9% and 6%, respectively. All SRU- malignancies were localized papillary carcinomas ≤14 mm. The SRU+ group included 22 malignancies with mean size of 2.9 cm and 17 cases of regional disease. There were no tumor recurrence or deaths in the study period. The total healthcare cost estimate over a 12-month period for SRU- patients with benign disease was $89,188 (biopsy $64,728, surgery $24,460).
Table 1. Categorization of biopsies, pathology and treatment for SRU positive and SRU negative encounters.

	SRU positive	SRU negative	Total
Biopsy episodes/encounters	313	87	400
Biopsy episodes with benign results	245	82	327
Thyroid carcinoma total	22	5	27
Localized	17	5	22
Regional	4	0	4
Metastatic	0	0	
Malignancy – other type	1	0	1
Resection for benign disease	58	5	63
Follow-up imaging for nodule surveillance	85	35	120

Conclusion
Utilizing SRU recommendations would reduce the number of thyroid FNA encounters by 21% and prevent five surgical procedures for benign disease, resulting in a savings of over $89,000 for workup of benign disease. Although there were missed malignancies in the SRU- group, they were not aggressive by histological type, size and stage. Society of Radiologists in Ultrasound recommendations captured all malignancies that were larger and/or with metastatic disease.

KEYWORDS: Thyroid, Malignancy

eP-138

18F Fluorodeoxyglucose Positron Emission Tomographic CT in the Evaluation of Residual/Recurrent Squamous Cell Carcinoma of the Oral Cavity and Oropharynx

Spampinato, M.·Matheus, M.·McLaughlin, C.·Kereshi, B.·Day, T.·Rumboldt, Z.
Medical University of South Carolina
Charleston, SC.

Purpose
Our goal was to assess the use of [18F] fluorodeoxyglucose positron emission tomographic CT (PET CT) in the assessment of recurrent or residual loco-regional disease in patients with previously treated oral cavity and oropharyngeal squamous cell carcinoma, with the hypothesis that maximal SUV measurements of the primary tumor site would be predictors of overall survival.
Materials & Methods

Note: Scanned images are included in the proceedings. Some submitted images were reduced during editing, thereby decreasing clarity. Also, refer to the Program Planner. Proceedings Content as of 3-29-2013.

We retrospectively reviewed records of 64 patients referred for PET CT imaging to evaluate for residual or recurrent cancer of the oral cavity and oropharynx over a two-year period [42 men, 57 Caucasian, 7 African American, median age 61 (range 27-82)]. After PET CT all patients either underwent a biopsy of the primary tumor site or had routine clinical followup of at least 12 months. Imaging data collection was conducted by two observers and discrepancies were resolved by consensus. Maximal SUV were recorded for the primary tumor site. Overall survival in days was recorded. Differences in SUV measurements and clinical characteristics between patients with and without disease recurrence were evaluated using Mann-Whitney and Pearson chi-square tests. Receiver operating characteristic (ROC) analysis provided potential cut-off values for identification of tumor recurrence. Subsequently, Kaplan-Meier survival curves also were generated for the dichotomized maximal tumor SUV values, based on the results of the ROC analysis. Results were considered statistically significant when $p < 0.05$.

Results

There were no significant differences between subjects with and without recurrent disease in gender ($p = 0.179$), racial distribution ($p = 0.684$), ethanol abuse ($p = 0.177$), history of smoking ($p = 0.503$), initial cancer staging (0.924), and age ($p = 0.137$). As expected, survival was significantly worse in patients with recurrent disease ($p < 0.001$). Maximal primary tumor site SUVs were significantly different between pathology-proven recurrent tumors and cases without disease at pathology or clinical followup ($p = 0.001$). The area under the ROC curve for maximal primary tumor site SUV was 0.74 (95% confidence interval: 0.60 - 0.88, $p = 0.001$). Thresholds of 4.3 and 4.5 for maximal primary tumor site SUV provided the best combination of sensitivity, specificity and accuracy for this parameter (respectively 80%, 51%, 70% and 76%, 55%, 70%). The Kaplan Meier analysis showed that maximal tumor SUV values > 4.3 and maximal tumor SUV values > 4.5 were significant predictors of overall survival (respectively chi square =13.40, $p < 0.001$; chi square =12.19, $p < 0.001$)

Conclusion

Quantitative SUV measurements and in particular maximal primary tumor site SUV can be a useful adjunct to the interpretation of [18F] PET CT studies in the detection of residual/recurrent disease and in predicting survival in squaumous cell carcinoma of the oral cavity and oropharynx.

KEYWORDS: Squamous cell carcinoma, Oropharynx

eP-139

MR Perfusion Findings in Head and Neck Masses

Aralasmak, A.·Yetis, H.·Yıldız, S.·Meric, A.·Pinarbasili, N.·Toprak, H.·Alkan, A.
Bezmialem Vakif University
Fatih/Istanbul, TURKEY.

Purpose

To define MR perfusion findings of head and neck masses.

Materials & Methods

Total 48 patients, referred to MR unit for head and neck imaging for mass lesion, were enrolled. T2 dynamic contrast-enhanced MR perfusion sequences were added following routine noncontract views, thereafter contrast-enhanced sequences of the neck region were completed. For MR perfusion, routine dose of gadolinium (0.1 mmol/kg body weight) was administrated after 7sn of data acquisition. The injection was performed by automatic injector in the right arm at a rate of 5 ml/s followed by 15 ml saline. During the postprocessing, vertebral arteries were chosen for reference artery. Following computation of CBV, CBF, MTT and TTP maps, measurements were performed from solid and mostly enhancing and hyperperfused part of the mass lesions. At the same slice, measurements from normal-appearing muscles also were measured. Normalized CBV (nCBV), CBF (nCBF), MTT (nMTT), and TTP (nTTP) values were calculated by dividing the perfusion values of the mass lesions to that of the skeletal muscles. Except three, pathology results of all were obtained and correlated with nCBV, nCBF, nMTT, nTTP values. Lymphadenopathies were accepted as mass lesions and grouped according to their pathology.

Results

Table shows the neck masses, their pathology results and their nCBV, nCBF, nMTT, nTTP values.

Head and Neck Masses	Number	nCBV	nCBF	nMTT	mTTP
Ectopic Thyroid Tissue	2	50.7	20.6	3.03	10.28
Squmaous Cell Cancer	10	45.15	16.03	3.25	1.17
Papillary Thyroid cancer	4	35.43	26.99	4.02	3.58
Glomus tumor	4	25.5	13	5.52	4.5
Parotid Warthin Tumor	1	22.82	19.08	2.3	1.52
Reactive Lymph node Hyperplasia	2	21.69	9.26	1.52	1.28
Parotid Myoepithelial Carcinoma	1	12.31	7.06	1.81	1.44
Granulamatous Lymphadenitis	3	7.39	6.71	1.72	2.16
Lymphoma	9	6.85	7.59	4.09	1.15
Giant Multinoduler Goiter	3	6.58	3.91	9.59	1.34
Sebaceous Carcinoma	1	3.72	19	1.45	1.69
Parathyroid Carcinoma	1	1.51	1.35	0.79	0.99
Lipoma	2	1.84	2.23	0.57	1.16
Venolymphatic malformation	1	0.58	50	1.07	0.98
Mucocele	1	0	0	0	0

Conclusion

Note: Scanned images are included in the proceedings. Some submitted images were reduced during editing, thereby decreasing clarity. Also, refer to the Program Planner. Proceedings Content as of 3-29-2013.

MR perfusion studies with conventional head and neck MR imaging will be helpful for characterization of head and neck masses. Ectopic thyroid masses, SCCs, papillary thyroid cancers and glomus tumors were well hyperperfused masses of neck region. Lymphomas usually were hypoperfused masses. Although we observed some SCC masses as minimally hyperperfused and some lymphoma masses as hyperperfused in our study. Granulomatous lymph nodes were usually hypoperfused compared to the reactive lymph nodes. Warthin and myopeithelial carcinoma of parotid gland were both hyperperfused masses. Giant multinoduler goiters were observed hypoperfused, although they are enhancing avidly on postcontrast views.

KEYWORDS: MR perfusion-weighted imaging, Neck masses

eP-140

Diffusion Restriction in the Paranasal Sinuses: Clinical and Computed Tomographic Correlation

Besachio, D. A.·Rassner, U.
University of Utah
Salt Lake City, UT.

Purpose
To identify any clinical significance of diffusion restriction in the paranasal sinuses seen on brain magnetic resonance imaging (MRI).
Materials & Methods
Brain MRI imaging interpreted by a single neuroradiologist over a one-year period was reviewed retrospectively. Diffusion restriction on DWI imaging was identified in the paranasal sinuses or nasal cavity in 29 patients. When computed tomography (CT) of the site demonstrating diffusion restriction was available, these findings were correlated with MRI findings. Any available clinical-pathologic correlation also was performed.
Results
The most commonly identified site of diffusion restriction is the maxillary sinus. We were able to correlate diffusion restriction with CT scan of the head, face or neck in 18 subjects performed within eight weeks of MRI. Thirteen of 18 (72%) demonstrated mucoperiosteal thickening on CT of the involved sinus wall. We identified two main patterns of diffusion restriction in the paranasal sinuses, central and mucosal. Although only three cases were seen, a mucosal pattern of diffusion restriction in the sphenoid sinus was noted with the diagnosis of invasive fungal sinusitis in two of three cases (66%). A single case of maxillary sinus mucosal diffusion restriction was present with a confirmed case of invasive fungal sinusitis. The single case of nasal cavity diffusion restriction demonstrated squamous cell carcinoma on follow-up resection of the associated soft tissue mass. Of note, no CT correlative cases demonstrated air-fluid levels, a finding often associated with acute sinusitis. T1- and T2-weighted imaging characteristics were variable but low or mixed low and intermediate T2 signal predominated (24/29) in areas of diffusion restriction, in concordance with previous literature. Of note, all cases of invasive fungal sinusitis and diffusion restriction were associated with high T1-weighted signal in the affected sinus.

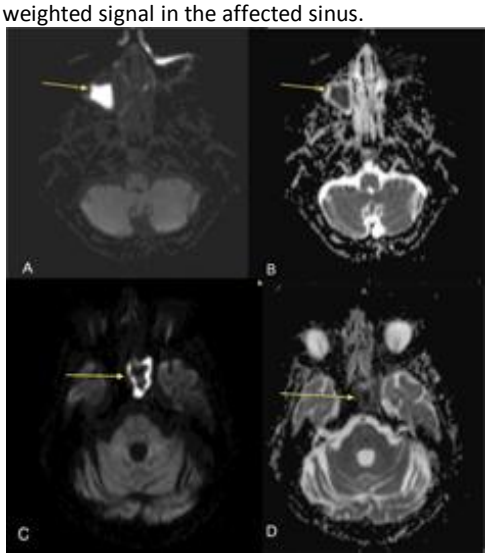

Conclusion
Diffusion restriction in the paranasal sinuses is an uncommon finding on brain MRI but likely represents a finding worthy of mention. The most common pattern identified is central restriction, which appears to be strongly associated with changes seen in chronic inflammatory sinonasal disease. A mucosal pattern was less common and in the sphenoid sinus may be associated with mucosal necrosis secondary to invasive fungal sinusitis.

KEYWORDS: Paranasal, Diffusion MR imaging

eP-141

One Low-Radiation Exposure MDCT of the Sinuses Can Be Used for Both Clinical Diagnosis and Be of Adequate Quality to Provide Safe Navigational Guidance for Sinus Surgery

Siegelman, J. R. Q. W.[1]·Supanich, M.[2]·Magri, A.[3]·Lesnik, G. T.[1]·Green, S. J.[1]·Donovan, W.[1]
[1]William W Backus Hospital, Norwich, CT, [2]Henry Ford Hospital, Detroit, MI, [3]Upstate Medical Physics - Landauer, Victor, NY.

Purpose
Given the recent changes announced by the International Commission on Radiological Protection (ICRP) related to tissue reactions from low levels of ionizing radiation, and new lowered threshold for absorbed dose in lens of .5 Gy, institutional dose and radiation exposure levels for sinus computed tomography (CT) studies using automatic exposure control (AEC) were examined across one institution's three unique scanner models. In addition, the adequacy of institutional protocols for endoscopic sinus

Note: Scanned images are included in the proceedings. Some submitted images were reduced during editing, thereby decreasing clarity. Also, refer to the Program Planner. Proceedings Content as of 3-29-2013.

surgical (FESS) surgical mapping was assessed. This work aims to assess radiation dose levels objectively. This research examines the use of $CTDI_{vol}$ and estimated organ dose.

Materials & Methods

Under IRB approval, retrospective radiation exposure levels and organ dose estimates from routine CT sinus studies using AEC on three volumetric MDCT scanners from three different manufacturers were carried out using a commercially available program eXposure ™. The software uses one phantom model from the Cristy set of models, and the UK National Radiation Protection Bureau (NRPB report R186) to complete the Monte Carlo simulation to estimate organ doses based on the area scanned and the scanner output. Mean organ dose of the lens and salivary glands were compared with the the scanner reported CTDI vol $_{vol}$, and DLP. Data from a total of 303 consecutive patients studies over a period of 10 months were identified for analysis. The same diagnostic scans also were utilized for surgical planning. The objective navigational ability of Functional Endoscopic Sinus Surgery software (Landmarx TM) for all 49 patients who underwent both sinus CT using these protocols was assessed.

Results

The data from the patient population was found to have a $CTDI_{vol}$ mean 11.8mSv, s.d. 2.1, lens dose 5.3mSv, sd 0.825, Salivary gland dose 8.5 mSv, sd 1.657. A linear relationship was found between $CTDI_{vol}$ and absorbed lens dose with a slope of 0.37 and a Pearson Correlation Coefficient of 0.92. The relationship between $CTDI_{vol}$ and the dose absorbed by the salivary glands was determined to have a linear relationship with a slope of 0.75 and a Pearson Correlation Coefficient of 0.93. FESS software was able to successfully navigate in all 49 of consecutive cases at our institution (n = 49).

Conclusion

Low radiation exposure MDCT, utilizing a radiation dose level, below the 25th percentile based on ACR Dose Index Registry for sinus CT and approaching radiation exposure levels obtained with cone beam CT, provides adequate anatomical detail for endoscopic sinus surgical navigation. Absorbed organ dose in sinus studies is provided utilizing the retrospective Monte Carlo simulation of absorbed organ doses from clinical CT studies and linear relationships between organ doses and $CTDI_{vol}$ were observed.

KEYWORDS: Screening, Sinonasal disease, Radiation

eP-142

Oval Window Dysplasia: Developmental Dynamics and Imaging Correlate

Raz, E.[1]·Gupta, D.[1]·Gangadhar, K.[1]·Hagiwara, M.[1]·Som, P.[2]·Yu, E.[3]·Fatterpekar, G.[1]
[1]New York University, New York, NY, [2]Mount Sinai Hospital, New York, NY, [3]University of Toronto, Toronto, ON, CANADA.

Purpose

Recent genetic and embryologic studies have demonstrated that the development of oval window is intimately dependent on the development of stapes footplate and the normal course of the tympanic segment of the facial nerve. The purpose of our study was to provide an imaging correlate to the normal and abnormal embryogenesis of these structures by: 1. Assessing the presence and size of the oval window in individuals with normal stapes. 2. Assessing the presence and size of the oval window in patients with dysplastic or absent stapes. 3. Evaluating the course of the facial nerve through the tympanic cavity in “normal” individuals, and in patients with dysplastic stapes.

Materials & Methods

Fifteen patients with absent or dysplastic stapes were identified retrospectively by searching the hospital database and radiology reports. Of these, three patients demonstrated opacified middle ear cavities making it difficult to assess the stapes. These three patients were therefore excluded from the study. Twelve age-matched individuals with normal high-resolution CT studies of the temporal bone, obtained for trauma were included as the control population. The studies were assessed for presence of stapes and oval window, size of oval window, and course of the facial nerve through the tympanic cavity.

Results

In the control population, the stapes and oval window were identified in all 12 individuals. The oval window measured 2.3 + 0.2 cm (mean 2.4 cm) in the axial plane, and 1.5 + 0.2 cm (1.4 cm) in the coronal plane. In the patient population, the stapes was absent in 10 patients, and dysplastic in two patients. In all 10 patients, where the stapes was absent, the oval window was completely atretic. Instead a bony plate was seen in the expected location of the oval window. In the remaining two patients with dysplastic stapes, in terms of its morphology and orientation, the oval window was seen to be dysplastic, being smaller in size, measuring 0.8 - 1.0 cm in the axial plane, and 0.5 - 0.8 cm in the coronal plane. A normal course of the facial nerve was seen in all 12 normal temporal bone CT studies. Instead, an anomalous course of the facial nerve was seen in all 12 patients.

Conclusion

Our study conclusively shows that a normal stapes is essential for the presence of a normal window. Likewise, an absent/dysplastic stapes results in an absent/dysplastic oval window, and is associated with an anomalous course

Note: Scanned images are included in the proceedings. Some submitted images were reduced during editing, thereby decreasing clarity. Also, refer to the Program Planner. Proceedings Content as of 3-29-2013.

of the tympanic segment of the facial nerve. These findings are consistent with recent embryologic and genetic studies which have demonstrated that the presence of oval window is largely dependent on induction signals from the stapes, and is influenced by the location of the facial nerve in the tympanic cavity.

KEYWORDS: Temporal bone, Dysplasia

eP-143

Paragangliomas and the Jugular Vein

Orru', E.·Aygun, N.·Blitz, A. M.·Carey, J. P.·Olivi, A.·Yousem, D. M.
Johns Hopkins Medical Institution
Baltimore, MD.

Purpose
Paragangliomas are neuroendocrine tumors originating from the extra-adrenal paraganglia of the nervous system, and arise in the head and neck region (H&N) in three percent of cases. The most common pathologic entity in this area is carotid body tumor (CBT), followed by glomus jugulare (GJ) and jugular tympanicum (JT), while the rarest is glomus vagale (GV). Surgery is the only definitive treatment, tailored on a patient-by-patient basis depending on symptoms and location of the lesions. These tumors are known to often involve neighboring structures, either invading or compressing them. Our aim was to determine the incidence of jugular vein (JV) invasion or compression by paragangliomas and to determine which modality [computed tomography (CT), magnetic resonance imaging (MRI) or digital subtraction angiography (DSA)] was most accurate in making this determination.
Materials & Methods
This study was HIPAA compliant and approved by the institutional IRB. We retrospectively reviewed the records and imaging studies of all the patients with H&N paragangliomas identified in the past five years via a radiology information system keyword search. Imaging studies of 31 patients who underwent surgical treatment were reviewed and compared with surgical reports regarding JV involvement.
Results
The study group consisted of 19 (61.3%) females and 12 (38.7%) males with an average age of 48 years (range: 26-69 years). Of these patients 18 (58.0%) had GJ, seven (22.6%) had CBT, three (9.7%) had JT and three (9,7%) had GV. Eight (25.8%) tumors were recurrent. Overall, imaging studies identified JV involvement in 20 cases (64.5%), of which 16/31 (51.6%) showed JV invasion and four of 31 (12.9%) JV compression. Only GJs showed JV invasion. MR imaging was performed in 19 patients and gave positive results in 15 cases, showing sensitivity (Se) of 93%, specificity (Sp) of 60%, positive predictive value (PPV) of 87% and negative predictive value (NPV) of 75%; accuracy was 84%. CT was performed in 17 patients with eight positive results showing Se of 89%, Sp of 100%, PPV of 100% and NPV of 89%; accuracy was 94% . DSA for purposes of pre-operative embolization was carried out in 20 patients and positive in eight patients, showing Se of 54%, Sp of 86%, PPV of 88%, NPV of 50%; accuracy was 65%.
Conclusion
The JV is involved in 64.5% of cases of H&N paraganglioma. Wall invasion is characteristic of the GJs, while JV displacement can be present with other tumors. For the evaluation of the JV in the presurgical management of H&N paragangliomas, MRI has the highest Se while CT has the highest Sp. Digital subtraction angiography alone is not reliable in assessing the JV involvement, but is very rarely performed as the only imaging modality.

KEYWORDS: Paraganglioma, Glomus tumors, Jugular vein invasion

eP-144

Redefining Normal Facial Nerve Enhancement: Healthy Subject Comparison of Typical Enhancement Patterns, Postcontrast Spin Echo versus Magnetization Prepared Rapid Acquisition Gradient-Echo Imaging

Lubarsky, M.·Aiken, A. H.·Saindane, A.·Kang, J.·Hudgins, P. A.·Dehkharghani, S.
Emory University
Atlanta, GA.

Purpose
Normal facial nerve contrast enhancement patterns have been described on conventional T1-weighted spin echo (SE) sequences. However, they have not been described on the more recently introduced and commonly employed magnetization prepared rapid acquisition gradient echo (MPRAGE) sequences. Advantages of MPRAGE are near-isotropic volumetric images that allow multiplanar reformations and robust contrast. In this investigation we compare the pre vs. postcontrast features of cranial nerve VII of both SE and MPRAGE sequences in a 23-patient cohort.
Materials & Methods
In this prospective IRB-approved study, 23 patients with no facial nerve symptoms comprised the study population, and 38 normal nerves were reviewed (eight nerves were excluded due to presence of a mass). Pre and postcontrast signal intensity (SI) on SE and MPRAGE of seven facial nerve segments (cisternal, canalicular, labyrinthine, geniculate, superficial petrosal, tympanic, and stylomastoid) were assessed independently by two neuroradiologists, following consensus read of a subset of cases. Corresponding pre and postcontrast multiplanar data sets were analyzed synchronously; signal intensities for each segment were assigned a value of 0-3 (0-no signal; 1-faint visualization; 2-signal equivalent to normal brain; 3-signal equivalent to enhancing dural sinus), with

Note: Scanned images are included in the proceedings. Some submitted images were reduced during editing, thereby decreasing clarity. Also, refer to the Program Planner. Proceedings Content as of 3-29-2013.

enhancement defined as the difference in signal intensity between pre and postcontrast images. Statistically significant differences in location and degree of SI and enhancement were assessed. Statistical significance was defined as a p-value:<0.05.
Results
1. Statistically significant higher precontrast SI was demonstrated in five segments (cisternal, canalicular, labyrinthine, geniculate and stylomastoid) on MPRAGE when compared to SE sequences. 2. Statistically significant higher postcontrast SI was demonstrated in cisternal, canalicular, labyrinthine, geniculate and superficial petrosal nerve segments on MPRAGE when compared to SE sequences. 3. In the SE series, statistically significant enhancement was demonstrated in labyrinthine, geniculate, superficial petrosal nerve, tympanic, and stylomastoid segments and lack of enhancement was demonstrated in cisternal and canalicular segments. 4. In the MPRAGE series, statistically significant enhancement was demonstrated in geniculate, superficial petrosal nerve, tympanic, and stylomastoid segments and lack of significant enhancement was demonstrated in cisternal, canalicular and labyrinthine segments.
Conclusion
Significantly greater facial nerve SI is observed on MPRAGE sequences, both with and without gadolinium administration among normal subjects in most facial nerve segments. Improved identification of the facial nerve and/or its circumneural plexus on MPRAGE is thus more likely, and may be misinterpreted as pathologic when evaluated in the context of existing paradigms of normal enhancement derived from past studies employing SE techniques. Postcontrast MPRAGE sequences may falsely suggest pathologic enhancement in intracanalicular or occasionally the cisternal segments, two segments that have been described as nonenhancing, likely due to the greater intrinsic SI of the nerve. True enhancement patterns differed only in the labyrinthine segments, seen only in SE, likely due to the insufficient resolution to identify the nerve/plexus on precontrast SE. As volumetric, high-resolution imaging becomes more commonplace, examiners should remain cognizant of normal deviation from expected "enhancement" patterns to avoid misdiagnosis and other interpretive pitfalls.

KEYWORDS: Facial nerve, MR imaging, enhancement

eP-145

Semicircular Canal Dehiscence in Children with Sensorineural Hearing Loss

Choudhri, A. F.[1,2]·Whitehead, M. T.[1,2]·MacDonald, C. B.[1]
[1]University of Tennessee Health Science Center, Memphis, TN, [2]Le Bonheur Children's Hospital, Memphis, TN.

Purpose
Imaging of sensorineural hearing loss (SNHL) often is performed with temporal bone CT, sometimes with MR and occasionally using both modalities; however many patients have no identifiable structural abnormality. An enlarged vestibular aqueduct is a commonly reported finding in children with SNHL; however the incidence of other communications between the labyrinthine system and the intracranial compartment is not known. We evaluated the incidence of dehiscence of the superior, lateral, and posterior semicircular canals (SSCC, LSCC, PSCC), respectively in children with SNHL.
Materials & Methods
One hundred consecutive temporal bone CT studies on children with SNHL were evaluated by two neuroradiologists. All studies were acquired volumetrically on a 320 detector CT scanner with 0.5 mm collimation. 0.5 mm axial source data were available for review in all cases, as well as 1 mm axial and coronal bone algorithm images. The osseous integrity of the semicircular canals was evaluated, as well as the morphology of the vestibule, cochlea, and the size of the vestibular aqueduct.
Results
There were 11 instances of semicircular canal dehiscence identified in eight patients, all of whom had normal size of the vestibular aqueduct and no CT evidence of cochlear dysplasia. This included seven PSCC, three SSCC, and one LSSC. Of the seven cases of PSCC dehiscence, three were only visible on the 0.5 mm images whereas four were visible on both 1.0 and 0.5 mm images. The cases of SSCC and LSSC dehiscence were visible on both data sets.
Conclusion
Semicircular canal dehiscence is not uncommon in children with SNHL, and may be related to SNHL by the same mechanisms as an enlarged vestibular aqueduct. Dehiscence of the PSCC may be easier to detect on source data as opposed to thicker sections. Close scrutiny of the vestibular system and semicircular canals, including use of thin-section data, may increase the diagnostic yield on CT of the temporal bone performed in children with SNHL.

KEYWORDS: Temporal bone, Hearing loss

eP-146

Head and Neck Endovascular Repair of Vascular Malformations

Yakes, W. F.
Vascular Malformation Center
Englewood, CO.

Purpose
To determine the efficacy of ethanol embolotherapy of extracranial head and neck vascular formations of all types, particularly after failures of other endovascular and surgical treatments.
Materials & Methods
One hundred sixty-six patients (64 males, 102 females; mean age 38 years) presented with extracranial arteriovenous malformations (AVMs) of the head and neck area. Over half of the patients had undergone previously

Note: Scanned images are included in the proceedings. Some submitted images were reduced during editing, thereby decreasing clarity. Also, refer to the Program Planner. Proceedings Content as of 3-29-2013.

failed therapies. All patients underwent ethanol embolotherapy under general anesthesia. Forty-five patients had AVMs and 121 patients had venous malformations (VM).
Results
Of 45 AVM patients, 26 patients are cured (mean followup 2½ years); of 121 venous malformation patients 65 are at end-therapy (mean followup 4½ years). The remaining patients are not at end-therapy and are being treated for their residual malformations. In AVM followup, arteriography is the main imaging modality to determine cure or residual AVM as MR is less sensitive in the evaluation of residual AVM. In VM followup, MR is the main imaging tool, particularly with T-2 fat suppression and/or STIR imaging. All patients demonstrated improvement post-therapy. Complications were 4.5%, to include bleeding self-limited partial 7th nerve palsy (with recovery), skin injury (not requiring skin grafts), infection and pain.
Conclusion
Ethanol has proven its consistent curative potential at long-term followup for high-flow AVMs and low-flow VM lesions at long-term followup as lesions in the periphery. Complication rates remain low. The procedures are tolerated well by the patients and done on an out-patient basis. Prior surgery and embolization procedures can cause difficulty in lesion access, but does not obviate further ethanol endovascular treatment.

KEYWORDS: Endovascular management

Monday, May 20 – Wednesday, May 22
6:30 AM – 9:00 PM
Thursday, May 23
6:30 AM – 3:00 PM
Hall B1

Electronic Posters (ePosters) 147 - 213

eP4-Interventional

Note: A missing printed number indicates an abstract has been withdrawn.

eP-147

Pipeline Embolization Device Strategies

Urdaneta-Moncada, A. R.[1]·Ziegler, J.[2]·Mowji, P.[3]·Feng, L.[1]·Chao, K.[1]
[1]Kaiser Permanente Los Angeles Medical Center, Los Angeles, CA, [2]Kaiser Permanente San Diego Medical Center, San Diego, CA, [3]Kaiser Permanente Orange County Medical Center, Anaheim, CA.

Purpose
Pipeline embolization device (PED) is a flow diversion stent for the treatment of large wide-neck aneurysms that are not well treated with coiling methods including stent assisting coiling. The PED material and design are relatively unique including its deployment. Objective: Evaluation of the PED procedures including issues during deployment and strategies to outcome problems.
Materials & Methods
Retrospective multicentered case series of 30 PED procedures for treatment of aneurysms. The cases were evaluated for issues that arose during PED deployment. The different strategies for managing problems were assessed for their effectiveness.
Results
There were eight major issues with PED deployment. 1. Detachment from capture coil, 2. Pipeline embolization device apposition to the vessel wall, 3. Torqueing or twisting of the PED, 4. Accurate placement of the PED, 5. Herniation of PED into aneurysm, 6. Advancing the microcatheter and removing the delivery system, 7. Accessing the distal outflow artery, and 8. Postprocedure stroke within three days. Successful treatment strategies for each of the major issues demonstrated reasonable success.
Conclusion
Pipeline embolization device is a 1st generation flow diversion stent with a variety of issues related to its deployment. However, familiarity with PED deployment strategies can result in a more successful deployment.

KEYWORDS: Aneurysm treatment, Interventional

eP-148

Endovascular Treatment of Complex Intracranial Aneurysms: Flow Diverter Silk Stent

Buyukkaya, R.[1]·Cebeci, H.[2]·Erdogan, C.[2]·Hakyemez, B.[2]
[1]Duzce University, Duzce, TURKEY, [2]Uludağ University, Bursa, TURKEY.

Purpose
Endovascular treatment of intracranial cerebral aneurysms is different from classic saccular aneurysms when they are wide-necked, blister-like, fusiform-shaped and large size (more than 20 mm). Treatment of these aneurysms are more difficult and mortality and morbidity rates are higher. Flow diverter stents are designed specifically for

Note: Scanned images are included in the proceedings. Some submitted images were reduced during editing, thereby decreasing clarity. Also, refer to the Program Planner. Proceedings Content as of 3-29-2013.

challenging aneursyms. They provide endovascular reconstruction in aneurysmal segment to induce cure. In this study flow diverter stent (Silk; BaltExtrusion) technique is used in the treatment of complex ruptured or unruptured aneurysms. Early and midterm results of treatment, technical approach, thromboembolic results and approach to ruptured aneurysms were evaluated.
Materials & Methods
Thirty-two patients [age range: 34-79 years; 23 female (71.8%), nine male (28.2%)], whose aneurysms were not eligible for conventional endovascular techniques or surgery, were treated with Silk stent. Forty Silk stents were placed in 34 aneurysms (32 radiologically and clinically diagnosed patients). Three of the aneurysms were ruptured anerysms. Twenty of the aneurysms were carotid-ophthalmic aneurysms (58.8%) and six were cavernous ICA aneurysms (17.6%). There were two supraclinoid aneurysms (5.9%), two petrosal ICA aneurysm (5.9%). There were only four posterior circulation aneurysms in our series (11.8%). Except for three patients (8.8%) who presented with subarachnoid hemorrhage, all patients were pretreated with dual antiplatelet medications for at least three days before intervention. Three patients who presented with subarachnoid hemorrhage were treated with dual antiplatelet medications at the time of intervention. All patients received antiplatelet medication at least for a three-month period after endovascular treatment.
Results
The Silk stents were placed in a proper position in all patients. Adjunctive therapies were performed in four (12%) patients. Intra-arterial abciximab was administered in two patients because of intra-arterial thromboembolic event and intrastent balloon modelling was done in two patients. There was one mortality (2.94%) and one transient morbidity (2.94%). Control angiographic studies were performed in 31 patients (one mortality) and 33 aneurysm at the mean time of 9 ± 3 months (3-15 mo) after treatment. Control angiographic results included 81.8% complete occlusion (27/33), 12.1% residual neck remnant (4/33) and 6.1% residual saccular filling (2/33).
Conclusion
Flow diverter Silk stent is an effective tool for endovascular treatment of ruptured and unruptured challenging aneurysms because it allows high total occlusion rates, it is safe and effective and has acceptable mortality and morbidity rates.

KEYWORDS: Aneursym, Flow diverter, silk stent

eP-149

Are 'AComs' "AComs"?

Hughes, N.·Shankar, J.
Dalhousie University
Halifax, NS, CANADA.

Purpose
In current literature, the term anterior communicating aneurysm (Acom) incorporates true anterior communicating artery, A1-A2 junction, A1 and A2 aneurysms. What proportion of Acoms are actually true Acoms?
Materials & Methods
We completed a retrospective imaging review of coiled Acom aneurysms in the Dalhousie neuroradiology department from January 1, 2007 to October 6, 2011 for a total of 57 patients. Of these, 47 had CT angiography (CTA) imaging available on the Nova Scotia PACS system. Only patients with CTA images were recategorized into one of the four subgroups. One patient's images were indeterminate. Classification was accomplished using 0.6, 1.5 or 2.5 mm axial source images with coronal and sagittal reconstructions.
Results
There were 39 A1-A2 junction aneurysms, four true Acom, two A2 and one with both A1-A2 and true Acom. Of the 40 A1-A2 junction aneurysms, 15 were males. Thirty-eight of the 46 presented with rupture. All of the eight elective coilings were A1-A2 aneurysms. For most of the aneurysms, the domes were projecting in two orientations, for example superior and anterior. The five true Acom aneurysms appeared to project in one plane, two superior, two inferior and one anterior.
Conclusion
The pathogenesis of the subgroups of Acom aneurysms is unclear and further research is needed. In our study, the vast majority of Acom aneurysms are A1-A2 junction aneurysms. Are these four subgroups, therefore, linked together inappropriately in the current literature?

KEYWORDS: Aneurysm classification, Aneursym

eP-150

Preliminary Results of Flow Diversion Device (Silk Stent) in the Treatment of Intracranial Aneurysms in Fifteen Subjects: Medium and Long-Term Followup

Morin, F.·La Piana, R.·Cortes, M.·Tampieri, D.
Montreal Neurological Institute
Montreal, QC, CANADA.

Purpose
Treated intracranial aneurysms have an approximately 30% rate of recanalization. In the last years, many technical advances, such as the balloon remodelling technique and stent-assisted coils, have improved the results obtainable with endovascular treatment. A new

Note: Scanned images are included in the proceedings. Some submitted images were reduced during editing, thereby decreasing clarity. Also, refer to the Program Planner. Proceedings Content as of 3-29-2013.

generation of stents has been introduced recently: the flow diversion devices. They have been developed especially for the treatment of giant, fusiform or wide-neck aneurysms. Flow diverters reduce intra-aneurysmal blood flow and eventually thrombosis of the aneurysm is achieved. The SILK stent is a self-expandable flexible stent with low porosity; it was approved for clinical use in Europe in 2007. The aim of our study is to analyze the preliminary results at medium and long-term followup of our experience with SILK stent in a series of 15 consecutive cases.

Materials & Methods

The use of SILK stent as flow diverter was introduced at our Department of Neuroradiology in April 2009. Since then, a series of 15 patients with a total of 16 intracranial aneurysms were treated endovascularly using SILK stents. Thirteen patients were female and two were male, with a mean age at treatment of 53.7 years (range between 42 and 63 years of age). There were 13 aneurysms located in the anterior circulation, two in the basilar artery and one in the vertebral artery. Thirteen of these aneurysms were saccular and three were dissecting. Neuroradiologic followup [DSA, CTA (320 row scanner, Toshiba Aquilion ONE) or MRI/A] was available for 14 patients at three months (100%), 11 patients (77.3%) at 8-12 months and seven patients (46.7%) at two years.

Results

Twelve patients were treated using one SILK stent; of these, in one patient one SILK stent treated two aneurysms. In four patients two SILK stents were required in a telescopic fashion. In five subjects coils were used in addition to the SILK stent. The mean duration of followup was 15.3 months (s.d. 7.9). Reduction of flow within the aneurysm was achieved and visualized in all 15 patients (100%) at the immediate post-treatment angiography. Complete occlusion of the aneurysm was observed in 12 cases at their latest neuroradiologic study (12/15; 80%). In the remaining three patients (20%) a residual flow in the aneurysm still was observed at their latest follow-up exam (one at eight-month followup, two at 24-month followup).

Conclusion

In our three years experience of SILK stent use, a total of 15 patients and 16 aneurysms were treated at our Institution. Our data showed good results in terms of complete occlusion of the aneurysms, which was achieved and maintained in 80% of cases as of their latest follow-up study.

KEYWORDS: Aneursym, Flow diverter

eP-151

Single Center Direct Comparison of Neuroform and Enterprise Stents in the Treatment of Wide-Necked Intracranial Aneurysms

Durst, C.[1]·Khan, P.[2]·Gaughen, J.[1]·Patrie, J.[1]·Jensen, M.[1]·Evans, A.[1]
[1]University of Virginia, Charlottesville, VA, [2]Batra Hospital and Medical Reseach Centre, New Dehli, INDIA.

Purpose

Individually, the technical successes, clinical outcomes, and complications for Neuroform and Enterprise stents have been well documented. However, few studies have directly compared the technical or clinical outcomes of both stents. This study represents only the second report of a direct comparison of not only the technical and clinical outcomes, but also the complications associated with the use of each stent at a single institution.

Materials & Methods

A retrospective chart review identified 109 patients who underwent stent-assisted coil embolization for the treatment of a wide-neck aneurysm, which was defined as an aneurysm with either a dome to neck ratio of less than two or a neck diameter greater than 4 mm. Immediate and long-term clinical and imaging outcomes were recorded for all patients.

Results

Our technical success rate of 95.8% is concordant with that reported in the literature. Primary occlusion rates were 15.6% while an additional 32.8% of the treated aneurysms showed delayed occlusion on follow-up imaging and an additional 12.5% demonstrated progressive but incomplete occlusion on later exams. There were 18.8% of the treated aneurysms recanalized with an equal distribution between the Neuroform and Enterprise stents. However, major complication rates were three-fold higher with Enterprise stents as compared to Neuroform stents, 15.4% versus 4.5%, respectively. In total, eight out of the 10 major complications experienced with Enterprise stents occurred in vessels deemed tortuous. Conversely, only one major complication occurred in tortuous vessels using the Neuroform stent.

Conclusion

Although this study is retrospective and nonrandomized, it represents one of the first direct comparisons of Enterprise and Neuroform stents, limiting intra-operator variability. Our technical and clinical outcomes were individually similar to those of other institutions. There is no significant difference in the immediate or long-term occlusion or recurrence rates between the Enterprise and Neuroform stents. However, our data suggest an increased risk of major complication, particularly infarction, when using an Enterprise stent.

KEYWORDS: Aneurysm embolization, Stents, complications

Note: Scanned images are included in the proceedings. Some submitted images were reduced during editing, thereby decreasing clarity. Also, refer to the Program Planner. Proceedings Content as of 3-29-2013.

eP-152

Endovascular Treatment of Intracranial Aneurysms: Occurrence of Thromboembolic Events

Lee, Y.·Yoo, W.
Catholic University of Korea
Bucheon, Wonmigu, Sosadong, KOREA, REPUBLIC OF.

Purpose
To evaluate the frequency and causes of thromboembolic events associated with endovascular embolization of intracranial aneurysms. Correlations between radiologic findings (aneurysm size, localization, embolization time, number of coils used, as well as patient age) were evaluated with the occurrence of thromboembolic events.
Materials & Methods
Three hundred sixty-eight patients treated with coil embolization (396 total procedures) between March 2007 and September 2012 were included. All patients underwent a routine diffusion-weighted magnetic resonance imaging (DWI) within the 72 hours after the intervention for the detection of ischemic complications.
Results
Thromboembolic complications were more common in patients with ruptured aneurysms (12/23, 51%) than in those with unruptured aneurysms (112/373, 30%).The incidence of DWI abnormalities was higher in older patients (≥60 years) when compared to younger patients (≤60 years). There was no correlation between aneurysm location and the occurrence of lesions or among the number of coils used, the size of the aneurysm, or embolization time.
Conclusion
In order to provide adequate and timely treatment, a routine DWI followup after coil embolization of intracranial aneurysms might be helpful, especially in older patients.

KEYWORDS: Aneurysm embolization, Diffusion-weighted imaging

eP-153

Curative Embolization of Brain Arteriovenous Malformations with Onyx: Patient Selection, Embolization Technique, and Outcome

Mansour, O.
Alexandria University
Alexandria, EGYPT.

Purpose
A new curative embolization technique with Onyx for selected small and medium-sized superficially located brain AVMs was developed, which consists of obliteration of the nidus, including incremental occlusion of the draining veins. We report our first clinical results.
Materials & Methods
Between June 2008 and July 2011, 24 patients (seven women, 17 men; mean age, 41 years; range, 6-74 years) with AVMs were selected for curative embolization with Onyx. Presentation was hemorrhage in 14 and seizures in 10 patients. AVM location was frontal in 11, occipital in six, parietal in four, and temporal in three. Arteriovenous malformation size was a mean of 2.2 cm (median, 2; range, 1-3 cm).
Results
Complete angiographic obliteration of the AVM with Onyx in a single session was achieved in all 24 patients. There were no hemorrhagic or ischemic complications (0%; 95% CI, 0%-16.3%), and no new deficits induced by the treatment. Of 14 patients with ruptured AVMs, one patient who presented with a large frontal hematoma died shortly after surgical evacuation of the hematoma following complete embolization of a micro-AVM. Follow-up angiography at three months in 23 patients demonstrated a small AVM remnant in one that was treated with gamma knife radiosurgery. The other 22 AVMs remained completely occluded.
Conclusion
In selected patients with small and medium-sized superficial brain AVMs, as defined in our study, injection of Onyx by using a curative embolization technique in a single session seems to provide a safe and effective alternative to radiosurgery or surgery.

KEYWORDS: Arteriovenous malformation, Embolization

eP-154

Color Doppler-Guided Percutaneous Sclerotherapy of Smaller Facial Arteriovenous Malformation

Bhalla, N.[1]·Bhalla, M.[2]
[1]Victoria Jubilee Hospital, Ahmedabad, INDIA, [2]Medical College of Wisconsin, Milwaukee, WI.

Purpose
To evaluate efficacy of percutaneous treatment of facial arteriovenous malformation (AVM) measuring less than 4 cm, using polidocanaol 3% under color doppler (CD) guidance in outpatient clinical settings.
Materials & Methods
Six patients with facial AVM identified and measured on CD examination as less than 4 cm were treated with CD-guided percutaneous foam sclerotherapy during July 2008 and February 2010 on clinic basis. Following informed consent, lesion site was prepped in routine fashion, and venous side of lesion was identified on CD and compressed manually. The lesions were percutaneously punctured under CD guidance using 21 gauge needle. Polidocanol 3% diluted 50% with distilled water was foamed using Tessari's technique and was injected into the lesion. Polidocanol (1-3 cc) was used depending on lesion size. Treated site was kept compressed for 20 minutes following the procedure. Up to three such sessions were performed. Results were considered as worsened, totally occluded, partially occluded and unsuccessful based on CD

Note: Scanned images are included in the proceedings. Some submitted images were reduced during editing, thereby decreasing clarity. Also, refer to the Program Planner. Proceedings Content as of 3-29-2013.

findings and clinical examination. None of the patients were admitted indoor or required hospital stay.
Results
Complete occlusion of AVM was achieved in four patients in up to three sittings, three of which showed reduced lesion size. Two of the six patients achieved partial occlusion with reduced vascularity. None of them worsened and none of the procedure-related complication was noted. All patients complained of transient swelling, tenderness and discoloration at local site for up to one week.
Conclusion
Percuatenous sclerotherpy of facial AVM measuring less than 4 cm on CD study, is a safe and effective procedure which is reasonably effective with very low morbidity or complication and gives good clinical improvement, even when performed on outpatient clinic basis.

KEYWORDS: Arteriovenous malformation, Doppler ultrasound, foam sclerotherapy

eP-155

A Multidisciplinary Team Approach to Treating Intracranial Arteriovenous Malformations in a Regional Neuroscience Center

Davis, E.·O'Leary, S.·Flynn, P.·Smyth, G.·McKinstry, S.·Abouharb, A.·Simms, H. N.·Rennie, I.
Royal Victoria Hospital
Belfast, UNITED KINGDOM.

Purpose
To evaluate the management and treatment of intracranial AVMs and their outcomes over a five-year period in a regional center. Intracranial arteriovenous malformations (AVMs) are a relatively uncommon entity but can prove fatal or result in serious neurologic sequelae. With advances in radiologic imaging techniques these lesions are increasingly recognized and there are myriad approaches to treatment with no defined gold standard and treatment protocols based on locally available expertise. The decision regarding treatment is complex and involves a number of factors including whether the lesion is ruptured or unruptured, how amenable it is to treatment based largely on the Spetzler-Martin grading system, patient wishes as well as compromise between risk versus benefit. In our institution we have adopted a multidisciplinary team approach with all treatment options considered.
Materials & Methods
Retrospective chart review of all patients with AVMs managed by our unit over the past five years. Patients charts were assessed and the following information extrapolated: (1) Spetzler-Martin grade of all patients. (2) Multidisciplinary team meeting notes were evaluated to see which treatment options were offered and (3) Whether a stereotactic radiosurgical opinion was sought. (4) What discussions were had with the patient. (5) What treatment plan was ultimately decided upon. (6) What the outcome of the treatment was. (7) Whether more than one treatment was employed and how many times and lastly (8) Morbidity and mortality.
Results
In our institution we have adopted a multidisciplinary team approach involving both neurosurgery and neuroradiology. This includes endovascular embolization with glue and onyx and surgical resection, with these options available locally. As well as this the majority of unruptured AVMs are referred for a Stereotactic Radio-Surgical opinion. This adjunct to our locally available expertise is invaluable and ensures that we are capable of offering a comprehensive service for the treatment of AVMs. All treatment options are carefully considered and often patients ultimately have a combination of treatment modalities with a common pathway being for embolization prior to completion stereotactic radiosurgery. In our institution over the past five years, we have treated over 100 patients - 33.6% of these were treated with embolization only, 32.7% had stereotactic radiosurgery only with a further 24% going on to have a combination of both embolization and stereotactic radiosurgery and 4.8% were managed conservatively. Of the remaining patients, two patients did not attend followup, one resolved spontaneously, one additional patient was deemed untreatable following review by the multidisciplinary team and another patient died from unrelated causes prior to treatment. Processes, complication rates, etc. to be included at a later date.
Conclusion
With the various treatment options available and lack of level I or II evidence available in the literature regarding treatment, we feel that a multidisciplinary team approach, as offered in our institution, is the optimum approach and most beneficial to the patient. This combined approach leads to thorough evaluation and input from all specialties involved in AVM treatment.

KEYWORDS: Arteriovenous malformation, multidisciplinary

eP-156

Novel Technique for Selective Ophthalmic Artery Infusion Chemotherapy of Retinoblastoma in Children with Retrograde Ophthalmic Artery Flow

Abruzzo, T. A.[1]·Kimbrough, D. A.[2]·Cornell, K.[1]·Augsburger, J.[1]·Geller, J.[1]
[1]Cincinnati Childrens Hospital Medical Center, Cincinnati, OH, [2]University of Cincinnati Medial Center, Cincinnati, OH.

Purpose
Selective ophthalmic artery (OA) infusion chemotherapy (SOAIC) is an alternative to enucleation for the treatment of advanced intra-ocular retinoblastoma. In many children, microcatheter placement in the OA causes flow reversal and precludes delivery of chemotherapeutic agents to the

Note: Scanned images are included in the proceedings. Some submitted images were reduced during editing, thereby decreasing clarity. Also, refer to the Program Planner. Proceedings Content as of 3-29-2013.

tumor. The purpose of this work was to develop an interventional technique for stable conversion of retrograde OA flow to anterograde during SOAIC.
Materials & Methods
Between June 2009 and December 2012, patients with unilateral or bilateral International Classification System group C and D retinoblastoma and intact visual function were treated by SOAIC using melphalan, topotecan, or combinations of melphalan, topotecan and carboplatin depending on prior systemic chemotherapy regimens. Treatment cycles were every three to four weeks until examination under anesthesia (EUA) revealed stable tumor remission. Adjunctive therapies including subconjunctival carboplatin injections and cryotherapy were administered depending on the initial response to treatment and the extent of vitreal seeding. All SOAIC treatments were administered by placing a 4 French introducer sheath in the femoral artery and a coaxial 4 French diagnostic catheter in the internal carotid artery on the side of the tumor. Systemic heparin anticoagulation was administered in addition to adjunctive nebulized albuterol, intravenous decadron and intranasal Afrin. Chemoinfusions were administered through coaxial 1.2-1.5 French microcatheters placed through the diagnostic catheter and into the OA ostium. Ophthalmic artery hemodynamics were assessed by microcatheter angiography. If OA flow was anterograde the age-adjusted dose of chemotherapy was administered through the microcatheter in a total volume of 30-45 ml over a period of 30-40 minutes. If retrograde OA flow was demonstrated, temporary balloon occlusion (TBO) of the ipsilateral external carotid artery (ECA) was performed using an over-the-wire balloon occlusion catheter. Anterograde OA flow was confirmed by microcatheter angiography before and after intra-arterial administration of chemotherapy.
Results
Thirteen eyes with retinoblastoma were treated in 12 patients (four male). Patients ranged in age from seven to 96 months. Each eye was administered 2-10 treatment cycles, (average five). Sixty-two procedures were performed. In six patients, OA flow became retrograde after microcatheter placement. In all six patients TBO of the ECA restored anterograde flow to the OA. Anterograde OA flow remained stable throughout each SOAIC procedure enabling effective delivery of the entire chemotherapy dose to the intraocular tumor target. Twenty-two SOAIC procedures were performed with TBO of the ECA. There was no serious morbidity or complications directly attributable to the balloon occlusion procedure. Two of the seven eyes treated by standard SOAIC technique were enucleated because of suspicious findings on EUA, both of which were histologically negative for tumor. One of the six eyes treated with adjunctive TBO of the ECA was enucleated because of treatment refractory vitreal seeds. Two patients managed with standard SOAIC technique still are actively being treated. One patient currently is being managed with the TBO technique. All remaining patients have been in tumor-free remission an average of five months.
Conclusion
Temporary balloon occlusion of the ECA is a safe and effective means of managing retrograde OA flow in children undergoing SOAIC.

KEYWORDS: Retinoblastoma, Balloon assistance, retrograde

eP-157

Carotid Blowout Syndrome: Endovascular Management by Stenting and Embolization

Tisnado, J.[1]·Fox, W. C.[1]·Amendola, M. A.[2]·Sydnor, M. K.[1]·Amendola, C.[3]·Ehlenberger, C. A.[1]·Tisnado, J.[4]
[1]Medical College of Virginia Hospitals/VCU Medical Center, Richmond, VA, [2]Innovative Cancer Institute, South Miami, FL, [3]Georgetown University, Washington, DC, [4]Hartford General Hospital, Hartford, CT.

Purpose
Carotid blow out syndrome (CBOS) is a catastrophic emergency associated with high morbidity and mortality (M&M). The usual causes are: head and neck malignant tumor invasion, postoperative, postradiation therapy, inflammatory and trauma, among others. The conventional surgical management, including carotid artery and/or branch ligation and/or carotid artery bypass, is fraught with high M&M, may be ineffective and result with limited success. With the advent of covered and uncovered, balloon-expandable or self-expandable metallic stents, the emergent management of CBOS has improved and currently a permanent or temporary success in the endovascular management is expected.
Materials & Methods
During the last few years, we have studied 15 patients (adults and children, male and female) with CBOS of different etiologies, considered difficult or not manageable by surgery. The insertion of different types of stents, covered or uncovered, self-expanding or balloon-expandable, has been successful. We have used Gore Viabahn® Endoprosthesis, iCast™ (Atrium), Fluency® Plus Stent-Graft (Bard), Wallstent and Wallgraft (Boston Scientific) and Protégé (Bard). All procedures have been done in the IR suite and were successful in temporarily managing CBOS. No major stenting or embolization complications occurred. The patients had a relatively long or a temporary survival in a short followup.
Results
The emergency insertion of stents is a safe, effective and relatively easy procedure to permanently or temporarily manage CBOS. A longer followup and more patients treated are necessary to determine the long-term role of stenting in CBOS.
Conclusion
The surgical management is difficult and may be ineffective. The placement of stents, with or without

Note: Scanned images are included in the proceedings. Some submitted images were reduced during editing, thereby decreasing clarity. Also, refer to the Program Planner. Proceedings Content as of 3-29-2013.

adjuvant embolization, must be considered the first choice to manage CBOS, particularly in desperate situations.

KEYWORDS: Carotid artery stenting, Mortality, head and neck tumor

eP-158

Impact of Pretreatment Diffusion-Weighted Imaging ASPECTS on the Outcomes of Mechanical Thrombectomy for Acute Anterior Circulation Stroke

Yoon, W.·Jung, M.·Jung, S.·Kang, H.
Chonnam National University Hospital
Gwangju, KOREA, REPUBLIC OF.

Purpose
Correlation between pretreatment lesion size on diffusion-weighted imaging (DWI) and functional outcome in acute ischemic stroke is still unclear. The aim of this study was to assess whether the Alberta Stroke Program Early CT Score (ASPECTS) on DWI can reliably predict clinical outcomes at three months following mechanical thrombectomy therapy in patients with acute anterior circulation stroke.
Materials & Methods
Fifty-four consecutive patients with anterior circulation stroke treated with mechanical thrombectomy using Solitaire stent system within six hours after symptom onset were enrolled. ASPECTS was assessed on DWI just prior to the mechanical thrombectomy. Diffusion-weighted imaging ASPECTS scores were either categorized into 0 to 6 (n = 27) or 7 to 10 (n = 27). The primary outcome measure was a modified Rankin Scale (mRS) score of 0-2 at three months.
Results
The median ASPECTS on DWI was 6.5. At three months, 21 (39%) had an mRS score of 0-2, and three patients (5.5%) had died. Patients with an mRS score of 0-2 (good outcome) were younger (61 ± 15.4) than other patients (73 ± 8.6, $p = 0.003$), had lower rates of previous coronary artery disease (0% vs 18.1%, $p = 0.038$), and had higher rate of recanalization (100% vs 51.5%, $p<0.001$). Of patients with DWI ASPECTS 7-10, 48.1% had good outcome. Of those with DWI ASPECTS 0-6, 29.6% had good outcome. There was no significant association between DWI ASPECTS and clinical outcome ($p = 0.163$). On multivariate regression analysis, independent predictor of good outcome (mRS 0-2) was patient's age (odds ratio = 0.922, $p = 0.02$).
Conclusion
Diffusion-weighted imaging ASPECTS does not seem to impact on clinical outcomes after mechanical thrombectomy in patients with acute anterior circulation stroke. Patient's age, history of coronary artery disease, and recanalization status were significantly associated with clinical outcomes after mechanical thrombectomy for acute anterior circulation stroke.

KEYWORDS: Actue stroke, Diffusion MR imaging, mechanical thrombectomy

eP-159

Emergent Carotid Artery Stenting within Six Hours after Onset of Acute Ischemic Stroke

Yoon, W.·Jung, M.·Jung, S.·Kang, H.
Chonnam National University Hospital
Gwangju, KOREA, REPUBLIC OF.

Purpose
Acute ischemic stroke attributable to atherosclerotic steno-occlusive disease of extracranial internal carotid artery (ICA) carries a poor prognosis. The purpose of this study was to investigate the recanalization rate and clinical outcomes following emergent carotid artery stenting for hyperacute ischemic stroke.
Materials & Methods
Carotid artery stenting was performed in 28 patients with acute atherosclerotic steno-occlusive disease of extracranial ICA within six hours of stroke onset. Of these patients, 23 patients had tandem intracranial arterial occlusion at the level of ICA terminus (n = 2), M1 segment of middle cerebral artery (MCA) (n = 14), M2 segment of MCA (n = 4), and M3 segment of MCA (n = 3). Treatment for intracranial occlusions included mechanical thrombectomy, or combination of mechanical clot disruption and intra-arterial urokinase infusion. Successful recanalization was defined as successful extracranial ICA stent placement plus intracranial thrombolysis in cerebral ischemia (TICI) grade 2b or 3 after the treatment. The primary outcome measure was a modified Rankin Scale (mRS) score of 0-2 at three months.
Results
Median patient age was 71 years, and median NIHSS score at presentation was 11. Overall, successful recanalization rate was in 57.1% (16/28). Symptomatic intracerebral hemorrhage occurred in one patient (3.6%). Sixteen patients (57.1%) had a good clinical outcome (mRS 0-2) at three months. Successfully recanalized patients had a significantly higher rate of good outcome than those without recanalization at three months (75% vs 33%, $P = 0.027$). Patients without intracranial tandem occlusion had a more favorable clinical outcome than those with intracranial occlusion (100% vs 47.8%, $P = 0.033$). Mortality was 0% (0/28) at three months.
Conclusion
Emergent carotid artery stenting in acute atherosclerotic extracranial ICA steno-occlusive disease has a relatively high recanalization rate with a good clinical outcome in more than half of the patients. Successful recanalization (extracranial and intracranial) is associated with a good outcome in our cohort of patients undergoing emergent carotid artery stenting.

KEYWORDS: Actue stroke, Carotid artery stenting, emergencies

Note: Scanned images are included in the proceedings. Some submitted images were reduced during editing, thereby decreasing clarity. Also, refer to the Program Planner. Proceedings Content as of 3-29-2013.

eP-160

Outcome of Mechanical Thrombectomy with the Solitaire Stent in Acute Intracranial Internal Carotid Artery Occlusion

Yoon, W.·Jung, M.·Jung, S.·Kang, H.
Chonnam National University Hospital
Gwangju, KOREA, REPUBLIC OF.

Purpose
Acute stroke from occlusion of the intracranial internal carotid artery (ICA) is associated with a poor clinical outcome despite intravenous or intra-arterial thrombolytic treatment. Mechanical thrombectomy using retrievable stents is a newly available modality for acute stroke therapy. The purpose of this study was to evaluate the safety and efficacy of mechanical thrombectomy using Solitaire stent in the treatment of patients with acute intracranial ICA occlusion.
Materials & Methods
Between November 2010 and March 2012, a total of 64 consecutive patients with acute ischemic stroke were treated with mechanical thrombectomy by using Solitaire stent at our center. Of those patients, we retrospectively reviewed 17 consecutive patients presented with acute stroke attributable to ICA terminus occlusion within six hours from symptom onset. Successful recanalization was defined as thrombolysis in cerebral ischemia (TICI) grade 2b or 3. The primary outcome measure was a modified Rankin Scale (mRS) score of 0-2 at three months.
Results
Median patient age was 70 years, and median NIHSS score at presentation was 14. Median procedure time was 54 minutes. Overall, successful recanalization was achieved in 64.7% (11/17). No symptomatic intracerebral hemorrhage occurred. Five patients (29.4%) had a good clinical outcome (mRS 0-2) at three months. Good outcome occurred in 46% of patients (5/11) with recanalization and in 0% of patients without recanalization (P = 0.049). Mortality was 5.9% (1/17) at three months.
Conclusion
Mechanical thrombectomy using Solitaire stent has a relatively high recanalization rate with a good outcome in one third of patients and a significantly low mortality rate in patients with acute ICA occlusion. Patients with successful recanalization by Solitaire thrombectomy have improved clinical outcome compared with those patients without recanalization.

KEYWORDS: Actue stroke, Mechanical thrombectomy

eP-161

Absorbed Dose Measurements of Flat Panel CT Acquisitions for Parenchymal Blood Volume Estimates in Interventional Radiology

Supanich, M. P.[1]·Theesen, H.[2]·Sanders, W.[1]
[1]Henry Ford Health System, Detroit, MI, [2]Siemens AG, Hoffman Estates, IL.

Purpose
The use of flat panel CT in interventional neuroradiology settings has increased in recent years due to the ability to acquire and display of CT-like images, CT angiograms (CTAs) and blood volume maps. The use of these image sets during a treatment holds particular promise in stroke management. To date, there has been no characterization of the absorbed dose to the brain from flat panel CT studies. Given the increased focus on radiation dose in the community and the fact that many patients undergoing an interventional procedure are subjected to multiple studies using ionizing radiation, assessing the radiation dose of these studies is important.
Materials & Methods
Absorbed radiation dose measurements were performed using a 0.6 cc ionization chamber and digital electrometer from Radcal Corporation. A modified anthropomorphic head phantom from Phantom Laboratory composed of tissue equivalent material and a human skull was utilized to obtain the absorbed dose measurements. Holes were drilled in the phantom to allow insertion of the ion chamber for measurements. Tissue equivalent rods were placed in the holes not used for the dose measurement. Absorbed dose measurements of a standard parenchymal blood volume technique using two consecutive spins were made on a Siemens Artis Zee biplane system. Each spin was acquired over eight seconds with the dose to the detector set at 0.36 uGy per view. The ionization chamber was placed in the center hole of the head phantom and located at the level of the eyes. Average tube potential and tube current reported for each spin were 72 kV and 528 mA, respectively. The system reported the Air KERMA for each spin was 114 mGy. Measurements of absorbed dose in both standard noncontrast CT, CTA and shuttle CT perfusion (CTP) of the head were performed on GE CT systems. The ionization chamber placement replicated that of the flat panel CT acquisition. The scan ranges were consistent with clinical practice. The acquisitions were performed using automatic exposure control and the scanner reported $CTDI_{vol}$ was 63.6 mGy(head-16cm), 29.4 mGy(head-16cm) and 120.5 mGy(head-16cm) for the CT, CTA and CTP studies, respectively.
Results
The measured absorbed dose in the center of the phantom's brain was recorded from the digital electrometer used to read out the ionization chamber. The total absorbed dose from the two spins of the flat panel CT acquisition was 29.1 mGy. The measured absorbed doses were 48.0 mGy, 21.4 mGy and 78.4 mGy for the CT, CTA

Note: Scanned images are included in the proceedings. Some submitted images were reduced during editing, thereby decreasing clarity. Also, refer to the Program Planner. Proceedings Content as of 3-29-2013.

and CTP studies, respectively.
Conclusion
The acquisition of flat panel CT data using a dual spin acquisition following the intravenous injection of contrast agent in an interventional setting provides whole brain noncontrast CT images, parenchymal blood volume maps and 3D images with enhancement of both arteries and veins. These three datasets can be acquired at an absorbed dose nearly equivalent to a standard head CTA, at 60% of the dose of a standard head CT, and at more than half the dose of our institution's CTP protocol.

KEYWORDS: Cerebral blood volume, Dose, 3D angiography

eP-162

Dose Reduction in 3D Rotational Angiography with Axial Collimation

Radvany, M. G.[1]·Banckwitz, R.[2]·Koehler, C.[2]·Ehtiati, T.[3]·Mahesh, M.[1]
[1]Johns Hopkins University School of Medicine, Baltimore, MD, [2]Siemens, Forcheim, GERMANY, [3]Siemens, Princeton, NJ.

Purpose
As 3D tomographic imaging in flat panel systems is used more frequently it is important to consider methods for limiting the total radiation dose during the procedure. Different operators perform 3D acquisitions using varying modes to acquire data including different degrees of magnification and axial collimation. In this paper we present a study to demonstrate that axial collimation significantly reduces the effective radiation dose to the patient without reducing the diagnostic quality of the image data.
Materials & Methods
Dose measurements were performed using Rando Alderson 73 kg anthropomorphic phantom. This phantom is equipped with slices of 2.5 cm thickness for carrying thermoluminescent dose meter (TLD). Thermoluminescent doses were inserted in different measurement locations inside the Alderson phantom. The phantom was examined under the C-arm angiographic system AXIOM Artis (Siemens Healthcare, Germany) with a 30 x 40 cm flat image detector, using 5s 3D DSA protocols (syngo 3D DSA, Siemens Healthcare, Germany) at 48 cm FOV and 42 cm FOV without axial collimation, and then repeated using axial collimation of approximately 30%. The dose area product (DAP) also was recorded for each acquisition. The radiation dose measurement in Sievert, averaged over the TLDs, then is converted to effective dose. Subsequently we searched the radiology database for patients who underwent cerebral angiography with 3D rotational angiography to find and compare image quality at different rates of magnification and collimation. When the angiography suite was installed, operators routinely obtained rotational angiograms without collimation at 48 cm and 42 cm FOV while gaining familiarity with the equipment. Subsequent software updates allowed collimation in the axial direction and a 30% collimation was adopted for all studies unless clinically indicated.
Results
The results of the measurements performed on Alderson phantom show that the 5s 3D DSA protocol without any axial collimation has an effective dose of 0.9 mSv for both zoom rates, while the same protocol with an axial collimation of about 30% of FOV has an effective dose of 0.7 mSv for both zoom rates. The DAP for the same acquisitions was 155.2 $mGym^2$ for 48 cm FOV, and 119.8 $mGym^2$ for 42 cm FOV. Using axial collimation the DAP was reduced to 73.9 $mGym^2$ and 50.6 $mGym^2$ at 48 and 42 cm FOV respectively. In clinical studies we found that the image quality was maintained using axial collimation. The mean DAP on 48cm FOV was 695.9 $mGym^2$ and 1230 $mGym^2$, with and without collimation respectively. The DAP on studies obtained at 42cm FOV was 392.3 $mGym^2$ and 1008.9 $mGym^2$, with and without collimation respectively.
Conclusion
Axial collimation can be used to reduce the effective dose by approximately 25% without sacrificing diagnostic image quality. The phantom experiment shows that the effective dose is not reduced by change in magnification rate, therefore changing FOV from 48 cm to 42 cm is not a reliable technique for reducing radiation dose and should be practiced carefully to avoid truncation artifacts.

KEYWORDS: 3D DSA, Radiation dose reduction

eP-163

Clinical Outcomes of Coiling Ruptured Aneurysms Have Significantly Improved: A Meta-Analysis of Outcome of Coiling in Hydrocoil Endovascular Occlusion and Packing Study and the Cerecyte Coil Trial Compared with the International Subarachnoid Aneurysm Trial

Molyneux, A. J.[1]·Graham, C.[2]·Williams, C.[3]·Sneade, M.[1]·Forrester, L.[2]·White, P.[4]
[1]Oxford University, Oxford, UNITED KINGDOM, [2]Edinburgh University, Edinburgh, UNITED KINGDOM, [3]Glasgow University, Glasgow, UNITED KINGDOM, [4]Newcastle University, Newcastle, UNITED KINGDOM.

Purpose
To determine clinical outcomes at discharge and three - six months in patients with subarachnoid hemorrhage from a ruptured aneurysm prospectively enrolled in the Hydrocoil Endovascular occlusion and Packing Study (HELPS) and the Cerecyte Coil Trial (CCT) and to compare with the one-year outcomes in similar patients in the International Subarachnoid Aneurysm Trial (ISAT).
Materials & Methods
A predefined protocol of the meta-analysis has been presented previously. The study included all patients enrolled in HELPS2 and CCT3 who were WFNS grade 1 and 2 at the time of randomization. These were compared with

Note: Scanned images are included in the proceedings. Some submitted images were reduced during editing, thereby decreasing clarity. Also, refer to the Program Planner. Proceedings Content as of 3-29-2013.

the comparable ISAT patients allocated to clipping and coiling and were good grade at the time of randomization and in good grade at the time of treatment; patients who died, rebled, deteriorated due to delayed ischemic deficit or who crossed over to the other treatment were excluded. We prespecified the same subgroups as in ISAT. We examined procedural complications, discharge outcomes, rebleeding rates and three and six months clinical outcomes in HELPS and CCT respectively and compared these with 12 months outcomes in ISAT. Of 999 patients enrolled in the HELPS and CCT randomized trials, 487 patients were enrolled and treated for a recently ruptured aneurysm were in good clinical grade, WFNS 1 & 2. In the ISAT cohort 832 of 1073 patients allocated to coiling, and 846 of 1070 allocated to clipping fulfilled the eligibility criteria.

Results

There were more large aneurysms and posterior circulation aneurysms in HELPS/CCT than ISAT- 15·3% versus 6·1% large (p<0·001) and 11·4% versus 2·4% posterior circulation respectively (p<0·001). Otherwise the baseline characteristics were similar. Procedural rupture was reported in 171/846 (20·2%) of the ISAT clipping group, 46/832 (5·5%) of the ISAT coiling group and 24/487 (4·9%) of the HELPS/CCT group (p = 0.7). Thrombo-embolic complication was reported in 22/846 (2·6%) of the ISAT clipping group, 38/832 (4·5%) of the ISAT coiling group and 11/487(2·2%) of the HELPS/CCT group, p = 0.86 (versus ISAT clipping) and p = 0.035 (versus ISAT coiling) respectively. Rebleeding after treatment occurred in 4/487 (0·8%), in HELPS/CCT, compared with a total of 23/832 in the ISAT coiling group (2·8%), (p = 0.015) and a rebleed rate of 10/846 (1·2%), (p = 0.78) in the ISAT clipping group. Discharge home was seen in 35·5% of the ISAT clipping group, 46·5% of the ISAT coiling and 69·2% of the HELPS/CCT group. (p = <0.001). Independent outcome (mRS 0-2) was observed at followup, (3/6 months HELPS/CCT, one year ISAT) in 630/846 (72.7%), 682/832 (81.8%) and 418/487 (88.2%) in ISAT clipping, ISAT coiling and HELPS/CCT respectively. The case fatality at one year was 6·2%, 4·9% and 3·4%, in ISAT clipping, ISAT coiling and HELPS/CCT respectively.

Conclusion

The recent clinical outcomes of coiling have significant improved compared with the period of ISAT enrollment from 1994 to 2002. These findings further reinforce the significant clinical benefit of coiling compared with clipping for suitable aneurysms.

KEYWORDS: Aneursym, Meta-analysis

eP-164

Comparison of 3D Rotational Angiography with Its Axial Source Images in the Evaluation of Intracranial Aneurysm Dimensions

Ferris, M.[1]·Stokum, C.[1]·Ashruf, S.[1]·Abu-Zahra, K. W.[1,2]
[1]University of Maryland, Baltimore, MD, [2]Mecklenburg Radiology Associates/Novant Healthcare, Charlotte, NC.

Purpose

3D rotational angiography (3DRA) is a staple in the evaluation of intracranial aneurysms for endovascular treatment. 3D rotational angiography is superior to 2D digital subtraction angiography (2D DSA) in determining an aneurysm's spatial relationships, but is inferior in its ability to accurately measure aneurysm dimensions due to postprocessing in the construction of 3DRA from axial source images (ASI). The purpose of this study is to further describe the measurement accuracy of 3DRA using ASI as a standard of reference.

Materials & Methods

A retrospective analysis of 49 patients with 52 intracranial aneurysms who underwent 3DRA for evaluation of previously untreated aneurysms was conducted. Two neuroradiologists measured the dimensions of each aneurysm using 3DRA and corresponding ASI. The mean difference in neck sizes and dome-to-neck ratios between 3D RA and ASI were calculated. The proportions of "wide-neck" aneurysms seen on 3DRA and ASI were compared using two different definitions of "wide-neck," including <1.5 and <2.0. Interobserver variability was calculated in all instances.

Results

For Observer A: the average difference in neck size was 0.78 mm. ± 0.90 (P < .0001); the average difference in dome-to-neck ratio was 0.32 ± 0.77 (P < .0001). For Observer B: the average difference in neck size was 0.87 mm. ± 0.61 (P < .0001); the average difference in dome-to-neck ratio was 0.23 ± 0.48 (P < .0001). The two readers demonstrated no significant difference (all P < .0001) and good correlation in their measurements of: neck size in 3DRA (r = 0.8428), neck size in ASI (r = 0.8764), and dome-to-neck ratio in 3DRA (r = 0.8085). The two readers demonstrated no significant difference (P = 0.0046) but weak correlation in their measurement of dome-to-neck ratio in ASI (r = 0.3869). With a definition of wide-neck as dome-to-neck ratio <1.5, no statistical difference was found between the two readers in their classification of aneurysms as wide-neck using either 3DRA (P = 1.0) or ASI (P = 0.6685); Observer A read 28 aneurysms(28/52; 53.8%) as wide-neck using 3DRA compared with 17 aneurysms (17/52; 32.7%) using ASI (P = 0.0477); Observer B read 27 aneurysms (27/52; 51.9%) as wide-neck using 3DRA compared with fourteen aneurysms (14/52; 26.9%) using ASI (P = 0.0156). With a definition of wide-neck as dome-to-neck ratio <2.0, there was no statistical difference between the two readers in their classification of aneurysms as wide-neck using either 3DRA (P = 1.0) or ASI

(P = 0.4224); Observer A read 41 (41/52; 78.8%) aneurysms as wide-neck using 3D compared with 29(29/52; 55.8%) using ASI (P = 0.0208); Observer B read 41 (41/52; 78.8%) aneurysms as wide-neck using 3DRA compared with 34(34/52; 65.4%) using ASI (P = 0.1891).
Conclusion
In this retrospective study, 3DRA measurements significantly overestimated aneurysm neck sizes and significantly underestimated dome-to-neck ratio, with good agreement between two readers. Aneurysm neck size and dome-to-neck ratio are essential determinants in the decision to treat endovascularly and in device selection. Axial source image analysis should supplement 3DRA in the evaluation of intracranial aneurysms for endovascular treatment.

KEYWORDS: 3D DSA, Aneurysm sizes

eP-165

Stent-Assisted Coil Embolization of Aneurysms with Small Parent Vessels (≤ 2 mm): Safety and Efficacy Analysis

Puri, A. S.·Kuhn, A.·Hou, S.·Gounis, M. J.·Wakhloo, A. K.
University of Massachusetts Medical Center
Worcester, MA.

Purpose
Stent-assisted coil embolization (SACE) is a new therapeutic approach for wide-neck intracranial aneurysms. Stent-assisted coil embolization however can be technically challenging in small cerebral vessels (≤2 mm). Only a limited number of case series are available in the literature that have studied the safety and efficacy profile. We present our experience with currently approved stents for SACE of aneurysms with small cerebral vessels.
Materials & Methods
We identified all patients who underwent SACE with either a Neuroform or an Enterprise stent at our institution between June 2006 and October 2012. Only patients with a parent artery diameter of ≤2 mm were included. Patient comorbidities (arterial hypertension, smoking, hyperlipidemia, and coronary artery disease) and aneurysm characteristics (ruptured versus nonruptured, incidental finding, recanalized) were documented and angiographic follow-up data were reviewed.
Results
A total of 41 patients with 44 aneurysms met our criteria and were included in the study. The mean age was 54.5 years. Mean parent artery diameter was 1.7 mm (range 1.2 mm to 2 mm). Aneurysms were detected as incidental findings in 34.1%. Most aneurysms were located in the anterior circulation (75%). Middle cerebral artery aneurysms were found in 29.6% and anterior communicating artery aneurysms in 34.1% of cases. Aneurysms associated with symptoms were seen in 31.8%. Fourteen aneurysms had been previously coiled but recanalized and thus were retreated with stent-assisted coil embolization. In 54.5% of cases (n = 24) a Neuroform stent was used. Stent placement was successful in 41 cases (93.2%). Periprocedural thromboembolic complications occurred in six interventions (13.6%) but all were treated successfully with IA lysis (abciximab). Aneurysm rupture with SACE and vessel straightening was seen in one case (2.3%) each. Near complete or complete aneurysm obliteration was seen in 37 aneurysms (84.1%). Six-month follow-up angiography was available for 28 patients (68.3%). Coil compaction was seen in three cases one of which also revealed an in-stent stenosis but not requiring a retreatment. One stent occlusion was seen at followup, but did not require any further intervention due to excellent collaterals. Longer-term followup at 12 to 20 months were available in 13 patients. In two cases coil compaction remained stable compared to the six-month followup and in two cases new aneurysm recanalization was noticed. No in-stent stenosis was found. Three-year follow-up angiography was available for four patients. Further coil compaction was seen in one patient who had previously shown stable recanalization at six and 12 month follow-up angiography. Retreatment was only necessary in this single case.
Conclusion
Our results suggest that SACE of aneurysms with parent vessels ≤2mm in diameter is feasible with acceptable periprocedural complications and excellent long-term patency rate of parent arteries. However, like with other locations, recanalization, although low, remains an issue.

KEYWORDS: Aneurysm treatment, Stents, Small parent vessel

eP-166

P2Y12 Assay Values in the Prediction of Thromboembolic Events after Neurointervention

Gingras, J.·Clopton, D.·Durst, C.·Schweickert, P.·Patrie, J.·Jensen, M. E.·Evans, A.
University of Virginia
Charlottesville, VA.

Purpose
Dual antiplatelet therapy has been established as the standard of care for prevention of in-stent thrombosis after placement of an intracranial stent. However, the desire to prevent in-stent thrombosis counters the need for the aneurysm to thrombose after coil embolization. Additionally, platelet inhibition predisposes patients to a number of complications, while the dose and treatment duration are not standardized. Expense, patient compliance, and associated complications demand the need for appropriate use of antiplatelet therapy in this patient population. The purpose of this study is to determine the odds of a patient having an adverse event as compared to the inhibition of aneurysm thrombosis based on the P2Y12 assay and Aspirin Reaction Unit (ARU) values.

Note: Scanned images are included in the proceedings. Some submitted images were reduced during editing, thereby decreasing clarity. Also, refer to the Program Planner. Proceedings Content as of 3-29-2013.

Materials & Methods
A retrospective analysis identified 110 patients who had undergone stent-assisted coil embolization of a wide-neck aneurysm. Patients were reviewed by members of the research team not involved in the initial treatment. Patients who were treated electively were initiated on standard dual anti-platelet therapy of aspirin 325 mg and clopidogrel 75 mg three to five days prior to the procedure. Six patients presenting acutely with subarachnoid hemorrhage received antiplatelet therapy of aspirin and/or clopidogrel just prior to or during the procedure, depending on when it was determined that a stent would be required. Enterprise and all generations of Neuroform stents were included in this study. The patients were continued on aspirin and clopidogrel after treatment. Platelet inhibition was assessed using aspirin response units (ARU), while the "VerifyNow" P2Y12 assay was used to determine patient response to clopidogrel. The degree of aneurysm thrombosis was sequentially assessed for thrombosis using follow-up cerebral angiograms, computed tomography angiography (CTA), or magnetic resonance angiography (MRA). All complications related to the procedure were recorded from careful chart review. The statistical analysis controlled for the stent manufacturer and the presence or absence of subarachnoid hemorrhage.
Results
Logistic regression statistical analysis was performed using univariate and multivariate adjusted odds ratios. Analysis demonstrated that aspirin and clopidogrel levels did not effect aneurysm thrombosis after stent placement. Additionally, it was shown that treatment with clopidogrel does not increase the likelihood of aneurysm recannulization. While aspirin response levels did not correlate with the likelihood of major complication, the odds of a major complication after stenting were inversely related to the P2Y12 assay value ($p = 0.039$).
Conclusion
This study demonstrates a statistically significant increase in major complications as the response to clopidogrel antiplatelet therapy decreases as determined by the P2Y12 assay values. However, ARU values did not correlate with major complications. Additionally, aspirin and clopidogrel demonstrated no effect on aneurysm thrombosis or recannulization. These findings suggest that the P2Y12 values should be monitored in patients after placement of an intracranial stent. A prospective study would be warranted to determine the optimum P2Y12 threshold values, which will prevent major complications without inhibiting aneurysm thrombosis.

KEYWORDS: Aneursym, Stents, P2Y12

eP-167

Noise Reduction Filter for Visualization of Enterprise VRD on High-Resolution CT-Like Imaging

Oishi, S.[1]·Yamada, M.[2]·Yokoyama, H.[2]·Shiraishi, K.[3]·Satow, T.[2]
[1]Toshiba Medical Systems Corp., Otawara, JAPAN, [2]National Cerebral and Cardiovascular Center Hospital, Suita, JAPAN, [3]Toshiba Medical Systems Engineering Co., Ltd., Otawara, JAPAN.

Purpose
Stent-assisted coiling is used as one of the treatment options for wide-neck aneurysms. Adaption of stent struts to vessel wall should be checked before starting coiling, but struts are almost invisible on x-ray acquisition data because of diameters of 60 μm in the case of Enterprise VRD. Stent imaging, high-resolution CT-like imaging, make those visible, but those are sometimes fragmented due to enhanced noise with high spatial resolution kernel. The fragmentation issues might cause difficulty in identifying kink of the struts. We have developed a dedicated noise reduction filter.
Materials & Methods
Existing noise reduction filter called coherence filter and the new noise reduction filter were applied to ten stent imaging data sets. The data were assessed independently by two experienced neuroradiologists/neurosurgeons, who were blinded to both images and patients, and a semiquantitative five-point grading scale (1 = poor, 5 = excellent) were used to score visibility of stent struts.
Results
The coherence filter and new noise reduction data were demonstrated on Figure 1(a) and Figure 1(b), respectively. Stent struts were clearly identified on Figure 1(b). Noise levels were decreased with the coherence filter and new noise reduction filter by 46.1% and 80.3% on average, respectively. Table 1 shows averaged five-point grading scale for each neuroradiologist/neurosurgeon.

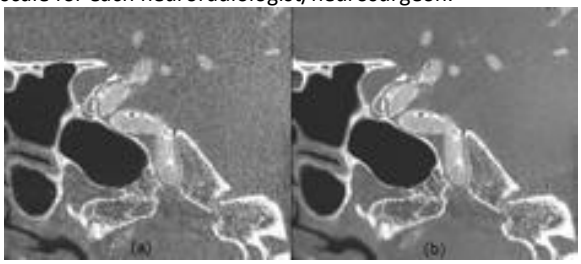

Note: Scanned images are included in the proceedings. Some submitted images were reduced during editing, thereby decreasing clarity. Also, refer to the Program Planner. Proceedings Content as of 3-29-2013.

Averaged five-point grading scale

	Coherence filter	New noise reduction filter
Neuroradiologist A	2.5	4.3
Neuroradiologist B	2.1	4.3

Conclusion
New noise reduction filter dramatically suppressed noise on high resolution CT-like imaging data without losing fine stent struts information. Kink of stent struts could be determined clearly with the new noise reduction data, and the well visualized struts will avoid unexpected complications at stent-assisted coiling.

KEYWORDS: 3D imaging, Aneurysm treatment, noise reduction

eP-168

Endovascular Management of Distal Posterior Inferior Cerebellar Aneurysms: Case Series

Boddu, S. R.·Noorian, A.·Schuette, A.·Tong, F. C.
Emory University Hospital
Atlanta, GA.

Purpose
Peripheral aneurysms of the posterior inferior cerebellar artery (PICA) are rare, and pre-existing literature concerning their endovascular treatment is limited. Posterior inferior cerebellar artery aneurysms are challenging, prone to procedural rupture and treatment strategies including surgical clipping and endovascular occlusion of the parent PICA are reported. In this study, we review endovascular management of five patients with distal PICA aneurysms, without sacrifice of the feeding artery.
Materials & Methods
Retrospective review of all the patients with treated peripheral PICA aneurysms at Emory University Hospital from May 2010 to May 2012 was performed. Clinical histories, radiologic images and operative reports were reviewed. Patients underwent emergent CT scan of the head if concerned for subarachnoid hemorrhage at presentation and 4-vessel diagnostic conventional angiography. CT scans were done postprocedure to insure the absence of PICA infarction. Patients were followed with conventional cerebral angiography.
Results
Five patients with a mean age at presentation: 60 years (range: 52-68 years). M:F-3:2. The clinical presentation was severe headache with nausea, vomiting and dizziness in all patients. None of them had seizures or focal motor neurologic deficits. Hunt and Hess scale at admission: Grade: 1 - one patient; Grade: 2 - one patient; Grade: 3 - two patients. Four of five (80%) patients had hydrocephalus; needed EVD and two of these patients had prolonged hospital stay from recurrent hydrocephalus and needed ventriculo-peritoneal shunt. Three of five patients had associated vascular malformations. Four patients had follow-up angiogram at three months and one patient at three and 12 months. One patient at three months followup had 30-40% recurrence and was treated with surgical clipping. Four of five patients had stable occlusion of the aneurysm at initial angiographic followup. No mortality or rebleeding was reported in the followup of patients as of this date.

Conclusion
We report a series of five distal PICA aneurysms with successful endovascular management and preservation of parent artery with no complication, good immediate and follow-up outcome. With rapid advances in endovascular techniques, the endovascular option can potentially be the first line to treat this critical condition with parent vessel preservation. Further large studies are warranted.

KEYWORDS: Endovascular embolization, Aneursym, posterior inferior cerebellar artery

eP-169

Cerebral Aneurysm Hemodynamic Alterations after Placement of a Flow-Diverter Stent

Takao, H.[1]·Suzuki, T.[1]·Tateshima, S.[2]·Masuda, S.[1]·Kadokura, S.[1]·Chein, A.[2]·Mohamed, A.[1]·Murayama, Y.[1]·Vinuela, F.[2]
[1]The Jikei University School of Medicine, Tokyo, JAPAN, [2]University of California Los Angeles, Los Angeles, CA.

Purpose
Currently, the placement of a stent as flow diverter (FD: Pipeline™) has been indicated as a treatment option, which has the potential to prevent aneurysm rupture by reducing hemodynamic forces and promoting aneurysm thrombosis. However, recent literature shows that some

Note: Scanned images are included in the proceedings. Some submitted images were reduced during editing, thereby decreasing clarity. Also, refer to the Program Planner. Proceedings Content as of 3-29-2013.

seemingly successful treatments have been complicated by late hemorrhage. We believe that flow changes after placement of FD may cause some complications. We assessed this hypothesis through quantification of changes in intracranial aneurysm flow dynamics resulting from the placement of Pipeline stents.

Materials & Methods

Starting from DSA images before treatment, the aneurysm geometry was extracted and analyzed using a mathematical formula for fluid flow under pulsatile blood flow conditions. Commercial software (ANSYS ICEM CFD 13) was used for both mesh generation and fluid simulation. Simulations were performed before and after virtual placement of the Pipeline flow diverter, and hemodynamic parameters were compared in some parameters.

Results

Our result shows reductions in aneurysm velocity and wall shear stress (WSS), and increased pressure within the aneurysm after placement of this stent. This pressure increase is related to effective resistance in the parent artery due to placement of the device. The blood velocity into aneurysms decreased. In the parent artery, our result indicated increase of pressure, velocity and WSS.

Conclusion

Flow diverter devices can cause intra-aneurysmal and parent artery pressure increase. These hemodynamic changes in the parent artery and aneurysm may lead to rupture or treatment complications. Patient-specific CFD models potentially may be a useful tool in estimating the risks of device use before treatment using the FD stent.

KEYWORDS: Stents, Aneursym, flow diverter

eP-170

Comparison of Contrast-Enhanced Time-Resolved MR Angiography and Digital Subtraction Angiography for Monitoring of Pipeline Embolization of Intracranial Aneurysms

Boddu, S.·Saindane, A. M.·Dehkharghani, S.·Tong, F.·Dion, J.
Emory University School of Medicine
Atlanta, GA.

Purpose

Endoluminal reconstruction and flow diversion using the pipeline embolization device is a novel treatment for cerebral aneurysms. Followup with digital subtraction angiography (DSA) has been reported following pipeline embolization; however, a noninvasive technique for monitoring extent of residual aneurysm filling, aneurysm recurrence, and in-stent stenosis is desirable. We hypothesize that contrast-enhanced time-resolved MRA (CE-TR-MRA) will provide a reliable and effective noninvasive method for following pipeline embolized aneurysms.

Materials & Methods

Over an 18-month period, patients with pipeline embolization of intracranial aneurysms who completed an initial follow-up evaluation with 3D time-of-flight (TOF) MRA, CE-TR-MRA, and DSA were reviewed. Twenty-nine pipeline embolized intracranial aneurysms in 21 patients were evaluated. Subjects underwent MRA on a 1.5T GE unit using both 3D-TOF-MRA and CE-TR-MRA using time-resolved imaging of contrast kinetics (TRICKS) with intravenous administration of a standard dose gadolinium-based contrast agent. Ten dynamic phases with submillimeter in-plane resolution and four-second temporal resolution were obtained. All patients underwent DSA within a median of 11.5 days(0-68 days) after the MRA. Three-dimensional TOF-MRA, CE-TR-MRA, and DSA images were evaluated for presence and size of residual aneurysm, and endolumenal stent diameter, with DSA used as the reference standard.

Results

Twenty of 21 CE-TR-MRA studies were of diagnostic quality; one patient had a nondiagnostic MRA due to artifact from a clipped contralateral aneurysm. Three aneurysms represented recurrence following prior endovascular coiling. The median MRA follow-up period was 177 days following pipeline placement (49-218 days). The sensitivity and specificity, positive predictive value (PPV), and negative predictive value (NPV) of the 3D-TOF-MRA relative to DSA for detection of residual/recurrent aneurysm filling were 79%/78%/88%/63%, and 95%/78%/90%/88% for CE-TR-MRA relative to DSA. The two aneurysms reported occluded on CE-TR-MRA that were patent on DSA demonstrated only minimal curvilinear filling measuring 1 mm in maximal depth. One aneurysm reported minimal interstitial filling on CE-TR-MRA showed complete occlusion on DSA performed on

Note: Scanned images are included in the proceedings. Some submitted images were reduced during editing, thereby decreasing clarity. Also, refer to the Program Planner. Proceedings Content as of 3-29-2013.

the same day. A major pitfall of 3D TOF MRA was failure to differentiate T1 hyperintense thrombus and residual aneurysm filling. Both MRA techniques overestimated the extent of narrowing of the pipeline stent lumen, 3D TOF MRA by a mean of 58%, and CE-TR-MRA by a mean of 27%. The figure demonstrates overestimation of stenosis on a CE-TR-MRA MIP versus DSA.

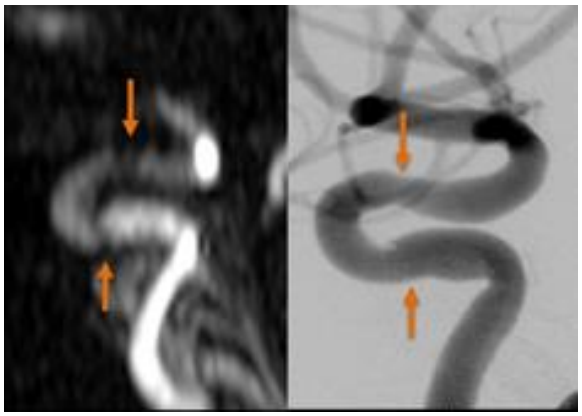

Conclusion
Contrast-enhanced TR-MRA is a promising noninvasive technique for monitoring pipeline-embolized intracranial aneurysms and is more sensitive and specific than 3D-TOF-MRA. Both 3D-TOF-MRA and TR-CE-MRA overestimate the extent of in-stent stenosis.

KEYWORDS: 4D MRA, Aneurysm embolization

eP-171

Second Catheter Angiography after Initially Negative Invasive and Noninvasive Imaging in Patients with Atraumatic Subarachnoidal Hemorrhage

Ringelstein, A.·Mueller, O.·Moenninghoff, C.·Goericke, S. L.·Sure, U.·Forsting, M.·Schlamann, M.
University Hospital Essen
Essen, GERMANY.

Purpose
This study aimed to determine the yield of DSA for the detection of causative vascular lesions in patients with atraumatic subarachnoidal hemmorhage (SAH) and negative initial noninvasive and invasive neurovascular examinations (CTA, DSA and MRA).
Materials & Methods
We retrospectively evaluated 7147 invasive catheter angiographies between 2004 and 2012 from our PACS System. Ninety patients presented with subarachnoidal hemorrhage and repetitive DSA because initial noninvasive and invasive imaging was negative concerning a causative vascular lesion. Two neuroradiologists reanalyzed the initial imaging and the result of repetitive DSA independently to find out if a second DSA might be helpful in detecting an initially occult bleeding source.
Results
Repetitive DSA demonstrated a causative vascular lesion in four patients (4.5%). In all other patients no causative vascular lesion was found. Since the implementation of 3D rotational DSA in 2008 only one more causative vascular lesion was found during repetitive DSA and the rate of initially negative imaging and accordingly the number of necessary reangiographies approximately halved although the number of acute SAH did not change significantly.
Conclusion
Repetitive DSA revealed a cause for SAH after initially negative imaging diagnostics in some rare cases and the detection rate decreased after implementation of 3D rotational DSA. But as these findings have a therapeutic and prognostic impact, we think that a repetitive DSA can be recommended in patients with SAH, even under consideration of the risk of a second invasive diagnostic angiography itself. Interdisciplinary evaluation and double reading of the initial imaging might be helpful to avoid repetitive DSA.

KEYWORDS: Aneursym, Catheter angiography

eP-172

Benefit of 3D Rotational Angiography Compared to Conventional Biplanar Digital Subtraction Angiography in Detecting Bleeding Sources after Subarachnoidal Hemorrhage

Ringelstein, A.·Mueller, O.·Goericke, S. L.·Moenninghoff, C.·Sure, U.·Forsting, M.·Schlamann, M.
University Hospital Essen
Essen, GERMANY.

Purpose
In about 85% of patients with subarachnoidal hemorrhage (SAH) a causative vascular lesions can be found during acute imaging diagnostics with CTA and DSA. In 15% the bleeding source cannot be cleared. Usually, a repetitive DSA is mandatory and includes the usual complication risk of an invasive angiography. The present study assesses if 3D rotational angiography may help to avoid a repetitive DSA.
Materials & Methods
From January 2004 till December 2012 we extracted 90 patients with acute nontraumatic SAH and negative initial imaging diagnostics concerning the bleeding source from our PACS system. All patients have received a second angiography on the basis of an interdisciplinary neuroradiologic and neurosurgical conference. Retrospective and independent double reading was performed. From 2004 until July 2008 only 2D DSA was available, since July 2008 until today 3D rotational DSA has been performed in every case during first and second DSA.
Results
In the second DSA, we found four aneurysms in four patients (4/90; 4.5%) that were treated subsequently. During the first 4.5 years of this study 60 patients needed a reangiography compared to 30 patients during the last

Note: Scanned images are included in the proceedings. Some submitted images were reduced during editing, thereby decreasing clarity. Also, refer to the Program Planner. Proceedings Content as of 3-29-2013.

4.5 years. The number of patients with acute nontraumatic SAH treated in our hospital did not change significantly. During the first phase we found three aneurysms, during the second phase of the study only one.
Conclusion
Using 3D rotational DSA during initial imaging diagnostics helps to reduce false negative results concerning the bleeding source during acute diagnostics and helps to avoid repetitive DSA. The usage of 3D DSA during second angiography does not reveal more aneurysms than conventional biplanar DSA. Three-dimensional rotational DSA should be an essential part of diagnostics after acute SAH.

KEYWORDS: Aneurysmal subarachnoid hemorrhage, Catheter angiography

eP-173

Transbrachial Coil Embolization of Cerebral Aneurysms in the Anterior Cerebral Circulation with a Novel Sheath Guide for Transbrachial Carotid Cannulation

Iwata, T.·Mori, T.·Miyazaki, Y.·Nakazaki, M.·Takahashi, Y.
Shonan Kamakura General Hospital Stroke Center
Kamakura, JAPAN.

Purpose
Transfemoral approach is a common technique for coil embolization of cerebral aneurysms in the anterior cerebral circulation. However, it is difficult to advance a guiding catheter into the carotid artery through the femoral route in patients with a tortuous aortic arch, an unfavorable supra-aortic takeoff, aortic diseases or occlusion of the femoral artery. The purpose of our study was to report our initial experiences of coil embolization of cerebral aneurysms in the anterior cerebral circulation with a novel sheath guide for transbrachial carotid cannulation.
Materials & Methods
A 6 Fr sheath guide designed specifically for transbrachial carotid cannulation was developed, transbrachial coil embolization for cerebral aneurysms was started in May 2011. Included for analysis were patients who underwent transbrachial coil embolization of cerebral aneurysms in the anterior cerebral circulation from May 2011 to July 2012. Adjuvant techniques, angiographic results, procedural success and periprocedural complications were investigated.
Results
Eighteen patients underwent transbrachial coil embolization of cerebral aneurysms in the anterior cerebral circulation. The locations of aneurysms were the internal carotid artery (ICA) paraclinoid (n = 7), ICA posterior communicating artery (n = 4), middle cerebral artery (n = 3), anterior communicating artery (n = 3) and anterior cerebral artery (n = 1). Transbrachial approach was never abandoned or switched to transfemoral approach in any cases. The stent-assist and balloon-assist techniques as adjuvant ones were used smoothly through the sheath guide in three patients and in nine patients, respectively. At the end of the coil embolization, complete occlusion was in 12 patients and near complete in six. All procedures were successful through the brachial route. Neither periprocedural complications nor access-site related complications occurred. Patients were free on their beds immediately after coil embolization even during hemostasis.
Conclusion
Transbrachial coil embolization of cerebral aneurysms in the anterior cerebral circulation with a novel sheath guide for transbrachial carotid cannulation was safe, feasible and useful.

KEYWORDS: Aneursym, Endovascular embolization

eP-174

Vision Outcomes and Major Complications after Endovascular Coil Embolization of Ophthalmic Artery Aneurysms

Durst, C.[1]·Nguyen, Q.[2]·Gaughen, J.[1]·Patrie, J.[1]·Jensen, M.[1]·Evans, A.[1]
[1]University of Virginia, Charlottesville, VA, [2]Franklin Square Hospital, Baltimore, MD.

Purpose
Ophthalmic artery aneurysms are difficult to treat surgically due to their location near the clinoid process and the proximity of the optic nerves. Furthermore, aneurysms arising from either the ophthalmic artery or the ophthalmic segment of the internal carotid artery have been known to cause visual disturbances or eye pain. The advent of endovascular treatment techniques has provided an alternate method for the treatment of these aneurysms. This paper aims to describe the inherent risks of endovascular treatment of these aneurysms and the likelihood of improvement or degradation of visual disturbances or eye pain after treatment.
Materials & Methods
A retrospective study identified 91 patients (78 female and 13 male) who underwent coil embolization of an ophthalmic artery aneurysm or an aneurysm of the ophthalmic segment of the internal carotid artery. All treatment data, immediate and long term imaging outcomes, and immediate and long term clinical outcomes were recorded.
Results
There was no difference in the rate of major complication between aneurysms arising from the ophthalmic artery and those arising from the ophthalmic segment of the internal carotid artery. Patients who presented with hemorrhage are more likely to have a major complication ($p = 0.003$). Patients with hypertension tended to have more major complications, though this did not reach statistical significance ($p = 0.100$). Of the 65 patients with greater than six months of follow-up imaging, 19 had a

Note: Scanned images are included in the proceedings. Some submitted images were reduced during editing, thereby decreasing clarity. Also, refer to the Program Planner. Proceedings Content as of 3-29-2013.

recurrence. The maximum dimension of the aneurysm dome (p = 0.003), the aneurysm neck (p = 0.031), and the dome to neck ratio (p = 0.002) correlate with the rate of recurrence. Patients who presented with hemorrhage were more likely to have an aneurysm recurrence (p = 0.018). When patients presented with a recurrence, they were more likely to present with a subsequent recurrence (p = 0.032). Patients who were symptomatic prior to treatment were likely to improve after treatment while those who were asymptomatic were likely to stay that way (p = 0.029). This is contrary to what has been published previously. Those with a smaller aneurysm neck diameter were more likely to have symptomatic improvement (either improvement in visual disturbance or eye pain) after treatment (p = 0.035).
Conclusion
Complication rates may be stratified according to the presence or absence of subarachnoid hemorrhage with hypertension possibly being a smaller contributor. The risk of recurrence after endovascular treatment also correlates with the presence or absence of hemorrhage and increases with the size of the aneurysm. Perhaps most importantly, patients who present with symptomatic visual disturbance or eye pain have significant improvement after treatment.

KEYWORDS: Ophthalmic artery, Aneursym, vision

eP-175

Endovascular Treatment of Small Wide-Neck Intracranial Aneurysms: Which Treatment Now?

Redjem, H.·Blanc, R.·Pistocchi, S.·Bartolini, B.·Nishido, H.·Piotin, M.
Fondation Adolphe De Rothschild
Paris, FRANCE.

Purpose
The aim of this study was to evaluate angiographic and three months clinical outcomes after endovascular treatment of little wide-neck aneurysms ≤ 3 mm.
Materials & Methods
Beetween January 2002 and November 2011, 1627 consecutive patients with 1963 aneurysms have been treated in our center by endovascular treatments. One hundred six aneurysms (33 ruptured) measuring less than 3 mm have been treated in 103 patients. Among them, 11 aneurysms have been treated by flow-diverter stents. We report procedural complications, immediate angiographic results and clinical and angiographic outcomes.
Results
No hemorrhagic or thrombo-embolic complication has been reported in the group of the aneurysms treated with flow diverter. In the group of aneurysms treated by coils or stent-assisted coiling, we report five (4.8%) vascular or aneurysm bag perforations and two (1.9%) thrombo-embolic complications. There were three (2.9%) permanent and three (2.9%) transient neurologic complications among which two deaths have been attributed to the intervention.
Conclusion
Endovascular treatment of small wide-neck intracranial aneurysms is not associated with a higher rate of complications than for larger ones despite a higher risk of vascular perforation. Treatment with stent-flow diverters may be a good choice for lesions of the "blister-like" type and offers a new approach in the endovascular treatment of microaneurysms.

KEYWORDS: Aneursym, Aneurysm treatment, small aneurysm

eP-176

Dyna-CT Atlas of Pipeline Device

Massari, F.·Chaudry, I.·Spiotta, A.·Miranpuri, A. S.·Hawk, H. E.·Turner, R. D.·Turk, A. S.
Medical University of South Carolina
Charleston, SC.

Purpose
A successful Pipeline (PED) (Covidien, Irvine, CA, USA) embolization procedure is dependent upon understanding the anatomical relations of the deployed PED to the parent vessel, aneurysm neck and surrounding anatomical structures, ensuring adequate neck coverage with the PED. We have created an Atlas of IA DYNA CT PED deployment demonstrating adequate wall apposition, poor wall apposition, neck coverage, poor apposition between telescoping stents and PED complications such as PED intussusception.
Materials & Methods
High anatomical detail of the PED in relation to the parent vessel, aneurysm neck and adjacent structures can be difficult to obtain with conventional or three dimensional (3D) rotational angiography. To obtain this detail, an intra-arterial dilute (20%) contrast-enhanced DYNA CT (Siemens, Forchheim, Germany) was performed using an Artis Zee flat panel biplane angiographic system with commercially available software and reconstructed on a commercially available Leonardo workstation (Siemens Medical Solutions, Erlangen, Germany). The images obtained give exquisite detail of the PED itself, its apposition to the parent vessel wall, neck coverage as well as complication of PED deployment.
Results
At our institution a total of 104 PEDs have been deployed. A total of 21 IA contrast-enhanced DYNA CTs (ICE DYNA CT) have been performed to evaluate PED deployment. In analyzing the acquired ICE DYNA CTs we have created an atlas of PED deployment, complication and artifacts. The atlas created demonstrates cases of incomplete stent apposition due to poor conformability of the PED due to tortuous cerebral vasculature, as well as stent deformation such as flattening of the stent midsection, kinking, or inward crimping of the proximal and distal ends, as well as

Note: Scanned images are included in the proceedings. Some submitted images were reduced during editing, thereby decreasing clarity. Also, refer to the Program Planner. Proceedings Content as of 3-29-2013.

an intussuscepted stent.

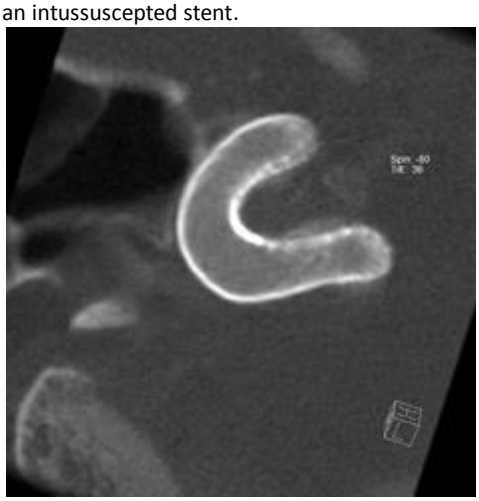

Conclusion
Our study presents an illustrative case atlas, in which information added by the ICE DYNA CT improves our understanding and visualization of PEDs that is superior to DSA an 3D DSA. It enhances understanding of stent behavior in clinical practice and improves the efficacy and safety of intracranial deployment of the PED device.

KEYWORDS: Dynamic CT angiogram, Endovascular flow diverter, aneurysm, Pipeline embolization device

eP-177

Stent Assistance as a Packing Density Determining Factor in Endovascular Aneurysmal Coiling

Darwish, M. M. N.·Ku, A.·Aziz, K. M.·Williams, R.
Allegheny General Hospital
Pittsburgh, PA.

Purpose
Techniques for aneurysmal coiling have been greatly improved recently and now they involve hydrocoils, balloon remodeling or stent assistance. We here compare the stent assistance to other methods regarding packing densities of the coiled aneurysms. Our purpose is to compare the packing densities of the aneurysms coiled with stent assistance versus those coiled with coils alone and/or with balloon assistance.
Materials & Methods
This is a retrospective study of our 354 interventionally coiled aneurysms. We have divided these aneurysms into ruptured and unruptured aneurysms and each group has been further subdivided into those treated with either Hydrogel or bare platinum coils. Volume fill is calculated by the Angiocalc program.
Results
As shown in the table, although the aneurysms treated with stent assistance were of larger sizes than those treated with coils alone or coils with balloon remodeling, they had greater packing densities especially if the stents were used with hydrogel coated coils. This may be explained technically by the fact that the stent acts as a barrier between the parent artery and the intra-aneurysmal coiling mass allowing insertion of more coil loops without fearing the backward herniation in the main vessel especially in the wide-necked aneurysms. Another unproved notice is that the stent may sometimes reduce the flow inside the aneurysm, especially with double stenting, and thus helps stagnation and intra-aneurysmal thrombosis.

		Bare Platinum Coils		Hydrogel Coated Coil	
No. of assisted coiling cases of treated aneurysms	Total	182		172	
	Differential	Ruptured	Unruptured	Ruptured	Unruptured
		95	87	85	87
No. of assisted coiling cases	Coils alone	70	35	56	14
	Balloon	22	33	17	21
	Stent	3	19	12	53
Aneurysmal Size (in mm^3)	Avg. (/ group)	148.98	165.55	272.64	424.68
	Avg. (Total)	156.75		349.55	
	Coils alone	176.04	189.36	298.78	452.9
	Balloon	59.71	88.82	203.74	164.2
	Stent	172.09	262.57	248.26	517.5
Percentage Of Packing Volume (%)	Avg. (Total)	49.20%		82.20%	
	Avg. (/ group)	46.37	52.36	80.64	83.72
	Coils alone	44.24%	47.26%	81.43%	80.88%
	With balloon remodeling	48.61%	53.58%	72.95%	83.64%
	With Stent Assistance	80.26%	59.48%	87.83%	83.58%

Conclusion
The use of stent assistance specifically increases the density of packing volumes when compared to coils alone or even coils with balloon remodeling techniques. For large aneurysms, we recommend hydrogel coated coils with stent assistance.

KEYWORDS: Aneursym, Endovascular coiling, stent assistance

eP-178

TOPSAT: A Single-Center Randomized Controlled Feasibility Trial of Management Strategies in Poor-Grade Aneurysmal Subarachnoid Hemorrhage Patients

Mitra, D.[1]·Gholkar, A.[1]·Jayakrishnan, V.[1]·Gregson, B.[2]·White, P.[2]·Vincent, A.[1]·Mitchell, P.[1]
[1]Royal Victoria Infirmary, Newcastle upon Tyne, UNITED KINGDOM, [2]Newcastle University, Newcastle upon Tyne, UNITED KINGDOM.

Purpose
Management of WFNS good-grade aneurysmal subarachnoid hemorrhage (SAH) is well established and

Note: Scanned images are included in the proceedings. Some submitted images were reduced during editing, thereby decreasing clarity. Also, refer to the Program Planner. Proceedings Content as of 3-29-2013.

based on high quality evidence. However for poor-grade SAH the evidence is primarily from small retrospective case series. We report a single-center randomized controlled pilot feasibility trial of two management strategies: early endovascular aneurysm treatment (early treatment arm) or aneurysm treatment after neurologic recovery (conventional treatment arm). The study - Treatment Of Poor-Grade Subarachnoid Hemorrhage Trial (TOPSAT) - looks at the feasibility of randomization, recruitment rate, safety profile including mortality rate and functional outcome.

Materials & Methods

Hemodynamically stable adult patients admitted to ITU with WFNS grade IV or V SAH were eligible for the study. Assent for the trial was obtained from next of kin. Major exclusion criteria were signs of irreversible brain death, patients requiring immediate clot evacuation, pure intraventricular hemorrhage, age over 75 years and lack of equipoise. Patients were randomized within 24 hours of admission to ITU on an intention-to-treat basis. Patients in the early treatment arm received endovascular treatment of aneurysm within 24 hours of randomization. Patients in the conventional arm received aneurysm treatment (endovascular/surgical as appropriate) after neurologic recovery to WFNS grade III or better. The randomization process ensured even distribution of patients with significant hydrocephalus in the two arms. Functional outcome was measured by Modified Rankin's Score (MRS) at discharge and at six months.

Results

Fifty-one patients were screened for the trial over a 29-month period. Fourteen patients met the eligibility criteria and eight were randomized. In the other six, assent for the trial was not obtained. The recruitment rate for the trial was 57% of patients eligible and 16% of patients screened. Main reasons behind ineligibility for the trial were improvement of WFNS grade to III or better before randomization (21.6%), requirement for emergency clot evacuation (13.5%), hemodynamic instability (13.5%) and delay before randomization (13.5%). Five patients were randomized to early treatment arm and three patients to conventional treatment arm. Six patients in the study died (mortality rate 75%). Two patients had good outcome (MRS 1 in one and MRS 0 in another). There were no endovascular procedure-related adverse event and no unexpected nonprocedure-related adverse event.

Conclusion

Many centers currently offer early endovascular treatment to a significant number of poor-grade SAH patients. Efficacy of this approach needs to be established through a randomized controlled trial. Our experience suggests that such a trial is feasible and safe. However recruitment rate is relatively low due to attrition by factors described above. A multicenter study is necessary to obtain the necessary patient recruitment.

KEYWORDS: Aneursym, SAH, poor-grade

eP-179

Multimodel Treatment of Dural Arteriovenous Fistula with Emphasis on Endovascular Embolization: Single Center Experience

Shahin, G. S.·Marin, H.·Sanders, W.·Kole, M.·Jung, M.
Henry Ford Hospital
Detroit, MI.

Purpose

Definitive treatment of dural arteriovenous fistulas (DAVFs) implies total disconnection of the fistula, and traditionally was done surgically. Endovascular treatment of DAVF had consistently gained ground during the last seven years, in particular since the widespread use of ethylene polyvinyl alcohol as embolic agent. We performed a retrospective analysis of our patients with DAVF, in order to identify the rate and predicting factors for endovascular cure.

Materials & Methods

Total of 40 consecutive patients referred to us with diagnosis of cerebral DAVF were anlayzed. Demographics, presenting symptoms, angiographic architecture, treatment and followup were reviewed. We excluded patients with cavernous carotid fistula and pial AVM.

Results

Total of 13 patients presented intracranial hemorrhage, 10 with pulsatile tinnitus, one with headache, 16 with various neurologic deficits (vertigo, memory loss, hydrocephalus, cranial nerve deficits). We have classified DAVFs by location in convexity (n = 7), anterior cranial fossa (n = 2), middle cranial fossa (n = 2), transverse/sigmoid sinus (n = 9), petroclival (n = 9), tentorial/vein of Galen (n = 4), posterior fossa (7). By angiography, there were grade I + IIA (n = 6), IIB (n = 7), III (n = 10), IV (n = 14), V(n = 3 patients) according to the Cognard classification. Ten patients were treated with endovascular embolization solely with 60% cure. In 17/24 patients where embolization was used, residual shunting was seen. Total of 14 patients were treated with combination endovascular embolization and surgery. Embolization was not successful in totally eliminating the fistula, because of the large, multihole fistulas in 12/24 patients and inability to position the microcatheter in the the proximity of the fistula site in 5/24 patients. Seven patients were treated with surgery alone and two with radiosurgery. Total of seven patients (presenting with pulsatile tinnitus alone) opted for conservative followup.

Conclusion

Endovascular embolization in combination with surgery are most effective in complete treatment of DAVFs. Embolization alone can be successful in treatment of small DAVFs when the microcatheter is positioned in proximity to the site of the fistula.

KEYWORDS: AVF, Embolization

Note: Scanned images are included in the proceedings. Some submitted images were reduced during editing, thereby decreasing clarity. Also, refer to the Program Planner. Proceedings Content as of 3-29-2013.

eP-180

MR Perfusion Findings in Patients with Symptomatic Posterior Fossa Venous Congestion

Hui, F. K.·Dyer, E.·Jones, S.
Cleveland Clinic
Cleveland, OH.

Purpose
Vascular lesions of the brain may result in venous hypertension that may or may not be clinically silent. Headaches, encephalopathy, seizures, infarction and hemorrhage may be associated as sequlae of venous hypertension. Causative factors may include dural sinus or venous thrombosis or arteriovenous fistulae. Developmental venous anomalies have been associated with perfusion abnormalities as well. This report reviews the perfusion findings in three patients with lesions that resulted in venous congestion in the posterior fossa.
Materials & Methods
Retrospective analysis of the case logs of the cerebrovascular center was performed yielding three patients with cerebellar venous congestion. Patient demographic, imaging and clinical information was obtained.
Results
The three patients are summarized in tabular form along with demographic, imaging findings included. One patient harbored a dural arteriovenous fistula of the left tentorium and two patients harbored developmental venous anomalies that drained the majority of a cerebellar hemisphere. The dural fistula was managed with embolization of the diseased sinus, and one of the developmental venous anomalies was treated conservatively given the intermittent nature of low grade, ipsilateral posterior headaches. The third patient was managed with anticoagulation and hydration, given recent development of 10 out of 10 headaches with worsening during valsalva in a patient with a known large venous anomaly. Two weeks following initiation of medical therapy, the patient reported return to baseline levels of discomfort. Imaging in the last case demonstrated high-grade venous outlet stenosis of the venous anomaly.

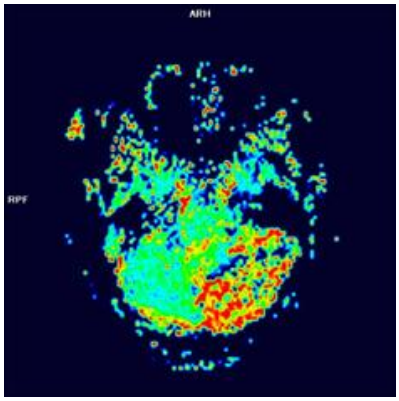

Conclusion
MR perfusion can help noninvasively assess the degree of venous stasis manifesting with prolonged mean transit time and increased cerebral blood volume. Resolution or improvement in relative perfusion parameters may correspond with clinical improvement. With sufficient experience, it may become possible to differentiate between clinically silent and pathologic developmental venous anomalies as well as assess the malignancy of dural fistulae.

KEYWORDS: MR perfusion-weighted imaging, Arteriovenous, Venopathy

eP-181

Craniovertebral Junction (Occiput-C2) Spinal Arteriovenous Dural Fistulas with Cranial and with or without Spinal Perimedullary Venous Drainage - A Potentially Dangerous Clinical Feature: A Case Series

Puri, A. S.[1]·Hou, S.[1]·Telischak, N.[2]·Thomas, A.[2]·Wakhloo, A.[1]
[1]University of Massachusetts Medical Center, Worcester, MA, [2]Beth Israel Deaconess Medical Center, Boston, MA.

Purpose
Spinal dural arteriovenous fistula (SDAVF) is an abnormal connection between arteries and veins in the dural covering. The venous drainage from these fistulas can be extradural in the suboccipital venous plexus or intradural. The intradural venous drainage is the dangerous variety as it can occur either cranially into the posterior fossa or caudally into the vertebral venous plexus or in both directions. Venous reflux into the posterior fossa can lead to intraparenchymal or subarachnoid hemorrhage. The caudally directed venous reflux can cause venous congestion and subsequent myelopathy. The skull base region, from the occiput to C2, is unique in its location for SDAVFs as both the brain and the spinal cord are at risk. We describe the clinical presentation, angioarchitecture, management and clinical follow up of FOUR cases with skull base SDAVFs and dangerous venous outflows.
Materials & Methods
We performed a retrospective review of the case logs of the University of Massachusetts Medical Center and Beth

Note: Scanned images are included in the proceedings. Some submitted images were reduced during editing, thereby decreasing clarity. Also, refer to the Program Planner. Proceedings Content as of 3-29-2013.

Israel Deaconess Medical Center between July 2011 and November 2012 in order to select patients with angiographically proven SDAVFs at the craniovertebral junction with cranial intradural venous reflux and/or caudal spinal perimedullary venous reflux in order to analyze the angiographic features, treatment strategy and clinical followup.

Results

Patient demographics included one male and three females, age range from 60-65 years. Three patients presented with symptoms likely related to the SDAVF, two with posterior fossa hemorrhage, and one with cervical cord myelopathy. One patient was incidentally discovered during workup and treatment of a ruptured supratentorial aneurysm. Angiography in all patients demonstrated a left-sided SDAVF located at the craniovertebral junction and supplied by the musculospinal branches of the V2 and/or V3 segments of the vertebral artery. The venous drainage in all four cases was into the intradural veins of the posterior fossa. In three cases additional venous reflux into the spinal perimedullary venous system was noticed. Endovascular treatment was attempted in two patients but due to the small size of the arterial feeders, an optimal microcatheter position could not be achieved for a safe liquid embolic injection. Three patients underwent surgical resection of the SDAVF. The two patients with posterior fossa hemorrhages are neurologically intact after surgery. The patient with cervical cord myelopathic symptoms is in a chronic rehabilitation facility. The patient with incidentally discovered SDAVF, treatment has been deferred for an endovascular treatment until she has recovered adequately from her aneurysmal subarachnoid hemorrhage and vasospasm.

Conclusion

This case series of patients with craniovertebral SDAVF with dangerous venous outflow on angiograms shows the potential morbidity of SDAVF and illustrates the need for an early and aggressive surgical or endovascular management to obliterate the arteriovenous shunt.

KEYWORDS: Arteriovenous fistulas, Spinal arteriovenous malformation, venous outflow

eP-182

Interest of Using a Spherical Convex Anamorphosis for a Better Understanding of the Angio-Architecture of Brain Arteriovenous Malformations

Clarençon, F.[1]·Maizeroi-Eugène, F.[2]·Gory, B.[3]·Sourour, N.[1]·Bresson, D.[4]·Mounayer, C.[5]
[1]Pitié-Salpêtrière Hospital, Paris, FRANCE, [2]Segmentix, Limoges, FRANCE, [3]Lyon University Hospital, Lyon, FRANCE, [4]Lariboisière Hospital, Paris, FRANCE, [5]Limoges University Hospital, Limoges, FRANCE.

Purpose

To elaborate an algorithm of convex spherical anamorphosis that could be applied on 3D rotational angiography (3D RA) acquisitions for the understanding of brain arteriovenous malformations (bAVMs).

Materials & Methods

The algorithm was elaborated on Matlab software (version R2009b). The data from 3D RA of 12 patients (six males, six females; 10 supratentorial bAVMs; two infratentorial bAVMs) treated with a previously described segmentation algorithm (ASNR 2012). The convex spherical anarmophosis is a barrel distortion that consists to apply a part of a plane surface on a convex hemisphere. This deformation may help to "spread" the nidus and the vessels close to the nidus. Two independent observers applied this algorithm on the volumes (nidus, arteries and veins) derived from the segmentation of bAVMs and semiquantitatively evaluated its quality (poor, fair and good). The number of arterial feeders to the nidus showed by this barrel distortion was compared with the images obtained from 6 f/s DSA in AP, lateral and oblique projections.

Results

The application of the convex spherical anamorphosis was possible in all cases. The quality of the deformation provided was evaluated as good by both observers in most cases. In average, convex spherical anamorphosis could depict one more arterial feeder than the six f/s DSA.

Conclusion

The algorithm of convex spherical anamorphosis elaborated is a promising tool for a better understanding of complex bAVMs.

KEYWORDS: Arteriovenous malformation, Algorithm

eP-183

Combined Treatment of Brain Arteriovenous Malformations with Onyx Embolization Followed by Radiosurgery

Pierot, L.·Kadziolka, K.·Lanoix, O.·Rousseaux, P.
Hopital Maison-Blanche
Reims, FRANCE.

Purpose

The treatment of cerebral arteriovenous malformations (AVMs) is complex, based on embolization, surgery, and radiosurgery, or a combination of modalities. Treatment by Onyx embolization followed by radiosurgery was not evaluated previously. The goal of our study is to evaluate in an homogeneous, monocentric series the long-term clinical and anatomical outcome of patients treated by this combination.

Materials & Methods

From April 2003 to June 2008, 20 patients (11 females and nine males, aged 10 to 55 years) were treated for a brain AVM by Onyx embolization followed by radiosurgery. Arteriovenous malformation size was < 3 cm in seven cases and ≥ 3 cm in 13 cases. Modalities and complications of the procedure were analyzed as well as long-term clinical and anatomical outcome (two - four years after

Note: Scanned images are included in the proceedings. Some submitted images were reduced during editing, thereby decreasing clarity. Also, refer to the Program Planner. Proceedings Content as of 3-29-2013.

treatment).
Results
Out of 17 patients evaluated by DSA after radiosurgery, 10 had a complete occlusion of AVM nidus (58.8%). Complete occlusion was observed in five of seven Spetzler-Martin grade 1-2 AVMs (71.4%) and in five of 10 Spetzler-Martin grade 3-4 AVM (50.0%). Complete occlusion was observed in four of five AVM with size < 3 cm (80.0%) and six of 12 AVM with size > 3 cm (50.0%). One out of 20 patients had significant worsening of their clinical status (mRS ≥ 2) at long-term followup.
Conclusion
In this series of patients with AVMs treated with Onyx embolization followed by radiosurgery, the safety and efficacy of this treatment combination is quite satisfactory with a 58.8% rate of complete obliteration and a low rate of clinical complications (5.0%).

KEYWORDS: Arteriovenous malformation, Embolization, radiosurgery

eP-184

Dose Reduction in Transarterial Melphalan Infusion for Intraocular Retinoblastoma

Cooke, D. L.·Stout, C. E.·Kim, W. T.·Hetts, S. W.·Higashida, R. T.·Dowd, C. F.·Halbach, V. V.·Gould, R. G.
University of California San Francisco
San Francisco, CA.

Purpose
Retinoblastoma (RB) is a rare and curable malignancy affecting the pediatric population. Intravenous chemotherapy is the long-standing delivery method, though intra-arterial (IA) is gaining popularity given the reduced side effects related to systemic administration. Intra-arterial infusion has demonstrated technical feasibility, few procedural complications, and robust tumor response. Given the sensitivity of the target organ, patient age, and secondary tumor susceptibility a premium has been placed on minimizing procedura- related radiation exposure.
Materials & Methods
To reduce patient dose during the IA infusion procedure, a combination of tailored surgical methods, including collimation, single plane usage, reduced source-to-image distance, and exclusion of the lens from the field of view, and customization of the fluoroscopic technique were performed. While the dose rate continued to be controlled by the automatic exposure control, the routine fluoroscopic settings were changed from the standard 7.5 pulses per second and a dose level to the detector of 36 nanoGy per pulse, to a pulse rate of four pulses per second and a detector dose to 23 nanoGy per pulse. The angiographic dose indicators [Reference Point air Kerma (RP) and fluoroscopy time] for cohort of 10 consecutive (12 affected eyes, 30 infusions) were analyzed.
Results
The mean RP per treated eye was 20.1 ± 11.9 mGy with a mean fluoroscopic time of 8.5 ± 4.6 minutes. Review of the data demonstrated three cases with elevated dose relative the mean dose (Figure 1). These outliers represented three different scenarios: 1) Unstable catheter position (treatment five) requiring usage of multiple microcatheter types; 2) External carotid supply (treatment 10) to the ophthalmic artery; and 3) Mixed use of the standard and low-dose settings (treatments 17 and 18) to better visualize the arterial anatomy. Subsequent treatments (treatments 15 and 22) in the patient with external carotid to the ophthalmic artery regressed toward the mean dose.

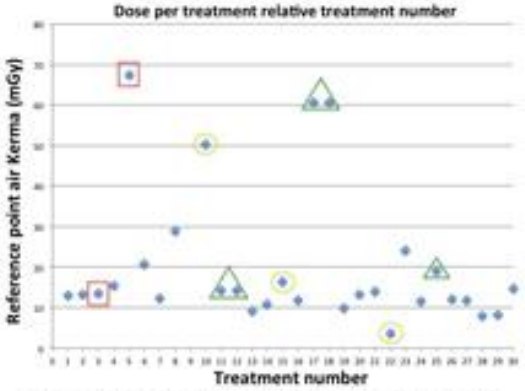

Figure 1. Scatter plot of treatment number relative reference point air Kerma (mGy) per treated eye. Treatments 3 and 5 (red), 11, 12, 17, 18, 25, 26 (green), and 1–, 15, and 22 (yellow) represent the three patients treated at different time points. Treatments 11-12 and 17-18 were performed at the same time given the patients' bilateral disease. The four highest doses represented three different scenarios: 1) unstable catheter position (treatment 5) secondary to an acute ophthalmic artery origin requiring usage of multiple microcatheter types; 2) External carotid supply (treatment 10) to the ophthalmic artery; and 3) Mixed use of the standard and low dose settings (treatments 17 and 18) to better visualize the arterial anatomy.

Conclusion
Ophthalmic arterial melphalan infusion is a safe and effective means to treat retinoblastoma. Modification to contemporary fluoroscopic systems combined with parsimonious fluoroscopy can minimize radiation exposure.

KEYWORDS: Retinoblastoma, Dose reduction

eP-185

C-Arm CT Measurement of Cerebral Blood Volume: Optimization of Injection Protocols and Steady State Analysis

Caroff, J.[1,2]·Jittapiromsak, P.[2]·Benachour, N.[2]·Pasco Papon, A.[1]·Ruijters, D.[3]·Aubé, C.[1]·Spelle, L.[2]·Moret, J.[2]
[1]CHU Angers, Angers, FRANCE, [2]Beaujon Hospital, Paris, FRANCE, [3]Philips, Best, NETHERLANDS.

Purpose
Cerebral volume measurement by flat panel detector CT in the angiography suite is a promising tool for patient management during endovascular early stroke therapy. A steady state of contrast agent distribution is mandatory during acquisition. To the best of our knowledge, this was the first time that steady state parameters were studied in clinical practice.
Materials & Methods

Note: Scanned images are included in the proceedings. Some submitted images were reduced during editing, thereby decreasing clarity. Also, refer to the Program Planner. Proceedings Content as of 3-29-2013.

Before the cerebral blood volume study, test injections were performed and analyzed to determine a customized acquisition delay from injection time for each patient. Three different injection protocols were used including peripheral and central venous injections. Seventy-two mL of contrast agent material was administrated at an injection rate of 4.0 mL/s followed by a 72 or 20-mL saline bolus at the same injection rate. Twenty-four patients were treated for different types of neurovascular diseases. From test injections and time attenuation curves were calculated: maximal attenuation, steady state length and delay from injection.

Results

With a 10% threshold from maximum attenuation, average steady state duration was less than 10 seconds. Maximum attenuation values and steady state durations with minimal delay variations were obtained with central injection protocol and the smallest amount of saline chase.

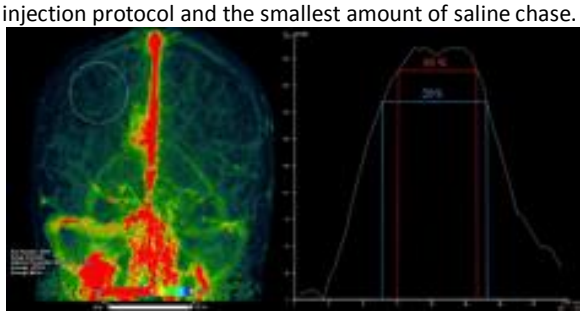

Conclusion

With clinically acceptable contrast agent volumes, steady state is a brief condition thus fast rotation speed acquisitions are needed. From this study it is possible for most patients to establish a probabilistic acquisition delay and then to avoid test injections.

KEYWORDS: C-arm CT CBV, Cerebral blood volume

eP-186

Update on the UK Flow Diverter Registry

White, P. M.[1]·Molyneux, A.[2]
[1]Institute for Ageing & Health, Newcastle upon Tyne, UNITED KINGDOM, [2]Oxford University, Oxford, UNITED KINGDOM.

Purpose

All flow diverters deployed in UK from 01/01/2010 have been entered into a prospective national audit. Audit is designed to determine procedural safety, early efficacy and medium term clinical outcome. Primary outcome is the modified Rankin score at one year and secondary outcomes are procedural complication rates, change in Rankin and angiographic occlusion.

Materials & Methods

All 31 UK neuroscience centers were contacted. Twenty-six centers responded, five centers did not respond (but three of these don't have an INR service). Two of responders have INR service but indicated they don't use FDs. Twenty-four active centers enrolling into registry. NICE guidelines now mandate use of Registry for all PED cases undertaken in the UK.

Results

We will present demographic and procedural data on the first 200 patients enrolled and data as it becomes available on 12-month followups. Two hundred sixteen aneurysms were treated in total. Eighty-seven percent were not ruptured recently (nearly all unruptured). Age range: 25-82 years, 57% <60 years, 75% female. Average number of FDs used was 1.7 (range 0-8) with more than one device used in 70 patients. Aneurysm type - 66% were saccular, 10% fusiform, 22% giant, 5% blister. Aneurysm location - 20% cavernous ICA, 60% other ICA and 8% posterior. Twelve percent were small, 21% medium, 45% large, 22% giant. Most were wide necked (79%). Forty-five technical problems were encountered (>1 in some patients). There were three periprocedural infarcts, eight cases of parent vessel occlusion and/or flow diverter thrombosis (three felt unrelated to FD device). There were nine "periprocedural" bleeds (within 30 days) - five first bleeds from target aneurysm, three cases of vessel perforation, one remote parenchymal bleed (ipsilateral). There were four cases of delayed hemorrhage - one from aneurysm (unruptured), two ipsilateral and one combined contralateral/ventricular bleed. Thirty-day mortality was 4.5% - but 4% in not recently ruptured versus 10% in recently ruptured aneurysms. There were five cases of progressive cranial nerve palsy. Eighty-two percent were discharged home. Clinical status at discharge was improved 10%, unchanged 76% and worse 10%.

Conclusion

This is a work in progress. However a National Registry of novel devices within the INR field is perfectly feasible. In the absence of RCTs, a comprehensive prospective Registry is perhaps the best way to rapidly establish safety and obtain some idea of device efficacy. An independent professionally run Registry may well be the optimum way to undertake postmarketing surveillance.

KEYWORDS: Flow diverter, Aneurysm treatment

eP-187

Phase-Contrast Synchrotron Radiography of Cerebral Protection Device Retrieved after Carotid Artery Stenting: Feasibility as ex vivo Evaluation of Device-Captured Embolic Debris

Youn, S.[1]·Kim, H.[1]·Kim, H.[2]
[1]Daegu Catholic University Medical Center, Daegu, KOREA, REPUBLIC OF, [2]Daegu Catholic University Medical School, Daegu, KOREA, REPUBLIC OF.

Purpose

To demonstrate the feasibility of phase-contrast synchrotron radiography as a tool for evaluating the embolic debris captured on cerebral protection device

Note: Scanned images are included in the proceedings. Some submitted images were reduced during editing, thereby decreasing clarity. Also, refer to the Program Planner. Proceedings Content as of 3-29-2013.

(CPD) retrieved after carotid artery stenting (CAS).
Materials & Methods
Five patients (four males, median age, 66 years; range, 55-82 years) with severe carotid artery stenosis underwent CPD-protected CAS. After CAS, the retrieved CPDs were emulsified in 4% formalin, and placed in front of synchrotron beam from 7B2 beamline at Pohang Light Source (PLS, Pohang, Korea). The 600 images of phase-contrast radiography were obtained by rotating CPD 360°. The three-dimensional reconstructed images were segmented into the embolic debris and CPD by visual analysis. Total volume of emboli was calculated by summing up each volume of emboli per scanning level. The surface area covering membrane pore was counted seen from outer surface, and the percentage of covered area was calculated.
Results
Embolic debris were clearly demonstrated within pore, outer and inner surface of CPD. The mean total volume of embolic debris was 538.832 x 10^{-6} mL (range, 225.275-965.484 x 10^{-6} mL). The average 61.46% of them were located at apical one third of CPD. The average 20.84% of the pore area were covered by the debris.
Conclusion
Phase-contrast synchrotron radiography allows us to better understand the detailed microscale appearance of debris with its quantitative information. The debris at outer surface may imply the potential risk of embolization during CAS, and necessitate modifying the design of CPD and procedural steps.

KEYWORDS: 3D visualization, Carotid stent-assisted angioplasty, phase-contrast; synchrotron radiography

eP-188

Metallic Artifacts Reduction of Post-Therapeutic Flat-Panel Detector CT Images

Hung, S.[1,2]·Lin, C.[1,2]·Guo, W.[1,2]·Wu, C.[1,2]·Luo, C.[1,2]·Chang, F.[1,2]·Chu, W.[1,2]
[1]Taipei Veterans General Hospital, Taipei, TAIWAN,
[2]National Yang Ming University, Taipei, TAIWAN.

Purpose
Most of angiography suites currently used for diagnostic and interventional neuroradiology are equipped with flat detectors, by which flat detector CT (FD CT) has been widely used. However, in FD CT, the artifacts caused by metallic implants obscure their surrounding structures-of-interest and degrade the imaging quality. We aimed to evaluate the efficacy of reducing the metallic artifacts in FD CT by a postprocessing method.
Materials & Methods
We retrospectively reprocessed FD CT scan volumes of 42 patients. The patients were treated with endovascular coiling (31/42), liquid embolization (9/42), or shunting surgery (2/42) since January 2009. The imaging slice of FD CT that was impaired worst by metallic artifacts was chosen as a target slice. A 1.5 x 1.5 cm^2 ROI was placed, respectively, on the target slice at the vicinity of metallic implants and the adjacent metallic artifact-free slice (as a control) to evaluate the imaging quality before and after applying a metallic artifacts reduction (MAR) prototype software (Siemens Healthcare). The range and standard deviation of CT densities in Hunsfield unit (HU) of the ROI were used as an indicator of imaging quality and noise for the current study. Two experienced neuroradiologists scored the images with consensus.
Results
The metallic artifacts were qualitatively reduced in all patients (Figure). Quantitatively, the range of HU and noise were reduced by 88% and 85% in 31 patients treated by coiling +/- stenting, 69% and 74% in nine patients by liquid embolization, and 70.1% and 60% in two patients by shunting surgery as compared with that before applying MAR. Of 31 patients treated with coiling, the noise reduced by 84.8%, 81.8%, 74.7% in supratentorial, skull base/juxtasellar regions, and posterior fossa by location of metallic implants respectively. The range of HU and noise increased by 30% in control slices after applying MAR ($P < .05$), irrespectively of the types and locations of metallic implants.

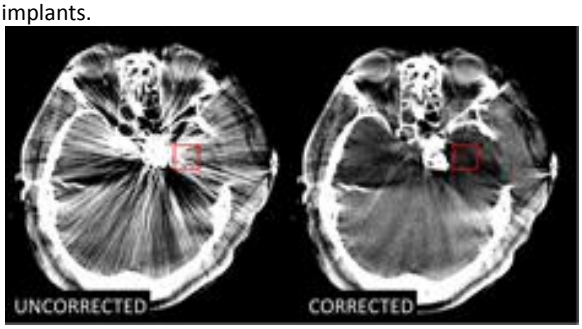

Conclusion
Artifacts, stemmed from metallic implants, in FD CT are feasibly and effectively reduced by postprocessing software. The reduction of artifacts significantly improves imaging quality both qualitatively and quantitatively for clinical interpretation and application.

KEYWORDS: Flat-detector cone-beam CT, Metal artifact

eP-189

Enhanced, Rapid Occlusion of Carotid and Vertebral Arteries Using the Amplatzer Vascular Plug II: The Duke Cerebrovascular Center Experience in Eight Patients with 22 AVP II Devices

Mihlon, F.·Agrawal, A.·Nimjee, S.·Ferrell, A.·Zomorodi, A.·Smith, T.·Britz, G.
Duke University Hospital
Durham, NC.

Purpose
Therapeutic embolization of the common carotid artery (CCA), internal carotid artery (ICA), and vertebral artery

Note: Scanned images are included in the proceedings. Some submitted images were reduced during editing, thereby decreasing clarity. Also, refer to the Program Planner. Proceedings Content as of 3-29-2013.

(VA) is necessary in the treatment of a subset of chronic arteriovenous fistulas (AVF), hemorrhages, highly vascularized neoplasms prior to resection, and giant aneurysms. There are currently no reports of the use of the Amplatzer Vascular Plug II (AVP II) to occlude the CCA, ICA, or VA. This article is a case series reporting the Duke Cerebrovascular Center experience using the AVP II in neurointerventional applications.

Materials & Methods

This case series is a retrospective review of all of the cases at Duke University Hospital where an AVP II was used in the CCA, ICA, or VA up to September 2012. The AVP II often was used in conjuction with embolization coils or as multiple AVP IIs deployed in tandem.

Results

Eight cases meeting criteria were performed between 2010 and 2012. These included two chronic VA to internal jugular (IJ) AVFs, one hemorrhagic CCA-IJ AVF secondary to invasive head and neck squamous cell carcinoma, one ICA hemorrhage secondary to invasive head and neck squamous cell carcinoma, one ICA hemorrhage secondary to trauma, one ruptured ICA aneurysm, one giant petrous ICA aneurysm, and one case of cervical vertebral sarcoma requiring preoperative VA embolization. Successful occlusion of the target vessel was achieved in all eight cases. There was one major complication that consisted of a watershed distribution cerebral infarct; however, this was related to emergent occlusion of the ICA in the setting of intracranial hemorrhage and not necessarily a problem intrinsic to the AVP II.

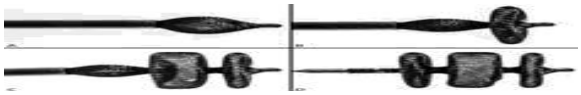

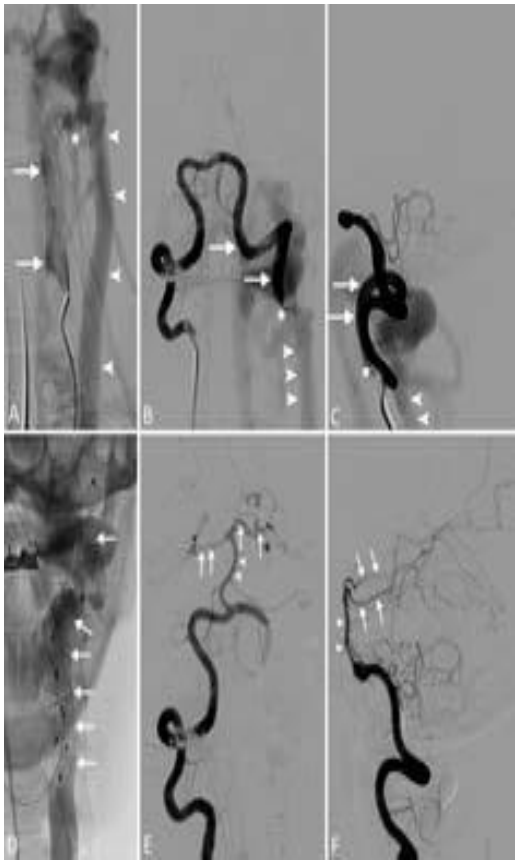

Conclusion

The AVP II is relatively large, self-expanding vascular occlusion device that safely allows enhanced, rapid take-down of carotid and vertebral arteries with low risk of distal migration.

KEYWORDS: Arteriovenous fistulas, Embolization, Amplatzer

eP-190

Cost Analysis of Aneurysmal Repair by Endovascular Coiling versus Flow Diversion

Nadarajah, M.
National Neuroscience Institute Singapore
Singapore, SINGAPORE.

Purpose

Flow diverters enable intracranial aneurysmal repair without the need to enter the aneurysmal sac. Concerns however have been raised regarding the cost compared to coiling techniques. The aim of this study was to evaluate the relative costs for different aneurysm sizes to ascertain if different sizes are more cost effectively treated by a particular method to establish which aneurysms are most cost effectively treated by each method.

Materials & Methods

Patients undergoing aneurysmal repair at two neurovascular referral centers between September 2005

Note: Scanned images are included in the proceedings. Some submitted images were reduced during editing, thereby decreasing clarity. Also, refer to the Program Planner. Proceedings Content as of 3-29-2013.

and August 2010 were included, bar patients who underwent coiling for recurrences of prior microneurosurgical clipping. These aneurysms were stratified into three size groups. The average and median number of coils or flow diverters and the average and median costs of treatment of each size category was calculated.
Results
Four hundred twenty-nine aneurysms were treated. Of these, 409 were coiled with or without assist devices. Forty-eight percent fell under Group A (<7 mm), 36% under Group B (7-12 mm) and 16% under Group C (>12 mm). Twenty aneurysms were flow diverted, and of these 14 were treated de novo, five previously coiled, and one previously clipped. Twenty percent belonged in Group A, 25% in Group B and 55% in Group C. The highest procedural costs in the coiling group were Group C aneurysms requiring stent assistance with an average of $24,563 (median $23,860). Using flow diversion, the average was $24,650 (median $16,490).
Conclusion
Given the price parity threshold crossed for aneurysms >12 mm requiring stent assistance and the relative ease of the flow diverter technique, we suggest that flow diversion should be considered the first-line treatment for aneurysms in this category.

KEYWORDS: Endovascular flow diverter, Endovascular management, Costs, cost analysis, Coiling

eP-191

Use of a Semipermeable Mesh Implant for Treating Painful Osteoporotic Vertebral Compress Fractures of the Thoracic and Lumbar Spine

Ortiz, A.[1]·de Venecia, C.[1]·Patel, B.[2]
[1]Winthrop University Hospital, Mineola, NY, [2]Stony Brook University School of Medicine, Stony Brook, NY.

Purpose
To assess the efficacy of a semipermeable mesh implant (Algea Therapies) in the treatment of painful thoracic and lumbar osteoporotic vertebral compression fractures.
Materials & Methods
Patients with painful thoracic and lumbar osteoporotic vertebral compression fractures which were refractory to conventional medical management and less than three months of age were considered possible candidates for this vertebral augmentation technique. Patients were excluded from this procedure if the fracture was chronic (greater than three months) if the vertebral pedicle could not accommodate the instrumentation and if the vertebral body height loss was more than 60%. Data recorded for the procedure included patient age, gender, fracture type (using the Magerl classification), fracture level, mesh stent size, amount of cement injected, cement extravasation, complications and pre and postprocedure pain scores and Oswestry Disability index scores.
Results
Nine patients were included in this study; seven females and two males, with an average age of 76.2 years. Each patient had one level treated with the mesh implant; two thoracic levels (T11 and T12) and seven lumbar levels (L1, L2 or L3). Anterior column with superior endplate fractures were treated. The 10 x 15 mm implant was used in six treated vertebrae, including the two thoracic vertebrae; the 10 x 20 mm implant was used to treat two lumbar vertebrae and a 10 x 25 mm implant was used to treat an L1 vertebra. An average of 2 mL of acrylic bone cement was injected and there was no fluoroscopic evidence of cement leakage. No patient-related complications were seen and there were no device failures. All patients, followed to at least three weeks, have shown major pain relief.
Conclusion
Vertebral augmentation with a semipermeable mesh stent implant can be used to effectively and safely treat osteoporotic vertebral compression fractures within the lower thoracic and lumbar spine.

KEYWORDS: Vertebral augmentation

eP-192

Chronic Occlusion of the Vertebrobasilar Vessels with Acute Clinical Deterioration: Endovascular Treatment and Clinical Outcome

Aguilar-Pérez, M.[1]·Kurre, W.[1]·Fischer, S.[1]·Niehaus, L.[2]·Bäzner, H.[1]·Schmid, E.[1]·Henkes, H.[1]
[1]Klinikum Stuttgart, Stuttgart, GERMANY, [2]Klinikum Winnenden, Winnenden, GERMANY.

Purpose
Chronic occlusion of the vertebrobasilar vessels may cause acute or chronic brainstem, cerebellar and cerebral ischemia, especially in the case of profound arterial hypotension or dehydration, which may cause failure of collateral blood supply. The spontaneous prognosis of this condition is known to be poor. These chronic occlusions, however, are mostly considered unsuitable for endovascular recanalization. The purpose of this study was to evaluate the efficacy of reopening a chronically occluded vertebrobasilar vessel during acute decompensation and describe technical issues occurring during the procedure and their potential solutions.
Materials & Methods
We retrospectively reviewed all patients who underwent endovascular recanalization of a chronic vertebrobasilar occlusion in our institution. All patients presented with acute clinical deterioration or with medically refractory symptoms and were treated with a combination of segmental balloon dilatation and oversized self-expanding stent deployment. Technical success was defined as the ability to reopen the chronically occluded vessel and improve the antegrade perfusion of the basilar artery. Clinical outcome was measured as mRS score.

Note: Scanned images are included in the proceedings. Some submitted images were reduced during editing, thereby decreasing clarity. Also, refer to the Program Planner. Proceedings Content as of 3-29-2013.

Results
Endovascular recanalization was attempted in 24 patients; recanalization was performed successfully in 21 of the 24 cases (87.5%). There were two procedural complications (8%): one vessel perforation during the catheterization and one retroperitoneal hemorrhage. After the procedure, eight patients were stable (33%), 13 patients improved (54%), and four patients were worse (16%). The mean angiographic followup was 16.4 months. Seven patients developed significant in-stent stenosis during this period, which was treated successfully with angioplasty and stenting.
Conclusion
This limited experience reveals that recanalization of chronically occluded vertebrobasilar arteries is technically feasible with current endovascular methods. These procedures can be challenging, they carry substantial risks and should be reserved for patients with medically refractory symptoms.

KEYWORDS: Acute basilar artery, Recanalization, angioplasty and stenting

eP-193

Pediatric Posterior Circulation Artery-to-Artery Thromboembolic Strokes Caused by Cervical Rotation Induced V3 Segment Vertebral Artery Dissection

Stout, C.·Kim, W.·McSwain, H.·Cage, T.·Cooke, D.·Fullerton, H.·Fox, C.·Lawton, M.·Hetts, S.·Higashida, R.·Dowd, C.·Halbach, V.
University of California San Francisco Medical Center
San Francisco, CA.

Purpose
Pediatric posterior circulation stroke is a rare cerebrovascular disease. The intimate relationship of the vertebral artery (VA) to the cervical spine, and the dynamic anatomical changes they undergo with head rotation (HR), predispose to rotational vascular disease, an idea first proposed by de Kleyn and Versteegh (1933). Vertebral artery dissection initiated by traumatic HR was first proposed by Swartz et al (1956). Since then, VA dissection from less traumatic and/or atraumatic HR has been reported including during swimming, archery practice and yoga. Approximately 53% of reported pediatric idiopathic VA dissections localize to the V3 VA segment (Fullerton et al., 2001), just distal to its exit from the C2 transverse foramen, as it wraps around the C1-C2 joint. In five pediatric patients who presented with progressive posterior circulation strokes and suggestion of VA dissection on cross-sectional imaging, we performed arteriography with HR to evaluate how cervical rotation can cause extrinsic compression and occlusion of this vulnerable segment of the VA, leading to dissection and artery-to-artery thromboembolism.
Materials & Methods
To safely use HR cerebral arteriograms to evaluate our patients, the maximal normal range of HR was established prior to induction of anesthesia, contralateral HR during arteriograms was brief, blood pressure under anesthesia was carefully controlled and, when appropriate, patients were anticoagulated with heparin. Posterior circulation arteriograms were performed first to evaluate for distal branch occlusions, followed by head neutral and HR VA arteriograms. 3D rotational arteriograms helped to evaluate the regional anatomy.
Results
In five sequential pediatric patients with posterior circulation strokes and suggestion of focal dissection at the proximal V3 VA segment, posterior circulation arteriograms demonstrate diffuse vertebrobasilar branch occlusions consistent with artery-to-artery embolic disease. Cervical VA arteriograms show subtle focal irregularity/dilation, some with superimposed intimal flaps, consistent with dissections of varying chronicity. Contralateral HR causes focal VA occlusion at the dissection site that is fully reversed with return to neutral head position. In several cases, each VA showed occlusion on contralateral HR. Many of these findings can be demonstrated on MRI/MRA and CT/CTA.

Conclusion
Focal extrinsic compression and occlusion of the proximal loop of the V3 VA segment at the limits of HR is a mechanism for dissection that acts as a nidus for posterior circulation thromboembolic strokes. This disease process, likely more prevalent than previously recognized, has characteristic findings on HR cerebral angiography, some of which can be seen on cross-sectional imaging.

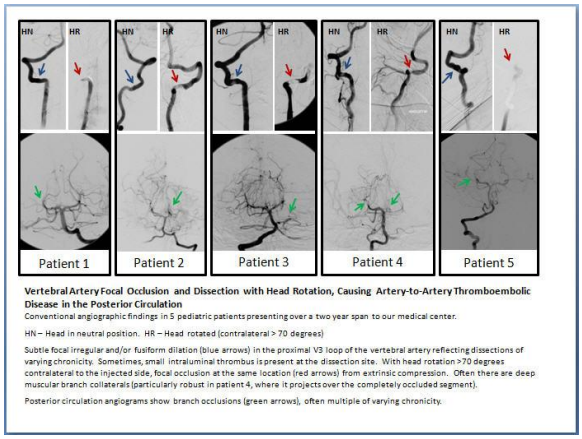

KEYWORDS: Stroke, Dynamic angiography, Cervical rotation

Note: Scanned images are included in the proceedings. Some submitted images were reduced during editing, thereby decreasing clarity. Also, refer to the Program Planner. Proceedings Content as of 3-29-2013.

eP-194

Outcomes of Mechanical Thrombectomy for Posterior Circulation Strokes: A Study of the Nationwide Inpatient Sample 2006-2010

Brinjikji, W.·Rabinstein, A. A.·Lanzino, G.·Kallmes, D. F.·Cloft, H. J.
Mayo Clinic
Rochester, MN.

Purpose
Acute posterior circulation occlusions are associated with high morbidity and mortality rates. Many studies have demonstrated that recanalization of posterior circulation occlusions using mechanical thrombectomy can improve patient outcomes. To date, there exist no large series of outcomes for patients with posterior circulation occlusions undergoing mechanical thrombectomy. We evaluated a large administrative database to determine trends and outcomes in the use of mechanical thrombectomy in patients with posterior circulation strokes.
Materials & Methods
Using the Nationwide Inpatient Sample, we evaluated outcomes of patients treated for acute ischemic stroke in the United States from 2006-2010. Patients who suffered acute ischemic stroke and underwent endovascular clot retrieval were selected. Those patients with posterior circulation occlusions were identified using International Classification of Disease 9 Codes 433.00, 433.01, 433.20, and 433.21 (occlusion of basilar artery with and without infarction and occlusion of vertebral artery with and without infarction). Primary outcomes were morbidity (discharge to a long-term facility) and mortality. Secondary outcomes were length of stay and intracranial hemorrhage (ICH) rate. Multivariate logistic regression analysis was performed to determine independent predictors of mortality. Variables included in this analysis were occlusion location (anterior versus posterior), gender, race, age, Charlson Co-morbidity Index, presence of intracranial hemorrhage and tissue plasminogen activator administration.
Results
From 2006-2010, 10,758 patients underwent mechanical thrombectomy for acute ischemic stroke (267 patients in 2006 and 4096 patients in 2010). A total of 631 patients underwent thrombectomy for posterior circulation strokes. Mortality rate among patients with posterior circulation occlusions was 40.5% (253/631). Morbidity rate was 33.6% (210/631). The rate of ICH for patients with posterior circulation occlusions was 15.7% (99/631). Mean length of stay was 11.9 ± 24.7 days. Mortality for patients <65 years old was 39.1% (155/398) compared to 43.0% (98/223) for patients ≥65 years old (P = 0.22). On multivariate analysis, posterior circulation occlusion (OR = 3.29, 95%CI = 2.71-3.98, P<.0001) and increasing age (OR = 2.10, 95%CI = 1.88-2.35, P<.0001) were significant predictors of increased mortality. Other significant predictors of increased mortality were male gender, white race, ICH and rt-PA administration.
Conclusion
Patients undergoing mechanical thrombectomy for posterior circulation occlusions suffered high morbidity and mortality rates. Posterior circulation occlusions are an independent risk factor for mortality amongst mechanical thrombectomy patients. More research is needed to improve outcomes among these patients and to determine which patients with posterior circulation occlusions will benefit from endovascular therapy.

KEYWORDS: Thrombectomy, Basilar artery occlusion, Endovascular

eP-195

Reduced Rates of Restenosis after Stent Angioplasty of Intracranial Atherosclerotic Stenoses with Drug Eluting Stents: Preliminary Experience with Taxus Element

Kurre, W.[1]·Aguilar-Pérez, M.[1]·Fischer, S.[1]·Arnold, G.[2]·Schmid, E.[3]·Bäzner, H.[3]·Henkes, H.[1]
[1]Katharinenhospital, Stuttgart, GERMANY, [2]Klinikum Sindelfingen-Böblingen, Sindelfingen, GERMANY, [3]Klinikum Stuttgart, Stuttgart, GERMANY.

Purpose
Stent angioplasty of intracranial atherosclerotic lesions is associated with high rates of restenosis. Small cases series with drug eluting stents (DES) showed promising results in terms of long-term stability but the high rigidity of DES was a major drawback. Modifications in stent design improved the flexibility of DES making them more suitable for the application in intracranial vessels. In this study we report our experience with the thin-strut paclitaxel eluting Taxus Element stent for the treatment of intracranial atherosclerotic lesions.
Materials & Methods
We retrospectively reviewed all patients having been treated with the Taxus Element DES in our institution for an intracranial atherosclerotic lesion. Patients treated in the setting of an acute vessel occlusion were excluded. Technical success was defined as the ability to place the Taxus Element at the desired location and reducing the degree of stenosis below 50%. To assess safety we reported procedure-related neurologic complications. Follow-up angiography was performed after six and 12 weeks, three and 12 months and yearly thereafter.
Results
Stent angioplasty with Taxus Element was attempted in 64 patients harboring 73 stenoses that were treated in 70 procedures. Nine of the target lesions were restenoses. The average degree of luminal narrowing was 73%. Thirty-four stenoses were located in the anterior, 39 in the posterior circulation. Seven lesions (9.6%) could not be accessed with Taxus Element and were treated by angioplasty alone or in combination with a self-expanding stent. The average degree of stenosis post-treatment was 21.5%. More than 50% luminal narrowing post-treatment

Note: Scanned images are included in the proceedings. Some submitted images were reduced during editing, thereby decreasing clarity. Also, refer to the Program Planner. Proceedings Content as of 3-29-2013.

was observed in two (2.7%) cases. Neurologic complications associated with the treatment occurred in six (9.4%) patients of whom one (1.6%) had a permanent deficit. Control angiography was available for 52 of 64 (81.3%) successfully treated lesions after a median of 131 days. Angiographic imaging revealed one asymptomatic stent occlusion and one restenosis (3.8%). One patient developed a minor stroke due to discontinuation of clopidogrel after nine months and one patient had a stroke in the contralateral hemisphere.

Conclusion

Taxus Element reduced the rate of restenoses after stenting of intracranial atherosclerotic lesions below 4%. The new stent design improved the technical feasability of DES implantation now being comparable to bare metal balloon-expandable and self-expanding stents. Major complications are rare.

KEYWORDS: In-stent restenosis, Stenosis, intracranial stenting

eP-196

Intraprocedural Cerebral Blood Volume Measurement Using C-Arm Computed Tomography for Acute Ischemic Stroke Management

Zhang, Y.[1]·Hong, B.[1]·Yang, Z.[1]·Liu, J.[1]·Ye, H.[2]
[1]Center of Clinical Neuroscience, Shanghai, CHINA, [2]Siemens China, Shanghai, CHINA.

Purpose

It is a challenge to make a clinical decision for an acute stroke patient with large intracranial artery occlusion. Brain perfusion images characterizing tissue viability are capable of providing a method to select patients who can benefit from endovascular treatment. This study is to investigate the value of intraprocedural cerebral blood volume (CBV) measurement using C-arm computed tomography (CA CT) in assessment of acute ischemic stroke and the effect of endovascular thrombolysis treatment.

Materials & Methods

Fifteen patients suffered from acute stroke were administrated in our hospital and were transferred to the cath lab for further diagnosis and treatment from August 2011 to October 2012. Nine out of fifteen patients diagnosed with digital subtract angiography (DSA) as big arteries occlusion in the anterior circulation were included in this study. Recanalization time from symptoms onset was from 115 min to eight hours. All these patients received endovascular thrombolysis therapy. Four patients accepted mechanical thrombectomy therapy, two received stenting treatment and three underwent both. C-arm CT was performed before and immediate after the treatment. Cerebral blood volume values were calculated with a commercial software (syngo DynaPBV Neuro, Siemens, Germany). Absolute CBV values of ipsilateral and contralateral areas, relative CBV values (rCBV = ipsilateral CBV/contralateral CBV) before and after treatment were statistically analyzed with paired t test.

Results

Vessel occlusions were in the middle cerebral artery (6/9), the internal carotid artery (ICA) (3/9). All patients underwent procedures uneventfully. There were obvious ischemic manifestations in CBV maps in eight patients. The mean ipsilateral CBV was 8.6 ± 3.5 ml/1000 ml, the mean contralateral CBV was 24.7 ± 7.4 ml/1000 ml before procedure ($P<0.01$). After endovascular thrombolysis, the ipsilateral and contralateral CBV values changed to 21.8 ± 8.8 and 24.0 ± 7.1 ($P = 0.19$), the rCBV increased dramatically from 0.32 to 0.96 ($P<0.01$). No symptomatic intracranial hemorrhage happened after procedures. mRS≤2 was observed in six patients three months later and no patient died and no major events occurred during the three-month followup.

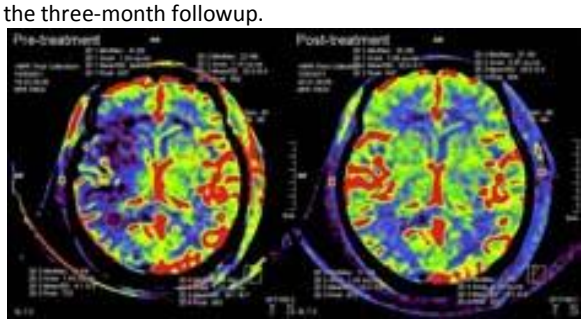

Conclusion

Intraprocedural CBV measurement by CA CT showed the ipsilateral CBV significantly decreased during the onset of acute ischemic stroke, and recovered to nearly normal level after recanalization (Graph). It facilitates the diagnosis of acute stroke and the assessment of effect of procedure.

KEYWORDS: Acute ischemic stroke, C-arm CT CBV

eP-197

Imaging-to-Stent Deployment Time Interval Is Shorter during Daytime versus after Hours in Endovascular Therapy for Acute Ischemic Stroke

Almekhlafi, M. A.[1,2]·Eesa, M.[1]·Nambiar, V.[1]·Volny, O.[3]·Mishra, S.[1]·Desai, J.[1]·Zimmel, L.[1]·Menon, B.[1]·Demchuk, A.[1,4]·Goyal, M.[1,4]
[1]University of Calgary, Calgary, AB, CANADA, [2]King Abdulaziz University, Jeddah, SAUDI ARABIA, [3]St. Anne´s Faculty Hospital, Brno, CZECH REPUBLIC, [4]Hotchkiss Brain Institute, Calgary, AB, CANADA.

Purpose

The importance of time to recanalization in the management of acute ischemic stroke cannot be overemphasized. The stentretrievers introduced a unique advantage of establishing immediate flow to the ischemic tissue once the stent is deployed. A potential factor for delays in achieving a fast imaging to stentretriever

Note: Scanned images are included in the proceedings. Some submitted images were reduced during editing, thereby decreasing clarity. Also, refer to the Program Planner. Proceedings Content as of 3-29-2013.

deployment time is the intervention timing. We assessed the feasibility of achieving a fast imaging to first stentretriever deployment during daytime hours.
Materials & Methods
This is a case series of acute ischemic stroke patients treated with endovascular therapy in a tertiary center. The imaging to first stentretriever deployment time was defined as the time from the completion of CT angiogram to the time of the first angiographic run showing the stentretriever deployment. This time interval was compared between patients treated during the daytime hours (0700-1800 hours) vs. outside these hours. CT perfusion, MR imaging was not used routinely. Endovascular procedures were done using local anesthesia.
Results
Ninety-nine patients with anterior circulation stroke were treated between January 2011 and October 2012. Of those, 62.9% were treated during daytime hours. The median imaging to first stentretriever deployment time was 86 minutes (80.5 minutes for daytime procedures vs. 97 minutes for procedures outside daytime hours; U-test p value 0.038). There was a trend towards shorter times likely due to streamlining of processes (Figure). The proportion of patients treated during daytime hours who achieved an imaging to first stentretriever deployment time under 120 minutes was 86% compared to 65.8% in procedures outside daytime hours (Chi-square test p 0.02). Outcome data were available for 50 patients (50%). The proportion of patients with a favorable discharge modified Rankin Scale (mRS <3) in the cohort that achieved an imaging to first stentretriever deployment time under 120 minutes was 65% compared to only 20% in the cohort who did not achieve that time interval (Chi-square test p 0.01). None of the patients who did not meet this target time achieved mRS score of one or less compared to 55% of those with an imaging to first stentretriever deployment time under 120 minutes (Chi-square test p 0.002).

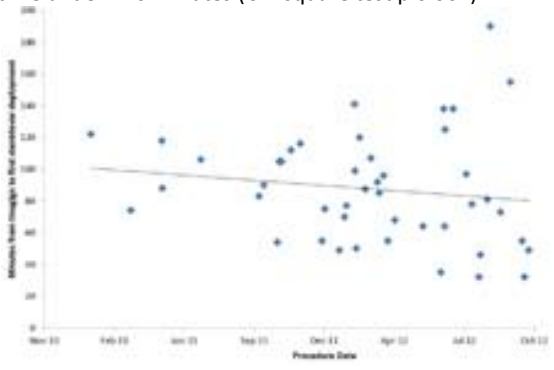

Conclusion
An imaging to first endovascular stentretriever deployment time under 120 minutes is feasible. Focusing on streamlining workflow has the potential to reduce these times further. However it is affected by time of day and may be associated with better functional outcome.

KEYWORDS: Thrombectomy, Endovascular therapy, Stroke

eP-198

Effective Patient Dose of Flat-Detector CT and Multislice CT Protocols: Comparative Measurements Using the Alderson Rando Phantom

Struffert, T.[1]·Hauer, M.[1]·Banckwitz, R.[2]·Koehler, C.[2]·Doerfler, A.[1]
[1]University Erlangen-Nuremberg, Erlangen, GERMANY, [2]Siemens AG, Healthcare Sector, Forchheim, GERMANY.

Purpose
Increasingly, flat detector CT (FD CT) is used for various applications in neuroradiology, such as brain visualization (DynaCT), intravenous FD CT angiography or petrous bone scanning, respectively. Additionally, intraarterial 3D DSA is used to supplement 2D angiographic studies. However, effective patient dose has not been sufficiently addressed in these new applications. The aim was to measure and compare the dose of 1) analogue FD CT and multislice CT (MS CT) protocols, and 2) standard 2D angiography protocols to intraarterial 3D DSA.
Materials & Methods
Using an Alderson Rando phantom effective patient dose (according to ICRP 103) was measured on a 128 row multislice CT (Siemens Somatom AS +) and a flat detector angiographic system (Siemens Axiom Artis dBA) using standard protocols as recommended by the manufacturer.
Results
1) Comparison of FD CT and MSCT (FD CT/MS CT): brain parenchyma imaging (Dyna CT) 2.9/1.4 mSv, perfusion imaging 2.3/4.2 mSv, petrous bone 0.4/0.2 mSv, angiography head 2.9 (using collimators 0.5)/0.5 mSv), respectively. 2) 2D angiography protocols: ap.-lat. standard series 1 mSv, enlarged oblique projection 0.3 mSv, intra-arterial 3D DSA 0.9 mSv (using collimators 0.3 mSv), respectively.
Conclusion
The effective dose of a brain DYNA CT is twice as high as for a MSCT, whereas other FD CT applications are in the dose range of MS CT. Using collimation for these FD CT applications, the dose may be reduced considerably up to 70%. Especially due to the low dose of 3D DSA, we recommend to use this technique primarily for visualization of aneurysms in order to reduce the number of 2D series to identify the ideal working position for endovascular therapy.

KEYWORDS: Flat-panel angiographic CT, Dosimetry, Alderson Rando Phantom

Note: Scanned images are included in the proceedings. Some submitted images were reduced during editing, thereby decreasing clarity. Also, refer to the Program Planner. Proceedings Content as of 3-29-2013.

eP-199

A Prospective, Multicenter Pilot Study for the Validation of Flat Panel Perfused Blood Volume Imaging in Patients with Cerebrovascular Disease

Fiorella, D. J.[1]·Turk, A.[2]·Woo, H.[1]·Deuerling-Zheng, Y.[3]·Sarmiento, M.[3]
[1]State University of New York at Stony Brook, Stony Brook, NY, [2]Medical University of South Carolina, Charleston, SC, [3]Siemens AG, Forchheim, GERMANY.

Purpose
Newer flat panel angiographic detector (FP) systems have the capability to generate perfused blood volume (PBV) maps. The ability to generate these maps in the angiographic suite has the potential to markedly expedite the treatment of patients with acute ischemic stroke. The present study compares FP PBV maps to cerebral blood volume (CBV) maps derived using standard dynamic computed tomographic perfusion (CTP) in a population of patients with cerebrovascular ischemic disease.
Materials & Methods
Fifty-two patients with cerebrovascular ischemic disease at two participating institutions prospectively underwent both standard dynamic CTP imaging followed by FP PBV imaging (syngo Neuro PBV IR; Siemens, Erlangen, Germany) under a protocol approved by both Institutional Review Boards (IRB). The feasibility of the FP system to generate PBV maps was assessed. The radiation doses for both studies were compared. The sensitivity and specificity of the PBV technique to detect (1) any blood volume deficit and (2) a blood volume deficit greater than one third of a vascular territory were defined using standard dynamic CTP CBV maps as the gold standard.
Results
Of 52 patients imaged, PBV maps were technically adequate in 38 (73.1%). The 14 inadequate studies were not interpretable secondary to patient motion/positioning (4), injection issue (2), or other (8). The average dose for FP PBV was 247 mGy (median 231) versus 208 (median 20) for CTP CBV. On CTP derived CBV maps 23 of 38 had a CBV deficit (60.5%) and 12 (31.6%) had a deficit that accounted for greater than one third of a vascular territory. FD PBV maps were 100% sensitive and 86.7% specific to detect any CBV deficit and 100% sensitive and 65.4% specific to detect any CBV deficit of greater than one-third of a territory.
Conclusion
Perfused blood volume maps can be generated using FP systems. The average radiation dose is similar to a standard CTP examination. Perfued blood volume maps have a high sensitivity for detecting CBV deficits defined by conventional CTP. Perfused blood volume maps tended to overestimate the size of CBV deficits. This overestimation most likely indicates that the FP protocol initiates parenchymal imaging prior to complete saturation of the blood volume in areas perfused via indirect pathways (i.e., leptomeningeal collaterals).

KEYWORDS: Stroke, Volumetric perfusion CT

eP-200

Thrombus Density Does Not Predict Angiographic Results of Mechanical Thrombectomy with Stentretrievers

Yilmaz, U.·Roth, C.·Reith, W.·Papanagiotou, P.
Saarland University Hospital
Homburg, GERMANY.

Purpose
Mechanical thrombectomy with stentretrievers in acute stroke has emerged as a promising new technique with the highest recanalization rate of the therapeutic procedures available so far. However, in up to 20% of the cases mechanical thrombectomy with stentretrievers results in poor angiographic outcomes with TICI-scores ≤ 2a. The purpose of this study was to investigate whether thrombus density on the initial CT scan can predict the angiographic outcome of the recanalization procedure in MCA occlusions.
Materials & Methods
The data of 70 patients with acute MCA-occlusions who underwent endovascular treatment with stentretrievers in our department were included. We analyzed thrombus densities, angiographic outcome and periprocedural thrombus fragmentation and embolization to a more distal position or branch.
Results
The mean thrombus density was 49.8 ± 7.8 HU and the mean difference to the density of the contralateral MCA was 9.9 ± 8.0 HU. There were no significant differences in the thrombus densities of occlusions that were successfully recanalized (mTICI ≥ 2b) and those that were not. Neither were there significant correlations of thrombus densities and periprocedural thrombus fragmentations and embolizations which occurred in 64.3% and 54.3% respectively. We found a nonsignificantly higher rate of recanalizations mTICI ≥ 2b when the difference to the density of the contralateral MCA was between 1 and 20 HU. This tendency increased in the group of patients who were treated by combined IV-rtPA and mechanical thrombectomy (86.2% versus 57.1%, P = 0.081) and disappeared in the group of patients who were treated by mechanical thrombectomy only (82.8% versus 80.0%, P = 0.881). Separately analyzing rates of thrombus fragmentation and embolization we found a nonsignificant increase in those rates in the cases with differences outside the range 1 to 20 HU who had been treated by combined IV-rtPA and mechanical thrombectomy.
Conclusion
In contrast to results of other revascularization procedures as published in a recent study, the angiographic result of mechanical thrombectomy with stentretrievers is not predicted by thrombus density. This might indicate that higher performance of stentretrievers is in part due to an insensibility of stentretrievers to different clot compositions. Yet when IV-rtPA and mechanical

Note: Scanned images are included in the proceedings. Some submitted images were reduced during editing, thereby decreasing clarity. Also, refer to the Program Planner. Proceedings Content as of 3-29-2013.

thrombectomy are combined there are nonsignificant differences in the rates of successful recanalization, thrombus fragmentation and embolization. These results raise the question whether IV-rtPA might lead to higher rates of thrombus fragmentation and embolization during mechanical thrombectomy in some cases with certain thrombus compositions. This will have to be addressed in studies with larger case numbers.

KEYWORDS: Mechanical thrombectomy, Stroke

eP-201

Angiographic Collateral Score as a Predictor of Clinical Outcome and Contrast Staining in Acute Large Vessel Ischemic Stroke

Amans, M. R.·Cooke, D. L.·Vella, M.·Hetts, S. W.
University of California San Francisco
San Francisco, CA.

Purpose
Improvements in endovascular techniques for revascularization in patients with acute ischemic stroke (AIS), have led to improved reperfusion rates. Both the thrombolysis in cerebral infarction (TICI) score and the extent of pial collateral circulation have been shown to predict clinical outcomes. Contrast staining when defined as high density without mass effect on CT after endovascular intervention in AIS patients has been shown to be an early indicator of parenchymal infarction, and these cases rarely undergo hemorrhagic transformation. We sought to determine if change in pial collateral circulation before and after revascularization predicts adequate reperfusion in AIS patients.
Materials & Methods
Retrospective review was performed of imaging and charts of patients with anterior circulation AIS who underwent cerebral angiogram and had at least one subsequent CT. Diagnostic cerebral angiograms were reviewed independently by 3 ACGME fellowship-trained neuroradiologists who also have had additional subspecialty training in neurointerventional radiology. Follow-up imaging was evaluated for contrast staining of brain parenchyma as a surrogate marker for parenchymal injury and hemorrhagic transformation. Change in modified Rankin score (ΔmRS, defined as mRS at discharge minus mRS at admission) was the primary measure of clinical outcome. Contributions of final TICI score after endovascular intervention, pial collateral circulation score prior to intervention, and change in pial collateral circulation (CiPC, defined as preintervention collateral score minus post intervention collateral score) to patient and imaging outcomes relative to known predictors of patient outcomes in AIS therapies (age, gender, presentation mRS, occlusion level, procedure length, time from stroke onset to intervention, tobacco use, alcohol use, diabetes, previously known vascular disease, hemorrhagic transformation after intervention, prior TIA, prior stroke, antecedent anticoagulation) were determined by logistic regression.
Results
Median admission mRS was three (0, 4) (25%ile, 75%ile), median discharge mRS was four (3, 5), and median ΔmRS was one (-1, 4). Parenchymal contrast staining on follow-up CT was evident in 63.4% of patients (45/71). Logistic regression analysis revealed that CiPC scores [odds ratio (OR): 0.678, 0.661, and 0.752 for readers 1, 2, and 3, respectively) and TICI scores after intervention (OR: 1.251, 1.784, and 1.697 for readers 1, 2, and 3 respectively) are independent predictors of ΔmRS (p = 0.006, 0.009, and 0.134; p = 0.257, 0.011, 0.023, readers 1, 2, and 3 for CiPC; TICI, respectively), and CiPC scores (OR: 1.106, 1.591, and 1.848 for readers 1, 2, and 3, respectively) and TICI scores after intervention (OR: 1.281, 1.451, and 1.714 for readers 1, 2, and 3 respectively) to be independent predictors of contrast staining on follow-up imaging (p = 0.53, 0.017, 0.031; p = 0.28, 0.14, 0.05, readers 1, 2, and 3 for CiPC; TICI, respectively).
Conclusion
Final TICI score (direct measure of antegrade flow to a vascular territory) and CiPC (regression of collateral circulation presumably secondary to improved antegrade flow to viable brain tissue) are independent predictors of patient outcomes as measured by improved mRS and imaging outcomes as measured by contrast staining in our patient cohort.

KEYWORDS: Collateral circulation, Stroke

eP-202

Update on the Pragmatic Ischemic Stroke Thrombectomy Evaluation Randomized Controlled Trial

White, P. M.[1]·Muir, K.[2]·Ford, G.[1]·Brown, M.[3]·Clifton, A.[4]·Murray, A.[5]·Ford, I.[5]
[1]Institute for Ageing & Health, Newcastle upon Tyne, UNITED KINGDOM, [2]Institute of Neurosciences, Glasgow, UNITED KINGDOM, [3]University College London, London, UNITED KINGDOM, [4]St. Georges Hospital, London, UNITED KINGDOM, [5]Glasgow University, Glasgow, UNITED KINGDOM.

Purpose
To provide early recruitment data arising from the UK-based Pragmatic Ischemic Stroke Thrombectomy Evaluation (PISTE) pragmatic randomized controlled trial [of mechanical thrombectomy plus IV thrombolysis (IVT) versus IVT in acute ischemic stroke] and an update on the progress of the trial.
Materials & Methods
Pragmatic Ischemic Stroke Thrombectomy Evaluation is a PROBE design multicenter randomized controlled trial with concealed allocation. Primary outcome is 90-day clinical outcome based on dichotomized modified Rankin Score. Groups are matched using appropriate minimization criteria. Secondary endpoints include ordinal shift analysis

Note: Scanned images are included in the proceedings. Some submitted images were reduced during editing, thereby decreasing clarity. Also, refer to the Program Planner. Proceedings Content as of 3-29-2013.

of Rankin, days at home by 90 days, procedural safety, SICH rate, recanalization rate (as adjudicated by an independent panel of reviewers blinded to allocation). Analysis of results is on an intention to treat basis. The funders (Stroke Association) and trial sponsor (Greater Glasgow Health Board on behalf of UK NHS) have no control over the running of the trial and no access to the trial data. Pragmatic Ischemic Stroke Thrombectomy Evaluation is actively recruiting.

Results

Information on early patient recruitment will be provided at the ASNR meeting as part of an update on trial progress.

Conclusion

Pragmatic Ischemic Stroke Thrombectomy Evaluation is the first RCT examining thrombectomy within the fairly homogenous UK NHS healthcare system and one of only two PROBE trials directly comparing the addition of thrombectomy to best medical therapy (IVT), which is the most relevant clinical question to answer.

KEYWORDS: Thrombectomy, Stroke, thrombolysis

eP-203

Multimodal Stroke Imaging Including Time-Resolved Whole Brain Perfusion Imaging within the Angio Suite: Preliminary Results of a Novel Flat-Detector CT Application

Struffert, T.[1]·Deuerling-Zheng, Y.[2]·Strother, C.[3]·Goelitz, P.[1]·Lang, S.[1]·Doerfler, A.[1]
[1]University Erlangen-Nuremberg, Erlangen, GERMANY,
[2]Siemens AG, Healthcare Sector, Forchheim, GERMANY,
[3]University of Wisconsin, Madison, WI.

Purpose

Flat-detector CT applications that are available during endovascular procedures are used in increasing numbers in the neurointerventional angio suite. Recently feasibility of multimodal flat-detector stroke imaging including time-resolved perfusion imaging could be demonstrated in the experimental setting. To demonstrate clinical feasibility we reviewed our first acquisitions in patients and compared to standard methods (MRI/CT).

Materials & Methods

Under an institutionally approved protocol the new FD CT application (10 consecutive bi-directional rotations) was used in six patients with acute stroke (M1 occlusion, 2 right, 4 left) following endovascular stroke treatment. Intravenous contrast medium injection was used. Using standard software brain parenchyma (FD CT) and vascular structures (FD CTA) were reconstructed. Using prototype software calculation of cerebral blood flow (CBF), blood volume (CBV), mean transit time (MTT and time to peak (TTP) maps was possible using a standard deconvolution-based algorithm for dynamic perfusion quantification. The images were reviewed in consensus reading by two experienced neuroradiologists and compared to MRI/CT images (MR/CT perfusion, MR/CT angiography), respectively.

Results

In all except in one case endovascular treatment resulted in complete recanalization (TICI 0 to TICI 3). Flat-detector CTA reconstructions confirmed recanalization of the M 1 segment in successfully treated patients and persistent occlusion in one case. In two cases subarachnoidal hemorrhage was visible on postinterventional FD CT, confirmed by follow-up CT. Evaluation of the MTT/TTP maps showed symmetric normalization after recanalization. In the successfully treated patients CBF normalized in two and was increased (hyperperfusion) in three cases, CBV normalized in three and increased in two cases, respectively. In the unsuccessful case CBF and CBV lesion showed an increase in volume.

Conclusion

Time-resolved whole brain perfusion imaging within the angio suite is feasible and demonstrated good correlation to standard perfusion methods and follow-up imaging. In addition, visualization of brain parenchyma and vascular structures is possible providing “multimodal stroke imaging” within the angio suite. Further evaluation is necessary.

KEYWORDS: Flat-panel angiographic CT, Stroke, time resolved perfusion imaging

eP-204

Increased Incidence of Intraprocedural Vasospasm with Use of Distal Protection Device during Carotid Stenting

Nazarian, J. P.·Vidal, L. L. M.·Badve, C. A.·Sunshine, J. L.·Blackham, K. A.
University Hospitals Case Medical Center
Cleveland, OH.

Purpose

A major risk of carotid artery stenting is dislodging and distal embolization of atherosclerotic plaque material. Intravascular distal protection devices have been introduced into clinical practice in an effort to address this problem. Multiple attempts to firmly establish that these devices reduce neurologic complications have met with mixed results. Furthermore, there has been only limited investigation of the relationship between use of a distal protection device and intraprocedural vasospasm. We studied the characteristics of patients who underwent cervical carotid stenting with and without use of a distal protection device.

Materials & Methods

Following approval by the institutional review board, a retrospective chart review was performed on 143 patients (median age 65.5 years, range 40-91 years) who underwent carotid stenting at our institution between February 2003 and November 2012. Demographic and clinical data, including age, sex, comorbidities, percent carotid stenosis, intra and postprocedural complications, and in-hospital mortality were obtained from paper charts

Note: Scanned images are included in the proceedings. Some submitted images were reduced during editing, thereby decreasing clarity. Also, refer to the Program Planner. Proceedings Content as of 3-29-2013.

and electronic medical records. Comorbidities examined included hypertension, diabetes mellitus, hyperlipidemia, coronary artery disease, prior stroke, and smoking history. Complications included intraprocedural vasospasm and stroke. Patients who underwent carotid stenting were divided into two groups: 66 patients in whom a distal protection device was placed (DPD group) and 77 in whom it was not (non-DPD group). Statistical analysis was performed using a z-test and unpaired two-tailed student's *t*-test to detect differences in complication rates, as well as demographic characteristics and patient comorbidities, between the two groups. Distal protection devices used included Cordis Angioguard® and Abbott Accunet®.

Results

Out of total 143 patients who underwent carotid stent placement, 66 had a distal protection device placed and 77 did not. There were four procedure-related strokes (6.1%) and no procedure-related deaths in the DPD group, with two strokes (2.6%) and no procedure-related deaths in the non-DPD group. These differences did not achieve statistical significant. Three patients in the non-DPD died during their hospital stay for reasons not related to their stenting procedure. No significant differences were found between the mean patient ages, gender proportions, or percent carotid stenoses of the two groups. Comparison of comorbidities between the two groups revealed an increased history of coronary artery disease in the non-DPD group which was statistically significant ($p = 0.004$). No other significant differences in rates of comorbid conditions were identified. Subgroup analysis performed on 31 patients in the nonprotection device group for whom electronic procedure notes were available revealed two incidences of notable intraprocedural vasospasm (6.45%), compared with 15/66 (22.7%) in the distal protection device group ($p = 0.02$).

Conclusion

Use of a distal protection device was associated with a statistically significant increase in the incidence of intraprocedural carotid vasospasm. No significant difference in procedure-related strokes or mortality rates was detected between the two groups. The ostensible benefit of the embolic protection device may be outweighed by the increased complexity of the procedure including longer procedural times, increased difficulty with exchange of catheters while maintaining embolic protection device position and direct vascular untoward effects such as vasospasm.

KEYWORDS: Carotid artery stenting, Vasospasm, distal protection device

eP-205

Use of Stentretrievers in Acute Ischemic Stroke: Performance Evaluation in a Patient-Specific Vascular Replica with and without Using a Balloon-Guide Catheter

Chueh, J. Y.[1]·Kuhn, A. L.[1]·Puri, A. S.[1]·Wilson, S.[2]·Wakhloo, A. K.[1]·Gounis, M. J.[1]

[1]University of Massachusetts Medical School, Worcester, MA, [2]Concentric Medical, Mountain View, CA.

Purpose

Expedited revascularization through mechanical thrombectomy is the principle goal of treatment of ischemic stroke, and may provide good clinical outcomes. In order to progress toward this goal, the latest stentretrievers were evaluated and compared to the Merci Retriever to understand their effectiveness under different clinical situations. Our hypothesis is that the mechanical properties of the embolism and the proximal flow control during thrombectomy contribute to successful recanalization and the potential for distal clot fragmentation.

Materials & Methods

Mechanical thrombectomy was performed with the use of the Trevo, Solitaire FR, and Merci Retriever in our in vitro MCA occlusion model. The occlusion model included proximal and distal collateral pathways in an effort to mimic functional human anatomy. The efficacy and safety of these thrombectomy devices were evaluated with and without temporary proximal balloon occlusion in both soft and hard clot analogues. Characterization of microemboli in the effluent was conducted by using the Coulter Principle.

Results

Partial flow restoration was observed immediately after deployment of the stentrievers (70.5 ± 26.6 and 46.2 ± 23.0 ml/min in the soft and hard clot occlusions, respectively). Applying aspiration during clot retrieval resulted in flow reversal. This phenomenon was more significant when proximal temporary occlusion with the balloon was used (-83.1 ± 66.7 versus -32.3 ± 48.8 ml/min, $P<0.0001$). All the soft occlusions were cleared successfully by mechanical thrombectomy regardless of device type and presence of proximal flow control (average thrombectomy attempt: 1.1). In the Trevo, Solitaire and Merci hard clot groups, all the procedures which were performed through a balloon-guide catheter (BGC) achieved complete flow restoration, giving a recanalization rate of 100% (average thrombectomy attempt: 1.1). In one out of eight hard occlusions in which BGC was not used, the Solitaire system was not able to retain the clot within the device during retrieval, resulting in a partial flow restoration (74.1%). Partial clot removal also occurred in one Merci experiment; however, the small residual clot did not obstruct any flow. The Merci device was less efficient in hard clot removal as compared to the Trevo and Solitaire devices (mean thrombectomy attempt: 1.5 versus 1.1). The rate of distal clot fragments with size greater

Note: Scanned images are included in the proceedings. Some submitted images were reduced during editing, thereby decreasing clarity. Also, refer to the Program Planner. Proceedings Content as of 3-29-2013.

than 1000 µm and between 200-1000 µm from the hard clot model was significantly reduced with the deployment of BGC ($p<0.05$). However, the BGC offered only slight reduction of clot fragmentation for soft clots. There was a significant increase in the number of particles having a diameter between 8-200 µm generated during thrombectomy using the soft clot model ($p<0.0001$) regardless of BGC assistance or device used as compared to that with the hard clot model. The average particle diameter in this range was less than 10 µm in all groups.
Conclusion
The amount of flow restoration can be quantified and the size and number of the distal emboli generated during the procedure can be characterized by using the in vitro model system of cerebrovascular occlusion. The risk of distal embolization is reduced with the use of temporary flow arrest with a BGC.

KEYWORDS: Stroke, Thrombectomy, embolization

eP-206

Utility of Temporary Balloon Occlusion Testing in Predicting Outcomes after Permanent Parent Vessel Occlusion

Whisenant, J. T.·Derdeyn, C. P.·Cross, D. T.·Moran, C. J.
Mallinckrodt Institute of Radiology
St. Louis, MO.

Purpose
To review the utility of the temporary balloon occlusion (TBO) test as it pertains to prediction of patient outcomes following permanent parent vessel occlusion. Patients often undergo TBO testing as part of the diagnostic workup prior to permanent parent vessel sacrifice. We perform a three-part test that includes intraprocedural neurologic assessment, neuroangiographic evaluation of the adequacy of collateral flow, and 99m-Tc-Bicisate administration during temporary balloon occlusion. Pending the TBO test results, parent vessel occlusion may be performed; and this patient population is at risk for postparent vessel sacrifice ischemic complications, such as TIA, stroke, and death.
Materials & Methods
Data were reviewed retrospectively from all patients who underwent ICA TBO from March 2002 to December 2011. Patients then were subdivided into those that underwent permanent ICA occlusion and those that did not. Data from those that underwent permanent ICA occlusion were collected over the succeeding six months for the occurrence of three primary outcomes: transient ischemic attack (TIA), ischemic stroke (CVA), and death. In the subgroup of patients with a CVA following the parent vessel occlusion, additional data were collected in the following areas: 1) type of parent vessel sacrifice (open versus endovascular), 2) timing of symptom onset (procedural, early postop, late postop), and 3) type/location of infarct. Based on these factors, a mechanism of the event was postulated (thromboembolic versus hemodynamic).
Results
One hundred fifty ICA TBOs were performed between March 2002 and December 2011. Thirty-six went on to have permanent endovascular or surgical ICA occlusion. In the group that had parent vessel sacrifice, there were the following outcomes: five TIAs (13.9%), six CVAs (16.7%), and three deaths (7.3% - all due to underlying malignancy). Of the nine patients with ischemic complications (i.e., TIA or CVA) after the parent vessel sacrifice, eight had SPECT performed and all eight were normal or had "fixed" defects, seven had angiography performed and sic of the seven were interpreted as normal, and all nine had clinical neurologic assessment performed and all nine passed. Of the six patients with CVA, four are postulated to be hemodynamic in etiology, one is postulated to be thromboembolic in etiology, and one is of indeterminate etiology (hemodynamic or thromboembolic).

Timing and Type of Ischemic Stroke Following Parent Vessel Sacrifice

PATIENT	AGE	TBO ANGIO RESULT	SPECT RESULT	TBO NEURO EXAM	METHOD OF SACRIFICE	TIME ONSET OF CVA	MECHANISM OF CVA	SYMPTOMS OF CVA
1	78	Not done	Pass	Pass	Endovascular	Early post-op (hours/days)	Hemodynamic/embolic - single centrum semiovale by CT	Mild RUE weakness
2	44	Pass	Pass	Pass	Open Surgical	Early post-op (hours/days)	Hemodynamic	Mild weakness - complete resolution at later followup
3	51	Pass	Not done	Pass	Endovascular	Early post-op (hours/days)	Hemodynamic - Centrum Semiovale	L hemiplegia, R facial droop
4	64	Fail	Pass	Pass	Open Surgical	Late post-op (weeks/months)	Hemodynamic - Centrum Semiovale	LUE weakness 4 months post op
5	86	Pass	Pass	Pass	Endovascular	Late post-op (weeks/months)	Thromboembolic - stump	LUE/LLE weakness and L sided neglect
6	73	Not done	Pass	Pass	Endovascular	Early post-op (hours/days)	Hemodynamic	R hemiplegia, R facial weakness, aphasia

Conclusion
The rate of ischemic stroke following ICA sacrifice in patients who have "passed" TBO testing is higher than expected. The majority of ischemic strokes affected the deep white matter of the centrum semiovale and occurred in the early or late postop period supporting a hemodynamic etiology. The SPECT and angiographic testing appears to be more effective in assessing cortical flow than assessing flow to the deep white matter.

KEYWORDS: Balloon test occlusion, Hemodynamics, temporary balloon occlusion

eP-207

Endovascular Treatment of Tandem Vascular Occlusions in Acute Ischemic Stroke

Puri, A. S.[1]·Kuhn, A.[1]·Hou, S.[1]·Khan, M.[1]·Kwon, H.[2]·Gounis, M. J.[1]·Wakhloo, A. K.[1]
[1]University of Massachusetts Medical Center, Worcester, MA, [2]Chungnam National University Hospital, Daejeon, KOREA, REPUBLIC OF.

Purpose
Tandem vascular occlusions represent a treatment

Note: Scanned images are included in the proceedings. Some submitted images were reduced during editing, thereby decreasing clarity. Also, refer to the Program Planner. Proceedings Content as of 3-29-2013.

challenge in acute ischemic stroke (AIS). Both revascularization of the proximal lesion followed by the treatment of the distal occlusion or vice versa, have shown advantages as well as disadvantages. However, the order in which the affected vessels should be treated to achieve rapid and permanent flow restoration has not been determined yet. Here we evaluate the safety and efficacy of our approach and clinical as well as angiographic results for different endovascular treatment combinations for tandem vascular occlusions.

Materials & Methods

All patients with AIS secondary to tandem lesions treated endovascularly were identified either at the University of Massachusetts Memorial Medical Center(n=18) or at the Chungnam National University Hospital(n=3) between June 2006 and November 2012 and their data were reviewed. We included patients who presented with extracranial internal carotid artery (ICA) occlusion and a concomittant occlusion of either the distal ICA 'T' occlusion, middle cerebral artey (MCA) or the anterior cerebral artery (ACA). We also included patient with occlusion of the proximal vertebral artery (VA) and a simultaneous occlusion of the basilar artery (BA). We collected the information of each patient's stroke risk factors, National Institute of Health Stroke Scores (NIHSS) and modified Rankin Scores (mRS) on admission and at discharge. Data also collected included: method of anesthesia during intervention, means of intracranial revascularization and use of cerebral protection devices. The final recanalization achieved was evaluated by using the Thrombolysis In Cerebral Infarction (TICI) score.

Results

A total of 21 patients were identified to have tandem vascular occlusions. The mean age was 50 years. Patient comorbidities included smoking (38.1%), hypertension (57.1%), dislipidemia (33.3%), diabetes (19%) and alcohol abuse (23.8%). Mean NIHSS and median mRS at admission was 17.9 and five respectively. In 76.2% of cases, the intervention was performed under general anesthesia. An ICA lesion with concommitant MCA occlusion was present in 90.5% of cases. Involvment of the VA with basilar BA occlusion was seen in 9.5%. In 81% of patients (n = 17) treatment of the proximal occlusion was initiated followed by the distal occlusion. Endovascular protection devices for the ICA occlusion were used in five cases. Six patients received IV tPA prior to the endovascular intervention. In 94.7% of cases ICA revascularization was achieved with stent placement. Intra-arterial lysis was used mostly to recanalize the MCA occlusion (84.2%); both BA occlusions were treated with endovascular thrombectomy. Thrombolysis In Cerebral Infarction 2B and 3 recanalization was achieved in 14 cases (66.7%). An mRS of ≤2 at discharge was achieved in 38.1%; mean patient NIHSS was 8.1. Four patients died.

Conclusion

Our results show that an aggressive recanalization of tandem lesions can be used safely with an excellent outcome in a subgroup of patients with AIS. This subgroup has a bad natural history with a high morbidity and mortality. We prefer the proximal occlusion using a stent followed by distal recanalization with either mechanical, pharmaceutical or combined thrombolysis. This approach has low periprocedural complications and can achieve excellent angiographic and clinical outcome.

KEYWORDS: Thrombolysis, Carotid artery stenting, tandem occlusions

eP-208

Simple and Easy Way Using Time-Intensity Curve of Perfusion-Weighted Images to Find Penumbra in Stroke Patients within Twelve Hours of Onset Due to the Carotid Artery Occlusion

Mori, T.･Iwata, T.･Miyazaki, Y.･Nakazaki, M.･Takahashi, Y.
Shonan Kamakura General Hospital
Kamakura, JAPAN.

Purpose

The aim of our retrospective study was to find indicators of time-intensity curve (TIC) of PWI indicating penumbra in stroke patients with acute carotid artery occlusion.

Materials & Methods

Included were acute stroke patients 1) who were admitted within 12 hours of onset between January 2005 and January 2012, and 2) in whom emergency MRA showed absolutely no visualization of the affected internal carotid artery (ICA). Patients who underwent intravenous tPA or endovascular treatment were excluded. We assessed, NIHSS on admission (NIH adm), NIHSS on the 7th day (NIH 7th), in-hospital death, the time to peak (TP) and the peak signal (PS) comparing the affected side (a) TIC with the contralateral side (c) TIC, which was generated on regions of interest set at symmetrical positions of the bilateral MCA territories. Time to peak delay was defined as TPa - TPc, PS% as PSa/PSc x 100. Early neurologic improvement (ENI) was defined as NIH adm - NIH 7th more than four or (NIH adm less than five and NIH 7th less than five). We evaluated relationship between TP delay, PS%, EMI and inhospital death.

Results

Fifty-nine patients were analyzed. Mean age was 78 years old. Thirty-one patients were women. Median NIH adm, NIH 7th, TP delay and PV% were 18, 24, 5.9 and 68.8, respectively. Twenty-two patients died during hospitalization. Thirteen patients had ENI. Time to peak delay ($p<0.01$) and PV% ($p<0.005$) were significant predictors of EMI. Receiver operating characteristics curves showed that cut-off points in TTP delay and PV% were 4.7 and 85, respectively. Time to peak delay ($p<0.05$) and PV% ($p<0.0005$) were significant predictors of inhospital death. Receiver operating characteristics curves showed that cut-off points in TP delay and PV% were 12 and 32, respectively. Among 40 patients without TP more than 4.7 and PV%less than 32, 11 patients had TP delay of 4.7 s and PS% of 32 or more and less than 85%, and only

Note: Scanned images are included in the proceedings. Some submitted images were reduced during editing, thereby decreasing clarity. Also, refer to the Program Planner. Proceedings Content as of 3-29-2013.

one of them achieved ENI.

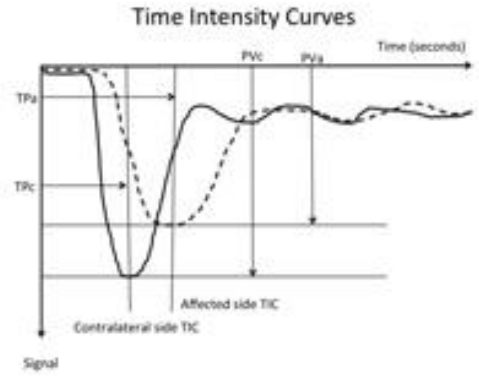

Conclusion
Time to peak delay more than 4.7 s and PS% of 32 or more and less than 85% were indicators of penumbra predicting neither early clinical improvement nor inhospital death.

KEYWORDS: Acute stroke, Diffusion-perfusion mismatch, time intensity curve

eP-209

One-Year Clinical Experience with the pREset 4/20 Stent Retriever for the Treatment of Acute Ischemic Stroke: A Review of 169 Consecutive Cases

Kurre, W.[1]·Aguilar-Pérez, M.[1]·Fischer, S.[1]·Schmid, E.[2]·Sperber, W.[3]·Bäzner, H.[2]·Henkes, H.[1]
[1]Katharinenhospital, Stuttgart, GERMANY, [2]Klinikum Stuttgart, Stuttgart, GERMANY, [3]Klinikum Esslingen, Esslingen, GERMANY.

Purpose
The purpose of this study was to evaluate the safety and efficacy of the pREset 4/20 stent retriever in a real world clinical setting.
Materials & Methods
We retrospectively analyzed all embolic cerebral vessel occlusions treated with pREset 4/20 between August 2011 and July 2012. Device-related complications, parenchymal hemorrhage type II (PHII) and diffuse SAH on follow-up imaging served as safety endpoints. In terms of efficacy, a TICI 2b and 3 score was regarded as successful recanalization and a mRS of 0-2 at 90 days was defined as good clinical outcome. In addition, we compared safety and efficacy between treatments performed with pREset alone and in combination with other devices.
Results
One hundred sixty-nine patients with 175 target vessels were included. Successful recanalization after the last pass with pREset was achieved in 78.9% of targets. The end of procedure successful recanalization rate was 91.4%. One vessel wall injury (0.8%) and 7.1% new emboli were related to pREset. PH II or diffuse SAH were observed in 8.9%. Good clinical outcome was achieved in 31.4%. Multiple devices were used in 29.7% of targets. Escalation of therapy was associated with an increased risk of vessel injury (p = 0.027) and a trend for lower recanalization rates, higher rates of hemorrhage on imaging and worse clinical outcome.
Conclusion
pREset 4/20 proved to be safe and effective with similar results compared to other stent retrievers. Escalation of therapy carries a higher procedural risk and should be performed only after a careful risk-benefit assessment.

KEYWORDS: Thrombectomy, Actue stroke, pREset

eP-210

Late Vertebro-Basilar Clot Retrieval: Angiographic and Clinical Outcomes

Djoukhadar, I. A.[1]·Alli, S.[2]·Hassan, A.[2]·Patankar, T.[1]·Goddard, A.[1]
[1]Leeds Radiology Academy, Leeds, UNITED KINGDOM, [2]Leeds Teaching Hospitals, Leeds, UNITED KINGDOM.

Purpose
To describe our experience in performing mechanical clot disruption and intra-arterial t-PA in patients presenting (>12 hours after ictus) with basilar thrombosis and rapidly deteriorating neurologic status.
Materials & Methods
Retrospective, single-center study of patients (N = 6, mean age of 44 years ranging from 10 to 78 years, 50% males) with basilar artery stroke with onset of symptoms at > 12 hours over two-year period (September 2010 - September 2012). Clot location, successful recanalization, device type, device-related complications, clinical outcomes (modified Rankin Scale score) and mortality at 90 days were assessed.
Results
Three patients had complete occlusion at the proximal basilar artery, two at the distal basilar artery (clot extension into right P1 and clot extension in both P1 segments) and one patient having left vertebral artery and proximal basilar artery thrombosis. The shortest time from symptom's onset to the angio-suite was 15 hours: 21 minutes and the longest was 74 hours: 33 minutes. None of our patients received intravenous t-PA bridging therapy. Devices used included five Solitaire stents (Three 6 x 30 and Two 4 x 20), three Revive Devices (4.5 x 22) and four Penumbra Devices (two 032, one 041 and one 054). The device-related complications included one case of stent collapse needing balloon angioplasty and a case of moderate vasospasm that was controlled with Nimodipine infusion. Complete recanalization (TICI 3) was achieved in three patients (50%) and partial recanalization (TICI 2B) but with good perfusion was achieved in the remaining three patients. The three-month outcome was favorable (mRS: 0 - 2) in three patients, poor (mRS: 4) in one patient and the mortality rate at three months was 33% (two

Note: Scanned images are included in the proceedings. Some submitted images were reduced during editing, thereby decreasing clarity. Also, refer to the Program Planner. Proceedings Content as of 3-29-2013.

patients died).
Conclusion
Mechanical clot retrieval beyond 12 hours achieves good recanalization rates. Good clinical outcomes can be achieved in carefully selected patients.

KEYWORDS: Thrombectomy, Basilar artery occlusion

eP-211

Post-Thrombectomy Hemorrhage: Ischemia on CT Angiography as a Predictor of Hemorrhage Rates

Nickell, L. T.·Hise, J. H.·Layton, K. F.
Baylor University Medical Center
Dallas, TX.

Purpose
Intracranial hemorrhage is a feared complication of mechanical endovascular thrombectomy and intra-arterial thrombolysis and causes significant morbidity and mortality. The purpose of this study is to identify if post-thrombectomy/thrombolysis hemorrhage rates could be predicted based on the extent of cerebral ischemia identified on CT angiographic source images.
Materials & Methods
We conducted a chart review of all neurointerventional cases of stroke treatment by mechanical thrombectomy and/or intra-arterial thrombolytic administration. The degree of ischemia was measured on source images from CT angiograms obtained immediately before intervention. Successful recanalization rate and postoperative hematoma formation is measured. Only cases involving the anterior circulation were considered. Clinical and imaging data were analyzed retrospectively.
Results
A total of 157 cases of neurointerventional stroke treatment were identified. Thirty-one cases were eliminated (18 involved the posterior circulation, 10 had no CT angiogram images, and four were complicated by aneurysm coiling), leaving 125 cases included in the dataset. Patients with very little to no ischemia on CTA source images (n = 64) demonstrated a hematoma formation rate of 6.3% (n = 4). Cases with marked ischemic changes (n = 61) showed a parenchymal hematoma rate of 16.4% (n = 10).
Conclusion
Evaluation of the source images from CT angiography for ischemic change can be a valuable tool in identifying a patient's risk of post-thrombectomy hemorrhage, as the rate of postoperative hemorrhage increases significantly if marked ischemic changes are seen on pretreatment scans.

KEYWORDS: Thrombectomy, Stroke

eP-212

Endovascular Management of Inoperative Meningiomas

Yakes, W. F.
Vascular Malformation Center
Englewood, CO.

Purpose
To determine the efficacy of ethanol embolization of single and multiple meningiomas in poor surgical candidates.
Materials & Methods
Eleven patients (eight female, three male; mean age 52 years) underwent clinical, MR, and angio evaluations. In patients who had postsurgical recurrence and/or were poor operative risks, ETOH embo was offered as an alternative procedure. Two patients had multiple meningiomas related to Von Recklinghausen's Neurofibromatosis Type II.
Results
All patients underwent ethanol embolization of single and multiple pedicles supplying the tumor. Four patients suffered complications (one patient minor late SAH without sequelae, two patients transient 6^{th} nerve palsy, one patient transient worsening of aphasia). MR imaging and CT demonstrated significant necrosis and shrinkage of the tumors at long-term followup (range: 6-72 mos; mean: 30 mos).
Conclusion
ETOH, being a liquid agent, penetrates to the capillary level causing necrosis and exclusion of collateral flow. This leads to tumor necrosis and shrinkage. Taking advantage of the slow-growing, non-metastasizing characteristics and increased vascularity of this tumor, ETOH is an attractive alternative therapy that is minimally invasive. This treatment can be offered in selected poor surgical patients. This procedure is efficacious in highly vascular tumors and in poorly vascularized meningiomas not possible to treat surgically.

KEYWORDS: Meningioma

eP-213

Mandibular Arteriovenous Malformation Diagnosis and Curative Treatment

Yakes, W. F.
Vascular Malformation Center
Englewood, CO.

Purpose
To determine optimal management strategies for the treatment of mandibular arteriovenous malformation (AVM).
Materials & Methods
Twelve patients (nine females, three males) age 9-14 years; mean age 10 years, underwent endovascular therapy to treat their mandibular AVMs. Nine patients had distinct intraosseous AVMs. Three had multiple facial and

Note: Scanned images are included in the proceedings. Some submitted images were reduced during editing, thereby decreasing clarity. Also, refer to the Program Planner. Proceedings Content as of 3-29-2013.

intramaxillary AVMs requiring treatment. Outside institutions recommended massive hemifacila resections in these patients. Four patients had prior PVA and gel foam embolization, one patient had a lip graft, one had prior mandible surgery, all that had failed.

Results

All twelve patients have demonstrated MR and angiographic cure of their AVMs. One patient's therapy is not completed and is on-going. The followup is 1 month - 41 months, with a mean followup of 29 months. No complications were noted.

Conclusion

Endovascular approaches to manage mandibular AVM can be curative. The intraosseous variety is largely a fistula between artery and vein within the bone. All responded well to endovascular ethanol therapy alone. Surgery was not required in any patient. Surprisingly no complications were encountered in this patient series. Long-term cures are noted in this patient series with endovascular approaches alone. No massive surgical resections in any patient, even in patients with multiple AVMs of the soft tissues, mandible and maxilla, were required to effect cure.

KEYWORDS: Interventional, Arteriovenous

Monday, May 20 – Wednesday, May 22
6:30 AM – 9:00 PM
Thursday, May 23
6:30 AM – 3:00 PM
Hall B1

Electronic Posters (ePosters) 214 – 262

ePS-Pediatrics

Note: A missing printed number indicates an abstract has been withdrawn.

eP-214

Apparent Diffusion Coefficient Histogram Analysis of the Normal-Appearing Brain in Sickle Cell Disease

Watanabe, M.·Buch, K.·Jara, H.·Sakai, O.
Boston Medical Center
Boston, MA.

Purpose

The purpose of this study is to investigate changes in apparent diffusion coefficient (ADC) histogram of the normal-appearing brain in patients with sickle cell disease (SCD), comparing with control population.

Materials & Methods

After acquiring IRB approval, this retrospective study included 41 SCD patients and 41 age-matched patient controls who underwent brain MR imaging for various clinical reasons during 2005-2008. All subjects showed no apparent abnormalities on conventional brain imaging. Both the SCD group and control group consisted of 22 males and 19 females (age range 2-48 years, average 20 years). All subjects were imaged at 1.5T (Achieva or Intera, Philips Medical Systems, Cleveland, OH) with our institutional clinical protocol that includes a single-shot diffusion-weighted echo-planar imaging pulse sequence (Key imaging parameters: 3899/74ms TR/TE, 89 EPI-factor and b = 0, 1000 smm^{-2}). Diffusion-weighted imaging data were DICOM transferred for processing, and the whole intracranial volume including the cerebrospinal fluid, gray and white matters, was segmented using a single-channel dual-clustering algorithm. Apparent diffusion coefficient histogram of the whole intracranial volume was generated and further modeled with Gaussian functions. Apparent diffusion coefficient peak values and histogram widths were derived from these histograms, and plotted as a function of age. The paired t-test was used to analyze the difference between the SCD subjects and the age-matched controls.

Results

The histogram widths were significantly wider in the SCD group for both males (p<0.01) and females (p<0.01). The peak values of the ADC histograms were elevated significantly in female SCD subjects (p<0.01), while there was no statistically significant difference in ADC peak values between male SCD subjects and controls (p = 0.06). The SCD group demonstrated increased inter-subject variance in both ADC peak values and histogram widths.

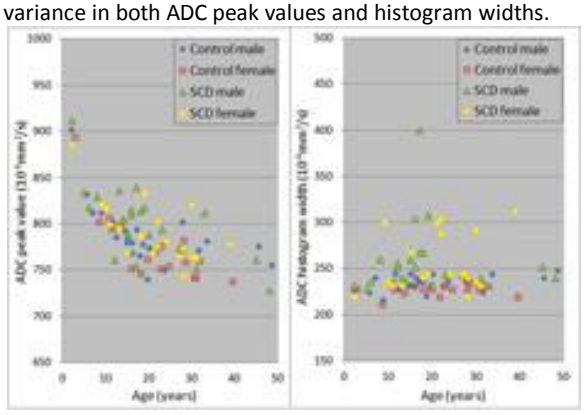

Conclusion

The ADC histogram analysis revealed its potentials to visualize subtle changes in normal-appearing brains in SCD patients, demonstrating wider histogram distribution and increased ADC peak values.

KEYWORDS: Sickle cell disease, Brain, apparent diffusion coefficient

Note: Scanned images are included in the proceedings. Some submitted images were reduced during editing, thereby decreasing clarity. Also, refer to the Program Planner. Proceedings Content as of 3-29-2013.

eP-215

Covert Hepatic Encephalopathy in Children with Liver Cirrhosis: Diffusion-Weighted MR Imaging and Proton MR Spectroscopy

Abdel Razek, A.·Ezzat, A.·Abdalla, A.·Megahed, A.
Mansoura University Hospital
Mansoura, EGYPT.

Purpose
To detect covert hepatic encephalopathy (CHE) in children with liver cirrhosis with diffusion-weighted MR imaging (DWI) and proton magnetic resonance spectroscopy (1H-MRS) of the brain.
Materials & Methods
Prospective study was conducted upon 30 consecutive children (age range 6-16 years, 21 boys and 9 girls) with liver cirrhosis and 15 age- and sex-matched healthy control children. Patients with CHE (n = 17) and with no CHE (n = 13) groups and control group underwent DWI, 1H-MRS, neuropsychologic tests (NPT) and electroencephalogram (EEG). The ADC values and integrals of glutamate or glutamine (Glx), myoinositol (mI), choline (Cho) and creatine (Cr) at the right ganglionic region were calculated. Metabolic ratio of Glx/Cr, mI/Cr, and Cho/Cr were calculated.
Results
There was significant difference between CHE, no CHE and control group in the ADC value (P = 0.001 for all groups), GLx/Cr (P = 0.001 for all groups), mI/Cr (P = 0.004, 0.001, 0.001 respectively), Ch/Cr (P = 0.001 for all groups), full scale IQ of NPT (P = 0.001, 0.001, 0.143 respectively) and EEG background frequency (P = 0.001, 0.001, 0.063 respectively). The NPT had negative correlation with ADC value (r = -0.872, P = 0.001) and GLx/Cr (r = -0.812, P = 0.001) and positive correlation with mI/Cr (r = 0.732, P = 0.001). The EEG background frequency had negative correlation with ADC value (r = -0.957, P = 0.001) and GLx/Cr (r = -0.855, P = 0.001) and positive correlation with mI/Cr (r = 0.775, P = 0.001).
Conclusion
We concluded that DWI and 1H-MRS are noninvasive imaging modalities that can be used to detect CHE in children with liver cirrhosis and correlated well with parameters of NPT and EEG.

KEYWORDS: 1H MRS

eP-216

Longitudinal MR Studies in a Patient with Medium-Chain Acyl-Coenzyme-A-Dehydrogenase Deficiency

Bernardi, B.·Figà-Talamanca, L.·Longo, D.·Verdolotti, T.
Bambino Gesù Pediatric Hospital
Rome, ITALY.

Purpose
We report serial brain MRI and H-MR spectroscopy (MRS) changes in patient with medium-chain acyl-coenzyme-A-dehydrogenase (MCAD) deficiency who developed acute encephalopathy. MCAD is an enzyme of the mitochondrial b-oxidation of fatty acids, an essential source of energy for cells during stress. Usually the first clinical presentation occurs by age of two with onset of acute hypoketotic hypoglycemia. Clinical features of this decompensated state include seizures and lethargy progressing to death if not treated prompty with dextrose infusion. Diagnosis is suspected on the basis of plasma acylcarnitine levels and altered urinary organic acid profile and confirmed through genetic analysis or demonstrating reduced enzyme activity. To the best of our knowledge, there are only a few reports describing brain MRI findings in MCAD deficiency and no systematic description of neuroimaging features has been reported.
Materials & Methods
A 12-month-old girl presented with sudden onset of acute encephalopathy. Baseline laboratory investigations revealed severe hypoglycemia, hyperammonemia and hyperchloremic metabolic acidosis. Patient was treated with glucose infusion that resulted in a progressive normalization of glucose and ammonia blood levels and gradual resolution of symptoms. The first conventional MR imaging, performed within six hours of onset, was normal, while there were bilateral symmetric restricted diffusion lesions on diffusion-weighted imaging (DWI) in the middle cerebellar peduncle, nucleus caudatus, putamen and periventricular white matter. To confirm visual assessment of DWI, a quantitative measurement of apparent diffusion coefficient (ADC) was calculated in eight different anatomical locations for each hemisphere. Resulting ADC values were significantly lower than those measured in five age-matched healthy subjects. Second MRI, 24 hours after onset, did not show conventional MRI or DWI abnormalities. Quantitative assessment of ADC confirmed the complete resolution of previously reported DWI abnormalities. The third MRI, at 72 hours, revealed bilateral symmetric hyperintensity on T2-weighted imaging in the middle cerebellar peduncle, nucleus caudatus, putamen and periventricular white matter. DWI showed low ADC values in both globus pallidus. Single-voxel H-MRS revealed higher than normal GABA and glutamine in nucleus lenticularis. Four weeks after first neuroimaging, MRI revealed widespread atrophy and high T2 in both globus pallidus. DWI did not reveal any notable signal abnormality and ADC was normal. Single-voxel MRS showed normalization of GABA and glutamine.
Results
MCAD usually appears acutely and has high morbidity-mortality rates; early diagnosis is therefore important to promptly begin treatment. Furthermore genetic counseling may provide useful information to prevent triggering events and assess genetic risk to siblings.
Conclusion
In our opinion the case described has several interesting aspects: - It demonstrates the role of MRI in early diagnosis of the decompensated state of the disease; in

Note: Scanned images are included in the proceedings. Some submitted images were reduced during editing, thereby decreasing clarity. Also, refer to the Program Planner. Proceedings Content as of 3-29-2013.

our case DWI revealed bilateral symmetric distribution of lesions that strongly suggested a metabolic disease. - Ours and other recent studies demonstrate that acute hypoglycemia may cause bilateral lesions not only in gray matter areas that are known to be more susceptible to injury, but also in white matter locations. - Severe hypoglycemia may cause reversible restricted diffusion that could be pathogenetically different from the irreversible cell necrosis observed in ischemia.

KEYWORDS: Metabolic, MR diffusion, MRS

eP-217

Proton MR Spectroscopy of the Brain in Children with Neuronopathic Gaucher Disease

Abdel Razek, A.·Abdalla, A.·Abdel Gaber, N.·Megahed, A.·Fathy, A.·Barakat, T.
Mansoura University Hospital
Mansoura, EGYPT.

Purpose
To assess the clinical usefulness of proton MR spectroscopy (1H-MRS) in children with neuronopathic Gaucher disease (NGD).
Materials & Methods
Prospective study was conducted upon 21 consecutive children with acute (n = 6) and chronic (n = 15) forms of NGD (14 boys, seven girls age range from 7 months to 72 months: mean 45 months) and for age- and sex-matched control group (n = 15). All patients and controls underwent single voxel 1H-MRS of the frontal white matter using short and intermediate TE (30 and 135 ms). The integrals of choline (Ch), creatine (Cr), myoinsoitol (mI) and lipid were assigned. The mI/Cr, Ch/Cr were calculated. The modified severity scoring tool (m-SST) of NGD was calculated and genotyping was performed for all patients. The metabolites correlated with clinical types, m-SST and genotyping.
Results
There was significant difference in Ch/Cr (P = 0.001) and mI/Cr (P = 0.001) between patients with NGD and control group. Lipid peak was detected in 14 patients with NGD. Patients with acute NGD revealed higher m-SST (P = 0.001), Ch/Cr (P = 0.001) and mI/Cr (P = 0.001) compared to the chronic form. Patients with homozygous gene mutation (L444P/L444P) mutation had significantly higher m-SST (P = 0.001), Ch/Cr (P = 0.001) and mI/Cr (P = 0.001) than those with heterozygous gene mutation (L444p/D409H). The Ch/Cr ratio was well correlated with m-SST (r = -0.727; P = 0.001) and genotying (r = -0.727; P = 0.001).
Conclusion
We concluded that 1H-MRS may be used to detect brain abnormalities in children with NGD and Ch/Cr and mI/Cr are well correlated with m-SST and genotyping.

KEYWORDS: MR spectrocopy

eP-218

Role of Contrast-Enhanced Brain and Spinal MR Imaging in Metachromatic Leukodystrophy

Alkan, O.·Saygi, S.·Pekoz, B.·Altinkaya, N.·Demir, S.
Baskent University
Adana, TURKEY.

Purpose
To present contrast-enhanced brain and spinal MR imaging findings a patient with metachromatic leukodystrophy (MLD).
Materials & Methods
Five-year-old female child presented with walking and speech disorders. The patient underwent contrast-enhanced brain MR, diffusion MR, MR spectroscopy and contrast-enhanced lumbar spine MR imaging.
Results
T2-weighted image of the brain showed abnormal hyperintensity in the deep and periventricular white matter and posterior limbs of the internal capsules. Diffusion-weighted imaging showed decreased water diffusivity in affected regions. Postcontrast T1-weighted image of the brain showed enhancement of the cranial nerves (Figure 1a, b). Postcontrast T1-weighted image of the lumbar spine displayed enhancement of the cauda equina (Figure 2). MR spectroscopy showed decreased N-acetylaspartate and elevated lactate.

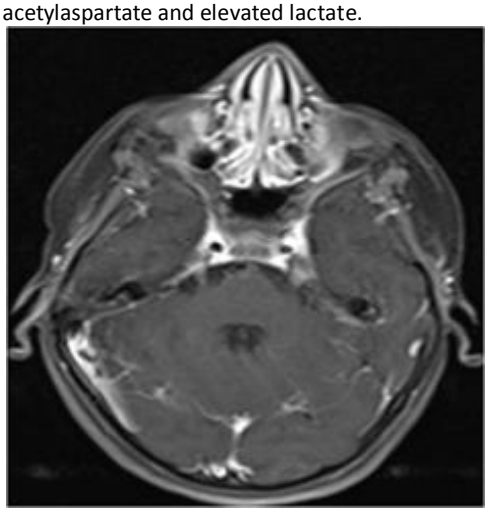

Note: Scanned images are included in the proceedings. Some submitted images were reduced during editing, thereby decreasing clarity. Also, refer to the Program Planner. Proceedings Content as of 3-29-2013.

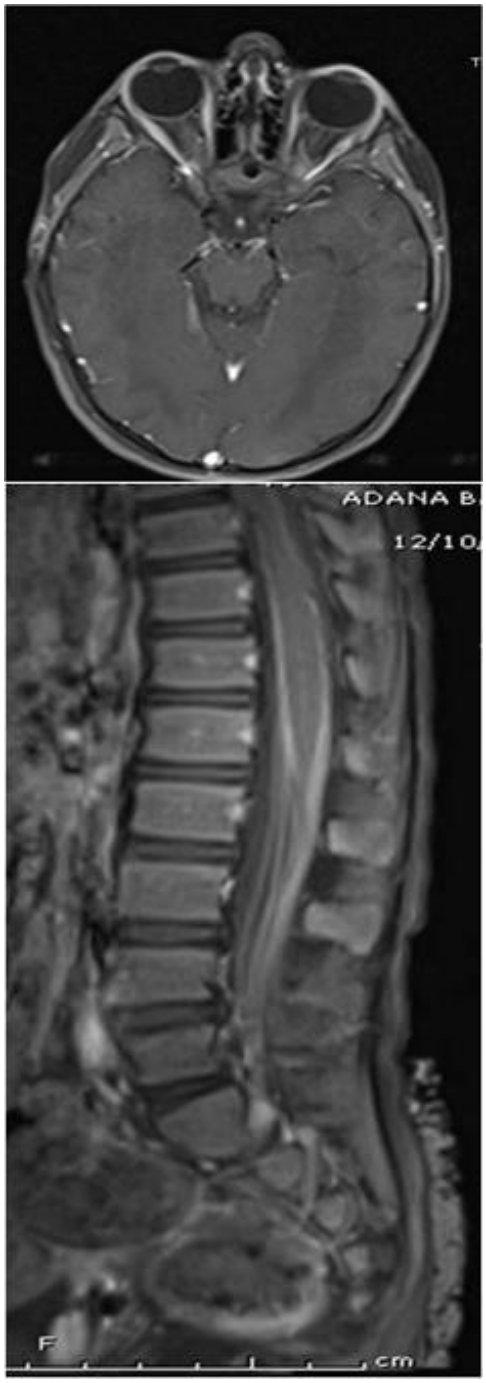

Conclusion
Metachromatic leukodystrophy is one of the more common leukodystrophies with well documented white matter findings. However, involvement of the cranial nerves and cauda equina on MR images are being reported only recently. The contrast enhancement of cranial nerves and cauda equina may accompany the white matter findings of MLD. Contrast-enhanced brain and spinal MR imaging may prove useful in diagnosing or differentiating the various leukodystrophies.

KEYWORDS: Contrast-enhanced MR imaging, Spinal imaging, metachromatic leukodystrophy

eP-219

Focal Cortical Dysplasia in Children and Adolescents: MR Features and Related Clinical Outcomes

Cheon, J.·Choi, Y.·Kim, I.·Kim, W.
Seoul National University
Seoul, KOREA, REPUBLIC OF.

Purpose
To analyze MRI features of children and young adolescents with focal cortical dysplasia (FCD) in order to identify predictive factors for clinical outcomes.
Materials & Methods
From January 2005 to March 2012, 372 children and young adolescents with partial or secondary generalized seizure had MRI performed using 1.5T or 3.0T MR equipment in our hospital. Among them, 76 patients with one identified area of seizure onset zone on MRI which correlated with clinical history, seizure semiology, EEG abnormalities or other imaging modalities were included in our study. Other patients with negative MRI findings, multiple epileptogenic lesions or other epileptogenic lesions such as tumor were excluded from our study. We evaluated cortical and subcortical signal abnormalities on T2-weighted image (T2WI), blurring of gray-white matter junction, thickening of the cortex, abnormal deep sulci or transmantle sign. More than 2 years free of seizures was defined as a good prognosis. We compared clinical features, seizure history and MR features between refractory group and two-year seizure-free group.
Results
Twenty-four patients had more than 2 years free of seizures suggesting good prognosis while 52 patients had refractory seizure. MR findings were subcategorized into four groups: predominantly involved subcortical white matter with hyperintensity on T2WI (n = 23), localized cortical thickening with deep sulci (n = 21), diffuse cortical abnormality with hyper or isointensity on T2WI (n = 24), diffuse cortical abnormality with hypointensity on T2WI (n = 8). Patients with both cortex and white matter abnormalities (p = 0.028), hypointensity of the involved cortex (p = 0.01), and hyperintense subcortical WM abnormalities (p = 0.028) showed poor clinical outcome.

Note: Scanned images are included in the proceedings. Some submitted images were reduced during editing, thereby decreasing clarity. Also, refer to the Program Planner. Proceedings Content as of 3-29-2013.

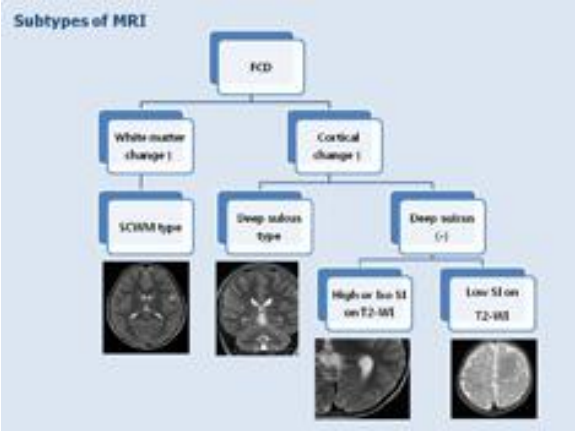

Conclusion
This study suggests that hypointensity on involved cortex on T2WI or concurrence of cortical and white matter abnormalities may be related to poor clinical features in patients with FCD.

KEYWORDS: Focal cortical dysplasia, MR imaging brain

eP-220

Ictal Hippocampal Metabolism in Experimental Prolonged Febrile Seizures

Clerk-Lamalice, O.[1]·Carmant, L.[2]·Lepage, M.[3]·Lecomte, R.[3]
[1]University of Sherbrooke, Sherbrooke, QC, CANADA, [2]Sainte-Justine Research Center - University of Montreal, Montreal, QC, CANADA, [3]Sherbrooke Molecular Imaging Center - University of Sherbrooke, Sherbrooke, QC, CANADA.

Purpose
Febrile seizures (FS) are the most common type of benign convulsions observed in young children. On the other hand, retrospective studies have demonstrated that candidates to temporal lobe epilepsy (TLE) surgery had higher prevalence of FS in childhood. Also, many patients with TLE and mesial temporal sclerosis have cortical dysplasia (CD). However, the link between CD, atypical FS and TLE remains unclear. Studies from our group demonstrated long-term hippocampal injury in animals with experimental CD and FS. In this study, we investigate ictal epileptic activity assessed by [18F]-FDG PET in a FS experimental rat model.
Materials & Methods
Ten male Sprague-Dawley rat pups were divided into four groups: naïve controls(NC, n=2), hyperthermic seizures controls (HSC, n=2), freeze-lesion controls (LC, n=2) and freeze-lesion pups with hyperthermic seizure(LHS, n=4). A freeze lesion was induced on the right frontoparietal cortex to mimic CD at postnatal day one (P1). At P10, [18F]-FDG was injected intraperitoneally(26.5±5.0 MBq). Animals then were placed in a box heated with warm dry air and removed after three minutes of generalized seizure. PET images then were acquired under anesthesia with a LabPET4 small animal scanner for a period of 60 minutes. Manual delimitation of the hippocampus, olfactory bulb, frontoparietal cortex, striatum, thalamus, brainstem and cervical spinal cord was performed with the help of an atlas using inhouse software. [18F]-FDG uptake ratios in each brain structure were calculated relative to the spinal cord uptake values. Statistical analysis between groups for each structure was performed with ANOVA Tukey posthoc test with p=0.05.
Results
Ictal [18F]-FDG uptake increased statistically between groups for all structures studied except in the hippocampus (Figure).

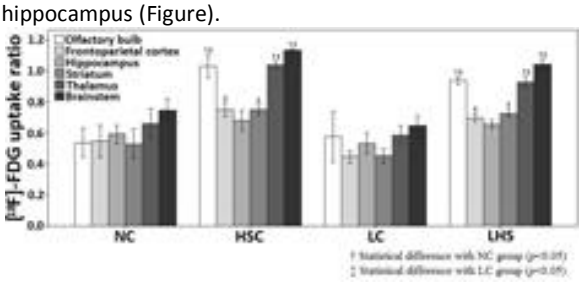

Conclusion
Interestingly, the absence of [18F]-FDG increase uptake in the seizing hippocampus is paradoxical. It has been demonstrated that hyperthermia-induced seizures have their onset and persist in limbic structures. Thus an increase uptake in this region was expected. Low brain protein expression of GLUT1 and GLUT3 and a failure of perfusion adaptation in the hippocampus secondary to inhomogeneous vascular bed may be the cause of an hypoxic-metabolic mismatch. CD did not play a role in this study probably because of the fixed length of generalized seizures for LHS and HSC groups. With nonsustained seizures, previous results showed that LHS rats have longer and more severe convulsions. These convulsions could be prone to hypoxic-metabolic mismatch and explain subsequent hippocampal atrophy, cognitive deficits as well as spontaneous recurrent seizures seen in LHS rats only.

KEYWORDS: PET, Epilepsy, febrile seizures

eP-221

Feasibility of Neonatal Thalamic Parcellation Based on Probabilistic Neocortical Connections

de Macedo Rodrigues, K.[1]·Ben-Avi, E.[2]·Choe, M.[1]·Drottar, M.[1]·Grant, P.[1]·Zöllei, L.[2]
[1]Children's Hospital Boston, Boston, MA, [2]A.A. Martinos Center for Biomedical Imaging/Massachusetts General Hospital, Boston, MA.

Purpose
The thalamus has a crucial role in integrating motor and somatosensory systems and special attention has been

Note: Scanned images are included in the proceedings. Some submitted images were reduced during editing, thereby decreasing clarity. Also, refer to the Program Planner. Proceedings Content as of 3-29-2013.

given to its significance in cognition. Comprehension of the normal thalamic structural and functional development could have a significant impact on our understanding of the thalamic physiology, how it is related to different brain areas. It also would be important as a reference when studying how the thalamus and its connections are affected in pathologic states. The purpose of this preliminary study is to provide a parcellation of the thalamus in clusters derived from thalamic connections to predefined neocortical targets determined by probabilistic diffusion tractography in a neonatal population. We anticipate that these clusters will retain an anatomical and functional correspondence to known thalamic nuclei. This approach has been demonstrated successfully previously for the adult population.

Materials & Methods

We selected magnetic resonance imaging (MRI) scans from five term neonates, whose study included three-dimensional multiecho magnetization-prepared rapid gradient-echo imaging with motion correction and diffusion tensor imaging (DTI) with 30 noncollinear directions and 5 low b-values. All scans were acquired in a 3T system with a 32-channel adult head coil. All the studies were interpreted as normal by a pediatric neuroradiologist. Tools from the FSL library were used to run probabilistic diffusion tractography. The thalamus was defined as seed region and pre-established neocortical areas were target regions. These comprised of the prefrontal cortex, premotor and primary motor areas, the somatosensory area, the posterior parietal cortex, as well as the occipital and temporal lobes. The seed and target areas were segmented manually using Freeview (http://surfer.nmr.mgh.harvard.edu/FreeviewGuide).

Results

We were able to regularly identify five main clusters for the thalamus, with the exception of the left thalamus in one subject, where four clusters were recognized. The identified clusters appear to bear anatomical and functional correspondence to the thalamic nuclei groups mediodorsal, ventral anterior and lateral, ventral posterior, pulvinar and geniculate bodies.

Conclusion

Our preliminary results suggest that parcellation of the neonatal thalamus based on neocortical connections obtained from probabilistic tractography is viable. We plan to expand the number of subjects studied, age range of subjects and compare normal development to pathologic states.

KEYWORDS: Thalamic, Probabilistic, parcellation

eP-222

Diffusion Tensor Imaging in Pediatric Hypertrophic Olivary Degeneration

Meoded, A.·Poretti, A.·Jallo, G.·Burger, P. C.·Huisman, T. A. G. M.·Izbudak, I.
Johns Hopkins Hospital
Baltimore, MD.

Purpose

The Guillain-Mollaret triangle (GMT) or dentato-rubro-olivary pathway is a functional brain stem neurologic circuit. The triangle consists of 1) olivary-dentato fibers from the hilum of one inferior olivary nucleus (ION) crossing the midline and traversing the inferior cerebellar peduncle (ICP) of the contralateral side to reach the contralateral dentate nucleus, 2) dentato-rubral fibers arising from the contralateral dentate nucleus, entering their own superior cerebellar peduncle (SCP) and decussating within the midbrain to reach the opposite red nucleus and 3) the ipsilateral central tegmental tract (CTT) or rubro-olivary tract descending from the red nucleus to the original ION. Disruptive lesions affecting components of the GMT may result in hypertrophic olivary degeneration (HOD). We present diffusion tensor imaging (DTI) findings in a six-year-old girl with HOD. To our knowledge, this is the first dedicated DTI analysis of the GMT in a child with HOD.

Materials & Methods

A six-year-old girl presented with a subtle intention tremor of the left hand three months after neurosurgical resection of a midbrain pilocytic astrocytoma. Brain MRI was performed three months after neurosurgery on a 1.5T scanner. Diffusion tensor imaging data were acquired with a single-shot, spin-echo, echo-planar (EPI) sequence. Balanced pairs of diffusion gradients were applied along 21 directions using *b*-values of 0 s/mm^2 and 1000 s/mm^2. Diffusion tensor imaging postprocessing was performed off-line using MRI Studio software. Regions of interest (ROIs) were manually positioned bilaterally within the ION, ICP, dentate nucleus, SCP, and red nucleus. For every ROI, calculated fractional anisotropy (FA), mean diffusivity (MD), axial (AD) and radial (RD) diffusivity values were collected. For the purpose of statistical analysis, the same DTI postprocessing was performed for three age/gender-matched children with normal neurologic exam and normal brain MRI.

Results

In our patient, conventional MRI demonstrated a T2-hyperintense signal in both IONs (more pronounced on the right side) and the right ION was slightly enlarged suggesting bilateral HOD. Follow-up MRI five months later, revealed increased T2-hyperintensity of both IONs and enlargement of the right ION. Diffusion tensor imaging analysis revealed higher FA and AD values of the ION and lower FA, but higher RD values of all other GMT components compared to age- and gender-matched controls.

Note: Scanned images are included in the proceedings. Some submitted images were reduced during editing, thereby decreasing clarity. Also, refer to the Program Planner. Proceedings Content as of 3-29-2013.

Conclusion
Diffusion tensor imaging analysis of the various components of GMT in pediatric HOD correlates with histopathologic findings. Increased FA values of the ION may be explained by increased packing of white matter fibers. However, associated hyperintense T2 signal is contradictory and the association between increased FA values and hyperintense T2 signal remains unclear. Low FA and high RD values of the other GMT components likely reflect additional demyelination associated with axonal degeneration. Selective evaluation of AD and RD may help to differentiate between the various components of myelin and axonal degeneration in HOD.

KEYWORDS: DTI, Pediatric brain, brain stem

eP-223

Role of Screening Sinus CT in Pediatric Hematopoetic Stem Cell Transplant Patients

Oppenheimer, A. G.[1]·Dave, H.[2]·Symons, H.[3]·Huisman, T. A. G. M.[3]·Izbudak, I.[3]
[1]Cleveland Clinic Florida, Weston, FL, [2]Children's National Medical Center, Washington, DC, [3]Johns Hopkins Hospital, Baltimore, MD.

Purpose
Purpose of this investigation is to evaluate the role of screening sinus CT prior to hematopoetic stem cell transplantation(HSCT) as a predictor of developing post-HSCT sinusitis and as a baseline examination from which to compare post-HSCT scans. Furthermore, we correlate CT findings with the presence of acute clinical sinusitis in this unique immunocompromised pediatric population.
Materials & Methods
Medical records and CT scans of 100 consecutive pediatric patients who received a screening sinus CT prior to HSCT at Johns Hopkins Hospital from 2006-2010 were reviewed. Seventy of these patients had a sinus CT following transplantation. Pre- and post-HSCT sinus disease was evaluated using two methods:a quantitative scoring system established by Lund and Mackay(LM) and the "common-practice" radiology reporting of sinusitis based on the presence of air fluid levels, frothy secretions or total opacification of any individual sinus.
Results
Overall, nine patients had clinical sinusitis pre-HSCT while 18 patients developed sinusitis post-HSCT. Fourteen percent of patients with normal screening sinus CT subsequently developed clinical sinusitis post-HSCT compared with 23% of asymptomatic patients with radiographic abnormalities alone and 22% of patients with clinical sinusitis(Table1). This higher rate of developing post-HSCT sinusitis was not statistically significant(p=0.20). Furthermore, subgroup analysis of patients with abnormal scans stratified by LM score(mild/moderate/severe) or the presence of particular "common-practice" findings also was not found to be significantly different(p=0.58). The PPV of having acute clinical sinusitis for a given radiographic abnormality was highest for total sinus opacification(56%), frothy secretions(53%), and fluid levels(47%) and lowest for mucosal thickening alone(13%). PPV was even greater(67%) with the combined presence of at least two abnormalities(fluid level, frothy secretions or total sinus opacification)(Table2). Using the screening sinus CT as a baseline examination, a significant difference was found in LM score change from baseline between patients who did and did not develop post-HSCT clinical sinusitis(10.4 vs. 4.2 p=<0.001). Furthermore, patients with a change in the LM score≥10 were 2.77 times more likely to have clinical sinusitis(CI:1.32-5.81).

Development of Post-HSCT Clinical sinusitis

Pre-HSCT CT findings	No. of patients	Post-HSCT sinusitis	%
Normal	***56***	***8***	***14***
Radiographic abnormalities alone			
Total	***35***	***8***	***23***
Mild Lund-Mackay	25	6	24
Mod/Severe Lund-Mackay	10	2	20
Mucosal disease alone	19	5	26
Fluid level/frothy secretion/total opacification	16	3	19
Clinical Sinusitis	***9***	***2***	***22***
Total	100	18	18

Note: Scanned images are included in the proceedings. Some submitted images were reduced during editing, thereby decreasing clarity. Also, refer to the Program Planner. Proceedings Content as of 3-29-2013.

Correlation of CT findings with clinical sinusitis in pediatric oncology patients

CT Finding	Sensitivity	Specificity	PPV	NPV
Mucosal thickening alone	19	71	***13***	78
Fluid level	26	94	***47***	87
Frothy secretion	37	94	***53***	89
Total-near total opacification	56	92	***56***	92
Multiple abnormalities	37	97	***67***	89

Conclusion
Neither the presence nor the severity of pre-HSCT radiographic sinus disease was found to significantly correlate with the development of clinical sinusitis later in the post-transplant period. However, Pre-HSCT CT scans can serve as a baseline from which subsequent scans may be compared--with LM score change≥10 a significant threshold. Radiographic findings of total sinus opacification, frothy secretions, or fluid levels have the strongest correlation with the presence of acute clinical sinusitis and may prompt further clinical workup.

KEYWORDS: Sinonasal disease, Pediatric head and neck,

eP-224

Concomitant Meningioma and Glioma within the Same Optic Nerve in Neurofibromatosis Type 1

Akça, A.·Büyükkapu Bay, S.·Karadoğan, M.·Çorapçıoğlu, F.·Anik, Y.
Kocaeli University School of Medicine
Kocaeli, TURKEY.

Purpose
We aimed to present an extraordinary case of neurofibromatosis type 1 with concomitant meningioma and glioma in the same optic nerve.
Materials & Methods
A 4-year-old boy was admitted to our hospital with right-sided proptosis. We performed ophthalmologic examination, physical examination and magnetic resonance imaging (MRI).
Results
Physical examination revealed numerous cafe-au-lait macules, axillary freckling and right-sided proptosis. On MRI a mass originating from the right optic nerve sheath with normal appearance of the optic nerve was observed which was consistent with optic nerve sheath meningioma. Another mass lesion was observed in the prechiasmatic region of the same optic nerve which was consistent with optic nerve glioma. Ophthalmologic examination revealed no abnormality.

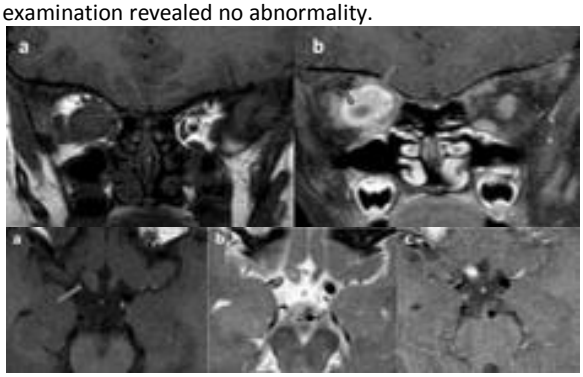

Conclusion
Neurofibromatosis type 1 is an inherited tumor predisposition syndrome. Diagnosis can be made using the National Institutes of Health diagnostic criteria. These patients are prone to developing both peripheral and central nervous system tumors. Gliomas are the most common primary central nervous system tumors that especially are seen in the optic pathways in children. MR imaging is an excellent method of choice in the followup of patients with neurofibromatosis, as well as detecting lesions in asymptomatic patients. The diagnosis of an optic nerve glioma and optic nerve sheath meningioma can be confirmed by computed tomography or magnetic resonance imaging. Two different types of optic pathway tumors in the same optic nerve is an extraordinary case. It is important to recognize imaging findings of these tumors and make correct diagnosis because the treatments differ between these two tumors.

KEYWORDS: Neurofibromatosis, Nerve sheath tumor, optic glioma

eP-225

Atypical Characteristics and Behavior of Dysembryoplastic Neuroepithelial Tumors

Daghistani, R.[1]·Miller, E.[2]·Kulkarni, A.[3]·Widjaja, E.[3]
[1]University of Toronto, Toronto, ON, CANADA, [2]Children's Hospital for Eastern Ontario, Ottawa, ON, CANADA, [3]Hospital for Sick Children, Toronto, ON, CANADA.

Purpose
Dysembryoplastic neuroepithelial tumors (DNET) classically are considered as benign, cortically based tumors that are stable. However, there were case reports that suggest DNET may not be as benign as previously thought of. The purpose of our study was to identify atypical location, characteristics and behavior of DNET in children.
Materials & Methods

Note: Scanned images are included in the proceedings. Some submitted images were reduced during editing, thereby decreasing clarity. Also, refer to the Program Planner. Proceedings Content as of 3-29-2013.

The MRI images of 51 patients with pathologically proven DNETs, were reviewed retrospectively. The following were assessed: tumor location, neuroimaging appearances including hemorrhage, calcification and edema, tumor growth preoperatively and after subtotal resection, tumor recurrence, malignant transformation and metastatic seeding.

Results

Two (3.9%) patients had intraventricular lesions, three (5.9%) had associated edema, three (5.9%) had calcifications and one (2%) had hemorrhage on preoperative CT and MRI. Sixteen of 51 (31.4%) of the lesions exhibited enhancement postgadolinium administration. Six of 29 (20.7%) of the preoperative lesions that had follow-up imaging were enlarging prior to surgery. In six of 18 (33.3%) with subtotal resection, there was an increase in size of the residual tumor. Tumor recurrence at the surgical bed occurred in three of 30 (10%) patients who had gross total resection. Two of 51 (3.9%) cases developed secondary lesions distant to the primary tumor, the secondary lesions were within the lateral ventricles.

Conclusion

In children, DNETs may have atypical location, characteristics and behavior, including growth of primary or residual lesions and multifocal tumor. These findings emphasize the need for followup of patients with DNET postresection.

KEYWORDS: Dysembryoplastic neuroepithelial tumor, recurrence

eP-226

Measurements of Normal Inner Ear in Children with Congenital Sensorineural Hearing Loss and a "Normal Temporal Bone CT Scan"

Bahador, F.·Darke, M.·Nabi, J.·Fallahian, A. H.
University of Missouri Health Care
Columbia, MO.

Purpose

Using standardized measurements of the inner ear to see whether there are subtle bony malformations in children with congenital sensorineural hearing loss whose temporal bone computed tomography are grossly normal.

Materials & Methods

IRB approval was obtained. Medical records and the pure-tone audiometric results of 339 patients, diagnosed with sensorineural hearing loss in our tertiary referral center were reviewed. Children with perinatal infections were excluded from the study. The high-resolution temporal bone CT scans of the remaining 112 patients were reviewed retrospectively. Patients with cochlear, labyrinthine, aqueductal or IAC anomalies also were excluded. Fifty-six patients with 90 ears, and grossly normal temporal bone CT scans met the eligibility criteria. The control subjects, who included 55 patients with 90 ears, had undergone CT for the evaluation of cholesteatoma, mastoiditis, external ear disease or trauma. The CT scans of the SNHL and the control groups were performed between June 2004 and September 2011 and between September 2005 and August 2011, respectively. Two readers including a PGY-4 radiology resident and a radiologist with 11 years experience who did not have any knowledge of the other reader's interpretations or audiometric results reviewed all CT scans independently. Standardized measurements including maximal height and length of cochlea and vestibule, canal lumen width and bony island width of superior semicircular canal (SSCC) and lateral semicircular canal (LSCC), canal lumen width and inferior limb length of posterior semicircular canal (PSCC) were made on axial and coronal CT images. Correlation was made with short and long axes to avoid error in measurements.

Results

Student's *t*-test was performed to compare the measurements of the two groups. Significant difference was noted only in width of the posterior semicircular canal between the SNHL and control groups for one of the readers, with a narrow margin of accuracy. No significant difference was noted in other nine measurements.

	Reader 1					Reader 2				
	SNHL		Control		*t* test	SNHL		Control		*t* test
	Mean (mm)	SD (mm)	Mean (mm)	SD (mm)	*P* value	Mean (mm)	SD (mm)	Mean (mm)	SD (mm)	*P* value
Cochlea length	8.88	0.54	8.86	0.55	0.84	8.77	0.76	8.8	0.56	0.74
Cochlea height	4.41	0.32	4.37	0.33	0.52	4.49	0.4	4.53	0.37	0.45
LSCC bony width	3.58	0.47	3.55	0.48	0.65	4.01	0.48	3.9	0.48	0.13
LSCC lumen width	1.34	0.14	1.3	0.15	0.14	1.33	0.17	1.3	0.14	0.21
PSCC inf. limb length	7.34	0.6	7.19	0.56	0.1	7.11	0.64	7.02	0.72	0.41
PSCC lumen width	1.06	0.17	1.01	0.16	0.04*	1.11	0.13	1.1	0.14	0.37
SSCC bony width	5.16	0.47	5.22	0.53	0.4	5.05	0.54	5.04	0.56	0.89
SSCC lumen width	1.02	0.12	1.1	0.85	0.41	1.17	0.16	1.17	0.17	0.99
Vestibule length	5.78	0.4	5.74	0.79	0.65	6.13	0.38	6.07	0.43	0.59
Vestibule width	3.3	0.3	3.39	0.64	0.2	3.5	0.31	3.54	0.36	0.41

	SNHL	Control
No.	55 Patients - 90 Ears	56 Patients - 90 Ears
Age range	5 months -16 years, 10 months	5 months -17 years, 10 months
Mean age	7 years and 11 months	8 years and 10 months

Conclusion

Current study does not support application of CT scan as a standard tool for measurements of bony labyrinth of inner ear to identify subtle abnormalities of inner ear in patients with proven congenital sensorineural hearing loss. Larger multicenter studies might be required to elucidate.

KEYWORDS: Sensorineural hearing loss, CT, inner ear

Note: Scanned images are included in the proceedings. Some submitted images were reduced during editing, thereby decreasing clarity. Also, refer to the Program Planner. Proceedings Content as of 3-29-2013.

eP-227

Diffusion-Weighted Imaging of Fetal Head, Neck and Spine Tumors

Mignone Philpott, C.[1]·Shannon, P.[2]·Ryan, G.[2]·Chitayat, D.[2]·Blaser, S.[1]
[1]Hospital for Sick Children, Toronto, ON, CANADA, [2]Mount Sinai Hospital, Toronto, ON, CANADA.

Purpose
Diffusion-weighted imaging can be used to characterize tumors of the head, neck and neural axis given its ability to assess the relative motion of molecules within tissue and hence degree of cell density and presumed tissue differentiation. The tumor cell type, for example, lymphoma versus carcinoma and degree of differentiation can also be inferred. MR imaging is used increasingly for better differentiation of sonographically detected tumors in the fetus, to assist in diagnosis and subsequent management. We sought to evaluate the potential utility of diffusion-weighted imaging in characterizing tumors of the head and neck in the fetus.
Materials & Methods
We identified fetuses who had MR imaging performed to evaluate a mass in the head, neck or spine in our institution over the last five years. The imaging was reviewed retrospectively with specific note made of T2, T1 signal characteristics, presence of signal drop on susceptibility-weighted sequences, size and location of the tumor. A region of interest within the tumor was drawn for assessment of ADC value. All follow-up imaging and pathology was reviewed, including postnatal biopsies and autopsies in cases where there had been termination. The ADC values of these masses were charted to see if there was any relationship between etiology and malignant potential and ADC values.
Results
There were 15 fetuses in total, 10 of whom had a pathology diagnosis, three who had postnatal MRI confirming the diagnosis and two others who were lost to postnatal followup. Three patients had a sacrococcygeal teratoma, two predominantly cystic with mature elements, the other immature, two had sarcomas: infantile hemangiopericytoma and infantile myofibromatoma, two, heterotopia, one, encephalomalacia postinfarction, another hematoma, and two, posterior fossa cystic lesions. The benign posterior fossa cystic lesions, encephalomalacia, cystic teratomas and vascular/lymphatic malformations all exhibited ADC values at least 1000 x 10-6mm2/s higher than the immature teratoma, sarcomas and the medulloblastoma (Figure 1). The T2 and SWI sequences help differentiate the heterotopic brain and hematoma from the latter cellular tumors.

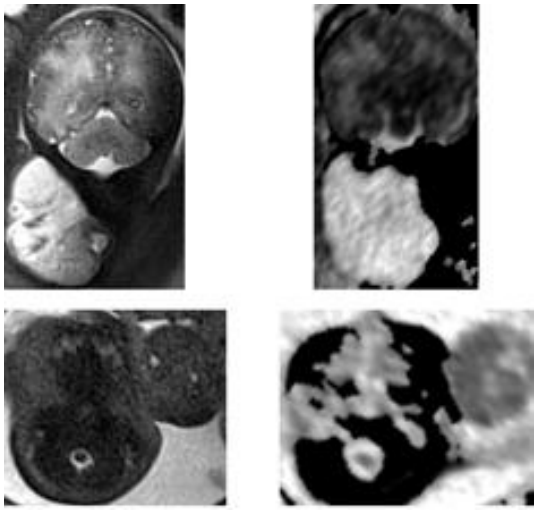

Conclusion
Apparent diffusion coefficient assessment, together with traditional MR sequences and SWI, appears to be a potentially useful tool in differentiating benign from potentially malignant neural axis masses in the fetus.

KEYWORDS: Fetal MR imaging, Masses, head, neck, spine

eP-228

Radiologic Approach to Pediatric Cervical Spine Trauma

Chopra, P. R.·Srivastava, V.·Halpin, J. S.
University of Missouri Kansas City
Kansas City, MO.

Purpose
Although cervical spine trauma is a rare occurrence in children it has the potential for severe neurologic consequences. However, if accurately diagnosed and managed, it is possible to minimize the extent of damage. This presentation will focus on the various types of cervical spine trauma and their characteristics and how to accurately diagnose cervical spine trauma in children by employing aspects of clinical history, physical examination, and appropriate imaging techniques. Our goal is to emphasize specific imaging studies that are the best tools for diagnosing cervical spine trauma, while also minimizing the amount of radiation exposure to our pediatric patients. Lateral radiographs are the initial radiographic study to screen for cervical trauma in children. When no significant finding is noted and no further clinical concern persists, no further radiographic evaluation is necessary. However, if clinical concern is present, MRI or flexion/extension radiographs are recommended.

KEYWORDS: Cervical

Note: Scanned images are included in the proceedings. Some submitted images were reduced during editing, thereby decreasing clarity. Also, refer to the Program Planner. Proceedings Content as of 3-29-2013.

eP-229

Delta Wave Detection in Magnetoencephalographic Data of High School Football Players

Davenport, E. M.[1]·Urban, J. E.[2]·Whitlow, C. T.[1]·Powers, A.[1]·Thompson, M. M.[2]·Rawley, J.[1]·McGowin, I.[2]·Alberto, G.[2]·Bungo, T.[2]·Godwin, D.[2]·Stitzel, J. D.[2]·Maldjian, J. A.[1]
[1]Wake Forest University School of Medicine, Winston-Salem, NC, [2]Wake Forest University, Winston-Salem, NC.

Purpose
The Head Impact Telemetry (HIT) system records kinematic data from impacts received from an encoder unit installed in player helmets during football practices and games. Magnetoencephalography (MEG) is a noninvasive form of functional brain imaging that is used to further understand brain function. Injured neural tissue can produce low-frequency magnetic signals (delta waves), which can be detected using advanced processing of MEG data. The purpose of this study is to determine if high numbers of impacts experienced in a season of high school football are associated with detectable changes in MEG delta waves.
Materials & Methods
An institutional ethics committee approved this study. The total number of head impacts of 18 normal male subjects aged 16-18 years were recorded over a football season using the HIT system. Eight minutes of eyes-open, resting-state MEG data were acquired for each subject using a 275-channel CTF whole-head system pre and postseason. In addition, structural anatomical MRI was acquired using a 3T Siemens Skyra scanner with a 32-channel head coil. Using an in-house automated pipeline, MEG data were baseline corrected, band-stop filtered at 60Hz, down-sampled to 100Hz, and band-pass filtered to 1-4Hz (delta spectrum). Artifacts from head motion, and muscles were removed. Magnetoencephalography data then were projected into standard source space at 5 mm resolution using a scalar beamformer with leadfield correction for noise normalization. The time-course for each voxel then was divided into 2.5-second epochs with 50% overlap, and each epoch was fourier transformed. The average delta spectrum amplitude was recorded for each epoch, and averaged across epochs. The group mean and standard deviation of the 18 subject's preseason delta spectrum for each voxel were found, creating a control group. Subjects were separated into a high-impact group (>600 impacts, two subjects), and a low-impact group (~250 impacts, two subjects) based on the HIT data. Postseason delta band amplitudes were compared to the control group by calculating voxel-wise Z-scores for the high-impact and low-impact subjects.
Results
Figure 1 demonstrates the Z-score maps of these four subjects, thresholded at two standard deviations. The low-impact players have few areas of significant delta wave difference from the control group. The high-impact players have large areas of significant increases in delta waves, particularly parasagittally around the falx.

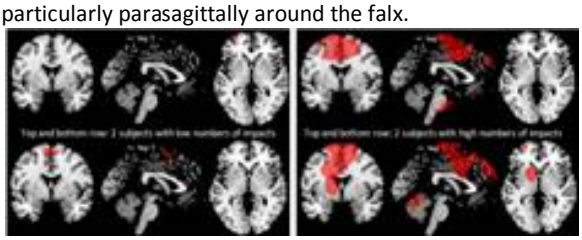

Conclusion
High school football players with a higher number of impacts per season may demonstrate functional changes in brain delta-wave activity that previously has been associated with head injury.

KEYWORDS: Concussion, MEG

eP-230

Prevalence of Subdural Collections in Children with Macrocrania

Richards, T.·Greiner, M. V.·Care, M.·Leach, J. L.
Cincinnati Children's Hospital Medical Center
Cincinnati, OH.

Purpose
To determine the prevalence of subdural collections (SDC) on cross-sectional imaging in children with macrocephaly correlating with subarachnoid space (SS) enlargement.
Materials & Methods
The radiology information system of a large pediatric medical center was reviewed for "macrocrania" and "macrocephaly" on reports of cranial MRI/CT examinations in children < 24 months of age, over a 24-month period. Head circumference (HC) was obtained from the clinical record. Studies were blind reviewed for: SDC presence and SS size. Children with prior cranial surgery, parenchymal abnormalities, hydrocephalus, or conditions predisposing to parenchymal volume loss were excluded. Chart review was performed on those with SDC.
Results
Imaging from 177 children with enlarged HC was reviewed. Nine were excluded for a final cohort of 168 subjects (108 with enlarged SS). Subdural collections were identified in six (3.6%), all with enlarged SS (6/108, 5.6%). In four, SDC were small, homogeneous, and not overtly hemorrhagic. In two cases, the collections were complex (septations or hemorrhage). Two children were reported as victims of child abuse (both with complex collections). No definitive etiology was established in the other cases.
Conclusion
The prevalence of SDC in imaged children with macrocrania is 3.6 %, all occurring in children with enlarged SS (6/108, 5.6%). Although limited by sample size, our results suggest that enlarged subarachnoid spaces are associated with some SDC in this cohort. Despite these findings, we feel strongly that every unexpected SDC in a young child, especially if complex in

Note: Scanned images are included in the proceedings. Some submitted images were reduced during editing, thereby decreasing clarity. Also, refer to the Program Planner. Proceedings Content as of 3-29-2013.

appearance, receive close clinical evaluation for underlying causes, especially abusive head trauma. Abbreviation Key: SS = subarachnoid spaces, SDH = subdural hemorrhage, SDC = subdural collections, CT = computed tomography, MRI = magnetic resonance imaging, HC = head circumference.

KEYWORDS: Subdural hemorrhage, Pediatric brain

eP-231

Minimizing Radiation Exposure in Evaluation of Pediatric Head Trauma: Utilization of Rapid MR Imaging

Ahmad, N.[1]·Patel, B.[1]·Hira, A.[2]·Jeevan, D.[1]·LeCompte, L.[1]·Mehta, H.[1]
[1]Westchester Medical Center, Valhalla, NY, [2]University of Pennsylvania, Philadelphia, PA.

Purpose
Among children who have sustained trauma, the central nervous system is the most commonly injured isolated system. Computed tomography (CT) has been the gold-standard of imaging for initial and follow-up evaluation of head trauma in the pediatric population. Given the rampant use of CT and the concern for radiation, the pediatric radiology community has been at the forefront of radiation dose reduction in CT, fluoroscopy and radiography. Recent studies have demonstrated utilization of a rapid MRI technique to minimize radiation. In an effort to reduce radiation exposure, we aim to demonstrate rapid magnetic resonance imaging as having equal and/or increased sensitivity compared to CT, for follow-up evaluation of extra-axial and/or intraparenchymal hemorrhage in pediatric patients who have sustained head trauma.
Materials & Methods
This is a retrospective case-control study reviewing imaging of patients who sustained head trauma at Westchester Medical Center from January 2010 through January 2012. The major inclusion criteria included patients who obtained an initial head CT and a follow-up rapid MRI. Our rapid MRI sequences include: axial echo-planar imaging (EPI) diffusion-weighted; axial EPI T2, axial turbo spin-echo T2; axial single-shot FLAIR; axial single-shot T2; and coronal turbo spin-echo T2-weighted. All imaging was blindly re-interpreted by a board-certified neuroradiologist for specific parameters including: extra-axial hemorrhage (epidural, subdural, subarachnoid, intraventricular); intraparenchymal contusion/shear injury; and skull fractures. The sensitivity and specificity of rapid MRI was calculated.
Results
There are a total of 49 pediatric patients (age range 0-19 years; 26 M and 23 F) who sustained head trauma. On average, the patients underwent a follow-up rapid MRI within 48 hours or less from time of initial head CT. Our results demonstrate that rapid MRI has a sensitivity of 94% and specificity of 93% for detection of extra axial hemorrhage. Rapid MRI is superior to CT in the detection of contusion/shear injury. In detection of calvarial fracture rapid MRI has a sensitivity of 72% and a specificity of 95%. Eight patients had hemorrhagic contusion and/or shear injury identified on follow-up rapid MRI but not on initial CT. Possible explanations for this include: rapid MRI is superior in detection of contusion/shear and/or contusions/shear injury may have developed in the interim time period between the CT and follow-up MRI.
Conclusion
MR imaging is an adequate examination for follow-up imaging in lieu of repeat CT in the management of acute traumatic brain injury in the pediatric population. Given the diminished sensitivity of rapid MRI in detection of fracture, it may not act as a replacement for initial CT examination.

KEYWORDS: Traumatic brain injury, MR imaging brain

eP-232

Role of Apparent Diffusion Coefficient Values in the Evaluation of Pediatric Head Injury: Abusive Head Trauma May Not Differ from Nonabusive Head Trauma

Siddiqui, A.·Ceschin, R.·Panigrahy, A.·Berger, R. P.·Zuccoli, G.
Children's Hospital of Pittsburgh
Pittsburgh, PA.

Purpose
Differences in the severity and mechanism of a traumatic brain injury suggest that the resulting biochemical response may differ. Apparent diffusion coefficient (ADC) changes in abusive head trauma (AHT) are usually felt to be at least in part secondary hypoxic-ischemic injury after apnea, hypotension, strangulation, or suffocation. To the contrary in nonabusive head trauma (NHT) changes in ADC values are reportedly associated with diffuse axonal injury (DAI). The purpose of this retrospective observational study is to investigate brain injuries on ADC MRI sequences in subjects with AHT and compare these findings with subjects with NHT.
Materials & Methods
This was an institutional board review protocol study of 88 patients. Excluding patients with a history of respiratory arrest/failure, cardiac arrest, profound hypotension before MR, left a NAT cohort of 25 patients with mean age of 5.89 months and AT cohort of 11 patients with a mean age of 12 months. First, ADC maps of the genu, splenium, caudate, thalamus and putamen were measured manually via a standard region of interest (ROI) through a DICOM receiver. Then whole brain ADC values were measured using Linux-based neuroimaging program software (FSL). Models were adjusted for age, age-squared and GCS.
Results
No structure or Glascow Coma Scale (GCS) factor held a p-value under 0.10. Thus, there was not a statistical difference between the two populations. For the AHT

Note: Scanned images are included in the proceedings. Some submitted images were reduced during editing, thereby decreasing clarity. Also, refer to the Program Planner. Proceedings Content as of 3-29-2013.

population, the ADC values (and standard deviations) were as listed: whole brain, 1.110 x 10^{-3} mm^2/s (194); genu, .974 x 10^{-3} mm^2/s (321); splenium, .890 x 10^{-3} mm^2/s (249); caudate, .968 x 10^{-3} mm^2/s (172); thalamus, .897 x 10^{-3} mm^2/s (147); and putamen, .963 x 10^{-3} mm^2/s (171). For the NHT population, the ADC values were as listed: whole brain, 1.084 x 10^{-3} mm^2/s (175); genu, .919 x 10^{-3} mm^2/s (236); splenium, .932 x 10^{-3} mm^2/s (252); caudate, .949 x 10^{-3} mm^2/s (173); thalamus, .916 x 10^{-3} mm^2/s (124); and putamen, .906 x 10^{-3} mm^2/s (176).

Conclusion

Our results displayed that ADC values between AHT and NHT do not differ. These findings suggest that ADC alone does not seem helpful in distinguishing AHT from NHT.

KEYWORDS: ADC, Pediatric brain, Abusive Head Trauma

eP-233

Automated Machine Learning Analysis of Systematic Radiologic Phenotyping in Diseases Associated with Intracranial Calcification

Stivaros, S. M.[1,2]·Mileva, R.[1]·Gledson, A.[1]·van der Knaap, M. S.[3]·Keane, J.[1]·Crow, Y.[1]·Livingston, J.[4]
[1]University of Manchester, Manchester, UNITED KINGDOM, [2]Royal Manchester Children's Hospital, Manchester, UNITED KINGDOM, [3]VU University Medical Center, Amsterdam, NETHERLANDS, [4]Leeds General Infirmary, Leeds, UNITED KINGDOM.

Purpose

Intracranial calcification (ICC) often is considered an epiphenomenon of low diagnostic specificity. It occurs in both acquired/genetic conditions and also may be seen in asymptomatic individuals. To our knowledge there has been no systematic modelling of the radiologic phenotypes associated with ICC. In the leukoencephalopathies such a strategy has enabled the characterization and earlier diagnosis of specific disorders and the identification of previously unrecognized diseases, which in turn has facilitated the identification of causative genes. We present a systematic language-based model for the radiologic phenotyping of ICC which, in combination with advanced machine learning techniques allows for automated diagnostic stratification, the performance of which exceeds that of individual experts alone.

Materials & Methods

Two hundred twenty-four CT scans from 184 patients were sent to our group for review due to our interest in ICC. Infective causes had been excluded prior to referral. A range of diagnoses were established after referral by a combination of radiologic, genetic and clinical assessment in 107 patients. In the remaining 77 cases the diagnosis remained unknown. By a process of iterative reporting a systematic language-based model of ICC appearances on CT was derived. This was used to capture the imaging appearances of all scans into a novel data-construct. Multiple data analysis techniques were applied to the imaging model including Automated Decision Tree analysis, Cluster analysis, Bayesian analysis and Support Vector Machine analysis. Diagnostic stratification was performed for AGS versus all other diagnoses as well as multiple stratifications including AGS vs Cerebroretinal Microangiopathy with Calcifications and Cysts (CRMCC) vs all other known vs all unknown diagnoses.

Results

The mean age of referred patients was 5.9 years with a median age of 1.33 years (range 0.02-59 years). The diagnostic accuracy of the referring centers was of the order of 26%. The systematic language-based radiologic phenotype model was comprised of a dataset of 80 binary nominal attributes. An Averaged One-Dependence Estimator performed best at classifying cases into either AGS versus all other diagnosis with a sensitivity of 87%, specificity of 90%, and area under ROC of 92%. For stratification into AGS vs CRMCC versus known versus unknown diagnoses a C4.5 algorithm with adaptive boosting yielded the best results with sensitivity and precision of 86% and ROC area of 93%.

Conclusion

Here we present data to illustrate that a systematic approach to the radiologic phenotyping of ICC with machine-learning analysis can yield significant improvements in radiologic diagnostic accuracy. Further work will include the integration of MRI data and a prospective analysis of diagnostic performance. Taken in clinical context such techniques allow for the identification of specific disorders associated with ICC. Whilst the number of pathognomonic patterns may be limited, we consider that this strategy will both aid the diagnosis of particular conditions, and allow for the exclusion of disorders incompatible with the observed neuroimaging pattern. Furthermore, new phenotypes may be identified and the underlying genetic basis may in the future be determined through the use of such methodologies.

KEYWORDS: Neurogenetics, Data mining

eP-234

Update on Neuroradiologic Findings in Aicardi-Goutières Syndrome: Expanding the Phenotype

La Piana, R.[1]·Orcesi, S.[2]·Olivieri, I.[2]·Crow, Y.[3]·Uggetti, C.[4]
[1]Montreal Neurological Institute, Montreal, QC, CANADA, [2]C. Mondino Neurological Institute, Pavia, ITALY, [3]University of Manchester, Manchester, UNITED KINGDOM, [4]San Carlo Borromeo Hospital, Milano, ITALY.

Purpose

Scientific understanding of Aicardi-Goutières syndrome (AGS) has increased dramatically in the last six years. Consequently, an increasing number of cases of AGS are being identified. The aim of our study was to review the neuroradiologic findings of AGS in light of recently acquired insights into disease pathogenesis and phenotype. In particular, our goals were: a) to verify the

Note: Scanned images are included in the proceedings. Some submitted images were reduced during editing, thereby decreasing clarity. Also, refer to the Program Planner. Proceedings Content as of 3-29-2013.

presence of neuroradiologic diagnostic criteria (leukodystrophy, atrophy, brain calcifications); b) to update the diagnostic neuroradiologic criteria by modifying the existing ones and/or by adding newly identified.
Materials & Methods
Patients were ascertained by referral to the C. Mondino Neurological Institute in Pavia, the International Aicardi-Goutières syndrome Association (IAGSA), and the Nuclease Immune Mediated Brain and Lupus-like conditions (NIMBL) project funded by the European Union (7th Framework Programme). The inclusion criteria were the following: genetic and/or clinical diagnosis of AGS; availability of at least one brain MRI study and one head CT scan of diagnostic image quality; availability of clinical information (age at onset, clinical presentation, clinical evolution, presence of extraneurologic features).
Results
We reviewed brain MRI and CT scans of 46 cases diagnosed with AGS. Of these, 36 had been reported in a previous study, whilst 10 cases (21.7%) were newly ascertained. In comparison to the previous reports, no new patterns of white matter alterations were observed. The two patterns (fronto-posterior gradient versus diffuse involvement) thus, are confirmed. In four cases with diffuse pattern, a relative sparing of the perirolandic region was defined. Brain calcifications were observed in all new diagnosed cases. Unusually, calcifications were limited to the cerebellar vermis in one subject with a clinical diagnosis of AGS (where genetic analysis of AGS1-6 was negative). In comparison to the previous reports, brain atrophy was not a relevant neuroradiologic finding in five new cases. New pathologic findings, not previously reported, were identified in the region of the basal ganglia in three patients (6.5%; 3/46), one with AGS1 mutation, two with AGS6.
Conclusion
Aicardi-Goutières syndrome was an underdiagnosed disease until the early 2000s. The availability of genetic testing, and the subsequent identification of new disease-associated genes, has led to a dramatic increase in the number of cases diagnosed since 2006. As a corollary of this, an expansion of the phenotype has been documented, both in clinical and neuroradiologic terms. We believe that the results of our study will prove helpful in directing diagnostic testing in patients with suspected AGS.

KEYWORDS: Leukodystrophy, Calcifications

eP-235

New Cerebellar Neuroimaging Findings in Mucopolysaccharidoses Types I and II

Alqahtani, E.[1]·Huisman, T. A. G. M.[1]·Boltshauser, E.[2]·Scheer, I.[2]·Güngör, T.[2]·Tekes, A.[1]·Maegawa, G. H.[1]·Poretti, A.[1]
[1]The Johns Hopkins University, Baltimore, MD, [2]University Children's Hospital of Zurich, Zurich, SWITZERLAND.

Purpose
The mucopolysaccharidoses (MPS) is a heterogeneous group of rare lysosomal storage diseases characterized by the accumulation of glycosaminoglycans. Common neuroimaging findings include enlargement of the perivascular spaces (PVS) mostly within the periventricular white matter, signal abnormalities of the supratentorial white matter, ventriculomegaly and cortical atrophy. Posterior fossa findings have been addressed less commonly in the neuroimaging literature. Our study aims to extend the spectrum of neuroimaging findings in patients with MPS focusing on the posterior fossa.
Materials & Methods
The inclusion criteria were 1) the diagnosis of MPS based on abnormal enzyme assays and/or genetic analysis and 2) the availability of at least one MRI study of diagnostic quality including 3D T1- and axial T2-weighted images. All available images were evaluated retrospectively with semiquantitative measurement and qualitative analysis of the PVS (size and location), ventriculomegaly (size), cerebral atrophy (degree of severity), supratentorial white matter (degree of signal abnormality), cerebellum and posterior fossa (size), the presence of a mega cisterna magna, acquired tonsillar ectopia, cranial vault hyperostosis and morphologic abnormalities of the sella, and stenosis at the level of the foramen magnum (degree of severity).
Results
Ten patients could be included in the study (nine males and one female). Seven patients have MPS type I; three patients have MPS type II. At the time of the most recent MRI, the median age was 9.9 years (mean age 10.1 years, range 1.8 to 28.8 years). Longitudinal MR studies were available for four patients. Supratentorial findings included enlarged PVS in all patients (mostly involving the parieto-occipital white matter) and ventriculomegaly, white matter signal abnormalities, and cerebal atrophy in six patients. Infratentorially, PVS were enlarged at the level of the brain stem in eight and at the level of the cerebellum in five patients (bilaterally in four, unilaterally in one patient). Over time, in two patients cerebellar PVS's enlargement increased, while it decreased in two other patients. In two patients we found a macrocerebellum, in one a mega cisterna magna. In one patient, a macrocerebellum became apparent over time. An acquired tonsillar ectopia or cerebellar atrophy was not found in any patient. Cranial vault hyperostosis was present in seven patients and stenosis of the foramen

Note: Scanned images are included in the proceedings. Some submitted images were reduced during editing, thereby decreasing clarity. Also, refer to the Program Planner. Proceedings Content as of 3-29-2013.

magnum and morphologic abnormalities of the sella in four.
Conclusion
Enlargement of the PVS in the cerebellar white matter was present in 50% of our study population and was variable over time. Macrocerebellum was found in two patients and developed over time in one. Both enlargement of the cerebellar PVS and macrocerebellum have not been reported previously in MPS patients. Neuroradiologists should be aware that posterior fossa involvement is not uncommon in MPS type I and II and consequently should carefully evaluate the cerebellum and brain stem in these patients. The clinical significance of cerebellar involvement in MPS patients is unclear and should be assessed in larger cohort of patients.

KEYWORDS: Cerebellum, Metabolic, Mucopolysaccharidoses; Perivascular spaces

eP-236

Neuroradiologic Findings of Biotin-Responsive Basal Ganglia Disease

Al Sheikh, F.[1]·Al Adwani, N.[1]·Al-Shafi, S.[1]·Al Shahwan, S.[1]·Tabarki, B.[1]·Zuccoli, G.[2]
[1]Prince Sultan Military Medical City, Kingdom of Saudi Arabia, SAUDI ARABIA, [2]Children's Hospital of Pittsburgh, Pittsburgh, PA.

Purpose
Biotin-responsive basal ganglia disease (BBGD, OMIM#607483) or thiamine transporter-2 deficiency is an inherited treatable neurometabolic disease resulting from mutations in the SLC19A3 gene. Early treatment with thiamine and biotin result in normal outcome. Severe neurodevelopmental outcome and even death is observed in untreated patients. The objective is to investigate the neuroradiologic features of BBGD, and to clarify the disease spectrum.
Materials & Methods
Thirteen patients with a genetically proven diagnosis of BBGD between 2009 and 2012 were investigated by MRI brain/MRS during the acute phase and followup.
Results
We enrolled 13 patients that met the diagnostic criteria for BBGD. The BBGD occurred predominantly in preschool/school aged patients. The typical clinical picture consisted of recurrent subacute encephalopathy leading to coma, seizures, and extrapyramidal manifestations. During the acute crisis, brain MRI revealed bilateral and symmetrical involvement of the striatum in all patients. Nine (70%) patients showed symmetric involvement of the medial dorsal nucleus of the thalamus. Seven (54%) patients showed involvement of the brainstem nuclei. Ten (77%) patients showed extensive involvement of the cortex. Nine (70%) patients showed alterations in the cerebellar cortex and vermis. One patient (6%) showed involvement of the periventricular regions of the third ventricle. None of our patients disclosed subcortical white matter involvement. Vasogenic edema was identified in the affected brain regions during the acute phase the disease. None of the patients showed cytotoxic edema. MR spectroscopy was obtained in six patients disclosing decreased N-acetyl-aspartate and increased lactate peaks. Follow-up MRI showed evolving brain lesions consistent with remote injury: gliosis and atrophy were present, particularly in the striatum.
Conclusion
Biotin-responsive basal ganglia disease is an under diagnosed pan-ethnic treatable condition. Clinicians treating patients for unexplained encephalopathy and neuroimaging showing vasogenic edema in the bilateral striatum, infra and supratentorial cortex and brainstem, should consider this disorder early in the hospital course as a therapeutic trial with biotin and thiamine can be lifesaving.

KEYWORDS: Metabolic, Diffusion-weighted imaging, Biotin-responsive basal ganglia disease

eP-237

Comparison of MR Imaging Characteristics at Time of Multiple Sclerosis Onset between Pediatric Patients and Adults: A Retrospective Data Analysis

Milos, R.[1]·Szimacsek, M.[1]·Pritsch, M.[2]·Penzien, J.[3]·Karenfort, M.[4]·Blaschek, A.[5]·Seidl, R.[1]·Rostasy, K.[6]·Bayas, A.[7]·Storm van's Gravesande, K.[8]·Prayer, D.[1]·Kornek, B.[1]
[1]Medical University of Vienna, Vienna, AUSTRIA, [2]DRK-Children's Hospital, Siegen, GERMANY, [3]Children's Hospital Klinikum Augsburg, Augsburg, GERMANY, [4]Heinrich Heine University Düsseldorf, Düsseldorf, GERMANY, [5]Dr. von Hauner's Children's Hospital - Ludwig-Maximilians University, Munich, GERMANY, [6]Innsbruck Medical University, Innsbruck, AUSTRIA, [7]Klinikum Augsburg, Augsburg, GERMANY, [8]Gottfried von Preyer Children Hospital, Vienna, AUSTRIA.

Purpose
There are many similarities between pediatric- and adult-onset multiple sclerosis (MS), however patients with disease onset before the age of 18 have a higher relapse rate and seem to present more often with brainstem symptoms. Only few studies have compared magnetic resonance imaging (MRI) findings at disease onset between patients with pediatric- versus adult-onset MS. Therefore the aim of this study was to compare the imaging characteristics of the brain and spinal cord between children and adults at MS onset. Furthermore we evaluated the 2010 McDonald criteria in both groups.
Materials & Methods
We analyzed retrospectively clinical and MRI data from 52 patients (33 women and 19 men) with pediatric-onset MS (mean age 14.36 ± 1.91 years) and 42 patients (22 women and 20 men) with adult-onset MS (mean age 29.97 ± 8.39

Note: Scanned images are included in the proceedings. Some submitted images were reduced during editing, thereby decreasing clarity. Also, refer to the Program Planner. Proceedings Content as of 3-29-2013.

years). The minimum MRI protocols required the following sequences: axial and sagittal T2-weighted or FLAIR, T1-weighted before and postgadolinium for brain and sagittal T2-weighted and T1-weighted before and postgadolinium for spinal cord. The following parameters were assessed: initial symptoms at disease onset, presence of oligoclonal bands in the cerebrospinal fluid, mean time from first demyelinating attack to first brain and spinal MRI, number of focal T2 hyperintense, T1-hypointense, gadolinium-enhancing, and giant (over 2 cm in diameter) lesions and lesions distribution in brain and spinal cord.
Results
All patients showed symptoms characteristic for MS, including optic neuritis, brainstem/cerebellar or spinal cord syndrome or a syndrome attributed to cerebral hemispheres (sensory and/or motor dysfunction). Oligoclonal bands were positive in 94% of children and 80% of adults. The time between symptoms onset and first brain scan was similar between children and adults (mean 0.76 versus 0.88 months), while for the spinal scan there was a longer delay in children (mean 1.56 versus 0.9 months). We found no significant differences in the number and distribution of cerebral lesions between the two groups, although there was a tendency for children to have more frequent an infratentorial involvement (59.61% versus 42.85% of patients). Likewise, there were no significant differences in the number and size of spinal lesions between the two groups. Adults more frequently had enhancing cord lesions (52.94% versus 24% of patients), as well as predominantly only thoracical located lesions (23.8% versus 3.84%). In contrast, children more often had simultaneous cervical and thoracic lesions (50% versus 28.57%). At clinical onset the 2010 McDonald criteria were fulfilled as follows: the dissemination in space (DIS) in 88.23% of children and in 87.5% of adults, the dissemination in time (DIT) in 54.16% of children and 39.39% of adults and both DIS and DIT in 52.08% of children and 40.62% of adults.
Conclusion
In our cohort of pediatric and adult onset MS we did not find a major difference in the initial MRI presentation, although a trend was noted for a higher infratentorial involvement in children and more frequent contrast-enhancing lesions in adults. With respect to the McDonald criteria the demonstration of DIT as well as both DIS and DIT was higher in pediatric patients.

KEYWORDS: Multiple sclerosis, McDonald criteria, Onset

eP-238

MR Imaging Findings in Childhood Posterior Reversible Encephalopathy Syndrome: What is Different Than the Adults?

Donmez, F. Y.·Guleryuz, P.·Agildere, M.
Baskent University
Ankara, TURKEY.

Purpose
Posterior reversible encephalopathy syndrome (PRES) is a clinical scene presenting with convulsion, vision abnormalities, altered mental status and headaches in the presence of an underlying etiology and diagnosis can be made by support of radiologic studies. In this study, we evaluated the MRI findings of PRES in children and compared our findings with that of the known features in adult patients, and find the pathophysiologic reason that may cause the difference.
Materials & Methods
Twenty-nine children (13 male, 16 female, aged 1-17 years, mean age 10 years) diagnosed as PRES clinically and by radiologic workup were reviewed retrospectively. Clinical records were analyzed for the clinical symptoms at the time of MRI study and the underlying etiology. MR images were evaluated for the distribution of the lesions, contrast enhancement, diffusion restriction and any complication such as hemorrhage.
Results
Twenty-four of the patients presented with seizure, five had altered mental status, one patient had vision abnormality and one had ataxia. Underlying etiologies were variable: Chronic renal disease (n:8), leukemia (n:3), lymphoma (n:3), Wilson's disease (n:3), acute hepatitis (n:3), liver transplant recipient (n:3), hemolytic uremic syndrome (n:2), hemophagocytic syndrome (n:2), aplastic anemia (n:1) and metastatic osteosarcoma on chemotherapy regimen (n:1). Mean blood pressure was 130/85. Parietal (90%) and occipital (72%) involvement are the most common findings as expected; however, frontal lobe (66%) edema also is not uncommon, with rates close to occipital involvement. Temporal lobes were only involved if the edema was extensive in all parts of the brain (21%). Isolated temporal lobe involvement in absence of parietooccipital edema was not seen. The most interesting finding was the cerebellar involvement which was present in almost half of the patients (48%) and which was also atypical in adult patients. There were two patients with atypical presentation, with involvement of the thalami and basal ganglia and the brainstem. Contrast enhancement is also another finding which was found more common than the adults (39%). Twenty-six patients had diffusion-weighted imaging, diffusion restriction was seen in four of them (15%) and four patients had hemorrhage (15%); which are almost the same frequencies as in the adults.
Conclusion
The explanation of the posterior involvement related to

Note: Scanned images are included in the proceedings. Some submitted images were reduced during editing, thereby decreasing clarity. Also, refer to the Program Planner. Proceedings Content as of 3-29-2013.

lack of sympathetic innervation of the arterioles supplied by the vertebrobasilary system also is not entirely correct in children with PRES. However, the increased incidence of cerebellar involvement may show that the posterior circulation in children is more vulnerable than the adults. The contrast enhancement which is seen more common than in the adults may show that the pathophysiology in children may be related to blood-brain barrier breakdown more commonly, which can support the theory of the toxic endothelial injury. Mean blood pressure was not very high in our study group, only some of the children with kidney diseases had hypertension, which also makes it not possible to explained the syndrome solely by hypertensive effects and promote the toxic endothelial injury theory to be more commonly encountered in children with PRES.

KEYWORDS: PRES, Childhood, MR imaging

eP-239

Neuroimaging Findings in Rare Case of Navajo Neurohepatopathy (MPV 17-Related Mitochondrial Depletion Syndrome)

Malhotra, A.·Kalra, V.·Rao, B.·Jubinski, P.·Mistry, P.
Yale University
New Haven, CT.

Purpose
To present the neuroimaging findings in a rare case of Navajo neurohepatopathy (MPV 17-related mitochondrial depletion syndrome).
Materials & Methods
MPV 17-related hepatocerebral mitochondrial depletion syndrome (MDS) is a rare congenital autosomal recessive disorder characterized by hepatic failure, failure to thrive and neurologic findings. Three phenotypes have been described based on age at onset - infantile (onset before age six months), childhood (onset between ages one and five years) and classic form (after age five). The classic form tends to have moderate liver dysfunction with progressive neuropathy. There are only a few cases described in the literature with description of involvement of cerebellar white matter, cerebellar peduncles, substantia nigra and dorsal brainstem.
Results
A 9-year-old girl presented with liver dysfunction due to cirrhosis and the initial liver biopsy showed abnormal copper deposits in the liver, although genetic testing was negative for Wilson's disease. She underwent liver transplant and did well on immunosuppression for eight months. She presented with ataxia and progressive decline in neurologic function. Initial MRI showed bilateral basal ganglia ring-enhancing lesions. Multiple nodular lesions were found in the lungs and kidneys, and the lung biopsy revealed post-transplant lymphoproliferative disorder (PTLD), likely polymorphic. The patient was treated with chemotherapy. The patient had sequential brain imaging over four months, which showed appearance of multiple scattered hemorrhagic lesions which were felt to be due to PTLD. The patient developed T2 hyperintense signal in the dorsal cervical cord and subsequently restricted diffusion in the bilateral pyramids and reticular formation extending cranially along the inferior cerebellar peduncles with additional foci in the periventricular white matter abutting the third ventricle, occipital horns and atria of lateral ventricles and in the corpus callosum. These findings progressively worsened over 6 weeks with persistent low ADCs, before the patient expired.
Conclusion
We present a very rare case of classic form of MPV 17-MDS with sequential neuroimaging findings. Merkle et al (AJNR Am J Neuroradiol 33:E34 -E35 Mar 2012) previously described the involvement of reticulospinal tracts and descending reticular activating system. Diffusion-weighted images were particularly helpful in our case in following the CNS involvement. Awareness of this entity and its neuroimaging findings will help in early identification and appropriate genetic counseling.

KEYWORDS: Mitochondrial disease, Demyelination, Navajo

eP-240

Obex Level in Normal Subjects Compared to Chiari 1 and Complex Chiari Malformation Patients

Moore, H. E.[1]·Moore, K. R.[2]
[1]Scripps College, Claremont, CA, [2]Primary Children's Medical Center, Salt Lake City, UT.

Purpose
The obex is used as a surgical landmark for the cervicomedullary junction, and it is detectable on MR imaging. Low obex level, indicative of hindbrain herniation, has been described in both Chiari 1 malformation (CM1) and complex Chiari malformation (CCM). We hypothesize that the obex level in CM1 and CCM brains is statistically significantly different from the obex level in normal brains.
Materials & Methods
Eight-four control subjects were identified during an institutional imaging database search using the search term "normal brain". Subjects 18 years of age were excluded. All control subject brain MRI exams were confirmed to be normal. Eighty-five CM1 and 66 CCM patient MRI exams also were evaluated. Obex level was measured in all 235 control and patient subjects. Cerebellar tonsil level, craniocervical angle (CXA), and odontoid retroflexion (pB-C2) also were compared among the control, CM1, and CCM brains.
Results
The obex resided above the foramen magnum in all control subjects. The obex was lower in the CM1 and CCM patients; however, with statistically significant inferior obex displacement as compared to normal control subjects. The cerebellar tonsils were normally positioned (< 5 mm below foramen magnum) in all control subjects. Cerebellar tonsillar descent (ectopia) was statistically

Note: Scanned images are included in the proceedings. Some submitted images were reduced during editing, thereby decreasing clarity. Also, refer to the Program Planner. Proceedings Content as of 3-29-2013.

significant in the CM1 and CCM patients as compared to controls. Within the control group, average pB-C2 measured 4.6 mm and CXA 160 degrees. CXA was statistically significantly smaller and pB-C2 larger between control and CCM patients but not between control and CM1 patients.

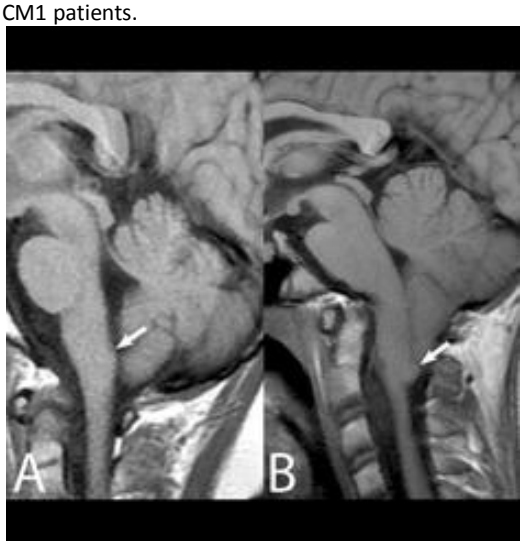

Conclusion
The obex level resides above the foramen magnum in normal subjects, but it is consistently displaced inferiorly in CM1 and CCM patients. Cerebellar tonsillar ectopia is always present in CM1 and CCM patients but not in normal subjects. Odontoid retroflexion and reduced CXA are common in CCM but less consistently observed in CM1 patients.

KEYWORDS: Chiari malformation type 1, Cerebellar tonsils, Complex Chiari malformation

eP-241

Apparent Diffusion Coefficient Value of Developing Normal Fetal Brain

Hoffmann, C.[1]·Katorza, E.[1]·Weisz, B.[1]·Tsarfati, G.[1]·Biegon, A.[2]
[1]Sheba Medical Center, Ramat-Gan, ISRAEL, [2]Brookhaven National Laboratory, New York City, NY.

Purpose
The apparent diffusion coefficient (ADC) value of the brain tissue changes during the maturation process of the brain. It is important to establish the normal values for each gestational week in order to distinguish the abnormal values from the normal ones.
Materials & Methods
Forty-eight women underwent MRI in the third trimester (26-33 weeks GA). The indication was siblings with metabolic diseases in previous pregnancies and normal US, and cases in which an anatomical abnormality was suspected, but the MRI excluded the condition. The ADC value was measured in nine locations on both hemispheres and in the posterior fossa.
Results
The ADC value declines during the third trimester in all the ROIs, excluding the frontal lobe. The difference is not significant between each consecutive week. The ADC value is lower in the gray matter and in the brain stem than in the white matter.

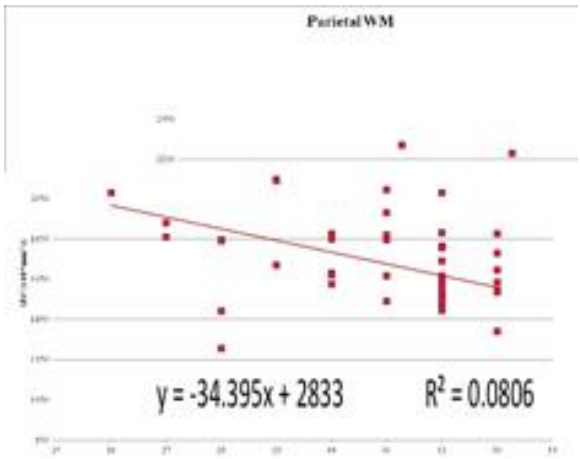

Conclusion
The ADC value in the white matter is higher than in the gray matter. During pregnancy the process of myelination takes place so the ADC value has a tendency to be lower.

KEYWORDS: Diffusion-weighted imaging, 1.5T, normal development

eP-242

Enlargement of the Internal Auditory Canal in PHACES Association

Meltzer, D. E.[1]·Blei, F.[2]·Robson, C.[3]·Holliday, R. A.[4]
[1]St. Luke's-Roosevelt Hospital Center, New York, NY, [2]Vascular Birthmark Institute of New York, New York, NY, [3]Boston Children's Hospital/Harvard Medical School, Boston, MA, [4]New York Eye and Ear Infirmary, New York, NY.

Purpose
Posterior fossa malformations, hemangiomas, arterial anomalies, cardiac defects, eye abnormalities, and sternal defects comprise the PHACES association. The segmental facial hemangiomas of PHACES association are frequently associated with ipsilateral cerebellar hypoplasia and ipsilateral anomalies of the intracranial internal carotid artery. Recently, attention has been drawn to the incidence of intracranial hemangiomas, especially in the internal auditory canal (IAC) and cerebellopontine angle cistern. In our experience with PHACES association patients, we have noticed several patients with enlargement of the IAC. We questioned whether this finding represented residual osseous enlargement secondary to an IAC hemangioma. The purpose of this

Note: Scanned images are included in the proceedings. Some submitted images were reduced during editing, thereby decreasing clarity. Also, refer to the Program Planner. Proceedings Content as of 3-29-2013.

study was to document the incidence and imaging appearance of anomalies of the IAC and posterior fossa in patients with PHACES association.
Materials & Methods
All 46 patients underwent MR imaging of the brain. Intravenous gadolinium was administered to 37 of these patients. Forty-two patients ranged in age from eight days to 10 years at the time of initial imaging. Four patients ranged in age from 16-25 years. CT examinations were available for review in 10 of patients. Three neuroradiologists with at least eight years of experience interpreting neuroradiologic imaging studies retrospectively reviewed images of the brain from patients with PHACES association. The focus was to document the presence of posterior fossa anomalies. Specifically, these included cerebellar hypoplasia, enlargement (and anomalous craniocaudad tilt) of the internal auditory canal (IAC), prominence of the posterior petrous ridge, and hypoplasia of the overlying occipital bone.
Results
Sixteen patients demonstrated a combination of cerebellar hypoplasia, ipsilateral enlargement of the IAC, and ipsilateral prominence of the posterior petrous ridge. Eight of these 16 patients also had ipsilateral hypoplasia of the overlying occipital bone. Five patients had ipsilateral posterior fossa enlargement with a prominent CSF space around the hypoplastic cerebellum. Three patients demonstrated a hemangioma in the IAC. Two patients demonstrated asymmetric IAC enhancement without definable mass. Of the five patients with abnormal IAC enhancement, one did not demonstrate enlargement of the IAC.
Conclusion
Thirty-five percent of the PHACES patients in this retrospective review had IAC enlargement, ipsilateral to their cerebellar hypoplasia, with associated anomalous tilt of the affected IAC, and mild ipsilateral prominence of the petrous ridge. Only nine percent of the PHACES patients demonstrated evidence for IAC hemangioma. The results do not support our original theory of a causative relation between IAC hemangioma and IAC enlargement. The results raise the alternative possibility that the enlarged IAC in PHACES is related to a generalized malformation of the osseous components of the posterior fossa in association with cerebellar hypoplasia. Associated ipsilateral hypoplasia of the overlying calvarium is an additional, less consistent, finding in these patients.

KEYWORDS: PHACES, Internal auditory canal, Infantile hemangioma

eP-243

Normal Calvarial Variants Portrayed by 320 Detector 3D Volumetric CT

Whitehead, M. T.·Choudhri, A.
University of Tennessee
Memphis, TN.

Purpose
Normal variant intrasutural ossicles, fissures, foramen, and asymmetries are commonplace in the developing calvarium. As CT technology has advanced, normal variant anatomy has become increasingly recognizable. Radiologists should be readily aware of normal variants so as to prevent misdiagnoses. We performed a retrospective review of 2D and 3D CT datasets to determine type, location, number, and symmetry of normal calvarial variations.
Materials & Methods
Two hundred eighty-eight consecutive CT scans performed on children under two years of age in a 12-month period at a single academic medical center were evaluated. Studies with craniofacial abnormalities, excessive motion artifact, ventricular shunts, prior intracranial surgery, and studies with no available 3D reconstructions were excluded. Two hundred thirty-five studies met inclusion criteria (ages 0.85+/-0.63 years, range 0.00 to 2.82 years, median 0.7 years). Three-dimensional CT data sets displayed at 18 degree intervals in tumble and rotation were reviewed for the location, number, and symmetry of intrasutural ossicles, fissures, and foramen. Studies were reviewed in a blinded manner by two fellowship-trained neuroradiologists with ABR subspecialty certificates in neuroradiology. A consensus reading was reached in all cases.
Results
The vast majority of patients had intrasutural ossicles (84%; 199/235; range 0 to 25, median 3), principally located in the lambdoid sutures (70%; 165/235; range 0 to 22, median 2). Intrasutural ossicles were not identified in the metopic, sphenotemporal, and parietosquamosal sutures in any patient. There was striking variability regarding number and symmetry of these intrasutural ossicles. Short segment parietal fissures were present in several patients (17%; 41/235) in two distinct locations, unilaterally or bilaterally terminating in the lambdoid sutures. Unilateral or bilateral parietal foramina near the vertex midline were present in some patient (37%, 86/235), most of which were tiny in size.

Note: Scanned images are included in the proceedings. Some submitted images were reduced during editing, thereby decreasing clarity. Also, refer to the Program Planner. Proceedings Content as of 3-29-2013.

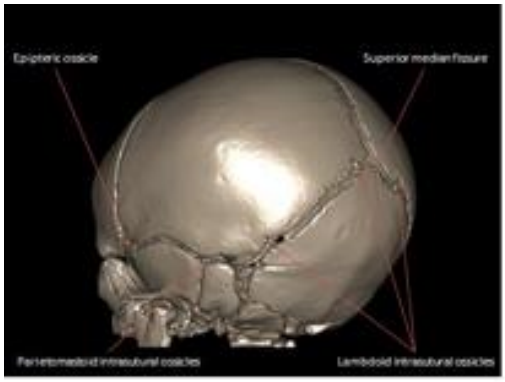

Conclusion
Normal variant intrasutural ossicles, fissures, and foramen are a very frequent occurrence in the developing calvarium and should not be mistaken for pathology. Most patients less than two years of age have intrasutural ossicles. Asymmetric ossicles and fissures can be distinguished from fractures by their characteristic locations and appearances. Deviations from the normal pattern of calvarial variants should raise suspicion for possible pathologic processes.

KEYWORDS: 320 detector row, Skull, Ossicles, anatomy

eP-244

Functional Neuroimaging of Patients with Posthemispherotomy Pre and Postintensive Gait Therapy

Salamon, N.·DeBode, S.·Bookheimer, S.
University of California Los Angeles
Los Angeles, CA.

Purpose
Many patients with intractable epilepsy underwent hemispherotomy for seizure control, plasticity and reorganization of the motor control may develop after surgery. We studied motor and gait functions pre- and post-body weight support treadmill (BWST) training, and correlate changes from training using functional MRI (fMRI) cortical activation from voluntary knee movements. Our goals are to exploit functional plasticity in the developing human brain by determining if age at injury/surgery, related to specific pathologies, predicts baseline motor/gait functions and response to BWST training.
Materials & Methods
Diffusion Tensor Imaging: An axial 2D EPI based diffusion-weighted sequence (Siemens Allegra 3.0T TE/TR 129/6000 ms, FOV 240 x 240 mm, Matrix 128 x 128 interpolated to 256 x 256, Slice thickness 2 mm, Number of slices 70) will be acquired with diffusion gradients along 32 noncollinear directions at two b values of 600 sec/mm2 and 1200 sec/mm2. Functional MR Imaging: Functional MRI analysis will be obtained using motor sensory testing using knee movement. Control and five posthemispherectomy patients had received BWST training and pre- and post-fMRI was performed. Data analysis was made using a statistical program (Stat View SAS Institute, Cary, NC). Differences between control and hemispherectomy patients were compared using t test and repeated-measured analysis of variance. Comparisons using nominal variables were performed using chi-square tests. Results were considered at a minimal level of significance of P<.05.
Results
For hemispherectomy patients, the increase in activation of the voxel was obtained in ipsilateral paretic and contralateral nonparetic movements (p<.02) after BWST. For control subjects, there was decrease in activity in the voxels after BWST. Attached image demonstrates pre- and post-BWST fMRI result of the right hemispherectomy patient with left foot movement activation.

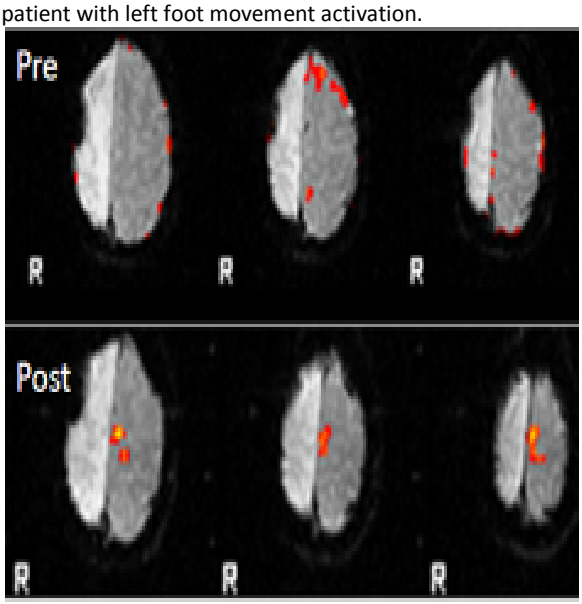

Conclusion
Locomotor therapy such as BWST can improve motor connectivity in hemispherectomy patients. Further study is needed to optimize motor functions of the residual corticospinal pathway and long term follow-up assessment with fMRI will be helpful in the future research.

KEYWORDS: Motor mapping, Functional brain mapping, hemispherotomy

Note: Scanned images are included in the proceedings. Some submitted images were reduced during editing, thereby decreasing clarity. Also, refer to the Program Planner. Proceedings Content as of 3-29-2013.

eP-245

Reproducibility of Metrics Derived from Diffusion Tractography in a Cohort of Pediatric Patients

Paldino, M. J.·Rodrigues, K. M.·Hedges, K.·Grant, P. E.
Children's Hospital Boston
Boston, MA.

Purpose
The reproducibility of parameters derived from diffusion tractography has not been widely studied and, in particular, there is very little data from the developing brain. The goal of this study is to quantify the test-retest repeatability of ADC and FA derived from tractography in a cohort of pediatric patients.
Materials & Methods
Patients were identified retrospectively from a database of pediatric epilepsy patients who met the criteria of having 1) a 3T brain MR examination and 2) Two separate but identical DTI sequences obtained in the same MR session. Patients were excluded for seizure during the examination or significant degradation to image quality such as by motion. Diffusion Toolkit was used for deterministic tract reconstruction(angular threshold: 35 deg). Two users experienced in tractography performed tract segmentation and analysis in Trackvis (www.trackvis.org). Tracts segmented included the corpus callosum as well as bilateral corticospinal tracts, inferior longitudinal fasciculi, inferior fronto-occipital fasciculi, and arcuate fasciculi (AF). Mean ADC and mean FA were calculated for each tract. For each patient, the two individual diffusion datasets were analyzed independently by different users, resulting in two observations for each parameter for every tract. Prior to considering the entire dataset in toto, the mean difference between observations across the following subgroups was compared using the Wilcoxon signed-rank test: 1. Tracts from structurally normal versus dysplastic brains; 2. Left- versus right-sided tracts. 3. Each tract versus the remaining aggregate of all other tracts (e.g., all corticospinal tracts versus all other tracts). Any potential difference between observations from the two users also was assessed using the Wilcoxon signed-rank test. For each parameter, we then calculated: 1. Mean coefficient of variation (CoV). 2. Regression coefficient; 3. Repeatability coefficient; 4. Ninety-five percent confidence limits (95%CL) for change. For any tracts not identified bilaterally in all patients, Cohen's kappa coefficient was calculated to assess agreement between the readers.
Results
Twenty patients were included (age range: 3-18 years). All tracts were identified bilaterally in all patients except for the AF, which was not identified on the right in eight subjects and not identified on the left in five subjects. Repeatability was consistent across the dataset; hence, the remaining tests were performed based on all identifiable tracts. No difference between observations was identified($p = 0.89$). Test-retest estimates of the reproducibility of mean ADC and mean FA are presented in Table 1. For the AF, Cohen's kappa coefficient for agreement between the readers (absent vs present) was 1.0 [95%CI (1.0, 1.0)].

Repeatability of mean ADC and mean FA derived from DTI tractography. Asterisk (*): $p < 0.01$.

	ADC	FA
mean CoV (%)	2.8	2.5
Regression Coefficient	0.952*	0.964*
Repeatability Coefficient	0.00015	0.014
95% CL for change (%)	10.3	8.6

Conclusion
These findings demonstrate good test-retest repeatability of mean ADC and FA derived from DTI tractography in a cohort of pediatric patients. Change greater than the repeatability coefficient or 95%CL for change are unlikely to be related to intrinsic variability of the method.

KEYWORDS: Reproducibility, Diffusion tensor image

eP-246

Neuroimaging Abnormalities Are Prevalent in Adolescents with Lupus at Time of Disease Quiescence

Hunter, J. V.·Canter, D. L.·Muscal, E.
Texas Children's Hospital
Houston, TX.

Purpose
Conventional neuroimaging abnormalities have been described in children and adults with active neuropsychiatric lupus (NPSLE). We hypothesized similar findings in children with inactive neurologic disease.
Materials & Methods
We acquired conventional MRI sequences on a 3T scanner as part of a prospective neuropsychology and novel neuroimaging study. A pediatric neuroradiologist (JVH) assessed white matter lesions and measures of parenchymal volume loss on conventional anatomical sequences while blinded to disease status.
Results
Imaging was acquired for N = 41 right-handed adolescents (mean age 15.6 $\pm$ 1.6 years; female 90%; Hispanic 41% and African-American 24%). Mean disease duration at time of imaging was 29.1 $\pm$ 26.7 months. Only five subjects (12.2%) had a history of NPSLE. Disease activity indices reflected well controlled and inactive disease for all subjects at the time of imaging. Most subjects were on prednisone (92.7%, mean dose 19.1 $\pm$ 12.0 mg) and 41.4% were on

Note: Scanned images are included in the proceedings. Some submitted images were reduced during editing, thereby decreasing clarity. Also, refer to the Program Planner. Proceedings Content as of 3-29-2013.

additional immunosuppressive agents (methotrexate, mycophenolate mofetil, or azathioprine) at imaging. Many of the adolscents had positive vasculopathy markers (39.0% with a lupus anticoagulant and 65.9% with a positive antiphospholipid antibody). T2 or FLAIR sequences revealed 18 subjects (43.9%) with small (2-3 mm) multifocal punctate white matter (WM) lesions. There were no gray matter lesions visualized. All subjects with WM lesions had at least one frontal lesion (50% with bifrontal lesions). Additional locations of WM lesions included parietal lobes (16.6%) and centrum semi-ovale (11.1%). Corpus colossal thinning was observed in 22.0% of subjects. Features suggestive of cerebral volume loss were common (sulcal widening 65.6% and ventricular dilation 34.1%). Cerebellar volume loss (foli prominence) was observed in 68.3% of subjects. Evidence of WM lesions or parenchymal volume loss was not associated with previous nephritis, hypertension, vasculopathy risk factor positivity, or cumulative prednisone dosing. Measurements of Evan's ratio, thickness of the corpus callosum and size of third ventricle were not associated with cumulative prednisone dosing. Measures of executive function were not significantly lower in adolescents with abnormal MRIs.
Conclusion
We observed a predominance of frontal WM lesions and parenchymal volume loss in a large percentage of adolescents with lupus. Conventional MR imaging abnormalities were documented early in disease courses and at times of disease inactivity. Evidence of nervous system involvement on advanced imaging may indeed predate clinical manifestations in adolescent lupus patients. These abnormalities appeared to be independent of corticosteroid burden and may reflect subclinical neuroinflammation or vascular disease in this population.

KEYWORDS: Pediatric brain, Lupus, white matter disease

eP-247

MR Anatomy of Developing Teeth in the Neonatal Period

Whitehead, M. T.·Choudhri, A.
University of Tennessee/Lebonheur Children's Hospital Memphis, TN.

Purpose
Odontogenesis is a complex process that initiates in the embryonic period and continues into adulthood. Primary and secondary teeth formation begin at six and 20 gestational weeks, respectively. Normal term neonates have 20 developing unereupted primary teeth. To our knowledge, there is no existing literature regarding normal MR imaging patterns of teeth in term neonates. Pathologic diagnoses require familiarity of normal anatomy. In this article, we will review the normal tooth embryology and anatomy and detail the normal MR appearance of developing neonatal teeth.
Materials & Methods
Fifty-nine consecutive neonatal patients' brain MRIs (ages 0 to 27 days) were reviewed by two pediatric neuroradiologists boarded by the ABR with CAQs in neuroradiology. Seven premature patients (<37 weeks gestation) and two patients with inadequate field of view were excluded. Mandibular and maxillary tooth anatomy was detailed on T1, T2, T2 FLAIR, and postcontrast T1-weighted images (when available) from the remaining 50 patients' MRIs.
Results
The imaging pattern of developing teeth in the neonate is remarkably consistent. In all patients, the primary teeth were in the early maturation stage with several distinct MRI regions. Hypointense surfaces represent the developing crowns partially envelope neural crest mesenchyma that will become the dentin, pulp, and periodontia. Permanent teeth anlagen were present in some locations along the lingual aspect of deciduous teeth. Medial incisor and lateral incisor permanent teeth in the bell stage of development were present in all patients bilaterally in the mandible and maxilla. Permanent teeth bells representing early developing molars resided posterior to the developing deciduous mandibular and maxillary teeth in all patients. The majority of patients (36/50) also had visible permanent bilateral maxilla and mandibular canine teeth buds.

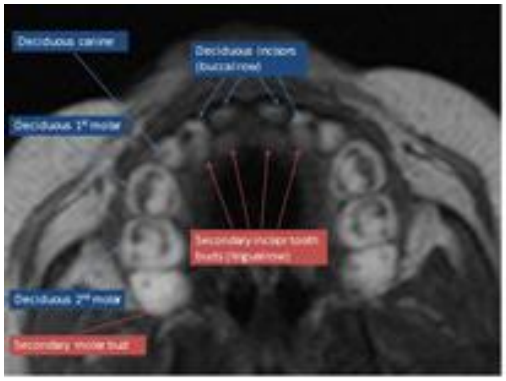

Conclusion
The developing primary and secondary unerupted teeth display characteristic MR appearances in normal neonates. Twenty developing primary teeth in the maturational stage are consistently present. Several unmineralized tooth bells of secondary teeth also are present.

KEYWORDS: Pediatric head and neck, Jaw, Teeth

Note: Scanned images are included in the proceedings. Some submitted images were reduced during editing, thereby decreasing clarity. Also, refer to the Program Planner. Proceedings Content as of 3-29-2013.

eP-248

Healthy Preterm Infants Have a Preserved Hemodynamic Response to Transient Elevation of Intracranial Pressure during Anterior Fontanelle Compression

Zamora, C. A.·Tekes, A.·Alqahtani, E.·Northington, F. J.·Kalayci, O.·Huisman, T. A. G. M.
Johns Hopkins University School of Medicine
Baltimore, MD.

Purpose
Abnormal cerebral autoregulation plays a major role in the development of a variety of neonatal neurologic complications. Particularly, the preterm infant is presumed to have abnormal autoregulation, although the available evidence is conflicting and not conclusive. We performed this study 1- to determine normative cerebral resistive index (RI) values in healthy preterm and term infants and 2- to establish whether or not the hemodynamic response to transient elevation in intracranial pressure during anterior fontanelle compression is different between these groups.
Materials & Methods
This retrospective study included healthy preterm and term infants less than three months of age with a normal first head ultrasound (US). Resistive indexes were measured in the anterior cerebral circulation at the beginning of the study, first at baseline and then following three-five seconds of fontanellar compression with the transducer. Patients were excluded on the basis of sepsis, hypoxic ischemic encephalopathy, subsequent intracranial adverse events, intracranial procedures, cardiac surgery, clinically significant cardiac shunts, cardiomyopathies, or congenital cardiac malformations. We calculated normal baseline values and ranges (mean ± two standard deviations) and percent change in RI between baseline and compression. Two-tailed unpaired t tests were utilized to separately compare mean baseline RI, mean compression RI, and mean percent change in RI between the two groups.
Results
A total of 129 healthy subjects were included in the study. Gestational age ranged from 25 to 41 weeks. Mean follow up (± standard deviation) was 200 ± 175 days. Mean baseline RI was 0.7 ± 0.08 in preterm (n = 67; normal range, 0.54 - 0.86) and 0.66 ± 0.07 in term infants (n = 62; normal range 0.52 - 0.8). This difference in mean RIs was statistically significant (P = .001). Mean RI during fontanellar compression was 0.71 ± 0.08 in preterm and 0.68 ± 0.07 in term infants. This difference in mean RIs was also statistically significant (P = .015). The mean percent change in RI between baseline and compression was 5.86% ± 4.2% in preterm and 7.47% ± 6.2% in term infants. This difference was not statistically significant (P = .092).
Conclusion
There was no difference in the hemodynamic response to fontanelle compression (as measured by percent change in RI from baseline) between healthy preterm and term infants. This suggests that cerebral autoregulation is preserved in the healthy preterm infant. In addition, we present the normative baseline and compression RI values for both groups in a large group of healthy term and preterm infants.

KEYWORDS: Ultrasonography, Autoregulation, Resistive index

eP-249

Systematic Radiologic Phenotyping and Decision Tree Analysis of Multiparametric MR Imaging Data in Pediatric Posterior Fossa Tumors

Kamaly-Asl, I.[1,2]·Cain, J.[1]·Gledson, A.[1]·Tang, V.[2]·Wright, N.[2]·Soh, C.[3]·Birch, J.[1]·Keane, J.[1]·Jackson, A.[1]·Stivaros, S. M.[1,2]
[1]University of Manchester, Manchester, UNITED KINGDOM, [2]Royal Manchester Children's Hospital, Manchester, UNITED KINGDOM, [3]Salford Royal Foundation NHS Trust, Manchester, UNITED KINGDOM.

Purpose
Imaging remains crucial to diagnosis, staging and treatment planning in pediatric posterior fossa tumors. Despite recent advances in multiparametric MRI techniques there still remains significant uncertainty in the radiologic phenotyping of a proportion of these tumors. In addition, specific histologic diagnosis and grading often guides surgical resection but is not always available pre/intraoperatively. We have developed a systematic reproducible descriptive imaging model that integrates advanced quantitative MRI imaging metrics into one data repository. This dataset underpins a radiologic decision support system (DSS) that facilitates more accurate radiologic phenotyping of these tumors.
Materials & Methods
Using the North West Children's Tumour Registry we collated available imaging, demographic and histological data on 115 pediatric patients presenting with posterior fossa tumors from 1953 to April 2012. A language-based systematic analysis and scoring system was devised to model the imaging phenotype with correlation to proven histology of these development cases. Computerized decision tree analysis of the imaging database was performed using multiple algorithms to derive an imaging phenotype classification system which could be used as a diagnostic DSS. The imaging of 40 patients with posterior fossa tumors presenting to our institution between January 2008 and January 2012 then was selected randomly and independently reported by one general neuroradiologist, two pediatric radiologists with an interest in pediatric neuroradiology and one dedicated pediatric neuroradiologist. Using the DSS the same cases were re-reported at a later date and a comparison made between the radiologic diagnostic accuracy with and without the systematic reporting schema and DSS.
Results

Note: Scanned images are included in the proceedings. Some submitted images were reduced during editing, thereby decreasing clarity. Also, refer to the Program Planner. Proceedings Content as of 3-29-2013.

The median patient age used to create the radiologic phenotype model was 7.2 years with a range of 2.6 - 15.3 years, of whom 49% were female. The descriptive model contained 30 major attributes which accommodated 120 variables giving just under one million variable permutations per patient. The most successful decision tree algorithm for diagnostic stratification was found to be Alternating Decision (AD) Tree with a true positive rate of 93% and an ROC area of 98%. The initial radiologic diagnostic accuracy varied between 68 - 75%. In the patients with disconcordant radiologic and histologic diagnoses four pilocytic astrocytomas were felt to be cystic ependymomas/medulloblastoma. Two medulloblastomas were felt to more closely resemble ependymomas. Two brainstem gliomas were found to be noncystic pilocytic astrocytomas. One atypical teratoid rhabdoid tumor was radiologically characterized as an ependymoma and two ependymomas were incorrectly called medulloblastoma/pilocytic astrocytoma. By contrast, repeat imaging analysis using the systematic schema in combination with the ADTree DSS yielded a diagnostic accuracy of 93%.

Conclusion

To our knowledge this study is the first systematic descriptive model of pediatric posterior fossa tumors integrating any radiologic metric. It validates the concept of decision tree analysis for diagnostic prediction using systematic phenotypic modelling and demonstrates the potential of an automated decision tree classification DSS. Validation will require the analysis of larger numbers of scans from patients with posterior fossa tumors of known and unknown etiology. We think this work points towards such techniques having a huge potential as diagnostic tools.

KEYWORDS: Pediatric brain tumors, Data mining

eP-250

Pediatric Pilocytic and Pilomyxoid Astrocytomas: MR Imaging Characteristics and a Comparison of Apparent Diffusion Coefficient and T2/Cerebrospinal Fluid Measurements

Lindsay, A. J.·Rush, S. Z.·Fenton, L. Z.·Stence, N. V.
Children's Hospital Colorado
Denver, CO.

Purpose

Pilocytic astrocytomas (PCAs) are the most common primary brain tumor in children. Pilomyxoid astrocytomas (PMAs) are a variant of PCAs that are characterized by a higher rate of recurrence and CSF dissemination. Imaging findings overlap in these tumors. MR diffusion-weighted imaging correlates with water diffusivity and cellularity and differs for some tumors, thus serving as a potential discriminatory tool . Our goal was to review MR imaging characteristics of PCAs and PMAs and compare quantitative apparent diffusion coefficient (ADC) and T2-weighted signal metrics for differences to facilitate distinguishing these tumors.

Materials & Methods

Following IRB approval, the neuro-oncology database at a tertiary care Children's Hospital was reviewed retrospectively for patients with pathology proven PCA and PMA from 2003 to 2012. Patients with neurofibromatosis I were excluded. Eleven patients with PCA and nine patients with PMA were identified. On MRI at presentation, tumor characteristics were recorded and regions of interest (ROIs) were drawn within solid tumor on T2-weighted images and ADC maps. Regions of interest were drawn within ventricular CSF to normalize the T2-weighted data and to provide a similar ratio for the ADC data. The mean T2/CSF, ADC, and ADC/CSF and minimum ADC values were recorded. A delta ADC value was recorded by obtaining the maximum difference of five ADC values within different areas of solid tumor. Tumor volume was measured by drawing ROIs around the solid portion of the tumor using TeraRecon.

Results

Results are summarized in Tables 1 and 2. Pilocytic astrocytomas patients were older (median age 5.4 years) than PMA patients (median 1.9 years). No PMAs were predominantly cystic, while 3/11 PCAs were predominantly cystic. PMAs more frequently homogeneously enhanced (78% versuss 27%) and were more frequently homogeneously T2 hyperintense (78% versus 18%). Excluding patients without an adequate follow-up interval, PMAs were more likely to become cystic with time (71% versus 30%). Mean T2/CSF, mean ADC, mean ADC/CSF, minimum ADC, delta ADC, and tumor volume were greater for PMAs than PCAs, though the differences were not statistically significant.

Note: Scanned images are included in the proceedings. Some submitted images were reduced during editing, thereby decreasing clarity. Also, refer to the Program Planner. Proceedings Content as of 3-29-2013.

Table 1: Demographics and Qualitative Results

		PCA (11 Patients)	PMA (9 Patients)	p value (* for < 0.05)
Age		6 months to 18 years (median 5.4 years)	3 months to 5 years (median 1.9 years)	0.028*
Gender		7 male (64%)	3 male (33%)	0.178
Tumor Location				
-	Optic Pathway	6 (55%)	6 (67%)	0.582
-	Posterior Fossa	5 (45%)	2 (22%)	0.279
-	Other	0	1 (11%)	0.257
Tumor Characteristics				
-	Solid	6 (55%)	5 (56%)	0.964
-	Cystic	3 (27%)	0	0.08
-	Mixed	2 (18%)	4 (44%)	0.202
-	Infiltrative	4 (36%)	5 (56%)	0.39
Enhancement				
-	Homogeneous	3 (27%)	7 (78%)	0.025*
-	Heterogeneous	8 (73%)	2 (22%)	0.025*
T2 Hyperintensity				
-	Homogeneous	2 (18%)	7 (78%)	0.008*
-	Heterogeneous	9 (82%)	2 (22%)	0.008*
Treatment		3/10 (30%)	5/7 (71%)	0.092

Table 2: Quantitative Results

	PCA (11 Patients)	PMA (9 Patients)	p value
Mean T2/CSF	0.656	0.767	0.16
Mean ADC [10(-6) mm2/sec]	1316	1394	0.64
Mean ADC/CSF [10(-6) mm2/sec]	0.447	0.464	0.78
Mean Minimum ADC [10(-6) mm2/sec]	1200	1280	0.72
Mean Delta ADC [10(-6) mm2/sec]	195.7	253.7	0.29
Mean Tumor Volume [mL]	27.64	36.04	0.5

Conclusion

Relative to PCAs, at diagnosis PMAs are less frequently cystic, and more often homogeneously T2 hyperintense and enhancing. Pilomyxoid astrocytomas were more likely than PCAs to become cystic with treatment over time. Although mean T2/CSF, mean ADC, mean ADC/CSF, minimum ADC, delta ADC, and tumor volume were greater for PMAs than PCAs, the differences were not statistically significant and could not reliably distinguish PMA from PCA.

KEYWORDS: Pilocytic astrocytoma, Pilomyxoid astrocytoma

eP-251

Low Grade Gliomas: Neuroimaging Findings of Pseudoprogression after Radiotherapy

Naftel, R.·Zuccoli, G.·Deutsch, M.·Jakacki, R.·Pollack, I. F.
Children's Hospital of Pittsburgh
Pittsburgh, PA.

Purpose
Increasing enhancement and mass effect following radiation therapy in patients with low-grade gliomas (LGG) can be mistaken for tumor progression and/or malignant degeneration. Differentiating this “pseudoprogression” from true progression is necessary to determine the need for alternative therapy. This study investigates the incidence, timetable, and changes in size of low-grade glioma after radiotherapy.
Materials & Methods
Retrospective chart review was performed on children treated with radiotherapy (RT) for LGG at the Children’s Hospital of Pittsburgh Neuro-Oncology program with at least one year of followup. A blinded neuroradiologist performed tumor measurements using the largest cross-sectional area.
Results
Twenty-nine children, median age 12, underwent RT (external beam-23, gamma knife-6) for tumor recurrence (2/29) progression (10/29), or as a primary treatment (14/29). Histologies included juvenile pilocytic astrocytoma (20/29), LGG (5/29), and radiologic diagnosis of LGG (4/29). Sixteen patients developed increased enhancement and/or mass effect following RT with a median time to maximum tumor enlargement of six months, with a range of four months up to 4.2 years. Twelve patients reached their peak size within eight months while four patients did not reach their peak until after 2.7 years. The pseudoprogression tumor size enlarged to a median maximum cross-sectional area of 154.9% of the pre-RT baseline. The pseudoprogression tumor size decreased to a median stable cross-sectional area of 72.8% of the pre-RT baseline. In comparison, all patients without pseudoprogression experienced decrease in size of the tumor and stabilization. The tumor size decreased to a median stable cross-sectional area of 15.3% of the pre-RT baseline. Ten children were symptomatic

Note: Scanned images are included in the proceedings. Some submitted images were reduced during editing, thereby decreasing clarity. Also, refer to the Program Planner. Proceedings Content as of 3-29-2013.

and treated with steroids (n = 10) and/or avastin (n = 3). Three children were operated upon, two for cyst fenestration, and one for debulking after concern for true progression; however, pathology showed treatment effect: radiation necrosis with scattered juvenile pilocytic astrocytoma tumor cells. In all 16 cases, the tumor eventually decreased in size without additional antitumor therapy. With a median followup of 4.8 years (range 1.0-12.4 years), all patients remain alive and only one patient experienced true progression.

Conclusion

Tumor pseudoprogression was seen in over half of patients with LGG. Most patients experienced pseudoprogression in the first eight months after RT; however, four patients experienced maximum pseudoprogression after 2.7 years. While both pseudoprogression and nonpseudoprogression patients experienced stability of their tumors, at the last followup pseudoprogression tumors were still on average larger than those without pseudoprogression.

KEYWORDS: Pediatric brain tumors, Pseudoprogression, Radiotherapy

eP-252

MR Imaging of Pleomorphic Xanthoastrocytomas in Children with Emphasis on Diffusion-Weighted Imaging

Moore, W.[1]·Mathis, D.[1]·Gargan, L.[2]·Klesse, L.[1]·Margraf, L.[1]·Bowers, D. C.[1]·Koral, K.[1,2]
[1]University of Texas Southwestern Medical Center at Dallas, Dallas, TX, [2]Children's Medical Center, Dallas, TX.

Purpose

To describe the imaging characteristics of pediatric pleomorphic xanthoastrocytoma (PXA) with particular attention paid to diffusion-weighted imaging characteristics.

Materials & Methods

Review of Neuro-Oncology database revealed 11 PXAs from 1/1998 through 4/2012. The pathology specimens were reviewed and diagnoses were confirmed according to the 2007 WHO Classification of Central Nervous System Tumors. Two patients did not have preoperative imaging performed at our institution. Remaining nine patients had preoperative MRI and seven had DWI performed with b values of 0 and 1000. The examinations were reviewed by a fourth-year radiology resident and a pediatric neuroradiologist. The location, size, signal and enhancement characteristics, presence of cyst(s), presence and size of the perilesional edema were recorded. On the ADC maps, the solid components of the tumors were sampled by placing as many as nonoverlapping region of interests (ROIs). One ROI was placed on the normal thalamus. Mean tumor ADC values and tumor: normal brain ADC ratios were calculated.

Results

Of the nine patients, two had anaplastic features. Eight tumors were supratentorial. The supratentorial tumor volumes varied from 1.73 cm^3 to 249.86 cm^3 (mean = 98.61, SD = 103.58). Six of the eight supratentorial tumors were associated with scalloping of the inner table. Six lesions had either multiple cysts or predominantly cystic. Seven of the nine patients had significant vasogenic edema about the solid tumor, defined as greater than 10 mm in diameter. Except for the smallest tumor in the temporal lobe, all tumors showed intense heterogenous enhancement. Tumor ADC values could be measured reliably in six patients. The ADC mean was 874 ± 214 x 10^{-6} mm^2/s (min-max: 617-1189). The tumor: normal brain ADC ratio was 1.12 ± 0.28 (min-max: 0.75-1.32).

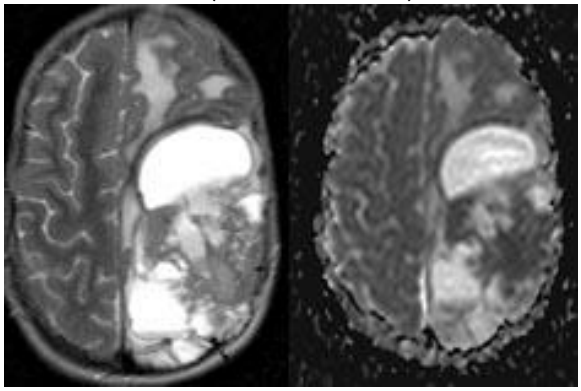

Figure: Axial T2-weighted and axial ADC map of a six-year-old male with pleomorphic xanthoastrocytoma.

Conclusion

Pleomorphic xanthoastrocytoma is a rare tumor of pediatric central nervous system. It can attain a relatively big size in the cerebral hemispheres until becoming symptomatic and its diffusion characteristics may be confused with aggressive tumors.

KEYWORDS: Pediatric neoplasms, Pleomorphic xanthoastrocytoma

eP-253

MR Diffusion and Perfusion Characteristics of Desmoplastic Infantile Ganglioglioma

Barad, U. H.·Ho, C. Y.·Kralik, S. F.
Indiana University
Indianapolis, IN.

Purpose

MR imaging using diffusion and perfusion has been used previously to differentiate low-grade and high-grade brain tumors; however, diffusion and perfusion imaging characteristic of desmoplastic infantile ganglioglioma (DIG) has not been described previously in the literature to our knowledge.

Materials & Methods

Two cases of DIG were diagnosed at our institute between October 2009 and March 2011. In addition to routine pre and postcontrast sequences including diffusion-weighted

Note: Scanned images are included in the proceedings. Some submitted images were reduced during editing, thereby decreasing clarity. Also, refer to the Program Planner. Proceedings Content as of 3-29-2013.

imaging, dynamic T2* perfusion images were performed on 1.5T superconducting Avanto (Siemens, Erlangen, Germany) with TR 1531 msec TE 30.6 msec, slice thickness of 5 mm and rate of injection 4 ml/sec.
Results
On perfusion images, the solid enhancing portion of tumor demonstrate rCBV equivalent to contralateral white matter and cystic areas has no increase in rCBV as expected. Diffusion appearance on ADC map of the solid enhancing portion is equivalent of the gray matter.
Conclusion
Brain tumor presenting within the first two year of life may be large in size and have a heterogeneous appearance on MRI. The use of advance MR imaging techniques including diffusion and perfusion imaging helpful to diagnose DIG, a low-grade tumor, from high-grade PNET or ATRT. Because complete surgical resection considered curative, preoperative surgical diagnosis is essential for favorable outcome.

KEYWORDS: Pediatric brain tumors, Desmoplastic infantile ganglioglioma

eP-254

MR Imaging in a Young Child without Removal of the Cochlear Implant Magnet: Technical Aspects

Jacob, R.[1,2]·Roland, P.[1,2]·Morriss, M.[1,2]
[1]Children's Medical Center, Dallas, TX, [2]University of Texas Southwestern Medical Center, Dallas, TX.

Purpose
Cochlear implants (CI) are used widely for treatment of sensorineural hearing loss. Over 30,000 children in USA have received cochlear implants. Traditionally if a patient with a CI needs an MRI, it necessitates surgical removal of the CI magnet and post-MRI surgical replacement of the magnet. In recent years MR has been performed safely in a limited number of adults and older children without removal of the CI magnet. This case describes the technical aspects and planning behind the performance of an MR study on a three-year seven-month-old child without removal of the CI magnet. This is the first report of a child this young undergoing such a procedure.
Materials & Methods
The patient required MR imaging of the brain to evaluate for leukodystrophy. He had previously undergone implantation of a Med El CI on the right. At the request of the child's parent and in consultation with the pediatric otologist, pediatric neuroradiologist - MRI safety officer, a decision was made to perform the MRI study without removal of the CI magnet. A preprocedure CT was performed to evaluate thickness of the bone well around the magnet. Informed consent was obtained from the parent. A mold was created by the otolaryngology department with hearing aid molding material to cover the scalp overlying the CI magnet. Gauze was tightly wound around the head to hold the mold in place over the magnet. The study was performed under general anesthesia. The patient was carefully moved in and out of the magnet bore under supervision of the MRI safety officer. MR imaging of brain was performed on a Philips 1.5T magnet. Low specific absorption rate axial T2, axial FLAIR and sagittal T1 sequences were obtained.
Results
The patient tolerated the study with no evidence of local heating, pain or malfunction of the CI. Clinical examination confirmed no dislocation of the magnet. The images were felt to be diagnostic. Artifacts from the CI were demonstrated in the right parietal, temporal and occipital lobes and lateral aspect of right cerebellar hemisphere. This corresponded to approximately 18% of the brain area at the level of the third ventricle. No artifacts were demonstrated in the bilateral internal auditory canal regions. The artifacts were of similar size on all sequences.
Conclusion
MR imaging on a young child with a CI was performed safely on a 1.5T magnet without removal of the cochlear implant magnet. This case describes the strict technical and safety measures to be followed. The study was of diagnostic quality with the artifact from the implant limited to a small portion of the brain.

KEYWORDS: MR imaging safety, Internal auditory canal, cochlear implant

eP-255

Quantitative Analysis of Cortical Thickness in Children Treated with Craniospinal Radiation versus Posterior Fossa Conformal Radiation Therapy

Stence, N. V.[1]·Plimpton, S. R.[2]·Mirsky, D. M.[1]·Foreman, N. K.[1]·Liu, A.[2]
[1]Children's Hospital Colorado, Aurora, CO, [2]University of Colorado Denver, Aurora, CO.

Purpose
Standard therapy for different posterior fossa tumors can include either craniospinal radiation (CSI) or conformal radiation therapy (CRT). Children who receive radiation therapy as part of treatment for posterior fossa tumors are known to experience long-term neurocognitive delays. Evidence suggests neurocognitive function may be relatively preserved in children treated with CRT versus CSI. Other recent research has attempted to correlate cortical thickness (CT) with measures of intelligence in patients with schizophrenia and in normal controls. In general, there is a positive correlation between CT and IQ. However, CT in various regions of the brain do change rapidly during childhood and adolescence, and the way CT changes over time is influenced by IQ. This study sought to determine if CT in children treated with CSI was measurably different than children treated with posterior fossa CRT.
Materials & Methods
Seventy-nine patients who received radiation therapy for

Note: Scanned images are included in the proceedings. Some submitted images were reduced during editing, thereby decreasing clarity. Also, refer to the Program Planner. Proceedings Content as of 3-29-2013.

the treatment of a brain tumor were included in the analysis. Fifty-one received CSI as standard therapy for their tumor (medulloblastoma, PNET, and nongerminomatous germ cell tumor). Twenty-eight received focal posterior fossa CRT for ependymoma. Analysis included MRI performed after completion of radiation therapy for tumor surveillance. Routine scanning included a noncontrast T1 MPRAGE sequence with isotropic 1 mm voxel size. Reconstruction of the cortical surfaces and measurement of cortical thickness were performed using the FreeSurfer toolkit (version 5.1). Cortical surfaces were reconstructed and parcellated. Patient surfaces were resampled onto an "average brain" for significance mapping. A general linear model was used in FreeSurfer via the QDEC toolbox for statistical analysis. Significance maps were smoothed with a 25 mm kernel. Differences between CSI and CRT were corrected to ignore age in model fitting (age was treated as a nuisance). ANCOVA was used to determine p-values for each CSI versus CRT lobe.

Results

Mean range of follow-up for CSI patients was 38.1 months, and for CRT patients was 23.3 months. Cortical thickness in CSI patients was significantly thinner in the left parietal and left occipital lobes ($p<0.001$), and trended towards significantly thinner in the left frontal lobe ($p<0.108$) (Figure 1). No other statistically significant differences were detected in CT between the two groups.

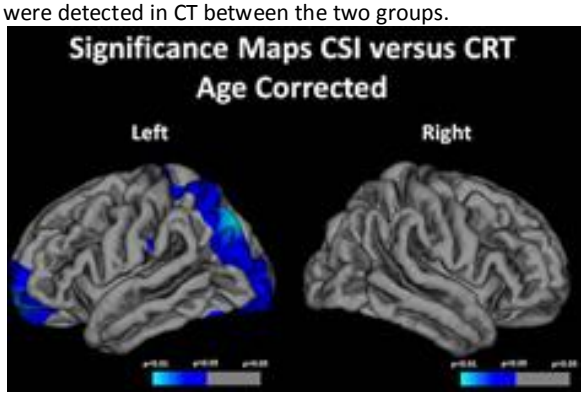

Conclusion

Cortical thickness in children treated with CSI was thinner in the left parietal and occipital lobes compared to children treated with CRT. Further research is needed to correlate CT differences with differences in specific neurocognitive outcomes in these two groups.

KEYWORDS: Cortical thickness, Neoplasm, FreeSurfer

eP-256

Are We Imaging Gently?: Radiation Dose to Children Undergoing Head and Cervical Spine CT at Nonpediatric Hospitals

Burgin, K.·Ramakrishnaiah, R. H.·Kumar, M.·Samant, R.·Shilpa, H.·Van Hemert, R.·Glasier, C. M.·Angtuaco, E.
University of Arkansas for Medical Sciences
Little Rock, AR.

Purpose

Children sustaining trauma are more likely to undergo head and cervical spine CT study at the nearest hospital which is likely a nonpediatric, adult hospital. The purpose of this study is to compare CT parameter and radiation dose to children undergoing CT studies of head and cervical spine at adult hospitals with the parameters and radiation dose at a dedicated tertiary care pediatric hospital.

Materials & Methods

This is a retrospective study at a tertiary care pediatric hospital and a tertiary care university hospital. Head and cervical spine trauma workup CT studies of children with ages between one day to 15 years that are imported via the emergency medical service (EMS) from various adult hospitals across the country to the PACs of a tertiary care pediatric hospital and a university hospital will be selected. Patients will be grouped under three age-specific groups (Group A: one day to five years, Group B: five years to 10 years and Group C: 10 years to 15 years). Ten head CT and 10 cervical spine CT studies will be included under each age group. Exact age-matched groups will be replicated with CT studies of head and cervical spine performed at the tertiary care pediatric hospital with optimized CT parameters compliant with American College of Radiology CT accreditation program requirements. All CT studies will be quality checked and nondiagnostic scans will be excluded from the study. The CT parameters (kVp and mAs), CTDI and DLP will be collected from the dose page of the CT studies. The corrected dose in mSv will be derived using recommended correction factor for patient weight and body size. Statistical analysis for added radiation dose and the significance will be determined.

Results

We expect a significantly higher radiation dose received by pediatric patients undergoing CT studies of head and cervical spine at nonpediatric hospitals without CT technique optimization.

Conclusion

This study emphasizes the role of the radiologist to establish strict protocols in both the pediatric and adult hospital setting to reduce radiation exposure to children.

KEYWORDS: Radiation dose reduction, Radiation safety, pediatric head and cervical spine CT study

Note: Scanned images are included in the proceedings. Some submitted images were reduced during editing, thereby decreasing clarity. Also, refer to the Program Planner. Proceedings Content as of 3-29-2013.

eP-257

Abnormal Findings on Brain MR Imaging in Neurologically Normal Children: Classification Scheme and Process for Reporting and Clinical Followup in a Research Study of Normal Brain Development

Leach, J. L.·Vannest, J.·Schapiro, M.·Holland, S.
Cincinnati Children's Hospital Medical Center
Cincinnati, OH.

Purpose
To describe the MRI findings in normal children recruited for an imaging study of normal development, and define a standardized classification and clinical follow-up process for these studies.
Materials & Methods
MR imaging from 114 subjects recruited for a study of normal brain development (Pediatric Functional Imaging Research Network, NICHD - HHSN275200900018C) formed the study group. Subjects and first degree relatives had a negative history for neurologic or psychiatric disease. Subjects were in normal school classes, reached normal developmental milestones, had no history of head trauma, GA < 37 or >42 weeks, BW >10th percentile, no chronic illness, and normal neurologic examinations. MR imaging was performed at 3T with 1mm isotropic T1-weighted and T2 FLAIR sequences. Imaging evaluation was performed by a board-certified pediatric neuroradiologist with 20 years' experience interpreting pediatric brain imaging. Imaging studies were classified as: 0-normal, 1- normal variant, 2 - possibly clinically significant, 3 - likely clinically significant, 4- cannot interpret (artifact). Studies also were assessed for alteration of normal anatomy (potentially important for grouped normative data) and need for clinical followup. A standardized procedure for image evaluation, reporting, and followup will be presented.
Results
There were 47 males and 67 females in the study group with a mean age of 8.3 years (2 months - 18 years). One hundred twelve studies were evaluated (two were uninterpretable - motion artifact). Fourteen (12.5%) had findings of possible (12) or likely (2) clinical significance. Clinical followup was recommended in 13 (11.7%). Six (5.4%) had distortion of normal anatomy that could impact group morphologic analyses. Likely clinically significant abnormalities included a small 4th ventricular mass, and extensive sinus disease with an obstructive antral choanal polyp. Possibly clinically significant abnormalities included: White matter abnormalities - six, Tonsillar ectopia - two, Callosal anomalies - two, Paranasal sinus opacification - two, Encephalomalacia - one.
Conclusion
Abnormalities were identified in 12.5% of normal children in a research study of normal brain development using MRI. Most required clinical or imaging followup. Six findings (43% of abnormal studies) involved the white matter, which may be difficult or impossible to detect on standard volumetric T1-weighted sequences. Performance of high-resolution FLAIR sequences in the research setting may demonstrate more potential brain pathology. Identified abnormalities may be clinically important and can impact utilization for normative studies. A well defined classification, reporting, and follow-up process is strongly recommended when imaging children in the research setting.

KEYWORDS: Abnormalities, Brain development, Normal language development

eP-258

Can Transcranial Doppler Ultrasound Predict Patient Stay?

Aw, J.·Burrowes, D.·Schoeneman, S. E.·Smith, C. M.·Wainwright, M. S.
Ann & Robert H Lurie Children Hospital of Chicago
Chicago, IL.

Purpose
Transcranial Doppler ultrasound (TCD) is a portable, noninvasive examination assessing measurements of cerebral blood flow velocities, from which the Resistive Index (RI) & Pulsatility Index (PI) can be calculated. The use of TCD has been used primarily with the Stroke Prevention Trial in Sickle Cell Anemia. The value of TCD also has been investigated in the setting of subarachnoid hemorrhage and occlusive carotid and vertebral artery disease. Its use in other indications has not been defined completely, particularly with respect to the value of resistive and pulsatility indices. The purpose of this study is to review the TCD RI and PI in acutely ill patients treated in the pediatric intensive care unit (PICU). The RI and PI were reviewed to determine if there are any statistical correlations between these indices and the patient's hospital stay.
Materials & Methods
IRB approval was obtained. Our limited TCD protocol includes the interrogation of the proximal, middle and distal segments of the middle cerebral artery (MCA). All patients who had undergone a limited TCD between June 1, 2010 and September 19, 2012 were identified on our PAC system. The standard deviations for the average RI and PI for each patient's MCA were correlated with hospital stay using the Pearson's test.
Results
There were 39 patients out of a total of 216 who had multiple TCD exams while in the ICU. Preliminary review of four out of 39 patients, who had multiple TCD's ranging from 4 - 8 TCD exams. The hospital stay in these patients ranged from 12 - 42 days. A strong positive correlation was found with the standard deviation for RI and hospital stay (Right RI r = 0.8, Left RI r = 0.4), a moderate positive correlation with the left PI (r = 0.2) and a moderate negative correlation with the right PI (r = -0.2).
Conclusion
Transcranial Doppler ultrasound has been a proven benefit

in the sickle cell, subarachnoid hemorrhage and occlusive carotid and vertebral artery disease patients. The preliminary data suggest the greater the standard deviation of the RI, the longer the patient remained in the hospital. The higher standard deviation could suggest greater clinical instability and in turn reflect the number of days the patient remained in the hospital. These preliminary data suggest that more work is required in this area to determine a standard deviation that may indicate clinical instability.

KEYWORDS: Ultrasonography, Clinical applications, Clinical outcome

eP-259

High-Resolution MR Imaging Evaluation of Obstetric Brachial Plexus Injury: A Promising Alternative to Traditional CT Myelography

Somashekar, D. K.·Parmar, H.·Ibrahim, M.·Yang, L.
University of Michigan
Ann Arbor, MI.

Purpose
Despite recent improvement in perinatal care, the incidence of obstetric brachial plexus injury (OBPI) is still up to three per 1000 births. Obstetric brachial plexus injuries vary from complete nerve disruption at the level of the brachial plexus (neurotmesis), or nerve root avuslions at the spinal cord level to milder form including neuropraxia (nerve stretching) and axonetmesis (disruption of axon sheath). Clinically it is difficult to characterize the lesion type, as patients may present with similar apparent deficiencies. CT myelography (CTM) currently is considered as the best imaging modality for evaluating nerve root avulsion, and continues to be the most widely practiced technique. Recent improvements in MRI techniques have made MRI an attractive alternative to evaluate nerve root avulsions. Our aim was to demonstrate utility of the novel MRI technique in evaluation of normal spinal nerve roots and in avulsion injuries of these roots.
Materials & Methods
Institutional review board approval was obtained and patient consent waived for this HIPAA-compliant, prospective study. All patients with clinically diagnosed OBPI and who underwent MRI between July 2011 and December 2012 were identified. MR imaging was performed using a high-resolution heavily T2-weighted T2 DRIVE sequence with 0.6 mm slice thickness and using uniform voxel size. MR imaging findings were reviewed by two board-certified neuroradiologists by consensus to document presence of any nerve root avulsion from C5 to T1 and for presence of pseudomeningocele. The operative findings of those patients that went to surgery were reviewed. The surgical findings were compared to the pre-operative MR diagnoses and the comparisons were labeled as either concordant or discordant.
Results
There were 13 patients (nine male, four female) with clinically diagnosed brachial plexus abnormality. Six out of 13 patients went on to surgery during which a total of 19 nerve roots were evaluated. A total of eight avulsions were found at surgery and in 11 other patient the injury was more distal (rupture). Six out of eight avulsions identified at surgery were at C5-6 level, consistent with existing surgical literature, while one nerve root avulsion was identified at C7 and C8 level respectively. The overall sensitivity and specificity of MRI for nerve root avulsion was 75% and 82% respectively. Interestingly, in two patients who had surgically positive nerve root avulsion but negative MRI had no pseudomeningocele at those levels.
Conclusion
Our preliminary results show that high-resolution MRI offers an excellent alternative to CTM in the evaluation of brachial plexus avulsion injuries with similar sensitivity compared to that of CTM. Unlike conventional CTM it is noninvasive and does not use ionizing radiation. Further refinement of the technique and validation of our findings in larger patient population will go a long way in making this as the primary imaging modality for evaluation of OBPIs.

KEYWORDS: Brachial plexus, Brachial plexopathy

eP-260

Age-Related Changes of the “Eye-of-the-Tiger“ Sign in MR Imaging

Stoeter, P.·Vilchez, C.·Roa, P.·Speckter, H.·Perez-Then, E.·Oviedo, J.
CEDIMAT
Santo Domingo, DOMINICAN REPUBLIC.

Purpose
To describe and quantify changes of the “eye-of-the-tiger” sign with increasing age in patients with pantothene-kinase associated neurodegeneration (PKAN), and to look for an imaging parameter which might be related to the progression of the disease.
Materials & Methods
Included were the MR data from 30 patients (four to 76 years old) and three genetically positive cases (seven to 11 years old) without clinical manifestation, all with a confirmed mutation of the PKAN2 gene. Evaluation was based mainly on T2-, T2*, diffusion- and T1-weighted scans including measurement of the extension of the hypointense part of the “tiger’s eye”.
Results
The youngest (4-year-old) patient presented with a hyperintensity in the globus pallidus in T2-weighted images, but without reduction of diffusion, and only the T2* sequences showed a tiny signal drop below this area. Whereas this patient was already symptomatic, the three “preclinical” cases presented the classical “tiger’s eye”. Six

Note: Scanned images are included in the proceedings. Some submitted images were reduced during editing, thereby decreasing clarity. Also, refer to the Program Planner. Proceedings Content as of 3-29-2013.

older patients, however, did not show the typical bright spot. The extent of the hypointense area was significantly ($p<0.01$) correlated to age, but not to the degree of dystonia ($p>0.05$). The maximum of signal loss was localized in the area below the "tiger's eye", corresponding exactly to a severe and circumscribed hypointensity in T1-weighted images in eight patients. Otherwise, the globus pallidus was diffusely hyperintense in T1-weighted except from the "tiger's eye". This area was iso- or slightly hypointense in T1-weighted sequences, but in four cases, it was seen as a bright spot in both T1- and T2-weighted imaging.

Conclusion

The changes of the "eye-of-the-tiger" sign with increasing age correspond well to the current hypotheses of an early lesion turning into an area of gliosis, and an accumulation of iron in the globus pallidus which starts below this lesion and increases over time. Its varying appearance in different MR sequences can be explained by the susceptibility effects of this paramagnetic substance. However, some questions about the preference of the lesion and the accumulation of iron to affect two different areas in the anterior part of the globus pallidus, and about the latency between the acute stage and the clinical manifestation remain open. Because the extent of the iron accumulation is not significantly correlated to the degree of dystonia, we cannot recommend use of it as a parameter for disease progression.

KEYWORDS: Iron deposition, Basal ganglia disease

eP-261

Arachnoid Cysts and Intracranial Arteriopathy as Hallmarks of Neural Crest Involvement in Tuberous Sclerosis

Boronat, S.·Thiele, E.·Johnson, J.·Caruso, P.
Massachusetts General Hospital
Boston, MA.

Purpose

Some clinical findings in tuberous sclerosis complex (TSC), such as hypomelanotic macules are related to maldevelopment of the neural crest (NC), which is also the origin of the cranial meninges and some of the intracranial vessels. The purpose of this study is to evaluate the frequency and characteristics of menigeal involvement and intracranial arteriopathy in TSC in a large cohort of patients and to review the pertinent literature.

Materials & Methods

We reviewed the brain MRIs of 220 patients with definite clinical diagnosis of TSC for arachnoid cysts, meningiomas, and intracranial arterial anomalies of neural crest origin. We then reviewed the literature with regard to these findings.

Results

Features of intracranial arteriopathy on MRI were detected in four of 220 (1.8%) patients with TSC higher than the frequency found on studies of incidental MRI findings in the normal asymptomatic population (0.5%,0.21% to 0.87%). The internal carotid artery (ICA) was the most frequently affected. 5.6% of patients (12 out of 220) had arachnoid cysts (ACs) higher than the prevalence found on MRI in asymptomatic individuals (0.35%, 0.13% to 0.67%). Three patients showed two or more ACs and two of these patients had associated autosomal dominant polycystic disease (ADPKD), which also predisposes to ACs and is also known to be associated with an increased risk for intracranial aneursyms. One patient had a meningioma. One patient presented with a clinical diagnosis of TSC, no intracranial tubers or subependymal nodules (SENs) on imaging, but showed an intracranial AC, a phenotype that we propose as the neural crest-specific phenotype of TSC. Arterial aneurysms, mostly aortic and intracranial, have been reported as a rare finding in TSC and two cases of arachnoid cysts (ACs) and two cases of meningiomas have been reported to date in TSC; however, the literature contains to date only case reports of these neural crest-related manifestations, and our study represents the only large systematic review.

Conclusion

Neural crest (NC) related pathology presents with a higher frequency in TSC than in the general population. Meninges, intracranial smooth vascular cells (SMCs), and pericytes of the forebrain are of NC origin. Arachnoid cysts and intracranial arteriopathy are part of the clinical spectrum of TSC and may be present in patients with the NC-specific phenotype.

KEYWORDS: Tuberous sclerosis

eP-262

Diffusion Tensor Imaging of the Pediatric Thoracic Spinal Cord Using a Short Echo Time Inner Field-of-View Sequence

Middleton, D. M.[1]·Mohamed, F. B.[1]·Barakat, N.[2]·Finsterbusch, J.[3]·Faro, S. H.[1]·Shah, P.[1]·Samdani, A.[2]·Mulcahey, M.[2]
[1]Temple University, Philadelphia, PA, [2]Shriners Hospital for Children, Philadelphia, PA, [3]University Medical Center Hamburg-Eppendorf, Hamburg, GERMANY.

Purpose

Studies of the cervical spinal cord (SC) in subjects with spinal cord injury (SCI) have shown good correlation between DTI values and clinical examination results. Extending this technique to the thoracic SC is challenging due to physiologic motion which is more prevalent in the thoracic region. In the cervical SC, use of an inner field-of-view (iFOV) sequence has been shown effective in producing good quality images. The purpose of this study was to implement and evaluate the iFOV DTI sequence for imaging of the pediatric thoracic SC in normal and injured subjects.

Materials & Methods

Note: Scanned images are included in the proceedings. Some submitted images were reduced during editing, thereby decreasing clarity. Also, refer to the Program Planner. Proceedings Content as of 3-29-2013.

Eight pediatric subjects, six typically developing (TD) subjects without evidence of SC pathology and two patients with SCI were recruited. Imaging was performed using a short echo iFOV echo-planar DTI sequence. This sequence was implemented on a 3.0T Siemens Verio MR scanner and optimized for imaging the thoracic SC. Images were acquired axially along the SC. Sequence parameters used were: 20 directions, b = 1000s/mm^2, voxel size = 1.2x1.2x3 mm^3, slices=50, TR=7400 ms, TE=89 ms, averages=3. Due to length of the thoracic SC, imaging was split into two slabs with acquisition time was approximately seven minutes per slab. Motion correction was applied and tensor estimation was performed on the corrected images. Regions of interest (ROIs) were drawn on each axial slice along the length of the thoracic SC in the center of the cord to minimize averaging of the SC with surrounding cerebrospinal fluid (CSF). Values for fractional anisotropy (FA), mean diffusivity (MD), axial diffusivity (AD), and radial diffusivity were calculated for each ROI.

Results

Images were acquired successfully using the iFOV sequence. Midline sagittal images reconstructed from axial slices showed good cord/CSF delineation in both TD subjects (Figure 1a:T1-T8,1b:T7-L1) and subjects with SCI (Figure 1c:T1-T10,1d:T7-L2). Mean indices for TD subjects were FA = 0.42 ± 0.05, MD = 0.52 ± 0.09, AD = 0.75 ± 0.09, RD = 0.40 ± 0.05. Subjects with SCI showed decreases in FA and increases in diffusivity indices (mean values FA = 0.24 ± 0.04, MD = 0.63 ± 0.10, AD = 0.79 ± 0.10, RD = 0.56 ± 0.09).

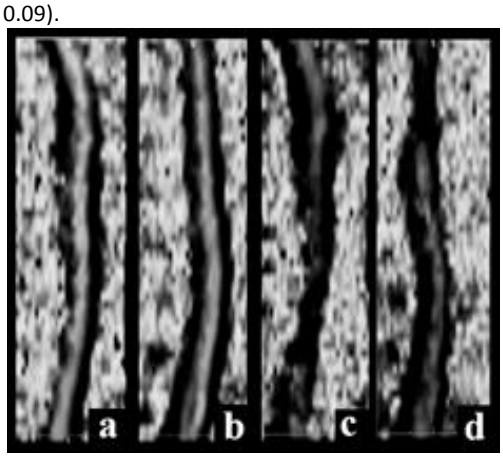

Conclusion

The iFOV sequence used was effective in acquiring DTI images of the pediatric TSC with less distortion. Subjects with SCI exhibited decreased FA and increased diffusivity indices when compared to TD subjects. These results are extremely promising and warrant data collection in a large group of subjects.

KEYWORDS: Diffusion tensor image, Spinal cord, Pediatric

Monday, May 20 – Wednesday, May 22
6:30 AM – 9:00 PM
Thursday, May 23
6:30 AM – 3:00 PM
Hall B1

Electronic Posters (ePosters) 263 – 272

ePosters-Socioeconomics

Note: A missing printed number indicates an abstract has been withdrawn.

eP-263

Match Day: Online Search Trends Reflect Real-Time Interest in Neuroradiology Training

Harsha, A.·Schmitt, J.·Mohan, S.
University of Pennsylvania
Philadelphia, PA.

Purpose

Internet search trends have been shown to parallel the growth of consumer interest in products and services across many industries. The purpose of this study is to identify and characterize temporal relationships between the growth in the neuroradiology fellowship applicant pool and related internet search engine queries.

Materials & Methods

From July 1, 2006 to July 1, 2011, the Google Trends tool was used to analyze search engine query data for "neuroradiology fellowship" and related terms to identify individuals seeking information regarding fellowship training. These terms returned a search volume index (SVI) representing the search frequency relative to the total search volume during the study interval and geographic region for the United States during each academic year. Results were compared with National Residency Match Panel Specialties Matching Services (NRMP-SMS) match data using a Pearson correlation analysis. Regression analysis was employed to characterize annual search trends and peak search activity.

Results

Normalized mean annual search traffic for neuroradiology fellowship increased by 46% over the 60-month study period. There was an annual mean SVI increase of 10% (range 7 - 32%; SD 17%), with a linear increase in yearly SVI over time. There was a similar increase in total neuroradiology fellowship applicants (57% increase) over

Note: Scanned images are included in the proceedings. Some submitted images were reduced during editing, thereby decreasing clarity. Also, refer to the Program Planner. Proceedings Content as of 3-29-2013.

the study interval. Annual SVI approached statistical significance in predicting the total number of applicants for that match year (R_2= 0.71, p = 0.17). Additionally, there were statistically significant differences in SVI by month (p = 0.041) with greatest increase in mean SVI observed in December (52% increase; range 16 - 69%; SD 22%).
Conclusion
There has been an overall increase in internet search traffic related to neuroradiology fellowship with a correlation to the annual growth in total number of fellowship applicants. Reflected in this trend is an annual peak in search traffic in December corresponding to the NRMP application cycle. In-depth analysis of internet search queries mirror real-time trends in radiology trainee professional interests and may provide useful information for fellowship directors to attract potential candidates.

KEYWORDS: Fellowship, Trend analysis, information technology

eP-264

Acute TeleStroke Management and Therapy System Using Mobile Phone and Tablet

Takao, H.[1]·Murayama, Y.[1]·Ishibashi, T.[1]·Karagiozov, K. L.[1]·Vinuela, F.[2]
[1]The Jikei University School of Medicine, Tokyo, JAPAN, [2]University of California Los Angeles, Los Angeles, CA.

Purpose
Physicians must quickly evaluate acute stroke patients to determine treatment. Prompt diagnosis and treatment of cerebral stroke patients are essential for their recovery. With the increasing demands for management of stroke, shortening the time of decision making through telemedicine is becoming important. Based on this hypothesis, we developed a telestroke system in Japan (called “Synapse ERm”) for faster access to diagnostic images and clinical information.
Materials & Methods
This system is based on transferring patient data, images, movies (Angio and/or operating room), and face-to-face meeting between hospital systems and participating medical staffs in and out of the hospital, using their standard, currently utilized mobile devices (iPhone, Andorid) and Tablet. The system is able to transfer clinical data, CT, MR, echo, angiographic and intraoperative images and expert opinion in real time like Facebook and Twitter. It also provides tools for management of diagnosis and treatment information, for example, simple calculation of appropriate drug dosage, modified Rankin Scale and perfusion diffusion mismatch.
Results
A pilot application of the system in our hospital showed adequate performance and proper information transfer, resulting in proper diagnosis and management of all stroke patients. This system was installed at our institution in August 2010, for communication with our affiliated hospitals. Over 161 stroke calls were initiated until the end of July 2012.

Conclusion
The telestroke system proved to be efficient for appropriate standard management in most time-demanding treatments of stroke. It is our belief that utilization of this system with handheld devices will make it possible to help and save the lives of more stroke patients.

KEYWORDS: Teleradiology, Structural network, telestroke

eP-265

Reports and Studies of Uncommon Conditions with Critical Intracranial Imaging Findings Are More Frequently Published in the Nonradiology Compared to the Radiology Literature

Doolittle, D.·Lehman, V. T.·Schwartz, K.·Eckel, L.
Mayo Graduate School of Medical Education
Rochester, MN.

Purpose
Imaging findings of CNS disease are reported both in the peer-reviewed radiology and in the clinical literature. Given changes in radiology journal preferences, we hypothesize that recent primary reports and studies of imaging features of several uncommon diseases with intracranial manifestations are more frequent in the nonradiology literature.
Materials & Methods
PubMed searches from 12/1/2007-12/1/2012 were performed for four uncommon CNS diseases with intracranial imaging manifestations using the following search terms: 1.) ‘Susac Syndrome OR Susac’s Syndrome’ 2.) ‘(transient lesion OR reversible lesion) AND corpus callosum’ 3.) ‘amyloid beta related angiitis OR ABRA OR amyloid vasculitis’ and 4.) ‘Parry Romberg Syndrome OR en coup de sabre’. Included case reports or series contained figures and text of imaging features; included original research contained, at minimum, descriptions of imaging findings of included patients. Exclusion criteria

Note: Scanned images are included in the proceedings. Some submitted images were reduced during editing, thereby decreasing clarity. Also, refer to the Program Planner. Proceedings Content as of 3-29-2013.

were: 1.) Non-English language, 2.) Review article and 3.) Non-target diagnosis captured by search terms. Articles were characterized as case reports, case series or original research. Original research was categorized as containing either: 1) Only description of imaging findings of study patients or 2) Specific assessment of an imaging technique or systematically studied imaging features of the disease were noted. Journals were categorized as radiology or nonradiology.

Results

One hundred twenty-one articles (95 case reports, 15 case series, and 11 original research) met inclusion criteria, 30 for Susac's Syndrome, 53 for transient lesion of the corpus callosum, 13 for amyloid beta related angiitis (ABRA), and 25 for Parry Romberg Syndrome. One hundred five articles were derived from nonradiology journals; 16 from radiology journals. Eight original research articles specifically assessed imaging techniques or imaging features, all eight in nonradiology journals. Two original research articles assessed imaging features of ABRA including leptomeningeal enhancement, one assessed mass-like lesions with ABRA, one characterized the intracranial imaging findings in Parry-Romberg Syndrome, two assessed diffusion tensor imaging findings with Susac's Syndrome, one assessed rate of lesions in the corpus callosum and rate of contrast enhancement with Susac's Syndrome, and one compared the appearance of Susac's lesions to multiple sclerosis lesions at 7T.

Conclusion

Reports and studies of the selected uncommon diseases with intracranial manifestations are far more frequent in clinical journals when compared to dedicated radiology publications. A substantial proportion of uncommon disease imaging findings are in the form of case reports, which frequently are published in nonradiology journals. Radiologists should review both radiology and nonradiology journals when searching for reports of imaging features of uncommon diseases affecting the brain. Radiologists should consider further study of these diseases with publications within the radiology literature.

KEYWORDS: Susac's syndrome, Amyloid, radiology literature

eP-266

Are NIH-Funded Articles Cited More? A Study of the American Journal of Neuroradiology

Davis, M. A.·Castillo, M.·Henderson, L.
University of North Carolina-Chapel Hill
Durham, NC.

Purpose

We evaluated whether or not funding through the National Institutes of Health (NIH) has any bearing on the citation counts of published works. We looked at papers published in the American Journal of Neuroradiology (AJNR) and hypothesize that papers without NIH funding are cited just as much as those with NIH funding.

Materials & Methods

Through the Thomson Reuters database "Web of Knowledge" we accessed all articles published in AJNR from 1997- 2007 using specific filters and keywords. Data then were filtered for NIH and non-NIH-funded studies. NIH funded AJNR publications also were accessed through the Research Portfolio Online Reporting Tools (RePORT) powered through the NIH. The number of citations per article was extracted from the "Web of Knowledge" database. We identified the total number of citations per article and per year, to date, and extracted these data into total AJNR publications, AJNR publications funded through NIH, and AJNR publications not funded through NIH. We defined a publication as having NIH funding if it was stated in the authors notes as having funding through the NIH or if the publication was stated as funded under the RePORT database. Only original, full-length, research articles were used. Using the raw data a t-test for significance was performed.

Results

A total of 3761 original research articles were published in the AJNR between 1997 and 2007. Of this number 169 articles were funded through NIH. NIH-funded articles showed an average of 32.79 citations per article with an average of 2.03 citations per year. Non-NIH-funded articles received an average of 24.74 citations per article and an average of 1.51 citations per year. NIH-funded publications comprised 6% of all citations for AJNR publications. These findings were statistically significant with p =.001.

Conclusion

In AJNR, NIH-funded publications were cited more often than those that were not funded.

KEYWORDS: AJNR, citations

eP-267

Moving Forward: Lessons Learned from a Multiphase Practice Quality Improvement Initiative Aimed at Addressing Appropriate Utilization of Screening CT in the Emergency Department

Griffith, B.·Vallee, P.·Krupp, S.·Jung, M.·Slezak, M.·Nagarwala, J.·Loeckner, C. P.·Jain, R.
Henry Ford Hospital
Detroit, MI.

Purpose

The purpose of this project is to discuss the lessons learned over the course of our multiphase practice quality improvement (PQI) initiative aimed at improving utilization of screening cervical spine CT in the emergency department. The project will address issues related specifically to improvements in appropriate utilization of cervical spine CT, as well as general issues of project development, implementation, and analysis as they relate to addressing appropriate utilization of all imaging.

Materials & Methods

Note: Scanned images are included in the proceedings. Some submitted images were reduced during editing, thereby decreasing clarity. Also, refer to the Program Planner. Proceedings Content as of 3-29-2013.

Despite the availability of screening criteria for cervical spine imaging [National Emergency X-Radiography Utilization Study (NEXUS) and Canadian Cervical Spine Rule (CCR)], many patients continue to be imaged without meeting these criteria. The goal of this multiphase PQI initiative was to assess appropriate utilization of screening cervical spine CT in the emergency department following blunt trauma and whether educating clinicians regarding these criteria could improve over-utilization rates. The study was designed in three phases: Phase 1 was a retrospective evaluation of all cervical spine CT examinations performed following blunt trauma. Phase 2 was a collaborative prospective study between the Departments of Radiology and Emergency Medicine, assessing utilization following introduction of an ordering clinician survey. Phase 3 was reassessment of utilization following implementation of an education initiative. Each phase evaluated appropriate utilization according to the NEXUS criteria with emphasis on the ACR Appropriateness Criteria in Phases 2 and 3. This exhibit will discuss the design, implementation, and results of the project's three phases, exploring potential reasons for "over-utilization", as well as methods for improving appropriate use of imaging. The exhibit also will discuss PQI requirements related to maintenance of certification (MOC) and provide a guide to implementing similar PQI projects at other institutions.

Results

Of 1524 patients without injury evaluated during Phase 1, 23.9% had no documentation of any of the five NEXUS low-risk criteria and therefore were potentially unnecessary examinations. Following introduction of an ordering clinician survey documenting study indication, the rate of "over-utilization" decreased to 16.1% in Phase 2. This rate further decreased to 13% following implementation of a clinical education program. The findings of our multiphase PQI project show that despite availability of screening tools for cervical spine imaging, many patients continue to be imaged without meeting these criteria. The findings also show that simply educating ordering clinicians regarding appropriate criteria is effective in decreasing unnecessary studies and improving patient care. Applying the methods used in this multiphase approach to utilization of other imaging studies has potential to significantly impact patient care across the healthcare spectrum.

Conclusion

The lessons learned from this study have important implications not only for radiology, but for the future of healthcare across the country. With limited resources and more patients, there is emphasis on appropriate utilization of all healthcare resources, with much attention directed towards medical imaging. Therefore, it is incumbent upon radiologists to take the lead in addressing appropriate use of all imaging studies. This project lays out an achievable method of assessing and improving appropriate utilization of imaging while also fulfilling maintenance of certification requirements.

KEYWORDS: Overutilization, Utilization management, cervical spine

eP-268

Discrepancies between Gender and Use of Brain MR Imaging: Analysis of Indications, Pathology, and Interventions

Lau, D.·Bentley, J. N.·Maher, C. O.·Shah, G. V.
University of Michigan Health System
Ann Arbor, MI.

Purpose

Ever since the use of magnetic resonance imaging (MRI), female patients tend to undergo more brain MRIs than males; the reason for this and its consequences remain unclear. In this study, we identified the most common indications and assess the indication differences between female and male. We also evaluate whether certain indications are more likely associated with pathology and/or interventions between males and females.

Materials & Methods

All brain MRIs from 1997 to 2009 were identified. Analysis for differences in frequency and number of brain MRIs between genders was performed. Next, 100 male and 100 female MRIs were randomly selected in seven age groups. Repeat MRIs and patients aged less than 18 were excluded. Data regarding indication, pathology, need for neurology and/or neurosurgery consultation, and intervention/surgery were collected. Descriptive statistics and chi-squared test were employed to assess outcome differences between genders by age and specific indications.

Results

A total of 48,417 brain MRIs were performed: 20,327 males and 28,090 females. Males underwent greater numbers of MRIs in patients 18 years and younger. But from 19 years and on, females underwent more MRIs; there were peaks in the third and eighth decade. After randomized selection, 1,236 patients remained. The three most common indications for brain MRI were neoplasia, headache, and cranial nerve deficit. When stratified by indications, males underwent significantly more MRIs than females for cranial nerve deficit (13.5% vs. 9.7%, $p=0.037$) and cognitive disorders (11.2% vs. 7.7%, $p=0.038$). Females underwent significantly more MRIs than males for headache (8.2% vs. 16.3%, $p<0.001$) and endocrine disorders (1.8% vs. 5.0%, $p=0.002$). However, among these four indications, there were no significant differences in pathology, consultation, and interventions between males and females. Rather males underwent significantly more neurosurgical interventions for an indication of neoplasia (28.7% vs. 12.2%, $p=0.010$), and males had significantly higher rates of major pathology for an indication of vascular concern (63.0% vs. 42.6%, $p=0.034$).

Note: Scanned images are included in the proceedings. Some submitted images were reduced during editing, thereby decreasing clarity. Also, refer to the Program Planner. Proceedings Content as of 3-29-2013.

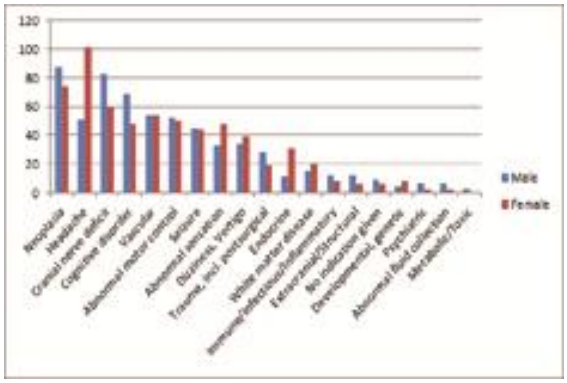

Conclusion

During childhood and adolescent ages, males tend to undergo more brain MRI studies, but after the first two decades females undergo more brain MRIs. The higher incidence of headaches possibly explains the higher rates and numbers of brain MRI; however, there is no difference in presence of pathology, need for consultation, and intervention. Rather a suspicion/indication for neoplasia in males was associated with higher rates of need for neurosurgical intervention. Decisive use of brain MRI is warranted, especially for patients with headache and without neurologic deficits.

KEYWORDS: Sex differences, MR imaging brain, indications

eP-269

Effect of Adaptive Statistical Iterative Reconstruction on Patient Dose in Neuroradiology Computed Tomographic Studies

Komlosi, P.·Zhang, Y.·Ornan, D.·Wintermark, M.
University of Virginia
Charlottesville, VA.

Purpose

Adaptive statistical iterative reconstruction (ASIR) is a signal processing method that can decrease image noise, thereby computed tomographic (CT) images of comparable diagnostic quality can be obtained using less radiation. The purpose of this study is to quantify the effect of systematic use of ASIR versus filtered back projection (FBP) for neuroradiology CT protocols on patients' radiation dose and image quality.

Materials & Methods

This retrospective, HIPAA-compliant study was approved by our institutional review board, with waiver of informed consent. We evaluated the effect of ASIR on six types of neuroradiologic CT studies: unenhanced brain CT in adult patients, unenhanced brain CT in pediatric patients, adult cervical spine CT, adult cervical and intracranial CT angiography, adult soft tissue neck CT with contrast, and adult lumbar spine CT. For each type of CT study, two series of 100 consecutive studies were reviewed: 100 studies performed with FBP and 100 studies performed with ASIR of 40%. Dose modulation was systematically used, with appropriate noise indices for FBP and ASIR. For each examination, the weighted volume CT dose index (CTDIvol) and dose-length product (DLP) were recorded and noise was measured. Each study also was reviewed for image quality by a board-certified neuroradiologist, and noise was measured as the standard deviation of the CT density in the patient's background. Continuous variables (CTDIvol, DLP, noise) were compared by using t-tests, and categorical variables (image quality) were compared by using Wilcoxon rank-sum tests.

Results

For adult cervical and intracranial CT angiograms, the CTDIvol and DLP, respectively, were reduced by 28.5% and 21.6%, respectively, by using ASIR versus FBP. Significant dose reductions ($P < .001$) also were observed for adult unenhanced brain CT and lumbar CT studies performed with ASIR. Analysis is ongoing for pediatric unenhanced, neck soft tissue and cervical spine CT studies, and complete results will be presented at the ASNR meeting. Image quality and noise were similar for both FBP and ASIR.

Conclusion

Use of advanced statistical iterative reconstruction for neuroradiology CT examinations affords significant dose reduction while maintaining image quality.

KEYWORDS: Dose reduction, CT, ASIR

eP-270

Prevalence of Subsequent Intracranial Neoplasms on Screening MR Imaging in Long-Term Survivors of Childhood Acute Lymphoblastic Leukemia

Sabin, N. D.·Santucci, A.·Klimo, P.·Zhang, N.·Srivastava, D.·Pui, C.·Hudson, M. M.·Krull, K. R.·Kun, L.·Krasin, M.·Reddick, W. E.·Hillenbrand, C.·Ogg, R.·Patay, Z.·Robison, L. L.·Armstrong, G. T.
St. Jude Children's Research Hospital
Memphis, TN.

Purpose

To determine the prevalence of intracranial neoplasms on screening magnetic resonance imaging (MRI) in a group of long-term survivors of childhood acute lymphoblastic leukemia (ALL) who presented with no overt neurologic complaints.

Materials & Methods

One hundred sixty-four long-term survivors of childhood ALL [including 125 treated with cranial radiation therapy (CRT)] underwent unenhanced screening MRI examination of the brain as part of a larger study of neurocognitive outcomes. The median age at the time of the study was 30.8 years (range 19-51 years) and the median time from diagnosis of ALL was 25.5 years (12-46 years). MRI examinations were reviewed by a single neuroradiologist. Demographic and treatment data were compared for survivors with and without subsequent neoplasms.

Results

Note: Scanned images are included in the proceedings. Some submitted images were reduced during editing, thereby decreasing clarity. Also, refer to the Program Planner. Proceedings Content as of 3-29-2013.

Eighteen of 164 survivors (11%) had a total of 30 subsequent intracranial or craniocervical junction neoplasms. All survivors who had a subsequent neoplasm had received CRT. Development of intracranial neoplasm was associated with CRT exposure (p=0.0076) but not with sex, race/ethnicity, age at diagnosis or chemotherapy exposure. Among the 125 patients who had received CRT, 18 (14.4%) developed subsequent tumors and 14 (78%) of those received CRT doses ≥ 20 Gy. All patients with subsequent neoplasms were greater than 20 years from their primary cancer diagnosis. Six patients had multiple tumors. All but two subsequent neoplasms were supratentorial. Notably, all patients presented with no overt neurologic complaints. Three tumors (17%) involved the superior sagittal sinus. A single craniocervical junction neoplasm displaced and deformed the upper cervical spinal cord. By noncontrast MRI, the neoplasms were most suggestive of meningiomas. Six tumors were resected. By histopathology, four of these were WHO grade 1 meningiomas, one was a WHO grade 2 atypical meningioma and one was a meningioma with unspecified grade. One lesion was treated with gamma knife radiotherapy without biopsy or resection. The remaining patients are being followed with serial imaging.

Conclusion

Adult survivors of childhood ALL who received CRT are at long-term risk of developing intracranial or craniocervical junction neoplasms and the prevalence of these neoplasms increases with length of time from primary cancer diagnosis. We detected a higher percentage of intracranial neoplasms in survivors treated with cranial RT than in earlier reports of such neoplasms in ALL survivors up to 20 years post-therapy. As all of our survivors with neoplasms were greater than 20 years post-diagnosis, this likely reflects the long latency period for the development of meningiomas resulting in increased detection over time. In addition, the prevalence may be underestimated since the MRI examinations for this series were obtained without intravenous contrast. The patients in our study presented with no overt neurologic complaints despite the fact that some tumors demonstrated significant mass effect or involved the superior sagittal sinus suggesting the need for periodic screening with brain MRI of long-term survivors of childhood ALL who received CRT.

KEYWORDS: Radiation effects, Leukemia, subsequent neoplasms

eP-271

Initial Utilization of a New MR Acute Stroke Protocol

Kubal, W. S.·Meshksar, A.·Nael, K.
University of Arizona
Tucson, AZ.

Purpose

We recently introduced a new MR acute stroke protocol in our institution. Following educational presentations and introduction of the new protocol into clinical practice, we noted a dramatic increase in utilization. We were concerned that the new procedure might be over utilized due to supplier-induced demand. Supplier-induced demand may occur when asymmetry of information exists between the supplier and the consumer particularly with the introduction of a new product or service. The purpose of this study is to compare utilization and incidence of positive results of the new protocol with the old protocol.

Materials & Methods

The former acute stroke protocol took approximately 20 minutes of imaging time. The new stroke protocol takes only approximately 10 minutes of imaging time. The time saving was largely achieved by replacing the time-of-flight MRA with a comprehensive contrast-enhanced MRA. The diffusion-weighted sequence in each protocol is comparable. The accuracy and efficiency of the new protocol has been reported previously. Forty-three consecutive patients underwent the old acute stroke protocol MR imaging between June 01 and August 30 and 156 consecutive patients underwent the new acute stroke protocol MR imaging between September 10 and December 9. An experienced neuroradiologist reviewed all patients. Inclusion criteria were history of an acute neurologic deficit and successful completion of the exam. The final groups consisted of 38 patients in the old protocol group and 141 patients in the new protocol group.

Results

The increase in utilization over a comparable time period was both dramatic and highly statistically significant. A positive result was defined as restricted diffusion compatible with acute infarct. In the old protocol group 10/38 = 26% and in the new protocol group 32/141 = 23% showed a positive result. These data were analyzed with a z-test for uncorrelated samples and $z = 6.88$, $p < 0.001$. This result is highly significant for the same incidence of positive results in each group despite a great increase in utilization.

Conclusion

The rapid growth of medical technology has provided physicians with an increased ability to diagnose abnormalities and treat patients. New technologies are strongly advocated and may become widely used without careful assessment of their appropriate role in the care of patients. When there is an asymmetry of information, there is potential for an artificial increase in demand. We were concerned that a new protocol we introduced for diagnosis and characterization of acute stroke might be over utilized. We found that although utilization had increased dramatically, the incidence of positive results was statistically unchanged both before and after introduction of the new scan protocol. We speculate that the increase in patients being scanned reflects adoption of the new protocol over less comprehensive imaging algorithms. Due to the shortened imaging time of the new protocol, there was a lower resource cost for each positive diagnosis.

Note: Scanned images are included in the proceedings. Some submitted images were reduced during editing, thereby decreasing clarity. Also, refer to the Program Planner. Proceedings Content as of 3-29-2013.

KEYWORDS: Utilization rates, Acute stroke

eP-272

Limited Headache Imaging Using an Axial FLAIR Pulse Sequence

Besachio, D. A.·Abele, T. A.·Davidson, H.·Quigley, E.·Rassner, U.
University of Utah
Salt Lake City, UT.

Purpose
Neuroimaging often is performed in the setting of non-acute, non-focal headache. Studies have shown that in the setting of non-acute headache magnetic resonance (MR) imaging demonstrates clinically significant findings in only 0.6-1.5% of cases. The fluid-attenuated inversion recovery (FLAIR) sequence has proven useful in evaluation of a broad array of intracranial pathologies and thus may be useful as a screening sequence for the evaluation of nonacute headache. The purpose of this study is to determine the feasibility of limited brain MR imaging using a single noncontrast axial FLAIR sequence to screen patients with nonacute, nonfocal headache.
Materials & Methods
A radiology information system search was performed for history of "headache" in brain MR imaging from May through November 2012. Subjects with an acute presentation, a history of malignancy, seizure, demyelinating disease or specifically stated focal neurologic findings were excluded. Imaging orders requested with a disease specific MRI protocol (e.g., multiple sclerosis protocol) also were excluded. A neuroradiologist with a certificate of added qualification blinded to the results of the complete MR scan independently reviewed the single axial FLAIR sequence of each study. The examiner was asked to identify abnormalities, indicate whether further examination was felt to be necessary, and why further imaging was needed. Findings from the single axial FLAIR sequence were compared to those from the full MR scan to assess the utility of FLAIR imaging as a screening sequence.
Results
A preliminary data set of 50 subjects was identified meeting inclusion criteria. Patient ages were 18-80 years (mean 41 years). Based on the single axial FLAIR sequence, the neuroradiologist requested additional imaging in 15 of 50 subjects. Based on the full examination, eight subjects had a finding that could explain their headache or had nonheadache-related findings requiring further evaluation (Table 1). All eight of these subjects were identified correctly in the 15 subjects for which additional imaging was requested. Sensitivity and specificity of the single axial FLAIR sequence for identification of a possible source of headache or other nonheadache-related finding requiring followup was 100% and 81%, respectively.

Findings in data set with (*) indicating a potential headache source or other important finding.

Intracranial pathology	Number	%
Nonspecific white matter disease	20	40
Normal	19	38
Anatomical variant	4	8
Chiari 1*	3	6
Neoplasm*	2	4
Demyelinating disease*	2	4
Parenchymal hemorrhage*	1	2

Conclusion
A single axial FLAIR sequence interpreted by a neuroradiologist may be adequate to screen patients with nonfocal, nonacute headache.

KEYWORDS: FLAIR, Headaches

Monday, May 20 – Wednesday, May 22
6:30 AM – 9:00 PM
Thursday, May 23
6:30 AM – 3:00 PM
Hall B1

Electronic Posters (ePosters)
273 – 304

ePT-Spine

Note: A missing printed number indicates an abstract has been withdrawn.

Note: Scanned images are included in the proceedings. Some submitted images were reduced during editing, thereby decreasing clarity. Also, refer to the Program Planner. Proceedings Content as of 3-29-2013.

eP-263

Practical MR Imaging Grading System for Cervical Foraminal Stenosis Based on Oblique Sagittal Images

Park, H. J.
Sungkyunkwan University School of Medicine, Kangbuk Samsung Hospital
Seoul, KOREA, REPUBLIC OF.

Purpose
To propose a new and practical MRI grading method for cervical neural foraminal stenosis and to evaluate its reproducibility.
Materials & Methods
We evaluated 50 patients (M:F = 37:13, mean 49 years) who visited our institution and underwent oblique sagittal MRI of the cervical spine. A total of 300 foramina and corresponding nerve roots in 50 patients were analyzed qualitatively from C4-5 to C6-7. We assessed the grade of cervical foraminal stenosis at the maximal narrowing point according to the new grading system based on T2-weighted oblique sagittal images. The incidence of each of the neural foraminal stenosis grades according to cervical level was analyzed by chi-square tests. Intra and interobserver agreements between two radiologists were analyzed using kappa statistics. Kappa value interpretations were poor ($k < 0.1$), slight ($0.1 \leq k \leq 0.2$), fair ($0.2 < k \leq 0.4$), moderate ($0.4 < k \leq 0.6$), substantial ($0.6 < k \leq 0.8$), and almost perfect ($0.8 < k \leq 1$).
Results
Significant stenoses (grades 2 and 3) were rarely found at the C4-5 level. The incidence of grade 3 at the C5-6 level was higher than at other levels, a difference that was statistically significant. The overall intraobserver agreement according to cervical level was almost perfect. The agreement at each level was almost perfect, except for only substantial agreement at the right C6-7 by reader 2. No statistically significant differences were seen according to cervical level. Overall kappa values of interobserver agreement according to cervical level were almost perfect. In addition, the agreement of each level was almost perfect. Overall intra and interobserver agreement for the presence of foraminal stenosis (grade 0 vs. grades 1, 2, and 3) and for significant stenosis (grades 0 and 1 vs. grades 2 and 3) showed similar results and were almost perfect. However, only substantial agreement was seen in the right C6-7.
Conclusion
A new grading system for cervical foraminal stenosis based on oblique sagittal MRI provides a reliable assessment and good reproducibility. This new grading system is a useful and easy method for the objective evaluation of cervical neural foraminal stenosis by radiologists and clinicians.

KEYWORDS: Spinal imaging, Disk degeneration

eP-274

Clinical Correlation of a New Practical MR Imaging Method for Assessing Central Lumbar Spinal Stenosis

Park, H. J.
Sungkyunkwan University School of Medicine, Kangbuk Samsung Hospital
Seoul, KOREA, REPUBLIC OF.

Purpose
To evaluate interobserver agreement and determine whether a new MRI grading system agrees with symptoms and neurologic signs.
Materials & Methods
We examined 160 patients (M:F = 72:88; mean age, 65 years) who underwent MRI of the lumbar spine at our institution and were evaluated by two musculoskeletal radiologists. The presence and grade of central lumbar spinal stenosis (CLSS) at L3-4, L4-5 and L5-S1 were assessed according to a new grading system, the Lee system. The results were correlated with clinical manifestations and neurologic examinations [positive neurologic manifestation (PNM), negative neurologic manifestation (NNM)]. Statistical analyses were performed using kappa statistics, and nonparametric correlation analysis (Spearman's correlation).
Results
Interobserver agreement in the grading of CLSS between the two readers was substantial (k value = 0.780). Interobserver agreement of the L4-5 level and older age group were high (0.789, 0.814). The correlation coefficient (R) of reader 1 between MRI grade (0, 1, 2, or 3) and neurologic manifestations (negative or positive) was 0.654; the R of reader 2 was 0.591. In the younger age group (<57 years), the R of reader 1 was 0.634 and the R of reader 2 was 0.500. In the older age group (≥ 57 years), the R of reader 1 was 0.650 and the R of reader 2 was 0.645. Correlation coefficients were higher at the level of L3-4 (0.612 - 0.678) than other levels but did not show statistical significance ($p > 0.05$).
Conclusion
Interobserver agreement for the new CLSS grading system was substantial. Grade 0 was associated with NNMs and grade 3 with PNMs in this cohort. Grade 2 demonstrates more cases of PNM than NNM but requires further evaluation. Correlations between MRI grade and clinical manifestations were moderate and slightly higher in older patients.

KEYWORDS: Spinal imaging, Disk herniation

Note: Scanned images are included in the proceedings. Some submitted images were reduced during editing, thereby decreasing clarity. Also, refer to the Program Planner. Proceedings Content as of 3-29-2013.

eP-275

Utility of CT-Guided Bone Biopsy for Vertebral Osteomyelitis

Bauml, J. A.·Bosman, S. A.·Hansra, N.·Saran, N.
University of Illinois at Chicago Medical Center
Chicago, IL.

Purpose
CT-guided bone biopsy has been advocated as a useful tool to aid in the diagnosis and treatment of suspected vertebral osteomyelitis. No large review study providing convincing evidence supporting this practice is available. This single institution retrospective study is aimed at providing concrete data to help guide the discussion and debate over the usefulness of image-guided bone biopsy for vertebral osteomyelitis.
Materials & Methods
Data pertaining to vertebral body bone biopsies performed from January 2003 to March 2011 at the University of Illinois Hospital Chicago was compiled. Antibiotic regimens/treatment plans (prebiopsy) for the patients undergoing biopsy were recorded. Alterations in treatment plan based on the results of these biopsies were analyzed. The study design was that of a retrospective chart review.
Results
Of the 109 total vertebral body biopsies performed during the study period, 72 were performed for clinically or radiologically suspected cases of vertebral osteomyelitis. Fifty of these patients with clinically diagnosed osteomyelitis had negative culture results. Of the patients with negative culture results, the biopsy changed management in one case, but that change was based on unexpected pathology rather than culture results. In seven patients the biopsies never yielded a diagnostic culture. The total number of positive culture results from these 72 biopsies was 15. Two of those patients were lost to followup. Out of the 13 remaining patients, the treatment plan for nine was changed based on the results. Four out of nine were not on prebiopsy antibiotics and were started on tailored therapy. Five out of nine patients' preexisting antibiotic regimens were tailored. Of the 65 specimens that were successfully cultured by microbiology, 15 cultures were positive. This corresponds to a culture positivity rate of 23%. In summary, nine patients who underwent biopsy had their management changed on the basis of the microbiology report. However, the other 57/72 (87.5%) patients who underwent biopsy for culture did not have their treatment changed as a result.

Vertebral biopsies performed by radiology for suspected osteomyelitis 1/2003 to 3/2011

	N	% of total	N Culture result changed treatment	% Treatment changed
Osteo suspected clinically and biopsy ordered	72		Sep-72	12.50%
Biopsy sample successfully obtained	70	97.20%	Sep-70	12.90%
Positive Culture	15	23.10%	15-Sep	60.00%
Negative Culture	50	76.90%	0/50	0.0%
Error in transfer*	4			
Improper preparation**	1			

*Pathology was performed on specimen but the specimen was not received by microbiology

** Specimen sent in formalin and unable to be used for culture

Conclusion
Because (1) image-guided bone biopsies fail to provide an etiologic microorganism in most cases of clinically suspected osteomyelitis-diskitis and (2) in the setting of positive culture results broad-spectrum antibiotics often are continued unchanged, and (3) osteomyelitis is a clinical diagnosis and therefore a negative culture does not allow one to cease antibiotics in suspected cases: bone biopsy may not be a useful tool to guide treatment except in cases in which there is high clinical suspicion of an atypical organism such as tuberculosis.

KEYWORDS: Osteomyelitis, Biopsies, CT-guidance

eP-276

Novel Approach to Teaching Fluoroscopic Neuroanatomy and Spine Injection Skills

Musco, J.·Nanda, A.·Davis, R.
University of Missouri
Columbia, MO.

Purpose
Learning and understanding fluoroscopic neuroanatomy and acquiring the skills to safely perform spine injections is an essential part of training for many radiology, neurology, neurosurgery, anesthesia, and physical medicine and rehabilitation residents. Unfortunately there are no inexpensive and easily accessible models available to simulate and teach this essential skill. Thus, much of the teaching and learning is done while the patient is on the fluoroscopy table using the "See one, do one, teach one" method.
Materials & Methods
We present a novel cost-effective approach to making a fluoroscopic simulator using a plastic spine model coated with a metallic adhesive. The adhesive was painted on the deconstructed plastic spine model and allowed to dry

overnight. The model then was reassembled and wrapped in a gel foam pillow to simulate placement of the needle in an actual patient.
Results
Although the plastic noncoated model was radiopaque we found it difficult to visualize smaller structures such as facet joints under fluoroscopy. Coating the plastic spine model with our metallic adhesive allowed for improved visualization of the plastic model under fluoroscopy. Improving visualization of smaller structures like facet joints allows the plastic model to become a useful tool for simulating and training residents to perform more advanced procedures like facet injections and nerve root blocks.
Conclusion
We were able to transform an inexpensive plastic model of the lumbar spine into a useful neuroanatomy fluoroscopic simulator device that can be used to teach fluoroscopic neuroanatomy and spine injection skills without subjecting patients to multiple needle placement attempts and unnecessary radiation.

KEYWORDS: Fluoroscopy, Interventional, simulator

eP-277

Diffusion-Weighted Imaging of the Spinal Cord: Pictorial Essay and Review of Its Applications in Spinal Cord Pathology

Yañez, A.·Fuentes, P.·Fassler, X.·Gonzalez, M.
Instituto de Neurocirugía Asenjo
Santiago, CHILE.

Purpose
Diffusion-weighted imaging (DWI) is a widespread used technique in cerebral diseases; nevertheless the anatomical issues regarding the spine and spinal cord hinder the application of that sequence in this particular region. This pictorial essay reviews and shows the applications of DWI in spine and spinal cord diseases.
Materials & Methods
The MR DWI studies of the spine and spinal cord obtained in our center between April to December 2012 with a 1.5T unit were reviewed restropectively. The acquisition parameters were: TR 2500; TE 65 ms; NEX 32; 250 x 250 mm; acquisition matrix 128, slice numbers 12; slice thickness 3 mm, with an acquisition time of 2 minutes and 50 seconds.
Results
We present only confirmed cases (clinical, pathologic or laboratory confirmation) including dorsal spinal cord infarct, conus medullaris infarct, subarachnoid epidermoid cyst, aortic dissection with dorsal spinal cord infarct, paraspinal abscess secondary to spondylodiskitis, and lymphoma of the vertebral bodies.
Conclusion
Diffusion-weighted imaging of the spine and spinal cord is a reliable tool that can improve diagnostic accuracy in spinal cord pathology.

KEYWORDS: Diffusion-weighted imaging, Spinal cord, spine

eP-278

Tailored Tube Current Reduction Strategy and Its Effect on Effective Patient Radiation Dose for CT-Guided Interventions

Swarnkar, A.[1]·Ezhapilli, S.[2]·Krishna, S.[1]·Ogden, K.[1]
[1]Upstate Medical University, Syracuse, NY, [2]Emory University, Atlanta, GA.

Purpose
CT is the preferred modality for many image-guided interventional procedures of the head, neck and spine. These procedures are associated with a high radiation dose to the patient due to multiple scans that are performed during the procedure. During performance of the scans sometimes limited information is required, such as location, depth and direction of the needle or catheter, and the tube current can be decreased significantly, thus decreasing the radiation dose. In this study we determined the magnitude of decrease in patient radiation dose without compromising the success of the image-guided procedure by using fractions of the tube current and tailoring it according to the extent of anatomical detail and information necessary.
Materials & Methods
We reviewed a total of 40 consecutive patients undergoing CT-guided interventional procedures such as biopsies, epidural blood patches, and abscess drainage. During each of these procedures, initially a diagnostic scan was performed using automatic mA setting on the scanner. Subsequent scans were performed with a fraction of the tube current (e.g., 1/2 the automated mA setting for discerning soft tissue detail like nerves, vessels or 1/16 the mA for identifying needle depth and direction). The actual dose length product (DLP) was recorded automatically at the end of each procedure. The estimated dose which the patient would have received if the dose was not reduced was calculated by scaling DLP by using the ratio of automated mA to actual mA used during the intervention. Dose length product was converted into the effective dose and the percentage reduction of the effective dose was calculated for each patient.
Results
The effective doses during the procedures ranged from 0.1mSV to 20mSV with an average of 5.19mSV (standard deviation of 4.33) whereas the estimated effective doses without such mA reduction strategy ranged from 0.2mSV to 30mSV with an average of 8.96mSV (SD 7.52). The average reduction of radiation dose was 38%.
Conclusion
Our study reveals that effective radiation doses during interventional procedures can be decreased without any negative impact and must be considered as a reasonable

Note: Scanned images are included in the proceedings. Some submitted images were reduced during editing, thereby decreasing clarity. Also, refer to the Program Planner. Proceedings Content as of 3-29-2013.

approach to reduce effective patient radiation dose during these procedures. The extent of acceptable reduction of tube current is variable and is tailored to suit the need for anatomical detail and essential information for each procedure being performed.

KEYWORDS: Radiation safety

eP-279

Improved Detection and Conspicuity of Multiple Sclerosis Spinal Cord Lesions by STIR Phase Imaging: A Retrospective Comparative Analysis

Nayak, N.[1]·Salah, R.[2]·Huang, J.[3,4]·Hathout, G.[1,3,4]
[1]University of California Los Angeles, Los Angeles, CA, [2]2David Geffen School of Medicine at University of California, Los Angeles, CA, [3]University of California Olive View Medical Center, Sylmar, CA, [4]Greater Los Angeles-West Los Angeles Veterans Administration Medical Center, Los Angeles, CA.

Purpose
Multiple sclerosis (MS) is the most common disabling CNS disease of young adults. MR imaging is used routinely to detect MS plaques in the brain and spinal cord. A significant portion of MS patients demonstrate spinal cord lesions at the time of initial workup, which are an important part of the McDonald criteria for diagnosis. However, whereas brain imaging sequences are now fairly standardized, debate continues regarding the optimal sequences for imaging the spinal cord. The short T1 inversion recovery (STIR) sequence has been shown in the current literature to improve lesion detection with its additive T1/T2 weighting, but current spinal cord imaging protocols from the Consortium on MS Center Consensus Guidelines do not include the STIR sequence. We demonstrate that not only do STIR sequences improve lesion detection compared directly to conventional T2-weighted sequences, but they also significantly improve lesion conspicuity, facilitating earlier positive diagnosis.
Materials & Methods
Dedicated MR spinal cord imaging of 29 sequential patients with clinically confirmed multiple sclerosis was analyzed retrospectively by two independent neuroradiologists in a novel study design. Sagittal T2-weighted and STIR sequence images from the same study for each patient were examined for MS plaques using a double-blinded review of individual images “separated in time and space,” such that STIR and T2 image pairs were never analyzed simultaneously. Number of lesions and individual lesion conspicuity, using a subjective scale (1-5), was tallied for each sequence. Averages for each observer were compared using a paired t-test analysis for statistical significance.
Results
Significantly more MS lesions were detected on STIR than on T2-weighted sequences for both observers ($p = 0.001$, and $p = .005$). In seven patients, the conventional T2 sequence detected no lesions at all, whereas STIR sequences showed significant cord involvement. Lesion conspicuity also was significantly better on STIR for both observers ($p < 0.0005$). For T2-weighted sequences, there was a statistically significant difference in the number of lesions detected between the two observers ($p = 0.003$), but there was no statistically significant difference on STIR ($p = 0.43$).

Conclusion
Short T1 inversion recovery sequence imaging not only significantly improves detection of MS lesions within the spinal cord, but also provides better contrast and conspicuity of visible lesions, creating a more confident diagnostic measure of MS extent and progression. STIR sequences of the spinal cord should be routinely obtained during initial and routine followup of MS.

KEYWORDS: Multiple sclerosis plaques, Spinal cord

eP-280

Pedicolaminar Fracture Separation: Validation of a Hyperextension-Rotation Mechanism by Biomechanical and Clinical Analysis

Gibbs, W. N.·Murphy, J. S.·Harris, J. H.·Heiserman, J. E.·Ross, J. S.·Dean, B. L.
Barrow Neurological Institute
Phoenix, AZ.

Purpose
The majority of cervical spine injury patterns have well described mechanisms of injury. The mechanism associated with pedicolaminar fracture separation (PLFS) remains controversial after five decades, since its original description. Pure PLFS is characterized by fracture of the ipsilateral pedicle and lamina, with tearing of the capsular ligaments allowing for rotation of the lateral mass. There is associated disruption of the anterior longitudinal ligament and intervertebral disk. Some authors have claimed that PLFS is a hyperextension-rotation injury, while others propose a hyperflexion-rotation, lateral hyperflexion, or pure axial rotation mechanism. We have evaluated the largest collection of PLFS cases reported to date utilizing advanced techniques in order to determine the dominant

Note: Scanned images are included in the proceedings. Some submitted images were reduced during editing, thereby decreasing clarity. Also, refer to the Program Planner. Proceedings Content as of 3-29-2013.

mechanism of injury.
Materials & Methods
Ninety-three cases of cervical spine trauma with a component of PLFS were reviewed. Computed tomography (CT) of the cervical spine, as well as magnetic resonance imaging of the cervical spine and CT of the head, when available, were analyzed to determine the dominant vector of force, site of impact, and additional injuries. A three-dimensional, anatomically accurate, finite element model of the cervical spine was generated from CT images of a cadaveric human cervical spine. The magnitude and location of stresses upon the pedicle, lamina, and intervening articular mass were analyzed during simulated hyperextension-rotation. Subsequently, the simulated mechanisms of injury were applied directly to two human cadaver cervical spine specimens, which were load tested utilizing strain gauges applied to pedicle and lamina.
Results
Sixty-two percent (58/93) of cases demonstrated features of pure PLFS. Of these, the majority, 46% (43/93), resulted from a hyperextension-rotation mechanism and 16% (15/93) resulted from lateral hyperflexion. Thirty-eight percent (35/93) demonstrated features of severe hyperflexion injury with pedicle and laminar fractures. There was a near perfect correlation between sites of greatest stress depicted by finite element analysis during hyperextension-rotation and fracture location in the clinical cases. Strain gauge analysis verified all tested mechanisms as potential causes of PLFS.

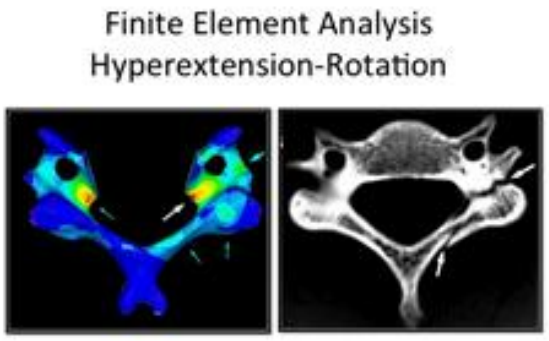

Conclusion
Biomechanical and clinical analysis validates hyperextension-rotation as the most common mechanism of injury associated with pure PLFS. Lateral hyperflexion is a less common cause of PLFS. Severe hyperflexion with pedicle and laminar fractures is a more severe injury, with different fracture patterns. It should be considered a separate entity and different terminology should be applied. These distinct injury types can differ in prognosis and surgical approach. Correctly identifying and describing the injury type facilitates appropriate patient care.

KEYWORDS: Spinal trauma

eP-281

Variations in Surgical Approaches to Lumbar Spine Disease: A Nationwide Survey and Analysis

Quencer, R. M.[1]·Modic, M. T.[2]·Obuchowski, N.[2]·Steinmetz, M. P.[3]·Wang, J. C.[2]·Williams, S.[1]·Lubelski, D.[2]·Mroz, T. E.[2]
[1]University of Miami Miller School of Medicine, Miami, FL, [2]Cleveland Clinic, Cleveland, OH, [3]Metro Health Medical Center, Cleveland, OH.

Purpose
Since it is widely recognized, but never documented, that surgical approaches to common lumbar spine disease are idiosyncratic, our primary purpose was to study treatment agreement among spine surgeons when faced with seven common spinal conditions. A secondary purpose was to see if there were significant differences between spine surgeons as a group versus subgroups such as specialty, geographic location, training, and time in practice.
Materials & Methods
An on-line survey containing seven cases of common lumbar spine pathology with a brief clinical history, representative conventional plain films, MR/CT imaging and surgical choices was sent to 3000 spine surgeons asking them to respond with their typical practice patterns. These cases included varying scenarios and manifestations of spondylolisthesis, recurrent disk herniation and mechanical back pain. Depending on the scenario, seven to ten potential treatment options were offered. The overall probability of two randomly chosen surgeons disagreeing on the treatment method given a particular scenario was computed. The probability then was computed within subgroups of surgeons and compared with overall levels of disagreement.
Results
Six hundred twenty-one of 3000 surgeons completed the survey. Treatment probability for disagreement for each survey scenario was: (1) two previous microdiskectomies with recurrence - 69%; (2) diskogenic pain 1 level - 76%; (3)degenerative spondylolisthesis without back pain - 73%; (4) degenerative spondylolisthesis with back pain 64%; (5) isthmic spondylolisthesis with L5 radiculopathy and back pain -69%; (6) one previous microdiskectomy with recurrence - 22%; (7) diskogenic pain 2 levels -75%. A representative scenario is included below. The highest probability for agreement (78%) was for a patient with one previous microdiskectomy with recurrent disk herniation. The lowest probability for agreement, 24%, was for a patient with diskogenic pain at one level. Given seven treatment choices for a scenario we would expect two surgeons to agree at least 14.3% of the time by chance alone.

Note: Scanned images are included in the proceedings. Some submitted images were reduced during editing, thereby decreasing clarity. Also, refer to the Program Planner. Proceedings Content as of 3-29-2013.

Conclusion

If a patient with a common lumbar spine problem were to consult two different spinal surgeons there is a high likelihood that there would be significant probability for disagreement in their treatment recommendations. These widely variable surgical approaches to the same conditions are important for the neuroradiologist to recognize.

KEYWORDS: Disk disease, Outcomes, surgical decisions

eP-282

Normalization of Fractional Anisotropy and Apparent Diffusion Coefficient Values Below Regions of Moderate to Severe Spinal Canal Stenosis in the Cervical Spine

Pan, L.[1]·Tseng, I.[1]·Kanfi, A.[1]·Bhat, H.[2]·Porter, D.[2]·Sze, G.[1]
[1]Yale-New Haven Hospital, New Haven, CT, [2]Siemens, Malvern, PA.

Purpose

Past work has suggested that fractional anisotropy (FA) and apparent diffusion coefficient (ADC) values change predictably in regions of spinal canal stenosis. Theoretically, one could postulate that FA and ADC values below regions of significant stenosis also might be abnormal. However, this hypothesis has yet to be investigated. Our purpose is to characterize the change below the site of stenosis, if any. Understanding of FA and ADC values below the site of stenosis will further research into the pathophysiology of compressive myelopathy and improve our ability to characterize potential concomitant lesions in patient with spondylosis.

Materials & Methods

Diffusion-weighted images (DWI) of 18 patients on a 3T Siemens magnet using readout-segmented echo-planar imaging sequences in a sagittal orientation were evaluated retrospectively on a separate postprocessing workstation. Coronal and sagittal reformats guided the placement of an ovoid region of interest (ROI) within the confines of the spinal cord on the axial projection. The ROI was placed at the C1 and C7 vertebral body levels above and below the stenosis in all patients. The calculated FA and ADC values were compared to the values in 18 normal patients with no spinal canal stenosis. Statistical significance between the two groups was obtained using a 2-sample T-test.

Results

The DTI sequences in patients with moderate to severe cervical spine stenosis demonstrated a mean FA value of 676.7 and ADC value of 886.0 at the C1 level and a mean FA value of 624.4 and ADC value of 886.0 at the C7 level. The DTI sequences in patients with normal cervical spines demonstrated a mean FA value 705.85 and ADC value of 851.48.0 at the C1 level and a mean FA value of 715.8 and ADC value of 927.6 at the C7 level. The FA values decreased 7.69% in the patients with cervical spine stenosis and 2.69% in the normal patients, and the ADC values increased 23.2% in the patients with cervical spine stenosis and 8.94% in the normal patients. Using a 2-sample T-test, there was no statistically significant difference in the change of the FA and the ADC values between the two groups.

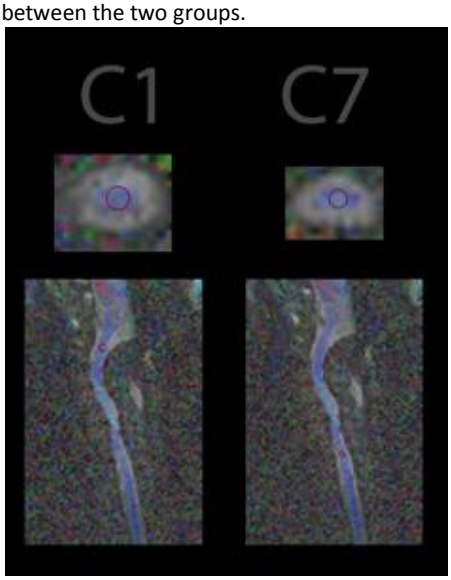

Conclusion

Normalization of FA and ADC values in the cervical spinal cord below the site of moderate to severe stenosis suggests recovery of diffusion properties in the cord.

KEYWORDS: DTI, Degenerative, FA ADC

eP-283

Fluoroscopic-Guided Myelogram - Fluoro Time and Patient Body-Mass Index: A Baseline Study

Boddu, S. R.·Corey, A. S.·Saindane, A. M.·Applegate, K.·Fountain, A. J.
Emory University Hospital
Atlanta, GA.

Purpose

Evaluation of postoperative spine is a challenging situation. Myelography is the investigation of choice for pre-operative planning and assessment in patients with contraindications for MRI. Also the supplementary information provided by myelography in the presence of

Note: Scanned images are included in the proceedings. Some submitted images were reduced during editing, thereby decreasing clarity. Also, refer to the Program Planner. Proceedings Content as of 3-29-2013.

metal hardware from spinal fixation prior to the revision surgery remains invaluable. There are no published guidelines for the acceptable range of fluoroscopic time for myelography. The study is aimed to obtain the baseline fluoroscopic time ranges for myelography involving different spinal levels and for varying body-mass index (BMI).

Materials & Methods

Retrospective review of all patients who underwent myelography at four hospitals over a one-year period (July 2011 - June 2012) was performed. Procedure logbooks, electronic medical records accessed for patient demographics, extent of myelography, prior history of spinal surgery, BMI, fluoroscopic time. Patients were categorized based on BMI and extent of myelography. Based on the federal obesity guidelines issued by National Heart, Lung and Blood Institute, patients were categorized into normal (18.5 - 24.9), over weight (25 - 29.9) and obese (≥ 30). Based on the extent of myelography patients were categorized into three subgroups: single level, two levels and whole spine. Logarithmic conversion of fluoroscopic times was performed to render normal distribution to the data. Fluoroscopic time was calculated for each subgroup and chi-square analysis was performed.

Results

Two hundred forty-seven successful (mean age 60 years, range 15-91 years, 51% male) fluoroscopic-guided lumbar approach procedures were performed. Six patients were excluded due to insufficient data. One hundred sixty patients had single level myelogram (5: cervical; 2: Thoracic; 153: Lumbar), 59 had two level myelogram (19: cervical +lumbar; 7: cervical +thoracic; 33: thoracic +lumbar) and 22 patients had total spine myelogram. Fourteen attending neuroradiologists and 14 fellows/residents participated. The mean fluoroscopic time for single level myelogram: 1.54 minutes (standard deviation: 0.79), for two level myelogram: 2.26 minutes (standard deviation: 0.89) and total spine myelogram: 2.32 minutes (standard deviation: 0.94). There was overall increased fluoroscopic time with increase in BMI as reported in Table 1. However the increase in the fluro time is not statistically significant (p = 0.43).

Table:1

BMI	Subgroups	Mean	95% CI
18.5 - 24.9	1 level2 LevelsWhole	1.42.091.65	1.13 - 1.671.57 - 2.612.48 - 4.42
25-29.9	1 level2 LevelsWhole	1.542.251.68	1.36 - 1.721.88 - 2.621.33 - 2.03
≥30	1 level2 LevelsWhole	1.62.392.57	1.39 - 1.812.03 - 2.751.12 - 4.02

Conclusion

In our study, fluoroscopic time for myelography increases with patient body-mass index (BMI) with no statistical significance. Baseline fluoroscopic times for single level; two levels and total spine myelography do not exceed five minutes. This study provides suggested fluoroscopy times based on the extent of myelography and patient body-mass index (BMI).

KEYWORDS: Fluoroscopy, Myelography, Body-Mass index

eP-284

Microwave Ablation of Spinal and Paraspinal Tumors: Initial Experience in Eleven Procedures

Kastler, A.[1,2]·Alnassan, H.[3]·Aubry, S.[4]·Kastler, B.[4,5]
[1]University Hospital, Clermont Ferrand, FRANCE, [2]I4S Laboratory EA 4268, Franche Comte University, Besançon, FRANCE, [3]I4S Laboratory EA 4268-IFR 133, Besançon, FRANCE, [4]University Hospital, Besançon, FRANCE, [5]I4S Laboratory EA 4268-IFR 133, Franche Comte University, Besançon, FRANCE.

Purpose

To evaluate the feasibility and efficacy of percutaneous microwave ablation (MWA) under CT guidance in the management of refractory pain in bone and soft tissue tumors in spinal and paraspinal locations.

Materials & Methods

Eleven MWA were performed in 10 adult patients using an Acculis MTA-2 Generator, 2.45GHz with a 17-gauge antenna. Topography of lesions were as follows: nine bone lesions (thoracic spine: 1, lumbar spine: 4, sacrum: 4) and two soft tissue lesions (paraspinal soft tissue). Six of eight bone lesions were osteolytic. All 11 ablated lesions were metastases (lung: 6, prostate: 2, leiomyosarcoma: 1, renal: 1). All procedures were performed with CT guidance under local anesthesia and nitrous oxyde. Followup was performed either by contrast ultrasound in case of soft tissue lesion or MRI in case of bone lesion. Pain prior procedure, immediately after and at distance was assessed using a VAS pain score.

Results

Lesion size ranged from 12 mm to 70 mm. Technical success was 100%. Mean ablation time was 4.75 minutes (1-13) with an average of 4.2 cycles per ablation lasting from 30 seconds to 3 minutes with a ablation power ranging from 30 to 160 W. Mean VAS before procedure was 7.11/10. Immediate pain relief was greater than or equal to 50% in 10/11 cases and lasted for an average of 4.85 months (range 0.5-15 months). No adverse events occurred during or after procedure.

Conclusion

Percutaneous MWA appears to be a feasible, safe, effective and fast technique for the management of refractory pain in spinal and parspinal tumors. Ablation time appears to be highly reduced compared to radiofrequency ablation.

Note: Scanned images are included in the proceedings. Some submitted images were reduced during editing, thereby decreasing clarity. Also, refer to the Program Planner. Proceedings Content as of 3-29-2013.

KEYWORDS: Spinal neoplasm, Pain, microwave thermal ablation

eP-285

Value of High Viscosity Cement in Augmentation of Advanced Malignant Compression Fractures

Padwal, J.[1]·Georgy, M.[2]·Georgy, B.[1,3]
[1]University of California San Diego, San Diego, CA, [2]Canyon Crest Academy, San Diego, CA, [3]San Diego Imaging, San Diego, CA.

Purpose
Vertebral augmentation in malignant compression fractures is associated with higher complication rates compared to benign fractures. High viscosity cement is associated with lower leakage rate. We are investigating the value of high viscosity cement in vertebroplasty performed in cases of advanced malignant compression fracture.
Materials & Methods
Institutional board approval was obtained for this retrospective study. Twenty-six patients (17 females and 9 females with average age of 73.9) underwent vertebroplasty for pain control due to underlying different metastatic diseases were evaluated. A total of 37 levels treated. Postprocedure CT and radiographs were evaluated for presence and location of leakage.
Results
All treated levels had epidural tumor extension or cortical bone disruption or both (8 levels) in preprocedure CT or MR studies. On postprocedure CT images, there were 25 cement leakages (67%), 15 venous, right diskal, three epidural, and one leak in a neural foramen. Two levels show two different leaks. Postprocedure radiographs show 16 leakages (43%), seven venous and nine diskal. None of those leaks were of any clinical significance and required any further intervention.
Conclusion
Vertebral augmentation using high-viscosity cement in advanced malignant vertebral compression fracture is relatively safe. Although, there is a high cement leakage in postprocedures CT, still less than published data in benign lesions. All leakage reported are minimal and does not appear to have any clinical consequences.

KEYWORDS: Vertebral compression fractures, Vertebral augmentation

eP-286

Role of Lumbar Diskography in the Surgical Management of Patients with Axial Back Pain: A Single Center Retrospective Study

Bhatnagar, P.·Birchall, D.·Gregson, B.·Butteriss, D.
Royal Victoria Infirmary
Newcastle upon Tyne, UNITED KINGDOM.

Purpose
The intervertebral disk has been shown to be a cause of chronic lumbar spine pain without disk herniation in 26% to 39% cases. However, there is a lack of consensus in the literature regarding the diagnosis and treatment of these intervertebral disk disorders. The selection of appropriate patients for lumbar disk surgery is a challenging task involving a highly variable, multifactorial decision process complicated by a lack of reliable, validated clinical signs and imaging findings. Lumbar provocation diskography, which includes disk stimulation and morphologic evaluation, often is used to distinguish a painful disk from other potential sources of pain. The aim of this study was to investigate the role of diskography in the selection of patients with disk-related pain for fusion surgery and also to determine if these patients had any symptomatic improvement after the spinal fusion.
Materials & Methods
We carried out a retrospective study of 91 patients who had a lumbar diskography at our institution between June 2007 to November 2010. All patients were referred for axial back pain not manageable by conservative/medical means, and were being considered for attempted surgical management because imaging showed single or two-level disk degeneration. We reviewed the imaging, clinical notes and letters and collected data regarding patient demographics, a positive or negative diskography (including a nonconcordant result (i.e., pain from a normal disk, and not from a degenerative disk is counted as a negative result in terms of surgical decision making) whether or not the patient was treated with a surgical fusion of the abnormal level, and whether or not the pain improved. Statistical analysis was performed using the Fisher's Exact two-sided test and the Mann-Whitney test.
Results
Of the 91 patients, diskogram was positive for 56 cases and negative for 35 cases. We found that if a patient had a positive diskogram then they were more likely to have surgery (67% of those with positive diskogram had surgery compared with 17% of those with a negative diskogram) [Fisher's exact (2-sided) $p < 0.0001$]. In patients who had a positive diskogram, surgery was associated with symptomatic improvement in 32% of patients compared to only 5% who did not have surgery (Fisher's exact $p = 0.004$). However, 68% patients with positive diskogram had ongoing back pain despite surgery. There was no evidence of a relationship between the patient's age and the result of diskogram (Mann-Whitney test $p = 0.343$), between the age and having surgery (Mann-Whitney test p

Note: Scanned images are included in the proceedings. Some submitted images were reduced during editing, thereby decreasing clarity. Also, refer to the Program Planner. Proceedings Content as of 3-29-2013.

= 0.346) or between the age and outcome of surgery (Mann-Whitney test p =0.971). There was some suggestion that women may be more likely to have a positive diskogram than men but more data would be needed to confirm this. Women also may be more likely to have surgery but again a larger sample would be needed to check.
Conclusion
Diskography is a useful investigation in the management of patients with diskogenic back pain and may contribute to improving the selection process of patients for spinal fusion surgery.

KEYWORDS: Diskography, Fusion

eP-287

Teaching Fluoroscopic Neuroanatomy and Spine Injection Skills on a Modified Plastic Model of the Lumbar Spine

Musco, J.·Nanda, A.·Davis, R.
University of Missouri
Columbia, MO.

Purpose
Learning and understanding fluoroscopic neuroanatomy and acquiring the skills to safely perform spine injections is an essential part of training for many radiology, neurology, neurosurgery, anesthesia, and physical medicine and rehabilitation residents. Unfortunately there are no inexpensive and easily accessible models available to simulate and teach this essential skill. Thus, much of the teaching and learning is done while the patient is on the fluoroscopy table using the “See one, do one, teach one” method.
Materials & Methods
We present a novel cost-effective approach to making a fluoroscopic simulator using a plastic spine model coated with a metallic adhesive. The model then is wrapped in a gel foam pillow to provide stability for the spinal needle and to block the trainees view of the model. After reviewing general lumbar neuroanatomy using images obtained from the model, the trainees were provided with instructions on use of the fluoroscopy camera and basic needle handling technique and placement. The trainees then performed a series of mock procedures using the model. The mock procedures were monitored for total procedure time, total fluoroscopy time, and accuracy of needle placement.
Results
All trainees showed a statistically significant improvement in total procedure time, total fluoroscopy time, and accuracy of needle placement. After performing the mock procedures, trainees were more confident and felt as though they were now better prepared to perform the procedures on actual patients.
Conclusion
We were able to transform an inexpensive plastic model of the lumbar spine into a useful neuroanatomy fluoroscopic simulator device that can be used to teach fluoroscopic neuroanatomy and spine injection skills without subjecting patients to multiple needle placement attempts and unnecessary radiation.

KEYWORDS: Fluoroscopy, Anatomy, injection skills

eP-288

Effect of Preprocedure Antibiotics on the Diagnostic Accuracy of Image-Guided Spinal Biopsy in Diagnosis of Vertebral Osteomyelitis and Diskitis

Gnerre, J. M.·Dickson, A.·Ortiz, A. O.
Winthrop University Hospital
Mineola, NY.

Purpose
To determine how pretreatment with antibiotics affects the diagnostic accuracy of image-guided biopsies of the spine exclusively for vertebral osteomyelitis and diskitis.
Materials & Methods
Data were examined from a retrospective case series of CT and fluoroscopically guided biopsies of 14 patients who received pretreatment with antibiotics for at least two consecutive days prior. The mean age of patients was 67 years, with a range of 38-83 years, including nine males and five females.
Results
In our series, only 23% of patients with confirmed vertebral osteomyelitis yielded a positive biopsy result (23% sensitivity, 100% specificity, 21% accuracy, 100% precision). And of those three patients, the condition usually was complicated by a severe infectious process that was grossly indicative of a spinal infection. One patient had a right psoas abscess, another had a lumbar abcess, which afforded these patients a larger sample area.
Conclusion
Image-guided biopsy of the spine is a safe and accurate tool for diagnosis of vertebral osteomyelitis and diskitis. Pretreatment with antimicrobial therapy prior to biopsy significantly reduces biopsy sensitivity and accuracy. Regardless of pretreatment, positive biopsy results are more likely when sampling patients with extensive infectious processes. Our results indicate that spinal biopsies should be performed as early as clinically possible in order to maximize its efficiency as a diagnostic tool for patients with suspected vertebral osteomyelitis and diskitis.

KEYWORDS: Osteomyelitis, Biopsies, diskitis

Note: Scanned images are included in the proceedings. Some submitted images were reduced during editing, thereby decreasing clarity. Also, refer to the Program Planner. Proceedings Content as of 3-29-2013.

eP-289

Interventional Neuroradiology Sympathetic Blocks

Massari, F.[1]·Tsai, N. T.[1]·Rumboldt, Z.[1]·Pedicelli, A.[2]·Bonaldi, G.[3]·Cianfoni, A.[4]
[1]Medical University of South Carolina, Charleston, SC, [2]Catholic University of Rome, A. Gemelli Hospital, Rome, ITALY, [3]Ospedali Riuniti, Bergamo, ITALY, [4]Neurocenter of Southern Switzerland, Lugano, SWITZERLAND.

Purpose
Aim of this presentation is to offer an overview on image-guided sympathetic blocks, focusing on specific indications, techniques, outcomes in four highly specialized medical center in USA and Western Europe, as well as comparison with literature.
Materials & Methods
Sympathetic blocks are used for diagnostic, prognostic and therapeutic purposes for painful and other conditions associated with sympathetic system dysfunctions. Main indications for sympathetic blockade are: Complex regional pain syndrome (CRPS), phantom limb pain, central pain, hyperhydrosis, acute pancreatitis, and abdominal viscera cancer pain. Stellate ganglion blocks are utilized for painful and nonpainful conditions related to sympathetic dysfunctions of head, neck and upper extremities. Thoracic sympathetic blocks are utilized for CRPS, postoperative analgesia, pain from fractured ribs, therapeutic control of hyperhydrosis of the upper limbs and torso, liver capsule pain after blunt trauma, acute postherpetic neuralgia, and premature ventricular contractions (PVCs). Coeliac plexus blocks are utilized in pain due to intra-abdominal cancer, stemming from organs innervated by coeliac plexus. Lumbar sympathetic blocks are utilized for CPRS of the lower extremities, herpes zoster, amputation stump pain and inoperable peripheral vascular vasospastic diseases of the lower limb. Superior hypogastric blocks are utilized for pelvic pain, and pelvic organs cancer pain (uterus, cervix, bladder, prostate, urethra, testes and ovaries). Impar ganglion blocks are utilized in coccydynia.
Results
The sympathetic nervous system has been implicated in numerous pain syndromes including neuropathic, vascular and visceral pain. In relation to this, in order to determine the sympathetic role in the transmission of pain and to manage these algic syndromes, sympathetic ganglia are targeted for local anesthetic blocks, for diagnostic, prognostic, and therapeutic purposes, balanced in a more complex pain treatment strategy, in the treatment of CRPS and other pain conditions. Safe and precise performance of these blocks requires knowledge of the loco-regional anatomy, accurate imaging guidance, and rigorous technique. Elements of relevant fluoroscopic and cross-sectional anatomy, procedural technique elements as well as outcomes are discussed and displayed.
Conclusion
This multicentric study summarizes indications, anatomy, techniques, outcomes in four highly specialized medical centers in USA and Western Europe, as well as comparison with literature, for the sympathetic blocks.

KEYWORDS: Neoplasm, Image-guided procedures, Pain, Injections, Autonomic system

eP-290

Retrograde Axonal Transport Is Impaired after Radiation Injury: Demonstration with Neurographic Molecular Imaging

Le Roux, L. G.·Bredow, S.·Grosshans, D.·Schellingerhout, D.
M. D. Anderson Cancer Center
Houston, TX.

Purpose
The goal of this study was to determine whether molecular imaging is a suitable technique to detect changes in the spinal cord in response to radiation injury.
Materials & Methods
The lower thoracic spinal cord of adult female BALB/c mice was irradiated with single doses of 2, 10, and 80 Gy. An optical imaging method utilizing the fluorescently labeled nontoxic C-fragment of tetanus toxin (TTc) was used to evaluate changes in the retrograde axonal transport mechanism, while Luxol fast blue staining served to assess demyelination in radiated cords.
Results
Transport of TTc in the thoracic spinal cord was impaired in a dose-dependent manner as early as two days after radiation. Transport was significantly decreased by 16 d in animals exposed to either 10 or 80, while animals exposed to 2 Gy remained unaffected. Further, animals exposed to the highest dose also experienced significant weight loss by nine d and developed posterior paralysis by 45 d. Demyelination in radiated cords could be observed after 30 d in mice exposed to 80 Gy.
Conclusion
Radiation of the spinal cord induces dose-dependent changes in the axonal transport mechanism which can be monitored by molecular imaging. This approach suggests a novel diagnostic modality to assess nerve injury and monitor therapeutic interventions.

KEYWORDS: Radiation toxicity, Spinal cord, molecular imaging

Note: Scanned images are included in the proceedings. Some submitted images were reduced during editing, thereby decreasing clarity. Also, refer to the Program Planner. Proceedings Content as of 3-29-2013.

eP-291

DYNA CT Myelography versus Multislice CT Myelography: Time for a Change?

Chaudry, I.[1]·Spiotta, A.[1]·Brooks, N.[2]·Turner, R.[1]·Fiorella, D.[3]·Turk, A.[1]
[1]Medical University of South Carolina, Charleston, SC, [2]University of Wisconsin School of Medicine and Public Health, Madison, WI, [3]Stony Brook University, Stony Brook, NY.

Purpose
There have been considerable improvements in C-arm angiographic flat-panel detectors and software reconstruction algorithms that allows for improved spatial resolution as well as osseous and soft tissue differentiation. Our goal was to compare multislice CT (MS CT) to angiographic CT (DYNA CT) in myelographic imaging, to evaluate the benefits of DYNA CT and its possible clinical applications.
Materials & Methods
In total, 70 consecutive patients with degenerative spine disease (cervical = 16, thoracic = 3, lumbar = 51) underwent DYNA CT and MS CT myelography. DYNA CT myelography was performed on a flat-panel Siemens Artis Zee biplane neuroangiography platform with images reconstructed on an independent Leonardo workstation. Multislice CT was performed on 16-slice Siemens or GE MSCT scanner with MPR images reconstructed locally. Four reviewers, two experienced neuroradiologists and two neurosurgeons will review all MS CT and DYNA CT source and MPR images for overall impression, contrast distribution, perceptibility of disks, perceptibility of bines, delineation of spinal canal, delineation of nerve roots, hardware artifact, overall diagnostic applicability. Images were scored on a 1-5 scale with 1 = very poor, 2 = poor, 3 = moderate, 4 = good and 5 = very good.
Results
Full data analysis is pending. To date, both CT and DYNA CT were found to be of diagnostic quality 98% and 95% of the time respectively. Fifty-one (71%) of the DYNA CTs were found to be of the same or better diagnostic quality while only 18 (26%) were found to be inferior but still of diagnostic quality. The DYNA CT scored better on perceptibility of bones, spinal canal and nerve roots when compared to MS CT. DYNA CT exceled at evaluation of nerve root evaluation but was limited by hardware artifact. We found that DYNA CT is comparable to MS CT and subjectively has better imaging quality in virgin spines but is inferior when orthopedic hardware is present.

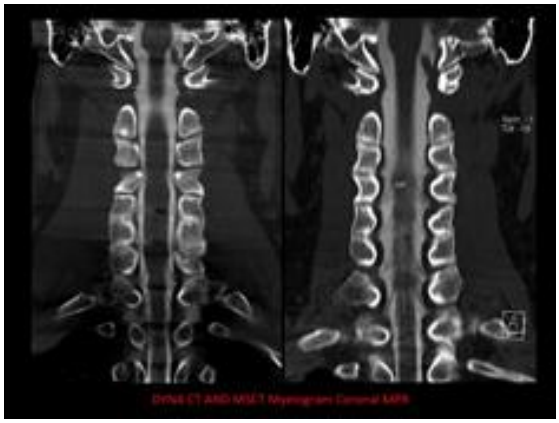

Conclusion
DYNA CT myelography maybe useful in the evaluation of degenerative spine disease in the virgin spine. Pending software improvements with metal artifact correction software will likely improve these results. The results will be updated at the time of the meeting.

KEYWORDS: Myelography, DYNA CT

eP-292

Comparison of Fractional Anisotropy and Apparent Diffusion Coefficient Values Measured on Axial versus Sagittally Acquired Cervical Spinal Cord Diffusion Tensor Imaging in Normal Subjects

Idowu, O.·Carrino, J.·Riley, L. H.·Izbudak, I.
Johns Hopkins Hospital
Baltimore, MD.

Purpose
Fractional anisotropy (FA) and mean diffusivity (MD) are commonly used quantitative parameters in diffusion tensor imaging (DTI) of the cervical spinal cord, subject to variability in regards to plane of imaging used for calculations and region of interest (ROI) placement. The aim of this study is to evaluate the differences in FA and MD values calculated at each cervical spine level when DTI analysis is performed on sagittal image acquisitions, versus axial image acquisitions in adult control subjects. On axial images the goal was to also evaluate the differences in FA and MD values between gray versus white matter, compared to the ROIs that contained both gray and white matter.
Materials & Methods
Diffusion tensor imaging was performed on five patients on a 3T Siemens MR system with imaging protocol consisting of a sagittal T1-weighted, sagittal T2-weighted and sagittal and axial DTI sequences. A total of 10 diffusion directions were applied with two b-values (0 and 1000 s/mm2). Diffusion tensor imaging analysis was performed using Siemens Neuro 3D software with FA and MD values calculated on both the axial and sagittal DTI acquisitions with ROIs that contained both gray and white matter. Region-specific FA and MD values also were calculated on

Note: Scanned images are included in the proceedings. Some submitted images were reduced during editing, thereby decreasing clarity. Also, refer to the Program Planner. Proceedings Content as of 3-29-2013.

axial imaging with ROI placement in the central gray matter, and dorsal white matter. Nonparametric statistical analysis utilizing the Friedman and Wilcoxon signed rank tests was performed.

Results

Average (±SD) FA values in the cervical spine calculated on axial acquisitions measured 0.66±.02 (C2-C3), 0.61±.06 (C3-C4), 0.65±.05 (C4-C5), 0.65±.08 (C5-C6), 0.72±.03 (C6-C7) and 0.74±.07 (C7-T1). Average (±SD) FA values in the cervical spine calculated on sagittal acquisitions measured 0.72±.05 (C2-C3), 0.77±.11 (C3-C4), 0.71±.06 (C4-C5), 0.64±.11 (C5-C6), 0.61±.10 (C6-C7) and 0.67±.04 (C7-T1). No statistically significant differences were found between whole spine FA values calculated in the axial plane versus the sagittal plane. Average (±SD) MD values in the cervical spine calculated on axial acquisitions measured 0.95±.07 (C2-C3), 0.96±.05 (C3-C4), 0.93±.06 (C4-C5), 0.97±.13 (C5-C6), 0.89±.05 (C6-C7), and 0.95±.08 (C7-T1). Average(±SD) MD values in the cervical spine calculated on sagittal acquisitions 1.00±.10 (C2-C3), 0.79±.16 (C3-C4), 0.96±.09 (C4-C5), 0.92±.14 (C5-C6), 0.98±.12 (C6-C7) and 1.00±.13 (C7-T1). No statistically significant differences were found between whole spine MD values calculated in the axial plane versus the sagittal plane. Average (±SD) FA values with regions of interest placed in the gray matter measured 0.63±.05 (C2-C3), 0.55±.05 (C3-C4), 0.54±.02 (C4-C5), 0.54±.05 (C5-C6), 0.62±.09 (C6-C7) and 0.60 ±.09 (C7-T1). FA values were significantly lower in the gray matter in the spinal cord measured on axial DTI data compared to whole cord values at C2-C3, C3-C4, C4-C5 and C5-C6 ($p<0.05$), and trended towards lower values at the remaining cervical spine levels.

Conclusion

Preliminary results suggest that fractional anisotropy and mean diffusivity values at each cervical spine level do not significantly vary based on the DTI acquisition plane. FA values measured in the gray matter are lower than whole cord FA values measured on axial or sagittal acquired DTI which correlates with the spinal cord DTI study results in the literature.

KEYWORDS: DTI, Cervical spine, diffusion tensor imaging

eP-293

MR Neurography in Thoracic Outlet Syndrome: Bony Anomalies or Fibrous Bands Causing Selective T2 Lesions

Baumer, P.[1]·Kele, H.[2]·Antoniadis, G.[3]·Heiland, S.[1]·Bendszus, M.[1]·Pham, M.[1]
[1]University of Heidelberg, Heidelberg, GERMANY, [2]Center for Neurology, Hamburg, GERMANY, [3]University of Tübingen, Günzburg/Tübingen, GERMANY.

Purpose

Neurologic diagnosis in thoracic outlet syndrome can be difficult. Until recently, neuroimaging has not offered more than confirmation or exclusion of cervical ribs in patients suspected with TOS. Visualization of fibrous bands in TOS has to our knowledge not been reliably achieved previously even though they are commonly found in-situ by surgeons and anatomists. We investigated whether MRI is able to visualize fibrous bands compressing the brachial plexus as well as T2 lesions within the affected roots or trunks.

Materials & Methods

High-resolution MR neurography was employed in 29 patients with a clinical diagnosis of true neurologic TOS or nonspecific TOS. The MRN protocol on a 3T unit (Verio, Siemens) included 3D SPACE STIR (TR/TE/TI 3800/267/180 ms, voxel size 0.781 x 0.781 x 0.8 mm^3, FoV 250, slices 72, averages 2) using a standard neck coil, sagittal-oblique T2 SPAIR (TR/TE 5530/45 ms, voxel size 0.469 x 0.469 x 3.0 mm^3, FoV 150, slices 51, averages 4) and 3D PD SPACE (TR/TE 1170/33 ms, voxel size 0.703 x 0.703 x 0.7mm^3, FoV 180, slices 51, averages 2) using custom made surface coils (NORAS GmbH, Würzburg, Germany) designed for imaging of the brachial plexus. SPACE sequences were used for 3D reconstruction of images.

Results

Five patients (17%) were identified with morphologic correlates of TOS. These included fibrous bands extending from cervical ribs to the first thoracic rib (Figure A), and pseudarthrosis or synostosis between ribs. A T2 lesion of the brachial plexus confirmed the diagnosis in all cases and was selective to the compressed portion (C8, inferior trunk, medial cord) (Figure B). Patients with true neurologic TOS as well as patients with nonspecific TOS exhibited these signal alterations.

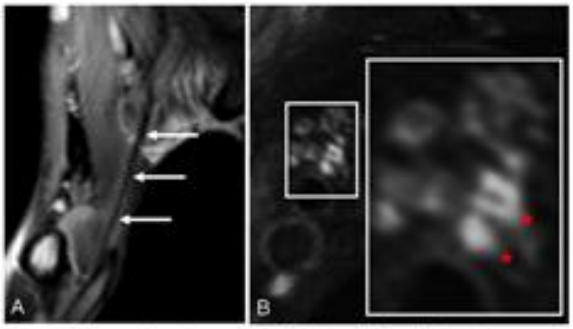

Conclusion

Diagnosis of TOS can be confirmed by MR neurography. Morphologic correlates of TOS may exist even in nonspecific ("disputed") TOS. Anatomical anomalies visualized by MRI include fibrous bands that lead to selective T2 lesions of the brachial plexus.

KEYWORDS: Thoracic outlet syndrome, MR neurography

Note: Scanned images are included in the proceedings. Some submitted images were reduced during editing, thereby decreasing clarity. Also, refer to the Program Planner. Proceedings Content as of 3-29-2013.

eP-294

Presurgical Location of the Adamkiewicz Artery in Thoracoabdominal Aortic Aneurysms: Comparison between Intra-Arterial CT Angiography and Intravenous CT Angiography

Gabrieli, J.[1,2]·Clarençon, F.[1]·Di Maria, F.[1]·Cormier, E.[1]·Sourour, N.[1]·Gaudric, J.[1]·Le Jean, L.[1]·Chiras, J.[1]
[1]Pitié-Salpêtrière Hospital Paris VI University, Paris, FRANCE, [2]University of Padua, Padua, ITALY.

Purpose
To compare the sensitivity of intra-arterial CT angiography (IA CTA) and intravenous CT angiography (IV CTA) for the presurgical location of the Adamkiewicz artery (AKA) in thoracoabdominal aortic aneurysms/dissections.
Materials & Methods
Retrospective study of 19 consecutive patients (median-age 67 years, age-range 42 to 81 years, six females) with thoracoabdominal aortic aneurysm (TAAA)/dissection (X TAAA, Y dissections). All patients underwent IA CTA on an hybrid angio-suite with injection of 100 cc of iodinated contrast material through a 5F pigtail catheter positioned at the origin of the descending aorta (injection rate 7 ml/s); the same patients also performed CTA with contrast administered through an antecubital vein at a rate of 5ml/s. Imaging findings were evaluated independently by two neuroradiologists with focus on the level of the origin of the AKA, on the visualization of the anterior spinal artery (ASA) and on its continuity with the aorta; the two latter also were assessed qualitatively by the readers as follows: no/poor visualization, fair visualization, good/excellent visualization.
Results
Adamkiewicz artery level was located in 74% of IA CTAs (14/19) versus 0% of CTA; ASA was visualized in 89% of IA CTAs (17/19) versus 47% of IV CTAs (9/19), a good/excellent visualization of the ASA was present on 58% of IA CTAs (11/19) which was never reported on IV CTAs; continuity with the aorta was seen on 84% of IA CTAs (16/19) versus 11% of IV CTAs (2/19), a good visualization of the continuity with the aorta was reported on 58% of IA CTAs (11/19) but never on IV CTAs.
Conclusion
Intra-arterial CTA is superior to conventional IV CTA for the location and visualization of the AKA and the ASA in patients with TAAA/aortic dissections; thus IA CTA seems to be a promising tool in the presurgical evaluation of these patients.

KEYWORDS: Adamkiewicz artery, Intra-arterial, CT angiography

eP-295

Multiple-Site Epidural Blood Patch Administration through a Single Lumbar Puncture for Treatment of Cerebral Spinal Fluid Hypovolemia

Gemmete, J. J.·Chaudhary, N.·Pandey, A. S.
University of Michigan Hospitals
Ann Arbor, MI.

Purpose
An epidural blood patch (EBP) is accepted as a standard procedure to treat CSF hypovolemia. In quite a few cases, the CSF leak is spread over a large area along the spinal epidural space, making it difficult to identify the true leakage points. In such cases, autologous blood can be infused at multiple spinal levels with multiple entries. In this paper, the authors have devised a multiple-site EBP method with a single lumbar entry point by way of using a 4F vertebral catheter for continuous infusion. In this report, we introduce a new, single-entry, continuous multiple-site EBP administration technique and report the results we have obtained.
Materials & Methods
An EBP was applied via a 4F vertebral catheter in five patients with spontaneous CSF hypovolemia (three women and two men; mean age 35 years, range 22-53 years). The detection of an epidural CSF leak was based on the findings of an MRI gadolinium myelogram. In all cases, however, the leakage sites could not be identified clearly. The main symptoms of these patients were recurrent spontaneous chronic subdural hematoma (two patients), and orthostatic headache (five patients). All patients were placed prone on the angiographic table and biplane fluoroscopy utilized for guidance. After administration of local anesthetic, a 19G single wall needle was inserted into the epidural space at L2 below the conus medullaris which was confirmed with a contrast injection. A 0.035 inch glidewire then was advanced into the epidural space followed by a 10 cm 4F sheath. A 4F vertebral catheter was advanced over the wire to the level of C4. A small amount of contrast was injected into the epidural space to confirm approach position. Autologous blood was obtained from the patient through a peripheral intravenous and injected through the catheter as it was slowly moved in a caudal direction. Approximately 1cc of blood was injected at each vertebral level as it was pulled in a caudal direction to L2. An average of 45 cc, range 40 - 55 cc of blood was injected into the epidural space.
Results
The two spontaneous chronic subdural hematomas resolved at followup. In four patients, the orthostatic headache disappeared completely, and it was nearly relieved in one patient.
Conclusion
This new application method of an EBP with the aid of a 4F vertebral catheter enables infusion of a sufficient amount of autologous blood into multiple epidural areas with a single lumbar entry point.

Note: Scanned images are included in the proceedings. Some submitted images were reduced during editing, thereby decreasing clarity. Also, refer to the Program Planner. Proceedings Content as of 3-29-2013.

KEYWORDS: Spinal CSF leak, Blood patch, catheter

eP-296

Prevention of Oxaliplatin-Induced Neuropathy by Minocycline: Demonstration by Imaging and Behavioral Assessment

Flores, L. G.·Vichaya, E. G.·Le Roux, L. G.·Schellingerhout, D.
M. D. Anderson Cancer Center
Houston, TX.

Purpose
The purpose of our study was to utilize neurography, a new imaging technology evaluating retrograde transport, to determine if minocycline can prevent oxaliplatin-induced neuropathy, by using imaging with loss of retrograde axonal transport and pain behavior as biological readouts.
Materials & Methods
Female BALB/c mice received one of four treatments vehicle/vehicle, vehicle/minocycline, oxaliplatin/vehicle, or oxaliplatin/minocycline (n = 8/group). A 30 mg/kg cumulative dose of oxaliplatin or dextrose vehicle was given in 10 divided intraperitoneal doses across three weeks using a five days of treatment, five days rest, five days treatment administration paradigm. Furthermore, animals were treated daily with 50 mg/kg minocycline or 0.9% saline vehicle by oral gavage throughout the experiment beginning 48 hours prior to the first oxaliplatin treatment. To assess the impact of minocycline on oxaliplatin-induced neuropathy, both imaging and behavioral (i.e., mechanical sensitivity) data were assessed at baseline and each week for three weeks. For each imaging session, animals received fluorescently labeled TTc-Alexa790 (15 ug/20 uL) via intramuscular injection into the calf muscle. Fluorescent imaging (Xenogen IVIS 200) was used to image the distribution of TTc over 60 minutes, with ROI measurements taken over the lower thoracic spine to quantitate fluorescent uptake. Region of interest measurements had background activity subtracted, and were normalized to the signal intensity at time = 0. Mechanical sensitivity was assessed through the use of von Frey nylon filaments that produce calibrated force on the footpads. The 50% hind paw withdrawal threshold was calculated. At the end of the study tissue was harvested for immunohistochemical analysis.
Results
Oxaliplatin/vehicle treated animals showed a decrease in transport of TTc during weeks two and three, while the TTc transport of the vehicle/vehicle and oxaliplatin/minocycline remained stable across the experiment. The vehicle/minocycline group saw an increase in transport of TTc during weeks two and three. Similarly, the behavioral data indicated that oxaliplatin treatment resulted in increased mechanical sensitivity, while minocycline treatment abrogated this effect, such that animals in the oxaliplatin/vehicle group showed increased sensitivity compared to all other groups. This effect emerged within the first week of treatment and remained throughout the study. At week three there was a significant correlation between pain behavior and TTc transport.
Conclusion
Oxaliplatin causes decrease in retrograde axonal transport in the sciatic nerves and spinal cord, consistent with prior demonstrations. In this study we show that this effect can be attenuated by minocycline pretreatment. Behavioral and imaging data were correlated. This suggests that minocyclin can prevent the painful neuropathy induced by oxaliplatin, and that the mechanism of this effect might be related to retrograde axonal transport.

KEYWORDS: Neurotoxicity, Neurography, Molecular Imaging

eP-297

Odontoid Process Posterior Inclination in the Normal Adult and Adult Chiari 1 Population

Besachio, D. A.·Khaleel, Z.·Shah, L.
University of Utah
Salt Lake City, UT.

Purpose
Posterior odontoid process inclination has been associated with Chiari 1 malformation in the pediatric population. It has been proposed these findings need to be addressed during surgical decompression to improve outcome. To date, there is no literature to support the presence of abnormal odontoid inclination in adults who are diagnosed with a Chiari 1 malformation relative to the normal population. The purpose of this study is to evaluate the normal adult measurements for odontoid retroflexion, retroversion, and pB-C2 (posterior basion - posterior C2) line relative to a cohort of adults with Chiari 1 malformation to facilitate future research addressing surgical planning and treatment outcomes of Chiari 1 malformations in the adult population.
Materials & Methods
We performed a retrospective analysis of noncontrasted cervical spine CT scans of 150 consecutive adult control subjects obtained for indications other than Chiari I malformation. Three neuroradiologists performed the following measurements: odontoid retroflexion, odontoid retroversion, odontoid length, pB-C2 line and clivus-canal angle. Patients with trauma, mass lesion, extensive arthopathy or congenital anomaly of the craniocervical junction were excluded from the analysis. Identical measurements then were performed in a retrospective fashion for a cohort of 42 adult Chiari 1 malformation subjects using MRI in the Chiari 1 population. Statistical analysis then was applied to these unpaired data sets to determine if a significant difference was present between the two groups.
Results

Note: Scanned images are included in the proceedings. Some submitted images were reduced during editing, thereby decreasing clarity. Also, refer to the Program Planner. Proceedings Content as of 3-29-2013.

One hundred twenty-five out of 150 control patients met the inclusion criteria. Of those, 80 were male and 45 were female with mean age of 52 years (range of 18 - 89 years). Odontoid retroflexion angle ranged from 70 to 89 degrees (mean 79.3), odontoid retroversion angle ranged from 57 to 87 degrees (mean 71.9) and clivus-canal angle ranged from 140 to 194 degrees. The range and mean of odontoid process length were 17.7- 26.2 mm and 21.7 mm, respectively. The mean of pB-C2 line was 6.5 mm with a range of 0 - 11.2 mm. A cohort of 42 subjects with Chiari 1 malformation was identified. Of those, 15 were male and 27 were female with a mean age of 34 years (range of 18-61 years). In female subjects, a significant difference between control and Chiari 1 subjects was identified with respect to odontoid retroversion (68 and 71 degrees), clivus-canal angle (164 and 158 degrees), and pb-C2 line (4 mm versus 5 mm). No difference was found in odontoid process retroflexion or length. No significant measured difference was found between male control and Chiari 1 subjects.

Conclusion

Our study suggests a significantly greater degree of odontoid retroflexion, retroversion, and difference in odontoid process length between normal adult males and females. Furthermore, retroversion of the odontoid process with more tissue projecting posterior to the pB-C2 line, and alignment of the craniovertebral junction is significantly different between adult female control subjects and adult female Chiari 1 patients. There may be a role for addressing these specific anatomical findings in surgical management of this subset of the Chiari 1 population.

KEYWORDS: Chiari malformation type 1, Odontoid

eP-298

Emergent MR Imaging of the Spine after Hours

Black, D. F.·Erickson, B. J.·Hunt, C.·Diehn, F. E.·Gilbertson, J.·Timothy, K. J.·Rydberg, C.·Morris, J. M.·Wood, C. P.
Mayo Clinic
Rochester, MN.

Purpose

Evaluate after-hours emergent spine MRI utilization trends and impact on patient management over the past 13 years at our tertiary care referral center. Specifically, determine how often emergent MRIs alter management and the timing of definitive therapies provided.

Material & Methods

Following approval by our internal review board, we obtained MRI reports from all emergent spine MRIs which at our institution were completed during weekdays from 10 pm - 6 am and weekends from 2 pm - 6 am over the last 13 years. We found 179 emergent, after-hour MRIs of the spine and reviewed each patients' medical record in order to record the spinal region imaged, patient age and gender, category of finding (ex: traumatic, neoplastic, infectious, etc…), presence of cord compression, type of intervention generated by the MRI result (surgery, radiation, antibiotics, steroids), and the time interval between finishing the MRI examination and administering therapy.

Results

The number of after-hours spine MRIs performed has increased steadily from eight per year to 23 per year over the 13-year period. Overall, 75/179 (42%) had no significant findings. Positive findings consisted of the following pathologic categories: 23% traumatic, 15% neoplastic, 7% infectious, and 3% had acute degenerative changes. Forty percent (72/179) of scans demonstrated an intramedullary (12/179) or extramedullary (60/179) lesion affecting either the cord or cauda equina. Of these, 56% went on to surgery, 43% had steroids, 11% had radiation, and 8% were treated with antibiotics. Overall, 29% (52/179) underwent surgery to treat pathologies identified on imaging. Only 2% (4/179) of patients went to surgery within three hours of completing their emergent MRI. Only 6% (10/179) went to surgery within six hours and 16% (29/179) had surgery within 12 hours of completing their MRI scan. Overall, only 5% (8/179) of patients undergoing emergent spine MRI had findings that were treated with urgent radiation therapy and most of these were within 12 to 24 hours of completing their MRI scan. Only 1% (2/179) of patients were treated with radiation within six hours of completing their MRI scan. Of those treated with steroids 39/179 (22%), 41% were treated within three hours of completion of their MRI scan. Of the 12/179 (7)% treated with antibiotics, 50% were treated within three hours of completion of their MRI scan.

Conclusion

Clinical use of emergent spine MRI is increasing steadily over the last 13 years at our institution. While MR imaging discerned significant clinical findings, performing emergent studies overnight rarely results in immediate surgical intervention which, most often, is undertaken six hours or more after completion of the MRI with only 6% of after-hours scans resulting in surgery within six hours of the MRI scan. Only 1% of patients were treated within three hours of completing the MRI with radiotherapy. While immediate surgical and radiation therapies are uncommon, patients that were treated with either steroid or antibiotics for their MRI findings were much more likely to receive these interventions within three hours.

KEYWORDS: Emergencies, Spinal imaging

Note: Scanned images are included in the proceedings. Some submitted images were reduced during editing, thereby decreasing clarity. Also, refer to the Program Planner. Proceedings Content as of 3-29-2013.

eP-299

Potential Biomechanical Implications of Thoracic Curvature Shape and Thoracic Kyphotic Angle in Elderly Women without Vertebral Compression Fracture

Enterkin, J.[1]·Bartynski, W.[1]·Petropoulou, K.[2]·Bartynski, S.[2]·Madrecha, J.[2]·Amrhein, T.[1]
[1]Medical University of South Carolina, Charleston, SC, [2]University of Pittsburgh, Pittsburgh, PA.

Purpose
The thoracic kyphotic angle (TKA) increases with age. A group of elderly patients (≥ 65 years old) has been identified with an increased TKA without evidence of a vertebral compression fracture (VCF) but with bimodal TKA distribution noted, high TKAs potentially increasing vertebral body stress. Exaggerated thoracic kyphosis is known to affect spine loads and balance in the elderly. The purpose of this study is to evaluate the thoracic curvature shape and TKA in senior women without compression fracture to better characterize potential biomechanical impact of TKA increase.
Materials & Methods
Ninety-six elderly women (≥ 65 years old) were identified without evidence of vertebral compression fracture/wedge deformity on digital lateral chest x-ray. The TKA (Cobb angle) was measured utilizing available PACS software (Stentor) from the T1-T2 level to the T12-L1 level based on endplate visualization. The shape of the thoracic curvature was classified into four distinct recognizable subgroups: 1) gentile-uniform curvature, 2) dominant-upper-thoracic curvature (between T1 and T5), 3) dominant-middle-thoracic curvature (between T4 and T8), and dominant-lower-thoracic curvature (between T8 and T12). Thoracic curve shapes and associated average TKAs were compared.
Results
Gentile-uniform shape was noted in 63 of 96 (65%) patients with dominant middle-thoracic curvature seen in 19 of 96 (20%), dominant upper-thoracic curvature in 12 of 96 (13%) and dominant lower-thoracic curvature in two of 96 (2%). A difference in TKA was noted between the observed curve shapes. Average TKA was greatest in patients with dominant middle-thoracic curvature (48°) with lower TKA in patients with gentile-thoracic curvature (44°) and dominant lower-thoracic curvature (41°). Surprisingly, average TKA was only 30° degrees in patients with dominant upper-thoracic curvature. Bimodal distribution was noted in the dataset when all curve shapes were combined, Bimodal distribution was noted in the patients with gentile-uniform curve shape, further suggesting a subgroup at risk even with gentile curvature.
Conclusion
Distinct differences in thoracic curvature shape and average TKA are noted in elderly women without evidence of compression fracture. Dominant focal middle-thoracic curvature and those with high TKA gentile curvature might have important implications in the development of thoraco-lumbar junction VCF and balance stability. Thoracic kyphotic angle and thoracic curve shape are likely important to consider when developing thoracic spine biomechanical loading models.

KEYWORDS: Anatomical variation, Fracture, Kyphosis

eP-300

Evaluation of the Upper Cervical Spine in MR Imaging of the Brain: A Frequently Overlooked Region

Raz, E.[1]·Saba, L.[2]·Ozsvath, J.[1]·D'Ambrosio, F.[3]·Knopp, E.[1]·Fatterpekar, G.[1]
[1]New York University, New York, NY, [2]University of Cagliari, Cagliari, ITALY, [3]Sapienza University, Rome, ITALY.

Purpose
The standard protocol for brain contrast MRI includes the high-resolution T1-MPRAGE which usually covers the upper cervical spine (UCS): the 3D slab can be extended inferiorly to cover the UCS without prolonging the scan time. We aim to describe the characteristics and frequency of positive findings in the UCS region in a consecutive cohort of patients undergoing a contrast brain MRI, in which the T1-MPRAGE sequence was performed.
Materials & Methods
One hundred consecutive patients that underwent a contrast brain MRI as part of their routine clinical care have been evaluated. Exclusion criteria were the lack of T1-MPRAGE sequence in the protocol and presence of substantial motion artifact. The following have been evaluated: reason for the exam, lower coverage of the T1-MPRAGE (expressed as spinal level), lower coverage of the conventional sequences, extra Z-axis coverage of the T1-MPRAGE in cm. Statistical analysis was performed to evaluate the incidence of findings in the UCS which can be visualized using the T1-MPRAGE of the brain and to evaluate the difference of coverage with respect to different reason for exam.
Results
Six patients were excluded (four cases for motion artifact and in two cases no T1-MPRAGE was obtained) with remaining 94 patients (64 F, 30 M) with a mean age of 45.8 (18.5) years included in the study. The reason for the exam was: followup for brain tumor (n = 35), followup for demyelinating disease (n = 30), vascular malformation (n = 4), various other reasons (n = 25), including, suspected mass, headaches, vertigo. The T1-MPRAGE on average allowed for an extra 3.7 (1.6) cm Z-axis coverage compared to the conventional sequences ($p<0.001$). In 15 cases (15.9% of the cases; Fisher's exact test: $p<0.0001$), the extended coverage allowed for visualization of additional findings: leptomeningeal disease (n = 2), intramedullary lesions (n = 1), nerve sheath tumors (n = 2) and degenerative disease involving the craniocervical junction (n = 9).
Conclusion
T1-MPRAGE, performed as part of the standard protocol

Note: Scanned images are included in the proceedings. Some submitted images were reduced during editing, thereby decreasing clarity. Also, refer to the Program Planner. Proceedings Content as of 3-29-2013.

for contrast brain MRI covers the UCS, not visible with the routine sequences. This can demonstrate additional findings that in some cases can be deemed clinically significant.

KEYWORDS: Spinal cord, Incidental findings

eP-301

Cerebrospinal Fluid Flow Disruption and the Presyrinx State: Imaging Findings and Pathophysiology of a Reversible Myelopathic Condition

Tamrazi, B.·Chin, C.
University of California San Francisco
San Francisco, CA.

Purpose
The purpose of this study is to discuss the pathophysiology, imaging findings, and management of the presyrinx state. The development of syringomyelia secondary to obstruction of CSF flow is well documented in the neuroradiology literature. However the concept of a presyrinx state is not well understood and exists as part of the spectrum of syringomyelia. We will demonstrate the distinct imaging findings and clinical presentation of this potentially reversible condition to help radiologists recognize this entity and ultimately clinicians to promptly manage the patient prior to the development of an irreversible myelopathy.
Materials & Methods
Three patients with imaging and clinical findings of myelopathy were examined in this retrospective review. The patients were found to have evidence of CSF flow disruption secondary to transverse myelitis with cord expansion as well as chronic subdural collections leading to spinal cord intraparenchymal T2 prolongation on MRI without cavitation/syrinx formation. These findings were seen to improve after surgical intervention to alleviate the underlying source of CSF flow obstruction supporting the concept of a potentially reversible myelopathic condition, previously described as a presyrinx state.
Results
Disturbances in CSF flow in the subarachnoid space can potentially lead to a spectrum of pathologies, ranging from reversible to irreversible myelopathy in the form of presyrinx and ultimately syrinx. Cerebrospinal fluid flows from the subarachnoid space into perivascular spaces of the spinal cord and ultimately into the interstitial spaces towards the central canal. Under certain conditions where there is an obstruction to CSF flow such as in cases of arachnoid adhesions, mass lesion, or transverse myelitis causing cord expansion, CSF flow is altered creating edema within the cord. This is distinct from a syrinx where there is formation of a cavity in the cord. Differences on MRI include T2 prolongation without evidence of cavitation, a central canal that is not enlarged, as well as evidence of mechanical obstruction to CSF flow such as degenerative spondylosis causing canal narrowing as well as extra-axial collections such as chronic subdural hematomas. These findings were seen to improve following surgical intervention to alleviate the obstruction with re-establishment of normal CSF flow (Figure 1).

Conclusion
Disturbances in CSF flow dynamics cause a spectrum of myelopathic conditions, including the potentially reversible presyrinx state. This study illustrates the underlying pathophysiology and imaging findings of the presyrinx in order to help radiologists identify this relatively unknown reversible condition to ultimately prevent further progression to permanent myelopathy.

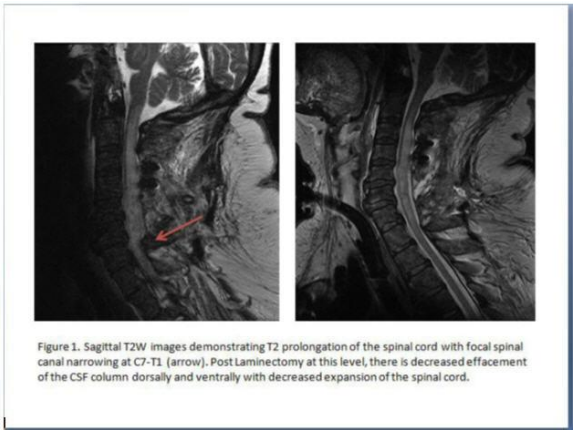

Figure 1. Sagittal T2W images demonstrating T2 prolongation of the spinal cord with focal spinal canal narrowing at C7-T1 (arrow). Post Laminectomy at this level, there is decreased effacement of the CSF column dorsally and ventrally with decreased expansion of the spinal cord.

KEYWORDS: Spinal cord, Syringohydromyelia

eP-302

Prevalence of Unsuspected Sacral Insufficiency Fractures in Patients Undergoing Lumbar Spine MR Imaging

Myneni, M. C.·Vinson, E. N.
Duke University Medical Center
Durham, NC.

Purpose
Sacral insufficiency fractures are an uncommon cause of low back pain and have an increased incidence in the elderly and in patients who have undergone prior external beam radiation therapy to the pelvis. Due to the widespread use of lumbar spine MR imaging to evaluate patients with low back pain and/or neurologic symptoms, unsuspected sacral insufficiency fractures occasionally are detected on the inferior-most axial images through the lumbar spine. The purposes of this study are to find the prevalence of sacral insufficiency fractures detected on routine MR of the lumbar spine and to determine the most sensitive routine sequence at detecting these fractures.
Materials & Methods
Two musculoskeletal-trained radiologists retrospectively reviewed 600 consecutive lumbar spine MR examinations and noted the presence or absence of signal abnormality at the superior sacrum. A fracture was diagnosed when signal abnormality was present and a linear component

Note: Scanned images are included in the proceedings. Some submitted images were reduced during editing, thereby decreasing clarity. Also, refer to the Program Planner. Proceedings Content as of 3-29-2013.

and/or abnormal morphology of the sacral cortex was visible on one or more imaging sequences. The original dictated report was reviewed in each case to determine if a sacral insufficiency fracture was diagnosed. If follow-up imaging was obtained to confirm or refute the presence of a sacral fracture, those images and reports were reviewed as well. In those patients with fractures, the signal characteristics, location, and most useful routine diagnostic sequence were recorded.
Results
Fractures of the superior sacrum were visualized in six (1%) of the 600 lumbar spine studies; five (83.3%) of them were unilateral, and one (16.7%) was bilateral. The average age of patients with sacral fractures was 61.5 years (range, 42-91 years). The most useful diagnostic sequence was the axial T1-weighted sequence. Review of the original dictated report revealed that the diagnosis of sacral insufficiency fracture was made in five (83.3%) of the cases.
Conclusion
Sacral insufficiency fractures are an important and likely under-recognized cause of low back pain. These fractures occasionally are seen on routine MR imaging of the lumbar spine, and were present in 1% of lumbar spine studies in this series. The axial T1-weighted images were more useful than the axial or sagittal T2-weighted images, likely due to the nonfat-suppressed nature of the axial T2-weighted images, and to the location of the fractures lateral to the typical field-of-view of the sagittal images. Paying particular attention to the bone marrow signal intensity in the superior sacrum on the most inferior axial T1-weighted images may improve one's ability to diagnose these fractures as a potential etiology of low back pain and thus improve the diagnostic utility of lumbar MR imaging in the evaluation of patients with nonspecific low back pain.

KEYWORDS: Insufficiency fractures, Sacrum

eP-303

Evaluation of the Intervertebral Disk Angle for the Assessment of Anterior Cervical Diskoligamentous Injury

Howell, M.·Fakhran, S.·Alhilali, L.
University of Pittsburgh Medical Center
Pittsburgh, PA.

Purpose
The anterior diskoligamentous complex (ADL) is important to cervical spinal stability. Subjective widening of the disk space after trauma has been used to gauge ADL disruption on CT, but no quantitative CT measurements exist to evaluate injury. The purpose of our study was to evaluate if an increased intervertebral disk angle (IDA) could serve as a more sensitive, reproducible indicator of ADL disruption compared to subjective assesment.
Materials & Methods
Intervertebral disk angle was measured retrospectively on CT for 122 disk levels with ADL disruption by MR and 1095 disk levels with an intact ADL by MR. Intervertebral disk angle was measured between the anterior superior endplate and anterior inferior endplate, with angle apex at the mid posterior disk. Area under the receiver operating characteristic curves (AUC) for subjective disk widening and specific angle values were obtained. Intervertebral disk angle reproducibility also was evaluated.
Results
Intervertebral disk angle measurements were "substantially reproducible". No disk with intact ADL had an IDA greater than 18° or two standard deviations (SD) from the average IDA of the remaining disks. Area under the receiver operating characteristic curves for a criterion of subjective disk widening was 0.58. Area under the receiver operating characteristic curves for objective criteria, IDA greater than 13 or IDA above one SD from normal values, was 0.85. Maximal AUC was achieved if IDA greater than two SD from the average IDA of the other disks was used (0.86).
Conclusion
Subjective disk widening does not accurately detect ADL disruption on CT; an elevated IDA provides a more sensitive and objective measurement to help to direct further imaging in trauma patients.

KEYWORDS: Spinal trauma, MR imaging spine, CT imaging spine

eP-304

Intraosseous Fluid Sign Predicts Dynamic Vertebral Fracture Mobility

Stein, J. M.·Shah, L. M.
University of Utah
Salt Lake City, UT.

Purpose
Corticocancellous disruption and weakened trabecular bone due to osteoporosis or a marrow replacement process may manifest as an intraosseous fluid sign on CT and/or MRI. This may predict mobility of vertebral body fractures with dynamic maneuvers. Awareness of this potential vertebral collapse may affect patient management.
Materials & Methods
Following IRB approval, the RIS was queried for "fracture" in CT of the thoracic or lumbar spine from March 2011 to 2012. Those CT cases with acute or subacute (< 1 month) fractures and follow-up lateral upright radiographs within one week, with or without MRI, were included. Flexion-distraction injuries were excluded. The fracture type and chronicity were categorized as compression or burst and acute or subacute, respectively. The CT and MRI exams, if available, were evaluated for intraosseous fluid attenuation and signal intensity, respectively. Lateral upright radiographs within one week of the initial imaging were assessed semiquantitatively for further vertebral height loss. A Fisher's exact test was performed.

Note: Scanned images are included in the proceedings. Some submitted images were reduced during editing, thereby decreasing clarity. Also, refer to the Program Planner. Proceedings Content as of 3-29-2013.

Results
The study population included 17 females and 16 males with an average age of 55 years. Spinal segmental locations of the fractures were thoracic and lumbar. There were 41 fractures, of which 23 were compression fractures and 18 burst-type fractures. Of these fractures, 17/41 (41%) had the fluid sign, 11 of which (59%) demonstrated dynamic vertebral height loss on upright radiographs. All of the fractures with a fluid sign and dynamic vertebral body height loss displayed less than 50% loss of height. Three cases showed dynamic vertebral height loss but did not have the fluid sign (13%). Dynamic vertebral body fractures demonstrated an average of 16.4% decreased vertebral body height and six degrees increased kyphosis on upright lateral radiographs compared to supine CT. Of those patients with dynamic loss of vertebral height, the majority (93%) were treated conservatively. Persistent back pain required kyphoplasty in one patient and spinal fixation in two patients. Fluid sign predictive of dynamic vertebral body mobility was found to be statistically significant ($p<0.05$).

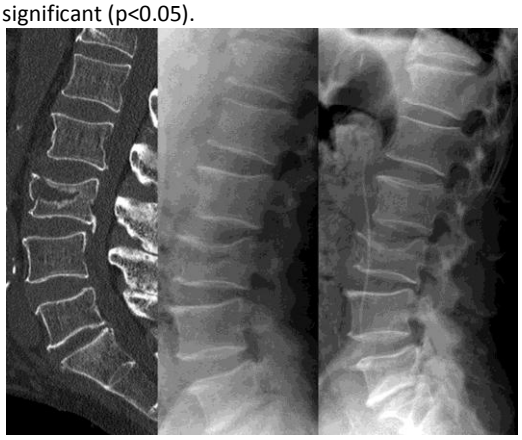

Conclusion
Those vertebral body fractures with an intraosseous fluid sign on CT +/- MRI have an increased risk of dynamic mobility on upright radiographs compared to those fractures without an intraosseous fluid sign. Vertebral body height loss was less than 50%. Radiologists need to be aware of the predictability of this dynamic vertebral body height loss, which can be suggested by the intraosseous fluid sign.

KEYWORDS: Fracture, Spinal imaging

Monday, May 20 – Wednesday, May 22
6:30 AM – 9:00 PM
Thursday, May 23
6:30 AM – 3:00 PM
Hall B1

Education Exhibits (EdE) 2 - 38

EdE1-Adult Brain

Note: A missing printed number indicates an abstract has been withdrawn.

EdE-02

Supporting Roles of Susceptibility-Weighted Imaging and Time-of-Flight MR Angiography Sequences in the Diagnosis and Characterization of Dural Arteriovenous Fistulas

Weisman, N. J.·Matouk, C.·Johnson, M.·Minja, F.
Yale New Haven Hospital
New Haven, CT.

Purpose
To demonstrate the corroboratory roles of susceptibility-weighted imaging (SWI) and time-of-flight MR angiography (TOF MRA) sequences in the diagnosis and characterization of dural arteriovenous fistulas (dAVFs).
Approach/Methods
We present a series of six dAVF patients imaged with both SWI and TOF MRA sequences. The fistulous site, degree of cortical venous reflux (CVR) and associated pseudophlebitic pattern (PPP) were evaluated and confirmed with digital subtraction angiography (DSA), the gold standard diagnostic technique.
Findings/Discussion
Recognition of hyperintense venous signal on SWI and TOF MRA images is an important clue in the diagnosis of dAVFs and fistulous point identification. The hyperintense signal noted on TOF MRA images is due to the “time-of-flight” effect of arterialized venous blood flow. Susceptibility-weighted imaging venous hyperintensity in dAVF patients may be secondary to a combination of this “time-of-flight” effect and diamagnetic oxygenated blood. Given these similarities, SWI and TOFMRA sequences may be regarded as complimentary in the diagnosis of dAVFs. In our study, the fistulous point was accurately identified in all six patients on SWI and TOF MRA images. In addition to fistulous point identification, SWI and MRA identified 100% (four of four) patients with CVR and PPP confirmed on DSA; features correlated with an increased risk of

Note: Scanned images are included in the proceedings. Some submitted images were reduced during editing, thereby decreasing clarity. Also, refer to the Program Planner. Proceedings Content as of 3-29-2013.

intraparenchymal hemorrhage. Both sequences tended to underestimate the degree of PPP when compared to DSA in three of the four patients with CVR.
Summary/Conclusion
Susceptibility-weighted imaging and TOF MRA are complementary noncontrast, noninvasive MRI sequences that can be used to accurately diagnose dAVFs. They also may be useful tools in the routine management and followup of patients with dAVFs.

KEYWORDS: Dural arteriovenous fistula

EdE-03

Pearls and Pitfalls of I-123 Ioflupane (DATscan) SPECT Imaging: What the Radiologist and Clinician Need to Know

Chaudhry, A. A.[1]·Gul, M.[2]·Matthews, R.[1]·Franceschi, D.[1]
[1]Stony Brook University Medical Center, Stony Brook, NY,
[2]Winthrop University Hospital, Mineola, NY.

Purpose
1. Review the anatomy, pathophysiology, and imaging findings including SPECT imaging (DATscan), CT, and MRI of various movement disorders including Parkinson disease and supranuclear palsy. 2. Review pearls and pitfalls of SPECT Imaging.
Approach/Methods
1. Review of nigrostriatum I-123 Ioflupane imaging highlighting study technique and clinical indications. 2. Review approach to SPECT study interpretation. 3. Review imaging findings of I-123 Ioflupane for various movement disorders and their respective differential diagnoses. 4. Review radiologic pitfalls and emphasize key points which can help in avoiding these pitfalls. 5. Review clinical and radiologic pearls that can help narrow the differential diagnosis.
Findings/Discussion
1. Detailed physiologic and pharmacologic discussion of I-123. 2. Case-based discussion of clinical features, pathophysiology, histology features, imaging findings (SPECT, CT and/or MRI) highlighting radiologic pearls, treatments and prognosis of various movement disorders. 3. Case-based discussion of various pitfalls of I-123 Ioflupane imaging along with reviewing clinical and radiology findings that can help in arriving at the correct diagnosis.

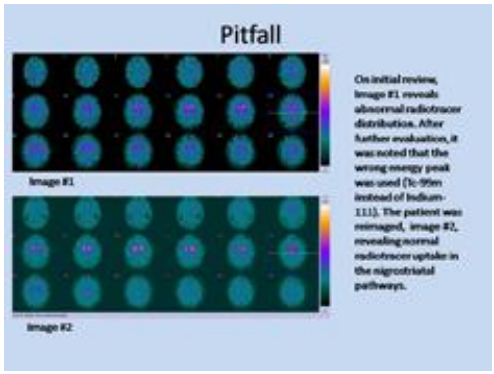

Summary/Conclusion
1. I-123 Ioflupane nigrostriaum imaging is a valuable functional imaging modality in evaluation of various movement disorders including Parkinson disease, essential tremor, pseudoparkinsonism, and progressive supranuclear palsy. 2. By the conclusion of this presentation, the radiologist should have a better understanding of I-123 Ioflupane findings of various movement disorders. 3. Differential diagnosis can be narrowed utilizing age, clinical findings and imaging characteristics on I-123 Ioflupane imaging to avoid common pitfalls.

KEYWORDS: Parkinson disease, Substantia nigra, DATscan

EdE-04

***"Put Your Money Where Your Temporal Lobe Is"*: The Unique Imaging Characteristics of CADASIL**

Morris, J.·Li, S.
Baystate Medical Center
Springfield, MA.

Purpose
CADASIL is the most common heritable cause of stroke and vascular dementia. Clinically, it presents with nonspecific symptoms including migraines, early-onset TIAs, mood disturbance, and progressive cognitive decline. Imaging of patients with CADASIL commonly yields white matter hyperintensity (WMH), a nonspecific finding seen in many disorders. This discussion will elucidate the MRI findings that differentiate CADASIL from imaging mimickers.
Approach/Methods
Compare the imaging findings associated with CADASIL to those of other disorders involving WMH.
Findings/Discussion
A constellation of unique MRI findings suggests the diagnosis of CADASIL. The typical MRI progression begins at age 20-30 with symmetric punctate or nodular periventricular and centrum semiovale WMH on T2-weighted and FLAIR sequences. Lesions increase in prevalence and extent with age, coalescing into larger patchy WMH at age 30-40, specifically in the external capsules (66% of cases) and anterior temporal lobes (60%

Note: Scanned images are included in the proceedings. Some submitted images were reduced during editing, thereby decreasing clarity. Also, refer to the Program Planner. Proceedings Content as of 3-29-2013.

of cases), but sparing the medulla; lacunar infarcts become apparent at this age as well. Microhemorrhages follow, and eventual T1-weighted hypointensities result from severe tissue damage. Other generic neuroimaging findings also are seen, including dilated perivascular spaces and age-incongruent brain atrophy. White matter hyperintensities are ubiquitous, and thus MRI mimickers of CADASIL are frequent. In many cases clinical history excludes CADASIL, but not always. Notably, none of the following disorders demonstrate symmetric WMH in the anterior temporal lobes or external capsules, but a short discussion of their imaging findings is still warranted. Small vessel ischemic disease WMH is asymmetric and subcortical/periventricular, generally seen in association with risk factors for ischemia. Multiple sclerosis presents with WMH, but lesions never involve the basal ganglia or thalamus, whereas CADASIL lesions do. Cerebral amyloid angiopathy causes WMH as well, but evidence of hemorrhage always parallels the finding. The WMH seen in posterior reversible encephalopathy syndrome are, as the name suggests, posteriorly based. Acute demyelinating encephalomyelitis produces WMH, but they are seen both supra and infratentorially. Finally, vasculitides and infectious causes of WMH are numerous, but the findings are asymmetric and the diagnosis generally can be made by clinical presentation and simple laboratory analysis.

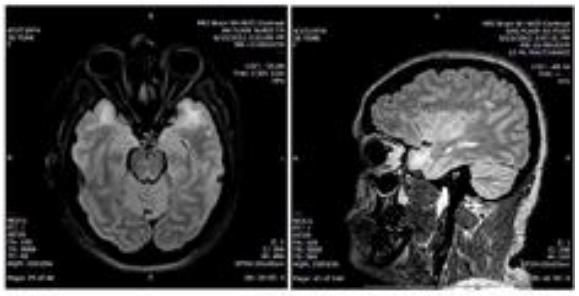

Summary/Conclusion
CADASIL remains elusive, as its symptomatology is nonspecific, but neuroimaging is paramount in its diagnosis. While genetic testing remains the gold standard and neuroimaging cannot make the diagnosis alone, characteristic MRI findings of CADASIL are relatively specific: symmetric T2-weighted and FLAIR hyperintensity in the white matter of the anterior temporal lobes and external capsules suggests a diagnosis of CADASIL.

KEYWORDS: MR imaging brain, White matter disease, CADASIL

EdE-05

Inadvertent Reset of a Programmable Cerebrospinal Fluid Shunt: Not Just a Theoretical Concern

Hira, A. S.·Macyszyn, L.·Mamourian, A.
University of Pennsylvania
Philadelphia, PA.

Purpose
Programmable ventriculoperitioneal shunt valves are used widely and represent an important tool for the treatment of both adult and pediatric cases of hydrocephalus. While inadvertent resetting of the magnetic valve due to an MR scanner's magnetic field has been suggested to offer a potential risk, there are no such cases reported in the literature. We present two such cases of MR scan-programmable shunt interaction to emphasize this risk in the MR environment.
Approach/Methods
We reviewed the literature regarding inadvertent magnet interaction and the recognition of programmable shunt valves. Two patients in whom their programmable valve settings changed during an MRI examination were identified retrospectively from our institution and reported here.
Findings/Discussion
Recent studies have demonstrated improved long-term effectiveness of programmable valves for the treatment of hydrocephalus compared with conventional fixed valves. Balancing any benefit, however, programmable valves represent a new risk for patients having an MRI. It is essential that these valves be recognized prior to the scan and the valve settings interrogated afterwards so that any change can be communicated promptly to the patient's physician. In this report, the setting of one patient's Strata valve was altered from 0.5 to 2.5 due to their MR scan. While this change was in fact recognized by the radiologist no action was taken. The patient's ventricular system subsequently enlarged sufficiently to cause a change in mental status that required hospital admission. In a second patient with a programmable shunt, a striking change in the ventricular size was noted between the start and finish of a single MRI examination of the brain. Recognition of this change led to an immediate valve reset by neurosurgery staff.
Summary/Conclusion
Due to the increasing use of programmable VP shunt valves, it is essential for radiologists and MR staff to develop a system to identify such patients, check postscan settings, and make appropriate arrangements when reset is necessary. We provide these two cases to illustrate that this is not a theoretical problem and suspect that this situation is either underreported or unrecognized at some sites.

KEYWORDS: Hydrocephalus, Shunt, malfunction

Note: Scanned images are included in the proceedings. Some submitted images were reduced during editing, thereby decreasing clarity. Also, refer to the Program Planner. Proceedings Content as of 3-29-2013.

EdE-06

Hypertrophic Olivary Degeneration: Review of Anatomy, Pathology, and Imaging

Ahmed, F. Y.·Telford, R.·Roberson, G. H.·Vattoth, S.
University of Alabama
Birmingham, AL.

Purpose
The aim of this presentation is to review the anatomy of dento-rubro-olivary pathway, the so called "Guillain-Mollaret Triangle", and discuss how lesions in its afferent fibers lead to hypertrophic olivary degeneration (HOD). Our teaching point is to learn how to diagnose HOD according to its MRI appearance, and differentiate it from other medullary lesions in order to avoid unnecessary concern and intervention.
Approach/Methods
The presentation will be organized anatomically by dento-rubro-olivary pathway and adjacent structures with the help of MRI images and graphic representation. Hypertrophic olivary degeneration MRI appearance as well as laterality, and location of lesions causing it also will be discussed. Finally, special emphasis will be made on other medullary lesions which could be misdiagnosed as HOD.
Findings/Discussion
Hypertrophic olivary gegeneration is a unique type of transneural degeneration. It is caused by primary lesions in dento-rubro-olivary pathway. The inferior olivary nucleus (ION) hypertrophy may lead to misdiagnosis of HOD as a medullary mass lesion. Hypertrophic olivary degeneration could be ipsilateral, contralateral or bilateral based on the location of primary lesion and usually present at six months or later from having the primary lesion. Understanding the anatomy of "Guillain-Mollaret Triangle" and its clinical and radiologic implication is very important to diagnose HOD and differentiating it from other medullary lesions.
Summary/Conclusion
Diagnosis of HOD is to be considered in patient with dento-rubro-olivary pathway lesions. It is also important to know the differentiation between HOD and other medullary lesions. Correct diagnosis is crucial to avoid unnecessary investigations and clinical concern. At the end of this review, the radiologist will be confident in diagnosing HOD based on the understanding of underlying anatomy and its characteristic MRI appearance.

KEYWORDS: Hypertrophic olivary degeneration, Inferior olivary nucleus

EdE-07

MR Imaging of Toxic and Metabolic Encephalopathies

Goldstein, A.·Samim, M.·Mahajan, A.
Yale University School of Medicine
New Haven, CT.

Purpose
Altered mental status is common in both the emergency and inpatient setting, ranging from confusion to coma. Initial workup often seeks to exclude catastrophic events such as stroke, infection/sepsis, and traumatic injury. Once these causes have been ruled out, a "secondary survey" usually includes an evaluation for toxic and metabolic etiologies, including drug intoxication, electrolyte abnormalities, hypoxemia, and uremia. In these conditions, noncontrast head CT can be nonspecific or unremarkable, and characteristic MR imaging findings may be helpful in narrowing the differential diagnosis. Since toxic-metabolic encephalopathies may be reversible, timely detection can help the referring clinician initiate early treatment to prevent further or permanent neurologic dysfunction. This educational exhibit reviews the MRI features of several more common toxic and metabolic encephalopathies to help the interpreting radiologist further contribute to the care of patients with such conditions.
Approach/Methods
This exhibit utilizes multisequential MR images from patients with clinical and laboratory findings consistent with specific metabolic and toxic encephalopathy syndromes to review their classic MR imaging features. Conditions to be discussed include hypoglycemia, hyperammonemia, hypernatremia, osmotic myelinolysis, and hyperalimentation, among others. Differences in the topographic distribution of signal abnormalities will be highlighted with a special emphasis placed on the underlying pathophysiology of the observed signal changes. Disorders with similar imaging findings will be compared and contrasted.
Findings/Discussion
Since various toxic and metabolic insults primarily affect different parts of the brain, specific imaging findings can suggest a diagnosis (or at least help narrow the differential diagnosis). For example, acute hyperammonemic encephalopathy typically results in T2 and FLAIR hyperintensities involving the insular cortex and cingulate gyrus, often with restricted diffusion. Osmotic demyelination classically involves the pons, as well as the cerebral white matter and basal ganglia, with hyperintense T2 and FLAIR lesions and possible restricted diffusion due to cytotoxic edema. Such imaging findings will be exemplified and further discussed in the exhibit.

Note: Scanned images are included in the proceedings. Some submitted images were reduced during editing, thereby decreasing clarity. Also, refer to the Program Planner. Proceedings Content as of 3-29-2013.

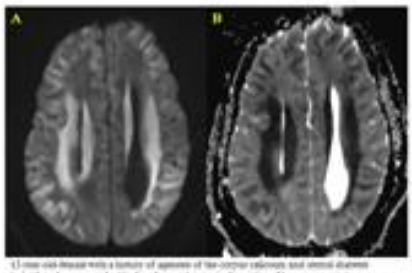

Summary/Conclusion
The diagnosis of toxic-metabolic encephalopathy often poses a difficult clinical challenge. While history and physical examination findings can be suggestive, MR imaging can be of further assistance when classic imaging findings are present and recognized by the interpreting radiologist. An understanding of the basic patterns of cortical, white matter, basal ganglia, thalamic, and brainstem involvement by specific toxic-metabolic encephalopathies can narrow the differential diagnosis. In turn, this can prevent unnecessary testing, expedite treatment, and aid in providing prognostic information.

KEYWORDS: Encephalopathy, Metabolic, toxic

EdE-08

Asymptomatic Focal Cortical Dysplasia: An Underreported Entity?

Butteriss, D. J. A.[1]·Joshi, A.[2]
[1]Regional Neurosciences Centre, Newcastle upon Tyne, UNITED KINGDOM, [2]Royal Victoria Infirmary, Newcastle upon Tyne, UNITED KINGDOM.

Purpose
Focal cortical dysplasia (FCD) is an increasingly important entity due to its association with intractable epilepsy. With improvements in imaging and surgical techniques, lesional surgery may be an appropriate treatment for some cases of epilepsy related to an underlying FCD. However, it remains unclear what proportion of FCDs are asymptomatic. A single neuroradiologist in a single setting has found a series of seven cases of cortical and subcortical lesions suggestive of an atypical or novel form of FCD not associated with intractable epilepsy. These lesions have been investigated as low grade neoplasms, with unnecessary anxiety and investigation, up to and including brain biopsy. This document will review the imaging and clinical features of these cases.
Approach/Methods
Since August 2008 the author has collected seven cases with similar appearances from an unselected cohort of patients referred to the regions neurosciences center for imaging. Initial radiologic diagnoses for the abnormalities included infarct and low-grade glioma. In one case the lesion was not reported and in another the lesion was described and no differential diagnosis was offered. Only one case was offered a primary diagnosis of focal cortical dysplasia, as it was reported by the author while collating this data. The majority of lesions seemed to be incidental findings. In only one case was the patient being investigated for epilepsy (case 5 WP). In this case the patient had had a first seizure at the age of 59, while on holiday, and had imaging in Greece, not available for review. The report was of an infarct. The seizures were controlled with standard anti-epilepsy medication.
Findings/Discussion
All of the lesions have a similar appearance, being increased T2 and low T1 signal, centered on the subcortical white matter, sometimes with involvement of the overlying cortex. The lesions have a typical "bubbly" or "spotty" appearance around the periphery. The findings typically associated with FCD including thickening of the cortex, indistinct gray/white matter interface and trans-mantle signal change, are not apparent in these cases.

Patient ID	DoB	Sex	Date of initial MRI	Reason for scan	Lesion location	special sequences	Follow up	Histology
1 JW	11.06.58	F	16.08.11	Headache	RT temporal	DWI – unrestricted MRS – high CHO low NAA Non-enhancing	1 year No change	
2 MO	16.05.66	F	29.01.08	LT SO myokymia	RT parietal	MRS elevated CHO, low NAA FA- decreased Non-enhancing	2.5 years No change	FCD
3 JM	25.04.53	F	14.11.09	SNHL	RT parietal	SWI – large vein assoc FA – decreased ASL - isoperfused	2.5 years No change	
4 DS	16.07.31	M	16.11.11	Encephalitis	LT temporal	DWI- unrestricted Non enhancing	6 months No change	
5 WP	23.07.47	M	05.08.06	New onset seizures	RT frontal	T2* - normal DWI –unrestricted Non-enhancing	6 years No change	Hamartoma/ dysplasia
6 RW	08.06.44	M	10.07.12	Cognitive decline	RT frontal	T2* - normal		
7 LL	26.11.55	F	12.05.07	Meningioma	RT posterior temporal	Non-enhancing	5.5 years No change	

Summary/Conclusion
The spectrum of focal cortical dysplasia may be larger than previously thought, with asymptomatic cases with a novel, but typical appearance being relatively common. These cases should and can be identified early so patients can be appropriately counselled, without need for extensive, expensive and invasive investigation.

KEYWORDS: Focal cortical dysplasia, asymptomatic

EdE-09

Adult Manifestations of Congenital Pediatric Brain Disorders

Reilly, C. B.·Tantiwongkosi, B.
University of Texas Health Science Center at San Antonio San Antonio, TX.

Purpose
Adult neuroradiologists may be unfamiliar with the imaging manifestations of pediatric brain insults presented

Note: Scanned images are included in the proceedings. Some submitted images were reduced during editing, thereby decreasing clarity. Also, refer to the Program Planner. Proceedings Content as of 3-29-2013.

in adulthood. The aim of this exhibit is to review adult manifestations of select common and uncommon congenital brain disorders, and how their radiologic appearance may be similar or different from a pediatric population.
Approach/Methods
Several cases of known or suspected congenital or acquired pediatric brain pathologies seen in the adult population on CT and MR examinations at our tertiary care academic institution over the last several years were selected for presentation. We performed a review of the literature to guide discussion of radiologic findings and the similarities and differences between adult and pediatric populations. When available, clinical pictures are presented to correlate with the imaging findings.
Findings/Discussion
We present a selection of cases collected from our institution of adult patients presenting with pediatric brain pathologies. Developmental brain disorders presented include Chiari malformation, neuronal migrational anomaly, posterior fossa malformation, etc. Some pediatric patients having toxic metabolic disorders survive till their adulthood with residual brain findings including hypoxic ischemic encephalopathy, adrenoleukodystrophy, mitochondrial diseases, etc. Neurocutaneous syndromes presented include neurofibromatosis, tuberous sclerosis, von Hippel-Lindau disease, and Sturge Weber syndrome. We discuss these conditions with an emphasis on appearance in the adult population and similarities and differences between the appearances in a pediatric population. Embryologic and pathologic basis of the diseases are discussed.
Summary/Conclusion
This exhibit demonstrates adult manifestations of pediatric brain diseases. For each of the conditions encountered, a relevant differential diagnosis is provided and the pertinent differences and similarities in imaging findings when encountered in pediatric versus adult populations are provided. We hope to provide a concise review and discussion after which the reviewer will feel more comfortable when encountering this selection of pediatric neurologic conditions when discovered in an adult population.

KEYWORDS: Congenital anomalies, Metabolic, neurocutaneous syndromes

EdE-10

Hippocampal Changes in Seizure and Status Epilepticus: The Spectrum of Findings You Need to Know

Sanghvi, T. S.·Young, S. J.·Patel, S. T.·Quisling, R. G.
University of Florida
Gainesville, FL.

Purpose
Evaluation of the hippocampus in the context of a recent seizure event (not known epilepsy) requires an understanding of the specific structures that make up the hippocampus. We will begin with a review of the relevant anatomy and subsequently describe abnormal hippocampal findings.
Approach/Methods
To call an exam normal one needs to identify all of the specific structures within norma- sized hippocampi. We will begin by reviewing critical anatomy, describing the specific internal locations of the major (pyramidal) cell bodies and the myelinated pathways, as well as describe structures such as the entorhinal cortex, dentate granular layer, mossy fiber region within the hilum of the hippocampus, the conru amonis (especially CA3 and CA1) and finally the subiculum. Details of these structures are presented on both anatomical and MRI images. Once normal anatomy is reviewed we will focus on the spectrum of hippocampal abnormalities seen with acute temporal lobe seizures correlated with animal modeling for status epilepticus.
Findings/Discussion
Once normal findings have been described we will describe the time dependent changes seen with temporal lobe epilepsy. Hippocampal injury during limbic seizure activity undergoes a process similar to that of an ischemic event and follows a similar evolution of the glutamate cascade. Thus, the severity of findings match the depth and duration of the ictus event. The hyperacute stage includes hippocampal edema and effacement of the internal white matter lamination. The range of acute and subacute findings extending to chronic mesial temporal sclerosis also will be discussed.
Summary/Conclusion
The consequence of untreated prolonged seizures and subclinical status epilepticus is often dire. The need to make the diagnosis quickly and accurately enables the clinical service to treat effectively. In order to make the diagnosis quickly and accurately the radiologist must first be familiar with normal hippocampal anatomy so that he/she may recognize the presented spectrum of abnormalities. This presentation hopefully will increase awareness of subtle abnormalities and increase confidence in reporting which may result in significant clinical implications.

KEYWORDS: Hippocampus, Seizure, epilepsy

EdE-11

Interpretation and Pitfalls in 18-F Florbetapir Imaging for the Evaluation of Dementia of the Alzheimer Type: A Pictorial Essay

Pamarthy, S.[1]·Bohnen, N. I.[1,2]·Gross, M. D.[2]·Fig, L. M.[2]
[1]University of Michigan, Ann Arbor, MI, [2]Department of Veterans Affairs, Ann Arbor Healthcare System, Ann Arbor, MI.

Purpose
18-F Florbetapir (Amyvid) was recently (April 2012)

Note: Scanned images are included in the proceedings. Some submitted images were reduced during editing, thereby decreasing clarity. Also, refer to the Program Planner. Proceedings Content as of 3-29-2013.

approved by the Food and Drug Administration (FDA) for imaging of patients with cognitive impairment who are being evaluated for dementia of the Alzheimer type (DAT) versus alternative etiologies of cognitive decline. The agent binds with high affinity to neuritic β-amyloid plaques and is used to estimate plaque density. Image interpretation, which should be performed only following the completion of the FDA-required company-sponsored training program, differs from that of conventional radionuclide brain imaging, and requires binary categorization of images as positive or negative. We review the methodology for image acquisition and the interpretative schema for 18-F florbetapir studies as an introduction for radiologists who may be contemplating the use of this agent.

Approach/Methods

This educational exhibit will: 1. Describe technical aspects of 18-F Florbetapir PET imaging; 2. Using multiple images, discuss the interpretative criteria for positive and negative scans and the clinical significance of each; 3. Demonstrate the limitations of the use of 18-F Florbetapir imaging and the interpretative pitfalls that may be encountered.

Findings/Discussion

The exhibit will detail important aspects of the imaging protocol, including dosage, timing, PET scan acquisition and processing. Case examples will demonstrate positive and negative florbetapir images; this determination depends on assessment of the gray to white matter contrast. It is important to note that a positive scan, while indicating moderate to frequent amyloid plaques does not unequivocally establish a diagnosis of DAT because positive scans also may be observed in the cognitively normal aging brain (as confirmed by neuropathologic investigation), and in patients with other neurologic diagnoses (e.g., dementia with Lewy bodies). On the other hand, a negative florbetapir scan indicating the absence (or rarity) of neuritic plaques is inconsistent with a current diagnosis of DAT. To date, florbetapir imaging is not clinically indicated in predicting future dementia or for monitoring therapeutic response. Difficulties in interpretation may be related to cortical atrophy leading to widening of the sulci with consequent reduction of gray to white matter contrast, other structures that may take up the tracer (e.g., salivary glands), suboptimal image quality and artifacts such as patient motion.

Summary/Conclusion

18-F Florbetapir PET imaging is now FDA approved for the evaluation of selected patients with cognitive impairment. This exhibit may help improve the neuroradiologist's understanding of the techniques, interpretation methods, and limitations of the test to more effectively guide referring clinicians in its appropriate use in suitable patients.

KEYWORDS: Alzheimer disease, PET, 18-F Florbetapir

EdE-12

FDG-PET Neuroimaging of Medically Refractory Epilepsy: An Illustrative Review

Thaker, A. A.·Dubroff, J. G.
Hospital of the University of Pennsylvania
Philadelphia, PA.

Purpose

Neuroimaging studies play an established role in the diagnosis and evaluation of epilepsy, particularly in patients with medically refractory temporal lobe epilepsy (TLE). While MRI is highly sensitive and specific for hippocampal sclerosis (HS), the most common pathologic basis of TLE, a limited but significant number of patients have no identifiable MRI lesion. F-18 flourodeoxyglucose positron emission tomography (FDG-PET) is an adjunct imaging modality which often reveals ipsilateral hypometabolism, which has been shown to predict a good prognosis post-temporal lobectomy. The purpose of this educational exhibit is to provide an illustrative review of the role of FDG-PET neuroimaging in the evaluation of patients with medically refractory TLE.

Approach/Methods

Epilepsy surgery in patients with refractory TLE is a well established and evidence-based treatment. High-resolution MRI plays a crucial role in identifying potential epileptogenic lesions, and is the initial imaging modality in these patients. This exhibit will first present typical case examples of mesial temporal sclerosis (MTS), the MRI correlate for HS, with side-by-side FDG-PET comparison, which often demonstrates concordant focal hypometabolism (MRI+/PET+ cases). Approximately 15-20% of patients with refractory TLE have no MRI abnormality, and many of these patients will have only asymmetric focal hypometabolism on interictal FDG-PET. A case series of these MRI-/PET+ patients will be presented with additional relevant clinical data, including postsurgical outcome by Engel class. Finally, case examples of TLE patients with MTS on MRI and normal brain FDG-PET will be presented (MRI+/PET-).

Findings/Discussion

In epileptic patients with disease refractory to drug therapy, the main aim of surgery is seizure control and thus improved quality of life. Postsurgical outcomes are stratified by Engel class (class I: free of disabling seizures, class II: rare disabling seizures, class III: worthwhile improvement, class IV: no worthwhile improvement). Several published case series have shown that patients with intractable TLE and MRI-/PET+ have no difference in surgical outcome than those patients with MRI+ mesial temporal sclerosis. This data will be referenced in this exhibit to underscore the important adjunct role of FDG-PET in intractable TLE patients (see case example in Figure 1).

Note: Scanned images are included in the proceedings. Some submitted images were reduced during editing, thereby decreasing clarity. Also, refer to the Program Planner. Proceedings Content as of 3-29-2013.

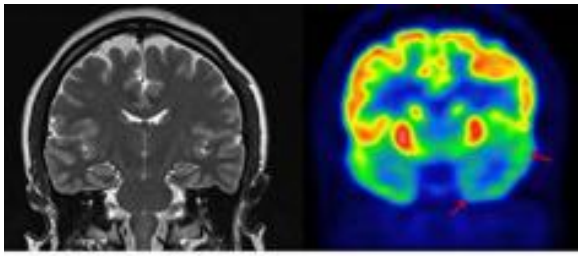

Figure 1.

Summary/Conclusion
FDG-PET neuroimaging has an increasing role in the presurgical evaluation of medically refractory TLE patients, and has been shown to identify patients who will have good surgical outcomes, regardless of whether MTS is identified on MRI. FDG-PET is an important modality in the armamentarium of the neuroradiologist who evaluates epilepsy patients.

KEYWORDS: PET, Epilepsy

EdE-13

MR Spectroscopy of Brain Tuberculomas: Findings and Literature Review

Morales, H.[1]·Gaskill-Shipley, M.[1]·Alfaro, D.[2]·Martinot, C.[3]·Castillo, M.[4]
[1]University of Cincinnati, Cincinnati, OH, [2]University Nacional Mayor de San Marcos, Lima, PERU, [3]Centro de Resonancia Magnetica, Lima, PERU, [4]University of North Carolina at Chapel Hill, Chapel Hill, NC.

Purpose
Central nervous system tuberculosis (TB) is a major health concern in developing countries, and is increasing in developed countries due to HIV/AIDS and multidrug-resistance. Our purpose is to describe the most common MR spectroscopic (MRS) findings in brain tuberculomas.
Approach/Methods
We describe the most common MRS findings in brain tuberculomas. Thirteen proven cases by histology and/or response to antimycobacterial therapy will be used to demonstrate the findings. The metabolic alterations are discussed in correlation with possible pathologic mechanisms, recent literature and spectroscopic findings of other common brain masses such as gliomas.
Findings/Discussion
Brain tuberculomas show a dominant peak of lipids. Most demonstrate an increase in glutamate/glutamine (Glx) and a serine peak at 3.8 ppm. Increased choline (Cho) is more common than previously thought. The presence of serine and lipids correlate with the make-up of the mycobacterium cell wall. Increased Glx is not a common finding in gliomas, its presence along with serine favors TB.

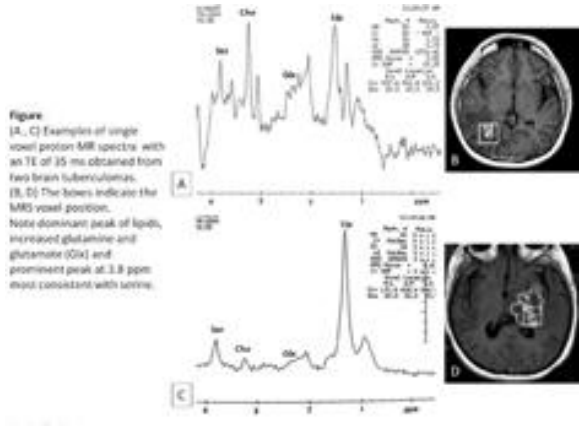

Figure

Summary/Conclusion
In absence of lipids, the diagnosis of brain tuberculoma is unlikely.

KEYWORDS: MR spectrocopy, Tuberculosis

EdE-14

Pictorial Review of the Various Clinical, Radiologic and Pathologic Findings of Chronic Lymphocytic Inflammation with Pontine Perivascular Enhancement Responsive to Steroids

Bhatnagar, P.·Karsandas, A.·Hall, J.·Birchall, D.·Butteriss, D.
Royal Victoria Infirmary
Newcastle upon Tyne, UNITED KINGDOM.

Purpose
1. To present the clinical and imaging findings of chronic lymphocytic inflammation with pontine perivascular enhancement responsive to steroids (CLIPPERS). 2. To aid better understanding of the pathogenesis and the histopathological findings of CLIPPERS. 3. To review the literature and enable the neuroradiologists in making the correct diagnosis.
Approach/Methods
Chronic lymphocytic inflammation with pontine perivascular enhancement responsive to steroids recently has been proposed as a rare chronic inflammatory central nervous system disorder which has a predilection to hindbrain and responds to immunosuppressive therapy. We present four cases encountered recently at our institution. Detailed laboratory workup and brain biopsy were performed. We describe the clinical features and MRI appearances of these cases. We also review the clinical and radiologic response to steroids. A brief differential diagnosis and review of literature will be presented.
Findings/Discussion
Patients with CLIPPERS mainly presented with ataxia, nystagmus, diplopia. MR imaging demonstrated characteristic pattern of punctate and curvilinear enhancement peppering the pons and extending variably into the medulla, brachium pontis and mid-brain. Lesions

Note: Scanned images are included in the proceedings. Some submitted images were reduced during editing, thereby decreasing clarity. Also, refer to the Program Planner. Proceedings Content as of 3-29-2013.

are typically less numerous and smaller as distance from the pons increases. One patient had involvement of the spinal cord, which has been described in literature. Lesions show patchy nonspecific increased T2 signal in the corresponding areas of contrast enhancement. The lesions do not have significant mass effect. Differential diagnoses that need to be considered and excluded include: neurosarcoidosis, lymphoma, vasculitis, Bickerstaff brainstem encephalitis, Bechet's, paraneoplastic and demyelinating diseases. On histopathology, there is marked lymphocytic infiltrate in the white matter with perivascular predominance and also a more diffuse parenchymal inflammatory infiltrate. Treatment with steroids leads to marked improvement with rapid improvement on the MRI. Rarely, cyclophosphamide is required for immunosuppression. Marked cerebellar atrophy often results and may contribute to long-term neurologic morbidity.

Summary/Conclusion

Chronic lymphocytic inflammation with pontine perivascular enhancement responsive to steroids is a newly described distinct inflammatory CNS disorder and probably more frequent than previously thought. It has characteristic MRI findings and there may be extrapontine involvement. Better understanding of this condition will enable the neuroradiologists in making a prompt diagnosis. This will help effective management, which may in turn limit permanent neurologic sequelae.

KEYWORDS: CLIPPERS

EdE-15

Pictorial Review and Differential Diagnosis of Common Choroid Plexus Lesions

Barret, W. A.[1]·Gaddamanugu, S.[2]·Vattoth, S.[1]
[1]University of Alabama Birmingham Radiology, Birmingham, AL, [2]Veterans Affairs Hospital, Birmingham, Birmingham, AL.

Purpose

Choroid plexus are present throughout the ventricles, but are most prominent in the body of the lateral ventricles. They are highly vascularized enhancing structures. Lesions involving the choroid plexus are diverse. The purpose of this exhibit is to review common choroid plexus pathology and to described imaging features which characterize and differentiate benign lesions from more malignant or obstructing pathology.

Approach/Methods

Anatomy and pathologies involving the choroid plexus will be reviewed. Computerized tomography and magnetic resonance images of choroid plexus pathologies will be illustrated. Imaging findings which help characterization of individual pathologies will be detailed.

Findings/Discussion

Pathology involving the choroid plexus is rare. The choroid plexus may be involved in systemic/generalized neurologic conditions or focally by tumors or cysts. The most common pathology involving the choroid plexus in adults are incidental simple or xanthogranulomatous cysts. The choroid plexus also can be involved by meningioma, metastasis, vascular malformations or lipoma. Temporal lobe surgery can alter choroid plexus morphology. In children or infants, the most common abnormality involving often is choroid plexus cysts or hemorrhage. Other rare pathology include choroid plexus papilloma or carcinoma. The choroid plexus can be secondarily involved in patients with syndromic disorders such as Sturge-Weber syndrome.

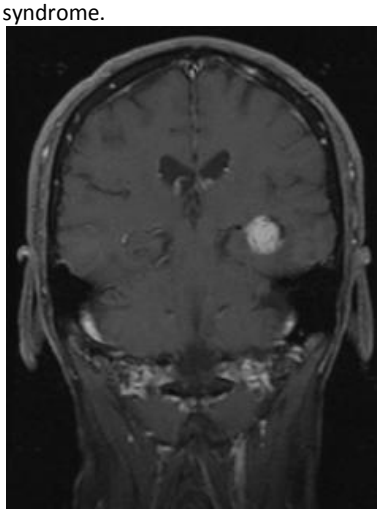

Image 1: Axial T2-weighted image of the brain reveals enlarged choroid plexus of the left temporal horn.

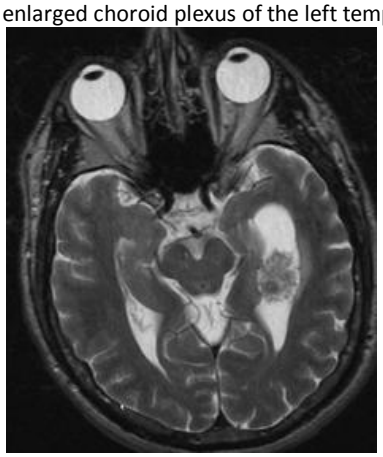

Image 2: Postcontrast images reveal significant enhancement of the choroid plexus mass. Patient had thyroid cancer and a iodine-131 posttreatment scan which revealed intense uptake in the left lateral ventricle, consistent with metastasis.

Summary/Conclusion

Knowledge of common incidental choroid plexus pathology is essential to avoid necessary investigations. More serious pathology of the choroid plexus is rare. This exhibit will review the common pathologies involving the choroid plexus.

KEYWORDS: Choroid plexus, Ventricles

Note: Scanned images are included in the proceedings. Some submitted images were reduced during editing, thereby decreasing clarity. Also, refer to the Program Planner. Proceedings Content as of 3-29-2013.

EdE-16

Extreme Pseudoprogression on MR Imaging of High-Grade Gliomas Treated with Paclitaxel Poliglumex: Comparison with Conventional Pseudoprogression and True Tumor Progression

Farnam, J.·Boxerman, J.·Jeyapalan, S.·Elinzano, H.·Goldman, M.·Safran, H.
Brown University Alpert School of Medicine
Providence, RI.

Purpose
High-grade gliomas (HGG) are the most common primary brain malignancies, with glioblastoma multiforme having a particularly dismal overall survival. Conventional first-line treatment includes resection plus targeted radiation in combination with chemotherapy. Chemoradiation with the radiosensitizing agent temzolomide (TMZ) has been associated with *pseudoprogression*, defined as progressive MRI enhancement following therapy that stabilizes or resolves over time without treatment modification. Paclitaxel poliglumex (PPX), a radiosensitizing agent previously investigated for treatment of esophageal cancer and more recently applied to the treatment of high-grade gliomas, has a radiosensitizing index 4-8 times that of TMZ and may similarly incite pseudoprogressive enhancement on post-treatment MRI examinations but to a much greater degree, and with durations exceeding that typically seen with TMZ. We aim to present examples of pseudoprogression with both agents, emphasizing the similar and distinguishing features, as well as examples demonstrating the similar appearance of true tumor progression.
Approach/Methods
A recent phase II study evaluated progression-free survival of patients with HGG treated with radiation and both PPX and TMZ. We will present the serial MR imaging of multiple patients from this study, demonstrating a spectrum of pseudoprogression and true tumor progression and compare this to examples of true progression and pseudoprogression in patients with HGG treated with TMZ and radiation therapy alone.
Findings/Discussion
Twenty-five patients were included in the above-mentioned study, 13 with post-PPX MRI findings consistent with pseudoprogression. Pathologic correlation with biopsy or repeat surgery was obtained in five of these patients. Onset of pseudoprogression occurred 2 to 174 days (mean 63 days) following completion of PPX, and persisted 18 to 719 days (mean 334 days). This “extreme” *pseudoprogression* persisted significantly longer than that typically seen with TMZ and radiation therapy alone. Pseudoprogression very closely resembles true tumor progression in appearance on postcontrast T1-weighted images.

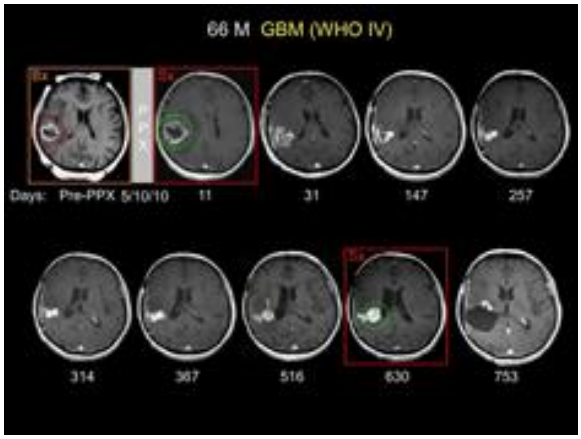

Figure 1. Extreme *pseudoprogression* with combined PPX/TMZ chemoradiation. Surgical excision at 630 days.
Summary/Conclusion
Pseudoprogression has been demonstrated in the setting of chemoradiation with combined PPX+TMZ with MRI findings that are more extensive and longer lasting than those seen with conventional radiosensitizing agents. Higher radiation sensitizers can therefore produce post-treatment imaging that appears increasingly worrisome to the neuroradialogist. Knowledge of the specific chemotherapeutic regimen therefore is essential when interpreting follow-up imaging and evaluating treatment response so as to not erroneously assume the presence of tumor progression. This will likely remain relevant to the neuroradiologist as additional highly radiation sensitizing agents are introduced clinically.

KEYWORDS: Pseudoprogression, Glioblastoma, paclitaxel poliglumex

EdE-17

Laser Interstitial Thermal Therapy for Brain Neoplasms: Imaging of Treatment Changes with Clinical Correlation

Bagade, S.[1]·Miller-Thomas, M.[1]·Mettenberg, J.[1]·Hawasli, A.[2]·Shimony, J.[1]·Leuthardt, E.[2]
[1]Mallinckrodt Institute of Radiology, St. Louis, MO, [2]Barnes Jewish Hospital, St. Louis, MO.

Purpose
1. To introduce the laser interstitial thermal therapy (LITT) technique to the neuroradiology community. 2. To report intraoperative, early and late post-treatment MRI findings in patients undergoing thermal ablation using LITT for brain tumors. 3. To review clinical outcome following the procedure.
Approach/Methods
A total of 15 patients with malignant brain neoplasms treated with thermal ablation using Monteris AutoLITT system at our institution were included in the study. Subjects included six females, nine males with ages between 34 to 78 years. These patients either had lesions

Note: Scanned images are included in the proceedings. Some submitted images were reduced during editing, thereby decreasing clarity. Also, refer to the Program Planner. Proceedings Content as of 3-29-2013.

not amenable to surgical resection or had medical comorbidities precluding traditional surgical treatment. Ten patients had primary glial neoplasms including glioblastoma multiforme (GBM) in five patients, high-grade astrocytoma in four patients and oligodendroglioma in one patient. The remaining five patients had metastatic brain lesions; three from lung carcinoma and one each from melanoma and colorectal cancer. One patient with GBM received repeat ablation of a lesion which had exhibited growth over 10 months in followup. A retrospective review of pre, intra, and postoperative imaging of these patients was performed, making note of volume of the enhancing tumor, presence of hemorrhage, necrosis, and extent of perilesional T2/FLAIR signal on imaging before and after ablation. Clinical outcome during the postoperative course was noted.

Findings/Discussion

On postoperative imaging, treated lesions showed increased T1 signal and susceptibility on blood-sensitive sequences consistent with hemorrhage and/or protein from coagulative necrosis. There was a surrounding new thin uniform rim of contrast enhancement following ablation. Most lesions showed mildly increased surrounding T2/FLAIR signal in the early postoperative course which decreased on delayed imaging. Significant number of patients had decrease in diffusion restriction as well as decrease in size of the enhancing portions of the lesion. The time course of these findings is currently under investigation. Six of 15 patients currently remain stable and recurrence free. Eight patients have experienced disease progression or recurrence since surgery (mean, five months progression-free). One patient had a clinical decline immediately after treatment.

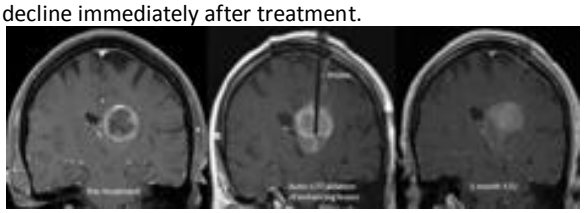

Summary/Conclusion

Laser interstitial thermal therapy is a minimally invasive treatment option for intracranial neoplasms to a subset of patients offering potentially decreased operative morbidity. Knowledge of imaging response to this treatment would be helpful to radiologists as this becomes a more commonly used neurosurgical treatment technique. Typical findings in the ablative zone include bright T1 signal with surrounding reactive ring enhancement accompanied by an initial increase in peritumoral edema which decreases later.

KEYWORDS: Neoplasm, Laser, laser interstitial thermal therapy

EdE-18

Illustrative Review of Cavernous Angiomas and their Variants

Meyer, M. A.·Shastri, R.·Shroff, S.·Khan, R.
University of Arizona
Tucson, AZ.

Purpose

To review the etiology/pathophysiology of sporadic and familial cavernous malformations and discuss the CT and MR imaging characteristics of cavernous malformations, including giant infiltrative cavernous malformation.

Approach/Methods

A literature review will be performed in order to accurately discuss the classification and various appearances of cavernous malformations. A pictorial essay of various appearances and classification of cavernous malformations will ensue.

Findings/Discussion

1. Introduction, 2. Pathogenesis and clinical manifestations of cavernous malformations, 3. Sporadic versus familial cavernous malformations, 4. CT and MR imaging characteristics, 5. Zambramski classification of cavernous malformations (with diagrams), 6. Associations and differential considerations.

Summary/Conclusion

At the end of this presentation, the viewer should be familiar with the unique and varied imaging appearance of cavernous malformations on both CT and MRI, their imaging classification system, mimicking lesions, as well as their natural history, pathogenesis, and clinical presentation. By reviewing the Zambramski classification as well as the varied etiology of these vascular malformations, the viewer will be better able to distinguish these lesions from arteriovenous malformations and hypervascular tumors.

KEYWORDS: Cavernous malformation, Zambramski classification

EdE-19

Plasmacytoma: Gamut of Neuroradiologic Imaging Findings

Marroquin, R.·Agarwal, A.
University of Missouri
Columbia, MO.

Purpose

To describe the spectrum of CT and MR imaging findings of solitary extramedullary and bone plasmacytomas in different locations related to neuroradiology.

Approach/Methods

Retrospective review of the imaging findings of all histopathologically proven cases of plasmacytomas from July 2009 until November 2012. A total of 11 cases were reviewed.

Note: Scanned images are included in the proceedings. Some submitted images were reduced during editing, thereby decreasing clarity. Also, refer to the Program Planner. Proceedings Content as of 3-29-2013.

Findings**/**Discussion
Plasmacytoma is considered a counterpart of multiple myeloma that is described as a solitary and discrete mass of monocolonal neoplastic plasma cells found in either bone or soft tissue. Plasmacytomas are divided into two groups according to their location: solitary bone plasmacytoma (when found in the skeletal system) and extramedullary plasmacytoma (EMP). Isolated EMP is very rare and comprises less than 4% of all plasma cellular disease of which more than 80% are localized to the submucosal lymphoid tissue of the nasopharyngeal and paranasal sinuses. This review will focus most on EMP as those are extremely rare and represent a diagnostic challenge. We will demonstrate the imaging findings of 11 cases of histopathologically confirmed plasmacytoma in different locations related to neuroradiology. Five cases were found to be in relation to the spine of which one presented as an isolated epidural mass in the lumbar spine with no definite bony involvement. Six cases were found to be in the head and neck region, of which two cases presented primarily as a nasal cavity soft tissue mass. One patient presented as an isolated nasopharyngeal mass with parapharyngeal extension.

Summary/Conclusion
Extramedullary and solitary bone plasmacytoma shows nonspecific CT and MR imaging features. MR imaging is the preferred modality for evaluation due to better soft tissue contrast. Features that may suggest the diagnosis of plasmacytomas are a bulky soft-tissue mass or infiltrative lesion.

KEYWORDS: Plasmacytoma, Brain neoplasms

EdE-20

Purpose of this Educational Exhibit is to Illustrate the MR Imaging Findings of Paraneoplastic Neurologic Syndromes, and Discuss the Clinical Manifestations of these Disease Entities

Bagga, S.·Eskey, C.·Fadul, C.
Dartmouth Hitchcock Medical Center
Lebanon, NH.

Purpose
Paraneoplastic neurologic syndromes (PNS) are remote effects of cancer that are not caused by the primary cancer or metastasis, or by infection, ischemia or metabolic disoders. These syndromes are being recognized more frequently because of longer patient survival, improved immunologic testing and use of advanced neuroimaging and improved knowledge amongst physicians. The neurologic disorder may develop before the cancer manifests clinically
Approach/Methods
This educational exhibit will discuss the clinical presentations, diagnostic testing including MRI imaging used for making the diagnosis of PNS.
Findings/Discussion
Some PNS are associated with antibodies directed against antigens expressed by both the tumor and the nervous system (onconeural antibodies). This association favors immune-mediation. However, the inability to find such antibodies does not rule out the diagnosis. The presence or the absence of paraneoplastic antibodies and the type of antibodies define different subtypes of PNS. Limbic encephalitis, subacute cerebellar ataxia, opsoclonus-myoclonus, retinopathies, sensory neuropathy, Lambert-Eaton myasthenic syndrome, Stiff-person syndrome are the most common syndromes.
Summary/Conclusion
The clinical manifestation and imaging findings of PNS will be reviewed.

KEYWORDS: Paraneoplastic, Encephalitis

EdE-21

Extracranial Manifestations of Glioblastoma: Thinking Outside the Box

Ginat, D.·Timpone, V.·Schaefer, P.
Massachusetts General Hospital
Boston, MA.

Purpose
To review the imaging manifestations of the various types

Note: Scanned images are included in the proceedings. Some submitted images were reduced during editing, thereby decreasing clarity. Also, refer to the Program Planner. Proceedings Content as of 3-29-2013.

of extracranial glioblastomas.
Approach/Methods
Retrospective review of our institution imaging database identified 20 cases of extracranial glioblastoma metastases, including 14 cases of drop metastases, one case of continuous extension into the cervical spinal cord from a brainstem glioblastoma, two cases of direct extension across the craniotomy into the dura and extradural soft tissues, one case of seeding in scalp along the surgical approach from prior craniotomy, one case of tumor dissemination via a ventriculoperitoneal shunt, and one case of systemic metastases. In addition, we encountered one case of glioblastoma that arose in conjunction with primitive neuroectodermal tumor in the ovary.
Findings/Discussion
Extracranial gliobastomas are uncommon entities. Most of these occur as metastases from primary intracranial glioblastoma. Mechanisms of dissemination include CSF spread into the spinal canal, direct extension through a craniotomy defect into the dura, direct extension from the brainstem into the spinal cord, seeding into the scalp during surgery or via shunt catheter, lymphatic spread, and hematogenous spread. Alternatively, glioblastomas can arise occasionally as primary tumors outside the brain, such as within the spinal cord and can even arise within ovarian teratomas. Imaging approaches for the spectrum of extracranial glioblastoma manifestations are further reviewed in this exhibit.
Summary/Conclusion
There is a wide spectrum in which extracranial glioblastoma metastases can manifest. Nevertheless, these typically display similar imaging features as their intracranial counterparts. The possibility of metastases should be considered upon review of follow-up brain MRI and imaging of the spine in patients with known glioblastoma.

KEYWORDS: Glioblastoma

EdE-22

"*At the Top of My Head*" - Mutimodality Imaging of Focal Protruding Masses of the Scalp and Skull in Adults and Children: A Pictorial Review of Pathology Causing *Bumps on the Head*

George, M.[1,2]·Li, S.[1,2]
[1]Baystate Medical Center, Springfield, MA, [2]Tufts University Medical School, Boston, MA.

Purpose
Focal protruding masses at the top of the head can become very large and disfiguring. They may cause social embarrassment and psychologic disturbance in the diseased. There is a wide spectrum of pathology that can cause *Bumps on the Head.* However there is no simple way to organize this group of diverse entities. The purpose of this exhibit is: to illustrate the imaging findings and their underling pathology of each disease entity with discussion of their differential diagnosis; to describe the related clinical presentations, relevant anatomy and treatment options.
Approach/Methods
1. These focal protruding masses of the skull and scalp can be evaluated with a multimodality imaging approach. CT and MR are most common utilized tools. Plain X-ray films, ultrasound and nuclear medicine studies sometimes are used. 2. To discuss their clinical presentations, etiology, differential diagnosis and treatment of each entity; To develop an organized search pattern from an anatomical approach. 3. The spectrum of those *Bumps on the Head* is different in adults and children. The most common ones in each group are presented and discussed.
Findings/Discussion
Focal skull and scalp masses can affect people of different age, from the newborn to adults. They range from benign to malignant as well. In children, the disease entities more commonly include an encephalocele, epidermoid, eosinphilic granuloma, exostoses, a hemangioma, etc. In adults, the disease entities include focal matastasis, lipoma, meningioma, neurofibroma, etc. Their imaging examples are displayed. CT and MR are the main imaging tools. The related clinical presentations, underline pathology, differential diagnosis and clinical management are discussed.

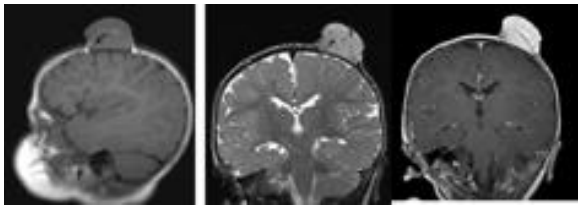

Summary/Conclusion
Bumps on the head can be caused by a diversity of diseases. These etiologies may be benign or malignant, syndromic or sporadic, bony or soft tissue in origin. They also occur in patients of different age. Considering the degree of variability and a wide spectrum of pathology, a broad and methodical approach is required for accurate and assured diagnosis. At the end of the presentation, the viewers will: 1. Become familiar with the different causes of focal protruding masses of the scalp and skull in adults and children, their clinical presentations and imaging characteristics so as to aid the radiologist in making appropriate and timely diagnoses and guiding further management. 2. Form a focused differential diagnosis based on the patient's clinical history and the physical appearance. 3. Understand their clinical presentations and underline radiologic-pathologic correlations.

KEYWORDS: Skull, Masses, CT and MR

Note: Scanned images are included in the proceedings. Some submitted images were reduced during editing, thereby decreasing clarity. Also, refer to the Program Planner. Proceedings Content as of 3-29-2013.

EdE-23

Pictorial Review of Various Diseases Causing Lactate Peak on MR Spectroscopy in Daily Practice

Nakamura, H.·Onodera, H.·Yoshida, Y.·Tanaka, Y.·Nakajima, Y.·Uchida, M.
St.Marianna University of Medicine
Kawasaki, JAPAN.

Purpose
The exhibit is to list the wide spectrum of diseases showing lactate peak and have enough knowledge about the etiology of lactate peak.
Approach/Methods
Although lactate cannot be resolved in the adult human brain under normal conditions, strongly enhanced concentrations of cerebral lactate often are seen in disease states associated with an increasing energy demand and/or impaired cellular capacity for oxidative phosphorylation. There are various conditions in which lactate peak can be resolved such as brain tumors, cerebral ischemia, demyelinating diseases and so on. For example in diagnosing brain tumor, lactate may be an indicator of malignancy, but it is not always true. Some benign brain tumors can show lactate peak. These confuse the radiologist. We reviewed retrospectively one thousand MR spectroscopy (MRS) and MRI studies from 2003-2012 and organized the information categorizing diseases according to the etiology.
Findings/Discussion
Lactate can be seen in the wide spectrum of diseases. These diseases include benign tumor (Lhermitte-Duclos diseases, pilocytic astrocytoma, desembroplastic neuroepithelial tumor) due to abnormal high glucose metabolism (glycolysis), malignant tumor (malignant lymphoma, metastatic tumor, high-grade glioma) due to both increased metabolic rate and the reduced clearance of lactate in the necrotic regions, radiation effect due to the ischemia underlying the mechanism for severe lesions, cerebral abscess due to the anerobic glycolysis of living cells, acute and subacute cerebral infarction due to anerobic glycolysis resulting from the decrease of oxygen supply, mitochondrial encephalopathy with lactic acidosis and stroke-like episodes (MELAS) and neonatal hypoxic encephalopathy due to the impairment of oxidative metabolism.

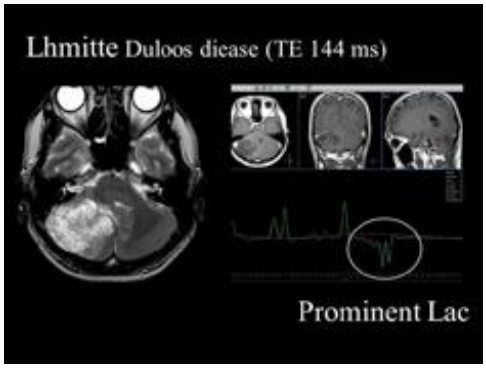

Summary/Conclusion
There are various diseases showing prominent lactate peak. It may be considered nonspecific but it is important to keep its variety in mind.

KEYWORDS: MR spectrocopy, Brain neoplasms

EdE-24

Imaging and Pathology Correlation of a Spectrum of Brain Tumors with Two Distinct Concomitant Pathologic Entities

Ramsewak, D.·Wang, A.·Patel, S.·Krishnan, A.·Donev, K.·Silbergleit, R.
Beaumont Health Systems
Royal Oak, MI.

Purpose
The occurrence of brain tumors with two different and distinct pathologic entities at the same location is rare, with only a few case reports in the literature. We aim to present four patients who harbored such "concomitant" or dual tumors, and review the neuroradiologic and pathologic findings.
Approach/Methods
Four pathology proven cases of concomitant brain tumors were identified and retrospectively reviewed. All of the patients had MR imaging of the brain performed with contrast. In addition, one of the patients also had MR spectroscopy and MR perfusion imaging. Corresponding pathology and related literature was reviewed.
Findings/Discussion
Two pathologically different tumors within the brain is a relatively rare occurrence; however, it is even more infrequent when the tumors arise simultaneously from the same location. Our four cases with such concomitant pathology include a glioblastoma occurring with a primitive neuroectordermal tumor (PNET), gliosarcoma occurring with a PNET, oligoastrocytoma occurring with metastatic B-cell lymphoma, and meningioma occurring with metastasis from lung adenocarcinoma. We also shall demonstrate the benefit of MR spectroscopy and MR perfusion in separating the two pathologies in the patient with the oligoastrocytoma and concomitant lymphoma.

Note: Scanned images are included in the proceedings. Some submitted images were reduced during editing, thereby decreasing clarity. Also, refer to the Program Planner. Proceedings Content as of 3-29-2013.

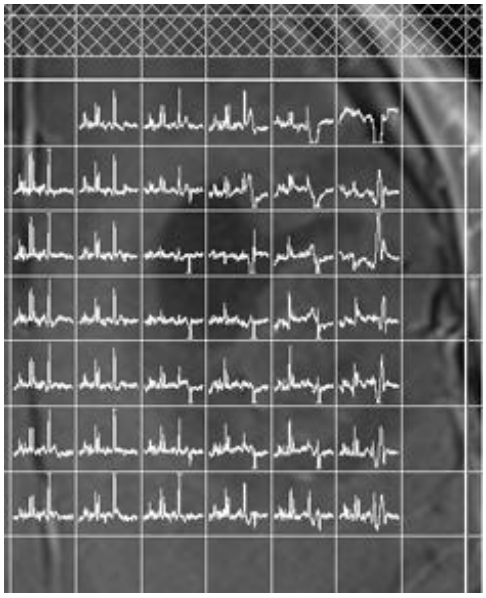

Figure 1. Multivoxel proton MR spectroscopy with TE 135 ms.

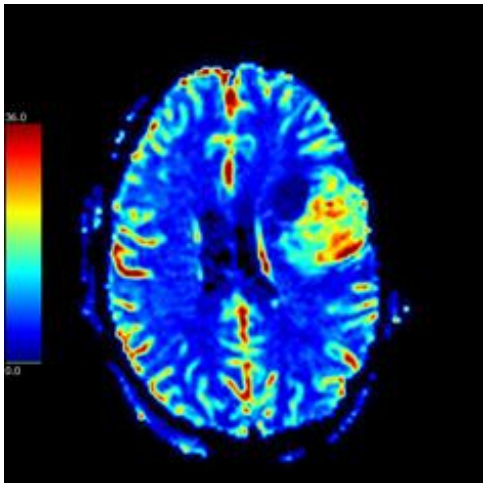

Figure 2. Dynamic contrast MR perfusion, show high malignant lymphoma with increased perfusion and increased choline peak contrasting with the concomitant oligoastrocytoma with decreased perfusion and decreased choline peak.

Summary/Conclusion

Brain tumors comprised of two distinct concomitant pathologic entities are rare and it is usually very difficult to determine the concomitant pathology from imaging findings alone. However, in our limited experience, MR perfusion and MR spectroscopy may help delineate different patterns within the tumor that correlate to their pathology.

KEYWORDS: Neoplasm, MR imaging brain, concomitant brain tumor

EdE-25

Tour 3T Intraoperative MR Imaging for Brain Tumor Treatment

Ginat, D.[1]·Swearingen, B.[1]·Curry, W.[1]·Cahill, D.[1]·Madsen, J.[2]·Herrington, J.[1]·Schaefer, P.[1]
[1]Massachusetts General Hospital, Boston, MA, [2]Boston Childrens Hospital, Boston, MA.

Purpose

1) To describe the appropriate selection of intraoperative MRI protocols for glioma and pituitary tumor resection, thermoablation, and related technical considerations. 2) To depict the unique intraoperative MRI findings. 3) To review the benefits and shortcomings of intraoperative MRI for brain tumor surgery.

Approach/Methods

Intraoperative MRI is performed at 3T at our institutions. For enhancing brain parenchymal tumor surgery, the following sequences are implemented: • Sag T2 SPACE FLAIR, • Axial Diffusion, • Axial T2, • Sagittal T1 MPRAGE precontrast with fat suppression, • Sagittal T1 MPRAGE postcontrast with fat suppression. For nonenhancing brain parenchymal tumor surgery, the following sequences are implemented: • Sag T2 SPACE FLAIR, • Axial Diffusion, • Axial T2, • Sagittal T1 MPRAGE. For pituitary tumor surgery, the following sequences are implemented: • Axial T2, • Coronal T2, • Coronal T1, • Sagittal T1 precontrast, • Coronal T1 postcontrast with fat suppression, • Sagittal T1 postcontrast with fat suppression, MR thermography can be used to monitor thermoablation of brain tumors.

Findings/Discussion

Intraoperative MRI is a valuable resource that can be performed efficiently with the proper sequence selection. The literature and our experience suggest that intraoperative MRI increases the likelihood of gross total resection for both pituitary tumors and gliomas, which in turn has significant prognostic implications. The use of intraoperative MRI can provide more accurate guidance in the setting of brain shift compared to other image-guided methods. In addition, intraoperative MRI can detect unsuspected complications earlier than routine postoperative imaging, potentially leading to improved outcomes. A unique consideration in the interpretation of intraoperative MRI is the presence of hyperacute hemorrhage, which may be almost indiscernible on T1 MPRAGE, but mildly hyperintense on T2 FSE. Another distinctive phenomenon is the presence of contrast leakage during surgery, which can be a potential confounder for residual tumor. MR imaging thermometry using a phase-sensitive sequence can accurately delineate the effects MRI-guided interstitial thermotherapy of brain tumors in real time.

Summary/Conclusion

As intraoperative MRI is increasingly utilized for brain tumor resection, it is important to be familiar with optimal sequence selection and the unique imaging findings that may be encountered.

Note: Scanned images are included in the proceedings. Some submitted images were reduced during editing, thereby decreasing clarity. Also, refer to the Program Planner. Proceedings Content as of 3-29-2013.

KEYWORDS: Brain neoplasms, Intraoperative imaging,

EdE-26

Strategies to Mitigate the Risks of MR Imaging on Patients with Implanted Spinal Cord Stimulation Systems

Safriel, Y.[1,2]·Breitenfeldt, M.[3]·Mashhadi, O.[3]·Orser, H.[3]·Welter, J.[3]·Manker, S.[3]
[1]Pharmascan, Wilmington, DE, [2]University of South Florida, Clearwater, FL, [3]Medtronic, Minneapolis, MN.

Purpose
Approximately 70% of spinal cord stimulation (SCS) patients are expected to need at least one MRI over the expected life of the device. Safe MRI scanning of patients with some SCS systems is possible under certain conditions. However, radiologists may not be aware of product differences and existing MRI labeling. We provide an overview of potential risks when conducting MRI of patients with SCS systems (table) and discuss mitigation strategies related to two main risks associated with MR imaging of patients with SCS implantable systems.

Potential Interactions of MRI on SCS Systems in a Patient

Modality	Energy	Patient Effect	Concern	Solution/Guidance
Lead Heating	RF	Electrode heating in epidural space	Thermal damage at lead electrodes	Limit RF levels and exposure to the head with use of a transmit/receive head coil. Lead is outside the MRI imaging area and risk is mitigated
Unintentional Implanted Device Interactions	Static Gradient RF	Permanent damage to INS or device memory issues	Device explant or reprogramming required	Electromagnetic compatibility protection: circuitry such as FFTs or no magnetic reed switch in newer INS models
Unintentional Stimulation	Gradient RF	Uncomfortable stimulation or shocking	Patient discomfort	Turn the stimulator off. Limit gradient exposure to 20T/sec
Magnetic Pull	Static	INS movement in the pocket or lead movement	Pulling/tugging sensation on lead or INS	Minimal or no ferromagnetic material in INS or lead. Recommend suturing the INS
Device Heating	Gradient	INS heating	Warm sensation at INS site	Limit gradient exposure. Monitor patient
Vibration	Gradient Static	Device explant or uncomfortable vibration	Uncomfortable vibration or device damage	Limit gradient exposure to 20T/sec Minimize size of stimulator. Monitor patient

Approach/Methods
Predominant risks in MR scanning of patients with SCS devices are: 1. RF-induced lead heating resulting in thermal injury to the spinal column and 2. Gradient, RF and static-induced device damage. Both heating and device damage risks associated with Medtronic SCS system were evaluated in a phantom torso scanned with 1.5T MRI. Lead heating was tested using a body RF coil with the landmark centered over the phantom torso or a transmit/receive head coil with the landmark centered over the head of the phantom. Temperature increases were measured at four different probe sites as a function of time. Device damage testing was performed using a body RF coil with the system lead and device configured to maximize exposure to gradient and RF fields.
Findings/Discussion
In order to mitigate risks to the patient, design and labeling strategies may be employed. *Labeling strategy:* Testing with a body RF coil showed a 16 - 21.7^{o}C temperature rise at the electrodes with a whole body SAR of 1.5 W/kg when the landmark was positioned over the center of the phantom torso. Testing with a transmit receive head coil only showed a 0.5^{o}C temperature rise at the electrodes with a head SAR of 1.79 W/kg with the MRI landmark centered over the center of the head of the phantom. The labeling strategy is therefore to limit MRI to head scan with a transmit/receive head coil. *Design Strategy:* Design strategies include minimal if any use of ferromagnetic material and incorporation of electromagnetic protection technology such as filtered feedthroughs (FFT) which dissipate RF energy away from the internal circuitry. A circuit configuration with a FFT capacitor will shunt, reflect or absorb EMI before it can enter the device housing and re-radiate into internal circuitry. The presence of the FFTs mitigates the EMI risk and results in fully functional devices following MRI exposure.
Summary/Conclusion
Currently, only the Medtronic line of products has regulatory approval (US FDA and CE) for an MRI conditionally safe scanning for head MRI. Patients can safely undergo head MRI scans with close adherence to the MRI requirements detailed in the device labeling.

KEYWORDS: Devices, Spinal instumentation, spinal cord stimulators

EdE-27

18F-Labeled Sodium Fluoride PET and Central Nervous System Imaging: Incidental Findings and the Potential of Hybrid PET/MR

Kessler, B. A.·Lee, Y.
University of North Carolina School of Medicine
Chapel Hill, NC.

Purpose
18F-labeled sodium fluoride (18F-NaF) is a bone-seeking agent primarily used in the evaluation of osseous metastatic disease. With the increasing availability of clinical PET/CT, imaging of bone disease with 18F-NaF may

Note: Scanned images are included in the proceedings. Some submitted images were reduced during editing, thereby decreasing clarity. Also, refer to the Program Planner. Proceedings Content as of 3-29-2013.

soon be a standard supplement or alternative to traditional bone scintography. Characterization of CNS pathology by 18F-NaF PET/CT has been largely unexplored. The increased clinical use of 18F-NaF PET/CT warrants an understanding of incidental CNS findings and the potential of 18F-NaF PET/CT as an adjunct to standard imaging of brain and spine pathology.
Approach/Methods
Retrospective overview of illustrative cases from UNC.
Findings/Discussion
Recent interest in 18F-NaF PET/CT for the evaluation of malignant and benign bone disease demonstrates its significant advantages over traditional bone scintography. As the availability of clinical PET/CT imaging increases, 18F-NaF PET/CT is likely to play a greater role in the diagnosis and management of bone disease. As such, the characterization of CNS pathology via 18F-NaF, both incidentally and as an adjunct to standard brain and spine imaging, is of great interest. Using illustrative cases, this educational exhibit reviews MRI of CNS pathology with concurrent 18F-NaF PET/CT imaging. Scans are fused when feasible to present the advantages and limitations of the modalities as separate and combined scans. Specific pathologies discussed include brain and skull metastases, spine metastases, cerebral artery infarcts, meningioma and crossed cerebellar diaschisis. Concurrent 18F-fluorodeoxyglucose (18F-FDG) PET/CT imaging is used for comparison in addition to a brief review of uptake mechanisms for both 18F-NaF and 18F-FDG. With the advent of hybrid PET/MR imaging, a discussion of the current state of clinical PET/MR is presented with preliminary hybrid PET/MR imaging. Finally a brief overview of the potential of clinical hybrid PET/MR using both 18F-NaF and 18F-FDG in the diagnosis and management of CNS pathology is presented.
Summary/Conclusion
As the use of 18F-NaF PET/CT for imaging of bone disease increases, its incidental characterization of CNS pathology is of great interest. 18F-NaF may provide additional information in certain CNS pathology, and has a potential role in hybrid PET/MR imaging of the brain and spine.

KEYWORDS: MR imaging/PET, Bone scan, sodium fluoride

EdE-28

Utility of Coregistered 3D MR Cisternography and 3D MR Angiography for Imaging Neurovascular Compression Syndromes of the Cranial Nerves

Alderfer, K.·Kim, P. E.·Law, M.·Go, J. L.·Shiroishi, M. S.·Boyko, O.·Lerner, A.
University of Southern California
Los Angeles, CA.

Purpose
• Review conventional MR imaging techniques for diagnosis and evaluation of neurovascular compression syndromes of the cranial nerves. • Describe advanced imaging techniques including coregistered 3D MR cisternography and 3D MRA for evaluation of these disorders. • Discuss utility and advantages of this technique in diagnosis and postoperative evaluation of neurovascular compression syndromes.
Approach/Methods
Review the characteristic MRI features of neurovascular compression syndromes of the cranial nerves. Review MR cisternography and MRA for diagnosis and evaluation of these disorders. Discuss challenges and limitations of conventional MR imaging. Demonstrate the utility and methods of coregistered 3D MR cisternography and 3D MRA for evaluation of these disorders. Discuss the role of this technique in diagnosis and postoperative evaluation of trigeminal neuralgia, glossopharyngeal neuralgia, and other neurovascular compression syndromes.
Findings/Discussion
Neurovascular compression of the cranial nerves can be visualized using conventional techniques such as MR cisternography and MRA. However, coregistration of 3D MR cisternography and 3D MRA allows for more precise evaluation of the complex relationship between cranial nerves, vascular structures and postsurgical changes such as Teflon sponge placement. This technique is particularly useful in differentiating arterial and venous structures in neurovascular compression.

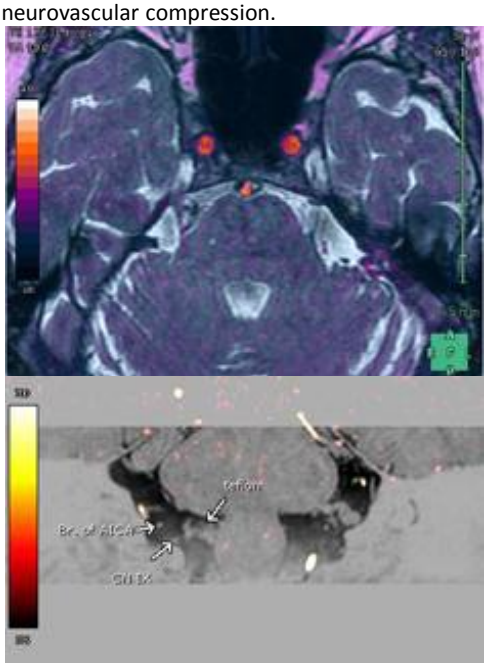

Summary/Conclusion
Imaging of the neurovascular compression disorders of the cranial nerves is challenging due to the complex relationship between cranial nerves and surrounding vascular structures. We describe our experience using coregistered 3D MR cisternography and 3D MRA, which allows more precise preoperative evaluation of these disorders and may assist in surgical planning. This technique is particularly useful in postsurgical setting and in evaluation of venous neurovascular compression.

Note: Scanned images are included in the proceedings. Some submitted images were reduced during editing, thereby decreasing clarity. Also, refer to the Program Planner. Proceedings Content as of 3-29-2013.

KEYWORDS: 3D imaging, Trigeminal neuralgia, coregistration

EdE-29

Strategies for Reduction of Radiation Dose and Contrast Media Volume in Neuro CT without Compromising the Image Quality

Shankar, J.·Pretty, L.
Queen Elizabeth II Health Science Centre
Halifax, NS, CANADA.

Purpose
Radiation from medical imaging has been a very important issue due to its long-term cumulative effects. There has been an impetus in reduction of radiation dose as much as possible without compromising the diagnostic quality of images. Similarly contrast nephropathy is a potential hazard from the computed tomography (CT) contrast media, which could potentially be dose related. We should also try to reduce the contrast media volume as much as practically possible without compromising the diagnostic quality of the images. The purpose of this study is to describe the various techniques/methods we used to reduce the radiation and contrast dose in different CT techniques used for neuroradiology.
Approach/Methods
On Siemens Definition Flash 128 slice dual energy scanner, we applied different techniques starting in June 2012 to reduce both radiation and contrast dose for neuroimaging. For plain head CT and CT angiograms (CTA), we utilized SAFIRE (Sinogram Applied Iterative Reconstruction), mA dose modulation and Care kV (modulation) to reduce the radiation dose. For postcontrast CT head, we used dual energy technique to potentially reduce the radiation dose. For CT perfusion (CTP), we used lower mA of 100 instead of 200 mAs to reduce the radiation dose despite prolonging the total time of imaging to include the permeability data acquisition. We reduced the dose of contrast media for all neuro CT angiograms.
Findings/Discussion
Application of all changes for reduction of radiation and contrast dose have maintained the image quality. For plain head CT, SAFIRE was applied with a strength of three for all scans - to compensate for reduction in mA, while maintaining image quality. We changed the slice thickness from 5 mm to 3 mm, to visually maintain the image quality. This has resulted in radiation dose reduction of 15%. Postcontrast head CT could be performed with dual energy mode and this can obviate the need of the plain head CT before contrast injection. This can virtually reduce the radiation dose by 50%. Computed angiography angiograms are performed using dual energy (DE). We reduced the quality reference mAs from 360 and 180 to 222 and 111 for kV of 80 and 140 respectively. This has resulted in a radiation dose reduction of 45%. We also reduced the dose of contrast media for CTAs of circle of Willis and carotids from 120 cc to 70 cc without any compromise of image quality. The reduction of mAs in CTP resulted in a radiation dose reduction of 35%. A further reduction of contrast media for CTP from 50 cc to 40 cc was applied. We also reconstruct the CTA from the optimal timing sequence of the CTP, which obviates the need of second acquisition and second bolus of contrast injection for CTA of circle of Willis. This resulted in further reduction of contrast and radiation dose.
Summary/Conclusion
By changing the technical parameters and adopting different strategies, overall radiation dose and contrast dose can be reduced significantly without compromising image quality.

KEYWORDS: Radiation dose reduction

EdE-30

Radiation Dose Reduction in Neuro CT: Clever Adaptation in a Lower Dose World

Tanenbaum, L. N.
Mount Sinai School of Medicine
New York, NY.

Purpose
Dose reduction technologies have gone from novelty to norm in a few short years. Techniques such as iterative reconstruction, x-y-z and selective in plane dose modulation, selectable and automated selection of reduced kV values, and utilization of reduced tube current are now in common use. However, application of the techniques has creating new challenges in day-to-day neuroradiology practice.
Approach/Methods
Based on our multivendor experience and the published literature, we review recent advancement in dose reduction techniques and share some potential solutions to the challenges posed by the application of dose reduction technologies.
Findings/Discussion
The first pass at clinical integration of iterative reconstruction (IR) to neuro CT led to dose reductions of up to 40% with quantitatively equivalent image quality (IQ); however, radiologist acceptance of these IR images has been somewhat variable. Recently we have seen adoption of higher levels of IR and achieved improvements in IQ acceptance, sometimes at dose reductions of 60% or more. Even more aggressive dose reductions are possible in susceptible populations as pediatric and neurosurgical ICU patients. Newer model-based IR techniques have enabled even greater dose reductions than the first wave of IR techniques while providing a beneficial boost in spatial resolution. Additional challenges and opportunities remain. As radiation doses for certain high contrast resolution studies, approach single view X-ray studies (e.g., paranasal sinuses, temporal bones), one must seek creative solutions so that the low contrast detectability of "soft tissue" windows is somewhat preserved. A fuller

Note: Scanned images are included in the proceedings. Some submitted images were reduced during editing, thereby decreasing clarity. Also, refer to the Program Planner. Proceedings Content as of 3-29-2013.

understanding of the relationship of reduced kV scanning to iodine visualization, low-contrast detectability, noise and net radiation dose is critical to designing protocols that are lower in CTDI. Reductions in contrast media doses are possible/desirable with lower kV techniques and the use of contrast agents with a higher iodine concentration.
Summary/Conclusion
Solutions are available to challenges inherent in associated with dose reduction techniques. These solutions can improve IQ, and may further reduce dose. Opportunities demand a re-thinking of acquisition parameters, contrast media application, and reconstruction techniques.

KEYWORDS: Radiation protection, Iterative reconstruction

EdE-31

Strategies to Safely and Reliably Perform MR Examinations in Patients with Electronic Implanted Devices

Watson, R. E.·Edmonson, H. A.·Patton, A.·Lindell, E. P.
Mayo Clinic
Rochester, MN.

Purpose
An increasing number of patients are receiving electronic implanted devices for treatment of various conditions. Many of these patients will need MR imaging due to ongoing or new medical issues. While some of these devices are MRI unsafe, and an MRI cannot be safely performed, an increasing number of implanted electronic devices are “MRI conditional”, and it is essential that radiologists fully understand the conditions that must be met to scan these patients safely as the potential for severe patient injury or even death is a possibility with some devices if scanning is performed without these conditions being met. The purpose of this presentation is to review the essential factors and required conditions that help ensure safe MRI scanning in these patients.
Approach/Methods
Up to date specific conditions permitting safe scanning of several electronic implanted devices, including several neurostimulators, cardiology-related implants including cardiac pacemakers and insertable loop recorders, and intrathecal infusion pumps are described, including prescanning device evaluation and preparation, specified MRI field strength, specific absorption rate (SAR) limitations, required coil types, value of MRI physicist participation, and postscanning evaluation.
Findings/Discussion
Specific conditions that help facilitate safe scanning of patients with deep brain stimulators, vagal nerve stimulators, spinal cord stimulators, sacral nerve stimulators, auditory brainstem implants, cochlear implants, cardiac pacemakers and defibrillators, insertable loop recorders, and intrathecal infusion pumps are reviewed. All prescanning evaluations must focus first on obtaining specific information about the implanted device, including make and model, and in the case of some sacral nerve stimulators, even the serial number of the device is important to determine whether safe scanning can occur. Prior to entering the MRI environment, several devices must be assessed, programmed, or turned off. Devices with leads must be assessed for lead integrity. With several devices, scanning must be performed with transmit/receive coils in which RF energy is contained to the scanned body part. These coils do not permit parallel or accelerated imaging. With some devices, limiting RF energy deposition (SAR limits) is a condition, and close collaboration with an MRI physicist can be beneficial to tailor the exam to create the best possible images within these constraints. Due to susceptibility artifacts from the devices, sequences need to be selected that will minimize image degradation in areas of interest. In the case of cochlear implants, due to concerns of potential infection, some work is proceeding in which the device magnet is left in place while scanning proceeds with the head tightly wrapped.
Summary/Conclusion
An increasing number of implanted electronic devices are being classified as MRI conditional, and with proper precautions, patients can benefit from MRI. However, it is imperative that radiologists fully understand all the factors that must be addressed to permit safe scanning in these patients.

KEYWORDS: MR imaging safety, Devices

EdE-32

Review of Stable Xenon Portable CT Perfusion Imaging of the Brain: Technical Factors, Safety and Clinical Applications

Mojtahed, A.·Hart, B. L.·Hayek, R. A.
University of New Mexico
Albuquerque, NM.

Purpose
To enhance the knowledge of practicing radiologists regarding: the principles behind, the safety and technical factors regarding, and the applications of stable xenon CT brain perfusion imaging in the clinical setting.
Approach/Methods
Selected cases of xenon perfusion imaging performed at an academic tertiary referral hospital over a six-year period were chosen to illustrate a variety of acute and nonacute neurovascular disease states.
Findings/Discussion
Discussion of technical factors of acquisition, discussion of safety concerns, and discussion of normal brain perfusion parameters including discussion of the autoregulatory processes encountered to maintain brain perfusion are illustrated in a case-discussion format. Cases presented include examples of normal brain perfusion, perfusion in moyamoya disease and balloon occlusion perfusion testing. Special emphasis is placed on portable xenon

Note: Scanned images are included in the proceedings. Some submitted images were reduced during editing, thereby decreasing clarity. Also, refer to the Program Planner. Proceedings Content as of 3-29-2013.

perfusion imaging in the ICU setting as a guide for medical management in treatment of vasospasm.
Summary/Conclusion
Stable xenon CT brain perfusion imaging is a safe and reliable method for acquiring quantitative cerebral perfusion information. Brain perfusion changes in many neurovascular disease states are clearly demonstrated using the stable Xenon CT perfusion technique, and portable stable xenon CT perfusion data can be used to alter patient management in the Neurointensive Care Unit setting. Through this exhibit we hope to enhance our readers' knowledge regarding stable xenon CT perfusion imaging.

KEYWORDS: CT brain perfusion, Cerebral vasospasm, xenon, moyamoya, balloon occlusion

EdE-33

Secondary Degeneration after Stroke: MR Imaging Features with Emphasis on Diffusion-Weighted Imaging Findings

Kinoshita, T.·Kinoshita, F.·Umetsu, A.·Miyata, H.
Research Institute for Brain and Blood Vessels-Akita
Akita, JAPAN.

Purpose
The purpose of this exhibit is to demonstrate MR imaging features of secondary degeneration after stroke. Slower water diffusion in the degeneration may be implicated in their hyperintensity at diffusion-weighted imaging (DWI). This exhibit will review DWI hyperintense lesions representing secondary degeneration.
Approach/Methods
A retrospective review of MR examinations of patients with subacute cerebral infarction or hemorrhage was undertaken. Findings of DWI and T2-weighted imaging were reviewed. Wallerian degeneration is anterograde axonal degeneration after proximal neuronal injury. Wallerian degeneration after middle cerebral artery (MCA) infarction involves the descending corticospinal tract, definable on MR imaging at the internal capsule, cerebral peduncle, basis pontis, and medullary pyramis. Pontine infarction can cause Wallerian degeneration of the pyramidal tract and pontocerebellar tract. Secondary degeneration of the substantia nigra in the midbrain is caused after striatal injury. Thalamic degeneration occurs after MCA infarction. Illustrative case material interpreted as secondary degeneration is presented with reference to DWI findings. One autopsy case of old pontine infarction with Wallerian degeneration was included in this exhibit.
Findings/Discussion
Wallerian degeneration after MCA infarction affects the ipsilateral descending cortiospinal tract. At one-two weeks, hyperintensity along the corticospinal tract can be seen at DWI. A coronal DWI taken along a straight line between the front edge and the deepest point of the interpeduncular cistern can clearly demonstrate the early change of Wallerian degeneration of the segment of the corticospinal tract between the internal capsule and the medulla oblongata. At one-two months, a well-defined band of low signal-intensity appears on T2-weighted images in the topographic distribution of the corticospinal tract. After 10-14 weeks, the signal becomes high signal. Over several years, accompanying corticospinal tract atrophy is seen. Wallerian degeneration after pontine infarction affects the ipsilateral pyramis of the medulla oblongata. Bilateral middle cerebellar peduncle lesions showing T2 high signal after pontine infarction involving the pontine nuclei are interpreted as Wallerian degeneration of the pontocerebellar tract. Coronal T2-weighted imaging can clearly display curvilinear high signal lesions in the bilateral pontocerebellar fibers adjacent to the pontine infarct. Occasionally, the corresponding middle cerebellar peduncle lesions show mild hyperintensity at DWI. In an autopsy case of pontine infarction, T2 high signal lesions in the pontocerebellar tracts corresponded to Wallerian degeneration histologically showing loss of myelinated fibers and fibrillary gliosis. In the subacute period of striatal stroke, MR imaging reveals secondary degeneration of the ipsilateral subasutantia nigra with abnormal T2 signal and restricted diffusion. In patients with MCA infarction in the late subacute period, DWI and T2-weighted imaging disclose involvement of the ipsilateral dorsomedial thalamus.
Summary/Conclusion
Awareness of DWI signal abnormalities in secondary neuronal degeneration due to the original infarct is clinically important. This should not be mistaken for other pathologic conditions, such as a new infarction.

KEYWORDS: Diffusion MR imaging, Wallerian degeneration, cerebral infarction

EdE-34

Cerebral Fat Embolism: Imaging Features Observed over Time in One Medical Center

Shreter, R.·Shreiber, R.·Barlavie, Y.·Goldsher, D.
Rambam Medical Center
Haifa, ISRAEL.

Purpose
This study reports a retrospective examination of the imaging findings of cerebral fat embolism (CFE) in the acute phase, and changes observed over time in follow-up studies.
Approach/Methods
A search of the database of Rambam Health Care Campus revealed seven patients who were diagnosed with CFE between the years 2006 and 2012. The study was approved by the institutional ethics committee, with exemption from informed consent. Of the seven patients, one was female and the rest were male, ages ranging between 20 - 64 years (average 40 years). Six were trauma

Note: Scanned images are included in the proceedings. Some submitted images were reduced during editing, thereby decreasing clarity. Also, refer to the Program Planner. Proceedings Content as of 3-29-2013.

patients with fractures of long bones and the seventh had sickle cell anemia. All patients initially underwent a brain CT indicated by neurologic or mental deterioration. One of them died shortly after the CT, and six went on to have an MRI examination one to five days following admission. Four of the six underwent a second MRI seven to 35 days after the first. Three patients had long-term follow-up MRIs performed five to 35 months later. Demographic and clinical data for each patient was collected from their charts. Imaging features from all the CT and MRI studies for each patient were reviewed.

Findings/Discussion

CT studies were interpreted as normal in three patients and abnormal in the other four. Of the abnormal CT studies, two had diffuse low attenuation regions in the white matter and the third had low attenuation lacunae demonstrated in the basal ganglia. One of the three died within several days. The second and third patients remained in a deep coma. MR imaging findings in the six surviving patients displayed two different patterns: 1. Miliary distribution pattern (previously described as "starfield pattern") of multiple punctuate lesions of high intensity on T2-weighted imaging (WI) and FLAIR, and restricted diffusion. This pattern was observed in four patients. 2. Scattered high-intensity lesions on T2WI without clear restricted diffusion, which appeared in two of the patients. In the follow-up exams, the hyperintense T2WI lesions shown in the acute phase tended to coalesce and then fade away. This feature was observed in five patients. Cerebral progressive atrophy developed in five of six patients. The one patient who initially had only a very few hyperintense T2WI lesions and no foci of restricted diffusion did not develop cerebral atrophy.

Summary/Conclusion

Cerebral fat embolism may present with two distinct imaging patterns on MRI (T2WI and DWI). The hyperintense T2WI lesions shown in the acute phase tend to coalesce and fade away over time. Cerebral atrophy may appear, and its severity directly correlates with the initial presentation. Low attenuation of the white matter on CT may predict a worse prognosis. Recognizing the typical imaging patterns on initial MRI is important to determine appropriate treatment to prevent further immediate and long-term neurologic deterioration.

KEYWORDS: Fat emboli

EdE-35

Complications of Intraventricular Shunts: A Review of Imaging and Pathology

Mabry, L. M.·Gaddamanugu, S.·Harris, A. L.·Vattoth, S.·Cure, J. K.·Sullivan, J. C.
University of Alabama Birmingham
Birmingham, AL.

Purpose

Intraventricular shunting is a common procedure performed to relieve hydrocephalus. In adults, the most common cause of hydrocephalus is normal pressure hydrocephalus or from prior meningitis. In children the most common cause is congenital aqueduct stenosis or from a brainstem tumor. Complications from intraventricular shunts are rare, but clinically significant.

Approach/Methods

Complications from intraventricular shunting may not present clinically. Both computerized tomography and magnetic resonance imaging are useful imaging techniques to assess complications. This exhibit will review the complications of intraventricular shunting by illustrating complications on cross-sectional imaging.

Findings/Discussion

Complications from intraventricular shunting are diverse. Common complications include shunt malposition which may lead to progressive hydrocephalus. Other common complications include intracranial hemorrhage, either in the cerebral parenchyma or within the ventricles. Less common complications include overshunting resulting in intracranial hypotension, ependymitis, intracranial foreign body, trapped ventricle or formation of intracranial inclusion cyst. Most of these complications are better assessed by magnetic resonance imaging. However CT is well utilized to demonstrate serial changes in ventricle size, which can identify under or overshunting.

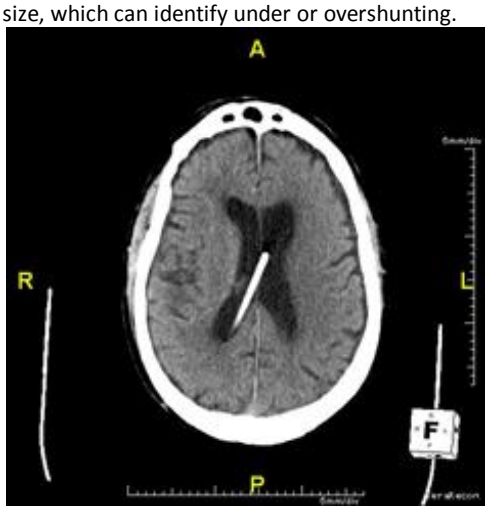

Figure 1: Overshunting of the ventricles leading to prominent extraaxial spaces.

Note: Scanned images are included in the proceedings. Some submitted images were reduced during editing, thereby decreasing clarity. Also, refer to the Program Planner. Proceedings Content as of 3-29-2013.

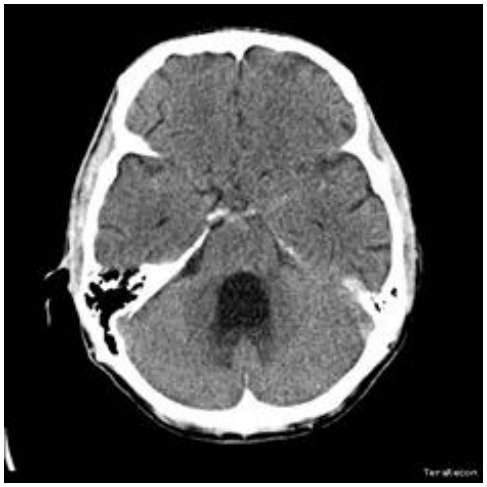

Figure 2 : Trapped 4th ventricle after lateral ventricle decompression. Patient had a history of ependymitis which caused fibrosis at the acqueduct.

Summary/Conclusion

Intracranial complications from intraventricular shunting are rare. However recognition of these complications is essential for patient management. Our exhibit will review these complications with various illustrations.

KEYWORDS: Ventricular decompression, Ventricles, complications

EdE-36

Neurovascular Dissections: Spectrum of CT and MR Imaging Findings

Mehdi, E.·Aralasmak, A.·Sharifov, R.·Asil, T.·Alkan, A.
Bezm-i Alem University
Istanbul, TURKEY.

Purpose

Craniocervical dissection is a crucial emergency state causing 20% of strokes in younger patients under the age of 45, usually resulting from hemorrhage into the vessel wall. The purpose of this educational exhibit is describing the imaging findings of craniocervical dissections in order to familiarize the radiologist with the range of entities.

Approach/Methods

Routinely performed computed tomography (CT) and magnetic resonance imaging (MRI) angiography of patients with craniocervical dissection findings were reviewed prospectively.

Findings/Discussion

Cases have been classified and illustrated into five types of Denver's criteria. The location of dissection, vessel lumen changes and possible hematomas were discussed and showed tricks to distinguish findings from similar pattern seen in other diseases.

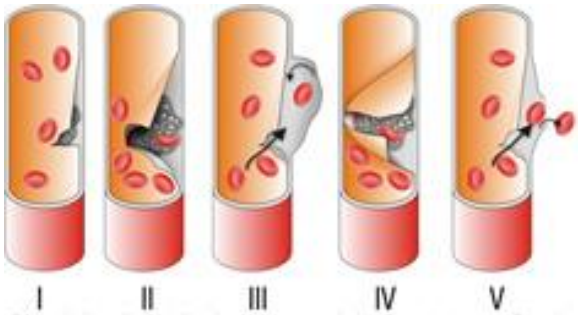

Schematic views of arterial dissection anatomy categorised by five grade, known as Denver's. I, intimal flap with <25% luminal narrowing. II, intimal flap with >25% luminal narrowing and thrombus. III, pseudoaneurysm. IV, occlusion. V Transection with extravasation.

Summary/Conclusion

MR imaging and CT have emerged as suitable alternatives to digital subtraction angiography (DSA) that can provide complementary information. Classification of imaging findings is the key role of management and treatment of dissections.

KEYWORDS: Dissection, Vessel wall, craniocervical

EdE-37

Current Understanding of Reversible Cerebral Vasoconstriction Syndrome

Trinh, V.·Chao, K.
Kaiser Permanente Los Angeles Medical Center
Los Angeles, CA.

Purpose

Headaches remain a leading symptom in acquiring medical imaging. Review the current literature regarding reversible cerebral vasoconstriction syndrome as a cause of recurrent headaches. Multimodality approach to illustrate the imaging findings of this diagnosis.

Approach/Methods

A relatively new known cause of recurrent thunderclap headaches is reversible cerebral vasoconstriction syndrome. We will review the various clinical presentations, possible associated causes including but not limited to medication- related, metabolic, and a postpartum state. Additionally we will review the key differential diagnoses including the absence of subarachnoid hemorrhage, underlying mass, or confirmed abnormal angiographic findings on two separate studies months apart in the setting of cerebral vasculitis. Finally we will discuss treatment strategies if and when they are needed including the use of calcium channel blockers, glucocorticoids, magnesium sulfate, and observation. The use of angioplasty also has been reported sparingly in the literature.

Findings/Discussion

Radiologists play an important role in the diagnosis of reversible cerebral vasoconstriction syndrome given the abnormal findings on an initial exam should reverse to a normal study on subsequent exam. Excluding the presence

Note: Scanned images are included in the proceedings. Some submitted images were reduced during editing, thereby decreasing clarity. Also, refer to the Program Planner. Proceedings Content as of 3-29-2013.

of subarachnoid hemorrhage or other possible intracranial diagnoses is important in the treatment of the patient's recurrent headache.
Summary/Conclusion
Understanding the diagnosis of reversible cerebral vascoconstriction syndrome will help the appropriate interepretation of CT/MR angiographic studies in the patient with recurrent headaches.

KEYWORDS: Headaches, Vasospasm, vasculitis

EdE-38

Many Faces of Cavernous Angiomas of the Central Nervous System

Marquez, J. C.[1,2]·Calle, S.[1]·Rodriguez, F.[1]·Castillo, M.[3]
[1]Pontificia Universidad Javeriana - Hospital Universitario San Ignacio, Bogota, COLOMBIA, [2]Resonancia Magnética del Country, Bogotá, COLOMBIA, [3]University of North Carolina at Chapel Hill, Chapel Hill, NC.

Purpose
Our purpose is to highlight the demographics, clinical presentation, and imaging features of cavernous angiomas (CA) of the CNS with special emphasis on their varying locations and appearances, including lesions found in the supratentorial region, brainstem, cerebellum, ventricles, and/or spine, in addition to those associated with radiotherapy or familial cavernous angiomatosis and with those that present with complications such as hemorrhage or edema, with the intention of providing key imaging findings that may aid the radiologist in detecting this potentially curable clinical entity.
Approach/Methods
We collected cases of CAs from the databases at our institutions. CT, MR and/or angiographic studies were evaluated and lesion size, location, imaging characteristics, multiplicity, and associated findings were recorded. The scientific literature pertinent to the subject was reviewed in order to illustrate a practical approach to identifying these malformations based on our personal experience in conjunction with currently available information.
Findings/Discussion
Cerebral CAs also known as cavernous hemangiomas, are a relatively common benign vascular neoplasm composed of sinusoid-type blood vessels that assemble into a compact mass that histologically shows little or no intervening neural parenchyma. They can occur anywhere in the spine or brain and account for approximately 8-15% of the vascular malformations in these locations. Cavernous angiomas may present as solitary or multiple masses with certain “alarming” characteristics that, to the inexperienced eye, may mimic more aggressive or malignant entities. The importance of recognizing these lesions lies in the potential for treatment, curability and a favorable prognosis in these patients. Understanding the typical features of CAs depending on their anatomical location within the brain is essential in order to provide a correct diagnosis.
Summary/Conclusion
Cavernous angiomas in the brain may display overlapping features with other CNS masses. Associated complications seen occasionally in these lesions, such as hemorrhage and surrounding edema, may further divert the radiologist from the accurate diagnosis. For this reason, detailed knowledge of the imaging characteristics encountered in patients with CAs is essential in order for the radiologist to not be misled by apparently suspicious findings.

KEYWORDS: Cerebral venous system, Venous malformations, benign vascular neoplasms

Monday, May 20 – Wednesday, May 22
6:30 AM – 9:00 PM
Thursday, May 23
6:30 AM – 3:00 PM
Hall B1

Education Exhibits (EdE) 39 - 52

EdE2-Anatomy

Note: A missing printed number indicates an abstract has been withdrawn.

EdE-39

On the Shoulders of Giants: “Elemental Brain Volumes” Derived from Modifications of Prior Parcellation Strategies Help to Explain Glial Tumor Spread

Hamilton, J. D.[1]·Hayman, L. A.[2]·Kumar, V.[1]·Schellingerhout, D.[1]·Shah, K.[1]·Chi, L.[1]·Hunter, J.[3]·Chavalli, L.[1]·Leeds, N. E.[1]·Prabhu, S.[1]·Kumar, A. J.[1]·Naidich, T. P.[4]
[1]M. D. Anderson Cancer Center, Houston, TX, [2]Anatom-e Information Systems, Houston, TX, [3]Texas Children's Hospital, Houston, TX, [4]The Mount Sinai Hospital, New York, NY.

Purpose
To utilize Brodmann areas and regional myeloarchitecture to define “elemental brain volumes” (EBV) that help to explain the patterns of growth of cerebral gliomas.
Approach/Methods
Glial tumor in the archicortex tends to stay in the archicortex until late in the disease process and we have observed the opposite to also be true. Brodmann used microscopic differences in the cortical lamination to define regional differences in cerebral architecture (cytoarchitecture) now designated Brodmann areas.

Note: Scanned images are included in the proceedings. Some submitted images were reduced during editing, thereby decreasing clarity. Also, refer to the Program Planner. Proceedings Content as of 3-29-2013.

Yasargil et al. defined zones of white matter situated deep to the cerebral gyri, conceptualized these zones as peduncles like unto the stalks of cauliflower, and defined specific sectors along the stalks in relation neighboring white matter tracts (sectorial anatomy). Mori et al. and Wedeen et al. utilized DTI-like techniques to demonstrate the locations and orientation of these regional white matter tracts with deep crossing fibers. Taken together, the Brodmann-defined "gyral" segments and segmental sectorial white matter anatomy may be used to define "elemental brain volumes" (EBV). Fractional anisotropy (FA) maps with directional color coding were superimposed on Brodmann defined gyral segments derived from a DTI of a normal subject. Using Yasargil's white matter classification for the "cauliflower-shaped" peduncle, we divided the white matter into superficial (cortical, subcortical, and subgyral sectors), neocortical deep (gyral and lobar sectors), and archicortex (capsular sector and deeper).
Findings/Discussion
The FA maps demonstrate that the superficial and archicortical white matter tend to run in parallel to each other, in contradistinction to the meshwork of crossing fibers in the deep white matter of the corona radiata and sagittal striatum. These crossing fibers may act as a barrier explaining the observations in the glioma behavior better than prior methods, and can provide the rationale for parceling the superficial white matter into Brodmann-defined segmental myeloarchitecture, the EBV. Almost all of the frontoparietal EBVs conform to a single superficial white matter "stalk" with the segmental myeloarchitecture running in parallel, even for areas that split a gyrus in half, such as Brodmann area 4 and 6 in the pre-central ("motor") gyrus. Additionally, subcortical "U-fibers" tended to connect gyri within Brodmann areas and not between them. Some areas such as the basal temporal and occipital lobes demonstrated an intermediate, transitional morphology with multiple short "stalks" of superficial fibers. (Please note that specific analysis of the survival data and the utility of EBVs for predicting patient survival are submitted to this meeting as a separate communication.)
Summary/Conclusion
Parcellation of the brain into gyral segments by Brodmann areas and defining the corresponding segmental sectorial myeloarchitecture establishes a set of "elemental brain volumes" that correlates to DTI and may help to define the patterns of local growth and spread of cerebral gliomas. This exhibit illustrates the patterns of these elemental brain volumes and their utility in clinical diagnosis.

KEYWORDS: Brain mapping, Diffusion tensor image, glioma spread

EdE-40

Hippocampus: A Pictorial Overview of the Embryonic Development, Normal Anatomy, Function and Pathology

Carranza, V. L.·Gupta, S.·Tuna, I.·Bhalla, M.·Mannem, R.·Leighton, M. P.·Ulmer, J. L.·Klein, A. P.
Medical College of Wisconsin Affiliated Hospitals
Milwaukee, WI.

Purpose
To provide a pictorial overview of the embryonic development, normal anatomy and function of the hippocampus, specifically its role in memory, and to present magnetic resonance imaging (MRI) of the most common hippocampal pathology.
Approach/Methods
A literature review was conducted to provide the information for this educational exhibit. Normal anatomy is presented in the form of illustrations, MR imaging and gross pathologic specimens. Magnetic resonance imaging of disease processes that affect the hippocampus is demonstrated.
Findings/Discussion
The hippocampus is a fascinating structure of the limbic system, with intricate anatomy and several vital functions, including consolidation of new memories, emotional responses, navigation and spatial orientation. With the help of illustrations, MRI and gross pathologic specimens, we have provided a closer look at the anatomy, which will help when looking for hippocampal abnormalities. A thorough understanding of the embryology, normal anatomy and function of the hippocampus is beneficial in making the imaging diagnosis of many disease processes that affect the hippocampus. The hippocampus is a vulnerable area affected or thought to be affected in many disease processes including Alzheimer disease, epilepsy, stress related illnesses, schizophrenia and amnesia; all of which have deficiencies in one or many of the functions of the hippocampus we have mentioned. Abnormalities in the hippocampus can be seen on imaging with these disease processes and others, and the key imaging features are important to know.
Summary/Conclusion
It is the hope that this educational exhibit will broaden the reader's understanding of the complexity of the hippocampus.

KEYWORDS: Hippocampus, Memory

EdE-41

Primer of Brainstem Anatomy and Pathology

Fitzgibbons, M.·Salamon, N.
University of California Los Angeles
Los Angeles, CA.

Purpose
To demonstrate detailed brain anatomy and pathology

Note: Scanned images are included in the proceedings. Some submitted images were reduced during editing, thereby decreasing clarity. Also, refer to the Program Planner. Proceedings Content as of 3-29-2013.

with MRI and DTI.
Approach/Methods
Part 1: A review of basic structural anatomy of the brainstem. - Major white matter pathways in the brainstem. - Pyramidal tracts. - Medial and lateral lemniscus. - MLF. - Central segmental tract. Part 2: A review of vascularization of the brainstem. Part 3: Pathology. - Congenital anomaly. - Infection. - Vascular malformation. - Stroke. - Neoplasm. - Degenerative disease. - Metabolic disease. - Transneuronal and Wallerian degeneration.

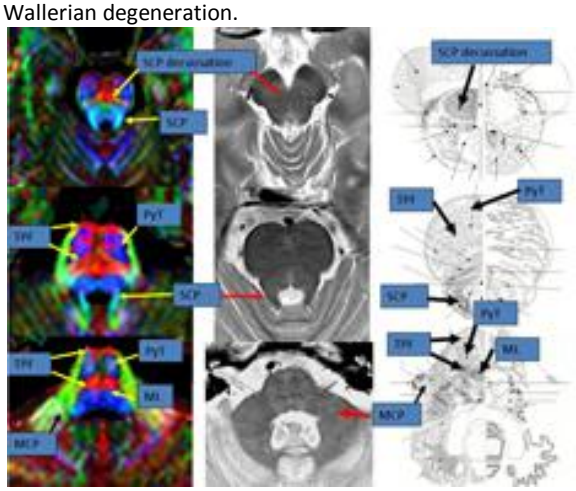

KEYWORDS: DTI

EdE-42

Angiographic Anatomy of the External Carotid Artery Branches and their Anastamoses with the Ophthalmic Artery

Shaikh, H.·Patel, N.·Pukenas, B.·Bagley, L.·Hurst, R.·Smith, M.
Hospital of the University of Pennsylvania
Philadelphia, PA.

Purpose
The aim of this exhibit is to illustrate the angiographic anatomy of the external carotid artery branches and their vascular anastamoses with the ophthalmic artery.
Approach/Methods
Evaluate common and external carotid artery angiograms performed at our institution in the last two years. Angiographic images and illustrations will be used to delineate the anatomy of the external carotid artery branches and some of their important anastamoses with the ophthalmic artery.
Findings/Discussion
The external carotid artery branches supply the face, scalp, dura and calvarium, but also have many important anastamoses with the internal carotid and vertebral arteries. These anastamoses help mantain blood flow in locations that are supplied by vessels that are diseased or congenital variants. Anastomoses to the ophthalmic artery may arise from the facial artery, superficial temporal artery, and internal maxillary artery. A diligent search for these anastamoses must be undertaken before performing embolization procedures involving these external carotid artery branches, as these branches are also potential conduits of embolization material to the ophthalmic artery, potentially causing blindness, stroke, and even death. Understanding the external carotid vascular anatomy, as well as paying close attention to the ophthalmic artery anastomoses will help guide neurointerventionalists during evaluation and treatment of diseases.
Summary/Conclusion
The external carotid artery angiographic anatomy is important to understand in order to diagnose diseases, understand vascular variants, and treat vascular abnormalities. Three of the external carotid artery branches often anastomose with the ophthalmic artery. Recognizing the angiographic appearance of these anastamoses is important for the neurointerventionalist in order to minimize risk of devastating complications including stroke, blindness, or death.

KEYWORDS: External carotid artery, Anastomosis

EdE-43

Pitfalls/Perils of Cross-Sectional Imaging: 40 Years of Mimics

Park, J.·Kagetsu, N.
St. Luke's-Roosevelt Hospital Center
New York City, NY.

Purpose
Due to increased utilization of cross-sectional imaging (MR, CT), numerous pitfalls have emerged that may mimic pathologies and result in misdiagnosis. The purpose of this study is to review common pitfalls that have been historically encountered, examine published literature on correlative cases, and evaluate ways to avoid errors in diagnosis.
Approach/Methods
We examined pitfalls commonly encountered during the advent of computed tomography in the 1970s and early 1980s and then during the era of magnetic resonance imaging (MRI) in the late 1980s to the present. The literature was reviewed for further information regarding the avoidance of misdiagnosis.
Findings/Discussion
With the advent of CT and MRI, normal anatomical variants were initially confusing to radiologists who had never seen these structures in three-dimensional imaging. Pitfalls that we evaluated and reviewed include: masslike appearance of the flocculus and nodulus on early CT, turbulent flow artifacts in thoracic spine MRI, petrous apex fat leading to misinterpretation of the contralateral normal petrous apex marrow on MRI, volume averaging leading to overdiagnosis of intramedullary and central

Note: Scanned images are included in the proceedings. Some submitted images were reduced during editing, thereby decreasing clarity. Also, refer to the Program Planner. Proceedings Content as of 3-29-2013.

pontine lesions on MRI, and pneumatization of the clinoid process mimicking an aneurysm on MRI.
Summary/Conclusion
Although the emergence of cross-sectional modalities such as computed tomography and magnetic resonance imaging provided increased diagnostic power, there initially was confusion with certain normal variants. We present several pitfalls that neuroradiologists have historically encountered and should be aware of when interpreting cross-sectional imaging. Understanding these commonly encountered variants and artifacts can improve the quality of diagnosis and decrease diagnostic misinterpretation.

KEYWORDS: Anatomy, Normal variant

EdE-44

Predicting the Spread of Glial Tumors: Lessons from the Auditory Cortex

Hunter, J. V.[1]·Hamilton, J.[2]·O'Donoghue, D.[3]·Pagani, J.[3]·Hayman, L.[4]·Kumar, V.[2]·Kumar, A. J.[2]·Naidich, T. P.[5]
[1]Texas Children's Hospital, Houston, TX, [2]M. D. Anderson, Houston, TX, [3]University of Oklahoma Health Science Center, Oklahoma City, OK, [4]Sunset Clinic, Houston, TX, [5]Mount Sinai Hospital, New York, NY.

Purpose
To describe the behavior of gliomas of the transverse temporal gyrus of Heschl.
Approach/Methods
Six cases of glioma involving the transverse gyrus were collected. The fiber connections of this gyrus with the surrounding superior temporal gyrus and insula were overlaid to indicate the relationship of the glioma to the long association fibers (arcuate), projection tract (corticothalamic to medial geniculate) and anterior commissural fibers. Four cerebral hemispheres were dissected to investigate the superficial white matter.
Findings/Discussion
Glial tumors of the auditory cortex have a predictable appearance. They do not spread along the known long association, projection or commissural fiber tracts. They do not expand or invade the adjacent superior temporal gyrus. Instead, gliomas beginning in the transverse gyrus enlarge the gyrus and then cross the inferior limiting sulcus of the insula to invade the posterior insular white matter. Gliomas beginning in the posterior insula spread along the same path into the auditory cortex. Anatomical dissection demonstrated this superficial white matter pathway between the insula and the transverse temporal gyrus.
Summary/Conclusion
Anatomical dissections and the natural behavior of gliomas identify superficial association fibers that interconnect the posterior insula with the transverse temporal gyrus of Heschl. These fibers define a discrete cortical segment which defines the limits of early tumor growth.

KEYWORDS: Neoplasm, Anatomical results, Heschl gyrus

EdE-45

Intracranial Hypotension: What Every Radiologist Needs to Know

Sanghvi, T. S.·Young, S. J.·Patel, S. T.·Bidari, S.·Bennett, J.·Quisling, R.
University of Florida
Gainesville, FL.

Purpose
Intracranial hypotension, an underdiagnosed treatable etiology of neurologic symptoms, remains to be well defined in the radiologic literature. The purpose of this educational exhibit it to describe the currently reported imaging findings of intracranial hypotension and define, in patients with those findings, relationships across the incisura and foramen magnum. The features of intracranial hypotension will be understood better and recognized by establishing the normal relationships between certain structures relative to the orienting planes of reference (i.e., the planes of the tuberculum sellae, incisura, and foramen magnum), defining the specific elements constituting central incisural, cervicomedullary and tonsillar herniation.
Approach/Methods
We describe normal and abnormal MRI measurements of the relationships of specific relevant displaceable structures (i.e., optic chiasm, tuber cinereum, mammilary body, interpeduncular fossa, etc.) with respect to specific planes (i.e., plane of the incisura, long axis of the visual pathway, plane of the diaphragma sella, etc.). Measurements described include distance of the chiasma above the diaphragma sella, angles of the optic pathway to the plane of the tuberculum sellae, distance of iter from the icisural line distance, height of the interpeduncular cistern at the plane of the mammilary body and foramen cecum, relationship of the tuber cinerum to the incisural line, the shape and width of the interpeduncular fossa and the position of the obex/decussation of the pyramids. Other findings noted include venous distension, the thickness of the basilar venous plexus at the mid clivus level and the presence of absence of subdural hematoma(s).
Findings/Discussion
Increasing awareness, and imaging detection, of intracranial hypotension can prevent errors in patient management. For example tonsillar descent in intracranial hypotension would not meet the same criteria for classification as a Chiari I malformation, and therefore posterior fossa decompressive surgery, and resultant cerebellar and brainstem prolapse, could be avoided. If, in this example, the correct diagnosis of intracranial hypotension could be made the patient may alternatively

Note: Scanned images are included in the proceedings. Some submitted images were reduced during editing, thereby decreasing clarity. Also, refer to the Program Planner. Proceedings Content as of 3-29-2013.

benefit from an epidural blood patch.
Summary/Conclusion
Intracranial hypotension is not an uncommon diagnosis described in the neurosurgical literature. Imaging is often the primary means of diagnosis; however, imaging manifestations may often be subtle and overlooked if proper measurements are not made. We present a few easily identified anatomical relationships to be aware of and systematically evaluate to increase confidence and accuracy in the diagnosis of intracranial hypotension. This systematic approach is critical as intracranial hypotension is a treatable cause of headache and more severe neurologic symptoms such as encephalopathy. Timely diagnosis, and aversion of unnecessary procedures resulting in increased patient morbidity, requires a knowledge of relevant normal and abnormal imaging anatomy.

KEYWORDS: Intracranial hypotension, Diagnostic accuracy

EdE-46

Predicting the Spread of Glial Tumors: Lessons from the Anterior Cingulate Cortex

Hunter, J. V.[1]·Hamilton, J.[2]·Hayman, L.[3]·O'Donoghue, D.[4]·Pagani, J.[5]·Kumar, V.[2]·Kumar, A. J.[2]·Naidich, T. P.[6]
[1]Texas Children's Hospital, Houston, TX, [2]M. D. Anderson, Houston, TX, [3]Sunset Clinic, Houston, TX, [4]Oklahoma Health Science Center, Oklahoma, OK, [5]University of Oklahoma, Oklahoma, OK, [6]Mount Sinai Hospital, New York, NY.

Purpose
To describe the behavior of gliomas of the anterior cingulate cortex.
Approach/Methods
Two cases of glioma in the superior frontal gyrus, five cases of glioma of the posterior cingulate gyrus and seven cases of glioma involving the anterior cingulate gyrus were collected. Four additional cases were identified from the literature. The fiber connections of the cingulate gyrus were overlaid to indicate the location of adjacent projection fibers (corticothalamic to anterior thalamic nucleus and corticostriate to the caudate nucleus). The anterior cingulate has no long association or commissural fibers, according to Krieg. Four cerebral hemispheres were dissected to investigate the superficial white matter.
Findings/Discussion
Glial tumors of the anterior cingulate have a predictable appearance. After substantial enlargement within the cingulate gyrus, they extend along the corticostriate fibers into the corpus callosum and expand into the lateral ventricle. They do not spread along the corticothalamic fiber tracts. Tumors of the superior temporal gyrus and posterior cingulate gyrus do not spread to the anterior cingulate gyrus.
Summary/Conclusion
Anatomical dissections and the natural behavior of gliomas identify patterns of spread from the anterior cingulate gyrus along the corticostriate fibers into the corpus callosum with later bulk growth within the lateral ventricle.

KEYWORDS: Anatomy, Neoplasm, cingulate

EdE-47

Pictorial and Educational Review of "Innominate" Anatomical Structures in Neuroimaging: Can You Name Them All?

Matys, T.[1]·Horsburgh, A.[1]·Ali, T.[1]·Antoun, N.[1]·Massoud, T. F.[2]
[1]Addenbrooke's Hospital, Cambridge, UNITED KINGDOM, [2]University of Cambridge, Cambridge, UNITED KINGDOM.

Purpose
In anatomy the term "innominate" is used to designate many parts of the body that are otherwise unnamed. Etymologically it is derived from the Latin meaning "nameless". In the brain and head and neck the use of the single expression "innominate" to describe several anatomical structures pertinent to neuroradiology causes confusion. To clarify this we review the anatomy of these diverse structures.
Approach/Methods
We analyzed publications on anatomy of the brain and head and neck to determine those structures designated as "innominate". This included aspects of neuroradiographic and neuroimaging anatomy.
Findings/Discussion
The term "innominate" is used to uniquely label the following anatomical structures that are indeed otherwise unnamed: 1) Innominate substance: this lies ventral to the anterior aspect of the lentiform nucleus extending from the lateral preoptico-hypothalamic zone over the optic tract towards the amygdala, and contains the basal nucleus of Meynert, whose cells distribute cholinergic fibers widely in the cerebral cortex, and perhaps undergo selective degeneration in Alzheimer disease; 2) Innominate fossa: a shallow depression between the false vocal cord and the aryepiglottic fold on either side of the larynx; 3) Innominate line: a diagonal line projected in the outer lateral third of the orbit in postero-anterior radiographs of the facial bones or the Caldwell projection of the skull, being a tangential projection of the temporal surface of the greater wing of the sphenoid; and 4) Panoramic innominate line: a vertical line crossing the outer third of the maxillary sinus on an orthopantomogram, corresponding to the intersection of the posterior surfaces of the zygomatic process of the maxilla and the frontal process of the zygoma. More confusingly, "innominate" is used as a synonym for several otherwise named structures. In addition to the relatively well known use of the term for 5) Brachiocephalic artery (first branch of the aortic arch), and 6) Brachiocephalic veins (formed by union of internal jugular and subclavian

Note: Scanned images are included in the proceedings. Some submitted images were reduced during editing, thereby decreasing clarity. Also, refer to the Program Planner. Proceedings Content as of 3-29-2013.

veins), it also has found its way into the nomenclature of 7) Foramen petrosum (innominate canaliculus or foramen of Arnold): an inconstant foramen in the greater wing of the sphenoid between foramen ovale and foramen spinosum, transmitting the lesser superficial petrosal nerve, and 8) Pterygoalar ligament (innominate ligament of Hyrtl-Calori): found in 1-10% of skulls and made of fibrous strands which, when ossified, form an "innominate" band extending from the undersurface of the greater wing of the sphenoid to the root of the lateral plate of the pterygoid process. This may form an ossified "innominate canal" under which the three deep temporal nerves or the motor part of the mandibular division of the trigeminal nerve pass.
Summary/Conclusion
Liberal use of the term "innominate" by anatomists to name diverse anatomical structures within the brain and head and neck leads to confusion, especially when some of these structures are otherwise named. In this educational exhibit we review and illustrate these structures pertinent to neuroimaging anatomy.

KEYWORDS: Anatomy

EdE-48

Learning and Remembering the Many Brainstem Syndromes

Zoltani, Z.·Zohrabian, V.
Thomas Jefferson University Hospital
Philadelphia, PA.

Purpose
To review the complex anatomy, organization, and pathology affecting the brainstem in order to more rapidly diagnose such lesions and to understand their complex and often devastating significance.
Approach/Methods
Utilizing a case-based, interactive, and self-study format the normal anatomy of the brainstem nuclei and fiber tracts will be reviewed through anatomical diagrams and corresponding MR images. Lesions affecting the midbrain, pons, and medulla will be reviewed with special attention to commonly encountered brainstem syndromes. The focus of each case will be to understand which cranial nerves are affected and what patient symptomatology may be expected. “The rule of 4” will be discussed as an aid to remembering the location and function of cranial nerve nuclei. Finally, extramedullary brainstem lesions will be briefly touched upon, namely those lesions affecting important passageways for exiting cranial nerves at the cavernous sinus, jugular foramen, and cerebellopontine angle.
Findings/Discussion
There are over 20 eponymously named cranial nerve syndromes, which have been historically well described, and typically result from stroke/ischemia, neoplasm, or demyelinating disease (MS/ADEM) with other less common causes being meningitis, osmotic demyelination syndrome, vascular malformations, and neurodegenerative diseases. We will focus on a few classic cases in addition to highlighting several vascular causes of syndromes caused by occlusion of the basilar and vertebral arteries and their perforating branches. In the midbrain, discussion will focus on the syndromes described by Weber, Benedikt, and Claude which all involve oculomotor nerve dysfunction and variations of weakness and ataxia. In the pons we will consider Millard-Gubler and Foville, which predominately affect the abducens nerve. Lastly, the well-known Wallenberg syndrome and the lesser-known Dejerine syndrome will be taken up and reviewed.
Summary/Conclusion
A thorough understanding of the anatomy, organization, and function of the brainstem can facilitate diagnosis of complex cranial nerve syndromes and allow for more complete recognition of the patient’s symptomatology.

KEYWORDS: Brainstem, Cranial nerve pathology

EdE-49

Real Estate Assessment: Brainstem Infarcts

Klein, A. P.[1]·Baruah, D.[1]·Maheshwari, M.[2]·Ceranske, A.[1]·Gupta, S.[1]·Mark, L. P.[1]·Ulmer, J. L.[1]
[1]Medical College of Wisconsin, Milwaukee, WI, [2]Children's Hospital of Wisconsin, Milwaukee, WI.

Purpose
A case-based educational exhibit created to explore the intricate anatomy of the brainstem with clinical correlation of function/dysfunction in the setting of acute infarction.
Approach/Methods
Nine unique patient cases have been accumulated with high quality MR images showing small focal acute infarcts within the brainstem. Each infarct is localized to a particular anatomical structure within the medulla, pons, or midbrain, and explains the patient’s presenting deficit. Axial diffusion-weighted images (DWI) and axial T2-weighted images from the cases are presented and supplemented with labeled, normal anatomical media including high-resolution cross-sectional photographs of brainstem post-mortem specimens, conventional MR images, and color-coded FA diffusion tensor images (when applicable, for white matter tracts).
Findings/Discussion
Solitary and isolated infarcts of brainstem nuclei and white matter tracts are not uncommonly seen. They often have excellent correlation with clinical dysfunction. Cases of isolated infarcts of the corticospinal tract, spinothalamic tract, oculomotor nucleus, abducens nucleus, motor/sensory nuclei of CN V, spinal nucleus of V, facial nucleus, medial longitudinal fasciculus, and medial lemniscus are presented.
Summary/Conclusion
Familiarity with brainstem anatomy is extremely helpful

Note: Scanned images are included in the proceedings. Some submitted images were reduced during editing, thereby decreasing clarity. Also, refer to the Program Planner. Proceedings Content as of 3-29-2013.

for a radiologist. Understanding the anatomical and functional relationships can optimize radiologic interpretations on both MRI and CT, in the setting of stroke, and beyond.

KEYWORDS: Brainstem, Infarct

EdE-51

Rare and Unusual Neurovascular Variants Arising from the Internal Carotid Artery

Gajjar, M.[1]·Patel, B. M.[1]·Seth, R.[2]·Hurley, M.[1]·Shaibani, A.[1]·Ansari, S. A.[1]
[1]Northwestern Memorial Hospital, Chicago, IL, [2]Baptist Hospital, Miami, FL.

Purpose
To explore anatomical variations along the internal carotid artery (ICA), and highlight unusual configurations that might be encountered during angiographic imaging. The angiographic appearances, embryologic development, prevalence, and associations of clinically relevant variants with neurovascular pathology will be discussed.
Approach/Methods
We review rare ICA variants, including occipital and ascending pharyngeal-ICA origins; aberrant or aplastic ICAs; persistent proatlantal, stapedial, hypoglossal, and trigeminal arteries; primitive maxillary and mandibular arteries, duplicated posterior communicating arteries with a persistent primitive fetal branch, infraoptic anterior cerebral artery, and dorsal/ventral ophthalmic arteries.
Finding/Discussion
The ICA features a straight cervical course up to the level of the skull base, typically without branch vessels. Ten to 40% of ICAs demonstrate anatomical variation. The occipital artery classically arises from the external carotid artery (ECA), coursing between the occipital bone and C1. Variations in the occipital artery may be due to the presence of abnormal growth factors during embryogenesis and regression of the first and second aortic arches. When the ascending pharyngeal artery originates from the cervical ICA, it represents a dorsal vestige of the third aortic arch. Congenital vascular variants of the middle ear are rare. These patients are at risk of injury during myringotomy or stapes surgery, requiring preoperative recognition. An aberrant ICA is formed by collateral blood flow, which substitutes the cervical and petrous portions of the ICA through branches of the ECA, and includes intratympanic and lateral pharyngeal variants. Persistence of the stapedial artery is rare, and can be associated with an aberrant ICA. The stapedial artery is a normal transient embryonic anastomosis between future ECA branches and ICA, with a prevalence of 0.48%. The persistent trigeminal artery is the most common and most cephalic of the persistent carotid-vertebrobasilar anastomoses (CVBA). Its prevalence is 0.1%-0.6%. Two types have been described and are equally common, lateral parasellar and medial transellar. The persistent hypoglossal artery is the second most common CVBA, with a prevalence of 0.02%-0.10%. It originates from the ICA at the C1-C3 level, traversing the hypoglossal canal, and anastomoses with the basilar artery. Primitive maxillary and mandibular artery are extremely rare and may be seen collateral pathways in the setting of ICA congenital occlusive disease. Duplication of the posterior communicating artery is uncommonly found, with a 2% prevalence of this anomaly found at surgical dissection. Unilateral partial and complete duplications have been described and associated fetal variations have not been entirely characterized. During early embryonic development, two primitive ophthalmic arteries are present, the ventral ophthalmic artery that persists, and the dorsal ophthalmic artery that regresses. In some instances, the opposite occurs, and the dorsal ophthalmic artery from the inferolateral trunk persists. An infraoptic course of the A1 segment of the anterior cerebral artery is a rare anomaly, with only 42 cases reported in the literature.
Summary/Conclusion
Variants of the ICA are rare, typically asymptomatic, and often incidental findings. However, these variants can occasionally influence surgical strategy, temporary occlusion time, embolic risk, and collaterals with potential impact on patient outcomes and postprocedural complications.

KEYWORDS: Anatomical variation, Internal carotid artery, angiography

EdE-52

From Rootlets to Rami: High-Resolution Imaging of Spinal Nerve Anatomy

Hynecek, R.[1]·Nidecker, A. E.[2]·Wasserman, B. A.[1]·Blitz, A. M.[1]
[1]Johns Hopkins, Baltimore, MD, [2]University of California Davis, Sacramento, CA.

Purpose
Constructive interference in the steady state (CISS) and volume interpolated breath hold examination (VIBE) are high-resolution isotropic gradient-echo MR techniques that are capable of producing exquisite detail of intradural and extradural spinal neuroanatomy. With images capable of submillimeter spatial resolution, it is important for the neuroradiologist to be familiar with the appearance of relevant structures that can be resolved using these techniques in the context of spine imaging.
Approach/Methods
During a 10-month period 39 patients were evaluated with high-resolution spine imaging. The cervical spine MRI protocol included 0.5-0.6 mm coronal isotropic CISS without and with contrast and 0.8 mm coronal isotropic VIBE without and with contrast. Similar parameters were applied to the lumbar and thoracic spine protocols in this series. Acquired data were reformatted into angled

Note: Scanned images are included in the proceedings. Some submitted images were reduced during editing, thereby decreasing clarity. Also, refer to the Program Planner. Proceedings Content as of 3-29-2013.

oblique views for optimal characterization of the structure being assessed utilizing standard MPR software on the PACS viewer.
Findings/Discussion
Surface anatomy of the spinal cord, dorsal and ventral roots/rootlets, dorsal root ganglia, dural root sleeves, spinal nerves, dorsal and ventral rami, rami communicantes, sympathetic ganglia, denticulate ligaments, and spinal canal structures including the dura, extradural venous system, and neural foramina, were reviewed systematically and are presented as image-based case examples with diagrammatic representations of normal anatomy.
Summary/Conclusion
Isotropic high-resolution imaging provides the capability of visualizing structures not typically seen with standard spine MRI techniques due to the constraints of conventional two-dimensional imaging. An image-based review of anatomical appearances and relationships of these structures is intended to familiarize radiologists with relevant anatomy.

KEYWORDS: High-resolution imaging, CISS, spine

Monday, May 20 – Wednesday, May 22
6:30 AM – 9:00 PM
Thursday, May 23
6:30 AM – 3:00 PM
Hall B1

Education Exhibits (EdE) 53 - 65

EdE3-Head and Neck

Note: A missing printed number indicates an abstract has been withdrawn.

EdE-53

CT and MR Imaging of Sialadenitis

Scher, D. J.·Joshi, A. S.·Taheri, M. R.
George Washington University
Washington, DC.

Purpose
1. To review the causes of sialadenitis. 2 . To review the imaging characteristics of acute and chronic sialadenitis on CT and MRI.
Approach/Methods
1. Patient chart review to identify examples of acute and chronic sialadenitis. 2. Imaging examples of acute and chronic sialadenitis. 3. Literature review of diagnostic imaging of sialadenitis.
Findings/Discussion
Inflammation of the salivary gland is called sialadenitis. Causes of sialadenitis can be broken down into three major categories: obstruction with sialolithiasis, obstruction without sialolithiasis and immunologic or inflammatory. In this educational exhibit, we will focus on cross-sectional image findings of specific examples of each of these categories. Image findings of obstruction with sialadenitis are further characterized using examples of acute, subacute and chronic stages. Obstruction without sialolithiasis is highlighted by idiopathic ductal stenosis of the Stensen's duct. Examples of the immunologic or inflammatory category include infectious adenitis, Sjogren's syndrome, and Kuttner's tumor. A literature review of each of these cases will be provided throughout this exhibit. The educational exhibit will end with several mimickers of sialadenitis, including HIV-related lymphoepithelial lesions and papillary cystadenoma lymphomatosum (Warthin's Tumor).
Summary/Conclusion
Multiple causes of sialadenitis exist, and imaging can play a critical role in honing the differential diagnosis. In this exhibit, the observer should become familiar with the different causes of sialadenitis and with their associated cross-sectional image findings.

KEYWORDS: Sialadenitis

EdE-54

Imaging Findings of Infectious Endophthalmitis

Radhakrishnan, R.[1]·Morales, H.[1]·Cornelius, R.[1]·Cunnane, M. E.[2]·Golnik, K.[1]·Rutty, A.[3]
[1]University of Cincinnati College of Medicine, Cincinnati, OH, [2]Massachusetts Eye and Ear Infirmary, Boston, MA, [3]University of Pittsburgh, Pittsburgh, PA.

Purpose
Endophthalmitis is a rare, but morbid inflammatory condition of the globe with imaging findings less well described. The aim of this exhibit is to illustrate the imaging features of infectious endophthalmitis, with appropriate MRI and CT images. We also will highlight the etio-pathogenesis of infectious endophthalmitis with the aid of easily understandable illustrations.
Approach/Methods
We reviewed our imaging database for illustrative cases of infectious endophthalmitis and also obtained clinical information from the patient's medical chart.
Findings/Discussion
Endophthalmitis is intraocular inflammation predominantly involving the anterior chamber, choroid or vitreous. Infection is often exogenous in etiology secondary to trauma or ocular surgery. Rarely, infection may be endogenous from hematogenous spread of organisms in susceptible individuals. Early disease may

Note: Scanned images are included in the proceedings. Some submitted images were reduced during editing, thereby decreasing clarity. Also, refer to the Program Planner. Proceedings Content as of 3-29-2013.

have normal imaging findings. There may be mild increase in enhancement of the uveoscleral layer on contrast-enhanced CT or MRI where the rich vascular supply of the choroid serves as a site for initial infection. Hyperdensity of the vitreous on CT or mild increased vitreous signal intensity on FLAIR and T1W MRI, also described as part of early disease, may reflect proteinaceous exudates into the vitreous. More fulminant endophthalmitis can present with ocular abscesses and focal exudates in conjunction with ocular membrane detachment. These focal exudates, which are demonstrated more easily with MRI, can show varying degrees of diffusion restriction and rim enhancement. Concomitantly, there can be edema or inflammation of the episcleral tissues, in the potential sub-Tenon space. Lacrimal gland enlargement often is associated. The end stage of unresolved endophthalmitis is phthisis bulbi, with collapse of the globe and loss of normal contour. Clinically, severity of infection is graded by degree of involvement of the intraocular structures; however, ophthalmoscopy may be suboptimal in these patients. Infectious endophthalmitis is often bacterial in etiology, but viruses, fungi and parasites also can cause ocular inflammation. Noninfectious endophthalmitis from autoimmune or granulomatous conditions such as sarcoid, Beçhet's disease, ANCA associated vasculitis, can have similar imaging appearance.

Summary/Conclusion

Initial diagnosis of endophthalmitis is made clinically and imaging is rarely needed. Imaging is indicated in the more complex, unresponsive patients, where assessment of disease extent and associated complications is needed to plan appropriate management. The radiologist should be aware of the imaging findings, particularly on MRI where the use of DWI can help to differentiate endophthalmitis from noninfectious inflammation of the globe.

KEYWORDS: Eye, Infections, globe

EdE-55

CT and MR Imaging Findings in Orbital Lymphoma

Carmody, R. F.·Khan, R.·Nael, K.·Shastri, R.
University of Arizona Medical Center
Tucson, AZ.

Purpose

To present a pictorial display of the many appearances of lymphoma when it involves the orbit. Other conditions that may resemble lymphoma also will be shown. Imaging clues that are helpful in distinguishing lymphoma from other diseases will be discussed.

Approach/Methods

The imaging findings in 23 patients with pathologically proven lymphoma, as well as two additional cases of acute lymphocytic leukemia, were reviewed retrospectively. The CT and MRI scans were examined as to the location of intraorbital disease, MR signal intensity, enhancement patterns, and presence or absence of bone destruction. Patient age and bilaterality of disease also were recorded. Where available, cell type also was noted.

Findings/Discussion

Most cases were non-Hodgkins B-cell lymphomas; two cases of T-cell lymphoma were found, as well as a single case of Hodgkins disease. Most patients were middle aged or elderly, although one case of T-cell lymphoma was in a six-year-old girl, and the other was in a 22-year-old man. Sixteen had bilateral and nine had unilateral involvement. The most common structure affected was the lacrimal gland (15 cases). Twenty-one individuals had extraconal disease, and seven had intraconal findings. The extraocular muscles were infiltrated in eight cases. Two patients had optic nerve sheath thickening. Only one patient had bone destruction. Conjunctival infiltration was seen in two cases. On MRI, lymphomatous tissue was isointense to gray matter on T1- and T2-weighted sequences, with strong enhancement. Restricted diffusion also was present. A characteristic feature of lymphoma was its propensity to "mold" itself to adjacent structures, such as the posterior globe. The entity that is most difficult to distinguish from lymphoma is idiopathic orbital inflammatory disease (pseudotumor), which typically has identical MR signal characteristics and can occur anywhere in the orbit. Metastatic disease also can have similar appearances when it involves the orbit, but is more likely to cause bone destruction. Lacrimal gland sarcoid is sometimes a differential diagnostic consideration, especially in young females. Other lymphoma mimics include primary rhabdomyosarcoma of the orbit, unilateral or asymmetrical Graves disease, and nerve sheath tumors.

Summary/Conclusion

B-cell lymphoma is a not uncommon cause of an orbital mass. Lymphoma often occurs in the lacrimal gland, is isointense on T1- and T2-weightefd imaging, shows restricted diffusion, and demonstrates strong contrast enhancement. A characteristic feature is its tendency to mold itself to the globe. Orbital pseudotumor may have an identical appearance. Lymphoma is unlikely to cause bone destruction.

KEYWORDS: Orbital tumor, Lymphoma

EdE-56

Ooh lala ! Who Has Seen This One Before?: A Medley of Unexpected Foreign Bodies Encountered by Neuroradiologists

Rehmani, R.·Gandhi, S.·Black, K.
North Shore-Long Island Jewish Health System
Manhasset, NY.

Purpose

To illustrate unusual and often unexpected incidental foreign bodies encountered by neuroradiologists in the head/neck. To increase awareness and highlight clinical relevance of such puzzling cases. A systemic imaging-based classification of such unfamiliar cases into emergent

Note: Scanned images are included in the proceedings. Some submitted images were reduced during editing, thereby decreasing clarity. Also, refer to the Program Planner. Proceedings Content as of 3-29-2013.

versus nonemergent categories is illustrated. This is supplemented by perplexing imaging appearance of certain exemplary postoperative cases. Multimodality approach is utilized.
Approach/Methods
We retrospectively reviewed unusual cases encountered at a tertiary care academic center in the department of neuroradiology, over a period of five years. These cases then were categorized systematically according to the urgency level requiring immediate management versus nonurgent incidentalomas.
Findings/Discussion
We present an assortment of cases of postfacial augmentation including chin augmentation (mentoplasty), cheek injections and augmentation (malarplasty) and rhinoplasy. We also present a case of multiple buttock augmentation resulting in much unexpected complication of florid multiple sclerosis. On one hand, we present a case of forgotten intracranial Mayfield pin postcraniotomy while on the other hand, we illustrate a case of accidental nail stuck in a patient's head. The normal postoperative imaging features of a case of post-glioblastoma multiforme (GBM) resection Gliadel wafer placement (for chemotherapy) are presented and contrasted from tumor recurrence, a common mimic. Additionally, we present exemplary cases of embedded foreign bodies in the esophagus such as ingested denture, swallowed battery, as well as a case of a very large pork chop stuck in the esophagus. Secondary complications of these often forgotten foreign bodies include walled-off abscesses and distal migration of the ingested material. Computed tomography imaging features of commonly encountered incidental intraoral edibles such as chewing gums and ginger mints also are presented.

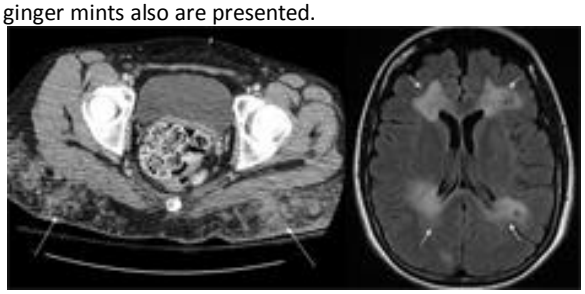

Summary/Conclusion
Radiology is at the heart of the modern day practice of medicine. Radiologic assessment of a non-native foreign body is oftentimes difficult in unexperienced hands. The clinical relevance and urgency of such a finding also is emphasized to allow correct and speedy management of patients. It is crucial that radiologists keep themselves abreast with ongoing newer surgical techniques especially in the field of plastic surgery as these patients may present for radiologic imaging at some point in their life for unrelated issues. This exhibit will create awareness and allow better understanding among the radiologists regarding the imaging features of currently prevalent augmentation techniques and their unexpected complications as well as imaging features of a multitude of other unusual foreign bodies in the head and neck.

KEYWORDS: Devices, Eye

EdE-57

More than Superficial: A Review of the Major Complications of Malignant Skin Neoplasms of the Head and Neck

Obeng, K. K.·Escott, E. J.·Valentino, J.·Aouad, R. K.·Ponting, J. M.
University of Kentucky
Lexington, KY.

Purpose
Nonmelanoma skin cancers (NMSCs) including squamous cell carcinoma (SCC) and basal cell carcinoma (BCC), and malignant melanoma frequently occur in the head and neck. However, the sometimes quite extensive local invasion and complications associated with these lesions often are not anticipated or well understood by the radiologist. The purpose of this review is to present the imaging findings of the major complications related to the invasion and locoregional metastases of malignant skin neoplasms of the head and neck.
Approach/Methods
Cases were collected by one of the following methods: a retrospective search of the radiology information system (RIS) for those patients who had undergone head and neck imaging (MRI, CT) at the University of Kentucky, Department of Radiology for the evaluation of head and neck skin malignancy, during the dates of January 2011 - July 2012; review of cases presented at the head and neck tumor board; and cases from the authors' personal collections.
Findings/Discussion
Detected complications included direct deep local invasion such as of the orbit, temporal bone or calvarium or parotid gland, especially for SCC. Perineural spread of tumor also was noted. Contrast enhancing nodularity of the surrounding subcutaneous fat and soft tissues about the primary skin lesion thought to reflect locoregional lymphatic invasion and regional lymphadenopathy also could be seen. Invasion of major vessels and other deep structures of the neck also is a feature of the disease.
Summary/Conclusion
Once NMSCs and malignant melanoma of the head and neck are diagnosed, and because of the variety of surgical and nonsurgical options that are available for treatment, careful preoperative assessment by an experienced surgeon, in consultation with a radiologist, pathologist and oncologist may be needed. Imaging frequently is requested to evaluate patients with deep invasion and locoregional metastases of primary skin malignant neoplasms of the head and neck. The noted complications of nonmelanoma skin cancers (NMSCs) and melanoma include deep local invasion such as of the temporal bone

Note: Scanned images are included in the proceedings. Some submitted images were reduced during editing, thereby decreasing clarity. Also, refer to the Program Planner. Proceedings Content as of 3-29-2013.

or orbit, perineural spread of tumor, metastases and/or invasion of the parotid gland, invasion of major vessels and other deep structures of the neck, and invasion of the skull or cranial vault depending on the type of tumor. The radiologist and clinician needs to be aware of these varied appearances, and therefore may better anticipate the immediate and latent complications following primary diagnosis, thereby facilitating early treatment with fewer complications.

KEYWORDS: Head and neck, Neoplasm, nonmelanoma skin cancers (NMSCs)

EdE-58

Horner's Syndrome: A Practical Approach to Critical Anatomy and Imaging

Parmar, H. A.·Ibrahim, M.·Cornblath, W.·Trobe, J.·Mukherji, S. K.
University of Michigan
Ann Arbor, MI.

Purpose
Horner's syndrome (HS) is a clinical triad of symptoms of ptosis, miosis and anhydrosis first described by Johann Horner in 1869. It results from interruption of oculosympathetic pathway (OSP) and a wide variety of benign and malignant entities can result in HS. While imaging patients with HS it is important for neuroradiologists to understand the anatomy of the OSP, to be aware of different entities within this pathway and choose correct imaging modality to arrive at the right diagnosis.
Approach/Methods
The goal of this exhibit is to give a brief overview of clinical features of HS, review the anatomy of the OSP, and provide the clinical and imaging approach while dealing with these patients. We also will present CT and MRI imaging features of different lesions that involve the OSP.
Findings/Discussion
The clinical approach for HS deals with knowing if it is acute or chronic and if it is isolated or nonisolated. Patients with nonisolated can have symptoms referred to hypothalamus/ brainstem, cervical cord, brachial plexus, carotid artery, neck or the cavernous sinus. On imaging, HS can be classified as preganglionic or postganglionic (with respect to the superior cervical ganglion). Preganglionic HS can be subdivided further into central (interruption of fibers from hypothalamus to spinal cord at C8-T2 level) and peripheral (interruption of fibers from C8- T2 to superior cervical ganglion). Typical lesions involving the preganglionic central pathway include lesions of the hypothalamus, brainstem and cervical cord. Lesions involving the preganglionic peripheral pathway include lesions like apical lung cancer, cervical rib, trauma and certain thyroid cancers. Lastly the lesions involving the postganglioic pathway include lesions of the superior cervical ganglion (trauma, iatrogenic neck dissection), internal carotid artery (dissection, aneurysm, arteritis), skull base and cavernous sinus (tumors, inflammation and cavernous sinus thrombosis).
Summary/Conclusion
Imaging interpretation of patients with HS is difficult due to varied spectrum of different entities producing HS and also due to lack of adequate knowledge of the OSP anatomy. Familiarizing with the critical anatomy of the OSP and the clinical and imaging approaches presented in this exhibit will provide a basic and useful framework for dealing with such patients and arrive at a correct diagnosis.

KEYWORDS: Horner's syndrome, Anatomy, pathology

EdE-60

Know your Notochord: Notochordal Remnants at the Central Skull Base

Conley, L. M.·Zlotchenko, G.·Shatzkes, D.
Lenox Hill Hospital
New York, NY.

Purpose
The notochord is a flexible rod-like structure that defines the axis of the embryo during intrauterine life. In addition to contributing to formation of normal anatomical structures such as the nucleus pulposis, a variety of remnants may persist resulting in a spectrum of lesions ranging from benign variants such as ecchordosis physaliphora to malignant chordomas. Our goal is to provide a radiologic review of notochordal remnants at the central skull base.
Approach/Methods
This educational exhibit will review notochordal embryology and the imaging findings of both normal and variant notochordal remnants at the central skull base. Lesions will be characterized both with regard to their anatomical location along the notochordal tract as well as their clinical significance and presentation. Companion cases emphasizing important differential considerations will be presented.
Findings/Discussion
Developmental variants and neoplasms tend to arise most frequently at the superior and inferior margins of the embryonic notochord (i.e., at the clivus and sacrum). At the central skull base, lesions may be located proximally within the postclival intradural (ecchordosis physaliphora) and extradural (chordoma) spaces, the clivus itself (persistent canalis basalis medianus, fossa navicularis magna) and in the central nasopharynx (Tornwaldt cyst). Characteristic CT and MRI features of these lesions are discussed, with the often difficult distinction between the benign ecchordosis physaliphora and malignant chordoma particularly emphasized. While most represent incidental "don't touch me" findings, those lesions that require further workup, intervention or continued followup are identified.

Note: Scanned images are included in the proceedings. Some submitted images were reduced during editing, thereby decreasing clarity. Also, refer to the Program Planner. Proceedings Content as of 3-29-2013.

Summary/Conclusion
Remnants of the notochord at the skull base range from the mundane (Tornwaldt cyst) to the esoteric (ecchordosis physaliphora). Understanding of the relevant embryology will aid in recognition of the characteristic location and imaging features of this diverse group of developmental variants and pathologic entities.

KEYWORDS: Skull base neoplasm, Normal variant, notochord remnants

EdE-61

Tales from the Crypts: Disease Processes of the Tonsillar Fossa

Zlotchenko, G.·Conley, L. M.·Shatzkes, D.
Lenox Hill Hospital
New York, NY.

Purpose
The tonsils have received enhanced attention recently due to the rise in incidence of human papillomavirus (HPV) related oropharyngeal squamous cell carcinoma. Their unique anatomy, with deep crypts and both epithelial and lymphoid elements, allows for a broad range of disease, and some unusual imaging features. Our goal is to provide a comprehensive review of the full spectrum of disease processes affecting the tonsillar fossa.
Approach/Methods
Normal anatomy and pathologic processes of the tonsils and related structures of the oropharynx will be reviewed, with an emphasis on CT, MRI and PET-CT imaging. Patterns of spread, unique imaging features, differential diagnoses, and imaging pitfalls will be addressed.
Findings/Discussion
Pathologic entities affecting the tonsillar fossa can be divided into three major categories: congenital, inflammatory/infectious and neoplastic. Congenital lesions include branchial cleft cysts and vasoformative anomalies such as venous or lymphatic malformations. Inflammatory/infectious lesions can be divided further into acute and chronic subtypes. Chronic processes include hyperplasia, chronic tonsillitis, tonsoliths, and mucous retention cysts. Acute processes represent a spectrum from tonsillitis to tonsillar/peritonsillar abscesses; while these are frequently bacterial or viral in etiology, some less common pathogens such as actinomycosis will be presented. Finally, neoplastic disease, with both common (squamous cell carcinoma, lymphoma) and uncommon (e.g., lymphoepithelioma, sarcoma) entities will be reviewed.
Summary/Conclusion
Though diminutive in size, the tonsillar fossa is disproportionately affected by a wide variety of relatively common disease processes. Knowledge of the details of its unique structural and functional anatomy, as well as characteristic patterns of spread and imaging pitfalls, will aid in formulating accurate and clinically useful differential diagnoses.

KEYWORDS: Oropharynx, Neck lesions, tonsillar fossa

EdE-62

Radiologic Evaluation of Endoscopic Endonasal Skull Base Surgery Candidates

Learned, K. O.·Lee, J. Y. K.·Newman, J. G.·Palmer, J. N.·Bagley, L. J.
University of Pennsylvania
Philadelphia, PA.

Purpose
Endoscopic endonasal approaches (EEA) have expanded beyond the paranasal sinus and sella to become the best surgical corridor to the entire ventral skull base. Using representative cases, we will discuss general principles, key skull base anatomy in relation to surgical access, the diversity of pathology, and the role of preoperative CT and MR imaging.
Approach/Methods
Our institutional and nationally published data on EEAs to skull base surgery are reviewed. The pathologies are categorized by anatomical locations and endoscopic surgical approaches. The preoperative CT and MR imaging are reviewed to illustrate the pertinent radiologic findings for surgical planning. Postoperative MR imaging and clinical followup demonstrate surgical results.
Findings/Discussion
Recent advancements in endoscopic techniques, instrumentation, intraoperative imaging navigation and cranial defect reconstruction enable endoscopic management of benign and malignant processes along the entire ventral skull base, petrous apex and infratemporal fossa as wells as in select cases within the cavernous sinus, suprasellar cistern, and anterior cranial fossa with similar results to those obtained with open craniofacial procedures but with beneficial lower rates of complication. Feasible and safe surgical access and reconstructive options depend upon the paranasal sinus and skull base anatomy of each patient. CT, MR and noninvasive angiographic studies should detail the location of the lesion, assess its relationship to adjacent neurovascular structures and note bony dehiscence, hyperostosis (potentially necessitating drilling) and anatomical variants (Onodi cells, heights of skull base, sphenoid sinus septum relationship with ICA), thus permitting safe surgical access. The endonasal corridor allows excellent access to the midline skull base from behind the frontal sinus to the clivus, permitting optimal lesion exposure and a direct surgical route to the lesion sparing critical neurovascular structures. Therefore, the ventral skull base lesions that are best addressed by the anterior endonasal approaches are located in the true midline without significant lateral extension over the orbital roof and optic nerve or extension posterolateral to

Note: Scanned images are included in the proceedings. Some submitted images were reduced during editing, thereby decreasing clarity. Also, refer to the Program Planner. Proceedings Content as of 3-29-2013.

the internal carotid artery. Superolateral location in the cavernous sinus, neurovascular encasement, pituitary stalk/hypothalamic involvement and brain invasion increase the difficulty of surgical resection and hence increase its risks. Preoperative radiologic assessment should include anatomical skull base locations based on EEA modules with attention to the above-mentioned critical assessments. Examples of surgical corridors and pathologies are transcribriform (esthesioneuroblastoma, olfactory meningioma), transphenoid (planum-tuberculum meningioma, craniopharyngioma), transclivus (chordoma, foramen magnum meningioma, ventral brain stem lesion) and trans-pterygoid (petrous apex cholesterol granuloma and petroclival chondrosarcoma).
Summary/Conclusion
In many cases, the preoperative radiographic evaluation is not only useful for diagnosis but is also useful for surgical mapping to warrant safe and optimal surgical outcome of EEAs. Both CT and MR imaging evaluation are required for appropriate patient selection and in guiding EEAs.

KEYWORDS: Skull base neoplasm, ENT, endoscopic

EdE-63

Skull Base Reconstruction: Demystifying Postoperative Imaging Evaluation

Learned, K. O.[1]·Maralani, P. J.[1]·Malloy, K. M.[2]·Loevner, L. A.[1]
[1]University of Pennsylvania, Philadelphia, PA, [2]University of Michigan, Ann Arbor, MI.

Purpose
The pathology of the skull base is challenging with complex anatomy and critical neurovascular structures. Collaboration of subspecialists including neuroradiologists, neurosurgeons, and head and neck surgeons is essential for safe and effective surgical resection and reconstruction. Postoperative imaging and clinical followup is even more challenging due to the alteration of normal anatomy. This presentation will review common surgical skull base reconstructions and illustrate a practical approach to postoperative imaging interpretation.
Approach/Methods
We review the commonly encountered skull base defect reconstructions by anatomical location, reconstructive tissues, and surgical techniques. The postoperative CT and MR imaging findings of normal reconstructions, and patterns of neoplastic recurrence will be discussed and illustrated.
Findings/Discussion
An arsenal of nonvascularized and vascularized tissues are employed to reconstruct surgically created skull base defects in order to achieve CSF sealant. For craniofacial resections, large tissue flaps and grafts are primarily utilized. For medium to large paramedian anterior skull base (ASB) defects such as craniofacial resection with bifrontal craniotomy, galeopericranial flap based on supraorbital or supratrochlear arteries is used routinely. CT and MR imaging show folds of tissue in the ASB defect with frontal sinus cranialization. Split thickness calvarial bone grafts rarely are used. Lateral ASB (infratemporal fossa) or lateral temporal bone defects are reconstructed routinely with temporo-parietal fascia with or without the temporalis muscle with preserved vascular pedicle of superficial temporal artery (STA) and/or deep temporal arteries and veins. Fasciocutaneous free tissue transfer has become the main stay for reconstructions with utilization of radial forearm free flaps with radial artery and accompanying vein microanastomosis to STA or facial artery and veins, respectively. These regional flaps and free flaps have characteristic striated muscle bundles, and variable MR signal intensity and enhancement due to multiple factors including scar maturation, resorption of fat, denervation, and in some cases sequel of postoperative adjuvant radiation. These flaps gradually lose tissue bulk due to atrophy. In endonasal endoscopic surgery, multilayer endoscopic reconstruction using pedicled nasoseptal flap is utilized to reconstruct the surgically created skull base defect. In the immediate postoperative period the pedicled flaps have a characteristic C-shaped arc configuration and an enhancing vascular pedicle on MR imaging. Over months the NSF retracts into the denuded skull base defect and sinonasal cavity but maintains its configuration. Neoplastic recurrences typically occur at the interface of the flap recipient bed and reconstructive tissue and appear as new or growing enhancing tissue.
Summary/Conclusion
Understanding the imaging appearance of skull base reconstruction is paramount for accurate postoperative assessment and delineation between normal reconstructive tissue and neoplasm.

KEYWORDS: Skull base neoplasm, Postoperative findings, skull base reconstruction

EdE-64

Hypoglossal Nerve: Anatomy and Causes of Palsy

Meyer, M. A.·Erly, W. K.
University of Arizona
Tucson, AZ.

Purpose
The hypoglossal nerve provides motor innervation to the tongue, and may be affected by pathology at multiple locations along its pathway. Knowledge of its anatomy and careful examination of the tongue are important in the diagnosis of lesions and determination of appropriate testing. Normal anatomy, clinical manifestations, and pathologic conditions that affect the hypoglossal nerve in its five segments will be reviewed.
Approach/Methods
An understanding of the intracranial and extracranial components of the hypoglossal nerve is fundamental in

Note: Scanned images are included in the proceedings. Some submitted images were reduced during editing, thereby decreasing clarity. Also, refer to the Program Planner. Proceedings Content as of 3-29-2013.

the evaluation of its pathology. A discussion of anatomy and the diseases that affect the nerve throughout its course from the medulla to the tongue will ensue.
Findings/Discussion
Dysfunction of the hypoglossal nerve may be a consequence of supranuclear, nuclear or infranuclear disease. The cortical center for lingual movement is located within the precentral gyrus, which sends fibers to the hypoglossal nucleus. The paired hypoglossus nuclei are located on the floor of the fourth ventricle within the medulla. The nuclear and infranuclear hypoglossal nerve can be divided into five segments: the medullary, cisternal, skull base, nasopharyngeal/oropharyngeal carotid space and sublingual segments. In evaluating the hypoglossal nerve, a segmental approach should be taken when assessing for nuclear and infranuclear involvement. Specific symptoms and findings related to tongue movement can be based in the specific location of the lesion. Hemiatrophy and weakness of the tongue can result in visible tongue deformity which can be recognized by the patient. In the clinical evaluation of the hypoglossal nerve, the clinician inspects the tongue to search for both difficulties in protrusion as well as any deviation of the tongue. The tongue deviates towards the side of weakness. A bilateral supranuclear lesion will result in a spastic tongue that cannot be protruded. A unilateral supranuclear lesion will cause the tongue to deviate away from the side of the lesion. A nuclear lesion causes the tongue to deviate toward the lesion. An infranuclear lesion distal to the C1 anastomosis has similar findings, but also produces involvement of the infrahyoid strap muscles. Tongue denervation in MRI can be viewed as chronic, subacute or acute. The radiologic findings of fatty infiltration and atrophy of the tongue may be the first clue that a hypoglossal process is present. In acute/subacute stage, abnormal enhancement, increased volume and T2 hyperintensity are present. In the early chronic stage there are changes of fatty replacement without loss of volume/atrophy. In the chronic stage there is extensive fatty replacement and loss of volume.
Summary/Conclusion
The hypoglossal nerve is the motor supply to the tongue. In order to create the most efficient imaging strategy one must be familiar with the anatomy of the hypoglossal nerve and the diseases that affect the nerve throughout the course from the medulla to the tongue.

KEYWORDS: Cranial nerve palsy, Hypoglossal nerve, anatomy

EdE-65

Three-Year Experience Using Cone Beam Computed Tomography in Temporal Bone Imaging

Kelly, H. R.[1,2]·Curtin, H. D.[1]
[1]Massachusetts Eye and Ear Infirmary, Boston, MA,
[2]Massachusetts General Hospital, Boston, MA.

Purpose
To review three years of experience of cone beam computed tomography (CBCT) in temporal bone imaging as utilized in a subspecialty hospital.
Approach/Methods
Cone beam computed tomography is an emerging technique with the ability to image fine bony structures with high spatial resolution and with the potential for lower radiation doses compared to conventional CT scans. Minimal data is available in the literature regarding the use of this technique in the temporal bone, with the majority of reports focused on cadaveric studies. All temporal bone studies performed on a 3D CBCT system (3D Accuitomo, J Morita Manufacturing) over a three-year period (400 total examinations) at a subspecialty eye and ear hospital were reviewed. Typical clinical indications, imaging findings and estimated radiation doses will be discussed, as will potential artifacts and problems faced with incorporating the system into the daily workload.
Findings/Discussion
In our opinion, CBCT in the temporal bone is particularly useful in evaluation of conductive hearing loss given its ability to clearly image the bony anatomy of the middle and inner ear, including the ossicles, oval and round windows and facial nerve canal. We also are inclined to use CBCT over conventional CT for evaluation of superior semicircular canal dehiscence. Examples of other entities diagnosed by CBCT will be provided, including otosclerosis, congenital ossicular anomalies, ossicular prostheses, bony erosions in the setting of cholesteatoma, spontaneous and postoperative tegmen defects and dehiscence of the facial nerve canal. Acquisition time for CBCT is longer than conventional CT, making CBCT more susceptible to motion artifact, the most common technical limitation that can interfere with diagnostic interpretation. Acquisition also places greater demands on the CT technologists, who must be trained in the new technique and typically spend more time performing a CBCT than a conventional CT of the same area. A “ghosting artifact” was present at times in the middle ear which can simulate soft tissue. While CBCT could theoretically provide high-resolution evaluation of inner ear congenital anomalies in children with sensorineural hearing loss, issues with upright acquisition and motion artifact currently preclude routine use of CBCT over conventional CT in younger pediatric patients. The radiation dose estimates for CBCT in the temporal bone are less than conventional CT, especially if only one side is evaluated.
Summary/Conclusion
Cone beam computed tomography may have advantages

Note: Scanned images are included in the proceedings. Some submitted images were reduced during editing, thereby decreasing clarity. Also, refer to the Program Planner. Proceedings Content as of 3-29-2013.

over conventional CT scans in certain pathologic entities in the temporal bone due to its high spatial resolution and capacity for depicting the fine bony structures. An understanding of the advantages as well as technical factors/limitations associated with this technique allow the head and neck radiologist to stratify patients to CBCT or conventional CT based on the clinical indication, patient history and age.

KEYWORDS: Cone-beam computed tomography, Temporal bone

Monday, May 20 – Wednesday, May 22
6:30 AM – 9:00 PM
Thursday, May 23
6:30 AM – 3:00 PM
Hall B1

Education Exhibits (EdE) 66 - 70

EdE4-Interventional

Note: A missing printed number indicates an abstract has been withdrawn.

EdE-66

Current Review of Treatment Strategies of Carotid Cavernous Fistulas

Trinh, V.·Chao, K.
Kaiser Permanente Los Angeles Medical Center
Los Angeles, CA.

Purpose
Carotid cavernous fistulas (CCFs) typically are classified as high flow/direct fistulas usually related to trauma or aneurysmal rupture or low flow/indirect fistulas secondary to spontaneous formation of dural fistulas. The educational abstract reviews the different treatment strategies regarding high and low flow CCFs primarily via arterial or venous endovascular approaches; however, with discussion of novel neurointerventional approaches notably through the foramen ovale in difficult situations in which endovascular access is not possible. Non-neurointerventional treatments including surgery and stereotactic radiosurgery also will be briefly mentioned. In regards to each treatment we will discuss the inherent risks of hemorrhage or other procedural complications and also the efficacy rates and/or need for reintervention when possible.
Approach/Methods
Review of the current literature and case series with longitudinal followup presented if available.
Findings/Discussion
The treatment of high flow direct fistulas is warranted given the typical earlier signs and clinical symptoms related to cranial nerve palsies, exophthalamos, or chemosis thought secondary to more acute venous hypertension. Endovascular approaches have long been utilized and historically an arterial approach using detachable balloons was considered the standard of care as of the 1980s. However problems arose including early detachment, deflation, or balloon rupture which led to the discontinuation in the U.S. market in 2003. Currently, there is wide acceptance in the use of liquid agents such as onyx, detachable coils, and endovascular stent graft placement with great success. Depending on the size of fistulous connection, covered stents, flow diverting stents, or porous stent-assisted coiling also are considered and now reported. Alternatively, a transvenous approach typically posteriorly through the internal jugular vein and inferior petrosal sinus are viable options. Often times the inferior petrosal sinus may be occluded and other avenues of venous access including through the ipsilateral superior petrosal sinus, facial vein, or superior ophthlamic vein through direct stick or surgical approach. In situations where no endovascular access is possible or safe, we have demonstrated a percutaneous approach through the foramen ovale to be an additional possible treatment approach to CCFs. Indirect CCFs may be asymptomatic and also can resolve on their own. In the absence of symptoms, the best treatment is considered to be conservative management. Current literature suggests that with the advent of ocular symptoms in indirect CCFs, the transvenous route of treatment is preferred for indirect fistulas given greater safety and efficacy.
Summary/Conclusion
Carotid cavernous fistulas have long been treated with great efficacy utilizing an endovascular approach. The goal in the treatment of carotid cavernous fistulas is to occlude the fistula and avoid occlusion of parent vessels, notably the native internal carotid artery. Knowledge of the type of fistulous connection and severity of the symptoms will help make an appropriate treatment decision. Understanding alternative venous approaches may assist in difficult cases. Finally, novel approaches for the treatment of CCFs such as a percutaneous approach through the foramen ovale also may be considered if an endovascular approach or open surgical approach are not feasible options.

KEYWORDS: Carotid cavernous fistula, Treatment assessment

Note: Scanned images are included in the proceedings. Some submitted images were reduced during editing, thereby decreasing clarity. Also, refer to the Program Planner. Proceedings Content as of 3-29-2013.

EdE-67

Percutaneous Access of the Superior Ophthalmic Vein in the Treatment of Carotid Cavernous Fistulae

Scott, C. J.·Heran, M. K. S.·McNeill, G. J.
Vancouver General Hospital
Vancouver, BC, CANADA.

Purpose
To illustrate a safe percutaneous method of accessing the superior ophthalmic vein to treat carotid cavernous fistulae.
Approach/Methods
We present four cases of carotid cavernous fistulae treated via percutaneous superior ophthalmic venous (SOV) approach. Access was performed using sonographic guidance in two of the cases. In the other two, sonographic-guided puncture was difficult and access was achieved using biplane angiographic roadmap technique. In all four cases, a micropuncture (Cook Medical, Bloomington, IN) kit was used for access and the four French sheath of the kit used as a working sheath for microcatheter access. In all four cases, coil embolization was performed of the carotid cavernous fistula with satisfactory angiographic result at completion. There were no significant orbital bleeding complications.
Findings/Discussion
Venous access to the cavernous sinus in the treatment of carotid cavernous fistulae typically is performed from a femoral approach when there is a patent inferior petrosal sinus. In cases where this approach is not possible, the SOV is a well recognized alternative approach. Traditionally, access to the SOV is achieved via surgical exposure and cannulation or via external jugular venous approach to the facial venous system. We have found that percutaneous access to the SOV is a safe and less invasive alternative. If able to be visualized by ultrasound, this is our preferred approach. In two of the cases, the arterialized vein was difficult to puncture in the supra-orbital region. In these cases using a biplane roadmap technique, percutaneous access was still possible.
Summary/Conclusion
Percutaneous puncture of the superior ophthalmic vein offers a safe and less invasive alternative to surgical exposure in the treatment of the carotid cavernous fistulae that cannot be accessed via traditional transvenous approach.

KEYWORDS: Carotid cavernous fistula, Ultrasonography

EdE-68

Intra-Arterial Carotid Imaging with Optical Coherence Tomography

Bhojwani, N.·Blackham, K.
University Hospitals Case Medical Center
Cleveland, OH.

Purpose
Optical coherence tomography (OCT) has recently been gaining recognition for assessment of atherosclerosis and treatment planning in the carotid circulation. The purpose of this exhibit is to concisely explain the technology and describe the potential benefits of OCT intravascular imaging of the carotid arteries and even the intracranial circulation.
Approach/Methods
We will present a concise review of the relevant OCT literature and underlying principles of the technology extrapolated from use in coronary imaging. The neuroradiologist and neurointerventionalist can provide more detailed and accurate diagnoses owing to the technical advantages relative to other modalities which, in turn, more accurately guides proper treatment. Like any type of imaging, inherent pitfalls and artifacts are present. Images will be provided from neurointerventional cases.
Findings/Discussion
Multiple modalities exist for carotid artery imaging such as intravascular ultrasound, catheter angiography, MRI, and CT. However, optical coherence tomography (OCT) provides superior resolution imaging of luminal arterial anatomy. Optical coherence tomography provides tissue resolution of up to 10 microns and, in addition, allows tissue characterization capabilities of different types of plaque and thrombus such as discernment between red and white thrombus, between plaque and neointimal hyperplasia and delineation of atherosclerotic ulceration. Vessel geometry can be obtained and stent assessment performed. Future advances of the technology include functional assessment with contrast enhancement and molecular OCT. Detection of Doppler-like signals would permit physiologic measurement.
Summary/Conclusion
Neuroendovascular OCT is a relatively new application of a technology already employed in cardiac imaging. Because of the high resolution and characterization capabilities, this modality can provide unparalleled detailed carotid imaging allowing for accurate diagnoses and superior guidance of neuroendovascular treatment. Optical coherence tomography is an important modality to become familiar with, since the technology has potential to become more widely used in the near future.

KEYWORDS: Carotid artery, Carotid stenosis, optical coherence tomography

Note: Scanned images are included in the proceedings. Some submitted images were reduced during editing, thereby decreasing clarity. Also, refer to the Program Planner. Proceedings Content as of 3-29-2013.

EdE-69

Embolic Protection Devices during Carotid Artery Endovascular Intervention

Bhojwani, N.·Blackham, K.
University Hospitals Case Medical Center
Cleveland, OH.

Purpose
Periprocedural athero and thromboembolic events are common complications resulting from endovascular treatment of carotid occlusive disease. Preventing such complications can be aided with embolic protection devices (EPD) of several types: distal protection in the form of balloon occlusion or filter, and proximal protection in the form of circulatory control devices. The purpose of this exhibit is to concisely delineate the different mechanisms of protection, which are considered a required component of carotid stenting.
Approach/Methods
We will review the three types of embolic protection devices in regard to available models, methods of use, advantages and disadvantages, and reported complications. The evidence basis for the use of these devices from the literature also will be reviewed. Example neurointerventional cases will be showcased to demonstrate application of use.
Findings/Discussion
Embolic protection devices are mandated by the Center for Medicare and Medicaid services during carotid artery stenting (CAS) in order for proper reimbursement. This decision is based not upon large randomized trials but upon a wealth of observational data and pooled results of small studies resulting in a consensus among experts suggesting that embolic protection devices can reduce the risk of stroke during CAS. Complications of embolic protecton devices include vasospasm, ischemia, and infarct. Disadvantages include cerebral flow impedance, trauma to vessel intima, vasospasm, and particle escape. Each device indication depends upon the difficulty in crossing the lesion, complexity of preparation, and safety of deployment. All the current designs are limited by severely stenotic lesions, tortuous vessels, and contralateral lesions. While there is no perfect EPD that can prevent all neurologic complications, the choice of EPDs should depend on the patient's anatomy and the operator's comfort.
Summary/Conclusion
Multiple embolic protection devices exist to decrease complications during endovascular treatment of carotid atherosclerosis with carotid artery stenting. Each device poses varying advantages and indications. Device complications and limitations are inherent of all three types.

KEYWORDS: Carotid artery, Endovascular management

EdE-70

MR Imaging and CT Findings on Postintervention Imaging after Mechanical Thrombectomy for Acute Ischemic Stroke

Jones, J. G. A.·Rastogi, S.
University of California Los Angeles
Los Angeles, CA.

Purpose
Mechanical thrombolysis for acute ischemic stroke is becoming increasingly more common. At our institution, we routinely obtain postintervention CT and MRI of the brain to evaluate both the results of the treatment as well as its complications. Several interesting and clinically relevant findings may be appreciated on a detailed analysis of the postoperative imaging based on the degree of recanalization, timing of recanalization, and the findings on the preintervention imaging.
Approach/Methods
We reviewed our institutional stroke database over the past ten years to identify cases demonstrating both typical and atypical postintervention findings on MRI and CT and correlated them with clinical presentation, preoperative imaging, timing of recanalization, degree of recanalization and patient outcomes.
Findings/Discussion
We will review several examples of contrast staining on CT and correlate them with MRI to demonstrate the difficulty of differentiating contrast staining on postoperative CT versus hemorrhage. The clinical significance of distinguishing between iodinated contrast and acute blood cannot be understated. We also will review the imaging findings indicating persistent vascular occlusion and ischemia such as: intravascular FLAIR hyperintensity, arterial GRE hypointensity indicating persistent thrombus and venous GRE hypointensity indicating persistent maximum oxygen extraction from ischemic tissue. We also will review postintervention MR perfusion findings demonstrating infarction, ischemia and luxury reperfusion. Lastly, we will discuss and demonstrate examples of FLAIR CSF hyperintensity seen in some cases postmechanical intervention known as hyperattenuation acute reperfusion marker (HARM).
Summary/Conclusion
This exhibit will increase the familiarity of radiologists with typical and atypical findings on the postoperative imaging findings on CT and MRI after mechanical intervention.

KEYWORDS: Educational, Actue stroke

Note: Scanned images are included in the proceedings. Some submitted images were reduced during editing, thereby decreasing clarity. Also, refer to the Program Planner. Proceedings Content as of 3-29-2013.

Monday, May 20 – Wednesday, May 22
6:30 AM – 9:00 PM
Thursday, May 23
6:30 AM – 3:00 PM
Hall B1

Education Exhibits (EdE) 71 - 80

EdE5-Pediatrics

Note: A missing printed number indicates an abstract has been withdrawn.

EdE-71

Early MR Imaging Evaluation of Suspected Nonaccidental Brain Injury

Palasis, S.·Messner, S.·Hayes, L. L.·Grattan-Smith, D.
Children's Healthcare of Atlanta
Atlanta, GA.

Purpose
To illustrate the benefit of performing early brain and cervical spine MRI for improved diagnosis and timing of injury in suspected nonaccidental trauma.
Approach/Methods
We have implemented a new nonaccidental trauma (NAT) protocol in cases of suspected child abuse and brain injury. The protocol consists of routine spin-echo imaging sequences, DTI, SWI, and fat saturated c-spine imaging. The goal was to perform the NAT protocol as soon as possible after arrival of the child to the emergency department and then perform a follow-up MRI within 10 days.
Findings/Discussion
The detection of nonaccidental brain injury rests heavily on neuroimaging. The recommendation of the American College of Radiology (ACR) and the American Academy of Pediatrics (AAP) has been to reserve early brain MRI for cases where the CT is abnormal or when abnormal neurologic findings are present and to perform cervical spine MRI only if there are clinical findings to suggest injury. Neurologic symptoms of trauma are not always readily obvious in the neonate/young infant and CT is often nonrevealing. The advent of new sensitive MR techniques have remarkably improved the sensitivity of MRI to early intracranial injury. We have found that MRI also can be useful in grossly estimating the timing of injury, mainly through detection of acute neuronal injury and delayed secondary neuronal injury using DTI. The identification of soft tissue edema in the cervical spine can refocus the imaging differential to trauma if the intracranial findings are indeterminate or in dispute.
Summary/Conclusion
We have found that the NAT protocol now being utilized at our institution has added new imaging information that is useful for detection of early intracranial injury and has helped with more accurate timing of the insult. Our exhibit will illustrate our experience since the implementation of this new protocol.

KEYWORDS: Pediatric brain, Traumatic brain injury, Child abuse

EdE-73

Revisiting Arachnoid Cyst: Atypical Imaging Findings, Unusual Presentation and Rare Complications

Ramakrishnaiah, R.·Schultz, K.·Samant, R.·Fitzgerald, R.·Burgin, K.·Hegde, S.·Van Hemert, R.·Angtuaco, E.
University of Arkansas for Medical Sciences
Little Rock, AR.

Purpose
Arachnoid cysts are common intracranial space-occupying lesions which are diagnosed incidentally on imaging studies. Arachnoid cysts typically present as extra-axial thin-walled cystic lesions which follow CSF signal intensity on all MRI sequences. Atypical presentation and complications of arachnoid cysts are relatively uncommon. The purpose of this scientific exhibit is to provide a pictorial review and discussion of unusual presentation and complications of arachnoid cysts in children.
Approach/Methods
Imaging studies of arachnoid cysts in children with unusual presentation or rare complications that having clinical significance and educational value will be selected from the extensive database of a tertiary care pediatric hospital over a period of eight years (2004 to 2012).
Findings/Discussion
A detailed pictorial review using high-resolution images and a brief discussion will be displayed under the following headings: 1. Complication and spontaneous variation of imaging characteristics: Rapid growth, spontaneous rupture, intracystic hemorrhage, spontaneous focal meningeal enhancement, subdural hygroma, raised intracranial pressure, obstructive hydrocephalus, encephalomalacia and significant bone remodeling occurring in association with arachnoid cysts. 2. Arachnoid cysts associated with other brain and spine lesions: schizencephaly, corpus callosal agenesis, Chiari I malformation, absent septum pellucidum, optic nerve hypoplasia, and multiple lateral spinal meningoceles. 3. Unusual location: Cyst of liliequist membrane, intraventricular cysts within the lateral, third and fourth ventricles, superior cerebellar cistern, ambient cistern, velum interpositum, septum pellucidum and spinal arachnoid cysts. 4. Miscellaneous: fetal arachnoid cyst, post-fenestration recurrence and arachnoid cyst CSF

Note: Scanned images are included in the proceedings. Some submitted images were reduced during editing, thereby decreasing clarity. Also, refer to the Program Planner. Proceedings Content as of 3-29-2013.

dynamics. 5. Differential diagnosis and cystic lesions mimicking arachnoid cyst.
Summary/Conclusion
Arachnoid cysts are common space-occupying lesions encountered in neuroimaging practice. Atypical presentation and complications of arachnoid cysts are relatively uncommon. But, a strong knowledge of rare and atypical imaging features of a common disease entity is necessary for accurate diagnosis, avoid potential pitfall, preempt unforeseen complication and improves patient management.

KEYWORDS: Arachnoid cyst, Complications, unusual presentation

EdE-74

Embryology and Imaging of Developmental Maxillofacial Anomalies: A Pictorial Review

Ramakrishnaiah, R. H.·Honnebier, B.·Kumar, M.·Samant, R.·Hegde, S.·Fitzgerald, R.·Van Hemert, R.·Angtuaco, E.
University of Arkansas for Medical Sciences
Little Rock, AR.

Purpose
Congenital maxillofacial anomalies are associated with a variety of syndromes that are encountered not infrequently in clinical practice. Imaging of those anomalies using high-resolution maxillofacial CT scan plays a key role in characterization of different bony dysplasia and in presurgical planning. The purpose of this scientific exhibit is to provide a pictorial review of embryogenesis of facial bones with brief discussion of various syndromes associated with maxillofacial anomalies and their associated imaging findings as well as imaging findings of isolated and syndromic maxiollofacial anomalies in children.
Approach/ Methods
Imaging studies of children with maxillofacial anomalies will be reviewed retrospectively and through an extensive data base search of a tertiary care pediatric hospital. All children were referred for imaging by the maxillofacial surgery division for presurgical assessment.
Findings/Discussion
A pictorial review would include a brief description of relevant embryology followed by a detailed description of characteristic imaging features. The imaging findings will be discussed with high-resolution multiplanar CT and MRI images. The following syndromes with maxillofacial anomalies and nonsyndromic isolated maxillofacial anomalies will be discussed: Nager syndrome, Pierre Robin syndrome, Parry-Romberg, Pfeiffer syndrome, Treacher Collins syndrome, Crouzon syndrome, Gorlin syndrome, Apert syndrome, external auditory canal atresia, maxillary hypoplasia, bilateral cleft lip, congenital facial defect, mandibular anomalies, hemifacial hypoplasia, dentofacial functional abnormalities, anodontia, hemifacial microsomia, microtia, choanal atresia, anopthalmia, and solitary central maxillary incisor syndrome.

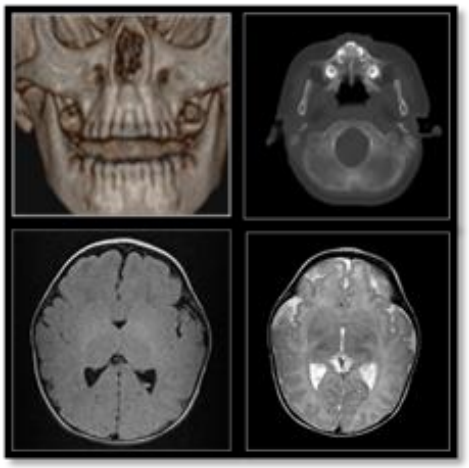

Figure: Patient with solitary midline maxillary incisor with an azygous anterior cerebral artery and lobar holoprosencephaly.
Summary/Conclusion
Maxillofacial anomalies are not infrequently encountered in neuroimaging practice. Knowledge of the different syndromes and their associated imaging findings is important for accurate assessment and better surgical planning and outcome for the patients.

KEYWORDS: Congenital anomalies, Face, syndromic maxillofacial anomaly

EdE-75

Thrombosis of Developmental Venous Abnormalities: Case Series and Review

Baradaran, H.·Tsiouris, A. J.
Weill Cornell Medical College
New York, NY.

Purpose
Developmental venous anomalies (DVA) are one of the most commonly encountered vascular malformations with an overall incidence of 2-4% of the population. While they are usually asymptomatic and incidental findings, rare complications are possible such as hemorrhage, nonhemorrhagic ischemia, or thrombosis of a draining vein. Thrombosis of a draining vein is very rare with less than 30 cases reported in the literature. Here, we present five cases of thrombosis of a draining vein in symptomatic pediatric patients.
Approach/Methods
A literature search of cases of thrombosis of developmental venous abnormalities was performed and relevant case reports were reviewed. The clinical histories and representative imaging findings for the five patients seen at our institution were reviewed. All five patients had MRI examinations. Of the five patients, one had a thrombosed DVA in the posterior fossa, two in the temporal lobe, and two in the frontal lobe.

Note: Scanned images are included in the proceedings. Some submitted images were reduced during editing, thereby decreasing clarity. Also, refer to the Program Planner. Proceedings Content as of 3-29-2013.

Findings/Discussion
We have five pediatric patients with complete or partial thrombosis of a draining vein in a DVA. The most severe case involved a large DVA in the left temporal lobe of a 12-year-old male. In this patient, there is a large collecting vein with intraluminal T1 hyperintensity, T2 hypointensity, and blooming artifact on susceptibility-weighted images with surrounding vascular structures consistent with thrombosis of a collecting vein of a large DVA. While this was the most obvious case, there were several other more subtle cases which demonstrated similar findings with areas of T2 hypointensity, T1 hyperintensity with blooming artifact on susceptibility-weighted images. In one case, the thrombus itself is not seen but an area of hemorrhagic infarction is seen with adjacent small enhancing vessels thought to be a DVA, so thrombosis of a draining vein was suspected.
Summary/Conclusion
The ability to recognize thrombosis of developmental venous anomalies is essential for appropriate treatment of symptomatic pediatric patients. When abnormalities do not conform to a vascular territory, thrombosis of DVA should be on the differential and should not be mistaken for a mass lesion. Recognizing these findings is essential to ensure appropriate treatment is initiated and further venous infarction is prevented if possible.

KEYWORDS: Developmental venous anomalies, Thrombosis

EdE-76

"What Lies Beneath": A Multimodality Approach to Imaging Congenital Spine Pathology Underlying Lumbosacral Cutaneous Lesions

Fox, L.·Li, S.
Baystate Medical Center
Springfield, MA.

Purpose
Children are commonly referred for imaging when a skin lesion is discovered in the lumbosacral region on physical examination because of the concern for underlying spinal malformations. The association exists because both skin and nervous tissue originate from ectoderm. The purpose of this exhibit is to review the imaging findings of congenital anomalies underlying midline lumbosacral cutaneous lesions (sacral dimple, skin tag, hypertrichosis) in multiple modalities.
Approach/Methods
1. Review of the normal lumbosacral spinal anatomy. 2. Describe the CT, ultrasound, MR, and plain film characteristics of congenital anomalies associated with lumbosacral skin lesions.
Findings/Discussion
Cases will be presented to illustrate imaging features of a broad array of disease entities including tethered cord, diastometomyelia, lipoma, dermal sinus, sacral agenesis, lumbar teratoma, etc. Relevant epidemiology, pathogenesis and clinical features will be discussed.

Summary/Conclusion
A knowledge and understanding of the various congenital spinal diseases affecting the pediatric patient will aid the radiologist in making appropriate and timely diagnoses. At the end of this presentation, the viewer should be familiar with the characteristic clinical and imaging features, epidemiology and pathogenesis of a variety of lumbosacral congenital malformations related to overlying cutaneous abnormalities.

KEYWORDS: Congenital anomalies, Lumbar spine

EdE-77

Imaging Manifestations of Uncommon Variants of Astrocytoma in Children

Stein, J. M.[1,2]·Santi, M.[1]·Vossough, A.[1]·Zimmerman, R. A.[1]·Feygin, T.[1]
[1]Children's Hospital of Philadelphia, Philadelphia, PA,
[2]Hospital of the University of Pennsylvania, Philadelphia, PA.

Purpose
The purpose of this presentation is to review uncommon imaging manifestations of astrocytoma in children.
Approach/Methods
We present a pictorial review of uncommon imaging manifestations of astrocytoma in children organized by several distinct locations: the cerebral hemispheres, the ventricles, the pineal region, the posterior fossa and the brainstem. Cases were obtained based on keyword searches of the radiology report database at our institution. Cases presented include MR images obtained at 1.5 or 3T, CT images, and pathologic correlation. Unusual imaging features in each location are identified. Highlights of this review include two cases of infantile astrocytomas with extensive leptomeningeal spread and multicystic involvement of the cerebral hemispheres mimicking congenital developmental anomaly or cerebral infarction, gliomatosis cerebri mimicking cortical dysplasia or inflammatory demyelination, exophytic astrocytoma at the cerebellopontine angle mimicking medulloblastoma or atypical teratoid-rhabdoid tumor, and exophytic brainstem

Note: Scanned images are included in the proceedings. Some submitted images were reduced during editing, thereby decreasing clarity. Also, refer to the Program Planner. Proceedings Content as of 3-29-2013.

astrocytoma mimicking ependymoma.
Findings/Discussion
Astrocytoma represents the most common type of primary central nervous system neoplasm in children and adults. Unusual manifestations of astrocytoma can mimic the typical appearances of more rare tumor types. A cystic appearance is a commonly recognized manifestation of pilocytic astrocytomas and pleomorphic xanthoastrocytomas. Infantile astrocytomas can have such an extensive infiltrative multicystic appearance that they may mimic developmental anomalies and infarct. Tumors that appear extra-axial, particularly in the posterior fossa, can represent exophytic astrocytomas. In our experience, high-resolution imaging sequences such as constructive interference in steady state (CISS) obtained in multiple planes can be helpful in identifying an attachement site to the adjacent cerebellar hemisphere or brainstem in these cases.
Summary/Conclusion
Astroctyomas can have diverse and unusual imaging manifestations and mimic more rare tumors. Imagers should be aware of these unusual manifestations, and astrocytoma should almost always be considered in the differential diagnosis of neoplasms at most intracranial locations in children.

KEYWORDS: Pediatric neoplasms, Astrocytoma

EdE-78

Pediatric Pineal Lesions: A Pictorial Review

Fang, A.·Meyers, S.
University of Rochester Medical Center
Rochester, NY.

Purpose
Pineal tumors are relatively rare tumors of the central nervous system and account for 3-8% of intracranial neoplasms in the pediatric population. The purpose of this educational poster is to highlight the anatomy and embryology of the pineal gland, as well as the pathology and characteristic imaging features of pineal lesions in pediatric patients.
Approach/Methods
A variety of pineal lesions will be presented illustrating their unique histology and imaging appearance on computed tomography (CT) and magnetic resonance imaging (MRI).
Findings/Discussion
This educational exhibit will discuss the differential of pineal region lesions including pineal parenchymal tumors, germ cell tumors, metastasis, and other pineal region masses arising from cell types adjacent to the pineal gland. The clinical and pathologic features of pineal lesions will be described. For each pineal region mass of varying origin, the unique imaging characteristics will be illustrated. A brief review of the therapeutic management of pineal lesions will be provided.
Summary/Conclusion
Lesions of the pineal gland can represent a variety of benign and malignant disease conditions. Knowledge of the clinical and pathologic features, and unique imaging characteristics of varying lesions, can assist in refining the differential diagnosis and help optimize patient treatment.

KEYWORDS: Pineal gland

EdE-79

MR Imaging Assessment of Cerebospinal Fluid Hydrodynamics with a Specific Focus on Children with Hydrocephalus

Hassan, E.·Cain, J.·Stivaros, S. M.
University of Manchester
Manchester, UNITED KINGDOM.

Purpose
There is much that we do not understand with regards to the pathophysiology of pediatric hydrocephalus. As a consequence our current clinical radiologic techniques for the assessment of hydrocephalus, such as the measurement of ventricular size/indices or the subjective assessment of cine phase contrast MRI, can be found lacking. Recent developments in advanced MRI-based perfusion and flow quantification techniques, such as phase contrast MRI (PCMRI) can be used to further our understanding of cerebrospinal fluid (CSF) flow in both normal and pathophysiologic states. These techniques are vital if we are to further our understanding of this disease process.
Approach/Methods
The exhibit will describe the prevalence and current understanding of the pathophysiology of pediatric hydrocephalus including a review of the literature on CSF pulsewave encephalopathy. We will provide a summary of current treatment and monitoring options as well as the current routine use of MRI in pediatric hydrocephalus diagnosis and assessment. In addition we will include an overview of the more advanced noninvasive MRI methodologies which have applications in CSF flow research, namely quantitative PCMRI. There with be an emphasis on the role of these techniques in the quantitative assessment of cerebral hemo/hydro dynamics, which can provide unique information regarding CSF flow in a variety of pathologic processes such as hydrocephalus. The exhibit also will cover the use of PCMRI in the premorbid and post-treatment assessment of third ventriculostomy for the management of children and adults with hydrocephalus.
Findings/Discussion
In order to develop an advanced understanding of CSF flow in children, comprehension must be gained about the complex physiologic mechanisms that exist in cerebral hydrodynamics. Using methodologies such as quantitative PCMRI, radiologic research is challenging some of the classical assumptions regarding CSF production and

absorption in children as well as adults. For example it has been postulated that some of the secretion of CSF must arise from the capillary bed through passive filtration, as the choroid plexus is unable to supply all of the fluid required to replace all of the CSF. In addition we are beginning to understand that CSF absorption may not in fact predominate across the arachnoid granulations, but be a process akin to the absorption of plasma filtrate through the subarachnoid capillaries.
Summary/Conclusion
Quantitative MRI methodologies now allow clinicians and researchers the ability to manage children more efficiently, with fewer invasive procedures. These methodologies also may be able to answer fundamental questions about the effect of hydrocephalus on cerebral perfusion. This exhibit will provide a summary of these methodologies and how they can be used in current clinical and research applications. In addition it is intended that this educational exhibit will provide the reader with the information necessary to guide them towards undertaking such imaging in both the clinical and academic settings, in what is undoubtedly an exciting clinical domain.

KEYWORDS: Hydrocephalus, Phase contrast imaging

EdE-80

Vascular Anomalies of the Head and Neck in Patients with Velocardiofacial Syndrome

Nayyar, R.·Das, K.·Nayyar, S.·Tatum, S. A.·Marrinan, E. M.·Swarnkar, A. S.
SUNY Upstate
Syracuse, NY.

Purpose
The purpose of our exhibit is to demonstrate the head and neck vascular abnormalities in patients with velo-cardio-facial syndrome (VCFS) and the importance to recognize these abnormalities for surgical planning. Our study is a review of 50 patients with velo-cardio-facial syndrome, with both a radiologists' perspective and otolaryngologists' perspective of the importance of these vascular abnormalities.
Approach/Methods
This is an IRB-approved, retrospective study of 50 patients with VCFS who underwent a MRA of the brain and neck.
Findings/Discussion
The study is currently ongoing; however, preliminary data demonstrates significant abnormalities of the carotid and vertebral arteries on the MRA examination. Medial displacement of the internal carotids, low carotid bifurcations, hypoplastic vertebral arteries, and tortuous or kinked internal carotids were common anomalies. The vascular abnormalities influence the surgical approach. Our discussion section will include images of these anomalies as well as a table tabulating the different anomalies. We also will have an otolaryngologist describe how these anomalies change his surgical approach and the importance of preoperative MRA examinations.
Summary/Conclusion
In summary, we will present and demonstrate the most common vascular abnormalities in patients with VCFS. The study is currently ongoing; however, preliminary data demonstrates a high percentage of an anomalous course of the internal carotid arteries. This presents a major risk for pharyngeal flap surgery. Our exhibit will demonstrate the importance of preoperative MRA examination for detecting these anomalies from both a radiologists and facial plastic surgeon's perspective.

KEYWORDS: Anatomical variation, Internal carotid artery, velo-cardio-facial syndrome (VCFS)

Monday, May 20 – Wednesday, May 22
6:30 AM – 9:00 PM
Thursday, May 23
6:30 AM – 3:00 PM
Hall B1

Education Exhibits (EdE) 81 - 82

EdE6-Socioeconomics

Note: A missing printed number indicates an abstract has been withdrawn.

EdE-81

Diagnostic Carotid Angiography CPT Codes Have Been Revised, and You Will Be Reimbursed Less: Why, How, and How Much

Donovan, W. D.[1]·Nicola, G. N.[2]·Bello, J. A.[3,4]·Hirsch, J. A.[5,6]·Tu, R. K.[7]·Morrow, M. J.[8]
[1]William W. Backus Hospital, Norwich, CT, [2]Hackensack University Medical Center, Hackensack, NJ, [3]Albert Einstein College of Medicine, The Bronx, NY, [4]Montefiore Medical Center, The Bronx, NY, [5]Massachusetts General Hospital, Boston, MA, [6]Harvard Medical School, Boston, MA, [7]Progressive Radiology, Washington, DC, [8]ASNR, Oak Brook, IL.

Purpose
Discuss why the cervicocerebral catheter angiography set came to be revised. Estimate the reimbursement impact of the carotid angiography code set revision and new valuation.
Approach/Methods
Review the CPT-RUC system that identified the carotid

Note: Scanned images are included in the proceedings. Some submitted images were reduced during editing, thereby decreasing clarity. Also, refer to the Program Planner. Proceedings Content as of 3-29-2013.

angiography codes as "potentially misvalued." (CPT = Current Procedural Terminology; RUC = Relative Value Scale Update Committee). Review the component coding scheme that previously described some typical carotid angiography procedures. Enumerate the new code structure. Describe the valuation process for the new codes: RUC review, CMS Final Rule. (CMS = Centers for Medicare and Medicaid Services, or Medicare).
Findings/Discussion
The component coding structure for reporting interventional procedures has been formally in place since 1992, with the advent of the RBRVS (Resource-Based Relative Value Scale). This system allowed detailed identification of a catheter angiography procedure by means of specific CPT codes for purposes of billing, research, resource allocation. Over the past few years, component coding has been increasingly marginalized through the concerted efforts of CMS, the RUC, and its subcommittee, the RAW (Relativity Assessment Workgroup). These efforts were rationalized as a means to achieve "efficiencies" in procedural reimbursement. Numerous radiologic supervision and interpretation (S&I) codes were identified as "potentially misvalued" through the "codes performed together" screen created by CMS. Creation of bundled codes was "recommended" through a joint CPT/RUC workgroup -- without workable alternatives. ASNR CPT physicians and staff participated in the creation of the new bundled code set. ASNR RUC physicians and staff participated in the RVU (relative value unit) valuation of the new code set. The RUC recommended values less than the involved societies requested; CMS decided to decrease those values further. The new codes are described, highlighting the changes from the previous system. Estimates of the RVU value and professional reimbursement for several representative cervicocerebral procedures will be provided.
Summary/Conclusion
Radiology societies have been compelled by CMS to rework component codes into bundled code sets. This has typically resulted in a decrease in RVU value, and the new carotid angiography codes are no exception. At abstract deadline, we estimate that the professional reimbursement for a typical carotid or vertebral diagnostic angiography procedure will be reimbursed 10-40% less than in 2012. Once CMS reimbursement policy is finalized for 2013, more
specific estimates of expected revenue decrease will be generated.

KEYWORDS: Medicare, Carotid angiography, vertebral angiography

EdE-82

ASNR at the RUC: A Case Study in Devaluation

Donovan, W. D.[1]·Barr, R. M.[2]·Silva, E.[3]·McGinty, G.[4]
[1]William W. Backus Hospital, Norwich, CT, [2]Mecklenburg Radiology, Charlotte, NC, [3]South Texas Radiology Group, San Antonio, TX, [4]NRAD Medical Imaging, Garden City, NY.

Purpose
Describe the Medicare RBRVS (Resource-Based Relative Value Scale) valuation process, using the complex example of recent revaluation of spine CT.
Approach/Methods
Review the mechanics of the RBRVS and the RUC (AMA/Specialty Society RVS Update Committee). Describe Medicare's recent attempts to target radiology CPT (Current Procedural Technology) code valuations, including the actions of the RAW (Relativity Assessment Workgroup). Using spine CT as an example, review ASNR's involvement in the identification of particular codes for review and preparation of RUC survey results for the thrice-yearly RUC meetings. Describe the process whereby RUC recommendations are assessed and sent to CMS (Centers for Medicare and Medicaid Services), and judged for the Final Rule. Describe the appeal process, and ultimate result.
Findings/Discussion
Spine CT represents a comprehensive example of the convoluted system for CMS reimbursement decisions. Cervical and lumbar spine CT exams were identified by the RAW as "potentially misvalued," meeting criteria as one of the "fastest-growing" procedures in the RUC database. Interested societies (including ASNR and ACR) were invited to present recommendations to the RUC as to the appropriate valuation of these procedures. ASNR and ACR conducted random surveys of their membership for the October 2009 RUC meeting. The societies recommended an increase in the then-extent RVU (Relative Value Unit) values of these procedures (as well as for thoracic spine CT); those RVU values dated back to the institution of the RBRVS in 1992. After vigorous discussion, the RUC recommended maintenance of the existing values. CMS disagreed with the decision of the RUC, and published a decrease in the RVU values of these procedures in the Final Rule. Radiology appealed the decision, which went to a CMS Refinement Panel for adjudication. This resulted in an increase in the RVU value for cervical spine, but not for thoracic or lumbar, instituted for the 2012 calendar year.
Summary/Conclusion
In recent years, CMS has pursued several strategies to decrease radiologists' reimbursement. Identification of "potentially misvalued" services is one method; interested societies are compelled to expend resources and ASNR physician volunteers' free time to seek appropriate valuations for the services its members provide. Even in the case of a straightforward diagnostic procedure, the elaborate system by which Medicare assigns RVUs to individual CPT codes can confound the hardiest payment

Note: Scanned images are included in the proceedings. Some submitted images were reduced during editing, thereby decreasing clarity. Also, refer to the Program Planner. Proceedings Content as of 3-29-2013.

policy veterans. The RUC survey process is the fundamental keystone of ASNR's efforts to achieve satisfactory valuation for the services its members provide.

KEYWORDS: Medicare, Overutilization, payment policy

Monday, May 20 – Wednesday, May 22
6:30 AM – 9:00 PM
Thursday, May 23
6:30 AM – 3:00 PM
Hall B1

Education Exhibits (EdE) 83 - 92

EdE7-Spine

Note: A missing printed number indicates an abstract has been withdrawn.

EdE-83

Tuberculous Spondylitis: A Pictorial Review of CT and MR Imaging Findings

Fukutomi, H.[1]·Okada, T.[1]·Oshima, S.[1]·Akasaka, T.[2]·Maekura, T.[1]·Koyama, T.[1]·Shiozaki, T.[1]·Todo, G.[1]·Tomihara, M.[1]
[1]Osaka Red Cross Hospital, Osaka, JAPAN, [2]Kishiwada City Hospital, Osaka, JAPAN.

Purpose
Tuberculous spondylitis requires early treatment since it causes severe deformation of the spine at advanced stages. Understanding of the typical findings of tuberculous spondylitis is clinically important, because the necessary antibiotic differs from pyogenic spondylitis. The purpose of this educational exhibit is to review computed tomography (CT) and magnetic resonance (MR) imaging findings of tuberculous spondylitis.
Approach/Methods
We retrospectively reviewed MR images of eight patients with tuberculous spondylitis (age: 42-88 years, mean: 69 years, five male and three female) diagnosed between 2005 and 2012 in our hospital. CT scans and MRI scans at 1.5T were performed in all patients. T2- and T1-weighted images, STIR (short-TI Inversion Recovery) images, pre and postcontrast fat-suppressed T1-weighted images were obtained.
Findings/Discussion
The etiology of tuberculous spondylitis is hematogenous or lymphatic spread from a pulmonary origin. The initial inoculum usually is located in one of the anterior vertebral bodies. The lesion spreads underneath the longitudinal ligament to adjacent vertebral bodies and more than three consecutive vertebral bodies often are affected (Figure 1). The intervertebral disks often are spared as mycobacterium tuberculosis does not have proteolytic enzymes. Congestion abscess and gravitation abscess are often observed (Figure 2). These abscesses are marked and progress far from the primary lesion, destroying vertebral bodies and presenting with severe symptoms. Calcifications and skip lesions often are observed. The clinical course often is longer than pyogenic spondylitis.

figure1

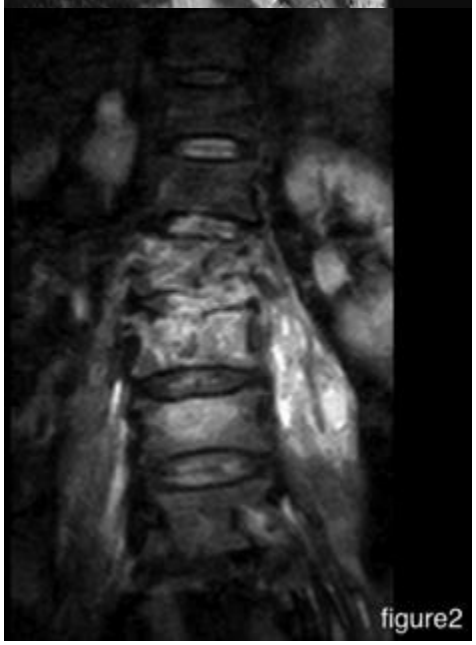
figure2

Summary/Conclusion
Awareness of the disease process and knowledge of the characteristic imaging findings of tuberculous spondylitis

are necessary in order to provide early appropriate treatment and prevent kyphosis.

KEYWORDS: Tuberculosis, Spondylitis

EdE-84

Facet Synovial Cyst Imaging Characteristics and Treatment

Cambron, S. C.·Guerin, S. J.·Pastel, D. A.
Dartmouth Hitchock Medical Center
Lebanon, NH.

Purpose
Lumbar facet synovial cyst formation is an important cause of treatable radiculopathy. Our aim is to present the imaging characteristics of spinal synovial facet cysts with MRI, CT, and CT myelogram. We also will review minimally invasive image-guided intervention of synovial cysts.
Approach/Methods
The imaging characteristics and location of facet synovial cysts of patients that underwent intervention at our institution from 2005-2012 will be reviewed retrospectively.
Findings/Discussion
Over 148 patients have been treated for lumbar synovial cysts at our institution with 199 facet cysts percutaneously. Of these patients, 110 had MR imaging available for review. Images demonstrating the anatomy and variable imaging characteristics of facet cysts on MRI, CT, and CT myelogram will be reviewed including examples of foraminal, lateral recess, central canal and bilateral cysts. Percutaneous treatment options and methods will be illustrated including CT-guided facet joint access and direct access to the synovial cyst with cyst rupture. The appearance of successful rupture also will be demonstrated.
Summary/Conclusion
Lumbar synovial formation is an important cause of treatable radiculopathy. With an understanding of the relevant anatomy and imaging characteristics of synovial cysts they can be successfully diagnosed and treated percutaneously.

KEYWORDS: Facet, CT guidance, synovial cyst

EdE-85

Radiofrequency Ablation of Spinal Metastases

Friedman, J.·Whittemore, A.·Chason, D. P.
University of Texas Southwestern Medical School
Dallas, TX.

Purpose
Spinal metastases are the most common site of osseous metastatic disease with a high incidence among patients with multiple different primary cancers. Treatment is aimed primarily at palliation with the primary goals of durable pain relief and amelioration of pain-related disability. Treatment options for spinal metastases include external beam radiation, chemotherapy, surgery and minimally invasive percutaneous techniques such as radiofrequency ablation.
Approach/Methods
This educational exhibit will serve as a tutorial for fellows and residents to learn how to perform percutaneous RFA of spinal metastatic lesions. The exhibit will discuss basic concepts of RFA as well as highlight newer techniques focused on single needle access that can be done in conjunction with biopsy and/or vertebroplasty.
Findings/Discussion
Learning points: 1. Identify criteria for patient selection, including indications and contraindications for RFA of spinal metastases, based on both clinical data and imaging studies. 2. Illustrate needle placements and approaches used to perform percutaneous RFA of spinal metastases. 3. Discuss the underlying thermal properties of RFA and how to utilize and monitor RFA probes to treat spinal metastases and minimize the risks of thermal injuries. 4. Describe newer devices, including navigational osteotomes and steerable RFA devices, that allow for a single needle approach and integration of concurrent biopsy and/or vertebral body augmentation.
Summary/Conclusion
Awareness of percutaneous RFA will allow training neuroradiologists to expand their services to include palliation of painful metastatic lesions.

KEYWORDS: Spinal instumentation, Spine interventions, spinal metastases

EdE-86

Value of the Epidurogram in Epidural Steroid Injections

Ortiz, A.
Winthrop University Hospital
Mineola, NY.

Purpose
To reinforce the importance of the epidurogram during the performance of lumbar epidural steroid injections.
Approach/Methods
Epidurograms from various lumbar epidural steroid injection procedures performed either through the interlaminar, transforaminal or caudal approaches are reviewed and used to demonstrate the importance of correlating the contrast distribution pattern with the patients' clinical presentation and history, as well as their therapeutic response to the procedure.
Findings/Discussion
The epidurogram should be used not only to confirm the location of the spinal needle tip within the spinal epidural space, but also to estimate the subsequent potential spread of injectate within the epidural space. Clinical scenarios are often encountered in which the distribution of contrast agent within the epidural space may be altered

Note: Scanned images are included in the proceedings. Some submitted images were reduced during editing, thereby decreasing clarity. Also, refer to the Program Planner. Proceedings Content as of 3-29-2013.

or confined due either to anatomical variation within the epidural space or to alteration of the epidural space by conditions such as lumbar stenosis, exit foramen stenosis, epidural adhesions and prior surgical interventions such as laminectomy or fusion. In these situations, the epidurogram should be evaluated carefully in order to ascertain the probable epidural spread of the subsequent injectate. Furthermore, the epidurogram may raise the possibility of a need for an alternative approach to access the area that correlates with the side and level of a patient's symptomatic presentation. Lastly, the epidurogram may explain why certain approaches result in symptomatic improvement, while other approaches may be associated with treatment failure.
Summary/Conclusion
A properly performed and analyzed epidurogram may facilitate improved patient outcomes following lumbar epidural steroid injection.

KEYWORDS: Epidural space, Anatomy

EdE-87

Notochord: Embryologic Anatomy and Notochord Derived Lesions

Patil, A. A.·Singh, J.·Kocak, M.·Jhaveri, M.·Bhabad, S.·Bachhav, V.
Rush University and Medical Center
Chicago, IL.

Purpose
The lesions of the notochord encompass a spectrum from notochord remnants, benign notochord tumor to aggressive lesions. Imaging plays an important role in lesion characterization and differentiating benign from malignant lesions. The aim of this exhibit is to illustrate the embryology of notochord, spectrum of malignant as well as benign notochord lesions, and anatomical variants.
Approach/Methods
A. Introduction. B. To review the embryologic anatomy of notochord using schematic illustration and CT/MR images. C. To review the imaging features of notochord derived lesions: 1. Clival chordoma, 2. Sacral chordoma, 3. Nasopharyngeal chordoma, 4. Benign notochordal cell tumors (BNCT), 5. Echordosis physilaphora. 6. Thornwaldt cyst, 7. Canalis basalis medianus, 8. Fossa navicularis magna.
Findings/Discussion
Notochord-derived lesions are interesting in terms of their typical location, imaging characteristics, clinical presentation and progression. Benign notochord lesions can be confused for more aggressive lesions.
Summary/Conclusion
An understanding of their typical radiologic appearance, expected location can help avoid unnecessary radiologic investigations and intervention.

KEYWORDS: Embryology, Anatomy, notochord lesions

EdE-88

Pediatric Spine Pathology Revealed with Readout Segmented EPI Diffusion Tensor Imaging

Hayes, L. L.[1]·Jones, R.[1,2]·Palasis, S.[1]·Grattan-Smith, D.[1]
[1]Children's Healthcare of Atlanta at Scottish Rite, Atlanta, GA, [2]Emory University, Atlanta, GA.

Purpose
To illustrate the utility (RS) EPI as a method for diffusion imaging of the spine to detect spinal pathology in pediatric patients.
Approach/Methods
Readout segmented DTI was performed on a 1.5T Avanto and a 3T Trio scanner with seven segments, a parallel imaging factor of 2, a b factor of 500 s/mm^2 and an in-plane resolution of 1.25 mm^2. The b factor was chosen to be lower than that used for studies of the brain to compensate for reduced SNR due to the smaller voxel dimensions used in this study and for a reasonable acquisition time of approximately five min. A sagittal slice orientation was chosen as it allows an entire section of the spine to be assessed with a single acquisition. In our initial studies of the C-spine, we evaluated both gated and nongated versions of the sequence but found that motion/pulsatility produced unacceptable artifacts in some subjects when gating was not used. Gating was used therefore for all subsequent studies. For the C-spine, a single slice was acquired on every third heartbeat and a delay for the peripheral trigger of approximately one third of the cardiac cycle was used. Gating was not used for the T or L spine. This sequence was added to standard protocols for imaging pediatric spines in various pathologic conditions, including drop metastases, spinal cord infarction, epidural abscesses, paraspinal neuroblastoma, bone metastases, and epidermoid cysts.
Findings/Discussion
(RS) EPI produced excellent image quality, nearly free from the artifacts plaguing other types of diffusion imaging of the spine. Traditional artifacts from the surrounding bone and motion of CSF, breathing, and arterial pulsations were drastically reduced, providing good spatial resolution and strong signal, thereby allowing identification of drop metastases from brain tumors such as medulloblastoma and germ cell tumors, some of which were not apparent on T1- and T2-weighted images. Additionally, diffusion-weighted imaging (DWI) was helpful in diagnosing spinal cord infarction, allowing differentiation from bland cord edema. It also was useful in defining the extent of epidural abscesses and helped distinguish them from other epidural collections. Additionally, DWI assisted in defining the margins of paraspinal neuroblastoma and detecting bony involvement. Furthermore, restricted diffusion within a cyst essentially clinched the diagnosis of an epidermoid.
Summary/Conclusion
(RS) EPI is a powerful method for diffusion imaging of the spine. Images presented in this exhibit demonstrate that this technique is exquisitely helpful in the workup of

Note: Scanned images are included in the proceedings. Some submitted images were reduced during editing, thereby decreasing clarity. Also, refer to the Program Planner. Proceedings Content as of 3-29-2013.

numerous pathologic conditions of the spine affecting children, including tumor, infarction, and infection.

KEYWORDS: Diffusion MR imaging, Pediatric spine

EdE-89

Spinal Extradural Fistula: A Pictorial Review

Chen, D.·Kuo, Y.·Kung, K.·Chen, C.
Taipei Medical University/Shuang Ho Hospital
Taipei, TAIWAN.

Purpose
Spinal extradural arteriovenous fistulas (AVFs) are rare conditions. They are characterized by the presence of an arteriovenous communication, localized to the paraspinal soft tissues and the epidural venous plexus. Rangel-Castilla et al divided spinal extradural AVFs into three types based on venous drainage pattern and clinical presentation. In Type A spinal extradural AVFs, arteriovenous shunting occurs in the epidural space and these types have an intradural draining vein causing venous hypertension and spinal cord edema with associated myelopathy or cauda equina syndrome. Type B1 malformations are confined to the epidural space with no intradural draining vein, causing compression of the spinal cord and/or nerve roots with myelopathy and/or radiculopathy. Type B2 malformations also are confined to the epidural space with no intradural draining vein and no mass effect, and are asymptomatic. The author aims to introduce these rare conditions with case demonstration.
Approach/Methods
The author will exhibit four cases of extradural AVFs to demonstrate the spectrum of the disease. Clinical findings, diagnostic evaluation, treatment and outcome are discussed.
Findings/Discussion
Two cases of type A spinal extradural AVFs have extradural fistulous locations (both at L3 level) and large epidural venous lakes with intradural venous drainage. They presented with progressive myelopathy. Transarterial embolization (TAE) with N-butyl cyanoacrylate (NBCA) was performed to occlude the fistula and the venous lake in both cases successfully. Regression of cord edema was noted and the symptoms were relieved in one patient and improved in another. The third case presents with cervical radiculomyelopathy. Angiography revealed a type B1 extradural AVF at T12 level with epidural venous drainage but without intradural venous drainage. Transarterial embolization with NBCA was performed to occlude the fistula successfully. The symptoms completely resolved. The fourth case was an incidental finding. A type B2 spinal extradural AVFs at cervical level was noted without intradural venous drainage or mass effect on surround tissue. No treatment was needed.
Summary/Conclusion
Spinal extradural AVFs are rare malformations which differ from dural AV fistulae in many ways. Careful differentiation and evaluation with selective spinal angiography was important before the treatment to be performed.

KEYWORDS: Spinal arteriovenous malformation

EdE-90

Spectrum of Neuroradiologic Findings in the Conus Medullaris and Filum Terminale: A Pictorial and Educational Review

Horsburgh, A.[1,2]·Antoun, N.[1]·Massoud, T. F.[1,3]
[1]Addenbrooke's Hospital, Cambridge, UNITED KINGDOM,
[2]Queen's Hospital, Romford, UNITED KINGDOM,
[3]University of Cambridge, Cambridge, UNITED KINGDOM.

Purpose
The term "conus" is derived from the Latin word for "cone", thus describing the morphologic shape of the spinal cord's caudal tip. However, the conus medullaris is not just a tapered continuation of the superior spinal cord segments. It represents a distinct entity within the spinal cord, with its own unique complex anatomical and physiologic features. The filum terminale, which often is considered as just a fibrous extension of the cord, recently has been shown to contain nerve bundles, which may play a functional role in some individuals. Lesions of the conus and filum terminale tend to present generically as back pain or cauda equina syndrome. Expedient MRI of the lumbar spine often is performed to image both these structures and to exclude a compressive lesion. However, there is a very wide range of clinical diseases that can affect this region. The breadth of lesions both common and uncommon, which can affect the conus, can often lead to controversies in clinical and radiologicl differential diagnosis. Management strategies differ substantially, depending on the type of lesion. In this region early diagnosis followed by timely medical or surgical treatment is favored to preserve neurologic functions. Thus it is important for neuroradiologists to be familiar with the spectrum of diseases in this region and their imaging manifestations.
Approach/Methods
We review the imaging findings in a wide spectrum of common and uncommon pathologic processes affecting the conus medullaris and filum terminale.
Findings/Discussion
We review the unique imaging anatomy of the conus medullaris and filum terminale, along with a pictorial review and discussion of the imaging findings in many of the conditions affecting this region. These include neoplastic lesions such as glial tumors (e.g., ependymoma, astrocytoma, glioblastoma and ganglioglioma), and nonglial tumors [e.g., schwannoma, neurofibroma, hemangioblastoma, primitive neuroectodermal tumor (PNET), lymphoma and primary CNS melanoma], and metastatic disease. We also consider non-neoplastic lesions including demyelinating lesions, granulomatous

Note: Scanned images are included in the proceedings. Some submitted images were reduced during editing, thereby decreasing clarity. Also, refer to the Program Planner. Proceedings Content as of 3-29-2013.

diseases (e.g., tuberculoma and sarcoidosis), infections including bacterial infections (e.g., pyogenic abscess) as well as parasitic infections (e.g., schistosomiasis, sparganosis and cysticercosis). We will discuss vascular abnormalities (e.g., cavernoma, arteriovenous malformations, arteriovenous fistula and conus infarction) and look at congenital lesions (e.g., spinal dysraphism, lipoma, epidermoid, dermoid cysts, teratoma and childhood tight filum syndrome). Very rare pathologies reported in the literature (e.g., intramedullary enterogenous cysts, endometriosis of the cauda equina) also are displayed.
Summary/Conclusion
Management strategies for conus medullaris and filum terminale abnormalities vary substantially, depending on the abnormalities revealed on neuroimaging. This presentation will aid in differentiating the often confusing imaging appearances of lesions in this region.

KEYWORDS: Conus, filum terminale

EdE-91

Occipital Condyle Fracture: An Under-Recognized Entity with Potentially Severe Sequelae: Review of Craniocervical Anatomy, Classification of Fracture and Ligamentous Injury, and Discussion of Imaging Techniques Aiding in Diagnosis

Myers, C.·Mehta, H.
Westchester Medical Center
Valhalla, NY.

Purpose
Occipital condyle fractures related to high-velocity head and neck trauma are rising in incidence with an increasing number of motor vehicle collisions. Evaluation of the skull base may be limited unless appropriate imaging technique is utilized, leading to missed diagnosis. This exhibit will discuss the relevant anatomy, classification of occipital condyle fractures, range of potential sequelae, how to focus on this region in clinical practice, as well as highlight current imaging techniques of the occipital condyle.
Approach/Methods
Multiple patients and associated imaging with CT and MRI of type I - III occipital condyle fractures as well as patients with ligamentous injury to the craniocervical junction are discussed. Anatomy and imaging of the skull base and craniocervical junction as well as occipital condyle fractures and associated ligamentous injury will be reviewed. Strategies and key regions of focus are discussed to increase the sensitivity and specificity of diagnosis for the interpreting radiologist.
Findings/Discussion
The Anderson and Montesano classification system describes type I - type III fractures, with increasing severity. Recognition and proper treatment is necessary to prevent spinal cord injury, particularly with type III fractures which often are associated with severe ligamentous damage and craniocervical instability. Recognition of injuries is vital to proper treatment.

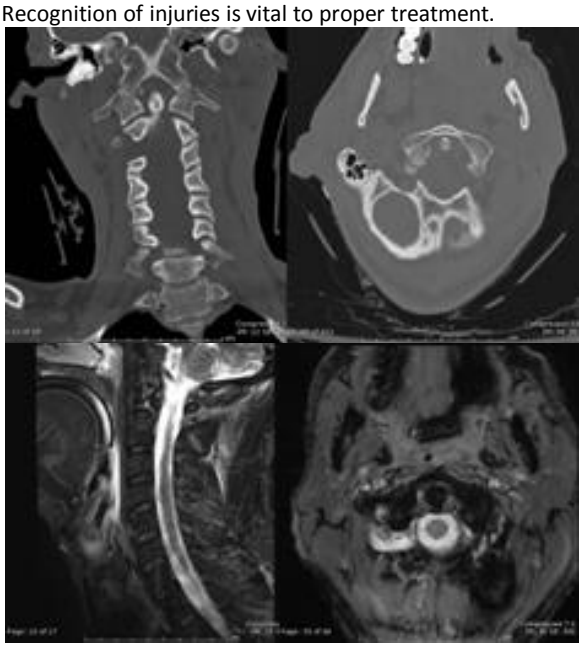

Summary/Conclusion
Educational goals: 1) Understanding the anatomy of the craniocervical junction as well as classification system, treatment options, and outcomes for occipital condyle fractures and associated ligamentous injury. 2) Review of current imaging techniques with CT and MRI to maximize dectection of craniocervical junction injury. 3) Review of the radiologic approach to evaluation of the craniocervical junction to ensure appropriate detection of fractures and ligamentous injury.

KEYWORDS: Occipital bone, Fracture, ligaments, occipital condyle, skull base

EdE-92

Clinical Correlations between Imaging Findings in Spinal Hemorrhage and Clinical Outcomes in Trauma Patients

Meyer, M. A.·Shastri, R.·Khan, R.
University of Arizona
Tucson, AZ.

Purpose
The purpose of this exhibit is 1. Review the importance of magnetic susceptibility imaging within the spinal canal and discuss artifacts that may be a source of obscuration. 2. Explore prognostic implications of cord hemorrhage as described in the literature and explain why spinal cord hemorrhage in the setting of trauma has been demonstrated to be associated with fixed defects or poor prognosis.
Approach/Methods
A comprehensive literature review will be performed in order to provide accurate prognostic implications of cord

Note: Scanned images are included in the proceedings. Some submitted images were reduced during editing, thereby decreasing clarity. Also, refer to the Program Planner. Proceedings Content as of 3-29-2013.

hemorrhage and its outcomes. A review of spinal anatomy, mechanisms of trauma and pictorial examples will ensue.
Findings/Discussion
We will review: 1. Illustrative review of anatomy of the spinal cord. 2. Neurologic deficits associated with spinal injury and key localization findings. 3. Mechanisms of traumatic spinal hemorrhage. 4. American spinal injury association grading system. 5. Key imaging findings on CT and MRI. 6. MRI and CT artifacts associated with spinal cord trauma. 7. Outcome scoring and prognostic benchmarks. 8. Case examples of cord hemorrhage associated with complete and incomplete neurologic impairment.
Summary/Conclusion
The viewer should gain an understanding of intrathecal hemorrhage as demonstrated on CT and MRI as well as understand the prognostic implication as it relates to associated neurologic deficits. By reviewing spinal cord anatomy as well as reviewing the American spinal injury association grading system, the viewer should have a better sense of the importance of identifying hemorrhage in these patients as well as the prognostic implications.

KEYWORDS: GRE, Spinal cord, spinal injury

Monday, May 20 – Wednesday, May 22
6:30 AM – 9:00 PM
Thursday, May 23
6:30 AM – 3:00 PM
Hall B1

Electronic Education Exhibits (eEdE) 1 - 70a

eEdE1-Adult Brain

Note: A missing printed number indicates an abstract has been withdrawn.

eEdE-01

Multimodality Imaging of Vertebrobasilar Dolichoectasia: Clinical Presentations, Imaging Spectrum, and Imaging Optimization

Samim, M.·Goldstein, A.·Mahajan, A.·Schindler, J.·Johnson, M.
Yale University School of Medicine
New Haven, CT.

Purpose
The purpose of this exhibit is to: -Review the current diagnostic criteria of vertebrobasilar dolichoectasia (VBD) utilizing CT, MR, and angiography (DSA) and discuss their limitations. -Demonstrate different presentations of VBD. -Review how to optimize imaging protocols. -Review available treatment options.
Approach/Methods
We will present cases of patients, both asymptomatic and with discrete neurologic syndromes diagnosed with VBD based on radiologic criteria (ectasia, lateral displacement, and height). The following will be reviewed: -The current and available diagnostic criteria, including “Smoker criteria”. -The technique of high-resolution CT and MR pulse sequences and angiography tailored for evaluation of VBD and the imaging interpretation. -Multimodality imaging features of compressive and vascular complications. -How to recognize imaging points of critical importance for treatment planning. -How to optimize imaging modalities.
Findings/Discussion
Imaging VBD is challenging due to the effects of turbulent flow, calcifications and thrombus formation that have different appearances on each imaging modality. Correlation of CT, MRI and DSA may provide a better understanding of both anatomy and pathophysiology in this complex disorder. Vertebrobasilar dolichoectasia can have various clinical presentations. For example, abnormal arterial dilatation can cause mechanical stress upon the surrounding brain structures, resulting in compressive symptoms. Alternatively, neurovascular symptoms can result from transient ischemic attack (TIA), ischemic stroke, or hemorrhagic stroke. In this exhibit, we illustrate cases of patients presenting with compressive symptoms including hydrocephalus and cranial nerve palsies, for example vertigo, hearing loss, facial palsy, and trigeminal neuralgia. Additionally, cases with vascular symptoms including acute stroke and intracranial hemorrhage will be presented. Dolichoectatic vessels with larger diameters seem to be associated with a greater risk of stroke, while those that exhibit marked tortuosity and elongation may be associated with compressive symptoms. Imaging pitfalls related to thrombus, calcification and flow disturbances are demonstrated and strategies for imaging optimization discussed. For example, MR flow effects in VBD due to abnormal vessel configuration can be better differentiated from intraluminal thrombosis by protocol optimization.

Note: Scanned images are included in the proceedings. Some submitted images were reduced during editing, thereby decreasing clarity. Also, refer to the Program Planner. Proceedings Content as of 3-29-2013.

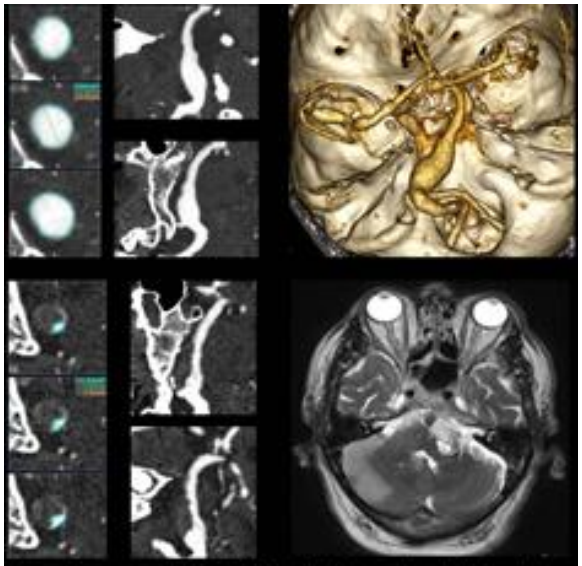

67 year old man presented with right sided facial and body weakness. Initial CT angiogram demonstrates basilar dolichoectasia with areas of narrowing and plaques within the vessel (Top). MR/MRA and repeat CTA within 1 day demonstrate extensive thrombus formation within the ventral aspect of the dolichoectatic basilar artery and acute infarct within the inferior half of the right cerebellum in an AICA/PICA territorial distribution (bottom).

Summary/Conclusion
Despite the lack of uniform diagnostic criteria, CT, multisequential MR, and angiography can be complimentary in the diagnosis of VBD and its compressive and vascular complications. By optimizing imaging protocols and recognizing imaging pitfalls, diagnostic accuracy can be improved. No standard treatment has been established to prevent the progression of the VBD; therefore, before the impact of any specific treatment can be addressed, a better understanding of the underlying pathophysiology of this disease is needed.

KEYWORDS: Basilar artery, Vertebral artery anomalies, dolichoectasia; stroke

eEdE-02

Atypical and Symptomatic Developmental Venous Anomalies

Trimble, C. R.·Fortes, M.·Jindal, G.·Miller, T.·Gandhi, D.
University of Maryland School of Medicine
Baltimore, MD.

Purpose
Developmental venous anomalies (DVAs) are the most common of the cerebrovascular malformations with an incidence of up to 2.6% in the general population. These are believed to occur as a result of an embryologic event that leads to interruption in normal development of the venous system. The congenital absence of normal pial or subependymal veins leads to an “anomalous venous disposition,” in which the venous drainage patterns are reversed. While a vast majority of DVAs are incidental and benign, there is growing realization that a small fraction of these lesions may be symptomatic. In this case-based educational exhibit, we highlight the imaging features and potential complications of atypical DVAs.
Approach/Methods
Multimodality imaging of 45 cases of atypical DVAs was collected from the authors’ teaching collection and report database query.
Findings/Discussion
Developmental venous anomalies in our collection presented with varying clinical symptoms including headaches, seizures, focal neurologic deficits, and intracranial hemorrhage. The clinical sequelae of DVAs were likely related to associated regional venous hypertension. In this exhibit, we will highlight atypical features associated with these DVAs, including draining vein thrombosis, loco-regional venous hypertension and draining vein stenosis. Additionally we will describe cases of giant DVAs, arterialized DVAs, and DVAs associated with cortical dysplasia.
Summary/Conclusion
Enhancing, linear, venous radicles draining into a collector vein constitute the pathognomonic “medusa head appearance” of DVAs. While the majority of these lesions are asymptomatic, a small fraction of DVAs result in symptoms which may be attributed to atypical associated lesions, including cavernous malformations, arteriovenous malformations, cortical dysplasia or loco-regional venous hypertension. Familiarity with the imaging findings of atypical DVAs can help facilitate correct diagnosis of this condition.

KEYWORDS: developmental venous anomaly

eEdE-03

TRICKS of the Trade: Time-Resolved Contrast-Enhanced MRA and Accelerated Phase Contrast MRA Improve the Detection and Characterization of Carotid-Cavernous Fistulas

Hartman, L. A.·Turski, P.·Kennedy, T.·Hartman, M.·Aagaard-Kienitz, B.
University of Wisconsin Hospital and Clinics
Madison, WI.

Purpose
The purpose of this exhibit is to use an interactive case-based review to illustrate improved delineation of the cavernous sinus and venous drainage of carotid-cavernous fistulas (CCFs) using high-resolution 4D contrast-enhanced time-resolved MR angiography (MRA) and accelerated phase contrast (PC) MRA. Together these MRA techniques provide vascular images that detect arteriovenous (AV) shunting and demonstrate arterial supply and venous drainage patterns. In some cases CCFs may be relatively mild presenting only with orbital pain. In these instances, MRA evaluation is key in establishing the diagnosis of CCF.
Approach/Methods
We will present cases of CCFs using clinical photographs, clinical presentation, MRI/MRA findings and DSA vascular

Note: Scanned images are included in the proceedings. Some submitted images were reduced during editing, thereby decreasing clarity. Also, refer to the Program Planner. Proceedings Content as of 3-29-2013.

anatomy. Current methods to improve spatial-temporal resolution of 4D contrast-enhanced MRA and PC MRA exams will be reviewed. Finally, a brief overview of treatment options for CCFs will be discussed including recent applications of focused radiation therapy.

Findings/Discussion

Carotid-cavernous fistula is an uncommon AV fistula that often initially presents as orbital pain. The diagnosis may be delayed as other causes of orbital pain are considered. Additional clinical symptoms include proptosis, chemosis, cranial neuropathies, decreased visual acuity and intracranial hemorrhage. Carotid-cavernous fistulas are characterized based on the Barrow classification. CT angiography and MRA can aid in depicting the arterial supply and venous drainage of CCFs. Findings associated with CCF on time-of-flight MRA include an enlarged cavernous sinus and a dilated superior ophthalmic vein with flow-related enhancement. With parallel imaging and 4D contrast-enhanced MRA (TRICKS and PC), a more definitive description of the venous drainage can be illustrated via early filling of the cavernous sinus and venous drainage pathway(s). These advanced MRA techniques can help identify the cortical venous drainage pattern (sphenoparietal sinus, cortical veins, petrosal veins, perimesencephalic veins), which places the patient at greater risk for intracranial hemorrhage and venous infarction, and often are treated more urgently. By demonstrating the venous drainage pathway(s) of a CCF, a preprocedure plan of treatment via endovascular route can be determined.

Figure 1A

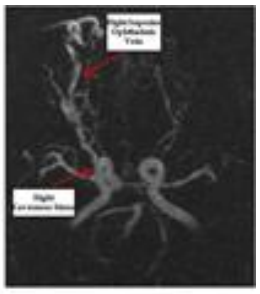

Figure 1B

Summary/Conclusion

We demonstrate representative cases of CCF based on DSA confirmed vascular pathophysiology. Advancements in temporal-spatial resolution of MRA allow important imaging features of CCF to be evaluated such as dominant arterial feeders, venous drainage pattern and morphologic changes in the orbit. We highlight the value of 4D MRA in the evaluation of patients presenting with orbital pain to establish the diagnosis early and avoid severe complications.

KEYWORDS: Cavernous carotid fistula, Dural arteriovenous fistula, magnetic resonance angiography

eEdE-04

Imaging Appearance of Intracranial Dural AV Fistulas

Fong, C.
Kaiser Permanente Los Angeles
Los Angeles, CA.

Purpose

The purpose of this exhibit is to review the imaging findings of intracranial dural arteriovenous fistulas. Dural AV fistulas are notoriously difficult to diagnose or confirm with CT and MR.

Approach/Methods

This review will highlight findings that can be seen on cross-sectional imaging including draining or prominent veins, abnormal enhancement, edema due to venous congestion, calcification and prior hemorrhage. We also will review the different types of dural AV fistulas and the clinical connotations associated with them.

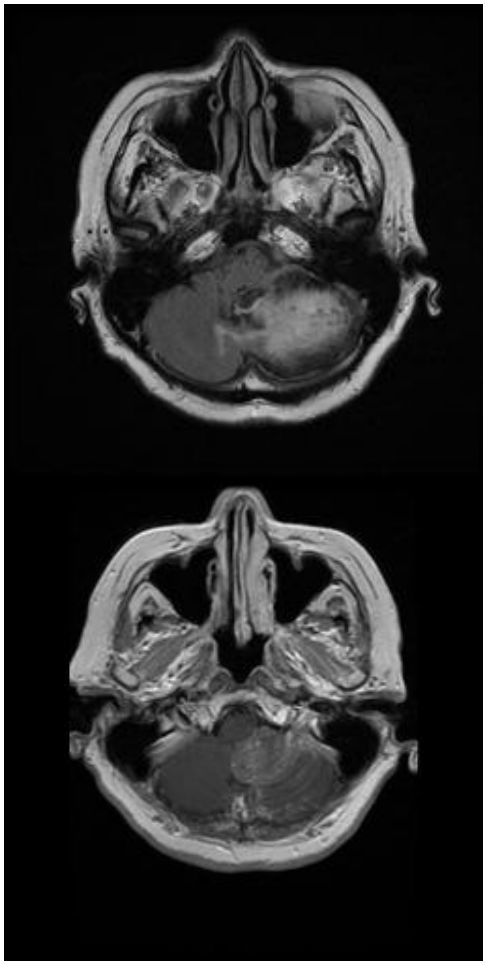

Note: Scanned images are included in the proceedings. Some submitted images were reduced during editing, thereby decreasing clarity. Also, refer to the Program Planner. Proceedings Content as of 3-29-2013.

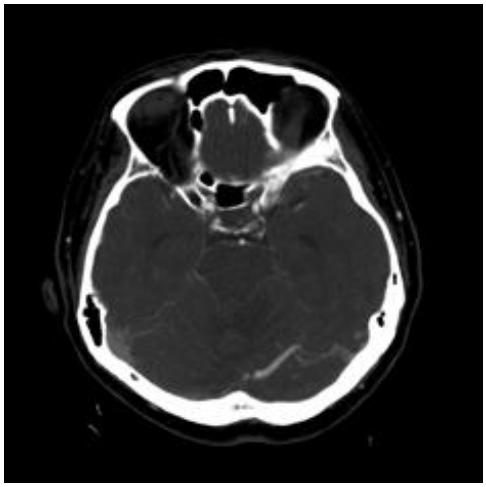

Summary/Conclusion
In summary, intracranial dural AV fistulas are difficult entities to diagnose, but awareness of this entity and its imaging findings can allow the astute radiologist to make this diagnosis.

KEYWORDS: Dural arteriovenous fistula, Arteriovenous fistulas

eEdE-05

Using Arterial Spin-Labeled MR Imaging to Identify Interictal Perfusion Abnormalities in Epilepsy

Raji, C. A.·Joe Qiao, J.·Wang, J.·Salamon, N.
University of California Los Angeles Medical Center
Los Angeles, CA.

Purpose
Epilepsy is a devastatingly chronic progressive neurologic disorder that affects one percent of the world population with an incidence of 70 per 100,000 per year. The number of new cases of pediatric epilepsy alone numbers approximately 300,000 per year. Despite the ability of MR imaging to identify structural lesions responsible for epilepsy cases, between 20-50% of patients with medically intractable epilepsy have no identifiable lesions on structural MR imaging. While brain SPECT offers important physiologic information in epilepsy diagnosis, it entails use of ionizing radiation that is less desirable particularly in the pediatric population. Perfusion imaging with arterial spin-labeled (ASL) MR imaging offers a powerful modality by which to noninvasively imaging and quantify cerebral perfusion without using ionizing radiation.
Approach/Methods
The purpose of our study is to illustrate how ASL can be clinically applied to identify perfusion defects in persons with epilepsy who have otherwise normal structural MR imaging. We possess a cohort of 361 individuals with epilepsy across the lifespan from infants to elderly aged 86. In this group, 32% (n = 117) had structural MR images that were interpreted as normal. The majority of this subgroup (n = 107) also received pulsed ASL MR imaging of the brain on a Siemens 3.0 T scanner during the interictal period. We will show examples of persons with epilepsy who have structurally normal MR scans such as in Figures 1-2.

Figure 1: One Year Old With Seizures

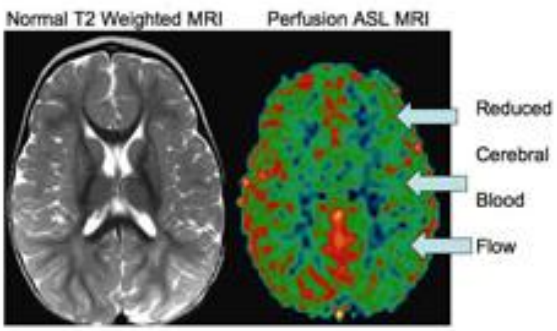

Figure 2: Three Year Old with New Onset Seizures

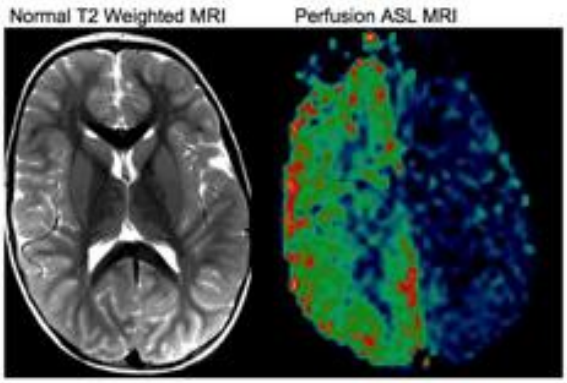

Findings/Discussion
We will summarize the imaging findings of this group with ASL, focusing on perfusion abnormalities. We hypothesize that ASL MR imaging in this epilepsy group with normal structural MR images will demonstrate hypoperfusion abnormalities in the interictal period.
Summary/Conclusion
This work will lend insight into the use of perfusion ASL MR imaging as a functional modality for improved diagnosis and classification of epilepsy.

KEYWORDS: Epilepsy, Arterial spin labeling

eEdE-06

Cerebellar Atrophy: Can I Say Something other than "Clinical Correlation Advised"?

Pereira, L. P.·Sair, H.·Ying, S.
Johns Hopkins Hospital
Baltimore, MD.

Purpose
To review the magnetic resonance imaging (MRI) patterns of various pathologies that are associated with cerebellar

Note: Scanned images are included in the proceedings. Some submitted images were reduced during editing, thereby decreasing clarity. Also, refer to the Program Planner. Proceedings Content as of 3-29-2013.

degeneration and to categorize these patterns according to anatomical involvement.
Approach/Methods
Cerebellar atrophy is a frequent finding in the typical neuroradiologic practice, and ataxia is a common presenting symptom. A wide variety of pathologies are related to regional or global reduction of cerebellar volume, which may or may not be accompanied by extracerebellar involvement. Here we present a radiologic approach to cerebellar intrinsic diseases associated with ataxia, with classic signs and less well recognized regional findings categorized according to anatomical involvement using conventional and advanced MRI.
Findings/Discussion
MR imaging frequently is performed in patients with ataxia. Neuroradiologists usually are well versed in ruling out structural lesions of the cerebellum, such as developmental abnormalities, vascular pathology, tumors, or trauma. However, in the remaining cases of cerebellar disease, it can be challenging to reach a more specific diagnosis, since patterns may overlap and have nonspecific appearances. In this review the authors classify conventional and advanced MRI findings according to the presence or absence of involvement in four major regions: 1) cerebellar cortex, 2) deep cerebellar nuclei and corpus medullare, 3) brain stem and cerebellar peduncles, and 4) other lesions outside the posterior fossa. Common pathologies that predominantly involve the cortical area include spinocerebellar ataxia (SCA) types 1 and 6, Friedreich ataxia (FA), Fragile X-Associated Tremor/Ataxia syndrome (FXTAS), the Autosomal Recessive Spastic Ataxia of Charlevoix-Saguenay (ARSACS), Neuropathy, Ataxia, and Retinitis Pigmentosa (NARP) syndrome, Cockayne syndrome, as well as paraneoplastic, alcohol, drug and gluten cerebellar damage. These pathologies can be subdivided further into regional patterns of involvement. Pathologies with prominent involvement of the deep cerebellar nuclei include FA, FXTAS and cerebrotendinous xanthomatosis (CTX). Pathologies with brain stem and/or cerebellar peduncle involvement are represented by multisystem atrophy, cerebellar type (MSA-c), SCA type 1 and 2, ARSACS and FXTAS. Pathologies that also demonstrate prominent CNS involvement outside of the posterior fossa include SCA type 3, MSA Parkinson type (MSA-p), NARP, ARSACS, Cockayne syndrome and ARSACS. We present a comprehensive classification schema for conventional and advanced MR findings, with brief clinical and imaging descriptions for each pathology.
Summary/Conclusion
Cerebellar atrophy is a diagnostic imaging challenge. Classification of imaging signs and predominant areas of involvement for the most frequent pathologies can be helpful in diagnostic evaluation and interpretation of conventional and advanced MRI.

KEYWORDS: Cerebellum, Degenerative, atrophy

eEdE-07

Basal Ganglia and Neurodegenerative Disorders

Bangiyev, L.[1]·Roudenko, A.[1]·Paydar, A.[1]·Milla, S.[1]·Naidich, T. P.[2]·Fatterpekar, G. M.[1]
[1]New York University Langone Medical Center, New York, NY, [2]Mount Sinai Medical Center, New York, NY.

Purpose
The purpose of this exhibit is to: 1. Discussing the anatomy and physiology of the basal ganglia. 2. Display the different “neurodegenerative" disease conditions involving the basal ganglia. 3. Providing imaging algorithms based on the age of the patient, location of the lesion in the basal ganglia, its morphologic appearance, and involvement of the other structures of the brain to help narrow the differential diagnosis.
Approach/Methods
Utilizing high-resolution T1-weighted images, T2-weighted images, and intermediate-weighted sequences and relevant graphic illustrations we will discuss in exquisite detail the anatomy and physiology of the basal ganglia. Normal and abnormal iron deposition will be discussed. Select CT and MR images will be used to display the different disease conditions involving the basal ganglia. Disease processes will be characterized into: - Deposition disorders: Wilson Disease, Hyperalimentation therapy (manganese), Pantothenate-kinase associated neurodegeneration (PKAN), Infantile Neuroaxonal Dystrophy, Parathyroid disorders and Fahr’s syndrome. - Toxic and Metobolic disorders: Kernicterus, Leigh syndrome, Hepatic encephalopathy, Carbon monoxide poisoning and Diabetic Striatopathy. - Infectious Diseases: TORCH, Creutzfeldt-Jacob disease, Cyptococcosis, and AIDS. - Movement disorders: Huntington Disease, Parkinson disease, and Parkinson-plus syndromes including Multiple System Atrophy. - Ischemic encephalopathy. - Traumatic Brain injury: Abnormal iron deposition.
Findings/Discussion
Lesions will first be distinguished based on their localization to the caudate nucleus, globus pallidus, putamen, subthalamic nucleus, and/or substantia nigra. Further differentiation will be made based on imaging characteristics, including density on CT as well as signal intensity on T1-weighted, T2-weighted/FLAIR, diffusion-weighted imaging, susceptibility-weighted and postcontrast sequences. In addition, involvement of other parts of the brain, such as the surrounding white matter structures, thalamus, cortex, cerebellum, and brainstem, also will be taken into account.
Summary/Conclusion
By utilizing a methodical approach we aim to provide the neuroradiologist an in-depth understanding of the anatomy and physiology of the basal ganglia. The information so gained along with a display of plethora of cases will assist in interpretation of and narrow the differential diagnoses for basal ganglia lesions based on

Note: Scanned images are included in the proceedings. Some submitted images were reduced during editing, thereby decreasing clarity. Also, refer to the Program Planner. Proceedings Content as of 3-29-2013.

their location, laterality, extent of disease, imaging characteristics on MR and CT, as well as presence of other abnormalities outside of the basal ganglia.

KEYWORDS: Basal ganglia, Neurodegenerative

eEdE-08

Multimodality Imaging of Degenerative Brain Diseases: Moving Beyond Degenerative Dementias with Conventional Imaging and Nuclear Medicine

Verdoorn, J. T.·Hunt, C. H.
Mayo Clinic
Rochester, MN.

Purpose
The purpose of the exhibit is to: 1) Review the common nuclear medicine studies used to image degenerative CNS diseases with an emphasis on new imaging techniques for atypical degenerative brain disease; 2) Correlate the findings of the nuclear medicine studies with those seen on MRI and at pathology; 3) Discuss the potential role of quantitation in increasing specificity for the diagnosis with FDG and amyloid imaging PET/CT.
Approach/Methods
After a brief review of the nuclear medicine options for imaging degenerative CNS disease, a series of patients will be presented to demonstrate the added value of these studies in evaluation of degenerative CNS disease, including Parkinsonism, motor neuron disease, and autoimmune processes. This series also will include cases which demonstrate the potential limitations of nuclear medicine with examples of how false positive and false negative studies can be obtained. All studies will be correlated with conventional imaging (CT, MRI) as well as pathologic findings.
Findings/Discussion
Nuclear medicine can be a powerful tool in the evaluation of degenerative CNS disease and provide important diagnostic and prognostic information. While its usefulness in documenting degenerative dementias such as Alzheimer disease, frontotemporal dementia, and Lewy body disease has been well document, nuclear medicine also can provide powerful insight into other degenerative CNS diseases such as Parkinsonism, motor neuron disease, autoimmune disorders, and atypical degenerative dementias such as corticobasilar degeneration. The addition of automated quantitation can increase the specificity of the findings as well.
Summary/Conclusion
Nuclear medicine can provided significant added value to the evaluation of degenerative CNS disease. The combination of nuclear medicine including PET/CT and scintigraphy and conventional imaging (CT and MRI) can improve diagnostic and prognostic accuracy.

KEYWORDS: PET/CT, Degenerative

eEdE-09

Imaging Differential Diagnosis of Conditions Other than Alzheimer Disease Presenting with Dementia

Patro, S. N.·Glikstein, R.·Chakraborty, S.
The Ottawa Hospital
Ottawa, ON, CANADA.

Purpose
The aim of this educational exhibit is: 1. To present various intra and extraaxial pathologic brain lesions we encountered in the workup of patients with dementia. 2. To discuss the different pathologies and their imaging features associated with dementia.
Approach/Methods
Twenty consecutive patients who underwent CT and MRI as part of the evaluation of dementia were reviewed in our hospital from November 2009 to November 2012.
Findings/Discussion
In this educational pictorial essay we are reviewing two patients with central pontine myelinolysis, two patients with multisystem atrophy-cerebellar variant, one patient with progressive supranuclear palsy, one patient with Creutzfeldt-Jakob disease, one patient with acute methanol toxicity, one patient with HIV encephalopathy, one patient with severe microangiopathic disease, two patients with CADASIL, one patient with Sjogren's syndrome, one patient with severe anoxic brain injury, one patient with bilateral chronic subdural hemorrhage, one patient with meningioma, one patient with olivoponto cerebellar atrophy and four patients with normal pressure hydrocephalus who presented with dementia. Dementia by definition is a gradual and progressive decline of cognition caused by various diseases of the brain. The global prevalence of dementia is estimated to be 24 million and likely to be double in the next 20 years. Alzheimer disease is the most common primary neurodegenerative disease. The less common causes are fronto-temporal dementia, diffuse lewy body disease, cerebrovascular disease, atypical Parkinsonism, CJD, HIV-related encephalopathy. It is also important to be aware of other treatable conditions like tumor, subdural hemorrhage and normal pressure hydrocephalus (NPH) which can produce features like dementia due to mass effect over the brain. Imaging is a part of the routine workup for all patients presenting with dementia. CT is the preliminary investigation to rule out treatable conditions. MR imaging with inherent high soft tissue resolutions helps in differentiating various types of dementia.
Summary/Conclusion
It is important to consider various etiologies in the workup of a patient with dementia. Imaging has now become a standard part of the diagnostic process in evaluating dementia.

KEYWORDS: MR imaging brain, Creutzfeldt-Jakob disease, hydrocephalus, HIV

Note: Scanned images are included in the proceedings. Some submitted images were reduced during editing, thereby decreasing clarity. Also, refer to the Program Planner. Proceedings Content as of 3-29-2013.

eEdE-10

"Change in Mental Status": Decoding Neuroimaging Clues for Systemic Processes of Excess and Deficiency

Liu, R.·Li, J.
Albert Einstein Medical Center
Philadelphia, PA.

Purpose
"Change in mental status" is perhaps the most commonly encountered indication for neuroimaging in a hospital setting for an increasingly complex group of conditions, which are often difficult to diagnosis clinically as they do not contribute to any focal neurologic signs and symptoms. Many of these conditions are due to systemic excesses or deficiencies in metabolites or in their regulation and have characteristic imaging findings. The ability to recognize and alert clinicians of these conditions can guide them to the proper diagnostic and laboratory examinations and lead to early, appropriate treatment. This educational exhibit outlines some of these conditions and highlights their characteristic imaging findings.
Approach/Methods
A search of the authors' teaching files and our PACS imaging archive was performed to identify potential patients with MR imaging of the following conditions: metabolic diseases of childhood, alcohol-related encephalopathy, vitamin deficiencies, toxic/metabolic diseases, hypertension/PRES, medication-induced encephalopathy, hypoxic/ischemic encephalopathy, and hypoglycemia. Images then were reviewed by authors to identify characteristic imaging features of these conditions. These then were displayed in an educational format via a PowerPoint presentation.
Findings/Discussion
Several of the systemic, inherited metabolic disorders of excess toxic metabolite accumulation are discussed including X-linked adrenoleukodystrophy, metachromatic leukodystrophy, and Canavan disease. In addition, excess accumulation of minerals leading to demyelination are discussed in the setting of alcoholism with examples of acute and chronic alcoholic encephalopathy as well as Marchiafava-Bignami disease. Cocaine abuse, methanol poisoning, and carbon monoxide poisoning are presented as examples of toxic metabolite accumulation. Methotrexate, tacrolimus, and metronidazole are displayed as examples of iatrogenic toxic effects. For the systemic deficiency disorders, we show characteristic imaging findings of thiamine and B12 vitamin deficiencies as well as those characteristic imaging findings present from lack of auto-regulation of blood pressure in posterior reversible encephalopathy syndrome. A lack of essential metabolites such as oxygen and glucose are demonstrated with acute hypoxic-ischemic injury, sub-acute hypoxic-ischemic encephalopathy, and hypoglycemia.
Summary/Conclusion
With prompt recognition of characteristic imaging findings in a variety of toxic and metabolic conditions, we can better serve our clinical colleagues by alerting them to the possibility of these diagnoses, guiding them to the proper laboratory examinations, and promoting early treatment as well as better patient outcome.

KEYWORDS: Encephalopathy, Metabolic

eEdE-11

Improved Detection of Cortical Malformations Using Curvilinear Reformatting of 3D Volumetric MR Imaging of the Cerebral Cortex in Combination with Diffusion Tensor Imaging

Campeau, N.·Patton, A.
Mayo Clinic
Rochester, MN.

Purpose
To illustrate the merits of using a 3D curvilinear reformatting postprocessing algorithm in combination with diffusion tensor imaging (DTI) for improved assessment of epileptogenic cortical malformations.
Approach/Methods
Three-dimensional (3D) volumetric T1-weighted data sets obtained from magnetic resonance imaging (MRI) studies performed for evaluation of individuals with epilepsy were postprocessed manually on a computer workstation using a 3D curvilinear reformatting algorithm to produce a flattened 2 dimensional rendition of the cortex of the entire brain. Reformatted images of the brain were obtained to depict the cortical surface, and serial reformatted curvilinear planes at varying depths/thickness from the cortical surface. All suspicious areas were correlated with diffusion tensor imaging (FA maps, tractography) when available.
Findings/Discussion
Pathology identified and processed with these techniques included focal cortical dysplasia, lissencephaly, pachygyria, polymicrogyria, and schizencephaly. The location of the pathology and extent of cortical involvement was improved with curved reformatting algorithm. Anatomical landmarks and their relationship to the location of abnormalities are determined more precisely with curved reformatting. Improved comparison of contralateral anatomy allows for more confident determination of subtle abnormalities. The specificity of imaging abnormalities seen with curvilinear reformatting is improved with use of DTI.
Summary/Conclusion
Curvilinear reformatting combined with DTI not only allows improved delineation of cortical malformations, but assists in identification of normal anatomical landmarks. These techniques provide an efficient and concise visual representation of pathology, useful for conveying imaging findings to referring clinicians for surgical planning and optimize the extent of pathologic resection.

KEYWORDS: Cortical malformation, 3D visualization

Note: Scanned images are included in the proceedings. Some submitted images were reduced during editing, thereby decreasing clarity. Also, refer to the Program Planner. Proceedings Content as of 3-29-2013.

eEdE-12

Spectrum of CT Perfusion Findings in the Post-Ictal State

Boyer, A. C.·Spear, D.·Wilson, B.·Gupta, G.·Kramer, J.·Bakalis, C.·Wilseck, J.
Oakland University William Beaumont School of Medicine
Royal Oak, MI.

Purpose
Diagnosing transient neurologic deficits following seizure compared to deficits due to cerebral ischemia can be difficult in the acute setting. CT perfusion (CTP) imaging commonly is used in the setting of suspected acute cerebral ischemia. During a seizure, cerebral perfusion initially increases in affected regions, which reverses to hypoperfusion in the post-ictal state. Other perfusion abnormalities including a state of mixed hypoperfusion and hyperperfusion as well as isolated focal hyperperfusion also have been reported in the post-ictal state. The purpose of this educational exhibit is to present the spectrum of CTP imaging findings seen in the post-ictal state and discuss useful tips to differentiate post-ictal perfusion abnormalities from acute cerebral ischemia.
Approach/Methods
The basics of CTP will be discussed briefly. Typical alterations in seizure-related cerebral perfusion will be reviewed followed by a pictorial review of the spectrum of CTP findings in the post-ictal state. Imaging examples provided were generated from a review of 425 consecutive patients who underwent CTP for acute stroke-like neurologic symptoms at our institution over a 17-month period. These patterns of abnormal perfusion will be compared to a typical example of hypoperfusion due to cerebral ischemia. Finally, key factors that can be used to differentiate seizure from cerebral ischemia on CTP will be reviewed.
Findings/Discussion
CT perfusion imaging abnormalities are common following seizure. The most common CTP pattern seen in the post-ictal state is hypoperfusion with prolonged mean transit time (MTT) and time to drain (TTD) with decreased cerebral blood volume (CBV) and cerebral blood flow (CBF). Other patterns include isolated hyperperfusion with abnormally decreased MTT and TTD and increased CBV and CBF as well as a mixed pattern consisting of areas of hyperperfusion and areas of hypoperfusion. In cases of hypoperfusion, defects of CBF and CBV are matched. Post-ictal perfusion abnormalties can be seen in a holo-hemispheric, multi-lobar, or cortical ribbon pattern. The basal ganglia typically are spared while involvement of the thalamus is common.

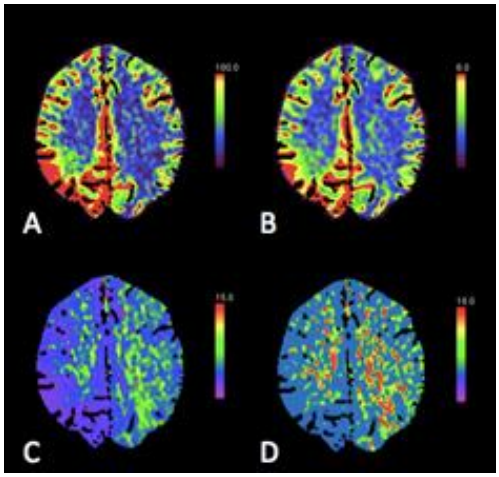

Summary/Conclusion
Post-ictal cerebral perfusion abnormalities can present as a spectrum of findings on CTP imaging. Matched perfusion abnormalities occurring in a distribution not classic for a vascular territory without an associated abnormality on CT angiography should raise the possibility of seizure as the cause of a patient's neurologic deficit.

KEYWORDS: CT perfusion, Seizure

eEdE-13

Perioperative and Postoperative Surgical Epilepsy Imaging: A Pictorial Essay

Venkatesh, R. M.·Hasso, A. N.·Hsu, F. P. K.·Lin, J. J.·Handwerker, J.
University of California Irvine Medical Center
Orange, CA.

Purpose
Medically intractable epilepsy is a challenging problem that often requires a multidisciplinary surgical approach involving neurologists, neurosurgeons, and neuroradiologists. A plethora of surgical techniques, divided into general categories of resective and disconnective procedures, are available to address this issue, each with unique perioperative and postoperative imaging features. Given the complexity of the cases, the increasing number of surgical epilepsy patients, as well as the confounding imaging features involving multiple modalities, neuroradiologists must become increasingly familiar with perioperative and postoperative imaging features.
Approach/Methods
Drawing on the approach of a large epilepsy center, imaging examples of lobectomy, hemispherectomy, corpus callosotomy, multiple subpial transection, and vagal nerve stimulator patients will be demonstrated. Multiple imaging modalities including 3D reconstructions, fusion of images for intraoperative guidance, PET/CT, fMRI and DTI as well as conventional CT and MRI all play important roles in the evaluation of the surgical epilepsy patient. Intraoperative

Note: Scanned images are included in the proceedings. Some submitted images were reduced during editing, thereby decreasing clarity. Also, refer to the Program Planner. Proceedings Content as of 3-29-2013.

images and detailed anatomical depictions that can help aid in understanding the characteristic radiologic appearances also will be shown. Numerous implantable devices are in use, and knowing the different types and their radiologic appearances is important for the neuroradiologist functioning as part of a multidisciplinary team.
Findings/Discussion
New techniques in imaging including 3D reconstruction and image coregistration for intraoperative guidance are allowing for a more thorough assessment and evaluation of the patient undergoing epilepsy surgery. Familiarity with these types of images is important to the future of epilepsy management. MR imaging findings of postsurgical patients should not be confused for other similar appearing entities and well known mimics. While difficult to interpret, imaging confounded by artifact from implantable devices still can provide valuable information. Lastly, examples of the common and uncommon complications from epilepsy surgery will be shown, such as the characteristic appearance of hemorrhage from subdural grid electrode placement for electrocorticography.
Summary/Conclusion
Given the increase in epilepsy surgery, neuroradiologists need to familiarize themselves with perioperative and postoperative imaging appearances of surgical epilepsy patients, especially in the setting of newer tools such as 3D imaging. As part of a multidisciplinary team, the neuroradiologist also should be familiar with common implantable devices. Anatomical drawings and intraoperative pictures correlating with radiologic findings can help with understanding the imaging appearances in epilepsy surgical patients.

KEYWORDS: Epilepsy, 3D imaging, postoperative findings

eEdE-14

Reversible Focal T2 Hypointensity in Seizures Associated with Nonketotic Hyperglycemia

Lee, E.[1]·Jeong, B.[1]·Kim, K.[1]
[1]Dongguk University Ilsan Hospital, Goyang-City, KOREA, REPUBLIC OF, [2]Dongguk University Ilsan Hospital, Goyang-City, KOREA, REPUBLIC OF.

Purpose
Hyperglycemia rarely may be seen with seizures. Hyperglycemia may reduce seizure threshold because of the increase in gamma-aminobutyric acid metabolism and may trigger epileptic discharges. We describe MRI abnormalities in five patients with nonketotic hyperglycemia (NKH) and seizures, and also attempt to characterize the pathogenesis of this unusual finding.
Approach/Methods
We retrospectively evaluated clinical and radiologic abnormalities in five patients with NKH.
Findings/Discussion
All patients presented with seizures and long-standing diabetes mellitus. The MRI abnormalities observed acutely were focal subcortical hypointensities on T2-WI and FLAIR imaging in all patients with overlying cortical gyral hyperintensities in three patients. Focal overlying cortical or leptomeningeal enhancement on contrast-enhanced T1-weighted imaging or CE-FLAIR imaging, was observed in all patients. Diffusion-weighted imaging showed mild restricted diffusion in three patients with cortical gyral T2 hyperintensities. On clinical recovery, the subcortical T2 hypointensity and overlying cortical hyperintensities reversed in all patients.
Summary/Conclusion
Patients with seizures in NKH may have transient MRI abnormalities that are characterized by subcortical T2 hypointensity with overlying cortical or leptomeningeal enhancement in addition to cortical T2 hyperintensity. Recognition of this radiologic abnormality in NKH is important in restricting unwarranted investigations and to institute early therapy.

KEYWORDS: Diabetes, Seizure, MR imaging

eEdE-15

Holy Grails of Epilepsy Imaging: The "Nonlesional" Patient, Multifocal and Extratemporal Epilepsy

Kim, P. E.[1]·Hazany, S.[2]·Liu, C. Y.[1]·Heck, C.[1]·Millett, D.[2]·Lerner, A.[1]·Rajamohan, A.[1]·Shiroishi, M.[1]·Go, J. L.[1]·Boyko, O.[1]·Henderson, R.[1]·Law, M.[1]
[1]University of Southern California Keck School of Medicine, Los Angeles, CA, [2]Rancho Los Amigos National Rehab Center, University of Southern California Keck School of Medicine, Los Angeles, CA.

Purpose
Epilepsy diagnosis and treatment is one of the most complex endeavors in the field of neuromedicine; thus, the role of neuroimaging in epilepsy often is poorly understood, even by neuroradiologists, unless one is intimately associated with a robust epilepsy surgical practice. The purpose of this educational exhibit is to familiarize the neuroradiologist with the role of imaging in the evaluation of the epilepsy patient, particularly those being considered for resective surgery, and to describe the advanced imaging strategies that must be employed for those patients with “normal” or nonlocalizing imaging studies and electrographically multifocal or extratemporal epilepsy.
Approach/Methods
Utilizing the experience of the University of Southern California Keck Medical Center Comprehensive Epilepsy Program, some of the most difficult diagnostic/therapeutic dilemmas, most often “nonlesional” or extratemporal epilepsy cases, were selected to illustrate the role of neuroimaging in such evaluations. The complex integration of advanced multimodality imaging, including PET-MRI coregistration, SISCOM, and 3D neuronavigation, with

Note: Scanned images are included in the proceedings. Some submitted images were reduced during editing, thereby decreasing clarity. Also, refer to the Program Planner. Proceedings Content as of 3-29-2013.

clinical Video-EEG correlation and operative Phase II EEG guidance is discussed.
Findings/Discussion
A significant proportion of epilepsy cases are nonlocalizing with conventional neuroimaging, and commonly multifocal or extratemporal in origin. These cases make epilepsy diagnosis and treatment an extremely complex and challenging endeavor, stemming largely from current limitations of methodologies that can be used to assess and localize brain function. Additionally, resective surgery is potentially curative, but is a high-stakes endeavor that requires a high degree of confidence in data derived from a battery of diagnostic evaluations. Neuroimaging maintains a critical role in this assessment and is integrated somewhat differently into the complex epilepsy evaluation matrix compared to imaging evaluation of other neuropathologies because interpretation is highly dependent on clinical and electrographic correlation. This ultimately has important implications for neuroimaging interpretation and utilization.
Summary/Conclusion
Imaging in difficult epilepsy cases is a challenging undertaking with several unique elements relative to other neuroradiologic pursuits. We illustrate the most diagnostically challenging epilepsy cases to describe the strategic role of neuroimaging within the larger matrix of epilepsy diagnosis and treatment.

KEYWORDS: Multimodality imaging, MR imaging brain, SISCOM

eEdE-16

The Hippocampus: A Review of the Imaging Characteristics that Differentiates the Pathology Affecting this Unique Component of the Limbic System

Elgethun, M. T.·Spearman, M. P.·Fukui, M. B.
Allegheny General Hospital
Pittsburgh, PA.

Purpose
The hippocampus is a component of the limbic system that can be affected by certain disorders due to its unique attributes. We will present an educational exhibit reviewing the unique anatomy of the hippocampus including its arterial supply, as well as reviewing disorders that can affect the hippocampus including mesial temporal sclerosis, infarction, infection, dementia disorders, seizure disorders and malignancy.
Approach/Methods
The education exhibit will review the anatomy and arterial supply of the hippocampus and its unique role as a component of the limbic system. The CT and MR imaging characteristic of the different pathologies will be presented in an interactive case review format. The exhibit will emphasize the critical importance of understanding the hippocampus to form an accurate differential diagnosis taking into consideration the patient history and imaging characteristics.
Findings/Discussion
Based on its specific characteristics, the hippocampus is susceptible to unique pathology. The exhibit will discuss how the location, history and imaging characteristics of pathology affecting the hippocampus can help to determine the etiology. The exhibit will use an interactive case review format to illustrate how the patient history and imaging characteristics can help narrow the differential. In addition, the cases will provide examples of the importance of understanding the anatomy, arterial supply and function of the hippocampus in regards to its unique pathologic disorders as listed above.
Summary/Conclusion
This education exhibit has reviewed the unique structure, arterial supply of the hippocampus and its function as a component of the limbic system. The exhibit has demonstrated the imaging findings on CT and MR of the different pathologies arising in the hippocampus. This exhibit is designed to reinforce and review the hippocampus to emphasize the importance of understanding its intricacies resulting in its unique susceptibility to pathology.

KEYWORDS: Limbic system, Anatomy, hippocampus

eEdE-17

Brain Mapping: How Much Do You Know?

Gupta, S.[1]·Klein, A.[1]·Bhalla, M.[2]·Carranza, V.[2]·Ulmer, J. L.[1]·Leighton, M.[1]·Maheshwari, M.[3]·Ceranske, A.[1]·Baruah, D.[1]
[1]Medical College of Wisconsin, Milwaukee, WI, [2]Medical College of Wisconsin Affiliated Hospitals, Milwaukee, WI, [3]Childrens Hospital, Medical College of Wisconsin, Milwaukee, WI.

Purpose
An interactive case-based electronic quiz utilizing preoperative functional MR imaging (fMRI) and diffusion tensor imaging (DTI) data obtained for localizing at-risk functional networks (language, motor, vision) prior to tumor resection.
Approach/Methods
CC-FA DTI maps for this review were obtained with a 1.5 T system (GE Medical Systems, Milwaukee, WI) by using a dual-refocused spin-echo technique, 3 mm slice thickness, 13 gradient-encoding directions, a b-value = 900, an NEX = 2, a TE = 70 ms, and a TR min = 11 s to acquire 40 contiguous slices with a 128 x 128 matrix and 240 mm field of view. Axial, coronal, and sagittal CC-FA maps are used in an interactive quiz. Bold fMRI data also were acquired with motor, speech/language, and vision paradigms. Knowledge of specific white matter tracts, functional cortical regions, structure/function relationships, and proposed clinical deficits are tested and reinforced using a multiple choice format.
Findings/Discussion

Note: Scanned images are included in the proceedings. Some submitted images were reduced during editing, thereby decreasing clarity. Also, refer to the Program Planner. Proceedings Content as of 3-29-2013.

Three separate brain-mapping cases are presented in the following sequence: clinical presentation, conventional CT and MR imaging, preoperative fMRI and DTI data, surgical correlation, and postoperative imaging. Multiple choice questions and point-and-click functionality are used to test the user's knowledge of relevant functional anatomy and concepts. Five questions per case have been created for a total of 15 questions. The user's correct answers are recorded, and a final tally is displayed at the conclusion of the quiz. Three summary slides at the end of the exhibit illustrate the important concepts.
Summary/Conclusion
The goal of this interactive electronic quiz is to teach and reinforce functional anatomical considerations in brain tumor patients prior to surgery. When used effectively, fMRI and DTI have a profound impact on the preservation of language, motor, and vision networks.

KEYWORDS: fMRI, Self-assessment, reporting

eEdE-18

Demystifying Clinical Applications of Functional MR Imaging

Badve, C. A.·Vidal, L. L. M.·Blackham, K. A.·Sunshine, J. L.
University Hospitals Case Medical Center
Cleveland, OH.

Purpose
The purpose of this exhibit is to present the clinical application of functional MR imaging (fMRI) by describing the physiologic basis, reviewing the typical imaging acquisition and standard processing techniques, as well as illustrating day-to-day interpretation through clinical cases.
Approach/Methods
The viewer will first undergo a short self-evaluation to assess level of his/her current knowledge on fMRI. Subsequently, a succinct and relevant discussion on eloquent cortex anatomy, BOLD effect physiology and a typical fMRI imaging protocol will be presented. Then we will present an interactive session utilizing routine but exemplar clinical cases that display the primary and accessory motor cortex, speech generation and comprehension areas as well as the visual cortex within a variety of presurgical lesions and clinical scenarios. At the conclusion of the module, the viewer will be offered a second self-evaluation to assess newly acquired knowledge. The viewer also will be able to explore several hyperlinks, which will provide additional reading sources and fMRI trivia.
Findings/Discussion
Functional MRI is an elegant tool for assessing cortical activation and delineating eloquent cortex, based on the phenomenon of increased cortical activity leading to increase in oxyhemoglobin concentration. This in turn leads to small yet detectable signal changes on T2* images acquired during resting state as well as with different tasks that cause cortical activation. Intricate statistical postprocessing techniques allow quantitative comparison of signal between these states which then is utilized for radiologic interpretation. Functional MRI can identify the primary motor, visual and speech areas in the cortex in cooperative patients. This information permits the assessment of the spatial relationship between brain lesions and these critical areas. Current fMRI applications may include surgical and radiotherapy planning for brain tumors, arteriovenous malformations and epileptic foci resection. This noninvasive technique can enable greater margin of safety in surgical planning so as to minimize collateral damage during the surgery.
Summary/Conclusion
The authors present an interactive educational exhibit on the basic methods of fMRI acquisition, processing and interpretation that can be applied to a range of typical clinical scenarios. This exhibit, with the pre and postevaluations, will serve as an engaging self-learning exercise for the viewers. Residents and fellows will have an opportunity to familiarize themselves with this unique technique. Practicing neuroradiologists will reinforce their confidence on this topic with this refresher module.

KEYWORDS: fMRI, Motor cortex

eEdE-19

Nuclear Imaging for Neuroradiologists: PET-CT and Beyond

Go, M.[1]·Mukhi, S. V.[2]·Donohoe, K.[1]·Moonis, G.[1]
[1]Beth Israel Deaconess Medical Center, Boston, TX,
[2]Michael E DeBakey VA Medical Center, Houston, TX.

Purpose
To review established and emerging nuclear imaging studies that may be encountered by the practicing neuroradiologist and head and neck radiologist.
Approach/Methods
We will present illustrative nuclear imaging cases with cross-sectional correlation for the following entities: 1. Fluorodeoxyglucose (FDG) positron emission tomography (PET) for diagnosing Alzheimer disease; 2. Amyloid ligand imaging with PET for diagnosing Alzheimer disease; 3. FDG PET for differentiating radiation necrosis from recurrent brain tumors; 4. Thallium scan for differentiating radiation necrosis from recurrent brain tumors; 5. FDG PET for evaluating brain metastases; 6. FDG PET scan for differentiating lymphoma from toxoplasmosis; 7. I-123 MIBG for imaging neuroendocrine tumors; 8. In-111 pentetreotide scan for imaging neuroendocrine tumors; 9. I^{123} ioflupane for diagnosing Parkinson disease; 10. FDG PET for diagnosing mesial temporal sclerosis; 11. Tc-99m red blood cell (RBC) blood pool imaging for diagnosing calvarial hemangioma;12. Tc-99m Sestamibi for detection of parathyroid adenoma; 13. In-111 DTPA cisternography for diagnosing cerebrospinal fluid (CSF) leaks and 14. Tc-99m DTPA for confirming brain death.

Note: Scanned images are included in the proceedings. Some submitted images were reduced during editing, thereby decreasing clarity. Also, refer to the Program Planner. Proceedings Content as of 3-29-2013.

Findings/Discussion
MR imaging (MRI) and CT are the most commonly used modalities for imaging the brain and head and neck. However, functional nuclear imaging is playing an increasingly important and expanding role for diagnosing certain lesions in the brain and head and neck. The most common nuclear study encountered by the neuroradiologist is FDG PET-CT for the evaluation of head and neck cancer; however, there are many other established and emerging scenarios where the use of nuclear imaging provides invaluable information that may not be obtained through conventional CT or MRI. We depict a wide range of nuclear imaging studies that the neuroradiologist may encounter, describe the indications, mechanisms of action, and expected imaging findings with cross-sectional correlation, where appropriate.
Summary/Conclusion
Our exhibit illustrates and elucidates a wide range of nuclear imaging examinations that may be encountered by the neuroradiologist or used as an adjunct when conventional CT or MRI does not or cannot provide a definitive diagnosis.

KEYWORDS: Brain neoplasms, CSF leak, neurodegenerative

eEdE-20

MEG Time-Frequency Activity during Attentional Conflict in Traumatic Brain Injury

Luks, T. L.·Dale, C. L.·Tarapore, P. E.·Cooper, S.·LaHue, S. C.·Findlay, A. M.·Lee, H. A.·Honma, S. M.·Mizuri, D.·Nagarajan, S.·Mukherjee, P.
University of California San Francisco
San Francisco, CA.

Purpose
Patients with traumatic brain injury (TBI) are known to have persistent cognitive deficits, particularly in attention and working memory functions. We used magnetoencephalography (MEG) to examine the millesecond timecourse of neural activity during a Stroop Attention Task in four frequency bands with a beamforming source localization.
Approach/Methods
Data were acquired from 19 adult patients with mild or moderate TBI and 13 healthy controls using a 275-channel whole-head biomagnetometer (CTF Systems, Vancouver, BC) and analyzed in the time-frequency domain using Nutmeg (bil.ucsf.edu/nutmeg). Activity at each voxel over time was calculated at four different time frequencies of interest (theta: 4-7 Hz, alpha:8-12, beta: 12-30 Hz, low gamma: 30-55 Hz, high gamma: 63-117 Hz). For each participant, activity in each voxel for incongruent versus congruent trials (i.e., Stroop Conflict-related activity) was calculated and submitted to within and between group analyses.
Findings/Discussion
Control subjects had significant conflict-related activity in prefrontal and temporal regions in all four frequency bands, including activity in Dorsolateral Prefrontal Cortex (DLPFC) and Anterior Cingulate Cortex (ACC), beginning as early as 50 msec post-stimulus and extending through our 700 msec window (the point at which motor responses begin to occur). In these regions with normal conflict-related activity (as defined by the control group), TBI patients had equivalent or reduced activity. However, TBI patients had extensive significantly increased activity in other frontal, temporal and occipital brain regions in each frequency band. High Gamma activity in right prefrontal cortex from 350-450 msec and right ACC from 350-400 msec was associated with neurocognitive conflict processing scores in TBI patients, and this activity in right prefrontal cortex also was associated with Extended Glascow Outcome Scale (GOSE) scores, a measure of clinical status.

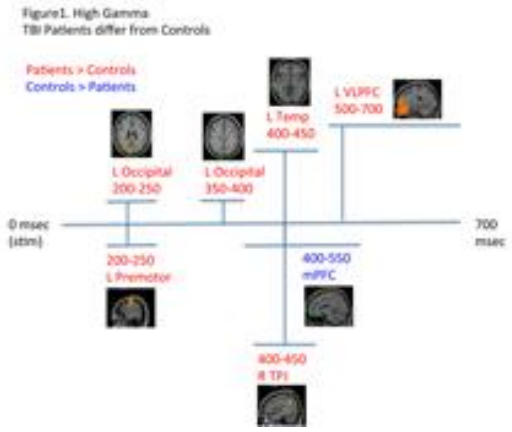

Summary/Conclusion
These results suggest that during attentional conflict, TBI patients had reduced activity in prefrontal attention networks, but increased compensatory activity in other regions, and that these cognitive changes were associated with clinical status.

KEYWORDS: Traumatic brain injury, MEG, attentional conflict

eEdE-21

Imaging of Viral Infection and White Matter Disease: Differential Diagnoses and Imaging Pitfalls

Moritani, T.·Kirby, P.
University of Iowa Hospitals and Clinics
Iowa City, IA.

Purpose
To demonstrate CT and MRI findings of white matter disease with various viral infections. To illustrate the pathology and pathophysiology and discuss the differential diagnosis.
Approach/Methods
We reviewed CT and MRI findings including diffusion-

Note: Scanned images are included in the proceedings. Some submitted images were reduced during editing, thereby decreasing clarity. Also, refer to the Program Planner. Proceedings Content as of 3-29-2013.

weighted imaging (DWI) in 46 patients with white matter involvement associated with viral infections. These cases are comprised of encephalitis/encephalopathy related to herpes simplex virus type 1 and 2, varicella zoster virus (VZV), Epstein-barr (EB) virus, cytomegalovirus, human herpes virus (HHV) type 6, human immunodeficiency virus (HIV), hepatitis virus, influenza virus, enterovirus, rotavirus, West Nile virus (WNV), progressive multifocal leukoencephalopathy (PML, JC virus), subacute sclerosing panencephalitis (SSPE, measles) and mild encephalitis/encephalopathy with a reversible splenial lesion (MERS). The diagnosis was based on antibody titers and MR imaging. Histopathology (biopsy or autopsy) was obtained in five patients.
Findings/Discussion
Herpes simplex encephalitis (HSE) is the most common cause of sporadic fatal encephalitis, accounting for 10-20% of encephalitic viral infections. Diffusion-weighted imaging was more sensitive than conventional MRI in detecting early changes of herpes encephalitis which is important for the treatment with acyclovir reducing the mortality. Pathologically, herpes encephalitis showed both cytotoxic and vasogenic edema associated with massive tissue necrosis and petechial or even confluent hemorrhage. The medial temporal lobes, inferior frontal lobes and insula commonly were involved. However, in infants and young children, the lesions tended to extend into frontoparietal lobes. In neonatal herpes simplex type 2 encephalitis, cerebral cortex and white matter were involved in a more global fashion. Human herpes virus-6-associated encephalitis has been recognized increasingly as a serious complication in immunocompromised patients. MR imaging often showed mesial temporal lobe involvement similar to HSE. However, ganciclovir and foscarnet are the treatment of choice. Multifocal cortical and white matter lesions were seen in VZV encephalitis and SSPE. Cytomegalovirus infection often involved periventricular white matter. Progressive multifocal leukoencephalopathy is characterized by demyelination, associated with oligodendrocytes infected with the JC virus. It usually is encountered in immunocompromised patients. West Nile virus develops meningoencephalitis. MR imaging showed mild hyperintense lesions on T2 and FLAIR in the basal ganglia, thalami, mesial temporal lobe, white matter, cerebellum, brain stem, especially the substantia nigra and medulla. Pathology demonstrated lymphocytic neutropholis perivascular lymphocytic cuffing, microglial nodules, spongiotic changes, and necrosis. White matter lesions in PML characteristically extended into the subcortical U-fibers. Cerebellar and brain stem involvements were common. The degree of lesion enhancement depended upon the patient's immunologic state. The pathologic hallmark of HIV encephalopathy/encephalitis is multinucleated giant cells in the white matter. MR imaging showed diffuse periventricular white matter lesions, but brain stem and basal ganglia also could be involved. Mild encephalitis/encephalopathy with a reversible splenial lesion secondary to viral infections (EB, influenza, rotavirus) also were demonstrated.
Summary/Conclusion
We demonstrate CT, MRI and DWI findings of viral encephalitis/encephalopathy with white matter involvement and various distributions. We discuss the differential diagnosis based on the characteristic distribution, and illustrate the underlying pathology and pathophysiology.

KEYWORDS: Encephalitis, Encephalopathy, viral

eEdE-22

Multidisciplinary Approach to Tropical and Subtropical Infectious Diseases: Imaging with Pathologic Correlation

Hanagandi, P. B.[1]·Goncalves, F. G.[2]·Amaral, L. F.[3]·Chong, J.[1]·Torres, C. I.[1]·Chankowsky, J.[1]·del Carpio, R.[1]
[1]Montreal General Hospital, McGill University, Montreal, QC, CANADA, [2]Radiologia Infinita - Brasilia Children's Hospital, Brasilia, BRAZIL, [3]Hospital da Beneficência Portuguesa de São Paulo & Hospital São José, São Paulo, BRAZIL.

Purpose
To highlight the diverse neuroimaging features of various endemic tropical and subtropical infectious diseases with serology and pathologic correlation.
Approach/Methods
We intend to describe the pathognomonic CT and MR imaging features of several tropical/subtropical CNS infections. We include a selection of both common and rare bacterial, granulomatous, viral, fungal and parasitic infections with interactive differential diagnosis.
Findings/Discussion
The spectrum of tropical/subtropical infections can present with a wide range of clinical symptoms ranging from fulminant to insidious onset, as well as chronic/progressive to relapsing/remitting course. Many of these diseases have pathognomonic imaging findings related to specific anatomical sites of CNS involvement. Others are less specific and require laboratory confirmation. Based on a high index of clinical suspicion, demographics and specific laboratory investigations one often can make an accurate diagnosis. This pictorial includes cases of tuberculosis, neurocysticercosis, toxoplasmosis, neurosyphilis, schistosomiasis, trypanosomiasis, hydatid disease, blastomycoses, cryptococcosis, amoebic encephalitis, poliomyelitis, Japanese encephalitis, cerebral Malaria, West Nile encephalitis, varicella, listeriosis and HIV differential diagnosis and brief interactive discussion.

Note: Scanned images are included in the proceedings. Some submitted images were reduced during editing, thereby decreasing clarity. Also, refer to the Program Planner. Proceedings Content as of 3-29-2013.

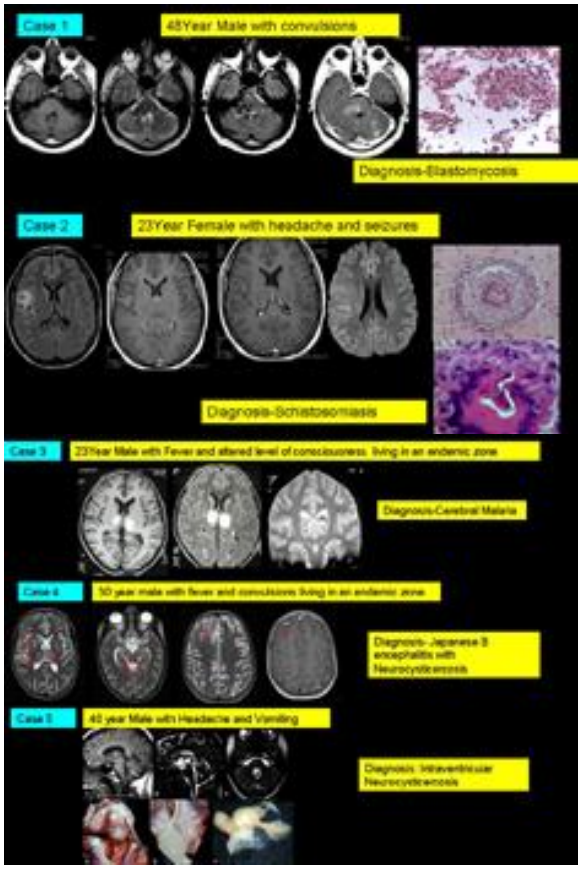

Summary/Conclusion
In view of the increasing immigration to Western countries as well as the popularity of world travel, many of these diseases are now evolving from endemic to worldwide phenomena. The radiologist needs to be aware of patients background and familiarize one's self with both the characteristic and unusual imaging features of these diseases to avoid diagnostic delay and complications.

KEYWORDS: Infections, 1.5T, tropical, bacterial, fungal, parasitic,viral

eEdE-23

MR Imaging and Clinical Characteristics of Anti-Aquaporin4 Antibody Positive NMO or NMO Spectrum Disorders

Kurobe, Y.·Maeda, M.·Umino, M.·Sakuma, H.
Mie University School of Medicine
Tsu, JAPAN.

Purpose
The anti-aquaporin4 (AQP4) antibody has been incorporated into diagnostic criteria for neuromyelitis optica (NMO). Some anti-AQP4-positive patients who do not match the diagnostic criteria are termed as NMO spectrum disorders. This exhibit presents characteristic MR imaging findings and clinical findings of anti-aquaporin4 antibody positive NMO or NMO spectrum disorders.

Approach/Methods
We recruited 11 patients with anti-aquaporin4 antibody positive NMO or NMO spectrum disorders at our hospital, including three patients with definite NMO, five patients with myelitis, and one patient with optic neuritis. However, two patients had neither myelitis nor optic neuritis. MR imaging and clinical characteristics of those patients were evaluated retrospectively.

Findings/Discussion
A summary of clinical and MR imaging findings is shown in the Table. All eight patients with myelitis had typical contiguous spinal lesion over three or more vertebral segments. Contrast-enhanced MR imaging revealed definite enhancement in four patients. The enhancement pattern was identical to that of spinal sarcoidosis in two of the four. Brain lesions were detected in 10 patients. Four patients showed characteristic NMO lesion locations such as the dorsal brainstem or hypothalamus. Among the four, one patient showed posterior reversible encephalopathy syndrome in her clinical course (Figure). Four patients showed nonspecific lesions, but two patients showed periventricular ovoid lesions resembling those of multiple sclerosis. MR spectroscopy showed decreased NAA/Cho in four patients.

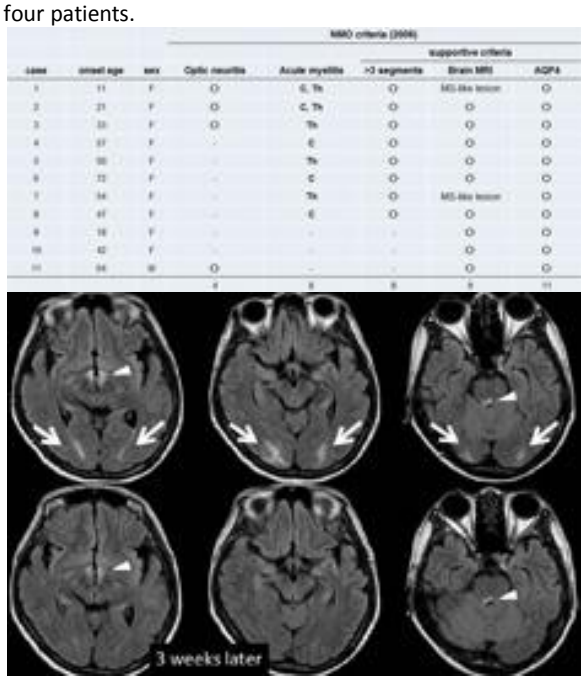

Summary/Conclusion
We will present typical and atypical MR imaging findings as well as clinical findings of anti-aquaporin4 antibody positive NMO or NMO spectrum disorders in light of the literature. This exhibit enhances knowledge related to anti-aquaporin4 antibody positive NMO or NMO spectrum disorders.

Note: Scanned images are included in the proceedings. Some submitted images were reduced during editing, thereby decreasing clarity. Also, refer to the Program Planner. Proceedings Content as of 3-29-2013.

KEYWORDS: MR imaging, Neuromyelitis optica, NMO spectrum disorders

eEdE-24

Neuroimaging of the Complications of Natalizumab Therapy in Multiple Sclerosis: A Pictorial Review

Honce, J. M.
University of Colorado
Aurora, CO.

Purpose
Natalizumab is an effective therapy for patients with multiple sclerosis (MS), and is being prescribed with increasing frequency, in some cases as a first line agent. With the increased utilization of natalizumab, complications associated with this therapy are seen more often in clinical practice. The primary complication of natalizumab therapy is the rare but devastating progressive multifocal leukoencephalopathy (PML). Fortunately, rapid drug withdrawal, usually by plasma exchange, has improved patient survival. Unfortunately, a new problem, PML associated immune reconstitution inflammatory syndrome (PML-IRIS), has emerged after drug withdrawal, and has a significant negative impact on patient outcomes. The IRIS phenomenon is not limited to PML treatment, and has been described recently in patients ceasing natalizumab therapy for other reasons (a phenomenon we term natalizumab rebound). The purpose of this exhibit is to discuss the MR imaging (MRI) features and clinical characteristics of natalizumab associated PML, PML-IRIS and natalizumab rebound, with emphasis on the early imaging features, allowing rapid diagnosis, treatment and/or modification of therapies to improve patient outcomes.
Approach/Methods
Using a case-based, interactive approach, cases of PML, PML-IRIS and natalizumab rebound that were diagnosed and/or treated at our institution are reviewed. The MRI features and clinical characteristics of natalizumab associated PML are detailed, focusing specifically on features of PML lesions very early in the disease when patients are asymptomatic or nearly asymptomatic, and before more classical PML lesions have developed. Imaging features that are predictive of earlier/more aggressive PML-IRIS are discussed, as are the MR findings of PML-IRIS itself. Finally the MRI features and clinical characteristics of natalizumab rebound are detailed, focusing on differentiating this phenomenon from conventional MS relapses.
Findings/Discussion
To limit the devastating impact of natalizumab associated PML and PML-IRIS it is crucial that neuroradiologists recognize their clinical and imaging spectrum, especially the earliest features of these disease processes. The shape, location and distribution of lesions, T1-weighted hypo or hyperintensity, microcyst/granular appearance on T2-weighted imaging, patterns of contrast enhancement, and hyperintensity on diffusion imaging are all key to making a confident, early diagnosis of PML and excluding differential considerations such as MS relapse, ADEM, or other infectious/inflammatory processes. Early contrast enhancement and widespread disease are associated with poorer patient outcomes, independent of delays in diagnosis, and predict earlier development/increased severity of PML-IRIS. Natalizumab rebound is an aggressive inflammatory response occurring months after drug cessation, and is characterized by an atypically high number of enhancing lesions in a widespread distribution, tending to occur at pre-existing T1 hypo intense lesions. Recognizing and differentiating natalizumab rebound from an MS relapse is critical as more aggressive therapies usually are needed.
Summary/Conclusion
After viewing this exhibit, the learner will: A - Recognize the clinical and imaging features of natalizumab associated PML, including features occurring early in the disease, when the patient is asymptomatic or near asymptomatic. B - Recognize the imaging features of PML-IRIS, and MR findings on initial imaging predictive of earlier/more aggressive PML-IRIS and poorer patient outcomes. C - Differentiate between conventional MS relapse and the aggressive inflammatory response of natalizumab rebound.

KEYWORDS: Multiple sclerosis, Medication, natalizumab

eEdE-25

Spectrum of Drug-Induced Complications in the Brain: A Primer for the Radiologist

Rohatgi, S.[1,2]·Hsu, L.[1,2]
[1]Brigham and Women's Hospital, Boston, MA, [2]Harvard Medical School, Boston, MA.

Purpose
1. To illustrate via examples, the various imaging characteristics of drug-induced complications in the brain.
2. Clinical management and prognostic implications of imaging changes.
Approach/Methods
In this exhibit, we will demonstrate and discuss the various drug-induced imaging findings in the brain, which often present as diagnostic dilemmas due to their rarity and lack of clinical familiarity. Key pertinent differential diagnosis and management issues also are included.
Findings/Discussion
Drug-induced central nervous system (CNS) findings are varied and may not be familiar to practices that commonly do not interact with certain patient populations such as oncological specialties and their multiple drug treatment protocols. Often the cases are made even more challenging due to a lack of appropriate history or misleading presentation. As the patients often are followed up at different imaging centers it is important for the radiologist to be aware of some of these findings, to

Note: Scanned images are included in the proceedings. Some submitted images were reduced during editing, thereby decreasing clarity. Also, refer to the Program Planner. Proceedings Content as of 3-29-2013.

provide better patient care especially in the outpatient settings. Central nervous system toxicity due to recreational drugs and alcohol are relatively common and well documented. Neuroimaging changes that are due to methotrexate, platinum derivatives, cyclosporin and metronidazole are less frequent. In the current era of molecular targeted therapy, especially in cancer patients with their many evolving treatment options, brain is at particular risk for side effects. Novel toxicities and new imaging appearances are seen in patients on antiangiogenic agents like bevacizumab (avastin), tyrosine kinase inhibitors, monoclonal antibodies like ipilimumab and natalizumab (Tysabri). Potential complications include hemorrhages, ischemic strokes, posterior reversible encephalopathy (PRES), hypophysitis and progressive multifocal leukoencephalopathy (PML). These drug-related sequelae vary from self limiting reversible manifestations to severe life-threatening conditions, thus early recognition is paramount so that appropriate therapy can be instituted promptly and misdiagnosis avoided.
Summary/Conclusion
We have reviewed the imaging spectrum of drug-induced complications in the brain using case-based examples. Awareness of these complications on imaging is important as it can improve outcomes by initiating the appropriate treatment as well as cessation of the offending drug. This exhibit is designed to provide a framework by which general and neuroradiologists may work in concert with clinicians to optimize patient care and treatment outcomes.

KEYWORDS: Brain, Drugs, complications

eEdE-26

Virchow-Robin Spaces also Known as Perivascular Spaces: Why Should I Care?

Patel, T. Y.·Blackham, K. A.·Coffey, M. D.·Badve, C. A.·Vidal, L. L. M.·Javadi, P.
University Hospitals Case Medical Center
Cleveland, OH.

Purpose
The purpose of this Educational Exhibit is twofold: a) to demonstrate the anatomy and physiology of Virchow-Robin spaces also known as perivascular spaces; and b) to discuss common pathology affecting these intracranial spaces.
Approach/Methods
Users will be exposed to an image-based format to appreciate the anatomy and physiology of perivascular spaces. This will be followed subsequently by a case-based discussion on the most common pathology affecting these spaces as well as the mimics of dilated perivascular spaces. To consolidate the concepts learned, users will have the chance to go through a self-assessment module at the end of each section.
Findings/Discussion
Virchow-Robin spaces are pial-lined perivascular spaces filled with interstitial fluid that surround perforating intracranial blood vessels as they travel from the subarachnoid space through the brain parenchyma. They follow CSF intensity on all MR sequences. Based on their characteristic location within the brain, these spaces are subdivided into three different types. While they are normal structures in the brain and can be seen with increasing frequency and size with advanced age, it is important to distinguish them from pathologic mimics giving the appearance of apparently dilated perivascular spaces such as lacunar infarcts, neurocysticercosis, arachnoid cysts, and cystic neoplasms. Furthermore, there are several important disease entities that cause abnormal enhancement as well as true lesions of these otherwise normal appearing perivascular spaces. Classic examples include neoplasms such as glioblastoma and lymphoma, vasculitis including primary cerebral angiitis, infectious etiologies such as meningitis, and inflammatory conditions such as sarcoidosis and amyloidosis.
Summary/Conclusion
This educational exhibit will be helpful for the residents and fellows to appreciate the nuances of perivascular spaces. Additionally, it will serve as a quick review for the more experienced neuroradiologists.

KEYWORDS: Virchow-Robin space, Anatomy, pathology

eEdE-27

A Case of CLIPPERS: A Rare, Recently Described Inflammatory Brainstem Condition with a Review of the Differential Diagnosis

Tarabishy, B.·Aho, T. R.
Henry Ford Hospital
Detroit, MI.

Purpose
Chronic lymphocytic inflammation with pontine perivascular enhancement responsive to steroids (CLIPPERS) is a recently described autoinflammatory disease of predominantly the brainstem and cerebellum with distinct clinical, radiologic and pathologic features. To date, approximately 30 cases have been reported in the literature. We report a case of CLIPPERS at our institution with follow-up imaging and supplement it with a thorough differential diagnosis with illustrative cases.
Approach/Methods
A detailed history along with physical exam, laboratory findings and imaging findings for a case of CLIPPERS at our institution is presented. Findings from recently published literature also are reviewed and presented. Finally, a detailed differential diagnosis is reviewed accompanied by illustrative cases.
Findings/Discussion
Our patient illustrates the unique clinical and imaging findings of CLIPPERS including nonspecific laboratory findings and a characteristic "salt and pepper"

Note: Scanned images are included in the proceedings. Some submitted images were reduced during editing, thereby decreasing clarity. Also, refer to the Program Planner. Proceedings Content as of 3-29-2013.

enhancement pattern on MRI with marked improvement after steroids. Review of the literature confirms these features as reliable indicators of CLIPPERS.
Summary/Conclusion
CLIPPERS is a newly described autoinflammatory disease of the brain with distinct and characteristic clinical, pathologic and imaging findings that should be included in the differential of interpreting physicians whenever the suggestive imaging findings are seen in the brainstem.

KEYWORDS: Brainstem, Inflammatory

eEdE-28

Pictorial Review of the Imaging Manifestations of Neurosarcoidosis

Nguyen, W.[1]·Ashruf, S.[1]· Endale, B.[1]·Stern, B.[1]·Steven, A.[1]
[1]University of Maryland Medical Center, Baltimore, MD,
[2]University of Maryland Medical Center, Baltimore, MD.

Purpose
Sarcoidosis is an idiopathic multisystem inflammatory disorder known to present with a wide variety of both clinical and imaging manifestations when affecting the neuraxis. By reviewing both the common and uncommon imaging findings of neurosarcoidosis, this exhibit seeks to raise awareness of this disease process.
Approach/Methods
Over 50 cases of neurosarcoidosis were collected to help with this presentation. Cases were collected prospectively in the radiology department, from medical records in the neurology clinic, and by utilizing a search engine to mine the PACS system, all at the University of Maryland Medical Center. All confirmed cases were cross-referenced with the clinical presentation, and clinical and imaging followup when available.
Findings/Discussion
Neurosarcoidosis has a multitude of imaging manifestations which may involve all spaces along the entirety of the neuraxis. Most commonly it presents as leptomeningeal enhancement with preference for the basilar cisterns. Other imaging manifestations include involvement of the cranial nerves resulting in cranial nerve deficits. Neurosarcoidosis also can demonstrate parenchymal involvement, most commonly involving the hypothalamus and brain stem. Spinal neurosarcoidosis is a relatively uncommon manifestation and can present as intramedullary, intradural extramedullary, extradural, vertebral or even disk space lesions. When there is both intra and extramedullary disease, sarcoidosis should be strongly considered as there are few entities which demonstrate both simultaneously. Correlation with imaging outside of the CNS, including the musculoskeletal system and thorax, can aid greatly in diagnosis as over 90% of these patients will have additional systemic findings.
Summary/Conclusion
Neurosarcoidosis has protean imaging and clinical manifestations and often is difficult to diagnose definitively. By understanding its variable imaging manifestations, the neuroradiologist may aid our clinical colleagues in further workup and subsequent management of these complex patients.

KEYWORDS: Sarcoid, Neurosarcoidosis

eEdE-29

Completing the Differential: A Comprehensive Discussion of Multiple Sclerosis Mimics

Jewells, V.·Horsley, L. C.
University of North Carolina - Chapel Hill
Chapel Hill, NC.

Purpose
This review will examine the imaging findings, symptoms, pathophysiology, laboratory, and treatment differences of multiple sclerosis (MS) and its many mimics in order to discuss the broad differential of diseases that should be considered during image interpretation.
Approach/Methods
Records were identified by searching an IRB-approved database of 783 patients with MS and MS-like symptomatology with selective review of MR images and clinic notes to address the pathology exhibited at our institution.
Findings/Discussion
Some patients presented with MS-like symptoms and ultimately were diagnosed with unusual medical conditions including chronic inflammatory demyelinating polyneuropathy (CIDP), dilitative arteriopathy (autopsy proven, Figure #1), and HTLV-1. Distinct imaging, laboratory, and clinical findings help pinpoint the correct diagnosis.

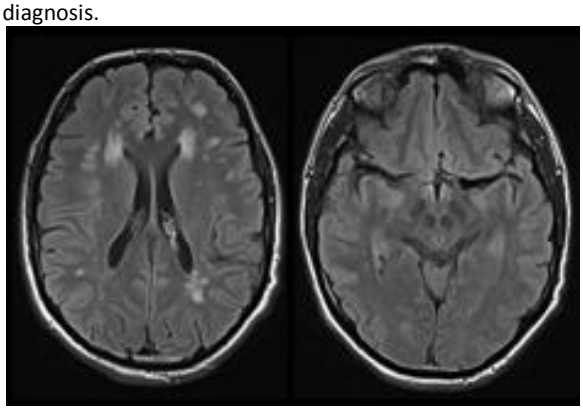

Figure. Thirty-one-year-old caucasian male who presented with MS symptoms, but was proven at autopsy to have no demyelinating lesions, but rather dilitative arteriopathy. FLAIR images are shown. The first image shows multiple abnormal FLAIR signal foci typical of MS lesions. The second image shows ectasia of the bilateral middle cerebral arteries.
Summary/Conclusion
Despite clinical criteria, laboratory tests, and specific

Note: Scanned images are included in the proceedings. Some submitted images were reduced during editing, thereby decreasing clarity. Also, refer to the Program Planner. Proceedings Content as of 3-29-2013.

brain/spine MRI findings, MS is a diagnosis of exclusion with a large number of disorders that mimic it. Some variants or forms of MS including Balos concentric sclerosis and neuromyelitis optica express positive complement resulting in a more aggressive course, and if suspected need to be addressed in the imaging report. In addition, acute disseminated encephalomyelitis (ADEM), CADASIL, Behçet's disease, progressive multifocal leukoencephalopathy (PML), Sussac's syndrome, HIV encephalopathy, sarcoidosis, systemic lupus erythematosus (SLE), Sjögren's syndrome, Lyme disease, toxoplasmosis, and neoplasms are typically mentioned in the literature as being misdiagnosed as MS, in addition to the rare conditions we also encountered. These processes will be described with regard to their imaging, pathophysiology, and laboratory differences to educate the audience about the many MS mimics.

KEYWORDS: Multiple sclerosis, Differential diagnosis

eEdE-30

RadioGenomics and Glioblastoma Multiforme: Update from the TCGA Glioma Phenotype Research Group

Flanders, A. E.[1]·Colen, R. R.[2]·Gutman,, D. A.[3]·Hwang, S. N.[3]·Wintermark, M.[4]·Jain, R.[5]·Jilwan-Nicolas, M.[4]·Chen, Y. J.[6,7]·Raghavan, P.[4]·Holder, C. A.[3]·Rubin, D.[8]·Erickson, B.[9]·Huang, E.[10]·Kirby, J.[10]·Freymann, K.[10]·Jaffe, C. C.[11]·TCGA Glioma Phenotype Research Group
[1]Thomas Jefferson University Hospital, Philadelphia, PA, [2]M. D. Anderson Cancer Center, Houston, TX, [3]Emory University, Atlanta, GA, [4]University of Virginia, Charlottesville, VA, [5]Henry Ford, Detroit, MI, [6]University of California San Diego Health System, San Diego, CA, [7]San Diego Medical Center, San Diego, CA, [8]Stanford University, Stanford, CA, [9]Mayo Clinic, Rochester, MN, [10]NCI/NIH, Bethesda, MD, [11]NCI/NIH, Rockville, MD.

Purpose
Imaging features of cancers are phenotypic expressions of the tumors genomic blueprint. The term "radiogenomics" or the phrase "genomic imaging" has been applied to the concept of bridging these relationships between imaging and genomics in clinical research. Opportunities to systematically marry the rich imaging features provided by MR imaging to genetics of cancer have been limited to small cohorts and exploration of limited imaging features. The Cancer Genome Atlas (TCGA) has been banking large volumes of tumors for comprehensive genomic analysis. The first tissue line collected by TCGA was glioblastoma multiforme (GBM). Concurrently, the Cancer Imaging Program (CIP) collected baseline MRI studies on each of the TCGA submissions into a secure repository known as the Cancer Imaging Archive (TCIA). The purpose of this exhibit is to summarize the collective work of the TCGA Glioma Phenotype Research Group - an ad hoc volunteer committee focused on advancing the complementary role of imaging in understanding the biological and clinical behavior of GBM.
Approach/Methods
The TCGA Glioma Phenotype Research group initially developed, vetted and tested a controlled vocabulary of comprehensive MRI features of GBM. This VASARI featureset captures 30 unique imaging characteristics that are familiar to neuroradiologists in the evaluation of brain tumors. Using this methodology, the baseline imaging features of over 130 glioblastomas have been recorded by three or more independent observers. Subsets of physiologic imaging characteristics such as dynamic susceptibility contrast (DSC perfusion) and diffusion tensor imaging (DTI) were utilized for related analyses.
Findings/Discussion
Through this unique collaborative effort, eight other distinct research arms have been initiated from this single project that focused on the interrelationship of the 30 subjective MRI features (VASARI featureset) and the genetics of GBM. These include: (1) DSC T2* MR perfusion analysis which examines the combination of perfusion metrics and molecular characteristics to improving ability to predict survival; (2) Forecasting disease-free interval and survival using combined modeling of clinical parameters, imaging and genomics; (3) Mapping of edema/cellular invasion to MR phenotypes using MRI volumetrics and large-scale gene and microRNA expression profiling in GBM; (4) A growth kinetic study to predict growth pattern of GBM based upon features on baseline MRI, (5) Man-machine correlation of cardinal MR imaging features scored between human and machine observers; (6) Prediction of histopathologic, genomic and clinical features from DTI characteristics of GBM; (7) A computer-aided detection (CAD) texture analysis which uses multispectral features including intensity, texture and morphology to identify important features that predict genetic patterns; and (8) Supervised and unsupervised clustering of GBM into semantically distinct categories using imaging derived features.
Summary/Conclusion
Imaging has a much greater role to play in oncology than just diagnosis and staging. There is a complementary role between clinical parameters, imaging and genetics that can improve upon current methods to predict disease type, response to treatment and overall survival in GBM. The collective work of the TCGA Glioma Phenotype Working Group serves as a model for efficient collaboration and discovery.

KEYWORDS: Glioblastoma, Genomic analysis, MR imaging

Note: Scanned images are included in the proceedings. Some submitted images were reduced during editing, thereby decreasing clarity. Also, refer to the Program Planner. Proceedings Content as of 3-29-2013.

eEdE-31

Spectrum of Neuroimaging Findings in Radiation-Related Central Nervous System Lesions

Gocmen, R.·Guler, E.·Guler, I.·Ozgen, B.·Oguz, K.
Hacettepe University
Ankara, TURKEY.

Purpose
To review the imaging features and discuss the approach to the differential diagnosis of radiation-induced injury in the central nervous system (CNS).
Approach/Methods
The computed tomography and magnetic resonance imaging findings of patients who had undergone radiation therapy and developed radiation-related lesions in CNS were reviewed for this educational exhibit.
Findings/Discussion
The various types of radiation-induced changes of brain will be described and characterized. These include: radiation necrosis, diffuse white matter injury, focal white matter lesion, vascular lesions (pseudoaneurysm, telangiectasia, cavernoma, arteriovenous malformation, vasculitis), mineralizing microangiopathy, transient focal contrast enhancement, secondary neoplasm, stroke-like migraine attacks after radiation therapy (SMART), necrotizing leukoencephalopathy.
Summary/Conclusion
Radiation therapy is used frequently for the treatment of neoplastic or nonneoplastic CNS disorders such as arteriovenous malformations. With the growing use of high dose radiation therapies such as cyberknife or gamma knife, radiation-induced injuries are increasingly encountered. The radiologists should be familiar with the imaging characteristics and differential diagnosis with essentially brain tumor in these lesions.

KEYWORDS: Radiation injury, Cerebral radiation necrosis, MR imaging

eEdE-32

3 Square Centimeters. Anatomy and Pathology of the Posterior Third Ventricle, Pineal and Quadrigeminal Plate Region: A Neuroradiographic Review

Fredriksen, J. R.·Morris, J. M.
Mayo Clinic
Rochester, MN.

Purpose
To demonstrate the imaging appearance of the normal anatomy and pathology of lesions occurring in the posterior third ventricle, pineal region, quadrigeminal plate, quadrigeminal plate cistern, velum interpositum, and internal cerebral veins.
Approach/Methods
After obtaining IRB approval we retrospectively searched the pathology, surgery, radiology, and clinical institutional databases for pathologic diagnosis of lesions in the above states regions over a 15-year time frame. Specifically search terms including the anatomical location as well as the varied pathologies that can occur in these locations were queried. This included but was not limited to pineal gland, internal cerebral veins, posterior commissure, Habenular commissure, Velum Interpositum, thalamus, choroid plexus, quadrigeminal plate, aqueduct of Sylvius, third ventricle, tectum, superior and inferior colliculus, epidermoid, teratoma, dermoid, quadrigeminal plate glioma, primary pineal neoplasm of indeterminate grade, pineocytoma, pineoblastoma, papillary tumor of the pineal gland, germinoma, mixed germ cell neoplasm, meningioma, ependymoma, subependymoma, choroid plexus papilloma, choroid plexus carcinoma, pilocytic astrocytoma, splenium corpus callosum, aqueductal stenosis, cavernous hemangioma, trilateral retinoblastoma, pineal cyst, lipoma, pineal metastasis, vein of Galen aneurysm, arteriovenous malformation, internal cerebral vein thrombosis, and dural arteriovenous fistula. We then reviewed the available imaging and detailed the distinguishing imaging characteristics, age and clinical history that allowed lesions to be differentiated from one another.
Findings/Discussion
Lesions that occur in the posterior third ventricle, pineal, and quadrigeminal plate region are often large at the time of diagnosis making site of origin difficult to pinpoint. Since many of the lesions ultimately go on to biopsy it is helpful to the referring neurosurgeon to have as much information as possible before performing a biopsy or if a biopsy is even necessary. We describe in this educational exhibit ways to help the neuroradiologist narrow the differential diagnosis using anatomical clues, age of the patient, available laboratory data, clinical history, and novel imaging techniques.

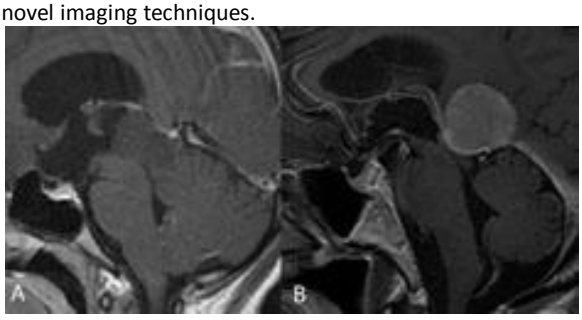

Summary/Conclusion
A wide array of pathologic entities and normal variants can occur in this 3 squared centimeter region of the brain. After the conclusion of viewing this educational exhibit the radiologist will be able to provide a meaningful, concise, and clinically relevant differential diagnosis to the referring clinicians.

KEYWORDS: Pineal gland, Third ventricle, quadrageminal plate

Note: Scanned images are included in the proceedings. Some submitted images were reduced during editing, thereby decreasing clarity. Also, refer to the Program Planner. Proceedings Content as of 3-29-2013.

eEdE-33

Mimics of Brain Tumor at Neuroimaging with Clinicopathologic Correlation

Starkey, J.·Tihan, T.·Cha, S.
University of California San Francisco
San Francisco, CA.

Purpose
To review the CT and MRI features that differentiate tumor mimics from brain tumors.
Approach/Methods
We retrospectively reviewed the CT and MR imaging of all patients without prior intracranial abnormality who were referred to our institution for resection of lesions initially interpreted as tumor and later proven non-neoplastic on pathology. For these cases, we reviewed the imaging findings that potentially aid in prospective diagnosis of tumor mimicking entities.
Findings/Discussion
Of 956 cases identified, 120 (12.6%) were pathologically proven to be non-neoplastic: 56 abscess/infection, 25 demyelination disease, 15 vascular (cavernous angioma, hemangioma, venous telangiectasia, organized hematoma), 8 radiation necrosis (with prior non-melanomatous head/neck or skin primary malignancy treated with external beam radiation), 7 subacute ischemia, 7 angiitis/vasculitis/nonspecific inflammation, and 2 astrogliosis. Five imaging findings suggestive of tumor mimics include 1) T1 hyperintensity, 2) smooth and complete rim of T2 hypointensity, 3) homogeneously reduced diffusion, 4) rim of leading edge reduced diffusion, and 5) incomplete ring enhancement in a cystic lesion. Prior history of radiation therapy that included irradiation of a part of brain was the most helpful in the diagnosis of radiation necrosis in a patient presenting with aggressive-appearing brain mass. We provide CT, MR, and histopathology images for representative cases, including gyral T1 shortening in subacute ischemia, smooth peripheral T2 shortening in cavernous angioma, homogeneously reduced diffusion within a ring enhancing mass including pyogenic abscess, tuberculoma, nocardia, and neurocysticercosis, leading edge peripheral reduced diffusion within an angioinvasive aspergillosis brain abscess, temporal lobe FLAIR hyperintensity with reduced diffusion in herpes encephalitis, incomplete ring enhancement in cystic tumefactive demyelination, and irregular rim enhancement with surrounding edema in radiation necrosis.

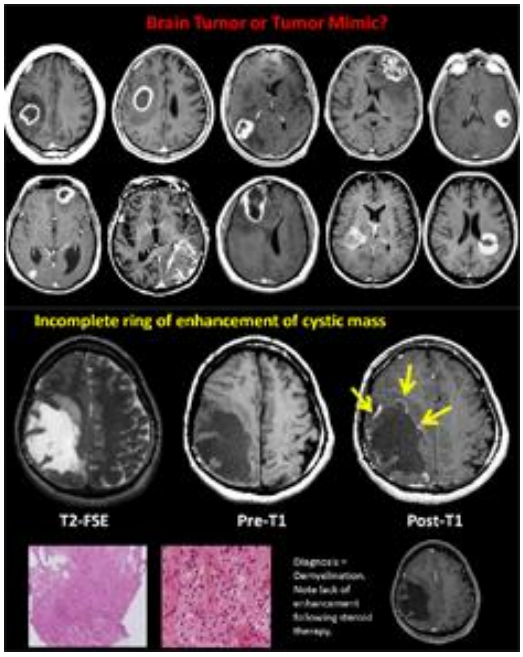

Summary/Conclusion
While tumor mimics share many imaging features with neoplastic brain lesions, they have specific MRI features that aid in preoperative diagnosis, avoiding unnecessary surgical resection and allowing appropriate clinical management.

KEYWORDS: Neoplasm, mimic

eEdE-34

Granulocytic Sarcoma: What the Radiologist Needs to Know Regarding Granulocytic Sarcoma and Other Associated Conditions

Chaudhry, A.[1]·Hoefling, N. L.[1]·Gul, M.[2]·Peyester, R.[1]
[1]Stonybrook University Medical Center, Stonybrook, NY,
[2]Winthrop University Hospital, Mineola, NY.

Purpose
Granulocytic (myeloid) sarcoma can be the initial presentation of aleukemic leukemia that either resulted from myelodysplastic syndrome conversion into leukemia, de novo aleukemic leukemia or leukemia relapse. It can present weeks to months before the peripheral presence of the leukemia. Although granulocytic sarcoma carries a broad differential diagnosis, it can be narrowed utilizing age, clinical features, and imaging characteristics of the lesion, such as location, enhancement pattern and presence of necrosis. By the conclusion of this presentation, the radiologist should have a better understanding of various clinical presentations of granulocytic sarcoma and relevant imaging and pathologic findings.
Approach/Methods
We present a case-based review of the clinical features, imaging, pathophysiology, histologic features, treatments

Note: Scanned images are included in the proceedings. Some submitted images were reduced during editing, thereby decreasing clarity. Also, refer to the Program Planner. Proceedings Content as of 3-29-2013.

and prognosis of granulocytic (myeloid) sarcoma also known as chloroma. We will describe the characteristic imaging (CT and MRI) features of granulocytic sarcoma. Information will be presented on the various conditions associated with granulocytic sarcoma such as myelodysplastic syndrome and acute myelogenous leukemia; clinical presentation and histopathologic findings of each entity are discussed.
Findings/Discussion
Multiple different presentations of granulocytic sarcoma will be shown, including brain parenchymal, ventricular, submandibular, orbital and spinal. We also will show cases of similar appearing entities such as lymphoma, metastases, infection, tuberculosis, astrocytoma, sarcoma, sarcoidosis, hemangiopericytoma and malignant fibrous histiocytoma, with an emphasis on differentiating these from granulocytic sarcoma. Additional processes resulting from infection, inflammation, injury and/or malignancy that may mask and/or mimic granulocytic sarcoma will be discussed with emphasis on key points which help to narrow the differential diagnosis.
Summary/Conclusion
Granulocytic sarcoma is a rare pathology that can be the initial manifestation of aleukemic leukemia. Knowledge of the imaging characteristics and differential considerations can play an important role and aid in the early diagnosis of this disease.

KEYWORDS: Cancer, Leukemia

eEdE-35

PET Parametric Response Maps as a Clinical Tool for Clinical Monitoring and Predicting Treatment Response in Diffuse Gliomas

Ellingson, B. M.·Harris, R. J.·Chen, W.·Czernin, J.·Phelps, M. E.·Cloughesy, T. F.·Pope, W. B.
David Geffen School of Medicine at University of California Los Angeles
Los Angeles, CA.

Purpose
PET tracers have demonstrated superior specificity for identifying regions of metabolically active brain tumors; however, single time-point evaluations of tumor tracer uptake fail to reflect temporal changes in tumor metabolic behavior and lack insight into the spatial heterogeneity of tumor growth and/or response to therapy. The purpose of this study is to highlight the value in 18F-FDG, 18F-FDOPA and 18F-FLT PET parametric response maps (PRMs) as a tool clinical evaluation of patients with diffuse gliomas.
Approach/Methods
PET PRMs are calculated by performing voxel-wise subtraction between tracer standard uptake value (SUV) on a current PET scan (e.g., during treatment) and a previous (baseline) scan after registration to the same image space. Specifically, baseline PET images are first aligned to a baseline MR images, the post-treatment MR image then is registered to the pretreatment MR image, and the registration matrix is applied to the corresponding post-treatment PET images. Voxel-wise subtraction between the uptake values then is performed on the PET images; alternatively, the percentage change in uptake can be calculated. Finally, a threshold for difference in tracer uptake based on normal variability in normal-appearing tissue is used to determine whether voxels are significantly different. The resulting volume and volume fraction of significantly increasing, decreasing, or changing voxels in a tumor region are used to define PET PRMs.
Findings/Discussion
PET PRMs using either 18F-FDG, 18F-FDOPA or 18F-FLT PET tracers can be used to quantify spatially-specific tumor growth characteristics and response to specific therapies in diffuse gliomas. PET PRMs show significantly better sensitivity for detecting regional metabolic changes compared with standard ROI-based and visual assessments of serial PET scans.

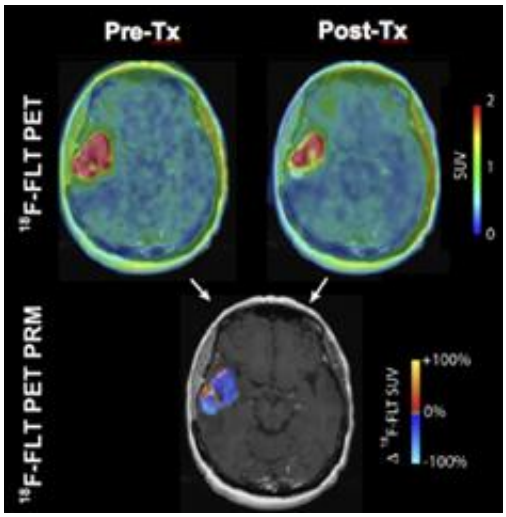

Summary/Conclusion
PET PRMs are a novel technique for automated quantification of metabolic changes during clinical evaluation and treatment of brain tumors. Future studies aimed at validating the spatial specificity are warranted.

KEYWORDS: Brain neoplasms, PET, imaging biomarker

eEdE-36

CT and MR Imaging of Intracranial Cystic Lesions: A Practical Location-Based Approach

Hakham, S.·Prober, A.·Madan, N.·Do-Dai, D. D.
Tufts Medical Center
Boston, MA.

Purpose
The purpose of our exhibit is to present a simplified, yet comprehensive and systematic approach for analyzing intracranial cystic lesions based on lesion location and CT and MR appearance. An appropriate differential diagnosis for each lesion is entertained, with specific discussion of

management: which lesions require intervention or followup, and which can be forgotten.
Approach/Methods
Sample cases from our institution are utilized to present a pictorial review of typical and atypical intracranial cystic lesions and provide a systematic, location-based algorithm to formulate an accurate differential diagnosis. Where appropriate, pitfalls, mimics, and complicating features will be discussed and histopathologic correlation will be reviewed.
Findings/Discussion
While some lesions, such as cystic neoplasms, require further intervention, numerous benign or probably benign lesions can be ignored or followed. However, developing a systematic approach can be useful in formulating an accurate differential diagnosis based on the lesion location, morphology, and presence or absence of complicating features. Moreover, such an approach can facilitate management decisions. Intra- and extra-axial cystic lesions including cystic neoplasms, infectious cysts, and true cysts are discussed, with specific attention to the next step in management. Additional emphasis is given to the location of the lesion as a clue for a more accurate diagnosis. For instance, while pineal cysts, dermoids, Rathke cleft cysts, and suprasellar arachnoid cysts are seen more often as midline extra-axial lesions, epidermoids, neurocysticercosis, arachnoid cysts, and neurenteric cysts are among diagnoses to be more expected as off-midline extra-axial cystic lesions. Intra-axial parenchymal lesions may present as porencephalic cysts, neuroglial cysts, or enlarged prevascular spaces. Lastly, choroid plexus cysts, ependymal cysts, and colloid cysts are seen most commonly as intra-axial, intraventricular cystic lesions.
Summary/Conclusion
Our educational exhibit aims to provide the practicing neuroradiologist with a framework for approaching the various intracranial cystic lesions in a systematic manner to effectively provide an appropriate differential diagnosis for each lesion and an approach to management.

KEYWORDS: Cyst, Intracranial

eEdE-37

Cerebellopontine Angle Mass: An Interactive, Case-Based Review

Thurlow, P. C.·Fukui, M. B.·Goldberg, M. F.
West Penn Allegheny Health System
Pittsburgh, PA.

Purpose
The differential diagnosis of common cerebellopontine angle (CPA) masses is one of the most well known in all of neuroradiology. These include: meningioma, schwannoma, epidermoid cyst, arachnoid cyst, and metastasis. However, the neuroradiologist must be aware of and recognize the less common pathology that can occur at the CPA. The purpose of this exhibit is to show the various disease processes that occur at the CPA via an interactive, case-based review.
Approach/Methods
This educational exhibit will: 1) Review normal CPA anatomy, including relevant osseous, vascular, and cranial nerve anatomy. 2) Review the common pathologic processes that occur at the CPA. Comment will be made on key
diagnostic clues and pitfalls, as well as important “do not touch” lesion mimics. 3) Review rare pathologic processes that occur at the CPA. These include, but are not limited to: fat necrosis, radiation necrosis, ganglioglioma and chrondrosarcoma. Comment will be made on key diagnostic clues and pitfalls. 4) Provide a diagnostic strategy that can be employed by the radiologist upon encountering a CPA mass. 5) Provide an interactive case-based review and self-assessment quiz to reinforce key teaching points.
Findings/Discussion
The participant will learn a strategy for diagnosing CPA masses that emphasizes identifying lesion location and extension to critical adjacent anatomy, typical imaging features, and imaging technique. The CPA is composed of multiple components, including subarachnoid/CSF space, osseous skull base, arterial and venous vasculature, cranial nerves, dura, cerebullum, and brainstem. With a greater understanding of this anatomy, as well as the use of conventional and advanced imaging techniques, the participant will be given a strategy for precisely identifying the wide range of common and uncommon pathologies that can occur at the CPA.
Summary/Conclusion
The diagnosis of CPA pathology can be challenging, at times, for the radiologist. Achieving the correct diagnosis is critical for therapeutic decision-making, prognostication, and improved patient outcomes. This interactive education exhibit provides a review of CPA anatomy and highlights key features to distinguish the various potential etiologies of CPA pathology.

KEYWORDS: Cerebellopontine angle, Differential diagnosis

eEdE-38

Cysts in the Brain: To Worry or Not to Worry?

Rohatgi, S.[1,2]·Hsu, L.[1,2]
[1]Brigham and Women's Hospital, Boston, MA, [2]Harvard Medical School, Boston, MA.

Purpose
1. To illustrate the imaging spectrum of cystic lesions in the brain using case-based examples. 2. Differential diagnosis and clinical presentation based on anatomical location. 3. Key imaging pearls of commonly encountered cysts and cystic lesions. 4. Recognize benign from neoplastic cysts, hence prevent unnecessary interventions.
Approach/Methods
We approached various cystic lesions, using an origin and

Note: Scanned images are included in the proceedings. Some submitted images were reduced during editing, thereby decreasing clarity. Also, refer to the Program Planner. Proceedings Content as of 3-29-2013.

location-based algorithm. Clinical features and imaging appearances on CT and MR are discussed with key pertinent differential diagnosis and management.
Findings/Discussion
Cysts or cystic lesions are often benign incidental findings and usually asymptomatic. Some cysts, however, are associated with tumors. Differential of cysts or cystic lesions can be approached according to their origin, pathogenesis or anatomical location. It is important to recognize and differentiate benign or developmental cysts from tumor-associated cysts as these have vastly different prognosis. Familiarity with the imaging spectrum may prevent unnecessary biopsy/surgery. MR imaging currently is the diagnostic modality of choice in characterization of cystic lesions, although there are instances where CT is complementary to MRI, especially in detection of calcification or hemorrhage.
Summary/Conclusion
Cystic lesions can at times pose a diagnostic dilemma because of their varied locations and appearances. Awareness of the imaging characteristics of these lesions is important for prognosis as well as prevention of unnecessary interventions. This educational exhibit reviews imaging spectrum of cystic lesions based on their location, diagnostic imaging pearls and their differential diagnosis.

KEYWORDS: Cysts, location, imaging

eEdE-39

T1-Weighted Dynamic Contrast-Enhanced and T2*-Weighted Dynamic Susceptibility Contrast MR Imaging - Physical Principles, Techniques and Clinical Applications in Neuro-Oncology: What the Neuroradiologist Needs to Know

Hoque, K. E.[1]·Huhdanpaa, H.[1]·Hwang, D. H.[1]·Muradyan, N.[2]·Booker, M. T.[1]·Russell, S.[1]·Sivasundaram, L.[1]·Naghi, I.[1]·Kim, P. E.[1]·Lerner, A.[1]·Law, M.[1]·Shiroishi, M. S.[1]
[1]University of Southern California, Los Angeles, CA, [2]iCAD, Inc., Los Angeles, CA.

Purpose
The purpose of this exhibit will be to provide a comprehensive overview of the physical principles, techniques and clinical applications of T1-weighted dynamic contrast-enhanced (DCE) and T2*-weighted dynamic susceptibility contrast (DSC) MRI in a case series of neuro-oncology patients.
Approach/Methods
1. Tumor biology. 2. Physical principles and techniques of DCE and DSC MRI. 3. Clinical applications of DCE and DSC MRI in neuro-oncology patients. 4. Pitfalls. 5. Future of DCE and DSC MRI.
Findings/Discussion
1. Tumor biology: An overview of tumoral angiogenesis and a focus on VEGF will be provided. 2. Physical principles and techniques of DCE and DSC MRI: Relevant concepts involving image acquisition, postprocessing and interpretation will be provided. 3. Clinical applications of DCE and DSC MRI in neuro-oncology patients: An overview of tumor diagnosis, prognosis, therapy selection and therapeutic evaluation will be provided. 4. Pitfalls: Common pitfalls and controversies regarding DCE and DSC MRI in neuro-oncology will be discussed. 5. Future of DCE and DSC MRI: A discussion of future applications and challenges facing DCE and DSC MRI in neuro-oncology will be provided.
Summary/Conclusion
This education exhibit will provide the neuroradiologist with an in-depth review of the relevant concepts underlying the technical and clinical aspects of DCE and DSC MRI in the context of the brain tumor patient through a case series. It is hoped that this will better enable integration of these functional MRI techniques into their clinical practice.

KEYWORDS: Dynamic contrast enhancement, Dynamic susceptibility contrast-enhanced

eEdE-40

Neuroradiology Jeopardy

Maralani, P. J.·Mohan, S.
University of Pennsylvania
Philadelphia, PA.

Purpose
In this interactive jeopardy game we will review the imaging findings of 31 important diagnoses in neuroradiology. The cases are presented the same way they were brought to our attention by the clinical services. It is designed to increase diagnostic accuracy of the trainees with particular emphasis on imaging findings. The game is at the level of a senior radiology resident or a neuroradiology fellow.
Approach/Methods
Our jeopardy game consists of six categories including: 1) Brain tumor; 2) Infectious, inflammatory and toxic/metabolic pathologies; 3) Vascular pathologies; 4) Head and neck pathologies; 5) Spine; and 6) Potpourri. In each category there are six cases in increasing order of complexity. There will be a final jeopardy case of traumatic brain contusion that involves multimodality imaging, with stress on CT diagnosis and review of the findings on MRI.
Findings/Discussion
Figure 1 demonstrates the format of the game. Table 1 demonstrates the cases that will be presented. In each case we will review the imaging and pertinent clinical

Note: Scanned images are included in the proceedings. Some submitted images were reduced during editing, thereby decreasing clarity. Also, refer to the Program Planner. Proceedings Content as of 3-29-2013.

findings that help narrow down the differential diagnosis.

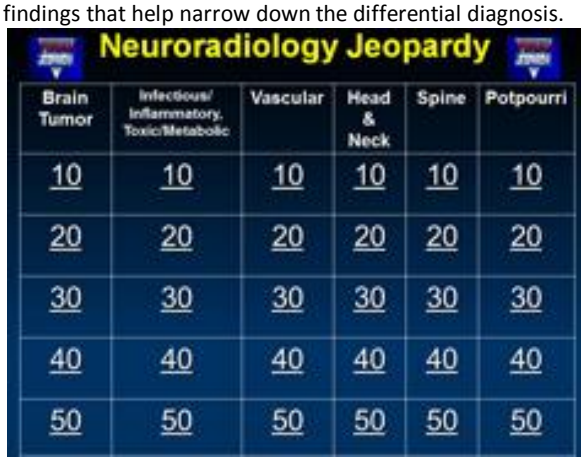

Table 1.

Brain Tumor	Infectious/Inflammatory, Toxic/Metabolic	Vascular	Head & Neck	Spine	Potpourri
GBM	Herpes encephalitis	Arteriovenous malformation	Peritonsillar abscess	Chance Fracture	Fibrous Dysplasia
Epidermoid	Global hypoxic injury	Vertebral artery aneurysm	Otosclerosis	Diskitis/Osteomyelitis	Tumefactive Perivascular Spaces
Lymphoma	Basal tuberculosis meningitis	Moyamoya disease	Venolymphatic Malformation	Dural AV fistula	Intracranial Hypotension
Gliomatosis cerebri	Progressive multifocal leukoencephalopathy	Capillary telangiectasia	Ameloblastoma	Devic's Disease	Thrombophlebitis superficial neck veins
Cardiac myxoma with hemorrhagic brain metastasis	Pseudohypoparathyroidism	CADASIL	Endolymphatic Sac Tumor	Myxopapillary Ependymoma	Hyperammonemia, Hepatic Encephalopathy

Summary/Conclusion
This presentation serves as an interactive teaching tool for senior radiology residents and fellows. It emphasizes on several important imaging findings in neuroradiology that will help reach the final diagnosis. This exposition also can be used as an evaluation tool for trainees to assess their readiness in diagnostic neuroradiology.

KEYWORDS: Brain, ENT, spine

eEdE-41

Meningiomas: Morphologic Manifestations and Mimics on MR and CT

Thuahnai, S. T.·Lindsay, A.·Boyer, P.·Rubenstein, D.
University of Colorado Denver
Denver, CO.

Purpose
Classically meningiomas are described as avidly enhancing dural-based extra axial masses, but the MRI and CT appearance may be variable. The purpose of this exhibit is to present the various MRI and CT findings of meningiomas.
Approach/Methods
We retrospectively reviewed the imaging of meningiomas and mimics that were biopsy proven in our institution. The imaging was reviewed for anatomical location, signal characteristics on MRI or density on CT, type of enhancement and involvement of adjacent structures. Imaging features were correlated with other pathologic diagnosis and grading.
Findings/Discussion
While the classic dural-based extra axial mass is a typical presentation for a meningioma, there are other variations. When dural-based they are found mostly supratentorially with clear attachment to the convexity, dura or falx. Infratentorial involvement can occur along the clivus, tentorium cerebelli, along the cerebellopontine angles, jugular foremen and in the spine. Less common locations are intraosseous, intranasal and intraventricular. Other dural-based or superficially located parenchymal neoplasms can mimic meningiomas.

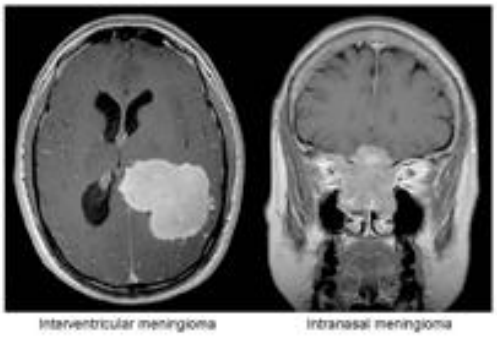

Summary/Conclusion
Meningiomas can have a variety of appearances on CT and MRI. They can occur in locations that are atypical and their typical appearance may be mimicked by lesions of other etiology. Imaging findings may not be suggestive of the WHO grade of the meningiomas.

KEYWORDS: Meningioma, Variants, mimics of dural-based lesions

eEdE-42

Ten Tumors Under the Tent: Posterior Fossa Masses

Linscott, L.·Wippold, F.·Miller-Thomas, M.
Mallinckrodt Institute of Radiology
St. Louis, MO.

Purpose
Present the imaging findings of common posterior fossa masses. Emphasis will be on characteristic imaging features of each diagnosis, important clinical discriminators, and pitfalls in diagnosis.
Approach/Methods
1. Cases will be identified from our clinical practice in both a large tertiary care adult medical center and large tertiary care children's hosptital. Imaging modalities presented will include MRI, CT, PET, and angiography. 2. Discuss differentiating imaging features and clinical pearls of the following posterior fossa masses: - Metastasis, - Hemangioblastoma, - Ependymoma, - Medulloblastoma, - Juvenile pilocytic astrocytoma, - Dysplastic gangliocytoma, - Brainstem glioma, - Meningioma, - Atypical Teratoid Rhabdoid Tumor, and - Dermoid/Epidermoid. 3. Present an

Note: Scanned images are included in the proceedings. Some submitted images were reduced during editing, thereby decreasing clarity. Also, refer to the Program Planner. Proceedings Content as of 3-29-2013.

interactive quiz based on the presented cases designed to reinforce key concepts.
Findings/Discussion
Posterior fossa masses are encountered commonly in both adults and children. While age plays an important role in determining the differential diagnosis, imaging features help to narrow the differential and often suggest a most likely diagnosis. Just a few examples of such imaging features to be discussed include; contrast enhancement equal to blood pool with flow voids strongly suggests hemangioblastoma rather than other cystic posterior fossa lesions; hyperattenuation on CT in a pediatric cerebellar mass suggests medulloblastoma as the most likely diagnosis; extension of tumor through the foramina of Luschka and Magendie strongly suggests ependymoma as the most likely diagnosis; Diffusion-weighted imaging is critical for the evaluation of cystic posterior fossa masses to differentiate such lesions as epidermoid and arachnoid cysts. Some examples of potential diagnostic pitfalls include; increased FDG radiotracer uptake in nonaggressive lesions such as dysplastic gangliocytoma; a dural tail is not pathognomonic for meningioma.
Summary/Conclusion
Posterior fossa masses are commonly encountered and many have distinctive imaging appearances. The workup and management of these entities varies greatly. Knowledge of distinctive imaging findings helps the radiologist to narrow the differential diagnosis, guide management decisions, and avoid diagnostic pitfalls.

KEYWORDS: Posterior fossa, Masses

eEdE-43

Multimodal Imaging of Neurocutaneous Syndromes: A Pictorial Review

Ibrahim, S. M.·Bokhari, S. J.·Bronen, R.·Mahajan, A.·Malhotra, A.
Yale University School of Medicine
New Haven, CT.

Purpose
The objective of this presentation is to discuss the pathophysiology, genetics, and clinical presentation of the following neurocutaneous syndromes: 1) Tuberous sclerosis (TS); 2) Neurofibromatosis types 1 (NF1) and 2 (NF2); 3) von Hippel-Lindau (VHL); and Sturge Weber syndrome (SW).
Approach/Methods
Cross-sectional imaging has become increasingly important in recognizing features of neurocutaneous syndromes. The role of CT, MRI, MR spectroscopy, PET and diffusion tensor imaging will be discussed in the diagnosis of these neurocutaneous syndromes. The characteristic features of each of these neurocutaneous syndromes will be highlighted.
Findings/Discussion
The pathophysiology and genetic basis for TS, NF1, NF2, VHL and SW will be discussed in addition to the imaging features. The diagnostic criteria will be highlighted with emphasis on the differential diagnoses specific to each neurocutaneous syndrome.
Summary/Conclusion
Multimodality imaging plays an important role in the diagnosis of neurocutaneous syndromes. It is important for the radiologist to recognize the complex and sometimes salient features of these rare entities.

KEYWORDS: VHL, Phakomatoses, NF1 and 2

eEdE-44

Primary Central Nervous System Lymphoma: An Interactive Pictorial Review of Common and Uncommon Imaging Presentations

Wang, Y.[1]·Hanagandi, P. B.[1]·Goncalves, F. G.[2]·Chong, J.[1]·Bessissow, A.[1]·Chankowsky, J.[1]·del Carpio-O'donovan, R.[1]
[1]Montreal General Hospital, McGill University, Montreal, QC, CANADA, [2]Radiologia Infinita - Brasilia Children's Hospital, Brasilia, BRAZIL.

Purpose
In this interactive educational exhibit, we emphasize the characteristic CT and MR imaging features depicting the presentation and evolution of primary CNS lymphoma.
Approach/Methods
After a review of imaging features, we present typical and atypical examples of primary CNS lymphoma in immunocompetent and immunocompromised patients, as wells as lymphoma mimics, in an interactive case-based format. Each case is accompanied by a brief discussion.
Findings/Discussion
Primary CNS lymphoma is a predominantly B-cell lymphoma, and represent over 6% of all primary brain tumors. It has a diffuse microscopic growth pattern, distinct perivascular extension, and a predilection for the basal ganglia or periventricular regions. On imaging, the high cellularity of tumors appears hyperattenuating on noncontrast-enhanced CT, with low to intermediate signal intensity on T2-weighted MR images and enhancement. Internal hemorrhage and necrosis present in immunocompromised individuals may create a diagnostic dilemma. Although sensitive to chemotherapy and radiotherapy, often with dramatic disappearance of lesions on follow-up radiologic studies, aggressive tumor recurrence is common and the overall prognosis is poor.
Summary/Conclusion
Primary CNS lymphoma is an increasingly prevalent intracranial neoplasm with nonspecific clinical presentation. Its imaging appearance, especially in immunocompromised individuals, may mimic other intracranial neoplasms and infectious or inflammatory etiologies. This interactive review from our institution will better familiarize radiologists with typical and atypical

imaging features, differential diagnosis, and locations of primary CNS lymphoma on CT and MRI.

KEYWORDS: Lymphoma, Brain neoplasms

eEdE-45

MR Imaging Findings of Ipilimumab-Related Hypophysitis

Jones, K. S.·Baykal, A.·Gabriel, R.
Virginia Commonwealth University Health System
Richmond, VA.

Purpose
Cytotoxic T-lymphocyte-associated antigen 4 (CTLA-4) blocking agents may cause adverse events related to their activity on the immune system. Ipilimumab, a monoclonal antibody effective in treating metastatic melanoma, has induced autoimmune syndromes such as enteritis, thyroiditis, dermatitis, and hypophysitis. We present the clinical and imaging findings of a patient with metastatic melanoma, who developed acute Addisonian crisis secondary to Ipilimumab-related autoimmune hypophysitis (AH).
Approach/Methods
A 58-year-old woman with metastatic melanoma postresection of a solitary brain metastasis and whole brain radiation developed progressive fatigue, headache, vomiting and subsequent acute mental status deterioration 3 months after initiating Ipilimumab treatment. She presented to the emergency room after becoming acutely aphasic, agitated, and immobile. Urgent brain MRI demonstrated enlargement of the pituitary gland with heterogeneous signal, enhancement, and possible hemorrhage. Upon admission she became rapidly hypotensive and was found to have marked hyponatremia, hypopituitarism, and adrenal crisis.
Findings/Discussion
Autoimmune hypophysitis can be divided into primary and secondary subtypes. Primary AH includes lymphocytic, the most common type often associated with pregnancy, granulomatous and xanthogranulomatous hypophysitis. Secondary AH occurs due to systemic disease such as sarcoid, Langerhans cell histiocytosis, or Wegeners granulomatosis, sequelae of adjacent intracranial masses or infection, or as most recently described by adverse drug effects such as from chemotherapy. The CTLA-4 gene functions to down regulate T-lymphocytes. Mutations in this gene are associated with a variety of autoimmune diseases. Similarly, antibody suppression of CTLA-4 can augment the body's immune response against tumor.Cytotoxic T-lymphocyte-associated antigen-4 blocking immunotherapies such as Ipilimumab have a demonstrated effect on metastatic melanoma and renal cell carcinoma. Previous reports of anti-CTLA-4 or Ipilimumab induced hypophysitis have described enlargement of the pituitary gland, usually with homogeneous enhancement on MRI. Imaging findings were generally nonspecific, including diffuse enlargement of the gland with loss of bright signal in the posterior pituitary and variable involvement of the infundibulum. By distinction, our patient presented with heterogeneous enlargement of the pituitary gland with possible hemorrhage. Since the brain lesion previously resected had been a hemorrhagic melanoma metastasis, initial differential considerations included primary pituitary processes such as hypophysitis or apoplexy versus a hemorrhagic metastatic lesion to the pituitary gland.Reported clinical presentations of AH have ranged from solitary hormonal derangements to panhypopituitarism. Isolated ACTH deficiency is the most common pituitary hormone defect, usually iatrogenic from glucocorticoid administration. This was the critical deficiency causing adrenal crisis and shock in our patient. The severity of our patient's hypophysitis and resulting adrenal crisis required ICU care including stress dose steroids and pressor support. She recovered over the course of several days, was discharged successfully, and has been treated as an outpatient with a long course of low dose steroids. On follow-up MRI, pituitary gland size returned to normal without evidence of residual hemosiderin thus excluding the possibility of apoplexy or hemorrhagic metastasis. While Ipilimumab was discontinued after the acute hospitalization, she has remained in remission to date.
Summary/Conclusion
This unique imaging presentation provides the radiologist insight into the complexities of a promising new chemotherapeutic agent.

KEYWORDS: Pituitary gland, Chemotherapy, MR imaging

eEdE-46

A Web-Based Mobile Application for Learning and Reviewing the Appearance of Intraventricular Masses Using a Multimodality Approach

Horn, C.·Kadoch, M. A.·Sicular, S.·Ward, T. J.·Fitzpatrick, D.·Naidich, T.
Mount Sinai Medical Center
New York, NY.

Purpose
The purpose of the exhibit is: 1. To provide quick and easy access to a web-based mobile application and reference guide that addresses most of the common intraventricular masses as evaluated by modern imaging modalities. 2. To provide a reference tool that addresses the limitations of other online reference tools, which can be cost-prohibitive, require log-ins or registration, lack interactivity, and are often slow to engage the end user. 3. To provide imaging of both the specific and nonspecific imaging features of a given intraventricular mass. 4. To provide a novel learning platform that is fully functional using either the internet alone or on most major handheld devices and tablets, which are becoming increasingly important as educational resources for fellows, trainees,

Note: Scanned images are included in the proceedings. Some submitted images were reduced during editing, thereby decreasing clarity. Also, refer to the Program Planner. Proceedings Content as of 3-29-2013.

and students.
Approach/Methods
All intraventricular masses encountered at our institution since 2001 were reviewed for potential inclusion in the exhibit.
Findings/Discussion
The major teaching points of this exhibit are: 1. Reviewing the diagnostic as well as nonspecific imaging findings of multiple intraventricular masses on modern imaging modalities. 2. Encouraging each user to expand on this review by linking each pathology to important AJNR articles that further discuss that specific pathology. 3. Measuring the success of this electronic educational exhibit by monitoring number of online views and traffic directed towards the supplied AJNR articles.
Summary/Conclusion
A web-based mobile application for learning and reviewing the appearance of intraventricular masses using a multimodality approach is presented.

KEYWORDS: Intraventricular, Neoplasm

eEdE-47

MR Imaging in the Evaluation of Brain Metastases Treated with Stereotactic Radiosurgery

Almeida-Freitas, D. B.[1]·Carvalho, S. C.[1]·Pinho, M. C.[2]·Leite, C. C.[1]
[1]Universidade de São Paulo, São Paulo, BRAZIL, [2]University of Texas Southwestern Medical Center, Dallas, TX.

Purpose
The purpose of this exhibit is to review and illustrate conventional and functional magnetic resonance imaging (MRI) findings after stereotactic radiosurgery (SRS) for metastatic brain tumors.
Materials & Methods
Review of imaging findings of metastatic brain tumors treated with SRS, using sample cases from a specialized tertiary oncologic hospital.
Results
Stereotactic radiosurgery for metastatic brain tumors: A) Clinical application, B) Biological effects, C) Conventional magnetic resonance imaging, D) Diffusion-weighted Imaging, E) Perfusion-weighted imaging, F) Permeability-weighted imaging, G) 1H-magnetic resonance spectroscopy.
Conclusion
Radiosurgery is a therapeutic modality of proven efficacy that has been applied increasingly in the management of metastatic brain tumors. The major teaching points of this exhibit are to review MRI findings after radiosurgery for metastatic brain tumors, and to present a strategy for imaging evaluation that potentially may aid in the differentiation of residual/recurrent tumor from radiation-induced lesions. Radiologists should be familiarized with these finding in order to provide more accurate follow-up results and to improve patient clinical outcome.

KEYWORDS: Metastases, Radiation therapy

eEdE-48

Two Common Image Appearances that Seem to Contradict MR-Physics

Fourgas, E.·Abele, T.·Rassner, U.
University of Utah
Salt Lake City, UT.

Purpose
Knowledge of MR-physics is important to understand findings on magnetic resonance (MR) imaging. However, occasionally appearances on MR images seem to contradict MR-physics: Lesions with higher signal on T2 fast spin-echo images than CSF and flow voids looking better on proton density (PD) than T2 images. The purpose of this presentation is to resolve these apparent contradictions.
Approach/Methods
Cystic brain lesions can have higher T2 signal than CSF despite water having the longest T2 time of all tissues. Flow voids look superior on proton density than T2-images, even though better flow voids should be seen on long TE sequences. A careful review of imaging parameters, detailed image appearance and MR-physics in respect to these phenomena was undertaken.
Findings/Discussion
Water has the longest T2 time (4-5 seconds at body temperature), but also the longest T1-time of all tissues. While most tissues fully recover with commonly used TR (4-5 seconds), water would need 20-25 seconds. Proteinaceous cysts will recover more longitudinal magnetization than CSF with commonly used long TR times and have more transverse magnetization after the 90 degree rf-pulse. Despite proteinaceous cysts having shorter T2 times than water, the more efficient T1-relaxation can overwhelm shorter T2 effects and result in higher T2 signal (T1 shine-through). This could be overcome by increasing TR or TE, however this would prolong the exam or produce a more myelographic appearance. Flow voids are said to be better with longer TEs (increased separation between the 90- and 180 rf-pulse). However, flow voids are more striking PD than T2 images despite a short TE. Region of interest measurements reveal that arterial flow voids are almost entirely devoid of signal on T2 and PD images (open arrows), while venous flow voids are darker on T2 than PD images (closed arrows), owing to the longer TE. However, short TE results in higher parenchymal signal and thus a larger signal difference between flow voids and parenchyma on PD compared to T2 images.

Note: Scanned images are included in the proceedings. Some submitted images were reduced during editing, thereby decreasing clarity. Also, refer to the Program Planner. Proceedings Content as of 3-29-2013.

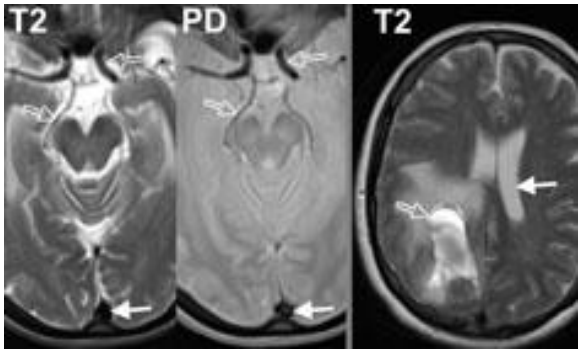

Summary/Conclusion
Lesion with higher T2 signal than CSF and flow voids looking better on proton density than T2 images do not contradict MR-physics. Understanding the underlying principles of these imaging findings can aid in clinical interpretation: Cysts with higher T2 signal than CSF must have T1 shortening. Flow voids are more robust on T2, however flow compromise will become apparent earlier on PD than T2 images.

KEYWORDS: Artifacts, MR imaging brain

eEdE-49

MR Imaging in the Differential Diagnosis of Intra-Axial Cervico-Medullary Junction Lesions

Patro, S. N.·Torres, C.·Nguyen, T.
The Ottawa Hospital
Ottawa, ON, CANADA.

Purpose
The goal of this educational exhibit is to present different common and infrequent intra-axial pathologies of the cervico-medullary junction. We will discuss the characteristic MR imaging features and we will provide an imaging approach to the different cervico-medullary junction lesions.
Approach/Methods
We reviewed the imaging findings and clinical history of eight patients who presented with lesions at the cervico-medullary junction, in our Institution. All of these patients underwent routine imaging including T1-weighted images before and after gadolinium administration and T2-weighted images. The lesions and the differentiating features were discussed in detail.
Findings/Discussion
The cervico-medullary junction is a very important part of the central nervous system and the lesions affecting this area can present with varied neurologic symptoms including lower cranial nerve deficits. In this educational pictorial essay we will be discussing various intra-axial lesions involving the cervico-medullary junction including tumoral lesions such as brain stem glioma and ganglioglioma, infectious processes such as listeria rhombencephalitis and viral myelitis, inflammatory processes such as neuromyelitis optica and ADEM, demyelinating lesions such as multiple sclerosis and neurodegenerative disease such as amyotrophic lateral sclerosis. We also have included one patient who was referred from another Institution with marked enlargement and T2 hypersignal of the cervico-medullary junction mimicking a tumor. Before a cord biopsy was done, the images were reviewed carefully; subtle flow voids were noted on the dorsal surface of the cervicomedullary junction leading to the diagnosis of spinal DAVF which was confirmed with catheter angiogram. We also will discuss the characteristic imaging findings and differentiating features of each entity.
Summary/Conclusion
Different intra-axial pathologies can involve the cervico-medullary junction with varied clinical presentation. In combination with clinical and laboratory findings, MR imaging plays a very important role in differentiating and characterizing these lesions.

KEYWORDS: Glioma, Multiple sclerosis, ganglioglioma, ADEM, meyelitis

eEdE-50

A Public and Scalable Neuroradiology Teaching File for Mobile Devices

Balkman, J. D.[1,2]·Prabhu, S. P.[2]·Belden, C. J.[1]
[1]Dartmouth-Hitchcock Medical Center, Hanover, NH,
[2]Boston Children's Hospital, Boston, MA.

Purpose
To develop an online neuroradiology case file for mobile devices that resembles the navigation capability of a PACS workstation. The mobile teaching file should be low-cost, universally accessible, connect to a real-time database, and have an intuitive and functional user interface.
Approach/Methods
The Eclipse open-source environment with Java software development kit (SDK) was used to develop frontend and backend software on a MacBook Pro computer. Local testing for handheld devices was performed using the XCode iOS simulator. The Google App Engine SDK plugin for Eclipse was utilized for deployment of the application to a unique and publicly available website hosted by Google, http://mobilerads.appspot.com. A Google Cloud SQL server was used to organize case information while Google Blobstore was used to host image data. Cases and image files were served to the end-user in a mobile-friendly format utilizing Java, jQuery and JavaScript programs, which provided the look and feel of a “native” handheld application. Navigation of the cases was evaluated on latest versions of both the iPad (2nd, 3rd, and 4th generations) and iPhone (4, 4S, 5) running iOS 6.
Findings/Discussion
A mobile application connected to a real-time case database was created with upfront costs of under 30 dollars per month. At the time of this writing, 26

Note: Scanned images are included in the proceedings. Some submitted images were reduced during editing, thereby decreasing clarity. Also, refer to the Program Planner. Proceedings Content as of 3-29-2013.

neuroradiology teaching cases were added to the database. Each teaching file consisted of image stacks from one or more sequences, annotated key images with captions, diagnostic reports, a discussion section, and set of "flashcards" for self-quizzing. Cases were available online immediately after uploading. The application was compatible with the latest iPhone and iPad mobile devices. Download times with Wifi connection averaged 3 seconds for each sequence. Navigation of cases using finger gestures allowed image zoom, pan, and image stack scrolling. Users were able to vote cases up/down, search the case database by diagnosis, compare and navigate two sequences simultaneously, and read reports while viewing images.

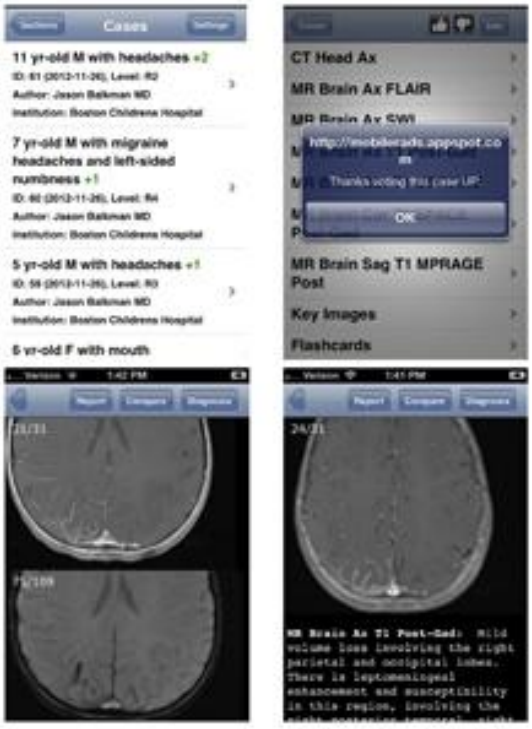

Summary/Conclusion
Current technology affords the ability to create public, low-cost, and scalable teaching files for mobile devices connected to real-time databases. These applications give users a similar interactive experience to a PACS workstation, allowing image panning, zooming, and stack scrolling by way of finger gestures. Image rich mobile device "apps" as the one described above are well suited for neuroradiology, allowing the user to compare intricate anatomy across multiple sequences simultaneously, while providing annotated images and online teaching.

KEYWORDS: Educational, Mobile technology, teaching file

eEdE-51

To Infinity and Beyond: Exploring the Future of Neuroradiology

Khan, M.·Hoeffner, E.·Srinivasan, A.
University of Michigan Health System
Ann Arbor, MI.

Purpose
The purpose of this exhibit is to discuss recent advances in neuroimaging and their associated clinical applications in an effort to paint a picture of the future of neuroradiology.
Approach/Methods
This exhibit is divided into two broad categories, CT and MRI, with focus on technical advances in each modality and their clinical applications. The exhibit will aim to briefly review some of the major emerging imaging techniques in these modalities, with straightforward explanations and the use of informative illustrations. Some examples of these emerging CT techniques include: dual energy CT, 4D CT perfusion analysis, adaptive and model-based iterative reconstruction, and phase-contrast CT. Examples of emerging MRI techniques that will be discussed include: parallel imaging, multiplexed echo planar imaging, advancements in perfusion imaging, diffusion tensor imaging, compressed sensing multi-spectral imaging, PET-MRI, and ultrahigh-field MRI (7.0 Tesla). Emphasis will be placed not only on the science behind these techniques, but the relevance to neuroimaging today. Where appropriate, prior published experiences with these new imaging techniques will be summarized and referenced.
Findings/Discussion
The variety of new imaging techniques in CT and MRI offer a pathway to improved diagnosis of subtle lesions by improving tissue characterization (in the case of ultrahigh-field MRI and phase-contrast CT), dramatically decreased image acquisition time (multiplexed echo planar imaging, parallel imaging), reduction of radiation dose (iterative reconstruction), and unique functional information (diffusion tensor imaging). These advances may not only provide valuable information and tangible benefit to the referring clinician and patient, but may expand the variety and appeal of the ever-growing field of neuroradiology.
Summary/Conclusion
The field of neuroradiology has progressed tremendously since the days of pneumoencephalography, and will continue to advance rapidly as newer imaging technologies emerge. This exhibit provides a concise and unified source of review of the advances in neuroimaging in an easily digestible format.

KEYWORDS: 4D CT, Dual-energy CT, compressed sensing

Note: Scanned images are included in the proceedings. Some submitted images were reduced during editing, thereby decreasing clarity. Also, refer to the Program Planner. Proceedings Content as of 3-29-2013.

eEdE-52

Image Coregistration: Quantitative Processing Framework for the Assessment of Brain Lesions

Huhdanpaa, H. T.·Hwang, D. H.·Cen, S.·Lerner, A.·Boyko, O. B.·Law, M.·Shiroishi, M. S.
University of Southern California
Los Angeles, CA.

Purpose
The quantitative, multiparametric assessment of brain lesions may require postprocessing steps which often consist of coregistering different parameters derived from MR imaging (MRI) sequences such as T1-weighted dynamic contrast-enhanced (DCE), T2*-weighted dynamic susceptibility contrast (DSC), and diffusion-weighted (DWI) and diffusion tensor (DTI) MRI, among others. This will be followed by analysis of the voxel values of the region of interest within the sequences and calculated parametric maps (ie., ADC, FA, permeability), and then deriving multiparametric models to help classify imaging data. For these approaches to scale to busy neuroradiology practices and to become more widely adopted among clinical neuroradiologists, there is a need for an intuitive quantitative processing framework which ideally may be constructed from commonly available and open-source components, and which will maximally automate the postprocessing steps. Additionally, such a framework should be generic and modular enough to adapt to different clinical and research questions without significant reworking.
Approach/Methods
One of the goals of the project is to construct a quantitative postprocessing framework with open source and commonly available software components as much as possible. With this goal in mind, Matlab, which is commonly available, was chosen for the actual postprocessing environment, and Statistical Parametric Mapping (SPM), which is open-source, was chosen for the coregistration portion of the framework. Matlab routines were designed and implemented to extract and concatenate the coregistration transforms, to take the coregistered MRI sequences as inputs to the process, allow the user to specify the region of interest (ROI), and then store the voxel values within the ROI to the database for further statistical analysis and multiparametric model creation (Figure 1). The functionality of the framework was validated using brain tumor MRI cases.

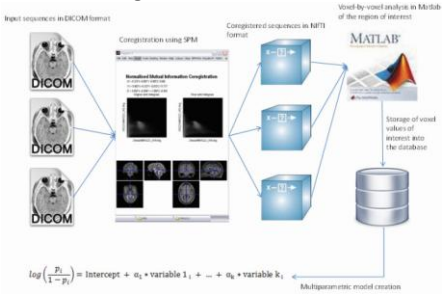

Findings/Discussion
The implementation of this quantitative postprocessing framework can enable a neuroradiologist to intuitively, without complex user interactions, create multiple parameters for each voxel, thus to facilitate in depth voxel-wise analysis. It also will reduce the postprocessing time to near real time.
Summary/Conclusion
This work supports the idea that common software components can be utilized to implement an intuitive real time quantitative postprocessing framework. It can result in improved scalability and hopefully increased adoption of the postprocessing steps needed to answer important neuroradiologic diagnostic questions.
Acknowledgments: NIH R21EB013456, NIH UL1RR031986-01.

KEYWORDS: Coregistration, Postprocessing, quantitative imaging

eEdE-53

Pitfalls in the Interpretation of Dynamic Contrast-Enhanced Cross-Sectional Imaging with Particular Attention to Perfusion Imaging

Patel, K. M.·Chen, J.
University of California San Diego
San Diego, CA.

Purpose
Contrast-enhanced cross-sectional imaging techniques (CT, MR angiography and perfusion) are used routinely in evaluation of neurovascular anatomy and brain functional and metabolic parameters. There are numerous pitfalls relating to these techniques that may lead to interpretive errors if the reader is not familiar with them.
Approach/Methods
Education Goals/Teaching Points - 1. Familiarize the reader with various potential pitfalls that may occur during interpretation of dynamically injected contrast-enhanced cross-sectional studies by using a case-based quiz format. 2. Provide the reader with practical strategies for accounting and avoiding these pitfalls including review of perfusion and angiographic source images. 3. Demonstrate how specific clinical data can significantly change initial interpretation and subsequent management (e.g., hyperperfusion therapy, chronic stenoses or occlusions, previous surgery). 4. Discuss basic principles and assumptions of perfusion imaging. 5. Discuss the effects of different postprocessing algorithms on accuracy of perfusion maps. 6. Discuss potential variability of perfusion maps based on postprocessing technique.
Findings/Discussion
Present key images from multiple clinical case examples such as: 1. Incorrect estimation of ischemic penumbra in setting of cerebral hyperperfusion. 2. Incorrect estimation of ischemic penumbra in setting of asymmetric inflow stenosis.

3. Suboptimal placement of region of interests (ROIs) and arterial input functions (AIFs). 4. Artifacts from retrograde flow such as retrograde venous perfusion in the setting of either functional or anatomical central venous stenosis.
Summary/Conclusion
Multiple potential pitfalls that may occur during interpretation of contrast-enhanced cross-sectional studies may be avoided by gaining better understanding of technical acquisition and postprocessing parameters, clinical information and review of source images.

KEYWORDS: Pitfalls, MR angiography, CT angiography

eEdE-54

It's a Bird!⋯It's a Plane!⋯Oh Wait, It's Just Artifact: A Pictorial Review of the Most Commonly Encountered Artifacts in High-Field Strength MR Imaging of the Central Nervous System for Beginners

Zohrabian, V. M.·Zoltani, Z.
Thomas Jefferson University Hospital
Philadelphia, PA.

Purpose
MR imaging (MRI) is a powerful, safe and noninvasive tool, which has become widespread in neurologic examinations owing to excellent soft-tissue contrast and spatial resolution. Despite advances in imaging protocols and updated hardware and software packages, MRI remains vulnerable to a host of imaging artifacts given inherent properties of the patient being scanned, data inconsistencies, and hardware imperfections. Imaging artifacts may confound interpretation and mimic pathologies when not recognized. The purpose of this education exhibit is to allow recognition of the most commonly encountered artifacts in MR imaging of the CNS, and may be especially useful for trainees and those novice to the interpretation of neurologic imaging studies. Through a review of clinical images, we hope to alleviate misunderstandings that may lead to misdiagnoses in high-field strength MR imaging of the CNS.
Approach/Methods
Through a case-based, interactive format, we will highlight artifacts that are commonly seen with high-field strength MRI of the head, neck and spine. The types of artifacts discussed will include but not be limited to ghosting artifact secondary to motion, J-coupling in T2-weighted fast spin-echo imaging, flow-related artifacts as may be seen in large vessels and cerebrospinal fluid, magnetic susceptibility artifacts such as with axial diffusion-weighted echo planar imaging, metallic-related artifacts, inhomogeneous or incomplete fat saturation, and chemical shift artifacts. The examples presented will focus on the potential for radiologic misinterpretation in the presence of such artifacts. When available, the appearances of image artifacts on 1.5T MRI will be compared with 3T MRI, with an additional focus on recognizing the increased sensitivity to contrast enhancement of leptomeningeal and pachymeningeal vessels afforded by 3T MR imaging.
Findings/Discussion
Recognition of various MR imaging artifacts is needed to efficiently and accurately interpret clinical cases. Furthermore, with some working knowledge of the physical bases of artifacts, strategies can be implemented to lessen their severity, and thus, increase diagnostic certainty.
Summary/Conclusion
The quality of MRI may be limited by a variety of artifacts that may prove particularly problematic for beginner readers of neurologic imaging. A better understanding of such artifacts is necessary not only for the appropriate interpretation of cases, but also for the implementation of measures to optimize MR image quality.

KEYWORDS: Artifacts, MR imaging

eEdE-55

Perfusion Imaging Deconvolved: A Primer on Theory, Analysis, and Interpretation for the Neuroradiologist

Bansal, V.[1]·Kudo, K.[2]·Dehkharghani, S.[1]
[1]Emory University, Atlanta, GA, [2]Iwate Medical University, Morioka, JAPAN.

Purpose
Numerous techniques have been proposed to measure cerebral blood flow (CBF) and noninvasively probe tissue perfusion. Applications include stroke diagnosis and prognostication, tumor grading, and characterization of normal physiology. While the development of a readily accessible yet truly quantitative measure of CBF remains enigmatic, several semiquantitative techniques employing CT/MRI dynamic bolus passage with rapid imaging, adapted from classic indicator dilution theory, have shown promise in widespread applications. An extensive body of literature has highlighted the significant variability in computed perfusion across various methodologies and analysis schemes, and between competing third party vendor perfusion analysis systems. While the variability and potential instabilities inherent to such techniques may impact profoundly clinical decision-making, the fundamental theories governing these techniques remain generally under appreciated by practicing radiologists, limiting insight into specific advantages or comparative attributes of available systems. The primary motivation for this exhibit was development of a perfusion imaging primer to expand accessibility and appreciation of perfusion theory to a broader audience, specifically underscoring the theoretical features most relevant to practicing neuroradiologists. The primer will expound those features at the intersection of mathematics, engineering, physiology, and cerebrovascular disease, in a systematic and methodical framework designed for imaging clinicians, using a graphical and case-based format highlighting data acquisition, postprocessing, and

Note: Scanned images are included in the proceedings. Some submitted images were reduced during editing, thereby decreasing clarity. Also, refer to the Program Planner. Proceedings Content as of 3-29-2013.

interpretation.
Approach/Methods
Using cases from our large local database and custom animations, we will explain the relevant physiology and graphically depict the theory underlying the computation of the most commonly encountered perfusion parameters. We will further demonstrate the effects of various postprocessing paradigms on final perfusion estimates, focusing on their potential clinical impact through sample cases and simulations.
Findings/Discussion
Noninvasive measurements of cerebral perfusion offer an invaluable probe of disease and normal physiology, and aid prognostication and treatment planning. This exhibit will focus on MR/CT-based perfusion methods utilizing exogenous nondiffusible tracers (NDT). The most commonly computed perfusion parameters include blood volume, blood flow, mean transit time, and T_{max}. The first three are related by the central volume theorem, and predicated upon a theoretically "instantaneous" bolus to a closed capillary system. Owing to the real-world bolus delay/dispersion inherent to the proximal IV injections of NDT, the tissue time-concentration curves observed in practice do not reflect tissue perfusion in any straightforward manner. To simulate the effects achieved from such a theoretically instantaneous bolus, many algorithms deconvolve an arterial input function (AIF) from the tissue-concentration curve, thus allowing recovery of the so-called tissue residue function, representing the tissue's response to such an impulse bolus. We will explain graphically the principles of convolution/deconvolution as it applies to perfusion imaging, as well as the physiologic significance of these common perfusion parameters. These techniques will be compared to simpler, nondeconvolution-based techniques, as well as to more complex parametric models of perfusion more recently gaining attention.
Summary/Conclusion
This perfusion imaging primer aims to provide neuroradiologists with critical insights related to perfusion imaging theory, acquisition, and postprocessing. Principles are presented by an illustrative and case-based exhibition of the scientific basis, with emphasis on practical clinical differences and limitations.

KEYWORDS: Brain perfusion, Deconvolution, primer

eEdE-56

Current Diagnostic Imaging of Carotid Artery Stenosis

Park, Y.·Nguyen, V.
Long Island Jewish Medical Center
New Hyde Park, NY.

Purpose
The purpose of this presentation is to provide a current multimodality review of carotid artery stenosis, its detection, calculation and characterization of the plaque morphology by ultrasound, computed tomography and magnetic resonance imaging. The diagnostic impact on the management of carotid artery stenosis will be examined. Concluding this presentation will be a focal refresher of the documentation of technique and recommended reporting for carotid artery stenosis.
Approach/Methods
This will be a case-based review of carotid artery disease characterization by ultrasound (US), computed tomography angiography (CTA), magnetic resonance angiography (MRA). Current literature review of the different stenosis percentage calculations and the impact on management will be discussed. We will discuss the methods used to assess the degree of internal carotid artery stenosis [e.g., North American Symptomatic Carotid Endarterectomy (NASCET) and European Carotid Surgery Trial (ECST)]. We will review additional findings in carotid disease, such as plaque ulceration and hemorrhage. Finally, we will compare current ICD-9 and the future ICD-10 report requirements for this disease evaluation. We will highlight the appropriate documentation of imaging technique and findings.
Findings/Discussion
Although historically conventional angiography is the gold standard with which noninvasive imaging (MRA, and CTA) are compared, its use has decreased with improved accuracy of noninvasive imaging. It now is utilized mainly in conjunction with revascularization in stent placement. Noninvasive imaging is now the preferred choice. Ultrasound is recommended in patients with moderate risk because of its availability and low cost but may overestimate the severity of stenosis. MR angiography or CTA are recommended when sonography is equivocal or indeterminate, particularly in symptomatic patients. MR angiography holds the advantage of lack of radiation whereas CTA is accessible with few contraindications. Conventional angiography is used for discordant results or if there is preference for limited contrast in cases with renal dysfunction. Accurate quantification of stenosis severity has ramifications in steering medical, endovascular or surgical treatment. Stenosis can be calculated with different methods, but may result in different percent stenosis for the same patient. Thus, it is particularly important to state the method used. The NASCET and ECST are the primary methods used to grade the stenosis, and will be discussed. We will discuss the use of imaging in characterization of plaque morphology. A clear and succinct report in compliance with ICD-10 will maximize reimbursements that the physician and hospital receives, as well as help protect against Medicare's recovery audit contractor (RAC).
Summary/Conclusion
As neuroradiologists we play a critical role in providing an accurate evaluation and description of the severity of carotid artery stenosis. Our reports are central to the management of patients as well as reimbursement ramifications.

Note: Scanned images are included in the proceedings. Some submitted images were reduced during editing, thereby decreasing clarity. Also, refer to the Program Planner. Proceedings Content as of 3-29-2013.

KEYWORDS: Carotid stenosis, NASCET

eEdE-57

Clinical Application of High-Resolution MR Intracranial Vessel Wall Imaging

Choi, J.·Kim, S.·Han, M.·Im, N.
Ajou Medical Center
Suwon, KOREA, REPUBLIC OF.

Purpose
Compared with conventional MR imaging (MRI) and MR angiography (MRA), high-resolution (HR) MR intracranial vessel wall imaging can acquire high quality images that could depict intracranial arterial wall. High-resolution MR intracranial vessel wall imaging could demonstrate the various intracranial conditions such as stable or unstable atherosclerotic stenosis, vasculitis, dissection and perforating artery disease. In this presentation, we will review the basics, protocols and clinical application of the HR contrast-enhanced MR intracranial vessel wall imaging.
Approach/Methods
**Basic and protocols for HR contrast-enhanced MR intracranial vessel wall imaging. HR 2D T1WI, T2WI, PDWI, 3D black blood T1WI, 3D black blood T1WI with contrast enhancement and 3D FLAIR VISTA
Findings/Discussion
**Unstable atherosclerotic stenosis. Eccentric intracranial artery stenosis is related to atherosclerotic disease and the enhancement that has been correlated with plaque inflammation and instability may represent unstable plaque. Expensive remodeling also was seen more frequently in patients with unstable plaque. **Stable atherosclerotic occlusion. Constrictive remodeling was seen more frequently in patients with stable stenosis, whereas expansive remodeling was observed more frequently in patients with unstable vascular disease. Constrictive remodeling, while playing a role in accelerating the narrowing of lumen, was associated with stable features. **Vasculitis. In contrast to the pattern seen in patients with atherosclerotic stenosis, patient with vasculitis showed a smooth, diffuse, concentric pattern of enhancement. **Intracranial artery dissection. Intracranial dissection had a similar pattern to atherosclerosis, including eccentric wall thickening with enhancement. High-resolution MRI could demonstrate dissecting flap and vascular ectasia at the segment of the arterial dissection. Another distinguishing feature is bright wall component on nonenhanced T1 and FLAIR sequences (indicating methemoglobin in the arterial wall), as well as visualization of a false lumen. **Normal-appearing angiography in patients with brain stem infarction on 3D TOF MRA. Occasionally, we can see the lenticulostriatal or brain stem infarction without any abnormality on TOF MRA by virtue of expensive remodeling or too small vessel wall disease. High-resolution MRI could demonstrate wall enhancement or thickening in some patients with these infarctions. **The usefulness of 3D FLAIR VISTA image for intracranial vessel wall imaging. 3D FLAIR VISTA MRI that can acquire high quality images is very sensitive for hemorrhage or fluid with high protein contents. On contrast-enhanced T1-weighted image, intraluminal flow stasis due to severe stenosis or dissection could be demonstrated as intraluminal high signal intensity that could cause misunderstanding of enhanced active plaque. 3D FLAIR VISTA MRI could be helpful to differentiate intravascular stagnant blood from plaque enhancement. 3D FLAIR VISTA MRI is also helpful to detect intramural hematoma or intraplaque hemorrhage.
Summary/Conclusion
High-resolution MR intracranial vessel wall image could depict intracranial vessel wall and its pathology in ischemic stroke and TIA patients. High-resolution multisequences have the potential to characterize the pathology in the intracranial artery and may be a useful modality for evaluating the degree of stenosis. Also, this sequence makes it possible to depict some pathology in the vessel wall without conventional angiographic abnormality.

KEYWORDS: High-resolution imaging, Intracranial vessel wall

eEdE-58

Stroke Mimics Imaging Atlas: Pearls and Pitfalls in Interpretation of Brain CT Perfusion Studies

Tamrazi, B.·Yuh, E.
University of California San Francisco
San Francisco, CA.

Purpose
In this educational exhibit, we demonstrate CT perfusion correlates of both common and unusual mimics of acute stroke. Prior studies have demonstrated that approximately 20% of patients who receive thrombolysis for acute ischemia ultimately are found to have an alternate clinical diagnosis. It is important for neuroradiologists to be aware of perfusion imaging correlates of these alternate diagnoses, as well as normal variants and anomalies in perfusion imaging studies. We provide an organized review of pearls and pitfalls in the interpretation of brain perfusion studies, employing numerous examples from our institution. The discussion also has relevance to MRI cerebral perfusion maps obtained using dynamic susceptibility contrast or arterial spin labeling perfusion imaging.
Approach/Methods
Using cases collected from clinical practice, we demonstrate brain perfusion normal variants and both common and uncommon correlates of mimics of acute ischemia and stroke. Cases are presented as unknowns with clinical history and exam, followed by initial neuroradiologist interpretation, and concluding with the final clinical diagnosis and follow-up information.
Findings/Discussion
Neuroradiologists can play a decisive role in the

Note: Scanned images are included in the proceedings. Some submitted images were reduced during editing, thereby decreasing clarity. Also, refer to the Program Planner. Proceedings Content as of 3-29-2013.

management and treatment of acute ischemia and stroke through prompt, accurate interpretation of brain perfusion studies. Familiarity with limitations and pitfalls associated with these studies can prevent unnecessary thrombolytic therapy in cases of clinical and imaging mimics of acute stroke. Cases to be discussed include perfusion alterations in seizure and postictal state, chronic high-grade carotid stenosis resulting in chronic oligemia (Figure 1), post-hemicraniectomy state, immediate post-carotid endarterectomy state, subtle primary brain tumor, transient ischemic attack, migraine headaches, and luxury perfusion in the setting of subacute infarct. Giant internal carotid artery aneurysms and other nonocclusive hemodynamically significant lesions that result in delayed flow to major vascular territories, and the impact of different perfusion postprocessing algorithms on perfusion maps in these cases, also will be discussed.

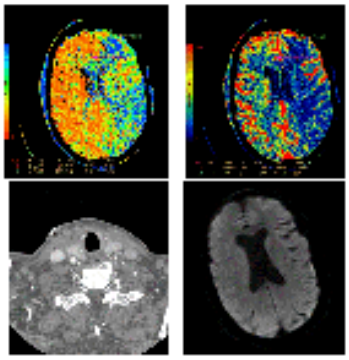

Summary/Conclusion

Brain perfusion studies are an important component of the imaging evaluation of acute ischemia and stroke. We review key examples of brain perfusion studies that mimic acute ischemia and stroke. Familiarity with these common pitfalls and variants in brain perfusion imaging can aid neuroradiologists in making prompt, decisive contributions to clinical management in suspected acute ischemia and stroke.

KEYWORDS: Actue stroke

eEdE-59

Suboptimal Contrast-Enhanced Head and Neck MR Angiography Due to Venous Reflux: Analysis of Causative Factors

Lee, E.·Shin, D.
Dongguk University Ilsan Hospital
Goyang-City, KOREA, REPUBLIC OF.

Purpose

Contrast-enhanced head and neck MR angiography (MRA) may be degraded by venous stasis or reflux of contrast into the jugular veins. The purpose of this study was to analyze the causative factors of venous stasis or reflux on contrast-enhanced head and neck MRA.

Approach/Methods

We retrospectively reviewed 300 consecutive patients who underwent contrast-enhanced head and neck MRA (right injection-150 patients, and left injection-150 patients). We also reviewed the age, sex, body mass index (BMI), history of hypertension, and history of diabetes mellitus (DM) of all patients. We measured the shortest width of left or right brachiocephalic vein (BCV), the diameter of aortic arch, the distance between sternum and vertebral body. The relationship between these factors and the venous stasis or reflux was analyzed.

Findings/Discussion

In all 300 patients, 45 (15%) patients showed venous stasis or reflux. Among the 45 patients, patients with left-arm injection were 30 and patients with right-arm injection were 15. And the difference was statistically significant (P = .015). Venous reflux into the jugular vein or cervical vein also was more severe in patients with left-arm injection. The mean age and the male-to-female ratio of patients with venous stasis or reflux was significantly higher than the patients without venous stasis or reflux. The BMI, history of hypertension and history of DM did not significantly differ. In 150 patients with left-arm injection, 30 (20%) patients had venous stasis or reflux. The mean shortest width of left BCV of the 30 patients with venous stasis or reflux was significantly narrower than that without venous stasis or reflux group (2.96 ± 0.29 mm vs. 4.80 ± 0.21 mm; P = .0001). After we adjusted for sex and age in the logistic regression model, the shortest width of left BCV still was associated significantly with venous stasis or reflux. There was no significant difference in the mean diameter of aortic arch (P = .21), and the mean shortest anteroposterior distance from the sternum to the vertebral body (P = .14) between the two groups. In 150 patients with right-arm injection, all variables did not differ significantly.

Summary/Conclusion

Compression of the left BCV can lead to venous stasis or reflux. To acquire an optimal image on contrast-enhanced head and neck MRA, left-arm injection should be avoided especially in the elderly patients.

KEYWORDS: MR angiography, Carotid angiography

eEdE-60

Brain Cortical Lesions: Ischemia and Beyond

Adapa, P.·White, M. L.·Helvey, J. T.·Keiper, M. D.
University of Nebraska Medical Center
Omaha, NE.

Purpose

Ischemic injury is the most common and a well recognized etiology for cortical abnormalities detected with brain MRI. However, nonischemic etiologies can mimic the appearance of cortical ischemia. Pattern recognition is

critical in arriving at a diagnosis to help the clinical teams in their management plans. In this exhibit, we present a clinical and imaging review of the various ischemic and nonischemic cortical lesions.
Approach/Methods
A review of our PACS database and personal teaching files was performed by the authors. Representative cases of various cortical lesions were selected. Conventional MRI features and additionally T1 dynamic enhancement, dynamic susceptibility enhancement, diffusion imaging and spectroscopy features of these cortical lesions will be reviewed. Emphasis is made on lesions with restricted diffusion abnormalities which have the greatest confounding appearance with ischemic lesions.
Findings/Discussion
We review the MRI findings of focal ischemia and the varying degrees of diffuse hypoxic-ischemia injury. Then, we discuss the imaging features of other cortical lesions including but not limited to viral encephalitis, Creutzfeldt-Jakob disease (CJD), glioma with cortical infiltration, mitochondrial diseases, leukemic cortical infiltration, hyperammonemia, hypoglycemia, electrolyte abnormalities and postictal changes. Symmetry and extent of cortical involvement on MRI and evaluation of perirolandic or watershed zone cortical involvement are two of the important imaging characteristics to differentiate ischemic versus nonischemic lesions. Other patterns of involvement, like temporal lobe involvement in herpes encephalitis or pontine changes associated with osmotic demyelination, can suggest an alternate diagnosis. Laboratory diagnostic information, including microbiologic and CSF analysis can sometimes be the key to differentiate cases of encephalitis, CJD, metabolic and electrolyte abnormalities. However, brain or muscle biopsy may be needed for mitochondrial diseases. Advanced imaging studies including T1 and T2* dynamic contrast enhancement, diffusion imaging and MR spectroscopy (as in identifying elevated lactic acid level in MELAS) can help differentiate these various cortical lesions and guide the clinician for appropriate work up to arrive at the correct diagnosis.
Summary/Conclusion
Through this educational exhibit, we provide a pictorial essay of the various ischemic and nonischemic cortical lesions. We explain the utility of using certain advanced imaging techniques, most importantly diffusion imaging, in differentiating these lesions to guide the clinicians appropriately for proper clinical management.

KEYWORDS: Cortical involvement, Ischemia, restricted diffusion, nonischemic lesions

eEdE-61

Head-to-Head Comparisons between MR Perfusion (Arterial Spin Labeling and Dynamic Susceptibility Contrast) and CT Perfusion in Seizures and Strokes

Baruah, D.·Raslau, F.·Gupta, S.·Klein, A.·Ulmer, J.
Medical College of Wisconsin and Affiliated Hospitals
Wauwatosa, WI.

Purpose
A variety of perfusion techniques have become commercially available, including MR perfusion methods such as arterial spin labeling (ASL) and dynamic susceptibility contrast (DSC) as well as CT perfusion (CTP). Due to differences in technique, software algorithm, color palette, and color scale, perfusion maps in the same patient may yield difference results. A head-to-head comparison between these perfusion techniques can reveal relative advantages and disadvantages, which can be used to optimize imaging strategies for different clinical needs.
Approach/Methods
The similarities and differences are reviewed between ASL, DSC, and CTP in terms of basic physics and technique. Then an array of head-to-head comparisons is illustrated in both seizure and stroke workups. Their relative advantages and disadvantages are identified, and suggestions are offered for optimizing the choice of perfusion technique for specific clinical contexts.
Summary/Conclusion
In seizures, ASL is superior for identifying peri-ictal activity and for differentiating stroke-mimicking seizures. In strokes, ASL has the highest negative predictive value. Consequently, ASL is the optimal imaging strategy when the clinical question requires the exclusion of perfusion abnormalities.

KEYWORDS: Arterial spin labeling, Dynamic susceptibility contrast-enhanced, computed tomography perfusion, stroke, seizure

eEdE-62

Why Is the Area Hyperperfused on CT Perfusion?

Patro, S. N.·Nguyen, T.·Torres, C.·Lum, C.·Chakraborty, S.
The Ottawa Hospital
Ottawa, ON, CANADA.

Purpose
Perfusion CT frequently is used in patients with ischemic stroke for assessment of core infarct and ischemic penumbra. However, it is not infrequent to see areas of increased CBV in the workup of patients with suspected stroke. The aim of this pictorial essay is to present and discuss different causes of increased CBV or CBF seen with CT perfusion in the workup of patients with acute or chronic cerebral ischemia.
Approach/Methods

Note: Scanned images are included in the proceedings. Some submitted images were reduced during editing, thereby decreasing clarity. Also, refer to the Program Planner. Proceedings Content as of 3-29-2013.

We reviewed clinical and imaging data from eight patients who underwent CT perfusion for acute or chronic cerebral ischemia who had areas of increased CBV or CBF.
Findings/Discussion
Causes of increased CBV can be classified as global or local. Global causes could be due to acetazolamide challenge. In patients with chronic cerebral ischemia related to underlying stenotic lesion, the acetazolamide challenge test is helpful in distinguishing areas with decreased CVR (tissue under hemodynamic stress) from areas with preserved CVR (tissue with reduced metabolic demand). Acetazolamide challenge fails to cause increased CBF and CBV in areas with decreased CVR and thus helps in selecting patients for revascularization. Local increase in CBV and CBF could be secondary to various causes. Luxury perfusion is a condition that can be encountered in patients after recanalization following acute ischemic stroke. There will be increased CBF and CBV in the infarcted tissue which predisposes it for hemorrhagic transformation. This also can be encountered following carotid endarterectomy and predicts the chances of postrevascularization intracranial bleed. An accidental intra-arterial injection of CT contrast into the brachial artery can cause focal rise of cerebral blood flow and volume. Cerebral blood flow and CBV also are markedly elevated within the AVM nidus and in the AVF, reflecting high vascularity; however, the perinidal/perifistula areas could demonstrate low CBV and CBF, suggesting ischemia. Perfusion imaging could differentiate focal seizures from ischemic stroke by demonstrating localized hypermic state in patients with seizure. High grade tumors like glioblastoma multiforme are inherently associated with increased perfusion of the tumor tissue secondary to underlying increased neoangiogenesis.
Summary/Conclusion
Clinical examination and close serial examination of the data volumes and of the dynamic CTangiogram often will provide clues to the right diagnosis when an area of increased perfusion is present.

KEYWORDS: CT perfusion, Stroke, tumor, seizure

eEdE-63

Challenges and Controversies of CT Perfusion in Acute Stroke

Vagal, A. S.·Khatri, P.
University of Cincinnati Medical Center
Cincinnati, OH.

Purpose
The purpose of this exhibit is to review the technical and pathophysiologic challenges of CT perfusion (CTP) and to assess existing literature for evidence-based medicine for use of CTP in acute stroke.
Approach/Methods
The exhibit will be divided into four main categories as follows: 1. Discussion of imaging biomarkers of patient outcome in acute stroke. 2. Sources of variability of CTP technique: patient, postprocessing algorithms, acquisition. 3. Thresholds used in the analysis of CTP: infarct core versus penumbral volume, penumbra versus benign oligemia, gray matter versus white matter thresholds. 4. Evidence-based guidelines for use of CTP in making acute stroke treatment decisions.
Findings/Discussion
Even after more than a decade of perfusion imaging, diagnostic and therapeutic efficacy of perfusion is an area of controversy and vigorous debate. To date, all published randomized controlled trials have used MR-based multimodal imaging for the thrombolytic treatment selection. No clinical trials have been conducted using CT-based multimodal imaging and currently evidence is lacking on the efficacy of CT perfusion in making acute stroke treatment decisions. Yet, due to wide spread accessibility of CT scanners, CTP is being rapidly assimilated into routine clinical practice of stroke evaluation and treatment.
Summary/Conclusion
Increasing utilization of CTP in acute stroke may be creating a paradigm shift and it is pertinent for the practicing neuroradiologist to be aware of the current controversies and challenges of CT perfusion.

KEYWORDS: Actue stroke, Brain perfusion

eEdE-64

Multimodal Approach of Intracranial Hypotension Syndrome: Pitfalls in Clinical Manifestations, Imaging Findings and Treatments

Pinzon, O.·Moritani, T.·Lai, L.·Capizzano, A.
University of Iowa Hospitals and Clinics
Iowa City, IA.

Purpose
To demonstrate multimodal imaging findings of intracranial hypotension syndrome correlated with clinical manifestations and post-treatment outcome. To discuss clinical and imaging pitfalls using cases with misdiagnosis leading to inappropriate or delayed management.
Approach/Methods
We reviewed 58 patients with intracranial hypotension syndrome with various clinical manifestations (postural headache, hearing complaints, vertigo, 6^{th} nerve palsy, facial numbness, seizure, hypersomnia, altered mental status and frontotemporal brain sagging syndrome). Imaging modalities included brain CT/MRI, total spine MRI, CT/MR myelography, and radioisotopic CSF leak study. Clinical management included bed rest, increased oral intake of fluids, caffeine, glucocorticoids, intrathecal saline infusion, lumbar epidural blood patch, epidural blood patch targeted to the leak level (cervical/thoracic) based on CT myelogram findings, and surgical ligation.
Findings/Discussion
The variety of symptoms is explained by the Monro-Kellie

Note: Scanned images are included in the proceedings. Some submitted images were reduced during editing, thereby decreasing clarity. Also, refer to the Program Planner. Proceedings Content as of 3-29-2013.

doctrine: the sum of brain, CSF, and intracranial blood volumes remain constant. Compensatory mechanisms, such as venous engorgement, take place during CSF hypovolemia. Brain sagging can place traction on cranial nerves or cause subdural hematomas by tearing bridging dural veins. Severe brain sagging can cause acute altered mental status, hypersomnia or cognitive impairment. In most cases of intracranial hypotension, defined MRI criteria were found: pachymeningeal enhancement, subdural fluid collections, venous and pituitary engorgement, basal cistern effacement, brain and brainstem sagging and tonsillar ectopia. However, normal MRI did not exclude the diagnosis of intracranial hypotension. Radionuclide cisternogram was more sensitive but less specific compared to CT myelography. Dynamic CT myelography could determine location and extension of CSF leak, thus guiding epidural blood patch. However, in many typical intracranial hypotension cases, leak studies only showed multiple meningeal cysts without evidence of CSF leak, and patients only temporarily improved after multiple blood patches. Lumbar intrathecal infusion with normal saline can be used to temporarily restore CSF volume in patients with consciousness alteration requiring emergent treatment. These illustrative cases demonstrate the spectrum of pitfalls encountered in the diagnosis and treatment of intracranial hypotension. Potential pitfalls include: 1) clinically misdiagnosed as migraine; cervical radiculopathy; transient ischemic attack; subdural hematomas; subarachnoid hemorrhage; meningitis 2) misdiagnosed as Chiari I malformation on MRI treated with decompression surgery and delayed appropriate treatment (blood patch and surgical ligation) causing intracranial hypertension 3) intracranial hypertension associated with pregnancy leading to CSF leak causing intracranial hypotension, 4) Intraspinal CSF leak after lumbar puncture misdiagnosed as epidural abscess in an infant resulting in unnecessary surgery, 5) clinically misdiagnosed as fronto-temporal dementia which was turned to be “frontotemporal brain sagging syndrome” (autopsy was performed in one case and was negative for primary neurodegeneration), 6) CSF leak due to osteophytes, 7) intracranial hypotension related to pseudomeningocele, 8) complicated with cerebral venous sinus thrombosis, 9) C1-C2 retrospinal fluid collection mistaken for actual site of CSF leakage.

Summary/Conclusion

We demonstrate multimodality imaging findings and discuss the pathophysiology of intracranial hypotension syndrome with various clinical manifestations and post-treatment outcome. We illustrate pitfalls using the cases with misdiagnosis leading to inappropriate or delayed management emphasizing the role of neuroradiologists in diagnosing and treating this important condition.

KEYWORDS: Intracranial hypotension, MR imaging, myelogram

eEdE-65

Would You Know It If It Hit You in the Face? Exploring the Radiological Link Between Facial Fractures and Intracranial Hemorrhage

Pan, Q.[1]·Holstad, J.[2]·Byrns, K.[2]·Penna, K.[2]·Lev, S.[2]
[1]American University of the Caribbean, Saint Martin, SAINT MARTIN, [2]Nassau University Medical Center, East Meadow, NY.

Purpose

We investigate maxillofacial fractures and associated intracranial hemorrhages with the intent to enhance the radiologist’s search pattern.

Approach/Methods

Trauma cases with concurrent imaging of the face and head were compiled from both our oral maxillofacial surgery clinics and our Level I trauma center ED. Patients with both traumatic maxillofacial injury and intracranial hemorrhage were categorized by mechanism of injury, age, gender, and sub-type of fracture or bleed. Isolated fractures considered were mandible, nasal, zygomatic, orbital, maxillary and frontal and fracture patterns were Lefort and zygomaticofacial complex. Intracranial hemorrhages were epidural, subdural, subarachnoid or intraparenchymal. We demonstrate illustrative cases and include literature highlights noting associations between traumatic maxillofacial injuries and intracranial hemorrhage.

Findings/Discussion

The facial skeleton, with its horizontal and vertical buttresses, may absorb significant energy during head trauma. When this capacity is surpassed, deleterious forces can be transmitted intracranially. There is immense variability (5.4 to 86%). in the literature concerning reported rates of concurrent maxillofacial fractures and intracranial hemorrhage. If we include only individuals with both head and maxillofacial CT exams, our original clinic list of 1682 patients is reduced to 131, while the ED list of 293 is narrowed to 139. Of the 270 total, 29 (10.7%) demonstrated at least one facial fracture with any intracranial hemorrhage. Mechanisms of injury include MVA, fall, assault, pedestrian struck and nonspecified trauma. Virtually all possible combinations of fracture and hemorrhage type were observed, though some trends were evident. Fractures involving the frontal bone revealed the strongest association with intraparenchymal hemorrhage. This observation is strongly supported and reflects the proximity of the frontal bone to the underlying brain. Lefort fractures demonstrated the strongest association with subarachnoid hemorrhage. Fractures of the sphenoid bone, involving the skull base, also had a relatively increased bleed association, reflecting the high energy forces involved.

Note: Scanned images are included in the proceedings. Some submitted images were reduced during editing, thereby decreasing clarity. Also, refer to the Program Planner. Proceedings Content as of 3-29-2013.

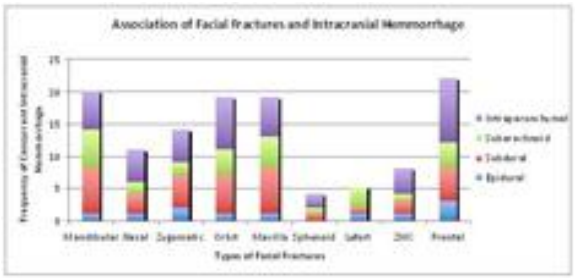

Summary/Conclusion
In the emergent setting it is important for radiologists, surgeons, and emergency physicians to be cognizant of the propensity of facial fractures and intracranial hemorrhages to simultaneously occur. A clearer understanding of the patterns of facial injuries will assist both the on-call radiologist's search pattern and care provider's management. Several trends emerge, particularly highlighting the deleterious nature of frontal and Lefort-type fractures. Although the statistical utility of this review is limited by sample size and selection methods, the patterns observed fall within the aforementioned broad range of published data and presents new avenues for exploring these associations.

KEYWORDS: Traumatic brain injury, Craniofacial findings

eEdE-66

Head Trauma: The Role of Imaging and What the Radiologist Needs to Know

Khorrami-Arani, N.[1]·Liang, T.[2]·Nicolaou, S.[1]
[1]Vancouver General Hospital, Vancouver, BC, CANADA,
[2]University of British Columbia, Vancouver, BC, CANADA.

Purpose
The etiologies of head trauma usually vary with the patient's age; in the elderly population, accidental falls are the most common causes, whereas in younger patients and children, motor vehicle collisions and abuse are common causes respectively. Regardless, traumatic brain injury (TBI) from post head trauma is a leading cause of mortality and morbidity in the world's population and it has been estimated that approximately 2% of the entire population currently lives with disabilities caused by TBI, and over 500,000 emergency department visits annually are accounted for by head trauma. Thus, it is important for the radiologist to rapidly and accurately diagnose the TBI and be aware of the potential complications. The purpose of this exhibit is to review the pathophysiology of these injuries, discuss the role of imaging with emphasis on the roles of MDCT and MRI, and review the spectrum and classification of injuries.
Approach/Methods
A retrospective review of head trauma cases at our institution will be conducted for imaging examples to demonstrate the spectrum of these injuries.
Findings/Discussion
This education exhibit will review the epidemiology, anatomy, pathophysiology and mechanism of injury, and parameters for clinical assessment of head trauma. The spectrum of injuries post head trauma including epidural and subdural hematomas, shear injuries, subarachnoid hemorrhage, parenchymal and skull base injuries will be reviewed and imaging examples as well as characteristic imaging findings of each will be demonstrated and discussed. The role of imaging and a review of imaging modalities available for head trauma including , MDCT, CTA, MRI will be reviewed. Emphasis on the role of MDCT will focus on the utility of reformats, the significance in the size of the midline shift, the swirl sign, role of CTA and CTV in evaluating vascular injuries, the ability to demonstrate perfused blood volume imaging and perfusion with emphasis on the traumatic penumbra. The clinical significance of these findings on MDCT will be reviewed. Emphasis on the role of MRI will focus on the new techniques available for head trauma imaging including, but not limited to spectroscopy, diffusion tensor imaging, susceptibility imaging and MRI perfusion. Finally, an imaging and management algorithm for head trauma will be proposed and reviewed to help aid the radiologist and trauma team act quickly and effectively.
Summary/Conclusion
Head trauma presents with a unique spectrum of injuries and characteristic imaging findings that are important for the radiologist to quickly recognize as it can have significant implications on prognosis and management. These injuries and their imaging examples have been reviewed in this exhibit. MDCT and MRI with new techniques available for imaging of head trauma and TBI are extremely useful and have been reviewed here. A useful algorithm for imaging and management of head trauma has been proposed, this algorithm will allow the radiologist to efficiently and successfully decide management and can be easily adapted to the radiologist's daily practice.

KEYWORDS: TBI, head trauma

eEdE-67

The Dynamic Appearance of Intracranial Hemorrhage on MR Imaging and the Physics Behind It

LoStracco, T. A.·Shrier, D. A.·Meyers, S. P.
University of Rochester
Henrietta, NY.

Purpose
Characterization of the MRI features of intracranial hemorrhage can be important for the diagnosis and treatment of various pathologic disorders. The purpose of this exhibit is to illustrate the various configurations and locations of intracranial hemorrhages, as well as the sequential MRI signal changes over time, while describing the basic physical principles behind the evolution of a hemorrhage. This will help provide a deeper

Note: Scanned images are included in the proceedings. Some submitted images were reduced during editing, thereby decreasing clarity. Also, refer to the Program Planner. Proceedings Content as of 3-29-2013.

understanding of these concepts.
Approach/Methods
Provide a brief summary of the biochemistry behind the evolution of hemorrhage and how these processes are exploited by MR physics to provide distinct imaging characteristics. This will be followed by numerous examples of high quality images of different types of intracranial hemorrhage, as well as all different stages of hemorrhage, ranging from hyperacute to chronic. These examples then will be correlated with the physical principles that were summarized previously.
Findings/Discussion
Often we learn about the evolution of intracranial hemorrhage through memorization of how each stage appears on each sequence. However, by understanding these principles at the microscopic level, one can develop a more profound understanding of how and why hemorrhage has the appearance it does. This will help provide more clear and confident interpretation of head MRs performed for intracranial hemorrhage.
Summary/Conclusion
It is easy to resort to memorization in order to understand a process as complex as evolution of intracranial hemorrhage. However, this is unnecessary if one has a working understanding of the biochemical and physical processes that are occurring.

KEYWORDS: Hemorrhage, MR imaging brain

eEdE-68

Be Prepared: The Spectrum of Neuroradiologic Emergencies of the Brain - A Primer for the On-Call Radiology Resident

Agrawal, J. P.·Lev, S.
Nassau University Medical Center
East Meadow, NY.

Purpose
Our educational exhibit aims to increase awareness and diagnosis of neuroradiologic emergencies of the brain. The interactive case-based discussion emphasizes common and unusual situations encountered on call. The viewer will discern subtle findings and consider more obscure diagnoses. Imaging pearls and take-home points are highlighted.
Approach/Methods
We present cases from our Level I Trauma and designated stroke center occurring during the past five years. Imaging modalities include CT, CTA/CTV, MRI, and MRA/MRV. We categorize emergencies by location and etiology. We also discuss the importance of mechanisms of injury. Each clinical scenario is followed by questions regarding the radiologic workup.
Findings/Discussion
Vascular emergencies can be ischemic, hemorrhagic, or both. Acute ischemic stroke necessitates prompt and accurate radiologic assessment. We ask the viewer to detect early subtle signs that can be missed. Pediatric stroke poses a unique challenge. It presents with unconventional symptoms and is due to varying etiologies. Without high suspicion, delays in stroke team activation may occur. Conditions that mimic stroke also must be considered. We present several cases of stroke mimickers, such as a glioblastoma multiforme that was misinterpreted as an infarct. Intracranial hemorrhage can be categorized by etiology (traumatic or nontraumatic) and location (intraparenchymal or extra-axial). Diffuse axonal injury results from rotational acceleration forces, accounting for lesion distribution. For contusions, the resident should evaluate for coup and contrecoup injuries. Mass effect and cisternal effacement must be communicated urgently. Subdural hemorrhages (SDH) result from low pressure venous bleeding. Intracranial brain motion may produce contralateral insult. Coronal reformats are useful in evaluating subtemporal, convexity, and tentorial hematomas. Low density areas within a heterogeneous SDH may represent unclotted blood. Epidural hemorrhages can not only be arterial but also, less commonly, venous, secondary to tears of the torcula or transverse sinus. Consider nonaccidental trauma in the pediatric population with extra-axial hemorrhages of varying ages. Subarachnoid hemorrhage (SAH) has many causes. Perimesencephalic nonaneurysmal SAH has a specific pattern and a benign course. Rarely, a ruptured aneurysm may present with intraparenchymal hemorrhage alone. Vascular injury is especially suspect with high velocity and rotational motions (MVA and athletic). Injury to vascular structures can be intracranial or extracranial and can produce pseudoaneurysms, A-V fistulas, and carotid dissections/occlusions. Assess for depressed calvarial, sphenoid (associated with carotid-cavernous fistulas), and petrous (carotid canal) fractures. Cervical fractures may produce vertebral injury. Nontraumatic vascular emergencies include intracranial hypertension/hypotension and vasculitides. Drug/toxin induced CNS injuries require a high index of suspicion. Posterior reversible encephalopathy syndrome is a rare condition that can be easily overlooked and requires prompt identification to prevent permanent damage. CNS infections differ in immunocompetent and immunocompromised individuals and can be categorized by location and pattern: extra-axial, ring-enhancing, temporal lobe, basal ganglia, and white matter lesions. Tumors, even benign ones, can be acutely life-threatening. We show an unusual case of a large colloid cyst, producing impending brain herniation secondary to hydrocephalus.
Summary/Conclusion
Neuroradiologic emergencies comprise a diverse array of conditions. The interpreting radiologist can actively participate in patient management with appropriate imaging recommendations, prompt diagnosis, and timely communication.

KEYWORDS: Emergencies, Educational, resident

Note: Scanned images are included in the proceedings. Some submitted images were reduced during editing, thereby decreasing clarity. Also, refer to the Program Planner. Proceedings Content as of 3-29-2013.

eEdE-69

Opening Pandora's Box? An Overview of Surgical Interventions on the Cranial Vault for the Radiologist

MacAdam, B. D.·Ambalathunkal, E.·Beecher, J.·Lev, S.·Lev, S.
Nassau University Medical Center
East Meadow, NY.

Purpose
We aim to provide an overview of the evaluation of the postoperative head. Using our experience with craniotomy, craniectomy, and cranioplasty at our institution, we discuss the indications, procedures, postoperative findings, and complications. We also relay surgical and pathophysiologic insights, focusing on what the neurosurgeon and radiologist need to know.
Approach/Methods
A list of all trauma patients undergoing craniotomy, craniectomy, or cranioplasty at our level I trauma center from January 2011 to present was obtained from the Department of Neurosurgery. Imaging was performed using a 320-slice CT scanner and reviewed by a board certified neuroradiologist. Only cases with both pre and postoperative imaging were included. The numbers of each type of procedure as well as complications and their temporal course were based on the imaging review in concert with clinical data. A review of the current neurosurgery and radiology literature regarding indications, techniques and complications was performed and summarized.
Findings/Discussion
The noncontrast head CT is the workhorse of pre and postoperative neurosurgical imaging. The radiologist must be aware of normal postoperative findings in order to quickly differentiate signs which may indicate potentially severe complications. Of the 38 cases ultimately included for review, there were 17 craniotomies, 18 craniectomies, and 2 cranioplasties. Three of the patients who initially underwent craniectomy required cranioplasty at a later date. We found a much higher number of complications following craniectomy (70.5% of cases) than either craniotomy (16.7%) or cranioplasty (0%). This ordering correlates to numerous reports in the literature. Our discussion includes a brief review of the relevant anatomy along with an overview of current and historical surgical perspectives.We highlight the various indications for neurosurgical intervention, including extra-axial and intraparenchymal hemorrhages, cerebral edema, and depressed skull fractures. The normal postoperative findings unique to each procedure are discussed in depth. We review the broad spectrum of potential complications as well as their expected time course. These range from the relatively benign to life-threatening and include extracranial herniations, tension pneumocephalus, hygromas, post-traumatic hydrocephalus, infection, new or expanded intraparencyhmal contusions/hemorrhage, extra-axial hemorrhages, and syndrome of the trephined. We discuss the controversies surrounding decompressive craniectomies as well as the pathophyisologic basis of unfavorable outcomes.
Summary/Conclusion
Timely recognition of complications following neurosurgical intervention on the cranial vault via craniotomy, craniectomy, and cranioplasty, is crucial to allow early intervention and prevent additional injury. The astute radiologist, equipped with a knowledge of anatomy and familiar with the expected postsurgical changes is better able to assist the neurosurgeon in the management of these often critically ill patients.

KEYWORDS: Postoperative findings, Traumatic brain injury

eEdE-70

Dural Venous Sinuses: Review of Normal/Variant Anatomy and Common Pathologic Conditions Resulting in Impaired Cerebral Blood Drainage

Rajsheker, S.·Williamson, K. M.·Bourekas, E. C.·Luttrull, M. D.·Nguyen, X.·Slone, H. W.
The Ohio State University Wexner Medical Center
Columbus, OH.

Purpose
The goal of this exhibit is to review dural venous sinus normal and variant anatomy with subsequent discussion regarding common pathology affecting the sinuses.
Approach/Methods
First the normal anatomy will be reviewed using computed tomography (CT) and magnetic resonance (MR) imaging followed by a review of the common normal variants and pitfalls leading to misdiagnosis of dural venous sinus pathology. Various common pathologic conditions affecting the dural venous sinuses then will be discussed with an emphasis on the importance and utility of thorough evaluation with CT and MR venography.
Findings/Discussion
To understand and recognize abnormal dural venous sinuses and the common pathology affecting them it is essential to first know the normal and variant anatomy of the drainage system of the brain and its typical appearance on both CT and MRI. With this knowledge one can easily see direct signs of dural venus sinus obstruction. In less obvious cases there are many indirect signs, such as diffuse brain edema, decreased ventricular size, and venous infarctions, that we must be familiar with in order to ensure a prompt and proper diagnosis of impaired dural venous sinus blood flow. Occlusion or stenosis, and subsequent symptomatology, of the dural venous sinuses can result from a number of pathologic conditions that result in either internal blockage, external compression, or frank invasion. Examples of such conditions include acute or chronic thrombi from such things as infection or trauma; intracranial, cranial, or extracranial masses; and developmental vascular abnormalities. Findings suggestive of dural venous sinus abnormalities may be visualized on

Note: Scanned images are included in the proceedings. Some submitted images were reduced during editing, thereby decreasing clarity. Also, refer to the Program Planner. Proceedings Content as of 3-29-2013.

standard noncontrast CT images and standard brain MR sequences though it is often imperative to confirm this suspicion with dedicated CT and MR venography, especially in more subtle cases with a coinciding nonspecific clinical presentation.
Summary/Conclusion
Dural venous sinus pathology is difficult to diagnosis because of its variable and nonspecific presentation. It most frequently manifests itself due to compression, invasion, or occlusion resulting in vague symptomatology from the delay of cerebral blood drainage. Delay in diagnosis may lead to high morbidity and mortality; whereas, prompt diagnosis can lead to proper treatment and significantly improve the patient prognosis. Thus, familiarity with the imaging plays a key role in the delineation of normal anatomy and normal variants and is vital in the diagnosis of dural venous sinus pathology.

KEYWORDS: Dural sinus, Dural sinus thrombosis

eEdE-70a

"Down and Out": Imaging of Various Etiologies of Third Cranial Nerve Palsy

Jarraya, M.[1]·Hayashi, D.[1]·Drissi, C.[2]·Murata, T.[1]·Guermazi, A.[1]·Sakai, O.[1]·Ben Hammouda, M.[2]·Mian, A.[1]
[1]Boston University, Boston, MA, [2]Institute of Neurology, Tunis, TUNISIA.

Purpose
The diagnosis and management of third cranial nerve (CNIII) palsy vary according to the age of the patient, clinical presentation, and associated symptoms. The purpose of our presentation is to review relevant anatomy of CNIII and to present the radiologic findings of CNIII palsy, using magnetic resonance imaging (MRI) and conventional arteriography. Such knowledge contributes to the appropriate clinical management of CNIII pathology.
Approach/Methods
Retrospective review of imaging examinations (brain MRI and arteriography) of patients presenting with CNIII palsy was performed at two tertiary referral centers. Imaging findings were reviewed and correlated with the neuro-ophthalmologic impairment to determine the site of the lesion along the CNIII pathway. Relevant anatomy is reviewed. Nuclear and fascicular arrangement within the midbrain is explained based on previous reports and experimental findings. Anatomical relationships and radiologic anatomy of the cisternal and cavernous portions also are presented. Subsequently examples of different presentations of CNIII palsy are displayed following a comprehensive classification based on the site of the lesion (central, cisternal, or cavernous).
Findings/Discussion
There are many potential causes for CNIII palsy. Anatomical localization of the abnormality is important and depends on the imaging findings and clinical presentation. Central causes include mesencephalic tuberculoma, cavernoma, tumors, and ischemia. Cisternal etiologies can be posterior communicating artery aneurysm, neuritis, sarcoid, and lymphoma. Cavernous etiologies include nasopharyngeal tumor extending to the cavernous sinus, internal carotid artery aneurysm, cavernous hemangioma of the cavernous sinus, pituitary apoplexy, and cavernous sinus thrombosis.
Summary/Conclusion
Third cranial nerve palsy is a common cause of diplopia, ptosis and mydriasis. MR imaging is typically the primary modality used in determining the site and the nature of the lesion. In some cases, conventional angiography also can be helpful. Knowledge of clinical presentation and imaging findings as well as important anatomical relationships of CNIII along its course is crucial in locating the site of the pathology, identifying the etiology and assisting in timely clinical management.

KEYWORDS: Cranial nerve palsy

Monday, May 20 – Wednesday, May 22
6:30 AM – 9:00 PM
Thursday, May 23
6:30 AM – 3:00 PM
Hall B1

Electronic Education Exhibits (eEdE) 71 - 85

eEdE2-Anatomy

Note: A missing printed number indicates an abstract has been withdrawn.

eEdE-71

Deep Brain Stimulation: A Comprehensive Pictorial Review

Bansal, V.·Chokshi, F. H.·Mewes, K.·Gross, R. E.·Riva Posse, P.·Mayberg, H. S.·Hudgins, P. A.
Emory University
Atlanta, GA.

Purpose
Deep brain stimulation (DBS) is used for treatment of medically refractory movement disorders and several neuropsychiatric conditions. Optimal outcomes depend on careful patient selection, accurate electrode targeting, and proper follow up for complications. Based on our institution's experience with DBS, we will provide a review of the principles behind DBS, discuss pre and

Note: Scanned images are included in the proceedings. Some submitted images were reduced during editing, thereby decreasing clarity. Also, refer to the Program Planner. Proceedings Content as of 3-29-2013.

postoperative magnetic resonance imaging (MRI) protocols, and findings that are important for radiologists to convey in their interpretation.
Approach/Methods
Over a six-year period, 370 patients received DBS at our institution. Representative images demonstrate key basal ganglia landmarks, expected stimulator locations, and although rare, surgical complications. MRI protocols that best show landmarks and limitations to imaging are presented.
Findings/Discussion
Deep brain stimulation is FDA-approved for the treatment of medically refractory essential tremor, Parkinson's disease, and - through a humanitarian device exemption - dystonia and obsessive-compulsive disorder. Additional indications under clinical investigation include epilepsy, treatment-resistant depression, chronic pain, Alzheimer disease and addictions. The procedure consists of implanting an electrode in the brain connected to a pulse generator located in a subcutaneous pocket over the upper chest. Precise localization of the electrode tip at the desired target correlates with successful clinical outcomes. Two methods are used for targeting the electrode tip; the *indirect method* relies on measurements, based on a standard atlas, using a coordinate system derived from the anterior and posterior commissures. Alternatively, to better account for variability in individual anatomy, the *direct method* relies on high resolution volumetric MR brain images to directly visualize the intended targets. Due to difficulty in direct visualization with current technologies, a hybrid indirect/direct system is often used. Final placement is ultimately confirmed via intraoperative activation of the electrode and observation of the intended treatment effect, or by direct imaging visualization with MRI and/or CT. For each clinical indication, there may be one to three possible targets for treatment-efficacy; for example, stimulators for Parkinson disease typically target the subthalamic nucleus (STN) or the globus pallidus pars interna (GPi). Additionally, we are one of a few institutions where DBS is being used for treatment-resistant depression, with 26 patients treated to date. In these patients, the subcallosal cingulate white matter is targeted. At our institution, three distinct MRI protocols have been developed for DBS patients: 1. Screening, 2. Preoperative, 3. Postoperative. Each includes the optimal sequences/planes for targeting specific regions and methods to reduce susceptibility on postoperative images. Perioperative complications of stimulator placement include seizure and intracranial hemorrhage. Delayed complications include lead fracture, migration, and infection. It is important to understand the appearance of the stimulator system as well as the expected tip location for proper identification of these complications.
Summary/Conclusion
Deep brain stimulation for medically refractory movement and neuropsychiatric conditions requires in-depth knowledge of neuroanatomy and careful attention to MR acquisition. As a member of the health care team, the neuroradiologist should understand the rationale for stimulator placement and the expected pre and postoperative imaging appearance for optimal patient outcomes.

KEYWORDS: Deep brain stimulator, Basal ganglia anatomy, complications

eEdE-72

Simulation-Based Training in Neuroradiology

Robertson, H. J. F.[1]·Yang, J.[1]·Wojak, J.[1]·Miranpuri, A.[2]
[1]Louisiana State University Health Sciences Center, New Orleans, LA, [2]Medical University of South Carolina, Charleston, SC.

Purpose
The rapid decrease in recent years of patient referrals for cerebral angiography necessitates alternative educational techniques for resident and fellow training in neuroradiology. Such remedial action is necessary now if angiography knowledge in depth is to remain an inherent part of neuroradiology. Simulation-based training (SBT) can be the effective solution to this dilemma.
Approach/Methods
Many neuroradiology training institutions already have a simulation laboratory, or at least access to a regional laboratory. Commercially available vascular procedural simulation devices of high fidelity have highly developed computer programs which can provide virtual reality angiography training and experience using simulated catheters, wire guides, coils and stents. Silastic arterial models can provide training and experience with actual catheters, wire guides and interventional materials for coiling of aneurysms, stent placement and blood clot extraction. An SBT program for individual or team training is developed around established educational principles. It includes an expert level lecture on the procedure and its risks and possible complications, a pretest of subject knowledge, a series of supervised simulations, a post-test and a proctor-trainee debriefing interview. Repeat SBT sessions at several weeks time intervals provide cumulative training metrics to assess individual knowledge and skills development in invasive procedures without risk of patient injury.
Findings/Discussion
Successful outcomes have been shown for SBT applied to subsequent patient procedures in laproscopic surgery, some aspects of orthopedic surgery, anesthesia, endovascular diagnostic and interventional procedures. Simulation-based training can be applied to all interventional procedures in neuroradiology. It can provide continuous assessment of resident and fellow procedural knowledge and manual skills.
Summary/Conclusion
Simulation-based training is an effective method of basic training in interventional procedures in neuroradiology

without risk of patient injury. Preliminary SBT combined with the subsequent patient procedures is expected to result in improved trainee skills and procedural outcomes with minimal technical errors, reduced procedure time and radiation exposure.

KEYWORDS: Educational, Arteriography, simulation

eEdE-73

Do You See What I See? Visual Field Deficits from Lesions along the Visual Pathway

Singh, V.[1]·Reede, D. L.[1]·Smoker, W. R. K.[2]
[1]SUNY Downstate University Hospital of Brooklyn Long Island College Hospital, Brooklyn, NY, [2]University of Iowa Hospital and Clinics, Iowa City, IA.

Purpose
• Review the anatomy of the visual pathway. • Learn the types of visual field defects and the location of lesions that produce them. • Develop an imaging-based approach for the evaluation of patients with visual field deficits.
Approach/Methods
Presented in a quiz format, using illustrations, and corresponding CT and MR images, the anatomy of the visual pathway is reviewed from the anterior chamber to the occipital lobe. A variety of lesions involving portions of the visual pathway (optic nerve, optic tract, optic chiasm, lateral geniculate ganglion), optic radiations (Myer's and Braun's loops) and occipital cortex are present including traumatic, neoplastic and inflammatory pathologies.
Findings/Discussion
Emphasis is placed on understanding the anatomical basis for the corresponding visual field deficits.
Summary/Conclusion
Imaging can be crucial in determining the cause, as well as correlating the location of a lesion along the visual pathway, with the type of visual deficit observed on clinical examination. After viewing this exhibit the viewer will be familiar with the anatomy of the visual pathway, the type of lesions encountered and expected visual field deficit based on a lesion's location.

KEYWORDS: Visual pathways, Visual loss, visual system

eEdE-74

In Limbo: A Review of the Limbic System Imaging Anatomy

Garcia, L. E.·Jay, A.
Georgetown University Hospital
Washington, DC.

Purpose
The limbic system is composed of a complex network of cortical and subcortical structures involved in many aspects of brain function, including learning, memory, and emotional behavior. It also is involved in many neuropathologic conditions, both isolated or as part of more diffuse processes due to its robust connections with the rest of the brain. Even though it plays an important role in both the structural composition and pathology affecting the brain, not many radiologists feel comfortable evaluating it. We aim to familiarize the participants of this educational exhibit with the normal imaging anatomy of the limbic system and review some common pathology affecting this region.
Approach/Methods
We begin by giving a brief overview of the limbic system embryology. We then proceed to show imaging anatomy of the limbic system divided into cortical and subcortical regions. Examples of pathology involving the limbic system in different disease categories will be shown.
Findings/Discussion
The limbic system's relation to memory and emotional aspects of brain function stems from its embryologic relation to primitive regions of the brain containing a trilaminar cortex architecture, and its communication with more modern regions containing a six-layer cortex. The limbic system's intricate and complex anatomy is best evaluated by magnetic resonance multiplanar imaging. The system is better understood when divided into cortical and subcortical structures. The cortical structures include the parahippocampal and cingulate gyri, hippocampus, and fornices. The subcortical structures include the amygdala, septal area, thalamus, hypothalamus, and mamillary body. The limbic system is involved by many disease categories, including congenital, malignant, infectious, neurodegenerative, ischemic, traumatic, and epileptogenic disorders. Involvement may be isolated to this region or may be secondarily involved by a more diffuse process originating in another region of the brain.
Summary/Conclusion
The limbic system is an important component of the brain and is involved in many disease processes. Therefore, familiarity with normal imaging anatomy of this region provides radiologists with an important tool in making diagnostic decisions and avoid remaining in limbo when it comes to helping both patients and referring physicians.

KEYWORDS: Anatomy, Limbic system

eEdE-75

Functional Anatomy and Pathology of the Corpus Callosum: Correlation with Diffusion Tensor Imaging

Lee-Felker, S.·Felker, E.·Salamon, N.
University of California Los Angeles
Los Angeles, CA.

Purpose
To highlight the use of diffusion tensor imaging (DTI) in understanding the functional organization of the corpus callosum, with anatomical-clinical correlation of corpus callosum pathology.
Approach/Methods

Note: Scanned images are included in the proceedings. Some submitted images were reduced during editing, thereby decreasing clarity. Also, refer to the Program Planner. Proceedings Content as of 3-29-2013.

First we will review the anatomy and functional topography of the corpus callosum on DTI. Then we will illustrate a variety of pathologic conditions affecting the corpus callosum, including congenital anomalies, demyelinating diseases, infarctions, neoplasms, and neurocognitive disorders.
Findings/DIscussion
The corpus callosum is the main white matter fiber bundle connecting the two brain hemispheres. Despite advances in modern neuroimaging techniques, we have yet to fully understand the functional organization of the corpus callosum and how it is altered in a variety of pathologic conditions. Diffusion tensor imaging is widely available with the ability to obtain both morphologic and quantitative values of structures such as the corpus callosum for assessing functional aspects of disease.
Summary/Conclusion
This exhibit demonstrates the functional topography of the corpus callosum with various pathologic conditions. Diffusion tensor imaging is helpful as an additional, practical imaging tool to illustrate functional mapping for correlation with clinical assessment and treatment planning.

KEYWORDS: Diffusion tensor image, Corpus callosum

eEdE-76

Optic Pathways from Anatomy to Pathology: A Pictorial Essay and Review

Aragao, M. F. V.[1]·Pereira, B. P. G.[1,2]·Lima, L. T. B.[1,2]·Morais, T. P.[1,2]·Araújo, A. C. C.[3]·Filho, E. A.[1,2]
[1]Multimagem, Recife, BRAZIL, [2]Hospital das Clinicas - UFPE, Recife, BRAZIL, [3]Hospital Esperanca, Recife, BRAZIL.

Purpose
Since the early stages of development of radiology, imaging of the visual pathways has been a challenge, and usually involved the use of plain radiographs, complex motion tomography, or invasive techniques such as orbital venography and pneumoencephalography. Nowadays, sectional imaging techniques have prevailed as the preferred examination. In this pictorial essay we intend to provide a practical and objective approach regarding the multiple pathologic conditions that affect the visual pathways, with special interest in the correlation between their CT, MR and advanced MR imaging findings, anatomical localization and clinical symptomatology.
Approach/Methods
The CT, MR and advanced MR images of congenital, tumoral, infectious, inflammatory, demyelinating and vascular conditions affecting the optic nerve, optic chiasm, optic tracts, optic radiations and visual cortex of multiple patients were obtained in our institution. All the cases were reviewed posteriorly and confirmed through histopathologic examination whenever feasible. The main patient characteristics (gender, age, familiar and pathologic history) and the main lesion characteristics (location, morphology, density, signal intensity and contrast enhancement) were described and extensively discussed.
Findings/Discussion
Usual indications for imaging of the visual pathways generally involve variable degrees of visual loss. Rapidity of onset of the symptoms alongside correct evaluation of specific visual field deficits and patient's epidemiologic characteristics usually allow a high degree of clinical suspicion regarding the wide array of possible underlying conditions. Sectional imaging techniques commonly are tailored to display the expected condition optimally. Anatomical location and lesion morphologic characteristics are essential information for the development of an accurate diagnosis.
Summary/Conclusion
In this electronic education exhibit we provide a concise yet complete description of the key imaging findings observed in the most common visual pathways pathologic processes. MR imaging has a major role in visual pathways imaging and as such is discussed more extensively.

KEYWORDS: Optic nerve, Orbits, optic chiasm

eEdE-77

Vascular Anatomy of the Deep Gray Matter: A Review of Normal Arterial and Venous Circulation, Anatomical Variants, and Associated Pathology of the Basal Ganglia and Thalami

Yam, B. L.·Maralani, P. J.·Mohan, S.
Hospital of the University of Pennsylvania
Philadelphia, PA.

Purpose
The deep gray matter arterial supply and venous drainage is complex with extensive variations. Thorough knowledge of this vascular anatomy is essential for localization of vascular pathology. The purpose of this exhibit is to review the arterial and venous circulation of the deep gray matter, correlate with cross-sectional and angiographic imaging techniques, demonstrate associated pathologic processes using a multimodality approach, and review the relevant imaging and anatomy literature.
Approach/Methods
We will discuss the relevant embryology and normal and variant vascular supply of the caudate, putamen, globus pallidus and thalamus through illustrations and correlative cross-sectional and angiographic techniques. The vascular supply of the internal and external capsules also will be addressed due to their proximity and clinical significance. We then will demonstrate arterial and venous pathology involving the deep gray matter nuclei using correlative multimodality imaging.
Findings/Discussion
The basal ganglia and thalami are clusters of paired deep gray matter structures that have an intricate vascular supply. Knowledge of the normal and variant vascular

Note: Scanned images are included in the proceedings. Some submitted images were reduced during editing, thereby decreasing clarity. Also, refer to the Program Planner. Proceedings Content as of 3-29-2013.

anatomy of these structures is important to help determine the etiology of associated vascular pathology, as well as to localize the involved vessels. Diseases of various intracranial arterial and venous branches cause distinctive patterns of ischemia or infarction of the basal ganglia and thalami. Following initial characterization by cross-sectional imaging, digital subtraction angiography may help improve characterization of vascular abnormalities of the deep gray matter and help narrow the differential diagnosis.
Summary/Conclusion
This review outlines the embryology, vascular anatomy and associated pathology of the basal ganglia and thalami. Imaging characteristics and patterns of vascular pathology affecting the deep gray structures are highlighted to demonstrate the anatomical basis of pathology.

KEYWORDS: Basal ganglia anatomy, Basal ganglia disease, vascular anatomy of the deep gray matter

eEdE-78

Basal Cisterns Revisited

Ratcliffe, M. R.·McCreary, R.·Siripurapu, R.·Herwadkar, A.
Salford Royal Hospital
Salford, UNITED KINGDOM.

Purpose
To demonstrate the anatomy of the basal cisterns, their contents and arachnoid membranes using modern high resolution imaging techniques with particular focus on correlating with pathologic processes affecting the vessels and nerves.
Approach/Methods
We present an electronic educational exhibit highlighting the basal cistern anatomy. We then will review pathologies that may be encountered in the basal cisterns as they affect various nerves and vessels as well as there relation to the adjacent arachnoid membrane. Tumor spread, patterns of SAH and surgical approaches will be discussed.
Findings/Discussion
The basal cisterns are a complex network of subarachnoid spaces separated from each other by a trabeculated porous wall with various sized openings. It is of clinical significance that cerebral arteries, veins and cranial nerves pass through these subarachnoid spaces. The anatomy is essential to understand the different direction of aneurysm growths and pattern of blood spread in patients with subarachnoid hemorrhage. The anatomy of various cranial nerves in the cisternal portion and their relation to the adjacent vessels is important when determining neurovascular conflicts. Tumor locations and extensions especially in the posterior fossa is predicted by the anatomy of the cisterns and the arachnoid.
Summary/Conclusion
This educational exhibit highlights the importance of understanding the normal basal cistern anatomy with particular focus on vascular and cranial nerve pathologies.

KEYWORDS: Anatomy, basal cisterns

eEdE-79

MR Angiography Evaluation of Anatomical Variants and Anomalies Affecting Circle of Willis

Baxi, A.·Jay, A.·Lee, C.·Berkowitz, F.
MedStar Georgetown University Hospital
Washington, DC, DC.

Purpose
1. To describe normal imaging appearance of circle of Willis on magnetic resonance (MR) angiography. 2. To describe potential collateral pathway and anastomosis between internal carotid (anterior) and vertebral arteries (posterior circulation). 3. To study normal variants and anomalies in circle of Willis and review their radiologic and clinical significance.
Approach/Methods
The circle of Willis is a major source of blood supply to the brain. A complete circle of Willis is seen only in 50% of cases. It is formed by anastomosis and collaterization between internal carotid (anterior) and vertebral arteries (posterior circulation).This communicating pathway allows adequate distribution of cerebral blood flow and perfusion not only between right and left side but also between anterior and posterior parts of the brain in the event of intra and extracranial carotid and vertebral artery occlusive disease. It is thus very important to know the embryonic development, prevalence and clinical relevance of various anatomical variants and anomalies of circle of Willis with respect to the pathology with which they are associated. An attempt is made in this educational exhibit to describe normal imaging appearance, anatomical variants and anomalies of circle of Willis on MR angiography. Magnetic resonance angiography of brain performed in patients for various clinical indications was reviewed and studied for normal circle of Willis, its anatomical variants and anomalies.
Findings/Discussion
The circle of Willis is formed when the internal carotid artery on each side divides into the anterior and middle cerebral arteries. The anterior cerebral arteries then are united by an anterior communicating artery. Posteriorly, the basilar artery which is formed by union of left and right vertebral arteries branches into right and left posterior cerebral arteries which communicates with the internal carotid system anteriorly via the right and left posterior communicating arteries respectively. Common anatomical variants and anomalies we encountered were: 1. Hypoplasia or absent arteries, 2. Fetal origins of PCA, 3. Infundibular dilatations, 4. Persistent carotid-basilar artery anastomoses such as primitive trigeminal, hypoglossal and otic arteries, 5. Fenestrations, duplications, accessory and early bifurcations of cerebral arteries, 6. Azygous and

Note: Scanned images are included in the proceedings. Some submitted images were reduced during editing, thereby decreasing clarity. Also, refer to the Program Planner. Proceedings Content as of 3-29-2013.

hemispheric ACA, median artery of corpus callosum, and 7. Aberrant and proatlantal anomalies of ICA.
Summary/Conclusion
The circle of Willis is an anastomotic system of arteries that sits at the base of the brain. It is very important for a radiologist to know normal anatomy, anatomical variants and anomalies of circle of Willis to understand physiology of blood redistribution and their significance in pathologies affecting brain. The major teaching points of this educational exhibit are: 1. Imaging appearance of normal circle of Willis, anatomical variants and anomalies on magnetic resonance angiography. 2. Identification of potential anastomotic collaterals between anterior and posterior circulation. 3. Clinical importance of normal variants and anomalies with respect to patient management.

KEYWORDS: MR angiography, Normal variant, circle of Willis

eEdE-80

The Veins of the Posterior Cranial Fossa in Health and Disease

McCreary, R.·Ratcliffe, M. R.·Siripurapu, R.·Herwadkar, A.
Salford Royal Hospital
Salford, UNITED KINGDOM.

Purpose
To review the posterior fossa venous anatomy in health and disease using contemporary cross-sectional and DSA techniques.
Approach/Methods
We present an electronic exhibit highlighting the posterior fossa venous anatomy and its relevance during neurovascular and open surgical procedures using cross-sectional imaging and catheter angiography. CT venography, MR venography and intra-arterial DSA studies are included in the discussion.
Findings/Discussion
The venous drainage of the posterior fossa is comprehensively discussed. We demonstrate the utility of understanding the venous drainage of the brainstem and cerebellum in evaluating various vascular and nonvascular pathologies affecting the posterior fossa. Various intracranial and skull base surgical cases are illustrated to highlight the relevance of understanding the venous anatomy and variations for surgical planning and understanding postoperative complications.
Summary/Conclusion
This educational exhibit highlights the importance of understanding the venous drainage of the posterior fossa in evaluating various vascular and nonvascular conditions.

KEYWORDS: Venous anatomy, Posterior fossa

eEdE-81

Test Your Knowledge: Anatomical Variations of the Cerebral Arterial Circulation - A Case-Based Review

Felker, E. R.·Lee-Felker, S. A.·Salamon, G. G.·Salamon, N.
David Geffen School of Medicine
Los Angeles, CA.

Purpose
Variations in the cerebral arterial circulation are common; with improvements in image quality and easy access to MR angiography (MRA) and CT angiography (CTA), they are being recognized more frequently. Knowledge of these variants is important for accurate interpretation, as some variants can influence surgical and interventional procedures. The purpose of this exhibit is to provide an interactive review of common cerebral arterial variants whereby viewers can test their knowledge in a quiz-based format.
Approach/Methods
We will briefly review the normal anatomy and embryology of the cerebral arterial circulation. Then we will provide examples of the most common and clinically relevant anatomical variants, highlighting the appearance, prevalence, and associations of each. Cases will be illustrated with MRA, CTA, and conventional catheter angiography. Each case will be followed by multiple-choice questions that highlight important aspects.
Findings/Discussion
Fenestrations, persistent carotid-vertebrobasilar anastomoses and aberrant arteries in the skull base comprise the majority of clinically important anatomical variants. They may be associated with other intracranial vascular abnormalities, most commonly aneurysms and cranial nerve symptoms. Embryologic remnant networks can be used as collaterals. Knowledge of anatomical variants, common anastomoses and potential vascular networks is important for radiologists to better understand pathophysiology and treatment planning.
Summary/Conclusion
Cerebral artery variants often are identified in daily vascular imaging. Precise knowledge of these anatomical variants not only can aid in the detection of other associated intracranial vascular abnormalities but also can lead to better understanding of collateral networks and suggest treatment planning for interventional and neurosurgical procedures.

KEYWORDS: Anatomical variation, circle of Willis

Note: Scanned images are included in the proceedings. Some submitted images were reduced during editing, thereby decreasing clarity. Also, refer to the Program Planner. Proceedings Content as of 3-29-2013.

eEdE-82

The Absent Carotid Artery: Congenital or Acquired?

Jung, M. W.·Griffith, B.·Kelly, M.·Shahin, G.·Sanders, W.·Kole, M.·Marin, H.
Henry Ford Hospital
Detroit, MI.

Purpose
The goal of this educational exhibit is to illustrate the fundamentals of internal carotid artery anatomy from an embryologic perspective, create a systematic approach for assessment of congenital internal carotid artery anomalies and demonstrate its relevance in the endovascular treatment of acquired arterial disease. Medical illustrations and selected angiography cases from our institution will be provided.
Approach/Methods
Various cases of congenital ICA anomalies from a segmental embryologic perspective will be shown using multimodal imaging and angiographic correlation. Patterns of collateral flow pathways will be discussed with regard to endovascular treatment. Cases of acquired internal carotid occlusions will be shown with regard to different pathways of collateral flow.
Findings/Discussion
Patterns of collateral flow from internal carotid artery occlusion/dysgenesis can be divided into three pathways: 1) circle of Willis anastomoses, 2) Persistent embryologic arteries and 3) External to internal carotid artery anastomoses. Persistent embryologic arteries include the trigeminal, hypoglossal and proatlantal intersegmental arteries, for which examples are provided. Understanding the embryologic origin of the internal carotid artery and potential collateral flow is important for differentiating congenital from acquired disease and for avoiding complications during endovascular procedures.
Summary/Conclusion
At the completion of this educational exhibit, the individual should be able to understand internal carotid anatomy from an embryologic perspective, congenital internal carotid artery anomalies, and differentiate acquired internal carotid artery occlusion from congenital anatomical variants.

KEYWORDS: Carotid artery, Congenital anomalies

eEdE-83

The Floor of the Third Ventricle: Anatomical, Physiologic, Pathologic and Surgical Review

Burgin, K.·Kumar, M.·Ramakrishnaiah, R.·Samant, R.·Fitzgerald, R.·Van Hemert, R.·Angtuaco, E.
University of Arkansas for Medical Sciences
Little Rock, AR.

Purpose
Hypothalamic dysfunction results in systemic symptoms that may have little to no neurologic deficits. Emotional disturbance, growth difficulties, water imbalance, sleeplessness and weight problems are oftentimes the primary clinical presentation. Our exhibit seeks to highlight the anatomy and physiology associated with this area and we will present pathologic entities associated with the hypothalamus in its primary location along the floor of the third ventricle. The surgical approach for abnormalities also will be reviewed.
Approach/Methods
A retrospective review for hypothalamic abnormalities was conducted using an extensive database search for the last ten years at tertiary adult and pediatric hospitals which were studied by both CT and MRI. Surgical correlative data with pathology were available in most of the cases. These pathologic entities are discussed with a review of the normal representative anatomy of the floor of the third ventricle. Each pathologic entity was reviewed with its effect on the normal anatomy of the third ventricle.
Findings/Discussion
A pictorial review of the normal anatomy and various pathologic entities affecting the floor of the third ventricle will be shown. Relevant imaging findings will be presented. Primary lesions of the floor of the third ventricle starting from the optic chiasm, pituitary infundibulum, tuber cinereum and mamillary bodies will be discussed. Pathologic entities to be shown are congenital, developmental, inflammatory, tumoral and vascular processes that primarily affect this area as well as adjacent lesions that secondarily distort the floor of the third ventricle. Discussion of the effect on the hormonal physiology important in this area will be discussed. Surgical approach to masses in this area also will be shown.

Summary/Conclusion
This review will highlight the important anatomy and specific pathology related to the third ventricle floor using

Note: Scanned images are included in the proceedings. Some submitted images were reduced during editing, thereby decreasing clarity. Also, refer to the Program Planner. Proceedings Content as of 3-29-2013.

modern neuroimaging studies to highlight their importance in defining the systemic symptoms that are associated with abnormalities in this critical part of the brain.

KEYWORDS: Third ventricle, Hypothalamus

eEdE-84

Anatomy of Neck Muscle Variations

Rubinstein, D.·Valladares Otero, A.
University of Colorado
Aurora, CO.

Purpose
The purpose is to describe the anatomy of neck muscle variations. Most neck muscle variations are asymptomatic, however it is important to be able to differentiate them from pathology such as lymphadenopathy or soft tissue metastasis. It also is important to identify them as a cause of palpable abnormality that a patient or a physician may encounter.
Approach/Methods
Retrospective evaluation of neck CT and MR scans performed for a broad variety of indications, excluding patients with neck surgery or neoplasm which could confound identification of neck muscles. We looked for supernumerary, anomalous and absent muscles, muscle defects and alternate origin/insertion of neck muscles.
Findings/Discussion
Multiple neck muscle variations and anomalous muscles were demonstrated, including but not limited to boutonniere defect in the mylohyoid muscle, anomalous muscles such as the cleidooccipital muscle and levator claviculae, accessory muscles such as anterior digastric muscle bundles, variations in muscle insertions such as a clavicular origin of the omohyoid inferior belly, absent muscle bellies such as an absent anterior digastric and absent inferior omohyoid inferior belly. These are some examples of the muscle variations we have encountered.

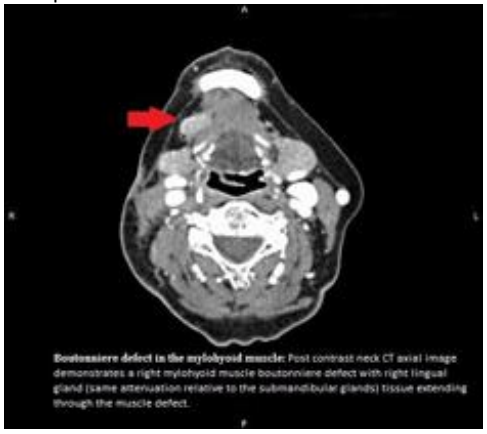

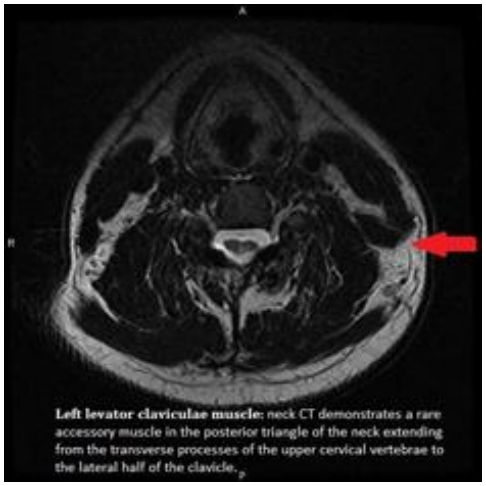

Summary/Conclusion
Numerous muscle variations have been described by anatomists, most tend to be asymptomatic; however, some may result in palpable abnormalities or potentially can be confused with pathology. The diagnosis of an anomalous muscle or neck muscle variation should be borne in mind when evaluating neck imaging.

KEYWORDS: Anatomical variation

eEdE-85

When Your Eye Goes in and the Sixth Nerve Goes Out: A Review of Sixth Cranial Nerve Anatomy and Pathology

Smittkamp, C.[1]·Smoker, W.[1]·Reede, D.[2]·Gentry, L.[3]
[1]University of Iowa, Iowa City, IA, [2]East Manhattan Diagnostic Imaging, New York, NY, [3]University of Wisconsin, Madison, WI.

Purpose
• Review the anatomical course of the sixth cranial nerve. • Be able to identify important anatomical landmarks on imaging studies. • Review various pathologies relevant to particular segments of the sixth cranial nerve.
Approach/Methods
This viewer-interactive, electronic exhibit breaks down the course of the sixth cranial nerve (abducens) from its nucleus to the lateral rectus muscle into six manageable anatomical segments: nuclear, cisternal, skull base, cavernous sinus, orbit, lateral rectus muscle. Each segment is assessed in the same three ways. First, a custom illustration highlighting important adjacent structures and anatomical landmarks is presented. This will help the reader develop a conceptual view of the region. Second, a set of corresponding MR and/or CT images illustrates the same anatomical region. This will help translate the conceptual view of the anatomy into the ability to identify key anatomical landmarks on cross-sectional imaging studies. Knowledge of adjacent structures is important in the ability to clinically localize pathology and, thereby, direct imaging to the appropriate location. Finally, multiple cases are presented that demonstrate the various

Note: Scanned images are included in the proceedings. Some submitted images were reduced during editing, thereby decreasing clarity. Also, refer to the Program Planner. Proceedings Content as of 3-29-2013.

pathologies that may occur in each of the anatomical segments.
Findings/Discussion
Pathologies exemplified include demyelination, tumor, inflammation, infection, trauma, vascular compression, and idiopathic causes.
Summary/Conclusion
Double vision secondary to sixth cranial nerve palsy is the most common isolated cranial nerve palsy, yet rarely addressed. It often is accompanied by other clinical findings, unique combinations of which may help localize lesions to the appropriate segment. Imaging assessment can best be achieved by a thorough understanding of the nerve's anatomical course and nearby structures. We aim to solidify this knowledge by providing a review of sixth cranial nerve anatomy through illustrations and cross-sectional imaging followed by viewer-interactive examples of various pathologies that affect the six segments of the sixth cranial nerve.

KEYWORDS: Anatomy, Cranial nerve pathology, sixth, VI

eEdE-85a

Behind the Name: Eponyms of Neuroradiology

Chow, D. S.·Miloushev, V.·Garger, A. A. V.·Dipoce, J.·Utukuri, P.·Filippi, C. G.·Lignelli, A.
Columbia University
New York, NY.

Purpose
There are numerous eponyms encountered within neuroradiology given its rich history. Eponyms are pervasive throughout medicine and are used to communicate complex pathologies while honoring an individual in a given field. The purpose of this exhibit is to review and define commonly used eponyms in neuroradiology.
Approach/Methods
This exhibit will categorize various eponyms encountered in neuroanatomy, neuropathology, and diagnostic techniques. Eponyms will be grouped anatomically: (1) cerebral hemispheres, (2) posterior fossa, (3) sella and pituitary, (4) vascular structures, and (5) spine. A pre and postinteractive quiz module will be provided for users to assess their knowledge.
Findings/Discussion
An organized and illustrative spectrum of eponyms relevant to neuroradiology is provided. A biographical sketch, representative imaging, and radiologic teaching points will accompany each described eponym. Familiarity with eponyms is important for understanding complicated disease processes and for accurate communication with other physicians.
Summary/Conclusion
There are numerous eponyms encountered in neuroradiology. Knowledge of these eponyms is important for minimizing confusion with colleagues and referring physicians. Additionally, it allows for an opportunity to remember individuals who have contributed to our field.

KEYWORDS: Educational, Differential diagnosis

Monday, May 20 – Wednesday, May 22
6:30 AM – 9:00 PM
Thursday, May 23
6:30 AM – 3:00 PM
Hall B1

Electronic Education Exhibits (eEdE) 86 - 122a

eEdE3-Head and Neck

Note: A missing printed number indicates an abstract has been withdrawn.

eEdE-86

"Am I Getting on Your Nerves?": Anatomy and Pathology of Nerves in the Infrahyoid Neck

Font, S.[1]·Reede, D.[1]·Smoker, W. R. K.[2]·Gentry, L.[3]·Holliday, R.[4]
[1]SUNY Downstate at Long Island College Hospital, Brooklyn, NY, [2]University of Iowa Hospitals and Clinics, Iowa City, IA, [3]University of Wisconsin Hospital and Clinics, Madison, WI, [4]The New York Eye and Ear Infirmary, New York, NY.

Purpose
1. Learn the location of major nerves in the infrahyoid neck. 2. Demonstrate the imaging findings of common lesions affecting the nerves. 3. Review clinical findings associated with nerve involvement.
Approach/Methods
Information is presented in a quiz format using illustrations and corresponding cross-sectional images to provide a comprehensive review of infrahyoid neck nerve anatomy. This is followed by case presentations with emphasis on the location of pathology with reference to nerves, imaging findings and clinical symptoms. Lesions discussed include: • Vagus nerve X-(Nerve sheath tumors, extrinsic compression of the recurrent laryngeal nerve-above and below the thoracic inlet). • Spinal Accessory nerve XI-(Nerve sheath tumors and secondary involvement by adjacent tumor). • Phrenic nerve-(Secondary involvement by tumor). • Brachial plexus-(Pancoast tumor, nerve sheath tumor, nerve root avulsion). • Sympathetic plexus-(Nerve sheath tumor, extrinsic compression).

Note: Scanned images are included in the proceedings. Some submitted images were reduced during editing, thereby decreasing clarity. Also, refer to the Program Planner. Proceedings Content as of 3-29-2013.

Findings/Discussion
A wide variety of pathology occurs in the infrahyoid neck where the anatomy is complex. A number of nerves from different origins (cranial, cervical, sympathetic and brachial plexuses) traverse this region. An understanding of the nerve anatomy enables one to identify primary and potential extrinsic nerve involvement based on lesion location and/or clinical symptoms. This information may have significant impact on treatment planning.
Summary/Conclusion
Nerve involvement may be due to intrinsic or extrinsic pathology. Knowledge of the location of the nerves in the infrahyoid neck and common pathologies encountered in this region will increase the accuracy of imaging interpretation. Upon completion of this module, the user will have improve his/her ability to interpret cross-sectional images of the infrahyoid neck including identifying lesions originating in or potentially involving, major nerves. This information is important for surgical planning and may improve patient outcomes.

KEYWORDS: Anatomy, Nerve imaging

eEdE-87

The Diagnostic Features on MR Imaging of Carcinoma ex Pleomorphic Adenoma

Yokota, H.･Motoori, K.･Horikoshi, T.･Mukai, H.･Inoue, K.･Higashide, T.･Okamoto, Y.･Uno, T.
Chiba University Hospital
Chiba, JAPAN.

Purpose
Pleomorphic adenoma is the most common benign neoplasm of salivary gland origin. The incidence of malignant transformation is about 10% in those present for more than 15 years. Observation is a selection on elderly patients. Carcinoma ex pleomorphic adenoma (CXPA) must be diagnosed before this selection. The usefulness of fine-needle aspiration cytology in salivary tumors continues to be a controversial subject. Radiologists should recognize that MR imaging also is useful for estimating the pathology of CXPA and demonstrating their morphology and extent.
Approach/Methods
Eighteen cases of CXPA (14 parotid gland, 2 submandibular gland, 2 minor salivary gland) were identified from our imaging database. Key imaging characteristics with histopathologic images of these cases are presented.
Findings/Discussion
Key sequences are T2-weighted image, dynamic study and diffusion-weighted image. The cases with ring-shaped hypointense nodule in the tumors on T2-weighted image are classified as invasive type of CXPA (9/18 cases). This ring nodule represented a capsule of pleomorphic adenoma. The cases without ring nodule are classified as noninvasive type. In half of these cases, malignant components can be detected in the tumors (5/18 cases).
Peak time and wash out ratio on time intensity curve of dynamic study are effective for differentiating salivary tumors. Low value of apparent diffusion coefficient (ADC) often presents malignant tumor. Combination of these techniques produces more accurate diagnosis of malignant salivary gland tumors. The residual half cases present normal patterns (4/18 cases).

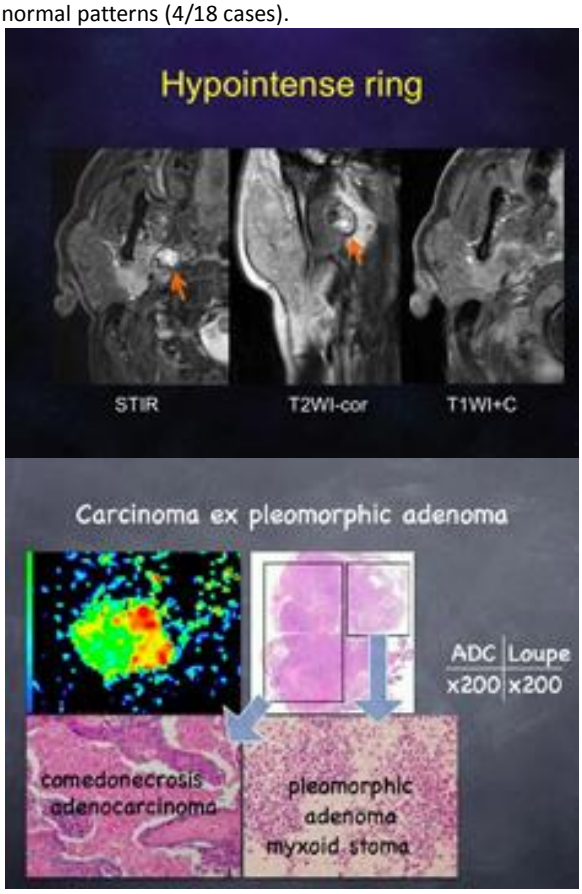

Summary/Conclusion
Carcinoma ex pleomorphic adenoma presents different patterns depending on invasion from capsule. The ring nodule in the tumor is a characteristic sign of invasive type of CXPA. Combination of dynamic study and ADC measurement is essential for diagnosing noninvasive type of CXPA.

KEYWORDS: Salivary gland, Carcinoma

Note: Scanned images are included in the proceedings. Some submitted images were reduced during editing, thereby decreasing clarity. Also, refer to the Program Planner. Proceedings Content as of 3-29-2013.

eEdE-88

Old is Gold: Role of Conventional Sialography in Modern Radiology - With Emphasis on Sjögren Syndrome and Sialoendoscopy

Chaudhry, U. S.·Maley, J. E.·Policeni, B.·Schularick, N.·Hoffman, H. T.
University of Iowa, Hospitals and Clinics
Iowa City, IA.

Purpose
A large segment of the population suffers from salivary gland disease, constituted by a wide array of pathology. One common cause is Sjögren syndrome, an autoimmune disorders affecting 0.5 to 3 million people in the U.S. alone. Conventional sialography was a standard diagnostic modality for such diseases, but preference shifted to noninvasive techniques such as MRI and CT sialography. With the advent of sialoendoscopy and related techniques, conventional sialography has seen a resurgence. Additionally, (our experience suggests) conventional sialography in diseases such as Sjögren syndrome may have competitive diagnostic accuracy as compared to new modalities. It therefore is more important than ever to have a good understanding of the procedure, findings, advantages and limitations of conventional sialography.
Approach/Methods
We performed a retrospective review at University of Iowa of a total of 103 sialograms performed at our tertiary care center from 2008 to 2012. We highlight several interesting cases, with a literature review of key pathologies evaluated through sialography.
Findings/Discussion
Conventional sialography was first established in 1904 by Carpy, and has not seen much of an evolution as far the technique of the study is concerned. Briefly, the study involves dilation of the ductal orifice, followed by insertion of a specialized catheter and injection of contrast. An advantage of this modality over MR sialography is that it gives better spatial resolution of the gland. Also dilatation of the ductal orifice helps determine the need for a papillotomy and also establishes the presence or absence of stenosis at the orifice. This is something that is particularly useful in preoperative planning. In our exhibit we present a brief summary of major salivary gland anatomy and basic technique in conventional sialography. Some normal examples are used for this illustration. Contrast agents and standardizing suggestions then are discussed. After which conditions such as Sjögren's, sialoliths and sialosis are reviewed with examples of cases. Special emphasis is given to Sjögren syndrome and the grading used in sialography.
Summary/Conclusion
Conventional sialography offers a unique insight in salivary gland pathology with advantages lacking in other available imaging modalities. With otolaryngologists utilizing and relying on this age-tested technique, it is more imperative than ever that neuroradiologists have a firm grasp of this modality.

KEYWORDS: Salivary gland, Sjögren's syndrome, sialography

eEdE-89

Imaging and Management of Maxillofacial Trauma: What the Surgeon Needs to Know

Khorrami-Arani, N.[1]·Liang, T.[2]·Nicolaou, S.[1]
[1]Vancouver General Hospital, Vancouver, BC, CANADA,
[2]University of British Columbia, Vancouver, BC, CANADA.

Purpose
Maxillofacial (MF) trauma presents with a unique spectrum of injuries and characteristic image findings. Imaging plays a critical role in identifying these injuries and influencing their management. Emerging technologies and techniques also have made imaging faster, more accurate, and safer by reducing radiation dose exposure. The purpose of this exhibit is to review the anatomy and mechanism of spectrum of the injuries, the various imaging modalities available and characteristic imaging findings. A management algorithm for evaluation of MF trauma from the maxillofacial surgeons perspective will be described.
Approach/Methods
A retrospective review of MF trauma cases at our institution will be conducted for imaging examples to demonstrate the spectrum of these injuries.
Findings/Discussion
This educational exhibit will review the epidemiology, anatomy, mechanism of injury, and parameters for clinical assessment of MF trauma. Imaging modalities for MF trauma including radiographs, MDCT, MRI will be reviewed, with the emphasis on MDCT with volume rendering as the imaging exam of choice. The spectrum of injuries including nasal, frontal sinus, orbital, zygoma, maxillary and mandibular fractures and globe injuries will be discussed. Additionally, the characteristic findings, imaging examples of MF trauma on MDCT, and their clinical significance will be demonstrated. Imaging mimics and diagnostic pitfalls will be discussed and imaging examples will be demonstrated to help readers avoid these diagnostic errors. A discussion of the usefulness and limitations of MDCT in the setting of determining management and surgical exploration for these injuries will be employed. Finally, an imaging and management algorithm for MF trauma from the surgeons perspective will be proposed and reviewed.
Summary/Conclusion
Maxillofacial trauma presents with a unique spectrum of injuries and characteristic imaging findings which have been reviewed in this exhibit. The utility of MDCT with volume rendering for imaging of MF trauma in both diagnosis and determination of a surgical versus conservative management have been demonstrated in this

exhibit. A useful algorithm for imaging and management of MF trauma has been proposed and can be adapted easily to radiologists' and trauma surgeon's practices.

KEYWORDS: Facial fractures, maxillofacial trauma

eEdE-90

Perineural Spread in the Head and Neck: Now You See It, Now You Don't!

Khledi, R. A.·Sheitt, H.·Gommsani, R. E.·Adas, R. A.
King Abdulaziz Medical City
Jeddah, SAUDI ARABIA.

Purpose
To review the clinical and radiologic features of perineural spread of disease in cross-sectional imaging and briefly discuss the common pathologies and sites.
Approach/Methods
We retrospectively reviewed the neck and skull base studies of adult patients with perineural spread of diseases in our institution from January 2012 to present. We also reexamined the different pathologies and most common sites of involvement in these patients.
Findings/Discussion
Our understanding of perineural spread of disease has evolved over the last century. Although it is seen more commonly in malignant rather than benign lesions, they can occur in a wide variety of pathologies. They may be radiographically evident before the onset of clinical silence. It is important to distinguish between perineural invasion and spread. Invasion occurs when microscopic cells are seen surrounding small nerve branches. As such it cannot be seen on imaging and it is an ominous prognostic sign associated with an increased local recurrence rate and decreased survival. The exact mechanism of perineural spread is still poorly understood. The most accepted current theory is that nerves provide a pathway of least resistance for lesion growth. The diagnosis of perineural spread is clinical. Imaging often is used to confirm the clinical suspicion. Computed tomography and MRI play a very important role in the evaluation of perineural spread, but MRI has become the modality of choice. MR imaging is superior to CT in providing more accurate assessment of intracranial spread to the Meckel's cave, the cavernous sinus, the internal auditory canal or cerebellopontine angle while CT scans are superior to MRI for evaluating bony changes, which are important because a substantial portion of the cranial nerves are contained within bony structures. Areas to look for bony changes include: the supraorbital foramen, pterygopalatine fossa, foramen rotundum, vidian canal, palatine foramen, foramen ovale, mandibular foramen, and stylomastoid foramen. Among the radiologic findings to look for are neural thickening and enhancement which may lead to foraminal enlargement and destruction, obliteration of the fat planes at foraminal openings, neuropathic atrophy, and convexity of the lateral cavernous sinus wall. Preoperative diagnosis of perineural spread/invasion is an important factor in guiding both surgical and radiation treatment planning. It also has serious staging and prognostic implications. Treatment guidelines differ according to the primary pathology and the sites involved, but radiation therapy is the main line of treatment following surgery.
Summary/Conclusion
Perineural spread/invasion in the head and neck is a serious entity that has important implications on prognosis and treatment of different diseases. Imaging plays an essential role in determining the site and extent of the disease, sometimes even before the onset of clinical symptoms.

KEYWORDS: Perineural, Cranial nerve pathology

eEdE-91

Spectrum of Temporomandibular Joint Pathology: A Pictorial Review

Nundkumar, A.·Shen, P.·Lee, P.
University of California Davis
Sacramento, CA.

Purpose
This is a pictorial review characterizing the wide range of pathology of the temporomandibular joint (TMJ) rarely encountered in practice. Our review includes, primary tumor, infection, and arthritides.
Approach/Methods
Retrospective multicenter analysis of cases with primary or secondary pathology involving the TMJ joint was performed. Specific educational cases with representative images were selected.
Findings/Discussion
In our experience, pathology of temporomandibular joint beyond trauma and osteoarthritis is infrequently encountered. However to add some clarity to the wide spectrum of TMJ disorders, the various TMJ entities were organized into categories of: trauma, infectious, arthropathies, vascular, benign and malignant masses. Arthropathies of the TMJ include rheumatoid arthritis, osteoarthritis and calcium pyrophosphate dehydrate arthropathy. Benign mass lesions of the TMJ include fibrous dysplasia, synovial chondromatosis and osteochondritis dessicans. Malignant primary and secondary mass lesions include osteosarcoma, chondrosarcoma, synovial sarcoma, squamous cell carcinoma, skull base giant cell tumor and secondary parotid tumors. In each category representative images of pathology with key radiologic findings and descriptions will be provided.
Summary/Conclusion
The wide spectrum of disease and imaging findings in the temporomandibular joint are reviewed in this pictorial review. Familiarity with the various entities is important to appropriate management.

Note: Scanned images are included in the proceedings. Some submitted images were reduced during editing, thereby decreasing clarity. Also, refer to the Program Planner. Proceedings Content as of 3-29-2013.

KEYWORDS: TMJ, Temporomandibular

eEdE-92

Imaging of Atypical Orbital Varices: Utilization of Contrast-Enhanced MR Angiography and Valsalva for Differentiation from Other Enhancing Orbital Lesions

Thompson, A. F.·Gentry, L. R.·Hartman, M. J.·Kennedy, T. A.·Lucarelli, M. J.·Reede, D. L.·Smoker, W. R. K.·Turski, P. A.
University of Wisconsin
Madison, WI.

Purpose
The imaging diagnosis of orbital varices is usually straightforward. This exhibit will demonstrate 10 orbital varices with atypical presentations where conventional imaging findings were not completely specific. The prospective utilization of a comprehensive MR imaging (MRI)/MR angiography (MRA) vascular mass protocol (VMP) was helpful in differentiating these atypical varices from other vascular orbital lesions. Many of these atypical cases presented with either loss of vision or cranial neuropathy, both of which are unusual with simple varices. Our goal is to highlight atypical clinical and imaging presentations of orbital varices and the distinguishing VMP features as compared to other avidly enhancing orbital masses.
Approach/Methods
The context will be set briefly by describing both the embryology and classification of vascular malformations as they relate to orbital varices. Ten cases will be used to illustrate the variable clinical presentations, visual complications, and types of disease progression associated with these lesions. The cases will illustrate the widely atypical forms of orbital varices on VMP imaging and the imaging features that distinguish them from other avidly enhancing orbital lesions. Finally, given the variable appearances of orbital varices and their ability to mimic many other enhancing orbital lesions, we will highlight the invaluable use of contrast-enhanced MRA (CE MRA) in differentiating orbital varices from other masses. Flow patterns on CE MRA, lesion distension with valsalva, or demonstration of intralesional thrombus all may be necessary for making the correct diagnosis. Not all features will be present for any given case, however.
Findings/Discussion
The long accepted criterion used to confidently diagnose orbital varices has been a change in lesion size on contrast-enhanced CT or MRI before and after valsava. As we will demonstrate, however, not all varices are distensible, and those that are can lose distensibility at any time in their course for no apparent reason. Contrast-enhanced MRA, on the other hand, may show pulsatile venous phase filling in these cases. Furthermore, this CE MRA appearance is markedly different from that of other avidly enhancing lesions in the differential diagnosis (meningioma, cavernous malformation, nerve sheath tumor, metastasis, hemangiopericytoma).
Summary/Conclusion
Orbital varices have a highly variable imaging appearance and also may demonstrate an atypical clinical presentation that may mimic other avidly enhancing orbital masses. Furthermore, the classical feature of orbital varices, their distensibility, is not always present. As such, these atypical varices are not always differentiated easily from other enhancing orbital lesions by standard imaging techniques. A comprehensive vascular mass protocol consisting of conventional pre and postcontrast MRI, CE MRA, and demonstration of lesion distensibility often is necessary to differentiate atypical orbital varices from other lesions when other conventional imaging is ambiguous.

KEYWORDS: Venous malformations, Orbital tumor, contrast-enhanced MR angiography

eEdE-93

MR Imaging Classification of Primary Choroidal Melanoma Using Surface Coil Technique and Imaging Features

Hanagandi, P. B.[1]·Gonçalves, F. G.[2]·Chong, J.[1]·Torres, C. I.[1]·Chankowsky, J.[1]·del Carpio, R.[1]
[1]Montreal General Hospital, McGill University, Montreal, QC, CANADA, [2]Radiologia Infinita - Brasilia Children's Hospital - Brazil, Brasilia, BRAZIL.

Purpose
1. To review and classify primary choroidal melanoma and emphasize the importance of dedicated surface coil imaging. 2. Illustrate various intraocular complications associated with choroidal melanoma.
Approach/Methods
Fifty patients were evaluated with 1.5T MR imaging (MRI) (GE Signa Excite) using a dedicated 3-inch surface coil, T1-weighted,T2-weighted and postcontrast fat-suppressed sequences were used for assessment. Depending on the degree of melanin content, most melanomas demonstrated T1 and T2 shortening. Postcontrast fat-suppressed technique plays a vital role in differentiating primary tumor from retinal detachment, subchoroidal effusion, vitreous hemorrhage and scleral invasion.
Findings/Discussion
Ultrasound is the most widely used imaging modality for the assessment of intraocular tumors. In recent years MRI has emerged successfully as a very promising tool particularly in the assessment of primary choroidal melanoma. Combination of dedicated surface coil imaging and thin slice acquisition generates high signal-to-noise ratio images thereby improving diagnostic accuracy. Ultrasound continues to remain an operator-dependent modality and subtle lesions may be overlooked or misinterpreted. We classified melanomas based on their morphology and location using multiplanar imaging which helps in accurate localization and effective radiotherapy planning and assessment of post-treatment response.

Note: Scanned images are included in the proceedings. Some submitted images were reduced during editing, thereby decreasing clarity. Also, refer to the Program Planner. Proceedings Content as of 3-29-2013.

Summary/Conclusion
We have attempted to classify melanomas based on their morphology and location which may help in radiotherapy planning and assessment of post-treatment response. Postcontrast images help in differentiating primary tumor from effusion, hemorrhage and scleral invasion. Lack of operator dependency reduces intra and interobserver discrepancies when measuring tumor burden.

KEYWORDS: 1.5T, Orbits, choroidal melanoma, surface coil imaging

eEdE-94

A Review of Differential Diagnosis of Restricted Diffusion in the Optic Nerves

Maralani, P. J.[1]·Mohan, S.[1]·Srinivasan, A.[2]·Arastoo Vossough, A.[1]
[1]University of Pennsylvania, Philadelphia, PA, [2]University of Michigan, Ann Arbor, MI.

Purpose
Restricted diffusion (RD) in the optic nerves (ON) is an uncommon finding, but when present, it can be helpful in narrowing the differential diagnosis during image interpretation. In addition to dedicated orbital MRI, this finding often can be assessed on routine brain MR imaging. In this exhibit we will review various etiologies and differential diagnosis of RD in the ONs.
Approach/Methods
The ONs are extensions of the brain into the orbits and attention to this fact will facilitate the understanding that similar pathologic processes producing RD in the brain can cause RD in the ONs. In this exhibit we will review: • The arterial supply and venous drainage of the ONs. • Various etiologies of RD in the ONs in detail and categorize the differential diagnoses into vascular, infectious, inflammatory and neoplastic causes, with case examples provided for each category. • Anterior nonischemic papillitis (ANIP) and its unique features. • Dedicated diffusion protocol pertaining to orbits.
Findings/Discussion
Understanding the vascular supply of the optic nerves is important since various segments of the optic nerve are supplied by different vessels. Details of the vascular supply will be provided in the educational exhibit. From a practical standpoint, the arterial supply can be classified into those supplying the optic nerve head and those supplying the remainder of the optic nerve. The venous drainage is predominantly to the central retinal vein and to a lesser degree to the ophthalmic venous system and cavernous sinus. The various etiologies of RD in the ONs can be categorized as follows: 1. Vascular: Acute ischemia due to arterial emboli, arteritis, or central retinal vein occlusion can cause RD in the ON due to acute ischemia or venous hypertension and venous infarction. Venous infarction shows a more extensive pattern of RD than arterial ischemia. The findings on fundoscopic examination (FE) are different in arterial and venous thrombosis. 2. Inflammatory/infectious: Active inflammation such as acute optic neuritis with or without demyelinating disease can cause RD. It also has been reported in viral infections. Fundoscopic examination can show optic disk edema and/or pallor. 3. Neoplastic: Involvement of the ONs by neoplasms with highly packed cells can cause RD. For example diffuse involvement of the ONs by lymphoma or perineural spread of retinoblastoma along the ONs. Fundoscopic examination shows optic disk edema or a retinal mass with or without hemorrhage. 4. Anterior nonischemic papillitis: This finding can be seen in patients with increased intracranial pressure (ICP) due to neoplasm, hydrocephalus and pseudotumor cerebri, and it resolves as ICP returns to normal. Fundoscopic examination shows optic disk edema and/or pallor.
Summary/Conclusion
Attention to the presence of RD in the optic nerves, the clinical scenario, and ophthalmologic exam can significantly help in narrowing the differential diagnosis of this imaging finding and help provide more accurate image interpretations. The etiologies often are similar to those causing RD in the brain.

KEYWORDS: Restricted diffusion, Optic nerve

Note: Scanned images are included in the proceedings. Some submitted images were reduced during editing, thereby decreasing clarity. Also, refer to the Program Planner. Proceedings Content as of 3-29-2013.

eEdE-95

Imaging of Neuro-Ophthalmology for Neuroradiologists

Tantiwongkosi, B.·Schneider, A.·Yu, F.·Schatz, M.
University of Texas Health Science Center San Antonio
San Antonio, TX.

Purpose
This pictorial review will illustrate the relevant anatomy, function and diseases in neuro-ophthamology that neuroradiologists should know. Radiologic and neuro-ophthalmologic correlation is emphasized.
Approach/Methods
Patients with neuro-ophthalmologic diseases often present with nonspecific symptoms, including eye pain, blurred or double vision, and changes in color perception. There are localizing signs detected on neurologic and ophthalmologic examination that are specific for certain anatomical locations, such as junctional visual field defects in anterior chiasmal syndrome. The neural pathways related to neuro-ophthalmic diseases are complicated, such that some neuroradiologists may find them too time-consuming to understand. However, appreciation for these specific localizing signs tremendously helps the neuroradiologists focus on particular anatomical regions, making image interpretation accurate and meaningful. Furthermore, some lesions have pathognomonic appearances on imaging, making further investigation or biopsy unnecessary. Computed tomography (CT), MRI, neuro-ophthalmologic findings (visual field perimetry, fundoscopic and eye movement exams) and simplified diagrams superimposed on CT/MRI are used to elucidate the anatomy, function, and the disorders themselves.
Findings/Discussion
This presentation covers both the afferent visual pathway and efferent papillary/oculomotor pathway. The anatomy and function of each pathway are illustrated by diagrams of nerve fibers and nuclei on MR images compared with gross anatomy specimens. The afferent visual pathway encompasses structures which perceive, relay, and process visual information: the eyes, optic nerves, optic chiasm, optic tracts, lateral geniculate nuclei, optic radiations, and striate cortex. The efferent pupillary/oculomotor pathway controls pupil size and eye movement: the pretectal region, the medial longitudinal fasciculus, the third, fourth, and sixth cranial nerves/nuclei. Specific neurologic and ophthalmologic signs caused by lesions at each subsite of the pathway are highlighted. Diseases vary by location to include neoplasms, demyelinating diseases, infection, and strokes. Imaging characteristics of each disease and differential diagnostic clues are discussed.
Summary/Conclusion
Familiarity with characteristic clinical and neuroimaging findings of neuro-ophthalmologic disease is invaluable for neuroradiologists in providing accurate diagnoses and management guidance.

KEYWORDS: Visual pathways, Oculomotor, neuro-ophthalmology

eEdE-96

A Web-Based Mobile Application for Learning and Reviewing the Appearance of Orbital Tumors Using a Multimodality Approach

Chorney, E. T.·Amin, V. B.·Sicular, S.·Ward, T. J.·Kadoch, M. A.·Pawha, P. S.
Mount Sinai Medical Center
New York, NY.

Purpose
The purpose of the exhibit is: 1. To provide quick and easy access to a web-based mobile application and reference guide that addresses most of the common orbital tumors as evaluated by modern imaging modalities. 2. To provide a reference tool that addresses the limitations of other online reference tools, which can be cost-prohibitive, require log-ins or registration, lack interactivity, and are often slow to engage the end user. 3. To provide imaging of both the specific and nonspecific imaging features of a given orbital tumor. 4. To provide a novel learning platform that is fully functional using either the internet alone or on most major handheld devices and tablets, which are becoming increasingly important as educational resources for fellows, trainees, and students.
Approach/Methods
All relevant orbital tumors encountered at our institution since 2001 were reviewed for potential inclusion in the exhibit.
Findings/Discussion
The major teaching points of this exhibit are: 1. Reviewing the diagnostic as well as non-specific imaging findings of multiple orbital tumors on modern imaging modalities. 2. Encouraging each user to expand on this review by linking each pathology to important AJNR articles that further discuss that specific pathology. 3. Measuring the success of this electronic educational exhibit by monitoring number of online views and traffic directed towards the supplied AJNR articles.
Summary/Conclusion
A web-based mobile application for learning and reviewing the appearance of orbital tumors using a multimodality approach is presented.

KEYWORDS: Orbital tumor

Note: Scanned images are included in the proceedings. Some submitted images were reduced during editing, thereby decreasing clarity. Also, refer to the Program Planner. Proceedings Content as of 3-29-2013.

eEdE-97

Seeing Is Believing: Optic Nerve Lesions and Their Symptomatology

Chung, R.·Tuan, A.·Dietrich, R.·Dorros, S.·Mafee, M.
University of California San Diego
San Diego, CA.

Purpose
To review the varied pathology of the optic nerve with particular attention paid to the clinical presentation and imaging characteristics.
Approach/Methods
1. Brief review of the normal anatomy of the optic nerve, comparing gross specimens to corresponding CT and MR images. 2. Review of images and symptomatology with quiz format of selected congenital, inflammatory, infectious, and neoplastic conditions of the optic nerve.
Findings/Discussion
Anatomy will be presented in a didactic format. Representative images of selected cases of congenital, inflammatory, infectious, and neoplastic conditions of the optic nerve will be shown with their clinical presentations and salient radiologic points will be made with each image. Each case will be followed by a short quiz to engage the viewer in active participation underscoring important points about clinical diagnosis and management. The following optic nerve lesions will be reviewed: multiple sclerosis of the optic nerve, sarcoidosis, tuberculosis, lymphoma, optic sheath meningioma, optic nerve glioma, metastatic disease to the optic nerve, infarct, hemangioma, neurofibroma, medullary epithelioma of the optic nerve, septo-optic dysplasia and perioptic nerve cyst.

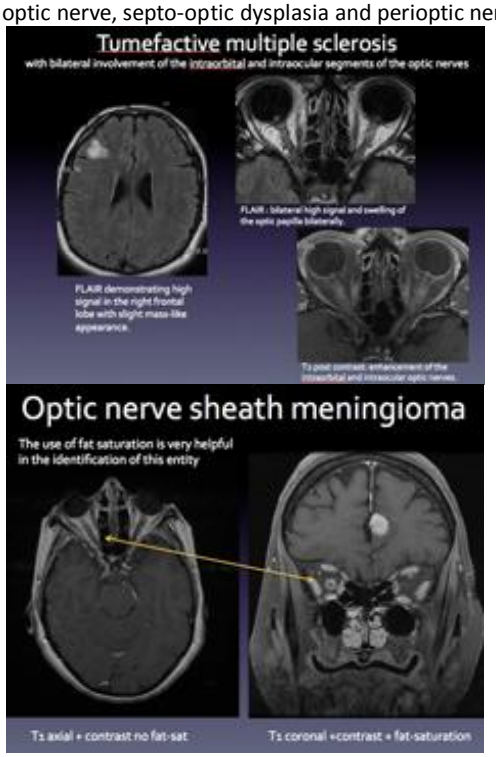

Summary/Conclusion
This educational exhibit will review the varied pathologies of the optic nerve, ranging from the relatively well-known to the exceptional and rare, emphasizing the clinical presentation and imaging characteristics that clinch the diagnosis. After completion of the exhibit, the viewer will have a solid clinical and radiologic understanding of the spectrum of optic nerve lesions to help differentiate between optic nerve pathologies in clinical practice.

KEYWORDS: Optic nerve

eEdE-98

Dual Energy CT Applications for Imaging of the Brain and Neck

Khorrami-Arani, N.[1]·Liang, T.[2]·Shewchuk, J.[1]·Nicolaou, S.[1]
[1]Vancouver General Hospital, Vancouver, BC, CANADA,
[2]University of British Columbia, Vancouver, BC, CANADA.

Purpose
Dual energy CT (DECT) refers to the simultaneous acquisition of low and high voltage CT data (most commonly 80/100 and 140 kVp), and is a technological advancement of CT for which multiple chest and abdominal imaging applications previously have been demonstrated. The purpose of this exhibit is to review the principles of DECT and review and demonstrate examples of potential applications of DECT for imaging of the brain and neck.
Approach/Methods
A retrospective review of patients scanned by the DECT head and DECT neck protocols at our institution will be conducted for imaging examples.
Findings/Discussion
This educational exhibit will review the basic principles and technique behind DECT, and the radiation dose considerations. The exhibit also will review the potential utility of DECT for imaging of the brain and neck. The following applications will be discussed in the exhibit: metal artifact reduction, differentiation between acute intracranial hemorrhage and iodine contrast in patients scanned for stroke and trauma, assessment of iodine distribution in stroke, optimization of kV for CT angiography (CTA), improving detection of acute bleeding (i.e., the dot sign), using iodine color-coded maps, and utility in visualization of the neck vasculature in difficult to assess regions at the base of the skull and heavily calcified vessels. Imaging examples of each of these applications will be demonstrated. In addition, the specific advantages and limitations of these applications of DECT for imaging of the brain and neck will be discussed.
Summary/Conclusion
Recent articles have demonstrated promising results for the application of DECT for imaging of the head and neck. We have demonstrated in our exhibit that DECT can be useful to help reduce metal artifact, differentiate hemorrhage and contrast, assess iodine distribution for

Note: Scanned images are included in the proceedings. Some submitted images were reduced during editing, thereby decreasing clarity. Also, refer to the Program Planner. Proceedings Content as of 3-29-2013.

stroke imaging, optimize CTA at a lower kV, increase detection of abnormal enhancement with iodine overlay maps, and improve visualization of neck vessels.

KEYWORDS: Dual energy spectral, Dual-energy CT

eEdE-99

Endoscopic versus Transcranial Approaches to Skull Base Tumors: What the Surgeon Wants to Know

Nickell, L. T.·Bhatki, A. M.·Coimbra, C. J.·Saad, A. F.·Gupta, M.·Opatowsky, M. J.
Baylor University Medical Center
Dallas, TX.

Purpose
The purpose of this educational exhibit is to review the imaging characteristics of sinonasal and skull base tumors pertinent to surgical planning, with particular emphasis on the imaging features, extent, and key landmarks critical in determining which lesions can be removed via an endoscopic endonasal surgical approach versus standard open approaches.
Approach/Methods
Using a quiz-based interactive approach, multiple cases of sinonasal and skull base tumors will be presented. The pertinent imaging characteristics and anatomy of each lesion will be reviewed, a differential diagnosis will be generated, and the diagnosis will be revealed. The surgical approach utilized (open transcranial versus endonasal endoscopic) and operative findings then will be discussed, enabling a full understanding of the surgical landmarks and anatomical relationships vital to otolaryngologists and neurosurgeons. Finally, a survey of the endonasal corridors to the skull base will be presented and the advantages of minimally invasive operations, such as the endoscopic endonasal approach, will be reviewed.
Findings/Discussion
The endoscopic endonasal approach is being utilized increasingly to access sinonasal as well as lesions of the skull base, including of the sellar and parasellar regions, anterior skull base, clivus, and petrous region. This surgical approach offers many advantages - the surgical literature describes decreased rates of collateral damage to adjacent neurovascular structures and faster recovery times. There are limitations to this approach, however, and not all skull base tumors can be approached in this manner. It is critical for the neuroradiologist to understand the anatomy of these regions, the characteristics and differential diagnoses of associated tumors, and the anatomical relationships and landmarks that determine if a tumor can be removed en total by an endonasal endoscopic technique. Furthermore, a working knowledge of these surgical techniques is required for accurate assessment of postoperative and longer-term follow-up studies.
Summary/Conclusion
As modern, minimally invasive surgical techniques for sinonasal and skull base tumors become more widespread, it is crucial for the neuroradiologist to have a working knowledge of these procedures and to know what information should be included in the radiology report. A systematic approach to lesions of the sinonasal region and skull base, with special consideration placed on the neurovascular structures and relationships critical to the surgeon, is the key to successful interpretation.

KEYWORDS: Skull base neoplasm

eEdE-100

Head and Neck Imaging of Chronic Recurrent Multifocal Osteomyelitis

Sargar, K.·Kao, S.·Sato, Y.·Singh, A.·Ferguson, P.
University of Iowa Hospitals
Iowa City, IA.

Purpose
1. To demonstrate various imaging features of chronic recurrent multifocal osteomyelitis (CRMO) in head and neck region. 2. To discuss key imaging features to differentiate CRMO from other differential diagnoses such as infection and neoplasms.
Approach/Methods
Chronic recurrent multifocal osteomyelitis is noninfectious osteomyelitis seen in pediatric population. Most common sites of involvement are metaphysis of long bones, clavicle, mandible, vertebrae and pelvis. Typical imaging pattern of involvement in clavicles and mandible is very helpful for the diagnosis of this entity. Though extremity involvement is common in CRMO, involvement of clavicles and mandible is important differentiating point between CRMO and infection. We are demonstrating radiographic,MR imaging (MRI), CT and nuclear scan imaging features of two prototype sites of CRMO (i.e., clavicles and mandibles). There are two phases of CRMO - active and reparative. Imaging appearance also can be helpful to suggest the phase of disease. Lack of abscess, fistula sequestrum and significant soft tissue involvement and aggressive periosteal reaction are key features to differentiate CRMO from infectious osteomyelitis and neoplasms.
Findings/Discussion
Though CRMO is diagnosis of exclusion, radiologists can suggest diagnosis based on imaging appearance. It is necessary to differentiate CRMO from infections and neoplasms as treatment approach and prognosis is entirely different.

Note: Scanned images are included in the proceedings. Some submitted images were reduced during editing, thereby decreasing clarity. Also, refer to the Program Planner. Proceedings Content as of 3-29-2013.

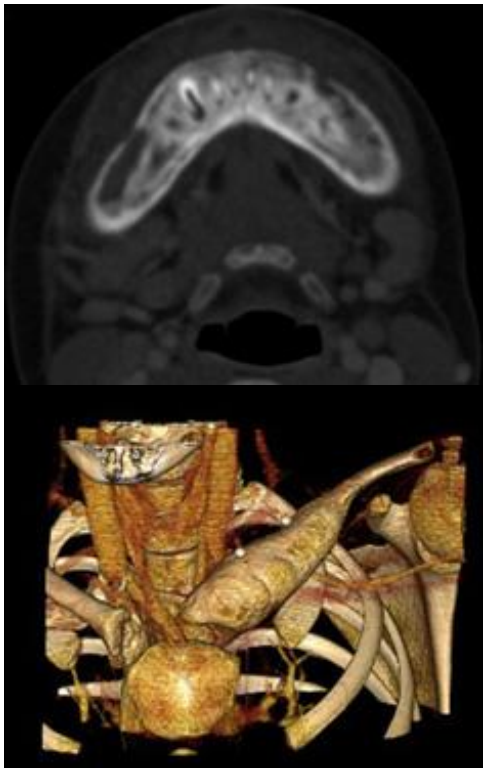

Summary/Conclusion
Chronic recurrent multifocal osteomyelitis is noninfectious osteomyelitis in pediatric population with typical involvement of clavicles and mandibles in head and neck region. Various key features on imaging of head and neck region are helpful to differentiate CRMO from infection and neoplasms. Differentiation of CRMO from these entities is essential in view of treatment and prognostication.

KEYWORDS: Head and neck, Osteomyelitis, chronic recurrent multifocal osteomyelitis

eEdE-101

Different Flavors of Advanced Imaging in the Head and Neck

Godfrey, W.·Brown, P. A.·Parmar, H.·Srinivasan, A.
University of Michigan Health System
Ann Arbor, MI.

Purpose
1. To briefly describe the principles of diffusion-weighted imaging (DWI) and perfusion imaging. 2. To illustrate with examples various clinical applications of DWI and perfusion in the head and neck.
Approach/Methods
Content organization: DWI: Principle. DWI: Technique in the head and neck. DWI: Clinical applications: • Differentiation of benign and malignant lesions. • Differentiation of recurrent malignancy and benign granulation tissues. • Identification of recurrent cholesteatoma. • Identification of ocular abscess. • Extraocular muscle involvement in thyroid ophthalmopathy. • Extraocular muscle metastases. • Acute optic neuritis. • Traumatic ocular injury. MR Perfusion: Principle. MR Perfusion: Technique in the head and neck. MR Perfusion: Clinical applications. • Differentiation of malignant from nonmalignant lesions. • Differentiation of recurrent tumors from post-therapy changes. • Monitoring and prediction of response to therapy.
Findings/Discussion
Advanced imaging in the head and neck is gaining increasing importance in head and neck radiology and is making inroads into clinical practice. Due to its unique ability to assess water motion at a molecular level, diffusion-weighted imaging (DWI) shows potential in differentiation of benign and malignant tumors, and post-therapy changes versus recurrent tumor (the latter entities show relative restriction of water motion due to their cellularity). In addition to helping determine benign from malignant lesions, apparent diffusion coefficient (ADC) also could be used for treatment followup. Early response to treatment is reflected in an ADC increase in the primary tumor and nodal metastasis; whereas nonresponding lesions tend to reveal only a slight increase or decrease in ADC during followup. Other clinical applications of DWI include recognition of recurrent cholesteatoma and acute optic neuritis amongst others. Along with DWI, MR perfusion imaging has proved promising in head and neck cancer in the differentiation of tumor and normal tissues, and to evaluate response to therapy. Patients who had local disease control following treatment demonstrating significantly increased blood volume and K^{trans} compared to those patients with local or regional failure.

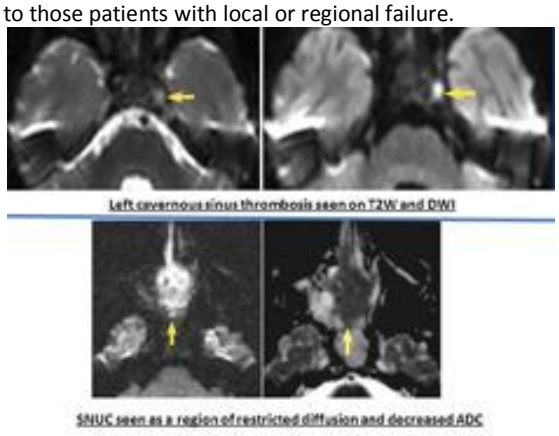

Left cavernous sinus thrombosis seen on T2W and DWI

SNUC seen as a region of restricted diffusion and decreased ADC

Summary/Conclusion
Advanced imaging frequently is being used in the head and neck for a variety of neoplastic and non-neoplastic clinical indications. The radiologist should be aware of its potential to best interpret day-to-day head and neck imaging.

KEYWORDS: Diffusion-weighted imaging, MR perfusion-weighted imaging

Note: Scanned images are included in the proceedings. Some submitted images were reduced during editing, thereby decreasing clarity. Also, refer to the Program Planner. Proceedings Content as of 3-29-2013.

eEdE-102

Dose Reduction Strategies in Head and Neck Imaging

Khorrami-Arani, N.[1]·Liang, T.[2]·Shewchuk, J.[1]·Nicolaou, S.[1]
[1]Vancouver General Hospital, Vancouver, BC, CANADA,
[2]University of British Columbia, Vancouver, BC, CANADA.

Purpose
Recent technologic advances in CT and new dual energy material characterization capabilities allow for dose reduction techniques that do not sacrifice image and diagnostic quality and can help minimize radiation exposure. The purpose of this exhibit is to review the current dose reduction strategies available for head and neck imaging.
Approach/Methods
A retrospective review of head and neck images from patients from our institution will be conducted.
Findings/Discussion
This educational exhibit will discuss dose reduction strategies available for head and neck imaging. The strategies discussed will include minimizing dose to thyroid and lens using tube current modulation, modulation of kVp based on topogram attenuation values, limiting z-overscanning by applying adaptive section collimation, and new iterative reconstruction techniques to help decrease image noise and artifacts and improve spatial resolution. Head and neck imaging examples of these techniques will be demonstrated, and the advantages of the application of each of these dose reduction techniques will be reviewed.
Summary/Conclusion
After reviewing this educational exhibit, the reader will be able to apply dose reduction techniques to minimize radiation exposure in head and neck imaging. Techniques such as iterative reconstruction, KV modulation, tube current modulation, and adaptive section collimation allow dose reduction in head and neck imaging while maintaining image quality and diagnostic performance.

KEYWORDS: Dose reduction

eEdE-103

Cranial Nerve Quiz Module: An Interactive Review of Cranial Nerve Imaging

Perni, K.·Parmar, H.·Ibrahim, M.·Mukherji, S. K.
University of Michigan
Ann Arbor, MI.

Purpose
Imaging of the cranial nerves is challenging due to the complex anatomy, as well the diversity of pathologic processes. It is important for neuroradiologists to understand the basic anatomy of the cranial nerves from the brainstem to their distal branches, firstly to correctly image them and secondly to understand the varied pathologies involving them. In addition, awareness of the clinical findings is important in this setting to guide image interpretation, to determine extent of disease, and subsequently to determine the range of treatment options. This electronic education exhibit is dedicated to demonstrating a critical anatomy of the cranial nerves and varied pathologies. This will be in an interactive way for the user to assess their own knowledge to facilitate long term retention of this information.
Approach/Methods
A retrospective review of the imaging findings in patients with both representative and unusual cranial nerve pathology, correlated with clinical symptomatology, was done using imaging studies of patients conducted at our institution. Modalities demonstrated include both MRI and CT imaging as appropriate in selected cases to best show cranial nerve pathology. In addition, interrogation of the patient's clinical record was performed to outline signs and symptoms pertinent to the imaging study. We observed that we could use the high resolution osseous detail provided by CT of the specific foramina and canals traversed by the various cranial nerves and their branches, combined with the soft tissue resolution of MRI, to demonstrate several different disease processes.
Findings/Discussion
Specific MRI findings such as signal abnormalities on T1- and T2-weight sequences, pattern, distribution and symmetry of contrast enhancement, and cranial nerve morphology proved beneficial for diagnosis, as well as classic CT signs such as expansion of skull base foramina and canals, and effacement of foraminal fat. The utilization of multiplanar MRI sequences and reformatted CT imaging in the coronal and sagittal plane also was important to elucidate complex anatomy and pathology that may be difficult to fully appreciate on axial images alone. Several different imaging sequences, including the use of fat suppressed and high resolution images proved to be very helpful as well. The clinical history was also extremely useful; such vital details included a history of primary malignancy, systemic or localized inflammatory processes, the duration of the patient's symptoms, and their specific focal neurologic deficits. In this exhibit we outlined the clinical presentation in combination with representative sequences and slices on MRI and CT of routine and unusual cranial nerve pathology, in order to help the user formulate a reasonable differential diagnosis.
Summary/Conclusion
There are a large number of specific structures and a wide variety of pathology involving the cranial nerves. Correlation with clinical symptoms, along with an interactive review of the anatomy and disease processes will help the user consolidate his or her knowledge, and apply this to clinical practice. This then could improve the referring physician's ability to adequately determine the extent of disease and develop strategies for further workup and treatment.

KEYWORDS: Cranial nerve palsy

Note: Scanned images are included in the proceedings. Some submitted images were reduced during editing, thereby decreasing clarity. Also, refer to the Program Planner. Proceedings Content as of 3-29-2013.

eEdE-104

Cone Beam CT: Imaging Techniques and Evaluation of Oral Pathology

Saad, A. F.[1]·Nickell, L. T.[1]·Benson, B. W.[2]·Flint, D. J.[2]·Liang, H.[2]·Opatowsky, M. J.[1]
[1]Baylor University Medical Center, Dallas, TX, [2]Texas A&M Health Science Center - Baylor College of Dentistry, Dallas, TX.

Purpose
The purpose of this educational exhibit is to present current technology and applications of cone beam computed tomography (CBCT) as well as review a spectrum of oral pathology evaluated with CBCT.
Approach/Methods
The principles of image generation and optimization using CBCT will be discussed with particular consideration of CBCT strengths and limitations compared with multidetector computed tomography (MDCT). Frequently encountered oral pathology will be reviewed to illustrate the clinical utility of current CBCT devices. The developing applications and limitations of CBCT in head and neck radiology will be addressed.
Findings/Discussion
Cone beam computed tomography is an emerging technology that has been used increasingly in dentomaxillofacial radiology. Images are created using an x-ray beam collimated with conical geometry and a flat panel detector. In contrast to conventional CT, where z-axis translation is needed to create an image set of multiple axial sections, CBCT requires one gantry rotation to obtain a volumetric dataset consisting of isometric voxels capable of submillimeter resolution. CBCT images can be reconstructed in any plane with theoretically reduced effects of partial volume averaging and improved spatial resolution. Additional strengths include decreased radiation dose and cost when compared to MDCT. CBCT does suffer from increased scatter and image noise, particularly at the periphery of images. Compared with MDCT, the primary limitation in the use of CBCT in diagnostic imaging is less robust characterization of soft tissue density structures. Review of literature generally shows a trend of increased utility of CBCT in the setting of treatment planning, intraoperative guidance, and lesion followup with decreased patient radiation dose. CBCT has been shown to be advantageous in the resolution and identification of small anatomical structures as compared with MDCT. CBCT is well suited to the evaluation of oral pathology; particularly with the availability, cost, and convenience of office-based systems. The evaluation of osseous and dental lesions is optimized due to the inherent high contrast of these structures. The decreased streak artifact obtained with CBCT is advantageous in evaluating lesions adjacent to dental amalgam.

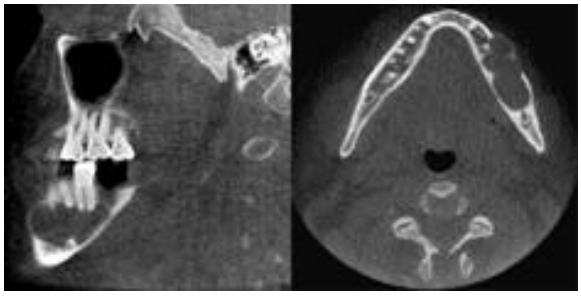

Summary/Conclusion
The utility of CBCT in dentomaxillofacial imaging has been established, with excellent evaluation and characterization of dental disease, jaw lesions, facial trauma, and dental implantology. Emerging applications of CBCT in head and neck radiology include skull base, temporal bone, and sinonasal imaging. The combination of increased spatial resolution with diminished patient radiation dose will be key factors in further applying CBCT to the broader field of neuroradiology.

KEYWORDS: Cone-beam computed tomography, Oral cavity

eEdE-105

Lytic Lesions of the Mandible and Maxilla: Imaging with Surgical Correlation

Cambron, S. C.·Addante, R. R.·McIntyre, J. J.
Dartmouth Hitchock Medical Center
Lebanon, NH.

Purpose
Lytic lesions of the mandible and maxilla present a common differential challenge, yet is infrequently taught in medical school or residencies. Although neuroradiologists often are presented with these lesions at CT, exposure to these lesions appearance on plan radiographs and surgical findings are limited. Our aim is to present the anatomy, imaging, and surgical findings of lytic lesions of the mandible and maxilla through an interactive series of cases with plain radiographs, CT, and intraoperative surgical images.
Approach/Methods
We review the imaging of lytic mandibular and maxillary lesions acquired at our institution with correlative surgical images acquired over a 7-year period. Findings are presented in an interactive electronic PowerPoint based format.
Findings/Discussion
The differential considerations of lytic lesions of the mandible and maxilla are presented. Images and illustrations of relevant anatomy including tooth and osseous structures, alveolar nerve, and sinuses will be reviewed. Specific images will be used to illustrate key differential features which can narrow the diagnosis including location relative to the teeth (periapical,

Note: Scanned images are included in the proceedings. Some submitted images were reduced during editing, thereby decreasing clarity. Also, refer to the Program Planner. Proceedings Content as of 3-29-2013.

periconal, interradicular), alveolar nerve, and solitary lesions. There also will be a discussion of lesion features such as degree of loculation, border definition, and matrix generation. Interactive features are included which allow participants to click on a location or lesion feature to bring up differential cases based on that location or feature. A summary of key teaching points also is included.
Summary/Conclusion
Lytic lesions of the mandible and maxilla present an interesting differential challenge. With an understanding of relevant anatomy and differential considerations we can accurately diagnose the etiology of these lesions and guide treatment decisions to improve patient care.

KEYWORDS: Mandible, Head and neck, dental

eEdE-106

Clival Tumors and Mimics: When It's Not a Chordoma

Noor, A.·Doshi, A.·Corcuera-Solano, I.·Fowkes, M.·Well, D.·Patel, K.·Pawha, P.·Nadich, T.·Som, P.
Mount Sinai Hospital
New York, NY.

Purpose
There are a variety of both common and uncommon lesions that can involve the clivus. A number of these entities have similar and often overlapping imaging appearances. The purpose of this exhibit is to review the imaging features of these lesions and provide a succinct differential diagnosis.
Approach/Methods
A retrospective review of our imaging cases of different clival lesions that had pathologic correlation was performed. Between 2010 and the present time, 10 cases were identified.
Findings/Discussion
In this group of patients the clinical presentations often were noncontributory to diagnosis. Symptomatology included headache, localized pain or in the case of pituitary lesions, pituitary-axis dysfunction. Therefore, imaging has become an important tool in differentiating these entities. Benign and malignant tumors involving the clivus often are difficult to differentiate as many of these lesions have overlapping features on CT and MRI. Location, local bony changes, signal characteristics and enhancement patterns may allow the radiologist to provide a narrowed differential diagnosis. Sphenoid mucocoele, meningioma, chondrosarcoma, ecchordosis physaliphora, a rare olfactory neuroblastoma, and invasive pituitary adenoma are some of the lesions that can have imaging findings similar to that of a chordoma; however, they are quite different in their treatment and prognosis. In this exhibit, the imaging appearance and underlying pathology of these entities will be reviewed. The imaging features that permit some distinction between these diagnoses will be emphasized.
Summary/Conclusion
Clinical presentations of patients with lesions in the clivus often are not helpful in identifying an underlying pathology. Imaging has become a very important tool. Because there are overlapping imaging features for many of these entities, arising at a pertinent and limited differential diagnosis is of utmost importance to the ordering clinician.

KEYWORDS: Chordoma, Clivus

eEdE-107

A Review of Benign and Malignant Pediatric Head and Neck Masses

Meesa, I.·Parmar, H.·Ibrahim, M.·Mukherji, S.
University of Michigan
Ann Arbor, MI.

Purpose
A broad spectrum of congenital and acquired solid and cystic masses can be encountered in the pediatric head and neck. Although most masses have a benign etiology, it is important for the radiologist to be apprised of potential malignant lesions, especially in the appropriate clinical context. The purpose of this poster is to describe and illustrate US, CT and MR imaging findings of various common/rare and benign/malignant pediatric head and neck masses encountered at our institution, followed by a brief presentation of the pathophysiology. Pertinent embryology for certain congenital lesions will be described, if relevant.
Approach/Methods
A retrospective review of pediatric head and neck masses encountered at our institution on US, CT, and MRI over the last 10 years will be performed. IRB approval was obtained.
Findings/Discussion
In this exhibit, we will classify common pediatric head and neck lesions into the following broad categories: orbits, nasal region lesions, salivary, thyroid, lymph node, nerve sheath, vascular, muscle and miscellaneous. Listed below are some of the common lesions we will present in each category: Orbits (gliomas, meningiomas), Nasal region masses (encephaloceles, nasal gliomas, dermoids-epidermoids, hemangiomas), maxillary/mandibular lesions (ameloblastoma), Nerve Sheath tumors [schwannoma (NF2), plexiform neurofibroma (NF1)], Salivary lesions (rannulas), Thyroid lesions (nodules, adenomas, colloid cysts, papillary carcinoma), Lymph nodes (inflammatory, infectious, lymphoma, metastases, Vascular [congenital hemangiomas, arteriovenous malformation, lymphangiomas, venous malformations vs acquired (aneurysm, thrombosis)], Muscle (fibromatosis coli, aggressive fibromatosis, rhabdomyosarcoma), and Miscellaneous [congenital anomalies of branchial apparatus, thyroglossal duct cyst, thymic cyst, teratomas/dermoid, glomus tumors (glomus jugulare), cervical lipoblastoma, cervical encephalocele].

Note: Scanned images are included in the proceedings. Some submitted images were reduced during editing, thereby decreasing clarity. Also, refer to the Program Planner. Proceedings Content as of 3-29-2013.

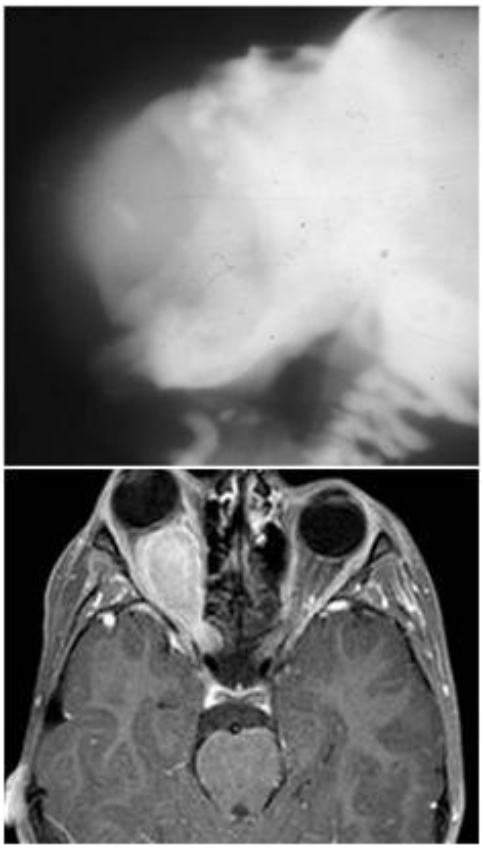

Summary/Conclusion
After reviewing the exhibit, the reader will have a better appreciation/understanding of the various pediatric head and neck tumors one might come across while reviewing/interpreting pediatric neuroimaging studies.

KEYWORDS: Head and neck, Pediatric head and neck, congenital

eEdE-109

Pseudotumors and Uncommon Lesions of the Infrahyoid Neck: How to Avoid Misinterpretation and Pitfalls

Noujaim, S.·Abel, N.·Cacciarelli, A.
William Beaumont Hospital
Royal Oak, MI.

Purposezi
Misdiagnosis and mischaracterization of these less common lesions within the infrahyoid neck may lead to unnecessary biopsies, procedures and additional imaging, exposing the patient to unwarranted complications. The purpose of this presentation is to familiarize the readers with the less common lesions and pseudotumors affecting the infrahyoid neck, how to recognize and diagnose them as well as how to narrow the differential diagnosis avoiding pitfalls in interpretation.
Approach/Methods
Numerous cases were collected from the archives of a major tertiary medical center. The best cases were reviewed and selected for purpose of this presentation. The cases presented here include but are not limited to congenital anomalies related to 3rd and 4th branchial apparatus (thymopharyngeal duct cyst, ectopic thymus, 4th branchial sinus tract and related thyroid abscess), pathology related to the brachial plexus (primary and metastatic tumors and hypertrophic neuropathies), lesions and pseudolesions of the neck muscles (levator claviculae muscle, hypertrophy of levator scapulae muscle, fibromatosis coli of newborn, calcific tendonitis of the longus coli muscle), foregut anomalies (foregut duplication cysts) and other congenital anomalies (dermoid cyst and teratomas).
Findings/Discussion
After a brief review and definition of the infrahyoid spaces of the neck using diagrams and illustrations, a number of less common lesions will be presented along with its differential diagnosis.
Summary/Conclusion
Misdiagnosis and mischaracterization of these less common lesions and pseudotumors within the infrahyoid neck may lead to unnecessary biopsies, procedures and additional imaging, exposing the patient to unwarranted complications.

KEYWORDS: Neck lesions, Congenital, tumor

eEdE-110

Imaging Features of Anaplastic Thyroid Carcinoma: An Unfamiliar Entity in Fatal Neoplasm. What's the Role of US and CT in Anaplastic Thyroid Carcinoma Patients?

Lee, A.·Kim, J.
Seoul National University Hospital
Seoul, KOREA, REPUBLIC OF.

Purpose
1. To present typical ultrasonographic (US) and computed tomographic (CT) features of anaplastic carcinoma. 2. To determine if useful imaging features of anaplastic carcinoma can predict prognosis.
Approach/Methods
We retrospectively reviewed the imaging and medical records of the 36 patients (9 men and 27 women) among 50 patients diagnosed with ATC from August 1995 to November 2011 at our hospital. Image analysis was performed according to the following US and CT parameters: size, echogenecity on US, presence of necrosis/calcification, perithyroidal invasion, lymph node (LN) metastasis and distant metastasis. Clinical data were sex, age, method for diagnosing ATC, treatment and survival duration. Statistical analysis (student t-test, Fisher's exact test and uni/multivariant analysis) was used.
Findings/Discussion
The mean age of patient at diagnosis was 61 years (range, 22-88 years). Anaplastic carcinomas appeared as large (average 3.9 cm) masses accompanied by necrosis (61.1%),

Note: Scanned images are included in the proceedings. Some submitted images were reduced during editing, thereby decreasing clarity. Also, refer to the Program Planner. Proceedings Content as of 3-29-2013.

calcification (91.6%), direct invasion into the adjacent organs (83.3%), and cervical lymph node involvement (77.8%) on US and CT. All lesions were shown as hypo/marked hypo-echoic mass on US. Multivariant analysis identified patient age (>70 years), tumor size, and extrathyroidal invasion as statistically significant predictors for anaplastic carcinoma (*p*-value< 0.05).

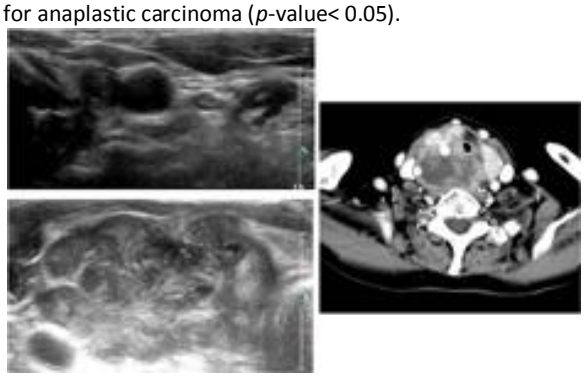

Summary/Conclusion
If an older patient has a large hypoechogenic thyroid mass with necrosis, calcification and extrathyroidal invasion, anaplastic carcinoma should be included in the differential diagnosis. Ultrasound and CT features also help to predict the prognosis of patients.

KEYWORDS: Thyroid, Carcinoma, anaplastic thyroid carcinoma

eEdE-111

Imaging Spectrum of Blunt Vascular Neck Injuries

Khorrami-Arani, N.[1]·Liang, T.[2]·Shewchuk, J.[1]·Nicolaou, S.[1]
[1]Vancouver General Hospital, Vancouver, BC, CANADA, [2]University of British Columbia, Vancouver, BC, CANADA.

Purpose
Blunt vascular neck injuries (BVNI) encompass injuries to the carotid and vertebral arteries, which can occur in the setting of polytrauma or injury to the craniocervical region. Although previously thought to be rare, recent literature has reported an incidence of up to 1.60% of injuries in blunt trauma patients. Complications such as stroke or cerebrovascular ischemia are a common cause of morbidity and mortality in BVNI and can appear 10-72 hours post-trauma after a latent phase. Thus, early detection and management of these injuries is crucial. The purpose of this exhibit is to review the utility of screening, discuss the imaging modalities available with emphasis on dose reduction and new imaging techniques, and review the grading and characteristic findings of BVNI and impact on therapeutic strategies.
Approach/Methods
A retrospective review of BVNI at our institution will be conducted for imaging examples to demonstrate the spectrum of these injuries.
Findings/Discussion
This educational exhibit will review the epidemiology, mechanism of injury, and clinical presentation and assessment of BVNI. The rationale of a potential screening algorithm involving multidetector CT (MDCT) will be discussed. Imaging modalities for BVNI including ultrasound, MR angiography, CT angiography, and catheter angiography will be reviewed. The spectrum of injuries and the injury grading system of BVNI on MDCT will be discussed with imaging examples. Imaging mimics and diagnostic pitfalls will be discussed and demonstrated to help readers avoid these diagnostic errors. This exhibit will show the utility of new artifact minimization and dose reduction techniques such as iterative reconstruction and dual energy imaging, particularly for vessels within the skull base and foramina transversaria, which are difficult regions to assess. Follow-up imaging, prognosis, and management will be reviewed. An imaging algorithm will be introduced for screening of BVNI and impact on treatment strategies such as when medical versus interventional/surgical management is required.
Summary/Conclusion
Blunt vascular neck injuries are associated with significant morbidity and mortality that may be prevented by early screening with MDCT. The imaging spectrum of BVNI and its mimics have been demonstrated in this exhibit. Prognosis and management is based on grading of BVNI. New artifact minimization and dose reduction techniques are useful for optimal diagnostic imaging of BNVI.

KEYWORDS: CTA, vascular neck injuries

eEdE-112

Role of CT and MR Imaging in Thyroid Cancer Patients: Who and When to Image, and Where to Look

Saito, N.[1]·Nakahira, M.[1]·Chang, Y.[2]·Sakai, O.[2]·Uchino, A.[1]·Kimura, F.[1]
[1]Saitama International Medical Center, Saitama, JAPAN, [2]Boston Medical Center, Boston University School of Medicine, Boston, MA.

Purpose
The purpose of this educational exhibit is: 1) To understand the role of CT and MR imaging in assessment of thyroid cancer. 2) To review various radiographic manifestations of thyroid cancer and potential pitfalls.
Approach/Methods
We retrospectively reviewed our patient database to identify patients with thyroid cancer. CT and MR imaging studies and clinical history were examined. Through illustrative case examples, we will demonstrate the clinical utility of CT and MR imaging for thyroid cancer.
Findings/Discussion
Evaluation of thyroid disease often is performed with ultrasound or nuclear medicine. Although it is difficult to reliably distinguish between benign and malignant lesions on CT and MR imaging, these modalities play highly important roles in the staging and treatment of thyroid

Note: Scanned images are included in the proceedings. Some submitted images were reduced during editing, thereby decreasing clarity. Also, refer to the Program Planner. Proceedings Content as of 3-29-2013.

cancer. The clinical utility of CT and MR imaging are: (A) evaluation of tumor burden and invasion to the adjacent structures, (B) assessment of lymph nodes, (C) assessment of distant metastasis, (D) differentiation of thyroid lesion from other pathologic lesions, (E) presurgical anatomical evaluation, and (F) posttreatment evaluation. Various characteristic imaging findings are reviewed and the indications for CT and MR imaging in the patients with thyroid cancer are discussed. The limitations of CT and MR imaging for thyroid lesions also are discussed.
Summary/Conclusion
The teaching points of this exhibit are: 1) CT and MR imaging can be helpful in making accurate diagnosis and surgical planning in patients with thyroid cancer, particularly in cases of bulky disease or tumor invasion resulting in symptoms such as hoarseness, difficulty of breathing and dysphagia. 2) Knowing who and when to image with CT and MR in the setting of thyroid cancer and recognizing the potential pitfalls is critical for accurate diagnosis.

KEYWORDS: Thyroid, CT, MR imaging

eEdE-113

Imaging Spectrum and Management of Penetrating Neck Trauma

Khorrami-Arani, N.[1]·Liang, T.[2]·Shewchuk, J.[1]·Nicolaou, S.[1]
[1]Vancouver General Hospital, Vancouver, BC, CANADA, [2]University of British Columbia, Vancouver, BC, CANADA.

Purpose
Penetrating neck injuries are associated with a high risk of clinically significant injury due to the presence of multiple vital structures within a small anatomical area. The mortality from penetrating neck injuries has been estimated to be up to 10%. Imaging allows for early diagnosis and can assist in management decisions for these injuries. The purpose of this exhibit is to review the mechanisms of penetrating neck trauma, available imaging modalities, characteristic findings on multidetector CT (MDCT), and the utility of MDCT for determination of surgical versus nonoperative management.
Approach/Methods
A retrospective review of cases of penetrating neck injuries from our institution will be conducted.
Findings/Discussion
This educational exhibit will review the anatomy, mechanism of injury, and clinical assessment of penetrating neck injuries to the neck. A review of the anatomical zones of the neck with correlation to imaging and implications for management will be conducted. Imaging modalities including ultrasound, angiography, MRI, and multidetector CT will be assessed for use in penetrating neck injuries. Imaging examples and MDCT characteristics will be reviewed for specific penetrating injuries, including arterial, venous, esophageal, tracheal, and laryngeal injuries. The utility of new techniques such as iterative reconstruction and mono-energetic spectral imaging for metal artifact reduction on CT will be reviewed. The usefulness and limitations of MDCT to determine wound trajectory and to guide appropriate intervention (surgical versus nonoperative) will be discussed. Our institution's protocol for imaging penetrating neck injuries will be described.
Summary/Conclusion
After reviewing this exhibit, the reader will understand the characteristic imaging findings and have reviewed imaging examples of various patterns of penetrating neck injury. Dose reduction and artifact minimization techniques can help minimize metal artifacts and can help limit radiation dose exposure to patients. Multidetector CT is useful in guiding appropriate management (surgical versus nonoperative).

KEYWORDS: Emergencies, penetrating neck trauma

eEdE-114

A Walking Tour of the Temporal Bone

Byrns, K.·Lev, S.
Nassau University Medical Center
East Meadow, NY.

Purpose
We provide the viewer with a virtual tour through the intricate architecture of the temporal bone, stopping along the way to examine areas of physiologic and pathologic interest, utilizing three-dimensional reformations of high-resolution MDCT studies.
Approach/Methods
High-resolution axial sections were obtained via 320-slice multidetector computed tomography. Vital Vitrea fx software was utilized to generate volumetric and flythrough reformations of the temporal bone in order to elucidate the complex anatomy. The anatomical review is supplemented by cases of traumatic and nontraumatic pathology from our community-based Level 1 trauma center. The images were postprocessed in Adobe Photoshop to provide colorization and labeling for further illustration.
Findings/Discussion
The temporal bone represents one of the most intricate regions of head and neck imaging, featuring complex and subtle anatomical details. It is crucial for the radiologist to properly orient him or herself and, in doing so, develop region-appropriate differential diagnoses. The ability to obtain thin collimation images via state-of-the-art multidetector computed tomography has proven invaluable for unlocking the elaborate three-dimensional relationships of the various key regions and associated structures. Furthermore, volumetric rendering software has enabled the radiologist to observe the anatomy in novel ways. In particular, virtual flythrough software can transform an area several orders of magnitude smaller than the observer into an environment to be explored. The

Note: Scanned images are included in the proceedings. Some submitted images were reduced during editing, thereby decreasing clarity. Also, refer to the Program Planner. Proceedings Content as of 3-29-2013.

journey begins at the entrance, the external auditory canal, which may be afflicted by various degrees of atresia as well as infectious and neoplastic processes, both benign and malignant. We then proceed into the middle ear, with its various recesses and prominences, housing the ossicular chain. The ossicles demand careful observation in order to detect improper development, erosive neoplasms, or disruption from longitudinal fractures. Gazing upward reveals Prussak's space, the classic location for an acquired cholesteatoma. Next, we transport the viewer into the inner ear, with its cochlear turns and labyrinthine chambers, observing the myriad congenital and acquired lesions that one might encounter. If one finds the structure unexpectedly simplified, the diagnosis lies along a spectrum extending from aplasia to incomplete partition, such as the Mondini deformity. Finally, the voyage culminates as we exit through the porus acusticus and vestibular aqueduct, where entities such as vestibular schwannomas or endolymphatic sac tumors may be encountered.

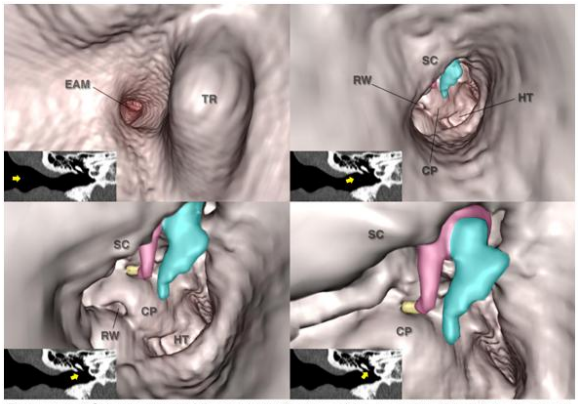

Flythrough of Outer Ear into Middle Ear highlighting the ossicles, the malleus (blue), incus (magenta), and stapes (yellow), as well as additional areas of interest, including the external acoustic meatus (EAM), tragus (TR), round window niche (RW), hypotympanum (HT), scutum (SC), and cochlear promontory (CP). The perspective of each panel is indicated by the arrow within the inset coronal CT images.

Summary/Conclusion
Virtual flythrough reconstructions provide a unique and powerful method to understand and appreciate the exquisite anatomy of the temporal bone and facilitate location-based differential diagnoses.

KEYWORDS: Temporal bone, 3D computed tomography

eEdE-115

The Preoperative Cholesteatoma: Beyond the Scutum and Prussak Space. Identification of Surgical Landmarks and Anatomical Variants that Could Have Implications on Surgical Method and Approach

Hakham, S.·Sillman, J.·Madan, N.·Bedi, H. S.
Tufts Medical Center
Boston, MA.

Purpose
1. Review the surgical anatomy of the ear, with CT correlation. 2. Identify landmarks within the temporal bone that radiologists should be familiar which could have implications on surgical approach. 3. Describe variants within the temporal bone which could have implications on the type of surgery and surgical approach.
Approach/Methods
The anatomical landmarks of the ear and temporal bone are reviewed in the order in which the structures are approached during surgery. Other surgically relevant details including anatomical variations and associated surgical complications are presented in pictorial and tabulated formats, where appropriate.
Findings/Discussion
Multiplanar high-resolution computed tomography (HRCT) is the reference standard for imaging examination of the temporal bone, providing the surgeon with a precise three-dimensional road map in preoperative evaluation of cholesteatoma. This examination has a crucial role on the specific surgical approach adopted by the surgeon and subsequently on the clinical outcome to reduce and potentially prevent intra and postoperative complications. A thorough knowledge of the surgical anatomy and pathology by the expert radiologist not only aids in adequate interpretation of such studies, but also aims the surgeon to avoid the unnecessary complications. Through a collaborative effort with otolaryngologists at our institution, we propose a comprehensive, yet systematic method for evaluation of the temporal bone, pointing out the essential components of an ideal dictation in preoperative evaluation of cholesteatoma.
Summary/Conclusion
CT examination of the temporal bone is instrumental in the diagnosis and preoperative evaluation of cholesteatoma. Our exhibit provides a structured format for interpretation of the preoperative cholesteatoma, with special attention to surgical landmarks and anatomical variants that could have implications on surgical method and approach.

KEYWORDS: Cholesteatoma, preoperative evaluation

eEdE-116

High-Resolution Ossicular Anatomy: Correlation with MicroCT and Otoscopy

Choudhri, A. F.[1,2]·Whitehead, M. T.[1,2]·Chatterjee, A. R.[1]·MacDonald, C. B.[1]
[1]University of Tennessee Health Science Center, Memphis, TN, [2]Le Bonheur Children's Hospital, Memphis, TN.

Purpose
Ossicles are tiny bones within the middle ear critical for conduction of pressure vibrations from the tympanic membrane to the oval window. Congenital and acquired abnormalities of the ossicles can impair hearing; however, due to their small size with features below clinical imaging resolution, a detailed understanding of their morphology can aid in evaluation.
Approach/Methods

Note: Scanned images are included in the proceedings. Some submitted images were reduced during editing, thereby decreasing clarity. Also, refer to the Program Planner. Proceedings Content as of 3-29-2013.

We obtained 8 micron isotropic resolution microCT scans of individual ossicles, as well as of an entire middle ear with the ossicular chain intact, to help provide a teaching tool about the morphology and orientation of the ossicles. Comparison with clinical CT scans performed at 0.5 mm isotropic resolution is provided, as well as otoscopic images to assist in understanding spatial orientation.
Findings/Discussion
An interactive viewer allows the user to scroll through microCT and clinical CT datasets, and navigate in a virtual 3D environment. This information is paired with detailed photographs of the ossicles and otoscopic images, with the goal of conveying an understanding of the morphology and orientation of the ossicles and their associated ligaments, as well as the margins of the mesotympanum and epitympanum.

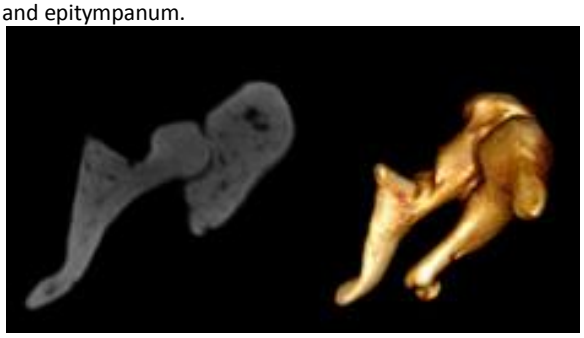

Summary/Conclusion
Interpretation of abnormalities in ossicular morphology and articulation requires a detailed understanding of the underlying anatomy. By reviewing the CT and microscopic appearance of the ossicles and their ligaments we feel that the reader will have an improved understanding of the anatomy and spatial orientation of the structures of the mesotympanum.

KEYWORDS: Temporal bone, Anatomy

eEdE-117

Views of the Third-Window Phenomenon: What a Radiologist Needs to Know

Torres, F.·Hoque, K.·Lerner, A.·Shiroishi, M.·Go, J. L.
University of Southern California
Los Angeles, CA.

Purpose
To provide an overview of lesions of the inner ear resulting in the third-window phenomenon.
Approach/Methods
Utilizing the teaching files from a major academic institution on the West Coast as well as an associated pre-eminent ototology clinic, the clinical manifestation, pathophysiologic basis, and diagnostic imaging features of lesions resulting in third-window phenomenon will be reviewed.
Findings/Discussion
Fistula formation associated with the inner ear may result in the "third-window" phenomenon. This exhibit will review the pathologic basis and current theories associated with this entity which leads to sensorineural hearing loss. Examples of this entity will be provided utilizing high-resolution CT and MR imaging. Additional reformatted planes of view on CT also will be described to aid the radiologist in making this diagnosis.
Summary/Conclusion
The third-window phenomenon is an uncommon cause for sensorineural hearing loss. A combination of the clinical symptomatology, audiometry examination, and imaging features will be reviewed to aid the radiologist in making this unique diagnosis.

KEYWORDS: Inner ear, Semicircular canal dehiscence, third window

eEdE-118

Intratympanic Masses: The Common, the Rare, and the Unheard of

Tuan, A. S.·Chung, R.·Farid, N.·Mafee, M. F.
University of California San Diego
San Diego, CA.

Purpose
The thrust of this exhibition is to review and to differentiate various intratympanic masses in adults and children.
Approach/Methods
The normal intratympanic anatomy will be reviewed, then selective images of pathologic intratympanic entities will be shown. A short quiz will follow to reinforce the concepts in this educational exhibit.
Findings/Discussion
Following a review of normal intratympanic anatomy, selective images of the following entities will be presented. 1. Intratympanic teratoma (choristoma). 2. Intratympanic papilloma and polyps. 3. Intratympanic meningioma (ectopic) and extension of intracranial en plaque meningioma into the middle ear (along vascular, neural, and natural channels). 4. Intratympanic extension of labyrinthine schwannoma. 5. Glomus tympanicum and its mimics (ectopic carotid, jugular bulb diverticulum, cholesterol granuloma, extramedullary hematopoiesis). 6. Primary cholesteatoma of the middle ear. 7. Intratympanic metastasis.
Summary/Conclusion
This educational exhibit will enhance our understanding of various intratympanic masses, emphasize the differing imaging characteristics of intratympanic masses, and increase our ability in differentiating these lesions. Imaging will play an important role in the clinical management of intratympanic lesions.

KEYWORDS: Middle ear, Temporal bone

Note: Scanned images are included in the proceedings. Some submitted images were reduced during editing, thereby decreasing clarity. Also, refer to the Program Planner. Proceedings Content as of 3-29-2013.

eEdE-119

Radiologic Evaluation of Congenital Aural Dysplasia: Spectrum and Associated Abnormalities

Nace, S. R.·Kennedy, T. A.·Gubbels, S. P.·Gentry, L. R.
University of Wisconsin
Madison, WI.

Purpose
To present an interactive display exhibiting the spectrum of congenital aural dysplasia as well as the complex cross-sectional anatomy of associated middle ear, mastoid, and inner ear anomalies.
Approach/Methods
Multiple cases of congenital aural dysplasia were collected and reviewed at the University of Wisconsin Hospital and Clinics. Selected high-resolution CT and 3D surface rendered reformatted images illustrate the spectrum of pinna and external auditory canal malformations, in addition to associated abnormalities of the middle ear, mastoid, and inner ear.
Findings/Discussion
Congenital aural dysplasia occurs on a spectrum, ranging from mild deformities resulting in isolated malformation of the pinna to complete absence of the external auditory canal with severe associated middle and inner ear defects. Due to the concurrent embryologic development of the first and second branchial arches, associated abnormalities of the middle ear and mastoid are disproportionately represented. Evaluation of the inner ear, ossicular chain, course of the facial nerve, and degree of development/ pneumatization of the middle ear cavity and mastoid antrum are crucial in preoperative assessment in this patient population. An understanding of these known associations, as well as the complex three-dimensional anatomy of the temporal bone on high-resolution CT is required for full appreciation of the extent of abnormalities beyond the clinically obvious, and those abnormalities which are critical in managing the patient from both clinical and surgical perspectives.
Summary/Conclusion
Radiologic evaluation of congenital aural dysplasia requires an understanding of the disease spectrum, known associated abnormalities due to embryologic origins, and the complex cross-sectional anatomy of the temporal bone on high-resolution CT.

KEYWORDS: Congenital aural atresia, Temporal bone

eEdE-120

A Web-Based Mobile Application for Learning and Reviewing the Appearance of Osseous Lesions of the Skull Using a Multimodality Approach

Cohen, M. G.·Kadoch, M. A.·Sicular, S.·Fitzpatrick, D.·Naidich, T. P.·Rosenberg, H. K.
Mount Sinai Medical Center
New York, NY.

Purpose
The purpose of the exhibit is: 1. To provide quick and easy access to a web-based mobile application and reference guide that addresses most of the common osseous lesions of the skull as evaluated by modern imaging modalities. 2. To provide a reference tool that addresses the limitations of other online reference tools, which can be cost-prohibitive, require log-ins or registration, lack interactivity, and are often slow to engage the end user. 3. To provide imaging of both the specific and nonspecific imaging features of a given osseous skull lesion. 4. To provide a novel learning platform that is fully functional using either the internet alone or on most major handheld devices and tablets, which are becoming increasingly important as educational resources for fellows, trainees, and students.
Approach/Methods
All relevant osseous lesions of the skull encountered at our institution since 2001 were reviewed for potential inclusion in the exhibit.
Findings/Discussion
The major teaching points of this exhibit are: 1. Reviewing the diagnostic as well as nonspecific imaging findings of multiple osseous skull lesions on modern imaging modalities. 2. Encouraging each user to expand on this review by linking each pathology to important AJNR articles that further discuss that specific pathology. 3. Measuring the success of this electronic educational exhibit by monitoring number of online views and traffic directed towards the supplied AJNR articles.
Summary/Conclusion
A web-based mobile application for learning and reviewing the appearance of osseous lesions of the skull using a multimodality approach is presented.

KEYWORDS: Skull, Neoplasm

eEdE-121

Conductive Hearing Loss: Common Etiologies and Key Imaging Features

Torres, F.·Lerner, A.·Shiroishi, M.·Hoque, K.·Go, J.
University of Southern California
Los Angeles, CA.

Purpose
This exhibit will review the characteristic imaging features of the most common etiologies of conductive hearing loss.

Note: Scanned images are included in the proceedings. Some submitted images were reduced during editing, thereby decreasing clarity. Also, refer to the Program Planner. Proceedings Content as of 3-29-2013.

Approach/Methods
Case material will be provided from the teaching files from a major academic institution on the west coast and associated pre-eminent ototology clinic. All cases were diagnosed utilizing the Weber-Rinne test and audiometry examination for which they were referred for potential conductive hearing loss without sensorineural hearing loss.
Findings/Discussion
Conductive hearing loss is due to an abnormality of conduction of sound waves to the oval window. This exhibit will examine a wide variety of pathologic processes that result in conductive hearing loss, including otodystrophies associated with the middle ear cavity including fibrous dysplasia and Paget's disease. In addition, primary ossicular anomalies including ossicular fixation and erosive processes will be reviewed, as well as congenital structural abnormalities which may involve the external auditory canal and middle ear cavity. In addition, the imaging features of acquired lesions within the middle ear that may cause impingement of the ossicular chain due to inflammation or infection will be presented, including space-occupying masses within the middle ear cavity that also result in conductive hearing loss.
Summary/Conclusion
Unlike sensorineural hearing loss, for which the cause may not be radiographically imaged, the underlying pathology is commonly determined by closely scrutinizing the external auditory canal, tympanic membrane, and the middle ear cavity and its contents and may be missed by the radiologist. This exhibit will educate the attendee of the imaging features that are the root cause of conductive hearing loss.

KEYWORDS: Conductive hearing loss, Temporal bone

eEdE-122

CT Evaluation of External Auditory Canal Atresia: What the ENT Wants to Know

Hu, J.·Nguyen, V.
North Shore Long Island Jewish Health System
New Hyde Park, NY.

Purpose
CT plays a central role in preoperative evaluation and planning for external auditory canal atresia. This exhibit will present the various findings of external auditory canal atresia and their implications in surgical planning.
Approach/Methods
We will review the CT findings of external auditory canal atresia, discuss imaging findings that may serve as surgical landmines, review the basic mechanism of surgical repair, and highlight the relevant findings that the surgeon uses to plan the surgical approach.
Findings/Discussion
CT is used to evaluate appropriate surgical candidates, and can be predictive of postoperative hearing results. Relevant CT findings include the degree of formation of the incudomalleolar complex, the integrity of the incudostapedial joint, the patency of the oval and round windows, temporal bone pneumatization, the integrity of the stapes, and the course of the facial nerve. Of note, external auditory canal atresia in association with several congenital malformation syndromes may be more severe, involving more middle ear and even inner ear deformities.
Summary/Conclusion
The CT findings of external auditory canal atresia that the radiologist conveys to the surgeon play a vital role in both the determination of appropriate surgical candidates and in preoperative planning.

KEYWORDS: Middle ear, Inner ear, external auditory canal

eEdE-122a

Problematic Pediatric Airway: Prenatal and Postnatal Imaging

Ferrante, M.·Steinklein, J. M.·Bittman, M.·Nguyen, V.
Long Island Jewish Medical Center
New Hyde Park, NY.

Purpose
Airway compromise is a potentially life-threatening condition that necessitates urgent medical attention. The pediatric population is particularly at risk as the pharyngeal and laryngeal spaces are smaller, and can be narrowed at baseline from lymphoid tissue. Narrowing can be due to a multitude of causes which are highlighted in this exhibit.
Approach/Methods
Select cases of airway compromise in the pediatric population have been included for review and educational exhibit, and categorized into congential masses, anomalies, infectious/inflammatory, and foreign bodies. Discussion of each case will follow with take-home points highlighted throughout the presentation. Methods of fetal MRI and the need for multiplanar series will be reviewed. Select cases collected at our institution include: CHAOS syndrome, Cleft palates and oral cavity narrowing, nasopharyngeal narrowing (choanal atresia and pyriform aperture stenosis), thryoglossal duct cyst at base of tongue, infections and abscesses (including MAI and Cat Scratch Fever), vascular malformations, lymphatic malformations, malignancies such as rhabdomyosarcoma, head and neck epidermoid and dermoid cysts, bony lesions with airway compromise, and foreign bodies.
Findings/Discussion
A wide assortment of diagnoses can compromise the pediatric airway and include congential malformations of the maxillofacial region, aerodigestive tract and subglottic airway, acquired mucosal diseases such as infection and inflammation, masses and adenopathy. While the patient may be asymptomatic, the finding of airway compromise could develop into dire consequences for the patient. In the setting of a prenatal diagnosis, the diagnostic exams

Note: Scanned images are included in the proceedings. Some submitted images were reduced during editing, thereby decreasing clarity. Also, refer to the Program Planner. Proceedings Content as of 3-29-2013.

we perform can alter the immediate postnatal care and necessitate multidisciplinary presence in the delivery room to provide necessary postnatal care to protect the airway. Congential anomalies can lead to airway narrowing or compromise. With fetal MRI better equipped to image this region of anatomy, a prenatal diagnosis can alter immediate postnatal care.
Summary/Conclusion
A wide assortment of pathologies in the pediatric head and neck can alter airway mechanics and have the potential for life-threatening consequences. In the prenatal and neonatal age group, careful sonographic evaluation and use of MRI for suspected fetal anomalies, immediate postnatal period can be optimized to ensure proper airway management and oxygenation of a newborn.

KEYWORDS: Pediatric head and neck, Neonatal MR imaging, pediatric airway

Monday, May 20 – Wednesday, May 22
6:30 AM – 9:00 PM
Thursday, May 23
6:30 AM – 3:00 PM
Hall B1

Electronic Education Exhibits (eEdE) 123 - 128

eEdE4-Interventional

Note: A missing printed number indicates an abstract has been withdrawn.

eEdE-123

Flow-Diverting Stents in the Treatment of Intracranial Aneurysms: What the Neuroradiologist Needs to Know

Thurlow, P. C.·Ku, A.·Goldberg, M. F.
West Penn Allegheny Health System
Pittsburgh, PA.

Purpose
The management of large and giant wide-necked intracranial aneurysms (IAs) historically has represented a significant challenge for neurointerventional radiologists, with a high rate of rupture without intervention, high surgical mortality rates, and high recurrence rates following intervention. Flow-diverting stents, of which the Pipeline Embolization Device (PED) (EV3/Covidien) is currently the only FDA-approved device, offer a novel approach to the treatment of large and giant wide-necked IAs. The introduction of the PED into clinical practice requires radiologists to be familiar with the unique imaging characteristics of IAs treated with flow-diverting stents. The purpose of this exhibit is to discuss the role of flow diverting stents in the management of large and giant wide-necked IAs and present a case-based review of the computed tomography (CT), magnetic resonance (MR), and angiographic imaging characteristics of IAs treated with flow diverting stents.
Approach/Methods
This educational exhibit will begin with a review of the classification system for IAs and the natural history of giant, wide-necked, and fusiform IAs. A brief review of the conventional treatment options for IAs then will be undertaken. An overview of the applications, mechanism of action, clinical data, and imaging features of the PED then will be presented, followed by an interactive, case-based review of the CT, MR, and angiographic imaging characteristics of IAs treated with the PED over time.
Findings/Discussion
The participant will be presented with the classification system by size and configuration for IAs and learn the features of large and giant wide-necked IAs that make flow-diverting stents particularly effective in their treatment. The mechanism of action of the PED is through flow diversion and re-endothelialization. Because the PED obviates intrasaccular aneurysm packing and allows thrombus mass to be resorbed, mass effect symptoms, including cranial nerve neuropathies and headaches, also are alleviated. These effects are manifest on follow-up imaging as a gradual decrease in the size of the excluded aneurysm sac. Complete preintervention characterization of the aneurysm and an understanding of the imaging characteristics of the aneurysm over time following treatment with the PED are essential for appropriate treatment and followup.
Summary/Conclusion
Flow-diverting stents represent an important development in the management of large and giant wide-necked IAs. An understanding of the role of flow-diverting stents in IA management, as well as the imaging appearance of IAs treated with the flow-diverting stents, is essential for the practicing radiologist. This interactive educational exhibit provides an overview of large and giant wide-necked IAs and highlights the key features of the flow-diverting stent in the treatment of IAs through an interactive, case-based review.

KEYWORDS: Flow diverter, Aneurysm treatment, pipeline

Note: Scanned images are included in the proceedings. Some submitted images were reduced during editing, thereby decreasing clarity. Also, refer to the Program Planner. Proceedings Content as of 3-29-2013.

eEdE-124

Demonstrating CTA Criteria for the Diagnosis of Dural Arteriovenous Fistula

Michalski, M. H.·Lawrence, D. A.·Minja, F.·Weisman, N.·Matouk, C.·Bulsara, K.·Johnson, M. H.
Yale New Haven Hosptial
New Haven, CT.

Purpose
Dural arteriovenous fistulas (dAVF), which consist of direct connections between dural arterial feeders and venous sinuses dural veins, are rare vascular abnormalities. While benign dAVFs rarely become symptomatic, aggressive lesions that involve the leptomeninges often present with significant neurologic symptoms or hemorrhage. On CTA studies performed in the emergent setting, these malformations can be mistaken for more common pial-based AVMs. However, diagnosis of dAVFs can be a critical distinction in the risk stratification and therapeutic management of these patients. Several imaging findings have been reported as being suggestive of dAVF; in this presentation, we demonstrate CTA imaging findings that have been useful tools in diagnosing dAVFs.
Approach/Methods
To explore methods for delineating dAVFs from pial AVMs, a review of angiographically confirmed cases of dAVF was conducted. Patients treated at a single academic institution over the past 10 years were assessed for the study. Patients who had inconclusive angiographic results, initially mixed AVF/AVM disease, or patients that did not have a CTA performed prior to their angiography were excluded. The resulting cases then were reviewed for CTA findings (and confirmatory correlates on other available modalities) unique to dAVFs to assist in their detection. These findings then were compared against several analogous studies of patients with pial AVMs in similar locations. In addition, a review of recent literature was performed to identify other reported dAVF imaging findings.
Findings/Discussion
After systematic review, several imaging findings were found which are suggestive dAVF. First, a intraparenchymal nidus of vessels, a characteristic finding of pial AVMs, could not be identified in dAVFs. Second, the presence of dilated cerebral veins without dilated feeding inflow vessels suggested a dural arterial source. Finally, venous sinus occlusions or blind ending venous pouches could reflect an underlying dAVF. Several examples of these findings in multiple locations within the cranial vault were obtained as examples for this presentation, along with matching negative examples with pial AVMs.

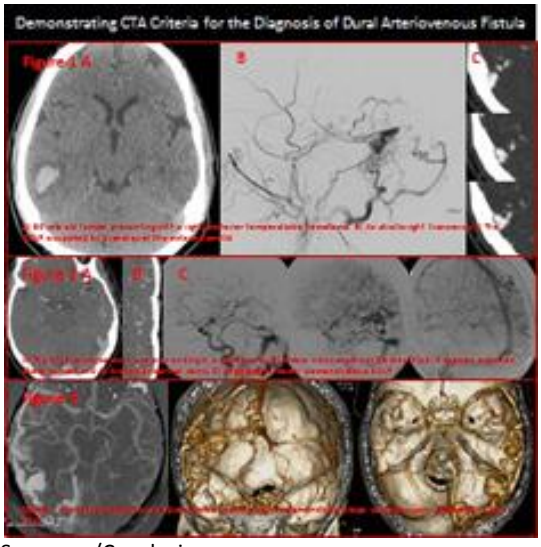

Summary/Conclusion
We demonstrate several CTA findings that can help in the diagnosis of dAVF, with multiple corresponding imaging examples of dAVFs juxtaposed with pial AVMs. These criteria can be helpful in the diagnosis, treatment and risk stratification of ambiguous AVMs that present in the emergent setting.

KEYWORDS: Dural arteriovenous fistula, Arteriovenous malformation

eEdE-125

A Web-Based Application for Learning and Reviewing the Appearance of Intracranial Vascular Lesions Using a Multimodality Approach

Ward, T. J.·Kadoch, M. A.·Sicular, S.·Horn, C.·Cohen, M. G.·Doshi, A.
Mount Sinai Medical Center
New York, NY.

Purpose
The purpose of the exhibit is: 1. To provide quick and easy access to a web-based application and reference guide that addresses most of the common intracranial vascular lesions as evaluated by modern imaging modalities. 2. To provide a reference tool that addresses the limitations of other online reference tools, which can be cost-prohibitive, require log-ins or registration, lack interactivity, and are often slow to engage the end user. 3. To provide imaging of both the specific and nonspecific imaging features of a given intracranial vascular lesion. 4. To provide a novel learning platform that is fully functional using either the internet alone or on most major handheld devices and tablets, which are becoming increasingly important as educational resources for fellows, trainees, and students.
Approach/Methods
All relevant intracranial vascular lesions encountered at our institution since 2001 were reviewed for potential

Note: Scanned images are included in the proceedings. Some submitted images were reduced during editing, thereby decreasing clarity. Also, refer to the Program Planner. Proceedings Content as of 3-29-2013.

inclusion in the exhibit.
Findings/Discussion
The major teaching points of this exhibit are: 1. Reviewing the diagnostic as well as nonspecific imaging findings of multiple intracranial vascular lesions on modern imaging modalities. 2. Encouraging each user to expand on this review by linking each pathology to important AJNR articles that further discuss that specific pathology. 3. Measuring the success of this electronic educational exhibit by monitoring number of online views and traffic directed towards the supplied AJNR articles.
Summary/Conclusion
A web-based application for learning and reviewing the appearance of intracranial vascular lesions using a multimodality approach is presented.

KEYWORDS: Arteriovenous malformation, Arteriovenous fistulas

eEdE-126

Basic Techniques of Neurointerventional Radiology: What the Neuroradiology Fellow Should Know

Shaikh, H.·Patel, N.·Bagley, L.·Pukenas, B.·Smith, M.·Hurst, R.
Hospital of the University of Pennsylvania
Philadelphia, PA.

Purpose
To illustrate and describe basic angiographic techniques that are important for neuroradiology fellows to learn.
Approach/Methods
Pictures and videos of neurointerventional physicians and fellows at our institution will be used in this exhibit to help illustrate basic neurointerventional techniques and their importance. Techniques of flush-line, catheter, wire, coil, stent, and embolic agent preparation will be discussed. Standard angiographic projections, rotational angiography, anatomical landmarks and hemostasis techniques will be reviewed. The Siemens' (Malvern, PA) Artis biplane angiography unit will be used for demonstration purposes. Various flow models also will be used to help illustrate basic vessel selection and contrast injection techniques.
Findings/Discussion
Integration to a neurointerventional service may be a daunting task, particularly for those fellows with limited prior angiographic experience. This exhibit hopes to develop a basic framework for understanding neurointerventional radiology and its role in the diagnosis and treatment of neurologic disorders. The exhibit will review pertinent elements of the preprocedural evaluation including patient symptomatology, physical exam, laboratory tests, prior imaging and anatomical variants. A systematic manner with careful attention to detail is required for each and every neurointerventional case. All catheters, lines, wires and other devices must be prepared and examined prior to usage in order to minimize risks (such as air emboli) to the patient. Optimizing radiographic projections, minimizing radiation dose, use of rotational angiography and 3D postprocessing techniques, and hemostasis techniques including use of closure devices will be covered. Techniques of obtaining arterial access as well as selective vascular catheterization, including road mapping techniques will be discussed. Postprocedural evaluation and assessment for possible complications are also imperative.
Summary/Conclusion
Appropriate preparation, careful attention to detail and mastery of basic techniques are essential in neurointerventional procedures to ensure patient safety. This exhibit attempts to detail basic neurointerventional techniques - in short, what every fellow should know.

KEYWORDS: Cerebral angiography, Educational, techniques

eEdE-127

Risk of Contrast-Induced Nephropathy in Patients Undergoing Treatment for Acute Stroke

Javadi, P.·Etesami, M.·Patel, T.·Blackham, K.
University Hospital Case Medical Center
Cleveland, OH.

Purpose
The purpose of this education exhibit is to discuss the rare incidence of and risk factors for contrast-induced nephropathy (CIN) after the use of iodinated contrast for endovascular treatment of acute ischemic stroke (AIS) as compared to the high risk of CIN in patients undergoing coronary angiography for myocardial infarction (MI).
Approach/Methods
A review of literature for the incidence and risk factors of CIN in patients receiving iodinated contrast for CT angiography or endovascular treatment in the setting of acute ischemic stroke was performed which was compared to the risk of CIN in patients receiving percutaneous intervention (PCI) for MI. Additionally, results from our institute for the incidence and risk factors for CIN in patients receiving endovascular treatment for AIS also have been included.
Findings/Discussion
There is an increased rate of 12-26% of CIN in patients with myocardial infarction who underwent PCI. Studies also have shown correlation of multiple risk factors including diabetes mellitus, previous history of chronic kidney disease, and amount of contrast used during the procedure with CIN. The majority of the studies showed higher incidence of CIN in patients with advanced renal disease, cardiogenic shock, volume depletion, poor ejection fraction and decreased cardiac output secondary to myocardial infarction. Association with poor clinical outcome and prolonged hospital stay have been well established. Previous studies have shown low incidence of CIN in acute stroke patients who underwent emergent multimodal CT scanning ranging from 2-3.7%. The only

Note: Scanned images are included in the proceedings. Some submitted images were reduced during editing, thereby decreasing clarity. Also, refer to the Program Planner. Proceedings Content as of 3-29-2013.

published cohort of 99 patients undergoing endovascular therapy for acute ischemic stroke reported an incidence of 3% for acute contrast-induced nephropathy. Most of these cases of acute kidney injury had resolved after hydration. No patients in these study groups needed dialysis at discharge. No clear correlation between risk factors have been established, although study samples are small compared to the acute coronary syndrome (ACS) group. Postulated differences in incidence and complications of CIN in patients receiving iodinated contrast medium in ACS and acute ischemic stroke include cardiogenic shock in setting of MI, higher underlying comorbidities in patients with ACS, and pre-renal azotemia which is correctable with hydration in AIS. In our cohort of patients, the risk of developing CIN was relatively low among acute stroke patients who underwent emergent endovascular treatment (1.5%). Eighty-four percent (161) patients had a baseline creatinine less than 1.5 mg/dl. All but two patients with baseline creatinine of 1.5 mg/dL developed CIN. Female gender, history of diabetes and additional preceding CT angiogram in 44 patients were not associated with higher risk of developing CIN.
Summary/Conclusion
The risk of developing CIN is low among acute stroke patients who undergo emergent endovascular intervention. Laboratory investigation should not delay as much as known renal insufficiency should not preclude intra-arterial treatment of stroke. A prospective randomized clinical trial is warranted to evaluate long-term effects of use of contrast and interval development of chronic kidney disease.

KEYWORDS: Stroke, Complications, contrast-induced nephropathy

eEdE-128

"Recreational Vasculopathy or Vasculitis": Not So Fun for Your Brain

Supsupin, E. P.[1]·Lee, P.[2]·Dahlin, B.[2]
[1]University of Texas Medical School at Houston, Houston, TX, [2]University of California Davis, Davis, CA.

Purpose
This is a pictorial essay of cerebrovascular manifestations resulting from abuse of recreational drugs. We recently observed the emergence of such conditions in our practice.
Approach/Methods
The vasculopathic/vasculitic changes associated with recreational substances of abuse gaining in popularity such as Bathsalts (street names: "Ivory Wave", "Purple Wave", "Vanilla Sky", and "Bliss") and Ecstasy (MDMA: 3,4-methylenedioxymethamphetamine) and the more familiar drugs such as marijuana, cocaine, and similar agents are the main focus of this discussion. Emphasis on the neuroimaging/neuroangiographic presentations of these cases, in correlation with their clinical manifestations on the basis of pharmacologic and toxicologic mechanisms will highlight this presentation.
Findings/Discussion
Newer recreational substances of abuse are designed to elude detection by routine UDS (urinary drug screen). The lack of awareness by the general medical community of their existence despite their rising popularity, and the similarity of angiographic features between primary CNS vasculitis and drug-induced vasculopathy/vasculitis, have contributed significantly to delayed diagnosis and treatment. Typically in our experience, an adolescent or young adult without clear or known risk factors presenting with acute hemorrhage or stroke raises the "red flag" that heralds the correct diagnosis. Awareness of this rising problem and its clinical and radiologic manifestations is important for early diagnosis and appropriate management, obviating the need for costly and sometimes invasive diagnostic procedures (i.e., brain biopsy). The distinction between secondary vasculopathy/vasculitis induced by recreational drugs and illicit substances versus primary central nervous system (CNS) vasculitides is important. Drug-induced vasculopathy is managed conservatively by identifying and removing the offending agent. While calcium channel blockers and angioplasty have been utilized to treat selected patients exhibiting rapid clinical deterioration, no established therapy exists. In contrast, primary CNS vasculitis is treated with immunosuppressive therapy.

Note: Scanned images are included in the proceedings. Some submitted images were reduced during editing, thereby decreasing clarity. Also, refer to the Program Planner. Proceedings Content as of 3-29-2013.

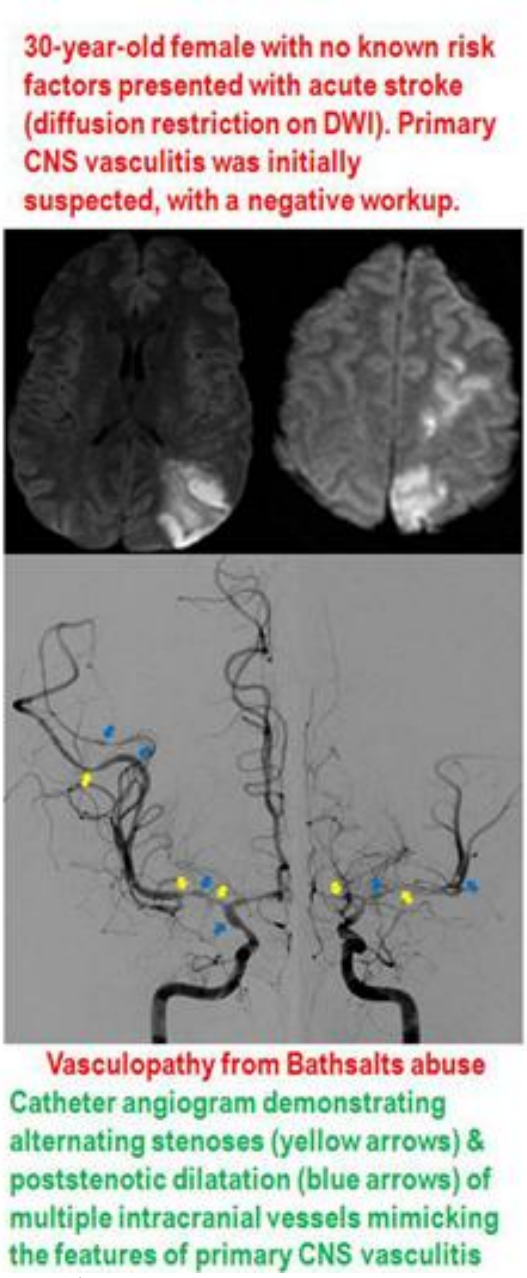

Summary/Conclusion
The cerebrovascular insults resulting from abuse of recreational substances are presented. The diagnosis of secondary vasculopathy/vasculitis must be suspected in a young patient without risk factors presenting with acute hemorrhage or stroke. Whereas angiography cannot reliably distinguish primary from secondary vasculitis/vasculopathy and because some recreational substances are undetectable on routine UDS, cognizance and prompt recognition are crucial in efficiently arriving at the correct diagnosis and timely institution of appropriate therapy.

KEYWORDS: Arteriopathy, Stroke, drug-induced vasculopathy or vasculitis

Monday, May 20 – Wednesday, May 22
6:30 AM – 9:00 PM
Thursday, May 23
6:30 AM – 3:00 PM
Hall B1

Electronic Education Exhibits (eEdE) 129 - 156a

eEdE5-Pediatrics

Note: A missing printed number indicates an abstract has been withdrawn.

eEdE-129

Brain Squids: Expanding the Imaging and Clinical Spectrum of Developmental Venous Anomalies in Children

Linscott, L.·Leach, J. L.·Jones, B. V.·Abruzzo, T.
Cincinnati Children's Hospital Medical Center
Cincinnati, OH.

Purpose
Developmental venous anomalies (DVAs) commonly are identified on imaging examinations and typically are treated as incidental findings with no significant clinical manifestations. Increasing imaging identification of DVAs has led to recognition of their association with a variety of conditions. This presentation will review the imaging spectrum of these common vascular anomalies, give multiple case examples using multimodality imaging, and review the suspected embryologic origin and pathophysiologic mechanisms of DVAs in the pediatric population.
Approach/Methods
Developmental venous anomalies were identified by searching the radiology information system using a database search engine for the terms "venous angioma" , "developmental venous anomaly", "angioma", and "venous" at a large tertiary care academic childrens hospital. Case material was obtained from identified cases for educational presentation. Imaging from MRI, SWI, MRV, CT, CTV, and angiography will be presented and correlative clinical information will be discussed. Information regarding the prevalence, distribution, and morphology of DVAs will be presented.
Findings/Discussion

Note: Scanned images are included in the proceedings. Some submitted images were reduced during editing, thereby decreasing clarity. Also, refer to the Program Planner. Proceedings Content as of 3-29-2013.

The spectrum of imaging findings associated with DVAs is more extensive than traditionally appreciated. Understanding the typical "squid-like" appearance of DVAs is important for accurate identification, and avoiding misdiagnosis. Most DVAs represent incidental variations in venous anatomy; however, they can be associated with other lesions and conditions. Restriction of flow through the collecting vein by thrombosis or stenosis may give rise to parenchymal injury. Identification of DVAs in planned surgical trajectories is of critical importance, as disruption may lead to significant parenchymal sequelae. Multiple case examples will be presented with emphasis on typical and atypical imaging appearances, associated parenchymal manifestations, as well as known associations with cavernous malformations, migrational anomalies, AVMs, and fistulas. The relationship of DVAs to head and neck venous malformations and important neurocutaneous syndromes will be presented.
Summary/Conclusion
Although most DVAs are incidental findings, a wide range of other brain lesions and conditions may be related to these vascular anomalies. Although imaging manifestations of DVAs are well known, a wide spectrum of sizes and drainage patterns are encountered, that should be understood when interpreting imaging exams.

KEYWORDS: , developmental venous anomaly

eEdE-130

Imaging Spectrum of Venous-Related Cerebral Injury in Children

Linscott, L.·Leach, J. L.·Abruzzo, T.
Cincinnati Children's Hospital Medical Center
Cincinnati, OH.

Purpose
To review the developmental anatomy, pathophysiology, and imaging patterns of venous-related cerebral injury in children. Emphasis will be placed on unifying concepts to better understand the effects of venous hypertension/insufficiency in the developing child, providing the imaging professional with a conceptual framework to better understand and confidently identify imaging patterns of venous-related cerebral injury.
Approach/Methods
Case material will be identified by clinical chart review and detailed imaging review using an automated radiology/pathology database application at a large tertiary care pediatric hospital. Modalities presented will include MRI (including perfusion, spectroscopy, SWI, and DTI), CT, CTA, MRA, MRV, MR perfusion, and angiography.
Findings/Discussion
Venous-related brain injury is a common form of cerebrovascular injury in children. The developmental and acquired causes of venous-related cerebral injury comprise a diverse, heterogeneous group of diagnoses. Examples include: germinal matrix hemorrhage in preterm neonates, periventricular hemorrhagic infarction, cerebral angiomatosis (Sturge-Weber syndrome), acute and chronic cerebral venous thrombosis, and congenital and acquired venous and arteriovenous malformations and fistulas. Despite the heterogeneity of these diagnoses, injury to the brain occurs along common pathways of venous hypertension/insufficiency, ischemia, and hemorrhage.
Summary/Conclusion
Venous-related injury to the developing brain is found in a heterogeneous group of cerebrovascular disorders. An improved understanding of common pathophysiologic pathways provides the imaging professional with a conceptual framework to correctly identify imaging patterns of venous-related brain injury, direct appropriate therapy, and avoid diagnostic pitfalls.

KEYWORDS: Venous obstruction, Venous malformations

eEdE-131

Pediatric Stroke: An Interactive Tutorial

Djoukhadar, I. A.·Macmullen-Price, J.·Warren, D. J.
Leeds Radiology Academy
Leeds, UNITED KINGDOM.

Purpose
We aim to review the imaging strategies and findings encountered in pediatric stroke. Ultimately the objective of this educational electronic exhibit is to enhance residents' confidence in making accurate and early diagnosis during oncall commitments.
Approach/Methods
The exhibit format will include case-based review of various pediatric strokes.
Findings/Discussion
Stroke in the pediatric population is relatively infrequent and the diagnosis often is delayed and occasionally missed. Early stroke diagnosis and treatment is essential in improving long-term functional outcome and preventing recurrence. We present a comprehensive review with a selected mix of cases, the imaging features of different stroke subtypes including arterial thrombosis, vasculitis, sinovenous thrombosis and hemorrhagic causes. Emphasis will be placed on the imaging features that allow early and accurate diagnosis. Some imaging mimics and potential pitfalls also will be highlighted. An interactive self-assessment exam will be presented at the end of the exhibit.

Note: Scanned images are included in the proceedings. Some submitted images were reduced during editing, thereby decreasing clarity. Also, refer to the Program Planner. Proceedings Content as of 3-29-2013.

Summary/Conclusion

In demonstrating the different stroke imaging features and in the common diagnostic pitfalls, this exhibit will enhance the residents' understanding and confidence in making accurate diagnosis. After reviewing this electronic exhibit, the learner will be able to test their understanding through an interactive self-assessment.

KEYWORDS: Pediatric stroke

eEdE-132

Review of Normal and Abnormal Intracranial Processes Leading to Various T2 and FLAIR White Matter Signal Alterations in the Pediatric Brain

Meesa, I.·Ibrahim, M.·Mukherji, S.
University of Michigan
Ann Arbor, MI.

Purpose

The purpose of this exhibit is to review the various physiologic and nonphysiologic processes that lead to T2 and FLAIR MRI signal alterations in the pediatric brain and how the radiologist can use clinical information (age, clinical history, and labs) along with various imaging sequences such as diffusion and imaging such as proton MR spectroscopy to distinguish one process from the other.

Approach/Methods

We will perform a retrospective review of the MRIs in infants and young children performed at our institution over the last 10 years with the following findings: normal myelination, abnormal myelination, inflammatory (ADEM), and infectious (encephalitis) conditions and determine how we used age, clinical data, and imaging to come to the right diagnosis.

Findings/Discussion

Both normal physiologic myelination and abnormal pathophysiology can lead to signal alterations. For example, in infants and young children, the deep cerebral white matter shows a triphasic sequence of white matter signal change. Additionally, because the temporal lobes are nearly the last to undergo myelination, the more peripheral white matter can remain hyperintense on FLAIR images beyond 24 months of age. Attention to age is important. Pathophysiologic mechanisms affecting myelin can lead to white matter abnormalities. Three main pathophysiologic mechanisms that would affect myelination are: hypomyelination, demyelination, and rarefaction. Because these processes often result in similar MR white matter findings, we will illustrate how proton MR spectroscopy can be used to help differentiate one process from the other. Additionally, inflammatory processes such as ADEM and infectious processes such as encephalitis also can lead to abnormal T2 and FLAIR signal.

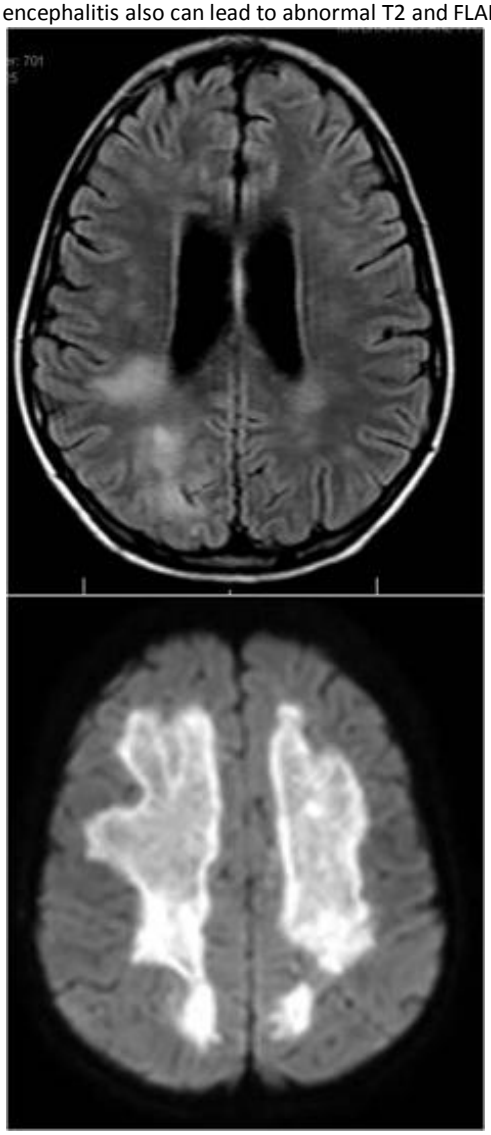

Summary/Conclusion

In conclusion, by using all available data [age, underlying medical conditions, clinical history (physical exam and labs)] and additional imaging sequences such as FLAIR, diffusion, and proton MR spectroscopy the radiologist will be able to arrive at an appropriate diagnosis.

KEYWORDS: Demyelination, Acute disseminated encephalomyelitis, encephalopathy

Note: Scanned images are included in the proceedings. Some submitted images were reduced during editing, thereby decreasing clarity. Also, refer to the Program Planner. Proceedings Content as of 3-29-2013.

eEdE-133

Congenital Brain and Spine Anomalies: Detection with Fetal MR Imaging and Postnatal Correlation

Supakul, N.·Kralik, S. F.·Ho, C. Y.
Indiana University School of Medicine
Indianapolis, IN.

Purpose
To demonstrate the spectrum of congenital malformations of the central nervous system (CNS) detected from fetal magnetic resonance imaging (MRI) and to correlate with postnatal imaging.
Approach/Methods
From our computerized radiology system (2008-2012), patients who had an abnormal obstetrics ultrasound (US) with MRI follow-up imaging were identified (n = 160). The fetal MRI study was reviewed for recognizable CNS pathology and correlated with postnatal imaging studies (n = 65) including US, computed tomography (CT) or MRI.
Findings/Discussion
We will demonstrate several cases of congenital pathologies of the brain and spine detected from fetal MRI with postnatal imaging correlation. These include neural tube closure defects [Chiari malformation (n = 11), encephalocele (n = 4), and myelomeningocele without Chiari (n = 5)], disorders of diverticulation [holoprosencephaly (n = 2) and corpus callosum anomalies (n = 4)], neuronal migration and sulcation abnormalities [schizencephaly (n = 2)], posterior fossa malformations [Dandy-Walker malformation (n=6)], and congenital tumors and vascular lesions [epignathus (n = 1), venolymphatic malformation (n = 2), sinus thrombosis (n=2)]. The imaging techniques, commonly missed diagnoses and key findings will be discussed.
Summary/Conclusion
Fetal MRI is a useful imaging modality, providing valuable clinical information not seen on US. This information will help parents make decisions during the pregnancy, and possible advanced treatment during the pre and postnatal period. Familiarity with fetal MRI imaging and diagnosable CNS pathology can improve accuracy and patient care.

KEYWORDS: Fetal MR imaging, Congenital brain malformations, congenital spine malformations

eEdE-134

Congenital Dermal Sinus Imaging: A Ten-Year Institutional Review of Pediatric Spinal MR Imaging

Cagley, J. R.·Figi, A. R.·Selden, N. R.·Pollock, J. M.
Oregon Health and Science University
Portland, OR.

Purpose
Dermal sinus tracts have a variety of imaging appearances ranging from the clinically and radiographically obvious to the occult. In this imaging-based review, we will present the common imaging features and diagnostic pearls regarding MRI evaluation of dermal sinus tracts.
Approach/Methods
A 10-year retrospective search of the radiologic information system was utilized to identify reports with mention of a dermal sinus tract on all MRI spine reports in a pediatric population at our institution. The results of this search were reviewed by the radiology staff. Dermal sinus tracts were classified on type, location, and associated imaging features.
Findings/Discussion
Seven hundred exams were searched yielding 614 instances of keywords associated with dermal sinus tracts. The 700 cases were reviewed by the authors yielding 25 positive cases. Twenty-two cases were observed in the lumbar spine, two cases were in the thoracic spine, and one case was in the sacrum. Common associations included dermoid or lipomas, diastematomyelia, and cord tethering. Most dermal sinus tracts were identified in the subcutaneous tissues on T1 and T2 sagittal imaging. The dura in most cases demonstrated a small notch at the point of communication between the dermal sinus tract and the thecal sac. The most pathognomonic cases will be presented here highlighting the imaging features and diagnostic pearls.
Summary/Conclusion
Dermal sinus tracts are an important entity in the pediatric population as delay in diagnosis may result in increased morbidity. In this educational exhibit, we have reviewed the common imaging features and diagnostic pearls identified from a retrospective search. Awareness of these imaging features and pearls may allow the practicing radiologist to more confidently diagnose these entities and associated pathologic features.

KEYWORDS: Congenital anomalies, Pediatric spine, dermal sinus

eEdE-135

Imaging Review of Congenital Inner Ear Anomalies

Singh, A. K.[1]·Bathla, G.[2]·Sato, Y.[2]·Tiwari, R.[3]
[1]University of Texas Health Science Center, San Antonio, TX, [2]University of Iowa Hospitals and Clinics, Iowa City, IA, [3]Bhopal Medical Center, Bhopal, INDIA.

Purpose
The purpose of this exhibit is to review the imaging findings of congenital inner ear anomalies in an interactive format.
Approach/Methods
We retrospectively reviewed the cases of congenital inner ear anomalies and their representative images were used for this exhibit.
Findings/Discussion
The etiology of profound sensorineural hearing loss in children is multifactorial with congenital inner ear anomalies being an important category which can be

Note: Scanned images are included in the proceedings. Some submitted images were reduced during editing, thereby decreasing clarity. Also, refer to the Program Planner. Proceedings Content as of 3-29-2013.

diagnosed by imaging. The cochleovestibular anomalies are classified in order of decreasing severity: labyrinthine aplasia, cochlear aplasia, common cavity deformities, cystic cochleovestibular malformations (IP-1), cochleovestibular hypoplasia, and incomplete partition type 2 (IP-2). Other inner abnormalities are associated with abnormal development of semicircular canal, cochlear nerve, vestibular aqueduct and internal auditory canal. The imaging appearance of these entities is reviewed in an interactive format with subsequent discussion. The figure shows cystic appearance of right cochlea and vestibule with partition in between consistent with incomplete partition type 1 anomaly.

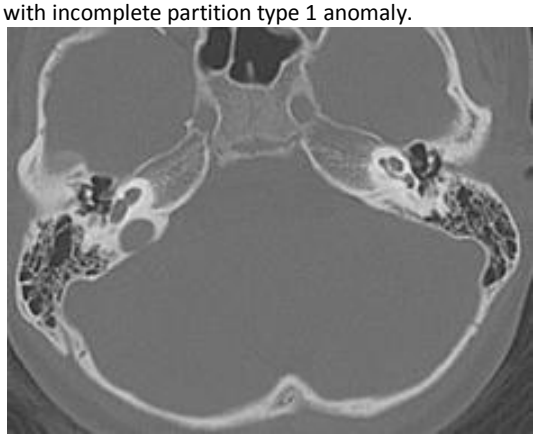

Summary/Conclusion
Congenital inner anomalies are an important cause of sensorineural hearing loss. Recognizing these anomalies on imaging is helpful in the management. Our goal is to review the imaging appearance of these anomalies in an interactive format.

KEYWORDS: Cochleovestibular malformations, Sensorineural hearing loss

eEdE-136

Cerebral Palsy

Izbudak, I.[1]·Poretti, A.[1]·Huisman, T. A. G.[1]·Lequin, M. H.[2]
[1]Johns Hopkins University, Baltimore, MD, [2]Sophia Children's Hospital, Erasmus, NETHERLANDS.

Purpose
Cerebral palsy (CP) is the most common physical disability in childhood and about 2-3 of every 1000 live born children in the Western world are affected. Although it is a clinical diagnosis neuroimaging plays an important role to identify the etiology and pathogenesis, to differentiate from mimickers, to predict the neuromotor and cognitive outcome, and to evaluate response to neuroprotective treatments. Our goal in this review is 1. to demonstrate conventional MRI and advanced neuroimaging findings in cerebral palsy; 2. to present the role of early neuroimaging to predict cerebral palsy.
Approach/Methods
We will present a wide spectrum of conventional brain MRI findings in children with cerebral palsy; emphasizing the relation between MRI pattern of lesions and different clinical phenotypes. We also will present brain MRI findings of CP mimickers. The advanced MR imaging techniques in recent decade [e.g., diffusion-weighted imaging (DWI), diffusion tensor imaging (DTI), magnetic resonance spectroscopy (MRS), susceptibility-weighted imaging (SWI), volumetric MRI, functional MRI (fMRI), resting state fMRI] have significantly improved our understanding of CP at microstructural level. We will present examples of these advanced neuroimaging results in children with cerebral palsy. Lastly we will emphasize the value of neuroimaging (fetal ultrasound and MRI) during fetal, neonatal and infantile period in predicting neuromotor outcome when there is suspicion of brain injury/malformation in early life.
Findings/Conclusion
Neuroimaging is not necessarily required for diagnosis of cerebral palsy because the disorder is based on clinical findings. The principal contribution of neuroimaging is to the understanding of etiology and pathogenesis, that may have implications for genetic counseling.
Summary/Conclusion
Earlier diagnosis of CP may be possible with implementation of early neuroimaging biomarkers that might allow early treatment interventions in the near future.

KEYWORDS: Cerebral palsy, Imaging biomarker, structural and functional neuroimaging

eEdE-137

Craniofacial Syndromes and Congenital Midface Anomalies: What the Radiologist and Clinician Need to Know Regarding Midfacial Anomalies and Other Associated Conditions

Gul, M.[1]·Chaudhry, A. A.[2]·Dunkin, J.[2]
[1]Winthrop University Hospital, Mineola, NY, [2]Stony Brook University Medical Center, Stony Brook, NY.

Purpose
1. Review of embryology, clinical findings, imaging features with histopathology correlation of congenital midface anomalies. 2. Enumerate the more common types of craniofacial syndromes with emphasis on their characteristic radiologic features and differential diagnostic considerations.
Approach/Methods
1. Review midfacial embryogenesis, normal development of anatomical structures and review factors that lead to abnormal development. 2. Identify imaging findings and review of treatments and prognosis of various nasal cavity/nasofrontal anamolies, craniofacial syndromes and congenital midline masses. 3. Case-based discussion of mimics resulting from infection, inflammation, injury and/or malignancy that may mask and/or mimic congenital anomalies will be discussed.

Note: Scanned images are included in the proceedings. Some submitted images were reduced during editing, thereby decreasing clarity. Also, refer to the Program Planner. Proceedings Content as of 3-29-2013.

Findings/Discussion
1. Detailed pictorial discussion (cartoon and/or radiographic demonstration) of craniofacial embryogenesis highlighting key embryologic and anatomical locations with emphasis of factors that lead to abnormal development. 2. Identify and describe radiographic, ultrasound, CT and/or MR imaging findings followed by discussion of treatments and prognosis of the following entities: a. Nasal cavity/nasofrontal anamolies: pyriform aperture stenosis, choanal atresia, nasolacrimal duct anomalies (nasolacrimal duct stenosis). b. Craniofacial syndromes: Crouzon syndrome, Treacher Collins syndrome, Pierre Robin syndrome, Apert syndrome, Cornelia de Lange syndrome, Hay Wells syndrome, Axenfeld syndrome. c. Congenital midline masses: Dermoid, epidermoid, nasal glioma, encephaloceles, chordoma. 3. Clinical findings, key imaging findings, histopathology, treatment and prognoses of the following will be discussed: a. Lymphoma, b. Metastases, c. Abscess, d. Tuberculosis, e. Hemangiopericytoma, f. Malignant fibrous histiocytoma, g. Fibrous dysplasia, h. Chloroma.
Summary/Conclusion
1. Congenital mid-facial anomalies are a common entity that requires early recognition and intervention. In order to provide an early diagnosis and appropriate therapy radiologists and clinicians must have a good understanding of mid-facial embryogenesis and normal development of anatomical structures. 2. By the conclusion of this presentation, the radiologist should have a better understanding of various clinical presentations of congenital mid-facial anomalies and relevant imaging findings. 3. Although numerous craniofacial syndromes exist, differential diagnosis can be narrowed utilizing age, clinical features, and imaging characteristics (e.g., lesion location, enhancement pattern, necrosis, etc).

KEYWORDS: Craniofacial findings, Pediatric head and neck, midline anomalies

eEdE-138

Functional Neuroimaging of Patients with Post Hemispherotomy Pre- and Post-Intensive Gait Therapy

Salamon, N.·Debode, S.·Bookheimer, S.
University of California Los Angeles
Los Angeles, CA.

Purpose
Many patients with intractable epilepsy underwent hemispherotomy for seizure control, plasticity and reorganization of the motor control may develop after surgery. We studied motor and gait functions pre- and post-body weight support treadmill (BWST) training, and correlate changes from training using functional MRI (fMRI) cortical activation from voluntary knee movements. Our goals are to exploit functional plasticity in the developing human brain by determining if age at injury/surgery, related to specific pathologies, predicts baseline motor/gait functions and response to BWST training.
Approach/Methods
Diffusion tensor imaging (DTI): An axial 2D EPI based diffusion-weighted sequence (Siemens Allegra 3.0T TE/TR 129/6000ms, FOV 240 x 240 mm, matrix 128 x 128 interpolated to 256 x 256, slice thickness 2 mm, number of slices 70) will be acquired with diffusion gradients along 32 noncollinear directions at two b values of 600 sec/mm2 and 1200 sec/mm2. fMRI: functional MRI analysis will be obtained using motor sensory testing using knee movement. Control and 5 posthemispherectomy patients had received BWST training and pre and postfMRI was performed. Data analyses were made using a statistical program (Stat View SAS Institute, Cary,NC). Differences between control and hemispherectomy patients were compared using t test and repeated-measured analysis of variance. Comparisons using nominal variables were performed using chi-square tests. Results were considered at a minimal level of significance of P<.05.
Findings/Discussion
For hemispherectomy patients, the increase in activation of the voxel was obtained in ipsilateral paretic and contralateral nonparetic movements (p<.02) after BWST. For control subjects, there was decrease in activity in the voxels after BWST. Attached image demonstrates pre and postBWST fMRI result of the right hemispherectomy patient with left foot movement activation.

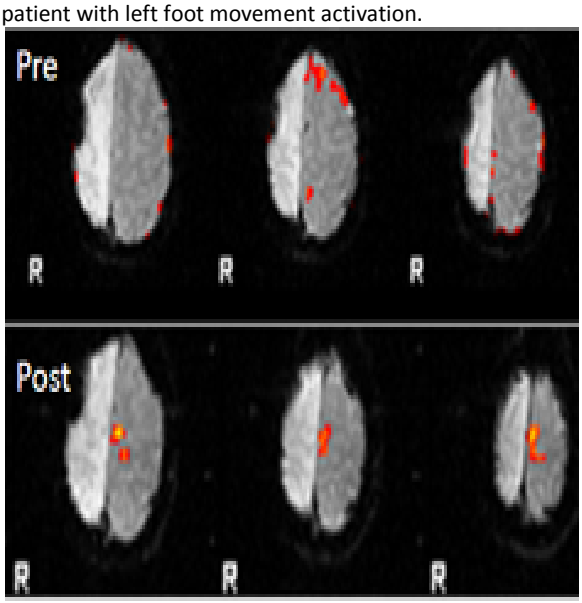

Summary/Conclusion
Locomotor therapy such as BWST can improve motor connectivity in hemispherectomy patients. Further study is needed to optimize motor functions of the residual corticospinal pathway and long term follow-up assessment with fMRI will be helpful in future research.

KEYWORDS: Hemimegalencephaly, Motor development, fMRI

Note: Scanned images are included in the proceedings. Some submitted images were reduced during editing, thereby decreasing clarity. Also, refer to the Program Planner. Proceedings Content as of 3-29-2013.

eEdE-139

Acute Ischemic Infarct in Neonates: The 3 Tesla MR Imaging Experience

Thompson, A. F.·Wang, Y. Y.
University of Wisconsin
Madison, WI.

Purpose
The purpose of this study is to share our initial findings of 3T MR imaging (MRI) studies performed on neonates presenting acutely with brain ischemia to a university-affiliated community hospital.
Approach/Methods
A brief outline of the known benefits and drawbacks of 3T MRI in neonates will be presented, as will the specific aspects of our 3T MRI neonatal brain protocol. Additional background information on the typical MRI findings of both acute ischemic infarct and hypoxic-ischemic injury in neonates also will be described briefly. We then have a selection of 26 3T MRI studies performed an average of two days from initial presentation on neonates with acute onset symptoms of infarct, most often including seizure, apnea, or focal neurologic deficit. The neonates were an average of six days old at the time of the first diagnostic 3T MRI study, and a variety of pathologies are exemplified on imaging, including acute unifocal and multifocal ischemic arterial infarcts, acute venous infarct, old prenatal infarct, acute hypoxic-ischemic insult, and germinal matrix hemorrhage.
Findings/Discussion
It is well known that the increased field strength of a 3T MR scanner causes a two-fold increase in the signal-to-noise ratio (SNR) when applied clinically. At our institution, it also decreases the scanning time for a given study by one third when compared to 1.5T MRI. While most patient populations ultimately can benefit from these key basic features of 3T MRI, the advantage to neonates is particularly significant. Our 26 cases demonstrate these benefits. Specifically, the higher resolution on standard MR sequences allows for better definition of both the neonatal neuroanatomy and any associated pathology. Higher resolution of apparent diffusion coefficient (ADC) maps may be more sensitive to penumbra and therefore to key prognostic findings such as pre-Wallerian degeneration in settings of stroke. Higher resolution susceptibility-weighted imaging (SWI) may be more sensitive to hemorrage. Ultimately, the increased resolution of the study as a whole may allow earlier disease detection. Furthermore, faster scan times reduce the need for sedation and the likelihood of motion artefact when compared to standard 1.5T MR imaging. At our institution we do not require sedation for a full 3T MRI study that includes pre and postcontrast sequences and even MR spectroscopy in some cases. It therefore bypasses all risk factors associated with anesthesia, unlike with our previous 1.5T MRI studies.
Summary/Conclusion
The increased magnetic field strength of a 3T MRI enables acquisition of higher resolution sequences in one-third of the time needed at 1.5T. In neonates, this has considerable potential, as exemplified in our cases, for disease detection as early as, or possibly earlier than, with 1.5T. Furthermore, even if disease is not detected earlier, the shortened scan times of 3T MRI allow for complete bypass of sedation, making it a safer, lower risk study than that performed with sedation at 1.5T. Because of this, quick brain studies are no longer needed at our institution, as 3T MRI scans can be performed instead.

KEYWORDS: 3T, Neonatal MR imaging, brain ischemia

eEdE-140

3T MR Imaging of Pre-Wallerian Degeneration in Neonates Presenting with Acute Infarct

Thompson, A. F.·Wang, Y. Y.
University of Wisconsin
Madison, WI.

Purpose
Pre-Wallerian degeneration (PWD) is a critical finding on brain MR imaging (MRI) in patients presenting with infarct, as it has significant, life-long prognostic implications. This case-based study highlights the benefits of using 3T MRI to detect PWD in neonates presenting with acute ischemic infarct.
Approach/Methods
Pre-Wallerian degeneration first will be defined, its typical imaging features in neonates described, and its impact on prognostication discussed. From the initiation of neonatal 3T MRI at the community hospital affiliated with our institution in February until December 2012, approximately 46 patients under the age of 28 days were scanned, 26 of whom had MRI findings consistent with acute ischemic brain injury, and 15 cases which showed extensive ischemia. The 26 patients were an average age of 6 days at the time of the MRI scan, and MRI was performed an average of 2 days after presentation. Of these 26 patients, 12 showed pre-Wallerian degeneration on MRI. Each of these 12 cases also were included in the 15 patients who presented with extensive ischemic infarct. These cases will be presented, including the commonalities and differences in their clinical presentations, their varied initial clinical courses, and their key imaging findings.
Findings/Discussion
3T MRI has the benefit of increased signal-to-noise ratio (SNR), which is particularly relevant to the imaging of neonatal neuroanatomy and neuropathology. The resulting high resolution of the 3T field is manifested on all MR sequences, including those most important to the diagnosis of infarct and PWD, diffusion-weighted imaging (DWI) and apparent diffusion coefficient (ADC) maps. 3T MRI has the added benefit of shortened scan times, so much so that our institution requires no sedation of

Note: Scanned images are included in the proceedings. Some submitted images were reduced during editing, thereby decreasing clarity. Also, refer to the Program Planner. Proceedings Content as of 3-29-2013.

neonates undergoing 3T MRI exams. Pre-Wallerian degeneration carries a poor neurodevelopmental prognosis, and as such its detection may alter clinical treatment, such as change in the type of rehabilitation used or earlier implementation of experimental therapies. Twenty-six neonates presented with ischemic infarct, 15 of whom had extensive ischemic infarct, and of these, 12 patients were found to have PWD. This suggests a high detection rate of PWD by 3T MRI in patients with extensive ischemic infarct. Current literature suggests a sensitivity of 83% for discovery of PWD in neonates presenting with acute arterial infarct scanned with a 1.5T MRI (Kirton et al.). The 3T MRI has the added benefit, however, of not requiring sedation, therefore making it a lower risk procedure than 1.5T MRI.

Summary/Conclusion

Discovering PWD on MR imaging is a key factor in determining the prognosis of infants presenting with ischemic infarct. Though 1.5T MRI has been shown to be effective in detecting PWD, its longer acquisition time predisposes the study to motion artifact, necessitating neonatal sedation for the study. Our experience shows that MR imaging at 3T is similarly effective in detecting the critical result of neonatal PWD in patients presenting with extensive ischemic infarct, while not using any sedation. Therefore, in an effort to minimize the risk to neonates undergoing MR imaging, we favor the use of 3T MRI when available.

KEYWORDS: 3T, Wallerian degeneration

eEdE-141

Leukemia in the Central Nervous System: Imaging of the Disease and the Collateral Damage

Bathla, G.·Policeni, B.·Sato, Y.
University of Iowa Hospitals and Clinics
Iowa City, IA.

Purpose

1) To briefly discuss the various early and late complications that may be encountered in patients with acute leukemia, both at presentation and as a result of therapy. 2) To review the imaging spectrum and classic neuroimaging appearances that may be seen, either as a consequence of the primary disease or secondary to the effects of treatment.

Approach/Methods

1) The exhibit aims to review the pertinent imaging findings in the central nervous system (CNS) through a brief yet concise review of the existing literature. 2) This is accompanied by a comprehensive review of the imaging manifestations of both the disease as well as the treatment complications that may be encountered.

Findings/Discussion

Leukemia is the most common malignancy in the pediatric population. Prior to the introduction of chemotherapy, CNS complications of leukemia rarely were encountered since the disease had an aggressive course and was almost uniformly fatal. Advance in medical care, including introduction of aggressive chemotherapy regimens have reduced significantly the associated mortality. However, the incidence of CNS complications has increased, both as a consequence of the longer survival and secondary to the aggressive chemoradiation. Neuroimaging findings in these patients can be subdivided as those secondary to the leukemia itself and those that occur as a result of therapy. The former include parenchymal hemorrhage, chloromas, meningeal and orbital disease. The latter can be further classified as those secondary to chemotherapy, radiotherapy and those resulting from immunosuppression. These include cerebrovascular complications, white matter disease, posterior reversible encephalopathy, microvascular angiopathy, parenchymal atrophy, vascular malformations and atypical infections. Finally, these patients also have a higher incidence of developing a second malignancy which may include a glioma, meningioma or sarcoma.

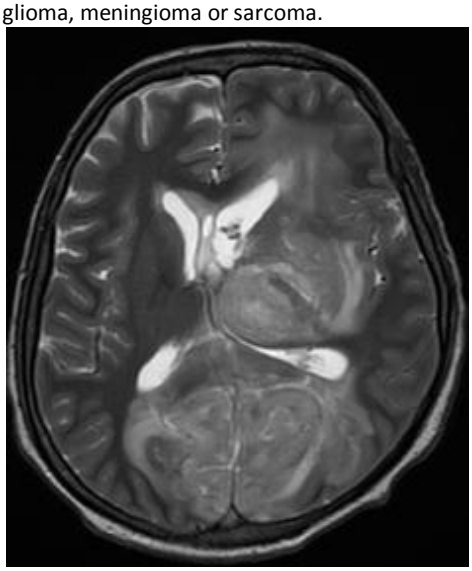

Summary/Conclusion

Advances in leukemia treatment have been accompanied by a higher incidence of CNS complications. Imaging not only plays a key role in diagnosis, but often affects management in select cases. Through this exhibit, we present a concise, but comprehensive, review of different CNS pathologies which may be encountered in leukemic patients.

KEYWORDS: Leukemia, Radiation effects, chemotherapy

Note: Scanned images are included in the proceedings. Some submitted images were reduced during editing, thereby decreasing clarity. Also, refer to the Program Planner. Proceedings Content as of 3-29-2013.

eEdE-142

Brain and Leukemia: The Common, the Rare and the Unexpected

Alsharief, A. N. A.·Batawi, A. A. A.·Adas, R.·Almehdar, A.
King Abdul-Aziz Medical City
Jeddah, SAUDI ARABIA.

Purpose
To present the imaging features of the broad spectrum of intracranial pathologies in leukemic patients as identified on both computed tomography (CT) and MR imaging (MRI).
Approach/Methods
We retrospectively reviewed the brain imaging studies of pediatric and adult leukemic patients in our institution performed from January 2012 to present to document and review the different intracranial pathologies in these patients.
Findings/Discussion
Leukemia is the most common childhood malignancy, accounting for one third of all new malignancies. Although these patients initially can present with neurologic symptoms, intracranial involvement can be discovered before clinical symptoms become evident. Generally, Intracranial findings in leukemia can be classified into two major categories; pathologies related to the primary disease, such as chloroma and leukemic cell infiltration; and findings related to complications of the disease and/or medication, including hemorrhage, thrombosis, secondary infections and drug toxicity. Some of these complications appear early in the course of the disease as posterior reversible encephalopathy syndrome and methotrexate-induced neurotoxicity, while other complications can appear later. It is crucial to inquire about the nature and onset of symptoms, the type and duration of chemotherapy and the immune status. Good history and thorough knowledge of this wide range of pathologies is the radiologist's key to reaching the proper imaging diagnosis and therefore aid hematologists and oncologists in optimizing their patient's care.
Summary/Conclusion
Early identification and correct diagnosis of intracranial abnormalities associated with leukemia are crucial for daily practice of radiologists, particularly those working in hematology and oncology centers. This is because the general overall long-term disease-free survival rate of leukemia is around 80% and many related intracranial complications are treatable.

KEYWORDS: Leukemia, Brain, intracranial, CT, MR imaging

eEdE-143

MR Imaging of Pediatric Pineal Gland Lesions

Gross Kelly, T. C.[1]·Cakmakci Midia, E.[2]·Guleria, S.[3]·Firat, S.[2]·Jogal, S.[2]·Maheshwari, M.[2]·Segall, H. D.[2]
[1]Children's Hospital of Wisconsin, Milwaukee, WI, [2]Children's Hospital of Wisconsin/Medical College of Wisconsin, Milwaukee, WI, [3]University of Alabama, Tuscaloosa, AL.

Purpose
The purpose of this educational exhibit is to provide a systematic diagnostic approach for the evaluation of pediatric pineal gland lesions. There are a wide range of lesions that may be seen in the pineal region. In order to facilitate diagnostic evaluation of pineal region masses, they can be grouped into 4 categories: (1) germ cell tumors (2) pineal parenchymal neoplasms, (3) neoplasms arising from adjacent tissues and (4) nonneoplastic masses.
Approach/Methods
In this exhibit we will review: (1) embryology, histology and anatomy of the developing pediatric pineal gland as well as (2) MR imaging (MRI) features of neoplastic and nonneoplastic lesions within and around the pineal gland.
Findings/Discussion
The MR appearance of pediatric pineal gland lesions such as pineal gland cysts, germ cell tumors, pineocytoma, teratoma, anlage tumors, papillary tumors and others will be reviewed. MR imaging features that can help differentiate neoplastic from non-neoplastic tumors will be highlighted.

Summary/Conclusion
Our goal is to provide a succinct review of the MRI appearance of neoplastic and non-neoplastic pineal gland lesions in order to facilitate detection and diagnosis of pineal gland abnormalities in the pediatric patient. We will achieve this goal by reviewing normal MR anatomy of the pineal gland followed by examples of lesions that can arise within or around the pineal gland.

Note: Scanned images are included in the proceedings. Some submitted images were reduced during editing, thereby decreasing clarity. Also, refer to the Program Planner. Proceedings Content as of 3-29-2013.

KEYWORDS: Pineal gland, Pediatric brain tumors, MR imaging

eEdE-144

Atypical Teratoid Rhabdoid Tumors: Review of Imaging Features

Mazumder, A. A.[1,2]·Adams, A.[1]·Paine, S. M. L.[3,1]·Jacques, T. S.[3,1]·Mankad, K.[1]
[1]Great Ormond Street Hospital for Children NHS Foundation Trust, London, UNITED KINGDOM, [2]The National Hospital for Neurology and Neurosurgery, London, UNITED KINGDOM, [3]Birth Defects Research Centre, UCL Institute of Child Health, London, UNITED KINGDOM, [4]Great Ormond Street Hospital for Children NHS Foundation Trust, London, UNITED KINGDOM.

Purpose
Pediatric atypical teratoid rhabdoid tumor (ATRT) of the brain is an aggressive and rare tumor. There are various imaging findings that assist with differentiating these from other tumors, for example medulloblastomas and choroid plexus papillomas. The pathologic characteristics of the tumor closely resemble those of the renal rhabdoid tumor of infancy. Cytomorphologic appearances of this tumor include hypercellularity with tissue fragments; large, round, and pleomorphic “plasmacytoid” cells; and “rhabdoid” cells with brightly eosinophilic cytoplasm; large, eccentrically placed nuclei; and single, prominent nucleoli with or without fibrillary globoid inclusion. The clinical outcomes from ATRT often are poor and thus recognizing, and differentiating these tumors on imaging is important to help guide treatment, as aggressive management may help alter the course of this tumor. The purpose of this study is to review the imaging findings of patients with ATRT of the brain, through the review of imaging of a local case series, describe common and subtle features based upon our review.
Approach/Methods
The various imaging features of ATRT tumors are reviewed and presented. A retrospective review of a case series with descriptions of various pertinent appearances of an ATRT tumor will be presented.
Findings/Discussion
The imaging findings of ATRT are varied, and differentiating them from other more common or less aggressive lesions can be problematic. However early recognition is important as it can help guide towards aggressive clinical management.
Summary/Conclusion
Atypical teratoid rhabdoid tumors are aggressive and difficult to diagnose tumors of pediatric patients, with features similar to other lesions. Recognition of the varied and rare imaging findings can help guide early management decisions.

KEYWORDS: ATRT

eEdE-145

A Web-Based Mobile Application for Learning and Reviewing the Appearance of Pineal Gland Lesions Using a Multimodality Approach

Amin, V. B.·Chorney, E. T.·Sicular, S.·Ward, T. J.·Horn, C.·Kadoch, M. A.
Mount Sinai Medical Center
New York, NY.

Purpose
The purpose of the exhibit is: 1. To provide quick and easy access to a web-based mobile application and reference guide that addresses most of the common pineal gland lesions as evaluated by modern imaging modalities. 2. To provide a reference tool that addresses the limitations of other online reference tools, which can be cost-prohibitive, require log-ins or registration, lack interactivity, and often are slow to engage the end user. 3. To provide imaging of both the specific and nonspecific imaging features of a given pineal gland lesion. 4. To provide a novel learning platform that is fully functional using either the internet alone or on most major handheld devices and tablets, which are becoming increasingly important as educational resources for fellows, trainees, and students.
Approach/Methods
All pineal gland lesions encountered at our institution since 2001 were reviewed for potential inclusion in the exhibit.
Findings/Discussion
The major teaching points of this exhibit are: 1. Reviewing the diagnostic as well as nonspecific imaging findings of multiple pineal gland lesions on modern imaging modalities. 2. Encouraging each user to expand on this review by linking each pathology to important AJNR articles that further discuss that specific pathology. 3. Measuring the success of this electronic educational exhibit by monitoring number of online views and traffic directed towards the supplied AJNR articles.
Summary/Conclusion
A web-based mobile application for learning and reviewing the appearance of pineal gland lesions using a multimodality approach is presented.

KEYWORDS: Pineal gland, Neoplasm

eEdE-146

Imaging Review of Pediatric Head and Neck Neoplasms

Singh, A. K.[1]·Sato, Y.[2]·Sato, S.[2]·Tiwari, R.[3]
[1]University of Texas Health Science Center, San Antonio, TX, [2]University of Iowa Hospitals and Clinics, Iowa City, IA, [3]Bhopal Medical Center, Bhopal, INDIA.

Purpose
The purpose of this exhibit is to review the imaging appearance of pediatric head and neck neoplasms,

Note: Scanned images are included in the proceedings. Some submitted images were reduced during editing, thereby decreasing clarity. Also, refer to the Program Planner. Proceedings Content as of 3-29-2013.

including in utero imaging.
Approach/Methods
We retrospectively reviewed the cases of pediatric and fetal head and neck neoplasms at our institution. The representative cases were selected and their images were used for this exhibit.
Findings/Discussion
Most of the head and neck lesions in the pediatric age group are of benign etiology like inflammatory and congenital lesions. Neoplasms are uncommon with only 5% of pediatric cancers arising in the head and neck region. These lesions are discussed with emphasis on the unique imaging features. Some of the examples are hemangioma, metastases, rhabdomyosarcoma, teratoma, juvenile angiofibroma, etc. Imaging not only helps in diagnosing these neoplasms but may help deciding the care of the patients. In the evaluation of fetal neck masses, MR is an important imaging tool which helps not only in the diagnosis but it also can evaluate the fetal airway compression which is essential in planning for EXIT (ex utero intrapartum treatment). Figure shows a large enhancing lesion in the left masticator space which proved to be a rhabdomyosarcoma.

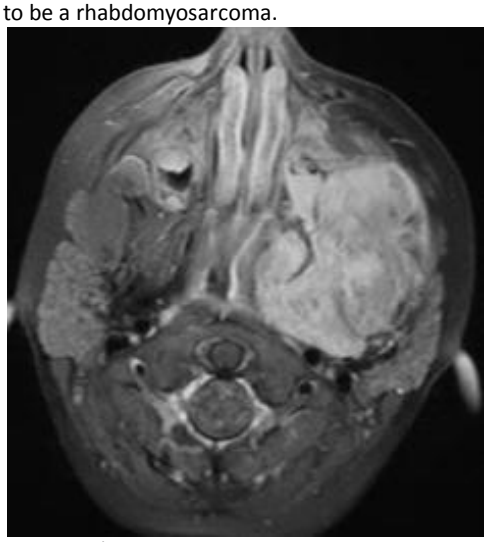

Summary/Conclusion
Imaging plays a key role in the diagnosis of head and neck neoplasms in pediatric age group and during intrauterine life. It is essential to be familiar with the characteristic imaging appearance of these lesions which is the goal of this exhibit.

KEYWORDS: Rhabdomyosarcoma, Hemangioma

eEdE-147

Common and Uncommon Pediatric Temporal Bone Lesions: Case-Based Teaching File

Patel, R.[1,2]·Jacob, R.[1,2]·Booth, T.[1,2]
[1]Children's Medical Center, Dallas, TX, [2]University of Texas Southwestern Medical School, Dallas, TX.

Purpose
Temporal bone lesions in pediatric population can be commonly secondary to infection (mastoiditis) and Langerhans cell histiocytosis. Uncommon lesions like cholesteatoma, metastatic neuroblastoma and rhabdomyosarcoma are occasionally encountered. Rare lesions include benign lesions like aneurysmal bone cyst, melanotic progonoma, arteriovenous malformation and malignant lesions like osteosarcoma, Ewing's sarcoma and lymphoma. This electronic presentation outlines the following: 1. Review the clinical presentations of temporal bone lesions. 2. Review the imaging features of common and uncommon temporal bone lesions in children.
Approach/Methods
A retrospective search of PACS was performed on studies performed at the Children's Medical Center, Dallas for the last 10 years. Imaging studies depicting lesions in the temporal bone were identified. All studies were de-identified, prior to image export.
Findings/Discussion
Over 10 representative cases of the different temporal bone lesions including but not limited to Langerhans cell histiocytosis, cholesteatoma, mastoiditis, rhabdomyosarcoma, metastatic neuroblastoma, lymphoma, osteosarcoma, Ewing's sarcoma, aneurysmal bone cyst, melanotic progonoma were selected for inclusion.
Summary/Conclusion
Familiarity with the imaging features of temporal bone lesions helps formulate a reasonable differential diagnosis. The knowledge of uncommon lesions will help in broadening the differential and ensuring they are considered while formulating a diagnosis.

KEYWORDS: Pediatric neoplasms, Temporal bone

eEdE-148

Pediatric Sellar and Suprasellar Pathology: A Tour Beyond "SATCHMOE"

Parekh, N. D.[1,2]·Chang, J.[1]·Ryan, M.[2]
[1]Northwestern Memorial Hospital, Chicago, IL, [2]Ann and Robert H Lurie Children's Hospital of Chicago, Chicago, IL.

Purpose
Sellar/suprasellar abnormalities often are encountered in the pediatric population, but the spectrum of disease and implications for treatment and management differ significantly from the adult population. The purpose of this educational exhibit is to discuss an approach to imaging

Note: Scanned images are included in the proceedings. Some submitted images were reduced during editing, thereby decreasing clarity. Also, refer to the Program Planner. Proceedings Content as of 3-29-2013.

this region in children, illustrate the normal development and anatomy, and review pathology present in the pediatric population, emphasizing the salient and differentiating imaging features.
Approach/Methods
1. Normal anatomy, embryology and development of the pituitary gland. 2. Diagnostic algorithm and optimization of computed tomography (CT) and MR imaging (MRI) techniques for imaging the sellar/suprasellar region. 3. Comprehensive review of the pediatric suprasellar/sellar pathology.
Findings/Discussion
Abnormalities of the sellar and suprasellar region can arise from many structures including the pituitary gland, infundibulum, hypothalamus, optic chiasm, or parasellar structures. Congenital abnormalities in this region are a particular concern in the pediatric population; pituitary hypoplasia or an ectopic posterior pituitary are rarely a consideration in the adult population, but can be critical for the appropriate growth and development of a child or adolescent. Empty sellas, though a common incidental finding in adults, are uncommon in children and may reflect intracranial hypertension. Additionally, some malformations - duplication of the stalk or absence of the optic chiasm - can be important indicators of more extensive midline abnormalities. Pediatric suprasellar lesions are predominantly neoplastic; although non-neoplastic, inflammatory, infectious and, rarely, demyelinating lesions also occur. Entities that are frequent concerns in adults, such as aneurysms, metastases or meningiomas, are rare in children; but other lesions such as craniopharyngiomas, germ cell tumors or Langerhans cell histiocytosis should be of greater consideration. Assessing the presence of the posterior pituitary bright spot also is important in assessing suprasellar and stalk lesions, and this can be optimized with specific imaging techniques, such as high resolution fat saturated T1 sequences to suppress any adjacent marrow fat. Intrasellar lesions such pituitary cysts or adenomas occur in children as in adults. However, in addition to special imaging techniques - dynamic contrast-enhanced imaging to unmask small lesions - knowledge of the vascularity in this region is important. Hypophyseal veins, rarely appreciated by imaging in adults, commonly are visualized in children and can be a source of false positives. Pituitary macroadenomas are rare in pediatrics, and often clinically evident, but their imaging appearance can be challenging in this population, especially since other cystic and solid lesions are more common.
Summary/Conclusion
A variety of lesions affect the sella and suprasellar region in the pediatric population. The frequency of disease differs significantly between adults and children. Metastases, aneurysms and other lesions commonly encountered in adults are typically only distant considerations in children, and thus popular adult mnemonics such as “SATCHMOE” should not be extrapolated to the pediatric population without consideration for the different prevalence of these lesions. Knowledge of the common pediatric lesions and their imaging appearance is important in generating meaningful and relevant diagnoses. Additionally, understanding the anatomy, embryology and differences in childhood disease also can help optimize the imaging technique in order to avoid pitfalls.

KEYWORDS: Pituitary gland, Pediatric brain

eEdE-149

Brain Destruction: Are Porencephaly, Cystic Encephalomalacia, Leucoencephalomalacia, Gliosis Synonyms?

Davila-Acosta, J. H.[1]·Miller, E.[1]·Hassan, D.[1]·Beltran-Marin, M.[2]
[1]Children Hospital of Eastern Ontario, Ottawa, ON, CANADA, [2]Erasme University Hospital, Brussels, BELGIUM.

Purpose
In neuroradiologic literature, there is a vicious use of terms that refer to differing patterns of brain damage or destruction. These differ largely in the pediatric and adult population with superimposed definition of the terms. This exhibit intends to: 1. Describe the pathophysiology of the different patterns of brain destruction at different ages and their long term result. 2. Provide a systematic definition of the patterns of brain destruction using pathology and imaging correlation. 3. Describe the relationship of the patterns of brain destruction with their causes and age of damage.
Approach/Methods
Depending on the etiology of an injury, age of occurrence of the event, severity and extension of the injury; different patterns of brain damage and destruction can affect the brain. We intend to review the pathologic definitions and findings of the main patterns of brain destruction and correlate with their imaging findings including porencephaly, hydrancephaly, cystic encephalomalacia, encephalomalacia, leucoencephalomalacia, gliosis, and others. The exhibit will present relevant information about the process of brain maturation including the differentiation and maturation of neuroblasts and oligodendrocites that play a key role in understanding brain injuries.
Findings/Discussion
Definitions of terms used to describe patterns of brain destruction are different among pathologists and radiologists. Through our review we will combine findings of pathology and imaging to clarify different entities and try to related the findings to causes, time of injury and outcome. The brain maturation process involves morphologic and brain composition changes. Morphologic changes include a decrease in the size of extraaxial and ventricular spaces and an increase in brain volume. Brain composition changes include changes in cellular density, increase in complex lipids content (myelination process),

Note: Scanned images are included in the proceedings. Some submitted images were reduced during editing, thereby decreasing clarity. Also, refer to the Program Planner. Proceedings Content as of 3-29-2013.

decrease in free fluid white matter water content, developing white matter and cortical fiber network and neurotransmitters, and neurotransmitters-receptors interactions. One of the most important events that occurs during brain maturation is given by the immature oligodendrocytes which are actively reproducing and forming myelin. This has a poor reparative function in younger ages. These changes can explain why similar brain pathology can have varying characteristics at different ages and the differences observed in brain disease in neonates, infants and older children. Examples of the different characteristic pattern of brain disease can be seen in ischemic process, metabolic disease, cortical development malformations, infectious process, tumors and genetic disorders.

Summary/Conclusion

Understanding the brain maturation process can help to recognize the different patterns in brain destruction and brain damage. This information can help to recognize causes and etiology of injury.

KEYWORDS: Brain abnormalities, Brain maturation, encephalomalacia

eEdE-150

MR Imaging Evaluation of Head, Neck and Spine Masses in the Fetus

Mignone Philpott, C.[1]·Shannon, P.[2]·Chitayat, D.[2]·Ryan, G.[2]·Blaser, S.[1]
[1]Hospital for Sick Children, Toronto, ON, CANADA, [2]Mt Sinai Hospital, Toronto, ON, CANADA.

Purpose

MR imaging is increasingly utilized to further evaluate cranial, neck and spine masses in the fetus. Our purpose is to illustrate the common tumors and tumor mimicks and their distinguishing imaging features, using conventional and advanced MR imaging (MRI) techniques and describe pertinent features to aid clinical management.

Approach/Methods

All fetal MRI cases of head, neck and spine masses performed in our institution were reviewed, in conjunction with follow-up postnatal imaging and pathologic correlation. Note was made of working diagnoses prior to and post MRI, and correlation made with final pathology diagnosis. We have reviewed other similar case series and case reports of fetal head, neck and spine masses, particularly those with pathologic correlation.

Findings/Discussion

The most common masses of the spine are sacrococcygeal teratomas and in the neck, lymphatic malformations. Soft tissue sarcomas comprise the majority of malignant neck neoplasms. Heterotopic and benign cystic lesions are the most common intracranial masses, with malignancies, such as medulloblastoma, more rare. The distinction of potentially malignant from benign entities appears to be aided by use of diffusion-weighted imaging. We demonstrate the key imaging characteristics of these tumors and their mimics: including heterotopia and infarctions. Heterogeneity of the tumor (i.e., hemorrhage and calcified components) appear well illustrated on conventional and susceptibility-weighted techniques and such features aid differential diagnosis. There was a high correlation with the final pathology diagnosis in all our cases. MR imaging also provides good anatomical definition of the tumor, key to planning ex utero intrapartum treatment (EXIT) procedures.

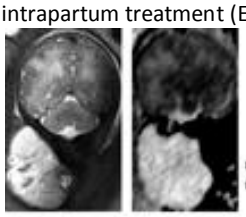

Coronal T2, coronal DWI sequences: Cervical lymphatic malformation

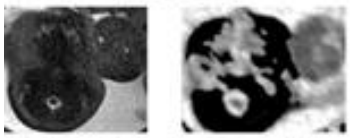

Coronal T2, coronal DWI sequences: Facial myofibroma

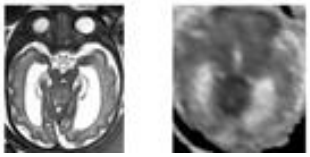

Axial T2, DW sequences: Medullonastoma

Summary/Conclusion

MR imaging is an essential tool for further evaluation of fetal head/neck and spinal masses, including defining their anatomical relationship with surrounding structures and distinguishing intracranial tumors from benign or destructive pathology. We illustrate examples of commonly encountered entities and key imaging points for lesion characterization and diagnosis, paramount in antenatal management and counselling.

KEYWORDS: Fetal MR imaging, Masses, head, neck, spine

eEdE-151

Disorders of the Cranial Nerves in Pediatrics

Vossough, A.·Dahmoush, H. M.
Children's Hospital of Philadelphia
Philadelphia, PA.

Purpose

Disorders of the cranial nerves often are seen in pediatric neuroradiology. While there are some common etiologies of cranial nerve dysfunction among children and adults, many disorders typically are seen only in children or are diagnosed during childhood. Clinical manifestations referable to cranial nerves often are encountered in children. Magnetic resonance (MR) imaging of cranial nerve pathologic conditions is challenging because of the relatively small size of most nerves. Demonstrating subtle abnormalities of these small neural structures requires tailored studies focusing on the specific nerve(s) that need evaluation. This ultimately results in earlier and more

Note: Scanned images are included in the proceedings. Some submitted images were reduced during editing, thereby decreasing clarity. Also, refer to the Program Planner. Proceedings Content as of 3-29-2013.

accurate diagnoses improving patient care. This educational exhibit will provide an illustrated review of a variety of cranial nerve conditions which predominantly present in the pediatric age group.
Approach/Methods
First, we will review briefly the various classes of thin-section high-resolution MR imaging techniques that will allow adequate visualization and evaluation of the cranial nerves in children. We then will review the various etiologies that are either uniquely or more commonly seen in children with cranial nerve dysfunction, using a systematic approach to each individual cranial nerve. Finally, we will discuss various disorders that often cause multiple cranial nerve disorders in children.
Findings/Discussion
Magnetic resonance imaging of pediatric cranial nerve pathologic conditions is challenging due to the relatively small size of most nerves. Demonstrating subtle abnormalities of these small neural structures requires tailored studies focusing on the specific nerve(s) that need evaluation. The use of focused high-resolution exams especially with use of higher field systems allows such assessment to be made in many instances. Various spin-echo and balanced gradient-echo techniques are available for optimal visualization of the cranial nerves in children. There are numerous etiologies of pediatric cranial nerve abnormalities. Congenital abnormalities specific to individual cranial nerves, including absence or hypoplasia of the nerve, either in isolation or as part of genetic or syndromic conditions commonly are seen in children. There can be involvement of the cranial nerves by demyelinating, inflammatory, metabolic, degenerative, or infectious processes that commonly affect children. Many cranial nerve-related masses also classically present in the pediatric population. Vascular variants and anomalies resulting in cranial nerve dysfunction can be seen in children. Various metabolic and multisystem disorders can involve multiple cranial nerves in children.
Summary/Conclusion
Disorders and abnormalities of the cranial nerves which commonly or exclusively present in the pediatric population will be demonstrated in this educational exhibit. This will include congenital, demyelinating, inflammatory, metabolic, degenerative, infectious, neoplastic, and vascular lesions. Tailored studies directed by the clinical presentation are important in delineation of the symptomatic cranial nerve and familiarity with such abnormalities can provide an important role in the overall management of these children.

KEYWORDS: Cranial nerves, Cranial nerve pathology

eEdE-152

Fetal MR Imaging: A Valuable Tool in Evaluation of Fetal Brain Pathology

Yazbek, S.[1]·Allmendinger, A.[2]·Grant, P. E.[1]
[1]Boston Children's Hospital, Harvard Medical School, Boston, MA, [2]Brigham and Women's Hospital, Harvard Medical School, Boston, MA.

Purpose
Obstetrical ultrasound remains the primary screening technique for the fetal central nervous system (CNS). However, over the last two decades, MRI has proven to be an extremely useful adjunctive tool in evaluating the developing brain.
We will describe the advantages of fetal MRI by exposing the findings of different CNS abnormalities on fetal MRI and on obstetrical ultrasound.
Approach/Methods
Abnormal fetal brain MRIs that were performed in our institution over a two-year period (2010-2012) were reviewed. The studies were performed on a 1.5T magnet and included multiplanar SSFSE T2, FIESTA, T1, T2* and diffusion-weighted images. We start by discussing the safety of MRI in pregnancy, its limitations and the different sequences and new techniques developed in fetal MRI. We then describe the different CNS pathologies encountered on fetal MRI and compare, in each case, the anomalies delineated on the MRI to the pathology demonstrated on an obstetrical ultrasound done the same day. We also compare the findings of the fetal MRI to the findings of a postnatal brain MRI when this is available.
Findings/Discussion
With respect to potential teratogenicity, the majority of reports suggest that MR is safe in the fetus. Fetal MRI is preferably performed after the first trimester, after organogenesis has occurred. MR imaging usually is performed on 1.5T scanners with ultrafast MR imaging techniques to reduce the likelihood of fetal movement during acquisition. MR imaging provides excellent image contrast by exploring multiple tissue properties such as T1 and T2. MR imaging also provides an assessment of diffusion changes, and can show changes over time in various metabolites in the brain through the use of MR spectroscopy. Diffusion tensor imaging and fMRI have been performed successfully in late gestation pregnancies when the fetal head is engaged in the maternal pelvis and relatively immobile. Fetal MRI permits prenatal evaluation of multiple CNS abnormalities. Examples of pathology illustrated include ventriculomegaly, aqueductal stenosis, interhemispheric cysts, posterior fossa abnormalities, corpus callosum abnormalities, cortical malformations, intracranial hemorrhages, infarctions, tuberous sclerosis, aicardi syndrome, piriform aperture stenosis, hemimegalencephaly, vascular malformations, chiari malformations as well as head and neck anomalies including cleft lip and palate. Fetal MRI allowed a better delineation of brain abnormality demonstrated on an

Note: Scanned images are included in the proceedings. Some submitted images were reduced during editing, thereby decreasing clarity. Also, refer to the Program Planner. Proceedings Content as of 3-29-2013.

obstetrical ultrasound done the same day and, sometimes, allowed finding additional anomalies. These anomalies were confirmed on the postnatal MRI, which also provided further evaluation and extra information.
Summary/Conclusion
This review illustrates the important value of MRI in the evaluation of fetal brain abnormalities and its significant role in prenatal counseling. Technical advances in MRI will further improve the evaluation of fetal brain. However, since fetal MRI usually is performed when an abnormality is suspected on the ultrasound or in case of prior abnormal pregnancy, a large number of “real” normal control fetal MRIs is not available. This is why, early diagnosis of some subtle brain abnormalities remains challenging.

KEYWORDS: Fetal MR imaging, Ultrasonography, brain

eEdE-153

Double Trouble. . . Occam's Razor Does Not ALWAYS Cut It!"

Mirsky, D. M.[1]·Bello, J. A.[2]
[1]Children's Hospital Colorado, Aurora, CO, [2]Montefiore Medical Center, Bronx, NY.

Purpose
Beyond the scope of "incidental findings", more than one finding may be apparent on a neuroimaging study. When two or more such findings are made, they may be viewed as being clinically significant or insignificant. Our goal is to present cases with dual distinct pathology that may be related and how to approach such cases in order to provide appropriate recommendations for followup.
Approach/Methods
Cases of dual (or more) pathology were collected from inpatient and outpatient imaging sources in both pediatric and adult populations. The cases were researched for clinical relevance of the multiple findings and recommended followup. In each case the findings were categorized according to their significance and relationship. The dual pathology was further categorized as: - distinct, but related (NF with optic glioma and "white spots"). - distinct and unrelated (glioblastoma and AVM). - distinct and possibly related (meningioma and white matter signal . . uncommon edema, venous congestion).
Findings/Discussion
A spectrum of distinct pathologies encountered on a single imaging study are reviewed. Various subtleties are presented and discussed in the context of their clinical significance and providing useful follow-up recommendations.
Summary/Conclusion
It is not uncommon for more than one finding to be discovered on a neuroimaging study. The difficulty that arises is trying to determine whether the findings are related and clinically significant or insignificant. The true challenge arises when one is faced with dual pathologies that are unrelated or not obviously related and how to handle such cases. At a time when imaging and reporting efficiency are paramount to streamlining healthcare, we present several examples of such cases, with recommendations for appropriate followup.

KEYWORDS: Incidental findings

eEdE-154

Imaging Spectrum of Encephalopathy in Children

Singh, A. K.[1]·Bathla, G.[2]·Sato, Y.[2]·Tiwari, R.[3]
[1]University of Texas Health Science Center, San Antonio, TX, [2]University of Iowa Hospitals and Clinics, Iowa City, IA, [3]Bhopal Medical Center, Bhopal, INDIA.

Purpose
The purpose of this exhibit is to review the imaging spectrum of encephalopathy in children.
Approach/Methods
We retrospectively reviewed the cases of encephalopathy in children with different etiologies and their representative images were used for this exhibit.
Findings/Discussion
Pediatric encephalopathy is an uncommon condition but it is associated with significant morbidity and mortality. There are different causes of encephalopathy in children which can be grouped into multiple categories like infections, toxic, metabolic, hypoxia, seizure, tumors, etc. These entities with their imaging features are discussed in this exhibit. Some of the examples are hypoglycemic encephalopathy, hypoxic-ischemic encephalopathy, kernicterus, MELAS, metastatic disease, herpes encephalitis, etc. Early diagnosis in these conditions is extremely important for proper management. Figure shows diffuse high FLAIR signal in the bilateral white matter in a patient diagnosed with methotrexate induced leukoencephalopathy.

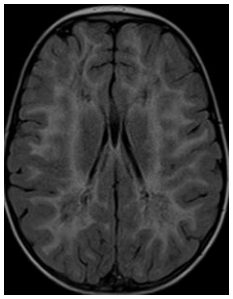

Summary/Conclusion
Imaging plays a key role in the management of pediatric encephalopathy and the radiologist may be the first one to suggest accurate diagnosis. It is essential to be familiar with the imaging appearance of different causes of pediatric encephalopathy which is the goal of this exhibit.

KEYWORDS: Encephalopathy

Note: Scanned images are included in the proceedings. Some submitted images were reduced during editing, thereby decreasing clarity. Also, refer to the Program Planner. Proceedings Content as of 3-29-2013.

eEdE-155

Common and Uncommon Imaging Manifestations of Langerhans Cell Histiocytosis in Children

Shifrin, A.[1]·Nabavizadeh, S. A.[2]·Feygin, T.[2]·Pollock, A. N.[2]·Vossough, A.[2]·Zimmerman, R. A.[2]
[1]Mount Auburn Hospital, Cambridge, MA, [2]The Children's Hospital of Philadelphia, Philadelphia, PA.

Purpose
To illustrate the spectrum of common and uncommon imaging manifestations of Langerhans cell histiocytosis (LCH) in children.
Approach/Methods
At our institution, imaging of suspected LCH in the brain, head, neck, and spine is performed either on MRI or CT and, in select cases, on US. MR imaging is performed using 1.5 or 3.0T magnets. Our protocols include T1- and T2-weighted, postcontrast thin sections through the region of interest in orthogonal planes, as well as diffusion-weighted imaging.
Findings/Discussion
The spectrum of common and uncommon imaging findings in multiple patients with LCH lesions will be illustrated. A wide variety of lesion locations includes the brain, head, skull base, neck, and spine. Special attention will be given to imaging techniques, including diffusion-weighted imaging, and the pathophysiology of LCH lesions. Additionally, several imaging findings not previously established as characteristic of LCH, including presence of restricted diffusion and fluid-fluid levels, will be described.
Summary/Conclusion
Langerhans cell histiocytosis can present with variable clinical and imaging manifestations, and familiarity with different patterns of this entity is necessary for timely and accurate diagnosis.

KEYWORDS: Langherans cell histiocytosis, Pediatric brain

eEdE-156

Neuroimaging in Tuberous Sclerosis Complex: Highlighting Changes in Cerebellar Tubers

Banker, P.·Rodrigues, D.·Salamon, N.
University of California Los Angeles
Los Angeles, CA.

Purpose
To describe cases of tuberous sclerosis complex (TSC) with cerebellar lesions that experienced changes in signal and morphology over time, including development of neovascularization, suggesting an alternate pathogenesis of cerebellar tubers that differs from the natural course of cerebral tubers.
Approach/Methods
A retrospective review of MR imaging (MRI) from 61 pediatric and young adult patients with TSC found 15 patients with cerebellar lesions (24.6%). Followup was obtained in 13 of the 15 patients (86.7%), mean age of 6.7 years at initial imaging and 14.3 years to final imaging. During a mean follow-up period of 7.6 years, an average of 7.1 MRI studies were performed. Four of the 13 patients had bilateral cerebellar tubers, accounting for a total of 17 lesions. Of the 17 total cerebellar tubers in the 13 patients, six underwent change over time (35.3%, 46.2% respectively). Amongst the six tubers that changed over time, the majority showed neovascularization, calcification, enhancement, T2/FLAIR hyperintensity, and focal parenchymal atrophy with time. One cerebellar tuber ultimately hemorrhaged after developing a prominent adjacent cortical vessel.
Findings/Discussion
Tuberous sclerosis complex is an inherited systemic disease with prominent CNS, cutaneous, and visceral manifestations. Cerebellar tubers have been described in 24%-28% of cases. While Vaughn et al have described these tubers to change with time, the development of adjacent vascularity and propensity for bleeding has not been reported. The majority of the cerebellar tubers that were followed up underwent neovascularization, calcification, and focal cerebellar atrophy. Neovascularization was seen in 11/17 (64.7%), calcification in 10/17 (58.8%), parenchymal atrophy in 17/17 (100%), enhancement in 7/17 (41.2%), and high T2/FLAIR signal in 14/17 (82.4%) of the cerebellar tubers. Hemorrhage within a cerebellar tuber was observed in one patient, described below. MR imaging of the brain in one particular patient at the time of presentation demonstrated at least 25 cerebral tubers, bilateral subependymal nodules, and a right cerebellar tuber. His right cerebellar tuber initially showed T1 hypointensity, T2/FLAIR hyperintensity, enhancement, but no calcification or prominent cortical vessels. Over time, this lesion developed a new cortical vessel, adjacent focal parenchymal atrophy, and calcification. This lesion ultimately hemorrhaged on his final follow-up MRI.
Summary/Conclusion
Tuberous sclerosis complex is a unique neurophakomatosis with diverse manifestations. We describe specific progressive changes in cerebellar lesions in TSC and propose that these changes may have prognostic importance, especially in the setting of neovascularization and hemorrhage. Unlike the cerebral tubers, which tend to remain stable, the morphologic evolution of cerebellar tubers suggests that an alternate pathogenesis may play a role in the development of these lesions.

KEYWORDS: Tuberous sclerosis, Cerebellum, epilepsy

Note: Scanned images are included in the proceedings. Some submitted images were reduced during editing, thereby decreasing clarity. Also, refer to the Program Planner. Proceedings Content as of 3-29-2013.

eEdE-156a

Pediatric Leukodystrophies: Utilizing Diffusion-Weighted Imaging and MR Spectroscopy to Refine the Conceptual Approach

Allmendinger, A.[1]·Viswanadhan, N.[1]·Yazbek, S.[2]·Prahbu, S.[2]
[1]Brigham and Women's Hospital, Harvard Medical School, Boston, MA, [2]Boston Children's Hospital, Harvard Medical School, Boston, MA.

Purpose
Pediatric leukodystrophies are complex group of diseases that result from abnormal primary myelination or secondary myelin/neuronal degeneration. MR imaging is now the modality of choice for detecting these white matter disorders; however, findings may be nonspecific with the use of conventional MR sequences. We will provide a systematic clinical-radiologic conceptual approach to pediatric leukodystrophies, and present cases of specific disorders with specific patterns of abnormality. In addition, we will elaborate the use of MR spectroscopy and diffusion-weighted imaging in the diagnostic algorithm, along with key clinical features that aid in making a more specific diagnosis, or at least narrow the differential diagnoses.
Approach/Methods
Imaging studies obtained for pediatric patients with proven pediatric white matter disease from our tertiary care institution over an eight-year period (2004 -2012). MR images were obtained on both 1.5 and 3T magnets (majority on 3T). We illustrate the diagnostic workup with emphasis on the utility of diffusion-weighted imaging and MR spectroscopy. We describe important imaging features of each disease narrowing the differential diagnosis of this complex group of diseases, which guides the radiologist and clinicians in planning the most appropriate workup and tailor laboratory tests, ultimately reducing overall costs and ensuring more prompt diagnosis.
Findings/Discussion
Use of a conceptual approach in conjunction with the clinical features can help narrow the differential diagnosis in these patients. In this clinical-radiologic approach, we divide the disorders into groups based on the relative degree of involvement of the gray and white matter, exact distribution of the abnormality, age of onset, head size, nature of lesions, organ and skeletal involvement, neurologic features and degree of temporal progression. MR spectroscopy and DWI data is merged with the structural and clinical characteristics to help refine the diagnosis pathway. Examples of grouped disorders include leukodystrophies presenting with macrocephaly, gray matter involvement with and without visceral storage, predominant white matter involvement, combined gray and white matter involvement, neonatal disorders mimicking gray matter degeneration (subdivided into epileptic syndromes, metabolic disorders and other deficiencies). Specific diagnostic patterns are seen in patients with metachromatic leukodystrophy, globoid cell leukodystrophy, Saposin B deficiency, Canavan disease, Alexander disease, Sulfite Oxidase deficiency, Leigh syndrome, glutaric aciduria Type-1, hydroxyl-glutaric aciduria, Pelizaeus-Merzbacher disease and mitochondrial encephalopathy, lactic acidosis, with stroke-like episodes (MELAS), hypomyelination with basal ganglia atrophy, LBSL, megalencephalic leukoencephalopathy with cysts, pyruvate carboxylase deficiency, fucosidosis, X-Linked adrenoleukodystrophy and maple syrup urine disease (MSUD). We emphasize utility of diffusion-weighted imaging and MR spectroscopy in diagnosing some of these conditions. We also highlight potential pitfalls in the diagnosis of these disorders, challenges in classifying more rare disorders and mention possible solutions for future research.
Summary/Conclusion
This review illustrates the value of the combined clinical and radiologic approach to pediatric leukodystrophies. We highlight specific MRI patterns of numerous common and unusual white matter diseases and provide a structured algorithm to aid in narrowing the differential, and in some cases, make an accurate, initial diagnosis. We show how judicious use of MR spectroscopy and diffusion-weighted imaging can help refine the diagnostic algorithm.

KEYWORDS: Leukodystrophy, DTI tractography

Monday, May 20 – Wednesday, May 22
6:30 AM – 9:00 PM
Thursday, May 23
6:30 AM – 3:00 PM
Hall B1

Electronic Education Exhibits (eEdE) 157 - 161

eEdE6-Socioeconomics

Note: A missing printed number indicates an abstract has been withdrawn.

Note: Scanned images are included in the proceedings. Some submitted images were reduced during editing, thereby decreasing clarity. Also, refer to the Program Planner. Proceedings Content as of 3-29-2013.

eEdE-157

NeuroRads.org: Integrating ASNR Resources with the ABR Core Exam of the Future

Kadoch, M. A.·Rydzinski, Y.·Horn, C.·Sicular, S.·Ward, T. J.·Cohen, M. G.
Mount Sinai Medical Center
New York, NY.

Purpose
The purpose of the exhibit is to present an educational resource to aid radiology residents preparing for the new ABR core exam. ASNR resources (AJNR, Neurographics, Case of the Week, etc.) are an invaluable resource for young trainees who may not yet be aware of their utility for board exam preparation. NeuroRads.org will integrate these resources with the specific neuroradiology expectations of the new ABR core exam as outlined in the official ABR core exam study guide. In addition, several web-based mobile applications will provide the user with opportunities to review the major imaging features of the most commonly tested entities.
Approach/Methods
All ASNR resources (AJNR, Neurographics, Case of the Week, etc.) were surveyed exhaustively for integration with the official ABR Diagnostic Radiology Core Examination Study Guide. Select cases from our institution were included in the development of web-based mobile applications.
Findings/Discussion
Neuroradiology training finds itself at a pivotal crossroads, with the ABR Core Exam of the Future expected to debut in the fall of 2014. It is critical that invaluable ASNR resources are not overlooked by young trainees who will be preparing for the new board examinations. By integrating the most relevant of these resources with the ABR's new exam expectations, the next generation of radiologists will be exposed to the outstanding educational resources available through the ASNR.
Summary/Conclusion
NeuroRads.org will integrate ASNR resources with the ABR core exam of the future to ensure that the next generation of young radiologists preparing for board examinations are exposed to the outstanding educational resources available through the ASNR.

KEYWORDS: Neuroradiology training

eEdE-158

Infinitely Variable On-the-Fly Real-Time Planar Interrogation of Volumetric CT and MR Imaging Data Sets Using Off-the-Shelf Game Controllers

Brunberg, J. A.[1]·Seibert, T.[1]·Teistler, M.[2]
[1]University of California Davis, Sacramento, CA, [2]Flensburg University of Applied Sciences, Flensburg, GERMANY.

Purpose
Currently available CT and MR imaging protocols allow for the derivation of high-resolution image data with isometric voxel dimensions. The interrogation of these 3D image data sets using fixed orthogonal planes, or single angulated planes, is, however, frequently insufficient for an optimal characterization of imaging findings. The purpose of this exhibit is to demonstrate the development of a small hand-held ultrasound-like probe that allows for on-the-fly infinitely adjustable interrogation of an MR or CT imaging data set in real time.
Approach/Methods
Software has been programmed to integrate with inexpensive computer game controllers, allowing for on-the-fly interrogation of high resolution volumetric CT or MR image data sets in a manner similar to the strategies used for a clinical ultrasound imaging procedure.
Findings/Discussion
These software and hardware adaptations allow for a more definitive observer-defined characterization of normal and abnormal structural relationships within the spine, within the head and neck, within orbits, and within the cranial vault. Regions of interest that are obscured by normal oblique relationships, by structural pathology, or by rotation or asymmetric patient positioning during CT or MR image acquisition, can be reformatted immediately and anatomically characterized. A software-enabled standard PC computer and game controllers will be available for demonstration.
Summary/Conclusion
The ability to achieve on-the-fly infinitely variable reformatted planar anatomical imaging improves the utility of volumetric CT and MR imaging data for the characterization of normal and abnormal structural findings. Versatility, low cost and clinical utility suggest that this capability should be incorporated as a routine tool that is available for diagnostic use in association with the radiologist's PACS workstation.

KEYWORDS: Informatics, Image processing

Note: Scanned images are included in the proceedings. Some submitted images were reduced during editing, thereby decreasing clarity. Also, refer to the Program Planner. Proceedings Content as of 3-29-2013.

eEdE-159

Self-Plagiarism in the American Journal of Neuroradiology versus Radiology: An Evaluation Using iThenticate

Kalnins, A. U.[1]·Chin, M.[1]·Halm, K.[2]·Castillo, M.[1]
[1]University of North Carolina at Chapel Hill, Chapel Hill, NC, [2]American Journal of Neuroradiology, Oakbrook, IL.

Purpose

Plagiarism is thought to be commonly encountered in medical journals. Multiple sporadic, similar phrases may be identified synthesizing what has been previously written and most editors accept this practice. Copying entire sections from prior manuscripts is, however, considered plagiarism. In order to evaluate similarities in academic work, programs such as iThenticate cross-reference manuscripts against databases of publications. The American Journal of Neuroradiology (AJNR) randomly uses iThenticate to evaluate 25% of published manuscripts/year for potential overlap. However, it is not clear if the program should be used to evaluate for plagiarism in all submissions. In order to review the scope of potential plagiarism, we analyzed all original research articles published in AJNR and Radiology in 2011 and randomly chose two AJNR issues from 2012 using iThenticate. Our goals were: to assess whether analyzing two randomly chosen issues from one journal provides similar information to analyzing an entire year, and to see if significant duplications are more common in a specialty journal (AJNR) or a general journal (Radiology).

Approach/Methods

All original research articles from AJNR and Radiology in 2011 were cross-referenced with those contained in the iThenticate publication database. We arbitrarily chose a 15% threshold for duplicated content and when it was exceeded, two individuals assessed the similarities and assigned them significance (sporadic phrases vs. large sections, the latter implying plagiarism). Two randomly chosen AJNR issues in 2012 (March, September) also were evaluated for similarities and differences with the statistical results obtained for the entire 2011 volume of AJNR.

Findings/Discussion

Table 1

	AJNR 2011*	AJNR Mar	AJNR Sep 2012
Number of original research articles per issue and standard deviation	27.45 (2.73)	25	27
Number of articles with >15% total overlap per issue	4.91 (1.92)	5	4
Number of articles with >15% overlap from a single source	1.09 (1.04)	3	1
Number of articles with significant overlap per issue	0.18 (0.40)	0	0

*Average number of articles per issue

Table 2

	AJNR 2011	Radiology 2011
Number of scientific research articles in 2011	302 from 11 issues, 27.5 per issue	343 from 12 issues, 28.6 per issue
Number of articles with >15% similarity	54 (17.9% of total articles)	12 (3.5% of total articles)
Number of articles with >15% similarity from a single source	12 (4.0% of total, 22.2% of articles with >15% similarity)	2 (0.6% of total, 16.7% of articles with >15% similarity)
Number of articles with significant overlap	2 (0.66% of total articles, 16.7% of articles with >15% similarity from a single source)	1 (0.29% of total articles, 50% of articles with >15% similarity from a single source)

Summary/Conclusion

Using our empiric 15% threshold, the number of articles found to have significant duplicated content was low for both AJNR and Radiology (0.66% vs. 0.29%). When the original research articles published in AJNR and Radiology in 2011 were evaluated for significant similarities, only two articles in AJNR and one in Radiology were deemed to have significant overlap with prior publications, in all instances judged as self-plagiarism. While AJNR had a greater percentage of articles demonstrating a greater than 15% overlap with prior publications when compared to Radiology, most were considered not significant. Additionally, analyzing two randomly chosen issues of AJNR yielded no significant differences in articles with >15% duplications when compared with those published during one entire year.

KEYWORDS: AJNR, Quality control, plagiarism

eEdE-160

Collaborative Web-Based Platform for the Creation of Diagnostic and Clinical Management Algorithms

Gibson, D.[1]·Bonneville, F.[2]·Belden, C.[3]·Wippold, F.[1]
[1]Mallinckrodt Institute of Radiology, St. Louis, MO, [2]Hôpital de Rangueil, Toulouse, FRANCE, [3]Dartmouth-Hitchcock Medical Center, Lebanon, NH.

Purpose

Emerging challenges for 21st century neuroradiology focus on resource utilization and decision support in an era of changing models of reimbursement, increasingly complex imaging studies and ever-expanding body of scientific literature.

Approach/Methods

Neuroradiology must adapt to these challenges and

Note: Scanned images are included in the proceedings. Some submitted images were reduced during editing, thereby decreasing clarity. Also, refer to the Program Planner. Proceedings Content as of 3-29-2013.

provide visionary leadership in the development of the content and context of objective measures of health care delivery. Towards this end, we have developed a web-based platform comprised primarily of 1) an intuitive graphical user interface allowing the creation of evidence-based clinical pathways and/or diagnostic algorithms within the context of a large scale relational database 2) network functionality for purposes of collaboration within recognized institutional or subspecialty frameworks, and 3) a filtered web and biomedical search engine facilitating rapid access to the most relevant clinical content. As an educational tool, the platform can supplement neuroradiologic training by providing searchable algorithms which may be used to generate more narrowed differential diagnoses than the traditional "gamuts" or location-based mnemonics.

Findings/Discussion

The platform also provides a means for neuroradiologists to collaborate with clinical colleagues in designing clinical pathways that guide rational usage of imaging resources, which is a high priority in accountable care reimbursement systems. With ultimate integration into electronic health record(s), diagnostic algorithms will be measured for accuracy as determined by pathologic diagnosis, thus creating the potential for data-driven probabilistic differential diagnoses in the future. Similarly, the quality of care pathways will be judged on clinical outcomes, measures of efficiency, and patient satisfaction.

Summary/Conclusion

We believe that by providing a transparent framework in which to measure the value of neuroimaging, we will preserve access to these often life-saving technologies, justify the large scale investments required for continued innovation, and more importantly provide the level of quality healthcare our patients deserve.

KEYWORDS: Quality improvement, Cost-effective, decision support

eEdE-161

CT Dose Measurement and Dose Reduction Strategies: A Primer and Self-Assessment for Neuroradiologists

Sampathu, D. M.·Mamourian, A. C.
Hospital of University of Pennsylvania
Philadelphia, PA.

Purpose

Surveys have demonstrated repeatedly that physicians have difficulty accurately predicting both the magnitude and relative radiation exposure of radiology exams. Furthermore, in spite of their training in medical physics, radiologists also have difficulty describing the radiation dose of common CT exams. As a result of the increasing utilization of CT exams, patients have become more knowledgeable and concerned about the potential for adverse effects from radiation. Given these dynamics, it is imperative that neuroradiologists become familiar with the language of radiation dose and understand the physics underlying modern multidetector scanners and new radiation dose reduction strategies.

Approach/Methods

This exhibit reviews basic terminology and definitions pertaining to radiation dose, summarizes the dose of common neuroradiologic CT exams, and explains the factors that contribute to it. Dose reduction strategies which can be introduced readily into daily practice are reviewed. A self-assessment tool is included in order to reinforce key facts and concepts; this tool has the potential to be adapted into a self-assessment module (SAM).

Findings/Discussion

The methods used to estimate CT radiation dose, including the common units of measurement such as CTDIvol and DLP are reviewed. The concepts of “absorbed dose” and “effective dose” are illustrated with images showing immediate and long-term adverse radiation effects. Typical radiation doses, expressed in mSv and DLP, associated with common neuroradiologic CT exams are summarized in a fashion to make them easy to recall. For example, a routine head has an effective dose that is less than background radiation in the USA and DLP of approximately 1000 mGy/cm. Next, the effects of varying CT scanning parameters such as kVp, mAs, pitch, and collimation on patient dose using a multidetector scanner are explained along with the rationale for adjusting these parameters based on patient attributes and desired dose limits. For example, the concepts of over-beaming and over-ranging are reviewed to explain why early single slice scanners, while now outdated, were surprisingly dose efficient. CT scanner hardware and reconstruction

Note: Scanned images are included in the proceedings. Some submitted images were reduced during editing, thereby decreasing clarity. Also, refer to the Program Planner. Proceedings Content as of 3-29-2013.

techniques, including iterative reconstruction, are reviewed with regard to their effects on patient dose and perceived image quality.
Summary/Conclusion
As both the utilization of CT exams and the broad awareness of potential adverse effects of medical radiation increase, it is essential that neuroradiologists understand both CT scanner principles and radiation physics. This exhibit provides a concise review of the terminology of dose, CT hardware and techniques, and radiation dose reduction strategies that should be of value as we all strive to create diagnostic images at the lowest possible dose.

KEYWORDS: Radiation dose reduction, Radiation exposure, CT

Monday, May 20 – Wednesday, May 22
6:30 AM – 9:00 PM
Thursday, May 23
6:30 AM – 3:00 PM
Hall B1

Electronic Education Exhibits (eEdE) 162 - 179

eEdE7-Spine

Note: A missing printed number indicates an abstract has been withdrawn.

eEdE-162

Intraspinal Masses: Don't Forget Sequestered Disk Fragment

Green, D. B.·Coopersmith, H.
North Shore University Hospital
Manhasset, NY.

Purpose
1. Review the evolution of disk herniation from bulge to sequestered fragment. 2. Illustrate the similar imaging findings of sequestered disk fragments and other spinal pathology. 3. Demonstrate the importance of recognizing a possible sequestered disk fragment.
Approach/Methods
We present a series of sequestered disk fragments from our institution and list a differential diagnosis for each case. A companion case of each item of the differential diagnosis then will be shown to highlight the differences and similarities in imaging findings.
Findings/Discussion
Sequestered disk fragments will be compared with meningioma, schwannoma, metastasis, nerve sheath tumor, epidural abscess, epidural hematoma, complex facet cyst, and scar tissue. Important features include location, morphology, signal characteristics, and presence of enhancement. Symptoms and patient history also will be considered, and potential differences in patient management will be discussed.
Summary/Conclusion
Sequestered disk fragments are rare and frequently overlooked but can mimic other spinal pathology and cause similar symptoms. Consideration of sequestered disk fragments as part of a differential diagnosis can impact patient management, surgical planning, and patient outcomes.

KEYWORDS: Disk displacement

eEdE-163

Nuclear Medicine for the Evaluation of Spine Infections: A Multimodality Review with MR Imaging and Pathologic Correlation

Sabby, T. L.·Hunt, C. H.·Diehn, F. E.
Mayo Clinic
Rochester, MN.

Purpose
The purpose of the exhibit is to: 1) Review the common nuclear medicine imaging studies used to image spine infections; 2) Correlate findings on these studies with those seen on MRI and at pathology; 3) Discuss the limitations related to nuclear medicine imaging of the spine and how to avoid potential pitfalls.
Approach/Methods
After a short review of the nuclear medicine options for imaging spine infections, a case series of patients will be presented demonstrating the utility of scintigraphy with and without SPECT/CT for the evaluation of spine infection. This series also will include cases which demonstrate the limitations of nuclear medicine, with emphasis on sources for both false negative and false positive results. All studies will be correlated with conventional imaging (CT, MRI) and pathologic findings.
Findings/Discussion
Nuclear medicine can be an effective tool when trying to problem-solve difficult spine infection cases. In addition to being available to patients who may not be able to undergo MRI, scintigraphy (especially with SPECT/CT) can help triage select patients appropriately and guide biopsies. Nevertheless, a thorough understanding of the potential pitfalls is needed in order to optimize patient management.
Summary/Conclusion
Nuclear medicine can provide significant added value to the evaluation of spine infections in select cases. The combination of scintigraphy with SPECT/CT, CT, and MRI is

Note: Scanned images are included in the proceedings. Some submitted images were reduced during editing, thereby decreasing clarity. Also, refer to the Program Planner. Proceedings Content as of 3-29-2013.

a powerful imaging tool. However, careful understanding of the limitations of scintigraphy in this setting is needed to avoid misinterpretation of findings.

KEYWORDS: Spinal imaging, Infections

eEdE-164

CT Sacroplasty for Treatment of Painful Sacral Fractures

Borowski, A. M.·Olmsted, J. E.·Thompson, P.
Providence Health Center
Waco, TX.

Purpose
Sacral insufficiency fractures (SIF) can be a source of significant low back and pelvic pain in the elderly population. Percutaneous sacroplasty is being advocated as a relatively safe and effective image-guided procedure for treatment of the pain and disability associated with these fractures. We have embraced this technique to treat our patients, and present our experience in performing these procedures with conscious sedation, utilizing CT guidance.
Approach/Methods
During the past 24 months, 15 patients were referred to our facility for treatment of painful sacral vertebral fractures. Fracture acuity was documented by clinical history, and concurrent CT or MRI studies of the sacrum. Treatment was performed by interventional radiologists, utilizing conscious sedation. These patients usually are elderly, with multiple co-morbidities, so minimal sedation was used. Typically, 25mg Benadryl (IV), and 50-100 micrograms Fentanyl (IV) were adequate. Sometimes, Versed (Midazolam), also was given (0.5-1.0 mg). Surgery was performed with the patients in prone position, under CT guidance. Polymethyl methacrylate (PMMA) bone cement was injected through either 11 or 13 gauge needles. Procedure termination points were either dense opacification of the sacral ala, extra-osseous PMMA extrusion, or migration of the bone cement into adjacent neuro-foramina. Clinical followup was performed postoperatively by the attending physician, and delayed followup was provided by our clinical nurse co-ordinator, using telephone interviews and a standardized visual analog pain scale (VAS).
Findings/Discussion
Of the 15 patients treated, 14 had documented osteoporosis. This, along with clinical history, suggested benign insufficiency as the etiology of their fractures. One patient had a known diagnosis of multiple myeloma. Average age was 74.5 (range 55-96). All 15 patients were female. The average procedure time was 50.4 minutes (range 18-86 minutes). Treatment was bilateral in 13 of the 15 patients. Only two patients had unilateral fractures augmented. Eleven patients had significant improvement within 24 hours (greater than 5 points on subjective VAS). Two patients had moderate relief after severn-day followup (3-5 points), one patient died later (unrelated to the surgery) without significant relief, and one was lost to followup. Improvement in ambulation was not assessed.

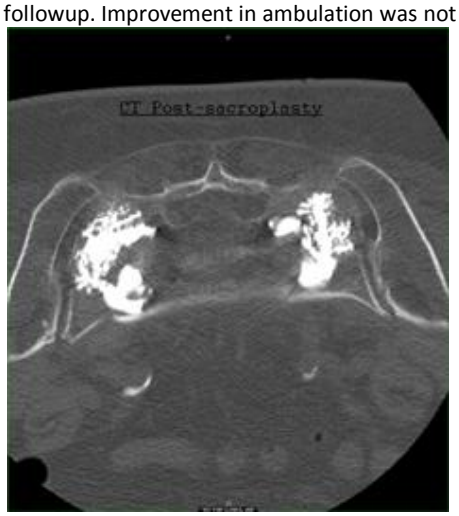

Summary/Conclusion
Percutaneous CT-guided sacroplasty seems to be an effective, time and cost-efficient means of pain reduction with the appropriate sub-set of patients. We have had very promising results over these past two years, and hope that this treatment algorithm continues to help our patients have a more productive and pain-free life-style in the future.

KEYWORDS: Sacroplasty, CT-guidance, fracture

eEdE-165

A Cross-Platform Mobile Web Application for Learning and Documenting Competency in Neuroradiology Procedures

Stein, J. M.·Mohan, S.
Hospital of the University of Pennsylvania
Philadelphia, PA.

Purpose
Learning and demonstrating competency in routine procedures is an important part of radiology training at the residency and fellowship levels. The smartphones and other mobile devices that many trainees already carry could be used to facilitate learning and rapid documentation of procedural experiences.
Approach/Methods
Using free and open source components, we developed a mobile web application to facilitate learning and documenting competency in fluoroscopy-guided lumbar puncture and myelogram procedures. The application uses the Sencha Touch JavaScript framework to mimic a native application on iPhone, Android and Blackberry smartphones as well as the Apple iPad and other tablets. It also runs on Mac and Windows desktop computers. The application presents a step-by-step guide for each procedure with illustrative figures and anatomical images as well as space for user notes. It incorporates a time-

Note: Scanned images are included in the proceedings. Some submitted images were reduced during editing, thereby decreasing clarity. Also, refer to the Program Planner. Proceedings Content as of 3-29-2013.

stamped procedure log with appropriate fields for procedure type, accession number, attending radiologist, complications, and other comments. Importantly, the application also includes evaluation forms that can be completed easily and electronically signed by the attending radiologist. The procedure log and attending assessment data may be stored locally or remotely. Finally, a summary page presents a graphical representation of procedures performed and trends and averages with respect to fluoroscopy time. This data can be made available to the program director for comparison across trainees. We are in the process of piloting the use of this application for training in our own department.
Findings/Discussion
Documenting procedural experience is necessary for radiology licensing and will be a focus of the new ACGME milestones for resident education in diagnostic radiology. Our application enables these activities to be rapidly documented at the time and location they are performed. By incorporating step-by-step reference guides, a procedure log, attending assessment and review into a single platform, the application should aid learning and help to ensure complete documentation. The application could be expanded to include additional procedures performed in neuroradiology as well as other radiology subspecialties.
Summary/Conclusion
A cross-platform application for mobile devices can be created to facilitate learning and documenting competency in neuroradiology procedures.

KEYWORDS: Lumbar puncture, Educational, mobile

eEdE-166

Dual Energy CT Imaging for the Spine

Khorrami-Arani, N.[1]·Liang, T.[2]·Shewchuk, J.[1]·Nicolaou, S.[1]
[1]Vancouver General Hospital, Vancouver, BC, CANADA,
[2]University of British Columbia, Vancouver, BC, CANADA.

Purpose
Dual-energy CT (DECT) refers to the simultaneous acquisition of low and high voltage CT data (most commonly 80 and 140 kVp), and is a technological advancement of CT for which multiple chest and abdominal imaging applications have been demonstrated previously. The purpose of this exhibit is to review the principles of DECT and review and demonstrate examples of the potential applications of DECT for imaging of the spine.
Approach/Methods
A retrospective review of patients scanned by the DECT spine protocol at our institution will be conducted for imaging examples.
Findings/Discussion
This educational exhibit will review the basic principles and technique behind DECT, and the radiation dose considerations. The exhibit also will review the potential utility of DECT for imaging of the spine. The following applications will be discussed in the exhibit: metal artifact reduction in the setting of penetrating injury or surgical instrumentation, identification and differentiation of crystal diseases such as gout and CPPD, diagnosis of spondylodiskitis, differentiation of acute fractures from old fractures by visualizing marrow edema, improved detection of abnormal epidural enhancement in the setting of infection and postoperative peridural fibrosis, and using DECT myelography to detect spinal cerebrospinal fluid (CSF) leaks. Imaging examples of each of these applications will be demonstrated. In addition, the specific advantages and limitations of these applications of DECT for imaging of the spine will be discussed.
Summary/Conclusion
Recent articles have demonstrated promising results for the application of DECT for imaging of the spine. This exhibit has demonstrated that DECT can be useful to help reduce metal artifact, identify crystal disease, rule out or confirm infection, recognize bone marrow edema, improve detection of epidural enhancement, and optimize detection of spinal CSF leaks.

KEYWORDS: Dual-energy CT, Dual energy spectral

eEdE-167

New Imaging Strategies to Detect Effects of Microgravity on the Intervertebral Disk of Astronauts

Riascos-Castaneda, R. F.[1]·Reza, H.[1]·Cotes, C.[1]·Heymann, J.[1]·Lotz, J.[2]·Hargens, A.[3]
[1]The University of Texas Medical Branch, Galveston, TX,
[2]University of California San Francisco, San Francisco, CA,
[3]University of California San Diego, San Diego, CA.

Purpose
Explain the theories behind the increased low back pain and disk degenerative changes after exposure to microgravity. Show the strategies used to reduce effects of microgravity in space. Explain how new advanced imaging techniques can aid the understanding of the disk degenerative changes and the early detection of them.
Approach/Methods
Educational Exhibit will show: 1. Back pain in space. 2. Effects of spaceflight on the spine. Risk of disk damage in space. 3. Hypothesized spinal unloading in microgravity. 4. Deficiencies of present exercise hardware for space. 5. Pre and postflight tests of crew on international space station. 6. Advanced imaging. 7. Spinal morphology with 3D imaging. 8. Measure water content with T2 mapping. 9. Intervertebral disk spectroscopy. 10. Lumbar spine compressibility tests. 11. In vivo kinematic test.
Summary/Conclusion
Exposure of the intervertebral disk to microgravity has shown to increase the risk of lumbago and disk herniations. We will show the proposed theories to explain these changes based on the microstructure of the

Note: Scanned images are included in the proceedings. Some submitted images were reduced during editing, thereby decreasing clarity. Also, refer to the Program Planner. Proceedings Content as of 3-29-2013.

intervertebral disk and the strategies that are used to research the causes and early detection of intervertebral disk changes pre and postflight in the astronaut population.

KEYWORDS: 3 T, Disk degeneration, astronaut

eEdE-168

Diffusion-Weighted Imaging of Usual and Unusual Tumor and Tumor-Like Lesions in the Spine

Smittkamp, C.·Moritani, T.·Kirby, P.·Kademian, J.
University of Iowa
Iowa City, IA.

Purpose
We address the utility of diffusion-weighted imaging (DWI) along with the corresponding apparent diffusion coefficient (ADC) maps in the evaluation of spinal lesions by assessing individual cases across a wide range of pathologies. By assessing common tumors, unusual tumors, and tumor-like lesions, we will show that diffusion-weighted imaging (DWI) can be a helpful tool in lesion detection, lesion assessment, and in distinguishing malignant from benign processes.
Approach/Methods
The DWI and ADC sequences from a total of 270 patient MRIs showing spinal lesions previously diagnosed through a combination of clinical, imaging, and pathologic findings were reviewed. The DWI images were of the spin-echo, echo-planar type with parallel imaging, and the ADC maps were calculated from b values of 0 and 1000 sec/mm2. The lesions evaluated included both primary and secondary malignant tumors as well as benign tumors and tumor-like lesions. They are comprised of lytic and sclerotic bone metastases from a variety of primary lesions (including lung, breast, prostate, glioblastoma, and clear cell meningioma), multiple myelomas, lymphomas, leukemia, osteosarcomas, chordomas, a variety of primary bone tumors (including osteoid osteoma, giant cell tumor, Langerhans histiocytosis), multiple hemangiomas (both atypical and infiltrating type), notochord rests, bone marrow edema with Schmorl's nodes, osteomyelitis with granuloma formations, bone necrosis, and traumatic bone lesions.
Findings/Discussion
Diffusion-weighted imaging often shows hyperintensity with low corresponding ADC values in various malignant bone tumors due to their hypercellularity. Benign conditions do not demonstrate the same hyperintensity. These findings can be useful in detection of a tumor as well as in differentiating malignant and benign conditions (such as typical from atypical/infiltrating hemangiomas). There were, however, some limitations to this result. First, sclerotic bone lesions, even when malignant, did not demonstrate the same DWI hyperintensity, and the ADC values were difficult to evaluate. Additionally, susceptibility artifacts such as nearby surgical devices sometimes inhibited interpretation. Finally, the calculation of ADC values were sometimes hampered due to lesional tissue containing bone or fat.
Summary/Conclusion
We show how DWI and ADC provide utility in the evaluation of the wide variety of spinal lesions. These sequences can aid in the initial detection of lesions; they can help decide the likelihood of a lesion's malignancy by demonstrating hyperintensity due to increased cellularity; and they can be especially helpful in distinguishing between malignant and benign processes that may otherwise appear similar, such as between a hemangioma and atypical/infiltrating hemangioma. We demonstrate these utilities through case examples of a variety of common tumors, unusual tumors, and tumor-like lesions in the spine.

KEYWORDS: Diffusion-weighted imaging, Spinal imaging, spinal lesions

eEdE-169

Brachial Plexus: Review of Anatomy, Imaging Protocol and Spectrum of Abnormalities

Subramanian, S.·Maheshwari, M.·Tolat, P.·Chandra, T.·Midia, E. C.·Kelly, T. G.·Segall, H.
Medical College of Wisconsin Milwaukee
Milwaukee, WI.

Purpose
Brachial plexus pathologies are relatively uncommon and diagnosis can be challenging. MR imaging is the imaging modality of choice for evaluating the brachial plexus for potential pathology. The purpose of this exhibit is to provide a fascile review of brachial plexus MRI anatomy, protocols and pathology.
Approach/Methods
In this educational exhibit, we will review the normal brachial plexus anatomy with MR image correlation, review MRI protocols for evaluation of brachial plexus, and discuss the different brachial plexus pathologies seen in pediatric and adult patients. Brachial plexus pathologies including traumatic, inflammatory, neoplastic processes and mechanical compression will be discussed with illustrative examples.
Findings/Discussion
Injury to brachial plexus may be related to birth trauma in infants or secondary to fall or other traction injuries in older individuals. Imaging findings in these cases could range from nerve root/trunk avulsion, pseudomeningocele, and brachial plexus (or spinal cord) edema/hematoma in the acute phase to denervation changes in the pectoral girdle muscles in subacute to chronic phase. Neoplastic processes affecting the brachial plexus range from primary neurogenic tumors (i.e., schwannoma, plexiform neurofibroma, malignant primary nerve sheath tumors, etc.) or secondary involvement by tumors (i.e., pancoast tumor or leukemic infiltration).

Note: Scanned images are included in the proceedings. Some submitted images were reduced during editing, thereby decreasing clarity. Also, refer to the Program Planner. Proceedings Content as of 3-29-2013.

Brachial plexus compression can be present due to cervical rib or fibrous bands (thoracic outlet syndrome), mass lesion, or fluid collection/hematoma in the axilla. CT angiography also plays a significant role in evaluation of thoracic outlet syndrome.
Summary/Conclusion
Imaging of brachial plexus is unique and technically challenging. MR imaging is the primary diagnostic modality of choice. It is important that the radiologist is aware of the optimal imaging protocol and common abnormalities in order to provide prompt and accurate diagnosis.

KEYWORDS: MR imaging, brachial plexus

eEdE-170

The Postoperative Spine: Hardware, Techniques, and Imaging Appearances

Ratcliffe, M. R.·McCreary, R.·Siripurapu, R.·Herwadkar, A.
Salford Royal Hospital
Salford, UNITED KINGDOM.

Purpose
1. To discuss the imaging techniques and protocols used in the assessment of the postoperative spine. 2. To review the normal imaging appearances of the postoperative status of the spine following various surgical procedures including stabilization, fusion, and disk replacement with various techniques and devices.
Approach/Methods
We present an electronic educational exhibit of the techniques and protocols used to image as well as the normal imaging appearances of the postoperative appearances of the spine.
Findings/Discussion
Spinal surgery is common and has extensively evolved into a complex, specialized field. The goal of this exhibit is to give an overview of common surgical procedures and approaches and discuss the normal postoperative state. Instrumentation is used to provide stability and restore anatomical alignment in the treatment of fractures, degenerative disease, infection, tumors, and congenital deformities. Various posterior and anterior surgical approaches may be used and instrumentation may involve a myriad of devices including screws, spinal wires, vertebral cages, and artificial ligaments and disks. As spinal procedures are becoming increasingly common, the instrumented spine is seen with increasing frequency in routine radiology practice and the radiologist should have an understanding of spinal biomechanics and the common approaches and devices used in spinal instrumentation.
Summary/Conclusion
Evaluating the postoperative spine is challenging due to the continual changes in both surgical technique and hardware. Radiologists, and in particular neuroradiologists, need to be familiar with the normal imaging appearances of the spine following stabilization, fusion, and disk replacement with various techniques and devices.

KEYWORDS: Spinal instumentation, Spinal imaging, postoperative spine

eEdE-171

Imaging of Spinal Cord Syndromes: from Brown-Sequard to Cauda Equina

Baer, A. H.·Parmar, H. A.·Ibrahim, M.
University of Michigan
Ann Arbor, MI.

Purpose
The purpose of this educational exhibit is to review the clinical presentation and neurologic examination of classic spinal cord syndromes and to correlate those with associated imaging characteristics.
Approach/Methods
The following syndromes were compared in terms of their etiologies, presenting neurologic examinations, and characteristic imaging features: Brown-Sequard syndrome, central cord syndrome, dorsal cord syndrome, segmental syndrome, ventral cord syndrome, pure motor syndrome, conus medullaris syndrome, and cauda equina syndrome. Patient cases were collected and graphic illustrations were generated to demonstrate the anatomical distribution of pathology, and a table was created to compare the relative frequency of associated signs and symptoms for each syndrome.
Findings/Discussion
There are eight classic syndromes associated with disorders of the spinal cord and cauda equina. These syndromes are defined by characteristic pain, sensory impairment, motor weakness, abnormal reflexes, altered muscle tone, and related organ (e.g., bowel and bladder) dysfunction. Magnetic resonance imaging in conjunction with clinical information, blood and CSF analysis, and occasionally conventional angiography often can provide a timely and accurate diagnosis.
Summary/Conclusion
Spinal cord syndromes, including acute and chronic processes, are a pathologically heterogeneous group of conditions with potential for permanent neurologic deficit if not diagnosed and managed expeditiously. In many cases, identifying the underlying cause is a diagnostic challenge. Dorsal cord syndrome, for example, has several possible causes (spirochete infection, multiple sclerosis, spinal cord metastases, etc.). Neuroimaging, with close attention to the clinical history and neurologic examination, can reduce the differential diagnosis substantially, often to a single etiology.

KEYWORDS: Spinal cord, Spinal imaging, spinal stroke

Note: Scanned images are included in the proceedings. Some submitted images were reduced during editing, thereby decreasing clarity. Also, refer to the Program Planner. Proceedings Content as of 3-29-2013.

eEdE-172

Longitudinally Extensive Myelopathy: The Spectrum of Pathology on MR Imaging

Eckart, D.[1]·Poretti, A.[1]·Boltshauser, E.[2]·Huisman, T. A.[1]·Izbudak, I.[1]
[1]Johns Hopkins Hospital, Baltimore, MD, [2]University Children's Hospital of Zurich, Switzerland, Zurich, SWITZERLAND.

Purpose
Abnormal intramedullary spinal cord signal abnormality on magnetic resonance imaging (MRI) in a longitudinally extensive distribution without cord expansion suggests a broad list of differential diagnostic considerations. Making the correct diagnosis requires attention to both the imaging features of the disease, the age of the patient, and the clinical context. This educational exhibit illustrates the spectrum of diagnoses with T2 hyperintense, intramedullary signal abnormality spanning three or more vertebral body segments (longitudinally extensive), including demyelination, cord infarct, metabolic abnormalities, viral and bacterial infection.
Approach/Methods
After obtaining internal review board (IRB) approval, a retrospective review of the clinical database at our institution was interrogated to find cases of longitudinally extensive, intramedullary T2 signal abnormality between 2009 and 2012. Tumor and trauma cases were excluded. Two neuroradiologists reviewed the images and the clinical record, categorizing the etiology as infection, inflammation/demyelination, infarction, edema, metabolic, or vascular abnormality. Images were evaluated for the presence or absence of contrast enhancement, restricted diffusivity if diffusion imaging was performed, presence of blood products, and associated imaging findings such as fracture or ligament injury, flow voids suggesting spinal dural arteriorvenous fistula (dAVF), or postsurgical changes. Additional studies including cerebrospinal fluid (CSF) analysis, spinal angiography, and diffusion tensor imaging were reviewed when available. Cases of demyelinating /inflammatory myelopathy were subcategorized further as neuromyelitis optica, multiple sclerosis, acute disseminated encephalomyelitis, or idiopathic transverse myelitis.
Findings/Discussion
The spectrum of pathology causing longitudinally extensive transverse myelopathy demonstrates considerable overlap. This exhibit explores the varying imaging appearances of both common and rare causes of longitudinally extensive T2 hyperintense signal abnormality as seen in approximately 40 patients with 110 MRI scans. A disproportionate number of our patients had a clinical diagnosis of transverse myelitis, reflecting our institutional bias as a referral center for transverse myelitis with a relatively low trauma volume. Representative images depicting viral and bacterial myelitis, cord abscess, demyelinating diseases (neuromyelitis optica, multiple sclerosis, and idiopathic transverse myelitis), cord infarction, transient cord edema related to hydrocephalus, metabolic derangement, and vascular lesions are presented in an interactive fashion.
Summary/Conclusion
Although many causes of longitudinally extensive spinal cord signal abnormality on MRI have similar imaging appearances, familiarity with the spectrum of clinical and imaging manifestations of these causes helps focus the differential diagnosis. With attention to the patient's age, careful review of the clinical record and CSF analysis, and knowledge of the imaging findings, an accurate diagnosis or limited differential diagnosis can be made prospectively to allow timely management decisions.

KEYWORDS: Myelopathy, Intramedullary, spinal cord

eEdE-173

Immune Related Disorders of the Spinal Cord: A Pictorial Review

Hoque, K. E.·Lerner, A.·Shiroishi, M.·Torres, F.·Go, J. L.
University of Southern California
Los Angeles, CA.

Purpose
To educate the attendee regarding immune related disorders of the spinal cord.
Approach/Methods
Utilizing the spine teaching files from a major academic institution on the West Coast, the causes of immune related disorders of the spinal cord will be demonstrated.
Findings/Discussion
Immune mediated disorders of the spinal cord are a group of disease processes which are multifactorial in origin. This exhibit will describe the pathophysiology, clinical manifestations, epidemiology, state of the art MR imaging, and briefly describe the treatment strategies for these disease processes. The disease processes to be discussed include multiple sclerosis, Devic's disease, ADEM, immune mediated vasculitis of the spinal cord, Guillain Barre syndrome, chronic inflammatory demyelinating polyneuropathy, and other less common disorders of the spinal cord.
Summary/Conclusion
Immune mediated disorders of the spinal cord are an uncommon but important group of disease processes which may involve the spinal cord. This exhibit serves to educate the attendee regarding this subset of disease entities.

KEYWORDS: Spinal imaging, Spinal cord

Note: Scanned images are included in the proceedings. Some submitted images were reduced during editing, thereby decreasing clarity. Also, refer to the Program Planner. Proceedings Content as of 3-29-2013.

eEdE-174

Imaging of Nontraumatic Spinal Cord Abnormalities

Montgomery, J. P.[1]·Haubrich, N.[2]·Blackham, K.[1]
[1]University Hospitals Case Medical Center, Cleveland, OH, [2]Boston College, Chestnut Hill, MA.

Purpose
Myelopathy is a common clinical indication for imaging of the spine with clinical presentations of extremity weakness, parasthesias or bowel and bladder dysfunction. There are many causes of myelopathy including trauma, inflammation, infection, neoplasm and degenerative changes which can become unwieldy to mentally organize and thereby inhibit learning. This exhibit presents a radiologic compartment approach that reduces the intimidation of generating a differential diagnosis.
Approach/Methods
Relevant normal spinal cord anatomy initially is reviewed by way of a labeled comparison of drawings and MR images. Spinal cord pathology then is discussed on the basis of anatomical location: intramedullary, extramedullary-intradural and extradural. These anatomical compartments are further subdivided by etiology including congenital abnormalities, neoplasms, inflammatory processes, infectious processes and vascular abnormalities. These etiologies will be illustrated with exemplar cases.
Findings/Discussion
Spinal cord pathology is complex and intimidating when viewed as a large list of congenital, infectious, inflammatory and degenerative etiologies. Beginning with the spinal cord and moving outward to the meninges and then the vertebral column, common clinical and classic radiologic disorders will be discussed and illustrated with clinical correlation. The discussion also will include the disease demographics and an emphasis on the MRI findings. Entities will include classic congenital malformations such as myelomeningocele, intramedullary pathologies such as astrocytoma, metastasis and demyelination, extramedullary tumors such as meningioma, neurofibroma and dropped metastases, as well as extradural manifestations of cord or nerve root compression such as diskitis-osteomyelitis, disk herniation and bone tumors.
Summary/Conclusion
This exhibit aims to engage the viewer in a focused and easy to understand review of nontraumatic spinal cord pathology utilizing a radiologic compartment approach with an emphasis on MR imaging findings. Topics will be classified by anatomical location and further subdivided by etiology in order to provide an organized approach to spinal cord anomalies that may contribute to the common clinical indication for spine imaging: “myelopathy”.

KEYWORDS: Spinal cord

eEdE-175

Value of MR Imaging and Diffusion Tensor Imaging as Biomarkers for Classifying Acute Spinal Cord Injury

Zoltani, Z.[1]·Zohrabian, V.[1]·Kamali, A.[2]·Gorniak, R. J. T.[1]·Dresner, M. A.[3]·Flanders, A. E.[1]
[1]Thomas Jefferson University Hospital, Philadelphia, PA, [2]Cooper Hospital, Camden, NJ, [3]Philips Medical Systems, Philadelphia, PA.

Purpose
Spinal cord injury (SCI) is a significant problem in the United States with approximately 11,000 new cases per year with an overall prevalence of 250,000 patients living with this condition. Lifetime cost of care averages two million dollars and U.S. expenditures for SCI exceed six billion dollars annually exclusive of lost wages and productivity. Currently there are no “cures” for SCI. The goal of this exhibit is to demonstrate the current role that MR imaging (MRI) plays in the assessment of spinal cord injury and the potential future role diffusion tensor imaging (DTI) could have in improving characterization of injury.
Approach/Methods
While most SCI patients will realize some spontaneous recovery in the first six months after injury, there are only crude metrics available to help discriminate and select for patients that have an intrinsic capacity for recovery versus those that would benefit from some form of novel medical/surgical therapy to promote neural regeneration. Clinical parameters have been used historically to infer the amount of damage sustained to the spinal cord after injury. However, the accuracy of this examination is totally dependent upon the patients ability to cooperate and skill level of the examiner. In the acute trauma setting, the reliability of this clinical exam diminishes and therefore other objective means are needed to directly assess the degree of damage to the spinal cord.
Findings/Discussion
MR imaging has been advocated as the only noninvasive means to directly evaluate the internal architecture of the spinal cord. Three cardinal spinal cord features of SCI on MRI include swelling, edema and hemorrhage. Lesion characteristics, location and length correlate with the neurologic deficit and potentially augment the clinical examination in assessing neurologic recovery. More recently, DTI has been applied to this problem by rendering data related to integrity of white matter tracts. There is both experimental and human data showing that SCI creates a relative decrease in longitudinal diffusivity and increase in radial diffusivity and generalized loss in anisotropy. There are a myriad of technical challenges in measuring these parameters in the human spinal cord using conventional clinical instruments. These include artifacts introduced by motion, the surrounding bony structures, the injury itself as well as limitations of the small target size, spatial resolution/signal and intrinsic time limitations imposed when imaging critical care

patients. The goal of this exhibit is to: (1) introduce the participant to the clinical problems associated with assessing the SCI patient, (2) understand the relationship between assessment and neurologic recovery, (3) review the scientific/clinical evidence on the additional value that MRI provides in directly interrogating the spinal cord architecture, (4) review the principles of DTI and its application to our understanding of SCI and recovery.
Summary/Conclusion
There are both quantitative and qualitative features provided through the combined use of MRI and DTI that can be used as biomarkers in the objective assessment of neurologic impairment in setting of acute SCI. This information could be used to counsel patients/families and as criteria for selective administration of novel therapies.

KEYWORDS: Spinal cord, Diffusion tensor image, neurologic recovery

eEdE-176

Cervical Spine Stability In Trauma: Mechanics, Imaging, and Controversies

Tenenbaum, M.·Alkalay, R.·Hackney, D.
Beth Israel Deaconess Medical Center
Boston, MA.

Purpose
To discuss the mechanics of cervical spine stability after trauma, indications for imaging, and interpretation of CT and MR findings.
Approach/Methods
Stability of the spine depends on integrity of its osseous and ligamentous elements. Spinal ligaments display nonlinear mechanical behavior, a function of their intrinsic tissue structure and visco-elastic nature. They allow mobility while providing increasing kinematic constraints towards the extremes of joint motion. In the upper cervical spine the alar ligament prevents excessive axial rotation at the atlanto-occipital joint, and the transverse ligament limits anterior translation of C1. These provide the primary sources of stability for C1-C2. Primarily due to motor vehicle accidents, alar ligament injury may result in the C0-C2 complex undergoing increased flexion, lateral bending, and axial rotational-based instability beyond the functional range of motion. In the middle to lower spine, the anterior longitudinal ligament (ALL) and posterior longitudinal ligament (PLL), contribute to support and stability of the anterior column. The posterior ligamentous complex (PLC) includes the facet joint capsules, ligamentum flavum and the supraspinous and interspinous ligaments. The PLC contributes to stability by providing resistance to tensile forces in flexion and form the "posterior tension band". High rate injury, resulting in partial or complete tear of the ligaments may result in a highly unstable spine demonstrating significant inter-level translational and rotational displacements, for which the muscular control of the neck cannot compensate in active or passive motion. Injuries to the capsular ligaments result in sagittal, axial, and lateral instability. Classifications have progressed beyond the Denis 3-column concept, and the importance of the posterior ligamentous complex has become increasingly clear. Indications for imaging, particularly for those patients who cannot undergo a full neurologic evaluation, have evolved as imaging technology has advanced. MR reveals apparently significant injuries in some patients with no evidence of fracture. The correlation of MR-apparent ligamentous injury with surgical findings is far less than perfect. The prevalence of destabilizing ligament injury in patients with normal CT scans is uncertain, with widely divergent values reported in the literature. Some studies have found near perfect sensitivity and negative predictive value of CT for detecting clinically significant post-traumatic spinal instability. The severity of ligamentous injury ranges from laxity to frank disruption, and there are as yet no proven criteria for MRI findings corresponding to functional insufficiency in the absence of frank tears. Consequently, the role of MR in acute evaluation also is controversial. Keeping ICU patients in collars for prolonged periods of time while awaiting imaging results or neurologic recovery can lead to complications, particularly for those with head injuries. This "conservative" approach may have significant detrimental effects.
Findings/Discussion
We will review the mechanical principles of spine trauma, indications for CT and MR imaging, and interpretation of these studies in terms of spinal stability.
Summary/Conclusion
The evaluation of cervical spine trauma is an essential topic in radiology practice. Introduction of progressively advanced imaging had lead to controversies over the role of imaging in management, which studies should be obtained, and how they should be interpreted.

KEYWORDS: Spinal trauma, Acute spinal trauma

eEdE-177

Imaging of the Thoracolumbar Spine Injuries in Trauma with the Introduction of New Concepts

Khorrami-Arani, N.[1]·Liang, T.[2]·Ouellette, H.[1]·Munk, P.[1]·Nicolaou, S.[1]
[1]Vancouver General Hospital, Vancouver, BC, CANADA,
[2]University of British Columbia, Vancouver, BC, CANADA.

Purpose
Each year, over 30,000 injuries to the spinal column occur from trauma, of which the majority are due to blunt trauma. These injuries often can result in neurologic damage; thus, it is important to recognize these injuries early to allow prompt diagnosis and management. The purpose of this exhibit is to review the imaging modalities and findings available for acute thoracolumbar spine injuries, defined as injuries involving the thoracic (T1-T12) and lumbar (L1-L5) spinal segments, and review and

Note: Scanned images are included in the proceedings. Some submitted images were reduced during editing, thereby decreasing clarity. Also, refer to the Program Planner. Proceedings Content as of 3-29-2013.

discuss the utility of a new classification scheme for the thoracolumbar spine for prognosis assessment and clinical management.
Approach/Methods
A retrospective review of cases of thoracolumbar spine injury from our institution will be conducted.
Findings/Discussion
This educational exhibit will review the pathophysiology and clinical presentation of acute thoracolumbar spine injuries, and discuss indications for acute thoracolumbar spine imaging. We will discuss the findings, strengths and weaknesses, and demonstrate examples of lateral radiographs, CT, and MR imaging (MRI) as imaging modalities for thoracolumbar injuries. A review of the classification systems available for imaging of thoracolumbar spine fractures will be conducted, with emphasis on the new thoraco-lumbar injury and classification scale (TLICS). The three main independent characteristics for assessing a thoracolumbar injury include morphology, integrity of posterior ligamentous complex and the neurologic status of the patient. The usefulness of each factor will be reviewed, and imaging examples of the application of the classification scale will be demonstrated. Finally, the efficacy and ability of TLICS to help guide the team towards either a surgical versus nonoperative management will be evaluated.
Summary/Conclusion
The TLICS system is a new and well accepted classification system for the diverse presentation of thoracolumbar injuries. It is based on three major components for assessment: the morphology of the injury, the integrity of the posterior ligamentous complex, and the neurologic status of the patient. An overall severity score is used in conjunction with the classification system, and allows determination of prognosis and helps guide management. After reviewing this exhibit, the reader will understand the TLICS classification and be able to quickly and accurately diagnose thoracolumbar injuries, and efficiently aid the trauma team in clinical management decisions.

KEYWORDS: Spinal trauma, thoracolumbar spine injury

eEdE-178

Localization of Spinal Subdural Hemorrhage: How Confident Are We?

Gandhe, A. R.·Flanders, A.·Patel, F.·Mohiuddin, J.·Chopade, T.·Patel, R.·Sharma, D. K.
Thomas Jefferson University Hospital
Philadelphia, PA.

Purpose
MR imaging (MRI) is considered to be investigation of choice for spinal hemorrhage. Even though MRI is able to evaluate the location, extent and compressive effects of hemorrhage, diagnosing the exact space of hemorrhage may be difficult. The purpose of the exhibit is to discuss those spinal hemorrhages which by imaging criteria appear to be in one space (i.e., epidural/subdural/subarachnoid) and found to be in another space intraoperatively.
Approach/Methods
Patients operated for spinal hemorrhage were evaluated retrospectively for location of hemorrhage. MR imaging was specific in location, extent, compressive effects, spinal cord changes, and to exclude associated lesion. There were few cases where spatial localization of hemorrhage on MRI did not match with intraoperative findings.
Findings/Discussion
Case 1. A 72-year-old male presented with intracranial and spinal hemorrhage after fall. He had history of DVT and was on heparin. MR imaging spine demonstrated extensive subdural hemorrhage dorsally from T1-T2 to L3-L4; causing anterior displacement of spinal cord. Intraoperative findings demonstrated subarachnoid hemorrhage. Case 2. A 75-year-old male presented with lower extremity pain after epidural injection. MR imaging lumbar spine demonstrated small epidural hemorrhage centered at L4-L5 with large associated subdural hemorrhage. Epidural fat was largely preserved, anterior margin was irregular and dura was not visualized. Postoperative findings demonstrated only epidural hematoma. Case 3. A 49-year-old patient presented with progressively increasing lower extremity weakness and numbness. He was on coumadin. MR imaging lumbar spine demonstrated crescent-shape dorsal extra-axial hemorrhage with largely preservation of epidural fat. Dura was not visualized. Postoperative findings demonstrated epidural hemorrhage.

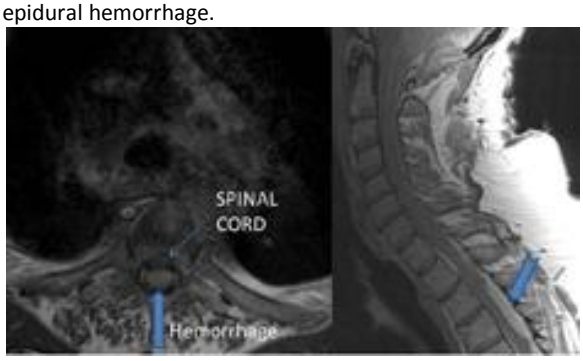

Note: Scanned images are included in the proceedings. Some submitted images were reduced during editing, thereby decreasing clarity. Also, refer to the Program Planner. Proceedings Content as of 3-29-2013.

Imaging Findings of Spinal Hemorrhage	
Spinal Epidural Hemorrhage (SEH)	Spinal Subdural Hemorrhage (SSH)
Involvement of epidural fat	Epidural fat preserved
Presence of curtain sign	Absence of curtain sign
Visualization of dura matter	Nonvisualization of dura matter
Lentiform shape	Crescent shape
Regular anterior margin	Irregular anterior margin
Tapering craniocaudal margins	Nontapering craniocaudal margins
Smaller craniocaudal extent	Long craniocaudal extent

Summary/Conclusion
Localization of space of hemorrhage has significant role in management of spinal hemorrhages. MR imaging is investigation of choice in evaluation of spinal hemorrhage; however, occasionally, exact localization of space of spinal hemorrhage especially subdural hemorrhage is not possible. One should always think possibility of spinal epidural and rarely subarachnoid hemorrhage, though imaging findings favor subdural hemorrhage.

KEYWORDS: Spinal trauma, Hemorrhage, subdural

eEdE-179

Imaging of Cervical Spine Injuries

Khorrami-Arani, N.[1]·Liang, T.[2]·Shewchuk, J.[1]·Nicolaou, S.[1]
[1]Vancouver General Hospital, Vancouver, BC, CANADA,
[2]University of British Columbia, Vancouver, BC, CANADA.

Purpose
Age-adjusted incidence rates in Canada for spinal cord have been estimated to be 50.87 per million per year. Of these injuries, the majority are caused by blunt trauma. Two to three percent of blunt trauma victims suffer cervical spine (C-spine) injuries, and 40-50% of these injuries result in neurologic damage. It is important to recognize these injuries early for prompt diagnosis and management. The purpose of this exhibit is to review the imaging modalities and findings for acute C-Spine injuries, review indications for imaging, and discuss the utility of a classification and scoring system for the cervical spine.
Approach/Methods
A retrospective review of cases of C-spine injury from our institution will be conducted.
Findings/Discussion
This educational exhibit will review the pathophysiology and clinical presentation of acute C-spine injuries, and discuss indications for acute C-spine imaging with review of the Canadian C-spine rule, NEXUS study criteria, and CCR study criteria. We also will review the subaxial injury classification (SLIC) and severity score for acute C-spine fractures. The utility of MDCT in assessing the C-spine in an obtunded patient will be demonstrated with imaging examples. We will discuss and demonstrate the findings of acute C-spine injuries on radiography, CT, and MRI, and review the strengths and weaknesses of each imaging modality.
Summary/Conclusion
There are limitations in detecting upper and lower C-spine skeletal injuries on radiographs. CT is the most useful and informative imaging tool for C-spine skeletal trauma, and MRI is the imaging modality of choice in investigating ligamentous and spinal cord injury. Criteria exist to indicate which patients need imaging to evaluate for possible acute C-spine injury, and we have reviewed a system for scoring injury severity.

KEYWORDS: Cervical spine

Index of Program Participants

Numbers refer to session and presentation numbers, *not to page numbers*.

Index Key: O = Scientific Paper (Oral Presentation); EE = Electronic Excerpta e; P = Scientific Poster (Print Format); eP = Electronic Scientific Poster (ePoster); EdE = Education Exhibit (Print Format); eEdE = Electronic Education Exhibit

A

Aagaard-Kienitz, B. eEdE-03
Aamodt, D. O-252
Abbott, D. O-308
Abbott, M. F. O-308
Abdalla, A. eP-215, eP-217
Abdel Gaber, N. eP-217
Abdel Razek, A. eP-11, eP-215, eP-217
Abdulhak, M. EE-87, O-129
Abdulla, A. eP-110
Abe, O. eP-93
Abel, N. eEdE-109
Abele, T. eEdE-48
Abele, T. A. eP-134
Abele, T. A. O-538
Abele, T. A. eP-272
Abellaneda, A. eP-55
Abello, M. O-204
Abouharb, A. eP-155
Abrol, T. O-285
Abrol, T. O-539
Abruzzo, T. eEdE-129, eEdE-130
Abruzzo, T. A. eP-156
Absinta, M. O-305
Abu-Zahra, K. W. eP-164
Adams, A. eEdE-144
Adams, P. O-27
Adapa, P. EE-65, eEdE-60, O-407
Adappa, N. D. O-532
Adas, R. eEdE-142
Adas, R. A. eEdE-90
Adas, R. A. A. EE-62
Addante, R. R. eEdE-105
Agarwal, A. EdE-19
Agarwal, V. eP-80, O-309, O-425
Aghakhanyan, G. P-7
Agid, R. O-274
Agid, R. O-419
Agildere, M. eP-238, O-42b
Agrawal, A. eP-189
Agrawal, J. P. eEdE-68
Aguilar-Pérez, M. eP-192, eP-195, eP-209, O-98
Ahlhelm, F. O-239
Ahmad, N. eP-231
Ahmed, F. Y. EdE-06
Ahmed, S. O-485, O-537
Ahmediev, M. M. O-244a
Ahn, K. P-45, P-48
Ahn, S. S. O-387
Ahn, S. S. O-113
Aho, T. R. eEdE-27
Aiken, A. O-250, O-487, O-491
Aiken, A. H. eP-144, O-530
Airan, R. O-240, O-59
Airan, R. D. O-427
Aitken, S. eP-92
Aizenberg, M. R. O-407
Akansel, G. O-41
Akao, J. eP-81, O-580
Akao, J. H. O-56
Akasaka, T. EdE-83
Akça, A. eP-224
Akhtar, E. P-95
Akhtar, N. P-95
Akiyama, Y. eP-54
Akiyama, Y. P-105a
Al Adwani, N. eP-236
Al Harbi, M. O-392
Al Shahwan, S. eP-236
Al Sheikh, F. eP-236
Alattas, F. O-117
Alazzaz, A. A. A. O-117
Albers, G. W. O-49, P-58
Alberto, G. eP-229, O-512
Alberts, M. J. O-229
Albom, M. O-221
Albright, H. W. O-282
Alden, T. D. EE-63
Alderfer, K. EdE-28
Alexander, M. D. eP-135, eP-99
Alfaro, D. EdE-13
Al-Hakim, M. Mazen. EE-4
Alhazzaa, M. O-227
Al-Helli, O. O-28
Alhilali, L. eP-303
Alhilali, L. M. O-306, O-422, O-529
Ali, S. eP-100
Ali, S. eP-68
Ali, S. O-429
Ali, T. EdE-47
Alimenti, A. O-221
Al-Jaber, A. EE-52, EE-7
Alkalay, R. eEdE-176
Alkan, A. EdE-36, eP-139, O-104
Alkan, O. eP-218
Al-Khalili, R. EE-5
Allegri, A. O-323
Allen, H. N. eP-18
Alli, S. eP-210
Allmendinger, A. eEdE-152, eEdE-156a
Almehdar, A. eEdE-142
Almehdar, A. S. EE-62
Almeida-Freitas, D. O-546
Almeida-Freitas, D. B. eEdE-47, O-569
Almekhlafi, M. A. eP-197, O-165
Almutairi, A. eP-69
Alnassan, H. eP-284
Alonso, J. eP-62
Alonso-Basanta, M. eP-120
Alorainy, I. A. eP-103
Alperin, N. eP-128, O-522
Alqahtani, E. eP-235, eP-248, O-433
Alsaadi, A. O-117
Al-Shafi, S. eP-236

Index of Program Participants

Numbers refer to session and presentation numbers, *not to page numbers*.
Index Key: O = Scientific Paper (Oral Presentation); EE = Electronic Excerpta e;
P = Scientific Poster (Print Format); eP = Electronic Scientific Poster (ePoster);
EdE = Education Exhibit (Print Format); eEdE = Electronic Education Exhibit

Alsharief, A. N. A. eEdE-142
Altaye, M. O-505
Alterman, R. O-42a
Altinkaya, N. eP-218
Altman, N. O-148
Alves-Leon, S. O-238, O-477
Alves-Leon, S. Vieira. eP-19
Alvisi, E. P-5
Amans, M. R. eP-201, O-555
Amaral, L. Faria do. eEdE-22
Amaro, E. P-26
Ambalathunkal, E. eEdE-69
Amendola, C. eP-157
Amendola, M. A. eP-157
Ametlli, V. P-107
Amin, V. B. eEdE-145
Amin, V. B. eEdE-96
Amrhein, T. eP-299
Amrhein, T. J. O-488, O-490
Anderson, J. C. eP-18
Anderson, J. S. O-24
Anderson, R. C. E. EE-68
Andrade, A. Ferreira. O-423
Andre, J. O-298
Andre, J. B. eP-46, O-205, P-49
Andreassen, O. O-21, O-29, O-31
Andreisek, G. O-128
Andrew, R. eP-92
Andrews, T. O-118, O-67
Andronesi, O. O-403
Angtuaco, E. EdE-73, EdE-74, eEdE-83, eP-256
Angtuaco, E. J. eP-65
Anik, Y. eP-224, O-41
Ansari, S. eP-36
Ansari, S. A. EdE-51, EE-36, EE-63
EE-73, eP-84
Ansari, S. A. O-228, O-229, O-277
O-295, O-301, O-504
Ansari, S. A. O-225
Antoniadis, G. eP-293
Antoun, N. EdE-47, EdE-90, EE-15
EE-54a, P-29, P-72, P-73, P-76, P-77, P-9
Antulov, R. O-116
Anumula, N. O-472
Anzai, Y. eP-117, eP-121, eP-46, O-298, P-49
Anzalone, N. O-283, O-540
Aoki, S. eP-30, P-23
Aouad, R. K. EdE-57
Applebee, A. O-118
Applegate, K. eP-283, O-307
Aragao, M. Fatima. Vasco. eEdE-76
Aralasmak, A. EdE-36, eP-139, O-104
Arastoo Vossough, A. eEdE-94
Araújo, A. Chiappetta. Correia de. eEdE-76
Arbab, A. eP-56
Arbab, A. S. eP-53
Argiolas, G. Maria. O-501
Arias, E. J. O-97
Armitage, P. O-325
Armstrong, G. T. eP-270
Armstrong-Wells, J. O-434
Arnold, G. eP-195
Arrighi, H. O-30
Ascencio, J. P-16
Ashe-McNally, C. O-479
Ashruf, S. eEdE-28
Ashruf, S. eP-164
Asil, T. EdE-36
Asıl, T. O-104
Atay, M. O-104
Atchie, B. eP-70
Aubé, C. eP-185
Aubry, S. eP-133, eP-284
Auger, C. eP-62
Augsburger, J. eP-156
Aulakh, M. O-115
Auschwitz, T. O-437
Avitsian, R. O-32
Aviv, R. O-119, O-120
Aviv, R. I. eP-98
Aviv, R. I. O-44, O-574
Aviv, R. I. O-125
Avner, S. O-38
Aw, J. eP-258
Awad, I. O-578
Awai, K. eP-54
Awane, A. P-50
Aydin, O. eP-23, eP-28
Ayeni, S. O-565
Aygum, N. P-55
Aygun, N. eP-143
Aymerich, F. X. eP-62
Ayoub, D. O-271, O-273
Azagra, A. O-242, O-577
Aziz, K. M. eP-177
Azizyan, A. eP-67
Azuma, M. eP-33, eP-5, O-516

B

Babb, J. S. O-536
Babiarz, L. S. O-251, O-253
Bachhav, V. EdE-87
Backes, W. H. P-15
Badan, M. O-221
Badve, C. O-279
Badve, C. A. eEdE-18, eEdE-26, eP-204
Baer, A. O-514
Baer, A. H. eEdE-171
Baeumer, P. O-73, O-74
Bag, A. K. O-521
Bagade, S. EdE-17
Bagci, A. O-522
Bagga, S. EdE-20, P-69
Bagher-Ebadian, H. eP-52, eP-53, eP-56
Bagley, L. EdE-42, eEdE-126

Index of Program Participants

Numbers refer to session and presentation numbers, *not to page numbers*.

Index Key: O = Scientific Paper (Oral Presentation); EE = Electronic Excerpta e; P = Scientific Poster (Print Format); eP = Electronic Scientific Poster (ePoster); EdE = Education Exhibit (Print Format); eEdE = Electronic Education Exhibit

Bagley, L. J. EdE-62, P-38
Bahador, F. eP-226
Bahia, P. O-477
Bahia, P. Valle. eP-8
Bahl, M. eP-137, O-415, O-418
Bakalis, C. eEdE-12
Bakshi, A. C. O-69
Balkman, J. D. eEdE-50
Balottin, U. O-511
Bammer, R. eP-79, O-205, O-49
Banckwitz, R. eP-162, eP-198
Banerjee, S. O-54
Bangiyev, L. eEdE-07, O-413
Banich, M. O-36
Banich, M. T. O-241
Banker, P. EE-17, EE-72, eEdE-156
Bannykh, S. eP-67
Bansal, A. P-113
Bansal, S. O-143
Bansal, V. eEdE-55, eEdE-71
Barad, U. H. eP-253
Baradaran, H. EdE-75, O-494, O-61, P-52
Barajas, R. P-33
Barakat, N. eP-262, O-438, O-439, O-440
Barakat, T. eP-217
Baratto, A. P-7
Barbe, C. O-226
Barest, G. O-513
Barker, P. eP-15, O-140, O-508
Barker, P. B. O-141, O-22, O-243, P-10
Barkhof, F. O-30
Barkovich, A. J. O-509, O-54
Barkovich, J. P-100
Barkovich, M. eP-69, O-549
Barlavie, Y. EdE-34
Barnes, R. O-426
Barnett, D. EE-25
Barnett, G. H. O-207
Barnwell, S. O-99
Barr, R. M. EdE-82
Barret, W. A. EdE-15
Barry, K. A. EE-4
Bartnik-Olson, B. L. P-102
Bartolini, B. eP-175
Bartsch, A. O-75
Bartynski, S. eP-299
Bartynski, W. eP-102, eP-299
Baruah, D. EdE-49, eEdE-17, eEdE-61
Basak, S. O-568
Bashir, M. O-417
Bastian, A. J. O-506, O-507
Bastianello, S. O-511, P-5
Batawi, A. A. A. eEdE-142
Batchelor, T. O-403
Batchelor, T. T. O-404
Bathla, G. eEdE-135, eEdE-141, eEdE-154
Batjer, H. O-295
Batjer, H. O-301
Batty, R. O-554
Baugnon, K. O-487, O-491
Baugnon, K. L. O-530
Baugnon, K. Lloyd. O-250
Baumer, P. eP-293
Bäumer, P. O-72
Baumer, P. O-75
Bauml, J. A. eP-275, P-114
Bawa, P. O-324
Baxi, A. eEdE-79
Bayas, A. eP-237
Bayer-Karpinska, A. O-499
Baykal, A. eEdE-45
Bäzner, H. eP-192, eP-195, eP-209, O-98
Beal, K. O-543
Becker, J. T. P-8
Becske, T. O-278
Bedi, H. S. eEdE-115
Beecher, J. eEdE-69
Behbahanian, Y. O-288
Belden, C. eEdE-160
Belden, C. J. eEdE-50
Bello, J. A. eEdE-153
Bello, J. A. EdE-81
Beltran-Marin, M. eEdE-149, O-242, O-577
Belzberg, A. J. O-128
Bembea, M. O-433
Ben Hammouda, M. eEdE-70a
Benachour, N. eP-185
Ben-Avi, E. eP-221
Bendok, B. O-301
Bendok, B. R. eP-84, O-295
Bendszus, M. eP-293, O-204, O-391
O-503, O-71, O-72, O-73, O-74, O-75
Benndorf, G. EE-57
Bennett, J. EdE-45
Benson, B. W. eEdE-104
Bentley, J. N. eP-268
Bentson, J. EE-86
Berberian, G. H. EE-37
Berger, R. P. eP-232
Bergey, G. O-140, O-141
Bergman, D. O-225
Bergsland, N. O-511
Berkowitz, F. EE-10, eEdE-79
Berkowitz, I. O-433
Berman, J. P-22
Bermudez Allende, M. Z. EE-8
Bernard, T. J. O-434
Bernardi, B. eP-216
Bernat, A.-L. O-101
Bernier Turmel, F. P-104
Bernstein, R. A. O-229
Bernstein, R. A. O-225
Bert, R. J. O-106
Bertini, E. O-322

Index of Program Participants

Numbers refer to session and presentation numbers, *not to page numbers*.

Index Key: O = Scientific Paper (Oral Presentation); EE = Electronic Excerpta e; P = Scientific Poster (Print Format); eP = Electronic Scientific Poster (ePoster); EdE = Education Exhibit (Print Format); eEdE = Electronic Education Exhibit

Berven, S. O-66
Besachio, D. A. eP-140, eP-272, eP-297, O-53
Besseling, R. M. H. P-15
Bessero, S. O-221
Bessissow, A. eEdE-44, eP-44
Bezerra, R. EE-10
Bhabad, S. EdE-87
Bhalla, M. EdE-40, eEdE-17, eP-154
Bhalla, N. eP-154
Bhat, H. eP-282
Bhatia, R. P-30
Bhatia, S. O-148
Bhatki, A. M. eEdE-99
Bhatnagar, P. EdE-14, eP-286, P-25
Bhattacharyya, P. O-32
Bhojwani, N. EdE-68, EdE-69
Bianchi Marzoli, S. O-410
Bidari, S. EdE-45
Biegon, A. eP-241
Bilaniuk, L. T. O-550
Bini, P. P-5
Biondi, A. O-101, O-280, O-515
Biousse, V. O-558
Birch, J. eP-249
Birchall, D. EdE-14, eP-286, P-25
Birks, J. O-94
Bittman, M. eEdE-122a
Bjelan, M. EE-44
Black, A. O-579
Black, D. F. eP-298
Black, K. eEdE-122b
Blackham, K. EdE-68, EdE-69
Blackham, K. EE-2, EE-9, eEdE-127
Blackham, K. eEdE-174
Blackham, K. A. eEdE-18, eEdE-26
eP-204, O-279
Blanc, R. eP-175
Blaschek, A. eP-237
Blaser, S. eEdE-150, eP-227
Blee, P. P-25
Blei, F. eP-242
Blitz, A. P-47
Blitz, A. M. EdE-52, eP-143, P-55
Block, T. O-413
Boada, F.
Boada, F. E. O-218
Bobinski, M. EE-22
Boddu, S. eP-170
Boddu, S. O-302
Boddu, S. O-68
Boddu, S. R. eP-101, eP-168, eP-283, O-307
Boe, D. L. P-113
Boggan, J. EE-22
Bohnen, N. I. EdE-11
Bokhari, S. J. eEdE-43
Boland, M. O-564
Boltshauser, E. eEdE-172, eP-235, O-321, O-322
Bonaldi, G. eP-289
Bonekamp, S. O-243
Bonifacio, S. P-100
Bonmassar, G. eP-97
Bonneville, F. eEdE-160
Bonvin, C. EE-31
Booker, M. T. eEdE-39
Bookheimer, S. eEdE-138, eP-244, O-544
Boop, F. A. O-147
Boop, F. A. O-437
Boop, F. A. O-435
Booth, T. eEdE-147
Borgie, R. C. eP-97, O-389
Bornemann, R. O-312, O-313, P-110
Boronat, S. eP-261, O-317
Borowski, A. M. eEdE-164
Borra, R. O-403
Borrego-Ruiz, P. O-206
Borri, M. Lucia. P-12
Borys, E. EE-22
Bosemani, T. O-321
Bosman, S. A. eP-275, P-114
Bouras, C. O-214
Bourekas, E. C. eEdE-70
Bower, L. P-107
Bowers, D. C. eP-252
Boxerman, J. EdE-16
Boyd, A. O-27
Boyer, A. C. eEdE-12
Boyer, L. eP-72
Boyer, P. eEdE-41
Boyko, O. EdE-28, eEdE-15
Boyko, O. B. eEdE-52, eP-66
O-244, O-246, O-254
Boyle, C. P-8
Brace, J. A. EE-6
Bradford, D. O-66
Branch, C. A. O-421
Branson, B. O-124
Branstetter, B. O-529
Branstetter, B. F. EE-42
Brashear, H. O-30
Brasic, J. eP-15
Brat, D. J. O-211, O-284
Braun, M. O-527
Bray, M. EE-14
Bredow, S. eP-107, eP-290, O-70
Breitenfeldt, M. EdE-26
Bresson, D. eP-182
Brewer, J. O-21, O-29, O-31
Brinjikji, W. eP-194, O-534, O-96
Britz, G. eP-189
Broderick, J. eP-37
Broderick, J. P. eP-98
Brodie, S. O-517
Brody, D. L. O-419
Bronen, R. eEdE-43, O-520

Index of Program Participants

Numbers refer to session and presentation numbers, *not to page numbers*.
Index Key: O = Scientific Paper (Oral Presentation); EE = Electronic Excerpta e;
P = Scientific Poster (Print Format); eP = Electronic Scientific Poster (ePoster);
EdE = Education Exhibit (Print Format); eEdE = Electronic Education Exhibit

Brooks, N. eP-291
Brost, A. eP-79
Brouwers, H. Bart. O-110
Brown, M. eP-202
Brown, P. A. eEdE-101
Bruce, B. B. O-558
Bruce, J. N. EE-90
Bruesewitz, M. R. P-105
Brugger, P. C. O-318
Brumback, R. O-565
Brunberg, J. A. eEdE-158, O-27
Bryan, R. O-64, P-46
Buch, K. eP-124, eP-214, O-498
Buchholz, M. O-499
Buckingham, C. L. eP-21
Buerki, S. O-321
Bukshpun, P. P-17, P-19, P-22
Bulacio, J. O-32
Bulsara, K. eEdE-124
Bungo, T. eP-229, O-512
Burd, D. A. EE-37
Burger, P. C. eP-222
Burgin, K. EdE-73, eEdE-83, eP-256, eP-65
Burke, A. G. eP-18
Burke, P. O-498
Burns, P. A. O-165
Burrowes, D. eP-258
Butman, J. A. eP-105, O-121, O-424, P-42, P-68
Butteriss, D. EdE-14, eP-286, P-25
Butteriss, D. J. A. EdE-08
Büyükkapu Bay, S. eP-224
Buyukkaya, R. eP-148, eP-23, eP-28
Byrns, K. eEdE-114, eEdE-65
Byun, H. O-398
Byun, J. P-74

C

Çabuk, G. EE-54
Cacciarelli, A. eEdE-109
Cage, T. eP-193
Cagley, J. R. eEdE-134
Cagnoli, P. O-40
Cahill, D. EdE-25
Cain, J. EdE-79, eP-249
Cain, J. R. O-517
Cakmakci Midia, E. eEdE-143
Callaghan, B. C. O-22, P-10
Calle, S. EdE-38
Callstrom, M. R. O-493
Calner, P. O-498
Cambron, S. C. EdE-84, eEdE-105
Campeau, N. eEdE-11
Canapicchi, R. P-7
Canoll, P. O-201
Canstein, C. O-488, O-490
Cantello, R. EE-18, eP-58, O-480
Canter, D. L. eP-246
Cantrell, C. P-56
Cantrell, C. G. O-45, P-61
Cao, C. P-91
Capizzano, A. eEdE-64
Capizzano, A. A. O-567
Capizzano, A. Andres. eP-47
Carai, A. eP-74
Cardinal, J. P-103
Care, M. eP-230
Carey, J. P. eP-143, P-86
Carigi, T. O-511
Carlos, R. C. O-22, P-10
Carmant, L. eP-220
Carmichael, O. T. P-8
Carmody, R. O-390, O-394
Carmody, R. F. EdE-55
Carneiro, F. EE-28
Carneiro, F. EE-28, eP-37, O-113, O-387
Caroff, J. eP-185
Carr, C. M. EE-74
Carranza, V. eEdE-17
Carranza, V. L. EdE-40
Carriero, A. EE-18, eP-58, O-480
Carrino, J. eP-292
Carroll, K. O-99
Carroll, T. O-119, O-120, O-301
Carroll, T. J. eP-36, eP-84
Carroll, T. J. O-295, O-45, O-50, P-56, P-61
Carroll, T. J. O-125
Carson, B. S. O-559
Carson, K. A. O-433
Carter, B. O-129
Caruso, P. eP-261, O-315, O-317
Caruso, P. A. eP-125, O-146
Carvalho, S. C. eEdE-47
Case, M. P-20
Castellano, A. O-283, O-540
Castillo, M. EdE-13, EdE-38, eEdE-159
eP-266, O-249, O-531, P-40, P-83
Castro, L. H. M. eP-16
Cattin, F. O-280
Cattin, F. O-515
Caverzasi, E. eP-48, P-5
Cebeci, H. eP-148, eP-23, eP-28
Cecava, N. O-481
Cen, S. eEdE-52, P-37
Ceranske, A. EdE-49, eEdE-17
Cerejo, R. P-70
Ceroni, M. P-5
Cerri, G. Guido. O-423
Ceschin, R. eP-232, O-436
Cha, J. O-398
Cha, S. eEdE-33
Cha, S. eP-68, P-33
Cha, S.-H. eP-42
Cha, S.-H. P-66
Chabert, E. eP-72
Chacon, M. eP-55, O-502, P-64

Index of Program Participants

Numbers refer to session and presentation numbers, *not to page numbers*.

Index Key: O = Scientific Paper (Oral Presentation); EE = Electronic Excerpta e; P = Scientific Poster (Print Format); eP = Electronic Scientific Poster (ePoster); EdE = Education Exhibit (Print Format); eEdE = Electronic Education Exhibit

Chai, B. B. P-109
Chai, J.-W. P-51
Chaibi, Y. O-582
Chaim, K. T. eP-16
Chakraborty, A. K. EE-20
Chakraborty, S. eEdE-09, eEdE-62
Chakravarthy, V. P-95
Chalak, L. O-431
Chaljub, G. EE-55, EE-56
Chamiraju, P. O-148
Chan, L. O-215, O-222
Chan, Q. eP-14
Chan, Y. eP-14
Chandra, T. eEdE-169
Chang Sen, L. eP-106
Chang, B. P-106
Chang, C.-I. P-51
Chang, C.-N. eP-17
Chang, E. I. P-79
Chang, F.-C. eP-188, O-223
Chang, J. eEdE-148
Chang, J. P. P-56
Chang, Y.-M. eEdE-112, O-492
Changlai, T. eP-132
Chankowsky, J. eEdE-22, eEdE-44, eEdE-93, eP-44
Chantraine, F. O-221
Chao, K. EdE-37, EdE-66, eP-147
Chao, R. P-94
Chapman, P. O-521
Chapuy, S. O-515
Chason, D. P. EdE-85
Chatterjee, A. R. eEdE-116
Chaudhary, N. eP-295, O-277, P-92
Chaudhry, A. EE-16
Chaudhry, A. eEdE-34
Chaudhry, A. A. EdE-03, eEdE-137
Chaudhry, U. O-567
Chaudhry, U. S. eEdE-88, eP-35, eP-87
Chaudry, I. eP-176, eP-291
Chavalli, L. EdE-39, O-402
Chazen, J. O-131
Chein, A. eP-169
Chen, A. O-487, O-491
Chen, B. T. eP-116
Chen, C. C. EE-50
Chen, C. C. C. P-51
Chen, C.-C. P-2
Chen, C.-J. EdE-89, O-237, O-42
Chen, D. EdE-89, O-237, O-42
Chen, H.-C. P-2
Chen, H.-L. P-27
Chen, H.-M. P-51
Chen, J. eEdE-53, eP-101b
Chen, J. Y. O-539, P-63
Chen, J. Y. EE-50, O-172
Chen, J.-K. P-3
Chen, M.-H. P-27
Chen, S.-K. P-11, P-54
Chen, T.-T. P-24
Chen, W. eEdE-35, O-406
Chen, W. P-33
Chen, W.-H. P-2
Chen, W.-S. O-573
Chen, Y. J. eEdE-30
Chen, Y.-L. eP-17, P-41
Chenevert, T. L. P-43
Cheng, Y.-C. P-2
Cheon, J.-E. eP-219
Cheung, W.-K. eP-34
Chez, M. P-97
Chhabra, A. O-128, P-111
Chi, L. EdE-39, O-402
Chi, T. Linda. P-39
Chia, T. L. eP-98
Chiang, G. C. O-213
Chien, A. O-303
Chin, C. eP-301, O-127
Chin, E. M. O-510
Chin, M. eEdE-159
Chin, M. S. O-249
Chinnadurai, P. eP-2
Chintalapani, G. eP-2, O-293
Chiras, J. eP-294, O-101, P-91
Chitayat, D. eEdE-150, eP-227
Chiu, C.-F. O-573
Chiu, P. eP-14
Chiu, W. eP-126
Choe, M.-S. eP-221
Choi, C. eP-24
Choi, C. O-217, O-562
Choi, C.-G. eP-76
Choi, H. P-45
Choi, H. P-48
Choi, J. eEdE-57
Choi, S. eP-31
Choi, S. eP-38
Choi, S. O-533
Choi, W. P-85
Choi, Y. eP-119
Choi, Y. eP-219
Choi, Y. O-533
Chokshi, F. H. eEdE-71, O-486
Chokshi, F. H. O-551
Chong, J. eEdE-22, eEdE-44, eEdE-93
Chong, J. J. R. eP-44
Chopra, P. R. eP-228
Chorney, E. T. eEdE-145
Chorney, E. T. eEdE-96
Choudhri, A. eP-243, eP-247
Choudhri, A. F. eEdE-116, eP-145, O-147
Choudhri, A. F. O-435, O-437, O-510
Choudhri, A. F. O-316
Choudhri, O. A. eP-135
Chow, D. O-548

Index of Program Participants

Numbers refer to session and presentation numbers, *not to page numbers*.
Index Key: O = Scientific Paper (Oral Presentation); EE = Electronic Excerpta e;
P = Scientific Poster (Print Format); eP = Electronic Scientific Poster (ePoster);
EdE = Education Exhibit (Print Format); eEdE = Electronic Education Exhibit

Chow, D. S. eEdE-85a, O-201, O-208
Chowdhury, R. O-288
Christoforidis, G. O-578
Christos, P. J. O-426
Chu, E. O-142
Chu, T. P-59
Chu, W.-F. eP-188, O-573
Chueh, J. Yu. eP-205
Chun, R. H. EE-39
Chung, G. O-519
Chung, M. EE-64
Chung, R. eEdE-118, eEdE-97
Chung, S.-Y. eP-38
Chung, W.-J. eP-83
Chunhua, Y. eP-101b
Chwang, W. B. eP-53, eP-56
Cianfoni, A. eP-289
Ciasca, P. O-410
Ciricillo, S. P-97
Ciura, V. A. O-110
Clarençon, F. eP-182, eP-294, O-101, P-91
Clark, K. H. EE-42
Clarke, A. O-103, O-94
Claude, J. O-66
Claus, E. O-36
Clerk-Lamalice, O. eP-220, O-160
Clifton, A. eP-202
Cloft, H. J. eP-194, eP-95, eP-96, O-534, O-96
Clopton, D. eP-166
Cloran, F. J. O-483
Close, O. eP-81
Cloughesy, J. N. O-541
Cloughesy, T. F. eEdE-35, O-210, O-287
O-288, O-401, O-406
O-541, O-544
Cobb, A. O-397
Coffey, M. EE-2, EE-9
Coffey, M. D. eEdE-26
Cognard, C. O-100
Cohen. G. eEdE-157
,
Cohen, M. G. eEdE-120, eEdE-125
Cohn, E. O-531
Coimbra, C. EE-25
Coimbra, C. J. eEdE-99
Colen, R. O-211
Colen, R. R. eP-130, eP-132, O-284
O-285, O-292, O-539, O-545
Colen, R. R. eEdE-30
Collins, M. W. O-425
Collins, P. O-30
Commins, D. L. P-37
Comunale, J. P. O-472
Conley, L. M. EdE-60, EdE-61
Connaughton, P. O-149
Conners, J. J. O-225, O-229
Connolly, D. J. A. O-319
Connor, S. O-132, O-566
Conrod, J. O-233
Cooke, D. eP-193
Cooke, D. L. eP-184, eP-201, O-555
Cooper, J. O-245
Cooper, L. O-211
Cooper, S. eEdE-20
Cooper, S. R. O-35
Cooper, S. R. O-37
Coopersmith, H. eEdE-162
Çorapçıoğlu, F. eP-224
Corcuera Solano, I. O-576, O-580
Corcuera-Solano, I. eEdE-106
Cordova, J. S. O-290
Corey, A. O-250, O-487, O-491
Corey, A. O-530
Corey, A. S. eP-283, O-307
Cormier, E. eP-294
Cornblath, W. EdE-58
Cornelius, R. EdE-54
Cornell, K. eP-156
Cornu, P. P-91
Cortes, M. eP-150
Cortes, M. D. P. P-87
Cortese, I. C. M. O-121
Cosgrive, J. EE-13
Costa, A. P-5
Coste, A. eP-72
Cotes, C. eEdE-167
Cotes, C. C. eP-128, O-526
Coughlin, J. M. O-427
Covington, A. eP-127
Covington, A. O-439
Crawley, A. O-105
Crawley, A. P. O-392
Cross, D. T. eP-206, O-97, P-93
Cross, J. O-25
Crow, Y. eP-233, eP-234
Crowley, H. eP-49
Cui, J. P-112
Culberton, S. P-49
Culbertson, C. J. P-62
Cunha, H. H. eP-9
Cunnane, M. O-412
Cunnane, M. E. EdE-54
Cupino, A. O-289
Cure, J. O-521
Cure, J. K. EdE-35
Curran, Y. O-229
Curry, W. EdE-25
Curtin, H. D. EdE-65
Curtis, L. O-221
Cuvinciuc, V. O-214
Czernin, J. eEdE-35, O-406

D

Dabbs, K. P-64
Daghistani, R. eP-225

Index of Program Participants

Numbers refer to session and presentation numbers, *not to page numbers*.

Index Key: O = Scientific Paper (Oral Presentation); EE = Electronic Excerpta e; P = Scientific Poster (Print Format); eP = Electronic Scientific Poster (ePoster); EdE = Education Exhibit (Print Format); eEdE = Electronic Education Exhibit

Dagis, A. eP-116
Daher Vaz, N. EE-28
Dahlin, B. eEdE-128
Dahmoush, H. M. eEdE-151
Dai, D. O-95
Dale, A. O-21, O-29, O-31
Dale, A. M. O-546
Dale, B. O-65
Dale, C. L. O-37
Dale, C. L. eEdE-20
Dalm, B. D. O-524
D'Ambrosio, F. eP-300
Damen, M. M. J. P-15
Danielian, L. E. eP-7
Danish, H. O-290
Danish, S. F. O-568
Darflinger, R. J. EE-46
Darke, M. eP-226
Darwish, M. M. N. eP-177
Das, K. EdE-80
Das, T. O-44
Dass, C. eP-100, O-429
Date, S. eP-54
Dave, H. eP-223
Davenport, E. M. eP-229, O-512
Davidson, H. eP-272
Davila-Acosta, J. H. eEdE-149
Davis, A. eP-85
Davis, E. eP-155
Davis, M. P-107
Davis, M. A. eP-266
Davis, R. eP-276, eP-287
Davis, S. M. eP-98
Davy-Jow, S. L. eP-104
Day, T. eP-138
De Bruin, D. E. eP-35, eP-87
De Cori, S. P-7
de Macedo Rodrigues, K. eP-221, O-432
De Marchi, D. P-7
de Venecia, C. eP-191
De vita, E. O-28
Dea, N. EE-58
Dean, B. L. eP-280
Debnam, J. Matthew. P-39
Debnam, J. Matthew. P-79, P-82
Debode, S. eEdE-138, eP-244
Decarie, J.-C. P-104
Decker, C. O-204
Decker, S. J. eP-104
Dehkharghani, S. eEdE-55, eP-101
eP-144, eP-170, O-302
O-388, O-58, O-62, O-68, P-53
Deible, C. R. eP-80
Deif, A. O-114
del Carpio, R. eEdE-22, eEdE-93
del Carpio-O'donovan, R. eEdE-44, eP-44
del Pilar Cortes, M. P-3
DeLano, M. C. eP-81
Delfyett, W. T. eP-106, eP-80, O-309, O-425
Delgado, D. O-494
Delman, B. N. eP-74
DeLoia, S. P. EE-42
DeLone, D. R. P-105
Demaerel, P. EE-26
Demaerschalk, B. M. P-63
Demchuk, A. eP-197
Demchuk, A. M. eP-98
Demehri, S. P-111
Demir, S. eP-218
Demirci, A. O-41
Demirci, D. O-41
Demtchouk, V. O-473
Denckla, M. O-508
Derdeyn, C. P. eP-206, O-97, P-93
Derkatch, S. O-207
Desai, J. eP-197
Desai, N. K. O-551, O-553, O-558
Desai, S. P-98
DeSalvo, M. O-139
Desco, M. O-206
Desikan, R. S. O-21, O-29, O-31
Deuerling-Zheng, Y. eP-199, eP-203
Deutsch, M. eP-251
Devulapalli, K. O-230
Dey, M. O-578
Di Maria, F. eP-294, P-91
Di Maria, F. I. O-101
Di Perri, C. O-511
Diaz, O. O-293
Dichgans, M. O-499
Dickson, A. eP-288
Diehn, F. E. eEdE-163
Diehn, F. E. O-252
Diehn, F. E. EE-74
Diehn, F. E. eP-298
Dietrich, A. O-26
Dietrich, J. P-36
Dietrich, R. eEdE-97
Dillon, W. P. O-131
Dineen, R. A. P-59
Ding, L. eP-6
Ding, Y. S. O-218
Ding, Y.-H. O-95
Dinkel, J. O-420, O-478
Dion, J. eP-170, O-302, O-68
Dipoce, J. eEdE-85a
Dittrich, E. O-318
Djoukhadar, I. A. EE-13, eEdE-131
eP-210, P-106
Dmytriw, A. A. O-419
Do, H. M. eP-135
Dobre, M. C. eP-79
Do-Dai, D. O-525
Do-Dai, D. D. eEdE-36

Index of Program Participants

Numbers refer to session and presentation numbers, *not to page numbers*.

Index Key: O = Scientific Paper (Oral Presentation); EE = Electronic Excerpta e; P = Scientific Poster (Print Format); eP = Electronic Scientific Poster (ePoster); EdE = Education Exhibit (Print Format); eEdE = Electronic Education Exhibit

Doerfler, A. eP-198, eP-203
Dolić, K. O-116
Dolinskas, C. A. P-38
Dombert, T. O-72
Domingues, R. O-238, O-477
Domingues, R. Cortes. eP-8
Donauer, E. O-98
Donev, K. EdE-24
Donmez, F. Y. eP-238, O-42b
Donohoe, K. eEdE-19
Donovan, W. eP-141
Donovan, W. D. EdE-81, EdE-82
Doolittle, D. eP-265
Doraiswamy, P. M. eP-10
Doring, T. eP-8
Dormont, D. O-166, O-582
Dorros, S. eEdE-97
Doshi, A. eEdE-106, eEdE-125
Douw, L. O-139
Dowd, C. eP-193
Dowd, C. F. eP-184, O-555
Dowlatshahi, D. eP-86, eP-98
Dowlatshahi, D. O-497
Dowling, M. O-556
Drazin, D. eP-67
Dresner, M. A. eEdE-175, O-137
Drissi, C. eEdE-70a
Drottar, M. eP-221
Druzgal, T. Jason. O-34
Du, X. O-176
Du, Y. O-36
Duan, S. O-496
Dubroff, J. G. EdE-12
Duffin, J. O-105
Dulay, M. F. O-235
Dumont, D. O-574
Duncan, C. T. O-67
Dunkin, J. eEdE-137
Dunn, W. O-211
Durst, C. EE-80, eP-151, eP-166 eP-174, O-289, O-416
Dwamena, B. A. P-10
Dyer, E. eP-180

E

Eastwood, J. O-484
Eastwood, J. D. eP-136, eP-137
Ebert, C. O-531
Eboli, P. eP-67
Eckart, D. eEdE-172, P-47
Eckel, L. eP-265
Eckel, L. J. O-252
Eckel, L. J. P-105
Edden, R. eP-15
Edden, R. A. E. O-22, O-243, P-10
Eddleman, C. S. O-295
Edeiken-Monroe, B. S. P-82
Edmonson, H. A. EdE-31
Eesa, M. eP-197, O-165
Ehlenberger, C. A. eP-157
Ehtiati, T. eP-162, O-60, P-86
Eibenberger, K. P-86
Eid, M. O-528
Eilaghi, A. O-119, O-120, O-125
Eilaghi, A. O-44
Einhaus, S. O-147
Eisenbeis, A. O-232
Ekholm, S. O-202, O-399, O-408
Elgethun, M. T. eEdE-16
Eliahou, R. eP-120
Elias, J. O-34
Elinzano, H. EdE-16
Elkhateb, M. eP-11
Ellika, S. K. O-411
Ellingson, B. O-475
Ellingson, B. M. eEdE-35, O-210, O-287 O-288, O-304, O-401 O-406, O-436, O-479, O-541, O-544
Elsayed, M. eP-11
Emblem, K. E. O-404
Enatsu, R. O-32
Endale, B. eEdE-28, O-161
Engel, C. W. eP-104
English, J. O-99
English, P. P-25
Enokizono, M. eP-108, eP-22, eP-3
Enterkin, J. eP-102, eP-299
Entezari, P. O-301
Erdogan, C. eP-148
Erickson, B. eEdE-30
Erickson, B. J. eP-298
Erickson, K. I. P-8
Erly, W. O-394
Erly, W. K. EdE-64
Ernstrom, K. P-63
Esclamado, R. O-484
Esclamado, R. M. eP-136, eP-137, O-418
Escorsi-Rosset, S. eP-13, eP-9
Escott, E. J. EdE-57
Eshetu, T. O-559
Eskey, C. EdE-20
Eskin, A. O-288
Esmaeli, B. P-79
Espinoza, F. V. O-531, P-83
Estrade, L. O-226
Etesami, M. EE-2, EE-9, eEdE-127
Evans, A. eP-151, eP-166, eP-174
Evans, D. T. O-282
Ezhapilli, S. eP-278
Ezzat, A. eP-215

F

Fadul, C. EdE-20
Fakhran, S. eP-303, O-306, O-422, O-529
Falini, A. O-283, O-410, O-540
Fallahian, A. H. eP-226

Index of Program Participants

Numbers refer to session and presentation numbers, *not to page numbers*.
Index Key: O = Scientific Paper (Oral Presentation); EE = Electronic Excerpta e;
P = Scientific Poster (Print Format); eP = Electronic Scientific Poster (ePoster);
EdE = Education Exhibit (Print Format); eEdE = Electronic Education Exhibit

Fang, A. EdE-78
Fanou, E. M. O-554
Farahani, S. J. P-111
Farahani, S. J. O-128
Faraji, F. O-102
Faria, A. V. O-506, O-507
Farid, N. eEdE-118, eP-69, O-546, O-549
Farnam, J. EdE-16
Faro, S. O-438, O-439, O-440
Faro, S. H. eP-262
Farquhar, T. P-113
Farrall, A. J. O-43
Fassler, X. eP-277
Fathy, A. eP-217
Fatterpekar, G. eP-142, eP-300, eP-45 eP-51, eP-61, O-26, O-500, O-501 O-570, P-35
Fatterpekar, G. M. eEdE-07
Fatterpekar, G. M. O-413, O-536 ,
Faul, D. O-218
Faulkner, M. P-107
Federer, G. E. EE-37
Feinstein, A. O-119, O-120, O-125
Felber, S. O-98
Feldman, E. L. O-22, P-10
Feldstein, N. A. EE-68
Feliciano, P. P-12
Felker, E. eEdE-75
Felker, E. R. eEdE-81
Felsberg, G. EE-33
Feltrin, F. Stewan. O-423
Feltus, W. Y. O-174
Feng, L. eP-147
Fenton, L. Z. eP-250, O-320
Ferguson, P. eEdE-100, P-81
Fernandez Alen, J. eP-43
Fernández-García, P. O-206
Ferrante, M. eEdE-122a
Ferrell, A. eP-189
Ferriero, D. P-100
Ferriero, D. M. O-509
Ferris, M. eP-164
Feygin, T. EdE-77, eEdE-155, O-550
Fiehler, J. O-232
Fig, L. M. EdE-11
Figà-Talamanca, L. eP-216
Figi, A. R. eEdE-134
Filho, E. Albuquerque. eEdE-76
Filippi, C. O-201, O-208, O-548
Filippi, C. G. EE-68, eEdE-85a, O-118, O-67
Filosto, M. O-76
Findlay, A. M. eEdE-20, O-37
Fink, K. R. eP-46, O-298
Finsterbusch, J. eP-262
Fiorella, D. eP-291
Fiorella, D. J. eP-199
Firat, S. eEdE-143
Firbank, M. P-25
Fisch, C. O-160
Fischbein, N. eP-79
Fischbein, N. J. O-112
Fischer, S. eP-192, eP-195, eP-209
Fishbein, L. O-483
Fisher, J. O-105
Fisher, J. A. O-392
Fisher, W. O-521
Fitzgerald, R. EdE-73, EdE-74, eEdE-83
Fitzgerald, R. T. eP-49, eP-65
Fitzgibbons, M. EdE-41
Fitzpatrick, D. eEdE-120
Fitzpatrick, D. eEdE-46
Flaherty, M. L. eP-98
Flanders, A. eEdE-178, O-211, O-292, O-539
Flanders, A. E. EE-77, EE-79, EE-88 eEdE-175, eEdE-30
Flanders, A. E. O-137, O-284
Flanders, A. E. eP-12
Fleetwood, I. O-300
Fleyscher, L. O-124
Fleysher, R. O-482
Flint, D. J. eEdE-104
Floca, R. O-503
Floeter, M. K. eP-7
Flores, L. G. eP-296
Flores-Sarnat, L. O-321
Florman, J. EE-24
Flynn, P. eP-155
Fodera, V. O-61, P-52
Foerster, B. R. O-22, P-10
Fogel, B. O-475
Fong, C. eEdE-04
Fong, C. L. EE-82
Fong, C. L. EE-66
Fons Estupina, M. O-432
Font, S. eEdE-86
Forbes, K. P. eP-92
Ford, G. eP-202
Ford, I. eP-202
Ford, J. M. eP-104
Foreman, N. K. eP-255
Forrester, L. eP-163
Förschler, A. O-224, O-93
Forsting, M. eP-171, eP-172, O-299
Fortes, M. eEdE-02
Fortes, M. C. EE-85
Fountain, A. J. eP-283, O-307
Fourgas, E. eEdE-48, O-523, O-528
Fourie, E. P-98
Fowkes, M. eEdE-106
Fox, A. J. O-103
Fox, C. eP-193
Fox, L. EdE-76
Fox, W. C. eP-157

Index of Program Participants

Numbers refer to session and presentation numbers, *not to page numbers*.
Index Key: O = Scientific Paper (Oral Presentation); EE = Electronic Excerpta e;
P = Scientific Poster (Print Format); eP = Electronic Scientific Poster (ePoster);
EdE = Education Exhibit (Print Format); eEdE = Electronic Education Exhibit

Franceschi, A. M. O-389
Franceschi, D. EdE-03
Francis, P. O-119, O-120
Francis, P. L. O-125
Fredriksen, J. R. eEdE-32, O-175
Freymann, J. eP-101b, O-292, O-539
Freymann, K. eEdE-30
Friedel, R. O-33
Friedman, D. P. O-248
Friedman, E. P-19
Friedman, J. EdE-85
Friedman, K. P. O-218
Friedrich, B. O-224, O-93
Frijia, F. P-7
Frölich, A. M. O-51
Fruehwald-Pallamar, J. O-116
Frysinger, R. O-34
Fu, R. O-286
Fu, R. O-405
Fuentes, P. eP-277
Fujii, H. EE-53
Fujimoto, M. P-50
Fujita, A. EE-53
Fujita, T. eP-122
Fukuda, S. eP-3
Fukui, M. B. eEdE-16, eEdE-37
Fukutomi, H. EdE-83
Fuller, G. O-167
Fullerton, H. eP-193
Fullerton, H. J. O-54
Fung, S. H. O-235
Furtado, A. D. O-436
Furukawa, M. eP-113, eP-117, eP-121 eP-122, P-18, P-65
Futatsuya, K. eP-64, O-219, O-63
Futterer, S. EE-8

G

Gabriel, R. eEdE-45
Gabriel, S. P-105
Gabrieli, J. eP-294
Gach, H. P-8
Gaddamanugu, S. EdE-15
Gaddamanugu, S. EdE-35
Gadde, J. O-547
Gaddipati, A. O-576
Gafton, A. R. O-414
Gagoski, B. O-149
Gahramanov, S. O-286, O-405
Gaikwad, S. P-30
Gaillard, W. D. O-143
Gailloud, P. EE-31, EE-37a
Gajjar, M. EdE-51
Galanaud, D. O-166, O-420, O-478, O-563, O-582
Gallagher, T. P-56
Gallucci, M. eP-49
Gandhe, A. R. EE-77, EE-79, EE-88, eEdE-178
Gandhi, D. EE-85, eEdE-02, O-281, P-89
Gandhi, S. EE-43, eEdE-122b
Gangadhar, K. eP-142
Gao, J.-H. O-578
Garcia, L. A. L. P-26
Garcia, L. E. eEdE-74
Garden, A. O-537
Garg, A. P-30
Gargan, L. eP-252
Garger, A. A. V. eEdE-85a
Garger, A. V. EE-68, EE-90
Garvin, J. EE-68
Gaskill-Shipley, M. EdE-13
Gasparetto, E. L. eP-19
Gasparetto, E. Leandro. eP-8, O-238, O-477
Gasparotti, R. O-76
Gass, A. O-30
Gaudric, J. eP-294
Gaughan, J. O-438, O-440
Gaughen, J. eP-151, eP-174
Gbucz, I. O-100
Ge, G. O-99
Ge, Y. O-518
Geibprasert, S. O-274
Geller, J. eP-156
Gemmete, J. J. eP-295, O-277, P-92
Gentry, L. eEdE-85, eEdE-86
Gentry, L. R. eEdE-92
Gentry, L. R. eEdE-119
George, A. O-220, O-23
George, A. E. O-218
George, M. EdE-22
Georgy, B. eP-285, O-310, O-311
Georgy, M. eP-285, O-310
Gerber, S. O-166, O-563
Germano, I. eP-74
Gersing, A. S. O-232
Gerstner, E. O-403
Gerstner, E. R. O-404, P-36
Geschwind, M. P-5
Geschwind, M. D. eP-48
Ghassemi, A. P-97
Gholkar, A. eP-178, O-99
Ghosh, S. EE-5
Ghostine, J. O-275
Giannakopoulos, P. O-214, O-216, O-221
Gibbs, W. N. eP-280
Gibson, D. eEdE-160
Gibson, J. EE-19, EE-81, EE-83
Gibson, T. EE-48
Gidley, P. O-537
Gilbertson, J. eP-298
Gillard, J. O-25
Gillen, J. O-243
Gillies, G. T. O-524
Ginat, D. EdE-21, EdE-25
Ginat, D. T. eP-131
Gingras, J.-M. eP-166

Index of Program Participants

Numbers refer to session and presentation numbers, *not to page numbers*.

Index Key: O = Scientific Paper (Oral Presentation); EE = Electronic Excerpta e; P = Scientific Poster (Print Format); eP = Electronic Scientific Poster (ePoster); EdE = Education Exhibit (Print Format); eEdE = Electronic Education Exhibit

Ginsberg, L. O-537
Ginsberg, L. E. EE-41, O-485
Ginsberg, L. E. P-79
Gladstone, D. J. eP-98
Glasier, C. M. eP-256
Glass, H. P-100
Glass, H. C. O-509
Glastonbury, C. M. O-538
Gleason, A. K. O-230
Gledson, A. eP-233, eP-249
Glielmi, C. O-218
Glikstein, R. eEdE-09
Gnerre, J. M. eP-288
Go, C. O-145
Go, J. EE-12, eEdE-121
Go, J. L. EdE-28
Go, J. L. O-244, P-37
Go, J. L. eEdE-117, eEdE-15, eEdE-173
Go, M. eEdE-19
Gobin, Y. P. O-99
Gocmen, R. eEdE-31
Goddard, A. eP-210, P-106
Godfrey, W. eEdE-101
Godwin, D. eP-229, O-512
Goelitz, P. eP-203
Goericke, S. Luise. eP-171, eP-172
Goff, D. eP-6
Goktekin, O. O-104
Gold, J. P-19
Goldberg, M. F. eEdE-123, eEdE-37, O-171
Goldman, M. EdE-16
Goldsher, D. EdE-34, eP-91
Goldstein, A. EdE-07, eEdE-01
Goldstein, J. N. O-110
Golfinos, J. , P-35
Golnik, K. EdE-54
Golomb, J. O-220, O-23
Golovac, S. O-314
Gomez, C. O-164
Gomez, P. eP-43
Gommsani, R. E. eEdE-90
Gomyo, M. eP-29, eP-94, O-108
Goncalves, F. G. eEdE-44
Goncalves, F. Guimarães. eEdE-22
Gonçalves, F. Guimarães. eEdE-93
Gonen, O. O-23
Gonyea, J. V. O-118, O-67
Gonzalez, M. eP-277
Gonzalez, R. O-245, O-255
Gonzalez, R. Gilberto. O-110
Gonzalez-Martinez, J. O-32
Gorman, D. P-14
Gornet, M. O-66
Gorniak, R. J. T. eEdE-175, O-137
Gory, B. eP-182
Gould, R. G. eP-184
Gounis, M. J. eP-165, eP-205, eP-207, eP-6
Goyal, M. eP-197, O-165
Goyal, V. P-30
Graf, M. O-503
Grafman, J. eP-7
Graham, C. eP-163
Grant, P. eP-221, O-432
Grant, P. E. eP-245
Grant, P. Ellen. eEdE-152
Grant, P. Ellen. O-149
Grattan-Smith, D. EdE-71, EdE-88
Green, D. B. eEdE-162
Green, S. J. eP-141
Greene, J. O-212
Greenstein, M. O-39
Greenwood, M. P-113
Gregg, L. EE-37a
Gregson, B. eP-178, eP-286
Greiner, H. O-144
Greiner, M. V. eP-230
Griauzde, J. P-92
Griffith, B. EE-87, eEdE-82, eP-267, eP-52, O-129
Griffiths, P. O-554
Griffiths, P. D. O-325, O-557, O-560
Grigg, A. EE-14
Grignon, L. O-247
Grinband, J. O-208
Grinstead, J. O-304
Gross Kelly, T. C. EE-39, eEdE-143
Gross, M. D. EdE-11
Gross, R. E. eEdE-71
Grosshans, D. eP-290
Grossman, J. AI. EE-64
Grossman, R. G. O-235, O-293
Grossman, R. I. O-124, O-518
Gubbels, S. P. eEdE-119
Guenzler, V. O-30
Guerin, S. J. EdE-84
Guermazi, A. eEdE-70a
Guha-Thakurta, N. P-39, P-79
Gui, D. O-576
Guidon, A. eP-10
Guirado, V. Monteiro. Paula. O-423
Gul, M. EdE-03, eEdE-137, eEdE-34
Guler, E. eEdE-31
Guler, I. eEdE-31
Guleria, S. eEdE-143
Guleryuz, P. eP-238, O-42b
Gundlack, F. O-60
Güngör, T. eP-235
Guo, W.-Y. eP-188, O-223, O-272, O-573
Guo, X. O-201, O-548
Guo, X. O-578
Gupta, A. O-294, O-494, O-61, P-52
Gupta, D. eP-142
Gupta, G. eEdE-12
Gupta, J. eP-55, O-502, P-64
Gupta, M. eEdE-99

Index of Program Participants

Numbers refer to session and presentation numbers, *not to page numbers*.

Index Key: O = Scientific Paper (Oral Presentation); EE = Electronic Excerpta e; P = Scientific Poster (Print Format); eP = Electronic Scientific Poster (ePoster); EdE = Education Exhibit (Print Format); eEdE = Electronic Education Exhibit

Gupta, N. O-537
Gupta, R. O-420, O-478
Gupta, S. EdE-40, EdE-49, eEdE-17, eEdE-61
Gutierrez, J. EE-87
Gutman, D. eP-101b, eP-132, O-284, O-292
Gutman, D. A. O-211
Gutman, D. A. O-539
Gutman, D. A. O-290
Gutman, , D. A. eEdE-30
Guzik, A. K. P-63
Guzman, R. O-475
Guzmán-De-Villoria, J. A. O-206

H

Ha, B. P-74
Haacke, E. O-518
Hackman, T. G. eP-126
Hackney, D. eEdE-176
Hackney, D. B. O-42a
Hadeishi, H. P-44
Hadjipanayis, C. G. O-290
Hadley, J. Rock. eP-134
Hagerman, P. O-27
Hagerman, R. O-27
Hagiwara, M. eP-142, O-413, O-536
Haithcock, J. A. EE-60
Hajj-ali, R. P-70
Hakham, S. eEdE-115, eEdE-36
Hakimelahi, R. eP-128, O-526
Hakyemez, B. eP-148
Hakyemez, B. eP-23
Hakyemez, B. eP-28
Halbach, V. eP-193
Halbach, V. V. eP-184, O-555
Hall, J. EdE-14
Haller, S. O-214, O-216, O-221
Halm, K. eEdE-159
Halpin, J. S. eP-228
Hamberg, L. M. eP-131
Hamilton, B. E. O-405
Hamilton, B. H. O-474
Hamilton, J. EdE-44, EdE-46, O-537
Hamilton, J. D. EdE-39
Hamilton, J. D. O-402, O-485
Hamilton, J. D. eP-77, O-282
Hammer, K. O-93
Han, J. O-105
Han, M. eEdE-57
Han, M. eP-31
Han, M. O-297, P-88
Han, S. S. P-38
Han, Z. eP-79
Hanagandi, P. B. eEdE-22, eEdE-44
Hanagandi, P. B. eP-44
Hanagandi, P. Baladev. eEdE-93
Handwerker, J. EE-29, eEdE-13, O-142
Haneda, J. P-75
Hanks, J. B. O-416
Hanley-Knutson, K. O-168
Hansra, N. eP-275, P-114
Hara, A. P-21
Harb, J. G. EE-7
Hargens, A. eEdE-167
Hargreaves, E. L. O-568
Harmening, K. O-93
Harnsberger, H. Ric. O-538
Harnsberger, R. O-528
Harris, A. L. EdE-35
Harris, J. P-98
Harris, J. H. eP-280
Harris, R. J. O-479
Harris, R. J. eEdE-35, O-288, O-401
Harris, R. J. O-541, O-544
Harrison, C. E. O-486
Harsha, A. eP-263
Harshman, B. P-32
Hart, B. EE-14
Hart, B. L. EdE-32
Härtl, R. O-426
Hartman, A. L. O-506, O-507
Hartman, A. L. O-321
Hartman, L. A. eEdE-03
Hartman, M. eEdE-03
Hartman, M. J. eEdE-92
Hartwigsen, G. O-239
Hartzog, J. P-107
Hasan, K. eP-12
Hasan, K. M. eP-128
Hash, S. O-282
Haslwanter, T. P-86
Hassan, A. eP-210
Hassan, A. O-117
Hassan, D. eEdE-149
Hassan, E. EdE-79
Hasso, A. O-142
Hasso, A. N. EE-29, eEdE-13
Hatch, N. O-123
Hathout, G. eP-110, eP-279
Hattori, N. P-23
Haubrich, N. eEdE-174
Hauer, M. eP-198
Haughton, V. O-130
Hawasli, A. EdE-17
Hawk, H. E. eP-176
Hayakawa, Y. eP-112
Hayashi, D. eEdE-70a
Hayashi, K. eP-3
Hayashi, T. eP-22
Hayek, R. A. EdE-32
Hayes, L. L. EdE-71, EdE-88
Hayman, L. EdE-44, EdE-46
Hayman, L. Anne. EdE-39
Hayman, L. Anne. O-402
Hazany, S. eEdE-15
Hebert, J. P-87

Index of Program Participants

Numbers refer to session and presentation numbers, *not to page numbers*.

Index Key: O = Scientific Paper (Oral Presentation); EE = Electronic Excerpta e; P = Scientific Poster (Print Format); eP = Electronic Scientific Poster (ePoster); EdE = Education Exhibit (Print Format); eEdE = Electronic Education Exhibit

Heck, C. eEdE-15
Hedges, K. eP-245
Hegde, S. EdE-73, EdE-74
Hegenbart, U. O-71
Hegi, M. eP-130
Heidary, G. O-411
Heier, L. P-101
Heiland, S. eP-293, O-204, O-391, O-503, O-75
Hein, A. eP-106
Heiserman, J. E. eP-280
Helmer, E. EE-32
Helpern, J. O-123, O-400
Helton, K. J. O-473
Helvey, J. T. eEdE-60
Helvey, J. T. EE-20
Hemmen, T. M. P-63
Henderson, L. eP-266
Henderson, R. eEdE-15
Henkel, D. O-144
Henkes, H. eP-192, eP-195, eP-209, O-98
Henley, D. P-20
Henry, C. O-166
Henry, L. O-425
Henry, R. G. eP-48
Heran, M. K. S. EdE-67, EE-30, EE-58
Herbert, J. eP-61, O-124
Herbst, T. P-113
Hermoye, L. eP-57
Hernandez Lain, A. eP-25
Hernandez, R. J. O-173
Herrington, J. EdE-25
Herrmann, F. O-214
Hershey, B. eP-100, O-429
Herskovits, E. H. O-64, P-46
Herwadkar, A. eEdE-170, eEdE-78, eEdE-80
Hess, C. P. eP-48, O-509, O-54
Hesselink, J. R. eP-69, O-549
Heth, J. P-43
Hetts, S. eP-193
Hetts, S. W. eP-184, eP-201, O-555, O-561, O-99
Heymann, J. eEdE-167
Heymann, J. C. eP-128, O-526
Heyne, R. O-431
Hiatt, M. D. O-246, O-254
Higaki, T. eP-54
Higashida, R. eP-193
Higashida, R. T. eP-184, O-555
Higashide, T. eEdE-87
Hijaz, T. EE-8
Hilario, A. eP-25, eP-43
Hild, M. P-28, P-31
Hildreth, K. O-106
Hill, P. O-251, O-253
Hill, S. P-98
Hillenbrand, C. eP-270
Hipko, S. O-118, O-67
Hippe, D. S. eP-46, O-205
Hira, A. eP-231
Hira, A. S. EdE-05
Hirai, T. eP-33, eP-5, O-516
Hiratsuka, Y. eP-40
Hirsch, J. O-245, O-255
Hirsch, J. A. EdE-81
Hise, J. H. eP-211
Hito, R. eP-131
Hiwatashi, A. eP-129, P-84
Ho, C. P-103
Ho, C. Y. eP-253, O-134
Ho, C. Yueh. eEdE-133
Hoang, J. K. eP-136, eP-137, O-308
O-415, O-417, O-418, O-484
Hoang, K. O-563
Hobbs, H. A. eP-137, O-418
Hoch, M. eP-100, O-429
Hochstetler, H. P-20
Hoeberigs, M. Christianne. P-15
Hoeffner, E. eEdE-51
Hoefling, N. EE-16
Hoefling, N. L. eEdE-34
Hoffman, H. T. eEdE-88
Hoffmann, C. eP-241
Hofman, P. A. M. P-15
Hofmeister, J. O-216
Hogarth, K. O-566
Holder, C. eP-101b, O-211
Holder, C. A. eEdE-30
Holder, C. A. O-284
Holder, C. A. O-539
Holder, C. A. O-290
Holdsworth, R. O-39
Holland, D. O-21, O-29, O-31
Holland, S. eP-257
Holland, S. K. O-505
Holland-Bouley, K. O-144
Holliday, R. eEdE-86
Holliday, R. A. eP-242
Holloway, W. P-95
Holly, L. T. O-304
Holmes, J. H. O-56
Holness, S. P-80
Holstad, J. eEdE-65
Honarmand, A. R. EE-36, EE-63, EE-73
Honarmand, A. R. O-228, O-229, O-277
O-301, O-504
Honarmand, A. R. O-225
Honce, J. M. eEdE-24
Honda, H. eP-129, P-84
Honda, S. eP-22
Honda, Y. eP-54
Hong, B. EE-1, eP-196
Hong, Y. O-162
Honma, S. M. eEdE-20, O-37
Honnebier, B. EdE-74
Hopf, N. O-98

Index of Program Participants

Numbers refer to session and presentation numbers, *not to page numbers*.

Index Key: O = Scientific Paper (Oral Presentation); EE = Electronic Excerpta e; P = Scientific Poster (Print Format); eP = Electronic Scientific Poster (ePoster); EdE = Education Exhibit (Print Format); eEdE = Electronic Education Exhibit

Hopkins, K. L. EE-67
Hoque, K. EE-12, eEdE-117, eEdE-121
Hoque, K. E. eEdE-173, eEdE-39
Horenstein, C. O-208
Hori, M. eP-30, P-23
Horie, N. eP-22, eP-3
Horikoshi, T. eEdE-87
Horn, C. eEdE-125, eEdE-145 eEdE-157, eEdE-46
Hornegger, J. eP-79
Hornung, B. O-71, O-74
Horsburgh, A. EdE-47, EdE-90, EE-54a P-29, P-72, P-73, P-76, P-77, P-9
Horska, A. O-508
Horsley, L. C. eEdE-29
Horsley, W. O-247
Hoshi, K. P-44
Hou, P. eP-77, O-282
Hou, S. EE-59, eP-165, eP-181, eP-207
Howard, E. A. O-164
Howard, M. A. O-524
Howell, L. L. O-62
Howell, M. eP-303
HR, A. eP-109
Hsieh, K.-C. eP-34
Hsu, D. O-230
Hsu, F. P. K. eEdE-13
Hsu, H.-L. O-237
Hsu, L. eEdE-25, eEdE-38
Hsu, N.-W. P-27
Hsu, Y.-H. O-276
Hu, J. eEdE-122
Hu, S. O-66
Hu, Y. P-112
Huang, A. P-11, P-54
Huang, B. O-531
Huang, E. eEdE-30
Huang, E. O-539
Huang, J. eP-110
Huang, J. eP-279
Huang, Q. EE-1
Huang, R. Y. P-109
Huang, S. eP-101b
Huang, Y. O-574
Huang, Y.-L. O-42
Hudgins, P. O-487, O-491, O-530
Hudgins, P. A. eEdE-71, eP-144, O-250, O-486
Hudson, M. M. eP-270
Huerga, E. eP-62
Huey, E. D. eP-7
Hughes, M. A. eP-80
Hughes, N. eP-149
Huhdanpaa, H. eEdE-39, P-37
Huhdanpaa, H. T. eEdE-52
Hui, F. P-70
Hui, F. K. eP-180, O-393
Huisman, T. A. G m. eEdE-136
Huisman, T. A. G. M. eP-222, eP-223
Huisman, T. A. G. M. eP-248
Huisman, T. A. G. M. O-506, O-507, O-559
Huisman, T. A. G. P-99
Huisman, T. A. G. M. eP-235
Huisman, T. A. G. M. O-321, O-322, O-433
Huisman, T. Agm. eEdE-172
Hund, E. O-71
Hung, S.-C. eP-188, O-223, O-573
Hunt, C. eP-298
Hunt, C. H. eEdE-08, eEdE-163, O-252
Hunter, G. J. eP-131
Hunter, J. EdE-39, O-402
Hunter, J. V. EdE-44, EdE-46, eP-246
Hurley, M. EdE-51, eP-36
Hurley, M. C. EE-36, EE-63, EE-73, eP-84
Hurley, M. C. O-228, O-229, O-277, O-504
Hurley, M. C. O-225
Hurst, R. EdE-42, eEdE-126
Hurtado Rua, S. O-294
Hurtado Rua, S. M. O-494
Huss, D. O-34
Huss, D. O-39
Hussain, A. O-399
Hussain, N. O-39
Hussain, S. O-393
Huynh, T. J. eP-98
Huynh, T. J. O-44
Huynh, T. J. O-574
Hwang, D. H. eEdE-39, eEdE-52, P-37
Hwang, S. O-388
Hwang, S. O-519
Hwang, S. N. eEdE-30
Hwang, S. N. O-539
Hwang, S. N. O-284, O-290, O-292
Hwang, W. D. P-49
Hyder, I. Z. P-38
Hygino da Cruz, L. O-570
Hynecek, R. EdE-52
Hynynen, K. O-574

I

Iadanza, A. O-410
Iaia, A. O-547
Iancu, D. O-227, O-497
Ibrahim, H. EE-40
Ibrahim, M. EdE-58, eEdE-103 eEdE-107, eEdE-132, eEdE-171 eP-259, O-514, O-571
Ibrahim, S. M. eEdE-43
Ibrahim, Y. O-114
Ichinose, N. P-90
Ide, S. eP-93, O-122, O-219, O-63
Ideguchi, R. eP-108, eP-22
Idowu, O. eP-292
Iida, E. eP-113, eP-122, P-18, P-65
Im, N. eEdE-57
Inaoka, T. EE-49

Index of Program Participants

Numbers refer to session and presentation numbers, *not to page numbers*.

Index Key: O = Scientific Paper (Oral Presentation); EE = Electronic Excerpta e; P = Scientific Poster (Print Format); eP = Electronic Scientific Poster (ePoster); EdE = Education Exhibit (Print Format); eEdE = Electronic Education Exhibit

Inglese, M. O-124
Inoue, K. eEdE-87
Inoue, K. eP-1
Intrapiromkul, J. eP-15
Iqbal, A. eP-92
Iqbal, M. eP-123
Iqbal, S. eP-123
Iryou, Y. O-516
Ishibashi, T. eP-264
Ishikawa, K. P-75
Ishiyama, M. eP-117, eP-121
Iskander, A. eP-56
Ison, C. eP-77
IST-3 Collaborative Group O-43
Itagiba, V. G. A. eP-8
Itokawa, H. P-50
Iv, M. O-112
Ivanidze, J. O-472
Iwata, T. eP-173, eP-208, eP-39, O-231, O-48
Iwata, Y. O-231
Iyer, V. R. P-78
Izbudak, I. eEdE-136, eEdE-172
eP-222, eP-223, eP-292, O-133

J

Jaberi, A. eP-86, O-497
Jackson, A. eP-249, O-517, O-542
Jackson, E. F. eP-77, O-282
Jacob, F. O-432
Jacob, R. eEdE-147, eP-254
Jacobson, J. O-396
Jacobson, S. O-69
Jacques, T. S. eEdE-144
Jafari-Khouzani, K. O-404
Jaffe, C. eP-101b, O-211, O-284, O-292
Jaffe, C. C. eEdE-30
Jaffe, C. Carl. O-539
Jaghadeesan, B. O-109
Jahng, G. P-85
Jahng, G.-H. eP-83
Jain, A. B. eP-116
Jain, R. eEdE-30
Jain, R. eP-267, eP-52, eP-53
eP-56, O-129, O-211, O-284
O-292, O-539, P-107
Jakacki, R. eP-251, O-436
Jakubovic, R. O-120, O-125
Jakubovic, R. O-44
Jallo, G. eP-222, O-506, O-507
Jallo, G. I. O-559
Jameison, s. EE-13
Jamjoom, D. Z. eP-103
Jamshidi, P. EE-50
Janowski, M. O-59
Jansen, J. F. A. P-15
Jansen, T. R. O-312, O-313, P-110
Januel, A.-C. O-100
Jara, H. eP-214
Jarafi-Khouzani, K. P-36
Jarquin, S. O-166
Jarraya, M. eEdE-70a
Jarvis, D. O-325
Javadi, P. EE-2, EE-9, eEdE-127, eEdE-26
Jay, A. eEdE-74, eEdE-79
Jayakrishnan, V. eP-178
Jean, B. eP-72
Jean, B. O-101
Jeeva, I. P-106
Jeevan, D. eP-231
Jensen, J. O-123, O-124, O-400
Jensen, M. eP-151, eP-174
Jensen, M. eP-55, O-502
Jensen, M. B. P-64
Jensen, M. Elizabeth. eP-166
Jeon, P. O-398
Jeong, B. eEdE-14
Jeong, Y. I. eP-84
Jewells, V. eEdE-29, eP-126
Jeyapalan, S. EdE-16
Jhala, N. C. EE-38
Jhaveri, M. EdE-87
Jiang, F. eP-70
Jiang, W.-J. O-393
Jilwan-Nicolas, M. eEdE-30
Jilwan-Nicolas, M. O-539
Jin, J. O-99
Jin, K. eP-38
Jindal, G. EE-85, eEdE-02, P-89
Jirari, M. O-280
Jissendi-Tchofo, P. O-242, O-577
Jittapiromsak, P. eP-185
Joe Qiao, J. eEdE-05
Jogal, S. eEdE-143
Johnathan, S. P-61
Johnson, C. E. O-472
Johnson, J. eP-261, O-315
Johnson, J. M. eP-125
Johnson, K. O-575
Johnson, M. EdE-02, eEdE-01
Johnson, M. H. eEdE-124
Johnstad, T. R. O-246
Johnston, S. C. O-99
Jonathan, S. V. eP-84
Jones, B. O-552
Jones, B. V. eEdE-129, O-505
Jones, J. O-282, O-485
Jones, J. G. A. EdE-70
Jones, J. R. O-282
Jones, K. S. eEdE-45
Jones, R. EdE-88
Jones, S. eP-180, O-32, P-70
Jones, S. S. O-393
Jordan, D. W. O-279
Joseph, N. M. eP-68
Joseph, O. O-115

Index of Program Participants

Numbers refer to session and presentation numbers, *not to page numbers*.
Index Key: O = Scientific Paper (Oral Presentation); EE = Electronic Excerpta e;
P = Scientific Poster (Print Format); eP = Electronic Scientific Poster (ePoster);
EdE = Education Exhibit (Print Format); eEdE = Electronic Education Exhibit

Joshi, A. EdE-08
Joshi, A. eP-123
Joshi, A. S. EdE-53
Jubinski, P. eP-239
Jubouri, S. O-143, O-409
Juliano, A. O-412
Juliano, A. F. EE-47
Junck, L. O-571
Junck, L. R. P-43
Jung, H. O-398
Jung, J. P-74
Jung, M. eP-158, eP-159, eP-160
Jung, M. eP-179, eP-267
Jung, M. W. eEdE-82
Jung, S. eP-158, eP-159, eP-160
Jung, S. O-297
Jung, S. P-45
Jung, S. P-48
Jung, S. P-88

K

Kabir, K. O-312, O-313
Kabir, K. P-110
Kademian, J. eEdE-168
Kadirvel, R. O-95
Kadivar, K. O-414
Kadoch, M. A. eEdE-120, eEdE-125, eEdE-145 eEdE-157, eEdE-46, eEdE-96
Kadokura, S. eP-169
Kadom, N. O-143, O-409
Kadziolka, K. eP-183, O-100, O-226
Kagetsu, N. EdE-43
Kai, Y. eP-5
Kaichi, Y. eP-54, eP-64
KajIwara, Y. eP-41
Kakeda, S. eP-64, eP-93, O-122, O-219, O-63
Kakigi, T. eP-27
Kalayci, O. eP-248
Kallmes, D. O-95
Kallmes, D. F. eP-194, eP-95, eP-96, O-534
Kallmes, D. F. O-96
Kalnins, A. U. eEdE-159
Kalpathy-Cramer, J. O-404, P-36
Kalra, V. EE-83, eP-239
Kalra, V. B. EE-19, EE-81
Kamagata, K. eP-30, P-23
Kamali, A. eEdE-175, eP-12, O-137
Kamalian, S. eP-97, O-389
Kamaly-Asl, I. eP-249
Kamer, A. P. O-134, P-103
Kaminsky, I. O-60
Kamiya, K. eP-30, P-23
Kane, P. O-66
Kaneda, T. eP-112, eP-114
Kanfi, A. eP-282
Kang, H. eP-158, eP-159, eP-160
Kang, H. eP-32
Kang, H. P-88
Kang, J. eP-144, O-551
Kang, S. O-562
Kao, S. eEdE-100, P-81
Kara, E. EE-54
Karadoğan, M. eP-224
Karagiozov, K. L. eP-264
Karagulle Kendi, A. Tuba. O-486
Karenfort, M. eP-237
Karmonik, C. O-235, O-293
Karolyi, D. R. O-115
Karr, L. O-118
Karsandas, A. EdE-14
Karwacki, G. O-239
Kasprian, G. J. O-318
Kassner, A. O-125
Kastler, A. eP-133, eP-284, O-515
Kastler, B. eP-133, eP-284, O-515
Kato, M. eP-113, eP-122, P-18
Katorza, E. eP-241
Katsaros, V. K. eP-57
Katz, J. S. O-64a
Katz, Z. O-60
Kaufmann, T. J. EE-74
Kawamura, Y. eP-20, P-44
Kaya, A. O-41
Kazlas, M. O-412
Kazmi, S. A. Jaffar. O-407
Keane, J. eP-233, eP-249
Keiper, M. O-247
Keiper, M. D. EE-65, eEdE-60
Keiper, M. D. EE-20
Kele, H. eP-293, O-73
Keller, I. A. O-568
Kelly, H. R. EdE-65, eP-131
Kelly, M. eEdE-82
Kelly, T. Gross. eEdE-169
Kemeny, J. Louis. eP-72
Kennedy, T. eEdE-03
Kennedy, T. A. eEdE-119, eEdE-92
Kereshi, B. eP-138, O-400
Kerr, R. O-94
Kertels, O. O-224
Kesari, S. eP-69, O-549
Kesser, B. O-535
Kessler, B. A. EdE-27
Ketonen, L. EE-21, eP-77, O-167, O-282
Ketonen, L. M. P-39
Ketter, N. O-30
Keyes, D. O-115
Khaled, M. O-34
Khaleel, Z. EE-11, eP-297
Khalil, K. eP-52, O-292
Khalil, T. eP-72
Khalilzadeh, O. O-420, O-478
Khan, M. eEdE-51
Khan, M. eP-207
Khan, P. eP-151

Index of Program Participants

Numbers refer to session and presentation numbers, *not to page numbers*.

Index Key: O = Scientific Paper (Oral Presentation); EE = Electronic Excerpta e; P = Scientific Poster (Print Format); eP = Electronic Scientific Poster (ePoster); EdE = Education Exhibit (Print Format); eEdE = Electronic Education Exhibit

Khan, R. EdE-18, EdE-55, EdE-92, O-390, O-394
Khatri, P. eEdE-63
Khledi, R. A. eEdE-90
Khorrami-Arani, N. eEdE-102, eEdE-111
eEdE-113, eEdE-166, eEdE-177
eEdE-179, eEdE-66, eEdE-89, eEdE-98
Khwaja, O. O-432
Kido, D. O-396, P-102, P-80
Kikuchi, K. eP-129
Kikuchi, K. eP-40
Kikuchi, K. P-84
Kikuchi, N. P-50
Kikuchi, Y. eP-20
Killiany, R. J. O-476
Kim, B. eP-111
Kim, B. O-398
Kim, B. P-45
Kim, B. P-48
Kim, D. eP-24, eP-83, O-217, O-562
Kim, E. P-4
Kim, E. Y. O-113, O-387
Kim, H. eP-187
Kim, H. eP-187
Kim, H. eP-24
Kim, H. eP-38
Kim, H. eP-76, eP-83
Kim, H. O-107
Kim, H. O-217
Kim, H. O-217
Kim, H. O-398
Kim, H. O-398
Kim, H. O-562
Kim, H. J. O-401, O-541
Kim, H.-J. P-74
Kim, I. eP-119
Kim, I.-O. eP-219
Kim, J. eEdE-110
Kim, J. eP-118, eP-119
Kim, J. eP-38
Kim, J. eP-47
Kim, J. P-74
Kim, J.-H. eP-31
Kim, J.-H. O-533
Kim, K. eEdE-14
Kim, K. eP-111
Kim, K. eP-118
Kim, K. O-398
Kim, N. eP-76, eP-83
Kim, N. O-38, O-421
Kim, P. E. EdE-28
Kim, P. E. eEdE-39, eP-66, O-244
Kim, P. E. eEdE-15
Kim, S. eEdE-57
Kim, S. eP-101a
Kim, S. eP-24, eP-76, eP-83, O-217
Kim, S. O-297
Kim, S. O-398
Kim, S. O-562
Kim, S. P-88
Kim, S. E. eP-134
Kim, S.-C. O-533
Kim, S.-E. O-495
Kim, W. eP-193
Kim, W. eP-219
Kim, W. T. eP-184, O-555
Kimbrough, D. A. eP-156
Kimmich, C. O-71
Kimura, F. eEdE-112, O-492
Kinder, K. O-168
King, K. eP-70, eP-81, O-46, O-580
King, K. F. O-56
Kinoshita, F. EdE-33, P-60
Kinoshita, T. EdE-33, P-60
Kirby, J. eEdE-30
Kirby, J. eP-101b, O-292, O-539
Kirby, P. EE-76
Kirby, P. eEdE-168
Kirby, P. eEdE-21, O-567
Kirchin, M. P-71
Kirollos, R. W. P-72, P-73, P-76
Kis, A. O-145
Kishi, T. eP-113, P-18
Kister, I. eP-61
Kitahara, H. P-21
Kitajima, M. eP-33, eP-5, O-516
Kitamura, G. P-102
KItamura, N. EE-49
Kiura, Y. P-90
Klatt-Cromwell, C. N. eP-126
Kleefisch, C. J. eP-55
Klein, A. eEdE-17
Klein, A. eEdE-61
Klein, A. P. EdE-49
Klein, A. P. EdE-40
Klein, D. P-3
Klenk, A. M. O-241
Klesse, L. eP-252
Klimo, P. eP-270, O-437
Kline-Fath, B. O-430
Kliot, M. O-127
Klisch, J. O-100
Klucznik, R. O-293
Knauth, M. O-51
Knisely, J. P. S. O-64a
Knopp, E. eP-300, , , O-570, P-35
Knudsen, J. M. O-252
Knutson, A. eP-105
Ko, N. O-102
Kobayashi, K. eP-29
Kocak, M. EdE-87
Kochunov, P. O-481
Koehler, C. eP-162
Koehler, C. eP-198
Kofler, J. M. P-105

Index of Program Participants

Numbers refer to session and presentation numbers, *not to page numbers*.

Index Key: O = Scientific Paper (Oral Presentation); EE = Electronic Excerpta e; P = Scientific Poster (Print Format); eP = Electronic Scientific Poster (ePoster); EdE = Education Exhibit (Print Format); eEdE = Electronic Education Exhibit

Koh, Y. eP-118, eP-119
Kohler, N. EE-33
Koike, H. eP-108
Koike, H. eP-3
Kole, M. eEdE-82, eP-179
Kolić, K. O-488
Kollasch, P. D. P-108
Kollmer, J. O-73, O-74
Kollmer, J. C. O-71, O-72
Komi, M. O-516
Komlosi, P. eP-269
Komlos-Kukreja, M. O-144
Komoto, D. eP-54
Konno, Y. EE-3
Kontos, A. P. O-425
Koo, B. Bon. O-476
Koohi, Y. EE-34, EE-51, EE-80
Koon, P. P-33
Koon, P. D. O-54
Koprivsek, K. EE-44
Koral, K. eP-252, P-96
Kornek, B. eP-237
Korogi, Y. eP-64, eP-93, O-122, O-219, O-63
Korosec, F. R. O-56
Korutz, A. W. eP-36
Kostic, V. S. P-6
Kosuge, M. P-23
Kouznetsov, E. O-275
Kovanlikaya, A. P-101
Kovari, E. O-214
Koyama, T. EdE-83
Koyanagi, M. eP-29
Kozic, D. EE-44, P-6
Kralik, S. F. eEdE-133, eP-253, O-134
Kramer, J. eEdE-12
Kramer, L. A. eP-128
Kranz, P. G. O-308, O-418
Krasin, M. eP-270
Krecke, K. N. P-105
Krings, T. O-274
Krishna, S. eP-278
Krishnan, A. EdE-24, EE-52
Krishnan, A. P-97
Krishnaraj, M. eP-55
Krmpotich, T. O-36
Krmpotich, T. D. O-241
Krueger, K. W. P-28, P-31
Krueger, P. P-28, P-31
Krull, K. R. eP-270
Krupp, S. eP-267
Ku, A. eEdE-123, eP-177
Ku, J.-W. O-42
Kubal, W. O-394
Kubal, W. S. eP-271, eP-60
Kudo, K. eEdE-55
Kudomi, S. eP-113
Kuhn, A. eP-165, eP-207, eP-6
Kuhn, A. Luisa. EE-59, eP-205
Kulkarni, A. eP-225
Kulkarni, G. B. EE-70
Kuller, L. H. P-8
Kumar, A. J. EdE-44, EdE-46
Kumar, A. J. eP-130
Kumar, A. J. EdE-39
Kumar, A. J. eP-77, O-282, O-402, O-485
Kumar, M. EdE-74, eEdE-83, eP-256, eP-65
Kumar, S. EE-41, P-82
Kumar, V. EdE-39
Kumar, V. EdE-44, EdE-46
Kumar, V. A. O-402
Kun, L. eP-270
Kundel, H. O-64, P-46
Kung, C.-T. P-27
Kung, K.-L. EdE-89
Kunitomi, Y. O-111
Kuno, H. eP-114
Kuo, Y.-S. EdE-89
Kurisu, K. P-105a
Kurisu, K. P-90
Kurobe, Y. eEdE-23
Kurre, W. eP-192, eP-195, eP-209, O-98
Kushnirsky, M. O-64a
Kutner, K. O-426
Kwak, B. P-74
Kwak, H. O-519
Kwan, J. Y. eP-7
Kwon, H.-J. eP-207
Kyogoku, S. eP-30
Kyosen, S. Obikawa. P-12

L

La Piana, R. eP-150, eP-234, P-3
La, C. O-502, P-64
Labrousse, M. O-527
Labus, J. S. O-479
LaFranchi, S. EE-48
Lagares, A. eP-25, eP-43
LaHue, S. C. O-35
LaHue, S. C. eEdE-20
LaHue, S. C. O-37
Lai, A. O-210, O-287, O-288
O-401, O-406, O-541
Lai, L. EE-76, eEdE-64, eP-47
Lam, B. B. O-522
Lane, J. I. EE-45
Lang, S. eP-203
Lange, D. O-212
Langlands, G. O-395
Langs, G. O-318
Langtangen, H. O-130
Lankford, D. EE-55, EE-56
Lanoix, O. eP-183
Lanzino, G. eP-194, eP-95, eP-96, O-96
Lassman, A. O-201
Latour, L. L. eP-105, P-68

Index of Program Participants

Numbers refer to session and presentation numbers, *not to page numbers*.

Index Key: O = Scientific Paper (Oral Presentation); EE = Electronic Excerpta e; P = Scientific Poster (Print Format); eP = Electronic Scientific Poster (ePoster); EdE = Education Exhibit (Print Format); eEdE = Electronic Education Exhibit

Lau, D. eP-268
Lau, H. P-62
Law, M. EdE-28, eEdE-15, eEdE-39, eEdE-52 eP-66, O-244, P-37
Lawrence, D. A. eEdE-124
Lawton, M. eP-193
Lawton, M. T. O-102
Layton, K. F. EE-25, EE-60, eP-211, O-162
Le Jean, L. eP-294
Le Roux, L. eP-107
Le Roux, L. G. eP-290, eP-296, O-70
Le, N. T. eP-21
Leach, J. L. eEdE-129, eEdE-130 eP-230, eP-257, O-144, O-552
Leake, D. R. EE-61
Learned, K. eP-120
Learned, K. O. EdE-62, EdE-63, O-532, P-38
Leclercq, D. O-166, O-563, O-582
LeCompte, L. eP-231
Lecomte, R. eP-220
Lee, A. eEdE-110, O-297
Lee, A. P-88
Lee, C. eEdE-79
Lee, C. O-217
Lee, C. P-66
Lee, C.-W. O-276, P-11
Lee, D. P-4
Lee, E. EE-10
Lee, E. eEdE-14, eEdE-59
Lee, H. eP-42
Lee, H. O-107
Lee, H. A. eEdE-20, O-37
Lee, J. O-107
Lee, J. H. O-568
Lee, J. S. eP-26
Lee, J. Y. P-38
Lee, J. Y. K. EdE-62
Lee, J.-H. eP-118, eP-119
Lee, K. P-85
Lee, L. O-119, O-120
Lee, L. Y. K. O-532
Lee, M. H. O-419
Lee, P. eEdE-128, eEdE-91
Lee, P. N. O-509, P-100
Lee, P. S. P-79
Lee, R. O-172
Lee, S. eP-42
Lee, S. eP-42
Lee, S. eP-76
Lee, S. P-57
Lee, S. P-66
Lee, S. R. EE-57
Lee, S.-K. P-51
Lee, S.-R. P-66
Lee, V. O-225
Lee, V. H. O-229
Lee, W. A. O-102
Lee, Y. EdE-27
Lee, Y. eP-111
Lee, Y. P-57
Lee, Y.-J. eP-152
Leeds, N. E. EdE-39
Leeds, N. E. O-402
Leeds, N. E. O-282
Lee-Felker, S. eEdE-75
Lee-Felker, S. A. eEdE-81
Lefton, D. EE-64
Lehman, V. T. eP-265
Leigh, R. O-251, O-253
Leighton, M. eEdE-17
Leighton, M. P. EdE-40
Leite, C. C. eEdE-47, eP-16
Leite, C. C. O-569
Leite, C. Costa. O-423
Lensing, F. D. O-136, O-523
Leon, S. Vieira. Alves. eP-8
Leoncini, G. O-283, O-540
Leone, M. EE-18
Lepage, M. eP-220
Lequin, M. H. eEdE-136
Lerner, A. EdE-28
Lerner, A. EE-12, eEdE-117, eEdE-121
Lerner, A. eEdE-15
Lerner, A. eEdE-173
Lerner, A. eEdE-39, eEdE-52
Lerner, A. eP-66, O-244
Lerner, A. P-37
Lesiuk, H. O-227
Lesnik, G. T. eP-141
Lester, M. EE-8
Leu, K. O-406
Leuthardt, E. EdE-17
Lev, M. H. eP-97, O-389
Lev, S. eEdE-114, eEdE-65, eEdE-68, eEdE-69, eEdE-69
Levy, M. O-133
Lewin, J. S. O-251, O-253
Lewis, D. O-95
Lewkowitz-Shpuntoff, H. O-421
Lewkowitz-Shpuntoff, H. M. O-38
Leypoldt, F. O-232
Lhuaire, M. O-527
Li, B. O-513
Li, C.-D. O-64, P-46
Li, J. eEdE-10
Li, L. O-578
Li, N. O-424
Li, S. EdE-04, EdE-22, EdE-76
Li, S.-H. P-27
Li, X. O-286
Li, X. P-112
Li, Y. P-19
Li, Y.-O. O-35
Li, Z.-H. P-24

Index of Program Participants

Numbers refer to session and presentation numbers, *not to page numbers*.
Index Key: O = Scientific Paper (Oral Presentation); EE = Electronic Excerpta e;
P = Scientific Poster (Print Format); eP = Electronic Scientific Poster (ePoster);
EdE = Education Exhibit (Print Format); eEdE = Electronic Education Exhibit

Liang, H. eEdE-104
Liang, T. eEdE-102, eEdE-111, eEdE-113, eEdE-166, eEdE-177, eEdE-179, eEdE-66, eEdE-89, eEdE-98
Liao, Y.-P. O-237, O-42
Libby, B. O-498
Licht, D. J. O-550
Lien, R. J. O-579
Lignelli, A. eEdE-85a, O-201, O-548
Lignelli, A. A. EE-90
Lim, Y. eP-24
Lima, L. Thayse. Barros. eEdE-76
Limbrisk, D. D. O-505
Lin, C.-J. eP-188
Lin, C.-J. O-223, O-573
Lin, D. eP-63, O-140, O-141
Lin, J. J. eEdE-13
Lin, L. Y. O-419
Lin, S. J. O-279
Lin, W.-C. P-27
Lin, W.-M. P-27
Lin, Y. O-473
Lindell, E. Paul. EdE-31
Lindley, R. O-43
Lindsay, A. eEdE-41, O-320
Lindsay, A. J. eP-250
Linendoll, N. O-525
Linscott, L. eEdE-129, eEdE-130, eEdE-42, O-552
Liouta, E. eP-57
Lipton, M. O-38, O-421
Lipton, M. L. O-482
Lipton, R. O-38
Lipton, R. B. O-421
Lirng, J.-F. O-223
Liu, A. eP-255
Liu, C. eP-10
Liu, C. Y. eEdE-15
Liu, C.-S.J. O-35
Liu, H.-H. EE-27
Liu, H.-H. P-39
Liu, H.-M. O-276, P-11
Liu, H.-M. P-54
Liu, J. EE-1, eP-196
Liu, J. K. EE-5
Liu, M.-Y. P-11, P-54
Liu, R. eEdE-10
Liu, R. T-k. O-574
Liu, T. eP-33, O-122, O-212, O-219, O-63
Liu, X. eP-50, O-202, O-399, O-408
Liu, X. O-572
Livingston, B. EE-24
Livingston, J. eP-233
Liying, Z. O-119
Lloyd Baugnon, K. O-486
Loecher, M. O-575
Loeckner, C. Patrick. eP-267
Loevner, L. eP-120, O-483
Loevner, L. A. EdE-63, EE-38, O-532
Loh, J. eP-61
Lombardo, F. P-7
Longo, D. eP-216
Longstreth, W. T. P-8
Loomba, J. O-34
Lopes, D. O-99
Lopes-Rueda, F. Cristina. eP-8
Lopez, M. EE-23
Lopez, O. P-8
Loredo, L. P-80
LoStracco, T. A. eEdE-67
Lotz, J. eEdE-167, O-66
Lou, X. O-393
Lovblad, K.-O. O-214, O-216, O-221
Lovell, M. O-320
Lu, C.-H. P-27
Lu, H. O-518
Lu, S. eP-24
Lubarsky, M. eP-144
Lubelski, D. eP-281
Lubicz, B. O-100
Lucarelli, M. J. eEdE-92
Lucic, M. EE-44
Lucignani, G. O-511
Luetmer, P. H. P-105
Lui, Y. W. eP-61, O-428
Luk, D.-K. P-112
Luks, T. L. eEdE-20
Luks, T. L. O-37
Lum, C. eEdE-62
Lum, C. eP-86, O-227, O-496, O-497
Lum, M. A. O-561
Lung, P. O-132
Luo, C.-B. eP-188, O-223
Lustig, R. eP-120
Luther, N. O-426
Luttrull, M. D. eEdE-70
Lutz, K. O-204
Lyden, P. D. P-63
Lyman, G. O-484
Lyman, G. H. eP-136
Lynch, M. C. O-64, P-46
Lyra, K. Paz. de. eP-16

M

Mabry, L. M. EdE-35
Mac Donald, C. L. O-419
MacAdam, B. D. eEdE-69
MacDonald, C. B. eEdE-116, eP-145
Machnowska, M. H. O-274
Maclaren, J. eP-79
Macmullen-Price, J. eEdE-131
Macovei, I. O-280
Macyszyn, L. EdE-05
Madan, G. O-531
Madan, N. eEdE-115, eEdE-36, O-525
Madrecha, J. eP-299

Index of Program Participants

Numbers refer to session and presentation numbers, *not to page numbers*.
Index Key: O = Scientific Paper (Oral Presentation); EE = Electronic Excerpta e;
P = Scientific Poster (Print Format); eP = Electronic Scientific Poster (ePoster);
EdE = Education Exhibit (Print Format); eEdE = Electronic Education Exhibit

Madsen, J. EdE-25
Maeda, M. eEdE-23, eP-1, eP-4
Maegawa, G. H. eP-235
Maekura, T. EdE-83
Mafee, M. eEdE-97
Mafee, M. F. eEdE-118
Maghami, E. eP-116
Maghnie, M. O-323
Magnus, T. O-232
Magrath, E. P-68
Magrath, R. P-53
Magrath, R. P. O-58, O-62
Magri, A. eP-141
Mahajan, A. EdE-07, eEdE-01, eEdE-43, O-414
Mahajan, B. eP-130
Maher, C. O. eP-268
Maher, E. eP-70
Mahesh, M. eP-162
Maheshwari, M. EdE-49, eEdE-143
eEdE-169, eEdE-17
Mahone, E. Mark. O-508
Mahoney, E. O-498
Mair, G. O-43
Mair, Y. H. EE-62
Maizeroi-Eugène, F. eP-182
Majumder, S. eP-130
Mak, H. eP-14
Maksimovic, J. O-575
Maksimovic, J. H. O-33
Maldjian, J. A. eP-229, O-512
Maley, J. E. eEdE-88
Malhotra, A. EE-19, EE-71
EE-81, EE-83, eEdE-43, eP-239
Malhotra, R. M. O-117
Malkan, P. R. O-254
Malloy, C. eP-70
Malloy, K. M. EdE-63
Mamourian, A. EdE-05
Mamourian, A. C. eEdE-161
Manchester, D. O-320
Mandell, D. M. O-105, O-392
Mangano, F. O-144
Mangano, F. T. O-505
Mangla, R. O-114
Mankad, K. eEdE-144
Manker, S. EdE-26
Manley, G. T. O-35
Mannem, R. EdE-40
Mansour, O. eP-153
Manto, M. O-242
Manzoni, P. O-515
Manzoor, M. O-400
Mao, H. O-58, O-62, P-53
Maralani, P. J. EdE-63, EE-38
eEdE-40, eEdE-77, eEdE-94
Marashi, K. B. EE-25
Maravilla, K. eP-90
Marco, E. P-98
Mardal, K.-A. O-130
Margraf, L. eP-252
Marin, H. eEdE-82, eP-179
Marjanska, M. O-403
Mark, L. P. EdE-49
Markl, M. O-295, O-301
Marquez, J. C. EdE-38, P-40
Marrinan, E. M. EdE-80
Marroquin, R. EdE-19
Martens, N. eP-55
Martin, A. O-102
Martin, A. J. O-561
Martin, C. P-95
Martin-Duverneuil, N. O-563
Martinez, C. R. eP-104
Martinez, N. O-543
Martino, N. P-7
Martinot, C. EdE-13
Martins, A. Maria. P-12
Martinuzzi, A. P-7
Masch, W. R. P-43
Mashhadi, O. EdE-26
Masodkar, K. eP-55
Mason, W. P. O-401
Masoud, H. P-62
Massari, F. eP-176, eP-289, O-488, O-490
Massey, L. O-28
Massoud, T. F. EdE-47, EdE-90
EE-15, EE-54a, P-29
P-72, P-73, P-76, P-77, P-9
Masuda, S. eP-169
Masutani, Y. eP-30
Mateos-Pérez, J. M. O-206
Matheus, G. eP-102
Matheus, M. eP-138
Mathew, N. O-548
Mathis, D. eP-252
Matouk, C. EdE-02, eEdE-124
Matsumoto, J. EE-34
Matsumoto, J. A. O-176
Matsumoto, N. P-84
Matsunaga, H. P-21
Matsunaga, N. eP-113, eP-122
Matsunaga, N. P-18
Matsunaga, N. P-65
Matsuo, T. eP-22
Matsushige, T. P-90
Matsuura, K. eP-4
Matthews, R. EdE-03
Mattox, D. E. O-250
Matys, T. EdE-47, EE-15, P-29
P-72, P-73, P-76, P-77
Mawad, M. E. eP-2
Maya, M. eP-67
Mayberg, H. S. eEdE-71
Mayer, E. O-479

Index of Program Participants

Numbers refer to session and presentation numbers, *not to page numbers*.
Index Key: O = Scientific Paper (Oral Presentation); EE = Electronic Excerpta e;
P = Scientific Poster (Print Format); eP = Electronic Scientific Poster (ePoster);
EdE = Education Exhibit (Print Format); eEdE = Electronic Education Exhibit

Mayer, R. R. P-39
Mazumder, A. A. eEdE-144
Mazura, J. C. O-54
Mazzini, L. eP-58, O-480
McCallum, S. eP-46, O-298
McClarty, B. O-207
McColl, R. O-46
McCollough, C. H. P-105
McComb, G. J. eP-59
McCreary, R. eEdE-170, eEdE-78, eEdE-80
McCune, J. O-40
McDonald, C. R. O-546
McDonald, J. S. eP-95, eP-96
McDonald, R. J. eP-95, eP-96
McDonnell, O. EE-11
McDougall, C. O-99
McEvoy, L. O-21, O-29, O-31
McGinty, G. EdE-82
McGorty, K. O-536
McGovern, M. O-30
McGowin, I. eP-229, O-512
McGreggor, A. O-147
McGuire, S. O-481
McIntyre, J. J. eEdE-105
McKean, E. L. P-92
McKeever, P. O-571
McKinney, A. M. eP-82
McKinney, A. M. O-135, P-78
McKinney, A. M. O-109
McKinnon, G. eP-81, O-580
Mckinnon, M. C. O-56
McKinstry, R. C. O-505
McKinstry, S. eP-155
McKnight, C. D. O-514
McLaughlin, C. eP-138
McLean, A. O-432
McNally, J. Scott. O-495
McNally, S. O-523
McNeill, G. J. EdE-67, EE-30, EE-58
McQuillan, H. O-325
McSwain, H. eP-193, O-555
McTaggart, R. A. eP-135
Meagher, S. P-94
Medina, F. J. P-40
Medina, L. O-148
Meerzaman, D. eP-101b
Meesa, I. eEdE-107, eEdE-132
Megahed, A. eP-215, eP-217
Mehan, W. O-317
Mehan, W. A. O-146
Mehdi, E. EdE-36
Mehta, H. EdE-91, eP-231
Meier, T. O-33
Melhem, E. R. eP-26
Melhem, E. R. EE-89
Meltzer, D. E. eP-242
Mendelsohn, D. B. EE-6
Mendes, C. Silvia. C. P-12
Mends, F. eP-85
Menezes, R. O-274
Mengesha, B. eP-46, O-298
Menon, B. eP-197
Menon, R. G. O-45, O-50, P-61
Menon, , R. G. eP-84
Meoded, A. eP-222, eP-7, O-506
O-507, O-559, P-99
Mercer, D. O-505
Meretoja, A. eP-98
Merhar, S. O-430
Meric, A. eP-139
Merlo, M. O-221
Merritt, T. Allen. P-102
Meshksar, A. eP-271, O-390, O-394
Messner, S. EdE-71
Mettenberg, J. EdE-17
Mettenburg, J. M. eP-80
Metting, S. W. eP-99
Metwalli, Z. A. EE-57
Mewes, K. eEdE-71
Meyer, B. O-93
Meyer, B. C. P-63
Meyer, M. A. EdE-18, EdE-64, EdE-92
Meyers, S. EdE-78
Meyers, S. P. eEdE-67
Mian, A. eEdE-70a, O-498, O-513, P-62
Mian, A. Z. O-476
Miaux, Y. O-30
Michalski, M. H. eEdE-124
Middleton, D. eP-127
Middleton, D. M. eP-262
Midia, E. Cakmakci. eEdE-169
Mignano, J. O-525
Mignone Philpott, C. eEdE-150, eP-227
Mihlon, F. eP-189, O-106
Mikati, A. O-578
Miki, H. eP-40
Mikkelsen, T. eP-52, O-211, O-292
Mikulis, D. O-105
Mikulis, D. J. O-392
Miles, L. O-144
Miletić, D. O-116
Mileva, R. eP-233
Milla, S. eEdE-07
Millan, J. M. eP-43
Millar, W. S. EE-68
Miller, B. L. eP-48
Miller, E. eEdE-149, eP-225
Miller, G. M. P-108
Miller, I. O-148
Miller, T. EE-85
Miller, T. eEdE-02
Miller, T. R. P-89
Miller, T. S. O-296
Miller-Thomas, M. EdE-17, eEdE-42

Index of Program Participants

Numbers refer to session and presentation numbers, *not to page numbers*.
Index Key: O = Scientific Paper (Oral Presentation); EE = Electronic Excerpta e;
P = Scientific Poster (Print Format); eP = Electronic Scientific Poster (ePoster);
EdE = Education Exhibit (Print Format); eEdE = Electronic Education Exhibit

Millett, D. eEdE-15
Mills, S. J. O-542
Milos, R.-I. eP-237
Miloslavsky, M. O-30
Miloushev, V. eEdE-85a, O-201, O-548
Mine, B. O-100
Minja, F. EdE-02, eEdE-124
Minja, F. J. O-173
Miraldi, F. eP-19, O-238, O-477
Miranpuri, A. eEdE-72
Miranpuri, A. S. eP-176
Mironov, A. O-565
Mironov, O. O-114
Mirsky, D. M. eEdE-153, eP-255, O-434
Mishra, N. K. P-30
Mishra, S. eP-197
Mistretta, C. O-575
Mistry, P. eP-239
Mitchell, C. H. O-133
Mitchell, P. eP-178
Mitchell, P. eP-98
Mitha, A. P. O-165
Mitjana, R. eP-62
Mitra, D. eP-178
Mitulescu, A. O-582
Miyata, H. EdE-33
Miyazaki, M. eP-59
Miyazaki, Y. eP-173, eP-208, eP-39, O-48
Mizuiri, D. O-37
Mizuri, D. eEdE-20
Mocco, J. O-99
Mochizuki, T. eP-40
Modic, M. T. eP-281
Moe, D. EE-39
Moenninghoff, C. eP-171, eP-172, O-299
Moghekar, A. P-47
Mohamed, A. eP-169
Mohamed, F. eP-127, O-438, O-439, O-440
Mohamed, F. B. eP-262
Mohamed, M. A. eP-15, O-22, P-10
Mohan, S. EE-38, EE-89, eEdE-165
eEdE-40, eEdE-77, eEdE-94
eP-26, eP-263, O-64, P-46
Mohiuddin, J. EE-77, EE-79, EE-88
Mojtahed, A. EdE-32
Mok, K. P-3
Mokhtari, K. O-563
Molyneux, A. eP-186
Molyneux, A. J. eP-163, O-103, O-94
Momoli, F. eP-86, O-497
Montalban, X. eP-62
Montanaro, D. P-7
Montechiari, M. O-410
Monteith, S. O-34
Montgomery, B. K. O-435
Montgomery, J. P. eEdE-174
Montisci, R. O-500
Moonis, G. EE-23, eEdE-19, O-174, O-412
Moore, H. E. eP-240
Moore, K. R. eP-240
Moore, W. eP-252
Morais, L. M. T. O-389
Morais, T. Peixoto. eEdE-76
Morales, H. EdE-13, EdE-54, eP-89
Morales, R. O-161
Moran, C. J. eP-206, O-97, P-93
Moreau, K. O-106
Moret, J. eP-185
Morgan, J. N. eP-125
Mori, S. O-506, O-507
Mori, T. eP-173, eP-208, eP-39, O-231, O-48
Morikawa, M. eP-108, eP-22, eP-3
Morin, F. eP-150
Moritani, T. EE-76, eEdE-168, eEdE-21
eEdE-64, eP-47, O-567
Moriya, J. eP-64, O-122, O-219, O-63
Moriya, M. P-50
Morozova, L. EE-48
Morris, J. EdE-04
Morris, J. M. eEdE-32
Morris, J. M. O-175, O-493
Morris, J. M. eP-298
Morris, K. O-30
Morrish, W. O-165
Morriss, M. eP-254
Morriss, M. C. O-431
Morrissette, A. eP-7
Morrow, M. J. EdE-81
Morsi, H. eP-2
Moseley, M. E. O-49
Mossa-Basha, M. EE-35, eP-46, O-298, P-49
Motoi, Y. P-23
Motomura, M. eP-108
Motoori, K. eEdE-87
Mouannes-Srour, J. O-119, O-120, O-125
Mounayer, C. eP-182, O-271, O-273
Mowji, P. eP-147
Mroz, T. E. eP-281
Mu, Y. O-27
Mucke, J. O-391, O-503
Mueller, O. eP-171, eP-172, O-299
Muherjee, S. O-416
Muir, K. eP-202
Mukai, H. eEdE-87
Mukherjee, P. eEdE-20, O-35, O-37
P-17, P-19, P-22, P-98
Mukherjee, S. EE-34, O-535
Mukherji, S. eEdE-107, eEdE-132
Mukherji, S. K. EdE-58, eEdE-103
Mukhi, S. V. eEdE-19
Mulcahey, M. eP-262, O-438, O-439, O-440
Muldoon, L. L. eP-73, O-286
Muller, K. A. O-546
Muller, S. O-530

Index of Program Participants

Numbers refer to session and presentation numbers, *not to page numbers*.
Index Key: O = Scientific Paper (Oral Presentation); EE = Electronic Excerpta e;
P = Scientific Poster (Print Format); eP = Electronic Scientific Poster (ePoster);
EdE = Education Exhibit (Print Format); eEdE = Electronic Education Exhibit

Munk, P. eEdE-177
Muradyan, N. eEdE-39
Muradyan, N. P-37
Murakami, Y. O-122, O-219, O-63
Murata, T. eEdE-70a
Murayama, Y. eP-169, eP-264, O-99
Murodova, D. O-244a
Murph, D. EE-55, EE-56
Murphy, J. S. eP-280
Murphy, R. O-247
Murray, A. eP-202
Muscal, E. eP-246
Musco, J. eP-276, eP-287
Mushlin, A. I. O-472
Muzaffar, M. O-415
Myers, C. EdE-91
Myers, J. N. O-485
Myneni, M. C. eP-302

N

Nabavizadeh, S. A. eEdE-155
Nabi, J. eP-226
Nace, S. R. eEdE-119
Nadarajah, M. eP-190
Nadgir, R. eP-124
Nadich, T. eEdE-106
Nadkarni, T. P-64
Naeini, K. M. O-288
Nael, K. EdE-55, eP-271, O-390, O-394
Naftel, R. eP-251
Nagarajan, S. eEdE-20
Nagarajan, S. S. O-37
Nagarwala, J. eP-267
Nagata, I. eP-22, eP-3
Naghi, I. eEdE-39
Nagpal, P. eP-52
Nagpal, S. O-205
Nahabet, E. O-230
Naidich, T. eEdE-46, O-379a
Naidich, T. P. EdE-44, EdE-46
eEdE-07, eEdE-120, O-402
Naidich, T. P. EdE-39
Naidich, T. P. O-579
Nair, D. O-32
Nair, G. O-305, O-69
Nair, V. A. eP-55, O-502
Nair, V. A. P-64
Najm, I. O-32
Nakahira, M. eEdE-112, O-492
Nakaji, S. eP-20
Nakajima, Y. EdE-23
Nakamura, H. EdE-23
Nakamura, J. eP-93
Nakamura, Y. eP-54
Nakanishi, A. P-23
Nakashima, H. eP-108
Nakatsuka, T. EE-49
Nakazaki, M. eP-173, eP-208, eP-39, O-231, O-48
Naliboff, B. O-479
Nambiar, V. eP-197
Nanda, A. eP-276, eP-287
Narayana, A. , , P-35
Nardone, R. eP-49
Narita, M. P-44
Narvid, J. O-127
Nascimento, S. O-423
Nash, T. O-505
Nasrallah, I. M. O-64, P-46
Nass Duce, M. EE-54
Nasseri, M. O-405
Nasuelli, N. eP-58, O-480
Nath, J. O-324
Nathanson, K. O-483
Nawroth, P. O-74
Nayak, N. eP-279
Nayak, N. B. eP-110
Nayyar, R. EdE-80
Nayyar, S. EdE-80
Nazarian, J. P. eP-204
Needle, M. EE-68
Neelakantan, A. eP-92
Neimark, M. O-324
Nejad-Davarani, S. eP-56
Nejad-Davarani, S. P. eP-53
Nelson, P. Kim. O-278
Nelson, R. C. eP-137, O-418
Nemeth, A. J. P-14
Nesbit, E. O-286
Nesbit, G. O-99
Nesbit, G. M. O-474
Nestadt, G. eP-15
Nestor, P. J. O-25
Neuwelt, E. A. eP-73, O-286, O-405
Newman, D. O-129
Newman, J. G. EdE-62, O-532
Newman, N. J. O-558
Newman, S. A. EE-89
Ng, J. D. O-474
Ng, K. O-215, O-222
Ng, S. Hang. O-489
Ng, S.-H. eP-17, P-41
Nghiemphu, P. L. O-210, O-287
O-288, O-401, O-406, O-541
Ngo, M. EE-82
Ngo, M. O-163
Nguyen, D. O-27
Nguyen, Q. eP-174
Nguyen, T. eEdE-49, eEdE-62, O-498, P-62
Nguyen, V. , eEdE-122
eEdE-122a, eEdE-56, O-64a
Nguyen, W. eEdE-28
Nguyen, X. eEdE-70, O-484
Nguyen, X. V. eP-136
Nicholson, A. O-388
Nickell, L. T. EE-25, eEdE-104, eEdE-99, eP-211

Index of Program Participants

Numbers refer to session and presentation numbers, *not to page numbers*.

Index Key: O = Scientific Paper (Oral Presentation); EE = Electronic Excerpta e; P = Scientific Poster (Print Format); eP = Electronic Scientific Poster (ePoster); EdE = Education Exhibit (Print Format); eEdE = Electronic Education Exhibit

Nickerson, J. P. O-236
Nicola, G. N. EdE-81
Nicolaou, S. eEdE-102, eEdE-111, eEdE-113, eEdE-166, eEdE-177, eEdE-179, eEdE-66, eEdE-89, eEdE-98
Nicolas-Jilwan, M. EE-80
Nicolasjilwan, M. eP-101b
Nidecker, A. EE-22
Nidecker, A. E. EdE-52
Niehaus, L. eP-192
Nikolaou, K. O-499
Nimjee, S. eP-189
Niogi, S. N. O-426, P-101
Nishido, H. eP-175
Nishimura, S.-I. O-516
Nishizawa, M. O-111
Nitatori, T. eP-29, eP-94, O-108
Nitta, S. eP-78, O-581
Njagulj, V. EE-44
Noor, A. eEdE-106
Noorian, A. eP-168
Norbash, A. M. P-62
North, P. E. EE-39
Northington, F. J. eP-248
Nosaka, R. P-105a
Nouet, A. P-91
Noujaim, S. eEdE-109
Novikov, D. S. O-428
Nowak, A. P-28, P-31
Nundkumar, A. eEdE-91
Nusbaum, A. O. O-536
Nutanson, I. O-220, O-23

O

O'Connor, P. O-119, O-120
O'Connor, P. W. O-125
Obara, M. eP-129, O-492, P-84
Obeng, K. K. EdE-57
Obrzut, M. O-60
Obuchowski, N. eP-281
Obusez, E. C. O-393, P-70
Ochoa, J. P-16
O'Connor, E. eP-100, O-429
O'Connor, J. C. O-162
O'Dell, M. C. P-32
O'Donoghue, D. EdE-44, EdE-46
O'Dowd, S. M. P-59
Oga, A. eP-122
Ogasawara, A. O-122, O-219, O-63
Ogden, K. eP-278
Ogg, R. eP-270
Ogg, R. O-473
Oguz, K. eEdE-31
Ohara, A. eP-29, eP-94, O-108
Ohnari, N. eP-64, O-219, O-63
Ohsone, F. P-21
Oikonomou, D. O-74
Oishi, S. eP-167
Okada, H. O-436
Okada, K. O-122, O-219, O-63
Okada, T. EdE-83
Okamoto, K. P-75
Okamoto, N. P-50
Okamoto, Y. eEdE-87
Okamoto, Y. eP-54
Okazaki, T. P-90
Okubo, T. P-21
O'Leary, S. eP-155
Olivi, A. eP-143
Olivieri, I. eP-234
Olmsted, J. E. eEdE-164
Olson, J. J. O-290
Olson, L. O-553
Omari, M. eP-61
Onana, Y. eP-133
O'Neill, D. P. O-134
Onodera, H. EdE-23
Opatowski, M. J. O-164
Opatowsky, M. J. EE-25, eEdE-104, eEdE-99, O-162
Oppenheimer, A. G. eP-223
Orcesi, S. eP-234
Ornan, D. eP-269, O-416
Orru', E. eP-143
Orser, H. EdE-26
Ortiz Lievano, J. C. O-110
Ortiz Teran, L. O-315
Ortiz, A. EdE-86, eP-191, O-314
Ortiz, A. O. eP-288
Orton, T. O-227
Osborn, A. G. O-47
Oshima, S. EdE-83
Oshinski, J. P-53
Oshinski, J. N. O-58, O-62
Otaduy, M. C. G. eP-16
Ottawa Hospital Research Institute O-496
Ottawa Stroke Research Group (OSRG) eP-86
Ottawa Stroke Research Group O-227, O-497
Otten, L. A. O-312
Ouellette, H. eEdE-177
Oustwani, C. EE-8
Oviedo, J. eP-260
Ow, T. J. O-485
Owen, J. P. P-17, P-19, P-22, P-98
Oyoyo, U. O-396
Oyoyo, U. P-102
Oyoyo, U. P-80
Ozdemir, T. O-104
Ozgen, B. eEdE-31
Ozgür, A. EE-54
Ozonoff, A. eP-124
Ozsvath, J. eP-300

P

Pacheco, E. O-148
Padua, A. O-65
Padwal, J. eP-285, O-310

Index of Program Participants

Numbers refer to session and presentation numbers, *not to page numbers*.

Index Key: O = Scientific Paper (Oral Presentation); EE = Electronic Excerpta e;
P = Scientific Poster (Print Format); eP = Electronic Scientific Poster (ePoster);
EdE = Education Exhibit (Print Format); eEdE = Electronic Education Exhibit

Pagani, J. EdE-44, EdE-46
Paine, S. M. L. eEdE-144
Palacios, W. EE-22
Palasis, S. EdE-71, EdE-88
Paldino, M. O-432
Paldino, M. J. eP-245
Paldino, M. J. O-411
Palesi, F. O-511
Paley, M. O-325
Palmer, C. O-109, O-135
Palmer, J. N. EdE-62, O-532
Pamarthy, S. EdE-11
Pan, H.-C. O-272
Pan, L. eP-282
Pan, M. P-5
Pan, Q. eEdE-65
Pandey, A. S. eP-295, O-277, P-92
Pandit, R. P. eP-99
Panigrahy, A. eP-232, O-436
Pantano, P. O-26
Papanagiotou, P. eP-200
Papanikolaou, N. eP-57
Paparella, G. P-7
Papasozomenos, S. EE-27
Papavassiliou, E. O-42a
Parekh, M. O-55
Parekh, N. P-56
Parekh, N. D. eEdE-148
Park, C. P-57
Park, D. P-57
Park, E. J. eP-16
Park, H. J. eP-115, eP-263, eP-274
Park, J. EdE-43, EE-64
Park, J. EE-78, O-475
Park, J. K. EE-84, EE-86
Park, S. P-74
Park, S.-W. eP-101a, O-533
Park, Y. eEdE-56
Parker, D. O-495
Parker, D. L. eP-134
Parker, E. , , P-35
Parker, J. R. P-71
Parker, L. O-248
Parmar, H. eEdE-101, eEdE-103 eEdE-107, eP-259, O-514
Parmar, H. A. EdE-58, eEdE-171, O-571
Parra, C. A. O-473
Parvathaneni, U. eP-117, eP-121
Pasco Papon, A. eP-185
Pascual, B. O-235
Pastel, D. A. EdE-84, P-69
Patankar, T. eP-210, P-106
Patay, Z. eP-270
Pate, K. P-53
Pate, K. S. O-58, O-62
Patel, B. EE-73
Patel, B. eP-191
Patel, B. eP-231
Patel, B. O-301
Patel, B. O-97
Patel, B. M. EdE-51
Patel, F. EE-77, EE-88
Patel, K. eEdE-106, O-379a
Patel, K. M. eEdE-53
Patel, M. R. eP-99
Patel, N. EdE-42, eEdE-126
Patel, R. eEdE-147
Patel, S. EdE-24
Patel, S. EE-87
Patel, S. H. EE-4
Patel, S. H. O-412
Patel, S. R. EE-4
Patel, S. T. EdE-45
Patel, S. T. EdE-10
Patel, T. EE-2, EE-9, eEdE-127
Patel, T. Y. eEdE-26
Patil, A. A. EdE-87
Patrie, J. eP-151, eP-166, eP-174, O-289, O-416
Patro, S. N. EE-75, eEdE-09, eEdE-49, eEdE-62
Patton, A. EdE-31, eEdE-11
Pawha, P. eEdE-106
Pawha, P. O-379a
Pawha, P. S. eEdE-96
Pawha, P. S. O-579
Payabvash, S. O-135, O-389
Paydar, A. eEdE-07
Peacock, J. C. O-66
Pearl, M. S. O-59
Pedicelli, A. eP-289
Pekcevik, Y. O-133
Pekoz, B. eP-218
Peng, Y. eP-17, P-41
Penna, K. eEdE-65
Penta, M. P-96
Penzien, J. eP-237
Perchinunno, M. EE-18, eP-58, O-480
Pereira, B. eP-72
Pereira, B. Perez. Guedes. eEdE-76
Pereira, L. P. eEdE-06, O-240
Perez Nuñez, A. eP-25
Perez, F. A. eP-46, O-298
Perez-Then, E. eP-260
Perlbarg, V. O-420, O-478
Perlman, J. P-101
Perlman, S. O-475
Perni, K. eEdE-103
Perry, A. eP-68
Perry, J. O-496
Peshock, R. O-46
Peters, T. L. eP-7
Peterson, R. B. O-250
Petrcich, W. eP-86, O-497
Petrella, J. R. eP-10

Index of Program Participants

Numbers refer to session and presentation numbers, *not to page numbers*.
Index Key: O = Scientific Paper (Oral Presentation); EE = Electronic Excerpta e;
P = Scientific Poster (Print Format); eP = Electronic Scientific Poster (ePoster);
EdE = Education Exhibit (Print Format); eEdE = Electronic Education Exhibit

Petropoulou, K. eP-299
Petrou, M. O-22, P-10
Petrović, I. P-6
Peverini, R. P-102
Peyester, R. eEdE-34
Peyster, R. EE-16
Pezeshk, P. eP-82
Pflugmacher, R. O-312, O-313, P-110
Pham, D. L. eP-105, O-424, P-68
Pham, M. eP-293, O-71, O-72, O-73, O-74, O-75
Phelps, M. E. eEdE-35
Phillips, H. S. O-288
Phillips, J. M. O-505
Phillips, M. O-32
Phillips, S. O-395, P-67
Piattella, C. O-26
Piccardi, B. P-3
Pichiecchio, A. O-511
Pieper, T. O-321
Pierot, L. eP-183, O-100, O-226
Piga, M. eP-45, eP-51, O-500, O-501, O-52
Pina, S. eP-126
Pinarbasili, N. eP-139
Pingue, V. P-5
Pinho, M. eP-70
Pinho, M. C. eEdE-47, O-569
Pinzon Jimenez, O. eP-47
Pinzon, O. eEdE-64
Piotin, M. eP-175
Piper, S. O-306
Pirovano, G. P-71
Pisapia, D. O-201
Pistocchi, S. eP-175
Pistorio, A. O-323

Plimpton, S. R. eP-255
Plumb, P. O-556
Poage, D. P. EE-20
Poisson, L. O-292
Pojman, N. P-17, P-22
Polaskova, P. O-404
Poliashenko, S. O-491
Poliashenko, S. M. O-487
Policeni, B. eEdE-141, eEdE-88
Policeni, B. A. eP-35, eP-87
Politi, L. S. O-410
Politi, L. Salvatore. O-283
Politi, L. Salvatore. O-540
Pollack, I. F. eP-251, O-436
Pollock, A. N. O-550
Pollock, A. N. eEdE-155
Pollock, J. EE-48
Pollock, J. M. EE-67, eEdE-134
Poloskova, P. P-36
Pomerantz, S. R. O-110
Pomero, E. O-280
Pomper, M. G. O-22, O-427, P-10
Ponomarjova, S. O-271, O-273
Ponting, J. M. EdE-57
Pope, W. B. eEdE-35, O-210, O-287
O-288, O-401, O-406, O-541, O-544
Poplawski, M. O-379a
Porcu, M. O-500
Poretti, A. eEdE-136, eEdE-172
eP-222, eP-235, O-321, O-322
O-506, O-507, O-559, P-99
Porter, D. eP-282
Poublanc, J. O-105, O-392
Powell, S. K. O-505
Powers, A. eP-229, O-512
Prabhakaran, S. O-504
Prabhakaran, S. K. O-225, O-228, O-229
Prabhakaran, V. eP-55, O-33, O-39, O-502, P-64
Prabhu, S. EdE-39, O-402
Prabhu, S. P. eEdE-50, O-149
Prager, A. J. O-543
Prahbu, S. eEdE-156a
Pravata, E. O-123
Prayer, D. eP-237, O-318
Prescott, J. W. eP-10
Prescott, S. L. P-108
Prestigiacomo, C. O-99
Pretty, L. EdE-29
Pride, L. O-556
Priest, R. O-474
Pritsch, M. eP-237
Prober, A. eEdE-36
Prola Netto, J. O-143, O-405
Prothmann, S. O-224
Provataris, J. O-38, O-421
Prust, M. J. P-36
Pryma, D. O-483
PS, B. EE-70
Psychogios, M.-N. O-51
Pucci, O. O-105
Pui, C.-H. eP-270
Pukenas, B. EdE-42, eEdE-126
Pulsifer, M. B. O-315
Purcell, D. O-30
Puri, A. S. eP-165, eP-181, eP-205, eP-207, eP-6
Puts, N. eP-15
Puybasset, L. O-420, O-478

Q

Qaddoumi, I. O-473
Qi, J. O-201, O-548
Qi, Z. eP-89
Quencer, R. M. eP-281
Quigley, E. eP-272
Quinlivan, M. P-20
Quiqley, E. O-523
Quisling, R. EdE-45
Quisling, R. G. EdE-10

R

Rabinstein, A. A. eP-194

Index of Program Participants

Numbers refer to session and presentation numbers, *not to page numbers*.

Index Key: O = Scientific Paper (Oral Presentation); EE = Electronic Excerpta e; P = Scientific Poster (Print Format); eP = Electronic Scientific Poster (ePoster); EdE = Education Exhibit (Print Format); eEdE = Electronic Education Exhibit

Radbruch, A. O-204, O-391, O-503
Radhakrishnan, R. EdE-54, eP-89
Radvany, M. G. eP-162, O-60
Raghavan, P. EE-51, EE-80
Raghavan, P. eEdE-30
Raghavan, P. eP-101b, O-289
O-416, O-535, O-539
Ragheb, J. O-148
Rahman, O. EE-63
Rahman, O. O-504
Rajagopal, A. O-505
Rajamohan, A. EE-12, eEdE-15
Rajamohan, A. O-244, O-244
Rajamohan, A. P-37
Raji, C. P-8
Raji, C. A. eEdE-05
Rajsheker, S. eEdE-70
Raju, A. O-316
Ralston, M. EE-24
Ramakrishnaiah, R. EdE-73, eEdE-83
Ramakrishnaiah, R. H. EdE-74, eP-256, eP-65
Raman, R. P-63
Ramos, A. eP-25, eP-43
Ramos, M. eP-46, O-298, P-49
Ramos, Y. M. O-430
Ramsewak, D. EdE-24
Rand, M. H. P-12
Rangel-Castilla, L. O-293
Rao, A. O-485
Rao, A. T. O-121
Rao, B. EE-19, eP-239
Rao, N. EE-77
Raslau, F. eEdE-61
Rassner, U. eEdE-48, eP-140, eP-272, O-53
Rastogi, S. EdE-70
Ratai, E.-M. O-146
Ratcliffe, M. R. eEdE-170, eEdE-78, eEdE-80
Rath, T. J. eP-106
Ratnanather, T. O-140, O-141
Rawley, J. eP-229, O-512
Raymond, J. O-275
Rayz, V. O-102
Raz, E. eP-142, eP-300, eP-45
eP-51, eP-61, , O-124, O-26
O-278, O-413, O-500, O-501, O-52, O-570
Reaume, J. O-536
Recht, L. O-205
Reddick, W. E. eP-270
Reddy, C. G. O-524
Redel, T. O-293
Redjem, H. eP-175
Reed, B. J. O-282
Reede, D. eEdE-85
Reede, D. eEdE-86
Reede, D. L. eEdE-92
Reede, D. L. eEdE-73
Rehani, B. O-245, O-255
Rehmani, R. EE-43, eEdE-122b
Reich, D. S. O-121, O-305, O-69
Reilly, C. B. EdE-09
Reina, V. O-582, P-91
Reinsberger, C. O-139
Reiser, M. F. O-499
Reiter, P. O-502, P-64
Reith, W. eP-200
Remer, S. P-107
Rennie, I. eP-155
Reynolds, J. O-36
Reza, H. eEdE-167
Rezek, I. O-95
Riascos, R. eP-128, O-526
Riascos-Castaneda, R. F. eEdE-167
Riccelli, L. P. eP-18
Richards, T. eP-117, eP-121
Richards, T. eP-230
Rideout-Gros, S. O-574
Rigamonti, D. P-47
Riina, H. O-278
Riina, H. A. O-472
Riley, L. H. eP-292
Rimkus, C. M. eP-16
Ringelstein, A. eP-171, eP-172, O-299
Riofrio, A. D. O-417
Ripellino, P. EE-18
Riva Posse, P. eEdE-71
Rivers-Bowerman, M. D. O-57
Roa, P. eP-260
Roberson, G. H. EdE-06
Roberts, J. O-495
Roberts, J. A. eP-134
Roberts, T. P-22
Robertson, H. J. F. eEdE-72
Robinson, C. L. O-294
Robison, L. L. eP-270
Robson, C. eP-242
Robson, C. D. O-411
Robusto, V. O-547
Rodeo, S. A. O-426
Rodrigues, D. EE-72, eEdE-156
Rodrigues, K. M. eP-245
Rodriguez, C. O-216
Rodriguez, E. O-134
Rodriguez, F. EdE-38
Roehm, P. C. O-536
Rohatgi, S. eEdE-25, eEdE-38
Rohde, S. O-391, O-503
Rojas, R. O-174, O-42a
Roland, J. Thomas. O-536
Roland, P. eP-254
Rollins, N. K. O-431, O-556
Rolo, J. eP-13
Roman, G. C. O-235
Romano, J. EE-17
Romero, J. O-245, O-255

Index of Program Participants

Numbers refer to session and presentation numbers, *not to page numbers*.

Index Key: O = Scientific Paper (Oral Presentation); EE = Electronic Excerpta e; P = Scientific Poster (Print Format); eP = Electronic Scientific Poster (ePoster); EdE = Education Exhibit (Print Format); eEdE = Electronic Education Exhibit

Romero, J. M. O-110
Romero, R. J. P-62
Roncarolo, F. P-87
Rondinoni, C. eP-13
Rontal, D. EE-52
Rooney, W. O-286
Rosand, J. O-110
Rosen, B. O-403
Rosen, B. R. O-404
Rosen, L. O-64a
Rosenbaum, D. P-101
Rosenbaum, S. O-38
Rosenbaum, S. B. O-421
Rosenberg, H. K. eEdE-120
Rosenthal, E. S. eP-97
Rosman, D. O-245, O-255
Ross, A. B. O-236
Ross, J. S. eP-280
Ross, M. eP-135
Ross, R. L. EE-90
Rossi, A. O-323
Rossi, G. O-511
Rostasy, K. eP-237
Roth, C. eP-200
Roudenko, A. eEdE-07
Rousseaux, P. eP-183
Roviglione, B. O-323
Rovira, A. eP-62
Rowland, L. M. O-243
Rowley, H. A. O-56
Roy Choudhury, K. eP-136, O-484
Roy, D. O-275
Rubenstein, D. eEdE-41
Rubin, D. eEdE-30
Rubin, D. O-292, O-539
Rubin, P. eP-125
Rubinstein, D. eEdE-84
Rueda, F. eP-19
Rueda-Lopes, F. C. O-238, O-477
Ruetters, M. O-75
Ruijters, D. eP-185
Rumboldt, Z. eP-138, eP-289, O-400, O-488, O-490
Rumpel, H. O-215, O-222
Rush, S. Z. eP-250
Rusinek, H. O-220, O-23
Russell, D. P. O-530
Russell, S. eEdE-39
Rutt, B. O-55
Rutty, A. EdE-54
Ryan, G. eEdE-150, eP-227
Ryan, M. eEdE-148
Ryan, M. O-508
Ryang, Y.-M. O-93
Rydberg, C. eP-298
Rydberg, C. H. EE-45
Rydzinski, Y. eEdE-157
Rykken, J. eP-82
Rykken, J. B. P-78
Rymer, M. P-95
Ryoo, I. O-533
Ryu, C.-W. P-85

S

Saad, A. F. EE-60, eEdE-104, eEdE-99
Saad, Z. O-69
Saam, T. O-499
Saba, L. eP-300, eP-45, eP-51, eP-61, O-500, O-501, O-52, O-570
Sabby, T. L. eEdE-163
Sabin, N. D. eP-270
Sadeghi, N. O-242, O-577
Safran, H. EdE-16
Safriel, Y. EdE-26, O-65
Saigal, G. O-177
Saindane, A. eP-101, eP-144
Saindane, A. M. eP-170, eP-283, O-302, O-307, O-553
Saindane, A. M. O-68
Saindane, A. M. O-558
Sair, H. eEdE-06, O-240
Sair, H. I. O-427
Saito, K. eP-64
Saito, N. eEdE-112, O-492
Saito, T. P-105a
Sajjadi, S. A. O-25
Sakae, T. eP-112
Sakai, O. EE-53, eEdE-112, eEdE-70a, eP-124, eP-214, O-492, O-513
Sakamoto, S. P-90
Sakuma, H. eEdE-23, eP-1, eP-4
Salah, R. eP-279
Salamon, G. G. eEdE-81
Salamon, N. EdE-41, EE-72, eEdE-05, eEdE-138, eEdE-156, eEdE-75, eEdE-81, eP-244, O-304, O-390, O-475
Salehi, B. O-396
Salehian, B. eP-116
Saleme, S. O-271, O-273
Salmon, C. E. G. eP-13, eP-9
Saloner, D. O-102, O-561
Saltz, J. O-284
Saltz, J. H. O-211
Salvador, E. eP-25, eP-43
Salzman, K. L. O-538
Sam, K. O-105
Samant, R. EdE-73, EdE-74, eEdE-83, eP-256
Samant, R. S. eP-65
Samdani, A. eP-262, O-438
Samim, M. EdE-07, eEdE-01
Sampathu, D. M. eEdE-161
San Millan, D. EE-31
San Millán, D. EE-37a
Sanchez, P. O-431
Sandercock, P. O-43
Sanders, W. eEdE-82, eP-161, eP-179

Index of Program Participants

Numbers refer to session and presentation numbers, *not to page numbers*.
Index Key: O = Scientific Paper (Oral Presentation); EE = Electronic Excerpta e;
P = Scientific Poster (Print Format); eP = Electronic Scientific Poster (ePoster);
EdE = Education Exhibit (Print Format); eEdE = Electronic Education Exhibit

Sandulache, V. C. O-485
Sanelli, P. O-61, P-52
Sanelli, P. C. O-294, O-472, O-494
Sanghvi, T. S. EdE-10, EdE-45
Santarosa, C. O-283, O-540
Santi, M. EdE-77
Santos, A. C. eP-13, eP-9
Santos, M. eP-48
Santos, M. O-227
Santucci, A. eP-270
Saran, N. eP-275, P-114
Sargar, K. eEdE-100, P-81
Sargsyan, A. eP-128
Sarkar, S. N. O-42a
Sarmiento, M. eP-199
Sarnat, H. B. O-321
Sasai, K. P-23
Satake, M. eP-114
Sathyan, P. eP-130, eP-132
Sato, K. eP-30
Sato, K. P-23
Sato, S. eEdE-146
Sato, T. O-122, O-219, O-63
Sato, T. P-75
Sato, Y. eEdE-100, eEdE-135
eEdE-141, eEdE-146, eEdE-154, P-81
Satow, T. eP-167
Sattin, J. eP-55, O-502, P-64
Sauer, D. EE-48
Savage, J. O-160
Savino, M. R. O-428
Saygi, S. eP-218
Sayre, J. O-475
Scarpace, L. eP-52, O-292, P-107
Schabel, A. O-523
Schaefer, P. EdE-21, EdE-25, O-245, O-255
Schaefer, P. W. O-389
Schapiro, M. eP-257
Schatz, M. eEdE-95
Scheer, I. eP-235
Schellingerhout, D. EdE-39, eP-107, eP-290
eP-296, eP-77, O-282
O-402, O-70
Schenning, R. C. EE-67
Scher, D. J. EdE-53
Scheri, R. P. O-415
Schindler, A. O-499
Schindler, J. eEdE-01
Schlamann, M. eP-171, eP-172, O-299
Schlemmer, H.-P. O-391, O-503
Schlobohm, K. O-67
Schmid, E. eP-192, eP-195, eP-209
Schmidt-Wilcke, T. O-40
Schmiedeskamp, H. O-205
Schmit-Hoffman, J. O-536
Schmitt, J. eP-263
Schneider, A. eEdE-95
Schneider, E. O-215
Schnell, S. O-295
Schob, S. eP-34
Schoeneman, S. E. EE-63, EE-73, eP-258
Schönland, S. O-71
Schramm, P. O-51
Schranck, F. O-66
Schreibmann, E. O-290
Schuette, A. eP-168
Schuff, N. O-213, O-572
Schularick, N. eEdE-88
Schulder, M. O-64a
Schultz, K. EdE-73
Schultz, L. eP-52, eP-53, eP-56
Schultz, T. O-40
Schwamm, L. H. eP-97
Schwartz, K. eP-265
Schwartz, K. M. O-252
Schwartz, M. O-274
Schwartz, R. O-106
Schweickert, P. eP-166
Schweitzer, A. D. O-212, O-494
Scoffing, D. O-25
Scoggins, M. O-473
Scott, C. J. EdE-67, EE-30, EE-58
Scott, H. D. EE-6
Sedrak, P. P-79
Seedial, S. O-212
Seeger, C. eP-79
Segal, A. Z. O-472
Segall, H. eEdE-169
Segall, H. D. eEdE-143
Seibert, T. eEdE-158
Seider, T. eP-48
Seidl, R. eP-237
Sekiya, K. eP-112, eP-114
Selden, N. R. eEdE-134
Senior, B. O-531
SENTIO Investigators Group eP-90
Seo, H. eP-38
Seo, S.-H. O-529
Seol, J. O-483
Sepahdari, A. EE-40
Sepulveda, J. eP-25
Seritan, A. O-27
Serre, I. O-226
Serulle, Y. O-220, O-23
Seshadri, R. EE-70, eP-109
Seth, R. EdE-51, EE-36
Sethi, V. eP-100, O-429
Setty, B. O-513
Severino, M. O-323
Seyama, G. eP-41
Sezaki, T. eP-20
Sha, S. J. eP-48
Shada, A. O-416
Shah, A. O-578

Index of Program Participants

Numbers refer to session and presentation numbers, *not to page numbers*.
Index Key: O = Scientific Paper (Oral Presentation); EE = Electronic Excerpta e;
P = Scientific Poster (Print Format); eP = Electronic Scientific Poster (ePoster);
EdE = Education Exhibit (Print Format); eEdE = Electronic Education Exhibit

Shah, G. V. eP-268
Shah, K. EdE-39, O-402
Shah, L. eP-297, O-136, O-523
Shah, L. M. eP-304, O-47
Shah, P. eP-100, eP-262, O-429
O-438, O-439, O-440
Shah, P. N. eP-127
Shah, R. R. eP-80
Shahbazi, M. O-212
Shahin, G. eEdE-82
Shahin, G. S. eP-179
Shahlaie, K. EE-22
Shaibani, A. EdE-51, EE-36, EE-63
EE-73, eP-36, O-225, O-228
O-229, O-277, O-504
Shaikh, H. EdE-42, eEdE-126
Shaltoni, H. eP-2
Shankar, J. EdE-29, eP-149, O-300
O-57, P-67
Shankar, J. J. S. eP-75, O-233, O-395, O-397
Shankaranarayanan, A. P-33
Shannon, P. eEdE-150, eP-227
Shapiro, M. eP-88
Shapiro, M. O-278
Sharifov, R. EdE-36
Sharma, M. O-227, O-496
Sharma, M. Chand. P-30
Shastri, R. EdE-18, EdE-55, EdE-92, eP-60
Shatzkes, D. EdE-60, EdE-61
Shebjam, S. O-401
Sheikh Bahaei, N. O-25
Sheitt, H. eEdE-90
Shen, C.-Y. P-24
Shen, P. eEdE-91
Shenkar, R. O-578
Shepherd, T. O-220, O-23
Shepherd, T. M. O-218
Sherin, C. O-245
Sherman, P. O-481
Sherr, E. P-17, P-19, P-22
Sherry, R. O-115
Shetty, T. O-426
Shewchuk, J. eEdE-102, eEdE-111
eEdE-113, eEdE-166
eEdE-179, eEdE-98
Shi, C. O-578
Shiau, C.-Y. O-272
Shibata, N. P-50
Shields, M. O-26
Shifrin, A. eEdE-155, O-550
Shigematsu, Y. eP-5, O-516
Shilpa, H. eP-256
Shim, H. O-290
Shim, J. P-74
Shimatani, N. O-108
Shimoji, K. P-23
Shimony, J. EdE-17
Shimony, J. S. O-505
Shimony, J. S. O-419
Shin, D. eEdE-59
Shin, N. Y. O-113, O-387
Shin, N.-Y. eP-118
Shinagawa, K. P-90
Shindo, M. EE-48
Shiodera, T. eP-78, O-581
Shiozaki, T. EdE-83
Shiraishi, K. eP-167
Shiroishi, M. eEdE-117, eEdE-121, eEdE-15
eEdE-173, eP-66, O-244
Shiroishi, M. S. EdE-28, eEdE-39, eEdE-52, P-37
Shonka, N. O-407
Shreiber, R. EdE-34, eP-91
Shreter, R. EdE-34, eP-91
Shrier, D. A. eEdE-67
Shroff, S. EdE-18
Shtilbans, A. O-212
Shu, H.-K.G. O-290
Shukla, G. P-30
Shulman, M. B. O-218
Sicular, S. eEdE-120, eEdE-125, eEdE-145
eEdE-157, eEdE-46, eEdE-96
Siddiqui, A. eP-232
Siegelman, J. R. Q. W. eP-141
Siemonsen, S. O-232
Silbergleit, R. EdE-24
Sillman, J. eEdE-115
Silva, C. F. EE-59
Silva, E. EdE-82
Simms, H. N. eP-155
Simpkin, W. P-67
Simpson, S. O-505
Sinanaj, I. O-216
Singh, A. eEdE-100, P-81
Singh, A. K. eEdE-135, eEdE-146, eEdE-154
Singh, J. EdE-87
Singh, V. eEdE-73
Sinha, R. O-517
Siotto, P. O-501
Siripurapu, R. eEdE-170, eEdE-78, eEdE-80
Sitartchouk, I. O-125
Sitton, C. W. EE-27
Sivasundaram, L. eEdE-39
Skinner, H. D. O-485
Sklar, E. O-522
Slasky, S. E. EE-5
Slezak, M. eP-267
Sloan, A. E. O-207
Slone, H. W. eEdE-70
Smith, C. M. eP-258
Smith, J. O-38, O-421
Smith, M. EdE-42, eEdE-126
Smith, M. O-145
Smith, P. W. O-416
Smith, T. eP-189

Index of Program Participants

Numbers refer to session and presentation numbers, *not to page numbers*.
Index Key: O = Scientific Paper (Oral Presentation); EE = Electronic Excerpta e;
P = Scientific Poster (Print Format); eP = Electronic Scientific Poster (ePoster);
EdE = Education Exhibit (Print Format); eEdE = Electronic Education Exhibit

Smittkamp, C. eEdE-168, eEdE-85
Smittkamp, C. A. O-524
Smoker, W. eEdE-85
Smoker, W. R. K. eEdE-86, eEdE-92
Smoker, W. R. K. eEdE-73
Smyth, G. eP-155
Snead, O. O-145
Sneade, M. eP-163, O-103, O-94
Snyder, A. Z. O-419
Sodagari, F. eP-124
Sogabe, T. eP-41
Soh, C. eP-249
Sohn, B. eP-119
Sohn, C.-H. eP-31, O-297, O-533, P-88
Soize, S. O-226
Solomon, D. P-47
Solomon, D. L. O-476
Solomon, M. A. O-476
Soltanolkoltabi, M. EE-63, EE-73, O-277
Soltanolkotabi, M. O-225, O-228, O-229, O-504
Som, P. eEdE-106, eP-142
Somashekar, D. K. eP-259
Soul, J. O-432
Sourour, N. eP-182, eP-294, P-91
Sourour, N. A. O-101
Spampinato, M. eP-138, O-123, O-400
Spann, B. M. O-235
Sparacia, B. O-547
Sparacia, G. O-547
Spear, D. eEdE-12
Spearman, M. P. eEdE-16
Speckter, H. eP-260
Spelle, L. eP-185
Sperber, W. eP-209
Sperling, S. O-34
Spiotta, A. eP-176, eP-291
Spirer, D. J. P-14
Spokoyny, I. P-63
Srinivasan, A. eEdE-101, eEdE-51, eEdE-94
Srivastava, D. eP-270
Srivastava, V. eP-228
Stamoulis, C. O-432
Stanton, C. L. eP-88
Starkey, J. eEdE-33, O-572
Staub, F. O-72
Staudt, M. O-321
Stecco, A. EE-18, eP-58, O-480
Steele, J. O-282, O-485
Steeman, R. R. M. P-15
Stefani, T. eP-72
Stefanski, P. eP-86, O-497
Stein, J. M. EdE-77, eEdE-165
Stein, J. M. eP-304
Steinklein, J. O-64a
Steinklein, J. M. eEdE-122a
Steinmetz, M. P. eP-281
Stemmer-Rachamimov, A. O-146
Stence, N. V. eP-250, eP-255, O-320, O-434
Stenzel, F. O-239
Stern, B. eEdE-28
Steven, A. eEdE-28, O-161
Stewart, D. O-66
Stickney, K. P-107
Stieg, P. E. O-472
Stippich, C. O-239
Stitzel, J. O-512
Stitzel, J. D. eP-229
Stivaros, S. O-517
Stivaros, S. M. EdE-79, eP-233, eP-249
Stoeter, P. eP-260
Stokum, C. eP-164
Stork, L. EE-48
Storm van's Gravesande, K. eP-237
Stormann, J. O-42a
Stout, C. eP-193, O-555
Stout, C. E. eP-184
Støverud, K. H. O-130
Straka, M. O-205
Stranjalis, G. eP-57
Strathearn, L. P-67
Strominger, Z. P-19
Strother, C. eP-203
Struffert, T. eP-198, eP-203
Stufflebeam, S. O-139
Stufflebeam, S. M. O-404
Stufflebeam, S. M. O-146
Su, J. O-55
Suarez, K. P-80
Subramanian, S. EE-39, eEdE-169
Suddarth, B. O-176
Suemitsu, M. eP-112, eP-114
Sugimoto, H. EE-53
Sugiyama, K. P-105a
Suh, C. eP-76, O-562
Suki, D. P-39
Sullivan, J. C. EdE-35
Sullivan, S. E. P-92
Sun, W. eP-81, O-580
Sunaert, S. EE-26
Sundblad, A. EE-24
Sundell, K. P-20
Sundgren, P. C. O-40
Sundgren, P. C. M. P-43
Sung, E. EE-53
Sunshine, J. L. eEdE-18, eP-204
Supakul, N. eEdE-133
Supanich, M. eP-141
Supanich, M. P. eP-161
Supsupin, E. P. eEdE-128
Sure, U. eP-171, eP-172, O-299
Suri, A. K. O-482
Suri, J. eP-45, eP-45, eP-51
Suri, J. S. O-501, O-52
Suwa, A. eP-1

Index of Program Participants

Numbers refer to session and presentation numbers, *not to page numbers*.
Index Key: O = Scientific Paper (Oral Presentation); EE = Electronic Excerpta e;
P = Scientific Poster (Print Format); eP = Electronic Scientific Poster (ePoster);
EdE = Education Exhibit (Print Format); eEdE = Electronic Education Exhibit

Suzuki, M. eP-30, P-23
Suzuki, T. eP-169
Swarnkar, A. eP-278
Swarnkar, A. S. EdE-80
Swartz, R. O-44
Swearingen, B. EdE-25
Sych, N. S. P-13
Sychra, V. O-100
Sydnor, M. K. eP-157
Symons, H. eP-223
Symons, S. P. eP-98
Symons, S. P. O-44
Sze, G. eP-282, O-414
Szikora, I. O-100
Szimacsek, M. eP-237
T
Tabarki, B. eP-236, eP-49
Tabesh, A. O-123, O-400
Tadanori Tomita, T. EE-73
Taeshineetanakul, P. O-274
Taheri, M. R. EdE-53
Tailor, D. R. eP-80, O-234
Takahashi, Y. eP-173, eP-208, eP-39, O-231, O-48
Takao, H. eP-169, eP-264
Takayasu, T. P-105a
Takechi, A. eP-41
Takeguchi, T. eP-78, O-581
Talekar, K. EE-88
Talkad, A. P-94
Tam, M. ,
Tamargo, R. J. EE-37a
Tampieri, D. eP-150, P-3, P-87
Tamrazi, B. eEdE-58, eP-301
Tan, E. O-215, O-222
Tanabe, J. L. O-241, O-36
Tanabe, M. eP-122
Tanaka, H. O-111
Tanaka, N. O-139
Tanaka, Y. EdE-23
Tanaka, Y. eP-64
Tanenbaum, L. O-576, O-580, O-66
Tanenbaum, L. N. O-379a
Tanenbaum, L. N. EdE-30
Tanenbaum, L. N. O-579
Tang, E. R. O-513
Tang, V. eP-249
Tang, Y. O-176
Tang, Y. O-300
Tantawy, A. eP-11
Tantiwongkosi, B. EdE-09, eEdE-95
Tanwar, M. O-64, P-46
Tanweer, O. O-278
Tarabishy, B. eEdE-27
Tarapore, P. E. eEdE-20, O-37
Tarulli, E. O-103
Tassone, F. O-27
Tateishi, H. eP-29, eP-94
Tateshima, S. eP-169
Tatum, L. S. O-282
Tatum, S. A. EdE-80
Tavares, F. C. O-564, P-55
Taylor, T. R. P-59
TCGA Glioma Phenotype Research Group eEdE-30, O-211, O-539
Teistler, M. eEdE-158
Teixeira, M. Jacobsen. O-423
Tekes, A. eP-235, eP-248, O-433
Telford, R. EdE-06
Telischak, N. eP-181
Tenenbaum, M. eEdE-176
Tenenbein, R. O-119
Teng, M. O-223
Terada, H. EE-49
Terbrugge, K. O-274
terBrugge, K. G. O-419
Terreni, M. Rosa. O-283, O-540
Thaker, A. A. EdE-12
Thakur, M. O-520
Thakur, S. O-220, O-23
Thawait, G. K. O-128, P-111
Thawait, S. K. O-128, P-111
The Alzheimer's Disease Neuroimaging Initiative eP-10
The IMS Investigators eP-37
The TCGA Glioma Phenotype Research Group O-284
Theesen, H. eP-161
Thibert, R. O-317
Thiele, E. eP-261
Thiele, E. A. O-315
Thielen, K. R. P-105
Thomas, A. eP-181
Thomas, A. O-306
Thomas, R. O-205
Thompson, A. F. eEdE-139, eEdE-140, eEdE-92
Thompson, G. O-542
Thompson, L. O-36
Thompson, L. L. O-241
Thompson, M. M. eP-229, O-512
Thompson, P. eEdE-164
Thompson, P. M. P-8
Thompson, W. O-21, O-29, O-31
Thornhill, R. eP-86, O-497
Thornton, F. J. O-56
Thornton, J. O-28
Thuahnai, S. T. eEdE-41
Thurlow, P. C. eEdE-123, eEdE-37, O-171
Thurnher, M. M. O-116
Tian, W. eP-50, O-202, O-399, O-408
Tihan, T. eEdE-33
Tillisch, K. O-479
Timchenko, O. O-299
Timothy, K. J. eP-298
Timpone, V. EdE-21
Ting, W.-Y. O-272

Index of Program Participants

Numbers refer to session and presentation numbers, *not to page numbers*.
Index Key: O = Scientific Paper (Oral Presentation); EE = Electronic Excerpta e;
P = Scientific Poster (Print Format); eP = Electronic Scientific Poster (ePoster);
EdE = Education Exhibit (Print Format); eEdE = Electronic Education Exhibit

Tintore, M. eP-62
Tisnado, J. eP-157
Tisnado, J. eP-157
Tiwari, R. eEdE-135, eEdE-146, eEdE-154
Toaff, J. EE-10
Todeschini, A. O-76
Todo, G. EdE-83
Togao, O. eP-129, P-84
Toh, C. eP-17, P-41
Toh, C. Hong. O-489
Tolat, P. eEdE-169
Tolete, P. O-220
Toma, S. O-216
Tomihara, M. EdE-83
Tomita, Y. P-50
Tomiyama, N. O-111
Tomlinson, G. A. eP-98
Tomm, A.-M. O-214
Tomsick, T. eP-37
Tong, F. eP-170, O-302, O-68, P-53
Tong, F. C. eP-168, O-58, O-62
Tonnelet, R. O-527
Toprak, H. eP-139, O-104
Torres, C. EE-75, eEdE-49, eEdE-62, eP-86
Torres, C. Ignacio. eEdE-22, eEdE-93
Torres, F. EE-12, eEdE-117, eEdE-121
eEdE-173, P-37
Tran, A. N. O-210
Tran, B. EE-56
Tregellas, J. R. O-241
Treiman, G. S. O-495
Trelles, M. O-499
Trevino, C. P-86
Trimble, C. R. eEdE-02, O-281
Trinh, H. O-140, O-141
Trinh, V. EdE-37, EdE-66, EE-66, O-163
Trobe, J. EdE-58
Troulis, M. eP-125
Troxell, M. L. EE-67
Truelsen, T. P-58
Trunet, S. O-166
Trunet, S. O-563
Truwit, C. O-109
Truwit, C. T. O-135
Tryggestad-Codispoti, K.-E. O-143
Trzepacz, P. P-20
Tsai, F.-Y. O-272
Tsai, N. T. eP-289
Tsai, N.-W. P-27
Tsai, T. O-555
Tsarfati, G. eP-241
Tseng, I. eP-282
Tseng, Y.-C. O-237
Tsien, C. P-43
Tsiouris, A. O-212
Tsiouris, A. J. EdE-75, O-426
Tsiouris, A. J. O-472
Tsuchiya, K. eP-29, eP-94, O-108
Tsuji, S. O-122, O-219, O-63
Tsukabe, A. O-111
Tu, R. K. EdE-81
Tuan, A. eEdE-97
Tuan, A. S. eEdE-118
Tuna, I. EdE-40
Turk, A. eP-199, eP-291, O-99
Turk, A. S. eP-176
Turner, R. eP-291
Turner, R. D. eP-176
Turski, P. eEdE-03
Turski, P. A. eEdE-92, O-56
Turski, P. A. O-575
Tustison, N. O-289
Twieg, D. B. O-45, O-50
Tyagi, V. O-220, O-23
Tyan, Y.-S. P-24
Tyc, R. O-207
Tymofiyeva, O. O-509, P-100
Tyndall, A. J. O-239

U

Uchida, M. EdE-23
Uchino, A. eEdE-112, O-492
Uchino, K. O-393
Ueda, I. O-122, O-219, O-63
Uetani, M. eP-108, eP-22, eP-3
Uggetti, C. eP-234
Ulmer, J. eEdE-61
Ulmer, J. L. eEdE-17
Ulmer, J. L. EdE-40, EdE-49
Umetsu, A. EdE-33, P-60
Umino, M. eEdE-23, eP-1, eP-4
Unal, S. EE-54
Underwood, M. L. O-282
Uno, T. eEdE-87
Upadhyay, N. EE-70
Urban, J. E. eP-229, O-512
Urdaneta-Moncada, A. R. EE-32, eP-147
Uribe Acosta, T. E. O-526
Urrutia, V. O-251, O-253
Utukuri, P. eEdE-85a
Uy, M. eP-15

V

Vachhani, J. P-94
Vagal, A. eP-89
Vagal, A. S. eEdE-63
Vajtai, P. L. EE-67
Vakil, P. eP-36, eP-84, O-295, O-301, P-61
Valencia, H. EE-64
Valentino, J. EdE-57
Valladares Otero, A. eEdE-84
Vallee, P. eP-267
van der Bom, I. M. J. eP-6
van der Knaap, M. S. eP-233
van Eeghen, A. M. O-315
Van Hemert, R. EdE-73, EdE-74, eEdE-83, eP-256, eP-65

Index of Program Participants

Numbers refer to session and presentation numbers, *not to page numbers*.

Index Key: O = Scientific Paper (Oral Presentation); EE = Electronic Excerpta e; P = Scientific Poster (Print Format); eP = Electronic Scientific Poster (ePoster); EdE = Education Exhibit (Print Format); eEdE = Electronic Education Exhibit

Van Slyke, P. O-574
VandenBerg, S. R. O-546
Vannest, J. eP-257
Vanslooten, A. eP-53, eP-56
Varallyay, C. G. eP-73, O-286, O-405
Vasani, D. EE-71
Vattoth, S. EdE-06, EdE-15, EdE-35
Vavla, M. P-7
Vavricek, J. O-247
Vavro, H. O-490
Velásquez, J. P-16
Vella, M. eP-201
Venkatesh, R. M. EE-29, eEdE-13
Verdolotti, T. eP-216
Verdoorn, J. T. eEdE-08
Viamonte, C. A. O-486
Vichaya, E. G. eP-296
Vidal, L. L. M. eEdE-18, eEdE-26, eP-204, O-279
Vigen, K. K. O-56
Vij, G. O-415
Vilchez, C. eP-260
Viljoen, S. O-524
Villablanca, J. P. EE-86
Villablanca, J. Pablo. EE-78, EE-84
Villanueva-Meyer, J. P-33
Vincent, A. eP-178
Vinson, E. N. eP-302
Vinuela, F. eP-169, eP-264, O-303
Viry, F. O-582
Viswanadhan, N. eEdE-156a
Vitali, P. P-5
Volny, O. eP-197
von Kummer, R. O-43
von Kummer, R. P-58
von Ritschl, R. EE-55, EE-56
Vora, A. P. P-1
Vora, L. eP-116
Vos, S. B. eP-79
Voss, J. O-33, O-39
Vossough, A. EdE-77, eEdE-151, eEdE-155, O-550

W

Wada, A. P-21
Wagshul, M. E. O-482
Wainwright, M. S. eP-258
Wakahiro, M. P-19, P-22
Wakhloo, A. eP-181
Wakhloo, A. K. EE-59, eP-165, eP-205, eP-207, eP-6
Walczak, P. O-59
Walker, B. S. O-47
Walsh, E. G. O-45, O-50
Wang, A. P-43
Wang, A. Ming. EE-4
Wang, A.-M. EdE-24
Wang, B. EE-21, O-167
Wang, H. O-408
Wang, H.-C. P-27
Wang, H.-Y. EE-50
Wang, J. eEdE-05
Wang, J. P-39
Wang, J. C. eP-281
Wang, K. O-56
Wang, P. O-40, P-43
Wang, S. EE-12
Wang, S. eP-26
Wang, W.-H. O-237, O-42
Wang, W.-T. O-424
Wang, X. O-508
Wang, Y. eEdE-44
Wang, Y. eP-31, eP-33, O-122, O-212, O-219
Wang, Y. O-63
Wang, Y. Y. eEdE-139, eEdE-140
Wang, Y.-H. O-276
Ward, T. J. eEdE-125, eEdE-145 eEdE-157, eEdE-46, eEdE-96
Wardlaw, J. M. O-43
Warren, D. J. EE-13, eEdE-131
Warren, M. O-46
Warren, R. F. O-426
Warshall, C. O-64a
Wasliewski, M. O-295
Wasserman, B. A. EdE-52
Watanabe, K. eP-93, O-122, O-219, O-63
Watanabe, M. eP-214
Watanabe, Y. O-111
Watanabe, Y. P-105a
Watcharotone, K. O-514
Waters, J. O-571
Watson, R. E. EdE-31, P-108
Watts, R. O-118, O-236, O-67
Wei, K.-C. eP-17, P-41
Wei, L. O-58, O-62, P-53
Wei, S. O-56
Wei, X.-C. O-321
Weiler, M. O-74, O-75
Weill, A. O-275
Weinberg, J. S. P-39
Weiner, M. O-213
Weiner, M. O-46
Weinstein, G. O-525
Weisman, N. eEdE-124
Weisman, N. J. EdE-02, O-520
Weiss, L. O-426
Weisz, B. eP-241
Welker, K. M. P-108
Well, D. eEdE-106
Welsh, R. C. O-22, P-10
Welter, J. EdE-26
Weng, J.-C. P-24
Weprin, L. S. O-164
Werner, J. D. eP-136
Wessman, B. P-107
Wheless, J. W. O-147
Whisenant, J. T. eP-206, P-93
White, M. L. EE-65, eEdE-60, O-407

Index of Program Participants

Numbers refer to session and presentation numbers, *not to page numbers*.
Index Key: O = Scientific Paper (Oral Presentation); EE = Electronic Excerpta e;
P = Scientific Poster (Print Format); eP = Electronic Scientific Poster (ePoster);
EdE = Education Exhibit (Print Format); eEdE = Electronic Education Exhibit

White, M. L. EE-20
White, N. S. O-546
White, P. eP-163, eP-178
White, P. M. eP-186, eP-202
Whitehead, M. T. eEdE-116, eP-145 eP-243, eP-247, O-147 O-316, O-435, O-437
Whitlow, C. T. eP-229, O-512
Whittemore, A. EdE-85
Wick, W. O-204
Widjaja, E. eP-225, O-145
Wiestler, B. O-204
Wiggins, R. O-136, O-523, O-528
Wiggins, R. H. eP-134
Wijtenburg, S. A. O-243
Williams, C. eP-163
Williams, F. O-319, O-325, O-557, O-560
Williams, R. eP-177
Williams, S. eP-281
Williams, S. C. O-177
Williamson, K. M. eEdE-70
Wilms, G. E. R. EE-26
Wilner, A. , , P-35
Wilseck, J. eEdE-12
Wilson, B. eEdE-12
Wilson, F. O-566
Wilson, M. O-473
Wilson, S. eP-205
Wilson, S. O-524
Wing, L. EE-15, P-29, P-77
Winston, L. O-69
Wintermark, M. eEdE-30
Wintermark, M. eP-269, O-284, O-289 O-292, O-34, O-416, O-539
Winters, R. R. EE-60
Wippold, F. eEdE-160, eEdE-42
Wirtz, D. C. O-312, O-313, P-110
Witkosky, M. EE-35
Witte, M. M. P-20
Wnuk, N. O-484
Wo, S. O-309, O-425
Wojak, J. eEdE-72
Wolosker, A. Maria. Borri. P-12
Wong, A. EE-32, EE-46
Wong, H. Fai. O-489
Wong, H.-F. eP-17, P-41
Wong, T. O-105, O-392
Woo, H. eP-199
Wood, C. P. O-252
Wood, C. P. P-108
Wood, C. P. eP-298
Wood, C. P. P-105
Woodworth, D. C. O-401, O-541
Wostrack, M. O-93
Wright, B. W. O-24
Wright, D. O-494
Wright, N. eP-249
Wright, R. O-514
Wrubel, G. L. EE-47
Wu, A. eP-135
Wu, C. O-301
Wu, C.-C. eP-188
Wu, C.-H. P-2
Wu, H.-M. O-223
Wu, J. O-525
Wu, S. O-570
Wu, T. eP-7
Wu, T.-H. O-573
Wu, X. O-536
Wu, Y. O-575
Wu, Y.-M. eP-17
Wu, Y.-M. P-41
Wunderlich, S. O-224
Wycliffe, N. P-102
Wycliffe, N. D. P-80

X

Xi, W. O-416
Xie, J. eP-50
Xin, W. O-289
Xu, D. O-509, P-100

Y

Yaeger, K. O-422
Yakes, W. F. eP-146, eP-212, eP-213
Yam, B. L. eEdE-77
Yamada, M. eP-167
Yamada, S. eP-59, eP-78, O-581
Yamahata, T. eP-1
Yamamoto, K. P-21
Yamamoto, T. eP-78, O-581
Yamasaki, F. P-105a
Yamashita, K. eP-129, P-84
Yamashita, Y. eP-33, eP-5
Yamashita, Y. eP-78
Yamashita, Y. O-516
Yamashita, Y. O-581
Yamawaki, S. eP-54
Yan, Z. EE-16
Yañez, A. eP-277
Yang, C.-W. P-51
Yang, C.-Y. P-11
Yang, C.-Y. P-54
Yang, J. eEdE-72
Yang, L. eP-259
Yang, Z. EE-1, eP-196
Yarnold, J. O-94
Yavin, D. O-165
Yazbek, S. eEdE-152, eEdE-156a, O-149
Ye, H. EE-1, eP-196
Yeoh, C. O-215
Yetis, H. eP-139
Yetkin, Z. F. EE-6
Yevich, S. M. EE-57
Yi, K. eP-42, P-66
Yıldız, S. eP-139

Index of Program Participants

Numbers refer to session and presentation numbers, *not to page numbers*.

Index Key: O = Scientific Paper (Oral Presentation); EE = Electronic Excerpta e; P = Scientific Poster (Print Format); eP = Electronic Scientific Poster (ePoster); EdE = Education Exhibit (Print Format); eEdE = Electronic Education Exhibit

Yilmaz, U. eP-200
Ying, H. eP-101b
Ying, H. O-564
Ying, S. eEdE-06, O-240
Yokota, H. eEdE-87
Yokoyama, H. eP-167
Yokoyama, K. eP-30
Yokoyama, R. eP-40
Yoneda, T. O-516
Yoo, A. J. O-389
Yoo, B. EE-78, EE-84
Yoo, B. Y. EE-86
Yoo, I. O-297, P-88
Yoo, W. eP-111
Yoo, W.-J. eP-152
Yoon, T. O-297, P-88
Yoon, W. eP-158, eP-159, eP-160
Yoshida, M. eP-30
Yoshida, S. P-99
Yoshida, Y. EdE-23
Yoshimura, R. eP-93
Yoshiura, T. eP-129, P-84
Yoshiya, K. O-111
You, K. P-42
Youn, S. eP-187, O-107
Young Poussaint, T. O-436
Young, B. O-502
Young, B. M. P-64
Young, R. O-543
Young, S. J. EdE-10, EdE-45
Young, W. L. O-102
Yousem, D. M. eP-143, O-251, O-253, O-564
Yousry, T. O-28
Yu, E. eP-142, O-413
Yu, F. eEdE-95, O-407
Yu, J. eP-106
Yu, L. P-105
Yu, P. P-20
Yuan, W. O-505
Yuh, E. eEdE-58
Yui, M. eP-78, O-581
Yun, J. O-201
Yun, T. eP-31
Yun, T. O-533

Z

Zaccagna, F. EE-15, P-29
Zacharia, B. E. EE-90
Zagzag, D. , O-570, P-35
Zaharchuk, G. O-112, O-205, O-49
Zakalik, K. EE-52
Zaman, O. O-518
Zamora, C. O-433
Zamora, C. A. eP-248
Zan, E. O-251, O-253, O-564, P-55
Zanation, A. O-531
Zaninotto, A. Luiza. Costa. O-423
Zaza, A. O-521
Zee, C. eP-66
Zeineh, M. M. O-55
Zeng, H. eP-55
Zessler, A. eP-63
Zhang, B. O-144
Zhang, L. O-120
Zhang, M. O-32
Zhang, N. eP-270
Zhang, X. O-62
Zhang, Y. EE-1
Zhang, Y. EE-65
Zhang, Y. eP-196
Zhang, Y. eP-269
Zhang, Y. O-407
Zhang, Y. J. O-293
Zhang, Z. O-543
Zhao, B. O-201, O-548
Zhao, L. O-578
Zheng, K. O-212
Zhong, J. O-202
Zhou, Y. O-218
Zhou, Y. O-428
Zhu, H. O-141
Zhu, X. O-393
Ziegler, J. eP-147
Zimmel, L. eP-197
Zimmer, C. O-224, O-232
Zimmerman, D. P-113
Zimmerman, M. O-38
Zimmerman, M. E. O-421
Zimmerman, R. A. EdE-77
Zimmerman, R. A. O-550
Zimmerman, R. A. eEdE-155
Zimmerman, R. D. O-426
Zimmerman, R. D. O-472
Zinn, P. O. eP-130, eP-132 O-285, O-539, O-545
Ziv, E. O-509, P-19, P-22
Zlotchenko, G. EdE-60, EdE-61
Zohrabian, V. EdE-48, eEdE-175, O-137
Zohrabian, V. M. eEdE-54, O-248
Zöllei, L. eP-221
Zoltani, Z. EdE-48, eEdE-175, eEdE-54, O-137
Zoltani, Z. A. O-248
Zomorodi, A. eP-189
Zou, P. O-473
Zuberi, A. eP-123
Zuccoli, G. eP-232, eP-236, eP-251, eP-49
Zulian, G. O-214
Zumofen, D. O-278
Zun, Z. O-49
Zwicker, J. EE-75